Acta Chemica Scandinavica A 30 (1976) 1—7

Hexamethylphosphoramide as Proton Acceptor. Part 1. A Near-infrared Study of Its Heteroassociation with Ordinary and Halogenated Alcohols

RITVA KUOPIO,[a] ANTTI KIVINEN[a] and JUHANI MURTO[b]

[a] Department of Pharmacy, University of Helsinki, Fabianinkatu 35, SF-00170 Helsinki 17, Finland and [b] Department of Physical Chemistry, University of Helsinki, Meritullinkatu 1 C, SF-00170 Helsinki 17, Finland

Values of the formation constants K_{11}, frequency shifts $\Delta\nu$OH and thermodynamic parameters ΔH, ΔG and ΔS have been determined by near-infrared spectrometry for the hydrogen-bonded 1:1 alcohol-base complexes formed between fifteen ordinary or halogenated alcohols and hexamethylphosphoramide and for the phenol-hexamethylphosphoramide complex in carbon tetrachloride solutions.

The pK_a values of the alcohols studied vary from about 19 to about 5, the most acidic alcohols being the two perhalogenated *t*-butyl alcohols. The spectrometric quantities K_{11}, ΔH and $\Delta\nu$OH vary almost linearly with the acidity of the alcohols, although the slopes for ordinary and for halogenated alcohols are slightly different. The complexation entropies for the different alcohol-base pairs are quite similar in magnitude, *i.e.*, the systems are essentially isoentropic. The frequency shifts vary with temperature. The Badger-Bauer relation holds with a few small deviations. In the case of the most acidic alcohols and the phenol there are several hydrogen-bonded OH absorption peaks, probably due to the interaction of νOH(bonded) vibrations with overtones or combinations of lower frequency vibrations.

Hexamethylphosphoramide, $[(CH_3)_2N]_3PO$ (HMPA), is a dipolar, aprotic solvent with excellent solvent properties.[1-4] In addition, HMPA has some interesting biological properties, which are not so widely known as its excellent solvent properties. HMPA has been considered as possibly the most suitable model compound for the study of certain anticancer (cytostatic) drugs and the general mechanism of chemosterilation.[5-8] The acute [9] as well as the chronic [10] toxicity of HMPA seems to be low.

The importance of hydrogen bonding in biological systems is nowadays generally recognized.[11,12] In addition to the carbonyl group, also the P=O group is a very efficient proton acceptor in these systems. The experimental data on the P=O group are still meagre, however. In this paper we wish to report the results obtained for the hydrogen bonding between HMPA and various alcohols and phenol, special attention being directed to the effects of the acidity and steric factors of alcohols and phenol.

EXPERIMENTAL

Chemicals. Hexamethylphosphoramide (zur Synthese, E. Merck AG) was refluxed under vacuum over CaO for about 20 h, decanted and distilled, b.p. 80 °C/2 mmHg. HMPA was stored over molecular sieves 4Å. Hexamethylphosphoramide-d_{18} [octadecadeuteriohexamethylphosphoramide, HMPA-d_{18}, $[(CD_3)_2N]_3PO$ (Uvasol, E. Merck AG)] was used as received. It was stored under nitrogen.

2,2,2-Tribromoethanol (*purum*, Fluka AG) and 1,1,1,3,3,3-hexachloro-2-propanol (Hynes Chemical Research Corp.) were crystallized from hexane. 2,2,2-Trichloroethanol (*purum*, Fluka AG) was distilled under vacuum, b.p. 87 °C/2 mmHg. 1,1,1-Trichloro-2-methyl-2-propanol (Ph. Nordica quality) contained about 5 % water, which was distilled away, after which the alcohol was sublimed at ordinary pressure. All other alcohols were purified as described previously.[13-17] The liquid alcohols were stored over molecular sieves 3A (methanol

Table 1. Spectral data for 1:1 hydrogen-bonded complexes between alcohols or phenol and HMPA in carbon tetrachloride at 25 °C and the pK_a values [16–22] of alcohols and phenol.

Alcohol [a] (Phenol)	K_{11} / M^{-1}	$-\Delta H°$ / kJ mol^{-1}	$\Delta\nu$ / cm^{-1}	pK_a	From literature $-\Delta H°$ / kJ mol^{-1}	From literature $\Delta\nu$ / cm^{-1}	
1 MeOH	39.0	22.8	275	15.09			
2 EtOH	30.5	19.8	271	15.93			
3 i-PrOH	21.2	19.0	263	17.1			
4 *t*-BuOH	16.0	17.6	252	> 19	23.8 [c]		
5 3-MP	9.77	17.2	242				
6 TBE	289	24.9	393	12.70			
7 TCE	406	26.1	396	12.25			
8 TFE	1230	34.2	394	12.39	32.1 [d]	405 [e]	
9 HCP	3960	33.5	> 553 [b]				
10 HFP	23600	37.3	> 519 [b]	9.3	41.4 [f]	540 [f]	
11 TCTB	64.8	21.3	357				
12 TFTB	199	24.8	372				
13 HFTB	4640	31.2	> 502 [b]	9.6			
14 TCHFB	20300	32.5	> 645 [b]	5.1			
15 PFTB	82600	40.5	> 651 [b]	5.4	43.9 [g]	770 [g]	
16 PhOH	1820	29.9	> 464 [b]	9.97	31.8 [c]	450 [h],	460 [i,j]

[a] 3-MP = 3-methyl-3-pentanol, TBE = 1,1,1-tribromoethanol, TCE = 1,1,1-trichloroethanol, TFE = 1,1,1-trifluoroethanol, HCP = 1,1,1,3,3,3-hexachloro-2-propanol, HFP = 1,1,1,3,3,3-hexafluoro-2-propanol, TCTB = 1,1,1-trichloro-2-methyl-2-propanol, $CCl_3(CH_3)_2COH$, TFTB = 1,1,1-trifluoro-2-methyl-2-propanol, $CF_3(CH_3)_2COH$, HFTB = 1,1,1,3,3,3-hexafluoro-2-methyl-2-propanol, $(CF_3)_2CH_3COH$, TCHFB = 2-trichloromethyl-1,1,1,3,3,3-hexafluoro-2-propanol, $CCl_3(CF_3)_2COH$, PFTB = perfluoro-*t*-butyl alcohol, $(CF_3)_3COH$, [b] complex band with several maxima, measured from the first maximum, [c] Ref. 23, [d] Ref. 24, [e] Ref. 25, [f] Ref. 26, [g] Ref. 27, [h] Ref. 28, [i] Ref. 29, [j] Ref. 30.

and ethanol) or 4A (other alcohols and CCl_4). It should be mentioned that the alcohols containing much chlorine are very hygroscopic.

Measurements. The near-infrared spectra were recorded on a Beckman DK-2A spectrophotometer equipped with a thermostated cell holder. The details of the measurements have been published previously.[13,17]

The IR spectra were recorded with a Perkin-Elmer 621 spectrometer at ambient temperature, using 5 mm cells with KBr windows (sealed cells from RIIC). The spectra of the alcohol-HMPA complexes in CCl_4 were scanned against HMPA in CCl_4. HMPA-d_{18} was also used as a proton acceptor to avoid the disturbing influence of the C–H stretching vibrations of HMPA on the hydrogen bonded OH stretching absorption.

Calculations were carried out as previously described.[17]

The $\Delta\nu$OH values are estimated to be accurate within $\pm 3-5$ cm^{-1}, ΔH values within ± 2 kJ mol^{-1} and K_{11} values within 10 %.

The non-SI units used were: 1 M = 1 mol dm^{-3}; 1 mmHg = 133.322 Pa.

RESULTS AND DISCUSSION

The experimental data obtained are presented in Table 1, which also contains the pK_a's of alcohols determined in water. The symbols used for the alcohols are explained in a footnote to Table 1. When the proton donor was an ordinary alcohol, TBE, TCE, TFE, TCTB or TFTB (for which the pK_a's are about 12 or greater), the absorption bands of the bonded νOH vibration were simple in form and the frequency shifts $\Delta\nu$OH were easy to estimate (see Fig. 1). No indication was found of the existence of a double maximum, frequently observed when the bonding occurs at the carbonyl group. This may be related to the fact that P=O groups are more polar than C=O groups. It has been estimated that in HMPA the P=O bond has about 50 % ionic character.[1,2,31,32] We assume that the hydrogen bonding occurs only to the lone pairs of oxygen of HMPA.

For complexes between the alcohols with pK_a values smaller than 12 or phenol and

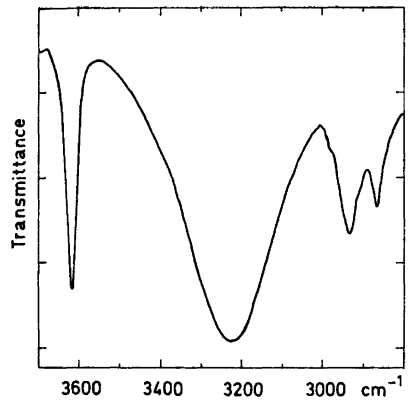

Fig. 1. Illustrative spectrum for the system TFE – HMPA-d_{18}. Solvent CCl_4, temperature ambient, 5 mm cells with KBr windows; concentrations: 0.0153 M TFE + 0.00772 M HMPA-d_{18}, 0.00772 M HMPA-d_{18} in the reference beam.

HMPA, the bonded OH absorption bands consist of several submaxima. Examples are the IR spectra of the HFP – HMPA and PFTB – HMPA complexes shown in Fig. 2. The existence of these submaxima is probably due to the coupling of νOH(bonded) vibrations with combinations or overtones of some other vibration of lower frequency. For the phenol – HMPA complex the substructure of the νOH-(bonded) band can be explained by assuming Fermi resonance between νOH(bonded) vibrations and suitable combination vibrations of the phenol.[33]

The free νOH absorption band of HFP, as of HCP, consists of two maxima (Fig. 2). In both cases the values of $\Delta\nu$OH were estimated from the higher frequency absorption peak.

For complexes with several νOH(bonded) absorption peaks only the lowest limit of $\Delta\nu$OH can be estimated (Table 1).

It has been stated that the values of $\Delta\nu$OH-(bonded) depend on the base concentration and, accordingly, a concentration-independent value should be determined by extrapolation to infinite dilution of the $\Delta\nu$OH values measured at varying concentrations.[34,35] For several alcohol – HMPA pairs the $\Delta\nu$OH's were measured by varying the concentration of HMPA. The small changes observed in $\Delta\nu$OH were within the range of experimental error. The values of $\Delta\nu$OH in Table 1 are unextrapolated values measured at relatively high dilution.

The values obtained in this work (Table 1) are in good accord with those reported in the literature. The only exception is the *t*-BuOH – HMPA system, for which the value of $-\Delta H°$, 23.8 kJ mol^{-1}, reported by Bogachev *et. al.*[23] is remarkably higher than our value. The value of Bogachev *et al.* appears too large when compared with $-\Delta H°$ values for other ordinary alcohols. The discrepancies in the $\Delta\nu$OH values for HFP, PFTB and phenol are explained by the fact that the absorption band of the complex is not simple and the $\Delta\nu$OH values are measured from different points in the spectra.

Acidity of alcohols and spectrometric quantities. Most studies of the influence of the acidity on hydrogen bond strength have been made

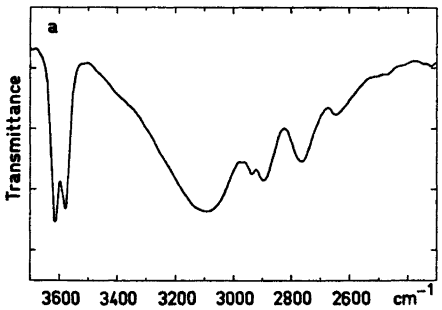

Fig. 2a. Illustrative spectrum for the system HFP – HMPA-d_{18}. Solvent CCl_4, temperature ambient, 5 mm cells with KBr windows; concentrations: 0.0186 M HFP + 0.00566 M HMPA-d_{18}, 0.00566 M HMPA-d_{18} in the reference beam.

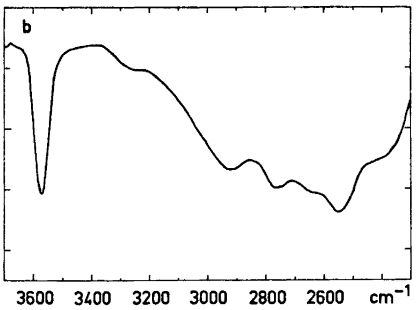

Fig. 2b. Illustrative spectrum for the system PFTB – HMPA-d_{18}. Solvent CCl_4, temperature ambient, 5 mm cells with KBr windows; concentrations: 0.0119 M PFTB + 0.00566 M HMPA-d_{18}, 0.00566 M HMPA-d_{18} in the reference beam.

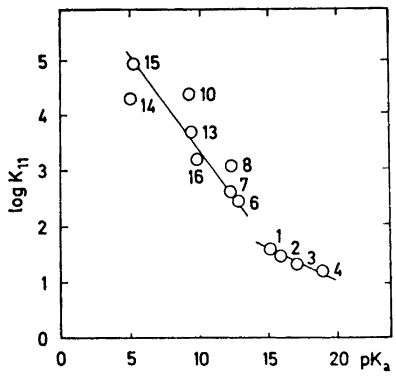

Fig. 3. The plot of log K_{11} against pK_a of the alcohol for the alcohol–HMPA systems at 25 °C.

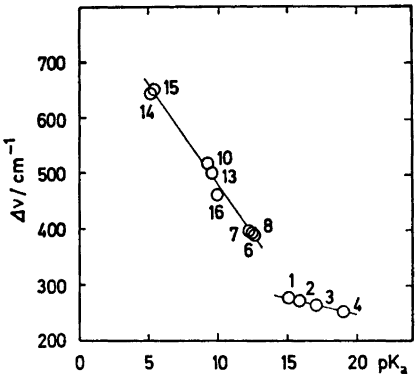

Fig. 4. The plot of $\Delta\nu$ against pK_a of the alcohol for the alcohol–HMPA systems at 25 °C.

with substituted phenols, for which the pK_a's can vary considerably. The pK_a values of ordinary alcohols vary only a few pK_a units and only recently have papers been published on more acidic alcohols. The influence of the acidity on the intermolecular (and intramolecular) hydrogen bonding has recently been reviewed by Rochester.[36] The Brønsted acidity can best be introduced in terms of the water acidity, pK_a, of the alcohols. Table 1 reveals that the more acidic an alcohol is, the more marked is the tendency to hydrogen bond. This usually leads to increased values of the spectrometric parameters K_{11}, $-\Delta H°$ and $\Delta\nu$OH.[20,37] In Figs. 3 and 4, K_{11} and $\Delta\nu$OH are plotted against the pK_a of the alcohols, and it can be seen that the dependence is linear in both cases. This is also true in the case of $-\Delta H°$. The slight scatter of a few points of K_{11} (and also of $-\Delta H°$) may be due to experimental inaccuracy inherent in the determination of these quantities. It seems, however, that the slopes for the ordinary alcohols differ somewhat from those for the halogenated alcohols. The situation is analogous to that found by Dierckx *et al.*[38] in their study on the influence of the acidity of proton donor on $\Delta\nu$OH values. They, too, obtained different slopes for phenols and for ordinary alcohols.

Our studies on the heteroassociation of substituted phenols with HMPA are in progress; preliminary results indicate that the behaviour of halogenated alcohols resembles more closely that of the phenols than that of the ordinary alcohols.

On the basis of the values of Figs. 3 and 4 we decided that the influence of steric effects on the hydrogen bonding is negligible.

Relations between spectrometric quantities. It has been stated that the value of $\Delta\nu$X–H is a better measure of the strength of a hydrogen bond than is K_{11} or ΔH.[39] This is true because, in the hydrogen-bonded system Z–X–H···Y–Z′, $\Delta\nu$X–H measures energetic changes in the formation of the hydrogen bond H···Y, while ΔH is a measure of the energies of different interactions between Z–X–H and Y–Z′. Also, recent force field calculations on hydrogen-bonded complexes indicate that $\Delta\nu$X–H is a good measure of the complex strength.[40] It is not therefore surprising that the Badger-Bauer relation, *i.e.* the linear dependence between ΔH and $\Delta\nu$OH, does not always hold. The experimental results obtained in this work and reproduced in Fig. 5 show the Badger-Bauer relation to be approximately valid.

The thermodynamic quantities for different alcohol–HMPA complexes are listed in Table 2. In many equilibrium and kinetic systems, ΔH is quite often found to be a linear function of ΔS. This relation is also common in the case of hydrogen-bonded systems. Thus Pimentel and McClellan[11] have discussed the significance of the ΔH *vs.* ΔS relation, and refer to cases in which the linearity of the enthalpy-entropy relation holds. The explanation given by Pimentel and McClellan[41] for hydrogen-bonded

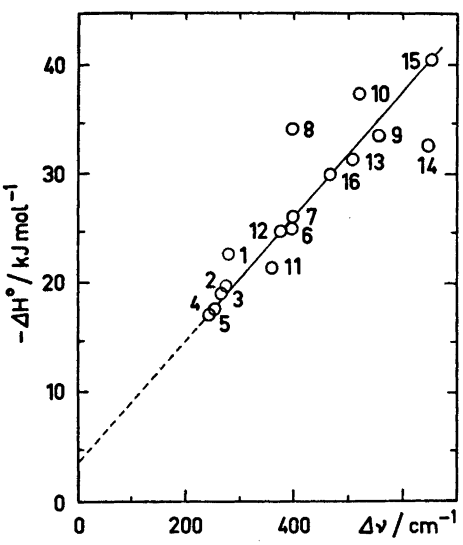

Fig. 5. The plot of $-\Delta H°$ against $\Delta\nu$ for the alcohol – HMPA systems at 25 °C.

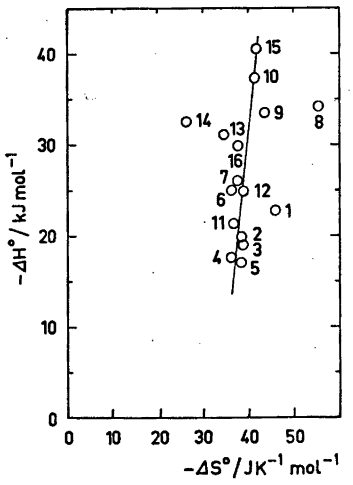

Fig. 6. The plot of $-\Delta H°$ against $-\Delta S°$ for the alcohol – HMPA systems at 25 °C.

systems, that "a higher value of $-\Delta H$ implies stronger bonding, with a more restricted configuration in the polymer, hence greater order leading to a larger value of $-\Delta S$", is widely cited.

In Fig. 6, $\Delta H°$ is expressed as a function of $\Delta S°$. We can see that the correlation, instead of being linear, illustrates rather the isoentropic case, *i.e.* ΔS values are roughly constant. There are only a few other systems, with substituted phenols as proton donors, where isoentropicity is also observed.[42–44]

Table 2. Thermodynamic quantities for 1:1 hydrogen-bonded complexes between alcohols or phenol and HMPA in carbon tetrachloride at 25 °C.

Alcohol (Phenol)	$-\Delta H°$ kJ mol^{-1}	$-\Delta G°$ kJ mol^{-1}	$-\Delta S°$ JK^{-1} mol^{-1}
MeOH	22.8	9.08	46.0
EtOH	19.8	8.45	38.2
i-PrOH	19.0	7.57	38.6
t-BuOH	17.6	6.86	36.2
3-MP	17.2	5.65	38.6
TBE	24.9	14.1	36.4
TCE	26.1	14.9	37.6
TFE	34.2	17.6	55.3
HCP	33.5	20.5	43.5
HFP	37.3	25.0	41.4
TCTB	21.3	10.3	36.8
TFTB	24.8	13.1	39.0
HFTB	31.2	20.9	34.6
TCHFB	32.5	24.6	26.4
PFTB	40.5	28.1	41.7
PhOH	29.9	18.6	37.7

At present, the experimental data are too meagre and to some extent too uncertain to allow us to decide whether there is any fundamental difference between those hydrogen-bonded acid-base systems that are isoentropic and those that are not. We expect, however, that the increase in order is of the same order of magnitude for most 1:1 hydrogen-bonded complexes when the geometries of the complexes are nearly the same, namely "linear" or open type configuration. This would favour isoentropicity. On the other hand, the stiffness of the complex, which increases with increasing hydrogen-bond strength, also affects the entropy term.

The double-scale enthalpy equation. Among many multiparameter equations for correlating acid-base behaviour the empirical double-scale enthalpy equation $-\Delta H = E_A E_B + C_A C_B$ proposed by Drago and Wayland [45] is perhaps the most useful in predicting the enthalpies of hydrogen-bond formation. Parameters E_A and E_B are interpreted as the susceptibility of the acid and base, respectively, to undergo electrostatic interaction; C_A and C_B are interpreted as the susceptibility of the acid and the base,

Table 3. The parameters E_A and C_A of alcohols and phenol, and experimental and calculated (see text) enthalpy values of the HMPA-proton donor systems. The E_B and C_B values of HMPA are 1.52 and 3.55, respectively.[47]

Alcohol (Phenol)	E_A	C_A	$-\Delta H°_{calc}$ / kJ mol^{-1}	$-\Delta H°_{exp}$ / kJ mol^{-1}
t-BuOH	2.04	0.300	17.4	17.6
TFE	3.88	0.451	31.4	34.2
HFP	5.93	0.623	46.9	37.3
PFTB	7.34	0.731	57.5	40.5
PhOH	4.33	0.442	34.1	29.9

respectively, to form a covalent bond.[45–48] Table 3 shows the experimental enthalpy values together with values calculated from the double-scale enthalpy equation using the parameters E_A and C_B (indicated in Table 3), which give the $-\Delta H$ values in the units of kcal mol^{-1}. It has been estimated that the difference between measured and calculated values should be less than 4 kJ mol^{-1} [45,46] (*cf.* also Ref. 44). In the present study the agreement is excellent for the *t*-BuOH–HMPA system and satisfactory for the TFE–HMPA and PhOH–HMPA systems. The marked difference between measured and calculated enthalpy values for HFP–HMPA and PFTB–HMPA systems may be attributed partly to the steric hindrance and partly to the high acidity, *i.e.*, strong hydrogen bonds of these alcohols. It has also been stated that because of the intramolecular hydrogen bonding in HFP and PFTB, one should add 4.6 kJ mol^{-1} and 4.2 kJ mol^{-1}, respectively, to the calculated negative enthalpy value.[47]

The values obtained in this study imply that the hydrogen bonding of halogenated alcohols resembles more closely the bonding of phenol than that of the ordinary alcohols. Work is in progress to obtain more information on the complexing of substituted phenols with HMPA.

REFERENCES

1. Normant, H. *Angew. Chem. 79* (1967) 1029.
2. Normant, H. *Russ. Chem. Rev. 39* (1970) 457.
3. Robert, L. *Properties and use of hexamethylphosphorotriamide*, Pierrefitte–Auby, Paris 1970.
4. Cox, B. G. and Parker, A. J. *J. Amer. Chem. Soc. 95* (1973) 408, and the references cited.
5. Chang, S. C., Terry, P. H. and Bořcovec, A. B. *Science 144* (1964) 57.
6. Bulyginskaya, M. A. and Vronskikh, M. D. *Russ. Chem. Rev. 39* (1970) 964, and the references cited.
7. Koshy, T. and Chandra, K. R. *J. Sci. Ind. Res. 31* (1972) 515.
8. Bořcovec, A. B. *Insect Chemosterilants*, Interscience, New York 1966.
9. Gaines, T. B. *Toxicol. Appl. Pharmacol. 14* (1969) 515.
10. Kimbrough, R. D. and Gaines, T. B. *Bull. Environ. Contam. Toxicol. 10* (1973) 225.
11. Pimentel, G. C. and McClellan, A. L. *Annu. Rev. Phys. Chem. 22* (1971) 347, and the references cited.
12. Vinogradov, S. N. and Linnell, R. H. *Hydrogen Bonding*, Van Nostrand-Reinhold, New York 1971, Chapter 9.
13. Kivinen, A. and Murto, J. *Suom. Kemistilehti B 40* (1967) 6.
14. Kivinen, A., Murto, J., Korppi-Tommola, J. and Kuopio, R. *Acta Chem. Scand. 26* (1972) 904.
15. Murto, J., Kivinen, A., Kajander, K., Hyömäki, J. and Korppi-Tommola, J. *Acta Chem. Scand. 27* (1973) 96.
16. Murto, J., Kivinen, A., Korppi-Tommola, J., Viitala, R. and Hyömäki, J. *Acta Chem. Scand. 27* (1973) 107.
17. Kivinen, A., Murto, J. and Kilpi, L. *Suom. Kemistilehti B 40* (1967) 301.
18. Murto, J. In Patai, S., Ed., *The chemistry of the hydroxyl group*, Wiley, London 1971, Chapter 20.
19. Filler, R. and Schure, R. M. *J. Org. Chem. 32* (1967) 1217 .
20. Zeegers-Huyskens, Th. *Spectrochim. Acta A 23* (1967) 855.
21. Nikiforov, G. A. and Ershov, V. V. *Russ. Chem. Rev. 39* (1970) 644.
22. Takahashi, S., Cohen, L. A., Miller, H. K. and Peake, E. G. *J. Org. Chem. 36* (1971) 1205.
23. Bogachev, Yu. S., Vasianina, L. K., Shapetko, N. N. and Yakushin, F. S. *Dokl. Akad. Nauk SSSR 206* (1972) 1142.
24. Sherry, A. D. and Purcell, K. F. *J. Phys. Chem. 74* (1970) 3535.
25. Sherry, A. D. Ph. D. *Thesis*, Kansas State University, 1971; *Diss. Abstr. B 32* (1971) 3288.
26. Purcell, K. F., Stikeleather, J. A. and Brunk, S. D. *J. Amer. Chem. Soc. 91* (1969) 4019.
27. Sherry, A. D. and Purcell, K. F. *J. Amer. Chem. Soc. 94* (1972) 1853.
28. Gramstad, T. *Spectrochim. Acta 20* (1964) 729.

29. Chen, T. and Morgan, L. O. *J. Phys. Chem. 76* (1972) 1973.
30. Gramstad, T. and Storesund, H. J. *Spectrochim. Acta A 26* (1970) 426.
31. Bell, J. V., Heisler, J., Tannenbaum, H. and Goldenson, J. *J. Amer. Chem. Soc. 76* (1954) 5185.
32. Larson, L. *Sv. Kem. Tidskr. 71* (1959) 336.
33. Kivinen, A., Murto, J. and Kuopio, R. *Finn. Chem. Lett.* (1974) 211.
34. Baitinger, W. F., Schleyer, P. von R., Murty, T. S. S. R. and Robinson, L. *Tetrahedron 20* (1964) 1635.
35. Joris, L. and Schleyer, P. von R. *Tetrahedron 24* (1968) 5991.
36. Rochester, C. H. In Patai, S., Ed., *The chemistry of the hydroxyl group*, Wiley, London 1971, Chapter 7.
37. Singh, S., Murthy, A. S. N. and Rao, C. N. R. *Trans. Faraday Soc. 62* (1966) 1056.
38. Dierckx, A.-M., Huyskens, P. and Zeegers-Huyskens, Th. *J. Chim. Phys. Physicochim. Biol. 62* (1965) 336.
39. Lutskii, A. E. *Zh. Strukt. Khim. 13* (1972) 534.
40. Cummings, D. L. and Wood, J. L. *J. Mol. Struct. 20* (1974) 1.
41. Pimentel, G. C. and McClellan, A. L. *The Hydrogen Bond*, Freeman, San Francisco 1960, pp. 220–221.
42. Ghersetti, S. and Lusa, A. *Spectrochim. Acta 21* (1965) 1067.
43. Stymne, B., Stymne, H. and Wettermark, G. *J. Amer. Chem. Soc. 95* (1973) 3490.
44. Arnett, E. M., Mitchell, E. J. and Murty, T. S. S. R. *J. Amer. Chem. Soc. 96* (1974) 3875.
45. Drago, R. S. and Wayland, B. B. *J. Amer. Chem. Soc. 87* (1965) 3571.
46. Drago, R. S., Vogel, G. C. and Needham, T. E. *J. Amer. Chem. Soc. 93* (1971) 6014.
47. Guidry, R. M. and Drago, R. S. *J. Amer. Chem. Soc. 95* (1973) 759.
48. Drago, R. S. *J. Chem. Educ. 51* (1974) 300, and the references cited.

Received June 4, 1975.

Acta Chemica Scandinavica A 30 (1976) 8—14

Magnetic Structures and Properties of $V_{1-t}Mn_tAs$

KARI SELTE,[a] ARNE KJEKSHUS,[a] GUNNAR VALDE,[a] and ARNE F. ANDRESEN[b]

[a] Kjemisk Institutt, Universitetet i Oslo, Blindern, Oslo 3, Norway and [b] Institutt for Atomenergi, Kjeller, Norway

The pseudo-binary VAs – MnAs system has been investigated by X-ray and neutron diffraction and magnetic susceptibility measurements. VAs and MnAs are completely soluble in each other and the crystal structure at and below room temperature is of the MnP type, except for a very small range near the composition MnAs where the NiAs type structure prevails. In the Mn rich region of $V_{1-t}Mn_tAs$ a second or higher order transition from MnP to NiAs type structure is observed at elevated temperatures. The temperature dependence of the magnetic susceptibility follows the Curie-Weiss Law in the region of the (high temperature) NiAs type structure. The low temperature phase with NiAs type structure exhibits ferromagnetism. In the region of the MnP type crystal structure a double, a axis type helimagnetic ordering of the spins is adopted at low temperatures ($\sim 0.60 \leqq t \leqq 0.95$ in $V_{1-t}Mn_tAs$). The spiral parameters depend both on composition and temperature.

Studies on the magnetic properties of phases with the MnP type structure are frequently rendered difficult by the small magnetic moments generally associated with such phases. The existence of cooperative, magnetic phenomena may therefore be difficult to detect and large uncertainties are necessarily attached to the interpretation of the experimental data. On turning to ternary phases it may be possible to improve the conditions somewhat by incorporating elements which carry or induce larger magnetic moments. A suitable element for this purpose is Mn. In line with this, the present paper concerns the magnetic structures and properties of $V_{1-t}Mn_tAs$, the work being greatly stimulated by the findings for $Cr_{1-t}Mn_tAs$ [1,2] and $Mn_{1-t}Fe_tAs$.[3]

EXPERIMENTAL

Samples of VAs and MnAs were made by heating weighed quantities of the elements [99.5 % V (A.D. Mackay), 99.9+ % Mn (The British Drug Houses; crushed powder from the commercial electrolytic grade material), and 99.9999 % As (Koch-Light Laboratories)] in evacuated, sealed quartz tubes, as described in Refs. 3 and 4. VAs and MnAs were mixed in proportions appropriate to the desired ternary compositions and subjected to a first annealing at 850 °C for one week. All samples were crushed and subjected to one or two further annealings for one week at 850 °C, then cooled to 600 °C over two days and finally quenched in ice water.

The experimental details concerning the X-ray and neutron diffraction and magnetic susceptibility measurements have been reported earlier.[5]

RESULTS

(i) *Chemical crystal structures.* The room temperature unit cell dimensions of $V_{1-t}Mn_tAs$ are shown in Fig. 1 as functions of the composition parameter t. The complete mutual solid solubility of VAs and MnAs is brought out in the continuous variation of all unit cell dimensions with t. The possible extension of the homogeneity range of $V_{1-t}Mn_tAs$ to metal/non-metal (atomic) ratios different from 1.00 has not been examined for $t \neq 0$ [4] and 1.[6]

At room temperature the MnP type atomic arrangement is stable in the interval $0 \leqq t \leqq 0.98$, whereas the NiAs type prevails for $0.98 < t \leqq 1$ (see Figs. 1 and 2). The X-ray and neutron diffraction data show that the substituted atoms are distributed at random in the metal sub-lattice, unit cell dimensions and positional parameters for $t = 0.50$, 0.60, 0.70, 0.90, and 0.95 being given in Table 1.

Table 1. Unit cell dimensions and positional parameters with standard deviations for some $V_{1-t}Mn_tAs$ samples as derived by least squares profile refinements of neutron diffraction data. (Space group *Pnma*; positions 4(*c*); overall profile reliability factors ranging between 0.035 and 0.052.)

t	T (K)	a (Å)	b (Å)	c (Å)	x_T	z_T	x_X	z_X
0.95	80	5.585(1)	3.500(1)	6.181(1)	0.0068(32)	0.2083(21)	0.1992(9)	0.5827(12)
	293	5.703(1)	3.625(1)	6.331(1)	0.0035(11)	0.2171(9)	0.2170(5)	0.5804(8)
0.90	4.2	5.616(1)	3.499(1)	6.210(1)	0.0078(15)	0.2167(45)	0.1957(9)	0.5804(12)
	80	5.619(1)	3.507(1)	6.215(1)	0.0003(19)	0.2062(23)	0.2022(8)	0.5811(10)
	293	5.710(1)	3.601(1)	6.318(2)	0.0025(20)	0.2120(18)	0.2141(7)	0.5868(10)
0.70	4.2	5.652(1)	3.462(1)	6.230(1)	0.0090(20)	0.2085(20)	0.2020(8)	0.5783(8)
	80	5.658(1)	3.465(1)	6.235(1)	0.0103(18)	0.2060(19)	0.2001(9)	0.5766(10)
	293	5.721(1)	3.525(1)	6.296(1)	0.0070(21)	0.2051(18)	0.2095(7)	0.5807(7)
0.60	5	5.683(2)	3.445(2)	6.254(2)	−0.0002(22)	0.1984(22)	0.2038(7)	0.5748(8)
	80	5.691(3)	3.451(2)	6.283(3)	−0.0015(28)	0.1951(27)	0.2054(9)	0.5760(9)
	293	5.735(3)	3.489(2)	6.311(3)	−0.0013(21)	0.2012(21)	0.2071(6)	0.5766(7)
0.50	5	5.709(2)	3.430(1)	6.260(2)	−0.0006(24)	0.1966(24)	0.2013(6)	0.5760(7)
	80	5.714(3)	3.435(2)	6.268(3)	0.0002(27)	0.1983(28)	0.2026(7)	0.5757(8)
	293	5.743(2)	3.464(1)	6.290(2)	0.0017(25)	0.1988(25)	0.2049(7)	0.5759(8)

All pseudo-binary systems of the type TAs $-$MnAs [2,3] contain the unusual feature of taking an NiAs type atomic arrangement as both low (I) and high (II) temperature forms, separated by a temperature interval in which the MnP type structure prevails. This peculiarity is associated with the magnetic behaviour of Mn-rich $T_{1-t}Mn_tAs$ samples; see ii. The second or higher order MnP⇌NiAs (II) type transition in $V_{1-t}Mn_tAs$ has been detected by the high temperature powder X-ray method ($0.70 \leqq t \leqq 1$; see Fig. 3) as well as the magnetic susceptibility data ($0.80 \leqq t \leqq 1$; see ii). The trend in the data, which are mutually consistent

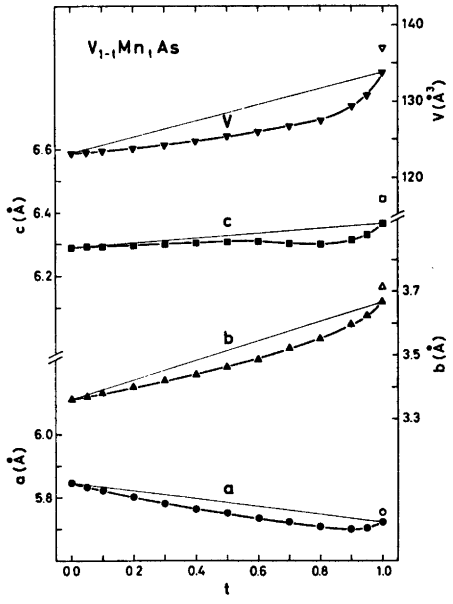

Fig. 1. Room temperature (extrapolated for MnAs) unit cell dimensions of ternary solid solution series VAs−MnAs *versus* composition. Error limits do not exceed size of symbols. Open symbols for MnAs represent data for its NiAs type structure at room temperature.

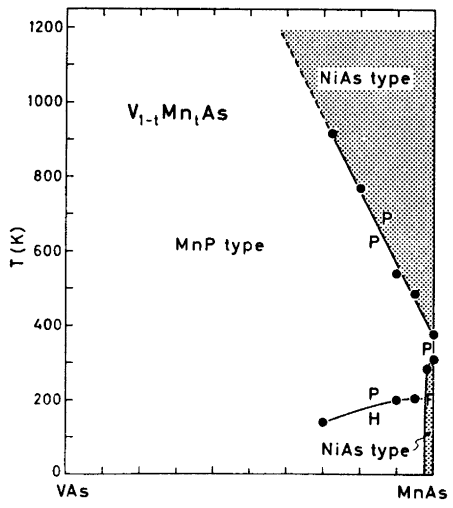

Fig. 2. Diagram of the phase relations in the pseudo-binary VAs−MnAs system. Phase boundaries indicated by broken lines are uncertain. Magnetic state is indicated by: P para, H helical, F ferro.

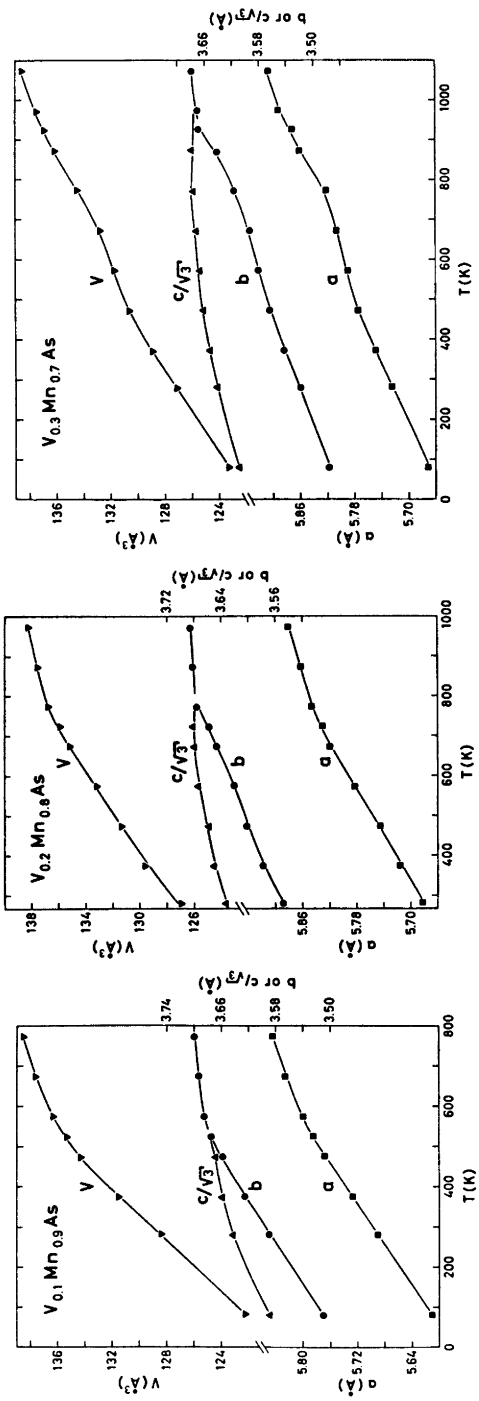

Fig. 3. Unit cell dimensions of three $V_{1-t}Mn_tAs$ samples *versus* temperature. Average relative expansion coefficients α_a [$=\alpha_T - \alpha_{T'}/a_{300}(T-T')$], α_b, α_c multiplied by 10^6 K are 39, 44, 29; 61, 69, 36; and 69, 107, 59 for $V_{0.30}Mn_{0.70}As$ (80 – 700 K), $V_{0.20}Mn_{0.80}As$ (300 – 600 K), and $V_{0.10}Mn_{0.90}As$ (80 – 450 K), respectively.

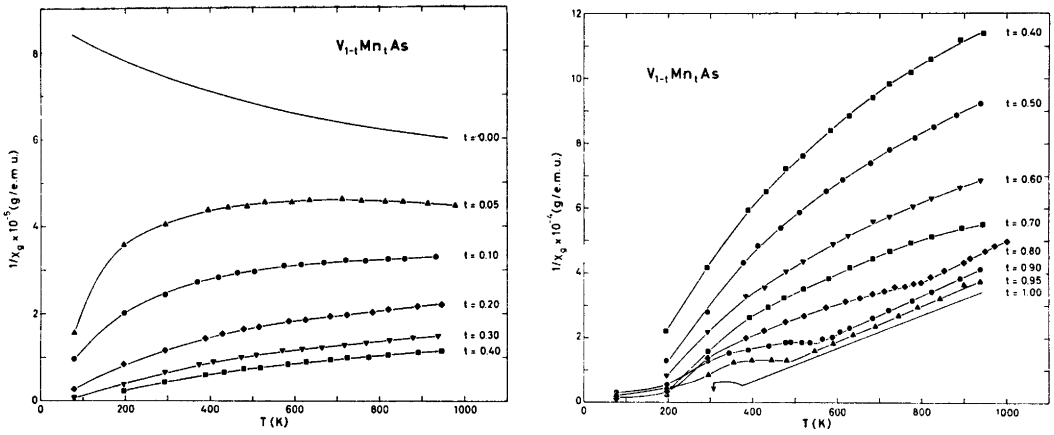

(a) (b)

Fig. 4. Reciprocal magnetic susceptibility as function of temperature for $V_{1-t}Mn_tAs$ samples with (a) $0 \leqq t \leqq 0.40$ and (b) $0.40 \leqq t \leqq 1$. Curves for $t = 0$ and 1 are quoted from Refs. 3 and 4.

for the two sets, suggests that the transition continues to take place in samples with $t < 0.70$, although it could not be followed with our equipment.

Mn-rich $T_{1-t}Mn_tAs$ samples have in common (*cf.* Refs. 2, 3, 7, and 8) a relatively low temperature for the MnP⇌NiAs (II) type transition, an appreciable temperature interval for the complete conversion from the NiAs type to the fully relaxed MnP type positional parameters, and unusually large thermal expansion coefficients in the changing region of the MnP type structure. These phenomena are intimately connected and have probably a common origin in the unique property of Mn, being capable of appreciable adjustments of size as a function of its electronic (*e.g.* high spin/low spin) state.

(ii) *Magnetic susceptibility.* As seen from Fig. 4 the reciprocal magnetic susceptibility *versus* temperature characteristics undergo a gradual change with the composition parameter t of $V_{1-t}Mn_tAs$. Among these thermomagnetic curves, that for $t = 0$ is unique in decreasing steadily with increasing temperature. All the other curves are characterized by having a shorter or longer convex portion towards the temperature axis. For samples with $0.80 \leqq t \leqq 1$ the convex portions are interrupted by linear sections on the high temperature side. The temperature at which the change-over takes place is that for the transition between the MnP and NiAs (II) type structures (see i). Thus, the fulfilment of Curie-Weiss Law is associated with the NiAs type structure. With decreasing content of Mn from $t = 1$ to $t = 0.80$ a small reduction is noted in paramagnetic moment and Curie constant (Table 2).

Non-linear $\chi^{-1}(T)$ curves may almost be taken as a trade mark for phases with the MnP type structure. The $\chi^{-1}(T)$ curves shown in Fig. 4 are no exception in this respect. The thermomagnetic curves for $V_{1-t}Mn_tAs$ show similarities with those for $Cr_{1-t}Mn_tAs$ [2] and $Mn_{1-t}Fe_tAs$,[3] low temperature ferromagnetic behaviour being observed for $t = 1$ and, rather weakly, for $0.40 \leqq t \leqq 0.70$ of the $V_{1-t}Mn_tAs$ phase. (Indication of the weak ferromagnetism was not found in the neutron diffraction data for samples with $t = 0.50$, 0.60, and 0.70.)

(iii) *Magnetic structures.* The ferromagnetic mode of MnAs,[9] with moments arranged

Table 2. Curie constant (θ), paramagnetic moment ($\mu_P = \sqrt{8C_M}$), and number of unpaired electrons ($n = 2S_T$; according to the "spin only" approximation) for $V_{1-t}Mn_tAs$ samples which fulfil Curie-Weiss Law.

t	θ (K)	μ_P (μ_B)	$2S_T$
1.00	270 ± 10	4.5 ± 0.3	3.6 ± 0.2
0.95	255 ± 15	4.3 ± 0.3	3.4 ± 0.2
0.90	240 ± 20	4.2 ± 0.4	3.3 ± 0.3
0.70	230 ± 20	4.0 ± 0.4	3.1 ± 0.3

Table 3. Parameters specifying the double, *a* axis helimagnetic ordering in $V_{1-t}Mn_tAs$. (Angle (β) between moment vector and spiral axis is assumed to be 90°.)

t	0.95	0.90		0.70	
T (K)	80	4.2	80	4.2	80
$\tau/2\pi a^*$	0.128(2)	0.116(2)	0.116(2)	0.080(3)	0.078(3)
μ_T (μ_B)	1.9(1)	1.9(1)	1.9(1)	1.6(1)	1.6(1)
ϕ (°)	65(1)	70(1)	75(1)	60(1)	56(1)
T_N (K)	206(1)	200(1)		142(1)	

perpendicular to the hexagonal *c* axis of its NiAs type atomic arrangement, extends slightly ($t > 0.98$) into the ternary region of $V_{1-t}Mn_tAs$ (*cf.* Fig. 2). The other binary end member, VAs, does not exhibit a cooperative magnetic phenomenon above 4.2 K.[4]

The double, *a* axis type helimagnetic ordering, which rather recently was observed for $Fe_{1-t}Mn_tAs$ ($\sim 0.88 < t < \sim 0.99$; MnP type structure),[3] is also found for $V_{1-t}Mn_tAs$ samples in the interval $\sim 0.60 \leqq t \leqq 0.95$. This helimagnetic mode [3] is, besides the Néel temperature (T_N) and the magnetic moment per metal atom (μ_T), specified by the spiral propagation vector (τ), the phase angle between independent spirals (ϕ), and the angle between the moment and the spiral axis (β). As evident from Fig. 2 and Table 3, T_N varies slowly over the composition range $0.70 \leqq t \leqq 0.95$. A similar statement applies roughly to the magnetic moment when the limited accuracy in the determination of this parameter is considered. For the $V_{0.40}Mn_{0.60}As$ sample, near the Mn-poor limit of the helical mode, T_N is reduced appreciably ($5 < T_N < 80$ K) and the low (almost insignificant) intensity of the magnetic reflections prevents meaningful estimates of the spiral parameters. The propagation vector and the phase angle are found to vary appreciably with composition and temperature (see Fig. 5 and Table 3), thus resembling

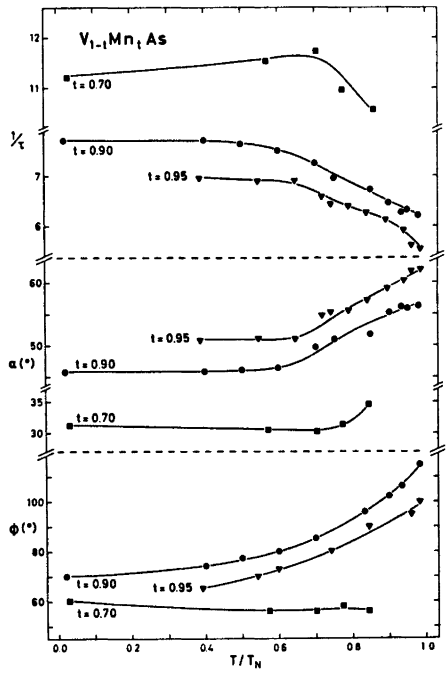

Fig. 5. Spiral turn angle per *a* length (α) and number of *a* lengths per spiral revolution ($1/\tau$) together with phase angle (ϕ) for $t = 0.70$, 0.90, and 0.95 of $V_{1-t}Mn_tAs$ as functions of reduced temperature.

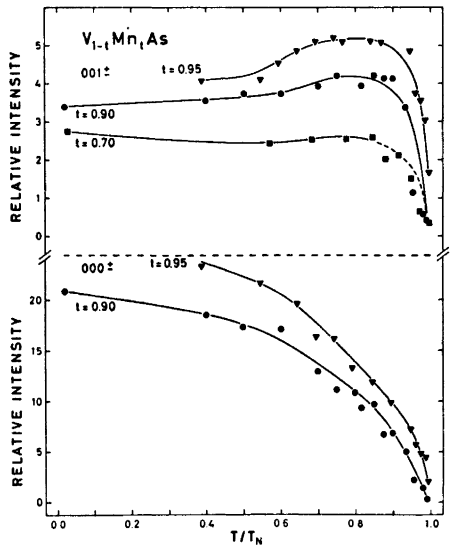

Fig. 6. Temperature dependence of relative, integrated intensities of $000^{\pm}$ and $001^{\pm}$ for $t = 0.70$, 0.90, and 0.95 of $V_{1-t}Mn_tAs$.

to some extent the findings for $Fe_{0.10}Mn_{0.90}As$.[3]

The integrated intensity *versus* reduced temperature relationships for the strongest satellites $000^{\pm}$ and $001^{\pm}$ of $V_{0.05}Mn_{0.95}As$, $V_{0.10}Mn_{0.90}As$ and $V_{0.30}Mn_{0.70}As$ are shown in Fig. 6. (Due to the small value of α for $V_{0.30}Mn_{0.70}As$ $000^{\pm}$ lies extremely close to the primary neutron beam, and the integrated intensity could only be inaccurately determined by subtraction of the background as obtained above T_N.) The marked difference in the temperature variation of the corresponding integrated intensities of $000^{\pm}$ and $001^{\pm}$ immediately suggests that there are changes in ϕ with temperature. The apparent reduction in magnetic moment with temperature for helimagnetic arrangements does not, in general, follow the Brillouin type relationships characteristic of collinear magnetic structures. This is also the case for the double, *a* or *c* axis type spiral structures occurring among the MnP type phases (*cf.* Refs. 3, 5, 10–13), where the disordering of the moments affects the temperature dependences of α, ϕ, and β in addition to μ_T. Lacking a suitable dynamic model for the description of the thermal movements of the moments in terms of the variables μ_T, α, ϕ, and β, the three latter parameters were assumed to be static temperature functions, and the hypothetical $\mu_T/\mu_{T,0K}$ *versus* T/T_N relationship shown in Fig. 7 was postulated. Although the magnetic susceptibility data for $V_{0.30}Mn_{0.70}As$ give indication of a small ferromagnetic component, probably due to deviation of β from 90°, the constraint $\beta = 90°$ was not relaxed. The temperature dependence of α follows from the location of the satellites in relation to the nuclear reflections, permitting this parameter to be established separately. Thus, using the temperature variations of μ_T from Fig. 7, α from Fig. 5, and $\beta = 90°$, the temperature dependence of ϕ shown in the bottom part of Fig. 5 could be deduced from the observed intensities of $000^{\pm}$ and $001^{\pm}$ shown in Fig. 6. As a check of the mutual consistency of the data, the smooth curves in Fig. 6 have been calculated on the deduced spiral parameters, μ_T, α, (β,) and ϕ. The calculated curves are seen to fit the experimental points remarkably well.

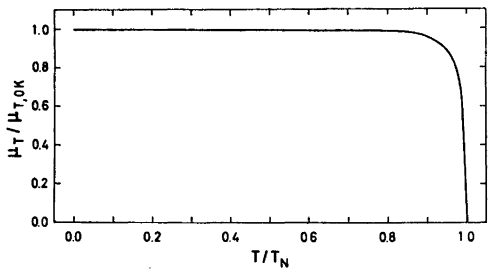

Fig. 7. Postulated temperature dependence of magnetic moments in helimagnetic modes of $V_{0.30}Mn_{0.70}As$, $V_{0.10}Mn_{0.90}As$, and $V_{0.05}Mn_{0.95}As$.

The carefully collected intensity data for $000^{\pm}$ at various temperatures were examined in order to unveil possible sample inhomogeneities of the type encountered for the magnetically isostructural $Mn_{0.90}Fe_{0.10}As$.[3] No such inhomogeneity was found for the $V_{1-t}Mn_tAs$ samples.

DISCUSSION

The phase diagram of the pseudo-binary VAs–MnAs system (Fig. 2) shows marked similarities to that of CrAs–MnAs,[2] but differs to some extent from that of MnAs–FeAs.[3] Since V and Cr precede Mn in the 3*d* series, it would be of interest to examine the phase relationships in the system MnAs–CoAs, where Co, like Fe, succeeds Mn.

The common feature of the high temperature portions of the CrAs–MnAs [2] and VAs–MnAs systems is the second or higher order crystallographic transitions between MnP and NiAs type structures. Similar MnP⇌NiAs type transitions are also found in a number of other binary and ternary phases.[13–17] Available information concerning such transitions are reasonably consistent with recent considerations on geometrical [15] and group theoretical [18] basis.

On substitution of another metal or nonmetal component into a binary MnP type compound which takes cooperative magnetic ordering, two different situations arise. If neither the solute nor the solvent metal atom is Mn, only small substitutions appear to destroy the cooperative magnetic phenomena.[17] Relatively large magnetic homogeneity ranges have, on the other hand, been observed for the pseudo-binary *T*As–MnAs systems studied so far.[2,3]

The magnetic data for the $T_{1-t}Mn_tAs$ phases (as well as $MnP_{1-x}As_x$) also have a number

of other features in common. Whenever the NiAs type structure occurs, the magnetic moments are appreciably higher than found for the corresponding MnP type state (3.1 – 3.7 *versus* 1.3 – 1.9 for the spin quantum number $2S_T$; Ref. 3 and *vide supra*). The terminology high spin/low spin may be used although these phrases have lost their clear-cut meaning here, where the electrons are, at least partly, delocalized and spread over a number of energy bands.

A theoretical investigation of the double, *a*-axis type helimagnetic mode is required in order to compare $V_{1-t}Mn_tAs$ and $Fe_{1-t}Mn_tAs$[3] in a meaningful manner. The starting point of Kallel *et al.*[19] may constitute a suitable basis for such an exploration.

Although $V_{1-t}Mn_t$ As ($\sim 0.60 \leqq t \leqq 0.95$), and $Fe_{1-t}Mn_tAs$ ($\sim 0.88 < t < \sim 0.99$)[3] are magnetically isostructural, the tendency towards conical deformation of the spiral arrangement is more prominent in the latter phase. In neither of the cases conical deformation is observed near the Mn-rich phase boundaries. In order to obtain more insight into the origin of the conical arrangements, attention should be focussed on the behaviour of these phases in magnetic fields.

Acknowledgement. The assistance of Ing. Stanislav Vratislav (I.A.E.A.-fellow from The Technical University of Prague, Czechoslovakia) in some of the neutron diffraction measurements is greatly appreciated.

REFERENCES

1. Watanabe, H., Kazama, N., Yamaguchi, Y. and Ohashi, M. *J. Appl. Phys. 40* (1969) 1128.
2. Kazama, N. and Watanabe, H. *J. Phys. Soc. Jap. 30* (1971) 1319.
3. Selte, K., Kjekshus, A. and Andresen, A. F. *Acta Chem. Scand. A 28* (1974) 61.
4. Selte, K., Kjekshus, A. and Andresen, A. F. *Acta Chem. Scand. 26* (1972) 4057.
5. Selte, K., Kjekshus, A. and Andresen, A. F. *Acta Chem. Scand. 26* (1972) 3101.
6. Grønvold, F., Snildal, S. and Westrum, E. F. *Acta Chem. Scand. 24* (1970) 285.
7. Selte, K. and Kjekshus, A. *Acta Chem. Scand. 27* (1973) 3195.
8. Selte, K., Kjekshus, A. and Andresen, A. F. *Acta Chem. Scand. 27* (1973) 3607.
9. Bacon, G. E. and Street, R. *Nature (London) 175* (1955) 518.
10. Boller, H. and Kallel, A. *Solid State Commun. 9* (1971) 1699.
11. Felcher, G. P., Smith, F. A., Bellavance, D. and Wold, A. *Phys. Rev. B 3* (1971) 3046.
12. Selte, K., Kjekshus, A., Oftedal, T. A. and Andresen, A. F. *Acta Chem. Scand. A 28* (1974) 957.
13. Selte, K., Hjersing, H., Kjekshus, A. and Andresen, A. F. *Acta Chem. Scand. A 29* (1975) 312.
14. Ido, H. *J. Phys. Soc. Japan 25* (1968) 1543.
15. Selte, K. and Kjekshus, A. *Acta Chem. Scand. 27* (1973) 3195.
16. Franzen, H. F. and Wiegers, G. A. *J. Solid State Chem. 13* (1975) 114.
17. Selte, K., Hjersing, H., Kjekshus, A., Andresen, A. F. and Fischer, P. *Acta Chem. Scand. A 29* (1975) 695.
18. Franzen, H. F., Haas, C. and Jellinek, F. *Phys. Rev. B 10* (1974) 1248.
19. Kallel, A., Boller, H. and Bertaut, E. F. *J. Phys. Chem. Solids 35* (1974) 1139.

Received June 2, 1975.

Acta Chemica Scandinavica A 30 (1976) 15—23

Thermodynamics of Metal Complex Formation in Aqueous Solution. XI. Equilibrium and Enthalpy Measurements on the Mercury(II) Azide System

STEN AHRLAND and EFRAIM AVŞAR*

Inorganic Chemistry 1, Chemical Center, University of Lund, S-220 07 Lund 7, Sweden

The thermodynamic functions for the stepwise formation of the mercury(II) azide complexes have been determined in aqueous sodium perchlorate medium of unit ionic strength at 25.00 °C. The stability constants have been found spectrophotometrically using iron(III) ion as an auxiliary central ion. The constants have been checked potentiometrically, by the redox Hg(II) – Hg(I) half-cell. Glass electrode measurements have also been applied in an attempt to determine the formation constants of the complexes beyond the second one. These are formed to such a slight extent, however, that no values could be obtained. The enthalpy changes have been determined by a direct calorimetric procedure.

The two complexes which predominate in the range studied are formed in fairly exothermic reactions, while the entropy changes, though positive, contribute only slightly to the stability of the complexes.

In two preceding papers of this series,[1,2] the complex formation of the azide ion has been studied. These investigations have now been extended to the mercury(II) azide system. Due to the nature of the system and to the very strong complex formation, the determination of the formation constants for the individual steps becomes rather difficult. An extra complication is also met in the calculations where the $\bar{n}/[L]$ *vs.* [L] plot turns out to have a maximum close to the $\bar{n}/[L]$-axis which makes the extrapolation to [L] = 0 uncertain. It is therefore desirable to check the result by applying independent methods of measurement. To this end, both a spectrophotometric method using the Fe(III) ion as an auxiliary central ion and a potentiometric method using the mercury(III) – mercury(I) couple have been applied for the determination of the constants. In order to determine the formation constants of the complexes beyond the second step, some redox titrations with mercury electrode as well as glass electrode measurements have also been performed. However, due to the rapid dissolution of mercury in solutions containing Hg^{2+}, N_3^- and Hg_2^{2+} ions according to the reaction $Hg(0) + Hg(II) \rightarrow 2Hg(I)$, redox measurements turned out to be impossible. A calorimetric study of the higher complexes was also unsuccessful as sufficiently high concentrations of Hg(II) could not be employed, due to the low solubility of $Hg(N_3)_2$.

The azide system of mercury(II) has previously been studied spectrophotometrically by Musgrave and Keller [3] at 28 °C and various ionic strengths. The intensely coloured FeN_3^{2+} ion was used as an indicator. No determination of the enthalpy changes has been carried out so far.

NOTATION AND MAIN EQUATIONS

The notation is the same as in parts IX and X of this series,[1,2] with the following additions:

A = absorbance

l = cell thickness

$a = A/l$ = linear absorption coefficient

ε = molar absorption coefficient

λ = wavelength

* Present address: Technical University of Istanbul, Chemical Engineering Faculty, Department of Physical Chemistry, Macka-Istanbul, Turkey.

C_{Fe}, C_{II} and C_I = total concentrations of iron(III), mercury(II) and mercury(I), respectively

$\alpha_0 = [Hg^{2+}]/C_{II}$ = fraction of the bivalent mercury present as Hg^{2+}.

$$-\Delta E_{corr} = E_0 - E + 29.58 \log\left(\frac{V_0+v}{V_0}\right) = -59.16 \log \alpha_0 \text{ (mV)}$$

E_0 = emf of the redox cell when $C_L = 0$

E = emf of the redox cell when $C_L \neq 0$

Calculation of formation constants from spectrophotometric measurements. First, the formation constant of FeN_3^{2+} has to be determined under the prevailing conditions. If only the first mononuclear complex is formed and the absorbance is measured at a wavelength where this complex is the only absorbing species, the following relation holds according to Beer's law:

$$a = \varepsilon[FeL] \quad (1)$$

Further, in such a case

$$\bar{n}_{Fe} = \frac{[FeL]}{C_{Fe}} = \frac{a}{\varepsilon C_{Fe}} = \frac{\beta_{1,Fe}[L]}{1+\beta_{1,Fe}[L]} \quad (2)$$

where $\beta_{1,Fe}$ is the formation constant of FeL. Hence

$$\frac{\varepsilon C_{Fe}}{a} = 1 + \frac{1}{\beta_{1,Fe}[L]} \quad (3)$$

For the association constant of HN_3 is valid

$$K = \frac{C_L - [L] - (a/\varepsilon)}{h\,[L]} \quad (4)$$

Substituting [L] from eqn. (4) in eqn. (3) and recognizing that $[FeL] = a/\varepsilon \ll (C_L + C_{Fe})$ we obtain

$$\frac{C_L C_{Fe}}{a} = \frac{1+hK}{\varepsilon\beta_{1,Fe}} + \frac{1}{\varepsilon}(C_L + C_{Fe}) \quad (5)$$

A plot of $(C_L C_{Fe}/a)$ *vs.* $(C_L + C_{Fe})$ at constant acidity should therefore give a straight line with intercept $(1+hK)/\varepsilon\beta_{1,Fe}$ and a slope of $1/\varepsilon$, permitting the evaluation of ε and $\beta_{1,Fe}$ when h and K are known.

For the determination of the formation constants of the mercury(II) azide complexes, corresponding values of [L] and $\bar{n}$ must be known. If two mononuclear complexes are formed, $\bar{n}$ is defined as

$$\bar{n} = \frac{[HgL] + 2[HgL_2]}{C_{II}} \quad (6)$$

As $[HgL] + 2[HgL_2] = C_L - [L] - [HL] - [FeL]$ and $[FeL] = a/\varepsilon$, eqn. (1), introduction of $[HL] = Kh[L]$ yields

$$\bar{n} = \frac{C_L - [a/\varepsilon + [L](1+hK)]}{C_{II}} \quad (7)$$

while [L] can be found from eqn. (3) once $\beta_{1,Fe}$ is known.

The constants have been evaluated both graphically and numerically. In the graphical calculation, the functions X are computed from a graphical integration of $\bar{n}/[L]$ *vs.* [L]. From corresponding values of X and [L], the formation constants are then obtained.[4]

The numerical calculations have been carried out by a high-speed computer according to two different programs, designed by Sandell [5] and by Karlsson,[6] respectively.

Mathematical treatment of $\bar{n}/[L]$ *vs.* [L] *curve.* The shape of the $\bar{n}/[L]$ *vs.* [L] curve will depend upon the ratio between the consecutive formation constants. Most often $\bar{n}/[L]$ decreases smoothly as [L] increases, but for extreme ratios a maximum will appear at a certain value of [L]. In such cases, extrapolation to $[L] = 0$ may easily result in an erroneous intercept especially if few experimental points, or none at all, are situated in the region of this maximum. This is in fact the case for the mercury(II) azide system investigated here.

The condition for the appearance of a maximum will be briefly discussed here. For the sake of simplicity, only two complexes are considered, but the conclusion is valid for N complexes as well. A necessary condition that a function $f(x)$ be an extremum at $x = x_0$ is that $f'(x_0) = 0$. For two mononuclear complexes

$$\bar{n}/[L] = \frac{\beta_1 + 2\beta_2[L]}{1+\beta_1[L]+\beta_2[L]^2}$$

Hence $d(\bar{n}/[L])/d[L] = 0$ when

$$2\beta_2 - \beta_1^2 = 2\beta_1\beta_2[L] + 2\beta_2^2[L]^2 \quad (8)$$

If $2\beta_2 - \beta_1^2 = 0$, *i.e.* $K_1/K_2 = 2$, the extremum is the point of interception. For $[L] \neq 0$ the condition is

$$2\beta_2 > \beta_1^2 \textit{ i.e. } K_1/K_2 < 2 \quad (9)$$

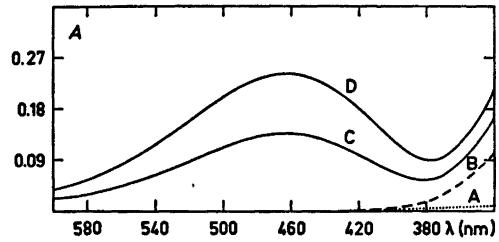

Fig. 1. Absorption spectra of FeN_3^{2+} at 25 °C and $I = 1.00$ M ($l = 2.001$ cm).
(A) 1.000 mM NaN_3, (B) 2.161 mM $Fe(ClO_4)_3$ + 79.11 mM $HClO_4$, (C) 2.161 mM $Fe(ClO_4)_3$ + 1.000 mM NaN_3 + 79.11 mM $HClO_4$, (D) 2.161 mM $Fe(ClO_4)_3$ + 2.000 mM NaN_3 + 79.11 mM $HClO_4$.

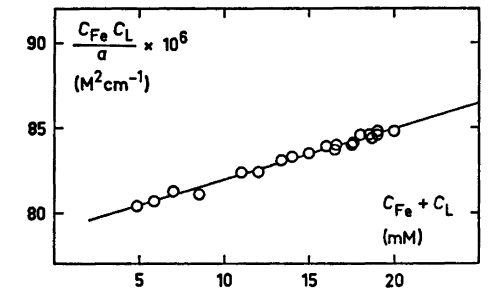

Fig. 2. The determination of $\beta_{1,Fe}$ and ε (see eqn. 5).

Solving eqn. (8) for [L]

$$[L]_0 = \frac{(4\beta_2 - \beta_1^2)^{\frac{1}{2}} - \beta_1}{2\,\beta_2} \qquad (10)$$

At this point, the value of $\bar{n}/[L]$ is

$$(\bar{n}/[L])_{ext} = \frac{(4\beta_2 - \beta_1^2)^{\frac{1}{2}}}{2 - (\beta_1^2/2\beta_2)} \qquad (11)$$

which for $[L]_0 = 0$, when $2\beta_2 = \beta_1^2$ of course is reduced to

$$(\bar{n}/[L])_{ext} = \beta_1$$

EXPERIMENTAL

Chemicals. A standard stock *mercury(II) perchlorate* solution was prepared by dissolving a weighed amount of red HgO (Mallinchrodt, *a.r.*) in a standard perchloric acid (Baker, *a.r.*) solution. *Mercury(I) perchlorate* solution was prepared from $Hg_2(ClO_4)_2.4H_2O$ (G. F. Smith, *p.a.*) and analyzed according to Pugh.[7] The solution always contains minute amounts of Hg^{2+} which were determined by measuring the redox potential of the solution after adding known amounts of $Hg(ClO_4)_2$, $HClO_4$ and $NaClO_4$ (see Ref. 8). Standard *iron(III) perchlorate* solutions were prepared according to Ref. 9. *Sodium azide* and *sodium perchlorate* were prepared and analyzed as described before.[1]

Table 1. Spectrophotometric measurements on FeN_3^{2+} at 25.0 °C and $I = 1.00$ M. For all points: $C_H = 200.0$ mM, $\lambda = 460$ nm and $l = 1.001$ cm.

C_{Fe} (mM)	C_L (mM)	a (cm^{-1})
5.463	0.500	0.032
4.002	1.000	0.047
5.463	1.000	0.064
6.403	1.000	0.075
16.01	0.500	0.090
8.004	1.000	0.093
4.002	2.000	0.094
5.463	1.500	0.096
4.322	2.000	0.101
5.463	2.000	0.127
12.01	1.000	0.137
6.403	2.000	0.149
8.004	2.000	0.185
5.463	3.000	0.190
18.11	1.000	0.203
9.605	2.000	0.221
12.01	2.000	0.274
8.004	3.000	0.277
16.01	2.000	0.361
18.11	2.000	0.405

Apparatus. The absorbance was measured with a Zeiss PMQ II spectrophotometer. The temperature was maintained at 25.0 ± 0.1 °C by using jacketed compartment in conjunction with a thermostatically controlled water-bath. A Hitachi recording spectrophotometer was used for the absorption spectra.

A Radiometer PHM 52 digital pH meter was used for the redox and pH measurements.

The calorimeter used in this study is of the model developed and described by Grenthe *et al.*[10]

Procedure. The technique of the calorimetric measurements has been described before.[11]

For the determination of $\beta_{1,Fe}$ and ε the following procedure has been applied. Aliquots of standard solutions of sodium azide and iron(III) perchlorate were added to 50 ml volumetric flasks that already contained perchloric acid and sodium perchlorate. In order to prevent hydrolysis the concentration of acid was kept high, $C_H = 200.0$ mM, and was checked after each absorbance measurements. The ligand concentration was always kept very low relative to the metal ion concentration (the so-called M-method [12]). Only the first complex is then

Table 2. Spectrophotometric data for the mercury(II) azide system. For all points: $C_H = 200.0$ mM, $\lambda = 460$ nm and $l = 1.001$ cm.

C_{II} (mM)	C_L (mM)	C_{Fe} (mM)	a (cm^{-1})	$[L] \times 10^7$ (M)	$\bar{n}$	$(\bar{n}/[L]) \times 10^{-6}$ (M^{-1})
1.465	2.000	8.004	0.038	0.720	1.085	15.07
4.194	5.620	8.004	0.045	0.851	1.224	14.38
1.465	2.000	9.605	0.046	0.725	1.081	15.07
3.822	4.000	12.01	0.054	0.680	0.944	13.88
4.194	6.744	8.004	0.062	1.17	1.499	12.39
1.398	2.000	12.01	0.063	0.793	1.103	13.91
0.699	1.000	17.23	0.068	0.596	0.929	15.59
2.796	5.000	8.004	0.073	1.38	1.507	10.92
3.822	5.000	12.01	0.075	0.943	1.165	12.35
2.796	5.620	8.004	0.094	1.77	1.649	9.316
2.796	4.000	16.32	0.098	0.905	1.241	13.71
7.323	10.00	17.20	0.106	0.929	1.291	13.90
1.398	3.372	12.01	0.148	1.86	1.643	8.833
2.796	5.000	16.32	0.148	1.37	1.501	10.96
2.796	6.744	8.004	0.159	3.01	1.798	5.973
4.194	10.00	8.004	0.214	4.06	1.831	4.510
1.398	4.000	12.01	0.216	2.73	1.731	6.341
1.911	6.000	8.004	0.229	4.35	1.842	4.235
2.796	6.000	16.32	0.231	2.14	1.695	7.921
0.699	4.000	8.004	0.257	4.88	1.745	3.576
2.796	8.000	8.004	0.260	4.94	1.853	3.751
1.911	5.000	16.01	0.286	2.71	1.784	6.583
1.398	5.000	12.01	0.336	4.25	1.817	4.275
0.699	5.000	8.004	0.347	6.62	1.745	2.636
1.398	4.496	17.23	0.382	3.36	1.802	5.363
1.465	5.000	16.32	0.434	4.02	1.802	4.483
0.699	6.000	8.004	0.440	8.42	1.718	2.040
2.796	10.00	8.004	0.442	8.45	1.856	2.196
1.398	6.000	12.01	0.467	5.93	1.838	3.100
1.398	5.000	17.23	0.477	4.21	1.810	4.299
2.796	10.00	16.32	0.864	8.10	1.878	2.319

formed and its formation constant can be determined as described above.

The absorbance measurements involving the Hg(II) azide complexes were performed in the same way. The solutions then contained known amounts of Hg(II) perchlorate besides Fe(III) perchlorate, perchloric acid and sodium azide. The measurements were made against a reference of 1.00 M $NaClO_4$.

The redox measurements were arranged as titrations as described by Sillén and his co-workers.[8,13] They were performed in an atmosphere of purified nitrogen. The titrations were interrupted when a precipitate of mercury(I) azide was noticed.

MEASUREMENTS AND RESULTS

Spectrophotometric measurements. Absorption spectra of iron(III) azide solutions are shown in Fig. 1. These are completely symmetrical for the two values of C_L chosen which confirms that only the first complex is formed. The absorbance of FeN_3^{2+} is measured for the absorption maximum at 460 nm, Table 1. The values are recorded in the order of increasing a. The plot of

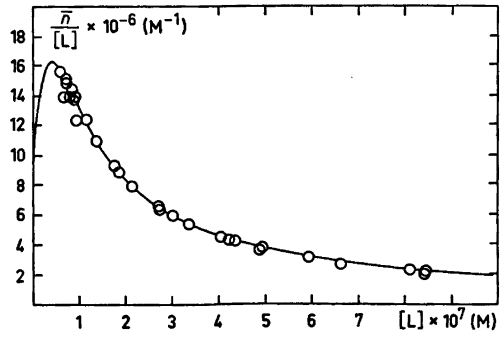

Fig. 3. $\bar{n}/[L]$ *vs.* [L] plot, the integration of which gives the X-functions, *cf.* Table 2. The curve has been computed from the values of β_j.

Table 3. The calculated values of K_{12} from the redox titrations. The symbols refer to Fig. 4.

○ S: 3.661 mM Hg^{2+}, 0.315 mM Hg_2^{2+}
T: 7.323 mM Hg^{2+}, 50.00 mM NaN_3

$-\Delta E_{corr}$ (mV)	α_0	$\bar{n}$	K_{12}
3.84	0.861	0.167	(0.511)
7.13	0.758	0.325	0.402
10.43	0.666	0.476	0.390
13.78	0.585	0.621	0.363
17.33	0.509	0.759	0.365
20.94	0.443	0.891	0.336
24.88	0.380	1.017	0.330
29.02	0.323	1.138	0.313
33.71	0.269	1.254	0.308
38.76	0.221	1.366	(0.284)

△ S: 7.323 mM Hg^{2+}, 1.05 mM Hg_2^{2+}
T: 14.645 mM Hg^{2+}, 50.00 mM NaN_3

$-\Delta E_{corr}$	α_0	$\bar{n}$	K_{12}
6.89	0.765	0.310	(0.446)
9.80	0.683	0.445	0.409
12.70	0.610	0.568	0.414
15.46	0.548	0.682	0.391
18.29	0.491	0.787	0.391
21.09	0.440	0.884	0.391
23.83	0.396	0.974	0.374
26.19	0.361	1.058	0.320
29.44	0.318	1.137	0.356
35.22	0.254	1.279	0.335
41.05	0.202	1.404	(0.301)
47.55	0.157	1.516	(0.274)

eqn. (5) is shown in Fig. 2. A value of $\varepsilon = (3.32 \pm 0.09) \times 10^3$ cm^{-1} M^{-1} is found for FeN_3^{2+}. With the value of $K = 2.77 \times 10^4$ M^{-1} determined earlier [1] the value of $\beta_{1,Fe} = (2.00 \pm 0.06) \times 10^4$ M^{-1} is finally found.

The spectrophotometric measurements pertaining to the mercury(II) azide system are collected in Table 2, where they are listed in the order of increasing values of a.

As the $\bar{n}/[L]$ *vs.* [L] plot has a maximum at $[L] \simeq 4 \times 10^{-5}$ mM, Fig. 3, the extrapolation to $[L] = 0$ and hence the graphical integration becomes difficult to carry out with precision. Therefore, the uncertainty in β_1 is high. The value of β_2 is not very much affected by the value of β_1, however, and will therefore nevertheless be fairly precise.

In the numerical calculations, concordant values of β_1 and β_2 have been obtained from both the programs used.[5,6] The results of these calculations are:

	$\beta_1(M^{-1})$	$\beta_2(M^{-2})$
Graphical	$(1.2 \pm 0.6) \times 10^7$	$(2.8 \pm 0.4) \times 10^{14}$
$\bar{n}$ *vs.* [L] fitting (Ref. 6)	$(1.1 \pm 0.6) \times 10^7$	$(2.44 \pm 0.57) \times 10^{14}$
$\bar{n}/[L]$ *vs.* [L] fitting (Ref. 6)	$(0.911 \pm 0.54) \times 10^7$	$(2.24 \pm 0.18) \times 10^{14}$
Ligand program (Ref. 5)	$(0.78 \pm 0.69) \times 10^7$	$(2.0 \pm 0.7) \times 10^{14}$

The errors given correspond to three standard deviations or to estimated errors, in the case of the graphical calculation.

Potentiometric measurements on the mercury(II) azide system

(a) *Redox titrations of mercury(II) – mercury(I) solutions with azide ions.* The equilibrium

$$Hg^{2+} + Hg(N_3)_2 \rightleftharpoons 2HgN_3^+,$$

$$K_{12} = \frac{[HgN_3^+]^2}{[Hg^{2+}][Hg(N_3)_2]} = \frac{\beta_1^2}{\beta_2} = \frac{K_1}{K_2}$$

has been studied by measuring the emf of a clear solution containing Hg^{2+}, N_3^- and a small known concentration of Hg_2^{2+} at constant acid concentration using the following cell:

$$+\text{Pt} \left| \begin{array}{l} C_{II}\ \text{mM} \\ Hg(ClO_4)_2 \\ C_I\ \text{mM} \\ Hg_2(ClO_4)_2 \\ C_L\ \text{mM} \\ NaN_3 \\ C_H\ \text{mM} \\ HClO_4 \\ C_{NaClO_4}\ \text{to} \\ I = 1.00\ \text{M} \end{array} \right| \begin{array}{l} \\ \\ \\ \\ \\ 1.00\ \text{M} \\ NaClO_4 \\ \\ \\ \\ \end{array} \left| \begin{array}{l} 25.0\ \text{mM} \\ NaCl \\ \\ \\ \\ \\ 975\ \text{mM} \\ NaClO_4 \end{array} \right| \text{Ag,AgCl} -$$

If it is assumed that the concentrations of free ligand and of azide complexes of mercury(I) are negligible the value of K_{12} can be found according to [13]

$$K_{12} = \frac{(2-\bar{n}-2\alpha_0)^2}{\alpha_0(\alpha_0+\bar{n}-1)} \qquad (13)$$

That no mercury(I) complexes are formed is proven by varying the C_I. The emfs measured were those expected if C_I was present as Hg_2^{2+}.

In the measurements, equal volumes of solutions T_1 and T_2 were added to $V_0 = 20.00$ ml of solution S. The solutions T_1, T_2 and S had the following compositions:

T_1: $C_L = 50.00$ mM NaN_3; $C_{NaClO_4} = 950$ mM

T_2: $2C_{II}$ mM $Hg(ClO_4)_2$; $C_H = 100.00$ mM $HClO_4$; $NaClO_4$ to $I = 1.00$ M

S: C_{II} mM $Hg(ClO_4)_2$; $_I$ mM $Hg_2(ClO_4)_2$; $_H = 50.00$ mM $HClO_4$; $NaClO_4$ to $I = 1.00$ M

The results of the redox measurements are collected in Table 3. In the beginning the values are somewhat high, presumably depending upon that the calculation of K_{12} from eqn. (13) is rather uncertain when α_0 is near 1. The gradual decrease at the end of the series may be ascribed to a beginning precipitation of $Hg_2(N_3)_2$, not yet noticeable to the eye. The value of K_1/K_2 has been calculated by the least squares computer program [6] and found to be 0.37 ± 0.03. In Fig. 4, $-\Delta E_{corr}$ as a function of $\bar{n}$, calculated with $K_1/K_2 = 0$, 0.37 and ∞, is compared with the values found experimentally. Obviously K_1/K_2 has a finite value, $\neq 0$.

By combining the value of K_1/K_2 with the fairly precise values of β_2 found above, better values of β_1 can be calculated. The spectrophotometric data are in fact best fitted by $\beta_1 = 9.50 \times 10^6$ M^{-1} and $\beta_2 = 2.44 \times 10^{14}$ M^{-1}. This set of constants is therefore considered to be the "best" one.

With $K_1/K_2 = 0.37$, the co-ordinates of the maximum of $\bar{n}/[L]$ *vs.* [L] plot will be (eqns. 10 and 11).

$$[L]_0 = 0.3945/\beta_1$$

and

$$(\bar{n}/[L])_{max} = 1.726\ \beta_1$$

or, for the value of $\beta_1 = 9.50 \times 10^6$ M^{-1} found above

$$[L]_0 = 4.15 \times 10^{-8}\ M$$

and

$$(\bar{n}/[L]_{max} = 1.64 \times 10^7\ M^{-1}\ (cf.\ Fig.\ 3)$$

(b) *Glass electrode measurements.* In an attempt to determine the formation constants of the complexes beyond the second one, measurements with glass electrode have been carried out at high ligand concentrations in a buffered medium. On account of the low solubility of $Hg(N_3)_2$ no high values of C_{II} could be used, however. Once formed, the precipitate of $Hg(N_3)_2$ is not dissolved even at very high azide concentrations, suggesting that the higher complexes, if formed at all, must be rather weak. For the low values of C_{II} that can be used, $\lesssim 10$ mM, the values of [L] and $\bar{n}$ found are very uncertain. Some measurements carried out at the most favourable $C_{II} = 9.556$ mM are collected in Table 4. In the range of [L] studied, no perceptible formation of higher complexes takes place. Of course such complexes might be formed at even higher ligand concentrations.

Calorimetric measurements. In all the series, a ligand solution, T, was added to $V_0 = 90.00$ ml of a mercury(II) solution, S. Every titration was as a rule carried out twice, with a reproducibility generally within 0.04 J. The data are given in Table 5.

The hydrolysis of mercury(II) has been suppressed by addition of perchloric acid. As a consequence, proton as well as mercury(II) azide complexes are formed during the titrations. However, since the formation of the mercury(II) azide complexes is very strong, up to $\bar{n} = 2$ the proton azide association is negligible

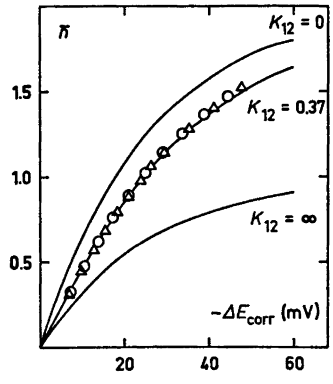

Fig. 4. Plot of $-\Delta E_{corr}$ as a function of $\bar{n}$ for $K_1/K_2 = 0$, 0.37 and ∞, *cf.* Table 3.

Table 4. Glass electrode measurements on the mercury(II) azide system at 25.00 °C and $I = 1.00$ M. For all points: $C_{II} = 9.556$ mM and $C_H = 30.88$ mM.

$-E_H$ (mV)	h (mM)	C_L (mM)	[L] (mM)	$\bar{n}$
2.6	0.0328	83.33	33.95	1.9
6.5	0.0282	88.71	39.52	1.9
9.5	0.0251	93.75	44.43	1.9
14.2	0.0209	102.9	53.31	2.0
17.9	0.0181	111.1	61.56	2.0
20.7	0.0162	118.4	68.78	2.0
23.0	0.0148	125.0	75.14	2.0
24.9	0.0138	131.0	80.93	2.0
26.6	0.0129	136.4	86.38	2.0
28.0	0.0122	141.3	91.34	2.0
29.2	0.0117	145.8	95.66	2.0
31.2	0.0108	153.9	103.2	2.1
32.8	0.0101	160.7	110.0	2.1
34.1	0.0096	166.7	115.8	2.1

and C_H remains almost the same. Beyond $\bar{n} = 2$, only formation of HN_3 takes place. When finally all perchloric acid had been converted into HN_3, the heats were practically zero.

To correct for the formation of hydrazoic acid, it is necessary to know the values of K and $\Delta H°$ for this reaction under the prevailing conditions. These quantities have been determined in an earlier investigation [1] as follows: $K = 2.77 \times 10^4$ M^{-1}, $\Delta H° = -12.76$ kJ mol^{-1}.

The enthalpy changes have been calculated by the least squares computer program "Letagrop Kalle".[14] The results are collected in Table 6.

DISCUSSION

The formation constant of FeN_3^{2+} has previously been determined under a variety of conditions.[3,15,16] In spite of the difference in the media used, the agreement with the present value, Table 6, is fairly good. Thus Bunn *et al.* have found $\beta_{1,Fe}K_a = 0.76$ at 20 °C and $I = 0.75$ M while the present value of this quantity is 0.722.

The study of the mercury(II) complexes by Musgrave and Keller [3] (at 28 °C) refers to the ionic strengths 0.05, 0.15 and 0.25 M. Their values of β_1 are compatible with the value found in the present investigation. Their values of β_2 are, on the other hand, much lower than the value of β_2 found here. This might be due to the difference in medium but a more reasonable explanation is perhaps that their calculation becomes very uncertain at $\bar{n} \approx 2$, and also at $\bar{n} \approx 1$, as they use the differences $(2/\bar{n} - 1)[L]^2$ and $(1 - 1/\bar{n})[L]$. Any small errors in $\bar{n}$ can thus cause quite erroneous estimates. Moreover, the number of experimental points is small which certainly further detracts from the precision of β_2.

The similar and strongly exothermic values of $\Delta H_1°$ and $\Delta H_2°$ for the mercury(II) azide system indicate the formation of two equivalent bonds of an essentially covalent character. Analogous complexes are of course well-known in most other halide and pseudo-halide systems of mercury(II) so far investigated.

Further azide ions are not co-ordinated within the range of the ligand concentrations used, however. In this respect, N_3^- is reminiscent of another nitrogen donor, *viz.* NH_3. Also in the ammonia system a very pronounced stop, comprising almost 6 powers of ten in [L], is observed after the co-ordination of the second ligand.[17] For most other halides and pseudo-halides this stop, though still prominent, is less marked. Only for the iodide system it is of nearly the same extension as for the much weaker nitrogen systems.[16]

The strong complex formation of the azide system is reflected mainly in the negative enthalpies. The driving force for the formation of the azide complexes of mercury(II) is the enthalpy decrease, caused by the formation of mainly covalent bonds between the metal ion and ligand. A minor contribution to the stability also comes from the entropy increase, *viz.* 24 % for the first and 12 % for the second step.

The nitrogen donors form complexes in aqueous solution with most soft acceptors and also with acceptors of medium hardness, such as Ni(II) and Zn(II). Nitrogen should therefore be classified as considerably softer than oxygen. The bonds from soft acceptors to nitrogen donors should therefore be more covalent than the bonds to oxygen donors. This ought to be reflected in more negative enthalpies for the formation of the nitrogen complexes. On the other hand, the azide ion is among the hardest of the pseudo-halides. For some of these, which

Table 5. The calorimetric data pertaining to the mercury(II) azide system. For all the series: $V_0 = 90.00$ ml and $V = (V_0 + v)$ ml.

S: $C_{II} = 0.955$ mM, $C_H = 3.09$ mM, $C_{NaClO_4} = 994$ mM
T: $C_L = 100.0$ mM, $C_{NaClO_4} = 900$ mM

v (ml), Q_{corr} (J), δQ_{corr} (J): 1.00, 3.254, 0.044; 5.00, 1.672, 0.103; 2.00, 2.743, 0.097; 8.00, 0.114, 0.024: 3.00, 1.277, −0.014.

S: $C_{II} = 0.955$ mM, $C_H = 53.09$ mM, $C_{NaClO_4} = 944$ mM
T: $C_L = 100.0$ mM, $C_{NaClO_4} = 900$ mM

v (ml), Q_{corr} (J), δQ_{corr} (J): 1.00, 3.058, 0.061; 5.00, 2.569, 0.039; 2.00, 2.523, 0.185; 7.00, 2.548, 0.015; 3.00, 1.448, 0.074.

S: $C_{II} = 1.911$ mM, $C_H = 6.18$ mM, $C_{NaClO_4} = 988$ mM
T: $C_L = 100.0$ mM, $C_{NaClO_4} = 900$ mM

v (ml), Q_{corr} (J), δQ_{corr} (J): 2.00, 6.475, 0.122; 4.00, 5.759, −0.070.

S: $C_{II} = 1.911$ mM, $C_H = 6.18$ mM, $C_{NaClO_4} = 988$ mM
T: $C_L = 100.0$ mM, $C_{NaClO_4} = 900$ mM

v (ml), Q_{corr} (J), δQ_{corr} (J): 1.00, 3.201, 0.047; 2.00, 3.467, −0.118; 3.00, 3.617, −0.234; 4.00, 2.095, 0.212; 6.00, 2.537, 0.018; 8.00, 2.337, 0.080; 11.00, 1.134, 0.210; 14.00, 0.137, −0.075.

S: $C_{II} = 1.911$ mM, $C_H = 56.18$ mM, $C_{NaClO_4} = 938$ mM
T: $C_L = 100.0$ mM, $C_{NaClO_4} = 900$ mM

v (ml), Q_{corr} (J), δQ_{corr} (J): 2.00, 6.363, 0.043; 4.00, 5.368, 0.173; 6.00, 2.838, 0.007; 9.00, 3.816, 0.061; 12.00, 3.744, 0.095.

S: $C_{II} = 1.911$ mM, $C_H = 56.18$ mM, $C_{NaClO_4} = 938$ mM
T: $C_L = 100.0$ mM, $C_{NaClO_4} = 900$ mM

v (ml), Q_{corr} (J), δQ_{corr} (J): 1.00, 3.114, 0.047; 2.00, 3.339, −0.094; 3.00, 3.151, −0.005; 4.00, 2.121, 0.274; 5.00, 1.426, 0.082; 6.00, 1.350, −0.013; 8.00, 2.545, 0.047; 10.00, 2.529, 0.037.

S: $C_{II} = 2.867$ mM, $C_H = 59.26$ mM, $C_{NaClO_4} = 932$ mM
T: $C_L = 100.0$ mM, $C_{NaClO_4} = 900$ mM

v (ml), Q_{corr} (J), δQ_{corr} (J): 1.00, 3.119, 0.039; 2.00, 3.341, −0.080; 3.00, 3.164, 0.116; 4.00, 3.314, −0.068; 6.00, 4.887, 0.252, 8.00, 2.801, 0.037, 11.00, 3.796, 0.098, 14.00, 3.795, 0.051.

S: $C_{II} = 2.867$ mM, $C_H = 59.26$ mM, $C_{NaClO_4} = 932$ mM
T: $C_L = 100.0$ mM, $C_{NaClO_4} = 900$ mM

v (ml), Q_{corr} (J), δQ_{corr} (J): 1.50, 4.713, 0.071; 3.00, 4.978, −0.062; 5.00, 6.274, −0.021; 7.00, 3.378, 0.243; 10.00, 3.845, 0.109.

S: $C_{II} = 4.778$ mM, $C_H = 15.44$ mM, $C_{NaClO_4} = 970$ mM
T: $C_L = 100.0$ mM, $C_{NaClO_4} = 900$ mM

v (ml), Q_{corr} (J), δQ_{corr} (J): 2.00, 6.379, 0.084; 4.00, 6.697, −0.033; 6.00, 6.856, −0.111; 8.00, 6.859, −0.124.

S: $C_{II} = 4.778$ mM, $C_H = 65.44$ mM, $C_{NaClO_4} = 920$ mM
T: $C_L = 100.0$ mM, $C_{NaClO_4} = 900$ mM

v (ml), Q_{corr} (J), δQ_{corr} (J): 1.00, 3.114, 0.030; 2.00, 3.287, −0.039; 3.00, 3.368, −0.083; 4.00, 3.383, −0.079; 5.00, 3.381, −0.068; 7.00, 6.622, −0.049.

S: $C_{II} = 4.778$ mM, $C_H = 65.44$ mM, $C_{NaClO_4} = 920$ mM
T: $C_L = 100.0$ mM, $C_{NaClO_4} = 900$ mM

v (ml), Q_{corr} (J), δQ_{corr} (J): 1.50, 4.770, −0.009; 3.00, 4.969, −0.054; 4.50, 5.039, −0.079; 6.00, 4.988, −0.025; 8.00, 6.464, −0.083.

Table 6. The overall formation constants and the values of $\Delta G°_j$, $\Delta H°_j$ and $\Delta S°_j$ for the consecutive steps of the mercury(II) azide system, and the values of β_1 and $\Delta G°_1$ of the iron(III) system, at 25.00 °C and $I = 1.00$ M. The errors given correspond to three standard deviations or to estimated errors.

System	j	β_j (M^{-j})	$-\Delta G°_j$ (kJ mol^{-1})	$-\Delta H°_j$ (kJ mol^{-1})	$\Delta S°_j$ (J mol^{-1} K^{-1})
$Hg^{2+} - N_3^-$	1	$(9.50 \pm 0.50) \times 10^8$	39.83 ± 0.13	30.4 ± 1.6	32 ± 5
	2	$(2.44 \pm 0.18) \times 10^{14}$	42.29 ± 0.22	37.1 ± 1.8	17 ± 6
$Fe^{3+} - N_3^-$	1	$(2.00 \pm 0.06) \times 10^4$	24.55 ± 0.07		

have been discussed in this connexion, the order of increasing softness is $N_3^- < SCN^- < SeCN^- < CN^-$. Among this series of donors, the covalency increases and the tendency to ionic bonding decreases. Their affinity for soft acceptors thus increases in the order given.

Acknowledgement. The support given to these investigations by Statens naturvetenskapliga forskningsråd (The Swedish Natural Science Research Council) and the Scientific and Technical Research Council of Turkey is gratefully acknowledged.

REFERENCES

1. Ahrland, S. and Avşar, E. *Acta Chem. Scand. A 29* (1975) 881.
2. Ahrland, S. and Avşar, E. *Acta Chem. Scand. A 29* (1975) 890.
3. Musgrave, T. R. and Keller, R. N. *Inorg. Chem. 4* (1965) 1793.
4. Fronæus, S. In Jonassen, H. B. and Weissberger, A. *Techniques of Inorg. Chem.*, Interscience, New York, London 1963, Vol. 1, Chapt. 1.
5. Sandell, A. *Acta Chem. Scand. 25* (1971) 2609.
6. Karlsson, R. *Private communication.*
7. Pugh, W. *J. Chem. Soc.* (1937) 1824.
8. Jonsson, A., Qvarfort, I. and Sillén, L. G. *Acta Chem. Scand. 1* (1947) 461.
9. Anton, A., Dodd, J. G. and Harvey, Jr., A. E. *Anal. Chem. 32* (1960) 1209.
10. Grenthe, I., Ots, H. and Ginstrup, O. *Acta Chem. Scand. 24* (1970) 1067.
11. Ahrland, S. and Kullberg, L. *Acta Chem. Scand. 25* (1971) 3471.
12. Johansson, L. *Acta Chem. Scand. 25* (1971) 3569.
13. Sillén, L. G. and Infeldt, G. *Sv. Kem. Tidskr. 58* (1946) 61.
14. Arnek, R. *Ark. Kemi 32* (1970) 81.
15. Bunn, D., Dainton, F. S. and Duckworth, S. *Trans. Faraday Soc. 57* (1961) 1131.
16. Wallace, R. M. and Dukes, E. K. *J. Phys. Chem. 65* (1961) 2094.
17. Bjerrum, J. *Metal Ammine Formation in Aqueous Solution*, Diss., University of Copenhagen, Copenhagen 1941.
18. Sillén, L. G. *Acta Chem. Scand. 3* (1949) 539.

Received June 9, 1975.

Acta Chemica Scandinavica A 30 (1976) 24—30

The Molecular and Crystal Structure of Tris(1,2-ethanediol)-cobalt(II) Sulfate: $[Co(C_2H_6O_2)_3]SO_4$

BRITT-MARIE ANTTI

Department of Inorganic Chemistry, University of Umeå, S-901 87 Umeå, Sweden

The crystal structure of $[Co(C_2H_6O_2)_3]SO_4$ has been determined and refined using three-dimensional X-ray diffraction data. The unit cell is monoclinic, $P2_1/c$, with $Z=4$ and cell dimensions $a=8.818(1)$ Å, $b=7.585(1)$ Å, $c=19.264(1)$ Å and $\beta=99.357(5)°$. The structure was solved by heavy-atom Patterson and Fourier methods and refined by full-matrix least-squares techniques based on 3130 independent intensities. The final R-value was 0.038. The structure consists of discrete $[Co(C_2H_6O_2)_3]^{2+}$-cations and SO_4^{2-}-anions. Co(II) is octahedrally surrounded by six glycol oxygens with the Co—O distances ranging between 2.054(2) and 2.108(2) Å. The sulfate ions connect these cations by means of hydrogen bonds.

This work forms part of a research program at this department which includes the investigation of the coordination changes in complexes between glycol* and a series of transition metal ions ($Mn^{2+}-Zn^{2+}$). Two series are considered, one with chloride as anion [1,2] and the other with sulfate as anion. This paper presents the structure of $[Co(C_2H_6O_2)_3]SO_4$, which is the third in the sulfate series, the other two being $[Cu(C_2H_6O_2)_3]SO_4$[3] and $[Ni(C_2H_6O_2)_3]SO_4$. The nickel compound has only been characterized from Weissenberg film data and was found to be isostructural with $[Cu(C_2H_6O_2)_3]SO_4$.[2] No further X-ray data have been collected so far.

EXPERIMENTAL

Crystal preparation and analyses. Pink, tabular (100), crystals separated when solutions of $CoSO_4.7H_2O$ in glycol (molar ratio 1:3) were kept in a desiccator over sulfuric acid for a few days. The cobalt content of the crystals was determined by titration with EDTA [4] to be 17.24 (weight-%). Calculated for $[Co(C_2H_6O_2)_3]SO_4$: 17.27. IR-spectra confirmed the absence of water in the structure.

Crystal data and space group. Rotation and Weissenberg photographs (zero and first layers) taken from crystals mounted around their b- and c-axes revealed that the crystals were monoclinic. The unit cell parameters measured from these photographs were refined using data obtained from powder photographs taken with a camera of Guinier-Hägg type with Cu$K\alpha$-radiation and Si ($a=5.43054$ Å) as internal standard. (Copper foil was used to avoid fluorescence.) The cell parameters, with estimated standard deviations in parentheses, are $a=8.818(1)$ Å, $b=7.585(1)$ Å, $c=19.264(1)$ Å and $\beta=99.357(5)°$. A density of 1.77 ± 0.01 g cm^{-3} was measured for $[Co(C_2H_6O_2)_3]SO_4$ with the flotation method using bromoform and xylene. The calculated value for four formula units was 1.78 g cm^{-3}. The systematic extinctions of intensities found for $h0l$ when $l=2n+1$ and for $0k0$ when $k=2n+1$ are characteristic for the space group $P2_1/c$ (No. 14).

Intensity data. A crystal with dimensions $0.08\times0.25\times0.14$ mm was chosen for the measurements. As it was hygroscopic, it was mounted in a capillary of Lindeman glass with its b-axis parallel to the rotation axis. 4227 diffracted intensities from $h0l-h10l$ were measured with the automatic linear diffractometer PAILRED using graphite-monochromated Mo$K\alpha$-radiation. The intensities were measured by omega-scan and the half scan interval for $h0l$ reflexions was 1.0° for $\theta>18°$ and 1.9° for $\theta\leq18°$. For $h1l$ reflexions the corresponding values were 1.0 and 2.0° and these values were then used for the remaining layers. Reflexions for which the total number of counts during one scan interval did not exceed 4000 were measured twice. Background intensities were measured for 40 s before and after each scan and the scan speed was 1°/min. 3130 independent intensities ($\sin\theta_{max}=0.58$), which were significantly above back-

* Throughout this paper 1,2-ethanediol will be referred to as glycol.

Table 1. Computer programs used for the crystallographic calculations.

Name	Program function	Authors
PIRUM	Indexing and refinement of cell parameters from powder data.	P.-E. Werner, Stockholm, Sweden.[11]
TAPESUSY	Primary reduction of PAILRED diffractometer data.	O. Mårtensson and B. Hedman, Umeå, Sweden.
ABSOT [a]	Lorentz, polarization and absorption corrections for data collected using Weissenberg geometry. Preparative calculations for isotropic extinction correction in subsequent least-squares program.	P. Coppens, L. Leiserowitz and D. Rabinovich; modified by J. O. Thomas, Uppsala, Sweden.
UPALS [a]	Full-matrix least-squares refinement of atomic positional and thermal parameters, scale factors, and isotropic or anisotropic extinction parameters according to P. Coppens and W. C. Hamilton.[13]	J.-O. Lundgren, Uppsala, Sweden.[12] The program is based on LALS, a revised version of UCLALS1 by P. K. Gantzel, R. A. Sparks and K. N. Trueblood.
DRF [a]	Fourier summations including routines for structure factor calculations.	A. Zalkin, Berkeley, USA; modified by R. Liminga, J.-O. Lundgren, Uppsala and O. Lindgren, Göteborg, Sweden.
DISTAN [a]	Calculation of distances and angles, with corresponding standard deviations.	A. Zalkin, Berkeley, USA; modified by R. Liminga and J.-O. Lundgren, Uppsala, Sweden.
PLANE [a]	Calculation of least-squares planes using the method suggested by D. Blow [14] and calculation of the distance from a point to a plane and dihedral angles between planes.	C.-I. Brändén, Uppsala; modified by J.-O. Lundgren, Uppsala, Sweden.
SFIG	Calculation of structure factors for possible reflexions in a preset part of the reflexion sphere.	R. Liminga, Uppsala, Sweden.
ORTEP	Thermal ellipsoid plot program for stereoscopic illustrations of crystal structures.	C. K. Johnson, Oak Ridge, USA.[15]
LAYOUT	Editing of structure factor tables.	O. Mårtensson, Umeå, Sweden.

[a] These programs have been modified for a CDC 3300 computer by B. Hedman, Umeå, Sweden.

ground at the 95 % level, *i.e.* had $\Delta I/I \leqq 0.5$,[1] were used in the refinements. Lp and absorption corrections were made. The linear absorption coefficient was 15.94 cm^{-1} and the transmission factor varied from 0.79 to 0.88. When the refinements were terminated, structure factors for all the unobserved intensities were calculated. They all had amplitudes lower than or equal to the corresponding threshold value.

The data programs used in the course of this structure determination are listed in Table 1. All calculations were performed on a CDC 3300 computer.

STRUCTURE DETERMINATION AND REFINEMENT

From a three-dimensional Patterson vector map the positions for the cobalt and sulfur atoms were found. A Fourier synthesis was calculated, based on these positions, and from this all the remaining non-hydrogen atoms were located. All atoms lie in general four-fold positions. The structure was refined by full-matrix least-squares techniques. When the positional

Table 2a. Atomic positional and thermal parameters for $[Co(C_2H_6O_2)_3]SO_4$. All parameters have been multiplied by 10^4. The anisotropic temperature factors have been calculated according to the formula $\exp[-(h^2\beta_{11}+k^2\beta_{22}+l^2\beta_{33}+2hk\beta_{12}+2hl\beta_{13}+2kl\beta_{23})]$. (Standard deviations are given in parentheses.)

	x	y	z	β_{11}	β_{22}	β_{33}	β_{12}	β_{13}	β_{23}
Co	2351(0.4)	1229(0.5)	3706(0.2)	53(0.4)	66(0.5)	12(0.1)	5(0.4)	3(0.1)	1(0.2)
O(1)	3090(2)	2946(3)	3007(1)	82(3)	158(5)	13(0.5)	−19(3)	1(1)	12(1)
O(2)	4580(2)	1812(3)	4235(1)	64(2)	93(4)	19(0.6)	10(2)	−0.2(1)	5(1)
O(3)	1485(2)	3218(3)	4276(1)	75(3)	89(3)	16(0.5)	13(2)	6(1)	−4(1)
O(4)	74(2)	1275(3)	3166(1)	64(2)	132(4)	18(0.6)	−8(3)	1(1)	−2(1)
O(5)	2892(2)	−1123(3)	3241(1)	86(3)	106(4)	18(0.6)	8(3)	11(1)	−7(1)
O(6)	1800(3)	−600(3)	4436(1)	122(3)	77(3)	14(0.5)	−2(3)	10(1)	−1(1)
C(1)	4692(4)	3389(5)	3166(2)	78(4)	126(6)	20(1)	21(4)	9(1)	6(2)
C(2)	5087(3)	3420(4)	3953(2)	76(4)	82(5)	22(1)	−14(3)	−0.1(1)	−4(2)
C(3)	−170(4)	3236(5)	4117(2)	70(4)	118(6)	26(1)	18(4)	14(2)	−6(2)
C(4)	−599(4)	2887(5)	3344(2)	70(4)	142(6)	24(1)	25(4)	−3(2)	9(2)
C(5)	2065(4)	−2531(4)	3508(2)	89(4)	80(5)	21(1)	1(3)	5(1)	−12(2)
C(6)	2225(4)	−2365(4)	4295(2)	148(5)	69(5)	19(1)	1(4)	12(2)	−3(2)
S	2775(1)	3267(1)	1141(0.3)	56(1)	83(1)	12(0.2)	−14(1)	4(0.3)	5(0.3)
O(7)	1832(3)	3586(4)	1696(1)	88(3)	193(6)	17(1)	41(3)	13(1)	18(1)
O(8)	2913(2)	4947(3)	760(1)	94(3)	93(4)	19(1)	−27(3)	0.5(1)	13(1)
O(9)	4298(2)	2668(3)	1478(1)	63(3)	137(5)	32(1)	13(3)	5(1)	16(2)
O(10)	2041(3)	1947(4)	649(1)	188(5)	143(5)	18(1)	−91(4)	3(1)	−2(1)

Table 2b. Atomic positional and thermal parameters for the hydrogen atoms. The fractional coordinates have been multiplied by 10^3. (Standard deviations are given in parentheses.)

	x	y	z	B
H(1)	273(4)	307(6)	262(2)	3.4(8)
H(2)	480(4)	633(6)	75(2)	3.4(8)
H(3)	172(4)	327(6)	469(2)	3.8(9)
H(4)	52(4)	554(6)	180(2)	4.0(9)
H(5)	361(5)	869(7)	326(2)	4.7(10)
H(6)	212(5)	964(6)	485(2)	4.0(10)
H(7)	466(3)	747(4)	203(1)	1.3(6)
H(8)	483(4)	445(6)	291(2)	3.3(8)
H(9)	389(4)	858(5)	91(2)	2.2(7)
H(10)	451(4)	422(6)	419(2)	3.6(9)
H(11)	64(5)	729(6)	60(2)	4.0(9)
H(12)	62(5)	939(7)	72(2)	5.2(11)
H(13)	30(4)	872(5)	194(2)	2.2(7)
H(14)	171(4)	786(6)	181(2)	3.2(8)
H(15)	247(4)	629(5)	338(2)	2.5(7)
H(16)	96(4)	763(5)	323(2)	2.0(7)
H(17)	160(3)	679(5)	450(2)	2.0(7)
H(18)	325(4)	738(6)	455(2)	3.5(9)

coordinates and the anisotropic temperature factors for all atoms were used as parameters, the refinement converged at an R-value of 0.049 ($R=[\sum||F_o|-|F_c||]/\sum|F_o|$). At this stage a difference electron density map was calculated, and, from this, probable positions for the hydrogen atoms were located. When their atomic positional and isotropic thermal factors were included as parameters, the refinement finally gave an R-value of 0.038. The weights were calculated by the method suggested by Cruickshank,[5] $w=1/(a+|F_o|+c|F_o|^2+d|F_o|^3)$ with $a=400$, $c=0.03$ and $d=0.001$. The final $R_w=[\sum w_i(|F_o|-|F_c|)^2/\sum w_i|F_o|^2]^{1/2}=0.034$. The scattering curves used for Co^{2+}, S, O, and C were those proposed by Cromer and Waber.[6] The anomalous dispersion corrections for Co^{2+} and S were selected from Cromer and Liebermans [7] calculations, and both $\Delta f'$ and $\Delta f''$ were taken into account. For the hydrogen atoms, the scattering curve given by Stewart *et al.*[8] was used. A final difference electron density map was almost flat (the highest peak corresponded to 0.44 e Å^{-3}).

The final atomic positional and thermal parameters are given in Tables 2a and b. The corresponding observed and calculated structure amplitudes can be obtained from the author, on request.

DESCRIPTION AND DISCUSSION OF THE STRUCTURE

The structure consists of discrete $[Co(C_2H_6O_2)_3]^{2+}$-cations and SO_4^{2-}-anions. These are mutually related in the way shown in Fig. 1, and are connected by means of hydrogen bonds between sulfate and glycol oxygens.

The coordination around Co(II). In the cation, Co(II) coordinates the six glycol oxygens with a slightly distorted octahedral arrangement with O(1) at the significantly shortest distance (2.054 Å); O(3), O(5) and O(6) at a mean distance of 2.086 Å, and O(2) and O(4) at the significantly longest distance (mean value 2.107 Å) to Co(II). The deviation of the four nearest ligands from the calculated least-squares plane around Co(II) is −0.073(3), 0.073(3), 0.083(3), −0.100(3) Å for O(1), O(3), O(5), and O(6), respectively, the atoms on which the calculation is based. Co(II) is situated 0.009(1) Å above the plane

The ligands. The glycol ligands, which act as bidentate ligands, all have *gauche* conformation with dihedral angles between connected O−C−C planes of 51.3, 55.9, and 51.8°, respectively, for ligands I, II, and III (for the labeling of ligands see Table 3). These values are

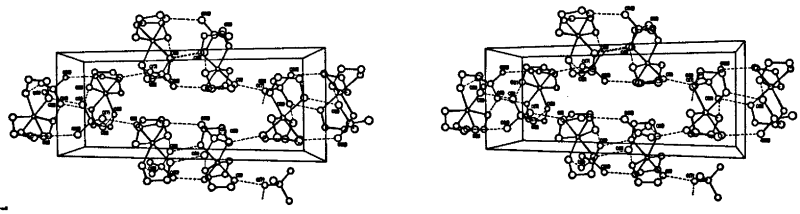

Fig. 1. A stereoscopic view of the molecular packing in $[Co(C_2H_6O_2)_3]SO_4$. Hydrogen bonds are marked with dashed lines.

Table 3. Dimensions of the $[Co(C_2H_6O_2)_3]^{3+}$-ion. (Standard deviations are given in parentheses.) The labelling of atoms is in accordance to Fig. 2.

Atoms	d (Å)	Atoms	Angle (°)	Atoms	Angle (°)
Co – O(1)	2.054(2)	O(1) – Co – O(2)	79.3(1)	O(3) – Co – O(4)	81.2(1)
Co – O(2)	2.108(2)	O(1) – Co – O(3)	93.9(1)	O(3) – Co – O(5)	167.2(1)
Co – O(3)	2.082(2)	O(1) – Co – O(4)	92.6(1)	O(3) – Co – O(6)	88.9(1)
Co – O(4)	2.106(2)	O(1) – Co – O(5)	98.2(1)	O(4) – Co – O(5)	93.9(1)
Co – O(5)	2.087(2)	O(1) – Co – O(6)	175.0(1)	O(4) – Co – O(6)	92.0(1)
Co – O(6)	2.088(2)	O(2) – Co – O(3)	89.2(1)	O(5) – Co – O(6)	79.4(1)
		O(2) – Co – O(4)	167.0(1)		
		O(2) – Co – O(5)	97.3(1)		
		O(2) – Co – O(6)	96.6(1)		

Ligand	Atoms	d_{O-C} (Å)	d_{C-C} (Å)	$\angle_{O-C-C}$ (°)	$\angle_{Co-O-C}$ (°)
I	Co < O(1) – C(1)	1.435(4)	1.500(5)	106.2(2)	114.5(2)
	Co < O(2) – C(2)	1.436(4)		109.5(3)	108.6(2)
II	Co < O(3) – C(3)	1.442(4)	1.500(5)	107.0(3)	109.9(2)
	Co < O(4) – C(4)	1.426(4)		110.0(3)	107.2(2)
III	Co < O(5) – C(5)	1.435(4)	1.503(5)	109.3(3)	108.5(2)
	Co < O(6) – C(6)	1.429(4)		106.6(3)	113.5(2)

Atoms	d (Å)	Atoms	d (Å)	Atoms	d (Å)
O(1) – H(1)	0.77(4)	C(1) – H(7)	1.01(3)	C(4) – H(13)	0.91(4)
O(2) – H(2)	0.66(4)	C(1) – H(8)	0.96(4)	C(4) – H(14)	0.97(4)
O(3) – H(3)	0.79(4)	C(2) – H(9)	0.90(3)	C(5) – H(15)	1.01(4)
O(4) – H(4)	0.77(4)	C(2) – H(10)	0.95(4)	C(5) – H(16)	1.04(3)
O(5) – H(5)	0.64(4)	C(3) – H(11)	1.03(4)	C(6) – H(17)	0.97(3)
O(6) – H(6)	0.82(4)	C(3) – H(12)	1.03(5)	C(6) – H(18)	0.97(4)

in good agreement with those previously determined for metal-glycol complexes where glycol functions as a bidentate ligand.[1–3]

In the five-membered $Co-O_2-C_2$ rings, the intramolecular distances show no significant deviations from other published values. The intra-ring angles show the same trend for all three rings; when the Co – O – C angle is larger than or almost equal to the tetrahedral angle the corresponding O – C – C angle is smaller than that value or *vice versa*. The O – H and C – H distances are normal for X-ray data and the angles around oxygen and carbon involving hydrogen atoms agree fairly well with the tetrahedral angle, they range between 98 and 128°. A list of distances and angles is presented in Table 3.

Conformational analysis. Using the terminology discussed by Raymond *et al.*[9] for tris-(ethylenediamine)-metal complexes and looking down the molecular three-fold axis, which almost parallels the crystallographic c-axis, the $[Co(C_2H_6O_2)_3]^{3+}$-ions have the $\Lambda\delta\delta\delta(=\Delta\lambda\lambda\lambda)$ conformation (Fig. 2). As the structure is centrosymmetric both enanthiomorphs Λ and Δ will be present in equal amounts. In $[Cu(C_2H_6O_2)_3]SO_4$[3] at least one of the glycol ligands has a $\Lambda\lambda(=\Delta\delta)$ conformation which was explained in terms of shorter hydrogen bond distances to sulfate oxygens from that ligand, compared to the other two. In this structure the hydrogen bond distances are all of about the same order of magnitude [2.614(3) – 2.683(4) Å] as would be expected

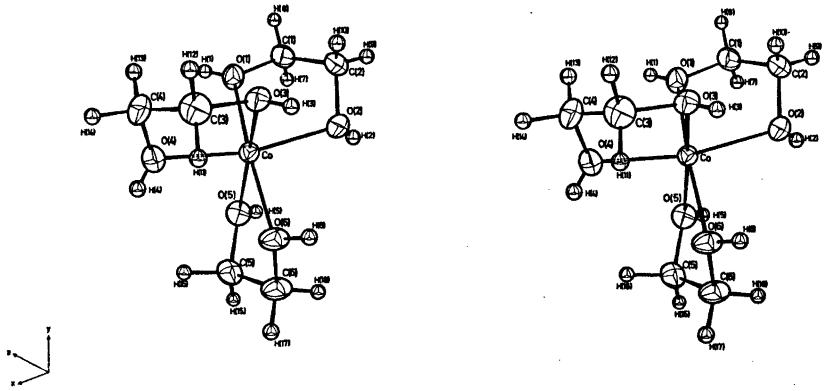

Fig. 2. A stereoscopic illustration of the $[Co(C_2H_6O_2)_3]^{2+}$-ion looking down [101] and showing the coordination around Co(II). Thermal ellipsoids are scaled to enclose 50 % probability.

from the conformational analysis. These values agree well with those found in $[Co(H_2O)_6]SO_4$,[10] where the O···O distances range between 2.65(3) and 2.93(3) Å. The $\Lambda\delta$-conformation of the glycol ligands in $[Co(C_2H_6O_2)_3]SO_4$, which means that the C–C bonds almost parallel [001], could be a reason for the elongation of the unit cell in the *c*-direction.

The sulfate ion and the hydrogen bond contacts. The sulfate group, like the rest of the molecule, seems to be essentially strain-free. The largest deviation from the tetrahedral angle is 1.3°. The S–O distances could be divided into two groups which differ slightly in length. O(7) and O(8) have a mean distance of 1.481 Å to the sulfur atom and show two hydrogen bonds each, while O(9) and O(10) having one hydrogen bond contact each are at a mean distance of 1.461 Å from the sulfur atom. As is indicated in Table 4, none of the hydrogen bonds deviate significantly from linearity.

Acknowledgements. I wish to express my sincere thanks to Professor Nils Ingri for much valuable advice and for all the facilities placed at my disposal. I also thank Dr. Britt Hedman for all the help concerning computational problems. The English of this paper has been corrected by Dr. Michael Sharp. This work forms part of a program supported by the Swedish Natural Science Research Council.

Table 4. Dimensions of the sulfate group and hydrogen bond contacts in $[Co(C_2H_6O_2)_3]SO_4$. (Standard deviations are given in parentheses.)

Atoms	*d* (Å)	Atoms	Angle (°)
S–O(7)	1.477(2)	O(7)–S–O(8)	108.5(1)
S–O(8)	1.485(2)	O(7)–S–O(9)	108.2(1)
S–O(9)	1.465(2)	O(7)–S–O(10)	110.0(2)
S–O(10)	1.456(3)	O(8)–S–O(9)	110.0(1)
		O(8)–S–O(10)	109.4(1)
		O(9)–S–O(10)	110.7(2)

Atoms	d_{O-H} (Å)	$d_{H\cdots O}$ (Å)	$d_{O\cdots O}$ (Å)	$\angle_{O-H\cdots O}$ (°)
O(1)–H(1)···O(7)	0.77(4)	1.87(4)	2.633(3)	174(5)
O(2)–H(2)···O(8)	0.66(4)	1.97(4)	2.623(3)	177(4)
O(3)–H(3)···O(10)	0.79(4)	1.83(4)	2.614(3)	170(5)
O(4)–H(4)···O(7)	0.77(4)	1.91(4)	2.683(4)	175(4)
O(5)–H(5)···O(9)	0.64(4)	1.99(4)	2.615(3)	165(6)
O(6)–H(6)···O(8)	0.82(4)	1.81(4)	2.628(3)	176(4)

REFERENCES

1. Antti, B.-M. *Acta Chem. Scand. 27* (1973) 3513.
2. Antti, B.-M. *Acta Chem. Scand. A 29* (1975) 76.
3. Antti, B.-M., Lundberg, B. K. S. and Ingri, N. *Acta Chem. Scand. 26* (1972) 3984.
4. Kolthoff, I. M., Sandell, E. B., Meehan, E. J. and Bruckenstein, S. *Quantitative Chemical Analysis*. 4th Ed., Macmillan, London 1969, p. 744.
5. Cruickshank, D. W. J. *Computing Methods in Crystallography*, Pergamon, London 1965, p. 114.
6. Cromer, D. T. and Waber, J. T. *Acta Crystallogr. 18* (1965) 104.
7. Cromer, D. T. and Lieberman, D. *J. Chem. Phys. 53* (1970) 1891.
8. Stewart, R. F., Davidson, E. R. and Simpson, W. T. *J. Chem. Phys. 42* (1965) 3175.
9. Raymond, K. N., Corfield, P. W. R. and Ibers, J. A. *Inorg. Chem. 7* (1968) 842.
10. Zalkin, A., Ruben, H. and Templeton, D. H. *Acta Crystallogr. 15* (1962) 1219.
11. Werner, P.-E. *Ark. Kemi 31* (1970) 513.
12. Lundgren, J.-O. *UPALS a Crystallographic Full-matrix Least-squares Refinement Program*. UUIC-B13-3. Inst. of Chemistry, Univ. of Uppsala, Sweden 1972.
13. Coppens, P. and Hamilton, W. C. *Acta Crystallogr. A 26* (1970) 71.
14. Blow, D. *Acta Crystallogr. 13* (1960) 168.
15. Johnson, C. K. (1965) *ORTEP*. ORNL-3794, Oak Ridge National Laboratory, Oak Ridge, Tennessee.

Received June 13, 1975.

Acta Chemica Scandinavica A 30 (1976) 31—38

Kinetics of Dissociation of the Tetracyanonickelate(II) Ion

HANS PERSSON* and CARL GUSTAV EKSTRÖM

Division of Physical Chemistry, University of Lund, Chemical Center, P.O.B. 740, S-220 07 Lund 7, Sweden

The acid dissociation of $Ni(CN)_4^{2-}$ has been studied spectrophotometrically mainly at 267.5 nm in the pH range $0 < pH < 3$. The ionic strength was kept at 3.00 M by means of sodium perchlorate. The temperature was 25.0 °C. The measurements show that the kinetics of dissociation can be adequately described by

$$-d[Ni(CN)_4^{2-}]/dt = k_{obs}[Ni(CN)_4^{2-}]$$

with

$$k_{obs}^{-1} = (k_{00} + k_{01}h)^{-1} + [HCN](k_{11}h + k_{12}h^2)^{-1}$$

which corresponds to the following stoichiometric mechanism

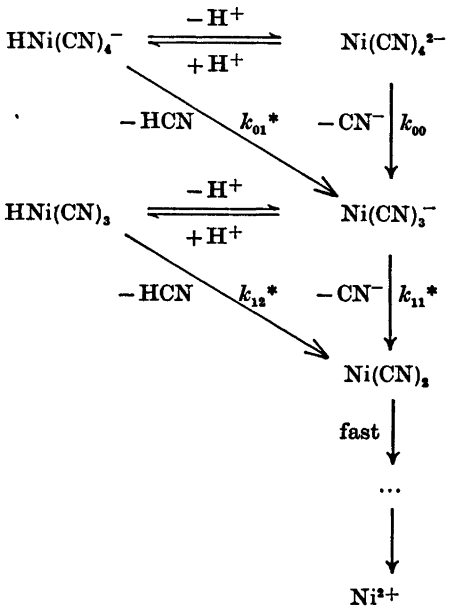

In this scheme horizontal arrows represent rapid protonations and deprotonations, and

$k_{00} = (3.4 \pm 0.6)10^{-4}$ s^{-1};
$k_{01} = (3.34 \pm 0.16)10^{-3}$ s^{-1} M^{-1}

$k_{11} = (1.55 \pm 0.15)10^{-5}$ s^{-1};
$k_{12} = (5.5 \pm 0.4)10^{-5}$ s^{-1} M^{-1}

(The error limits are given as three times the standard deviations). While k_{00} is a true rate constant, k_{01}, k_{11} and k_{12} are products of rate constants and equilibrium constants:

$k_{01} = k_{01}^* K_{h0}$; $k_{11} = k_{11}^* K_{00} K_a^{-1}$;
$k_{12} = k_{12}^* K_{00} K_{h1} K_a^{-1}$

where $K_{h0} = \dfrac{[HNi(CN)_4^-]}{[Ni(CN)_4^{2-}]h}$;

$K_{00} = \dfrac{[Ni(CN)_3^-]_{eq}[CN^-]_{eq}}{[Ni(CN)_4^{2-}]_{eq}}$;

$K_{h1} = \dfrac{[HNi(CN)_3]}{[Ni(CN)_3^-]h}$

are equilibrium constants. (K_a = dissociation constant for HCN). Since the values of the equilibrium constants K_{h0}, K_{00} and K_{h1} are unknown the pure rate constants k_{01}^*, k_{11}^* and k_{12}^* cannot be determined.

The kinetics of the formation and dissociation of the tetracyanonickelate(II) ion have previously been investigated by Kolski and Margerum.[1] These authors report an extensive formation of acid nickel cyanide species, $H_xNi(CN)_4^{x-2}$, analogous to those reported, *e.g.* for the iron(II)-cyanide system.[2] According to Kolski and Margerum protonated nickel cyanide complexes should in fact be the dominating species at equilibrium at $pH < 5$.

Our study of the system $Ni^{2+} - CN^-$ at equilibrium shows that the only complex existing

* Correspondence to be adressed to this author.

in appreciable concentrations is $Ni(CN)_4^{2-}$ and that concentrations of $NiCN^+$, $Ni(CN)_2$ and $Ni(CN)_3^-$ are negligible.[3]

Our analyses of potentiometric data do not support the suggestion that protonated nickel cyanide species exist at equilibrium and certainly exclude a formation of acid complexes to the extent claimed by Kolski and Margerum.[1]

Since we have not been able to find those protonated species which are fundamental parts of the kinetic model proposed by Kolski and Margerum, we considered it important to investigate the kinetics as well.

The acid dissociation of $Ni(CN)_4^{2-}$ is a rather slow process and is well suited for study by conventional spectrophotometric techniques. In our studies of the association reaction, to be published in a later paper, stopped-flow methods have been used in addition.

The present paper describes the dissociation measurements.

EXPERIMENTAL

Chemicals. Perchloric acid, sodium perchlorate, sodium cyanide, and nickel(II) perchlorate were obtained as described in previous papers.[3,4] Stock solutions of $Na_2Ni(CN)_4$ were prepared in two ways: (1) directly from calculated amounts of sodium cyanide and nickel(II) perchlorate solution and (2) from solid $Na_2Ni(CN)_4$ prepared by a modification of the procedure described by Fernelius *et al.*[5] Since the precipitate of $Ni(CN)_2$ was difficult to filter, centrifugation was used instead.

No difference between the results obtained using the different stock solutions could be found.

Measurements. An absorption spectrum for $Ni(CN)_4^{2-}$ was recorded as described previously [3] using a Hitachi EPS-3T spectrophotometer. This spectrum showed three absorbance peaks at 267.5, 285 and 310 nm, respectively. 267.5 nm was chosen as a suitable wavelength for measurements. At 267.5 nm CN^-, HCN and Ni^{2+} have negligible absorbances.

For the kinetic measurements a Zeiss PMQ II spectrophotometer equipped with 1 – 5 cm Beckman quartz cuvettes was used. The molar absorptivity for $Ni(CN)_4^{2-}$ at 267.5 nm was determined to 1.06×10^4 M^{-1} cm^{-1}.

The rate dependence on the species $Ni(CN)_4^{2-}$, H^+, Ni^{2+} and HCN (or CN^-) has been investigated.

In the first series of measurements $[H^+]$ was kept constant within each series. The solutions were obtained by mixing equal volumes of two solutions S and T by means of a glass syringe.

$$S:\begin{cases} C_M\ Na_2Ni(CN)_4 \\ 3M - 3C_M\ NaClO_4 \end{cases} \qquad T:\begin{cases} C_H\ HClO_4 \\ 3M - C_H\ NaClO_4 \end{cases}$$

C_M was about $2 \times 10^{-5} - 2 \times 10^{-4}$ M and C_H was varied from 2×10^{-3} M to 2 M. These measurements indicated an approximate first order reaction with respect to $Ni(CN)_4^{2-}$. When the logarithm of the absorbance was plotted against the reaction time, however, a systematic deviation from linearity was obtained. This deviation might be suspected to depend on HCN being formed in the course of the reaction which might retard the dissociation.

Measurements with varying initial concentrations of HCN showed that HCN strongly retarded the reaction.

A check showed that the presence of Ni^{2+} did not affect the reaction rate.

The measurement solutions were now designed in the following way:

$$S:\begin{cases} C_M\ Na_2Ni(CN)_4 \\ 3M - 3C_M\ NaClO_4 \end{cases} \qquad T:\begin{cases} C_A\ HCN \\ C_H\ HClO_4 \\ 3M - C_H\ NaClO_4 \end{cases}$$

The values of C_M and the cuvette length l were chosen so that an initial absorbance between 0.4 and 0.8 was obtained.

The measurement series were performed at the following hydrogen ion concentrations: $[H_3O^+]$: 1.000 M; 0.750 M; 0.500 M; 0.375 M; 0.250 M; 0.1000 M; 0.0750 M; 0.0500 M; 0.0250 M; 0.0100 M; 0.00750 M; 0.00500 M; 0.00250 M; 0.00100 M. Since the values of C_M have been kept very low compared to C_H the hydrogen ion concentration can be regarded as constant within each series. For each value of $[H_3O^+]$ about 5 – 10 measurements were performed with different values of the initial hydrogen cyanide concentration, C_A. The absorbance A was measured as a function of the reaction time t until $A \approx 0.1$ and corrected for the small absorbance A_∞ measured after completion of the reaction.

CALCULATIONS AND RESULTS

The calculations have been based upon a general model described by Ekström.[6] The reaction scheme (Fig. 1) is valid for both dissociation and association.

This reaction scheme may be regarded as composed of fast protonation equilibria (vertical rows) and slower reactions implying gain or loss of cyanide ions (horizontal rows). (In Fig. 1 only the arrows corresponding to dissociation have been marked).

It should be noticed that it is not possible to distinguish between on the one hand a successive loss of CN^- and H^+ and on the other

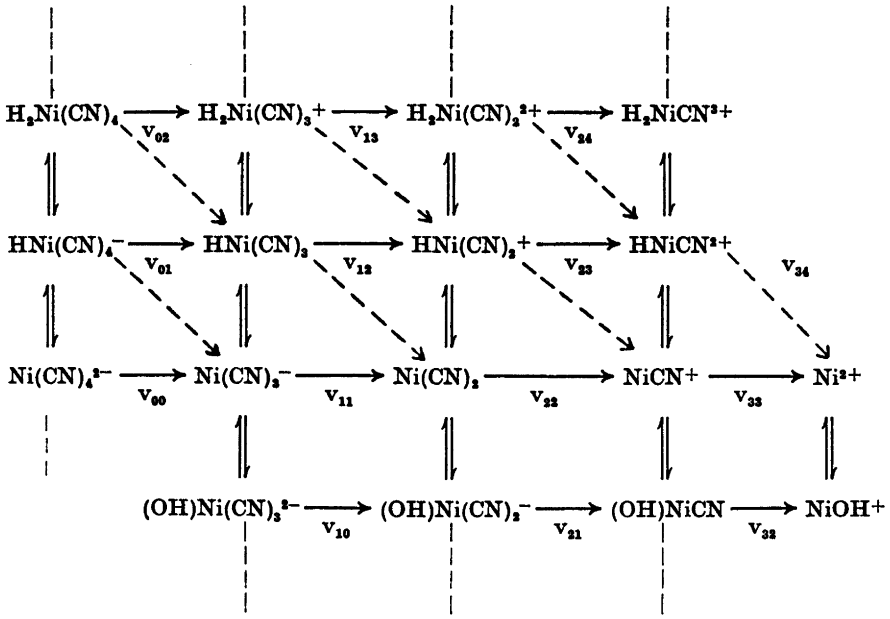

Fig. 1. A general model for possible dissociation and association reactions $Ni^{2+} - Ni(CN)_4^{2-}$.

hand a direct loss of HCN. Thus for instance the reactions

$$HNi(CN)_4^- \xrightarrow{-CN^-} HNi(CN)_3 \overset{-H^+}{\rightleftharpoons} Ni(CN)_3^-$$

may be substituted by $HNi(CN)_4^- \dashrightarrow Ni(CN)_3^- + HCN$ (note the dashed arrows in Fig. 1).

With the assumption that all species except $Ni(CN)_4^{2-}$ and Ni^{2+} are in a steady state it can be shown [6] that the total reaction rate, v, is given by:

$$v = [(v_{00} + v_{01} + \cdots)^{-1} + (v_{10} + v_{11} + \cdots)^{-1} + (v_{20} + v_{21} + \cdots)^{-1} + (v_{30} + v_{31} + \cdots)^{-1}]^{-1} \quad (1)$$

where $v = -\dfrac{d[Ni(CN)_4^{2-}]}{dt}$ and

$$v_{ij} = k_{ij} h^j [HCN]^{-i} [Ni(CN)_4^{2-}](1 - Q\,K^{-1})$$

$$v = \frac{[Ni(CN)_4^{2-}]}{N} - \frac{[Ni(CN)_4^{2-}]Q}{NK} \quad (2)$$

where $N = \dfrac{1}{k_{00} + k_{01}h + k_{02}h^2 + \cdots} +$

$$\frac{[HCN]}{k_{10} + k_{11}h + \cdots} + \frac{[HCN]^2}{k_{20} + k_{21}h + \cdots} + \frac{[HCN]^3}{k_{30} + k_{31}h + \cdots}$$

$Q = \dfrac{[Ni^{2+}][CN^-]^4}{[Ni(CN)_4^{2-}]}$ and K is the corresponding equilibrium constant (*i.e.* $K = 1/\beta_4$); ($h = [H_3O^+]$).

In the right hand member of eqn. (2) the first term represents the forward reactions (the dissociation reactions) and the second term the backward reactions (the association reactions). If the backward reactions can be neglected we thus obtain for the dissociation reactions:

$$v_d = -\frac{d[Ni(CN)_4^{2-}]}{dt} = k_{obs}[Ni(CN)_4^{2-}] \quad (3)$$

where $k_{obs} = \dfrac{1}{N([HCN], h)}$ (4)

Analogously we obtain for the association reactions:

$$v_a = \frac{[Ni(CN)_4^{2-}]Q\beta_4}{N([HCN], h)} = \frac{\beta_4[Ni^{2+}][CN^-]^4}{N([HCN], h)} =$$

$$= \frac{\beta_4 K_a^4 [HCN]^4 [Ni^{2+}]}{h^4 N([HCN], h)} \text{ or}$$

$$v_a = -d[Ni^{2+}]/dt = k_{obs}[Ni^{2+}] \quad (5)$$

where $k_{obs} = \dfrac{\beta_4 K_a^4 [HCN]^4}{h^4 N([HCN], h)}$ (6)

Integration of eqn. (3) yields $\ln [Ni(CN)_4^{2-}]_t = \ln [Ni(CN)_4^{2-}]_0 - k_{obs}t$, if k_{obs} is constant. At the

Table 1. Corresponding values of initial hydrogen cyanide concentration, $[HCN_0]$, and observed rate constant, $k°_{obs}$, for the different measurement series. (Within every series the hydrogen ion concentration h is constant). $\Delta k = 100 \times (k_{obs} - k_{calc})/k_{calc}$.

$[HCN]_0$/mM	$k°_{obs}/s^{-1}$	Δk/%
$h = 1.000$ M		
30.0	1.456×10^{-3}	+1.8
20.0	1.814×10^{-3}	+1.0
15.0	2.027×10^{-3}	−1.6
8.00	2.584×10^{-3}	−0.4
5.00	2.862×10^{-3}	−1.9
3.00	3.160×10^{-3}	−0.7
1.000	3.330×10^{-3}	−4.8
0.400	3.260×10^{-3}	−9.6
0	3.580×10^{-3}	−2.7
$h = 0.750$ M		
30.0	9.47×10^{-4}	+0.3
20.0	1.165×10^{-3}	−4.1
15.0	1.402×10^{-3}	−1.1
8.00	1.880×10^{-3}	+1.5
5.00	2.200×10^{-3}	+3.3
3.00	2.435×10^{-3}	+2.8
1.000	2.661×10^{-3}	−0.2
$h = 0.500$ M		
30.0	5.15×10^{-4}	−2.4
20.0	6.67×10^{-4}	−4.6
15.0	7.42×10^{-4}	−11.1
8.00	1.049×10^{-3}	−8.7
5.00	1.294×10^{-3}	−5.5
3.00	1.516×10^{-3}	−3.4
1.000	1.753×10^{-3}	−4.7
0	1.954×10^{-3}	−2.8
$h = 0.375$ M		
30.0	3.487×10^{-4}	−0.7
20.0	4.47×10^{-4}	−5.7
15.0	5.70×10^{-4}	−0.9
8.00	7.58×10^{-4}	−7.6
5.00	1.011×10^{-3}	−0.9
3.00	1.094×10^{-3}	−7.0
1.000	1.358×10^{-3}	−4.7
$h = 0.250$ M		
30.0	2.019×10^{-4}	+0.2
20.0	2.772×10^{-4}	−0.4
15.0	3.404×10^{-4}	−1.1
8.00	4.94×10^{-4}	−3.8
5.00	6.16×10^{-4}	−5.4
3.00	7.65×10^{-4}	−3.5
1.000	9.55×10^{-4}	−5.8
0	1.139×10^{-3}	−3.2
$h = 0.1000$ M		
50.0	4.21×10^{-5}	+6.7
40.0	4.95×10^{-5}	+1.7
30.0	6.58×10^{-5}	+3.8
20.0	9.42×10^{-5}	+3.8
10.0	1.717×10^{-4}	+7.3
8.0	2.064×10^{-4}	+9.3
6.50	2.420×10^{-4}	+10.9
5.00	2.593×10^{-4}	+0.4
4.00	3.274×10^{-4}	+11.0
3.00	3.695×10^{-4}	+7.6
2.00	4.50×10^{-4}	+9.7
1.000	5.45×10^{-4}	+6.7
0.500	6.20×10^{-4}	+6.6
0.100	7.06×10^{-4}	+8.0
0	7.08×10^{-4}	+4.8
$h = 0.0750$ M		
20.0	6.87×10^{-5}	+5.1
15.0	8.76×10^{-5}	+4.2
8.00	1.412×10^{-4}	+0.7
5.00	2.091×10^{-4}	+6.5
3.00	2.918×10^{-4}	+8.9
1.00	4.54×10^{-4}	+7.6
$h = 0.0500$ M		
20.0	4.43×10^{-5}	+6.0
15.0	5.77×10^{-5}	+6.4
8.00	9.91×10^{-5}	+6.4
5.00	1.440×10^{-4}	+7.3
3.00	2.012×10^{-4}	+5.8
1.000	3.388×10^{-4}	+3.9
0	5.11×10^{-4}	+0.7
$h = 0.0250$ M		
20.0	2.102×10^{-5}	+4.7
15.0	2.803×10^{-5}	+6.3
8.00	5.11×10^{-5}	+9.1
5.00	7.72×10^{-5}	+9.7
3.00	1.200×10^{-4}	+13.6
1.000	2.566×10^{-4}	+21.3
0	5.22×10^{-4}	+22.9
$h = 0.0100$ M		
15.0	1.027×10^{-5}	−1.2
12.0	1.229×10^{-5}	−4.8
8.00	1.840×10^{-5}	−3.4
6.00	2.557×10^{-5}	+2.4
5.00	3.265×10^{-5}	+10.5
4.00	3.728×10^{-5}	+2.9
2.00	6.77×10^{-5}	+2.5
1.00	1.138×10^{-4}	+1.3
0.800	1.306×10^{-4}	−0.0
0.600	1.555×10^{-4}	−0.3
0.400	2.006×10^{-4}	+3.6
0.200	2.690×10^{-4}	+5.4
0.100	3.299×10^{-4}	+8.7
0	3.988×10^{-4}	+6.5

Table 1. Continued.

$[HCN]_0$/mM	k°_{obs}/s^{-1}	Δk/%
$h = 7.50 \times 10^{-3}$ M		
2.00	5.37×10^{-5}	+4.6
1.50	6.75×10^{-5}	+3.4
0.800	1.101×10^{-4}	+3.9
0.300	2.076×10^{-4}	+8.9
$h = 5.00 \times 10^{-3}$ M		
2.00	3.517×10^{-5}	−1.0
1.50	4.46×10^{-5}	−2.8
0.800	7.47×10^{-5}	−3.3
0.500	1.044×10^{-4}	−4.6
0.300	1.471×10^{-4}	−2.9
0	3.45×10^{-4}	−3.6
$h = 2.50 \times 10^{-3}$ M		
2.00	1.708×10^{-5}	−7.7
1.50	2.136×10^{-5}	−11.9
0.800	3.817×10^{-5}	−11.0
0.500	6.10×10^{-5}	−4.5
0.300	7.67×10^{-5}	−19.2
0	2.992×10^{-4}	−14.4
$h = 1.00 \times 10^{-3}$ M		
3.00	5.00×10^{-6}	−2.2
2.00	8.62×10^{-6}	+13.3
1.50	1.119×10^{-5}	+11.2
1.00	1.338×10^{-5}	−10.1
0.800	1.572×10^{-5}	−14.6
0.600	2.104×10^{-5}	−12.7
0.400	3.050×10^{-5}	−12.7
0.200	5.27×10^{-5}	−17.0
0.100	8.41×10^{-5}	−21.5
0	2.873×10^{-4}	−16.6

actual wavelength only $Ni(CN)_4^{2-}$ absorbs light and the absorbance

$$A = \varepsilon_{Ni(CN)_4^{2-}}[Ni(CN)_4^{2-}]l$$

Thus

$$\ln A_t = \ln A_0 - k_{obs}t \qquad (7)$$

If $\ln A_t$ is plotted as a function of t a straight line with the slope k_{obs} is obtained for every measurement series, provided that h and [HCN] are constant within the series. While h can be considered to be constant to a good approximation, [HCN] varies somewhat since it is formed from $Ni(CN)_4^{2-}$. If HCN has been added initially, the deviation from linearity can be kept very small. However, k_{obs} was determined both at $t = 0$ corresponding to $[HCN] = [HCN]_0$

Table 2. Supplementary values of (h, k°_{obs}, Δk) at $[HCN]_0 = 0$. (For definitions see Table 1).

h/M	0.800	0.660	0.400	0.0800	0.0660	0.0400	0.0066	0.0040
k°_{obs}/s^{-1}	3.105×10^{-3}	2.583×10^{-3}	1.729×10^{-3}	5.88×10^{-4}	6.01×10^{-4}	5.20×10^{-4}	4.02×10^{-4}	3.37×10^{-4}
Δk/%	+3.0	+1.5	+3.1	−3.3	+7.1	+9.6	+10.7	−4.9

and $k_{obs} = k^{\circ}_{obs}$, and also after a few half times when $[HCN] \approx [HCN]_0 + 4[Ni(CN)_4^{2-}]_0$ and $k_{obs} \approx k^{\infty}_{obs}$.

Within the measurement errors both sets of ([HCN], k_{obs}) gave the same set of rate constants, k_{ij}, see below. In Table 1 the corresponding values of (h, $[HCN]_0$ and k°_{obs}) for the different series have been collected. Table 2 contains some complementary values of (h,k°_{obs}) at $[HCN]_0 = 0$

For series with the same hydrogen ion concentration k_{obs}^{-1} was plotted as a function of [HCN]. These plots yielded straight lines, *i.e.* at constant h: $k_{obs}^{-1} = A + B$ [HCN] where A and B are constants whose values depend on h.

When A^{-1} was plotted as a function of h (Fig. 2) a straight line was obtained implying that $k_{0i} = 0$ for $i \geq 2$. From the intercept and slope of this line k_{00} and k_{01} were determined.

The corresponding analyses of B as a function of h showed that only k_{11} and k_{12} were significant *i.e.* $(Bh)^{-1} = k_{11} + k_{12}h$ (Fig. 3).

The results can be summarized in the following equation

$$k_{obs} = \{(k_{00} + k_{01}h)^{-1} + [HCN](k_{11}h + k_{12}h^2)^{-1}\}^{-1} \quad (8)$$

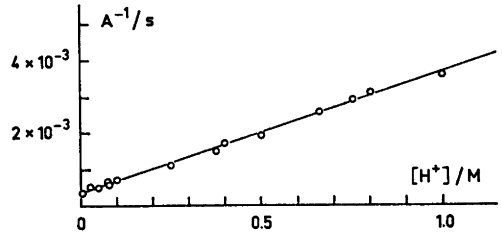

Fig. 2. Determination of k_{00} and k_{01} from a plot of A^{-1} as a function of [H$^+$]. (A is defined from $k_{obs}^{-1} = A + B$[HCN]).

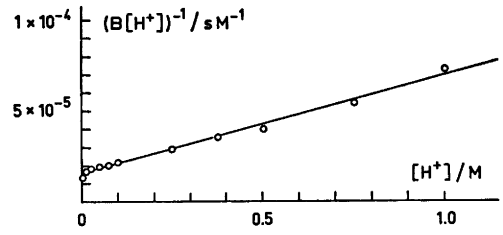

Fig. 3. Determination of k_{11} and k_{12} from a plot of $(B[H^+])^{-1}$ as a function of [H$^+$]. (B is defined from $k_{obs}^{-1} = A + B$[HCN]).

with

$k_{00} = (3.41 \pm 0.6)10^{-4}$ s^{-1};
$k_{01} = (3.34 \pm 0.16)10^{-3}$ s^{-1} M^{-1}
$k_{11} = (1.55 \pm 0.15)10^{-5}$ s^{-1};
$k_{12} = (5.47 \pm 0.4)10^{-5}$ s^{-1} M^{-1}

(The errors are given as three times the standard deviations in the constants obtained from the linear plots described above). The corresponding reaction scheme is shown in Scheme 1.

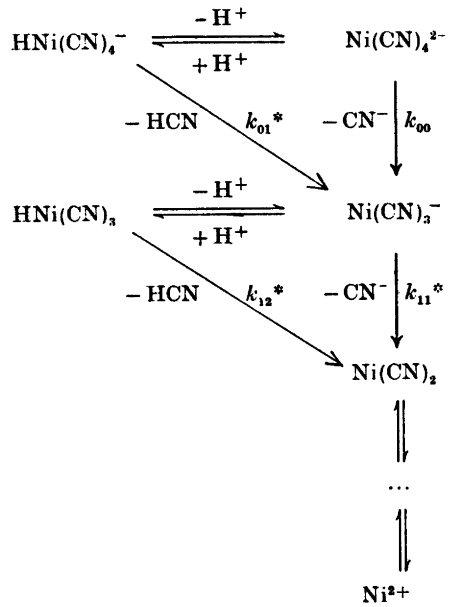

Scheme 1.

In order to check how close the constants $k_{00} - k_{12}$ describe the measurement data k_{calc} were calculated from eqn. (8) for the actual values of h and HCN and were compared to the values of k_{obs} obtained experimentally (Tables 1, 2).

The experimental errors can be expected to be about $\pm(5-10)$ %. (At the lowest values of h the errors can be assumed to be larger). From Table 1 it is obvious that the experimental material is well described by the calculated constants.

(The values of k_{obs} could alternatively be calculated from the integrated rate expression. Combining eqns. (3) and (8) and integrating we get

$$\ln x - k_1 x = -k_2 t + \ln a - k_1 a$$

Here x = concentration of $Ni(CN)_4^{2-}$ at time t. a = concentration of $Ni(CN)_4^{2-}$ at $t = 0$. k_1 and k_2 contain the constants $k_{00} - k_{12}$ as parameters and are functions of h. k_1 and k_2 can be determined for each experiment (h being constant within each experiment). From the corresponding values of h, k_1 and k_2 the constants $k_{00} - k_{12}$ can be determined.

However, in the present measurements the cyanide concentration was approximately constant within each series. Hence, nearly linear plots were obtained at the determination of the values of k_{obs} permitting a good accuracy in the evaluation of both k°_{obs} and k^{∞}_{obs}. The numerically more simple method using initial rates was therefore preferred for the calculations).

Our previous measurements [3] show clearly that the species $H_xNi(CN)_4^{x-2}$ ($i = 1-4$) exist at most to a very small extent at equilibrium. Our present kinetic measurements, however, indicate that $HNi(CN)_4^-$ is kinetically significant. Therefore, we decided to make a supplementary investigation of the formation of $HNi(CN)_4^-$. According to Kolski and Margerum,[1] the equilibrium constant for the reaction

$$Ni(CN)_4^{2-} + H_3O^+ \rightleftharpoons HNi(CN)_4^- + H_2O$$

is

$$K_H = 2.5 \times 10^5 \text{ M}^{-1}$$

Thus $Ni(CN)_4^{2-}$ should possess obvious base properties. We added $Na_2Ni(CN)_4$ to a solution of perchloric acid for which pH had been measured and measured pH in the solution soon after mixing. The concentration of the perchloric acid was chosen so that only a slow disintegration of $Ni(CN)_4^{2-}$ could be expected. The concentrations before possible reaction were: $[H_3O^+] = 0.50$ mM; $[Ni(CN)_4^{2-}] = 1.00$ mM.

Before addition of $[Ni(CN)_4^{2-}]$ we measured $-\lg [H_3O^+] = 3.30$. Accepting the value of K_H postulated by Kolski and Margerum we should expect a value of $-\lg [H_3O^+] \approx 5.40$ after addition of $Na_2Ni(CN)_4$ corresponding to a change in electromotive force of about 124 mV. We measured a change in emf of less than 1 mV, indicating a negligible formation of $HNi(CN)_4^-$. The results of this experiment thus support the results from our previous equilibrium measurements.[3]

DISCUSSION

The results from our experiments thus show that the acid dissociation of $Ni(CN)_4^{2-}$ can be described by a rather simple model with two types of reaction paths, implying loss of HCN and loss of CN^-, respectively. As mentioned above it is not possible to distinguish between a loss of HCN and successive losses of CN^- and H^+. The former model, however, seems to be more attractive from a chemical point of view.

Our measurements show further that protonated nickel cyanide species are not present in detectable concentrations. Hence, the results from our measurements on the dissociation of $Ni(CN)_4^{2-}$ indicate a kinetic model quite different from that proposed by Kolski and Margerum.[1]

When our investigations of the dissociation of $Ni(CN)_4^{2-}$ were completed, and we were analyzing the results from our measurements on the association reactions, the results of an investigation of the kinetics of the tetracyanonickelate(II) ion by Crouse and Margerum [7] were published. In this paper a study of the dissociation of $Ni(CN)_4^{2-}$ by means of I_2 as a scavenger for cyanide is described. The authors find that the rate constant for this reaction does not depend on pH when pH > 3. Their method is not applicable at lower values of pH.

Crouse and Margerum propose the following reaction model.

$$Ni(CN)_4^{2-} \underset{k_{34}}{\overset{k_{43}}{\rightleftharpoons}} Ni(CN)_3^- + CN_T$$

$$Ni(CN)_3^- \underset{k_{03}}{\overset{k_{30}}{\rightleftharpoons}} Ni^{2+} + 3CN_T$$

A steady state approximation in $Ni(CN)_3^-$ leads to $k_{obs} = k_{43}k_{30}/(k_{34}[CN]_T + k_{30})$ where k_{30}, k_{34} and k_{43} may depend on $[H^+]$. However, Crouse and Margerum have not determined the dependence on $[H^+]$ or the corresponding mechanism. From their measurements a constant value of $k_{43} = 4.8 \times 10^{-4}$ s^{-1} is obtained at pH > 3. The expression above may be rearranged to

$$k_{obs}^{-1} = \left(\frac{1}{k_{43}} + \frac{k_{34}}{k_{43}k_{30}}[CN_T]\right) \qquad (9)$$

A comparison of our eqn. (8) with Crouse's and Margerum's eqn. (9) shows that they are

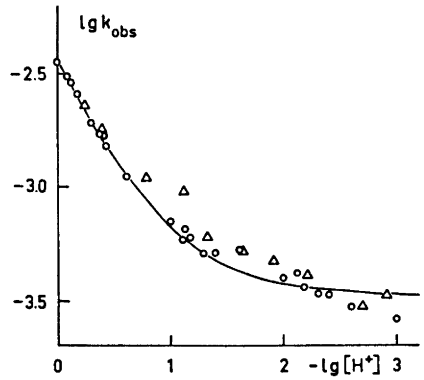

Fig. 4. The hydrogen ion dependence of the rate constant k_{obs} at zero hydrogen cyanide concentration. The full-drawn curve represents lg k_{calc} calculated from eqn. (8). The experimental values of k_{obs} are denoted by ○ (this work) and △ (according to Kolski and Margerum [1]). ([H+] in M and k_{obs} in s^{-1}).

identical if the following relations between their parameters hold:

$$k_{43} = k_{00} + k_{01}h \text{ and } k_{34}/k_{43}k_{30} = (k_{11}h + k_{12}h^2)^{-1}$$

When cyanide is removed by iodine the association reactions can be neglected and $k_{obs} \approx k_{43}$. At low values of h, $k_{43} \approx k_{00}$. Thus under the experimental conditions used by Crouse and Margerum only the reaction $Ni(CN)_4^{2-} \rightarrow Ni(CN)_3^-$ is significant. This explains the constant value of k_{obs} obtained by these authors. The agreement between the values of $k_{43} = 4.8 \times 10^{-4}$ s^{-1} at pH > 3 given by Crouse and Margerum and our value of $k_{00} = 3.82 \times 10^{-4}$ s^{-1} is good considering the large differences in the ionic media.

In Fig. 4 experimental and calculated values of lg k_{obs} at [HCN] = 0 are plotted against $-\lg [H^+]$. The experimental values obtained by Kolski and Margerum are plotted in the same diagram showing on the whole a good agreement.

The experiments performed by Kolski and Margerum,[1] as well as those performed by Crouse and Margerum [7] can be satisfactorily explained using the reaction model described in the present paper.

In our investigations of the association reactions to $Ni(CN)_4^{2-}$ (Ref. 8), k_{11}', k_{22}' and k_{33}' were determined ($k_{ii}' = \beta_4 K_a^4 k_{ii}$). We obtained $\beta_4 K_a^4 k_{11} = 2.16 \times 10^{-12}$ s^{-1}. Using $K_a = 3.28 \times 10^{-10}$ M (Ref. 4) and $k_{11} = 1.55 \times 10^{-5}$ s^{-1} from the dissociation reactions we get $\beta_4 = (1.20 \pm 0.12) \times 10^{31}$ M^{-4} from our kinetic measurements, in excellent agreement with the value $(1.25 \pm 0.09) \times 10^{31}$ M^{-4} obtained from the equilibrium measurements.[3]

Acknowledgements. We owe our gratitude to Professor Ido Leden for his kind interest in this work and valuable advice and to Miss Bodil Jönsson for skilful assistance with the measurements.

REFERENCES

1. Kolski, G. B. and Margerum, D. W. *Inorg. Chem. 7* (1968) 2239.
2. Jordan, J. and Ewing, G. J. *Inorg. Chem. 1* (1962) 587.
3. Persson, H. *Acta Chem. Scand. A 28* (1974) 885.
4. Persson, H. *Acta Chem. Scand. 25* (1971) 543.
5. Fernelius, W. C. and Burbage, J. J. *Inorg. Synth.* (1946) 227.
6. Ekström, C. G. *To be published.*
7. Crouse, W. C. and Margerum, D. W. *Inorg. Chem. 6* (1974) 1437.
8. Persson, H. *Acta Chem. Scand. A 30* (1976) 39.

Received May 30, 1975.

Acta Chemica Scandinavica A 30 (1976) 39—42

Kinetics of Formation of the Tetracyanonickelate(II) Ion

HANS PERSSON

Division of Physical Chemistry, University of Lund, Chemical Center, Box 740, S-220 07 Lund 7, Sweden

The formation of $Ni(CN)_4^{2-}$ has been investigated spectrophotometrically mainly at 267.5 nm in the pH-range 4.7 – 7.0. Both conventional spectrophotometry and stopped-flow methods have been applied. The ionic medium was 3.00 M $NaClO_4$ and the temperature 25.0 °C. The kinetics of the association reactions can in the actual pH-range be described by the following scheme:

$$Ni^{2+} \xrightarrow[+CN^-]{} NiCN^+ \xrightarrow[+CN^-]{} Ni(CN)_2 \xrightarrow[+CN^-]{} Ni(CN)_3^- \xrightarrow[+CN^-]{\text{fast}} Ni(CN)_4^{2-}$$

On the assumption that all species except $Ni(CN)_4^{2-}$ and Ni^{2+} are in a steady state the results from both the association and dissociation [1] measurements can be summarized in:

$$-dX/dt = k_{obs}X \qquad (1)$$

where

$X = [Ni(CN)_4^{2-}]$ for dissociation and $[Ni^{2+}]$ for association and

$$k_{obs} = (1 + \beta_4 K_a^4 [HCN]^4 h^{-4})/\{(k_{00} + k_{01}h)^{-1} + [HCN](k_{11}h + k_{12}h^2)^{-1} + [HCN]^2(k_{22}h^2)^{-1} + [HCN]^3(k_{33}h^3)^{-1}\} \qquad (2)$$

and the corresponding reaction scheme shown beside. (Only the arrows corresponding to dissociation have been marked).

$k_{00} = (3.4 \pm 0.6)10^{-4}$ s^{-1}; $k_{01} = (3.34 \pm 0.16)10^{-3}$ s^{-1} M^{-1}; $k_{11} = (1.55 \pm 0.15)10^{-5}$ s^{-1}; $k_{12} = (5.5 \pm 0.4)10^{-5}$ s^{-1} M^{-1}; $k_{22} = (0.169 \pm 0.020)$ s^{-1}; $k_{33} = (5.6 \pm 1.0)10^3$ s^{-1}

While k_{00} is a true rate constant, $k_{01} - k_{33}$ are products of rate constants and equilibrium constants. Since the values of these equilibrium constants are unknown the pure rate constants $k_{01}^* - k_{33}^*$ cannot be determined.

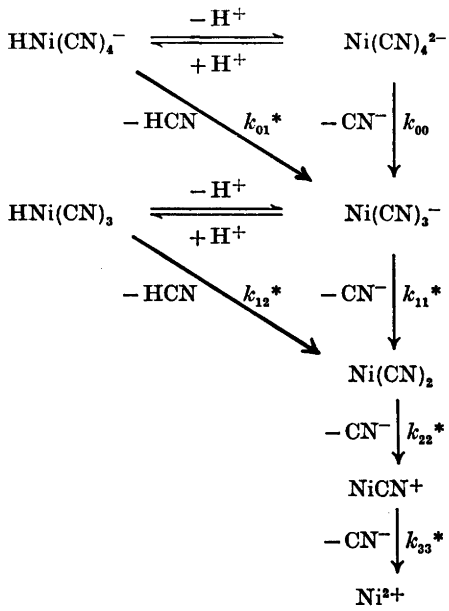

The kinetic measurements yield a value of the overall stability constant for $Ni(CN)_4^{2-}$ which is in excellent agreement with the value obtained in previous equilibrium studies.[2]

Results from equilibrium measurements on the complex system $Ni^{2+} - CN^-$ and kinetic studies of the acid dissociation of $Ni(CN)_4^{2-}$ have been presented in previous papers.[2,1]

The kinetics of the dissociation and the association of $Ni(CN)_4^{2-}$ have been investigated earlier by Kolski and Margerum.[3] The reaction model proposed by these authors, however, presupposes the existence of protonated nickel cyanide species in high concentrations even at rather low concentrations of hydrogen ions.

This assumption was not confirmed by our equilibrium measurements.[2] Since the reaction rate varies strongly in the pH-range examined, both conventional spectrophotometry and stopped-flow techniques have been used. The choice of the pH-interval, $4.7 < pH < 7.0$, was based on the following grounds: (i) At $pH > 4.7$ the association to $Ni(CN)_4^{2-}$ is complete at equilibrium and the reaction is not inconveniently slow, (ii) at $pH > 7$ the reactions are so fast that the accuracy in determining k_{obs} is seriously lowered.

EXPERIMENTAL

Chemicals. Acetate buffers were prepared from acetic acid (Merck *p.a.*) and sodium acetate (BDH) *p.a.*). Phosphate buffers were prepared from $NaH_2PO_4.2H_2O$ (BDH *p.a.*) and $Na_2HPO_4.12H_2O$ (Merck *p.a.*). Acetate buffers were used in measurements at which $pH < 6$ and phosphate buffers at higher values of pH. As to other chemicals see Ref. 1.

Measurements. In the spectrophotometric measurements a Zeiss spectrophotometer PMQ II was used and in the stopped-flow investigations a modified Durrum-Gibson equipment.

The studies were mainly performed at the wavelength 267.5 nm,[1] but a few series were also carried out at 285 nm yielding concordant results.

Within each experimental series pH was kept as constant as possible by means of buffers, while the initial concentration of hydrogen cyanide was varied. The initial nickel concentration was so small, that the concentration of HCN can be regarded as approximately constant in most experimental series. The measurement solutions were obtained by mixing equal volumes of two solutions S and T by means of a glass syringe:

S: $\begin{cases} C_M \quad Ni(ClO_4)_2 \\ NaClO_4 \text{ to } 3.00 \text{ M} \\ \text{ionic strength} \end{cases}$

T: $\begin{cases} C_A \quad HCN \\ \text{buffer} \\ NaClO_4 \text{ to } 3.00 \text{ M ionic strength} \end{cases}$

Some measurements with buffer in S as well as in T gave concordant results C_M was about $4 \times 10^{-6} - 8 \times 10^{-5}$ M and C_A was varied from 1×10^{-2} to 5×10^{-2} M. The total concentration of buffer in T was about $1 \times 10^{-2} - 5 \times 10^{-2}$ M. In this region (but not at higher buffer concentrations) the values of k_{obs} were found to be independent of the total buffer concentration within the experimental errors.

The reaction rate is strongly dependent upon the hydrogen ion concentration, h. Although h is maintained approximately constant by means of the buffers, small deviations may cause substantial changes in reaction rate. Therefore pH was measured in each solution, and the experimental values of the rate constant k_{exp} were corrected to the same value of h, k_{obs}, for corresponding series.

The association reaction showed first order dependence with respect to the nickel(II) ion concentration. Corresponding values of h, [HCN] and k_{obs} have been collected in Table 1.

CALCULATIONS AND RESULTS

The calculations have been based upon a general reaction scheme proposed by Ekström,[4] which has been described briefly in an earlier paper.[1] If the dissociation reactions can be neglected, the following general expression can be deduced:

$$k_{obs} = \left[\frac{\beta_4 K_a^4 [HCN]^4}{h^4}\right] \left[\frac{1}{k_{00} + k_{01}h + \cdots} + \frac{[HCN]}{k_{10} + k_{11}h \cdots} + \frac{[HCN]^2}{k_{20} + k_{21}h \cdots} + \frac{[HCN]^3}{k_{30} + k_{31}h + \cdots}\right]^{-1} \quad (3)$$

While k_{00} is a true rate constant, $k_{01} - k_{33}$ are products of rate constants and equilibrium constants:

$k_{01} = k_{01}^* K_{h0}$; $k_{11} = k_{11}^* K_{00} K_a^{-1}$; $k_{12} = k_{12}^* K_{00} K_{h1} K_a^{-1}$; $k_{22} = k_{22}^* K_{00} K_{11} K_a^{-2}$; $k_{33} = k_{33}^* K_{00} K_{11} K_{22} K_a^{-3}$ where

$$K_{h0} = \frac{[HNi(CN)_4^-]}{[Ni(CN)_4^{2-}]h}; \quad K_{00} = \frac{[Ni(CN)_3^-]_{eq}[CN^-]_{eq}}{[Ni(CN)_4^{2-}]_{eq}};$$

$$K_{h1} = \frac{[HNi(CN)_3]}{[Ni(CN)_3^-]h}; \quad K_{11} = \frac{[Ni(CN)_2]_{eq}[CN^-]_{eq}}{[Ni(CN)_3^-]_{eq}};$$

$$K_{22} = \frac{[NiCN^+]_{eq}[CN^-]_{eq}}{[Ni(CN)_2]_{eq}}$$

are equilibrium constants. K_a = dissociation constant for HCN. Since the values of the equilibrium constants above except K_a are unknown the pure rate constants $k_{01}^* - k_{33}^*$ cannot be determined. (Only those of the constants k_{ij} in the general expression (3) that have been found to be relevant in the actual dissociation – and association measurements have been defined above in terms of rate constants and equilibrium constants.)

Some preliminary calculations showed that the term $(k_{00} + k_{01}h + \ldots)^{-1}$ can be neglected

Table 1. Corresponding values of hydrogen cyanide concentration and observed rate constant, k_{obs}, for the different measurement series. (Within each series the hydrogen ion concentration, h, is constant.)

[HCN]/ mM	k_{obs}/s^{-1}	[HCN]/ mM	k_{obs}/s^{-1}
$h = 1.932 \times 10^{-5}$ M		$h = 1.500 \times 10^{-6}$ M	
4.85	3.35×10^{-5}	5.00	5.18×10^{-2}
9.85	2.85×10^{-4}	10.00	0.334
14.85	1.000×10^{-3}	15.00	0.981
19.85	2.27×10^{-3}	20.00	1.94
24.85	4.56×10^{-3}	25.00	3.09
$h = 1.545 \times 10^{-5}$ M		$h = 9.68 \times 10^{-7}$ M	
4.85	7.3×10^{-5}	5.00	0.170
9.85	5.42×10^{-4}	10.00	1.00
14.85	1.95×10^{-3}	15.00	2.62
19.85	4.45×10^{-3}	20.00	4.95
24.85	8.69×10^{-3}	25.00	7.70
$h = 9.66 \times 10^{-6}$ M		$h = 8.41 \times 10^{-7}$ M	
4.85	2.79×10^{-4}	5.00	0.283
9.70	1.99×10^{-3}	10.00	1.68
14.85	7.16×10^{-3}	15.00	4.13
19.85	1.71×10^{-2}	20.00	7.69
		25.00	11.3
$h = 7.73 \times 10^{-6}$ M		$h = 6.17 \times 10^{-7}$ M	
4.85	3.95×10^{-4}	5.00	0.688
9.85	3.45×10^{-3}	10.00	3.25
14.85	1.17×10^{-2}	15.00	7.64
19.85	2.60×10^{-2}	20.00	13.9
25.00	5.50×10^{-2}	25.00	18.1
$h = 4.56 \times 10^{-6}$ M		$h = 4.14 \times 10^{-7}$ M	
4.85	2.30×10^{-3}	5.00	1.52
9.85	1.54×10^{-2}	10.00	6.62
15.00	5.14×10^{-2}	15.00	13.6
20.00	1.18×10^{-2}	20.00	21.3
25.00	0.219		
$h = 2.324 \times 10^{-6}$ M		$h = 2.208 \times 10^{-7}$ M	
5.00	1.85×10^{-2}	5.00	5.31
10.00	0.120	10.00	18.8
15.00	0.332	15.00	34.3
20.00	0.698	20.00	49.3
25.00	1.215		
		$h = 9.04 \times 10^{-8}$ M	
		5.00	16.4
		10.00	42.9
		15.00	70.6
		20.00	95.5

in the used pH-range $4.7 < pH < 7$. Eqn. (3) can then be transformed to

$$\frac{[HCN]^3}{k_{obs}h^4} = \frac{1}{k_{10}' + k_{11}'h + \ldots} + \frac{[HCN]}{k_{20}' + k_{21}'h + \ldots} + \frac{[HCN]^2}{k_{30}' + k_{31}'h + \ldots}$$

where $k_{ij}' = \beta_4 K_a^4 k_{ij}$ or

$$[HCN]^3/k_{obs}h^4 = A + B[HCN] + C[HCN]^2 \qquad (4)$$

where A, B and C are constants with values depending on h.

From eqn. (4) values of A, B and C were first determined for series of measurements with the same value of h. Then A^{-1} was plotted against h yielding a straight line through the origin, indicating that among all k_{ij}' only k_{11}' is detectable in the investigated pH-range. Analogous analyses of B^{-1} and C^{-1} as functions of h indicated that among the possible constants k_{2j}' and k_{3j}' only k_{22}' and k_{33}' were significant.

The following constants were obtained from the graphical calculations:

$k_{11}' = (2.16 \pm 0.20)10^{-12}$ s^{-1}; $k_{22}' = (2.36 \pm 0.30)$ 10^{-8} s^{-1}; $k_{33}' = (7.8 \pm 1.5)10^{-4}$ s^{-1}.

The error limits represent graphically determined maximum errors. From the dissociation measurements [1] $k_{11} = 1.55 \times 10^{-5}$ s^{-1} was calculated.

The values of k_{11} and k_{11}' above yield $\beta_4 K_a^4 = 1.394 \times 10^{-7}$ which gives $k_{22} = (0.169 \pm 0.020)$ s^{-1} and $k_{33} = (5.6 \pm 1.0)10^3$ s^{-1}.

Furthermore, using the value $K_a = 3.28 \times \times 10^{-10}$ M, determined in earlier measurements,[2] we get a value of the overall stability constant for $Ni(CN)_4^{2-}$: $\beta_4 = (1.20 \pm 0.12)10^{31}$ M^{-4} in very good agreement with the value $(1.25 \pm 0.09) \times 10^{31}$ M^{-4} obtained in earlier equilibrium studies.[2]

For the association reactions eqn. (3) can be rearranged to give k_{obs} as a function of $[CN^-]$:

$$k_{obs} = \beta_4[CN^-]^3 \left[\frac{1}{K_a k_{11}} + \frac{[CN^-]}{K_a^2 k_{22}} + \frac{[CN^-]^2}{K_a^3 k_{33}}\right]^{-1} \qquad (5)$$

Using the values of the constants β_4, K_a, k_{11}, k_{22} and k_{33}, k_{obs} was computed as a function of $[CN^-]$ from eqn. (5). In Fig. 1 the calculated curve $\lg k_{obs} = f(\lg[CN^-])$ is represented and in the same diagram some experimental data are plotted.

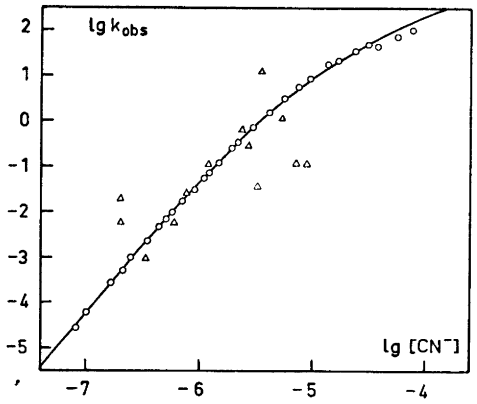

Fig. 1. The full-drawn curve represents lg k_{obs} calculated from eqn. (5). The experimental values of (lg [CN^-], lg k_{obs}) are denoted by O (this work) and △ (from the work of Kolski and Margerum [3]). (k_{obs} in s^{-1} and [CN^-] in M).

From results of the kinetics reported by Kolski and Margerum [3] for the formation of $Ni(CN)_4^{2-}$ some values of (lg[CN^-], lg k_{obs}) were calculated. These values have been plotted in Fig. 1 for comparison.

DISCUSSION

The results from the equilibrium and kinetic measurements on the nickel cyanide system can be summarized as follows: At equilibrium only Ni^{2+} and $Ni(CN)_4^{2-}$ exist in substantial concentrations. Although the complexes $NiCN^+$, $Ni(CN)_2$ and $Ni(CN)_3^-$ are so weak compared to $Ni(CN)_4^{2-}$, that they cannot be proved to exist at equilibrium, they are undoubtedly kinetically significant.

A description of the dissociation measurements also requires reaction paths *via* $HNi(CN)_4^-$ and $HNi(CN)_3$ existing either as intermediate species or as activated complexes. The studies at equilibrium, however, clearly indicate that protonated species do not occur in measurable amounts. Nor can any sign of intermediates be detected from the change of light absorption spectrum during a kinetic run. These spectra indicate the presence of only Ni^{2+} and $Ni(CN)_4^{2-}$.

The results from the measurements on the association from Ni^{2+} to $Ni(CN)_4^{2-}$ can be described within the experimental errors by means of a model, where only successive additions of CN^- are assumed to take place. It cannot be excluded that a minor part of the reaction might occur with addition of HCN, *i.e. via* the species $HNiCN^{2+}$ and $HNi(CN)_2^+$. Fig. 1 shows, however, that the experimental material is well described without assuming the formation of such species.

The path *via* $HNi(CN)_3$ which was found in the dissociation measurements [1] cannot be detected in the association studies. The reason for this is immediately clear from an inspection of eqn. 2, in which $k_{11}h \gg k_{12}h^2$ in the whole range $4.7 < pH < 7.0$ (The term $k_{12}h^2$ corresponds to the reaction path *via* $HNi(CN)_3$ and $k_{11}h$ to the direct loss or uptake of CN^-).

In Fig. 1 a comparison can be drawn between the values of (lg [CN^-], lg k_{obs}) obtained in the present work and by Kolski and Margerum.[3] From Fig. 1 it can be concluded that their results can be satisfactorily described by the present reaction model in the range of cyanide concentration where the scattering of their data is moderate.

The value of β_4 determined kinetically agrees closely with the value obtained in the equilibrium measurements.

Thus the present investigations on dissociation and association give results considerably different from those obtained by Kolski and Margerum concerning both the kinetics and the complex species existing at equilibrium.

Acknowledgements. I express my gratitude to Professor Ido Leden and Dr. Carl Gustav Ekström for valuable discussions and to Miss Bodil Jönsson for skilful assistance with the measurements.

REFERENCES

1. Persson, H. and Ekström, C. G. *Acta Chem. Scand. A 30* (1976) 31.
2. Persson, H. *Acta Chem. Scand. A 28* (1974) 885.
3. Kolski, G. B. and Margerum, D. W. *Inorg. Chem. 7* (1968) 2239.
4. Ekström, C. G. *To be published.*

Received May 30, 1975.

Acta Chemica Scandinavica A 30 (1976) 43—46

A CNDO/2 Study of Bipyridyls. I

ODD BORGEN, BRYNHILD MESTVEDT and INGE SKAUVIK

Division of Physical Chemistry, The University of Trondheim, The Norwegian Institute of Technology, N-7034 Trondheim-NTH, Norge

The binding energies of 2,2′-bipyridyl and its di-cation have been calculated as a function of the interplanar angles by the CNDO/2 method. The potential energy curve of 2,2′-bipyridyl has a pronounced energy maximum at the planar *cis*-form. For interplanar angles less than 70° from the planar *trans*-configuration the energy varies within narrow limits. This is in fair agreement with the results from previous experimental work. The di-cation of 2,2′-bipyridyl has a marked energy minimum around the stable planar *trans*-configuration. For both systems the electron distributions and the dipole moments at different interplanar angles have been computed.

The determination of the relation between the interplanar angle and the energy of 2,2′-bipyridyl, in the following denoted by BP, presents an interesting problem. Electron diffraction studies of the free molecule [1] indicate that the interplanar angle is not limited in the same way as in biphenyl and 4,4′-bipyridyl. In these molecules the planar configuration is counteracted by steric hindrance and the interplanar angle can vary within narrow limits only. In BP steric effects of this kind are not expected to exist, and one will expect the planar *trans*-form to be most stable. This configuration is, *e.g.*, the one found in the solid state.[2] For the free molecule, however, an experimental dipole moment of 0.61 Debye is found,[3] a fact that indicates a non-centrosymmetrical structure. Electron-diffraction studies of this and related compounds have been carried out by Almenningen and Bastiansen.[1] The results indicate a rather flat potential-energy curve with no considerable minima or maxima except for a significant maximum at the planar *cis*-configuration of the BP-molecule.

The di-cation of BP, hereafter denoted by BPH_2, is only known from highly acidic solutions. According to Nakamoto [4] the planar *trans*-form of this molecule is most stable. This is reasonable because of steric hindrance and also the expected distribution of charge in the molecule. In the crystalline state two different modifications of the di-hydrochloride are known.[5] In modification I there is an angle of about 17° between the ring planes. Modification II, however, shows an interplanar angle of 0° (planar *trans*-configuration).

This work has mainly been concerned with the shape of the potential-energy function by means of the CNDO/2-method. In addition the results from the electronic distribution calculations are presented. The energy levels of the compounds are not presented here as the original CNDO/2 method has proved to be rather unsuccessful from a spectroscopist's point of view. For this purpose other parametrizations have proved to give more satisfactory results[6,7]

Similar studies have been carried out for biphenyl by Gropen and Seip [10] and more recently by Tajiri *et.al.*[11]

METHOD

The original CNDO/2-method was used.[8] The calculations were performed on a UNIVAC 1108 computer using the program system QCPE 242,[9] adapted for the UNIVAC computer by the authors. The parametrization used is the same as the one used in the original program. Throughout this work the notation for the atoms in the molecules is that shown in Fig. 1a.

The atoms H_1 and H_1' are of interest in

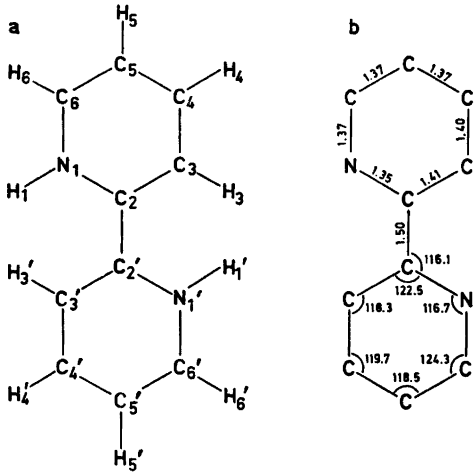

Fig. 1. a. Notation of the atoms in the molecules. b. The bond lengths and angles used for the CNDO/2-calculations of bipyridyl (BP) and its di-cation (BPH_2).

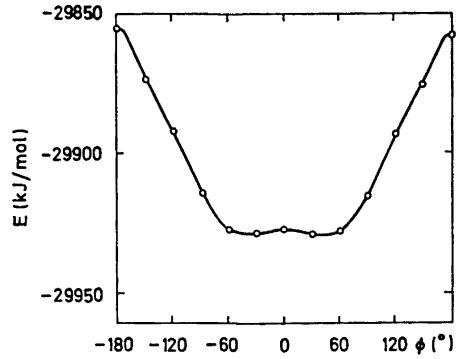

Fig. 2. The calculated binding energy of bipyridyl (BP) as a function of the interplanar angle.

connection with the di-cation only. The interplanar angle is denoted ϕ, with the *trans*-configuration corresponding to $\phi = 0°$. The calculations were based upon crystal data for the BP-molecule [2] and the di-hydrochloride of the BP-molecule.[5] Bond lengths and angles are given in Fig. 1b.

RESULTS AND DISCUSSION

1. 2,2'-Bipyridyl. The binding energy of the compound as a function of the interplanar angle is presented in Table 1, and graphically in Fig. 2. The most prominent feature of the calculated potential-energy curve is a pronounced maximum at $\phi = 180°$. In the region between approximately $-70°$ and $+70°$ interplanar angle, the energy is constant within some 500 J. Very shallow minima are found about $\pm 45°$ from the planar *trans*-form. The explanation of the fact that the absolute energy minimum is not located at the perfectly planar *trans*- configuration, may, in a qualitative sense, be attributed to repulsive effects between hydrogen atoms and the lone pair electrons of nitrogen.

The mean value of the interplanar angle $\langle\phi\rangle = 30.1°$ has been calculated, assuming a Bolzmann distribution. The connection between the interplanar angle and the dipole moment is presented in Table 1, and graphically in Fig. 3. The average value of the dipole moment is found to be $\langle\mu\rangle = 1.0$ D. This is somewhat larger than the observed value (0.61 D). The calculated bond densities are given in Table 2. The overall picture is rather complex and will not be described in detail here. However, the central bond ($C_2 - C_2'$) is of special interest as to the variations with

Table 1. The binding energy and dipole moment of BP and the binding energy of BPH_2 for different values of the interplanar angle.

	BP			BPH_2	
Angle (°)	E (A.U.)	E (kJ/mol)	μ (D)	E (A.U.)	E (kJ/mol)
0	−11.399	−29927	0.00	−10.30034	−27044
30	−11.399	−29928	1.02	−10.28774	−27010
60	−11.399	−29927	1.92	−10.26171	−26942
90	−11.394	−29914	2.66		
120	−11.385	−29892	3.18		
150	−11.379	−29874	3.52		
180	−11.372	−29856	3.66		

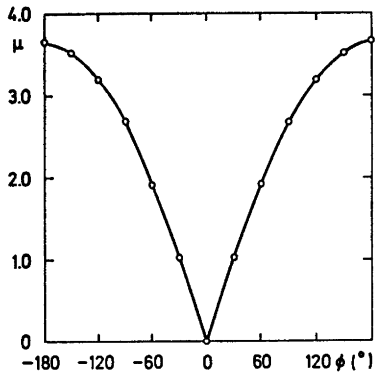

Fig. 3. The calculated dipole moment of bipyridyl (BP) as a function of the interplanar angle.

increasing interplanar angle. The bond density decreases as ϕ is increased from 0 to 90°. This is followed by a decrease for higher values of ϕ. The explanation of this is probably that the π-bond between the carbon atoms, C_2 and C_2' changes with the angle. At $\phi = 90°$ the p_z-orbitals of these atoms are orthogonal, and give, theoretically, no contribution to the bond. In other words, there is a gradual change from double- to single-bond character for the central bond. This indicates that the bond length should be varied with the interplanar angle in order to determine a more correct energy function.

In Table 3, the charge densities on atoms are shown. The most prominent feature is

Table 2. The bond densities of BP and BPH_2.

	BP							BPH_2		
Bond	0°	30°	60°	90°	120°	150°	180°	0°	30°	60°
N_1-C_2	1.676	1.674	1.670	1.668	1.663	1.661	1.660	1.558	1.528	1.627
N_1-C_6	1.652	1.653	1.656	1.664	1.671	1.689	1.691	1.678	1.661	1.670
C_5-C_6	1.986	1.986	1.962	1.916	1.863	1.819	1.793	1.928	1.914	1.968
C_4-C_5	1.938	1.932	1.940	1.966	1.997	2.029	2.050	1.892	1.870	1.925
C_3-C_4	1.910	1.909	1.902	1.893	1.882	1.871	1.866	1.935	1.949	1.894
C_2-C_3	1.864	1.873	1.898	1.932	1.968	1.998	2.007	1.805	1.776	1.923
C_2-C_2'	1.511	1.509	1.501	1.496	1.498	1.503	1.505	1.726	1.680	1.584
N_1-H_1								1.320	1.322	1.317
C_6-H_6	1.403	1.406	1.412	1.420	1.432	1.433	1.436	1.561	1.560	1.561
C_5-H_5	1.310	1.310	1.310	1.310	1.310	1.309	1.309	1.535	1.534	1.536
C_4-H_4	1.355	1.356	1.359	1.362	1.365	1.366	1.366	1.502	1.503	1.500
C_3-H_3	1.416	1.416	1.411	1.417	1.418	1.417	1.417	1.532	1.532	1.534

Table 3. The charge densities on atoms of BP and BPH_2. The unit is 10^{-3} electrons. Positive values to electronic excess.

	BP							BPH_2		
Atom	0°	30°	60°	90°	120°	150°	180°	0°	30°	60°
C_2	−99	−101	−107	−109	−106	−100	−96	−130	−103	−169
N_1	+158	+160	+161	+159	+153	+147	+146	+31	+57	−17
C_6	−95	−96	−96	−93	−86	−81	−77	−208	−209	−180
C_5	+22	+24	+27	+29	+25	+20	+17	−61	−101	−9
C_4	−44	−44	−46	−46	−43	−38	−38	−67	−115	−129
C_3	+39	+40	+41	+41	+36	+31	+28	−58	−102	+7
H_6	+15	+15	+11	+8	+3	+2	−0	−81	−81	−83
H_5	+6	+6	+7	+8	+9	+10	+10	−97	−96	−98
H_4	+11	+10	+8	+7	+6	+6	+7	−83	−84	−82
H_3	−13	−11	−7	−2	+1	+3	+2	−66	−68	−80
H_1								−180	−176	−187

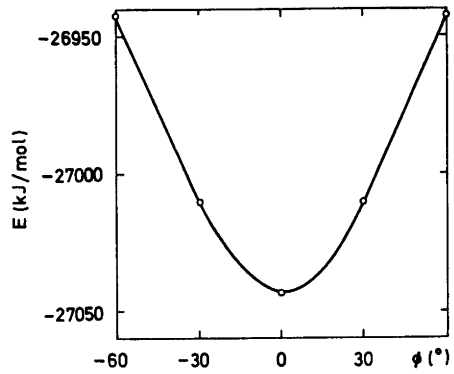

Fig. 4. The calculated binding energy of the di-cation of bipyricyl (BPH_2) as a function of the interplanar angle.

the transfer of electrons to the nitrogen atoms. Another conspicuous effect is that every second atom of the pyridyl rings is negatively charged, the others being positively charged. This effect is quite typical for heterocyclic rings containing one atom which is more electronegative than the other atoms and corresponds with what is found from, *e.g.*, the study of organic fluorides by the CNDO-method.[8] The hydrogen atoms are found to have rather small charges, to a certain extent reflecting the charges of the carbon atoms to which they are connected.

II. The di-cation of 2,2'-bipyridyl. The energy function of this compound is less complex than that of BP. The results of the calculations are presented in Table 1 and graphically in Fig. 4. Calculations have been made for ϕ-values of 0, 30, and 60° only, this being sufficient to determine the energy minimum. As might be expected, a sharply defined energy minimum is located at 0° interplanar angle (*trans*-configuration).

In Table 2, the bond densities for this system are presented. Comparing with the results for the neutral molecule one will find that the bond densities are not very different. It should be remarked that the bond densities for the C–H-bonds are found to be greater for this compound that for BP. This may be an artifact arising from the fact that somewhat smaller values for the C–H-distances have been used for this compound. The charge densities on atoms may be found in Table 3. These also show common features with the neutral molecule. In addition it may be remarked that the positive charge is fairly evenly distributed over the entire molecule, leaving only the nitrogen atoms negatively charged.

REFERENCES

1. Almenningen, A. and Bastiansen, O. *K. Nor. Vidensk. Selsk. Skr.* (1958) 4.
2. Merritt, L. L. and Schröder, E. D. *Acta Crystallogr. 9* (1956) 801.
3. Kranbühl, R., Klug, D. and Vaugham, W. *Nat. Acad. Sci. Nat. Res. Counc. Publ.* (1969) No. 1705.
4. Nakamoto, K. *J. Phys. Chem. 64* (1960) 1420.
5. Borgen, O. and Mestvedt, B. *To be published.*
6. Del Bene, J., and Jaffe, H. H. *J. Chem. Phys. 48* (1968) 1807.
7. Ellis, R., Kühnlenz, G. and Jaffe, H. H. *Theoret. Chim. Acta 26* (1972) 131.
8. Pople, J. A., and Beveridge, D. L. *Approximate Molecular Orbital Theory*, McGraw-Hill, New York 1970.
9. Loew, G. H. and Berkowitz, D. S. CNINDO with bond density calculation, QCPE, Indiana University, Bloomington, Ind.
10. Gropen, O. and Seip, H. M. *Chem. Phys. Lett. 11* (1971) 445.
11. Tajiri, A., Takagi, S. and Hatano, M. *Bull. Jap. Chem. Soc. 46* (1973) 1067.

Received May 29, 1975.

Acta Chemica Scandinavica A 30 (1976) 47—53

A Potentiometric Study of the Complex Formation between Cd(II) and *N*-Alkylsubstituted Thiosemicarbazides

PER B. TRINDERUP *

Chemistry Department I, The H. C. Ørsted Institute, Universitetsparken 5, DK-2100 Copenhagen Ø, Denmark

The stability constants between Cd(II) and a series of *N*-alkylsubstituted thiosemicarbazides in 1 M sodium nitrate solution have been determined.

The variation of the two first consecutive stability constants K_1 and K_2 for a number of 4-alkylsubstituted thiosemicarbazides can be rationalized semi-quantitatively in terms of the Hammett linear free energy relationship.

The constants K_3 are identical within the uncertainty of measurements for the whole series of systems investigated regardless of substitution in the thiosemicarbazides. This fact may reflect a change in configuration around the central metal ion when a *bis* thiosemicarbazide complex takes up a third ligand.

The purpose of the present investigation is to elucidate the ligating properties of a series of ligands as a function of various substituents. Thiosemicarbazide

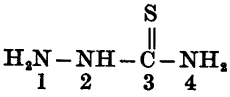

is well suited for this purpose. It is acting as a bidentate ligand, coordinating *via* the N(1) and the S atoms, towards several metal ions [1–10] and this makes it possible to study the influence of substitution on a coordinating atom, N(1), on an atom in a chelate ring, N(2), and on an atom in a side chain, N(4). The choice of the thiosemicarbazide ligand system is moreover based on the fact that most alkylsubstituted thiosemicarbazides are easily prepared, and a vast number of these are described in the literature.[11]

The choice of a suitable central metal ion was less obvious. Potentiometric measurements, using a metal electrode, were considered most promising, since the thiosemicarbazides exhibit only very weak basic properties in aqueous solution.[12] Thus the metals Cu, Zn, Cd, and Hg were considered. The stability constants for the unsubstituted thiosemicarbazide towards zinc,[12] cadmium,[12–15] mercury,[12,16] and silver [13,16] have been determined already. The constants for the cadmium system are of such an order of magnitude as to ensure a good determination of similar systems. The Cu(II)-thiosemicarbazide system cannot be determined, since the Cu^{2+} ion is reduced by the ligand.

EXPERIMENTAL

Chemicals. Demineralized water was distilled twice in an all quartz apparatus with small amounts of sodium permanganate added during the first distillation. The following commercial chemicals were of analytical grade and used without purification: sodium nitrate, cadmium nitrate tetrahydrate, cadmium sulfate 8/3-hydrate, ammonium nitrate, and thiosemicarbazide.

The cadmium metal (Fluka) was an especially pure product, impurities less than 0.0002 %. All mercury used was redistilled.

The ligands except thiosemicarbazide itself were prepared as described by Jensen *et al.*[11]: 4-methylthiosemicarbazide, 4-allylthiosemicarbazide, 4-*tert*-butylthiosemicarbazide, 2,4-dimethylthiosemicarbazide, 1,1,4-trimethylthiosemicarbazide, and 2-isopropyl-4-methylthiosemicarbazide were prepared from hydrazine

* Present address: NEUCC, Building 305, Technical University of Denmark, DK-2800 Lyngby, Denmark

or an alkylsubstituted hydrazine and the appropriate alkylisothiocyanate.[11] 2-Methylthiosemicarbazide was prepared by treating 4-*tert*-butyl 2-methylthiosemicarbazide with hot concentrated hydrochloric acid, a general way of preparing thiosemicarbazides unsubstituted in the 4-position.[11] 1-Methylthiosemicarbazide was prepared from 1-*tert*-butoxycarbonyl-4-*tert*-butyl-1-methyl-thiosemicarbazide.[11]

The crude products were recrystallized from water and ethanol. In case of coloured impurities charcoal was used, until pure products, as shown from the melting points and microanalysis, were obtained. The unsubstituted thiosemicarbazide was treated in the same way.

The cadmium amalgam was prepared in two different ways, which gave equally good products. First a suitable amount of cadmium metal was dissolved in the calculated amount of mercury under nitrogen atmosphere and applying gentle heating (about 60 °C) to give by cooling a two phase system with an overall content of cadmium of 10 % w/w. The second method used was to generate the cadmium metal electrolytically using a mercury cathode and a platinum anode. The electrolyte used was a solution of saturated cadmium sulfate, 0.1 M with respect to sulfuric acid. A current density of 0.125 A/cm² was employed as recommended by Treadwell.[17] With an anode with an active surface of 8 cm² 100 g of amalgam was prepared in *ca* 5 h.

The cadmium amalgams were stored under an oxygen-free atmosphere.

Measurements were made using the following elements:

Hg	Hg_2Cl_2	sat. KCl		sat. NH_4NO_3
10^{-4} M HNO_3 1 M KNO_3 *L* M Ligand *M* M $Cd(NO_3)_2$		Cd,Hg		Hg

Temperature 25 ± 0.1 °C. The total metal ion concentration M was varied between 4×10^{-2} and 10^{-3} M. The total ligand concentration L was varied from 2×10^{-3} M and upwards. The maximal L is limited by the solubility of the individual ligands. Thus a total ligand concentration of 10^{-1} M was obtained for the most soluble ligand 1,1,4-trimethylthiosemicarbazide, whilst 4-*tert*-butylthiosemicarbazide, which is the least soluble ligand investigated, only gave $L_{max} = 6 \times 10^{-3}$ M. Oxygen-free nitrogen was passed through the solution 15 min before and during the measurements to exclude oxygen from the solution and to stir it.

The Nernst equation for this element was shown to be valid in the interval from 10^{-1} to 10^{-4} M Cd^{2+} and $L = 0$.

Fresh solutions were prepared for each measurement from stock solutions of cadmium nitrate and sodium nitrate. The ligand was added as the solid. The stock solutions of cadmium nitrate were standardized against EDTA by potentiometric titrations using the cadmium amalgam electrode and by titration using Eriochrome-T as an indicator.

For 2-isopropyl-4-methylthiosemicarbazide only a very small amount was available (about 0.4 g) and so it was necessary to use another technique. In the element the ammonium nitrate solution was substituted by an agar bridge, containing 1 M sodium nitrate, and a solution of 1 M sodium nitrate, 10^{-4} M nitric acid and 2-isopropyl-4-methylthiosemicarbazide was titrated with a cadmium nitrate solution, adjusted to ionic strength 1 with sodium nitrate.

The EMF of the elements were measured by means of the Radiometer potentiometers PHM25SE or PHM52 and followed until the potential drift was less than 0.1 mV in 15 min. This value was taken as the equilibrium potential.

In the titration experiments a 2.5 ml Radiometer ABU11 automatic burette was used.

Calculations were performed using a least squares minimization computer program outlined in the appendix. Activity coefficients were assumed to be constant and only mononuclear complexes were considered. Moreover it was assumed that the basic properties of the ligands can be neglected. The only ligand, for which the basic properties have been studied is the unsubstituted thiosemicarbazide for which Goddard *et al.* have reported a value of 1.50 for the pK value of the ionization of the protonated ligand.[12] To test the validity of the last assumption the stability constants have been calculated for the Cd^{2+} – thiosemicarbazide system using a modified version of the computer program, performing the required corrections. The results of this calculations were: log $\beta_1 = 2.60(1)$, log $\beta_2 = 4.68(2)$, and log $\beta_3 = 5.85(2)$. These values are indistinguishable from those obtained without corrections (Table 1).

RESULTS AND DISCUSSION

The following thiosemicarbazides were investigated: 1-methyl (*2*), 2-methyl (*3*), 4-methyl (*4*), 4-allyl (*5*), 4-*tert*-butyl (*6*), 2,4-dimethyl (*7*), 1,1,4-trimethyl (*8*), and 2-isopropyl-4-methylthiosemicarbazide (*9*). The ligands have been chosen so that the series includes substitution on all nitrogen atoms and examples on substitution in several positions in the ligand. The number of possible ligands has been limited, however, by the slight solubility of several substituted thiosemicarbazides in aqueous solution.

In addition, the experimental data of Nørlund Christensen and Rasmussen[15] for the

Table 1. The logarithm to the consecutive and cumulative stability constants for the determined Cd^{2+}-alkylsubstituted thiosemicarbazide systems. The standard deviations $\times 10^2$ are given in parentheses. The number of independent experiments (N) for each ligand is given in the last column.

	Thiosemicarbazide	log β_1	log β_2	log β_3	log K_2	log K_3	N
(*1*)	Unsubstituted	2.60(1)	4.68(2)	5.86(2)	2.08(2)	1.18(3)	
(*2*)	1-Methyl	2.34(8)	4.48(11)	5.84(17)	2.14(13)	1.36(20)	12
(*3*)	2-Methyl	2.31(2)	4.22(4)	5.53(5)	1.91(4)	1.31(6)	24
(*4*)	4-Methyl	2.75(2)	5.09(2)	6.30(6)	2.34(3)	1.21(6)	19
(*5*)	4-Allyl	2.60(2)	4.81(3)	5.95(9)	2.21(4)	1.14(9)	18
(*6*)	4-*tert*-Butyl	2.86(6)	5.36(16)		2.50(17)		11
(*7*)	2.4-Dimethyl	2.18(3)	3.88(5)	4.92(10)	1.70(6)	1.04(11)	16
(*8*)	1,1,4-Trimethyl	1.76(4)	3.17(3)		1.41(5)		19
(*9*)	2-Isopropyl-4-methyl	1.51(5)					10

cadmium – thiosemicarbazide (*1*) system were treated by the program described in the appendix.

The results of the calculations are listed in Table 1 as the logarithm to the overall stability constants β_i with the standard deviations in parenthesis. The cadmium(II) ion probably in all cases takes up a maximum of three thiosemicarbazides, but due to limited solubility of the ligands (*6*) and (*8*) it has been possible only to determine the first two stability constants for these systems and only one constant for ligand (*9*).

Substitution in the 4-position. A number of stability constants, involving thiosemicarbazides, substituted in the 4-position only, have been determined and makes it possible to investigate the inductive effect on complex formation from a substituent in this place, since the steric effects from substituents are expected to be of minor importance in this position, away from the reaction sites. Empirical correlations of this type are usually termed linear free energy relationship [18] and owes its name to the fact that, for a series of structurally closely related ligands, a plot of the logarithm of the stability constants (proportional to the free energy of complex formation ΔG°) *versus* a parameter representing the inductive effect of the substituent, usually gives a straight line. This technique, which also holds for, *e.g.*, kinetic data of several organic compounds has been widely used in organic chemistry [18–20] and was used already in 1934 by Larsson [21] for complex formation. It has later been used by several authors [22–25] to correlate the complexing ability of related ligands or metal ions.

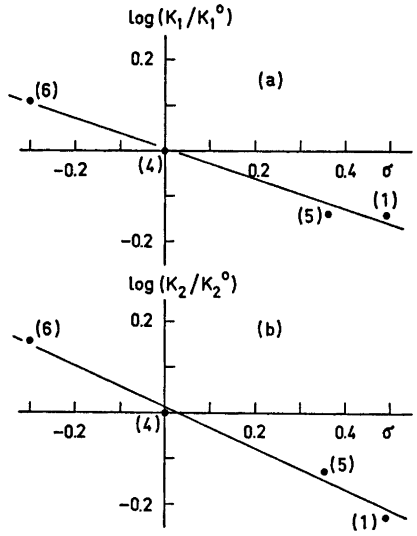

Fig. 1. The Hammet plots for the first (a) and second (b) stability constant for some Cd(II) – 4-alkylsubstituted thiosemicarbazide systems. The ligands are: (*1*) unsubstituted, (*4*) 4-methyl-, (*5*) 4-allyl- and (*6*) 4-*tert*-butyl-thiosemicarbazide.

Using a ligand with acid or basic properties, the best correlations are usually obtained, plotting log K for complex formation *vs.* pK for protonation of the ligand.[21–24] Fair plots are, however, also frequently obtained, using an empirical parameter σ, suggested by Hammet [26] instead of pK.[24,25] This parameter is introduced through the Hammet equation:

$$\log (K/K_0) = \sigma\varrho$$

which relates the equilibrium (or rate) constant K relative to the constant (K_0) for a parent compound to a parameter ϱ, characteristic for the specific reaction and σ, the substituent parameter.

For the Cd^{2+} – 4-alkylthiosemicarbazide systems 4-methylthiosemicarbazide was taken as the reference ligand and σ-values, determined by Taft [19] from kinetic studies of esters of carboxylic acids, were used. The Hammett plots for K_1 and K_2 for these systems are shown in Fig. 1. In both cases fairly good linear relationships are found. The slopes of the lines, found from a least squares fit are $\varrho = -0.35(5)$ and $-0.45(5)$, respectively.

The negative slope of the lines indicates, that the complex formation is promoted by an enhanced negative charge on the ligating sulfur atom adjacent to the substituent. This is what one would intuitively expect and such results are found in many cases. Examples of the opposite behaviour are known, however, and have been interpreted as due to extensive π back donation from the metal ion to the ligand [24,25,27] This interpretation has, however, recently been criticized.[28]

Within the interval of confidence, the slopes of the two lines can be considered identical. Since ϱ is very sensitive to the type and strength of the bonds between donor and acceptor atoms,[23,24] this indicates, that the first and the second ligand is coordinated to the cadmium ion in the same manner, and that only minor steric effects are involved in the series.

The logarithm to the third consecutive stability constants K_3 does not fall in with the scheme mentioned above. The variation of K_3 is discussed later.

Substitution in the 2-position. One might expect the same type of dependence of stability constants on substitution in the 2- and in the 4-position. Reversal behaviours are, however, observed. Introduction of a methyl group in the 4-position increases log K_1 from 2.60 to 2.75. (Only the variations in log K_1 are discussed. The variations in log K_2 are similar). However, a methyl group in the 2-position makes the complex formation less favourable (log $K_1 = 2.31$). When the ligand is substituted in both the 2- and the 4-positions at the same time the complexes are even less stable. This decrease in stability is a function of the bulkiness of the substituents: log $K_1 = 2.18$ for 2,4-dimethylthiosemicarbazide and only 1.51 for 2-isopropyl-4-methylthiosemicarbazide.

This indicates a steric hindrance, presumably because the conformation of the ligand necessary for chelating complex formation is hindered in the case of substitution in the 2-position, this effect being more pronounced in case of a further substitution on the N(4).

This point is illustrated by a study by Jensen *et al.*[29] of the conformation of alkylsubstituted thiosemicarbazides in solution by means of ^1H NMR spectroscopy in $CDCl_3$ and DMSO-d_6. The conclusion is that the C – N bonds of thiosemicarbazide have partly double bond character such that C, N(2), N(4), S and the substituents on these atoms are co-planar, however, with rather low barriers of rotation in these solvents. For N(2)-substituted thiosemicarbazides it was found that the substituent was *s-cis* to the sulfur atom. For 2,4-disubstitution this conformation is even more pronounced. Since chelation demands *s-trans* configuration, the free energy difference between the two conformations may be reflected in the stability constants measured here for the cadmium complexes.

Substitution in the 1-position. Like in the 2-position, introduction of a substituent on N(1) lowers the stability of the complex. log K_1 for 1-methylthiosemicarbazide is 2.34 and for 1,1,4-trimethylthiosemicarbazide log K_1 is only 1.76. Since N(1) is one of the reaction sites in the chelating ligand, this variation is to be expected.

From qualitative judgements of the colour of solutions of Ni^{2+} and a number of 1-substituted thiosemicarbazides, Jensen and Rancke-Madsen have concluded [30] that no complex formation takes place contrary to the behaviour for ligands unsubstituted in this position. Since in case of 1-substitution N(1) is sterically hindered, the difference between the two metal ions towards this type of ligands is mainly due to the difference in the metal-sulfur bond strength. Although Christensen and Rasmussen have argued, that thiosemicarbazide is bound to cadmium mainly through the N(1) atom

and that the S–Cd bond is rather weak [15] this bond is still expected to be stronger than the Ni–S bond.

Variation of K_3. The values of log K_3 together with their estimated standard deviations have been collected in Table 1.

It should be noticed that the values of log K_3 are much smaller than for the two first stepwise stability constants and that their absolute values are surprisingly independent of substitution in the ligands contrary to variations found for K_1 and K_2 (Fig. 1). Within the uncertainty of the measurements log K_3 is constant and identical to the value obtained for the unsubstituted ligand. The great ratio of K_2/K_3 for the cadmium–thiosemicarbazide system ($\log K_2 = 2.08$ and $\log K_3 = 1.18$), led Christensen and Rasmussen to postulate that a change in configuration from a tetrahedral bis complex to an octahedral tris complex takes place with uptake of the third ligand.[15]

From an X-ray structure determination, bis(thiosemicarbazide) cadmium(II) sulfate has recently been shown to contain cadmium ions in an octahedral environment.[31] The unit cell contains two independent complex ions both with octahedral coordination and the two chelating thiosemicarbazides nearly coplanar, in one complex *cis* and in the other *trans* to each other. The two remaining axial coordination sites are occupied by oxygen from the sulfato groups.

One should, however, be careful deducing structures of labile metal complexes in solution from the structure in the solid state and the results of the present investigation support the idea proposed [15] that the bis(thiosemicarbazide) cadmium(II) ion is 4-coordinated in solution.

APPENDIX

Several authors have discussed the use of digital computers in the treatment of complex formation data.[32–36] The program developed for the present study is based on a conventional nonlinear regression technique as described by Demig [37] and Wentworth.[38] In its present state it is designed to treat potentiometric data only. Moreover, it is presumed that only monomeric species are formed.

Notation. For convenience, the most important definitions are collected below:

M, m: total and free metal concentrations, respectively.
L, l: total and free ligand concentrations, respectively.
$\beta_i = [ML_i]/m\,l^i$: the overall stability constant of the i'th mononuclear complex.
E: experimentally measured EMF difference of the cells in which $L=0$ and $L=L$, $E = -k \log m/M$
F = $F(E, M, L, \log \beta_1 ... \log \beta_N)$ function, relating the three variables E, M, and L to the N parameters $\log \beta_n$ $(1 \leq n \leq N)$
σ: Standard deviation.
$k = (RT/zF) \ln 10$

The error square sum to be minimized can be expressed as

$$\sum (E(\log \beta_i)_{calc} - E_{obs})^2 \Big/ \left(\sigma_E^2 + \frac{\delta E}{\delta M} \sigma_M^2 + \frac{\delta E}{\delta L} \sigma_L^2 \right)$$

The required partial derivatives F′ (Demig's nomenclature [37]) are found from the well-known relations:[39]

$$M = m + \sum_{n=1}^{N} \beta_n m l^n$$

$$L = l + \sum_{n=1}^{N} n \beta_n m l^n$$

and from the definitions of E and β_i.

$$F'_M = \frac{\delta E}{\delta M} = -\frac{k}{mM \ln 10} \frac{\delta m}{\delta M} M - m$$

$\frac{\delta m}{\delta M}$ (and $\frac{\delta l}{\delta M}$) is found by solving the two equations:

$$\frac{\delta M}{\delta M} = 1 = \frac{\delta M}{\delta m}\frac{\delta m}{\delta M} + \frac{\delta M}{\delta l}\frac{\delta l}{\delta M}$$

$$\frac{\delta L}{\delta M} = 0 = \frac{\delta L}{\delta m}\frac{\delta m}{\delta M} + \frac{\delta L}{\delta l}\frac{\delta l}{\delta M}$$

$$\left(1 + \sum_{n=1}^{N} \beta_n l^n\right)\frac{\delta m}{\delta M} + \left(\sum_{n=1}^{N} n \beta_n m l^{n-1}\right)\frac{\delta l}{\delta M} = 1$$

$$\left(\sum_{n=1}^{N} n \beta_n l^n\right)\frac{\delta m}{\delta M} + \left(1 + \sum_{n=1}^{N} n^2 \beta_n m l^{n-1}\right)\frac{\delta l}{\delta M} = 0$$

F'_L is found in a similar manner:

$$F'_L = \frac{\delta E}{\delta L} = -\frac{-k}{m \ln 10}\frac{\delta m}{\delta L}$$

$$\frac{\delta M}{\delta L} = 0 = \frac{\delta M}{\delta m}\frac{\delta m}{\delta L} + \frac{\delta M}{\delta l}\frac{\delta l}{\delta L}$$

$$\frac{\delta L}{\delta L} = 1 = \frac{\delta L}{\delta m}\frac{\delta m}{\delta L} + \frac{\delta L}{\delta l}\frac{\delta l}{\delta L}$$

And finally $F'_{\log \beta_n}$ is found thus:

$$F'_{\log \beta_n} = \frac{\delta E}{\delta \log \beta_n} = -\frac{k\beta_n}{m}\frac{\delta m}{\delta \beta_n}$$

$\frac{\delta m}{\delta \beta_n}\left(\text{and } \frac{\delta l}{\delta \beta_n}\right)$ is found in analogy with $\frac{\delta m}{\delta L}$ and $\frac{\delta m}{\delta M}$:

$$\frac{\delta M}{\delta \beta_n} = 0 = \frac{\delta M}{\delta m}\frac{\delta m}{\delta \beta_n} + \frac{\delta M}{\delta l}\frac{\delta l}{\delta \beta_n} + \frac{\delta M}{\delta \beta_n}\frac{\delta \beta_n}{\delta \beta_n}$$

$$\frac{\delta L}{\delta \beta_n} = 0 = \frac{\delta L}{\delta m}\frac{\delta m}{\delta \beta_n} + \frac{\delta L}{\delta l}\frac{\delta l}{\delta \beta_n} + \frac{\delta L}{\delta \beta_n}\frac{\delta \beta_n}{\delta \beta_n}$$

since $\frac{\delta M}{\delta \beta_n} = ml^n$ and $\frac{\delta L}{\delta \beta_n} = nml^n$.

The initial guesses on the parameters $\log \beta_1$ ...$\log \beta_N$ are then corrected with the calculated $\Delta \log \beta_i$ or a fraction of them and the whole calculation is repeated until the limit of the iteration is reached. The sum of squares of the weighted residuals is calculated in each cycle and the iteration is stopped, when the relative difference between two such numbers, arising from two subsequent iterations, is less than 10^{-4}. The standard deviations are assumed to be $\sigma_E = 0.2$ mV and σ_L and $\sigma_M = 1.0$ %.

An ALGOL as well as a FORTRAN version of the program (for the RC4000 from Regnecentralen A/S Copenhagen and the IBM 370/165 computer respectively) has been written.*

Acknowledgements. The author wishes to express his sincere thanks to Professor K. A. Jensen for supplying several of the ligands, to Dr. E. Larsen for numerous stimulating discussions and to Dr. O. Mønsted for valuable suggestions concerning methods of calculation.

* A punched tape listing or a card deck of the program is available from the author upon request.

REFERENCES

1. Hazell, R. G. *Acta Chem. Scand. 26* (1972) 1365.
2. Hazell, R. G. *Acta Chem. Scand. 22* (1968) 2809.
3. Hazell, R. G. *Acta Chem. Scand. 22* (1968) 2171.
4. Grønbæk, R. Rasmussen, S. E. *Acta Chem. Scand. 16* (1962) 2325.
5. Cavalca, L., Nardelli, M. and Fava, G. *Acta Crystallogr. 15* (1962) 1139.
6. Villa, A. C., Manfredotti, A. G. and Guastini, C. *Cryst. Struct. Commun 1* (1972) 125.
7. Gastaldi, L. and Forta, P. *Cryst. Struct. Commun. 1* (1972) 353.
8. Cavalca, L., Nardelli, M. and Branchi, G. *Acta Crystallogr. 13* (1960) 688.
9. Nardelli, M., Fava Gasparri, G., Giraldi Bottistini, G. and Musatti, A. *Chem. Commun* (1965) 187.
10. Canzolari Cappacchi, L., Fava Gasparri, G., Ferrari, M. and Nardelli, M. *Chem. Commun.* (1968) 910.
11. Jensen, K. A., Anthoni, U., Kägi, B., Larsen, Ch. and Pedersen, C. Th. *Acta Chem. Scand. 22* (1968) 1.
12. Goddard, D. R., Lodam, B. D. and Ajayi, S. O. *J. Chem. Soc. A* (1969) 506.
13. Ajayi, S. O. and Goddard, D. R. *J. Chem. Soc. Dalton* (1973) 1751.
14. Toropova, V. F. and Naimushina, K. V. *Russ. J. Inorg. Chem. 5* (1960) 421.
15. Nørlund Christensen, A. and Rasmussen, S. E. *Acta Chem. Scand. 17* (1963) 1315.
16. Toropova, V. F. and Kirillova, L. S. *Russ. J. Inorg. Chem. 5* (1960) 276.
17. Treadwell, F. P. *Helv. Chim. Acta 4* (1921) 551.
18. Shorter, J. *Quart. Rev. Chem. Soc. 24* (1970) 433.
19. Taft, R. W. In Newman, M. S., Ed., *Steric Effects in Organic Chemistry*, Wiley, New York 1956, Chapter 13.
20. Jaffe, H. H. *Chem. Rev. 53* (1953) 191.
21. Larsson, E. *Z. Phys. Chem. A 169* (1934) 207.
22. Irving, H. and Rosotti, H. *Acta Chem. Scand. 10* (1956) 72.
23. Tucci, E. R., Ke, C. H. and Li, N. C. *J. Inorg. Nucl. Chem. 29* (1967) 1657.
24. May, W. R. and Jones, M. M. *J. Inorg. Nucl. Chem. 24* (1962) 511.
25. Irving, H. and Da Silva, J. J. R. F. *Proc. Chem. Soc. London* (1962) 250.
26. Hammett, L. P. *Chem. Rev. 17* (1935) 125.
27. Murmann, R. K. and Basolo, F. *J. Am. Chem. Soc. 77* (1955) 3484.
28. Yingst, A. and McDaniel, D. H. *J. Inorg. Nucl. Chem. 28* (1966) 2919.
29. Jensen, K. A., Buchardt, O., Carlsen, N. G., Ettlinger, M. G. and Svanholm, U. *Acta Chem. Scand. To be published.*
30. Jensen, K. A. and Rancke-Madsen, E. *Z. Anorg. Allgem. Chem. 219* (1934) 243.

31. Larsen, E. and Trinderup, P. *Acta Chem. Scand. A 29* (1975) 481.
32. Rydberg, J. In Kirschner, S., Ed., *Advances in the Chemistry of Coordination Compounds*, Macmillan, New York 1961.
33. Sullivan, J. C., Rydberg, J. and Miller, W. F. *Acta Chem. Scand. 13* (1959) 2023.
34. Sillén, L. G. *Acta Chem. Scand. 16* (1962) 159.
35. Ingri, N. and Sillén, L. G. *Acta Chem. Scand. 16* (1962) 173.
36. Sillén, L. G. *Acta Chem. Scand. 18* (1964) 1085.
37. Demig, W. E. *Statistical Adjustment of Data*, Wiley, New York. 1944.
38. Wentworth, W. E. *J. Chem. Educ. 42* (1965) 96.
39. Bjerrum, J. *Metal Ammine Formation in Aqueous Solution*. Haase, Copenhagen 1941.

Received June 13, 1975.

Acta Chemica Scandinavica A 30 (1976) 54—58

Molecular Structure of Gaseous Bis(methylthio)methylborane

S. LINDØY, H. M. SEIP and R. SEIP

Department of Chemistry, University of Oslo, Oslo 3, Norway

Bis(methylthio)methylborane has been studied by gas electron diffraction. The molecular skeleton was found to be at least nearly planar, and only a *syn-anti* form was observed. The average B—S and C—S bond distances are 1.796(7) and 1.818(6) Å, respectively.

A series of compounds with BS bonds, *i.e.* $(CH_3)_2B_2S_3$,[1] $Cl_2B_2S_3$,[2] $(CH_3)_2BSCH_3$,[3] $B(SCH_3)_3$,[4] and $(CH_3)_2BSSB(CH_3)_2$,[5] has been investigated by gas electron diffraction at this institute. As a natural extension of these investigations we have now studied bis(methylthio)methylborane. From the previous investigations of boron-sulfur compounds both conformers I and II seem possible, and we were particularly interested in determining which is the more stable one.

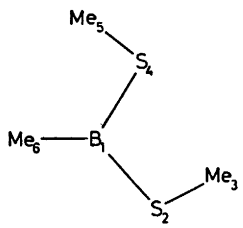

I

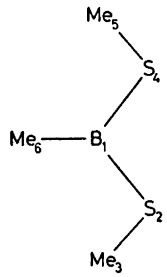

II

EXPERIMENTAL AND STRUCTURE ANALYSIS

Two sets of photographic plates were recorded with Balzers' eldigraph KD-G2.[6,7] Set 1 consisted of 5 plates, made at an electron wavelength of 0.05847 Å, and a nozzle-to-plate distance of 579.69 mm; set 2 of 4 plates, wavelength 0.05853 Å, and distance 189.78 mm. The nozzle temperature was about 50 °C. The data were treated in the usual way using the modification function $s/(|f_C'||f_B'|)$.[8] The scattering amplitudes were those used previously.[3] Two average intensity curves were computed, one from each set of plates. The curves covered the s intervals 1.0 – 13.75 Å^{-1} and 3.25 – 40 Å^{-1}, respectively. Finally a composite intensity curve was computed (see Fig. 1). The data for $s > 35$ Å^{-1} were discarded in the refinements because of noise.

The experimental radial distribution (RD) function[8] calculated by Fourier inversion of the composite intensity curve given in Fig. 1, is shown in Fig. 2. The outer part of the curve is particularly interesting since it shows that form I must be the dominant one: In conformer II the distances S2 ... C5 and S4 ... C3 would be equal and cause a larger peak near 4.5 Å than found in the experimental curve.

To carry out least-squares refinements some assumptions about the geometry were necessary. Convenient and plausible ones, shown by the RD curve to be essentially correct, were:

(1) planar arrangement of C6B1S4S2,
(2) the S—B distances are equal,
(3) the S—C distances are equal,
(4) all C—H distances are equal,
(5) local C_{3v} symmetry for the SCH_3 groups and for the BCH_3 group
(6) equal SCH angles.

The fifteen parameters given in Table 1 are then necessary to describe the molecular geometry.

The results of least-squares refinement with a diagonal weight matrix are given in Tables 1 and 2. Only a few of the mean amplitudes (u) could be refined simultaneously with the geometrical parameters. The other u values were either kept at values close to those calculated from spectroscopic data (see the next section) or adjusted somewhat in separate calculations.

The perpendicular amplitude correction coefficients calculated as described in the next section, were used to find the r_α structure[9] which is geometrically consistent. The shrinkage effect is therefore included in the calculation of the results given in the Tables 1 and 2.

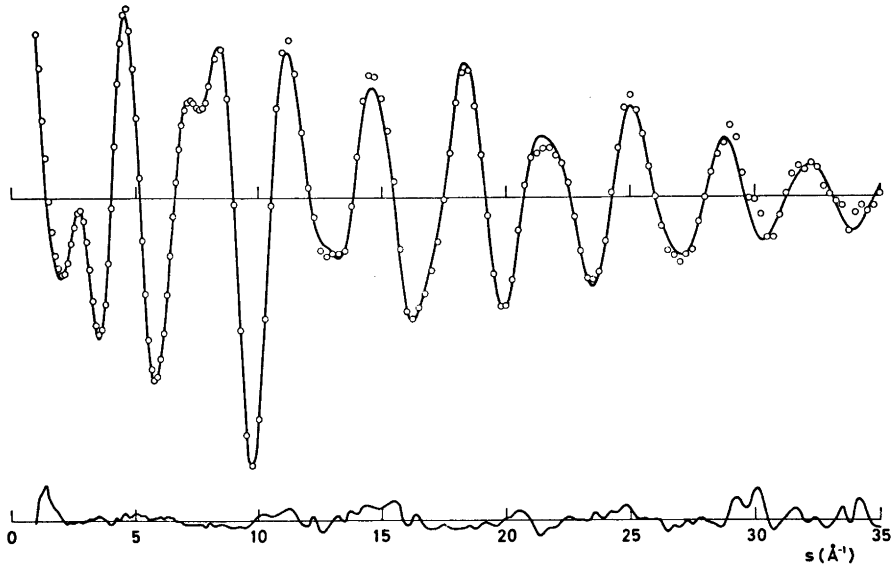

Fig. 1. Comparison of the experimental intensity values (circles) and the corresponding theoretical ones (full line) calculated with the parameters in Tables 1 and 2. The differences between experimental and theoretical values are also shown.

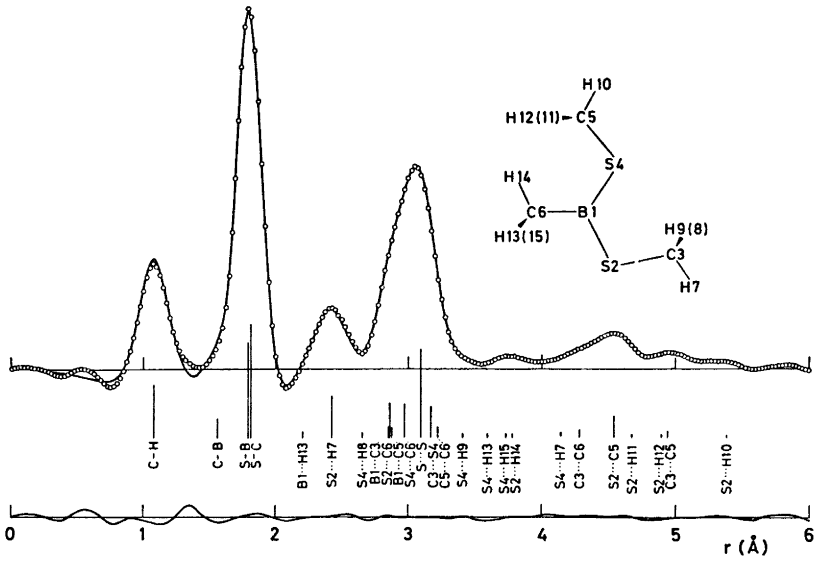

Fig. 2. Experimental (circles) and theoretical (full line) radial distribution functions calculated with an artificial damping constant [8] $k = 0.003$ Å^2. The differences between experimental and theoretical values are also shown. The positions and approximate areas of the peaks corresponding to the most important interatomic distances are indicated.

Table 1. Bond distances, the corresponding mean amplitudes of vibration and angle parameters in bis(methylthio)methylborane.[a]

	Distances and amplitudes r_a (Å)[a]	u^{ED} (Å)[b]	u^S (Å)[c]
C–H	1.086(5)	0.074(5)	0.079
C–B	1.567(10)	0.053(10)	0.056
S–B	1.796(7)	0.052 (2)[d]	0.055
S–C	1.818(6)	0.050	0.053
	Angles (degrees)		(degrees)
∠S2BC	116.4(4)	ϕ(CBS2C)	196.7(55)
∠S4BC	124.4(4)	ϕ(CBS4C)	−17.3(66)
∠BS2C	104.5(10)	ϕ(BS2CH7)	200.0[e]
∠BS4C	106.2(14)	ϕ(BS4CH10)	190.0[e]
∠SCH	112.0(5)	ϕ(S2BCH13)	75.0[e]
∠BCH	112.5[e]		

[a] The standard deviations given in parentheses correspond to the last digit given. The values were corrected for the correlation between the intensity data as described in Ref. 10. For C–H an asymmetry constant $\varkappa = 0.00002$ Å^3 was applied, in all other cases $\varkappa = 0$. [b] Mean amplitudes from the electron-diffraction investigation. [c] Mean amplitudes calculated from spectroscopic data as described in the text for model I with planar skeleton. [d] The difference between the u values was assumed. [e] The value was not refined simultaneously with the other parameters.

Table 2. Non-bonded distances and the corresponding mean amplitudes of vibration.[a]

	r_a (Å)	u^{ED} (Å)	u^S (Å)
S···S	3.096	0.073(3)	0.072
S2···C5	4.550	0.099(10)	0.089
S2···C6	2.858	0.073	0.079
S4···C3	3.163	0.126	0.136
S4···C6	2.974	0.070	0.075
B···C3	2.849	0.099	0.090
B···C5	2.882	0.100	0.091
C3···C5	4.938	0.099(27)	0.139
C3···C6	4.284	0.100(25)	0.092
C5···C6	3.242	0.147	0.139
S2···H7	2.431	0.090(8)	0.106
S2···H10	5.381	0.082	0.117
S2···H11	4.648	0.147	0.175
S2···H12	4.942	0.138	0.175
S2···H13	3.222	0.218	0.194
S2···H14	3.779	0.137	0.112
S2···H15	2.999	0.208	0.184
S4···H7	4.134	0.145	0.156
S4···H8	2.629	0.236	0.266
S4···H9	3.423	0.249	0.266
S4···H13	3.579	0.193	0.167
S4···H14	3.051	0.183	0.157
S4···H15	3.757	0.162	0.138
B···H13	2.216	0.106	0.108

[a] The u values with standard deviations given in parentheses have been refined with the geometrical parameters; *cf.* Table 1.

However, since the torsional frequencies are not known, some of the correction terms are rather uncertain.

MEAN AMPLITUDES OF VIBRATION AND PERPENDICULAR AMPLITUDE CORRECTION COEFFICIENTS

The IR and Raman spectra of $CH_3B(SCH_3)_2$ have been studied by Vahrenkamp.[11] We computed the fundamental frequencies (see Table 3) by the program written by Gwinn,[12] and the mean amplitudes and correction coefficients as described by Stølevik *et al.*,[13] starting with force constants obtained for $(CH_3)_2BSCH_3$ [3] and $B(SCH_3)_3$.[4] Table 4 gives the values used in the final calculations. Vahrenkamp assigned the frequencies near 280 cm^{-1} and 295 cm^{-1} to torsions about the BS bonds. Using the force constants given in Table 4, these frequencies became 103 and 129 cm^{-1}, respectively, which seems more reasonable. We believe δ_{as} (CBS_2) and δ_{as} (BSC) to be about 295 and 332 cm^{-1}, respectively. The weak band near 383 cm^{-1} is then unexplained. The value seems too high to correspond to methyl torsion which is more likely to be about 250 cm^{-1}, and may possibly be a combination band.

Table 3. Vibration spectrum (frequencies in cm^{-1}) of bis(methylthio)methylborane.[a]

Tentative assignment		IR	Raman	Calculated
τ(BS)				103
τ(BS)				129
$\delta_s(CBS_2)$			165 s	167
δ_s(BSC)			235 s	223
$\tau(SCH_3)$?	[τ(BS)]		280 w	248, 267
$\delta_{as}(CBS_2)$	[τ(BS)]	295 vw	292 s	293
δ_{as}(BSC)	[$\delta_{as}(CBS_2)$]	332 w	331 s	330
combination?	[δ_{as}(BSC)]	384 w	382 w	
$\gamma(CBS_2)$			431 vw	423
$\nu_s(BS_2)$		519 m	517 vs	504
ν(CS)		708 m	713 vs	709, 718
$\nu_{as}(BS_2)$		1026/1052 vs	1029 vw	1057/1082
ν(BC)		1073/1105 s	1074 w	1078/1116

[a] Most of the frequencies corresponding to hydrogen vibrations have not been included here. The observed values are taken from Vahrenkamp's work.[11] In some cases our proposed assignment differs from that of Vahrenkamp (given in square brackets).

Table 4. Force constants used in the calculations of frequencies, mean amplitudes of vibration and correction coefficients.[a]

Stretching (mdyn/Å)		Bending (mdyn Å/rad²)		Repulsion (mdyn/Å)	
B–S	2.50(2)	BSC	1.05(2)	S···H	0.54(6)
C–S	1.80(2)	SBS	0.95(1)	B···H	0.46(3)
B–C	2.20(1)	SBC	0.80(2)	H···H	0.20(9)
C–H[b]	4.20(3)	SCH	0.35(6)	C3···S4	0.07(1)[d]
C–H[c]	4.30(6)	BCH	0.35(3)	C5···C6	0.04(1)
		HCH	0.35(9)		
Coupling (mdyn/Å)		**Torsional (mdyn Å/rad²)**		**Out-of-plane (mdyn Å/rad²)**	
BC/BS	0.25(2)	CBSC	0.10(2)	BS/CBS[e]	0.06(2)
BS/BS	0.40(1)	SBSC	0.10(2)	BC/SBS	0.05(1)
		BSCH	0.04(6)		
		SBCH	0.01(6)		

[a] The number of contributions is given in parentheses. [b] B–CH_3 group. [c] S–CH_3 group. [d] This value was also applied for $B(SCH_3)_3$. The value given in Table 4 of Ref. 4 is a misprint. [e] BS bond out of the CBS plane.

Table 5. Comparison of BS and CS bond lengths.

	$(CH_3)_2BSCH_3$	$CH_3B(SCH_3)_2$	$B(SCH_3)_3$
B–S	1.779(5)	1.796(7)	1.805(2)
C–S	1.825(4)	1.818(6)	1.825(3)
Average	1.802	1.807	1.815

DISCUSSION

The investigation shows conformer I to be the dominant one. Radial distribution curves calculated for mixtures of I and II showed that the amount of conformer II must certainly be less than 20 %. Preliminary results obtained by electron diffraction for $N_3B(OCH_3)_2$[14] and by *ab initio* calculations for $HB(OH)_2$[15] show that these molecules also prefer form I; in the latter case the energy difference is about 2 kcal/mol.

The skeleton of bis(methylthio)methylborane is certainly nearly planar. Table 1 shows that when the torsional angles about the BS bonds are refined, deviations of about 17° from planarity are obtained. A least-squares refinement was also carried out with these torsional angles fixed at 180° and 0°, respectively. The ratio between the R factors was 1.021. According to Hamilton's test [16] the model with a planar skeleton can therefore not be rejected at the 5 % significance level. When in addition the assumptions made about the structure and the rather large uncertainties in the perpendicular amplitude correction coefficients are considered, we conclude that an essentially planar skeleton is consistent with the experimental data.

The bond lengths in $(CH_3)B(SCH_3)_2$ are similar to the values found in $(CH_3)_2BSCH_3$ and $B(SCH_3)_3$ (Table 5). The slight tendency for an increase in the BS bond lengths with increasing number of SCH_3 groups is in agreement with the results of Kroner *et al.*[17] obtained by photoelectron spectroscopy and semi-empirical MO calculations. It should be noted, however, that the very similar lengths of the BS and CS bonds makes it difficult to determine the individual values with high accuracy, except in $B(SCH_3)_3$ where the BS distance follows from the value found for the S···S distance. The uncertainties in the BS stretching force constants in the three compounds are too large to justify a discussion of the variation.

Acknowledgements. The authors are grateful to Prof. W. Siebert, Fachbereich Chemie der Philipps Universität, Marburg/Lahn, for the sample of bis(methylthio)methylborane. Financial support from the Norwegian Research Council for Science and Humanities is gratefully acknowledged.

REFERENCES

1. Seip, H. M., Seip, R. and Siebert, W. *Acta Chem. Scand. 27* (1973) 15.
2. Almenningen, A., Seip, H. M. and Vassbotn, P. *Acta Chem. Scand. 27* (1973) 21.
3. Brendhaugen, K., Nilssen, E. W. and Seip, H. M. *Acta Chem. Scand. 27* (1973) 2965.
4. Johansen, R., Nilssen, E. W., Seip, H. M. and Siebert, W. *Acta Chem. Scand. 27* (1973) 3015.
5. Johansen, R., Seip, H. M. and Siebert, W. *Acta Chem. Scand. A 29* (1975) 644.
6. Zeil, W., Haase, J. and Wegmann, L. *Z. Instrumentenk. 74* (1966) 84.
7. Bastiansen, O., Graber, R. and Wegmann, L. *Balzers' High Vacuum Report 25* (1969) p. 1.
8. Andersen, B., Seip, H. M., Strand, T. G. and Stølevik, R. *Acta Chem. Scand. 23* (1969) 3224.
9. Kuchitsu, K. and Cyvin, S. J. In Cyvin, S. J. Ed., *Molecular Structures and Vibrations*, Elsevier, Amsterdam 1972, Chapter 12.
10. Seip, H. M. and Stølevik, R. In Cyvin, S. J., Ed., *Molecular Structures and Vibrations*, Elsevier, Amsterdam 1972, Chapter 11.
11. Vahrenkamp, H. *J. Organomet. Chem. 28* (1971) 181.
12. Gwinn, W. D. *J. Chem. Phys. 55* (1971) 477.
13. Stølevik, R., Seip, H. M. and Cyvin, S. J. *Chem. Phys. Lett. 15* (1972) 263.
14. Gundersen, G. *To be published.*
15. Gundersen, G., Jonvik, T. and Seip, H. M. *To be published.*
16. Hamilton, W. C. *Acta Crystallogr. 18* (1965) 502.
17. Kroner, J., Nölle, D. and Nöth, H. *Z. Naturforsch. B 28* (1973) 416.

Received June 19, 1975.

Acta Chemica Scandinavica A 30 (1976) 59—62

A Calorimetric Investigation of Bromo and Iodo Complexes of Mercury(II) in Dimethyl Sulfoxide

R. ARNEK and D. POCEVA *

Department of Inorganic Chemistry, Royal Institute of Technology, Stockholm, Sweden

The equilibrium constants and enthalpy changes for the reactions between HgX_2 and X^-, where X = Br and I, in dimethyl sulfoxide (1 M $NaClO_4$, 25 °C) have been obtained from calorimetric data. The stepwise formation constants for $HgBr_3^-$ and $HgBr_4^{2-}$ are $K_3 = 10^{5.6 \pm 0.1}$ M^{-1} and $K_4 = 10^{2.65 \pm 0.03}$ M^{-1} and the enthlapy changes $\Delta H°_3 = -26.9 \pm 0.2$ kJ mol^{-1} and $\Delta H°_4 = -22.7 \pm 0.5$ kJ mol^{-1}. The corresponding values for HgI_3^- and HgI_4^{2-} are $K_3 = 10^{6.1 \pm 0.1}$ M^{-1}, $K_4 = 10^{2.58 \pm 0.03}$ M^{-1}, $\Delta H°_3 = -26.8 \pm 0.1$ kJ mol^{-1} and $\Delta H°_4 = -22.8 \pm 0.3$ kJ mol^{-1}.

Solutions of mercury(II) halide complexes in dimethyl sulfoxide (DMSO) are being studied in this laboratory by X-ray diffraction.[1] The iodide complexes have been found to be mononuclear with HgI_4^{2-} regularly tetrahedral, HgI_3^- pyramidal and HgI_2 approximately linear.[2] The related calorimetric investigation reported here was performed in order to obtain thermodynamic data for the mercury(II) bromide and iodide complexes in DMSO. As the solvating properties of the dipolar aprotic solvent DMSO are markedly different from those of a protic medium, such as water, it is of considerable interest to compare the thermodynamic parameters for complex formation in the two media, DMSO and water. Data for the mercury(II) halide complexes in aqueous solution are available in literature.[3]

Earlier investigations of mercury(II) iodide complexes in DMSO have been made by Buckingham and Gasser [4] (conductance and spectrophotometry), Peterson, Lingane and Reynolds [5] (spectrophotometry), Foll, Le Demézét and Courtot-Coupez [6] (potentiometry), Gorenbein *et al.*[7–9] (freezing point depression and calorimetry) and Samoilenko *et al.*[10] (potentiometry).

Data on mercury(II) bromide complexes in DMSO have been reported by Le Demézét *et al.*,[6] Gorenbein *et al.*[9] and Samoilenko *et al.*[10]

EXPERIMENTAL

Chemicals. The solvent *dimethyl sulfoxide* (Mallincrodt, analytical reagent) was distilled under reduced pressure at about 60 °C over calcium hydride, the first and the last fraction of the distillate being dicarded. The water content of the DMSO, measured by Karl Fischer titration, was found to be less than 0.05 %.

Sodium perchlorate was prepared by neutralizing sodium carbonate with perchloric acid. The crystals obtained were recrystallized once from water and then dried to constant weight at 125 °C.

Mercury(II) bromide and *iodide*, *sodium bromide* and *iodide* were all of analytical grade and were carefully dried before using.

Apparatus. The measurements were carried out with an automatic calorimeter of the isothermal jacket type.[11] The calorimeter is wholly immersed in a thermostat bath of type LKB 7603A, maintained at 25.000 ± 0.001 °C. The calorimeter was initially charged with 100.0 cm^3 (V_0) of a solution S containing HgX_2 and usually in addition some amount of NaX. Successive additions were made to the solution S of v cm^3 of another thermostated solution T containing NaX. Before each addition from the buret the same amount of solution (v cm^3) was removed from the calorimeter vessel, as should be added, so that the final volume was always 100.0 cm^3. The solutions used in the experiments were prepared by dissolving weighed amounts of the reagents in DMSO. The concentration range of HgX_2 studied was 0.005 – 0.200 M for

* Present address: Faculty of Technology and Metallurgy, Skoplje, Yugoslavia.

$HgBr_2$ and 0.005 – 0.040 M for HgI_2.* The concentration of NaX in the buret solution T was 0.2 – 0.35 M for NaBr and 0.2 – 0.5 M for NaI. The ionic strength was kept constant at 1 M by using sodium perchlorate as ionic medium.

The heat of dilution of the solution T, always less than 0.5 M in NaX, in DMSO with sodium perchlorate as ionic medium, was found by experiments to be negligible.

RESULTS AND CALCULATIONS

The reactions which have been studied are

$$HgX_2 + X^- \rightleftharpoons HgX_3^- \quad (1)$$

$$HgX_3^- + X^- \rightleftharpoons HgX_4^{2-} \quad (2)$$

with X = Br and I.

For reactions (1) and (2) we denote the equilibrium constants K_3 M^{-1} and K_4 M^{-1} and the enthalpy changes ΔH°_3 and ΔH°_4 kJ/mol.

The zero superscripts used with ΔH (and also with ΔG and ΔS in the following) mean that the standard states are hypothetical ideal one molar solutions of the solutes in DMSO (1 M $NaClO_4$).

The experimental data from the enthalpy titrations are pairs of (v,Q) values, where Q J is the heat evolved for an addition of v cm^3. The (v,Q) values for two representative titrations are given in Tables 1 and 2. (In total 11 series of measurements were performed, including 160 Q-values). By means of the least-squares program LETAGROP/KALLE [12] (calorimetric version of LETAGROP) the values for the parameters K_3, K_4, ΔH°_3 and ΔH°_4 were searched for which minimize the error square sum U defined by

$$U = \sum (Q_{calc} - Q)^2$$

The values for the equilibrium constants K_3 and K_4 and the enthalpy changes ΔH°_3 and ΔH°_4 which give a minimum in the error square sum U are given in Table 3.

The errors given correspond to three standard deviations. σ_Q is the standard deviation in the Q-measurements. It was found during the calculations that the function $U(K_3)$ (for both Br^- and I^-) has a rather shallow minimum. Conse-

* Throughout this paper M = mol dm^{-3}.

Table 1. Experimental results for a typical titration in the Hg(II) – Br^- system.[a]

S: $C_{HgBr_2} = 20.445 \times 10^{-3}$ M; $C_{Br^-} = 1.298 \times 10^{-3}$ M
T: $C_{Br^-} = 0.2595$ M

v/cm³	Q/J	ΔQ/J
0.500	3.464	0.020
0.499	3.495	−0.019
0.500	3.490	−0.007
0.499	3.504	−0.028
0.499	3.505	−0.030
0.498	3.507	−0.039
0.500	3.504	−0.023
0.999	6.946	0.004
0.997	6.936	−0.015
0.997	6.847	0.003
0.499	3.227	0.046
0.500	2.909	0.029
0.999	5.246	0.003
0.998	4.964	−0.054
0.998	4.626	−0.038
0.997	4.211	−0.036
0.998	3.668	0.002
0.998	3.075	0.008
0.999	2.438	0.040

[a] The complete set of experimental data are available from the authors upon request.

Table 2. Experimental results for a typical titration in the Hg(II) – I^- system.[a]

S: $C_{HgI_2} = 20.63 \times 10^{-3}$ M;
$C_{I^-} = 2.542 \times 10^{-3}$ M
T: $C_{I^-} = 0.5114$ M

v/cm³	Q/J	ΔQ/J
0.500	6.838	0.008
0.500	6.833	0.012
0.500	6.814	0.031
0.498	6.819	−0.003
0.499	6.830	−0.003
0.498	6.807	−0.007
0.500	6.552	0.030
0.498	5.179	0.043
0.500	4.862	0.036
0.498	4.642	−0.021
0.499	4.302	0.007
0.499	3.939	−0.028
0.500	3.438	0.007
0.498	2.943	−0.028
0.500	2.442	−0.035
0.999	3.422	0.028
0.999	2.167	−0.016

[a] The complete set of experimental data are available from the authors upon request.

Table 3. Computed values of K_3, K_4, $\Delta H°_3$ and $\Delta H°_4$ in DMSO (1 M $NaClO_4$, 25 °C).

System	X = Br	X = I
log K_3	5.6 ± 0.1	6.1 ± 0.1
log K_4	2.65 ± 0.03	2.58 ± 0.03
$\Delta H°_3$, kJ	−26.85 ± 0.15	−26.78 ± 0.11
$\Delta H°_4$, kJ	−22.68 ± 0.28	−22.84 ± 0.27
σ_Q, J	0.04	0.04

quently the values for log K_3 are relatively uncertain. In fact the constants K_3 are somewhat too high to be safely determined from calorimetric titration data. The most favourable range for determining equilibrium constants by calorimetry is usually considered to be $0 < \log K < 3$.

In Tables 1 and 2 the experimental data (v,Q) and the differences $\Delta Q = (Q_{calc} - Q)$ are given for two typical experiments

PREVIOUS DATA. DISCUSSION

The values for K_3 and K_4 obtained by us from calorimetric data are in reasonable agreement with those obtained by le Demézét *et al.*[6] from potentiometric measurements in 0.1 M Et_4NClO_4 (log $K_3 = 5.8$, log $K_4 = 2.4$ for Hg(II) − Br^-; log $K_3 = 6.2$, log $K_4 = 2.2$ for Hg(II) − I^-). The values for Hg(II) − I^- reported by Peterson *et al.*[5] are markedly lower (log $K_3 = 5.74 \pm 0.1$, log $K_4 = 1.88 \pm 0.02$); however, those values were obtained from measurements without a supporting electrolyte and with a total mercury(II) concentration not exceeding 5×10^{-5} M. Samoilenko *et al.*[10] reported in 1 M $NaClO_4$ log $K_4 = 0.9$ for Hg(II) − Br^- and log $K_4 = 2.0$ for Hg(II) − I^-; the former value seems rather low.

Gorenbein *et al.*[8,9] reported calorimetric values for ΔH_3 and ΔH_4 in DMSO without ionic medium ($\Delta H_3 = -23.4$ kJ mol^{-1}, $\Delta H_4 = -13.8$ kJ mol^{-1} for Hg(II) − Br^-; $\Delta H_3 = -32.2$ kJ mol^{-1}, $\Delta H_4 = -11.3$ kJ mol^{-1} for Hg(II) − I^-). Our values for $\Delta H°_3$ and $\Delta H°_4$ differ considerably from those reported by Gorenbein *et al.*[8,9] Unfortunately the latter do not give the complex constants used in the computation of the ΔH-values.

A value $\Delta H_3 + \Delta H_4 = -43.8$ kJ mol^{-1} in DMSO without ionic medium has been reported by Buckingham and Gasser.[4]

The thermodynamic parameters $\Delta G°$, $\Delta H°$ and $\Delta S°$ for the formation of the complexes HgX_3^- and HgX_4^{2-} in DMSO are collected in Table 4 together with the corresponding quantities for aqueous solution. For comparison the values of K_3 and K_4 in DMSO and water are also in Table 5. Comparing the thermodynamic parameters in DMSO for the formation of Hg(II) − bromide and iodide complexes, we find that they are strikingly similar (in aqueous solution there is a considerable difference). For both ligands the values of K_3 and K_4 are higher in DMSO than in water, the increase being most pronounced for K_3. For the bromide complexes this is mainly an effect of the more favourable enthalpy terms in DMSO. For the iodide complexes, where the material for comparison

Table 4. The values of $\Delta G°$, $\Delta H°$ and $\Delta S°$ at 25 °C in DMSO and water for the reactions studied: (A) Hg(II) − Br^-, (B) Hg(II) − I^-.

Reaction	DMSO, 1 M $NaClO_4$ [a]			H_2O, 0.5 M $NaClO_4$		
	$\Delta G°$/ kJ mol^{-1}	$\Delta H°$/ kJ mol^{-1}	$\Delta S°$/ J mol^{-1} K^{-1}	$\Delta G°$/ kJ mol^{-1}	$\Delta H°$/ kJ mol^{-1}	$\Delta S°$/ J mol^{-1} K^{-1}
A. Hg(II) − Br^-						
$HgBr_2 + Br^- \rightleftharpoons HgBr_3^-$	−32.0	−26.9	+17	−12.0[b]	−12.6[b]	−2[b]
$HgBr_3^- + Br^- \rightleftharpoons HgBr_4^{2-}$	−15.1	−22.7	−25	−9.7[b]	−17.1[b]	−25[b]
$HgBr_2 + 2Br^- \rightleftharpoons HgBr_4^{2-}$	−47.1	−49.6	−8	−21.7[b]	−29.7[b]	−27[b]
B. Hg(II) − I^-						
$HgI_2 + I^- \rightleftharpoons HgI_3^-$	−34.8	−26.8	+27	−21.6[c]	−	−
$HgI_3^- + I^- \rightleftharpoons HgI_4^{2-}$	−14.7	−22.8	−27	−12.7[c]	−	−
$HgI_2 + 2I^- \rightleftharpoons HgI_4^{2-}$	−49.5	−49.6	0	−34.2[c]	−42.0[d]	−26

[a] Present work. [b] Ref. 13. [c] Ref. 14. [d] Ref. 15, 16.

Table 5. Values of K_3 and K_4 in DMSO and water at 25 °C.

	DMSO		H_2O [a]	
	X=Br	X=I	X=Br	X=I
log K_3	5.6	6.1	2.1	3.8
log K_4	2.65	2.58	1.7	2.2
log $K_3 K_4$	8.25	8.68	3.8	6.0

[a] Ref. 13, 14.

is not complete, the difference in the entropy terms seems to be as important as the difference in the enthalpy terms.

To explain, at least qualitatively, the difference in stability between the complexes in DMSO and in water one has to take into account the different solvating properties of the two media. In general anions, and especially those able to form hydrogen bonds, are more strongly solvated in water than in DMSO. The halide ions have in a protic solvent such as water, capacity to form hydrogen bonds. The capacity is more pronounced the smaller the ion; the iodide ion is probably rather weakly hydrogen bonding. In an aprotic solvent such as DMSO no hydrogen bonds can be formed.

One might thus expect the bromide ion, which can form hydrogen bonds in water, to form stronger mercury(II) complexes in DMSO than in water, provided there is not too big a difference in solvation of Hg(II) in the two media. For the iodide ion, on the other hand, which probably forms no hydrogen bonds in water, one might expect less difference in stability between the mercury(II) complexes in water and DMSO. One would furthermore expect the difference in stability between the mercury(II) – bromide and iodide complexes to be smaller in DMSO than in water. The observed stabilities of the complexes give support to the model outlined briefly above.

The stabilities of several metal halide complexes in dimethyl sulfoxide have been discussed in a recent paper by Ahrland and Björk.[17]

Acknowledgements. This work has been supported by the Swedish Natural Science Research Council. The English was revised by Dr. D. Lewis.

REFERENCES

1. Johansson, G. and Sandström, M. *Personal communication.*
2. Gaizer, F. and Johansson, G. *Acta Chem. Scand. 22* (1968) 3013.
3. Sillén, L. G. and Martell, A. E., Eds., *Stability Constants*, The Chemical Society, Special Publications Nos. 17 and 25, London 1964, 1971.
4. Buckingham, A. and Gasser, R. P. H. *J. Chem. Soc. A* (1967) 1964.
5. Peterson, R. J., Lingane, P. J. and Reynolds, W. L. *Inorg. Chem. 9* (1970) 680.
6. Foll, A., Le Demézét, M. and Courtot-Coupez, J. *Bull. Soc. Chim. Fr.* (1972) 1207.
7. Gorenbein, E. Y., Vainshtein, M. N., Trofimchuk, A. K., Abarbarchuk, I. L. and Skorobogatko, E. P. *Zh. Obshch. Khim. 43* (1973) 495.
8. Gorenbein, E. Y., Vainshtein, M. N., Skorobogatko, E. P. and Trofimchuk, A. K. *Zh. Obshch. Khim. 44* (1974) 1558.
9. Gorenbein, E. Y., Vainshtein, M. N. and Skorobogatko, E. P. *Ukr. Khim. Zh. 9* (1974) 923.
10. Samoilenko, V. M., Lyashenko, V. I. and Polishchuk, N. V. *Zh. Neorg. Khim. 19* (1974) 2984.
11. Arnek, R. and Holmqvist, E. *To be published.*
12. Arnek, R. *Ark. Kemi 32* (1970) 81.
13. Björkman, M. and Sillén, L. G. *Trans. Roy. Inst. Technol. (Stockholm)* 1963.
14. Sillén, L. G. *Acta Chem. Scand. 3* (1949) 539.
15. Gallagher, P. K. and King, E. L. *J. Amer. Chem. Soc. 82* (1960) 3510.
16. Christensen, J. J., Izatt, R. M., Hansen, L. D. and Hale, J. D. *Inorg. Chem. 3* (1964) 130.
17. Ahrland, S. and Björk, N.-O. *Coord. Chem. Rev. 16* (1975) 115.

Received June 26, 1975.

Acta Chemica Scandinavica A 30 (1976) 63—68

Acid-catalyzed Hydrolyses of Bridged Bi- and Tricyclic Compounds. VII. Kinetics of 2-Methyl-2-norbornenols in Isotopically Different Waters *

MARTTI LAJUNEN and HEIKKI LYYTIKÄINEN

Department of Chemistry and Biochemistry, University of Turku, SF-20500 Turku 50, Finland

Solvent deuterium isotope effects have been measured for the hydrolysis of 2-methyl-*exo*-2-norbornenol (VII) and 2-methyl-*endo*-2-norbornenol (VIII) in deuterium oxide-protium oxide mixtures. The data are best in accordance with the *A*-1 hydrolysis, in which a proton (deuteron) rapidly attacks the hydroxylic oxygen of the substrate and the rate-determining departure of a water molecule produces a carbocation, which yields, by reaction with the solvent, VII and rearranged alcohols (mainly 1-methyl-3-nortricyclanols). Besides, rate-determining protonation (deuteration) of the double bond occurs in the hydrolysis of VIII. Activation parameters support the same mechanism.

In recent papers [1–4] kinetics of acid-catalyzed hydrolysis of two epimeric 2-norbornenols (I and II) and four 3-nortricyclanols (III – VI) was discussed. Marked solvent effects,[1] slightly negative activation entropies,[1,4] and solvent deuterium isotope effects ($k_D/k_H < 1$) [1,3,4] are in accordance with the rate-determining protonation of the double bond of I and II and of the three-membered carbon ring of III – V ($A-S_E2$ mechanism).[5] A slight general acid catalysis occurring in the hydration of I and II also supports the same mechanism.[2] In the case of III no general acid catalysis was observed in phosphoric acid-dihydrogen phosphate buffers (implying an *A*-1 mechanism), but its verification (< 10 % of the total disappearance rate) beside the dominating hydronium ion catalysis may have failed owing to experimental inaccuracy.[2] The results are in agreement with the transition state structures which closely resemble the carbocation intermediates (*cf.* hydration of simple olefins).[5] The protonation of the hydroxylic group was, however, observed in the hydration of VI ($k_D/k_H = 2.1$, $\Delta S^{\neq} = 32$ J mol^{-1} K^{-1}) and to some extent also in the hydrolysis of I yielding the rearranged tricyclic product III ($k_D/k_H \approx 1.6$).[1,3] In this work acid-catalyzed hydrolysis of two epimeric tertiary alcohols, 2-methyl-*exo*-2-norbornenol (VII) and 2-methyl-*endo*-2-norbornenol (VIII), was investigated in protium oxide-deuterium oxide mixtures under catalysis of perchloric acid. The corresponding

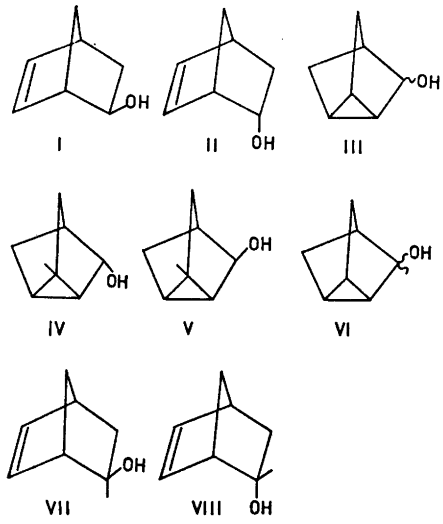

* Part VI, see Ref. 4.

study concerning 3-methyl-3-nortricyclanol (VI) is under way.

EXPERIMENTAL

2-Norbornenone was prepared by hydrolyzing the Diels-Alder adduct of cyclopentadiene and 2-chloroacrylonitrile in alkaline dimethyl sulfoxide.[6] The Grignard reaction between 2-norbornenone and methyl magnesium iodide produced 2-methyl-*endo*-2-norbornenol,[7] which also contained 8 – 10 % of the *exo* alcohol. The isomers were separated by repeated distillations through an efficient column. The purity of the *endo* alcohol was *ca.* 99 % and that of the *exo* alcohol *ca.* 97 % (3 % *endo* alcohol) as analyzed by GLC. The alcohols were identified on the basis of their IR and NMR spectra.[7–9]

Deuterium oxide was from Norsk Hydro (99.8 atom-% of D) and deuterioperchloric acid from E. Merck AG (*ca.* 70 % of $DClO_4$ in D_2O, > 99 atom-% of D).

Gas-chromatographic methods used for measuring the disappearance rates of the substrates and for evaluating the formation rates of unstable intermediate products (B) in consecutive reactions A→B→C (when A also yields other unstable products) were described earlier.[10]

RESULTS AND DISCUSSION

The acid-catalyzed hydrolysis of 2-methyl-*exo*-2-norbornenol (VII in Scheme 1) produces in $H_2O - D_2O$ mixtures containing 0.1 M $LClO_4$ (L = H,D) 1-methyl-3-nortricyclanols (*trans* and *cis* isomers, IV and V, in an approximate ratio of 14/1)[11] as major intermediate products, which are hydrated by solvent water to methyl-substituted norbornanediols (these were not identified).[4] Two unknown minor intermediate products were also observed to form; their retention times were between those of VII and VIII when an FFAP column was employed for the GLC analyses. The formation of elimination products, diolefins, could not be detected.

The hydrolysis of 2-methyl-*endo*-2-norbornenol (VIII in Scheme 1) yields the same products as the *exo* isomer, but also VII is a probable intermediate product (a small GLC peak with the proper retention time could be seen), which, however, transforms so fast into IV + V (they had the same retention times) and into minor products that its concentration remains small. (Even half of VIII may hydrolyze *via* VII according to rough iterative calculations, which evaluated k_A in the consecutive reactions VIII $\xrightarrow{k_A}$ VII $\xrightarrow{k_B}$ IV + V + minor products. The formation rate of VII is roughly included in the formation rate of IV + V, because $k_A \ll k_B$ and the portion of the unknown products yielded by VII is small.)

The disappearance rates of VII and VIII and the formation rates of IV + V from VII and VIII are presented in Table 1. (In the iterative calculations of the formation rates of IV + V, the disappearance rate of the *trans* alcohol, IV, was used,[4] since it is the main product[11] and the disappearance rates of V differ only slightly (10 – 20 %) from those of IV.)[4]

The difference between the disappearance rates and the formation rates presented in Table 1 represents the part of reaction which occurs either *via* other intermediate products than IV and V or produces directly norbornanediols. In the hydrolysis of VII, these differences (< 10 % of the total rate) can be

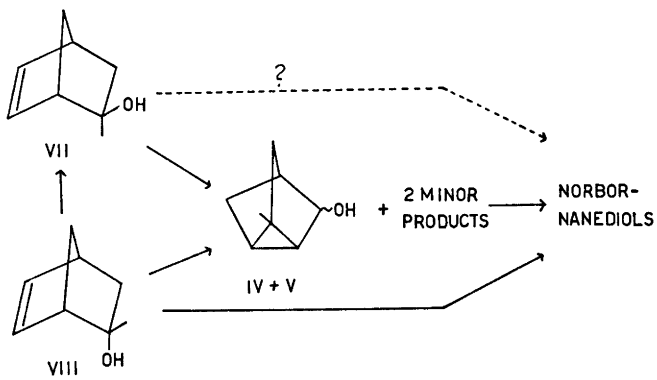

Scheme 1.

Table 1. Total disappearance rates (k_{tot}) of 2-methyl-*exo*- and -*endo*-2-norbornenols (VII and VIII) and formation rates (k_f) of 1-methyl-3-nortricyclanols (IV and V) from VII and VIII in solutions of perchloric acid (0.10 M) in protium oxide-deuterium oxide mixtures (n = deuterium atom fraction) at 75 °C.

Substrate	n	$k_{tot}/10^{-5}$ s^{-1}	$k_f/10^{-5}$ s^{-1}	k_f/k_{tot}
VII	0.0	311 ± 8	298 ± 3	0.96
	0.2	369 4	341 5	0.92
	0.4	437 6	408 5	0.93
	0.6	518 6	452 7	0.87
	0.8	633 8	589 8	0.93
	1.0	737 9	688 18	0.93
VII–OAc [a]	0.0	10.1 ± 0.2		
	1.0	24.8 0.5		
VIII	0.0	7.17 ± 0.03	3.25 ± 0.11	0.45
	0.2	7.61 0.05	4.17 0.06	0.55
	0.4	8.42 0.06	5.16 0.09	0.61
	0.6	9.66 0.08	6.24 0.13	0.65
	0.8	11.12 0.06	7.45 0.17	0.67
	1.0	12.88 0.04	9.20 0.16	0.71

[a] 2-Methyl-*exo*-2-norbornenyl acetate, measured at 25 °C.

Table 2. Observed and calculated (eqn. 2) solvent deuterium isotope effects on the total disappearance rates (tot) of VII and VIII, on the formation rates (f) of IV + V from VII and VIII, and on the differences (d) of the two rates in the D_2O-H_2O mixtures (0.1 M $LClO_4$) at 75 °C.

Substrate	n	$(k_n/k_H)_{tot}$ obs.[a]	calc.	$(k_n/k_H)_f$ obs.	calc.	$(k_n/k_H)_d$[b] obs.
VII	0.0	1.00	1.00	1.00		
	0.2	1.19	1.17	1.14		
	0.4	1.40_5	1.37	1.37		
	0.6	1.67	1.64	1.52		
	0.8	2.03_5	1.98	1.98		
	1.0	2.37	2.43	2.31		
VII–OAc[c]	1.0	2.46				
VIII	0.0	1.00	1.00	1.00	1.00	1.00
	0.2	1.06	1.10	1.28	1.21	0.82
	0.4	1.17	1.22	1.59	1.47_5	0.83
	0.6	1.35	1.37	1.92	1.82	0.87
	0.8	1.55	1.55	2.29	2.28	0.94
	1.0	1.80	1.77	2.83	2.90	0.94

[a] The maximum errors calculated from the standard errors of the rate coefficients in Table 1 are 1–5 % (av. 2.5 %). [b] $(k_n/k_H)_d = (k_{tot} - k_f)_n/(k_{tot} - k_f)_H$. [c] 2-Methyl-*exo*-2-norbornenyl acetate, measured at 25 °C.

explained by the formation of the minor products (and experimental error), but in the case of VIII the differences varying steadily with deuterium fraction (55 % in H_2O and 29 % in D_2O) seem too large to be explained in this way. (Rough iterative calculations were performed to evaluate the formation rates of the minor products by setting their disappearance rates to zero. In this way their portions were estimated to be a few per cent. The

increase in the formation rates with the increasing deuterium fraction was detected.)

The isotope effects (Table 2) measured on the differences of the disappearance rates and the formation rates are larger than unity in the case of VII (very rough values, not listed in Table 2), but they are regularly a little smaller than unity in the case of VIII. These results agree with the idea that in the hydrolysis of VII the difference is due to the formation of the minor rearranged products, but in the hydrolysis of VIII, in addition to the formation of the minor products, a marked part of the reaction yields directly norbornanediols (see Scheme 1) by hydration of the homoallylic double bond. The isotope effect on this kind of addition reaction was measured to be 0.5 – 0.65 in the hydration of the secondary 2-norbornenols (I and II).[1,3] Separation of the reaction occurring *via* the minor products from the reaction yielding directly the norbornanediols was not attempted owing to inaccuracy in the experimental data, but an increase in the rates of the former reaction occurring with increasing deuterium fraction (see above) causes a decrease in the isotope effects of the latter reaction. Thus the k_D/k_H value for the latter will be fairly similar to those observed for the $A-S_E2$ hydration of substrates I – V.[1,3,4] The hydration of the double bond of *exo* alcohol VII is probably an insignificant part of its hydrolysis (*cf.* hydration rates of I and II, Ref. 1).

The deuterium isotope effects observed (Table 2) can also be employed for discussing the reaction mechanism of the change of VII and VIII to the intermediate products. The total disappearance rates have been considered in the case of VII and the formation rates of IV + V have been included in the case of VIII unless otherwise noted. The isotope effects ($k_D k_H = 2.4 - 2.8$) are similar to that measured for the hydrolysis of 2-methyl-*exo*-2-norbornenyl acetate (Table 2), which hydrolyzes *via* an $A_{AL}1$ mechanism[10] (rapid equilibrium in the protonation of an oxygen atom before the rate-determining unimolecular reaction).[12] Thus the protonation of the hydroxylic oxygen is evident.

The total solvent deuterium isotope effect, k_n/k_H, for proton (deuteron) transfer reactions in aqueous medium with deuterium atom fraction n can be expressed by eqn. (1).[13,14]

$$\frac{k_n}{k_H} = \frac{\prod (1-n+n\phi_j)}{\prod (1-n+n\phi_i)} \exp[\Delta(\Delta G^{\ominus})/RT] \qquad (1)$$

In the equation ϕ_i is the fractionation factor of an exchangeable proton (deuteron) in the initial state, ϕ_j is that in the transition state, and $\Delta(\Delta G^{\ominus})$ represents the standard free energy of transfer for the transition state from light to mixed water minus that for the initial state transferred in the same way.

Eqn. (1) can be transformed to eqn. (2) in the case of an A-1 mechanism, if the rate-

$$\frac{k_n}{k_H} = \frac{(1-n+n\phi_3)^2}{(1-n+n\phi_1)\,(1-n+nl)^3} \qquad (2)$$

determining step is assumed to be the elimination of a water molecule from the protonated substrate (fractionation factors are presented above the formulas):

$$\mathrm{ROL} \overset{\phi_1}{+} \mathrm{L_3O^+} \underset{\mathrm{L_2O}}{\overset{l}{\rightleftharpoons}} \mathrm{ROL_2^+} \overset{\phi_2}{\rightarrow}$$

$$[\mathrm{X\cdots OL_2}]^+ \underset{\mathrm{TS}}{\overset{\phi_3}{\rightarrow}} \mathrm{X^+} + \mathrm{OL_2} \overset{1.0}{}$$

or to eqn. (3), if the rate-determining step is assumed to be

$$\frac{k_n}{k_H} = \frac{1}{(1-n+n\phi_1)\,(1-n+nl)^3} \qquad (3)$$

a rearrangement of the intermediate X^+ into another intermediate Y^+ with no exchangeable protons (deuterons) in either of them. Besides, we must assume that the structure of the hydronium ion is L_3O^+ (L = H,D) and that the free energy term $\Delta(\Delta G^{\ominus}) = 0$ (*cf.* Ref. 3). The A-2 and $A-S_E2$ mechanisms (slow proton transfer at the hydroxylic oxygen in the latter case) have been excluded since the former is improbable due to the activation entropies (see later) and marked solvent effects[10,11] and since the latter did not give any agreement between the observed and calculated isotope effects (*cf.* Ref. 15).

Eqn. (2) has been used for calculation of the values of the fractionation factor ϕ_3 (ϕ_1 was fixed as unity, *i.e.* the same as that of water, and the fractionation factor of the lyonium ion, l, was fixed as 0.72)[3] by search-

ing the best fits between the observed and calculated isotope effects by the method of least squares. Factor ϕ_3 is 0.952 ± 0.002 for VII and 1.041 ± 0.006 for VIII; 0.813 ± 0.002 was calculated for the total disappearance rate of VIII. The calculated isotope effects are presented in Table 2 and they are regularly some per cent smaller than the observed ones in mixed water (*i.e.* $0.2 \leq n \leq 0.8$) in the hydrolysis of VII and in the formation reaction of IV + V from VIII (the occurrence of VII as a short-living intermediate product may cause an error in the latter case), but some per cent larger than the observed ones in the total disappearance of VIII. In the hydration of 3-methyl-3-nortricyclanol (VI) under the same conditions, the calculated (eqn. 2) isotope effects are also regularly some per cent smaller than the observed ones ($\phi_3 = 0.902$).[15] Hence, this behavior is probably "normal" and is possibly due to several approximations made.[3,13,14] That the value of ϕ_1 is some per cent larger or smaller than unity has no marked effect on the value of ϕ_3. The behavior observed in the total disappearance of VIII is evidently "abnormal", agreeing with two competing reactions mentioned; thus the fractionation factor 0.813 has no meaning. The ϕ_3 value of VII seems reasonable ($\phi_2 \lesssim \phi_3 \lesssim \phi_{L,O}$ or $0.72 \lesssim \phi_3 \lesssim 1.0$), but that of VIII (1.041) is possibly too large due to experimental inaccuracy.

The fractionation factor of the hydroxylic hydrogen of the substrates (ϕ_1) can be calculated from eqn. (3) in the $H_2O - D_2O$ mixtures, if the transition states do not contain exchangeable protons (deuterons). In the hydrolysis of VII, ϕ_1 increases from 1.01 to 1.13 rather regularly with increasing deuterium content of the medium and in the formation of IV + V from VIII the increase is still more marked (from 0.64 to 0.95), which makes this mechanism improbable. The magnitude of ϕ_1 for VII, however, seems quite reasonable ($\approx 1 = \phi_{L,O}$).

The solvent deuterium isotope effects thus agree best with the *A*-1 mechanism in which elimination of a water molecule from the substrate, protonated at the hydroxylic oxygen, is the rate-determining step of the reaction. The value of ϕ_3 is probably a measure of the degree of departure of the water molecule (*i.e.* $\phi_3 \approx 0.72$ in the beginning and $\phi_3 \approx 1$ in the end). The values of ϕ_3 measured for

Table 3. Total disappearance rates (k_a^{tot}), formation rates of IV + V (k_a^f), and their differences (k_a^d) for the hydrolysis of 2-methyl-2-norbornenols in 1.00 M perchloric acid, and the activation parameters at 25 °C.

Substrate	t/°C	$k_a^{tot}/10^{-5}$ M^{-1} s^{-1}	$k_a^f/10^{-5}$ M^{-1} s^{-1}	$k_a^d/10^{-5}$ M^{-1} s^{-1} [a]
VII	25	13.2 ± 0.7 [b]	12.8 ± 0.8 [b]	0.4 ± 1.1 [c]
	25	13.2 ± 0.3	12.5 ± 0.2	0.7 ± 0.4
	35	54.2 0.4	51.7 1.2	2.5 1.3
	45	231 3	209 5	22 6
	55	737 12	662 13	75 18
$\Delta H^{\ddagger}$/kJ mol^{-1}		107.6 ± 1.1	104.4 ± 2.7	
$\Delta S^{\ddagger}$/J mol^{-1} K^{-1}		42 ± 7	31 ± 9	
VIII	25	0.125 ± 0.002 [b]	0.033 ± 0.002 [b]	0.097 ± 0.003 [b]
	35	0.617 ± 0.003	0.185 ± 0.007	0.432 ± 0.008
	45	2.72 0.01	1.06 0.05	1.66 0.05
	55	10.98 0.11	4.58 0.15	6.40 0.19
	65	41.8 0.4	20.3 1.3	21.5 1.4
$\Delta H^{\ddagger}$/kJ mol^{-1}		119.3 ± 0.4	132.5 ± 2.1	110.9 ± 1.0
$\Delta S^{\ddagger}$/J mol^{-1} K^{-1}		42 ± 1	75 ± 6	11 ± 3

[a] Errors are calculated from eqn. $\delta_a = (\delta_{tot}^2 + \delta_f^2)^{1/2}$. [b] Calculated from the activation parameters. [c] $(k_a^d)_{calc.} = (k_a^{tot})_{calc.} - (k_a^f)_{calc.}$

VII and VIII are thus in accordance with the Hammond principle [16] which states that the structure of the transition state at an energetically higher level is closer to that of an intermediate (formed in the rate-determining step) than is the structure of the transition state at an energetically lower level. However, the fact that ϕ_3 measured for one *exo* substrate is smaller than that measured for the corresponding *endo* substrate may be fortuitous and necessitates more studies. The carbocation X^+ formed produces VII (also in the hydrolysis of VII) and rearranged products (mainly IV and V) in its reaction with the solvent.

The activation parameters have been measured for the hydrolyses of the substrates in aqueous 1.00 M perchloric acid. The results are presented in Table 3. The activation parameters calculated for the total disappearance rates are typical of the A-1 mechanism as are also those calculated for the formation of IV+V. However, the activation entropy computed for the difference of the former two rates in the case of VIII is only slightly positive and the subtraction of the formation rates of the minor products from the difference of the total disappearance rates of VIII and the formation rates of IV+V easily makes the activation entropy slightly negative, which is typical of the $A-S_E2$ hydration of the double bond and the three-membered carbon ring.[1,4]

The *exo*/*endo* rate ratios calculated for the formation rates of IV+V from VII and VIII are *ca.* 80 in D_2O-H_2O mixtures (0.1 M $LClO_4$) at 75 °C and *ca.* 390 in aqueous perchloric acid (1 M) at 25 °C, which are typical of the solvolysis reactions of 2-norbornyl and 2-norbornenyl esters.[17,18]

Acknowledgements. We wish to thank Prof. P. Salomaa, Ph.D., for valuable discussions and Mr. M. Hotokka, B.Sc., for the calculation of the fractionation factors on a Univac 1108 computer.

REFERENCES

1. Lajunen, M. and Hirvonen, P. *Finn. Chem. Lett.* (1974) 245.
2. Lajunen, M. and Wallin, M. *Ibid.* (1974) 251.
3. Lajunen, M. and Wallin, M. *Ibid.* (1975) 18.
4. Lajunen, M. and Lyytikäinen, H. *Ibid.* (1975) 97.
5. Williams, J. M. and Kreevoy, M. M. *Advan. Phys. Org. Chem. 6* (1968) 63, with refs.
6. Freeman, P. K., Balls, D. M. and Brown, D. J. *J. Org. Chem. 33* (1968) 2211.
7. Paasivirta, J. *Ann. Acad. Sci. Fennicae A II 116* (1962) 1.
8. Mälkönen, P. J. and Toivonen, N. J. *Suom. Kemistilehti B 33* (1960) 53.
9. Paasivirta, J. and Mälkönen, P. J. *Suom. Kemistilehti B 44* (1971) 230.
10. Lajunen, M. *Acta Chem. Scand. A 28* (1974) 919, 939.
11. Lajunen, M. and Lyytikäinen, H. *Acta Chem. Scand. A 30* (1976) 69.
12. Euranto, E. K. In Patai, E., Ed., *The Chemistry of Carboxylic Acids and Esters*, Interscience, London 1969, pp. 549–569, with refs.
13. Salomaa, P. *Acta Chem. Scand. 23* (1969) 2095, with refs.
14. Salomaa, P., Hakala, R. Vesala, S. and Aalto, T. *Acta Chem. Scand. 23* (1969) 2116, with refs.
15. Lajunen, M. *Finn. Chem. Lett.* (1975) 153.
16. Hammond, G. S. *J. Amer. Chem. Soc. 77* (1955) 334.
17. Sargent, G. D. In Olah, G. A. and Schleyer, P. v. R., Eds., *Carbonium Ions*, Vol. 3, Interscience, London 1972, Chapter 24.
18. Brown, H. C., Ravindranathan, M. and Peters, E. N. *J. Amer. Chem. Soc. 96* (1974) 7351, with refs.

Received June 27, 1975.

Acta Chemica Scandinavica A 30 (1976) 69—75

Acid-catalyzed Hydrolyses of Bridged Bi- and Tricyclic Compounds. VIII.* Kinetics of 2-Methyl-*exo*-2-norbornenyl Acetate and Its Intermediate Products in Dioxane—Water Mixtures

MARTTI LAJUNEN and HEIKKI LYYTIKÄINEN

Department of Chemistry and Biochemistry, University of Turku, SF-20500 Turku 50, Finland

Solvent effects on the hydrolysis of 2-methyl-*exo*-2-norbornenyl acetate (*exo*-II-OAc) and its intermediate products, 2-methyl-*exo*-2-norbornenol (*exo*-II-OH) and 1-methyl-3-nortricyclanols (*trans*- and *cis*-III-OH), have been measured with 1-methyl-cyclopentyl and 1-methylcyclohexyl acetates as reference substrates in dioxane-water mixtures under catalysis of perchloric acid. The ratio of the formation rates of the unrearranged bicyclic and rearranged tricyclic intermediate products does not significantly change with changing dioxane content. Formation of the tricyclic products is stereoselective: *trans*-III-OH:*cis*-III-OH = 14:1 (0 and 55.5 wt.% dioxane). The results agree better with a bridged homoallylic carbocation than with equilibrating classical bi- and tricyclic carbocations.

Former papers [1,2] dealt with the acid-catalyzed hydrolyses of several secondary and methyl-substituted tertiary norbornyl and norbornenyl acetates, which were investigated in dioxane-water mixtures. By employing the modified Foote-Schleyer relationship for estimation of the "normal" hydrolysis rates of the tertiary acetates, anchimeric increase of rate was evaluated in the case of 2-methyl-*exo*-2-norbornyl (*exo*-I-OAc) and 2-methyl-*exo*-2-norbornenyl (*exo*-II-OAc) acetates. The *exo/endo* rate ratios were measured to be 630 and 130, respectively, at 25 °C (only the $A_{AI}1$ mechanism was included).

Criticism has been presented against employing both the "normal" rates, estimated by the Foote-Schleyer method, and the *exo/endo* rate ratios as measures of the anchimeric assistance.[3] However, an increase in the *exo/endo* rate ratios has been observed in the solvolysis of 5-methyl-2-aryl-norbornenyl esters with increasing π participation as measured from the amount of the rearranged tricyclic products.[4] Hence, the *exo/endo* rate ratio of 130 measured for 2-methyl-2-norbornenyl acetates seems to be rather small. Therefore, more studies were carried out in order to determine the character of the transition state and of carbocation intermediate(s) in the hydrolysis of 2-methyl-*exo*-2-norbornenyl acetate (*exo*-II-OAc). The solvent effects on its disappearance rates and on the formation and disappearance rates of its intermediate products, 2-methyl-*exo*-2-norbornenol (*exo*-II-OH) and 1-methyl-3-notricyclanols (III-OH), were investigated in dioxane-water mixtures and the results were compared with those of 1-methylcyclopentyl (Pen-OAc) and 1-methylcyclohexyl (Hex-OAc) acetates.

EXPERIMENTAL

The preparation of 2-methyl-*exo*-2-norbornenol (purity 97 % by GLC)[5] and 1-methyl-3-nortricyclanols (purity of *trans* isomer was 98 % and that of *cis* isomer 76 % by GLC; the impurity consisted of the other isomer and both of them had the same retention times)[6] has been presented earlier. 2-Methyl-*exo*-2-norbornenyl acetate was obtained by heating the corresponding alcohol in a pyridine—acetic anhydride mixture.[7] The product contained about 10 % of the *endo* acetate. The reaction media consisting of water, dioxane

* Part VII, see Ref. 5.

(purified),[8] and perchloric acid (1.00 mol dm^{-3}) were prepared by weighing the components.

The gas-chromatographic methods used for measuring the disappearance rates of the substrates and for evaluation of the formation rates of the unstable intermediate products (B) in consecutive reactions A→B→C (when A also yields other unstable products) were described earlier.[1] The effect of impurities on the disappearance rates of the substrates was eliminated by subtracting the GLC peak area of the impurity from the common peak area if they had the same retention time. The peak area of the impurity during the run was evaluated from its mol fraction in the substrate and from its reaction rate which was measured separately.

The portions of the *trans* and *cis* isomers of 1-methyl-3-nortricyclanol were measured in the intermediate products as follows. The tricyclic alcohol, obtained in the hydrolyses of the bicyclic acetate and alcohol, was separated from other components on a Perkin-Elmer F 21 preparative gas chromatograph with a Carbowax 20 M column. The alcohol was analyzed on a Perkin-Elmer Model R 10 NMR (60 MHz) spectrometer by measuring the intensities of the 1-methyl signals.[9] Other protons, however, disturbed the analyses and the results were only approximate. More accurate results were achieved by acetylating the alcohol mixtures in acetyl chloride–N,N-dimethyl aniline (in mol ratio 1:1) at room temperature and by analyzing the acetates by GLC (retention times of the acetates were different enough when applying, *e.g.*, a Carbowax 20 M column). The procedure was not observed to change the *cis/trans* ratio in a control experiment: III-OAc (*cis/trans* = 76/24) $\xrightarrow[Et_2O]{LiAlH_4}$ III-OH (*cis/trans* ≈ 80/20, by NMR)→ III-OAc (*cis/trans* = 76/24).

RESULTS AND DISCUSSION

2-Methyl-*exo*-2-norbornenyl acetate (*exo*-II-OAc) yields in its hydrolysis (Scheme 1) both the unrearranged alcohol, 2-methyl-*exo*-2-norbornenol (*exo*-II-OH), and the rearranged alcohols, 1-methyl-3-nortricyclanols (*cis*- and *trans*-III-OH), and possibly two minor products (*cf.* Refs. 1 and 5). These alcohols are unstable in acidic aqueous solutions and react with the medium producing methyl-substituted norbornanediols (these were not identified).[5,6] The formation of elimination products, diolefins, was not observed. The disappearance rates of *exo*-II-OAc and the formation and disappearance rates of *exo*-II-OH, *cis*-III-OH, and *trans*-III-OH were measured in dioxane-water mixtures containing perchloric acid, 1.00 mol dm^{-3}. The hydrolysis of 1-methylcyclopentyl acetate (Pen-OAc) and 1-methylcyclohexyl acetate (Hex-OAc; the rate coefficients have been presented earlier)[2] was studied under the same conditions and the amount of olefins was measured in the hydrolysis products. The results are listed in Table 1.

The results of this work are in good accordance with the rate coefficients measured in Ref. 1 for two substrates ($k_a^{tot} = 18.2 \times 10^{-5}$ M^{-1} s^{-1} for *exo*-II-OAc and 37.9×10^{-5} M^{-1} s^{-1} for Pen-OAc at 25 °C in 60 wt.% dioxane-water containing perchloric acid, 1.00 mol dm^{-3}). The reaction rates depend similarly on the dioxane content of the medium in the $A_{AL}1$ hydrolyses[1] of *exo*-II-OAc, Hex-OAc, and Pen-OAc, in the A-1 rearrangement[5] of *exo*-II-OH, and in the A-S_E2 hydration[6] of *cis*- and *trans*-III-OH. This kind of similarity has been observed earlier in other hydrolytic reactions proceeding *via* A-1 and A-S_E2 mechanisms.[10]

The logarithms of the rate coefficients *versus* H_0 acidity functions of the dioxane–water

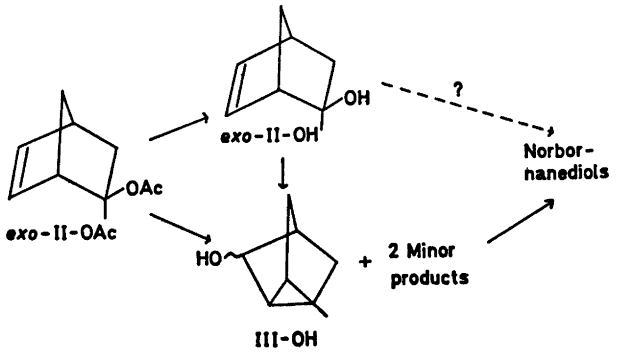

Scheme 1.

Table 1. Total disappearance rates of the substrates (k_a^{tot}) and formation rates of *exo*-II-OH from *exo*-II-OAc and of III-OH from *exo*-II-OH (k_a^f) in dioxane-water mixtures (1.00 mol dm^{-3} $HClO_4$) at 25 °C. Approximate amounts of olefins formed in the hydrolyses are also presented.

Substrate	Wt. % of dioxane	k_a^{tot}/ 10^{-5} M^{-1} s^{-1}	k_a^f/ 10^{-5} M^{-1} s^{-1}	k_a^f/k_a^{tot}	% olef.
exo-II-OAc	0.0	220 ± 3	144 ± 3	0.65	
	18.5	132 2	89.3 1.6	0.68	
	37.0	62.0 0.9	40.7 1.1	0.66	
	55.5	23.4 0.3	15.6 0.4	0.67	
	74.0	15.2 0.2	11.0 0.2	0.72	
	88.4	107 3	73.6 1.6	0.69	
	90.0	183 6	127 3	0.69	
exo-II-OH	0.0	13.2 ± 0.3	12.5 ± 0.2	0.95	
	18.5	6.76 0.08	6.44 0.08	0.95	
	37.0	2.91 0.06	2.70 0.08	0.93	
	55.5	1.28 0.01	0.97 0.02	0.76 ?	
	74.0	0.776 0.010	0.713 0.006	0.92	
	88.4	7.21 0.10	7.24 0.12	1.00	
	90.0	15.0 0.3	12.8 0.2	0.85	
	92.0	55.9 0.7			
	93.0	122 2			
cis-III-OH	0.0	1.27 ± 0.02			
	18.5	0.653 0.009			
	37.0	0.312 0.007			
	55.5	0.129 0.001			
	74.0	0.0743 0.0008			
	88.4	0.250 0.007			
	90.0	0.412 0.005			
trans-III-OH	0.0	1.77 ± 0.08			
	18.5	0.864 0.012			
	37.0	0.389 0.009			
	55.5	0.162 0.004			
	74.0	0.0946 0.0018			
	88.4	0.314 0.007			
	90.0	0.531 0.008			
Pen-OAc	0.0	439 ± 12			8
	18.5	205 4			7
	37.0	99.5 1.6			19
	55.5	42.5 0.9			23
	74.0	27.7 0.6			28
	90.0	450 9			29
Hex-OAc [a]	0.0	65.7 ± 1.3			4
	10.0	43.1 0.8			10
	20.0	23.5 0.5			12
	40.0	9.22 0.05			20
	60.0	3.65 0.06			33
	79.2	3.73 0.06			50
	89.1	38.5 0.6			68

[a] The rate coefficients have been presented in Ref. 2.

Table 2. Slopes and intercepts for the plots of log k_a^{tot} *vs.* H_0 and (log $k_a^{tot}+H_0$) *vs.* H_0 for the hydrolyses of the substrates in dioxane–water mixtures (0–55.5 wt. % of dioxane, 1.00 mol dm^{-3} $HClO_4$) at 25 °C.

Substrate	– slope for log k_a^{tot} *vs.* H_0	– slope for (log $k_a^{tot}+H_0$) *vs.* H_0	– intercept
exo-II-OAc	1.08± 0.11	0.08± 0.11	2.84± 0.04
exo-II-OH	1.14 0.04	0.14 0.04	4.11 0.02
cis-III-OH	1.10 0.05	0.10 0.05	5.12 0.02
trans-III-OH	1.15 0.04	0.15 0.04	4.99 0.01
Pen-OAc	1.12 0.03	0.12 0.03	2.60 0.01

mixtures and the terms (log k_a+H_0) *versus* H_0 [11] give fairly straight lines with parameters presented in Table 2 (H_0 functions for dioxane contents of 0–60 wt.% are interpolated linearly from those presented by Paul and Long).[12] The slopes are very similar for all three types of reactions studied and do not give information about the classical or non-classical characters of the transition states (*cf.* Ref. 2). The H_0 range employed is, however, quite narrow. (The H_0 functions have also been determined for mixtures richer in dioxane, but they are greatly scattered.)[13]

More information about the characters of the transition states and intermediates in the hydrolysis of *exo*-II-OAc and *exo*-II-OH were achieved by examination of their intermediate products. *Exo*-II-OAc produces 65–72 % (the percentage of *exo*-II-OH = 100k_a^f/k_a^{tot}) of the unrearranged alcohol, *exo*-II-OH, the portion of which obviously does not depend on the dioxane content (Table 1). The remainder consists of the rearranged alcohols, III-OH, and possibly of two unknown minor products. *exo*-II-OH yields 93± 2 % of III-OH and two minor products; neither does the ratio of these products change with changing dioxane content. Analysis of the isomeric ratios of III-OH in the products yielded by *exo*-II-OAc and *exo*-II-OH (Table 3) gives interesting results: the *cis*-III-OH/*trans*-III-OH ratios are about 7/93 in solutions consisting of 0 and 55.5 % dioxane, but are distinctly larger in 95.6 % dioxane. 2-Methyl-*endo*-2-norbornenyl acetate (*endo*-II-OAc) also produces mainly *trans*-III-OH in 95.6 % dioxane (Table 3; the *cis*/*trans* ratio is probably still smaller than the observed *ca.* 14/86 in solutions richer in water; *cf. exo*-II-OAc). In order to check that the ratios are not affected by equilibration between *cis*- and *trans*-III-OH, two different III-OH mixtures were submitted to similar treatment (Table 3). Marked isomerization could be seen only in 95.6 % dioxane during the reaction times employed for the bicyclic substrates. *trans*-III-OH hydrates about 30 % faster than *cis*-III-OH (Table 1), which decreases the apparent portion of the *trans* isomer in the tricyclic products. The results presented in Table 3 are not corrected with regard to these differences in the disappearance rates, but they are the observed ratios when the concentration of III-OH is approximately at its maximum.

Table 3. Amount of the *cis* isomer in 1-methyl-3-nortricyclanols (III-OH) produced in the hydrolyses of the substrates in dioxane–water mixtures (1.00 mol dm^{-3} $HClO_4$) at 25 °C.

Substrate	Reaction time/h	Wt. % of dioxane	% of *cis* isomer
exo-II-OAc	4.3	0.0	6
	26	55.5	7
	0.2	95.6	11
endo-II-OAc [a]	0.1	95.6	*ca.* 14
exo-II-OH	5	0.0	5
	64	55.5	8
	3	95.6	37
III-OH(*cis*/*trans* = 76/24)	4.5	0.0	81
	3	95.6	65
	0.2	95.6	78
III-OH (*cis*/*trans* = 2/98 [b]	0.6	0.0	7

[a] 45 °C, NMR analysis. [b] 75 °C, 0.1 M $HClO_4$ (the reaction rates under these conditions are approximately similar to those in 1.00 M $HClO_4$ at 48 °C).

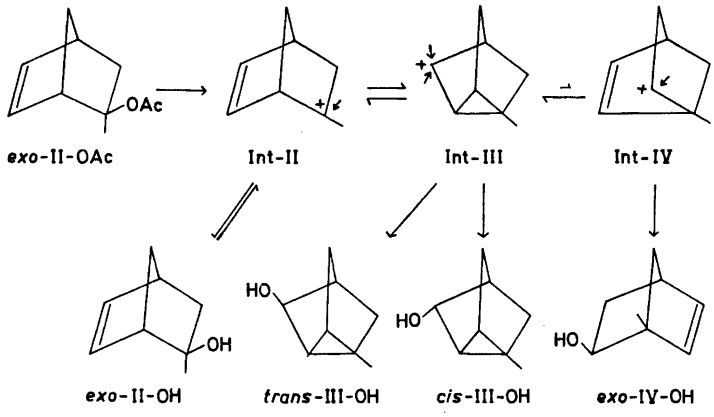

Scheme 2.

The monocyclic esters, 1-methylcyclopentyl acetate (Pen-OAc) and 1-methylcyclohexyl acetate (Hex-OAc), produce in their hydrolysis corresponding alcohols and *exo*-olefins (*i.e.* methylenecycloalkanes, by NMR), the ratios of which change fairly regularly with changing dioxane content of the medium: the apparent olefin portion increases with decreasing water concentration. (The percentages of the olefins expressed in Table 1 are only approximate averages during the two first half-lives of the reactions. Equilibration between the alcohols and the olefins was not eliminated and decomposition of the alcohols and acetates occurred slightly in GLC analyses yielding the olefins mentioned; but these effects cannot be very marked.) The increase of the olefinic portion in the products with increasing dioxane content indicates a decrease of solvent nucleophilicity, which makes the lifetime of the intermediate carbonium ions longer in solutions richer in dioxane, thus giving time for proton elimination.

The decrease of solvent nucleophilicity has, however, no obvious effect on the *exo*-II-OH/III-OH ratio (Table 1). This eliminates the possibility that the reaction intermediate would consist of slowly (as compared with solvent attack) equilibrating classical carbocations, (Int-II, Int-III, and Int-IV in Scheme 2). If the equilibrium between the ions takes place much faster than the attack of water, occurrence of the classical carbocations is, however, possible from this point of view. The occurrence of the secondary cation, Int-IV, does not seem very probable beside the more stable tertiary cation, Int-II. The formation of *exo*-II-OH and III-OH can also take place *via* bridged homoallylic carbocations (Int-II-π, Int-III-π, and Int-IV-π in Scheme 3; geometric structures closer to norbornene than nortricyclane are assumed for the first and last and

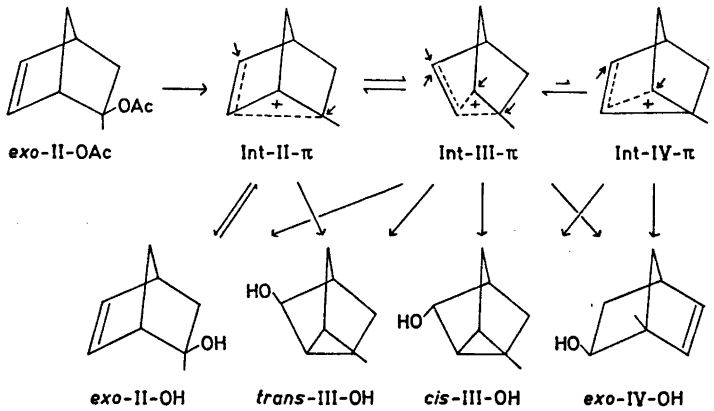

Scheme 3.

a structure closer to nortricyclane than norbornene for the middle). The *exo*-II-OH/III-OH ratio depends on the energies of the transition states yielding the rearranged and unrearranged products.[3] According to the results of this work (Table 1), the difference between the free energies is slight (*ca.* 2 kJ mol^{-1}; it is supposed that no equilibration of the products occurs). Hence, the carbocation produces also the substrate itself in the hydrolysis of *exo*-II-OH, which retards its reaction as compared with *exo*-II-OAc.

The attack of a water molecule at C(3) of intermediates Int-III and Int-III-π can take place from two directions, *cis* and *trans*. A factor, which can control the ratio of these attacks, is the methyl group, which has a steric crowding effect on the transition state of the *cis* attack. However, this effect seems very slight, because the $LiAlH_4$ reduction of 1-methyl-3-nortricyclanone produces *trans*- and *cis*-III-OH (*cis* and *trans* attacks, respectively) in the ratio 46:54,[7] and in the reduction with $LiAlH(OCH_3)_3$ the ratio is 41:59 (performed in dry ether at 0 °C). The shielding effect of the departing acetic acid or water molecule cannot be significant either, because the departure and water attack occur on opposite sides of the moiety. Thus intermediates Int-III and Int-III-π would probably yield *cis*- and *trans*-III-OH in the approximate 1:1 ratio, which differs markedly from the observed ratio *ca.* 7/93 in 0 and 55.5 % dioxane. This fact eliminates the possibility of the rapidly equilibrating classical carbocations to yield the products in the proper ratio.

The intermediate Int-IV-π is probably also unstable as compared with Int-II-π since it requires a delocalization of the positive charge on the secondary carbon, but prevents its delocalization on the tertiary carbon. Besides, the formation of 1-methyl-*exo*-2-norbornenol (*exo*-IV-OH in Scheme 3) over *exo*-II-OH and *cis*-III-OH over *trans*-III-OH would be preferred. Two unidentified minor GLC peaks were detected in the hydrolysis of *exo*-II-OH, but their portion must be smaller than 10 % evaluated on the basis of the differences between the disappearance rates of *exo*-II-OH and the formation rates of III-OH in Table 1. Hence, the only dominating carbocation is evidently Int-II-π, which also explains well the *cis*/*trans* ratio observed: much of the norbornene geometric structure remains in this cation and therefore the *exo* attack (=*trans* attack), of C(3) is more probable than the *endo* attack (=*cis* attack), but the ratio of *exo*/*endo* attacks may be smaller than in the cases of norbornane and norbornene skeletons.[3,14]

The larger *cis*/*trans* ratios in the products of the hydrolyses of *exo*-II-OAc and *exo*-II-OH in 95.6 % dioxane than in 0 or 55.5 % dioxanes are probably partly due to equilibration of the tricyclic alcohols (Table 3), but they may be partly due to the occurrence of carbocations other than Int-II-π. This is made possible by the low nucleophilicity of the medium rich in dioxane (see above), which lengthens the lifetime of the cations and allows the isomerization of Int-II-π to other intermediates (*e.g. endo*-II-OH yields *trans*- and *cis*-III-OCHO in the ratio 66/33 in formic acid).[7]

In the product analysis of the solvolysis reactions of the secondary 2-norbornenyl esters (labelled properly by ^2H or ^{14}C), attention has been paid to the bicyclic compounds, which form the minority of the solvolysis products, whereas analysis of the majority of the solvolysis products, *i.e.* the tricyclic compounds, has mostly been omitted.[15] However, mass spectrometric and NMR analyses have recently been performed for 3-nortricyclyl acetate-*d* produced by acetolysis (125±5 °C, 48 h) of 2-deuterio-*endo*-2-norbornenyl brosylate.[16] The results suggest an approximately fifty-fifty attack from the "*exo*" and "*endo*" sides of the intermediate carbocation. Unfortunately, a possible equilibration of the *cis* and *trans* isomers of 3-nortricyclyl acetate-*d* during the long treatment in refluxing acetic acid has, however, not been investigated.

The results of this work are in agreement with those of Ref. 1. The latter imply the occurrence of π participation in the transition state of the acid-catalyzed hydrolysis of 2-methyl-*exo*-2-norbornenyl acetate and the former suggest the occurrence of π participation in the intermediate (and evidently in the transition state of the product-yielding step) in the hydrolyses of both the *exo* acetate and the corresponding alcohol. Thus, the π participation of the homoallylic double bond causes both the increase of reaction rate and the

formation of rearranged products (*cf.* Brown *et al.*).[4] The *exo*/*endo* rate ratios seem, however, to have marked individual differences, and hence they cannot be used as such to separate classical and nonclassical mechanisms.

REFERENCES

1. Lajunen, M. *Acta Chem. Scand. A 28* (1974) 919.
2. Lajunen, M. *Ibid. A 28* (1974) 939.
3. *E.g.* Brown, H. C. *Account. Chem. Res. 6* (1973) 373, with refs.
4. Brown, H. C., Ravindranathan, M., and Peters, E. N. *J. Amer. Chem. Soc. 96* (1974) 7351.
5. Lajunen, M. and Lyytikäinen, H. *Acta Chem. Scand. A 30* (1976) 63.
6. Lajunen, M. and Lyytikäinen, H. *Finn. Chem. Lett.* (1975) 97.
7. Paasivirta, J. *Ann. Acad. Sci. Fennicae A 116* (1962) 1.
8. Vogel, A. I. *Practical Organic Chemistry*, 3rd Ed., Longmans, London 1970, p. 177.
9. Paasivirta, J. *Suom. Kemistilehti B 44* (1971) 135.
10. Kankaanperä, A. and Merilahti, M. *Acta Chem. Scand. 26* (1972) 685.
11. Bunnett, J. F. and Olsen, F. P. *Can. J. Chem. 44* (1966) 1917.
12. Paul, M. A. and Long, F. A. *Chem. Rev. 57* (1957) 1, with refs.
13. Bunton, C. A. and Hendy, B. N. *J. Chem. Soc.* (1962) 2562.
14. Peters, E. N. and Brown, H. C. *J. Amer. Chem. Soc. 94* (1972) 7920.
15. Lee, C. C. and Ko, C. F. *J. Amer. Chem. Soc. 96* (1974) 8032, with refs.
16. Vogel, P., Delseth, R., and Quarroz, D. *Helv. Chim. Acta 58* (1975) 508.

Received June 27, 1975.

Acta Chemica Scandinavica A 30 (1976) 76—78

Short Communications

Transfer and Exchange Effects in the Dissociation of 3-Nitrobenzoic Acid in H_2O and D_2O and in Their DMSO Mixtures

ANTTI VESALA and ERKKI SALOMA

Department of Chemistry, University of Turku, SF-20500 Turku 50, Finland

The effect of including the transfer terms in the equations of the simple equilibrium theory of acetic acid dissociation in H_2O and D_2O has been studied by Gold [1] applying the so-called transfer activity factors. The free energy of transfer amounts to about 10 % of the total effect in this case. Salomaa [2] has separated the transfer and exchange effects in the dissociation of picric acid using the assumption that the free energy of transfer of undissociated picric acid from H_2O to D_2O equals that of 1,3,5-trinitrobenzene. The magnitude of the transfer effect is about 15 % of the total change in the free energy in this case. The study of carbonic and sulfurous acids made by Salomaa *et al.*[3] has also revealed a transfer contribution of 15 – 25 %.

The dissociation constants of 3-nitrobenzoic acid have been determined by potentiostatic titration.[4] Because of the scarce solubility of the acid in water, the titrations were carried out in water – DMSO mixtures. Therefore, it is possible to study and compare the transfer effects when the acid and its dissociation products are transferred in the following cyclic process:

$$\begin{array}{ccc} \text{acid}(H_2O) & \xrightarrow{\text{I}} & \text{acid}(D_2O) \\ \downarrow \text{II} & & \downarrow \text{IV} \\ \text{acid}(H_2O\text{-DMSO}) & \xrightarrow{\text{III}} & \text{acid}(D_2O\text{-DMSO}) \end{array}$$

The mol fractions of DMSO in H_2O and D_2O were chosen in such a way that the total change in the acid dissociation had the magnitude of $(pK_{D_2O} - pK_{H_2O}) = \Delta pK$ also in processes II, III, and IV. The mol fractions of DMSO in the aqueous solutions are 0.096 and 0.090 in H_2O and D_2O, respectively, when the conditions mentioned above are fixed.

The transfer and exchange effects cannot be separated by measuring only the pK values. Therefore, the free energies of transfer of methyl ester and the barium salt of 3-nitrobenzoic acid from one solvent to another have been determined. The former compound represents the undissociated acid and the latter the dissociation products of the acid in the transfer from one solvent to another. These assumptions seem to be relevant, although the barium salt in itself is a rather crude model for H^+A^-. On the other hand there are enough previous data, especially concerning the transfer free energies from H_2O to D_2O, making it quite possible to use the barium salt for this purpose.[2,5a]

The barium salt of 3-nitrobenzoic acid was prepared by mixing equal amounts of $Ba(OH)_2$ and the acid in water. The product was twice recrystallized from water. The methyl ester of 3-nitrobenzoic acid was prepared by the standard method.[6] The product was treated with charcoal and recrystallized three times from absolute methanol. The treatment of other chemicals and reagents has been described earlier.[4]

The free energies of transfer of barium 3-nitrobenzoate were determined by solubility measurements. The solubility was analyzed conductometrically using a method described elsewhere.[5b] The solubility products were then extrapolated to zero ionic strength by the aid of the Debye-Hückel equation (1).

$$\log y_{\pm} = \frac{2 \times 3^{1/2} A c^{1/2}}{1 + 3^{1/2} Ba c^{1/2}} \qquad (1)$$

In this equation A is calculated as described in the previous paper,[4] c is the concentration of the salt, and the ionic size parameter Ba was assumed to be of the same magnitude in all solutions ($= 1.81$).[7] The solubility product at zero ionic strength is calculated by eqn. (2). The K_s values are

$$K_s = 4(y_{\pm})^3 c^3 \qquad (2)$$

seen in Table 1.

The free energies of transfer of metyl 3-nitrobenzoate were determined by distributing the ester between cyclohexane and aqueous phases. The concentration in the two phases were analyzed spectrophotometrically. The free energies of transfer of methyl ester and barium salt in processes I, II, III, and IV are tabulated in Table 2.

Table 1. Solubilities and solubility products of Ba 3-nitrobenzoate in H_2O and D_2O and their DMSO mixtures.

Solvent	c/mol dm^{-3} 10^{-3}	$-\log y_\pm$	$K_s/10^{-7}$	$\Delta G^\ominus$/kJ mol^{-1}
H_2O	6.322	0.1126	4.644	36.153
D_2O	5.177	0.1045	2.696	37.501
H_2O–DMSO	6.447	0.1161	4.808	36.068
D_2O–DMSO	5.728	0.1110	3.492	36.861

Table 2. Free energies of transfer of methyl 3-nitrobenzoate and Ba 3-nitrobenzoate and transfer contributions of total $\Delta G^\ominus$ in the dissociation of 3-nitrobenzoic acid for processes I, II, III, and IV (for assumptions, see text).

Process	$\Delta G^\ominus_t$ J mol^{-1} for Me-ester (for HA)	$\Delta G^\ominus_t$ J mol^{-1} for Ba-salt (for $2H^+$ A^-)	Total transfer contribution
I	110	1350	560
II	−2010	−85	1970
III	550	795	−150
IV	−1570	−640	1250

A procedure analogous to that described by Salomaa was applied when transfer and exchange effects in the H_2O-D_2O system were evaluated.[2] The following equilibria are included in this procedure (concentration scale is applied throughout):

$$D_3O^+(D_2O) + A^-(D_2O) + H_2O + HA(H_2O) = H_3O^+(H_2O) + A^-(H_2O) + D_2O + DA(D_2O) \quad (3)$$

$$\tfrac{1}{2}Ba^{2+}(H_2O) + A^-(H_2O) = \tfrac{1}{2}Ba^{2+}(D_2O) + A^-(D_2O) \quad (4)$$

$$\tfrac{1}{2}Ba^{2+}(H_2O) + Cl^-(H_2O) = \tfrac{1}{2}Ba^{2+}(D_2O) + Cl^-(D_2O) \quad (5)$$

$$H_3O^+(H_2O) + Cl^-(H_2O) = H_3O^+(D_2O) + Cl^-(D_2O) \quad (6)$$

$$\text{Me-ester}(H_2O) = \text{Me-ester}(D_2O) \quad (7)$$

$$HA(H_2O) = HA(D_2O) \quad (8)$$

$$H_3O^+(H_2O) + Cl^-(H_2O) + \tfrac{3}{2}D_2O = D_3O^+(D_2O) + Cl^-(D_2O) + \tfrac{3}{2}H_2O \quad (9)$$

$$H_3O^+(aq) + \tfrac{3}{2}D_2O = D_3O^+(aq) + \tfrac{3}{2}H_2O \quad (10)$$

$$H_3O^+(H_2O) + A^-(H_2O) = H_3O^+(D_2O) + A^-(D_2O) \quad (11)$$

$$HA(D_2O) + \tfrac{1}{2}D_2O = DA(D_2O) + \tfrac{1}{2}H_2O \quad (12)$$

The corresponding free energies are reported in Table 3. The transfer free energy for the dissociation products of the acid (eqn. 11) calculated from the basis of eqns. (4), (5), and (6) is $\Delta G^\ominus_t = 475$ J mol^{-1}. The total transfer free energy is obtained if eqn. (8) is taken into account and is $475 - 110 = 365$ J mol^{-1}. The total reaction of isotopic exchange is formed by adding eqn. (10) and the reverse of eqn. (12). The free energy for eqn. (12) is obtained from the free energies of eqns. (3), (4), (9), (5), and (8). The total free energy of isotopic exchange equilibrium is thus $2770 - 855 = 1915$ J mol^{-1}. Thus the contribution of the transfer effect is $(365/2280)100 = 16$ % from the total effect. This is of the same magnitude as that for picric acid which is reasonable.

Table 3. Free energies for equilibria (3)–(12).

Eqn.	$\Delta G^\ominus$/J mol^{-1}	Ref.
(3)	−2280	This work
(4)	675	This work
(5)	1040	5a
(6)	840	8
(7)	110	This work
(8)	110	This work
(9)	3610	8
(10)	2770	8,9
(11)	475	This work
(12)	855	This work

The transfer and exchange effects may also be studied in the whole cyclic process in the

following rather naive way. It is assumed that the free energies of transfer for H^+A^- and $\frac{1}{2}Ba^{2+}A^-$ and for HA and methyl ester are equal when passing from one solvent to another. The $\Delta G^\ominus$ values as well as the transfer free energy contributions calculated therefrom are reported in Table 2.

It is difficult to conclude whether the deviations from total $\Delta G^\ominus$ in passing from H_2O or D_2O to their DMSO mixtures are due to experimental errors or some structural features of the system. Anyway, the $\Delta G^\ominus$ values are clearly lower when the exchange effects are included (processes I and III). The liquid structure of the DMSO mixtures where the mol fraction of DMSO is low, deviates somewhat from that of pure water although there are some controversial opinions on that. The effect of experimental errors on the determined $\Delta G^\ominus$ values is considerable, especially in distribution measurements. More extensive investigation has to be made especially at different temperatures and solvent compositions.

1. Gold, V. and Lowe, B. M. *J. Chem. Soc. A* (1968) 1923.
2. Salomaa, P. *Suomen Kem. B 45* (1972) 149.
3. Salomaa, P., Vesala, A., and Vesala, S. *Acta Chem. Scand. 23* (1969) 2107.
4. Vesala, A. and Saloma, E. *Acta Chem. Scand. 30* (1976). *In press.*
5. Kellomäki, A. *Ann. Acad. Sci. Fenn. Ser A II* (1970) a. p. 40; b. p. 25.
6. Gilman, H. and Blatt, A. H. *Org. Synth. Coll. Vol. I.* (1956) 372.
7. Kielland, J. *J. Amer. Chem. Soc. 59* (1937) 1675.
8. Salomaa, P. *Acta Chem. Scand. 25* (1971) 365.
9. Gold, V. *Advan. Phys. Org. Chem. 7* (1969) 281.

Received October 27, 1975.

Acta Chemica Scandinavica A 30 (1976) 79—97

Bis(2,2′-bipyridine) and Bis(1,10-phenanthroline) Complexes of Chromium(III) and Cobalt(III)

MARTIN PAUL HANCOCK,[a] JENS JOSEPHSEN [b] and CLAUS ERIK SCHÄFFER [a]

[a] Chemistry Department I (Inorganic Chemistry), University of Copenhagen, H.C. Ørsted Institute, Universitetsparken 5, DK-2100 Copenhagen Ø, Denmark and [b] Present address: Roskilde University Centre, P.O.Box 260, DK-4000 Roskilde, Denmark

A number of complexes of the type $[M(N-N)_2XY]^{n+}$ (M = Cr(III) or Co(III); N−N = 2,2′-bipyridine (bipy) or 1,10-phenanthroline (phen); X,Y = F, Cl, H_2O, OH or $\frac{1}{2}C_2O_4$; $n = 1$, 2 or 3) have been subjected to a critical preparative study. The new complex ions *cis*-$[M(phen)_2(H_2O)Cl]^{2+}$ have been isolated as their perchlorate salts and their stability relative to the corresponding *cis*-diaqua complexes determined as $K_1 \simeq 9$ l mol^{-1} (M = Cr) and $K_1 \simeq 40$ l mol^{-1} (M = Co) at an ionic strength of *ca.* 0.11 M.

In the absence of trace impurities of the corresponding metal(II) species the dichloro complexes *cis*-$[M(N-N)_2Cl_2]^+$ are unusually robust with respect to acid hydrolysis. The otherwise rather slow anation of *cis*-$[M(N-N)_2(H_2O)_2]^{3+}$ by chloride ion is also greatly accelerated by traces of appropriate M(II) species.

Base hydrolysis of the cobalt(III) dichloro complexes is fast even in the absence of added catalyst, but this is not the case with the chromium(III) analogues.

Although some of the complex salts studied exist in a variety of polymorphic forms, only one geometric isomer has been found in each case. The interconversion of many of the chromium(III) complexes has been examined and the cleavage reactions of the racemic and optically active di-μ-hydroxobis {bis(N−N)-chromium(III)} complexes have been included in these interconversion studies to substantiate the assertion that all the complexes have the *cis*-configuration. The latter cleavage reactions have led to the preparation of a number of optically active chromium(III) species, including the previously unreported ions $(-)_{589}$-*cis*-$[Cr(phen)_2X_2]^+$ (X = F or Br), and $(-)_{589}$-*cis*-$[Cr(bipy)_2Br_2]^+$.

Their molar rotations at the Na D-line and circular dichroism spectra in the visible region have been measured.

The accumulated evidence indicates the generality of the *cis*-configuration for bis(N−N) complexes of the trivalent metal ions Cr(III), Co(III), Rh(III), and Ir(III).

No evidence for the existence of *trans* complexes of the title types has presented itself during the present study.

I. INTRODUCTION

The chemistry of a great variety of complexes with the heterocyclic ligands 2,2′-bipyridine * and 1,10-phenanthroline * has been the subject of many studies with different aims.[1,2] Many years ago Jaeger and Van Dijk [3] reported the preparation of several cobalt(III) bipy complexes, including chloride salts of the supposed *cis*-(violet) and *trans*-(green) isomers of $[Co(bipy)_2Cl_2]^+$. Pfeiffer and Werdelmann [4] prepared, among other complexes, cations of the type $[M(phen)_2Cl_2]^+$ (M = Cr(III) or Co(III)), including the supposed *trans*-chromium(III) complex.

Our studies providing evidence for the *cis*-configuration of bis(N−N) complexes of Cr(III), Co(III), Rh(III), and Ir(III) were first presented [5] in 1968 and published as a communication [6] in 1969. It was decided to divide the detailed documentation for our claims [6] into two parts. The first part, giving details of the X-ray powder photograph studies, has been published previously.[7] The second part is included in the present paper.

We originally studied complexes of these heterocyclic ligands from a spectroscopic view-

* 2,2′-Bipyridine and 1,10-phenanthroline will be abbreviated in the following as bipy and phen, respectively, or by the common designation N−N.

point [8] and it was hoped that octahedral *trans*-bis(N–N) complexes of chromium(III) and cobalt(III) could give information about the ligand-field parameters of these ligands. However, as implied above, such *trans*-complexes do not appear to exist, the cause of this apparently being a large steric repulsion between opposing pairs of protons in bis(N–N) complexes, when two such ligands are coplanar.[9]

There have been a few cases of bis(N–N) complexes of divalent metal ions reported in the literature, for which a coplanar arrangement of the two heterocyclic ligands would have been expected on the basis of the general coordination properties of the metal ions. The most noteworthy of these are $[Pt(bipy)_2]^{2+}$,[10] $[Pd(bipy)_2]^{2+}$ and $[Pd(phen)_2]^{2+}$.[11] The low kinetic stability of $[Pd(phen)_2]^{2+}$,[11] the fact that the formation constant for [Pd(phen) (en)]$^{2+}$ is *ca.* 10^8 times greater than that for $[Pd(phen)_2]^{2+}$,[12] and the rather special acid-base behaviour of $[Pt(bipy)_2]^{2+}$,[13] are properties which are explicable in terms of a large steric repulsion in these complexes and which are consistent with X-ray structure analyses on salts of $[Pd(N-N)_2]^{2+}$,[14–16] which show appreciable deviations from coplanar arrangements of the ligands.

From a study of the ligand-field spectra of aqueous bis(bipy) and bis(phen) copper(II) complexes, Jørgensen [17] has shown that, in contrast to the bis(ethylenediamine)copper(II) species, they do not have the *trans*-configuration. The X-ray structures of several bis(bipy)-copper(II) species have shown that they all contain distorted trigonal bipyramidal cations of the type $[Cu(bipy)_2X]^{n+}$.[18–22]

In the present paper our chemical interconversions and correlations in the bis(N–N)-chromium(III) and cobalt(III) systems are described and the ambiguous literature on this area of chemistry is reviewed experimentally, including such properties as polymorphism and the kinetic and thermodynamic stability of some of the complexes.

II. EXPERIMENTAL

A. General

Materials. The following chemicals of analytical grade were used: 1,10-phenanthroline hydrate (BDH), 1,10-phenanthroline hydrochloride hydrate and 2,2′-bipyridine (Riedel de Haën). The 2,2′-bipyridine used for the large scale preparation of $[Cr(bipy)_2OH]_2(ClO_4)_4 \cdot 2H_2O$ (employed in prep. 42 below) was obtained by recrystallisation of a product of technical quality kindly donated by I.C.I. Ltd. All other chemicals were of reagent grade and were used without further purification.

Magnetic measurements. The magnetic susceptibility of sample 11*a* was measured at 25 °C, using the Faraday method with $Hg[Co(SCN)_4]$ as reference.[23]

Analyses. Metal analyses were performed by Dr. Hans Buchwald of this laboratory, using extremely accurate procedures developed by him and later to be published. C, H, N, and Cl analyses were carried out by the microanalytical laboratory of this institute, using standard procedures. For an unknown reason H analyses gave difficulties with some of the present complexes.

Circular dichroism measurements. The CD data in the region 400–650 nm were obtained using a Roussell-Jouan Model I Dichrographe. Data for maximum deflections are given in Table 3 as (λ_{CD}, $\Delta\varepsilon_{CD}$), with λ_{CD} in nm and $\Delta\varepsilon_{CD} = \varepsilon_l - \varepsilon_r$, in l mol^{-1} cm^{-1}.

Optical rotation measurements. Optical rotation was measured at 25 °C and 589 nm using a Perkin-Elmer Model 141 Spectropolarimeter. Data are given in Table 3 as molar rotation, $[M]_{589}^{25}$, in degree l mol^{-1} m^{-1}.

^1H NMR spectra. Spectra were measured at 30 °C on a Varian Model HA-100 instrument.

Absorption spectra. Absorption spectra in the region 400–650 nm, recorded using a Cary Model 14 spectrophotometer, were used for characterisation and identification of the complexes. Data for maxima (max), minima (min) and shoulders (sh) are given in Tables 2 and 3, with the wavelength, λ, in nm and the molar absorptivity, ε, in l mol^{-1} cm^{-1}. Identifying spectral data given in section IIB below are, unless otherwise indicated, given in the same order as in the columns of Table 2.

B. Preparations

The preparations of the following complexes have been described previously by us, together with their visible absorption spectra: *cis*-$[Cr(bipy)_2F_2]ClO_4$ and *cis*-$[Cr(phen)_2F_2]ClO_4 \cdot H_2O$,[24] $[(bipy)_2Cr(OH)_2Cr(bipy)_2](ClO_4)_4 \cdot 2H_2O$, $[(phen)_2Cr(OH)_2Cr(phen)_2]Cl_4 \cdot 9H_2O$, and $[(phen)_2Cr(OH)_2Cr(phen)_2](NO_3)_4 \cdot 4H_2O$.[25] With the exception of the new complex ions *cis*-$[M(phen)_2(H_2O)Cl]^{2+}$ (M = Cr or Co) and the optically active species $(-)_{589}$-*cis*-$[Cr(phen)_2F_2]^+$ and $(-)_{589}$-*cis*-$[Cr(N-N)_2Br_2]^+$, complexes of the same formulation as those described in this section have, apart from some differences in solid-state counter-ion, been reported in the literature. However, the preparative methods for the vari-

ous complexes have been examined more critically in the present work than before and in most cases are described in greater detail. The methods of preparation of the *cis*-dichlorobis(N–N)cobalt(III) complexes have been improved to give chloride salts which exhibit a much greater kinetic stability in aqueous solution than previously reported.

1. *cis*-$[Cr(bipy)_2Cl_2]Cl.2H_2O$. *a*. This compound was prepared according to the literature method [26] (*cf.* prep. 4). The crude product is often brownish but the pure dihydrate is olivegreen when obtained by recrystallisation from 0.1 M hydrochloric acid and washing with 96 % ethanol until the filtrate is green. (Yield 70 %). Anal. $[Cr(C_{10}H_8N_2)_2Cl_2]Cl.2H_2O$: C, H, N, Cl. The characterising spectral data are given in Table 2. This compound and the corresponding nitrate and perchlorate salts are soluble in dimethylformamide (DMF).

b. The same compound was prepared by the reaction of chromium(III) chloride hexahydrate with bipyridine in methanol.[27] Bipyridine (3.2 g, 20.5 mmol) and chromium(III) chloride hexahydrate (2.67 g, 10 mmol) were dissolved in methanol (50 ml) and the green solution heated under reflux for 3 h. The red-brown solution was concentrated to 20 ml and cooled at −15 °C. The almost black crystals, which separated from a red solution, were washed with methanol (precooled to −15 °C) and when dried in air crumbled to an olivegreen product (yield 3.3 g, 65 %). Identifying spectral data (0.1 M HCl, *cf.* Table 2): (553, 474, 445, −, −, −, 0.46, 0.23).

2. *cis*-$[Cr(bipy)_2Cl_2]Cl.HCl.3H_2O$ and $HCl.2H_2O$. *cis*-$[Cr(bipy)_2Cl_2]Cl.2H_2O$ (0.5 g) was almost dissolved by gentle heating for 5 min with conc. hydrochloric acid (30 ml). The mixture was filtered hot, leaving a brown residue(I) which was washed with conc. hydrochloric acid and dried over $CaCl_2.2H_2O$. (Yield 0.1 g). The filtrate was cooled slowly to 0 °C and the brown crystals that separated were filtered off and washed and dried as above. (Yield 0.3 g, 55 %). Anal. $[Cr(C_{10}H_8N_2)_2Cl_2]Cl.HCl.3H_2O$: C, H, N, Cl. Identifying spectral data (H_2O, *cf.* Table 2): (553, 474, 445, 43.7, 19.0, 91.0, 0.435, 0.209).

The brown residue(I) was analysed. Anal. $[Cr(C_{10}H_8N_2)_2Cl_2]Cl.HCl.2H_2O$: C, H, N, Cl. Identifying spectral data (H_2O, *cf.* Table 2): (553, 474, 445, 43.7, 21.0, 89, 0.48, 0.24).

3–7. *cis*-$[Cr(phen)_2Cl_2]^+$ salts. The characterising spectral data for a carefully purified sample of *cis*-$[Cr(phen)_2Cl_2]Cl.2H_2O$ have been given previously [25] (*cf.* Table 2).

3. The chloride dihydrate, *cis*-$[Cr(phen)_2Cl_2]Cl.2H_2O$, was prepared as in Ref. 4. Anal. $[Cr(C_{12}H_8N_2)_2Cl_2]Cl.2H_2O$: C, H, N, Cl. Identifying spectral data (H_2O, *cf.* Table 2): (558, 478, −, −, 0.450). The X-ray powder photograph of this compound showed it to be the *δ* polymorph of Ref. 28.

4. The chloride tetrahydrate, *cis*-$[Cr(phen)_2Cl_2]Cl.4H_2O$. The second preparative method [29] was analogous to prep. 1*a*. The red tetrahydrate was obtained after drying in air. Anal. $[Cr(C_{12}H_8N_2)_2Cl_2]Cl.4H_2O$: C, H, N, Cl, Cr. Identifying spectral data (H_2O, *cf.* Table 2): (558, 478, 40.2, 17.6, 0.437).

5. The chloride hydrogen chloride,[4] *cis*-$[Cr(phen)_2Cl_2]Cl.HCl.3H_2O$. *cis*-$[Cr(phen)_2Cl_2]Cl.2H_2O$ (0.5 g) was dissolved in conc. hydrochloric acid (50 ml) at room temperature, whereupon the red-violet hydrogen chloride adduct began to precipitate almost immediately. The mixture was boiled gently for 1 min. After cooling, the red-violet crystals were isolated by filtration and washed with conc. hydrochloric acid, the last few drops of which were left on the filter. The moist product was dried in a desiccator over $CaCl_2.2H_2O$ for three days. Anal. $[Cr(C_{12}H_8N_2)_2Cl_2]Cl.HCl.3H_2O$: C, H, N, Cl^-, Cr. Identifying spectral data (H_2O, *cf.* Table 2): (558, 478, 40.1, 17.4, 0.435).

6. The nitrates, *cis*-$[Cr(phen)_2Cl_2]NO_3.3\frac{1}{2}H_2O$ and $\frac{1}{2}H_2O$. *cis*-$[Cr(phen)_2Cl_2]Cl.2H_2O$ (0.25 g, 0.45 mmol) was dissolved in water (17 ml, 90 °C). 0.1 M nitric acid (5 ml) was added to the hot, green solution which was then allowed to cool slowly. Red needles precipitated gradually. These were filtered off, washed with 0.1 M nitric acid and air-dried. (Yield 0.21 g, 77 %). They were recrystallised from water, giving the pure nitrate $3\frac{1}{2}$ hydrate. Anal. $[Cr(C_{12}H_8N_2)_2Cl_2]NO_3.3\frac{1}{2}H_2O$: C, H, N, Cl, Cr. Identifying spectral data (DMF, *cf.* Table 2): (578, 492, 42.5, 22.5, 0.530). When recrystallised from 0.1 M nitric acid a mixture of red and green crystals was obtained, the green crystals being the nitrate with lower water content. Anal. $[Cr(C_{12}H_8N_2)_2Cl_2]NO_3.\frac{1}{2}H_2O$: C, H, N, Cl.

7. The nitrate hydrogen nitrate, *cis*-$[Cr(phen)_2Cl_2]NO_3.HNO_3$. *cis*-$[Cr(phen)_2Cl_2]Cl.2H_2O$ (0.3 g) was dissolved in boiling conc. nitric acid (10 ml) and the solution cooled to room temperature. The almost quantitative precipitate of red needles was filtered off and washed with 4 M nitric acid. The product was recrystallised by dissolving it in boiling conc. nitric acid (10 ml) and cooling the filtered solution to 20 °C. The crystals were filtered off, washed with 0.1 M nitric acid and dried over $CaCl_2.2H_2O$. (Yield 0.3 g). Anal. $[Cr(C_{12}H_8N_2)_2Cl_2]NO_3.HNO_3$: C, H, N, Cl. Identifying spectral data (DMF, *cf.* Table 2): (578, 491, 42.5, 22.4, 0.527).

8. *cis*-$[Co(bipy)_2Cl_2]Cl.2H_2O$.[3] We employed a procedure which is essentially that used for the preparation of *trans*-dichlorotetrakis(pyridine)cobalt(III) chloride.[30] The use of liquid chlorine as an oxidising agent prevents the formation of green by-products containing cobalt(II) (*cf.* prep. 11).

Bipyridine (4.68 g, 30 mmol) was dissolved in methanol (110 ml) under reflux. To the solution was then added blue anhydrous

cobalt(II) chloride (1.95 g, 15 mmol) in portions, over a period of 5 min. The initially yellow solution gradually became red-brown. The solution was cooled to −60 °C and liquid chlorine (6 ml, 150 mmol) added with stirring. A grey precipitate immediately began to form. Under continued stirring the temperature was allowed to rise to −20 °C. The grey product was then quickly filtered from the green solution and washed with ice-cold 1 M hydrochloric acid. (Yield 5.7 g, 75 %). The product was recrystallised twice from 0.1 M hydrochloric acid saturated with chlorine, but it can also be recrystallised as in prep. 9. Anal. $[Co(C_{10}H_8N_2)_2Cl_2]Cl.2H_2O$: C, H, N, Cl, Co. The characterising spectral data are given in Table 2. The spectrum remained unchanged during a fortnight when the solution was kept in the dark at 25 °C.

9. *cis*-$[Co(phen)_2Cl_2]Cl.3\frac{1}{2}H_2O$. Ablov's method[31] gives a product slightly contaminated with $[Co(phen)_2Cl_2]$. An alternative method [4] (heating $[Co(phen)_3]Cl_3$ in chloroform) seemed not to work without the cobalt(II) compound present as a redox catalyst.[32] The procedure used here is essentially that for the bipyridine analogue (prep. 8).

Phenanthroline hydrate (4.2 g, 20.1 mmol) was dissolved in methanol (200 ml) under reflux and to the solution was then added anhydrous blue cobalt(II) chloride (1.3 g, 10 mmol). The initially yellow solution gradually became red, and the resulting solution of $[Co(phen)_2Cl_2]$ was then cooled to about −60 °C. To the cold red solution was added liquid chlorine (5 ml, 120 mmol) in aliquots of 1 ml, resulting in almost immediate oxidation, as indicated by the precipitation of a grey powder.

The mixture was allowed to warm up to 20 ° C. It was then heated with 10^{-3} M hydrochloric acid (100 ml) to 65 °C, resulting in complete dissolution, and cold 4 M hydrochloric acid (100 ml) was added. The resulting mixture was cooled to −5 °C and filtered. The precipitate was washed with a little ice-cold water and then acetone, and dried in air. (Yield 4.1 g, 70 %). Recrystallisation was effected by dissolving the product on the filter in 10^{-3} M hydrochloric acid (250 ml) saturated with chlorine gas and preheated to 60 °C, and then adding an equal volume of cold 2 M hydrochloric acid. The solution was then cooled at 0 °C and filtered. The violet precipitate was washed and dried as above. Anal. $[Co(C_{12}H_8N_2)_2Cl_2]Cl.3\frac{1}{2}H_2O$: C, H, N, Cl, Co. Characterising spectral data are given in Table 2. The spectrum remained unchanged during a fortnight when the solution was kept in the dark at 25 °C.

The green dihydrate was prepared by heating the violet compound for 3 h at 110 °C and then leaving it to stand in air (rel. humidity ~40 %). Anal. $[Co(C_{12}H_8N_2)_2Cl_2]Cl.2H_2O$: C, H, N, Cl. The X-ray powder pattern of this salt was very similar to that of the violet parent complex; its kinetic stability towards hydrolysis was considerably lower than that of the latter.

10. *cis*-$[Co(phen)_2Cl_2]NO_3.3H_2O$. This salt was originally reported to be a tetrahydrate.[31] The chloride (0.2 g, 0.35 mmol) was dissolved in water (25 ml) at room temperature and 0.1 M nitric acid (6 ml) was added dropwise to the stirred solution. The fine grey-violet crystals which rapidly separated were filtered off, washed with ethanol and air-dried. (Yield 0.18 g, 85 %). Anal. $[Co(C_{12}H_8N_2)_2Cl_2]NO_3.3H_2O$: C, N, Cl, Co.

11. *cis*-$[Co(phen)_2Cl_2]_2$ $[CoCl_4].2H_2O$. *a*. This green complex was prepared exactly as reported previously.[33] Its constitution has been discussed earlier.[34] Anal. $[Co(C_{12}H_8N_2)_2Cl_2]_2$ $[CoCl_4].2H_2O$: C, H, N, Cl, Co. Identifying spectral data (1.2 M HCl, *cf.* Table 2): (542, 472, −, −, 0.48). Since cobalt(II) ions in 1.2 M hydrochloric acid solution have a very small molar absorptivity at 542 nm, the molecular weight of the present sample could be calculated, from $\varepsilon_{max} = 56.6$ for *cis*-$[Co(phen)_2Cl_2]^+$ (Table 2), to be 605 (Theor. 608.5). The characterising spectral data for a nitromethane solution are given in Table 2. The magnetic susceptibility was determined as $\chi^{298} = 7850 \times 10^{-6}$ cgs per mol Co(II) which, with a diamagnetic correction of 525×10^{-6} cgs,[35] corresponds [23] to $\mu_{eff} = 4.47$ (± 0.03) B.M.

b. The same complex, with identical X-ray powder photograph to sample *a*, was prepared directly by the addition of a hot blue solution of $CoCl_2.6H_2O$ (4 g) in conc. hydrochloric acid (10 ml) to a solution of *cis*-$[Co(phen)_2Cl_2]Cl.3\frac{1}{2}H_2O$ (0.55 g) in boiling water (10 ml). The solution was then left until the temperature was about 20 °C. The green crystals were filtered off, washed with 6 M hydrochloric acid until the filtrate was no longer blue but green, and air-dried. (Yield 0.50 g). Anal. $[Co(C_{12}H_8N_2)_2Cl_2]_2[CoCl_4].2H_2O$: C, H, N, Cl, Co. Identifying spectral data (nitromethane, *cf.* Table 2): (693, 667, 633, 588; 678, 647, 598, 477; 650, 611, 485, 215; 585, 405, 249, 59).

12. Mixed dichloro chloride, *cis*-[(Cr, Co)$(phen)_2Cl_2]Cl.2H_2O$. The initial compounds (prep. 3 and 9, 0.1 g of each) were dissolved in 0.02 M hydrochloric acid (25 ml) and the solution left to stand at room temperature. Almost black crystals separated, and were filtered off and washed with 0.1 M hydrochloric acid. (Yield 0.11 g). Anal: Cr 5.61; C 51.9; H 3.6; N 10.2; Cl 18.4, corresponding to about 60 % chromium(III) complex. The addition of a sodium sulfide solution to an aqueous solution of the product resulted in the formation of a black precipitate, demonstrating the presence of cobalt in quantity. The X-ray powder photograph of the mixed complex was very similar to that of the pure chromium complex with the same water content.

13. *cis*-$[Cr(bipy)_2(H_2O)OH](ClO_4)_2$. The *cis*-diaqua complex was prepared by known meth-

ods,[36] but since this compound is very soluble it was most conveniently isolated as its corresponding base. The easiest preparative method was the cleavage of the di-μ-hydroxobis-{bis(2,2'-bipyridine) chromium(III)} perchlorate [25] (the bipy-diol perchlorate). Diol perchlorate (1.9 g, 3.2 mmol Cr) was dissolved in 70 % perchloric acid (10 ml) and the solution heated at 60 °C for 24 h. The orange solution was cooled and partially neutralised with a solution of sodium carbonate decahydrate (14 g) in hot water (10 ml). It was further neutralised to pH ~4 with 2 M sodium hydroxide (7 ml). At this point the aquahydroxo complex precipitated almost quantitatively. It was filtered off, washed with cold water and ethanol, and dried at 60 °C for 2 h. (Yield 1.6 g, 85 %). To purify the product it was dissolved on the filter in cold 1 M perchloric acid (10 ml), a saturated solution of sodium perchlorate (10 ml) was added to the filtrate, and finally 2 M sodium hydroxide (5 ml) added dropwise with cooling and stirring. Filtration, washing and drying were performed as above. By this procedure the unreacted diol, if any, remained on the filter. (Recrystallisation yield 85 %). Anal. $[Cr(C_{10}H_8N_2)_2(H_2O)OH](ClO_4)_2$: C, H, N, Cl. The characterising spectral data are given in Table 2.

14. $[Co(bipy)_2(H_2O)OH](ClO_4)_2$. *a. cis*-$[Co(bipy)_2(H_2O)_2](ClO_4)_3.2H_2O$ was prepared by a procedure analogous to that for the phen analogue [37] (yield 25 %), but it was more convenient to isolate its corresponding base. *cis*-$[Co(bipy)_2Cl_2]Cl.2H_2O$ (2.05 g, 4.0 mmol) was ground with a suspension of silver oxide [precipitated from silver nitrate (2.8 g, 16 mmol) in water (20 ml) using 2 M sodium hydroxide (10 ml)] and the mixture placed in the dark. After 2 h the red suspension was filtered and the silver chloride washed with cold water (2 ml). To the filtrate was added a saturated solution of sodium perchlorate (5 ml), and it was then acidified with 6 M perchloric acid to pH ~5. After cooling the solution, the resulting red precipitate was filtered off, washed with a little cold water and with ethanol, and then dried for 2 h at 60 °C in air. (Yield 2.1 g, 90 %). To purify the product it was dissolved on the filter in 1 M perchloric acid (20 ml), saturated sodium perchlorate solution (20 ml) was added to the filtered solution, and finally 2 M sodium hydroxide (10 ml) added dropwise with stirring. The red crystals were isolated by filtration and washed and dried as above. The product exhibited the same spectrum as the unrecrystallised complex. Anal. $[Co(C_{10}H_8N_2)_2(H_2O)OH](ClO_4)_2$: C, H, N, Cl. The characterising spectral data are given in Table 2.

b. More elegantly, $[Co(bipy)_2Cl_2]^+$ may be hydrolysed with hydroxide ions, as described in prep. 16 for the phen analogue.

15. *cis*-$[Cr(phen)_2(H_2O)_2](NO_3)_3.2H_2O$. This was prepared by a method similar to that previously reported.[36] Chromium(III) nitrate enneahydrate (4.0 g, 10 mmol) and phen hydrate (4.47 g, 22 mmol) were dissolved in 0.7 M nitric acid (40 ml), and the solution heated under reflux. After half an hour 2 M LiOH (8 ml) was added to the red solution, which was heated under reflux for a further 5 h and then cooled in ice to give orange needles which were filtered off, washed with ice-cold water and heated at 60 °C in air. (Yield 5 g, 75 %). For recrystallisation, the product was dissolved on the filter in 0.1 M nitric acid preheated to 100 °C, and the solution was filtered and cooled in ice. The crystals were washed and dried as above. (Yield 4 g). Anal. $[Cr(C_{12}H_8N_2)_2(H_2O)_2](NO_3)_3.2H_2O$: C, H, N, Cr. The characterising spectral data are given in Table 2.

16. $[Co(phen)_2(H_2O)OH](ClO_4)_2$. *a*. The corresponding acid to this complex ion was prepared according to Ref. 37 but the compound was isolated here in the same way as the bipy analogue (for experimental details see prep. 14). Anal. $[Co(C_{12}H_8N_2)_2(H_2O)OH](ClO_4)_2$: C, H, N, Cl, Co. The characterising spectral data are given in Table 2.

b. More elegantly, one of the qualitative kinetic observations [32] (see section III C) could be used preparatively. *cis*-$[Co(phen)_2Cl_2]$-$Cl.3\frac{1}{2}H_2O$ (1 g, 1.7 mmol) in 1 M sodium hydroxide (10 ml) was stirred for 2 h. The solution was treated with a saturated solution of sodium perchlorate (5 ml), cooled in ice and titrated with 6 M perchloric acid until precipitation was complete. The crystals were filtered off, washed with ice-cold water and air dried. The product was recrystallised by dissolving it in 1 M perchloric acid (10 ml) and adding saturated sodium perchlorate solution (20 ml) to the filtered solution followed by addition of 2 M sodium hydroxide (*ca.* 5 ml) to give pH ~5. Washing and drying were performed as above. (Yield 1 g, 90 %.) Anal. $[Co(C_{12}H_8N_2)_2(H_2O)OH](ClO_4)_2$: C, H, N, Cl, Co. Identifying spectral data (0.1 M $HClO_4$ and 0.1 M NaOH, respectively, *cf.* Table 2): (496, 448, 63, 44; 512, 447, 73, 32).

17. *cis*-$[Co(phen)_2(H_2O)_2](NO_3)_3.2H_2O$. This was prepared according to Ref. 37. Anal. $[Co(C_{12}H_8N_2)_2(H_2O)_2](NO_3)_3.2H_2O$: C, H, N.

18. Mixed diaqua nitrate, *cis*-[(Cr, Co)-$(phen)_2(H_2O)_2](NO_3)_3.2H_2O$. 0.2 g of each of the initial compounds (prep. 15 and 17) were dissolved in hot water (4 ml). To the hot solution was added 4 drops of 14 M nitric acid and the solution was left to stand at room temperature. The resulting orange crystals were isolated by filtration and washed with cold water and cold 96 % ethanol. (Yield 0.2 g). Anal: Cr 3.97; C 42.28; H 3.71; N 14.43, corresponding to about 50 % chromium(III) complex. The cobalt content was qualitatively demonstrated as for the mixed dichloro chloride (prep. 12). As with the latter the X-ray powder photograph was very similar to that of the pure chromium complex.

19. *cis*-$[Cr(phen)_2(H_2O)Cl](ClO_4)_2.H_2O$. *cis*-$[Cr(phen)_2Cl_2]Cl.2H_2O$ (2.2 g, 4 mmol) was heated under reflux in 0.3 M hydrochloric acid (167 ml) for 3 h and the solution was then cooled in ice. Methanol (75 ml) and then 70 % perchloric acid (10 ml) were added and the solution cooled at −15 °C. The reddish precipitate was filtered off and washed with methanol. The green compound remaining on the filter is the dichloro complex as the perchlorate. The combined mother-liquor and methanol washings were treated with a saturated solution of sodium perchlorate (50 ml) and cooled at −15 °C. The light-red crystals were filtered off, washed with cold 1 M perchloric acid and water, and air-dried at 70 °C. (Yield 1.5 g). The product was recrystallised from 1 M perchloric acid to give red crystals. Anal. $[Cr(C_{12}H_8N_2)_2(H_2O)Cl](ClO_4)_2.H_2O$: C, H, N, Cl. The characterising spectral data are given in Table 2.

20. *cis*-$[Co(phen)_2(H_2O)Cl](ClO_4)_2.2\frac{1}{2}H_2O$. *a.* To a solution of *cis*-$[Co(phen)_2Cl_2]Cl.3\frac{1}{2}H_2O$ (1.16 g, 2 mmol) in hot water (20 ml) was added dropwise a solution of silver nitrate (0.75 g, 4.5 mmol) in water (1.5 ml). The solution was stirred and allowed to cool slowly to room temperature. The silver chloride was removed by filtration and the red filtrate diluted with methanol (30 ml). 6 M perchloric acid (10 ml) was then added, and by vigorously scratching the glass, whilst cooling the solution in ice, red-brown crystals separated. They were filtered off, washed with ice-cold water and dried at 60 °C in air for 4 h. (Yield 1.1 g, 80 %). The product was recrystallised from 0.1 M perchloric acid to give red-brown crystals. Anal. $[Co(C_{12}H_8N_2)_2(H_2O)Cl](ClO_4)_2.2\frac{1}{2}H_2O$: C, H, N, Cl. The characterising spectral data are given in Table 2.

b. *cis*-$[Co(phen)_2Cl_2]Cl.3\frac{1}{2}H_2O$ (0.5 g, 0.85 mmol) was dissolved in 10^{-3} M hydrochloric acid (50 ml) at room temperature. 2 M aqueous trimethylamine (1 ml) was added with vigorous stirring, when the solution rapidly became red. After 5−10 s 12 M perchloric acid (2 ml) was added, resulting in the immediate formation of a dense pinkish precipitate. The mixture was allowed to stand at 0 °C for *ca.* 2 h and the now crystalline red precipitate was filtered off and washed with a little ice-cold water. The product was purified by dissolving it on the filter in hot 0.1 M perchloric acid (25 ml) and filtering the solution, leaving a grey residue of unreacted insoluble *cis*-$[Co(phen)_2Cl_2]ClO_4$. The deep-red filtrate was cooled at 0 °C for 2 h and the resulting red crystals filtered off, washed with ice-cold water and dried in air. (Yield 0.35 g, 60 %). Identifying spectral data (0.1 M HNO_3, *cf.* Table 2): (520, 462, −, −, 0.528).

21. $[Cr(bipy)_2C_2O_4]Cl.4H_2O$; *cis*-$[Cr(bipy)_2Cl_2]^+ \rightarrow [Cr(bipy)_2ox]^+$.[38] *cis*-$[Cr(bipy)_2Cl_2]Cl.2H_2O$ (5.7 g, 11 mmol) was added with stirring to a boiling solution of potassium oxalate (2.1 g, 11 mmol) in water (22 ml). After boiling for 4 min, the red solution was cooled in ice to give a red solid. This was filtered off, washed with ice-cold ethanol and air-dried. (Yield 3.8 g). The inhomogeneous product was extracted with a little boiling water, giving an orange solution and leaving a brownish residue. The filtered orange solution was cooled in ice and the resulting crystals washed and dried as above. (Yield 1.9 g, 30 %). Anal. $[Cr(C_{10}H_8N_2)_2C_2O_4]Cl.4H_2O$: C, N, Cl. The characterising spectral data are given in Table 2. Note that in Ref. 38 a printing error appeared for this compound. On p. 1392 the first absorption maximum is tabulated as 510 nm, whereas the curve on the same page clearly demonstrates that it is a little below 500 nm.

22. $[Cr(bipy)_2C_2O_4]ClO_4$; $[(bipy)_2Cr(OH)_2Cr(bipy)_2]^{4+} \rightarrow [Cr(bipy)_2ox]^+$. A mixture of $[Cr(bipy)_2OH]_2(ClO_4)_4.2H_2O$ [25] (2.0 g, 1.7 mmol), sodium oxalate (0.23 g, 1.7 mmol) and oxalic acid dihydrate (0.42 g, 3.3 mmol) in water (30 ml) was stirred at 70 °C until all the solids has dissolved. The flask was then stoppered tightly and heated in an oven at 80 °C for 2 h. After allowing the mixture to cool to *ca.* 50 °C, the orange crystals were filtered off, washed with cold water and methanol, and air-dried (Yield 1.2 g, 65 %). Anal. $[Cr(C_{10}H_8N_2)_2C_2O_4]ClO_4$: C, H, N, Cl. Identifying spectral data (H_2O, *cf.* Table 2): (497, 464, −, −, −, −, 0.722).

23. $[Cr(bipy)_2C_2O_4][Cr(bipy)(C_2O_4)_2].4H_2O$. The brownish residue from prep. 21 was dissolved in a larger quantity of boiling water, and the filtered red solution was cooled in ice to give red crystals which were filtered off, washed with ethanol and air-dried. (Yield 60 %). Anal. $[Cr(C_{10}H_8N_2)_2C_2O_4][Cr(C_{10}H_8N_2)(C_2O_4)_2].4H_2O$: C, H, N, Cr. The spectrum of an aqueous solution showed $(\lambda, \varepsilon)\max = (518,130)$; $(\lambda, \varepsilon)\min = (462,70)$, to be compared with maxima at 497 and 535 nm [38] for $[Cr(bipy)_2ox]^+$ and $[Cr(bipy)ox_2]^-$, respectively.

24. $[Cr(phen)_2C_2O_4]Cl.4H_2O$; *cis*-$[Cr(phen)_2Cl_2]^+ \rightarrow [Cr(phen)_2ox]^+$.[38] *cis*-$[Cr(phen)_2Cl_2]Cl.2H_2O$ (3.9 g, 7 mmol) was added with stirring to a boiling solution of potassium oxalate (1.3 g, 7 mmol) in water (38 ml). The solution was boiled for 3 min. Isolation and recrystallisation were performed as in prep. 21. (Yield 2.6 g, 60 %). Anal. $[Cr(C_{12}H_8N_2)_2C_2O_4]Cl.4H_2O$: C, N, Cl. Characterising spectral data are given in Table 2.

25−27. *cis*-$[Cr(bipy)_2F_2]^+$ prepared from different initial materials. The quoted compounds were treated in each case with liquid hydrogen fluoride (50 ml) in a polythene beaker and the mixture stirred and left overnight. The red residue was dissolved (prep. 25 and 26) in water or methanol (5 ml), or extracted (prep. 27) with methanol (10 ml). The filtered solution was then treated with lithium perchlorate (*ca.* 0.2 g per mmol Cr), giving violet crystals on standing which were filtered off, washed with ethanol and air-dried. Identifying spectral data, given after each preparation, are to be

compared with the characterising data of Table 2.

25. $[Cr(bipy)_2ox]^+ \rightarrow cis\text{-}[Cr(bipy)_2F_2]^+$. Initial material $[Cr(bipy)_2C_2O_4]Cl.4H_2O$ (0.56 g, 1 mmol). (Yield 0.40 g, 80 %). (519, 445, 415, 461, −, −, −, −, 0.45, 0.38).

26. $[(bipy)_2Cr(OH)_2Cr(bipy)_2]^{4+} \rightarrow cis\text{-}[Cr(bipy)_2F_2]^+$. Initial material $[Cr(bipy)_2OH]_2(ClO_4)_4.2H_2O$ [25] (1.0 g, 1.7 mmol Cr). (Yield 0.56 g, 65 %). (519, 443, 416, 461, −, −, −, −, 0.47, 0.39).

27. $cis\text{-}[Cr(bipy)_2Cl_2]^+ \rightarrow cis\text{-}[Cr(bipy)_2F_2]^+$. Initial materials $cis\text{-}[Cr(bipy)_2Cl_2]Cl.2H_2O$ (0.5 g, 1 mmol) and mercuric acetate (0.95 g, 3 mmol). (Yield 0.32 g, 65 %). (519, 443, 415, 461, −, −, −, −, 0.45, 0.38).

28 − 30. $cis\text{-}[Cr(phen)_2F_2]^+$ prepared from different initial materials. The quoted compounds were treated in each case with liquid hydrogen fluoride (50 ml) in a polythene beaker and the mixture stirred and left overnight. The red residue was dissolved (prep. 28 and 29) in water or methanol (10 ml), or extracted (prep. 30) with methanol (10 ml). The product was isolated as in prep. 25 − 27 and recrystallised in each case from 0.01 M perchloric acid, giving violet crystals. Identifying spectral data, given after each preparation, are to be compared with the characterising data of Table 2.

28. $[Cr(phen)_2ox]^+ \rightarrow cis\text{-}[Cr(phen)_2F_2]^+$. Initial material $[Cr(phen)_2C_2O_4]Cl.4H_2O$ (0.61 g, 1 mmol). (Yield 0.46 g, 80 %). (522, 455, 420, −, −, −, 0.37, 0.24).

29. $[(phen)_2Cr(OH)_2Cr(phen)_2]^{4+} \rightarrow cis\text{-}[Cr(phen)_2F_2]^+$. Initial material $[Cr(phen)_2OH]_2Cl_4.9H_2O$ [25] (2.2 g, 3.7 mmol Cr). (Yield 1.9 g, 85 %). Anal. $[Cr(C_{12}H_8N_2)_2F_2]ClO_4.H_2O$: C, H, Cl. (522, 455, 420, −, −, −, 0.38, 0.25).

30. $cis\text{-}[Cr(phen)_2Cl_2]^+ \rightarrow cis\text{-}[Cr(phen)_2F_2]^+$. Initial materials $cis\text{-}[Cr(phen)_2Cl_2]Cl.2H_2O$ (0.6 g, 1.1 mmol) and mercuric acetate (0.8 g, 2.5 mmol). (Yield 0.4 g, 65 %). Anal. $[Cr(C_{12}H_8N_2)_2F_2]ClO_4.H_2O$: C, H, Cl. (522, 455, 420, −, −, −, 0.38, 0.25).

31 − 34. $cis\text{-}[Cr(bipy)_2Cl_2]^+$ prepared from different initial materials. Identifying spectral data, given after each preparation, are to be compared with the characterising data of Table 2.

31. $[(bipy)_2Cr(OH)_2Cr(bipy)_2]^{4+} \rightarrow cis\text{-}[Cr(bipy)_2Cl_2]^+$. The wine-red solution of $[Cr(bipy)_2OH]_2(ClO_4)_4.2H_2O$ [25] (1.0 g, 1.7 mmol Cr) in conc. hydrochloric acid (10 ml) was cooled to 0 °C and saturated with hydrogen chloride gas. Heating at 50 °C in a sealed tube overnight gave red-brown needles, separated from an orange solution. These were filtered off, washed with water and ethanol, and air-dried. (Yield 0.7 g, 75 %). (DMF: 572, 488, −, −, 0.512).

32. $cis\text{-}[Cr(bipy)_2F_2]^+ \rightarrow cis\text{-}[Cr(bipy)_2Cl_2]^+$. The red solution of $cis\text{-}[Cr(bipy)_2F_2]ClO_4$ (0.6 g, 1.2 mmol) in conc. hydrochloric acid (10 ml) was heated in a sealed tube at 100 °C for 5 h. The red-brown salt, separated from a green solution, was isolated as above. (Yield 0.5 g, 80 %). (DMF: 572, 488, −, −, 0.510).

33. $cis\text{-}[Cr(bipy)_2(H_2O)_2]^{3+} \rightarrow cis\text{-}[Cr(bipy)_2Cl_2]^+$. The orange solution of $cis\text{-}[Cr(bipy)_2(H_2O)\,OH](ClO_4)_2$ (0.65 g) in conc. hydrochloric acid (10 ml) was heated at 70 °C overnight. The red-brown crystals, separated from a green solution, were isolated as above. (Yield 0.52 g, 80 %). (DMF: 572, 488, −, −, 0.509).

34. $[Cr(bipy)_2ox]^+ \rightarrow cis\text{-}[Cr(bipy)_2Cl_2]^+$. $[Cr(bipy)_2C_2O_4]Cl.4H_2O$ (0.56 g, 1 mmol) was partially dissolved in conc. hydrochloric acid (10 ml). The mixture was cooled to 0 °C and saturated with hydrogen chloride gas, after which complete dissolution occurred. The orange solution was heated in a sealed tube at 50 °C overnight and the cooled mixture was filtered to separate the brown crystals from a red solution. While drying in air the crystals crumbled to a green powder of $cis\text{-}[Cr(bipy)_2Cl_2]Cl.2H_2O$. (Yield 0.40 g, 80 %). (H_2O: 553, 473, 445, −, −, −, 0.440, 0.212).

35 − 38. $cis\text{-}[Cr(phen)_2Cl_2]^+$ prepared from different initial materials. The crude product was in all cases heated at 70 °C for 1 h, when it became green, and was then recrystallised from 0.1 M hydrochloric acid to give the pure chloride dihydrate. The identifying spectral data, given after each preparation, are to be compared with the characterising data of Table 2.

35. $[(phen)_2Cr(OH)_2Cr(phen)_2]^{4+} \rightarrow cis\text{-}[Cr(phen)_2Cl_2]^+$. The wine-red solution of $[Cr(phen)_2OH]_2Cl_4.9H_2O$ [25] (0.5 g, 0.86 mmol Cr) in conc. hydrochloric acid (5 ml) was cooled to 0 °C and saturated with hydrogen chloride gas. Heating at 50 °C in a sealed tube overnight gave red needles which were filtered off from an orange solution. (Yield 0.4 g, 80 %). (H_2O: 558, 478, −, −, 0.447).

36. $cis\text{-}[Cr(phen)_2F_2]^+ \rightarrow cis\text{-}[Cr(phen)_2Cl_2]^+$. The red solution of $cis\text{-}[Cr(phen)_2F_2]ClO_4.H_2O$ (1.0 g, 1.8 mmol) in conc. hydrochloric acid (50 ml) was cooled to 0 °C and saturated with hydrogen chloride gas. Heating for 2 days in a sealed tube at 50 °C gave red needles. (Yield 1.0 g, 90 %). (H_2O: 558, 478, −, −, 0.447).

37. $cis\text{-}[Cr(phen)_2(H_2O)_2]^{3+} \rightarrow cis\text{-}[Cr(phen)_2Cl_2]^+$. The orange solution of $cis\text{-}[Cr(phen)_2(H_2O)_2](NO_3)_3.2H_2O$ (0.6 g, 0.9 mmol) in conc. hydrochloric acid (10 ml) was heated at 80 °C in a sealed tube overnight. Red needles (0.4 g, 75 %) were separated from a green solution. (H_2O: 558, 478, −, −, 0.452).

38. $[Cr(phen)_2ox]^+ \rightarrow cis\text{-}[Cr(phen)_2Cl_2]^+$. $[Cr(phen)_2C_2O_4]Cl.4H_2O$ (0.61 g, 1 mmol) was partly dissolved in conc. hydrochloric acid (10 ml). The mixture was cooled to 0 °C and saturated with hydrogen chloride gas, after which complete dissolution occurred. The orange solution was heated in a sealed tube at 50 °C overnight, and red needles (0.51 g, 80 %) were separated from a green solution. (H_2O: 558, 478, −, −, 0.447).

39. *cis*-$[Cr(bipy)_2Cl_2]^+ \rightarrow$ *cis*-$[Cr(bipy)_2(H_2O)_2]^{3+}$. $[Cr(bipy)_2Cl_2]Cl.2H_2O$ (0.6 g, 1.2 mmol) was ground with moist silver oxide and water (10 ml) and left overnight in the dark [the silver oxide was prepared, as in prep. 14, from silver nitrate (0.8 g, 4.6 mmol)]. The filtered red solution was acidified with conc. nitric acid to pH ~1. The very slight precipitate was filtered off, and the orange solution was concentrated until precipitation began, when it was readjusted to pH ~1 with solid lithium hydroxide hydrate and cooled at 0 °C (in more strongly acid solution crystallisation did not take place). The orange precipitate of the nitrate salt was filtered off, washed with ice-cold 96 % ethanol, and air-dried. (Yield 0.25 g, 35 %). Identifying spectral data (0.1 M HNO_3, *cf.* Table 2): (492, 468, −, −, 0.87). Later it was found that the aquahydroxo complex was much easier to isolate in good yield (*cf.* prep. 13).

40. *cis*-$[Cr(phen)_2Cl_2]^+ \rightarrow$ *cis*-$[Cr(phen)_2(H_2O)_2]^{3+}$. *cis*-$[Cr(phen)_2Cl_2]Cl.2H_2O$ (0.56 g, 1 mmol) was ground with moist silver oxide and water (50 ml) and left in the dark overnight. [The silver oxide was prepared, as in prep. 14, from silver nitrate (0.6 g, 3.5 mmol)]. The filtered red solution was acidified with conc. nitric acid to pH ~1. The slight precipitate was filtered off, and the orange solution concentrated to 10 ml and readjusted to pH ~1 with solid lithium hydroxide hydrate. Cooling at 0 °C produced orange crystals of the nitrate salt which were filtered off, washed with ice-cold 96 % ethanol and air-dried. (Yield 0.35 g, 55 %). Identifying spectral data (0.1 M HNO_3, *cf.* Table 2): (496, 458, −, −, 0.69).

41. $[(phen)_2Cr(OH)_2Cr(phen)_2]^{4+} \rightarrow$ *cis*-$[Cr(phen)_2(H_2O)_2]^{3+}$. This hydrolysis, using nitric acid, has been reported previously [39] and studied kinetically.[40] When the chloride salt of the diol was used we found that chloro complexes were formed together with diaqua complex. However, when the diol nitrate was used, pure diaqua complex was obtained (see also prep. 51).

42 – 52. Preparation of optically active complexes. Identifying absorption spectral data are given as (λ_{max}, λ_{min}, $\varepsilon_{min}/\varepsilon_{max}$) and, unless otherwise indicated, are to be compared with characterising spectral data given in Table 2. CD and optical rotation data are given in Table 3.

42. Resolution of chromium(III)(bipy)diol. A. $[Cr(bipy)_2OH]_2(ClO_4)_4.2H_2O$ [25] (50 g, 41.8 mmol) and potassium trifluoroacetate (32 g, 210 mmol) were stirred in methanol (300 ml) for 1 h at 25 °C. The deep-red solution was filtered and the precipitate of potassium perchlorate washed with a little methanol. The combined filtrate and washings were then added to a stirred 25 °C solution of sodium $(+)_{589}$ antimonyl tartrate (25.8 g, 83.5 mmol: equivalent to 50 % of the diol in solution) in 10^{-3} M hydrochloric acid (300 ml), whereupon a dense pink precipitate was rapidly formed. The mixture was stirred for 15 min and then filtered, and the diastereoisomer washed with cold 10^{-3} M hydrochloric acid, then methanol, and air-dried. (Yield 16.6 g (crop A1)).

The mother-liquor from the above mixture was then treated with a 25 °C solution of a further portion of sodium $(+)_{589}$ antimonyl tartrate (25.8 g) in 10^{-3} M hydrochloric acid (150 ml), as before, and left to stand overnight. The resulting crop of crystals was filtered off and washed and dried as above. (Yield 22.4 g (crop A2)). Treatment of the mother-liquor with a further portion of resolving agent, as above, gave (after standing for 24 h) a further, very small crop of diastereoisomer. (Yield 0.55 g (crop A3)).

Addition of a fourth portion of resolving agent (25.8 g) in 10^{-3} M hydrochloric acid (150 ml) produced no further precipitation, even after prolonged standing at 25 °C. However, on cooling the solution at 5 °C for 2 days, a good crop of large red-brown crystals was obtained and was isolated by filtration. These crystals were much more soluble in cold 10^{-3} M hydrochloric acid than the three crops isolated previously, and so were washed only with methanol and air-dried. (Yield 23.6 g (crop A4)). This difference in solubility strongly suggests that crop A4 contains predominantly the second diastereoisomer.

B. Crops A1, A2 and A4 were converted, in each case, to the perchlorate salt by the following procedure (crop A3 was very small and was not converted). The total crop was dissolved, with stirring, in the minimum volume of cold 2 M sodium acetate solution and the red solution filtered. Addition of excess saturated aqueous sodium perchlorate solution then resulted in essentially quantitative precipitation of the perchlorate salt, which was filtered off, washed with cold 1 M perchloric acid and then methanol, and air-dried. The yields from the three crops of $(+)_{589}$ antimonyl tartrate salt were as follows: – crop B1, 9.74 g; crop B2, 13.23 g; crop B4, 13.60 g. Analysis indicated, in each case, that the dihydrate was obtained. Identifying spectral data (10^{-3} M HCl, *cf.* Ref. 25): (For B1: 537, 467, 0.443; for B2: 537, 467, 0.429; for B4: 537, 467, 0.430). The molar rotation of crop B4 (+ 9132° l mol^{-1} m^{-1}) was opposite in sign but lower in magnitude than those of crops B1 and B2 (which were virtually identical: see Table 3) and so the former was recrystallised once from hot water containing a little 2 M perchloric acid.[25] The measured molar rotation then improved to a value almost identical in magnitude to that of the first 2 crops (see Table 3). The analytical data indicate that crops B1 and B2 ($(-)_{589}$ enantiomer) comprise 46 % of the total original amount of racemic bipy diol, and this fact, together with the solubility observations on the various diastereoisomer fractions and the observed molar rotations of

the corresponding crops of perchlorate salt, suggests that essentially complete resolution has been effected.

43. Resolution of chromium(III)(phen)diol. A. The procedure employed was analogous to that for the resolution of the bipy diol. $[Cr(phen)_2OH]_2(NO_3)_4.4H_2O$ [25] (34.5 g, 29.3 mmol) was stirred with potassium trifluoroacetate (22.3 g, 147 mmol) in methanol (150 ml) for 30 min at 25 °C. The filtered red solution was then added to a 25 °C solution of sodium $(+)_{589}$ antimonyl tartrate (18.1 g, 58.6 mmol) in 10^{-3} M hydrochloric acid (100 ml). The resulting dense precipitate was filtered off, washed with cold 10^{-3} M hydrochloric acid and then 96 % ethanol, and air-dried (the washings were added to the mother-liquor). (Yield 19.85 g (crop A1)). The mother-liquor was then left to stand overnight, giving a further crop of red-brown needles which were isolated as above. (Yield 5.50 g (crop A2)). After further treatment of the mother-liquor with a second portion of resolving agent (18.1 g) in 10^{-3} M hydrochloric acid (100 ml), as before, the solution was left to stand for *ca.* 1 h and the resulting fine precipitate isolated as previously. (Yield 5.85 g (crop A3)).

On leaving the filtrate to stand overnight, a good yield of large red-brown flaky crystals was obtained. These proved to be much more soluble in 10^{-3} M hydrochloric acid than the three previous crops and were therefore washed only with 96 % ethanol and air-dried. (Yield 17.8 g (crop A4)). Addition of a third portion of the resolving agent to the residual mother-liquor, as before, followed by cooling of the solution at 5 °C for 3 days, resulted in the formation of a further crop of large crystals with solubility properties as for crop A4. (Yield 8.92 g (crop A5)).

B. Crops A1-A5 were converted to the very insoluble perchlorate salt as for the bipy analogue (prep. 42). Yields were: crop B1, 10.72 g; crop B2, 2.96 g; crop B3, 3.32 g; crop B4, 10.48 g; crop B5, 5.52 g. Analysis indicated, in each case, that the trihydrate was obtained.

For rotation, CD and absorption spectrum measurements, solutions of portions of crops B1 and B2 ($(-)_{589}$ enantiomer), and crop B4 ($(+)_{589}$ enantiomer) were prepared in nitromethane, a solvent in which the phen diol appears to be quite stable. The middle crop (crop B3) and the final crop (crop B5) were not examined. Measurements were not made in acidic aqueous solution because the chromium(III) phen diol is known to be somewhat unstable in this medium.[25] Characterising spectral data, measured for crop B1 (nitromethane; *cf.* in 0.1 M HNO_3, Ref. 25): (λ_{max} 540, 422 (sh); ε_{max} 113.9, 302.6; λ_{min} 462; ε_{min} 42.9; $\varepsilon_{min}/\varepsilon_{max}$ 0.386). Identifying spectral data for B2 and B4: (For B2: 540, 462, 0.421; for B4: 540, 462, 0.398). The analytical data indicate that crops B1, B2 and B3 comprise 49 % of the total original amount of diol and this fact, together with the virtually identical magnitudes of molar rotation observed for crops B1, B2 and B4 (Table 3) and the solubility observations, again indicates essentially complete resolution.

44. $(-)_{589}$-$[(bipy)_2Cr(OH)_2Cr(bipy)_2]^{4+}$ → $(-)_{589}$-*cis*-$[Cr(bipy)_2Cl_2]^+$. This conversion was effected in the same way as for the racemic bipy diol (prep. 31), using $(-)_{589}$-$[Cr(bipy)_2OH]_2(ClO_4)_4.2H_2O$ (2.0 g, crop B1 from prep. 42). (Yield 1.31 g, 70 %). Anal. $[Cr(C_{10}H_8N_2)_2Cl_2]ClO_4.\frac{1}{2}H_2O$: C, H, N, Cl. Identifying spectral data (DMF): (572, 488, −, −, 0.504).

45. $(-)_{589}$-$[(phen)_2Cr(OH)_2Cr(phen)_2]^{4+}$ → $(-)_{589}$-*cis*-$[Cr(phen)_2Cl_2]^+$. This reaction was performed as in prep. 35, using $(-)_{589}$-$[Cr(phen)_2OH]_2(ClO_4)_4.3H_2O$ (1.0 g, crop B1 from prep. 43) in conc. hydrochloric acid (25 ml). After cooling the final reaction mixture at 5 °C for 24 h, the fine grey-green crystals were filtered off, washed with water and methanol, and air-dried. (Yield 0.50 g, 55 %). Identifying spectral data (DMF): (578, 493, −, −, 0.562).

46. $(-)_{589}$-$[(bipy)_2Cr(OH)_2Cr(bipy)_2]^{4+}$ → $(-)_{589}$-*cis*-$[Cr(bipy)_2Br_2]^+$. $(-)_{589}$ $[Cr(bipy)_2OH]_2$-$(ClO_4)_4.2H_2O$ (2.0 g, 1.67 mmol: crop B1 from prep. 42) and potassium trifluoroacetate (1.2 g, 7.90 mmol) were stirred in methanol (20 ml) for 30 min at 25 °C. The precipitated potassium perchlorate was removed by filtration, washed with a little methanol, and the washings added to the bulk filtrate. The methanol solution was then evaporated to dryness on a rotary evaporator and the solid dissolved in conc. hydrobromic acid (20 ml, *d* 1.73). The deep-red solution was then cooled to 0 °C, saturated with HBr gas, and the tightly sealed flask placed in an oven at 50 °C for 24 h. The reaction mixture was then cooled at 5 °C overnight and the fine green crystals of the bromide hydrobromide salt were removed by filtration, washed twice with conc. hydrobromic acid (*d* 1.73) and then liberally with ether, and air-dried. (Yield 0.93 g, 35 %). Anal. $[Cr(C_{10}H_8N_2)_2Br_2]Br.HBr.3H_2O$: C, H, N, Br. An aqueous solution of the complex gave a strongly acid reaction. Characterising spectral data (H_2O): λ_{max} 574, 518, 445 (sh); ε_{max} 52.7, 45.6, 132: λ_{min} 526, 484; ε_{min} 43.9, 29.0).

47. $(-)_{589}$-$[(phen)_2Cr(OH)_2Cr(phen)_2]^{4+}$ → $(-)_{589}$-*cis*-$[Cr(phen)_2Br_2]^+$. $(-)_{589}$-$[Cr(phen)_2OH]_2(ClO_4)_4.3H_2O$ (1.0 g, crop B1 from prep. 43) was dissolved in conc. hydrobromic acid (25 ml, *d* 1.73) and the solution saturated, at 0 °C, with HBr gas. The tightly sealed flask was then placed in an oven at 50 °C for 24 h. After cooling the reaction mixture to 0 °C an ice-cold solution of lithium perchlorate (2.0 g) in water (20 ml) was added, giving an immediate green precipitate of the perchlorate salt of the product. This was filtered off, washed with water and ethanol, and air-dried. (Yield 0.86 g, 85 %). Anal. $[Cr(C_{12}H_8N_2)_2Br_2]ClO_4$: C, H, N, Cl, Br. Characterising spectral data (DMF):

(λ_{max} 598, 522, 421 (sh); ε_{max} 49.8, 42.8, 227: λ_{min} 538, 495; ε_{min} 36.5, 32.0).

48. Attempted conversion $(-)_{589}$-$[(bipy)_2Cr(OH)_2Cr(bipy)_2]^{4+}$ → optically active *cis*-$[Cr(bipy)_2F_2]^+$. Repeated attempts to perform this reaction on $(-)_{589}$-$[Cr(bipy)_2OH]_2(ClO_4)_4.2H_2O$, by the procedure described in prep. 26, or by stirring the complex in liquid hydrogen fluoride in a closed polythene bottle for varying periods of time and then isolating the product as in prep. 26, gave only the racemic difluoro complex in good yield (both unrecrystallised and recrystallised products were inactive). Anal. $[Cr(C_{10}H_8N_2)_2F_2]ClO_4$: C, H, N. Identifying spectral data (H_2O): *e.g.* (519, 461, −, −, 0.438).

49. $(-)_{589}$-$[(phen)_2Cr(OH)_2Cr(phen)_2]^{4+}$ → $(-)_{589}$-*cis*-$[Cr(phen)_2F_2]^+$. This reaction was performed essentially as in prep. 29 for the racemic complex, using $(-)_{589}$-$[Cr(phen)_2OH]_2(ClO_4)_4.3H_2O$ (1.0 g, crop B1 from prep. 43) stirred with anhydrous hydrogen fluoride (*ca.* 80 ml). After leaving the crimson solution to evaporate overnight, the red residue was dissolved in 1:1 aqueous-methanol (40 ml) and the product isolated as in prep. 29. The complex was recrystallised from warm (*ca.* 50 °C) water by addition of lithium perchlorate (1.0 g) in water (10 ml). The crystals were filtered off, washed with 96 % ethanol, and air-dried. (Yield 0.47 g, 55 %). Identifying spectral data (H_2O): (522, 455, −, −, −, −, 0.352, −).

50. $(-)_{589}$-$[(bipy)_2Cr(OH)_2Cr(bipy)_2]^{4+}$ → $(-)_{589}$-*cis*-$[Cr(bipy)_2(H_2O)_2]^{3+}$. This conversion was effected as in prep. 13 for the racemic complex, using $(-)_{589}$-$[Cr(bipy)_2OH]_2(ClO_4)_4.2H_2O$ (2.0 g, crop B2 from prep. 42). The optically active complex appears to be considerably more soluble than the racemic (prep. 13) and the percentage yield of the former is thus correspondingly lower than that of the latter. (Yield 0.70 g, 35 %). Anal. $[Cr(C_{10}H_8N_2)_2(H_2O)OH](ClO_4)_2.2H_2O$: C, H, N, Cl. Identifying spectral data (0.1 M HCl): (492, 468, −, −, 0.877).

51. $(-)_{589}$-$[(phen)_2Cr(OH)_2Cr(phen)_2]^{4+}$ → $(-)_{589}$-*cis*-$[Cr(phen)_2(H_2O)_2]^{3+}$. The procedure employed here was as in prep. 13, using $(-)_{589}$-$[Cr(phen)_2OH]_2(ClO_4)_4.3H_2O$ (1.0 g, crop B1 from prep. 43) and 70 % perchloric acid (10 ml). (Yield 0.55 g, 50 %). Anal. $[Cr(C_{12}H_8N_2)_2(H_2O)OH](ClO_4)_2.2H_2O$: C, N, Cl. Identifying spectral data (0.1 M HCl): (496, 458, −, −, 0.695).

52. Attempted conversion $(-)_{589}$-$[(bipy)_2Cr(OH)_2Cr(bipy)_2]^{4+}$ → optically active $[Cr(bipy)_2ox]^+$. This attempted conversion was performed exactly as in prep. 22 for the racemic complex except that $(-)_{589}$ diol perchlorate (2.0 g, crop B1 from prep. 42) was used. The product, however, exhibited no rotation at 589 nm or CD in the region 650 − 400 nm, although its absorption spectrum in aqueous solution was identical with that of the complex from prep. 22.

C. Equilibrium experiments

The heterocyclic ligands are so robustly bound in the bis(N − N) complexes of both chromium(III) and cobalt(III) that the partial equilibria involving chloride and water in the last two coordination sites could be studied. The equilibrated solutions were prepared starting from both sides of the equilibrium, *i.e.* from the dichloro and the diaqua complexes. Solutions containing *cis*-$[Cr(phen)_2Cl_2]^+$ (I), *cis*-$[Cr(phen)_2(H_2O)_2]^{3+}$ (II), *cis*-$[Co(phen)_2Cl_2]^+$ (III) and *cis*-$[Co(phen)_2(H_2O)_2]^{3+}$ (IV) were prepared by dissolving *cis*-$[Cr(phen)_2Cl_2]Cl.2H_2O$, *cis*-$[Cr(phen)_2(H_2O)_2](NO_3)_3.2H_2O$, *cis*-$[Co(phen)_2Cl_2]Cl.3\frac{1}{2}H_2O$ and *cis*-$[Co(phen)_2(H_2O)OH](ClO_4)_2$, respectively, in 0.10 M hydrochloric acid and adding solid sodium chloride so as to give final concentrations: $C_{complex} = 3.00 \times 10^{-3}$ M and $C_{Cl^-} = 0.109$ M in each case. These concentrations were chosen so as to permit a reasonable estimate of the first complexity constant for chloride, K_1, preliminary experiments having indicated that the fraction of dichloro species in the equilibrated solutions was small for both the chromium(III) and cobalt(III) systems at the above chloride concentration. After heating the solutions for 3 days at 60 °C, they were cooled to 25 °C and their absorption spectra recorded. The two chromium(III) solutions (I and II) exhibited identical spectra: $(\lambda, \varepsilon)_{max}$ = (505, 40); $(\lambda, \varepsilon)_{min}$ = (458, 23). The spectra of the two cobalt(III) solutions (III and IV) were likewise identical: $(\lambda, \varepsilon)_{max}$ = (516, 56); $(\lambda, \varepsilon)_{min}$ = (462, 33). Further heating at 60 °C did not produce any further change in the positions of the absorption maxima but the intensities of the bands decreased very slowly, possibly due to displacement of phenanthroline.

From the recorded spectra of the equilibrium mixtures, the absorptivities were measured at every 10 nm between 600 and 460 nm and the resulting sets of data were fitted, by the least-squares method, to a linear combination of the corresponding data for the appropriate diaqua, aquachloro, and dichloro systems. The resulting complexity constants calculated for the chromium(III) system were $K_1 = 8.7 \pm 0.5$ and $K_2 = 0.3 \pm 0.2$ l mol^{-1}, whilst for the cobalt(III) system the calculated values were $K_1 = 38 \pm 2$ and $K_2 = 0.5 \pm 0.1$ l mol^{-1} (K_1 and K_2 being defined as given in section III C). These complexity constants are valid at 60 °C and an ionic strength of *ca.* 0.11 M, but are expected to be rather sensitive to the medium and decrease with increasing ionic strength.

III. DISCUSSION OF DICHLORO COMPLEXES

A. Polymorphism and colour variation

The dichlorobis(N−N) complexes of chromium(III) and cobalt(III) [section II B, prep. 1−10] exhibit remarkably dichroic properties. In daylight, aqueous solutions of all these ions appear in low concentrations green to olive-green but in higher concentrations violet to red. However, solutions of these ions in various organic solvents (*e.g.* dimethylformamide, dimethyl sulfoxide) maintain their colours, *viz.* green (chromium) and violet (cobalt), irrespective of concentration.

The solid salts also give varying colour impressions. In many cases the anhydrous salts and lower hydrates are green to brown whereas higher hydrates or acid hydrates are violet to red.*

It is also often observed that samples which are green in daylight show a pronounced colour change on going to normal artificial light (whose intensity distribution is shifted toward the red), when they appear red-brown (chromium) or red-violet (cobalt). However, many of the crystals are extremely pleochroic and much more so than crystals of corresponding aliphatic amine complexes.

The two hydrates of dichlorobis(phen)chromium(III) chloride that we have encountered have strange stability relations. When crystallised from methanolic solution and dried in air the red tetrahydrate [section II B, prep. 4] is obtained, but crystallisation from aqueous solution gives a green dihydrate [section II B, prep. 3] with a different X-ray powder photograph. At room temperature the latter salt is the stable one of the two hydrates, the red tetrahydrate turning green and reverting to the dihydrate even when (and particularly rapidly when) kept over water in a desiccator. The $[Co(phen)_2Cl_2]^+$ cation may be crystallised into the stable hydrate, $[Cr(phen)_2Cl_2]Cl.2H_2O$,[7] and likewise the cation $[Co(phen)_2(H_2O)_2]^{3+}$ may be crystallised into $[Cr(phen)_2(H_2O)_2](NO_3)_3.2H_2O$ [section II B, prep. 18].

B. *cis*-Dichlorobis(1,10-phenanthroline)cobalt(III) tetrachlorocobaltate(II)

We previously reported evidence [34] to show that one [33] of the several green phen- (or bipy-) containing cobalt(III) complexes which had been believed to contain a *trans*-$[Co(N-N)_2Cl_2]^+$ cation* actually is *cis*-$[Co(phen)_2Cl_2]_2[CoCl_4].2H_2O$ [section II B, prep. 11]. We also stated that the apparent difference [33] between its ^1H NMR spectrum and that of the violet *cis*-$[Co(phen)_2Cl_2]Cl.3\frac{1}{2}H_2O$ in DMSO solution could be explained partly by a difference in the resolution of the two reported spectra, and partly by a difference in the internal standards relative to which the chemical shifts were given. Further details of our ^1H NMR results are given here and are compared with those reported previously [33] (Table 1).

It was previously stated and qualitatively explained by us [34] that the ^1H NMR spectra of green *cis*-$[Co(phen)_2Cl_2]_2[CoCl_4].2H_2O$ in DMSO-d_6 and aqueous (D_2O) solution are completely different, partly because one chloride ligand in the cation is hydrolysed rather rapidly in aqueous solution when appropriate cobalt(II) species are present [32] and partly because the paramagnetic anion, $[CoCl_4]^{2-}$, which persists in DMSO, reacts with water to give the hexaaquacobalt(II) cation which, although still paramagnetic, is less likely to interact with the investigated cation because of its positive charge. It would appear that the effect of the presence of the paramagnetic anion is only small, since the ^1H NMR spectra of low concentration DMSO solutions of *cis*-$[Co(phen)_2Cl_2]_2[CoCl_4].2H_2O$ and *cis*-$[Co(phen)_2Cl_2]Cl.3\frac{1}{2}H_2O$ are virtually identical (Table 1). However, line broadening is observed in the spectrum of the former salt when the concentration exceeds *ca.* 10^{-2} M, presumably because ion-pairing then becomes significant. Fig. 1 shows the ^1H NMR spectrum of *cis*-

* For the chlorides of $[Co(phen)_2Cl_2]^+$ four differently coloured salts have been reported [41] and five chlorides of $[Cr(phen)_2Cl_2]^+$ have been characterised by having different X-ray powder photographs.[28,42] However, the experimental conditions for preparing these different salts have not been specified in detail.

* All of these green complexes have been shown by various methods not to contain such a cation.[9,43,44]

Table 1. Chemical shifts for protons in bis(phen)cobalt(III) complexes, in ppm relative to the signal for the methyl protons of *tert*-butanol (except in the fourth row).

Solvent	Proton assignments according to Ref. 33 (apart from last 2 rows)						
	2	4	7	3	5+6	8	9
cis-$[Co(phen)_2Cl_2]Cl.3\frac{1}{2}H_2O$							
D_2O[a,b]	−8.76, −8.71	−7.88, −7.79	−7.36, −7.27	−7.16[c]	−6.99[c]	−6.20[c]	−6.03[c]
d_6-DMSO[a]	−8.98, −8.94	−8.26, −8.18	−7.77, −7.68	−7.47	−7.36[c]	−6.54[c]	−6.42[c]
DMSO[d]	−8.92	−8.20	−7.71	−7.45	−7.36	−6.56	−6.44
Proposed *trans*-$[Co(phen)_2Cl_2]^+$salt							
DMSO[d,e]	−0.29, −0.25	0.3 to 0.6	0.8 to 1.05	1.20		2.20	
DMSO[d,f]	−9.19, −9.15	−8.6 to −8.3	−8.1 to −7.85	−7.70		−6.70	
DMSO[d,g]	−9.01, −8.97	−8.4 to −8.1	−7.9 to −7.65	−7.52		−6.52	
cis-$[Co(phen)_2Cl_2]_2[CoCl_4].2H_2O$							
d_6-DMSO[a,h]	−8.94, −8.88	−8.20 to −8.12	−7.74 to −7.64	−7.44	−7.34	−6.53	−6.41
D_2O[a,b,i]	−8.95, −8.26, −7.98, −7.25, −6.30, −5.99						
cis-$[Co(phen)_2(H_2O)Cl](ClO_4)_2 2\frac{1}{2}H_2O$							
D_2O[a,b]	−8.98, −8.29, −8.02, −7.27, −6.34, −6.01						

[a] Measured at 30 °C using a Varian HA-100. [b] Slightly acidic solution. [c] Band-group centre positions. [d] Given in Ref. 33, measured at 35 °C using either a Varian HR-100 or a Perkin-Elmer R10. [e] Apparently given in the τ scale ($\tau_{TMS} = 10.0$) [f] Translated to the present scale using the fact that the methyl protons of *tert*-butanol give a signal 1.10 ppm downfield from that of TMS (*i.e.* at τ 8.90) when both compounds are dissolved in d_6-DMSO. The numbers in the fifth row are thus obtained by subtracting 8.90 from those in the fourth row. [g] Translated to the present scale using a table value [45] of τ 8.72 for the methyl proton signal of *tert*-butanol. The numbers in the sixth row are thus obtained by subtracting 8.72 from those in the fourth row. [h] 5.6×10^{-3} formula units per litre. [i] 9.3×10^{-3} formula units per litre. Only band group maxima of the highly-resolved spectrum obtained by accumulation over 22 scans are given; species present: *cis*-$[Co(phen)_2(H_2O)Cl]^{2+}$.

$[Co(phen)_2Cl_2]_2[CoCl_4].2H_2O$ in DMSO at two concentrations. It is remarkable that a variation in concentration by a factor of less than two can produce such a pronounced effect. More dilute solutions give, of course, less intense spectra which exhibit, however, the same number of peaks at the same positions and with essentially the same line-widths as the lower spectrum of Fig. 1.

It can be seen from Table 1 that the present and previous [33] ^1H NMR results for DMSO solutions of the violet *cis*-$[Co(phen)_2Cl_2]Cl.3\frac{1}{2}H_2O$ and the green *cis*-$[Co(phen)_2Cl_2]_2[CoCl_4].2H_2O$ are consistent. In a previous communication [34] we also stated that our ^1H NMR results for aqueous (D_2O) solutions of the green species were in agreement with those reported previously.[33] The latter statement is now known to be incorrect, the error arising from an incorrect calibration of the relevant spectra with respect to the reference signal. We have subsequently re-examined the spectrum of the green species in D_2O and find it to be quite different to that reported by the previous authors [33] (Table 1). Furthermore, our previous contention [34] that the cation in green *cis*-$[Co(phen)_2Cl_2]_2[CoCl_4].2H_2O$ undergoes aquation to *cis*-$[Co(phen)_2(H_2O)Cl]^{2+}$ in aqueous solution is clearly supported by a comparison of the ^1H NMR spectra of D_2O solutions of the green complex and of pure *cis*-$[Co(phen)_2(H_2O)Cl](ClO_4)_2.2\frac{1}{2}H_2O$ (Table 1).

The present samples of the green complex have been prepared both by the previous pro-

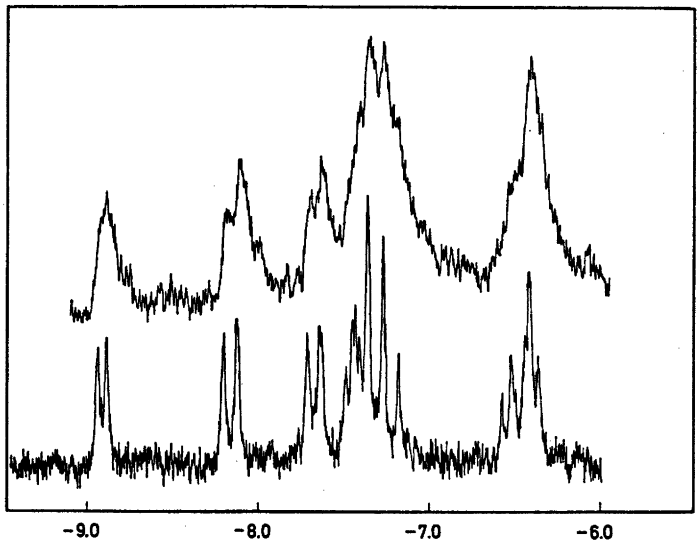

Fig. 1. ^{1}H NMR spectra of *cis*-$[Co(phen)_2Cl_2]_2[CoCl_4].2H_2O$ at two different concentrations in DMSO-d_6. The scale is given in ppm relative to the signal for the methyl protons of *tert*-butanol. Lower spectrum: 7.4×10^{-3} formula units per litre; upper spectrum 12.3×10^{-3} formula units per litre. A pronounced line-broadening effect is observed on going from the more dilute to the more concentrated solution. The concentration difference is very small but the effect is still considerable, probably because of increased interaction of the cation with the paramagnetic anion.

cedure [33] and by a method involving direct addition of a solution containing $[CoCl_4]^{2-}$ ion to an aqueous solution of pure *cis*-$[Co(phen)_2Cl_2]Cl.3\frac{1}{2}H_2O$ [section II B, prep. 11]. Both methods gave products exhibiting identical X-ray powder photographs and absorption spectra.

C. Kinetic and thermodynamic stability

In the absence of catalysts, the *cis*-dichlorobis(N−N) complexes of cobalt(III) are remarkably robust [32] relative to the ethylenediamine analogue *cis*-$[Co(en)_2Cl_2]^+$,[46] at least with respect to acid hydrolysis of the cobalt-to-chloride bonds. There has been considerable disagreement in the literature concerning the robustness of the metal-chloride bonds in the dichlorobis(N−N)cobalt(III) complexes.[3,4,28,31,32,47–55] It has been shown that these conflicting results are caused by the action of catalytic impurities.[32]

A method of preparation has been devised here which yields samples of the *cis*-dichlorobis(N−N)cobalt(III) salts for which the hydrolysis of the first chloride, in 10^{-3} M hydrochloric acid, could not be detected spectrophotometrically within two weeks. However, this was only the case when the solutions were kept in the dark. When exposed to diffuse daylight the solutions underwent a colour change within one day. This light sensitivity of the acid hydrolysis reaction was not appreciated by us at the time of publication of our previous communication.[32]

Moreover, the robustness with respect to loss of the heterocyclic ligands in acidic solution exceeds that towards loss of chloride ion by several orders of magnitude, so that the latter reactions can effectively be studied independently of the former.

The robustness of the pure *cis*-$[Co(N-N)_2Cl_2]^+$ species towards acid hydrolysis does not hold for base hydrolysis.[32] For example, treatment of aqueous solutions of *cis*-$[Co(N-N)_2Cl_2]Cl.aq$ with ammonia results in a rapid change in colour at room temperature from the violet to violet-green colour of the dichloro

complexes to pinkish red, and in the phen case the absorption spectrum of the resulting solution, made strongly acidic after a few minutes with hydrochloric acid, is very similar to that of the *cis*-$[Co(phen)_2(H_2O)Cl]^{2+}$ cation (*cf.* Table 2). When similar experiments are performed using sodium hydroxide a rapid colour change also takes place. The resulting solutions, on acidifying after *ca.* 5 min with hydrochloric acid, are orange-red in colour and exhibit absorption spectra agreeing closely with those of the species *cis*-$[Co(N-N)_2(H_2O)_2]^{3+}$ (*cf.* Table 2).

The influence of pH on the hydrolysis behaviour of the *cis*-$[Co(N-N)_2Cl_2]^+$ cations is further exemplified by the fact that solutions of *cis*-$[Co(bipy)_2Cl_2]^+$ in a pyridine buffer (pH 4.4) were found to undergo no change in absorption spectrum within 24 h at room temperature, whereas solutions of the complex in a buffer of 2,4,6-trimethylpyridine (pH 7.5) showed spectral evidence of hydrolysis within a few minutes under the same conditions.

Hydrolysis reactions of the type described above were adapted for use in the preparation of the complexes *cis*-$[Co(phen)_2(H_2O)Cl](ClO_4)_2.2\frac{1}{2}H_2O$ [section II B, prep. 20 *b*] and *cis*-$[Co(N-N)_2(H_2O)OH](ClO_4)_2$ [section II B, prep. 14 *b* and 16 *b*] in good yield. Since the use of ammonia for the synthesis of *cis*-$[Co(phen)_2(H_2O)Cl]^{2+}$ was found to give an impure perchlorate salt, the poorly-coordinating base trimethylamine (which has a pK value very close to that of ammonia) was employed instead in prep. 20 *b*.

It would be expected that a conjugate-base (CB) mechanism for the base induced hydrolysis of *cis*-$[Co(N-N)_2Cl_2]^+$ would not be operative, since it would involve a deprotonation of the aromatic ring system of the N–N ligand. This expectation was borne out by means of ^{1}H NMR experiments. Almost saturated solutions of the *cis*-$[Co(N-N)_2Cl_2]Cl.aq$ complexes in D_2O were basified by addition of sodium hydroxide and, after 5 min, acidified with hydrochloric acid. The ^{1}H NMR spectra of the resulting solutions were found to be identical with those of the appropriate pure *cis*-$[Co(N-N)_2(H_2O)_2]^{3+}$ species in acidic D_2O. If some kind of CB mechanism for base hydrolysis were operating, involving the exchange of a proton of the heteroaromatic ring system of the N–N ligands with a deuterium ion, the ^{1}H NMR spectra of the resulting deuterated diaqua species should be different from those of the non-deuterated.

For the *cis*-dichlorobis(N–N)chromium(III) complexes, as with the Co(II)-free cobalt(III) complexes, the robustness of the metal-to-chloride bonds towards acid hydrolysis is also orders of magnitude greater than for the corresponding *cis*-dichlorobis(ethylenediamine)-chromium(III) [52] complex. The chromium(III) species, however, exhibit no special behaviour in basic solution. For example, the visible spectrum of *cis*-$[Cr(phen)_2Cl_2]^+$ in 0.1 M sodium hydroxide solution, at room temperature, is identical to that in 0.1 M hydrochloric acid.

It seems possible that the catalytic effect of hydroxide ion on the hydrolysis of the *cis*-$[Co(N-N)_2Cl_2]^+$ ions arises because of reduction by the former, a phenomenon which is known to be operative in the reaction of $[Fe(N-N)_3]^{3+}$ with hydroxide ion.[53] The failure of the *cis*-$[Cr(N-N)_2Cl_2]^+$ ions to exhibit base hydrolysis behaviour comparable to that displayed by the cobalt(III) analogues is in keeping with this hypothesis, since the chromium(III) complex ions are expected to be much less easily reduced than the cobalt(III) species.

Because of the particular electronic characteristics of the heterocyclic ligands we have made some attempt to assess whether or not the greater robustness of the *cis*-$[M(N-N)_2Cl_2]^+$ ions than their *cis*-$[M(en)_2Cl_2]^+$ analogues (M = Cr or Co) towards acid hydrolysis is accompanied by a greater thermodynamic stability. This was done spectrophotometrically by heating acidic aqueous solutions of the *cis*-diaqua- and dichlorobis(phen) chromium(III) or cobalt(III) complexes, containing the same complex concentration and chloride ion concentration, at 60 °C for 3 days and monitoring their absorption spectra. Since the spectra of the solutions prepared from both types of complex of a given metal became identical, equilibrium was believed to have been attained. Assuming the resulting spectra to be linear combinations of those for the *cis*-diaqua, aquachloro and dichloro complexes, the value of $K_1 = \{[M(phen)_2(H_2O)Cl]^{2+}\}/\{[M(phen)_2(H_2O)_2]^{3+}\}\{Cl^-\}$, could be estimated to be about 9 l mol^{-1} for the chromium(III) system and about 40 l mol^{-1} for the cobalt(III) system (for the estimated

values of $K_2 = \{[M(phen)_2Cl_2]^+\}/\{[M(phen)_2(H_2O)Cl]^{2+}\}\{Cl^-\}$, see section II C). Whilst no corresponding data appear to have been reported for the strictly analogous *cis*-bis(ethylenediamine) systems, the above values for K_1 do not appear to be more than *ca.* one order of magnitude greater than those reported for the comparable chromium(III) [54] and cobalt(III) [55] pentaammine systems. The indication is, therefore, that the metal-to-chloride bonds in these bis(N – N) complexes are not especially thermodynamically stable.

As communicated previously,[32] the *cis*-$[Cr(N-N)_2Cl_2]^+$ cations undergo catalysed acid hydrolysis reactions under appropriate conditions. For example, addition of fresh zinc amalgam (prepared by addition of zinc powder to a dilute mercury(II) chloride solution) to a small aliquot of a *ca.* 10^{-2} M stock solution of *cis*-$[Cr(phen)_2Cl_2]Cl.2H_2O$ in 10^{-3} M hydrochloric acid, without agitation, results in a fairly rapid colour change from red-violet to yellow-green (owing to reduction to Cr(II) species). Careful withdrawal of this solution and its addition to a 20-fold volume of the same stock chromium(III) solution which has been briefly bubbled with nitrogen gas causes a very rapid colour change from red-violet to orange-red. After allowing this solution to oxidise in air and acidifying it with nitric acid the visible absorption spectrum exhibits a maximum at λ_{max} 507 nm, indicating a mixture of *cis*-$[Cr(phen)_2(H_2O)Cl]^{2+}$ and *cis*-$[Cr(phen)_2(H_2O)_2]^{3+}$ species (*cf.* Table 2). This result is thus in agreement with the results of the equilibrium experiments described above, in that the thermodynamically less stable chromium-to-chloride bonds become hydrolysed to a greater extent than in the cobalt(III)[32] system.

As well as examining the effect of catalysis on the rate of aquation of *cis*-$[M(N-N)_2Cl_2]^+$,[32] we have made a qualitative comparative study of the anation of the complexes *cis*-$[M(N-N)_2(H_2O)_2]^{3+}$ by chloride ion under catalytic and non-catalytic conditions. Approximately 10^{-2} M solutions of *cis*-$[Co(N-N)_2(H_2O)_2]^{3+}$ in 0.05 M perchloric acid containing a very large excess of lithium chloride ($[Cl^-] \simeq 7$ M) undergo no apparent change within several hours at room temperature. However, addition to such solutions of a minute quantity of the cobalt(II) complex $[Co(phen)_2Cl_2]$ results in gradual but essentially quantitative precipitation of the *cis*-dichlorobis(N – N)cobalt(III) complexes within *ca.* 1 h under the same conditions. Similar behaviour is observed for the chromium(III) analogues: Approximately 10^{-2} M solutions of *cis*-$[Cr(N-N)_2(H_2O)_2]^{3+}$ in 10^{-3} M hydrochloric acid containing lithium chloride ($[Cl^-] \simeq 7$ M) undergo no apparent change on prolonged standing at room temperature. Addition to such solutions, however, of a little freshly prepared zinc amalgam results in the rapid precipitation of the *cis*-dichlorobis(N – N) chromium(III) complexes under the same conditions.

The catalytic influence of the lower oxidation state species on the acid hydrolysis and anation reactions is, however, not very useful for the study of the chloride-water coordination equilibria, since these species also catalyse equilibration with respect to the heterocyclic N – N ligands themselves, and thereby complicate the issue.[32] Although the aquation-anation equilibria are established much faster in the absence of a catalyst than the equilibria involving the N – N ligands, the two types of reactions take place simultaneously when the lower oxidation state catalysts are present.

IV. CHEMICAL CORRELATIONS AND DISCUSSION OF CONFIGURATION IN BIS(N – N)CHROMIUM(III) COMPLEXES

The classical demonstration of *cis*-configuration, which in the chemistry of chromium(III) has always been confirmed by subsequent work, is the chemical correlation with the corresponding oxalato or di-μ-hydroxo ("diol") complexes. For example, Pfeiffer *et al.*[56] treated

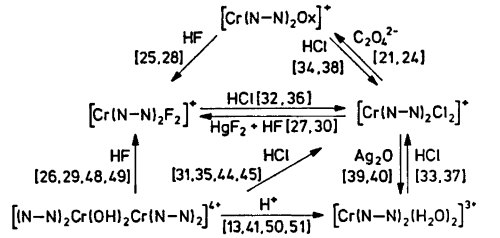

Fig. 2. Chemical interconversions of bis(N – N) chromium(III) complexes. The numbers in square brackets refer to the preparations in section II B.

Table 2. Spectral data characterising the compounds.

Complex ion	Ref.	λ_{max}	λ_{min}	λ_{sh}	ε_{max}	ε_{min}	ε_{sh}	$\varepsilon_{min}/\varepsilon_{max}$ [a]	$\varepsilon_{min}/\lambda_{sh}$	Medium
cis-$[Cr(bipy)_2Cl_2]^+$	prep. 1a	553	474	445	43.7	18.9	90.0	0.433	0.210	H_2O or 0.1 M HCl
cis-$[Cr(bipy)_2Cl_2]^+$	prep. 1a	572	488		47.3	24.0		0.507		DMF
cis-$[Cr(phen)_2Cl_2]^+$	25	558	478		40.1	17.5		0.437		H_2O or 0.1 M HCl
cis-$[Cr(phen)_2Cl_2]^+$	25	578	492		42.5	22.8		0.537		DMF
cis-$[Co(bipy)_2Cl_2]^+$	prep. 8	538	458		57.8	18.1				10^{-3} M HCl
cis-$[Co(phen)_2Cl_2]^+$	prep. 9	542	472		56.6	23.6		0.416		10^{-3} M HCl
cis-$[Cr(bipy)_2(H_2O)_2]^{3+}$ [b]	prep. 13	492	468		44.8	39.2		0.875		0.1 M $HClO_4$
		448	442		94.2	89.2		0.947		
cis-$[Cr(phen)_2(H_2O)_2]^{3+}$	prep. 15	496	458		43.7	29.4		0.673		0.1 M HNO_3
cis-$[Cr(bipy)_2(OH)_2]^+$	prep. 13	517	465	440	42.0	35.1	69.7			0.1 M NaOH
				424			160			
cis-$[Cr(phen)_2(OH)_2]^+$	prep. 15	519	468		41.5	34.8				0.1 M NaOH
cis-$[Co(bipy)_2(H_2O)_2]^{3+}$	prep. 14	489	428		60.7	25.2				0.1 M $HClO_4$
cis-$[Co(phen)_2(H_2O)_2]^{3+}$	prep. 16a	496	448		62.2	41.9				0.1 M HCl
cis-$[Co(bipy)_2(OH)_2]^+$	prep. 14	505	441		73.8	33.4				0.1 M NaOH
cis-$[Co(phen)_2(OH)_2]^+$	prep. 16a	512	447		74.5	32.0				0.1 M NaOH
cis-$[Cr(phen)_2(H_2O)Cl]^{2+}$	prep. 19	522	461		41.2	17.0				0.1 M HNO_3
cis-$[Co(phen)_2(H_2O)Cl]^{2+}$	prep. 20	520	462		59	31		0.525		0.1 M HNO_3
cis-$[Cr(bipy)_2F_2]^+$	24	519	461		48.6	22.0		0.452		H_2O
		443			57.3			0.384		
		415			144					
cis-$[Cr(phen)_2F_2]^+$	24	522	455	420	46.5	16.6	69.2	0.357	0.240	H_2O
cis-$[Co(phen)_2Cl_2]_2$-$[CoCl_4].2H_2O$	prep. 11a	693	678		655	585				nitromethane
		667	648		613	407				
		633	598		489	258				
		589	477		209	64				
$[Cr(bipy)_2ox]^+$	prep. 21	497	464	448	66.5	48.7	90.4	0.732		H_2O
				417			220			
$[Cr(phen)_2ox]^+$	prep. 24	501	454		62.6	33.0				H_2O

[a] When ratios between molar absorptivities are given, ε for the first minimum is always measured relative to ε for the first maximum and eventually, where applicable, relative to ε for the second maximum (or shoulder). [b] Data in the second line here are not included in any identifying spectral data for this complex (see prep. 39 and 50).

$[Cr(en)_2ox]^+$ salts with concentrated hydrochloric acid at 40 °C and isolated a violet *cis*-dichloro salt. By treatment of the latter with oxalate ions they were then able to regenerate the initial cation, but this was not possible with the green *trans*-dichloro complex. Correlations of this type have been established [6] for bis(bipy) and bis(phen) chromium(III) complexes of the types $[Cr(N-N)_2F_2]^+$, $[Cr(N-N)_2Cl_2]^+$ and $[Cr(N-N)_2(H_2)O)_2]^{3+}$ and the interconvertibility of these mononuclear complexes has, in general, been demonstrated. The interconversion reaction scheme is shown in Fig. 2, with numbers referring to the preparations in the Experimental (section II B). All the conversions have been performed in satisfactory yield, thereby demonstrating that the isolated species at least comprise the major reaction products.

A number of different preparative routes to the dichloro complexes exist in the literature (see references in section II B). These have all been put to the test and it has been shown that they all give a single, identical, dichlorobis-(N-N)chromium(III) complex ion. The same is true for the diaqua and difluoro complexes. The method of identification of reaction products has, in addition to chemical analysis, been the measurement of the visible absorption spectrum under specified conditions.

The ligand-field spectra of complexes of the type $[M(N-N)_2X_2]^{n+}$ (M = Cr or Co) (Table 2)

Table 3. Chiroptical data for optically active bis(N—N) chromium(III) complexes.

Complex	Prep. No.	Solvent	[Complex][a] for [M] and CD	$[M]_{589}^{25}$	Absorption λ_{max}	Absorption ε_{max}	Circular dichroism λ_{CD}	Circular dichroism $\Delta\varepsilon_{CD}$
$(-)_{589}$-$[Cr(bipy)_2OH]_2(ClO_4)_4.2H_2O$	42							
crop B1			1.539×10^{-3}	−9 510			not measured	
crop B2			1.992×10^{-3}[b]	−9 528			615	+0.18
		10^{-3} M HCl			537[f]	106.2	518	−6.62
					447	158.0	402	+0.79[c]
$(+)_{589}$-$[Cr(bipy)_2OH]_2(ClO_4)_4.2H_2O$	42							
crop B4			1.568×10^{-3}	+9 464			615	−0.19
							518	+6.65
							402	−1.29[c]
$(-)_{589}$-$[Cr(phen)_2OH]_2(ClO_4)_4.3H_2O$	43							
crop B1			2.193×10^{-3}[d]	−14 080			529	−6.89
							409	+1.18
crop B2		nitro-methane	1.669×10^{-3}	−14 120	540[g]	114	529	−7.13
					422(sh)	303	409	+1.17
$(+)_{589}$-$[Cr(phen)_2OH]_2(ClO_4)_4.3H_2O$	43							
crop B4			1.554×10^{-3}	+14 080			528	+7.10
							409	−1.16
$(-)_{589}$-*cis*-$[Cr(bipy)_2Cl_2]ClO_4.\frac{1}{2}H_2O$	44	DMF	3.848×10^{-3}	−3 412	572[h]	47.3	607	+0.79
							530	−0.45
							452	+0.43
$(-)_{589}$-*cis*-$[Cr(phen)_2Cl_2]ClO_4$	45	DMF	4.618×10^{-3}	−6 676	578[h]	43.2	612	+1.12
					420(sh)	178	533	−0.78
							453	+0.42
$(-)_{589}$-*cis*-$[Cr(bipy)_2Br_2]Br.HBr.3H_2O$	46	H_2O	5.055×10^{-3}	−2 820	574[h]	52.7	600	+0.76
					518	45.6	522	−0.36
					445(sh)	132	427	−0.27
$(-)_{589}$-*cis*-$[Cr(phen)_2Br_2]ClO_4$	47	DMF	5.221×10^{-3}	−6 863	598[h]	49.8	622	+1.17
					522	42.8	541	−0.65
					421(sh)	227	521(sh)	−0.56
							470	+0.13
$(-)_{589}$-*cis*-$[Cr(phen)_2F_2]ClO$	49	H_2O	6.280×10^{-3}	−3 207	522	46.5[i]	565	+1.15
					420(sh)	69.2	494	−1.33
							415	+0.22
$(-)_{589}$-*cis*-$[Cr(bipy)_2(H_2O)_2]^{3+}$[e]	50	0.1 M HCl	8.240×10^{-3}	−1 510	492	44.8	523	+0.42
					448	94.2	464	−0.68
							420(sh)	−0.27
$(-)_{589}$-*cis*-$[Cr(phen)_2(H_2O)_2]^{3+}$[e]	51	0.1 M HCl	5.910×10^{-3}	−3 460	496	43.7	574	−0.04
					422(sh)	141	531	+0.07
							475	−0.80
							428(sh)	−0.30

[a] In mol litre^{-1}, determined from molar absorptivity of longest wavelength absorption band, unless otherwise stated. [b] Concentration for CD = 2.095×10^{-3} M. [c] $\Delta\varepsilon_{CD}$ value not very accurate because of large slit-width. [d] Concentration for CD = 0.975×10^{-3} M. [e] Solution of aquahydroxo complex, as perchlorate salt, in 0.1 M HCl. [f] Spectrum taken from Ref. 25. [g] Spectrum measured for sample of crop B1. [h] Spectrum measured for this sample. [i] ε_{max} values from Ref. 24.

with a particular ligand X are so similar that one may safely conclude that each set of four complexes have the same configuration. Furthermore, there is a conspicuous system in the relationship between these spectra and those of the corresponding *cis*- and *trans*-bis(ethylenediamine) complexes as far as the first spin-allowed cubic parentage ligand-field transition is concerned,[8] although the second transition of this type is masked in the bis(N—N) com-

plexes. This observation can, on the basis of Yamada's and Tsuchida's empirical concept of hyperchromism/hypochromism,[57] be used to assign the configuration of the bis(N−N) complexes.

We have found [8] that the first spin-allowed ligand-field bands of the bis(N−N) complexes of chromium(III) and cobalt(III) which unquestionably have the *cis*-configuration, *i.e.* the chromium(III) diols, the carbonato complexes of cobalt(III), and the oxalato complexes of both metals, all exhibit lower molar absorptivities than those of the corresponding *cis*-bis(ethylenediamine) complexes, and we conclude that both N−N ligands are hypochromic relative to ethylenediamine. When the molar absorptivities of the first spin-allowed ligand-field bands of our other bis(N−N) chromium(III) and cobalt(III) complexes are compared [8] with those of the corresponding *cis*- and *trans*-bis(ethylenediamine) complexes it is found that this hypochromism of the N−N ligands relative to ethylenediamine is borne out for the *cis*-configuration but not for the *trans*.

A more sophisticated classical "proof" of the *cis*-configuration of such octahedral complexes would be their resolution into optical enantiomers. However, in the systems under discussion, such a resolution does not, in itself, constitute irrefutable evidence for the *cis*-configuration, since a slight out-of-plane twist, relative to one another, of the two N−N ligands in a distorted (hypothetical) *trans*-bis(N−N) complex would produce the symmetry properties necessary for the existence of enantiomeric forms. Amongst bis(N−N) complexes of chromium(III) and cobalt(III), a direct resolution into enantiomers has been reported for the chromium(III) diols [58,59] and for the complexes $[M(N-N)_2ox]^+$ (M = Cr or Co).[38,59,60] Another publication [61] also reports the resolution of $[M(bipy)_2Cl_2]^+$ (M = Cr or Co) and $[Cr(phen)_2Cl_2]^+$, but gives no quantitative data. The optically active diols were further cleaved with dilute nitric acid to give the optically active diaqua complexes, but no detailed procedures or data were given.[58]

In the present work, as well as studying the cleavage of the racemic bipy and phen diols, we have re-examined their resolution and studied the cleavage, by concentrated hydrochloric, hydrobromic and perchloric acids and by liquid hydrogen fluoride, of their $(-)_{589}$ enantiomers, giving the $(-)_{589}$ enantiomers of the *cis*-dichloro-, dibromo- and diaquabis(N−N)chromium(III) and the *cis*-difluorobis(phen)chromium(III) mononuclear complexes (we were unable to prepare optically active difluorobis(bipy)chromium(III) by this method). The circular dichroism and optical rotation data in the visible region for the optically active complexes obtained in this work are reported in Table 3. The CD and rotation data for the bipy diol indicate a comparable degree of resolution to that reported earlier [58,59,62] and from other observations we believe that essentially complete resolution of both the bipy and phen diols has been effected (see Experimental, section II B). Since the configuration of the heterocyclic ligands in the diols is *cis*,[25,63] the chemical identity of the cleavage products with complexes of the same formulation obtained by other preparative routes provides very strong evidence for the *cis*-configuration of the ligands in bis(N−N)chromium(III) complexes.

Thus, when the above conclusions concerning the configuration of bis(N−N) chromium(III) and cobalt(III) complexes are taken together with the results of our X-ray powder photograph studies [7] on bis(N−N) M(III) complexes (M = Cr, Co, Rh, or Ir) and with the results of previous X-ray structure analyses of $[Co(bipy)_2Cl_2]_2[CoCl_4]$ [44] and $[Co(phen)_2Cl_2]Cl.3H_2O$,[64] the combined conclusions are readily seen to be complementary and to provide extremely strong evidence for the generality of the *cis*-configuration of bis(N−N) complexes of these four trivalent metals, both in the solid state and in solution.

Acknowledgement. One of us (M.P.H.) is very grateful to the Royal Society for the award of a European Exchange Programme Research Fellowship.

REFERENCES

1. Brandt, W. W., Dwyer, F. P. and Gyarfas, E. C. *Chem. Rev. 54* (1954) 959.
2. McWhinnie, W. R. and Miller, J. D. *Advan. Inorg. Chem. Radiochem. 12* (1969) 135.
3. Jaeger, F. M. and van Dijk, J. A. *Z. Anorg. Allg. Chem. 227* (1936) 311.
4. Pfeiffer, P. and Werdelmann, B. *Z. Anorg. Allg. Chem. 263* (1950) 31.

5. Josephsen, J. and Schäffer, C. E. 13.ende Nordiske Kemikermøde, København 1968, p. 58.
6. Andersen, P., Josephsen, J., Nord (Waind), G., Schäffer, C. E. and Tranter, R. L. *Chem. Commun.* (1969) 408.
7. Andersen, P. and Josephsen, J. *Acta Chem. Scand. 25* (1971) 3255.
8. Josephsen, J. and Schäffer, C. E. *To be published.*
9. McKenzie, E. D. *Coord. Chem. Rev. 6* (1971) 187.
10. Morgan, G. T. and Burstall, F. H. *J. Chem. Soc.* (1934) 965.
11. Livingstone, S. E. *J. Proc. Roy. Soc., N. S. Wales 85* (1951) 151; *86* (1952) 32.
12. Parthasarathy, V. and Jørgensen, C. K. *Chimia 29* (1975) 210.
13. Nord, G. *Acta Chem. Scand. A 29* (1975) 270.
14. Rund, J. V. *Inorg. Chem. 7* (1968) 24.
15. (a) Cartey, A. J. and Chieh, P. C. *Chem. Commun.* (1972) 158. (b) Chieh, P. C. *J. Chem. Soc. Dalton Trans.* (1972) 1643.
16. Hinamoto, M., Ooi, S. and Kuroya, H. *Chem. Commun.* (1972) 356.
17. Jørgensen, C. K. *Acta Chem. Scand. 9* (1955) 1362.
18. Barclay, G. A., Hoskins, B. F. and Kennard, C. H. L. *J. Chem. Soc.* (1963) 5691.
19. Procter, I. M. and Stephens, F. S. *J. Chem. Soc. A* (1969) 1248.
20. Nakai, H., Ooi, S. and Kuroya, H. *Bull. Chem. Soc. Jap. 43* (1970) 577.
21. Nakai, H. *Bull. Chem. Soc. Jap. 44* (1971) 2412.
22. Stephens, F. S. *J. Chem. Soc. Dalton Trans.* (1972) 1350.
23. Figgis, B. N. and Nyholm, R. S. *J. Chem. Soc.* (1958) 4190.
24. Glerup, J., Josephsen, J., Michelsen, K., Pedersen, E. and Schäffer, C. E. *Acta Chem. Scand. 24* (1970) 247.
25. Josephsen, J. and Schäffer, C. E. *Acta Chem. Scand. 24* (1970) 2929.
26. Burstall, F. H. and Nyholm, R. S. *J. Chem. Soc.* (1952) 3570.
27. Bayazitova, E. A., Zelentsov, V. V. and Spitsyn, V. I. *Russ. J. Inorg. Chem. 13* (1968) 249.
28. Gibson, J. G. and McKenzie, E. D. *J. Chem. Soc. A* (1969) 2637.
29. Baker, W. A. and Phillips, M. G. *Inorg. Chem. 4* (1965) 915.
30. Glerup, J. and Schäffer, C. E. *To be published.*
31. Ablov, A. V. *Russ. J. Inorg. Chem. 6* (1961) 157.
32. Josephsen, J. and Schäffer, C. E. *Chem. Commun.* (1970) 61.
33. Miller, J. D. and Prince, R. H. *J. Chem. Soc. A* (1969) 519.
34. Josephsen, J. and Schäffer, C. E. *Acta Chem. Scand. 23* (1969) 2206.
35. (a) Figgis, B. N. and Lewis, J. In *Modern Coordination Chemistry*, Interscience, New York 1960, 403. (b) Griffith, J. S. *The Theory of Transition Metal Ions*, Cambridge Univ. Press, London 1964, 279.
36. Inskeep, R. G. and Bjerrum, J. *Acta Chem. Scand. 15* (1961) 62.
37. Ablov, A. V. and Palade, D. M. *Russ. J. Inorg. Chem. 6* (1961) 567.
38. Broomhead, J. A., Dwyer, M. and Kane-Maguire, N. *Inorg. Chem. 7* (1968) 1388.
39. Inskeep, R. G. and Benson, M. *J. Inorg. Nucl. Chem. 20* (1961) 290.
40. Wolcott, D. and Hunt, J. B. *Inorg. Chem. 7* (1968) 755.
41. Negoiu, D., Panait, C. and Marica, M. *An. Univ. Bucaresti, Ser. Stiint Natur. Chim. 16* (1967) 115.
42. Gibson, J. G. and McKenzie, E. D. *Inorg. Nucl. Chem. Lett. 5* (1969) 683.
43. Gibson, J. G., Laird, R. and McKenzie, E. D. *J. Chem. Soc. A* (1969) 2089.
44. Hinamoto, M., Ooi, S. and Kuroya, H. *Bull. Chem. Soc. Jap. 44* (1971) 58.
45. Varian Catalogue of NMR Spectra 1963.
46. Pearson, R. G., Boston, C. R. and Basolo, F. *J. Amer. Chem. Soc. 75* (1953) 3089.
47. Vlček, A. A. *Inorg. Chem. 6* (1967) 1425.
48. Farina, R. and Wilkins, R. G. *Inorg. Chem. 7* (1968) 514.
49. Pearson, R. G., Meeker, R. E. and Basolo, F. *J. Inorg. Nucl. Chem. 1* (1955) 341.
50. Ablov, A. V. and Palade, D. M. *Russ. J. Inorg. Chem. 6* (1961) 306.
51. Yamasaki, K. *Bull. Chem. Soc. Jap. 13* (1938) 538.
52. McDonald, D. J. and Garner, C. S. *J. Amer. Chem. Soc. 83* (1961) 4152.
53. Nord, G. and Wernberg, O. *J. Chem. Soc. Dalton Trans.* (1972) 866.
54. Duffy, N. V. and Earley, J. E. *J. Amer. Chem. Soc. 89* (1967) 272.
55. Taube, H. *J. Amer. Chem. Soc. 82* (1960) 524.
56. Pfeiffer, P., Koch, P., Lando, T. G. and Trieschmann, A. *Ber. Deut. Chem. Ges. 37* (1904) 4255.
57. Yamada, S. and Tsuchida, R. *Bull. Chem. Soc. Jap. 26* (1953) 15.
58. Mason, S. F. and Wood, J. W. *Chem. Commun.* (1968) 1512.
59. Kaizaki, S., Hidaka, J. and Shimura, Y. *Inorg. Chem. 12* (1973) 135.
60. Ferguson, J., Hawkins, C. J., Kane-Maguire, N. A. P. and Lip, H. *Inorg. Chem. 8* (1969) 771.
61. Broomhead, J. A. and Grumley, W. *Inorg. Chem. 10* (1971) 2002.
62. Mason, S. F. *Inorg. Chim. Acta Rev. 2* (1968) 89.
63. Veal, J. T., Hatfield, W. E. and Hodgson, D. J. *Acta Crystallogr. B 29* (1973) 12.
64. Ablov, A. V., Kon, A. Yu. and Malinovski, T. I. *Proc. Akad. Sci. (USSR) 167* (1966) 410.

Received July 10, 1975.

Acta Chemica Scandinavica A 30 (1976) 98—102

A Calorimetric Study of the Relative Strain Enthalpies in Some *C*-Methyl-substituted Tris(ethylenediamine)cobalt(III) Complexes

SVEN BAGGER, OLE BANG and FLEMMING WOLDBYE

Chemistry Department A, The Technical University of Denmark, Building 207, DK-2800 Lyngby, Denmark

Strain enthalpies for a series of complexes have been determined from calorimetric measurements of decomposition reactions with sodium sulfide in aqueous solution. The experimental data are correlated with the stereochemistry of the complexes and are compared with some theoretical results from the literature.

In recent decades metal complexes with chelate rings have been extensively studied by application of the methods of conformational analysis.[1]

One chief objective for these studies has been to evaluate the relative strain energies of geometrical and conformational isomers of octahedral complexes with three diamine ligands.

The concept of strain in a molecule has a long history in chemistry [2] and although its definition is rather vague it has proved to be very useful.

In theoretical approaches the strain energy (or conformational energy) is often treated as a sum of four potentials, representing bond length distortion strain, bond angle distortion strain ("Baeyer strain"), torsional energy of rotation about bonds ("Pitzer strain"), and nonbonded interactions.

Energy differences obtained from such calculations, where entropy is not taken into account, may be equated with enthalpy differences, ΔH, since at constant pressure, P,

$$\Delta H = \Delta E + P\Delta V \simeq \Delta E$$

where ΔV, the volume change between isomers, normally is considered to be negligible.

In the present experimental approach we have attempted to obtain the relative strain enthalpies of some tris(diamine)cobalt(III) complexes by calorimetry.

We have looked at the effect of *C*-methyl-substitution in the five-membered chelate rings of 1,2-ethanediamine, a theme which has been treated theoretically in a recent paper from our laboratory.[3]

NOMENCLATURE

The diamine ligands used are abbreviated as follows: 1,2-ethane-diamine (or ethylenediamine) = en, $(-)_D$-(*R*,*R*)-1,2-dimethyl-1,2-ethanediamine (or *l*-butanediamine) = lbn, (*R*,*S*)-1,2-dimethyl-1,2-ethanediamine (or *meso*-butanediamine) = mbn, and 1,1-dimethyl-1,2-ethanediamine (or isobutanediamine) = ibn.

An unspecified diamine is designated by aa. For simplicity the complexes are sometimes referred to by the numbers I—X (see Table 2).

The Greek letters Δ, Λ, δ, and λ are used to specify configurations and conformations as recommended by IUPAC;[4] ξ is used instead of δ and λ if the ring conformation is unspecified.

A five-membered ring in an octahedral tris(diamine) complex is puckered and may have its C—C axis either almost para*llel* or *ob*lique relative to the C_3-axis (or pseudo C_3-axis) of the complex; these two situations are denoted *lel* and *ob*.[5] A *C*-methyl-substituent in the ring may be either equatorially or axially oriented, and these two possibilities are indicated by *eq* and *ax*.

METHOD

The experimental basis of the method employed was in part adopted from the literature.[6—8] It amounts to measuring the heat of reaction for the decomposition of the amine

complexes by excess sodium sulfide in aqueous solution.

If a solution of $[Co(aa)_3]Cl_3$ is added to a solution of Na_2S, the complex ion will decompose quantitatively in a reaction with the following stoichiometry

$$[Co(aa)_3]Cl_3 + \tfrac{3}{2}Na_2S \rightarrow \tfrac{1}{2}Co_2S_3(s) + 3aa + 3NaCl$$

We have determined ΔH for such reactions by calorimetry at 25.0 °C.

The experimental ΔH-values, ΔH_{exp}, for the tris(diamine) complexes I–X are taken as indications of their relative strain enthalpies.

For lack of an obvious, "strainfree" reference molecule we have chosen to normalize our results relative to $[Co(en)_3]^{3+}$ by defining a strain parameter, H_{strain}, as

$$H_{strain} \equiv \{\Delta H_{exp} \text{ for } [Co(en)_3]^{3+}\} - \{\Delta H_{exp} \text{ for } [Co(aa)_3]^{3+}\}$$

This means that H_{strain} equals ΔH for the hypothetical process

$$[Co(en)_3]_{aq}^{3+} + 3aa_{aq} \rightarrow [Co(aa)_3]_{aq}^{3+} + 3en_{aq}$$

in dilute aqueous solution.

Evidently, H_{strain} includes differences in solvation enthalpies in addition to the differences in strain enthalpy. But in the interpretation of our results we have assumed solvational differences to be negligible. Recent experimental results [9] support the validity of this approximation if the argument is restricted to 1,2-ethanediamine and its *C*-alkyl-substituted derivatives.

EXPERIMENTAL

Calorimeter. The calorimeter used (Type 8721-1 from LKB-Instruments, Sweden) is of the constant environment-temperature type, designed for work at atmospheric pressure. It has a thin-walled 100 ml Pyrex glass reaction vessel with a built-in thermistor as temperature sensor. A gold stirrer also serves as a holder for a 1 ml cylindrical ampoule. The breaking of the ampoule against a sapphire-tipped rod is accomplished by activating a motor-driven mechanism. The reaction vessel is contained in a chromium plated brass case which is submerged in a water thermostat with a temperature constancy better than 10^{-3} K.

Temperature *vs.* time curves were registered by a Beckman ten-inch potentiometric recorder (Full scale deflection 0.15 K; reading accuracy $\pm 6 \times 10^{-4}$ K).

Calibrations were performed on the system after each reaction using a built-in electrical heater.

In order to check the experimental uncertainty of the set-up, the heat of solution of a recommended [10] test substance, tris(hydroxymethyl)aminomethane (200 mg in 100 ml 0.1 M HCl), was determined at 25.0 °C. The result from five runs was 29.68 ± 0.10 kJ mol^{-1} to be compared with the very accurately determined value [10] of 29.70 ± 0.025 kJ mol^{-1}.

Thermochemical experiments. The quantity ΔH_{exp} at 25.0 °C for a certain complex, $[Co(aa)_3]Cl_3$, was determined in two steps from a molar reaction enthalpy, ΔH_1, and a molar solution enthalpy, ΔH_2.

$$\underset{8 \times 10^{-1}\,M}{[Co(aa)_3]^{3+}} + \tfrac{3}{2}S^{2-} \rightarrow \tfrac{1}{2}Co_2S_3(s) + \underset{3 \times 8 \times 10^{-3}\,M}{3aa} \qquad \Delta H_1$$

$$\underset{8 \times 10^{-1}\,M}{[Co(aa)_3]^{3+}} \rightarrow \underset{8 \times 10^{-3}\,M}{[Co(aa)_3]^{3+}} \qquad \Delta H_2$$

$$\underset{8 \times 10^{-3}\,M}{[Co(aa)_3]^{3+}} + \tfrac{3}{2}S^{2-} \rightarrow \tfrac{1}{2}Co_2S_3(s) + \underset{3 \times 8 \times 10^{-3}\,M}{3aa} \qquad \Delta H_{exp}$$

$$\Delta H_{exp} = \Delta H_1 - \Delta H_2$$

For determinations of ΔH_1 and ΔH_2 the ampoule always contained 0.8 mmol accurately weighed complex chloride in 1 ml aqueous solution. The reaction vessel was filled with 100 ml 80 mM aqueous Na_2S to obtain ΔH_1, and with 100 ml H_2O to obtain ΔH_2.

It was checked by spectrophotometry that the decomposition was quantitative under the conditions used.

Some typical temperature curves for sulfide reactions are presented in Fig. 1. The temperature change was evaluated by a graphical procedure based on "Dickinson's method".[11]

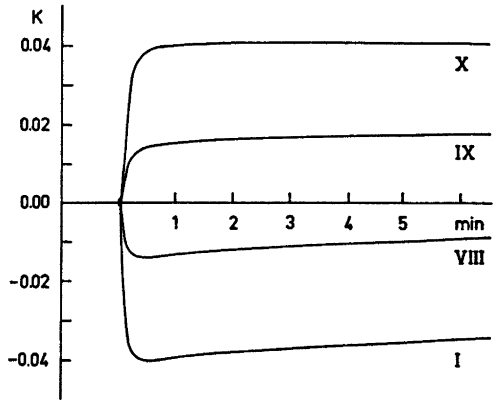

Fig. 1. Temperature *vs.* time curves for the sulfide reactions of complexes I, VIII, IX, and X.

Table 1.

		Molecular weight (see text)	ΔH_1 kJ mol^{-1}	ΔH_2 kJ mol^{-1}
I	*rac*-$[Co(en)_3]^{3+}$	409	21.51 21.63 21.30 21.63	3.10 3.10
II	Δ-$[Co(en)_2(lbn)]^{3+}$	387	22.05 21.76	2.38
III	Δ-$[Co(en)(lbn)_2]^{3+}$	432	25.94 26.23	2.13
IV	Δ-$[Co(lbn)_3]^{3+}$	448	24.35 24.60	1.13
V	*rac*-$[Co(en)_2(mbn)]^{3+}$	399	12.43 12.22	3.18
VI	*rac*-$[Co(en)(mbn)_2]^{3+}$	415	5.56 5.86	3.93
VII	*rac*-$[Co(mbn)_3]^{3+}$	457	0.62 0.59	3.10
VIII	*rac*-$[Co(en)_2(ibn)]^{3+}$	382	7.07 7.47	2.75
IX	*rac*-$[Co(en)(ibn)_2]^{3+}$	437	−7.91 −7.82	2.59
X	*rac*-$[Co(ibn)_3]^{3+}$	499	−20.83 −20.92	1.80

The results from determinations of ΔH_1 and ΔH_2 are given in Table 1.

Preparation of complexes. The complexes were prepared in aqueous solution by aerial oxidation of $CoCl_2 \cdot 6H_2O$, the pertinent amine(s), and HCl (molar ratio 1:3:1) in the presence of active charcoal.

Purification and separation was carried out by descending paper chromatography using Whatman 3 MM paper with a mixture of water saturated butanol and butylchloride (98 vol %:2 vol %) as eluent.

The general procedure has previously been described in more detail.[12]

Analyses. The molecular weights of the chlorides, $[Co(aa)_3]Cl_3.nH_2O$, given in Table 1 were obtained from cobalt analyses on the samples actually used in the calorimetric experiments. These determinations were performed in the following way. The complexes were fumed to dryness with conc. H_2SO_4; after dilution with water cobalt(II) in the resulting clear solutions was determined by addition of excess EDTA and back-titration with zinc(II) following the method of Kiss.[13]

The number of methyl-substituents relative to the number of ring protons was in each case verified by the integrated ^1H NMR spectra.

Description of the samples. All the complexes were isolated as the chlorides, $[Co(aa)_3]Cl_3.nH_2O$.

Samples II, III, and IV each consist of only one geometrical isomer, as defined by their formulae in Table 2.

I, V, and VIII each consist of one Δ/Λ-pair.

VII and X are equilibrium mixtures of the two possible Δ/Λ-pairs. This is illustrated for the ibn case in Fig. 2; the situation is analogous for mbn, where one ring carbon has *R*-configuration and the other has *S*-configuration.

VI and IX are equilibrium mixtures of the three possible Δ/Λ-pairs. See Fig. 3.

Table 2.

		ΔH_{exp} kJ mol^{-1}	H_{strain} kJ mol^{-1}	Number of axial CH_3-groups
I	*rac*-$[Co(en)_3\xi\xi\xi]^{3+}$	18.4	0	0
II	Δ-$[Co(en)_2(lbn)\xi\xi\lambda]^{3+}$	19.5	−1.1	0
III	Δ-$[Co(en)(lbn)_2\xi\lambda\lambda]^{3+}$	24.0	−5.6	0
IV	Δ-$[Co(lbn)_3\lambda\lambda\lambda]^{3+}$	23.4	−5.0	0
V	*rac*-$[Co(en)_2(mbn)\xi\xi\xi]^{3+}$	9.2	9.2	1
VI	*rac*-$[Co(en)(mbn)_2\xi\xi\xi]^{3+}$	1.8	16.6	2
VII	*rac*-$[Co(mbn)_3\xi\xi\xi]^{3+}$	−2.5	20.9	3
VIII	*rac*-$[Co(en)_2(ibn)\xi\xi\xi]^{3+}$	4.5	13.9	1
IX	*rac*-$[Co(en)(ibn)_2\xi\xi\xi]^{3+}$	−10.5	28.9	2
X	*rac*-$[Co(ibn)_3\xi\xi\xi]^{3+}$	−22.7	41.1	3

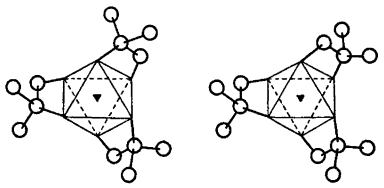

Fig. 2. Possible geometrical isomers of Δ-$[Co(ibn)_3\xi\xi\xi]^{3+}$ (only carbon atoms are shown).

RESULTS AND DISCUSSION

The final results are given in Table 2, and the experimental values of the strain parameter are presented diagrammatically in Fig. 4.

By examination of molecular models it clearly appears that in tris(diamine) complexes with five-membered rings the axial methyl-substituents must be subject to a considerable steric hindrance, which in part is caused by interactions with neighbouring rings. It is also apparent from models that equatorial substituents, which point away from the rest of the molecule, hardly will affect the molecular strain.

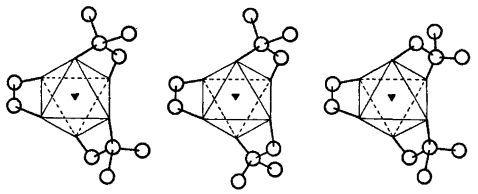

Fig. 3. Possible geometrical isomers of Δ-$[Co(en)(ibn)_2\xi\xi\xi]^{3+}$ (only carbon atoms are shown).

These simple considerations are sufficient to rationalize the main features of the pattern observed in Fig. 4.

In chelate rings with mbn or ibn one methyl group will always adopt axial orientation in λ- as well as δ-conformation (see Table 3), and in accordance with this the molecular strain enthalpy, H_{strain}, increases with increasing number of mbn or ibn ligands.

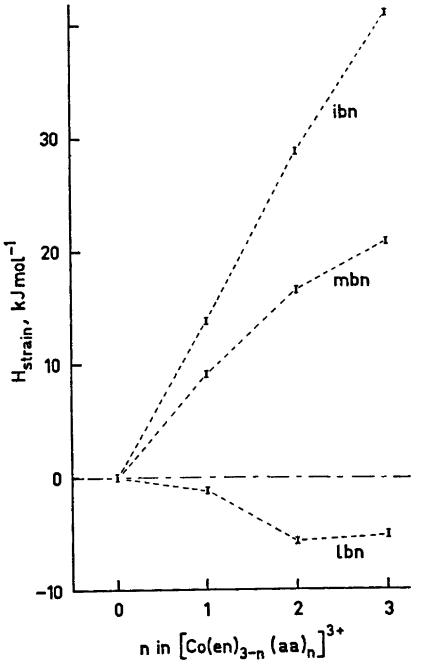

Fig. 4. The experimental strain enthalpies of complexes I−X in diagrammatical representation. Uncertainties are indicated.

Table 3. Key to structures of diamine ligands.

	Δ-configuration	Λ-configuration
δ-conformation		
en	*ob*	*lel*
lbn	*ob*/2 *ax*	*lel*/2 *eq*
mbn	*ob*/1 *eq*, 1 *ax*	*lel*/1 *eq*, 1 *ax*
ibn	*ob*/1 *eq*, 1 *ax*	*lel*/1 *eq*, 1 *ax*
λ-conformation		
en	*lel*	*ob*
lbn	*lel*/2 *eq*	*ob*/2 *ax*
mbn	*lel*/1 *eq*, 1 *ax*	*ob*/1 *eq*, 1 *ax*
ibn	*lel*/1 *eq*, 1 *ax*	*ob*/1 *eq*, 1 *ax*

In the three lbn complexes studied all methyl groups are equatorial; this explains that H_{strain} is close to zero in these cases.

Corey and Bailar [5] stated that in tris(1-methyl-1,2-ethanediamine) complexes the energy difference between a ring conformation with an axial methyl group and a conformation with an equatorial methyl group probably is in excess of 8 kJ mol^{-1} per CH_3-group.

Niketić and Woldbye [3] arrived at 9.2 kJ mol^{-1} per CH_3-group for the *ax*−*eq* difference in lbn complexes.

For comparison the data in Table 2 yields *ca.* 8 kJ mol^{-1} in mbn rings and *ca.* 14 kJ mol^{-1} in ibn rings for the average value of H_{strain} per axial CH_3-group.

So far the experimental results have been discussed in terms of the orientation of methyl groups. For a more detailed analysis differences between *lel* and *ob* conformations should also be taken into account.[1,3]

It is generally accepted that in, *e.g.*, $[Co(en)_3]^{3+}$ a *lel* conformation is energetically favoured relative to an *ob* conformation, and an evaluation by Corey and Bailar [5] led to *ca.* 2.5 kJ mol^{-1} per ring for this *ob-lel* strain enthalpy difference.

Studies by Sudmeier *et al.*[10] indicate that in solution $[Co(en)_3lel_2ob]^{3+}$ is the most abundant form as a result of combined enthalpy and entropy effects. This might explain the fact that the experimental strain enthalpy for $[Co(en)_3]^{3+}$ is found to be higher than for, *e.g.*, $[Co(lbn)_3lel_3]^{3+}$. But it should be noted that equatorial *C*-methyl-substitution in itself may lower the strain enthalpy, as it was shown in a theoretical study of $[CoCl_4(en)]^-$.[15]

In the discussion given here it has been assumed that ring conformations are either λ or δ. Although this assumption may seem reasonable it should be remembered that for the present some intermediate compromise between λ and δ cannot be excluded in all cases.

Acknowledgement. This work has been supported by Statens naturvidenskabelige Forskningsråd.

REFERENCES

1. For detailed treatments and literature references see: a. Buckingham, D. A. and Sargeson, A. M. In Allinger, N. L. and Eliel, E. L., Eds., *Topics in Stereochemistry*, Wiley-Interscience, New York 1971, Vol. 6, p. 219. b. Hawkins, C. J. *Absolute Configuration of Metal Complexes*, Wiley-Interscience, New York 1971. c. Brubaker, G. R. *J. Chem. Educ. 51* (1974) 608.
2. Baeyer, A. *Ber. Deut. Chem. Ges. 18* (1885) 2269.
3. Niketić, S. R. and Woldbye, F. *Acta Chem. Scand. 27* (1973) 3811.
4. *IUPAC Nomenclature of Inorganic Chemistry*, 2nd Ed., Butterworths, London 1971.
5. Corey, E. J. and Bailar, Jr., J. C. *J. Amer. Chem. Soc. 81* (1959) 2620.
6. Lamb, A. B. and Simmons, J. P. *J. Amer. Chem. Soc. 43* (1921) 2188.
7. Ovenston, T. C. J. and Terrey, H. *J. Chem. Soc.* (1936) 1660.
8. Yatsimirskii, K. B. and Pankova, L. L. *Zh. Obshch. Khim. 19* (1949) 617.
9. Bianchini, C., Fabbrizzi, L., Paoletti, P. and Lever, A. B. P. *Inorg. Chem. 14* (1975) 197.
10. Irving, R. J. and Wadsö, I. *Acta Chem. Scand. 18* (1964) 195.
11. Wadsö, I. *Sci. Tools 13* (1966) 33.
12. Bang, O., Engberg, A., Rasmussen, K. and Woldbye, F. *Proc. 3rd Symp. Coord. Chem.*, Akadémiai Kiado, Budapest 1970, p. 63.
13. Kiss, T. A. *Z. Anal. Chem. 208* (1965) 334.
14. Sudmeier, J. L., Blackmer, G. L., Bradley, C. H. and Anet, F. A. L. *J. Amer. Chem. Soc. 94* (1972) 757.
15. DeHayes, L. J. and Busch, D. H. *Inorg. Chem. 12* (1973) 1505.

Received July 7, 1975.

Acta Chemica Scandinavica A 30 (1976) 103—108

The Molecular and Crystal Structure of Tris(1,2-ethanediol)-zinc(II) Sulfate: $[Zn(C_2H_6O_2)_3]SO_4$

BRITT-MARIE ANTTI

Department of Inorganic Chemistry, University of Umeå, S-901 87 Umeå, Sweden

The crystal structure of $[Zn(C_2H_6O_2)_3]SO_4$ has been determined and refined using three-dimensional X-ray diffraction data. The unit cell is orthorhombic, $Ac2a(C_{2v}^{17})$, with $Z=4$ and the following cell parameters: $a=9.544(1)$ Å, $b=14.198(1)$ Å and $c=9.180(1)$ Å. The structure was solved by heavy-atom Patterson and Fourier methods. The refinement using full-matrix least-squares techniques was based on 1364 reflexions and converged at an R-value of 0.042. The structure consists of discrete $[Zn(C_2H_6O_2)_3]^{2+}$-cations and SO_4^{2-}-anions. Zn(II) is octahedrally surrounded by the six glycol oxygens, with a mean Zn—O distance of 2.091 Å. The sulfate ions connect the cations by means of hydrogen bond contacts thus forming a three-dimensional network.

This work forms part of a research program at this department, which aims at elucidating the coordination behaviour of glycol* towards different transition metal ions ($Mn^{2+}-Zn^{2+}$) especially with chloride [1,2] and sulfate as anions. This structure is the fourth in the series with sulfate as anion, the other three being $[Cu(C_2H_6O_2)_3]SO_4$,[3] $[Ni(C_2H_6O_2)_3]SO_4$ and $[Co(C_2H_6O_2)_3]SO_4$.[4]

EXPERIMENTAL

Crystal preparation and analyses. The crystals were prepared by dissolving $ZnSO_4.7H_2O$ in glycol on a water-bath (molar ratio 1:3) and leaving the solution in a desiccator over sulfuric acid. After a few days colourless, thick tabular, hygroscopic crystals separated. The zinc content of the crystals was determined by titration with EDTA [5] to 18.2 (weight-%). Calculated for $[Zn(C_2H_6O_2)_3]SO_4$: 18.6. IR-spectra indicated that no water was present in the structure.

Crystal data and space group. Weissenberg and precession photographs revealed that the crystals were orthorhombic. The cell parameters measured from these photographs were refined using data obtained from a powder film, taken in a camera of Guinier-Hägg type using $CuK\alpha_1$-radiation and Si ($a=5.43054$ Å) as internal standard. The final cell parameters with estimated standard deviations are: $a=9.544(1)$ Å, $b=14.198(1)$ Å and $c=9.180(1)$ Å. The density of the crystals was determined by the flotation method using xylene and bromoform. The experimentally determined density is 1.84 ± 0.01 g cm^{-3} and the calculated value with $Z=4$ is 1.856 g cm^{-3}. The systematic extinctions found (for hkl when $k+l=2n+1$, for $0kl$ when k and $l=2n+1$ and for $hk0$ when $h=2n+1$) are characteristic for the space groups $Ac2a(C_{2v}^{17}$; No. 41) and $Abma(D_{2h}^{18}$; No. 64). In standard setting these space groups are $Aba2$ and $Cmca$ respectively, but in order to label the axes so as to get $c<a<b$, which is consistent with international convention, $Aba2$ was transformed to $Ac2a$ by the matrix $100/00\bar{1}/010$ and $Cmca$ to $Abma$ by the matrix 001/100/010. The general eight-fold positions for $Ac2a$ become: x,y,z; $\bar{x},y,\bar{z}$ $1/2-x,y,$ $1/2+z$; $1/2+x,y,$ $1/2-z$, and A-centering. In $Abma$ a center of symmetry is added to these positions. As $Z=4$ in this structure both Zn and S must be in a fourfold position. The only way this can be achieved with a reasonable Zn-S distance is by choosing the acentric space group $Ac2a$. The correctness of this choice is further supported by the successful refinement and the lack of high correlation coefficients between any of the atoms.

Intensity data. A crystal with the dimensions $0.19\times0.19\times0.19$ mm was mounted in a capillary of Lindeman glass to protect it from moisture. Intensities for $hk0-hk7$ were measured on the automatic diffractometer PAILRED using graphite-monochromated $MoK\alpha$-radiation. During the seventh layer the crystal started to decompose and a new crystal with

* Throughout this paper 1,2-ethanediol will be referred to as glycol.

Table 1a. Atomic positional and vibrational parameters for $[Zn(C_2H_6O_2)_3]SO_4$. All parameters have been multiplied by 10^4. The anisotropic temperature factors have been calculated according to the expression $\exp[-(h^2\beta_{11}+k^2\beta_{22}+l^2\beta_{33}+2hk\beta_{12}+2hl\beta_{13}+2kl\beta_{23})]$. (Standard deviations are given in parentheses.)

	x	y	z	β_{11}	β_{22}	β_{33}	β_{12}	β_{13}	β_{23}
Zn	0	1500	0	41(0.5)	21(0.2)	52(0.7)	0	4(0.6)	0
O(1)	1381(3)	363(3)	88(5)	39(2)	28(1)	129(6)	4(2)	11(3)	1(3)
O(2)	1573(3)	2502(3)	−384(4)	49(3)	24(1)	71(4)	−4(2)	−1(3)	5(2)
O(3)	39(4)	1585(3)	2271(4)	58(2)	34(2)	61(3)	13(2)	3(3)	10(2)
C(1)	725(5)	4497(4)	4686(7)	60(4)	26(2)	104(7)	5(2)	11(4)	−4(3)
C(2)	3236(6)	2700(4)	3089(6)	82(5)	39(3)	80(6)	20(3)	−33(4)	−5(3)
C(3)	3687(6)	1879(5)	2214(6)	90(6)	46(3)	79(6)	23(4)	−28(5)	−12(3)
S	0	4708(1)	0	36(1)	20(0.5)	49(2)	0	−3(1)	0
O(4)	901(3)	4114(3)	921(4)	66(3)	29(1)	57(3)	8(2)	−19(3)	6(2)
O(5)	923(3)	311(3)	4109(5)	50(3)	39(2)	106(5)	−3(2)	2(3)	31(3)

the dimensions $0.20 \times 0.22 \times 0.37$ mm was used to collect the intensities for $hk7-hk12$. Altogether 2552 intensities were measured from the first crystal and 1215 from the second. The intensities were measured by omega-scan. The half scan interval for $hk0$ reflexions was 1.2° for $\theta > 20°$ and 1.7° for $\theta < 20°$ and it was gradually increased to 1.3 and 1.9° ,respectively, for $hk7$ reflexions (first crystal). For the second crystal the intervals were 1.4 and 2.0° for $hk7$ reflexions, the latter being gradually increased to 2.3° for $hk12$ reflexions. Reflexions for which the total number of counts during one scan interval did not exceed 10 000 were remeasured. Background intensities were measured 40 s before and after each scan and the scan speed used was 1°/min.

After Lp- and absorption corrections [μ(MoKα) = 22.17 cm^{-1}] had been applied to all intensities in the two data materials the hkl and $\bar{h}kl$ reflexions were averaged by taking the arithmetic mean value of their respective F^2-values. The intensity data at this stage consisted of two separate sets; I($hk0-hk7$) with 1132 independent intensities and II($hk7-hk12$) with 565 independent intensities. Since the first crystal had started to decompose during the seventh layer and there were large differences between the two $hk7$ layers, that of data I was deleted, leaving 1019 intensities. At the end of the refinements, structure factors for all the unobserved reflexions were calculated and they all had amplitudes lower than the corresponding threshold values. The computer programs used were the same as those described in an earlier paper by the author.[4]

Table 1b. Atomic positional coordinates for the hydrogen atoms. The fractional coordinates have been multiplied by 10^3. An overall temperature factor $B = 4$ Å^2 was used throughout the refinement. (Standard deviations are given in parentheses.)

	x	y	z
H(1)	288(8)	44(6)	475(9)
H(2)	154(8)	291(6)	−6(9)
H(3)	22(9)	119(6)	222(11)
H(4)	85(8)	439(6)	371(10)
H(5)	125(9)	393(6)	500(9)
H(6)	382(7)	327(6)	288(9)
H(7)	235(8)	283(6)	311(8)
H(8)	387(8)	217(6)	129(9)
H(9)	286(7)	131(6)	230(8)

STRUCTURE DETERMINATION AND REFINEMENT

Data I was used to calculate a three-dimensional Patterson synthesis. Both Zn and S were found in the special fourfold position 0,y,0. From subsequent three-dimensional Fourier and difference Fourier syntheses the rest of the non-hydrogen atoms could be located. Least-squares refinements with individual scale factors and the positional coordinates and isotropic thermal factors for all atoms as parameters yielded an R-value of 0.069.

Subsequently an overall scale factor was used in the refinement and data was further reduced by omitting those reflexions for which $\Delta I/I \geq 0.5$[1] which left 891 independent intensities (sin $\theta_{max} = 0.66$). When anisotropic thermal factors for all atoms were introduced, the R-value decreased to 0.044. From a difference Fourier synthesis reasonable positions for the nine hydrogen atoms were found and their positional

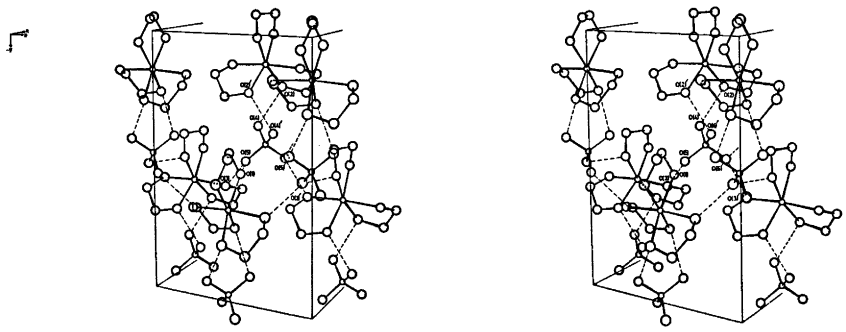

Fig. 1. A stereoscopic view of the molecular packing in $[Zn(C_2H_6O_2)_3]SO_4$. Hydrogen bonds are indicated with dashed lines. For the sake of clarity only one unique repeating unit in the [100]-direction has been illustrated.

coordinates refined. The data sets were then brought together and the refinement continued until convergence at an R-value of 0.043. As the space group is polar and the calculated structure amplitudes include the effect of anomalous scattering, two orientations of the structure had to be considered. In this case it was sufficient to change k to $-k$ in order to change the orientation and the decrease in the conventional R-factor from 0.0432 to 0.0418 (R_w: 0.0508→ 0.0491) is significant with more than 99 % certainty.[6] The scattering curves used for Zn^{2+}, S, O, and C were those proposed by Cromer and Waber [7] and the dispersion correction terms ($\Delta f'$ and $\Delta f''$) for Zn^{2+} and S were selected from Cromer and Lieberman's [8] calculations. For the hydrogen atoms the scattering curve proposed by Stewart *et al.*[9] was used. The weights were calculated according to the relation suggested by Cruickshank [10]

$w = 1/(a + |F_o| + c|F_o|^2 + d|F_o|^3)$ using the constants $a = 250$, $c = -0.02$ and $d = 0.0003$. The final weighted R-value

$$R_w = [\sum w_i(|F_o| - |F_c|)^2 / \sum w_i|F_o|^2]^{\frac{1}{2}} = 0.047.$$

The isotropic temperature factors for the hydrogen atoms were included as parameters for some additional cycles of refinement. Due to the fact that the data set is comprised from two different materials being scaled together, there was no physical significance in the values obtained and they are not published.

In a final difference Fourier synthesis nothing abnormal could be detected. The highest peaks were in the vicinity of Zn and S and there were some additional peaks at the oxygen atoms which possibly could arise from small errors in the scattering factors. The final atomic positional and vibrational parameters are listed in Table 1. The observed and calculated struc-

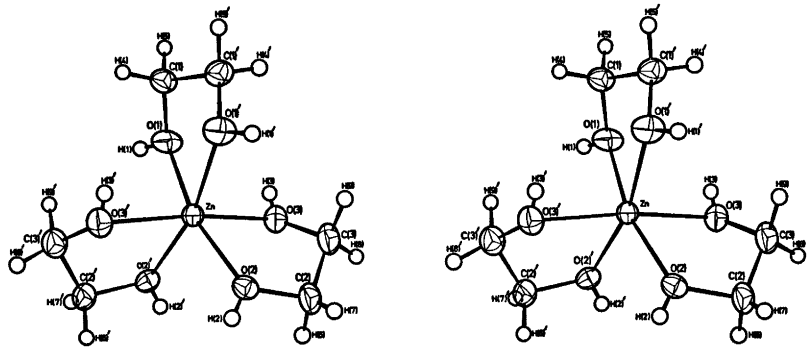

Fig. 2. A stereoscopic illustration of the $[Zn(C_2H_6O_2)_3]^{2+}$-ion. Thermal ellipsoids are scaled to enclose 50 % probability.

Table 2. Dimensions of the $[Zn(C_2H_6O_2)_3]^{2+}$-ion. For the labelling of atoms, see Fig. 2. (Standard deviations are given in parentheses.)

Ligand	Atoms	d_{Zn-O}(Å)	d_{O-C}(Å)	d_{C-C}(Å)	$\angle_{O-C-C}$(°)	$\angle_{Zn-O-C}$(°)
I	Zn(O(1)–C(1))(O(1)′–C(1)′)	2.086(4)	1.428(6)	1.499(10)	107.8(4)	112.3(3)
II, II′	Zn(O(2)–C(2))(O(3)–C(3))	2.099(4) 2.089(3)	1.441(7) 1.436(7)	1.480(9)	109.7(5) 108.2(5)	112.7(3) 109.2(3)

Atoms	Angle(°)	Atoms	Angle (°)
O(1)–Zn–O(1)′	78.6(2)	O(2)–Zn–O(2)′	94.6(2)
O(1)–Zn–O(2)′	94.6(1)	O(2)–Zn–O(3)′	96.7(2)
O(1)–Zn–O(2)	166.1(2)	O(2)–Zn–O(3)	78.8(2)
O(1)–Zn–O(3)	89.7(2)	O(3)–Zn–O(3)′	173.4(2)
O(1)–Zn–O(3)′	95.4(2)		

Atoms	d (Å)	Atoms	Angle (°)	Atoms	Angle (°)
O(1)–H(1)	0.78(8)	Zn–O(1)–H(1)	117(6)	O(3)–C(3)–H(8)	104(5)
O(2)–H(2)	0.65(8)	Zn–O(2)–H(2)	119(7)	O(3)–C(3)–H(9)	111(4)
O(3)–H(3)	0.59(8)	Zn–O(3)–H(3)	83(9)	C(1)′–C(1)–H(4)	120(5)
C(1)–H(4)	0.91(9)	C(1)–O(1)–H(1)	114(6)	C(1)′–C(1)–H(5)	111(5)
C(1)–H(5)	0.99(8)	C(2)–O(2)–H(2)	106(7)	C(3)–C(2)–H(6)	112(4)
C(2)–H(6)	1.00(8)	C(3)–O(3)–H(3)	124(9)	C(3)–C(2)–H(7)	118(5)
C(2)–H(7)	0.86(8)	O(1)–C(1)–H(4)	109(5)	C(2)–C(3)–H(8)	102(5)
C(3)–H(8)	0.96(8)	O(1)–C(1)–H(5)	114(5)	C(2)–C(3)–H(9)	106(4)
C(3)–H(9)	1.15(8)	O(2)–C(2)–H(6)	106(4)	H(4)–C(1)–H(5)	95(7)
		O(2)–C(2)–H(7)	98(5)	H(6)–C(2)–H(7)	112(7)
				H(8)–C(3)–H(9)	124(6)

ture amplitudes can be obtained from the author on request.

DESCRIPTION AND DISCUSSION OF THE STRUCTURE

The structure is built up from discrete $[Zn(C_2H_6O_2)_3]^{2+}$-cations and SO_4^{2-}-anions. The SO_4^{2-}-ions connect the cations by means of hydrogen bonds forming a three-dimensional network as shown in Fig. 1.

The coordination around Zn(II). The six coordinated glycol oxygens form an almost regular octahedron around Zn(II); there are no significant differences between the Zn–O distances which range between 2.086(4) and 2.099(4) Å. This is consistent with what would be expected for an ion with a closed d-shell and six equivalent ligands. The mean Zn–O distance of 2.091 Å agrees well with the Zn–O distances measured in five different octahedral hexaquozinc complexes, where the weighted mean value of $Zn-OH_2$ is 2.099 ± 0.020 Å.[11]

The angular distribution in the octahedron around Zn is not so ideal as in the hexaquo complexes. As glycol acts as a bidentate ligand (see below) the dimensions of the glycol molecules will determine the O–Zn–O angles, which in all the complexes investigated so far fall considerably below 90° (Fig. 2 and Table 2)

The ligands. The glycol molecules have *gauche* conformation with dihedral angles between connected O–C–C planes of 50.7 and 48.2° for ligands I and II(II′), respectively. (For the

labelling of ligands, see Table 2). Because of the twofold rotation axis, ligand I possesses C_2-symmetry and ligands II and II′ are symmetry-related. As a consequence the carbon atoms in ligand I are situated at equal distances above and below the Zn – O – O plane, 0.330(7) Å, while ligand II shows more unsymmetric behaviour, C(2) being 0.118(6) Å above the Zn – O – O plane and C(3) 0.403(7) Å below it. In the three puckered five-membered $Zn-O_2-C_2$ rings the angles around the oxygen and carbon atoms do not differ significantly from the tetrahedral angle of 109.5° (Table 2). The C – C and C – O distances as well as the O – H and C – H distances in the five-membered rings all agree well with earlier reported values for this kind of complex.[1–4]

Conformational analysis of the $[Zn(C_2H_6O_2)_3]^{2+}$ *ion.* In the $[Zn(C_2H_6O_2)_3]^{2+}$-ion none of the ligands have their C – C bond parallel to the molecular three-fold axis (Fig. 2). Using the terminology derived for tris(ethylenediamine)-metal complexes and discussed by Raymond *et al.*,[12] and later by Hawkins,[13] the conformation for the $[Zn(C_2H_6O_2)_3]^{2+}$-ion thus becomes $\Lambda\lambda\lambda\lambda(-\Delta\delta\delta\delta)$. As the point group is *m2m*, both enantiomorphs Λ and Δ will be present in equal amounts.

In $[Cu(C_2H_6O_2)_3]SO_4$,[3] where one of the ligands has a $\Lambda\lambda$-conformation, this was explained by the fact that this ligand showed shorter hydrogen bond distances to sulfate oxygens than the other two. This is not consistent with the conditions found in this structure, where ligand I shows two hydrogen bond distances of 2.726(5) Å, while the corresponding values for ligand II (II′) are 2.613(6) and 2.661(5) Å, *i.e.* significantly shorter although all three ligands have $\Lambda\lambda$-conformation. In the compound $[Zn(H_2O)]_6$-$SO_4[(NH_4)_2SO_4]$ (Tutton's salt),[14] where the Zn – O distances are comparable to those found in this structure (mean value = 2.105 ± 0.025 Å), the hydrogen bond distances between water oxygens and sulfate oxygens vary between 2.71 and 2.85 Å. A comparison between these values and those found in $[Zn(C_2H_6O_2)_3]SO_4$ reveals that ligand I shows quite normal hydrogen bond distances, while ligand II (II′) is involved in significantly shorter hydrogen bond contacts. Evidently there must be some additional factors besides hydrogen bond contacts that influence the ring conformation, probably molecular packing conditions.

The sulfate group and hydrogen bond contacts. There are no significant differences between the S – O distances which show a mean value of 1.474 Å. The O – S – O angles are in good agreement with the expected value of 109.5°; the largest deviation being 1.9°. The sulfate ions function as connecting groups between the $[Zn(C_2H_6O_2)_3]^{2+}$-cations by means of hydrogen bond contacts. O(4) has one hydrogen bond contact to O(2) with an O···O distance of 2.661(5) Å, and O(5) has hydrogen bond contacts to O(1) and O(3) with the corresponding O···O distances of 2.726(5) and 2.613(6) Å. A complete list of distances and angles within the sulfate ion is presented in Table 3. The bond O(3) – H(3)···O(5) is far from linear, while the other two do not differ significantly from 180°.

Table 3. Dimensions of the sulfate group and hydrogen bond contacts in $[Zn(C_2H_6O_2)_3]SO_4$.

Atoms	d(Å)	Atoms	Angle(°)
S – O(4)	1.471(3)	O(4) – S – O(4)′	110.1(3)
S – O(5)	1.476(4)	O(4) – S – O(5)	107.6(2)
		O(4) – S – O(5)′	111.3(2)
		O(5) – S – O(5)′	109.0(3)

Atoms	d_{O-H}(Å)	$d_{H\cdots O}$(Å)	$d_{O\cdots O}$(Å)	$\angle_{O-H\cdots O}$(°)
O(1) – H(1)···O(5)	0.78(8)	1.96(8)	2.726(5)	166(9)
O(2) – H(2)···O(4)	0.65(8)	2.02(8)	2.661(5)	165(9)
O(3) – H(3)···O(5)	0.59(8)	2.24(9)	2.613(6)	124(11)

Acknowledgements. My sincere thanks are due to Professor Nils Ingri for much valuable advice and for all the facilities placed at my disposal. I also thank Dr. Britt Hedman for many stimulating discussions and for valuable help concerning computational problems. The English of this paper has been corrected by Dr. Michael Sharp. This work forms part of a program supported by the Swedish Natural Science Research Council.

REFERENCES

1. Antti, B.-M. *Acta Chem. Scand. 27* (1973) 3513.
2. Antti, B.-M. *Acta Chem. Scand. A 29* (1975) 76.
3. Antti, B.-M., Lundberg, B. K. S. and Ingri, N. *Acta Chem. Scand. 26* (1972) 3984.
4. Antti B.-M. *Acta Chem. Scand. A 30* (1976) 24.
5. Kolthoff, I. M., Sandell, E. B., Meehan, E. J. and Bruckenstein, S. *Quantitative Chemical Analysis*, 4th Ed. Macmillan, London 1969, p. 744.
6. Hamilton, W. C. *Acta Crystallogr. 18* (1965) 502.
7. Cromer, D. T. and Waber, J. T. *Acta Crystallogr. 18* (1965) 104.
8. Cromer, D. T. and Lieberman, D. *J. Chem. Phys. 53* (1970) 1891.
9. Stewart, R. F., Davidson, E. R. and Simpson, W. T. *J. Chem. Phys. 42* (1965) 3175.
10. Cruickshank, D. W. J. *Computing Methods in Crystallography*, Pergamon, London 1965, p. 114.
11. Ferrari, A., Braibanti, A., Manotti Lanfredi, A. M. and Tiripicchio, A. *Acta Crystallogr. 22* (1967) 240.
12. Raymond, K. N., Corfield, P. W. R. and Ibers, J. A. *Inorg. Chem. 7* (1968) 842.
13. Hawkins, C. J. *Absolute Configuration of Metal Complexes*, Wiley-Interscience, New York 1971, Chapter 3.
14. Montgomery, H. and Lingafelter, E. C. *Acta Crystallogr. 17* (1964) 1295.

Received June 13, 1975.

Acta Chemica Scandinavica A 30 (1976) 109—114

NMR Studies on Cyclic Arsenites. ^{1}H NMR Spectral Analysis and Conformational Studies of 1,3,2-Diazarsolanes, 1,3,2-Oxazarsolanes and 1,3,2-Dioxarsolanes

DAGFINN W. AKSNES, FATHY A. AMER * and KNUT BERGESEN

Department of Chemistry, University of Bergen, Allégaten 70, N-5014 Bergen-Univ., Norway

This paper reports preparation and ^{1}H NMR studies of ten arsolanes of which seven have been fully analyzed in terms of chemical shifts and coupling constants. Approximate values of the ring torsional angles have been obtained by means of the *R*-value method. The NMR data are adequately explained on the basis of rapidly interconverting twist-envelope conformations which, however, show several features of specific steric interactions and favoured conformations.

^{1}H NMR investigations on a series of arsolanes have been reported in preceeding papers.[1–3] The NMR data of these five-membered rings were adequately explained on the basis of rapidly interconverting non-planar conformations. Although the precise conformation adopted by a five-membered ring compound is dependent on the number and nature of substituents,[4] we have observed that the steric requirements of the arsolane ring are as important as those of the substituents. Our previous results [2,3] also demonstrated the tendency of a sulfur atom, as compared to oxygen, to increase the puckering of the ring. Similar observations have also been reported for 1,3,2-dithiaphospholanes,[5] 1,3-dithiolanes,[6,7] and 1,3-oxathiolanes.[8]

Although the ^{1}H NMR spectra of a series of 1,3,2-diazaphopholanes [9] and 1,3,2-oxazaphospholanes [10,11] have been analyzed, no NMR analyses of the analogous arsolanes have been reported. In order to investigate the effect of nitrogen as hetero-atom in arsolanes we have prepared compounds I–V and investigated their ^{1}H spectra.

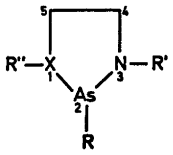

X=N; *1,3,2-diazarsolanes.*
I; R′=R″=CH_3, R= OCH_3
II; R′=R″=CH_3 R=OPh

X=O, R″=lone pair; *1,3,2-oxazarsolanes.*
III; R′=Ph, R=OCH_3
IV; R′=Ph, R=OPh
V; R′=CH_3, R=OCH_3

Trigonal inversion about the nitrogen atom and a possible preference of the substituent at nitrogen for either the one or other side of the ring,[12] complicate the conformational assignment of these systems.

The chloro-compounds (see experimental) have also been prepared. However, only exchange-averaged NMR spectra resulting from rapid exchange of chlorine were observed.

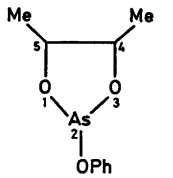

VI; *cis* (4,5-dimethyl)
VII; *trans* (4,5-dimethyl)

* Present address: Department of Chemistry, Faculty of Science, Mansoura University, Mansoura, Egypt.

We have also extended our previous studies on 4,5-dimethyl-1,3,2-dioxarsolanes[1] by analyzing the ^{1}H NMR spectra of VI and VII.

EXPERIMENTAL

The general procedure for the preparation of 2-chloro-1,3-dimethyl-1,3,2-diazarsolane, 2-chloro-3-phenyl-1,3,2-oxazarsolane, and 2-chloro-3-methyl-1,3,2-oxazarsolane as starting materials for the syntheses of I–V is given:[13] A solution of *N*,*N*-dimethyl-ethylenediamine, *N*-phenyl-ethanolamine or *N*-methylaminoethanol in dried diethyl ether was added dropwise, while stirring, to a solution of trichloroarsine and triethylamine in dried diethyl ether. The triethylamine hydrochloride was filtered off and the diethyl ether was removed by rotary evaporation. The oily residue was distilled at reduced pressure in a heated jacket column.

2-Chloro-1,3-dimethyl-1,3,2-diazarsolane, $b.p._{0.5}$ 65 °C, yield 55 %.

2-Chloro-3-phenyl-1,3,2-oxazarsolane, $b.p._{0.5}$ 132 °C, yield 40 %.

2-Chloro-3-methyl-1,3,2-oxazarsolane, $b.p._{0.1}$ 50 °C, yield 45 %.

The 2-methoxy and 2-phenoxy compounds were prepared from the appropriate chloro-compounds and methanol or phenol, respectively, in diethyl ether using triethylamine as base. The yield varied and was at most 40 %. The boiling points (°C) at 0.1 mmHg pressure of compounds I through VII are as follows: 37, 97, 105, 154, 27, 48–50, and 48–50, respectively.

The ^{1}H NMR spectra were examined in benzene, deuteriochloroform, and deuteriochloroform/benzene solutions (*ca.* 50 % v/v). A small amount of TMS was added to the samples and used as internal standard and lock signal source. The 100 MHz spectra were run at ambient probe temperature (*ca.* 30 °C) on a VARIAN HA-100 spectrometer. Line positions were obtained by averaging the results of two frequency-calibrated spectra recorded at 100 Hz sweep width (2 Hz/cm).

The ^{1}H NMR spectra were analyzed by means of the computer programs LAOCN3,[14] UEAITR,[15] and KOMBIP.[16] The computations were performed on a UNIVAC 1110 computer. The graphical output was obtained using a Calcomp Plotter.

SPECTRAL ANALYSIS

The largest chemical shift difference between geminal methylene protons in compounds I and II was achieved by using benzene as solvent. The ^{1}H NMR spectra for the CH_2-CH_2 fragment in I and II show a close resemblance and are symmetrical about their mid-points. The detailed spectral analyses were carried out successfully on the basis of an AA'BB' spin system. The spectrum is most conveniently characterized by linear combinations K, L, M, and N of the four coupling constants.[17] Explicit equations may be given for twelve lines in AA'BB' spectra.[17] If these lines can be recognized $|\nu_A-\nu_B|$, $|L|$, $|M|$, and $|N|$ are directly obtainable from the spectrum. We approached the problem using a mixture of computations and direct assignment. We estimated values of the coupling constants from the literature and assumed that $L=J_{AA'}$

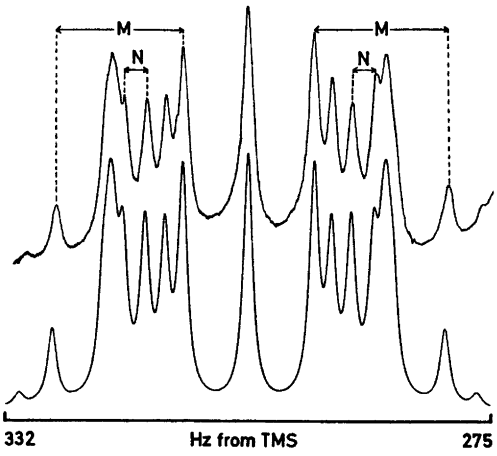

Fig. 1. Experimental (upper trace) and calculated (lower trace) 100 MHz spectrum of the methylene protons in compound I. $N=J_{AB}+J_{AB'}$ and $M=J_{AB}-J_{AB'}$, are directly obtainable from the spectrum when $J_{AA'}=J_{BB'}$.

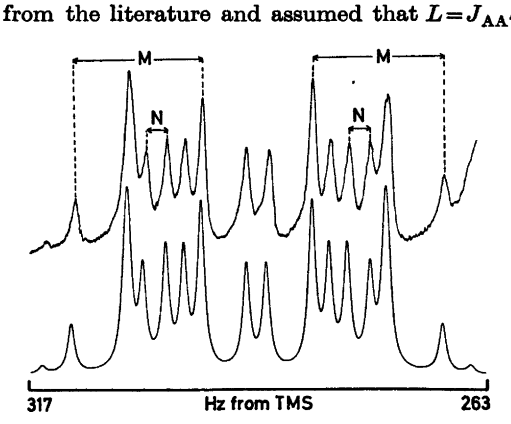

Fig. 2. Experimental (upper trace) and calculated (lower trace) 100 MHz spectrum of the methylene protons in compound II. N and M are defined in Fig. 1.

Table 1. 100 MHz NMR parameters (in Hz) and ring torsional angles of compounds I–VII.[a]

Compound Solvent	I C_6H_6	II	III $C_6H_6/CDCl_3$, 1:1	IV	V	VI $CDCl_3$	VII
ν_A	316.93	301.49	310.22	282.93	318.56	453.97	389.94
ν_B	290.30	277.66	298.95	280.16	291.64		390.93
ν_K			417.18	400.71	448.59	113.86	128.76
ν_L			406.44	393.55	417.73		128.91
$J_{AA'}$	6.00	6.29				5.29	
$J_{BB'}$	5.91	6.21					
J_{AB}	−8.94	−8.97	−9.27	−9.26	−8.72		8.81
$J_{AB'}$	6.35	6.29					
J_{AK}			6.46	6.57	6.17	6.31	5.98
$J_{AK'}$						−0.19	
J_{AL}			2.91	3.07	4.89		−0.17
J_{BK}			5.77	6.23	6.10		−0.19
J_{BL}			9.62	9.53	7.65		5.97
J_{KL}			−9.24	−9.67	−8.88		
Assigned transitions	15	21	28	20	32	151	122
RMS error	0.098	0.096	0.053	0.078	0.061	0.068	0.044
R-value	1.07	1.01	1.85	1.73	1.26		
φ (deg.)	47	45	55	54	49		

[a] Chemical shifts downfield from TMS. K and L represent the $O-CH_2$ or CH_3 protons, as appropriate.

$-J_{BB'}=0$ thereby reducing the number of explicit lines to eight (with degeneracy). We were able to pick out these eight lines after some trial and error analyses, thus providing good values of $|M|$ and $|N|$ directly from the spectrum as shown in Figs. 1 and 2. Once $|N|$ is known $|\nu_A-\nu_B|$ is obtained indirectly from the two N-"doublets". Computations with variation of K then enabled a complete assignment to be made. Computer iteration gave the refined parameters listed in Table 1. Good fits between the observed and calculated spectra were obtained as demonstrated in Figs. 1 and 2.

The ^{1}H NMR spectra of compounds III–V were broad and showed little fine structure when pure benzene or deuteriochloroform were used as solvents. A considerable improvement in the resolution was achieved, however, by using a 1:1 mixture of benzene and deuteriochloroform as solvent.

The methylene protons of compounds III–V give rise to NMR spectra of the ABKL type owing to the relatively large chemical shift differences between the two signal groups. Since the AB region of the spectrum is almost a mirror image of the KL region (Figs. 3 and 4) it follows that $J_{AB}\approx J_{KL}$.

The ABKL spin system can be partially broken down into two ab sub-spectra and two kl sub-spectra.[18] These sub-spectra are characterized by the coupling constants of the full system, that is, J_{AB} and J_{KL}, but by effective chemical shifts:

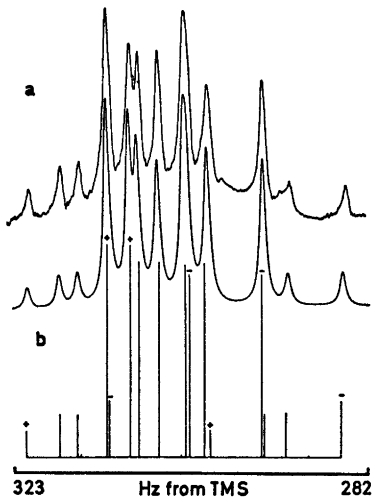

Fig. 3. Experimental (a) and calculated (b) 100 MHz spectrum of the $O-CH_2$ protons (KL region) in compound III. The two kl sub-spectra are indicated in the stick-plot.

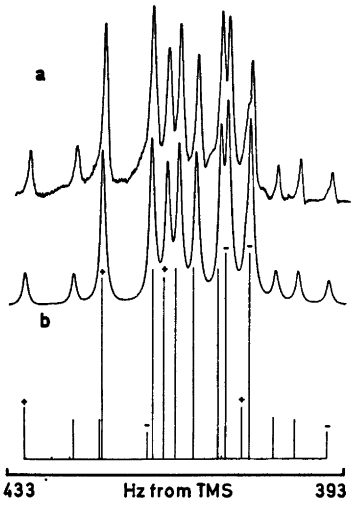

Fig. 4. Experimental (a) and calculated (b) 100 MHz spectrum of the $N-CH_2$ protons (AB region) in compound III. The two ab sub-spectra are indicated in the stick-plot.

$$\nu_{a\pm} = \nu_A \pm \tfrac{1}{2}(J_{AK} + J_{AL})$$
$$\nu_{b\pm} = \nu_B \pm \tfrac{1}{2}(J_{BK} + J_{BL})$$
$$\nu_{k\pm} = \nu_K \pm \tfrac{1}{2}(J_{AK} + J_{BK})$$
$$\nu_{l\pm} = \nu_L \pm \tfrac{1}{2}(J_{AL} + J_{BL})$$

The extreme lines in the AB and KL spectra must originate from the ab and kl sub-spectra since the weak coupling constants have the same sign (Figs. 3 and 4). Furthermore, since $J_{AB} \approx J_{KL} \approx -9$ Hz two more lines originating from the ab and kl sub-spectra are readily picked out. By manipulating these lines acceptable trial values of the parameters were obtained. A fresh computation then allowed the remaining lines to be assigned. The final computer iteration gave the refined parameters for the 1,3,2-oxazarsolanes listed in Table 1. Figs. 3 and 4 show excellent fit between the experimental and calculated spectra of III.

The NMR signals originating from the $CHCH_2-CHCH_2$ protons in compounds VI and VII were analyzed on the basis of $AA'K_2K_2'$ and ABK_2L_2 spin systems, respectively. When $J_{KK'} = 0$ all the spectral parameters of the $AA'K_2K_2'$ system may be obtained directly from the experimental spectrum with the limitation that $|J_{AK} + J_{AK'}|$ is found instead of the two individual coupling constants.[19] Reasonable trial parameter of the *trans* molecule (VII) were obtained directly from the experimental spectrum or by comparison with related systems.[1] The refined parameters of VI and VII obtained from the iterative computer analysis are listed in Table 1.

DISCUSSION

It may be confidently concluded, on the basis of the coupling constants, that the molecular conformations of I and II are very similar. The 2-substituted 1,3-dimethyl-1,3,2-diazarsolanes may, in principle, exist in *trans* and *cis* forms with respect to the *N,N*-dimethyl groups. The *trans* form is unique whereas the *cis* form may exist as *anti* and *syn* conformers. All these forms are, however, readily interconverted by inversion at nitrogen. Inspection of molecular models suggests, however, that the *anti* form predominates strongly over the *syn* form.

The type of spin system observed for I and II implies that the heterocyclic ring is planar or, more likely, undergoes rapid interconversions between equivalent nonplanar forms, like A and B below with X=N, at rates that are large on the NMR time scale. At any rate, only the *cis* form can explain the observed symmetrical spin system. The NMR data for I and II are thus consistent with a strong predominance of the *anti* form possessing *cis* *N,N*-dimethyl groups. Moreover, the similarity of the *cis* and *trans* vicinal coupling constants together with the steric requirements of the heterocyclic ring (*cf.* rabbit-ear effect [18]), suggest firmly that the ring is non-planar. It follows that the NMR results are adequately explained only in terms of rapidly interconverting twist-envelope conformations, A and B, possessing one pseudo-axial and one pseudo-equatorial *N*-methyl group. This conclusion is supported by earlier results on analogous systems.[1-3,5,20] Furthermore, the preferred conformation of the related 2-alkyl-*N,N*-dimethyl-1,3-diazanes con-

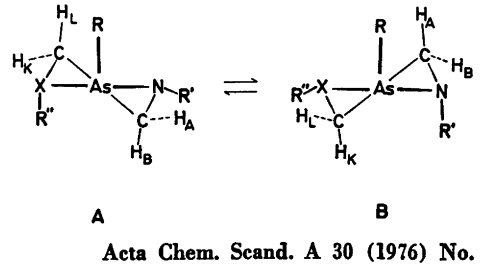

tains one axial and one equatorial *N*-methyl group.[12]

Our NMR data for compounds III–V can also be satisfactorily explained on the basis of the A and B pseudo-rotamers above. However, comparable contributions of the A and B pseudo-rotamers would result in similar values of J_{AK} and J_{BL}, contrary to experiment. The large value of J_{BL} in III and IV indicates a strong predominance of one particular conformation. Dreiding stereomodels readily showed that the A pseudo-rotamer possessing a pseudo-equatorial phenyl group at nitrogen, is the most probable conformation. However, replacement of the bulky phenyl substituent at nitrogen by a methyl group reduces significantly the diaxial interactions between the pseudo-axial hydrogen at carbon 5 and the pseudo-axial substituent at nitrogen. In accordance with this observation the reduced difference between J_{AK} and J_{BL} indicates that the A and B pseudo-rotamers are more equally populated.

It can be anticipated from Dreiding stereomodels and the Karplus relationship,[21] that the largest vicinal coupling constant in compounds III–V involves the pseudo-axial protons of the predominating conformation (A). From this assumption it follows that the resonance signals of the pseudo-axial protons appear at higher field than the geminal pseudo-equatorial protons in agreement with previous results on 1,3,2-oxathiarsolanes [2] and 1,3-oxathiolanes.[22]

The chemical shift assignments of I and II, made by analogy with the 1,3,2-oxazarsolanes, are consistent with the reported downfield shifts of protons *cis* rather than *trans*, to a pseudo-axial substituent at arsenic or phosphorus in arsolanes [1–3] and phospholanes.[20,23] The validity of this rule has been disputed, however.[5,23] At any rate, the reverse assignment of *cis* and *trans* O–CH_2 protons in 1,3,2-oxazarsolanes and 1,3,2-oxathiarsolanes [2] has been made.

It is seen that replacement of the *N*-methyl group by phenyl produces a substantial decrease in the internal shift difference $|\nu_A - \nu_B|$ on the adjacent methylene protons. The reduced shift is presumably caused by a combination of conformational effects and the anisotropy of the equatorial *N*-phenyl group.

Geminal coupling constants in CH_2 groups α to a nitrogen atom cover a wider range of values, even in apparently closely related structures, than in any other type of CH_2 groups.[24] On this basis the magnitude of the geminal coupling constants of the N–CH_2 moiety in I–V is remarkably similar and close to the values reported for the analogous 1,3,2-diazaphospholanes [9] and 1,3,2-oxazaphospholanes.[10,11] The geminal coupling constants of the O–CH_2 protons are within the expected range.[24]

The two *cis* coupling constants, $J_{AA'}$ and $J_{BB'}$ in I and II are virtually identical in accordance with the situation in 1,3,2-dithiarsolanes,[2] 1,3,2-dioxaphospholanes,[23,25] and ethylene sulfite.[23] However, the two *cis* coupling constants differ considerably in some 1,3,2-diazaphospholanes [9] and 1,3,2-dithiaphospholanes.[5]

The near-equality of the *cis* and *trans* coupling constants in I and II is in contrast to the reported situation in the analogous diazaphospholanes [9] and dioxaphospholanes [23,25] ($J_{trans} < J_{cis}$) as well as in dithiarsolanes [2] and dithiaphospholanes [5] ($J_{trans} > J_{cis}$). The large variation in the vicinal coupling constant reflects changes in the X–C–C–X torsional angle (X = O, N, S) in these five-membered rings.

The X–C–C–N torsional angle, ψ, has been calculated from the vicinal coupling constants of the CH_2–CH_2 moiety using the *R*-value method due to Buys and Lambert [26] (Table 1). It should be emphasized, however, that the obtained torsional angles characterize only the mean geometry of the heterocyclic ring. Similar calculations based on the reported coupling constants for 1,3,2-diazaphospholanes [9] and 1,3,2-oxazaphospholanes [10] give torsional angles in the ranges 37–43° and 41–43°, respectively. This indicates that the diazarsolane and oxazarsolane rings are more puckered than their phosphorus counterparts. It also seems that the steric requirements of the *N*-phenyl substituent, as compared to an *N*-methyl group, increase the puckering of the oxazarsolane ring by about 5°.

The vicinal coupling constants found in the *cis* and *trans* isomers of 2-phenoxy-4,5-dimethyl-1,3,2-dioxarsolane, VI and VII, respectively, are fairly close to the corresponding parameters in 2-chloro- and 2-phenyl-4,5-dimethyl-1,3,2-dioxarsolane.[1] This observation

indicates that the conformations of corresponding isomers are similar and little affected by the substituent at arsenic.

The large value of J_{AB} in the *trans* form indicates that this coupling constant mainly involves the pseudo-axial protons, that is, the conformation possessing pseudo-equatorial methyl groups predominates. This conclusion is also reasonable on steric grounds since the 2-phenoxy substituent probably occupies a pseudo-axial position.

The steric requirements of the methyl groups are certainly more important in the *cis* molecule and are expected to produce a highly puckered conformation. The resulting enlarged H–C–C–H angle should produce a fairly small vicinal coupling constant [21,26] contrary to experiment. It seems that a compensating reduction in the electronegativity effect of the adjacent oxygen atoms is operating. This is reasonable since the magnitude of the electronegativity effect depends on the dihedral angle, and empirically it is found that the effect is greatest when the electronegative group (atom) is *trans* to one of the coupled protons.[27]

In accordance with previous assignments, we believe that the methine and methyl signals at lower and higher field arise from protons *cis* and *trans* to the pseudoaxial phenoxy group at arsenic.

Acknowledgement. One of us (F.A.A.) thanks The Royal Norwegian Council for Scientific and Industrial Research for a fellowship.

REFERENCES

1. Aksnes, D. W. and Vikane, O. *Acta Chem. Scand. 26* (1972) 835, 2532.
2. Aksnes, D. W. and Vikane, O. *Acta Chem. Scand. 27* (1973) 1337, 2135.
3. Aksnes, D. W. and Bjorøy, M. *Acta Chem. Scand. A 29* (1975) 672.
4. Booth, H. *Progr. Nucl. Magn. Resonance Spectrosc. 5* (1969) 149.
5. Peake, S. C., Fild, M., Schmutzler, R., Harris, R. K., Nichols, J. M. and Rees, R. G. *J. Chem. Soc. Perkin Trans. 2* (1972) 380.
6. Sternson, L. A., Coviello, D. A. and Egan, R. S. *J. Amer. Chem. Soc. 93* (1971) 6529.
7. Keskinen, R., Nikkilä, A. and Pihlaja, K. *J. Chem. Soc. Perkin Trans. 2* (1973) 1376.
8. Keskinen, R., Nikkilä, A. and Pihlaja, K. *J. Chem. Soc. Perkin Trans. 2* (1974) 466.
9. Albrand, J. P., Cogne, A., Gagnaire, D. and Robert, J. B. *Tetrahedron 28* (1972) 819.
10. Devillers, J., Roussel, J. and Navech, J. *Org. Magn. Resonance 5* (1973) 511.
11. Devillers, J., Cornus, M., Roussel, J. and Navech, J. *Org. Magn Resonance 6* (1974) 205.
12. Hutchins, R. O., Kopp, L. D. and Eliel, E. L. *J. Amer. Chem. Soc. 90* (1968) 7174.
13. Scherer, O. J. and Schmidt, M. *Angew. Chem. 76* (1964) 787.
14. Bothner-By, A. A. and Castellano, S. *LAOCN3*, Mellon Institute, Pittsburgh, Penn., U.S.A.
15. Johannesen, R. B., Ferretti, J. A. and Harris, R. K. *J. Magn. Resonance 3* (1970) 84.
16. Aksnes. D. W. *KOMBIP, Progr. No. 205*, Quantum Chemistry Program Exchange, Indiana University, Chemistry Department, Bloomington, Ind., U.S.A.
17. Emsley, J. W., Feeney, J. and Sutcliffe, L. H. *High Resolution Nuclear Magnetic Resonance Spectroscopy*, Vol. 1, Pergamon, New York 1965.
18. Diehl, P. and Chuck, R. J. *Mol. Phys. 13* (1968) 417.
19. Diehl, P., Harris, R. K. and Jones, R. G. *Progr. Nucl. Magn. Resonance 3* (1967) 1.
20. Bergesen, K., Bjorøy, M. and Gramstad, T. *Acta Chem. Scand 26* (1972) 2156, 3037.
21. Karplus, M. *J. Chem. Phys. 30* (1959) 11.
22. Pasto, D. J., Klein, F. M. and Doyle, T. W. *J. Amer. Chem. Soc. 89* (1967) 4368.
23. Haake, P., McNeal, J. P. and Goldsmith, E. J. *J. Amer. Chem. Soc. 90* (1968) 715.
24. Cahill, R., Cookson, R. C. and Crabb, T. A. *Tetrahedron 25* (1969) 4681.
25. Gagnaire, R. D., Robert, J. B., Verrier, J. and Wolf, R. *Bull. Soc. Chim. Fr.* (1966) 3719.
26. Lambert, J. B. *Accounts Chem. Res. 4* (1971) 87.
27. Lynden-Bell, R. M. and Harris, R. K. *Nuclear Magnetic Resonance Spectroscopy*, Nelson, London 1969.

Received July 19, 1975.

Acta Chemica Scandinavica A 30 (1976) 115—120

Remarks on the Problem of Finding Best Set Conductance Parameters for Electrolyte Solutions

PER BERONIUS

Division of Physical Chemistry, University of Umeå, S-901 87 Umeå, Sweden

Three conductance equations in current use, the expanded forms of the Fuoss-Hsia and Pitts equations and a recent equation of Fuoss including the Chen effect, have been used to analyze conductance data for several univalent electrolytes in pure solvents and binary solvent mixtures. The method of handling the conductance data is based on determination of the values of the limiting molar conductivity and the ion-pair association constant which minimize $\sigma(\Lambda)$, the standard deviation between experimental and computed Λ values, for a range of values of the distance parameter, R, the maximum centre-to-centre distance between the ions in the ion-pair. For each equation the graph of $\sigma(\Lambda)$ *vs.* R is frequently observed to exhibit two minima with almost equal $\sigma(\Lambda)$'s, one minimum often appearing at a value of R close to the Bjerrum radius, q, the other minimum deviating considerably from the Bjerrum q value. Though not in obvious contradiction with the position taken by Justice that the distance parameter should be numerically identified with the Bjerrum radius, the present observations suggest that the Justice point of view might be questioned.

The dependence of the molar conductivity, Λ, on electrolyte concentration, c, for electrolytes which are subject to ion-pair formation may be described by means of equations of the type,

$$\Lambda = \alpha[\Lambda_\infty - S(c\alpha)^{1/2} + Ec\alpha\ {}^{10}\log(c\alpha) + J_1 c\alpha - J_2(c\alpha)^{3/2}] \quad (1)$$

where α is the degree of dissociation of the ion-pairs and Λ_∞ is the molar conductivity at infinite dilution. The other symbols in eqn. (1) will be defined below. Let us merely remark here that the J coefficients depend upon, among other factors, a distance parameter, R, the maximum centre-to-centre distance between the ions in the ion-pair.

From eqn. (1), combined with the mass action law for the equilibrium between unpaired and paired ions (ion-pair association constant, K_A), and the Debye-Hückel equation [1]

$${}^{10}\log\ \gamma \simeq -A(c\alpha)^{1/2}/[1 + BR(c\alpha)^{1/2}] \quad (2)$$

for the mean molar activity coefficient, γ, of free ions, the parameters Λ_∞, K_A, and R may be iteratively computed, *cf.* Ref. 2. That combination of Λ_∞, K_A, and R which minimizes $\sigma(\Lambda)$, the standard deviation between observed and computed Λ values, is usually adopted as the "best set".

In a preceding investigation [3] conductance data for numerous univalent electrolytes in pure and mixed solvents were analyzed by means of the Fuoss-Hsia conductance equation [4,5] in the form developed by Fernandez-Prini [6] ("FHFP" equation). The method of calculation used involves iterative determination of those values of Λ_∞ and K_A which minimize $\sigma(\Lambda)$ for selected values of the distance parameter, R, over a range of the latter (usually from 1 to 25 Å); *cf.* Ref. 7.

Very frequently the $\sigma(\Lambda) - R$ curve was found to exhibit two minima with almost identical $\sigma(\Lambda)$'s, one minimum appearing rather close to the Bjerrum radius,[8] q, the other minimum appearing at a value of $R \ll q$. This indicates that the Justice point of view that R should be numerically identified with the Bjerrum radius, *cf.* Refs. 9 and 10, may be questioned. Compare the conflicting positions concerning the physical interpretation of the distance parameter taken by Fuoss [11] and Justice.[12]

The preceding investigation [3] of non-unique sets of conductance parameters, restricted to

the FHFP equation, has been now extended to two other important conductance equations, *viz.* the Pitts equation [13] in the expanded form of Fernandez-Prini and Prue,[14] ("PFPP" equation) and a recent equation of Fuoss as developed by Justice [15] ("FJ" equation) in which the so-called Chen effect [16] is taken into account. Some typical results for univalent electrolytes in pure solvents and binary solvent mixtures will be discussed in the present paper.

CALCULATIONS

The three conductance equations studied in the present investigation are all of the form given in eqn. (1) in which S is the Onsager limiting law coefficient.[17] In the FHFP and PFPP equations $E = E_1\Lambda_\infty - E_2$, while in the FJ equation $E = E_1\Lambda_\infty - 2E_2$. The coefficients E_1 and E_2 are given in Ref. 17. The σ coefficients appearing in the J terms of eqn. (1), in which $J_1 = \sigma_1\Lambda_\infty + \sigma_2$ and $J_2 = \sigma_3\Lambda_\infty + \sigma_4$, were taken from Ref. 6 for the FHFP equation, from Ref. 14 for the PFPP equation, and from Ref. 15 for the FJ equation.

Solvent permittivities, ε, and viscosities, η, used in the calculations are the same as in the original investigations.[18-22]

A detailed account of the method of computation developed to find the values of Λ_∞ and K_A which minimize $\sigma(\Lambda)$ for some assigned value of the distance parameter in the conductance equation, eqn. (1), and in the Debye-Hückel equation, eqn. (2), has been previously given.[3,7]

The calculations of Λ_∞, K_A, and $\sigma(\Lambda)$ were repeated by means of a CDC 3300 computer for a selected range of R values and a graph of the conditional minimum $\sigma(\Lambda)$ as a function of association distance prepared. The R value of the minimum * (or minima) of the $\sigma(\Lambda) - R$ curve was established with an uncertainty of less than 0.02 Å by repeated calculations around the minimum using successively smaller increments in R.

* Throughout the text the association constant, K_A, is given on the molar scale. The units of Λ_∞ and $\sigma(\Lambda)$ are $cm^2\ \Omega^{-1}\ mol^{-1}$.

DISCUSSION

Conductance parameters derived according to the FHFP and FJ equations are almost identical. This statement may be illustrated by means of Fig. 1 in which Λ_∞, K_A, and $\sigma(\Lambda)$ have been plotted *vs.* R for cesium iodide in a dioxane-water mixture [18] ($\varepsilon = 12.81$) at 25 °C for the three equations concerned. For the FHFP and FJ equations the curves representing the dependence of Λ_∞ and of K_A on R practically overlap and the shapes of the $\sigma(\Lambda) - R$ curves are very similar in character.

Conductance data at 25 °C for cesium iodide in seven different dioxane-water mixtures with permittivities in the range $12.81 \leq \varepsilon \leq 60.18$ are reported by Lind and Fuoss.[18] Graphs of $\sigma(\Lambda)$ *vs.* R according to the PFPP and FJ equations for these systems are shown in Figs. 1 and 2. Because of the close resemblance of the $\sigma(\Lambda) - R$ curve according to the FHFP equation with that of the FJ equation any graphical representation for the FHFP equation is omitted in Fig. 2.

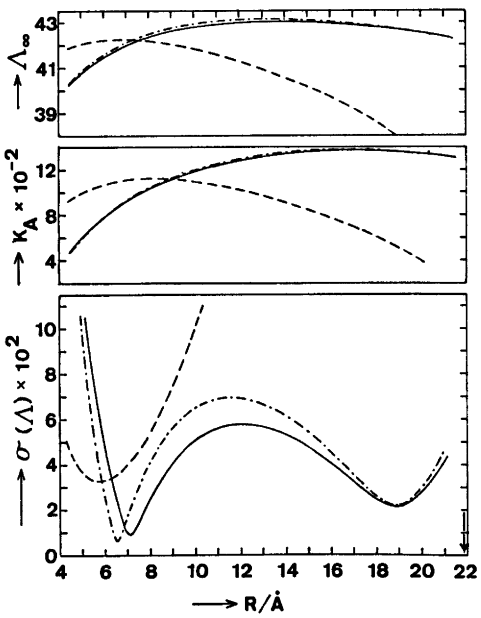

Fig. 1. Graphs of Λ_∞, K_A, and $\sigma(\Lambda)$ *vs.* R for CsI in a dioxane–water mixture [18] ($\varepsilon = 12.81$) at 25 °C for PFPP equation (- - -), FHFP equation (- · -), and FJ equation (———), *cf.* Table 1. The arrow indicates the Bjerrum radius, q.

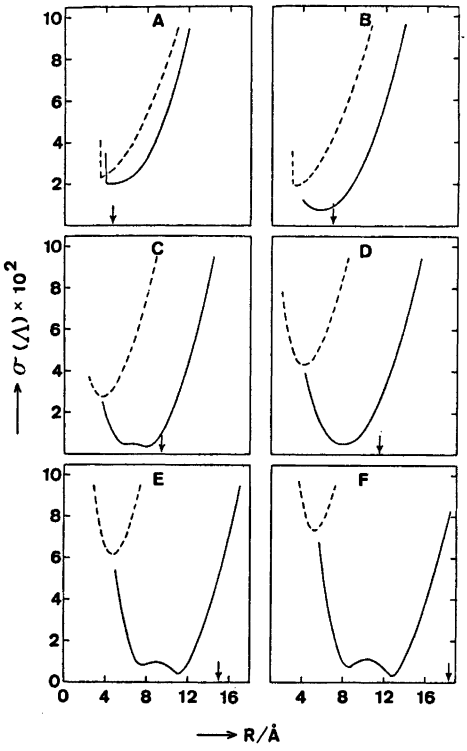

Fig. 2. Graphs of $\sigma(\Lambda)$ *vs.* R for CsI in dioxane – water mixtures [18] at 25 °C for PFPP equation (- - -) and FJ equation (———). The diagrams A – F refer to solvent mixtures with permittivities equal to 60.18, 40.57, 29.79, 24.44, 18.68, and 15.29, respectively, *cf.* Table 1. The arrows indicate the Bjerrum radius.

Given in Table 1 is a compilation of the conductance parameters corresponding to the minima of the $\sigma(\Lambda) - R$ curves (*cf.* Figs. 1 and 2) according to the PFPP and FJ equations for the cesium iodide dioxane – water systems. Since the FJ and FHFP equations yield almost identical values of the conductance parameters no results for the FHFP equation are tabulated. Two sets of values for Λ_∞, K_A, R, and $\sigma(\Lambda)$ are listed for those $\sigma(\Lambda) - R$ curves exhibiting double minima. Included in this table are also the values of the Bjerrum radius [8]

$$q = |z_+ z_-| e^2/(2\varepsilon \mathbf{k} T) \qquad (3)$$

where z_+ and z_- are the valencies of the ions, e is the electronic charge, $\mathbf{k}$ is Boltzmann's constant, and T is the absolute temperature.

For these systems it is found that the PFPP equation yields $\sigma(\Lambda) - R$ curves with a single minimum, *cf.* Figs. 1 and 2, while the FJ and FHFP equations, in most instances, yield curves with two minima (Table 1).

Hughes and Price [19] report conductance data for several quaternary ammonium bromides in ethyl methyl ketone at 25 °C. In general curves with two minima are obtained according to all three equations studied (Table 2).

Hughes and White [20] report conductance data at 25 °C for potassium iodide in seven different acetone – water mixtures. With the exception of that solvent mixture containing 3.304 per cent of water, the graphs of $\sigma(\Lambda)$ *vs.* R exhibit double minima for all three conductance equations investigated (Table 3).

Table 1. Parameters for CsI in dioxane-water mixtures at 25 °C derived from conductance data in Ref. 18.

Diox. wt %	ε	η/cP	Λ_∞/cm² Ω^{-1} mol^{-1} PFPP	FJ	K_A/M^{-1} PFPP	FJ	R/Å PFPP	FJ	q/Å	$\sigma(\Lambda)$/cm² Ω^{-1} mol^{-1} PFPP	FJ
22.1	60.18	1.328	99.39	99.40	0.00	0.5	3.49	4.52	4.66	0.023	0.020
44.6	40.57	1.820	66.82	66.86	0.5	3.9	3.24	5.84	6.91	0.019	0.008
57.1	29.79	1.982	56.38	56.51	8.0	20.8	3.69	8.03	9.41	0.027	0.003
				56.49		13.8		5.99			0.005
63.7	24.44	1.986	52.13	52.32	29.0	47.8	4.16	8.10	11.46	0.043	0.005
70.7	18.68	1.922	48.06	48.49	119	187	4.71	11.16	15.00	0.061	0.004
				48.39		145		7.63			0.008
75.2	15.29	1.839	45.30	45.97	384	533	5.22	12.85	18.33	0.073	0.003
				45.76		439		8.50			0.008
78.5	12.81	1.754	42.19	42.02	1054	937	5.73	7.11	21.87	0.033	0.009
				42.69		1362		18.86			0.022

Table 2. Parameters for electrolytes in ethyl methyl ketone at 25 °C derived from conductance data in Ref. 19. $\varepsilon = 18.014$; $\eta = 0.3774$ cP; $q = 15.55$ Å.

Salt[a]	Λ_0/cm² Ω^{-1} mol^{-1}		K_A/M^{-1}		R/Å		$\sigma(\Lambda)$/cm² Ω^{-1} mol^{-1}	
	PFPP	FJ	PFPP	FJ	PFPP	FJ	PFPP	FJ
Et_4NBr	158.24	158.25	976	1006	5.81	11.60	0.032	0.026
Pr_4NBr	146.60	146.53	965	976	3.32	6.39	0.012	0.010
	146.89	146.83	1048	1089	8.55	16.81	0.023	0.020
Bu_4NBr	139.79	139.67	826	831	4.02	7.02	0.009	0.008
	140.02	140.00	878	927	7.08	15.50	0.012	0.011
Pe_4NBr	135.09	134.94	813	810	4.94	7.70	0.011	0.010
		135.28		886		13.98		0.011
Hex_4NBr	131.19	131.14	684	694	3.05	5.58	0.013	0.012
	131.44	131.41	777	825	9.34	18.00	0.024	0.023
$Hept_4NBr$	128.42	128.37	678	689	3.32	6.00	0.009	0.008
	128.65	128.62	761	810	8.96	17.56	0.016	0.015
Oct_4NBr	126.26	126.19	678	687	3.57	6.29	0.008	0.008
	126.47	126.45	751	800	8.43	17.02	0.011	0.011

[a] For Me_4NBr no reevaluation of the conductance data was undertaken because of the narrow concentration range investigated (from 0.01791 to 0.03993 mM).

Table 3. Parameters for KI in acetone-water mixtures at 25 °C derived from conductance data in Ref. 20.

H_2O wt %	ε	η/cP	Λ_0/cm² Ω^{-1} mol^{-1}		K_A/M^{-1}		R/Å		q/Å	$\sigma(\Lambda)$/cm² Ω^{-1} mol^{-1}	
			PFPP	FJ	PFPP	FJ	PFPP	FJ		PFPP	FJ
0.179	20.23	0.301	197.20	197.17	61.8	67.5	1.67	2.98	13.85	0.14	0.14
			197.35	197.34	163	198	13.39	21.28		0.15	0.14
0.291	20.29	0.302	195.85	195.83	67.3	74.4	1.43	2.63	13.81	0.14	0.14
			195.97	195.96	178	212	15.02	22.63		0.15	0.15
1.175	20.76	0.309	190.54	190.51	62.9	68.7	1.60	2.87	13.50	0.081	0.079
			190.69	190.68	158	191	13.39	21.02		0.097	0.096
2.012	21.21	0.316	185.60	185.56	83.7	87.1	2.66	4.34	13.21	0.083	0.081
			185.74	185.74	140	173	9.49	17.45		0.095	0.096
2.817	21.64	0.324	180.54	180.51	75.3	79.3	2.53	4.20	12.95	0.027	0.027
			180.67	180.67	133	164	10.34	17.93		0.028	0.028
3.304	21.90	0.329	177.20	177.26	117	139	5.94	10.85	12.79	0.14	0.12
3.574	22.04	0.332	171.59	171.57	115	142	14.58	21.45	12.71	0.050	0.051
			171.37	171.33	14.7	20.6	0.98	1.75		0.057	0.057

Table 4. Parameters for LiBr in acetone-methanol mixtures at 25 °C derived from conductance data in Ref. 21.

MeOH wt %	ε	η/cP	Λ_0/cm² Ω^{-1} mol^{-1}		K_A/M^{-1}		R/Å		q/Å	$\sigma(\Lambda)$/cm² Ω^{-1} mol^{-1}	
			PFPP	FJ	PFPP	FJ	PFPP	FJ		PFPP	FJ
0.1	20.6	0.300	193.56	193.01	3467	3441	5.11	10.41	13.60	0.12	0.15
0.3	20.6	0.300	190.88	190.68	2648	2660	3.98	10.01	13.60	0.15	0.15
1.0	20.7	0.301	185.72	185.90	1571	1649	2.85	13.58	13.54	0.057	0.057
			186.10	185.63	1636	1583	7.18	6.17		0.065	0.061
2.0	20.8	0.301	181.57	181.52	1087	1098	2.71	5.50	13.47	0.16	0.15
			181.87	181.78	1149	1171	7.03	13.86		0.19	0.17
5.0	21.1	0.301	174.45	174.42	663	695	5.64	12.85	13.28	0.073	0.071
			174.26	174.12	631	632	3.30	5.54		0.078	0.095
10.0	21.6	0.304	166.43	166.65	354	397	4.35	11.47	12.97	0.099	0.065
				166.42		353		6.01			0.11
20.0	22.7	0.314	154.00	154.02	132	131	3.93	5.11	12.34	0.14	0.078
				154.27		175		11.06			0.087
50.0	26.3	0.370	128.56	128.80	18.1	40.9	3.88	8.73	10.65	0.18	0.087

Table 5. Parameters for electrolytes in ethylene glycol at 25 °C derived from conductance data in Ref. 22. $\varepsilon = 37.70$; $\eta = 0.1619$ P; $q = 7.43$ Å.

Salt[a]	Λ_∞/cm² Ω⁻¹ mol⁻¹		K_A/M⁻¹		R/Å		$\sigma(\Lambda)$/cm² Ω⁻¹ mol⁻¹	
	PFPP	FJ	PFPP	FJ	PFPP	FJ	PFPP	FJ
Me_4NBr	7.954	7.960	4.0	11.8	3.35	8.31	0.0044	0.0039
		7.954		1.5		3.33		0.0046
Et_4NBr	7.172	7.174	2.5	9.8	3.90	8.88	0.0039	0.0038
		7.173		1.1		4.16		0.0039
Pr_4NBr	6.718	6.722	3.6	8.1	3.49	6.39	0.0036	0.0027
Bu_4NBr	6.488	6.493	2.4	7.4	3.43	6.49	0.0042	0.0036
Me_4NI	7.578	7.579	8.0	14.2	5.16	9.85	0.0053	0.0053
	7.575	7.574	0.0	0.0	1.81	2.69	0.0054	0.0054
Et_4NI	6.798	6.797	10.5	15.5	9.41	13.24	0.0025	0.0025
	6.808	6.807	0.0	0.0	1.94	2.81	0.0046	0.0046
Pr_4NI	6.347	6.345	14.3	0.0	8.22	1.78	0.0044	0.0041
	6.348	6.347	0.0	19.6	1.16	12.29	0.0043	0.0044
Bu_4NI[a]	6.060	6.059	14.6	19.4	11.04	14.55	0.0041	0.0040
	6.071	6.069	0.0	0.0	1.18	1.80	0.0060	0.0056

[a] The point at $c = 2.3781$ mM was omitted because it deviated by -1 % from the curve fitted according to eqn. (1) to the remaining points.

Similar results are obtained for lithium bromide in eight different acetone-methanol mixtures [21] (Table 4).

Conductance data referring to four quaternary ammonium bromides and the corresponding iodides in ethylene glycol at 25 °C are reported.[22] With some exceptions (Me_4NBr and Et_4NBr according to FJ and FHFP equations) the present analysis results in $\sigma(\Lambda) - R$ curves with a single minimum for the bromides (Table 5). For the iodides two minima are obtained for all three conductance equations. One minimum, appearing for some value of R within the 1 – 3 Å range, which is in fact less than the sum of the crystallographic radii for the iodide ion and quaternary ammonium ions concerned,[23]

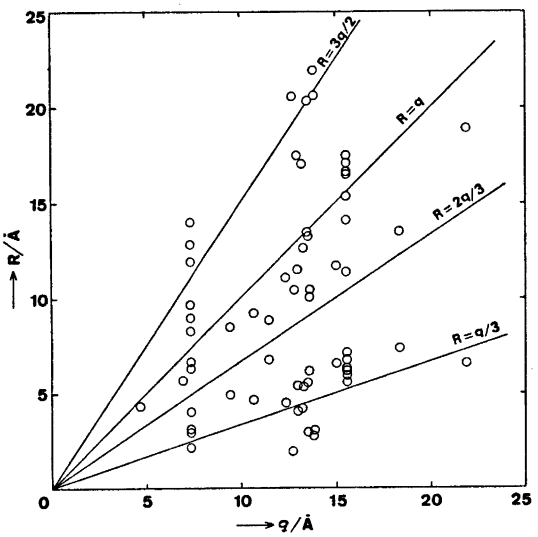

Fig. 3. Association distance, according to FHFP equation, *vs.* Bjerrum radius for the electrolyte systems listed in Tables 1 – 5. For the $\sigma(\Lambda) - R$ curves exhibiting two minima, *cf.* Figs. 1 and 2, the R values of both have been plotted.

corresponds to $K_A = 0$ (no association to ion-pairs). The other minimum, appearing within the 5 – 15 Å range (Table 5), corresponds to small positive values of K_A. These results do not seem to indicate that the quaternary ammonium halides discussed behave like strong electrolytes [22] in ethylene glycol. Compare the discussions [24,25] concerning the difficulty of establishing association constants uniquely from electrical conductance data for only slightly associated electrolytes.

The examples given in the present paper show conclusively that for the PFPP equation as well as for the FJ and FHFP equations the goodness of the fit of the conductance equation to the experimental points is of little help in determining the "exact" value of the distance parameter. This is so not only for highly dissociated salts, *cf.* Ref. 24, but also for electrolytes showing considerable association to ion-pairs, *e.g.* lithium bromide with $K_A = 1.6 \times 10^3$ in the acetone-methanol mixture with $\varepsilon = 20.7$, *cf.* Table 4. There is an obvious demand for supplementary methods to establish the value of the distance parameter.

In Fig. 3 the values of the association distance according to the FHFP equation for the systems listed in Tables 1 – 5 have been plotted *vs.* Bjerrum radius. For the systems giving $\sigma(\Lambda) - R$ curves with two minima the R values of both have been plotted. From this graph it is found that some sets of data may be represented by $R = q$, which is in accord with the Justice point of view.[9,10] However, other sets may be represented by $R = q/3$, $R = 2q/3$, $R = 3q/2$ *etc.* Similar graphs of R *vs.* q are obtained for the PFPP and FJ equations.

Although these results do not disprove that the distance parameter should be numerically identified with the Bjerrum radius [9,10] it is obvious that such a point of view cannot be accepted without reservation.

Acknowledgement. Financial support from the Swedish Natural Science Research Council is gratefully acknowledged.

REFERENCES

1. Robinson, R. A. and Stokes, R. H. *Electrolyte Solutions*, Butterworths, London 1965, pp. 229 – 230.
2. Kay, R. L. *J. Amer. Chem. Soc. 82* (1960) 2099.
3. Beronius, P. *Acta Chem. Scand. A 29* (1975) 289.
4. Fuoss, R. M. and Hsia, K.-L. *Proc. Nat. Acad. Sci. U. S. 57* (1967) 1550.
5. Fuoss, R. M. and Hsia, K.-L. *Proc. Nat. Acad. Sci. U. S. 58* (1968) 1818.
6. Fernández-Prini, R. *Trans. Faraday Soc. 65* (1969) 3311.
7. Beronius, P. *Acta Chem. Scand. A 28* (1974) 77.
8. Bjerrum, N. *Kgl. Dan. Vidensk. Selsk. Mat. Fys. Medd. 7* (1926) No 9.
9. Justice, J.-C. *Electrochim. Acta 16* (1971) 701.
10. Renard, E. and Justice, J.-C. *J. Solution Chem. 3* (1974) 633.
11. Fuoss, R. M. *J. Phys. Chem. 78* (1974) 1383.
12. Justice, J.-C. *J. Phys. Chem. 79* (1975) 454.
13. Pitts, E. *Proc. Roy. Soc. London A 217* (1953) 43.
14. Fernández-Prini, R. and Prue, J. E. *Z. Phys. Chem. (Leipzig) 228* (1965) 373.
15. Barthel, J., Justice, J.-C. and Wachter, R. *Z. Phys. Chem. (Frankfurt am Main) 84* (1973) 100.
16. Chen, M. S. *Thesis*, Yale University 1969.
17. Fuoss, R. M. and Accascina, F. *Electrolytic Conductance*, Interscience, New York 1959, Chap. XV.
18. Lind, Jr., J. E. and Fuoss, R. M. *J. Phys. Chem. 65* (1961) 1414.
19. Hughes, S. R. C. and Price, D. H. *J. Chem. Soc. A* (1967) 1093.
20. Hughes, S. R. C. and White, S. H. *J. Chem. Soc. A* (1966) 1216.
21. Nilsson, A.-M. *Acta Chem. Scand. 27* (1973) 2722.
22. DeSieno, R. P., Greco, P. W. and Mamajek, R. C. *J. Phys. Chem. 75* (1971) 1722.
23. Robinson, R. A. and Stokes, R. H. *Electrolyte Solutions*, Butterworths, London 1965, pp. 125 and 461.
24. Duer, W. C., Robinson, R. A. and Bates, R. G. *J. Chem. Soc. Faraday Trans. 1* (1972) 716.
25. Barker, B. J., Huffman, Jr., H. L. and Sears, P. G. *J. Phys. Chem. 78* (1974) 2689.

Received August 13, 1975.

Acta Chemica Scandinavica A 30 (1976) 121—124

The Acid Hydrolysis and Related Reactions of Oxalatobis(2,2′-bipyridine)chromium(III) and Oxalatobis(1,10-phenanthroline)-chromium(III) Ions

OLE FARVER[a] and GWYNETH NORD[b]

[a] Department of Chemistry AD (Inorganic and Physical Chemistry), Royal Danish School of Pharmacy and [b] Chemical Laboratory I (Inorganic Chemistry), H. C. Ørsted Institute, University of Copenhagen, DK-2100 Copenhagen Ø, Denmark

The kinetics of the acid hydrolysis of Cr(ox)-(bipy)$_2^+$ * and Cr(ox)(phen)$_2^+$ have been studied. The rate expression is rate $= k_{aqn}$[H$^+$] [complex]. At 25 °C and unit ionic strength the respective second order rate constants are: $k_{aqn} = 9.0 \times 10^{-7}$ M^{-1} s^{-1} and 5.9×10^{-7} M^{-1} s^{-1}. The activation parameters have been measured, and the enthalpies of activation are the same as those reported for the racemisation of the same complexes. This is consistent with the major contribution to $\Delta H^{\neq}$ being the breaking of a Cr—O bond in a common intermediate.

Although much studied [1,2] the mechanisms of reactions involving transition metal complexes containing coordinated oxalate still pose problems. In particular, it has recently been shown [2] that the oxygen-18 exchange and the racemisation of the title complexes follow different rate laws. The activation parameters for the ^{18}O exchange, unlike the racemisation, differ very little on substitution of Cr^{3+} for Co^{3+} [3] or for Pt^{2+} [4] or on substitution of L-L for oxalate.[2] The exchange thus reflects the *ligand reactivity* and has been rationalised [1,2] in terms of proton attack on the carbonyl oxygen of the complexed oxalate.

Analogous solvent or proton attack on the coordinated oxygen would lead to *disruption of the octahedral structure* (Cr—O bond stretching) with racemisation through an idealised five coordinate, or, if extra solvated water is available, through a seven coordinate intermediate. The latter but not the former would accord with the now accepted associative mechanism [5] for substitution in Cr^{3+} complexes, and on further proton or solvent attack would lead to disruption of both metal—oxygen bonds and aquation. The title complexes are known on aquation to give the *cis*-diaqua-(L-L)$_2$ complexes although more slowly than the rate at which racemisation occurs.

Since the major contribution to the activation energy would, following the above mechanism, in *both cases* be the stretching of the metal—oxygen bond, similarities in the activation energies of the two processes might be expected. The extra step after racemisation and leading to dissociation of oxalate depend on rapid equilibria involving solvent molecules brought into the transition state by proton or metal ion attack on the coordinated oxygen. We present here the kinetic data for the acid hydrolysis and discuss this together with the data for the related reactions given in the literature.

EXPERIMENTAL

[Cr(ox) (bipy)$_2$] Cl.4H$_2$O and [Cr(ox) (phen)$_2$] CF$_3$COO.2H$_2$O were prepared from the respective "diols" by treating the diols for about 12 h with equimolar amounts of oxalic acid and potassium oxalate at 50 °C. The products were

* The following abbreviations are used in this paper: phen = 1,10-phenanthroline, bipy = 2,2′-bipyridine, ox = oxalate ion, and L—L = bipy or phen.

recrystallised from water and the purity was confirmed by means of the visible spectra of the aqueous solutions:

$Cr(ox)(bipy)_2^+$: $(\lambda,\varepsilon)_{max} = (497,\ 66.5)$, $(\lambda,\varepsilon)_{min} = (464,\ 48.7)$

$Cr(ox)(phen)_2^+$: $(\lambda,\varepsilon)_{max} = (501,\ 62.6)$, $(\lambda,\varepsilon)_{min} = (454,\ 33.0)$ [6]

Due to the low solubilities of the perchlorate complex salts, nitric acid (Merck *pro analysi*) was used throughout. Preliminary experiments showed that this acid gave the same results as did hydrochloric acid. The ionic strength was kept constant at 1.0 M with either sodium nitrate or lithium nitrate, neither of these cations giving specific rate effects. Water redistilled twice in an all quartz apparatus was used for making up all the stock and experimental solutions.

The spectra of the complexes were measured in the range 600 – 350 nm using a Zeiss DMR 10 double grating spectrophotometer. An accurately weighed amount of the solid complex was quickly dissolved in a thermostatted solution of the other reagents, making the concentration of the complex $1-7\times10^{-3}$ M. The solutions were then immediately transferred to the thermostatted spectrophotometer cell and the reaction was followed by measuring the absorbancies at λ_{max} (497 nm for $Cr(ox)(bipy)_2^+$ and 501 nm for $Cr(ox)(phen)_2^+$).

The kinetic data were collected on punched paper tape by means of an automatic data sampling system and fed into a UNIVAC 1110 computer for analysis. The reactions were, with the exception of the lowest temperature, followed for at least two half lives and there were always at least 2000 measurements per kinetic run.

RESULTS

The spectra of the final solutions were those of the *cis*-diaqua complexes, and the overall reaction is therefore

$$Cr(ox)(L\text{-}L)_2^+ + 2H^+ \xrightarrow{k_{obs}} cis\text{-}(H_2O)_2Cr(L\text{-}L)_2^{3+} + C_2O_4H_2$$

Pseudo first order rate constants, k_{obs} were determined by minimising the error square sum, $s^2 = \sum_{i=1}^{n} (A_{obs} - A_{calc})^2$ where n is the number of measurements, A_{obs} is the measured absorbancy at the fixed wavelength, and A_{calc} the absorbancies calculated from

$$A_{calc} = (A_0 - A_\infty)\exp(-k_{obs}t) + A_\infty$$

where A_0 and A_∞ are the absorbancies at $t=0$ and $t=\infty$, respectively. The minimum of s^2 with respect to k_{obs} was found by means of a random search procedure written in NU-algol.

The above procedure was possible as the experiments were always performed under conditions in which the acid concentrations were held virtually constant during the reaction. The results from the computer analysis showed that the reactions were first order in complex. This was further confirmed by determining the rate constants with different initial concentrations of the complexes under otherwise identical conditions.

Examples of the effect of acid concentration on the rate of aquation are shown in Fig. 1. The results show that the reaction is first order in H^+ both for the phen and the bipy complex – in contrast to the racemisation reaction (see discussion below). Since the straight lines in all cases within experimental error go through the origin there is no detectable acid independent dissociation reaction.

Addition of oxalic acid to the reaction mixtures had no influence on the reaction rates, *i.e.* the reverse reaction is negligible.

Table 1 gives the second order rate constants, k_{aqn} determined from the slopes of the straight lines at the different temperatures, together with the enthalpies and entropies of activation calculated from the Eyring plots shown in Fig. 2. Errors are the standard deviations of the least squares plots. The activation parameters for the racemisation reactions of the same complexes under analogous con-

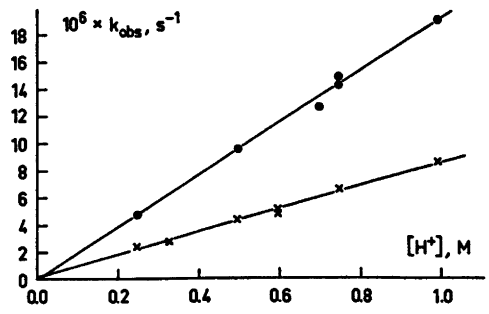

Fig. 1. Acid concentration dependence of aquation rate constants for $Cr(ox)(bipy)_2^+$ at 46.0 °C and unit ionic strength (×) and for $Cr(ox)\ phen)_2^+$ at 55.8 °C (●).

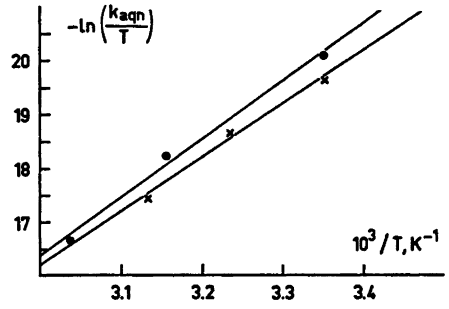

Fig. 2. Eyring plots for aquation of Cr(ox)(bipy)$_2^+$ (×) and Cr(ox)(phen)$_2^+$ (●).

ditions calculated from Ref. 2 are given in parentheses.

Table 1. Second order rate constants and activation parameters for the acid hydrolysis of the chromium(III) complexes.

$k_{aqn} \times 10^6$ M^{-1} s^{-1}	T K	$\Delta H^{\ddagger}$ kJ mol^{-1}	$\Delta S^{\ddagger}$ J K^{-1} mol^{-1}
Cr(ox)(bipy)$_2^+$			
0.90(6)	298.2	82.4(30)	−84(6)
2.5(1)	309.0	[79.5(10)][a]	[−61(3)][a]
8.5(4)	319.2		
Cr(ox)(phen)$_2^+$			
0.59(3)	298.2	88.9(50)	−67(8)
3.9(2)	316.7	[82.9(10)][a]	[−57(3)][a]
19.2(6)	329.0		

[a] Activation parameters for the racemisation of the same chromium (III) complexes calculated from Ref. 2.

DISCUSSION

The mechanism given below can explain that, although the rate laws are different for the racemisation and aquation reactions, the activation enthalpies are within the experimental error the same. It is analogous to that suggested for the reactions of $Cr(ox)_3^{3-}$.[5]

$$[(L\text{-}L)_2Cr(ox)]^+ + H_2O \underset{k_b}{\overset{k_f}{\rightleftharpoons}} [X]^+$$

$$[X]^+ + H_3O^+ \xrightarrow{k_a} C_2O_4H_2 + cis[(L\text{-}L)_2Cr(OH_2)(OH)]^{2+}$$

$$cis[(L\text{-}L)_2Cr(OH_2)(OH)]^{2+} \overset{\pm H^+}{\rightleftharpoons} cis[(L\text{-}L)_2Cr(OH_2)_2]^{3+}$$

In this scheme the major contribution to $\Delta H^{\ddagger}$ arises from the breaking of a Cr−O bond following attack of water on the metal centre. The intermediate $[X]^+$ could either reform into the opposite optical isomer or react further by addition of H_3O^+ to a carbonyl oxygen followed by rapid proton transfer. Following this scheme and using both a steady state treatment for $[X]^+$ and the assumption that $k_a[H^+] \ll k_b$ gives

$$k_{rac} = k_f \text{ and } k_{aqn} = k_f k_a / k_b$$

For $[Cr(phen)_2(ox)]^+$ at 55 °C from Ref. 2, k_{rac} is available. Combining this with our value for k_{aqn} gives $k_b/k_a = 26$. The assumption made above is therefore valid as, under our experimental conditions, $k_a[H^+]$ would never be greater than about 4 % of k_b.

The racemisation of $[Cr(bipy)_2(ox)]^+$ occurs through two reaction paths. From the data given in Ref. 2 we calculate that at 45 °C

$$k_{obs} = k_{rac} + \frac{k'K[H^+]}{1 + K[H^+]}$$

$k_{rac} = 1.6 \times 10^{-4}$ s^{-1}, $k' = 4.0 \times 10^{-4}$ s^{-1}, $K = 1.4$ M^{-1}, where k_{obs} is the total constant, k_{rac} is that for the hydrogen ion independent path analogous to that above, and k' that for the hydrogen ion dependent path. It seems reasonable that this latter reflects a transition state with a bipy ligand protonated in the *trans* form allowing racemisation but with the Cr−N bond rapidly reforming (*cf.* Ref. 3). Combining the acid *independent* rate at 55 °C with k_{aqn} at the same temperature gives for this complex $k_b/k_a = 29$. This is nearly the same as that calculated above for $[Cr(phen)_2(ox)]^+$.

Finally we have found that just as for the racemisation of the monooxalato complexes [2] and in contrast to the bisoxalato complexes,[1] no specific cation effects are observed for the aquation reaction using the following cations in concentrations *ca.* 5×10^{-2} M: Ce^{3+}, Nd^{3+}, Yb^{3+}, In^{3+}, Zn^{2+}, Mn^{2+}, Cd^{2+}, Hg^{2+}.

With Tl^{3+}, however, oxidation of the oxalate accompanies a more rapid aquation as would be expected from attack on a carbonyl oxygen

of the coordinated ligand, so that the mechanism would thus involve a step analogous to that suggested in Ref. 2 to explain the $[H^+]$ dependence of the ^{18}O exchange. Details of this redox reaction will be given in a later publication.

REFERENCES

1. Broomhead, J. A., Kane-Maguire, N. and Lauder, I. *Inorg. Chem. 9* (1970) 1243 and references therein.
2. Broomhead, J. A., Kane-Maguire N. and Lauder, I. *Inorg. Chem. 10* (1971) 955.
3. Broomhead, J. A., Kane-Maguire, N., Lauder, I. and Nimmo, P. *Chem. Commun.* (1968) 747.
4. Teggins, J. E. and Milburn, R. M. *Inorg. Chem. 4* (1965) 793.
5. Edwards, J. O., Monacelli, F. and Ortaggi, G. *Inorg. Chim. Acta 11* (1974) 47.

Received July 10, 1975.

Acta Chemica Scandinavica A 30 (1976) 125—132

The Molecular Structure of 4,4′-(*R*-Propylene-diiminato)-di-(3-penten-2-one)copper(II) Studied by X-Ray Diffraction Methods and Circular Dichroism

ERIK LARSEN,[a] SINE LARSEN,[b] S. RØEN[a] and K. J. WATSON[b]

[a] Chemistry Department I and [b] Chemistry Department IV, University of Copenhagen, The H. C. Ørsted Institute, Universitetsparken 5, DK-2100 Copenhagen Ø, Denmark

Absorption and circular dichroism spectra of the title compound have been measured for the complex dispersed in KBr discs. The interpretation of these spectra by the molecular exciton theory showed that the complex is tetrahedrally distorted with the absolute configuration *Λ*. These conclusions have been confirmed by determination of the crystal structure by X-ray diffraction methods. The crystals are orthorhombic, space group $P2_12_12_1$, $Z=8$, with unit cell dimensions $a=12.452$ Å, $b=21.032$ Å and $c=10.766$ Å. The final least squares refinement using 2521 observed reflections gave unit weighted and weighted residuals of 0.047 and 0.058, respectively.

The two crystallographically independent molecules in the structure are not significantly different and have a tetrahedrally distorted planar coordination of the copper(II) atoms. The angle between the two acetylacetone planes is 10° with the absolute configuration *Λ*. The *R*-propylene part of the ligand has its methyl group in an axial position and the ethylene bridge in a *gauche* conformation.

The stereochemical results from the structure determination are in qualitative agreement with the exciton interpretation of the solid state circular dichroism spectra.

Transition metal complexes of the condensation products between diamine and conjugated dioxo compounds have received great attention and work has been done using a variety of techniques. Currently there is great interest in the ability of cobalt(II) complexes to reversibly bind molecular oxygen. If such systems are to be used as models for biological oxygen carriers it is desirable to obtain knowledge about all the factors which influence molecular and electronic structures. The crystal and molecular structures of ethylenebis(acetylacetoneiminato)copper(II) and a series of adducts have been determined.[1–4] It was found that the complex as a whole deviates only slightly from planarity. Jensen and Larsen [5] found that the title compound, also called *R*-propylenebis(acetylacetoneiminato) copper(II), [Cu *R*-pn(acac)$_2$], in solution is very distorted and they estimated by means of the exciton theory that the two acetylacetonato parts form an angle of some 40°.

This geometry of the complex including the absolute configuration of [Cu *R*-pn(acac)$_2$] was used within a simple MO scheme to combine ligand π-orbitals with metal 3*d* orbitals and thus explaining the signs of the rotatory strengths of the $d-d$ transitions. The exciton model as applied to such complexes is a very crude model which only considers the weak coupling of the π-transitions on the two acetylacetone parts of the ligand and ignores the presence of the copper ion. Therefore, it is of importance to obtain independent information about the structure and also to measure the absorption and circular dichroism under conditions where the structure is known.

EXPERIMENTAL

Crystallographic examination. The title compound was prepared [5] from $Cu(OH)_2$ and the acid form of the ligand in acetone and recrystallized from cyclohexane to obtain single crystals

suitable for the X-ray diffraction studies. The crystals grow as red-brown rhombic plates. In polarized light they appear red and green when the electric vector is parallel to the two rhombic diagonals.

Preliminary photographs showed that the crystals are orthorhombic. The space group is uniquely determined to be $P2_12_12_1$ from the systematically absent reflections. A single crystal of the dimensions $0.29 \times 0.36 \times 0.15$ mm^3 was chosen for the data collection and for the accurate determination of the unit cell parameters. The reflections from the crystal were very broad, so to get good resolution of the diffraction peaks, Cu$K\alpha$ radiation obtained from a graphite monochromator was used for the data collection on a Picker FACS-1 diffractometer. The setting angles for 12 relatively high angle reflections were located automatically on the diffractometer and these angles were used in a least squares refinement to determine the cell parameters. The density of the crystals was determined by flotation in a mixture of chlorobenzene and bromobenzene.

The intensity data were measured at 22 °C by a $\theta-2\theta$ scan performed at a rate of 1° per minute. The scan range was increased with 2θ. Background counts were made for 20 s at each end of the scan range. The intensities of three standard reflections were measured after every 40 reflections. These measurements indicated that no deterioration or misalignment of the crystal had occurred during the data collection.

The 4039 reflections with $\sin\theta/\lambda \leq 0.580$ measured during the data collection were reduced to 2521 independent observed reflections which had $I/\sigma(I) > 1.5$, where $\sigma(I)$ is the standard deviation of the intensity calculated from counting statistics. The data set was corrected for Lorentz and polarization effects but not for absorption.

The following computer programs were employed during this work: The Vanderbilt System [6] for all diffractometer operations, a local modification of the program NRC-2A[7] for data reduction, ORTEP II [8] for illustrations and The X-RAY System [9] for the crystal structure analysis.

The atomic scattering factors used in the calculations were those of Cromer and Mann.[10] The anomalous dispersion corrections to the scattering factor of the copper atom were by Cromer and Liebermann.[11]

Spectral measurements. The circular dichroism spectra were obtained on Roussell-Jouan dichrographs I and II and absorption spectra were recorded on a Cary 14 spectrophotometer. [Cu *R*-pn(acac)$_2$] was treated in a ball mill with KBr for 2–5 h. For measurements in the UV region various dilutions were made. The KBr-complex mixture was pressed into plates by standard techniques used for IR spectroscopy. Plate thickness was measured by micrometer. The plates for UV measurements were sufficiently dilute to be completely transparent to the eye whereas the KBr-suspensions for visible spectra invariably gave turbid plates due to the relatively high complex concentration (2×10^{-2} – 10^{-3} mol/dm^3). The visible absorption of many plates was measured and qualitative equality with solution spectra was found. The experimental shortcomings exclude quantitative comparisons in this region. The UV absorption of the plates indicated little disturbance from internal reflections. The circular dichroism measurements on KBr-disks were performed on a number of plates of varying complex concentrations ($2 \times 10^{-2} - 10^{-5}$ M) and widths (1 – 2 mm). Maximum uncertainties on UV measurements are estimated to ± 10 % judged as the reproducibility of independent measurements.

CRYSTAL DATA

4,4′-(*R*-Propylenediiminato)di(3-penten-2-one)copper(II); $C_{13}H_{20}N_2O_2Cu$; M = 299.9. Orthorhombic, $a = 12.452(6)$ Å, $b = 21.032(12)$ Å, $c = 10.766(7)$ Å, $U = 2819(5)$ Å^3. $D_m = 1.41 \pm 0.02$ g cm^{-3}, $Z = 8$, $D_c = 1.413(3)$ g cm^{-3}. μ(Cu$K\alpha$) = 21.2 cm^{-1}, $F(000) = 1256$. Systematically absent reflections: $h00$ when h odd, $0k0$ when k odd, $00l$ when l odd; space group $P2_12_12_1$ (D_2^4, No. 19). Developed faces {010} and {101}.

STRUCTURE DETERMINATION AND REFINEMENT

The coordinates for the two independent copper atoms could be deduced from the three-dimensional Patterson function. The positions of the other non-hydrogen atoms of the structure were determined from two successive Fourier syntheses phased from the partial structure.

This structure has been refined by the method of least squares minimizing $R = \sum w(|F_o| - K|F_c|)^2$ using the 2521 observed reflections.

Initially a unit weighted full matrix refinement of the scalefactor, the atomic coordinates and individual, isotropic temperature factors was performed. Later when anisotropic temperature factors were introduced the parameters were varied in blocks corresponding to the two independent molecules. The weights employed during the last cycles of least squares refinement were of the form $w = X \cdot Y$. The

two factors X and Y in the product are defined as follows, for $\sin\theta > 0.4700$ $X = 1.0$ otherwise $X = \sin\theta/0.4700$, for $|F_o| < 15.0$ $Y = 1.0$ otherwise $Y = 15.0/|F_o|$.

The asymmetric carbon atom in the amine part of the ligand has previously been shown to have the *R*-configuration,[12] and this was used to decide between the two possible enantiomeric structures. Though the anomalous dispersion correction to the scattering factor of copper is small with Cu$K\alpha$ radiation the absolute configuration was confirmed by least squares refinement. Refinement of the structure corresponding to the *R*-configuration of the asymmetric carbon atom converged when the unit weighted and weighted residuals were 4.7 and 5.8 %, respectively, while the refinement of the mirror image of the structure corresponding to the *S*-configuration of the carbon atom converged when the equivalent residuals were 4.8 and 6.0 %. Application of Hamiltons *R*-factor test [13] to these results indicates that the structure corresponding to the *S*-configuration can be rejected at a level of significance of 0.005. No attempt was made to locate the hydrogen atoms in the structure.

The final coordinates and anisotropic thermal parameters for the non-hydrogen atoms in the structure are listed in Tables 1 and 2, respectively. A list of observed and calculated structure amplitudes with phases may be obtained from the authors upon request.

Table 1. Final atomic coordinates. The estimated standard deviations × 10^4 are given in parentheses. The first number in the numerical label distinguishes between the two molecules in the structure. The other numbers in the label are illustrated in Fig. 1.

Atom	*x*	*y*	*z*
Cu1	0.59326(0.6)	0.48096(0.3)	−0.01492(0.6)
O11	0.5458(4)	0.4109(2)	−0.1140(4)
C11	0.5687(5)	0.3523(3)	−0.0942(6)
C12	0.6281(5)	0.3297(3)	0.0038(7)
C111	0.5250(8)	0.3065(4)	−0.1908(8)
C13	0.6721(5)	0.3654(3)	0.1006(6)
C131	0.7312(9)	0.3287(5)	0.1999(9)
N11	0.6632(4)	0.4273(2)	0.1053(4)
C14	0.7057(5)	0.4646(3)	0.2109(5)
C15	0.7428(4)	0.5296(3)	0.1600(6)
C151	0.8520(4)	0.5231(4)	0.0940(7)
N12	0.6606(4)	0.5512(2)	0.0713(4)
C16	0.6461(5)	0.6115(3)	0.0479(6)
C161	0.7075(6)	0.6629(3)	0.1175(8)
C17	0.5708(5)	0.6330(3)	−0.0433(6)
C18	0.5104(5)	0.5949(3)	−0.1199(5)
C181	0.4328(6)	0.6258(3)	−0.2096(7)
O12	0.5117(3)	0.5346(2)	−0.1227(3)
Cu2	0.40468(0.6)	0.49875(0.3)	0.24570(0.6)
O21	0.4548(4)	0.4300(2)	0.3473(4)
C21	0.4383(4)	0.3705(3)	0.3264(6)
C22	0.3836(5)	0.3459(3)	0.2271(7)
C211	0.4855(7)	0.3267(3)	0.4238(8)
C23	0.3364(5)	0.3804(3)	0.1296(6)
C231	0.2859(8)	0.3445(4)	0.0217(9)
N21	0.3367(4)	0.4429(2)	0.1275(4)
C24	0.2896(5)	0.4788(3)	0.0237(5)
C25	0.2526(4)	0.5439(3)	0.0699(5)
C251	0.1458(5)	0.5394(4)	0.1394(7)
N22	0.3371(3)	0.5671(2)	0.1541(4)
C26	0.3550(5)	0.6278(3)	0.1691(6)
C261	0.2959(6)	0.6778(3)	0.0935(7)
C27	0.4295(5)	0.6524(3)	0.2584(6)
C28	0.4861(4)	0.6152(3)	0.3436(5)
C281	0.5595(6)	0.6489(3)	0.4336(6)
O22	0.4840(3)	0.5547(2)	0.3531(4)

DESCRIPTION AND DISCUSSION OF THE STRUCTURE

Table 3 lists the bond lengths and bond angles for the two crystallographically independent molecules. By inspection of the table it is apparent that there are only minor differences between the molecules. The average numerical difference in the bond lengths is 0.92 and in the bond angles it is 1.24 measured in units of the estimated standard deviation from the least squares refinement. A normal probability plot of the ranked deviates in bond lengths and bond angles shows that these follow a normal distribution. Therefore it is concluded that the structure contains two not significantly different molecules. Some average values of important bond lengths and bond angles are shown in Fig. 1.

It is of interest to compare the conformation of the bridging propylene group with the conformation found for the corresponding complexes derived from ethylenediamine. Hall and Waters have determined the crystal structure for ethylenebis(acetylacetoneiminato) copper(II),[1] [Cu en(acac)$_2$], where the ethylene bridge takes an unsymmetric *gauche* conformation. A *gauche* conformation is likewise found for the hemihydrate,[2] whereas eclipsed conformations were found for the hydrate [3] and

Table 2. The thermal parameters, U_{ij}, in units of $Å^2 \times 10^4$. The expression for the temperature factor is $\exp\{-2\pi^2(U_{11}h^2a^{*2}+U_{22}k^2b^{*2}+U_{33}l^2c^{*2}+2U_{12}hka^*b^*+2U_{13}hla^*c^*+2U_{23}klb^*c^*)\}$. The estimated standard deviations from the least squares refinement are given in parentheses. The labelling is the same as in Table 1.

Atom	U_{11}	U_{22}	U_{33}	U_{12}	U_{13}	U_{23}
Cu1	472(4)	470(4)	466(4)	8(3)	−34(3)	−7(3)
O11	859(28)	511(22)	602(24)	30(21)	−189(22)	−63(19)
C11	601(33)	486(28)	623(33)	−21(26)	66(28)	−41(26)
C12	733(38)	488(29)	862(45)	39(27)	145(37)	109(33)
C111	1201(64)	574(37)	882(50)	−72(42)	−36(51)	−174(37)
C13	519(30)	639(35)	650(35)	−43(28)	1(28)	221(30)
C131	1143(65)	1001(60)	937(57)	121(55)	−186(55)	437(51)
N11	454(23)	639(28)	497(24)	−41(21)	−10(20)	88(21)
C14	523(31)	815(40)	481(28)	−49(29)	−57(25)	14(28)
C15	399(27)	789(38)	567(30)	−75(27)	−38(24)	−91(30)
C151	391(27)	964(47)	818(42)	16(32)	91(30)	49(41)
N12	426(23)	565(25)	554(25)	10(20)	−28(21)	−60(21)
C16	497(28)	594(33)	677(36)	−89(26)	157(28)	−160(29)
C161	802(45)	620(37)	1009(54)	−176(36)	1(44)	−248(39)
C17	539(31)	481(26)	699(35)	0(24)	77(28)	−4(26)
C18	537(30)	554(31)	521(30)	22(25)	77(27)	60(25)
C181	845(46)	686(37)	736(41)	124(36)	−55(37)	213(33)
O12	591(21)	476(20)	536(21)	6(17)	−96(19)	18(17)
Cu2	414(3)	540(4)	406(3)	−57(3)	−28(3)	−22(3)
O21	613(22)	536(22)	522(21)	−15(18)	−75(20)	−8(18)
C21	406(26)	617(33)	578(32)	4(24)	71(25)	−27(27)
C22	631(36)	565(32)	789(42)	16(28)	16(34)	−97(31)
C211	865(47)	634(38)	800(40)	104(35)	−43(41)	113(36)
C23	457(29)	631(34)	611(35)	−63(26)	14(28)	−199(29)
C231	989(54)	858(49)	923(55)	−142(46)	−170(52)	−383(46)
N21	462(25)	684(30)	449(24)	−88(22)	7(21)	−73(22)
C24	549(30)	805(38)	465(27)	−120(30)	−64(26)	7(30)
C25	386(28)	716(36)	493(28)	−124(24)	−47(24)	87(27)
C251	402(28)	919(48)	744(40)	−71(30)	101(30)	146(37)
N22	380(22)	561(26)	485(23)	−74(19)	−45(20)	51(21)
C26	481(28)	651(36)	574(33)	13(27)	−8(28)	47(28)
C261	800(46)	627(36)	800(45)	−94(34)	−164(41)	101(34)
C27	522(30)	584(30)	601(32)	−69(24)	−12(29)	−66(28)
C28	482(28)	596(33)	481(28)	−96(25)	35(26)	−86(26)
C281	771(41)	773(40)	582(35)	−227(35)	−111(33)	−126(32)
O22	632(23)	549(22)	512(20)	−95(19)	−104(20)	10(18)

the methylammonium perchlorate adduct.[4] In [Cu en(acac)$_2$].$CH_3NH_3ClO_4$ the ethylene carbon atoms are co-planar with the four ligating atoms whereas in [Cu en(acac)$_2$].H_2O these atoms are situated on one side of the plane of the ligators. An ORTEP drawing of [Cu *R*-pn(acac)$_2$] (Fig. 2) shows the *gauche* conformation of the ethylene bridge with the methyl group in the axial position. The dihedral angle defined by N1, C4, C5, and N2 is 42.3(6)° and 41.5(6)° for the two molecules. This conformation is surprisingly close to the conformation determined [14] by ^1H NMR for the corresponding diamagnetic complex [Ni *R*-pn(acac)$_2$]. In most cases chelate rings of 1,2-propanediamine have the methyl group in an equatorial position, but in [Cu *R*-pn(acac)$_2$] this would lead to a severe interaction with the methyl group on the nearest acetylacetone part. The conformation of the Cu−pn ring is δ as also proposed by Downing and Urbach [14] on the basis of the circular dichroism of the $d-d$ transitions. A similar conformation was found by X-ray diffraction for the salicylaldimine complex [Cu pn(sal)$_2$].[15]

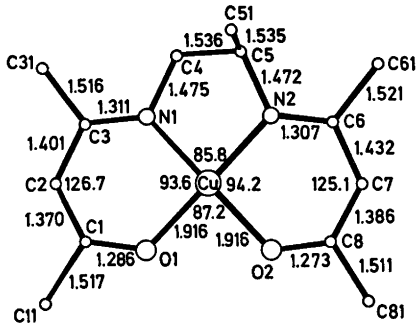

Fig. 1. An ORTEP drawing viewed perpendicular to the mean coordination plane. The shown bond lengths and bond angles are mean values for the two independent molecules of the asymmetric unit.

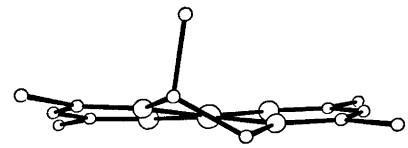

Fig. 2. The molecule viewed along the molecular pseudo two-fold axis.

To illustrate the overall geometry of [Cu *R*-pn(acac)$_2$] Table 4 lists the distances of the atoms from some characteristic planes. The complex is grossly planar but with a significant tetrahedral distortion as may be seen from the distribution of atoms above and below the plane (I) defined by the four ligators. The two acetylacetoneimine parts are nearly planar with the angle between the planes of 10 and 11° for the two molecules.

Table 3. Bond lengths (Å) and bond angles (°). The labelling corresponds to Fig. 1. Standard deviations in parentheses in terms of the last digit.

	1	2		1	2
Cu–O1	1.913(4)	1.918(4)	O1 –Cu–O2	87.2(2)	87.2(2)
Cu–O2	1.910(4)	1.922(4)	O1 –Cu–N1	93.6(2)	93.5(2)
Cu–N1	1.925(5)	1.928(5)	N1 –Cu–N2	85.9(2)	85.7(2)
Cu–N2	1.935(5)	1.936(5)	O2 –Cu–N2	94.1(2)	94.3(2)
O1–C1	1.283(7)	1.289(7)	Cu –O1–C1	125.3(4)	125.5(4)
C1–C2	1.373(10)	1.368(9)	O1 –C1–C2	125.4(6)	125.7(6)
C2–C3	1.397(10)	1.405(10)	O1 –C1–C11	114.5(6)	114.0(5)
C3–C31	1.510(11)	1.522(11)	C11–C1–C2	120.0(6)	120.3(6)
C3–N1	1.307(8)	1.315(8)	C1 –C2–C3	126.8(6)	126.6(6)
N1–C4	1.479(8)	1.470(8)	C2 –C3–N1	122.0(6)	121.9(6)
C4–C5	1.543(10)	1.529(9)	C2 –C3–C31	116.4(6)	119.1(6)
C5–C51	1.540(8)	1.529(8)	C31–C3–N1	121.6(6)	118.9(6)
C5–N2	1.472(7)	1.472(7)	Cu –N1–C3	126.6(4)	126.7(4)
N2–C6	1.307(8)	1.306(8)	Cu –N1–C4	111.5(4)	111.3(4)
C6–C7	1.430(9)	1.433(9)	N1 –C4–C5	107.7(5)	109.5(5)
C7–C8	1.375(8)	1.397(9)	C4 –C5–N2	107.1(5)	106.3(4)
C8–C81	1.513(10)	1.509(9)	C51–C5–C4	110.5(6)	111.4(5)
C8–O2	1.269(7)	1.277(7)	C51–C5–N2	110.0(5)	109.9(5)
C6–C61	1.521(10)	1.520(10)	C5 –N2–Cu	112.1(4)	112.3(4)
C1–C11	1.519(10)	1.514(10)	C6 –N2–Cu	126.1(4)	126.1(4)
			N2 –C6–C7	122.0(5)	123.1(6)
			N2 –C6–C61	121.7(6)	121.9(6)
			C61–C6–C7	116.3(5)	115.0(6)
			C6 –C7–C8	125.8(5)	124.4(6)
			C7 –C8–O2	126.3(5)	127.0(5)
			C7 –C8–C81	118.8(5)	117.7(6)
			C81–C8–O2	115.0(5)	115.4(5)
			C8 –O2–Cu	125.6(4)	124.9(4)

Table 4. Distances in Å of the atoms from the least squares planes.[a]

Atom	I		II		III	
	1	2	1	2	1	2
Cu	−0.02	0.01	0.08	0.00	−0.02	−0.10
O1	0.12*	0.11*	0.00*	0.01*	0.26	0.05
N1	−0.12*	−0.11*	0.00*	−0.00*	−0.25	−0.37
O2	−0.12*	−0.11*	−0.04	−0.19	0.01*	0.00*
N2	0.12*	0.11*	0.44	0.24	−0.02*	−0.01*
C1	0.20	0.24	0.00*	0.01*	0.32	−0.03
C2	0.15	0.02	0.01*	0.01*	0.15	−0.25
C11	0.37	0.25	0.00	0.02	0.61	0.15
C3	−0.02	−0.11	−0.01*	−0.01*	−0.14	−0.44
C31	−0.09	−0.31	−0.04	−0.12	−0.32	−0.79
C4	−0.36	−0.28	−0.08	−0.04	−0.62	−0.61
C5	0.36	0.41	0.75	0.65	0.10	0.15
C51	1.87	1.92	2.25	2.17	1.58	1.63
C6	0.15	0.04	0.55	0.18	0.02*	0.01*
C61	0.33	0.17	0.91	0.42	−0.09	0.11
C7	−0.01	−0.12	0.34	0.08	−0.01*	−0.01*
C8	−0.13	−0.16	0.06	−0.23	−0.01*	0.00*
C81	−0.31	−0.31	−0.17	−0.47	−0.07	0.00

[a] The displacements marked with an asterisk are those of the atoms used in determining the least squares plane.

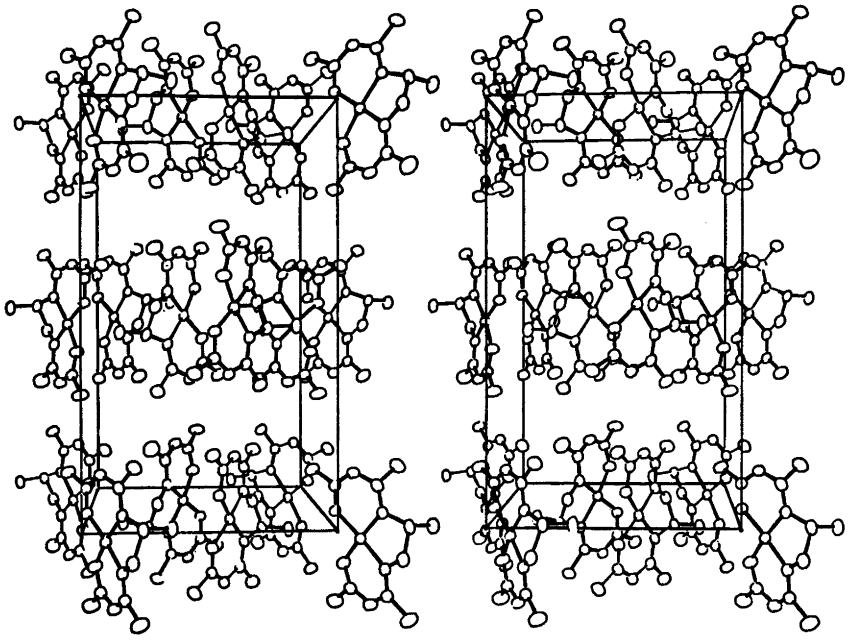

Fig. 3. Stereo pair of the packing viewed along the *c* axis.

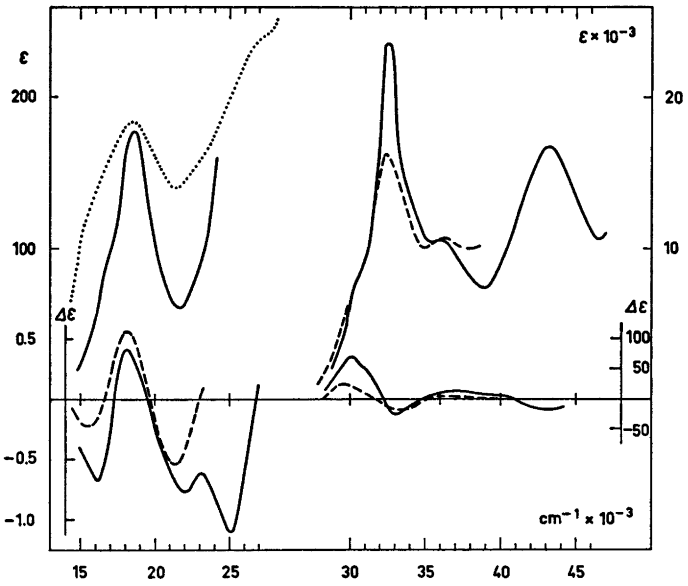

Fig. 4. Absorption and circular dichroism spectra of [Cu *R*-pn(acac)$_2$] in methanol solution (———) and dispersed as crystals in KBr-discs (- - -).

The absolute configuration of the two lines connecting N and O within an acetylacetoneimine is *A* thus confirming the qualitative result based on the circular dichroism spectrum of the crystalline compound dispersed in KBr.

The bond lengths and bond angles of the two conjugated acetylacetoneiminato parts differ only insignificantly indicating that the propylene methyl group interacts weakly with the rest of the molecule. All the molecular dimensions are similar to those found for other acetylacetoneiminato complexes. The C–C bond length closest to the nitrogen atom is greater than the C–C distance adjacent to the oxygen atom. This difference is rationalized by assuming that the inner complex is derived from the tautomer form of the ligand where the hydrogen atom is bonded to the nitrogen atom. This is the tautomer found by ^{1}H NMR for the free ligand in solution.[16,17] However, judged by the low value of the C–N bond length, 1.31 Å, it is evident that the conjugation is quite extensive.

The molecular packing in the crystal is determined by van der Waals interactions between adjacent complexes. The two independent molecules are nearly co-planar (angle ~2°) and parallel to the *b* axis. The packing is illustrated in Fig. 3 by a stereo pair seen from the *c* axis. There are only negligible interactions between molecules in the direction of the *b* axis with the shortest distance of 3.9 Å between two methyl carbon atoms.

The complex has earlier been claimed to be more tetrahedrally distorted in solution than found here for the crystalline state.[5] This difference could possibly be a consequence of the packing forces.

SPECTRAL RESULTS AND DISCUSSION

The absorption and circular dichroism spectra of [Cu *R*-pn(acac)$_2$] in methanol [5] are shown in Fig. 4 together with the circular dichroism curve obtained from the complex dispersed in KBr discs. The latter technique has severe limitations as described in the experimental section and only for allowed transitions in the region 29 000 – 34 000 cm^{-1} are the measurements on KBr discs considered truly quantitative. The two circular dichroism curves for this region do show interesting similarities and differences. Firstly, it is noticed that the two Cotton effects attributed to the exciton coupled internal $\pi \rightarrow \pi^*$ transitions have the same sign in solution and in KBr.

This shows that in the complex the acetylacetonate units are distributed with the same absolute configuration in methanol solution and in the solid. The absolute configuration predicted [5] from the chiroptical properties is in agreement with this X-ray diffraction study. Secondly, it is noteworthy that the solution Cotton effects are considerably larger than for the crystalline state. This effect may be explained by a difference in the angle between the two acetylacetonate planes. A larger angle ($\sim 40°$) was earlier estimated for solution conformation compared to the angle found for the complex in crystals ($\sim 10°$).

It is unfortunate that the spectral results of the visible region are too disturbed by internal reflections to be of quantitative use. Instead single crystal linear and circular dichroism measurements can be done giving additional information on the polarization effects.[18]

REFERENCES

1. Hall, D., Rae, A. D. and Waters, T. N. *J. Chem. Soc.* (1963) 5897.
2. Hall, D., Morgan, H. J. and Waters, T. N. *J. Chem. Soc. A* (1966) 677.
3. Clark, G. R., Hall, D. and Waters, T. N. *J. Chem. Soc. A* (1969) 823.
4. Baker, E. N., Hall, D. and Waters, T. N. *J. Chem. Soc. A* (1970) 396.
5. Jensen, H. P. and Larsen, E. *Acta Chem. Scand. 25* (1971) 1439.
6. Lenhert, P. G. *The Vanderbilt Disk Oriented Diffractometer System.*
7. Ahmed, F. R. *N.R.C. Crystallographic Program System*, National Research Council, Ottawa 1968.
8. Johnson, C. K. ORTEP: *A Fortran Ellipsoid Plot Program for Crystal Structure Illustrations*, Report ORNL-3794, Second Rev., Oak Ridge National Laboratory, Oak Ridge 1970.
9. Stewart, J. M. *et al. The X-Ray System 1972*, Technical Report Tr-192, Computer Science Center, University of Maryland.
10. Cromer, D. and Mann, J. B. *Acta Crystallogr. A 24* (1968) 321.
11. Cromer, D. and Liebermann, D. *J. Chem. Phys. 53* (1970) 1891.
12. Saito, Y. and Iwasaki, H. *Bull. Chem. Soc. Jap. 35* (1962) 1131.
13. Hamilton, W. C. *Acta Crystallogr. 18* (1965) 502.
14. Downing R. S. and Urbach, F. L. *J. Am. Chem. Soc. 91* (1969) 5977.
15. Llewellyn, F. and Waters, T. N. *J. Chem. Soc.* (1960) 2639.
16. Dudek, G. O. and Holm, R. H. *J. Am. Chem. Soc. 83* (1961) 209.
17. Larsen, E. and Schaumburg, K. *Acta Chem. Scand. 25* (1961) 962.
18. Jensen, H. P. *Acta Chem. Scand. A 30* 1976) 137.

Received August 6, 1975.

Acta Chemica Scandinavica A 30 (1976) 133—136

Hydrothermal Preparation and Magnetic Properties of α-CrOOH, β-CrOOH, and γ-CrOOH

A. NØRLUND CHRISTENSEN

Department of Inorganic Chemistry, University of Aarhus, DK-8000 Aarhus C, Denmark

The chromium oxide hydroxides, α-CrOOH, β-CrOOH, and γ-CrOOH were prepared using hydrothermal techniques. The unit cell parameters at 293 K were determined for α- and β-CrOOH. All samples of γ-CrOOH were X-ray amorphous and chemical analysis showed a smaller chromium content (55.0 %) than corresponding to the formula γ-CrOOH (61.3 %). The infra red spectra of γ-CrOOH indicate that the compound contains water of hydration.

The magnetic properties of the three compounds have been investigated between 75 and 293 K using the Faraday method. α-CrOOH is paramagnetic and the magnetic moment of Cr^{3+} is 3.74 ± 0.05 μ_B. β-CrOOH shows a deviation from the Curie-Weiss law at temperatures below 225 K. The magnetization has a broad maximum in the temperature range 90 to 140 K corresponding to a Néel temperature of approximately 120 K. In the paramagnetic temperature range the magnetic moment of Cr^{3+} is 3.91 ± 0.10 μ_B. γ-CrOOH is paramagnetic in the investigated temperature range and the magnetic moment of Cr^{3+} is 3.71 ± 0.05 μ_B.

The oxide hydroxide of chromium, CrOOH, can be prepared in three polymorphic forms, using hydrothermal techniques.[1–9] α-CrOOH has a layer structure with short hydrogen bonds.[10–11] β-CrOOH has an indium oxide hydroxide structure,[12] and is a dense phase with short hydrogen bonds.[8,13] γ-CrOOH is assumed to have the same structure as lepidocrocite, γ-FeOOH.[9] Unit cell parameters and space group for two modifications of CrOOH are listed in Table 1. The magnetic properties of β-CrOOH and γ-CrOOH have not been investigated before. The magnetic properties of α-CrOOH have been investigated in the temperature range 66 to 530 K using the Gouy method.[14] In this work samples were prepared for investigations of hydrogen bonding and magnetic properties of the three compounds.

Table 1. Unit cell parameters and magnetic data for chromium oxide hydroxides.

Compound	Unit cell parameters in Å			Space group	θ_N (K)	θ_P (K)	Molar Curie Constant C_M Exp.	Magnetic moment in μ_B	Ref.
	a	*b*	*c*						
α-CrOOH	2.979(5)	2.979(5)	13.37(2)			−170.9	1.74	3.74(5)	This work
	2.976(1)	2.976(1)	13.36(1)	$R\bar{3}m$					11
						−276	1.9342	3.93	14
β-CrOOH	4.862(2)	4.298(2)	2.955(1)		120	−102.1	1.91	3.91(10)	This work
	4.861	4.292	2.960	$P2_1nm$					5,13
γ-CrOOH						−106.9	1.72	3.71(5)	This work

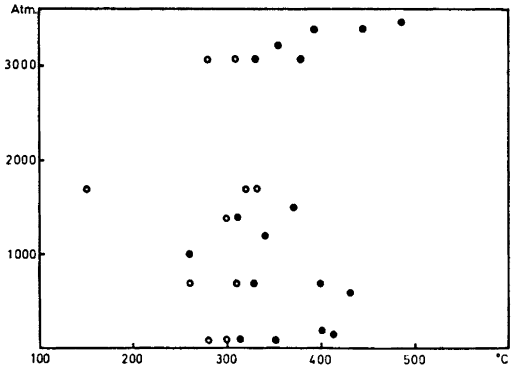

Fig. 1. Pressure temperature region used in the preparation of γ-CrOOH, open circles, and α-CrOOH, filled circles.

EXPERIMENTAL

Chemistry and X-ray technique. α-CrOOH and γ-CrOOH were obtained by reduction of chromate with formate under hydrothermal conditions. The solution used was 1 M with respect to Na_2CrO_4 and 1.5 M with respect to HCOONa. A conventional hydrothermal technique was used.[15] Fig. 1 shows the pressure-temperature region used. At temperatures below 250 °C pure γ-CrOOH is formed and at temperatures above approximately 320 °C pure α-CrOOH is formed. In a temperature range from 250 to 320 °C γ-CrOOH contaminated with α-CrOOH is obtained, and the α-CrOOH content is increasing with increasing temperature used in the hydrothermal preparation. X-Ray powder patterns were taken of all products from the hydrothermal preparation using a Guinier camera with Cu$K\alpha_1$ radiation, $\lambda = 1.54051$ Å, or Co$K\alpha_1$ radiation, $\lambda = 1.78892$ Å, and sodium chloride ($a_{NaCl} = 5.6389$ Å) or germanium ($a_{Ge} = 5.6576$ Å) as internal standards. The unit cell parameters for α-CrOOH obtained from such a measurement are listed in Table 1. All samples of pure γ-CrOOH were amorphous. Chemical analyses were made of α-CrOOH and γ-CrOOH using a standard thiosulfate-iodine titration of chromate. (Found for α-CrOOH: Cr 60.3. Calc.: Cr 61.3. Found for γ-CrOOH: Cr 55.0. Calc.: Cr 61.3). A thermogravimetric analysis of γ-CrOOH shows a weight loss in the temperature range 80 to 240 °C corresponding to a 7 % water content of the sample. The weight loss in the temperature range 240 to 430 °C corresponds to the formation of Cr_2O_3 from the chromium oxide hydroxide, (see Table 2). A Guinier powder pattern of a sample of γ-CrOOH heated to 715 °C for 24 h had only lines of Cr_2O_3.

β-CrOOH was prepared from CrO_3 by reduction under hydrothermal conditions. CrO_2 was obtained from CrO_3 by dry decomposition. CrO_3 was sealed in gold ampoules and heated from 375 to 415 °C at an external hydrostatic pressure up to 300 MPa for 75 h. Approximately 650 mg of CrO_3 was then sealed in gold ampoules with 2 g of oxalic acid, $(COOH)_2 . 2H_2O$, and 1 ml of water, and was treated hydrothermally at temperatures from 350 to 405 °C and pressure from 170 to 230 MPa for 73 h. Guinier powder patterns of the products were obtained as described above, and the unit cell parameters obtained are listed in Table 1. Chemical analyses of β-CrOOH were made using the same procedure as for α-CrOOH. (Found: Cr 59.5. Calc.: Cr 61.3).

Infra red spectra. The IR spectra of the three chromium compounds were recorded over the frequency range 4000 to 300 cm^{-1} with a Perkin-Elmer 180 spectrophotometer using pellets of mixtures of 1 mg of sample and 200 mg of KBr. The spectra are shown in Fig. 2.

Magnetic measurements. The magnetization of α-CrOOH, β-CrOOH, and γ-CrOOH was measured at temperatures from 75 to 293 K using the Faraday method. The sample was placed in a flow cryostat cooled with liquid nitrogen, and the magnetization was recorded with an electrobalance. The magnetic field was calibrated using Mohrs salt, $(NH_4)_2 Fe(SO_4)_2 . 6H_2O$, $\chi_g = 32.2 \times 10^{-6}$, and erbium

Table 2. Experimental conditions for hydrothermal preparation of samples of γ-CrOOH and chromium content. (Theoretical value for γ-CrOOH: 61.3 %).

Exp. No.	Temp. °C	Pressure MPa	Time in	Guinier powder pattern	Chromium content in %
1	260	70	24	amorphous	56.35
2	300	8	26	amorphous	54.70
3	310	170	72	traces of α-CrOOH	54.56
γ-CrOOH containing 7 % of water					56.8
γ-CrOOH corrected for the water content					61.0

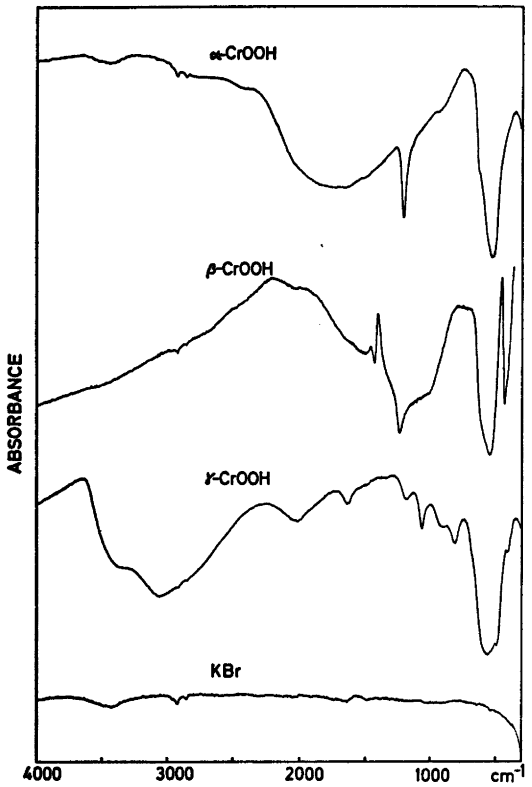

Fig. 2. Infra red spectra of α-CrOOH, β-CrOOH, γ-CrOOH, and KBr.

oxide hydroxide, ErOOH, $\chi_g = 181.8 \times 10^{-6}$, as standards. Fig. 3 shows χ_{mol}^{-1} *vs.* temperature for α-CrOOH and for γ-CrOOH. The two compounds are paramagnetic in the temperature range investigated and the susceptibilities follow the Curie-Weiss law, $\chi_{mol} = C_M/(T-\theta_p)$.

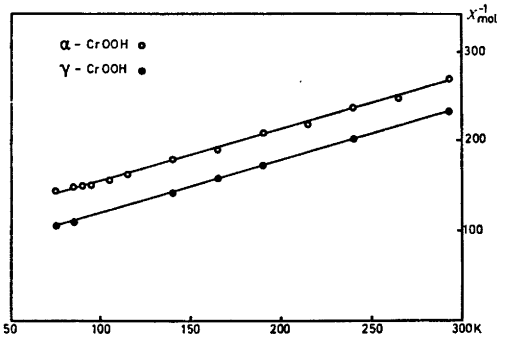

Fig. 3. χ_{mol}^{-1} *vs.* temperature for α-CrOOH and γ-CrOOH.

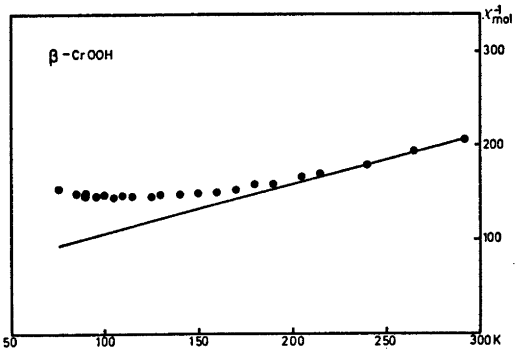

Fig. 4. χ_{mol}^{-1} *vs.* temperature for β-CrOOH.

The magnetic data for the two compounds are listed in Table 1. Fig. 4 shows χ_{mol}^{-1} *vs.* temperature for β-CrOOH. The susceptibility follows the Curie-Weiss law from room temperature to approximately 225 K and below this temperature the deviation from the Curie-Weiss law is significant. The magnetization has a broad maximum in the temperature range 90 to 140 K corresponding to a Néel temperature of approximately 120 K. The magnetic data for β-CrOOH are listed in Table 1.

CONCLUSIONS

The hydrothermal investigation yielded the three chromium compounds α-CrOOH, β-CrOOH, and γ-CrOOH. The two compounds α-CrOOH, and β-CrOOH could be identified *via* chemical analysis and their X-ray diffraction powder patterns, that were indexed with unit cell parameter very similar to previously reported values (see Table 1). γ-CrOOH could only be made as X-ray amorphous samples. The chemical analysis is not in satisfactory agreement with the formula γ-CrOOH suggested by Hund,[9] who reported the X-ray powder pattern for γ-CrOOH and showed it to be similar to that of γ-FeOOH. No chemical analysis are given in Ref. 9 for γ-CrOOH. The results of some chemical analyses on samples of γ-CrOOH are listed in Table 2. A content of water in the samples may explain the low values of the chromium analysis.

The infra red spectra of the three compounds are different from each other (see Fig. 2). α-CrOOH has a broad absorption band in the frequency range 2000 – 1400 cm^{-1} with a minimum at 1700 cm^{-1}. A short hydrogen

bond of 2.49 ± 0.02 Å has been reported for α-CrOOH.[11] β-CrOOH shows a broad and rather weak absorption band in the frequency range $1850 - 1450$ cm^{-1}, and the structure of the compound will have a short hydrogen bond of 2.4 ± 0.2 Å.[13] γ-CrOOH shows a broad absorption band at 3500 cm^{-1}, characteristic for free water. The lack of characteristic OH^--absorption bands in α-CrOOH and β-CrOOH are possibly due to the short hydrogen bonds.

The magnetic data for α-CrOOH found in this investigation are different from the previously reported values; the greatest differences are found for θ_p (see Table 1). The crystal structure of β-CrOOH is very similar to that of CrO_2 and can be described as a deformed rutile structure. The magnetic data for the two compounds are, however, very different from each other, and the magnetic superexchange must have different character in the two compounds. CrO_2 becomes ferromagnetic with a Curie temperature of 118 °C [16] and β-CrOOH shows an antiferromagnetic nature below 120 K. γ-CrOOH is paramagnetic in the temperature range investigated.

Acknowledgements. I am indebted to Carlsbergfondet for the use of some of the high pressure equipments and to Statens Naturvidenskabelige Forskningsråd for the use of the Faraday magnetometer. Mr. N. J. Hansen and Miss G. Petersen are acknowledged for valuable assistance in measuring magnetic data and in recording IR spectra. Mrs. B. Saustrup Kristensen is acknowledged for the thermogravimetric analysis.

REFERENCES

1. Simon, A., Fischer, O. and Schmidt, Th. *Z. Anorg. Allg. Chem. 185* (1930) 107.
2. Laubengayer, A. W. and McCune, H. W. *J. Am. Chem. Soc. 74* (1952) 2362.
3. Shafer, M. W. and Roy, R. *Z. Anorg. Allg. Chem. 276* (1954) 275.
4. Ipatiew, W. and Kisselew, A. *Ber. Dtsch. Chem. Ges. 59* (1926) 1418.
5. Thamer, B. J., Douglass, R. M. and Staritzky, E. *J. Am. Chem. Soc. 79* (1957) 547.
6. Tombs, N. C., Croft, W. J., Carter, J. R. and Fitzgerald, J. F. *Inorg. Chem. 3* (1964) 1791.
7. Shibasaki, Y. *Mat. Res. Bull. 7* (1972) 1125.
8. Christensen, A. N. *Mat. Res. Bull. 6* (1971) 691.
9. Hund, F. *Naturwissenschaften 46* (1959) 320.
10. Douglass, R. M. *Acta Crystallogr. 10* (1957) 423.
11. Hamilton, W. C. and Ibers, J. A. *Acta Crystallogr. 16* (1963) 1209.
12. Lehmann, M. S., Larsen, F. K., Poulsen, F. R., Christensen, A. N. and Rasmussen, S. E. *Acta Chem. Scand. 24* (1970) 1662.
13. Christensen, A. N. *Inorg. Chem. 5* (1966) 1452.
14. Meisenheimer, R. G. and Swalen, J. D. *Phys. Rev. 123* (1961) 831.
15. Christensen, A. N. *J. Solid State Chem. 4* (1972) 46.
16. Flippen, R. B. *J. Appl. Phys. 34* (1963) 2026.

Received July 29, 1975.

Acta Chemica Scandinavica A 30 (1976) 137—142

Crystal Linear and Circular Dichroism of the Copper(II) Complex of the Schiff Base from *R*-1,2-Propanediamine and Acetylacetone

HANS PETER JENSEN *

Institute of Molecular Biology, University of Oregon, Eugene, Oregon 97403, U.S.A.

The crystal LD and CD spectra in the visible range have been studied for the copper(II) complex of the Schiff base from *R*-1,2-propanediamine and two molecules of acetylacetone. The results have been used to assign possible ligand field transitions to absorption bands of known polarizations. It is shown that the dipole strength of a given absorption band need not have the same origin as a whole, as part of the absorption in the visible range can be accounted for by $d_{yz} \rightarrow d_{xy}$ and $d_{yx} \rightarrow \pi^*$ transitions. Furthermore, the instrumentation used to obtain LD and CD spectra of an anisotropic crystal is discussed.

Much work has been devoted to gain insight into the crystalline, molecular and electronic structure of copper(II) complexes of β-diketones and of Schiff base derivatives from β-diketones. *E.g.*, the crystalline structure of the anhydrate, the hemihydrate, and the monohydrate of the copper(II) complex with 4,4′-(ethylenediimino)-di(3-pentene-2-one) [Cu en(acac)$_2$] was determined a number of years ago [1–3] and recently the crystalline structure of the copper(II) complex of 4,4′-(*R*-1,2-propanediimino)di(3-pentene-2-one) [Cu Rpn(acac)$_2$] has been determined.[4]

By studying absorption and circular dichroism (CD) spectra of Cu Rpn(acac)$_2$, it has been concluded that this type of compound in solution has a structure somewhere between tetrahedral and planar arrangements;[5,6] in this specific case it was also possible to give the chiralty of the dominating structure later confirmed by the X-ray structural analysis.[4]

Recently it has been shown from linear dichroism (LD) and CD measurements that the nonplanar structure of Cu en(acac)$_2$ observed in the crystalline structure is also present in solution.[7] While there is a fair degree of consistency among structural assignments for this type of compound, the situation becomes a little more confused with respect to electronic configuration and assignments to absorption bands in the visible and near ultraviolet (UV) range. Extended Hückel calculations on the molecular orbitals in bis(β-ketoenolate) complexes of copper(II) assuming a planar structure of the compounds indicated the relative energies of the ligand π-orbitals and the metal ion 3*d*-orbitals to be $3\pi \gtrsim 3d < 4\pi$ with $3d_{xy}$ as the half-filled orbital in the metal $3d^9$-system.[8] It seems to be generally accepted that $3d_{xy}$ is the high energy orbital of the metal ion even when these complexes are nonplanar and twisted towards a tetrahedral structure,[5,6,9] but when it comes to assignments of the electronic transitions in the ligand field range, certain ambiquities are evident. There are three bands of interest for the complexes Cu en(acac)$_2$ and Cu Rpn(acac)$_2$, a shoulder at $\sim$16 000 cm^{-1} (I) on the main peak in the visible at $\sim$18 000 cm^{-1} (II) and a band hidden in the foot of the internal ligand $\pi \rightarrow \pi^*$ transitions at $\sim$22 000 – 23 000 cm^{-1} (III). The earlier assignments to these bands have been summarized in Table 1.

Some of the ambiguity stems from the fact that different approaches have been used in the papers cited. The argument of Downing and Urbach for II being $d_{z^2} \rightarrow d_{xy}$ is based on the experimental fact that II is shifted rather

* On leave from Chemistry Department A, Technical University of Denmark, DK-2800 Lyngby, Denmark.

Table 1. Assignments of visible range bands in Cu Rpn(acac)$_2$ and Cu en(acac)$_2$.

Compound	Band	Assignment	Treated in point group [a]	Polarization [b]	Ref.	Phase
Cu Rpn(acac)$_2$	I	$(x^2-y^2)\rightarrow(xy)$	C_{2v}	y		
	II	$(z^2)\rightarrow(xy)$	C_{2v}	y	5	solution
	III	$(xz)\rightarrow(xy)$	C_2	x		
Cu Rpn(acac)$_2$	I	$(x^2-y^2)\rightarrow(xy)$	D_2	z		
	II	$(xz)\rightarrow(xy)$	D_2	x		
		$(xy)\rightarrow 4\pi$	D_2	x and z	6	solution
	III	or				
		$n\rightarrow\pi^*$	D_2	x and z		
Cu en(acac)$_2$	I	$(x^2-y^2)\rightarrow(xy)$	C_{2v}	y		
	II	$(z^2)\rightarrow(xy)$	C_{2v}	y	9	crystalline
	III	not a $d\rightarrow d$				

[a] The point group of Cu diamine(acac)$_2$ cannot be higher than C_2; on the other hand, one can obtain a better group to work in if one either takes the deviation from planarity to be small (C_{2v}) or puts the N and O equal and forgets the ethylene bridge (D_2). [b] Polarization direction in an orthogonal molecular coordinate system where (a), the ligators define the xy-plane (least mean squares); (b), the x-axis is the projection in this plane of the line passing the midpoints between the two oxygens and the two nitrogens; (c), the z-axis is normal to the xy-plane and passes through the metal ion; see fig. 2 of Ref. 6.

much by adding pyridine to the complex in solution. The assignments of Jensen and Larsen are based on interpretations of CD spectra assuming that the $d\rightarrow d$ transitions "borrow" electric transition dipole moments from the internal ligand $\pi\rightarrow\pi^*$ transitions, and the assignments of Olson *et al.* come from a study of the polarized crystal spectra interpreted in an oriented gas model. From the crystal structure of Cu Rpn(acac)$_2$[4] it is seen that the molecules in the unit cell are oriented in such a way that measurements with linearly polarized light along the **a** and **c** axes would give rise to very weak absorptions of y-polarization in the molecular coordinate system (Table 2). Therefore in the case of Cu Rpn(acac)$_2$ it is possible to study the x- and z-polarized bands specifically contrary to Olson *et al.* dealing with Cu en(acac)$_2$.

SPECTRAL PROPERTIES OF ANISOTROPIC CRYSTALS

A crystal of Cu Rpn(acac)$_2$ is an anisotropic medium capable of showing LD because of the orientation of the molecules in the crystal and CD because of the molecular asymmetry. Also, because of the Kronig-Kramers relationships, linear birefringence (LB) and circular birefringence (CB) have to be taken into consideration. Consequently, the linearly polarized light used in measuring polarized absorption spectra of an oriented crystal of, *e.g.*, Cu en(acac)$_2$ (without molecular asymmetry) will generally be subjected to both LD and LB effects. The crystal may be considered as a stack of slices of infinitesimal pathlengths,[10] and the linearly polarized light in slice 1 will then be subjected to a LD effect associated with a rotation, α_1,

Table 2. Squares of direction cosines in Cu Rpn(acac)$_2$ crystal.

Direction of unit vector	Squares of components of unit electric vector along molecular axes as defined in Table 1					
	Molecule 1[a]			Molecule 2[a]		
	x	y	z	x	y	z
Along **a**	0.360	0.007	0.633	0.373	0.008	0.619
Along **b**	0.015	0.984	0.001	0.009	0.988	0.003
Along **c**	0.625	0.008	0.367	0.617	0.003	0.380

[a] Orthorhombic crystal $P2_12_12_1$ with four equivalent positions, every position has two molecular units.

of the vibration direction; therefore the polarized absorption in slice 2 is measured in a different direction than in slice 1. In a crystal of Cu Rpn(acac)$_2$, this might get even worse since furthermore we have a CB effect which also has a rotation of the vibrational direction of linearly polarized light as result. Thus it turns out that we have to consider the influence of all the possible effects of the anisotropic crystal on polarized light in designing the experiment by which we will determine the specific effects. A way of handling this problem is shown by Gō [11] who demonstrates that in writing the incoming light as a Stokes vector, the different effects of a general media can be expressed in a 4×4 Mueller matrix $\mathbf{F}(l)$ which again is related to another 4×4 Mueller matrix $\mathbf{H}$ through the relation

$$\mathbf{F}(l) = \exp(-2\eta l \mathbf{H})$$

where η is the number density of active molecules (in this case $\eta = 1$) and l is the pathlength. The elements in the $\mathbf{H}$ matrix have been related to the phenomenological parameters LD, LB, CD, and CB by Troxell and Scheraga.[12]

INSTRUMENTATION

As the mathematical apparatus for handling the effects of a general anisotropic medium on light is available, the subject will now be the selection of a particular effect by instrumentation. A phase modulation spectrophotometer capable of selecting any one of the four effects (LD, LB, CD, CB) has been described in principle by Hofrichter and Schellman,[13] and we shall only briefly describe the instrumentation for measuring LD and CD on microscopic samples.

Light from a double monochromator passes through a polarizer and then through an optical modulator with principal axes at 45° to that of the polarizer. The modulator [14] is a piece of fused silica, which is driven to oscillation by mechanical coupling to a quartz crystal cut so that it has a resonance frequency of 50 kHz. The oscillation is selected so that it provides a periodically varying birefringence in the silica plate with an amplitude that is determined by the strength of the signal from the driving oscillator. Light which is polarized 45° to the axes of a birefringent plate emerges with a variety of polarizations depending on the magnitude of the birefringence. If the phase difference introduced by the modulator sweeps back and forth between $-\pi/2$ and $+\pi/2$, the light switches between the two orthogonal forms of circularly polarized light with the same frequency as the oscillator (50 kHz) and if the phase difference sweeps between $-\pi$ and $+\pi$, the light switches between the two orthogonal forms of linearly polarized light at twice the frequency of the oscillator (100 kHz).

After leaving the modulator, the light passes through the sample which is centered in the light beam on the stage of a microscope and with the image of the sample focused at the photomultiplier position. The photocurrent is then sent through a lock-in-amplifier, selecting either a 50 kHz or 100 kHz AC current. To calculate the light intensity proportional to the photocurrent, the following procedure may be used:

$$\mathbf{s}_o = \mathbf{F}_{\text{medium}}\mathbf{F}_{\text{modulatior}}\mathbf{F}_{\text{polarizer}}\mathbf{s}_i$$

where $\mathbf{s}_i$ and $\mathbf{s}_o$ are the Stokes vectors of the incoming and outgoing light beam, respectively, and the F's Mueller matrices.[15] It should be noted that $\mathbf{F}_{\text{medium}}$ from Troxell and Scheraga is arranged to match a Stokes vector developed on basis of Pauli spin matrices.[16] Multiplying the matrices together determines the output intensity (matrix-element 1 in $\mathbf{s}_o$). The result has terms containing $\cos(\delta_{\max} \sin \omega t)$ and $\sin(\delta_{\max} \sin \omega t)$ due to modulation. These may be expanded in Fourier series:

$$\cos(\delta_{\max} \sin \omega t) = J_0(\delta_{\max}) + 2\sum_{k=1}^{\infty} J_{2k}(\delta_{\max}) \cos 2k\omega t$$

$$\sin(\delta_{\max} \sin \omega t) = 2\sum_{k=1}^{\infty} J_{2k-1}(\delta_{\max}) \sin(2k-1)\omega t$$

where J_n are Bessel functions of order n.

For the LD and CD effects keeping only DC, ω, and 2ω terms and using only the expansion of $\mathbf{H}$ to the second order, then

$$I(\text{photocurrent}) \propto \tfrac{1}{2}e^{-\text{Abs}}[1 + \tfrac{1}{2}(\text{CD}^2 + \text{LD}^2) - \text{LD}J_0(\delta_{\max}) + 2\text{CD}J_1(\delta_{\max}) \sin \omega t - 2\text{LD}J_2(\delta_{\max}) \cos 2\omega t]$$

To detect LD, a modulation of $\pi \sin \omega t$ (maxi-

mizes J_2) should be used and signals at 2ω (100 kHz) should be observed, thus:

$$\frac{\langle I_{AC}\rangle}{I_{DC}} \propto \frac{-2LD\,J_2(\delta_{max})}{1+\frac{1}{2}(CD^2+LD^2)-LD\,J_0(\delta_{max})}$$

To detect CD a modulation of $\pi/2\cdot\sin\omega t$ (maximizes J_1) should be used and signals at ω(50 kHz) should be observed, thus:

$$\frac{\langle I_{AC}\rangle}{I_{DC}} \propto \frac{2CD\,J_1\delta(_{max})}{1+\frac{1}{2}(CD^2+LD^2)-LD\,J_0(\delta_{max})}$$

As may be seen from these expressions it is important to keep $LD(\lambda)=0$ when measuring $CD(\lambda)$ in case $LD > CD$.

EXPERIMENTAL

Cu Rpn(acac)$_2$ and Cu en(acac)$_2$ were prepared and crystals grown as previously described.[4,9] The identity of the compounds was established from chemical analysis. Suitable crystals (app. size 0.5 mm × 0.5 mm × 0.1 mm) were glued to cover glasses and the position of the unit cell axes in the tabular faces of the crystals was determined by the Buerger precession method. The signs of the LD curves as well as the absorption scales were established by using a standard made from pseudoisocyanin-*N*,*N'*-diethyl iodide in a stretched PVA-film.[17] The sign and absorption scale of the CD curve was established by using a solution of Cu Rpn(acac)$_2$ as standard, furthermore the CD curve of the crystalline material was measured under the condition $LD(\lambda)=0$ maintained by turning the microscope stage during the measurement.

The spectral response of the detector system (an E.M.I. 6256S PM tube mounted in a PAR model PM tube housing) is negligible above 610 – 620 nm.

RESULTS

The LD curves and CD curve of Cu Rpn(acac)$_2$ and the LD curve of Cu en(acac)$_2$ are given in Figs. 1, 2 and 3, respectively. Looking at the LD of Cu Rpn(acac)$_2$ and refering to Table 2, it is seen that the band at 620 nm has *x*-polarization and the band at 540 nm has *z*-polarization in the molecular coordinate system.

The crystal CD of Cu Rpn(acac)$_2$ is seen to be in agreement with the CD spectrum of Cu Rpn(acac)$_2$ in KBr [4] both with respect to shape and magnitude; this is certainly expected since the only difference between the spectra is that

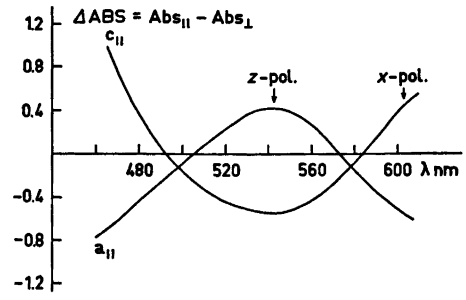

Fig. 1. LD-spectra of Cu Rpn(acac)$_2$. c∥ is absorption along the **c**-axis minus absorption along the **a**-axis of the crystal. The total absorbance of the crystal at 540 nm is ~ 6 measured in the microscopic set-up without use of polarizer and modulator and scaled against a Cu Rpn(acac)$_2$ solution.

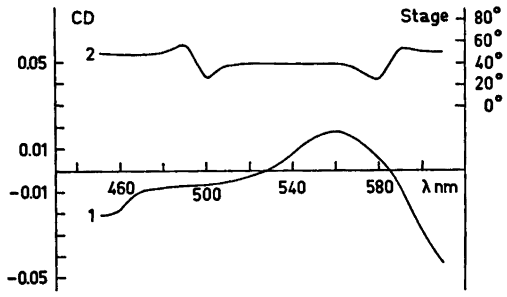

Fig. 2. 1, CD spectrum of Cu Rpn(acac)$_2$ in the crystalline phase. 2, Programming function of the microscope stage to keep $LD(\lambda)=0$ given relative to stage position = 0° for the crystal **a**-axis parallel to the vibration direction of the incoming linearly polarized light.

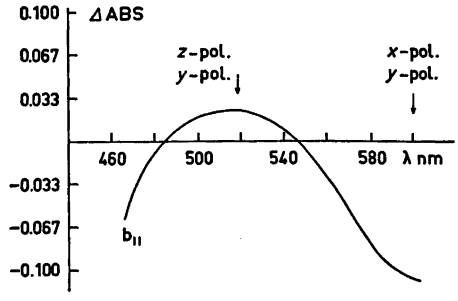

Fig. 3. LD-spectrum of Cu en(acac)$_2$. b∥ is absorption along the **b**-axis minus absorption along the **c**-axis of the crystal. The total absorbance of the crystal at 540 nm is ~ 6.

in KBr the LD is zeroed by random orientation of the molecules whereas in the crystals, the LD is zeroed by rotating the microscope stage.

To check the instrument LD of Cu en(acac)$_2$ was also measured and referring to Table 1 of Ref. 9, it is seen that the band at 620 nm may be x- and y-polarized and the band at 520 nm z- and y-polarized, which is in agreement with the assignments of Olson *et al.*[9]

DISCUSSION

Larsen *et al.*[4] state that the angle between the two chromophoric parts of Cu Rpn(acac)$_2$ in the crystalline phase is 10° as compared to an estimated angle of 45° in solution.[6] As the $\pi\rightarrow\pi^*$ transition parts (29 000 – 35 000 cm^{-1}) in the solution spectra of Cu Rpn(acac)$_2$ and Cu en(acac)$_2$ are quite similar, we may expect the same magnitude for the angle in Cu en(acac)$_2$ since the estimation is based purely on the ratio of the dipole strengths of the split components in the $\pi\rightarrow\pi^*$ transition band.[6,18] The angle between the chromophoric parts of Cu en(acac)$_2$ in the solid state may be calculated from the crystal data and is found to be 4°. Although the symmetry of either molecule cannot be higher than C_2 (and even C_1 for Cu Rpn(acac)$_2$ because of the methyl group on the ethylene bridge), it is advantageous to use either C_{2v} or D_2.

Certainly the geometry of the molecules changes on going from solution into the solid form and as this change is towards a planar configuration for both of the two complexes, it is reasonable to assign contributions in $C_{2v}(x)$. On the other hand, it is still a fact that the molecules are not exactly planar so there may also be contributions to account for in a D_2 representation. The representations of the valence shell molecular orbitals in $C_{2v}(x)$ as well as D_2 are given in Table 3.

Transitions of x- and z-polarizations giving electric transition dipole moments are sought since the Cotton effects under the absorption bands and the y-polarized part of the absorption spectrum have been accounted for.[6,9] The z-polarized transition at 540 nm (for Cu Rpn(acac)$_2$ in solution assigned to $(xz)\rightarrow(xy)$ with x-polarization and gaining electric transition dipole moment for the rotational strength from the x-polarized $\pi\rightarrow\pi^*$ transition [6]) could very well have its origin in the $(yz)\rightarrow(xy)$ electronic transition, which when accounted for in C_{2v}, has z-polarization. This assignment of the z-polarized part of band II is furthermore in agreement with the expectation put forward earlier,[6,8] namely that $3d_{xz}$ and $3d_{yz}$ at the copper ion in a planar or nearly planar complex would have almost the same orbital energy; consequently there is no ambiguity in assigning band II partly to $(xz)\rightarrow(xy)$ and partly to $(yz)\rightarrow(xy)$.

Table 3. Transformations of molecular orbitals in Cu Rpn(acac)$_2$.

$C_{2v}(x)$	Orbital	D_2
a_2	$4\pi_+ = 4\pi_1 + 4\pi_2$[a]	a
b_1	$4\pi_- = 4\pi_1 - 4\pi_2$	b_2
b_2	(xy)	b_1
a_1	(x^2-y^2)	a
a_2	(yz)	b_2
b_1	(xz)	b_2
a_1	(z^2)	a
b_1	$3\pi_+ = 3\pi_1 + 3\pi_2$	b_1
a_2	$3\pi_- = 3\pi_1 - 3\pi_2$	b_2
a_1	x	b_2
b_2	y	b_2
b_1	z	b_1

[a] The two chromophoric parts of the molecules are numbered 1 and 2 respectively in consistency with the numbering in Ref. 6.

In looking for an x-polarized electronic transition, the only obvious candidate is found to be the transition $(xy)\rightarrow(4\pi)$ in D_2, and therefore the x-polarized part of band I may be tentatively assigned to that transition. This certainly presents a problem since the assignment to band III has been given as either $3\pi\rightarrow(xy)$[19] or $(xy)\rightarrow 4\pi$[20] for bis(β-ketoenolate) complexes of copper(II). However, as Cotton *et al.* state, as possible assignment to band III (the shoulder at 26 000 cm^{-1} in copper(II) bis(acetylacetonate)) could also be $\sigma^n\rightarrow\pi^*$, an assignment which was discussed further by Jensen and Larsen [6] in the sense that the $\sigma^n\rightarrow\pi^*$ transitions produce excited states with the same symmetries as the π-excited states thereby making a coupling between the two kinds of transitions possible.

An alternative assignment to band III is the one given by Downing and Urbach (see

Table 1), but this is in conflict with the assignment given to the x-polarized part of band II, and also with the generally accepted notion that band III is not a $d \rightarrow d$ transition.

Therefore, it is seen that accepting the assignment $\sigma^n \rightarrow \pi^*$ of Jensen and Larsen to band III, it is possible to have $(xy) \rightarrow 4\pi$ at a somewhat lower energy than 23 000 cm^{-1}, supporting the above given assignment of $(xy) \rightarrow 4\pi$ to the 16 000 cm^{-1} x-polarized absorption band, an assignment which is furthermore in accordance with the calculations of Cotton *et al.*

Acknowledgements. The author is most grateful to Professor J. A. Schellman for the opportunity to visit his laboratory on grants from the National Institutes of Health (GM 20195, GM 15423) and the National Science Foundation (GB 41459), and also to Statens Naturvidenskabelige Forskningsråd (511-3785) for providing the travelling funds. The access to the crystal data of Drs. S. Larsen, E. Larsen, E. Røen and K. J. Watson prior to publication, the PVA-film provided by Dr. B. Nordén and the positioning of unit cell axes in actual crystals by Dr. R. Fenna are highly appreciated.

REFERENCES

1. Hall, D., Rae, A. D. and Waters, T. N. *J. Chem. Soc.* (1963) 5897.
2. Clark, G. R., Hall, D. and Waters, T. N. *J. Chem. Soc. A* (1968) 223.
3. Hall, D., Morgan, H. J. and Waters, T. N. *J. Chem. Soc. A* (1966) 677.
4. Larsen, E., Larsen, S., Røen, S. and Watson, K. J. *Acta Chem. Scand. A 30* (1976) 125.
5. Downing, R. S. and Urbach, F. L. *J. Amer. Chem. Soc. 91* (1969) 5977.
6. Jensen, H. P. and Larsen, E. *Acta Chem. Scand. 25* (1971) 1439.
7. Jensen, H. P., Davidsson, Å. and Nordén, B. *Inorg. Nucl. Chem. Lett. 11* (1975) 67.
8. Cotton, F. A., Harris, C. B. and Wise, J. J. *Inorg. Chem. 6* (1967) 909.
9. Olson, C. D., Basu, G. and Linn Belford, R. *J. Coord. Chem. 1* (1971) 17.
10. Jones, R. C. *J. Opt. Soc. Am. 38* (1948) 671.
11. Gō, N. *J. Phys. Soc. Jap. 23* (1967) 88.
12. Troxell, T. C. and Scheraga, H. A. *Macromolecules 4* (1971) 519.
13. Hofrichter, H. J. and Schellman, J. A. *Jerusalem Symposia on Quantum Chemistry and Biochemistry V*. The Israel Academy of Sciences and Humanities, Jerusalem, 1973.
14. Kemp. J. *J. Opt. Soc. Am. 59* (1969) 950.
15. Shurcliff, W. A. *Polarized Light*, Harvard Univ. Press., Cambridge, Mass. 1962.
16. Schmieder, R. W. *J. Opt. Soc. Am. 59* (1969) 297.
17. Nordén, B. *Acta Chem. Scand. 27* (1973) 4021.
18. Larsen, E. *Acta Chem. Scand. 23* (1969) 2158.
19. Jørgensen, C. K. *Acta Chem. Scand. 16* (1962) 2406.
20. Cotton, F. A. and Wise, J. J. *Inorg. Chem. 6* (1967) 917.

Received June 9, 1975.

Acta Chemica Scandinavica A 30 (1976) 143—151

The Bis[di(2-aminoethyl)sulfide]cobalt(III) Ion. Existence of only the Unsymmetrical-facial Geometric Isomer and Its Optical Resolution.

GRAEME H. SEARLE* and ERIK LARSEN

Chemistry Department I, The H. C. Ørsted Institute, Universitetsparken 5, DK-2100 Copenhagen, Denmark

Bis[di(2-aminoethyl)sulfide]cobalt(III) was prepared by a variety of methods. The products from all preparations were the same geometric isomer exclusively, as established by Sephadex ion-exchange chromatography and NMR spectra. From comparisons of CD spectra with the spectra of the isomers of the analogous $[Co(dien)_2]^{3+}$ system, the resolved complex $(-)_D$-$[Co(daes)_2]^{3+}$ was assigned the *unsymmetric-facial* geometry, and it probably has the absolute configuration Δ. It racemises rapidly on charcoal (complete within 10 min at 20 °C). The observed ion-association effects and the NMR spectrum are also consistent with the geometry being *u-facial*. The two other possible geometric isomers, *s-facial* and *meridional* could not be detected. Some sulfur-sulfur interaction is possible, and this might confer rigidity on the chelate ring conformations and thus account for the multiple NH_2 resonances observed in the ^1H NMR spectrum.

A number of metal complexes of various thioether ligands are known. When the thioether donor atom bridges two chelate rings, there exists the possibility of two coordination modes, *facial* and *meridional*, for the tridentate moiety. Although there have been several detailed studies over recent years of the stereochemistry associated with coordination of flexible multidentate linear thia-amine ligands, a *meridional* topology of five-membered chelate rings about donor sulfur has not yet been demonstrated in any complex. By comparison, such *meridional* coordination appears to be common at coordinated secondary amine sites.

It was the purpose of this work to attempt to establish the *meridional* coordination mode for donor sulfur coupling five-membered chelate rings in the complex system $[Co(daes)_2]^{3+}$ where daes represents the tridentate ligand di(2-aminoethyl) sulfide, $H_2N-CH_2-CH_2-S-CH_2-CH_2-NH_2$.

The investigation reported here of the complex system $[Co(daes)_2]^{3+}$ was prompted by our recent studies on the closely analogous bis(diethylenetriamine)cobalt(III) complex system.[1,2] Both these systems can potentially exist in three topological forms designated[1] *s-fac*, *u-fac* and *mer* and shown in Fig. 1. In addition the *u-fac* and *mer* forms are dissymmetric and can exist in optical forms. All these isomeric forms of $[Co(dien)_2]^{3+}$ (dien = diethylenetriamine) have been isolated and characterized.[1,3]

The three geometric isomers of $[Co(dien)_2]^{3+}$ coexist at equilibrium, and each separate iso-

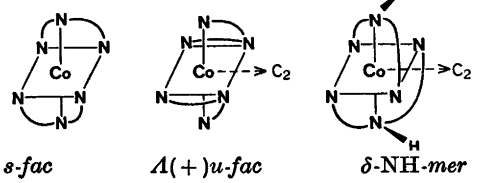

s-fac $\Lambda(+)$*u-fac* δ-NH-*mer*

Fig. 1. The geometric isomers of $[Co(dien)_2]^{3+}$. The possible isomers of $[Co(daes)_2]^{3+}$ are analogous to those above, with S replacing NH. The nomenclature is elaborated in Ref. 1.

* On leave from Department of Physical and Inorganic Chemistry, University of Adelaide, South Australia.

mer isomerizes slowly to the same equilibrium mixture under similar conditions. The equilibrium proportions in aqueous solution at 18 °C and with singly charged anions (halide, nitrate, perchlorate) are *mer:u-fac:s-fac* = 65:27:8, so that the *meridional* topology of coordinated dien is clearly preferred over the *facial* arrangements.[1,2]

The difference between the three isomers of $[Co(dien)_2]^{3+}$ or those of $[Co(daes)_2]^{3+}$ (Fig. 1) can be broadly defined in terms of the planar or angular stereochemistry about the secondary nitrogen or thioether donor atoms,[4] but the description of donor atom bond angles as *angular* or *planar* (corresponding to the descriptions of topology as *facial* or *meridional*) does not necessarily make these angles key angles in determining relative isomer stabilities. It has been appreciated for some time that any strain arising from departures of bond angles about the metal and donor atoms from their natural octahedral and tetrahedral values should be alleviated by a "levelling-out" process over all the bond angles of the structure.[4] More recently it has been realized from energy minimization calculation that the energetics of a molecular system is a function of *all* its degrees of freedom (bond angles, bond lengths, non-bonded interactions and bond torsions),[5] and it follows therefore that the separation of any one structural parameter as contributing more or less to the energetics is not valid.

Full energy minimization calculations for each of the $[Co(dien)_2]^{3+}$ isomers have indicated that in the energy minimized structures the C–N–C bond angles do not differ greatly over the three isomers, and that the energies associated with the departures of these angles from tetrahedral (at most $\sim 5°$ for the *mer* isomer) are relatively minor contributions to the total energies.[5]

The isomeric distribution in $[Co(daes)_2]^{3+}$ was of some interest therefore, and on the basis of the above results for $[Co(dien)_2]^{3+}$ there seemed reasonable likelihood of being able to obtain the *mer* isomer of $[Co(daes)_2]^{3+}$ having a donor sulfur in a pseudo-planar arrangement. The immediate aim of the present work therefore was to prepare $[Co(daes)_2]X_3$ by various methods and to isolate, characterize and identify the geometric isomers present.

Some metal complexes of daes coordinated in a tridentate manner have been isolated previously. The cobalt(III) complexes $[Co(daes)_2]Cl_3$, $[Co(daes)(dien)]Cl_3$ and $[Co(daes)Cl_3]$ were reported recently by Hori [6] but the isomeric compositions were not investigated. For $[Pt(daes)Cl_3]Cl$ only one of the two possible isomers could be detected but its structure was not established,[7] and $[Ni(daes)_2]X_2$ was suggested to consist at least largely of the *s-fac* isomer from the tetragonal splitting observed in the electronic spectrum.[8] Thus the detailed coordination behaviour of daes is essentially unknown.

EXPERIMENTAL

Instrumentation. Absorption spectra, circular dichroism spectra, and optical rotations, were measured on a Cary 14 spectrophotometer, a Roussel-Jouan Dicrograph model II, and a Perkin-Elmer 141 polarimeter, respectively. ORD curves were measured on a Perkin-Elmer 141 MC polarimeter. ^1H NMR spectra were measured on Varian A-60A and Bruker JX-90 NMR spectrometers.

Preparation of daes. The diamine was prepared by modification of literature methods.[9–11] Hydrogen sulfide (about 55 g, J. T. Baker Chemical Co., New Jersey, 98.5 % pure) was bubbled in a slow stream (2 h) through a stirred solution of ethylenimine monomer (93 g, Koch-Light Laboratories Ltd., England) in methanol (100 ml, Analar) in a flask cooled in an ice bath. The solvent was removed on a rotary evaporator, and some 2-aminoethylthiol by-product also sublimed off. The crude product was distilled under pressure when more 2-aminoethylthiol was removed first, and the required diamine was then collected separately. Yield: 73 g (56 %). The diamine was redistilled, b.p. 124–126 °C/17 mmHg (uncorr.), and comparisons of ^1H NMR spectra in D_2O indicated that it was free of the monomer by-product.

Preparation of daes.2HCl. HCl (59 ml of 11.3 M) in ethanol was added to a stirred solution of daes (40.0 g) in ethanol cooled in an ice bath. The solution was concentrated on a rotary evaporator, and the product crystallized on standing in a refrigerator. The hygroscopic product was filtered off, washed with ethanol, and dried in a vacuum desiccator. Yield: 57.0 g (88 %). M.p. 123–124 °C. (Found: C 24.8; H 7.3; N 14.3; Cl 36.7; S 16.9. Calc. for $C_4H_{14}N_2Cl_2S$: C 24.9; H 7.3; N 14.5; Cl 36.7; S 16.6).

Preparations of the $[Co(daes)_2]^{3+}$ complex. Method A, aerial oxidation. To a solution of $CoCl_2.6H_2O$ (2.38 g, 0.01 mol) in water (300

ml), a solution of daes.2HCl (4.25 g) and $LiOH.H_2O$ (1.39 g) in water was added. Powdered charcoal (1 g) was added, and the solution was aerated for 40 h. The charcoal was filtered from the red-orange solution. After reserving a small sample for Sephadex chromatography, the solution was diluted three-fold, and absorbed on a short column of Bio-Rex 70 weak acid cation exchange resin (analytical grade, 50 – 100 mesh) in the Li^+ form. After washing the column with water, the complex was eluted with 0.1 M HBr. Evaporation of the effluent solution to dryness in a rotary evaporator gave orange-red crystals of crude $[Co(daes)_2]Br_2.H_2O$. Yield after standing in a hygrostat: 5.51 g (98 %).

Method B, aerial oxidation with added phosphate. To $CoCl_2.6H_2O$ (2.38 g) in water (500 ml) was added $Na_3PO_4.12H_2O$ (19 g). Charcoal (1 g) was added to the mixture followed by daes (2.41 g) and HCl (10 ml of 1 M). After aeration (40 h) the charcoal was removed leaving a dark orange-brown solution of pH ~ 11. This solution contained a substantial proportion of polynuclear complex species which remained as a grey-green band at the column head during passage of the $[Co(daes)_2]^{3+}$ product down a column of SP-Sephadex C-25 with sodium $(+)_D$-antimonyl tartrate solution. The presence of polymeric material precluded isolation of the required complex by the weak acid cation exchange procedure as in method A, and isolation of product was not pursued.

Method C, from $[Co(NH_3)_6]Cl_3$. This was similar to the method used by Hori.[13] A mixture of $[Co(NH_3)_6]Cl_3$ (2.68 g, 0.01 mol), daes.2HCl (4.2 g), $LiOH.H_2O$ (1.85 g) and powdered charcoal (0.5 g) in water (80 ml) was warmed over a steam bath for 2 h, when evolution of ammonia had ceased. The solution was diluted and the charcoal was filtered off. A small volume was reserved for Sephadex chromatography. The product was obtained as the bromide salt using Bio-Rex 70 cation exchange resin as in method A. A small amount of some brownish-green product, probably $[Co(daes)Cl_3]$ obtained on evaporation of the effluent solution was extracted with warm ethanol. The orange crystals of $[Co(daes)_2]Br_3.H_2O$ were filtered off from the ethanol solution, washed with 96 % ethanol, air-dried, then treated in a hygrostat. Yield: 4.70 g (85 %).

In another preparation by this method the solution left after removing the charcoal was concentrated to a small volume and the product crystallized on addition of ethanol. The orange crystals of $[Co(daes)_2]Cl_3,2H_2O$ were filtered off, washed with 96 % ethanol and ether, and air-dried. Yield: 3.84 g (87 % calculated as dihydrate).

Isolation of complex as the perchlorate salt was carried out from another batch using a column of SP-Sephadex C-25 cation exchange resin. The product was passed down the column as a single band using 0.5 M $NaClO_4$ solution.

Method D, from trans-$[Co(py)_4Cl_2]Cl.6H_2O$ *in methanol solvent.* *trans*$[Co(py)_4Cl_2]Cl.6H_2O$ [12] (2.95 g, 0.005 mol) was dissolved in methanol (80 ml, Analar) by warming. A solution of daes (1.35 g) in methanol (20 ml) was added dropwise to the above stirred solution, when a greyish precipitate commenced to settle out immediately. The solution was heated to boiling over a steam bath when the suspended solid became orange, and the solution was then evaporated to dryness on a rotatory evaporator. The resulting orange solid was dissolved in water, and the solution was filtered and made up to 500 ml. After reserving a small sample (3 ml) for Sephadex chromatography, the solution was applied to a column of Bio-Rex 70 cation exchange resin. The complex was recovered as bromide (as in method A) and some purplish-grey by-products were retained on the resin.

In another preparation by this method, the crude $[Co(daes)_2]Cl_3.2H_2O$ was filtered off from the methanol solution after cooling, washed with ethanol and ether, and air-dried. Yield: 2.05 g (93 % calculated as dihydrate).

Method E, from trans-$Co(py)_4Cl_2]Cl.6H_2O$ *in pyridine solvent.* This was carried out in a similar manner to that in method D. On evaporation to dryness the solid was greenish-yellow, but formed a red-brown solution in water. Some solution was reserved for Sephadex chromatography, and $[Co(daes)_2]Br_3.H_2O$ was isolated as in method D. More by-products were apparent from this method than in the methanol preparation, but these were essentially retained on the BioRex 70 resin and in the ethanol. Yield: 2.12 g (76 % calculated as monohydrate).

Method F, from $Na_3]Co(CO_3)_3].3H_2O$. To an ice-cold stirred slurry of $Na_3[Co(CO_3)_3].3H_2O$ [13] (3.62 g, 0.01 mol) in water (30 ml) was added daes.2HCl (3.86 g) and HCl (20 ml of 1 M). The mixture was warmed over a steam bath (30 min) and gradually became red-brown, and the solution was filtered. A sample was chromatographed on Sephadex with 0.3 M sodium (+)-antimonyl tartrate eluent and produced two bands. A carmine band ran just ahead of the single yellow-orange band of $[Co(daes)_2]^{3+}$ so that it was probably a 3+ charged complex. Its visible absorption spectrum did not correspond with that expected for a $[Co(daes)_2]^{3+}$ complex.

The $[Co(daes)_2]^{3+}$ product was isolated by the weak acid cation exchange procedure as in method A, but it could not be completely separated from the carmine complex by this procedure. Evaporation of the 0.1 M HBr effluent solution gave a solid containing two compounds. Water then dissolved the orange $[Co(daes)_2]Br_3$ and left an insoluble green powder which was removed. Its analysis

(Table 1) was consistent with $[Co(daes)Br_3]$. Yield of $[Co(daes)_2]Br_3.H_2O$: 4.93 g (88 %).

Sephadex chromatographic analysis of complex products from preparations. The solutions in all the above preparations were made sufficiently dilute to retain all the complex products in solution. A suitable aliquot of each product solution (~0.02 g of product complex) was applied to a column (60 × 1.8 cm) of SP-Sephadex C-25 cation exchange resin in the Na^+ form, washed with water and chromatographed with 0.3 M sodium (+)-antimonyl tartrate solution. From each preparation the same single yellow-orange band corresponding to a 3+ charged ion was obtained. This single $[Co(daes)_2]^{3+}$ band was eluted from the column and collected in a number of 10 ml fractions. The CD spectra recorded for all fractions from all preparations were of the same form with opposite maxima at 512 and 457 nm, but changed sign over each set of fractions demonstrating a partial optical resolution within the band.

For some runs, optical densities at the maximum 485 nm were also measured for the fractions. Using $\varepsilon_{485} = 215$ the values of $\Delta\varepsilon_{512}$ could be calculated, and the values of $\Delta\varepsilon_{512}$ so obtained for the fractions in order from preparative method A were: ~ -5.3, -3.4, -2.6, -1.5, 0, $+1.0$, $+2.1$, $+2.6$, $+3.0$, $+3.4$, $\sim +3.7$.

From most preparations, small amounts of by-products were also evident during the above chromatography procedures.

The use of 0.3 M $NaClO_4$, 0.1 M Na_3PO_4 and 0.3 M sodium $(+)_D$-tartrate solutions as eluents likewise produced only a single $[Co(daes)_2]^{3+}$ band.

Recrystallization and analyses of complexes. The chloride, bromide and perchlorate salts of $[Co(daes)_2]^{3+}$ had high solubilities in water. The chloride and bromide salts were recrystallized from 50 % aqueous methanol (10 g complex in 40 ml) by gradually adding ethanol while stirring. After standing at 6 °C overnight, the orange crystals were filtered off, washed with 96 % ethanol, air-dried, and then left in a hygrostat of 45 weight-% H_2SO_4 (50 % relative humidity approximating to normal room conditions) over 1 day.

All the salts showed variable water content dependent on the mode of drying, so that treatment in a hygrostat was employed to give reproducible analyses (Table 1). Thermogravimetric analyses showed that removal of hydrate water commenced at low temperatures (*e.g.* 35 °C at a slow heating rate, 2 °C per min) indicating loosely bound hydrate water reminiscent of $[Co(en)_3]^{3+}$ salts.[14]

Resolution of $[Co(daes)_2]Cl_3.2H_2O$. To a boiling, stirred solution of $[Co(daes)_2]Cl_3.2H_2O$ (4.42 g, 0.01 mol) in water (25 ml), solid sodium $(+)_D$-arsenyl tartrate (4.10 g, 0.016 mol) was added and dissolved. Crystallization commenced shortly after the solution was left to cool to room temperature and after 2 h in an ice bath $(-)_D$-$[Co(daes)_2](+)_D$-$[AsO(tart)]_3.H_2O$ were filtered off, washed with cold water and methanol, and air-dried. Yield: 3.9 g (80 % of one optical form). This diastereoisomer had specific rotations $[\alpha]_\lambda^{25}$ of -224, $+162$, $+401°$ at the mercury wavelengths 546, 436, 364 nm, respectively. The diastereoisomer was recrystallized by dissolution in hot water (~200 ml), filtration and concentration to ~50 ml. After seeding, the mixture was left to crystallize in an ice bath for 1 h, and the fine plates were filtered off, washed with ice-water, 96 % ethanol, and air-dried. After four recrystallizations the specific rotations (0.1 % solution, 1 dm tube) had become constant at $[\alpha]_{589}^{25}$ $-129°$; $[\alpha]_{578}^{25}$ $-170°$; $[\alpha]_{546}^{25}$ $-345°$; $[\alpha]_{436}^{25}$ $+237°$; $[\alpha]_{364}^{25}$ $+596°$. Analyses of recrystallized compounds are listed in Table 1.

The recrystallized diastereoisomer was converted into fine orange needles of $(-)_D$-$[Co(daes)_2]Br_3.2H_2O$ using Bio-Rex cation exchanger. The specific rotations (0.04 % solution, 1 dm tube), which were unchanged on recrystallization, were $[\alpha]_{589}^{25}$ $-256°$; $[\alpha]_{578}^{25}$ $-359°$; $[\alpha]_{546}^{25}$ $-735°$; $[\alpha]_{436}^{25}$ $+501°$; $[\alpha]_{364}^{25}$ $+1620°$.

After removing the diastereoisomer, the filtrate containing $(+)_D$-$[Co(daes)_2]^{3+}$ was heated to near boiling and further $(+)_D$-sodium arsenyl tartrate (4.0 g, 0.0156 mol) was added. After filtration 10 ml 96 % ethanol was added to the warm solution and the mixture was allowed to cool to room temperature. 5.7 g (5.4 mmol ~110 % of the $(+)_D$-stereoisomer) $(+)_D$-$[Co\ daes_2]$-$(+)_D$-$[AsO\ (tart)]_3$ precipitated. This diastereoisomer had specific rotations $[\alpha]_\lambda^{25}$ of 127, -46 and $-890°$ at the mercury lines 546, 436, 364 nm, respectively. The diastereoisomer was recrystallized three times. The last recrystallization did not change the specific rotations: $[\alpha]_{578}^{25}$ 164°; $[\alpha]_{546}^{25}$ 301°; $[\alpha]_{436}^{25}$ $-153°$; $[\alpha]_{364}^{25}$ $-579°$. $(+)_D$-$[Co(daes)_2]Br_3.2H_2O$ was obtained analogously to the antipode and with the same optical purity.

The racemic bromide monohydrate could be resolved in an analogous manner to that above.

RESULTS AND DISCUSSION

In seeking the three possible geometric isomers of $[Co(daes)_2]^{3+}$ the complex was prepared by a number of different methods as described above.

Preparation of the complex by the dimethyl sulfoxide oxidative procedure [15] was unsuccessful; no reaction was apparent when solutions of $CoCl_2$ and 2(daes.2HCl) + 3LiOH in dimethyl sulfoxide were mixed and warmed.

Table 1. Analytical data for $[Co(daes)_2]^{3+}$ complexes prepared.

Complex [a]	C		H		N		S		Halogen		Molar ratio
	Calc.	Found	Calc.	Found	Calc.	Found	Calc.	Found	Calc.	Found	H_2O:Co [b]
$[Co(daes)_2]Br_3.H_2O$	17.2	17.0	4.7	4.6	10.1	10.1	11.5	11.3	43.0	43.2	1.1
$[Co(daes)_2]Cl_3.2H_2O$	21.7	21.5	6.4	6.4	12.7	12.6	14.5	14.4	24.1	24.3	2.3
$[Co(daes)_2](ClO_4)_3.H_2O$	15.6	15.7	4.3	4.1	9.1	9.1	10.4	10.6	17.3	16.7	1.0
$[Co(daes)Br_3]$	11.5	11.7	2.9	3.0	6.7	6.9	7.7	7.7	57.2	56.2	
$(-)_D$-$[Co(daes)_2]$-$(+)_D$-$(AsOC_4H_4O_6)_3.H_2O$	23.2	23.1	3.7	3.6	5.4	5.4	6.2	6.5			[c]
$(-)_D$-$[Co(daes)_2]Br_3.2H_2O$	16.7	16.4	4.9	4.8	9.7	9.6	11.2	11.6	41.7	41.7	2.1
$(+)_D$-$[Co(daes)_2]$-$(+)_D$-$(AsOC_4H_4O_6)_3.H_2O$	23.2	23.8	3.7	3.5	5.4	5.5					
$(+)_D$-$[Co(daes)_2]Br_3.2H_2O$	16.7	16.5	4.9	4.8	9.7	9.7	11.2	11.5	41.7	41.4	
$(+)_D$-$[Co(daes)_2]$-$(ClO_4)_3.H_2O$	15.6	15.8	4.3	4.3	9.1	9.2	10.4	10.5	17.3	17.0	

[a] daes = $C_4H_{12}N_2S$. [b] By thermogravimetric analysis. [c] Uncertain due to decomposition.

The preparations with charcoal would be expected to give equilibrium mixtures of the geometric isomers, whereas different isomer distributions might be expected from the other methods. Moreover, isomer proportions can be modified by changes of solvent,[2] and different isomers can be the main products isolated from reactions under such different conditions.[16]

The product from all the above preparations appeared to be a single geometric isomer, however, and two approaches were used to check this.

Samples of the product solutions from all the preparations were separately chromatographed on columns of SP-Sephadex C-25 cation exchange resin using 0.3 M sodium $(+)_D$-antimonyl tartrate as eluent. In each case only a single yellow-orange band was obtained, and this was eluted and collected totally in a number of fractions. The optical activity showed a regular change over all the fractions, with $\Delta\varepsilon_{max,512}$ of early fractions negative, the $(-)_D$ optical isomer, and of later fractions positive. These observations are consistent with the band on Sephadex containing a single geometric isomer which is partially optically resolved within the band during the elution with $(+)_D$-antimonyl tartrate. This separation of optical isomers provides substantial evidence that only one geometric isomer

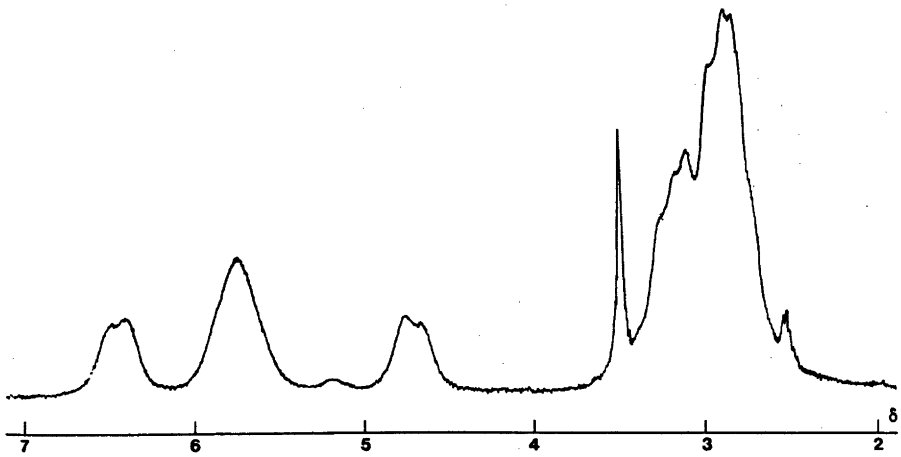

Fig. 2. 90 MHz ^1H NMR spectrum of *u-fac*-$[Co(daes)_2]^{3+}$ in DMSO-d_6 with tetramethylsilane as internal reference.

was present in all these preparative mixtures, as a chromatographic procedure which can separate optical isomers would be expected to discriminate even more readily between geometric isomers if more than one of these were present.[1]

The second approach was to isolate the $[Co(daes)_2]^{3+}$ products from the various preparations in the maximum possible yields and to compare their ^1H NMR spectra. The product complex from each preparative method was isolated almost quantitatively as $[Co(daes)_2]Br_3.H_2O$ using a weak acid cation exchange resin procedure, and all these products had identical ^1H NMR spectra (Fig. 2). The three geometric isomers of $[Co(daes)_2]^{3+}$ should have substantially different ^1H NMR spectra, as do the isomers of $[Co(dien)_2]^{3+}$,[1,2] so that any second isomer of $[Co(daes)_2]^{3+}$ has been beyond the limits of detection from NMR variations.

The isolated complex was resolved into optical isomers using sodium $(+)_D$-arsenyl tartrate. Through recrystallization of the diastereoisomer to maximum rotation, optically pure $(-)_D$-$[Co(daes)_2]Br_3.2H_2O$ was obtained whose ^1H NMR spectrum (Fig. 2) was identical to those of the crude products from all preparations. This reinforces the above evidence for the existence of only one geometric isomer.

Absorption and CD spectra, and assignment of the isomer as u-fac. The resolution of the complex excludes the centrosymmetric *s-fac* isomer (symmetry C_{2h}) but does not distinguish the dissymmetric isomers *u-fac* and *mer* which both have C_2 symmetry. However, several lines of evidence, particularly the CD spectrum, indicate that it is *u-facial.*

The absorption, ORD and CD spectra of the $(-)_D$-isomer of the resolved complex are shown in Fig. 3 and data are listed in Table 2. The visible absorption spectrum exhibits a maximum at 485 nm (20 600 cm^{-1}, $\varepsilon = 215$) with a band half-width $\bar{\nu}_{\frac{1}{2}}$ of 3200 cm^{-1}. The corresponding low energy band of *u-fac*-$[Co(dien)_2]^{3+}$ has maximum at 468 nm (21 400 cm^{-1}, $\varepsilon = 96$) and $\bar{\nu}_{\frac{1}{2}}$ 3400 cm^{-1}.[1] There are no signs of splitting in these bands, and the second octahedral absorption bands (at 359 nm for $[Co(daes)_2]^{3+}$, 338 nm for *u-fac*-$[Co(dien)_2]^{3+}$ are apparent single transitions

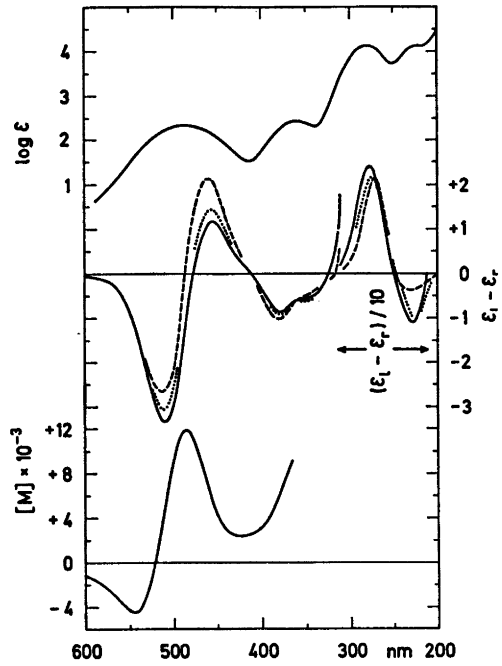

Fig. 3. The absorption, CD and ORD spectra of $(-)_D$-*u-fac*-$[Co(daes)_2]Br_3.2H_2O$ in water (approx. 10^{-3} M solution), and the CD in 0.2 M Na_2SeO_3 (- - -) and in 0.2 M Na_2SO_4 (. . .).

also. The circular dichroism spectrum of the $[Co(daes)_2]^{3+}$ isomer shows two components under the first absorption band with an energy separation of 2400 cm^{-1}. For *u-fac*-$[Co(dien)_2]^{3+}$ a similar pattern has been found with an energy separation of 2500 cm^{-1} between the two CD components.[3,17] These data indicate that daes lies somewhat lower in the spectrochemical series than dien. From the relative positions of the first ligand field bands in the absorption spectra of $[Co(daes)_2]^{3+}$ (Fig. 3) and $[Co(NH_3)_6]^{3+}$, $[Co(en)_3]^{3+}$ and *cis*-$[Co(en)_2(H_2O)_2]^{3+}$,[18] we deduce that daes lies between H_2O and NH_3 (and near dien) in the spectrochemical series in accord with some previous proposals.[6,19,20]

On the basis of all these spectral comparisons, the visible spectra of the three possible geometric isomers of $[Co(daes)_2]^{3+}$ might be expected to exhibit maxima at similar energies, so that the positions of bands and the degree of splitting may not distinguish between these arrangements.

Table 2. Electronic band maxima for $(-)_D$-$[Co(daes)_2]Br_3.2H_2O$ in water.

Unpolarised absorption		Circular dichroism		CD in 0.2 M Na_2SeO_3		Optical rotary dispersion	
λ(nm)	ε	λ	$(\varepsilon_l-\varepsilon_r)$	λ	$(\varepsilon_l-\varepsilon_r)$	λ	[M]
						545	−4 420 (trough)
		512	−3.35	515	−2.68	521	0
485	215						
		457	+1.18	461	+2.15	461	+11 980 (peak)
						425	+2 430 (trough)
		379	−0.88	381	−1.04		
359	274						
		~340	~−0.55	~340	inflexion		
279	14 000	276	+24.3	271	+21.1		
224	14 500	227	−11.3	232	−3.8		

The CD spectrum of $(-)_D$-$[Co(daes)_2]^{3+}$ shows a close correspondence to that of $(-)_D$-*u-fac*-$[Co(dien)_2]^{3+}$ over the ligand field and charge-transfer regions, in respect of both the relative positions of the component CD bands and their sign.[21] In particular both complexes show lower-energy negative and higher-energy positive components under the $^1A_{1g}\rightarrow{}^1T_{1g}$ absorption band (parent O_h), a negative component in the region of the $^1A_{1g}\rightarrow{}^1T_{2g}$ band (two negative components are shown here for $(-)_D$-$[Co(daes)_2]^{3+}$; two similarly-signed components may merely be less well resolved in the $(-)_D$-*u-fac*-$[Co(dien)_2]^{3+}$ complex), and lower-energy positive and higher-energy negative components in the charge-transfer region. There is also a correspondence in the relative magnitudes of the component bands within each complex, although $\Delta\varepsilon$ for the bands of $(-)_D$-$[Co(daes)_2{}^{3+}$ are larger than for the corresponding component bands of $(-)_D$-*u-fac*-$[Co(dien)_2]^{3+}$ by factors of about two or three. The effect of added selenite is to diminish and enhance, respectively, the lower- and higher-energy components of the $^1A_{1g}\rightarrow{}^1T_{1g}$ bands in both complexes (Fig. 3).

The CD of $(-)_D$-$[Co(daes)_2]^{3+}$ thus differs from that expected for a *mer* structure in each of the three respects mentioned, the high intensity of the charge-transfer components ($\Delta\varepsilon = +24, -11$) being particularly noteworthy. The close correspondence of the spectrum with that of $(-)_D$-*u-fac*-$[Co(dien)_2]^{3+}$ and the similar effects of selenite thus allow the present structure to be assigned as *u-facial*. On this basis also $(-)_D$-*u-fac*-$[Co(daes)_2]^{3+}$ probably has the same absolute configuration as $(-)_D$-*u-fac*-$[Co(dien)_2]^{3+}$, which has been assigned previously as Δ.[3,17,21]

ORD spectrum and optical stability of the complex. The Cotton effect which crosses zero at 521 nm is clearly associated mainly with the negative CD transition at 512 nm (Fig. 3). The positive section of the ORD will have contributions also from positive tails of component anomalies associated with the positive CD transitions at 457 nm and in the ultraviolet, so that the peak is very large.

The resolved complex has a high optical stability. The optical rotations (mercury lines) of a solution in water had not decreased measureably after 30 h at 50 °C. On the other hand addition of charcoal caused complete loss of activity within 10 min at 20 °C. After removal of the charcoal, this racemized solution gave the same single yellow-orange chromatography band when eluted down a Sephadex column using sodium $(+)_D$-antimonyl tartrate.

These features are similar to the properties of $(+)_D$-$[Co(en)_3]^{3+}$, and the rapid racemization on charcoal indicates the facility of bond rearrangement, albeit possibly in a Co(II) intermediate.[22] There would seem to be no mechanistic barrier therefore to the formation of the other two geometric isomers accompanying racemization of $(-)_D$-*u-fac*-$[Co(daes)_2]^{3+}$, and the fact that there has been no evidence throughout this work for the existence of the *s-fac* and *mer* isomers must indicate their relatively low thermodynamic stabilities.

The effect of phosphate in preparations of amine complexes. The equilibrium geometric

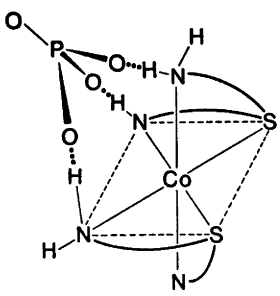

Fig. 4. The proposed ion-pair between *Λu-fac*-$[Co(daes)_2]^{3+}$ and PO_4^{3+}.

isomer proportions of $[Co(dien)_2]^{3+}$, *mer*:*u-fac*:*s-fac* = 65:28:7 under "normal" conditions, are considerably modified by the presence of phosphate to become 12:29:59.[2] This enhanced proportion of the *s-fac* isomer at the expense of *mer* has been ascribed to the differential specific associations between the PO_4^{3-} anion and the three isomeric cations, with the interaction magnitudes being in the order *s-fac* > *u-fac* > *mer*. In the $[Co(daes)_2]^{3+}$ system, *only* the *u-fac* isomer has three amine donor groups suitably disposed to permit hydrogen bonding with three oxygens of a tetrahedral oxyanion in the manner previously proposed[2] (Fig. 4). On this rationale the order of the magnitudes of interactions of $[Co(daes)_2]^{3+}$ with PO_4^{3-} should thus be *u-fac* ≫ *s-fac* ~ *mer*.

It would be expected that if the other two isomers were present, their separation from *u-fac*-$[Co(daes)_2]^{3+}$ should be effected readily on Sephadex by ion-associating eluents such as Na_3PO_4. The single $[Co(daes)_2]^{3+}$ chromatographic band always obtained, under all chromatography conditions and from all preparations (including particularly the aerial oxidation preparation carried out in 0.1 M Na_3PO_4 solution), is then consistent with the *u-facial* isomer being the exclusive product.

The pronounced effect of selenite on the CD spectrum (Fig. 3) demonstrates significant ion-association, so that this effect provides additional evidence for the *u-facial* geometry.

^1H NMR spectra. ^1H NMR spectra were studied at both 60 and 90 MHz, and some chemical shift data are given in Table 3.

The isolated $[Co(daes)_2]^{3+}$ products (and various fractions from some recrystallizations) all had essentially identical ^1H NMR spectra in dimethyl sulfoxide-d_6, showing three broad NH_2 signals integrating in the ratio 1:2:1, and the same CH_2 characteristics. The region of the CH_2 protons was complicated but showed little distinct fine structure.

The CH_2 region was essentially invariant with the different anions used (Br^-, Cl^-,

Table 3. Chemical shifts δ of *u-fac*-$[Co(daes)_2]^{3+}$ in dimethyl sulphoxide-d_6 (ppm downfield from internal TMS).

Complex	CH_2[a]	NH_2	NH_2	NH_2	NH_2
$[Co(daes)_2]Br_3$ (90 MHz)	2.87, 2.91, 3.00, 3.12 3.19, 3.27	4.67, 4.77[b] (1) (1)	5.17 (weak)	5.76 (4)	6.41, 6.49 (1) (1)
$[Co(daes)_2]Br_3$ (60 MHz)	2.92, 3.15	4.68, 4.83		5.70, 5.82	6.33, 6.50
$[Co(daes)_2]Br_3$ + added LiCl (60 MHz)	2.88, 3.17	5.27, 5.40[b] (1) (1)	5.70 (2)	6.30 (2)	6.73, 6.87 (1) (1)
$[Co(daes)_2]Cl_3$ (90 MHz)	2.87, 2.99, 3.15	5.36, 5.46[b] (1) (1)	5.84 (2)	6.26 (2)	6.90, 6.96 (1) (1)
$[Co(daes)_2]Cl_3$ (60 MHz)	2.92, 3.15	5.32, 5.48		5.97, 6.08	6.77, 6.87
$[Co(daes)_2]Cl_3$ in D_2O/D_2SO_4 (60 MHz)	3.07, 3.25, 3.43	~4.5[c]		5.2	5.8
$[Co(daes)_2](ClO_4)_3$ (90 MHz)	2.91, 3.10, 3.20	4.04, 4.17	4.71 (weak)	5.10, 5.21	5.56, 5.64
u-fac-$[Co(dien)_2]I_3$ (60 MHz)[d]	2.7–3.0	4.68 (2)	5.08 (2)	6.40 (1) (>NH)	
u-fac-$[Co(4\text{-methyldien})_2]Br_3$ (60 MHz)	2.6–3.1 (CH_3 at 2.79)	5.00 (1)	5.30 (1)		

[a] Peak positions above complex background. [b] Figures in parentheses are relative peak areas. [c] Obscured by HOD peak. [d] From Ref. 3.

ClO_4^-), but the NH_2 resonances showed a considerable anion dependence.

With $[Co(daes)_2]Br_3$ in DMSO-d_6 at 60 MHz, each of the three NH_2 signals seems split into doublets. At 90 MHz a fourth very weak NH_2 signal at δ 5.17 was observed, and the major signal now appears as a single resonance at δ 5.76 (Fig. 2). Spin-decoupling indicated that the weak NH_2 resonance at δ 5.17 is coupled to the NH_2 resonances at $\delta \sim 4.7$ (doublet) and at 5.76 but is not coupled to the NH_2 resonances at $\delta \sim 6.4$.

The NH_2 pattern for the perchlorate is similar, although it has shifted upfield from the bromide situation. The chloride salt shows four distinct NH_2 signals (intensity ratio 1:1:1:1), downfield from those of the bromide, and the NH_2 signals at highest and lowest fields show similar splitting to the signals at corresponding positions in the other salts.

This variation in the NH_2 resonances is indicative of differential ion-association effects, and when LiCl was added to the tube of $[Co(daes)_2]Br_3$ the resulting NH_2 pattern was similar to that of the chloride salt. However, INDOR and tickling experiments also indicate that smaller fractions than 1/8 of the total number of an equivalent N-bound protons are distinguishable. This observation may point to slow (by the NMR time scale) conformational interconversions. Computer simulation (LAOCOON II) seems to exclude that these effects arise from the coupling within the six protons of a given chelate ring.

We expect to clarify this point in the near future when better equipment is placed at our disposal.

It is noted that the NH_2 splitting is considerably greater in the present complex than in the *u-fac* and *mer* isomers of $[Co(dien)_2]^{3+}$ and of $[Co(4\text{-methyl dien})_2]^{3+}$ where only two NH_2 resonances are observed in each instance (Table 3).[3,23] This may reflect the larger difference between *equatorial vs. axial* character expected for the substituents on the ring atoms of the $[Co(daes)_2]^{3+}$ rings which are expanded relative to the rings of $[Co(dien)_2]^{3+}$.

Acknowledgements. G.H.S. is indebted to Prof. Jannik Bjerrum and Dr. Erik Larsen for the opportunity of spending a study leave in Copenhagen. We acknowledge financial support from the National Science Foundation, Copenhagen, for this work and for the purchase of a Bruker NMR spectrometer. We are grateful also for microanalyses carried out by Chemistry Department II, The H. C. Ørsted Institute, and for some circular dichroism measurements at Chemistry Department A, The Technical University of Denmark, Lyngby. We also thank Dr. Erik Pedersen, Chemistry Department I, The H. C. Ørsted Institute, for thermogravimetric analyses, and Dr. K. Hori, Yamagata University, Japan, for correspondence concerning his work.

REFERENCES

1. Keene, F. R. and Searle, G. H. *Inorg. Chem. 11* (1972) 148.
2. Keene, F. R. and Searle, G. H. *Inorg. Chem. 13* (1974) 2173.
3. Yoshikawa, Y. and Yamasaki, K. *Bull. Chem. Soc. Jap. 45* (1972) 179.
4. Dwyer, F. P. *Aust. J. Sci. 24* (1961) 97.
5. Dwyer, M. and Searle, G. H. *Chem. Commun.* (1972) 726.
6. Hori, K. *Nippon Kagaku Zasshi 91* (1970) 62.
7. Mann, F. G. *J. Chem. Soc.* (1930) 1745.
8. Taylor, L. T. and Barefield, E. K. *J. Inorg. Nucl. Chem. 31* (1969) 3831.
9. Nathan, A. H. and Bogert, M. T. *J. Amer. Chem. Soc. 63* (1941) 2361.
10. Barnett, J. W. *J. Chem. Soc.* (1944) 5.
11. Marxer, A. and Miescher, K. *Helv. Chim. Acta 34* (1951) 924.
12. Glerup, J. and Springborg, J. *To be published.*
13. Bauer, H. C. and Drinkard, W. C. *Inorganic Syntheses*, McGraw-Hill, New York 1966, Vol. VIII, p. 202.
14. Galsbøl, F. *Inorganic Syntheses*, McGraw-Hill, New York 1970, Vol. XII, p. 269.
15. Woldbye, F. *Studier over Optisk Aktivitet*, Thesis, Danmarks Tekniske Højskole 1968, p. 138.
16. Michelsen, K. *Acta Chem. Scand. 24* (1970) 2003.
17. Keene, F. R., Searle, G. H. and Mason, S. F. *Chem. Commun.* (1970) 839.
18. Jørgensen, C. K. *Absorption Spectra and Chemical Bonding in Complexes*, Pergamon Press, Oxford, 1962, p. 293.
19. Jørgensen, C. K. *Inorganic Complexes*, Academic, New York 1963, p. 143.
20. Livingstone, S. E. *Quart. Rev. 19* (1965) 386.
21. Konno, M., Marumo, F. and Saito, Y. *Acta Crystallogr. B 29* (1973) 739.
22. Dwyer, F. P. In Kirschner, S., Ed., *Advances in the Chemistry of Coordination Compounds*, Macmillan, New York, 1961, p. 21.
23. Keene, F. R., Searle, G. H. and Teague, S. G. *Unpublished work.*

Received July 5, 1975.

Acta Chemica Scandinavica A 30 (1976) 152—156

Short Communications

About the Space Group of $H_3Mo_{12}PO_{40}(H_2O)_{29-31}$; a Discussion

RUDOLF ALLMANN

Department of Geosciences, University of Marburg, D 355 Marburg, Germany

Recently Strandberg [1] has reported the structure of a hydrated dodecamolybdophosphoric acid. He reports a tetragonal cell with $a = 16.473(5)$ and $c = 23.336(7)$ Å, space group $I4_1/amd$, whereas for the analogous tungsto compound, $H_3W_{12}PO_{40}(H_2O)_{29}$, Noe-Spirlet *et al.*[2] report a cubic structure with $a = 23.272(5)$ Å, space group $Fd3m$. For the title compound we measured a cubic cell too with $a = 23.33(1)$ Å.

Therefore I looked a bit closer at the data reported by Strandberg and it turned out that this structure can be described just as much as a cubic one. This will be shown by applying the transformation matrix $(-\frac{1}{2}\ -\frac{1}{2}\ 0/-\frac{1}{2}\ \frac{1}{2}\ 0/0\ 0\ -1)$ to the reported coordinates after shifting the origin to $\bar{4}2m$ (*i.e.* P in 0, 0, 0). By this transformation the space group symbol changes from $I4_1/amd$ into $F4_1/ddm$, which better shows its subgroup relation to $Fd3m$. The transformed lattice constants become about equal: $a_F = a_I 2^{\frac{1}{2}} = 23.296(7) \approx c = 23.336(7)$ (average = 23.31 Å). Furthermore the coordinates achieve the form xxz ↷ or xxx and are about identical for the atoms paired in Table 1. The last fact is the essential proof for the cubic structure of $H_3Mo_{12}PO_{40}(H_2O)_{29-31}$. The averaged coordinates compare well with those of $H_3PW_{12}O_{40}(H_2O)_{29}$ [2] (see Table 1).

As for the triclinic $H_3Mo_{12}PO_{40}(H_2O)_{13-14}$ the pseudo-symmetry of the polyanion is reduced to 23 instead of $\bar{4}3m$,[3] we will try to check whether a similar reduction does occur for the 29-hydrate, *i.e.* whether the space group may be $Fd3$ instead of $Fd3m$, which means that $F_{hkl} = F_{khl}$ does not hold. For the about isomorphous tungsto-compound $NaH_2W_{12}PO_{40}(H_2O)_{13-14}$, however, the pseudo-symmetry remains $\bar{4}3m$.[4]

Table 1. Transformed atomic coordinates for $H_3PMo_{12}O_{40}(H_2O)_{29-31}$ (original data from Strandberg, 1975) compared with those of $H_3PW_{12}O_{40}(H_2O)_{29}$ (absolute coordinates from Noe-Spirlet *et al.* 1975).

	$H_3PMo_{12}O_{40}(H_2O)_{29-31}$ $F4_1/ddm$			$Fd3m(a = 23.31)$		$H_3PW_{12}O_{40}(H_2O)_{29}$ $Fd3m(a = 23.272(5))$			
Atom	x	y	z	$x = y$	z	Atom	$x = y$		z
P	0	0	0	0	0	P	0	0	0
Mo1	0.00430	0.10805	0.10807	0.10806	0.00431	W	0.10803		0.00400
Mo2	0.10807	0.10807	0.00432						
OP(11'2)	0.0382	0.0382	0.0382	0.0382	0.0382	O(1)	0.03794		0.03794
O(11')	0.0488	0.0488	−0.1279	0.0488	−0.1278	O(2)	0.04873		−0.12736
O1(12)	0.12775	0.04865	−0.0489						
O(11'')	0.0640	−0.0640	−0.1441	0.0639	0.1442	O(3)	0.06342		0.14369
O2(12)	0.1442	−0.0639	−0.0639						
O(1)	0.1581	0.0079	−0.1582	0.1582	−0.0078	O(4)	0.15873		−0.00765
O(2)	0.15835	0.15835	−0.0077						
Aq1	−0.250	0.250	0.0010	0.250	−0.0011	not reported			
Aq2	0.0011	0.250	−0.250	≡(0	0.2511)				

1. Strandberg, R. *Acta Chem. Scand. A 29* (1975) 359.
2. Noe-Spirlet, M.-R., Brown, G. M., Busing, W. R. and Levy, H. A. *Acta Crystallogr. A 31* S80 (Amsterdam meeting).
3. d'Amour, H. and Allmann, R. *Z. Kristallogr. In press.*
4. Allmann, R. and d'Amour, H. *Z. Kristallogr. 141* (1975) 161.

Received November 27, 1975.

A Theoretical Study of Conformational Stability in Molecules with Two or Three Si—O Bonds

I. HARGITTAI* and H. M. SEIP

Department of Chemistry, University of Oslo, Oslo 3, Norway

The anomeric effect in compounds with C—O bonds [1] has been studied by *ab initio* calculations, *e.g.* on fluoromethanol [2] and methanediol.[3] In the present work we give the results of some *ab initio* calculations on silanediol and silanetriol. This investigation was initiated partly for comparison with previous results on methanediol [3] and partly for supplementing electron diffraction studies on methyl methoxy silanes [$(CH_3)_3SiOCH_3$,[4] $(CH_3)_2Si(OCH_3)_2$,[5] $CH_3Si(OCH_3)_3$,[6] $Si(OCH_3)_4$[7]].

The calculations were carried out with the program MOLECULE [8] which solves the Roothaan-Hall equations for a Gaussian type basis. The functions proposed by Roos and Siegbahn [9] were used for silicon and oxygen, *viz.*

Si: (10*s*, 6*p*, 1*d*) contracted to (6, 4, 1), (*d* exponent 0.30) O: (7*s*, 3*p*) contracted to (4, 2). For hydrogen (4*s*) contracted to (2*s*) was used with a scale factor of 1.2 for all the exponents.[10]

The results for the four staggered forms of $H_2Si(OH)_2$ (I—IV) shown in Fig. 1 are given in Table 1. In methanediol only the most stable form (similar to I, Fig. 1) was found to correspond to a minimum in the potential energy surface. The relative energies for silanediol are seen to be in the same order as for methanediol, but the values are considerably smaller. This difference between the silicon and carbon compounds is apparently not related to the use of *d*-orbitals on silicon; the value obtained for the relative energy for form III is nearly the same when the *d* orbitals are not included in the calculations.

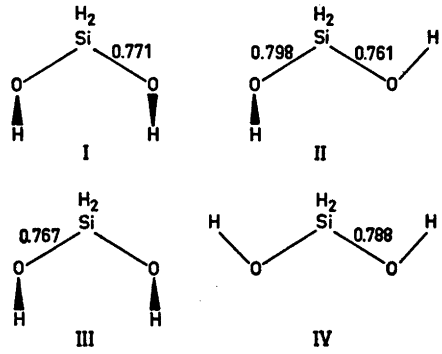

Fig. 1. The four conformations considered for silanediol. The overlap populations obtained for the Si—O bonds are given.

The simplest explanation for the smaller relative energies for the silicon compound seems to be that the longer Si—O bond, as compared with the C—O bond, decreases the dipole-dipole interaction between the oxygen lone pairs, and also decreases the contribution of the threefold component to the total potential of internal rotation.

The overlap populations obtained for the Si—O bonds are also given in Fig. 1. Their variations correlate well with the bond length variations found in the analogous conformers of methanediol,[3] except that our results indicate a slightly longer bond length in III than in I.

For silanetriol, calculations were first carried out for models with C_s symmetry (V, Fig. 2). Table 2 shows the results. The minimum is in the vicinity of $\phi = 60°$. Thus the eclipsed form ($\phi = 60°$) of $HSi(OH)_3$ appears to have greater stability than the staggered form ($\phi = 120°$). On the other hand, the electron diffraction data of methyltrimethoxy silane were found

* On leave from the Central Research Institute for Chemistry, Hungarian Academy of Sciences, Budapest, H-1088, Puskin utca 11—13.

Table 1. Total and relative energies for conformations I—IV of silanediol.[a] Relative energies for methanediol [3] are given for comparison.

Form	Silanediol Total energy (a.u.)	Rel. energy (kcal/mol)	Methanediol Rel. energy (kcal/mol)
I	−440.73123	0	0
II	−440.73017	0.67	4.4
III	−440.72830	1.85(1.96)[b]	5.5
IV	−440.72625	3.14	11.0

[a] Assumed bond lengths and angles Si—H 1.48 Å, Si—O 1.63 Å, O—H 0.97 Å, H—Si—H 109.5°, O—Si—O 109.5°, Si—O—H 123.0°. [b] Obtained when *d*-orbitals on silicon were not included in the basis set.

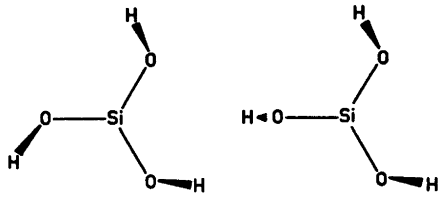

Fig. 2. Symmetric and asymmetric conformations considered for silanetriol.

to be consistent with a C_3 model, the prevailing forms of which having rotation angles between 100 and 155°, essentially a staggered conformation probably with large amplitude torsional motion. However, the structures of $HSi(OH)_3$ and $CH_3Si(OCH_3)_3$ need not necessarily be the same. The non-bonded O···H interactions in $HSi(OH)_3$ are favourable in the eclipsed form, while the oxygen···methyl interactions in $CH_3Si(OCH_3)_3$ seem to favour the staggered form. Apart from these non-bonded interactions, the dipole-dipole interactions, the electron delocalization, and the threefold component of the total potential of internal rotation must also be considered (*cf.* Ref. 3). The last term is certainly more favourable in the staggered form, but its relative magnitude is probably small in $HSi(OH)_3$.

Of the possible staggered conformations of $HSi(OH)_3$, form VI of Fig. 2 would be the most likely to display the anomeric effect.[11] As the relevant result shows (Table 2), this form indeed appears to be slightly more stable than the symmetric staggered form, but somewhat less stable than the eclipsed conformation.

These tentative comparisons do not allow far-reaching conclusions. The present results show the anomeric effect in silanediol but to considerably less extent than in methanediol. On the other hand, our calculations provide no indication of the anomeric effect in silanetriol. In this connection it may be of interest to mention that the length of the Si–O bond in methyl trimethoxy silane (1.632 ± 0.004 Å)[5] was found to be nearly the same as in trimethyl methoxy silane (1.639 ± 0.004 Å).[4] In case of an appreciable anomeric effect more shortening would have been expected in the trimethoxy derivative.

Table 2. Total and relative energies for silanetriol.[a]

$\phi_1=\phi_2=\phi_3$ (°)[b]	Total energy (a.u.)	Rel. energy (kcal/mol)
0	−515.53998	5.27
30	−515.54397	2.76
60	−515.54835	0.0
90	−515.54771	0.40
120	−515.54575	1.64 (1.05)[c]
150	−515.54108	4.58
180	−515.53725	6.99

[a] Assumed bond lengths and angles Si–H 1.48 Å, Si–O 1.63 Å, O–H 0.97 Å, H–Si–O 109.5°, Si–O–H 123.7°. [b] The *anti* position of the H–Si–O–H chain corresponds to $\phi = 0°$. [c] Obtained for a model with $\phi_1 = 0°$, $\phi_2 = \phi_3 = 120°$ (see Fig. 2).

Acknowledgements. One of us (I. H.) expresses appreciation to Professors O. Bastiansen, S. J. Cyvin and H. Viervoll for an invitation to Norway and to Norges almenvitenskapelige forskningsråd for a Fellowship.

1. Romers, C., Altona, C., Buys, H. R. and Havinga, E. In Eliel, E. L. and Allinger, N. L., Eds., *Topics in Stereochemistry*, Vol. 4, Interscience, New York 1969.
2. Wolfe, S., Rauk, A., Tel, L. M. and Csizmadia, I. G. *J. Chem. Soc. B* (1971) 136.
3. Jeffrey, G. A., Pople, J. A. and Radom, L. *Carbohydr. Res. 25* (1972) 117.
4. Csákvári, B., Wagner, Zs., Gömöry, P., Hargittai, I., Rozsondai, B. and Mijlhoff, F. C. *Acta Chim (Budapest). Submitted for publication.*
5. Gergö, É., Hargittai, I., Schultz, Gy. and Mijlhoff, F. C. In progress in the Budapest laboratory.
6. Gergö, E., Hargittai, I. and Schultz, Gy. *J. Organometal. Chem. Submitted for publication.*
7. Boonstra, L. H., Mijlhoff, F. C., Renes, G., Spelbos, A. and Hargittai, I. *J. Mol. Struct. 28* (1975) 129.
8. Almlöf, J. USIP Report 72–09, University of Stockholm, 1972.
9. Roos, B. and Siegbahn, P. *Theor. Chim. Acta 17* (1970) 209.
10. Huzinaga, S. *J. Chem. Phys. 42* (1965) 1923.
11. Mijlhoff, F. C. *Kém. Közl. 43* (1975) 399.

Received December 9, 1975.

Crystal Structure of Cyclotetradecane at −157°C

P. GROTH

Department of Chemistry, University of Oslo, Oslo 3, Norway

A recent study of cyclotetradecanone, $C_{14}H_{26}O$,[1] revealed a disordered structure with respect to the oxygen atoms while the ring skeleton had the "rectangular" diamond-lattice conformation (without observable disorder). For cyclotetradecane, $C_{14}H_{28}$, this conformation has the lowest calculated enthalpy [2] as well as being the observed one in liquid and solution.[3] It has been stated that it is also the experimental crystal conformation.[2] However, to the best of the author's knowledge no results have yet been published on the conformation in the solid state, and will therefore now be presented.

The crystals of $C_{14}H_{28}$ are triclinic with cell dimensions (for Dirichlet's reduced cell) $a=5.340(4)$ Å, $b=8.041(6)$ Å, $c=8.424(7)$ Å, $\alpha=64.4(1)°$, $\beta=89.5(1)°$, $\gamma=82.0(1)°$. There is one molecule in the unit cell and the space group is $P\bar{1}$.

894 observed reflections were measured on an automatic four-circle diffractometer at −157 °C (Mo$K\alpha$-radiation). No corrections for absorption or secondary extinction were carried out (crystal size = (0.1 × 0.2 × 0.4) mm³).

The structure was solved by direct methods [4] and refined by full-matrix least-squares technique.[5]* Anisotropic temperature factors were introduced for the carbon atoms. Weights in least squares were obtained from the standard deviations in intensities, $\sigma(I)$, taken as

$$\sigma(I)=[C_T+(0.02C_N)^2]^{\frac{1}{2}}$$

where C_T is the total number of counts and C_N the net count. The R-value arrived at was 5.1 % (weighted value $R_w=5.2$ %) for 894 observed reflections.

Final fractional coordinates with estimated standard deviations are given in Table 1. Maximum root-mean-square anisotropic thermal amplitudes for the carbon atoms range from 0.16 to 0.18 Å. No rigid-body analysis has been performed. Interatomic distances, bond angles, and dihedral angles are given in Table 2 together with standard deviations, computed from the final correlation matrix. Fig. 1, a schematic drawing of the molecule, illustrates the "rectangular" conformation of the 14-membered ring.

From Table 2 it may be seen that the C−C bond lengths are equal within limit of error (mean value 1.534 Å). The bond angle C2−C3−C4 (112.3°) is significantly smaller than the others which are equal with an average of 114.6°. This value corresponds closely to those of cyclotetradecanone [1] (114.4°) and cycloundecanone [6] (114.6°). Fig. 1 shows that C3 is

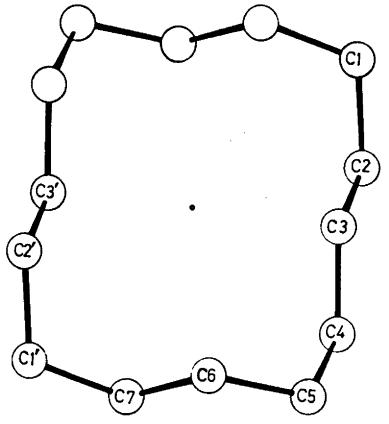

Fig. 1. Schematic drawing of the molecule.

* All programs used (except those for phase determination) are included in this reference.

Table 1. Final fractional coordinates and thermal parameters with estimated standard deviations. The expression for anisotropic vibration is exp [$-2\pi^2(h^2a^{*2}U11+..+2klb^*c^*U23)$]. Atom Hmn is bonded to atom Cm.

ATOM	x	y	z	U11	U22	U33	U12	U13	U23
C1	.76758(43)	.13041(29)	.79436(26)	.0295(12)	.0228(11)	.0179(11)	.0003(9)	-.0028(9)	-.0067(9)
C2	.75636(38)	.15557(30)	.59558(26)	.0244(11)	.0209(11)	.0201(11)	-.0010(9)	.0019(8)	-.0105(9)
C3	.49516(37)	.24515(29)	.58176(25)	.0247(11)	.0207(11)	.0172(10)	-.0038(9)	.0015(8)	-.0092(9)
C4	.49943(39)	.30767(30)	.38218(26)	.0280(12)	.0209(11)	.0168(10)	-.0029(9)	.0014(8)	-.0086(9)
C5	.24602(39)	.41099(29)	.19893(26)	.0262(11)	.0273(12)	.0148(11)	-.0063(9)	-.0001(8)	-.0087(9)
C6	.14111(39)	.58705(28)	.22006(27)	.0212(11)	.0259(12)	.0163(11)	-.0001(9)	-.0020(8)	-.0076(9)
C7	.31337(40)	.73767(28)	.15645(26)	.0267(12)	.0247(11)	.0132(10)	-.0032(9)	.0017(8)	-.0067(9)

ATOM	x	y	z	B	ATOM	x	y	z	B
H11	.6438(39)	.0055(29)	.8498(27)	1.8(4)	H12	.9427(44)	.8409(31)	.8469(29)	2.8(4)
H21	.8159(37)	.0432(29)	.5751(26)	1.6(4)	H22	.8809(35)	.2398(26)	.5401(23)	.9(3)
H31	.4382(34)	.3458(28)	.5318(24)	1.3(4)	H32	.3643(37)	.1572(27)	.5490(25)	1.4(3)
H41	.5421(38)	.2002(31)	.2779(27)	2.1(4)	H42	.6407(36)	.3862(26)	.2594(24)	1.0(3)
H51	.1092(36)	.3277(26)	.2287(24)	1.1(3)	H52	.2656(39)	.4441(29)	.0734(31)	2.1(4)
H61	.1077(36)	.5547(27)	.3433(29)	1.5(4)	H62	-.0279(43)	.6365(29)	.1564(28)	2.2(4)
H71	.3169(36)	.7977(27)	.0192(29)	1.8(4)	H72	.4931(38)	.6794(25)	.2042(25)	1.2(3)

Table 2. Bond distances, bond angles, and dihedral angles with estimated standard deviations.

DISTANCE	(Å)	DISTANCE	(Å)
C1 - C2	1.535(3)	C2 - C3	1.528(3)
C3 - C4	1.533(3)	C4 - C5	1.536(3)
C5 - C6	1.531(3)	C6 - C7	1.538(3)
C7 - C1'	1.536(3)		

ANGLE	(°)	ANGLE	(°)
C1 - C2 - C3	114.7(2)	C2 - C3 - C4	112.3(2)
C3 - C4 - C5	114.7(2)	C4 - C5 - C6	114.6(2)
C5 - C6 - C7	114.2(2)	C6 - C7 - C1'	114.4(2)
C7 - C1' - C2'	114.7(2)		

DIHEDRAL ANGLE	(°)
C1 - C2 - C3 - C4	176.6(2)
C2 - C3 - C4 - C5	-176.8(2)
C3 - C4 - C5 - C6	58.8(3)
C4 - C5 - C6 - C7	61.8(2)
C5 - C6 - C7 - C1'	-178.1(2)
C6 - C7 - C1' - C2'	64.4(3)
C7 - C1' - C2' - C3'	58.6(3)

the middle atom at the long "edge" of the "rectangle". Since this is the least strained position, one would expect an angle more close to 109.5° at C3 than at any other atom. In cyclotetradecanone the corresponding angle is 112.7°. The dihedral angles of Table 2 are also in very good agreement with the values found for cyclotetradecanone: 177.4, −174.9, 57.8, 60.7, −170.4, 64.8, 59.0°. C−H bond distances range from 0.95 to 1.04 Å. No short *inter*-molecular distances are observed.

A list of observed and calculated structure factors is available from the author.

Acknowledgement. The author would like to thank cand.real. T. Ledaal for supplying the crystals.

1. Groth, P. *Acta Chem. Scand. A 29* (1975) 374.
2. Dale, J. *Acta Chem. Scand. 27* (1973) 1115.
3. Borgen, G. and Dale, J. *Chem. Commun.* (1970) 1340.
4. Germain, G., Main, P. and Woolfson, M. M. *Acta Crystallogr. A 27* (1971) 368.
5. Groth, P. *Acta Chem. Scand. 27* (1973) 1837.
6. Groth, P. *Acta Chem. Scand. A 28* (1974) 294.

Received November 27, 1975.

Acta Chemica Scandinavica A 30 (1976) 157—162

The Crystal Structure of Tetraphenylphosphonium Bis(tetrathiomolybdato)nickelate(II)

INGER SØTOFTE

Chemistry Department B, The Technical University of Denmark, DTH 301. DK-2800 Lyngby, Denmark

The crystal structure of tetraphenylphosphonium bis(tetrathiomolybdato)nickelate(II), $[P(C_6H_5)_4]_2[Ni(MoS_4)_2]$, has been determined by three-dimensional X-ray methods. The crystals are triclinic with unit cell dimensions $a=12.60(3)$ Å, $b=12.75(3)$ Å, $c=9.41(2)$ Å, $\alpha=113.3(3)°$, $\beta=96.4(3)°$, $\gamma=108.5(3)°$ and space group $P\bar{1}$. The structure was refined by full-matrix least-squares procedures to an R factor of 0.074 using 3867 independent, statistically significant reflections collected on an automatic diffractometer. The nickel atom has planar coordination, and the molybdenum atom has distorted tetrahedral coordination. In the NiS_2Mo ring the Ni – S and the Mo – S distances are all 2.23 Å. Outside the ring the Mo – S distances are 2.15 Å. The NiS_2 and MoS_2 planes are inclined at 169°. The Ni – Mo contact of 2.80 Å is rationalized in terms of the constraint and not in terms of a metal-metal interaction.

Thioanions of the type MS_4^{2-}, M = Mo or W, are known to form complexes, $M'(MS_4)^{2-}$, with ions of the first transition series. The complexes can be isolated in the form of tetraphenylphosphonium salts. For the $Ni(MS_4)_2^{2-}$ complex Müller [1] suggests a planar coordination of the Ni atom and a tetrahedral arrangement for the MS_4 group. Recently [2] the crystal structures of two trinuclear complexes, $\{[(\pi\text{-}C_5H_5)_2M(SCH_3)_2]Ni\}^{2+}$, M = Mo and Nb, have been reported. In the Mo-compound the Ni atom has planar coordination and the Ni – Mo contact is 3.39 Å. However, in the Nb complex the Ni atom has tetrahedral coordination and the Ni – Nb contact is short, 2.78 Å, which was rationalized as metal-metal bonding. An X-ray investigation of the compound, $[P(C_6H_5)_4]_2[Ni(MoS_4)_2]$, was carried out in order to see if the tetrahedral coordination of the Mo atom would cause a metal-metal bonding.

EXPERIMENTAL

Preparation. The compound was prepared by Erik Larsen, Chemistry Department I, University of Copenhagen. In order to obtain crystals sufficiently large for an X-ray investigation, 10^{-4} mol of $[P(C_6H_5)_4]_2MoS_4$ were dissolved in acetonitrile and 5×10^{-5} mol of nickel acetate in acetonitrile were added. The operation was carried out in a glove box under nitrogen. Well developed, red-brownish crystals were formed.

X-Ray technique. A crystal of dimensions 0.07 mm × 0.17 mm × 0.20 mm was used. Space group and preliminary unit cell dimensions were obtained from Weissenberg and precession photographs taken with Cu$K\alpha$- and Mo$K\alpha$-radiation. A set of three-dimensional intensity data was collected by a $\theta-2\theta$ scanning technique on a Picker FACS-1 single crystal X-ray diffractometer. Mo$K\alpha$-radiation was selected using a graphite monochromator. Harmonics were excluded by means of a pulse height discriminator. Reflections within a hemisphere of radius $\sin\theta/\lambda=0.707$ Å^{-1} were measured. 3511 of the 7378 independent reflections showed net intensities less than twice their estimated standard deviation and were designated as "unobserved". They were not included in the refinement of the structure.

Computer programmes. A FORTRAN programme [3] evaluated intensities, calculated standard deviations and Lorentz and polarization corrections. The prepolarization of the incident beam was included. No absorption correction was made ($\mu_{Mo}=12.6$ cm^{-1}). The crystal structure analysis computations were performed on an IBM 370/165 computer using the X-Ray crystallographic programme system of Stewart *et al.*[4] and the drawing programme ORTEP written by Johnson.[5] The atomic scattering factors used were for molybdenum and nickel those computed from relativistic Dirac-Slater wave functions [6] and for sulfur, phosphorus and carbon those computed from numerical Hartree-Fock wave functions.[7]

Table 1a. Atomic coordinates. The estimated standard deviations ($\times 10^4$) are given in parentheses. For phosphorus and carbon isotropic temperature parameters, $U(\times 10^2)$ in Å^2 are given. The estimated standard deviations ($\times 10^3$) are given in parentheses.

Atom	x	y	z	U
Ni	0.0000(0)	0.0000(0)	0.0000(0)	
Mo	0.1192(1)	0.2588(1)	0.1629(1)	
S1	0.0512(3)	0.1345(2)	−0.1004(3)	
S2	0.0884(2)	0.1220(2)	0.2614(2)	
S3	0.0220(2)	0.3717(2)	0.2446(3)	
S4	0.3007(2)	0.3760(3)	0.2294(5)	
P	0.3344(2)	0.7493(2)	0.1641(2)	2.9(1)
C1	0.2459(6)	0.6127(7)	−0.0220(9)	3.3(1)
C2	0.2780(8)	0.6048(8)	−0.1634(11)	4.5(2)
C3	0.2137(8)	0.4974(8)	−0.3102(11)	4.6(2)
C4	0.1210(8)	0.4033(9)	−0.3117(11)	4.8(2)
C5	0.0893(8)	0.4114(9)	−0.1717(11)	4.9(2)
C6	0.1529(7)	0.5172(8)	−0.0251(10)	4.1(2)
C7	0.2598(6)	0.7693(7)	0.3198(9)	3.2(1)
C8	0.2410(7)	0.6876(8)	0.3881(10)	4.2(2)
C9	0.1887(8)	0.7086(9)	0.5158(11)	4.9(2)
C10	0.1578(8)	0.8092(9)	0.5729(12)	5.1(2)
C11	0.1761(9)	0.8901(10)	0.5058(13)	5.9(2)
C12	0.2271(8)	0.8702(9)	0.3760(11)	4.9(2)
C13	0.3671(6)	0.8836(6)	0.1305(8)	3.0(1)
C14	0.2778(7)	0.8940(7)	0.0403(10)	3.8(2)
C15	0.2994(7)	1.0055(8)	0.0296(11)	4.5(2)
C16	0.4072(8)	1.1038(8)	0.1098(11)	4.7(2)
C17	0.4954(8)	1.0935(8)	0.1956(10)	4.2(2)
C18	0.4766(7)	0.9825(7)	0.2070(9)	3.4(2)
C19	0.4688(7)	0.7396(7)	0.2330(9)	3.6(2)
C20	0.5195(8)	0.7944(9)	0.3979(11)	4.8(2)
C21	0.6276(9)	0.7946(10)	0.4540(13)	5.8(2)
C22	0.6832(10)	0.7432(11)	0.3450(14)	6.4(3)
C23	0.6337(11)	0.6888(12)	0.1802(15)	6.9(3)
C24	0.5240(9)	0.6837(10)	0.1226(13)	5.7(2)

Table 1b. Anisotropic temperature factor parameters, $U_{ij}(\times 10^4)$ in Å^2. The estimated standard deviations ($\times 10^4$) are given in parentheses.
The form of the temperature factor expression is $\exp[-2\pi^2\sum_{ij}h_ih_ja_i^*a_j^*U_{ij}]$.

Atom	U_{11}	U_{22}	U_{33}	U_{12}	U_{13}	U_{23}
Ni	381(07)	280(06)	270(06)	144(05)	75(05)	106(05)
Mo	454(04)	360(03)	426(04)	154(03)	120(03)	137(03)
S1	1023(22)	385(11)	341(11)	156(13)	161(12)	194(10)
S2	614(14)	357(10)	296(09)	174(10)	2(09)	117(08)
S3	481(12)	384(11)	672(15)	231(10)	203(11)	214(10)
S4	430(14)	570(16)	1049(25)	122(12)	234(15)	196(16)

CRYSTAL DATA

Crystal system: triclinic
Unit cell: $a = 12.60(3)$ Å, $b = 12.75(3)$ Å, $c = 9.41(2)$ Å,
$\alpha = 113.3(3)°$, $\beta = 96.4(3)°$, $\gamma = 108.5(3)°$.

$d_{obs} = 1.58$ g/cm^3, $d_{calc} = 1.56$ g/cm^3.
One molecule of $[P(C_6H_5)_4]_2[Ni(MoS_4)_2]$ per unit cell.
No piezoelectric effect could be detected.
Possible space groups: $P1$ and $P\bar{1}$.

STRUCTURE DETERMINATION

Since there is only one formula unit per cell the Ni atom was chosen to lie in the special position (0,0,0). The coordinates of the Mo atom were readily deduced from a three-dimensional Patterson function. The position of the remaining non-hydrogen atoms were derived from successive Fourier syntheses. Least-squares refinement of coordinates and isotropic temperature factor coefficients gave an R factor of 0.08. Further refinement with anisotropic temperature factor parameters for Mo, Ni, and S lowered the R-value to 0.074 ($R_w = 0.082$).

Table 2a. Some interatomic distances in Å. The estimated standard deviations ($\times 10^3$) are given in parentheses.

Ni – Mo	2.798(08)
Ni – S1	2.228(05)
Ni – S2	2.230(07)
Mo – S1	2.222(06)
Mo – S2	2.232(05)
Mo – S3	2.148(05)
Mo – S4	2.153(06)
P – C1	1.806(08)
P – C7	1.804(09)
P – C13	1.792(10)
P – C19	1.806(10)
Mean P – C	1.802(5)
C1 – C2	1.409(14)
C2 – C3	1.410(11)
C3 – C4	1.378(14)
C4 – C5	1.393(16)
C5 – C6	1.400(11)
C6 – C1	1.384(12)
C7 – C8	1.400(15)
C8 – C9	1.407(15)
C9 – C10	1.380(17)
C10 – C11	1.381(20)
C11 – C12	1.414(17)
C12 – C7	1.397(15)
C13 – C14	1.406(14)
C14 – C15	1.406(16)
C15 – C16	1.389(11)
C16 – C17	1.372(16)
C17 – C18	1.408(15)
C18 – C13	1.404(10)
C19 – C20	1.393(13)
C20 – C21	1.404(17)
C21 – C22	1.376(18)
C22 – C23	1.390(18)
C23 – C24	1.400(19)
C24 – C19	1.399(15)
Mean C – C	1.396(4)

Table 2b. Some interatomic angles (°). The estimated standard deviations ($\times 10$) are given in parentheses.

Ni – S1 – Mo	77.9(2)
Ni – S2 – Mo	77.7(2)
S1 – Ni – S2	101.7(2)
S1 – Mo – S2	101.8(2)
S1 – Mo – S3	111.2(2)
S1 – Mo – S4	111.8(2)
S2 – Mo – S3	110.3(2)
S2 – Mo – S4	111.8(2)
S3 – Mo – S4	109.7(2)
C1 – P – C7	111.7(4)
C1 – P – C13	108.8(4)
C1 – P – C19	110.6(4)
C7 – P – C13	108.0(4)
C7 – P – C19	108.8(4)
C13 – P – C19	108.9(4)
Mean C – P – C	109.5(2)
C6 – C1 – C2	121.2(6)
C1 – C2 – C3	118.9(8)
C2 – C3 – C4	119.3(10)
C3 – C4 – C5	121.6(7)
C4 – C5 – C6	119.6(9)
C5 – C6 – C1	119.3(9)
C12 – C7 – C8	121.0(9)
C7 – C8 – C9	119.0(10)
C8 – C9 – C10	120.0(11)
C9 – C10 – C11	121.1(11)
C10 – C11 – C12	120.1(12)
C11 – C12 – C7	118.6(11)
C18 – C13 – C14	120.4(9)
C13 – C14 – C15	119.0(7)
C14 – C15 – C16	119.8(10)
C15 – C16 – C17	121.4(10)
C16 – C17 – C18	120.0(7)
C17 – C18 – C13	119.3(9)
C24 – C19 – C20	120.7(9)
C19 – C20 – C21	119.7(10)
C20 – C21 – C22	119.3(10)
C21 – C22 – C23	121.4(13)
C22 – C23 – C24	119.8(12)
C23 – C24 – C19	118.9(10)
Mean C – C – C	120.0(4)

Unit weights were used. The weights used in the final least-squares refinement were $w = xy$, where, if $0.33F_{obs} > |F_{calc}|$, then $w = 10^{-9}$, else if $\sin\theta > 0.19$, then $x = 1$, else $x = (\sin\theta)/0.19$ and if $50 > F_{obs}$, then $y = 1$, else $y = 50/F_{obs}$. The resulting agreement factor R was unchanged 0.074 ($R_w = 0.082$).

The contributions of the hydrogen atoms were neglected. The space group $P\bar{1}$ was assumed in all calculations. The refinement confirms that this choice is correct. The final positional and thermal vibration parameters

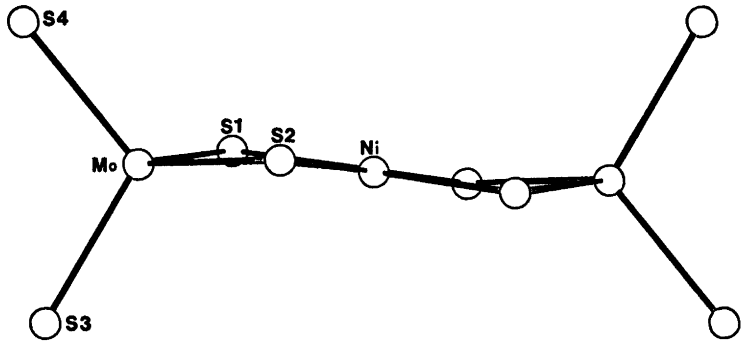

Fig. 1. The $[Ni(MoS_4)_2]^{2-}$ ion.

with their estimated standard deviations are listed in Table 1. Bond distances and angles with their estimated standard deviations are given in Table 2. A list of observed and calculated structure factors may be obtained from the author or the department upon request.

DESCRIPTION AND DISCUSSION OF THE STRUCTURE

The crystals are built up from isolated anions about symmetry centres and cations in general positions in the cell. In the anion four sulfur atoms form two double bridges between the nickel atom and the two molybdenum atoms (Fig. 1). Each molybdenum atom is coordinated to four sulfur atoms at the corners of a distorted tetrahedron. The NiS_4 group is rigorously planar and the Mo···Ni···Mo system linear owing to the fact that the nickel atom lies at a center of symmetry. The results therefore confirm that the compound has a planar structure around Ni as suggested by Müller.[1] However, the MoS_2NiS_2Mo system is not planar. The molybdenum atoms are displaced 0.26 Å from the NiS_4 plane. The angle between the NiS1S2 plane and the MoS1S2 plane is 169.0° and that between the plane of NiS1Mo and NiS2Mo 171.1°. Within the NiS_2Mo ring there are no significant differences between the Ni–S and Mo–S bonds (Table 2a). The Ni–S distance is that commonly found in other planar NiS_4 complexes.[8] The Mo–S(bridge) distance is somewhat longer and the two Mo–S distances outside the ring are somewhat shorter than 2.18 Å, which is found for the MoS_4^{2-} ion.[9] The coordination polyhedron of the molybdenum is slightly distorted from the tetrahedron because of the small angle in the ring. Therefore all angles involving S1 and S2 are greater than the tetrahedral value while the angle S3–Mo–S4 is equal to it (Table 2b). Neither the two M–S–M angles nor the two S–M–S angles have significantly different values within the fourmembered ring (Table 2b). The obtuse angle at the nickel atom is due to the tetrahedral coordination at the molybdenum atom and to the strain imposed by the planarity of the NiS_4 unit.

The anisotropic mean-square amplitudes of vibration of the two sulfur atoms in the ring are decidedly enlarged in the directions normal to the plane of the ring (Table 1b). Within the ring the Ni-Mo contact is short, 2.798 (0.008) Å. The obtuse angle at the nickel atom makes the dimensions of the NiS_2Mo ring satisfy the Dahl [10] criteria for metal-metal bonding. However, the interaction is perhaps not so substantial as the Ni–Nb bonding in $\{[(\pi\text{-}C_5H_5)_2Nb(SCH_3)_2]_2Ni\}(BF_4)_2.2H_2O$.[2] The two $\{[(\pi\text{-}C_5H_5)_2M(SCH_3)]_2Ni\}^{2+}$-complexes, with M = Mo or Nb are prepared by adding $NiCl_2$ to a solution of $(\pi\text{-}C_5H_5)_2M(SCH_3)_2$. Therefore the compounds would be expected to contain M(IV) and Ni(II). In this case the formal description of the valency state for the Mo-compound will be d^2-d^8-d^2, and for the Nb-compound d^1-d^8-d^1. By transferring one electron from niobium to nickel the situation of fully occupied shells are obtained, d^0-d^{10}-d^0, which is a more favourable state. Since nearly all Ni(0) complexes are tetrahedral molecules, the nickel atom in the above Ni–Nb complex should

Table 3. Least-squares planes for phenyl rings and deviations of the constituent atoms in Å × 10^4. The estimated standard deviations of the atoms from the plane are 0.002 Å for 1, 0.005 Å for 2, 0.009 Å for 3, and 0.013 Å for 4.

Atom	Ring 1	Atom	Ring 2	Atom	Ring 3	Atom	Ring 4
C1	−8	C7	40	C13	91	C19	94
C2	−16	C8	23	C14	−6	C20	71
C3	20	C9	−54	C15	−99	C21	−135
C4	0	C10	24	C16	120	C22	33
C5	−26	C11	38	C17	−33	C23	129
C6	29	C12	−71	C18	−73	C24	−191

have tetrahedral coordination, which the structure determination confirms. In the $\{[(\pi\text{-}C_5H_5)_2Nb(SCH_3)_2]Ni\}^{2+}$ and the $[Ni(MoS_4)_2]^{2-}$ complexes one of the metal ions has a tetrahedral environment. This seems to be enough to make the ring dimensions satisfy the Dahl criteria for metal-metal bonding. The two $[(\pi\text{-}C_5H_5)_2M(SCH_3)_2Ni]^{2+}$-complexes have M−S bond lengths about 2.49 Å while the Mo−S distance in $[Ni(MoS_4)_2]^{2-}$ is only 2.23 Å. In all three compounds the Ni−S bonds are about 2.20 Å. Therefore, the longer Ni−Mo distance in $[(\pi\text{-}C_5H_5)_2Mo(SCH_3)_2Ni]^{2+}$ can be rationalized in terms of small S−M−S angles rather than in terms of an effect from the bond length variation.

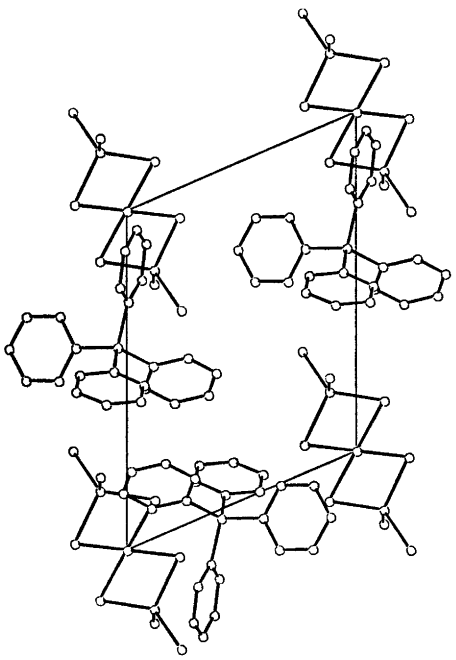

Fig. 2. The projection of the structure viewed perpendicular to the *bc*-plane.

Table 4. The shortest van der Waals distances in Å. The estimated standard deviations (× 10^3) are given in parentheses.

C16−C18 (1−*x*, 2−*y*, −*z*)	3.410(15)
C4−C22 (1−*x*, 1−*y*, −*z*)	3.506(20)
C4−C10 (−*x*, 1−*y*, −*z*)	3.536(15)
S3−C8	3.671(13)
S3−C9	3.711(14)
S3−C5 (−*x*, 1−*y*, −*z*)	3.718(15)
S1−C5	3.743(15)
S3−C10 (−*x*, 1−*y*, 1−*z*)	3.753(14)
S2−C21 (1−*x*, 1−*y*, 1−*z*)	3.784(15)

The bond distances and angles in the tetraphenylphosphonium ion agree with previous studies on structures containing this ion.[11] The angles around the phosphorus atom are close to the tetrahedral value (Table 2b). Average C−C bond lengths are 1.396 Å and average bond angles 120.0°. The least squares planes were calculated for the four rings and, as can be seen from Table 3, all the rings are approximately planar. Plane I (C4−C1−P−C13−C16) and plane II (C10−C7−P−C19−C22) make an angle of 87.1°. The angles between plane I and ring 1 and ring 3 are 45.0 and 41.0° and those between plane II and ring 2 and ring 4 are 56.9 and 20.1°, respectively. Therefore the tetraphenylphosphonium ion does not approximate any symmetrical conformation.

The tetraphenylphosphonium ions are located in the space between the anions (Fig. 2). The cations and the anions are separated by normal van der Waals distances, of which the shortest are shown in Table 4.

Acknowledgements. The data were collected at Chemistry Department IV, the University of Copenhagen, on a diffractometer granted by Statens almindelige Videnskabsfond. The author is indebted to Dr. K. J. Watson and Mr. F. Hansen for collecting the data, and to Dr. E. Larsen for discussions.

REFERENCES

1. Müller, A., Ahlborn, E. and Heinsen, H.-H. *Z. Anorg. Allg. Chem. 386* (1971) 102 and references therein.
2. Prout, K., Critchley, S. R. and Rees, G. V. *Acta Crystallogr. B 30* (1974) 2305.
3. Alcock, N. W. and Watwon, K. *An extensive modification of the programme NRC-2A* written by F. R. Ahmed, National Research Council, Ottawa, Canada.
4. Stewart, J. M., Kundell, F. A. and Baldwin, J. C. *The X-Ray System, Version 1970*, Chemistry Department, University of Maryland, College Park, Maryland 20740, U.S.A.
5. Johnson, C. K. *ORTEP, Report ORNL-3794*, Oak Ridge National Laboratory, Oak Ridge 1965.
6. Cromer, D. T. and Waber, J. T. *Acta Crystallogr. 18* (1965) 104.
7. Cromer, D. T. and Mann, J. B. *Acta Crystallogr. A 24* (1968) 321.
8. Holm, R. H. and O'Connor, M. J. *Prog. Inorg. Chem. 14* (1971) 306.
9. Koz'min, P. A. and Popova, Z. V. *Zh. Strukt. Khim. 12* (1971) 99.
10. Dahl, L. F., deGil, E. R. and Feltham, R. D. *J. Amer. Chem. Soc. 91* (1969) 1653.
11. Textor, M., Duhler, E. and Oswald, H. R. *Inorg. Chem. 13* (1974) 1361 and references therein.

Received August 29, 1975.

Acta Chemica Scandinavica A 30 (1976) 163—170

The Crystal and Molecular Structure of Indium and Iron(III) Complexes with 1-(2-Thienyl)-4,4,4-trifluoro-1,3-butanedione

H. SOLING

Chemistry Department B, Technical University of Denmark, DK-2800 Lyngby, Denmark

Single crystals of the title compounds, $In(TTA)_3$ and $Fe(TTA)_3$, have been investigated by X-ray diffractometry. The compounds are isostructural $In(TTA)_3$: $a = 8.803(15)$ Å, $b = 17.67(3)$ Å, $c = 19.63(4)$ Å, $\beta = 110.2(1)°$. $Fe(TTA)_3$: 8.865(9) Å, $b = 17.46(2)$ Å, $c = 19.69(2)$ Å, $\beta = 110.8(1)°$. Space group $P2_1/c$. The structures were refined to $R = 0.069$ and 0.078, respectively. The unit cell contains two pairs of *meridional-tris-β*-diketonate complexes centered on the special positions $\frac{1}{2}$, 0,0 and $\frac{1}{2},\frac{1}{2},\frac{1}{2}$. The metal atom is at the center of gravity of the six coordinating oxygen atoms, which form the apices of a slightly deformed octahedron. The average In—O distance is 2.13(2) Å, the Fe—O distance is 1.99(2) Å. Contrary to other *tris-β*-diketonates the two C—C bonds of the chelate ring are of unequal length, the C—C bond closest to the CF_3 group being the shorter. Fluorine atoms apart, each ligand may roughly be represented by a plane pivoted around an edge of the coordination polyhedron.

The crystal structure analysis, reported in this paper, is the second of a current series of structure investigations [1] of metal compounds of 1-(2-thienyl)-4,4,4-trifluoro-1,3-butanedione, (trivial name thenoyltrifluoracetone). The structure formula of this unsymmetric β-diketone, henceforth designated HTTA, is shown in Fig. 1.

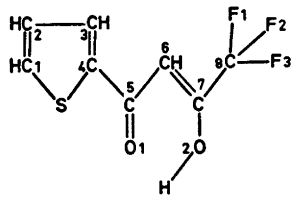

Fig. 1. Structure formula of 1-(2-thienyl)-4,4,4-trifluoro-1,3-butanedione, displaying the labelling scheme.

The compounds $In(TTA)_3$ and $Fe(TTA)_3$, which are the topics of this paper, are isostructural.

EXPERIMENTAL

Preparation and analysis

$In(TTA)_3$ 6.6 g of $InCl_3$ (BDH) was dissolved in 130 ml of 50 % ethanol, (v/v). 15.9 g of the β-diketone (Merck), freshly sublimed *in vacuo*, were dissolved in 320 ml of 50 % ethanol and neutralized with ammonia. The former solution was slowly poured into the latter under vigorous stirring. The stirring was continued for half an hour, then the precipitation was completed by addition of 450 ml of water. The white, microcrystalline raw product was washed with water and dried in the air. Colourless, tabular crystals were grown from a solution of the raw product in nitromethane. The melting point, determined on a microscope hot stage (Mettler FP52/5), was 164.6 ± 0.8 °C. After destruction of the complex with concentrated nitric acid, indium was determined by microtitration with EDTA according to Schwarzenbach.[2] (Found: In 14.68. Calc. for $In(C_8H_4F_3O_2S)_3$: 14.75).

$Fe(TTA)_3$ was prepared as described by Berg and Truemper.[3] Single crystals were grown from a solution of the raw material in a 50 % (v/v) mixture of diethylether and cyclohexane. The well-developed, garnet red, prismatic crystals melt at 162.6 ± 0.5 °C on the hot stage microscope; m.p. lit.[3] 159—160 °C. Iron was determined by microtitration with EDTA [2] after appropriate destruction of the complex. (Found: Fe 7.78. Calc. for $Fe(C_8H_4F_3O_2S)_3$: 7.76).

Collection and treatment of intensity data

Intensity data were collected by means of a semi-automatic two-circle diffractometer, run in the ω-scan mode. Net intensities were con-

verted to relative structure factors by application of the usual Lorentz and polarization corrections.

In(TTA)$_3$. Monochromatized (graphite) Mo*K*α radiation ($\lambda = 0.71069$ Å) was used to measure the reflections from all unique planes in the sin θ/λ range from 0.06 to 0.6 Å^{-1}. Two different crystals had to be used. During the scanning of the *h*8*l* zone, the first crystal became opaque, and its reflecting power decreased more than 10 % within a few hours. A second crystal sufficed for the remainder of the data collection. For scaling purposes the *h*0*l* reflections of the second crystal were also measured. The dimensions of the two crystals were $0.250 \times 0.060 \times 0.375$ mm^3 and $0.375 \times 0.070 \times 0.400$ mm^3, respectively. Since the platey crystals were mounted with their shortest dimension (the *b*-axis) along the direction of the Weissenberg spindle, corrections for absorption [4] were made. A Gaussian grid of 864 sample points was found suitable. Each F_o was assigned a standard deviation based on counting statistics. Reflections with $F_o < 3\sigma(F_o)$ were rejected, leaving 2759 reflections for the structure analysis, *i.e.* more than 6 observations per adjustable parameter.

Fe(TTA)$_3$. The sin θ/λ range was 0.06 to 0.45 Å^{-1}, (LiF-monochromator). No corrections were made for absorption. The yield of $F_o < 3\sigma(F_o)$ was 1178, *i.e.* approximately 5 observations per refined parameter. (Fe and F atoms only were assigned anisotropic temperature parameters).

CRYSTAL DATA

$In(C_5H_4F_3O_2S)_3$ (FW = 778.3) and $Fe(C_5H_4F_3O_2S)_3$ (FW = 719.4) both crystallize in the space group $P2_1/c$ (No. 14). Unit cell dimensions were determined from several independent precession photographs.

In(TTA)$_3$: $a = 8.803(15)$ Å, $b = 17.67(3)$ Å, $c = 19.63(4)$ Å, $\beta = 110.2(1)°$, at 22 °C. Volume of the cell = 2867 Å^3. $F(000) = 1528$. $D_x(Z=4) = 1.788$ g cm^{-3}, D_m(flot.) = 1.788(5) g cm^{-3}. μ(Mo*K*a) = 11.3 cm^{-1}.

Fe(TTA)$_3$: $a = 8.865(9)$ Å, $b = 17.46(2)$ Å, $c = 19.69(2)$ Å, $\beta = 110.8(1)°$, at 22 °C. Volume of the cell = 2848 Å^3. $F(000) = 1436$. $D_x(Z=4) = 1.678$ g cm^{-3}, D_m(flot.) = 1.675(5) g cm^{-3}. μ(Mo*K*α) = 8.60 cm^{-1}.

SOLUTION AND REFINEMENT OF THE STRUCTURES

In(TTA)$_3$. The structure was solved for all non-hydrogen atoms by application of the heavy atom method. At the later stages of

Table 1. In(TTA)$_3$. Fractional atomic coordinates and anisotropic thermal parameters of the observed atoms. Standard deviations are in parentheses. The form of the temperature factor expression is exp $[-2\pi^2 \sum_{ij} h_i h_j a_i^* a_j^* U_{ij}]$. See Fig. 1 for labelling of the atoms.

	X	*Y*	*Z*	U_{11} or U	U_{22}	U_{33}	U_{12}	U_{13}	U_{23}
In	0.4544(1)	0.21043(5)	0.08363(2)	0.050(1)	0.028(1)	0.033(1)	0.000(5)	0.020(5)	0.001(5)
S(1)	0.2994(6)	0.1463(2)	0.2933(2)	0.096(4)	0.056(2)	0.055(2)	0.003(2)	0.028(2)	0.006(2)
F(11)	0.119(2)	0.4577(7)	0.0940(7)	0.27(2)	0.082(9)	0.12(1)	0.10(1)	0.131(15)	0.057(8)
F(12)	0.074(2)	0.4137(2)	−0.0074(7)	0.168(15)	0.076(9)	0.10(1)	0.038(9)	−0.03(1)	0.030(8)
F(13)	0.2970(15)	0.4560(5)	0.0507(8)	0.12(1)	0.062(8)	0.198(15)	0.005(7)	0.05(1)	0.060(9)
O(11)	0.338(1)	0.1982(4)	0.1630(4)	0.083(8)	0.029(5)	0.044(6)	0.010(5)	0.043(6)	0.002(4)
O(12)	0.287(1)	0.3000(5)	0.0446(4)	0.078(8)	0.040(6)	0.030(5)	0.017(5)	0.021(5)	−0.001(4)
C(11)	0.236(2)	0.168(1)	0.3633(8)	0.090(15)	0.07(1)	0.05(1)	−0.02(1)	0.04(1)	0.00(1)
C(12)	0.171(2)	0.236(1)	0.357(1)	0.06(1)	0.08(1)	0.09(1)	0.00(1)	0.04(1)	−0.03(1)
C(13)	0.1576(15)	0.2774(5)	0.2935(6)	0.038(8)	0.033(7)	0.035(7)	−0.005(6)	0.023(6)	−0.006(5)
C(14)	0.2367(15)	0.2314(8)	0.2532(6)	0.036(9)	0.048(9)	0.032(7)	−0.010(6)	0.005(6)	0.000(6)
C(15)	0.2665(15)	0.2493(7)	0.1863(6)	0.044(9)	0.045(8)	0.016(6)	−0.007(7)	0.017(6)	−0.002(5)

Table 1. Continued.

C(16)	0.218(2)	0.3195(7)	0.1512(6)	0.06(1)	0.033(7)	0.034(8)	0.009(7)	0.020(7)	−0.002(6)
C(17)	0.2313(15)	0.3374(7)	0.0868(7)	0.036(9)	0.043(8)	0.033(7)	−0.001(6)	0.005(6)	0.019(6)
C(18)	0.180(2)	0.4158(8)	0.0581(8)	0.07(1)	0.048(9)	0.047(9)	0.024(9)	0.019(9)	−0.003(8)
S(2)	0.6329(6)	0.2040(2)	−0.1275(2)	0.100(4)	0.067(3)	0.049(2)	0.007(3)	0.028(3)	−0.008(2)
O(21)	0.571(1)	0.2229(4)	0.0048(4)	0.075(7)	0.030(5)	0.034(5)	−0.006(5)	0.025(5)	−0.010(4)
O(22)	0.624(1)	0.2947(5)	0.1409(4)	0.059(7)	0.042(5)	0.043(5)	−0.009(5)	0.017(5)	−0.014(5)
F(21)	0.768(3)	0.4718(7)	0.1205(7)	0.034(2)	0.070(8)	0.114(9)	−0.10(1)	0.113(8)	−0.040(6)
F(22)	0.867(2)	0.4015(8)	0.2066(8)	0.138(15)	0.12(1)	0.14(1)	0.00(1)	−0.05(1)	−0.07(1)
F(23)	0.637(2)	0.4391(7)	0.1815(8)	0.15(1)	0.11(1)	0.18(1)	−0.044(9)	0.11(1)	−0.11(1)
C(21)	0.704(3)	0.2443(15)	−0.1887(9)	0.091(15)	0.14(2)	0.030(9)	0.022(15)	0.010(9)	0.02(1)
C(22)	0.754(3)	0.3132(15)	−0.172(1)	0.095(15)	0.14(2)	0.081(15)	0.00(2)	0.05(1)	0.048(15)
C(23)	0.750(2)	0.3396(7)	−0.1062(6)	0.045(9)	0.050(8)	0.023(7)	−0.021(7)	0.008(6)	0.013(6)
C(24)	0.677(2)	0.2821(8)	−0.0740(7)	0.06(1)	0.056(9)	0.028(7)	0.005(8)	0.015(7)	0.008(7)
C(25)	0.639(2)	0.2807(7)	−0.0082(6)	0.053(9)	0.038(8)	0.035(7)	0.003(7)	0.016(7)	0.000(6)
C(26)	0.686(2)	0.3442(8)	0.0403(7)	0.08(1)	0.043(8)	0.034(8)	−0.008(8)	0.029(8)	−0.006(6)
C(27)	0.674(2)	0.3459(7)	0.1059(6)	0.05(1)	0.042(8)	0.027(7)	−0.007(7)	0.018(7)	−0.020(6)
C(28)	0.737(3)	0.4150(9)	0.1527(9)	0.105(15)	0.05(1)	0.06(1)	−0.02(1)	0.03(1)	−0.016(8)
S(3)	0.0260(6)	0.0640(2)	−0.0977(2)	0.056(3)	0.077(3)	0.048(2)	−0.008(2)	0.010(2)	0.004(2)
F(31)	0.642(2)	−0.0691(5)	0.1785(9)	0.178(15)	0.046(7)	0.170(15)	0.013(8)	−0.07(1)	0.028(8)
F(32)	0.588(2)	0.08(1)	0.2475(8)	0.155(15)	0.24(2)	0.12(1)	0.093(15)	0.08(1)	0.136(15)
F(33)	0.7945(15)	0.0198(7)	0.2220(5)	0.065(7)	0.12(1)	0.079(8)	0.019(7)	0.001(6)	0.037(7)
O(31)	0.301(1)	0.1287(5)	0.0118(4)	0.065(7)	0.033(5)	0.032(5)	−0.009(5)	0.009(5)	0.003(4)
O(32)	0.597(1)	0.119(5)	0.1385(4)	0.060(7)	0.036(5)	0.030(5)	0.003(5)	0.012(5)	−0.005(4)
C(31)	−0.066(2)	−0.016(1)	−0.1363(6)	0.059(15)	0.105(16)	0.05(1)	−0.03(1)	0.012(9)	0.02(1)
C(32)	0.015(2)	−0.077(1)	−0.1014(9)	0.080(15)	0.084(15)	0.065(15)	−0.05(1)	0.02(1)	−0.02(1)
C(33)	0.161(2)	−0.0620(8)	−0.0426(8)	0.07(1)	0.06(1)	0.054(9)	−0.016(9)	0.045(9)	−0.025(8)
C(34)	0.179(2)	0.0154(7)	−0.0329(7)	0.06(1)	0.03(8)	0.050(9)	−0.005(7)	0.019(8)	−0.001(7)
C(35)	0.3030(15)	0.0570(5)	0.0218(6)	0.037(9)	0.030(15)	0.037(7)	−0.001(6)	0.027(7)	−0.010(5)
C(36)	0.4172(15)	0.0191(8)	0.0773(7)	0.05(1)	0.043(8)	0.047(9)	0.008(7)	0.013(8)	−0.014(7)
C(37)	0.5455(15)	0.0520(8)	0.1314(8)	0.026(8)	0.040(8)	0.07(1)	0.010(7)	0.013(7)	0.002(7)
C(38)	0.641(2)	0.0015(9)	0.1947(9)	0.058(15)	0.05(1)	0.07(1)	0.011(9)	0.02(1)	0.015(8)
H(11)	0.24(2)	0.14(1)	0.40(1)	0.069					
H(12)	0.12(3)	0.26(1)	0.39(1)	0.078					
H(16)	0.17(2)	0.354(9)	0.175(8)	0.039					
H(21)	0.65(2)	0.24(1)	−0.24(1)	0.101					
H(22)	0.80(3)	0.36(1)	−0.20(1)	0.089					
H(26)	0.73(2)	0.39(1)	0.022(9)	0.049					
H(31)	−0.17(2)	−0.021(1)	−0.17(1)	0.065					
H(32)	0.00(2)	−0.12(1)	−0.12(1)	0.062					
H(36)	0.41(2)	−0.04(1)	0.076(9)	0.049					

refinement an empirical weight function, $w^{\frac{1}{2}} = (5.0 + 0.0140\ F_o)^{-\frac{1}{2}}$, was used. When the refinement was nearly completed, the sites of the hydrogen atoms, except those attached to the C(3) atoms, could be localized on a Fourier difference map. Each hydrogen atom was assigned an (invariant) isotropic temperature factor corresponding to that of the carrier atom. A few more cycles of least squares calculations brought the refinement to a conclusion, where all shifts were less than 1/10 of the estimated standard deviation. The final R value was 0.069, and the error of fit quotient was 1.15.

Fe(TTA)$_3$. The structure was solved and refined for all non-hydrogen atoms, the indium compound being used as a starting model. $w^{\frac{1}{2}} = 14.1/F_o$ maximum allowed $w = 0.1$. The refinement terminated at $R = 0.078$. The error of fit quotient was 1.09.

Atomic form factors for the neutral atoms were used throughout. For indium the form factors were those given by Cromer and Waber.[5] The other form factors, as well as corrections for the anomalous dispersion of In and Fe, were taken from *International Tables for X-Ray Crystallography*.[6] Fractional coordinates and thermal parameters of the observed atoms are listed in Tables 1 and 2. Lists of observed and calculated structure factors may be obtained from this institute.

All crystallographic calculations have been performed with the X-RAY program system edited by Stewart.[7] The stereo drawing Fig. 2 has been made by means of the ORTEP II program of Johnson.[8]

RESULTS AND DISCUSSION

Both structures consist of pairs of *meridional tris-β*-diketonate molecules, centered around the special positions ½,0,0 and ½,½,½ (Fig. 2). The separation of the two enantiomorphous molecules in terms of the metal to metal distance is 8.28 Å for In(TTA)$_3$ and 8.22 Å for Fe(TTA)$_3$. The next shortest metal to metal distance is the a translation.

The metal atom is almost exactly at the common center of gravity of the six coordinating oxygen atoms, which form the apices of a slightly deformed octahedron. Metal to oxygen distances, oxygen to oxygen distances and some

Table 2. Fe(TTA)$_3$. Fractional atomic coordinates and thermal parameters of the observed atoms. Standard deviations are in parentheses. The form of the temperature factor expression is $\exp[-2\pi^2\sum_i\sum_j h_i h_j a_i^* a_j^* U_{ij}]$. See Fig. 1 for labelling of the atoms.

	X	Y	Z	U_{11} or U	U_{22}	U_{33}	U_{12}	U_{13}	U_{23}
Fe	0.4601(3)	0.2117(1)	0.0830(1)	0.065(2)	0.040(2)	0.036(2)	0.003(2)	0.192(1)	0.004(1)
S(1)	0.3132(8)	0.1436(4)	0.2859(3)	0.086(2)					
F(11)	0.112(3)	0.456(1)	0.079(1)	0.27(2)	0.102(15)	0.196(15)	0.127(15)	0.144(15)	0.087(1)
F(12)	0.100(2)	0.412(1)	−0.0209(8)	0.150(15)	0.130(15)	0.09(1)	0.05(1)	−0.016(9)	0.024(9)
F(13)	0.305(2)	0.459(1)	0.047(1)	0.13(1)	0.09(1)	0.192(15)	0.00(1)	0.05(1)	0.06(1)
O(11)	0.3548(15)	0.2000(7)	0.1578(6)	0.049(3)					
O(12)	0.3069(15)	0.2986(7)	0.0445(6)	0.059(3)					
C(11)	0.253(3)	0.1618(15)	0.357(1)	0.075(6)					
C(12)	0.179(3)	0.2308(15)	0.350(1)	0.084(7)					
C(13)	0.161(2)	0.2761(9)	0.2851(8)	0.025(4)					
C(14)	0.247(2)	0.229(1)	0.2464(9)	0.048(5)					
C(15)	0.277(2)	0.247(1)	0.1812(9)	0.042(5)					
C(16)	0.228(2)	0.320(1)	0.147(1)	0.055(5)					

Table 2. Continued.

C(17)	0.245(2)	0.338(1)	0.082(1)	0.046(5)					
C(18)	0.187(3)	0.413(1)	0.048(1)	0.071(6)					
S(2)	0.6194(9)	0.2018(4)	−0.1260(4)	0.096(2)					
F(21)	0.800(3)	0.464(1)	0.1308(9)	0.40(3)	0.112(15)	0.120(5)	−0.13(2)	0.11(2)	−0.07(1)
F(22)	0.860(2)	0.393(1)	0.2160(9)	0.165(15)	0.120(15)	0.13(1)	0.02(1)	−0.05(1)	−0.06(1)
F(23)	0.640(2)	0.440(1)	0.183(1)	0.124(13)	0.14(1)	0.189(15)	−0.02(1)	0.066(1)	−0.12(1)
O(21)	0.5624(15)	0.2237(7)	0.0070(6)	0.049(3)					
O(22)	0.6182(14)	0.2898(7)	0.1393(6)	0.053(3)					
C(21)	0.691(3)	0.2358(15)	−0.189(1)	0.080(7)					
C(22)	0.754(3)	0.3029(15)	−0.1681(15)	0.106(8)					
C(23)	0.762(2)	0.331(2)	−0.1029(8)	0.023(4)					
C(24)	0.671(2)	0.276(1)	−0.070(1)	0.057(5)					
C(25)	0.641(2)	0.278(1)	−0.003(9)	0.044(5)					
C(26)	0.693(2)	0.343(1)	0.042(1)	0.056(5)					
C(27)	0.682(2)	0.340(1)	0.111(1)	0.051(5)					
C(28)	0.735(3)	0.4114(15)	0.1587(15)	0.081(7)					
S(3)	0.0293(8)	0.0718(4)	−0.0946(3)	0.077(2)					
F(31)	0.662(2)	0.063(1)	0.180(1)	0.20(2)	0.07(1)	0.157(15)	0.04(1)	−0.05(1)	0.021(9)
F(32)	0.605(2)	0.012(1)	0.2476(8)	0.15(1)	0.27(2)	0.09(1)	0.103(15)	0.06(1)	0.12(1)
F(33)	0.802(2)	0.0288(9)	0.2226(7)	0.09(1)	0.127(15)	0.01(1)	0.01(1)	0.01(1)	0.059(6)
O(31)	0.3157(15)	0.1347(7)	0.0172(6)	0.047(3)					
O(32)	0.5959(15)	0.1268(7)	0.1351(6)	0.049(3)					
C(31)	−0.069(3)	−0.0103(15)	−0.135(1)	0.084(7)					
C(32)	0.013(3)	−0.0740(15)	−0.1018(15)	0.099(8)					
C(33)	0.163(3)	0.058(1)	−0.040(1)	0.064(6)					
C(34)	0.181(2)	0.023(1)	−0.0309(9)	0.050(5)					
C(35)	0.310(2)	0.062(1)	0.022(1)	0.053(5)					
C(36)	0.424(2)	0.021(1)	0.080(1)	0.055(5)					
C(37)	0.550(2)	0.058(1)	0.1315(9)	0.505(5)					
C(38)	0.652(3)	0.092(1)	0.196(1)	0.068(6)					

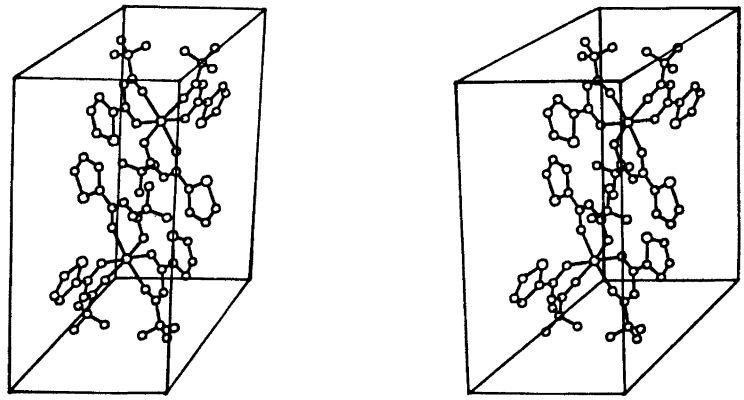

Fig. 2. Stereo drawing of one enanthiomorphous pair of $In(TTA)_3$ molecules centered around ½, ½, ½. The *b* axis is pointing upward.

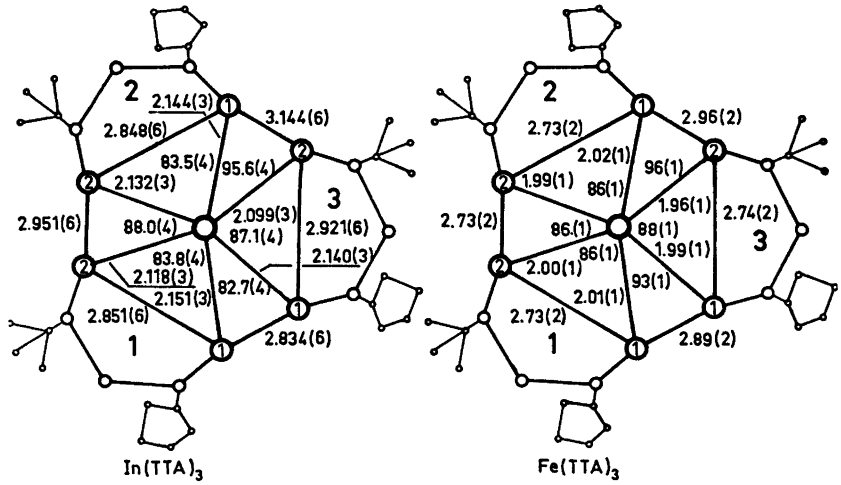

Fig. 3. Schematic representation of the complexes showing distances and (some) angles of the octahedron of coordination. Standard deviations are in parentheses.

oxygen-metal-oxygen bond angles are shown in Fig. 3.

The average Fe–O distance is 1.99(2) Å*. The same average distance 1.992(6) Å, has been found in ferric *tris*-acetylacetonate.[9] Also the average oxygen to oxygen "bite" distances of the chelate rings are virtually the same in the two ferric compounds, *viz.* 2.740(15) Å in the present compound and 2.732(2) Å in the acetylacetonate. The average In–O distance is 2.13(2) Å. No structure determinations of β-diketonates or similar compounds have been reported as yet. In–O distances ranging from ~2.1 to ~2.2 Å have been found in some purely inorganic compounds, *e.g.* 2.171(8) Å in $In(OH)_3$[10].

As far as bond lengths and bond angles of the ligand are concerned the compounds investigated resemble each other closely. Average values for each compound are listed in Tables 3 and 4. The results compare well with those found for the Cs salt [1] and with those reported for $NH_4Pr(TTA)_4.2H_2O$.[11]

A certain lack of regularity of the chelate ring is expected, due to the electronegative

* Standard deviations of averages quoted in this section are sample deviations.

Table 3. In(TTA)$_3$ and Fe(TTA)$_3$. Average lengths, in Å, of chemically equivalent bonds. The standard deviations (in parentheses) have been calculated from the formula $\sigma_l=[\sum_i(l_i-\bar{l})^2/(n-1)]^{\frac{1}{2}}$. The typical standard deviation of individual bonds as estimated from the least squares refinement is 0.02 Å for In(TTA)$_3$ and 0.03 Å for Fe(TTA)$_3$.

Atoms	In(TTA)$_3$ Average	Range	Fe(TTA)$_3$ Average	Range
S–C(1)	1.688(9)	0.015	1.70(2)	0.04
S–C(4)	1.709(15)	0.032	1.68(3)	0.05
C(1)–C(2)	1.32(2)	0.04	1.34(4)	0.07
C(2)–C(3)	1.41(2)	0.03	1.43(7)	0.12
C(3)–C(4)	1.44(2)	0.08	1.49(5)	0.09
C(4)–C(5)	1.45(1)	0.02	1.43(1)	0.03
C(5)–C(6)	1.41(3)	0.06	1.430(5)	0.01
C(6)–C(7)	1.35(3)	0.05	1.38(1)	0.03
C(7)–C(8)	1.52(1)	0.02	1.51(3)	0.05
C(8)–F	1.29(2)	0.05	1.28(4)	0.11
C(5)–O(1)	1.27(1)	0.03	1.26(2)	0.05
C(7)–O(2)	1.28(2)	0.04	1.269(5)	0.009
C(1)–H(1)	0.93(6)	0.10		
C(2)–H(2)	0.93(15)	0.32		
C(6)–H(6)	0.99(4)	0.11		

Table 4. In(TTA)$_3$ and Fe(TTA)$_3$. Average bond angles, in degrees. The standard deviations (in parentheses) have been calculated from the formula $\sigma_a=[\sum_i(a_i-\bar{a})^2/(n-1)]^{\frac{1}{2}}$. In most cases the standard deviation of the individual angles as estimated from the least squares refinement is 1 or 2 degrees.

Atoms	In(TTA)$_3$ Average	Range	Fe(TTA)$_3$ Average	Range
C(1)–S–C(4)	92.2(3)	0.6	95(2)	3.9
S–C(1)–C(2)	112(1)	2.7	110(2)	2.3
C(1)–C(2)–C(3)	115.9(7)	2.3	118(3)	5.0
C(2)–C(3)–C(4)	108(1)	2.4	107(3)	5.2
C(3)–C(4)–S	111(1)	2.4	111(4)	6.9
S–C(4)–C(5)	119(1)	1.7	120(3)	4.2
C(3)–C(4)–C(5)	130(2)	3.1	129(3)	6.1
C(4)–C(5)–C(6)	120(1)	2.1	120(2)	2.8
C(5)–C(6)–C(7)	125(1)	2.0	120(2)	2.5
C(6)–C(7)–C(8)	117.4(4)	0.8	117(2)	3.7
O(1)–C(5)–C(4)	116(2)	3.0	118(1)	2.3
O(1)–C(5)–C(6)	123.7(9)	1.6	123(2)	3.9
O(2)–C(7)–C(8)	118.8(7)	1.4	114(2)	3.1
O(2)–C(7)–C(6)	130.9(6)	1.1	133(6)	9.8
F–C(8)–C(7)	113(2)	6.9	114(3)	8.0
F–C(8)–F	105(2)	5.3	104(4)	10.9

Table 5. Comparison of chelate C–C bond lengths (Å) in some TTA compounds.

Compound	C(5)–C(6)	C(6)–C(7)	Ref.
CsTTA	1.427(9)	1.380(8)	1
mer-Fe(TTA)$_3$	1.430(5)	1.38(1)	present work
mer-In(TTA)$_3$	1.41(3)	1.35(3)	present work
fac-Cr(TTA)$_3$	1.406(6)	1.363(8)	unpubl.
Average [a]	1.418(7)	1.367(8)	
Weighted Average [a]	1.414(4)	1.370(5)	

[a] Based on individual observations and standard deviations from the least squares refinement.

character of the terminal CF_3 group. The data collected in Table 5 suggest, that the C(6)–C(7) bond is shorter than the C(5)–C(6) bond. This is supported by statistical tests.[12] The pooled set of observed C(5)–C(6) distances show no significant differences, (5 % level). The same is true for the set of C(6)–C(7) distances. The difference between the averages of the sets, however, is highly significant, (0.5 % level).

The essential features of the molecular conformation are visible on the stereo drawing Fig. 2. The non-hydrogen atoms of each thiophene group are coplanar (5 % level). Roughly, each ligand may be represented by a plane defined by the five atoms C(4) through C(8). The standard deviation from the plane of the atoms defining it is ~0.04 Å. The pivoting of the ligand plane around the O(1)–O(2) line is a well-known characteristic of β-diketonate complexes.

The conformation of the two ligands, facing each other in Fig. 2, deviates slightly from that of the other four. The rotation (~25°) of the CF_3 group around the C(7)–C(8) bond is distinct.

In keeping with the high volatility of the β-diketonates,[13] intermolecular distances less than 0.2 Å + sum of van der Waals radii are scarce. No obvious pattern of contacts can be disentangled.

REFERENCES

1. Soling, H. *Acta Chem. Scand. A 29* (1975) 523.
2. Schwarzenbach, G. *Die komplexometrische Titration*, Ferdinand Enke, Stuttgart 1956.
3. Berg, E. W. and Truemper, J. T. *J. Phys. Chem 64* (1960) 487.
4. Coppens, B., Leiserowitz, L. and Rabinovich, D. *Acta Crystallogr. 18* (1965) 1035.
5. Cromer, D. T. and Waber, J. T. *Acta Crystallogr. 18* (1965) 104.
6. *International Tables for X-Ray Crystallography, Vol. III*, Kynoch Press, Birmingham 1962.
7. *X-RAY Program System for X-Ray Crystallography 1972*, Computer Science Center, University of Maryland.
8. Johnson, C. K. *ORTEP, Report ORNL 3794*, Oak Ridge National Laboratory, Oak Ridge 1965.
9. Iball, J. and Morgan, C. H. *Acta Crystallogr. 23* (1967) 239.
10. Christensen, A. N., Grønbæk, R. and Rasmussen, S. E. *Acta Chem. Scand. 18* (1964) 1261.
11. Lalancette, R. A., Cefola, M., Hamilton, W. C. and La Placa, S. J. *Inorg. Chem. 6* (1967) 2127.
12. Hamilton, W. C. *Statistics in Physical Sciences*, The Ronald Press Company, New York 1964.
13. Berg, E. W. and Reed, K. P. *Anal. Chim. Acta 42* (1968) 207.

Received September 2, 1975.

Acta Chemica Scandinavica A 30 (1976) 171—181

Binuclear Complexes of Chromium(III). I. Thermodynamics and Kinetics of the Equilibrium between μ-Hydroxo and Di-μ-hydroxo Binuclear Complexes of Chromium(III) with Ethylenediamine as a Ligand

JOHAN SPRINGBORG [a] and HANS TOFTLUND [b]

[a] Chemistry Department, The Royal Veterinary and Agricultural University, DK-1871 Copenhagen V., Denmark and [b] Department of Chemistry, University of Odense, DK-5000 Odense, Denmark

The binuclear ion *meso*-$[(en)_2Cr(OH)_2Cr(en)_2]^{4+}$-(diol) is shown in acid solution to give very fast an equilibrium mixture with the corresponding mono-hydroxo bridged ions $[(H_2O)(en)_2Cr(OH)Cr(en)_2(OH)]^{4+}$ (aquahydroxo mono-ol) and $[(H_2O)(en)_2Cr(OH)Cr(en)_2(H_2O)]^{5+}$ (diaqua mono-ol). The aquahydroxo mono-ol as well as its basic form, $[(OH)(en)_2Cr(OH)Cr(en)_2(OH)]^{3+}$ (dihydroxo mono-ol) were isolated as their perchlorate salts. The equilibrium constant K_{eq} = [aquahydroxo mono-ol]/[diol] was determined at $\mu = 1.00$ M, to be 0.84 at 0.8 °C and 0.76 at 20 °C. The acid dissociation constants, K_{a1} and K_{a2}, of the diaqua mono-ol were determined spectrophotometrically ($pK_{a1} = 0.67$) and potentiometrically ($pK_{a2} = 7.94$), respectively, at $\mu = 1.00$ M, at 0.8 °C. The kinetics of the equilibrium reaction between diol and mono-ol was studied spectrophotometrically at 0.8 °C and $\mu = 1.00$ M in the $[H^+]$ range $10^{-5} - 1.00$ M, the rate expression being $-d[diol]/dt = d[mono-ol]/dt = k_1[diol] - k_{-1}K_{a1}/(K_{a1} + [H^+])[mono-ol]$, where $k_1 = 0.0221$ min^{-1} is the pseudo first-order rate constant for the reaction of diol to aquahydroxo mono-ol and $k_{-1} = 0.0254$ min^{-1} is the true first-order rate constant for the reverse reaction. From kinetic data at 0.8 °C and 20 °C, the activation parameters $E_a(k_1) = 19.6$ kcal/mol and $E_a(k_{-1}) = 20.7$ kcal/mol were determined. The influence of ionic strength on K_{eq}, k_1 and k_{-1} was shown to be small.

In strongly basic solution, the diol deprotonates to give the blue μ-hydroxo-μ-oxo complex, which was isolated as its perchlorate salt, $[(en)_2Cr(O)(OH)Cr(en)_2](ClO_4)_3.2H_2O$.

Binuclear chromium(III) compounds with hydroxyl as a bridging ligand are known in cases with one, two or three hydroxo groups as bridging ligands, *i.e.* binuclear compounds belonging to the class of bridged structures called *mono-ols*, *diols*, and *triols*. So far most attention has been shown the mono-ols and the diols of chromium(III).

The classical mono-ols are the rhodo ion, $[(NH_3)_5Cr(OH)Cr(NH_3)_5]^{5+}$, and the erythro ion, $[(NH_3)_5Cr(OH)Cr(NH_3)_4(H_2O)]^{5+}$, which were both isolated by Jørgensen [1,2] in 1882. Later, a number of so-called acido erythro ions, $[(NH_3)_5Cr(OH)Cr(NH_3)_4X]^{4+}$ (X = Cl, Br, F, SCN, NO_2) have been reported.[3-6] The binuclear hydroxo-bridged structure of these compounds is now well established.[3-5,7-10]

Diols have been known since Pfeiffer [11] and Dubsky [12] nearly 70 years ago isolated salts of the ammonia diol, $[(NH_3)_4Cr(OH)_2Cr(NH_3)_4]^{4+}$, and of the ethylenediamine diol, $[(en)_2Cr(OH)_2Cr(en)_2]^{4+}$. The ethylenediamine diol, which is built up of two optically active units, is capable of existing in isomeric forms, *i.e.* a *meso* form and two optically active forms. It has recently been shown by an X-ray structure analysis on the salt $[(en)_2Cr(OH)_2Cr(en)_2](ClO_4)_2Cl_2.2H_2O$,[13] that the isomer isolated by Pfeiffer is the *meso* form. Two other Cr(III) diols have had their structure determined by X-ray structure analysis, *meso*-$[(gly)_2Cr(OH)_2Cr(gly)_2]$ and *racemic*-$[(phen)_2Cr(OH)_2Cr(phen)_2]Cl_4.6H_2O$.[14,15]

Both mono-ols and diols are known to undergo acid cleavage of the μ-hydroxo bridges giving the monomeric diaqua species. The acid cleav-

age reaction of the rhodo ion and of several acido erythro ions has been studied kinetically and was found in perchlorate media to be independent of the hydrogen ion concentration.[5,6,16–18] Analogously, the acid cleavage reaction of the ethylenediamine diol has been shown in perchlorate media to be independent of the hydrogen ion concentration in the $[H^+]$ range 0.2 – 1.0 M,[19] whereas a first order dependence on $[H^+]$ has been reported for the rate of acid cleavage of the 1,10-phenanthroline diol in nitrate media.[20] Furthermore, the acid cleavage reactions of the aqua diol,[21] $[(H_2O)_4Cr(OH)_2Cr(H_2O)_4]^{4+}$, and the oxalato diol,[22] $[(ox)_2Cr(OH)_2Cr(ox)_2]^{4-}$, have been studied. The rate-laws showed a complex dependence on the hydrogen ion concentration.

To explain the kinetics of these cleavage reactions, a mono hydroxo bridged intermediate has been proposed. The intermediate is analogous to that proposed for interpreting the kinetics of the cleavage of analogous diols of Co(III).[23–26] In neither the Cr(III) nor the Co(III) systems has the mono-ol intermediate been isolated. Kinetic and thermodynamic data for the equilibrium between diol and mono-ol have been reported only for the equilibrium between the $[(H_2O)_5Cr(OH)Cr(H_2O)_5]^{5+}$ cation and the more well-characterized $[(H_2O)_4Cr(OH)_2Cr(H_2O)_4]^{4+}$ cation.[21]

In the present paper the equilibrium between *meso*-$[(en)_2Cr(OH)_2Cr(en)_2]^{4+}$ and the corresponding mono-ols is studied.

A preliminary report has been published.[27]

EXPERIMENTAL

Materials. Sodium perchlorate and 70 % perchloric acid with the descriptions "*puriss. p.a.*" were purchased from Fluka AG. Sodium hydroxide solutions were made from 'Titrisol' ampoules purchased from Merck. All other chemicals were analytical grade. For all spectrophotometric and potentiometric measurements carbon-dioxide-free, distilled water was used.

Instruments. A Zeiss DMR 21 spectrophotometer was used for all spectrophotometric measurements in the visible region. For the spectrophotometric data given below the absorbancy ε has been given in l mol^{-1} cm^{-1} and the wavelength λ has been given in nm. The molarity of solutions of the dimers was always defined as the number of mol of dimer and not the number of mol of chromium(III) per litre of solution. Infrared spectra of the compounds in potassium bromide discs were recorded on a Perkin-Elmer 457 grating infrared spectrophotometer.

The pH-measurements were made with a GK 2301 C combined glass and calomel electrode connected to a PHM 52 digital pH-meter, all from Radiometer, Copenhagen. The saturated potassium chloride calomel electrode was modified to 1 M sodium chloride in order to avoid precipitation of $KClO_4$ in the boundary between the medium and the electrode. The lower part of the electrode was placed in a flow-cell, which was cooled in an ice-bath. It was checked that the glass-electrode had an almost theoretical slope in the actual medium.

Analysis. Chromium analysis determined by atomic absorption spectrophotometry was performed by K. Jørgensen, Chemistry Department I, H. C. Ørsted Institute, and C, N, H, and Cl analyses were made by the microanalytical laboratory at the H. C. Ørsted Institute, Copenhagen.

Table 1. Spectral data in different media at 0 °C.

Sample	Medium	$(\varepsilon, \lambda)_{max}$	$(\varepsilon, \lambda)_{max}$
meso-$[(en)_2Cr(OH)_2Cr(en)_2](ClO_4)_4$	1 M $NaClO_4$	(199,539.5)	(107.386)
	1 M $HClO_4$	(199,539.5)	(107,385)
$[(OH)(en)_2Cr(OH)Cr(en)_2(OH)](ClO_4)_3.2H_2O$	1 M $NaClO_4$	(162,527.5)	(134,387)
	0.01 M NaOH, 1 M $NaClO_4$	(160,526.5)	(133,387)
$[(H_2O)(en)_2Cr(OH)Cr(en)_2(OH)](ClO_4)_4$	0.01 M NaOH, 1 M $NaClO_4$	(158,526.2)	(134,387)
	1.0 M NaOH	(159,525.2)	(135,384)
	1.0 M $NaClO_4$	(169,515.5)	(130,380.5)
	0.001 M $HClO_4$, 1 M $NaClO_4$	(169,515.0)	(129,380.5)
	0.005 M $HClO_4$, 1 M $NaClO_4$	(170,515.0)	(129,381.0)
	1 M $HClO_4$	(162,505.5)	(105,379)
$[(H_2O)(en)_2Cr(OH)Cr(en)_2(H_2O)]^{5+}$	–	(161,503)[a]	(100,378)[a]

[a] Calculated, see text. The concentrations of complex were always $\sim 4 \times 10^{-3}$ M.

Preparations. 1. meso-*Di-μ-hydroxobis[bis(ethylenediamine)chromium(III)] perchlorate* and other salts of the diol. $[(en)_2Cr(OH)_2Cr(en)_2]X_4.nH_2O$ ($X_4.nH_2O = Cl_4.2H_2O$; $(ClO_4)_4$, and $(ClO_4)_3Cl_2.2H_2O$). The perchlorate and chloride salts were prepared and their purity checked as described in the literature.[38] Visible spectra of the perchlorate salt in different media are given in Table 1. The salt, *meso*-$[(en)_2Cr(OH)_2Cr(en)_2](ClO_4)_3Cl_2.2H_2O$, which has been used for X-ray crystal-structure determination[13] was prepared in the following way. To a solution of *meso*-di-μ-hydroxobis[bis(ethylenediamine)chromium(III)]chloride dihydrate (0.4 g, 0.72 mmol) in water (10 ml) was added a mixture of 1.2 M hydrochloric acid (0.5 ml), a saturated solution of sodium perchlorate (1 ml), and ethanol (2 ml). The solution was slowly cooled to 0 °C, and after 1 h the blue-violet crystals were filtered off and washed with 96 % ethanol. (Found: Cr 15.08; C 14.01; N 16.64; H 5.53; Cl 20.80. Calc. for $[(en)_2Cr(OH)_2Cr(en)_2](ClO_4)_3Cl_2.2H_2O$: Cr 15.20; C 14.04; N 16.38; H 5.60; Cl 20.72).

2. meso-*μ-Hydroxo-μ-oxo-bis[bis(ethylenediamine)chromium(III)] perchlorate.* $[(en)_2Cr(O)(OH)Cr(en)_2](ClO_4)_3.2H_2O$.*meso*-Di-μ-hydroxobis[bis(ethylenediamine)chromium(III)] perchlorate (2.0 g, 2.6 mmol) was dissolved in 0 °C cold 2 M sodium hydroxide (80 ml). To the filtered solution was added, with stirring and cooling in ice, a saturated solution of sodium perchlorate (40 ml, room temperature). These operations were performed within 4 min in order to avoid hydrolysis. Green crystals of the perchlorate salt of the μ-hydroxo-μ-oxo complex precipitated almost instantaneously. The precipitate was filtered and washed with 96 % ethanol and dried in air. Yield 1.25 g (68 %). (Found: Cr 14.48; C 13.52; N 15.72; H 5.37; Cl 14.87. Calc. for $[(en)_2Cr(O)(OH)Cr(en)_2](ClO_4)_3.2H_2O$: Cr 14.61; C 13.50; N 15.75; H 5.24; Cl 14.94). The solid salt, if kept dry, is stable for months at room temperature. In aqueous solution the colour changes rapidly and within minutes becomes reddish owing to the formation of the μ-hydroxo bridged cation, $[(OH)(en)_2Cr(OH)Cr(en)_2(OH)]^{3+}$. By addition of perchloric acid to freshly prepared solutions, the perchlorate salt of the *meso* diol re-formed instantaneously and nearly quantitatively. $[(en)_2Cr(O)(OH)Cr(en)_2](ClO_4)_3.2H_2O$ (0.5 g, 0.70 mmol) was dissolved in water (10 ml) at 0 °C. To the blue solution was immediately added ice-cold 3 M perchloric acid (10 ml). The colour instantaneously turned violet and within seconds the perchlorate salt of *meso* diol precipitated. The precipitate was filtered off and washed with 96 % ethanol and ether. Drying in air yielded 0.47 g (yield 86 %) of pure *meso*-$[(en)_2Cr(OH)_2Cr(en)_2](ClO_4)_4$, identified by its infrared spectrum in the region 4000 to 250 cm^{-1}.

3. *μ-Hydroxobis[bis(ethylenediamine)hydroxochromium(III)] perchlorate dihydrate.* $[(OH)(en)_2Cr(OH)Cr(en)_2(OH)]ClO_4)_3.2H_2O$. *meso*-Di-μ-hydroxobis[bis(ethylenediamine)chromium (III)] perchlorate (7.76 g, 10 mmol) was added to 1 M sodium hydroxide (11 ml) at 33 – 35 °C. A green precipitate of μ-hydroxo-μ-oxobis[bis(ethylenediamine)chromium(III)] perchlorate and a blue solution of the μ-hydroxo-μ-oxo cation were formed instantaneously. The suspension was kept at 33 – 35 °C with stirring for 12 – 14 min. Within half a minute the colour of the solution shifted to red owing to the formation of the μ-hydroxobis[bis(ethylenediamine)hydroxochromium(III)] ion and after 10 min all the μ-hydroxo-μ-oxo salt had dissolved. To the resulting red solution, from which precipitation of red crystals of μ-hydroxobis[bis(ethylenediamine)hydroxochromium(III)] perchlorate had commenced, was added a saturated solution of sodium perchlorate (5 ml) and the suspension was cooled in ice for half an hour. The precipitate was filtered and washed with 96 % ethanol (four 10 ml portions). Drying in air yielded 4.50 g (62 %). The crude product was dissolved in 0.01 M sodium hydroxide (26 ml) at room temperature and a saturated solution of sodium perchlorate (13 ml) was added to the filtered solution with stirring and cooling in ice. After 10 min the precipitate was filtered, washed with 96 % ethanol and dried in air. Yield 3.5 g (78 %). The sample reprecipitated twice was pure. (Found: Cr 14.23; C 13.32; N 15.55; H 5.52; Cl 14.70. Calc. for $[(OH)(en)_2Cr(OH)Cr(en)_2(OH)](ClO_4)_3.2H_2O$: Cr 14.25; C 13.16; N 15.36; H 5.39; Cl 14.57). Visible spectral data in different media are given in Table 1. The solid salt is stable for months at room temperature. In aqueous solution the diol is re-formed nearly quantitatively as follows. $[(OH)(en)_2Cr(OH)Cr(en)_2(OH)](ClO_4)_3.2H_2O$ (0.729 g, 1.00 mmol) was dissolved at room temperature in 0.12 M perchloric acid (10 ml). The solution was kept at room temperature for 7 min and then a saturated solution of sodium perchlorate (10 ml) was added portionwise to the stirred solution during 3 min. After a further 10 min the precipitate was filtered off and washed with 96 % ethanol and ether. Drying in air yielded 0.72 g of pure *meso*-$[(en)_2Cr(OH)_2Cr(en)_2](ClO_4)_4$. Yield 93 %. The product was identified by its infrared spectrum in the region 4000 to 250 cm^{-1} and its visible absorption spectrum in 1 M $NaClO_4$ at 0 °C.

4. *Aquatetrakis(ethylenediamine)-μ-hydroxo-hydroxodichromium(III) perchlorate* $[(H_2O)(en)_2Cr(OH)Cr(en)_2(OH)](ClO_4)_4$. μ-Hydroxobis-[bis(ethylenediamine)hydroxochromium(III)] perchlorate (2.00 g, 2.74 mmol) was cooled in ice. To the cold solid was then added ice-cold 0.6 M perchloric acid (6 ml). The mixture was vigorously shaken to obtain a solution which then immediately was filtered into an ice-cold mixture of water (3 ml) and a saturated (at room temperature) solution of sodium perchlorate (6 ml) with cooling in ice and stirring. These

operations were performed within 5 s. The precipitation of the aquahydroxo mono-ol salt instantaneously commenced. The solution was filtered after a further 30 s and immediately washed with 96 % ethanol (three 20 ml portions) and then with ether. The product was sucked dry in a vacuum-desiccator for 15 min, weighed and stored at −15 °C. Yield 1.6 g (73 %). (Found: Cr 13.00; C 12.21; N 14.16; H 4.60; Cl 17.70. Calc. for $[(H_2O)(en)_2Cr(OH)Cr(en)_2(OH)](ClO_4)_4$: Cr 13.10; C 12.10; N 14.11; H 4.57; Cl 17.85). As a contamination of diol is likely and cannot be observed by the elementary analysis, a check of the purity was made spectrophotometrically. The spectrum was measured in 0.01 M NaOH, 1 M $NaClO_4$ (0 °C) and found to be identical to the spectrum of dihydroxo mono-ol (see Table 1).

At 60 °C the solid perchlorate salt gives diol very fast. Thus, heating of solid $[(H_2O)(en)_2Cr(OH)Cr(en)_2(OH)](ClO_4)_4$ at 60 °C for 10 min yielded a violet product identified as nearly pure *meso*-$[(en)_2Cr(OH)_2Cr(en)_2](ClO_4)_4$ by comparing its visible absorption spectrum in 1 M $NaClO_4$ at 0 °C, $(\varepsilon, \lambda)_{max} = (198,539)$ and (108,386), with that of authentic diol (see Table 1). The product showed an IR spectrum in the region 4000 − 250 cm^{-1} very similar but not identical to that of authentic *meso*-$[(en)_2Cr(OH)_2Cr(en)_2](ClO_4)_4$. At room temperature the perchlorate salt gives diol within a week, but at −15 °C it is stable for weeks. The perchlorate salt is very soluble in water. An aqueous solution gives nearly quantitatively the perchlorate salt of the diol as follows. $[(H_2O)(en)_2Cr(OH)Cr(en)_2(OH)](ClO_4)_4$ (0.794 g, 1.00 mmol) was dissolved at room temperature in 0.012 M perchloric acid (10 ml). The solution was kept at room temperature for 7 min and then a saturated solution of sodium perchlorate (10 ml) was added portionwise to the stirred solution during 3 min. After a further 10 min the precipitate was filtered off and washed with 96 % ethanol and ether. Drying in air yielded 0.70 g of pure *meso*-$[(en)_2Cr(OH)_2Cr(en)_2](ClO_4)_4$. Yield 90 %. The product was identified by its infrared spectrum in the region 4000 to 250 cm^{-1} and by its visible absorption spectrum in 1 M $NaClO_4$ at 0 °C.

Potentiometric determination of the acid dissociation constant of the aquahydroxo mono-ol. Solutions of $[(OH)(en)_2Cr(OH)Cr(en)_2(OH)](ClO_4)_3.2H_2O$ in 5×10^{-3} M $HClO_4$, 1.00 M $NaClO_4$ at 0 °C were prepared as described below for the spectrophotometric measurements and then immediately transferred to the flow-cell with suction. Reliable readings on the pH-meter could then be obtained about 1 min after the time of dissolution. The measurements were continued over a period of 5 min and the pH at the time of dissolution was then calculated by linear extrapolations. The definition $pH = -\log[H^+]$ was employed throughout, and concentration pH standards were made in the actual salt medium. Experimental results are given in Table 2.

Table 2. Determination of the second acid dissociation constant of $[(H_2O)(en)_2Cr(OH)Cr(en)_2(H_2O)]^{5+}$ in 1 M $NaClO_4$ at 0 °C. See text.

$10^3 \times C_{mono-ol}$ mol/l	pH	$\bar{n}$	pK_{a2}
3.254	2.768	1.008	
4.332	3.212	1.009	
4.691	3.605	1.010	
7.177	7.660	0.695	8.018
8.293	7.703	0.601	7.881
10.09	7.887	0.494	7.877
11.53	8.077	0.432	7.958
12.97	8.146	0.384	7.941
15.85	8.272	0.315	7.935
		pK_{a2}(av)	7.94

Spectra and kinetic runs. Nearly all spectrophotometric measurements were made in perchlorate medium with constant ionic strength at $\mu = 1.00$ M adjusted with $NaClO_4$. Owing to the rapid equilibrium between the diol and the mono-ols it was important that the interval between the time of dissolution of the complex (t_0) and the time for the first measurement on the spectrophotometer should be as short as possible. In solutions with $[ClO_4^-] = 1.00$ M, however, the perchlorate salts of the dimers dissolved slowly and this dictated the following method of preparation of the solutions. The solid dimer perchlorate was added to a known volume of water at the temperature of study. The mixture was then immediately vigorously shaken to give complete dissolution of the sample within 10 s of the addition of the complex. To the solution was then added the requisite amount of a solution of $NaClO_4$ (or $HClO_4 + NaClO_4$ *etc.*) by use of a thermostated syringe. The two media were mixed as fast as possible and the solution was rapidly transferred to the flow-cell with suction. A commercial 1 cm QS flow-cell (Helma) was used. Following the above procedure it was possible to make and transfer the solutions to the flow-cell within 25 s. The response of the spectrophotometer was a few seconds, which means that reliable measurements of the absorbancy could be obtained 30 s after the dissolution of the complex.

The temperature of the cell was kept constant by thermostating of the cell compartment of the Zeiss DMR 21 spectrophotometer. The temperature in the inner part of the cell was measured with a thermocouple. Nearly all measurements were performed at 0 °C. A small deviation between the temperature of the ice-bath and the equilibrium temperature (0.70 ± 0.05 °C) of the inner part of the cell was found. The temperature of the solutions, immediately

after they had been prepared and transferred to the cell ($t = 60$ s) was always slightly higher (0.9 °C) to decrease to the equilibrium temperature within 15 min. So, following strictly the same procedure for each measurement, the temperature could be reproduced throughout as 0.8 ± 0.1 °C.

The diol and the three mono-ols were all characterized by their absorption spectra in the region 650 – 340 nm at 0 °C and with $\mu =$ 1.00 M adjusted with $NaClO_4$. The spectra of the perchlorate salts of the diol and of the aquahydroxo mono-ol in neutral or acid solution changed rapidly with time, and extrapolations back to the time of dissolution (t_0) were therefore required. These were performed either logarithmically or linearly. Logarithmical extrapolations were calculated using eqn. 1 given below. Linear extrapolations were based on curves taken 30 and 60 s, respectively, after t_0 and were never greater than 2 %. The spectra of the perchlorate salts of the aquahydroxo or dihydroxo mono-ols in basic solutions at 0 °C were constant for 10 min after t_0 and could, therefore, be measured without difficulty.

The kinetic measurements were performed by following the change of the absorbancy in the region 650 – 340 nm of solutions initially composed either of diol or mono-ol. The changes in absorbancy at the wavelengths 570, 560 and 550 nm, respectively, were used for the calculations of the rate constants, as in this region the greatest differences between the absorbancies of the diol and the diaqua or aquahydroxo mono-ols are found.

Treatment of kinetic data. With the exception of the measurements in pure 1 M $NaClO_4$, all kinetic measurements were made under pseudo first-order conditions, *i.e.* the change in the hydrogen ion concentration during a kinetic run was never greater than 2 %. Pseudo first-order rate constants for the equilibration reaction were determined by plotting $\log(A_t - A_\infty)$ against time. Such plots were linear for more than 3 half-lives. The deviations observed after 3 $t_{\frac{1}{2}}$ were unsystematic and certainly due to an experimental error in the determination of the small differences $A_t - A_\infty$ in absorbancy. Rate constants were calculated from the slope of the plots using the relationship

$$\ln(A - A_\infty) = -k_{obs}t + \ln(A_0 - A_\infty) \quad (1)$$

The infinite time values, A_∞, were excellently defined for all kinetic runs in the acid solutions, *i.e.* absorption curves taken at $7t_{\frac{1}{2}}$ and $8t_{\frac{1}{2}}$, respectively, were identical within the experimental accuracy. For the kinetic runs in pure 1 M $NaClO_4$, constant absorption curves were never achieved, *i.e.* a very slow decrease of the absorbancy in the region 600 – 500 nm after $7t_{\frac{1}{2}}$ was observed. The readings of the absorbancy at $7t_{\frac{1}{2}}$ were then used as A_∞ values. Values of k_{obs} are given in Tables 3 and 4.

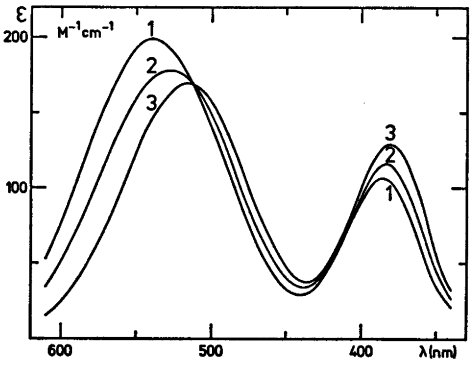

Fig. 1. Visible absorption spectra of *meso*-$[(en)_2Cr(OH)_2Cr(en)_2](ClO_4)_4$ (1) and $[(H_2O)(en)_2Cr(OH)Cr(en)_2(OH)](ClO_4)_4$ (3) in 10^{-3} M $HClO_4$, 1 M $NaClO_4$ at 0 °C extrapolated to the time of dissolution. The spectra of *meso*-$[(en)_2Cr(OH)_2Cr(en)_2](ClO_4)_4$ and $[(H_2O)(en)_2Cr(OH)Cr(en)_2(OH)](ClO_4)_4$, respectively, in 10^{-3} M $HClO_4$, 1 M $NaClO_4$ after 110 min were identical and nearly constant (2).

Table 3. Observed and calculated rate constants for the equilibrium between the diol and the mono-ols at 0.8 °C. See text. k_{calc} from eqn. (10).

C_{HClO_4} mol/l	$10^3 k_{obs}$(D) min^{-1}	$10^3 k_{obs}$(M) min^{-1}	$10^3 k_{obs}$(av) min^{-1}	$10^3 k_{calc}$ min^{-1}
$\simeq 10^{-5}$	4.35	4.65	4.50	4.75
1.00×10^{-3}	4.65	4.73	4.69	4.74
4.00×10^{-3}	4.38	4.29	4.34	4.35
1.00×10^{-1}	3.83	3.97	3.90	3.95
3.00×10^{-1}	3.37	3.33	3.35	3.27
5.00×10^{-1}	3.03	3.11	3.07	2.98
1.00	2.81	2.48	2.65	2.66

Table 4. Kinetic and thermodynamic data in various media.

Medium	T °C	$10^3 k_{obs}$(D) min^{-1}	$10^3 k_{obs}$(M) min^{-1}	$10^3 k_{obs}$(av) min^{-1}	$10^3 k_1$ min^{-1}	$10^3 k_{-1}$ min^{-1}	K_{eq}
10^{-3} M $HClO_4$, 1 M $NaClO_4$	20.0	52.9	55.7	54.3	23.5	30.8	0.763
$\mu = 1.00$ M	0.8	–	–	–	2.21[a]	2.54[a]	0.835[b]
10^{-3} M $HClO_4$	0.8	4.24	4.02	4.13	1.94	2.19	0.885

[a] Taken from Table 3 and Fig. 4. [b] Taken from Fig. 3.

RESULTS

Diol. The absorption spectra of aqueous solutions of salts of the diol, *meso*-$[(en)_2Cr(OH)_2Cr(en)_2]^{4+}$, change rapidly with time owing to a fast equilibrium with the corresponding mono-ols, *i.e.* μ-hydroxo bridged, binuclear cations. In order to obtain the spectrum of the diol it was therefore necessary, even at 0 °C, to extrapolate these absorption curves to the time of dissolution (see Fig. 1). In Table 1 it is seen that the spectra in 1 M $NaClO_4$ and in 1 M $HClO_4$ at 0 °C are identical. Protonation of the diol to form a μ-aqua-μ-hydroxo complex in 1 M $HClO_4$ at 0 °C is, therefore, assumed not to occur to any considerable extent (probably less than 3 %). The lower limit to the acid dissociation constant, K_a, of the μ-aqua-μ-hydroxo complex is then estimated as $K_a \geq 30$ M. When the diol is dissolved in strongly basic solution, it gives a blue solution of its deprotonated form,

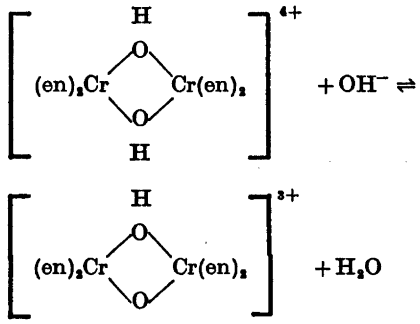

(2)

The μ-hydroxo-μ-oxo complex was isolated as a green perchlorate salt. From potentiometric and spectrophotometric measurements, the acid dissociation constant of the diol in pure water is roughly estimated as $pK_a \simeq 12$ at 20 °C.

Mono-ols. At room temperature, the colour of the basic solution of the blue μ-hydroxo-μ-oxo cation changes rapidly and within minutes becomes reddish owing to the formation of the μ-hydroxo bridged cation, $[(OH)(en)_2Cr(OH)Cr(en)_2(OH)]^{3+}$, hereafter referred to as the dihydroxo mono-ol. This cation was isolated as a reddish brown perchlorate salt, $[(OH)(en)_2Cr(OH)Cr(en)_2(OH)](ClO_4)_3.2H_2O$, in high yield (62 %). One of the corresponding acid forms, the aquahydroxo mono-ol, was also isolated as a salt. So, when the perchlorate salt of the dihydroxo mono-ol was dissolved fast in perchloric acid and immediately added to a strong solution of sodium perchlorate, the aquahydroxo mono-ol precipitated as $[(H_2O)(en)_2Cr(OH)Cr(en)_2(OH)](ClO_4)_4$ (yield 73 %). The isolation of the aquahydroxo mono-ol had to be performed fast, even at 0 °C, owing to the rapid formation of diol. The diaqua mono-ol, $[(H_2O)(en)_2Cr(OH)Cr(en)_2(H_2O)]^{3+}$, was not isolated as a salt, but characterized by its visible absorption spectrum and its acid dissociation constant as discussed later.

While the solid perchlorate salt of the dihydroxo mono-ol at room temperature is stable for months, the solid perchlorate salt of the aquahydroxo mono-ol gives almost quantitatively that of the diol within approximately a week at room temperature. At 60 °C solid aquahydroxo mono-ol gives diol within 10 min.

In aqueous solution these mono-ols can be transformed back to diol quantitatively. Thus, slightly acidified aqueous solutions of the mono-ols were left for 10 min at room temperature to ensure that equilibrium between mono-ol and diol had been established and $NaClO_4$ was then slowly added. By this the perchlorate salt of the diol, which is less soluble

than the perchlorate salt of the aquahydroxo mono-ol, precipitated quantitatively. For other anions, *i.e.* bromide, chloride, and dithionate, the salts of the diol are again the less soluble. This lower solubility of salts of the diol seems to be general.

The first and second acid dissociation constants, K_{a1} and K_{a2}, of the diaqua mono-ol were studied potentiometrically and spectrophotometrically. From the potentiometric measurements K_{a2} was determined as described below, whereas only a lower limit to K_{a1} could be estimated from these measurements. However, K_{a1} was then determined spectrophotometrically as shown in the following section.

The determination of pK_{a2} was performed by measuring pH in partly acidified solutions of $[(OH)(en)_2Cr(OH)Cr(en)_2(OH)](ClO_4)_3.2H_2O$. Because of the rapid conversion into diol a normal acidometric titration could not be performed. Therefore, solutions of $[(OH)(en)_2Cr(OH)Cr(en)_2(OH)](ClO_4)_3.2H_2O$ in 5×10^{-3} M $HClO_4$, 1 M $NaClO_4$ were made as rapidly as possible and the pH at the time of dissolution, pH_0, was then obtained by a linear extrapolation from the pH measurements within the first 5 min. For solutions with $\bar{n}<1$, where $\bar{n}$ is defined as below, an increase of pH with time was observed and the rate of change was in the order of 0.01 pH unit per min. For solutions with $\bar{n}>1$, pH was constant within the experimental accuracy.

K_{a2} was calculated by means of the equation:

$$pK_{a2} = -\log[H^+] + \log\left[\frac{\bar{n}}{1-\bar{n}}\right] - \log\left[1+\frac{[H^+](2-\bar{n})}{K_{a1}(1-\bar{n})}\right] \quad (3)$$

where $\bar{n}$ equals the average number of protons taken up by the dihydroxo mono-ol and is given by

$$\bar{n} = (C_{HClO_4} - [H^+] + [OH^-])/C_{mono\text{-}ol} \quad (4)$$

where $C_{mono\text{-}ol}$ = stoichiometric concentration of the complex and C_{HClO_4} = stoichiometric concentration of perchloric acid added. The last term of eqn. 3 was ignored in the calculations of pK_{a2}. From the measurements with $0<\bar{n}<1$, the average value $pK_{a2}=7.94$ was calculated as shown in Table 2.

A lower limit estimate of K_{a1} was obtained from the measurements with $\bar{n}>1$. Using the equation

$$pK_{a1} = -\log\frac{[H^+]^2(2-\bar{n})}{K_{a2}\bar{n}+[H^+](\bar{n}-1)} \simeq pH + \log\frac{(\bar{n}-1)}{(2-\bar{n})} \quad (5)$$

and an estimated accuracy (±0.02 unit in pH) in the measured pH values, it is calculated that $pK_{a1}<1.3$. This is in agreement with the spectrophotometrically determined value of $pK_{a1}=0.67$.

The spectra (extrapolated to $t=t_0$) of $[(H_2O)(en)_2Cr(OH)Cr(en)_2(OH)](ClO_4)_4$ in 1 M $NaClO_4$ and in slightly acid solutions at 0 °C were identical as shown in Table 1. These observations are in agreement with the low pK_{a1} of the diaqua mono-ol, and the spectra in these media therefore represent the spectrum of the aquahydroxo mono-ol cation (see also Fig. 1). In stronger acid solutions, a blue-shift of the first absorption band was observed, but even in 1 M $HClO_4$ (0 °C), the mono-ol is not fully protonated to diaqua mono-ol (see Table 1). The spectrum of the pure diaqua mono-ol shown in Fig. 2 (see also Table 1) was calculated from the spectra in 1 M $HClO_4$ and 10^{-3} M $HClO_4$, 1 M $NaClO_4$ (0 °C) by means of the spectrophotometrically determined value of $pK_{a1}=0.67$.

The spectra of basic solutions (0.01 M NaOH, 1 M $NaClO_4$) of $[(H_2O)(en)_2Cr(OH)Cr(en)_2(OH)]$-

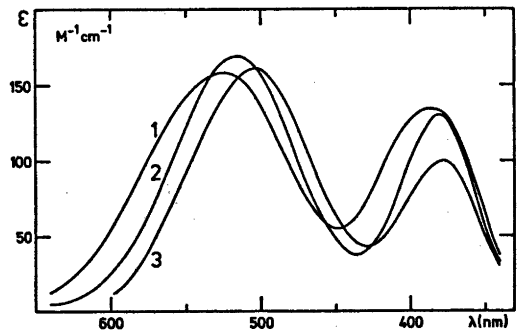

Fig. 2. Visible absorption spectra at 0 °C of 4×10^{-3} M solutions of $[(H_2O)(en)_2Cr(OH)Cr(en)_2(OH)](ClO_4)_4$ in 0.01 M NaOH, 1 M $NaClO_4$ (1) and in 10^{-3} M $HClO_4$, 1 M $NaClO_4$ (2), and the calculated spectrum of $[(H_2O)(en)_2Cr(OH)Cr(en)_2(H_2O)]^{5+}$ (3).

$(ClO_4)_4$ and $[(OH)(en)_2Cr(OH)Cr(en)_2(OH)](ClO_4)_3.2H_2O$ are identical and represent pure dihydroxo mono-ol (Table 1, Fig. 2). The spectrum of $[(OH)(en)_2Cr(OH)Cr(en)_2(OH)](ClO_4)_3.2H_2O$ in 1 M $NaClO_4$ without additional base is nearly identical to the spectrum of pure dihydroxo mono-ol in agreement with $pK_{a2}=7.94$. The spectrum of $[(H_2O)(en)_2Cr(OH)Cr(en)_2(OH)](ClO_4)_4$ in 1 M NaOH is nearly identical to the spectrum in 0.01 M NaOH, 1 M $NaClO_4$. The small blue-shift (1 nm) of the first absorption band observed in 1 M NaOH is most probably due to medium effects and not to a deprotonation of the mono-ol to a μ-oxo dimer. An upper limit to the acid dissociation constant of the dihydroxo mono-ol is, therefore, estimated as $pK_{a2}>16$ ($pK_w\simeq 15$ at 0°C).

The equilibria between aquahydroxo mono-ol, diaqua mono-ol, and diol. The equilibria between the diol and the mono-ols at 0 °C were studied spectrophotometrically in the region 650 – 340 nm. The hydrogen ion concentration was varied from 10^{-3} M to 1.00 M and the ionic strength, $\mu=1.00\pm0.03$ M, was kept constant with sodium perchlorate. In this $[H^+]$ region the aquahydroxo mono-ol is partially protonated to diaqua mono-ol, while protonation of the diol does not need to be considered, as mentioned above. The spectra of solutions initially composed of either diol or mono-ol changed with time and became constant within one and a half to three hours. At low acidity one and at high acidity three, well-defined isosbestic points were observed. For each hydrogen ion concentration the final curves and the isosbestic points were identical for solutions initially composed by either diol or mono-ol. The final spectra thus represent an equilibrium mixture between diol, aquahydroxo mono-ol and diaqua mono-ol.

The equilibrium curves for $[H^+]=10^{-3}$ and 5×10^{-3} M were nearly identical corresponding to an equilibrium between diol and aquahydroxo mono-ol alone (see Fig. 1). At higher $[H^+]$ a blue-shift of the first absorption band was observed and corresponds to an additional equilibrium involving the diaqua mono-ol. The equilibria which need to be considered are, therefore,

$$[(en)_2Cr(OH)_2Cr(en)_2]^{4+}+H_2O \underset{k_{-1}}{\overset{K_{eq}}{\underset{k_1}{\rightleftharpoons}}} [(H_2O)(en)_2Cr(OH)Cr(en)_2(OH)]^{4+} \quad (6)$$

$$[(H_2O)(en)_2Cr(OH)Cr(en)_2(OH)]^{4+}+H^+ \overset{(K_{a1})^{-1}}{\rightleftharpoons} [(H_2O)(en)_2Cr(OH)Cr(en)_2(H_2O)]^{5+} \quad (7)$$

where $K_{eq}=k_1/k_{-1}=$ [aquahydroxo mono-ol]/[diol] and K_{a1} is the first acid dissociation constant of the diaqua mono-ol. K_{eq} and K_{a1} were determined spectrophotometrically as follows. Considering solutions with identical hydrogen ion concentration, we denote the molar absorbancies at the wavelength λ extrapolated back to $t=0$ and at equilibrium, respectively, as $\varepsilon_0(\lambda)$ and $\varepsilon_{eq}(\lambda)$. Then $\varepsilon_0^D(\lambda)$ and $\varepsilon_0^M(\lambda)$ refer to solutions of diol and mono-ol, respectively. The mol fraction of diol, X, at equilibrium can then be expressed as

$$X=\frac{[\text{Diol}]}{[\text{Diol}]+[\text{Mono-ol}]}=\frac{\varepsilon_{eq}(\lambda)-\varepsilon_0^M(\lambda)}{\varepsilon_0^D(\lambda)-\varepsilon_0^M(\lambda)} \quad (8)$$

The dependence of X on the hydrogen ion concentration is then expressed by

$$X=\frac{1}{1+K_{eq}}-\frac{K_{eq}}{K_{a1}(1+K_{eq})}(X[H^+]) \quad (9)$$

The expression gives a linear relationship for X against $X[H^+]$. In Fig. 3 such a plot has been made for $[H^+]=10^{-3}-1.00$ M. In the calculation of X, the mean value obtained for the wavelength $\lambda=550$, 560, and 570 nm was used. From the slope, $-K_{eq}/[K_{a1}(1+K_{eq})]$, and the intercept, $1/(1+K_{eq})$, the values $K_{a1}=0.216$ M and $K_{eq}=0.835$ were then calculated.

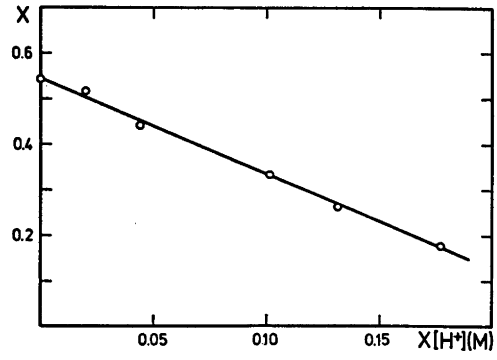

Fig. 3. Spectrophotometric determination of K_{a1} and K_{eq} at 0.8 °C and $\mu=1.00$ M. See text.

For the medium 1 M $NaClO_4$ (pH = 5 – 6), the equilibrium curves were not well defined as further hydrolysis of unknown character proceeds faster in neutral solutions than in acid solutions. However, using the absorption curves at 7 $t_{\frac{1}{2}}$ for the equilibrium curves, and eqn. (9), which at low $[H^+]$ reduces to $K_{eq} = (1-X)/X$, the value $K_{eq} = 0.91$ was calculated. This value is in reasonable agreement with the more accurate value $K_{eq} = 0.84$ determined above.

Additional spectrophotometric measurements in the media 10^{-3} M $HClO_4$ at 0 °C and 10^{-3} M $HClO_4$, 1 M $NaClO_4$ at 20 °C, respectively, showed identical equilibrium curves for solutions initially composed by either diol or mono-ol. The equilibrium constants calculated for these media using the expression $K_{eq} = (1-X)/X$ are given in Table 4. The values of $\varepsilon_0^M(\lambda)$ and $\varepsilon_0^D(\lambda)$, ($\lambda = 570$, 560, and 550 nm) were remeasured for each medium and temperature and small differences (up to 3 %) relative to the ε-values measured at $\mu = 1.00$ M and 0 °C were observed.

The kinetics of the equilibrium between mono-ol and diol. The kinetics of the equilibria between the diol and the aquahydroxo and diaqua mono-ols was investigated spectrophotometrically by following the change of the absorbancy of solutions initially composed of either the diol or the mono-ols. The pseudo first-order rate constants, k_{obs}, were obtained by plotting $\log(A_t - A_\infty)$ against time [eqn. (1)]. In Table 3, the values of k_{obs} (at $\mu = 1.00$ M and 0.8 °C) are seen to be nearly identical for solutions with identical hydrogen ion concentration, but initially composed of either diol [k_{obs}(D)] or mono-ol [k_{obs}(M)]. At low hydrogen ion concentration, k_{obs} is almost independent of the hydrogen ion concentration, but as the hydrogen ion concentration increases, a decrease of k_{obs} is observed. As discussed above, the stoichiometry of the reaction can be expressed by eqns. (6) and (7). Neglecting other equilibria, *e.g.* bridge formation and cleavage through a protonated diol, the following rate-law is predicted from eqns. (6) and (7),

$$k_{calc} = k_1 + \frac{K_{a1}}{[H^+] + K_{a1}} \times k_{-1} \qquad (10)$$

where K_{a1} is the first acid dissociation constant of the diaqua mono-ol, and k_1 and k_{-1} are the pseudo first-order and true first-order rate constants, respectively, in eqn. (6). The expression (10) gives a linear relation for k_{obs} against $K_{a1}/(K_{a1} + [H^+])$. Such a plot has been made in Fig. 4 using the k_{obs}(av) values from Table 3 and $K_{a1} = 0.216$ M as found above. From the slope, k_{-1}, and the intercept, k_1, the (pseudo) first-order rate constants are found to be $k_1 = 2.21 \times 10^{-2}$ min^{-1} and $k_{-1} = 2.54 \times 10^{-2}$ min^{-1}. From these values and the relation $K_{eq} = k_1/k_{-1}$, it is found that $K_{eq} = 0.87$, which within the experimental accuracy is in fair agreement with the more accurate value 0.84 as found above.

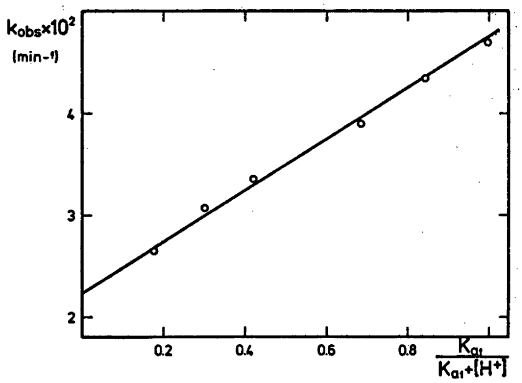

Fig. 4. The observed rate constants for the equilibrium reaction between diol and mono-ol as a function of $K_{a1}/K_{a1} + [H^+])$ at 0.8 °C and $\mu = 1.00$ M ($K_{a1} = 0.216$ M). The solid line represents the calculated values of k_{obs} given in Table 3.

For the media 10^{-3} M $HClO_4$ at 0.8 °C and 10^{-3} M $HClO_4$, 1 M $NaClO_4$ at 20 °C, respectively, the values of k_{obs} for solutions initially composed of either diol or mono-ol again were found to be nearly identical, as seen in Table 4. The values of k_1 and k_{-1} given in Table 4 are calculated from the expression $k_{obs} = k_1 + k_{-1}$, which is valid for acid solutions with $[H^+] \ll K_{a1}$ [see eqn. (10)]. The Arrhenius activation energies $E_a(k_1) = 19.6$ kcal/mol and $E_a(k_{-1}) = 20.7$ kcal/mol were then calculated from the rate constants at $\mu = 1.00$ M given in Table 4.

DISCUSSION

The μ-hydroxo bridged structure proposed for the three mono-ols is strongly supported by the values of the ligand field parameter Δ of

these species. From the spectral data given in Table 1, the Δ values for the diaqua mono-ol, the aquahydroxo mono-ol, and the dihydroxo mono-ol, respectively, are calculated to 19.88, 19.42, and 19.00 kK. In agreement with the average environment rule the Δ value for the aquahydroxo mono-ol within the experimental accuracy is equal to the average of the Δ values of the diaqua mono-ol and the dihydroxo mono-ol ($\Delta_{obs} = 19.42$ kK and $\Delta_{calc} = 19.44$ kK). The observed decrease in Δ by the replacement of H_2O by OH^- follows the spectrochemical series. Furthermore, the replacement of one H_2O by OH^- per Cr(III), is seen to correspond to a decrease of Δ by 0.88 kK. This is in excellent agreement with the corresponding value 0.86 kK obtained from the Δ values of *cis*-$[Cr(en)_2(H_2O)_2]^{3+}$ and *cis*-$[Cr(en)_2(OH)_2]^+$ (Δ = 20.58 kK and 18.87 kK, respectively).[28]

The equilibrium constant, K_{eq}, for the equilibrium between *meso*-$[(en)_2Cr(OH)_2Cr(en)_2]^{4+}$ and $[(H_2O)(en)_2Cr(OH)Cr(en)_2(OH)]^{4+}$ is nearly 40 times greater than K_{eq} for the corresponding equilibrium between $[(H_2O)_4Cr(OH)_2Cr(H_2O)_4]^{4+}$ and $[(H_2O)_5Cr(OH)Cr(H_2O)_4(OH)]^{4+}$ ($K_{eq} = 0.02$ at 25 °C in 2 M $LiClO_4$, calculated from the data given in Ref. 21). In both systems the variation of K_{eq} with temperature is small. In the ethylenediamine system the standard enthalpy change, $\Delta H°$, for the cleavage reaction of diol to aquahydroxo mono-ol was calculated from the data in Table 4 to be $\Delta H° = -0.7$ kcal/mol (1 M $NaClO_4$). The influence of ionic strength on K_{eq} is seen from Table 4 to be very small as would be expected for equilibria only involving reactions between one ion and one neutral molecule. It is noted that the small decrease of K_{eq} with increasing ionic strength corresponds closely to the change in water activity ($a_{H_2O} = 52.9$ M in 1 M $NaClO_4$ and $a_{H_2O} = 55.5$ M in 5×10^{-6} M $NaClO_4$ at 20 °C).[29]

The equilibrium between diol and aquahydroxo mono-ol is established very fast and k_1 as well as k_{-1} are several orders greater than the rate constant for water exchange in $[Cr(H_2O)_6]^{3+}$.[30] Furthermore, k_1 is about 10^3 times greater than the corresponding rate constant for the aqua diol, $k_1(aq) = 9 \times 10^{-4}$ min^{-1} at 25 °C.[21] The corresponding value for the phenanthroline diol has been estimated to be 2×10^{-3} min^{-1} at 20 °C.[20] At present we have no clear understanding why k_1 apparently is so much greater when ethylenediamine is the non-bridging ligand. In connection with the acid cleavage of diols it has been discussed to which extent the cleavage of the bridge to form mono-ol occurs through direct aquation or through an intermediate involving protonation of the hydroxo bridge. The observation that no hydrogen ion dependent term in the $[H^+]$ region $10^{-3} - 1.0$ M was found for the ring-opening reaction of the ethylenediamine diol supports the mechanism with direct aquation as proposed for the phenanthroline diol and the aqua diol.[19-21]

The large value of k_{-1} is probably due to proximity effects. As the k_{-1} path corresponds to an intramolecular nucleophilic attack by coordinated OH^-, one would expect a great enhancement in reactivity relative to a corresponding intermolecular nucleophilic attack. Analogously the ring-closure of $[(H_2O)_5Cr(OH)Cr(H_2O)_4(OH)]^{4+}$ to form diol is reported to be fast ($k_{-1} = 0.05$ min^{-1}, 25 °C).[21]

The observation that the $[(H_2O)(en)_2Cr(OH)Cr(en)_2(H_2O)]^{5+}$ cation is approximately a 10^3 times stronger acid than the *cis*-aqua erythro ion, $[(NH_3)_5Cr(OH)Cr(NH_3)_4(H_2O)]^{5+}$ ($pK_a = 3.5$ in 1 M $NaNO_3$ and 2.8 in 0.14 M $NaClO_4$ at at 25 °C)[21,4] is hardly explained in terms of the difference in the electronic properties of the *N*-ligators. We suggest that the low pK_{a1} of the diaqua mono-ol is due to a strong hydrogen-bonded stabilization of the corresponding base, aquahydroxo mono-ol, as outlined below.

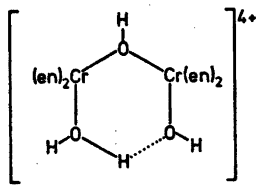

In a following paper in this series it is shown that, analogously to the *meso* isomer, the *racemic* isomer of the $[(en)_2Cr(OH)_2Cr(en)_2]^{4+}$ cation very fast gives an equilibrium mixture of diol and mono-ol.

Acknowledgement. We wish to express our gratitude to Brigitte Søndergaard Sørensen for her invaluable assistance during the experimental work.

REFERENCES

1. Jørgensen, S. M. *J. Prakt. Chem.* [2] *25* (1882) 321.
2. Jørgensen, S. M. *J. Prakt. Chem.* [2] *25* (1882) 398.
3. Linhard, M. and Weigel, M. *Z. Anorg. Allgem. Chem. 299* (1959) 15.
4. Schwarzenbach, G. and Magyar, B. *Helv. Chim. Acta 45* (1962) 1425.
5. Hoppenjans, D. W. and Hunt, J.B. *Inorg. Chem. 8* (1969) 505.
6. Matts, T. C., Moore, P., Ogilvie, D. M. W. and Winterton, N. *J. Chem. Soc. Dalton Trans.* (1973) 992.
7. Wilmarth, W. K., Graff, H. and Gustin, S. T. *J. Amer. Chem. Soc. 78* (1956) 2683.
8. Yevitz, M. and Stanko, J. A. *J. Amer. Chem. Soc. 93* (1971) 1512.
9. Veal, J. T., Jeter, D. Y., Hempel, J. C., Eckberg, R. P., Hatfield, W. E. and Hodgson, D. J. *Inorg. Chem. 12* (1973) 2928.
10. Urushiyama, A., Nomura, T. and Nakahara, M. *Bull. Chem. Soc. Jap. 43* (1971) 3971.
11. Pfeiffer, P. and Stern, R. *Z. Anorg. Chem. 58* (1908) 272.
12. Dubsky, J. V. *J. Prakt. Chem.* [2] *90* (1914) 61.
13. Kaas, K. *Acta Crystallogr. To be published.*
14. Veal, J. T., Hatfield, W. E., Jeter, D. Y., Hempel, J. C. and Hodgson, D. J. *Inorg. Chem. 12* (1973) 342.
15. Veal, J. T., Hatfield, W. E. and Hodgson, D. J. *Acta Crystallogr. B 29* (1973) 12.
16. Po, H. N. and Enomoto, H. *J. Inorg. Nucl. Chem. 35* (1973) 2581.
17. Po, H. N., Chung, Y. H. and Davis, S. R. *J. Inorg. Nucl. Chem. 35* (1973) 2849.
18. Gearon, I. E. *Ph.D. Dissertation*, The Catholic University of America, Washington, D.C. 1973.
19. Wolcott, D. *Ph.D. Dissertation*, The Catholic University of America, Washington, D.C. 1965.
20. Wolcott, D. and Hunt, J. B. *Inorg. Chem. 7* (1968) 755.
21. Thompson, G. Lawrence Radiation Laboratory Report, UCRL-11410, Berkeley, California 1964.
22. Grant, D. M. and Hamm, R. E. *J. Amer. Chem. Soc. 80* (1958) 4166.
23. Rasmussen, S. E. and Bjerrum, J. *Acta Chem. Scand. 9* (1955) 735.
24. de Maine, M. M. and Hunt, J. B. *Inorg. Chem. 10* (1971) 2106.
25. El-Awady, A. A. and Hugus, Jr., Z. Z. *Inorg. Chem. 10* (1971) 1415.
26. Ellis, J. D., Scott, K. L., Wharton, R. K. and Sykes, A. G. *Inorg. Chem. 11* (1972) 2565.
27. Springborg, J. and Toftlund, H. *Chem. Comm.* (1975) 422.
28. Springborg, J. and Schäffer, C. E. *Inorg. Syn. To be published.*
29. D'Ans, L. *Taschenbuch für Chemiker und Physiker*, Springer Verlag, Vol. 1, p. 813.
30. Hunt, J. P. and Plane, R. A. *J. Amer. Chem. Soc. 76* (1954) 5960.
31. Andersen, P. *Private communication.*

Received August 28, 1975.

Acta Chemica Scandinavica A 30 (1976) 182—186

Partial Molal Volumes and Additivity of Group Partial Molal Volumes of Alcohols in Aqueous Solution at 25 and 35 °C

HARALD HØILAND and EINAR VIKINGSTAD

Department of Chemistry, University of Bergen, N-5000 Bergen, Norway

The densities in aqueous solution of homologous series of alcohols have been measured at 25 and 35 °C. The systems were primary alcohols from propanol to hexanol; secondary alcohols from 2-propanol to 2-heptanol, 3-pentanol and 3-heptanol; the diols 1,2-propanediol, 1,3-, 1,4-, and 2,3-butanediol, 1,5- and 2,4-pentanediol, 1,7-heptanediol, and also mannitol.

Group partial molal volumes have been calculated confirming the additivity relation. They have been compared with van der Waals group volumes and group partial molal volumes in pure liquids and discussed in relation to a clathrate-like solvation model.

The additive properties of group partial molal volumes in homologous series of organic solutes, electrolytes or non-electrolytes, are of interest in solution theory and as an aid in the construction of simple models for numerical simulation work.

The first investigation of such additivity relations in aqueous solution was made by Traube.[1] Recent measurements of partial molal volumes of alcohols,[2] carboxylic acids and their salts,[3–5] and alkylamine hydrobromides [6] have been utilized to calculate the group partial molal volume of the methylene group, average value 16.0 cm^3 mol^{-1}, in agreement with Traube's results. This value is constant from series to series as long as the alkyl chain is straight.

The partial molal volumes of the carboxylic acids and their salts have been used to calculate the group partial molal volumes of the carboxyl and the methyl groups.[4] In these series the group partial molal volumes are additive with a precision better than ± 1 %. The additive nature of group partial molal volumes in pure organic liquids has also been demonstrated.[7]

EXPERIMENTAL

The alcohols were all supplied by Fluka. 2-Hexanol, 2-heptanol, 3-heptanol, and 1,7-heptanediol were *purum* grade, the rest *puriss.* grade. D-(−)-Mannitol was supplied by Merck.

The alcohols were all checked for impurities by gas-liquid chromatography. The impurity level was 1 − 2 parts per thousand for most alcohols. This was considered satisfactory and these alcohols were used without further purification. 1-Propanol and 2-propanol had a slightly higher impurity level, and they were distilled *in vacuo*, boiling points as given in the literature.[8]

D-(−)-Mannitol was dried *in vacuo* at 120 °C.

Water was passed through an ion exchange column, distilled and boiled. A portion of the water was doubly distilled as a check. No difference in density was observed.

The densities were measured by a Paar density meter (DMA O2C) as previously described.[9] Temperature was measured by a Hewlett-Packard quartz thermometer.

The temperature was controlled to ± 0.007 °C with an oil thermostat. Estimated error in the density $\pm 5 \times 10^{-6}$ g cm^{-1}.

RESULTS

Infinite dilution values. For each alcohol solutions were made at 4 − 7 concentrations in the range 0.02 − 0.5 mol kg^{-1}. Densities were measured, apparent molal volumes were calculated and extrapolated to infinite dilution assuming a linear concentration dependence. Typical plots are shown in Fig. 1. The error in the partial molal volumes at infinite dilution has been estimated to ± 0.10 cm^3 mol^{-1}.

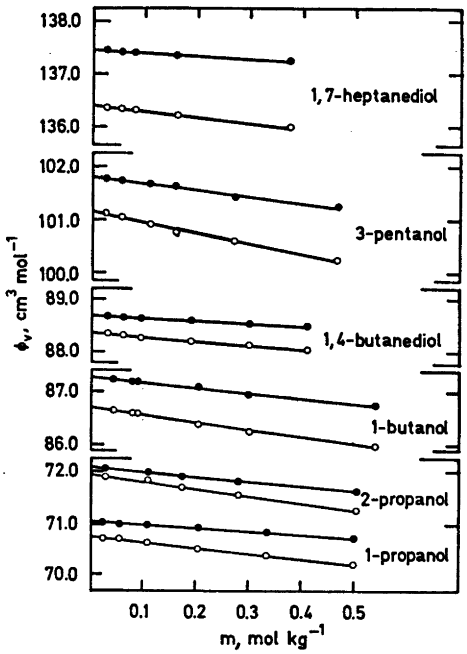

Fig. 1. Apparent molal volume *versus* concentration. The open circles are at 25 °C, the closed at 35 °C.

This linear extrapolation method has been critically investigated by Franks and Smith.[10] It was pointed out that linear plots do not necessarily give correct values of the partial molal volumes at infinite dilution, mainly due to a point of inflection in density as a function of concentration at higher concentrations. However, it appears that in the concentration range covered in this work the linearity is very good, and the final result for 1- and 2-butanol is in excellent agreement with the values of Franks and Smith evaluated from a more elaborate method of extrapolation.

Literature values for the partial molal volumes at infinite dilution were found for 1-propanol, 1- and 2-butanol, 1- and 3-pentanol at 25 °C.[2,10,11] No data were found at 35 °C. In all these cases the values at 25 °C agree. Friedman and Scheraga [12] report values for some primary and secondary alcohols at 1, 20, 40, and 50 °C. By interpolation of these data the two sets may be compared at 25 and 35 °C. Apparently for 2-propanol and 2-butanol the agreement is excellent. However, for 1-propanol, 1-butanol, and 1-pentanol the interpolated values from Friedman and Scheraga's work are 0.4 – 0.6 cm³ mol⁻¹ lower at 25 °C and 0.6 – 1 cm³ mol⁻¹ lower at 35 °C.

Calculations of group partial molal volumes. The group partial molal volume of the methylene group is easily determined by subtraction:

$$\overline{V}^\circ(CH_2) = \overline{V}^\circ(n+1) - \overline{V}^\circ(n) \qquad (1)$$

$\overline{V}^\circ(n)$ represents the partial molal volume of the solute molecule containing n methylene groups.

The values calculated from eqn. (1) are given in Table 1, the average being 16.0 cm³ mol⁻¹ in excellent agreement with previous determinations.[2-7].

With a knowledge of the group partial molal volume of the methylene group it is possible to proceed and calculate the group partial molal volume of the hydroxymethyl group, CH_2OH, from the data for 1,4-butanediol, 1,5-pentanediol and 1,7-heptanediol. It is assumed that the two hydroxymethyl groups are equivalent with respect to group partial molal volumes. The result given in Table 1c shows that a remarkably constant value of 28.2 cm³ mol⁻¹ is found.

The group partial molal volume of the methyl group may then be calculated from the homologous series of primary alcohols. The sum of the group partial molal volumes of the hydroxymethyl and the methylene groups can be subtracted from the total partial molal volume. This yields an average value for the methyl group $\overline{V}^\circ(CH_3) = 26.5$ cm³ mol⁻¹. Previous calculations of this quantity based on carboxylic acid series gave $\overline{V}^\circ(CH_3) = 26.1$ cm³ mol⁻¹. Taking all series into account the average group partial molal volume turns out to be: $\overline{V}^\circ(CH_3) = 26.4 \pm 0.3$ cm³ mol⁻¹.

Since all the other group partial molal volumes have been determined, the value of the hydroxymethylene group may be calculated from the secondary alcohols, Table 1b. Apparently the group partial molal volume of the hydroxymethylene group depends on the position it occupies in the molecule. In 2-position the value is 1.4 cm³ mol⁻¹ higher than in 3- or 4-position, and in 2-position relative to a carboxyl group the value has been calculated to 17.2 cm³ mol⁻¹.[4]

Table 1. Partial molal volumes and group partial molal volumes at infinite dilution, $cm^3\ mol^{-1}$.

	$V^{\circ}(\pm 0.1)$ 25 °C	35 °C	$V^{\circ}(CH_2)$ 25 °C	35 °C	$V^{\circ}(R)$ 25 °C	35 °C
(a) Primary alcohols					$R=CH_3$	
1-Propanol	70.75	71.08			26.6	26.7
1-Butanol	86.62	87.28	15.9	16.2	26.4	26.7
1-Pentanol	102.62	103.46	16.0	16.2	26.4	26.5
1-Hexanol	118.65	119.64	16.0	16.2	26.5	26.6
(b) Secondary alcohols					$R=CHOH$	
2-Propanol	71.93	72.10			19.1	19.3
2-Butanol	86.64	87.04	14.7	14.9	17.9	18.0
2-Pentanol	102.55	103.33	15.9	16.3	17.8	18.1
2-Hexanol	118.49	119.40	15.9	16.1	17.8	18.0
2-Heptanol	134.39	135.65	15.9	16.2	17.7	18.1
3-Pentanol	101.16	101.81			16.4	16.6
3-Hexanol	117.14[a]		16.0		16.3	
3-Heptanol	133.3	134.4	16.2	16.2	16.5	16.8
4-Heptanol	133.2[a]		16.1		16.4	
(c) Diols					$R=CH_2OH$	
1,4-Butanediol	88.35	88.69			28.2	28.2
1,5-Pentanediol	104.35	104.95	16.0	16.1	28.2	28.2
1,7-Heptanediol	136.40	137.45	16.0	16.2	28.2	28.2
1,2-Propanediol	71.22	71.68				
1,3-Butanediol	88.32	88.66	17.1	16.9		
2,3-Butanediol	86.56	86.96				
2,4-Pentanediol	104.64	105.10	18.0	18.1		
(d) Mannitol	119.33	120.37				

[a] Literature values from Ref. 2.

Table 2. Group partial molal volumes in aqueous solution and in pure liquids, van der Waals volumes and excess volumes, all in $cm^3\ mol^{-1}$.

Groups	Aqueous Solution 25 °C	35 °C	Pure liquids 20 °C	Van der Waals volumes	Excess Volumes
CH_3	26.4	26.5	31.48	13.67	−5.1
CH_2	16.0	16.2	16.58	10.23	−0.6
COOH	25.8	26.1	27.24	19.74	−1.4
CH_2OH	28.2	28.2	26.83	18.27	1.4
CHOH	17.8[a]	18.0[a]		14.82	
	16.4[b]	16.7[b]			
	17.2[c]				
CH_2COO^-	33.6[d]				
$CHOHCOO^-$	34.9[d]				

[a] Hydroxymethylene group in 2-position, [b] in 3- or 4-position, and [c] in 2-position to a carboxyl group. [d] Ref. 3.

Since the group partial molal volume of the methyl group has been redetermined from a larger number of data, some recalculated group partial molal volumes in Table 2 differ slightly from those previously published.[3] However, the differences are largely within the limits of experimental error.

DISCUSSION

The group partial molal volumes in aqueous solution may be compared with group partial molal volumes in pure liquid alcohols [7] and also with van der Waals group volumes.[13] The data for pure liquids compiled in Table 2

is at 20 °C. However, the densities of the pure liquids change but little with temperature in this region,[8] and the difference of 5 °C does not seem significant for qualitative comparisons.

The difference between the partial molal volume in aqueous solution and in the pure liquid has been termed the excess volume of the solute.[14] Excess group partial molal volumes are given in Table 2. However, the pure liquid is not satisfactory as a standard state and the excess volume may, it seems, just as well reflect specific volume effects in the pure liquid rather than solute – solvent interaction effects in water. For instance, the excess volume is negative for all the groups except the hydroxymethylene group. In pure primary alcohols extensive hydrogen-bonding takes place [14] forming long chains of hydrogen-bonded alcohol molecules which could reduce the group volume of the hydroxymethyl group, and in consequence lead to a positive excess volume. However, a large negative excess volume may still be taken to reflect stabilization of solvent structure,[15] and in this respect the methyl group is unique, having a much more negative excess volume than any other group. The methylene group has a small negative excess volume. Nevertheless it means that the excess volume of the solute as a whole decreases with the length of the molecule, suggesting increased stabilization of water structure with solute size.

The group partial molal volumes in aqueous solutions compared with van der Waals volumes, show that the void volume around the methyl group must be larger than the void around the other groups. NMR-data [16] on dilute alcohol solutions have been interpreted in terms of the solute in a clathrate-like environment where the hydroxyl group hydrogen-bonds into the water lattice thus helping to form the cavity wall. In this model the methyl group seems to be rotating freely in a large void, and the larger group molal volume of the hydroxymethylene group in 2-position compared with 3- or 4-positions, is probably due to this large void around a rotating methyl group. Hydrogen-bonding between water and the hydroxy-methylene group in 2-position may also be made difficult.

The volume increment per methylene group deviates substantially from 16.0 cm^3 mol^{-1} in three instances: (1) from 2-propanol to 2-butanol, (2) from 1,2-propane-diol to 1,3-butanediol, and (3) from 2,3-butanediol to 2,4-pentanediol. The observed partial molal volumes of these alcohols may be compared with the partial molal volume calculated from the group partial molal volumes. The comparison reveals that 2-propanol has an observed partial molal volume that is 1.3 cm^3 mol^{-1} higher than expected from the additivity relation, and 1,2-propane-diol and 2,3-butanediol have observed partial molal volumes that are lower than expected, 1.2 and 1.8 cm^3 mol^{-1}, respectively.

2-Propanol has two methyl groups separated only by a hydroxymethyl group. The large void volumes around the methyl group seem to interfere with each other and increase the total void by about 1 cm^3 mol^{-1}. In 1,2-propanediol and 2,3-butanediol two polar hydroxyl groups occupy neighbouring positions. The two polar groups apparently have a mutual effect on the surrounding water that reduces the partial molal volume, possibly through extensive hydrogen-bonding. This mutual interaction between neighbouring polar groups and water is also observed for a carboxyl and a hydroxymethylene group in neighbouring positions.[4] Such reductions in the volume requirements are clearly demonstrated by the partial molal volume of mannitol. If the partial molal volume of mannitol. is estimated from adding the group partial molal volumes in Table 2, the result is $\overline{V}^\circ$ (mannitol) = 124.8 cm^3 mol^{-1}, more than 5 cm^3 mol^{-1} higher than the observed value. The many neighbouring polar groups reduce the partial molal volume.

Mannitol is essentially a hydrophilic molecule and no clathrates are known to exist for hydrophilic solutes.[17] The group partial molal volumes in Table 2 are based on data for alcohol solutions where a clathrate-like structure is a possibility. Thus the difference between calculated and observed partial molal volume for mannitol may be related to different volume requirements between a clathrate-like structure on one hand, and a model where short-range solute-water interactions are dominating on the other.

The effect of temperature on the group partial molal volumes is small in the range 25 – 35 °C. The hydroxymethyl group is appar-

ently not affected at all, and the other group partial molal volumes increase by 0.1 – 0.3 cm^3 mol^{-1}. This increase is of the same order of magnitude as the experimental error in the partial molal volume determinations, and consequently no great significance can be attached to these group molal expansibilities.

REFERENCES

1. Traube, J. *Samml. Chem. Vortr. 4* (1899) 255.
2. Cabani, S. Conti, G. and Lepori, L. *J. Phys. Chem. 78* (1974) 1030.
3. Høiland, H. *Acta Chem. Scand. A 28* (1974) 699.
4. Høiland, H. and Vikingstad, E. *J. Chem. Soc. Faraday Trans. 1 71* (1975) 2007.
5. Sakurai, M. *Bull. Chem. Soc. Jap. 46* (1973) 1596.
6. Desnoyers, J. E. and Arel, M. *Can. J. Chem. 45* (1967) 359.
7. Exner, O. *Collect. Czech. Chem. Commun. 32* (1967) 1.
8. Timmermanns, J. *Physico-Chemical Constants of Pure Organic Compounds*, Elsevier, New York 1950, p. 313.
9. Høiland, H. *J. Chem. Soc. Faraday Trans. 1. 71* (1975) 797.
10. Franks, F. and Smith, H. T. *Trans. Faraday Soc. 64* (1968) 2962.
11. Alexander, O. M. *J. Chem. Eng. Data 4* (1959) 252.
12. Friedman, M. E. and Scheraga, H. A. *J. Phys Chem. 69* (1964) 3795.
13. Bondi, A. *J. Phys. Chem. 68* (1964) 441.
14. Franks, F. and Ives, D. J. G. *Quart. Rev. Chem. Soc. 20* (1966) 1.
15. Franks, F. and Reid, D. S. In Franks, F., Ed., *Water, a Comprehensive Treatise*, Plenum Press, New York 1973, Vol. 2, p. 323.
16. Glew, D. N., Maks, H. D. and Rath, N. S. *Chem. Commun.* (1968) 264.
17. Franks, F. In Covington, A. K. and Jones, P., Eds., *Hydrogen Bonded Solvent Systems*, Taylor and Francis, London 1968, p. 31.

Received September 22, 1975.

Acta Chemica Scandinavica A 30 (1976) 187—192

The Structure of the δ-Phase in the Cu—Sn System. A Phase of γ-Brass Type with an 18 Å Superstructure

LARS ARNBERG, ARNE JONSSON and SVEN WESTMAN

Departments of Inorganic and Structural Chemistry, Arrhenius Laboratory, University of Stockholm, Fack, S-104 05 Stockholm, Sweden

The gamma brass-like phase with the approximate composition $Cu_{41}Sn_{11}$ is face centered cubic, with a lattice parameter of ~17.96 Å. The space group is $F\bar{4}3m$. The structure may be described in terms of four different types of "cluster"; each cluster consisting of an inner tetrahedral, an outer tetrahedral, an octahedral and a cubo-octahedral position. The Sn atoms occupy one cubo-octahedral, one octahedral and one outer tetrahedral position of three different clusters, respectively. There are no Sn—Sn contacts in this idealized structure model. Some of the Sn atoms in the cubo-octahedral position of the model may, in the actual structure, be located at the inner tetrahedral position of the same cluster and at the octahedral position of the all-Cu cluster of the model.

The Cu—Sn system contains a γ-brass-like phase, called δ, with face-centered cubic superstructure. This phase, first described by Westgren and Phragmén,[1] has a very narrow homogeneity range around 20.5 atom % Sn. Knödler [2] investigated it by means of X-ray powder and Laue photographs and proposed a partially ordered structure with the nominal composition $Cu_{31}Sn_8$ (20.6 atom % Sn), having a valence electron concentration of 21 electrons/13 atoms. He based the model on a description of the related high-temperature γ-phase, in which all atoms were supposed to be situated at the lattice points of the body-centered cubic subcell ($a \sim 3$ Å). The shortest Sn—Sn contact, 4.2 Å, in the γ structure is the face diagonal of the subcell. The ideally ordered γ model has the stoichiometry Cu_3Sn, which lies within the homogeneity range of this phase.

In the δ phase, $Cu_{31}Sn_8$, some copper has been substituted for tin, and Knödler assumes this substitution to be completely random. Furthermore, the atomic arrangement described above is collapsed around the vacancies at 000 *etc.*, $\frac{1}{2}\frac{1}{2}\frac{1}{2}$ *etc.*, $\frac{1}{4}\frac{1}{4}\frac{1}{4}$ *etc.*, and $\frac{3}{4}\frac{3}{4}\frac{3}{4}$ *etc.*, yielding a normal γ-phase structure, which may be expressed in terms of atomic clusters: A, B, C, D, centered at the sites mentioned. Each cluster is built up of an inner tetrahedral (IT), an outer tetrahedral (OT), an octahedral (OH) and a cubo-octahedral (CO) point complex.[3,4] In Knödler's model, then, the IT position in cluster C is occupied by Sn. Its position parameter ($x = \frac{1}{4} + 0.0515$), given by Knödler, implies an Sn—Sn distance of 2.6 Å within this cluster; to be compared with Schubert's [5] tabulated value: $2r_{Sn} = 3.16$ Å.

Since it is possible to redistribute the atoms in this model into a completely ordered arrangement without Sn—Sn contacts and with a stoichiometry approximating the experimental value, we decided to collect single-crystal X-ray data in order to compare the "improved" model with Knödler's original proposal. The investigation is part of an inventory of possible variations on the gamma brass structural theme.[4]

EXPERIMENTAL

Weighed amounts of copper (granular, Mallinckrodt Analytical Reagent) and tin (E. Merck, Darmstadt) were melted together in a sealed evacuated silica capsule at 1150 °C for 24 h to a homogeneous alloy containing 20.6 atom % Sn. After the heat treatment the capsule was quenched in water, reheated

at 550 °C for seven days and again quenched in water. The density of the alloy specimen was calculated from its weight in air and in benzene.

Guinier photographs were taken with Cu$K\alpha_1$ radiation ($\lambda = 1.54050$ Å) and with KCl ($a = 6.2919$ Å) as an internal standard.[6] Single crystal X-ray diffractometer data were collected with a PW 1100 (Philips Automatic Diffractometer) from an irregular crystal fragment measuring approximately 0.05³ mm³.

202 independent intensities (out of 260 measured), with $\sigma(I)/I < 0.4$, were used in the final refinement. The measured intensities have been corrected for absorption, with the crystal assumed to be a sphere of diameter 0.05 mm ($\mu r = 4.3$). Atomic scattering factors were taken from Cromer and Waber [7] and corrected for dispersion according to Cromer.[8] Least squares structure refinements were carried out with the program LALS on the IBM 360/75 computer at the Stockholm Data Center.

In the final stages of refinement Cruickhank's weighting scheme [11] with $w = (1000 + 0.0002 |F_o|^2)^{-1}$ was employed. The extinction proved to be negligible; an attempt to correct for it resulted in extinction factors ranging between 0.98 and 1.00.

REFINEMENT AND RESULTS

The Guinier record could be completely indexed on the basis of a face-centered cubic lattice with $a = 17.9646(6)$ Å at 20.6 % Sn (*cf.* Knödler's[2] value, $a = 17.9550(3)$ Å at 20.51 % Sn). The density and composition values yield 416 ± 1 atoms per unit cell; almost exactly $= 8 \times 52$. This is, thus, a gamma phase structure without "extra" vacancies.

Both Knödler's structure model and our own proposal are formulated in space group $F\bar{4}3m$ (No. 216), but we started the structure refinement with models of the "ordinary gamma brass cell", *i.e.* a subcell with $a = 8.9823$ Å. When we refined such a model in space group $I\bar{4}3m$ ($h+k+l=4n$), with all atoms assumed to be Cu, very low values for B_{OT} and B_{OH} strongly indicated a preferred concentration of Sn at the OT and OH sites. The value of $R = 100 \sum||F_o| - |F_c|| / \sum|F_o|$ was 10 %.

On the basis of this first result we tested several models with a stoichiometry approximating the experimental one. Eventually we obtained fairly uniform values of the thermal parameters, and a value of $R = 9.7$ %, for the IT position containing only Cu; the OT, OH and CO positions all containing Cu and Sn in the proportion 3:1. We tested the atomic distribution further, using subcell diffraction data pertaining to space group $P\bar{4}3m$ (h, k and l all even). The best refinement ($R = 13.8$ %) produced a model containing Sn at the OH and CO positions around the origin of the subcell (averaging the A and B clusters), and at the OT position around $\frac{1}{2}\frac{1}{2}\frac{1}{2}$ (averaging clusters C and D). This corresponds to our proposed modification of Knödler's structure.

Finally, we refined the following complete models ($a = 17.9646$ Å) in space group $F\bar{4}3m$:

Table 1. Atomic distributions and parameters of the refined structure. Standard deviations in parentheses.

		a/Å	17.9646 (6)		
		Cluster A	Cluster B	Cluster C	Cluster D
IT	Atom	Cu(Sn)	Cu	Cu	Cu
16(*e*)	x	0.0508(8)	0.5540(11)	0.3001(10)	0.8079(8)
	B/Å²	1.9(4)	2.3(5)	1.9(5)	1.7(4)
OT	Atom	Cu	Cu	Cu	Sn
16(*e*)	x	−0.0836(12)	0.4142(10)	0.1664(9)	0.6609(5)
	B/Å²	2.5(7)	1.3(4)	0.9(5)	1.6(2)
OH	Atom	Cu	Sn	Cu(Sn)	Cu
24(*f*)	x	0.1751(14)	0.6809(6)	0.4272(11)	0.9264(18)
24(*g*)	B/Å²	2.7(4)	1.3(2)	0.8(4)	2.7(6)
CO	Atom	Sn(Cu)	Cu	Cu	Cu
48(*h*)	x	0.1580(4)	0.6592(6)	0.3945(9)	0.9062(6)
	z	0.0186(4)	0.5121(7)	0.2779(10)	0.7706(8)
	B/Å²	2.1(2)	1.5(3)	2.9(4)	1.2(3)

I. Our model, described in the introduction, in which the clusters A, C, B, D, situated along the body diagonal of the cell in the order mentioned, contain Sn at the CO(A), OH(B) and OT(D) positions. The R value obtained was 9.9 %.

II. A rearrangement of that model, containing Sn at CO(A), OH(B) and OT(C). Model II refined to $R = 12.4$ % and yielded $B_{OT(D)} = -1.7$ Å² (*cf.* Table 1). All other rearrangements of Sn_{OT}, Sn_{OH} and Sn_{CO} over three different clusters are identical with either I or II.

III. Knödler's model, *i.e.* Sn at CO(A), OH(B), IT(C) and OT(D), which refined to $R = 10.1$ %. The thermal parameter of the Sn atom at IT(C), $B = 5.0$ Å², became very high in relation to the others (1.0 – 2.6 Å²).

We then tested model I by means of F_o and difference Fourier syntheses in the ($\bar{1}10$) plane. The difference map was essentially featureless; the most prominent maxima had a height of 10 % of those in the F_o synthesis.

Nevertheless, the scatter of thermal parameter values was still considerable (0.4 – 2.8 Å²); this seemed to warrant a special investigation of whether some Sn might be located, *e.g.*, at OH(C), with $B = 0.4$. The following strategy proved to be effective: First, we refined isotropic extinction correction, over-all temperature factor and over-all scale factor separately, whereupon, having found extinction to be negligible, we refined the over-all scale and temperature factors together. Then we calculated and refined the occupancy parameters and, finally, occupancies and over-all temperature factors jointly. The fact that none of these changed in the last run supports the correctness of the result. Moreover, a similar refinement of Knödler's structure proposal converged to exactly the same final model.

The resulting structural parameters closely approximate those of our proposed model I. The difference between the refined structure and the idealized model is a redistribution of 6.8 Sn atoms per unit cell from the CO(A) type sites (= 14 % of the atoms) to the IT(A) (2.7 atoms/cell = 17 % substitution) and OH(C) (4.6 atoms/cell = 19 % substitution) sites. The Sn content of the refined model is 21.3 atom %, with an uncertainty of around ± 4 % estimated from the standard deviations of the occupancy parameters; this is indistinguishable from the experimental value of the synthetic composition: 20.6 % Sn.

Table 2. Structure factors for the refined $Cu_{41}Sn_{11}$ model. $R = 8.2$ %.

H	K	L	|FO|	|FC|
6	0	0	1983	1709
12	0	0	3237	3448
16	0	0	609	666
18	0	0	704	795
20	0	0	714	847
6	2	0	340	280
8	2	0	415	405
10	2	0	986	863
18	2	0	491	462
8	4	0	699	576
16	4	0	982	953
20	4	0	363	331
6	6	0	6552	6714
10	6	0	391	331
12	6	0	1256	1157
14	6	0	580	556
16	6	0	248	261
18	6	0	1241	1191
20	6	0	131	153
8	8	0	425	467
12	8	0	703	641
16	8	0	298	195
10	10	0	2173	1940
12	10	0	261	237
14	10	0	197	173
12	12	0	2714	2339
14	12	0	168	173
16	12	0	316	300
14	14	0	329	214
5	1	1	472	482
9	1	1	327	325
11	1	1	646	592
15	1	1	264	282
17	1	1	233	224
21	1	1	132	134
5	3	1	244	231
9	3	1	271	261
11	3	1	511	503
19	3	1	398	365
5	5	1	597	602
7	5	1	228	189
9	5	1	334	287
11	5	1	615	517
15	5	1	215	179
17	5	1	384	392
7	7	1	353	338
19	7	1	159	152
13	9	1	347	369
11	11	1	423	397
15	11	1	175	209
17	11	1	483	430
13	13	1	242	229
17	13	1	164	174
4	2	2	402	470
6	2	2	318	309
8	2	2	3621	3589
12	2	2	904	929
14	2	2	443	441
16	2	2	313	277
18	2	2	233	237
20	2	2	1043	1017
8	4	2	694	723
16	4	2	332	302
10	4	2	429	394
12	4	2	215	282
14	4	2	1953	1832
16	4	2	321	306
18	4	2	408	391
20	4	2	208	218
8	6	2	628	355
12	6	2	1068	1033
14	6	2	243	156
16	6	2	334	382
20	6	2	130	81
8	8	2	456	455
12	8	2	256	209
14	8	2	1996	1958
18	8	2	630	678
10	10	2	353	406
12	10	2	467	475
16	10	2	265	252
18	10	2	182	169
14	12	2	214	178
16	12	2	148	109
14	14	2	654	553
16	14	2	405	395
3	3	3	1599	1487
7	3	3	275	226
9	3	3	799	801
13	3	3	215	255
15	3	3	540	570
17	3	3	249	238
19	3	3	334	321
21	3	3	209	219
5	5	3	365	326
7	5	3	209	52
11	5	3	245	212
19	5	3	186	167
13	5	3	180	195
7	7	3	390	360
13	7	3	608	569
19	7	3	383	372
9	9	3	898	820
11	9	3	188	170
13	9	3	199	212
15	9	3	270	268
11	11	3	221	252
17	11	3	147	138
13	13	3	249	241
15	13	3	149	127
15	15	3	180	146
4	4	4	1775	1799
8	4	4	1232	1335
10	4	4	330	368
12	4	4	403	367
14	4	4	205	254
16	4	4	668	666
18	4	4	195	188
20	4	4	968	914
6	6	4	1526	1478
8	6	4	511	527
10	6	4	476	527
12	6	4	227	136
14	6	4	554	556
18	6	4	250	276
20	6	4	109	62
8	8	4	1711	1599
12	8	4	491	550
14	8	4	426	431
16	8	4	186	173
10	10	4	897	900
14	10	4	679	678
16	10	4	343	325
18	10	4	343	344
12	12	4	987	953
16	12	4	402	409
14	14	4	767	646
5	5	5	946	987
9	5	5	206	223
11	5	5	712	670
15	5	5	387	413
17	5	5	428	468
7	7	5	213	184
11	7	5	516	553
13	7	5	240	230
17	7	5	268	319
9	9	5	197	202
11	9	5	335	322
13	9	5	180	176
17	9	5	150	105
11	11	5	665	717
15	11	5	230	227
17	11	5	211	229
13	13	5	149	117
6	6	6	1191	1414
8	6	6	402	467
12	6	6	2669	2810
16	6	6	528	554
18	6	6	452	443
10	8	6	485	544
14	8	6	411	367
18	8	6	274	261
12	10	6	461	579
16	10	6	1089	1096
12	12	6	533	532
16	12	6	226	269
9	7	7	526	358
13	7	7	177	229
15	7	7	175	167
17	7	7	134	143
19	7	7	128	156
17	9	7	152	92
11	11	7	343	352
17	11	7	116	194
13	13	7	167	220
15	13	7	164	187
8	8	8	2918	3385
10	8	8	273	299
12	8	8	701	773
14	8	8	596	630
16	8	8	175	198
18	8	8	126	116
10	10	8	337	427
14	10	8	657	695
16	10	8	292	377
12	12	8	321	308
14	14	8	1668	1667
9	9	9	193	184
15	9	9	296	315
17	9	9	125	129
11	11	9	292	255
15	11	9	280	268
13	13	9	396	423
10	10	10	331	377
12	10	10	159	207
16	10	10	412	430
14	12	10	220	264
11	11	11	157	217
13	13	11	149	161
12	12	12	1036	1100

DISCUSSION

The idealized structure model arrived at has the stoichiometry $Cu_{41}Sn_{11}$. It is a modification, without Sn – Sn contacts, of Knödler's proposal.[2] Table 3 shows that the IT(C) – IT(C) distance, 2.55 Å, represents a Cu – Cu contact

Table 3. Coordination, number and type of contacts, interatomic distances (Å) with standard deviations.

3	IT(A)–IT(A)	Cu(Sn)–Cu(Sn) 2.582(33)
3	–OT(A)	–Cu 2.554(31)
3	–OH(A)	–Cu 2.579(23)
3	–CO(A)	–Sn(Cu) 2.785(20)
3	OT(A)–IT(A)	Cu–Cu(Sn) 2.554(31)
3	–OH(A)	–Cu 2.686(19)
3	–CO(A)	–Sn(Cu) 2.636(11)
[1	–IT(D)	–Cu 3.375(45)]
3	–CO(D)	–Cu 2.632(29)
2	OH(A)–IT(A)	Cu–Cu(Sn) 2.579(23)
2	–OT(A)	–Cu 2.686(19)
4	–CO(A)	–Sn(Cu) 2.875(6)
1	–OH(B)	–Sn 2.587(28)
[2	–CO(C)	–Cu 3.256(26)]
2	–CO(D)	–Cu 2.576(18)
1	CO(A)–IT(A)	Sn(Cu)–Cu(Sn) 2.785(20)
1	–OT(A)	–Cu 2.636(11)
2	–OH(A)	–Cu 2.875(6)
[2	–CO(B)	–Cu 3.328(12)]
1	–OT(C)	–Cu 2.665(19)
1	–OH(C)	–Cu(Sn) 2.531(12)
2	–CO(C)	–Cu 2.823(15)
1	–OH(D)	–Cu 2.863(21)
2	–CO(D)	–Cu 2.655(10)
3	IT(B)–IT(B)	Cu–Cu 2.743(45)
3	–OT(B)	–Cu 2.638(26)
3	–OH(B)	–Sn 2.661(9)
3	–CO(B)	–Cu 2.778(26)
[1	–OT(D)	–Sn 3.329(38)]
3	OT(B)–IT(B)	Cu–Cu 2.638(26)
3	–OH(B)	–Sn 2.769(11)
3	–CO(B)	–Cu 2.564(15)
3	–CO(C)	–Cu 2.499(29)
1	OH(B)–OH(A)	Sn–Cu 2.587(28)
2	–IT(B)	–Cu 2.661(9)
2	–OT(B)	–Cu 2.769(11)
4	–CO(B)	–Cu 2.895(9)
2	–CO(C)	–Cu 2.781(22)
2	–CO(D)	–Cu 2.878(17)
[2	CO(B)–CO(A)	Cu–Sn(Cu) 3.328(12)]
1	–IT(B)	–Cu 2.778(26)
1	–OT(B)	–Cu 2.546(15)
2	–OH(B)	–Sn 2.895(9)
1	–OH(C)	–Cu(Sn) 2.764(18)
2	–CO(C)	–Cu 2.582(15)
1	–OT(D)	–Sn 2.676(16)
1	–OH(D)	–Cu 2.557(20)
2	–CO(D)	–Cu 2.746(14)
3	IT(C)–IT(C)	Cu–Cu 2.547(24)
3	–OT(C)	–Cu 2.547(24)
3	–OH(C)	–Cu(Sn) 2.614(17)
3	–CO(C)	–Cu 2.430(31)
3	OT(C)–CO(A)	Cu–Sn(Cu) 2.665(19)
3	–IT(C)	–Cu 2.547(24)
3	–OH(C)	–Cu(Sn) 2.708(14)
3	–CO(C)	–Cu 2.531(20)

Table 3. Continued.

2	OH(C)–CO(A)	Cu(Sn)–Sn(Cu) 2.531(12)
2	–CO(B)	–Cu 2.764(18)
2	–IT(C)	–Cu 2.614(17)
2	–OT(C)	–Cu 2.708(14)
4	–CO(C)	–Cu 2.708(13)
1	–OH(D)	–Cu 2.629(38)
[1	CO(C)–OH(A)	Cu–Cu 3.256(26)]
2	–CO(A)	–Sn(Cu) 2.823(15)
1	–OT(B)	–Cu 2.499(29)
1	–OH(B)	–Sn 2.781(22)
2	–CO(B)	–Cu 2.582(15)
1	–IT(C)	–Cu 2.430(31)
1	–OT(C)	–Cu 2.531(20)
2	–OH(C)	–Cu(Sn) 2.708(13)
2	–CO(C)	–Cu 2.961(35)
[1	IT(D)–OT(A)	Cu–Cu 3.375(45)]
3	–IT(D)	–Cu 2.944(34)
3	–OT(D)	–Sn 2.755(14)
3	–OH(D)	–Cu 2.588(27)
3	–CO(D)	–Cu 2.584(23)
[1	OT(D)–OT(A)	Sn–Cu 3.329(38)]
3	–CO(B)	–Cu 2.676(16)
3	–IT(D)	–Cu 2.755(14)
3	–OH(D)	–Cu 2.753(19)
3	–CO(D)	–Cu 2.606(16)
2	OH(D)–CO(A)	Cu–Sn(Cu) 2.863(21)
2	–CO(B)	–Cu 2.557(20)
1	–OH(C)	–Cu(Sn) 2.629(38)
2	–IT(D)	–Cu 2.588(27)
2	–OT(D)	–Sn 2.753(19)
4	–CO(D)	–Cu 2.853(11)
1	CO(D)–OT(A)	Cu–Cu 2.632(29)
1	–OH(A)	–Cu 2.576(18)
2	–CO(A)	–Sn(Cu) 2.655(10)
1	–OH(B)	–Sn 2.878(17)
2	–CO(B)	–Cu 2.746(14)
1	–IT(D)	–Cu 2.584(23)
1	–OT(D)	–Sn 2.606(16)
2	–OH(D)	–Cu 2.853(11)
[2	–CO(D)	–Cu 3.444(27)]

in our model ($2r_{Cu} = 2.56$ Å) and an Sn–Sn contact in Knödler's ($2r_{Sn} = 3.16$ Å). The shortest Cu–Cu distance in the structure, *viz.* IT(C)–CO(C), is 2.43 Å, which is not remarkable; such a distance, 2.48 (1) Å, occurs, *e.g.*, in the Cu_9Al_4 structure.[9] The IT(A)–IT(A) and CO(A)–OH(C) distances, which might contain some element of Sn–Sn contact in the real structure (defect model I), are longer: 2.58 and 2.53 Å, respectively.

The sum of the copper and tin radii is 2.86 Å, according to Schubert,[5] but the copper-tin distance observed [10] in the high temperature γ phase (Cu_3Sn composition) is only 2.65 Å. In the δ structure the Sn–Cu contacts range from 2.90 (OH(B)–CO(B)) down to 2.53 Å (CO(A)–OH(C)), which is shorter than the Cu_3Sn value. All the other distances from the Sn atoms in CO(A) to the surrounding Cu atoms are ≥2.64 Å, however. From Sn at OT(D) there are three fairly short contacts to Cu at CO(D) and one short distance from Sn at OH(B) to Cu at OH(A), but the remaining contacts are all longer than 2.65 Å.

Acknowledgements. This investigation was sponsored by the Swedish Natural Science Research Council. We wish to express our gratitude to Professor Arne Magnéli for his

critical evaluation of our work, to Professor Peder Kierkegaard for kindly allowing us to use the diffractometer and to Dr. Anne-Marie Pilotti and Mr. Bengt Karlsson for introducing us to its proper use. We are extremely grateful to Dr. Don Koenig for practical help and instructive discussions. Finally, we wish to acknowledge the technical assistance of Mrs. Gunvor Winlöf.

REFERENCES

1. Westgren, A. and Phragmén, G. *Z. Anorg. Allg. Chem. 175* (1928) 80.
2. Knödler, H. *Metall 18* (1964) 1172.
3. Johansson, A. and Westman, S. *Acta Chem. Scand. 24* (1970) 3471.
4. Westman, S. *Chem. Commun. Univ. Stockholm* (1972) No. 4.
5. Schubert, K. *Kristallstrukturen Zweikomponentiger Phasen*, Springer Verlag, Berlin 1964.
6. Hambling, P. G. *Acta Crystallogr. 6* (1953) 98.
7. Cromer, D. T. and Waber, J. T. *Acta Crystallogr. 18* (1965) 104.
8. Cromer, D. T. *Acta Crystallogr. 18* (1965) 17.
9. Heidenstam, O. von, Johansson, A. and Westman, S. *Acta Chem. Scand. 22* (1968) 653.
10. Hendus, H. and Knödler, K. *Acta Crystallogr. 9* (1956) 1036.
11. Cruickshank, D. W. I. Lecture at the Summer School of Modern Methods of X-Ray Crystallography, Manchester 1960.

Received September 11, 1975.

Acta Chemica Scandinavica A 30 (1976) 193—197

Complexes between Gaseous Gallium Chloride and Cobalt Chloride

A. ANUNDSKÅS,* A. E. MAHGOUB ** and H. A. ØYE

Institutt for uorganisk kjemi, Norges tekniske høgskole, Universitetet i Trondheim, N-7034 Trondheim-NTH, Norway

In gaseous gallium chloride, Co^{2+} is found as $CoGa_2Cl_8$ with the following thermodynamic functions of formation at 673 K:

$CoCl_2(s) + Ga_2Cl_6(g) = CoGa_2Cl_8(g)$
$\Delta H^\circ = 43.9 \pm 0.7$ kJ, $\Delta S^\circ = 36.9 \pm 1.1$ J K^{-1}

The structure of $CoGa_2Cl_8$ is discussed, and a coordination of $CoCl_2$ to the Ga_2Cl_6 molecule, without breaking the double bond in Ga_2Cl_6, is suggested. An octahedral coordination of Co^{2+} is considered unlikely.

As an extension of a general study of gas complexes between $AlCl_3$ and divalent 3*d*-metal chlorides [1-3] it was decided to investigate the complexing properties of $GaCl_3$ with respect to $CoCl_2$.

Gaseous $GaCl_3$ and $AlCl_3$ have very similar structural and thermodynamic properties, both being subject to the equilibrium

$$A_2Cl_6(g) = 2ACl_3(g), \quad A = Al, Ga \qquad (1)$$

which is shifted to the right with increasing temperature. However, in spite of their similarities it is of interest to determine how the heavier Ga^{3+} ion compares to Al^{3+} for the general complexing reaction:

$$MCl_2(s,g) + n_2A_2Cl_6(g) = MA_{2n_2}Cl_{6n_2+2}(g) \qquad (2)$$

with $CoCl_2$ as the metal chloride in the present study. Although $GaCl_3$ is more difficult to handle than $AlCl_3$, the experiments were expected to benefit from the shift to the left of the side reaction:

$$2A_2Cl_6(g) + 3SiO_2(s) = 2A_2O_3(s) + 3SiCl_4(g) \qquad (3)$$

when substituting Ga_2Cl_6 for Al_2Cl_6.

The chosen experimental method was absorption spectroscopic determination of the pressure of the gas complex in closed quartz cells according to eqn. (2). This method has been described in detail previously.[1,4]

The molar absorption of a known amount of MCl_2 in the gas phase is first determined by the equation:

$$\varepsilon^i_{Co-Ga-Cl} = A^i V/nl \qquad (4)$$

whereafter the pressure of the gas complex in the presence of $MCl_2(s)$ is determined by

$$P_{Co-Ga-Cl} = \frac{A^i R\overline{T}}{\varepsilon^i_{Co-Ga-Cl} l} \qquad (5)$$

$\varepsilon^i_{Co-Ga-Cl}$: molar absorptivity of the gas complex at wavelength i, A: optical density at wavelength i, V: volume, n: mol of gas complex, l: optical path length, P: pressure of gas complex, R: gas constant and $\overline{T}$: mean cell temperature.

The pressure of Ga_2Cl_6 as well as the temperature were varied so that the stoichiometry and the thermodynamic functions for the reaction corresponding to eqn. (2) could be obtained.

EXPERIMENTAL

Anhydrous $GaCl_3$ was obtained in ampoules as 99.99 % (Schuchardt, München, DBR) and no further purification was performed. Anhydrous $CoCl_2$ was prepared from $CoCl_2.6H_2O$ "pure" (Koch-Light Labs., Colubrook, England) by heating under vacuum at 120 °C for 4 h,

* Present address: Forskningssenteret, Norsk Hydro a/s, 3901 PORSGRUNN, Norway.
** Present address: Chemistry Department, Faculty of Science, Cairo University, Giza, CAIRO, Egypt.

followed by purging with HCl for 2 h at 450 °C, and then repeated sublimation.

The experimental procedure has been described previously.[1,5] Equilibrium was found to be established within 30 min, at which time the spectrum was recorded.

RESULTS

Spectrophotometrically the gas complex formation between $CoCl_2(s)$ and $GaCl_3$ was detected above 280 °C by the appearance of two composite absorption bands at about 15.6 and 7.1 kK (Fig. 1). By analyzing the spectrum in detail, absorption maxima and shoulders were observed at the following wave numbers [expressed in kK with the molar absorptivities at 400 °C given in parenthesis (Exp. 2, Table 1)]: 14.9(85), 15.6(150), 16.8(140), 17.6(sh), 18.5(sh), 7.1(30), 5.9(−).

Due to the composite nature of the two main absorption regions, individual spectral half-widths could not be given, but would probably not exceed 2 kK.

The molar absorptivity for the strongest peak was determined in three experiments specified in Table 1. The molar absorptivity decreased with increasing temperature and did not reveal any dependence on the pressure of Ga_2Cl_6 above 400 °C. Between 300 and 400 °C a small decrease in molar absorptivity with increasing Ga_2Cl_6 pressure may be present, similar to what is observed by Dell'Anna and Emmenegger [6] for the $CoCl_2-Al_2Cl_6$ gas complex. Statistically, however, the pressure dependence was not significant on a 90 % confidence level, and all the molar absorptivity data were fitted to the following pressure-independent equation with a 2.5 % standard deviation:

$$\varepsilon^{15.6}{}_{\text{Co–Ga–Cl}} = -36.4 + 0.685\bar{T} - 6.017 \times 10^{-4}\bar{T}^2 \quad (6)$$

Eqn. (6) was used for determining the vapour pressure of the complex in the experiments with excess $CoCl_2$ (Table 1, Exp. 4 – 9).

Using a non-linear regression analysis program by Hertzberg,[7] previously described by Øye and Gruen,[4] the experiments were best described by the following complexing equilibrium:

$$CoCl_2(s) + Ga_2Cl_6(g) = CoGa_2Cl_8(g)^* \quad (7)$$

$$P_{CoGa_2Cl_8} = P_{Ga_2Cl_6} \exp_{10}\left(1.936 - \frac{2295}{T_{min}}\right) \quad (8)$$

corresponding to $\Delta H° = 43.9 \pm 0.7$ kJ and $\Delta S° = 36.9 \pm 1.1$ J K^{-1} at 673 K. The standard deviation in the estimate was 9.5 %. The pressure of the dimer, $P_{Ga_2Cl_6}$, was calculated by the ideal-gas law using the weighed-in amount of $GaCl_3$ and correcting for the amount consumed in the complexing and dissociation reaction:[8]

$$Ga_2Cl_6(g) = 2GaCl_3(g),$$
$$\log_{10}K(\text{atm}) = -4595/T + 7.066 \quad (9)$$

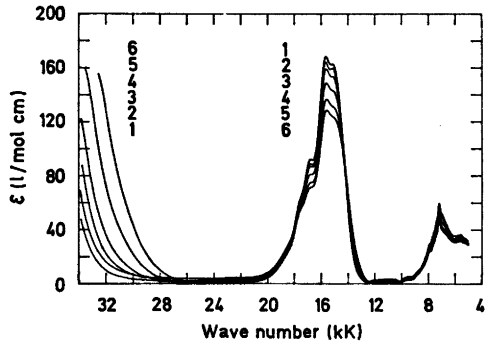

Fig. 1. Absorption spectra of $CoCl_2$ in gaseous Ga_2Cl_6 (Exp. 2). Temperatures are given in K. Curves 1, 575; 2, 625.5; 3, 678; 4, 726.5; 5, 782; 6, 821.

DISCUSSION

The expected absence of the side reaction due to attack of the quartz cuvette [eqn. (3)] by using $GaCl_3$ instead of $AlCl_3$ was experimentally verified. A loaded cell was left at 425 °C for 5 days without any detectable spectral changes. Even with this excellent stability and good reproducibility shown by repeated experiments, the fit to the model equations was not any better than the results with $AlCl_3$.[1] The reason may be that some $GaCl_3$ after all did evaporate at the filling of the cell.

Assuming constant temperature and a one-species model, the stoichiometric constant according to eqn. (2) may be calculated by using

* The method does not unambigously exclude the presence of polynuclear Co-species as $Co_2Ga_2Cl_{10}$,[4] but they are considered unlikely.

Table 1. Co–Ga–Cl gas complexes. Molar absorptivity at 15.6 kK (Exp. 1–3) and calculated vapour pressure in presence of $CoCl_2$(s) (Exp. 4–9).

Exp. No.	Specification	T_{min} (K)	$\bar{T}$ (K)	Optical density A	Molar absorptivity $\varepsilon_{Co-Ga-Cl}$ (l/mol cm)	$P_{Co-Ga-Cl}$ (atm)
	$P^\circ_{Ga_2Cl_6} = 1.276 \times 10^{-3}\bar{T}$	671	677	0.275	158.8	
1	$l = 14.2$ cm	721.5	728.5	0.255	147.2	
	$V = 76.73$ cm³	770	778	0.230	132.8	
	$w_{CoCl_2} = 1.215$ mg	808	817	0.210	121.3	
	$P^\circ_{Ga_2Cl_6} = 3.417 \times 10^{-3}\bar{T}$	571	575	0.560	162.3	
		620.5	625.5	0.555	160.9	
2	$l = 14.2$ cm	672	678	0.520	150.7	
	$V = 76.73$ cm³	719.5	726.5	0.490	142.0	
	$w_{CoCl_2} = 2.42$ mg	774	782	0.445	129.0	
		812	821	0.420	121.8	
	$P^\circ_{Ga_2Cl_6} = 7.34 \times 10^{-3}\bar{T}$	570	571	0.520	153.6	
		600	601	0.530	156.5	
3	$l = 5.0$ cm	653	654	0.510	150.6	
	$V = 14.22$ cm³	708	709	0.480	141.7	
	$w_{CoCl_2} = 1.26$ mg	762	763	0.450	132.9	
		817.5	818.5	0.415	122.6	
	$P^\circ_{Ga_2Cl_6} = 0.303 \times 10^{-3}\bar{T}$	492.5	495.5	0.017	155.3	2.97×10^{-4}
		540.5	544.5	0.032	158.2	6.03×10^{-4}
4	$l = 15.0$ cm	588.5	593.5	0.051	158.2	10.50×10^{-4}
	$V = 58.04$ cm³	640.5	646.5	0.063	155.0	14.30×10^{-4}
		692	699	0.059	148.4	15.20×10^{-4}
		743	751	0.047	138.7	13.90×10^{-4}
		796	805	0.0355	125.1	12.50×10^{-4}
	$P^\circ_{Ga_2Cl_6} = 0.71 \times 10^{-3}\bar{T}$	522	525	0.065	157.4	1.19×10^{-3}
		574.5	578.5	0.125	158.5	2.50×10^{-3}
5	$l = 15.0$ cm	632.5	637.5	0.200	155.8	4.48×10^{-3}
	$V = 55.86$ cm³	693.5	699.5	0.230	148.3	5.93×10^{-3}
		738	745	0.215	140.0	6.26×10^{-3}
		790	798	0.180	127.1	6.18×10^{-3}
	$P^\circ_{Ga_2Cl_6} = 1.455 \times 10^{-3}\bar{T}$	535	538	0.180	155.0	3.40×10^{-3}
		583	587	0.325	158.4	6.55×10^{-3}
6	$l = 15.1$ cm	628	633	0.495	156.1	10.91×10^{-3}
	$V = 44.06$ cm³	677	683	0.630	150.8	15.51×10^{-3}
		726	733	0.675	142.4	18.88×10^{-3}
		774.5	782.5	0.645	131.2	20.91×10^{-3}
		817	826	0.580	118.9	21.90×10^{-3}
	$P^\circ_{Ga_2Cl_6} = 1.50 \times 10^{-3}\bar{T}$	585	586	0.115	158.4	6.98×10^{-3}
		643.5	644.5	0.190	155.1	12.96×10^{-3}
7	$l = 5.0$ cm	700	701	0.250	148.1	19.42×10^{-3}
	$V = 15.12$ cm³	756	757	0.235	137.3	21.26×10^{-3}
		810.5	811.5	0.210	123.2	22.70×10^{-3}
	$P^\circ_{Ga_2Cl_6} = 2.94 \times 10^{-3}\bar{T}$	541	542	0.160	158.1	9.00×10^{-3}
		591.5	592.5	0.290	158.2	17.83×10^{-3}
8	$l = 5.0$ cm	646	647	0.470	154.9	32.22×10^{-3}
	$V = 14.84$ cm³	699	700	0.625	148.3	48.42×10^{-3}
		706	707	0.620	147.1	48.91×10^{-3}
		752	753	0.700	138.2	62.60×10^{-3}
		808	809	0.690	124.0	73.88×10^{-3}
	$P^\circ_{Ga_2Cl_6} = 7.42 \times 10^{-3}\bar{T}$	564	568	(2.27)[a]	158.6	(4.45×10^{-2})
		604.5	609	(3.10)	157.6	(6.55×10^{-2})
9	$l = 15.0$ cm	643.5	649	(4.05)	154.7	(9.29×10^{-2})
	$V = 5$ cm³	672	678	(4.50)	151.4	(11.02×10^{-2})

[a] Uncertain values.

the experiments with excess $CoCl_2$ at different Ga_2Cl_6 pressures. Referred to exp. 8 (Table 1), typical values between 0.96 and 1.08 are obtained at 394 °C, while slightly higher values were found at the lowest temperatures. In spite of these deviations from the value $n_2 = 1$, corresponding to $CoGa_2Cl_8(g)$, a two-species model [*e.g.* $CoGa_2Cl_8(g) - CoGa_3Cl_{11}(g)$ or $CoGa_2Cl_8(g) - CoGa_4Cl_{14}(g)$] did not improve the standard deviation relative to a one-species model with $CoGa_2Cl_8(g)$ present. In conclusion, $CoGa_2Cl_8(g)$ is considered to be the main gas species, but small amounts of $CoGaCl_5(g)$, $CoGa_3Cl_{11}(g)$ or $CoGa_4Cl_{14}(g)$ may be present.

Referring to Table 1, Exp. 4 and 5, it may seem curious that $P_{CoGa_2Cl_8}$ is decreasing with increasing temperature for the very highest temperatures in spite of a positive ΔH of the reaction given by eqn. (7). This is, however, consistent with the present model given by eqns. (7) and (8) and is simply due to dissociation of Ga_2Cl_6 [eqn. (9)].

The spectral data do not lend themselves to any unambiguous conclusion as to the geometric arrangement of chloride around the cobalt. The molar absorptivity is between the values one might expect for the octahedral and tetrahedral geometries, however, closer to those of octahedral geometry. The variation with temperature, however, is similar to that for a tetrahedral species,[9,10] and thus the octahedral coordination of Co^{2+} is considered highly unlikely. However, the possibilities of other geometries cannot be excluded.

The present experimental results for $CoCl_2 - GaCl_3$ are parallel to some very recent results on $CoCl_2 - AlCl_3$ gas complexes by Dell'Anna and Emmenegger,[6] Papatheodorou,[11] Thistlethwaite and Ciach,[12] as well as a previous study by Dewing.[13] They all find the main gas complex to be $CoAl_2Cl_8$ (as compared to $CoGa_2Cl_8$), and the spectral results are all very similar for the Al as well as the Ga containing complex. The main peak is found around 16 kK with a decrease in molar absorptivity with increasing temperature.

Table 2 gives the thermodynamic functions for gas complexation of $CoCl_2(s)$ as well as the dissociation of $Al_2Cl_6(g)$ and $Ga_2Cl_6(g)$. The entropy of dissociation of $Al_2Cl_6(g)$ and $Ga_2Cl_6(g)$ is seen to be the same. The entropy of complexation of $CoCl_2(s)$ with either $Al_2Cl_6(g)$ or $Ga_2Cl_6(g)$ is also seen to be equal, confirming the assumption of a similar structure of the two gas complexes. The remarkable feature of Table 2, however, is that the enthalpy of complexation is equal for the Al and the Ga containing complexes, in spite of the fact that the enthalpies of dissociation of $Al_2Cl_6(g)$ and Ga_2Cl_6 differ by 30 kJ. This suggests that the Al_2Cl_6 and Ga_2Cl_6 molecules remain essentially intact and do not dissociate, the $CoCl_2$ co-

Table 2. Thermodynamic functions for gas complex formation and dissociation reactions.

Ref.	Temp. K	$\Delta H°$ kJ	$\Delta S°$ J K^{-1}	K atm.
$Al_2Cl_6(g) = 2AlCl_3(g)$				
14	673	118	135	0.008
$Ga_2Cl_6(g) = 2GaCl_3(g)$				
8	673	88	135	1.7
$CoCl_2(s) + Al_2Cl_6(g) = CoAl_2Cl_8(g)$				
13	750	53.5	51.9	11.4×10^{-2}
6[a]	673	43.1 ± 2.2	39.3 ± 2.8	5.1×10^{-2}
11	673	41.8 ± 0.8	41.0 ± 1.3	7.9×10^{-2}
12	673	42.0 ± 0.7	45.0	12.3×10^{-2}
$CoCl_2(s) + Ga_2Cl_6(g) = CoGa_2Cl_8(g)$				
This work	673	43.9 ± 0.7	36.9 ± 1.1	3.3×10^{-2}

[a] Mean value of three methods.

ordinating at the end of the molecule, for instance approximately tetrahedrally in fashion II rather than I:

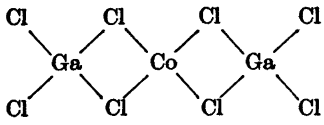

I

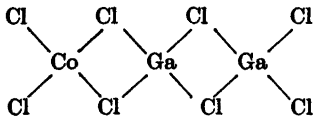

II (10)

Dell'Anna and Emmenegger [6] describe the Co coordination in $CoAl_2Cl_8$ as tetrahedral, whereas Papatheodorou [11] and Thistlethwaite and Ciach [12] describe it as mainly octahedral. Papatheodorou [11] explains the increase of molar absorptivity with decreasing temperature as due to small amounts of tetrahedrally coordinated Co^{2+} in equilibrium with the octahedral form, the tetrahedral coordination being more prevalent at lower temperatures.

We are at variance with this interpretation because it infers that the equilibrium

$$Co(tetr)Al_2Cl_8(g) = Co(oct)Al_2Cl_8(g) \quad (11)$$

has $\Delta H > 0$ and, since $K > 1$, $\Delta S > 0$. The signs of the thermodynamic functions are both opposite to what is expected. Whether structure I or II is assumed for a tetrahedral structure, a tetrahedral-octahedral transformation will result in the formation of two additional Co – Cl bonds with an expected negative ΔH. The vibrational entropy cannot be anticipated to counteract the negative rotational entropy [11] for eqn. (11). The main contribution to the vibrational entropy is given by the low frequency torsional vibrations and they are expected to be lower for the more loosely bonded $AlCl_4^-$ in the tetrahedral coordination, hence resulting in $\Delta S < 0$ for eqn. (11) both due to rotational and vibrational entropy.

It should, however, be stressed that the coordination equilibria in liquid and gaseous aluminium chloride still are intriguing. Co^{2+} and Ti^{2+} both have a similarly low octahedral site stabilization energy, but Ti^{2+} coordinates octahedrally in both the liquid and gaseous aluminium chloride,[2] while octahedral coordination of Co^{2+} is only found in liquid aluminium chloride.[10]

From a practical point of view it should be mentioned in conclusion that in spite of the similar thermodynamic properties of gas complex formation, Ga_2Cl_6 becomes less effective at higher temperatures due to its ease of dissociation relative to Al_2Cl_6. The greater stability of Ga_2Cl_6 in the presence of SiO_2 may, however, make it more attractive for detailed optical studies.

Acknowledgements. We gratefully acknowledge experimental assistance from Mr. Morten Sørlie and thereby support from Norges Almenvitenskapelige Forskningsråd. We have benefitted from discussions with Dr. J. Brynestad, Oak Ridge National Laboratory. Dr. A. E. Mahgoub expresses gratitude to the Norwegian Agency for International Development for a fellowship grant.

REFERENCES

1. Anundskås, A. and Øye, H. A. *Inorg. Nucl. Chem. 37* (1975) 1609.
2. Sørlie, M. and Øye, H. A. *To be published.*
3. Sutakshuto, S. and Øye, H. A. *To be published.*
4. Øye, H. A. and Gruen, D. M. *J. Am. Chem. Soc. 91* (1969) 2229.
5. Anundskås, A., Mahgoub, A. E. and Øye, H. A. *Egypt. J. Chem. In print.*
6. Dell'Anna, A. and Emmenegger, T. P. *Helv. Chim. Acta 58* (1975) 1145.
7. Hertzberg, T. "MODTLP" Report. Inst. for kjemiteknikk, Norges tekniske høgskole, Trondheim 1970.
8. Fischer, W. and Jübermann, O. *Z. Anorg. Allgem. Chem. 227* (1936) 227.
9. Gruen, D. M. and McBeth, R. L. *Pure Appl. Chem. 6* (1963) 23.
10. Øye, H. A. and Gruen, D. M. *Inorg. Chem. 4* (1965) 1173.
11. Papatheodorou, G. N. *Z. Anorg. Allgem. Chem. 411* (1975) 153.
12. Thistlethwaite, P. J. and Ciach, S. *Inorg. Chem. 14* (1975) 1430.
13. Dewing, E. W. *Metall. Trans. 1* (1970) 2169.
14. *JANAF Thermochemical Tables*, (Directors Stull, D. R. and Prophet, H.) Nat. Stand. Ref. Data Sci., Nat. Bur. Stand. 37, Washington 1971.

Received August 27, 1975.

Acta Chemica Scandinavica A 30 (1976) 198—202

The Crystal Structure of Cesium Sulfate, β-Cs_2SO_4

ANDERS G. NORD

Departments of Inorganic and Structural Chemistry, Arrhenius Laboratory, University of Stockholm, S-104 05 Stockholm 50, Sweden

The crystal structure of the room temperature modification of cesium sulfate, β-Cs_2SO_4, has been studied by X-ray diffraction techniques. At 25 °C the orthorhombic (*Pnam*) unit cell has the dimensions: $a = 8.239(1)$, $b = 10.944(1)$, and $c = 6.258(1)$ Å; $Z = 4$ and $d_{calc} = 4.260$ g cm^{-3}. The structure has been refined by least squares to $R = 0.038$ on the basis of 1330 independent reflections. The cesium ions are surrounded by eleven or by nine oxygen atoms with average metal-oxygen distances of 3.309(2) and 3.188(2) Å, respectively. The sulfate tetrahedra are almost regular with an average S – O distance of 1.477(2) Å. The compound is isostructural with β-K_2SO_4 and β-Rb_2SO_4.

The first X-ray diffraction studies of alkali sulfates were reported in 1916 by Ogg and Hopwood.[1] They had determined the unit cell dimensions for $(NH_4)_2SO_4$, β-K_2SO_4, β-Rb_2SO_4, and β-Cs_2SO_4, and thereby verified Tutton's suggestion [2] that the four sulfates were isomorphous. Later (in 1928) Ogg published a paper on the crystal structure of the four isomorphous sulfates.[3] The structures of $(NH_4)_2SO_4$ and β-K_2SO_4 have been reexamined several times, whereas a redetermination of the β-Rb_2SO_4 structure has not been carried out until recently.[4] A precise determination of the β-Cs_2SO_4 structure is reported in this investigation, which is a part of a program concerning the dimensions of the sulfate ion and the configuration of alkali-oxygen polyhedra.[4–8]

EXPERIMENTAL

The crystals used in this investigation were of *pro analysi* quality from Merck, Darmstadt. The X-ray powder pattern of the sample was in good agreement with the data published by Pannetier, Gaultier, and Tabrizi.[9] Values for the unit cell dimensions were calculated from the reflections of a photograph taken at 25 °C with strictly monochromatized Cu$K\alpha$ radiation ($\lambda = 1.5405$ Å) in a Guinier-Hägg type focusing camera. Potassium chloride ($a = 6.29294$ Å) [10] was used as an internal standard. The intensities and positions of the reflections on the photograph were determined by use of a computer-controlled SAAB film scanner and associated programs.[11] The lattice parameters were refined from 27 single-indexed reflections by the method of least squares as implemented in the program PIRUM.[12] The dimensions of the orthorhombic (*Pnam*) unit cell at 25 °C are: $a = 8.239(1)$, $b = 10.944(1)$, $c = 6.258(1)$ Å, and $V = 564.2$ Å^3. $Z = 4$ gives a calculated density of 4.260 g cm^{-3}. The values above are very close to those given by Pannetier *et. al.*;[9] *i.e.* $a = 8.235(1)$, $b = 10.940(3)$, and $c = 6.257(1)$ Å at room temperature.

Single crystal data. Single crystals of β-Cs_2SO_4 were prepared by the evaporation of an aqueous solution of the salt at about 0 °C over one week. The crystals were filtered off and washed with cold water. A small prismatic crystal with the approximate dimensions $0.07 \times 0.045 \times 0.12$ mm in the axial directions was mounted along the *c* axis and used for the collection of the intensity data.

The systematic absences are: $h0l$, $h \neq 2n$; and $0kl$, $k + l \neq 2n$, which is characteristic of the space group $Pna2_1$ and its centrosymmetric equivalent *Pnam*. Since β-Rb_2SO_4 (*cf.* Ref. 4) as well as β-K_2SO_4 (*cf.* Ref. 13) belong to space group *Pnam*, there is very little reason to believe that this should not be so for β-Cs_2SO_4 too. Moreover, the $N(z)$ test [14] applied to the complete data set clearly indicated a centric distribution. The space group *Pnam* (No. 62) was therefore chosen as the most probable.

Single-crystal data were collected on a Siemens automatic four-circle diffractometer equipped with a scintillation detector and a graphite monochromator, with Mo$K\alpha$ radiation ($\lambda = 0.7107$ Å). The $\theta - 2\theta$ scan technique was employed, with the five-values measuring procedure. The count was taken in steps of 0.01° with a step time of 1.2 s. Three strong reflections were measured every 5 h. Their

Table 1. Atomic coordinates and temperature factors for β-Cs_2SO_4 (*Pnam*). General equivalent positions 8(*d*): $\pm(x,y,z)$; $\pm(-x,-y,\frac{1}{2}+z)$; $\pm(\frac{1}{2}+x,\frac{1}{2}-y,\frac{1}{2}-z)$; $\pm(\frac{1}{2}-x,\frac{1}{2}+y,-z)$. The estimated standard deviations (within parentheses) refer to the last digit of the respective values. The anisotropic temperature factors are of the form $\exp[-(B_{11}h^2+B_{22}k^2+B_{33}l^2+2B_{12}hk+2B_{13}hl+2B_{23}kl)]$. The B_{ij} values below are multiplied by 10^4.

Atom	x	y	z	B_{11}	B_{22}	B_{33}	B_{12}	B_{13}	B_{23}
Cs(1)	0.6771(1)	0.4093(1)	$\frac{1}{4}$ [a]	70(1)	36(1)	92(1)	−1(1)	0 [a]	0 [a]
Cs(2)	−0.0112(1)	0.7015(1)	$\frac{1}{4}$ [a]	55(1)	35(1)	108(1)	1(1)	0 [a]	0 [a]
S	0.2411(2)	0.4172(1)	$\frac{1}{4}$ [a]	44(2)	23(1)	64(2)	0(1)	0 [a]	0 [a]
O(1)	0.0620(6)	0.4127(5)	$\frac{1}{4}$ [a]	34(5)	54(4)	217(15)	0(4)	0 [a]	0 [a]
O(2)	0.2973(7)	0.5460(4)	$\frac{1}{4}$ [a]	87(6)	25(3)	121(10)	−8(3)	0 [a]	0 [a]
O(3)	0.3035(4)	0.3558(3)	0.0570(5)	90(4)	40(2)	100(7)	4(2)	24(5)	−19(3)

[a] Parameter fixed by symmetry.

intensity variations lay within ±1 % during the complete run. All lattice points with h, k, $l \geq 0$ and $5° \leq \theta \leq 35°$ were measured. Of the 1330 independent non-extinct reflections, 803 (60 %) had $\sigma(I)/I \leq 0.10$ while 185 (14 %) had $\sigma(I)/I > \frac{1}{2}$ [$\sigma(I)/I$ is defined as $(I_{tot}+I_{back})^{\frac{1}{2}}/(I_{tot}-I_{back})$]. The net intensities were corrected for Lorentz, polarization, and absorption (μ = 133 cm^{-1}) effects with the program DATAPH (Coppens, Leiserowitz, Rabinovich, and Hamilton). The transmission factor A ($I = I_{obs}/A$) ranged from 0.350 to 0.567.

A general survey of the IBM 360/75 computer programs used in this work has been reported.[15]

STRUCTURE REFINEMENT

The structure was refined with the atomic parameters of rubidium sulfate [4] as a start. The program FALFA was used for the refinement; it is a local modification [16] of the full-matrix least-squares program LINUS (Busing, Martin, Levy, Hamilton, and Ibers). The atomic scattering factors for Cs^+, S^0, and O^-, with corrections for the real and imaginary part of the anomalous dispersion, were taken from the *International Tables*.[17-18]

The R value, $R = \sum||F_o|-|F_c||/\sum|F_o|$, dropped to 0.069 for the isotropic model and to 0.058 for the anisotropic model. However, inspection of the structure factor list showed that extinction effects were pronounced for some of the strongest, low-angle reflections. The most severe extinction occurred for the reflections (002) [$Q = |F_o/F_c| = 0.52$], (031) [Q = 0.61], (004), [$Q = 0.67$], and (211) [$Q = 0.67$].

From this stage, an isotropic secondary extinction parameter g [19] was included in the refinement, and the R value dropped to 0.038 for the model with anisotropic temperature factors. The refined value of the parameter g was 0.54 ± 0.04. The discrepancy between the observed and calculated structure factors for the above-mentioned four reflections decreased considerably [*e.g.* for reflection (002), Q = 0.956]. Refinements including anisotropic secondary extinction parameters [19] were also performed. However, the large correlation coefficients now appearing between some of the refined parameters, in addition to the insignificant improvement of the result, lead the author

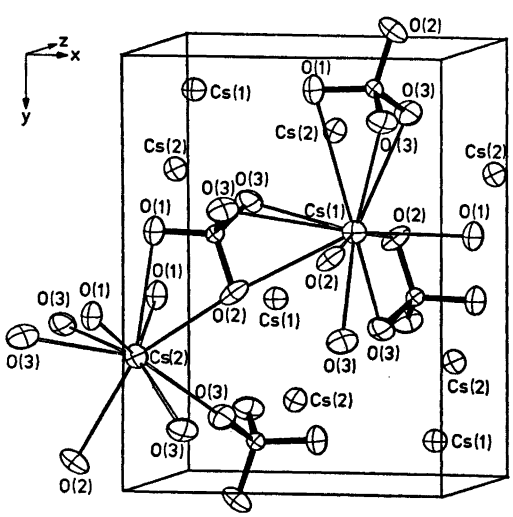

Fig. 1. ORTEP plot of the β-Cs_2SO_4 structure. The small ellipsoids represent sulfur atoms. For clarity only two cesium-oxygen polyhedra are shown.

Table 2. Interatomic distances (Å) and angles (°). Standard deviations are quoted in parentheses. All Cs–O distances <4.2 Å are given below. The S–O distances in square brackets have been corrected for thermal vibrations of the atoms according to the riding-motion model.[22]

Cs(1)–O(1)		3.172(5)		Cs(2)–O(2)		3.059(5)
–O(2)	(×2)	3.174(2)		–O(3)	(×2)	3.077(3)
–O(3)	(×2)	3.213(3)		–O(3′)	(×2)	3.144(3)
–O(3′)	(×2)	3.311(3)		–O(2′)		3.182(5)
–O(3″)	(×2)	3.358(3)		–O(1)		3.218(6)
–O(2′)		3.468(6)		–O(1′)	(×2)	3.395(2)
–O(1′)		3.649(6)		Average:		3.188(2)
Average:		3.309(2)				
S–O(1)		1.476(5)	[1.493]	O(1)–O(2)		2.426(7)
S–O(2)		1.484(5)	[1.493]	O(1)–O(3)	(×2)	2.409(5)
S–O(3)	(×2)	1.475(3)	[1.486]	O(2)–O(3)	(×2)	2.407(5)
Average:		1.477(2)	[1.490]	O(3)–O(3′)		2.416(6)
				Average:		2.412(3)
O(1)–S–O(2)		110.1(3)				
O(1)–S–O(3)	(×2)	109.5(2)				
O(2)–S–O(3)	(×2)	108.9(2)				
O(3)–S–O(3′)		110.0(3)				
Average:		109.5(1)				

Table 3. Comparison among three isostructural compounds β-M_2SO_4 (M = K, Rb, and Cs). Values calculated by the author from parameters given in Refs. 4 and 13 are denoted by asterisks.

Compound	β-K_2SO_4 [a]	β-Rb_2SO_4 [b]	β-Cs_2SO_4 [c]
Unit cell dimensions			
a (Å)	7.476(3)	7.813(1)	8.239(1)
b (Å)	10.071(4)	10.426(2)	10.944(1)
c (Å)	5.763(2)	5.969(1)	6.258(1)
V (Å³)	433.9*	486.2*	564.2
Uncorrected distances (Å)			
Metal-oxygen			
M(1)–O, average (11-coord.)	3.030(2)*	3.143(3)	3.309(2)
M(2)–O, average (9-coord.)	2.865(2)*	3.003(3)	3.188(2)
Sulfur-oxygen			
S–O(1)	1.459(4)	1.492(9)	1.476(5)
S–O(2)	1.473(4)	1.473(9)	1.484(5)
S–O(3) (×2)	1.472(5)	1.466(7)	1.475(3)
S–O average distance	1.469(2)	1.474(4)	1.477(2)
Oxygen-oxygen			
Average O–O in the SO_4 group	2.399(2)*	2.408(5)*	2.412(3)
Corrected distances (Å) Riding-motion model, S–O average distance	1.481*	1.487	1.490
R.m.s. radial thermal displacements (Å)			
M(1)	0.262*	0.236*	0.253
M(2)	0.249*	0.251*	0.247
S	0.211*	0.183*	0.204
O(1)	0.293*	0.280*	0.296
O(2)	0.273*	0.266*	0.263
O(3)	0.291*	0.272*	0.274

[a] Ref. 13. [b] Ref. 4. [c] This work.

to regard the isotropic-extinction model as the most reliable one. In this refinement Hughes' weighting function [20] with $h=4$ and $F_{o,min}=20$ was used for the 1145 "significant" reflections with $\sigma(I)/I \leq \frac{1}{3}$, while zero weights were assigned to the 185 "insignificant" reflections with $\sigma(I)/I > \frac{1}{3}$. The atomic parameters obtained in the refinement are listed in Table 1. The structure factor list can be obtained at request.

DESCRIPTION AND DISCUSSION OF THE STRUCTURE

The present work shows that Ogg's atomic positions [3] from 1928 were essentially correct. β-Cs_2SO_4 is isostructural with β-Rb_2SO_4, β-K_2SO_4, and many other compounds.[21] An ORTEP [22] plot of the structure is shown in Fig. 1. The structure is pseudo-hexagonal with $b/c = 1.7488 \approx 3\frac{1}{2}$.

Some interatomic distances (uncorrected) and angles are listed in Table 2. The S – O distances have also been corrected for the thermal vibrations of the atoms according to the riding-motion model [23] by use of the program ORFFE (Busing, Martin, and Levy). The sulfate tetrahedra are almost regular with an average S – O distance of 1.477(2) Å (uncorrected). They have a crystallographically imposed m symmetry. The cesium ions are surrounded in an irregular way by either eleven or nine oxygen atoms. The average Cs – O distances are 3.309(2) Å (11-coordination) and 3.188(2) Å (9-coordination), respectively.

Table 3 contains a comparison of the three isostructural compounds β-K_2SO_4 (Ref. 13), β-Rb_2SO_4 (Ref. 4), and β-Cs_2SO_4 (this work). It comprises the unit cell dimensions, some interatomic distances, and the r.m.s. radial thermal displacements of the atoms. The table shows a strong correlation between the increase in metal-oxygen distances and the increase in unit cell dimensions. As the metal-oxygen distances increase about 5 %, there is a corresponding increase in the order of 4 – 6 % for each unit cell edge. There is also a slight, though hardly significant, indication that the dimensions of the sulfate ions should increase a little as the size of the cations in the β-M_2SO_4 structure increases. An accurate structure analysis of the isostructural compound Tl_2SO_4, where the cations are about the same size as Rb^+, might be of interest in this respect.

The r.m.s. radial thermal displacements are rather similar for all crystallographically analogous atoms in the three β-M_2SO_4 structures; the analogous atoms vibrate almost identically. It should be noted, however, that the reflection data for β-K_2SO_4 were not corrected for absorption [$\mu(MoK\alpha) = 24.9$ cm^{-1}].[13] The data for β-Rb_2SO_4 have been treated in almost the same manner as described here for β-Cs_2SO_4.

Acknowledgements. The author would like to thank Professor Peder Kierkegaard for encouraging and valuable discussions concerning this work. Sincere thanks are also due to Dr. Donald F. Koenig, who carefully revised the English of this article. Finally the author is most grateful to Mrs. Stina Nord for her skilful technical assistance in the photographic X-ray recordings.

This work has been financially supported by the Swedish Natural Science Research Council.

REFERENCES

1. Ogg, A. and Hopwood, F. L. *Phil. Mag. 32* (1916) 518.
2. Tutton, A. E. H. *Crystalline Structure and Chemical Constitution*, McMillan, London 1910.
3. Ogg, A. *Phil. Mag. 5* (1928) 354.
4. Nord, A. G. *Acta Crystallogr. B 30* (1974) 1640.
5. Nord, A. G. *Chem. Commun. Univ. Stockholm* (1973) No. 3.
6. Nord, A. G. *Acta Chem. Scand. 27* (1973) 814.
7. Nord, A. G. Dissertation, *Chem. Commun. Univ. Stockholm* (1974) No. 12.
8. Nord, A. G. *Acta Crystallogr. A 31* Part S3 (1975) S 79.
9. Pannetier, G., Gaultier, M. and Tabrizi, D. *Bull. Soc. Chim. Fr.* (1968) 935.
10. Hambling, P. G. *Acta Crystallogr. 6* (1953) 98.
11. Malmros, G. and Werner, P. E. *Acta Chem. Scand. 27* (1973) 493.
12. Werner, P. E. *Ark. Kemi 31* (1969) 513.
13. McGinnety, J. A. *Acta Crystallogr. B 28* (1972) 2845.
14. Howells, E. R., Phillips, D. C. and Rogers, D. *Acta Crystallogr. 3* (1950) 210.
15. Nord, A. G. *Chem. Commun. Univ. Stockholm* (1973) No. 15.
16. Koenig, D. F. *Private communication.*
17. *International Tables for X-ray Crystallography*, Kynoch Press, Birmingham 1974, Vol. IV, Table 2.2A.
18. *Ibid.* 1968, Vol. III, Table 3.3.2C.
19. Coppens, P. and Hamilton, W. C. *Acta Crystallogr. A 26* (1970) 71.

20. Hughes, E. W. *J. Amer. Chem. Soc. 63* (1941) 1737.
21. Wyckoff, R. W. G. *Crystal Structures*, 2nd Ed., Wiley, New York 1965, Vol. 3.
22. Johnson, C. K. *AEC Accession No. 33516*, ORNL-3794, Oak Ridge 1965.
23. Busing, W. R. and Levy, H. A. *Acta Crystallogr. 17* (1964) 142.

Received August 8, 1975.

Acta Chemica Scandinavica A 30 (1976) 203—208

Reaction Rate Studies of the Acid Hydrolysis of Some Chromium(III) Complexes. VI. Acid Dissociation and Structure of 1,4,7,10-Tetraazadecanechromium(III) Complexes in Aqueous Perchloric Acid

L. MØNSTED and O. MØNSTED

Chemistry Department I (Inorganic Chemistry), University of Copenhagen, H. C. Ørsted Institute, Universitetsparken 5, DK-2100 Copenhagen Ø, Denmark

The chromium(III) 1,4,7,10-tetraazadecane ($H_2NCH_2CH_2NHCH_2CH_2NHCH_2CH_2NH_2$) species postulated by earlier workers to be the *mer*-triaqua(1-azonia-4,7,10-triazadecane) chromium(III) ion has been shown by potentiometric titrations to be the *cis*-diaqua(1,4,7,10-tetraazadecane)chromium(III) ion. Acidity constants and visible absorption spectra of this tetraamine ion are reported and compared with values for other tetraaminediaquachromium(III) species. Reinterpretation of earlier kinetic data necessitated by the above reformulation reveals not only that dechelation in acid solution of the 1,4,7,10-tetraazadecane ligand bound to chromium(III) takes place preferentially from the secondary amino groups, but also that the species thus initially formed reacts rapidly further to give a diaminetetraaquachromium(III) species.

For chromium(III) hydrolysis and isomerization reactions quantitative kinetic data exist in the literature for complexes of amine ligand pairs of the type RR'NH and $RR'NCH_2CH_2NH_3^+$. A summary of these data is given in Table 1. The pronounced difference between the kinetic behaviour of the first three reactant pairs and that attributed to the *mer* complexes is noteworthy. To us, this difference appeared difficult to explain in terms of the accepted structures of the reactants, and therefore it was decided to investigate the chromium(III) 1,4,7,10-tetraazadecane complexes in greater detail.

EXPERIMENTAL

Chemicals. Most chemicals employed have been described earlier.[5,6] *cis*-$[Cr(trien)Cl_2]Cl$ [7] and *cis*-$[Cr(trien)F_2]ClO_4$ [8] were prepared according to literature methods and the latter compound converted to *cis*-$[Cr(trien)Cl_2]ClO_4$ and *cis*-$[Cr(trien)Br_2]ClO_4$ by reacting the difluorido compound with concentrated hydrochloric or hydrobromic acid, respectively.[9]

Preparation of solutions. Preparation of the tetraammine- and the bis(1,2-ethanediamine)-chromium(III) solutions employed in the titration experiments have been described earlier.[5,6]

cis-*Diaqua(1,4,7,10-tetraazadecane)chromium(III).* About 100 mg of solid *cis*-dibromido(1,4,7,10-tetraazadecane)chromium(III) perchlorate was treated with 1 ml 1 M sodium hydroxide solution for 3 min at room temperature. The resulting solution was cooled in ice and acidified with 70 % perchloric acid. Unreacted dibromidoperchlorate complex was filtered off, and after dilution to about 10 ml with water the solution containing the complex was charged onto a 2 cm × 10 cm SP-Sephadex C-25 column. The column was operated at 0 °C and 0.75 M sodium perchlorate solution made 1 – 3 mM acid with perchloric acid eluted the different chromium(III) 1,4,7,10-tetraazadecane complexes essentially as described by Garner *et al.*[10] except that these authors used 1.25 to 4 M perchloric acid and Dowex AG50 W-X2 columns.

fac-*Triaqua(1-azonia-4,7,10-triazadecane)-chromium(III).* A mixture of this ion and the *cis*-diaminetetraaquachromium(III) isomers of the tetraamine ligand was prepared by rapidly heating an acid solution of impure tetraaminediaquachromium(III) ions, prepared by the method described above, to 100 °C and then

Table 1. Rate constants for reactions of some amine aqua chromium(III) complexes.

Complex [a]	10^6k (60 °C) (s^{-1})	Rate constant ratio	Ref.
Hydrolysis reactions			
$[Cr(a)(aq)_5]^{3+}$	0.31	0.17	1
$[Cr(enH)(aq)_5]^{4+}$	1.9		2
$[Cr(en)(aq)_4]^{3+}$	3.0	0.14	2
$[Cr(dienH)(aq)_4]^{4+}$	22		3
fac-$[Cr(dien)(aq)_3]^{3+}$	59	0.45	3
fac-$[Cr(trienH)(aq)_3]^{4+}$	130		4
mer-$[Cr(dien)(aq)_3]^{3+}$	16 000	13	3
mer-$[Cr(trienH)(aq)_3]^{4+}$	1 200		4
Isomerization reactions			
mer-$[Cr(dien)(aq)_3]^{3+}$	unobserved		3
mer-$[Cr(trienH)(aq)_3]^{4+}$	370		4

[a] The following abbreviations for the names of the ligands are used throughout this paper: a = ammonia, aq = water, en = 1,2-ethanediamine, enH = 2-aminoethylammonium ion, dien = 1,4,7-triazaheptane, dienH = 1-azonia-4,7-diazaheptane, trien = 1,4,7,10-tetraazadecane, and trienH = 1-azonia-4,7,10-triazadecane.

rapidly cooling the solution. From this mixture the individual complexes were prepared pure in solution by the chromatographic method described above for the tetraaminediaqua complex.

The visible absorption spectra of the solutions prepared by the above methods are given in Fig. 1. From the spectral characteristics in Table 2 it is concluded that the species generated by base hydrolysis of the *cis*-dibromido-(1,4,7,10-tetraazadecane)chromium(III) ion is identical to the one produced either by base hydrolysis or by mercury(II) accelerated chloride ligand hydrolysis of the *cis*-dichlorido-(1,4,7,10-tetraazadecane)chromium(III) ion.[10]

Spectral measurements. All visible absorption spectra were measured on a modified Cary 118C spectrophotometer at room temperature (23 ± 2 °C).

Potentiometric measurements. The pH measurements were carried out using a Radiometer PHM52 pH-meter equipped with a G202C glass electrode and a K401 calomel electrode both also from Radiometer. In the latter electrode the initial saturated potassium chloride electrode solution was replaced with 1.0 M sodium chloride solution. All measurements were carried out at 25.00 ± 0.05 °C, by titrating 25 ml of solutions 1 to 4 mM in chromium complex and 1.0 M in sodium perchlorate by 1.0 M sodium hydroxide solution. Since the complexes studied decompose noticeably at 25 °C fast titrations and consequently rapid electrode response were essential. For the electrode used pH measurements less than a 0.001 pH-unit from the final reading was obtained in less than 5 s. Consequently full titration curves of approximately 30 to 40 individual measurements could be obtained in 5 – 10 min.

Methods of analysis were essentially as described previously.[1]

Method of calculation. The primary experimental material for one titration curve con-

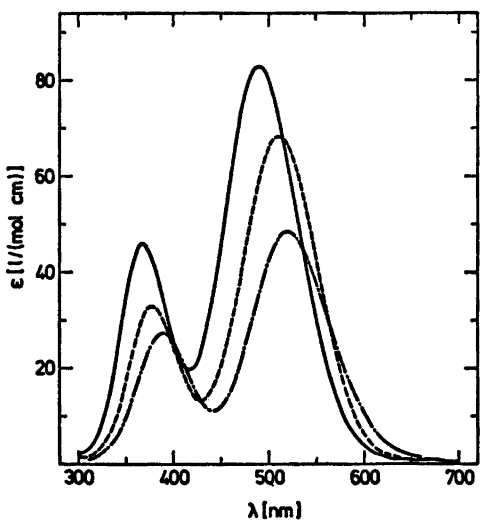

Fig. 1. Visible absorption spectra of compounds prepared and purified as described in the text. ——, *cis*-$[Cr(trien)(aq)_2]^{3+}$; - - -, *fac*-$[Cr(trienH)(aq)_3]^{4+}$; and ···, *cis*-$[Cr(trienH_2)(aq)_4]^{5+}$.

Table 2. Comparison with literature values of spectral characteristics of compounds prepared and purified as described in the text.

Complex	Medium[a]	λ_1 max (nm)	ε_1 max [l/(mol cm)]	λ_2 max (nm)	ε_2 max [l/(mol cm)]	ε_1 max/ ε_2 max	Ref.
cis-[Cr(trien)(aq)$_2$]$^{3+}$	A	490	82.7	367	45.4	1.82	[b]
	B	493	82.9	368	45.5	1.82	10[c]
fac-[Cr(trienH)(aq)$_3$]$^{4+}$	A	511	67.8	375	32.9	2.06	[b]
	B	513	72.0	375	35.6	2.02	10
cis-[Cr(trienH$_2$)(aq)$_4$]$^{5+}$	A	520	48.2	388	27.1	1.78	[b]
	B	522	48.7	389	27.5	1.77	10

[a] A, 0.5 M $HClO_4$ + 0.4 M $NaClO_4$; B, 2 M $HClO_4$. [b] This work. [c] Reported as *mer*-[Cr(trienH)(aq)$_3$]$^{4+}$ in this reference.

sisted of one initial volume, one base titrator concentration, and a series of potential differences (E) measured as function of the volume of added base (v), as well as estimated variances upon these same quantities (σ_E^2,σ_v^2).

Parameters were estimated by regression analysis, which for practical purposes for these data is equivalent to minimization of:

$$s^2 = \sum[\{E(\text{obs}) - E(\text{calc})\}^2/\{\sigma_E^2 + \left(\frac{dE}{dv}\right)^2 \sigma_v^2\}]$$

where the summation extends over all experiments of one titration curve.

The potential differences were calculated from the hydrogen ion concentrations of the solutions, and the hydrogen ion concentrations were calculated from the acidity constants of the weak acid investigated, the ionic product of water and the concentrations of weak acid and excess strong acid in the initial solution. Combination of the relevant mass action expressions with the expression for the potential differences in terms of the hydrogen ion concentrations in the initial solution (h_0) and in the i'th solution (h_i):

$$E_i = \Delta E + \alpha RT \ln \{(h_i + \gamma)/(h_0 + \gamma)\}/F \qquad (1)$$

yielded a nonlinear equation which was solved by Newtons algoritm. In eqn. 1 α and γ are measures of glass electrode deviations from ideal behaviour in terms of a reduced response ($\alpha RT/F$) relative to that expected theoretically (RT/F), and sodium ion error (γ), taken to be constant since only solutions with the sodium ion concentration equal to 1.0 mol/l were investigated. The term governed by the ΔE parameter is necessary as a fitting term since standardized potentials were not measured, as we were only interested in concentration acidity constants. For a divalent acid eight parameters were consequently to be determined. This was accomplished without difficulty from initial parameter values estimated by inspection of the titration curves. In Fig. 2 is shown the agreement between the experimental and the calculated titration curves for the *cis*-diaqua(1,4,7,10-tetraazadecane)chromium(III) complex.

It was not attempted to estimate the absolute magnitudes of σ_E and σ_v. The variances were, however, assumed to be constant for all titration points. Then only the ratio $\sigma_E\sigma_v$ was essential to the calculations and it was estimated to have the value 1.5 mV/μl (*cf.* Fig. 2). Since

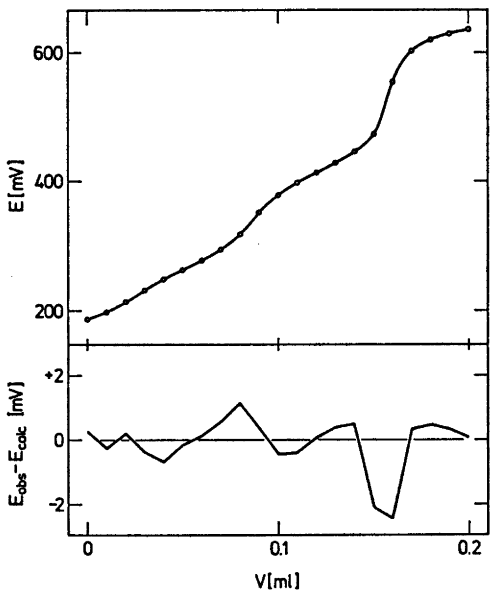

Fig. 2. Upper part: Experimental (O) and calculated (——) titration curve for *cis*-[Cr(trien)(aq)$_2$]$^{3+}$. Lower part: Differences between experimental and calculated titration curves.

absolute values for the variances were not estimated, a χ^2 test of the goodness of the fit between experiments and model could not be carried out. A reverse estimation is however possible, and it was found that in order to have $P\{\chi^2 < s^2\} \sim 50$ %, a value of σ_E about 0.4 mV is estimated. This value is not unreasonable, in particular if the somewhat unstable systems are borne in mind.

The calculational approach outlined above parameterizes a fair amount of possible systematic errors as, *e.g.*, strongly acid or basic impurities in the medium or the solid salts employed. Also the utilization of concentration acidity constants as well as the direct determination of the α parameter from the titration curves eliminates all systematic errors associated with the use of standard buffer solutions. It was also attempted to parameterize possible systematic errors due to absorbed carbon dioxide in solvent and sodium hydroxide titrator solution. For this the acid dissociation constants of carbon dioxide measured by Sillén *et al.*[11] ($pK_1 \sim 6.04$ and $pK_2 \sim 9.57$) in 1 M sodium perchlorate solution at 25 °C were used. The agreement between model and experiments was, however, not significantly improved, and from the estimated parameter values it seemed as if the parameter values rather than arising from carbon dioxide should be attributed to minor amounts of ammonia or amines generated by decomposition reactions of the investigated complexes. It was, however, reassuring to note the independence of the estimated acid dissociation constants upon this kind of systematic error.

These estimated concentration acid dissociation constants, determined from at least two full titration curves for each complex, are given in Table 3. In addition to these parameters the following ones, common to all the experiments were estimated: $\alpha \sim 0.964 \pm 0.008$, $\gamma \sim 10^{-12.08 \pm 0.09}$ mol/l and $K_w \sim 10^{-13.82 \pm 00.7}$ mol^2/l^2. Of these parameters the first two appear reasonable and the last is essentially in agreement with the values $10^{-13.80}$ mol^2/l^2 [12] and $10^{-13.95}$ mol^2/l^2,[13] earlier determined in a 1.0 M sodium perchlorate medium. By inspection of thse parameters and those of Table 3 the estimated standard deviations of both the log K_w and log K_2 values are seen to be somewhat larger than those estimated for the log K_1 values, as is to be expected.

RESULTS AND DISCUSSION

The titration curve, given in Fig. 2, of the species generated by base hydrolysis of the *cis*-dibromido(1,4,7,10-tetraazadecane)chromium(III) ion shows that it is a divalent acid. The close similarity between the acid dissociation constants of this ion and the *cis*-tetraamminediaqua- and the *cis*-diaquabis(1,2,-ethanediamine)chromium(III) ions given in Table 3 confirms our hypothesis that the species in question is not a *mer* triaqua complex as claimed earlier, but rather the *cis*-diaqua(1,4,7,10-tetraazadecane)chromium(III) ion.

Additional but less conclusive evidence comes from comparisons between elution behaviour and spectral characteristics of 1,4,7,10-tetraazadecane- and 1-azonia-4,7,10-triazadecane complexes which might reasonably be expected to resemble bis(1,2-ethanediamine)- and (2-aminoethylammonium)(1,2-ethanediamine) complexes, respectively.

Since the *mer*- and *fac*-(2-aminoethylammonium)triaqua-(1,2-ethanediamine)chromium(III) complexes are only partly separated by the technique which clearly separates these two ions from the *cis*-diaquabis(1,2-ethanediamine)chromium(III) complex and also separates the *fac*-triaqua(1-azonia-4,7,10-triazadecane)chromium(III) ion from the complex ion in question, a tripositive tetraaminediaqua structure of the latter complex is a reasonable

Table 3. Estimated concentration acidity constants (mean values ± standard deviations of the mean values) for some *cis*- and *trans*-tetraaminediaquachromium(III) complexes in 1.0 M sodium perchlorate solution at 25 °C.

Complex	$-\log K_1$[a]	$-\log K_2$[a]
cis-$[Cr(a)_4(aq)_2]^{3+}$	4.961 ± 0.015	7.53 ± 0.03
cis-$[Cr(en)_2(aq)_2]^{3+}$	4.75 ± 0.03	7.35 ± 0.05
cis-$[Cr(trien)(aq)_2]^{3+}$	4.47 ± 0.03	7.14 ± 0.05
trans-$[Cr(a)_4(aq)_2]^{3+}$	4.376 ± 0.014	7.78 ± 0.04
trans-$[Cr(en)_2(aq)_2]^{3+}$	4.118 ± 0.015	7.71 ± 0.05

[a] The K's are measured in mol/l.

Table 4. Comparison between spectral characteristics of some *cis*-bis(1,2-ethanediamine)- and some *cis*-(1,4,7,10-tetraazadecane)chromium(III) complexes.

Complex	λ_1 max (nm)	λ_2 max (nm)	Ref.
cis-$[Cr(en)_2F_2]^+$	517	378	14
cis-$[Cr(trien)F_2]^+$	523	374	8
cis-$[Cr(en)_2Cl_2]^+$	528	401	[a]
cis-$[Cr(trien)Cl_2]^+$	534	397	[a]
cis-$[Cr(en)_2(aq)_2]^{3+}$	486	368	6
cis-$[Cr(trien)(aq)_2]^{3+}$	490	367	[a]

[a] This work.

Table 5. Comparison between the position of the second spin-allowed absorption band of some isomeric triaminetriaqua chromium(III) complexes.

Complex	λ_2 *fac* (nm)	λ_2 *mer* (nm)	Ref.
$[Cr(a)_3(aq)_3]^{3+}$	374	376	5
$[Cr(en)(enH)(aq)_3]^{4+}$	378	380	6
$[Cr(dien)(aq)_3]^{3+}$	375	390	10
$[Cr(trienH)(aq)_3]^{4+}$	375	[367][a]	10

[a] This value refers to *cis*-$[Cr(trien)(aq)_2]^{3+}$ which in Ref. 10 is supposed to be the *mer*-$[Cr(trienH)(aq)_3]^{4+}$ ion.

supposition. This view is also supported by the fact that spectral differences similar to those observed for the difluorido and dichlorido tetraamine pairs both of known constitution are also found when the supposed *cis*-diaqua-(1,4,7,10-tetraazadecane) complex is compared to the *cis*-diaquabis(1,2-ethanediamine) complex. In all three cases the first spin allowed absorption band is shifted towards the red and the second towards the blue when the 1,4,7,10-tetraazadecane complexes are compared to the bis(1,2-ethanediamine) complexes (Table 4). Further evidence comes from a comparison between some isomeric triaminetriaquachromium(III) complexes. For the isomer pairs of known constitution a spectral shift towards the red of the second spin-allowed absorption band of *mer* isomers compared to the corresponding *fac* isomers has been observed (Table 5). This fact also makes it less likely that the species investigated is a *mer*-triaminetriaqua isomer.

The reformulation of the structure of the initial reactant species of the earlier kinetic investigations necessarily leads to a modification of the reaction scheme. The fact that both *fac*-triamine- and *cis*-diaminechromium(III) ions are produced simultaneously from the tetraamine isomer, combined with the generally accepted hypothesis that multiple metal ligand bond breaking reactions occur stepwise, makes it necessary to postulate the existence of a triamine species different from the one actually isolated from hydrolyzed tetraamine solutions. The simplest hypothesis about the structure of this species is, that it is a triamine isomer formed by hydrolysis of a secondary amine nitrogen atom. Intuitively this hypothesis rationalizes the high reactivity because of which this species has so far escaped detection. The reformulated reaction scheme is shown in Fig. 3. It should be noted that this modification of the reaction scheme in no way affects the numerical values for rate constants or activation energies but assigns these values to other reactions. The possibility may now be envisaged that a reinterpretation similar to the one given here

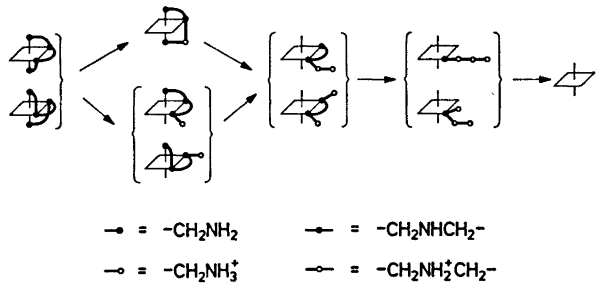

Fig. 3. Reaction scheme so far elucidated for the acid hydrolysis of 1,4,7,10-tetraazadecane complexes of chromium(III) (see text).

for the aqua-1,4,7,10-tetraazadecane complexes may also apply to the kinetic results for the aquaazido-1,4,7,10-tetraazadecane complexes,[15] in which system the initial reaction is said exclusively to be a *mer* to *fac* isomerization reaction.

REFERENCES

1. Mønsted, L. and Mønsted, O. *Acta Chem. Scand. 27* (1973) 2121.
2. Childers, Jr., R. F., Vander Zyl, Jr., K. G., House, D. A., Hughes, R. G. and Garner, C. S. *Inorg. Chem. 7* (1968) 749.
3. Lin, D. K. and Garner, C. S. *J. Amer. Chem. Soc. 91* (1969) 6637.
4. Kamp, D. A., Wilder, R. L., Tang, S. C. and Garner, C. S. *Inorg. Chem. 10* (1971) 1396.
5. Mønsted, L. and Mønsted, O. *Acta Chem. Scand. A 28* (1974) 23.
6. Mønsted, L. and Mønsted, O. *Acta Chem. Scand. A 29* (1975) 29.
7. House, D. A. and Garner, C. S. *J. Amer. Chem. Soc. 88* (1966) 2156.
8. Glerup, J., Josephsen, J., Michelsen, K., Pedersen, E. and Schäffer, C. E. *Acta Chem. Scand. 24* (1970) 247.
9. Pedersen, E. *Acta Chem. Scand. 24* (1970) 3362.
10. Wilder, R. L., Kamp, D. A. and Garner, C. S. *Inorg. Chem. 10* (1971) 1393.
11. Frydman, M., Nilsson, G., Rengemo, T. and Sillén, L. G. *Acta Chem. Scand. 12* (1958) 878.
12. Fischer, R. and Byé, J. *Bull. Soc. Chim. Fr.* (1964) 2920.
13. Anderegg, G. *Helv. Chim. Acta 50* (1967) 2333.
14. Glerup, J. *Unpublished measurements.*
15. Tang, S. C., Lum, S., Kamp, D. A., Wilder, R. L. and Garner, C. S. *J. Inorg. Nucl. Chem. 34* (1972) 3177.

Received August 18, 1975.

Acta Chemica Scandinavica A 30 (1976) 209—218

Conformational Analysis. XI. The Molecular Structure, Torsional Oscillations, and Conformational Equilibria of Gaseous Tetrakis-(bromomethyl)methane, $C(CH_2Br)_4$, as Determined by Electron Diffraction and Compared with Molecular-Mechanics Calculations

STEINAR RUSTAD and REIDAR STØLEVIK

Department of Chemistry, University of Oslo, P.O.Box 1033, Blindern, Oslo 3, Norway

Gaseous $C(CH_2Br)_4$ has been studied by electron diffraction. Two conformers named *D* (D_{2d} symmetry) and *S* (S_4 symmetry) were detected. The results are presented with error limits (2σ). The following values for distances (r_g) and angles ($\angle_\alpha$) are appropriate for the structure of both conformers: $r(C-H) = 1.09(5)$ Å, $r(C-C) = 1.554(9)$ Å, $r(C-Br) = 1.951(8)$ Å, $\angle CCBr = 114.2°(0.8)$, $\angle CCH = 111.7°(3.2)$. *D* and *S* have a tetrahedral arrangement of carbon atoms and all-staggered (1:2) conformations which do not possess parallel (1:3) Br···Br interactions. Torsional force constants and vibrational frequencies for both conformers have been estimated. The composition at 140 °C is 42(2) % of *S* and 58(2) % of *D*. As predicted by the molecular-mechanics calculations, conformers possessing parallel (1:3) Br···Br interactions are not present in detectable amounts. To a large extent the structural parameters obtained by the molecular-mechanics calculations reasonably agree with the experimental results.

I. INTRODUCTION

This work is part of a systematic conformational study of halogenated propanes and related molecules by electron diffraction in the gas phase. Results for the following molecules have been published: $[CH_2Br-CHBr-CH_2Br]$,[1] $[C(CH_2Cl)_4]$,[2] $[(CH_3)_2C(CH_2Cl)_2]$,[3] $[CH_3-C(CH_2Cl)_3]$,[4] $[CH_2Br-CH_2-CH_2Br]$,[5] $[CH_2Cl-CHCl-CH_2Cl]$,[6] $[CCl_3-CCl_2-CCl_3]$,[9] $[CCl_3-CCl_2-CHCl_2]$,[6] $[CCl_3-CH_2-CHCl_2]$,[8] $[CHCl_2-CCl_2-CHCl_2]$.[10]

$C(CH_2X)_4$(X = F, Cl, Br, I) compounds will be referred to in general as TMX. The number of possible staggered conformers in TMX is 81, but only six are spectroscopically distinguishable.[2] All conformers, except two, have one or more parallel (1:3) X···X interactions. The two exceptions are shown in Fig. 1, and these conformers will be referred to as **D** (possessing D_{2d} symmetry) and **S** (possessing S_4 symmetry), respectively.

$TMCl$[2] has been studied by electron diffraction. Only two conformers (**D** and **S**) were detected. **D** and **S** are present in *equal* amounts at a temperature of 105 °C. References to structural work on TMBr, spectroscopic studies, and measurements of dipole moments, are found in Ref. 2. However, the conformational equilibria of TMBr were not quantitatively described before the present work.

II. CALCULATION OF CONFORMATIONAL ENERGIES, GEOMETRIES, BARRIERS, AND TORSIONAL FORCE CONSTANTS

The semi-empirical energy model corresponds to molecular-mechanics calculations, including atom-atom potentials and valence force constants as described in Ref. 1. Energy parameters were taken from the work of Abraham and Parry,[11] and the valence force constants in Table 4 were used. The "normal" values of the geometry parameters are given in Table 1. In minimizing the energy, the geometry was constrained in the same way as described in Sect. V-A, except that all torsion angles were ad-

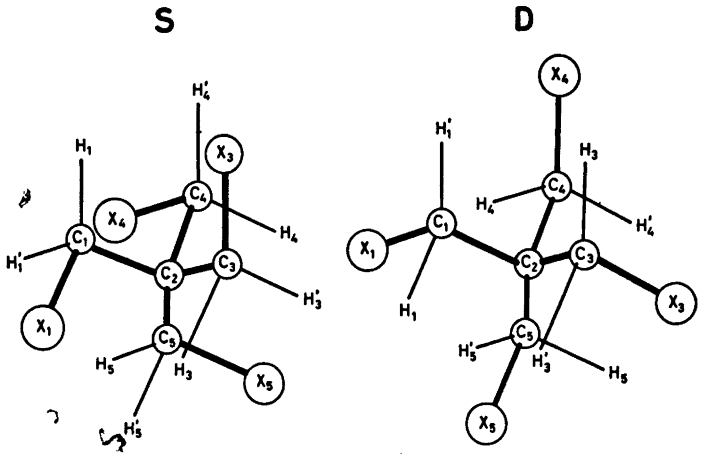

Fig. 1. Numbering of atoms in the two conformers **D** and **S** of $C(CH_2X)_4$. The conformer **D** has D_{2d} symmetry: three C_2 (mutually perpendicular), one S_4 (coincident with one C_2), two σ_d (through S_4). The **S** conformer has S_4 symmetry: one S_4 coincident with one C_2.

justed as independent variables. The conformational geometries derived from the semi-empirical energy model are present in Table 1. Calculated structure parameters indicate small deviations from staggered geometry in the conformer **S**, while there are no such deviations indicated for conformer **D**. Moreover, small deviations from a tetrahedral carbon framework are indicated for both **D** and **S**. The same indications were observed for TMCl.[3]

According to the present energy model, conformer **S** is 0.51 kcal/mol (Table 2) more stable than conformer **D**, while the corresponding value for TMCl [3] is 0.75 kcal/mol.

The conformers with *one* parallel (1:3) X···X interaction have their torsion angles displaced from staggered values. The energy of these conformers is thereby considerably lowered. However, the lowest energy obtained by minimalization was still more than 5 kcal/mol higher than the value for the conformer **D**. The calculations also lead to the conclusion that the *eclipsed* conformer of lowest energy is about 5 kcal/mol less stable than conformer **D**.

Some of the torsional barriers have to be high, and probably all of them are too high to be detected by electron diffraction. Nevertheless, NMR studies might lead to some information. Therefore, it is of interest to estimmate the value of the *lowest* barrier height when a conformation **S** is changed into **D** by rotations of $-CH_2X$ groups around the C–C

Table 1. Calculated geometries for the conformers **D** and **S** of $C(CH_2Br)_4$.

Type of parameter	"Normal" value	D	S
C–H (Å)	1.094	1.093	1.093
C–C (Å)	1.513	1.537	1.536
C–X (Å)	1.935	1.945	1.945
$C_1C_2C_3$ (°)	109.47	107.7	110.9
CCX (°)	109.47	113.0	112.9
CCH (°)	109.47	110.1	110.1
ϕ_{1-2} (°)	(−)[a]	0.0[b]	+123.5[c]
ϕ_{2-2} (°)	(−)	0.0	+123.5
ϕ_{4-2} (°)	(−)	0.0	−123.5
ϕ_{5-2} (°)	(−)	0.0	−123.5

[a] Torsion angles were adjusted as four independent variables for each conformer. [b] No deviation from staggered values. [c] Staggered values $|\phi| = 120°$.

Table 2. Calculated conformational energies (in kcal/mol) in $C(CH_2Br)_4$.

Type of energy	D	S
E (bonded)	2.70	2.58
E (van der Waals)	2.22	2.17
E (polar: X···H)	−15.50	−15.66
E (polar: X···X)	8.66	8.48
E (total)	−1.92	−2.43

bonds. If high barriers are to be avoided, then conformational minima, corresponding to conformers of low symmetry (C_1), are always reached before **S** is changed into **D** by rotations around C–C bonds. The conformers **S** and **D** are thus separated by double-maxima as indicated below:

S(0)→MAX(10.7)→C_1(5.6)→MAX(10.7)→**D**(0.5)

The energy values (kcal/mol) relative to the conformer **S** are shown in parentheses. The corresponding values for TMCl [2] are:

0→18→6→18→0.8.

Valence force constants were *numerically* computed from the energy model. Torsional force constants are given in Table 3.

III. CALCULATION OF VIBRATIONAL QUANTITIES

Valence force constants, except for the torsional part, were taken from the works of Schachtschneider [12] and Snyder.[13] The final force constant values used are shown in Table 4.

The normal coordinate program described by Gwinn [14] was used in computing vibrational frequencies.

Table 3. Calculated torsional force constants (in mdyn Å(rad)²) for conformers of $C(CH_2Br)_4$.

	D	**S**
F_ϕ (diagonal)[a]	0.26	0.25
$F_{\phi\phi'}$ (AA)[b]	−0.012	–
$F_{\phi\phi'}$ (AG)[b]	–	−0.040
$F_{\phi\phi'}$ (GG)[b]	−0.048	−0.032
$F(++++)$[c]	0.62	0.57
$F(++--)$[c]	1.38	1.21
$F(+-00)$[c]	0.54[d]	–
$F(+-+-)$[c]	–	1.13[d]

[a] $F_\phi(1\text{-}2)=F_\phi(3\text{-}2)=F_\phi(4\text{-}2)=F_\phi(5\text{-}2)=F_\phi$. [b] In the conformer **D** are two different kinds of $F_{\phi\phi'}$, interaction constants (AA and GG) corresponding to XCCCX fragments having their X···X distances AA or GG, respectively; in the **S** conformer are constants of type AG as well as GG. [c] $F(++++)$, $F(++--)$, $F(+-00)$, and $F(+-+-)$ are second order derivatives of the energy with respect to ϕ, under the constraints of the torsional modes approximately), as follows:

$(++++)$; $\Delta\phi_{3-2}=\Delta\phi_{3-2}=\Delta\phi_{4-2}=\Delta\phi_{5-2}=\Delta\phi$
$(++--)$; $\Delta\phi_{1-2}=\Delta\phi_{3-2}=\Delta\phi$ and $\Delta\phi_{4-2}=\Delta\phi_{5-2}=-\Delta\phi$
$(+-00)$; $\Delta\phi_{1-2}=\Delta\phi_{3-2}=\Delta\phi$ and $\Delta\phi_{4-2}=\Delta\phi_{5-2}=0$
$(+-+-)$; $\Delta\phi_{1-2}=\Delta\phi_{4-2}=\Delta\phi$ and $\Delta\phi_{3-2}=\Delta\phi_{5-2}=-\Delta\phi$

[d] Degenerate mode belonging to species E.

Table 4. Valence force constants for $C(CH_2Br)_4$.

Stretch (mdyn/Å)
C–C = 4.534
C–H = 4.850
C–X = 2.630
HCH = 0.500
HCX = 0.690
CCH = 0.670

Bend (mdyn Å/rad)²)
CCX = 0.910
CCC = 1.086

Stretch/stretch (mdyn/Å)
(C common): C–C/C–X = 0.35, C–C/C–C = 0.101, C–H/C–H = −0.007
Stretch/bend (mdyn/rad)
(C–C common): C–C/CCC = 0.417, C–C/CCX = 0.030, C–C/CCH = 0.260
(C–X common): C–X/HCX = 0.26, C–X/CCX = 0.49
Bend/bend (combination of two angles with the central C atom common, mdyn Å/(rad)²)
(C–X common): HCX/HCX = 0.05, (C–H common): HCC/HCX = 0.074
(C–C common): HCC/HCC = −0.026, (C common): HCC/HCX = 0.029
Bend/bend (combination of two angles with C–C common and dihedral angle *anti* or *gauche*)
anti: CCC/CCX = 0.093, HCC/CCC = 0.072
gauche: CCC/CCX = −0.024, HCC/CCC = −0.058
Torsion (mdyn Å/(rad)²), see also Sect. V-B
$F_\phi(S)_v = 0.86$; for conformer *S*
$F_\phi(D)^a = 0.33$; for conformer *D*

[a] The torsional force constants have been defined in the following way: each fragment A–C–C–C (A = H, X see Fig. 1) has been assigned an equal torsional force constant. The total force constant for the torsional coordinate ϕ_{i-2} (i = 1,3,4,5) is thus the sum of *nine* equal contributions, one from each fragment $A-C_i-C_2-C$.

Table 5. Calculated u and (K) values (Å) for internuclear distances in $C(CH_2Br)_4$ at 140 °C. The valence force field given in Table 4 was used.

Distance type	r (Å)	$F_\phi = 0.33$	$F_\phi = 0.55$	$F_\phi = 0.86$
C–H	1.077	0.078(0.0235)	0.078(0.0201)	0.078(0.0180)
C–C	1.544	0.052(0.0052)	0.052(0.0047)	0.052(0.0043)
C–X	1.942	0.057(0.0188)	0.057(0.0143)	0.057(0.0116)
$C_1 \cdots C_3$	2.52	0.077(0.0048)	0.076(0.0041)	0.074(0.0036)
$C_1 \cdots C_4$	2.52	0.077(0.0056)	0.076(0.0051)	0.075(0.0047)
C···X	2.95	0.081(0.0137)	0.080(0.0107)	0.080(0.0088)
C···H	2.13	0.111(0.0157)	0.110(0.0133)	0.110(0.0118)
X···H	2.49	0.114(0.0282)	0.113(0.0212)	0.112(0.0172)
H···H	1.78	0.125(0.0318)	0.124(0.0260)	0.124(0.0226)
X···X(GG)	4.17	0.284(0.0100)	0.242(0.0086)	0.213(0.0077)
X···X(AG)	5.11	0.187(0.0087)	0.175(0.0066)	0.167(0.0053)
X···X(AA)	5.89	0.113(0.0065)	0.112(0.0046)	0.112(0.0035)
C···X(g)	3.31	0.164(0.0112)	0.153(0.0089)	0.145(0.0075)
C···X(a)	4.32	0.079(0.0087)	0.078(0.0067)	0.078(0.0055)
X···H(GG)	2.79	0.254(0.0198)	0.238(0.0156)	0.227(0.0131)
X···H(AG)	4.27	0.184(0.0138)	0.174(0.0113)	0.168(0.0098)
X···H(AG)	4.55	0.166(0.0127)	0.160(0.0098)	0.156(0.0081)
X···H(GG)	3.63	0.242(0.0144)	0.214(0.0120)	0.195(0.0106)
X···H(AA)	5.07	0.128(0.0120)	0.128(0.0095)	0.127(0.0079)
C···H(g)	2.71	0.160(0.0121)	0.154(0.0100)	0.149(0.0087)
C···H(a)	3.44	0.106(0.0123)	0.106(0.0108)	0.106(0.0097)

Mean amplitudes of vibration corresponding to three different values of the torsional force constants were calculated as described in Ref. 15. In Table 5 are given u and K values [15] for internuclear distances. Some of these quantities are quite sensitive to the values of torsional force constants, which have been adjusted to fit the experimental intensities, as described in Sect. V-B.

Several other vibrational quantities in a molecule like TMBr also vary with the torsional force constants. To illustrate this point, some of these quantities have been calculated using different values of the torsional force constants, and the results are found in Tables 6 and 7.

The best estimates of the torsional force constants (see Sect. V-B) are 0.33 and 0.86 mdyn Å(rad)$^{-2}$ for the conformers **D** and **S**, respectively. Calculated frequencies corresponding to force constants within this range have been shown in Table 6. Frequency values in the range 40 – 60 cm^{-1} have to be expected for the conformers **D** and **S**. Generally the lowest frequency values correspond to torsional oscillations, however, bending frequencies down to *ca.* 50 cm^{-1} have to be expected for both con-

Table 6. Calculated frequencies in the range 40 – 335 cm^{-1} for conformers of $C(CH_2Br)_4$. Frequencies corresponding to torsional oscillations are indicated by (ϕ), and degenerate frequencies (species E) by *d*.

$F_\phi = 0.33$		$F_\phi = 0.55$		$F_\phi = 0.86$	
D	**S**	**D**	**S**	**D**	**S**
40(ϕ)	41(ϕ)	47(ϕ)	49(ϕ)	54.1(ϕ)	55
52(ϕ)[a]	49(ϕ)	54	53	54.3	56(ϕ)
53	56	62(ϕ)[d]	63(ϕ)	71(ϕ)[d]	71(ϕ)
110	73(ϕ)[d]	111	80(ϕ)[d]	113	85(ϕ)[d]
178	137	178	137	179	138
191[d]	192[d]	200[d]	219[d]	211[d]	245[d]
220(ϕ)	291	234	303	239	316
231	295	276(ϕ)	312	335(ϕ)	328

Table 7. Ratios ($q = Q_D/Q_S$) between vibrational partition functions (Q) for conformers of $C(CH_2Br)_4$ at 140 °C. Q is referred to the conformational energy minimum, and F_ϕ is the torsional force constant in mdyn Å (rad)$^{-2}$.

F_ϕ(S)	F_ϕ(D)	0.33	0.55	0.86
0.33		1.054	0.156	0.019
0.55		7.107	1.054	0.127
0.86		58.83	8.724	1.054

formers. Clearly some of the vibrational modes correspond to a rather complicated mixture of bending as well as torsional motion.

In order to calculate the conformational energy difference an estimate of the vibrational partition functions (Q) of the conformers are needed (Sect. VII). The ratio (q) between Q-values varies dramatically with the value of the torsional force constant as shown in Table 7. The difference in zeropoint vibrational energy is included in these ratios.

IV. EXPERIMENTAL AND DATA REDUCTION

TMBr was obtained from FLUKA. After recrystallization from CH_3CH_2OH and sublimation of the crystals, the sample melted at 162 – 163 °C.

Electron diffraction photographs were made at a nozzle temperature of 140 °C in the Oslo apparatus [16] under the following conditions.

Nozzle-to-plate, distance (mm)	480.78	481.22	201.22
Electron wavelength (Å)	0.06460	0.06458	0.06458
Number of plates	6	5	5
Range of data, in s(Å^{-1})	1.50– 19.125	1.375– 19.125	7.00– 43.00
Data interval, Δs(Å^{-1})	0.125	0.125	0.25
Estimated uncertainty in the s-scale (%)	0.14	0.14	0.14
Sector-to-plate distance (mm)	14.12	15.30	15.30

The electron wavelength was determined by calibration against gold, and corrected by an experiment with CO_2 giving a correction of +0.1 % in the s-scale. The data were reduced in the usual way to yield an intensity curve for *each plate*. Average curves for each set of distances were formed. The two 48 cm curves were then averaged. A composite curve was made by connecting the 48 cm and 20 cm average curves after scaling. The final experimental intensity curve is shown in Fig. 2. The intensities have been modified by $s/|f_{Br}'|^2$. The scattering amplitudes were calculated by the partial wave method [18] using Hartree-Fock atomic potentials.[19]

Contributions to the theoretical intensities from H···H distances, the H atoms bonded to different carbon atoms, were not included.

The radial distribution curve obtained by Fourier transformation of the final experimental intensity is presented in Fig. 3.

For the final least-squares refinements data from $s = 1.50$ Å^{-1} to $s = 23.50$ Å^{-1} were used. The data beyond this range were of lower quality.

V. STRUCTURE ANALYSIS AND REFINEMENTS

The calculated conformational energies suggest that only two conformers, **D** and **S**, are present in detectable amounts at 140 °C. From the areas under the two peaks (see Fig. 3) corresponding to the distances X···X(AG) and X···X(AA) it was easily concluded that **D** and **S** have to be present in nearly equal amounts.

A. Least-squares refinements. The least-squares program is a modified version of the program explained in Ref. 17. Several conformers may be included in the refinements with the present version of the program.

Models for the conformers were constructed with the following geometrical assumptions: (1) the C-atom framework possess D_{2d} symmetry, with $\angle C_1C_2C_3 = \angle C_4C_2C_5 = 109.47° - \theta_C$ for the **D** conformer and $\angle C_1C_2C_3 = \angle C_4C_2C_5 = 109.47° + \theta_C$ for the **S** conformer; (2) all four $C-CH_2X$ groups are equal; (3) each of the $C\text{-}CH_2X$ groups possess C_s symmetry, and the projection of the angle HCH′ on a plane perpendicular to the C – C axis is 120°; (4) the conformers **D** and **S** have identical structures except for the C – C torsion angles and the CCC angles.

Models were defined in terms of the following average parameters: C – H, C – C, C – X, ∠CCX, ∠CCH and θ_C. The torsion angles of the **S** conformer were defined as follows: $\phi_{1-2} = \phi_{3-2} = 120° + \phi_s$ and $\phi_{4-2} = \phi_{5-2} = -120° - \phi_s$. The deviation angle ϕ_s was refined. All torsion angles for the **D** conformer are equal to 0°. The exact staggered conformers thus have

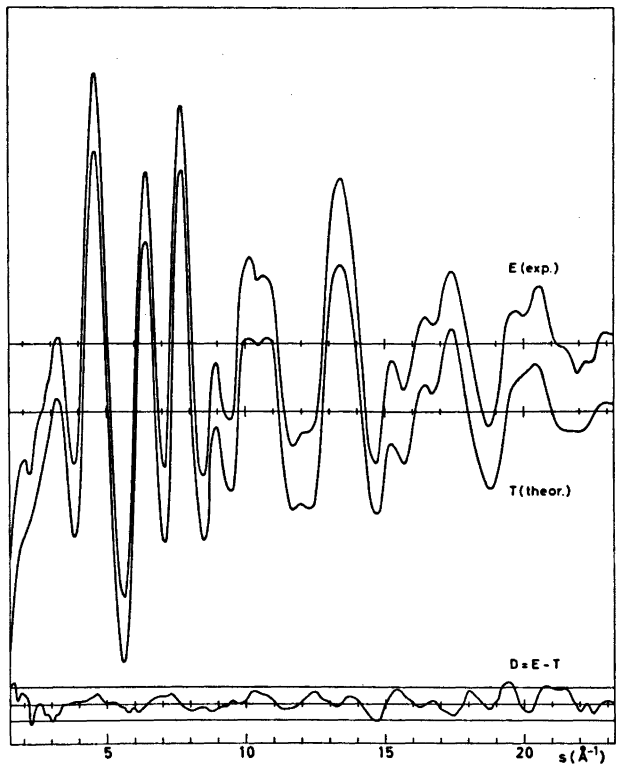

Fig. 2. Intensity curves for $C(CH_2Br)_4$ at 140 °C. Curve E shows the experimental intensity, and curve T the theoretical intensity corresponding to the final least-squares parameters. Curve D is the experimental minus theoretical, and the straight lines give the experimental uncertainty ($\pm 3 \times$ experimental standard deviation).

torsion angles: 120, 120, −120, −120° for **S** and 0, 0, 0, 0° for **D**.

Also adjusted was the composition parameter, the relative amount of conformer **S**.

In the first part of the structure analysis a number of refinements were carried out, in which selected combinations of parameters were allowed to vary, while others were held constant at plausible values. At some stages the background had to be corrected, however, none of the important conclusions about the structure and composition were changed thereby.

All important parameters could be simultaneously refined. The combination of all geometry variables, the u values for bond distances and for non-bonded distances of the kinds C···C, X···X and X···C, the composition parameter, and a scale factor refined to give convergence.

B. Determination of torsional force constants. The torsional modes of vibration contribute substantially to the mean amplitudes of several distances. Therefore, since a reasonable force field is known, except for the torsional part, the torsional force constants can be adjusted to fit the electron-diffraction data. The procedure used for TMCl [2] was used in order to estimate the diagonal torsional force constants of the conformers of TMBr. The most probable torsional force constants, as determined from the electron-diffraction data, are:

For **D**: $F_\phi = 0.33(-0.05, +0.15)$ mdyn Å(rad)$^{-2}$

For **S**: $F_\phi = 0.86(-0.25, +0.10)$ mdyn Å(rad)$^{-2}$

The error limits are subjective to a certain degree. Not all combinations of F_ϕ values are equally probable. Combinations of values [F_ϕ(D), F_ϕ(S)] within a triangle having corners

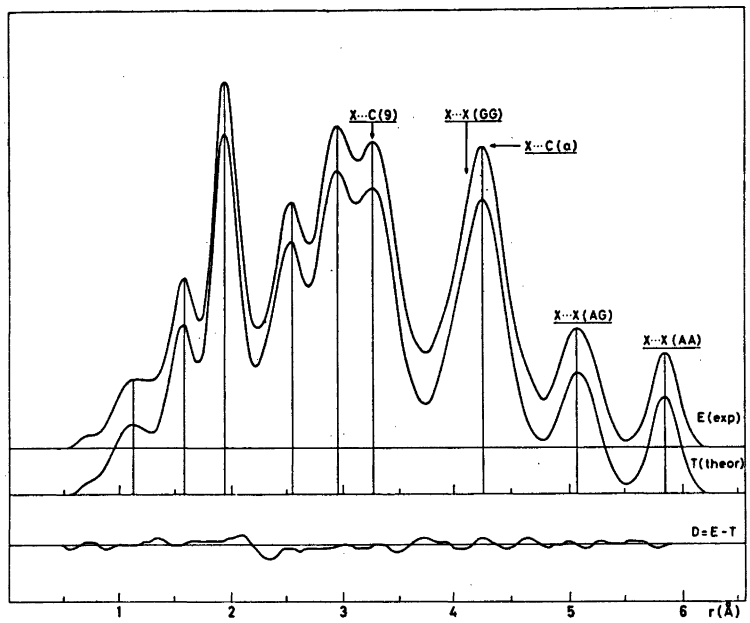

Fig. 3. Radial distributions for $C(CH_2Br)_4$ at 140 °C. Experimental (E) and theoretical (T) radial distribution curves and difference curve (D). The RD curves were calculated from the intensity curves of Fig. 2 with an artificial damping constant 0.0020 Å^2.

[0.27, 0.94], [0.34, 0.94], and [0.40, 0.61] are very probable. Error limits as indicated here do not allow for *systematic* errors in the remainder of the force field, nor in the temperature. These points have been discussed in a previous paper.[7]

VI. FINAL RESULTS

Results from the least-squares refinements, and standard deviations (σ) corrected for correlation in the experimental data,[20] are given. All intensities were given equal weights in the final refinements.

Non-bonded distances were restricted under the geometrical constraint of r_α parameters, by including correction terms $D=r_\alpha-r_a$ ($D=(u^2/r)-K$) for all distances.[21,22] Calculated u and K values, corresponding to final torsional force constants, are shown in Table 5. Structure parameters are given in Table 8. The uncertainty in the s-scale (0.14 %) has been included in the σ values. An experiment with CO_2 gave a correction of +0.1 % in the s-scale, therefore the bond lengths in Table 8 are 0.1 % longer than those obtained directly by refinements. The values of the deviation parameters, θ_c and θ_s, are not significantly different from zero.

The relative amounts of the conformers **D** and **S** were determined by refining the composition parameter α(S) with the restriction that $\alpha(S)+\alpha(D)=100$. The best least-squares estimate was $\alpha(S)=42$ % with $\sigma=1$ %.

Several u values have been refined and compared to those computed using the final torsional force constants. (see Table 9) Both sets of u values are experimental, but the calculated values combine information from spectroscopy as well as from electron diffraction. Some u values get very small contributions from the torsional modes of vibration. Such u valuès are those corresponding to bond distances, distances over *one* bond angle, the distances X···X(AA), and the distance X···C(a). The fact that these u values are generally in good agreement with those refined directly, is important. The force field used for TMBr thus seems reasonable. The value of u(C−X), determined directly by least-squares refinements,

Table 8. Structure parameters for $C(CH_2Br)_4$.

Bond lengths (Å)	r_a	σ
C–H	1.082	0.024
C–C	1.552	0.005
C–Br	1.949	0.004
Bond angles (°)	$\angle_\alpha$	σ
CCBr	114.2	0.4
CCH	111.7	1.6
CCC	(109.5)[a]	(0.9)[a]
HCBr	105.8[b]	1.6
Torsional deviation	ϕ_s (°)	σ (°)
angle in conformer **S**	+0.1[c]	0.8

[a] $\theta_c = +0.8°$ $\sigma(\theta_c) = 0.9°$, see Sect. V–A. [b] Dependent parameter. [c] See Sect. V–A for definition.

is significantly different from the spectroscopic value, probably due to an error in blackness correction. It is, however, unlikely that other u values are significantly disturbed by this type of error. The average deviation between the two sets of u values, $\langle|\Delta|/u\rangle$, is ca 17 %, while the average relative uncertainty, $\langle\sigma/u\rangle$, of the refined u values is ca 20 %. If only torsion dependent u values are included then $\langle|\Delta|/u\rangle = 10$ % and $\langle\sigma/u\rangle = 15$ %. In conclusion, the vibrationally consistent set of u and K values in Table 5 are considered the final ones for TMBr.

Parameter correlation coefficients (ϱ) with absolute values larger than 0.5 were obtained for the following parameter combinations:

Combination	ϱ-Value
CCX/C–X	−0.52
θ_c/CCX	−0.60
θ_c/ϕ_s	−0.84
u[X···C(a)]/u[X···C(g)]	−0.95
α(S)/u[X···X(AG)]	+0.60
scale/u(C–X)	+0.54

VII. DISCUSSION

The percentages α(D) and α(S) of the two conformers are related to the expression for the equilibrium constant as given in eqn. (1)

$$\alpha(D)/\alpha(S) = \tfrac{1}{2}(Q_D/Q_S)^{vib}\exp(-\Delta E^m RT) \quad (1)$$

(The *classical* rotational partition functions for the two conformers are very nearly equal.) Q^{vib} is the vibrational partition function, referred to the *minimum* of potential energy, for a conformer. $\Delta E^m = E_D{}^m - E_S{}^m$ is the difference in potential energy between the two conformers, and the difference is measured between energy *minima*. The difference in zero-point vibrational energy is thus included in the ratio between the vibrational partitions functions. R and T have their usual thermodynamic meanings.

If the vibrational partition functions for the conformers are known, then ΔE^m may be estimated from eqn. (1). The *ratio* between the

Table 9. Refined and calculated mean amplitudes (u) of vibration for $(CH_2Br)_4$ at 140 °C.

Type of distance	Dist. (Å)	Calculated[a] u-value (Å)	Refined[b] u-value	σ (Å)
C–H	1.082	0.078	0.098	0.034
C–C	1.552	0.052	0.053	0.010
C–X	1.949	0.057	0.024	0.008
C···C	2.53	0.076	0.065	0.029
$X···X_2$	2.94	0.080	0.068	0.007
$X_1···H_1$	2.47	0.113	0.102	0.036
X···C(g); **D**	3.29	0.164	0.144	0.048
X···C(g); **S**	3.29–3.31	0.145	0.125	(–)[c]
X···C(a)	4.31	0.078	0.088	0.014
X···X(AG); **S**	5.10	0.167	0.152	0.006
X···X(GG); **D**	4.13	0.284	0.270	0.017
X···X(GG); **S**	4.14	0.213	0.199	(–)[c]
X···X(AA); **D**	5.86	0.113	0.099	0.005

[a] The u values correspond to the force field in Table 5. [b] Values obtained by the least-squares refinements. [c] Refined together with the previous value as *one* parameter.

Table 10. Calculations of ΔE^m according to eqn. (1). See text.

	I	II	III
F_ϕ(D), mdyn Å (rad)$^{-2}$	0.33	0.45	0.55
F_ϕ(S), mdyn Å (rad)$^{-2}$	0.86	0.65	0.55
$q=(Q_D/Q_S)^{vib}$	58.8	5.20	1.05
ΔE^m, kcal/mol	+2.51	+0.51	−0.79

partition functions depends on the *difference* in torsional force constants as demonstrated in Table 7. Calculations of ΔE^m using three different sets of torsional force constants are summarized in Table 10. The combination I (0,33, 0.86) corresponds to the torsional force constants determined from the electron diffraction data. The combination II (0.45, 0.65) leads to the value of ΔE^m (0.51 kcal/mol) predicted by the semiempirical energy model. Both experiment and semi-empirical calculations thus indicate that conformer **D** is *less* stable than conformer **S**, but the ΔE^m values do not agree. The possibility III [$F_\phi(D)=F_\phi(S)$] seems less likely, however, a negative value of ΔE^m is not ruled out. The partition-function ratio also depends on conformational differences between non-torsional force constants. Assuming equal values of the vibrational partition functions of the conformers in this molecule could be very wrong.

The difference (**D**−**S**) in zero-point vibrational energy (ΔE_0^{vib}) is −2.1 kcal/mol, while the difference in vibrational energy at 413 K is −1.6 kcal/mol, as calculated from the expression $\Delta E_T^{vib}=RT^2\mathrm{d}(\ln q)/\mathrm{d}T$, with $q=(Q_D/Q_S)^{vib}$ corresponding to the force field in Table 4. The difference (**D**−**S**) in vibrational entropy is +4.3 cal(deg. mol)$^{-1}$ at 413 K, as calculated according to the expression $\Delta S_T^{vib}=R\ln q+RT\mathrm{d}(\ln q)/\mathrm{d}T$. If *equal* values of the conformational force constants are assumed, then ΔE_T^{vib} and ΔS_T^{vib} are temperature *independent* quantities with values close to zero ($q\simeq 1$). The corresponding quantities (ΔE_0^{vib}, ΔE_T^{vib}, and ΔS_T^{vib}) for TMCl [2] have approximately equal values to those reported here for TMBr.

According to the experimental findings the molecules TMCl [2] and TMBr have very nearly a tetrahedral arrangement of C atoms and approximately all-staggered (1:2) low-energy conformations. Conformers possessing parallel (1:3) X···X interactions have significantly higher energies and may deviate considerably from the all-staggered (1:2) form.

The molecular-mechanics calculations reasonably predict the structural parameters for TMBr and TMCl,[2] while the large value of the torsional force constant of the conformer **S** is not predicted by these calculations.

Acknowledgements. We are grateful to cand. real. A. Almenningen for recording the diffraction photographs. Financial support from Norges almenvitenskapelige forskningsråd is gratefully acknowledged.

REFERENCES

1. Stølevik, R. *Acta Chem. Scand. A 28* (1974) 299.
2. Stølevik, R. *Acta Chem. Scand. A 28* (1974) 327.
3. Stølevik, R. *Acta Chem. Scand. A 28* (1974) 455.
4. Stølevik, R. *Acta Chem. Scand. A 28* (1974) 612.
5. Farup, P. E. and Stølevik, R. *Acta Chem. Scand. A 28* (1974) 680.
6. Farup, P. E. and Stølevik, R. *Acta Chem. Scand. A 28* (1974) 871.
7. Fernholt, L. and Stølevik, R. *Acta Chem. Scand. A 28* (1974) 963.
8. Johnsen, J. P. and Stølevik, R. *Acta Chem. Scand. A 29* (1975) 201.
9. Johnsen, J. P. and Stølevik, R. *Acta Chem. Scand. A 29* (1975) 457.
10. Fernholt, L. and Stølevik, R. *Acta Chem. Scand. A 29* (1975) 651.
11. Abraham, R. J. and Parry, K. J. *J. Chem. Soc. Perkin Trans. 2* (1970) 539.
12. Schachtschneider, J. H. and Snyder, R. G. *Vibrational Analysis of Polyatomic Molecules.* IV (force constants for the haloparaffins). Project No. 31450, Technical Report No. 122-63 of Shell Development Company.
13. Snyder, R. G. and Schachtschneider, J. H. *Spectrochim. Acta 21* (1965) 169.
14. Gwinn, W. D. *J. Chem. Phys. 55* (1971) 477.
15. Stølevik, R., Seip, H. M. and Cyvin, S. J. *Chem. Phys. Lett. 15* (1972) 263.
16. Bastiansen, O., Hassel, O. and Risberg, E. *Acta Chem. Scand. 9* (1955) 232.
17. Andersen, B., Seip, H. M., Strand, T. G. and Stølevik, R. *Acta Chem. Scand. 23* (1969) 3224.
18. Peacher, J. and Willis, J. C. *J. Chem. Phys. 46* (1967) 4809.

19. Strand, T. G. and Bonham, R. A. *J. Chem. Phys. 40* (1964) 1686.
20. Seip, H. M. and Stølevik, R. In Cyvin, S. J., Ed., *Molecular Structures and Vibrations*, Elsevier, Amsterdam 1972.
21. Morino, Y., Kuchitsu, K. and Oka, T. *J. Chem. Phys. 36* (1962) 1108.
22. Kuchitsu, K. *J. Chem. Phys. 49* (1968) 4456.

Received August 29, 1975.

Acta Chemica Scandinavica A 30 (1976) 219—224

Preparation and Crystal Structure of β-Nb_2N and γ-NbN

A. NØRLUND CHRISTENSEN

Department of Inorganic Chemistry, Aarhus University, DK-8000 Aarhus C, Denmark

Samples of the niobium nitrides β-Nb_2N and γ-NbN have been obtained from the elements by sintering of niobium in nitrogen at 2100 °C (γ-NbN) or by zone melting of δ-NbN in nitrogen. In the zone melting δ-NbN is converted to β-Nb_2N and γ-NbN.

Based on a neutron diffraction powder pattern of a sample containing β-Nb_2N and γ-NbN the structures are proposed for the two compounds.

β-Nb_2N is trigonal, the space group is $P\bar{3}1m$ (No. 162) with $a = 5.267(2)$ Å, $c = 4.988(1)$ Å and three formula units per unit cell. The composition of the sample investigated is $NbN_{0.46(1)}$. γ-NbN is tetragonal, the space group is $P4/m$ (No. 83) with $a = 8.742(3)$ Å, $c = 8.592(3)$ Å, and 32 formula units per unit cell. The composition of the sample investigated is $NbN_{0.64(1)}$.

The phase diagram for the system niobium-nitrogen is complex and only partly investigated.[1] The crystal data for three of the phases found in the system are listed in Table 1.[1] All three compounds are non-stoichiometric. β-Nb_2N is trigonal, but the structure of the phase has not been investigated. The lattice parameter a of the hexagonal cell is almost independent of the composition, whereas the lattice parameter c increases rapidly from 4.955 Å for $Nb_2N_{0.8}$ to 4.995 Å for Nb_2N.[2] A structure for Nb_2N has been proposed with the niobium atoms in a hexagonal closepacking and the nitrogen atoms randomly distributed in the octahedral holes of the packing.[2]

Table 1. Unit cell parameters for β-Nb_2N, γ-NbN, and δ-NbN, Ref. 1. (Room temperature).

Phase	Crystal structure	Lattice parameters in Å N-poor boundary	N-rich boundary
β-Nb_2N	trigonal	$a = 3.056$ → $c = 4.955$ →	$a = 3.056$ $c = 4.996$
γ-NbN	tetragonal	$a = 4.385$ → $c = 4.310$ →	$a = 4.386$ $c = 4.335$
δ-NbN	cubic	$a = 4.382$ →	$a = 4.395$[a]

[a] corresponds to the stoichiometric composition.

γ-NbN is tetragonal and has a distorted sodium chloride structure,[3] but the structure of the phase has not been investigated. The unit cell parameter ratio c/a approaches 1 with increasing temperature and nitrogen content. The lattice parameter a of the tetragonal cell is almost independent of the composition, whereas the lattice parameter c increases with increasing nitrogen content, see Table 1. δ-NbN is cubic and has the sodium chloride structure.[3] The lattice parameter a increases from 4.382 Å for $NbN_{0.86}$ to 4.395 Å for NbN. It is possible to increase the stability of δ-NbN at high nitrogen pressures to the composition $NbN_{1.062}$. For this composition the niobium sub-lattice is defective,[4] and the unit cell parameter is smaller than 4.395 Å. δ-NbN is metallic and becomes superconductive at $T_c = 17.3$ K. The purpose of this investigation was to produce well characterized specimens of β-Nb_2N, γ-NbN and δ-NbN, so that crystal structures and other physical properties could be investigated. In the following the formulae β-Nb_2N, γ-NbN, and δ-NbN will be used for the nonstoichiometric compounds.

EXPERIMENTAL

Sample preparation and X-ray technique. Attempts have been made to prepare single crystals of β-Nb_2N, γ-NbN, and δ-NbN by a

floating zone crystal growth technique. The starting materials for the crystal growth experiments were powders of Nb of the nominal purity 99.8 % and nitrogen gas of the nominal purity 99.99 %. The metal powder was placed in rubber moulds which were sealed, evacuated and pressed at an isostatic pressure of 5000 atm to produce rods. The rods were either sintered in pure nitrogen to produce rods of niobium nitride or were zone melted in pure helium (99.99 % He) to produce solid bars of niobium. The experimental conditions for sintering are listed in Table 2.

The rods of niobium nitride were zone melted in an ADL MP crystal growth furnace using the zone melting procedure previously reported.[5] The experimental conditions for these crystal growth experiments are listed in Table 3.

Table 2. Experimental conditions for the preparation of rods of δ-NbN by sintering. Raw material Nb.

Preform No.	A[a]	B	C	D	E
1	8.3	*	30	–	2
2	10	2	11.8	1700	4
3	1.7	5	7	–	3.5

[a] A: N_2 gas pressure in atm. B: R.F. sintering coil No. * indicates the use of a zone melting coil. C: Power kW. D: Temperature of specimen measured with pyrometer. E: Duration of sintering in h.

Table 3. Experimental conditions for the zone melting of niobium nitrides. Preform of NbN.

Experiment No.	A[a]	B	C	D	E
NbN 1	17.0	2	13.7	64	50
NbN 2	19.5	2	15.9	130	10
NbN 3[b]	15.5	5	20.0	45	10
NbN 4	1.3	9	13.6	38	7.5
NbN 5[b]	11.5	9	15.0[c]	30	20
	16.5	9	11.4[d]		7.5
NbN 6[b]	16.5	9	9.0 to 13.0	55	10
NbN 7	2.0	9	13.4[c]	30	20
	17.0	9	17.0[d]	16	2.0

[a] A: N_2 gas pressure in atm. B: R.F. coil No. C: Power kW. D: Length of zone melted specimen. E: Growth rate in mm h^{-1}. [b] Preform of Nb. [c] First pass. [d] Second pass.

Guinier powder photographs obtained with a Guinier powder camera with $CuK\alpha_1$, $\lambda = 1.54051$ Å or $CoK\alpha_1$, $\lambda = 1.78892$ Å and with sodium chloride, $a_{NaCl} = 5.6389$ Å or germanium, $a_{Ge} = 5.6576$ Å as an internal standard, and optical metallography have been used to characterize the specimens. The results indicated that single crystals of δ-NbN cannot be obtained with a zone melting technique at the experimental conditions used. The sintered rods of δ-NbN are converted to specimens containing β-Nb_2N and γ-NbN in the zone melting procedure.

The solid bars of niobium were sintered in pure nitrogen using the experimental conditions listed in Table 4. The specimens were examined using optical metallography, and Guinier powder patterns were taken of the specimens as well. The results indicate that niobium by this treatment is converted to γ-NbN.

All the lines in the X-ray diffraction powder pattern of γ-NbN can be indexed with a tetragonal cell with $a_\gamma = 4.392(2)$ Å and $c_\gamma = 4.321(3)$ Å. However, precession photographs of a multidomain twinned specimen of γ-NbN show weak additional reflections corresponding to the unit cell parameters $a_T = 2a_\gamma$, and $c_T = 2c_\gamma$.

X-Ray powder patterns of a sample containing β-Nb_2N and γ-NbN were obtained with a powder diffractometer at temperatures from room temperature to 1700 °C. From these powder patterns the unit cell parameters for

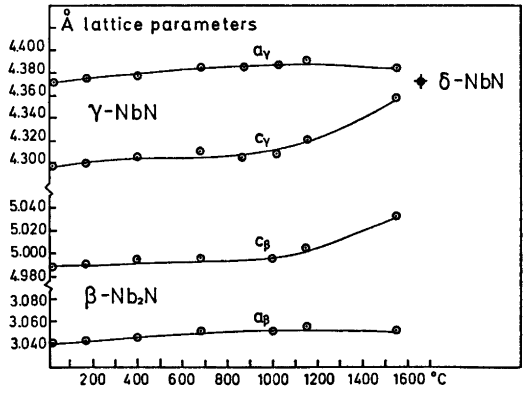

Fig. 1. The variation of the unit cell parameters of β-Nb_2N and γ-NbN with temperature. The values given are for the two subcells that can index the X-ray powder patterns but not the neutron powder patterns.

When heated to 1663 °C the diffraction lines from γ-NbN have disappeared and the diagram has lines of δ-NbN ($a = 4.372$ (5) Å). When the sample is cooled to room temperature the diffraction diagram shows again the lines from γ-NbN without any diffraction lines from δ-NbN.

Table 4. Experimental conditions for sintering of rods of niobium and niobium nitride.

Exp. No.	A[a]	B	C	D	E
NbN 8[c]	15.7	1350	24	γ-NbN+β-Nb_2N	unchanged
NbN 9[b]	17.0	1480	89	γ-NbN+Nb	main product Nb
NbN 10[b]	17.0	2000	66	γ-NbN	crystal twinned
NbN 11[b]	20.00	2100	112	γ-NbN	crystal twinned
NbN 12[c]	20.0	2100	90	γ-NbN	crystal twinned

[a] A: N_2 gas pressure in atm. B: Temperature of specimen °C measured with pyrometer. C: Duration of sintering in h. D: Composition of specimen. E: Comments. [b] Niobium. [c] Niobium nitride.

the two compounds were calculated, and the results of these measurements are shown in Fig. 1. No internal standard has been used in the determination of these unit cell parameters.

Neutron diffraction technique. A neutron diffraction powder pattern of a sample containing β-Nb_2N and γ-NbN was measured at room temperature using a triple-axis spectrometer with an energy analyser at the DR3 reactor at Risø. This instrument was chosen to obtain a low background intensity of the diagram. The sample was placed in a 12 mm diameter cylindrical vanadium container. The neutron wave length was 1.6886 Å (reflection from a (111) plane of a Ge monochromator). The diffraction pattern is shown in Fig. 2.

Crystal data and structure refinement. The diffraction pattern showed only reflections belonging to the two compounds β-Nb_2N and γ-NbN. The reflections from β-Nb_2N could be indexed with a hexagonal unit cell with $a_H = \sqrt{3}a_\beta$, and $c_H = c_\beta$, where a_β and c_β are comparable with the unit cell parameters for β-Nb_2N listed in Table 1. The reflections from γ-NbN could be indexed with a tetragonal unit cell with $a_T = 2a_\gamma$ and $c_T = 2c_\gamma$, where a_γ and c_γ are comparable with the unit cell parameters for γ-NbN listed in Table 1. The unit cell parameters for the two components are listed in Table 5.

The reflections for β-Nb_2N (except those within brackets in Fig. 2) could be completely

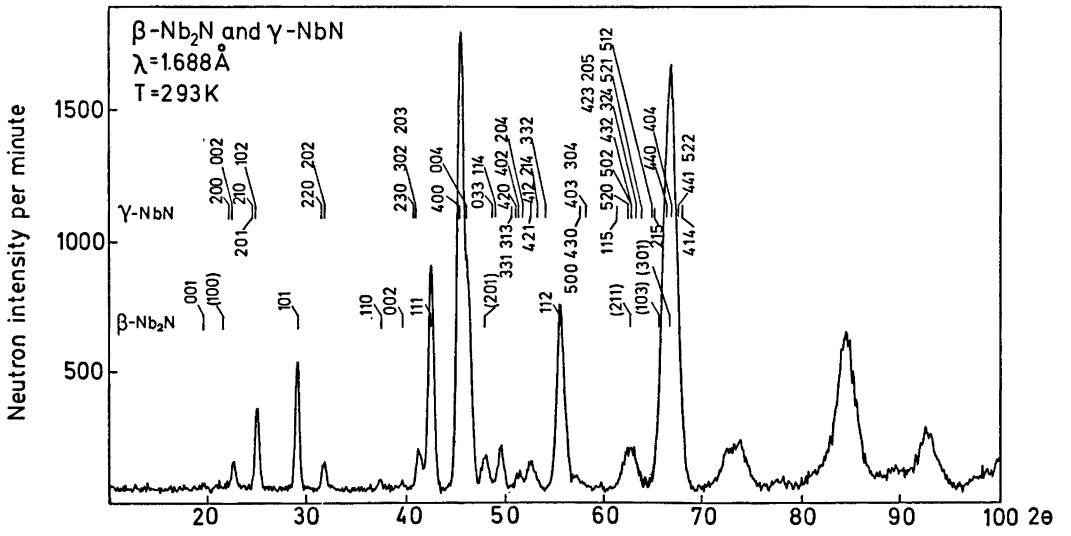

Fig. 2. Neutron diffraction powder pattern of a sample containing β-Nb_2N and γ-NbN.

Table 5. Composition, unit cell parameters and space group for β-Nb_2N and γ-NbN.

Formula	Composition	Unit cell parameters in Å		Space group
		a	*c*	
β-Nb_2N	$NbN_{0.46(1)}$	5.267(2)	4.988(1)	$P\bar{3}1m$ (No. 162)
γ-NbN	$NbN_{0.64(1)}$	8.742(3)	8.592(3)	$P4/m$ (No. 83)

resolved from reflections belonging to γ-NbN, and were used in the refinement of the structure of β-Nb_2N. The program F418 by Rietveld using a refinement on the profile intensities of the reflections was used.[6] The size of the unit cell for β-Nb_2N indicates that the cell contains three formula units and that the structure is of the ε-Fe_2N type [7] with space group $P\bar{3}1m$. In this space group the metal atoms can be placed in the 6*k* site with $x = 0.3333$ and $z = 0.25$, and the nitrogen atoms can be placed in the 2*d* and in the 1*a* sites. The diffraction data were not sufficient to permit a refinement of all possible parameters in the structure. The positional parameters of niobium have been fixed at the values mentioned above and all temperature factor parameters have been given the value zero. The parameters refined are a scale factor and two occupancy factors for site 6*k* and 2*d*. The results of the refinement are listed in Table 6. The niobium site and one of the nitrogen sites are only partly occupied corresponding to the composition of the β-Nb_2N sample investigated: $Nb_2N_{0.93(2)}$. The results of the refinement have been used to calculate all possible contributions from β-Nb_2N to the diffraction pattern (Fig. 2) from $2\theta = 10°$ to $2\theta = 70°$. These calculated contributions have been subtracted from the diffraction pattern to give a difference pattern with contributions only from γ-NbN.

The reflections of γ-NbN shown in Fig. 2 have been used in the refinement of the structure of γ-NbN, using the same refinement program as for β-Nb_2N. The composition of γ-NbN has been reported to be in the range $NbN_{0.75-0.79}$,[2,3] and the structure has been assumed to be a distorted sodium chloride structure. The formula Nb_4N_3 has been proposed for γ-NbN.[9] The size of the unit cell for γ-NbN indicates that the cell contains 32 formula units (assuming the composition NbN). The distortion of the sodium chloride structure is most likely related to the non-stoichiometry of the compound. For γ-NbN the space group $P4/m$ has been assumed with the possible positions of the atoms listed in Table 7. As the unit cell has a shorter *c*-axis than *a*-axis, the distortion of the structure is likely to be due to nitrogen vacancies in planes parallel to the 001 plane and to deviations of the *z*-parameters for the atoms from the values 0,1/4, 1/2, and 3/4.

The diffraction data were not sufficient to permit a refinement of all possible parameters in the structure. The temperature factor parameters have been set to zero and some positional parameters have been given fixed values (Table 7). The *z*-parameter for Nb9 and Nb10 and for the nitrogen atoms N1, N6, N7, and N8 have been refined, as well as occupancy factors for all the nitrogen atoms and a scale factor. The final values of parameters giving an acceptable agreement between the observed and the calculated diffraction pattern are listed in Table 7. The nitrogen site 8*l* (N1) is only partly occupied, and the two nitrogen sites 4*k* (N3) and 2*g* (N7) are vacant. From this the composition of the sample of γ-NbN investigated is $NbN_{0.64(1)}$.

In the refinement of the structure for the two compounds the atomic scattering length

Table 6a. Results of the refinement of the structure of β-Nb_2N.[a]

Atom	Atom site	*x*	*y*	*z*	Multiplicity Theor.	Calc.
Nb	6*k*	0.3333	0	0.2500	0.5	0.385(6)
N1	2*d*	1/3	2/3	1/2	0.16667	0.095(6)
N2	1*a*	0	0	0	0.08333	0.08333

[a] Scale factor = 0.0717, $R = 10.6$ %, $R(F^2) = 13.1$ %. (For definition of R (profile) and $R(F^2)$ (nuclear) see Ref. 8).

Table 6b. Observed and calculated intensities for β-Nb_2N and γ-NbN. Reading from left to right the columns are: *hkl* I_{calc} I_{obs}.

BETA	NIOBIUM	NITRIDE				4	2	0	307	309
0	0	1	21	183		4	0	2	428	441
1	0	1	5529	5011		2	0	4	419	556
1	1	0	121	288		4	2	1	57	105
0	0	2	365	231		4	1	2	595	1026
1	1	1	11146	11447		2	1	4	402	347
1	1	2	10687	12538		3	3	2	100	30
						5	0	0	0	25
						4	3	0	0	48
GAMMA	NIOBIUM	NITRIDE				4	0	3	206	983
2	0	0	705	472		3	0	4	13	66
0	0	2	479	768		1	1	5	60	72
2	1	0	1297	2125		5	2	0	256	218
2	0	1	110	167		5	0	2	227	211
1	0	2	1124	1107		4	3	2	453	423
2	2	0	360	559		4	2	3	310	317
2	0	2	785	562		3	2	4	308	333
2	3	0	520	370		2	0	5	261	262
3	0	2	458	684		5	2	1	159	142
2	0	3	311	868		5	1	2	154	127
4	0	0	26517	25952		2	1	5	237	154
0	0	4	11435	11591		4	4	0	14600	15468
0	3	3	376	503		4	0	4	25620	27174
1	1	4	193	298		4	4	1	261	282
3	3	1	5	3		5	2	2	2	2
3	1	3	83	48		4	1	4	21	23

for Nb and N were 0.711 and 0.940 ($\times 10^{-12}$ cm), respectively.[10]

CONCLUSION

The crystal growth investigation indicates that single crystals of δ-NbN cannot be obtained from sintered rods of δ-NbN using a zone melting technique at the experimental conditions used. It also shows that single crystals of β-Nb_2N or γ-NbN cannot be obtained in a floating zone crystal growth experiment as this always results in formation of a specimen containing β-Nb_2N and γ-NbN in a lamella structure. The pure phase γ-NbN can, however, be obtained by sintering of niobium in pure nitrogen.

The neutron diffraction investigation shows that β-Nb_2N has the ε-Fe_2N structure (Fig. 4). A model for the structure of γ-NbN where some of the niobium-nitrogen layers are completely occupied, and where some of the layers have vacancies at the nitrogen atom positions (see Fig. 3), fits best to the diffraction data. This model can yield an explanation of the fact that the unit cell parameter c for γ-NbN is increasing and the unit cell parameter a is constant with increasing nitrogen content of γ-NbN. The unit cell parameter a is fixed by the fully occupied layer for $z=0$. When the

Table 7. Results of the refinement of the structure of γ-NbN.[a]

Atom	Atom site	x	y	z	Multiplicity Theor.	Calc.
Nb1	1*a*	0	0	0	0.125	0.125
Nb2	1*b*	0	0	1/2	0.125	0.125
Nb3	1*c*	1/2	1/2	0	0.125	0.125
Nb4	1*d*	1/2	1/2	1/2	0.125	0.125
Nb5	2*e*	0	1/2	0	0.250	0.250
Nb6	2*f*	0	1/2	1/2	0.250	0.250
Nb7	4*j*	0.2500	0.2500	0	0.500	0.500
Nb8	4*k*	0.2500	0.2500	1/2	0.500	0.500
Nb9	8*l*	0.2500	0.0	0.243(7)	1.000	1.000
Nb10	8*l*	0.5000	0.2500	0.256(7)	1.000	1.000
N1	8*l*	0.2500	0.2500	0.202(6)	1.000	0.29(2)
N2	4*k*	0.2500	0.0	1/2	0.500	0.500
N3	4*k*	0.5000	0.2500	1/2	0.500	0.0
N4	4*j*	0.2500	0.0	0	0.500	0.500
N5	4*j*	0.5000	0.2500	0	0.500	0.500
N6	2*h*	1/2	1/2	0.288(7)	0.250	0.250
N7	2*g*	0	0	0.2500	0.250	0.0
N8	4*i*	0	1/2	0.253(5)	0.500	0.500

[a] Scale factor = 1.8156, $R = 8.6$ %, $R(F^2) = 5.6$ % (for observed and calculated intensities see Table 6b). Coordinates that may be used as parameters are listed as decimal fractions with standard deviations in brackets. Where no standard deviations are listed the coordinates have not been refined.

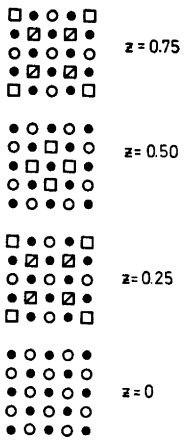

Fig. 3. Niobium-nitrogen layers in the structure of γ-NbN. Filled circles indicate niobium atom positions, and open circles nitrogen atom positions. Open squares are vacant nitrogen atom positions and partly filled squares are partly occupied nitrogen atom positions. The atomic layer for $z = 0$ is complete. In the layer for $z = 1/4$ approximately three nitrogen atoms are missing, and in the layer for $z = 1/2$ four nitrogen atoms are missing.

occupancy of the nitrogen atom sites of the layers for $z = 1/4$, $1/2$, and $3/4$ is increased, the spacing between these layers will increase, and the unit cell parameter c will be longer. The nitrogen content in the sample investigated of γ-NbN is low, $NbN_{0.64}$, compared to the values reported previously.[2,3,9]

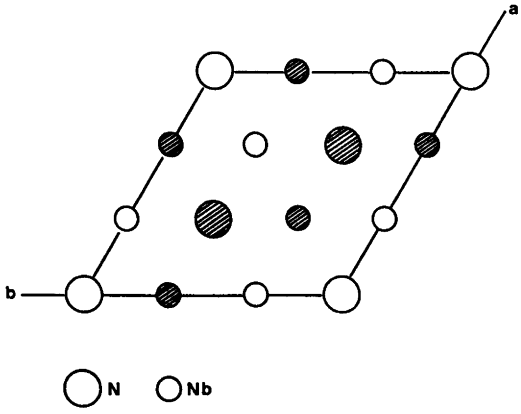

Fig. 4. Projection of the structure of β-Nb_2N along the [001] direction. Nitrogen atoms with $z = 0.5$ and niobium atoms with $z = 0.75$ are hatched.

This is possible because the sample investigated has been prepared at a temperature higher than that for the samples from Refs. 2 and 3. As the neutron diffraction powder pattern was made on a sample containing both compounds, the structures arrived at for β-Nb_2N and γ-NbN have not been obtained by a traditional refinement procedure. The diffraction data available are not sufficient to permit a refinement of all possible parameters, and the parameters are strongly correlated. Therefore the two structures should only be regarded as structural proposals. The high temperature X-ray powder diffraction investigation shows, that at temperatures between 1550 and 1660 °C and nitrogen gas pressures of 1 atm γ-NbN transforms to δ-NbN as the c/a ratio approaches unity. The transformation from δ-NbN to γ-NbN involves an order-disorder reaction. δ-NbN is cubic and substoichiometric in nitrogen with the vacancies randomly distributed at the nitrogen sites. The transformation from δ-NbN to γ-NbN on cooling of specimens results in formation of samples with a lamella structure and twinning (see Table 4) similar to the twinning formed in a Martensitic phase transformation.

Acknowledgements. The author is indebted to Mrs. B. Lebech, Department of Physics, Risø, for measuring the neutron diffraction powder pattern. Statens naturvidenskabelige Forskningsråd is acknowledged for the high temperature X-ray diffractometer.

REFERENCES

1. Toth, L. E. *Transition Metal Carbides and Nitrides*, Academic Press, New York and London, 1971.
2. Brauer, G. and Esselborn, E. *Z. Anorg. Allg. Chem. 309* (1961) 151.
3. Brauer, G. and Jander, J. *Z. Anorg. Allg. Chem. 270* (1952) 160.
4. Brauer, G. and Kirner, H. *Z. Anorg. Allg. Chem. 328* (1964) 34.
5. Christensen, A. N. *J. Crystal Growth. Submitted.*
6. Rietveld, H. M. *Program F418 – Fortran IV Version*, Reactor Centrum Nederland, Petten (N.H.), The Netherlands.
7. Burdese, A. *Metallurg. Ital. 49* (1957) 195.
8. Rietveld, H. M. *J. Appl. Cryst. 2* (1969) 65.
9. Guard, R. W., Savage, J. W. and Swarthorst, D. G. *Trans. AIME 239* (1967) 643.
10. Shull, C. G. *Coherent Neutron Scattering Amplitudes*, Massachusetts Institute of Technology, Cambridge, Mass. 1972.

Received August 29, 1975.

Acta Chemica Scandinavica A 30 (1976) 225—228

Crystal and Molecular Structure of Dicarbonylnitrosyl[hydrotris-(pyrazol-1-yl)borato]molybdenum, $HB(C_3N_2H_3)_3Mo(CO)_2NO$

ELIZABETH M. HOLT,[a] SMITH L. HOLT,[a] FRANK CAVALITO [b] and KENNETH J. WATSON [c]

[a] Chemistry Department, University of Wyoming, Laramie, Wyoming 82071, U.S.A., [b] Polytechnic Institute of Brooklyn, 333 Jay Street, Brooklyn, New York 11201, U.S.A., and [c] Kemisk Laboratorium IV, H. C. Ørsted Institut, DK-2100 København, Denmark

The crystal structure of dicarbonylnitrosyl-[hydrotris(pyrazol-1-yl)borato]molybdenum, $HB(C_3N_2H_3)_3Mo(CO)_2NO$, has been determined from X-ray single crystal diffractometer data and refined to a final R factor of 4.7 % (1572 independent reflections). The material crystallizes in a unit cell $a=b=11.435(5)$, $c=8.054(4)$ Å of space group $P\bar{3}$, $Z=2$. Coordination of the molybdenum is roughly octahedral and that of the boron tetrahedral. The dicarbonyl, nitrosyl disorder has been described using a composite scattering factor.

The structures of a series of metal complexes with the tridentate pyrazolyl borate ligand have been reported. Two of these have involved coordination to molybdenum: $HB(pz)_3(C_4H_7)(CO)_2Mo$ [1] and $HB(pz)_3Mo(CO)_2NNC_6H_5$ [2] and three have involved tridentate coordination of a trispyrazolyl borate ligand to other metals: $[HB(pz)_3]_2Co$,[3] $HB(pz)_3(COCH_3)(CO)_2Fe$,[4] and $HB(pz)_3(CF_3C{\equiv}CCF_3)(CH_3)Pt$.[5] In several of these materials a skewing of the planes of the pyrazolyl rings relative to the metal-boron axis has been noted. This skewing has been observed to take different forms. The structure determination of dicarbonylnitrosyl[hydrotris-(pyrazol-1-yl)borato]molybdenum was undertaken to provide a structure in which the geometry of the pyrazolyl ring system might be observed without the steric interference of other bulky coordination groups.

EXPERIMENTAL

Crystal data. $HB(C_3N_2H_3)_3Mo(CO)_2NO$, M = 384.22, trigonal, $P\bar{3}$, $a=b=11.435(5)$, $c=8.054(4)$ Å, $V=912.0(3)$ Å^3, $D_m=1.55$ (by flotation), $Z=2$, $D_c=1.50$ g cm^{-3}, no systematic absences, Mo$K\alpha$ radiation, $\lambda=0.71069$ Å, μ(Mo$K\alpha$) = 8.066 cm^{-1}.

Preliminary photography showed the material to crystallize in a trigonal space group with no systematic absences. The determination of $Z=2$ established that the molybdenum and boron atoms must lie on a line of three-fold symmetry with the two carbonyls and one nitrosyl disordered. A crystal needle-like in shape and of approximate size $0.20\times0.20\times0.30$ mm^3 was mounted on a Picker automated four circle diffractometer. Cell parameters were determined by least squares refinement of the angular positions of 12 independent reflections measured during alignment procedures.

3664 Bragg positions were measured with Mo$K\alpha$ radiation using a 1.66° 2θ-scan at a speed of 1° min^{-1} with backgrounds counted for 10 s at each extreme of the scan range. Three standard reflections were measured after every 50 reflections and their intensities were constant to within 5 % over the whole data measurement period. Of the data, 1557 were classed as non-zero $[|F_o|/\sigma|F_o|>1.5]$. Corrections for Lorentz and polarization factors were made in the usual manner.

Of the possible trigonal space groups in accord with $Z=2$ and the lack of systematic absences, $P\bar{3}$ was chosen. Solution and refinement proceeded without difficulty.[6] Examination of the Harker line 2/3,1/3,w for the special position 1/3,2/3,z allowed assignment of the z coordinate for the heavy atom. Three cycles of refinement of this coordinate ($R=27.9$ %) and a subsequent difference Fourier allowed location of the other eight unique non-hydrogen atoms. Anomalous dispersion corrections were made for molybdenum. Three cycles of least squares refinement of the positional and isotropic thermal parameters for all nine atoms gave an agreement factor of 11.4 %. Because a difference Fourier showed the presence of thermal motion, the isotropic temperature

factors were converted to their anisotropic equivalents and were refined for three cycles. The anisotropic thermal parameters for molybdenum and boron were constrained by the relationships $B_{11}=B_{22}=2B_{12}$, $B_{23}=B_{13}=0$.

Until this point the nitrosyl dicarbonyl disorder was approximated by one full occupancy carbon and one full occupancy oxygen. Because the parameters are so closely correlated, refinement using one nitrogen at one-third occupancy and one carbon at two-thirds occupancy was not successful. Final refinement was carried out designating the disordered position as CN and using for that atom a weighted averaged form factor (the carbon scattering factor plus one-third of the difference between carbon and nitrogen scattering at each $\sin\theta/\lambda$). In as much as the difference between a nitrosyl NO bond and a carbonyl CO bond is 0.03 Å, the oxygen was refined as a single and full occupancy atom.

In the final cycles of refinement a weighting scheme was introduced to reduce the weight of the high-intensity observations. Unit weights were retained for reflections $|F_o|<15.0$ and weights of $(15.0/|F_o|)^2$ were applied to those of greater intensity. At the conclusion of the analysis, the values of $\sum(|F_o|-|F_c|)^2$ for the reflections grouped in 20 sets of increasing $|F_o|$ did not differ by more than a factor of 2.0.

The final R factor was 4.7 %. The maximum ratio of the shift of a parameter to its corresponding estimated standard deviation was 0.003. A final difference Fourier map showed no peak greater than 0.3 e Å^{-3}. No attempt was made to locate the hydrogen atoms.

DISCUSSION OF THE STRUCTURE

Fig. 1 shows the structure in projection on the *ac* plane from the positional parameters of Table 1. Table 2 gives the anisotropic temperature factors and Table 3 the pertinent bond lengths and angles. Standard deviations were calculated from the least squares matrix. Lists of observed and calculated structure factors may be obtained from the authors on request.

Coordination of the boron is roughly tetrahedral. Coordination to molybdenum is close to octahedral as evidenced by bond angles

Table 1. Positional parameters, with estimated standard deviations in parentheses.

Atom	*x/a*	*y/b*	*z/c*
Mo	0.3333	0.6666	0.21881(6)
O	0.1153(5)	0.4445(5)	−0.0026(6)
N1	0.2108(3)	0.6732(3)	0.5629(4)
N2	0.1876(3)	0.6696(3)	0.3972(4)
CN	0.1948(4)	0.5278(5)	0.0812(5)
C1	0.1129(4)	0.6817(4)	0.6457(6)
C2	0.0240(4)	0.6833(4)	0.5311(7)
C3	0.0734(4)	0.6744(4)	0.3777(6)
B	0.3333	0.6666	0.6309(8)

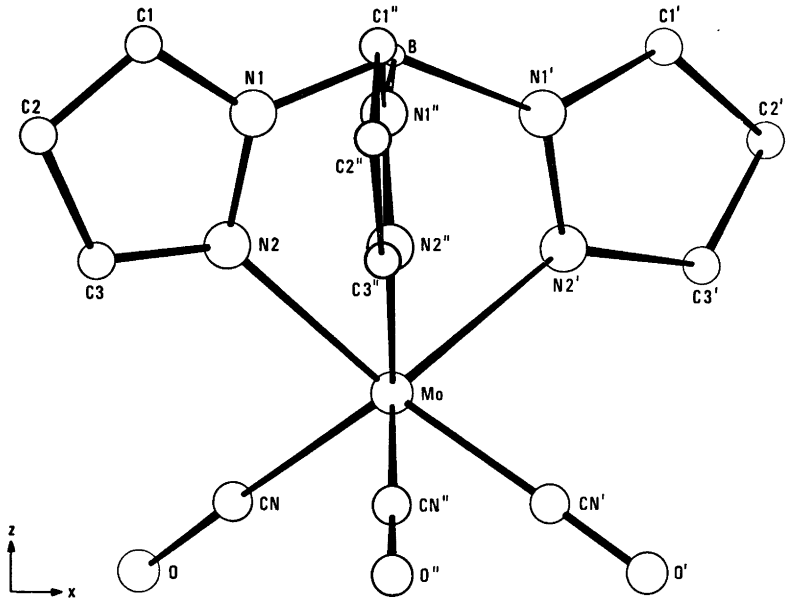

Fig. 1. The molecular conformation as viewed down the *b* axis.

Table 2. Thermal parameters. exp $[-(B_{11}h^2+B_{22}k^2+B_{33}l^2+2B_{12}hk+2B_{13}hl+2B_{23}kl)]$ with estimated standard deviations in parentheses.

Atom	B_{11}	B_{22}	B_{33}	B_{12}	B_{13}	B_{23}
Mo	0.00663(7)	0.00663	0.0657(7)	0.00331	0.0	0.0
O	0.0133(5)	0.0154(6)	0.0157(7)	0.0022(4)	−0.0041(5)	−0.0057(5)
N1	0.0055(2)	0.0059(2)	0.0081(4)	0.0027(2)	−0.0007(2)	−0.0002(2)
N2	0.0055(2)	0.0063(3)	0.0083(4)	0.0032(2)	0.0010(2)	−0.0007(2)
CN	0.0100(4)	0.0110(5)	0.0084(5)	0.0050(4)	−0.0005(4)	−0.0007(4)
C1	0.0061(3)	0.0075(4)	0.0136(6)	0.0032(3)	0.0026(4)	−0.0002(4)
C2	0.0049(3)	0.0078(4)	0.0193(9)	0.0030(3)	0.0010(4)	−0.0008(4)
C3	0.0051(3)	0.0067(3)	0.0158(7)	0.0028(3)	−0.0021(4)	−0.0010(4)
B	0.0066(5)	0.0066	0.0065(7)	0.0033	0.0	0.0

near to 90° at molybdenum. The bond lengths and angles in this structure are consistent with those in other structures of molybdenum pyrazolyl borates.

A calculation of the planarity of the pyrazolyl ring by least squares planes shows the ring to be planar (max. dev. 0.004 Å) with the molybdenum atom 0.113 Å on one side of the plane and the boron atom 0.021 Å on the other side of the plane. Thus the tridentate pyrazolyl borate ligand observed in a situation free of the steric effects of other bulky ligands still shows a skewing of the rings relative to the molybdenum-boron axis.

Table 3. Bond lengths (Å) and angles (°), with estimated standard deviations in parentheses.

Mo−N2	2.213(4)
N2−N1	1.357(4)
N1−B	1.546(4)
N2−C3	1.344(6)
C3−C2	1.383(7)
C2−C1	1.380(7)
C1−N1	1.347(6)
Mo−CN	1.930(4)
CN−O	1.150(6)
CN−Mo−CN′	90.45(30)
CN−Mo−N2	94.02(33)
N2−Mo−N2′	82.42(33)
Mo−N2−N1	120.11(34)
N2−N1−B	121.05(36)
C3−N2−N1	107.04(35)
N2−N1−C1	109.39(36)
N1−C1−C2	108.32(41)
C1−C2−C3	105.40(44)
C2−C3−N2	109.83(41)
C3−N2−Mo	132.81(40)
C1−N1−B	129.55(37)
O−CN−Mo	177.88(35)
N1−B−N1′	107.81(28)

It may be noted that whereas the two other molybdenum complexes with a tris pyrazolyl borate ligand tend to show this type of skewing of the pyrazole planes relative to the molybdenum-boron axis, two of the tris pyrazolyl borate complexes with other metals show a skewing of the plane of the coordinated ring such that the metal and the boron lie on the same side of the plane of the ring. In $HB(pz)_3(C_4H_7)(CO)_2Mo$ [1] two of the three rings show this twisted skewing [Ring A, max. dev. of ring members from plane (max. dev.) 0.001 Å, Mo 0.010 Å, B −0.078 Å; Ring B, max. dev. 0.006 Å, Mo −0.039 Å, B 0.176 Å] while the third ring (max. dev. 0.011 Å, Mo −0.193 Å, B −0.098 Å) has both coordinated atoms on the same side of the plane. Calculations performed on the position parameters for $HB(pz)_3Mo(CO)_2NNC_6H_5$ [2] show this same pattern. Ring A, max. dev. 0.004 Å, Mo −0.050 Å, B 0.016 Å; Ring B max. dev. 0.006 Å, Mo −0.006 Å, B −0.014 Å and ring C max. dev. 0.005 Å, Mo 0.103 Å, B 0.002 Å.

In contrast the tris pyrazolyl borate complexes with other metals seem to show a flapping type of skewing. The structure of $[HB(pz)_3]_2Co$ [3] shows the cobalt atom to be 0.042−0.227 Å from the plane of the pyrazolyl rings and the boron atom to be 0.022−0.180 Å from that plane on the same side of the ring. (Deviation of ring members from plane 0.001−0.013 Å). Calculations of planes performed on data published for $HB(pz)_3(COCH_3)(CO)_2Fe$ [4] show a similar situation: Ring 1, max. dev. 0.002 Å, Fe 0.129 Å, B 0.087 Å; Ring 2, max. dev.

0.015 Å, Fe 0.090 Å, B 0.008 Å; and Ring 3, max. dev. 0.002 Å, Fe 0.043 Å, B 0.095 Å. In a third non-molybdenum structure, the structure of $HB(pz)_3(CF_3C{\equiv}CCF_3)(CH_3)Pt$,[5] the choice of space group has forced one of the pyrazolyl rings to lie on a mirror plane with the platinum and boron. The other two rings are related by the mirror plane. Thus it does not seem valid to look at the skewing of the rings in this structure.

The single crystal structure of $HB(C_3N_2H_3)_3$-$Mo(CO)_2NO$ is consistent with the other published structures of molybdenum pyrazolyl borates in showing a twisted skewing of the pyrazolyl rings relative to the molybdenum-boron axis as opposed to the flapping type of skewing observed in structures of the ligand coordinated to other metals.

The authors express their gratitude to the Danish National Research Council for Natural Sciences for financial support towards the cost of the diffractometer system.

REFERENCES

1. Holt, E. M., Holt, S. L. and Watson, K. J. *J. Chem. Soc. Dalton Trans.* (1973) 2444.
2. Avitabile, G., Ganis, P. and Nemiroff, N. *Acta Crystallogr. B 27* (1971) 725.
3. Churchill, M. R., Gold, K. and Maw, C. E. Jr. *Inorg. Chem. 7* (1970) 1597.
4. Cotton, F. A., Frenz, B. A. and Shaver, A. *Inorg. Chim. Acta 7* (1973) 161.
5. Davies, B. W. and Payne, N. C. *Inorg. Chem. 13* (1974) 1843.
6. Scattering factors were taken from *International Tables for X-Ray Crystallography*, Vol. III, Kynoch Press, Birmingham, 1962, pp. 202–203. Computations were performed on an XDS Sigma 7 using modifications of the full matrix least squares program written by W. R. Busing, K. O. Martin and M. A. Levy and the Fourier program written by W. G. Sly, D. P. Shoemaker and J. H. Van den Hende, and on an IBM 360/75 computer at the Northern European Universities Computing Center, Lundtofte, Denmark, using the programs of J. M. Stewart, F. A. Kundell and J. C. Baldwin: *The X-RAY System 1970*, and local modifications of the data reduction program NRC-2A written by Ahmed, F. R.: *NRC Crystallographic Program System*, Ottawa 1968.

Received September 2, 1975.

Acta Chemica Scandinavica A 30 (1976) 229—234

Short Communications

On the Crystal Structure of $NH_4SnBr_3.H_2O$

JAN ANDERSSON

Department of Inorganic Chemistry, Chalmers University of Technology and the University of Göteborg, P. O. Box, S-40220 Göteborg 5, Sweden

From a solution of tin(II) bromide and ammonium bromide in water a compound with the stoichiometric composition $NH_4SnBr_3.H_2O$ can be crystallized. The translucent needle-like crystals rapidly become opaque in air. All "single crystals" investigated consisted of two crystals grown together along the *a* axis.

An X-ray investigation using Weissenberg techniques showed the crystals to have monoclinic symmetry. Possible space groups are No. 4, $P2_1$ and No. 11, $P2_1/m$.[1] The cell dimensions, as refined from Guinier powder diffraction data, are (21 °C):

$a = 9.4476 \pm 0.0008$ Å, $b = 4.4637 \pm 0.0005$ Å,
$c = 9.6242 \pm 0.0007$ Å, $\beta = 100.714 \pm 0.007°$,
$V = 398.79 \pm 0.06$ Å^3

There are two formula units of $NH_4SnBr_3.H_2O$ in the unit cell.

A comparison between a three-dimensional Patterson synthesis and theoretical vectors calculated from the point position $P2_1/m$:2(e) *i.e.* $\pm(x,\frac{1}{4},z)$ yielded the tin and bromine positions. Difference Fourier calculations showed possible ammonium and water positions. Both positions are remote from tin; water cannot therefore be a ligand. Least squares refinement of *h0l* and *h1l* data yielded an *R*-value of 15.3 %. The structure investigation is to be continued.

Table 1. Approximate atomic parameters for $NH_4SnBr_3.H_2O$.

Atom	*x*	*y*	*z*
Sn	0.146	0.250	0.131
Br(1)	0.359	0.250	0.349
Br(2)	0.990	0.250	0.725
Br(3)	0.699	0.250	0.996
NH_4	0.382	0.250	0.731
H_2O	0.765	0.250	0.394

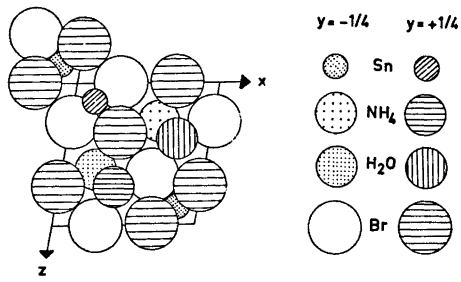

Fig. 1. A projection of the structure of $NH_4SnBr_3.H_2O$ on the *xz* plane.

Fig. 1 shows a projection of the structure on the *xz* plane. Tin has five bromine atoms as nearest neighbours, four of which form a somewhat distorted square with Sn—Br distances of 3.04—3.05 Å. These four bromine atoms are in the same plane. The tin atom is only slightly displaced from this plane. The fifth bromine atom is on the other side of the plane, 2.62 Å from tin. This distance is the shortest found in the five tin(II)-bromine compounds hitherto investigated.[2]

Tin is thus surrounded by a tetragonal pyramide of bromide ions. The crystal structure can be visualized as chains, parallel to the *b* axis, of such tetragonal pyramids sharing edges. Between these chains water molecules and ammonium ions form rows in the *y*-direction.

This work has been supported financially by the Swedish Natural Science Research Council, Contract No. 2318.

1. *International Tables for X-Ray Crystallography*, 2nd Ed., Kynoch Press, Birmingham 1952, Vol. I.
2. Andersson, J. *Acta Chem. Scand. A 29* (1975) 956.

Received December 8, 1975.

On the Force Field and Mean Amplitudes of Vibration of Germanium Dichloride

JON BRUNVOLL and ISTVÁN HARGITTAI *

Division of Physical Chemistry, The University of Trondheim, N-7034 Trondheim-NTH, Norway

In a recent communication [1] a preparation technique, mass spectrometric and infrared (matrix isolation) spectroscopic studies and electron diffraction investigation of germanium dichloride, $GeCl_2$, were reported. The vapour sample of the electron diffraction investigation, in fact, consisted of approximately equal amounts of $GeCl_2$ and $GeCl_4$. The earlier results [2] for the tetrachloride structure have been reproduced, and the bond angle in $GeCl_2$ was determined to be $107 \pm 5°$. Whereas the non-bond distances for the two molecular species were treated independently, only mean values for the Ge – Cl bond length and amplitude of vibration could be determined. The results are summarized in Table 1. That the mean values for r(Ge – Cl) and l(Ge – Cl) referring to the two molecular species were essentially the same as found for $GeCl_4$ by Morino *et al.* suggested that the r_g and l values for the Ge – Cl bond in $GeCl_2$ are little different from those in $GeCl_4$. We found it of interest to examine how different the bond strength is in these molecules, and accordingly, decided to determine the bond stretching force constant for $GeCl_2$. The bond stretching force constant in $GeCl_4$ has been reported earlier (2.79 mdyn/Å).[2] By establishing the force field for $GeCl_2$, it was also possible to see whether a difference in the l(Ge – Cl) values for $GeCl_2$ and $GeCl_4$ could be detected in the calculations. For this purpose, the available information in the literature [2,3] was extended calculating the l values for $GeCl_4$ at the temperature of the electron diffraction experiment of the mixture, *viz.* 80 °C (see below).

* Permanent address: Central Research Institute for Chemistry, Hungarian Academy of Sciences, H-1088 Budapest, Puskin utca 11 – 13, Hungary.

Table 1. Structural parameters (Å) determined by electron diffraction [1] for a mixture of $GeCl_2$ and $GeCl_4$.

$r_g(Ge-Cl)_{av}$	2.110 ± 0.004
$l(Ge-Cl)_{av}$	0.048 ± 0.001
$r_g(Cl\cdots Cl)_{GeCl_2}$	3.387 ± 0.096
$l(Cl\cdots Cl)_{GeCl_2}$	0.095 ± 0.010
$r_g(Cl\cdots Cl)_{GeCl_4}$	3.447 ± 0.014
$l(Cl\cdots Cl)_{GeCl_4}$	0.098 ± 0.010

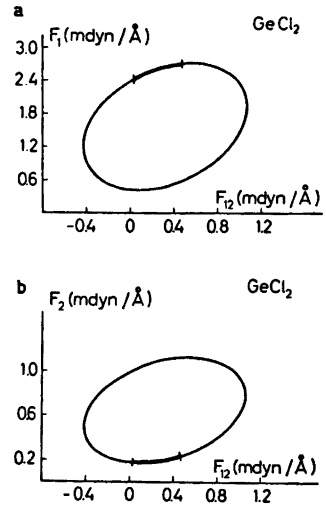

Fig. 1. Force constants for germanium dichloride, consistent with observed frequencies. The thicker portions of the graphs are consistent with the electron diffraction results. *a*, F_1 *vs.* F_{12}; *b*, F_2 *vs.* F_{12}.

The secular equation technique described by Cyvin [4] was used for establishing the force field of $GeCl_2$. The three frequencies were taken from the following sources:

ν_1 398.6 cm^{-1}, argon matrix infrared spectroscopy;[1,5] ν_2 159 cm^{-1}, gas phase Raman spectroscopy;[6] ν_3 373.4 cm^{-1}, argon matrix infrared spectroscopy.[1,5]

The force field of the A_1 species was varied within such limits that all force constants take real values. The results are presented graphically in Fig. 1. For each set of F values (F_1, F_{12}, F_2) expressions given by Cyvin [4] for the bent symmetrical XY_2 molecular model were used to find the l values. These calculated mean amplitudes of vibration were compared with the electron diffraction results. Computed l and F values consistent with the electron diffraction l(Cl···Cl) value for $GeCl_2$ are given in Table 2 and Fig. 2 (see also the thick portions

Table 2. Force fields and mean amplitudes of vibration for some combinations of force constants of $GeCl_2$.

F_1	F_2	F_{12}	l(Ge – Cl)	l(Cl···Cl)
2.439	0.182	0.026	0.0532	0.1112
2.581	0.183	0.174	0.0532	0.1037
2.676	0.204	0.322	0.0543	0.0960
2.726	0.244	0.470	0.0563	0.0881

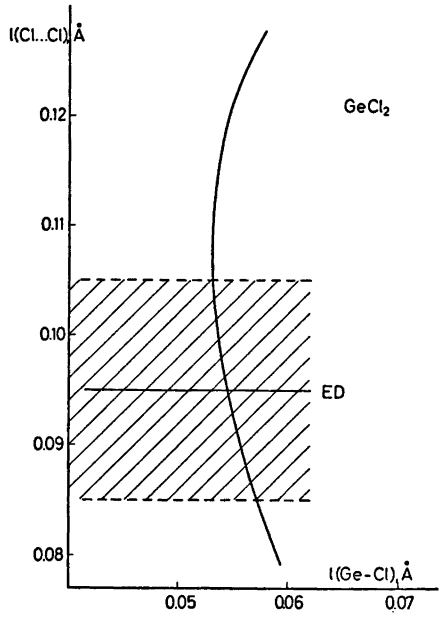

Fig. 2. Part for the mean amplitude of vibration ellipse for germanium dichloride at 80 °C. The electron diffraction value (ED) with error limit (shaded area) is also shown.

of the graphs in Fig. 1). As l(Ge−Cl) is plotted against l(Cl···Cl) in Fig. 2, it is seen that l(Cl···Cl) = 0.095 Å, *i.e.* the electron diffraction value, corresponds to l(Ge−Cl) = 0.054 Å. The calculated l (and K) values for $GeCl_2$ using $F_1 = 2.676$, $F_{12} = 0.322$, and $F_2 = 0.204$ mdyn/Å are given for three temperatures in Table 3.

If the contribution of the Ge−Cl bond of $GeCl_2$ is subtracted from the composite maximum of the radial distribution curve of the mixture, using l(Ge−Cl) = 0.054 Å, the remaining part corresponding to $GeCl_4$ yields l(Ge−Cl) = 0.046 Å. This is then in excellent agreement with the calculated l(Ge−Cl) value for $GeCl_4$, *viz.* 0.0468 Å at 80 °C.*

As for the force constants, the electron diffraction result for $GeCl_2$, l(Cl···Cl) = 0.095 ± 0.010 Å, is consistent with $2.58 < F_1 < 2.73$ mdyn/Å and $F_3 = 1.79$ mdyn/Å. The bond stretching force constant for $GeCl_2$, $f_r = \frac{1}{2}(F_1 + F_3)$ will then be between 2.18 and 2.26 mdyn/Å.

The bond stretching force constants indicate a weaker bond in $GeCl_2$ than in $GeCl_4$ while the bond lengths seemed to be little if any different from the electron diffraction results. The weaker bond is consistent with the calculated larger l value for the Ge−Cl bond in $GeCl_2$ *vs.* that in $GeCl_4$.

One of the authors (I.H.) expresses appreciation to Professors O. Bastiansen, S. J. Cyvin and H. Viervoll for an invitation to Norway and to Norges almenvitenskapelige forskningsråd for a fellowship (October−December, 1975).

Table 3. Mean amplitudes of vibration (l) and K values [a] for $GeCl_2$.

	$T = 0$ K	$T = 298$ K	$T = 353$ K
l(Ge−Cl)	0.0433	0.0514	0.0543
l(Cl···Cl)	0.0608	0.0893	0.0960
K(Ge−Cl)	0.0012	0.0033	0.0039
K(Cl···Cl)	0.0002	0.0002	0.0003

[a] $K = [\langle(\Delta x)^2\rangle + \langle(\Delta y)^2\rangle]/2r$

1. Vajda, E., Hargittai, I., Kolonits, M., Ujszászy, K., Tamás, J., Maltsev, A. K., Mikaelian, R. G. and Nefedov, O. M. *J. Organometal. Chem. In press.*
2. Morino, Y., Nakamura, Y. and Iijima, T. *J. Chem. Phys. 32* (1960) 643.
3. Bürger, H. and Ruoff, A. *Spectrochim. Acta 24 A* (1968) 1863.
4. Cyvin, S. J. *Molecular Vibrations and Mean Square Amplitudes*, Universitetsforlaget, Oslo, and Elsevier, Amsterdam 1968.
5. See also Ozin, G. A. and Van der Voet, A. *J. Chem. Phys. 56* (1972) 4768.
6. Beattie, I. R. and Perry, R. O. *J. Chem. Soc. A* (1970) 2429.

Received December 5, 1975.

* The other calculated values for $GeCl_4$ include l(Cl···Cl) = 0.1056 Å, K(Ge−Cl) = 0.0034 Å, and K(Cl···Cl) = 0.0027 Å.

The Crystal Structure of Antimony(III) Pyrogallate, $Sb(C_6H_3O_3).H_2O$

BENGT AURIVILLIUS and
CHRISTER SÄRNSTRAND

Division of Inorganic Chemistry 2, Chemical Center, University of Lund, P. O. Box 740, S-220 07 Lund 7, Sweden

Pyrogallol, $C_6H_6O_3$, has been used as an analytical reagent for antimony and bismuth because colourless $Sb(C_6H_3O_3).H_2O$ and yellow $Bi(C_6H_3O_3)$ are only slightly soluble in water solution.[1] The reagent may be used for quantitative determination of Sb^{3+} and Bi^{3+} either alone or in presence of ions of Zn, As or Pb.[2] Geometrical considerations show that one Sb or Bi cannot be bonded to all three oxygen atoms of one pyrogallate ion. For the Sb compound the structural formula may be

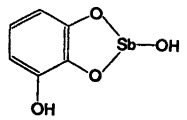

with three-coordinated Sb as proposed by Feigl[1] or a structure with four-coordinated Sb bonded to two or more pyrogallate ions. The second alternative seems to be the most probable.

$Sb(C_6H_3O_3).H_2O$ and $Bi(C_6H_3O_3)$ were synthesized according to the method of Vogel.[2] The X-ray powder photographs were interpreted by orthorhombic unit cells. The diffractograms indicate that the Sb and Bi compounds are very similar in spite of their different water content. The following lattice parameters were obtained with the aid of least-squares calculations.

	$Sb(C_6H_3O_3).H_2O$	$Bi(C_6H_3O_3)$
a/Å	8.4168(12)	8.5515(11)
b/Å	15.982(3)	16.063(3)
c/Å	4.7871(9)	4.6799(7)
V/Å^3	643.9(2)	642.8(2)

Single crystal measurements were made for the antimony pyrogallate compound. Weissenberg photographs showed the following conditions limiting possible reflexions: hkl only with $k+l=2n$ and $h0l$ only with $h=2n$, which are characteristic for the space groups $Amam$ (No. 63), $Ama2$ (No. 40) and $A2_1am$ (No. 36). The observed density (by floation) is 2.62 g cm^{-3}, in good agreement with the calculated density of 2.71 g cm^{-3} for four formula units per unit cell. Thus the unit cell contains four Sb atoms. Because of the very low observed intensity of all reflexions with $h=2n+1$, the positions

Table 1. Final positional and thermal parameters for Sb(III) pyrogallate. Standard deviations are given within parentheses. The anisotropic thermal parameters are based on the expression $\exp[-(h^2\beta_{11}+k^2\beta_{22}+l^2\beta_{33}+2hk\beta_{12}+2hl\beta_{13}+2kl\beta_{23})]$.

Atom	x	y	z	B/Å^2	β_{11}	β_{22}	β_{33}	β_{12}	β_{13}	β_{23}
Sb	0	0	0		.00459(7)	.00151(2)	.0156(3)	.0002(1)	0	0
O1	¼	.0309(6)	−.113(3)		.0037(10)	.0016(2)	.031(6)	0	0	.003(1)
O3	¼	.3946(8)	−.278(5)		.0114(16)	.0037(6)	.030(13)	0	0	.003(2)
O2	−.0298(7)	.0904(4)	−.291(2)		.0043(10)	.0020(2)	.040(6)	.0009(3)	.0008(13)	.0024(8)
C1	¼	.0934(8)	−.307(6)	1.48(23)						
C4	¼	.2179(8)	−.701(4)	1.81(21)						
C2	.1028(11)	.1238(5)	−.401(2)	1.47(12)						
C3	.1059(12)	.1868(5)	−.599(3)	1.82(14)						
H4	¼	.2643	−.845	2						
H3	.0118	.2087	−.670	2						

4(c) in *Amam*, 4(b) in *Ama*2 and 4(*a*) in $A2_1am$ did not seem probable for the Sb atoms. The positions 4(*a*) and 4(*b*) in *Amam* are not compatible with the presence of the stereochemically active lone pair of the Sb atoms, since their point symmetry is 2/*m*. Thus space group *Ama*2 was used and the four Sb atoms were assumed to occupy the position 4(*a*) with $z = 0$ whereby the origin of the unit cell was fixed.

A single crystal ($0.065 \times 0.014 \times 0.283$ mm^3) was mounted on a Pailred diffractometer along the crystallographic *c* axis (the 0.283 mm direction). Totally 1041 reflexions were collected using Mo$K\alpha$ radiation ($\lambda = 0.71069$ Å). The conditions for recording and reducing the intensities were mainly the same as described by Aurivillius and Malmros.[3] 417 intensities were considered unobserved, being weaker than 2.58 $\sigma(I)$, where $\sigma(I)$ is the standard deviation of the intensity based on counting statistics. 4 weak intensities were rejected because of uneven backgrounds. The remaining 620 intensities contained both *hkl* and $h\bar{k}l$ reflexions. After corrections for Lorentz, polarization and absorption effects ($\mu_{MoK\alpha} = 42.9$ cm^{-1}), the corresponding observed reflexions were average and 309 independent reflexions thus remained from the diffractometer measurements.

Having fixed the positions of the Sb atoms, the positions of the C and O atoms were found from difference Fourier maps. Least-squares refinements were made using anisotropic temperature factors for the Sb and O atoms and isotropic ones for the C atoms. The positions of the non-water hydrogen atoms were deduced from geometrical considerations and their temperature factors were fixed to agree with those of the corresponding carbon atoms. The parameters of the hydrogen atoms were not varied during the least-squares calculations. Anomalous dispersion was finally introduced for the Sb atoms and the weighted *R*-value was 0.0332. The signs of all *z* coordinates were reversed together with the signs of the terms β_{13} and β_{23} belonging to the anisotropic temperature factors. A new refinement gave the value 0.0327 for the weighted *R*-factor. Thus the structure of the single crystal used could best be described by the last-mentioned parameters. The final conventional *R*-factor is 0.023 for 309 reflexions. The antimony atoms do not contribute to 25 reflexions with $h = 2n + 1$. The separate *R*-factor for these reflexions is 0.066. Positional and thermal parameters are listed in Table 1. Lists of $|F_o|$ and $|F_c|$ are available on request.

The crystal structure of antimony pyrogallate is mainly as could be expected from the present knowledge of the coordination of antimony(III).[4] Each antimony atom is coordinated to four oxygen atoms belonging to two pyrogallate ions (*cf.* Fig. 1) in such a way that endless isolated chains of composition $Sb(C_6H_3O_3)$ parallel to the crystallographic *a* axis are formed. The Sb–O distances and

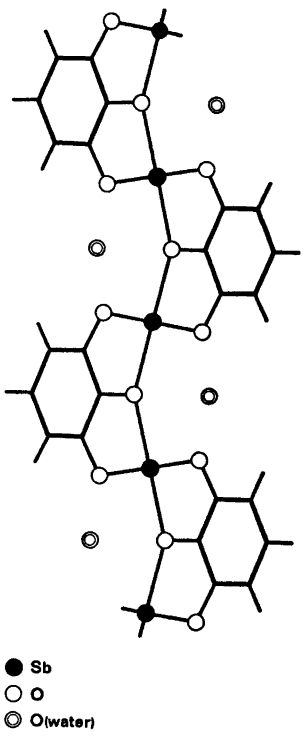

Fig. 1. A projection along the *c*-axis of an endless chain of composition $Sb(C_6H_3O_3).H_2O$. The chain is parallel to the *a*-axis. The water molecules are also indicated.

O–Sb–O angles agree well with the ones found for other four-coordinated Sb(III)-oxygen compounds. In addition to the four oxygen atoms at close distances, the Sb atom has two water molecules as next nearest neighbours at the distance 2.91(1) Å (*cf.* Fig. 1). Hydrogen bonds may be present between the water oxygen and the pyrogallate oxygens at the distance 2.71(2), 2.99(2) and 2.99(2) Å. Two antimony atoms, and one water oxygen atom

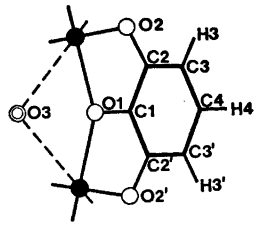

Fig. 2. A projection along the *c*-axis showing a part of the endless chain and a water molecule in order to illustrate the formation of the chelate rings.

Table 2. Distances (Å) and angles (°) in the SbO_4-polyhedron. The labeling of the atoms is given in Fig. 2.

	Present compound	$K_2[Sb_2(C_4H_2O_6)_2].3H_2O$[5]	$Fe(C_{12}H_8N_2)_3Sb_2(C_4H_2O_6)_2.8H_2O$[6]
Distances			
Sb–O2	2.022(9)	2.06(3), 2.01(3)	1.94(1)
Sb–O2′		2.05(2), 1.91(3)	1.94(1)
Sb–O1	2.228(4)	2.25(3), 2.22(3)	2.11(2)
Sb–O1′		2.17(3), 2.16(3)	2.16(2)
Angles			
O1–Sb–O1′	151.8(8)	147(1), 151(1)	153.5(7)
O1–Sb–O2	78.0(3)	77(1), 79(1)	79.7(6)
O1–Sb–O2′	82.7(4)	78(1), 80(1)	82.7(5)
O1′–Sb–O2	82.7(4)	82(1), 81(1)	84.9(5)
O1′–Sb–O2′	78.0(3)	79(1), 86(1)	79.1(5)
O2–Sb–O2′	92.9(9)	94(1), 103(1)	100.3(6)

are situated close to the plane formed by the corresponding pyrogallate ion (Fig. 2). The largest deviation from the best plane through the pyrogallate ring is 0.04 Å for the Sb atoms and 0.35 Å for the water oxygen atom. In this way three rings are formed which are nearly coplanar with the benzene ring, namely two five-membered chelate rings SbO_2C_2 and one four-membered ring containing two antimony atoms, one pyrogallate oxygen atom and one water oxygen atom. In Table 2 selected distances and angles of the present compound are compared to corresponding values for two other compounds where Sb also takes part in two five-membered chelate rings.

This investigation is a part of a research project financially supported by the Swedish Natural Science Research Council.

1. Feigl, F. and Ordelt, H. *Z. Anal. Chem. 65* (1924–25) 448.
2. Vogel, A. I. *A Text-Book of Quantitative Inorganic Analysis*, 3rd Ed., Longmans 1960, pp. 133, 490, 403.
3. Aurivillius, B. and Malmros, G. *Acta Chem. Scand. 27* (1973) 3167.
4. Bovin, J. O., Svensson, C. and Särnstrand, C. *Collected Abstracts from Second European Crystallographic Meeting*, Keszthely, Hungary, 1974, 206.
5. Kamenar, B., Grdenić, D. and Prout, C. K. *Acta Crystallogr. B 26* (1970) 181.
6. Zalkin, A., Templeton, D. H. and Ueki, T. *Inorg. Chem. 12* (1973) 1641.

Received December 16, 1975.

Acta Chemica Scandinavica A 30 (1976) 235—240

Metal Halide and Pseudohalide Complexes in Dimethyl Sulfoxide Solution. II. The Crystal Structure of Bisdimethyl Sulfoxide Silver(I) Perchlorate

NILS-OLOF BJÖRK and ANDERS CASSEL

Inorganic Chemistry 1, Chemical Center, University of Lund, P.O.B. 740, S-220 07 Lund, Sweden

The crystal structure of $Ag[(CH_3)_2SO]_2ClO_4$ has been determined from three-dimensional, photographic X-ray intensity data and refined from data collected with a four-circle diffractometer. The space group is $P2_1/n$ with $Z=4$ and the unit cell dimensions $a=10.336(1)$ Å, $b=18.188(2)$ Å, $c=6.523(1)$ Å and $\beta=98.56(1)°$. The structure is built up by infinite chains of silver atoms joined by double-bridging dimethyl sulfoxide oxygens. Each silver is also coordinated to a perchlorate ion, in which the oxygens are affected by great thermal motions. The coordination polyhedron of silver can be described as a distorted trigonal bipyramide, with Ag—O distances ranging between 2.36 and 2.74 Å.

This series of investigations mainly deals with metal complexes in solutions of dimethyl sulfoxide (DMSO). However, the structure determination of some crystallized metal dimethyl sulfoxide solvates are planned as they give important information about the coordination properties of the metal ions. With due caution, the structures which most plausibly exist in solution may also be inferred from these investigations. In this paper the structure of $Ag(DMSO)_2ClO_4$ is reported.

EXPERIMENTAL

Preparation and analysis. The preparation and analysis of $Ag(DMSO)_2ClO_4$ have been described elsewhere.[1] The compound was dissolved in acetone and colourless needles were obtained at room-temperature on slow evaporation of excess solvent.

Single crystal work. The compound is decomposed by traces of moisture. The needles are generally twinned and sufficiently good single crystals could not be obtained directly.

From large twinned crystals, however, single crystals of irregular shape were cut out and mounted in capillaries. A crystal, mounted along the c-axis, was used in recording preliminary Weissenberg data (Cu$K\alpha$, 1053 independent reflexions, visually estimated). Another crystal was used for collecting intensity data on a computer-controlled four-circle diffractometer of type CAD-4, using graphite-monochromatized Mo$K\alpha$ radiation ($\lambda=0.71069$ Å). Intensity data were recorded at a take-off angle of 5°. The $\omega-2\theta$ scan technique was used, with a scan interval $\Delta\omega=(0.7+0.5\tan\theta)°$. A fast prescan was used in order to determine the scan speed at which a predetermined minimum number of counts (3000) for each reflexion was received. The recording time was limited to 3 min. The intensities of 2780 reflexions were measured in the range $3°<\theta<27°$. Of these, 841 were below background, while 613 had intensities $I<3\sigma(I)$, where $\sigma(I)$ is the standard deviation of the intensity based on counting statistics. In all, 1454 reflexions were therefore discarded. After every 50th reflexion the intensities of three control reflexions were measured. A decrease of their intensities were found during the course of data collection. All intensities were therefore scaled with a first-order polynomial determined by least-squares. The values of I and $\sigma(I)$ were corrected for Lorentz and polarization effects. No correction for absorption was made [μ(Mo$K\alpha$) = 22.0 cm^{-1}].

Unit cell and space group. $Ag(DMSO)_2ClO_4$ crystallizes in the monoclinic system. Preliminary cell parameters and systematically absent reflexions were obtained from oscillation and Weissenberg photographs. From the systematically absent reflexions $h0l$: $h+l=2n+1$ and $0k0$: $k=2n+1$ the only possible space group is $P2_1/n$. The cell parameters were refined from Guinier-Hägg powder diffraction data by the method of least-squares. The density was deter-

Table 1. Crystal data for $Ag[(CH_3)_2SO]_2ClO_4$.

Space group $P2_1/n$

$a = 10.336(1)$ Å, $b = 18.188(2)$ Å, $c = 6.523(1)$ Å, $\beta = 98.56(1)°$, $V = 1213$ Å^3, $Z = 4$, $M = 363.6$, $D_m = 1.99$ g cm^{-3}, $D_x = 1.99$ g cm^{-3}, $\mu(MoK\alpha) = 22.0$ cm^{-1}.

Table 2a. Final fractional coordinates, multiplied by 10^4, and isotropic thermal parameters. Estimated standard deviations are given in parentheses. The occupancy numbers of the oxygen atoms are 1.0 for O(4), and 0.5 for O(3), O(5)–O(8).

Atom	x	y	z	B (Å^2) [a]
Ag	5737(1)	5261(1)	2647(1)	
S(1)	2604(3)	5867(2)	0588(5)	
S(2)	5535(3)	3417(2)	4073(5)	
O(1)	6143(7)	4411(4)	0080(11)	
O(2)	5365(9)	4185(4)	4846(11)	
O(3)	7508(23)	6098(19)	2351(51)	
O(4)	9671(17)	6369(9)	2423(33)	
O(5)	7998(30)	7055(24)	2884(89)	
O(6)	8198(45)	5774(14)	4085(48)	
O(7)	8629(37)	7014(19)	4543(57)	
O(8)	8859(42)	6366(36)	5404(43)	
Cl	8594(3)	6412(2)	3376(5)	4.4(1)
C(1)	1932(14)	5089(8)	1810(21)	5.7(3)
C(2)	8545(15)	4078(8)	1735(22)	6.5(3)
C(3)	4099(14)	3236(8)	2223(22)	6.5(3)
C(4)	4774(14)	7175(8)	3873(20)	5.8(3)

[a] For β_{ij}, *cf.* Table 2b.

mined from the loss of weight in benzene. Some crystal data are given in Table 1.

DETERMINATION AND REFINEMENT OF THE STRUCTURE

The positions of the silver, sulfur, chlorine, and DMSO oxygen atoms were determined by conventional methods, the calculations based on the Weissenberg data.

For the refinement counter intensities for 1326 non-zero reflexions were available. The positional and thermal parameters of the silver, sulfur, chlorine, and DMSO oxygen atoms obtained above were used as preliminary parameters. The resulting discrepancy factor $R = \sum||F_o| - |F_c||/\sum|F_o|$ was 0.095. From a subsequent three-dimensional difference synthesis six oxygen atom positions around the chlorine atom could be found.

With the positional and thermal parameters of silver, chlorine, carbon, and the DMSO-oxygens obtained in the last least-squares calculations, a further refinement was performed, where the only quantities varied were the scale factor, the positional and thermal parameters of the perchlorate oxygens and their occupancy numbers. The resulting R-value was 0.054. No oxygen atom gave converging occupancy numbers, but the values of five of them were approximately 0.5 and of the sixth 0.8. It was thus not possible to locate all perchlorate oxygen atoms in the structure. An additional calculation was made where the occupancy numbers were fixed to 0.5 for

Table 2b. Vibrational parameters, multiplied by 10^5, for silver, sulfur and oxygen. The expression used for the anisotropic thermal parameters is $\exp[-(h^2\beta_{11} + k^2\beta_{22} + l^2\beta_{33} + 2hk\beta_{12} + 2hl\beta_{13} + 2kl\beta_{23})]$.

Atom	β_{11}	β_{22}	β_{33}	β_{12}	β_{13}	β_{23}
Ag	129(1)	35(0)	202(2)	−8(1)	37(1)	0(1)
S(1)	83(3)	33(1)	278(8)	6(2)	39(4)	−10(2)
S(2)	120(4)	24(1)	256(8)	4(2)	45(4)	−9(2)
O(1)	75(8)	48(3)	234(19)	13(4)	25(10)	−1(6)
O(2)	207(13)	24(2)	248(21)	4(5)	86(14)	−9(6)
O(3)	133(26)	118(18)	780(114)	−73(18)	−77(45)	−190(38)
O(4)	379(31)	77(7)	1775(127)	−6(12)	689(57)	−26(24)
O(5)	160(41)	130(23)	1789(286)	59(25)	291(92)	345(72)
O(6)	661(96)	51(11)	532(99)	−124(27)	196(84)	37(26)
O(7)	302(60)	74(15)	590(115)	−16(25)	94(69)	−158(39)
O(8)	399(74)	208(39)	363(99)	25(47)	−273(69)	−1(50)

five and to 1.0 for the sixth, and the isotropic temperature factors replaced by anisotropic ones. The resulting conventional R-value was 0.052 and the weighted R_w-value, defined by $R_w = [\sum w_i(|F_o| - |F_c|)^2 / \sum |F_o|^2]^{\frac{1}{2}}$, 0.066. The quantity minimized was $w_i(|F_o| - |F_c|)^2$, with $w_i^{-1} = \sigma^2(|F_o|) + a|F_o|^2 + b$, where $a = 0.0015$ and $b = 2.0$ were used in the last refinement. The average values of $w_i(|F_o| - |F_c|)^2$ were nearly constant in different $|F_o|$ and sin θ intervals. A final difference electron density map gave no peaks larger than 2 e Å^{-3}. Scattering factors for neutral silver were taken from Cromer *et al.*[2] and for neutral sulfur, oxygen, chlorine, and carbon from Hanson *et al.*[3]

The final positional and thermal parameters are given in Table 2a, b. A table of observed and calculated structure factors can be obtained from the authors on request. All calculations were made on the Univac 1108 computer in Lund and short accounts of the program system have been given.[4,5]

DESCRIPTION AND DISCUSSION OF THE STRUCTURE

Stereoscopic views of the structure of $Ag(DMSO)_2ClO_4$ are given in Figs. 1 and 2. Selected interatomic distances and angles are presented in Table 3. The structure may be described as built up by infinite chains of the same formula, running along the c-axis. The silver atoms are joined by doubly bridging DMSO oxygens. Each silver is also coordinated to a perchlorate ion. Only weak interactions exist between the chains.

The coordination of silver. Silver is surrounded by six oxygen atom positions at distances 2.35 – 2.74 Å. Four of these refer to the DMSO oxygens and two to the perchlorate oxygens.

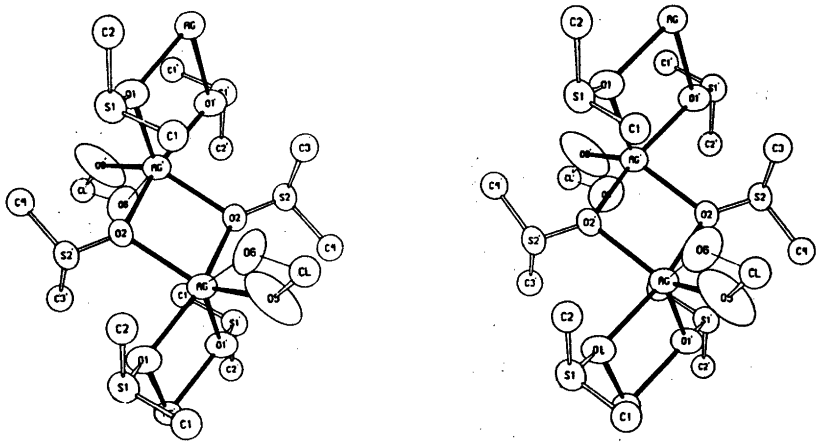

Fig. 1. Stereo view of the silver-oxygen coordination in one infinite chain. For notation, see Table 3a. The oxygen atoms O(4), O(5), O(7) and O(8) are omitted.

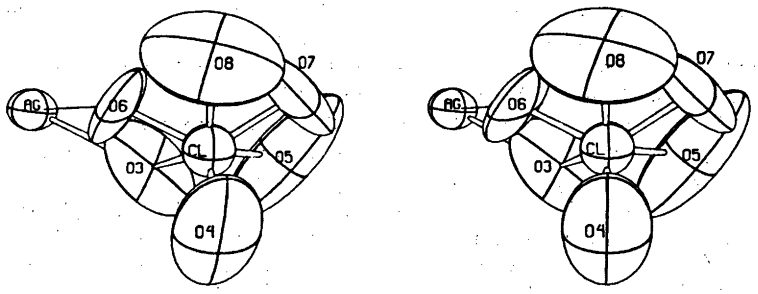

Fig. 2. Stereo view of the perchlorate-silver interaction.

Table 3. Selected interatomic distances (Å) and angles (°). Standard deviations are given in parentheses. For notations, see Figs. 1, 2 and Table 2a. An atom denoted with a prime is related to the unprimed through $\bar{1}$.

The coordination of silver

Ag–O(1)	2.362(7)	O(1)–Ag–O(6)	102.2(7)
–O(1′)	2.504(7)	O(1′)–Ag–O(2)	89.2(3)
–O(2)	2.354(8)	O(1′)–Ag–O(2′)	115.3(3)
–O(2′)	2.489(7)	O(1′)–Ag–O(3)	108.1(8)
–O(3)	2.411(29)	O(1′)–Ag–O(6)	138.1(7)
–O(6)	2.741(43)	O(2)–Ag–O(2′)	78.7(3)
		O(2)–Ag–O(3)	103.7(8)
O(1)–Ag–O(1′)	81.6(3)	O(2)–Ag–O(6)	97.9(7)
O(1)–Ag–O(2)	158.1(3)	O(2′)–Ag–O(3)	136.6(8)
O(1)–Ag–O(2′)	87.3(3)	O(2′)–Ag–O(6)	106.6(6)
O(1)–Ag–O(3)	98.0(8)	O(3)–Ag–O(6)	30(1)

The DMSO molecules

S(1)–O(1)	1.514(8)	O(1)–S(1)–C(1)	105.5(6)
–C(1)	1.812(14)	O(1)–S(1)–C(2)	105.4(6)
–C(2)	1.783(15)	C(1)–S(1)–C(2)	99.6(7)
S(2)–O(2)	1.504(7)	O(2)–S(2)–C(3)	105.6(6)
–C(3)	1.799(15)	O(2)–S(2)–C(4)	105.4(5)
–C(4)	1.784(14)	C(3)–S(2)–C(4)	99.8(7)

The perchlorate ion

Cl–O(3)	1.34(3)	O(4)–Cl–O(5)	109(2)
–O(4)	1.36(2)	O(4)–Cl–O(6)	115(2)
–O(5)	1.34(4)	O(4)–Cl–O(7)	111(2)
–O(6)	1.34(3)	O(4)–Cl–O(8)	113(2)
–O(7)	1.33(4)	O(5)–Cl–O(6)	133(3)
–O(8)	1.31(3)	O(5)–Cl–O(7)	52(3)
O(3)–Cl–O(4)	115(2)	O(5)–Cl–O(8)	108(4)
O(3)–Cl–O(5)	86(2)	O(6)–Cl–O(7)	120(2)
O(3)–Cl–O(6)	62(2)	O(6)–Cl–O(8)	68(3)
O(3)–Cl–O(7)	126(2)	O(7)–Cl–O(8)	60(3)
O(3)–Cl–O(8)	120(3)		

Silver-silver

Ag–Ag 3.685(2) and 3.746(2)

The occupancy numbers of the coordinating perchlorate oxygens O(3) and O(6) are 0.5 and the angle O(3)–Cl–O(6) is 62°. The two positions cannot be occupied simultaneously.

The coordination polyhedron can be described as a distorted trigonal bipyramide, with the two shortest silver oxygen bonds Ag–O(1) (2.36 Å) and Ag–O(2) (2.35 Å) as the axis. The angle O(1)–Ag–O(2) which should ideally be 180° is in fact 158.1°. The silver-oxygen distances of the equatorial plane are 2.49 and 2.50 Å for the DMSO oxygens and either 2.41 or 2.74 Å for the perchlorate oxygen; Table 3 and Fig. 1. Only five of the silver-oxygen distances are within the limits of the sums of covalent and ionic radii, 2.18 and 2.66 Å, respectively.[8] Distances larger than 2.66 Å do not imply bonds between the atoms, but up to 2.90 Å weak interactions may well exist.[7–9]

Similar approximately linear O–Ag–O fragments with short silver-oxygen distances are reported in the structures of $NH_2CH_2COOH.AgNO_3$,[10] $(AgC_2F_3O_2)_2C_6H_6$[11] and Ag_2SO_3.[12] In these structures the two short silver oxygen distances and the angle O–Ag–O are 2.22(2), 2.25(2) Å, 163.1(7)°; 2.22, 2.28 Å, 161.6° and 2.23(2), 2.30(3) Å, 155.1(9)°, respectively.

In aprotic solvents like acetone and nitroethane, silver is reported to be surrounded by four DMSO molecules.[13] In pure DMSO, the same coordination is likely to occur.

The perchlorate ion. The six oxygen positions O(3) to O(8) belong to the perchlorate ion. One of them, O(4), is given an occupancy number of 1.0 while the others are assigned 0.5. The distances Cl – O are all between 1.31 and 1.36 Å. In cases where oxygen atoms of the perchlorate ion are bonded to silver atoms, Cl – O(bonded) distances in the range 1.41(1) – 1.49(2) Å are reported.[7,8,14] On the other hand, for uncoordinated perchlorate oxygens distances between 1.22(3) and 1.52(2) Å are found.[7–9,14–16] The great deviations in these distances must be caused by the fact that there is no adequate way of describing the thermal motions of the oxygen atoms. Neither a spherical nor an ellipsoidal approximation of the electron density is satisfactory. In the present structure the perchlorate ion can be described as rotating around the Cl – O(4) axis. A similar model has been applied earlier.[16,17] The positions O(3) and O(6) with occupancy numbers 0.5 may be preferred positions but no acceptable tetrahedron can be derived using them as starting points because it is not possible to use the O(5) position in any tetrahedron involving O(3) or O(6), Fig. 2.

Many types of disordered perchlorate structures are known. In $AgClO_4.3$dioxane,[18] the ClO_4^--group is supposed to rotate completely around the chlorine position. Strong disorder also occurs in $(C_6H_6)_3CClO_4$.[15] As expected, perchlorate oxygens involved in bonding are often in fixed positions, while uncoordinated ones are disordered.[8,14] The present result seems to indicate, however, that the opposite also may occur, *viz.* a non-coordinated oxygen is fixed, while coordinated ones do rotate.

The DMSO molecules. The electronic structure of the S – O bond may be represented as a hybrid of the canonical forms (I), (II) and (III):

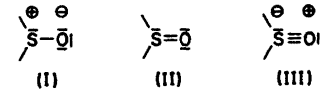

(I) (II) (III)

The structure of pure DMSO is most closely described by (II).[19] In the gas phase the S – O distance is 1.48 Å.[19] Coordination *via* oxygen means increased contribution of (I) which causes a decrease of the bond order. Conversely if coordination *via* sulfur occurs, the contribution of (III) would increase. The S – O distances found here, 1.50 and 1.51 Å, are lengthened relative to pure DMSO, as expected. They also agree well with values reported for other metal-DMSO complexes with oxygen coordination, *viz.* $La(NO_3)_3(DMSO)_4$,[20] 1.50(3) Å; $SnCl_4$-$(DMSO)_2$,[21] 1.51 and 1.54 Å and $FeCl_3(DMSO)_2$,[22] 1.541(6) Å. In cases where metal-sulfur coordination occurs the distances S – O found are, as expected, generally shorter, *viz.* $PdCl_2$-$(DMSO)_2$,[23] 1.475(5) Å; $Pd(NO_3)_2(DMSO)_2$,[24] 1.463(7) Å, and $C_{15}H_{13}OIrCl_2(DMSO)_2$,[25] 1.44 and 1.47 Å.

For DMSO, coordination *via* oxygen is far more common than coordination *via* sulfur.[19] The latter occurs only with very soft acceptors, such as the platinum metals in the compounds just mentioned. As silver(I) is also quite a soft acceptor the oxygen coordination in its DMSO solvate is certainly unexpected, the more so as sulfur coordination occurs in such a compound as silver(I) sulfite.[12] It should be noted, however, that also silver-oxygen coordination occurs in this compound.

Acknowledgements. Our sincere thanks are due to Professor Sten Ahrland and Dr. Karin Aurivillius for the kind interest they have taken in these investigations. The support of Statens naturvetenskapliga forskningsråd (the Swedish Natural Science Research Council) is also gratefully acknowledged.

REFERENCES

1. Ahrland, S. and Björk, N. O. *Acta Chem. Scand. A 28* (1974) 823.
2. Cromer, D. T. and Waber, J. T. *Acta Crystallogr. 18* (1965) 104.
3. Hanson, H. P., Herman, F., Lea, I. D. and Skillman, S. *Acta Crystallogr. 17* (1964) 1040.
4. Oskarsson, Å. *Acta Crystallogr. B 29* (1973) 1747.
5. Stålhandske, C. *Acta Crystallogr. B 30* (1974) 1586.
6. Pauling, L. *Nature of the Chemical Bond*, Cornell University Press, Ithaca, N.Y. 1960, p. (246) 514.
7. Rodesiler, P. F., Hall Griffith, E. A. and Amma, E. L. *J. Amer. Chem. Soc. 94* (1972) 761.

8. Hall Griffith, E. A. and Amma, E. L. *Ibid. 96* (1974) 743.
9. Nassimbeni, L. R. and Thackeray, M. M. *Acta Crystallogr. B 30* (1974) 1072.
10. Mohana Rao, J. K. and Viswamitra, M. A. *Acta Crystallogr. B 28* (1972) 1484.
11. Hunt, G. W., Lee, T. C. and Amma, E. L. *Inorg. Nucl. Chem. Lett. 10* (1974) 909.
12. Larsson, L. O. *Acta Chem. Scand. 23* (1969) 2261.
13. Luehrs, D. C., Nicholas, R. W. and Hamm, D. A. *J. Electroanal. Chem. 29* (1971) 417.
14. Rodesiler, P. F. and Amma, E. L. *Inorg. Chem. 11* (1972) 388.
15. Gomes de Mesquita, A. H., MacGillavry, C. H. and Eriks, K. *Acta Crystallogr. 18* (1965) 437.
16. Sundaralingam, M. and Jensen, L. H. *J. Amer. Chem. Soc. 88* (1966) 198.
17. Aurivillius, B. *Acta Chem. Scand. B 28* (1974) 681.
18. Prosen, R. J. and Trueblood, K. N. *Acta Crystallogr. 9* (1956) 741.
19. Reynolds, W. L. *Progr. Inorg. Chem. 12* (1970) 1.
20. Krishna Bhandary, K. and Manohar, H. *Acta Crystallogr. B 29* (1973) 1093.
21. Lindqvist, I. *Inorg. Adduct Molecules of Oxo-Compounds*, Springer-Verlag, Berlin 1963, p. 73.
22. Bennett, M. J., Cotton, F. A. and Weaver, D. L. *Acta Crystallogr. 23* (1967) 581.
23. Bennett, M. J., Cotton, F. A. and Weaver, D. L. *Ibid. 23* (1967) 788.
24. Langs, D. A., Hare, C. R. and Little, R. G. *Chem. Commun.* (1967) 1080.
25. McPartlin, M. and Mason, R. *Chem. Commun.* (1967) 545.

Received September 24, 1975.

Acta Chemica Scandinavica A 30 (1976) 241—248

The Crystal Structures of $Tl_3[Hg(SO_4)_2][HgSO_4Cl]$ and $Rb_3[Hg(SO_4)_2][HgSO_4Cl]$

BENGT BOSSON

Division of Inorganic Chemistry 2, Chemical Center, The Lund Institute of Technology, P.O. Box 740, S-220 07 Lund 7, Sweden

The crystal structures of $M_3[Hg(SO_4)_2][HgSO_4Cl]$, M = Tl(I), Rb have been determined from single-crystal diffractometer data. The compounds are isostructural, crystallizing in the monoclinic space group $P2_1$ with $Z = 2$. The unit-cell dimensions are

$a = 7.870(1)$, $b = 9.752(1)$, $c = 9.945(1)$ Å, $\beta = 110.72(1)°$ and
$a = 7.862(2)$, $b = 9.790(4)$, $c = 10.002(1)$ Å, $\beta = 111.12(2)°$

for the thallium and rubidium compounds, respectively. The structures may be considered as ionic, made up of $Hg(SO_4)_2^{2-}$, $HgSO_4Cl^-$ and M^+ ions. There is no reason to assume the presence of a stereochemical inert electron pair for the Tl^+ ion in the present structure.

The present investigation was undertaken to study the coordination polyhedra of univalent thallium and rubidium. A study in the same field has been reported previously.[1] Work is in progress on $RbZnSO_4Cl$, $TlZnSO_4Cl$ (a refinement) and $Tl_2S_2O_3$.

EXPERIMENTAL

Preparation. Single crystals of $Tl_3[Hg(SO_4)_2][HgSO_4Cl]$ and $Rb_3[Hg(SO_4)_2][HgSO_4Cl]$ were prepared by melting MCl, M_2SO_4 (M = Tl, Rb) and anhydrous $HgSO_4$ in a mol ratio of 1:1:2 in a sealed gold tube at a temperature of 700 °C. The crystals are in the form of transparent thin plates. The homogeneity of the crystalline samples was checked by X-ray Guinier-Hägg powder photographs.

Crystal data and space group. Preliminary Weissenberg photographs showed that the present thallium and rubidium salts are isostructural. The compounds crystallize in the monoclinic system. The only systematic absences found were $0k0$ with $k = 2n + 1$, which are characteristic of the space groups $P2_1$ (No. 4) and $P2_1/m$ (No. 11). An $N(z)$ test showed the structure to be noncentrosymmetric, thus indicating the space group $P2_1$.

The unit-cell dimensions were determined for $Tl_3[Hg(SO_4)_2][HgSO_4Cl]$ from powder photographs taken in a Guinier-Hägg focusing camera with $CuK\alpha_1$ radiation ($\lambda = 1.5405$ Å) and potassium chloride as an internal standard (cubic, $a = 6.2929$). Refinement of the cell parameters was performed by a least-squares program. The lattice constants for $Rb_3[Hg(SO_4)_2][HgSO_4Cl]$ were obtained from a least-squares analysis of the settings of 30 reflexions measured on a four-circle diffractometer with $MoK\alpha_1$ radiation ($\lambda = 0.70926$ Å).

The densities of the compounds were observed by measuring the loss of weight in benzene. Some crystal data are presented in Table 1.

Collection and reduction of intensity data

$Tl_3[Hg(SO_4)_2][HgSO_4Cl]$. A crystal with the dimensions $0.16 \times 0.03 \times 0.13$ mm³ along a, b

Table 1. Crystallographic data for $M_3[Hg(SO_4)_2][HgSO_4Cl]$ where M = Tl or Rb.

	M = Tl	M = Rb
a (Å)	7.870(1)	7.862(2)
b (Å)	9.752(1)	9.790(4)
c (Å)	9.945(1)	10.002(1)
β (°)	110.72(1)	111.12(2)
V (Å³)	713.9(1)	718.0(4)
Z	2	2
M (g mol^{-1})	1337.93	981.22
D_m (g cm^{-3})	6.22	4.45
D_x (g cm^{-3})	6.10	4.48
μ(MoKα) (cm^{-1})	565	334

and c, respectively, was chosen for the data collection. The intensity data were recorded on a computer-controlled Enraf-Nonius four-circle diffractometer (CAD4) using graphite-monochromatized Mo$K\alpha$ radiation ($\lambda = 0.71069$ Å). The $\omega - 2\theta$ scan technique was used with a scan interval $\Delta\omega°$, of $0.9 + 0.5 \tan\theta$. One fourth of reciprocal space out to $(\sin\theta)/\lambda = 0.985$ Å^{-1} was examined. Instrumental stability and crystal setting were checked using two standard reflexions remeasured every 90 min. No significant variation in their intensities could be observed.

The total number of reflexions was 1544, of which 79 were considered unobserved, being weaker than $3\sigma(I)$, where I is the intensity and $\sigma(I)$ its standard deviation based on counting statistics. The remaining 1465 intensities were corrected for Lorentz, polarization and absorption effects. The polarization factor used was that for ideally mosaic crystals. The crystal could be described by eight planes and the transmission factors, evaluated by numerical integration, were in the range 0.018 – 0.121.

Rb$_3$[*Hg*(*SO*$_4$)$_2$][*HgSO*$_4$*Cl*]. A crystal with the dimensions $0.17 \times 0.22 \times 0.09$ along a, b and c, respectively, was used for the data collection on the diffractometer with the same experimental conditions as described above. Of the 2046 independent reflexions recorded, 75 were excluded as $I < 3\sigma(I)$. The remaining 1971 reflexions were treated as mentioned above. For calculating the absorption corrections, the crystal was described by seven planes. The transmission factors were in the range 0.025 – 0.113.

STRUCTURE DETERMINATION

Tl$_3$[*Hg*(*SO*$_4$)$_2$] [*HgSO*$_4$*Cl*]. The positions of the heavy metal atoms were found from a combination of a three-dimensional Patterson function and direct methods. The chlorine, sulfur and oxygen atoms were located from a three-dimensional electron density difference synthesis. All atoms occupy the general point position 2(*a*) in the space group $P2_1$.

A full-matrix least-squares refinement minimizing $\sum w_i(|F_o| - |F_c|)^2$ was performed with weights $w_i^{-1} = \sigma^2(F_o^2)/4F_o^2 + aF_o^2 + b$. In the last cycle of refinement, the values $a = 0.0003$ and $b = 2.0$ were used. The convergency was followed by the agreement indices R and R_w, defined by $R = \sum||F_o| - |F_c||/\sum|F_o|$ and $R_w = [\sum w_i(|F_o| - |F_c|)^2/\sum w_i|F_o|^2]^{1/2}$. A refinement of the atomic coordinates with anisotropic temperature factors for thallium and mercury converged to $R = 0.051$ and $R_w = 0.052$. In this refinement the effect of anomalous dispersion was included, moreover a correction for extinction was applied. The value of the isotropic extinction parameters g was 2.2×10^{-5}.

Rb$_3$[*Hg*(*SO*$_4$)$_2$][*HgSO*$_4$*Cl*]. The positional and thermal parameters for the thallium compound were used as preliminary parameters for the rubidium salt. An exactly similar refinement was employed here as for $Tl_3[Hg(SO_4)_2]$-[$HgSO_4Cl$]. Weights used in the last cycle of the refinement were $w_i^{-1} = \sigma^2(F_o^2)/4F_o^2 +$

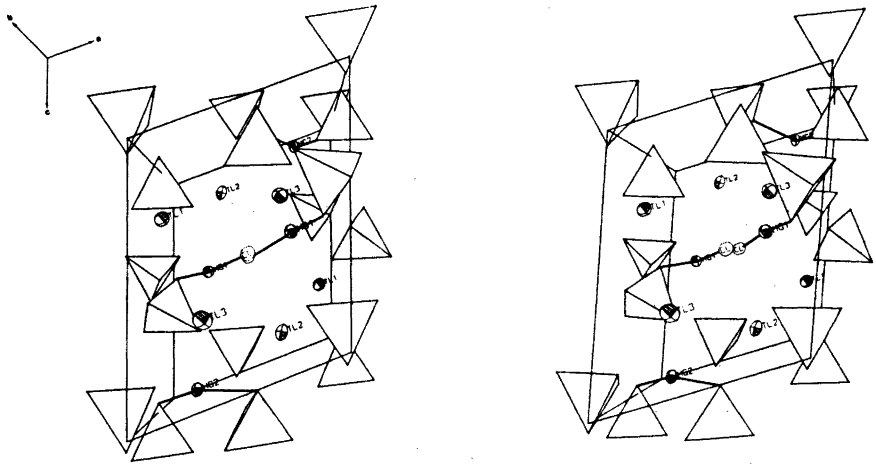

Fig. 1. A stereoscopic pair of drawings showing the ions $Hg(SO_4)_2^{2-}$, $HgSO_4Cl^-$ and Tl^+. The tetrahedra denote the sulfate groups.

Table 2. Final positional parameters and isotropic temperature factors in $Tl_3[Hg(SO_4)_2][HgSO_4Cl]$ and $Rb_3[Hg(SO_4)_2][HgSO_4Cl]$. Standard deviations are given in parentheses.

Atom	x	y	z	B (Å^2)
$Tl_3[Hg(SO_4)_2][HgSO_4Cl]$				
Tl(1)	0.9036(2)	0.2500(0)	0.7300(2)	–
Tl(2)	0.3166(2)	0.1183(2)	0.1422(2)	–
Tl(3)	0.6761(2)	0.4415(3)	0.3016(2)	–
Hg(1)	0.2688(2)	0.3516(3)	0.4966(2)	–
Hg(2)	0.7600(2)	0.0711(2)	0.0445(2)	–
Cl	0.484(1)	0.208(1)	0.488(1)	2.7(2)
S(1)	0.912(1)	0.116(1)	0.391(1)	1.7(2)
S(2)	0.014(1)	0.415(1)	0.110(1)	1.6(2)
S(3)	0.443(1)	0.301(1)	0.859(1)	1.8(2)
O(1A)	0.972(3)	0.256(3)	0.446(3)	1.6(4)
O(1B)	0.737(3)	0.122(3)	0.266(3)	1.8(4)
O(1C)	0.873(3)	0.049(3)	0.513(3)	2.3(5)
O(1D)	0.046(3)	0.045(3)	0.352(3)	2.3(4)
O(2A)	0.016(3)	0.461(3)	0.960(3)	1.9(5)
O(2B)	0.121(4)	−0.003(4)	0.862(4)	3.9(7)
O(2C)	0.967(4)	0.266(4)	0.092(3)	3.5(6)
O(2D)	0.199(3)	0.438(3)	0.214(3)	2.5(5)
O(3A)	0.580(4)	0.364(4)	0.816(3)	3.7(6)
O(3B)	0.264(3)	0.290(3)	0.746(3)	3.0(5)
O(3C)	0.504(4)	0.153(3)	0.912(4)	3.7(6)
O(3D)	0.426(4)	0.370(4)	0.981(3)	3.4(6)
$Rb_3[Hg(SO_4)_2][HgSO_4Cl]$				
Rb(1)	0.8986(3)	0.7500(0)	0.7314(3)	–
Rb(2)	0.3188(3)	0.8787(4)	0.1328(3)	–
Rb(3)	0.6734(4)	0.5539(4)	0.3035(4)	–
Hg(1)	0.2653(1)	0.6507(3)	0.4983(1)	–
Hg(2	0.7635(1)	0.9290(3)	0.0512(1)	–
Cl	0.481(1)	0.805(1)	0.481(1)	2.6(1)
S(1)	0.907(1)	0.892(1)	0.391(1)	1.3(1)
S(2)	0.028(1)	0.596(1)	0.110(1)	1.3(1)
S(3)	0.451(1)	0.710(1)	0.859(1)	1.4(1)
O(1A)	0.964(3)	0.754(2)	0.449(2)	1.9(3)
O(1B)	0.734(3)	0.883(2)	0.267(2)	1.9(3)
O(1C)	0.869(3)	0.963(2)	0.513(2)	2.0(3)
O(1D)	0.040(2)	0.963(2)	0.352(2)	1.7(2)
O(2A)	0.027(3)	0.554(2)	0.965(2)	2.2(3)
O(2B)	0.104(3)	0.016(3)	0.855(3)	3.0(4)
O(2C)	0.981(4)	0.742(3)	0.088(3)	3.4(4)
O(2D)	0.216(3)	0.577(2)	0.213(2)	2.5(3)
O(3A)	0.590(3)	0.655(2)	0.810(2)	2.8(3)
O(3B)	0.270(3)	0.719(2)	0.740(2)	2.1(3)
O(3C)	0.501(3)	0.854(2)	0.913(3)	3.0(4)
O(3D)	0.436(3)	0.634(2)	0.979(3)	2.7(3)

$0.008F_o^2$. This gave $R=0.077$, $R_w=0.089$, and a smooth weighting scheme. The extinction parameter g was 4.4×10^5.

Because of the space group a determination of the absolute configuration was possible for the crystal used.[3] The refinement of a structure with an absolute configuration opposite in the y-direction to the one chosen for $Tl_3[Hg(SO_4)_2][HgSO_4Cl]$ converged for the single crystal used for $Rb_3[Hg(SO_4)_2][HgSO_4Cl]$. Hamilton's R-test[3] indicates the absolute configuration for the rubidium crystal actually investigated up to a 0.005 significance level.

In all refinements, the atomic scattering

Table 3. Final anisotropic temperature factors for the heavy atoms in $Tl_3[Hg(SO_4)_2][HgSO_4Cl]$ and $Rb_3[Hg(SO_4)_2][HgSO_4Cl]$. The form of the anisotropic temperature factor is: $\exp[-(\beta_{11}h^2+..+2\beta_{12}hk+..)]$. Standard deviations are given in parentheses.

Atom	β_{11}	β_{22}	β_{33}	β_{12}	β_{13}	β_{23}
$Tl_3[Hg(SO_4)_2][HgSO_4Cl]$						
Tl(1)	0.01088(29)	0.00620(19)	0.00716(21)	−0.00048(19)	0.00293(19)	−0.00078(18)
Tl(2)	0.00889(26)	0.00574(18)	0.00857(24)	0.00028(18)	0.00154(20)	−0.00028(18)
Tl(3)	0.01592(35)	0.00771(22)	0.01062(28)	0.00304(23)	0.00603(26)	0.00279(21)
Hg(1)	0.00832(26)	0.00662(18)	0.00612(20)	0.00160(19)	0.00300(19)	0.00043(18)
Hg(2)	0.00626(24)	0.00511(17)	0.00718(21)	0.00056(16)	0.00220(18)	−0.00042(17)
$Rb_3[Hg(SO_4)_2][HgSO_4Cl]$						
Rb(1)	0.00755(36)	0.00583(21)	0.00469(21)	−0.00073(22)	0.00183(22)	−0.00104(18)
Rb(2)	0.00674(37)	0.00642(21)	0.00648(25)	0.00018(24)	−0.00001(24)	−0.00030(22)
Rb(3)	0.01332(51)	0.00737(26)	0.00813(30)	0.00278(30)	0.00407(32)	0.00291(25)
Hg(1)	0.00630(15)	0.00622(10)	0.00471(11)	0.00143(9)	0.00171(9)	0.00005(7)
Hg(2)	0.00484(14)	0.00532(8)	0.00447(10)	0.00061(8)	0.00127(8)	−0.00022(7)

Table 4. Selected distances (Å) and bond angles (°) with standard deviations in parentheses in the structures of $M_3[Hg(SO_4)_2][HgSO_4Cl]$, where M= Tl or Rb.

	M=Tl	M=Rb
Distances		
M(1)−O(3B)	2.80(3)	2.91(2)
M(1)−O(1C)	2.90(3)	2.97(2)
M(1)−O(2A)	2.96(3)	2.91(2)
M(1)−O(2B)	3.03(4)	3.08(3)
M(1)−O(1D)	3.03(3)	3.02(2)
M(1)−O(1A)	3.08(3)	3.05(2)
M(1)−O(3A)	3.14(4)	2.96(2)
M(1)−O(2D)	3.25(3)	3.43(2)
M(1)−Cl	3.35(1)	3.38(1)
M(1)−O(2C)	3.45(4)	3.39(3)
M(2)−O(3A)	2.60(4)	2.81(2)
M(2)−O(2A)	2.87(3)	3.06(2)
M(2)−O(2B)	2.94(4)	3.00(3)
M(2)−O(2C)	3.00(4)	2.86(3)
M(2)−O(1B)	3.09(3)	3.05(2)
M(2)−O(3C)	3.14(4)	3.03(2)
M(2)−O(3D)	3.21(4)	3.16(2)
M(2)−Cl	3.34(1)	3.32(1)
M(2)−O(2D)	3.40(3)	3.24(2)
M(3)−O(2B)	2.68(4)	2.78(3)
M(3)−O(1A)	2.89(3)	2.96(2)
M(3)−O(3C)	2.95(4)	2.87(2)
M(3)−O(3D)	3.16(4)	3.20(2)
M(3)−O(1B)	3.20(3)	3.30(2)
M(3)−O(3B)	3.44(4)	3.36(2)
M(3)−O(1C)	3.54(3)	3.52(2)
M(3)−O(1D)	3.53(3)	3.49(2)
M(3)−O(2D)	3.55(3)	3.38(2)
M(3)−Cl	3.60(1)	3.66(1)

Table 4. Continued.

Hg(1)−O(1C)	2.17(3)	2.10(2)
Hg(1)−Cl	2.24(1)	2.32(1)
Hg(1)−O(1A)	2.40(2)	2.46(2)
Hg(1)−O(3B)	2.58(3)	2.50(2)
Hg(1)−O(2D)	2.80(3)	2.83(2)
Hg(2)−O(2A)	2.09(3)	2.10(2)
Hg(2)−O(3C)	2.16(4)	2.16(2)
Hg(2)−O(1B)	2.34(3)	2.30(2)
Hg(2)−O(2C)	2.42(4)	2.44(3)
Hg(2)−O(3D)	2.42(4)	2.50(2)
Angles		
Cl−Hg(1)−O(1A)	116.2(0.8)	113.2(0.5)
Cl−Hg(1)−O(1C)	158.6(0.7)	158.6(0.6)
Cl−Hg(1)−O(2D)	92.1(0.7)	85.9(0.5)
Cl−Hg(1)−O(3B)	98.3(0.8)	98.2(0.5)
O(1A)−Hg(1)−O(1C)	83.6(1.03)	85.3(0.7)
O(1A)−Hg(1)−O(2D)	93.8(0.9)	97.5(0.6)
O(1A)−Hg(1)−O(3B)	76.5(0.9)	76.2(0.6)
O(1C)−Hg(1)−O(2D)	77.9(1.1)	80.9(0.7)
O(1C)−Hg(1)−O(3B)	94.1(1.1)	96.7(0.7)
O(2D)−Hg(1)−O(3B)	168.1(0.9)	173.5(0.6)
O(1B)−Hg(2)−O(2A)	118.4(1.0)	122.3(0.7)
O(1B)−Hg(2)−O(2C)	85.9(1.1)	90.9(0.8)
O(1B)−Hg(2)−O(3C)	97.2(1.1)	97.8(0.8)
O(1B)−Hg(2)−O(3D)	91.3(1.1)	89.9(0.7)
O(2A)−Hg(2)−O(2C)	83.7(1.2)	85.5(0.8)
O(2A)−Hg(2)−O(3C)	144.2(1.2)	138.0(0.9)
O(2A)−Hg(2)−O(3D)	94.3(1.2)	90.0(0.8)
O(2C)−Hg(2)−O(3C)	103.8(1.3)	107.4(0.9)
O(2C)−Hg(2)−O(3D)	175.2(1.2)	175.1(0.8)
O(3C)−Hg(2)−O(3D)	80.4(1.3)	77.3(0.8)

factors as well as the real ($\Delta f'$) and imaginary ($\Delta f''$) anomalous dispersion terms were those given by Cromer *et al.*[4,5]

The final positional parameters and isotropic temperature factors for both structures are given in Table 2. Anisotropic temperature factors for the thallium, mercury and rubidium atoms are presented in Table 3. In Table 4 selected interatomic distances and angles are given. Observed and calculated structure amplitudes are available on request.

All computations were made on the UNIVAC 1108 computer in Lund. A short account of the program system used has been given.[6]

DESCRIPTION AND DISCUSSION OF THE STRUCTURES

$Tl_3[Hg(SO_4)_2][HgSO_4Cl]$. The structure may be considered as ionic, made up of $Hg(SO_4)_2^{2-}$, $HgSO_4Cl^-$ and Tl^+ ions. The group $Hg(SO_4)_2^{2-}$ has previously been reported to exist in solution.[7] A stereoscopic view of the structure is presented in Fig. 1.

The sum of the ionic radii of Tl^+ and O^{2-} for eight-coordination is 3.00 Å and of Tl^+ and Cl^- 3.41 Å according to a summary.[8] A value of 3.33 Å is also reported [9] for Tl^+ to Cl^-. In the structure there are three kinds of thallium(I) atoms, denoted Tl(1), Tl(2) and Tl(3) in Fig. 1. The shortest thallium to oxygen distances, 2.80, 2.60 and 2.68 Å, and thallium to chlorine distances, 3.35, 3.34 and 3.60 Å, for Tl(1), Tl(2) and Tl(3), respectively, may indicate that they are mainly ionic in character.

All thallium atoms have irregular environments. The Tl(1) atom is surrounded by eight oxygen atoms at distances between 2.80 and 3.25 Å (mean value 3.02 Å), and by one chlorine atom at 3.35 Å. A ninth oxygen atom is situated at a distance of 3.45 Å (Fig. 2a). Tl(2) has seven oxygen neighbours at distances between 2.60 and 3.21 Å (mean value 2.98 Å) and one chlorine atom at 3.34 Å. An eighth oxygen atom is situated at a distance of 3.40 Å (Fig. 2b). Tl(3) is surrounded by five oxygen atoms, the distances ranging from 2.68 to 3.20 Å (mean value 2.98 Å) and by an addi-

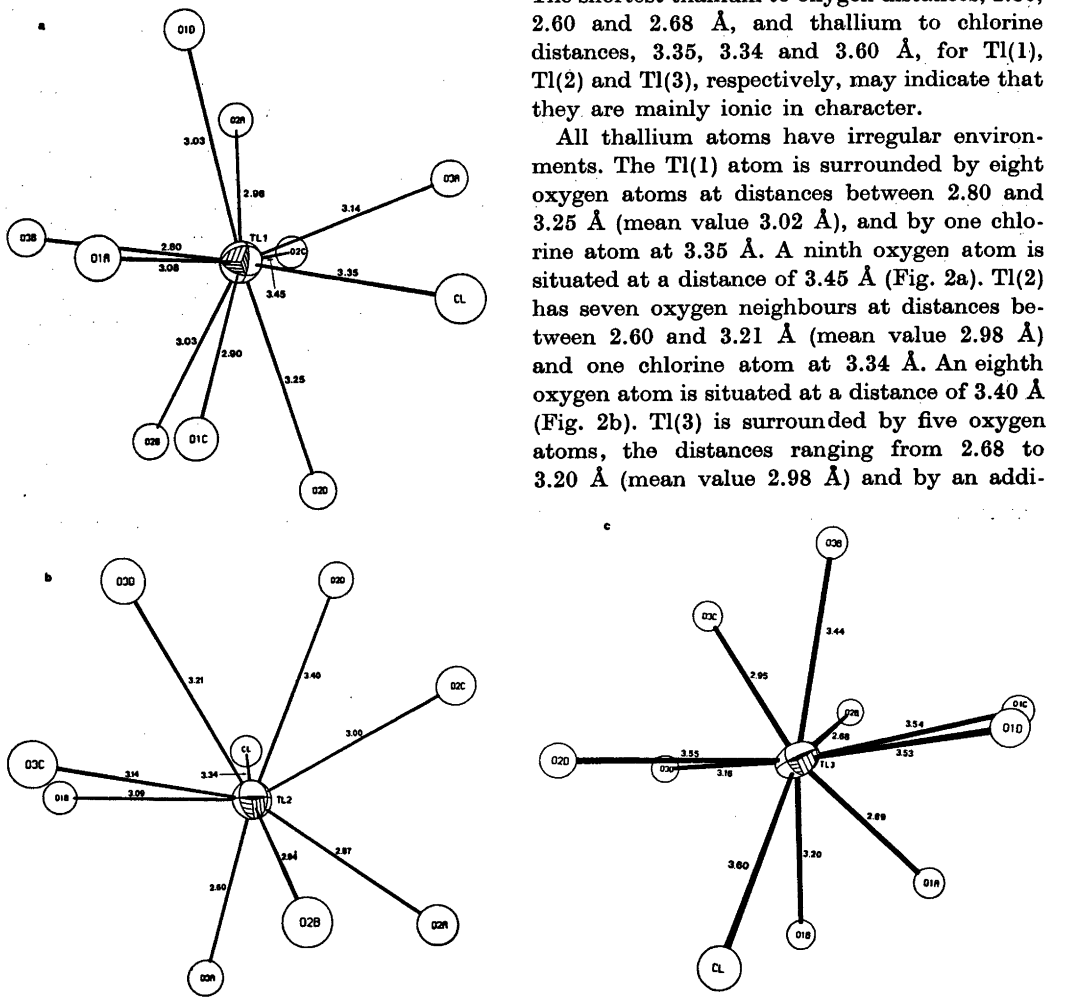

Fig. 2a–c. The environments of the Tl(1), Tl(2) and Tl(3) atoms.

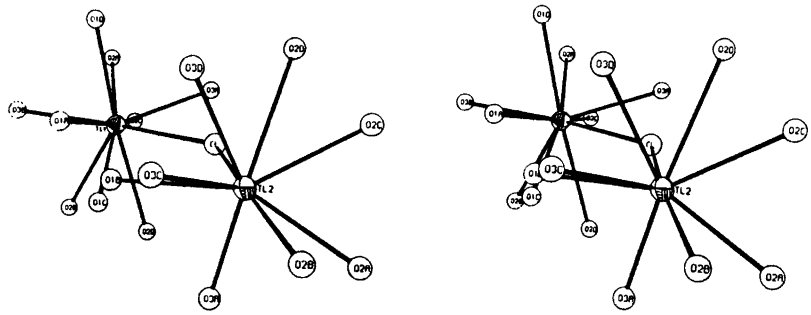

Fig. 3. Stereoscopic illustration showing the environments of the Tl(1) and Tl(2) atoms.

tional four, at distances varying between 3.44 to 3.55 Å. The chlorine – thallium distance is 3.60 Å. (Fig. 2c). Several thallium to oxygen distances are reported for different structures in the literature, *e.g.* 2.91 – 3.24 Å[1] for eight-coordination and 2.82 – 3.04 Å[10] for seven-coordination. In all of these structures, additional oxygen atoms are situated 3.4 – 3.5 Å from thallium. The environments of the Tl(1) and Tl(2) atoms are shown in a stereo view (Fig. 3).

In the structure there are two kinds of mercury atoms, denoted Hg(1) and Hg(2) in Fig. 1. The Hg(1) atom has two close ligands, in a nearly linear geometry, one oxygen atom at the distance 2.17 Å and one chlorine atom at 2.24 Å, the angle O – Hg – Cl being 158.6°. Thus a $HgSO_4Cl^-$ ion is formed. Three additional oxygen atoms from three other sulfate tetrahedra at the distances 2.40, 2.58 and 2.80 Å complete a distorted trigonal bipyramid (Fig. 4a).

The mercury atom Hg(2) has also two close ligands, one oxygen atom belonging to the S(2) sulfate group at 2.09 Å and another oxygen atom belonging to the S(3) sulfate group at 2.16 Å. The bond angle is 149°. In this way a $Hg(SO_4)_2^{3-}$ ion is formed. Three additional oxygen atoms are situated at the larger distances of 2.34 and 2.42(× 2) Å. The polyhedron thus formed may be described as a deformed trigonal bipyramid (Fig. 4b). Both mercury atoms of the asymmetric part of the unit cell thus occur as discrete complexes $HgSO_4Cl^-$ and $Hg(SO_4)_2^{3-}$. To our knowledge, only one discrete mercury sulfate complex has previously been found in the solid state, namely the finite $Hg_3(OH)_2(SO_4)_2$ chain in the crystal structure

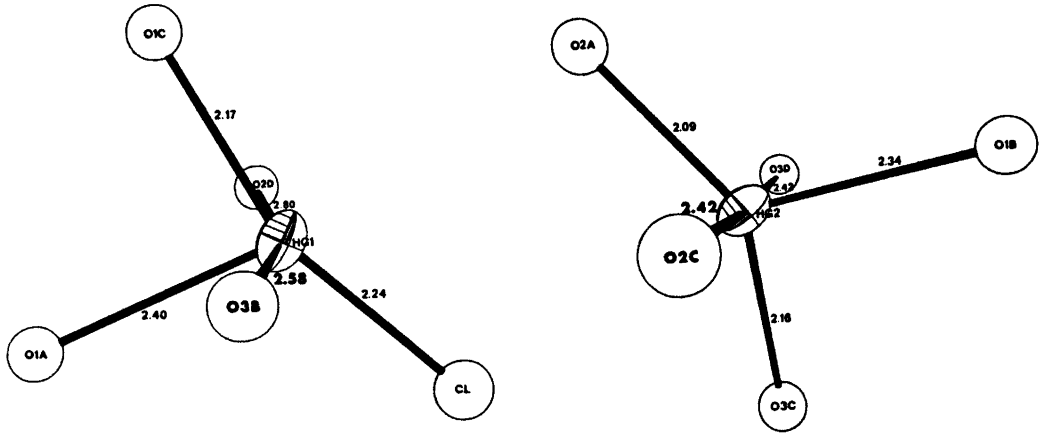

Fig. 4 a – b. The environments of the Hg(1) and Hg(2) atoms.

of $Hg_3(OH)_2(SO_4)_2.H_2O$.[11,12] It may be noted that all chlorine atoms of the unit cell are bonded to mercury. The tendency of mercury to coordinate a chlorine atom is thus larger than to coordinate a sulfate oxygen atom in the solid state. The fact that the present compound has been synthesized under water-free conditions, and the presence of large cations as Tl^+ or Rb^+ may have contributed to the occurrence of discrete mercury complexes in the crystal structure.

Twofold coordination is prevalent among mercury(II) compounds. As an example, in Hg_3OCl_4[13] the mercury atom forms two nearly colinear bonds to one oxygen and one chlorine atom, the distances Hg–O and Hg–Cl being 2.06(3) and 2.30(2) Å, respectively. The structures of $HgCrO_4.\frac{1}{2}H_2O$[14] and $Hg_3(OH)_2(SO_4)_2.H_2O$[11] have recently been refined to a high degree of accuracy, the calculations being based on neutron diffraction data.[12,15] In $HgCrO_4.\frac{1}{2}H_2O$ the mercury atom has two close oxygen neighbours belonging to two different chromate tetrahedra at the distances 2.055(1) and 2.064(1) Å, the O–Hg–O angle being 179.95(5)°. In the finite complex $Hg_3(OH)_2(SO_4)_2$ in the structure of $Hg_3(OH)_2(SO_4)_2.H_2O$ the distances mercury to a sulfate oxygen atom and an hydroxide oxygen atom are 2.058(2) and 2.087(2) Å, respectively, the angle O–Hg–O being 168.79(4)°. The complex formation of mercury is thus less pronounced in the compounds now investigated, also containing the big cations Tl^+ or Rb^+ than in compounds where the metals atoms are only mercury.

The dimensions of the three different sulfate groups are in good agreement with those reported (1.44–1.53 Å).[9] The mean S–O distances are 1.47, 1.48 and 1.51 Å. The S–O distances for the oxygen atoms bonded to mercury seem to be somewhat elongated (Table 4).

$Rb_2[Hg(SO_4)_2][HgSO_4Cl]$. In $Rb_2[Hg(SO_4)_2][HgSO_4Cl]$, isostructural with the thallium compound, the rubidium ions have the same coordinations as the thallium ions in the structure described above. The sum of the ionic radii for Rb^+ and O^{2-} and for Rb^+ and Cl^- are 3.00 and 3.41 Å,[8] respectively, the same radii sum as for the corresponding thallium salt. The distance Rb–Cl of 3.29 Å is reported for six-coordination.[9] If the rubidium salt is compared with the corresponding thallium salt, slight differences in the distances and angles are found (Table 4). The Rb(1) atom is surrounded by seven oxygen atoms at distances between 2.91 and 3.08 Å (mean value 2.99 Å) and by one chlorine atom at 3.38 Å. An eighth and a ninth oxygen atom are situated 3.39 and 3.43 Å apart, respectively. Rb(2) is surrounded by eight oxygen atoms at distances between 2.81 and 3.24 Å (mean value 3.03 Å) and by one chlorine atom at 3.32 Å. Rb(3) has an environment of nine oxygen atoms ranging from 2.78 to 3.52 Å and one chlorine atom at 3.66 Å.

In the compound Rb_2SO_4[16] there are two different sites of Rb atoms, denoted Rb(1) and Rb(2), both of them having irregular environments of oxygen atoms. The Rb(1) atom has ten oxygen atoms within the range 2.91 to 3.31 ($\sigma \approx 0.01$) Å, and Rb(2) has nine oxygen atoms at distances ranging from 2.88 to 3.24 ($\sigma \approx 0.01$) Å. The rubidium ion in $RbH_3(SeO_3)_2$[17] is surrounded by eight oxygen atoms forming a distorted cube. The Rb–O distances are between 2.939(6) and 3.192(5) Å.

The two mercury atoms, Hg(1) and Hg(2), in the rubidium salt have the same surroundings as in the thallium salt (Table 4). The mean S–O distances for the three different sulfate groups in the rubidium compound are 1.47, 1.48 and 1.48 Å, respectively.

Only a few structures of chlorides and sulfates containing thallium(I) or rubidium ions have so far been investigated. Large coordination numbers and varying bonding distances are common for the metal ions in these systems. The lone electron pair of thallium(I) is stereochemically inactive in the compounds $Tl_2[Cu(SO_3)_2]$[10] and $TlZnSO_4Cl$.[1] In the compound $Tl_2[Hg(SO_4)_2][HgSO_4Cl]$ the inert pair of electrons of thallium(I) may also be stereochemically inactive. This is supported by the fact that the rubidium ion, with the noble gas electron configuration, has the same surroundings as the thallium ions in the isotypical compound.

Acknowledgements. I wish to express my sincere thanks to Professor Bengt Aurivillius for his valuable advice and stimulating interest. I also thank Dr. Karin Aurivillius for much valuable help. The work forms part of a pro-

gram supported by the Swedish Natural Science Research Council.

REFERENCES

1. Bosson, B. *Acta Chem. Scand. 27* (1973) 2230.
2. Ibers, J. A. and Hamilton, W. C. *Acta Crystallogr. 17* (1969) 781.
3. Hamilton, W. C. *Acta Crystallogr. 18* (1965) 502.
4. Cromer, D. T. and Libermann, D. *J. Chem. Phys. 53* (1970) 1891.
5. Cromer, D. T. and Mann, J. B. *Acta Crystallogr. A 24* (1968) 321.
6. Stålhandske, C. *Acta Crystallogr. B 30* (1974) 1586.
7. Infeldt, G. and Sillén, L. G. *Sven. Kem. Tidskr. 58* (1946) 104.
8. Shannon, R. D. and Prewitt, C. T. *Acta Crystallogr. B 25* (1969) 925.
9. *International Tables for X-Ray Crystallography*, Kynoch Press, Birmingham 1965, Vol. III.
10. Hjertén, I. and Nyberg, B. *Acta Chem. Scand. 27* (1973) 345.
11. Björnlund, G. *Acta Chem. Scand. A 28* (1974) 169.
12. Aurivillius, K. and Stålhandske, C. *Z. Kristallogr. To be published.*
13. Aurivillius, K. *Ark. Kemi 22* (1964) 537.
14. Aurivillius, K. *Acta Chem. Scand. 26* (1972) 2113.
15. Aurivillius, K. and Stålhandske, C. *Z. Kristallogr. To be published.*
16. Nord, A. G. *Acta Crystallogr. B 30* (1974) 1640.
17. Tellgren, R., Ahmad, D. and Liminga, R. J. *Solid State Chem. 6* (1973) 250.

Received November 13, 1975.

Acta Chemica Scandinavica A 30 (1976) 249—256

Metal Halide and Pseudohalide Complexes in Dimethyl Sulfoxide Solution. III. Equilibrium Measurements on the Cadmium(II) Chloride, Bromide, Iodide, and Thiocyanate Systems

STEN AHRLAND and NILS-OLOF BJÖRK

Inorganic Chemistry 1, Chemical Center, University of Lund, P.O.B. 740, S-220 07 Lund, Sweden

The formation of chloride, bromide, iodide, and thiocyanate complexes of cadmium(II) in dimethyl sulfoxide has been studied at 25 °C by central ion measurements. An approximately constant ionic medium of an ionic strength = 1 M has been provided by the addition of ammonium perchlorate. In the case of chloride, measurements have also been performed in a lithium perchlorate trihydrate medium of the same ionic strength. All the complexes formed are more stable in DMSO than in water, but the difference is smaller the less prone the ligand is to form hydrogen bonds.

As stated in the first paper of this series,[1] the aim of the present investigations is to compare the strength of the halide and pseudohalide complexes formed in protic and aprotic solvents by acceptors of different bonding characteristics. As the protic solvent of reference water is the obvious choice, while dimethyl sulfoxide (DMSO) has been selected as the aprotic solvent. In the present paper, the formation of chloride, bromide, iodide, and thiocyanate complexes of cadmium(II) in the two solvents is compared. The aqueous systems have been very extensively, and carefully, investigated before. In DMSO, on the other hand, it seems that only the cadmium chloride system has been studied,[2] and moreover in a most exploratory manner.

In the present study, the stabilities of the cadmium(II) systems in DMSO have been determined potentiometrically by means of a cadmium amalgam electrode. A salt medium of an ionic strength $I = 1$ M has been employed. The corresponding measurements in aqueous solution refer to sodium perchlorate media which would therefore *per se* have been the best choice also for the DMSO measurements. Though sodium perchlorate is certainly soluble enough in DMSO,[3] this is nevertheless impossible on account of the low solubility of sodium chloride[3] (0.09 M) which would allow only fairly low concentration of free chloride ion in a 1 M sodium ion solution. For the ammonium[4] and the lithium ions,[3] on the other hand, not only the perchlorates but also the halides (except the fluorides) and the thiocyanates are sufficiently soluble. The present measurements have therefore been performed in ammonium and lithium perchlorate media. The temperature has been 25 °C.

The cadmium amalgam electrodes work very well in DMSO solutions of anhydrous ammonium perchlorate, yielding very stable and reproducible potentials; see below. In solutions of anhydrous lithium perchlorate, on the other hand, the amalgam is rapidly oxidized. No oxidation occurs, however, in 1 M solutions of the hydrate $LiClO_4.3H_2O$ in DMSO. As it is of primary interest to study the conditions in a completely anhydrous medium, all the systems have been measured in ammonium perchlorate solutions. In order to find out, however, how the stability of the complexes is influenced by a change of medium, the chloride system has also been measured in a solution of the lithium perchlorate hydrate.

Calculations of stability constants from potentiometric measurements of the free central ion con-

centration. The formulas used have been derived previously [5,6] and only a summary will therefore be given here. The overall stability constant β_{ji} for the complex M_iL_j is defined as

$$\beta_{ji} = [M_iL_j]/[M]^i[L]^j \quad (1)$$

The stepwise stability constant for the jth mononuclear complex is defined as

$$K_j = [ML_j]/[ML_{j-1}][[L] \quad (2)$$

If polynuclear complexes are formed as well, the following formulas are valid for the simplest case, that of dinuclear complexes:

$$C_M = [M]X + 2[M]^2Y \quad (3)$$

$$C_L = [L] + [M][L]\frac{dX}{d[L]} + [M]^2[L]\frac{dY}{d[L]} \quad (4)$$

where $X = 1 + \sum_{j=1}^{N} \beta_j[L]^j$ and $Y = \sum_{j=1}^{P} \beta_{j2}[L]^j$ (5,6)

If only mononuclear complexes are formed, $Y = 0$.

The emf of the following cell

$$-\mathrm{Cd(Hg)}\left|\begin{array}{l}C_M\text{M Cd-}\\(ClO_4)_2\\C_L\text{M}\\NH_4L\\NH_4ClO_4\\\text{to}\\I=\\1.00\text{ M}\end{array}\right|1.00\text{ M } NH_4ClO_4\left|\begin{array}{l}C_{M'}\text{M Cd-}\\(ClO_4)_2\\NH_4ClO_4\\\text{to}\\I=\\1.00\text{ M}\end{array}\right|\text{Cd-(Hg)}+$$

can be expressed as

$$E = E_k - (RT/2F)\ \ln\ [M] \quad (7)$$

where E_k includes the potential of the reference electrode and the liquid junction potentials. For the initial solutions where $C_L = 0$ and $[M] = C_M$, $E = E'$. Hence

$$E_M = E - E' = (RT/2F)\ \ln\ (C_M/[M]) = (RT/2F)\ \ln\ (X + 2[M]Y)$$

If only mononuclear complexes are formed E_M is evidently a function of [L] only. The functions $C_L(C_M)_{E_M}$ are then straight lines with intercepts $C_L = [L]$ for $C_M = 0$ and slopes equal to the ligand number $\bar{n} = (C_L - [L])/C_M$. Corresponding values of [L] and X can thus be obtained, and hence the stability constants β_j (and K_j), provided that the complexes are not so strong that the extrapolated values of [L] are $\simeq 0$.

If polynuclear complexes are also formed E_M is a function of [M] as well, and the curves $C_L(C_M)_{E_M}$ will no more be straight lines with a slope $= \bar{n}$. Extrapolated to $C_M = 0$ they will nevertheless yield [L], and from $X([L])$ the mononuclear constants β_j can still be calculated. For $C_M = 0$, the slopes of the $C_L(C_M)_{E_M}$-curves will be

$$k(E_M) = \left(\frac{\delta C_L}{\delta C_M}\right)_{C_M=0} = \bar{n}_I - \frac{2Y}{XX'} \quad (9)$$

where $\bar{n}_I$ is the ligand number referring to the mononuclear complexes. At least in principle, the function Y and hence the stability constants of the dinuclear complexes present can be calculated from eqn. (6) once the constants of the mononuclear complexes are known.[7] In practice, however, it is fairly difficult to determine the slopes $k(E_M)$ with the necessary precision.

If only mononuclear complexes are formed, or generally after extrapolation to $C_M = 0$, the Bodländer equation is valid

$$\bar{n}_I = \frac{d\log X}{d\log [L]} \simeq \frac{\Delta \log X}{\Delta \log [L]} \simeq \frac{2F}{RT\ln 10}\frac{\Delta E_M}{\Delta \log [L]} \quad (10)$$

implying that $\bar{n}_I$ can be calculated from the slope of the function $E_M([L])$.

When the complex formation is so strong that no reliable values of [L] are obtained by the extrapolarion described above, [L] can be found from the integrated Bodländer equation.

$$\log ([L]_0/[L]_j) = \int_{X([L]_j)}^{X([L]_0)} \frac{1}{\bar{n}_I}\, d\log X \quad (11)$$

provided that the complexes are mononuclear so that $\bar{n}_I$ can be found from the slopes of the $C_L(C_M)_{E_M}$-lines.

It must further be practicable to extend the measurements to an upper limit $[L]_0$ possible to determine independently, *e.g.* by extrapolation. For very strong complexes, a value of $[L]_0 > NC_M$ has then to be chosen.

From the functions $X([L])$ and $Y([L])$ thus found, preliminary evaluations of the constants β_j have been performed both graphically and by means of the computer program NPA ("Numerical Polynomial Approximation").

The final values of the constants have been determined numerically from eqn. (8) by means of the computer program EMK developed at this Center. Similar programs [9] have been used before for the treatment of emf and calorimetric data [10,11] but these have been confined to systems of mononuclear complexes.

The program EMK requires information about the formulas of the complexes formed. The best values of the various β_{ji} involved are found by minimizing the error square sum

$$U(\beta_j) = \sum_{i=1}^{N} w_i (E_{M,i,calc} - E_{M,i})^2 \qquad (12)$$

where w_i is a weighting term, here always = 1. For this calculation values of [L] and [M] are computed by simultaneous solvation of eqns. (3) and (4). This procedure is started by the introduction of suitable initial values of β_{ji}, obtained by the preliminary evaluations described above. Good initial values of β_{ji} very much facilitate the attainment of the final values satisfying eqn. (12). Especially when several complexes, among them also polynuclear ones, exist simultaneously the progress to the final values of β_{ji} is otherwise fairly slow.

EXPERIMENTAL

Chemicals. The hexasolvate $Cd(DMSO)_6(ClO_4)_2$ has been prepared and analyzed as described previously.[1]

The *lithium* and *ammonium chlorides* (BDH), the *ammonium bromide* (B & A) and the *ammonium iodide* (Baker Analyzed) were dried at 120 °C and their halide content checked titrimetrically. The *ammonium thiocyanate* (Merck) was dried at 110 °C, and the thiocyanate content determined titrimetrically. The *ammonium perchlorate* (Baker Analyzed) was dried at 110 °C. The *lithium perchlorate* (G. F. Smith) contained 2.97 mol water per mol perchlorate, as determined by heating to 150 °C.

Dimethyl sulfoxide was purified as described before.[1] The stock solutions of the various ligands contained < 0.2 % water by volume while the ammonium perchlorate solution contained < 0.07 %. These determinations of traces of water were performed by a modified Karl Fischer method.[12]

Cadmium amalgam containing 7 % cadmium was prepared and stored as described by Persson,[13] except that the dissolution took place at 80 °C.

Small variations in the cadmium content are of no importance as at 25 °C a two phase amalgam is formed [14] between 6 and 14 % Cd.

Apparatus. To keep the hygroscopic DMSO as dry as possible all measurements were performed in a glove-box, containing the Linde molecular sieve 4A XW. Further, predried nitrogen gas, presaturated with DMSO, was led through the box in order to prevent any moisture from entering. The relative humidity in fact never exceeded 4 %.

The nitrogen gas which had also been freed from oxygen was led through the electrode solutions in order to protect the amalgam electrodes from oxidation and to ensure a good mixing. Cadmium amalgam was used also for the reference electrodes as the otherwise very useful silver halide electrodes are easily dissolved in excess halide, on account of the ready formation in DMSO of higher soluble silver halide complexes.[19]

Commercial Ingold vessels were used for the electrode solutions, which were kept at 25.0 ± 0.1 °C by means of water circulating in an outer jacket around the vessels. The ligand solutions were added from a Metrohm piston burette. All parts of the apparatus in contact with DMSO were made from either glass or teflon. The measurements were performed with a Leeds & Northrup 7555 type K-5 potentiometer combined with a 9828 D.C. null detector, allowing a precision of ± 0.01 mV.

Procedure. Ligand solution T of the concentration C_L' (v ml) was added to a cadmium solution S of the initial concentration C_M' (V_0 = 10.00 ml) in the left half-cell. In the resulting solution, the total concentration of cadmium(II), C_M, decreases to $C_M = C_M' V_0/(V_0+v)$. The emf E actually measured is therefore due not only to the complex formation but also to the dilution. In order to find the E_M of eqn. (8), the following correction has to be introduced

$$E_M = E - E' - (RT/2F) \ln [(V_0+v)/V_0] \qquad (13)$$

Series were performed with at least three different values of C_M' and two different values of C_L'. Each series was repeated at least twice. The reproducibility was in general better than ± 0.04 mV for low values of C_L and better than ± 0.4 mV for high ones. Complete potentiometric data are obtainable from the authors.

To check that the cadmium amalgam electrode behaved according to Nernst's law in the DMSO solution, the emf's of cells containing no ligand were measured as a function of the metal ion concentration. These measurements were arranged as titrations where the metal ion solution was titrated into the initial 1.00 M NH_4ClO_4 solution. The value of E_k calculated varied within ± 0.4 mV for 2 mM ≤ C_M ≤ 40 mM.

In one of the series, a direct analytical determination of C_M was carried out at the end of the titration by means of atomic absorption.

No significant deviation was found from the calculated value, implying that neither had any amalgam been dissolved, nor had any evaporation of solvent taken place.

MEASUREMENTS AND RESULTS

Cadmium chloride in 1 M ammonium perchlorate. Both the graphical and the NPA evaluation of the data formally indicate no less than six complexes though the last two only at quite high chloride concentrations. If these exist at all, they are in any case much weaker than the previous ones. Within the limits of error, the same set of constants is obtained by both methods. A difference is apparent between $k(E_M)$ and $\bar{n}_I$ which might mean that polynuclear complexes exist. The corresponding values of Y and [L] can in fact be fitted with a complex M_2L_9. The constants obtained have then been employed as initial values in the EMK program. The final values resulting from this calculation do not differ very much from the initial ones except that $\beta_5 = 0$. This is not unexpected, since already the provisional value of β_5 had an error $\simeq 100$ %. If the dinuclear complex is excluded, the value of β_5 becomes significant but that of β_6 insignificant. However, as the error square sum (eqn. 12) was $\simeq 85$ % higher for this last set of complexes, the first set tried is preferred so far. The first four mononuclear constants are found to be the same in both cases.

The complex formation function computed from the preferred set of constants (Table 1) is plotted in Fig. 1. The values of $\bar{n}_I$ calculated from the Bodländer equation (eqn. 10) agree well with this function, and so do the slopes

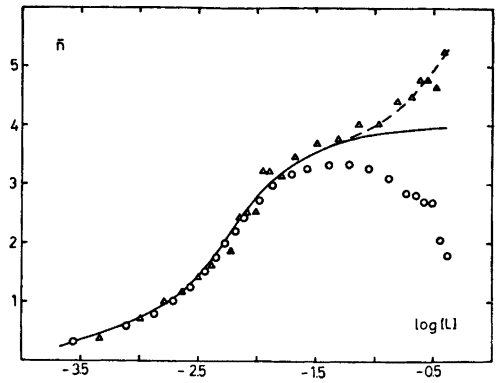

Fig. 1. The complex formation function of the cadmium(II) chloride system in 1 M NH_4ClO_4. The fulldrawn curve calculated from the constants β_1 to β_4. If the constants β_6 and β_{92} are included, the deviation indicated by the dashed curve results (for the average $C_M' = 10$ mm). Values of $k(E_M)$ denoted by circles, values of $\bar{n}_I$ from eqn. (10) by triangles. [L] in M.

from the $C_L(C_M)E_M$ for low values of [L]. The deviation due to the hypothetical complex M_2L_9 becomes perceptible for $[L] \gtrsim 30$ mM. For the highest value of C_M used, its maximum concentration would reach $\simeq 26$ %, at $[L] \simeq 163$ mM.

Cadmium bromide. Graphical and NPA evaluation of the measurements indicate five mononuclear complexes. For high values of [L], a difference exists between $k(E_M)$ and $\bar{n}_I$, though not at all as marked as in the chloride system.

The difference could be fitted with either of the complexes M_2L_8 and M_2L_9. The EMK program gives the best fit with the same set of

Table 1. The overall stability constants, β_j, for the cadmium(II) systems. The limits of error given correspond to three standard deviations, as obtained by the computer, or as estimated.

Medium → Ligand →	NH_4ClO_4, 1 M Cl^-	Br^-	I^-	SCN^-	$LiClO_4.3H_2O$, 1 M Cl^-
β_1/M^{-1}	1600 ± 100	850 ± 80	156 ± 10	64 ± 1	4150 ± 150
β_2/M^{-2}	$(1.2 \pm 0.7)10^5$	$(5 \pm 3)10^4$	$(4 \pm 2)10^3$	520 ± 30	$(1.5 \pm 0.3)10^6$
β_3/M^{-3}	$(5.2 \pm 0.8)10^7$	$(3.6 \pm 0.5)10^7$	$(3.2 \pm 0.2)10^6$	850 ± 90	$(2.0 \pm 0.2)10^9$
β_4/M^{-4}	$(2.7 \pm 0.5)10^9$	$(1.6 \pm 0.2)10^9$	$(4.9 \pm 0.2)10^7$	–	$(4.5 \pm 0.7)10^{11}$
β_6/M^{-6}	$(2.8 \pm 0.8)10^{10}$	$(3.7 \pm 1.8)10^9$	–	–	$(6 \pm 3)10^{12}$
β_{92}/M^{-10}	$(6 \pm 2)10^{21}$	$(3.7 \pm 1.5)10^{20}$	–	–	$\simeq 10^{26}$

The complexes ML_6 and M_2L_9 should be considered as hypothetical, *cf.* p. 256.

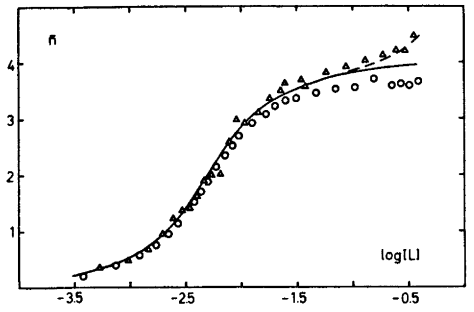

Fig. 2. The complex formation function of the cadmium(II) bromide system. Symbols, see Fig. 1.

complexes as was preferred for the chloride system.

The complex formation function calculated from the parameters given in Table 1 is drawn in Fig. 2. The $\bar{n}_I$ values from eqn. 10 agree well with the curve. The concentration of the hypothetical complex Cd_2Br_9 would never exceed $\simeq 16$ %.

Cadmium iodide. In the iodide system only the first four mononuclear complexes are indicated by the graphical evaluation as well as by the NPA. Much the same constants are found by both methods and these agree well with the final values calculated by the EMK program, Table 1. From the final constants, the complex formation function in Fig. 3 has been calculated. In this case, not only the values of $\bar{n}_I$ calculated from the Bodländer equation but also the values found from the slopes of the $C_M(C_L)_{E_M}$ lines fall on the curve for all values of [L].

On standing the originally almost colourless ammonium iodide solution developed an increasingly deeper colour as DMSO slowly oxidized iodide to iodine.[15] No significant differences in the emfs measured were found, however, if freshly prepared iodide solutions were used or if the solutions had been kept for two weeks. The change during such a period evidently does not matter.

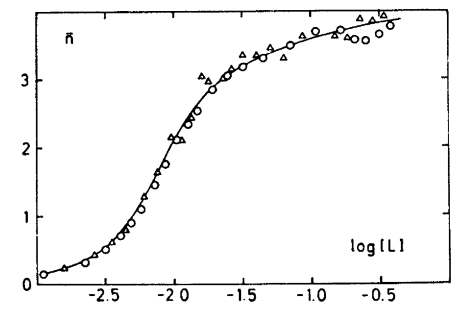

Fig. 3. The complex formation function of the cadmium(II) iodide system. Symbols, see Fig. 1.

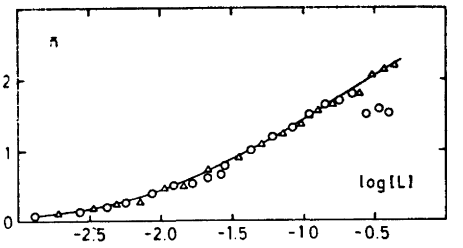

Fig. 4. The complex formation function of the cadmium(II) thiocyanate system. Symbols, see Fig. 1.

Cadmium thiocyanate. The graphical evaluation indicated only the first three mononuclear complexes. The constants found agreed well with the final ones calculated by the EMK program. These are given in Table 1 and the resulting complex formation function in Fig. 4. The values of $\bar{n}_I$ (eqn. 10) fit well to the curve and so do the $C_L(C_M)_{E_M}$ slopes except for a few points at the highest ligand concentrations.

Cadmium chloride in 1 M lithium perchlorate trihydrate. In order to keep the water content constant during the titrations, also the 1 M lithium chloride solution used as a titrant had

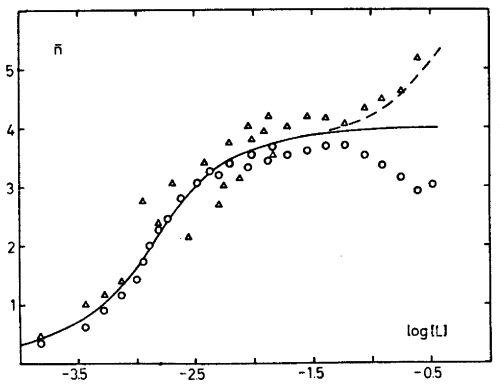

Fig. 5. The complex formation function of the cadmium(II) chloride system in 1 M $LiClO_4.3H_2O$. Symbols, see Fig. 1.

a concentration of water = 3.00 M. In the series employing 0.1 M lithium chloride, where the ligand solution already contained 2.70 M water from the supplementary lithium perchlorate no further water was added. In these cases the water content of the cell solution therefore varied between 2.70 and 3.00 M. It was checked separately that this variation did not bring about any significant change of the emf measured.

The value of [L] cannot be accurately determined from extrapolations of the $C_L(C_M)_{E_M}$ lines. A preliminary graphical evaluation using eqn. (11) gives $\beta_1 \approx 4000$ M^{-1}. Since the system might not be strictly mononuclear (*cf.* the $\bar{n}_I$ (log [L]) plot in Fig. 5) the integrated Bodländer equation (11) should not be used in the evaluation of the constants. Nor is it possible to employ Hedström's method,[5] which presupposes constant values of C_M in each series in order to ensure a reasonably simple treatment. In the beginning of the titrations, however, the values of $\bar{n}_I$ from eqn. (10) do not differ significantly from the $C_L(C_M)_{E_M}$ slopes. Consequently only mononuclear complexes exist in this region, and values of the constants β_1 to β_4 can be calculated with the EMK program. In the upper region where the values of $\bar{n}_I$ and $k(E_M)$ do differ, the values of [L] can, on the other hand, be found by extrapolation. The function X_4 is then calculated[5,6] from the values of β_1 to β_3 already found, and hence the values of β_4 to β_6. The value of β_4 thus found agrees well with that found before by means of the EMK program.

The resulting set of β_j is introduced in eqn. 6 and the Y polynomial calculated. The corresponding values of Y and [L] can be fitted with a complex M_2L_9. Finally all the data are introduced in the EMK program, with the values of β_1 to β_4 fixed. The β_6 value does not change appreciably from that obtained earlier, while β_5 vanishes. The final result (Table 1) is thus concordant with those reported above for the chloride and bromide systems in 1 M ammonium perchlorate (*cf.* also Figs. 1, 5 and 6).

DISCUSSION

As stated previously,[1] complexes formed by ligands able to form strong hydrogen bonds should be much more stable in aprotic solvents than in water relative to complexes formed by ligands not able to form such bonds. Moreover, if the solvation of the metal ion is not much stronger in the aprotic solvent, the complexes formed by hydrogen bonding ligands must be not only relatively but also absolutely stronger in aprotic solvents. This tendency is further strengthened if the activity of the solvent is lower in the aprotic medium. Whether this is the case for DMSO relative to water is uncertain. The lower concentration of solvent molecules in DMSO (14.0 M, as against 55.3 M in water, at 25 °C) acts in this direction but the strong hydrogen bonding between the water molecules might well more than compensate this effect. On the other hand the lower di electric constant of DMSO ($D = 46.4$, as against 78.4 for water, at 25 °C) will certainly tend to increase the stability of all complexes in DMSO relative to water.

As is obvious from the values of K_j collected in Table 2, a large increase of the stability relative to water occurs for the chloride complexes and a somewhat smaller for the bromide ones while the changes in stability for the iodide and thiocyanate complexes are modest. All the systems are stronger in DMSO than in water, however.

The differences between the halides in this respect are nevertheless so profound that a switch of the affinity sequence takes place between water and DMSO. In water, (*b*)-sequences $Cl^- < Br^- < I^-$ are found almost invariably for all the stepwise constants K_1 to K_3, Table 2 (though the trends are not very strongly marked; Cd^{2+} being a rather typical border line acceptor). In DMSO on the other hand the values of K_1, K_2 and though less marked, also K_4, follow (*a*)-sequences $Cl^- > Br^- > I^-$. Only in the case of K_3, a (*b*)-sequence still persists. Like in water, the complex formation curves get steeper from chloride to iodide, *cf.* Fig. 6. This certainly indicates that the bonds become increasingly covalent as the ligand becomes larger, and softer. The first complexes which are formed between oppositely charged ions are obviously more favoured relative to the

Table 2. Stability of cadmium halide and pseudohalide complexes in DMSO and water, at 25 °C.

Ligand	Cl^-	Br^-	I^-	SCN^-	Cl^-	Br^-	I^-	SCN^-
	DMSO, 1 M NH_4ClO_4				DMSO, 1 M $LiClO_4.3H_2O$			
K_1	1600	850	156	64	4150			
K_2	75	59	26	8.1	360			
K_3	430	720	800	1.6	1300			
K_4	52	44	15		230			
K_1/K_2	21	14	6	8	12			
K_2/K_3	0.17	0.08	0.03	5	0.28			
K_3/K_4	8.3	16	53		5.7			
	Water, 1 M $NaClO_4$				Water, 3 M $NaClO_4$			
K_1	22.3	36.5	75	20.7	38.5	57	121	24.5
K_2	2.7	2.9	6	4.7	4.4	3.9	5	3.9
K_3	0.43	1.7	49	1.1	1.5	9.5	137	4.0
K_4		2.6	19	0.70		2.4	40	
K_1/K_2	8.3	12	13	4.4	8.7	15	24	6.3
K_2/K_3	6.3	1.7	0.12	4.3	2.9	0.41	0.04	0.98
K_3/K_4		0.7	2.6	1.6		4.0	3.4	
Ref.	20	21	22		8,16			

latter ones, the stronger the electrostatic attraction exerted by the ligand. Conversely, the latter complexes are more favoured relative to the first ones, the larger the covalent contribution to the bonding.

The increase of covalency in the sequence stated also manifests itself in the circumstance

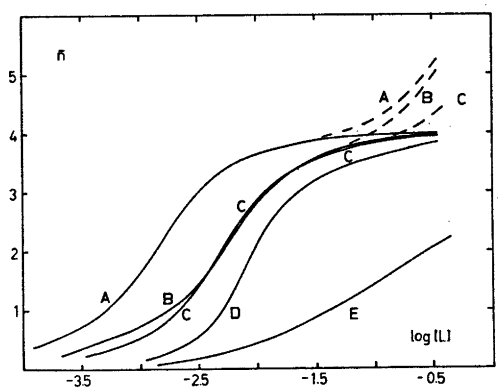

Fig. 6. The complex formation functions for: chloride (B), bromide (C), iodide (D) and thiocyanate (E), all in 1 M NH_4ClO_4, and for chloride in 1 M $LiClO_4.3H_2O$ (A). The fulldrawn curves calculated from β_1 to β_4 (E from β_1 to β_3). The dashed curves refer to the deviations found when the hypothetical β_5 and β_{92} are included.

that, in aqueous solution, the formation reactions become increasingly exothermic.[16,17]

The complex formation of the chloride system is considerably stronger in 1 M lithium perchlorate trihydrate than in 1 M ammonium perchlorate in spite of the fact that the presence of water in a concentration as high as 3 M would *per se* tend to lower the complexity. The most probable reason for the somewhat unexpected increase seems to be that the ammonium ions are associated to the chloride ions via hydrogen bonds which would make the ligand less available for complex formation. This is of course equivalent to a statement that at the present conditions ammonium chloride is far from completely dissociated in DMSO.

The water molecules added with the lithium perchlorate do not seem to interfere extensively with Cl^- in DMSO. Most plausibly they are taken care of by the cations present, presumably in the first hand by the hydrophilic Li^+. For this ion, DMSO may not compete so strongly as it certainly does for Cd^{2+}.

As seen from the low values of K_2/K_3, the second complex of the halide systems has a narrow range of existence in DMSO. This is also the case in aqueous solution though much less marked. From the thermodynamic functions of the aqueous systems it has been in-

ferred that a change from octahedral to tetrahedral coordination takes place, and moreover mainly at the third step.[18] A similar change of coordination is the most likely cause of the peculiarities in the relative stabilities of the complexes observed in DMSO. However, a good understanding of the processes involved presupposes that all the thermodynamic functions for the formation of the complexes are known. The next logical step is therefore to determine the enthalpy changes ΔH°_j of the consecutive formation reactions and from these, and the stability constants already known, also the entropy changes ΔS°_j. Such a determination, foreseen already at the planning of the present investigations, has in fact already been performed and the results will be reported in the next paper of this series. It may be mentioned already now, however, that a switch from an octahedral to a tetrahedral coordination is very clearly indicated for all the halide systems also in DMSO. In view of the narrow range of existence of the second complex found for both DMSO and water, Table 2, it is somewhat surprising, however, that the main part of the coordination change takes place at different steps in the two solvents, *viz.* already at the second step in DMSO while, as stated earlier, at the third step for water. This result shows that for a meaningful discussion of structure and bonding in solution based on thermodynamic data, a complete knowledge of all pertinent functions is necessary.

The calorimetric measurements also shed new light on the question of the complexes beyond the fourth one indicated in the chloride and bromide systems. Those effects which have been interpreted as possibly due to the formation of such complexes seem after all rather to be due to changes in the activity conditions, as will be fully discussed in the next paper. For all the systems investigated, the complex finally formed is most probably the mononuclear tetrahedral ML_4^{2-}.

Acknowledgements. Our sincere thanks are due to Professor Sture Fronæus for the kind interest he always has taken in these investigations. The support of Statens naturvetenskapliga forskningsråd (The Swedish Natural Science Research Council) is also gratefully acknowledged.

REFERENCES

1. Ahrland, S. and Björk, N. O. *Acta Chem. Scand. A 28* (1974) 823.
2. Burrus, R. T. *Polarographic studies in dimethyl sulfoxide*, Diss., University of Tennessee, 1962.
3. Kenttämaa, J. *Suom. Kemistilehti 33 B* (1960) 179.
4. Maxey, B. W. and Popov, A. I. *J. Amer. Chem. Soc. 89* (1967) 2230; *91* (1969) 20.
5. Fronæus, S. In Jonassen, H. B. and Weissberger, A., Eds., *Technique of Inorg. Chem.* Interscience, New York, London 1963, Vol. 1, Chapter 1.
6. Ahrland, S., Chatt, I., Davies, N. R. and Williams, A. A. *J. Chem. Soc.* (1958) 264.
7. Fronæus, S. *Komplexsystem hos koppar*, Diss., University of Lund, 1948.
8. Leden, I. *Potentiometrisk undersökning av några kadmiumsalters komplexitet*, Diss., University of Lund, 1943.
9. Karlsson, R. and Kullberg, L. *Chem. Scr. 9* (1976) 54.
10. Ahrland, S., Avsar, E. and Kullberg, L. *Acta Chem. Scand. A 28* (1974) 855.
11. Kullberg, L. *Acta Chem. Scand. A 28* (1974) 829, 897.
12. Karlsson, R. and Karrman, K. J. *Talanta 18* (1971) 459.
13. Persson, H. *Acta Chem. Scand. 24* (1970) 3739.
14. Hansen, M. *Constitution of Binary Alloys*, 2nd Ed., 1958, p. 420 as quoted in *Gmelin* 8th Ed., Nr *34* [*A*] Quecksilber, 1962, p. 1100.
15. Reynolds, W. L. *Progr. Inorg. Chem. 12* (1970) 1 (p. 58).
16. Gerding, P. *Acta Chem. Scand. 20* (1966) 79.
17. Ahrland, S. *Helv. Chim. Acta 50* (1967) 306.
18. Ahrland, S. *Struct. Bonding 15* (1973) 167.
19. Le Demezet, M., Madec, C. and L'Her, M. *Bull. Soc. Chim. Fr.* (1970) 365.
20. Vanderzee, C. E. and Dawson, H. J. *J. Amer. Chem. Soc. 75* (1953) 5659.
21. Kivalo, P. and Ekari, P. *Suom. Kemistilehti B 30* (1957) 116.
22. Gerding, P. *Acta Chem. Scand. 22* (1968) 1283.

Received September 24, 1975.

Acta Chemica Scandinavica A 30 (1976) 257—264

Metal Halide and Pseudohalide Complexes in Dimethyl Sulfoxide Solution. IV. Enthalpy Measurements on the Cadmium(II) Chloride, Bromide, Iodide, and Thiocyanate Systems

STEN AHRLAND and NILS-OLOF BJÖRK

Inorganic Chemistry 1, Chemical Center, University of Lund, P.O.B. 740, S-220 07 Lund, Sweden

The enthalpy changes for the formation of cadmium(II) chloride, bromide, iodide, and thiocyanate complexes in dimethyl sulfoxide have been determined by means of a calorimetric titration method. From the measured enthalpy changes, and the free energy changes computed from the stability constants, the entropy changes have been calculated. All data refer to 25.0 °C and an ammonium perchlorate medium of ionic strength 1.00 M.

For the halide systems ΔH_2 and ΔS_2 are particularly high, indicating that a change of coordination takes place at this very step. For the thiocyanate system the energy changes are rather small throughout.

It is also found that the total entropy gains on complex formation are much higher in DMSO than in water.

In order to elucidate the nature of the bonds involved in the formation of metal ion complexes in solution it is important to know all the thermodynamic functions for the pertinent reactions.[1,2] The free energy changes $\Delta G°_j$ for the stepwise formation of cadmium(II) chloride, bromide, iodide, and thiocyanate complexes in the protic solvent water and in the aprotic solvent dimethyl sulfoxide (DMSO) can be calculated from the stability constants reported previously.[2] The corresponding enthalpy changes ΔH_j are already known for water.[3–6] In the present investigation, the values of $\Delta H°_j$ for DMSO have been determined by direct calorimetric measurements. From the data thus available the corresponding entropy changes $\Delta S°_j$ can be calculated according to

$$\Delta G°_j = \Delta H°_j - T\Delta S°_j \qquad (1)$$

Enthalpy changes can be determined either by measuring the stability constants as a function of the temperature or calorimetrically, as here. The former method requires very precise measurements of K_j over a wide temperature range if the values of $\Delta H°_j$ are to be as reliable as those obtained by calorimetry.[7,8] Such a wide range is hardly accessible for DMSO of m.p. 18.5 °C. Further, within this range the change in heat capacity ΔC_p has to be negligible. The calorimetric method has also the advantage that fewer measurements are needed in order to achieve a certain precision.[9]

In most cases, the values of β_j have to be known already for the calculations of $\Delta H°_j$, as the calorimetric data as a rule do not allow a precise determination of both β_j and $\Delta H°_j$ from the experimental function Δh_v.[10,11] In certain well conditioned systems, however, it is possible to perform such a simultaneous determination.[10,12,13] This is in fact the case for the halide systems investigated here. If the values of β_j thus obtained agree with those found independently by potentiometric measurements, the result can of course be considered as very reliable.

The simultaneous determination of β_j and $\Delta H°_j$ for systems involving more than two complexes has until recently been a rather time-consuming task. The new program "Kalori" developed by Karlsson and Kullberg has very much eased this situation.[12,14] This program has been used for all calculations in the present paper.

Only a very exploratory calorimetric investigation of these systems has been performed previously.[15] In this study, which involved only the higher complexes, it was assumed that the dissolution of the solid halides results in a solution of the neutral complex ML_2. As this is certainly not true, the results reported are hardly correct.

NOTATION AND GENERAL EQUATIONS

Q_{exp} = heat change after addition of titrant (> 0 if heat is evolved)

Q_{dil} = heat of dilution

$Q_{corr} = Q_{exp} - Q_{dil}$ = heat change corrected for heat of dilution.

V_0 = initial volume of the solution in the calorimeter vessel.

v = volume of titrant added.

V = total volume of the solution of the calorimeter vessel.

ε_v = heat equivalent (J/ohm) of the calorimeter at the volume V.

$\Delta h_v = -\sum_v \frac{Q_{corr}}{C_M V}$ = total molar heat change after addition of v ml titrant.

The quantity Δh_v is related to the stepwise enthalpy change as follows:

$$\Delta h_v = \sum_{j=1}^{N} \sum_{k=1}^{j} \beta_j [L]^j \Delta H^\circ_k / X \qquad (2)$$

In the program "Kalori" applied here, a set of parameters is obtained which results in a minimum of the error square sum

$$U(\beta_j, \Delta H_j) = \sum_{i=1}^{N} w_i (Q_{i,calc} - Q_{i,corr})^2 \qquad (3)$$

where $w_i = 1$ is used.

EXPERIMENTAL

Chemicals. Hydrochloric acid, THAM (tris-(hydroxymethyl)aminomethane) and sodium hydroxide used for testing the calorimeter were of analytical grade. All other chemicals were prepared and analyzed as described before.[1,2]

Apparatus. A titration calorimeter of the isothermal jacket type was used. Its main features have been described by Ots.[16] To make work with DMSO solutions possible, some modifications had to be introduced, however. Thus all parts in contact with DMSO have been made from either gold, glass, teflon, or trifluorochloropolyethen. The inner vessel, which holds 100 ml, is inserted in an outer can which is wholly immersed in a water thermostat bath. The water content of DMSO increased slightly during the titration, but never exceeded 0.12 vol % (analyzed according to Ref. 17). The LKB precision thermostat used maintained its temperature at 25.000 ± 0.001 °C. For shorter periods (1 – 2 h) the temperature was, as a rule, stable even within $\pm 2 \times 10^{-4}$ °C. The room temperature was kept at 25.0 ± 0.2 °C.

Procedure. Initially 80 ml of a solution S in the inner vessel is equilibrated in the thermostat over night. Before the titration is started, the solution S is cooled (by air) to a temperature a little below that of the surrounding bath. The stirring necessary to bring about good mixing causes the temperature to rise slowly. Solution T, passing a heat-exchanger placed in the bath, is added (at most 5 ml) by a piston burette. The addition is made at a special "addition temperature", defined as the temperature where 1 M NH_4ClO_4 in DMSO can be added to an identical solution without any temperature change. All additions are made at a standard rate of 1 ml/min.

When the reaction is completed, the addition temperature is restored by either cooling or heating, depending upon whether the reaction is exothermic or endothermic. A new cycle is then started.

The calibration constant ε_v was determined as reported by Ots.[16] It was found to depend upon V according to $\varepsilon_v = a + b(V - 80)$ J ohm^{-1} where $a = 0.9780 \pm 0.0020$ J ohm^{-1} and $b = (1.236 \pm 0.020)10^{-2}$ J ohm^{-1} ml^{-1}.

Totally eight or nine titration series were performed for each system. In series 1 – 6, ligand solution T, of $C_L = 1.000$ M, was titrated into metal ion solutions S, with C_M varying from $\simeq 10$ to $\simeq 40$ mM. For series 7 – 9 solution T of $C_M \simeq 100$ mM was titrated into ligand solutions of $C_L \simeq 0.25$, 0.50 and 1.00 M. If only mononuclear complexes exist, the function $\Delta H_v(\bar{n})$ should be independent of C_M.

For all S solutions containing metal ions the heats of dilution on addition of ammonium perchlorate solution were negligible. For S solutions containing ligand as well as for all T solutions such dilutions gave quite large heat effects, at most 0.27 J per ml added T solution.

In eqn. (3), the input data are V_0, v, Q_{corr} and the initial concentrations of the metal ion and ligand solutions. The potentiometrically determined values of β_j were always taken as initial values in the calorimetric evaluation. The values of β_j determined calorimetrically have almost always larger errors than those found potentiometrically. This applies especially to the thiocyanate system, where the variation in Δh_v is fairly modest (*cf.* Fig. 1). In this case the potentiometrically determined values of β_j have been inserted in the program and not allowed to vary during the calculations.

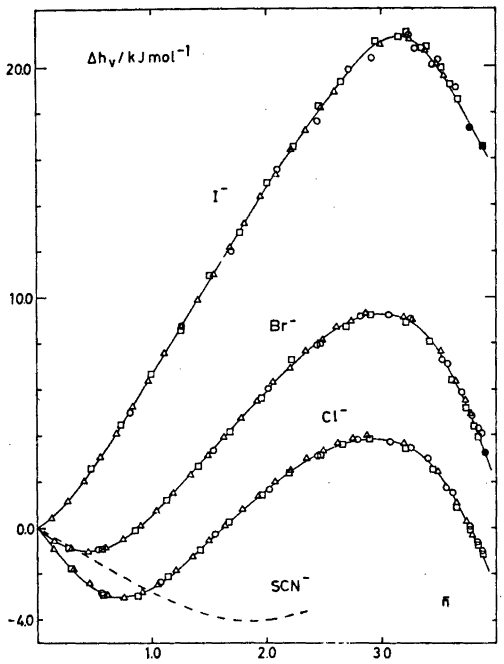

Fig. 1. The total molar enthalpy change Δh_v as a function of $\bar{n}$ for the halide systems. The fulldrawn curves are calculated from the mean values of β_j given in Table 1 and $\Delta H°_j$ from Table 2. The thiocyanate curve is dashed for comparison.

When values of β_j are determined both calorimetrically and potentiometrically, a weighted mean of these was used for the final calculations of $\Delta H°_j$ and $\Delta S°_j$. The complete calorimetric data are available from the authors.

Testing the calorimeter. To check the accuracy of the calorimeter, the heat of protonation of THAM and the heat of neutralisation of sodium hydroxide have been determined. In the first test THAM ($C_T = 20.0$ mM and $C_{TH^+} = 10.0$ mM) was protonated by 100.25 mM hydrochloric acid. The value found, $\Delta H_{corr} = 46.92 \pm 0.07$ J mol^{-1}, is significantly lower than those found by Öjelund and Wadsö,[18] -47.48 ± 0.03 kJ mol^{-1} or by Grenthe *et al.*,[19] -47.44 ± 0.05 kJ mol^{-1}.

Since the use of protonation of THAM as standard reaction has been somewhat in doubt,[20] no further attempts to obtain better values have been made.

In the second test 9.87 mM hydroxide solution was neutralized by the same hydrochloric acid as above. The value found, $\Delta H_{W\infty} = -55.84 \pm 0.04$ kJ mol^{-1} agrees very well with other determinations (Grenthe *et al.*,[19] -55.84 ± 0.05 kJ mol^{-1}; Vanderzee and Swanson,[21] -55.84 kJ mol^{-1}; Ots[16] -55.83 ± 0.02 kJ mol^{-1}). Corrections for the dilutions have been made according to SVCTP.[22,23]

RESULTS

The chloride system. Even when only the first four mononuclear constants, as determined potentiometrically, were applied in the "Kalori" program, no significant discrepancy was found between the series of different C_M. Only for the highest C_L (series 9) a very slight difference, at most 0.2 J, corresponding to $\simeq 3\sigma_Q$, was observed. When the values of β_j were allowed to vary an even better fit resulted though a slight difference at the higest C_L still persisted. The complexes ML_6 and M_2L_9 indicated by the potentiometric measurements should exist in perceptible amounts already in the calorimetric series 1 – 7 where, however, an excellent fit was obtained without them. The slight discrepancy in series 9 might well

Table 1. The stability constants of cadmium(II) chloride, bromide, iodide, and thiocyanate complexes in DMSO at 25 °C, determined by potentiometric and calorimetric methods. The errors given correspond to three standard deviations. Ionic medium 1 M ammonium perchloride.

j	Pot.	Cal.	Mean
Chloride (β_j, M^{-j})			
1	1600 ± 100	1800 ± 160	1680 ± 90
2	$(1.2 \pm 0.7)10^5$	$(1.8 \pm 0.5)10^5$	$(1.6 \pm 0.4)10^5$
3	$(5.2 \pm 0.8)10^7$	$(6.9 \pm 1.3)10^7$	$(5.9 \pm 0.8)10^7$
4	$(2.7 \pm 0.5)10^9$	$(4.3 \pm 0.8)10^9$	$(3.3 \pm 0.5)10^9$
Bromide (β_j, M^{-j})			
1	850 ± 80	820 ± 60	830 ± 50
2	$(5 \pm 3)10^4$	$(8 \pm 2)10^4$	$(6.8 \pm 1.8)10^4$
3	$(3.6 \pm 0.5)10^7$	$(4.0 \pm 0.5)10^7$	$(3.8 \pm 0.4)10^7$
4	$(1.6 \pm 0.2)10^9$	$(2.0 \pm 0.3)10^9$	$(1.8 \pm 0.2)10^9$
Iodide (β_j, M^{-j})			
1	156 ± 10	142 ± 26	152 ± 14
2	$(4 \pm 2)10^3$	$(3.4 \pm 3)10^3$	$(3.8 \pm 1.8)10^3$
3	$(3.2 \pm 0.2)10^6$	$(3.1 \pm 0.4)10^6$	$(3.2 \pm 0.2)10^6$
4	$(4.9 \pm 0.2)10^7$	$(4.0 \pm 0.9)10^7$	$(4.7 \pm 0.5)10^7$
Thiocyanate (β_j, M^{-j})			
1	64 ± 1	(79 ± 18)	
2	520 ± 30	(490 ± 240)	
3	850 ± 90	(2500 ± 2500)	

Table 2. Thermodynamics of the stepwise coordination of chloride, bromide, iodide, and thiocyanate to cadmium(II) in DMSO at 25 °C, in 1 M ammonium perchlorate medium. The errors given correspond to three standard deviations.

j	ΔG°_j (kJ mol^{-1})	ΔH°_j (kJ mol^{-1})	ΔS°_j (J K^{-1} mol^{-1})
Chloride			
1	−18.4 ± 0.2	−6.3 ± 0.1	40.6 ± 0.7
2	−11.2 ± 0.7	15 ± 2	88 ± 7
3	−14.7 ± 0.7	1 ± 2	53 ± 7
4	−10.0 ± 0.5	−12.2 ± 0.3	−7 ± 2
2+3	−25.9 ± 0.3	15.5 ± 0.4	139 ± 3
Bromide			
1	−16.7 ± 0.2	−3.9 ± 0.2	43.0 ± 0.9
2	−10.9 ± 0.7	17 ± 2	94 ± 7
3	−15.7 ± 0.7	2 ± 3	59 ± 10
4	−9.5 ± 0.4	−13.0 ± 0.2	−12 ± 2
2+3	−26.6 ± 0.3	18.9 ± 0.5	153 ± 3
Iodide			
1	−12.5 ± 0.2	2.4 ± 0.1	50.0 ± 0.8
2	−7.8 ± 1.4	27 ± 2	117 ± 8
3	−16.8 ± 1.4	−5 ± 2	40 ± 8
4	−6.7 ± 0.3	−9.54 ± 0.08	−10 ± 1
2+3	−24.6 ± 0.2	22.6 ± 0.2	158 ± 2
Thiocyanate			
1	−10.31 ± 0.04	−2.97 ± 0.02	24.6 ± 0.2
2	−5.2 ± 0.2	−2.8 ± 0.2	8 ± 1
3	−1.2 ± 0.5	4.2 ± 0.6	18 ± 3

be caused by the great change in ionic medium. In the final calculation series 9 was excluded, as well as series 8, where also a small systematic deviation was observed. The resulting set of β_j is given in Table 1. The final stepwise enthalpy changes were determined by use of an error weighted mean value from the two sets $\beta_{j,\mathrm{pot.}}$ and $\beta_{j,\mathrm{cal.}}$ (Table 1). The result is given in Table 2. In accordance with this result, the function $\Delta h_v(\bar{n})$ is independent of C_M, Fig. 1.

The bromide system. Also in this system, the potentiometric measurements indicated the existence of the complexes ML_6 and M_2L_9, though to a much less degree than for the chloride system. Just as for chloride, however, no trace of any complexes beyond the first four mononuclear ones were found calorimetrically, see Tables 1 and 2 and Fig. 1.

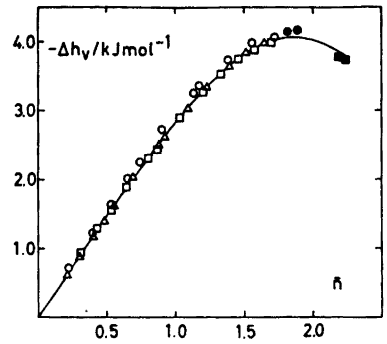

Fig. 2. The total molar enthalpy change Δh_v as a function of $\bar{n}$ for the thiocyanate system. Approximately the half of the experimental points, chosen at random, have been plotted. The fulldrawn curve is calculated from the sets of β_j and ΔH°_j given in Tables 1 and 2.

The iodide system. In this case, only the first four mononuclear complexes were indicated by the potentiometric investigation. Even at the highest ligand concentrations such a set of complexes also fit the calorimetric data excellently. Within the larger errors that are unavoidably connected with values of β_j determined calorimetrically, the constants moreover agree very well with these found potentiometrically, Table 1. This applies even to the second complex, the concentration of which never exceeds 6 %. The value of β_2 found calorimetrically is, at least formally, hardly significant but it still agrees with that found potentiometrically. The results for the iodide system are collected in Tables 1 and 2 and Fig. 1.

The thiocyanate system. An excellent fit was obtained with the values of β_j determined potentiometrically for the first three mononuclear complexes. For this system, however, the function Δh_v did not allow any simultaneous determination of β_j and ΔH°_j. The precision of the constants obtained in this way was very poor (Table 1) and it was therefore decided to use only the potentiometrically determined set of β_j for the final calculation of ΔH°_j. The results are reported in Tables 1 and 2 and Figs. 1 and 2.

DISCUSSION

The emf measurements on the chloride [2,24] and bromide [2] systems indicate that the complex formation might extend beyond the fourth mononuclear complex, and that polynuclear complexes might be formed, especially in the chloride system. The calorimetric measurements do not bear this out. The most likely cause of this discrepancy is that, at high concentrations of chloride and bromide, activity changes take place and/or liquid junctions potentials change, influencing the emf's measured in a way that can formally be interpreted as a formation of higher complexes. Such phenomena have been observed in several instances, and also in the case of other chloride and bromide systems.[25,26] Calorimetric measurements need not be at all affected by a corresponding change of medium.

In the following, it seems therefore most reasonable to consider only the first four mononuclear complexes for all the halide systems. The existence and strength of these complexes have, on the other hand, been amply confirmed by the calorimetric measurements.

A most remarkable feature of all the halide systems is that the second complex has a very narrow range of existence in DMSO, as reflected by the small values of $-\Delta G^\circ_2$ relative to $-\Delta G^\circ_3$. The same effect, though less marked is also observed in water, Table 3. This has already been discussed in the preceding paper of this series where it was also pointed out that such a peculiarity generally indicates a change of structure, taking place mainly at a certain step of the complex formation.[2] For the cadmium halides, the change most probably involves a switch from an octahedral coordination in the solvated ion to a tetrahedral coordination in the tetrahalide complexes. The step of the main change is indicated by the peculiar trends of ΔS°_j and ΔH°_j of the consecutive complexes. As long as the complex formation only implies the substitution of a solvent molecule in the inner coordination sphere by a halide ion, a monotonous decrease of ΔS°_j is expected to take place between each step.[27] If, on the other hand, a switch from octahedral to tetrahedral coordination takes place, more solvent molecules are set free, resulting in a large increment of ΔS°_j. Simultaneously, the energy needed for desolvation increases which results in a more positive, or less negative, value of ΔH°_j. The interaction of these two changes results in the peculiarities in ΔG°_j, *i.e.* K_j, originally observed.[2]

In water, the values of ΔS°_3 are abnormally high for all the halide systems, indicating that the change of structure takes place mainly at the third step. At least for chloride and bro-

Table 3. Thermodynamics of cadmium halide and thiocyanate complexes in DMSO and water, at 25 °C, in the media stated. ΔG°_j and ΔH°_j in kJ mol^{-1}, ΔS°_j in J mol^{-1} K^{-1}.

	DMSO				Water				
	1 M NH_4ClO_4				3 M $NaClO_4$				1 M $NaClO_4$
	Cl^-	Br^-	I^-	SCN^-	Cl^-	Br^-	I^-	SCN^-	I^-
ΔG°_1	−18.4	−16.7	−12.5	−10.3	−9.0	−10.0	−11.9	−8.0	−10.7
ΔG°_2	−11.2	−10.9	−7.8	−5.2	−3.7	−3.3	−4.0	−4.8	−4.6
ΔG°_3	−14.7	−15.7	−16.8	−1.2	−1.0	−5.6	−12.2	−1.3	−9.6
ΔG°_4	−10.0	−9.5	−6.7			−2.1	−9.2	0.0	−7.6
ΔH°_1	−6.3	−3.9	2.4	−3.0	−0.4	−4.1	−9.5	−8.1	−10.2
ΔH°_2	15	17	27	−2.8	0.1	−2.4	−0.8	−7.2	−2.1
ΔH°_3	1	2	−5	4.2	7.7	7.2	−3.1	−6.6	−5.9
ΔH°_4	−12.2	−13	−9.5			1.3	−15.9	−4	−16.8
ΔS°_1	41	43	50	25	29	20	8	0	2
ΔS°_2	88	94	117	8	13	3	10	−8	8
ΔS°_3	53	59	40	18	29	43	31	−18	12
ΔS°_4	−7	−12	−10			11	−23	−15	−33
ΔH_{β_2}	10	15	24	−2	7	1	−13	−22	−18
ΔS_{β_2}	182	196	207	51	77	66	49	−26	22

mide, this is also corraborated by very positive values of $\Delta H°_3$, Table 3. In DMSO, on the other hand, the values of $\Delta S°_2$ and $\Delta H°_2$ stand out as exceedingly high. In this solvent, therefore, the change of structure mainly takes place already at the second step.

As the solvent molecules must be considerably more crowded in the DMSO hexasolvate then in the hexahydrate, it is not surprising that a disrupture occurs at an earlier stage in DMSO than in water. The hydrate is likely to accomodate more halide ions, even in awkward positions, before the situation becomes impossible.

By means of X-ray diffraction, the hydrated cadmium(II) ion has recently been shown to be a regular octahedron in aqueous solution,[28,29] while CdI_4^{2-} is a regular tetrahedron.[29] In water, a change of coordination therefore certainly takes place, and the thermodynamics of the formation reactions indicate that this change preferably takes place at a certain step, *viz.* at the third one. In DMSO, like in water, a solid hexasolvate is formed.[1] The structure of this compound is still unknown, as well as that of the solvated ion in solution, but in all probability they are both octahedral. Also, the structures of the highest complexes formed, all of the formula CdL_4^{2-}, are probably tetrahedral. The peculiarities in $\Delta H°_j$ and $\Delta S°_j$ should therefore naturally be interpreted along the same lines as for aqueous solution.

Strikingly enough, the narrow range of existence of the second complex is caused by a change of coordination at the third step in water but at the second step in DMSO. The range of existence of a complex is conveniently expressed by the maximum molar ratio $(\alpha_j)_{max}$ that it reaches in equilibrium with its neighbours. For most systems where besides ML_j only ML_{j-1} and ML_{j+1} exist in appreciable amounts at $(\alpha_j)_{max}$, this quantity is well approximated by (cf. eqn. 18 of Ref. 30)

$$(\alpha_j)_{max} = 1/[1 + 2(K_{j+1}/K_j)^{\frac{1}{2}}] \quad (4)$$

Thus, the range of existence of the jth complex is determined by the ratio between two consecutive equilibrium constants, *viz.* K_j for the formation of the complex from the preceding one, and K_{j+1} for its conversion into the succeeding one. Moreover, the range becomes narrower, *i.e.* $(\alpha_j)_{max}$ smaller, the smaller the ratio K_j/K_{j+1}.

The ratio K_j/K_{j+1} depends upon the corresponding changes of enthalpy and entropy according to

$$K_j/K_{j+1} = \exp\ (RT)^{-1}[\Delta H°_{j+1} - \Delta H°_j - T(\Delta S°_{j+1} - \Delta S°_j)] \quad (5)$$

For the systems discussed K_2/K_3 is abnormally small. This may occur either because $\Delta H°_2 \gg \Delta H°_3$ or because $\Delta S°_3 \gg \Delta S°_2$, or because these conditions are both fulfilled at the same time. The condition for a ratio $K_2/K_3 < 1$ is evidently that $\Delta H°_2 + T\Delta S°_3 > \Delta H°_3 + T\Delta S°_2$.

In water, the low values of K_2/K_3 observed for the bromide and iodide systems are due to the high values of $\Delta S°_3$ which are not compensated by commensurate increases in $\Delta H°_3$. In DMSO, on the other hand, the low values of K_2/K_3 observed for all the halide systems are due to the very high values of $\Delta H°_2$ relative to $\Delta H°_3$, which are not compensated by the *per se* high value of $\Delta S°_2$ relative to $\Delta S°_3$.

At the coordination change, the gain of entropy thus dominates over the desolvation energy in aqueous solution which makes the complex mainly connected with the change, *i.e.* the third one, especially stable relative to its predecessor, *i.e.* K_2/K_3 becomes small. In DMSO, on the other hand, the desolvation energy dominates over the entropy gain which makes the complex mainly connected with the change, in this case the second one, especially unstable relative to its successor. Again K_2/K_3 becomes small, but for a different reason than in water.

An experimental consequence of the narrow range of existence of the second complex is that only the sums of the thermodynamic functions of the second and third steps can be very precisely determined, but not the individual functions, Table 2.

Another remarkable difference between the thermodynamics in aqueous and DMSO solution is that the entropy gains on complex formation are generally much higher in DMSO. This stands out very clearly from a comparison of the sums $\Delta S_{\beta_3} = \sum_{j=1}^{3} \Delta S°_j$ which for both solvents include most of the gains due to desolvation, Table 3. The difference is not un-

expected, however, in view of the higher degree of order that ought to prevail in water relative to DMSO, on account of the strong hydrogen bonds between the water molecules which have no counterpart in DMSO. On dehydration, the water molecules therefore move from a well-ordered hydrate shell to a fairly well-ordered bulk solvent, resulting in a relatively modest increase of entropy. On desolvation in DMSO, on the other hand, the solvent molecules move from a well-ordered solvate shell to a much less well-ordered bulk solvent, resulting in a much larger increase of entropy. The solvation of Cd^{2+} is moreover certainly stronger in DMSO than in water [31] which also contributes to the increased entropy gains in DMSO. The relative importance of the two factors considered is at present difficult to assess.

In water, $\Delta S°_{\beta_3}$ decreases in the sequence $Cl^- > Br^- > I^-$, Table 3, as expected from the decrease of hydration [32] of the halide ions in the same sequence. In DMSO, on the other hand, ΔS_{β_3} increases in the sequence mentioned. The solvation of Cl^- is presumably weaker in DMSO than in water, and that of I^- stronger, which evidently acts in the direction observed.[31,33] Still, even if the differences between the solvation energies are much smaller in DMSO than in water, the sequence remains $Cl^- < Br^- < I^-$. It seems therefore not possible to account for the actual *reversal* of ΔS_{β_3} only by this factor.

Analogously, the total enthalpy change $\Delta H_{\beta_3} = \sum_{j=1}^{3} \Delta H_j$ decreases in water in the sequence $Cl^- > Br^- > I^-$, as expected from the decrease of the dehydration energies of the ligands in the same sequence.[32] In DMSO, on the other hand, ΔH_{β_3} increases in the order mentioned, as does ΔS_{β_3}. The reason must evidently be the same, though still obscure.

In both solvents, thiocyanate behaves very differently from the halides, Table 3. The entropy changes are all small, slightly positive in DMSO and slightly negative (or zero) in water. The decrease of entropy relative to the halides is certainly accounted for by the losses of vibrational and rotational entropy on coordination of the triatomic SCN^-. The lack of extraordinarily high values of $\Delta S°_j$ and $\Delta H°_j$ at any particular step might indicate that the coordination change presumably taking place also in this system is spread out fairly evenly over several steps.[27] Another possibility would be that the rather weakly coordinating thiocyanate ion does not bring about any coordination change. In DMSO, a change might conceivably still occur at the fourth step which has not been reached in the present measurements.

Acknowledgements. We are indebted to Dr. Heikki Ots who put the calorimeter at our disposal. Dr. Lennart Kullberg has most generously shared his great experience of calorimetric measurements while introducing one of us (N.O.B.) into this field. The support of Statens naturvetenskapliga forskningsråd (The Swedish Natural Science Research Council) is gratefully acknowledged.

REFERENCES

1. Ahrland, S. and Björk, N. O. *Acta Chem. Scand. A 28* (1974) 823.
2. Ahrland, S. and Björk, N. O. *Acta Chem. Scand. A 30* (1976) 249.
3. Gerding, P. *Acta Chem. Scand. 20* (1966) 79.
4. Gerding, P. and Jönsson, I. *Acta Chem. Scand. 22* (1968) 2247.
5. Gerding, P. and Johansson, B. *Acta Chem. Scand. 22* (1968) 2255.
6. Gerding, P. *Acta Chem. Scand. 20* (1966) 2771.
7. Mc Auley, A. and Nancollas, G. H. *J. Chem. Soc.* (1963) 989.
8. Jones, A. D. and Choppin, G. R. *Actinides Rev. 1* (1969) 311; Choppin, G. R. and Schneider, J. K. *J. Inorg. Nucl. Chem. 32* (1970) 3283.
9. Schlyter, K. and Sillén, L. G. *Acta Chem. Scand. 13* (1959) 385.
10. Kullberg, L. *Thermodynamics of Metal Complex Formation in Aqueous Solution* Diss, Lund 1974 p. 14.
11. Cabani, S. and Gianni, P. *J. Chem. Soc. A* (1968) 547.
12. Kullberg, L. *Acta Chem. Scand. A 28* (1974) 829.
13. Christensen, J. J., Ruckman, J., Eatough, D. J. and Izatt, R. M. *Thermochim. Acta 3* (1972) 203.
14. Karlsson, R. and Kullberg, L. *Chem. Scr. 9* (1976) 54.
15. Gorenbein, E. J., Vainstein, M. N. and Skorobogatko, E. P. *Ukr. Khem. Zh. 9* (1974) 923.
16. Ots, H. *Acta Chem. Scand. 26* (1972) 3810.
17. Karlsson, R. and Karrman, K. J. *Talanta 18* (1971) 459.
18. Öjelund, G. and Wadsö, I. *Acta Chem. Scand. 22* (1968) 2691.
19. Grenthe, I., Ots, H. and (in part) Ginstrup, O. *Acta Chem. Scand. 24* (1970) 1067.

20. Hansen, L. D. and Lewis, E. A. *J. Chem. Thermodyn.* (1971) 35.
21. Vanderzee, C. E. and Swanson, J. A. *J. Phys. Chem. 67* (1963) 285.
22. Wagman, D. D., Bailey, S. M. and Schumm, R. H. *Selected Values of Chemical Thermodynamic Properties*, N.B.S. Technical Note 270-3 Jan. 1968.
23. Rossini, F. D. *Selected Values of Chemical Thermodynamic Properties*, Natl. Bur. Std. Circ. 500, U.S. Government Printing office, Washington 1952.
24. Burrus, R. T. *Polarographic studies in dimethyl sulfoxide*, Diss., University of Tenessee 1962.
25. Sandell, A. *Acta Chem. Scand. 24* (1970) 3391; *25* (1971) 1795.
26. Ahrland, S. and Johansson, L. *Acta Chem. Scand. 18* (1964) 2125.
27. Ahrland, S. *Struct. Bonding (Berlin) 15* (1973) 167.
28. Bol, W., Gerrits, G. J. A. and van Panthaleon van Eck, C. L. *J. Appl. Crystallogr. 3* (1970), 486.
29. Ohtaki, H., Maeda, M. and Ito, S. *Bull. Chem. Soc. Jap. 47* (1974) 2217.
30. Fronæus, S. In Jonassen, H. B. and Weissberger, A., Eds., *Technique of Inorg. Chem.* Interscience, New York, London, 1963, Vol. 1, Chapter 1.
31. Ahrland, S., Kullberg, L. and Portanova R. *To be published.*
32. Halliwell, H. F. and Nyburg, S. C. *Trans. Faraday Soc. 59* (1963) 1126.
33. Criss, C. M. and Salomon, M. In Covington, A. K. and Dickinson, T., Eds., *Physical Chemistry of Organic Solvent Systems*, Plenum Press, London, New York 1973, Chapter 2, Part 4, Appendices 2.11.3 and 2.11.15.

Received September 24, 1975.

Acta Chemica Scandinavica A 30 (1976) 265—269

Metal Halide and Pseudohalide Complexes in Dimethyl Sulfoxide Solution. V. Equilibrium Measurements on the Zinc(II) Chloride, Bromide, Iodide and Thiocyanate Systems

STEN AHRLAND and NILS-OLOF BJÖRK

Inorganic Chemistry 1, Chemical Center, University of Lund, P.O.B. 740, S-220 07 Lund, Sweden

The formation of chloride, bromide, iodide, and thiocyanate complexes of zinc(II) in dimethyl sulfoxide has been studied at 25 °C by central ion measurements. An approximately constant ionic medium of ionic strength = 1 M has been provided by means of ammonium perchlorate. All complexes formed are stronger in DMSO than in water and more so the harder the ligand, i.e. the more prone the ligand is to form hydrogen bonds. Consequently, the (*a*)-character of zinc(II) becomes even more marked in DMSO than in aqueous solutions.

In previous parts of this investigation, the changes of free energy, enthalpy and entropy accompanying the stepwise formation of chloride, bromide, iodide, and thiocyanate complexes of cadmium(II) have been measured and the results compared with those obtained earlier for the analogous reactions in aqueous solution.[1] The measurements have now been extended to the corresponding complexes of zinc(II). Though both zinc(II) and cadmium(II) are divalent d^{10} acceptors and consequently often react in much the same way, their coordinating properties are nevertheless rather different. Contrary to cadmium(II), zinc(II) very much prefers the light donor atoms to the heavy ones in aqueous solution, i.e. zinc(II) is a hard acceptor, much harder than the mildly soft cadmium(II). A comparison between the behaviour of these two acceptors in DMSO and water is therefore of considerable interest.[2]

In the present study, the stabilities of the zinc(II) chloride, bromide, iodide, and thiocyanate complexes in DMSO have been determined potentiometrically by means of a zinc amalgam electrode at 25 °C.

As in the cadmium(II) measurements,[1] an ammonium perchlorate medium of ionic strength $I = 1$ M has been employed. The corresponding measurements in aqueous solution [3,4] have been performed in sodium perchlorate media but as sodium chloride is not very soluble in DMSO,[5] such media are not practical in the present measurements.

Seemingly, no investigations of the stability of the zinc(II) complexes in DMSO have been reported so far.

CALCULATIONS

The notation is the same as before.[1] The stability constants have been calculated from the potentiometric measurements of the free central ion concentration, both graphically and numerically. The graphical method has earlier been discussed in detail. Only the final expressions will therefore be given here.

In the cells measured, the stable and reproducible cadmium amalgam electrode has been used as a reference:

$$-\mathrm{Zn(Hg)}\;\Big|\begin{array}{l}C_M\ \mathrm{M\ Zn(ClO_4)_2}\\ C_L\ \mathrm{M\ NH_4L}\\ \mathrm{NH_4ClO_4\ to}\ I = 1.00\mathrm{M}\end{array}\Big|\begin{array}{l}1.00\ \mathrm{M}\\ \mathrm{NH_4ClO_4}\end{array}\Big|\begin{array}{l}10.00\ \mathrm{mM\ Cd(ClO_4)_2}\\ \mathrm{NH_4ClO_4\ to}\\ I = 1.00\ \mathrm{M}\end{array}\Big|\;\mathrm{Cd(Hg)}+$$

The difference E_M between an emf E measured at a certain value of C_L and the emf E' at $C_L = 0$, where $C_M = [\mathrm{M}]$, is

$$E_M = (RT/2F) \ln (C_M/[M]) \quad (1)$$

If only mononuclear complexes are formed

$$C_M/[M] = X = 1 + \sum_{j=1}^{N} \beta_j [L]^j \quad (2)$$

which with (1) yields

$$E_M = (RT/2F) \ln X \quad (3)$$

The ligand number is given by

$$\bar{n} = \sum_{j=1}^{N} j\beta_j [L]^j / X \quad (4)$$

or approximatively by

$$\bar{n} = \frac{2F}{RT \ln 10} \frac{\Delta E_M}{\Delta \log [L]} \quad (5)$$

The functions $C_L(C_M)_{E_M}$ will be straight lines with the intercepts $C_L = [L]$ for $C_M = 0$ and the slopes $= \bar{n}$. For the numerical calculations the least-squares program EMK [6] has been used. This program is a simplified and faster version of the program used earlier. The present version is restricted to calculations on systems of mononuclear complexes. The best set of β_j is found by minimizing the following error square sum

$$U(\beta_j) = \sum_{i=1}^{N} w_i (E_{M,i,calc} - E_{M,i})^2 \quad (6)$$

where w_i is a weighting term, here = 1.

It may reasonably be assumed that the liquid junction potentials are negligible in the cells measured. From the values of E', it is then possible to calculate the difference $\Delta E°$(DMSO) between the formal standard potentials of the cadmium and zinc amalgam electrodes, on the concentration scale and in a medium of $I = 1$ M (NH_4ClO_4):

$$\Delta E°(DMSO) = E°\{Cd(Hg)\} - E°\{Zn(Hg)\}$$
$$= E' + \frac{RT}{2F} \ln \frac{C_M}{0.01} \quad (7)$$

For water, the corresponding difference $\Delta E°$(aq) has not been measured in the medium stated. The very similar activity functions [7] found for such salts of cadmium(II) and zinc(II) which are extensively dissociated in aqueous solution (nitrates, sulfates) indicate, however, that the activity coefficients of Cd^{2+} and Zn^{2+} varies in much the same way with the medium, as might also be expected. The difference $\Delta E°$(aq) should therefore be approximately the same for $I = 1$ M (NH_4ClO_4) and for $I = 0$ where it is very accurately known.[8] Hence $\Delta E° = \Delta E°(aq) - \Delta E°(DMSO)$ referring to $I = 1$ M (NH_4ClO_4) can be calculated with fair accuracy. This quantity is the change between water and DMSO for the difference between the formal standard potentials of cadmium and zinc amalgam. An identical change occurs, of course, between the standard potentials of cadmium and zinc metal as these differ from the amalgam electrodes only with respect to the activity of the metal in the electrode phase. The quantity $\Delta E°$ is in fact the emf of a cell with the cell reaction

$$Cd^{2+}(aq) + Zn^{2+}(DMSO) \rightarrow Cd^{2+}(DMSO) + Zn^{2+}(aq) \quad (8)$$

which is evidently independent of the electrode material. The free energy change of this exchange reaction is

$$\Delta G°_{ex} = -2F\Delta E° \quad (9)$$

EXPERIMENTAL

Chemicals. The hexasolvate $Zn(DMSO)_6(ClO_4)_2$ and all *ligand solutions* were prepared and analyzed as described previously.[1,2]

Zinc amalgam was prepared and stored as described by Persson.[9] The amalgam contained $\simeq 2.5$ % zinc. The exact concentration is not critical since a two-phase amalgam is formed [10] between 2.18 and 45 % at 25 °C.

The *apparatus* and the *procedure* have been the same as before.[1] The reproducibility of the emf's measured was generally better than ± 0.04 mV for low values of C_L. At values of $C_L \simeq 50$ mM, it was still better than ± 0.2 mV for all the systems. For higher values of C_L, the emf's were increasingly less reproducible. The reason for this is that the higher complexes predominating in this concentration range do not contribute to the exchange current, as has been shown by measurements of the electrode kinetics.[11] At $C_L \simeq 500$ mM, the reproducibility had decreased to about ± 2mV for the chloride and thiocyanate systems and to ± 1 mV for the bromide. For the weak iodide system the reproducibility was better than ± 0.1 mV even at the highest values of C_L used ($\simeq 500$ mM).

The final values of E were reached within 30 min and were extremely stable. Within the

next 5 h, the variation generally did not exceed ± 0.02 mV. If left for 24 h, the values changed by $\simeq 0.3$ mV. Also at high values of C_L (>50 mM), a similar change was observed when the cell was left standing.

The validity of Nernst's law has been checked[1] in the range 5 mM $\leq C_M \leq$ 40 mM. The value of $E°$(DMSO) was constant within ± 0.3 mV.

MEASUREMENTS AND RESULTS

The difference between the standard potentials of cadmium and zinc in DMSO and water. A value of $\Delta E°$(DMSO) = 363.9 mV is found. In water, at $I = 0$, $E°${Cd(Hg)} = -352.0 mV, *i.e.* 50.5 mV more positive than $E°$(Cd) = -402.5 mV,[8] while no perceptible difference exists between the potentials of zinc and zinc amalgam[18], $E°${Zn(Hg)} = $E°$(Zn) = -762.8 mV.[9] A value of $\Delta E°$(aq) = 410.8 mV results, judged to be approximately valid also at $I = 1$. Hence $\Delta E° = 46.9$ mV, and $\Delta G°_{ex} = -9.05$ kJ (eqn. 9), implying that Cd^{2+} is favoured relative to Zn^{2+} by a transfer from water to DMSO, *cf.* eqn. 8. Evidently, the solvation in DMSO relative to water is markedly more favourable for Cd^{2+} than for Zn^{2+}.

Zinc chloride and zinc bromide. If data referring to the highest values of C_L employed ($\lesssim 60$ mM) are included in the calculations, the error square sum of eqn. 6 becomes much higher than if they are omitted. If the high values are included, the first three mononuclear complexes are unambiguously identified. The fourth one cannot be positively proved, especially as the random errors are so large in that upper range of concentration where it might possibly exist. The upper limit of the stability constant is given in Table 1.

Since other evidence[1,13,14] also indicates that central ion measurements at high ligand concentrations may be subject to serious systematic errors, no data for $C_L \lesssim 60$ mM are included in the final calculations.

In the range of C_L thus chosen, both the numerical and the graphical evaluation indicates only the first three complexes. The constants calculated by the two methods agree very well. The complex formation function calculated from β_1 to β_3, eqn. 4, coincides well both with the values of $\bar{n}$ calculated from eqn. 5 and with those found from the slopes of the $C_L(C_M)$-lines, Fig. 1.

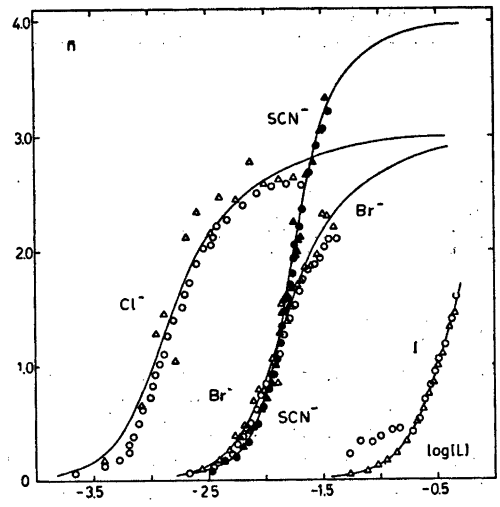

Fig. 1. The complex formation functions of the zinc(II) systems. The curves are calculated from eqn. (4). The slopes of the $C_L(C_M)_{E_M}$-lines are denoted by circles, values from eqn. (5) by triangles. The symbols are filled for the thiocyanate system. The potentiometric measurements reach as far as $\bar{n} = 2.80$ for Cl^-, 2.45 for Br^- and 3.5 for SCN^-. The parts of the curves extending beyond these values of $\bar{n}$ are based on the calorimetric measurements described in the next paper.

Zinc iodide. Graphical and numerical evaluation of the measurements indicate three mononuclear complexes. The sets of β_j found by the two methods of calculation agree very well. The complex formation function calculated from the set given in Table 1 coincides well with the values of $\bar{n}$ found from eqn. 5 but not so well with those found from the slopes of the $C_L(C_M)$-lines. For such a weak complex system as the present one this is not very surprising, however, as the $E_M(C_L)$-functions vary only little with C_M.

Zinc thiocyanate. As for the chloride and bromide systems, no data for $C_L \lesssim 60$ mM are included in the final calculations of the thiocyanate system. In this system, however, both the graphical and the numerical evaluation indicate four mononuclear complexes, with good agreement between the two sets of β_j. The complex formation function calculated from the numerical set (Table 1) is fulldrawn in Fig. 1. Both the values of $\bar{n}$ from eqn. 5 and those found from the slopes of the $C_L(C_M)$-lines fit very well to this function.

Table 1. The overall stability constants β_j for the halide and thiocyanate systems of zinc(II) investigated. The limits of error given correspond to three standard deviations. Medium: 1 M NH_4ClO_4.

	Cl^-	Br^-	I^-	SCN^-
β_1/M^{-1}	86 ± 25	7 ± 2	0.20 ± 0.04	24 ± 2
β_2/M^{-2}	$(6.8 \pm 0.2)10^5$	$(5.4 \pm 0.4)10^3$	5.1 ± 0.3	630 ± 430
β_3/M^{-3}	$(1.18 \pm 0.04)10^8$	$(1.2 \pm 0.1)10^5$	7.2 ± 0.5	$(1.6 \pm 0.3)10^5$
β_4/M^{-4}	$(<10^9)$	$(<2 \times 10^5)$	–	$(7.2 \pm 0.6)10^6$

DISCUSSION

As pointed out in the introductory paper of this series,[1] complexes formed by ligands able to participate in hydrogen bonding should be relatively more stable in the aprotic solvent DMSO than in water. All the systems investigated here are in fact stronger in DMSO than in water, Table 2. Particularly the chloride, but also the bromide complexes are much stronger. For the iodide and thiocyanate complexes the increase is relatively modest. The stabilities thus increase as expected, *viz.* more the harder the ligand. The result is, of course, that zinc(II) acquires an even more marked (*a*)-character in DMSO than in water.

For all the zinc halide systems, the first complex has a very narrow range of existence in DMSO, as shown by the very low value of the ratio K_1/K_2, Table 2. Also in the cadmium halide systems,[1] one of the complexes has a very narrow range of existence in DMSO, but in these systems the second complex is the disfavoured one.

Table 2. Stability of zinc halide and thiocyanate complexes in DMSO and water, at 25 °C.

	Cl^-	Br^-	I^-	SCN^-
	DMSO, 1 M NH_4ClO_4			
K_1	86	7	0.20	24
K_2	7900	770	26	26
K_3	170	22	1.4	250
K_4	< 10	< 2		45
K_1/K_2	0.011	0.009	0.008	0.92
K_2/K_3	46	35	19	0.10
K_3/K_4	> 17	> 11		5.6
	Water, 3 M $NaClO_4$		1 M $NaClO_4$	
K_1	0.65	0.27	0.03	5.10
K_2	0.38	0.15		2.2
K_3	5.6	3.3		1.4
K_4				2.1
K_1/K_2	2	2		2.3
K_2/K_3	0.07	0.05		1.6
K_3/K_4				0.67
Ref.	3	18	18	4

For the cadmium systems the thermodynamics of the formation of the consecutive steps indicate that the narrow range of the second complex most probably depends upon a change of coordination.[1] This change mainly takes place at this very step.

It has been proved by X-ray analysis [15] that the zinc ion in aqueous solution exists as a hexahydrate, of regular octahedral structure. For the DMSO solvate in solution no such structure determination has been performed. A solid solvate $Zn(DMSO)_6(ClO_4)_2$ is easily prepared,[2] however. The hexacoordination most probably persists in solution, with the solvent molecules in a regularly octahedral arrangement. On the other hand, solid halide complexes containing discrete tetrahedral groups ZnL_4^{2-} and $XnL_3(H_2O)^-$ are known,[16,17] indicating a preferance for tetrahedral coordination in zinc halide complexes. It is therefore likely that the narrow range of existence of the first complex in the zinc halide systems is due to a change from octahedral to tetrahedral coordination. A closer scrutiny of this must await the determination of the enthalpy and entropy changes of the complex formation, however, which will be the theme of the next paper in this series.

The thiocyanate systems of cadmium(II) and zinc(II) behaves quite differently. In the former,[1] none of the three complexes is disfavoured, while in the latter the second complex has a fairly narrow range of existence, Table 2. In water,[4] the third zinc complex is the weakest. Also for the thiocyanate system, a full dis-

cussion can be undertaken only when the changes of enthalpy and entropy for the various steps have been measured.

Acknowledgements. The support of Statens naturvetenskapliga forskningsråd (The Swedish Natural Science Research Council) is gratefully acknowledged.

REFERENCES

1. Ahrland, S. and Björk, N. O. *Acta Chem. Scand. A 30* (1976) 249, 257.
2. Ahrland, S. and Björk, N. O. *Acta Chem. Scand. A 28* (1974) 823.
3. Sillén, L. G., Liljeqvist, B. *Sv. Kem. Tidskr. 56* (1944) 85.
4. Ahrland, S. and Kullberg, L. *Acta Chem. Scand. 25* (1971) 3692.
5. Kenttämaa, J. *Suom. Kemistil. B 33* (1960) 179.
6. Karlsson, R. and Kullberg, L. *Chem. Scr. 9* (1976) 54.
7. Robinson, R. A. and Stokes, R. H. *Electrolyte Solutions*, Butterworth, London 1955.
8. Sillén, L. G. and Martell, A. E., Eds., *Stability Constants of Metal-Ion Complexes*, Chemical Society, Special Publications Nos. 17 and 25, London 1964, 1971.
9. Persson, H. *Acta Chem. Scand. 24* (1970) 3739.
10. Hansen, M. *Constitution of Binary Alloys*, 2nd Ed., 1958, p. 846, as quoted in *Gmelin*, 8th Ed. Nr *34* [*A*] Quecksilber, 1962, p. 1062.
11. Fronæus, S. and Johansson, C. L. *J. Electroanal. Chem. In press.*
12. Clayton, W. J. and Vosburgh, W. C. *J. Amer. Chem. Soc. 58* (1936) 2093.
13. Sandell, A. *Acta Chem. Scand. 24* (1970) 3391; *25* (1971) 1795.
14. Ahrland, S. and Johansson, L. *Acta Chem. Scand. 18* (1964) 2125.
15. Bol, W., Gerrits, G. I. A. and van Panthaleon van Eck, C. L. *J. Appl. Crystallogr. 3* (1970) 486.
16. Follner, H. and Brehler, B. *Acta Crystallogr. B 24* (1968) 1339.
17. Wells, A. F. *Structural Inorganic Chemistry* 4th Ed., Clarendon Press, Oxford 1975, pp. 390 and 394.
18. Gerding, P. *Acta Chem. Scand. 23* (1969) 1695.

Received October 1, 1975.

Acta Chemica Scandinavica A 30 (1976) 270—276

Metal Halide and Pseudohalide Complexes in Dimethyl Sulfoxide Solution. VI. Enthalpy Measurements on the Zinc(II) Chloride, Bromide, Iodide, and Thiocyanate Systems

STEN AHRLAND, NILS-OLOF BJÖRK and ROBERTO PORTANOVA

Inorganic Chemistry 1, Chemical Center, University of Lund, P.O.B. 740, S-220 07 Lund, Sweden

The enthalpy changes for the formation of zinc(II) chloride, bromide, iodide, and thiocyanate complexes in dimethyl sulfoxide have been determined calorimetrically. From the measured enthalpy changes, and the free energy changes computed from the stability constants, the entropy changes have been calculated. All data refer to 25.0 °C and an ammonium perchlorate medium of 1 M ionic strength.

For the chloride and bromide systems ΔH°_1 and ΔS°_1 are particularly high, while for the iodide and thiocyanate ΔH°_2 and ΔS°_2 are the highest. These high values are interpreted as due to a change of coordination. The total entropy gains found in DMSO are much higher than for the corresponding systems in water.

The thermodynamic functions governing the formation of cadmium(II) chloride, bromide, iodide, and thiocyanate systems in the aprotic solvent dimethyl sulfoxide (DMSO) have been reported in part IV of this series and the results compared with those previously obtained for the analogous reactions in aqueous solution.[2] As the complex formation depends much upon the acceptor characteristics of the metal ion, it is of great interest to extend the investigations to other metal ions which differ markedly from cadmium(II) in this respect. To facilitate the comparison, it is advisable to choose, in the first instance, ions analogous to cadmium(II), *i.e.* divalent d^{10} acceptors. Zinc(II) has therefore been the next acceptor to be investigated [1] and the stabilities of its chloride, bromide, iodide and thiocyanate complexes in DMSO have been reported in part V of this series.[3] For zinc(II), a much harder acceptor than the mildly soft cadmium(II), an (*a*)-sequence $Cl^- > Br^- > I^-$ is found already in water and it becomes much more marked in DMSO.

This paper deals with the determination of the enthalpy changes, ΔH°_j, for the stepwise formation of complexes within the zinc(II) systems mentioned. The results have been obtained by direct calorimetric measurements (*cf.* part IV). From the values of ΔH°_j and ΔG°_j thus available, the entropy changes have been found.

As previously, the measurements refer to a 1 M ammonium perchlorate medium of 25 °C. Recently, a very exploratory calorimetric investigation of these systems has been performed.[3] It was then assumed that the dissolution of the solid halides yields the neutral complex ML_2 in solution. From the present investigation it is obvious that this is not true. Consequently, the result is hardly correct, and in any case not comparable with the present ones.

EXPERIMENTAL

Chemicals. The hexasolvate $Zn(DMSO)_6(ClO_4)_2$ and all *ligand solutions* were prepared and analyzed as described previously.[1,2]

Apparatus. The calorimeter and the technique used have been described previously.[2] In each titration series a solution T was titrated into the reaction vessel initially containing V_0 ml of a solution S.

The heats of dilution were determined by analogous titration series where one of the reactant solutions was exchanged for 1 M ammonium perchlorate solution.

The notation is the same as before.[2] The calculations have been performed by the least

squares program "Kalori".[4,5] The complete calorimetric data are available from the authors.

MEASUREMENTS AND RESULTS

The chloride and bromide systems. First, values of $\Delta H°_j$ were calculated with the potentiometrically determined β_j, including a value of β_4 equal to the upper limit (part V). In the next run, where all constants were treated as unknowns (with the sets of β_j and $\Delta H°_j$ already determined as initial values), no significant values of β_4 were obtained, Table 1, in spite of the fact that the calorimetric measurements were extended to [L]≃375 mM. Though this value is much higher than the highest ones that could be applied in the potentiometric measurements ([Cl^-]≃30 mM and [Br^-]= 50 mM) the data are nevertheless well fitted by the first three complexes. The extension of the range of [L] also means a sizable increase in the highest value of $\bar{n}$ reached. For chloride this value is increased from 2.80 to 2.98, for bromide from 2.45 to 2.89, *cf.* Fig. 1 of part V.

In the final calculation of $\Delta H°_1$ to $\Delta H°_3$ for the chloride system, weighted mean values of β_1 to β_3 were used, Table 1. For the bromide system, on the other hand, where the calorimetric data did not provide any significant value of β_1 it was considered most appropriate to use the potentiometrically determined values of β_1 to β_3 for the final calculation. The thermodynamic functions found are given in Table 2. The function $\Delta h_v(\bar{n})$ is independent of C_M, again [2] indicating the absence of polynuclear complexes.

The iodide system. When both β_j and $\Delta H°_j$ were treated as unknowns, the values of β_j had quite large errors, Table 1. This applies particularly to β_1. The potentiometrically determined constants were therefore used for the final calculations of the thermodynamic functions, Table 2. The function $\Delta h_v(\bar{n})$ is given in Fig. 1.

Table 1. The stability constants of zinc(II) chloride, bromide, iodide, and thiocyanate complexes in DMSO at 25 °C, determined by potentiometric and calorimetric methods. The errors given correspond to three standard deviations. Ionic medium 1 M ammonium perchlorate.

j	Pot.	Cal.	Mean
Chloride (β_j, M^{-j})			
1	86 ± 25	89 ± 45	87 ± 26
2	$(6.8 \pm 0.2)10^5$	$(7.2 \pm 0.8)10^5$	$(6.9 \pm 0.4)10^5$
3	$(1.18 \pm 0.04)10^8$	$(1.7 \pm 0.3)10^8$	$(1.24 \pm 0.15)10^8$
4	$< 10^9$	$(1 \pm 4)10^7$	
Bromide (β_j, M^{-j})			
1	7 ± 2	1 ± 3	
2	$(5.4 \pm 0.4)10^3$	$(5.0 \pm 0.3)10^3$	
3	$(1.2 \pm 0.1)10^5$	$(1.3 \pm 0.2)10^5$	
4	$< 2 \times 10^5$	0	
Iodide (β_j, M^{-j})			
1	0.20 ± 0.04	0.05 ± 0.21	
2	5.1 ± 0.3	5.0 ± 1.8	
3	7.2 ± 0.5	6.5 ± 3.0	
4			
Thiocyanate (β_j, M^{-j})			
1	24 ± 2	24 [a]	
2	$(6 \pm 4)10^2$	$(6 \pm 9)10^2$	
3	$(1.6 \pm 0.3)10^5$	$(1.7 \pm 0.5)10^5$	
4	$(7.2 \pm 0.6)10^6$	$(9.6 \pm 2.4)10^6$	

[a] No variation.

Table 2. Thermodynamics of the stepwise coordination of chloride, bromide, iodide, and thiocyanate to zinc(II) in DMSO at 25 °C, in 1 M ammonium perchlorate. Errors correspond to three standard deviations.

Step, j	$\Delta G°_j$ (kJ mol^{-1})	$\Delta H°_j$ (kJ mol^{-1})	$\Delta S°_j$ (J K^{-1} mol^{-1})
Chloride			
1	-11.1 ± 0.8	22.3 ± 3.8	112 ± 13
2	-22.2 ± 0.9	0.8 ± 4.3	77 ± 15
3	-12.9 ± 0.2	-10.2 ± 0.2	9.1 ± 0.9
1+2	-33.3 ± 0.2	23.1 ± 0.4	189 ± 2
Bromide			
1	-4.8 ± 0.8	27.8 ± 5.2	110 ± 17
2	-16.5 ± 2.0	9.1 ± 5.4	85 ± 19
3	-7.7 ± 0.3	-4.2 ± 0.4	12 ± 2
1+2	-21.3 ± 0.2	36.9 ± 0.5	195 ± 3
Iodide			
1	4.0 ± 0.6	19.0 ± 7.5	50 ± 25
2	-8.0 ± 0.7	29.4 ± 7.8	127 ± 26
3	-0.9 ± 0.3	12.7 ± 2.3	45 ± 8
Thiocyanate			
1	-7.9 ± 0.2	5.5 ± 0.7	45 ± 3
2	-8.1 ± 2.1	23.5 ± 3.7	105 ± 15
3	-13.7 ± 2.2	-17.8 ± 3.7	-13 ± 15
4	-9.4 ± 0.5	-10.7 ± 0.6	-4 ± 3

The thiocyanate system. When all parameters were treated as unknowns the values of β_1 and $\Delta H°_1$, and also those of β_2 and $\Delta H°_2$, were so strongly interdependent that no significant results ensued. If the well determined $\beta_{1,pot}$ was introduced, however, reasonable values were obtained for β_2 to β_4, though the error in β_2 is still extremely large, Table 1. Like for the chloride and bromide systems, much higher values of [L] can be applied in the calorimetric measurements than in the potentiometric ones. In the former, a value of [SCN] $\simeq$ 470 mM was reached, corresponding to $\bar{n} \simeq 3.95$, while in the latter the range is limited to [SCN] $\lesssim$ 50 mM, and hence to $\bar{n} \lesssim 3.5$, (*cf.* Fig. 1 of part V).

In the final calculations of the thermodynamic functions the potentiometrically determined values of β_j have been used, Table 2. The function $\Delta h_v(\bar{n})$ is given in Fig. 1.

DISCUSSION

In the halide systems of zinc(II) the first complex has a narrow range of existence in DMSO solution (*cf.* part V). Also for the systems of weak chloride and bromide complexes formed in aqueous solution, a similar phenomenon occurs, though in these cases the second step is disfavoured.[6,7] Quantitatively, this is expressed by low values of the ratios K_1/K_2 and K_2/K_3, respectively. In Table 3, summarizing the thermodynamic functions, these conditions are reflected in the very positive values of $(\Delta G°_1 - \Delta G°_2)$ for DMSO and of $(\Delta G°_2 - \Delta G_3)$ for water. A narrow range of existence of a certain complex thus depends upon an interaction between the changes of enthalpy and entropy which in the case of a suppressed first complex, *i.e.* when $\Delta G°_1 \gg \Delta G°_2$, can be expressed as follows (*cf.* part IV).

$$\Delta H°_1 + T\Delta S°_2 \gg \Delta H°_2 + T\Delta S°_1$$

From the present measurements it is obvious that the first complex is disfavoured for different reasons in the chloride and bromide systems on the one hand and in the iodide system on the other. In the two former systems $\Delta H°_1$ is so much more positive than $\Delta H°_2$ that the decrease of the entropy gain from $\Delta S°_1$ to $\Delta S°_2$ is completely outweighed. In the iodide system, on the other hand, $\Delta S°_2$ is so much larger than $\Delta S°_1$ that the increase of the enthalpy change from $\Delta H°_1$ to $\Delta H°_2$ is completely outweighed. For the chloride and bromide systems in water [7] the narrow range of existence of the second complex is due to the very high values of $\Delta H°_2$, Table 3.

Due to the narrow range of existence of the first complex, only the sums of the thermodynamic functions for the first two steps can be precisely determined but not the individual functions, Table 2 (*cf.* also part IV).

The zinc(II) hydrate is a regular octahedron in aqueous solution.[8] No structural studies of the weak halide complexes formed in water have been performed, however. In DMSO, no direct information exists at all about the structures. The solvate is presumably hexacoordinated, however, both in the solid state and also in the solution. This inference is strengthened by the fact that in the closely related solid solvate $Zn(m\ DTSO)_6(ClO_4)_2$, where m DTSO stands

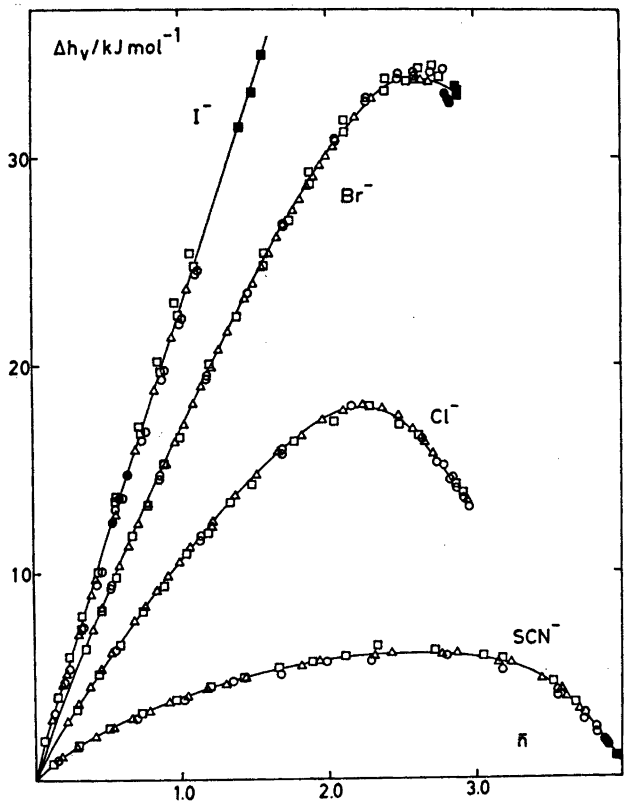

Fig. 1. The total molar enthalpy change Δh_v as a function of $\bar{n}$ for the halide systems. The fulldrawn curves are calculated from the mean values of β_j in the case of the chloride system. For the other systems the potentiometrically determined sets are used, *cf.* Table 1. The corresponding ΔH°_j are given in Table 2. Some of the experimental points are excluded at random.

for 1,3-dithian-monosulfoxide, the zinc ion is octahedrally surrounded by the sulfoxide molecules (coordinated, *via* oxygen, as expected).[9] On the other hand, all solid trihalido and tetrahalido complexes of zinc so far investigated contain discrete tetrahedral units, with water in the fourth position in the case of the trihalides.[10,11] A change of coordination thus certainly occurs in the course of the complex formation just as it does for the cadmium(II) halide system.[2]

The thermodynamic irregularities connected with certain steps of the complex formation should thus no doubt be interpreted along the same lines as for these, especially as the effect observed is so obviously of the same nature in both cases.

As indicated by the abnormally high entropy gains, the change of coordination for the zinc chloride and bromide systems mainly takes place already at the first step in DMSO but at the second step in water. This is different from the corresponding cadmium systems where the coordination change mainly takes place at the second step in DMSO and at the third step in water. For the zinc iodide system, on the other hand, the change evidently takes place mainly at the second step in DMSO, just as for the cadmium iodide system, *cf.* part IV, Table 3. In water, the zinc iodide system is too weak for a safe determination of the pertinent functions.[7]

For steric reasons it is not unexpected that the structural change occurs at an earlier step for zinc(II) than for cadmium(II) and also that a solvate of bulky DMSO molecules breaks up at an earlier step than a hydrate. The chloride and bromide systems throughout

Table 3. Thermodynamics of zinc halide and thiocyanate complexes in DMSO and water, at 25 °C, in the media stated. $\Delta G°_j$ and $\Delta H°_j$ in kJ mol^{-1}, $\Delta S°_j$ in JK^{-1} mol^{-1}.

	DMSO				Water		
	1 M NH_4ClO_4				3 M $NaClO_4$		1 M $NaClO_4$
	Cl^-	Br^-	I^-	SCN^-	Cl^-	Br^-	SCN^-
$\Delta G°_1$	−11.1	−4.8	4.0	−7.9	1.1	3.3	−4.0
$\Delta G°_2$	−22.2	−16.5	−8.0	−8.1	2.4	4.7	−1.9
$\Delta G°_3$	−12.9	−7.7	−0.9	−13.7	−4.3	−3	−0.8
$\Delta G°_4$	–	–	–	−9.4	–	–	−1.9
$\Delta H°_1$	22.3	27.8	19.0	5.5	5.5	1.5	−5.8
$\Delta H°_2$	0.8	9.1	29.4	23.5	38	42	−2
$\Delta H°_3$	−10.2	−4.2	12.7	−17.8	0	−8	−1
$\Delta H°_4$	–	–	–	−10.7	–	–	−8
$\Delta S°_1$	112	110	50	45	15	−5.9	−6
$\Delta S°_2$	77	85	127	105	120	125	0
$\Delta S°_3$	9.1	12	45	−13	8	−17	0
$\Delta S°_4$	–	–	–	−4	–	–	−20
$\Delta H°_{\beta_3}$	13	33	61	11	44	36	−9
$\Delta S°_{\beta_3}$	198	207	222	137	143	102	−6

behave according to this expectation. Also for cadmium iodide in DMSO and water, the rule holds. A very striking exception is found, however, *viz.* that the iodide systems of zinc and cadmium both change their coordination at the second step. This is the more remarkable as one would rather expect the rule to be more strictly valid for the large iodide ion than for its lighter congeners. Some other influence must evidently also be at work. Most likely, the unexpected trend depends upon that the effective charge on the central zinc ion increases in the sequence $Cl^- < Br^- < I^-$, the neutralization being more extensive the higher the charge density on the halide ion. With increasing effective charge, the central ion will more easily keep an extensive solvation, hence the retarded desolvation in the iodide system. For the cadmium systems, on the other hand, where the metal to ligand bonds are increasingly covalent in the sequence $Cl^- < Br^- < I^-$, the neutralization of the cationic charge is presumably more extensive, the more polarizable the halide ion. In this case, the charge on the central cadmium ion should therefore *decrease* from Cl^- to I^-. Consequently, no retarded desolvation is to be expected for the cadmium iodide system.

The inferences put forward above as to the variation with the halide of the effective charge on the central ion have in fact been verified by direct measurements [15] of the solvation enthalpies of the neutral complexes ML_2.

For the zinc thiocyanate system in DMSO, the change of coordination mainly takes place at the second step, as for iodide. This is different to the cadmium thiocyanate system where no very striking increases in entropy occur in the course of formation of the first three complexes, part IV, Table 3. The same also applies to both zinc and cadmium thiocyanate in aqueous solution.[13–14]

A most remarkable feature of the chloride and bromide systems of zinc(II) is that no fourth complex exists even at the highest ligand concentrations reached here. If such complexes can be formed at all they are in any case extremely weak relative to their predecessors as is evident from the complex formation curves which show quite marked shelves for $\bar{n}=3$ (*cf.* V, Fig. 1). The fourth tetrahedral position is clearly not at all attractive which is in marked contrast not only to the cadmium halides (*cf.* III, Fig. 6) but also to the zinc thiocyanate (V, Fig. 1). For all these systems, $\bar{n}=4$ is approached without any previous stops. The zinc iodide and the cadmium thiocyanate systems are too weak to allow any conclusions about their behaviour in this respect.

For all the zinc systems, the total gain of entropy is much higher in DMSO than in water, as is found by comparing $\Delta S°_{\beta_3} = \sum_{j=1}^{3} \Delta S°_j$ for the two solvents, Table 3. The corresponding cadmium systems behave in the same way, part IV, Table 3. As suggested in part IV, this difference is most probably due to the higher degree of order prevailing in water, on account of the strong hydrogen bonding between the water molecules which has no counterpart in DMSO. A desolvation thus implies a larger loss of order, and hence a larger gain of entropy, in DMSO than in water. The stronger solvation [15] of Zn^{2+} and Cd^{2+} in DMSO also contributes to the higher total gain of entropy, however.

As for the cadmium halides, the values of $\Delta S°_{\beta_3}$ in DMSO increase for the zinc halides in the sequence $Cl^- < Br^- < I^-$ which means a reversal of the sequence observed in aqueous solution. The difference of solvation between the halides in DMSO [15] and in water certainly acts in the direction observed, but is hardly large enough to account for the whole effect produced, as discussed in part IV.

For the thiocyanate system, the value of $\Delta S°_{\beta_3}$ is much lower than for any of the halides, a phenomenon that in an even higher degree was observed for the corresponding cadmium systems, part IV. As suggested there, the relatively low thiocyanate values are certainly due to losses of vibrational and rotational freedom sustained by the triatomic thiocyanate ion on coordination. These losses have of course no counterpart in the reactions of the halide ions.

For a closer comparison of the entropies involved in the formation of zinc and cadmium complexes in DMSO, the differences between the total entropy changes, $\Delta S°_{\beta_n} = \sum_{j=1}^{n} \Delta S°_j$, have been calculated. These differences $\Delta S°_{\beta_n}(Zn-Cd)$ give the entropy changes of the reactions

$$Zn(II)(solv) + Cd(II)L_n(solv) \rightarrow Zn(II)L_n(solv) + Cd(II)(solv) \quad (1)$$

As the abnormally high entropy increases occur at earlier steps for all the zinc systems, except the iodide, (*cf.* p. 273) the reaction (1) must involve a rather large gain of entropy for $n = 1$ and 2 in the case of chloride, bromide and thiocyanate. For iodide on the other hand, no large gain is to be expected. At the end of the complex formation, where the coordination change is certainly complete for both zinc and cadmium, $\Delta S°_{\beta_n}(Zn-Cd)$ should be very similar for all the ligands. The values of $\Delta S°_j$ even suggest that the coordination change is virtually completed with the third step. If so, already $\Delta S°_{\beta_3}(Zn-Cd)$ should not differ very much between the various systems. Since zinc(II) is more strongly solvated than cadmium(II) in DMSO [15] ΔS_{β_3} is moreover expected to be positive.

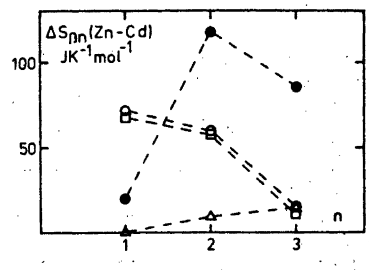

Fig. 2. The entropy change $\Delta S°_{\beta_n}(Zn-Cd)$ plotted against the number of participating ligands [*cf.* reaction (1)]. The signs refer to: Cl^-, ○; Br^-, □; I^-, △ and SCN^-, ●.

The values of $\Delta S_{\beta_n}(Zn-Cd)$ have been plotted in Fig. 2. For $n = 1$ and 2, the values found for chloride and bromide are, as expected, very different from those found for iodide. In contrast to this, the values for $n = 3$ are practically the same, $\simeq 14$ J K^{-1}, as would also be expected provided that the coordination change is really completed for all the halides as the third ligand enters the inner sphere. It is further striking that for chloride and bromide the values of $\Delta S°_{\beta_n}(Zn-Cd)$ are much the same for each step. For thiocyanate, the values are for all steps remarkably different from those found for the halides. It is especially noticeable that the value for $n = 3$ is so much higher, 86 J K^{-1}. This most probably implies that the change to a tetrahedral coordination has not been completed for the cadmium thiocyanate system with the third step.

REFERENCES

1. Ahrland, S. and Björk, N. O. *Acta Chem. Scand. A 28* (1974) 823.
2. Ahrland, S. and Björk, N. O. *Acta Chem. Scand. A 30* (1976) 249, 257, 265.
3. Gorenbein, E. I., Vainstein, M. N. and Skorobogatko, E. P. *Ukr. Chem. Zh. 9* (1974) 923.
4. Karlsson, R. and Kullberg, L. *Chem. Scr. 9* (1976) 54.
5. Kullberg, L. *Acta Chem. Scand. A 28* (1974) 829.
6. Sillén, L. G. and Liljeqvist, B. *Svensk Kem. Tidskr. 56* (1944) 85.
7. Gerding, P. *Acta Chem. Scand. 23* (1969) 1695.
8. Bol, W., Gerrits, G. J. A. and van Panthaleon van Eck, G. L. *J. Appl. Crystallogr. 3* (1970) 486.
9. Driessen-Fleur, T. *Cyclic Sulfoxides as Ligands*, Diss., Univ. of Leiden 1975.
10. Follner, H. and Brehler, B. *Acta Crystallogr. B 24* (1968) 1339.
11. Wells, A. F. *Structural Inorganic Chemistry*, 4th Ed., Clarendon Press, Oxford 1975, pp. 390 and 394.
12. Ahrland, S. and Kullberg, L. *Acta Chem. Scand. 25* (1971) 3692.
13. Gerding, P. and Johansson, B. *Acta Chem. Scand. 22* (1968) 2255.
14. Gerding, P. *Acta Chem. Scand. 20* (1966) 2771.
15. Ahrland, S. Kullberg, L. and Portanova, R. *To be published.*

Received October 1, 1975.

Acta Chemica Scandinavica A 30 (1976) 277—280

The Dissociation Constant of 3-Nitrobenzoic Acid in H_2O and D_2O and in their DMSO Mixtures

ANTTI VESALA and ERKKI SALOMA

Department of Chemistry, University of Turku, SF-20500 Turku 50, Finland

The dissociation constant of 3-nitrobenzoic acid was determined in H_2O-DMSO and D_2O-DMSO mixtures up to the DMSO mol fraction of 0.18 by potentiostatic titration. The Debye-Hückel treatment was used to correct the observed dissociation constants to zero ionic strength. Also a direct treatment characteristic of potentiostatic titration was applied in the extrapolation of thermodynamic constants and a good fit with the values obtained by the Debye-Hückel treatment was obtained.

The plot of pK *versus* the mol fraction of DMSO was observed to be linear both in H_2O and D_2O. By the aid of these linear relationships the pK values in pure H_2O and D_2O could be extrapolated.

The method of potentiostatic titration in determining dissociation constants is useful, especially when the measurements are carried out in different solvents as all empirical corrections due to the transfer of electrodes from one medium to another can be avoided. By this method it is possible to determine concentration dissociation constants by which thermodynamic constant of sufficient accuracy can be obtained.[1]

The solubility of 3-nitrobenzoic acid in water is relatively low so that the acid solution needed for the titrations had to be prepared in a properly chosen organic solvent. Since the pK values in light and heavy water were determined the solvent had to be such that it did not contain any exchangeable hydrogen. Dimethyl sulfoxide proved to be an excellent solvent in both respects. The pK value of 3-nitrobenzoic acid (approx. 3.5) is appropriate when the best possible applicability of the titration method is concerned.

One aim has been to determine the difference $pK_{D_2O} - pK_{H_2O}$ $(= \Delta pK)$ for 3-nitrobenzoic acid as accurately as possible. The dependence of the pK value on the mol fraction of DMSO is also expected to be of interest although the measurements cover only the mol fractions of DMSO up to 0.18. An important aspect is the search for such mixtures H_2O-DMSO and D_2O-DMSO, where the pK values compared with those in H_2O and D_2O, respectively, have changed with the value of ΔpK.

EXPERIMENTAL

Reagents. The light water employed was distilled water. The heavy water was purchased from Norsk Hydro. Its deuterium mol fraction was 0.998. Both light and heavy water were degassed under reduced pressure. The 3-nitrobenzoic acid was a purissimum product of Koch-Light Laboratories Ltd. It was recrystallized from water and dried at 373 K for 6 h. The observed melting point was 415.7 – 416.2 K (lit. value [2] 415.25). The acid used in the titrations was in a DMSO solution having a concentration of 0.500 mol/dm³. The potassium hydroxide solution was prepared in light water from Merck's ampoule. Its concentration was 0.1997 mol/dm³. The potassium hydroxide solution in D_2O was prepared by dissolving potassium hydroxide pellets (Merck *p.a.*) in D_2O. The pellets were rinsed with D_2O before dissolving. The concentration of the prepared KOD was 0.2149 mol/dm³ and its deuterium mol fraction 0.994. The other chemicals were of analytical grade and used as received.

Titration procedure. The zero instrument was a Metrohm Compensator E 388 equipped with a combined glass silver-silver chloride electrode. The titration procedure B described by Kankare was employed.[3] The volumes of acid and base were added to the solution using an Agla micrometer syringe. The titrations were car-

ried out in a thermostated jacketed vessel under nitrogen atmosphere. A Lauda thermostat was used to control the temperature within ±0.05 K. The titration mixtures were prepared by weighing proper amounts of water and DMSO. The initial volume, V_0, of the titration mixture was 20×10^{-3} dm³ in all experiments. The added volumes of the acid were of constant magnitudes in all experiments ($a_0 = 1.00 \times 10^{-5}$ mol and $a_1 = 1.00 \times 10^{-4}$ mol).

Evaluation of dissociation constants. The concentration dissociation constants of 3-nitrobenzoic acid were calculated from eqn. (1) where Z is the degree of deprotonation

$$K' = Z[H^+]/(1-Z) \quad (1)$$

and $[H^+]$ the hydrogen-ion concentration. Both of these can be evaluated from the slope and intercept of the titration curve in the usual manner. The ionic strength at the end of the titration was calculated to be aZ/V, where a is the total amount of the added acid and V is the total volume of the titration mixture. In addition to this the ionic strength was increased by known amounts of potassium chloride so that the constants were usually determined at five different ionic strengths in each water-DMSO mixture.

The thermodynamic dissociation constants were evaluated by the aid of the Debye-Hückel

$$pK = pK' - 2 \log y_\pm = pK' + \frac{2Az^2I^{1/2}}{1+Ba\ I^{1/2}} \quad (2)$$

extrapolation (2). In the above equation $y_\pm$ denotes the mean molar activity coefficient, I the ionic strength, and z the ionic charge. The ionic size parameter Ba was chosen as 2.5.[4] The parameter A was calculated separately for each titration mixture of a certain mol fraction of DMSO. The value of A at 298.15 K is known to be $354.42/D^{3/2}$, where D is the macroscopic dielectric constant of the solvent.[5] This constant was evaluated by the aid of the values measured in several H_2O-DMSO mixtures by Lindberg and Kenttämaa.[6] The obtained equations of least squares were then modified for H_2O and D_2O with the values determined by Vidulich *et al.*[7] to give formulas (3) and (4).

$$D_{H_2O} = 78.39 - 8.711\ x_{DMSO} - 47.46\ x_{DMSO}^2 \quad (3)$$

$$D_{D_2O} = 78.06 - 8.711\ x_{DMSO} - 47.46\ x_{DMSO}^2 \quad (4)$$

In these equations x_{DMSO} denotes the mol fraction of DMSO in the solvent. The assumption made here that the dielectric constant of D_2O-DMSO mixtures varies in a similar way as that in H_2O-DMSO mixtures is justified, because the measurements were carried out at a moderately low DMSO content.

For the sake of comparison the thermodynamic constants were also determined in the following direct way. The measured Z values and $[H^+]$ values (as pH) were plotted against the square root of the ionic strength by the aid of the method of least squares. The thermodynamic constant, K, can then be calculated from eqn. (1) with the aid of the values of Z and $[H^+]$ at zero ionic strength.

RESULTS AND DISCUSSION

The necessary data and the determined constants in H_2O have been tabulated in Table 1 as an example. From these values the thermodynamic constant can be obtained by extrapolation. This is shown in Table 2.

If pK is evaluated from the values in Table 1 by the direct method, the values of (0.5427 ± 0.0035) and $(2.721 \pm 0.003) \times 10^{-4}$ are obtained for Z and $[H^+]$ at zero ionic strength. From these values, eqn. (1) gives the value of 3.491 for pK.

The plots of pK_{H_2O} and pK_{D_2O} *versus* x_{DMSO} are given in Fig. 1. Linear regression analysis can be applied to determine pK_{H_2O} and pK_{D_2O} values

Table 1. The values of the concentration dissociation constants of 3-nitrobenzoic acid in H_2O ($x_{DMSO} = 0.00279$ at the end of the titration).

c_{KCl} /mol dm^{-3}	b_1[a] /10^{-5} mol	$[H^+]$[a] /10^{-4} mol dm^{-3}	Z[a]	I	pK'[a]
0.0500	6.181	3.095	0.6197	0.05337	3.297 ± 0.006
0.0250	5.918	2.963	0.5933	0.02823	3.364 ± 0.006
0.0100	5.809	2.909	0.5823	0.01317	3.392 ± 0.010
0.0075	5.785	2.902	0.5799	0.01066	3.397 ± 0.005
0.0050	5.685	2.847	0.5699	0.00810	3.423 ± 0.004
0.0025	5.649	2.828	0.5662	0.00558	3.433 ± 0.003

[a] Mean values from at least three determinations.

Table 2. The thermodynamic dissociation constant of 3-nitrobenzoic acid in H_2O ($x_{DMSO} = 0.00279$; $A = 0.5109$).

$I^{1/2}$	$-2 \log y_{\pm}$	pK'	pK
0.2310	0.1503	3.297	3.447
0.1680	0.1213	3.364	3.485
0.1148	0.0913	3.392	3.483
0.1032	0.0840	3.397	3.481
0.0900	0.0752	3.423	3.498
0.0747	0.0644	3.433	3.497

in respective pure waters. The results obtained are tabulated in Table 3, from which the ΔpK values, *i.e.* the values of $pK_{D_2O} - pK_{H_2O}$, can be calculated. These are within the experimental error of equal magnitude *viz.* (0.412 ± 0.010) and (0.401 ± 0.017) as calculated by means of the Debye-Hückel approximation and the direct method, respectively. The ΔpK value has been determined earlier by McDougall and Long.[8] The value 0.50 obtained by them is somewhat higher than ours. However, their pK_{H_2O} value is also higher (3.62) and seems to be the only one of this magnitude among the reported ones. Dippy and Lewis [9] report 3.493, Briegleb and Bieber [10] 3.450, and Peltier and Pichevin [11] 3.53. The agreement between these values and ours is satisfactory.

The agreement between the pK values obtained by the Debye-Hückel method and by the direct method is excellent especially in H_2O. This means that the direct method can be applied as a purely empirical method, at least in this case, when thermodynamic constants are evaluated.

As for the values in Table 3 it is observed that there exists a linear correlation between the pK values and the mol fraction of DMSO.

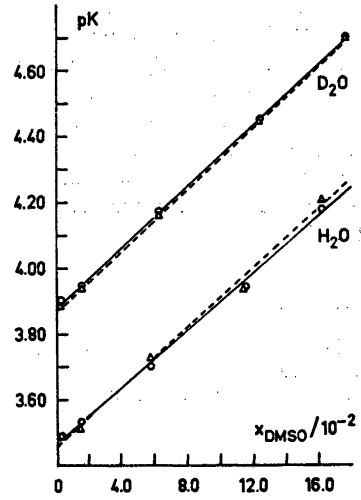

Fig. 1. The plot of pK of 3-nitrobenzoic acid *versus* x_{DMSO} in H_2O and D_2O. (The circles denote the points obtained by the Debye-Hückel treatment and the triangles those obtained by the direct method. Solid lines refer to the circles and dotted lines to the triangles.)

A roughly similar behavior is observed with benzoic acid, although the measurements are extended up to $x_{DMSO} = 0.8$ in this case.[12] There are insufficient data to test the variation of the pK value with the inverse of the dielectric constant as predicted by the Born equation. However, it seems that these plots are curved, but the amount of data does not give justification for any conclusions. It thus seems that this acid falls into the same category as those studied by Bell in dioxane-water mixtures.[13]

As can be seen from Fig. 1, the mol fraction of DMSO in the H_2O-DMSO mixture which corresponds to pure D_2O with respect to the dissociation of 3-nitrobenzoic acid is approx-

Table 3. The slopes and intercepts of the linear plots of pK *versus* x_{DMSO} (Fig. 1). (The intercepts refer to pK values in pure H_2O or D_2O.)

	Method	Slope	Intercept	Coeff. of correlation
H_2O	D−H	4.311 ± 0.077	3.465 ± 0.007	0.9995
D_2O	D−H	4.594 ± 0.071	3.877 ± 0.007	0.9996
H_2O	"Direct"	4.468 ± 0.182	3.462 ± 0.017	0.9975
D_2O	"Direct"	4.707 ± 0.001	3.863 ± 0.001	0.999993

imately 0.096. The mol fraction of DMSO in the D_2O-DMSO mixture which causes an increase of magnitude of ΔpK in pK is approximately 0.090. Low mol fractions of DMSO bring about an increase in the structural order of the system.[14] The above mol fractions thus indicate the well-known fact that there is more order in the structure of D_2O than in that of H_2O.

REFERENCES

1. Vesala, A. and Koskinen, V. *Finn. Chem. Lett. 2* (1975) 145.
2. *Handbook of Chemistry and Physics*, The Chemical Rubber Company, Cleveland Ohio, 50th Ed., p. C-191.
3. Kankare, J. J. *Anal. Chem. 44* (1972) 2376.
4. Kielland, J. *J. Amer. Chem. Soc. 59* (1937) 1675.
5. Robinson, R. A. and Stokes, R. H. *Electrolyte Solutions*, Butterworths, London 1970, p. 230.
6. Lindberg, J. J. and Kenttämaa, J. *Suom. Kemistilehti B 33* (1960) 104.
7. Vidulich, G. A., Evans, D. F. and Kay, R. L. *J. Phys. Chem. 71* (1967) 656.
8. McDougall, A. O. and Long, F. A. *J. Phys. Chem. 66* (1962) 429.
9. Dippy, J. F. J. and Lewis, R. H. *J. Chem. Soc.* (1937) 1008.
10. Briegleb, G. and Bieber, A. *Z. Elektrochem. 55* (1951) 250.
11. Peltier, D. and Pichevin, A. *Bull. Soc. Chim. Fr.* (1960) 1141.
12. Fiordiponti, P., Rallo, F. and Rodante, F. *Gazz. Chim. Ital. 104* (1974) 649.
13. Bell, R. P. and Robinson, R. R. *Trans. Faraday Soc. 57* (1961) 965.
14. Cox, B. G. *J. Chem. Soc. Perkin Trans. 2* (1973) 607.

Received September 10, 1975.

Acta Chemica Scandinavica A 30 (1976) 281—284

Lecithin—Diglyceride Interaction in Surface Films on Water and in Aqueous Systems

ROSALIND FAIMAN, KÅRE LARSSON * and BALAZS SZALONTAI

Lipid Chemistry Laboratory, University of Göteborg, CTH, Rännvägen 6, S-402 20 Göteborg 5, Sweden.

The interaction between the diglyceride 1-oleyl-3-stearin and L-α-dipalmitoyllecithin in monomolecular surface films at the air/water interface was studied by the surface balance technique. This diglyceride exhibits a condensed phase with extended molecules, which means that the methyl end groups form the contact surface with water. The diglyceride-lecithin mixtures form one phase with the polar groups in contact with water over the whole composition interval. At high pressures molecular segregation occurs at a diglyceride content above the 1:1 molecular ratio and the extended molecular conformation is adopted for diglyceride molecules above the 1:1 composition. Three-dimensional aqueous phases were examined by Raman spectroscopy, with emphasis on the hydrocarbon chain structure. It was found that in liposomes a few degrees below the chain melting temperature, the transition tilted to vertical hydrocarbon chains is influenced by small amounts of diglyceride, and that these effects are closely related to the monolayer phase behavior.

The interaction between different lipid components is important for the structure and function of biological membranes. The cholesterol-lecithin interaction has therefore been extensively studied, but it is somewhat surprising that almost no other components have been examined in detail in this respect. The diglyceride-lecithin interaction is interesting from many points of view. Diglycerides are naturally present in the membranes (sometimes about 10 %). The molecular geometry is the same as in the dominating membrane lipids, and therefore variations in, for example, the lecithin-diglyceride ratio corresponds mainly to variations in the strength of the water association. Furthermore the existence of one free hydroxyl group in the diglyceride molecule, which can act as a hydrogen bonding donor, relates it to cholesterol, and effects due to the rigid steroid skeleton can therefore be obtained by comparison with the well known cholesterol-lecithin interaction. Finally, the existence of an extended molecular conformation of the saturated diglycerides as a transition state in surface films on water was reported earlier.[1] It was therefore considered of interest to see whether this form is favoured in a mixed saturated/unsaturated diglyceride and whether some lecithin can participate in the formation of this type of surface film.

The surface balance technique was used in order to study the diglyceride-lecithin interaction at the air/water interface. In order to correlate the phase transitions in monolayers with aqueous bulk phases Raman spectroscopy was used.

MATERIALS AND METHODS

Standard methods were used in the synthesis of L-α-dipalmitoyl-lecithin (DPL) and the 1-oleoyl-3-stearoyl diglyceride (OHS). The purity was checked by TLC (no 1,2-diglyceride isomer was found to be present). A continuously recording surface balance of the vertical Wilhelmy type was used, and experimental details are given in Ref. 1. A Cary 82 Raman spectrophotometer with argon ion laser excitation was used. The samples were kept in a temperature controlled cell,[2] and other experimental details have been given earlier.[3] Mixtures of OHS-DPL differing by 10 % (w/w) were prepared and the solvent used in the monolayer work was hexane-ethanol 9:1. A few corresponding bulk samples with excess water were prepared, and

* Present address: Div. of Food Science, Chemical Center, Box 740, S-220 07 Lund 7, Sweden.

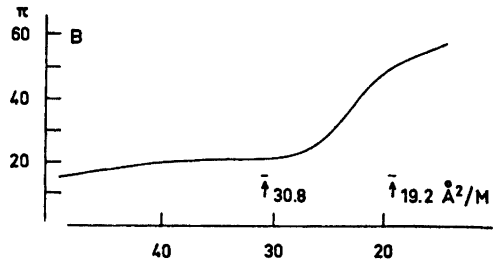

Fig. 1. Surface pressure isotherm of OHS at 20 °C. The photographically recorded isotherm is shown with surface value calibration points.

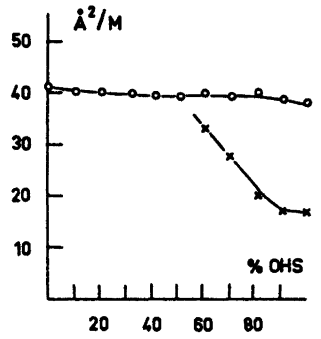

Fig. 2. Average molecular area at the collapse point *versus* composition of DPL-OHS mixtures. The collapse point corresponding to the extended molecular conformation is also shown.

owing to the limited amount of available diglyceride the three most interesting compositions were selected. The samples contained about 75 % (w/w) of water, which means that the lipids form a dispersion of liposomes (in a gel or liquid crystalline state depending upon the temperature).

RESULTS AND DISCUSSION

The pressure-area isotherm of OHS at 20.0 °C is shown in Fig. 1. It is important to notice that the molecular area corresponding to what normally is described as a collapse point of 18.2 Å² per molecule corresponds to extended molecules in this monolayer phase. There is a plateau starting at a molecular area of 38.5 Å² per molecule. It is evident from these values that a monolayer with the glycerol group in contact with water is formed first, and on further compression an extended conformation is adopted. As mentioned earlier it is known from similar studies of saturated diglycerides that an extended conformation can be obtained as a state of transitory existence.[1] The possibility of chain segregation into a chain layer occurring with saturated chains and another with unsaturated chains means such a reduction in free energy arising from better molecular close-packing that the extended conformation is a stable state at the water/air interface. It is believed that this transition between the extended form and the ordinary bilayer structure might have relevance for certain transport functions of membranes. Most membrane lipids have the same molecular geometry (one saturated and one unsaturated chain), and a conformational change of any protein present at the water interface can in principle result in a hydrophobic environment of the polar group. Ordinary membrane lipids might under such conditions be expected to behave as the diglyceride described above.

The average molecular area at collapse of the monolayer *versus* composition of binary mixtures DPL-OHS is shown in Fig. 2. The solid-condensed form with the two chains of the molecules laterally arranged has a molecular area at collapse of about 40 Å². This is a characteristic value of vertical chains in the hexagonal form, and it corresponds to the gel phase in aqueous lecithin bulk systems (*cf.* Ref. 4). No particular condensation effect is observed at the collapse pressure as well as at lower pressure values. This is interesting with regard to cholesterol-lecithin interaction. The well-known condensation effect in this case is usually ascribed to an effect from the rigid skeletons on the hydrocarbon chain mobility. Another explanation might be hydrogen bonding. As lecithin only contains hydrogen bonding acceptors it should be expected that any hydrogen bonding donor (such as the cholesterol hydroxyl group) would stabilize the mixed bilayer structure, the strongest effect corresponding to a 1:1 ratio. A consequence of this could be condensation of mixed monolayers. The diglyceride can like cholesterol act as a hydrogen bonding donor, and as will be seen below there is evidence for the occurrence of a 1:1 complex, and the lack of condensation effects indicates therefore that cholesterol-lecithin condensation is more due to the rigid steroid skeleton.

The collapse point of the extended form discussed above for pure OHS is also shown

in Fig. 2. It can be seen that there is no such phase at a diglyceride content of less than the 1:1 molecular ratio. The linear behavior of this collapse curve (see Fig. 2) shows that all the diglyceride molecules above this limit are segregated, so that above the collapse pressure of the mixed monolayer the excess of diglyceride molecules (above the 1:1 molecular ratio) is squeezed out to form separate film regions with an extended structure. The shape of the collapse curve at low lecithin content indicates that a minor proportion of the lecithin molecules are solved in the segregated diglyceride phase. It is proposed that the explanation for this behavior at high pressures is that there is a DPL-OHS hydrogen bonded molecular compound. As the lecithin molecules have many hydrogen bonding acceptors it seems probable that there is steric hindrance to hydrogen bonding associated with more than one diglyceride molecule per lecithin molecule.

It has recently been reported that DPL in excess water shows a transition from tilted to vertical chains at about 34 °C, and chain melting (gel→liquid crystal) at about 42 °C[4]). Related monolayer phases were also observed. In the binary DPL-OHS monolayer mixtures it was found that the tilted phase of DPL was stabilized at higher temperatures by the addition of OHS. An isotherm demonstrating this effect is shown in Fig. 3. The solid-condensed phase with tilted chains, which is formed at low pressures and which shows high compressibility, exists over a wide pressure range. In the case of pure DPL this tilted phase has a very narrow range of existence, whereas the high-pressure phase with vertical chains exists at a broader pressure range.[4]

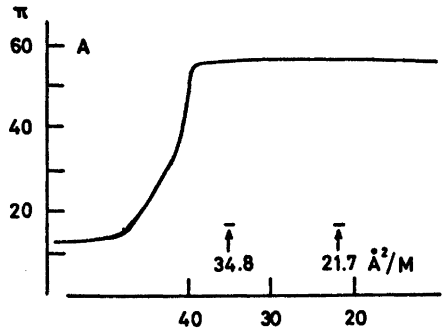

Fig. 3. Surface-pressure isotherm of a DPL-OHS 70:30 (w/w) mixture at 20 °C.

The Stokes Raman spectra DPL and DPL-OHS mixtures, in the proportions 90:10, 80:20, and 70:30 (w/w) in the presence of excess water were recorded at various temperatures in the region of vertical chain→tilted chain→disordered chain transitions, *i.e.* between 30 – 45 °C.[4] It has been shown earlier that the band intensity ratio I_{1090}/I_{1130} in the vibrational skeletal stretching region is highly sensitive to the conformation of the hydrocarbon chains particularly for the cooperative chain melting process when the all- or nearly all-*trans* configuration of the chains collapses to form the liquid crystalline state.[5,6] The ratio I_{1090}/I_{1130} for aqueous DPL is shown in Fig. 4, together with the errors allowed in the positioning of each point. There is some indication of a minor increase in this ratio, I_{1090}/I_{1130} in the temperature range of 34 – 42 °C, where the vertical →tilted chain transition is known to occur in the crystalline state [4] but the uncertainties in the experimental values, shown in Fig. 4, are too large to detect the lower temperature of this transition. The chain melting temperature at 39.5 – 41 °C is, however, clearly shown by the steep gradient of the curve, indicating that a co-operative chain melting process is occurring in this region.[5,6]

The I_{1090}/I_{1130} intensity ratio *versus* temperature was also plotted for each of the DPL-

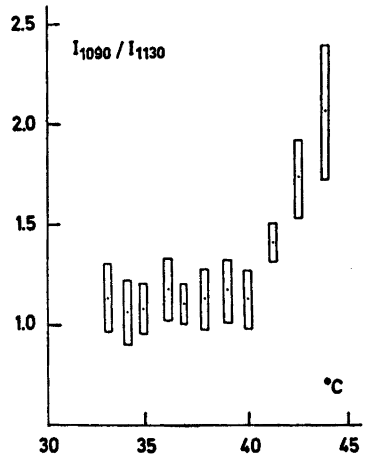

Fig. 4. Intensity ratio *versus* temperature of the 1090/1130 cm^{-1} bands in the Raman spectra of pure DPL. The experimental errors are indicated.

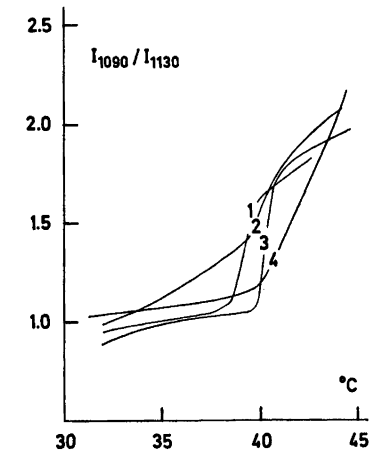

Fig. 5. The intensity ratio 1090/1130 cm^{-1} *versus* temperature of mixtures of DPL-OHS 10:90 (1), 20:80 (2), 30:70 (3) and of pure DPL (4).

OHS ratios and are shown in Fig. 5. The 90:10 ratio is designated 1, the 80:20 ratio 2, the 70:30 ratio 3, and the pure DPL curve is included for a comparison and designated 4.

Two interesting effects are observed from the addition of diglyceride to DPL, as can be seen in the Fig. 4. Firstly, there are significant shifts in the chain melting temperatures for each ratio. The magnitude of this shift may be taken as a measure of the lattice disturbances introduced by the presence of the diglyceride. This is because the gradient of the curve produced can be related to the degree of purity of the lipid and hydrocarbon chain saturation.[2,6] This result can be correlated with the features observed in the monolayer behavior described above. That is, the existence range of the vertical chain phase appears to be reduced by the presence of the diglyceride, *e.g.* in the case of the addition of 10 % (w/w) of diglyceride (curve 1) there is a shift of 1.5 – 2.0 °C to a lower temperature.

Secondly, there is a reduction in the gradient of the crystalline→liquid crystalline transition in the presence of 10 % OHS (curve 1) and 20 % OHS (curve 2) compared with the pure DPL (curve 4) but not with the addition of 30 % OHS (curve 3). The presence of *cis* C=C double bonds is known to disturb the chain packing in the crystalline state so that there is some degree of disorder already inherent in the crystalline form before transition to the liquid crystalline state occurs.[2,6] The magnitude of this disturbance in the all-*trans* conformation appears to be largest in the case of the addition of 20 % OHS (curve 2) where the gradient of I_{1090}/I_{1130} *versus* temperature is least.

In the case of the 70:30 ratio of DPL:OHS the gradient of the curve 3 is steeper than in the case of the other mixtures and, moreover, than in the case of the pure DPL (curve 4). This suggests an increase in the hydrocarbon chain order as the concentration of diglyceride is increased towards the 1:1 molecular ratio.

In conclusion it is interesting to note that this Raman spectroscopic behavior displayed by DPL-OHS mixtures at concentrations ≥70:30 is found to be contrary to the Raman spectroscopic behaviour observed in DPL-cholesterol mixtures and in fact other lipid-cholesterol mixtures.[2,7] In the case of the DPL-cholesterol mixture, the gradient of the curve I_{1090}/I_{1130} *versus* temperature decreases linearly with increasing concentrations of cholesterol even when the ratio of DPL-cholesterol is 1:1. This evidence tends to suggest that whereas the diglyceride forms a 1:1 molecular complex with the lipid in the bilayer, the presence of cholesterol in the ratio of 1:1 appears to form a looser type of association with the lipid.

Acknowledgement. The authors would like to acknowledge grants from the Natural Science Research Council, a UNESCO fellowship (for B.S.) and an EMBO fellowship (for R.F.) which made the work for this publication possible.

REFERENCES

1. Larsson, K. *Biochim. Biophys. Acta 318* (1973) 1.
2. Faiman, R. *Thesis*, University of Bradford 1974.
3. Larsson, K. and Rand, R. P. *Biochim. Biophys. Acta 326* (1973) 245.
4. Rand, R. P., Chapman, D. and Larsson, K. *Biophys. J. In press.*
5. Lippert, J. L. and Peticolas, W. L. *Proc. Nat. Acad. Sci. USA 68* (1971) 1572.
6. Faiman, R. and Long, D. A. *J. Raman Spectrosc. In press.*
7. Faiman, R., Larsson, K. and Long, D. A. *To be published.*

Received September 18, 1975.

Acta Chemica Scandinavica A 30 (1976) 285—288

Kinetics of Formation of Anhydroretinol from Retinyl Acetate in Acetic Acid, and from Retinyl Acetate and Retinol in Ethanol and Ethanol—Water Mixtures Containing Hydrogen Chloride

LAURI PEKKARINEN,[a] PÄIVI AUTIO [a] and AINO PEKKARINEN [b]

[a] Central Laboratory of OTK, SF-00500 Helsinki 50, Finland and [b] Department of Chemistry, Helsinki University of Technology, SF-02150 Espoo 15, Finland

The rate constant for the formation of anhydroretinol from retinyl acetate in acetic acid has been measured at 30, 40, 50 and 60 °C. In addition, the effects of sodium acetate, pyridine, acetic anhydride, and water on the rate constant have been studied at 50 °C. Only the addition of water had a pronounced effect, accelerating the rate of the reaction.

Also the rate constants for the HCl-catalyzed formation of anhydroretinol from retinyl acetate and from retinol in ethanol and ethanol-water mixtures have been measured at 15, 25, and 35 °C. The rate is about ten times higher with retinol than with retinyl acetate. In both cases the rate constants decrease markedly when water is added to ethanol. The changes in log k are correlated to changes in the acidity function H_0 (0.1 M HCl).

The mechanism of the reactions is discussed and the A-1 mechanism seems probable, the slowest stage being the dissociation of the protonated substrate to carbonium ion (retinylic cation) and acetic acid (with retinyl acetate) or water (with retinol).

Anhydroretinol is formed from retinol and retinyl acetate in an acid catalyzed reaction, which is typical of these compounds and which takes place easily.

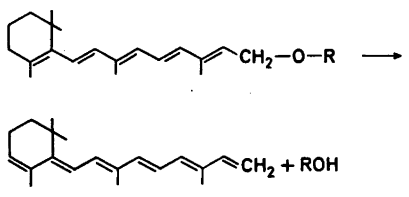

R = H, retinol; R = Ac, retinyl acetate

This reaction was first studied by Edisbury and his co-workers.[1] They found that vitamin A_1 (retinol) in anhydrous ethanol and in the presence of hydrogen chloride is transformed to a product which was called cyclized vitamin A. Shantz [2] prepared a pure anhydrovitamin A_1 (anhydroretinol) using a reaction catalyzed by p-toluenesulfonic acid in benzene. Methods have been developed for the quantitative determination of vitamin A based on the formation of its anhydroform.[3]

The kinetics of the formation of anhydroretinol has been studied to only a limited extent. Barnholdt [4] performed some measurements in the presence of HCl in ethanol with all-*trans* and 13-*cis* vitamin A_1. Higuchi and Reinstein [5] investigated the kinetics of the formation of anhydroretinol from retinol and retinyl acetate in ethanol, ethanol-water mixtures and ethanol-heptane mixtures, usually in the presence of HCl. The rate constants, calculated on the basis of the initial rate of formation of anhydroretinol, were measured only in the case of retinyl acetate in ethanol, catalyzed by HCl. They found that the reaction catalyzed by HCl slowed down abruptly when water was added to the ethanol. As far as we know, no other kinetic studies have been carried out on the formation of anhydroretinol.

We have previously studied the polymerization of retinyl acetate in acetic acid-water mixtures.[6] It was found that both the rate of polymerization and the rate of the formation of anhydroretinol were accelerated when water

was added to acetic acid. We present now, more precisely, measurements pertaining to the formation of anhydroretinol from retinyl acetate in pure acetic acid. The effect of the addition of water and some other compounds to acetic acid has also been studied. Experiments have been carried out with retinol and retinyl acetate in ethanol and ethanol-water mixtures with hydrochloric acid as catalyst. In particular, we wanted to compare the rate constants with the acidity function (H_0) because it is well known [7] that H_0 changes greatly when water is added to ethanol. The purpose of this work has been to elucidate the mechanism of the formation of anhydroretinol from retinol and retinyl acetate.

EXPERIMENTAL

Method. The experiments were carried out in a special reaction vessel constructed so that flushing with nitrogen was possible. The nitrogen was saturated with the solvent. In the experiments in acetic acid, 1 ml samples were withdrawn at appropriate intervals, while nitrogen was flowing through the vessel. The 1 ml sample was added to 20 ml cold (about 0 °C) absolute ethanol and the absorbance was measured immediately at the wavelengths 390, 342, and 326 nm with a Beckman DU-2 spectrophotometer. In ethanol and in ethanol-water mixtures the progress of the reaction was followed by taking 5 ml samples and adding them to 20 w % water-ethanol mixtures and measuring the absorbance at the wavelengths 390, 342, and 324 nm or 326 nm. The absorbance reading at 342 nm (isosbestic point) did not change appreciably during the reaction, indicating that there were no significant side reactions. The rate constants were calculated from the absorbance readings measured at 390 nm according to the equation

$$k = \frac{2.303}{t} \log \frac{A_e}{A_e - A}$$

where A is the absorbance reading at time t (initially equal to zero) and A_e is the final absorbance reading. It should be noted that A_e/A_r [A_r = absorbance of retinyl acetate or retinol at the beginning of the reaction at wavelength 326 nm (retinyl acetate) or 324 nm (retinol)] did not change significantly when the temperature was altered. The following values were obtained for the ratio A_e/A_r in the case of retinyl acetate in acetic acid: at 60 °C, 0.99 (15 experiments); at 50 °C, 1.1 (15 experiments); at 40 °C, 1.1 (4 experiments): at 30 °C 1.2 (2 experiments). These figures indicate that about 58 – 70 % of the retinyl acetate is converted into anhydroretinol according to the absorbance values given by Shantz [8] and 70 – 85 % according to those given by Oroshnik, Karmes and Mebane [8] and Bulgrin and Lookhart.[9]

The initial concentration of retinyl acetate in acetic acid was varied from 0.7×10^{-4} M to 7×10^{-4} M. In this concentration range, the rate constant was independent of the initial concentration of retinyl acetate. In ethanol and in ethanol-water mixtures the initial concentrations of retinol and retinyl acetate were about 1.8×10^{-4} M.

Chemicals. Retinol and retinyl acetate were products from F. Hoffmann-La Roche & Co Ltd. Ethanol was dried using Al-powder and Hg_2Cl_2 as a catalyst. The water content of dried ethanol was less than 0.01 w % (Karl Fischer) and that of the acetic acid, on the average, 0.1 w %. When the reaction was carried out in pure ethanol, HCl gas was introduced to dry ethanol by the usual method.[10] Solvent mixtures were made by weighing.

DISCUSSION

The rate constants k_1 ($\times 10^4/s^{-1}$) for the formation of anhydroretinol from retinyl acetate in pure acetic acid were found to be 0.372, 1.24, 3.85, and 11.9 at 30, 40, 50, and 60 °C, respectively. The corresponding activation energy was 97.0 kJ/mol and the value of log A 12.29.

Table 1 presents the other results pertaining to the formation of anhydroretinol from retinyl acetate in acetic acid. According to these results the effect of sodium acetate, acetic anhydride and pyridine on the rate of formation is slight. On the other hand, water has clearly an accelerating effect. Bruckenstein and Kolthoff [11] found that upon addition of water to a solution of a basic indicator like *p,p*-dimethylaminoazobenzene in acetic acid, the colour changes in favour of the acid species, even though water

Table 1. The formation of anhydroretinol from retinyl acetate in acetic acid at 50 °C.

Compounds added to acetic acid Comp.	M	H_2O (M)	Rate constant $k_1 \times 10^4/s^{-1}$
NaOAc	0.18	–	3.63
NaOAc	0.18	1.1	6.25
NaOAc	0.17	–	3.67
NaOAc	0.17	2.6	8.37
NaOAc	0.17	1.1	6.55
–	–	0.55	4.93
Ac_2O	0.085	–	3.77
Pyridine	0.24	–	4.17
Pyridine	0.24	1.1	6.30

is a base. This problem has been dealt with quite recently by de la Mare and Singh.[12] They studied, for example, the protonation of *p*-bromo-*N*,*N*-dimethylaniline in acetic acid when sodium acetate or sodium acetate and water were added. At the beginning, sodium acetate caused a slight decrease in the protonation power. When water was added to this solution, the protonation power clearly increased. These results suggest that the accelerating effect of water on the formation of anhydroretinol is caused by the stronger protonation of retinyl acetate and not by the other effects of water on the reaction. This interpretation is confirmed by the experiments in ethanol and ethanol-water mixtures, where the addition of water greatly retards the reaction catalyzed by HCl. Similar results have been obtained earlier by Higuchi and Reinstein.[5] Water does not seem to be necessary for the formation of anhydroretinol from retinyl acetate. The reaction which takes place by acyl-oxygen fission producing first retinol is therefore not very likely, but the rate-determining stage would be the same as in the acid catalyzed ester hydrolysis which takes place by the mechanism A_{AL}-1. For vinyl acetate, evidence[13] has been presented that the hydrolysis reaction is of A_{AC}-2 type, but the alcohol part of the ester in retinyl acetate is quite different. The assumption that the formation of anhydroretinol from retinyl acetate is an *A*-1 reaction is strengthened by the relatively high value of the activation energy and by the small negative value of the activation entropy (97.0 kJ mol^{-1}; −18 J mol^{-1} K^{-1}).

Table 2. The formation of anhydroretinol from retinol in ethanol and in ethanol-water mixtures.

Solvent wt % H_2O	Conc. of HCl M	Rate constant $k_2 \times 10^3$/M^{-1}s^{-1} 15 °C	25 °C	35 °C	*E* kJ/mol
0	0.002	–	230	–	–
0	0.004	89.0	269	655	74.0
5	0.025	–	8.30	–	–
5	0.050	1.95	8.77	29.1	99.9
10	0.050	–	4.82	–	–
10	0.10	–	4.85	–	–
20	0.050	–	3.85	–	–
20	0.075	–	3.79	–	–
20	0.100	1.06	3.81	12.5	91.1

Table 3. The formation of anhydroretinol from retinyl acetate in ethanol and in ethanol-water mixtures.

Solvent wt % H_2O	Conc. of HCl M	Rate constant $k_2 \times 10^3$/M^{-1}s^{-1} 15 °C	25 °C	35 °C	*E* kJ/mol
0	0.010	–	23.7	68.3	–
0	0.012	–	21.9	–	–
0	0.020	6.95	24.3	67.5	84
0	0.052	–	25.4	–	–
0	0.089	–	27.3	–	–
5	0.250	–	1.37	4.36	–
5	0.360	0.403	1.60	4.96	92.8
10	0.250	–	0.741	–	–
10	0.500	–	1.01	–	–
20	0.250	–	0.631	–	–
20	0.500	0.214	0.813	2.45	90.3
20	0.670	–	0.839	–	–

The results for the hydrogen-chloride-catalyzed formation of anhydroretinol from retinol and from retinyl acetate in ethanol and in ethanol-water mixtures are presented in Tables 2 and 3. The rate of the formation of anhydroretinol is about ten times higher with retinol than with retinyl acetate. It is further interesting to note that, in the case of retinol, when the concentration of HCl is low, a rather good second-order rate constant is obtained. In the case of retinyl acetate, HCl concentrations were higher and the second-order rate constant increased with the HCl concentration, especially in solvent mixtures where water was present. This may be due to the fact that, at higher concentrations of acid, the rate is no longer proportional to the molar concentration of acid but the rate follows the acidity function.

With retinol and retinyl acetate the rate decreases greatly when water is added to ethanol. Taking the H_0 values from the work of

Table 4. Values log $k_{0,1}+H_0$ for retinyl acetate and retinol in ethanol and ethanol-water mixtures at 25 °C.

Solvent wt % H_2O	H_0	log $k_{0,1}+H_0$ Retinol	Retinyl acetate
0	0.61	−1.01	−2.01
5	1.99	−1.11	−1.84
10	2.15	−1.18	−1.91
20	2.26	−1.16	−1.88

Braude and Stern,[7] we obtained the values presented in Table 4 for log $k_{0.1}+H_0$ (log $k_{0.1}$ represents the first-order rate constant when the hydrochloric acid concentration is 0.1 M, H_0 refers to the same concentration of HCl, $t=25$ °C).

It can be seen that log $k_{0.1}+H_0$ is constant, and it can therefore be assumed that the rate constant is proportional to the acidity function h_0 in the case of both retinol and retinyl acetate. Because the rate of formation of anhydroretinol is higher with retinol, one might assume that retinyl acetate first hydrolyses to retinol, but this is improbable on the basis of the results presented in Table 4.

The formation of anhydroretinol from retinol and retinyl acetate most probably follows the reaction scheme (R=H or Ac):

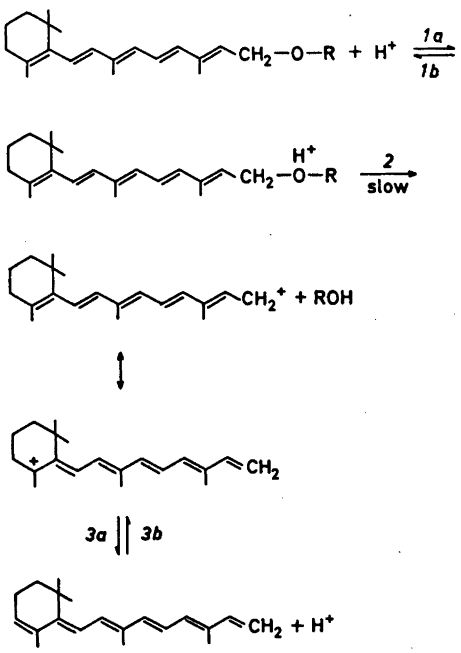

The carbonium ion in the above reaction scheme is the retinylic cation, a coloured compound absorbing at about 600 nm. This has been studied by Blatz *et al.*[14] We have obtained the spectra of anhydroretinol and not observed any colour formation in the reactions. Consequently, we assume that the concentration of retinylic cation was low. It seems probable, therefore, that the rate-determining stage is the dissociation of the protonated form (reaction 2) and that the mechanism is the *A*-1.

REFERENCES

1. Edisbury, J. R., Gilliam, A. E., Heilbron, I. M. and Morton, R. A. *Biochem. J. 26* (1932) 1164.
2. Shantz, E. M. *J. Biol. Chem. 182* (1950) 515.
3. Budowski, P. and Bondi, A. *Analyst 82* (1957) 751 and references cited there.
4. Barnholdt, B. *Acta Chem. Scand. 11* (1957) 909.
5. Higuchi, T. and Reinstein, J. A. *J. Am. Pharm. Ass. 48* (1959) 155.
6. Pekkarinen, L. and Uutela, P. *Suom. Kemistil. B 46* (1973) 127.
7. Braude, E. A. and Stern, E. S. *J. Chem. Soc.* (1948) 1976.
8. Oroshnik, W., Karmes, G. and Mebane, A. D. *J. Am. Chem. Soc. 74* (1952) 295.
9. Bulgrin, V. C. and Lookhart, G. L. *J. Am. Chem. Soc. 96* (1974) 6077.
10. Vogel, A. I. *Practical Organic Chemistry*, 3rd Ed., Longmans, Green and Co., London 1956, p. 180.
11. Bruckenstein, S. and Kolthoff, I. M. *J. Am. Chem. Soc. 78* (1956) 10.
12. de la Mare, P. B. D. and Singh, A. *J. Chem. Soc. Perkin Trans. 2* (1973) 59.
13. Yrjänä, T. *Suom. Kemistil. B 36* (1966) 81.
14. Blatz, P. E., Baumgartner, N., Balasubramaniyan, V., Balasubramaniyan., P. and Stedman, E. *Photochem. Photobiol. 14* (1971) 531 and references cited there.

Received November 14, 1975.

Acta Chemica Scandinavica A 30 (1976) 289—293

The Molecular Structure of Bis(chloromethyl) Ether, $ClH_2C—O—CH_2Cl$, in the Gas Phase

E. E. ASTRUP and A. M. AOMAR

Department of Chemistry, University of Oslo, Oslo 3, Norway

The structure of bis(chloromethyl) ether has been studied by the electron diffraction method in the vapour phase. Both chlorine atoms are found to have the same *gauche* relation (g^+g^+ or g^-g^-) to the COC chain, the dihedral angles δ(ClCOC) being 69.6°. The following structure parameters have been determined: $r(C-O) = 1.393(3)$ Å, $r(C-Cl) = 1.800(3)$ Å, $r(C-H) = 1.100(12)$ Å, $\angle COC = 114.2(1.5)°$, $\angle OCCl = 112.2(0.8)°$, $\angle OCH = 111.6(2.2)°$.

This electron diffraction investigation of bis(chloromethyl) ether (Fig. 1) is part of a study of the structures of cyclic and acyclic ethers.

Molecules of the type XCH_2-O-CH_2X may have four distinguishable conformers: *aa*, *ag*, $g^\pm g^\pm$, and g^+g^-. Of these the g^+g^- conformer may be disregarded because of the short Cl···Cl distance. The three different conformations which may be present in the gas phase are therefore the following for bis(chloromethyl) ether:

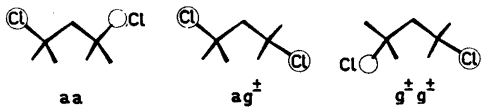

aa $\quad$ $ag^\pm$ $\quad$ $g^\pm g^\pm$

The conformational problem of this molecule has been investigated earlier by dipole moment investigations in the gas phase [1] and in non-polar solution,[2] and by Raman [3] and infrared [4] spectroscopy. The conclusion obtained from these methods is that the molecule has a shallow minimum about its equilibrium position, which suggests a distribution of slightly different conformers to be present. Chiba [1] has found, based on temperature dependent dipole moment measurements, that the $g^\pm g^\pm$ conformer possesses the lowest energy, determined to be 1.3 kcal below the $ag^\pm$ conformation.[5]

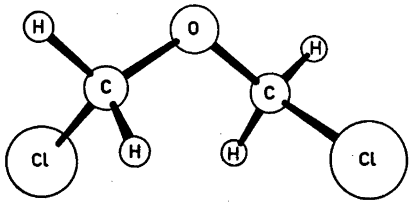

Fig. 1. Bis(chloromethyl) ether.

EXPERIMENTAL

A commercial sample of bis(chloromethyl) ether was obtained from Fluka. The electron diffraction diagrams were taken on a Balzer Eldigraph KDG2. The sample temperature was kept at about 10 °C during the exposures, and the pressure in the apparatus was approximately 1×10^{-5} Torr. The diffraction diagrams were recorded at 25.00 and 50.00 cm nozzle-to-plate distances, the electron wavelengths being 0.05852 and 0.05847 Å, respectively. Five selected plates were analysed for each nozzle-to-plate distance. The intensities were modified by $s/|f_C'||f_O'|$, where $|f'|$ is the scattering amplitude [6,7] for carbon and oxygen.

The experimental data were analysed in the usual way.[8] The experimental data obtained cover scattering angles corresponding to an s-range of $1.75-29.75$ Å^{-1}. The molecular intensity curve is shown in Fig. 2. A least-squares procedure was used to refine the distances and vibrational amplitudes estimated from the experimental radial distribution (RD) curve.

The calculations have been carried out on CDC 3300 and CDC 7400 (CYBER) computers.[8]

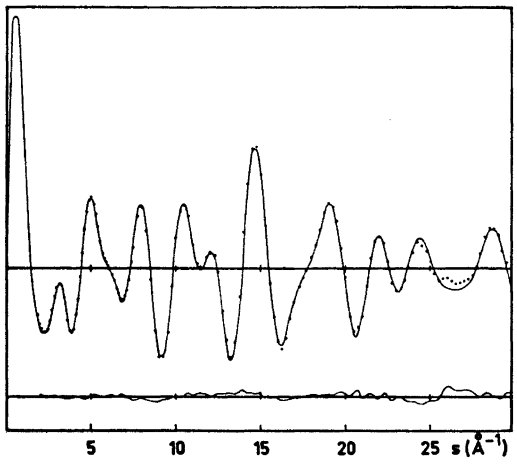

Fig. 2. Bis(chloromethyl) ether. Theoretical molecular intensity curve. The dots show the experimental values. The lower curve shows the difference between the experimental and theoretical values.

STRUCTURE ANALYSIS AND RESULTS

Approximate values for the parameters used in the least-squares analysis are determined from the experimental RD curve on Fig. 3.

The three first well separated peaks in the RD curve at about 1.1, 1.4, and 1.8 Å correspond to the C–H, C–O, and C–Cl bond distances, respectively. The next two peaks at 2.3 and 2.7 Å represent mainly distances over one angle, the most important contributions being C(1)···C(2), Cl(1)···H(1), and Cl···O. Also the three shortest Cl···H distances between different chloromethyl groups contribute to these peaks.

The two outer peaks in the RD curve at about 3.2 and 4.2 Å contain information about the conformation of the molecule. The C···Cl and Cl···Cl distances come in this region.

If the peak at 3.2 Å represented the Cl···Cl distance, this would be considerably shorter than the sum of the van der Waals' radii. It is therefore reasonable to assume that the Cl···Cl distance corresponds to the 4.2 Å peak. If this is so, the peak at 3.2 Å represents one or both of the non-bonded C···Cl distances. The remaining distances in the outer part of the RD-curve are Cl···H and H···H distances. However, their contribution is too small to give any indication of which conformers could be present. The theoretical models used in these investigations are all based on the assumption that the valence angles and bond distances are equal in both of the $-O-CH_2Cl$ groups of the molecule.

Fig. 4 shows the outer part of the experimental RD-curve compared with the corre-

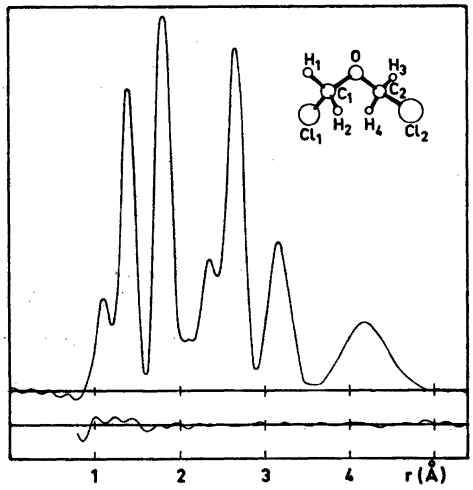

Fig. 3. Bis(chloromethyl) ether. Experimental radial distribution curve. The lower curve shows the difference between the experimental and the theoretical values. Artificial damping constant $k = 0.0015$ Å.

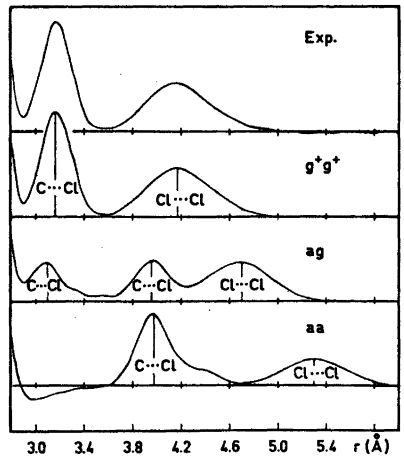

Fig. 4. Bis(chloromethyl) ether. The outer part of the experimental radial distribution curve compared with the corresponding part of the theoretical radial distribution curves for the three conformations: $g^{\pm}g^{\pm}$, *ag*, and *aa*.

Table 1. Structure parameters for bis(chloromethyl) ether. Distances (r_a-values) and mean amplitudes of vibration (u-values) are given in Å, angles in degrees. The standard deviations given in parentheses have been corrected to take into account data correlation. The uncertainty arising from error in the electron wavelength is included. (For numbering system of the atoms see Fig. 3.)

Distances	r	u
C–O	1.393(3)	0.043(6)
C–H	1.100(12)	0.070
Cl–C	1.800(3)	0.052(5)
$Cl_1 \cdots Cl_2$	4.232(36)	0.269(32)
Cl···O	2.660(6)	0.064(6)
Cl···C	3.150(10)	0.111(9)
$C_1 \cdots C_2$	2.340(21)	0.084(33)
$Cl_1 \cdots H_1$	2.367(19)	0.078
$Cl_1 \cdots H_4$	2.700(32)	0.135
$Cl_1 \cdots H_3$	4.035(26)	0.149
O···H	2.069(37)	0.097
$C_1 \cdots H_4$	2.573(28)	0.077
$C_1 \cdots H_3$	3.293(43)	0.101
Angles		
∠COC	114.2(1.5)	
∠OCCl	112.2(0.8)	
∠OCH	111.6(2.2)	
δ(ClCOC)[a]	69.6(1.6)	

[a] δ is the dihedral angle ClCOC.

sponding part of the theoretical RD-curves for the three conformers: the $g^{\pm}g^{\pm}$ (dihedral angle Cl–C–O–C, $\delta = 69.60$), *ag* ($\delta = 60.0$ and 180.0°) and *aa*. The *anti-anti* conformation is seen to result in a Cl···Cl distance outside the range of the experimental distances. Also the Cl···C distances at about 3.9 Å are too long to fit the peak at 3.2 Å, although the shapes of these peaks are comparable. This conformer does not seem to be present.

Also in the *anti-gauche* conformation the Cl···Cl distance is seen to be too long. The Cl···C distances in this conformation are separated into two peaks, due to the unequal dihedral angles Cl–C–O–C. A comparison of the area underneath these peaks with the experimental RD-curve suggests that the Cl···C distances should be of almost equal lengths in order to fit the experimental curve. The third possibility – the staggered conformation $g^{\pm}g^{\pm}$ – shows a good fit to the experimental curves. A least-squares refinement of the twist angles about the C–O bonds results in a Cl–C–O–C dihedral angle of 69.6°. The two Cl···C distances are then 3.150 Å and the corresponding vibrational amplitudes 0.111 Å. A refinement of the two twist angles independently is, for convergency reasons, only

Table 2. Correlation matrix (×100) for the parameters. (The coefficients having absolute values less than 30 are not given.)

Parameters	1	2	3	4	5	6	7	8	9	10	11	12	13	14	15
1 r(C-O)	100														
2 ∠COC		100													
3 r(C-H)			100												
4 r(Cl-C)				100											
5 ∠OCH		62	-32	43	100										
6 ∠OCCl	-37	-48	31	-61	-78	100									
7 δ(ClCOC)		88			45		100								
8 u(C-O)			-39		47	-35		100							
9 u(Cl-C)					53	-43		65	100						
10 u(Cl···Cl)					35				32	100					
11 u(Cl···O)		48			59	-45	41	50	58	31	100				
12 u(Cl···C)												100			
13 u(C···C)			-32		44	-32		30					100		
14 u(O···H)					-36	32		-39	-32				-40	100	
15 scale			-40		63	-48		75	77	39	67		37	46	100

possible when the u-values for the Cl···C distances are kept at fixed values. From the experimental curves there is no evidence of any admixture of other conformers of bis-(chloromethyl) ether in the gas phase.

It was necessary during the least-squares refinement to keep the u-values for non-bonded Cl···H, C···H, and H···H at fixed values in order to obtain convergency.

The final structural parameters are found in Table 1. The correlation matrix is given in Table 2.

As was expected, the molecule possesses a C_2 symmetry and a *gauche-gauche* conformation. An all-*anti* conformation would result in unfavourable interactions between non-bonded electrons on the oxygen and the halogen atoms. For comparison it may be mentioned that also 1,3-dibromopropane,[9] where the ether oxygen is replaced by an electrophile CH_2 group, contains 67 % of the *gauche-gauche* conformation, 3 % of the all-*anti* conformation, and 30 % of the *anti-gauche* conformation. In that compound a certain contribution of the *anti* conformer may be explained by a possible stabilization due to a bromine-hydrogen interaction. Such a stabilization is not present in bis(chloromethyl) ether.

The C–O bond distances in this molecule (1.393 ± 0.003Å) are somewhat smaller than usually found in aliphatic ethers.[10] Comparison with the gas phase structure of $ClCH_2-O-CH_3$ determined by electron diffraction by Planje *et al.*[11] shows, however, an even shorter C–O bond length (1.368 Å) for the chloromethoxy group. As pointed out in their article, two different C–O bond distances are presented in the same unresolved peak in their RD-curve. By fixing the vibrational amplitudes to what they assume a reasonable value for C–O bond distances, they determined the two C–O bond lengths to be 1.368 and 1.414 Å. However, a large uncertainty is connected with this procedure and standard deviations for these distances are not given.

The structure of chloromethyl methyl ether has also been investigated by Akishin *et al.*[12] with the electron diffraction method. It seems from their article that only an average C–O bond distance (1.42 ± 0.03 Å) is determined.

The Cl–C bond lengths in this work (1.800 ± 0.003 Å) are in good agreement with that found by Planje *et al.*[11] (1.813 Å), but appreciably smaller than the 1.87 Å, determined by Akishin *et al.*[12] It is seen that the C–O and C–Cl bond lengths in $ClCH_2-O-CH_2Cl$ are somewhat shorter and longer, respectively, than the corresponding distances in chloroalkanes and aliphatic ethers. This observation is by no means new, and it has been explained by Lucken[13] in 1959 and further supported by Williams in 1961[14] and 1962[15] as a partial double-bond due to charge migration from the reactive lone pair electron orbital to the anti-bonding σ-orbital of the C–Cl bonds. Williams concludes that such double-bonding in saturated aliphatic compounds is enhanced by increase in electronegativity of the acceptor atom and becomes more pronounced as the reactivity of the lone pair increases (N > O > F > Cl, Br > I).

The dihedral angle Cl–C–O–C of $69.6 \pm 1.6°$ found in this investigation of bis(chloromethyl) ether is in reasonably good agreement with the corresponding dihedral angles in chloromethyl methyl ether determined by Planje *et al.* and Akishin *et al.* to 74.3 and $76 \pm 5°$, respectively.

Acknowledgement. We are grateful to Dr. R. Seip and Mr. K. Brendhaugen for recording the photographic plates.

REFERENCES

1. Chiba, T. *Bull. Chem. Soc. Jpn 28* (1955) 295.
2. Morino, Y., Shiio, H. and Miyagawa, I. *Repts. Radiation Chem. Res. Inst. Tokyo Univ. 5* (1950) 6.
3. Katayama, M. and Morino, Y. *Repts. Radiation Chem. Res. Inst. Tokyo Univ. 4* (1949) 1.
4. Mizushima, S., Shimanouchi, T., Miyazawa, T. and Hayashi, M. *Unpublished.*
5. Miyagawa, I. *J. Chem. Soc. Jpn. (Pure Chem. Sect.) 75* (1954) 970.
6. Peacher, J. and Wills, J. C. *J. Chem. Phys. 46* (1967) 4809.
7. Strand, T. G. and Bonham, R. A. *J. Chem. Phys. 40* (1964) 1686.
8. Andersen, B., Seip, H. M., Strand, T. G. and Stølevik, R. *Acta Chem. Scand. 23* (1969) 3224.
9. Farup, P. E. and Stølevik, R. *Acta Chem. Scand. A 28* (1974) 680.
10. Blukis, U., Kasai, P. H. and Myers, R. J. *J. Chem. Phys. 38* (1963) 2753.

11. Planje, M. C., Toneman, L. H. and Dallinga, G. *Recl. Trav. Chim. Pays-Bas 84* (1965) 232.
12. Akishin, P. A., Vilkov, L. V. and Sokolova, N. P. *Isvest. Sibir. Otdel. Akad. Nauk. SSSR 5* (1960) 59.
13. Lucken, E. A. C. *J. Chem. Soc.* (1959) 2954.
14. Williams, J. F. A. *Trans. Faraday Soc. 57* (1961) 2989.
15. Williams, J. F. A. *Tetrahedron 18* (1962) 1477.

Received October 7, 1975.

Acta Chemica Scandinavica A 30 (1976) 294—296

Crystal Structure of Cyclodecanone at —160 °C. Some Crystal Data for Cyclopenta- and Cyclohexadecanone

P. GROTH

Department of Chemistry, University of Oslo, Oslo 3, Norway

The crystals of $C_{10}H_{18}O$ are monoclinic with space group $P2_1/c$, cell dimensions $a = 7.023(2)$ Å, $b = 5.418(2)$ Å, $c = 23.456(4)$ Å, $\beta = 95.16(2)°$, and four molecules in the unit cell. The structure was solved by direct methods and refined by full-matrix least-squares technique to an R-value of 3.4 % ($R_w = 4.1$ %) for 1392 reflections recorded on an automatic four circle diffractometer. The ten-membered ring has the "rectangular" diamond-lattice conformation. Crystal data for cyclopentadecanone and cyclohexadecanone are reported.

Strain-minimization calculations of medium and large cycloalkanes have been performed for more than ten years.[1–4] Detailed structure information of some cyclic ketones have been obtained by single crystal X-ray analyses.[5–8]

The crystals of $C_{10}H_{18}O$ are monoclinic with space group $P2_1/c$ and four molecules in the unit cell ($\varrho_c = 1.15$ g cm^{-3}, $\varrho_o = 1.17$ g cm^{-3}). The intensities were measured (at −160 °C) on a Syntex $P\bar{1}$ diffractometer with Enraf-Nonius liquid nitrogen cooling device (modified by H. Hope). With an observed-unobserved cutoff at $2.0\sigma(I)$, 1392 reflections were recorded as observed. The radiation was Mo$K\alpha$ and $\theta_{max} = 50°$. The crystal size was $(0.6 \times 0.04 \times 0.3)$ mm^3 and no corrections for absorption or secondary extinction have been carried out.

The structure was solved by direct methods [9] and refined by full-matrix least-squares technique.[10]* Anisotropic temperature factors were introduced for oxygen and carbon atoms.

* All programs used (except those for phase determination) are included in this reference.

Table 1. Final fractional coordinates and thermal parameters with estimated standard deviations. Expression for anisotropic vibration is: exp $[-2\pi^2(h^2a^{*2}U11 + \cdots + 2klb^*c^*U23)]$. Hmn is bonded to Cm.

ATOM	X	Y	Z	U11	U22	U33	U12	U13	U23
O	.45857(11)	.93633(16)	.38856(3)	.0173(4)	.0258(5)	.0253(4)	.0058(3)	.0012(3)	.0085(3)
C1	.60183(15)	.80687(22)	.31022(4)	.0156(5)	.0177(6)	.0122(5)	-.0008(5)	-.0022(4)	-.0030(4)
C2	.76808(16)	.87994(24)	.27698(5)	.0193(6)	.0171(6)	.0154(6)	.0069(5)	.0019(4)	.0006(5)
C3	.97179(16)	.85888(23)	.30645(4)	.0168(6)	.0174(6)	.0176(6)	.0089(4)	.0063(4)	.0081(5)
C4	1.02247(16)	1.04643(23)	.35424(5)	.0139(6)	.0168(6)	.0197(6)	-.0016(4)	.0025(4)	.0002(5)
C5	.89574(16)	1.03596(22)	.40396(5)	.0162(6)	.0143(6)	.0168(5)	-.0005(4)	.0006(4)	-.0006(5)
C6	.91313(16)	.79545(23)	.43855(5)	.0179(6)	.0166(6)	.0157(5)	-.0003(5)	-.0014(4)	-.0001(5)
C7	.74235(17)	.73895(24)	.47291(5)	.0259(6)	.0193(7)	.0163(6)	-.0006(5)	.0049(5)	.0006(5)
C8	.54219(17)	.74718(23)	.44077(5)	.0208(6)	.0175(6)	.0218(6)	-.0006(5)	.0007(5)	.0007(5)
C9	.49301(17)	.95331(23)	.39488(5)	.0179(6)	.0161(6)	.0241(6)	-.0022(5)	.0033(5)	.0007(5)
C10	.66743(17)	.86201(22)	.34133(5)	.0152(6)	.0149(6)	.0195(6)	-.0011(4)	-.0005(4)	-.0002(5)

ATOM	X	Y	Z	B	ATOM	X	Y	Z	B
H21	.7458(19)	1.0479(29)	.2625(5)	1.1(2)	H22	.7573(18)	.7684(28)	.2428(6)	1.3(2)
H31	1.0633(18)	.8815(23)	.2767(5)	1.0(2)	H32	.9937(17)	.6866(27)	.3211(6)	1.2(2)
H41	1.0134(17)	1.2174(26)	.3571(5)	1.2(2)	H42	1.1572(19)	1.0243(23)	.3683(5)	.9(2)
H51	.7613(16)	1.0627(28)	.3889(4)	.3(2)	H52	.9228(17)	1.1789(25)	.4298(5)	1.0(2)
H61	1.0279(18)	.8440(25)	.4668(5)	1.0(2)	H62	.9344(17)	.6526(25)	.4131(5)	1.1(2)
H71	.7428(19)	.8630(27)	.5057(6)	1.4(2)	H72	.7619(22)	.5759(31)	.4985(6)	1.6(3)
H81	.5210(17)	.9157(25)	.4239(5)	1.0(2)	H82	.4481(20)	.7258(27)	.4782(6)	1.6(2)
H91	.3563(20)	.5727(24)	.3814(5)	1.1(2)	H92	.5078(18)	.3868(27)	.4118(5)	1.3(2)
H101	.5532(20)	.4452(26)	.3131(5)	1.3(2)	H102	.7496(20)	.5135(24)	.3505(5)	.7(2)

Table 2. Interatomic distances, bond angles and dihedral angles with estimated standard deviations.

Distance	(Å)	Distance	(Å)
O – C1	1.220(1)	C1 – C2	1.518(2)
C2 – C3	1.537(2)	C3 – C4	1.531(2)
C4 – C5	1.530(2)	C5 – C6	1.534(2)
C6 – C7	1.535(2)	C7 – C8	1.535(2)
C8 – C9	1.534(2)	C9 – C10	1.535(2)
C10 – C1	1.513(2)		

Angle	(°)	Angle	(°)
O – C1 – C2	120.2(1)	O – C1 – C10	120.6(1)
C10 – C1 – C2	119.1(1)	C1 – C2 – C3	118.7(1)
C2 – C3 – C4	115.2(1)	C3 – C4 – C5	114.9(1)
C4 – C5 – C6	114.2(1)	C5 – C6 – C7	114.7(1)
C6 – C7 – C8	117.4(1)	C7 – C8 – C9	117.9(1)
C8 – C9 – C10	117.0(1)	C9 – C10 – C1	114.9(1)

Dihedral Angle	(°)
C1 – C2 – C3 – C4	-70.2(1)
C2 – C3 – C4 – C5	59.6(1)
C3 – C4 – C5 – C6	65.2(1)
C4 – C5 – C6 – C7	-158.6(1)
C5 – C6 – C7 – C8	51.4(2)
C6 – C7 – C8 – C9	66.1(2)
C7 – C8 – C9 – C10	-64.6(1)
C8 – C9 – C10 – C1	-56.0(1)
C9 – C10 – C1 – C2	152.3(1)
C10 – C1 – C2 – C3	-49.1(2)

Weights in least squares were obtained from the standard deviations in intensities, $\sigma(I)$, taken as

$$\sigma(I) = [C_T + (0.02C_N)^2]^{\frac{1}{2}}$$

where C_T is the total number of counts, and C_N the net count. The atomic form factors were those of Hanson *et al.*[11] except for hydrogen.[12] The R-value arrived at was 3.4 % (weighted value $R_w = 4.1$ %) for 1392 observed reflections.

Final fractional coordinates and thermal parameters with estimated standard deviations are given in Table 1. Maximum root mean squares anisotropic thermal amplitudes for oxygen and carbon range from 0.14 to 0.17 Å. No rigid-body analyses have been performed.

Interatomic distances, bond angles, and dihedral angles are given in Table 2 together with standard deviations, computed from the final correlation matrix. Fig. 1, a schematic drawing of the molecule, illustrates the "rectangular" diamond-lattice conformation of the ten-membered ring. Bond distances are normal.

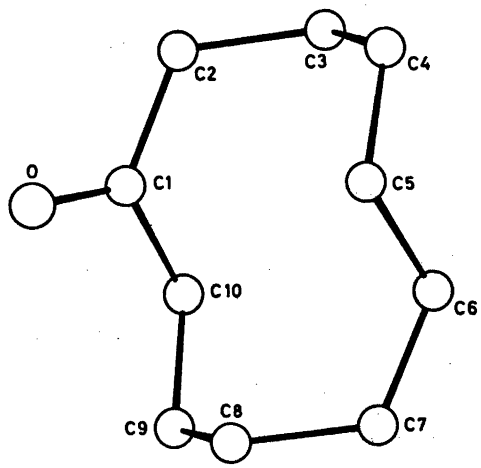

Fig. 1. Schematic drawing of the molecule.

The average C – C – C angle (excluding C10 – C1 – C2) of 116.1° is somewhat larger than in cycloundecanone (114.6°).[7]

A list of observed and calculated structure factors is available from the author.

Intensity data from single crystals of cyclopentadecanone and cyclohexadecanone have also been collected at –160 °C.

The crystals of $(CH_2)_{14}C=O$ are orthorhombic $a = 5.589(3)$ Å, $b = 7.814(4)$ Å, and $c = 15.990(8)$ Å. The number of molecules in the unit cell is two ($\varrho_c = 1.06$ g cm^{-3}). The systematic absences, $0kl$: $k + l = 2n$, correspond (by changing axes) to space groups No. 31, $Pmn2_1$, and No. 59, $Pmmn$, with four and eight equivalent positions, respectively. With $Z = 2$ both space groups demand a disordered structure. 512 reflections were recorded as observed.

The crystals of $(CH_2)_{15}C=O$ are also orthorhombic. The cell dimensions are $a = 5.395(2)$ Å, $b = 8.315(6)$ Å, and $c = 16.926(11)$ Å and $Z = 2$ ($\varrho_c = 1.04$ g cm^{-3}). The extinctions lead to the space group No. 17, $P222_1$, (with four equivalent positions), again demanding a disordered structure. 734 observed reflections were recorded.

Attempts to solve these structures by direct methods were not successful.

Lists of observed structure factors are available from the author.

Acknowledgement. The author would like to thank cand.real. T. Ledaal for supplying the compounds.

REFERENCES

1. Hendrickson, J. B. *J. Amer. Chem. Soc. 83* (1961) 4537; *86* (1964) 4854; *89* (1969) 7036.
2. Bixon, M. and Lifson, S. *Tetrahedron 23* (1967) 769.
3. Dale, J. *Acta Chem. Scand. 27* (1973) 1115.
4. Wiberg, K. B. J. *J. Amer. Chem. Soc. 97* (1965) 1070.
5. Dehli, J. and Groth, P. *Acta Chem. Scand. 23* (1969) 587.
6. Dahl, S. and Groth, P. *Acta Chem. Scand. 25* (1971) 1114.
7. Groth, P. *Acta Chem. Scand. A 28* (1974) 294.
8. Groth, P. *Acta Chem. Scand. A 29* (1975) 374.
9. Germain, G., Main, P. and Woolfson, M. M. *Acta Crystallogr. A 27* (1971) 368.
10. Groth, P. *Acta Chem. Scand. 27* (1973) 3131.
11. Hanson, H. P., Herman, F., Lea, J. D. and Skillman, S. *Acta Crystallogr. 17* (1964) 1040.
12. Stewart, R. F., Davidson, E. R. and Simpson, W. T. *J. Chem. Phys. 42* (1965) 3175.

Received September 24, 1975.

Acta Chemica Scandinavica A 30 (1976) 297—302

Theory for the Determination of Vapour Pressures by the Transpiration Method

HALVOR KVANDE and P. G. WAHLBECK*

Division of Inorganic Chemistry, The Norwegian Institute of Technology, The University of Trondheim, 7034 Trondheim-NTH, Norway

Equations valid for coupled diffusion and viscous flow are applied to the case of the transpiration experiment. The results presented in this paper do not assume a uniform total pressure in the apparatus, in contrast with the theory developed by Merten. A theory is presented for the diffusion of the sample vapour in opposition to the flow of carrier gas in the carrier gas entrance. Results from this theory are compared with those of Merten. Recommendations for users of the transpiration method are given.

The transpiration method is one of the simplest and most versatile methods for vapour pressure determinations at high temperatures.[1-3] The apparatus is simple and is shown schematically in Fig. 1. In principle, a carrier gas, which may be inert or reactive, is passed over or through the condensed sample under investigation in a constant temperature zone and with a constant flow rate of carrier gas. The flow is desired to be sufficiently slow so that the carrier gas is saturated with the vapour, which is condensed at some point "downstream" from the sample. The vapour pressure may be found by determination of the mass of vapour carried away by a known volume of carrier gas in a known time period, provided the molecular weight of the vapour is known. Conversely, when the molecular weight of the vapour is not known, it may be evaluated from observations by the transpiration method in combination with vapour pressure measurements by some other method. Thus, the transpiration method represents a valuable adjunct to the "boiling point" method, the theory of which is discussed in a subsequent paper.[4] Although

* Permanent address: Department of Chemistry, Wichita State University, Wichita, Kansas 67208, USA.

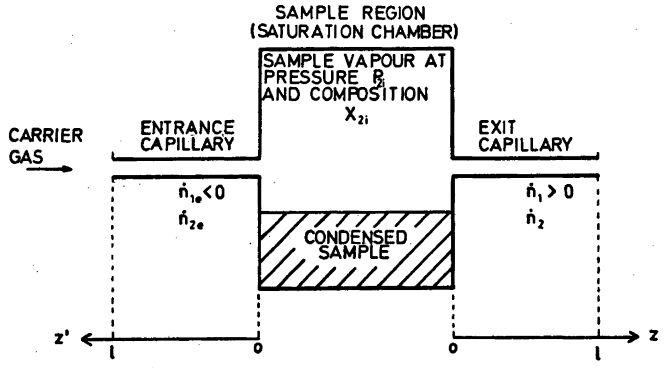

Fig. 1. Schematic diagram of the isothermal part of the apparatus used in a transpiration experiment.

experimentally quite different, the theories of these two methods have several features in common. It is the purpose of the present paper to present a consistent theory of the transpiration method.

As the flow rate of carrier gas, $\dot{n}_1$, is varied, three regions of interest can be described. They are: *1.* very small $\dot{n}_1$, a considerable amount of sample vapour is transported by a diffusion mechanism as well as by bulk hydrodynamic flow, *2.* moderate $\dot{n}_1$, most vapour transport is dependent on bulk hydrodynamic flow, and *3.* large $\dot{n}_1$, the gas in the sample compartment is not saturated with sample vapour.

The case in which the flow of carrier gas is so rapid that it is no longer saturated in the sample compartment, region *3* above, has been considered in detail by Hofmeister, Haeseler, and Glemser.[5] Merten and Bell [3] have discussed the kinetic aspects of the transpiration method, and found that at high flow rates, saturation of the carrier gas may be prevented by incomplete mixing in the gas stream or by insufficiently rapid vaporization of the sample. For the latter case these authors considered the application of the Langmuir equation, including a vaporization coefficient, for values of the rate of vaporization of the condensed sample. This case will not be considered further in this paper.

The flow of sample vapour in regions *1* and *2* can be considered together in the treatment to be presented since, in addition to bulk hydrodynamic flow, diffusive flow always occurs. This diffusion increases the total mass transport from the condensed sample, and is consequently of importance for the vapour pressure determination.

Several attempts have been made to give a quantitative description of the diffusion effects in the transpiration method.[3,5-8] In the present paper we will discuss the theory of this method, based on the proper definitions of diffusion and laminar viscous flow. Furthermore, diffusion in both the "upstream" and "downstream" directions will be considered.

THEORY

Case 1. Flow of vapour through exit capillary. We have discussed elsewhere [4] the equations for coupled diffusion and viscous flow. The appropriate equation for a binary system is

$$J_i = -Dc(dx_i/dz) + cx_iv \qquad (1)$$

where J_i is the flux of species i in mol s^{-1} cm^{-2} in the z direction, x_i is the mol fraction of species i, c is the total gas concentration in mol cm^{-3}, v is the mean molecular velocity in the z direction, and D is the gaseous diffusivity coefficient.[4,9,10]

Let subscripts 1 and 2 represent the two gaseous species in the transpiration experiment, carrier gas and sample vapour, respectively.

Experimentally one considers the case of a uniform temperature and a uniform flow rate of carrier gas. One wishes to interrelate the flux of sample vapour, J_2, to the equilibrium vapour pressure of the sample.

One may solve the differential equation (1) and obtain as a solution

$$x_{2z} = (J_2/cv)[1 - \exp(cvz/Dc)] + x_{2i} \exp(cvz/Dc) \qquad (2)$$

where x_{2z} is the value of the mol fraction of the vapour at $z=z$ and x_{2i} is the value at $z=0$. Consider the case of $z=l$, and assume that the sample vapour is dissipated completely at the end of the capillary. This assumption may be represented by $x_{2l}=0$. For this case, rearrangement of eqn. (2) gives

$$J_2 = x_{2i}cv/[1 - \exp(-cvl/Dc)] \qquad (3)$$

In our subsequent paper,[4] we show that v is the sum of two velocities; *i.e.*, v_d and v_v, where v_d is a velocity caused by diffusion and v_v is a velocity caused by a pressure gradient. These velocities are

$$v_d = \frac{D(1-\gamma)}{\gamma + x_1(1-\gamma)}(dx_1/dz) \qquad (4)$$

and

$$v_v = (-r^2/8\eta)(dP/dz) \qquad (5)$$

where $\gamma = \sqrt{M_2/M_1}$, M_i is the molecular weight, P is the pressure, r is the capillary radius and η is the viscosity. Replacing v in the numerator of eqn. (3) with eqns. (4) and (5), one has

$$J_2 = \frac{x_{2i}c\left(\frac{D(1-\gamma)}{\gamma + x_1(1-\gamma)}(dx_1/dz) - (r^2/8\eta)(dP/dz)\right)}{1 - \exp(-cvl/Dc)} \qquad (6)$$

Eqn. (6) may be rearranged and integrated over z, x_1 and P with values valid from the capillary entrance to the capillary exit. Assume that both gases are ideal, and that D and η are independent of z. With Dalton's law applied to the sample compartment, the ratio of the sample equilibrium vapour pressure to the total pressure is $P_{2i}/P_i = x_{2i}$, and one obtains

$$P_{2i}^2 = x_{2i}^2 P_f^2 + (16\eta RT x_{2i} l/r^2)\{J_2[1-\exp(-(J_1+J_2)l/Dc)] + (x_{2i}D'/lRT)\ln[1-x_{2i}(1-\gamma)]\} \quad (7)$$

where P_f is the pressure at the exit of the capillary and D' is DP. Replacing cv in the numerator of eqn. (3) by the equation

$$J_1 + J_2 = cv \quad (8)$$

which may be derived from eqn. (1) by use of the simple properties of the mol fraction, one has

$$x_{2i} = (J_2/(J_1+J_2))[1-\exp(-cvl/Dc)] \quad (9)$$

We identify terms assumed to be constant in eqns. (7) and (9) by

$$A = \pi r^2 D'/RTl \quad (10)$$

and

$$C = \pi r^4/(16RTl\eta) \quad (11)$$

Introducing also the equation

$$J_i = \dot{n}_i/(\pi r^2) \quad (12)$$

where $\dot{n}_i$ is the flow rate of species i in mol s^{-1}, we may rewrite eqns. (7) and (9) as

$$P_{2i}^2 = x_{2i}^2\{P_f^2 + (\dot{n}_1+\dot{n}_2)/C + (A/C)\ln[1-x_{2i}(1-\gamma)]\} \quad (13)$$

and

$$x_{2i} = [\dot{n}_2/(\dot{n}_1+\dot{n}_2)][1-\exp(-(\dot{n}_1+\dot{n}_2)/A)] \quad (14)$$

Eqns. (13) and (14) give a relationship valid for the calculation of the sample equilibrium vapour pressure, P_{2i}, at temperature T as determined by the two flow rates $\dot{n}_1$ and $\dot{n}_2$. These equations consider flow of materials only through the exit capillary of the apparatus. A direct application could be made to the experimental case in which the sample vapour transport, $\dot{n}_2$, is determined from the condensate in the "downstream" cold region of the apparatus. In this case the only measured values of $\dot{n}_2$ are for flow in the exit capillary.

It is of interest to discuss the value of $\dot{n}_2$ when the flow of carrier gas goes to zero, $\dot{n}_1 = 0$. In this case from eqns. (13) and (14) one has

$$P_{2i}^2 = x_{2i}^2\{P_f^2 + \dot{n}_2/C + (A/C)\ln[1-x_{2i}(1-\gamma)]\} \quad (13z)$$

and

$$x_{2i} = 1-\exp(-\dot{n}_2/A) \quad (14z)$$

These equations are exactly the same as those derived by us in a subsequent paper,[4] in which we consider the experimental case of $\dot{n}_1 = 0$.

Case 2. Flow of sample vapour through both entrance and exit capillaries. In addition to the flow and diffusion of carrier gas and sample vapour in the exit capillary, sample vapour may diffuse "upstream" through the entrance capillary. This effect may be important in experimental cases in which the sample vapour transport, $\dot{n}_2$, is determined by measuring the mass loss of the sample.

For the entrance capillary we consider the z' coordinate as shown in Fig. 1. It is to be noted that when sample vapour leaves the apparatus through the entrance capillary with this choice of z' coordinate, $\dot{n}_2 > 0$, whereas $\dot{n}_1 < 0$ because the carrier gas is flowing toward negative z'. For the entrance capillary, equations (13) and (14) should be applicable with the replacement of $\dot{n}_1$ by $-\dot{n}_1$. Thus,

$$P_{2i}^2 = x_{2i}^2\{P_{fe}^2 + (\dot{n}_{2e}-\dot{n}_1)/C_e + (A_e/C_e)\ln[1-x_{2i}(1-\gamma)]\} \quad (13e)$$

and

$$x_{2i} = [\dot{n}_{2e}/(\dot{n}_{2e}-\dot{n}_1)][1-\exp(-(\dot{n}_{2e}-\dot{n}_1)/A_e)] \quad (14e)$$

A subscript e has been added to quantities which will be different for the entrance capillary from those of the exit capillary. The quantities x_{2i} and P_{2i} are the same for both sets of equations since these quantities apply to the sample compartment. It is assumed that the gas in the sample compartment is of uniform composition and pressure.

By equating (14) and (14e) one obtains a relationship between $\dot{n}_2$ and $\dot{n}_{2e}$, and one is able to calculate the amount of sample vapour transported by diffusion through the entrance capillary.

Two cases are of interest:

Case A. $\dot{n}_1 = 0$. This gives

$$\dot{n}_{2e}/A_e = \dot{n}_2/A \quad (15)$$

With equal capillary dimensions, $A_e = A$ and $\dot{n}_{2e} = \dot{n}_2$.

Case B. $\dot{n}_1 \gg 0$, $\dot{n}_2$, $\dot{n}_{2e}$. In this case one has

$$-(\dot{n}_{2e}/\dot{n}_1)[1-\exp(\dot{n}_1/A_e)] = (\dot{n}_2/\dot{n}_1)[1-\exp(-\dot{n}_1/A)] \quad (16)$$

and if $\dot{n}_1 \gg A$, then

$$\dot{n}_{2e} = \dot{n}_2 \exp(-\dot{n}_1/A_e) \quad (17)$$

Clearly the equation resulting from the addition of (13) to (13e) is very complex, and its application is not practical since it contains too many unknown parameters.

DISCUSSION

Reduction to Merten's theory. Merten [8] has presented a theoretical approach to the transpiration experiment. He assumed that the pressure is uniform throughout the transpiration apparatus. One may obtain Merten's equation from equations (13) and (14) by assuming that $C = \infty$ and that $\dot{n}_1 \gg \dot{n}_2$. The assumption that $C = \infty$ is equivalent to assuming that $\eta = 0$; *i.e.*, the gas has no viscosity. With no viscosity there would be no resistance to flow of gas, and no pressure gradient would result. From the assumption that $\dot{n}_1 \gg \dot{n}_2$, one neglects $\dot{n}_2$ in terms in which the sum of $\dot{n}_1$ and $\dot{n}_2$ appears. Thus, equations (13) and (14) reduce to

$$\dot{n}_2 = \dot{n}_1 \frac{P_{2i}}{P_f}\left[1-\exp(-\dot{n}_1/A)\right]^{-1} \quad (18)$$

which is Merten's equation.

The main advantage of the present theoretical development is that no assumption regarding uniform pressure is made. In most experiments pressure gradients are not evaluated, and it would be extremely difficult to make the necessary measurements. In order to have large flow rates of carrier gas, a pressure gradient is required. The assumption of no pressure gradient appears to be somewhat unrealistic.

Comparison of results of theories. In Fig. 2 are given calculated curves of the vapour flow rate $\dot{n}_2$ *vs.* carrier gas flow rate $\dot{n}_1$ which were generated by the equations for the following cases: *1*, the present theoretical development considering only vapour flow from the exit capillary, eqns. (13) and (14); *2*, the results given in case *1* above with the addition of sample vapour transport through the carrier gas entrance capillary, assuming the same A value for both capillaries and *3*, the results given by Merten's eqn. (18) assuming that there is no pressure drop in the apparatus. The same values for P_{2i}, P_f and A were used for all three curves.

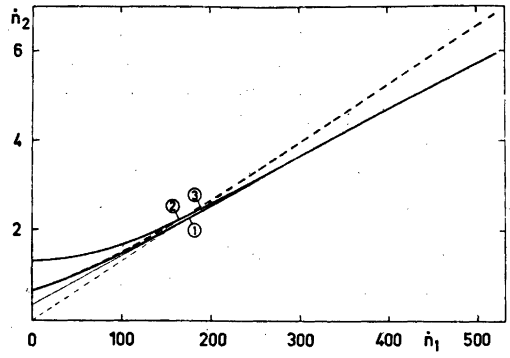

Fig. 2. Calculated curves of vapour flow rate $\dot{n}_2$ *vs.* carrier gas flow rate $\dot{n}_1$ in a transpiration experiment.
1. Present theory, diffusion through exit capillary only.
2. Present theory, diffusion through both entrance and exit capillaries.
3. Merten's [8] theory, diffusion through exit capillary only, and assuming no pressure drop in the apparatus.

In comparing the resulting curves of cases *1* and *3*, one notes that the curves are identical at small flow rates of carrier gas, $\dot{n}_1$ small. This is a reasonable result since the effect of viscous flow caused by a pressure gradient should be small when $\dot{n}_1$ is small.

At large flow rates of carrier gas, $\dot{n}_1$ large, the neglect of the viscosity of the vapour causes a difference between the two curves. It is reasonable that the difference between the two curves increases with increasing $\dot{n}_1$ since a larger pressure gradient is needed to cause the flow, and the effect of viscous flow will increase.

At larger flow rates of carrier gas, one may neglect the effect of vapour transport by diffusion. In the equations this may be done by setting $A = 0$. Eqn. (13) then reduces to

$$\dot{n}_2 = \dot{n}_1 \frac{P_{2i}}{\left(P_f^2 + \frac{\dot{n}_1 + \dot{n}_2}{C}\right)^{\frac{1}{2}} - P_{2i}} \quad (19)$$

and Merten's equation, eqn. (18), reduces to

$$\dot{n}_2 = \dot{n}_1 \frac{P_{2i}}{P_f} \quad (20)$$

With fixed values of P_f, P_{2i} and C, one may see that the dependence of $\dot{n}_2$ on $\dot{n}_1$ in our theory is non-linear, whereas there is a linear dependence in Merten's theory.

Thus, with the present theoretical development, data in the large $\dot{n}_1$ range are not linear. A straight line through this apparently linear range will have a non-zero intercept. This is contrasted with an actual zero intercept in Merten's theory.

Merten's assumption that $C = \infty$ gives a too low value for P_{2i}, while his assumption that $\dot{n}_1 \gg \dot{n}_2$ causes a too high value. In most practical cases the former effect is the larger. From the calculated curve 1 in Fig. 2 the difference between the pressure values from the two theories is about 10 %. Since C is proportional to r^4 [eqn. (11)], a smaller capillary radius will favour our theory.

We are presently performing measurements to determine experimentally the significance of our theory in relation to that of Merten.

The effect of diffusion. Diffusion of vapour through the entrance capillary in opposition to the flow direction of the carrier gas has been mentioned by Merten and Bell.[3] In the present paper the first attempt has been made to evaluate the contribution of the back diffusion.

In viewing curves *1* and *2* in Fig. 2, one notes that the gaseous diffusion through the entrance capillary does make a significant contribution to the vapour flow rate at small values of $\dot{n}_1$. For $\dot{n}_1 = 0$, the transport of sample vapour is increased with a factor of 2, when the capillary dimensions are equal.

At large flow rates of carrier gas, however, the diffusion contribution becomes very small. In both Merten's [8] and the present theoretical development terms of the type $[1 - \exp(-\dot{n}_1/A)]$ or $[1 - \exp(-(\dot{n}_1 + \dot{n}_2)/A)]$ are related to the diffusion transport mechanism. Thus, when the exponential expression is small compared to unity, diffusion may be neglected, *e.g.*, diffusion contributes less than 5 % to the transport of sample vapour when $\dot{n}_1/A > 3$.

From this discussion the nearly linear range of carrier gas flow rates for which the diffusion contribution is small, is determined by the parameter A. According to eqn. (10), A is dependent on r, l, T, and D'. From the kinetic theory of gases it is expected that D' is proportional to $T^{3/2}$, but is independent of pressure. Thus, the parameter A should be dependent on $r^2 T^{\frac{1}{2}}/l$, and the nearly linear range of carrier gas flow rates should depend on the capillary dimensions and the square root of temperature. This means that the equilibrium vapour pressure of the sample is of little importance for the determination of this range.

Recommendations for users of the transpiration method. In using the transpiration method for determining equilibrium vapour pressures, one should do the following.

1. One should determine experimentally a curve of the type shown in Fig. 2. This requires experimental determinations of $\dot{n}_2$ at varying $\dot{n}_1$ with fixed temperature T and hence fixed P_{2i}. This curve will delineate the nearly linear range, which is desired for laboratory measurements, from the diffusion range at small $\dot{n}_1$ and from the desaturation range at large $\dot{n}_1$. (In principle, by avoiding the desaturation range, the equilibrium vapour pressure P_{2i} and the parameters A and C could be determined from any set of $\dot{n}_1$, $\dot{n}_2$ and P_f data by fitting eqns. (13) and (14) to the data.)

2. From the data acquired above for the nearly linear range (small diffusion and no desaturation), determine the values of P_{2i} and C by a non-linear least squares computer program using eqn. (19).

3. Restrict measurements for vapour pressure determinations to $\dot{n}_1$ values in the nearly linear range. Rearranging eqn. (19), one has

$$P_{2i} = \frac{\dot{n}_2}{\dot{n}_1 + \dot{n}_2}\left(P_f^2 + \frac{\dot{n}_1 + \dot{n}_2}{C}\right)^{\frac{1}{2}} \quad (21)$$

Use eqn. (21) to calculate the equilibrium vapour pressure at other temperatures.

In case the vapour pressure is known, the data can be used to determine the molecular weight of the vapour. One may use the equation

$$\dot{n}_2 = \dot{m}_2/M_2 \quad (22)$$

where $\dot{m}_2$ is the measured mass of vapour carried away from the sample per unit time, and M_2 is the molecular weight of the vapour. By inserting eqn. (22) into eqn. (21), one may use the same procedure as described above to determine the molecular weight of the vapour.

Acknowledgements. The authors wish to express their appreciation for Grant 836 from the NATO Research Grants Programme to PGW which made it possible for the authors to collaborate on this research. The authors also wish to express their appreciation to Professor Ketil Motzfeldt for several discussions.

REFERENCES

1. Nesmeyanov, A. N. *Vapor Pressures of the Elements*, Academic, New York 1963.
2. Kubaschewski, O., Evans, E. L. and Alcock, C. B. *Metallurgical Thermochemistry*, 4th Ed., Pergamon Press, London 1967.
3. Merten, U. and Bell, W. E. In Margrave, J. L. *The Characterization of High-temperature Vapors*, Wiley, New York 1967, p. 91.
4. Motzfeldt, K., Kvande, H. and Wahlbeck, P. G. *Acta Chem. Scand. To be published.*
5. Hofmeister, H. K., Haeseler, R. v. and Glemser, O. *Z. Elektrochem. 64* (1960) 513.
6. Wagner, C. and Stein, V. *Z. Phys. Chem. (Leipzig) 192* (1943) 129.
7. Lepore, J. V. and Van Wazer, J. R. *A Discussion of the Transpiration Method for Determining Vapor Pressure*, MDDC-1188, U. S. Atomic Energy Commission, 1948.
8. Merten, U. *J. Phys. Chem. 63* (1959) 443.
9. Present, R. D. *Kinetic Theory of Gases*, McGraw-Hill, New York 1958, p. 49.
10. Geankoplis, C. J. *Mass Transport Phenomena*, Holt, Rinehart and Winston, New York 1972, p. 38.

Received June 19, 1975.

Acta Chemica Scandinavica A 30 (1976) 303—305

The Solubility of Chromium in Chromium(II) Chloride

S. SEETHARAMAN and L.-I. STAFFANSSON

Department of Metallurgy, Royal Institute of Technology, S-100 44 Stockholm, Sweden

The depression of the freezing point of anhydrous $CrCl_2$ has been determined by DTA and solubility measurements. The melting point of pure $CrCl_2$ was found to be 822 ± 1 °C and the eutectic was obtained at 806 °C and 3.4 ± 0.1 mol % Cr. From the saturation solubility curve, a value of 57.0 kJ/mol for the heat of solution of Cr in $CrCl_2$ was determined.

An understanding of the solution process of metals in their molten salts is of great importance technologically as well as theoretically. Considerable efforts have been made to study various metal-metalhalide systems, the chlorides in particular, to determine the type of ionic species present in such systems. Of these, the solution of Cr in $CrCl_2$ has received very little attention so far. This system is, however, of considerable technological interest, *e.g.* in the process for chromizing iron from a salt melt. The only reported work on this system is that of Corbett, Clark and Munday.[1] These authors measured the depression of the freezing point of $CrCl_2$ by the addition of Cr and found this to be 6 °C at the eutectic composition. The melting point of pure $CrCl_2$, according to their work was 824 °C and the eutectic composition was given as 3 – 4 mol % Cr. As a freezing point depression of 6 °C is incompatible with the existing models of solution of metals in their molten salts [2] and as the melting point of pure $CrCl_2$ has also been variously reported between 815 and 824 °C in literature, the present work was undertaken to clarify the uncertainties existing in this system.

EXPERIMENTAL

Materials. Electrolytic chromium with a purity of 99.99 wt % was used. The $CrCl_2$ was prepared by passing pure chlorine gas from a cylinder containing liquid chlorine over pieces of Cr metal in a quartz boat, kept in a quartz reaction tube and heated in a horizontal tube furnace to 900 °C. The chlorine was dried by conc. H_2SO_4 and P_2O_5. Approximately 20 g of the metal were used in each batch of the $CrCl_2$ synthesis and the reaction was normally complete in about 24 h. $CrCl_2$, condensed in the form of violet crystals in the colder parts of the furnace, was collected and stored in a closed glass vessel in a dry-box under an argon atmosphere. To avoid the absorption of moisture the $CrCl_2$ crystals thus prepared were handled only in the dry-box. This salt did not dissolve in water, which may be taken as an indication of high purity.

For the DTA measurements accurately known weights of $CrCl_2$ (approximately 400 mg) were transferred into thinwalled vycor tubes of 1 cm diameter in the dry-box. To this, proper proportions of Cr were added on top so that ultimately different ratios of $Cr/CrCl_2$ could be obtained. The volume above the Cr metal was closed by a tight-fitting quartz plunger tube and sealed under a vacuum of less than 10^{-3} Torr, by fusion in an oxy-hydrogen flame. The samples were pre-heated in a vertical furnace at 900 °C for 24 h to ensure that the formation of the dichloride and the solution of the metal in the fused dichloride were complete. Some of the samples were made to correspond to stoichiometric $CrCl_2$. To be sure of the purity of the $CrCl_2$ used for the preparation of the $CrCl_2$ some experiments were also carried out using resublimed $CrCl_2$. This procedure did, however, not alter the melting point of the pure $CrCl_2$.

DTA measurements. The DTA measurements were made in a Mettler Thermoanalyzer No. 59 with Pt/10 % Rh-Pt thermocouples. The reference was a vycor tube filled with crystalline quartz powder and sealed in the same way as the Cr-$CrCl_2$ capsules. The thermocouples were calibrated with pure aluminium and pure, dehydrated and pre-melted NaCl, sealed in vycor tubes under vacuum. The reference as well as the calibration capsules were nearly of the same dimension as the $CrCl_2$-Cr capsules. The quartz middle-range furnace supplied by

Mettler was used for heating the samples. The melting and freezing points could be accurately read with the aid of the five-fold magnification of the temperature scale provided in the thermoanalyzer.

Solubility measurements. Supplementing the DTA studies, the solubility of Cr in $CrCl_2$ was directly measured by equilibrating pieces of Cr metal of known weight with known amounts of $CrCl_2$ at fixed temperature and measuring the weight loss of Cr after equilibration. The samples were prepared in the same way as for DTA studies except that a large, single piece of chromium metal was used for each sample. The sample was kept inside a copper block and heated in a vertical tube furnace having a large constant temperature zone in the centre. The temperature was measured along the entire length of the sample by two Pt/10 % Rh-Pt thermocouples. The furnace was controlled by a Eurotherm thyristor regulator to ±1 °C, with a Pt/10 % Rh-Pt thermocouple embedded very close to the furnace windings. The equilibration was carried out for 72 h with repeated shaking of the sample. The sample was cooled fast, broken and the chromium piece was recovered. It was repeatedly boiled with distilled water, washed with pure alcohol, dried and the weight loss was determined.

RESULTS AND DISCUSSION

Twenty-five samples having compositions from 0 to 70 mol % chromium were studied by the DTA method. The composition corresponding to pure $CrCl_2$ gave identical melting and freezing points corresponding to 822±1 °C. This is somewhat higher than the results of Shiloff,[3] Seifert and Klatyk [4] and Kühnl and Ernst [5] but is slightly lower than the value obtained by Corbett *et al.*[1] and Fischer and Gewehr,[6] as can be seen in Table 1. The value of 815 °C reported by Doerner [6] could possibly be low due to contamination of the chloride.

Table 1. Melting point of chromium(II) chloride.

Melting point °C	Stated accuracy °C	Ref.
824	±1	1
820	±3	3
820.5	±1	4
820.5	±1	5
815	–	6
816	–	7
824	±2	8
822	±1	This work

While it appeared that the true liquidus of $CrCl_2$ could be observed in the DTA measurements, in some samples with very low amounts of excess Cr (up to 1 mol %), the runs with higher chromium content indicated that the solution process was often incomplete. Heating of the samples in inverted position prior to the DTA experiments often improved the results but because the capsules could not be shaken in the DTA apparatus the solution process was so slow that the measured liquidus values could hardly be relied upon. In such runs, there was a first melting peak corresponding to the eutectic at 806 °C, followed closely by a larger peak. On cooling the freezing always started much earlier, often only 2 or 3 °C lower than that of pure $CrCl_2$. This was not the case with pure $CrCl_2$. This point was clarified by the thermal analysis of samples containing a very large excess of Cr (of the order of 70 mol %). In these cases, Cr pieces extended through the entire height of the melt and thus Cr was available for solution at all heights. In these instances, only the eutectic peak was observed during heating as well as cooling. The eutectic temperature of 806 °C, observed in the present work corresponds to a depression of the freezing point of 16 °C. The lower value of 6 °C observed

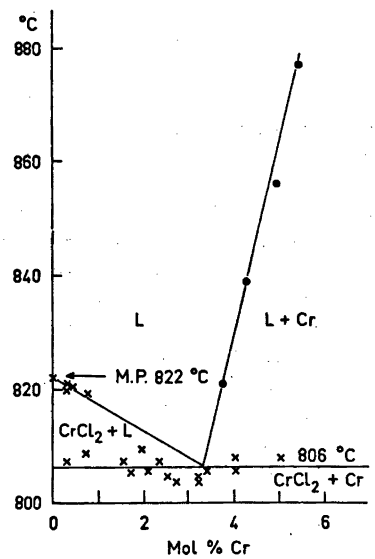

Fig. 1. The solubility of Cr in $CrCl_2$. ×, DTA; ●, Solubility measurements.

by Corbett *et al.*[1] can probably be explained on the basis of the slow rate of solution of chromium in $CrCl_2$ which might lead to non-equilibrium conditions. This appears to be a likely explanation particularly as the discrepancy in melting point of pure $CrCl_2$ between their work and this work is small and within the experimental error.

The eutectic composition was determined from an extrapolation of the saturation solubility curve which was established by solubility measurements. The results are summarized in Fig. 1, in which, however, the values obtained for samples with a Cr-content of more than 5 mol % are not shown. The intersection of the solubility line and the eutectic line gives the eutectic composition as 3.4 ± 0.1 mol % Cr which is within the range of 3 to 4 mol % Cr given by Corbett *et al.*

As the saturated salt melt is in equilibrium with pure solid chromium the heat of solution of chromium in the melt can be evaluated from the slope of the solubility curve. This gave a value of 57.0 kJ/mol.

The depression of the freezing point of $CrCl_2$ provides a means to estimate the number of foreign particles that enters the melt for each chromium atom added and will in this way give an indication of the mechanism by which the metal dissolves in the melt. In dilute solutions the two most likely models for dissolution of the metal as ions in its salt are the following:

$$Cr + Cr^{2+} \rightarrow Cr_2^{2+} \quad \text{(A)}$$

$$Cr + Cr^{2+} \rightarrow 2\ Cr^{+} \quad \text{(B)}$$

Assuming Cr being insoluble in solid $CrCl_2$ these two models will give the following ideal Temkin activity for $CrCl_2$ expressed by the mol fraction x of $CrCl_2$.

$$a_{CrCl_2} = (2x-1)/x \quad \text{(A)}$$

$$a_{CrCl_2} = 2x-1 \quad \text{(B)}$$

ΔT can be computed from the equation

$$\Delta T = -\frac{RT_0T}{\Delta H_f} \ln a_{CrCl_2}$$

where T_0 is the melting point in degree K of pure $CrCl_2$, T is the eutectic temperature, $\Delta T = T_0 - T$ and ΔH_f the heat of fusion. With $\Delta H_f = 7.7 \pm 1.5$ kcal/mol[9] it is found that model A gives $\Delta T = 10.5$ K, while model B gives $\Delta T = 20.5$ K at the eutectic, which is much higher than the value suggested by Corbett *et al.*[1] Unfortunately, the uncertainty in ΔH_f is too large to permit a choice between the two models.

Acknowledgements. The authors are indebted to the Axel Johnson Institute for Industrial Research, Nynäshamn, Sweden, for analytical help and for supply of the chromium metal used. We also want to thank Mr. O. Grinder for valuable discussions.

REFERENCES

1. Corbett, J. D., Clark, R. J. and Munday, T. F. *J. Inorg. Nucl. Chem. 25* (1963) 1287.
2. Corbett, J. D., Chapter 6 in *Fused Salts*, Sundheim, B. R., Ed., McGraw, New York 1964, p. 341.
3. Shiloff, J. C. *J. Phys. Chem. 64* (1960) 1566.
4. Seifert, H. J. and Klatyk, K. *Z. Anorg. Allg. Chem. 334* (1964) 113.
5. Kühnl, H. and Ernst, W. *Z. Anorg. Allg. Chem. 317* (1962) 84.
6. Doerner, H. A. *Chemistry of the Anhydrous Chlorides of Chromium*, U.S. Dep. of Interior, Bur. Mines, Tech. Paper 577 (1937).
7. Shkolnikov, S. N. *Trans. Leningrad Polytech. Inst. 272* (1967) 30.
8. Fischer, W. and Gewehr, R. *Z. Anorg. Allg. Chem. 222* (1935) 303.
9. Kubaschewski, O., Evans, E. Ll. and Alcock, C. B. *Metallurgical Thermochemistry*, 4th Ed., Pergamon Press, London 1967.

Received November 28, 1975.

Acta Chemica Scandinavica A 30 (1976) 306—312

Short Communications

Correction to "Ionic Concentrations in Calcium Phosphate Solutions. II. The Solubility of Hydroxylapatite in Water or Salt Solutions at 37 °C"

H. E. LUNDAGER MADSEN

Chemistry Department, Royal Veterinary and Agricultural University, Thorvaldsensvej 40, DK-1871 Copenhagen V, Denmark

We have found an error in the program for solubility calculations which means that the values in Table 2 (*Acta Chem. Scand. A 29* (1975) 745, 747) are wrong. The corrected table is given below.

Table 2. Calcium and total phosphate concentration in mmol/l.

I_0 =	0				0.15			
pK_{sp}' =	6.5		7.5		6.5		7.5	
pH	$[Ca^{2+}]$	[P]	$[Ca^{2+}]$	[P]	$[Ca^{2+}]$	[P]	$[Ca^{2+}]$	[P]
5.0	3.426	6.791	2.455	4.868	6.910	13.568	5.122	10.058
5.1	2.717	5.375	1.956	3.871	5.622	10.990	4.175	8.164
5.2	2.163	4.268	1.563	3.086	4.585	8.914	3.411	6.633
5.3	1.727	3.399	1.253	2.467	3.747	7.236	2.791	5.392
5.4	1.384	2.714	1.007	1.976	3.070	5.879	2.289	4.385
5.5	1.113	2.171	.812	1.586	2.520	4.778	1.881	3.568
5.6	.897	1.741	.656	1.275	2.075	3.885	1.550	2.903
5.7	.725	1.398	.532	1.026	1.712	3.160	1.280	2.362
5.8	.588	1.124	.432	.827	1.418	2.570	1.060	1.922
5.9	.478	.905	.352	.667	1.178	2.091	.881	1.565
6.0	.390	.730	.288	.539	.982	1.702	.735	1.274
6.1	.319	.589	.236	.435	.822	1.386	.615	1.038
6.2	.262	.476	.194	.352	.691	1.130	.518	.846
6.3	.216	.385	.160	.285	.584	.923	.437	.691
6.4	.179	.311	.133	.231	.496	.756	.372	.566
6.5	.149	.252	.111	.187	.423	.621	.317	.465
6.6	.125	.205	.092	.152	.363	.512	.272	.384
6.7	.105	.166	.078	.124	.313	.424	.235	.318
6.8	.088	.136	.066	.101	.271	.354	.203	.265
6.9	.075	.111	.056	.082	.236	.297	.177	.222
7.0	.064	.091	.048	.068	.206	.250	.154	.188
7.1	.055	.075	.041	.056	.180	.213	.135	.159
7.2	.047	.062	.035	.046	.158	.182	.119	.136
7.3	.041	.052	.031	.039	.139	.156	.105	.117
7.4	.036	.044	.027	.033	.123	.135	.092	.102
7.5	.031	.037	.023	.028	.109	.118	.082	.088
7.6	.027	.032	.020	.024	.096	.103	.072	.077
7.7	.024	.027	.018	.020	.085	.090	.064	.068
7.8	.021	.023	.016	.017	.076	.079	.057	.059
7.9	.019	.020	.014	.015	.067	.070	.051	.052
8.0	.016	.018	.012	.013	.060	.062	.045	.046

Received March 10, 1976.

The Molecular Structure of *C,C'*-Diiodine-*p*-carborane, 1,12-$C_2I_2B_{10}H_{10}$, Determined by Gas Phase Electron Diffraction

A. ALMENNINGEN,[a] O. V. DOROFEEVA,[b] V. S. MASTRYUKOV[b,*] and L. V. VILKOV[b]

[a] Department of Chemistry, University of Oslo, Blindern, Oslo 3, Norway, and [b] Laboratory of Electron Diffraction, Department of Chemistry, Moscow State University, Moscow 117234, USSR

The present work is a part of our systematic study of polyhedral carboranes and their derivatives. In the course of previous work we became interested in the stereochemistry of six-coordinate carbon and especially in its exopolyhedral distances. In order to measure them with sufficient accuracy it is expedient to avoid overlap with the many B – C and B – B distances in the icosahedral skeleton C_2B_{10}. Perhaps the most suitable bond distance for such a study is the C – I distance. In this connection *C,C'*-diiodine-*p*-carborane (DIPC), 1,12-$C_2I_2B_{10}H_{10}$, seems to be the simplest representative of the series of isomeric carboranes $C_2H_2B_{10}H_{10}$ with carbon atoms labelled by heavy substituents. The experimental part of this study has been carried out with the same sample in Oslo and in Moscow in order to achieve a reliable value of the C – I distance and to check experimental and computational procedures used in different laboratories, as advised by the Commission on Gas Electron Diffraction formed at the Ninth IUCr Congress.

Experimental and calculation procedure. DIPC was kindly supplied by A. F. Zhigach and V. N. Syryatskaya who prepared it in analogy to the synthesis of $C_2IHB_{10}H_{10}$;[1] its purity was checked by mass-spectrometry. The electron scattering patterns were recorded on the Oslo electron diffraction unit [2] and in Moscow on EG-100A, at nozzle-tip temperatures of approximately 230°. The data obtained cover the s-ranges from 1.5 to 30.25 Å^{-1} (Oslo) and from 3.0 to 29.0 Å^{-1} (Moscow). The different sets of experimental data were then analysed in Moscow according to the procedures normally used in our laboratories. The main difference between them lies in the type of modification of observed intensities. The Oslo-data were modified by the function $s/|f_I'|^2$, whereas s/BT was used for the Moscow data. The scattering factor, $f'(s)$, and the theoretical background, $BT(s)$, are defined in Ref. 3, which also contains other details of the structure analysis. Asymmetry constants,[3] $\varkappa_{ij} = au_{ij}^2/b$, were introduced for the bond distances using $a = 3$ Å^{-1} for r(B – H) and $a = 2$ Å^{-1} for the other bonded interactions. The structure refinements were carried out by the method of least squares based upon intensity data on the modified forms using a program written by H. M. Seip.[3]

Structure refinement. Molecular model of DIPC is shown in Fig. 1. It was assumed that the molecule has D_{5d} symmetry. Then its structure is determined by six parameters:

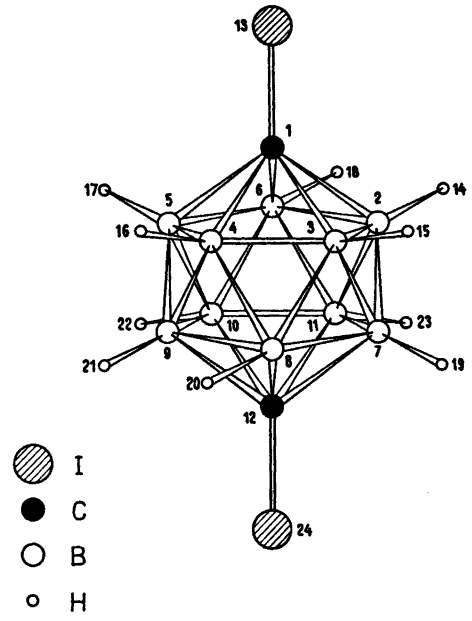

Fig. 1. Molecular model for 1,12-$C_2I_2B_{10}H_{10}$ molecule (DIPC).

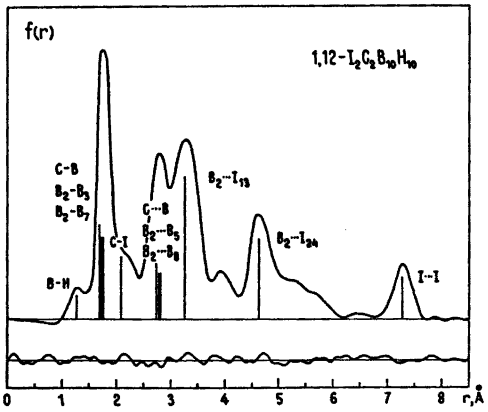

Fig. 2. Experimental radial distribution curve for DIPC molecule. The lower curve represents residual $\Delta f(r) = f(r)_{expl} - f(r)_{calc}$. Vertical bars correspond to principal internuclear distances. A damping factor, exp ($-0.002\ s^2$), was used.

* Address correspondence to this author.

Table 1. Molecular parameters of 1,12-$C_2I_2B_{10}H_{10}$ obtained on the basis of experiments carried out in Moscow (A) and in Oslo (B) and their comparison with values (C) reported for 1,12-$C_2H_2B_{10}H_{10}$ (Ref. 4). Internuclear distances (r_a) and vibrational amplitudes (u) in Å and angles in degrees with estimated standard deviations (3σ) in parenthesis.

Distance type	A r_a	u	B [a] r_a	u	C [a] r_a	u
C1 – B2	1.708(8)		1.703(10)		1.710(11)	
B2 – B3	1.777(8)	0.057(6)	1.780(8)	0.058(8)	1.792(7)	0.063(5)
B2 – B7	1.775(11)		1.780(13)		1.772(13)	
C1 – I13	2.082(14)	0.044(29)	2.107(18)	0.071(39)	–	–
B2 – H14	1.205(21)	0.091(41)	1.215(23)	0.071(40)	1.216(21)	0.093(17)
C1· ·B7	2.757(9)					
B2· ·B5	2.875(8)	0.080(9)		0.070(11)		0.075(5)
B2· ·B8	2.874(6)					
C1· ·C12	3.101(25)	0.060(28)		0.072(33)		0.071(14)
B2· ·B9	3.379(7)					
C1· ·H14	2.557(15)					
B2· ·H15	2.603(14)	0.121(16)		0.124(18)		0.127(33)
B2· ·H19	2.654(18)					
C1· ·H19	3.873(21)					
B2· ·H16	3.924(18)	0.105(20)		0.106(23)		0.129(24)
B2· ·H20	3.957(12)					
B2· ·H21	4.581(14)	0.075(53)		0.078(58)		0.098(61)
B2· ·I13	3.251(7)	0.108(10)		0.088(8)		–
B2· ·I24	4.640(6)	0.087(9)		0.085(10)		–
I13· ·I24	7.266(8)	0.115(9)		0.098(9)		–
I13· ·H14	3.412(28)	0.138(25)		0.086(22)		–
C1· ·I24	5.184(13)	0.118		0.065		–
I24· ·H14	5.611(20)	0.148		0.096		–
∠B7B2H14	124.8(3.6)	–	125.3(2.4)	–	130.0(1.8)	–
R-factor	0.087		0.101		0.077	

[a] Dependent internuclear distances in A and B are practically the same; they are not reported for C (Ref. 4).

Table 2. The C – I distances (Å) in different molecules.

Type of distance	Coordination number of carbon	Molecule	C – I	Ref.
Exopolyhedral	6	DIPC	2.09	This work
Aliphatic	4	CH_3I	2.139	7
Ethylenic	3	$I_2C=CI_2$	2.106	8
Acetylenic	2	I – C≡N	1.995	9
		I – C≡C – Br	1.985	10

bond distances C – I, C – B, B – B(basal), B – B(belt), B – H and bond angle C – B – H. These were refined with the most important vibrational amplitudes shown in Table 1. The observed radial distribution curve is shown in Fig. 2. One notes, in particular, a pronounced peak at ≃7.3 Å, which is due to the longest distance I···I in this molecule.

Discussion. 1. *C_2B_{10} cage.* There is satisfactory agreement between different sets of data concerning dimensions of C_2B_{10} cage as can be seen from Table 1. These geometrical parameters are also close to the values reported for 1,12-$C_2H_2B_{10}H_{10}$,[4] indicating that the substitution has negligible effect, if any.

2. *The C–I bond.* The parameter of greatest interest is obviously the C–I distance. Unfortunately, different values were obtained in two sets, although statistically the difference cannot be regarded significant. One of the possible reasons is the different atomic scattering factors used which may be important especially for heavy atoms. The Norwegian school computes atomic factors by the partial wave method (details see in Ref. 3), while in Moscow they are taken from the tables of Cox and Bonham.[5] Indeed, when the "hybrid" attempt was made to refine the Norwegian intensity data according to the procedure adopted in Moscow, the result was $C-I=2.09\pm0.01$ Å. Because this corresponds to the arithmetic mean of values cited in Table 1, we regard it as our final result. An associated amplitude of vibration measured in Moscow is lower than might be expected. A similar phenomenon has been observed by Beagley and McAloon [6] in studies of a number of tin compounds. The authors attributed it to overdamping of calculated intensities by the Cox and Bonham scattering factors.

The C–I distance obtained for DIPC is compared to C–I distances measured in different molecules in Table 2. One might anticipate the C–I distance in DIPC to be *larger* than aliphatic types due to a higher coordination number for the exopolyhedral carbon. This is, however, not the case and in fact, the C–I bond distance in question is practically equal to the ethylenic type. The chemical behaviour of carboranes as strong electron acceptors toward substituents on carbon atoms [11] provides a reasonable explanation of this remarkable feature, as pointed out earlier.[12] There is also additional evidence for "short" exopolyhedral bonds formed by six-coordinate carbon:

(1) The C–H stretch frequency in carboranes $C_2H_2B_{10}H_{10}$ falls into the region which is characteristic for the ethylenic bond.[13]

(2) The frequency of Cl in nuclear quadrupole resonance spectra for Cl-substituted carboranes is quite similar to those compounds where chlorine is bonded to the group with strong acceptor properties as in $ClCH(NO_2)_2$.[14]

It should be noted that in contrast exopolyhedral distances in carboranes formed by boron are *longer* than in corresponding reference compounds.[15]

Acknowledgements. We are indebted to Dr. A. Haaland for participating in the experimental part of this study and for his critical reading of the manuscript. We thank Dr. T. G. Strand for communication of his electron diffraction data prior to publication.

1. Grafstein, D., Bobinski, J., Dvorak, J., Smith, H., Schwartz, N., Cohen, M. S. and Fein, M. M. *Inorg. Chem. 2* (1963) 1120.
2. Bastiansen, O., Hassel, O. and Risberg, E. *Acta Chem. Scand. 9* (1955) 232.
3. Andersen, B., Seip, H. M., Strand, T. G. and Stølevik, R. *Acta Chem. Scand. 23* (1969) 3224.
4. Bohn, R. K. and Bohn, M. D. *Inorg. Chem. 10* (1971) 350.
5. Cox, H. L. and Bonham, R. A. *J. Chem. Phys. 47* (1967) 2599.
6. Beagley, B. and McAloon, K. T. *Chem. Phys. Lett. 10* (1971) 78.
7. Costain, C. C. *J. Chem. Phys. 29* (1958) 864.
8. Strand, T. G. *Acta Chem. Scand. 21* (1967) 2111.
9. Smith, A. G., Ring, H., Smith, W. V. and Gordy, W. *Phys. Rev. 74* (1948) 370.
10. Strand, T. G. *Acta Chem. Scand. In press.*
11. Grimes, R. N. *Carboranes*, Academic, New York and London 1970.
12. Mastryukov, V. S., Vilkov, L. V. and Dorofeeva, O. V. *J. Mol. Struct. 24* (1975) 217.
13. Leites, L. A., Vinogradova, L. E., Kalinin, V. N. and Zakharkin, L. I. *Izv. Akad. Nauk SSSR Ser. Khim.* (1968) 1016.
14. Bryukhova, E. V., Stanko, V. I., Klimova, A. I., Titova, N. S. and Semin, G. K. *Zh. Strukt. Khim. 9* (1968) 39.
15. Mastryukov, V. S., Vilkov, L. V., Osina, E. L., Golubinsky, A. V., Zhigach, A. F. and Siryatskaya, V. N. *J. Struct. Chem. USSR. Submitted.*

Received March 10, 1976.

The Crystal Structure of Ethylenediammonium Bromide

INGER SØTOFTE

Chemistry Department B, The Technical University of Denmark, DTH 301, DK-2800 Lyngby, Denmark

Infrared and far infrared spectra of normal and *C*-deuterated 1,2-ethylenediammonium difluorides, dichlorides, and dibromides have been measured.[1] A number of bands found for the fluorides and the chlorides have no analogues in the spectra of the bromides. Some of these bands may be due to the hydrogen-bonding in the crystals. However, only the crystal structure of the chloride has been reported.[2,3] The present X-ray investigation was carried out in order to find the hydrogen-bonding system of the bromide.

2. *The C–I bond.* The parameter of greatest interest is obviously the C–I distance. Unfortunately, different values were obtained in two sets, although statistically the difference cannot be regarded significant. One of the possible reasons is the different atomic scattering factors used which may be important especially for heavy atoms. The Norwegian school computes atomic factors by the partial wave method (details see in Ref. 3), while in Moscow they are taken from the tables of Cox and Bonham.[5] Indeed, when the "hybrid" attempt was made to refine the Norwegian intensity data according to the procedure adopted in Moscow, the result was $C-I=2.09\pm0.01$ Å. Because this corresponds to the arithmetic mean of values cited in Table 1, we regard it as our final result. An associated amplitude of vibration measured in Moscow is lower than might be expected. A similar phenomenon has been observed by Beagley and McAloon [6] in studies of a number of tin compounds. The authors attributed it to overdamping of calculated intensities by the Cox and Bonham scattering factors.

The C–I distance obtained for DIPC is compared to C–I distances measured in different molecules in Table 2. One might anticipate the C–I distance in DIPC to be *larger* than aliphatic types due to a higher coordination number for the exopolyhedral carbon. This is, however, not the case and in fact, the C–I bond distance in question is practically equal to the ethylenic type. The chemical behaviour of carboranes as strong electron acceptors toward substituents on carbon atoms [11] provides a reasonable explanation of this remarkable feature, as pointed out earlier.[12] There is also additional evidence for "short" exopolyhedral bonds formed by six-coordinate carbon:

(1) The C–H stretch frequency in carboranes $C_2H_2B_{10}H_{10}$ falls into the region which is characteristic for the ethylenic bond.[13]

(2) The frequency of Cl in nuclear quadrupole resonance spectra for Cl-substituted carboranes is quite similar to those compounds where chlorine is bonded to the group with strong acceptor properties as in $ClCH(NO_2)_2$.[14]

It should be noted that in contrast exopolyhedral distances in carboranes formed by boron are *longer* than in corresponding reference compounds.[15]

Acknowledgements. We are indebted to Dr. A. Haaland for participating in the experimental part of this study and for his critical reading of the manuscript. We thank Dr. T. G. Strand for communication of his electron diffraction data prior to publication.

1. Grafstein, D., Bobinski, J., Dvorak, J., Smith, H., Schwartz, N., Cohen, M. S. and Fein, M. M. *Inorg. Chem. 2* (1963) 1120.
2. Bastiansen, O., Hassel, O. and Risberg, E. *Acta Chem. Scand. 9* (1955) 232.
3. Andersen, B., Seip, H. M., Strand, T. G. and Stølevik, R. *Acta Chem. Scand. 23* (1969) 3224.
4. Bohn, R. K. and Bohn, M. D. *Inorg. Chem. 10* (1971) 350.
5. Cox, H. L. and Bonham, R. A. *J. Chem. Phys. 47* (1967) 2599.
6. Beagley, B. and McAloon, K. T. *Chem. Phys. Lett. 10* (1971) 78.
7. Costain, C. C. *J. Chem. Phys. 29* (1958) 864.
8. Strand, T. G. *Acta Chem. Scand. 21* (1967) 2111.
9. Smith, A. G., Ring, H., Smith, W. V. and Gordy, W. *Phys. Rev. 74* (1948) 370.
10. Strand, T. G. *Acta Chem. Scand. In press.*
11. Grimes, R. N. *Carboranes*, Academic, New York and London 1970.
12. Mastryukov, V. S., Vilkov, L. V. and Dorofeeva, O. V. *J. Mol. Struct. 24* (1975) 217.
13. Leites, L. A., Vinogradova, L. E., Kalinin, V. N. and Zakharkin, L. I. *Izv. Akad. Nauk SSSR Ser. Khim.* (1968) 1016.
14. Bryukhova, E. V., Stanko, V. I., Klimova, A. I., Titova, N. S. and Semin, G. K. *Zh. Strukt. Khim. 9* (1968) 39.
15. Mastryukov, V. S., Vilkov, L. V., Osina, E. L., Golubinsky, A. V., Zhigach, A. F. and Siryatskaya, V. N. *J. Struct. Chem. USSR. Submitted.*

Received March 10, 1976.

The Crystal Structure of Ethylenediammonium Bromide

INGER SØTOFTE

Chemistry Department B, The Technical University of Denmark, DTH 301, DK-2800 Lyngby, Denmark

Infrared and far infrared spectra of normal and *C*-deuterated 1,2-ethylenediammonium difluorides, dichlorides, and dibromides have been measured.[1] A number of bands found for the fluorides and the chlorides have no analogues in the spectra of the bromides. Some of these bands may be due to the hydrogen-bonding in the crystals. However, only the crystal structure of the chloride has been reported.[2,3] The present X-ray investigation was carried out in order to find the hydrogen-bonding system of the bromide.

Table 1. Positional and thermal parameters ($U_{ij} \times 10^4$ Å^2) with their estimated standard deviations. The form of the temperature factor expression is $\exp[-2\pi^2 \sum_{ij} h_i h_j a_i^* a_j^* U_{ij}]$.

Atom	x	y	z	U_{11}	U_{22}	U_{33}	U_{12}	U_{13}	U_{23}
Br	0.1510(1)	0	0.1722(2)	313(6)	306(6)	269(6)	0	60(4)	0
N	0.3746(7)	0	0.3618(23)	235(35)	362(49)	321(43)	0	41(31)	0
C	0.4698(7)	0	0.3537(21)	229(38)	379(52)	202(36)	0	44(29)	0

Experimental. Lattice type and space group were established from Weissenberg and precession photographs using Cu$K\alpha$- and Mo$K\alpha$-radiation. Three-dimensional data were measured on a semi-automatic equi-inclination diffractometer (Stoe & Cie, Darmstadt, DBR) using graphite monochromated Mo$K\alpha$-radiation and ω-scan technique. Harmonics were excluded by means of a pulse height discriminator. The crystal was mounted with its [010] axis as rotation axis. Reflections between a cylinder of radius $Y = 5.4°$ and a hemisphere with sin θ/λ < 0.7 Å were measured ($0 \leq k \leq 6$) giving 561 independent reflections of which 469 had $I > 2\sigma(I)$, where $\sigma(I) = [(1+k^2)PC + BC]$. The constant k was 0.04. The diffractometer output was processed by means of a programme which takes into account the polarization of the incident beam.

The dimensions of the crystal used were $0.32 \times 0.16 \times 0.01$ mm. No correction was made for absorption since the crystal was small. All symmetry related reflections were averaged.

The computations described below were performed on an IBM 370/165 computer using the X-RAY system [4] and the drawing programme ORTEP.[5] The atomic scattering factors used were those given by Cromer and Mann.[6]

Crystal data. $(CH_2NH_3)_2Br_2$, M = 221.9 Monoclinic, $a = 15.24(2)$ Å, $b = 4.79(3)$ Å, $c = 4.86(3)$ Å, $\beta = 101.9(5)°$, $V = 347.2$ Å^3, $Z = 2$, $D_c = 2.12$, $D_o = 2.12$, $F(000) = 212$, μ(Mo$K\alpha$) = 122.3 cm^{-1}. Systematic absences: hkl when $h+k$ odd. The possible space groups are $C2/m$, Cm and $C2$.

Structure determination. The coordinates of the bromide ion were found from a 3-dimensional Patterson map, and the positions of the carbon and nitrogen atoms revealed themselves in a subsequent fourier map. The structure was refined by full matrix least squares minimizing the function $\sum w(|F_o| - |F_c|)^2$. With anisotropic temperature factors and $w = 5.934 - 0.094|F| + 0.006|F|^2 - 7.309 \sin\theta/\lambda$ the refinement resulted in $R = 0.078$ ($R_w = 0.096$). The contributions of the hydrogen atoms were neglected in all calculations. The initial assumption that the structure has the space group $C2/m$ was confirmed by the convergence of the refinement.

Description and discussion of the structure. The final positional and thermal parameters are given in Table 1. The donor–acceptor distances and relevant angles where hydrogen bonding is assumed to take place are given in Table 2. A list of the observed and calculated structure factors may be obtained from the author or the department upon request.

Table 2. Distances and angles for possible N···Br hydrogen-bonded contacts. Br1 is at $(\frac{1}{2}-x, \frac{1}{2}, 1-z)$, Br2 at $(\frac{1}{2}-x, -\frac{1}{2}, 1-z)$.

N–Br	3.34(1)
N–Br1	3.37(2)
C–N–Br	162.8(8)
C–N–Br1	105.7(4)
Br–N–Br1	86.1(3)
Br1–N–Br2	90.4(6)
N–Br–N1	93.8(3)
N1–Br–N2	90.4(5)

The structure is shown in Fig. 1. All the atoms, Br^-, N and C, lie in the special position $x,0,z$ with the centre of the C–C bond at the centre of symmetry. Thus the ethylenediammonium ion has *trans* configuration with planar N–C–C–N chain, and in this respect the structure is similar to that of the chloride analogue.[2,3]

The C–C and C–N bond lengths of the present structure, 1.53(2) and 1.46(1) Å, respectively, agree with those found for ethylenediamine at −60 °C [1.51(2) and 1.47(1) Å, respectively].[7] The latter molecule too has the *trans* configuration. The C–N bond length is somewhat shorter than those found in the *gauche* isomers [1.49(1) Å] [8,9] but agree with those found in other *trans* isomers [1.47(1) Å] [7,8,10] and with the mean value of 1.472(5) Å found in other structures.[11] The C–C–N angle of 112.7(9)° is slightly larger than the tetrahedral angle, a feature which the present structure has in common with ethylenediamine. In the chloride analogue the angle between these atoms is equal to the tetrahedral angle.[2,3]

The N-Br donor–acceptor distances where hydrogen bonding is assumed to take place, are 3.34, 3.37 and 3.37 Å, respectively. They are shown as broken lines in Fig. 1. In addition

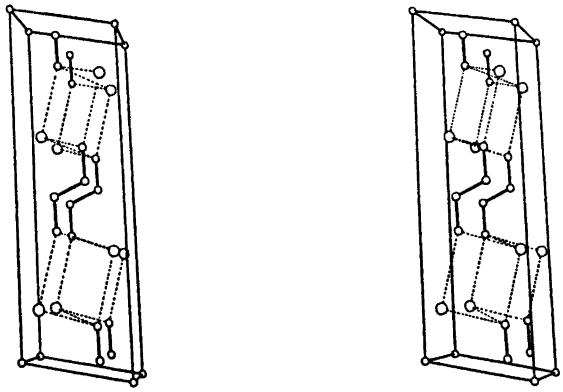

Fig. 1. Stereoscopic view of the structure of ethylenediammonium bromide along the *b* axis. The longest axis is the *a* axis. The hydrogen bonds are shown as broken lines.

there are two longer N-Br distances of 3.49(2) Å to Br^-3 and Br^-4, and the Br^- ions 1, 2, 3, and 4 form a planar rectangular arrangement with the N atom 0.38 Å from this plane.

The ethylenediammonium ions are stacked above each other in the *y* direction, and two of the hydrogen bonds link the ions in this direction. The third hydrogen bond links the ions in the *x* direction. This hydrogen bonding system between two ethylenediammonium ions along the *b* axis occurs twice in the unit cell (Fig. 1). There is no bonding along the *a* axis between these two hydrogen bonding systems. However, along the *c* axis the N – Br distances of 3.49 Å make contacts between the hydrogen bonding systems of two neighbouring unit cells.

The hydrogen bonds (3.12, 3.20, and 3.22 Å) in the chloride $(P2_1/a)$[2,3] form helices along the *b* axis between the ethylenediammonium ions. In the unit cell there are two such helices linked together by hydrogen bonds in the *c* direction. In the *a* direction there are N – Cl distances of 3.48 Å. In the bromide the N – Br distance of 3.49 Å is slightly longer than the sum of the van der Waals radii,[12] 3.45 Å, whereas in the chloride the difference between the observed value of 3.48 Å and the calculated of 3.30 Å is larger. The main difference between the hydrogen bonding systems in the two structures is the lack of hydrogen bonding coupling between the two hydrogen bonding systems along the *a* axis in the bromide. This may be the reason why the infrared spectra of the chloride show a number of strong and medium bands in addition to those found in the bromide.

Acknowledgement. The author wishes to thank Rolf W. Berg, who provided the single crystal, and Kjeld Rasmussen, both of Chemistry Department A, for discussions.

1. Christensen, L. C. and Rasmussen, K. *Spectrochim. Acta Part A 31* (1975) 895.
2. Ashida, T. and Hirokawa, S. *Bull. Chem. Soc. Jpn. 36* (1963) 704.
3. Koo, C. H., Kim, M. I. and Yoo, C. S. *J. Korean Chem. Soc. 7* (1963) 293.
4. Stewart, J. M., Kundell, F. A. and Baldwin, J. C. *The X-Ray System, Version 1972*, Chemistry Department, University of Maryland, U.S.A.
5. Johnson, C. K. *ORTEP*, Report ORNL-3794, Oak Ridge National Laboratory, Oak Ridge 1965.
6. Cromer, D. T. and Mann, J. B. *Acta Crystallogr. A 24* (1968) 321.
7. Jamet-Delcroix, S. *Acta Crystallogr. B 29* (1973) 977.
8. Dunand, A. and Gerdil, R. *Acta Crystallogr. B 31* (1975) 370.
9. Sakurai, K. *J. Phys. Soc. Jpn. 16* (1961) 1205.
10. Perez, S., Leger, J. M. and Housty, J. *Cryst. Struct. Commun. 2* (1973) 303.
11. Kennard, O., Watson, D. G., Allen, F. H., Isaacs, N. W., Motherwell, W. D. S., Petterson, R. C. and Town, W. G. *Molecular Structures and Dimensions, Vol A1* Utrecht, Oosthoek 1972.
12. Pauling, L. *Nature of the Chemical Bond*, Cornell University Press, Ithaca 1960, p. 260.

Received December 16, 1975.

A Ternary Germanium Tungsten Oxide of the Mo_5O_{14} Type

THOMMY EKSTRÖM,[a] E. IGUCHI [b,*] and R. J. D. TILLEY[b]

[a] Department of Inorganic Chemistry, Arrhenius Laboratory, University of Stockholm, S-104 05 Stockholm, Sweden and [b] School of Materials Science, University of Bradford, Bradford BD7 1DP, Yorkshire, England

During recent years attempts have been made to understand the factors which govern the formation of oxides with crystallographic shear (CS), bronze or pentagonal column (PC) structure types, particularly in oxide systems having tungsten or molybdenum as a major component.[1] The present authors have been systematically mapping a series of ternary M – W – O systems in the phase region close to WO_3. Some results for the Ti,[2] Zr,[3] V,[4] Cr,[5] Nb and Ta [6] systems have already been presented. In addition it is known that non-transition elements can also induce the formation of some of the structure types listed above.[7–9] With this background we thought it of interest to study the Ge – W – O system.

Samples were heated for up to five weeks in sealed, evacuated silica tubes at 1400 K. It was found by electron microscopy and X-ray diffraction analysis that samples of gross composition between WO_3 and $(Ge,W)O_{2.9}$ were essentially made up of CS phases, regardless of heating time. For compositions in the range $(Ge,W)O_{2.9}$ to $(Ge,W)O_{2.7}$ several compounds containing PC's as well as CS phases were found. The proportion of PC structures formed depended upon heating times and it appears that at least some of these phases form very slowly at this temperature.

One of the PC phases observed in these preparations is a ternary phase possessing the Mo_5O_{14} structure.[10] Monophasic samples of an oxide $(Ge,W)_5O_{14}$ were obtained in samples of gross compositions where about 5 atomic % of the metal content was Ge, heated for 5 weeks at 1400 K. The new $(Ge,W)_5O_{14}$ phase has been characterized using Guinier-Hägg X-ray powder photographs. A visual comparison of the X-ray pattern of this new oxide and that of the binary Mo_5O_{14} oxide clearly shows that the two phases are isostructural. The two patterns have the same indexed diffraction lines and the same intensity distribution. A powder pattern of the observed $(Ge,W)_5O_{14}$ oxide extracted from a sample of overall composition $Ge_2W_{16}O_{49}$, which only contained minor amounts of other oxides, gave the unit cell dimensions $a = 23.27(1)$ Å and $c = 3.791(1)$ Å.

This is the first time this structure type has been observed to be formed in any system other than a binary or ternary molybdenum oxide.[1] In addition, it appears to be quite stable at 1400 K once having formed. All the molybdenum oxides form very quickly, but prove to be of rather low stability and decompose at temperatures of the order of 900 – 1200 K. The stability of the $(Ge,W)_5O_{14}$ oxide is therefore somewhat surprising, and it is possible that the germanium has a particular role to play in this context.

The existence of this phase suggests that PC or tunnel compounds may be more prevalent in the binary and ternary tungsten oxides than previously thought. Already one new oxide of this type has been found in the binary W – O system [11] in samples heated for several weeks. The present result suggests that others may be found in binary and ternary systems if long heating times are employed. This is an interesting difference with the closely related molybdenum oxides where the PC structures tend to form at low temperatures and to decompose rather easily at moderate temperatures.[1]

Further experiments need to be carried out in ternary systems involving non-transition metals from groups 3B, 4B and 5B of the periodic table and such studies are planned. In addition the role that Ge plays in substituting for W and thus stabilizing the Mo_5O_{14} structure of $(Ge,W)_5O_{14}$ is not yet clear. To this end, a careful study of the homogeneity range of the $(Ge,W)_5O_{14}$ phase is at present being completed. These and other relevant results from the Ge – W – O system will be the subject of a further communication.

Acknowledgements. Part of this investigation has been conducted within a research program sponsored by the Swedish Natural Science Research Council. R.J.D.T. and E.I. would also like to thank the Science Research Council (London) for financial support.

1. Ekström, T. *Chem. Commun. Univ. Stockholm* No. 7 (1975).
2. Ekström, T. and Tilley, R. J. D. *Mater. Res. Bull. 9* (1974) 705.
3. Ekström, T. and Tilley, R. J. D. *Mater. Res. Bull. 9* (1974) 999.
4. Ekström, T. and Tilley, R. J. D. *J. Solid State Chem. 16* (1976) 141.
5. Ekström, T. and Tilley, R. J. D. *Mater. Res. Bull. 10* (1975) 1175.
6. Ekström, T. and Tilley, R. J. D. *J. Solid State Chem. In press.*
7. Pouchard, M., Berdoulay, F. and Vandeven, D. *C. R. Acad. Sci. Ser. C 266* (1968) 1066.
8. Parmentier, M., Gleitzer, C. and Courtois, A. *Mater. Res. Bull. 10* (1975) 341.
9. Steadman, R., Tilley, R. J. D. and McColm, I. J. *J. Solid State Chem. 4* (1972) 199.
10. Kihlborg, L. *Ark. Kemi 21* (1963) 427.
11. Pickering, R. and Tilley, R. J. D. *J. Solid State Chem. 16* (1976) 247.

* On leave from: Department of Metallurgical Engineering, Yokohama National University, Ohka, Minami-ku, Yokohama, 233 Japan.

Received January 16, 1976.

Acta Chemica Scandinavica A 30 (1976) 313—321

Studies on the Solvent Extraction of Europium(III) by Di-(2-ethylhexyl)phosphoric Acid (HDEHP) in Toluene

MANUEL AGUILAR and DJIET HAY LIEM

Department of Inorganic Chemistry, Royal Institute of Technology (KTH), S-100 44 Stockholm 70, Sweden

The extraction of Eu(III) from 0.10 M (Na,H)ClO_4 aqueous solution by di-(2-ethylhexyl)-phosphoric acid, HDEHP (=HA), in toluene has been studied. The distribution of Eu(III) between the two phases was measured by a radiometric method using Eu(III) labelled with the radioactive isotopes Eu-152(154). The distribution data has been analyzed by a graphical method as well as by the computer program LETAGROP-DISTR. The results may be explained by the formation of the following Eu(III)-di-(2-ethylhexyl)phosphoric acid species:

$Eu(III) + 3H_2A_2(org) \rightleftharpoons EuA_3(HA)_3(org) + 3H^+$;

$\log(K \pm 3\sigma) = 0.053 \pm 0.016$.

The possibility of the formation of Eu(III)-HDEHP species in the aqueous phase is indicated. The formation of $EuClO_4^{2+}$ is indicated, tentative values for the equilibrium constants being $\log K_1 = -0.35$ in 1.0 M (Na,H)ClO_4 and $\log K_1 = -0.23$ in 0.1 M (Na,H)ClO_4 solution. A general expression for calculating the equilibrium constant K for the extraction of Eu(III) by HDEHP into toluene from a given aqueous ionic medium is described.

Dialkylphosphoric acids are effective complexing agents for the extraction of lanthanides and actinides.[1–3] One which has been used extensively is di(2-ethylhexyl)phosphoric acid, HDEHP (=HA), primarily due to its excellent complexing properties over a wide pH range, its low solubility in aqueous solution and its commercial availability. HDEHP is used in the Dapex process for the recovery of uranium from leach liquors [4] and is being studied as a potential extractant for the reprocessing of spent nuclear fuel as an alternative to the established Purex process.[5,6] Recently, the potential use of HDEHP for the extraction of metals in non-nuclear industries, *e.g.* Zn,[7] Co, Ni,[16] V,[8,16] Mo [16,34] was also reported. By infrared spectroscopy and molecular weight determinations [9,10] distribution studies [11–13,30] and NMR studies,[14] dialkylphosphoric acids were shown to form strong dimeric species in nonpolar organic solvents. Previous studies [15,16] have shown that the metal extraction equilibria, when a dialkylphosphoric acid is used as extractant, are strongly influenced by the distribution and dimerization equilibria of HA. The use of HDEHP for the extraction of lanthanides and actinides has been previously reported.[17,18] In general there is agreement as to which metal species were formed. However, the reported values of the formation constants of the metal HDEHP species vary [17] (*cf.* Table 4). These deviations may in part be explained, because most authors have based their conclusions on the assumption that HDEHP is completely dimerized in all organic solvents over the whole range of concentration studied. However, these assumptions do not apply strictly for HDEHP and other dialkylphosphoric acids.[18] In this work we report the extraction of Eu(III) by HDEHP from 0.10 M (Na,H)ClO_4 in toluene. In the analysis of the data we used the equilibrium constants for the distribution, dimerization and dissociation of HDEHP in the two-phases system.[18]

Symbols and equilibrium constants

[ ] = equilibrium concentration in the aqueous phase

$[\ ]_{org}$ = equilibrium concentration in the organic phase

C_A = initial total concentration of di-(2-ethylhexyl)-phosphoric acid

HDEHP = di-(2-ethylhexyl)phosphoric acid

K_{pqr}^{org} = formation constant of the complex $(H^+)_p(Eu^{3+})_q(HA)_r$ in the organic phase, *cf.* eqn. (1)

K_{lmn}^{aq} = formation constant of the complex $(H^+)_l(Eu^{3+})_m(HA)_n$ in the aqueous phase, *cf.* eqn. (2)

I_{aq}, I_{org} = γ-activity of ^{152,154}Eu(III) in the aqueous and organic phases, given in cpm for equal volumes of samples.

D = $\sum[Eu]_{org}/\sum[Eu]_{aq} = I_{org}/I_{aq}$, net distribution of Eu(III)

$\sigma(y)$ = standard deviation in y (*cf.* Ref. 27, eqn. 17)

$K(X,I)$ = equilibrium constant for the extraction of Eu(III) by HDEHP from the ionic medium (Na,H)X with the ionic strength I into the organic phase, *cf.* eqn. (8)

$K(corr,0)$ = equilibrium constant for the extraction of Eu(III) by HDEHP into toluene from infinite diluted aqueous solution.

EXPERIMENTAL

HDEHP, di(2-ethylhexyl)phosphoric acid, $(C_8H_{17}O)_2P(OH)O$, was purified as described previously.[12,13] *$NaClO_4$* stock solution was prepared from Na_2CO_3 and $HClO_4$ as in Ref. 19. *$HClO_4$*, Merck, *p.a.*, free of Fe(III) was used without further purification. The stock solution was standardized against NaOH solution. Four 0.1 M (Na,H)ClO_4 solutions, where $2.5 > -\log[H^+] > 1.0$, were prepared. *Toluene*, Merck *p.a.*, was purified by washing with dilute solutions of NaOH and HCl and finally with distilled water.

Distribution experiments. The distribution of Eu(III) between two solutions S1 = H mM H^+, $(100-H)$ mM Na^+, 100 mM ClO_4^- and S2 = C_A mM HDEHP in toluene was measured as a function of the total concentration of HDEHP in toluene, at different constant H levels. The experiments were performed by equilibrating in a rotating rack equal volumes of solutions S1 and S2 in glass-stoppered centrifuge tubes in a thermostated room at 25 ± 0.5 °C. After equilibrium was attained, the tubes were centrifuged and aliquot samples were drawn from both phases for radiometric analysis of the metal distribution. The activity of the Eu-152(154) isotope was determined in a Tracerlab SC-57 low background Scintillation Counter with a Tl-activitated NaI crystal, connected with a Tracerlab SC-70 COMPU/MATIC V scaler. As a rule a minimum of 10^4 counts of activity was measured giving a statistical error less than 1 %. Toluene was found not to extract Eu(III) under the experimental conditions. In order to estimate the time necessary for attaining equilibrium, D was measured as a function of time for constant values of $C_A = 18.2$ mM and $-\log[H^+] = 2.3$ (*cf.* Fig. 1). No appreciable changes in the value of D can be observed after equilibration over a period of 4 h. In all the experiments the two phases were consequently equilibrated by shaking for at least 4 h. The $[H^+]$ in the aqueous phase was measured potentiometrically as described previously.[13]

Basic assumptions on the chemical model. In the analysis of the distribution data for Eu(III) we assume the formation of the species $(H^+)_p(Eu^{3+})_q(HA)_r$ in the organic phase and $(H^+)_l(Eu^{3+})_m(HA)_n$ in the aqueous phase. We denote these species by (p,q,r)(org) and (l,m,n)(aq); *e.g.* $(-3,1,6)$(org) represents $EuA_3(HA)_3$(org) and $(-1,0,1)(aq) = A^-(aq)$. The formation constant of these species is expressed by:

$$K_{pqr}^{org} = [(H^+)_p(Eu^{3+})_q(HA)_r]_{org}[H^+]^{-p} \times [Eu^{3+}]^{-q}[HA]^{-r} \quad (1)$$

$$K_{lmn}^{aq} = [(H^+)_l(Eu^{3+})_m(HA)_n][H^+]^{-l} \times [Eu^{3+}]^{-m}[HA]^{-n} \quad (2)$$

Using (1) and (2) we derive the expression for the distribution ratio:

$$D = \sum[Eu]_{org}/\sum[Eu] = \frac{\sum qK_{pqr}^{org}[H^+]^p[Eu^{3+}]^q[HA]^r}{\sum mK_{lmn}^{aq}[H^+]^l[Eu^{3+}]^m[HA]^n} \quad (3)$$

We make the assumptions that the extracted species are uncharged and that the activity factors for the different species are kept constant by the constant ionic strength of the aqueous solution. We now describe the two-phase system by a model containing the species denoted by sets of (p,q,r) and (l,m,n).

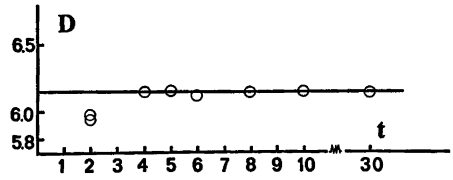

Fig. 1. The distribution of Eu(III) in the two-phase system Eu(III) – 0.1 M (Na,H)ClO_4/HDEHP-toluene as a function of shaking time t (in h). $-\log [H^+] = 2.30$ and $C_A = 18.2$ mM. The speed of the rotating rack is approximately 20 rpm.

DATA ANALYSIS

Graphical analysis. The distribution data for Eu(III) are given in Table 1 and represented in Fig. 2 as log D *versus* $-\log (\frac{1}{2}C_A)$ for different constant values of log $[H^+]$. The experimental points fall practically on straight lines with the slope approximately equal to -3. This indicates the predominant extraction of Eu-HDEHP species with the composition $(H^+)_p(Eu^{3+})_q(H_2A_2)_3$. This conclusion follows from the following relationship and the predominant formation of HDEHP dimers in the organic phase:[13]

$$C_A = 2[H_2A_2]_{org} + [HA]_{org} + 2[H_2A_2] + [HA] + [A^-] \approx 2[H_2A_2]_{org} \quad (4)$$

Assuming that Eu(III) exists as mononuclear species in both phases which is reasonable for the tracer concentration range used ($C_{Eu} < 10^{-6}$ M), we derive the following expression for the distribution ratio D:

$$D = \frac{[(H^+)_p(Eu^{3+})(H_2A_2)_r]_{org}}{[Eu^{3+}]} = K^*_{p1r}[H^+]^p[H_2A_2]_{org}^r \quad (5)$$

where K^*_{p1r} represents the equilibrium constant for the following reaction:

$$pH^+ + Eu^{3+} + rH_2A_2(org) \rightleftharpoons (H^+)_p(Eu^{3+})(H_2A_2)_r(org)$$

Introducing (4) into (5) the following relationship can be written:

$$\log D = \log K^*_{p1r} + p \log [H^+] + r \log [\tfrac{1}{2}C_A] \quad (6)$$

Table 1. The distribution of ^{152,154}Eu(III) between solutions of HDEHP – toluene and 0.10 M (Na,H)ClO_4 at 25 °C. Data given as C_A M and log D_{exp}. The initial concentration of Eu(III) in the aqueous phase $C_{Eu} < 10^{-6}$ M. The volume ratio $V_{org}V_{aq}^{-1} = 1$.

log $[H^+] = -2.417$							
0.0605,	2.6102;	0.0567,	2.5095;	0.0529,	2.4476;	0.0506,	2.4492;
0.0416,	2.1517;	0.0371,	2.0294;	0.0361,	2.0135;	0.0302,	1.7499;
0.0289,	1.6837;	0.0227,	1.3112;	0.0151,	0.7806;	0.0144,	0.7949;
0.0130,	0.6593;	0.0116,	0.4864;	0.0101,	0.2995;	0.0094,	0.2000;
0.0087,	0.1133;	0.0080,	−0.0353;	0.0072,	−0.1077;	0.0058,	−0.3868;
0.0043,	−0.7915;	0.0029,	−1.2711;	0.0015,	−2.1307.		
log $[H^+] = -2.097$							
0.0756,	2.0450;	0.0681,	1.9471;	0.0605,	1.7659;	0.0529,	1.5884;
0.0454,	1.3870;	0.0378,	1.1232;	0.0302,	0.8196;	0.0265,	0.6310;
0.0227,	0.4370;	0.0189,	0.2203;	0.0151,	−0.0613;	0.0144,	−0.1006;
0.0136,	−0.1493;	0.0129,	−0.2184;	0.0121,	−0.3193;	0.0106,	−0.4893;
0.0091,	−0.7032;	0.0076,	−0.9401.				
log $[H^+] = -1.500$							
0.1690,	1.3082;	0.1521,	1.1615;	0.1352,	1.0216;	0.1143,	0.7959;
0.1029,	0.6520;	0.0914,	0.5174;	0.0800,	0.3327;	0.0686,	0.1345;
0.0572,	−0.1001;	0.0457,	−0.3791;	0.0343,	−0.7572;	0.0229,	−1.2528.
log $[H^+] = -1.000$							
0.1690,	−0.2338;	0.1521,	−0.3713;	0.1352,	−0.5183;	0.1183,	−0.6915;
0.1143,	−0.7421;	0.1029,	−0.8693;	0.1014,	−0.9219;	0.0914,	−1.229;
0.0883,	−1.0811;	0.0800,	−1.1801;	0.0756,	−1.2263;	0.0686,	−1.386;
0.0605,	−1.5172;	0.0572,	−1.5976.				

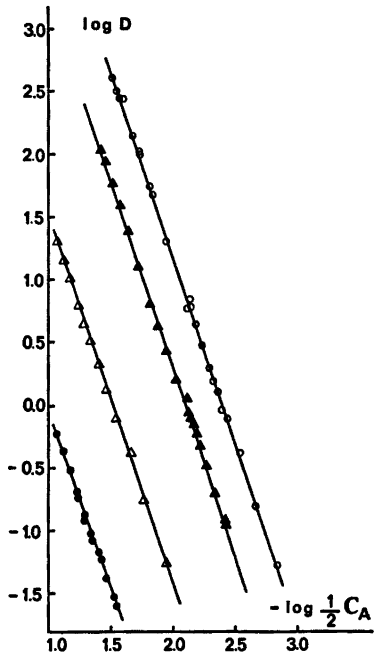

Fig. 2. The distribution of Eu(III) in the two-phase system 0.1 M (Na,H)ClO_4/HDEHP-toluene as a function of the initial total concentration of HDEHP in the organic phase, C_A M, for different constant values of $-\log h =$ 1.000 (●), 1.500 (△), 2.097 (▲), and 2.417 (○). The curves have been calculated (*cf.* Ref. 29), assuming the HDEHP species in Ref. 13 and Eu(III)-HDEHP species with the equilibrium constants given in Table 2, model 1.

A plot of log D *versus* $-\log(\frac{1}{2}C_A)$ will, according to (6) for a given constant $[H^+]$ give a straight line with a slope $-r$, which agrees with $r=3$ found in Fig. 2. In Fig. 3 the plot $\log D = f(-\log [H^+])$ for a set of constant values of C_A give straight lines with a slope of $+3$, which agrees with (6) for $p=-3$. In Fig. 4 we plot $\log D[H^+]^3$ *versus* log [HA], and find that all points practically fall on a straight line with a slope equal to 6, which indicates the predominant extraction of the species $EuA_3(HA)_3$(org). Our results thus agree with those obtained previously for similar systems (*cf.* Table 3).

Computer analysis of the data. The distribution data ($Np=69$ points) has been analyzed with the LETAGROP-DISTR program.[27,28] Using this program the computer calculates the set of constants $K_1, K_2, \ldots . K_n$ for the formation of the $(H^+)_l(Eu^{3+})_m(HA)_n$(aq) and $(H^+)_p(Eu^{3+})_q(HA)_r$(org) species which will minimize the error-square sum $U=\sum_1^{Np}(\log D_{calc}-\log D_{exp})^2$ for the Np experimental points available. The results of the computer analysis is given in Table 2. The assumption of the formation of $EuA_3(HA)_3$(org) (model 1) gives a better description of the data than when $EuA_3(HA)_2$(org) is assumed (model 2). No significant improvement in both U_{min} and $\sigma(\log D)$ is found when the additional formation of $EuA_3(HA)_4$(org) is assumed (model 3). For model 5 we assumed the additional formation of EuA_2^+(aq) and found a significant decrease in U_{min} and $\sigma(\log D)$. A similar effect was found in model 4 in which the additional formation of EuA^{3+}(aq) was assumed. Assuming the additional formation of both EuA^{3+} and EuA_2^+ in the aqueous phase (model 6) the calculations resulted in the rejection of the

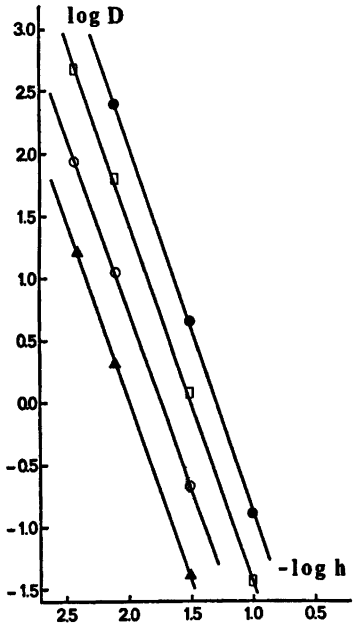

Fig. 3. The distribution of Eu(III) between HDEHP-toluene and 0.1 M (Na,H)ClO_4 as a function of $-\log h$ for various constant values of $C_A=0.020$ M (▲), 3.55×10^{-2} M (○), 6.32×10^{-2} (□) and 0.100 M (●). The points were taken from the curves in Fig. 2 for the given values of C_A. The straight lines in the figure have a slope of -3.

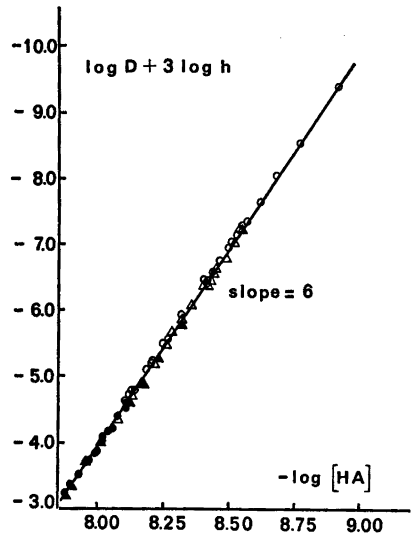

Fig. 4. The distribution of Eu(III) in the two-phase system 0.10 M (Na,H)ClO_4/HDEHP-toluene given as log Dh^{-3} *versus* log [HA] for various constant values of $-\log h = 1.000$ (●), 1.500 (▲), 2.097 (△) and 2.417 (○). The [HA] was calculated assuming the formation of HDEHP species with the equilibrium constants given by Liem.[18] The drawn line has been calculated (*cf.* Ref. 29), by assuming the formation of Eu(III)-HDEHP species and equilibrium constants given in Table 2, model 1.

EuA^{3+}(aq) species as seen from the reduction of its formation constant to zero. No improvement of U_{min} and $\sigma(\log D)$ is found in model 7, in which the formation of the species $(-3,1,5)$(org) and $(-1,1,1)$(aq) are assumed as well as those of model 5. Assuming model 5 and minimizing the following different error-square sums, gives practically the same values for log K_{pqr}

$\sum(\log D_{calc}D_{exp}^{-1})^2$: $(-2,1,2)$(aq)10.78; $(-3,1,6)$-(org)44.10

$\sum(D_{exp}D_{calc}^{-1}-1)^2$: $(-2,1,2)$(aq)10.78; $(-3,1,6)$-(org)44.10

$\sum(D_{calc}D_{exp}^{-1}-1)^2$: $(-2,1,2)$(aq)10.79; $(-3,1,6)$-(org)44.09

This means that the assignment of the same weight factor to the distribution data is reasonable. In the present work the weight factor has been given the value $w=1$. In Fig. 5 the error-function, log $(D_{calc}D_{exp}^{-1})$ is given as a function of C_A for model 5. The data are seen to show no systematic deviations.

Conclusions. The results thus show that Eu(III) is extracted by HDEHP in toluene predominantly as $EuA_3(HA)_3$. They also give indications for the formation of the species EuA_2^+ or EuA^{2+} in the aqueous phase. However, this should be considered as not confirmed, since within the experimental error, the data may satisfactorily be explained by the formation of $EuA_3(HA)_3$(org) alone with the equilibrium constant

Table 2. Equilibrium constants [a] log β_{pqr} for the formation of $(H^+)_p(Eu^{3+})_q(HA)_r$ species in the system Eu(III) – 0.10 M (Na, H)ClO_4/HDEHP-toluene for various assumptions of chemical models which minimize the error-square sum $U=\sum_1^{69}(\log D_{calc}-\log D_{exp})^2$.

Model No.	$(H^+)_p(Eu^{3+})_q(HA)_r$(aq)	$(H^+)_p(Eu^{3+})_q(HA)_r$(org)	U_{min}	$\sigma(\log D)$
1		$(-3,1,6)$ 44.08 ± 0.02	0.125	0.048
2		$(-3,1,5)$ 35.84 ± 0.09	3.883	0.239
3		$(-3,1,5)$ 34.00, max. 34.64 $(-3,1,6)$ 44.07 ± 0.03	0.123	0.043
4	$(-1,1,1)$ 5.04, max. 5.25	$(-3,1,6)$ 44.11 ± 0.02	0.088	0.035
5 [b]	$(-2,1,2)$ 10.78 ± 0.25	$(-3,1,6)$ 44.10 ± 0.02	0.085	0.035
6	$(-1,1,1)$ $\beta=0$; $(-2,1,2)$ 10.71, max. 11.00	$(-3,1,6)$ 44.10 ± 0.02	0.085	0.036
7	$(-1,1,1)$ 4.12, max. 5.43 $(-2,1,2)$ 10.73, max. 11.26	$(-3,1,5)$ 33.81, max. 34.61 $(-3,1,6)$ 44.10 ± 0.04	0.085	0.036

[a] The equilibrium constant $\beta_{pqr}=[(H^+)_p(Eu^{3+})_q(HA)_r]_t\,[H^+]^{-p}[Eu^{3+}]^{-q}[HA]^{-r}$, where the lower index t indicates the phase referred to in the reaction. The limits given correspond to approximately log $[\beta \pm 3\sigma(\beta)]$ and if $\sigma(\beta)>0.2\ \beta$, the maximum value log $[\beta+3\sigma(\beta)]$ is given.
[b] The "best" model assumed.

Table 3. Equilibrium constant log K for the reaction: $Eu(III) + 3H_2A_2(org) \rightleftharpoons EuA_3(HA)_3(org) + 3H^+$, in the two-phase system aqueous solution/dialkylphosphoric acid-toluene. Temperature 25 °C if not otherwise stated:

Two-phase system	log K	Ref.
1.0 M $(H^+,Na^+)ClO_4$/HDBP-toluene	1.73	31
1.0 M $(H^+,Na^+)NO_3$/HDBP-toluene	1.25	31
1.0 M $(H,Na)ClO_4$/HDAP-toluene	1.79	21
1.0 M $(H,Na)NO_3$/HDAP-toluene	1.31	21
1.0 M $(H,Na)ClO_4$/HDIAP-toluene	1.50	21
1.0 M $(H,Na)NO_3$/HDIAP-toluene	1.02	21
1.0 M $(H,Na)ClO_4$/HDOP-toluene	1.68	21
1.0 M $(N,Na)NO_3$/HDOP-toluene	1.20	21
1.0 M $(H,Na)ClO_4$/HDEHP-toluene	−0.35	21
1.0 M $(H,Na)NO_3$/HDEHP-toluene	−0.83	21
0.5 M HCl/HDEHP-toluene [a]	−0.44 [b]	24, 1
0.1 M $(H,Na)ClO_4$/HDEHP-toluene	0.053	This work
0.01 M $HClO_4$/HDEHP-toluene	1.57	33
1.0 M $(Li,H)ClO_4$/HDEHP-toluene	−0.92	35

[a] Temperature 22 °C. [b] Calculated from the single experimental point available.

$$Eu^{3+} + 6HA(aq) \rightleftharpoons EuA_3(HA)_3(org) + 3H^+;$$
$$\log (K \pm 3\sigma) = 44.10 \pm 0.02 \quad (7)$$

$$Eu^{3+} + 3H_2A_2(org) \rightleftharpoons EuA_3(HA)_3(org) + 3H^+;$$
$$\log (K \pm 3\sigma) = 0.053 \pm 0.016 \quad (8)$$

DISCUSSION

The formation of $EuA_3(HA)_3(org)$ found in this work thus agrees with the results found by other authors for comparable extraction systems (*cf.* Table 3). The formation of Eu(III)-HA species in the aqueous phase may be expected to increase with increasing pH and C_A. An indication of the formation of Hf(IV)-HDBP aqueous species in sulfate and perchlorate medium for $C_A > 10^{-3}$ M has been reported previously.[20] The value log $K = -0.83$ for the formation of $EuA_3(HA)_3(org)$ in the system Eu(III) − 1.0 M $(Na,H)NO_3$/HDEHP-toluene, given by Kolarik and Pankova [21] was calculated by neglecting the formation of $Eu(NO_3)^{2+}(aq)$. As has been shown,[22,23] Eu(III)-nitrate species are formed in significant concentrations at 1 M NO_3^- solutions, and this may explain the lower value of $K = 10^{-0.83}$ for 1.0 M NO_3^- medium compared with $K = 10^{-0.35}$ for 1.0 M ClO_4^- medium for the reaction (8), (*cf.* Table 3). Using the value given by Choppin and Strazik [22] for the formation of $EuNO_3^{2+}$ at the ionic strength $I = 1.0$ M, $K_1 = 10^{0.31}$ M^{-1}, we calculate for (8) the equilibrium constant for the extraction of Eu(III) from an ionic medium of $I = 1.0$ M:

$$K(\text{corr},1) = K(NO_3,1)(1 + K_1[NO_3^-]) \quad (9)$$

Substituting $K(NO_3, 1) = 10^{-0.83}$ and $K_1 = 10^{0.31}$ in (9), we obtain $K(\text{corr}, 1) = 10^{-0.35}$, in excellent agreement with the value $10^{-0.35}$ found experimentally for the extraction from 1.0 M $HClO_4$ medium,[21] where only weak complex formation between Eu(III) and ClO_4^- is expected. In Table 3 the value of $K(Cl, 0.5) = 10^{-0.44}$ from Peppard's data [24,1] (*cf.* remark in Table 3), applied for 0.5 M ionic chloride medium, was calculated by neglecting the

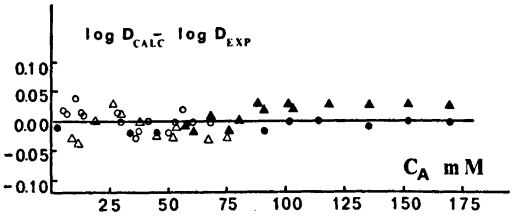

Fig. 5. The error log $(D_{calc}D_{exp}^{-1})$ as a function of C_A for the distribution of Eu(III) in the two-phase system Eu(III) − 0.10 M $(Na,H)ClO_4$/HDEHP-toluene, assuming the formation of $(H^+)_p(Eu^{3+})_q(HA)_r$ species and equilibrium constants given in Ref. 13 and Table 2, model 1. $-\log h = 1.000$ (●), 1.500 (▲), 2.097 (△) and 2.417 (○).

formation of Eu(III) – Cl^- species in the aqueous phase. Since Eu(III) is in tracer concentration, we assume that the ratios of the activity factors $f(EuCl^{2+})f^{-1}(Eu^{3+})$ and $f(EuCl_2^+) \times f^{-1}(Eu^{3+})$ do not vary significantly with the ionic strength for $I = 0.5$ to 1.0 M. This assumption is supported by the value found for the ratio of $f(EuNO_3^{2+})/f(Eu^{3+})$ at $I = 1.0$ and 0.2 M. Using the values $K_1 = 10^{0.31}$ at $I = 1.0$ and $K_1 = 10^{0.43}$ M^{-1} at $I = 0.2$ M for the formation of $EuNO_3^{2+}$ in Ref. 22 and $f(NO_3, 1) = 0.615$, $f(NO_3, 0.2) = 0.698$ (*cf.* Ref. 26), we may calculate the following value:

$$[f(EuNO_3^{2+},1)/f(Eu^{3+},1)][f(EuNO_3^{2+},0.2)/f(Eu^{3+},0.2)]^{-1} = K(NO_3,0.2).$$

$$K^{-1}(NO_3,1.0)f(NO_3,1.0)f^{-1}(NO_3,0.2) = 1.1 \approx 1.$$

Using the values $K_1(Cl,1) = 10^{-0.1}$ M^{-1} and $K_2(Cl,1) = 10^{-0.6}$ M^{-2} for the formation of $EuCl^{2+}$ and $EuCl_2^+$ for 1.0 M H(Cl,ClO_4) given by Choppin and Unrein [25] and $f(Cl,1) = 0.556$ and $f(Cl,0.5) = 0.615$ (*cf.* Kielland [26]), we calculate the values of the formation constants of these species at $I = 0.5$ M:

$$K_1(Cl,0.5) = f(Cl,0.5)f^{-1}(Cl,1)K_1(Cl,1) = 10^{-0.056}\ M^{-1},$$ and

$$K_2(Cl,0.5) = f^2(Cl,0.5)f^{-2}(Cl,1)K_2(Cl,1) = 10^{-0.512}\ M^{-2}$$

Using these values we calculate from Peppard's data:

$$K(corr,0.5) = K(Cl,0.5)(1 + K_1(Cl,0.5)[Cl^-] + K_2(Cl,0.5)[Cl^-]^2) = 10^{-0.44}[1 + 10^{-0.056} \times 0.5 + 10^{-0.512} \times (0.5)^2] = 10^{-0.26},$$

for the extraction of Eu(III) by HDEHP into toluene as given by (8) from a medium of ionic strength $I = 0.5$ M.

Test for the formation of europium(III) perchlorate complex. The significant difference between the values of K for the extraction of Eu(III) in toluene from 1.0, 0.1, and 0.01 M ClO_4^- medium (*cf.* Table 3) may be due to the formation of Eu(III)-perchlorate complexes. Assuming that for $C_{ClO_4} < 1$ M the predominant species formed is $EuClO_4^{2+}$, the following relationship applies:

$$f(Eu^{3+})f^{-3}(H^+)K^{-1}(ClO_4,I) = K^{-1}(corr,0)K^*(K^{*-1} + a_{ClO_4}) \quad (10)$$

where $K(ClO_4,I)$ is the experimentally found extraction constant for Eu(III) for a ClO_4^- medium of ionic strength I, $K(corr,0)$ the extraction constant for infinite diluted aqueous solution, $K^* = K_1(ClO_4,0)f(Eu^{3+}) \times f^{-1}(EuClO_4^{2+})(K_1(ClO_4,0))$ is the formation constant of $EuClO_4^{2+}$ at infinite dilution, and $a_{ClO_4} = f(ClO_4^-)[ClO_4^-]$. In (10) $K(corr, 0)$ and K^* may be assumed constant since as discussed previously the ratio of the activity factors $f(Eu^{3+})/f(EuClO_4^{2+})$ is expected to be constant in the range of ionic strength studied. In Fig. 6 we plot $\log Y = F(\log a_{ClO_4})$, where $Y = f(Eu^{3+}) \times f^{-3}(H^+)K^{-1}(ClO_4,I)$, and find that the points fall on a line of slope *approximately* +1 which agrees with (10). The constant for the formation of the $EuClO_4^{2+}$ may be calculated from:

$$K(corr,0) = K(ClO_4,1)f^3(H^+,1)f^{-1}(Eu^{3+},1) \times (1 + K_1(ClO_4,1) \times 1) = K(ClO_4,0.1)f^3(H^+,0.1) \times f^{-1}(Eu^{3+},0.1)(1 + K_1(ClO_4,0.1) \times 0.1) \quad (11)$$

where $K(ClO_4,1) = 10^{-0.35}$ and $K(ClO_4,0.1) = 10^{0.053}$ are the extraction constants and $K_1(ClO_4,1)$, $K_1(ClO_4,0.1)$ the constants for the formation of $EuClO_4^+$(aq) for 1.0 M and 0.1 M perchlorate medium, respectively. As discussed previously the ratio of the activity factors $f(EuClO_4^{2+})/f(Eu^{3+})$ is assumed to be constant for $I = 0.1 - 1$ M. One may then express the relationship:

$K_1(ClO_4, 1)/K_1(ClO_4, 0.1) = f(ClO_4, 1)/f(ClO_4, 0.1)$, where $f(ClO_4, 1) = 0.582$ and $f(ClO_4, 0.1) = 0.763$

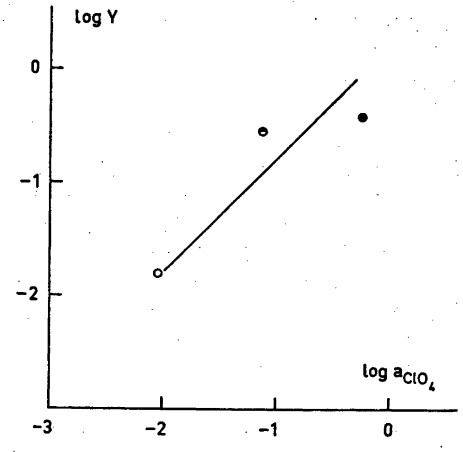

Fig. 6. The extraction of Eu(III) by HDEHP into toluene from 0.01 M ClO_4^- (○, Chiarizia *et al.*[33]), 0.1 M ClO_4^- (◒, this work) and 1.0 M ClO_4^- medium (●, Kolarik and Pankova [21]) (*cf.* text).

are the activity factors for ClO_4^- at $I = 1.0$ and 0.1 M (*cf.* Ref. 26). Substituting $K_1(ClO_4,1)/K_1(ClO_4,0.1) = 0.763$ and $f(Eu^{3+},1) = 0.071$, $f(H^+,1) = 0.745$, $f(Eu^{3+},0.1) = 0.180$ and $f(H^+,0.1) = 0.827$ (*cf.* Kielland [26]) into (11) we obtain:

$$Eu^{3+} + ClO_4^- \rightleftharpoons EuClO_4^{2+}; \quad K_1 = 10^{-0.35}\ M^{-1}$$
$$(I = 1.0\ M);\ K_1 = 10^{-0.23}\ M^{-1}\ (I = 0.1\ M).$$

From (11) we may calculate $K(\text{corr}, 0) = 10^{0.58}$ for the extraction of Eu^{3+} by HDEHP into toluene from infinite diluted aqueous solution. The extraction constant from a medium with non-complexing ligands and an ionic strength I can thus be expressed by:

$$K(\text{corr}, I) = f(Eu^{3+}, I) f^{-3}(H^+, I) \times 10^{0.58} \qquad (12)$$

Given the activity factors for Eu^{3+} and H^+, *e.g.* from Kielland's relationship [26] and the constant $K_n = [EuX_n^{3-n}][Eu^{3+}]^{-1}[X^-]^{-n}$ for the formation of complexes between Eu^{3+} and the ionic ligand X^- (*e.g.* NO_3^-, Cl^-) in the aqueous phase, we may express the equilibrium constant $K(X,I)$ for the extraction of Eu(III) by HDEHP into toluene from the ionic medium, *e.g.* (Na, H)X, with a given ionic strength I and containing the EuX_n^{3-n} (aq) species:

$$K(X,I) = f(Eu^{3+},I) f^{-3}(H^+,I) \times$$
$$(1 + \sum K_n[X^-]^n)^{-1} \times 10^{0.58} \qquad (13)$$

Using $f(Eu^{3+}, 1) = 0.071$, $f(H^+, 1) = 0.745$ and $K_1 = 10^{0.31}\ M^{-1}$ for the formation of $EuNO_3^{2+}$ (*cf.* Ref. 22), we calculate, from (13), the equilibrium constant for the extraction of Eu(III) by HDEHP from 1.0 M (Na, H)NO_3 into toluene, $K(NO_3, 1) = 10^{-0.67}$. This value is in fair agreement with the value $10^{-0.83}$ found experimentally by Kolarik and Pankova [21] for the same extraction system. Using $f(Eu^{3+}, 0.5) = 0.091$, $f(H^+, 0.5) = 0.766$, and $K_1 = 10^{-0.056}$, $K_2 = 10^{-0.512}$ for the formation of $EuCl^{2+}$ and $EuCl_2^+$ at 0.5 M (Na, H)Cl calculated previously, we calculate using (13) the equilibrium constant for the extraction of Eu(III) from 0.5 M Cl^- medium $K(Cl^-, 0.5) = 10^{-0.30}$, in agreement with the value $10^{-0.44}$ found experimentally for the same system (*cf.* Peppard *et al.*[24] and Baes [1]).

Acknowledgements. The work has been financially supported by the Swedish National Science Research Council and the Swedish Board for Technical Development. We are much obliged for the criticism given by Prof. Ingmar Grenthe. Dr. Derek Lewis and Mr. Ian Duncan, B.Sc. have revised the English text.

REFERENCES

1. Baes, Jr. C. F., *J. Inorg. Nucl. Chem. 24* (1962) 707.
2. Liem, D. H. *Inaugural Dissertation, Royal Institute of Technology*, Stockholm 1971 (available on request).
3. Peppard, D. F. *Annu. Rev. Nucl. Sci. 21* (1971).
4. Blake, Jr., C. A., Baes, Jr., C. F., Brown, K. B., Coleman, C. F. and White, J. C. *2nd Int. Conf. Peaceful Uses Atomic Energy*, Paper 1550, Geneva 1958; *ORNL-2171, Oak Ridge* 1956.
5. Flanary, J. R. *Progr. Nucl. Energy Ser. 3, Process Chemistry* I (1956) 195.
6. Goldschmidt, B., Regnaut, P. and Prevot, I. *Int. Conf. Peaceful Uses Atomic Energy*, Geneva 1955, Paper No. P/349.
7. Riele, W. A. M., Cloete, F. I. D., Haines, A. K., Sampson, T. D. and Tunley, T. F. *TMS Paper No. A74-17, Metallurgical Society of AIME*, 1974.
8. Fletcher, A. W. *U.S. Patent* 3,055,754 (1962).
9. Peppard, D. F., Ferraro, J. R. and Mason, G. W. *J. Inorg. Nucl. Chem. 4* (1957) 334.
10. Peppard, D. F., Ferraro, J. R. and Mason, G. W. *J. Inorg. Nucl. Chem. 7* (1958) 231.
11. Dyrssen, D. *Acta Chem. Scand. 11* (1957) 1771.
12. Dyrssen, D. and Liem, D. H. *Acta Chem. Scand. 14* (1960) 1091.
13. Liem, D. H. *Acta Chem. Scand. 26* (1972) 191.
14. Ferraro, J. R. and Peppard, D. F. *J. Phys. Chem. 67* (1963) 2639.
15. Dyrssen, D. and Liem, D. H. *Acta Chem. Scand. 14* (1960) 1100.
16. *Solvent Extraction Chemistry, Proc. Int. Conf. Solvent Extraction Chem. (ISEC) Gothenburg*, Dyrssen, D., Liljenzin, J. O. and Rydberg, J., Eds., North-Holland, Amsterdam 1967.
17. Marcus, Y., Kertes, A. S. and Yanir, E. *Equilibrium Constants of Liquid-Liquid Distribution Reactions, International Union of Pure and Applied Chemistry*, Butterworths, London 1974.
18. Marcus, Y. and Kertes, A. S. *Ion Exchange and Solvent Extraction of Metal Complexes*, Wiley-Interscience, New York 1969.
19. *Some Laboratory Methods in Current Use at the Department of Inorganic Chemistry, Royal Institute of Technology, Stockholm, Mimeograph* 1959.
20. Liem, D. H. and Sinegribova, O. *Acta Chem. Scand. 25* (1971) 277.

21. Kolarik, Z. and Pankova, H. *J. Inorg. Nucl. Chem. 28* (1966) 2325.
22. Choppin, G. R. and Strazik, W. F. *Inorg. Chem. 4* (1965) 1250.
23. Bansal, B. M. L., Patil, S. K. and Sharma, H. D. *J. Inorg. Nucl. Chem. 26* (1964) 993.
24. Peppard, D. F., Mason, G. W., Maier, J. L. and Driscoll, W. J. *J. Inorg. Nucl. Chem. 4* (1957) 334.
25. Choppin, G. R. and Unrein, P. J. *J. Inorg. Nucl. Chem. 25* (1963) 387.
26. Kielland, J. *J. Am. Chem. Soc. 2* (1937) 1675.
27. Ingri, N. and Sillén, L. G. *Ark. Kemi 23* (1964) 97; Sillén, L. G. and Warnqvist, B. *Ark. Kemi 31* (1969) 315; Sillén, L. G. and Warnqvist, B. *Ark. Kemi 31* (1969) 341; Arnek, R., Sillén, L. G. and Wahlberg, O. *Ark. Kemi 31* (1969) 353.
28. Liem, D. H. *Acta Chem. Scand. 25* (1971) 1521.
29. Ingri, N., Kakolowicz, W., Sillén, L. G. and Warnqvist, B. *Talanta 14* (1967) 1261.
30. Duyckaerts, G., Dreze, Ph. and Simon, A. *J. Inorg. Nucl. Chem. 13* (1960) 332.
31. Kuča, L. *Collect. Czech. Chem. Commun. 32* (1967) 288.
32. Brown, K. B., Coleman, C. F., Crouse, D. J. and Ryon, A. D. *Oak Ridge National Laboratory Progress Report* 1957, ORNL-2268.
33. Chiarizia, R., Danesi, P. R., Raieh, M. A. and Scibona, G. *J. Inorg. Nucl. Chem. 37* (1975) 1495.
34. Liem, D. H. *Unpublished work.*
35. Moulin, N., Hussonnois, M., Brillard, L. and Guillaumont, R. *J. Inorg. Nucl. Chem. 37* (1975) 2521.

Received October 3, 1975.

Acta Chemica Scandinavica A 30 (1976) 322—326

Crystal Structure of Nickel Bis-*N*,*N*-diethylphenylazothioformamide, $Ni[(C_6H_5)NNCSN(C_2H_5)_2]_2$

RITA GRØNBÆK HAZELL

Department of Inorganic Chemistry, University of Aarhus, DK-8000 Aarhus C, Denmark

Nickel bis-*N*,*N*-diethylphenylazothioformamide crystallizes in the tetragonal system, space group $P4_12_12$, $a = 10.38(2)$ Å, $c = 22.60(4)$ Å; $Z = 4$; three-dimensional X-ray data for a hemisphere of reflections with sin $\theta/\lambda \leq 0.7$ were collected on a semiautomatic diffractometer. *R*-value 0.045 for 1592 significant reflections after least squares refinement. Nickel is tetrahedrally coordinated by sulfur and hydrazinic nitrogen atoms. The tetrahedron is slightly flattened so that the N – Ni – N angle is 144°; the angle between the planes of the two ligands is 70.4°.

The compound under investigation was prepared by Jensen *et al.*[1] by oxidation of bis(1-phenyl-4,4-diethylthiosemicarbazidato)nickel(II), and also by reaction of the corresponding phenylazothioformamide with $Ni(CO)_4$. The present investigation was part of the attempt to clarify the bonding in this and similar compounds, the result of which was described by Jensen, Bechgaard, and Pedersen.[2]

EXPERIMENTAL

The crystals are elongated tetragonal bipyramids (bounded by {101}). The one used for intensity measurements was $0.15 \times 0.15 \times 0.3$ mm^3 and mounted along the *a*-axis. Cell dimensions and space group were obtained from precession photographs taken with Cu$K\alpha$ radiation ($\lambda = 1.5418$ Å). All reflections within a hemisphere ($h \geq 0$) with sin $\theta/\lambda \leq 0.7$ were measured on an automatic Supper-Pace diffractometer using Mo$K\alpha$ radiation obtained from a graphite monochromator.[3] Corrections for Lorentz and polarization effects but not for absorption were applied and the four symmetry related reflections were averaged leaving 1592 independent, significant reflections [$I > 2\sigma(I)$].

CRYSTAL DATA

$Ni(C_{11}H_{15}N_3S)_2$; M = 501.4;
Tetragonal; $a = 10.38(2)$ Å, $c = 22.60(4)$ Å; $V = 2435$ Å^3; $Z = 4$; $d_m = 1.37$ g/cm^3; $d_c = 1.38$ g/cm^3; $\mu_{MoK\alpha} = 9.9$ cm^{-1};

Systematic absences: $00l$: $l \neq 4n$
$h00$: $h \neq 2n$

Space group: $P4_12_12$ (No. 92) (or the enantiomorph, No. 96).

Final coordinates and temperature factor parameters are given in Tables 1 and 2. A list of observed and calculated structure factors can be obtained from the author.

STRUCTURE DETERMINATION AND REFINEMENT

The space group, unit cell and density indicated that Ni had to be on the diagonal twofold axis in the tetragonal unit cell. The Patterson projection, $P(vw)$, was solved to give the nickel and sulfur positions and the Fourier based on this showed all the lighter atoms. The structure was refined by the method of least squares using the 3-dimensional data. The ALGOL program used on the GIER computer at Aarhus University works in the block diagonal approximation and allows anisotropic temperature factor refinement and extinction correction according to Zachariasen [4] in the approximation given by Larson,[5] formula 3. The final value of the extinction coefficient, *g*, was 2.4×10^{-7}. The hydrogen atoms were found in a difference Fourier synthesis calculated at $R = 0.07$, those of the methyl groups being

Table 1. Final atomic coordinates (in fractions) with standard deviations in terms of the last digit in parentheses. For hydrogen atoms the isotropic temperature factor parameters, B (Å^2), are given.

	x	y	z	B
Ni	0.64663(7)	0.35397(7)	0.75000(0)	
S	0.4833(1)	0.3421(1)	0.68711(5)	
N1	0.5765(3)	0.2049(3)	0.7839(1)	
N2	0.4629(3)	0.1555(3)	0.7692(1)	
N3	0.2974(3)	0.1662(3)	0.7019(1)	
C1	0.4094(4)	0.2137(4)	0.7215(2)	
C2	0.2306(4)	0.0602(4)	0.7315(2)	
C3	0.1322(5)	0.1069(5)	0.7765(2)	
C4	0.2314(5)	0.2239(5)	0.6504(2)	
C5	0.2746(5)	0.1608(7)	0.5924(2)	
C6	0.6304(4)	0.1503(4)	0.8368(2)	
C7	0.5549(4)	0.0911(4)	0.8804(2)	
C8	0.6140(5)	0.0464(4)	0.9319(2)	
C9	0.7451(5)	0.0559(4)	0.9393(2)	
C10	0.8192(4)	0.1133(4)	0.8957(2)	
C11	0.7615(4)	0.1608(4)	0.8448(2)	
H1	0.4609(35)	0.0829(36)	0.8761(16)	3.3(0.8)
H2	0.5566(51)	0.0086(43)	0.9646(20)	6.8(1.3)
H3	0.7849(57)	0.0310(39)	0.9761(16)	4.1(0.9)
H4	0.9147(34)	0.1186(33)	0.9012(15)	3.1(0.8)
H5	0.8187(36)	0.2039(34)	0.8152(15)	3.3(0.8)
H6	0.2993(44)	0.0012(43)	0.7534(19)	5.9(1.1)
H7	0.1920(53)	0.0074(53)	0.7021(22)	7.6(1.4)
H8	0.2474(41)	0.3257(44)	0.6479(18)	5.5(1.2)
H9	0.1410(40)	0.2019(42)	0.6572(18)	5.0(1.0)
H10	0.2425(69)	0.0800(70)	0.5914(30)	13.3(2.4)
H11	0.3677(49)	0.1659(49)	0.5894(21)	7.5(1.3)
H12	0.2360(53)	0.2027(54)	0.5637(22)	8.5(1.5)
H13	0.0728(48)	0.0314(48)	0.7946(22)	7.6(1.4)
H14	0.0552(51)	0.1607(50)	0.7568(24)	8.4(1.5)
H15	0.1907(60)	0.1414(57)	0.8044(26)	10.6(1.7)

Table 2. Mean square vibration amplitudes, U_{ij}, in Å$^2 \times 10^{-4}$. Standard deviations in parentheses. The expression for the temperature factor is: $\exp[-2\pi^2(U_{11}(ha^*)^2 + \ldots 2U_{23}klb^*c^*)]$

	U_{11}	U_{22}	U_{33}	U_{12}	U_{13}	U_{23}
Ni	389(2)	389(2)	417(3)	−101(2)	0(0)	0(0)
S	476(5)	544(6)	476(5)	−145(4)	−56(4)	129(5)
N1	328(15)	348(15)	381(16)	−53(12)	−10(14)	−12(14)
N2	362(15)	355(15)	438(16)	−98(12)	−29(14)	−11(14)
N3	389(16)	588(22)	473(18)	−93(16)	−80(15)	75(18)
C1	343(19)	434(21)	407(20)	−34(16)	11(17)	−4(18)
C2	434(23)	501(25)	633(27)	−195(18)	−54(21)	21(22)
C3	662(32)	833(35)	658(28)	−269(27)	68(27)	−2(29)
C4	493(27)	620(31)	558(23)	−66(17)	−94(20)	64(22)
C5	648(32)	1328(54)	558(27)	42(35)	−36(26)	−22(34)
C6	401(19)	326(16)	418(19)	−2(15)	−17(16)	−53(15)
C7	421(22)	491(23)	511(23)	−80(19)	13(19)	20(21)
C8	703(31)	556(26)	483(24)	−116(25)	−19(24)	113(22)
C9	758(32)	452(24)	510(25)	−7(22)	−197(24)	6(21)
C10	493(25)	409(22)	683(28)	27(19)	−157(23)	−62(22)
C11	374(19)	447(22)	486(22)	−63(17)	−23(18)	15(19)

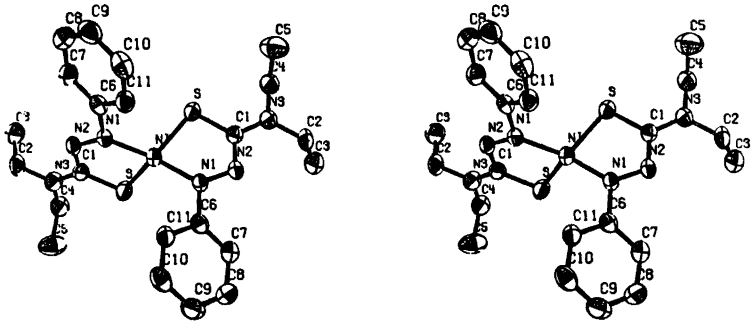

Fig. 1. Stereo view of a molecule of nickel bis-*N*,*N*-diethylphenylazothioformamide.

fitted to small positive regions with considerable uncertainty. These groups have large thermal movements compared to the rest of the molecule. Because no absorption correction had been made, and because we could not hope that a simple model like rigid body or riding motion would account for the thermal movements of this molecule, the temperature factors were not examined except to check that they looked reasonable. The weights in the refinement were $w=[\sigma(F)]^{-2}=\{[\sigma_c(F^2)+(1+k)F^2]^{\frac{1}{2}}-|F|\}^{-2}$ where $\sigma_c(F^2)$, the standard deviation from counting statistics, was supplemented with a contribution kF^2 to take account of other possible errors; k was adjusted during refinement so that the average of $w|\,|F_o|-|F_c|\,|^2$ was independent of $|F|$, ($k=0.016$). The final value of $R=\sum|\,|F_o|-|F_c|\,|/\sum|F_o|$ was 0.045.

DESCRIPTION OF THE STRUCTURE

The coordination around nickel is a somewhat flattened tetrahedron of two sulfur and two nitrogen atoms as illustrated in Fig. 1. The dimensions of the azothioformamide determine that the in-ring N–Ni–S angles are smaller than the tetrahedral value. The other angles around Ni are normal except the N–Ni–N angle, which is as big as 144°. The angle between the two ligand planes is 70.4° compared to 90° in a regular tetrahedron. In primary zinc dithizonate [6] the interplanar angle is 85°, and the N–Zn–N angle is 110°, *i.e.* much closer to regular tetrahedral coordination. In bis(acetophenone thioacethydrazonato)-nickel(II) [7] the interplanar angle is 21.6° and the N–Ni–N angle is 101.6°, *i.e.* close to *cis*-planar configuration; a planar structure is also reported for nickel dithizonate.[8] The steric requirements of the present complex seem similar to those of these two compounds and do not explain why it does not assume either

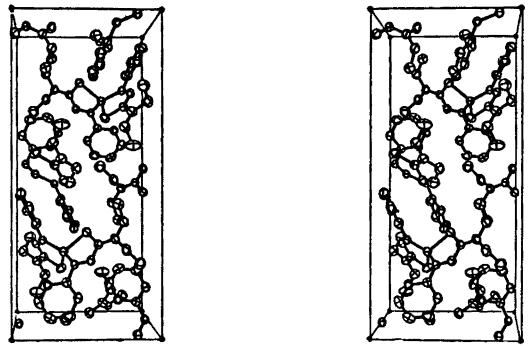

Fig. 2. Stereo view of the contents of a unit cell down the *a* axis.

Table 3. Bond lengths (Å) and angles (°). Standard deviations in parentheses.

Ni–S	2.215(2)	C2–H6	1.06(5)
Ni–N1	1.869(3)	C2–H7	1.05(5)
S–C1	1.723(4)	C4–H8	1.07(5)
N1–N2	1.328(4)	C4–H9	0.98(4)
N2–C1	1.356(5)	C3–H13	1.08(5)
N3–C1	1.338(5)	C3–H14	1.07(5)
N3–C2	1.463(6)	C3–H15	0.95(6)
N3–C4	1.478(6)	C5–H10	0.90(8)
C2–C3	1.521(7)	C5–H11	0.97(5)
C4–C5	1.531(7)	C5–H12	0.88(5)
N1–C6	1.435(5)	C7–H1	0.98(4)
C6–C7	1.401(6)	C8–H2	1.03(5)
C7–C8	1.395(6)	C9–H3	0.96(4)
C8–C9	1.375(7)	C10–H4	1.00(4)
C9–C10	1.385(6)	C11–H5	1.00(4)
C10–C11	1.387(6)		
C11–C6	1.377(5)		
S–Ni–S	119.5(1)	C1–N3–C2	122.6(3)
S–Ni–N1	85.5(1)	C1–N3–C4	120.9(4)
S–Ni–N1	112.9(1)	C2–N3–C4	116.4(3)
N1–Ni–N1	144.2(1)	N3–C2–C3	112.6(4)
Ni–S–C1	95.3(1)	N3–C4–C5	111.4(4)
Ni–N1–N2	124.2(2)	N1–C6–C7	122.7(3)
Ni–N1–C6	121.0(2)	N1–C6–C11	117.6(3)
C6–N1–N2	113.7(3)	C7–C6–C11	119.7(4)
N1–N2–C1	113.0(3)	C6–C7–C8	119.1(4)
N2–C1–S	121.5(3)	C7–C8–C9	120.9(4)
N2–C1–N3	117.0(3)	C8–C9–C10	119.6(4)
S–C1–N3	121.5(3)	C9–C10–C11	120.2(4)
		C10–C11–C6	120.5(4)

a regular tetrahedral arrangement or a nearly planar one. In zinc dithizonate the phenyl groups are coplanar with the rest of the ligand, in bis(acetophenone thioacethydrazonato) nickel the phenyl groups form an angle of 26° with the rest of the ligand making the two phenyl groups parallel. In the present compound the corresponding angle is 29° but in such a direction that the two phenyl groups get closer together; this deformation must be due to intermolecular packing forces, see Fig. 2. It is worth noticing that similar compounds without a bulky group at this nitrogen atom are too unstable to be isolated [1,2] whereas the present compound is very stable so the extra steric strain seems to be easily offset by some stabilizing effect.

The Ni–S and Ni–N bonds (Table 3) are longer than those of planar thiosemicarbazide complexes of divalent nickel [9–11] but shorter than the distances expected from tetrahedral divalent nickel. In a diamagnetic, tetrahedral Ni^0 complex,[12] $[(C_5H_5)_2Nb(SMe)_2]$ $Ni(BF_4)_2 \cdot 2H_2O$, the Ni–S distances (2.20 Å) are similar to the ones found in the present investigation. The ligand can be derived from thiosemicarbazide by removal of two protons from N1 and N2 (and substitution of bulky groups for other hydrogen atoms). As could be anticipated, this leads to a short N–N bond (1.33 Å) though not as short as expected for a localized double bond. The N2–C bond is significantly longer than in the thiosemicarbazides probably because of the participation of N2 in a nearly double bond to N1. The C–S and C–N3 bonds are also long although the differences are hardly significant. The coordination is so far from regular that simple ligand field considerations cannot predict the electronic structure, but Bechgaard [13] has presented a qualitative molecular orbital diagram in accordance with the observed spectra and magnetic properties, according to which the highest occupied orbital is a π^* orbital of the ligand.

Acknowledgements. Professor K. A. Jensen and Dr. K. Bechgaard are thanked for suggesting the problem and supplying good crystals and also for interesting discussions during this work. Statens Almindelige Videnskabsfond supplied the diffractometer, and F. R. Poulsen and T. la Cour wrote the programs used for datacollection and datareduction.

REFERENCES

1. Jensen, K. A., Bechgaard, K. and Pedersen, C. T. *Acta Chem. Scand. 22* (1968) 3341.
2. Jensen, K. A., Bechgaard, K. and Pedersen, C. T. *Acta Chem. Scand. 26* (1972) 2913.
3. Rasmussen, S. E. and Henriksen, K. *J. Appl. Crystallogr. 3* (1970) 100.
4. Zachariasen, W. H. *Acta Crystallogr. 16* (1963) 1139.
5. Larson, A. C. *Acta Crystallogr. 23* (1967) 664.
6. Mawby, A. and Irving, H. M. N. H. *J. Inorg. Nucl. Chem. 34* (1972) 109.
7. Larsen, S. *Acta Chem. Scand. A 28* (1974) 779.
8. Laing, M. and Alsop, P. A. *Talanta 17* (1970) 242.
9. Grønbæk, R. and Rasmussen, S. E. *Acta Chem. Scand. 16* (1962) 2325.
10. Hazell, R. G. *Acta Chem. Scand. 22* (1968) 2171.
11. Hazell, R. G. *Acta Chem. Scand. 26* (1972) 1365.
12. Douglas, W. E., Green, M. L. H., Prout, C. K. and Rees, G. V. *Chem. Commun.* (1971) 896.
13. Bechgaard, K. *Acta Chem. Scand. A 28* (1974) 185.

Received August 6, 1975.

Acta Chemica Scandinavica A 30 (1976) 327—334

NMR Studies on Cyclic Arsenites. ^{1}H NMR Spectral Analysis and Conformational Studies of Fifteen Ring-substituted 2-Chloro-, 2-Methoxy- and 2-Phenoxy-1,3,2-dioxarsenanes

DAGFINN W. AKSNES, JENS ANDERSEN* and KNUT BERGESEN

Department of Chemistry, University of Bergen, Allégaten 70, N-5014 Bergen-Univ., Norway

This paper reports preparation and ^{1}NMR investigations of fifteen six-membered arsenites. Nonequilibrium mixtures of two geometrical isomers have been observed for the methoxy-compounds. However, the present spectral analyses have only been performed on the thermodynamically more stable forms which predominated strongly in aged samples. The 4,6-dimethyl compounds constitute complex ten-spin systems. However, the methylene spectral regions of these compounds have been completely broken down into ab sub-spectra. This procedure facilitated the acquirement of trial values for the iterative computer analysis. The NMR data are adequately explained in terms of two chair conformations differing essentially in the configuration at arsenic. The predominant isomers of all compounds except those possessing *trans*-4,6-dimethyl groups, appear to exist almost entirely in one chair conformation with axially and equatorially oriented substituents at arsenic and carbon, respectively. In the *trans*-4,6-dimethyl compounds we have found strong evidence for a conformational equilibrium between two chair forms. The reduced stability of the diaxial conformer is probably a result of severe *syn*-axial interactions between the axial substituents at arsenic and C(6).

The ^{1}H NMR spectra of several six-membered arsenites have been investigated in two previous papers.[1,2] It has been shown that the preferred orientation of the substituent at arsenic is axial.[1–3] However, the conformational preferences of other exocyclic substituents on such rings have not been thoroughly studied.[3,4] This is in marked contrast to the considerable attention given the corresponding phosphites.[5–11]

Arbuzov *et al.*[3] report in a study based on measurements of dipole moments and Kerr constants, that the experimental and calculated data of 2-chloro-4-methyl-1,3,2-dioxarsenane are consistent with a chair conformation with axial chlorine and equatorial methyl. In more highly substituted systems, however, it is conceivable that the steric requirements of the substituents may force a dominance of another configuration at arsenic or confine the ring into a non-chair form.

In order to obtain more information about externally substituted arsenanes we have prepared the following fifteen arsenites and investigated their ^{1}H NMR spectra. However, a complete spectral analysis has only been performed on the predominant isomers.

EXPERIMENTAL

The eight cyclic chloro-compounds were prepared from the appropriate 1,3-butanediols and trichloroarsine in ether solution using triethylamine as base.[4,12] Treatment of the chloro-compounds with methanol or phenol in ether solution in the presence of excess triethylamine yielded the corresponding methoxy or phenoxy derivatives.[4] The boiling and melting points which have not been reported previously,[4] and the yields are as follows: B.p.$_{0.3}$ 42 °C (54 %); m.p. 97 °C (80 %); m.p. 79 °C (94 %); b.p.$_{0.05}$ 80 °C (75 %) and m.p. 45 °C (49 %) for compounds I, II, III, VIII and IX, respectively.

The ^{1}H NMR spectra were examined in benzene, deuteriochloroform, carbon disulfide

* J. A.'s contribution is limited to the data of Table 1.

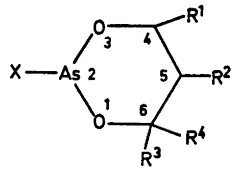

I:	X = Cl,	$R^1 = R^3 = R^4 = H$,	$R^2 = CH_3$
II:	X = Cl,	$R^1 = R^3 = R^4 = H$,	R^2 = *tert*-Bu
III:	X = Cl,	$R^1 = R^3 = R^4 = H$,	R^2 = Ph
IV:	X = OCH_3,	$R^1 = R^3 = R^4 = H$,	R^2 = Ph
V:	X = OPh,	$R^1 = R^3 = R^4 = H$,	R^2 = Ph
VI:	X = Cl,	$R^2 = R^3 = R^4 = H$,	$R^1 = CH_3$
VII:	X = OCH_3,	$R^2 = R^3 = R^4 = H$,	$R^1 = CH_3$
VIII:	X = OPh,	$R^2 = R^3 = R^4 = H$,	$R^1 = CH_3$
IX:	X = Cl,	$R^2 = R^3 = R^4 = H$,	R^1 = Ph
X:	X = Cl,	$R^2 = R^3 = H$,	$R^1 = R^4 = CH_3$ (*cis* methyl)
XI:	X = OCH_3,	$R^2 = R^3 = H$,	$R^1 = R^4 = CH_3$ (*cis* methyl)
XII:	X = Cl,	$R^2 = R^4 = H$,	$R^1 = R^3 = CH_3$ (*trans* methyl)
XIII:	X = OCH_3,	$R^2 = R^4 = H$,	$R^1 = R^3 = CH_3$ (*trans* methyl)
XIV:	X = Cl,	$R^2 = H$, $R^1 = R^3 = R^4 = CH_3$	
XV:	X = OCH_3,	$R^2 = H$, $R^1 = R^3 = R^4 = CH_3$	

and dichlorofluoromethane solutions (*ca.* 50 % v/v). A small amount of TMS was added to the samples and used as internal standard and lock signal source. The 60 MHz and 100 MHz spectra were recorded on JEOL-C-60H and VARIAN HA-100 spectrometers, respectively. Line positions were obtained by averaging the results of two frequency-calibrated spectra run at about 100 Hz sweep widths.

The ^{1}H NMR spectra were analyzed by means of the computer program LAOCN3,[13] UEAITR [14] and KOMBIP.[15] The computations were performed on a UNIVAC 1110 computer. The graphical output was obtained using a Calcomp Plotter.

SPECTRAL ANALYSIS

The methylene regions of the 100 MHz spectra of compounds I-V were initially analyzed by hand as AKL systems. (The methine and methylene protons are labelled A and KL, respectively). The hand-calculated spectral parameters ν_K, ν_L, J_{AK}, J_{AL}, and J_{KL} were employed as input parameters for iterative AKK'LL'X_3 or AKK'LL' analyses of the complete spectra.[13,14] The remaining trial parameters were readily obtained from the methine and methyl spectral regions.

The detailed spectral analyses of compounds VI-IX were carried out on the basis of ABKLMX$_3$ or ABKLM spin systems. The 100 MHz spectra of these compounds consist, apart from the methyl signals, of three main regions.

Trial parameters were obtained by analyzing, in part, the experimental spectra on a first-order basis. The refined parameters of I–IX resulting from iterative computer analyses,[13,14] of the complete spin systems (less the substituent at arsenic) are listed in Table 1. The spectra generated [15] from the refined parameters fit closely the experimental ones in each case as demonstrated for VI in Fig. 1.

The $CHCH_3-CH_2-CHCH_3$ moieties of compounds X–XIII constitute ABKK'X_3X_3' and ABKLX_3Y_3 spin systems for the *cis* and *trans* molecules, respectively. However, since the long-range methyl-methylene proton couplings are zero simplifications occur in the methylene (AB) region of these spectra. It is thus seen that the methylene spectral region of the *cis* and *trans* compounds constitutes the AB part of ABKK' or ABKL spin systems, respectively.

The AB part of the ABKK' spin system [16] has been broken down into three different ab sub-spectra by means of the procedure due to Diehl.[17,18] These sub-spectra are characterized by $J_{ab} = J_{AB}$ and the effective chemical shifts:

Symmetric, $m(KK') = \pm 1$

$$\nu_a = \nu_A \pm J_{AK};\ \nu_b = \nu_B \pm J_{BK} \quad (1)$$

Symmetric and antisymmetric, $m(KK') = 0$

$$\nu_a = \nu_A;\ \nu_b = \nu_B \quad (2)$$

The ab sub-spectrum corresponding to $m(KK') = 0$ has twice the intensity of the other

Table 1. 100 MHz NMR parameters (in Hz) of compounds I–IX measured in deuteriochloroform solution at 30 °C [a].

Compound	I [b]	II	III	IV	V	VI	VII	VIII	IX
Spin system	AKK'LL'X$_3$		AKK'LL'			ABKLMX$_3$			ABKLM
ν_{4a}	413.43	424.74	453.54	448.23	465.50	467.02	457.59	461.07	553.32
ν_{5a}						463.71	452.27	454.88	480.00
ν_{4e} [c]	396.09	389.81	406.04	378.20	388.59	124.26	114.88	114.20	
ν_{6e}						413.27	389.29	384.29	419.33
ν_{5a}	234.59	188.64	327.81	327.22	334.04	205.72	196.93	193.21	234.88
ν_{5e} [c]	75.55					164.92	154.50	144.09	178.41
J_{4a4e} [d]	−11.69	−10.86	−11.19	−10.71	−10.80	6.19	6.11	6.25	
J_{5a5e} [d]						−11.42	−11.04	−11.20	−11.52
J_{5a5e} [d]	6.66					−14.38	−14.22	−14.08	−14.52
J_{4a5a}	11.17	10.90	10.68	11.18	11.43	10.82	10.24	10.97	11.12
J_{5a6a}						12.26	12.19	12.42	12.19
J_{5a5e}	3.90	3.56	3.77	3.77	3.87	3.76	3.63	4.01	3.99
J_{4a5e}						1.85	2.02	2.07	2.00
J_{5e6a}						1.98	2.06	2.02	2.07
J_{5e6e}						2.45	2.53	2.53	2.39
J_{4a6a}	0.23	0.00	−0.14	0.12	−0.12	0.05	−0.01	0.02	0.00
J_{4a6e}	−0.33	−0.08	−0.54	−0.10	−0.48	0.09	0.13	0.00	0.00
J_{4e6e}	−0.37	0.00	0.90	0.47	0.67				
Assigned transitions	205	25	32	26	30	222	217	455	66
RMS error	0.091	0.087	0.079	0.108	0.091	0.092	0.087	0.074	0.080

[a] Chemical shifts downfield from TMS. [b] Measured in $CHFCl_2$ solution at −110 °C. [c] Methine or methyl shift as appropriate. [d] Geminal or vicinal coupling constants as appropriate.

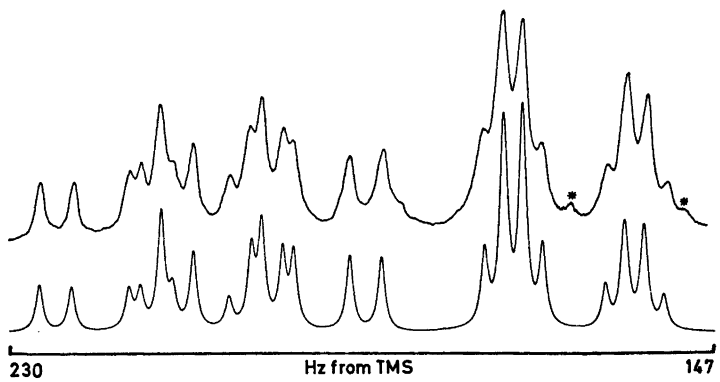

Fig. 1. Experimental (upper trace) and calculated (lower trace) 100 MHz spectrum at 30 °C of the methylene protons at C(5) in compound VI. The asterisks indicate impurities.

two ab sub-spectra. The four lines originating from the former spectrum were readily picked out since $J_{AB} \approx -14$ Hz (Fig. 2). Furthermore, the extreme high-frequency line in Fig. 2 must originate from the ab sub-spectrum corresponding to $m(KK')=1$ since J_{AK} and J_{BK} are both positive. The splitting patterns ($J_{AB} \approx -14$ Hz) and intensity distribution then yielded the three missing lines in this sub-spectrum. By manipulating the identified lines good trial values of ν_A, ν_B, J_{AB}, J_{AK} and J_{BK} were obtained. The remaining trial values were obtained from the methine and methyl spectral regions.

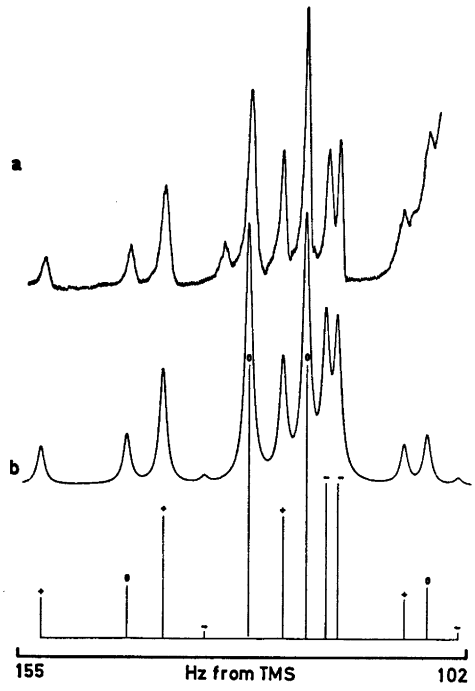

Fig. 2. Experimental (a) and calculated (b) 100 MHz spectrum of the methylene protons at C(5) in X. The breakdown into three ab sub-spectra corresponding to m(KK′) = 1, 0 and −1, is shown by the +, 0 and − signs, respectively.

The methylene regions of XII and XIII can, as already mentioned, be analyzed on the basis of an ABKL system. However, since $|\nu_K - \nu_L| \gg |J_{KL}| \approx 0$ a further reduction into an ABKX system occurs. That is, the AB part can be completely broken down into four ab sub-spectra,[18] one for each sign combination of $m_K = \pm\frac{1}{2}$ and $m_X = \pm\frac{1}{2}$. The ab sub-spectra are characterized by $J_{ab} = J_{AB}$ and the following effective chemical shifts:

$$\nu_a = \nu_A + m_K\,(J_{AK} \pm J_{AX})$$
$$\nu_b = \nu_B + m_K\,(J_{BK} \pm J_{BX}) \qquad (3)$$

The upper and lower signs in the parentheses correspond to equal and opposite signs, respectively, of m_K and m_X.

The two ab sub-spectra corresponding to equal sign of m_K and m_X were identified by using a similar procedure as described for the *cis* compounds (Fig. 3). This assignment provided good values of ν_A, ν_B, $(J_{AK} + J_{AX})$ and

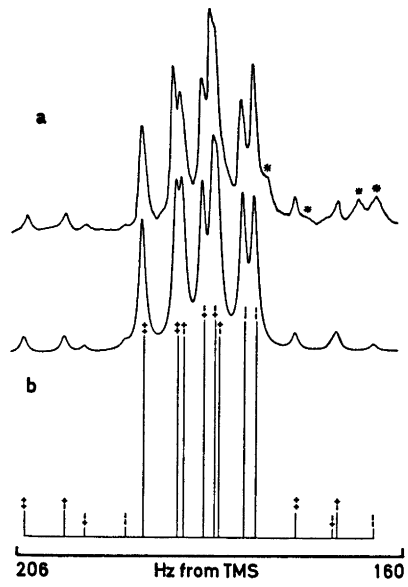

Fig. 3. Experimental (a) and calculated (b) 100 MHz spectrum of the methylene protons at C(5) in XIII. The breakdown into four ab sub-spectra, one for each sign combination of m_K and m_X, is shown by the + and − signs. The asterisks indicate impurities.

$(J_{BK} + J_{BX})$. Computation of ab sub-spectra with variation of $J_{ab}/|\nu_a - \nu_b|$ then enabled us to identify the two remaining ab sub-spectra, thus providing good values of the individual coupling constants. The remaining trial parameters were obtained directly from the methyl and methine spectral regions.

The 100 MHz spectra of the CH_2-$CHCH_3$ moiety in XIV and XV were analyzed as $ABKX_3$ spectra. An approximate first-order analysis yielded trial parameter for the iterative calculations.

The spectral parameters of X−XV listed in Table 2 were obtained from iterative computer analyses of the complete spin systems.[14] Good fits between the observed and calculated spectra [15] were obtained in each case as demonstrated in Figs. 2 and 3 for compounds X and XIII.

DISCUSSION

Several of the methyl-substituted 2-methoxy-1,3,2-dioxarsenanes examined in this work have been found to exist as a mixture of two

Table 2. 100 MHz parameters (in Hz) of compounds X–XV measured at 30 °C.[a]

Compound	X	XI	XII[b]	XIII	XIV	XV
Spin system	$ABKK'X_3X_3'$		$ABKLX_3Y_3$		$ABKX_3$	
Solvent	C_6H_6	$CDCl_3$	CS_2	$CDCl_3$	$CDCl_3$	$CDCl_3$
ν_{4a} [c]	439.79	456.13	466.88	461.44	458.93	463.09
ν_{5a} [c]			152.34	142.08		
ν_{4e} [c]	100.58	105.97	126.65	123.90	126.35	121.67
ν_{5e} [c]			452.71	435.88		
ν_{5a}	132.29	154.74	203.75	187.86	192.98	170.18
ν_{5e}	116.84	154.76	174.10	179.02	163.39	155.90
J_{4a4e} [d]	6.30	6.26	6.33	6.27	6.29	6.22
J_{5a5e} [d]			6.72	6.57		
J_{5a5e}	−14.27	−14.13	−13.75	−13.97	−14.11	−14.05
J_{4a5a}	10.91	10.88	9.54	8.36	11.04	11.03
J_{4a5e}	1.86	1.90	2.08	3.12	1.62	1.37
J_{5a5e}			4.82	4.70		
J_{5e5e}			3.09	4.97		
Assigned transitions	325	244	322	349	85	82
RMS error	0.080	0.074	0.068	0.066	0.076	0.062

[a] Chemical shifts downfield from TMS. All long-range coupling constants are negligible. [b] 60 MHz spectrum measured at −60 °C. The chemical shifts have been converted to 100 MHz values. [c] Methine or methyl shift as appropriate. [d] Vicinal $CHCH_3$ coupling constant.

geometrical isomers.[4] The existence of non-equilibrium isomer mixtures implies that thermal atomic inversion of arsenic is slow at room temperature as expected owing to the high barrier (25–42 kcal/mol).[19,20] However, the ^{1}H NMR spectra of aged samples of I–XV showed measurable amounts of only one isomer which is believed to be the thermodynamically more stable form. The present spectral analyses have therefore only been performed on the predominant isomers.

The ^{1}H NMR spectra of I in benzene and carbon disulfide solutions at ambient probe temperature, showed a broad octet and doublet for the methine and methylene protons, respectively. The corresponding methine and methylene NMR signals of XII recorded at ambient probe temperature in benzene and carbon disulfide solutions, displayed a broad sextet and triplet, respectively. However, at low temperature in carbon disulfide solution, the NMR spectra of I and XII proved to be almost identical to the spectra of the analogous methoxy-compounds. These observations imply that a process which leads to exchange of the nuclear magnetic environments of the methylene as well as the methine hydrogens, is taking place in these chloro-compounds. We believe, in accordance with previous conclusions,[3,8,21] that this process is an intermolecular chlorine exchange rather than a thermal inversion at arsenic.

The large vicinal coupling constant (10.2–12.4 Hz) observed in all compounds except XII and XIII, is typical for an axial-axial coupling in a chair conformation.[1,2,6–10] This value together with characteristic values of the remaining parameters, indicate strongly that these molecules, less XII and XIII, exist almost entirely in one chair conformation. The NMR data of the present compounds are adequately explained (*vide infra*) on the basis of two chair conformations, A and B, differing essentially in the configuration at arsenic. The chloro-compounds are formed in the main in one preferred configuration believed to be the more stable form A.[4] However, replacement of chlorine by methoxy in these compounds yielded, initially, the unstable isomer B which unless special care was taken, readily isomerized into A under the reaction conditions.[8]

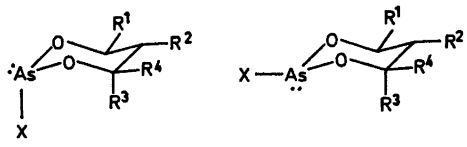

A B

It is noted in Tables 1 and 2 that the axial protons appear at lower field than the geminal equatorial protons in agreement with previous results for trimethylene sulfites [23–24] and 1,3,2-dioxaphosphorinanes [6–10,25] possessing axial 2-substituents. This observation thus indicates, in accordance with previous conclusions,[2–4] that the preferred orientation of the substituent at arsenic is axial, that is, the A conformation is the thermodynamically more stable form.

In the following discussion it is convenient to divide the investigated compounds into five groups according to their substitution patterns, *viz.* Group 1, 5-substituted; group 2, 4-substituted; group 3, *cis*-4,6-dimethyl-substituted; group 4, *trans*-4,6-dimethyl-substituted; and group 5, 4,6,6-trimethyl-substituted compounds. It can be concluded, on the basis of the coupling constants, that the molecular conformations are very similar within a given group and also, to some extent, in between different groups.

The large vicinal coupling constant (*ca.* 11 Hz) observed in the group 1 compounds shows that the substituent a C(5) occupies an equatorial position as expected. The value of J_{4a5a} in compounds I–V is about 1 Hz smaller than in the unsubstituted 1,3,2-dioxarsenanes.[3] The value of J_{5a5e} is, however, hardly affected by substitution at C(5). Similar effects or lack thereof, on the vicinal coupling constants upon substitution at C(5) have also been observed in 1,3,2-dioxaphosphorinanes [10] and trimethylene sulfites.[23] The reduction in J_{4a5a} is probably caused by the exocyclic substituent at C(5) rather than by a considerable reduction in ring puckering.

The NMR parameters of the group 2 compounds VI–IX, are consistent with an equatorial position of the substituent at C(4). This observation is in agreement with previous results for 2-chloro-4-methyl-1,3,2-dioxarsenane [3] and its phosphorus analogue.[10]

The values of J_{4a5a} and J_{5a5e} in group 2 are close to the corresponding parameters in group 1. Apparently, a substituent at C(4) produces a similar reduction in J_{4a5a} as a substituent at C(5). The value of J_{5a5a} on the unsubstituted side of the ring is, however, quite close to the axial-axial coupling constant in the almost staggered conformation of unsubstituted 2-X-1,3,2-dioxarsenanes (X = Cl, Br, OMe, OPh).[3] On this basis, an essentially staggered conformation of the O–C(4)–C(5)–C(6)–O portion of the ring is expected in VI–IX. This assumption is supported by calculations of the C(4)–C(5)–C(6)–O torsional angle based upon the *R*-value method due to Lambert [26] in that the calculated torsional angles range from 59.6 to 60.4°.

Inspection of Table 1 shows that the equatorial phenyl group at C(4) or C(5) gives rise to a considerable downfield shift of the ring protons in comparison with methyl or *tert*-butyl. This shift effect is largest at the geminal methine proton and decreases rapidly with the distance from the phenyl group. It is thus evident that the low-field shift is caused by the ring current effect of the phenyl group. It is also noted in Table 1 that the chlorine substituent at arsenic produces, in general, a considerably larger paramagnetic shift effect than the methoxy and phenoxy groups. A similar trend in the chemical shifts of 2-X-1,3,2-dioxarsenanes (X = Cl, OMe and OPh) [3] and their phosphorus analogues [27] is also noted upon inspection of the published data.

The measured values of J_{4a5a} and J_{4a5e} in the group 3 compounds X and XI, are very close to those in group 2. For the analogous phosphites [25] and *cis*-4,6-dimethyl-1,3-trimethylene sulfite with an axial S = O group,[24] ranges of J_{4a5a} 11.4–11.6 Hz and J_{4a5e} 2.1–2.4 Hz have been reported. These parameters are thus fairly close to those in X and XI. We conclude that these systems exist in similar chair conformations with axial 2-substituents and equatorial methyl groups.[8,11]

Comparison of the chemical shifts of X and XI is not relevant since these compounds have been examined in different solvents. The apparent upfield proton shifts in X as compared to XI, are obviously caused by the benzene solvent.

The NMR data of the group 4 compounds XII and XIII, are not so readily interpreted. The remarkably small value of J_{4a5a} together

with fairly large values of J_{5a6e} and J_{5e6e} cannot be explained on the basis of a single chair conformation like A or B. However, if it is assumed that the observed coupling constants are time-averaged values resulting from an equilibrium between conformers C and D in which C is the predominant form, then J_{4a5a} would be reduced by the inclusion of a fair amount of equatorial-equatorial coupling whereas J_{5e6e} would gain a similar increase from the axial-axial coupling. The two axial-equatorial coupling constants would not be appreciably changed by this process since $J_{ae} \approx J_{ea}$. The stereoisomers C and D differ essentially in the orientation of the substituent on arsenic. For the analogous 2-methoxy-*trans*-4,6-dimethyl-1,3,2-dioxaphosphorinane White *et al.*[8] also found evidence for a conformational equilibrium. In this context, it should be remembered that chair-chair conversions in the arsenites and phosphites may be influenced by vicinal-pair electron repulsions called into play on rotation about the O – As or O – P bonds.[7]

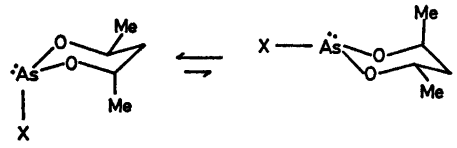

C D

The axial-axial and equatorial-equatorial coupling constants for the equilibrium C⇌D can be expressed by eqn. (4).

$$J_{4a5a} = pJ_{aa} + (1-p)J_{ee}$$
$$J_{5e6e} = pJ_{ee} + (1-p)J_{aa} \quad (4)$$

where p is the relative weight of the predominant conformer. Eqn. (5) is obtained by eliminating J_{ee} from eqn. (4).

$$p = \frac{J_{aa} - J_{5e6e}}{2J_{aa} - J_{4a5a} - J_{5e6e}} \quad (5)$$

On the assumption that the C and D conformers have the same partition function it follows that

$$p = \frac{1}{1 + \exp(-\Delta G^\circ/RT)} \quad (6)$$

where ΔG° is the free energy difference between the two conformers.

Unfortunately, J_{aa} is not known for the individual C and D conformers of XII and XIII. However, a fair estimate of J_{aa} is the average value of J_{4a5a} in the six investigated compounds possessing an equatorial methyl group at C(4) or C(5). By inserting the obtained value of $J_{aa} \approx 10.9$ Hz, and the measured values of J_{4a5a} and J_{5e6e} in XII and XIII, into eqn. (5) we obtain $p \approx 0.85$ and 0.70 at −60 and 30 °C, respectively. These values of p yield by means of eqn. (6), $\Delta G^\circ(-60\ ^\circ\text{C}) \approx 0.7$ kcal/mol and $\Delta G^\circ(30\ ^\circ\text{C}) \approx 0.9$ kcal/mol.

Hardly measurable amounts of the less stable isomer have been observed for most of the other arsenanes at thermal equilibrium. This indicates that the conformational free energy difference between axial and equatorial substituents at arsenic, is greater than about 2 kcal/mol in these compounds. Similar free energy differences in favour of an axial P – OMe orientation have been reported for the related 1,3,2-dioxaphosphorinanes.[7,8,11] The low value of ΔG° in XII and XIII indicates a reduced stability of the C conformer. We believe that this is a result of severe *syn*-axial or 1,3-diaxial interactions between the axial As – X group and the axial methyl group at C(6).

The average torsional angle of the O – C(4) – C(5) – C(6) – O portion in the *trans*-dimethyl rings has been calculated using the *R*-value method. The calculated values (54 – 55°) indicate that these rings are less puckered by *ca.* 3° than their mono- and disubstituted analogues possessing only equatorial ring substituents on the carbon skeleton. This observation probably reflects a tendency of the axial methyl group at C(6) to move away from the axial As – X bond and the axial methylene hydrogen at C(4) thereby reducing the *syn*-axial interactions in conformer C. A further reduction in the 1,3-steric interactions is expected owing to a flattening of the ring about arsenic in XII and XIII with respect to the analogous phosphites.[8]

The NMR data of the group 5 compounds show clearly that the major isomers exist almost entirely in a single chair conformation with one axial and two equatorial methyl groups. The conformation possessing diaxial methyl groups can be rejected on steric grounds. A fair amount of the less stable isomer of XV was observed at thermodynamic equilibrium. This observation again reflects a reduction in

the free energy difference between the A and B isomers owing to the 1,3-diaxial interactions in the former.

It is worthwhile to note that the relative shifts of the methylene and methyl hydrogens are the same in compounds XII–XV in that the axial signal appears downfield of the equatorial one. The general downfield shift of axial hydrogens as compared to equatorial ones, is mainly attributed to the anisotropy effect in these systems.

The measured values of the geminal coupling constants in I–XV cover the ranges −10.7 to −11.7 Hz and −13.7 to −14.5 Hz for the O–CH_2–C and C–CH_2–C moieties, respectively. These values are quite close to those reported for unsubstituted 1,3,2-dioxarsenanes [2] and variously substituted 1,3,2-dioxaphosphorinanes[6,7,10,27] and trimethylene sulfites.[22–24] The oxygen heteroatom thus gives rise to a positive increase of *ca.* 3 Hz in comparison with carbon. Molecular models of the six-membered arsenites indicate that both lone pairs of electrons on the oxygen heteroatom roughly bisect the CH_2 group (*i.e.* the H–H intermolecular axis). The contribution to J_{4a4e} and J_{4a4e} from the lone electron pairs is thus expected to be minimal and the positive contribution to the coupling is mainly attributed to inductive removal of σ-electrons from the CH_2 orbitals by the adjacent oxygen.[28,29]

REFERENCES

1. Aksnes, D. W. and Vikane, O. *Acta Chem. Scand. 26* (1972) 4170.
2. Aksnes, D. W. *Acta Chem. Scand. A 28* (1974) 1175.
3. Arbuzov, B. A., Anonimova, I. V., Vul'fson, S. G., Yuldasheva, L. K., Chadaeva, N. A. and Vereshchagin, A. N. *Phosphorus 5* (1974) 17.
4. Aksnes, D. W. and Tögersen, S. *Acta Chem. Scand. A 29* (1975) 376.
5. Denney, D. Z. and Denney, D. B. *J. Am. Chem. Soc. 88* (1966) 1830.
6. Hargis, J. H. and Bentrude, W. G. *Tetrahedron Lett. 51* (1968) 5365.
7. Bentrude, W. G. and Hargis, J. H. *J. Am. Chem. Soc. 92* (1970) 7136, and references therein.
8. White, D. W., Bertrand, R. D., McEwen, G. K. and Verkade, J. G. *J. Am. Chem. Soc. 92* (1970) 7125, and references therein.
9. Bentrude, W. G., Yee, K. C., Bertrand, R. D. and Grant, D. M. *J. Am. Chem. Soc. 93* (1971) 797.
10. Bergesen, K. and Albriktsen, P. *Acta Chem. Scand. 26* (1972) 1680.
11. Haemers, M., Ottinger, R., Zimmermann, D. and Reisse, J. *Tetrahedron 29* (1973) 3539, and references therein.
12. Kamai, G. and Chadaeva, N. A. *Dokl. Akad. Nauk. SSSR 81* (1951) 837.
13. Bothner-By, A. A. and Castellano, S. *LAOCN3*, Mellon Institute, Pittsburgh, Penn., U.S.A.
14. Johannesen, R. B., Ferretti, J. A. and Harris, R. K. *J. Magn. Reson. 3* (1970) 84.
15. Aksnes, D. W. *KOMBIP, Progr. No. 205*, Quantum Chemistry Program Exchange, Indiana University, Chemistry Department, Bloomington, Ind., U.S.A.
16. Kowalewski, V. J. and de Kowalewski, D. G. *J. Chem. Phys. 37* (1962) 2603.
17. Diehl, P. *Helv. Chim. Acta 48* (1965) 567.
18. Diehl, P., Harris, R. K. and Jones, R. G. *Progr. Nucl. Magn. Reson. Spectrosc. 3* (1967) 1.
19. Casey, J. P. and Mislow, K. *Chem. Commun.* (1970) 999.
20. Sénkler, G. H. Jr. and Mislow, K. *J. Am. Chem. Soc. 94* (1972) 291.
21. Fontal, B. and Goldwhite, H. *Tetrahedron 22* (1966) 3275.
22. Albriktsen, P. *Acta Chem. Scand. 25* (1971) 478.
23. Albriktsen, P. *Acta Chem. Scand. 26* (1972) 1783.
24. Cazaux, L. and Maroni, P. *Bull. Soc. Chim. Fr.* (1972) 773.
25. Albrand, J.-P., Gagnaire, D., Robert, J.-B. and Haemers, M. *Bull. Soc. Chim. Fr.* (1969) 3496.
26. Lambert, J. B. *Acc. Chem. Res. 4* (1971) 87.
27. Bergesen, K. and Albriktsen, P. *Acta Chem. Scand. 25* (1971) 2257.
28. Pople, J. A. and Bothner-By, A. A. *J. Chem. Phys. 42* (1965) 1339.
29. Chahill, R., Cookson, R. C. and Crabb, T. A. *Tetrahedron 25* (1969) 4681, 4711.

Received November 14, 1975.

Acta Chemica Scandinavica A 30 (1976) 335—339

The Crystal Structure of Thallium(I) Dibutyldithiocarbamate

ERIK ELFWING,* HELGA ANACKER-EICKHOFF, PER JENNISCHE and ROLF HESSE

Institute of Chemistry, University of Uppsala, Box 531, S-751 21 Uppsala, Sweden

The crystal structure of thallium(I) dibutyldithiocarbamate, $TlS_2CN(C_4H_9)_2$, has been determined from three-dimensional X-ray data. The crystals are monoclinic, space group $P2_1/c$. Unit cell parameters: $a = 14.108(2)$ Å, $b = 10.186(2)$ Å, $c = 9.647(2)$ Å, $\beta = 104.35(2)°$, $Z = 4$. The structure is built from centrosymmetric dimeric molecules linked by thallium-sulfur coordination to form layers parallel to the bc plane. The butyl ligands cover both sides of the layer so that only van der Waals interactions exist between adjacent layers. Thallium coordinates four sulfur atoms (2.97 – 3.16 Å) within the same dimer and two more distant sulfur atoms (3.98 – 4.19 Å). The structure resembles the structure of the corresponding cesium compound. The small differences between the two structures are discussed.

A number of thallium(I) dialkyldithiocarbamates have been investigated at this Institute.[1–5] They all contain dimeric molecules of the same type but the arrangement of the dimers is different. The linkage of the dimers is strongly influenced by the size and the kind of the alkyl groups. Since the coordination number of thallium decreases with increasing length of the ligands, a delicate balance evidently exists between packing and coordination requirements.

Thallium(I) dibutyldithiocarbamate has a lower melting point [6] than the corresponding isobutyl compound (75 – 76 °C and 166 – 168 °C (decomp.), respectively) and the crystals are much softer indicating a crystal structure with lower interaction between the building stones. The structure was expected to give additional information on the interaction between metal coordination and molecular packing.

* Present address: c/o NIFE Jungner AB, 57200 Oskarshamn, Sweden.

UNIT CELL AND SYMMETRY

Formula unit: $TlS_2CN(C_4H_9)_2$
Crystal system: monoclinic
Space group: $P2_1/c$ (No. 14)
$a = 14.108(2)$ Å, $b = 10.186(2)$ Å, $c = 9.647(2)$ Å,
$\beta = 104.35(2)°$
$Z = 4$, $D_m = 2.026(3)$ g cm^{-3}, $D_c = 2.021(1)$ g cm^{-3}

EXPERIMENTAL

Crystals of thallium(I) dibutyldithiocarbamate were prepared by Åkerström.[6] They were obtained from benzene and ethanol (1:1) as pale yellow square plates.

The density was measured by flotation in an aqueous solution of K_2HgI_4. The unit cell dimensions were determined from a Guinier-Hägg powder photograph using $CrK\alpha_1$ radiation with silicon ($a = 5.4305$ Å)[7] as internal standard.

489 independent reflections were recorded in the layers $0 \leq k \leq 8$ on equi-inclination Weissenberg photographs using $CuK\alpha$ radiation. The low upper θ limit, about 40°, was expected because of the low melting point and the softness of the crystals. The multiple film technique with four films was used. The crystals decomposed in the X-ray beam, so that each crystal could be used for one layer only. The relative intensities of the reflections were measured with an automatic film scanner SAAB AFS MK II,[8,9] connected on-line to an IBM 1800 processor controller. Process and integration programs by Werner [9] were used. The indexing was performed by a program of our own. The parameters for the integration procedure were the same as those used in two previous determinations.[1,5] A correction factor for the intensities of the strong reflections was applied as suggested by Werner.[10] Corrections were made for absorption as well as for Lorentz and polarization effects. Interlayer scale factors were determined from data obtained by recording the layers $hk0$ and $hk1$.

Table 1. Atomic coordinates and thermal parameters, listed as isotropic B or anisotropic b_{ij}. The anisotropic temperature factor is defined as $\exp(-b_{11}hh-2b_{12}hk..)$. The standard deviation corresponding to the last digit is shown in parentheses.

Atom	x	y	z	B(Å^2)
Tl	0.0174(3)	0.1759(7)	0.0079(5)	
S1	0.176(2)	−0.044(3)	0.087(3)	3.0(7)
S2	0.037(2)	−0.016(3)	0.272(4)	5.9(9)
C0	0.151(5)	−0.041(7)	0.255(8)	1(2)
N	0.227(8)	−0.066(11)	0.368(12)	8(3)
C11	0.329(7)	−0.068(10)	0.370(11)	4(2)
C12	0.355(5)	−0.210(13)	0.352(14)	7(3)
C13	0.468(9)	−0.222(13)	0.356(14)	8(4)
C14	0.505(11)	−0.361(15)	0.325(18)	11(5)
C21	0.211(7)	−0.071(10)	0.516(11)	4(2)
C22	0.249(7)	0.075(10)	0.605(11)	4(2)
C23	0.230(6)	0.054(9)	0.746(9)	3(2)
C24	0.263(9)	0.190(16)	0.838(15)	8(3)
	b_{11}	b_{22}	b_{33}	
Tl	0.0042(3)	0.0062(30)	0.0080(6)	
	b_{12}	b_{13}	b_{23}	
Tl	0.0017(8)	−0.0013(3)	0.0038(10)	

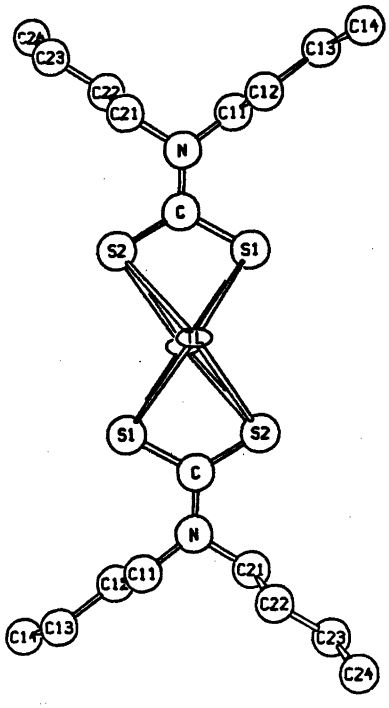

Fig. 1. The dimeric molecule in thallium(I) dibutyldithiocarbomate. The sulfur plane coincides with the paper plane.

DETERMINATION OF THE ATOMIC POSITIONS

Approximate positions of the thallium and sulfur atoms were found from a three-dimensional Patterson synthesis and adjusted by least squares calculations. Five of the carbon atoms were located from a three-dimensional difference synthesis and the temperature factor of thallium was refined anisotropically. The nitrogen atom and the remaining carbon atoms could then be located from a difference synthesis. No attempt was made to locate the hydrogen atoms.

The coordinates and isotropic temperature factors of all atoms were refined by full matrix least squares minimizing $\sum\omega(|F_o|-|F_c|)^2$. The weights, ω, were calculated according to Cruickshank [11] ($a=90.0$, $c=0.010$, $d=0.0$). Atomic scattering factors were taken from Hanson *et al.*[12] The nine scale factors were included in the refinement.

The least squares calculations were continued until the shifts on the parameters were less than 10 % of the estimated standard deviations. The final discrepancy index $R=\sum|(|F_o|-|F_c|)|/\sum|F_o|$, was 0.105.

The final atomic and thermal parameters are shown in Table 1. Tables of observed and

Table 2. Distances and angles in the dibutyldithiocarbamate ligand. The notation used is shown in Fig. 1. Atoms related by centrosymmetry are denoted by a bar.

Atoms	Distance (Å)	Atoms	Angle (°)	Atoms	Angle (°)
S1 – C0	1.74(8)	Tl – S1 – C0	85(3)	$\overline{\text{Tl}}$ – S1 – C0	85(3)
S2 – C0	1.67(8)	Tl – S2 – C0	85(3)	$\overline{\text{Tl}}$ – S2 – C0	83(3)
C0 – N	1.35(13)	S1 – C0 – S2	121(4)	S1 – C0 – N	116(7)
N – C11	1.44(15)	S2 – C0 – N	123(7)	C11 – N – C21	112(9)
N – C21	1.50(15)	C0 – N – C11	128(10)	C0 – N – C21	120(9)
C11 – C12	1.51(17)	N – C11 – C12	107(9)	N – C21 – C22	110(8)
C12 – C13	1.58(17)	C11 – C12 – C13	110(10)	C21 – C22 – C23	103(7)
C13 – C14	1.57(20)	C12 – C13 – C14	117(11)	C22 – C23 – C24	106(8)
C21 – C22	1.73(14)				
C22 – C23	1.47(13)				
C23 – C24	1.65(18)				
S1···S2	2.96(4)				

calculated structure amplitudes may be obtained on request from the Institute of Chemistry, University of Uppsala, Box 531, S-751 21 Uppsala 1, Sweden.

DESCRIPTION AND DISCUSSION

The structure of thallium(I) dibutyldithiocarbamate consists of dimeric molecules $[TlS_2CN(C_4H_9)_2]_2$, Fig. 1, which also gives the atomic notation. The distances and angles are given in Table 2. There are two molecules in the unit cell.

The thallium atoms are situated on either side of a sulfur parallelogram with edges 2.96(4) and 4.03(3) Å; the shorter edges connect the sulfur atoms within the ligands. The thallium-thallium distance is 3.62(1) Å. The SSCNCC parts of the ligands are planar with a maximum deviation of 0.1 Å from the least squares planes. The butyl groups have planar zig-zag carbon chains (maximum deviation 0.04 Å) situated on opposite sides of the central ligand plane.

A related dimeric molecule with similar shape and overall dimensions was found in the compound of cesium with the same ligand.[13] The metal-sulfur distances in the two compounds differ more than expected from metal ion radii. The intermolecular Cs – S distances, 3.53 – 3.62 Å, agree well with the sum of the ionic radii,[14] $r(Cs^+) = 1.69$ Å, $r(S^{2-}) = 1.84$ Å, but the corresponding distances in the thallium compound are 0.2 Å shorter than the radial sum ($r(Tl^+) = 1.44$ Å). Since thallium(I) is highly polarizable [15] it may be assumed that

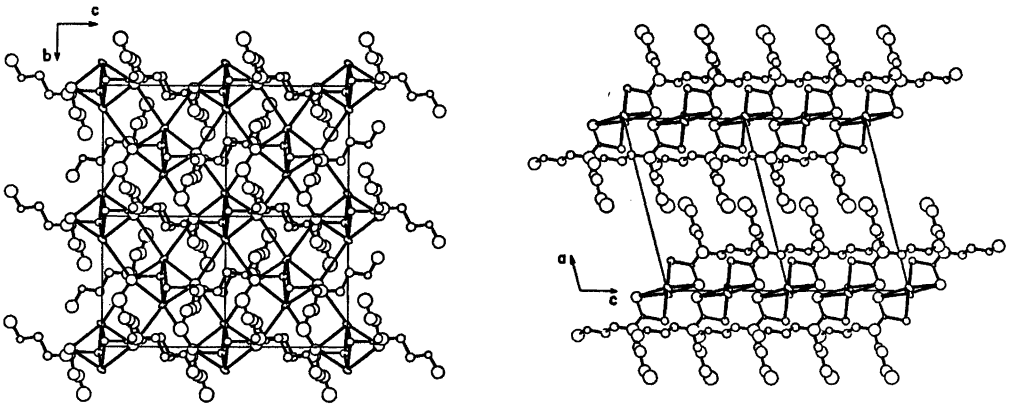

Fig. 2. The *yz* projection and the *zx* projection of two and four unit cells, respectively.

Table 3. Distances of coordination. The relationship between the coordinates of the sulfur atoms and those given in Table 2 is shown.

Atoms		Distance (Å)
Tl – S1	$-x,-y,-z$	2.97(3)
Tl – S2	$-x,-y,-z$	3.08(3)
Tl – S1	x,y,z	3.12(3)
Tl – S2	x,y,z	3.16(3)
Tl – S2	$-x,\frac{1}{2}+y,\frac{1}{2}-z$	3.98(4)
Tl – S2	$x,\frac{1}{2}-y,-\frac{1}{2}+z$	4.19(4)

such short thallium-sulfur distances require a displacement of the thallium electron clouds towards the exterior of the molecule. The dimers are linked by thallium-sulfur coordination in layers parallel to the *bc* plane. The butyl ligands project from both sides of this plane (Fig. 2). The layers are stacked upon one another in the *a* direction with only van der Waals interaction between them.

Within a sphere of radius 5 Å the thallium atom is surrounded by six sulfur atoms forming a distorted trigonal prism, Table 3 and

Table 4. Distances, D, and angles, A, in the thallium(I) dialkyldithiocarbamates listed in order of increasing D(Tl – Tl). D* refers to intermolecular distances. Values in Ångström and degrees.

Alkyl	D(Tl – Tl)	D(Tl – S)	D*(Tl – Tl)	D*(Tl – S)	Ref.
Isopropyl	3.58	2.98, 3.03, 3.04, 3.05	3.64	3.86	4
Ethyl (dimer B)	3.60	3.02, 3.05, 3.07, 3.10	3.47	3.80, 3.89	2
Ethyl (dimer A)	3.62	3.03, 3.07, 3.10, 3.12	3.54	3.71, 3.81	2
Butyl	3.62	2.97, 3.08, 3.12, 3.16	5.05	3.98, 4.19	
Isobutyl	3.68	2.97, 3.04, 3.12, 3.18	5.19	3.42	5
Methyl	3.85	2.99, 3.03, 3.28, 3.44	3.64	3.46, 3.52, 3.74	1
Propyl	3.98	2.88, 2.91, 3.02, 3.11, 3.12, 3.12, 3.29, 4.37	4.00	3.38, 3.52, 3.59, 3.69	3

Alkyl	A(Tl_2 vector – $-S_4$ plane normal)	A(S_2CNC_2 plane – $-S_4$ plane)	D(S – S)		A(S – S – S)
Iso-propyl	0	1	2.88	3.93	89.4
Ethyl (dimer B)	1	5	2.95	3.97	89.1
Ethyl (dimer A)	1	16	2.95	4.02	88.4
Butyl	3	3	2.96	4.03	87.7
Iso-butyl	2	7	2.95	3.96	87.9
Methyl	10	30	2.98	4.13	88.0

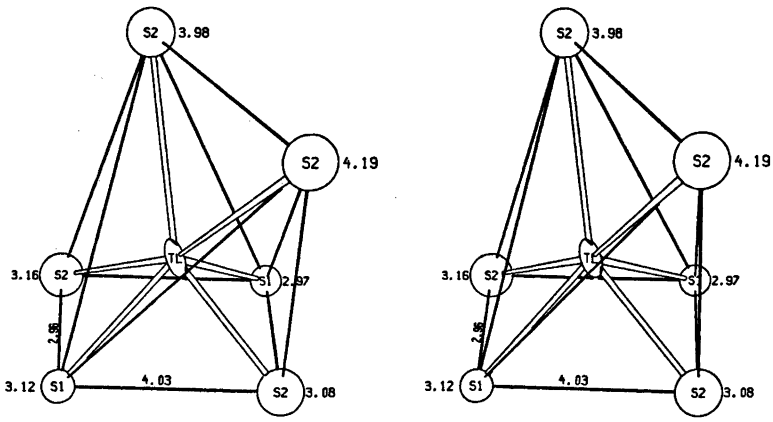

Fig. 3. Stereoscopic view of the coordinate polyhedron.

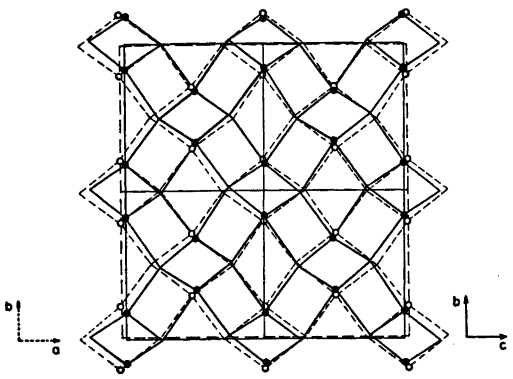

Fig. 4. The four-connected coordination net of the thallium and sulfur atoms in thallium(I) dibutyldithiocarbamate (full lines) superimposed on the corresponding net in cesium(I) dibutyldithiocarbamate (broken lines). Only the thallium atoms (dark circles) and the cesium atoms (light circles) are indicated.

Fig. 3. The four closest sulfur atoms belong to the same dimer, the two more distant atoms S2 to two other dimers. The Tl and S2 atoms are situated close to the *bc* plane (< 0.5 Å) and the S1 atoms, which do not participate in the linkage between the molecules, are situated 2.4 Å above and below this plane. The linkage can thus be described by a slightly puckered four-connected net of metal and sulfur atoms corresponding to that found in cesium dibutyldithiocarbamate.[13]

Although the dimensions of the two nets are similar, because of the similar shape and overall dimensions of the large molecules, the metal coordination geometries are different. Whereas the cesium atom is almost equidistant from all the coordinated sulfur atoms, the thallium atom is closer to the sulfur atoms in its own dimer than to the other two. The thallium atom polarization discussed above cannot alone explain the considerable length of the thallium-sulfur bonds between the molecules, since these bonds are shorter in other thallium dialkyldithiocarbamates, Table 4.

It appears that only the larger cesium atom is capable of achieving full contact with all six sulfur atoms. This difference between thallium and cesium was also observed in the dimethyldithiocarbamates,[1,16] where cesium has eightfold and thallium sevenfold coordination.

The effect of the linkage on the molecular geometry. The symmetry of the central part of the thallium dibutyldithiocarbamate molecule deviates only slightly from the *mmm* symmetry expected in an isolated dimer. Geometric data for the dimeric molecules in this and other thallium dialkyldithiocarbamates have been compiled in Table 4. The different degrees of distorsion from the ideal symmetry are clearly related to the interaction between the dimers in the crystal. The most regular dimers are found in the isopropyl compound, which has the lowest coordination number. Somewhat more distorted dimers occur in the butyl, isobutyl and ethyl compounds. The most distorted dimers are found in the propyl and methyl compounds which have high coordination numbers and short coordination distances between the molecules.

Acknowledgements. We thank Professor Ivar Olovsson for the facilities placed at our disposal and Dr. Åke Olin for valuable instruction and many stimulating discussions.

This work has been supported financially by grants from the Swedish Natural Science Research Council.

REFERENCES

1. Jennische, P. and Hesse, R. *Acta Chem. Scand. 27* (1973) 3531.
2. Pritzkow, H. and Jennische, P. *Acta Chem. Scand. A 29* (1975) 60.
3. Nilson, L. and Hesse, R. *Acta Chem. Scand. 23* (1969) 1951.
4. Jennische, P., Olin, Å. and Hesse, R. *Acta Chem. Scand. 26* (1972) 2799.
5. Anacker-Eickhoff, H., Jennische, P. and Hesse, R. *Acta Chem. Scand. A 29* (1975) 51.
6. Åkerström, S. *Ark. Kemi 24* (1965) 495.
7. Parrish, W. *Acta Crystallogr. 13* (1960) 838.
8. Abrahamsson, S. *J. Sci. Instrum. 43* (1966) 931.
9. Werner, P.-E. *Ark. Kemi 31* (1969) 505.
10. Werner, P.-E. *Acta Chem. Scand. 25* (1971) 1297.
11. Cruickshank, D. W. J., Pilling, D. E., Bujosa, A., Lovell, F. M. and Truter, M. R. *Computing Methods and the Phase Problem in X-Ray Analysis*, Pergamon Press, Oxford 1961, p. 32.
12. Hanson, H. P., Herman, F., Lea, J. D. and Skillman, S. *Acta Crystallogr. 20* (1966) 1040.
13. Aava, U. and Hesse, R. *Ark. Kemi 30* (1968) 149.
14. Wells, A. F. *Structural Inorganic Chemistry*, Oxford Clarendon Press, Oxford 1962, p. 71.
15. Lee, A. G. *Coord. Chem. Rev. 8* (1972) 289.
16. Wahlberg, A. *Acta Chem. Scand. A 30* (1976). *In press.*

Received November 18, 1975.

Acta Chemica Scandinavica A 30 (1976) 340—342

^{57}Fe Mössbauer Studies of $Fe_{1-t}T_tAs$ Phases with MnP Type Structure

KARI SELTE, ARNE KJEKSHUS and TROND RAKKE

Kjemisk Institutt, Universitetet i Oslo, Blindern, Oslo 3, Norway

Room temperature ^{57}Fe Mössbauer data for the ternary $Fe_{1-t}T_tAs$ phases (T = V, Cr, Mn, or Co) are reported and discussed in relation to their MnP type structure.

A comprehensive research programme on binary and ternary phases with the MnP type structure has been carried out to gain insight into their chemical bonding situation and to elucidate the factors governing the MnP *versus* NiAs type relationships. In the present work, solid solutions of the type $Fe_{1-t}T_tAs$ (T = V, Cr, Mn, or Co) have been investigated by Mössbauer spectroscopy at room temperature in order to study the variation of the ^{57}Fe Mössbauer parameters with composition.

EXPERIMENTAL

The samples were prepared as described in Refs. 1 – 5, their homogeneity being ascertained from powder X-ray (Guinier) photographs. Details concerning the ^{57}Fe Mössbauer experiments (at room temperature) and data reduction are given in Ref. 6. Chemical shift values are reported relative to $Na_2[Fe(CN)_5NO].2H_2O$ which was run before and after each sample and also used for velocity calibration.

RESULTS AND DISCUSSION

The ^{57}Fe Mössbauer chemical shift (δ) and quadrupole splitting (Δ) parameters for the $Fe_{1-t}T_tAs$ phases are shown in Fig. 1, the present values for FeAs being in reasonable agreement with those given in Refs. 7 and 8. The interval of t values studied varies: for T = Mn the two-phase field of the MnAs – FeAs system constitutes the limitation ($0 \leqq t \leqq 0.35$),[3] whereas the inherent statistical fluctuations (due to the lowered Fe-content) prevented unambiguous data reduction for large t in the other systems.

The overall decreasing tendency in δ on going from the left to the right of FeAs on Fig. 1 may be given an analogous interpretation to that proposed for the CrX_2 – FeX_2 – NiX_2 (X = As or Sb) series in Ref. 9. This implies that there should occur an effective transfer of d electron density (through the T – As bonds) from T = V, Cr, or Mn to Fe and from Fe to T = Co. The interpretation allows the metal atoms, randomly distributed over the metal sublattices, to be of adjustable size, and concurs with the decreasing average metal – non-metal bond lengths that must be established (*viz.* as inferred from structural data in Refs. 1 – 5, 10 – 12) in the series VAs – FeAs, CrAs – FeAs, MnAs – FeAs, and FeAs – CoAs. In addition to the more indirect effective transfer of electrons through the metal – non-metal bonds, the MnP type structure (as opposed to the FeS_2-m type discussed in Ref. 9) permits adjustments of the d-electron distribution through the direct metal – metal exchange routes in the atomic arrangement.

The parameter Δ reflects the degree of asymmetry of the overall electron density around the observer nuclei. A detailed account of Δ requires a comprehensive knowledge of the electronic states, and the very qualitative band structure information on phases with the MnP type structure will necessarily give the following discussion a rather speculative character.

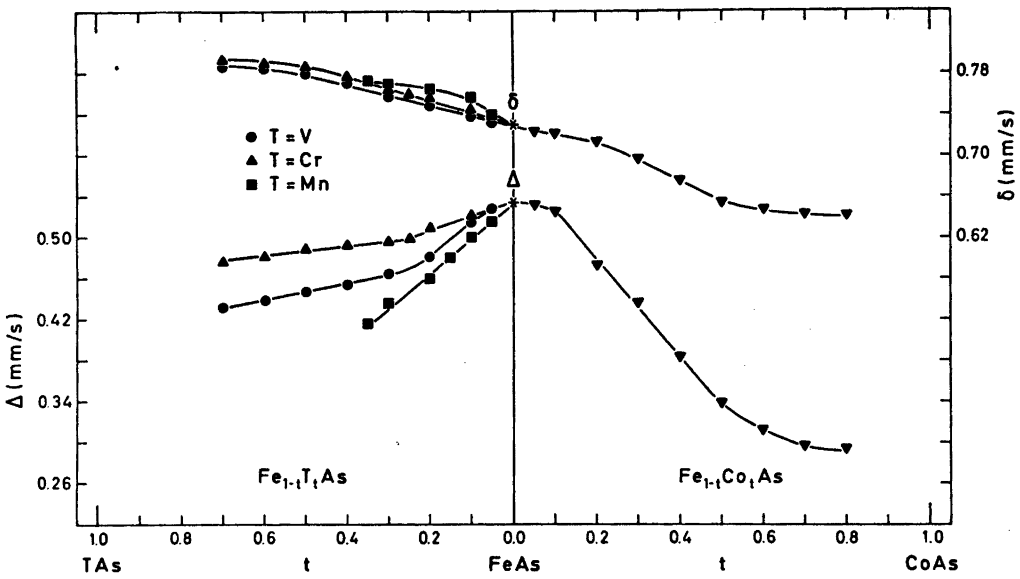

Fig. 1. Variation in ^{57}Fe Mössbauer chemical shift (δ) and quadrupole splitting (Δ) parameters with composition for $Fe_{1-t}T_tAs$ at room temperature. Estimated error limits do not exceed size of symbols.

In fact, even more crucial parameters for the interpretation, such as number of unpaired electrons in the paramagnetic state ($2S$; "spin only" approximation) and the intra-atomic exchange splitting energy ($E_{ex.}$), are lacking for the phases in question.

The influence on Δ by delocalized electrons must be comparatively small since these spend less time near the observer nuclei than localized. For the MnP type phases in particular, it should also be recalled that binary as well as ternary representatives show remarkable constancy in the unit cell proportions and positional parameters.[13] Moreover, due to the similarity in atomic arrangement, any difference in the effective atomic charges (which may be crucial in relation to δ) gives rise to only second order effects in the overall electronic asymmetry. Since contributions from localized bonding electrons in MnP type phases are likely to be insignificant, the variation in Δ must arise from corresponding distinctions in the metal–metal interactions and/or the non-bonding electrons on the metal atoms.

General band theoretical considerations as well as experience from special cases, suggest that bands representing metal–non-metal interactions are broad for both binary and ternary phases. On turning from binary to ternary MnP type phases, the band structure parameters that describe the bonding characteristics, may undergo changes which are compatible with the assumption of "averaged" metal atoms, as outlined in Ref. 9. Corresponding considerations lead to the suggestion that non-bonding states are to be represented by narrow bands, this common picture being somewhat modified for the MnP type phases for which the metal–metal interactions lead to broadening of the bands designated as "non-bonding" (*cf.* the discussion on MnAs in Ref. 14). In situations where the term "non-bonding" is fully applicable, no distinction between well defined compounds and solid solution phases is needed. Even in cases where the "non-bonding" states are not strictly non-bonding (*e.g.* resulting from perturbations due to metal–metal interactions as in MnP type phases), band descriptions for the binary end members cannot be mixed into an average "non-bonding" band picture for a given ternary composition. On the contrary, the "non-bonding" states of the $Fe_{1-t}T_tAs$ phases may be assumed to maintain much of their original

identity as FeAs and TAs states in the ternary composition region.

The use of ionic formulae provides a convenient tool in the evaluation of valence states even in cases where a covalent description should be more adequate (*cf.*, *e.g.*, Ref. 15). Thus, for phases with the MnP type structure, a valence state of three appears reasonable for the metal component (three electrons per metal atom engaged in metal–non-metal bonding). One therefore arrives at 2, 3, 4, 5, and 6 "non-bonding" d electrons for V, Cr, Mn, Fe, and Co in their monoarsenides. (This assumption concurs with that of Menyuk *et al.*[14] for MnAs.) Essentially the same number of "non-bonding" electrons must be associated with the individual metal atoms throughout the solid solution series. This constitutes a constraint on the mixing of bands in the ternary regions.

One factor which greatly influences the "non-bonding d^5 manifold" for Fe in $Fe_{1-t}T_tAs$ is the parameter $E_{ex.}$, which is reflected in the number of unpaired electrons. (Data referring to cooperative states are used below.) Following the schematic one-electron band description given for MnAs by Menyuk *et al.*[14], the situation in VAs and CoAs is assumed to be governed by $E_{ex.} \approx 0$, whereas $E_{ex.} \neq 0$ for CrAs, MnAs, and FeAs. Thus, the substitution of V or Co for Fe in FeAs may simulate a decrease in $E_{ex.}$ of FeAs, leading to a gradually more symmetrical (*viz.* with respect to α and β spin splitting, *cf.* Fig. 13 in Ref. 14) population of the Fe "d^5 manifold". The substitution of Cr or Mn for Fe in FeAs is, on the other hand, expected to increase $E_{ex.}$ of FeAs. Starting from the hypothetical FeAs band diagram, an increase in $E_{ex.}$ will lift the energies of the β spin states, thus promoting a more complete filling of the α spin states, and consequently a more symmetrical distribution of the "non-bonding" electrons of Fe. The decreasing tendency of Δ with t for all four $Fe_{1-t}T_tAs$ phases is accordingly explicable on the basis of this type of band model consideration. The individuality of the curves reflects distinctions in the population and symmetry of the "d^5 manifold".

The present discussion for the ^{57}Fe Mössbauer parameters of $Fe_{1-t}T_tAs$ is, in principle, also applicable to the corresponding data for $Fe_{1-t}T'_tP$ (T' = W, Mn, or Co) given in Ref. 7.

Acknowledgements. The authors wish to thank cand.real. Tor A. Oftedal for assistance in some of the ^{57}Fe Mössbauer measurements and Norges almenvitenskapelige forskningsråd for financial support.

REFERENCES

1. Selte, K., Kjekshus, A. and Andresen, A. F. *Acta Chem. Scand. 26* (1972) 3101.
2. Selte, K., Kjekshus, A. and Andresen, A. F. *Acta Chem. Scand. A 28* (1974) 61.
3. Selte, K., Kjekshus, A. and Oftedal, T. A. *Acta Chem. Scand. A 28* (1974) 803.
4. Selte, K., Kjekshus, A., Aaby, S. and Andresen, A. F. *Acta Chem. Scand. A 29* (1975) 810.
5. Selte, K., Kjekshus, A. and Andresen, A. F. *To be published.*
6. Kjekshus, A., Nicholson, D. G. and Mukherjee, A. D. *Acta Chem. Scand. 26* (1972) 1105.
7. Maeda, Y. and Takashima, Y. *J. Inorg. Nucl. Chem. 35* (1973) 1219.
8. Isaev-Ivanov, V. V., Kolchanova, N. M., Masterov, V. F., Nasledov, D. N. and Yarmarkin, V. K. *Soviet Phys.-Solid State 15* (1974) 2058.
9. Kjekshus, A. and Rakke, T. *Acta Chem. Scand. A 28* (1974) 1001.
10. Selte, K., Kjekshus, A., Jamison, W. E., Andresen, A. F. and Engebretsen, J. E. *Acta Chem. Scand. 25* (1971) 1703.
11. Selte, K. and Kjekshus, A. *Acta Chem. Scand. 25* (1971) 3277.
12. Selte, K., Kjekshus, A. and Andresen, A. F. *Acta Chem. Scand. 26* (1972) 4057.
13. Selte, K. and Kjekshus, A. *Acta Chem. Scand. 27* (1973) 3195.
14. Menyuk, N., Kafalas, J. A., Dwight, K. and Goodenough, J. B. *Phys. Rev. 177* (1969) 942.
15. Kjekshus, A. and Rakke, T. *Struct. Bonding (Berlin) 19* (1974) 45.

Received December 8, 1975.

Acta Chemica Scandinavica A 30 (1976) 343—350

Metal Ammine Formation in Solution. XVII. Stability Constants of Copper(II) Methylamine and Diethylamine Complexes Obtained from Solubility Measurements with Gerhardtite, $Cu(OH)_{1.5}(NO_3)_{0.5}$

LILIANA ILCHEVA* and JANNIK BJERRUM

Chemistry Department I, Inorganic Chemistry, H. C. Ørsted Institute, University of Copenhagen, DK-2100 Copenhagen Ø, Denmark

The solubility curve for the slightly soluble basic copper(II) nitrate gerhardtite ($Cu(OH)_{1.5}(NO_3)_{0.5}$) in 2 M methylammonium nitrate and 2 M diethylammonium nitrate, at 25 °C and in the pH range 4 to 9, has been determined by atomic absorption spectroscopy. From the data it was possible to estimate all of the consecutive stability constants in the methylamine-aqua system ($K_1 = 10^{4.11}$, $K_2 = 10^{3.40}$, $K_3 = 10^{2.70}$, $K_4 = 10^{1.87}$) and the orders of magnitude of the first stability constants in the diethylamine system. The constants differ only slightly from those in the copper(II) – ammonia system. The ammine formation with the aliphatic amines is somewhat influenced by hydroxo complex formation, for which a correction was introduced.

The solubility product of gerhardtite $K_s = [Cu^{2+}][OH^-]^{1.5}[NO_3^-]^{0.5}$ and the saturation constant $s = [Cu^{2+}][am]^{1.5}$ were found to be $10^{-15.75}$ and $10^{-10.50}$, respectively, in 2 M methylammonium nitrate and $10^{-16.12}$ and $10^{-11.35}$, respectively, in 2 M diethylammonium nitrate.

Ammonia and aliphatic amines behave rather similarly in their complex formation with silver(I) and mercury(II) ions.[1–3] The steric requirements of the amines thus appear to be only slightly greater than for ammonia, and it is of some interest to see to what extent this is the case for metal ions with a higher characteristic coordination number.[4] For this purpose we have in the present work studied the complex formation of copper(II) ions with methylamine and diethylamine in 2 M solutions of the corresponding alkylammonium nitrates. These particular amines are such strong bases that they almost completely precipitate the copper(II) ions in the pH-range in which the ammine complexes are formed, even in the presence of high concentrations of the alkylammonium salts. The usual method of determining the stability constants, involving the determination of the formation curve by means of pH-measurements, cannot therefore be used. One has to look for an alternative method, and one obvious possibility is to try to combine pH-measurements with solubility measurements on the basic precipitate formed. This method was found to work well in the present case where the precipitate is a basic copper(II) nitrate ($Cu(OH)_{1.5}(NO_3)_{0.5}$) found in nature as "gerhardtite". It has been shown earlier [5] by one of the present authors that gerhardtite has a well-defined solubility in ammonium nitrate solutions. Saturation is slow but equilibrium is reached after 1 – 2 weeks.

EXPERIMENTAL

Chemicals. All reagents were of analytical grade or of good commercial quality. 40 % aqueous methylamine (Riedel-de Haën) and pure diethylamine (Fluka, *puriss. p.a.*) were used.

Solutions. The various solutions were prepared in volumetric flasks by weighing or pipetting from stock solutions. 2.5 M stock solutions of the alkylammonium nitrates were prepared by neutralizing, *e.g.*, 1000 ml of 5.00 M HNO_3 with strong solutions of the amines, with

* On leave from Chemico-Technological Institute, Analytical Chemistry Department, Sofia 56, Bulgaria.

stirring and cooling in ice, and then diluting to 2000 ml with redistilled water. The working solutions (2.00 M) of the alkylammonium nitrates were made from the stock solutions by 4/5-dilution in volumetric flasks, the diluent being water, aqueous amine or nitric acid as required. The equivalence of acid and base in the 2 M alkylammonium nitrate solutions was determined by pH-measurements, and a correction was made, where necessary, for the self-dissociation of the protonated amine.

Acid-base constants of the amines. The concentration acid dissociation constants of the amines were determined by measuring the potential difference ΔE between 0.01 M solutions of HNO_3 and amine, respectively, in 2 M alkylammonium nitrate medium by means of a glass electrode. The constant for the methylammonium ion, $K_{CH_3NH_3^+}$, was determined to be $10^{-10.80 \pm 0.01}$ in 2 M $CH_3NH_3NO_3$,[6] whilst that for the diethylammonium ion, $K_{(C_2H_5)_2NH_2^+}$, was found to be $10^{-11.18 \pm 0.01}$ in 2 M $(C_2H_5)_2NH_2NO_3$.

Glass electrode measurements were performed in a jacketed vessel with thermostatted water flow. A selected Radiometer glass electrode (Type G 202 B) with the theoretical pH-dependence was used, and a specially constructed 1 M KCl-calomel electrode was employed as reference.[7] The potentiometer used was a Radiometer PHM 52 digital pH Meter, the mV-scale being preferred to the direct reading pH-scale.

Preparation of gerhardtite. To a mixture of 400 ml of 10 M NH_4NO_3 and 100 ml of 0.5 M $Cu(NO_3)_2$ in a 4 l Erlenmeyer flask was added, with stirring, 50 ml of 1.5 M aqueous ammonia and 1300 ml of distilled water, in that order. The solution was then placed on an electric hot plate with magnetic stirring and kept at about 60 – 70 °C. After some hours the solution became turbid and green crystals began to separate. The heating and stirring were continued for a day or more before the crystals were separated from the mother liquor. The crystals were washed several times with water, then with 96 % ethanol and dried at 80 °C. The yield was about 5 g.

Analysis of gerhardtite. Several portions were analyzed for copper by electrolysis in ammoniacal solutions, and for hydroxide by dissolution in standardized HCl and back titration with NaOH.[5] The copper content found (52.8 to 53.2 %) was close to the theoretical value of 53.0 %, and the number of OH-groups per Cu-atom was found to be 1.50 within a precision of about 1 %.

Solubility measurements were performed as follows: 2 M alkylammonium nitrate solutions, containing known added amounts of HNO_3 or of amine, were made up in 100 ml volumetric flasks. After addition of about 0.3 g of gerhardtite the solutions were transferred into pyrex flasks with tight fitting stoppers and placed to rotate in a thermostatted water bath at 25 °C. Then, after a sufficient lapse of time, the saturated solutions were separated from undissolved gerhardtite by filtration through a fine porosity glass sinter filter. After measurement of $pH = -\log[H^+]$, the saturated solutions were kept in a thermostatted room at 25 °C, sometimes for a few days, before being

Table 1. Solubility data for gerhardtite in 2 M methylammonium nitrate at 25 °C. $pH = 10.50 - p[CH_3NH_2]$.

No.	$C^\circ_{HNO_3}$	C°_{am}	h	ps_{Cu}	$p[Cu^{2+}]$	p[am]	pS	α_{CuOH}	$\bar{n}$
1	5.0×10^{-3}	–	439	2.45	2.37	5.35	10.40	0	~0
2	9.9×10^{-4}	–	475	3.12	3.09	4.90	10.43	0	0.14
3	7.4×10^{-4}	–	475	3.22	3.22	4.80	10.42	0	0.16
4	2.3×10^{-4}	–	335	3.63	3.80	4.48	10.52	0.01	0.32
5	1.0×10^{-4}	–	409	3.76	3.94	4.31	10.40	0.01	0.42
6	–	2.2×10^{-5}	574	3.95	4.32	4.22	10.64	0.02	0.50
7	–	4.8×10^{-5}	553	4.02	4.45	4.15	10.67	0.02	0.55
8	–	1.2×10^{-5}	575	4.11	4.75	3.98	10.72	0.02	0.84
9	–	2.5×10^{-4}	550	4.20	5.01	3.82	10.70	0.03	1.00
10	–	5.2×10^{-4}	549	4.24	5.54	3.47	10.75	0.04	1.43
11	–	1.1×10^{-3}	478	4.17	6.42	3.08	11.04	0.05	1.91
12	–	2.1×10^{-3}	478	3.97	7.07	2.78	11.24	0.06	2.38
13	–	1.1×10^{-2}	336	3.55	7.10	2.49	10.84	0.07	2.90
14	–	1.4×10^{-2}	360	3.18	7.58	2.28	11.00	0.09	3.00
15	–	3.5×10^{-2}	503[a]	2.57	–	1.86	–	0.14	3.30
16	–	4.7×10^{-2}	502[a]	2.23	–	1.76	–	0.17	–
Mean							10.50		

[a] $C^\circ_{Cu} = 0.0104$, gerhardtite precipitated after mixing.

Table 2. Solubility data for gerhardtite in 2 M diethylammonium nitrate at 25 °C. $pH = 10.82 - p[(C_2H_5)_2NH]$.

No.	$C°_{HNO_3}$	$C°_{am}$	h	ps_{Cu}	$p[Cu^{2+}]$	p[am]	pS	α_{CuOH}	$\bar{n}$
1	7.5×10^{-3}	–	357	2.31	2.30	5.99	11.29	0	0
2	5.0×10^{-3}	–	356	2.50	2.47	5.89	11.31	0	0
3	2.5×10^{-3}	–	356	2.79	2.79	5.72	11.38	0	0
4a	1.0×10^{-3}	–	312	3.18	3.21	5.43	11.36	–	–
4b	1.0×10^{-3}	–	363	3.17	3.21	5.47	11.43	0	~0
5	5.0×10^{-4}	–	362	3.47	3.52	5.29	11.46	0	~0
6a	5.0×10^{-6}	–	240	4.19	4.48	4.70	11.53	–	–
6b	5.0×10^{-6}	–	408	4.19	4.48	4.73	11.59	0.01	0.15
7a	–	2.4×10^{-4}	259	4.94	–	4.11	–	0.04	0.70
7b	–	2.4×10^{-4}	333	4.67	4.88	4.38	11.45	0.03	0.40
8a	–	4.8×10^{-4}	260	5.14	5.97	3.71	11.53	0.06	1.10
8b	–	4.8×10^{-4}	334	5.03	5.63	3.89	11.46	0.05	0.98
Mean							11.35		

analyzed for total and free copper(II).

The total copper(II) concentration (C_{Cu}) was determined by atomic absorption spectroscopy (Perkin-Elmer, Model 403), after dilution to $C_{Cu} \simeq 10^{-5}$ M, by comparison with standard solutions of copper(II) in the same medium.

The free copper(II) ion concentration [Cu^{2+}] was tentatively measured with a Radiometer Cupric Selectrode (F 1112 Cu). The electrode gave tolerably good results when the copper(II) ion concentration was not too small.

THE SOLUBILITY DATA

A selection of the solubility data is presented in Tables 1 and 2. The quantities $C°_{HNO_3}$ and $C°_{am}$ in the tables denote the initial concentrations of nitric acid and amine, respectively. For the equilibrated solutions saturated with gerhardtite we have tabulated the exponent ps_{Cu} of the solubility [$s_{Cu} = C_{Cu}(sat.)$], that of the free copper(II) ion, $p[Cu^{2+}]$, and that of the free amine p[am], calculated from the relationship

$$p[am] = pK_{amH^+} - \log 2 - pH$$

or, in the case of the most basic solutions, measured directly relative to an amine standard in the medium used. The 4th column in the tables ("Hours") indicates the length of time in which the solutions have been shaken with gerhardtite. Establishment of the equilibrium was somewhat faster in the more acid solutions, but seems always to be reached after 300 – 400 h. However, it should be mentioned that in the case of saturated solutions close to the solubility minimum, with copper concentrations of the order $10^{-4} - 10^{-5}$ M, the composition of the solutions moves somewhat towards lower p[am], along the solubility curve, by prolonged equilibrium adjustment. This is probably due to reaction with traces of CO_2 in the solutions (see, *e.g.*, Nos. 7 and 8 in Table 2).

The solubility curves are shown in Fig. 1. All the experimental data are plotted in the figure and an explanation of the plotted points is given in the figure text. For comparison, Fig. 1 also gives the solubility curve for gerhardtite in 2 M NH_4NO_3, as determined by one of the present authors in 1931.[5] The great similarity of the shape of this curve to that found for gerhardtite in 2 M $CH_3NH_3NO_3$ should be noted. In the 2 M diethylammonium nitrate solutions, in which gerhardtite is even less soluble than in 2 M $CH_3NH_3NO_3$, the solubility continues to decrease with increasing pH in the concentration range which could be studied. However, the solubility curve shows a decreasing slope and a minimum may be reached for $s_{Cu} \sim 0.5 \times 10^{-5}$ M at p[am] ~ 3, but it should be mentioned that the solubility of the basic salt in this case shows little tendency to increase again, colourless solutions being formed throughout the whole range up to high amine concentration.

The curve for 2 M NH_4NO_3 continues, for $p[NH_3] \leqq 2.2$, into a solubility curve for the dark violet tetrammine copper(II) nitrate. For the 2 M $CH_3NH_3NO_3$ medium the solubility

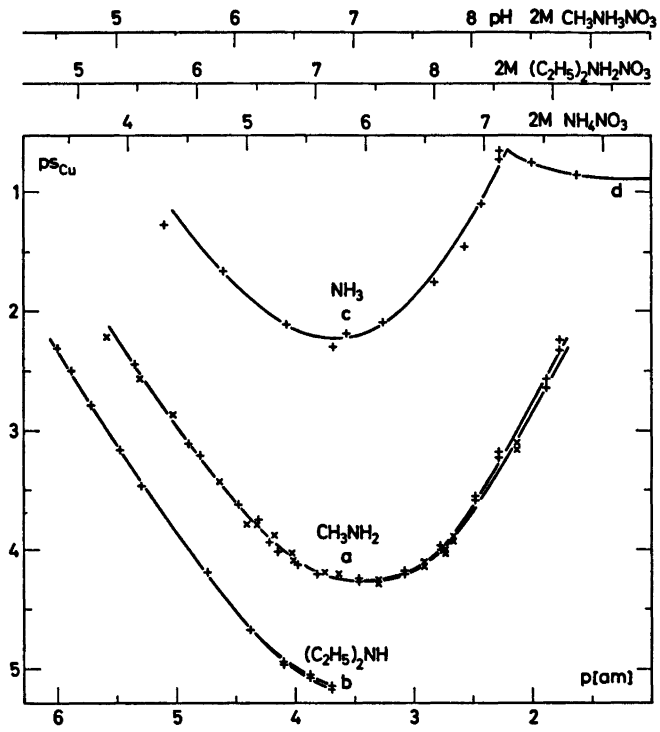

Fig. 1. The solubility curves for gerhardtite in 2 M methylammonium nitrate (curve a) and in 2 M diethylammonium nitrate (curve b) at 25 °C. All experimental results are shown. The points marked + correspond to the data tabulated in Tables 1 and 2. The data for the points marked × have not been tabulated, so as to reduce the size of the tables. In those cases where two points (either + or ×) are placed vertically above each other, the upper point represents the experimentally determined solubility and the lower point the solubility corrected for hydroxo complex formation. For comparison purposes the previously determined solubility curves for gerhardtite (curve c) [5] and tetrammine copper(II) nitrate (curved) [8] in 2 M NH_4NO_3 at 18 °C are also shown in the figure.

curve for gerhardtite passes over at a definite (but undetermined) value of $p[CH_3NH_2]$ into a curve for $Cu(OH)_2$ This was noticed because the precipitate from a solution of the composition $C°_{Cu} = 0.04$ M, $C°_{CH_3NH_2} = 0.14$ M turned, after some time, to black CuO. It was further noticed that a very soluble dark violet salt, probably $[Cu(CH_3NH_2)_4][(NO_3)_2$, is the stable solid phase at high amine concentrations.

THE SOLUBILITY PRODUCT OF GERHARDTITE

In 2 M alkylammonium nitrate solutions saturated with $Cu(OH)_{1.5}(NO_3)_{0.5}$, $S = [Cu^{2+}][am]^{1.5}$ is a solubility constant. In Tables 1 and 2 are given values for $pS = -\log S$. These values increase somewhat with increasing values for $p[Cu^{2+}]$, but this can be ascribed to the fact that the commercial Cu(II)-Selectrode used is not completely ideal in behaviour and shows deviations from Nernst's law. For this reason the values of pS in the acid range where the copper(II) ions are mainly present as aqua ions are assumed to be the most reliable, and the average values for pS given in Tables 1 and 2 are estimated in accordance with this assumption.

The exponent of the solubility product for gerhardtite: $K_s = [Cu^{2+}][OH^-]^{1.5}[NO_3^-]^{0.5}$ in 2 M alkylammonium nitrate solutions can be expressed as follows:

$$pK_s = pS + 1.5 \log \left(\frac{2 \times K_{amH^+}}{K_w} \right) - 0.5 \log 2.$$

Using the values found for pK_{amH^+} (10.80 for $CH_3NH_3^+$, and 11.12 for $(C_2H_5)_2NH_2^+$) and Harned's value for the ionic product of water in 2 M KCl at 25 °C ($pK_w = 14.10$),[9] pK_S is calculated to be 15.75 in 2 M $CH_3NH_3NO_3$, and 16.12 in 2 M $(C_2H_5)_2NH_2NO_3$ at 25 °C.

A value of $pS = 8.77$ for gerhardtite in 2 M NH_4NO_3 at 18 °C has previously been found.[5] In this medium $pK_{NH_4^+} = 9.40$ at 18 °C [10] and using Harned's value of $pK_w = 14.34$ in 2 M KCl at 18 °C,[9] one obtains $pK_s = 16.03$, to be compared with the values for pK_s in the other media at 25 °C.

THE INFLUENCE OF HYDROXO COMPLEX FORMATION

Methylamine and diethylamine are considerably stronger bases than ammonia and the possibility of hydroxo complex formation influencing the copper(II) – amine formation in the alkylammonium salt solutions must therefore be taken into account. The main products of the hydrolysis of copper(II) ions in dilute aqueous solutions are $CuOH^+$ and $Cu_2(OH)_2^{2+}$.[11-13] Denoting the hydrolysis constants as in "Tables of Stability Constants",[14] the concentrations of these species are given by the expressions:

$$[CuOH^+] = {}^*K_1[Cu^{2+}]/[H^+]$$
$$[Cu_2(OH)_2^{2+}] = {}^*\beta_{2,2}[Cu^{2+}]^2/[H^+]^2$$

and the fraction of copper(II) bound as hydroxo complex by the expression

$$\alpha_{OH} = \frac{{}^*K_1[H^+] + 0.5\,{}^*\beta_{2,2}[Cu^{2+}]}{[H^+]^2 + {}^*K_1[H^+] + 0.5\,{}^*\beta_{2,2}[Cu^{2+}]}$$

From the data of Pedersen [11] and Perrin [13] the hydrolysis constants in 2 M nitrate solutions at 25 °C can be estimated to be ${}^*K_1 \cong 10^{-8}$ and ${}^*\beta_{2,2} = 2 \times 10^{-11}$. The values of the hydrolysis constants for the aqua ammine systems are unknown, although ${}^*K_1$ for $Cu(NH_3)_3H_2O^{2+}$ can be estimated from data in the literature.[15,16] Reeves and Bragg [15] have titrated dilute solutions of $Cu(NH_3)_4^{2+}$ in 1 M aqueous ammonia with NaOH and found for the uptake of the first OH^-:

$$K_{OH} = \frac{[Cu(NH_3)_3OH^+][NH_3]}{[Cu(NH_3)_4^{2+}][OH^-]} = 10^{2.40}$$

${}^*K_1$, the acid dissociation constant for $Cu(NH_3)_3OH_2^{2+}$, is related to K_{OH} by the expression:

$${}^*K_1 = K_{OH} \times K_4 \times K_w = 10^{2.40} \times 10^{2.05} \times 10^{-14.10} = 10^{-9.65}$$

In this expression $K_4 = 10^{2.05}$ l mol^{-1} is the stability constant for binding the fourth ammonia, and $K_w = 10^{-14.10}$ is the ionic product of water. The values of ${}^*K_1$ for the aliphatic amine complexes cannot be very different from those for the ammonia complexes and are perhaps somewhat lower. We have therefore corrected for the hydroxo complex formation by assuming that ${}^*K_1$ increases smoothly from $10^{-9.5}$ for Cu $am_3H_2O^{2+}$ to 10^{-8} for Cu aq^{2+}. The value for ${}^*\beta_{2,2} = 2 \times 10^{-11}$ has been used without correction since the corresponding hydrolysis reaction only contributes to a slight extent to the hydrolysis at the low copper concentrations involved in the solubility measurements. The estimated values for α_{OH} are presented in Tables 1 and 2. In Table 1, ${}^*K_1$ was taken to be 10^{-8} for Nos. 1 – 8, 0.5×10^{-8} for Nos. 9 – 10, 2×10^{-9} for No. 11, 10^{-9} for No. 12, 0.5×10^{-9} for Nos. 13 – 14, and 0.3×10^{-9} for Nos. 15 – 16, whereas in Table 2 a value of 10^{-8} was used for Nos. 1 – 6, and 0.5×10^{-8} for Nos. 6 – 7. It can be seen that the correction for hydroxo complex formation is really significant – more than 10 % – only at relatively high amine concentrations (pH $\gtrsim$ 9).

ESTIMATION OF THE STABILITY CONSTANTS

A closer examination of the solubility data shows that the best way to estimate the stability constants is by means of the formation curve $\bar{n}$ *vs.* p[am]. Values of $\bar{n}$ can be obtained directly from the slope of the solubility curve at any p[am] by means of the formula:

$$\frac{\mathrm{d} \log s_{Cu}}{\mathrm{d} \log [am]} = \frac{\mathrm{d}\, ps_{Cu}}{\mathrm{d}\, p[am]} = n - 1.5$$

This formula can be derived as follows: Introducing $\alpha_0 = [Cu^{2+}]/s_{Cu}$ into the simple Bodländer formula,[10] one obtains:

$$\frac{\mathrm{d} \log \alpha_0}{\mathrm{d} \log [am]} = \frac{\mathrm{d} \log [Cu^{2+}]}{\mathrm{d} \log [am]} - \frac{\mathrm{d} \log s_{Cu}}{\mathrm{d} \log [am]} = -\bar{n}$$

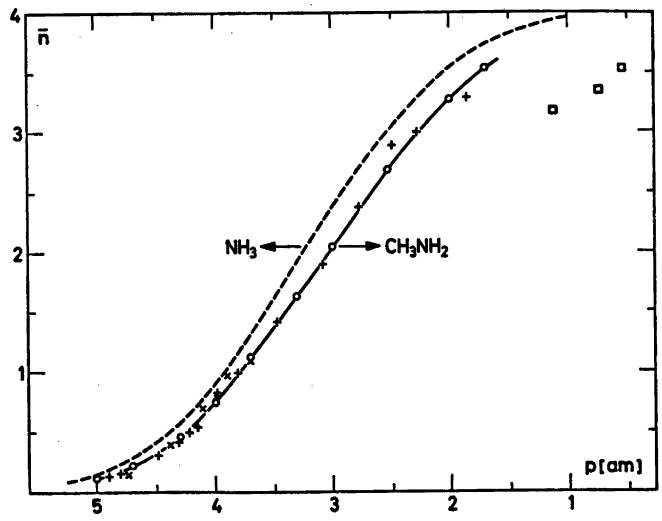

Fig. 2. The formation curve for the copper(II) methylamine system in 2 M $CH_3NH_3NO_3$ at 25 °C. The + points represent the experimental values from Table 1, and the ○ points represent values calculated using the computed stability constants given in Table 3. The □ points are uncorrected values obtained from the relationship $\bar{n} = (C_{am} - [am])/C_{Cu}$ by means of glass electrode measurements on 0.05 – 0.10 M $Cu(NO_3)_2$, 2 M $CH_3NH_3NO_3$ solutions with sufficiently high concentrations of CH_3NH_2 to prevent basic precipitation. The × points close to the methylamine curve represent the data for the diethylamine system from Table 2. The dashed formation curve in the figure is the curve for the copper(II) ammonia system under the same conditions (2 M NH_4NO_3 at 25 °C).[10]

From the expression for the saturation constant $S = [Cu^{2+}][am]^{1.5}$, one obtains d log $[Cu^{2+}] = -1.5$ d log [am], which inserted in the Bodländer formula gives the required expression.

The derived expression shows directly that the solubility curve has a minimum for $\bar{n} = 1.5$. However, strictly speaking the formula is only valid for a pure aqua-ammine formation. In order to use it correctly it is necessary first to correct the solubility for hydroxo complex formation. In our case this is done simply by multiplying s_{Cu} by $(1 - \alpha_{OH})$. In Fig. 1 the corrected values for ps_{Cu} are plotted vertically below the experimental solubilities, and it can be seen that the correction is generally small and for methylamine results in only a small decrease in the slope of the ascending branch of the solubility curve for pH > 7.

Values for the ligand number $\bar{n}$ derived from the slopes of the corrected solubility curves are tabulated in Tables 1 and 2. The formation curve for the copper(II) methylamine system, drawn from the data given in Table 1 (points marked +), is shown in Fig. 2. The data for the diethylamine system, taken from Table 2 (points marked ×), are also shown. These points are seen to lie rather close to the methylamine complex formation curve. It is also notable that the stabilities of the aliphatic amine complexes are only slightly smaller than those of the ammonia complexes; this can be seen by comparison with the dotted curve in the figure, which represents the formation curve for the copper(II) – ammonia system under the same conditions (2 M NH_4NO_3 at 25 °C).[10]

The stability constants for the methylamine system have been computed from the experimental data and the values are given in Table 3. The ○ points in Fig. 2 are calculated by means of these constants, and it can be seen how well the curve drawn through these points agrees with the experimental + points. The limited data given for the diethylamine system (the × points in the figure) show that the first stability constants for this system must have about the same values as those for the methylamine system, but the uncertainty in the measurements is too great to justify giving values for these constants.

Table 3. Comparison of the consecutive stability constants for some metal-ion methylamine systems with those for the analogous ammonia systems under similar conditions at 25 °C.

System	Medium	log K_1	log K_2	log K_3	log K_4	Ref.
Cu(II), CH_3NH_2	2 M $CH_3NH_3NO_3$	4.11	3.40	2.70	1.87	This paper
Cu(II), NH_3	2 M NH_4NO_3	4.22	3.57	2.95	2.20	10
Cd(II), CH_3NH_2	2 M $CH_3NH_3NO_3$	2.75	2.06	1.13	0.61	4
Cd(II), NH_3	2 M NH_4NO_3	2.69	2.14	1.48	0.97	10
Hg(II), CH_3NH_2	0.5 M $CH_3NH_3NO_3$	8.7	9.2	0.3	0.3	3
Hg(II), NH_3	2 M NH_4NO_3	8.8	8.7	1.0	0.8	10
Ag(I), CH_3NH_2	0.5 M $CH_3NH_3NO_3$	3.15	3.53			1,14
Ag(I), NH_3	0.5 M NH_4NO_3	3.30	3.93			10

DISCUSSION OF RESULTS AND COMPARISON WITH LITERATURE DATA

In Table 3 our stability constants for the copper(II)-methylamine system are compared with those for some other metal-ion methylamine systems, as well as with the constants for the corresponding metal-ion ammonia systems under similar conditions. The constants given for the mercury(II) and silver(I) systems are all taken from earlier work by one of the present authors.[1,3,10] The constants for the cadmium(II) methylamine system are taken from a paper of Spike and Parry.[4] The basic precipitates have a rather high solubility with the latter system, and it is the only methylamine system with the characteristic coordination number higher than two for which stability constants have hitherto been obtained.

The data collected in Table 3 show that ammonia and methylamine have nearly the same affinity towards complex formation. The greater steric bulk of methylamine has a slight influence only on the uptake of the last amine molecules. Thus, the values for K_1 in the copper(II)- and cadmium(II)-methylamine systems are almost the same as in the ammonia systems, whilst the values of K_4 decrease to about half of those in the latter. In the case of diethylamine only the first part of the solubility curve could be determined, but it is noteworthy that the much larger bulk of this amine does not seem to have any appreciable influence on the uptake of the first amine molecule (see the × points in Fig. 2). However, a steric effect must be expected for the uptake of subsequent diethylamine molecules. By extrapolation to the supposed minimum in the solubility curve (see Fig. 1) it can be estimated that $\bar{n} = 1.5$ for p[am] ~ 3, which is consistent with a considerable steric effect (*cf.* the formation curves in Fig. 2). However, the influence of hydroxo complex formation and possibly precipitation of copper(II) hydroxide is so pronounced in this case that a detailed study is difficult.

Bjerrum and Lamm [6] have previously estimated that K_4 for the copper(II)-methylamine system should be 20 – 25 times less than for the ammonia system. This result was obtained from the relationship: $\bar{n} = (C_{am} - [am])/C_{Cu}$, using glass electrode measurements on solutions stabilized with relatively high concentrations of copper(II) and methylamine relative to the methylammonium nitrate in the medium. However, such measurements only give approximate values for $\bar{n}$ which have to be corrected for salt effects.[3,10] If the activity coefficient of methylamine increases with concentration, as is the case for ammonia, one should expect to obtain values of $\bar{n}$ which are too low. We have made a few measurements on solutions with $C_{Cu} \sim 0.05 - 0.10$ M and $C_{CH_3NH_3} \sim 0.2 - 0.5$ M in 2 M $CH_3NH_3NO_3$ and confirmed that such measurements result in values for $\bar{n}$ which are too low (see the □ points in Fig. 2).

Finally we wish to draw attention to an error in "Tables of Stability Constants".[14] In Supplement No. 1 are erroneously given stability constants for diethylamine complexes of Cd(II), Co(II), Ni(II), and Zn(II). The authors con-

cerned [17,18] have not understood that when one titrates with diethylamine in 2 M NH_4NO_3, it is the constants for the ammonia complexes and *not* the diethylamine complexes which are obtained.

Acknowledgement. The authors thank Dr. Martin Hancock for correcting the English manuscript.

REFERENCES

1. Bjerrum, J. *Chem. Revs. 46* (1950) 381.
2. Bjerrum, J. and Refn, S. *Suom. Kemistil. B 29* (1956) 68.
3. Bjerrum, J. *Acta Chem. Scand. 26* (1972) 2734.
4. Spike, C. G. and Parry, R. W. *J. Am. Chem. Soc. 75* (1953) 2726.
5. Bjerrum, J. *K. Dan. Vidensk. Selsk., Mat.-Fys. Medd. 11* (1931) No. 5.
6. Bjerrum, J. and Lamm, C. G. *Acta Chem. Scand. 4* (1950) 997.
7. Lewis, G. N., Brighton, T. B. and Sebastian, R. L. *J. Am. Chem. Soc. 39* (1917) 2245.
8. Bjerrum, J. *K. Dan. Vidensk. Selsk., Mat.-Fys. Medd. 11* (1932) No. 10.
9. Harned, H. S. and Hamer, W. I. *J. Am. Chem. Soc. 55* (1933) 2194.
10. Bjerrum, J. *Metal ammine formation in aqueous solution*, P. Haase and Son, Copenhagen 1941; reprinted 1957.
11. Pedersen, K. J. *K. Dan. Vidensk. Selsk., Mat.-Fys. Medd. 20* (1943) No. 7.
12. Berecki-Biedermann, C. *Ark. Kemi 9* (1956) 175.
13. Perrin, D. D. *J. Chem. Soc.* (1960) 3189.
14. Sillén, L. G. and Martell, A. E. *Stability Constants, Chem. Soc. Spec. Publ. 17* (1964), and *Suppl. 25* (1970).
15. Reeves, R. E. and Bragg, P. *J. Am. Chem. Soc. 84* (1962) 2491.
16. Fisher, J. F. and Hall, J. L. *Anal. Chem. 39* (1967) 1550.
17. Popa, G. and Magearu, V. *Rev. Roum. Chim. 12* (1967) 1107.
18. Popa, G., Magearu, V. and Luca, C. *J. Electroanal. Chem. 17* (1968) 335.

Received December 19, 1975.

Acta Chemica Scandinavica A 30 (1976) 351—357

The Crystal and Molecular Structures of 5-Phenyl-1,2,3,4-thiatriazole and its 3-Oxide and 3-Ethyl Derivatives

T. OTTERSEN

Department of Pharmacy, University of Oslo, Oslo 3, Norway

The structures of I: 5-phenyl-1,2,3,4-thiatriazole, II: 5-phenyl-(1,2,3,4-thiatriazolio)-3-oxide, and III: 3-ethyl-5-phenyl-1,2,3,4-thiatriazolium tetrafluoroborate have been determined by X-ray methods using 1617, 1502 and 1514 reflections, respectively, collected on a counter diffractometer. Data for the first two compounds were collected at −165 °C and for the third compound at 19 °C. The crystal data are as follows:

I: Monoclinic, space group $P2_1/c$, $a = 9.806(2)$ Å; $b = 7.184(1)$ Å; $c = 11.204(2)$ Å; $\beta = 115.85°(1)$; $Z = 4$

II: Monoclinic, space group $P2_1/c$, $a = 7.591(4)$ Å; $b = 13.337(6)$ Å; $c = 14.667(7)$ Å; $\beta = 96.65°(4)$; $Z = 8$

III: Orthorhombic, space group $Pbca$, $a = 19.551(4)$ Å; $b = 19.755(4)$ Å; $c = 13.187(2)$ Å; $Z = 16$.

The structures were refined to conventional R-factors of 0.035 (I), 0.072 (II) and 0.091 (III). The standard deviations in bond lengths and angles involving only nonhydrogen atoms are: 0.002 Å and 0.1° (I), 0.005–0.009 Å and 0.3–0.6° (II), and 0.014–0.040 Å and 0.7–2.0° (III) excluding the tetrafluoroborate groups.

The thiatriazole rings are planar and the planes of the benzene rings are tilted 18.0° (I), 13.9° (II.A), 3.6° (II.B), 15.5° (III.A), and 11.5° (III.B), respectively, to the planes of the thiatriazole rings.

The chemistry of the heteroaromatic 1,2,3,4-thiatriazoles has attracted considerable interest during the last decades,[1,2] and both their physical and chemical properties have been investigated. On the basis of a series of theoretical calculations a set of structural parameters has been suggested for the parent ring.[2]

Several structural studies of thiadiazoles have been reported (see, *e.g.*, Refs. 3–8), and structural models of 1,2,3-, 1,2,5- and 1,3,4-thiadiazoles and/or derivatives thereof have been derived. However, no structural investigations of the thiatriazoles have been reported. An X-ray diffraction study of 5-phenyl-1,2,3,4-thiatriazole (I) was therefore carried out in order to establish a structural model of this heteroaromatic ring.

Since a confirmation of the oxidation [9] and alkylation [10] sites of the thiatriazole ring was wanted, the structures of 5-phenyl-(1,2,3,4-thiatriazolio)-3-oxide (II) and 3-ethyl-5-phenyl-1,2,3,4-thiatriazolium tetrafluoroborate (III) have also been studied in the present investigation.

EXPERIMENTAL, STRUCTURE DETERMINATION AND REFINEMENTS

Space groups were determined by film methods. A computer-controlled Syntex P$\bar{1}$ four-circle diffractometer with graphite-monochromatized Mo$K\alpha$ radiation, and in the cases of low-temperature work equipped with an Enraf-Nonius liquid nitrogen cooling device (modified by H. Hope), was utilized in the determination of unit cell parameters and the collection of intensity data. Unit cell parameters and their standard deviations were determined by a least-squares treatment of the angular coordinates of fifteen symmetry-independent reflections with 2θ-values between 32–45° (I), 25–40° (II) and 18–26° (III). The temperatures at crystal site were −165 °C (I), −165 °C (II) and 19 °C (III).

The computer programs utilized are part of a local assembly and are described in Refs. 11 and 12. Atomic scattering factors used were those of Doyle and Turner [13] for S, F, O, N, C, and B, and of Stewart *et al.*[14] for H.

The crystals used were plates of approximate dimensions 0.4 × 0.2 × 0.05 mm (I), 0.4 × 0.2 × 0.15 mm (II) and 0.3 × 0.2 × 0.05 mm (III). Three-dimensional intensity data were recorded

utilizing the $\omega - 2\theta$ scanning mode with scan speed variable between $2-8°$ min^{-1} (I and II) and $3-8°$ min^{-1} (III), depending on the intensity of the reflection. Background counting time was equal to $0.35 \times$ scan time on each side of the reflections. The intensity variations of three standard reflections which were remeasured after every hundred reflections were random for all data-sets collected. Accordingly no corrections were applied to the intensity data for these variations.

The estimated standard deviations were taken as the square root of the total count with an addition of 2 % of the net intensity for experimental uncertainties. The intensities were corrected for Lorentz and polarization effects.

The phase problems were solved by the MULTAN [12] program package, and the structure models were refined by full-matrix least-squares refinements. The final atomic parameters for nonhydrogen atoms are listed in Table

Table 1. Fractional atomic coordinates and thermal parameters with estimated standard deviations for non-hydrogen atoms. The temperature factor is given by $\exp\{-2\pi^2[u_{11}(a^*h)^2 + u_{22}(b^*k)^2 + u_{33}(c^*l)^2 + u_{12}(a^*b^*hk) + u_{13}(a^*c^*hl) + u_{23}(b^*c^*kl)]\}$.

Atom	x	y	z	u_{11}	u_{22}	u_{33}	u_{12}	u_{13}	u_{23}
Compound I									
S1	.2912(0)	.3983(0)	.9227(0)	.0133(2)	.0305(2)	.0168(2)	-.0026(1)	.0034(1)	-.0045(1)
N2	.4138(1)	.3824(2)	.8548(1)	.0133(5)	.0387(8)	.0283(7)	-.0011(5)	.0076(5)	.0014(6)
N3	.3424(1)	.3602(2)	.7288(1)	.0156(6)	.0338(8)	.0269(7)	-.0001(5)	.0111(5)	-.0003(5)
N4	.1889(1)	.3536(2)	.6772(1)	.0152(6)	.0304(8)	.0182(5)	.0010(4)	.0001(4)	.0005(4)
C5	.1424(1)	.3729(2)	.7712(1)	.0119(5)	.0182(7)	.0155(5)	-.0004(4)	.0042(4)	.0002(4)
C7	-.0179(1)	.3745(2)	.7442(1)	.0124(5)	.0167(7)	.0143(5)	-.0001(4)	.0057(4)	.0001(4)
C8	-.0025(1)	.3459(2)	.8459(1)	.0119(6)	.0203(7)	.0148(6)	.0017(5)	.0006(4)	.0006(5)
C9	-.2163(2)	.3475(2)	.8165(1)	.0193(6)	.0273(8)	.0241(7)	.0006(5)	.0141(5)	.0004(5)
C10	-.3253(1)	.3775(2)	.8871(1)	.0153(5)	.0242(8)	.0273(7)	.0017(5)	.0187(5)	.0003(6)
C11	-.2803(1)	.4092(2)	.9863(1)	.0134(5)	.0277(7)	.0262(6)	.0018(6)	.0058(4)	.0005(6)
C12	-.1266(1)	.4082(2)	.9148(1)	.0137(5)	.0248(7)	.0157(5)	.0012(5)	.0059(4)	.0005(5)
Compound II									
S1A	.4647(2)	.2058(0)	.2349(1)	.0313(8)	.0116(6)	.0181(7)	-.0005(4)	.0094(4)	.0050(4)
N2A	.4442(8)	.3237(3)	.2661(3)	.0324(28)	.0149(19)	.0173(19)	.0018(18)	.0096(17)	.0004(16)
N3A	.5233(7)	.3606(3)	.2186(3)	.0246(22)	.0139(20)	.0129(17)	.0011(16)	.0034(15)	-.0012(15)
N4A	.6035(7)	.3361(3)	.1488(3)	.0227(23)	.0120(17)	.0165(19)	-.0022(15)	.0044(16)	-.0003(14)
C5A	.5833(7)	.2366(3)	.1467(3)	.0199(23)	.0118(20)	.0126(18)	-.0018(15)	.0021(15)	.0008(15)
C6A	.5387(7)	.4739(3)	.2191(3)	.0309(29)	.0099(16)	.0241(18)	.0016(16)	.0095(16)	-.0002(15)
C7A	.6492(8)	.1667(3)	.0842(3)	.0251(27)	.0122(19)	.0238(20)	-.0003(17)	.0038(17)	-.0000(16)
C8A	.7897(8)	.1991(4)	.0819(3)	.0269(28)	.0143(20)	.0168(21)	-.0019(18)	.0054(18)	-.0002(17)
C9A	.7719(9)	.1365(4)	-.0572(4)	.0343(31)	.0176(23)	.0189(21)	.0017(21)	.0101(20)	-.0001(19)
C10A	.7765(10)	.0288(5)	-.0354(4)	.0351(33)	.0188(25)	.0239(25)	.0031(21)	.0044(22)	-.0005(20)
C11A	.7183(11)	-.0042(4)	.0472(4)	.0422(36)	.0114(19)	.0244(26)	.0021(20)	.0068(23)	-.0004(17)
C12A	.6525(9)	.0042(4)	.1863(3)	.0362(32)	.0107(19)	.0171(21)	.0013(18)	.0054(19)	.0000(16)
S1B	-.8335(2)	.0230(0)	.7389(1)	.0302(8)	.0113(6)	.0188(7)	.0024(4)	.0102(4)	.0001(4)
N2B	-.8423(8)	-.0945(3)	.7654(3)	.0268(25)	.0134(18)	.0188(21)	.0006(17)	.0063(17)	.0006(16)
N3B	.0519(7)	-.1500(3)	.7151(3)	.0257(26)	.0141(20)	.0168(18)	-.0017(16)	.0017(17)	.0002(15)
N4B	.1331(8)	-.1841(3)	.6471(3)	.0309(29)	.0131(18)	.0154(18)	-.0005(17)	.0024(17)	.0002(14)
C5B	.0985(7)	-.0875(4)	.6479(3)	.0192(23)	.0155(22)	.0145(19)	.0008(16)	.0047(16)	-.0002(15)
C6B	.8668(8)	-.2415(3)	.7273(3)	.0439(28)	.0109(16)	.0223(18)	.0011(16)	.0071(17)	.0004(14)
C7B	.1595(7)	.0648(3)	.5821(3)	.0195(24)	.0188(18)	.0141(18)	-.0004(16)	.0016(16)	.0008(16)
C8B	.2573(8)	.0384(3)	.5142(3)	.0245(25)	.0184(19)	.0170(20)	.0012(17)	.0039(17)	-.0002(16)
C9B	.3188(9)	.0989(4)	.4586(3)	.0279(28)	.0178(22)	.0146(20)	-.0009(19)	.0041(18)	.0000(17)
C10B	.2648(9)	.2002(4)	.4564(4)	.0251(27)	.0157(23)	.0189(20)	-.0025(18)	.0041(18)	.0001(17)
C11B	.1652(9)	.2328(3)	.5243(4)	.0314(29)	.0192(19)	.0206(22)	-.0008(18)	.0059(20)	.0001(16)
C12B	.1185(9)	.1651(4)	.5878(3)	.0308(28)	.0183(19)	.0167(21)	.0004(18)	.0053(18)	-.0001(16)
Compound III									
S1A	.3392(2)	.3322(2)	.4481(3)	.104(3)	.061(2)	.078(2)	-.014(2)	.016(2)	-.002(2)
N2A	.2941(6)	.3285(7)	.5491(18)	.094(7)	.074(7)	.083(7)	-.014(6)	.013(7)	.006(7)
N3A	.2978(6)	.3809(8)	.5976(9)	.071(7)	.083(9)	.072(7)	-.005(7)	.001(6)	.002(7)
N4A	.3362(6)	.4309(5)	.5635(8)	.074(6)	.063(6)	.068(6)	-.007(6)	.008(6)	-.002(5)
C5A	.3647(6)	.4119(7)	.4784(9)	.061(6)	.069(7)	.064(8)	.005(6)	.011(6)	.006(6)
C7A	.4115(6)	.4541(6)	.4203(18)	.057(7)	.065(8)	.066(8)	.008(7)	.021(7)	.003(7)
C8A	.4166(7)	.5226(6)	.4488(11)	.072(8)	.059(8)	.065(8)	.005(7)	.001(8)	.009(7)
C9A	.4636(9)	.5641(7)	.3673(14)	.093(9)	.060(7)	.102(11)	-.009(8)	.007(11)	.017(8)
C10A	.5032(9)	.5386(9)	.3152(12)	.096(11)	.101(14)	.059(8)	-.010(10)	.015(8)	.029(9)
C11A	.4972(12)	.4652(10)	.2944(2)	.159(17)	.089(13)	.075(9)	-.022(11)	.025(11)	-.031(8)
C12A	.4522(7)	.4238(8)	.3481(12)	.083(9)	.084(8)	.067(7)	-.010(8)	.001(8)	.009(8)
C13A	.2691(10)	.3939(7)	.6923(13)	.106(15)	.093(11)	.096(10)	-.015(9)	.034(10)	.013(8)
C14A	.1896(15)	.3728(22)	.6889(16)	.126(19)	.268(29)	.093(12)	-.013(21)	.048(12)	-.026(16)
S1B	.3221(2)	.4153(2)	.1487(3)	.098(3)	.088(2)	.075(2)	.006(2)	.008(2)	-.012(2)
N2B	.3948(6)	.4181(6)	.0881(18)	.085(8)	.074(8)	.083(8)	.011(6)	.009(6)	.008(6)
N3B	.3982(6)	.3819(7)	.0897(18)	.064(8)	.081(7)	.074(8)	-.002(7)	.009(6)	-.001(7)
N4B	.3329(6)	.3503(6)	-.0111(8)	.088(10)	.088(7)	.061(6)	.020(7)	.020(7)	.004(5)
C5B	.2875(7)	.3627(6)	.0599(10)	.068(9)	.061(6)	.063(8)	.006(6)	.014(8)	.012(6)
C7B	.2179(8)	.3356(6)	.0632(12)	.098(11)	.064(7)	.080(10)	.012(8)	.007(9)	.002(8)
C8B	.1933(18)	.3044(9)	-.0218(14)	.109(16)	.084(8)	.109(12)	.021(11)	.016(13)	.003(9)
C9B	.1253(13)	.2776(10)	-.0286(21)	.107(16)	.109(13)	.139(20)	.014(11)	.035(16)	.009(11)
C10B	.0839(12)	.2840(12)	.0068(31)	.101(14)	.118(14)	.173(25)	.043(11)	.030(20)	.019(15)
C11B	.1124(13)	.3140(12)	.1478(22)	.107(17)	.121(15)	.158(19)	.011(14)	.058(17)	.018(16)
C12B	.1784(9)	.3434(7)	.1483(14)	.071(10)	.088(9)	.101(18)	.004(8)	.025(9)	.014(8)
C13B	.4468(10)	.3718(13)	-.0610(14)	.084(12)	.168(16)	.093(10)	.016(11)	.036(10)	.007(12)
C14B	.5099(12)	.3969(10)	-.0254(21)	.105(16)	.123(15)	.185(21)	.010(11)	.074(15)	.038(14)
S1SA	.4243(9)	.2382(8)	.1985(15)	.099(18)	.065(10)	.075(14)	-.010(8)	-.038(9)	.002(8)
F16A	.4126(6)	.1742(5)	.1955(10)	.165(8)	.094(6)	.101(8)	-.009(6)	.046(7)	-.016(6)
F17A	.3735(16)	.2744(7)	.2284(15)	.343(29)	.131(8)	.288(14)	.062(12)	.045(14)	-.027(8)
F18A	.4644(19)	.2547(17)	.2758(20)	.372(35)	.307(24)	.216(18)	-.194(28)	-.148(22)	.063(17)
F19A	.4399(14)	.2595(13)	.1854(15)	.246(14)	.235(16)	.158(11)	-.099(13)	.043(12)	.051(11)
S1SB	.1813(28)	.4614(30)	.3878(18)	.308(61)	.332(73)	.069(14)	.276(64)	.085(24)	.088(25)
F16B	.1499(7)	.4996(11)	.3474(12)	.133(7)	.286(18)	.178(11)	.060(19)	-.038(8)	.079(11)
F17B	.1918(8)	.4662(13)	.4877(9)	.176(11)	.340(28)	.097(7)	.052(13)	.028(7)	.049(13)
F18B	.1716(34)	.3947(9)	.3922(28)	.359(65)	.140(18)	.223(19)	-.081(29)	.032(31)	.024(11)
F19B	.2427(8)	.4571(12)	.3329(9)	.155(9)	.385(18)	.122(7)	.094(11)	.024(7)	-.013(9)

Table 2. Fractional atomic coordinates and thermal parameters for hydrogen atoms (see text).

Atom	x	y	z	B
Compound I				
HC8	008(2)	.322(2)	.933(2)	1.7(3)
HC9	-.246(2)	.323(3)	.887(2)	2.5(4)
HC10	-.431(2)	.377(2)	.667(2)	2.0(4)
HC11	-.354(2)	.434(2)	.496(2)	2.0(4)
HC12	-.095(2)	.431(2)	.548(2)	2.2(4)
Compound II				
HC8A	.718	.273	.012	
HC9A	.810	154	-.116	
HC10A	.827	-.021	-.077	
HC11A	719	-.076	063	
HC12A	.616	.041	165	
HC8B	293	-.040	511	
HC9B	386	.074	402	
HC10B	302	249	409	
HC11B	135	304	529	
HC12B	046	189	.639	
Compound III				
HC8A	386	544	491	
HC9A	.469	610	404	
HC10A	.538	559	.277	
HC11A	.526	446	.240	
HC12A	.450	373	336	
H1C13A	.260	444	706	
H2C13A	.284	370	749	
H1C14A	168	.381	755	
H2C14A	190	.321	.676	
H3C14A	166	.395	.633	
HC8B	.222	.300	-.084	
HC9B	107	.255	-.083	
HC10B	.036	.265	.069	
HC11B	.084	.317	.210	
HC12B	196	.368	.208	
H1C13B	.435	.394	-.125	
H2C13B	.450	.322	-.072	
H1C14B	.545	.387	-.077	
H2C14B	.522	.373	.040	
H3C14B	.506	446	-.013	

1 and those for hydrogen atoms in Table 2. Standard deviations in molecular parameters were calculated from the correlation matrix ignoring standard deviations in cell parameters.

Compound I. Reflections with 2θ-values larger than 45° which had integrated counts of less than 8 cps determined in a 2s scan over the peak, were not measured. Of the 1975 reflections measured ($2\theta_{max} = 60°$), 1617 had intensities larger than twice their standard deviations. These were regarded as "observed" reflections, and the remaining were excluded from further calculations.

The structure model was refined to a conventional R of 0.07. At this point hydrogen atoms were included, and anisotropic thermal parameters were introduced for nonhydrogen atoms. Refinement of all positional and thermal parameters converged to a conventional R of 0.033 and a weighted R_w of 0.035.

In order to reduce the influence of the asphericity of the valence electrons all reflections with $\sin\theta/\lambda < 0.5$ were excluded from the final refinement [15] (leaving 935 F_o's). Refinement of all parameters involving nonhydrogen atoms resulted in a weighted R_w of 0.032, a conventional R of 0.035 and an R_t for the total data-set of 0.036. The standard deviation of an observation of unit weight, $(\sum W\Delta F^2/(m-s))^{\frac{1}{2}}$, was 1.18.

The r.m.s. difference between the observed U_{ij}'s and those calculated from the "rigid body" model [16] is 0.0007 Å², which indicates that the molecule may be regarded as a rigid body. The atomic positions were accordingly corrected for the librational motion. The eigenvalues of T are 0.13, 0.12 and 0.11 Å², and the r.m.s. librational amplitudes are 4.3, 2.1 and 1.7°.

Compound II. The unit cell volume found indicated eight formula units in the unit cell, *i.e.* two molecules in the asymmetric unit (space group $P2_1/c$); these will be denoted A and B, respectively.

Unfortunately, the crystal used in the first recording of intensity data cracked during the collection. This data-set (low-angle data, $2\theta_{max} = 45°$) was later used in the structure determination (987 reflections above 3σ level). A new data-set consisting of all reflections with 2θ-values between 42.5 and 60° which had integrated counts of more than 7 cps, determined in a $2s$ scan, were collected. Of the 1831 reflections measured, 1502 had intensities larger than 2.5 times their standard deviations. These were regarded as "observed" reflections, and the remaining were excluded from further calculations.

Refinement of positional and isotropic thermal parameters for all nonhydrogen atoms yielded, after inclusion of the hydrogen atoms in calculated positions with a common isotropic temperature factor of 2.0 Å², a conventional R of 0.09, using the low-angle data-set.

Refinement of positional and anisotropic thermal parameters for all nonhydrogen atoms, using the high-angle data-set, converged to an R of 0.072 and a weighted R_w of 0.080. The standard deviation of an observation of unit weight was 2.51.

The r.m.s. difference between the observed U_{ij}'s and those calculated from the "rigid-body" model [16] is 0.0012 Å² for molecule A and 0.0014 Å² for molecule B, which indicate that both molecules may be regarded as rigid

Table 3. Molecular parameters with estimated standard deviations.

	I		II.A		II.B		III.A	III.B
Bond lengths (Å). The values listed in the second column for compound I and II are the corrected lengths.								
S1–N2	1.677(2)	1.680	1.661(5)	1.664	1.662(5)	1.664	1.644(14)	1.618(13)
S1–C5	1.698(2)	1.702	1.717(6)	1.721	1.714(6)	1.718	1.700(14)	1.713(14)
N2–N3	1.283(2)	1.287	1.308(8)	1.312	1.313(8)	1.317	1.225(17)	1.261(17)
N3–N4	1.358(2)	1.359	1.383(7)	1.385	1.375(7)	1.375	1.320(16)	1.311(18)
N4–C5	1.326(2)	1.329	1.314(6)	1.317	1.315(7)	1.318	1.309(16)	1.306(18)
C5–C7	1.465(2)	1.467	1.455(7)	1.457	1.469(7)	1.470	1.456(19)	1.463(21)
C7–C8	1.403(2)	1.407	1.408(7)	1.411	1.383(8)	1.386	1.381(19)	1.370(24)
C8–C9	1.396(2)	1.397	1.381(8)	1.382	1.400(8)	1.400	1.370(22)	1.429(32)
C9–C10	1.393(2)	1.397	1.395(9)	1.397	1.401(8)	1.404	1.357(24)	1.406(40)
C10–C11	1.398(2)	1.402	1.407(10)	1.410	1.386(9)	1.389	1.327(26)	1.343(39)
C11–C12	1.398(2)	1.399	1.390(8)	1.391	1.394(8)	1.394	1.394(26)	1.412(33)
C7–C12	1.396(2)	1.399	1.406(7)	1.409	1.405(7)	1.408	1.378(21)	1.369(24)
N3–O6			1.252(7)	1.254	1.238(7)	1.240		
N3–C13							1.472(21)	1.449(22)
C13–C14							1.441(40)	1.417(36)
B15–F16							1.302(21)	1.227(28)
B15–F17							1.348(32)	1.337(38)
B15–F18							1.281(26)	1.333(70)
B15–F19							1.318(26)	1.404(44)
Bond angles (°)								
N2–S1–C5	90.6(1)		91.9(3)		91.8(3)		91.2(7)	91.4(7)
S1–N2–N3	111.0(1)		108.5(4)		108.8(4)		108.3(10)	109.4(10)
N2–N3–N4	116.0(1)		118.9(5)		118.2(5)		121.6(11)	119.5(12)
N3–N4–C5	111.1(1)		108.2(5)		109.0(5)		108.6(11)	110.1(12)
S1–C5–N4	111.2(1)		112.5(4)		112.2(4)		110.1(9)	109.4(11)
S1–C5–C7	125.7(1)		123.4(4)		124.1(4)		126.3(10)	124.3(12)
N4–C5–C7	123.1(1)		124.1(5)		123.6(5)		123.7(12)	126.3(14)
C5–C7–C8	121.1(1)		120.4(5)		119.8(5)		120.5(13)	117.5(16)
C5–C7–C12	118.8(1)		119.7(5)		118.7(5)		118.5(11)	121.1(15)
C8–C7–C12	120.1(1)		119.9(5)		121.4(5)		120.9(12)	121.4(16)
C7–C8–C9	119.6(1)		120.2(5)		119.2(5)		118.9(14)	119.0(19)
C8–C9–C10	120.5(1)		120.2(6)		119.8(6)		120.3(13)	120.8(21)
C9–C10–C11	119.8(1)		120.0(6)		120.4(6)		120.9(16)	116.5(19)
C10–C11–C12	120.2(1)		120.2(6)		120.3(6)		121.4(16)	124.6(22)
C7–C11–C12	119.8(1)		119.6(6)		118.8(5)		117.5(14)	117.5(19)
N4–N3–O6			118.9(5)		120.0(6)			
N2–N3–O6			122.2(5)		121.8(5)			
N2–N3–C13							121.9(13)	124.2(14)
N4–N3–C13							116.3(13)	116.3(15)
N3–C13–C4							113.7(15)	113.8(15)
F16–B15–F17							109.7(18)	118.9(25)
F16–B15–F18							113.6(18)	122.2(67)
F16–B15–F19							108.8(19)	112.2(23)
F17–B15–F18							94.0(28)	92.8(24)
F17–B15–F19							103.9(18)	112.4(41)
F18–B15–F19							124.4(19)	94.8(31)
Dihedral angles (°) The angles are positive in a right-hand screw								
N3–N4–C5–C7	178.9(2)		179.5(5)		177.8(5)		−178.9(10)	−178.9(11)
N2–S1–C5–C7	−179.0(2)		179.3(5)		177.4(5)		179.0(10)	−179.5(10)
S1–C5–C7–C8	−18.2(2)		165.7(5)		−176.3(5)		165.6(10)	169.0(11)
S1–C5–C7–C12	160.9(1)		−14.4(8)		1.3(8)		−16.8(14)	−9.6(16)
N4–N3–C13–C14							134.3(21)	−168.5(16)
N2–N3–C13–C14							−40.7(24)	11.4(25)

bodies. The atomic positions were accordingly corrected for the librational motion. The eigenvalues of T are 0.14, 0.12 and 0.10 Å² for both molecules, and the r.m.s. librational amplitudes are 4.1, 2.0 and 1.5° for molecule A, and 4.3, 1.3 and 1.3° for molecule B.

Compound III. The unit cell volume found indicated sixteen formula units in the unit cell, *i.e.* two molecules in the asymmetric unit (space group *Pbca*); these will be denoted A and B, respectively.

Three-dimensional intensity data at −165 °C were recorded using scan speed variable between 6 and 8° min⁻¹. A check showed that the intensity data only had monoclinic symmetry, and, further, the systematic absences were those corresponding to the space group $P2_1/c$. This may indicate a phase transition. This data-set was later used in the structure determination while a new data-set was collected. Of the 5995 reflections measured ($2\theta_{max} = 55°$) 2763 had intensities larger than twice their standard deviations. These were regarded as observed.

A new data-set was collected at 19 °C consisting only of reflections with an integrated count larger than 9 cps determined in a 2s scan. Of the 1805 reflections measured ($2\theta_{max} = 55°$) 1514 had intensities larger than twice their standard deviations. These were regarded as "observed" reflections, and the remaining were excluded from further calculations.

The phase problem was solved using the low-temperature data-set and the space group *Pbca*. Refinement of positional and isotropic thermal parameters for all nonhydrogen atoms yielded a conventional R of 0.19. Attempts to refine anisotropic thermal parameters resulted in several negative U_{ii}'s.

Refinement of positional and anisotropic thermal parameters for all nonhydrogen atoms, using the room-temperature data-set, converged after inclusion of the hydrogen atoms in calculated positions with a common isotropic temperature factor of 7.0 Å², to a conventional R of 0.115 and a weighted R_w of 0.119. In the final refinement all structure factors with $\sin\theta/\lambda < 0.3$ were excluded (leaving 1018 F_o's). Refinement of all parameters involving nonhydrogen atoms yielded a weighted R_w of 0.081, a conventional R of 0.091 and an R_t for the total data-set of 0.118. The standard deviation of an observation of unit weight was 2.00.

The thermal motion of the molecules or parts of them could not be described by the "rigid-body" model.[16]

CRYSTAL DATA

Compound I. 5-Phenyl-1,2,3,4-thiatriazole, $C_7H_5N_3S$, M = 163.2 amu, space group $P2_1/c$, $a = 9.806(2)$ Å, $b = 7.184(1)$ Å, $c = 11.204(2)$ Å,

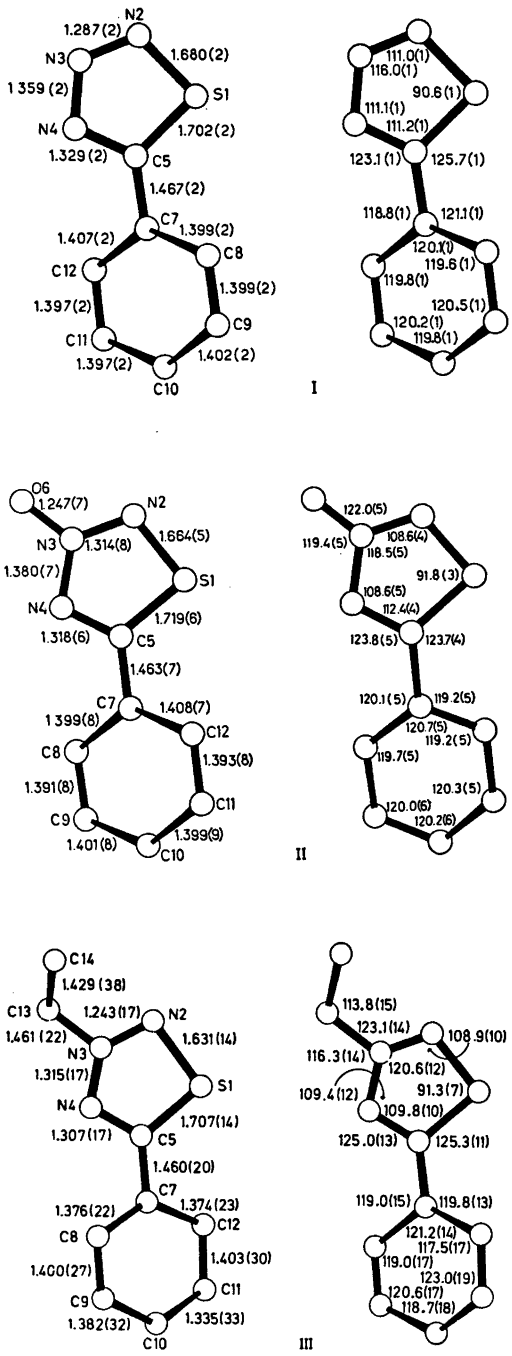

Fig. 1. Bond lengths (Å) (corrected for thermal libration effects for I and II), and bond angles (°) with estimated standard deviations. All parameters given for II and III including e.s.d.'s are mean values.

Table 4. Deviations from least-squares planes (Å × 10^3). The deviations for those atoms used to define the plane are given in italicized figures.

Atom	Compound I		Compound II				Compound III			
	I.1	I.2	II.A.1	II.A.2	II.B.1	II.B.2	III.A.1	III.B.2	III.B.1	III.B.2
S1	*0*	422	*−2*	−351	*1*	−113	*6*	−273	*−2*	275
N2	*−1*	138	*2*	−145	*3*	−182	*−23*	−10	*7*	101
N3	*1*	−248	*2*	163	*4*	−131	*22*	335	*−6*	−155
N4	*−1*	−350	*6*	252	*−3*	−53	*−7*	361	*1*	−213
C5	*1*	−13	*8*	7	*1*	−28	*−8*	49	*3*	3
O6			24	394	12	−158				
C7	22	*−8*	*−5*	*1*	−51	*6*	−14	*0*	12	*−4*
C8	−330	*3*	−297	*5*	−124	*2*	−321	*−11*	225	*−5*
C9	−302	*5*	310	*−3*	−207	*−3*	−253	*9*	231	*1*
C10	70	*8*	−22	*−3*	−216	*4*	78	*5*	1	*13*
C11	441	*2*	286	*9*	−155	*0*	343	*−16*	−260	*−24*
C12	420	*5*	277	*−8*	−78	*−5*	340	*14*	−228	*19*
C13							−3	633	−33	−400
C14							−927	−280	−298	−580

$\beta = 115.85°(1)$, $V = 710.3$ Å^3 ($t = -165$ °C), $Z = 4$, $D_{calc} = 1.525$ g/cm^3, $F(000) = 336$.

Compound II. 5-Phenyl-(1,2,3,4-thiatriazolio)-3-oxide, $C_7H_5N_3OS$, M = 179.2 amu, space group $P2_1/c$, $a = 7.591(4)$ Å, $b = 13.337(6)$ Å, $c = 14.667(7)$ Å, $\beta = 96.65°(4)$, $V = 1474.9$ Å^3 ($t = -165$ °C), $Z = 8$, $D_{calc} = 1.613$ g/cm^3, $F(000) = 736$.

Compound III. 3-Ethyl-5-phenyl-1,2,3,4-thiatriazolium tetrafluoroborate, $C_9H_{10}N_3S^+BF_4^-$, M = 279.0 amu, space group *Pbca*, $a = 19.551(4)$ Å [19.497(12) Å], $b = 19.755(4)$ Å [19.221(8) Å], $c = 13.187(2)$ Å [13.021(7) Å], $V = 5092.9$ Å^3 ($t = 19$ °C), $Z = 16$, $D_{calc} = 1.455$ g/cm^3, $F(000) = 2272$.

Numbers in brackets are cell dimensions at −165 °C.

DISCUSSION

Bond lengths and bond angles are listed in Table 3. The numbering of the atoms is indicated in Fig. 1, where also the mean values of bond lengths and bond angles found for the two crystallographically nonequivalent molecules in II and III are given, together with the values obtained for I. The largest differences in equivalent bond lengths between the two molecules (A and B) in II and III, excluding the tetrafluoroborate groups, are about three times the mean estimated standard deviations. Some selected dihedral angles are given in Table 3 and deviations from planarity in Table 4.

The accuracy in the molecular parameters found for III is poor and this structure will not be discussed in detail.

The five-membered rings are planar and the bond lengths indicate a considerable resonance stabilization, as has also been found for the 1,2,5- and 1,3,4-thiadiazoles.[3–5,17] However, there are two noteworthy changes in the parent thiatriazole ring (I) compared with the thiadiazoles. The S1–C5 bond is shortened by 0.02 Å compared with 1,3,4-thiadiazole,[4,5] and the S1–N2 bond is lengthened by 0.05 Å compared with 1,2,5-thiadiazoles.[3,17]

The angles between the benzene and thiatriazole rings are small [18.0° (I), 13.9° (II.A), 3.6° (II.B), 15.5° (III.A) and 11.5° (III.B)] and the C5–C7 bond lengths (1.46–1.47 Å) indicate conjugation between the rings.

The N2–S7–C5 angle of 90.6° is between the N–S–N angle [3,17] of 99.6° and the C–S–C angle [4,5] of 86.4°, and is close to the N–S–C angle of 91.6° found in 2,4-dimethyl-3,5-di-(phenylimino)-1,2,4-thiazolidine.[18]

The introduction of an oxygen atom at N3 in I, giving II, results in significant lengthenings of the N2–N3 and N3–N4 bonds, and an opening of the N2–N3–N4 angle by 2.5°. The angles S1–N2–N3 and N3–N4–C5 decrease by about 2.5°. Small changes in the other bond lengths are also indicated, implying charge redistributions over the whole ring.

The same angular changes as is found in II are also indicated in III.

For all these compounds the intermolecular forces in the crystals are of van der Waals type. The shortest intermolecular distances are mainly compatible with normal van der Waals contacts.

Acknowledgement. The author wishes to thank Dr. A. Holm for supplying the crystals.

REFERENCES

1. Jensen, K. A. and Pedersen, C. A. *Adv. Heterocyclic Chem. 3* (1964) 263.
2. Holm, A. *Adv. Heterocyclic Chem. In press.*
3. Dobyns, V. and Pierce, L. *J. Amer. Chem. Soc. 85* (1963) 3553.
4. Bak, B., Nygaard, L., Pedersen, E. J. and Rastrup-Andersen, J. *J. Mol. Spectrosc. 19* (1966) 283.
5. Markov, P. and Stølevik, R. *Acta Chem. Scand. 24* (1970) 2525.
6. Downie, T. C., Harrison, W. and Raper, E. S. *Acta Crystallogr. B 28* (1972) 1584.
7. Andreetti, G. D., Bocelli, G. and Sgarabotti, P. *Cryst. Struct. Commun. 3* (1974) 11.
8. La Cour, T. *Acta Crystallogr. B 30* (1974) 1642.
9. Holm, A., Carlsen, L., Lawesson, S.-O. and Kolind-Andersen, H. *Tetrahedron 31* (1975) 1783.
10. Holm, A., Schaumburg, K., Dahlberg, N., Christophersen, C. and Snyder, J. P. *J. Org. Chem. 40* (1975) 431.
11. Groth, P. *Acta Chem. Scand. 27* (1973) 1837.
12. Germain, G., Main, P. and Woolfson, M. M. *Acta Crystallogr. A 27* (1971) 368.
13. Doyle, P. A. and Turner, P. S. *Acta Crystallogr. A 24* (1968) 390.
14. Stewart, R. F., Davidson, E. R. and Simpson, W. T. *J. Chem. Phys. 42* (1965) 3175.
15. Ottersen, T. *Acta Chem. Scand. A 28* (1974) 661.
16. Shoemaker, V. and Trueblood, K. N. *Acta Crystallogr. B 24* (1968) 63.
17. Bonham, R. A. and Momany, F. A. *J. Amer. Chem. Soc. 83* (1961) 4475.
18. Christophersen, C., Ottersen, T., Seff, K. and Treppendahl, S. *J. Amer. Chem. Soc. 97* (1975) 5237.

Received October 14, 1975.

Acta Chemica Scandinavica A 30 (1976) 358—362

Addition of Hydrogen Sulfite to Bicyclo[2.2.1]heptenes. I. Kinetics of Some 2-Norbornenols and 2-Norbornenylmethanols in Aqueous Sodium Hydrogen Sulfite Solutions

MARTTI LAJUNEN and KATRIINA LEHTONEN

Department of Chemistry and Biochemistry, University of Turku, SF-20500 Turku 50, Finland

Addition rates of sodium hydrogen sulfite to the double bond of some 2-norbornenols and 2-norbornenylmethanols measured in aqueous solutions at pH 5.0 were observed to be surprisingly high for olefins having no carbonyl or cyano groups conjugated with the ethylenic linkage (half-lives were from 14 to 140 min at 25 °C when $[HSO_3^-]_0 = [\text{olefin}]_0 = 0.01$ M). The apparent second- and third-order rate coefficients were measured and corresponding activation parameters calculated. The order of the reaction was concluded to be between two and three, and an oxygen-initiated free-radical mechanism, which is in agreement with the formal kinetics, was proposed.

It has been known for a long time that sodium hydrogen sulfite easily reacts with oxygen-carbon double bonds, if they are not sterically hindered, and it also adds fairly easily to carbon-carbon double bonds conjugated with carbonyl or cyano groups, but ordinary ethylenic double bonds have generally been found to react with hydrogen sulfite slowly.[1–10] However, some 2-norbornenols and 2-norbornenylmethanols, dissolved in ether, were recently found to disappear quite rapidly when they were shaken with one molar aqueous hydrogen sulfite.[11] The addition probably takes place *via* a free-radical mechanism, since a free-radical inhibitor, such as hydroquinone, prevents it from occurring.[11] Hence the mechanism differs from the usual ionic addition reactions which occur at the ethylenic linkage of α,β-unsaturated aldehydes, ketones, acids, esters, and nitriles.[1–6]

In this work the rates of addition of sodium hydrogen sulfite to four 2-norbornenols [*exo*-2-norbornenol (I), *endo*-2-norbornenol (II), 2-methyl-*exo*-2-norbornenol (III), and 2-methyl-*endo*-2-norbornenol (IV)] and to four 2-norbornenylmethanols [*exo*-2-norbornenylmethanol (V), *endo*-2-norbornenylmethanol (VI), 2-meth-

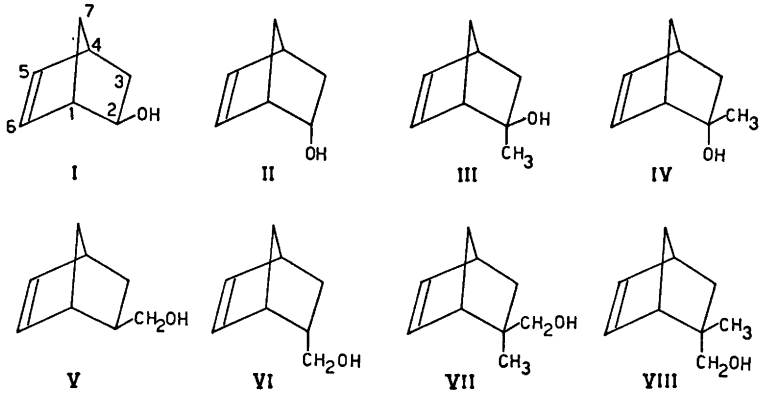

I II III IV

V VI VII VIII

yl-*exo*-2-norbornenylmethanol (VII), and 2-methyl-*endo*-2-norbornenylmethanol (VIII)] were measured under homogeneous conditions at varying temperatures and in one case (IV) by changing systematically the concentration of hydrogen sulfite.

EXPERIMENTAL

Preparations. The syntheses of the substrates I and II,[12] III and IV,[13,14] as well as V, VI, VII, and VIII,[15] have been described earlier. The purities were measured by gas chromatography (FFAP and Carbowax 1500 columns) and found to be ≥ 99 % for I, II, IV, VI, and VII, 97 % (3 % of IV) for III, and 95 % (5 % of VI and VII, respectively) for V and VIII. The saturated alcohols, which were used as inert internal standards in GLC analyses of the kinetic runs, were prepared as follows. *exo*-2-Norborneol was obtained by hydrolyzing the *exo* formate formed by addition of formic acid to norbornene.[16] 2-Norbornylmethanol (*exo*:*endo* = 1:2, the isomers gave a common peak in GLC) was obtained by catalytic hydrogenation of a mixture of 2-norbornenylmethanols. The synthesis of 3-nortricyclanol has been reported earlier.[12] The purities of the internal standards were ≥ 99 %.

Kinetic measurements. The reaction medium consisted of 20 cm³ of an acetic acid-0.2 M sodium acetate buffer solution of pH 5.0 and of such amounts of 0.2 M sodium chloride and 0.2 M hydrogen sulfite solutions that the total volume was 40 cm³. (The concentration of HSO_3^- is at its maximum at pH 4.4 and $[SO_3^{2-}] \leq 0.01\ [HSO_3^-]$ at pH 5.0.[17]) The water used for reaction media was saturated with air. The ionic strength of the medium was 0.20 M and the hydrogen sulfite concentration was usually from 0.009 to 0.014 M. The kinetic measurements were carried out under similar exposure to light. The internal standard (0.003 – 0.005 M) was added into the thermostated medium and the reaction was started by adding the substrate (0.003 – 0.009 M) as neat or as dissolved in 1 cm³ of purified[18] dioxane. Samples of 2 cm³ (10 – 12 in numbers) were rapidly transferred into a separatory funnel, which contained 5 cm³ of heptane. After shaking the organic phase was separated and analyzed by GLC. The heights of the peaks (h) of the substrate and the internal standard were measured from chromatograms (2 – 5 measurements per sample) and their ratios were calculated ($r = h_{substrate}/h_{standard}$).

The ratio calculated for the first sample (r_0') taken shortly after the initiation of the reaction was preliminarily fixed to correspond to the initial substrate concentration ($[ROH]_0$). The substrate and hydrogen sulfite concentrations ($[ROH]_t$ and $[HSO_3^-]_t$) of samples taken after time t had elapsed from removal of the first sample are given by:

$$[ROH]_t = \frac{r_t}{r_0'}[ROH]_0 \quad (1)$$

$$[HSO_3^-]_t = [HSO_3^-]_0 - ([ROH]_0 - [ROH]_t) \quad (2)$$

The second-order rate coefficient was calculated from the equation

$$k_2 t = \frac{1}{[HSO_3^-]_0 - [ROH]_0} \ln \frac{[ROH]_0\,[HSO_3^-]_t}{[HSO_3^-]_0\,[ROH]_t} \quad (3)$$

In all cases the substrate disappeared totally giving zero value for the final concentration.

The corrected initial ratio for the substrate was calculated from the equation

$$r_0 = r_0'(1 + [HSO_3^-]_0\, \Delta t k_2) \quad (4)$$

where Δt is the time elapsed from the addition of the substrate into the flask ($r = r_0$) to taking the first sample ($r = r_0'$). The corrected rate coefficients were calculated from eqns. (1) – (3) by replacing r_0' by r_0 and t by $t + \Delta t$.

The third-order rate coefficient was calculated from the equation

$$(t + \Delta t)k_3 = \frac{1}{([HSO_3^-]_0 - [ROH]_0)^2} \ln \frac{[ROH]_0\,[HSO_3^-]_t}{[HSO_3^-]_0\,[ROH]_t} \quad (5)$$

$$+ \frac{1}{[HSO_3^-]_0 - [ROH]_0}\left(\frac{1}{[HSO_3^-]_0} - \frac{1}{[HSO_3^-]_t}\right)$$

RESULTS AND DISCUSSION

The experimental second- and third-order rate coefficients were calculated and the results are listed in Table 1. In most cases the second-order rate coefficients decreased and the third-order rate coefficients increased slightly (more clearly in the former case) towards the end of the runs, which suggests that the real order of the reaction is between two and three. The same idea is supported by the fact that when the initial concentration of hydrogen sulfite was altered systematically in the case of 2-methyl-*endo*-2-norbornenol (IV, Table 1), k_2 again increased and k_3 decreased with increasing HSO_3^- concentration, the trend being more distinct in the former case: $k_2 = (2.0 \pm 0.3)\ [HSO_3^-]_0 + (0.006 \pm 0.004)$ and $k_3 = -(60 \pm 20)\ [HSO_3^-]_0 + (3.85 \pm 0.25)$. The same kind of variation of the second-order rate coefficient with varying HSO_3^- concentrations has also

Table 1. Apparent second- and third-order rate coefficients for disappearance of 2-norbornenols and 2-norbornenylmethanols in aqueous sodium hydrogen sulfite solutions (pH = 5.0).

Substrate	Temp. °C	$[ROH]_0$ 10^{-3} M	$[HSO_3^-]_0$ 10^{-3} M	k_2 10^{-3} M^{-1} s^{-1}	k_3 M^{-2} s^{-1}
I	15	6.51	10.42	3.50 ± 0.07	4.24 ± 0.12
	15	6.74	10.79	3.21 0.07	4.02 0.09
	25	6.58	10.55	6.20 0.13	7.90 0.11
	25	6.81	10.86	7.35 0.14	9.06 0.27
	35	6.76	10.00	6.02 0.22	7.64 0.13
	35	6.56	10.48	6.58 0.07	8.00 0.27
	35	6.70	10.69	5.85 0.07	7.23 0.22
II	15	8.33	13.32	0.85 ± 0.03	0.77 ± 0.03
	25	8.62	13.81	1.92 0.04	1.81 0.07
	35	8.53	13.63	4.71 0.05	4.00 0.10
III	15	7.71	12.35	2.23 ± 0.08	2.85 ± 0.21
	25	7.81	12.48	3.47 0.05	3.94 0.17
	35	7.71	12.35	5.93 0.09	6.21 0.14
	35	7.71	12.35	6.00 0.18	6.56 0.20
IV	5	8.50	13.58	0.66 ± 0.02	0.59 ± 0.02
	15	8.01	12.84	1.26 0.06	1.28 0.04
	25	4.99	5.00	1.57 0.06	3.53 0.18
	25	5.27	5.27	1.56 0.09	3.59 0.18
	25	5.62	10.00	3.03 0.10 [a]	3.68 0.10 [a]
	25	7.27	11.63	2.17 0.07 [b]	2.74 0.11 [b]
	25	7.55	12.09	2.85 0.14	2.90 0.14
	25	4.93	15.00	3.93 0.15	3.04 0.09
	25	7.13	22.83	5.01 0.21	2.54 0.08
	35	6.06	9.69	4.57 0.15	5.69 0.21
V	5.3	3.02	9.93	4.13 ± 0.08 [b]	4.82 ± 0.10 [b]
[redacted]	15	3.24	10.00	7.33 0.11 [b]	8.56 0.23 [b]
	25	3.18	9.93	14.8 0.2 [b]	17.9 0.4 [b]
VI	15	3.78	9.55	2.22 ± 0.05 [b]	2.59 ± 0.11 [b]
	25	4.73	9.34	4.09 0.15 [b]	5.00 0.21 [b]
	35	3.83	10.00	7.48 0.17 [b]	8.60 0.22 [b]
VII	15	4.70	10.00	2.78 ± 0.02 [b]	3.27 ± 0.12 [b]
[redacted]	25	4.56	10.00	5.93 0.16 [b]	6.58 0.12 [b]
	35	4.03	10.00	12.7 0.2 [b]	15.6 0.5 [b]
VIII	15	3.83	10.00	3.67 ± 0.18 [b]	3.81 ± 0.33 [b]
	25	3.82	6.11	6.22 0.27 [a,b]	11.6 0.4 [a,b]
	35	3.80	6.08	9.89 0.20 [b]	20.1 0.6 [b]

[a] Addition of hydroquinone (0.01 M) stopped the reaction. [b] The volume of 1 cm^3 of dioxane was added into 39 cm^3 of the reaction medium.

been observed in the reaction of hydrogen sulfite (or sulfite) ion with methacrylonitrile and methyl methacrylate.[5]

The rate coefficients increased generally with elevating temperature giving fairly linear log k *vs.* $1/T$ plots in most cases. A clear exception to this was observed in the reaction of *exo*-2-norbornenol (I, Table 1), where the rate coefficients (both k_2 and k_3) were smaller at 35 °C than at 25 °C. The observation requires further investigation. In the reaction of 2-methyl-*endo*-2-norbornenylmethanol (VIII, Table 1) the log k_3 *vs.* $1/T$ plot was also curved, but in this case the reason may be that the initial HSO_3^- concentration at 15 °C differs from those at 25 and 35 °C. A curved Arrhenius plot has also been reported for acrylonitrile.[5]

The apparent activation parameters are given in Table 2 together with the rate coefficients at 25 °C computed from them. They are of the same order of magnitude as those calculated for the second-order ionic addition of SO_3^{2-} ion to acrylonitriles and methyl acrylates.[5] The rates are thus surprisingly high for simple olefins (half-lives are from 14 to 140 min when calculated from the k_3

Table 2. Apparent activation parameters for the addition of sodium hydrogen sulfite to the double bond of some 2-norbornenols and 2-norbornenylmethanols and apparent rate coefficients at 25 °C calculated from them.

Substrate	$\Delta H^{\ddagger}$/kJ mol^{-1} from k_2	from k_3	$\Delta S^{\ddagger}$/J mol^{-1} K^{-1} from k_2	from k_3	k_2 / 10^{-2} M^{-1} s^{-1}	k_3 / M^{-2} s^{-1}
I[a]	47.5±6.8	48.8±5.2	−108±23	−64±18	6.57±0.46	8.46±0.44
II	60.8±2.9	58.2±0.0	−74±10	−45± 0	2.01±0.07	1.81±0.01
III	33.8±2.8	27.2±3.9	−159±10	−142±13	3.63±0.11	4.19±0.18
IV	44.2±1.6	52.4±2.4	−127± 5	−60± 8	2.53±0.07	2.89±0.12
V	42.2±3.1	42.7±4.1	−120±11	−78±14	14.4 ±0.8	17.3 ±1.3
VI	42.3±0.7	41.8±1.6	−129± 2	−91± 5	4.14±0.03	4.88±0.09
VII	53.5±1.1	55.1±4.6	−89± 4	−44±15	6.04±0.08	7.07±0.36
VIII	34.1±0.7	39.5[b]	−153± 2	−92[b]	6.16±0.04	11.6

[a] Calculated from the rate coefficients at 15 and 25 °C. [b] Calculated from the rate coefficients at 25 and 35 °C.

values at 25 °C in Table 2 by employing 0.01 M initial concentrations for the reactants). The effect of the substituent(s) at C-2 upon the addition rates of HSO_3^- seems to be fairly small, as was also observed in the proton addition to the double bond of the same substrates in aqueous perchloric acid.[12,14,15]

A formal kinetics for the addition of hydrogen sulfite *via* an oxygen-initiated free-radical mechanism to olefins, such as 2-norbornenols and 2-norbornenylmethanols, was derived by assuming the following scheme (*cf.* Refs. 1–5, 9–11, and 19):

$$HSO_3^- + \cdot A \underset{k_{-a}}{\overset{k_a}{\rightleftharpoons}} \cdot SO_3^- + AH \qquad (6)$$

$$\cdot SO_3^- + \underset{\text{OL}}{\rceil\!\lfloor} \underset{k_{-b}}{\overset{k_b}{\rightleftharpoons}} \underset{\text{RI}}{{}^{-}O_3S\rceil\!\lfloor\cdot} \qquad (7)$$

$$\underset{\text{RI}}{{}^{-}O_3S\rceil\!\lfloor\cdot} + HSO_3^- \underset{k_{-c}}{\overset{k_c}{\rightleftharpoons}} \underset{\text{P}}{{}^{-}O_3S\rceil\!\lfloor H} + \cdot SO_3^- \qquad (8)$$

where ·A is an initiating agent, *e.g.* oxygen dissolved in the reaction medium, OL is an olefinic substrate, RI is a free-radical intermediate, and P is a product. By assuming all steps (6)–(8) reversible and by employing the steady-state approximation for the concentrations of $\cdot SO_3^-$ and the intermediate RI, the following expression was obtained for the disappearance rate of the olefinic OL:

$$-\frac{d[OL]}{dt} = \frac{k_a[\cdot A][HSO_3^-](k_b k_c[HSO_3^-][OL] - k_{-b}k_{-c}[P])}{k_{-a}[AH](k_{-b} + k_c[HSO_3^-])} \qquad (9)$$

Since the reaction proceeded to the end completely and addition of acid or base did not regenerate any of the substrate, it can be concluded that $k_{-b}k_{-c}[P] \ll k_b k_c[HSO_3^-][OL]$. Since the initiating agent ·A is probably important only at the beginning of the run (the concentration of oxygen in the air saturated water is 2.5×10^{-4} M at 25 °C and thus 2–5 % of the initial concentration of HSO_3^-) [20] and AH is probably an unstable intermediate, the following approximation can be made: $k_a[\cdot A]/k_{-a}[AH] = K =$ constant. Thus eqn. (9) is simplified to

$$-\frac{d[OL]}{dt} = \frac{K k_b k_c [OL][HSO_3^-]^2}{k_{-b} + k_c[HSO_3^-]} \qquad (10)$$

This rate equation agrees well with the experimental data, since the second-order rate coefficient

$$k_2 = \frac{K k_b k_c [HSO_3^-]}{k_{-b} + k_c[HSO_3^-]} \qquad (11)$$

decreases with decreasing HSO_3^- concentration and the third-order rate coefficient

$$k_3 = \frac{K k_b k_c}{k_{-b} + k_c[HSO_3^-]} \qquad (12)$$

increases with decreasing HSO_3^- concentration. Thus the k_2 and k_3 values listed in Tables

1 and 2 are some kind of "apparent average" rate coefficients and are dependent on the HSO_3^- concentration in a way which depends on the mutual values of k_{-b} and k_c.

A rough estimate can be made for the ratio of $k_{-b}/k_c[HSO_3^-]$ by plotting $1/k_2$ *vs.* $1/[HSO_3^-]_0$ and by calculating the ratio *slope/intercept* $(=k_{-b}/k_c)$. In the case of 2-methyl-*endo*-2-norbornenol (IV; correlation coefficient = 0.95) this kind of estimation gives the value of 0.03 ± 0.01 for the ratio, which suggests that k_{-b} and $k_c[HSO_3^-]$ are of the same order of magnitude, if $[HSO_3^-] \approx 0.01$ M. Thus the order of reaction is really between two and three, which is in agreement with other kinetic data. Additional work on the subject is being carried out.

REFERENCES

1. Kharasch, M. S., May, E. M. and Mayo, F. R. *J. Org. Chem. 3* (1939) 175, with refs.
2. Kharasch, M. S., Schenck, R. T. E. and Mayo, F. R. *J. Am. Chem. Soc. 61* (1939) 3092.
3. Suter, C. M. *The Organic Chemistry of Sulfur*, Wiley, New York 1948, pp. 94–194.
4. Schenck, R. T. E. and Danishefsky, I. *J. Org. Chem. 16* (1951) 1683, with refs.
5. Morton, M. and Landfield, H. *J. Am. Chem. Soc. 74* (1952) 3523.
6. Finch, H. D. *J. Org. Chem. 27* (1962) 649.
7. Daeniker, H. U. v. and Druey, J. *Helv. Chim. Acta 45* (1962) 1972.
8. *Pat. DOS* 2224304, Ref. *Angew. Chem. 13* (1974) 555.
9. Miyata, T., Sakumoto, A., Washino, M. and Abe, T. *Chemistry Letters (Jpn)* (1975) 181, 367.
10. Sakumoto, A., Miyata, T., and Washino, M. *Chemistry Letters (Jpn)* (1975) 563.
11. Lajunen, M. and Lehtonen, K. *Acta Chem. Scand. B 29* (1975) 795.
12. Lajunen, M. and Hirvonen, P. *Finn. Chem. Lett.* (1974) 245.
13. Bly, R. S., DuBose, C. M., Jr. and Konizer, G. B. *J. Org. Chem. 33* (1968) 2188.
14. Lajunen, M. and Lyytikäinen, H. *Acta Chem. Scand. A 30* (1976) 63.
15. Lajunen, M. and Peuravuori, J. *Finn. Chem. Lett.* (1976). *In press.*
16. Kleinfelter, D. C. and Schleyer, P. v. R. *Org. Synth. 42* (1962) 79.
17. Perrin, D. D., Ed., *Dissociation Constants of Inorganic Acids and Bases in Aqueous Solutions*, Butterworths, London 1969, p. 203.
18. Vogel, A. I. *Practical Organic Chemistry*, 3rd Ed., Longman, London 1970, p. 177.
19. Tyutyunnikov, B. N., Bukhshtab, Z. I., Yushchenko, E. P. and Gasyuk, L. V. Ref. *Chem. Abstr. 78* (1973) 28836m.
20. Gordon, A. J. and Ford, R. A. *The Chemist's Companion*, Wiley, New York 1972, p. 39.

Received November 28, 1975.

Acta Chemica Scandinavica A 30 (1976) 363—369

The Crystal Structures of β-V_5As_3, γ-V_5As_3 and Cr_5As_3

ROLF BERGER

Institute of Chemistry, University of Uppsala, Box 531, S-751 21 Uppsala, Sweden

The crystal structures of two V_5As_3 modifications and Cr_5As_3 have been determined using single-crystal methods (β-V_5As_3) or powder methods (γ-V_5As_3 and Cr_5As_3). The symmetry is orthorhombic (space group *Pnma*). β-V_5As_3 is isotypic with Y_5Bi_3 and has a range of homogeneity. The cell dimensions for a crystal of composition $V_{4.94}As_3$ are $a = 6.440$ Å, $b = 7.677$ Å, $c = 9.285$ Å. γ-V_5As_3 and Cr_5As_3 are isotypic with β-Yb_5Sb_3. The cell dimensions for γ-V_5As_3 are $a = 9.464$ Å, $b = 7.520$ Å, $c = 6.471$ Å, and for Cr_5As_3: $a = 9.266$ Å, $b = 7.449$ Å, $c = 6.396$ Å. The two structure types are very similar and are closely related to Rh_5Ge_3.

The occurrence of a phase of the W_5Si_3 structure type in the V—As system was reported by Boller and Nowotny.[1] They observed [1,2] that the composition of this phase deviated appreciably from the ideal crystallographic formula. In the following text, this phase is denoted by α-V_5As_3.

The formation at high temperatures of two additional phases of compositions approximating V_5As_3 was mentioned in an earlier communication.[3] A complete crystal-structure analysis of one of them, denoted by β-V_5As_3 (previously [3] by β), is reported in the present paper. β-V_5As_3 has the ideal crystallographic formula V_5As_3, but a moderate range of homogeneity is indicated. The second phase, denoted by γ-V_5As_3 (previously [3] by γ), has been found only in arc-melted alloys. X-Ray powder and single-crystal data show that γ-V_5As_3 is isotypic with β-Yb_5Sb_3.[4] A β-Yb_5Sb_3 phase has also been found in the Cr—As system.

EXPERIMENTAL

Preparation of β-V_5As_3. The single crystal of β-V_5As_3 used for collecting the X-ray intensity data was selected from a sample prepared in the following manner.

Vanadium turnings (Vanadium Corp. of America, purity 99.5 %) and arsenic (Koch-Light Laboratories Ltd., claimed purity 99.99 %) were reacted in a silica tube at 900 °C for two days and heated for another four days at 1000 °C. A powder photograph of the sample showed the presence of α-V_5As_3, β-V_5As_3 and tetragonal V_3As_2.[5] Single crystals and crystal aggregates of β-V_5As_3 and V_3As_2 were formed. Normally, crystal formation is slow in this system. Traces of an oxide impurity were also detected, indicating that a chemical vapour-transport reaction involving oxygen-containing molecular species might be responsible for the enhanced crystal growth.

Preparation of γ-V_5As_3 and Cr_5As_3. Since there is an unavoidable loss of arsenic on arc-melting, both these compounds were synthesized by arc-melting material richer in arsenic than that corresponding to the stoichiometric formulae. The chromium used for the syntheses was labelled as Elektrolyt-Reinstchrom manufactured by Gesellschaft für Elektrometallurgie m.b.H., Nürnberg. A single-phase specimen of γ-V_5As_3 could be obtained but in other samples this phase occurred together with β-V_4As_3,[5] β-V_5As_3 or α-V_5As_3. Since the solidification process occurs under a very large temperature gradient, these phase-analytical observations cannot serve as any reliable evidence for the phase relationships under equilibrium conditions.

In the arc-melted Cr—As samples, Cr_5As_3 occurred together with CrAs. Heat treatment in a silica tube at 1000 °C for three days yielded CrAs and Cr_4As_3. No well-formed single crystals could be obtained.

X-Ray powder investigations. The cell dimensions were determined using a Guinier-Hägg type focussing camera with strictly monochromatic Cr$K\alpha_1$ radiation [$\lambda = 2.28975$ Å] and with silicon ($a = 5.431065$ Å) [6] or germanium ($a = 5.657906$ Å) [7] as internal calibration standards. Cell parameters were refined by the least-squares method. The powder photograph of β-V_5As_3 was indexed using approximate cell dimensions from Weissenberg and oscillation

Table 1. Powder diffraction data for β-$V_{4.94}As_3$. Cell dimensions: $a = 6.4402(3)$ Å, $b = 7.6767(4)$ Å, $c = 9.2846(5)$ Å.

hkl	Q×10⁵ (Å⁻²) obs.	calc.	Intensity obs.	calc.	hkl	Q×10⁵ (Å⁻²) obs.	calc.	Intensity obs.	calc.
011	2858	2857	-	0	301	22857	22859	-	7
101	3566	3571	-	1	311	24552	24556	27	27
002		4640	-	0	230	24919[a]	24916	-	9
111	5265	5268	-	2	024	25344	25348	23	33
020	6787	6787	-	0	033	25711	25712	4	13
102		7051	-	0	231	[c]	26076	1	1
112	8743	8748	2	2	302	26339	26339	18	12
200	9640	9644	9	3	223	26879	26872	6	6
121	10352	10359	32	20	040	27156[b]	27150	46	54
201	10802	10804	18	9	124	27762	27759	4	5
210	11338	11341	-	2	312	28052	28036	-	3
022	11425	11428	16	5	133	28121	28123	-	5
013	12135	12137	3	2	204		28205	-	0
211		12501	-	0	232		29556	-	0
103	12845	12851	39	23	321	29646	29647	-	4
122	13852	13839	-	0	214		29902	-	0
202	14286	14284	2	1	015	30713	30698	5	5
113		14548	-	0	141		30721		1
212		15981	-	1	105	31420	31417	6	7
220	16431	16432	6	6	042	31795	31790	-	1
031		16432		0	303	32151	32140	-	1
221	17591	17592	57	62	115	33138	33109	60	3
004	18556	18561	-	5	322		33127		56
131	18844	18843	20	24	313	33844	33837	-	5
123	19638	19639	47	48	142	34207	34201	-	3
203	20082	20085	10	13	224	35002[c]	34992	-	4
104	20977	20972	49	46	233	35366[c]	35356	-	0
222	21079	21072	90	100	134	36243[c]	36244	15[c]	17
213	21780	21781	17	19	240	36786	36794	3	11
132		22323	-	1	241		37954	-	5
114	22669	22669	4	5	331		38131	-	3

a) Overlapped by Ge b) Overlapped by Si c) Overlapped by α-V_5As_3

photographs. The powder photographs of γ-V_5As_3 and Cr_5As_3 were successfully indexed by comparison with β-V_5As_3, since the cell dimensions are very nearly equal despite structural differences. Powder intensity data were measured densitometrically with a SAAB film scanner using a method similar to that described by Malmros and Werner.[8] The intensity values obtained were slightly inaccurate due to difficulties in avoiding preferred orientation in the powder samples. Powder diffraction data are given in Table 1 (β-V_5As_3), Table 2 (γ-V_5As_3) and Table 3 (Cr_5As_3).

Single-crystal diffractometry. A many-faceted and well-shaped crystal of β-V_5As_3, with approximate dimensions $0.135 \times 0.098 \times 0.076$ mm, was selected for collecting the intensity data. These were recorded on a computer controlled Stoe-Philips four-circle diffractometer using graphite monochromatized Mo$K\alpha$ radiation. A step-scan procedure was used for recording the reflexions to a maximum in 2θ of 89°. The part of reciprocal space covered was limited by $-12 \leq h \leq 12$, $0 \leq k \leq 14$ and $-16 \leq l \leq 18$. Instrumental stability and crystal setting were checked regularly using three standard reflexions remeasured every 50 reflexions. The strongest of these three, (040), was found to vary somewhat erratically, while the other two remained within expected fluctuations.

Calculations. The calculations were performed on IBM 370/155 and IBM 1800 computers. The crystallographic programs are listed in Ref. 9. The LINNE film scanner program is a modification of the PILT program devised by G. Malmros.[8] Absorption corrections, with an approximate description of the crystal using 14 limiting faces, were applied to the single-crystal data. The minimum and maximum transmission factors were 0.0891 and 0.1775, using a calculated linear absorption coefficient of 329 cm^{-1}.

DETERMINATION OF THE β-V_5As_3 STRUCTURE

The data obtained from Weissenberg films indicated orthorhombic symmetry, with systematic absences corresponding to the space groups *Pnma* or $Pn2_1a$. The symmetry and the cell volume together with phase-analytical data suggested a unit-cell content of 20 vanadium and 12 arsenic atoms.

In the preliminary structure analysis, the Harker sections $P(u,0,w)$, $P(u,\frac{1}{2},w)$ and $P(u,v,\frac{1}{2})$ of the Patterson function were calculated, the intensity material being uncorrected for absorption and averaged intensity values being used for sets of reflexions that should be equivalent according to the orthorhombic symmetry.

The interpretation of the Patterson function was facilitated by the following considerations. The very strong (040) reflexion indicated that the atoms must be essentially confined to planes approximately $b/4$ apart. Moreover, the very weak (020) reflexion indicated that these planes scatter approximately equally. These observations, together with the fact that the scattering power of an arsenic atom is roughly twice that of vanadium, led to the assumption that vanadium and arsenic occupy one 8*d* position each, with $y \sim 0$, and the rest of the atoms are distributed in 4*c* positions in the space group *Pnma*.

The coordinates from the Harker sections, together with distance considerations, gave a reasonable model of the structure. F_o-syntheses were made and the positional parameters found, together with one scale-factor and six individual isotropic temperature factors, were refined using a full-matrix least-squares method. The atomic scattering factors were taken from Ref. 10 and the dispersion correction factors from Ref. 11. After four cycles a conventional *R*-value of 0.046 was obtained based on the 1538 strongest reflexions. Now that the assumed composition was confirmed, a linear absorption coefficient was calculated,

Table 2. Powder diffraction data for γ-V_5As_3. Cell dimensions: $a = 9.4640(3)$ Å, $b = 7.5204(2)$ Å, $c = 6.4712(2)$ Å.

hkl	$Q \times 10^5$ (Å^{-2}) obs.	calc.*	Intensity obs.	calc.	hkl	$Q \times 10^5$ (Å^{-2}) obs.	calc.*	Intensity obs.	calc.
101	3505	3504	-	1	231	22771	22767	-	9
011	4156	4156	-	3	013	23254	23260	-	6
200		4466	-	0	113		24376	-	0
111		5273	-	0	420	24935	24936	61	66
210		6234	-	1	203	25962	25958	35	20
201		6854	-	0	132	26588	26582	2	6
020	7073	7073	-	0	322	26675	26673	-	4
211	8622	8622	6	4	421	27324	27324	10	7
002	9553	9552	-	5	402		27416	-	1
121	10577	10577	43	20	213	27723	27726	35	35
102	10666	10668	15	6	040	28292	28290	50	70
220	11537	11538	20	8	331		28350	-	3
301	12438	12436	66	32	412		29184	-	1
112		12436		2	123		29681	-	2
221		13926	-	4	232	29931	29931	-	6
202	14012	14018	-	1	501	30300	30300	-	3
311		14204	-	1	303		31540	-	2
212	15791	15786	-	3	141		31795	-	1
022		16624	-	0	511	32068	32068	-	3
122	17743	17741	108	95	240		32756	-	0
400	17869	17864	-	6	223	33028	33030	34	45
031	18303	18301	7	21	313		33308	-	1
131	19427	19418	6	9	430	33773	33777	5	10
321	19506	19509	49	50	422	34489	34488	6	8
302		19600		23	241	35134	35144	-	2
410	19606	19632	16	1	332	35510	35513	23	15
401	20249	20252	14	48	431	36156	36165	-	2
230	20380	20379	-	2	521		37372		41
222	21092	21090	86	100	033	37379	37405	66	6
312	21365	21368	14	4	502		37464	-	3
411	22018	22020	3	9	042	37832	37842	8	9
103	22611	22608	9	20					

*) Atomic coordinates taken from β-Yb_5Sb_3

Table 3. Powder diffraction data for Cr_5As_3. Cell dimensions: $a = 9.2655(4)$ Å, $b = 7.4493(3)$ Å, $c = 6.3959(2)$ Å.

hkl	$Q \times 10^5$ (Å^{-2}) obs.	calc.*	Intensity obs.	calc.	hkl	$Q \times 10^5$ (Å^{-2}) obs.	calc.*	Intensity obs.	calc.
101	3615	3609	2	1	411	c	22884	-	9
011	4245	4247	-	3	103	23168	23166	23	21
200		4659	-	0	231		23322	-	9
111		5411	-	0	013	23801	23803	5	6
210		6461	-	1	113		24968	-	0
201		7104	-	0	420	25847	25846	62	66
020		7208	-	0	203	26660	26660	33	19
211	8911	8906	4	4	132	27166[a]	27161	4	6
002	9779	9778	4	4	322	27487	27470	-	4
121	10814	10818	28	16	421	28290	28290	19	7
102	10947[c]	10943	-	5	402		28416	-	1
220	11865	11868	15	5	213	28459	28462	51	34
112	12746	12745	3	2	040	28835	28833	56	70
301	12926	12928	45	27	331		29147	-	3
221	14301	14312	-	6	412		30218	-	1
202		14437	-	3	123		30374	-	2
311		14730	-	1	232	30657	30656	-	6
212		16239	-	2	501		31566	-	3
022		16986	-	0	141		32442	-	1
122	18147	18151	85	94	303		32484	-	2
400		18637	-	6	511		33368	-	2
031	18662	18663	39	21	240		33492	-	0
131	19829	19828	11	7	223	33878	33868	33	44
321	20137	20136	39	50	313	34286[b]	34286	-	1
302	20257	20262	11	24	430	34854	34856	-	10
410	20443	20439	12	1	422		35624	-	7
230	c	20878	-	2	241	c	35937	-	2
401	21086	21082	29	48	332	36479	36480	30	15
222	21647	21646	92	100	431	37308	37300	3	2
312	22059	22064	10	3					

*) Atomic coordinates taken from β-Yb_5Sb_3

a) Overlapped by Si b) Overlapped by Ge c) Overlapped by CrAs

and an absorption correction applied. In order to correct for extinction effects only reflexions having identical indices were averaged.

A series of least-squares refinements was started. The function minimized was

$$w(|F_o| - |F_c|)^2, \text{ where } w^{-1} = \sigma^2 + (p|F_o|)^2$$

σ is the standard deviation of F_o, based on counting statistics, and $p = 0.01$ is an empirical factor. Eleven reflexions were excluded due to obviously misread data, and the (040) reflexion was excluded because it behaved inconsistently during measurement and because it was probably strongly influenced by extinction effects. Reflexions with 'negative intensities' were omitted. An extinction correction according to Coppens and Hamilton,[12] based on approximations introduced by Zachariasen, was applied to the rest of the material. The isotropic temperature factors of two vanadium atoms were found to be somewhat larger than expected; the occupancy factors of these two positions were allowed to vary as the observation of cell parameter variations had indicated the probability of structure defects. Finally, anisotropic temperature factors were introduced. After convergence, the following discrepancy indices were obtained (3547 reflexions):

$$R(F) = 0.035, \text{ where } R(F) = \sum||F_o| - |F_c||/\sum|F_o|$$

and

$$R_w(F) = 0.035, \text{ where } R_w(F) = [\sum w(|F_o| - |F_c|)^2/\sum w|F_o|^2]^{\frac{1}{2}}$$

In line with the suggestion of Hirshfeld and Rabinovich [13] a final refinement was made based on F^2 rather than on F, including reflexions with 'negative intensities' to preserve the assumed normal distribution in the intensity data. For the 3645 reflexions refined the following R-values were obtained, $R(F^2) = 0.038$ and $R_w(F^2) = 0.059$, defined in a similar manner as above, only that F^2 replaces F in the formulae. The corresponding $R(F)$ was 0.034. No significant change in parameter values was found, but the standard deviations were somewhat lower than for the F refinement.

At this stage it was felt, that because of expected strong correlations between many of the parameters, any further refinement assuming the non-centrosymmetric $Pn2_1a$ symmetry would not be worthwhile. The very close agreement between the observed and

Table 4. Structure data for β-$V_{4.84}As_3$, including anisotropic thermal parameters $\beta_{ij}(\times 10^5)$. The form of the temperature factor is $\exp(-\beta_{11}h^2-\beta_{22}k^2\ldots-2\beta_{12}hk\ldots)$. Standard deviations within brackets.

Atom	Position	Occupancy (%)	x	y	z	β_{11}	β_{22}	β_{33}	β_{12}	β_{13}	β_{23}
V(1)	8*d*	100	0.20848(4)	0.55282(4)	0.06395(3)	243(4)	230(3)	159(2)	21(3)	−21(2)	11(2)
V(2)	4*c*	99.1(2)	0.14603(6)	1/4	0.78443(4)	364(7)	303(5)	158(3)	0	−33(4)	0
V(3)	4*c*	94.6(2)	0.28572(7)	1/4	0.26722(4)	333(7)	365(6)	142(4)	0	−46(4)	0
V(4)	4*c*	100	0.45513(6)	1/4	0.01131(4)	275(6)	193(4)	127(3)	0	−14(3)	0
As(1)	8*d*	100	0.07048(2)	0.50822(2)	0.32661(2)	290(3)	229(2)	126(1)	−25(2)	13(1)	−1(1)
As(2)	4*c*	100	0.05788(4)	1/4	0.04406(3)	248(4)	219(3)	148(2)	0	−28(2)	0

calculated structure factors implies that any deviation from centrosymmetry must be negligibly small, and the final structure is accordingly described in the terms of *Pnma* symmetry as presented in Table 4 (with parameter values taken from the F^2 refinement). A list of observed and calculated structure factors can be obtained from the author on request.

THE STRUCTURES OF γ-V_5As_3 AND Cr_5As_3

When the β-V_5As_3 structure had been determined it was seen to resemble closely the β-Yb_5Sb_3 structure,[4] the two compounds nevertheless representing different structure types. It appeared, however, that β-Yb_5Sb_3 might be truly isotypic with γ-V_5As_3 and Cr_5As_3. Powder intensity calculations were accordingly performed for the two arsenides, assuming this isotypism and using the atomic coordinates of β-Yb_5Sb_3 as given by Brunton and Steinfink.[4] A satisfactory agreement was found between observed and calculated intensities for both arsenides as presented in Tables 2 and 3, leaving no doubt that the three compounds are isostructural.

STRUCTURAL DESCRIPTIONS AND DISCUSSION

A projection of the β-V_5As_3 structure along the *b*-axis is illustrated in Fig. 1*a*. The coordination around As(1) may be characterized by a trigonal prismatic arrangement of metal atoms with three further atoms outside the prism faces. A closer look at the distances reveals that the trigonal prism is indeed very distorted; from this point of view the coordination is characterized better by the coordination number 8. The coordination polyhedron around As(2) is much more regular, a bisdisphenoidal arrangement with coordination number 8. Interatomic distances are presented in Table 5. The distances between unlike atoms in β-V_5As_3 are similar to those found in α-V_4As_3 [14] and β-V_4As_3.[5] The V(3) – V(4) distance of 2.61 Å is rather short, but the V(3) site is not fully occupied. Still shorter metal contacts are found in α-V_5As_3 (2.40 Å) and V_3As (2.38 Å).[15] In these two arsenides the metal atoms form straight infinite chains, but there are no data, as to the occupancy in these phases albeit cell parameter

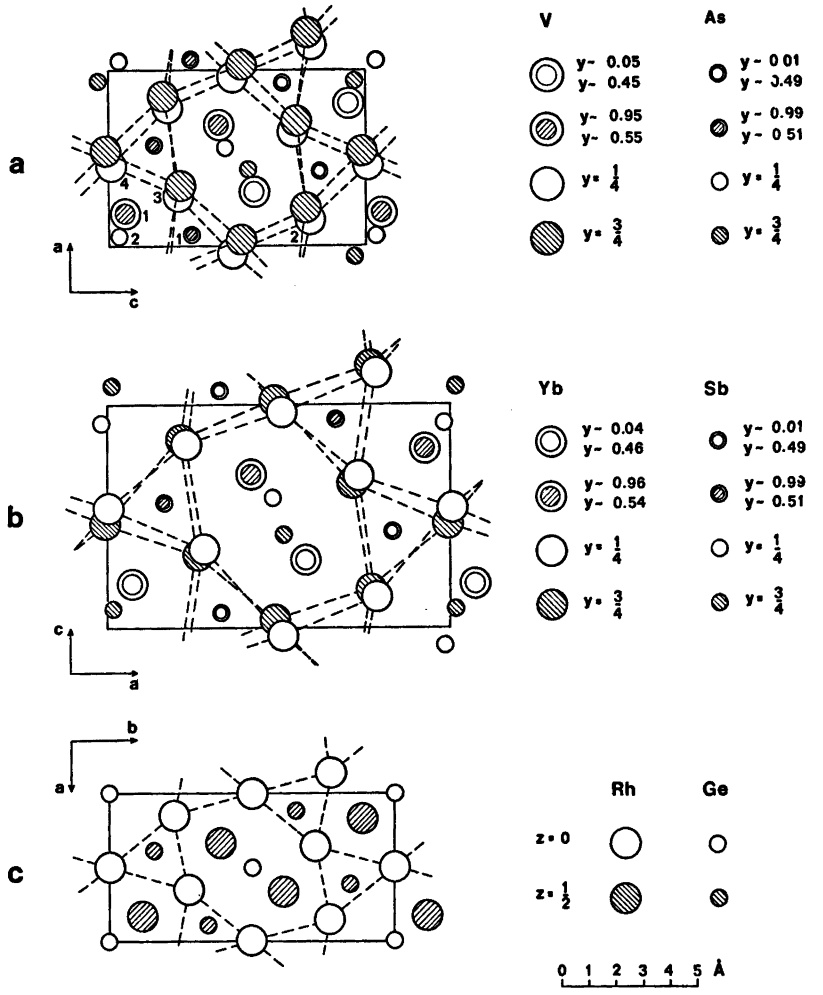

Fig. 1. The crystal structures of (a) β-V_5As_3 and (b) β-Yb_5Sb_3 projected along the *b*-axes, and c) Rh_5Ge_3 projected along the *c*-axis.

variations indicate the possibility of vacancies in both.

There is a striking resemblance between the β-V_5As_3 structure and the β-Yb_5Sb_3 structure, the latter being illustrated in Fig. 1*b*. There is also a close relationship to the Rh_5Ge_3 structure [16] illustrated in Fig. 1c; this fact was already recognized by Brunton and Steinfink in the case of β-Yb_5Sb_3. Owing to the lack of positional parameter data for γ-V_5As_3, no closer comparison can be made as regards distances and coordination in the orthorhombic V_5As_3 polymorphs.

Cell dimension variations [8] of β-V_5As_3 indicated a homogeneity range. In quenched specimens the cell volume was smaller, which could be interpreted as an increasing tendency to vacancy formation at higher temperatures. The *a* and *b* axes decrease and the *c* axis increases with decreasing volume. The structure refinement supported this view, indicating vanadium deficiency, the composition of the investigated crystal being $V_{4.94}As_3$.

β-V_5As_3 is most probably isotypic with Y_5Bi_3 reported by Schmidt *et al.*,[17] as well as with a further number of rare-earth bismuthides

Table 5. Interatomic distances (Å) for β-$V_{4.94}As_3$. The maximum standard deviation obtained was 0.0006 Å. Distances shorter than 3.5 Å are listed.

V(1) –	As(8)	2.492	V(4) – 2	As(1)	2.532
	As(2)	2.526		As(2)	2.576
	As(1)	2.566	2	As(1)	2.597
	As(1)	2.665		V(3)	2.615
	As(1)	2.618	2	V(1)	2.734
	V(2)	2.713	2	V(1)	2.858
	V(4)	2.734		V(2)	2.898
	V(4)	2.858		V(3)	2.960
	V(1)	3.027		V(2)	3.009
	V(3)	3.035			
	V(1)	3.046	As(1) –	V(3)	2.481
	V(2)	3.080		V(4)	2.532
	V(3)	3.144		V(2)	2.540
				V(1)	2.566
				V(4)	2.597
V(2) –	As(2)	2.477		V(1)	2.618
2	As(1)	2.540		V(2)	2.633
2	As(1)	2.633		V(1)	2.665
2	V(1)	2.713		V(3)	2.838
	V(4)	2.898		As(2)	3.289
	V(4)	3.009		As(1)	3.348
2	V(1)	3.080			
2	V(2)	3.283			
			As(2) –	V(2)	2.477
				V(3)	2.478
V(3) –	As(2)	2.478	2	V(1)	2.498
2	As(1)	2.481	2	V(1)	2.526
	As(2)	2.539		V(3)	2.539
	V(4)	2.615		V(4)	2.576
2	As(1)	2.838	2	As(1)	3.289
	V(4)	2.960			
2	V(1)	3.035			
2	V(1)	3.144			
2	V(3)	3.236			

recently reported by Yoshihara *et al.*[18] Schmidt *et al.* gave the composition of 37.8 at.% Bi (corresponding to the formula $Y_{4.94}Bi_3$) for a homogeneous single phase sample. This indicates that analogous metal vacancy distributions might occur in β-V_5As_3 and Y_5Bi_3. Yoshihara *et al.*, however, assign the formula $R_{5+x}Bi_3$ to their compounds, indicating deviations from the ideal composition towards the metal-rich side.

No range of homogeneity was detectable for γ-V_5As_3. This corresponds to the results for the isostructural β-Yb_5Sb_3, which was found to be strictly stoichiometric.[4]

The small amounts of homogeneous material available did not permit a conventional chemical analysis. An attempt to perform microprobe analyses on the very crystal examined and on γ-V_5As_3 failed to detect any significant deviations from the stoichiometric composition. The relative error of a microprobe analysis is of the same magnitude as the proposed deviation in composition.

α-V_5As_3 appears to form narrow two-phase regions with β- and γ-V_5As_3, with α-V_5As_3 as the most metal-rich component. Its cell volume is considerably smaller than that of the orthorhombic phases and has been found to vary, indicating non-stoichiometry. The variations affect the *c*-axis to the greatest extent. It is therefore likely that a vacancy mechanism involving a variable occupancy of the 4*a* or 4*b* positions (space group *I*4/*mcm*) is responsible for this behaviour. A complete single-crystal analysis has been started in order to study this problem. The results will be presented in a forthcoming paper.

In comparing the V – As and Cr – As systems it is notable that, when vanadium arsenide polymorphs exist, only the structure types adopted by the high-temperature phases are represented in the Cr – As system. This is illustrated by the couples Cr_4As_3 – β-V_4As_3 (Cr_4As_3 type) and Cr_5As_3 – γ-V_5As_3 (β-Yb_5Sb_3 type).

Acknowledgements. The author wishes to thank Professor Ivar Olovsson for all facilities put at his disposal and is indebted to Professor Stig Rundqvist for valuable discussions and comments. This work has been financially supported by the Swedish Natural Science Research Council.

REFERENCES

1. Boller, H. and Nowotny, H. *Monatsh. Chem. 97* (1966) 1053.
2. Boller, H. and Nowotny, H. *Monatsh. Chem. 98* (1967) 2127.
3. Berger, R. *Acta Chem. Scand. A 29* (1975) 641.
4. Brunton, G. D. and Steinfink, H. *Inorg. Chem. 10* (1971) 2301.
5. Berger, R. *Acta Chem. Scand. A 28* (1974) 771.
6. Deslattes, R. D. and Henins, A. *Phys. Rev. Lett. 31* (1973) 972.
7. Baker, J. F. C. and Hart, M. *Acta Crystallogr. A 31* (1975) 364.
8. Malmros, G. and Werner, P.-E. *Acta Chem. Scand. 27* (1973) 493.
9. Lundgren, J.-O., Ed., *Crystallographic Computer Programs*, Institute of Chemistry,

University of Uppsala, Uppsala 1975 UUIC-B13-04-2.
10. Hanson, H. P., Herman, F., Lea, J. D. and Skillman, S. *Acta Crystallogr. 17* (1964) 1040.
11. *International Tables for X-Ray Crystallography*, Kynoch Press, Birmingham 1968, Vol. III.
12. Coppens, P. and Hamilton, W. C. *Acta Crystallogr. A 26* (1970) 71.
13. Hirshfeld, F. L. and Rabinovich, D. *Acta Crystallogr. A 29* (1973) 510.
14. Yvon, K. and Boller, H. *Monatsh. Chem. 103* (1972) 1643.
15. Bachmayer, K. and Nowotny, H. *Monatsh. Chem. 86* (1955) 741.
16. Geller, S. *Acta Crystallogr. 8* (1955) 15.
17. Schmidt, F. A., McMasters, O. D. and Lichtenberg, R. R. *J. Less-Common Met. 18* (1969) 215.
18. Yoshihara, K., Taylor, J. B., Calvert, L. D. and Despault, J. G. *J. Less-Common Met. 41* (1975) 329.

Received November 18, 1975.

Acta Chemica Scandinavica A 30 (1976) 370—374

Some Oxidation Properties of Manganese and its Lower Oxides

ROBERT POMPE

Department of Inorganic Chemistry, Chalmers University of Technology and University of Göteborg, P.O. Box, S-402 20 Göteborg 5, Sweden

Oxidation of the pulverised samples of Mn, MnO and the equilibrium Mn_2O_3-Mn_3O_4 have been studied. The investigations were made in the temperature range 200 – 1000 °C and at oxygen partial pressures of 0.01, 0.20 and 1 atm. The techniques employed were thermogravimetry and differential thermal analysis. Mn_2O_3 was found to be the oxide finally formed by oxidation of the metal, MnO and Mn_3O_4 in the temperature range from 400 °C to the equilibrium temperature of decomposition. The equilibrium temperature for the system Mn_2O_3-Mn_3O_4 could be determined by decomposing the partially oxidized MnO or Mn_3O_4 using the TG-DTG technique. The thermodynamic aspects are discussed.

The ability of manganese to appear in different oxidation states gives rise to the existence of various solid oxide phases. The methods of preparation and the properties of these phases have been comprehensively described by Moore *et al.*[1] It was further established [2–5] that the oxide phases appeared as crystalline compounds which might be represented by ideal formulae MnO Mn_2O_3, Mn_3O_4 and MnO_2. MnO and Mn_3O_4 were shown to exhibit a considerable non-stoichiometry. The higher oxides were found to be convertible to the lower ones and *vice versa*, by a proper choice of temperature and oxygen pressure.[6–9]

The experimental results of many authors, however, differ somewhat as to which type of the oxide is formed and which temperature corresponds to the equilibrium value of decomposition. Mn_2O_3 or Mn_3O_4 are thus reported to form from MnO up to *ca.* 850 °C, while MnO_2 should be the product up to *ca.* 500 °C. Similarly, Mn_2O_3 is said to decompose to Mn_3O_4 at 920 – 970 °C. Hahn and Muan [10] found the equilibrium Mn_2O_3-Mn_3O_4 to be attainable in both directions and determined approximately the equilibrium temperatures as indicated in Fig. 1. Kim *et al.*[11] confirmed by a different method their values.

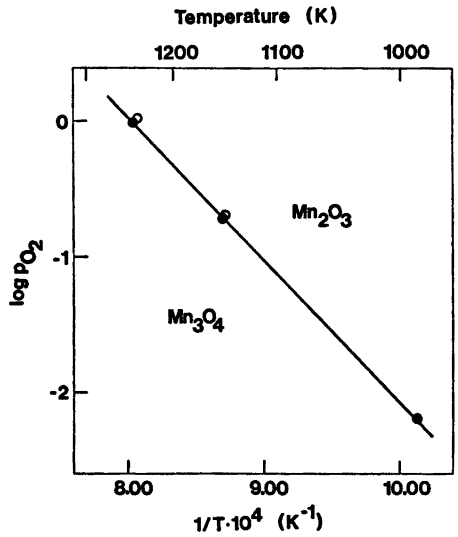

Fig. 1. Diagram showing the equilibrium oxygen pressure of the system $Mn_2O_3 - Mn_3O_4$ as a function of reciprocal temperature. ● This work, ○ Hahn and Muan.[10]

The oxidation of pure manganese in air was studied by Baldwin and co-workers.[12] By X-ray and metallographic analysis they identified MnO, Mn_3O_4 and Mn_2O_3 in the oxide scale below 825 °C and MnO with some Mn_3O_4 above this temperature. According to Païdassi and Echeverria [13] the oxide scale up to 850 °C consists of MnO, Mn_2O_3 and MnO_2, while at 900 – 1200 °C the oxides present are MnO and Mn_3O_4.

The purpose of the present work was to determine what kind of oxide is formed at various oxygen partial pressures (p_{O_2}) in the temperature range 200 – 1000 °C when samples of pulverized Mn metal or MnO are heated either continuously or at selected temperatures. A further objective was to explore the possibility of investigating the equilibrium Mn_2O_3-Mn_3O_4 by the TG-DTG technique.

EXPERIMENTAL

Starting materials. MnO was prepared by heating manganese powder in the nitrogen atmosphere containing about 100 ppm oxygen at 800 °C for 18 h. The product was obtained as a hard grey-green mass containing 4.1 weight % manganese metal. Mn_2O_3 and Mn_3O_4 were produced by complete oxidation of Mn, MnO or Mn_3O_4, and by decomposition of Mn_2O_3, respectively.

The grain size of the manganese powder and the oxides varied between 1 and 3 μ for about 90 % of the grains.

Apparatus and experimental procedure. The investigations were made using a micro-thermobalance (Mettler) with the additional equipment enabling TG, DTG and DTA curves to be simultaneously recorded as a function of temperature and time. The experimental and instrumental parameters used were as follows: Weight of the samples: 50 – 80 mg; reference substance: Cr_2O_3, $BaCO_3$ (estimation of ΔH for the reactions); crucibles of S platinum; sensitivity of the measurements: TG, 5×10^{-2} mg; DTG, 10 mg/min; DTA, 100 μV (Pt-Rh thermocouples); temperature control: ±1.5 °C; the heating rates used: 1 – 15 °C/min; the gas atmospheres employed: O_2; $Ar + O_2$, $p_{O_2} = 0.20$ atm; $N_2 + O_2$, $p_{O_2} = 0.01$ atm; gas flow: 6 l/h.

In studying the oxidation of MnO, Mn_3O_4 and Mn_2O_3, TG, DTG and DTA curves were recorded during heating of the samples up to 1000 °C. Systematic runs were made then at temperatures corresponding to the maxima of the appearing exothermic peaks, as well as some other selected temperatures.

Manganese powder was oxidized continuously up to 1000 °C and also at some lower, constant temperatures in the atmospheres of $p_{O_2} =$ 0.20 atm and 0.01 atm.

Each run was terminated when the DTG curve essentially stabilized close to its initial value. This indicated either a zero or insignificant weight change of the sample. The heating of the furnace was then interrupted and the samples were cooled as quickly as possible in the furnace atmosphere.

The products were examined by X-ray diffractometry, IR-spectroscopy and optical microscopy. Calculations, where feasible, were also made on the basis of weight gain or loss (TG) or the peak areas of the DTA curves.

RESULTS

Oxidation of Mn. On continuous heating of the samples up to 1000 °C the thermograms were such as schematically depicted in Fig. 2. The data for the subsequent runs are presented in Table 1. The weight increase appeared to be most pronounced in the temperature range of about 400 – 600 °C. At $p_{O_2} = 0.01$ atm the weight gain in this range was a linear function of time because of the limited oxygen supply. At the temperatures following from the figure a well-defined decomposition of the higher oxide took place. The diffraction patterns of the products before and after this decomposition were those of α-Mn_2O_3 and Mn_3O_4, respectively. One or two strongest reflections for Mn_3O_4 often appearing in the Mn_2O_3 pattern suggested the occurrence of a layer of Mn_3O_4 beneath that of Mn_2O_3. The IR spectra taken on Mn_2O_3 and Mn_3O_4 agreed with those published.[14]

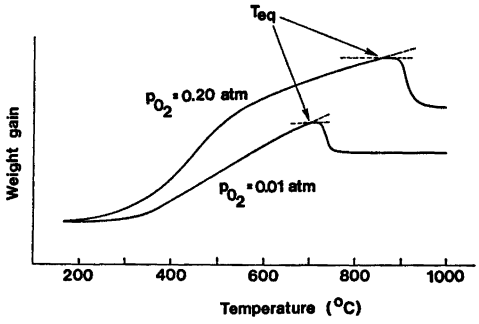

Fig. 2. The TG curves obtained in oxidizing the pulverized Mn up to 1000 °C at $p_{O_2} = 0.20$ atm and 1 atm.

Table 1. Oxidation of Mn powder up to 1000 °C at $p_{O_2} = 0.20$ atm and 0.01 atm.

p_{O_2} (atm)	Temp. (°C)	Time at const. temp. (h)	Products
0.20	1000	(heat. rate 1 °C/min)	Mn_3O_4
0.01	1000	(12 at 600 °C)	Mn_3O_4
0.01	600	16	Mn_2O_3
0.20	470	18	Mn_2O_3

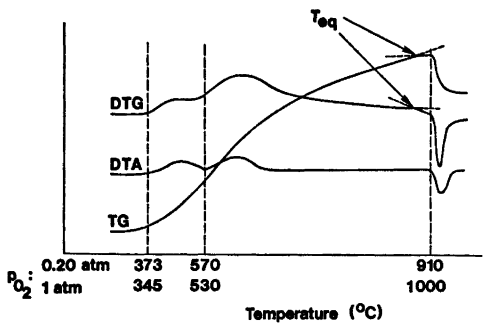

Fig. 3. The TG, DTG and DTA curves obtained in oxidizing MnO up to 1000 °C at $p_{O_2} = 0.20$ atm and 1 atm.

Oxidation of MnO. The essential appearance of the thermograms when oxidizing MnO at $p_{O_2} = 1$ atm and 0.20 atm at 1000 °C is shown in Fig. 3. Two exothermic peaks and one endothermic peak are apparent on the DTA curves at the temperatures indicated in the figure. The data characteristic of the constant temperature runs at $p_{O_2} = 0.20$ atm are given in Table 2.

In the run made at a temperature corresponding to the first exothermic reaction (480 °C) the DTG curve levelled off after *ca.* 1 h. X-Ray analysis revealed the presence of a small amount of Mn_2O_3 and the weight gain corresponded to almost complete oxidation of the Mn metal present in MnO, to Mn_2O_3.

The reaction corresponding to the second exothermic peak was suggested by X-ray patterns and thermogravimetrical calculations to be that of oxidation of MnO over Mn_3O_4 to Mn_2O_3.

Table 2. Oxidation of MnO at constant temperatures and $p_{O_2} = 1$ atm and 0.20 atm.

Temp. (°C)	Time at const. temp. (h)	Products
480	1	MnO, Mn_2O_3
610	4	Mn_2O_3, some MnO
780	6	Mn_2O_3
450	23	Mn_2O_3, MnO
330	12	MnO (some Mn_3O_4 and Mn_2O_3 of strongly distorted X-ray patterns)

The product after the endothermic reaction was always found to be Mn_3O_4.

Mn_2O_3–Mn_3O_4 system. Mn_3O_4 was oxidized at a heating rate of 10 °C/min up to 870 °C at $p_{O_2} = 0.20$ atm. The oxygen uptake was most rapid in the range of 650–770 °C. Increasing the temperature out of this range produced a decreased oxidation rate. Mn_3O_4 could be converted into Mn_2O_3 within 2 h at 700 °C.

When the temperature of a partially oxidized sample of MnO or Mn_3O_4 attained the value determined as the equilibrium temperature (T_{eq}), the DTG curve showed an abrupt change in the slope. The TG curve, at the same time, formed a small plateau before the onset of an observable decomposition. The plateau was more prolonged when Mn_2O_3, prepared by incomplete oxidation of MnO, was decomposed.

The values of the equilibrium temperature of decomposition obtained at $p_{O_2} = 1$ atm, 0.20 atm and 0.01 atm corresponded to 1246 K, 1151 K and 983 K, respectively, with a mean deviation of 3 K. The plot of their reciprocal values *versus* log p_{O_2} is shown in Fig. 1. $\Delta H°$ for the reaction $3Mn_2O_3 \rightarrow 2Mn_3O_4 + \frac{1}{2}O_2$ was evaluated from the peak area of the DTA curve. Using the reference value of 4.3 kcal/mol for $BaCO_3$ [16] the $\Delta H°$ value was found to be 24.6 kcal/3 mol Mn_2O_3. The value obtained from the slope of the plot in Fig. 1 was 21.8 kcal/3 mol Mn_2O_3 being thus close to that commonly accepted (21.6 kcal/3 mol Mn_2O_3)[11,15]

DISCUSSION AND CONCLUSIONS

The solid oxide phases obtainable by oxidation of Mn or MnO may be summarily written as MnO_{1+x}, where, for ideal stoichiometric molar ratios, x equals to $0.3\overline{3}$, 0.50 and 1.00. Using the tabulated data [15] and the formula for the computation of $\Delta G°$ in the form

$$\Delta G° = \Delta H_0 + (2.303a \log T + I)T + b \times 10^{-3}T^2 + c \times 10^5/T \quad \text{(A)}$$

a comparison was made of the thermodynamic stability of the oxides. ΔG-values per mol MnO were calculated at 700 K and $p_{O_2} = 0.20$ atm for Mn_3O_4, Mn_2O_3 and MnO_2 and also at 600 K and 800 K for the latter two oxides. The formula used was

$$\Delta G = x\Delta G°(MnO_{1+x}) - \Delta G°(MnO) - (x/2)RT \ln p_{O_2} \quad \text{(B)}$$

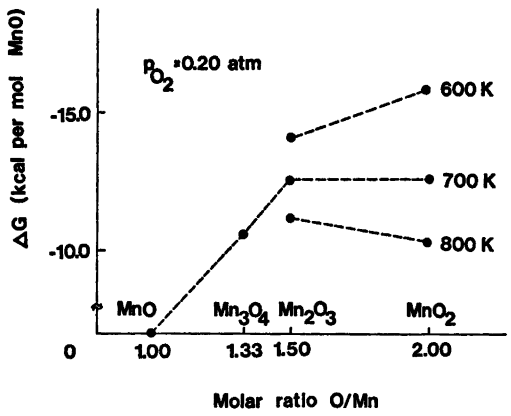

Fig. 4. The free enthalpy of formation per mol MnO for the higher manganese oxides at $p_{O_2}=0.20$ atm.

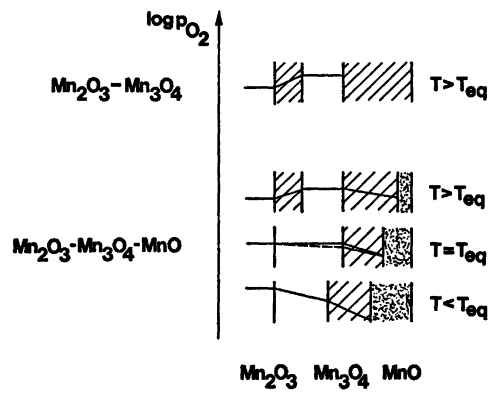

Fig. 5. The profiles of the oxygen pressure inside the grains of incompletely oxidized samples of Mn_2O_3 in the region of the equilibrium temperature of decomposition (T_{eq}) of Mn_2O_3 to Mn_3O_4.

and the values obtained were plotted in Fig. 4. Above 700 K Mn_2O_3 appears to be the most stable oxide while below this temperature the existence of MnO_2 should be favoured. The limiting value of p_{O_2} estimated for the system Mn_2O_3-Mn_3O_4 from the formula (B) is of the order of 10^{-6} atm at 700 K.

The experimental results obtained tend to confirm that Mn_2O_3 is the only oxide finally formed above 700 K. The yield of Mn_2O_3 per unit time is then a function of the grain size, the operating time and the oxygen supply. No evidence of the formation of MnO_2 has been found. The oxidation, however, proceeds extremely slowly at lower temperatures (< 700 K) and a considerably longer time is therefore required to attain equilibrium.

In studying the system $Mn_2O_3-Mn_3O_4$ Hahn and Muan [10] equilibrated the samples side by side at selected temperatures for between 40 and 300 h. In this investigation the duration of the measurements was reduced to less than 2 h. The change in the slope of the TG and DTG curves during heating was used to indicate the attainment of equilibrium. In order to obtain observable slope changes on the curves, partially oxidized samples of Mn_2O_3 were employed. Prepared by the oxidation of Mn, MnO or Mn_3O_4 they consisted of grains containing layers of MnO, Mn_3O_4 and Mn_2O_3 or Mn_3O_4 and Mn_2O_3, respectively.

The presumed oxidation mechanism behind this method of determining the T_{eq} values is outlined in Fig. 5. When approaching the region of equilibrium the profiles of p_{O_2} within a grain are assumed to be approximately as illustrated in the figure. At temperature $T < T_{eq}$ the oxidation of Mn_3O_4 to Mn_2O_3 and MnO to Mn_3O_4 takes place and the weight change occurs continuously. On reaching the equilibrium temperature T_{eq} the oxidation of Mn_3O_4 to Mn_2O_3 is stopped resulting in the slope change of the DTG curve.

In the presence of only Mn_3O_4 the oxygen pressure gradient (∇p_{O_2}) is removed and the TG curve stabilizes since no more oxygen can be taken up. When, however, MnO is also present a certain Δp_{O_2} still exists through the Mn_2O_3 layer. The TG curve then increases slightly giving rise to a prolonged plateau at a low heating rate. At temperatures $T > T_{eq}$ a negative p_{O_2} is built up within the Mn_2O_3 layer and the decomposition of Mn_2O_3 to Mn_3O_4 is then a rather rapid process.

From the data compiled [15] the value of T_{eq} can be evaluated. Using the formula (A) T_{eq} at $p_{O_2}=1$ atm is calculated to be about 1530 K. The experimentally determined $T_{eq}=1246$ K at $p_{O_2}=1$ atm gives a value of ΔG° equal to 1.6 kcal/mol Mn_2O_3. This is about 1 % of the ΔG° values for Mn_2O_3 or Mn_3O_4 and may represent a measure of the error in the determination of these values. Since the ΔG° ($Mn_2O_3-Mn_3O_4$) is calculated as a difference of ΔG° values for the oxides this formula may be in-

appropriate to an accurate calculation of T_{eq}.

The values of T_{eq} obtained in this investigation compare well with those reported.[10,11] This indicates that the above TG-DTG technique may provide a simple method for investigating solid oxide equilibria.

Acknowledgements. I wish to express my warmest thanks to Prof. Nils-Gösta Vannerberg for many helpful discussions and to Dr. John Wood for correction of the English text.

The investigation was performed in connection with a research project on nitrides in steel supported financially by the Swedish Board for Technical Development (Contr. No. EKB-U-287-74/75).

REFERENCES

1. Moore, T. E., Elis, M. and Selwood, P. W. *J. Am. Chem. Soc. 72* (1950) 856.
2. LeBlanc, M. and Wehner, G. *Z. Phys. Chem. Abt. A 168* (1934) 59.
3. Holtermann, X. X. *Ann. Chim. (Paris) 14* (1940) 121.
4. Dubois, P. *C. R. Acad. Sci. 199* (1934) 1416.
5. Drucker, C. and Hüttner, R. *Z. Phys. Chem. Leipzig 131* (1927) 237.
6. Hed, A. Z. and Tannhauser, D. S. *J. Electrochem. Soc. 114* (1967) 314.
7. Bergstein, A. and Vintera, I. *Chem. Listy 50* (1956) 1530.
8. Mackenzie, R. C. *The Diff. Therm. Inv. of Clays*, Mineral. Soc., London 1957, p. 320.
9. Dollimore, D. and Tonge, K. H. *Thermal Analysis 2* (1971) 91.
10. Hahn, W. C. and Muan, A. *Am. J. Sci. 258* (1960) 66.
11. Kim, D. O., Wilbert, Y. and Marion, F. *C. R. Acad. Sci. Paris Ser. C 262* (1966) 756.
12. Evans, E. B., Phalnikar, C. A. and Baldwin, W. M. *J. Electrochem. Soc. 103* (1956) 367.
13. Païdassi, I. and Echeverria, A. *Acta Metall. 7* (1959) 293.
14. Gattow, G. and Glemser, O. *Z. Anorg. Allg. Chem. 309* (1961) 143.
15. *Handbook of Chemistry and Physics*, 47th Ed., The Chem. Rubber Co., Cleveland.
16. Mackenzie, R. C. and Ritchie, P. F. S. *Thermal Analysis 1* (1971) 442.

Received November 19, 1975.

Acta Chemica Scandinavica A 30 (1976) 375—380

The Crystal and Molecular Structure of *endo*-3-Benzylsulfinylbicyclo[2.2.1]heptane-*endo*-2-carboxylic Acid

S. ABRAHAMSSON and HARRY M. ZACHARIS

Department of Structural Chemistry, Faculty of Medicine, University of Göteborg, Fack, S-400 33 Göteborg 33, Sweden

The title compound ($C_{15}H_{18}O_3S$) crystallizes in space group $C2/c$, with 8 molecules in a unit cell of dimensions $a=24.768$, $b=10.116$, $c=12.611$ Å and $\beta=118.05°$. The structure determination was accomplished *via* the heavy-atom method and led to a refined set of parameters with $R=0.042$ for 1461 observed reflexions. The compound investigated is the more reactive of two configurational isomers. The sulfinyl and carboxyl groups of different molecules are hydrogen-bonded. An intramolecular non-bonded close contact of 2.80 Å between the sulfur atom and the carbonyl oxygen provides an intramolecular proximity between these two groups, with an O−S···O angle of 173°. The study gives structural evidence for the anchimeric effects used to explain the solution kinetics of this and similar compounds.

The crystal structure of *endo*-3-benzylsulfinylbicyclo[2.2.1]heptane-*endo*-2-carboxylic acid (Ia) was determined in connection with kinetics studies of certain sulfinyl derivatives being investigated by Allenmark.[1,2]

In the hydriodic acid reduction of a sulfoxide the rate-accelerating effect of a neighbouring carboxyl group has been demonstrated. The reaction proceeds with formation of a cyclic sulfonium intermediate as the rate determining step. There is also strong evidence for an inversion mechanism in forming the cyclic intermediate.

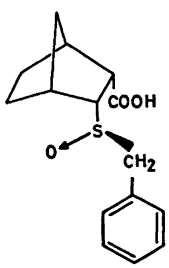

Ia

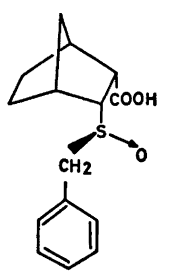

Ib

For the particular case involving (I), one of the diastereoisomers showed a rate constant more than 3000 times greater than the other.[3b] The diastereoisomers Ia and b differ only in their configuration about sulfur, but for each of them there exists a pair of mirror image isomers. This X-ray analysis concerns the racemate of the more reactive diastereoisomer.

EXPERIMENTAL

Good single crystals were found in samples kindly supplied by Dr. Stig Allenmark of Uppsala University. The compound had been recrystallized from a water-ethanol solution. The specimen chosen for investigation was a colourless rectangular prism of approximate dimensions $0.3\times0.25\times0.1$ mm. The systematic absences observed were for the hkl reflexions with $h+k$ odd, and for the $h0l$ reflexions with l odd. As the compound is a racemate and had a measured density in agreement with eight molecules in the unit cell of the two possible spacegroups, Cc or $C2/c$, the latter was the more logical choice. Later refinement of the structure verified that this choice was correct. The lattice constants given below were obtained from least squares refinement of the diffractometer setting angles of 12 reflexions. The intensity data were taken on Picker FACS I diffractometer supplied with a graphite monochromator using Cu$K\alpha_1$ radiation. The $\theta-2\theta$ scanning mode at a rate of 1°/min and a scan width of 2° adjusted for dispersion were used. Two ten-second background counts were taken at each end of the scan. Attenuation was used where reflexions exceeded 10.000 cps.

Measuring all reflexions out to a 2 θ of 110° provided 1461 independent reflexions greater than 2 σ above background. Three reflexions were monitored following every 50 measurements. The standard showing the greatest change had a root-mean-square deviation of 2.5 %.

Changes in the sum of the standard intensities were interpolated in a linear fashion and applied as scaling factors to the rest of the data. The intensities were also corrected for Lorentz and polarization effects but not for absorption.

CRYSTAL DATA

Molecular formula	$C_{15}H_{18}O_3S$
Molecular weight	278.373 g/mol
Space group	$C2/c$ (No. 15)
Cell constants	$a = 24.768(5)$,
	$b = 10.116(2)$,
	$c = 12.611(2)$ Å,
	$\beta = 118.05(5)°$
Unit cell volume	2788.46 Å^3
Calculated density ($Z = 8$)	1.326 g cm^{-3}
Measured density	1.31 g cm^{-3}
Linear absorption coefficient (Cu$K\alpha$)	20.1 cm^{-1}

STRUCTURE DETERMINATION

The sulfur coordinates were readily obtained from a three-dimensional Patterson synthesis. A subsequent three-dimensional Fourier synthesis based on the observed data and the phases obtained from the sulfur position, yielded the coordinates of seven additional atoms in the vicinity of the sulfur atom. The remaining non-hydrogen atoms were obtained at heights of 2–5 e$^-$/Å^3, from an electron density map based on the positions of the eight atoms previously found. Three cycles of least squares refinement, using anisotropic thermal parameters for the sulfur atom, gave $R = 0.12$. At this point a difference Fourier was calculated from which all but one of the hydrogens could be identified near their calculated positions and at heights from 0.5 to 1 e$^-$/Å^3. Using these hydrogen positions only in the structure factor calculations, anisotropic refinement of all non-hydrogen atoms led to an $R = 0.052$. With these positions fixed, subsequent isotropic refinement of only the hydrogen positions resulted in an $R = 0.044$. On the resulting difference Fourier a single peak appeared at a height of about 0.4 e$^-$/Å^3, in the region between the hydroxyl and sulfinyl oxygens. Assignment of this peak as a hydrogen atom and repeating the difference synthesis gave an electron density map with no point greater than 0.2 e$^-$/Å^3.

Since several of the largest structure factors with a sin θ/λ less than 0.2 were systematically as much as 10 % lower than the corresponding calculated values, it was assumed that these 28 reflexions suffered from extinction. They were removed from the last three cycles of refinement, which led to a final $R = 0.042$. Since the largest shift in either a coordinate or temperature factor was less than three-tenths of its corresponding standard deviation, the structure determination was now considered complete.

The atomic scattering factors for all atoms except hydrogen were taken from the International Tables for X-ray Crystallography.[3] The scattering factor for sulfur was corrected for the effect of anomalous dispersion (real part). The hydrogen scattering factor used was that given by Stewart, Davidson and Simpson.[4] The weighting scheme used in the refinement was that of Mills and Rollett.[5]

RESULTS AND DISCUSSION

A list of the final structure factors can be obtained from this laboratory. Coordinates

Table 1. Fractional coordinates with standard deviations in parentheses.

	x	y	z
S(1)	0.2370(1)	0.1310(2)	0.1489(1)
O(1)	0.2407(2)	0.2209(4)	0.2484(4)
O(2)	0.2402(3)	−0.0111(6)	−0.0383(5)
O(3)	0.3017(2)	−0.1765(5)	−0.0267(4)
C(1)	0.3638(3)	0.1293(7)	0.2789(6)
C(2)	0.3076(3)	0.0362(7)	0.2237(5)
C(3)	0.3250(3)	−0.0657(7)	0.1529(6)
C(4)	0.3902(3)	−0.0204(8)	0.1804(7)
C(5)	0.3855(3)	0.1089(9)	0.1133(8)
C(6)	0.3664(4)	0.2109(8)	0.1796(7)
C(7)	0.4151(3)	0.0289(9)	0.3085(7)
C(8)	0.2840(3)	−0.0792(7)	0.0209(6)
C(9)	0.1837(3)	0.0011(7)	0.1400(7)
C(10)	0.1231(3)	0.0614(7)	0.1081(7)
C(11)	0.1089(4)	0.0980(9)	0.1978(8)
C(12)	0.0543(5)	0.1584(11)	0.1705(12)
C(13)	0.0135(5)	0.1828(10)	0.0554(13)
C(14)	0.0256(4)	0.1484(11)	−0.0357(10)
C(15)	0.0812(4)	0.0862(9)	−0.0101(8)

Table 2. Anisotropic thermal parameters ($\times 10^4$) in the form $\exp[-2\pi^2(h^2a^{*2}U_{11}+k^2b^{*2}U_{22}+l^2c^{*2}U_{33}+2klb^*c^*U_{23}+2hla^*c^*U_{31}+2hka^*b^*U_{12})]$. Standard deviations are given in parentheses.

	U_{11}	U_{22}	U_{33}	U_{23}	U_{31}	U_{12}
S(1)	418(9)	347(9)	452(9)	25(7)	22(7)	2(7)
O(1)	594(32)	368(27)	512(27)	−17(22)	307(25)	47(23)
O(2)	695(36)	695(37)	519(31)	−75(28)	197(28)	158(31)
O(3)	709(35)	475(30)	555(30)	−23(25)	373(28)	72(26)
C(1)	453(40)	514(42)	453(41)	−45(35)	138(34)	−32(35)
C(2)	423(38)	407(39)	406(36)	43(31)	224(31)	−2(31)
C(3)	484(40)	370(38)	482(39)	62(31)	277(33)	11(31)
C(4)	464(43)	573(49)	676(48)	−20(41)	311(38)	40(37)
C(5)	659(53)	721(58)	738(55)	0(46)	440(46)	−168(45)
C(6)	550(49)	515(48)	707(50)	−1(40)	295(42)	−127(39)
C(7)	432(43)	685(55)	648(49)	8(42)	184(38)	8(40)
C(8)	526(41)	414(38)	521(41)	31(34)	301(35)	−40(34)
C(9)	481(42)	389(40)	729(50)	31(36)	313(39)	−39(33)
C(10)	436(42)	363(39)	682(48)	52(35)	260(38)	−70(32)
C(11)	484(47)	660(56)	919(63)	−106(48)	361(46)	−86(41)
C(12)	688(61)	798(70)	1667(109)	−277(72)	732(71)	−136(54)
C(13)	564(62)	628(64)	2148(144)	217(79)	577(76)	−10(50)
C(14)	611(57)	820(70)	1231(87)	568(65)	55(57)	−130(53)
C(15)	561(50)	727(59)	729(57)	246(48)	165(44)	−133(45)

Table 3. Fractional atomic coordinates and isotropic temperature factors for the hydrogen atoms. Estimated standard deviations in parentheses.

	x	y	z	B(Å^2)
H(1,1)[a]	0.369(3)	0.175(6)	0.343(5)	4.1(1.3)
H(2,1)	0.303(2)	−0.008(6)	0.286(5)	2.9(1.2)
H(3,1)	0.327(2)	−0.150(5)	0.189(5)	2.6(1.2)
H(4,1)	0.411(3)	−0.087(6)	0.168(5)	5.6(1.5)
H(5,1)	0.358(3)	0.104(6)	0.034(5)	4.8(1.5)
H(5,2)	0.426(3)	0.128(7)	0.120(6)	7.4(1.9)
H(6,1)	0.328(3)	0.255(6)	0.132(5)	6.2(1.5)
H(6,2)	0.396(3)	0.281(8)	0.215(7)	6.9(2.0)
H(7,1)	0.417(3)	−0.035(7)	0.365(6)	5.1(1.6)
H(7,2)	0.454(3)	0.066(7)	0.336(6)	5.8(1.7)
H(9,1)	0.199(3)	−0.034(6)	0.212(5)	4.7(1.5)
H(9,2)	0.183(3)	−0.162(6)	0.080(6)	4.8(1.5)
H(11,1)	0.140(3)	0.079(7)	0.276(6)	5.4(1.6)
H(12,1)	0.046(4)	0.177(9)	0.240(8)	8.4(2.3)
H(13,1)	−0.028(5)	0.221(10)	0.035(9)	11.5(2.9)
H(14,1)	0.000(4)	0.160(9)	−0.115(8)	9.1(2.5)
H(15,1)	0.092(4)	0.057(9)	−0.071(8)	9.4(2.4)
H(16)[b]	0.276(5)	−0.192(11)	−0.107(9)	11.5(3.1)

[a] The first number refers to the bonded atom. [b] Carboxyl hydrogen.

and anisotropic temperature factors for the non-hydrogen atoms are given in Tables 1 and 2, respectively. Hydrogen atom parameters are given in Table 3.

The atomic numbering and distances and angles for non-hydrogen atoms are shown in Fig. 1. The C−H distances range from 0.87 to 1.02 Å.

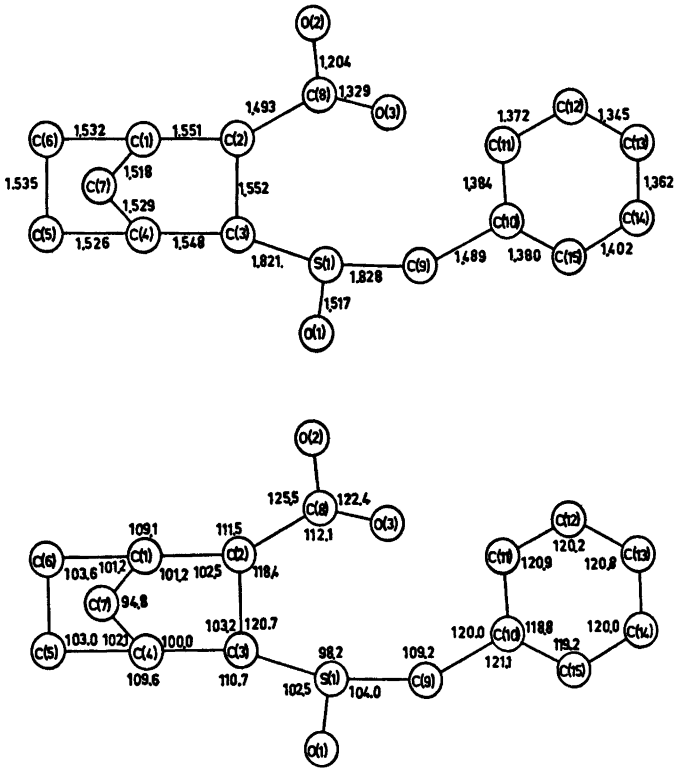

Fig. 1. Bond distances and angles. The average standard deviations are for the bonds S–C 0.005, S–O 0.003, C–C 0.007 and C–O 0.006 Å and for the angles C–S–C 0.2, C–S–O 0.2, C–C–C 0.4 and C–C–O 0.3°.

Table 4. Comparison of parameters about the sulfur atom.

Compound	C–S (Å)	S–O (Å)	C–S–O (°)	C–S–C (°)	O···S–O (°)	S···O (Å)	Ref.
o-Carboxyphenyl-methyl sulfoxide	1.788(5) 1.800(3)	1.517(2)	103.1(0.1) 104.6(0.2)	97.8(0.2)	176	2.78	8
(–)-*o*-Carboxyphenyl-methyl sulfoxide	1.782(6) 1.800(5)	1.517(3)	103.7(0.2) 104.3(0.2)	98.8(0.2)	173	2.73	9
endo-3-Benzylsulfinyl-bicyclo[2.2.1]heptane-*endo*-2-carboxylic acid	1.821(6) 1.828(8)	1.517(6)	102.5(0.3) 104.0(0.4)	98.2(0.3)	173	2.80	This study

Except for the three slightly longer bonds involving the substituted ring carbon atoms C(2) and C(3), the distances and angles in the norbornyl portion of the molecule are within 1.5 σ of the parameters for norbornane found from a microwave study.[6] The distances C(2)–C(8) and C(9)–C(10) exhibit the expected shortening for a C–C single bond adjacent to a multiple bond. The parameters about the sulfur are in good agreement with those found for similar compounds, and the relevant values are listed for comparison in Table 4.

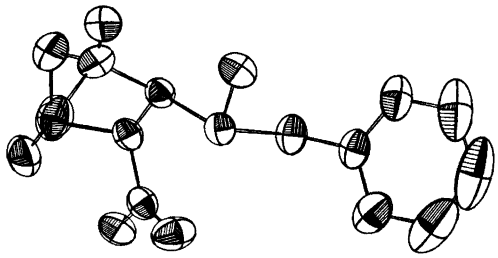

Fig. 2. Thermal ellipsoids at 50 % probability level.

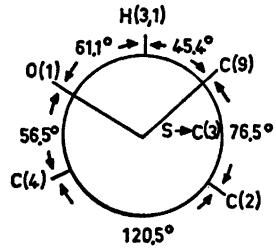

Fig. 3. Newman projection along the S(1)–C(3) bond.

The bond distances in the phenyl ring have an average value of 1.375 ± 0.013 Å (av. dev.), significantly shorter than the normal value of 1.394 Å. The shorter distances in the phenyl ring, particularly the two distances C(12) – C(13) and C(13) – C(14) are explained as an experimental artifact of the pronounced thermal motion in that region of the molecule (Fig. 2). The phenyl ring is planar to within ± 0.003 Å, and the internal angles are all within 1σ of 120°.

A Newman projection of one of the mirror image pairs of the structure viewed down the S(1) – C(3) bond is shown in Fig. 3 and establishes the configuration of the more reactive isomer as that of Ia. The molecular conformation is also illustrated in Fig. 4. The sulfur atom is situated as far as possible from the plane of the benzene ring, the torsion angle C(15) – C(10) – C(9) – S(1) being – 93.3°.

An intramolecular non-bonded contact of 2.80 Å between S(1) and O(2) is significantly shorter than the sum, 3.25 Å, of the van der Waals radii (*cf.* Abrahamsson *et al.*[7]) indicating a strong interaction of the negatively polarized carbonyl oxygen with the positively charged sulfur. The oxygen lies along the S – O dipole axis, the O···S – O angle being 173°. In the light of the reaction kinetics presented earlier for this and similar compounds, and the important role of anchimeric assistance in explaining those results, the geometry observed about

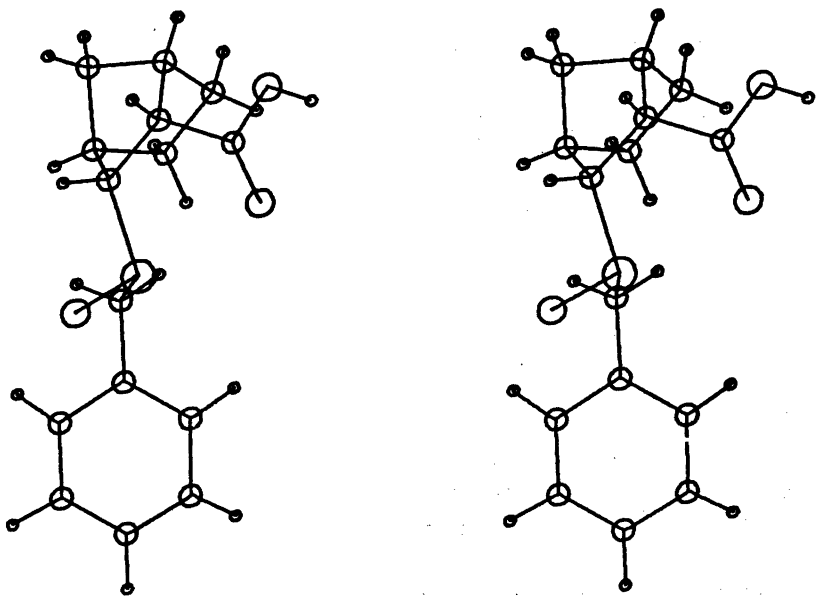

Fig. 4. Stereopair showing the molecular conformation.

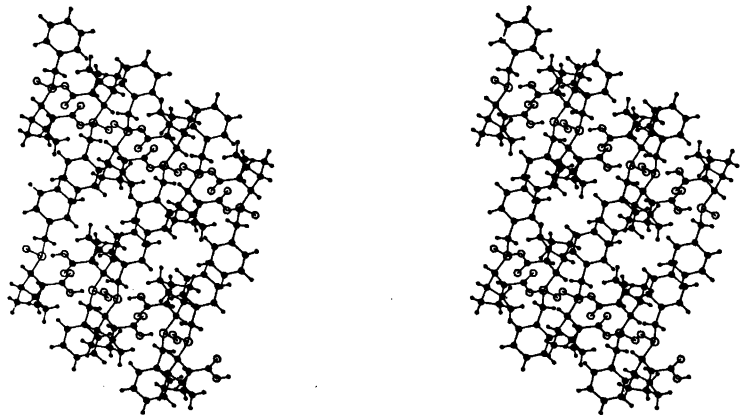

Fig. 5. Molecular packing.

the sulfur atom and especially the spatial relationship between the sulfinyl group and the carbonyl oxygen are consistent with the conclusions arrived at from solution kinetics studies.

The molecular packing is shown in Fig. 5. The O(1)···O(3) contact distance of 2.55 Å, the location of H(16) at a distance of 0.92 Å from O(3) and 1.64 Å from O(1) with an O–H···O angle of 169° indicate the presence of a rather strong hydrogen bond between pairs of molecules. Benzene rings pack in regions both with parallel and perpendicular ring planes whereas in other regions norbornyl rings are in van der Waals contact.

Grants in support of the Department were obtained from the Swedish Medical Research Council, the Swedish Board for Technical Development, the Wallenberg Foundation, and the U.S. Public Health Service (GM-11653).

REFERENCES

1. Allenmark, S. and Hagberg, C.-E. *Acta Chem. Scand. 24* (1970) 2225.
2a. Allenmark, S. and Johnsson, H. *Acta Chem. Scand. 25* (1971) 1860.
2b. Johnsson, H. and Allenmark, S. *Chem. Scr. 8* (1975). *In press.*
3. *International Tables for X-Ray Crystallography*, Kynoch Press, Birmingham 1962, Vol. III, p. 202.
4. Stewart, R. F., Davidson, E. R. and Simpson, W. T. *J. Chem. Phys. 42* (1965) 3175.
5. Mills, O. S. and Rollett, J. S. *Computing Methods and the Phase Problem in X-Ray Crystal Analysis*, Pergamon Press, London 1961, p. 107.
6. Allinger, N. L. *J. Am. Chem. Soc. 90* (1968) 1199.
7. Abrahamsson, S., Rehnberg, G., Liljefors, T. and Sandström, J. *Acta Chem. Scand. B 28* (1974) 1109.
8. Dahlén, B. *Acta Crystallogr. B 29* (1973) 595.
9. Dahlén, B. *Acta Crystallogr. B 30* (1974) 642.

Received November 20, 1975.

Acta Chemica Scandinavica A 30 (1976) 381—385

On the Formation and Properties of Tetrakis(acetylacetonato)-thorium(IV) Hemibenzene

BERT ALLARD

Department of Nuclear Chemistry, Chalmers University of Technology, Fack, S-402 20 Göteborg 5, Sweden

Lattice parameters have been determined for tetrakis(acetylacetonato)thorium(IV) hemibenzene, $[Th(C_5H_7O_2)_4.\frac{1}{2}C_6H_6]$. The unit cell is triclinic with the dimensions $a = 9.234(4)$ Å, $b = 11.093(6)$ Å, $c = 16.602(10)$ Å, $\alpha = 119.06(4)°$, $\beta = 120.16(3)°$, $\gamma = 74.81(3)°$ and $Z = 2$. The infrared spectrum has been measured. The bonding interaction between the chelate complex and the benzene molecule is very weak as indicated by thermogravimetric analysis and solution behaviour. The solvate can probably best be described as a clathrate. Similar compounds were not found, however, if the central atom was changed to Zr(IV), Ce(IV), Hf(IV), U(IV), or Np(IV), nor could any solvate formation be found with other aromatic compounds like toluene, pyridine, or with solvents with a smaller molecular volume or with acetylacetone.

In the course of preparing and studying the acetylacetonates of tetravalent metals[1] it was observed that crystals obtained from a benzene solution of $Th(AA)_4$ (AA = the acetylacetonate ligand) contained one molecule of the solvent for every two molecules of $Th(AA)_4$. Since an investigation of the molecular packing of such a solvated species would be of considerable interest, especially with regard to the influence of the benzene molecule on the geometry of the coordination sphere around the thorium atom, a structure determination was begun. Some other properties were also studied in order to find out if there were any indications of bonding interactions between the benzene molecule and the conjugated ring system of the ligand. In order to determine if the benzene coordinating ability of $Th(AA)_4$ is unique, a search for similar solvates with other tetravalent metal acetylacetonates and with other solvents were performed.

EXPERIMENTAL

Preparation of the compound. $Th(AA)_4$ was precipitated by mixing an aqueous solution of $Th(NO_3)_4$ and an aqueous solution of ammonia and acetylacetone.[2] In a similar way or by using an extraction procedure previously described[3] $Zr(AA)_4$, $Ce(AA)_4$, $Hf(AA)_4$, $U(AA)_4$, and $Np(AA)_4$ were also prepared. The complexes were crystallized from benzene at room temperature.

In the search for other solvates crystallization of $Th(AA)_4$ was performed from both aromatic and non-aromatic diluents with molecular volumes similar to or less than the volume of benzene (148.4 Å³/molecule at 25 °C). The following solvents were used (molecular volumes within parentheses obtained from density data): Water (30.0), ethanol (97.4), carbon disulfide (101.3), acetone (122.9), chloroform (133.9), pyridine (134.3), tetrahydrofuran (134.6), carbon tetrachloride (161.2), acetylacetone (171.0), diethyl ether (173.9), toluene (177.4), cyclohexane (180.5) and hexane (218.5)

Analysis. The thorium content of the complex was determined by α-counting in a TriCarb Liquid Scintillation Spectrometer on tracer amounts of ^{230}Th, which was added before preparation of the complex. The amount of solvated benzene was determined from thermogravimetrical measurements and by absorbance measurements of the solvated complex at ~ 675 cm^{-1} in carbon tetrachloride solutions.

Thermogravimetrical measurements. TGA and DTA curves were recorded with a Mettler Recording Vacuum Thermoanalyzer for the solvated and unsolvated $Th(AA)_4$.

Structure investigations. Preliminary lattice parameters were determined from diffraction measurements using the Weissenberg single crystal technique. X-Ray photographs were

taken of the solvated and unsolvated $Th(AA)_4$ using a Guinier focusing camera with Cu$K\alpha$ radiation.

Infrared spectra. Infrared spectra of the solvated and unsolvated $Th(AA)_4$ were recorded in the range 4000 – 400 cm^{-1} with a Perkin-Elmer 337 Grating IR Spectrophotometer, using a KBr pellet technique.

Density measurements. The density of dilute solutions of $Th(AA)_4$ in benzene and toluene was measured pycnometrically.

Solubility measurements. The solubility of $Th(AA)_4$ in hexane, carbon tetrachloride, hexone (4-methyl-2-pentanone), benzene, toluene, and chloroform was determined from measurements of the $Th(AA)_4$ concentration in saturated solutions using liquid scintillation technique and ^{230}Th.

PROPERTIES

Properties and stability in the solid state. The only solvate that was obtained was $Th(AA)_4 \cdot \frac{1}{2}C_6H_6$. Freshly made crystals of the solvate became opaque within a few hours exposure to air at room temperature, due to the loss of benzene and destruction of the structure. Because of this rapid decomposition of the solvate and since any non-stoichiometric solvent inclusions in the crystals had to be removed by washing and drying of the crystals before analysis, definitive reproducible values of the Th/C_6H_6 ratio were difficult to obtain. The measured values of this ratio were, however, close to and never less than two and did not exceed three indicating a solvate with the composition $Th(AA)_4 \cdot \frac{1}{2}C_6H_6$.

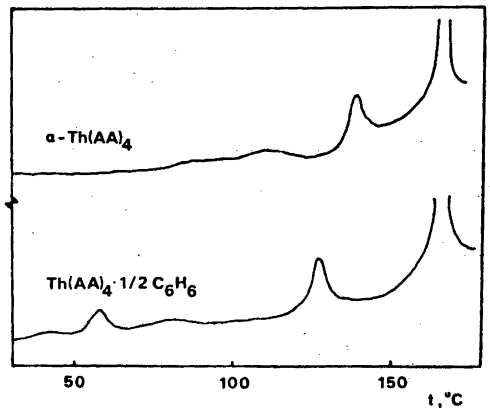

Fig. 1. DTA recording for α-$Th(AA)_4$ and $Th(AA)_4 \cdot \frac{1}{2}C_6H_6$.

Two forms of $Th(AA)_4$ exist, both being monoclinic.[1,4] The formation of a new stoichiometric compound distinguishable from the unsolvated $Th(AA)_4$ was confirmed from comparison of Guinier photographs.

The suggested composition of the solvate was confirmed by thermogravimetric measurements. The weight decrease due to decomposition and to evaporation of benzene began already at room temperature and was complete at about 70 °C (*cf.* the boiling point of benzene: 80.1 °C). A small endothermic peak was observed in the DTA recording at a temperature just below the point of complete loss of benzene, as can be seen in Fig. 1. Another endothermic peak around 130 °C was also found, possibly due to destruction of the lattice, and after this point a loss of weight which increased rapidly after the melting point, around 170 °C, began and indicated a sublimation. For the unsolvated α-$Th(AA)_4$ complex an endothermic transition occurred around 140°C, after which sublimation was noticeable. This reaction might be due to a destruction of the high-density α-$Th(AA)_4$ lattice. The low-density β-$Th(AA)_4$ form is more stable at high temperatures and is usually obtained by sublimation

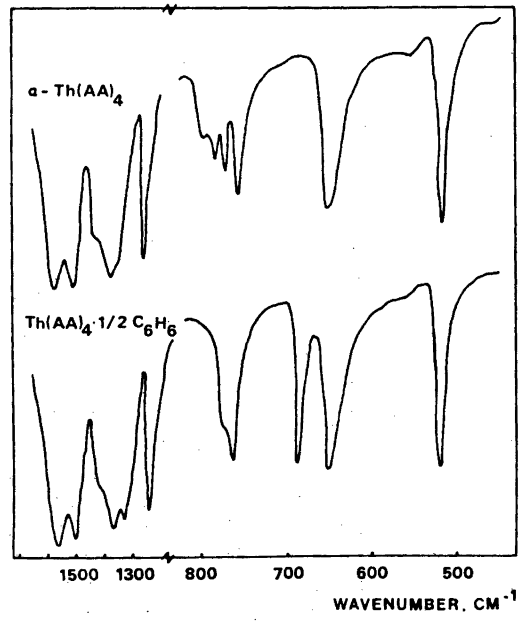

Fig. 2. Infrared spectra of α-$Th(AA)_4$ and $Th(AA)_4 \cdot \frac{1}{2}C_6H_6$.

of $Th(AA)_4$ at low pressure just below the melting point.[1]

From the preliminary structure investigation, the cell volume 1284.8 Å^3 was calculated for two formula units. A possible set of lattice parameters for the triclinic cell is $a = 9.234(4)$ Å, $b = 11.093(6)$ Å, $c = 16.602(10)$ Å, $\alpha = 119.06(4)°$, $\beta = 120.16(3)°$, $\gamma = 74.81(3)°$ and $Z = 2$. A full three-dimensional structure investigation is in progress,[5] and possibly a better choice of unit cell parameters will be selected. The molecular volume of benzene based on the density of the liquid at 25 °C is 148.4 Å^3 and from structure data 122.2 Å^3. The molecular volume of two molecules of the unsolvated α-$Th(AA)_4$ molecule, as given by structure data,[1] is 1187.0 Å^3. The sum of these volumes is 1335.5 and 1309.2 Å^3, respectively, which is greater than the measured 1284.8 Å^3 and thus suggests that the efficiency of packing of the molecule is better in the solvated than the unsolvated structure.

Infrared spectra have been recorded for solvated and unsolvated $Th(AA)_4$ and portions of these spectra are shown in Fig. 2. The assignment of the bands in the infrared spectrum of $Th(AA)_4$ is given in the literature.[6] Some minor differences between the two spectra are noticeable. A new peak appearing around 690 cm^{-1} in the spectrum of $Th(AA)_4 \cdot \frac{1}{2}C_6H_6$ and corresponding to the solvated benzene is shifted towards a higher frequency in comparison to the value for free benzene. The band around 1350 cm^{-1} due to CH_3 deformation is shifted to a lower frequency and the band around 1021 cm^{-1} assigned to CH_3 rocking is split. The slightly metal sensitive band around 660 cm^{-1} probably corresponding to ring deformation is shifted to a lower frequency. The bands around 750 – 800 cm^{-1} corresponding to CH out-of-plane bending appear as a single peak with shoulders while four peaks are distinguishable for the unsolvated species. Neither the bands at 530 cm^{-1} and 400 cm^{-1} which are sensitive to M – O vibrations, nor the bands around 1500 – 1600 cm^{-1} from C = C and C = O vibrations or any other pure in-plane stretchings have changed significantly. This indicates that the ligand ring geometry is more or less unperturbed in the presence of benzene molecules in the crystal lattice. Any change of the inner coordination would have caused shifts at least in the C = C and C = O vibrations.[7] It may be concluded that any interaction between the solvated benzene and the metal or ligand ring must be weak.

Properties in solution. From density measurements of dilute $Th(AA)_4$-solutions the apparent molar volume could be estimated. With the assumption that the solutions of $Th(AA)_4$ in the inert solvents benzene and toluene could be regarded as regular,[8] a simple mass balance consideration would give.

$$v_A = (m_m/\varrho_m - m_S/\varrho_S)M_A/m_A \quad (1)$$

where v, m, ϱ and M are molar volume, weight, density and formula weight, respectively, and subscripts A, S and m denote the complex, the pure solvent and the mixture of solute and solvent, respectively. Any interaction would of course give a volume change. Significant changes of the molar volume v_A as defined above for solutions of the same concentration but consisting of different solvents would be an indication of differences in the solvent-solute interaction.

For a dilute solution of $Th(AA)_4$ a molar volume of 350 ± 10 cm^3/mol was measured in benzene and 370 ± 10 cm^3/mol in toluene which possibly indicates a slightly stronger interaction or smaller intermolecular distances in benzene than in toluene. (In solid state the molar volumes obtained from structure investigations[1] are 357 and 368 cm^3/mol, for α- and β-$Th(AA)_4$, respectively.) The only conclusion of these measurements is that any difference that might exist between the coordination of $Th(AA)_4$ in benzene, which is capable of forming solid solvates, and $Th(AA)_4$ in toluene, which does not form solid solvates, is small.

From comparative studies of the distribution of tetravalent acetylacetonates ($Th(AA)_4$, $U(AA)_4$, $Np(AA)_4$, and $Pu(AA)_4$) between an aqueous phase and benzene it was found that $Th(AA)_4$ differs from the others.[9] A slightly different coordination for the $Th(AA)_4$ complex might be the explanation for this phenomena. If, however, there is an explicit interaction between benzene and $Th(AA)_4$, possibly due to some favourable steric circumstances, which does not occur with the other tetravalent acetylacetonates (with smaller molecular volumes), then this behaviour might be detected from solubility data. For this reason the solu-

bility of $Th(AA)_4$ was measured in hexane, carbon tetrachloride, hexone, benzene, toluene, and chloroform. Solvent-solute interaction with hexane and carbon tetrachloride would be small, while hexone and chloroform are very likely to interact with $Th(AA)_4$.[10,11]

According to the theory of regular solutions, the following relation should be valid:[8,12]

$$RT \ln a_2 = RT \ln x_2 + v_2\phi_1^2(\delta_1 - \delta_2)^2 \quad (2)$$

where R is the gas constant, T is the absolute temperature, a is the activity, x is the mol fraction, ϕ is the volume fraction, v is the molar volume, and δ is the solubility parameter. Subscript 2 denotes solute and 1 solvent. In a regular solution interactions between solvent and solute are mainly of a dispersion type. The heat of mixing and solution is non-zero while the entropy is that of an ideal solution. Significant interactions between solvent and solute, *e.g.* hydrogen bonding, would violate the basic postulates in the theory and hence would be expected to cause deviations. Deviations from eqn. (2) would consequently indicate the degree of solvent-solute interaction. [13]

The solubility parameter of a chelate, ML_n, may be estimated by the relation [14]

$$\delta_{ML_n} = (n/n')^{1/2}\delta_{HL} \quad (3)$$

where $v_{ML_n} = n'v_{HL}$. From eqn. (3) the value $\delta_{Th(AA)_4} = 11.38$ is obtained when using the molar volume of the chelate as given by the lattice parameters. [All δ-values in this report are given in $(cal\ mol/cm^3)^{1/2}$]. Eqn. (3) is in fact based on the assumption that the heat of evaporation of the chelate is simply obtained by addition of the contributions from the ligands. This is not unreasonable due to the additive nature of the molar cohesive energy which has been demonstrated in other cases.[15] Since the ligands in the complex are partly shielded the heat of evaporation should, however, be less than the value obtained from addition of the ligand contributions, which would change eqn. (3) to give

$$\delta_{ML_n} = (n''/n')^{1/2}\delta_{HL} \quad (4)$$

where $n'' \lesssim n$. For some tris acetylacetonates values of $n''/n \approx 0.73$ have been obtained.[16] For the somewhat less symmetric tetrakis-acetylacetonates a higher value might be expected. For $n''/n = n'/n \approx 0.87$ the value for $\delta_{Th(AA)_4} = \delta_{HAA} = 10.6$ would simply be obtained by assuming a volume reduction and a shielding effect of the same order.

In Table 1 calculated solubilities according to eqn. (2) are given using $\delta_{Th(AA)_4} = 10.6$. In order to eliminate the activity a_2 in eqn. (2) only relative values have been calculated using hexane as an inert reference diluent. Good agreement between measured and calculated solubilities is obtained for carbon tetrachloride, toluene, and benzene, while deviations are found for hexone and chloroform. The requirements for regularity are not violated and any specific interaction with benzene is not indicated. As already stated, chloroform is known to interact strongly with $Th(AA)_4$,[11] and mixed complexes with the composition $[Th(AA)_n.hexone]^{4-n}$ are also known from distribution experiments.[10] For both these solvents the calculated solubility values differ significantly from the measured values, due to a solvent-solute interaction. Evidently the basic postulates of the regular solution concept are not valid, and in order to obtain

Table 1. Measured and calculated solubilities. (For $\delta_{Th(AA)_4} = 10.6$) (v from lattice parameters.[1])

Solvent	δ [a]	Meas. log x	Meas. log x [b]	Calc. log x [b]
Hexane	7.27	−3.84	Ref.	Ref.
Carbon tetrachloride	8.58	−1.92	1.92	1.84
Hexone	8.65	−2.61	1.23	1.91
Toluene	8.99	−1.65	2.19	2.23
Benzene	9.16	−1.47	2.37	2.36
Chloroform	9.53	−1.43	2.41	2.61

[a] Calculated from $\delta = [(\Delta H^v - RT)/v]^{1/2}$. [8] [b] With hexane chosen as an inert reference solvent.

agreement between measured and calculated values the molar volumes and solubility parameters must be empirically modified.

CONCLUSIONS

Solid solvates between β-diketone complexes and benzene are not unique. Solvates with different solvent molecules including benzene are known for many rare earth complexes. A structure investigation of $[Yb(AA)_3H_2O.\frac{1}{2}C_6H_6]$ [17] shows that the benzene molecule in this compound is simply interstitially incorporated in the crystal lattice, the closest distance to any other carbon or oxygen atom from a benzene carbon atom being 3.53 Å. The volume of the solvate is very close to the sum of the volumes of the unsolvated complex and benzene indicating an efficiency of packing that is about equal.

In the case of $Th(AA)_4.\frac{1}{2}C_6H_6$ a volume reduction occurs, but only with a few per cent. The incorporation of benzene in the solid lattice seems to be mainly due to fortuitous packing relations in the solid state. Evidently the size of the central atom is of importance, since solid adducts of similar composition are not formed with the other, smaller tetravalent ions investigated. Benzene seems to have exactly the right size and geometry for entering the lattice, since no other of the studied solvents, including flat aromatics of smaller size, would form solid solvates. Thus no interaction responsible for the previously observed [9] very pronounced differences between partition coefficients of tetravalent actinide acetylacetonates in the benzene/water system could be found, and these anomalies are consequently due either to changes in the aqueous phase or to some other parameter related to the distribution equilibrium.

A systematic investigation of the thermodynamics of the distribution process of these complexes in different two-phase systems is in progress.

Acknowledgements. The skilfull experimental help by Mrs. B. Hjorth with the solubility measurements is gratefully acknowledged. The author is also indebted to Professor Jan Rydberg for fruitful discussions and suggestions and Dr. I Svedung for help with the thermogravimetric measurements. The English text was revised by E. Ratti-Moberg.

Support by the Swedish Atomic Research Council is gratefully acknowledged.

REFERENCES

1. Allard, B. *J. Inorg. Nucl. Chem. In press.*
2. Young, R. C. and Kovitz, J. *Inorg. Synth. 2* (1946) 123.
3. Titze, H. and Allard, B. *Acta Chem. Scand. 24* (1970) 715.
4. Grdenić, D. and Matković, B. *Acta Crystallogr. 12* (1959) 817.
5. Allard, B. *To be published.*
6. Yoshimura, T., Miyake, C. and Imoto, S. *Bull. Chem. Soc. Jap. 46* (1973) 2096.
7. Ginsberg, C. S. *Diss.*, Ohio University, 1964.
8. Hildebrand, J. H. and Scott, R. L. *Solubility of Non-electrolytes*, Dover Publ. Inc., New York 1964.
9. Liljenzin, J. O. and Rydberg, J. *Physico-Chemie du Protactinium*, Edition du C.N.R.S. *No. 154*, Paris 1966, p. 255.
10. Rydberg, J. *Ark. Kemi 8* (1955) 113.
11. Biltz, W. *Justus Liebigs Ann. Chem. 331* (1904) 334.
12. Jones, M. M., Davila, A. T., Hix Jr., J. E. and Dilts, R. V. *J. Inorg. Nucl. Chem. 25* (1963) 369.
13. Allard, B., Johnsson, S. and Rydberg, J. *Proc. Int. Solvent Extraction Conf.*, Lyon 1974, p. 1419.
14. Tanaka, M. *Proc. Int. Solvent Extraction Conf.*, Hague 1971, p. 18.
15. Small, P. S. *J. Appl. Chem. 3* (1953) 71.
16. Smith, J. S. *Diss.*, University of Leeds, 1968.
17. Watkins II, E. D., Cunningham, J. A., Phillips II, T., Sands, D. E. and Wagner, W. F. *Inorg. Chem. 8* (1969) 29.

Received November 5, 1975.

Acta Chemica Scandinavica A 30 (1976) 386—390

Short Communications

Two New Zirconium Arsenides, Zr_3As_2 and Zr_8As_5

BERTIL CARLSSON,* MARGARETA GÖLIN and STIG RUNDQVIST

Institute of Chemistry, University of Uppsala, Box 531, S-751 21 Uppsala, Sweden

In connection with previous studies of the Hf–As, Nb–As and Ta–As systems,[1–3] an examination of the Zr–As system was begun, but subsequently left unfinished. The studies provided some information on two new compounds discovered, however, and the results obtained are reported in the present communication.

Turnings of zirconium (claimed purity 99.9 %) and arsenic (claimed purity 99.99 %), both *ex* Koch-Light Laboratories Ltd., England, were heated in evacuated and sealed silica tubes at 900 °C for periods up to three days. The reaction products, consisting of mixtures of $ZrAs_2$, ZrAs and unreacted zirconium, were arc-melted under purified argon. The resulting alloys were crushed and examined by powder and single crystal X-ray diffraction methods.

Powder diffraction films were recorded in Hägg-Guinier type cameras, using Cu$K\alpha_1$ or Cr$K\alpha_1$ radiation. Silicon ($a = 5.431065$ Å)[4] was used for internal calibration. Single crystal fragments were examined in a Weissenberg camera using filtered Mo$K\alpha$ radiation. Single crystal intensity data were collected on a computer-controlled Stoe Philips four-circle diffractometer, using graphite-monochromatized Mo$K\alpha$ radiation. An $\omega - 2\theta$ step scan procedure was used in the measurements, and instrumental stability was checked by remeasuring three standard reflexions at regular intervals. The calculations were performed on IBM 370/155 and IBM 1800 computers using standard-type crystallographic programs described in Ref. 5.

The powder diffraction studies showed that the arc-melted alloys were generally inhomogeneous and often contained more than two phases. In alloys with high zirconium contents, the presence of Zr_3As, previously described by Lundström,[6] was observed. The lattice parameters of Zr_3As were found to agree closely with those reported earlier.[6] In more arsenic-rich preparations, two new phases were discovered. The first phase, Zr_3As_2, was found to be isostructural with Hf_3As_2 and Hf_3P_2 by comparing its powder pattern with that for Hf_3As_2,[1] and by comparing the Weissenberg films recorded for a Zr_3As_2 crystal fragment with those obtained for Hf_3P_2 by Lundström.[7] The second phase, Zr_8As_5, was characterized in a corresponding manner by comparison with the powder and single crystal data for the phosphide Nb_8P_5, investigated by Anugul *et al.*[8] The unit cell dimensions for Zr_3As_2 and Zr_8As_5 are given in Table 1. Some of the powder diffraction patterns of the arc-melted alloys contained lines, which did not belong to Zr_3As_2, Zr_8As_5, or any of the previously reported zirconium arsenides Zr_3As, ZrAs and $ZrAs_2$.[6,9] This indicates the presence of further phases in the Zr–As system.

The crystal structure of Zr_8As_5 was subjected to a closer examination, and diffractometer data were recorded for a single crystal fragment. Unfortunately, the crystal was accidentally lost before its dimensions had been measured, and no absorption correction could therefore be applied to the intensity values. A least-squares structure refinement was nevertheless performed using the uncorrected data. Atomic scattering factors and dispersion corrections were taken from Refs. 10 and 11, respectively. In the least-squares routine, the function $\sum[w(|F_o| - |F_c|)^2]$ was minimized, where the weights w were assigned according to the formula $w^{-1} = \sigma^2(F_o) + (0.05\ F_o)^2$ with $\sigma(F_o)$ obtained from counting statistics. One scale factor, 26 positional parameters and 14 isotropic temperature factors were varied; initial

Table 1. Crystallographic data for Zr_3As_2 and Zr_8As_5.

Compound	Zr_3As_2	Zr_8As_5
Structure type	Hf_3P_2	Nb_8P_5
Space group	*Pnma*	*Pbam*
a (Å)	10.5348(6)	28.3335(25)
b (Å)	3.7185(4)	10.2052(5)
c (Å)	10.3103(18)	3.7743(3)
Cell volume (Å^3)	403.9	1091.3

* Present address: Surahammars Bruks AB, S-735 00 Surahammar, Sweden

Table 2. Structure data for Zr_5As_5. (x and y parameters $\times 10^4$, isotropic temperature factors $\times 10^2$ Å^2).

Atom	Position	x	y	z	B
Zr1	2*a*	0	0	0	59(10)
Zr2	4*g*	2155(1)	2495(5)	0	69(8)
Zr3	4*g*	3275(2)	4105(5)	0	65(8)
Zr4	4*g**	0557(4)	4954(10)	0	80(15)
Zr5	4*h*	4936(2)	2414(5)	0.5	80(8)
Zr6	4*h*	0835(2)	0080(5)	0.5	45(7)
Zr7	4*h*	1209(2)	3224(6)	0.5	99(9)
Zr8	4*h*	2660(2)	0030(5)	0.5	47(6)
Zr9	4*h*	3731(2)	1643(5)	0.5	93(9)
As1	4*g*	0627(2)	2092(5)	0	65(8)
As2	4*g*	1616(2)	4811(5)	0	70(8)
As3	4*g*	4228(2)	3074(5)	0	65(8)
As4	4*h*	1724(2)	1003(5)	0.5	63(8)
As5	4*h*	2843(2)	2637(5)	0.5	63(8)

* Position filled to only 50 %.

values for the positional parameters were taken from the structure of Nb_5P_5. The Zr4 position was assumed to be occupied to 50 % only, in analogy to the situation in Nb_5P_5. The refinement converged, with the final conventional R-value of 0.14 for all 1272 reflexions measured. An attempt to refine the occupancy of the Zr4 position resulted in a value of 65 %, with a simultaneous increase in the isotropic temperature factor by a factor of two, the calculated correlation between the two parameters being of the order of 0.8. In view of the deficiencies in the intensity data, further refinements including, for instance, anisotropic thermal parameters were not considered worthwhile. The results of the refinement assuming a 50 % occupancy of the Zr4 position are presented in Table 2. The values of the isotropic temperature factors as given in Table 2 should be regarded with caution, while the values of the positional parameters can be treated with greater confidence.

Acknowledgement. Financial support from the Swedish Natural Science Research Council is gratefully acknowledged.

1. Rundqvist, S. and Carlsson, B. *Acta Chem. Scand. 22* (1968) 2395.
2. Rundqvist, S., Carlsson, B. and Pontchour, C.-O. *Acta Chem. Scand. 23* (1969) 2188.
3. Carlsson, B. and Rundqvist, S. *Acta Chem. Scand. 25* (1971) 1742.
4. Deslattes, R. D. and Henins, A. *Phys. Rev. Lett. 31* (1973) 972.
5. Lundgren, J.-O., Ed., *Crystallographic Computer Programs*, Institute of Chemistry, University of Uppsala, Uppsala 1975, UUIC-B13-04-2.
6. Lundström, T. *Acta Chem. Scand. 20* (1966) 1712.
7. Lundström, T. *Acta Chem. Scand. 22* (1968) 2191.
8. Anugul, S., Pontchour, C.-O. and Rundqvist, S. *Acta Chem. Scand. 27* (1973) 26.
9. Trzebiatowski, W., Weglowski, S. and Lukaszewicz, K. *Rocz. Chem. 32* (1958) 189.
10. Hanson, H. P., Herman, F., Lea, J. D. and Skillman, S. *Acta Crystallogr. 17* (1964) 1040.
11. Cromer, D. T. *Acta Crystallogr. 18* (1965) 17.

Received March 25, 1976.

The Crystal Structure of V_2P

ROLF BERGER and LARS-ERIK TERGENIUS

Institute of Chemistry, University of Uppsala, Box 531, S-751 21 Uppsala 1, Sweden

In a previous communication the existence of V_2P was reported.[1] A complete single-crystal analysis has been performed, which shows that this compound is isotypic with Co_2P (*anti*-$PbCl_2$) as suggested. No deviation from the crystallographic formula was detected, but the phase may nevertheless be identical with the compound ascribed the approximate composition $V_{2.4}P$ reported by Boller.[2]

Experimental details. The compound was prepared in the following manner. Vanadium (Materials Research Corp., 99.95 % purity) and red phosphorus (KEBO, at least 99 % purity) were heated in an evacuated silica ampoule at 900 °C for 8 days and subsequently melted in an arc furnace under an argon atmosphere. The alloy was finally heat-treated in an alumina crucible for 8 h at 1175 °C under an argon atmosphere using an induction furnace. The X-ray powder pattern showed only the lines of V_2P together with blurred lines interpreted as belonging to traces of cubic VO_{1-x}.

The existence of V_2P had not been reported in earlier surveys of the V–P system, and the possibility could not be excluded that this phase was in fact a ternary compound. The alloy had been in contact with silica in the preliminary stages of the synthesis, and a small P–Si substitution would escape detection in the X-ray structure refinement. Therefore it was considered worthwhile to determine the silicon content by chemical analysis.

In all stages of the analysis glassware was avoided, using platinum or teflon vessels. The samples were dissolved in nitric acid, and vanadium and phosphorus were removed from the slightly acidic solution as vanadate and

Table 2. Structure data for Zr_5As_5. (x and y parameters $\times 10^4$, isotropic temperature factors $\times 10^2$ Å^2).

Atom	Position	x	y	z	B
Zr1	2*a*	0	0	0	59(10)
Zr2	4*g*	2155(1)	2495(5)	0	69(8)
Zr3	4*g*	3275(2)	4105(5)	0	65(8)
Zr4	4*g**	0557(4)	4954(10)	0	80(15)
Zr5	4*h*	4936(2)	2414(5)	0.5	80(8)
Zr6	4*h*	0835(2)	0080(5)	0.5	45(7)
Zr7	4*h*	1209(2)	3224(6)	0.5	99(9)
Zr8	4*h*	2660(2)	0030(5)	0.5	47(6)
Zr9	4*h*	3731(2)	1643(5)	0.5	93(9)
As1	4*g*	0627(2)	2092(5)	0	65(8)
As2	4*g*	1616(2)	4811(5)	0	70(8)
As3	4*g*	4228(2)	3074(5)	0	65(8)
As4	4*h*	1724(2)	1003(5)	0.5	63(8)
As5	4*h*	2843(2)	2637(5)	0.5	63(8)

* Position filled to only 50 %.

values for the positional parameters were taken from the structure of Nb_5P_5. The Zr4 position was assumed to be occupied to 50 % only, in analogy to the situation in Nb_5P_5. The refinement converged, with the final conventional R-value of 0.14 for all 1272 reflexions measured. An attempt to refine the occupancy of the Zr4 position resulted in a value of 65 %, with a simultaneous increase in the isotropic temperature factor by a factor of two, the calculated correlation between the two parameters being of the order of 0.8. In view of the deficiencies in the intensity data, further refinements including, for instance, anisotropic thermal parameters were not considered worthwhile. The results of the refinement assuming a 50 % occupancy of the Zr4 position are presented in Table 2. The values of the isotropic temperature factors as given in Table 2 should be regarded with caution, while the values of the positional parameters can be treated with greater confidence.

Acknowledgement. Financial support from the Swedish Natural Science Research Council is gratefully acknowledged.

1. Rundqvist, S. and Carlsson, B. *Acta Chem. Scand. 22* (1968) 2395.
2. Rundqvist, S., Carlsson, B. and Pontchour, C.-O. *Acta Chem. Scand. 23* (1969) 2188.
3. Carlsson, B. and Rundqvist, S. *Acta Chem. Scand. 25* (1971) 1742.
4. Deslattes, R. D. and Henins, A. *Phys. Rev. Lett. 31* (1973) 972.
5. Lundgren, J.-O., Ed., *Crystallographic Computer Programs*, Institute of Chemistry, University of Uppsala, Uppsala 1975, UUIC-B13-04-2.
6. Lundström, T. *Acta Chem. Scand. 20* (1966) 1712.
7. Lundström, T. *Acta Chem. Scand. 22* (1968) 2191.
8. Anugul, S., Pontchour, C.-O. and Rundqvist, S. *Acta Chem. Scand. 27* (1973) 26.
9. Trzebiatowski, W., Weglowski, S. and Lukaszewicz, K. *Rocz. Chem. 32* (1958) 189.
10. Hanson, H. P., Herman, F., Lea, J. D. and Skillman, S. *Acta Crystallogr. 17* (1964) 1040.
11. Cromer, D. T. *Acta Crystallogr. 18* (1965) 17.

Received March 25, 1976.

The Crystal Structure of V_2P

ROLF BERGER and LARS-ERIK TERGENIUS

Institute of Chemistry, University of Uppsala, Box 531, S-751 21 Uppsala 1, Sweden

In a previous communication the existence of V_2P was reported.[1] A complete single-crystal analysis has been performed, which shows that this compound is isotypic with Co_2P (*anti*-$PbCl_2$) as suggested. No deviation from the crystallographic formula was detected, but the phase may nevertheless be identical with the compound ascribed the approximate composition $V_{2.4}P$ reported by Boller.[2]

Experimental details. The compound was prepared in the following manner. Vanadium (Materials Research Corp., 99.95 % purity) and red phosphorus (KEBO, at least 99 % purity) were heated in an evacuated silica ampoule at 900 °C for 8 days and subsequently melted in an arc furnace under an argon atmosphere. The alloy was finally heat-treated in an alumina crucible for 8 h at 1175 °C under an argon atmosphere using an induction furnace. The X-ray powder pattern showed only the lines of V_2P together with blurred lines interpreted as belonging to traces of cubic VO_{1-x}.

The existence of V_2P had not been reported in earlier surveys of the V–P system, and the possibility could not be excluded that this phase was in fact a ternary compound. The alloy had been in contact with silica in the preliminary stages of the synthesis, and a small P–Si substitution would escape detection in the X-ray structure refinement. Therefore it was considered worthwhile to determine the silicon content by chemical analysis.

In all stages of the analysis glassware was avoided, using platinum or teflon vessels. The samples were dissolved in nitric acid, and vanadium and phosphorus were removed from the slightly acidic solution as vanadate and

Table 1. Structure data for V_2P from refinement based on F^2. Standard deviations are given in parentheses. Space group *Pnma* (No. 62). All atoms in 4(c) positions. Full occupancy. $a = 6.2045(2)$ Å, $b = 3.3052(1)$ Å, $c = 7.5440(2)$ Å, $V = 154.70(1)$ Å^3; $Z = 4$. The anisotropic temperature factor is of the form: $\exp[-2\pi^2(U_{11}h^2a^{*2} + U_{22}k^2b^{*2} + U_{33}l^2c^{*2} + 2U_{13}hla^*c^*)]$; $U_{12} = U_{23} = 0$.

Atom	Positional parameters			$U_{ij} \times 10^5$ (Å^2)			
	x	y	z	U_{11}	U_{22}	U_{33}	U_{13}
V(1)	0.86148(8)	1/4	0.05891(7)	446(20)	558(20)	392(20)	−4(16)
V(2)	0.96041(9)	1/4	0.66624(7)	620(21)	584(22)	605(21)	−11(17)
P	0.24723(14)	1/4	0.14183(10)	524(29)	455(31)	570(31)	−4(25)

phosphate by anion exchange on Dowex 2 in its acetate form. The silicon content was determined spectrophotometrically.[3]

The silicon content was found to be 0.018 % in a crushed 43 mg sample and 0.013 % for the main part of the alloy (95 mg). The agreement between different aliquots was excellent. The discrepancy between the two samples might be due to inhomogeneity or due to the difference in specimen preparation and thus exposure to silicon-containing impurities. Preliminary tests of the analysis method using vanadate, phosphate and silicate indicated an accuracy better than 5 %.[4]

The cell dimensions were determined with a Guinier-Hägg type focussing camera, using strictly monochromatic Cu$K\alpha_1$ radiation and silicon ($a = 5.431065$ Å) [5] as internal calibration standard. The cell parameters given in Table 1 were refined using a least-squares method.

A small irregular fragment of the approximate dimensions $0.060 \times 0.020 \times 0.010$ mm picked from the final alloy proved to be a single crystal. A computer-controlled Stoe four-circle diffractometer equipped with a graphite monochromator to yield Mo$K\alpha$ radiation was used for collecting the single-crystal intensity data. An $\omega - 2\theta$ step-scan technique was utilized, and three standard reflexions were remeasured every 40 reflexions as a check of the stability. Reflexions were recorded up to 70° in 2θ, corresponding to $0 \leq h \leq 10$, $-5 \leq k \leq 5$ and $-12 \leq l \leq 12$. Because of the small size of the crystal and the calculated linear absorption ($\mu = 131$ cm^{-1}) it was considered that an absorption correction was not necessary.

The calculations were performed on IBM 370/155 and IBM 1800 computers. The crystallographic programs used have been described by Lundgren.[6]

Structure refinement. Reflexions that are equivalent according to the orthorhombic symmetry were averaged, and the structure was refined by a full-matrix least-squares method. As starting values for the positional parameters the coordinates of Co_2P were used.[7] The atomic scattering factors were taken from Hanson *et al.*[8] and the dispersion corrections from Cromer.[9] Refinements on both F and F^2 were performed, where the function minimized was $w(|F_o^n| - |F_c^n|)^2$ with $n = 1$ or 2, respectively. The weights were assigned in accordance with the formula $w^{-1} = \sigma^2(F_o^n) + (p_n|F_o^n|)^2$; $\sigma^2(F_o^n)$ is based on counting statistics, and the empirical factor p_n was set to $p_1 = 0.007$ and $p_2 = 0.015$ for the two refinements. Anisotropic temperature factors were introduced, but there was no need for extinction corrections since the effects even on the very strongest reflexion were negligible. No significant differences in parameter values were found between the results of the two refinements. The F^2 refinement is recommended [10] in order to preserve the assumed normal distribution in the intensity measurement, and the standard deviations obtained from the F^2 refinement were less than for the F refinement. The agreement factors were $R(F^2) = 0.029$, $R_w(F^2) = 0.039$ with the corresponding $R(F) = 0.032$ (371 reflexions), where

$$R(F^n) = \sum||F_o^n| - |F_c^n|| / \sum|F_o^n|$$

and

$$R_w(F^n) = [\sum w(|F_o^n| - |F_c^n|)^2 / \sum w|F_o^n|^2]^{\frac{1}{2}}$$

There were no indications of any appreciable deviation from the crystallographic formula. The isotropic temperature factors were quite similar to those obtained for other phosphides of this structure type.[7,11] The occupancy factors were varied but the refinements invariably terminated with full occupancy. The parameter values from the final F^2 refinement are given in Table 1 together with refined cell parameters. A table of observed and calculated structure factors can be obtained from the authors on request.

A thorough discussion of the Co_2P structure and its features were given by Rundqvist,[12] who made a sub-division of the *anti*-$PbCl_2$ structure type into two subclasses according to slightly different atomic arrangement. Typical representatives for the two sub-classes are Co_2P and Co_2Si, respectively. In the Co_2P sub-class the phosphorus atoms have nine near neighbours. A classifying feature [12,13] is the axial ratio a/c, which in V_2P is 0.823, consistent with the Co_2P sub-class. The complete

Table 2. Interatomic distances in V_2P (Å units). Distances shorter than 3.5 Å are listed. The estimated standard deviations are smaller than 0.001 Å for all distances.

V(1) – 2P	2.341	V(2) – 2P	2.461
– P	2.366	– 2P	2.547
– P	2.474	– P	2.674
– 2V(1)	2.545	– 2V(1)	2.716
– 2V(2)	2.716	– 2V(1)	2.872
– 2V(2)	2.872	– V(1)	3.013
– V(2)	3.013	– V(1)	3.025
– V(2)	3.025	– 2V(2)	3.043
– 2V(1)	3.305	– 2V(2)	3.305
		– 2V(2)	3.349
P – 2P	3.305		

single-crystal analysis showed that V_2P is indeed a new member of this class.

It is interesting to compare the atomic arrangement of V_2P with that of the isotypic Ru_2P,[7] since the metal radii are approximately equal. Different arrangements are found, which implies that the radius ratio is not the governing factor. The *b*-axis of Ru_2P is 3.859 Å while that of V_2P is only 3.305 Å. Thus the trigonal prisms in V_2P are contracted compared to those in Ru_2P, which demand the metal atoms outside the prism faces to be positioned further away from the central phosphorus atom. These M – P distances are then longer while within the prisms the M – P distances as well as the M – M distances are shorter than in Ru_2P. This leads to a more even distribution of the M – P distances but a larger spread of the M – M distances in V_2P. These geometrical aspects were introduced and thoroughly discussed by Rundqvist.[12] The interatomic distances in V_2P are presented in Table 2, using the same notation as Rundqvist. The mean V(1) – P distance is 2.38 Å and the mean Ru(1) – P distance is 2.34 Å. Corresponding averages for the M(2) – P distances are 2.54 and 2.61 Å for V_2P and Ru_2P, respectively. The shortest M – M distance in Ru_2P is 2.74 Å as compared to 2.55 Å in V_2P, the latter distance being shorter than a normal metal contact. Short intermetallic distances are not uncommon in vanadium-rich compounds with Group 4 or 5 elements.

Acknowledgement. Financial support from the Swedish Natural Science Research Council is gratefully acknowledged.

1. Berger, R. *Acta Chem. Scand. A 29* (1975) 641.
2. Boller, H. *Monatsh. Chem. 104* (1973) 48.
3. Andrew, T. R. *Analyst 82* (1957) 423.
4. Gustafsson, L. University of Uppsala. *Private communication.*
5. Deslattes, R. D. and Henins, A. *Phys. Rev. Lett. 31* (1973) 972.
6. Lundgren, J.-O., Ed., *Crystallographic Computer Programs*, Institute of Chemistry, University of Uppsala, Uppsala 1975, UUIC-B13-04-2.
7. Rundqvist, S. *Acta Chem. Scand. 14* (1960) 1961.
8. Hanson, H. P., Herman, F., Lea, J. D. and Skillman, S. *Acta Crystallogr. 17* (1964) 1040.
9. Cromer, D. T. *Acta Crystallogr. 18* (1965) 17.
10. Hirshfeld, F. L. and Rabinovich, D. *Acta Crystallogr. A 29* (1973) 510.
11. Rundqvist, S. *Acta Chem. Scand. 15* (1961) 342.
12. Rundqvist, S. *Ark. Kemi 20* (1962) 67.
13. Shoemaker, C. B. and Shoemaker, D. P. *Acta Crystallogr. 18* (1965) 900.

Received February 5, 1976.

On the Compound $La_4Co_3O_{10}$

M. SEPPÄNEN and M. H. TIKKANEN

Department of Mining and Metallurgy,
The Helsinki University of Technology,
SF-02150 Espoo 15, Finland

Some binary oxides, of general formulae AO and BO_2, form ternary compounds $AO(ABO_3)_n$, where one at the one end finds the perovskite ABO_3 ($n=\infty$) type structure and at the other the A_2BO_4 ($n=1$) the K_2NiF_4 type. Two further members of a series are known, *viz.* $A_3B_2O_7$ ($n=2$) and $A_4B_3O_{10}$ ($n=3$), but none has reported examples for n between 3 and ∞. The structure of $AO(ABO_3)_n$ contains n perovskite sheets separated by an AO sheet of NaCl like structure. Such series are known in the systems $CaO-MnO_2$, $CaO-TiO_2$, $SrO-MnO_2$, $SrO-TiO_2$, and $SrO-ZrO_2$.[1]

In the system La – Co – O $LaCoO_3$ and La_2CoO_4 with rhombohedrally modified perovskite and orthorhombic K_2NiF_4 type structures [2,3] are known. We have prepared $La_4Co_3O_{10}$,[4] which also has been reported quite recently by Janecek and Wirtz.[5]

Experimental. Initial batches of $LaCoO_3$ and La_2CoO_4 were prepared from 99.99 % La_2O_3 (Kemira OY) and 99.95 % CoO (Sheritt Gordon). Powder mixtures were coldpressed at 9.8 kN/cm². $LaCoO_3$-specimens were fired for one week at 1100 °C in oxygen atmosphere and La_2CoO_4-tablets for four days at 1300 °C in argon ($P_{O_2} \approx 10^{-6}$ bar) with frequent inter-

Table 2. Interatomic distances in V_2P (Å units). Distances shorter than 3.5 Å are listed. The estimated standard deviations are smaller than 0.001 Å for all distances.

V(1) – 2P	2.341	V(2) – 2P	2.461
– P	2.366	– 2P	2.547
– P	2.474	– P	2.674
– 2V(1)	2.545	– 2V(1)	2.716
– 2V(2)	2.716	– 2V(1)	2.872
– 2V(2)	2.872	– V(1)	3.013
– V(2)	3.013	– V(1)	3.025
– V(2)	3.025	– 2V(2)	3.043
– 2V(1)	3.305	– 2V(2)	3.305
		– 2V(2)	3.349
P – 2P	3.305		

single-crystal analysis showed that V_2P is indeed a new member of this class.

It is interesting to compare the atomic arrangement of V_2P with that of the isotypic Ru_2P,[7] since the metal radii are approximately equal. Different arrangements are found, which implies that the radius ratio is not the governing factor. The *b*-axis of Ru_2P is 3.859 Å while that of V_2P is only 3.305 Å. Thus the trigonal prisms in V_2P are contracted compared to those in Ru_2P, which demand the metal atoms outside the prism faces to be positioned further away from the central phosphorus atom. These M – P distances are then longer while within the prisms the M – P distances as well as the M – M distances are shorter than in Ru_2P. This leads to a more even distribution of the M – P distances but a larger spread of the M – M distances in V_2P. These geometrical aspects were introduced and thoroughly discussed by Rundqvist.[12] The interatomic distances in V_2P are presented in Table 2, using the same notation as Rundqvist. The mean V(1) – P distance is 2.38 Å and the mean Ru(1) – P distance is 2.34 Å. Corresponding averages for the M(2) – P distances are 2.54 and 2.61 Å for V_2P and Ru_2P, respectively. The shortest M – M distance in Ru_2P is 2.74 Å as compared to 2.55 Å in V_2P, the latter distance being shorter than a normal metal contact. Short intermetallic distances are not uncommon in vanadium-rich compounds with Group 4 or 5 elements.

Acknowledgement. Financial support from the Swedish Natural Science Research Council is gratefully acknowledged.

1. Berger, R. *Acta Chem. Scand. A 29* (1975) 641.
2. Boller, H. *Monatsh. Chem. 104* (1973) 48.
3. Andrew, T. R. *Analyst 82* (1957) 423.
4. Gustafsson, L. University of Uppsala. *Private communication.*
5. Deslattes, R. D. and Henins, A. *Phys. Rev. Lett. 31* (1973) 972.
6. Lundgren, J.-O., Ed., *Crystallographic Computer Programs*, Institute of Chemistry, University of Uppsala, Uppsala 1975, UUIC-B13-04-2.
7. Rundqvist, S. *Acta Chem. Scand. 14* (1960) 1961.
8. Hanson, H. P., Herman, F., Lea, J. D. and Skillman, S. *Acta Crystallogr. 17* (1964) 1040.
9. Cromer, D. T. *Acta Crystallogr. 18* (1965) 17.
10. Hirshfeld, F. L. and Rabinovich, D. *Acta Crystallogr. A 29* (1973) 510.
11. Rundqvist, S. *Acta Chem. Scand. 15* (1961) 342.
12. Rundqvist, S. *Ark. Kemi 20* (1962) 67.
13. Shoemaker, C. B. and Shoemaker, D. P. *Acta Crystallogr. 18* (1965) 900.

Received February 5, 1976.

On the Compound $La_4Co_3O_{10}$

M. SEPPÄNEN and M. H. TIKKANEN

Department of Mining and Metallurgy,
The Helsinki University of Technology,
SF-02150 Espoo 15, Finland

Some binary oxides, of general formulae AO and BO_2, form ternary compounds $AO(ABO_3)_n$, where one at the one end finds the perovskite ABO_3 ($n=\infty$) type structure and at the other the A_2BO_4 ($n=1$) the K_2NiF_4 type. Two further members of a series are known, *viz.* $A_3B_2O_7$ ($n=2$) and $A_4B_3O_{10}$ ($n=3$), but none has reported examples for n between 3 and ∞. The structure of $AO(ABO_3)_n$ contains n perovskite sheets separated by an AO sheet of NaCl like structure. Such series are known in the systems $CaO-MnO_2$, $CaO-TiO_2$, $SrO-MnO_2$, $SrO-TiO_2$, and $SrO-ZrO_2$.[1]

In the system La – Co – O $LaCoO_3$ and La_2CoO_4 with rhombohedrally modified perovskite and orthorhombic K_2NiF_4 type structures [2,3] are known. We have prepared $La_4Co_3O_{10}$,[4] which also has been reported quite recently by Janecek and Wirtz.[5]

Experimental. Initial batches of $LaCoO_3$ and La_2CoO_4 were prepared from 99.99 % La_2O_3 (Kemira OY) and 99.95 % CoO (Sheritt Gordon). Powder mixtures were coldpressed at 9.8 kN/cm². $LaCoO_3$-specimens were fired for one week at 1100 °C in oxygen atmosphere and La_2CoO_4-tablets for four days at 1300 °C in argon ($P_{O_2} \approx 10^{-6}$ bar) with frequent inter-

Table 1. X-Ray powder data of $La_4Co_3O_{10}$.

d_o	d_c	*hkl*	I_o	d_c	d_c	*hkl*	I_o
3.816	3.814	111	16	1.712	1.712	311	2
3.560	3.557	113	5	1.688	1.687	313	2
3.480	3.476	008	10	1.684	1.684	228	4
3.171	3.166	115	3	1.670	1.670	11 15	10
2.763	2.765	117	100	1.607	1.607	02 14	
2.734	2.735	020	32	1.602	1.602	20 14	10
2.710	2.710	200	32	1.586	1.585	137	
2.410	2.410	119	7	1.583	1.583	22 10	35
	2.356	026		1.574	1.575	317	9
2.348			3				
	2.340	206		1.509	1.508	139	2
2.148	2.149	028	19		1.506	11 17	
				1.503			1
2.137	2.137	208	10		1.500	319	
2.114	2.113	11 11	3	1.467	1.467	02 16	6
	1.950	02 10		1.464	1.463	20 16	
1.946			3				
	1.941	20 10		1.382	1.382	22 14	11
1.925	1.925	220	38	1.368	1.368	11 19	4
1.738	1.738	00 16	3	1.355	1.355	400	4
1.725	1.725	131	2	1.345	1.345	02 18	1

mediate grindings. $La_4Co_3O_{10}$-specimens were finally prepared from $LaCoO_3$ and La_2CoO_4 powders kept at 1130 °C in nitrogen atmosphere ($pO_2 = 10^{-3.95}$ bar) for five days.

The powder pattern of $La_4Co_3O_{10}$ was run by X-ray diffractometer PW 1410/20 using graphite monochromatized Cu$K\alpha$-radiation ($\lambda = 1.5418$ Å) at a scanning speed of 0.25°/min and a silicon powder ($a = 5.4301$ Å) as an internal standard.

The powder pattern of $La_4Co_3O_{10}$ was satisfactorily indexed with orthorhombic unit cell parameters, $a = 5.42$ Å, $b = 5.47$ Å and $c = 27.81$ Å. The measured density, 7.1 g cm^{-3}, corresponds to four formula units per cell ($D_x = 7.21$ g cm^{-3}). All indexes are unmixed, Table 1, so a possible space group is *Fmmm* (No. 69).

In our investigation of the La–Co–O-system we have obtained no evidence for $La_3Co_2O_7$. We shall later report on thermodynamic investigations of the system La–Co–O and also the powder pattern of $La_4Ni_3O_{10}$.

Acknowledgements. This research has been performed with financial support from the Finnish Natural Science Research Foundation and the Jenny and Antti Wihuri Fund.

1. Goodenough, J. B. and Longo, J. *Landolt-Börnstein Tabellen* Neue Serie III/4a, p. 203, Springer (Berlin) 1970.
2. Rabenau, A. and Eckerlin, P. *Acta Crystallogr. 11* (1958) 304.
3. Lehuede, P. and Daire, M. *C. R. Acad. Sci. 276* (1973) 1783.
4. Tikkanen, M. H. and Seppänen, M. *Research Report for the Academy of Finland*, Part 1, Febr. 1975.
5. Janecek, J. J., Wirtz, G. P. *Am. Ceram. Soc. Bull. 54* (1975) 739.

Received February 16, 1976.

Acta Chemica Scandinavica A 30 (1976) 391—396

Base-catalyzed Detritiation of Some Bicyclo[2.2.1]heptanones

MARTTI LAJUNEN and HEIKKI PILBACKA

Department of Chemistry and Biochemistry, University of Turku, SF-20500 Turku 50, Finland

Detritation-protonation rates have been measured for *exo* and *endo* hydrogens at the 3-position of norcamphor, 1-methylnorcamphor, camphor, and dehydronorcamphor in aqueous sodium hydroxide solutions and the activation parameters have been calculated. The *exo/endo* rate ratios, 30 (81), 34, 2.6 (4), and 8.5 (19) at 75 °C (extrapolated to 25 °C within parentheses), are of the same order of magnitude as those measured earlier for dedeuteration-protonation reactions of norcamphor and camphor. The discussion of the rate ratios has been based on a mechanism presented earlier.

Base-catalyzed hydrogen exchange at the 3-position of bicyclo[2.2.1]heptanones has been the subject of intensive studies during the last decade.[1–10] The *exo/endo* rate ratios of deprotonation-deuteration reactions have been observed to be almost of the same order of magnitude as the *exo/endo* solvolysis (*via* carbocations) rate ratios of bicyclic esters.[11–12] The rate ratios in the hydrogen exchange have been explained to be caused by angle strains, torsional strains, nonbonded repulsions as well as hybridization effects and orbital overlapping.[5–10] A mechanism for the reaction has been presented by Abad, Jindal, and Tidwell.[9] The *exo/endo* rate ratios of the opposite reaction, dedeuteration-protonation, have recently been measured to be approximately one tenth of that measured for the deprotonation-deuteration reactions.[10] The mechanism mentioned above also explains these data.

The technique employed for measuring the exchange rates of the α-hydrogens of bicyclic ketones has mostly been mass spectrometry,[5–10] which is, however, quite laborious. An easier technique, tritium counting, has been utilized for measuring the exchange rates of hydrogens at the equivalent α-sites of some symmetrical aliphatic ketones[13] and more recently at the nonequivalent α-sites of an unsymmetrical ketone.[14] The latter technique was now employed for measuring detritiation-protonation rates of norcamphor (I), 1-methylnorcamphor (II), camphor (III), and dehydronorcamphor (IV) in aqueous base solutions.

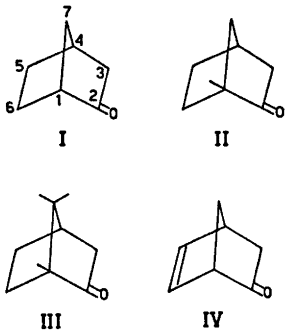

I II III IV

EXPERIMENTAL

Tritium labeling. One gram of the ketone was dissolved in 10 cm³ of a tritiation solution containing dimethyl sulfoxide, ordinary water, tritiated water (0.8 Ci/cm³), and tetramethylammonium hydroxide in the volume ratios 91:9:0.01:0.4. The tritiation times of the ketones were 3 h for I and II, 5 h for III, and 31 h for IV at room temperature. The times were estimated on the basis of the data reported by Tidwell,[5] by employing an acceleration effect of dimethyl sulfoxide measured in this laboratory.[15] Labeling per mol of camphenilone and fenchone was after 48 h 4 and 2 % of that measured for the substrates I–IV under the same conditions; thus labeling occurred dominantly at the 3-position of I–IV. The mol ratio of the ketone to tritium was *ca.* 10^5 in the tritiation solution; thus the exchange of only one protium to tritium per molecule was probable.

After tritiation the solution was neutralized by addition of dilute sulfuric acid and shortly after that extracted three times with 10 cm³ of pentane. The pentane layers were washed two times with water and dried over anhydrous sodium sulfate. Pentane was distilled off and the residues were used without further purification. The purities of the ketones were analyzed by GLC (FFAP column) to be > 99.5 % for I, III and IV, and 95.6 % for II (4.4 % of bicyclic alcohols).

Kinetic measurements. The reaction medium (130 cm³ of 0.01 – 0.1 M aqueous sodium hydroxide) was thermostated in a narrow-necked flask equipped with a ground-glass stopper. The reaction was started by adding the ketone (0.002 – 0.003 M) to the flask, shaking vigorously, and replacing the flask into the thermostated bath. The samples, 5 cm³ in volume and *ca.* 20 in number, were transmitted after appropriate intervals into glass cylinders, which contained 10 cm³ of cyclohexane and equivalent amounts (as compared with hydroxide ion) of nitric acid. The ketone was extracted into the organic phase by shaking for 2 min, after which the layers were allowed to separate over the night. Aliquots of 5 cm³ were pipetted from the organic layer and transferred into counting vials containing 10 cm³ of the scintillation liquid (0.1 g of *p*-bis(*o*-methylstyryl)benzene and 4 g of diphenyloxazole in 1.0 dm³ of toluene). The samples were analyzed on a Wallac 81000 scintillation counter. The final samples were taken after the reaction had continued for ten halflives from the first samples.

In the case of norcamphor (I) and 1-methylnorcamphor (II) the detritiation rates of the *exo* and *endo* hydrogens were measured consecutively since their rates were different enough and the first-order rate coefficients were calculated from the usual equation. In the case of camphor (III) and dehydronorcamphor (IV) the exchange rates of the *exo* and *endo* hydrogens were measured concurrently and the first-order rate coefficients were calculated from the equation [14]

$$\frac{N_0 - N_t}{N_0 - N_\infty} = x_{exo}[1 - \exp(-k_{exo}t)] + x_{endo}[1 - \exp(-k_{endo}t)] \quad (1)$$

In the equation N_0, N_t and N_∞ refer to the activities of the first sample, the sample taken after time t had elapsed from the first sample and the final sample, respectively, x_{exo} and x_{endo} are the fractions of labeling at the *exo*-3 and *endo*-3 positions in the first sample ($x_{exo} + x_{endo} = 1$), and k_{exo} and k_{endo} are the first-order rate coefficients for the detritiation from the *exo*-3 and *endo*-3 positions. For all sub-

Table 1. Observed detritiation-protonation rates of *exo*-3 and *endo*-3 hydrogens of some bicyclo[2.2.1]heptanones in aqueous 0.01 – 0.1 M sodium hydroxide solutions at different temperatures. Method A: the *exo* and *endo* rates were measured consequtively, method B: the rates were measured concurrently (eqn. 1).

Substrate	Method [a]	Temp./°C	$k_{b,exo}/10^{-4}$ M^{-1} s^{-1}	$k_{b,endo}/10^{-4}$ M^{-1} s^{-1}
I	A	45	52.8 ± 0.7	–
	A	55	125 1	–
	B	55	119 1	2.54 ± 0.01
	A	65	253 4	6.34 0.06
	A	75	510 7	15.6 0.1
	A	85	–	36.2 0.2
II	A	75	362 ± 3	9.51 ± 0.14
III	B	55	3.45 ± 0.01	1.04 ± 0.01
	B	65	6.94 0.01	2.84 0.01
	B	75	15.0 0.1	6.26 0.01
	B	85	36.9 0.1	13.6 0.1
IV	B	55	5.14 ± 0.01	0.464 ± 0.008
	B	65	12.3 0.02	1.27 0.01
	B	75	28.1 0.02	3.08 0.03
	B	85	52.3 0.01	7.38 0.02

[a] [NaOH] = 0.01 M for the *exo* exchange and 0.1 for the *endo* exchange in method A; [NaOH] = 0.1 M in method B.

In method B x_{exo} was between 0.45 and 0.52 in eqn. (1).

Table 2. Observed detritiation-protonation rates of hydrogen at the *exo*-3 position of norcamphor (I) in different sodium hydroxide solutions at 45 °C.

[NaOH]/M	$k_{exo}/10^{-4}$ s^{-1}	$k_{b,exo}/10^{-3}$ M^{-1} s^{-1} [a]
0.01	0.524 ± 0.007	5.28 ± 0.07
0.03	1.56 0.02	5.24 0.03
0.07	3.44 0.05	4.95 0.07
0.10	4.70 0.03	4.74 0.03

[a] $k_{b,exo} = k_{exo}/[NaOH]$.

strates k_{exo} was assumed to be greater than k_{endo} (*cf.* Refs 1 – 10). The parameters x_{exo}, x_{endo}, k_{exo}, and k_{endo} and their standard errors were calculated from the experimental data on a computer by the method of least squares. The second-order rate coefficients were calculated by dividing the first-order ones with the sodium hydroxide concentration.

RESULTS AND DISCUSSION

The detritiation-protonation rates of hydrogens at the *exo*-3 and *endo*-3 positions of norcamphor (I), 1-methylnorcamphor (II), camphor (III), and dehydronorcamphor (IV) were measured in aqueous 0.01 – 0.1 M sodium hydroxide solutions at different temperatures with the exception of II which was studied only at one temperature. The *exo* and *endo* exchange rates of I and II were measured consecutively (method A) and these of III and IV were measured concurrently (method B).[14] The results are collected in Table 1.

In order to check that the methods employed give equivalent results, the detritiation rates of hydrogens at the 3-position of norcamphor were measured in both ways. The rate coefficients in the 0.1 M solution at 55 °C measured by methods A and B for the *exo* exchange, 0.0112 (estimated from a measurement in the 0.01 M solution by the aid of the rate coefficients in Table 2) and 0.119, and for the *endo* exchange; 0.000245 (extrapolated from the rates measured by method A at 65, 75 and 85 °C) and 0.000254, respectively, (all with the dimension M^{-1} s^{-1}) are fairly the same.

The effect of the base concentration upon the exchange rate was studied by measuring the detritiation rate of the *exo* hydrogen of norcamphor in different base concentrations in the range 0.01 to 0.1 M. The second-order rate coefficients in Table 2 show that a negative salt effect is observable, but not marked. The same kind of effect can also be seen in the dedeuteration-protonation rates of the *exo*-3 and *endo*-3 hydrogens of norcamphor.[10]

The activation parameters of the exchange reactions are given in Table 3. In the calculations all the rates were corrected to correspond with the base concentration 0.1 M. The activation parameters are of the same order of magnitude as those observed for the deprotonation-deuteration reactions of the bicyclic ketones.[9] The rate coefficients calculated from the activation parameters (Table 3) allow

Table 3. Activation parameters of the detritiation-protonation of *exo*-3 and *endo*-3 hydrogens of some bicyclo[2.2.]heptanones and the rate coefficients at 75 °C calculated from them. [NaOH] = 0.1 M.

Tritium/ substrate	$\Delta H^{\ddagger}$/kJ mol^{-1}	$\Delta S^{\ddagger}$/J mol^{-1} K^{-1}	$k_b/10^{-4}$ M^{-1} s^{-1}
exo/I	66.3 ± 1.4	−81 ± 4	461 ± 13
endo/I	83.8 0.6	−59 2	15.6 0.1
exo/II	–	–	*ca.* 324 [a]
endo/II	–	–	*ca.* 9.51 [a]
exo/III	74.0 4.5	−87 13	16.3 0.9
endo/III	80.3 2.4	−77 7	6.24 0.19
exo/IV	73.3 2.7	−85 8	26.4 0.9
endo/IV	86.9 0.8	−64 2	3.11 0.03

[a] The values have been taken from Table 1 and the correction from the 0.01 to 0.1 M base concentration has been made for the *exo* rate coefficient according to Table 2.

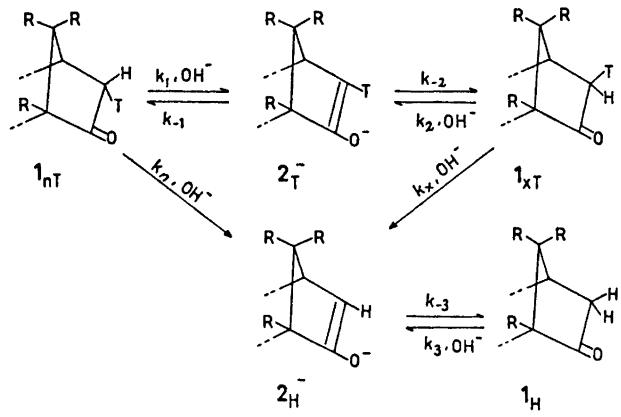

Scheme 1.

the comparison of the rates. The *exo*/*endo* rate ratios at 75 °C (extrapolated to 25 °C within parentheses): 30 ± 1 (81 ± 8) for I, *ca.* 34 for II, 2.6 ± 0.2 (4 ± 1) for III, and 8.5 ± 0.4 (19 ± 4) for IV, are clearly smaller than those measured for the deprotonation-deuteration reactions (660 – 715 for I, 18 – 21 for III, and 120 for IV in dioxane-water mixtures at 25 °C)[5,9,10] but of the same order of magnitude as those measured for the dedeuteration-protonation reactions (72 for I and 2 for III in dioxane-water mixtures at 25 °C).[10] The data support the idea that the hydrogen exchange reactions of the bicyclic ketones are not simple processes.[10]

Scheme 1, which is in agreement with the mechanism presented by Abad, Jindal, and Tidwell [9] and later by Banerjee and Werstiuk,[10] leads to eqn. (2) when estimating the rate of detriation from the *exo*- position

$$k_{exo}(\mathrm{T}\rightarrow\mathrm{H}) = k_x + k_2 - \frac{k_2 k_{-2}(k_n + k_1)}{(k_n + k_1)(k_{-1} + k_{-2}) - k_1 k_{-1}}$$

$$= k_x + k_2\left(1 - \frac{k_{-2}}{k_{-1} + k_{-2} - \dfrac{k_1 k_{-1}}{k_n + k_1}}\right) \qquad (2)$$

of the ketone (1_{xT}) if the steady-state approximation is made for the concentrations of intermediate enolate ions (2_T^- and 2_H^-) and for the *endo*-3 tritiated ketone (1_{nT}; the last approximation may be somewhat invalid for camphor). The scheme leads to eqn. (3) when estimating the rate of detritiation from the *endo*-3 position of the ketone (1_{nT})

$$k_{endo}(\mathrm{T}\rightarrow\mathrm{H}) = k_n + k_1 - \frac{k_1 k_{-1}(k_x + k_2)}{(k_x + k_2)(k_{-1} + k_{-2}) - k_2 k_{-2}} \qquad (3)$$

if the steady-state approximation is made for the concentrations of enolate ions (2_T^- and 2_H^-) and for the *exo*-3 tritiated ketone (1_{xT}) (*cf.* Ref. 10).

In the cases of norcamphor, 1-methylnorcamphor and dehydronorcamphor the approximation $k_1 \gg k_n$ can be made, since the primary isotope effect of tritium [13,16] further retards the slow departure of *endo*-tritium and the secondary isotope effect of tritium is probably small on the fast departure of *exo* protium.[9,16] The retarding effect of the *syn*-methyl group on k_1 is marked, but k_1 is evidently so much greater than k_n that the same approximation is valid for camphor. Thus, eqn. (2) is simplified to the form (*cf.* Ref. 10)

$$k_{exo}(\mathrm{T}\rightarrow\mathrm{H}) \approx k_x \qquad (4)$$

particularly, since $k_x > (>) k_2$ in the cases of I, II and IV and $k_x \sim k_2$ in the case of III.

The following approximation can also be made in the cases of I, II and IV: $(k_x + k_2)(k_{-1} + k_{-2}) \gg k_2 k_{-2}$, since $k_{-1} \gg k_{-2}$ and $k_x > (>) k_2$. Thus $k_{endo}(\mathrm{T}\rightarrow\mathrm{H})$ gets the simpler form (*cf.* Ref. 10)

$$k_{endo}(\mathrm{T}\rightarrow\mathrm{H}) \approx k_n + k_1\left(1 - \frac{k_{-1}}{k_{-1} + k_{-2}}\right) \qquad (5)$$

In these cases $k_1 \gg k_n$ and therefore the term $k_{-1}/(k_{-1} + k_{-2})$ ($\lesssim 1$) is important. In the case

of camphor (III), the approximation may not be valid, since the departure of *exo*-tritium (k_x) is retarded by both the primary isotope effect of tritium and the steric effect of the *syn*-7 methyl group and the rate ratio k_{-1}/k_{-2} is also decreased by the steric effect on k_{-1}.

The *endo*/*exo* rate ratio

$$\frac{k_{endo}(T\rightarrow H)}{k_{exo}(T\rightarrow H)} \approx \frac{k_n}{k_x} + \frac{k_1}{k_x}\left(1 - \frac{1}{1+\frac{k_{-2}}{k_{-1}}}\right) \qquad (6)$$

can be used for evaluation of values for k_x/k_n and k_{-1}/k_{-2} if we assume that $k_x/k_n \approx (k_1/k_2 \approx) k_{-1}/k_{-2}$ and estimate a value for k_1/k_x, which is the primary isotope effect (k_H/k_T) on the departure of hydrogen from the ketone as corrected for the secondary isotope effect of the hydrogen atom at the same carbon. The isotope effects on the rate coefficients in the other terms of eqn. (6) cancel out if the isotope effects (both primary and secondary) of the similar hydrogens at the *exo* and *endo* positions are equal.

If we assume the rough value of 13 for k_1/k_x ($13 = 6^{1\cdot44}$; the secondary effects are assumed to be unity, since 6 is a very rough mean for the primary deuterium isotope effect, k_H/k_D),[13,16] we get the following values for k_x/k_n at 25 °C (at 75 °C within parentheses; $k_1/k_x = 8.7$ as extrapolated [13] to 75 °C): 1100 (290) for I, (330 for II), 50 (25) for III and 270 (80) for IV, which seem quite reasonable (*cf.* Ref. 17). However, if eqn. (6) is applied for the evaluation of the ratio k_x/k_n in dedeuteration-protonation and deprotonation-deuteration reactions [5,10] by employing the k_{exo}/k_{endo} values presented above and the appropriate estimates for k_1/k_x (6 and 1/6, respectively), the values (500 – 800 for I, 15 – 25 for III and 140 for IV at 25 °C) are obtained, which are of the same order of magnitude, but regularly smaller than those calculated for the detritiation-protonation reactions. The values of k_x/k_n estimated in this way are, however, sensitive to the primary isotope effects, which may vary markedly with varying substrates and also with varying solvents.[13,16] The systematic differences may be caused by these facts, as well as by the approximations made, and do not conflict with the mechanism presented.

According to eqns. (4) and (5) the *exo* detritiation rates [$k_{exo}(T\rightarrow H)$] are approximately the same as the departure rates of *exo* tritium (k_x), but the *endo* detritiation rates $k_{endo}(T\rightarrow H)$ are greater than the departure rates of *endo* tritium (k_n). Thus the comparison of the departure rates (k_n) is more reasonable than that of the detritiation rates in the case of the *endo* exchange. The relative rates of departure of *exo* tritium are (1.0 for I) *ca.* 0.70 for II, 0.035 for III, and 0.057 for IV and the approximate relative rates of departure of *endo* tritium [$= (k_n k_{exo}(T\rightarrow H)/k_x)_i/(k_n k_{exo}(T\rightarrow H)/k_x)_I$, i = I, II, III or IV] are (1.0 for I), 0.6 for II, 0.4 for III, and 0.2 for IV at 75 °C (the values calculated directly from $(k_{endo}(T\rightarrow H))_i/(k_{endo}(T\rightarrow H))_I$ are, however, approximately equal).

The retarding effect of the 1-methyl group is slight as can be seen from the relative rates of II (*exo*- and *endo*-T) and is probably inductive by nature, since carbon 2 preserves its sp^2 hybridization at all the stages of the exchange reaction. The steric retarding effect of the *syn*-7 methyl group of III on the *exo*-T departure is *ca.* 0.09 (0.035/0.4), which seems reasonable (*cf.* Ref. 17; in the noncyclic two-stage free-radical addition of thiophenol to norbornene and 7,7-dimethylnorbornene $k_{latter}/k_{former} = 0.03$ at 0 °C). The retarding effect of the homoallylic double bond of IV is significant, although acceleration was expected due to the inductive effect and a possible homollylic stabilization effect of the ethylenic linkage. The same observation in the deprotonation-deuteration reaction of dehydronorcamphor has not got a satisfactory explanation from the differences in steric characters of the ethano ($-CH_2-CH_2-$) and etheno ($-CH=CH-$) bridges.[5,10] The effect of the hybridization change at carbon 3 ($sp^3 \rightarrow sp^2$) upon torsional strain and homoconjugation in the transition state of IV is unknown.[5] However, some kind of initial-state homoconjugation may occur in dehydronorcamphor, but not in norcamphor, and this may decrease the relative rate of IV.[18]

Acknowledgements. The authors wish to thank (the late) Professor Pentti Salomaa, Ph.D., and Professor Alpo Kankaanperä, Ph.D., for valuable advice concerning the tritium counting technique and Mr. Matti Hotokka, M.Sc., for kind advice concerning the calculations of the rates of the parallel reactions with the computer program written by him.

REFERENCES

1. Thomas, A. F. and Willhalm, B. *Tetrahedron Lett.* (1965) 1309.
2. Jerkunica, J. M., Borčić, S. and Sunko, D. E. *Tetrahedron Lett.* (1965) 4465.
3. Thomas, A. F., Schneider, R. A. and Meinwald, J. *J. Am. Chem. Soc. 89* (1967) 68.
4. Barraclough, P. and Young, D. W. *Tetrahedron Lett.* (1970) 2293.
5. Tidwell, T. T. *J. Am. Chem. Soc. 92* (1970) 1448.
6. Werstiuk, N. H. and Taillefer, R. *Can. J. Chem. 48* (1970) 3966.
7. Jindal, S. P., Sohoni, S. S. and Tidwell, T. T. *Tetrahedron Lett.* (1971) 779.
8. Jindal, S. P. and Tidwell, T. T. *Tetrahedron Lett.* (1971) 783.
9. Abad, G. A., Jindal, S. P., and Tidwell, T. T. *J. Am. Chem. Soc. 95* (1973) 6326.
10. Banerjee, S. and Werstiuk, N. H. *Can. J. Chem. 53* (1975) 1099, with refs.
11. Story, P. R. and Clark, B. C. In Olah, G. A. and Schleyer, P. v. R., Eds., *Carbonium Ions*, Interscience, New York 1972, Vol. 3, Chapter 23, with refs.
12. Sargent, G. D. *Ibid.*, Chapter 24, with refs.
13. Lynch, R. A., Vincenti, S. P., Lin, Y. T., Smucker, L. D. and Subba Rao, S. C. *J. Am. Chem. Soc. 94* (1972) 8351.
14. Kankaanperä, A., Oininen, L. and Salomaa, P. *Acta Chem. Scand. A 29* (1975) 153.
15. Salomaa, P. and Kankaanperä, A. *Unpublished results.*
16. Jones, J. R. *Trans. Faraday Soc. 61* (1965) 95; *65* (1969) 2138.
17. Brown, H. C., Kawakami, J. H. and Liu, K-T. *J. Am. Chem. Soc. 95* (1973) 2209.
18. Werstiuk, N. H., Taillefer, R., Bell, R. A. and Sayer, B. *Can. J. Chem. 51* (1973) 3010.

Received January 12, 1976.

Acta Chemica Scandinavica A 30 (1976) 397—404

Structures of Linear Multisulfur Systems. X. Sulfur-Sulfur Bonding in Compounds with Four and Five Collinear Sulfur Atoms. A Discussion Based on MO-Calculations

JORUNN SLETTEN

Department of Chemistry, University of Bergen, N-5014 Bergen-Univ., Norway

CNDO/2 calculations have been performed on a series of molecules containing four and five collinear sulfur atoms. The equilibrium geometries and charge distributions have been calculated. The theoretical results are compared with experimental data from X-ray crystallographic structure determinations. It is found that the CNDO/2 method is able to predict reasonably well in which cases partial bonding between sulfur atoms occurs. It is furthermore shown that the geometrical arrangements predicted for the sulfur sequences are closely related to those predicted for linear polyhalogen compounds.

It is well known that in structures of thiathiophthenes (I) and related compounds (*e.g.* II) the S–S bonds are found to be longer

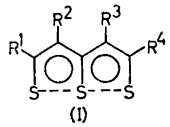

(I)

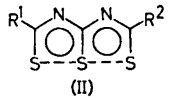

(II)

than corresponding single bonds.[1] Bonding schemes in which the central sulfur atom forms localized σ-bonds with the terminal sulfur atoms, utilizing *pd* or pd^2 hybrid orbitals, have been suggested.[2,3] Another of the proposed bonding schemes involves delocalized σ-bonding across the three sulfur atoms, 3-centre-4-electron bonding, in the following shortened 3c–4e bonding.[4,5] The description may be used with or without involving *d*-orbitals on the sulfur atoms. If *d*-orbitals are not included, this σ-bonding scheme is analogous to that suggested for trihalide ions by Hach and Rundle [6] and by Pimentel.[7]

Compounds including four and five collinear sulfur atoms, *e.g.* III and IV, may be described as extended thiathiophthenes. Several such

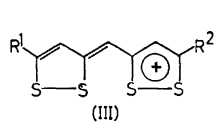

(III)

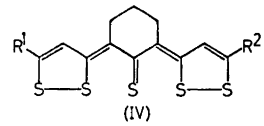

(IV)

compounds have been synthesized [8–11] and investigated by X-ray crystallographic methods.[12–23] In some of the compounds studied all S–S bonds have been found to be longer than single bonds, while in other compounds bond lengths comparable to those in five-membered cyclic dithioles are found.

The 3c-4e concept may be extended and generalized to give a description of *n*-centre bonds, (*nc-ve* bonds) as pointed out by Carpenter [24] and by Müller.[25] The general system under consideration by these authors is an array of *n* collinear equal atoms equally spaced. It is concluded that when $n \geqslant 4$, *n*-centre bonding is only to be expected if other forces keep the atoms in favourable positions.[25] In the higher homologues of thiathiophthenes, and related compounds, the carbon skeleton will tend to keep the sulfur atoms in favourable positions for delocalized *n*-centre σ-bonding.

In the present paper the results of CNDO/2 calculations on some selected model four- and five-sulfur compounds are given and compared with experimental results.

CALCULATIONS

The calculations have been performed with the CNDO/2 method, using standard parameters.[26–28] A slightly modified CNDO/2 program was employed.[29] *d*-Orbitals have not been included, due to the large number of additional parameters required in the calculations. Recent *ab initio* calculations give rather low *d*-orbital populations on the sulfur atoms in thiathiophthenes.[30] It is thus probable that the 3*d*-orbitals on sulfur in these compounds do not participate in building hybrid orbitals in the usual sense, but rather serve as polarizing functions on *s*- and *p*-orbitals so as to improve the occupied molecular orbitals without significantly changing their character.[31] On this background it seems reasonable to assume that the essential features of the bonding in the four- and five-sulfur compounds may be described by inclusion of only *s*- and *p*-orbitals.

It has been observed that CNDO/2 calculations with standard parameters and without *d*-orbitals predict too long S–S bonds in, *e.g.*, dithioles;[32,33] while calculations with *d*-orbitals yield too short S–S bonds.[32] Thus, when comparing experimental bond lengths with those predicted theoretically, the relative changes rather than the absolute values are relevant in the discussion.

In the various model compounds studied by CNDO/2 the valence electron energy of the system has been calculated for different S–S bond lengths. The S–S distances have been varied by moving the sulfur atoms along the sulfur row, keeping other bond lengths and angles constant. This mode of calculation is somewhat artificial, as the geometry in general is affected when the S–S distances are changed. *E.g.* a C–S bond adjacent to a "short" S–S contact is invariably longer than a C–S bond adjacent to a "long" S–S contact. However, in calculating the energies for different S–S configurations, the effect of ignoring the overall geometrical changes will to a first approximation cancel when multi-centre and two-centre molecules are compared. If the synchronous changes in geometry should be fully taken into account, the amount of calculations required would be prohibitive.

If delocalized *n*-centre bonding is present in an *n*-centre system, all the bond distances along the array would be expected to be longer than a corresponding bond in a two-centre system. Therefore the equilibrium S–S distances arrived at for the four- and five-sulfur compounds, are compared with the corresponding distances calculated for closely related two-centre models, *i.e.* isolated five-membered cyclic disulfides.

RESULTS AND DISCUSSION

A. Four-sulfur compounds

1. *Model compound "a"*. The geometry as determined experimentally for compound V[14] was used as a basis for model "a" (Fig. 1).

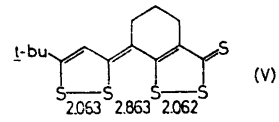

(V)

The model was constructed exactly planar, hence the slight deviations in corresponding C–C and C–S bond lengths between V and "a". C–H bond lengths were set equal to 1.08 Å. The variation in energy for "a" as a function of the S3–S4 distance is plotted in Fig. 2. In the calculations S2 and S3 were moved symmetrically along the sulfur row, so as to leave S1–S2 equal to S3–S4. S–S distances corresponding to minimum energy

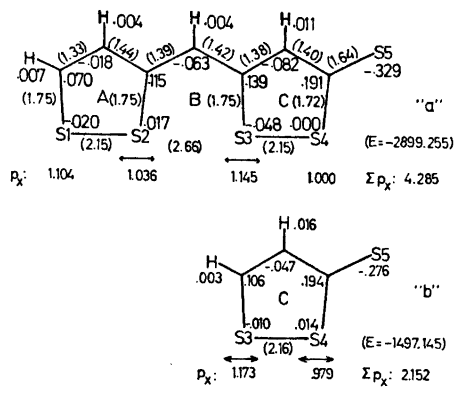

Fig. 1. Atomic charges and sulfur p_x population as calculated for models "a" and "b" at equilibrium geometries. Bond distances are shown in parentheses on "a". Bond lengths in "b" are as in ring C of "a". The minimum valence electron energies are given in units of eV.

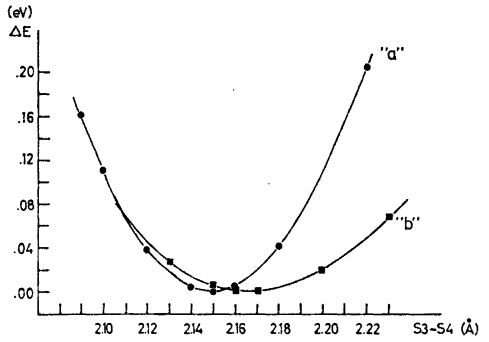

Fig. 2. The change ΔE in CNDO/2 valence electron energy for models "a" and "b" as a function of the S3–S4 bond length.

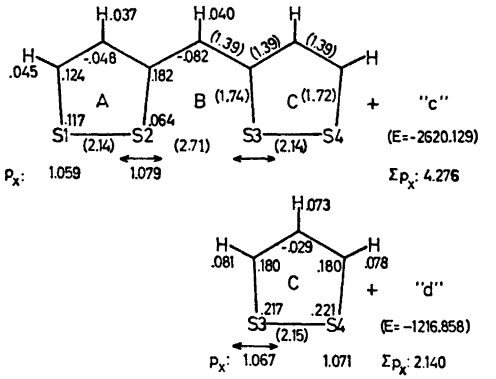

Fig. 3. Atomic charges, valence electron energy and sulfur p_x population as calculated for model compounds "c" and "d" at equilibrium geometries. Bond distances are given in parentheses on "c".

were derived by interpolation according to a second order polynomial fit. In order to compare the outer S–S bond distances arrived at in "a" with that in an isolated 1,2-dithiole ring of comparable geometry, calculations were carried out on 1,2-dithiole-3-thione (model "b").

In this calculation only one of the sulfur atoms, S3, was moved in order to mimic the calculations on "a". The optimized S–S distance in "b" is 2.16 Å while the outer distances in "a" are 2.15 Å. Hence, according to the CNDO results, the interaction between S2 and S3 does not lengthen the terminal S–S bonds in this four-sulfur compound relative to those of a dithiole. This is in agreement with experimental results which show the terminal distances in V to be of approximately the same lengths as the S–S bonds found in cyclic 1,2-dithioles.[14] According to the CNDO/2 calculations, both *s*- and *p*-orbitals are involved in the S–S σ-bonding; with *p*-orbitals giving the major contribution. Considering p_x-orbitals only as taking part in the S–S σ-bonding, there is a system with four centres and four electrons. The energetically most favourable arrangement apparently is two essentially localized 2c-2e bonds.

2. *Model compound "c".* The structure of the positive four-sulfur ion, VI, has been determined.[22] The outer S–S bond lengths determined experimentally do not differ significantly

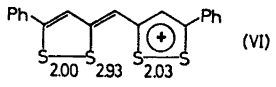

(VI)

from those of isolated 1,2-dithiolium ions.

For the calculations a model four-sulfur cation with twofold symmetry was constructed, model "c" (Fig. 3). As each of the outer rings in this molecule carries a formal charge of +0.5, it is not possible to find an exactly equivalent two-centre model for comparison. Instead a 1,2-dithiolium cation ("d") with geometry like ring C was used. The calculations give equilibrium S–S distances of 2.15 in "d" and 2.14 Å for the outer distances in "c". Both theoretical and experimental results thus suggest a bonding scheme in the four-sulfur cation equivalent to that in the neutral four-sulfur model "a".

3. *Model compound "e".* A negatively charged four-sulfur molecule has not yet been isolated. In such a compound there would be formally six p_x electrons in the sulfur array; *i.e.* a 4c-6e system. For the calculations on this anion an "unbiased" model "e" was constructed, with S–C = 1.72 Å, C–C = 1.39 Å, C–H = 1.08 Å, and bond angles at carbon atoms equal to 120°. S2 and S3 were moved as in the previous calculations. The equilibrium geometry arrived at is shown in Fig. 4. In this case the central S–S bond is the shorter one. The two-centre model used for comparison, model "f", is arrived at by a 180° rotation around each of the outer C–C bonds in "e". The optimum S–S bond length arrived at in the four-centre model is 0.04 Å longer than that in the two-centre

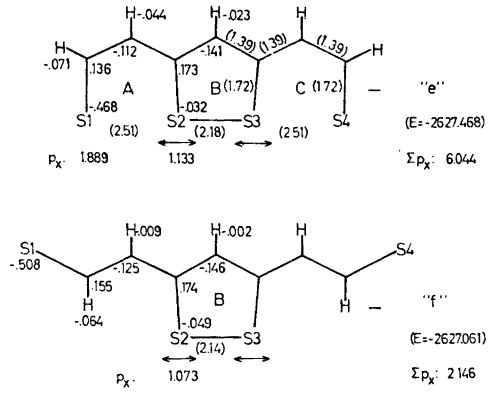

Fig. 4. Atomic charges, valence electron energy and sulfur p_x population as calculated for models "e" and "f" at equilibrium geometry. Bond lengths are shown in parentheses.

model. The calculations thus indicate that the interactions S1···S2 and S3···S4 are strong enough to have a lengthening effect on the central S–S bond, in agreement with the idea of σ-electron delocalization in electron-rich systems.

4. *Model compounds "g1", "g2" and "g3".* A neutral molecule isoelectronic to "e" is obtained by introducing nitrogen into the ring system in the manner illustrated in formula VII.

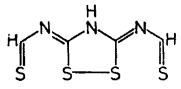

(VII)

Compounds analogous to VII have been synthesized,[10,11] and the structures of four of these have been determined by X-ray crystallographic methods.[19,20,23] The experimental results show that the central S–S bond is significantly longer than a single bond.

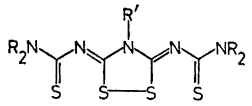

VIII (ref. 19)	2.763	2.167	2.763	R=i-pr, R'=Me
IX (ref.20)	2.745	2.196	2.676	R=i-pr, R'=p-NO_2-ph
	2.745	2.194	2.697	
	2.751	2.193	2.675	
X (ref.23)	2.742	2.161	2.785	R=Me, R'=Me
XI (ref.23)	2.784	2.171	2.784	R=Me, R'=ph

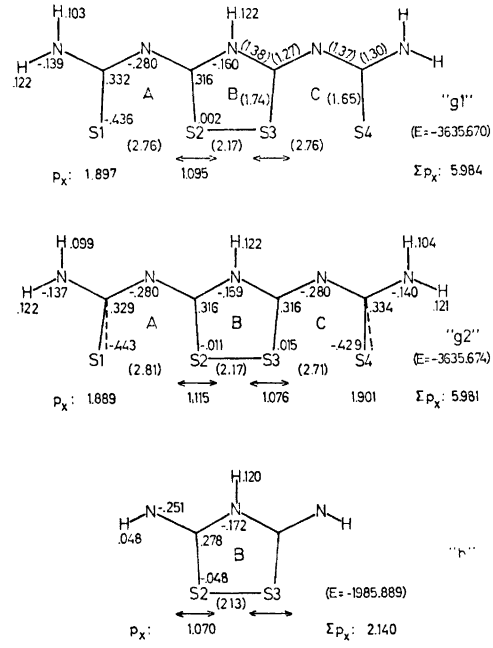

Fig. 5. Models "g1", "g2" and "h" with calculated atomic charges and sulfur p_x populations. N–H bonds = 1.04 Å, other bond distances are shown in parentheses.

CNDO/2 calculations were performed on a symmetrical model "g1" (Fig. 5). Optimal energy was found with the three S–S distances 2.76, 2.17 and 2.76 Å, respectively. The central distance is 0.04 Å longer than the S–S distance calculated for a reference cyclic disulfide, "h". Energy curves of the two models are shown

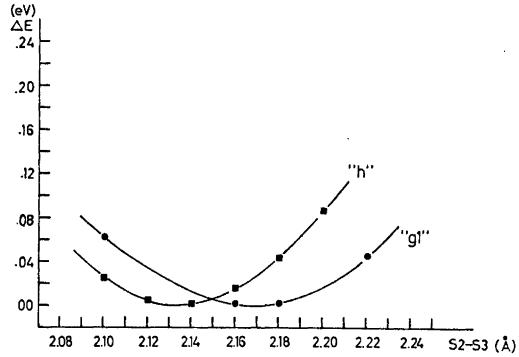

Fig. 6. The change ΔE in CNDO/2 valence energy for models "g1" and "h" as a function of the S2–S3 bond length.

in Fig. 6. As mentioned above the S–S bond lengths calculated by CNDO/2 for disulfides have been found to be approximately 0.1 Å longer than the experimental value. The calculated central S–S bond length in the four-sulfur model "g1" is, however, close to those observed experimentally in VIII–XI. The increase in S–S bond length by going from an isolated cyclic disulfide to the central ring of "g1" is hence underestimated in the calculations. Similarly, it has been found that CNDO/2 calculations not including *d*-orbitals on sulfur underestimate the variations in S–S bond lengths of open disulfides, R–S–S–R.[32]

The lengthening calculated for S2–S3 of "g1" is significant, and indicate that the three S–S bonds are partial bonds; as in the case of the four-sulfur anion (model "e"). As noted above, Müller has concluded that four-centre bonding is not very likely to occur.[25] Looking at Müller's energy calculations, however, it is seen that a four-centre bond has a significantly more favourable energy than a four-centre array with only *one* localized bond, while the energy difference between a four-centre bond and a system with *two* localized bonds, is minor.

In compounds VIII and XI the sulfur sequences have two-fold symmetries due to crystallographic requirements. In IX and X, which are also symmetrically substituted, the sulfur arrays are unsymmetrical. This is probably caused by differences in the crystallographic environments of atoms S1 and S4. In IX each of the S4 atoms (there are three molecules per asymmetric unit) has a close contact to the molecular plane of a neighbouring molecule, while the S1 atoms have no such short contacts.[20] This indicates that the S–S bonds in these four-sulfur molecules are easily perturbed by weak intermolecular forces.

An unsymmetrical model "g2" (Fig. 5) was constructed by shifting S1 and S4 in model "g1" 0.05 Å along the sulfur row. Calculations were carried out, moving S2 and S3 as described earlier. A minimum energy, not significantly different from that of the symmetrical model, was obtained. The calculations show a small displacement of the atomic charges in "g2" compared to "g1". S1 and S2 carry slightly larger negative charges than S4 and S3, respectively. Such an electronic displacement might be introduced in IX, *e.g.* due to the relatively close contact of S4 to the π-electron cloud of a neighbouring molecule; and hence an asymmetric sulfur sequence would be favourable.

It is well known that in trihalides, with delocalized 3c-4e bonding, the X_3^- sequence is more asymmetric the longer the total $[X-X-X]^-$ sequence.[34] By analogy one would expect that in these 4c-6e systems a shorter S···S···S···S sequence would correspond to a longer central S–S bond. From the experimental results (VIII–XI) it is seen that the variations in the four compounds studied are small and not systematic. The short total S···S arrays in IX do, however, correspond to central S–S bonds which are significantly longer than those found in the three other compounds. CNDO/2 calculations predict a barely detectable lengthening of the central S–S bond when S1···S4 is shortened (from 2.168 Å in "g2" to 2.173 Å in "g3" where the S1···S4 sequence is shortened by 0.30 Å).

B. Five-sulfur compounds

5. Model compounds "i1" and "i2". The structures of three compounds, each with five approximately collinear sulfur atoms, have been determined by X-ray crystallography (XII, XIII, XIV).[12,16,21] Molecule XII which is unsymmetrically substituted, shows a slight asymmetry in the sulfur sequence. The symmetrically substituted molecule XIII has, within experimental error, twofold symmetry, while compound XIV which is also symmetrically substituted, shows a large deviation from symmetry in the sulfur sequence. In each compound all four S–S distances are significantly longer than S–S bonds in cyclic dithioles.

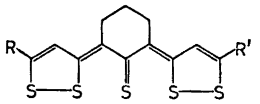

XII (ref.12)	2.14	2.62	2.55	2.16	R=ph, R'=t-bu
XIII (ref.16)	2.183	2.580	2.583	2.173	R=R'=t-bu
XIV (ref.21)	2.113	2.626	2.396	2.271	R=R'=p-MeO-ph

CNDO/2 calculations on a model with two-fold symmetry (model "i1") have been performed for various S···S distances (Fig. 7). The

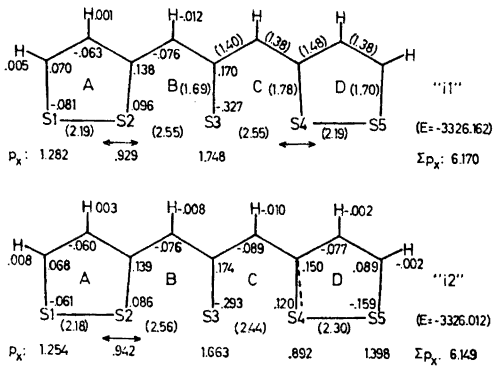

Fig. 7. Model compounds "i1" and "i2" with atomic charges and sulfur p_x population at equilibrium geometry. Bond distances are listed in parentheses.

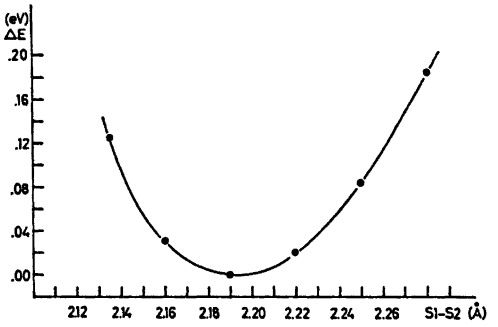

Fig. 8. ΔE plotted for model "i1" as a function of the S1 – S2 distance.

energy curve is plotted in Fig. 8. The results show that all S – S bonds are predicted to be longer than in dithioles; with the outer S – S bonds being the shorter ones, in good agreement with the experimental results. The calculated increase in S1 – S2 and S4 – S5 above the dithiole value, is, however, underestimated, as in the case of the four-sulfur compounds, "g1". In analogy with the notation used for the four-sulfur molecules, the partial bonding in the five-sulfur array may be described as 5c-6e bonding.

An unsymmetrical model "i2" was constructed by shifting S4 towards S3 such that S3 – S4 = 2.44 Å and S4 – S5 = 2.30 Å. In subsequent calculations these bond lengths were kept fixed, while moving S2. The CNDO results indicate that a lengthening of S4 – S5 will cause a slight shortening of S1 – S2. The experimental results show the same trend, however, much more pronounced (XIV).

As the two *p*-methoxyphenyl substituents in XIV have similar twist angles, the observed asymmetry in the sulfur array is probably induced by intermolecular forces. By studying the crystallographic packing it is found that the environments of the two outer disulfide rings are rather different. Dithiole ring A is sandwiched between the corresponding ring, A′, of another molecule and a phenyl group; while ring D's closest contacts are to a trimethylene bridge of another molecule.[21] It is possible that electronic repulsion between the π-electron clouds of ring A and its neighbours induces a migration of electronic charge from S1 towards S5. According to the calculations such an electronic displacement favours the asymmetric geometry observed where S1 – S2 is shorter than S4 – S5 (Fig. 7).

C. Models of polyhalides and polyhalogens

As mentioned in the introduction, the σ-bonding in thiathiophthenes apparently is similar to that in the trihalides. By analogy the σ-bonding in a linear X_4 (X = halogen)

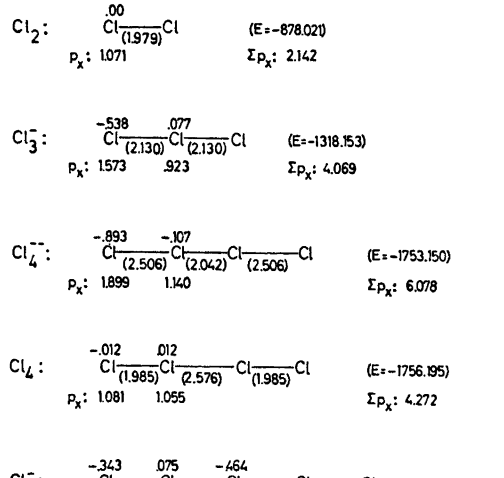

Fig. 9. Interatomic distances (in parentheses), atomic charges and p_x population in Cl_2,Cl_3^-, Cl_4^{2-}, Cl_4 and Cl_5^- at equilibrium geometries.

molecule might be of the 4c-4e type; while the bonding in X_4^{2-} and X_5^- may constitute delocalized 4c-6e and 5c-6e systems, respectively. In order to compare bonding patterns in the linear multisulfur compounds and linear polyhalogens, a series of CNDO/2 calculations were carried out on halogen model compounds. As the computer program available could not handle atoms with main quantum number larger than three, chloride compounds were used. Descriptions of the models and some results are summarized in Fig. 9. In the "free" Cl_2 molecule an interatomic distance of 1.978 Å is predicted by CNDO/2 in good agreement with the covalent single bond length of 1.98 Å.[35] Evidently the standard CNDO/2 parameterization gives a better fit for Cl_2 than for disulfides. The structure of a Cl_3^- ion is not known. Structures of Br_3^- and I_3^- ions, however, have been determined in several compounds (*e.g.* Refs. 36 – 39). Calculations were carried out for various Cl1···Cl3 distances. For each total length used, Cl2 was moved to find the lowest energy of the system. According to these calculations the optimal geometry of Cl_3^- is a symmetrical ion with Cl···Cl distances of 2.13 Å. For a symmetrical Cl_4^{2-} ion the calculations predict that all three bonds are significantly longer than a single bond. The equilibrium geometry is compatible to that of the sulfur arrays in models "e" and "g" suggesting a close similarity in bonding descriptions of these four-centre arrays.

The geometry of Cl_4^{2-} has not been determined experimentally. However, the homologous Br_4^{2-} ion has been observed in the crystal structure of W_6Br_{16}.[40] The ion is linear with a Br – Br distance of 2.43 Å for the central bond, and 2.98 Å for the two outer bonds. Similar four-centre arrays have been found in the compounds dimethylammonium bromide-bromine (2:1) and dimethylammonium chloride-iodine (2:1).[41] The average Br···Br distance of 2.8 Å is somewhat longer than that found in symmetrical Br_3^- (2.54 Å).[38] This is also in qualitative agreement with the average Cl···Cl distances of 2.35 and 2.13 Å predicted by CNDO/2 for Cl_4^{2-} and Cl_3^-, respectively. The halogen chains in the compounds mentioned above, have been interpreted as charge-transfer addition complexes formed by two halogen ions (donors) and one halogen molecule (acceptor).[42] The 4c-6e delocalized bonding concept describes the same system in terms of molecular orbital theory.

In a neutral four-centre model compound, Cl_4, CNDO/2 equilibrium geometry is calculated for a configuration with two short outer bonds and a long central distance. The outermost Cl – Cl bonds are almost identical to that predicted for Cl_2. This indicates that the σ-bonding in Cl_4 is equivalent to that in the four-sulfur array of model "a".

Calculations on a symmetrical linear Cl_5^- ion predict that all bonds will be longer than single bonds; – the outer bonds being the shorter ones, quite analogous to what has been found in the symmetrical five-sulfur sequences. X_5^- and YX_4^- halides known so far are nonlinear with two three-centre systems at right angles.[43,44] However, a linear polyiodide array has been recognized in a channel inclusion complex of trimesic acid polyiodide.[45]

CONCLUSION

CNDO/2 calculations have been performed on model compounds of linear multisulfur molecules, V – XIV. These calculations predict that relative to the S – S bond in an isolated cyclic disulfide, there will be a lengthening of S – S bonds in VII – XIV, but not in V and VI. This is in qualitative agreement with the experimental results.

Considering only p_x-orbitals as taking part in the S – S σ-bonding, a maximum of two *localized* S – S bonds may be formed both in a four-sulfur and a five-sulfur array. In four-sulfur compounds with four p_x-electrons, (V and VI), two localized S – S bonds are formed, while in four-sulfur compounds with six p_x-electrons, (VII-XI), there exists a delocalized 4c – 6e σ-bond. Analogously, in the five-centre compounds XII-XIV there exists a 5c – 6e bond. Thus, the results suggest that σ-delocalization occurs in these molecules when the number of p_x-electrons exceeds the number of atomic centres in the linear row.

REFERENCES

1. Hansen, L. K., Hordvik, A. and Sæthre, L. J. In Sterling, C. J. M., Ed., *Organic Sulphur Chemistry*, Butterworths, London 1975.

2. Maeda, K. *Bull. Chem. Soc. Jpn. 33* (1960) 304; *34* (1961) 785; 1166.
3. Johnstone, R. A. W. and Ward, S. D. *Theor. Chim. Acta 14* (1969) 420.
4. Giacometti, G. and Rigatti, G. *J. Chem. Phys. 30* (1959) 1633.
5. Gleiter, R. and Hoffmann, R. *Tetrahedron 24* (1968) 5899.
6. Hach, R. J. and Rundle, R. E. *J. Am. Chem. Soc. 73* (1951) 4321.
7. Pimentel, G. C. *J. Chem. Phys. 19* (1951) 446.
8. Klingsberg, E. *J. Heterocycl. Chem. 3* (1966) 243; *Chem. Ind. (London)* (1968) 1813.
9. Stavaux, M. and Lozac'h, N. *Bull. Soc. Chim. Fr.* (1967) 3557; (1968) 4273; (1969) 4184.
10. Goerdeler, J. and Ulmen, J. *Chem. Ber. 105* (1972) 1568; and personal communications.
11. Oliver, J. E. and Stokes, J. B. *Int. J. Sulfur Chem. A 2* (1972) 105.
12. Sletten, J. *Acta Chem. Scand. 24* (1970) 1464.
13. Sletten, J. *Acta Chem. Scand. 25* (1971) 3577.
14. Sletten, J. *Acta Chem. Scand. 26* (1972) 873.
15. Sletten, J. *Acta Chem. Scand. 27* (1973) 229.
16. Kristensen, R. and Sletten, J. *Acta Chem. Scand. 27* (1973) 2517.
17. Sletten, J. and Velsvik, M. *Acta Chem. Scand. 27* (1973) 3881.
18. Sletten, J. *Acta Chem. Scand. A 28* (1974) 499.
19. Sletten, J. *Acta Chem. Scand. A 28* (1974) 989.
20. Sletten, J. *Acta Chem. Scand. A 29* (1975) 317.
21. Sletten, J. *Acta Chem. Scand. A 29* (1975) 436.
22. Hordvik, A. *Acta Chem. Scand. 19* (1965) 1253; and Hordvik, A., Sletten, E. and Sletten, J. Paper given at The 6th Nordic Structure Chemistry Meeting in Århus, January 1967.
23. Flippen, J. L. *J. Am. Chem. Soc. 95* (1973) 6073.
24. Carpenter, G. B. *J. Chem. Educ. 40* (1973) 385.
25. Müller, H. *Z. Chem. 7* (1967) 81.
26. Pople, J. A., Santry, D. P. and Segal, G. A. *J. Chem. Phys. 43* (1965) S 129.
27. Pople, J. A. and Segal, G. A. *J. Chem. Phys. 44* (1966) 3289.
28. Santry, D. P. and Segal, G. A. *J. Chem. Phys. 47* (1967) 158.
29. Siegbahn, K., Nordling, C., Johansson, G., Hedman, J., Hedén, P. F., Hamrin, K., Gelius, U., Bergmark, T., Werme, L. O., Manne, R. and Baer, Y. *ESCA applied to free molecules*, North-Holland, Amsterdam, 1969.
30. Palmer, M. H. and Findlay, R. H. *J. Chem. Soc. Perkin Trans. 2* (1974) 1885.
31. Coulson, C. A. *Nature (London) 221* (1969) 1106.
32. Sæthre, L. J. *Acta Chem. Scand. A 29* (1975) 558.
33. Kiers, C. Th. and Vos, A. *Recl. Trav. Chim. Pays-Bas 91* (1972) 126
34. Gabes, W. *Ph. D. Thesis*, University of Amsterdam, 1973.
35. Pauling, L. *The Nature of the Chemical Bond*, Cornell Univ. Press, Ithaca 1960, 3rd Ed. pp. 224.
36. Runsink, J., Swen-Walstra, S. and Migchelsen, T. *Acta Crystallogr. B 28* (1972) 1331.
37. Cheesman, G. H. and Finney, A. J. T. *Acta Crystallogr. B 26* (1970) 904.
38. Lawton, S. L. and Jacobson, R. A. *Inorg. Chem. 7* (1968) 2124.
39. Breneman, G. L. and Willett, R. D. *Acta Crystallogr. B 25* (1969) 1073.
40. Siepmann, R. and Schnering, H. B. *Z. Anorg. Allg. Chem. 357* (1968) 289.
41. Strømme, K. O. *Acta Chem. Scand. 13* (1959) 2089.
42. Hassel, O. *Mol. Phys. 1* (1958) 241.
43. Broekema, J., Havinga, E. E. and Wibenga, E. H. *Acta Crystallogr. 10* (1957) 596.
44. Sly, W. G. and Marsh, R. E. *Acta Crystallogr. 10* (1957) 378.
45. Herbstein, F. H. and Kapon, M. *Acta Crystallogr. A 28* (1972) 575.

Received December 19, 1975.

Acta Chemica Scandinavica A 30 (1976) 405—410

The Molecular and Crystal Structures of $[CuCl_2(C_2H_6O_2)]$ and $[CuCl_2(C_2H_6O_2)].\frac{1}{2}H_2O$; Two Compounds Containing Neutral Dichloro(1,2-ethanediol)copper(II) Molecules

BRITT-MARIE ANTTI

Department of Inorganic Chemistry, University of Umeå, S-901 87 Umeå, Sweden

The crystal structures of the title compounds have been determined and refined using X-ray diffraction data. $[CuCl_2(C_2H_6O_2)]$ is monoclinic, space group $P2_1/c$, $Z=4$ and unit cell $a=7.424$ (1) Å, $b=10.939(5)$ Å, $c=7.518(1)$ Å and $\beta=95.666(9)°$. $[CuCl_2(C_2H_6O_2)].\frac{1}{2}H_2O$ is orthorhombic, space group $Pcnb$ (D_{2h}^{14}), with $Z=8$ and cell dimensions $a=10.198(1)$ Å, $b=18.769$ (1) Å and $c=7.043(1)$ Å. The structures were refined by full-matrix least-squares techniques to R-values of 0.042 (1739 reflexions) and 0.047 (2388 reflexions) for $[CuCl_2(C_2H_6O_2)]$ and $[CuCl_2(C_2H_6O_2)].\frac{1}{2}H_2O$, respectively. Both structures are built from discrete $CuCl_2(C_2H_6O_2)$ molecules with approximately planar coordination around Cu. The Cu—Cl distances range between 2.232 and 2.267 Å and the Cu—O distances between 1.958 and 2.004 Å. Adjacent molecules are connected by longer Cu···Cl contacts thus forming infinite layers in $[CuCl_2(C_2H_6O_2)]$ and chains in $[CuCl_2(C_2H_6O_2)].\frac{1}{2}H_2O$.

In two recent papers the structures of $[MnCl_2(C_2H_6O_2)_2]$ [1] and $[Me_2Cl_2(C_2H_6O_2)_4]Cl_2$ (Me = Co, Ni) [2] were presented. In the manganese compound the structure consists of discrete neutral molecules $[MnCl_2(C_2H_6O_2)_2]$ whereas the isostructural cobalt and nickel compounds are built from dimeric $[Me_2Cl_2(C_2H_6O_2)_4]^{2+}$-ions and Cl^--ions. The present work was undertaken in order to elucidate what structural changes would occur if copper was introduced as metal ion.

EXPERIMENTAL

The compounds were prepared by dissolving as much as possible of $CuCl_2.2H_2O$ in 1,2-ethanediol (glycol) (molar ratio 1:2) on the waterbath and placing the solution obtained in a desiccator over sulfuric acid. The space groups were derived from Weissenberg films and the densities determined by the flotation method using bromoform and xylene.

Tabular, light green and extremely hygroscopic crystals of $[CuCl_2(C_2H_6O_2)]$ separated after several weeks. IR-spectrum was recorded on a sample, which had been mulled in nujol and placed between NaCl-plates. From the spectrum it was clear that the sample had taken up water; the spectrum was in fact identical with that of $[CuCl_2(C_2H_6O_2)].\frac{1}{2}H_2O$ in the recorded wavenumber region (4000 – 625 cm^{-1}). Because of the extreme hygroscopicity, no analyses have been made so far. The systematic extinctions corresponded to space group $P2_1/c$ (No. 14). The cell parameters were refined from rotation photographs (a, b and c) and from omega scan on the diffractometer (a, c and β). The following parameters were obtained: $a=7.424(1)$ Å, $b=10.939(5)$ Å, $c=7.518(1)$ Å and $\beta=95.666(9)°$. The density is 2.14(1) g cm^{-3}; calc. for $[CuCl_2(C_2H_6O_2)]$ 2.148 g cm^{-3}.

$[CuCl_2(C_2H_6O_2)].\frac{1}{2}H_2O$ separated overnight as light-green, tabular crystals. If they were kept over sulfuric acid too long they lost their water content. Systematic extinctions uniqely determined the space group to be $Pcnb$ (D_{2h}^{14} No. 60) with the following coordinates for the general eightfold position: $\pm(x,y,z;\ \frac{1}{2}-x,y,\frac{1}{2}+z;x,\frac{1}{2}+y,\bar{z};\ \frac{1}{2}-x,\frac{1}{2}+y,\frac{1}{2}-z)$. From data obtained from a powder film taken in a camera of Guinier-Hägg type, the following cell parameters were refined: $a=10.198(1)$ Å, $b=18.769(1)$ Å and $c=7.043(1)$ Å. The density is 2.04(1) g cm^{-3}; calc. for $[CuCl_2(C_2H_6O_2)].\frac{1}{2}H_2O$ 2.03 g cm^{-3}. The crystals were analyzed for copper and chlorine. Found Cu 30.62 (electrolytically): Cl 33.3 (gravimetrically). Calc. for $[CuCl_2(C_2H_6O_2)].\frac{1}{2}H_2O$ Cu 30.92; Cl 34.5. IR-spectra indicated that water was present in the structure.

The intensity measurements were made using the automatic linear diffractometer PAILRED and graphite monochromated MoKα-radiation. Both crystals were sealed in glass capillaries during the data collection. The dimensions of the crystals were $0.09 \times 0.10 \times 0.25$ mm and $0.21 \times 0.25 \times 0.50$ mm for $[CuCl_2(C_2H_6O_2)]$ and $[CuCl_2(C_2H_6O_2)].\frac{1}{2}H_2O$ and they were rotated around their *b*- and *c*-axes, respectively. The omega-scan technique was used with scan speed 1°/min and weak reflexions (< 4000 counts) were measured twice. The half scan intervals were $1.5-1.6°$ ($1.5-1.6°$) for Ω_1 and $1.9-2.4°$ ($2.3-2.5°$) for Ω_2. The values in parentheses refer to those used for the crystal of $[CuCl_2(C_2H_6O_2)].\frac{1}{2}H_2O$ and Ω_1 was used for $\theta > 20°$ and Ω_2 for $\theta \leq 20°$. For the crystal of $[CuCl_2(C_2H_6O_2)]$ 2616 reflexions from $h0l - h15l$ were measured and for that of $[CuCl_2(C_2H_6O_2)].\frac{1}{2}H_2O$ 6634 from $hk0 - hk11$. From these 1739 ($\sin\theta_{max} = 0.55$) and 4385 ($\sin\theta_{max} = 0.60$), respectively, had $\Delta I/I \leq 0.5$.[1] Absorption correction was applied; $\mu_{MoK\alpha} = 44.7$ and 40.9 cm^{-1} for $[CuCl_2(C_2H_6O_2)]$ and $[CuCl_2(C_2H_6O_2)].\frac{1}{2}H_2O$, respectively. For $[CuCl_2(C_2H_6O_2)].\frac{1}{2}H_2O$ the *hkl* and $\bar{h}kl$ reflexions were averaged, leaving 2388 independent reflexions. As a final check, structure amplitudes were calculated for the unobserved reflexions. They all had values lower than or equal to the corresponding threshold values. The data programs used are described earlier.[5]

STRUCTURE ANALYSIS

The structures were solved by routine heavy-atom Patterson and Fourier methods and refined by full-matrix least-squares techniques to *R*-values of 0.042 ($R_w = 0.051$) and 0.047 ($R_w = 0.058$) for $[CuCl_2(C_2H_6O_2)]$ and $[CuCl_2(C_2H_6O_2)].\frac{1}{2}H_2O$, respectively. Anisotropic temperature factors were applied to the non-hydrogen atoms while for the hydrogen atoms the thermal vibrations were assumed to be isotropic. The function $\sum w(||F_o| - |F_c||)^2$ was minimized using weights calculated according to the function $w = 1/(a + |F_o| + c|F_o|^2 + d|F_o|^3)$ [6] using the constants $a = 400$, $c = -0.015$ and $d = 0.003$ for $[CuCl_2(C_2H_6O_2)]$ and 450, 0.005 and 0.003 for $[CuCl_2(C_2H_6O_2)].\frac{1}{2}H_2O$. The scattering curves for Cu, Cl, O, and C were those proposed by Cromer and Waber [7] and dispersion correction ($\Delta f'$, $\Delta f''$) was applied for Cu and Cl.[8] For the hydrogen atoms the scattering curve proposed by Stewart *et al.*[9] was used. As a final check a difference Fourier synthesis was calculated, from which nothing abnormal could be detected. The highest peak was found in the vicinity of copper. The final positional and thermal parameters are given in Tables 1 and 2. The list of observed and calculated structure amplitudes will be supplied by the author on request.

DESCRIPTION AND DISCUSSION OF THE STRUCTURES

The structures are built from near planar discrete molecules $CuCl_2(C_2H_6O_2)$ which are arranged in different ways in the two struc-

Table 1. Atomic positional and thermal parameters for $[CuCl_2(C_2H_6O_2)]$. For the non-hydrogen atoms all parameters have been multiplied by 10^4. The anisotropic temperature factor is $\exp[-(h^2\beta_{11} + k^2\beta_{22} + l^2\beta_{33} + 2hk\beta_{12} + 2hl\beta_{13} + 2kl\beta_{23})]$. For the hydrogen atoms the positional parameters have been multiplied by 10^3. The labelling of atoms is shown in Fig. 3. (Standard deviations in parentheses.)

	x/a	*y/b*	*z/c*	β_{11}(*B*)	β_{22}	β_{33}	β_{12}	β_{13}	β_{23}
Cu	73(1)	1208(0.5)	3282(1)	105(1)	62(0.4)	169(1)	−6(0.4)	30(1)	−20(0.5)
Cl(1)	−2108(1)	−197(1)	3288(1)	109(1)	63(1)	194(2)	−7(1)	23(1)	−7(1)
Cl(2)	−1292(1)	2609(1)	4847(1)	160(2)	68(1)	126(2)	12(1)	21(1)	−9(1)
O(1)	1528(5)	152(4)	1881(6)	139(6)	90(3)	287(9)	−14(3)	62(6)	−68(4)
O(2)	2329(4)	2200(3)	3269(4)	124(5)	66(2)	166(5)	−5(3)	6(4)	12(3)
C(1)	3405(6)	333(5)	2182(9)	104(6)	108(5)	278(13)	5(5)	50(7)	−33(7)
C(2)	3756(6)	1649(5)	2364(8)	127(7)	99(5)	242(11)	−6(5)	47(7)	10(6)
H(1)	142(9)	−49(8)	164(9)	6(2)					
H(2)	235(8)	290(6)	291(8)	4(1)					
H(3)	376(9)	−22(8)	341(10)	7(2)					
H(4)	403(8)	−10(6)	137(9)	5(1)					
H(5)	389(9)	213(7)	114(9)	6(2)					
H(6)	487(8)	197(6)	281(8)	4(1)					

Table 2. Atomic positional and thermal parameters for $[CuCl_2(C_2H_6O_2)].\frac{1}{2}H_2O$. For the labelling of atoms see Fig. 4.

	x/a	y/b	z/c	$\beta_{11}(B)$	β_{22}	β_{33}	β_{12}	β_{13}	β_{23}
Cu	1773(0.4)	1274(0.2)	239(1)	52(0.3)	17(0.1)	126(1)	2(0.1)	6(0.4)	−6(0.2)
Cl(1)	2852(1)	2073(0.4)	2078(1)	64(1)	19(0.2)	98(1)	−1(0.3)	5(1)	1(0.3)
Cl(2)	3461(1)	553(0.5)	−400(1)	75(1)	28(0.3)	164(2)	19(0.4)	−6(1)	−18(0.5)
O(1)	565(2)	641(1)	−1241(4)	68(2)	19(1)	163(5)	−3(1)	16(3)	−8(1)
O(2)	68(2)	1675(1)	995(4)	61(2)	25(1)	180(5)	3(1)	10(3)	−20(2)
O(3)	0	25	4081(5)	81(4)	43(2)	119(6)	28(2)	0	0
C(1)	4244(4)	4067(2)	3633(7)	66(3)	26(1)	237(10)	2(1)	−21(4)	18(3)
C(2)	1037(4)	3776(2)	568(8)	58(3)	27(1)	263(10)	0.4(1)	−30(4)	17(3)
H(1)	424(6)	60(4)	276(12)	6(2)					
H(2)	−14(5)	184(3)	218(9)	4(1)					
H(3)	63(6)	229(3)	486(12)	7(2)					
H(4)	418(4)	370(2)	267(7)	3(1)					
H(5)	366(5)	448(3)	335(8)	4(1)					
H(6)	98(5)	420(3)	147(8)	4(1)					
H(7)	186(5)	345(3)	41(9)	5(1)					

tures. In $[CuCl_2(C_2H_6O_2)]$ each molecule has Cu almost at $x=0$ and the packing of the molecules makes possible two longer contacts from each Cu to chlorines of adjacent molecules. These longer Cu---Cl contacts connect the near planar molecules in infinite layers parallel to (100) as is indicated in Fig. 1. In $[CuCl_2(C_2H_6O_2)].\frac{1}{2}H_2O$ the longer Cu---Cl contacts connect the molecules in infinite chains along [001]. These chains are further connected in pairs *via* the water molecules by means of hydrogen bonds in infinite layers extending parallel to (010). This arrangement is shown in Fig. 2.

The arrangement around the Cu-atoms. Around each copper atom there is a near planar arrangement with the two glycol oxygens and the two chlorine atoms from the formula unit as coordinated ligands (Figs. 3 and 4). The deviations from the calculated least-squares plane, defined by the coordinated ligands, are −0.007(2) [0.008(1)], 0.006(1) [−0.015(1)], 0.129(5) [0.159(3)], −0.069(4) [−0.159(3)] and 0.057(1) [0.113(1)] Å for Cl(1), Cl(2), O(1), O(2), and Cu, respectively. (The values in square brackets refer to those found in $[CuCl_2(C_2H_6O_2)].\frac{1}{2}H_2O$.) The Cu−O distances ranging between 1.958(4) and 2.004(3) Å agree well with other reported

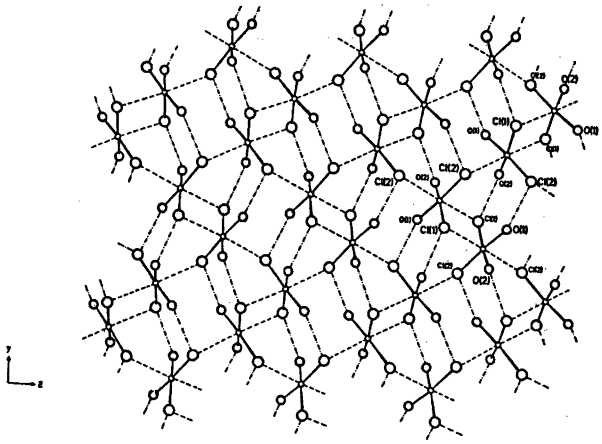

Fig. 1. The molecular packing in $[CuCl_2(C_2H_6O_2)]$. The carbon and hydrogen atoms are omitted. The dashed lines indicate the 'nonbonded' Cu---Cl contacts and the ·-· lines the hydrogen bond contacts.

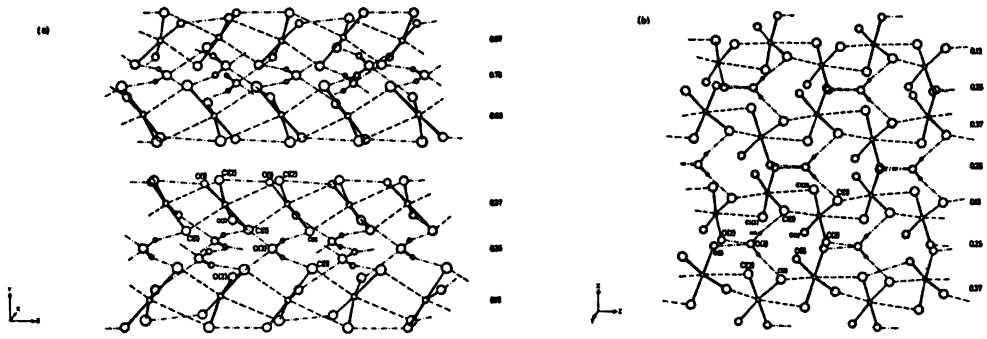

Fig. 2. The molecular packing in $[CuCl_2(C_2H_6O_2)].\frac{1}{2}H_2O$. Viewed along (a) the x-axis and (b) the y-axis. The numerals at the right correspond to the y-value of the Cu and O(3) atoms respectively. Legend as for Fig 1.

Cu – O bond lengths.[10]

The near planar $CuCl_2(C_2H_6O_2)$ molecules are connected *via* longer 'nonbonded' Cu---Cl contacts, in order to achieve the favoured tetragonally distorted, octahedral (4+2) arrangement around each Cu(II) (Figs. 1 and 2). Thus in the structure of $[CuCl_2(C_2H_6O_2)]$ planar four-membered rings $Cu<^{Cl(1)}_{Cl(1)}>Cu$ centered around a crystallographic inversion center are formed. The Cu – Cl(1)---Cu angle is 87.29(4)°, the Cl – Cl distance 3.875(2) Å and the Cu – Cu distance 3.704(1) Å. Furthermore, there is another type of connecting arrangement Cu-Cl(2)---Cu with a corresponding angle of 128.45(5)° and a Cu – Cu distance of 4.704(1) Å.

In $[CuCl_2(C_2H_6O_2)].\frac{1}{2}H_2O$ the four-membered ring arrangement $Cu<^{Cl(1)}_{Cl(2)}>Cu'$ is not planar and the deviations from the calculated least-squares plane are 0.062(1), 0.077(1), −0.305(1), and −0.394(1) Å for Cu, Cu', Cl(1), and Cl(2), respectively. The Cu – Cu' contact is 3.821(1) Å, well in excess of the value corresponding to Cu – Cu bonding (2.63 – 2.99 Å).[11,12] The Cl(1) – Cl(2) separation of 3.618(1) Å is in good agreement with the sum of the van der Waals radii for Cl (3.60 Å).[13]

The bonded Cu – Cl distances in the two structures as well as the longer Cu---Cl contacts in $[CuCl_2(C_2H_6O_2)]$ are in agreement with those reported by Willett and Rundle [14] for some copper chloride complexes. The great inequality in the 'nonbonded' Cu---Cl contacts in the hydrated compound $[CuCl_2(C_2H_6O_2)].\frac{1}{2}H_2O$ must be due to the insertion of half a water molecule per unit cell as in the water-free analogue the two 'nonbonded' Cu---Cl contacts

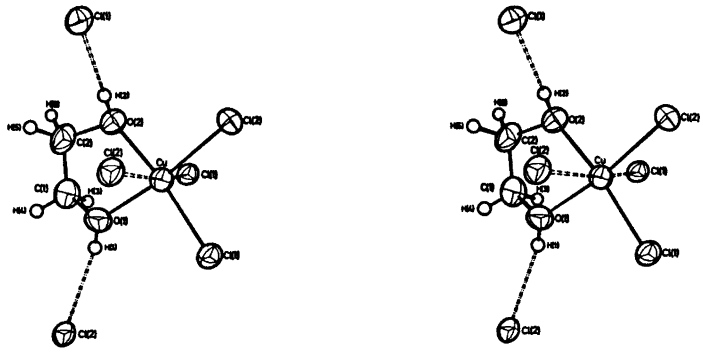

Fig. 3. A stereoscopic view of the coordination around Cu(II) in $[CuCl_2(C_2H_6O_2)]$. The ellipsoids are scaled to enclose 50 % probability. (Dashed lines indicate 'nonbonded' Cu---Cl contacts and the hydrogen bond directions are shown with -·- lines.)

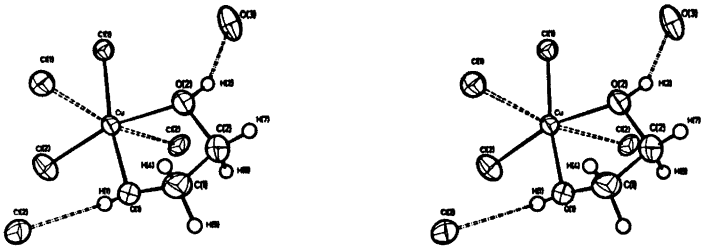

Fig. 4. A stereoscopic view of the coordination around Cu(II) in $[CuCl_2(C_2H_6O_2)]\cdot\frac{1}{2}H_2O$. Legend as for Fig. 3.

are almost equal (mean value 3.020 Å). Distances and angles in the two compounds are given in Table 3.

The glycol ligand. As in the earlier reported glycol complexes [1–5] the glycol ligand acts as a bidentate chelating agent and has *gauche* conformation in relation to the C–C bond. The dihedral angle is 35.7 and 51.6° for $[CuCl_2(C_2H_6O_2)]$ and $[CuCl_2(C_2H_6O_2)]\cdot\frac{1}{2}H_2O$, respectively, the former value being much smaller than those found earlier (45.9–56.1°).[1–5] The dihedral angles seem to be correlated to the deviations of the carbon atoms from the O–Cu–O plane. They are 0.510(7) [0.365(5)] for C(1) and 0.043(6) [−0.351(5)] Å for C(2). (The values in square brackets refer to $[CuCl_2(C_2H_6O_2)]\cdot\frac{1}{2}H_2O$.) This difference in ring symmetry might account for the greater stability

Table 3. Distances (Å) and angles (°) in $[CuCl_2(C_2H_6O_2)]$ and $[CuCl_2(C_2H_6O_2)]\cdot\frac{1}{2}H_2O$. Standard deviations in parentheses.

	$[CuCl_2(C_2H_6O_2)]$	$[CuCl_2(C_2H_6O_2)]\cdot\frac{1}{2}H_2O$
Cu–O(1)	1.958(4)	2.004(3)
Cu–O(2)	1.996(3)	1.968(3)
Cu–Cl(1)	2.232(1)	2.267(1)
Cu–Cl(2)	2.235(1)	2.235(1)
Cu···Cl(1)	3.064(1)	2.712(1)
Cu···Cl(2)	2.976(1)	3.365(1)
Cl(1)–Cl(2)	3.320(2)	3.402(1)
O(1)–O(2)	2.518(5)	2.551(4)
O(1)–C(1)	1.404(6)	1.457(5)
O(2)–C(2)	1.446(6)	1.442(5)
C(1)–C(2)	1.468(8)	1.497(7)
O(1)–H(1)	0.73(8)	0.74(9)
O(2)–H(2)	0.81(7)	0.91(6)
C(1)–H(3)	1.11(8)	0.96(5)
C(1)–H(4)	0.93(6)	0.99(5)
C(2)–H(5)	1.07(7)	1.02(6)
C(2)–H(6)	0.93(6)	1.05(6)
O(1)–C(1)–C(2)	108.5(4)	105.0(3)
O(2)–C(2)–C(1)	108.7(4)	104.8(3)
Cu–O(1)–C(1)	115.0(4)	112.1(2)
Cu–O(2)–C(2)	115.5(3)	114.2(2)
Cl(1)–Cu–Cl(2)	95.97(5)	98.14(3)
Cl(1)···Cu···Cl(2)	170.03(3)	169.07(3)
Cl(1)–Cu–O(1)	92.0(1)	171.1(1)
Cl(1)–Cu–O(2)	169.4(1)	91.2(1)
Cl(2)–Cu–O(1)	172.1(1)	90.5(1)
Cl(2)–Cu–O(2)	93.1(1)	165.1(1)
O(1)–Cu–O(2)	79.1(1)	79.9(1)

found for the hydrated compound compared to the water-free analogue. The intraring dimensions agree with those previously found for this kind of complex. The angles around oxygen and carbon involving hydrogen atoms agree fairly well with the tetrahedral angle; they range between 88 – 130 and 102 – 125° for $[CuCl_2(C_2H_6O_2)]$ and $[CuCl_2(C_2H_6O_2)].\frac{1}{2}H_2O$, respectively.

Hydrogen bond contacts. Within the infinite layers, from which $[CuCl_2(C_2H_6O_2)]$ is comprised, there is a pattern of hydrogen bond contacts between different molecules as indicated in Fig. 1. Each of the two chlorine atoms accepts one hydrogen bond from a glycol hydroxyl and the Cl··O distances are 3.077(4) and 3.068 (4) Å for Cl(1) and Cl(2), respectively. The corresponding O – H··Cl angles of 173(6) and 165(7)° indicate that the bonds do not deviate significantly from linearity.

In the hydrated compound both inter- and intrachain hydrogen bonds are found. The interchain contacts, which give rise to the layer formation, are formed *via* the water molecules. Each water oxygen shows four hydrogen bonds, tetrahedrally arranged; two as hydrogen bond donor to chlorine atoms, 3.146(3) Å, and two as hydrogen bond acceptor from the glycol hydroxyls, 2.669(4) Å. This arrangement is shown in Fig. 2. The bond O – H··Cl does not deviate significantly from linearity (∠O – H··O 164(6)°) and the acceptor Cl lies approximately in the plane of the water molecule. On the other hand, the O – H··O bond seems to be bent; the O – H··O angle is 152(5)°. Within the chains there are also hydrogen bond contacts between different molecules. They are of the O – H··Cl type with the glycol hydroxyls as donors. The Cl··O distance of 3.098(3) Å is in good agreement with other reported Cl··O distances and the O – H··Cl bond shows no significant deviation from linearity (∠O – H··Cl 175(7)°).

This increase of hydrogen bond contacts in the hydrated compound compared to the water-free compound will, in addition to the release of strain in the chelate ring, be of significant importance when the stability of the compounds is considered.

Acknowledgements. I wish to express my gratitude to Professor Nils Ingri for much valuable advice and for the facilities placed at my disposal. The English of this paper has been corrected by Dr. Michael Sharp. This work is part of a program supported by The Swedish Natural Science Research Council.

REFERENCES

1. Antti, B.-M. *Acta Chem. Scand. 27* (1973) 3513.
2. Antti, B.-M. *Acta Chem. Scand. A 29* (1975) 76.
3. Antti, B.-M. *Acta Chem. Scand. A 30* (1976) 103.
4. Antti, B.-M., Lundberg, B. K. S. and Ingri, N. *Acta Chem. Scand. 26* (1972) 3984.
5. Antti, B.-M. *Acta Chem. Scand. A 30* (1976) 24.
6. Cruickshank, D. W. J. *Computing Methods in Crystallography*, Pergamon, London 1965, p. 114.
7. Cromer, D. T. and Waber, J. T. *Acta Crystallogr. 18* (1975) 104.
8. Cromer, D. T. and Lieberman, D. *J. Chem. Phys. 53* (1970) 1891.
9. Stewart, R. F., Davidson, E. R. and Simpson, W. T. *J. Chem. Phys. 42* (1965) 3175.
10. Orgel, L. E. *An Introduction to Transition Metal Chemistry*, Methuen, London 1960, p. 60.
11. Barclay, G. A. and Kennard, C. H. L. *J. Chem. Soc.* (1961) 1544.
12. Barclay, G. A. and Hoskins, B. F. *J. Chem. Soc.* (1965) 1979.
13. Pauling, L. *The Chemical Bond*, Cornell University Press, Ithaca 1967.
14. Willett, R. D. and Rundle, R. E. *J. Chem. Phys. 40* (1964) 838.

Received December 16, 1975.

Acta Chemica Scandinavica A 30 (1976) 411—417

Isotope Effects in Proton-transfer Reactions. VI.* Base-catalysed Racemization of 2-Phenylpropionitrile in Dimethyl Sulfoxide-Methanol Solutions

NILS-ÅKE BERGMAN and INGER KÄLLSSON

Department of Organic Chemistry, University of Göteborg and Chalmers University of Technology, Fack, S-402 20 Göteborg, Sweden

The primary kinetic isotope effect in the racemization of 2-phenylpropionitrile with sodium methoxide as base has been determined in mixtures of methanol and dimethyl sulfoxide (DMSO) at +10 °C. A rather large increase in the strength of the isotope effect with increasing amount of DMSO has been observed. In methanol $k_D/k_H = 0.37 \pm 0.02$ and in 62 % methanol – 38 % DMSO $k_D/k_H = 0.18 \pm 0.01$. The variation and the magnitude of the primary kinetic isotope effect is believed to reflect an increasing symmetry of the transition state for the proton-transfer reaction with increasing concentration of DMSO in the solution. Brønsted's β determined by the acidity-function method equals 0.9. This, together with an observed curvature in the Brønsted plot, are facts which make it credible that 2-phenylpropionitrile does not behave as a Hammett base under the prevailing conditions.

The study of proton-transfer reactions has lately become a field of increasing interest, and efforts have been made to obtain detailed information on the transition-state structure in such reactions. A review of the work in the field has recently been published,[1] and can be consulted for references. The experimental quantities most frequently used as measures of the transition-state symmetry are the primary kinetic hydrogen isotope effect and Brønsted's β for the reactions. However, the validity of these quantities as indices of transition-state symmetry has recently been seriously questioned.[2,3] These doubts have mainly developed after the observation of anomalous Brønsted coefficients (see Ref. 2 and references cited there).

The compounds hitherto found to give rise to such deviations are all nitro compounds, and anomalies are observed when substituent changes are made in the substrate instead of in the catalysing base.[3] Brønsted β's less than zero as well as greater than unity are observed. Bordwell and Boyle [4] have suggested a two-step mechanism for the deprotonation of nitroalkanes to rationalize these effects.

For cyanocarbon acids, which in general are thought to behave as almost normal acids in the Eigen sense,[5,6] no anomalies have hitherto been reported, and we have now extended our investigations of proton transfers from cyanocarbon acids with an investigation of the base-catalyzed recemization of 2-phenylpropionitrile (I). In an earlier investigation,[7] a very weak kinetic isotope effect was found for the racemization of 2-methyl-3-phenylpropionitrile (II) in methanol. A Brønsted β equal to unity within the error limits was also determined by use of an acidity-function approach.

The present substrate, 2-phenylpropionitrile (I), is interesting from the point of view that there exists a possibility of delocalizing the negative charge into the phenyl group in the

* For Part V of this series, see Bergman, N.-Å. and Melander, L. *Acta Chem. Scand. A 28* (1974) 747.

transition state and in the resulting carbanion, a possibility which is missing in II. The consequences of this for the magnitude and variation of the kinetic primary isotope effect seemed to be worth investigating.

EXPERIMENTAL

(±)-2-Phenylpropionitrile was synthesized according to Wideqvist,[8] b.p. 66–67 °C/0.27 kPa. Lit [8] b.p. 99.8 °C/1.06 kPa.

(±)-2-Phenylpropionic acid was prepared by hydrolysis of the nitrile to the acid. In a typical run, 29.5 g (225 mmol) of 2-phenylpropionitrile, 30 ml of water, 30 ml of glacial acetic acid and 30 ml of concentrated sulfuric acid were refluxed for 1 h. The mixture was poured onto ice. The oil layer was separated off and the aqueous layer was extracted with ether. The organic layers were combined and washed with water. The ether solution was dried over anhydrous magnesium sulfate. The solvent was evaporated and the residue gave upon distillation *in vacuo* 27.4 g (81 %) of the acid, b.p. 137–138 °C/0.87 kPa.

(−)-2-Phenylpropionic acid was obtained according to Pettersson.[9] The specific rotation of the acid was $[\alpha]_D^{25}$ −76.5° (*c* 0.0177, ethanol), lit.[10] $[\alpha]_D^{25}$ −79.1° (*c* 0.0157, ethanol).

(+)-2-Phenylpropionic acid was also obtained according to Pettersson.[9] The specific rotation of the acid was $[\alpha]_D^{25}$ +75.5° (*c* 0.0849, ethanol). lit.[10] $[\alpha]_D^{25}$ +79.0° (*c* 0.0167, ethanol).

(−)-2-Phenylpropionamide and (+)-2-phenylpropionamide were prepared according to Pettersson.[9]

(+)-2-Phenylpropionitrile. The optically active nitriles used in this investigation were all prepared by dehydration of the corresponding amide, and in a typical run 3.7 g (24.8 mmol) of the (−)-2-phenylpropionamide and 8 g (56.35 mmol) of P_2O_5 were mixed and heated *in vacuo*. The optically active nitrile distilled at 85 °C/0.4 kPa and the yield was 2.1 g (64.6 %). The specific rotation was $[\alpha]_{436}^{25}$ +39.7° (*c* 0.035, methanol).

(−)-2-Phenylpropionitrile. The nitrile was prepared in the same way as described for (+)-2-phenylpropionitrile. The specific rotation was $[\alpha]_{436}^{25}$ −43.4° (*c* 0.025, methanol).

(±)-2-Phenylpropionitrile-2-d was prepared according to Cram and Uyeda.[11] Deuterated nitrile was hydrolyzed to acid in the same way as the undeuterated nitrile.

The *(+)-* and *(−)-2-phenylpropionic-2-d acids* were obtained by resolution[9] of the racemic deuterated acid. The specific rotations were $[\alpha]_D^{25}$ +75.1° (*c* 0.0225, ethanol) and −75.3° (*c* 0.0278, ethanol), respectively.

(+)-2-Phenylpropionitrile-2-d and *(−)-2-phenylpropionitrile-2-d* were prepared in the same way as described above for the undeuterated optically active nitriles. The specific rotations were $[\alpha]_{436}^{25}$ +42.6° (*c* 0.0059, methanol) and −42.7° (*c* 0.0508, methanol), respectively.

Purity of optically active nitriles. The products were all pure according to gas-liquid chromatography. The analyses were performed on a Perkin-Elmer 900 gas chromatograph fitted with a flame ionization detector. The outer diameter of the column used was 3 mm and the length 2 m. The stationary phase was 3 % of SE-30 silicon gum rubber on Gaschrom Q 100–120 mesh and the flow rate of nitrogen was 30 ml/min.

IR analysis of the neat liquid in a sodium chloride cell on a Beckmann IR 9 instrument showed a strong absorption at 2240 cm^{-1}.

^1H NMR analysis on a Varian A 60 (CCl_4): δ 7.25 (5 H, s), 3.80 (1 H, q), 1.50 (3 H, d).

Mass spectrometry on an AEI MS 902 instrument using the glass heated inlet system showed 95 % D in position 2 in the deuterated nitriles. The following conditions were used: sample temp. 100 °C, source temp. 200–300 °C, electron energy 10 eV, accelerating voltage 8 kV and emission 20 μA.

Methanol. Commercial methanol with a water content less than 0.05 % (Merck Methanol zur Analyse) was dried in the following way. Clean dry magnesium turnings were warmed with methanol in a flask until all of the magnesium had been converted into methoxide. More methanol was added, and after refluxing the methanol was distilled into a receiver equipped with a syringe needle which made it possible to transfer the methanol to a glass bottle closed with a rubber plug and metal closure. The entire procedure was performed under an atmosphere of nitrogen and in dried glassware. The bottles with purified methanol were stored in a desiccator.

In later kinetic runs commercial methanol (May & Baker Methanol anhydrous) was used without further purification. The water content in each batch of the methanol was determined by gas chromatography [12,13] using a Perkin-Elmer F11 instrument fitted with a hot wire detector. The outer diameter of the column used was 9 mm and the length 2 m. The column was filled with Porapak Q: column temp. 120 °C, carrier gas helium, flow rate 50 ml/min. The water content in the methanol was always less than 0.033 % by weight.

Dimethyl sulfoxide (DMSO) was dried over Linde type 4 A molecular sieves, distilled under reduced pressure and stored under an atmosphere of nitrogen.

Sodium-methoxide. A 20–100 mM stock solution of sodium methoxide was made by dissolving clean sodium metal in the above methanol under an atmosphere of dry nitrogen. The solution was titrated using a Radiometer Titrigraph, diluted with dry methanol and used for the kinetic runs. The error in the base concentration was less than 3 %. Titration of some of the solutions before and after the

kinetic run gave good agreement, within the experimental error.

All kinetic runs were performed on a Zeiss Old 5 digital polarimeter using the wave length 436 nm and with an accuracy in the reading of ±0.001°. The reactions were performed in a thermostated 10 cm polarimeter cell, equipped with vacuum windows. The temperature measurements were made, just outside and after the cell, in the circulating water from the thermostat, using a calibrated thermistor connected to a FLUKE 8300 A digital voltmeter. The thermistor was calibrated against a Hewlett Packard 2801 A quartz thermometer to a precision of 0.1 °C and was capable of measuring temperature changes of less than 0.002 °C. The temperature was maintained by a Hetofrig cooling bath, type CB6, together with a Hetotherm Ultrathermostat O2 Pt 623 UO. The temperature fluctuation within each run was less than 0.1 °C at 0 °C and less than 0.02 °C at higher temperatures. A Compucorp 425 G Scientist calculator, interfaced on line with the polarimeter and the voltmeter, collected polarimeter data, temperatures, and times, and evaluated rate constants using a least-squares program.

In a typical run, 0.023 g (0.176 mmol) of the nitrile and 1 ml of the pre-thermostated sodium methoxide solution were mixed and added to the polarimeter cell by means of a syringe. In the case of the fastest reactions, the polarimeter cell was first charged with methoxide solution by means of a syringe. Using another syringe, charged with a proper amount of the nitrile, the methoxide solution was withdrawn from the cell. The syringe was rapidly shaken and the mixture added to the cell. The reactions were followed for 2 – 3 half-lives and readings were made every two seconds.

Both the (+)- and (−)-form of the nitriles was used, and no difference was found between the racemization rates of the two forms.

Some of the kinetic runs were examined to completion, and no residual optical activity could be detected. After some of the kinetic runs the reaction mixture from the polarimeter cell was poured into aqueous HCl solution. Extraction with pure pentane and analysis of the pentane layer with gas chromatography showed no other products than the nitrile.

The base concentrations were corrected to the kinetic temperatures using published data on the density of methanol at different temperatures.[14]

RESULTS

Table 1 gives the results of a comparison between the racemization rate and the exchange rate for the nitrile in methanol solution. Deuterated optically active nitrile was allowed to react for about 10 min. The reaction was quenched with aqueous HCl solution and the nitrile isolated and analysed for the deuterium content by mass spectrometry and for the optical activity by polarimetry. Within the experimental errors the racemization rate is the same as the exchange rate. Thus the rate of racemization is a true measure of the rate of the proton transfer in methanol, and the same should be still more likely to hold in the mixtures containing DMSO.

Table 1. Comparison between racemization and exchange rates for (+)-2-phenylpropionitrile-2-*d* ($[\alpha]_{436}^{25}$ initially +43.48°, deuterium content initially 95 %) in methanol with sodium methoxide (0.012 M) as base. Reaction time about 10 min. Concentration of substrate: 0.06 – 0.15 M. Temperature: 25 °C.

$[\alpha]_{436}^{25}$ [a]	Racem. %	Deuterium content in substrate [b] %	Exch. %	Racem./ Exch.
23.17	47	52	45	1.04
25.51	41	54	43	0.95
24.80	43	55	42	1.02
25.42	42	58	39	1.08
27.35	37	59	38	0.97
			Mean value	1.01

[a] Obtained from recovered (+)-2-phenylpropionitrile-2-*d*, dissolved in methanol. [b] The initial and final deuterium contents of 2-phenylpropionitrile-2-*d* were determined by mass spectrometry. See Experimental.

The results from the measurements of the racemization rate for the nitrile in methanol using different base concentrations are shown in Table 2. Two different temperatures have been used in order to cover a base-concentration range as large as possible. The second-order rate constant (k_2), obtained by dividing the racemization rate constant (pseudo first-order rate constant) by the corresponding base concentration, is given. A small increase in k_2 with increasing base concentration is observed, and a plot of the logarithm of the pseudo first-order rate constant of the racemization *versus* the logarithm of the base concentration gives a straight line with a slope of 1.14 ± 0.02 (25.02 °C) and 1.05 ± 0.01 (0.05 °C), *i.e.*, the reaction order in methoxide ion deter-

Table 2. Racemization rates for 2-phenylpropionitrile in methanol with sodium methoxide as base. Concentration of substrate: 0.15 – 0.18 M.

[Base]/ mM	k_{obs}/ 10^{-4} s^{-1}	k_2/ 10^{-2} M^{-1} s^{-1} [a]
t = 25.02 °C		
10.8	25.0[b]	23.1
8.3	19.1[b]	23.0
5.3	11.4[b]	21.5
5.3[c]	11.3[b]	21.3
5.3[d]	11.4[b]	21.5
2.8	5.50[b]	19.6
t = 0.05 °C		
103	15.6[e]	1.51
68	10.2[e]	1.50
35	4.92[e]	1.41
35[f]	4.88[e]	1.39
17.3	2.36[e]	1.36

[a] Second-order rate constant. Error limits are less than 3 % including uncertainty in the base concentration. [b] Mean value obtained from two or three runs. The maximum deviation from the quoted mean values is less than 1.5 %. Standard deviation in each run is less than 0.5 %. [c] 0.24 mol % water added to the solution. [d] 1.10 mol % water added to the solution. [e] Obtained from only one run. Standard deviation in this run is less than 0.5 %. [f] Solution was 65 mM in NaCl.

mined in this way is somewhat above unity. This observation can be rationalized by assuming that the methoxide probably exists partly as ion-pairs in methanol at the concentrations concerned and that the ion-pairs is a more effective catalyst than the free ion.

Evidence for ion-pair formation in methanol solutions at very low base concentrations (0.4 – 6.7 mM) has also been given by Leffek and Suszka,[15] but their conclusion was that the reactivity of the ion pair was much less than that of the free methoxide ion in the combination of sodium methoxide with 4,4'-bis(dimethylamino)triphenylmethyl tetrafluoroborate in methanol.

On the contrary, Cram *et al.*[16] assumed that the base is completely dissociated at low concentrations (5.5 – 37.6 mM) and that the methoxide ion is the active catalytic species in the racemization of (–)-2-phenylbutyronitrile in methanol.

Evidently the idea put forward in the present investigation should be investigated further.

Changing the ionic strength of the reaction solution by the addition of NaCl has no significant influence on the racemization rate, as can be seen in Table 2.

Addition of small amounts of water to the

Table 3. The primary kinetic isotope effect in the racemization of 2-phenylpropionitrile in mixtures of DMSO and methanol with sodium methoxide as base. Concentration of the substrate: 0.15 – 0.18 M. Temp. 10.0 ± 0.1 °C; difference between any runs maximum 0.01 °C (*cf.* EXPERIMENTAL).

[DMSO]/ mol %	[Base]/ mM	Substrate[a]	k_2/ 10^{-2} M^{-1} s^{-1} [b]	k_D/k_H
		D	1.53 ± 0.05	
0	5.8	H	4.1 ± 0.1	0.37 ± 0.02
		D	1.69 ± 0.05	
0	50	H	4.6 ± 0.1	0.37 ± 0.02
		D	3.5 ± 0.1	
8.9	5.3	H	10.6 ± 0.3	0.33 ± 0.02
		D	14.3 ± 0.4	
21.6	5.3	H	48 ± 1	0.30 ± 0.02
		D	74 ± 2	
38.0	5.3	H	411 ± 13	0.18 ± 0.01

[a] H = 2-phenylpropionitrile, D = 2-phenylpropionitrile-2-*d*. [b] Second-order rate constant. Weighted average from at least two runs.

sodium methoxide solution has likewise no significant effect on the reaction rate (Table 2).

The racemization rate and k_D/k_H at different concentrations of DMSO in the solvent are given in Table 3.

The observed increase in the second-order rate constant in the experiments using different base concentrations indicates that a nearly constant base concentration is necessary if different experiments are to be compared. In any case, the isotopic nitriles in the same solvent mixture should be racemized with the same base concentration to minimize the errors in k_D/k_H. Hence, most of the runs in Table 3 refer to almost the same base concentration. However, a nearly tenfold increase in the base concentration in methanol has no measurable effect on k_D/k_H.

The rate constants for the heavy nitrile were obtained by using 2-phenylpropionitrile-2-*d* with a deuterium content at position 2 of 95 %. No correction for the protium content has been applied.

The large increase in the racemization rate with increasing concentration of DMSO in the solutions made measurements impossible in mixtures with more than 38 mol % DMSO. Thus, a reaction with a half-life of about 30 s was obtained at 10 °C in a solvent with 38 % DMSO and 62 % methanol. This is close to the lower limit for measurable rates with the present method. The increased viscosity of DMSO – methanol solutions complicated measurements at lower temperatures.

DISCUSSION

As can be seen from Table 3 the isotope effect is rather weak in methanol. The strength of the isotope effect increases rather rapidly with increasing proportion of DMSO in the solution. In 38 mol % DMSO an almost "normal" isotope effect is obtained. We have not been able to demonstrate the existence of a possible maximum in the strength of the isotope effect owing to the difficulty of measuring racemization rates for the present substrate in media still richer in DMSO.

The rather rapid strengthening of the isotope effect observed in the present investigation differs from what was obtained earlier with 2-methyl-3-phenylpropionitrile.[7] A comparison

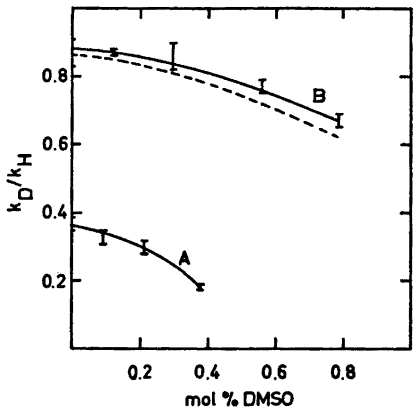

Fig. 1. Comparison between k_D/k_H obtained for 2-phenylpropionitrile at 10 °C (A) and for 2-methyl-3-phenylpropionitrile at 60 °C (B). Dashed curve indicates the effect of a temperature correction (assuming a pure zero-point-energy isotope effect) to 10 °C applied to curve B.

of the two investigations is made in Fig. 1. As can be seen, k_D/k_H for 2-methyl-3-phenylpropionitrile is closer to unity and varies considerably less than that for 2-phenylpropionitrile in the same composition range for the solvent.

Taking the magnitude of k_D/k_H as a measure of the symmetry of the transition state and ignoring a possible contribution from tunnelling, the results mean that the proton abstraction from 2-phenylpropionitrile by methoxide ion in 38 % DMSO – 62 % methanol is likely to have a nearly symmetrical transition state.

We have also tried to determine a Brønsted's β for this reaction. Although sometimes questioned as a reliable measure of the transition-state structure, it would be of interest to compare this magnitude with the β-value obtained for 2-methyl-3-phenylpropionitrile.[7]

The method of determining β when the free-energy change for the reaction is controlled by a solvent variation was devised by Bell and Cox,[17] and later used in determining β for the racemization of 2-methyl-3-phenylpropionitrile.[7]

The result for 2-phenylpropionitrile can be seen in Fig. 2. The points are more likely to be situated on a curved line than on an expected straight line, which was the case for 2-methyl-3-phenylpropionitrile. The best straight line

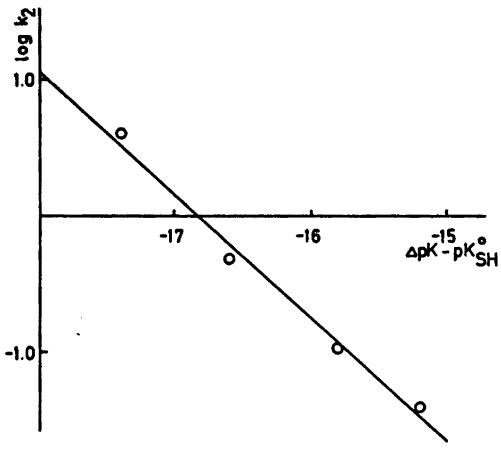

Fig. 2. Plot of the logarithm of the second-order rate constant for the racemization of 2-phenylpropionitrile in mixtures of methanol and DMSO at 10 °C *versus* $\Delta pK - pK°_{SH}$, obtained as in Ref. 7.

for the present results found by a least-squares treatment gives $\beta = 0.9$. This is a rather high value considering the strength of the kinetic isotope effect, and this together with the observed trend toward a curvature probably indicates that the underlying assumption in this treatment fails, *i.e.*, that the substrate (2-phenylpropionitrile) does not behave as the substituted anilines used in establishing the H_- acidity function.

The acidity-function method of determining Brønsted's β used here has recently been claimed to give abnormal β-values.[18] The addition of DMSO to a protic solvent is suggested[18] to raise the activity of the catalysing ion as well as the carbanion resulting from the carbon acid by similar amounts relative to the larger and perhaps also more polarisable transition-state anion. The result will be a large increase in the rate of the reaction when DMSO is added, but not necessarily a large change in ΔpK (difference in pK_a of the substrate and the conjugate acid of the catalysing base). This has been shown to be the case in, for instance, acetate-catalysed proton transfers from nitroparaffins.[18] The catalysing ion (acetate ion) and the nitronate ion have rather similar structures, and it is difficult to say what the effect would be if the resulting ion is a carbanion with a more or less localized charge, a[8] with our compound. In any case it is evident that a reliable simple relationship between rate and equilibrium is difficult to obtain in this way.

The only safe way to test the validity of the acidity-function method is to directly determine the pK's concerned. Unfortunately, such a determination has not been made for the present case, but the following estimates could be made.

The use of the acidity-function method to determine ΔpK is founded on the assumption that the substrate (in the present case 2-phenylpropionitrile) behaves as the indicators used to establish the H-scale. This also means that no dramatic change in the pK of the nitrile should be observed when the medium is changed from pure methanol to DMSO.[19] Assuming a constant pK of 2-phenylpropionitrile between 0 and 38 mol % DMSO means that the whole change in $\Delta pK - pK°_{SH}$ (2.2 units according to Fig. 2) is ascribed to an increase in pK for methanol. Such an increase does not seem unlikely in view of the fact that pK for methanol is known [20] to increase from 18.3 in methanol to 27.0 in pure DMSO.

However, the assumption of a constant pK for the nitrile, being a consequence of an assumed similarity to certain Hammet bases, is worth some consideration.

It is known [20] that 9-cyanofluorene becomes more acidic by almost 6 pK units when the medium is changed from methanol to DMSO. 2-Phenylpropionitrile very much resembles 9-cyanofluorene with respect to the possibility of delocalizing the negative charge of the anion into the phenyl group. On structural grounds it seems probable therefore that 2-phenylpropionitrile will become more acidic when the DMSO content of the medium is increased. As an example, a decrease in pK for 2-phenylpropionitrile by some 2 units together with some 2 units increase in pK for methanol over the composition range 0 – 38 mol % DMSO would be sufficient to make $\beta = 0.5$. A somewhat less rapid decrease in pK for 2-phenylpropionitrile would correspond to a somewhat higher β, of course.

At the present stage, when the pK_a of 2-phenylpropionitrile in different mixtures of methanol and DMSO is unknown, it is impos-

sible to determine a definite value of β. It does not seem unlikely, however, that the true β could be reconcilable with the isotope-effect evidence concerning the symmetry of the transition state.

Acknowledgements. We wish to thank Professor Lars Melander for his interest in this work and for many useful suggestions during the preparation of the manuscript. Many thanks are due to Mr. W. Pimlott (Department of Medical Biochemistry, University of Göteborg) for technical aid in the determination of the mass spectra. Financial support from the Swedish Natural Science Research Council is gratefully acknowledged.

REFERENCES

1. Davies, M. H., Robinson, B. H. and Keeffe, J. R. *Annu. Rep. Progr. Chem. 70 A* (1973) 123.
2. Hanna, S. B., Jermini, C., Loewenschuss, H. and Zollinger, H. *J. Am. Chem. Soc. 96.* (1974) 7222.
3. Kresge, A. J. *Can. J. Chem. 52* (1974) 1897.
4. Bordwell, F. G. and Boyle, J. W., Jr. *J. Am. Chem. Soc. 97* (1975) 3447.
5. Margolin, Z. and Long, F. A. *J. Am. Chem. Soc. 95* (1973) 2757.
6. Eigen, M. *Angew. Chem. 75* (1963) 489.
7. Melander, L. and Bergman, N.-Å. *Acta Chem. Scand. 25* (1971) 2264.
8. Wideqvist, S. *Sv. Kem. Tidskr. 55* (1943) 125.
9. Pettersson, K. *Ark. Kemi 10* (1956) 283.
10. Fredga, A. *Ark. Kemi 7* (1954) 241.
11. Cram, D. J. and Uyeda, R. T. *J. Am. Chem. Soc. 86* (1964) 5466.
12. Hogan, J. M., Engel, R. A. and Stevenson, H. F. *Anal. Chem. 42* (1970) 249.
13. Sellers, P. *Acta Chem. Scand. 25* (1971) 2295.
14. Timmermans, J. *Physico-Chemical Constants of Pure Organic Compounds*, McGraw-Hill, New York 1962, pp. 204–227.
15. Leffek, K. T. and Suszka, A. *Can J. Chem. 53* (1975) 1537.
16. Cram, D. J., Rickborn, B., Kingsbury, C. A. and Haberfield, P. *J. Am. Chem. Soc. 83* (1961) 3678.
17. Bell, R. P. and Cox, B. G. *J. Chem. Soc. B* (1970) 194.
18. Cox, B. G. and Gibson, A. *Chem. Commun.* (1974) 638.
19. Bowden, K. *Chem. Rev. 66* (1966) 119.
20. Ritchie, C. D. In Coetzee, J. F. and Ritchie, C. D., Eds., *Solute-Solvent Interactions*, Marcel Dekker, New York and London 1969, Chapter 4.

Received January 13, 1976.

Acta Chemica Scandinavica A 30 (1976) 418—420

A Study of Magnetic Properties of $V_xMo_{2-x}O_5$ ($1 \leq x \leq 1.14$)

B. BLOM and M. NYGREN

Department of Inorganic Chemistry, Arrhenius Laboratory, University of Stockholm, S-104 05 Stockholm, Sweden

Magnetic susceptibility measurements and X-ray powder analysis show that vanadium can substitute for molybdenum in $VOMoO_4$ according to the formula $V_{2-x}^{4+}V_{2(x-1)}^{5+}Mo_{2-x}^{6+}O_5$, $1 \leq x \leq 1.14$. All samples studied exhibit antiferromagnetic behaviour with Néel temperatures around 110 K.

Eick and Kihlborg [1] determined the crystal structure of $VOMoO_4$ and found it isostructural with $MoOPO_4$.[2] The structure may be described as consisting of strings of cornersharing VO_6-octahedra running parallel to the c axis of the tetragonal unit cell. The chains are coupled together by MoO_4-tetrahedra so that each tetrahedron joins four different chains of octahedra. The oxygen atoms surrounding a vanadium atom form an almost regular octahedron. The vanadium atom is displaced from the centre of the octahedron, which gives rise to a short vanadium-oxygen distance (1.677 Å).

The existence of a homogeneity range in the system $V_xMo_{2-x}O_5$ was demonstrated by Eick and Kihlborg [1] who suggested that x may differ from 1 by a few percent, at most. Later Darriet *et al.*[3] determined the homogeneity range to be $1 \leq x \leq 1.14$.

The present investigation of the magnetic properties of $V_xMo_{2-x}O_5$ has been conducted within a research program intended to elucidate the physical properties of $AOBO_4$ compounds.

EXPERIMENTAL

The starting materials were MoO_3 (Mallinckrodt, Anal. Reag.) and V_2O_5 (Fisher, *p.a.*). V_2O_3 and MoO_2 were prepared by hydrogen reduction of V_2O_5 at 1175 K and of MoO_3 at 725 K. The products were characterized by their X-ray powder patterns.

Samples of gross composition $V_xMo_{2-x}O_5$ with $0.95 \leq x \leq 1.20$ were prepared by heating appropriate mixtures of the oxides for six days in evacuated silica tubes at a temperature of 875 K. X-ray powder patterns of the specimens were recorded in a Guinier-Hägg focusing camera with $CuK\alpha_1$ radiation ($\lambda = 1.54051$ Å) and with KCl ($a = 6.2919$ Å) as an internal standard.

The magnetic susceptibility measurements were performed according to the Faraday method with a Cahn R. G. electrobalance. $HgCo(SCN)_4$ was used as standard.[4,5] The measurements were made in the temperature range 78 – 700 K with a heating rate of 2 – 4 degrees per minute. One of the samples ($VOMoO_4$) was also studied in the range 4.2 – 120 K. The apparatus used in this experiment also applied

Table 1. A summary of experimental data.

x in $V_xMo_{2-x}O_5$	Cell parameters (Å) at 298 K		C	θ	μ_{eff} per vanadium(IV)
	a	c			
1.00	6.6087(11)	4.2634(8)	0.415	−235	1.82
1.03	6.6060(8)	4.2648(5)	0.436	−235	1.90
1.05	6.5962(12)	4.2675(10)	0.414	−150	1.87
1.07	6.6033(10)	4.2666(8)	0.400	−220	1.85
1.10	6.5917(9)	4.2698(7)	0.371	−200	1.82
1.14	6.5875(7)	4.2709(5)	0.386	−235	1.90

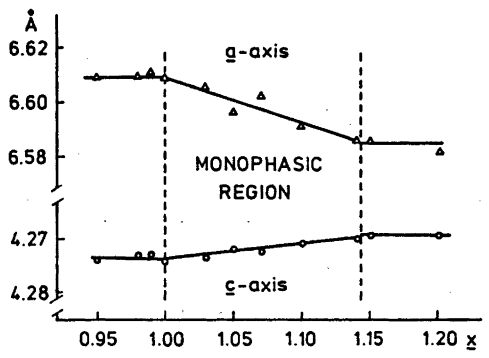

Fig. 1. Cell parameters for $V_xMo_{2-x}O_5$.

the Faraday method but the susceptibility values were obtained from an absolute determination of the field gradient. The two series of measurements yielded susceptibility values in the overlapping temperature region which were in agreement with each other within ±0.5 %.

RESULTS AND DISCUSSION

The X-ray photographs showed monophasic powder patterns for $1 \leq x \leq 1.14$. The cell parameters are given in Table 1 and Fig. 1. The *c* axis exhibits a small increase while the *a* axis decreases for increasing x values. Our findings are in good agreement with previously reported data for $VOMoO_4$ and $V_{1.10}Mo_{0.90}O_5$.[1,3]

A representative plot of the inverse susceptibility *versus* the temperature is given in Fig. 2 for the composition $VOMoO_4$. The susceptibility exhibits a maximum value at 110 K (*viz.* a Néel point) and obeys the Curie-Weiss law $[\chi_M = C/(T-\theta)]$ for temperatures above 225 K. The Curie constant, C, was calculated from the slope of the straight line shown in Fig. 2. The relation $\mu_{V^{4+}} = 2.83[C/(2-x)]^{\frac{1}{2}}$ yielded a Bohr magneton number of 1.82 for $VOMoO_4$; compared with the spin only value of 1.73 for V^{4+} this confirms that the vanadium atoms are tetravalent and, consequently, the molybdenum atoms hexavalent. The increase of the susceptibility below 10 K is probably due to impurities. A summary of the magnetic susceptibility data is given in Table 1.

Doyle *et al.*[6] have reported the molar susceptibility of $VOMoO_4$ at 293 K to be 7.67×10^{-4} emu per mol which compares favourably with our value 7.94×10^{-4}. (The conversion factor to SI units is $4\pi \times 10^{-6}$.)

When x becomes greater than 1 an amount of $x-1$ pentavalent vanadium atoms per formula unit will replace hexavalent molybdenum atoms in the tetrahedra. To keep the crystal electrically neutral $x-1$ vanadium

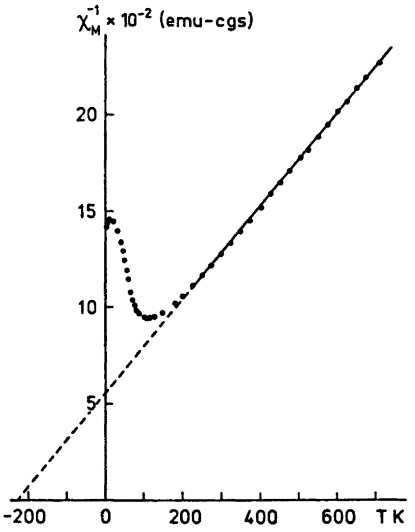

Fig. 2. The inverse molar susceptibility plotted *versus* the temperature for $V_xMo_{2-x}O_5$ with $x = 1.00$ ($VOMoO_4$).

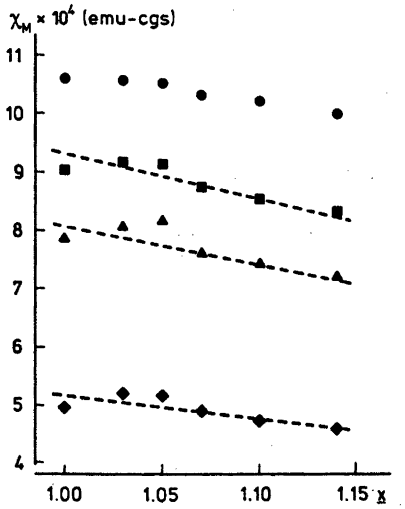

Fig. 3. The molar susceptibility plotted *versus* x in $V_xMo_{2-x}O_5$ at the Néel temperature (●), 225 K (■), 298 K (▲) and 600 K (◆). The dotted lines are calculated values with $\theta = -215$ K and $\mu_{V^{4+}} = 1.73$ in eqn. 1.

atoms within the octahedra will increase their oxidation number to plus five. This substitution mechanism would cause a decrease in the Curie constant with increasing x values while the number of Bohr magnetons per mol tetravalent vanadium atom should be constant. This is in satisfactory agreement with our observations (*cf.* Table 1).

The susceptibility should decrease with increasing x for a fixed temperature according to the formula

$$\chi_M = \frac{2\mu_{V^{4+}}(1-x)}{2.83^2(T-\theta)} \quad (1)$$

In Fig. 3 χ_M is plotted *versus* x for three temperatures. It is evident that a fairly linear relationship exists between χ_M and x. The dotted lines are obtained from equation 1 with θ equal to the mean value of those given in Table 1 and $\mu_{V^{4+}}$ equal to the spin only value for V^{4+} (1.73).

All samples showed antiferromagnetic behaviour with Néel temperatures around 110 K. The susceptibility at the Néel temperature varied between 1.06×10^{-3} and 1.00×10^{-3} emu per mol within the homogeneity range as shown in Fig. 3.

The magnetic susceptibility data thus show that vanadium substitutes for molybdenum in $VOMoO_4$ according to the formula V_{2-x}^{4+}-$V_{2(x-1)}^{5+}Mo_{2-x}^{6+}O_6$ over the compositional region $1 \leq x \leq 1.14$.

This result evidently confirms the mechanism of substitution put forward by Eick and Kihlborg [1] from considerations of the variation of the cell parameters. Our findings, however, do not support the possibility that x might assume values below 1, *i.e.* that molybdenum might substitute for vanadium in the octahedra.

Acknowledgements. The authors wish to thank Professor Arne Magnéli and Dr. Lars Kihlborg for their advice in connection with this work. Drs. S. Humble and K. Svensson of the Department of Solid State Physics, Royal Institute of Technology in Stockholm, are gratefully thanked for their kind assistance with the susceptibility measurements in the temperature region 4.2 – 90 K. This investigation has been supported by the Swedish Natural Science Research Council.

REFERENCES

1. Eick, H. and Kihlborg, L. *Acta Chem. Scand.* *20* (1966) 722.
2. Kierkegaard, P. and Westerlund, M. *Acta Chem. Scand.* *18* (1964) 2217.
3. Darriet, J., Galy, J. and Hagenmuller, P. *J. Solid State Chem.* *3* (1971) 596.
4. Kizhaev, S. A., Usachev, P. V. and Yudin, V. M. *Fiz. Tverd. Tela (Leningrad)* *13* (1971) 2829.
5. Räde, H.-St. *J. Phys. Chem.* *77* (1973) 424.
6. Doyle, W. P., McGuire, G. and Clark, G. M. *J. Inorg. Nucl. Chem.* *28* (1966) 1185.

Received December 19, 1975.

Acta Chemica Scandinavica A 30 (1976) 421—424

Isotope Effects in Proton-transfer Reactions. VII.* Deuterium Solvent Isotope Effect and Primary Kinetic Isotope Effect on the Racemization of 2-Phenylpropionitrile in Methanol/Methanol-*O*-*d*

NILS-ÅKE BERGMAN and INGER KÄLLSSON

Department of Organic Chemistry, University of Göteborg and Chalmers University of Technology, Fack, S-402 20 Göteborg, Sweden

The deuterium solvent isotope effect in mixtures of methanol and methanol-*O*-*d* has been determined for the methoxide-catalysed racemization of optically active 2-phenylpropionitrile at 25 °C. The limiting value of the ratio of the rate constants is $k_{MeOD}/k_{MeOH} = 2.10 \pm 0.03$. Application of the fractionation-factor theory leads to some discrepancy from the accepted solvation number of the methoxide ion. The primary kinetic isotope effect in different mixtures of methanol and methanol-*O*-*d* has been found to be constant, $k_D/k_H = 0.41 \pm 0.04$.

Solvent isotope effects are often considered useful in the investigation of reaction mechanisms.[1,2] In particular the information obtained from experiments in mixtures of light and heavy solvents has been considered to be of value in such studies.[3] A simple correlation between the solvent isotope effect and the involvement of solvent in the transition state has, however, been questioned.[3,4]

A rather strong solvent isotope effect was found in a recent investigation of the racemization of 2-methyl-3-phenylpropionitrile.[5] The limiting value of the ratio of the rate constants was $k_{CH_3OD}/k_{CH_3OH} = 2.11 \pm 0.05$ at 60 °C. The β-value derived from this ratio was somewhat low compared to the previously determined β which was obtained from a Brønsted plot based on an acidity function for methanol-dimethyl sulfoxide solutions. (The latter had been established by means of substituted anilines as indicator bases.) This together with some collected literature data from other reactions strongly emphasized the apparent absence of a simple relationship between the solvent isotope effect and the transition-state symmetry.

In the present work we have investigated the variation of the kinetic solvent isotope effect and the primary kinetic isotope effect on the racemization of 2-phenylpropionitrile in mixtures of methanol and methanol-*O*-*d*. A comparison with the related results for 2-methyl-3-phenylpropionitrile [5] is made.

EXPERIMENTAL

2-Phenylpropionitrile. The preparation of optically active and isotopic nitriles has been described previously.[6] Both enantiomers of the nitriles were used.

Methanol and methanol-O-d. The purification of the methanol and the determination of the water content were carried out as before.[6] Commercial methanol-*O*-*d* (CIBA) with an isotopic purity > 99 % D was used without further purification.

Kinetic runs. The preparation of solutions and the kinetic runs were carried out as previously described.[6] In order to minimize the inter-experimental errors, an effort was made to evaluate the rate constants for the light and heavy nitrile from the same run using 2-phenylpropionitrile with a deuterium content at position 2 of about 50 %. The rate constants were calculated using the program PROGA-EXP.[7] Unfortunately the uncertainty in the rate constants obtained for the light nitrile was too large. Hence these rate constants were obtained from runs with undeuterated nitrile.

* For Part VI of this series, see Ref. 6.

RESULTS

Table 1 shows the kinetic solvent isotope effect in mixtures of methanol and methanol-*O-d*. The k_n values for $n = 0.00$, 0.20 0.40, 0.60, and 0.80 were obtained in solutions prepared from the same stock solution of sodium methoxide. Another stock solution prepared from methanol-*O-d* was used for $n = 0.99$. A small error in the determination of the stock base concentration could thus have caused an extra error in the $k_{0.99}/k_0$ ratio. To check this, one value in 80 % methanol/20 % methanol-*O-d* was measured using the latter stock solution. The values of k obtained by means of the two different solutions showed no significant difference.

The limiting kinetic solvent isotope effect has been determined by means of a polynomial expression, which represents the least-squares fit of the experimental values. This polynomial is: $k_n/k_0 = 1.00 + 0.72n + 0.38n^2$, giving $k_1/k_0 = 2.10 \pm 0.03$ when the accuracy of the determination in 99 mol % methanol-*O-d* is taken into account.

The primary kinetic isotope effect in methanol and in mixtures of methanol and methanol-*O-d* is shown in Table 2. As can be seen from the table, k_D/k_H is constant within the experimental errors.

Table 1. Kinetic solvent isotope effect on the racemization of 2-phenylpropionitrile in mixtures of methanol and methanol-*O-d*. Temperature: 25.15 ± 0.05 °C. Concentration of substrate: 0.16 – 0.18 M. n = mol fraction of methanol-*O-d*.

n	[Base]/ mM	k_n/ 10^{-1} M^{-1} s^{-1} [a]	k_n/k_0 [b]
0	4.0	2.17 ± 0.03	1.00 ± 0.02
0.199	4.0	2.46 ± 0.03	1.13 ± 0.02
0.199	5.1	2.42 [c]	
0.399	4.0	2.93 ± 0.05	1.35 ± 0.03
0.599	4.0	3.40 ± 0.03	1.57 ± 0.02
0.799	4.0	3.92 ± 0.02	1.81 ± 0.02
0.99	5.1	4.53 ± 0.03	2.09 ± 0.03

[a] k_n is the mean of the second-order rate constants from at least 3 runs. Error limits are standard deviations of the mean values. [b] k_n/k_0 is the ratio between the second-order rate constants obtained in a solvent with a fractional content n of methanol-*O-d* and in ordinary methanol, respectively. [c] Obtained from one kinetic run using the same stock solution of sodium methoxide as for $n = 0.99$, (*cf.* Results).

Table 2. Primary kinetic isotope effect on the racemization of 2-phenylpropionitrile in mixtures of methanol and methanol-*O-d*. Temperature: 25.14 ± 0.05 °C. Concentration of base: 4.0 mM. Concentration of substrate: 0.15 – 0.18 M.

Mol fraction of methanol-*O-d* (n)	k_D/k_H [a]
0.0	0.42 ± 0.02
0.199	0.41 ± 0.01
0.399	0.41 ± 0.03
0.599	0.42 ± 0.02
0.99	0.40 ± 0.02

[a] k_D obtained from kinetic runs with a deuterium content in the nitrile of about 50 %. See Experimental.

DISCUSSION

The interpretation of the experimental results obtained in the present investigation is given in terms of the fractionation theory.[8] According to this theory,

$$k_n/k_0 = (1 - n + n\phi^{\ddagger})^p/(1 - n + n\phi_{MeO})^m$$

where k_n is the rate constant for a reaction in a mixture of methanol-*O-d* and methanol with the fractional deuterium content n and k_0 is the rate constant for the corresponding reaction in methanol. $\phi^{\ddagger}$ and ϕ_{MeO} are the fractionation factors for the transition state and the methoxide ion, respectively. The number of methanol molecules solvating the methoxide ion and the transition state are denoted m and p, respectively.

The fractionation factor for the methoxide ion has been determined experimentally,[9,10] and we have started from the value $\phi_{MeO} = 0.73_6$ determined at 33.5 °C.[9] Assuming a pure zero-point energy effect, the value at 25.15 °C would be 0.73_0 which is the value used in the present paper.

In order to enable a comparison to be made, the results from our previous investigation on 2-methyl-3-phenylpropionitrile [5] are shown together with the results from the present in-

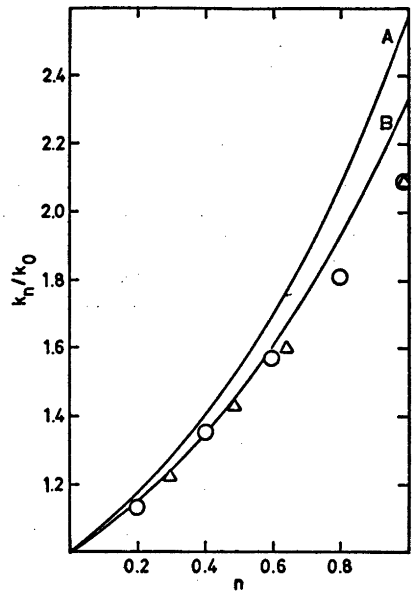

Fig. 1. Plot of k_n/k_0 *versus* n. ○: 2-phenylpropionitrile, experimental values at 25 °C. △: 2-methyl-3-phenylpropionitrile, experimental values at 60 °C. Solid curves: theoretical curves $k_n/k_0 = (1-n+n\phi_{MeO})^{-3}$ for $\phi_{MeO} = 0.73_0$ (A) and $\phi_{MeO} = 0.75_4$ (B).

vestigation in Fig. 1, where k_n/k_0 is plotted *versus* the fractional deuterium content in the solution. The solvent isotope effect is rather strong in both cases, but as the two investigations refer to two different temperatures, it should be somewhat stronger for 2-methyl-3-phenylpropionitrile than for 2-phenylpropionitrile at comparable temperatures.

In Fig. 1 two curves, A and B, are also drawn corresponding to $m = 3$ and $\phi^{\ddagger} = 1$ at 25 and 60 °C, respectively. These curves correspond to the assumption that the methoxide ion is solvated by three methanol molecules and that the transition state contains no methanol molecules with properties different from those in the bulk of the solution. In other words, the interaction between the transition state and the solvent would be negligible for a reaction which gives a curve like A or B. The only interaction with the solvent would be that of the methoxide ion. The experimental results for the two compounds, although referring to different temperatures, show a remarkable conformity, but the corresponding limiting curves deviate rather much due to the different values of ϕ_{MeO} at 25 °C (0.73_0) and 60 °C (0.75_4). From this comparison it can be concluded that the interaction between the solvent and the transition state is weaker in the reaction of 2-methyl-3-phenylpropionitrile than for 2-phenylpropionitrile. This idea of a rather weak interaction between the transition state and the solvent in the reaction of 2-methyl-3-phenylpropionitrile has previously been suggested.[5]

In the previous investigation of 2-methyl-3-phenylpropionitrile, $\phi^{\ddagger}$ (at 60 °C) was computed from k_1/k_0 for different combinations of m and p,[5] but in the present paper we have adopted a somewhat different method and applied it to the experimental data obtained with both nitriles.

The expression for k_n/k_0 can be transformed into:

$$[(1-n+n\phi_{MeO})^m k_n/k_0]^{1/p} = 1+n(\phi^{\ddagger}-1)$$

As we know ϕ_{MeO}, we are able to calculate the left-hand member for each experimental k_n/k_0 value and each set of m and p and plot it *versus* n. The best straight line through the points gives $\phi^{\ddagger}$. The results for some combinations of m and p are given in Table 3 together with the correlation coefficients obtained from the least-squares treatment.

Table 3. Transition-state fractionation factors $\phi^{\ddagger}$ for different numbers of methanol molecules solvating the methoxide ion (m) and the transition state (p). Numbers in italics are the correlation coefficients obtained from the least-squares treatment. I denotes 2-phenylpropionitrile, II 2-methyl-3-phenylpropionitrile. (Primary data for the latter have been taken from Ref. 5.)

	$m=1$		$m=2$		$m=3$	
	I	II	I	II	I	II
$p=1$						
	1.549	1.592	1.136	1.202	0.831	0.907
	0.998	*0.997*	*0.954*	*0.994*	*0.967*	*0.951*
$p=2$						
	1.246	1.262	1.066	1.097	0.911	0.953
	0.998	*0.999*	*0.953*	*0.993*	*0.965*	*0.949*
$p=3$						
	1.158	1.168	1.044	1.063	0.940	0.968
	0.998	*0.999*	*0.953*	*0.993*	*0.964*	*0.949*

It has been shown in other investigations [9a,b,10] that $m=3$ is a very reasonable assumption. We have thus to confine ourselves first-hand to $m=3$ and different values of p. As can be seen in Table 3, the fit is rather poor (to judge from the correlation coefficient) for at least 2-methyl-3-phenylpropionitrile independently of the value of p. A slightly better fit is obtained for 2-phenylpropionitrile. The reverse is true for $m=2$ but for both compounds the fit becomes best with $m=1$. However, a value of m less than 3 results in $\phi^{\ddagger} > 1$ which is somewhat difficult to interpret as we expect $\phi^{\ddagger}$ to lie between the value of ϕ_{MeO} and 1.

Fractionation factors greater than unity have been called upon recently to explain experimental evidence in amide methanolysis.[11] A fractionation factor $\phi^{\ddagger} = 1.2$ for the methanol molecules in the solvation shell of the transition state was found to be consistent with the experimental values. The methanol molecules in the solvation shell were thought to be trapped in a "gas-like" state during the existence of the transition state.

Due to the rather limited experimental data in the present investigation and also to the demand for very high accuracy of the data it is not easy to decide whether the present results could be explained in such terms. On the other hand, a definite discrepancy seems to exist between the results obtained and the predictions from a conventional application of the fractionation-factor theory. The deviations seem to be somewhat larger for 2-phenylpropionitrile. Whether the difference between the two carbon acids is caused by their different ability of delocalizing the developing negative charge in the transition state is a question which must be further investigated.

Provided that the number of methanol molecules solvating the transition state is the same for both compounds, the fact that the limiting solvent isotope effect for 2-methyl-3-phenylpropionitrile is probably stronger than that for 2-phenylpropionitrile at comparable temperatures means that the value of $\phi^{\ddagger}$ must be greater for the former substrate than for the latter.

The primary kinetic isotope effect has been found to be independent of the deuterium content of the solvent. This was also the case for 2-methyl-3-phenylpropionitrile.[5] A finding deviating from this behavior has been reported for the proton transfer from 2-nitropropane to hydroxide ion or methoxide ion. In these cases a weak interdependence was found.[4,9b]

Acknowledgements. We wish to thank Professor Lars Melander for his interest in this work and for many useful suggestions during the preparation of the manuscript. Many thanks are due to Docent Svante Wold who provided his computer program PROGAEXP. Financial support from the Swedish Natural Science Research Council is gratefully acknowledged.

REFERENCES

1. Schowen, R. L. *Progr. Phys. Org. Chem. 9* (1972) 275.
2. Albery, W. J. and Davies, M. H. *J. Chem. Soc. Faraday Trans. 1* (1972) 167.
3. Hammet, L. P. *Physical Organic Chemistry*, Mc Graw-Hill, New York 1970, p. 131.
4. Gold, V. and Grist, S. *J. Chem. Soc. Perkin Trans. 2* (1972) 89.
5. Bergman, N.-Å. and Melander, L. *Acta Chem. Scand. A 28* (1974) 747.
6. Bergman, N.-Å. and Källsson, I. *Acta Chem. Scand. A* 30 (1976) 000.
7. Wold, S. *Acta Chem. Scand. 21* (1967) 1986.
8. Kresge, A. J. *Pure Appl. Chem. 8* (1964) 243.
9. Gold, V. and Grist, S. *J. Chem. Soc. B* (1971) a. 1665; b. 2282.
10. More O'Ferrall, R. A. *Chem. Commun.* (1969) 114.
11. Hopper, C. R., Schowen, R. L., Venkatasubban, K. S. and Jayaraman, H. *J. Am. Chem. Soc. 95* (1973) 3280.

Received January 13, 1976.

Acta Chemica Scandinavica A 30 (1976) 425—428

Crystal Structure of the Phase $Pd_{32}S_{14}$

CHRISTIAN RØMMING and ERLING RØST

Department of Chemistry, University of Oslo, Oslo 3, Norway

The crystal structure of the title compound has been determined by X-ray diffraction methods using 229 observed reflections (sin $\theta/\lambda < 0.9$) collected on a counter diffractometer. The crystals are cubic, space group $I\bar{4}3m$ with the cell dimension $a = 8.954(2)$ Å. The structure was refined to a conventional R-factor of 0.037.

The structure contains Pd – Pd-contacts of lengths 2.79 and 2.94 Å; the Pd – S bond lengths are from 2.27 to 2.49 Å. The coordination around the palladium and sulfur atoms is discussed.

The existence of a phase of approximate composition Pd_4S has been reported by several authors (Ref. 1 and references therein). According to Grønvold and Røst the crystals of this phase are body-centered cubic with lattice constant $a = 8.930$ Å;[1] the composition was found to be near $Pd_{4.3}S$ and the density 8.68 g cm^{-3} corresponding to 30.7 palladium and 13.9 sulfur atoms per unit cell. Samples show a weak paramagnetic susceptibility between liquid air temperature and 460 °C. Fischmeister found that this phase has a low electrical resistivity with a positive temperature coefficient indicating a metallic type conductivity.[2] According to Raub *et al.* $Pd_{4.3}S$ is superconducting below 1.63 K.[3]

EXPERIMENTAL

Various samples of binary palladium – sulfur alloys were prepared by melting together calculated amounts of the elements in sealed evacuated silica tubes. The ground samples were annealed for one week at *ca.* 600 °C. Guinier X-ray powder photographs indicated that the composition of the resulting phase was approximately $Pd_{4.25}S$. Several fairly well developed crystals were obtained by slowly cooling a powdered sample which had been annealed at 630 °C for several days. One of these (approximate dimensions $0.03 \times 0.05 \times 0.08$ mm^3) proved to be suitable for intensity data collection.

Determination of unit cell dimensions and collection of intensity data were carried out on a SYNTEX $P\bar{1}$ four-circle diffractometer using graphite crystal monochromated Mo$K\alpha$-radiation. The $\theta/2\theta$ scanning mode was employed with the 2θ scan speed of 1° min^{-1} from 0.65° below $2\theta(\alpha_1)$ to 0.65° above $2\theta(\alpha_2)$; background counts were taken for 0.35 times the scan time at each of the scan range limits. Three standard reflections were measured after every 40 reflections; they showed no significant variation in intensity.

Of the 254 unique reflections with sin $\theta/\lambda < 0.9$, 229 were measured to be larger than 2.5 $\sigma(I)$ and were regarded as observed. The data set was corrected for Lorentz and polarization effects and also for absorption and secondary extinction.

The atomic form factors used were those of Hanson *et al.*[4] and the calculations were performed using the computer programs described in Ref. 5. The full-matrix least-squares refinement program minimizes the quantity $\sum w \Delta F^2$ where w is the inverse of the variance of the observed structure factors.

CRYSTAL DATA

$Pd_{4.286}S$, cubic, $a = 8.954(2)$ Å; $V = 717.7$ Å^3. Unit cell content: 32 palladium and 14 sulfur atoms. Calculated density 8.916 g cm^{-3}. μ(Mo$K\alpha$) = 201 cm^{-1}. Absent reflections: (hkl) for $h+k+l$ odd. Possible space groups: $I23$ (No. 197), $Im3$ (No. 204), $I432$ (No. 211), $I\bar{4}3m$ (No. 217), and $Im3m$ (No. 229).

STRUCTURE DETERMINATION

The space groups $Im3$ and $Im3m$ were excluded because statistical tests favoured a non-centric structure. The structure was solved

Table 1. Fractional atomic coordinates and thermal parameters with estimated standard deviations ($\times 10^5$). The temperature factor is given by $\exp -(B11h^2+B22k^2+B33l^2+B12hk+B13hl+B23kl)$.

Atom	x	y	z	$B11$	$B22$	$B33$	$B12$	$B13$	$B23$
Pd I	11624(13)	11624	11624	311(8)	311	311	−57(16)	−57	−57
Pd II	16979(8)	41829(11)	16979	245(7)	210(9)	245	8(11)	104(17)	8
S I	34392(40)	34392	34392	245(22)	245	245	−12(53)	−12	−12
S II	0	50000	0	154(36)	296(65)	154	0	0	0

by Patterson methods and a model was found which could be refined according to the space group $I\bar{4}3m$ (No. 217) in which eight palladium atoms (Pd I) are found in positions 8c and 24 (Pd II) in 24 *g*; eight sulfur atoms (S I) are situated in 8c and six (S II) in position 6*b*.

The final least-squares calculations with the refinement of positional and anisotropic thermal parameters converged to a conventional *R*-factor of 0.037 ($R_w=0.041$) including all observed reflections; the overdetermination ratio is 16 and the goodness of fit ($S=(\sum w\Delta F^2/n-m)^{\frac{1}{2}}$) is 1.68. Final parameters are listed in Table 1; the structure factor listing is available from the authors.

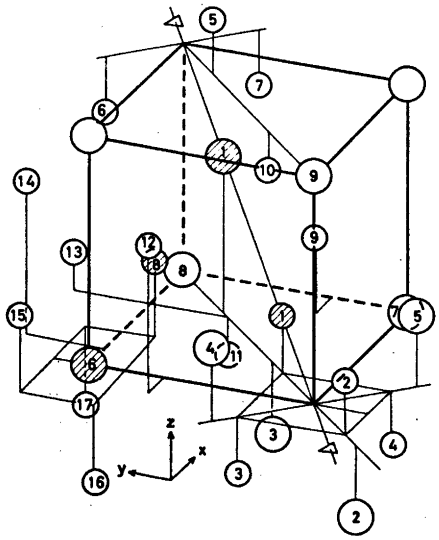

Fig. 1. One octant of the unit cell of $Pd_{32}S_{14}$. Small and large circles represent palladium and sulfur atoms, respectively. The hatched circles are atoms referred to in Tables 1 and 2. The numbering is as follows: S I: 1–5; S II: 6–9; Pd I: 1–7; Pd II: 8–17.

DESCRIPTION AND DISCUSSION OF THE STRUCTURE

It has been shown by the structure determination that the phase has a stoichiometric composition containing 32 palladium and 14 sulfur atoms per unit cell, corresponding to 69.57 atomic-% palladium or a formula of $Pd_{2.286}S$.

The thermal parameters indicate nearly isotropical vibration for all atoms; the average root mean square amplitudes of vibration are 0.11, 0.10, 0.10, and 0.09 Å for Pd I, Pd II, S I, and S II, respectively.

A perspective figure of one octant of the unit cell is presented in Fig. 1. In order to illustrate the various environments some atoms external to this volume are included. Interatomic distances are listed in Table 2. In the following discussion only interatomic distances less than 3.0 Å will be considered.

The coordination about S I and Pd I may be seen from Fig. 2 where a projection of a part of the structure into the mirror plane (1,1,0) is shown. Around the space diagonal

Table 2. Interatomic distances (Å). Estimated standard deviations are less than 0.002 Å for Pd–Pd and 0.004 Å for Pd–S bond lengths. Numbering of atoms may be seen from Figs. 1, 2 and 3.

Pd I	(1)–Pd I	(2,3,4)	2.944
	–Pd II	(8,9,10)	2.788
	–S I	(3,4,5)	2.490
Pd II	(8)–Pd I	(1)	2.788
	–Pd II	(11,12,13,14)	2.785
	–S I	(1)	2.303
	–S II	(6)	2.271
S I	(1)–Pd I	(5,6,7)	2.490
	–Pd II	(8,9,10)	2.303
S II	(6)–Pd II	(8,15,16,17)	2.271

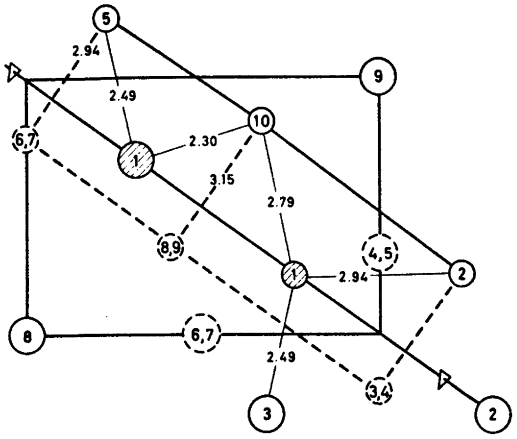

Fig. 2. Projection of the structure into the mirror plane (1,1,0) showing the atomic environments of Pd I and S I. Atoms in the mirror plane are drawn with solid lines.

[1,1,1], a three-fold axis, one finds slightly deformed trigonal prisms with palladium atoms in the corners: Pd I (2,3,4); Pd II (8,9,10); Pd I (5,6,7) *etc.* The Pd I – Pd I distances are 2.944 Å and the Pd II – Pd II distances 3.147 Å. Pd I and S I are situated alternately near the centers of every second of the prisms. The distances from this Pd I atom to the six surrounding palladium atoms are 2.944 Å [of the Pd I-type, forming a regular tetrahedron around the empty corner (0,0,0)] and 2.788 Å (Pd II). In addition the Pd I atom is bonded to three S I atoms (3,4,5) outside the quadrangular faces of the prism at distances of 2.490 Å. The S I atoms in prismatic centers are

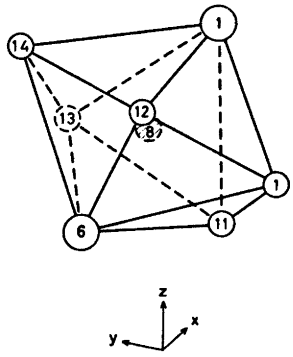

Fig. 3. The pentagonal bipyramidal coordination of Pd II (8). Symbols as in Fig. 1.

bonded to three Pd I-type atoms and three Pd II-type atoms at distances of 2.490 Å and 2.303 Å, respectively. No other atoms are closer than 3.50 Å to S I.

The coordinations of S II and Pd II are quite different from those of S I and Pd I. Atom S II (*cf.* Fig. 1, sulfur atom No. 6) is coordinated by four palladium atoms (8,15,16, 17) in a flattened tetrahedral arrangement; the Pd – S distances are 2.271 Å. The arrangement about Pd II is visualized in Fig. 3. To a central palladium atom (8) are bonded five palladium atoms (1,11,12,13,14) in a nearly planar pentagonal arrangement in distances of 2.788 Å (1) and 2.785 Å (11 – 14). The central palladium atom is also bonded to two sulfur atoms which form the apices of a pentagonal bipyramid with distances 2.271 Å (S II, 6) and 2.303 Å (S I, 1). The palladium atoms of the equatorial plane are coplanar within 0.2 Å; the central bond angles are in the range 68.8 – 74.6° and the S – Pd II (8) – Pd angles are from 84 to 97°.

The crystal structures of the following palladium – sulfur compound have so far been determined: PdS_2,[6] PdS,[7] $Pd_{2.286}S$ (present work), Pd_3S[8] and Pd_4S,[9] all of which seem to be stoichiometric. Accordingly no extended range of homogeneity has been found.

Short S – S distances corresponding to covalent bonds are found only in PdS_2, whereas intermetallic Pd – Pd bonds exist in all compounds richer in palladium than PdS; these are all longer than the Pd – Pd bond (2.751 Å) in metallic palladium. The coordination polyhedra around both sulfur and palladium atoms are irregular.

A distorted tetrahedral arrangement of palladium atoms around a sulfur atom is found in PdS with bond lengths within the range 2.26 to 2.45 Å; the corresponding bond length is 2.271 Å for the tetrahedral environment of S II in the present structure. A trigonal prismatic coordination comparable to that about S I is not found in any of the other palladium sulfides. This arrangement is, however, observed in several other palladium compounds, such as in PdTe (NiAs-type structure) and in palladium-rich phosphides.

REFERENCES

1. Grønvold, F. and Røst, E. *Acta Chem. Scand. 10* (1956) 1620.
2. Fischmeister, H. *Acta Chem. Scand. 13* (1959) 852.
3. Raub, Ch. J., Zachariasen, W. H., Geballe, T. H. and Matthias, B. T. *J. Phys. Chem. Solids 24* (1963) 1093.
4. Hanson, H. P., Herman, F., Lea, J. D. and Skillman, S. *Acta Crystallogr. 17* (1964) 1040.
5. Groth, P. *Acta Chem. Scand. 27* (1973) 1837.
6. Grønvold, F. and Røst, E. *Acta Crystallogr. 10* (1957) 329 and Munson, R. A. and. Kasper, J. S. *Inorg. Chem. 8* (1969) 1198.
7. Gaskell, T. F. *Z. Kristallogr. 96* (1937) 203.
8. Røst, E. and Vestersjø, E. *Acta Chem. Scand. 22* (1968) 819.
9. Grønvold, F. and Røst, E. *Acta Crystallogr. 15* (1962) 11.

Received January 13, 1976.

Acta Chemica Scandinavica A 30 (1976) 429—432

Surface Tension in Alkali Halide Mixtures

K. GRJOTHEIM,[a] T. NATERSTAD[b] and H. A. ØYE[b]

[a] Chemistry Department, University of Oslo, Oslo 3, Norway and [b]The University of Trondheim, Institute of Inorganic Chemistry, N-7034 Trondheim-NTH, Norway

The surface tension in binary molten mixtures of NaF – NaCl, NaF – NaBr, and NaCl – NaBr was measured by the pin detachment method.

The surface tension isotherm of each system at 900 °C was compared to isotherms calculated by applying an equation derived by Guggenheim for ideal mixtures and two modified forms of this equation as well as a model proposed by Eberhart. The observed values were represented within 1 % by the Eberhart model, while the values predicted by the other equations were found to be as much as 27 and 10 % too high, respectively.

As part of a general study of the physicochemical properties of molten binary alkali halide systems, surface tension measurements were carried out in NaF – NaCl, NaF – NaBr, and NaCl – NaBr.

The pin detachment method, which has been shown to be an absolute method [1] was combined with density measurements [2] using a Pt-10 % Rh sinker. The sinker was attached to a thermobalance [3] at the top of the furnace by means of a thin Pt-wire (diameter 0.2 mm).

Equating the detachment force of the pin, ΔW, to the weight of the liquid being lifted above the surface plane by the pin prior to its detachment from the melt surface, the surface tension was calculated by expressing ΔW as a function of the surface tension, the pin radius and the density of the bulk liquid, using a general Laplace equation for a liquid surface around a vertical rod.[1]

EXPERIMENTAL

The furnace and thermobalance together with the vacuum system of the apparatus applied have been described in detail elsewhere.[3,4]

The salts used (Baker Anal. 99.3 % NaF, 99.8 % NaCl, and 99.8 % NaBr, J. T. Baker, Holland) were dried under vacuum and recrystallized from the molten state in a nitrogen atmosphere. To ensure homogeneous mixtures, the weighed portion of the salts were melted in a closed Pt-crucible and were then finely crushed prior to each experiment.

Having inserted the salt to be investigated in a Pt- or vitreous carbon crucible in the furnace, the furnace was evacuated to $\sim 10^{-4}$ Torr and N_2-gas fed in to give a small overpressure (the N_2-gas rate being 0.2 l/h).

The crucible was raised or lowered relative to the sinker by means of a reversible DC-motor connected to a gear box from which an extended shaft drove the furnace up or down at a continuously adjustable speed of 0 – 1 cm/min.

On lifting the furnace until contact between the pin and the melt surface, a sudden increase of the recorded weight of the sinker was observed. By slowly lowering the furnace from this position, the recorded weight passed through a well-defined maximum before a reproducible minimum corresponding to the weight of the sinker in nitrogen atmosphere was attained. Weight changes were read to ± 0.1 mg. The recorded detachment weight, ΔW, ranged between 60 and 100 mg depending on the surface tension of the system investigated. The measurement of ΔW was repeated four times at each temperature. With few exceptions the values obtained corresponded within the accuracy of the recorder.

RESULTS

The surface tensions measured at different temperatures were fitted to the linear function

$$\gamma = \gamma_0 - \beta(t - t_0) \quad (1)$$

where γ and γ_0 are the surface tensions at temperature t and t_0, respectively, and β the temperature coefficient (Table 1). The experimental standard deviation in γ is denoted σ_γ.

Table 1. Surface tension [a] in alkali halide systems. $\gamma = \gamma_0 - \beta(t - t_0)$ (N m^{-1}).

System	Mol fraction	t_0	$\gamma_0 \times 10^3$ N m^{-1}	$\beta \times 10^6$ N m^{-1} degree^{-1}	σ_γ %	Temp. range °C
	X_{NaF}					
NaCl – NaF	0.00	800	115.7	69	0.3	839 – 912
	0.25	800	123.4	94	0.9	719 – 857
	0.50	800	132.8	78	0.1	806 – 896
	0.75	900	141.1	81	0.1	918 – 943
	1.00	1000	187.6	100	0.1	996 – 1052
NaBr – NaF	0.00	800	99.9	71	0.1	753 – 828
	0.25	800	106.2	64	0.1	701 – 849
	0.50	800	116.4	89	0.3	814 – 893
	0.75	900	128.4	54	0.1	915 – 949
	X_{NaCl}					
NaBr – NaCl	0.25	800	101.5	67	0.3	770 – 857
	0.35	800	102.5	66	0.3	747 – 812
	0.50	800	105.6	71	0.2	771 – 891
	0.60	800	107.4	72	0.1	715 – 805
	0.75	800	109.8	68	0.1	807 – 889
	0.85	800	113.2	85	0.2	783 – 839

a The isothermal surface tension is plotted *versus* the bulk mol fraction for each system in Fig. 1.

DISCUSSION

According to Guggenheim,[5] the following expression applies to the surface tension, γ, of an ideal solution of two components 1 and 2, with molar fractions X_1 and X_2 and a surface area per mol a:

$$\exp(-\gamma a/RT) = X_1 \exp(-\gamma_1 a/RT) + X_2(-\gamma_2 a/RT) \quad (2)$$

Usually the value of a is calculated by assuming equal packing density in the surface and the bulk phase. But this approach may seem somewhat crude in terms of ionic interactions. However, in binary and ternary alkali earth chloride mixtures,[6] and in binary alkali halide systems [7] the equation has been found to give reasonable estimates when mol fractions are replaced by volume fractions, ϕ:

$$\exp(-\gamma A/RT) = \phi_1 \exp(-\gamma_1 A/RT) + \phi_2 \exp(-\gamma_2 A/RT) \quad (3)$$

$$\phi_1 = \frac{V_1 X_1}{V_1 X_1 + V_2 X_2}$$

$$\phi_2 = 1 - \phi_1$$

$$A = [\phi_1 V_1 + \phi_2 V_2]^{2/3}$$

where A is taken to be the surface area per mol anion-cation pair, and V is the molar volume.

Assuming the molar surface area, A_i, for each component in a mixture to be the same as for the pure state:

$$A_i = \left[\frac{M_i}{\varrho_i}\right]^{2/3}$$

where M_i is the molar weight and ϱ_i the density of the component i, a second modification of eqn. (2) may be written:

$$\exp(-\gamma A/RT) = \phi_1 \exp(-\gamma_1 A_1/RT) + \phi_2 \exp(-\gamma_2 A_2/RT) \quad (4)$$

In a different approach Eberhart [8] assumed the surface tension to be a linear function of the surface mol fraction, X_i^r, defined in terms of experimental parameters by the equations:

$$\gamma = X_1^r \gamma_1 + X_2^r \gamma_2 \quad (5a)$$

$$X_1^r + X_2^r = 1 \quad (5b)$$

Assuming equilibrium between the bulk and surface phase, a concentration independent enrichment factor, S_{12}, is defined by

$$S_{12} = (f_1^r X_1^r / f_2^r X_2^r)/(f_1 X_1 / f_2 X_2) \quad (6)$$

where f is the activity coefficient and the superscript τ, as before, denotes the surface phase.

Setting the activity coefficient ratios in eqn. (6) equal to unity

$$S_{12}=(X_1^\tau/X_2^\tau)(X_1X_2) \tag{7}$$

Combining eqns. (5) and (7)

$$\gamma=\frac{S_{12}X_1\gamma_1+X_2\gamma_2}{S_{12}X_1+X_2} \tag{8a}$$

or rearranged:

$$S_{12}=(X_2/X_1)[(\gamma_2-\gamma)/(\gamma-\gamma_1)] \tag{8b}$$

The assumed temperature independent factor, S_{12}, can be determined from eqn. (8a) by a least squares fitting procedure or by testing the linearity of the rearranged eqn. (8b):[3]

$$\frac{\gamma-\gamma_1}{\gamma_2-\gamma_1}=-S_{12}\frac{X_1}{X_2}\left[\frac{\gamma-\gamma_1}{\gamma_2-\gamma_1}\right]+1 \tag{9}$$

Another consequence of the model is that if we have determined this enrichment factor experimentally for a mixture of components 1 and 2, S_{12}, and of components 2 and 3, S_{23}, then according to eqn. (7):

$$S_{13}=S_{12}S_{23} \tag{10}$$

Fig. 1 gives the experimental surface tension compared with the Guggenheim model, eqn. (2), the modified Guggenheim model, eqn. (3), and the Eberhart model, eqn. (8a). The model corresponding to eqn. (4) gives essentially the same results as eqn. (3). The enrichment factors, S_{ij}, are calculated from a least square fit of eqn. (8a) and are given in the second column of Table 2.

Eqns. (2) and (3) which in principle contain no adjustable parameters do predict the direction of the deviation from additivity, but tend

Table 2. Enrichment factor and standard deviation in fit of γ at 900 °C.

System i	j	S_{ij} Eqn. (8b)	σ_γ, %	S_{ij} Eqn. (10)
NaCl	NaF	5.05±0.25	0.97	3.14
NaBr	NaF	5.84±0.17	1.03	9.39
NaBr	NaCl	1.86±0.60	0.36	1.16

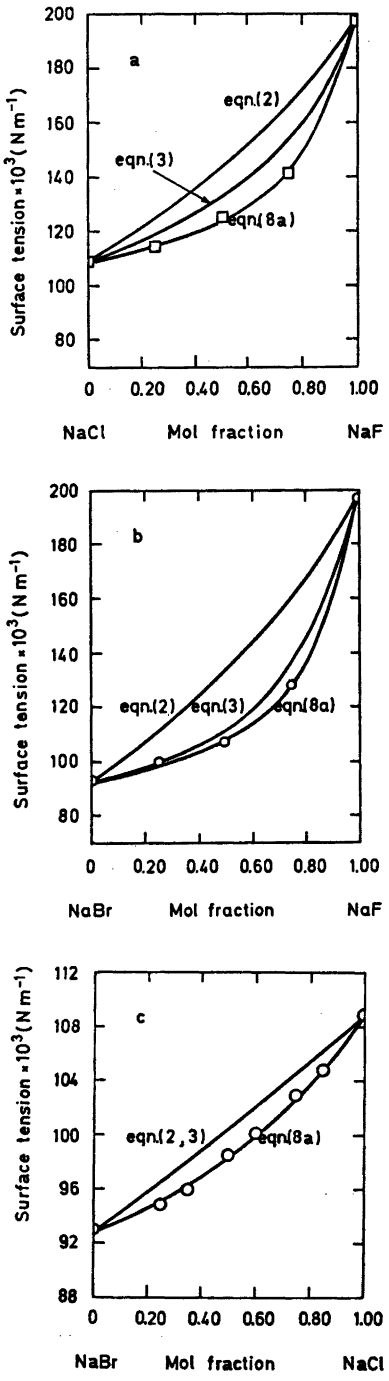

Fig. 1. Surface tension of sodium halide mixtures at 900 °C, compared with models according to eqn. (2), eqn. (3) and eqn. (8a). (a) NaCl–NaF; (b) NaBr–NaF; (c) NaBr–NaCl.

to underestimate it, although eqn. (3) gives a significant improvement over eqn. (2). This is probably because the volume fractions are more directly related to the packing efficiency of each species than the molar fractions.

The Eberhart model which introduces the parameter S_{ij} is seen to give a very satisfactory fit of the experimental surface tension values, the standard deviation being 0.4 – 1 % (Table 2) and hence of the same order of magnitude as the experimental standard deviation (Table 1).

The test of consistency according to eqn. (10) is, however, not satisfactory (Table 2, last column) but it should be stressed that S_{ij} is very sensitive towards small errors in the measured surface tension, especially in systems like NaBr – NaCl where differences between almost equal numbers enter the calculation of S_{ij} according to eqn. (8b).

In conclusion the Eberhart model seems to be acceptable for representing the surface tension of the investigated binary molten mixtures, and is able to accommodate larger deviations from additivity than the Guggenheim models. The neglect of the activity coefficients, however, limits the Eberhart model to systems with medium chemical interactions and it may not be suitable for such strongly interacting systems as, for instance the $MgCl_2$ – AlkCl systems.[6] The reported good fit [8] to eqn. (10) is not found, but a larger quantity of material is needed to draw possible chemical conclusions from these deviations.[9]

Acknowledgement. Thanks are expressed to ing. Th. Tharaldsen for carrying out some of the experimental work.

Financial support from The Royal Norwegian Council for Scientific and Industrial Research (Grant B 581) is gratefully acknowledged.

REFERENCES

1. Lillebuen, B. *Acta Chem. Scand. 24* (1970) 3287.
2. Grjotheim, K., Naterstad, T. and Øye, H. A. *To be published.*
3. Bratland, D., Grjotheim, K., Krohn, C. and Motzfeldt, K. *Acta Chem. Scand. 20* (1966) 1811.
4. Grjotheim, K., Lillebuen, B. and Øye, H. A. *Trans. Faraday Soc. 67* (1971) 640.
5. Guggenheim, E. A. *Mixtures*, Oxford at the Clarendon Press, London 1952, p. 181.
6. Grjotheim, K., Holm, J. L., Lillebuen, B. and Øye, H. A. *Acta Chem. Scand. 26* (1972) 2050.
7. Berge, B. and Holm, J. L. *Rapport til Norges Tekniske Høgskoles Fond*, NTH, Trondheim 1970.
8. Eberhart, J. G. *J. Phys. Chem. 70* (1966) 1183.
9. Guggenheim, E. A. *Thermodynamics*, 5th Ed., North-Holland, Amsterdam 1967, p. 207 – 213.

Received November 3, 1975.

Acta Chemica Scandinavica A 30 (1976) 433—436

The Crystal Structure of Cesium Dimethyldithiocarbamate, $CsS_2CN(CH_3)_2$

ANDERS WAHLBERG

Institute of Chemistry, University of Uppsala, Box 531, S-751 21 Uppsala 1, Sweden

The crystal structure of the titel compound was determined from three-dimensional diffractometer X-ray data. The crystals are orthorhombic with $a = 9.836(2)$ Å, $b = 11.138(2)$ Å, $c = 6.797(1)$ Å and $Z = 4$. The most probable space group is *Cmcm*, $R = 0.053$. The metal atoms and the ligand groups are packed in chains parallel to *c*. Within a chain each cesium atom has two sulfur atoms at a distance of 3.636(1) Å and four at 3.713(1) Å. The chains are connected by two long Cs–S bonds of 4.099(1) Å from each cesium so that a three-dimensional coordination net is formed with cesium in eight-coordination. The dimethyldithiocarbamate ligand has *mm* symmetry.

Compounds of the composition *AX* are being studied at this Institute. *A* is a monovalent cation and *X* is an organic ligand containing sulfur, *e.g.* dialkyldithiocarbamate $[S_2CNR_2]^-$, dtc. Hitherto *A* has usually been Cu(I), Ag(I), Au(I), or Tl(I). A dtc with the alkyl group R is abbreviated: M (methyl), E (ethyl), nP (propyl), iP (1-methylethyl), nB (butyl), iB (2-methylpropyl). In many cases compounds of Tl(I) and the alkali metals are similar. In the crystal structures of TlM [1] and TlnB [2] layers, and of TlE,[3] TlnP,[4] TliP,[5] and TliB [6] chains are formed. CsnB [7] is a layer structure related to TlnB. Uhlin [8] has studied dtc of the alkali metals in solution.

EXPERIMENTAL

Crystal preparation. The titel compound, CsM, was prepared by the general procedure described by Uhlin.[8] The solid residue was recrystallized from 2-propanol. This solvent had been prepared by drying 99.5 % 2-propanol with Union Carbide Molecular Sieves 3 Å.

Crystal data. The crystals appear as long yellow prisms elongated along [001] with the faces (110) and (1$\bar{1}$0) developed. The density was measured by flotation in a mixture of $CHCl_3$ and $CHBr_3$. The unit cell dimensions were found from a powder photograph taken on an IRDAB XCD 700 camera using Cr$K\alpha_1$ radiation ($\lambda = 2.28962$ Å) with silicon ($a = 5.43054$ Å) as an internal standard. The cell parameters were refined by the least-squares method using 22 observed θ-values. *Crystal data*: Orthorhombic, space groups: *Cmcm* (No. 63), *C2cm* (No. 40) or *Cmc*2_1 (No. 36), $a = 9.836(2)$ Å, $b = 11.138(2)$ Å, $c = 6.797(1)$ Å, $V = 744.7$ Å^3, $Z = 4$, $D_m = 2.26$ gcm^{-3}, $D_x = 2.257$ gcm^{-3}, m.p. = 169 – 173 °C, μ(Mo$K\alpha$) = 54.8 cm^{-1}.

Intensity data. A crystal of dimensions 0.060 × 0.058 × 0.150 mm^3 was mounted in a thin-walled glass capillary. The measurements were made on a Stoe-Philips four-circle PDP8/I computer-controlled diffractometer with a graphite monochromator using Mo$K\alpha$ radiation ($\lambda = 0.71069$ Å) and an ω-2θ scan technique. Automatic filter selection (one filter having a cutdown of 2:1 was inserted for the five strongest reflexions) and automatic scan-speed selection (× 1, × 2 or × 4) was used. 1283 intensities giving 1137 independent reflexions were collected in one octant in the reciprocal space up to $\sin\theta/\lambda = 0.862$. Three standard reflexions 004, 042 and 510 were monitored every 40 reflexions. $\omega - 2\theta$- and χ-scan over some reflexions before and after the experiment showed mechanical stability of the crystal mounting and the diffractometer system, and verified the quality of the detector crystal.

Corrections were made for background, Lorentz and polarization effects (including monochromator polarization) and for absorption. The transmission factor varied between 0.70 and 0.75. Isotropic extinction corrections were applied during the least-squares refinement.

Structure determination and refinements. The positions of cesium and sulfur were obtained from the three-dimensional Patterson function.

Table 1. Atomic coordinates and thermal parameters. The anisotropic factor is defined as $\exp(-\beta_{11}h^2-\beta_{22}k^2-\beta_{33}l^2-2\beta_{12}hk-2\beta_{13}hl-2\beta_{23}kl)$. $\beta_{13}=\beta_{23}=0.0$. Estimated standard deviations (in parentheses) are given for the last digits.

Atom	x	y	z	B
Cs	0.0	0.15042(3)	0.25	
S	0.34797(8)	0.35292(7)	0.25	
C	0.5	0.2773(3)	0.25	
N	0.5	0.1569(3)	0.25	
Cl	0.3734(4)	0.0891(3)	0.25	
H1	0.388(8)	0.011(6)	0.25	9.9(2.1)
H2	0.317(4)	0.113(3)	0.367(6)	5.4(8)

Atom	β_{11}	β_{22}	β_{33}	β_{12}
Cs	0.00981(4)	0.00750(3)	0.01396(6)	0.0
S	0.00697(6)	0.00659(6)	0.01997(16)	0.00157(5)
C	0.0063(3)	0.0051(3)	0.0116(6)	0.0
N	0.0061(3)	0.0052(2)	0.0244(9)	0.0
Cl	0.0075(3)	0.0068(3)	0.0375(13)	−0.0009(2)

The nitrogen and carbon atoms were then located in an F_o-synthesis, assuming the centrosymmetric space group *Cmcm*. Atomic positions and isotropic temperature factors were refined by full matrix least-squares calculations. After introduction of anisotropic temperature factors and of an isotropic extinction parameter, the hydrogen atoms were found in a Fourier difference synthesis. In the final cycles of the refinement, the coordinates for all atoms, the thermal parameters, anisotropic for the non-hydrogen atoms and isotropic for the hydrogen atoms were allowed to vary (33 parameters in all). The final shifts were all smaller than 1 % of σ. The resulting positional and thermal parameters are given in Table 1. A list of observed and calculated structure amplitudes is available on request. The quantity minimized in the least-squares refinements was $\sum w(|F_o^2|-|F_c^2|)^2$. The reflexions were weighted according to the formula $w^{-1}=\sigma_c^2(F^2)+0.03|F_o^2|=\sigma^2(F^2)$. Using all the 1137 reflexions, the refinement converged at $R(F^2)=\sum||F_o^2|-|F|_c^2|/|F_o^2|=0.064$ and $R_w(F^2)=(\sum w(|F_o^2|-|F_c^2|)^2/\sum w|F_o^4|)^{\frac{1}{2}}=0.073$ corresponding to a conventional $R(F)$ based on F of 0.053. This resulted in 49 reflexions having $||F_o^2|-|F_c^2||/\sigma(F^2)>2.0$ with the extreme value of 20 for the strongest reflexion 002. The value $q=$ (number of observations)/(number of parameters) = 34. The scattering factors for Cs were taken from the tables provided by Cromer and Waber,[9] and for S, N and C those suggested by Hanson *et al.*[10] The spherical scattering factors proposed by Stewart *et al.*[11] were used for H. Anomalous dispersion corrections[12] ($\Delta f'$ and $\Delta f''$) were applied for Cs and S.

Attempts were made to break the symmetry and to perform the refinement in the space groups $C2cm$ and $Cmc2_1$. No reasonable structure alternative was, however, obtained by these efforts. The space group used, *Cmcm*, gives good agreement between observed and calculated intensities and very satisfactory atomic positions even for the hydrogen atoms.

All large calculations were performed using the IBM 370/155 computer in Uppsala. The following major programs were used: CELNE, DATAPH, SORTA, DRF, UPALS, DISTAN and ORTEP. These programs have been described by Lundgren.[13] Small calculations were performed using the departmental IBM 1800 computer.

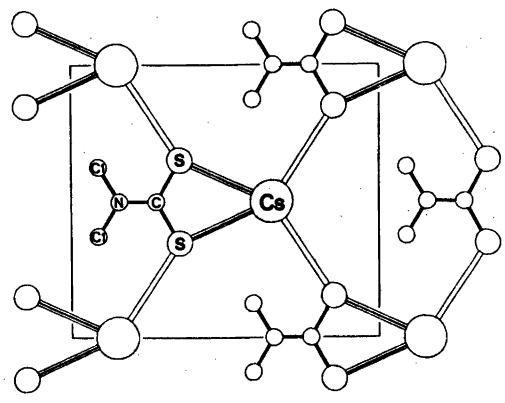

Fig. 1. Arrangement of the non-hydrogen atoms in the mirror plane $z=1/4$.

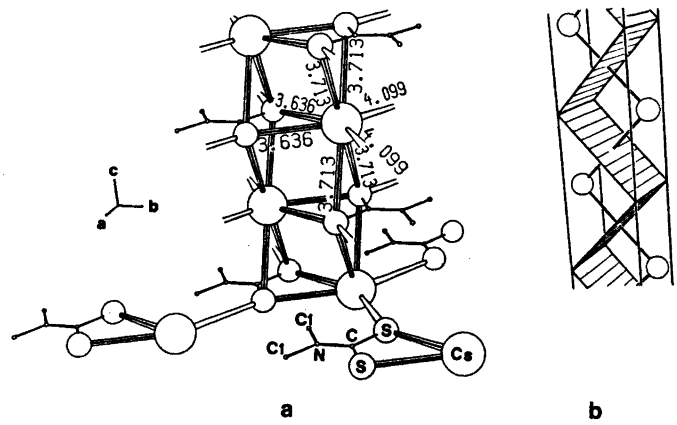

a b

Fig. 2. a. A chain perpendicular to the layer in Fig. 1. b. A schematical representation of the cesium and sulfur atom arrangement in a chain.

RESULTS AND DISCUSSION

General. The non-hydrogen atoms are situated in mirror planes (Fig. 1). Two such layers ($z=1/4$, $z=3/4$) related by a centre of symmetry ($\frac{1}{2},\frac{1}{2},\frac{1}{2}$) give the contents of the unit cell. The crystal structure can be described as built up of chains, perpendicular to these layers. The chains are thus parallel to *c* (Fig. 2). Cesium is coordinated to sulfur atoms in three dithiocarbamate ligands giving six Cs – S bonds within the chain. Two further sulfur atoms situated in adjacent chains are coordinated at an appreciably longer distance. Thus, cesium coordinates eight sulfur atoms. The coordination polyhedron for cesium is a distorted cube. Interatomic distances and angles are collected in Table 2.

Intermolecular contacts. There are no intermolecular distances shorter than the sum of the radii defined by Bondi [14] or those recommended by van der Helm *et al.*[15] The distances to nonbonding atoms in the vicinity of cesium are reported, as no values are given for Cs^+ by the cited authors. Short distances can be expected between atoms in adjacent mirror planes, as the distance between the mirror planes $z=1/4$ and $z=3/4$ is 3.40 Å. Distances Cs – N (4.02 Å) and Cs – C (3.49 Å) are of this type. Methyl hydrogen H2 are situated 3.25 Å from cesium (in adjacent chains). The corresponding Cs – Cl distance is 3.74 Å.

Table 2. Interatomic distances (Å) and angles (°).

Cs – Cs	4.773(1)	S – C – S	121.2(2)
Cs – S	3.636(1)	S – C – N	119.4(2)
Cs – S	3.713(1)	C – N – Cl	121.2(2)
Cs – S	4.099(1)	Cl – N – Cl	117.5(4)
S – S	2.991(2)	N – Cl – H1	112(5)
C – S	1.716(2)	N – Cl – H2	110(2)
C – N	1.342(5)	H1 – Cl – H2	110(3)
N – Cl	1.456(4)	H2 – Cl – H2	105(4)
Cl – Cl	2.490(8)		
H1 – Cl	0.88(6)		
H2 – Cl	1.00(4)		

Coordination. The coordinating distances exceed the sum of the Pauling ionic radii, 3.53 Å. The two shortest Cs – S distances [3.656(1) Å] are found in the dithiocarbamate plane and four slightly longer [3.713(1) Å] in the chain direction. These six distances, which are longer than those found for six-coordinated cesium in CsnB,[13] average value 3.62 Å, agree well with the mean Cs – S distance, 3.66 Å, in $Cs_2CS_3.H_2O$,[16] where cesium coordinates nine atoms (sulfur and oxygen). A mean value of 3.67 Å for eight-coordination is found in $Cs_2Pd_3S_4$ [17] and $Cs_2Mn_3S_4$.[18] The same value appears in Cs_2S_6 [19] for distances less than 4 Å. The non-substituted dithiocarbamates of cesium, rubidium, potassium, and ammonium are isostructural.[20,21] The cation is eight-coordinated as in CsM, but the coordination problems are quite different since the shielding bulks are replaced by hydrogens suitable for hydrogen bonds.

The chain. Fig. 2b shows the sulfur atoms in a chain represented by a series of rectangles. The cesium atoms are situated 0.04 Å outside the columns of sulfur atoms, and form a planar equidistant zigzag chain with Cs–Cs–Cs angles of 90.8°. The Cs–Cs distance, 4.773 Å, is longer than the one found in CsnB, 4.29 Å. In the cesium halides, the metal-metal distances have values of 4.1 Å to 4.3 Å, whereas the distance is 5.265 Å in solid cesium.[22] The present type of chain is also found in TlE.[3]

The linkage of the chains. The bonds from the chain in Fig. 2a demonstrate how adjacent chains are connected. Cesium coordinates one sulfur atom in each of two neighbouring chains at a distance of 4.099(1) Å. Although these two distances are significantly longer than those previously discussed, all the eight bonds contribute to the lattice energy because of the ionic character of the Cs–S interaction.

The ligand. The dimethyldithiocarbamate ligand has *mm* symmetry. In CsM the C–N distance is about 0.02 Å longer, and the S–C–S angle is about 10° larger than in the ligand in CuM_2,[23] TiM_3Cl,[24] CoM_2NO,[25] and FeM_2NO (−80 °C).[26]

Acknowledgements. I wish to express my gratitude to Professor Ivar Olovsson for his interest in my work and for the facilities put at my disposal. I am indebted to Dr. Rolf Hesse and Dr. Per Jennische for encouraging discussions. This work has been supported by grants from the Swedish Natural Science Research Council.

REFERENCES

1. Jennische, P. and Hesse, R. *Acta Chem. Scand. 27* (1973) 3531.
2. Elfwing, E., Anacker-Eickhoff, H., Jennische, P. and Hesse, R. *Acta Chem. Scand. A 30* (1976) 335.
3. Pritzkow, H. and Jennische, P. *Acta Chem. Scand. A 29* (1975) 60.
4. Nilson, L. and Hesse, R. *Acta Chem. Scand. 23* (1969) 1951.
5. Jennische, P., Olin, Å. and Hesse, R. *Acta Chem. Scand. 26* (1972) 2799.
6. Anacker-Eickhoff, H., Jennische, P. and Hesse, R. *Acta Chem. Scand. A 29* (1975) 51.
7. Aava, U. and Hesse, R. *Ark. Kemi 30* (1968) 149.
8. Uhlin, A. and Åkerström, S. *Acta Chem. Scand. 25* (1971) 393.
9. Cromer, D. T. and Waber, J. T. *Acta Crystallogr. 18* (1965) 104.
10. Hanson, H. P., Herman, F., Lea, J. D. and Skillman, S. *Acta Crystallogr. 17* (1964) 1040.
11. Stewart, R. F., Davidson, E. R. and Simpson, W. T. *J. Chem. Phys. 42* (1965) 3175.
12. Cromer, D. T. *Acta Crystallogr. 18* (1965) 17.
13. Lundgren, J.-O. (1974) *Crystallographic Computer Programs*, UUIC-B13-4-01, Inst. of Chemistry, Univ. of Uppsala, Sweden.
14. Bondi, A. *J. Phys. Chem. 68* (1964) 441.
15. van der Helm, D., Lessor, A. E. and Merritt, L. L. *Acta Crystallogr. 15* (1962) 1227.
16. Philippot, E. and Lindqvist, O. *Rev. Chim. Miner. 8* (1971) 491.
17. Bronger, W. and Huster, J. *J. Less-Common Metals 23* (1971) 67.
18. Bronger, W. and Böttcher, P. *Z. Anorg. Allg. Chem. 390* (1972) 1.
19. Abrahams, S. C. and Grison, E. *Acta Crystallogr. 6* (1953) 206.
20. Hahnkam, V., Kiel, G. and Gattow, G. *Z. Anorg. Allg. Chem. 368* (1966) 127.
21. Capacci, L., Villa, A. C., Ferrari, M. and Nardelli, M. *Ric. Sci. 37* (1967) 993.
22. Pearson, W. B. *A Handbook of Lattice Spacings and Structures of Metals and Alloys*, Pergamon Press, London 1958.
23. Einstein, F. W. B. and Field, J. S. *Acta Crystallogr. B 30* (1974) 2928.
24. Lewis, D. F. and Fay, R. C. *J. Am. Chem. Soc. 96* (1974) 3843.
25. Enmark, J. H. and Feltham, R. D. *J. Chem. Soc. D* (1972) 718.
26. Davies, G. R., Jarvis, J. A. J., Kilbourn, B. T., Mais, R. H. B. and Owston, P. G. *J. Chem. Soc. A* (1970) 1275.

Received December 1, 1975.

Acta Chemica Scandinavica A 30 (1976) 437—447

On the Structure of Highly Hydrolyzed Thorium Salt Solutions

M. MAGINI,[a] A. CABRINI,[a] G. SCIBONA,[a] G. JOHANSSON [b] and M. SANDSTRÖM [b]

[a] Laboratorio Chimica Fisica, Divisione Materiali CNEN, CSN-Casaccia, Italy, and [b] Department of Inorganic Chemistry, Royal Institute of Technology, S-100 44 Stockholm, Sweden.

The structure of highly hydrolyzed thorium salt solutions has been investigated by large and small-angle X-ray scattering techniques. It is shown that the hydrolysis complexes formed at room temperature contain a small number of Th atoms probably situated at the corners of slightly distorted face-sharing tetrahedra. Hydrolysis at higher temperatures leads to the formation of small crystallites (~40 Å), which have the ThO_2 structure. The arrangement of Th atoms in the hydrolysis complexes formed at room temperature differs from that found in ThO_2, although the Th atoms in both of the structures are joined by double oxygen bridges and form tetrahedral arrangements with Th—Th distances of 4.0 Å.

The hydrolytic reactions of the Th(IV) ion have been extensively investigated.[1–6] The hydrolysis leads to the formation of polynuclear complexes probably containing from two up to about six thorium atoms. X-Ray diffraction investigations of crystalline basic thorium salts [7] and of hydrolyzed thorium salt solutions [8] have clarified the structure of the dinuclear complex which is first formed. The two thorium atoms which are situated 4.0 Å apart are held together by two bridging oxygen atoms. Although the previously reported solution X-ray scattering data [8] did not result in unambiguous structure determinations of the complexes containing more than two Th atoms, they indicated that the structures are based on tetrahedral arrangements of the Th atoms within the complexes.

The hydrolysis of the solutions investigated previously was carried out by addition of HO^- to a thorium salt solution or by dissolving aqueous thorium oxide in the solutions. A maximum number of about 3 HO^- per Th^{4+} ion can be introduced in this way without the formation of a permanent precipitate. In the present paper results are reported from investigations of thorium nitrate solutions hydrolyzed by the extraction of HNO_3 with a primary amine. By combining this with heat treatment of the solution the hydroxide number, n_{HO} can be increased beyond 3 HO^- per Th^{4+}. This is a procedure which is commonly used in CNEN hydrometallurgical processes for the transformation of solutions containing Th, U, or Pu into gel microspheres, which are then used for the preparation of ceramic oxides for nuclear fuels.[9] Because of these technological applications the structures o the metal ion complexes in the strongly hydrolyzed solutions are of interest.

EXPERIMENTAL

Preparation and analysis of the solutions. An acidic thorium nitrate solution (solution A) was prepared by dissolving a weighed amount of $Th(NO_3)_4$ (Carlo Erba reagent grade) in 1 M nitric acid. A hydrolyzed solution was prepared from a 1 M thorium nitrate solution by extracting HNO_3 into an organic phase by means of a primary amine RNH_2.[10] The formation of the amine salt, RNH_3NO_3, is strongly favoured, which allows the preparation of solutions of a known average hydroxyl number, n_{HO}, by using known amounts of amine in the starting solution. The organic phase was prepared by dissolving a long chain primary amine (Primene JMT by General Mills Inc.) in Solvesso 100 (aromatic diluent manufactured by Esso-Chemical).

A solution B with $n_{HO} \simeq 2.9$ was prepared in this way. An aliquot of solution B was refluxed for about 1 h at 80—90 °C and a new solution, B′, with the same value of n_{HO}, was obtained. By further extraction of HNO_3 with Primene at 40—50 °C from the solution

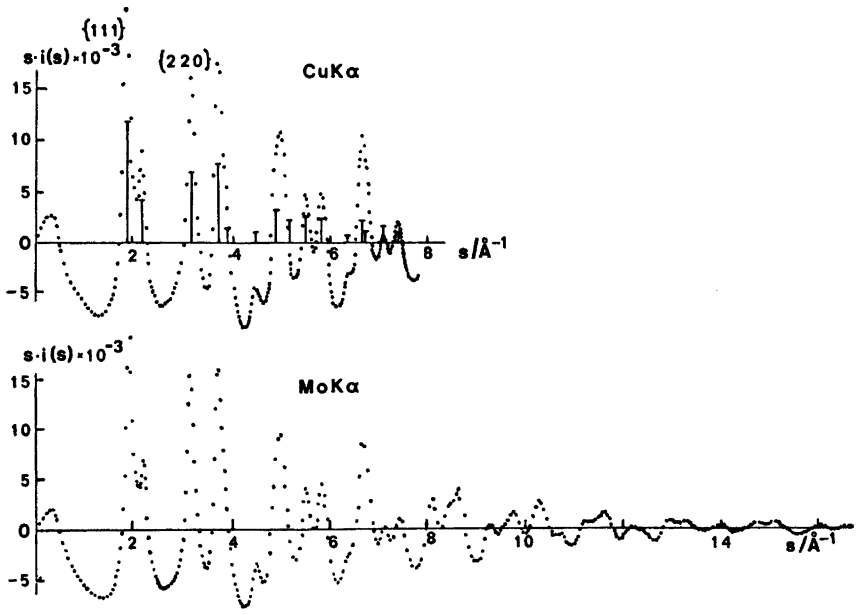

Fig. 1. Reduced intensity functions $i(s)$ in electron units e.u., multiplied by s, for solution B′ measured with Cu$K\alpha$ and Mo$K\alpha$ radiation. The ThO_2 powder pattern is indicated by vertical lines. The height of each line is proportional to the relative intensity of the reflection (ASTM-card No. 4-0556).

B′ a more hydrolyzed solution, having $n_{HO} \simeq 3.6$ was prepared (solution C).

These three hydrolyzed solutions (B, B′ and C) were filtered through an ultrafine filter (Jena-Glass G5) with a pore size of about 1 μm. In contrast to solution B, which was clear, the two solutions B′ and C were opaque but seemed to be stable for an indefinite period of time. This is shown by the essentially identical scattering curves in Fig. 1 which were obtained for the same solution B′ with a time interval of about one year.

The solutions were analyzed by titrating Th^{4+} with standard EDTA using pyrocatechol violet as indicator.[11] The hydrolyzed solutions were first depolymerized by boiling with concentrated nitric acid.

The nitrate content was determined by amperometric titration using iron(II) ammonium sulfate solution in a concentrated sulfuric acid medium.[11] The densities were determined both by a pycnometer and a digital precision densimeter (Anton Paer K.G.). The compositions of the four solutions are given in Table 1.

X-Ray scattering measurements. For the *large-angle X-ray scattering measurements* two different diffractometers were used. Both use the Bragg-Brentano semifocusing arrange-

Table 1. Compositions of the four solutions A, B, B′ and C.

Solution	A (acid)		B ($n_{HO}=2.88$)		B′ ($n_{HO}=2.88$)		C ($n_{HO}=3.57$)	
Concentration	mol/l	atoms/V	mol/l	atoms/V	mol/l	atoms/V	mol/l	atoms/V
Th	0.888	1	1.023	1	1.127	1	1.298	1
O	62.75	70.66	58.58	57.20	58.74	52.12	57.41	44.23
N	4.04	4.54	1.151	1.12	1.269	1.12	0.56	0.43
H	101.5	114.3	110.2	107.7	109.8	97.4	111.5	85.9
Stoichiometric volume V/Å^3	1869.7		1622.9		1473.2		1279.1	
Absorption coefficient μ/cm^{-1} (Cu$K\alpha$)	80.4		89.5		97.3		109.8	

ment with a focusing monochromator in the diffracted beam and with the X-ray tube and the scintillation counter moving in opposite directions around the stationary sample. The first one, which has been described in a previous paper,[12] was used with Mo$K\alpha$ radiation ($\lambda = 0.7107$ Å), mainly for measurements on the solution B′. The second one, manufactured by Rich. Seifert & Co., was used with Cu$K\alpha$ radiation ($\lambda = 1.5418$ Å) for measurements on all the solutions. The θ range covered ($2\theta =$ the scattering angle) was from 2 to 70 degrees corresponding to an s range ($s = (4\pi/\lambda) \sin\theta$) of about 0.3 to 7.7 (Cu$K\alpha$) or 0.6 to 16.6 Å^{-1} (Mo$K\alpha$). Measurements were performed at discrete points with intervals of 0.2° for Cu$K\alpha$ and 0.25° ($\theta < 25°$) or 0.5° for Mo$K\alpha$. Three combinations of opening, receiving and scatter slits were used to cover the complete θ-range. The data were recalculated to a common slit width using the measurements in overlapping regions. The fraction of incoherent radiation reaching the counter was estimated from the spectrum of the X-ray tube and the resolving power of the monochromator.

For the *small-angle measurements*, a commercial Kratky camera with Ni-filtered Cu$K\alpha$ radiation was used. The sample-detector distance, L, was 219.3 mm. A source slit of 0.08 mm and a detector slit of 0.15 mm were used for all measurements. The solutions were contained in thin-walled Lindemann-type glass capillaries with diameters of 0.5 mm. Of the four solutions A, B, B′ and C, only B′ and C gave appreciable intensities in the observable small-angle region. In order to estimate the influence of interparticle interference and of instrumental effects for these highly absorbing solutions (see Table 1), two more solutions were studied. These were prepared by diluting solution C with water to 1/2 and 1/10 of its original concentration and they will here be denoted C/2 and C/10, respectively.

DATA TREATMENT

Large-angle scattering. The observed intensity values, corrected for background radiation and for polarization in the solution and in the monochromator, were normalized to a stoichiometric unit of volume, V, containing one Th atom (Table 1). The normalization was done by comparing the corrected intensities in the high angle region, with the sum of the independent coherent scattering ($\sum_V n_i f_i^2$) and the incoherent scattering. The normalization was also done by an integration method.[13,14] The scattering factors given by Cromer and Waber[15] for neutral Th, O, and N atoms were used. For H they were taken from the International Tables.[16] Anomalous dispersion corrections were applied to thorium.[17] The incoherent intensity for Th, O and N was obtained from Cromer [18] or Cromer and Mann [19] and for H from Compton and Allison.[20] Corrections were made for the Breit-Dirac [21–23] effect. The normalized intensities, I'_{obs}, were corrected for the incoherent part of the radiation, and the reduced intensity function, $i(s)$, was calculated from the resulting values, I_{obs}, according to the expression: $i(s) = I_{obs} - \sum_V n_i f_i^2$.

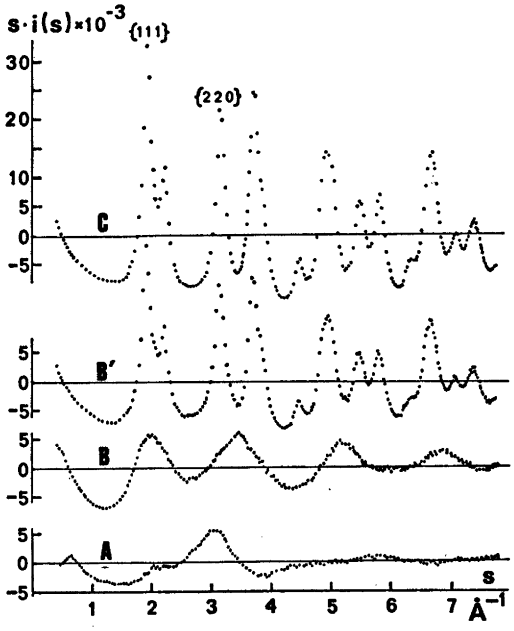

Fig. 2. Reduced intensity functions $i(s)$ in e.u., multiplied by s, for the four solutions A, B, B′ and C, obtained by Cu$K\alpha$ radiation.

Figs. 1 and 2 show the intensity data for the solutions investigated.

The radial distribution functions, $D(r)$, were calculated by a Fourier transformation of the diffraction data according to the expression:

$$D(r) = 4\pi r^2 \varrho_0 + (2r/\pi) \int_0^{s_{max}} si(s)\ M(s)\ \sin(rs)\ ds$$

where ϱ_0 is calculated as $[\sum_V n_i f_i(0)]^2/V$, and $M(s)$ is a modification function of the form $M(s) = [f_{Th}(0)/f_{Th}(s)]^2 \exp(-Ks^2)$, where $\exp(-Ks^2)$ is a damping factor. The K values of 0.02 and

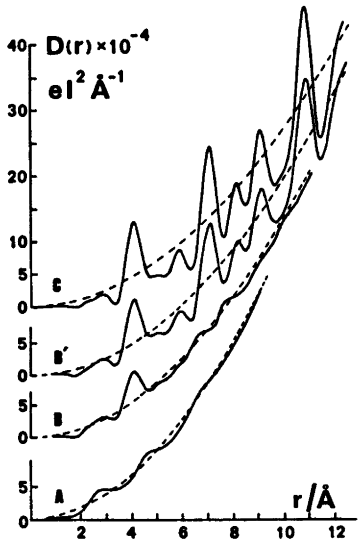

Fig. 3. Radial distribution functions, $D(r)$ (continuous lines), and the corresponding $4\pi r^2\varrho_0$ functions (dashed lines), for A, B, B' and C with Cu$K\alpha$ radiation.

0.01 were used for Cu$K\alpha$ and Mo$K\alpha$ radiations, respectively; the larger value for Cu$K\alpha$ was chosen to reduce the greater truncation errors.

The experimental intensity values were extrapolated to $s = 0$. The $D(r)$ curves were corrected for spurious peaks below 1 Å.[24] Fig. 3 shows the distribution functions obtained for the four solutions A, B, B' and C.

All calculations were carried out by means of computer programs which have been described in a previous paper.[25]

Line-broadening measurements. The pronounced peaks in the scattering curves for the solutions B' and C indicate the presence of small crystalline particles of ThO_2 (see Fig. 1). The average size of these was estimated by comparing the widths of two well-separated peaks ({111} and {220}) with those obtained for a standard specimen consisting of a crystalline powder UO_2, as shown in Fig. 4a. The estimate was made using the formula for spherical particles [26]

$$D = 0.92\lambda/[\Delta(2\theta)\cos\theta]$$

D is the average diameter of the crystallites, λ is the wavelength and 2θ is the scattering angle. The half-maximum line width, $\Delta(2\theta)$ in radians, was corrected for instrumental broadening by means of the expression [27]

$$\Delta(2\theta) = (B-b)^{1/2}(B^2-b^2)^{1/4}$$

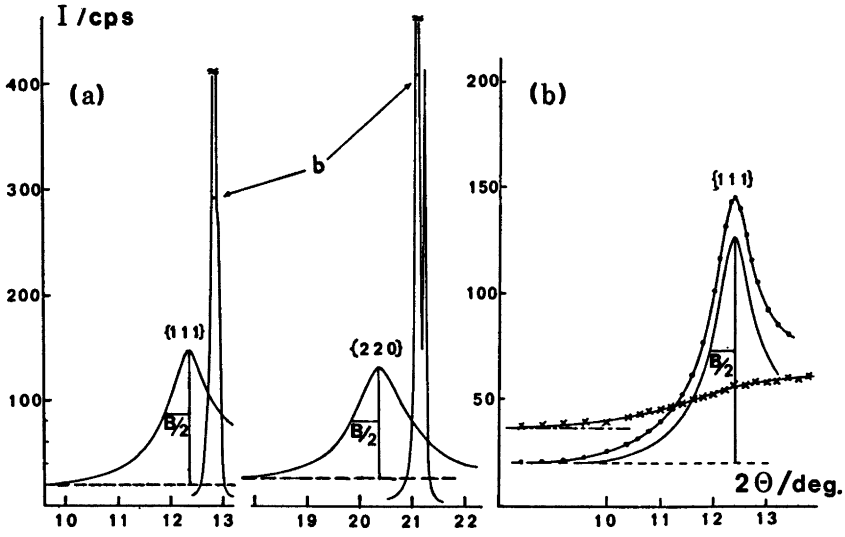

Fig. 4. (a) The {111} and {220} peaks of solution C and corresponding peaks from a crystalline powder of a UO_2 standard specimen. (*b*) Correction for the diffuse scattering for solution C/2. The background scattering from a non-polymerized solution of the same Th concentration (continuous line with crosses) is subtracted from the experimental peak (continuous line with dots). The B value is obtained from the resulting corrected peak (continuous line).

Table 2. Average diameters, D, of the crystallites estimated by line broadening measurements for solutions C, C/2, C/10 and B′ for the two wavelengths used. All B and b values correspond to $\Delta(2\theta)$-values measured in degrees.

Wave-length	2θ/deg.	{hkl}	Sol. C/10 B	D/Å	Sol. C/2 B	D/Å	Sol. C B	D/Å	Sol. B′ B	D/Å
Mo$K\alpha$	12.4	{111}	0.90	43.8	0.96	41.0	1.04	37.6	1.20	32.5
(b=0.08)	20.3	{220}	1.04	38.2	1.00	39.8	0.96	41.4	1.20	32.8
Cu$K\alpha$	27.0	{111}					1.90	44.7	2.20	38.5
(b=0.06)	45.0	{220}					2.00	44.7	2.40	37.1

Here B is the measured line width for the particles in the solution and b is the corresponding value for the standard substance. Correction for the α-doublet separation on the observed B values was found to have a negligible effect.

For the diluted solutions $C/2$ and C/10 a correction for the diffuse scattering from the solution was found to be necessary in order to obtain symmetrical peak shapes. The scattering from a non-polymerized acidic Th solution of the same Th concentration, was subtracted from the experimental intensity curves as shown in Fig. 4b for solution C/2. The results obtained for the four solutions are given in Table 2.

Small-angle scattering. The purpose of the small-angle X-ray scattering (SAXS) investigation was to compare the actual size of the particles in solution with the average size of the crystallites found from the line broadening and large-angle scattering measurements. The following approximate analysis of the data was then considered to be sufficient.

The measured intensities were corrected for parasitic scattering by subtracting intensity values, obtained by the same measuring procedure, for a non-polymerized solution having the same Th concentration. Slit-height corrections were not applied. As shown by Neilson [28] this should not affect to any great extent the results obtained. The scattering curves are shown in Fig. 5a.

For the analysis of the SAXS data the particles were assumed to be spherical. The Guinier approximation for spherical particles of uniform size and scattering density [29] can be written as $I(s)=I(0)\exp[-(sR)^2/5]$, where R is the actual radius of the particles. The intensity values $I(s)$, are in arbitrary units and $s=(4\pi/\lambda)\sin\theta\approx(2\pi x)/(\lambda L)$, where x is the vertical distance from the primary beam as measured on the instrument scale. The Guinier plots, which are shown in Fig. 5b, indicate a non-uniform size distribution for the particles in the solutions. An approximate analysis was made by selecting two different regions of the curves from which a "largest" value (R) and a "smallest" value (r) for the

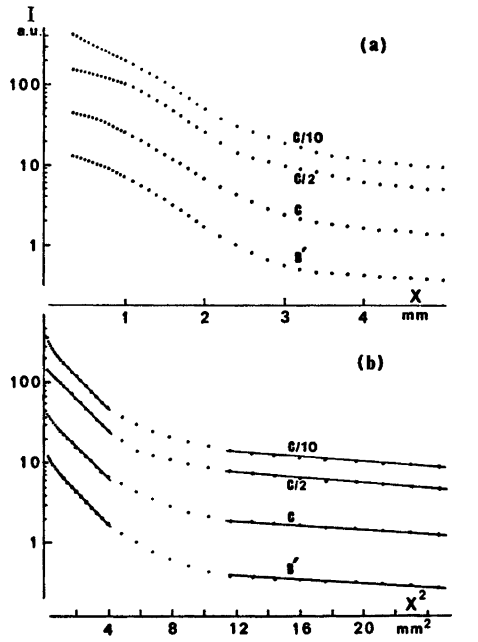

Fig. 5. (a) Experimental small-angle intensities (in arbitrary units a.u.) as a function of the vertical distance x on the instrument scale for solutions C, C/2, C/10 and B′. (b) Guinier plots (log I *versus* x^2) for the same solutions. The lines represent the best fit obtained in the two selected regions. (The intensity values for the solution B′ have been plotted on a different arbitrary scale than that used for the solutions C).

Table 3. Actual particle radii obtained by the Guinier approximation (R and r) and by the Hosemann treatment (r_H). Errors have been estimated by a least squares method (R and r) or by a graphical evaluation (r_H).

Solution	R/Å	r/Å	r_H/Å
C/10	82.9(8)	22.2(6)	62(3)
C/2	83.0(2)	24.0(1)	66(3)
C	81.5(7)	23.8(6)	58(3)
B′	83.7(8)	19.0(6)	64(3)

particle radii were calculated. These values are given in Table 3.

An attempt to determine the particle size distribution by the Hosemann method [29] was also made. In this method the distribution of the radii of gyration of the particles is represented by a Maxwellian distribution of the form

$$F(R_0) = 2R_0^n \exp(-R_0^2/r_0^2)/[r_0^{(n+1)}\Gamma(n/2+1/2)]$$

where Γ is the gamma function. The two parameters n and r_0 defining the Maxwellian distribution were calculated from the expressions $(s_0'/2s_m' - 1) = \frac{1}{2}(n+1)^{-1/2}$ and $r_0 = \frac{3}{\pi s'}(n+2)^{-1/2}$ after a graphical evaluation (Fig. 6a) of s_0' and $s_m'(s' = (2/\lambda)\sin\theta)$.

The arithmetic mean of the actual radii assuming sperical particles of uniform scattering density calculated from $r_H = (5/3)^{1/2} r_0 \times \Gamma(n/2+1)/\Gamma(n/2+1/2)$ is given in Table 3. All of the four values obtained are within 6 %, which does not exceed the precision to be expected from this determination. A Maxwellian distribution curve valid for all four solutions, could then be calculated from the average s_0' and s_m' values, and is given in Fig. 6 b.

INTERPRETATION OF THE DATA

Large-angle scattering. The reduced intensities and the radial distribution curves (RDF) for the four solutions investigated are shown in Figs. 1–3.

The acidic solution, A, and the solution hydrolyzed at room temperature, B, give scattering curves typical of true solutions. For solution B′, which has nearly the same stoichiometric composition as B (Table 1), from which it was obtained by heat treatment, the scattering curve is radically different. Sharp peaks similar to those of a powder pattern occur at the positions expected from the cubic ThO_2 structure (Fig. 1). This change is further accentuated in solution C.

The scattering data were analyzed by comparing peaks in the RDF's with peak shapes calculated for assumed interatomic interactions.[25] The results obtained for solutions A and B are given in Table 4.

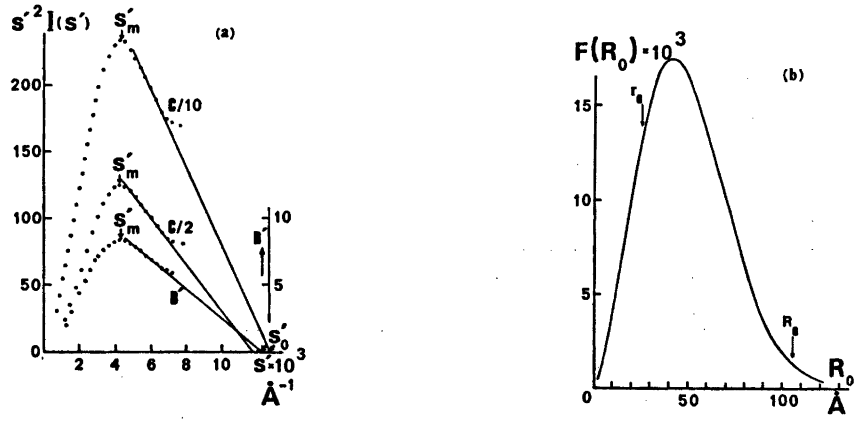

Fig. 6. (a) Values of $(s')^2 I$ *versus* the $s' = (2/\lambda)\sin\theta$ for solutions C/2, C/10 and B′. The value s_m' corresponds to the maximum of the curve. The s_0' value is given by the intersection with the s'-axis of the tangent to the curve at the inflection point. (b) The Maxwellian distribution curve, $F(R_0)$, *versus* the radius of gyration R_0, In the $F(R_0)$ function the gyration radii from the Guinier plots, R_G, and r_G are indicated for comparison.

Table 4. Results of the comparison of calculated peak shapes with the experimental distribution curves for solutions A and B; r_{nm} is the interatomic distance, n_d is the number of distances per Th atom, and b_{nm} is one-half of the mean square variation of the distance.

Interaction	Sol. A (acid) r_{nm}/Å	n_d	b_{nm}/Å²	Sol. B ($n_{HO}=2.88$) r_{nm}/Å	n_d	b_{nm}/Å²
1st Th–O	2.55	5.5	0.01	2.55	7.0	0.01
Th–NO_3 Th–N	3.10	3.5	0.01	3.10	1.1$_5$	0.01
Th–NO_3 Th–O	2.70	7.0	0.01	2.70	2.3	0.01
Th–Th	–	–	–	3.96	4.3	0.008
Coordination number of Th	5.5+7.0=12.5			7.0+2.3=9.3		

For the non-hydrolyzed solution A the analysis leads to the same conclusions as those reported previously.[8] The thorium ion is coordinated to about twelve water and nitrate oxygens, with the nitrate group bonded as a bidentate ligand. In the hydrolyzed solution B($n_{HO} \simeq 2.9$) the coordination number has decreased to a value of about nine, which reflects the decreased coordination of nitrate groups. As shown previously [8] the large peak at 4.0 Å in the RDF can be related to the shortest Th–Th distance within the polynuclear hydrolysis complexes. Each Th atom has an average of about 4 Th neighbours at this distance (Table 4). Two more peaks in the distribution curves – at about 6.5 and 7.5 Å – probably contain major contributions from Th–Th and Th–O interactions within the polynuclear complexes. However, these are much less pronounced than the peak at 4.0 Å.

In the crystal structures of basic thorium salts [7] and in thorium dioxide, which has the cubic fluorite structure [30] the shortest Th–Th distance is close to 4.0 Å, as is also found in the solutions, and occurs between Th atoms joined by two bridging oxygens. In the ThO_2 structure (Fig. 7a) each Th atom is surrounded by 12 other Th atoms at this distance. Eight oxygen atoms arranged at the corners of a cube are coordinated to each thorium. Since heating of solution B leads to the formation of particles, which have the ThO_2 structure, as shown by the scattering curve for solution B′, it would seem reasonable to expect similarities also between the structures of the hydrolysis complexes formed at room temperature in solution B and the structure of ThO_2. However, the long distances at 6.5 and 7.5 Å, indicated in the RDF for the solution B, do not seem to be consistent with distances found in the ThO_2 structure.

The large average number (≥ 4) of Th atoms joined at 4.0 Å to each Th atom in the hydrolysis complexes in solution B (Table 4) and the absence in its RDF of peaks between 4.0 and 6.5 Å, which can reasonably be related to Th–Th interactions, leads to the conclusion that the basic unit in the structure contains a tetrahedron of Th atoms.[8] Since the number of neighbours in a tetrahedron is only three, further Th atoms must be attached to this unit.

In the ThO_2 structure, tetrahedra of Th atoms can be distinguished and the structure may be described as being built up from tetrahedra sharing Th–Th edges or Th corners (Fig. 7a). In such fragments of the structure the longer Th–Th distances occur at 5.60, 6.86, and 7.95 Å, which are inconsistent with those found for the hydrolysis complexes even if we allow for Th–O interactions and for possible distorsions from the regular arrangement in the ThO_2 structure. It seems, therefore, that the bonding of further Th atoms to the basic tetrahedral unit in the hydrolysis complexes differs from that in the ThO_2 structure.

Face-sharing between the tetrahedra would be a conceivable arrangement, but does not occur in the ThO_2 structure. It has, however, been found in hydrolysis complexes of lead(II) [31,32] and tin(IV).[33] In $Pb_6O(OH)_6$ the lead atoms are linked by double oxygen bridges and the complex is built up from three slightly distorted tetrahedra of lead atoms sharing faces. If we use the same model for the thorium

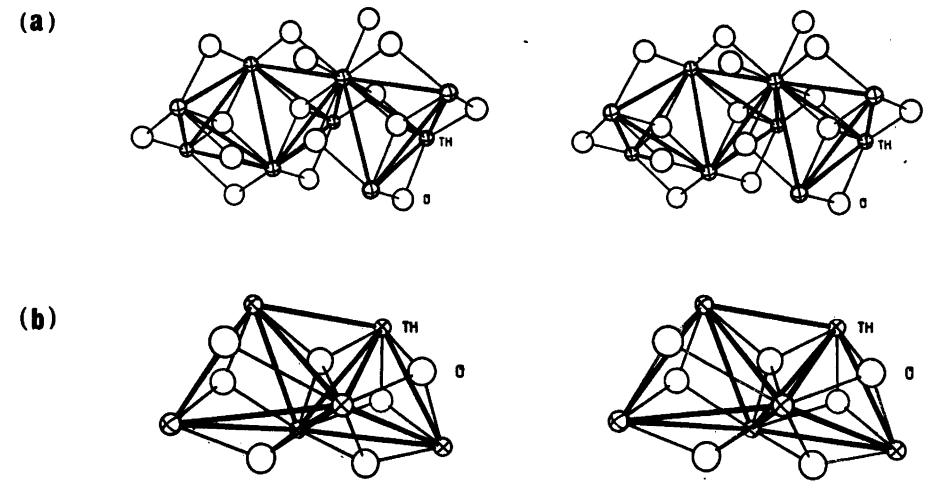

Fig. 7. (a) Fragments of the ThO_2 structure, showing Th tetrahedra sharing corners or edges. (b) The Th_6O_7 complex (analogous to the $Pb_6O(OH)_6$ complex) consisting of three face-sharing tetrahedra of Th atoms.

complexes (Fig. 7b), slightly enlarged to give an average of the short Th–Th distances of 3.96 Å, and calculate the corresponding peak shapes for this complex, we find their positions to be consistent with the peaks in the observed RDF for solution B (Fig. 8). It is possible, therefore, that the hydrolysis complexes formed at room temperature are built up from tetrahedra sharing faces.

Each tetrahedron in the ThO_2 structure contains an oxygen atom at its center. In a structure built up from face-sharing tetrahedra two neighbouring tetrahedra cannot both contain an oxygen. If the double oxygen bridges between the Th atoms are to be retained, as indicated by the short Th–Th distance of 4.0 Å, it can easily be shown that an addition of further face-sharing tetrahedra can occur only in one direction, leading to linear complexes. In an infinite complex of this type the average number of Th neighbours around each Th atom is 6. In a complex containing only three tetrahedra this number is 4 (Fig. 7b). These values, when compared with the value of about 4.3 found from the RDF for solution B, indicate a very limited number of face-sharing tetrahedra in the hydrolysis complexes. This is supported by the absence of pronounced peaks at larger r values in the RDF.

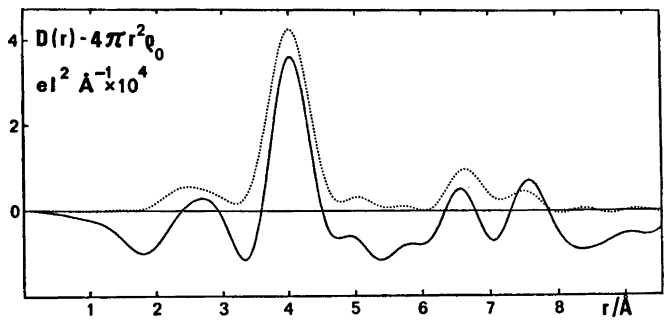

Fig. 8. Comparison between the RDF for solution B (full-drawn line) and the peak shapes (dotted line) calculated for the complex Th_6O_7 in Fig. 7b.

For solutions B′ and C, obtained from B by heat treatment, the scattering data show the presence of large fragments of the ThO_2 structure in the solutions. An analysis of the data, analogous to that carried out for solutions A and B, shows the average number of nearest Th neighbours around each Th atom to be about 7.5 for solution B′ and about 9.6 for solution C, compared to the value of 12 for the "inifinite" ThO_2 structure. Without knowledge of the possible presence of non-crystalline material in the solutions these values cannot be directly used to estimate the size of the particles. However, if the crystallites are sufficiently small, the longer of the interatomic distances occurring in the ThO_2 structure should fall outside a crystallite relatively more frequently than the shorter distances and this can be used to make a rough estimate of the size of the particles. For a distance, d, in the ThO_2 structure the variation of its frequency, n_d, with the size of the crystallite, measured as the number of unit cells along an edge of a cubically shaped particle, is shown in Fig. 9. The ratios $n_d/n(\infty)$, where $n(\infty)$ represents the frequency of the distance in the infinite structure and n_d is estimated from the RDF for solution C, are also shown in Fig. 9. The ratios are seen to decrease approximately as expected for a crystallite size corresponding to 4.5 unit cell edges. As there are no significant differences between the relative sizes of the peaks for B′ and C the same result is obtained for solution B′.

The crystallite size corresponding to 4.5 unit cells is marked by a vertical line in Fig. 9. The corresponding n_d values for the various distances are in agreement with the values determined from the RDF for solution C. It would seem, therefore, that in solution C, but not in solution B′, all thorium is present as ThO_2. In Fig. 10 a comparison is given between the RDF for solution C and peak shapes calculated for all Th–Th and Th–O interactions using different assumptions for the size of the crystallites.

The large-angle scattering data thus indicate that the crystallites in solutions B′ and C have an average size of around 28 Å, which is equivalent to a diameter of about 35 Å for a spherical particle. Although, in this derivation, the very probable occurrence of a distribution of particle sizes and shapes has not been taken into account, calculations based on reasonable assumptions about such distributions show that this will not be critical and the conclusions will still be approximately valid for the average size of the crystallites.

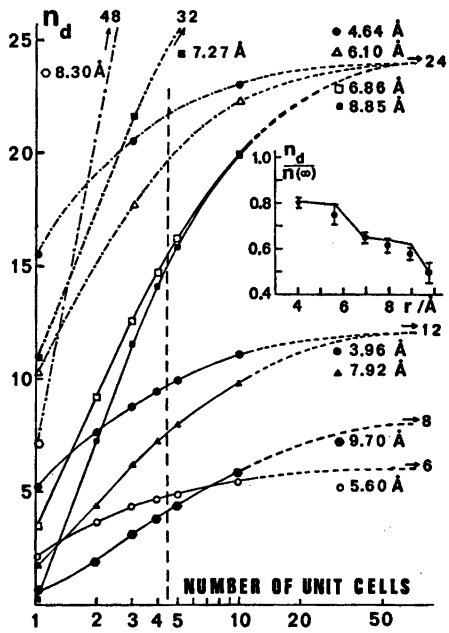

Fig. 9. Variation of the number of neighbours per Th atom, n_d, for distances, d, occurring in the ThO_2-structure as a function of the size of a cube-shaped crystallite measured as the number of unit cells along the crystallite edge. Full and dashed-dotted lines, identified by different symbols, give the n_d values for the first Th–Th and Th–O distances respectively; the limiting values, $n(\infty)$, correspond to the "infinite" ThO_2 structure. The vertical dashed line corresponds to an edge length of 4.5 unit cells. The inset shows the ratio $n_d/n(\infty)$ for the Th–Th distances. The line gives calculated values for a size corresponding to 4.5 unit cells, the dots give the experimental values with the estimated errors for solution C.

Line-broadening measurements. The results are given in Table 2. The diameters found for the crystallites all fall in the range 32 to 45 Å, and thus are of the same order of magnitude as those derived from the large-angle scattering data.

Small-angle measurements. Although solutions B′ and C are stable for a long period of

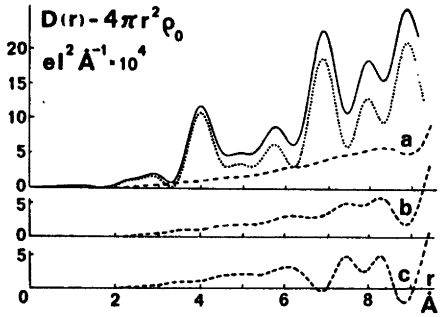

Fig. 10. $D(r)$-curve (full-drawn line) and calculated peak shapes (dots) for solution C(λ = Cu$K\alpha$). The peak shapes are calculated assuming all the Th atoms to be present as cube-shaped crystallites of ThO_2 with an edge length corresponding to 4.5 unit cells; the dashed line, a, represents the difference curve $D(r)$ – peak shapes. Two other difference curves are shown: b, peak shapes calculated assuming 93 % of all Th atoms to occur as cube-shaped crystals of ThO_2 with an edge length of 6 unit cells and c, assuming 80 % of all Th atoms to occur as "infinite" crystals of ThO_2.

time they are strongly opaque and it seems likely that the actual size of the particles in solution is larger than that determined for the crystallites. This is confirmed by the small-angle scattering measurements, which indicate that a range of particle sizes, generally larger than that determined for the crystallites, occurs in the solutions (see Table 3). Thus, each such particle must contain a number of crystallites joined together without any orientational relationship. The parameters s_m' and s_0' defining the distribution of particle sizes, are almost the same for all the solutions investigated (Fig. 8a) which implies that neither further hydrolysis nor dilution affect the particle sizes. The results for the diluted solutions also show that concentration-dependent scattering effects such as interparticle scattering are negligible.

CONCLUSIONS

The X-ray scattering data show that the method used in the present work for the hydrolysis of a thorium nitrate solution, *i.e.* the extraction of HNO_3 from the thorium solution by means of a primary amine, leads to the formation of the same hydrolysis complexes as those obtained by peptization, i.e. by dissolving aqueous thorium oxide in the solution. When the hydrolysis is carried out at room temperature the structures of the hydrolysis complexes formed are based on tetrahedral arrangements of Th atoms in which a Th atom shares two oxygens with each of its neighbors. Similar tetrahedra of thorium atoms with the same Th – Th distance can be distinguished in the ThO_2 structure but the linking of these tetrahedra in the hydrolysis complexes seems to be different from that found in the ThO_2 structure. In ThO_2 the tetrahedra are joined by common corners or edges. In the hydrolysis complexes the scattering data can be interpreted as indicating face-sharing between the tetrahedra. The structure of the hydrolysis complexes formed at room temperature cannot, therefore, be described merely as fragments of the ThO_2 structure, although the basic units in the structures are the same.

The heat treatment leads to the formation of crystallites which have the ThO_2 structure. The combination of large-angle and small-angle measurements has made it possible to distinguish between the actual size of the particles in the solution and the size of the crystallites. It is found that the crystallites have an average size of about 30 – 40 Å and can be joined together, without any orientational relationship, into larger particles.

The structural differences between the hydrolysis complexes formed at room temperature and thorium dioxide may explain the observation that precipitates from solutions hydrolyzed at increased temperature can be sintered into the ThO_2 microspheres used for the preparation of nuclear fuels at considerably lower temperatures (~1100 °C) than those required for precipitates obtained at room temperature (~1600 °C).[9]

Acknowledgements. The authors wish to thank Dr. P. Maltzef for the information given about the sol-gel CNEN process, Messr. A. di Bartolomeo and G. Casavola of Casaccia CNEN for technical assistance in the experimental work, and Dr. D. Lewis and Mr. I. Duncan for linguistic corrections.

Computer time was made available by Casaccia-CNEN and by the Computer Division of the National Swedish Office for Administrative Rationalization and Economy. Two of

the authors (GJ and MS) wish to thank The Swedish Natural Science Research Council for its support.

REFERENCES

1. Hietanen, S. *Acta Chem. Scand. 8* (1954) 1626.
2. Kraus, K. A. and Holmberg, R. W. *J. Phys Chem. 58* (1954) 325.
3. Baes, C. F., Meyer, N. J. and Roberts, C. E. *Inorg. Chem. 4* (1965) 518.
4. Danesi, P. R., Magini, M., Margherita, S. and D'Alessandro, G. *Energ. Nucl. (Milan) 15* (1968) 3359.
5. Hietanen, S. and Sillén, L. G. *Acta Chem. Scand. 22* (1968) 265.
6. Milic, N. B. *Acta Chem. Scand. 25* (1971) 2487.
7. Johansson, G. *Acta Chem. Scand. 22* (1968) 389.
8. Johansson, G. *Acta Chem. Scand. 22* (1968) 399.
9. Scibona, G., Bazzan, A., Cabrini, A., Chiarizia, R., Danesi, P. R., Magini, M. and Mezi, E. *CNEN Nuclear Symposium*, Torino 1967.
10. Baroncelli, F. Scibona, G. and Zifferero, M. *J. Inorg. Nucl. Chem. 24* (1962) 405.
11. Vogel, A. I. *A Text-book of Quantitative Inorganic Analysis*, Longmans, London 1961.
12. Johansson, G. *Acta Chem. Scand. 20* (1966) 553.
13. Krogh-Moe, J. *Acta Crystallogr. 9* (1956) 951.
14. Norman, N. *Acta Crystallogr. 10* (1957) 370.
15. Cromer, D. T. and Waber, J. T. *Acta Crystallogr. 18* (1965) 104.
16. *International Tables for X-Ray Crystallography*, Kynoch Press, Birmingham 1962, Vol. 3.
17. Cromer, D. T. *Acta Crystallogr. 18* (1965) 17.
18. Cromer, D. T. *J. Chem. Phys. 50* (1969) 4857.
19. Cromer, D. T. and Mann, J. B. *J. Chem. Phys. 47* (1967) 1892.
20. Compton, A. H. and Allison, S. K. *X-Rays in Theory and Experiment*, van Nostrand, New York 1935.
21. Breit, G. *Phys Rev. 27* (1926) 362.
22. Dirac, P. A. M. *Proc. Roy. Soc. London Ser. A 111* (1926) 405.
23. Dwiggins, C. W., Jr. and Park, D. A. *Acta Crystallogr. A 27* (1971) 264.
24. Levy, H. A., Danford, M. D. and Narten, A. N. *Data Collection and Evaluation with an X-Ray Diffractometer Designed for the Study of Liquid Structure*, Report ORNL-3960, Oak Ridge National Laboratory, Oak Ridge 1966.
25. Johansson, G. and Sandström, M. *Chem. Scr. 4* (1973) 195.
26. Klug, H. P. and Alexander, L. E. *X-Ray Diffraction Procedures*, Wiley, New York 1974.
27. Taylor, A. *X-Ray Metallography*, Wiley, New York 1961.
28. Neilson, G. F. *J. Appl. Crystallogr. 6* (1973) 386.
29. Guinier, A., Fournet, G., Walker, C. B. and Yudowitch, K. L. *Small-angle Scattering of X-Rays*, Wiley, New York 1955.
30. Wyckoff, R. W. G. *Crystal Structures, Interscience, New York 1963, Vol. 1.*
31. Spiro, T. G., Templeton, D. H. and Zalkin, A. *Inorg. Chem. 8* (1969) 856.
32. Johansson, G. and Olin, Å. *Acta Chem. Scand. 22* (1968) 3197.
33. Wernfors, G. *Acta Chem. Scand. 15* (1961) 1007 and in *Thesis*, Gothenburg 1970.

Received January 26, 1976.

Acta Chemica Scandinavica A 30 (1976) 448—452

Fluoroalcohols. Part 24. Infrared, Matrix Infrared, and Raman Spectra of 1,1,1-Trichloro-3,3,3-trifluoro-2-propanol

JUHANI MURTO,[a] ANTTI KIVINEN[b] and PEKKA SAARINEN[a]

[a] Department of Physical Chemistry, University of Helsinki, Meritullinkatu 1, SF-00170 Helsinki 17, Finland and [b] Department of Pharmacy, University of Helsinki, Fabianinkatu 35, SF-00170 Helsinki 17, Finland

The alcohol 1,1,1-trichloro-3,3,3-trifluoro-2-propanol has been synthesized and its infrared spectra recorded in the gaseous and liquid phases and in argon and nitrogen matrices. In addition the Raman spectrum of the liquid alcohol was recorded. Assignments of the vibration bands are made. The discussion deals especially with vibrations related to the OH group. Two conformers are present in the gaseous and liquid phases. A reversible interconversion between two species of the alcohol occurs in nitrogen matrices when the temperature is varied.

We have previously studied the spectra of the hexahalogenated 2-propanols 1,1,1,3,3,3-hexafluoro-2-propanol (HFP) [2-4] and 1,1,1,3,3,3-hexachloro-2-propanol (HCP) [5] and found significant differences in their behaviour in the OH stretching and torsion regions. Upon temperature variation, reversible changes were observed for these alcohols in nitrogen matrix medium, the most marked changes being in the case of HCP[6]. In the present paper we report results for an alcohol having both a CF_3 and a CCl_3 group, *viz.*, 1,1,1-trichloro-3,3,3-trifluoro-2-propanol (TCTFP). Spectral data for the corresponding ketone (CCl_3COCF_3) will be published elsewhere.[7]

EXPERIMENTAL

1,1,1-Trichloro-3,3,3-trifluoro-2-propanol (a new compound) was synthesized from CCl_3COCF_3 (obtained from PCR, Inc., Gainesville, Florida, U.S.A.) and $LiAlH_4$ (*cf.* HFP, Ref. 8). After several crystallizations (without solvent, or from pentane) the product melted at 29 – 30 °C (long, colourless needles). ^1H and ^{19}F NMR spectra indicated the product to be at least 99 % pure.

The IR spectra were recorded with a Perkin-Elmer 621 spectrometer,[9] the matrix spectra as previously reported,[5,10] varying the matrix to absorber (M/A) ratio between 1000 and 50. The Raman spectra were recorded with a Jarrell-Ash 25 – 305 spectrometer and argon ion laser [9,10] (488 nm exciting line; a slit servo system kept the spectral slit width constant at about 2 cm^{-1}).

RESULTS AND DISCUSSION

The alcohol molecule has 30 fundamental modes of vibration. The molecule has no symmetry, and thus all Raman bands are more or less polarized. The experimental results and assignments are given in Table 1.

Bands related to the OH group. OH conformers. The νOH band of TCTFP is a doublet in the IR spectra of the vapour (peaks at 3629 and 3599 cm^{-1}) and CCl_4 solution (peaks at 3600 and 3560 cm^{-1}). Two conformers are thus obviously present to an appreciable extent. Comparison with other alcohols having CF_3 and/or CCl_3 groups leads us to conclude that the higher-frequency peak is due to conformer II, the lower-frequency peak to conformer I (Fig. 1).

There are two νOH peaks in argon and nitrogen matrix spectra (Figs. 2, 4 and 5), similar to those of HCP. In argon the separation of these groups is only 14 cm^{-1}, whereas in nitrogen it is 50 cm^{-1}. In both matrices there are small irreversible changes in this region on warming the matrix (decrease of the 3586 cm^{-1} band relative to the 3572 cm^{-1} band in

Table 1. The observed frequencies (cm^{-1}) for $CCl_3CHOHCF_3$.

Vapour IR [a]	Argon matrix IR [b]	Nitrogen matrix IR [b,c]	Liquid Raman [d]	Assignment Fundam.	Approximate description [e]
3629 w II		3619, 3614 mw II	3605 [f] (4)	ν_1	νOH
		3592 II			ν_1, end group
	3592 sh	3574 sh I		ν_1	
3599 m I	3586 w	3572 sh I	3560 [f] (4)		νOH
	3578 sh	3568, 3566 m I, Ia			
	3572 m				
	3550	3546 I			ν_1, end group
		3500 II			ν_1, dimer
	3450 br	3465 I			
	3350 br	3350 br			ν_1, polymer
2965 vw I	2960 br, vvw	2960 br, vvw	2960 [f,g] (10) 0.2	ν_2	νCH
2920 vw II			2926 [f,g] (8) 0.2		
		1416 mw II			
	1399 sh			ν_3	
~1395 w	1396 w	1394 w I	1400 (1) >0.5		δ_aCH
	1394 sh				
	1392 sh				
	1348 sh			ν_4	
1343	1344 sh	1349 m	1343 (1)		δ_sCH
	1342 m	1346 sh			
		1286 s II	1285 (2) >0.5	ν_5	
	1256 s	1259 s Ia			δOH
1263 s		1243 w II			
		1235 w II			
	1270 vs	1274 m		ν_6	νCF_3
	1208 sh			ν_7	
1208 vs	1206 s	1204 vs Ia	1185 (1)		νCF_3
	1196 vvs	1187 vvs II			
1160 vvs	1160 vvs	1154 vvs Ia	1146 (2)	ν_8	νCF_3
	1155 vs	1145 vs II			
		1126 m II		ν_9	
1111 s	1112, 1110 s	1117 m I	1110 (3) <0.5		ν_aCCC
		1114 sh I			
		1043 w II		ν_{10}	
1030 w	1033, 1031 w	1036 mw I	1034 (5) 0.5		νCCO
		1030 sh I			
860 sh	864 m	864, 860 m	862 (13) 0.2	ν_{11}	νCCl_3
	861 sh				
840 s	842 sh	839 sh	835 (5) 0.7	ν_{12}	νCCl_3
	839 s	836 s Ia			
790 m	793 sh	791 m I	787 (6) 0.7	ν_{13}	ν_sCCC
	791 s				
		785 m II			
690 s	691 m		689 (6) 0.5	ν_{14}	$\delta_s CF_3$ ("umbrella")
	687 s	688 vs			

Table 1. Continued.

655 s	656 m 649 w 646 s	659 s 656 m 649 sh	658 (35)	0.10	ν_{15}	$\nu_s CCl_3$
~570 w	572 w	576 w	574 (2)	0.8	ν_{16}	δCF_3
~525	526 w 524 sh	524 w	525 (5)	<0.1	ν_{17}	δCF_3
~455 vw	456 w	458 w	461 (39)	0.08	ν_{18}	$\delta_s CCO$, $\nu_s CCl_3$
	402 vw		404 (100)	0.04	ν_{19}	$\delta_s CCl_3$ ("umbrella")
		420 sh 418 w Ia 410 m 396 w 394 w			ν_{20}	τOH
	333 m 326 ms 322 vs	325 br, w II				
	346 s	345 w	343 (9)	0.5	ν_{21}	$\delta_a CCO$
	290 w	290 w	295 (21)	0.75	ν_{22}	δCCl_3
	284 sh	282 sh	287 sh		ν_{23}	$\delta_s CCC$
	261 vw	269 vvw	264 256 (7)	0.6	ν_{24} ν_{25}	ϱCF_3 ϱCF_3
			215 (20)	0.6	ν_{26}	δCCl_3
			190 (10)	0.8	ν_{27}	ϱCCl_3
			154 (9)	0.7	ν_{28}	ϱCCl_3
			N.O.		ν_{29}	τCF_3
			N.O.		ν_{30}	τCCl_3

[a] Incomplete data due to low vapour pressure. [b] Intensities refer to matrices with large M/A ratios (before warming). [c] The two species are designated by I and II (see text), Ia relating to the strongest νOH band of species I. [d] The relative intensities are given in parentheses. The figures after these are the depolarization ratios. N.O. = not observed. [e] ν = stretching, δ = bending, ϱ = rocking, τ = torsion; s = symmetric, a = asymmetric vibration (local symmetry). [f] 9.1 Wt. % in CCl_4. [g] Only one peak is seen in the neat liquid [2950 (16) 0.2].

argon, decrease of the shoulders at 3574 and 3568 cm^{-1} in nitrogen).

In argon it is not clear, whether there are one or two OH conformers present (see Refs. 5 and 2). It seems possible that the conformer ratio changes during the deposition and that the νOH splitting is not due to OH conformers. No marked changes due to the IR beam occurred in the νOH region during the time interval 20 s to several hours (after opening the beam shutter) (*cf.* 2-fluoroethanol and 2-chloroethanol,[11] for which a change from the *gauche* conformer to the *trans* conformer was observed in the IR beam).

Marked reversible changes occur in the nitrogen matrix with changes in temperature:[6] with increasing temperature the peak at 3566 cm^{-1} increases, while that at about 3617 cm^{-1} decreases (Fig. 4). Similar, but still more marked changes have been observed for HCP.[5,6]

The energy difference of the two species was found to be about 150 J mol^{-1},[6] with the species giving rise to the higher νOH frequency being that of the lower energy. Since the peak height ratios change fast in response to changes in temperature, the energy barrier between the two species is obviously low. We found [6] the

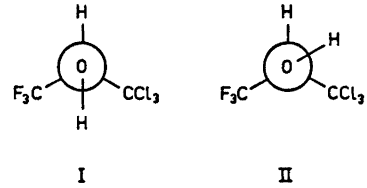

Fig. 1. The conformers of TCTFP.

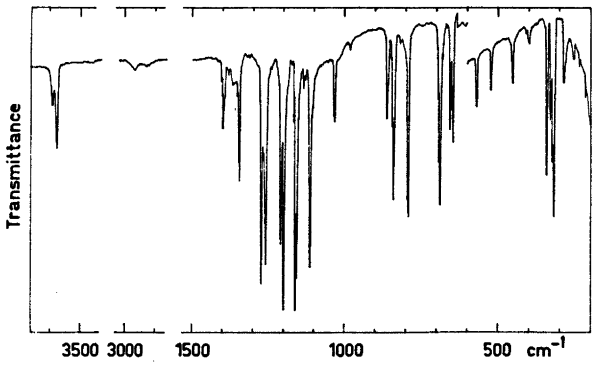

Fig. 2. IR spectrum of TCTFP in argon, M/A= 1000, 16 μmol TCTFP deposited during 2½ h at 13 K. The spectrum was recorded at 10 K.

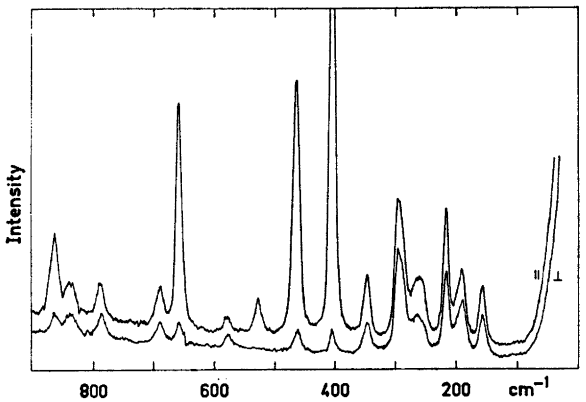

Fig. 3. Raman spectrum of liquid TCTFP in the region 900 – 0 cm^{-1}, single-pass cell.

formation of species II from species I to involve one nitrogen molecule in the cases of HCP and HFP, and the same is probably true also for TCTFP. Species I and II in nitrogen are probably related to the conformers I and II shown in Fig. 1, although the species in nitrogen may more properly be considered as nitrogen complexes of TCTCP.[5]

The changes in the νOH region of the nitrogen spectrum are paralleled by changes in the δOH and τOH regions (Fig. 4). The positions of the νOH, δOH and τOH bands of species II indicate a more "free" OH group than in the case of species I.

TCTFP has less tendency to associate than HFP, but considerably more than HCP. In the IR spectrum of the pure liquid the monomer absorption band is at 3550, 3600 sh cm^{-1} and

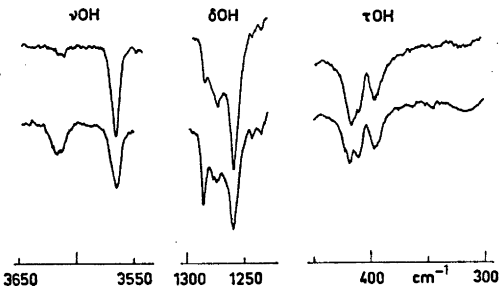

Fig. 4. νOH, δOH and τOH regions of TCTFP in a nitrogen matrix (M/A=500, 16 μmol TCTFP deposited during 1 h). The matrix was deposited at 13 K, annealed by warming to 27 K and the spectra were then recorded at 10 K (lower curves) and at 22 K (upper curves).

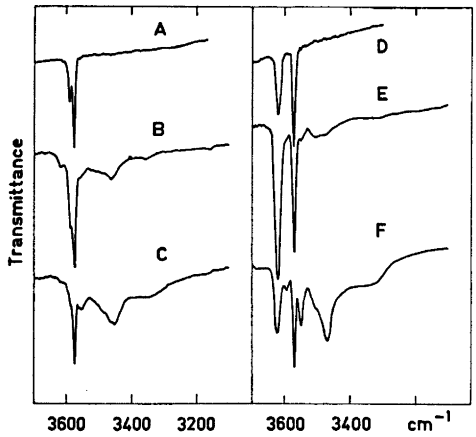

Fig. 5. IR spectra of the νOH region of TCTFP in argon (A, B and C) and nitrogen (D, E and F) matrices, recorded at 10 K. A, M/A = 1000, 16 μmol TCTFP deposited; B M/A = 50, 45 μmol deposited; C, the same as B, but after warming to 37 K; D, M/A = 1000, 12 μmol deposited; E, M/A = 50, 45 μmol deposited; F, the same as E, but after warming to 32 K.

the dimer absorption (equal in intensity to the monomer absorption but somewhat broader) at 3470 cm^{-1}.

Fig. 5 deals with the association in matrices. Separate "dimer end group" absorptions are observed for the two forms of TCTFP in nitrogen (Fig. 5F). Their intensity indicates a considerable fraction of "linear" dimers to be present.

Only one δOH peak is seen in the argon spectrum, although this region shows several bands in nitrogen (see Fig. 4).

The τOH band is the usual triplet in argon (Fig. 2), being much less intense than in the case of HCP. In nitrogen it consists of three relatively sharp peaks at 418, 410 and 395 cm^{-1}, somewhat like those found for HFP (but differing from the spectrum of HCP), and of a broader absorption at about 325 cm^{-1}, which obviously corresponds to species II. In CCl_4 the broad τOH band is at about 330 cm^{-1}, as in the case of HCP.[5]

Other fundamentals. The νCH absorption is a doublet in vapour and CCl_4 spectra (in both cases the peaks are at 2965 and 2920 cm^{-1}).

The assignment of the other bands is indicated in Table 1. As is usual with polychloro compounds, the group frequency approximation is relatively poor. Some band splitting may occur in the matrix spectra because of the chlorine isotope effect.[5]

The most intense band of the Raman spectrum is that at 404 cm^{-1}, which must thus refer to the CCl_3 group.

Our assignment of the vibrations of the CF_3 and CCl_3 groups is similar to that given for 1,1,1-trichlorotrifluoroethane.[12]

Acknowledgements. Miss Tuula Suontausta is thanked for preliminary work on TCTFP. We gratefully acknowledge financial support from the Jenny and Antti Wihuri Foundation of the Finnish Academy of Science, and from the Science Research Council of Finland.

REFERENCES

1. Part 23: Kivinen, A., Murto, J., Liljeqvist, S. and Vaara, S. *Acta Chem. Scand. A 29* (1975) 911.
2. Barnes, A. J. and Murto, J. *J. Chem. Soc. Faraday Trans. 2* (1972) 1642.
3. Murto, J., Kivinen, A., Viitala, R. and Hyömäki, J. *Spectrochim. Acta 29 A* (1973) 1121.
4. Murto, J., Kivinen, A., Näsäkkälä, M., Viitala, R. and Hyömäki, J. *Suom. Kemistil. B 46* (1973) 76.
5. Murto, J., Kivinen, A., Räsänen, M. and Perttilä, M. *Spectrochim. Acta. In press.*
6. Murto, J., Kivinen, A. and Mutikainen, I. *Chem. Phys. Lett. 36* (1975) 369.
7. Murto, J., Kivinen, A. and Suontausta, T. *Finn. Chem. Lett.* (1976) 50.
8. Middleton, W. J. and Lindsey, R. V., Jr. *J. Am. Chem. Soc. 86* (1964) 4948.
9. Murto, J., Kivinen, A., Kajander, K., Hyömäki, J. and Korppi-Tommola, J. *Acta Chem. Scand. 27* (1973) 96.
10. Murto, J., Kivinen, A., Edelmann, K. and Hassinen, E. *Spectrochim. Acta 31 A* (1975) 479.
11. Murto, J., Kivinen, A., Halonen, L. and Perttilä, M. *Unpublished results.*
12. Laloraya, R. K. and Laloraya, K. *J. Chem. Phys. 61* (1974) 1918.

Received February 26, 1976.

Acta Chemica Scandinavica A 30 (1976) 453—456

Thermodynamics of Transfer of Nonelectrolytes from Light to Heavy Water. III. Transfer Free Energies of Tertiary Aromatic Amines

ANTTI VESALA and JUKKA KAIKKONEN

Department of Chemistry, University of Turku, SF-20500 Turku 50, Finland

The free energies of transfer from H_2O to D_2O for pyridine, eight substituted pyridines, quinoline, and acridine have been determined by distribution and solubility measurements. Correlations between the transfer free energy and different solvation properties are presented. The properties concerned here are the basicity, the so-called hydrophilic character, and the relative amount of hydrogen atoms in the solute molecule.

Studies of aqueous solutions by means of replacing H_2O by its isotopic form D_2O have been increasing lately. Two main approaches have been applied to explain the changes in solution properties between H_2O and D_2O. The first approach is based on a statistical model for the solute in the solvent water. The other treats the problem by trying to find correlations with various other solution properties in the transfer from H_2O to D_2O. These two methods of operation have a strong thermodynamical basis, although the latter also involves some extra-thermodynamic assumptions and correlations.

Recently Ben Naim [1] published a paper using the first approach. He applies statistical mechanics to relate the isotopic effect in the standard free energy in light and heavy water with the change in the average number of hydrogen bonds in the solvent. Although the model is simple, it is possible to classify some solutes as structure breakers and structure promoters.

With the second approach it is difficult to find universal correlations giving additional knowledge about water solutions. Several attempts, including the ones made by the present writers, have been made to solve the problem with the aid of the thermodynamic transfer properties from H_2O to D_2O.[2–5] The transfer free energy, which, in practice, is the only thermodynamic quantity that can be investigated without calorimetric measurements in this context, is very sensitive to many influences.

We have here determined the transfer free energies from H_2O to D_2O for a limited group of compounds, namely tertiary aromatic amines. These are slightly polar compounds with no exchangeable hydrogens. In pyridine the substituents are mainly at positions 2 and/or 6. The main focus of interest has been to study the substituent effect on the values of $\Delta G_t^\ominus$, the standard free energy of transfer from H_2O to D_2O. The solubilities of pyridines in water, in general, are of such magnitude that the distribution measurements were the only possible means for determining the transfer free energies. This, on the other hand, caused greater experimental errors than if the $\Delta G_t^\ominus$ values had been determined by some direct method, *e.g.* by solubility measurements. However, some distinct features are found in the correlations between $\Delta G_t^\ominus$ and other solution properties.

EXPERIMENTAL

Light and heavy water (Norsk Hydro, deuterium mol fraction 0.997) was treated as described earlier.[4] The pyridines were commercial products of *purissimum* grade. 2-Pentylpyridine was synthesized from 2-methylpyridine and 1-chlorobutane with sodamide in anhydrous

xylene.[6a] Quinoline was synthesized in the conventional way.[6b] Both the commercial and synthesized products were redistilled before use. Acridine was purified by recrystallizing twice from ethanol.

The free energies of transfer from H_2O to D_2O of 2-pentylpyridine and acridine were determined by solubility measurements. For the others the free energy values were determined by distribution measurements. The third solvent used in the partitioning of the solutes was 2,2,4-trimethylpentane (BDH, special for spectroscopy).

The analysis of the pyridines was carried out in either of the two following ways. In connection with the distribution measurements a titration method was used. Samples were taken from the organic phase and weighed and transferred to approximately 40 cm^3 of glacial acetic acid and titrated in a Metrohm Combi Titrator Type 3D with perchloric acid of known molarity. The second method of analysis was spectrophotometrical using a Beckman DK-2A Ratio Recording Spectrophotometer. A standard solution was first prepared in water and proper amounts of it were injected with an Agla micrometer syringe directly into the tared spectrophotometer cell filled with water. The absorbances were measured and plotted *versus* concentration to obtain a standard curve. The samples were taken from the aqueous phase and transferred with the Agla syringe to the spectrophotometer cell. The absorbances were then measured and the corresponding concentrations read on the standard curve.

In the distribution measurements the equilibrium was allowed to settle for at least three days. In the solubility measurements a longer time *viz.* one week was needed. The equilibration vessels were sealed flasks, which were kept in complete darkness to prevent a possible decomposition by light. These flasks were kept in a water bath of constant temperature of 298.15 ± 0.05 K. The contents of the flasks were mixed during the equilibration by a magnetic stirrer.

RESULTS AND DISCUSSION

The free energy of transfer from H_2O to D_2O for solubility measurements can be evaluated in the way described earlier.[4] In the distribution measurements the simple calculations presented below are needed. Moderately low concentrations ($< 10^{-2}$ mol/dm^3) were used to assure the ideality of the system. The following equilibria prevail in the distribution experiments (the third solvent, 2,2,4-trimethylpentane, is denoted by S):

$$\text{solute}(m_H, H_2O) = \text{solute}(m_S, S) \quad (1)$$

$$\text{solute}(m_D, D_2O) = \text{solute}(m_S', S) \quad (2)$$

The partition coefficients are as follows

$$k_1 = m_S/m_H \quad (3)$$

$$k_2 = m_S'/m_D \quad (4)$$

If the solution in the third solvent is assumed to behave ideally, the partition coefficient (6) for the wanted equilibrium (5) is obtained.

$$\text{solute(hypoth. 1 m soln, } H_2O) = \text{solute(hypoth. 1 m soln, } D_2O) \quad (5)$$

$$K = k_1/k_2 = (m_S m_D)/(m_H m_S') \quad (6)$$

Table 1. Partition coefficients k_1 and k_2 and free energies of transfer from H_2O to D_2O of some tertiary aromatic amines.

Compound	k_1[a]	k_2[a]	$\Delta G_t^\ominus$/J mol^{-1}
1. Pyridine	41.79 ± 0.58	47.14 ± 1.76	306 ± 90
2. 2-Methyl-pyridine	157.7 ± 1.1	172.2 ± 1.4	218 ± 27
3. 2-Ethyl-	848.7 ± 2.2	896.0 ± 2.1	134 ± 11
4. 2-Pentyl-[b]	$(3.037 \pm 0.006)10^{-3}$	$(3.169 \pm 0.008)10^{-3}$	-104 ± 10
5. 2,6-Dimethyl-	544.8 ± 2.1	584.2 ± 2.1	174 ± 13
6. 2,4,6-Trimethyl-	1703 ± 19	1786 ± 25	118 ± 45
7. 2-Methoxy-	1344 ± 13	1536 ± 9	329 ± 28
8. 2,6-Dimethoxy-	15780 ± 107	17352 ± 71	235 ± 20
9. 2-Vinyl-	787.5 ± 8.9	903.4 ± 7.0	340 ± 35
10. Quinoline	1586 ± 9	1873 ± 17	412 ± 33
11. Acridine[b]	$(1.601 \pm 0.006)10^{-4}$	$(1.372 \pm 0.001)10^{-4}$	382 ± 18

[a] ($\pm$)-Values are standard errors. [b] Solubility values (aquamolal scale).

The free energy of transfer from H_2O to D_2O is then calculated from the well-known equation (7).

$$\Delta G_t^{\ominus} = -RT \ln (m_S m_D)/(m_H m_S') \quad (7)$$

The measured partition coefficients and the free energies of transfer calculated therefrom are tabulated in Table 1. The values for m_H and m_D are expressed in aquamolal scale. The m_S values are for practical reasons expressed as mg/g, which has no effect on the $\Delta G_t^{\ominus}$ values being calculated in aquamolal scale.

The error limits reported in connection with the $\Delta G_t^{\ominus}$ values are based on standard deviations of the mean values. Therefore, the real absolute errors may be of greater magnitude. These data together with the previous results indicate that the values of standard free energies of transfer can be measured with an accuracy of ± 10 %.

Not enough data exist for a correlation similar to the one described in an earlier paper, *i.e.* the correlation of the transfer free energy from H_2O to D_2O *versus* the free energy of dissolution in water of the compounds in question.[4] Instead, the increments of the so-called intrinsic hydrophilic character, reported by Hine and Mookerjee have been applied.[7] In practice, this correlation (Fig. 1) is similar to that described in paper I in this series.[4] It shows that the increments of Hine and Mookerjee are useful at least within a certain group of compounds.

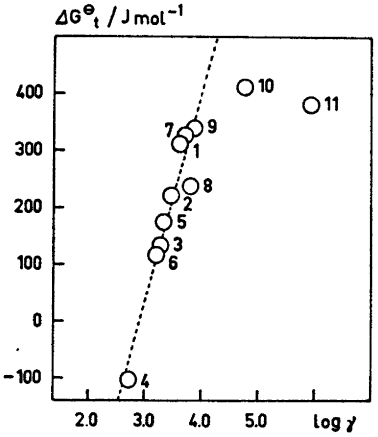

Fig. 1. Correlation between the free energy of transfer from H_2O to D_2O ($\Delta G_t^{\ominus}$) and the so-called hydrophilic character of some tertiary amines.

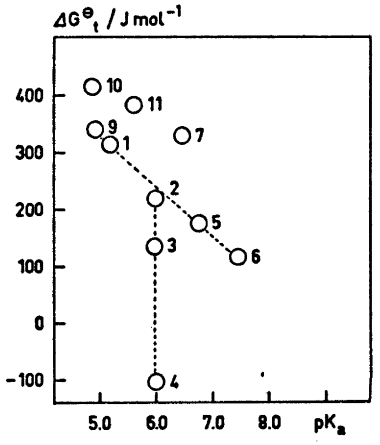

Fig. 2. Correlation between the free energy of transfer from H_2O to D_2O ($\Delta G_t^{\ominus}$) and the pK_a values of protonated tertiary aromatic amines.

Quinoline and acridine which deviate from the correlation line do not belong to the pyridine series.

Polar effects naturally play a marked role in the solvation of the solute in water. Therefore, one might expect that the basicity of the nitrogen atom would correlate with a quantity reflecting the dissolution phenomenon, *viz.* $\Delta G_t^{\ominus}$. Fig. 2 shows the plot of $\Delta G_t^{\ominus}$ *versus* pK_a the acidity constants of the conjugated acids having been taken from literature.[8] The cor-

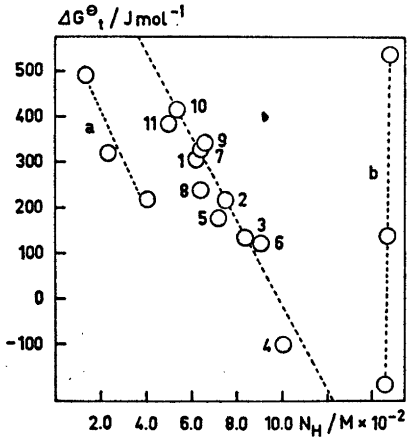

Fig. 3. Correlation between the free energy of transfer from H_2O to D_2O ($\Delta G_t^{\ominus}$) and the number of hydrogen atoms relative to molecular weights of solutes (a. the nitrobenzene group, b. the aliphatic amine group; Ref. 4.)

relation obtained is good especially for methylpyridines. Quinoline and acridine show small deviations which are to be expected considering their structures. There is, however, one striking feature in this plot, namely, the effect of the lengthening of the carbon chain of the substituent at position 2 in the pyridine ring (points 2, 3, and 4). A clear tendency towards lower free energies is observed when the length of the chain increases. This suggests that the polar effects, although important, are not the only ones operating in the dissolution phenomenon. We can call these additional effects hydrophobic or structure making. This same tendency is clearly observed in triethyl-, tripropyl-, and tributylamines. It can thus be said that in the dissolution of these compounds there exists a struggle between hydrophilic and hydrophobic characters.

One measure for the hydrophobic character is the number of hydrogen atoms in the solute molecule interacting with the solvent water. If this number is calculated on a relative basis, that is to say, if the number of hydrogen atoms divided by the molecular weight is chosen for this measure, the correlation in Fig. 3 is obtained. For this kind of limited group of compounds the correlation is satisfactory. No universal correlation is obtained on this basis. This can be seen in Fig. 3, where besides the pyridine group a nitrobenzene group and a tertiary aliphatic amine group are plotted as examples. These two last-mentioned groups deviate structurally from pyridines and also markedly from each other which is also indicated by the plots. This correlation can be used, however, as a good method of approximation for compounds whose structures closely resemble each other.

REFERENCES

1. Ben Naim, A. *J. Phys. Chem. 79* (1975) 1268.
2. Dahlberg, D. B. *J. Phys. Chem. 76* (1972) 2045.
3. Jolicoeur, C. and LaCroix, G. *Can. J. Chem. 51* (1973) 3051.
4. Vesala, A. *Acta Chem. Scand. A 28* (1974) 839.
5. Vesala, A. *Acta Chem. Scand. A 28* (1974) 851.
6. Vogel, J. A. *Textbook of Practical Organic Chemistry*, 3rd Ed., Longmans, London 1970, *a*. p. 845, *b*. p. 828.
7. Hine, J. and Mookerjee, P. K. *J. Org. Chem. 40* (1975) 292.
8. Katritzky, A. R., Ed, *Physical Methods in Heterocyclic Chemistry*, Vol. I, Academic, London 1963, p. 67.

Received December 19, 1975.

Acta Chemica Scandinavica A 30 (1976) 457—460

Conformational Analysis XV.* Preparation of Some Alkyl-substituted 5-Oxo-1,3-oxathiolans and Their Characterization with the Aid of Chemical Equilibration, ^{1}H NMR and IR Spectra

KALEVI PIHLAJA, ALPO NIKKILÄ, KARI NEUVONEN and RAIMO KESKINEN

Department of Chemistry, University of Turku, SF-20500 Turku 50, Finland

5-Oxo-1,3-oxathiolan and seven alkyl-substituted derivatives were prepared and their ^{1}H NMR and IR spectra recorded. 2,4-Dimethyl- and 2-*t*-butyl-4-methyl-5-oxo-1,3-oxathiolans which were mixtures of *cis* and *trans* forms were chemically equilibrated and the obtained thermodynamic parameters used to determine the conformational energies of 2a-Me, 2a-*t*-Bu, and 4a-Me groups (7.6, 9.8, and 1.2 kJ mol^{-1}, respectively). All the collected data are in agreement with a ring conformation where the sulfur atom is situated at the tip of an envelope form.

In spite of the fact that the 5-oxo-1,3-oxathiolan system has been frequently studied [1-7] only two of these reports [1,2] consider simple alkyl-substituted derivatives. Farines [1] has prepared compounds *1* – *7* but her configurational and conformational conclusions seem to need some revision. Satsumabayashi *et al.*[2] report the preparation of *2* and (*5* + *6*) only but do not pay any attention to the isomerism of 2,4-dimethyl-5-oxo-1,3-oxathiolan (*5* + *6*).

The above observation together with our earlier studies on the 1,3-oxathiolan system [8-10] prompted us to investigate the conformational and configurational properties of alkyl-substituted derivatives in some detail using ^{1}H NMR, IR and chemical equilibration as tools.

* For Part XIV see Nikander, H., Mukkala, V.-M., Nurmi, T. and Pihlaja, K. *Org. Magn. Reson. 8* (1976). *In press.*

EXPERIMENTAL

The compounds were synthesized from a suitable aldehyde or acetone and thioglycolic acid (E. Merck, *reinst*) or thiolactic acid (Fluka, *practicum*).[1,2] Their physical constants are collected in Table 1.

We were not able to separate *cis* and *trans* forms of 2,4-dimethyl- (*5* + *6*) and 2-*t*-butyl-4-methyl-5-oxo-1,3-oxathiolans (*9* + *10*). In the former case, however, their existence was revealed by the ^{1}H NMR spectrum and in the latter case also by gas chromatographic analysis (a 2 m × 3 mm stainless steel column containing 5 % Carbowax 20M on Chromosorb G, 60/80 mesh). Chemical equilibration of these epimer pairs was carried out in CCl_4 solutions at several temperatures (from 9 to 46 days) following the procedure described earlier.[9,10] The equilibrium ratios (Table 2) of the isomers were determined from the area of the 4-Me ^{1}H NMR signals (*5* + *6*) or from the gas chromatographic peak areas (*9* + *10*).

The ^{1}H NMR spectra were recorded with a Perkin-Elmer R-10 60 MHz NMR spectrometer (10 % v/v CCl_4 or C_6H_6 solutions) on a precalibrated paper with TMS as an internal standard. The obtained chemical shifts and coupling constants which are means of at least six separate scans are given in Table 3.

IR spectra were recorded on a PE-180 IR spectrometer using a capillary film between KBr windows. The IR results are listed in Table 4. The accuracy of the carbonyl bands is ±0.5 cm^{-1} and of the other bands ±3 cm^{-1}.

RESULTS AND DISCUSSION

We agree with Farines [1] that due to the lactone grouping –C–O–C(=O)–C–, the only significant conformation of the 5-oxo-1,3-oxathiolan ring (*1*) is the one with the sulfur

Table 1. Physical constants for the prepared 5-oxo-1,3-oxathiolans.

Substitution		B.p., K/kPa	M.p., K	n_D^{293}	d_{277}^{293}	Yield, %
Nil	(1)	357/1.60		1.5181		47
2-Me	(2)	343/1.20		1.4972		41
4-Me	(3)	352/1.47		1.4988	1.256	74
2,2-diMe	(4)	349–359/1.07		1.4835		30
2,4-diMe[a]	(5+6)	349/1.73		1.4804	1.159	66
2,2,4-triMe	(7)	355/1.87		1.4722		50
2-*t*-Bu	(8)	365–367/1.60	289	1.4803		85
2-*t*-Bu-4-Me[a]	(9+10)	371–373/1.60	297	1.4733[b]	1.104	86

[a] Mixtures of *cis* and *trans* forms. [b] At 298 K.

Table 2. ^{1}H NMR spectral data for the studied 5-oxo-1,3-oxathiolans.

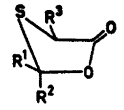

				Chemical shift (δ_{CCl_4}) and $\Delta = (\delta_{CCl_4} - \delta_{C_6H_6})$								Coupling const.(Hz)		
R^1	R^2	R^3		H(2)	Δ	H(4)	Δ	Me(2)	Δ	Me(4)	Δ	$J_{2,4}$	$J_{2,Me}$	$J_{4,Me}$
H	H	H	*1*	5.21	0.61	3.52	0.50							
Me	H	H	*2*	5.58	0.47	3.66	0.45	1.69	0.43				6.1	
H	H	Me	*3*	5.15	0.53	3.81	0.37			1.55	0.27	0.5[a,d]		7.2
Me	Me	H	*4*			3.75	0.37	1.75	0.35					
Me	H	Me	*5*	5.47	0.53	3.97	0.48	1.76	0.56	1.53	0.26	0.4	6.0	7.1
H	Me	Me	*6*	5.57	0.57	3.91	0.43	1.76	0.56	1.55	0.30	0.6	5.9	7.3
Me	Me	Me	*7*			4.09	0.34	1.75	0.35	1.56	0.22			7.2
t-Bu	H	H	*8*[b]	5.20	0.36	3.50[c]	0.38[c]	1.01	0.21			0.7		
						3.61	0.49					0.6		
t-Bu	H	Me	*9*	5.19	0.40	3.92	0.37	1.03	0.18	1.53	0.22	0.45[d]		7.1
H	*t*-Bu	Me	*10*	5.18	0.29	3.80	0.32	1.03	0.21	1.58	0.26	0.75[d]		7.3

[a] In α-bromonaphthalene where $J_{2,2'} = -6.9$ Hz, [b] $J_{4,4'} = -16.5$ Hz, [c] R^3, [d] Based on 300 MHz spectra.

Table 3. Equilibria between isomeric 2,4-dimethyl- and 2-*t*-butyl-4-methyl-5-oxo-1,3-oxathiolans at different temperatures and thermodynamic quantities for the studied isomer equilibria.

T	$K = [cis]/[trans]$ 2,4-diMe	2-*t*-Bu-4-Me
288	1.680±0.038	1.416±0.014
303	1.624±0.082	1.398±0.008[a]
303		1.398±0.039[a]
318	1.571±0.025	1.359±0.020
334	1.511±0.033	1.330±0.031[b]
334		1.334±0.030[b]
356		1.297±0.012[c]
356		1.303±0.014[c]
358		1.289±0.018
$-\Delta H°$, kJ mol^{-1}	1.84±0.08	1.18±0.05
$-\Delta S°$, J mol^{-1} K^{-1}	2.07±0.27	1.16±0.16
$-\Delta G°(298)$, kJ mol^{-1}	1.22	0.83

[a,b,c] Parallel experiments.

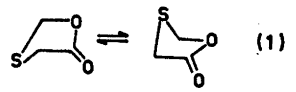

(1)

atom at the tip of an envelope form. However, we do not agree with her proposal that 2-methyl-5-oxo-1,3-oxathiolan (*2*) exists predominantly in the envelope form with an axial methyl group (*2b*). On the basis of our earlier knowledge of 1,3-oxathiolans [8–10] the interaction due to an axial methyl group in the position 2 should at least exceed 4 kJ mol^{-1} which is supported by our results dealing with 4-vinylbutyrolactone.[11] In the light of our present

(2)

(*2b*) (*2a*)

Table 4. The characteristic bands in the IR spectra of the studied 5-oxo-1,3-oxathiolans.

	Substitution	Peaks, cm^{-1} [a]
1	Nil	2910w, 2895w, *1831*shw, *1771s*, *1730*shm, 1462w, 1403m, 1121m, 1020s, 633w
2	2-Me	2925m, *1774s*, *1752.5*shs, 1449w, 1439w, 1408m, 1124m, 1103w, 1069s, 1018m 940m, 900m, 616w
3	4-Me	2930m, 2895m, 2870m, *1817*shm, *1768*s, 1462m, 1448m, 1087m, 1052m, 1021s, 994m, 946w, 660w, 627w, 606m
4	2,2-diMe	2930m, 2870w, *1790*shs, *1769.5s*, 1457m, 1439m, 1413m, 1110shm, 1094s, 1030w, 979s, 937s, 910w, 623w, 595w, 565w
5+6	2,4-diMe	2930m, 2870w, *1769*s, 1446m, 1078s, 1065shm, 1045s, 1015m, 995m, 928s, 607w 592w
7	2,2,4-triMe	2930m, 2870w, *1766s*, 1448m, 1107s, 1088m, 1051s, 1004m, 967s, 603w, 588m
8	2-*t*-Bu	2930shs, 2900m, 2865m, *1776.5s*, *1697*shm, 1476s, 1462m, 1407m, 1121m, 1037s, 1012s, 937m, 916m, 900m, 655w, 576w
9+10	2-*t*-Bu-4-Me	2930m, 2900m, 2865m, *1772*s, 1477m, 1462shm, 1448m, 1082w, 1058shm, 1033s, 1011s, 938m, 918m, 610w

[a] The accuracy of the line positions is ± 3 cm^{-1} except the carbonyl bands (italics) ± 0.5 cm^{-1}.

results the equatorial form (*2a*) really is greatly favoured. 4-Methyl-5-oxo-1,3-oxathiolan (*3*) also favours slightly the conformation with an equatorial methyl group in agreement with the postulation of Farines [1] (Tables 2 and 4). The ^1H NMR results confirm this conclusion since *3* gives an average signal for H(2), δ 5.15, that is 0.06 ppm shielding when compared with *1*. 2-Me has a 0.37 ppm deshielding effect on H(2). In other words the average of the H(2) signals of *5* and *6* should be δ 5.52 in excellent agreement with the experimental findings. The same situation prevails in the case of H(4) for both *5+6* and *9+10*.

Otherwise the ^1H NMR spectra serve mainly as an analytical tool only except the $^4J_{2,4}$ coupling constants for *5+6* and *9+10*. The *cis* forms (*5* and *9*) show clearly smaller $^4J_{2,4}$ values than the *trans* forms, an observation which is in excellent agreement with the $^4J_{2,5}$ values in correspondingly substituted 4-oxo-1,3-dioxolans.[12]

To determine the thermodynamic quantities for the equilibria (3) we equilibrated *5+6* and *9+10* at several temperatures. The values of the equilibrium constants at several temperatures are shown in Table 3 together with the thermodynamic quantities derived from them. In agreement with the observations in the case of 2,4-disubstituted 1,3-oxathiolans [10] the predominant conformation of the *trans* isomers is *6a* or *10a*. *Cis* isomers have anancomeric diequatorial envelope forms (*5a* and *9a*).

By assuming that the small but definite entropy differences for the epimer equilibria are mainly due to mixing of *6a* and *6b* or *10a* and *10b* we estimate $x_{6a} \sim 0.93$ and $x_{10a} \sim 0.97$. Since the entropy difference between the *trans* envelopes is likely to be negligible we obtain $\Delta H°_{obs} = 0.93x + 0.07(x + 6.4)$ for *5+6* and $\Delta H°_{obs} = 0.97x + 0.03(x + 8.6)$ for *9+10* from which we obtain $-\Delta H°(4a-Me) = 1.2 \pm 0.5$ kJ mol^{-1}. Consequently, $-\Delta H°(2a-Me) = 7.6 \pm 1.0$ and $-\Delta H°(2a-t\text{-}Bu) = 9.8 \pm 1.0$ kJ mol^{-1} in reasonable agreement with similar estimates for 1,3-oxathiolans.[10,13]

Let us finally inspect the IR results (Table 4). All compounds give main carbonyl bands in the

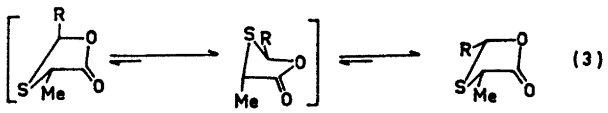

(3)

(*5b*) R = Me (*6a*) (*5a*) R = Me

(*10b*) R = *t*-Bu (*10a*) (*9a*) R = *t*-Bu

range 1766 – 1774 cm^{-1} typical of γ-lactones.[14] The values for single compounds show some additivity but the variation is too small to allow any further discussion. The bands arising from C – S linkages are found between 565 and 660 cm^{-1} and depend clearly on the degree of substitution at C(2) and C(4). Strong absorption in the range 900 – 1100 cm^{-1} is also typical of various sulfur compounds.[14] The deformation vibrations around 1450 cm^{-1} and the $\delta(SCH_2)$ bands around 1405 cm^{-1} are also characteristic for the compounds in question. The location of the bands in the range 2860 – 2930 cm^{-1} is also clearly modified from that found for C – H bonds in hydrocarbon radicals.[14]

Acknowledgements. The authors wish to thank Mr. Markku Kivimäki for some technical assistance and the Science Research Council of the Finnish Academy and the Emil Aaltonen Foundation for financial support. We are also indebted to Professor Marc Anteunis from the State University of Gent for providing the 300 MHz spectra of *3* and *9* + *10*.

REFERENCES

1. Farines, M. *Contribution a l'etude de quelques heterocycles a cinq elements*, University of Perpignan, France, 1973.
2. Satsumabayashi, S., Irioka, S., Kudo, H., Tsujimoto, K. and Matoki, S. *Bull. Chem. Soc. Jpn. 45* (1972) 913.
3. Pailer, M., Streicher, W., Takacs, F. and Moersdorf, K. *Monatsh. Chem. 99* (1968) 891.
4. Romo de Vivar, A. and Romo, J. *J. Org. Chem. 24* (1959) 1490.
5. Pedersen, C. Th. *Acta Chem. Scand. 20* (1966) 2314; *22* (1968) 247; *23* (1969) 489.
6. Møller, J. and Pedersen, C. Th. *Acta Chem. Scand. 24* (1970) 2489.
7. Okada, Y., Japan 6825,497, 4 November 1968, Appl. 13 July 1963, *Chem. Abstr. 70* (1969) 57812.
8. Pihlaja, K. *Suom. Kemistil. B 43* (1970) 143 and *J. Am. Chem. Soc. 94* (1972) 3333.
9. Keskinen, R., Nikkilä, A. and Pihlaja, K. *Tetrahedron 28* (1972) 3943.
10. Keskinen, R., Nikkilä, A., Pihlaja, K. and Riddell, F. G. *J. Chem. Soc. Perkin Trans 2* (1974) 466.
11. Pihlaja, K., Riddell, F. G., Jalonen, J., Rinta-Panttila, P. and Anteunis, M. *Org. Magn. Reson. 6* (1974) 301.
12. Asabe, Y., Takitani, S. and Tsuzuki, Y. *Bull. Chem. Soc. Jpn. 48* (1975) 966.
13. Pihlaja, K., Nikkilä, A. and Keskinen, R. *Bull. Soc. Chim. Belg. In press.*
14. Abram, M. and Mateescu, Gh. D. *Infrared Spectroscopy*, Wiley-Interscience, Bukarest 1972, Chapter II. 4, 290.

Received January 29, 1976.

Acta Chemica Scandinavica A 30 (1976) 461—467

The Crystal and Molecular Structure of α-Tetrakis (acetylacetonato)thorium(IV)

BERT ALLARD

Department of Nuclear Chemistry, Chalmers University of Technology, Fack, S-402 20 Göteborg 5, Sweden

The crystal and molecular structure of α-tetrakis-(acetylacetonato)thorium(IV), molecular formula $[Th(C_5H_7O_2)_4]$, has been determined from three-dimensional X-ray intensity data. The unit cell is monoclinic and belongs to the space group $P2_1/c$ with the lattice parameters $a = 11.768(2)$ Å, $b = 12.792(2)$ Å, $c = 17.039(3)$ Å, $\beta = 112.24(2)°$ and $Z = 4$. The structure determination was based on 1358 reflexions which were collected with the Weissenberg multiple-film technique. The structure was refined to a final R-value of 0.078. The coordination polyhedron around the thorium atom is a distorted dodecahedron (D_{2d}-$\bar{4}2m$). The Th – O bond distances range from 2.35 to 2.43 Å with a mean value of 2.38 Å. In contrast to most other dodecahedral structures involving bidentate ligands, the ligands, in this structure span adjacent vertices between the two orthogonal trapezoids in the dodecahedron. The over-all D_2 symmetry is nearly achieved. The ligands are folded 18° about the line joining the oxygen atoms within the ligand.

As a part of a systematic study of the properties of tetravalent actinide acetylacetonates [1–3] the α-form of thorium(IV) acetylacetonate (in this report denoted by α-$Th(AA)_4$) has been synthesized and investigated. Based on previous structure investigations,[3] theoretical considerations [4] and solution experiments [5] it has been suggested, that a change from a predominantly antiprismatic coordination (for the β-form) to a dodecahedral coordination (for the α-form) of the tetrakis acetylacetonates tend to occur with increasing radius of the central atom. The thorium complex would be the best choice for the study of such an effect, since thorium is the largest atom of the actinides and group IVb elements in the tetravalent state. Preliminary structure data from electron density projections have been previously given for α-$Th(AA)_4$ [6,7] but these data do not conclusively establish the nature of the inner coordination polyhedron. Lattice parameters and ligand configuration have also been suggested for the isomorphous α-$Ce(AA)_4$.[8]

EXPERIMENTAL

Preparation of the crystals. α-$Th(AA)_4$ was prepared by precipitation from an aqueous thorium nitrate acetylacetone solution, by addition of ammonia,[9] or by an extractive procedure previously used for β-$Np(AA)_4$.[10] By recrystallization from an organic solvent at room temperature, the α-form was almost exclusively formed. The β-form could sometimes be obtained from polar solvents at elevated temperature or by vacuum sublimation carried out just below the melting point. Recrystallization from benzene, however, yielded a solvate with the composition $Th(AA)_4 \cdot \frac{1}{2}C_6H_6$, which will be described in a following communication. For the complex α-$Th(AA)_4$ the metal content was determined radiometrically (α-counting using liquid scintillation technique) and the purity was checked by comparing recorded infrared spectra with spectra obtained from the literature.[12]

X-Ray methods. The structure investigation was based on single crystal X-ray diffraction measurements using an integrated Weissenberg equi-inclination multiple-film technique. A freshly prepared crystal with the dimensions $0.09 \times 0.11 \times 0.31$ mm^3 was mounted along the longest crystal axis denoted as the c-axis in a 0.2 mm glass capillary. Weissenberg photographs of the layers $hk0 - hk13$ were taken, using Cu$K\alpha$ radiation. The intensities were measured with an optical densitometer. The intensities of the four films recorded for each layer were brought to a common scale by a least squares procedure and were corrected

for Lorentz and polarization effects. When a preliminary structure had been found, a correction for absorption was performed.

The unit cell dimensions were obtained from X-ray powder photographs by using a Guinier focusing camera with $CuK\alpha$ radiation and an internal standard of potassium chloride.

The computations were carried out on an IBM 360/65 computer. The programs used were POWDER, SCALE, DATAP2, DRF, BLOCK, LALS, LINUS, DISTAN, PLANEFIT and ORTEP.[12]

STRUCTURE DETERMINATION AND REFINEMENT

The lattice parameters were obtained by a least-squares refinement of powder data. Preliminary values from single crystal measurements were used as starting parameters.

Cellparameters are given in Table 1. The systematic absences corresponded to the space group $P2_1/n$. After the refinement, the atomic parameters and unit cell dimensions were transferred to $P2_1/c$ in order to facilitate direct comparison with the isomorphous α-$Ce(AA)_4$. (Values given in Table 3 and Fig. 2 correspond to $P2_1/c$).

The positions of the thorium atoms were deduced from the three-dimensional Patterson synthesis. From a three-dimensional electron density difference synthesis the positions of the eight chelated oxygen atoms were found. A difference synthesis based upon the positions of the atoms located revealed the positions of the carbon atoms. The positions of the hydrogen atoms were not determined.

The inter-layer scale factors and preliminary parameters were improved by full-matrix least-squares refinement. The quantity $\sum w(|F_o| - |F_c|)^2$ was minimized with weights $w = (a + |F_o| + c|F_o|^2)^{-1}$ chosen according to Cruickshank.[14] Only reflexions with $0.70 < |F_o|/|F_c| < 1.40$ were refined. The scattering factors given by Cromer and Waber [15] were used for thorium and those of Doyle and Turner [16] for oxygen and carbon. An analysis of the weighting scheme is given in Table 2.

After refinement with only the thorium atom localized the conventional discrepancy index $R = \sum||F_o| - |F_c||/\sum|F_o|$ had a value of 0.21, which indicates the dominance of the heavy atom. Refinement with all non-hydrogen atoms localized without correction for absorption and with isotropic thermal parameters gave the value $R = 0.09$. After correction for absorption the value $R = 0.078$ was obtained. When allowance was made for unisotropic thermal parameters and with an over-all scale factor refinement, the value $R = 0.72$ was obtained, but since the ratio between the number of reflexions and the number of refined parameters in this case was low (5.2) very high values of the standard deviations were obtained. In Table 3 only the isotropic thermal parameters are given.

An attempt to introduce correction for extinction and anomalous scattering in the

Table 1. Crystallographic data for α-$Th(AA)_4$.

Unit cell:[a]	Monoclinic with $a = 16.664(2)$ Å $b = 12.792(2)$ Å $c = 17.039(3)$ Å $\beta = 40.88(2)°$ $V = 2374.0(8)$ Å^3 $Z = 4$
Formula weight:	$M = 628.48$
Density:	$\varrho_{obs} = 1.74$ g cm^{-3} $\varrho_{calc} = 1.758$ g cm^{-3}
Systematic absences:	$h0l$ when $h+l = 2n+1$ $0k0$ when $k = 2\ n+1$
Space group:	$P2_1/n$
General point positions:	4 *e*: $\pm(x,y,z;\ \pm(\frac{1}{2}+x,\ \frac{1}{2}-y,\ \frac{1}{2}+z)$
Linear absorption coefficient:	$\mu_{CuK\alpha} = 220$ cm^{-1}

[a] For $P2_1/c$ the lattice parameters $a = 11.768(2)$ Å, $b = 12.792(2)$ Å, $c = 17.039(3)$ Å and $\beta = 112.24(2)$ Å are obtained.

Table 2. Analysis of the weighting scheme $w=(20.0+|F_o|+0.016\,|F_o|^2)^{-1}$.

F_o interval	$w\Delta^2$	Number of reflexions	$\sin\theta$ interval	$w\Delta^2$	Number of reflexions
0–24	0.71	132	0.00–0.46	1.50	351
24–29	0.71	133	0.46–0.59	1.22	324
29–33	0.89	136	0.59–0.67	0.93	246
33–37	1.01	135	0.67–0.74	1.20	166
37–43	0.92	134	0.74–0.79	1.15	119
43–49	1.03	134	0.79–0.84	1.31	79
49–56	0.72	134	0.84–0.88	1.00	44
56–64	1.20	132	0.88–0.93	1.51	6
64–79	1.21	131	0.93–0.96	0	0
79–195	1.41	134	0.96–1.00	0	0

Table 3. Atomic coordinates, expressed as fractions of unit cell edges, and isotropic thermal parameters with their standard deviations (in parenthesis) for α-Th(AA)$_4$.

Atom	x	y	z	B, Å^2
Th	0.1903(1)	0.1464(1)	0.2003(1)	3.25(1)
O1	0.0618(25)	0.1791(21)	0.0562(19)	5.7(6)
O2	0.0398(19)	0.0150(18)	0.1535(17)	4.0(5)
O3	0.2108(22)	0.3323(16)	0.2005(18)	4.2(5)
O4	0.0098(19)	0.2219(18)	0.2061(14)	3.3(5)
O5	0.1888(23)	0.1200(19)	0.3379(16)	4.1(5)
O6	0.3885(22)	0.1914(21)	0.3011(15)	4.6(6)
O7	0.3010(17)	−0.0141(17)	0.2275(15)	3.3(4)
O8	0.3297(20)	0.1361(19)	0.1256(20)	5.0(5)
C1	−0.0858(34)	0.2295(20)	−0.0668(25)	4.2(8)
C2	−0.0514(28)	0.1637(22)	−0.0007(17)	2.4(5)
C3	−0.1182(35)	−0.0761(32)	0.0196(28)	5.5(9)
C4	−0.0645(28)	0.0118(25)	0.0991(26)	3.4(7)
C5	−0.1623(33)	−0.0773(31)	0.0967(29)	4.5(8)
C6	0.1837(36)	0.5057(26)	0.1704(30)	4.9(8)
C7	0.1377(29)	0.4091(33)	0.1865(30)	5.9(9)
C8	−0.0018(37)	0.4048(30)	0.1633(29)	5.7(9)
C9	−0.0524(36)	0.2988(34)	0.1811(28)	4.9(8)
C10	−0.1971(32)	0.3070(38)	0.1699(22)	5.2(9)
C11	0.2233(41)	0.0994(39)	0.4882(30)	5.1(9)
C12	0.2597(35)	0.1093(28)	0.4078(31)	5.0(8)
C13	0.3880(27)	0.1353(34)	0.4352(29)	4.0(7)
C14	0.4339(26)	0.1844(46)	0.3667(31)	5.0(9)
C15	0.5737(43)	0.1931(45)	0.4095(41)	5.4(9)
C16	0.4478(45)	−0.1447(38)	0.2789(26)	5.1(9)
C17	0.4071(28)	−0.0492(35)	0.2303(26)	4.8(8)
C18	0.4571(33)	−0.0010(31)	0.1776(32)	5.0(8)
C19	0.4270(28)	0.0811(26)	0.1329(25)	3.6(7)
C20	0.4842(33)	0.1256(33)	0.0735(31)	5.4(8)

refinement afforded no improvement. The parameters obtained in the last cycle of refinement are given in Table 3. Observed and calculated structure factors are available on request. A final difference synthesis, calculated by using the refined parameters given in Table 3 did not show any unexpected maximum or minimum.

DESCRIPTION AND DISCUSSION OF THE STRUCTURE

The coordination polyhedron composed of eight chelated oxygen atoms around the thorium atom in α-Th(AA)$_4$ is a distorted dodecahedron (D_{2d}-$\bar{4}2m$) as shown in Fig. 1. The ligand rings are essentially planar, while the thorium atom is displaced from this plane, producing a fold with an average value of 18° across the O – O line of the 6-membered ring. The packing of the molecules is illustrated in Fig. 2.

From the parameters in Table 3 distances and angles defining the geometry of the α-Th(AA)$_4$ molecule were calculated and are given in Table 4. The geometry of one ligand with average geometrical parameters is shown in Fig. 3. These average values are in line with previously obtained parameters for other acetylacetonates,[1-3] indicating a C – C single bond and C – CH and C – O bonds with significant double bond character.[17] The C – CH bonds seem, however, to be unexpectedly long.

The differences between measured and average values are sometimes large and are in cases larger than 3σ. There is, however, no systematic deviation which would indicate a lower ligand symmetry than the expected C_{2v}. Discrepancies in bond lengths and angles must be interpreted as indicative of systematic errors in the data, such as uncorrected absorption, rather than an actual distortion of the molecule. Another reason for the poor accuracy can be the unfavourable proportion between the heavy and light atoms in the molecule. The single thorium atom constitutes 37 % of the total molecular weight and the $Z_{heavy}^2/\sum Z_{light}^2$ ratio is 6.4. Moreover, the complex

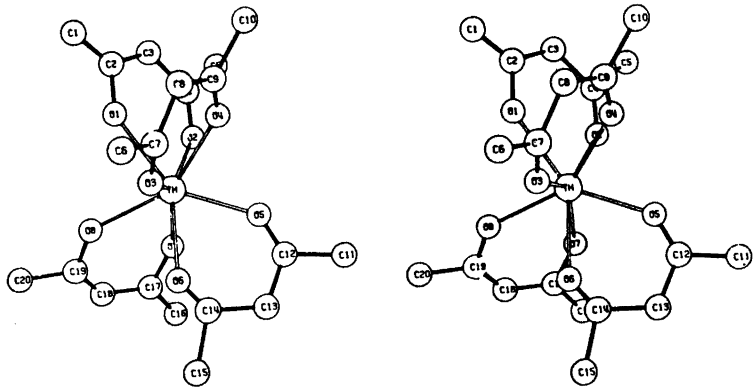

Fig. 1. The α-Th(AA)$_4$ formula unit (stereoscopic drawing).

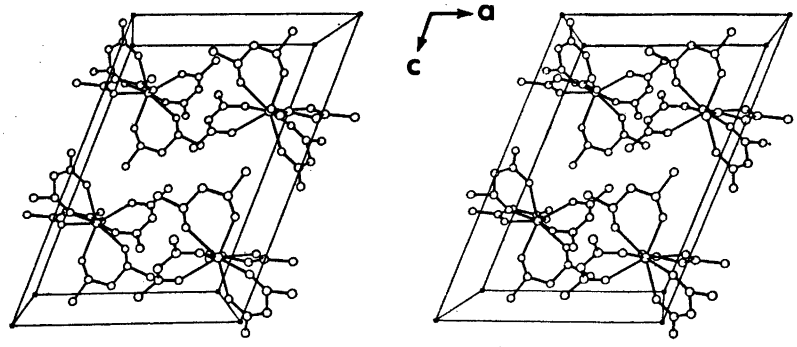

Fig. 2. The unit cell of α-Th(AA)$_4$ (stereoscopic drawing).

Table 4. Distances and angles for α-Th(AA)$_4$ (in Å and °) with their standard deviations (in parenthesis). The notation is in accordance with Fig. 1.

	Distance		Angle
Th–O1	2.38(2)	O1–Th–O2	70.9(9)
Th–O2	2.35(2)	Th–O1–C2	143(2)
O1–C2	1.33(4)	Th–O2–C4	134(2)
O2–C4	1.23(4)	O1–C2–C3	115(3)
C1–C2	1.34(4)	O2–C4–C3	128(3)
C2–C3	1.48(5)	C2–C3–C4	123(3)
C3–C4	1.50(5)	O1–C2–C1	115(3)
C4–C5	1.60(5)	O2–C4–C5	123(3)
O1–O2	2.75(3)	C1–C2–C3	131(3)
Th–C3	3.87(4)	C3–C4–C5	109(3)
Th–O3	2.39(2)	O3–Th–O4	71.6(8)
Th–O4	2.37(2)	Th–O3–C7	135(2)
O3–C7	1.27(4)	Th–O4–C9	139(3)
O4–C9	1.21(4)	O3–C7–C8	127(4)
C6–C7	1.41(5)	O4–C9–C8	124(4)
C7–C8	1.53(6)	C7–C8–C9	116(3)
C8–C9	1.55(6)	O3–C7–C6	116(4)
C9–C10	1.64(5)	O4–C9–C10	124(4)
O3–O4	2.79(3)	C6–C7–C8	116(4)
Th–C8	3.91(4)	C8–C9–C10	113(3)
Th–O5	2.38(2)	O5–Th–O6	72.1(8)
Th–O6	2.38(2)	Th–O5–C12	138(3)
O5–C12	1.18(5)	Th–O6–C14	136(3)
O6–C14	1.15(5)	O5–C12–C13	124(4)
C11–C12	1.58(6)	O6–C14–C13	130(3)
C12–C13	1.44(5)	C12–C13–C14	117(3)
C13–C14	1.58(5)	O5–C12–C11	124(4)
C14–C15	1.53(6)	O6–C14–C15	122(4)
O5–O6	2.80(3)	C11–C12–C13	110(4)
Th–C13	3.79(3)	C13–C14–C15	107(4)
Th–O7	2.38(2)	O7–Th–O8	68.1(8)
Th–O8	2.43(2)	Th–O7–C17	139(2)
O7–C17	1.31(4)	Th–O8–C19	136(3)
O8–C19	1.31(4)	O7–C7–18	117(4)
C16–C17	1.45(6)	O8–C19–C18	123(4)
C17–C18	1.39(6)	C17–C18–C19	131(4)
C18–C19	1.26(5)	O7–C17–C16	114(3)
C19–C20	1.52(6)	O8–C19–C20	109(3)
O7–O8	2.70(3)	C16–C17–C18	128(4)
Th–C18	3.80(3)	C18–C19–C20	128(3)

slowly disintegrated by X-ray irradiation.

For the dodecahedral coordination three different stereoisomers corresponding to different ligand attachments are possible for bidentate ligands with a fixed ring span. These are, with the notations given by Hoard,[4] I*d*-*mmmm*, II*d*-*gggg* and III*d*-*gggg* where *g* and *m* denotes edges of the polyhedron according to Fig. 4. Only I*d* and III*d* have the overall D_2 symmetry, which makes formation of polyhedron hybrides with antiprismatic coordinated isomers possible. So far only eight-coordinate chelates with dodecahedral configuration of type I*d* and III*d* are known. The isomer I*d* seems to be by far the most common configuration,[18] although lately β-diketonates of type III*d* have been found.[19,20] The configuration of α-Th(AA)$_4$ corresponds to isomer III*d* although a significant antiprismatic feature is observed. (Previously, α-Ce(AA)$_4$ has been denoted as

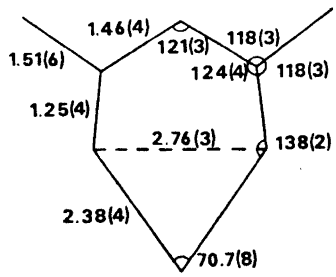

Fig. 3. The geometry of the acetylacetonate ligand in α-Th(AA)$_4$ (average values with standard deviations, in Å and °).

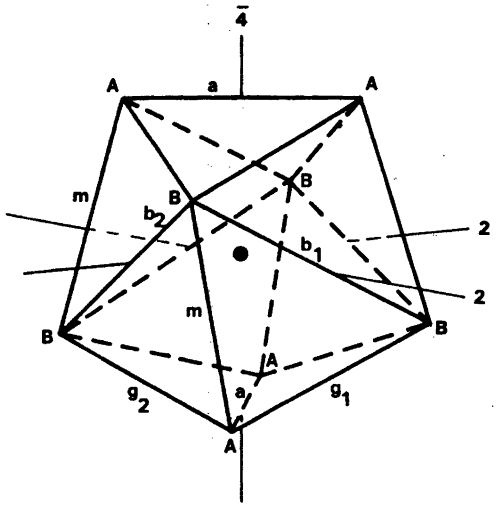

Fig. 4. The dodecahedron (D_{2d}-$\bar{4}2m$). Notations according to Hoard.[4]

predominantly antiprismatic.[8]) In Table 5 distances between the oxygen atoms in the coordination polyhedron are given.

For the dodecahedron orthogonality between the two trapezoids is required.[21] This criterion is very poorly fulfilled. Nevertheless description of the coordination as dodecahedral seems appropriate since the individual shape parameters, not the average values, for the whole polyhedron show the best correspondence with isomer III*d* when compared with values of the most favourable polyhedron.[4] This is, however, surprising, since the I*d* isomer should be more probable if ligand atom repulsion is considered as having the main influence on the choice of configuration.[22] Moreover, the β-form of tetravalent acetylacetonates, which is antiprismatic in the II*a* configuration,[3] show dodecahedral distortion towards I*d*, as would be expected, and not towards III*d*. This steric divergence between the two forms may be due to different bonding interaction, or intermolecular interaction due to a fortuitous packing in the solid state of the α-form. Different bond strength in the two forms, *e.g.* caused by various degrees of π overlap between ligand and metal, would be likely to influence the ligand geometry and would cause changes in the infrared spectrum. No significant differences between α- and β-Th(AA)$_4$ indicating such an effect have, however, been found.[23] Packing relations could be the main factor determining the preferred coordination polyhedron. Any short intermolecular distances indicating interaction between adjacent molecules have not been found. The closest intermolecular distances

Table 5. Distances between oxygen atoms within the dodecahedral coordination polyhedron for α-Th(AA)$_4$ (average values, in Å), with III*d* configuration, and distances in the most favourable polyhedron,[4] calculated for Th–O = 2.38 Å. Notations according to Fig. 4.

Polyhedron edge	Measured values	Calculated values (most favourable polyhedron) III*d*	I*d*	II*a*
a	2.91(2)	2.79	3.55	3.00
b_1[a]	3.80(20)	3.55	4.90	4.00
b_2	3.30(7)	3.55	2.79	3.00
m	2.85(9)	2.79	2.95	2.84
g_1[b]	2.76(5)	2.95	2.79	2.84
g_2	3.01(16)	2.95	2.95	3.00

[a] The edges b_1 and b_2 are unequal. This is consistent with a distortion towards the antiprosmatic isomer II*a*, when b_1 corresponds to a diagonal of the square face, giving $b_1 > b_2$. [b] The edge spanned by ligands.

between non-bonded atoms are 3.32 Å (C4 – C2) and 3.45 Å (C2 – O2).

For acetylacetonates with the small central atoms zirconium and hafnium only the β-form is known,[22] while for thorium acetylacetonate, which has the largest central atom of all possible tetravalent acetylacetonates, the α-form is far more easily prepared than the β-form, which decomposes rapidly at room temperature. This is an indication that the size of the central atom has a marked influence on the choice of coordination polyhedron. For the more bulky dibenzoylmethanates only one form is known for different tetravalent metals.[23] The inner coordination corresponds to the dodecahedral I*d* isomer, which is completely in agreement with the predicted most favourable polyhedron.[22] The effect of substituting the acetylacetonate ligand with the still larger dipivaloylmethanate ligand on the inner coordination would be of considerable interest, and a structure investigation of thorium dipivaloylmethanate is in progress.

Acknowledgements. The X-ray measurements were performed at the Department of Inorganic Chemistry, Chalmers University of Technology and the University of Göteborg. I am greatly indebted to Professor G. Lundgren and Professor N.-G. Vannerberg for all facilities put at my disposal and for helpful encouragement. Thanks are also due to Professor J. Rydberg and Doc. O. Lindqvist for stimulating interest and advice. I am also indebted to Mrs. B. Hjorth for skilfull experimental help and never failing optimism. The English text was revised by E. Ratti-Moberg. Support by the Swedish Atomic Research Council is gratefully acknowledged.

REFERENCES

1. Titze, H. *Acta Chem. Scand. 23* (1969) 399.
2. Titze, H. *Acta Chem. Scand. 24* (1970) 405.
3. Allard, B. *Acta Chem. Scand. 26* (1972) 3492.
4. Hoard, J. L. and Silverton, J. V. *Inorg. Chem. 2* (1963) 235.
5. Liljenzin, J. O. and Rydberg, J. *Physico-Chemie du Protactinium*. Editions du C. N. R. S. No 154, Paris 1966, p. 255.
6. Grdenić, D. and Matković, B. *Croat. Chem. Acta 30* (1958) 95.
7. Grdenić, D. and Matković, B. *Nature (London) 182* (1958) 465.
8. Titze, H. *Acta Chem. Scand. A 28* (1974) 1079.
9. Young, R. C. and Kovitz, J. *Inorg. Syn. 2* (1946) 123.
10. Titze, H. and Allard, B. *Acta Chem. Scand. 24* (1970) 715.
11. Allard, B. *Acta Chem. Scand. A 30* (1976) 381.
12. Yoshimura, T., Miyake, C. and Imoto, S. *Bull Chem. Soc. Jpn. 46* (1973) 2096.
13. Computer programs available in the program library of the Department of Inorganic Chemistry, Göteborg.
14. Cruickshank, D. W. J. In Rollet, S. J., Ed., *Computing Methods in Crystallography*, Pergamon, Glasgow 1965, p. 99.
15. Cromer, D. T. and Waber, J. T. *Acta Crystallogr. 18* (1965) 104.
16. Doyle, P. A. and Turner, P. S. *Acta Crystallogr. A 24* (1968) 390.
17. *Table of Interatomic Distances and Configuration in Molecules and Ions*, The Chemical Society, London 1965.
18. Lippard, S. J. *Progr. Inorg. Chem. 8* (1967) 109.
19. Lalancette, R. A., Cefola, M., Hamilton, W. C. and La Placa, S. J. *Inorg. Chem. 6* (1967) 2127.
20. Bennet, M. J., Cotton, F. A., Ledzdins, P. and Lippard, S. J. *Inorg. Chem. 7* (1968) 1770.
21. Lippard, S. J. and Russ, B. J. *Inorg. Chem. 7* (1968) 1686.
22. Allard, B. *J. Inorg. Nucl. Chem. In press.*
23. Wolf, L. and Bärnighaussen, H. *Acta Crystallogr. 13* (1960) 778.

Received October 31, 1975.

Acta Chemica Scandinavica A 30 (1976) 468—474

Magnetic Structures and Properties of $Mn_{1-t}Co_tAs$

KARI SELTE,[a] ARNE KJEKSHUS,[a] GUNNAR VALDE[a] and ARNE F. ANDRESEN[b]

[a] Kjemisk Institutt, Universitetet i Oslo, Blindern, Oslo 3, Norway and [b] Institutt for Atomenergi, Kjeller, Norway

The pseudo-binary MnAs—CoAs system has been investigated by X-ray and neutron diffraction and magnetic susceptibility measurements. $Mn_{1-t}Co_tAs$ exhibits slightly temperature dependent regions of limited solid solubility ($0 \leqq t \leqq 0.20 \pm 0.03$, $0.50 \pm 0.05 \leqq t \leqq 1$ below 350 °C). At lower temperatures the crystal structure is of the MnP type, except for a very small range near the composition MnAs, where the NiAs type structure prevails. At higher temperatures the NiAs type structure predominates. In both structure types the substituted atoms are randomly distributed over the metal sub-lattices.

The temperature characteristics of the magnetic susceptibility show a consistent trend in their changes with t above room temperature, the Curie-Weiss Law being fulfilled in the region of the high temperature NiAs type structure.

The low temperature NiAs type phase exhibits ferromagnetism. A double, a-axis helimagnetic mode is found below 196—152 K for Mn-rich $Mn_{1-t}Co_tAs$ samples ($0.05 \leqq t \leqq 0.15$) with MnP type structure. The spiral parameters depend both on composition and temperature.

Earlier communications consider the interesting magnetic properties of $V_{1-t}Mn_tAs$,[1] $Cr_{1-t}Mn_tAs$,[2,3] and $Mn_{1-t}Fe_tAs$,[4] all of which take the MnP type structure with random distribution of the two kinds of metal atoms over the metal sub-lattice. Since CoAs [5] (like VAs,[6] CrAs,[7] MnAs (40—120 °C),[8] and FeAs [9]) takes this structure type, "symmetry considerations" suggest that it may be rewarding to explore the magnetic properties of $Mn_{1-t}Co_tAs$.

EXPERIMENTAL

The binary compounds MnAs and CoAs were prepared by heating weighed quantities of the elements [(99.9+ % Mn (The British Drug Houses; crushed powder from commercial, electrolytic grade material), 99.99+ % Co (Johnson, Matthey & Co.; turnings from rods), and 99.9999 % As (Koch-Light Laboratories)] in evacuated, sealed quartz tubes as described in Refs. 4 and 5. The binary arsenides were mixed in proportions according to the desired ternary compositions and subjected to a series of annealings at 850 or 1000 °C, interrupted by intermediate crushings. The samples were then cooled to 600 °C over 2 d and finally quenched in ice water.

The applied experimental techniques (X-ray and neutron diffraction and magnetic susceptibility measurements) have been described earlier.[10]

RESULTS

(i) *Homogeneity ranges and atomic arrangements.* An isothermal cross-section of the pseudo-binary MnAs—CoAs system at room temperature (as derived from samples quenched from 600 °C) shows that this system exhibits a two-phase miscibility gap for $0.20 \pm 0.03 < t < 0.50 \pm 0.05$ of the formula $Mn_{1-t}Co_tAs$. The limits of the solid solubility ranges have been determined from the variations in the unit cell dimensions with t (Fig. 1), and further confirmed by application of the disappearing phase principle to the X-ray powder data. Samples with atomic (Mn + Co)/As ratios different from 1.00 have not been examined in this study. As evident from Fig. 1 the NiAs and MnP type structures are alternating as the stable atomic arrangement at room temperature in the Mn-rich region of $Mn_{1-t}Co_tAs$. Thus, the NiAs type structure prevails for $0.00 \leqq t < \sim 0.01$ and $0.10 \pm 0.01 \leqq t \leqq 0.20 \pm 0.03$, whereas the MnP type governs the rest of the single phase fields stated above.

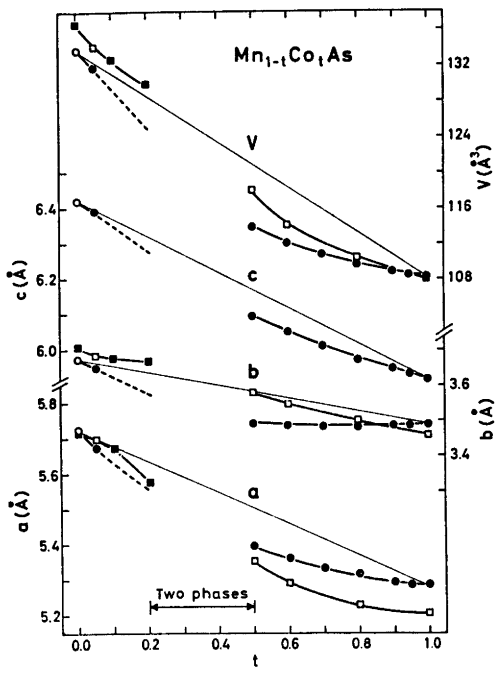

Fig. 1. Room temperature unit cell dimensions of $Mn_{1-t}Co_tAs$ as functions of t for samples quenched from 600 °C (filled symbols). Open symbols represent values derived by extrapolation from high temperature data. Circles and squares refer to MnP and NiAs type structures, respectively.

The crystallographic and magnetic phase relationships in the MnAs–CoAs system are illustrated in Fig. 2, where data for the system VAs–MnAs [1] are included for the purpose of comparison. Apart from a slight broadening of the two-phase field, the most prominent feature of the high temperature portion of the phase diagram is the complete predominance of the NiAs type structure. Since the NiAs type atomic arrangement occurs as both low and high temperature forms in MnAs, the designations I and II, respectively, introduced in Ref. 1, are conveniently adopted here. The second or higher order MnP⇌NiAs(II) type transition in $Mn_{1-t}Co_tAs$ is detected by low and high temperature neutron and X-ray (Fig. 3) diffraction methods, as well as by magnetic susceptibility measurements (see ii).

X-Ray and neutron diffraction data show that the substituted atoms are randomly distributed over the metal sub-lattices in both the MnP and NiAs type atomic arrangements at all temperatures. The unit cell dimensions and positional parameters for the samples studied by neutron diffraction are listed in Table 1.

(ii) *Magnetic susceptibility.* The temperature characteristics of the reciprocal magnetic susceptibility show a consistent trend in their changes with the composition parameter t

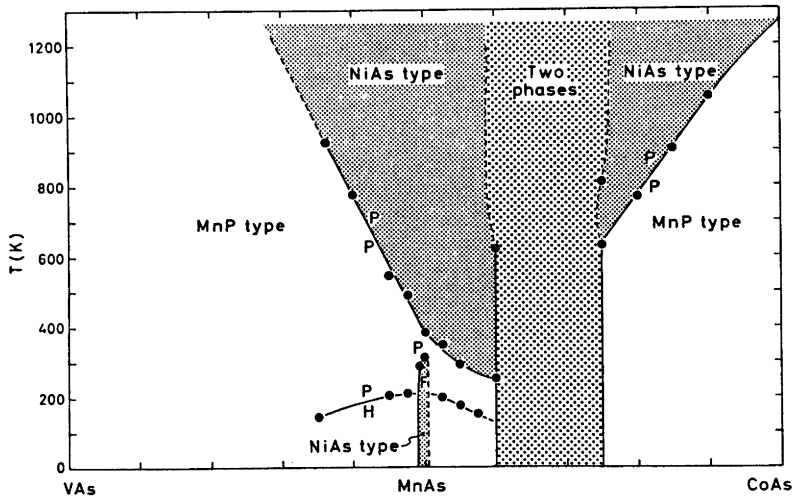

Fig. 2. Composite phase diagrams for the pseudo-binary VAs–MnAs [1] and MnAs–CoAs systems. Boundaries indicated by broken lines are uncertain. Magnetic state is indicated by: P para., F ferro., H helical.

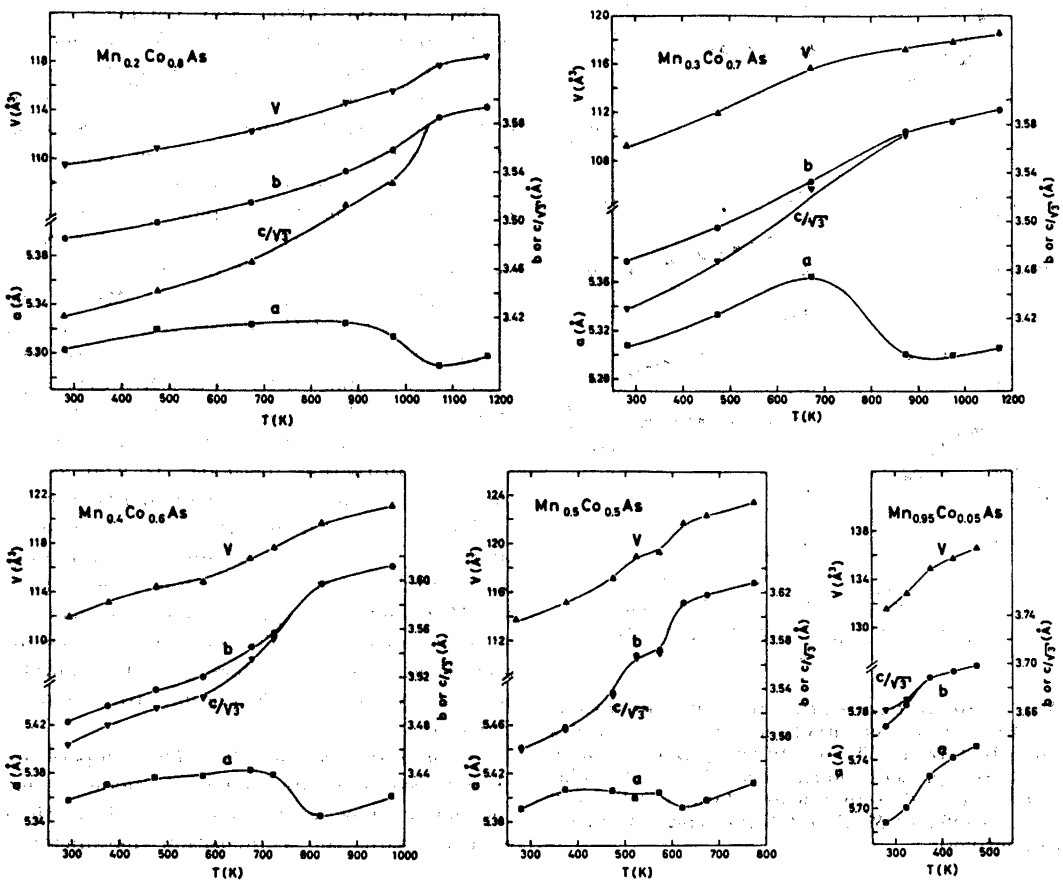

Fig. 3. Unit cell dimensions of selected $Mn_{1-t}Co_tAs$ samples *versus* temperature. Average relative expansion coefficients $\alpha_a[=(a_T-a_{T'})/a_{300}(T-T')]$, α_b, α_c multiplied by 10^6 K are 68, 125, 74; 9, 90, 90; 14, 41, 42; 35, 56, 80; and 4, 26, 41 for $Mn_{0.95}Co_{0.05}As$ (280–350 K), $Mn_{0.50}Co_{0.50}As$ (300–500 K), $Mn_{0.40}Co_{0.60}As$ (300–600 K), $Mn_{0.30}Co_{0.70}As$ (300–600 K), and $Mn_{0.20}Co_{0.80}As$ (300–800 K), respectively.

Table 1. Unit cell dimensions and positional parameters with standard deviations for some $Mn_{1-t}Co_tAs$ samples as derived by least squares profile refinements of neutron diffraction data. (Space group *Pnma*; positions 4(c); overall profile reliability factors ranging between 0.039 and 0.061.)

t	T (K)	a (Å)	b (Å)	c (Å)	x_T	z_T	x_X	z_X
0.05	4.2	5.5662(7)	3.5151(4)	6.1825(11)	−0.005(3)	0.222(4)	0.189(2)	0.587(1)
	79	5.5755(9)	3.5254(6)	6.1964(14)	0.006(3)	0.214(4)	0.198(1)	0.584(2)
	293	5.6875(18)	3.6541(19)	6.3494(25)	0.009(2)	0.226(3)	0.220(1)	0.590(3)
0.10	4.2	5.5539(8)	3.5252(5)	6.1843(12)	0.008(8)	0.215(3)	0.191(2)	0.584(2)
	79	5.5591(8)	3.5322(5)	6.1928(12)	0.013(3)	0.214(3)	0.197(1)	0.587(2)
	293 [a]	5.6702(11)	3.6764(5)	[6.3679]	[0]	[1/4]	[1/4]	[7/12]
0.15	5	5.5429(7)	3.5359(5)	6.1843(12)	0.014(2)	0.218(2)	0.194(1)	0.583(2)
	79	5.5461(8)	3.5417(6)	6.1969(14)	0.013(3)	0.216(3)	0.198(1)	0.584(2)
	293 [a]	5.6241(11)	3.6722(5)	[6.3603]	[0]	[1/4]	[1/4]	[7/12]

[a] NiAs type structure.

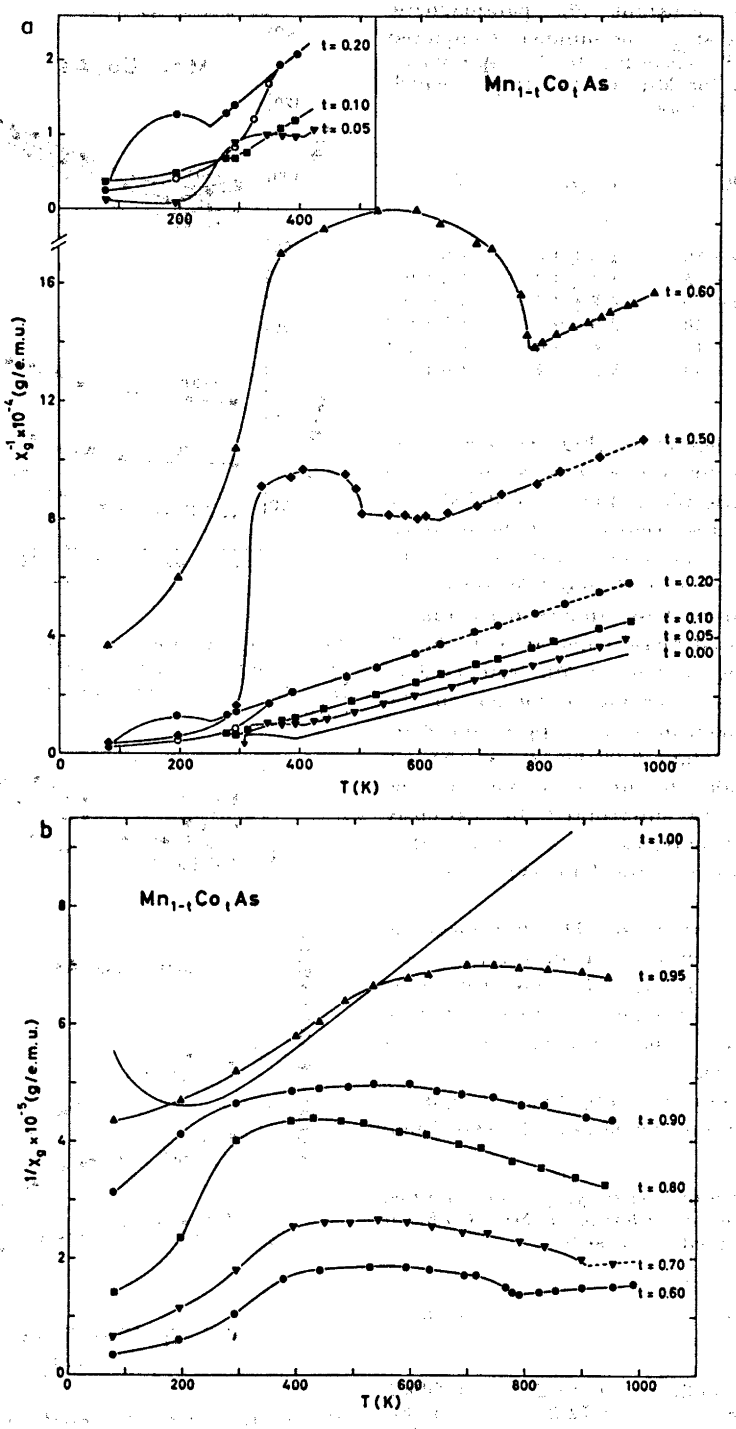

Fig. 4. Reciprocal magnetic susceptibility for typical $Mn_{1-t}Co_tAs$ samples: (a) $0 \leqq t \leqq 0.60$ and (b) $0.60 \leqq t \leqq 1$.

Table 2. Curie constant (θ), paramagnetic moment ($\mu_P = \sqrt{8C_M}$), and number of unpaired electrons ($n = 2S_T$; according to the "spin only" approximation) for $Mn_{1-t}Co_tAs$ samples which fulfil Curie-Weiss Law.

t	θ (K)	μ_P (μ_B)	$2S_T$
0.00	270 ± 10	4.5 ± 0.3	3.6 ± 0.2
0.05	235 ± 15	4.3 ± 0.3	3.5 ± 0.2
0.10	200 ± 15	4.2 ± 0.3	3.3 ± 0.2
0.20	100 ± 20	3.9 ± 0.3	3.1 ± 0.2
0.50	-320 ± 40	3.6 ± 0.4	2.7 ± 0.3
0.60	-750 ± 50	3.5 ± 0.4	2.6 ± 0.3

above room temperature (Fig. 4). The linear χ^{-1}(T) portions for single phase samples with $0 \leqq t \leqq 0.70$ (Curie-Weiss Law is fulfilled) are associated with the occurrence of the NiAs(II) type structure. The broken sections on the characteristics for $t = 0.20$ and 0.50 refer to a two-phase status of these samples in accordance with the indicated phase boundaries in Fig. 2. With decreasing content of Mn from $t = 0$ to $t = 0.60$ there is a gradual reduction in the paramagnetic moment, and an appreciable drop in the Curie constant θ (Table 2). At the low temperature side the linear sections of the χ^{-1}(T) curves are interrupted by variously shaped, curved portions, thus evincing that the transformation to the MnP type structure has occurred.

(iii) *Magnetic structures.* The ferromagnetic mode of MnAs,[11] with moments arranged perpendicular to the hexagonal c axis of its NiAs type atomic arrangement, extends slightly ($t < \sim 0.01$) into the ternary region of $Mn_{1-t}Co_tAs$ (*cf.* Fig. 2).

At low temperatures, $Mn_{1-t}Co_tAs$ samples in the composition range $0.05 \leqq t \leqq 0.15$ were found

Table 3. Parameters specifying the double, a-axis helimagnetic ordering in $Mn_{1-t}Co_tAs$ at 79 K (β is assumed to be 90°).

t	0.05	0.10	0.15
$\tau/2\pi a^*$	0.166(2)	0.184(2)	0.209(2)
$\mu_T(\mu_B)$	1.80(3)	1.72(3)	1.66(3)
ϕ(°)	95(3)	100(3)	104(3)
T_N(K)	196(1)	174(1)	152(1)

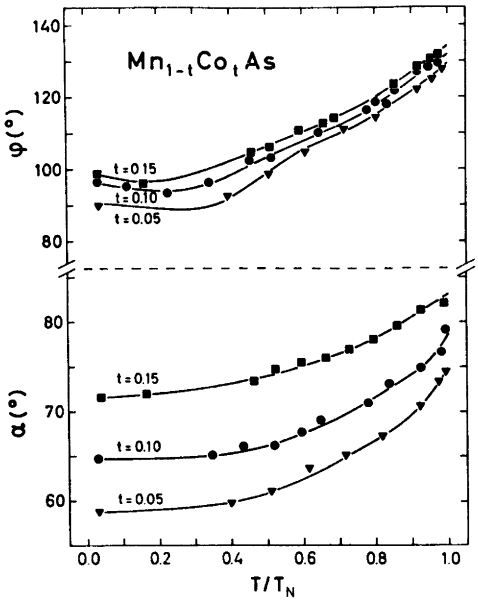

Fig. 5. Spiral turn angle per a-length (α) and phase angle (ϕ) for $t = 0.05$, 0.10, and 0.15 of $Mn_{1-t}Co_tAs$ as functions of reduced temperature.

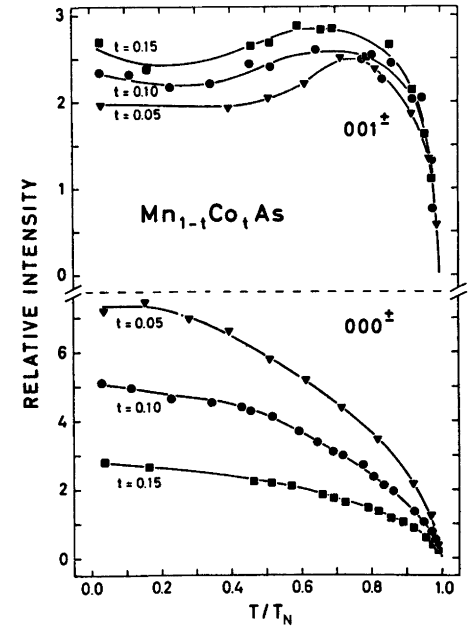

Fig. 6. Relative, integrated intensities of 000± and 001± *versus* reduced temperature for $t = 0.05$, 0.10, and 0.15 of $Mn_{1-t}Co_tAs$.

to take the double, *a*-axis type helimagnetic mode earlier observed for $V_{1-t}Mn_tAs$ ($\sim 0.60 \leqq t \leqq 0.95$) [1] and $Mn_{1-t}Fe_tAs$ ($\sim 0.01 < t < \sim 0.12$).[4] Parameters describing this helimagnetic arrangement, are magnetic moment per metal atom (μ_T), spiral propagation vector (τ), phase angle between independent spirals (ϕ), and angle between moment and spiral axis (β), numerical values being given in Table 3 together with the Néel temperatures (T_N) for samples with $t = 0.05$, 0.10, and 0.15. As seen from Fig. 2 and Table 3, T_N and μ_T decrease with increasing t. These results are in conformity with those for $V_{1-t}Mn_tAs$ ($0.70 \leqq t \leqq 0.95$). All MnP type phases with the double, *a*-axis type helimagnetic mode studied [1,4] so far have shown substantial variation of the propagation vector and phase angle with composition and temperature. As seen from Fig. 5 and Table 3, the $Mn_{1-t}Co_tAs$ phase ($0.05 \leqq t \leqq 0.15$) makes no exception in this respect. However, as opposed to the situation for $V_{1-t}Mn_tAs$, where α decreases with increasing V-content, α increases with t in $Mn_{1-t}Co_tAs$.

The (reduced) temperature dependence of the integrated intensity for the strongest satellites 000± and 001± of $Mn_{0.95}Co_{0.05}As$, $Mn_{0.90}Co_{0.10}As$, and $Mn_{0.85}Co_{0.15}As$ are shown in Fig. 6. Following the procedure outlined in Refs. 1 and 4 and utilizing a similar $\mu_T/\mu_{T,0K}$ *versus* T/T_N relationship to that postulated in Ref. 1, the calculated curves for ϕ *versus* T/T_N in Fig. 5 are obtained. This demonstrates an internal consistency between the various data.

DISCUSSION

Neglecting the magnetic aspects, the phase diagrams of the pseudo-binary systems *T*As–*T'*As (*T* or *T'*: V, Cr, Mn, Fe, or Co) with MnP type structure fall into two categories, according to whether there is complete or limited solid solubility. Consultations of unit cell volumes and interatomic distances for the binary compounds [5–9] show that the Hume-Rothery [12] 15 % criterion is not governing the distinction between these categories. Since MnAs–FeAs [4] and MnAs–CoAs are the only systems which exhibit regions of limited solid solubility, the guiding principle appears to be that of incompatibility of electronic band structures (*cf.* Ref. 13). The implications are accordingly that MnAs has an electronic band structure which differs from those of FeAs and CoAs.

A common feature of all MnAs–*T*As systems is a second (or higher) order crystallographic transition between MnP and NiAs type structures.[1,3,4] Consistent with geometrical [14] and group theoretical [15] considerations, similar MnP⇌NiAs type transitions are also found in a number of other binary and ternary phases,[14,16–19] but the conversion is there found at much higher temperatures. In this connection it is interesting to note that MnAs–CoAs is the only combination which results in a lowering of the temperature for the MnP⇌NiAs transition. Among the *T*As compounds CoAs also provides the only example of an MnP type phase with an axial ratio $c/b < \sqrt{3}$ ($c/b \equiv \sqrt{3}$ for the NiAs type atomic arrangement). $Mn_{0.5}Co_{0.5}As$ provides an interesting example, where c/b stays constant at 1.732 at all temperatures (Fig. 3), also in the region where the MnP type structure prevails.

The question of whether the double, helimagnetic ordering propagates in the *a* or *c* direction is also connected with the particular combination of the binary monoarsenides. The fact that *a* axis spirals only have been observed for Mn-rich $Mn_{1-t}T_tAs$ samples (*T* = V, Fe, Co) has led us to reconsider the available information on MnAs more carefully. (Revaluation of the data presented by Kazama and Watanabe [3] for $Cr_{1-t}Mn_tAs$ ($0.7 \leqq t \leqq 0.9$) suggests very strongly that this phase also takes the double, *a*-axis type helimagnetic structure. Work is in progress to verify this suggestion.) The magnetic exchange interactions are the factors which rule the cooperative magnetic arrangements, but these key parameters are in turn governed by *inter alia* the interatomic distances in the chemical structure. It may therefore be significant to note that just MnAs has the largest difference between the nearest and next nearest *T*–*T* distances among the MnP type *T*As compounds. Thus, bearing in mind that the *T*–*T* distances along the *a* direction in the MnP type MnAs structure are appreciably shorter than those in the *b*,*c* planes, and that the orientation of the ferromagnetic moments is perpendicular to the corresponding (*c*) direction in the NiAs(I) modification of MnAs, the arrangement of the moments in

planes perpendicular to *a* appears to be a natural consequence. The tendency towards spiral formation seems to originate from the zig-zag arrangement of the *T* atoms in the two mutually perpendicular directions. This observation together with a more careful analysis of the details of the various cooperative arrangements adopted by MnP type phases may lead to a resolution of the relation between the magnitudes of the exchange interaction parameters and the helical modes.

Acknowledgements. The assistance of Ing. Stanislav Vratislav (I.A.E.A.-fellow from The Technical University of Prague, Czechoslovakia) and cand.mag. Per G. Peterzens in the neutron diffraction measurements and the financial support of The Norwegian Research Council for Science and the Humanities are greatly appreciated.

REFERENCES

1. Selte, K., Kjekshus, A., Valde, G. and Andresen, A. F. *Acta Chem. Scand. A 30* (1976) 8.
2. Watanabe, H., Kazama, N., Yamaguchi, Y. and Ohashi, M. *J. Appl. Phys. 40* (1969) 1128.
3. Kazama, N. and Watanabe, H. *J. Phys. Soc. Jpn. 30* (1971) 1319.
4. Selte, K., Kjekshus, A. and Andresen, A. F. *Acta Chem. Scand. A 28* (1974) 61.
5. Selte, K. and Kjekshus, A. *Acta Chem. Scand. 25* (1971) 3277.
6. Selte, K., Kjekshus, A. and Andresen, A. F. *Acta Chem. Scand. 26* (1972) 4057.
7. Selte, K., Kjekshus, A., Jamison, W. E., Andresen, A. F. and Engebretsen, J. E. *Acta Chem. Scand. 25* (1971) 1703.
8. Wilson, R. H. and Kasper, J. S. *Acta Crystallogr. 17* (1964) 95.
9. Selte, K. and Kjekshus, A. *Acta Chem. Scand. 23* (1969) 2047.
10. Selte, K., Kjekshus, A. and Andresen, A. F. *Acta Chem. Scand. 26* (1972) 3101.
11. Bacon, G. E. and Street, R. *Nature 175* (1955) 518.
12. Hume-Rothery, W. *The Structure of Metals and Alloys*, Institute of Metals, London 1936.
13. Furuseth, S., Selte, K. and Kjekshus, A. *Acta Chem. Scand. 21* (1967) 527.
14. Selte, K. and Kjekshus, A. *Acta Chem. Scand. 27* (1973) 3195.
15. Franzen, H. F., Haas, C. and Jellinek, F. *Phys. Rev. B 10* (1974) 1248.
16. Ido, H. *J. Phys. Soc. Jpn. 25* (1968) 1543.
17. Selte, K., Hjersing, H., Kjekshus, A. and Andresen, A. F. *Acta Chem. Scand. A 29* (1975) 312.
18. Franzen, H. F. and Wiegers, G. A. *J. Solid State Chem. 13* (1975) 114.
19. Selte, K., Hjersing, H., Kjekshus, A., Andresen, A. F. and Fischer, P. *Acta Chem. Scand. A 29* (1975) 695.

Received January 29, 1976.

Acta Chemica Scandinavica A 30 (1976) 475—484

Short Communications

The Crystal Structure of Bromidobis(ethylenediamine)pyridinecobalt(III) Nitrate, $[CoBr(en)_2py](NO_3)_2$

OLLE BÖRTIN

Department of Inorganic Chemistry, University of Göteborg and Chalmers University of Technology, P.O. Box, S-402 20 Göteborg 5, Sweden

The crystal structure of bromidobis(ethylenediamine)pyridinecobalt(III) nitrate has been determined. The cell dimensions were obtained from powder diffraction photographs taken with a Guinier focusing camera using lead nitrate ($a = 7.8566$ Å)[1] as an internal standard and refined by the method of least squares using the program POWDER. Bromidobis(ethylenediamine)pyridinecobalt(III) nitrate was found to be monoclinic with $a = 13.141(3)$ Å, $b = 14.982(5)$ Å, $c = 9.075(3)$ Å, $\beta = 94.27(2)°$, $V = 1781$ Å^3, $Z = 4$, space group $P2_1/n$.

The positions of the cobalt and bromine atoms were obtained from Patterson calculations and the other atoms from successive electron density calculations. The structure was refined by least squares using the program BLOCK. The atomic scattering factors used were those calculated by Cromer and Waber.[2] The structure factors were weighted according to Cruickshank[3] with $a = 60.0$ and $c = 0.01$. Anisotropic thermal parameters of the atoms were introduced in the last cycles and the reliability index $R = \sum||F_o| - |F_c||/\sum|F_o|$ finally converged to 0.11. Some of the light atoms, however, were not positive definite. The resulting parameters are given in Table 1. A list of observed and calculated structure factors is available on request. The distances and angles were calculated with the program DISTAN and are listed in Tables 2 and 3.

Table 1. Final atomic parameters for $[CoBr(en)_2py](NO_3)_2$ (standard deviations in parentheses).

Atom	x	y	z
Co	0.0643(4)	0.2725(4)	0.3174(5)
Br	0.0109(4)	0.1648(5)	0.1266(5)
N(1)	0.1145(18)	0.3600(19)	0.4626(26)
C(1)	0.2200(32)	0.3871(31)	0.4363(38)
C(2)	0.2771(32)	0.3086(34)	0.3733(48)
N(2)	0.2081(19)	0.2565(24)	0.2624(29)
N(3)	0.0385(16)	0.3641(18)	0.1707(26)
C(3)	-0.0735(28)	0.3885(43)	0.1452(41)
C(4)	-0.1217(29)	0.3721(37)	0.2957(48)
N(4)	-0.0775(17)	0.2895(23)	0.3599(27)
N(5)	0.0864(18)	0.1695(18)	0.4593(22)
C(5)	0.0537(22)	0.1859(22)	0.6006(38)
C(6)	0.0580(26)	0.1131(31)	0.7126(50)
C(7)	0.1095(26)	0.0339(32)	0.6733(58)
C(8)	0.1479(39)	0.0292(39)	0.5336(55)
C(9)	0.1350(31)	0.0964(28)	0.4311(49)
N(6)	0.3941(18)	0.0933(17)	0.1993(27)
O(1)	0.4484(16)	0.0430(17)	0.1257(29)
O(2)	0.3528(21)	0.0518(22)	0.3008(31)
O(3)	0.3785(21)	0.1659(19)	0.1743(32)
N(7)	0.1975(13)	0.3308(16)	0.8610(18)
O(4)	0.2455(19)	0.3262(20)	0.9767(28)
O(5)	0.2359(24)	0.3119(26)	0.7487(32)
O(6)	0.1116(27)	0.3550(23)	0.8578(28)

Table 2. Bond distances and angles in $[CoBr(en)_2py](NO_3)_2$ (standard deviations in parentheses).

Distance (Å)		Angle (°)	
Co - Br	2.431(8)	Co - N(1) - C(1)	111(2)
Co - N(1)	1.939(27)	N(1) - C(1) - C(2)	110(3)
Co - N(2)	2.004(27)	C(1) - C(2) - N(2)	111(3)
Co - N(3)	1.925(26)	C(2) - N(2) - Co	108(2)
Co - N(4)	1.948(23)	Co - N(3) - C(3)	113(2)
Co - N(5)	2.016(26)	N(3) - C(3) - C(4)	106(3)
N(1) - C(1)	1.48(5)	C(3) - C(4) - N(4)	108(4)
C(1) - C(2)	1.53(7)	C(4) - N(4) - Co	113(2)
C(2) - N(2)	1.52(5)	Co - N(5) - C(5)	114(2)
N(3) - C(3)	1.52(4)	Co - N(5) - C(9)	125(2)
C(3) - C(4)	1.57(6)	N(5) - C(5) - C(6)	120(3)
C(4) - N(4)	1.47(6)	C(5) - C(6) - C(7)	116(4)
N(5) - C(5)	1.40(4)	C(6) - C(7) - C(8)	119(4)
C(5) - C(6)	1.49(6)	C(7) - C(8) - C(9)	123(4)
C(6) - C(7)	1.42(6)	C(8) - C(9) - N(5)	121(4)
C(7) - C(8)	1.40(7)	C(9) - N(5) - C(5)	121(3)
C(8) - C(9)	1.37(7)	O(1) - N(6) - O(2)	113(3)
C(9) - N(5)	1.30(5)	O(1) - N(6) - O(3)	125(3)
N(6) - O(1)	1.26(4)	O(2) - N(6) - O(3)	123(3)
N(6) - O(2)	1.27(4)	O(4) - N(7) - O(5)	120(2)
N(6) - O(3)	1.13(4)	O(4) - N(7) - O(6)	119(2)
N(7) - O(4)	1.19(3)	O(5) - N(7) - O(6)	121(2)
N(7) - O(5)	1.20(4)		
N(7) - O(6)	1.18(4)		

Table 3. Packing distances less than 3.2 Å in $[CoBr(en)_2py](NO_3)_2$.

Distance (Å)	
Br - N(4)	3.11
N(1) - O(1)	3.09
N(1) - O(1)	2.96
N(1) - O(5)	3.03
C(1) - O(5)	3.04
C(2) - O(3)	3.16
N(2) - O(3)	2.79
N(2) - O(4)	2.87
N(3) - O(2)	3.16
N(3) - O(6)	3.07
N(4) - O(3)	3.03
N(4) - O(4)	3.15
N(4) - O(5)	3.00
N(6) - O(6)	3.20

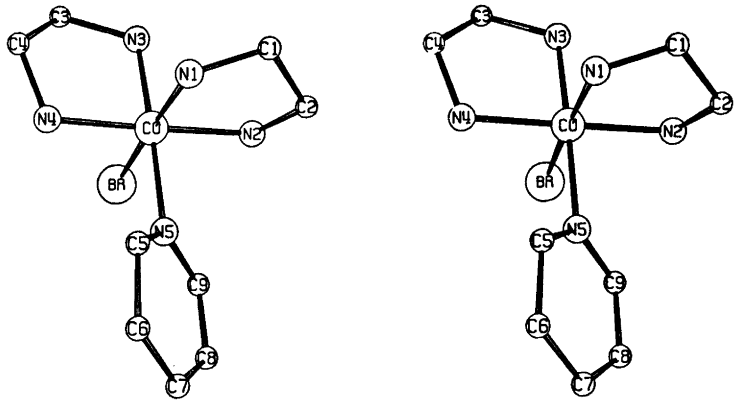

Fig. 1. A stereoscopic view of the ion $[CoBr(en)_2py]^{2+}$.

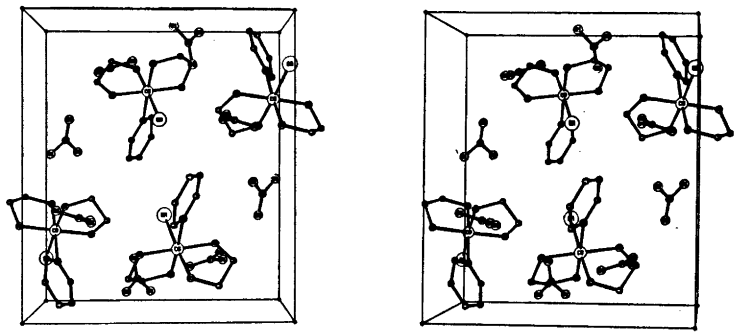

Fig. 2. A stereoscopic view of the structure.

The cobalt atom is octahedrally coordinated by one bromine atom and five nitrogen atoms with the bromine atom and the pyridine group in *cis* position to each other. The Co – Br bond distance is 2.43 Å and the Co – N bond distances are 2.02 Å (to py) and 1.93 – 2.00 Å (to en) with the shorter distances to the nitrogen atoms in *trans* position to the bromido and pyridine groups. The bond angles Co – N5 – C5 of 114° and Co – N5 – C9 of 125° indicate that the pyridine group is repelled by the bromine atom. The distance from Br to C9 is 3.27 Å and the calculated distance from Br to a hydrogen atom bonded to C9 is 2.85 Å.

The large bromidobis(ethylenediamine)pyridinecobalt(III) ions are arranged in a close-packed manner. The nitrate ions occupy holes between the cations. The two different nitrate ions are situated rather close to each other with the shortest distance 3.2 Å between the atoms N6 and O6. Some distances between oxygen atoms of the nitrate ions and nitrogen atoms of the ethylenediamine groups indicate that the structure is held together by hydrogen bonds. The shortest of these distances are 2.8 – 3.0 Å.

The ion $[CoBr(en)_2py]^{2+}$ is shown in Fig. 1 and the unit cell in Fig. 2.

Acknowledgements. This work has been supported by Chalmers University of Technology, which has supplied a grant to cover the costs of the computer work, which was performed at the Göteborg Universities' Computing Centre.

1. *International Tables for X-Ray Crystallography*, 2nd Ed., Kynoch Press, Birmingham 1952, Vol. III.
2. Cromer, D. T. and Waber, J. T. *Acta Crystallogr. 18* (1956) 104.
3. Cruickshank, D. W. J. *The Equation of Structure Refinements*, Glasgow 1964.

Received January 20, 1976.

Kinetic Salt Effect in Ion — Molecule Reactions. I. The Isotopic Exchange between Tetraethylammonium Iodide and Methyl Iodide in Ethylene Glycol at 25 °C

P. BERONIUS and R. P. GUPTA*

Department of Physical Chemistry, University of Umeå, S-901 87 Umeå, Sweden

Kinetic salt effect is one of the various factors that have to be considered in analyzing kinetic data for ion–molecule reactions.[1] For such reactions in organic solvent media unequivocal quantitative evaluation of the kinetic salt effect is usually rendered difficult because of association of the ionic reactant to higher aggregates such as ion pairs and triple ions, *cf.* Refs. 2–3.

The present study of the isotopic exchange reaction between a quaternary ammonium iodide and methyl iodide in ethylene glycol constitutes part of an investigation initiated to obtain quantitative information about the kinetic salt effect. Qualitatively the effect of ionic strength on reactions involving ions and dipolar molecules may be predicted.[4]

Reagents. Ethylene glycol (Merck, *p.a.*) was flushed with nitrogen to remove dissolved oxygen. Methyl iodide (Merck) was purified by distillation in a column filled with copper turnings and stored over mercury in the dark. The iodine content of the tetraethylammonium iodide used (Merck) was found to be ≥ 99 % according to isotope dilution analysis. The salt was labelled using carrierfree radioiodide (^{131}I). Solutions were prepared at 25 °C.

Kinetic procedure. The electrodeposition method,[5] was used to follow the exchange reaction,

$$(C_2H_5)_4N^{131}I + CH_3I \rightleftharpoons (C_2H_5)_4NI + CH_3{}^{131}I$$

at 25.00 ± 0.05 °C. The rate of exchange, R, was iteratively calculated[6] from the McKay equation,[7]

$$\ln (1-F) = -Rt(a+c)/ac \qquad (1)$$

where F is the fractional exchange, t is the reaction time, a is the concentration of methyl iodide, and c is the concentration of tetraethylammonium iodide.

A typical graph obtained upon plotting $\ln (1-F)$ *vs.* t according to eqn. (1) is shown in Fig. 1.

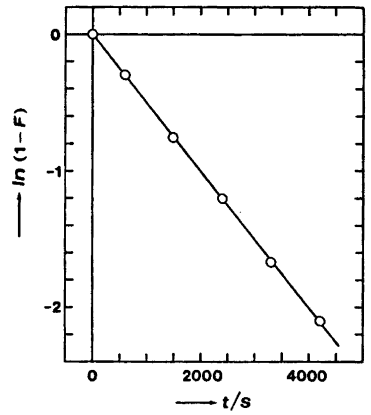

Fig. 1. Graphic representation of eqn. (1) for the exchange reaction studied at $c = 6.004$ mM.

Discussion. A compilation of the results of the kinetic measurements is given in Table 1 in which the observed rate constant, k, in the last column is defined by the expression, $k = R/ac$.

The value of k shows a slight tendency to decrease with increasing concentration of tetraethylammonium iodide (column 2) but is within experimental errors independent of the concentration of methyl iodide (column 1). As briefly discussed below this effect may be given various explanations.

In a previous investigation[8] of the exchange reaction between sodium iodide and methyl iodide in ethylene glycol using ^{125}I as a radioactive indicator no S_N1 contribution to the reaction rate could be detected. The reaction appeared to be of purely S_N2 type. The results of the present study confirm the absence of S_N1 exchange. This may be seen from Fig. 2, where R/a has been plotted *vs.* c according to the equation

$$R/a = k_1 + kc \qquad (2)$$

Table 1. Kinetic data for the exchange of ^{131}I between tetraethylammonium iodide and methyl iodide in ethylene glycol at 25 °C.

$a \times 10^2$ M	$c \times 10^4$ M	$R \times 10^8$ M s^{-1}	$k \times 10^3$ M^{-1}s^{-1}
5.109	100.06	416.61	8.150
5.174	80.05	347.00	8.378
5.289	60.04	270.49	8.518
5.530	40.04	190.34	8.596
5.450	30.03	141.16	8.625
5.365	20.02	92.289	8.592
3.087	12.30	33.150	8.731
6.561	10.01	57.642	8.777
5.284	10.01	45.612	8.623
5.232	5.003	22.848	8.729

* On leave from Banaras Hindu University, Varanasi-5, India.

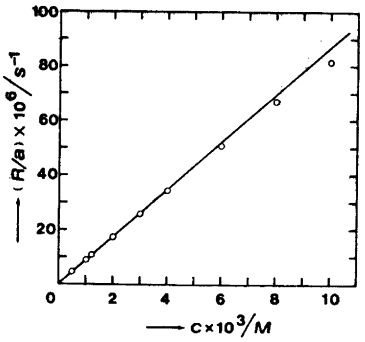

Fig. 2. Graphic representation of eqn. (2).

for a mixed S_N1-S_N2 reaction. In eqn. (2), which is applicable provided that the ionic reactant behaves like a strong electrolyte, k_1 is the rate constant for S_N1 exchange. The straight line in Fig. 2 passes within experimental errors through the origin, *i.e.* k_1 is zero.

In the higher concentration range investigated the points of R/a *vs.* c show negative deviations from the limiting tangent. These deviations might be described in terms of the extended Acree equation,[9]

$$k = \gamma k_f^{\infty}\alpha + k_p(1-\alpha) \qquad (3)$$

where γ is a salt effect correction factor, k_f^{∞} is the rate constant at infinite dilution for the exchange reaction between free iodide ion and methyl iodide, k_p is the corresponding rate constant for the exchange reaction involving paired iodide ion, and α is the degree of dissociation of the salt.

In the case of complete dissociation, that is $\alpha = 1$, eqn. (3) reduces to, $k = \gamma k_f^{\infty}$, *i.e.* the total change in k, which amounts to about 6 % for the concentration interval of the salt, would represent the kinetic salt effect.

Application [9] of various conductance equations to electrical conductance data [10] for tetraethylammonium iodide in ethylene glycol at 25 °C suggests that the salt may be subject to a slight ion-pair formation though complete dissociation cannot be ruled out. Hence, the possibility that the change in the observed rate constant with concentration of the ionic reactant is due to ion-pair formation and a lower reactivity of paired ions as compared with free ions cannot be ruled out.

Let us, for the purpose of calculation, assume the extreme case that the kinetic salt effect is negligible ($\gamma = 1$) and that the exchange with the organic reactant proceeds solely *via* free iodide ions ($k_p = 0$). In this case the expression,

$$1/k = 1/k_f^{\infty} + c\gamma_{\pm}^{2}kK_A/(k_f^{\infty})^2 \qquad (4)$$

can be derived.[11] In eqn. (4) K_A is the ion-pair association constant and $\gamma_{\pm}$ is the mean molar activity coefficient of free ions. The latter quantity was estimated [11] from the Debye-Hückel equation putting the distance parameter equal to the Bjerrum radius [12] ($q = 7.43$ Å at 25 °C for ethylene glycol).

A graph of $1/k$ *vs.* $c\gamma_{\pm}^{2}k$ according to eqn. (4) is shown in Fig. 3. From the equation of the least squares fitted straight line we obtain $k_f^{\infty} = (8.80 \pm 0.04) \times 10^{-3}$ M^{-1} s^{-1} and $K_A = 12 \pm 2$ M^{-1}, where the errors are standard deviations. This value of K_A is of the same magnitude as can be derived [9] from electrical conductance data.[10]

Further studies of kinetic salt effect in ethylene glycol as solvent are in progress.

Acknowledgement. Financial support from the Swedish Natural Science Research Council is gratefully acknowledged. R. P. Gupta thanks the Swedish Institute for a scholarship.

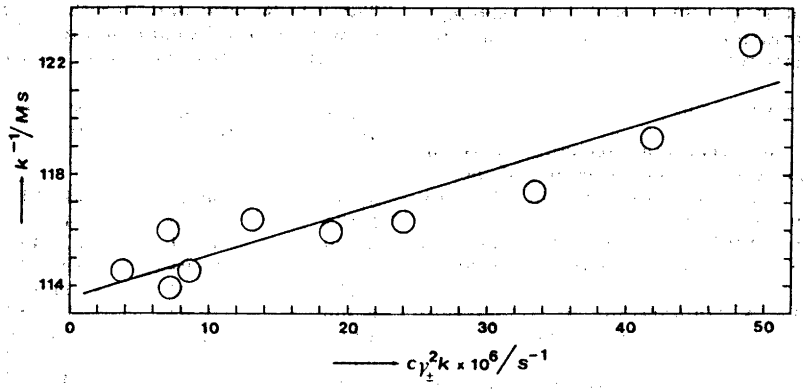

Fig. 3. Graphic representation of eqn. (4).

1. Gordon, J. E. *The Organic Chemistry of Electrolyte Solutions*, Wiley, New York 1975.
2. Beronius, P. and Pataki, L. *J. Am. Chem. Soc. 92* (1970) 4518.
3. Beronius, P. and Pataki, L. *Acta Chem. Scand. 25* (1971) 3705.
4. Benson, S. W. *The Foundations of Chemical Kinetics*, McGraw-Hill, New York 1960, pp. 536–537.
5. Beronius, P. *Sven. Kem. Tidskr. 76* (1964) 646.
6. Beronius, P. *Z. Phys. Chem. (Frankfurt am Main) 40* (1964) 33.
7. McKay, H. A. C. *J. Am. Chem. Soc. 65* (1943) 702.
8. Beronius, P. and Lindbäck, T. *Radiochem. Radioanal. Lett. 10* (1972) 107.
9. Beronius, P. *Acta Chem. Scand. A 30* (1976) 115.
10. DeSieno, R. P., Greco, P. W. and Mamajek, R. C. *J. Phys. Chem. 75* (1971) 1722.
11. Beronius, P. *Acta Chem. Scand. 23* (1969) 1175.
12. Bjerrum, N. *Kgl. Dan. Vidensk. Selsk. Mat.-Fys. Medd. 7* (1926) No. 9.

Received April 23, 1976.

Synthesis of Areneselenenyl Benzenesulfinates and Benzenethiosulfonates, and Tetraphenylarsonium Areneselenenyl Sulfites and Thiosulfates

TOR AUSTAD*

Department of Chemistry, University of Bergen, N-5014 Bergen-Univ., Norway

A large number of stable aromatic selenenyl sulfur compounds, ArSeSR, have been isolated (for a review see Ref. 1). Many of these compounds have an NO_2-group in the *ortho* position of the areneselenenyl group.[2] The ability of Se(II) to achieve coordination numbers higher than two probably serves to make these compounds more stable due to an intramolecular bonding between the selenium atom and one of the oxygen atoms of the nitro group.[3]

In this note we present the synthesis of some new aromatic selenenyl sulfur compounds which do not have any stabilizing groups in the *ortho* position. The various compounds are listed in Table 1.

Aromatic selenenyl benzenesulfinates were prepared from the corresponding aromatic selenenyl bromides and sodium benzenesulfinate in carbon tetrachloride, eqn. 1.

$$p\text{-XPhSeBr} + \text{PhSO}_2\text{Na} \rightarrow p\text{-XPhSeS(O)}_2\text{Ph} + \text{NaBr} \quad (1)$$

(X = H, Cl, and Me).

Aromatic selenenyl benzenethiosulfonates could be prepared from the corresponding aromatic selenenyl bromides and sodium benzenethiosulfonate in carbon tetrachloride, eqn. 2.

$$p\text{-XPhSeBr} + \text{PhS(O)}_2\text{SNa} \rightarrow p\text{-XPhSeSS(O)}_2\text{Ph} + \text{NaBr} \quad (2)$$

(X = H, Cl, and Me).

Analogous sulfur compounds, which have an NO_2-group in the *ortho* position of the arenesulfenyl group, have been isolated.[4]

Tetraphenylarsonium salts of aromatic selenenyl sulfites. A number of organic selenosulfates, seleno Bunte salts, have been prepared by the action of selenosulfate on alkyl chlorides or bromides in water or aqueous ethanol, eqn. (3) (see Ref. 1, p. 151).

$$\text{R–X} + \text{SeSO}_3^{2-} \rightarrow \text{R–SeSO}_3^- + \text{X}^- \quad (3)$$

However, in most cases the resultant organic selenosulfate was converted *in situ* to the corresponding diselenide. Until now, no aromatic seleno Bunte salt has been reported. We found that tetraphenylarsonium salts of aromatic selenosulfates could be prepared according to eqn. 4, from the corresponding areneselenenyl benzenesulfinates dissolved in ether, by reaction with a mixture of sodium sulfite and tetraphenylarsonium chloride dissolved in water:

$$p\text{-XPhSeS(O)}_2\text{Ph} + \text{SO}_3^{2-} \rightarrow p\text{-XPhSeSO}_3^- + \text{PhSO}_2^-$$

$$\text{Ph}_4\text{AsCl} \downarrow \quad \text{H}_2\text{O} \quad (4)$$

$$[\text{Ph}_4\text{As}^+][p\text{-XPhSeSO}_3^-]$$

(X = H, Cl, and Me)

The aromatic selenosulfate formed is immediately precipitated as a tetraphenylarsonium salt prior to the formation of any diaryldiselenide.

Pyridinium *S*-aryl thiosulfates have been prepared by Baumgarten.[5]

* Present address: Rogaland Regional College, Dept. of Science and Engineering, N-4001 Stavanger, Norway.

1. Gordon, J. E. *The Organic Chemistry of Electrolyte Solutions*, Wiley, New York 1975.
2. Beronius, P. and Pataki, L. *J. Am. Chem. Soc. 92* (1970) 4518.
3. Beronius, P. and Pataki, L. *Acta Chem. Scand. 25* (1971) 3705.
4. Benson, S. W. *The Foundations of Chemical Kinetics*, McGraw-Hill, New York 1960, pp. 536–537.
5. Beronius, P. *Sven. Kem. Tidskr. 76* (1964) 646.
6. Beronius, P. *Z. Phys. Chem. (Frankfurt am Main) 40* (1964) 33.
7. McKay, H. A. C. *J. Am. Chem. Soc. 65* (1943) 702.
8. Beronius, P. and Lindbäck, T. *Radiochem. Radioanal. Lett. 10* (1972) 107.
9. Beronius, P. *Acta Chem. Scand. A 30* (1976) 115.
10. DeSieno, R. P., Greco, P. W. and Mamajek, R. C. *J. Phys. Chem. 75* (1971) 1722.
11. Beronius, P. *Acta Chem. Scand. 23* (1969) 1175.
12. Bjerrum, N. *Kgl. Dan. Vidensk. Selsk. Mat.-Fys. Medd. 7* (1926) No. 9.

Received April 23, 1976.

Synthesis of Areneselenenyl Benzenesulfinates and Benzenethiosulfonates, and Tetraphenylarsonium Areneselenenyl Sulfites and Thiosulfates

TOR AUSTAD*

Department of Chemistry, University of Bergen, N-5014 Bergen-Univ., Norway

A large number of stable aromatic selenenyl sulfur compounds, ArSeSR, have been isolated (for a review see Ref. 1). Many of these compounds have an NO_2-group in the *ortho* position of the areneselenenyl group.[2] The ability of Se(II) to achieve coordination numbers higher than two probably serves to make these compounds more stable due to an intramolecular bonding between the selenium atom and one of the oxygen atoms of the nitro group.[3]

In this note we present the synthesis of some new aromatic selenenyl sulfur compounds which do not have any stabilizing groups in the *ortho* position. The various compounds are listed in Table 1.

Aromatic selenenyl benzenesulfinates were prepared from the corresponding aromatic selenenyl bromides and sodium benzenesulfinate in carbon tetrachloride, eqn. 1.

$$p\text{-XPhSeBr} + \text{PhSO}_2\text{Na} \rightarrow p\text{-XPhSeS(O)}_2\text{Ph} + \text{NaBr} \quad (1)$$

(X = H, Cl, and Me).

Aromatic selenenyl benzenethiosulfonates could be prepared from the corresponding aromatic selenenyl bromides and sodium benzenethiosulfonate in carbon tetrachloride, eqn. 2.

$$p\text{-XPhSeBr} + \text{PhS(O)}_2\text{SNa} \rightarrow p\text{-XPhSeSS(O)}_2\text{Ph} + \text{NaBr} \quad (2)$$

(X = H, Cl, and Me).

Analogous sulfur compounds, which have an NO_2-group in the *ortho* position of the arenesulfenyl group, have been isolated.[4]

Tetraphenylarsonium salts of aromatic selenenyl sulfites. A number of organic selenosulfates, seleno Bunte salts, have been prepared by the action of selenosulfate on alkyl chlorides or bromides in water or aqueous ethanol, eqn. (3) (see Ref. 1, p. 151).

$$\text{R–X} + \text{SeSO}_3^{2-} \rightarrow \text{R–SeSO}_3^- + \text{X}^- \quad (3)$$

However, in most cases the resultant organic selenosulfate was converted *in situ* to the corresponding diselenide. Until now, no aromatic seleno Bunte salt has been reported. We found that tetraphenylarsonium salts of aromatic selenosulfates could be prepared according to eqn. 4, from the corresponding areneselenenyl benzenesulfinates dissolved in ether, by reaction with a mixture of sodium sulfite and tetraphenylarsonium chloride dissolved in water:

$$p\text{-XPhSeS(O)}_2\text{Ph} + \text{SO}_3^{2-} \rightarrow p\text{-XPhSeSO}_3^- + \text{PhSO}_2^-$$

$$\text{Ph}_4\text{AsCl} \downarrow \quad \text{H}_2\text{O} \quad (4)$$

$$[\text{Ph}_4\text{As}^+][p\text{-XPhSeSO}_3^-]$$

(X = H, Cl, and Me)

The aromatic selenosulfate formed is immediately precipitated as a tetraphenylarsonium salt prior to the formation of any diaryldiselenide.

Pyridinium *S*-aryl thiosulfates have been prepared by Baumgarten.[5]

* Present address: Rogaland Regional College, Dept. of Science and Engineering, N-4001 Stavanger, Norway.

Table 1. New selenenyl sulfur compounds prepared in this work.

Compound	Mp. °C	Sulfur, % Calc.	Found [a]
p-MePhSeS(O)$_2$Ph	54	10.3	10.5
PhSeS(O)$_2$Ph	51	10.7	11.2
p-ClPhSeS(O)$_2$Ph	75 – 77	9.7	10.2
p-MePhSeSS(O)$_2$Ph	89 – 90	18.7	19.0
PhSeSS(O)$_2$Ph	43 – 45	19.5	19.9
p-ClPhSeSS(O)$_2$Ph	84	17.6	18.0
[Ph$_4$As$^+$][*p*-MePhSeSO$_3^-$]	206	5.1	5.4
[Ph$_4$As$^+$][PhSeSO$_3^-$]	160	5.2	5.7
[Ph$_4$As$^+$][*p*-ClPhSeSO$_3^-$]	179	4.9	5.0
[Ph$_4$As$^+$][*p*-MePhSeSSO$_3^-$]	171	9.6	10.0
[Ph$_4$As$^+$][PhSeSSO$_3^-$]	164	9.8	10.2
[Ph$_4$As$^+$][*p*-ClPhSeSSO$_3^-$]	130	9.3	10.5

[a] The analyses were performed at Ilse Beetz, Mikroanalytisches Laboratorium, 8640 Kronach/OFR., West Germany.

Tetraphenylarsonium salts of aromatic selenenyl thiosulfates. Foss [2] has prepared the potassium salt of *o*-nitrobenzeneselenenyl thiosulfate, and we earlier have prepared the tetraphenylarsonium salt of the analogous sulfenyl thiosulfate.[6] Tetraphenylarsonium salts of *para* substituted benzeneselenenyl thiosulfates were synthesised in an analogous way as described for the aromatic seleno Bunte salts, eqn. 5.

$$p\text{-XPhSeS(O)}_2\text{Ph} + \text{S}_2\text{O}_3^{2-} \rightarrow p\text{-XPhSeSSO}_3^- + \text{PhSO}_2^-$$
$$\text{Ph}_4\text{AsCl} \downarrow \text{H}_2\text{O} \qquad (5)$$
$$[\text{Ph}_4\text{As}^+][p\text{-XPhSeSSO}_3^-]$$
$$(\text{X} = \text{H, Cl, and Me})$$

The product immediately separates as a tetraphenylarsonium salt prior to the formation of any diselenide.

Due to the fact that [Ph$_4$As$^+$][PhSO$_2$S$^-$] is nearly insoluble in water,[7] selenenyl thiosulfonates, *p*-XPhSeSS(O)$_2$Ph, were not used as the starting materials in the synthesis of aromatic selenenyl sulfites and thiosulfates. [Ph$_4$As$^+$]-[PhSO$_2^-$] is easily soluble in water.

Experimental. Water-free PhSO$_2$Na was obtained from Fluka. Water-free PhS(O)$_2$SNa was prepared by dissolving the salt in absolute ethanol containing some benzene. The solvent was removed in vacuum, and the residue was dried carefully.

p-*XPhSeCN*. The aromatic selenocyanates were prepared from diazotized anilines and potassium selenocyanates: PhSeCN,[8] *p*-MePhSeCN,[9] and *p*-ClPhSeCN.[9]

(p-*XPhSe*)$_2$. The aromatic diselenides were prepared from the respective selenocyanates and potassium hydroxide in ethanol.[10]

p-*XPhSeBr*. The aromatic selenenyl bromides were synthesised from the diselenides and bromide in dry chloroform.[11] The compounds were recrystallized from light petroleum (40 – 60 °C) and stored in a freezer.

p-*XPhSeS(O)*$_2$*Ph*. The general procedure is analogous to the one used by Foss [12] to prepare aromatic sulfinates of divalent selenium. It consists in dissolving 2.0×10^{-3} mol of the aromatic selenenyl bromide in 45 ml of dry CCl_4. 2.2×10^{-3} mol, *i.e.*, 10 % excess of finely powered, dry sodium benzenesulfinate was added to the deep red selenenyl bromide solution. The mixture was stirred at room temperature until the solution became yellow. Sodium bromide and excess of sodium benzenesulfinate were filtered off, and the solvent was removed in vacuum. The product, which appeared as a semi-solid oil, was dissolved in about 25 ml of ether. About 5 ml of light petroleum (40 – 60 °C) was added, and the solution was left in a freezer and then in a dry-ice acetone mixture. The product crystallized as a stable yellowish-green compound. Yield 80 – 85 % based on the amount of aromatic selenenyl bromide.

p-*XPhSeSS(O)*$_2$*Ph*. The procedure for the preparation of aromatic selenenyl benzenethiosulfonates is analogous to the one described for the selenenyl sulfinates. 7.3×10^{-3} mol of the aromatic selenenyl bromide was dissolved in about 20 ml of CCl_4, and 8.0×10^{-3} mol of finely powered, dry sodium benzenethiosulfonate was added. The solution was

stirred at room temperature until it became yellowish-green. The product was recrystallized from 10 ml of ether. Yield 70–75 % based on the amount of the selenenyl bromide.

[Ph_4As^+][p-$XPhSeSO_3^-$]. The aromatic seleno Bunte salts were prepared from the corresponding selenenyl benzenesulfinates, $Na_2SO_3.7H_2O$, and $Ph_4AsCl.2H_2O$ according to the following procedure. A solution, made by dissolving 3.4×10^{-3} mol of the aromatic selenenyl sulfinate in 15 ml of ether, was added under vigorous stirring at room temperature to a solution containing 3.8×10^{-3} mol of each of the reagents $Na_2SO_3.7H_2O$ and $Ph_4AsCl.2H_2O$ in 25 ml of water. The reaction mixture was stirred for 5 min, and the product separated as a white crystalline compound. The salt was filtered off, washed carefully with cold water and drained well. The product was recrystallized from about 10 ml of warm acetonitrile by the addition of some ether. Yield *ca.* 85 % based on the amount of selenenyl sulfinate.

[Ph_4As^+][p-$XPhSeSSO_3^-$]. The tetraphenylarsonium salts of aromatic selenenyl thiosulfates were prepared from the corresponding selenenyl benzenesulfinates, $Na_2S_2O_3.5H_2O$, and $Ph_4AsCl.2H_2O$. The procedure is analogous to that described above for the preparation of the corresponding selenenyl sulfite salts. The products, which appeared as yellowish-green compounds, were recrystallized from acetonitrile by the addition of some ether. Yield 85–90 % based on the amount of the selenenyl benzenesulfinate.

1. Klayman, D. L. *Organic Selenium Compounds*, Wiley, New York 1973, pp. 144–157.
2. Foss, O. *J. Am. Chem. Soc. 69* (1947) 2236.
3. Eriksen, R. and Hauge, S. *Acta Chem. Scand. 26* (1972) 3153.
4. Loudon, J. D. and Livingston, A. *J. Chem. Soc.* (1935) 896.
5. Baumgarten, P. *Ber. Dtsch. Chem. Ges. 63* (1930) 1330.
6. Austad, T. *To be published.*
7. Austad, T. *Acta Chem. Scand. A 29* (1975) 241.
8. Behaghel, O. and Seibert, K. *Ber. Dtsch. Chem. Ges. 65* (1932) 812.
9. Challenger, F., Peters, A. T. and Halévy, J. *J. Chem. Soc.* (1926) 1648.
10. Rheinboldt, H. In Houben-Weyl, *Methoden der Organischen Chemie*, 4th Ed., G. Thieme, Stuttgart 1955, Band IX, p. 1095.
11. Ref. 10, p. 1164.
12. Foss, O. *Acta Chem. Scand. 6* (1952) 508.

Received March 12, 1976.

On Comparisons of Structural Information Obtained from Microwave Spectroscopy and from Electron-diffraction Studies of Gaseous Chlorobutatriene and Chlorobutenynes

MATS GRANBERG,[a] GRETE GUNDERSEN[b] and FRED KARLSSON[a]

[a] Department of Physical Chemistry, University of Stockholm, Arrhenius Laboratory, Fack, S-104 05 Stockholm, Sweden and [b] Department of Chemistry, University of Oslo, Oslo 3, Norway

In recent electron-diffraction studies on the molecular structures of gaseous C_4H_3Cl isomers[1–4] the moments of inertia calculated from the structural results were compared to values obtained from microwave spectroscopy.[5–9] The comparisons were based upon the assumption that the average distances r_α and r_z[10] are comparable quantities, and the corresponding moments of inertia are given in Table 1. They were derived from the operational parameters, respectively, for electron diffraction (r_a) and microwave spectroscopy (r_o)[10] using similar force fields for computation of the necessary correction terms as described previously.[1–9]

However, r_α should be corrected to r_α^0 in order to represent the distance between the mean positions of a pair of atoms in the zero-point level as does the r_z parameter.[10]

$$r_\alpha^0 = r_\alpha + (K - K_0) - \tfrac{3}{2}a(l^2 - l_0^2) \qquad (1)$$

where K_0 and l_0 are the perpendicular amplitude correction coefficient and the root-mean-square amplitude of vibration at absolute zero, and a is an anharmonicity constant which for bond distances is usually about 2 Å^{-1}.[10] The correction is dominated by the $K - K_0$ term and r_α is therefore smaller than r_α^0 by an amount which was assumed to be negligible. A closer examination of the moments of inertia for all five isomers (Table 1) reveals, however, that those obtained from the electron-diffraction data (r_α) are all smaller than the corresponding microwave ones (r_z). Although the discrepancies are smaller than the estimated error limits,[1–4] the similar trend indicates the presence of some systematic error. The approximation applied by using r_α rather than r_α^0 was therefore reconsidered. The K_0- and l_0-values were computed from the force fields described previously for the five compounds[1–4] and the corresponding moments of inertia based upon r_α^0-parameters ($a = 2$ Å^{-1}) are given in Table 1. The correction introduced removed

stirred at room temperature until it became yellowish-green. The product was recrystallized from 10 ml of ether. Yield 70–75 % based on the amount of the selenenyl bromide.

[Ph_4As^+][p-$XPhSeSO_3^-$]. The aromatic seleno Bunte salts were prepared from the corresponding selenenyl benzenesulfinates, $Na_2SO_3.7H_2O$, and $Ph_4AsCl.2H_2O$ according to the following procedure. A solution, made by dissolving 3.4×10^{-3} mol of the aromatic selenenyl sulfinate in 15 ml of ether, was added under vigorous stirring at room temperature to a solution containing 3.8×10^{-3} mol of each of the reagents $Na_2SO_3.7H_2O$ and $Ph_4AsCl.2H_2O$ in 25 ml of water. The reaction mixture was stirred for 5 min, and the product separated as a white crystalline compound. The salt was filtered off, washed carefully with cold water and drained well. The product was recrystallized from about 10 ml of warm acetonitrile by the addition of some ether. Yield *ca.* 85 % based on the amount of selenenyl sulfinate.

[Ph_4As^+][p-$XPhSeSSO_3^-$]. The tetraphenylarsonium salts of aromatic selenenyl thiosulfates were prepared from the corresponding selenenyl benzenesulfinates, $Na_2S_2O_3.5H_2O$, and $Ph_4AsCl.2H_2O$. The procedure is analogous to that described above for the preparation of the corresponding selenenyl sulfite salts. The products, which appeared as yellowish-green compounds, were recrystallized from acetonitrile by the addition of some ether. Yield 85–90 % based on the amount of the selenenyl benzenesulfinate.

1. Klayman, D. L. *Organic Selenium Compounds*, Wiley, New York 1973, pp. 144–157.
2. Foss, O. *J. Am. Chem. Soc. 69* (1947) 2236.
3. Eriksen, R. and Hauge, S. *Acta Chem. Scand. 26* (1972) 3153.
4. Loudon, J. D. and Livingston, A. *J. Chem. Soc.* (1935) 896.
5. Baumgarten, P. *Ber. Dtsch. Chem. Ges. 63* (1930) 1330.
6. Austad, T. *To be published.*
7. Austad, T. *Acta Chem. Scand. A 29* (1975) 241.
8. Behaghel, O. and Seibert, K. *Ber. Dtsch. Chem. Ges. 65* (1932) 812.
9. Challenger, F., Peters, A. T. and Halévy, J. *J. Chem. Soc.* (1926) 1648.
10. Rheinboldt, H. In Houben-Weyl, *Methoden der Organischen Chemie*, 4th Ed., G. Thieme, Stuttgart 1955, Band IX, p. 1095.
11. Ref. 10, p. 1164.
12. Foss, O. *Acta Chem. Scand. 6* (1952) 508.

Received March 12, 1976.

On Comparisons of Structural Information Obtained from Microwave Spectroscopy and from Electron-diffraction Studies of Gaseous Chlorobutatriene and Chlorobutenynes

MATS GRANBERG,[a] GRETE GUNDERSEN[b] and FRED KARLSSON[a]

[a] Department of Physical Chemistry, University of Stockholm, Arrhenius Laboratory, Fack, S-104 05 Stockholm, Sweden and [b] Department of Chemistry, University of Oslo, Oslo 3, Norway

In recent electron-diffraction studies on the molecular structures of gaseous C_4H_3Cl isomers[1–4] the moments of inertia calculated from the structural results were compared to values obtained from microwave spectroscopy.[5–9] The comparisons were based upon the assumption that the average distances r_α and r_z[10] are comparable quantities, and the corresponding moments of inertia are given in Table 1. They were derived from the operational parameters, respectively, for electron diffraction (r_a) and microwave spectroscopy (r_o)[10] using similar force fields for computation of the necessary correction terms as described previously.[1–9]

However, r_α should be corrected to r_α^0 in order to represent the distance between the mean positions of a pair of atoms in the zero-point level as does the r_z parameter.[10]

$$r_\alpha^0 = r_\alpha + (K - K_0) - \tfrac{3}{2}a(l^2 - l_0^2) \qquad (1)$$

where K_0 and l_0 are the perpendicular amplitude correction coefficient and the root-mean-square amplitude of vibration at absolute zero, and a is an anharmonicity constant which for bond distances is usually about 2 Å^{-1}.[10] The correction is dominated by the $K - K_0$ term and r_α is therefore smaller than r_α^0 by an amount which was assumed to be negligible. A closer examination of the moments of inertia for all five isomers (Table 1) reveals, however, that those obtained from the electron-diffraction data (r_α) are all smaller than the corresponding microwave ones (r_z). Although the discrepancies are smaller than the estimated error limits,[1–4] the similar trend indicates the presence of some systematic error. The approximation applied by using r_α rather than r_α^0 was therefore reconsidered. The K_0- and l_0-values were computed from the force fields described previously for the five compounds[1–4] and the corresponding moments of inertia based upon r_α^0-parameters ($a = 2$ Å^{-1}) are given in Table 1. The correction introduced removed

Table 1. Comparison of moments of inertia (in au Å²) for chlorobutatriene and chlorobutenynes obtained from microwave spectroscopy (MW) and electron-diffraction (ED) studies.

		r_s(MW) [5–9]	r_α(ED) [1–4]	r_α^0(ED) [b]
Chlorobutatriene [1,5]	I_a	–	20.5 (20.1) [a]	20.6 (20.2) [a]
ClHC=C=C=CH₂	I_b	326.01	322.9 (325.8)	324.5 (327.4)
	I_c	346.20	343.4 (345.8)	345.2 (347.6)
cis-1-Chlorobutenyne [2,6]	I_a	56.60	56.2	56.4
ClHC=CH–C≡CH	I_b	196.86	196.6	197.2
	I_c	253.40	252.8	253.6
trans-1-Chlorobutenyne [2,7]	I_a	–	11.1	11.1
ClHC=CH–C≡CH	I_b	334.88	333.5	334.8
	I_c	345.33	344.6	345.9
2-Chlorobutenyne [3,8]	I_a	73.63	73.5	73.7
H_2C=CCl–C≡CH	I_b	163.41	163.2	163.6
	I_c	237.05	236.7	237.3
4-Chlorobutenyne [4,9]	I_a	–	11.5 (11.5) [a]	11.6 (11.6) [a]
H_2C=CH–C≡CCl	I_b	358.49	356.2 (357.3)	358.7 (359.8)
	I_c	370.60	367.7 (368.8)	370.3 (371.4)

[a] The values for models III and I are given for chlorobutatriene [1] and 4-chlorobutenyne,[4] respectively, while parenthesized values represent models IV and II. [b] The valence angles are assumed to be equl to those of the r_α-models.

the systematic discrepancy between values obtained from the two methods, as seen from Table 1, and a better overall agreement was obtained. The comparisons of the moments of inertia still rest upon approximations as assumed force fields were applied in the computation of the various correction terms. In particular these are sensitive to changes in the force constants associated with the lower fundamental frequencies which are not well known. The uncertainty of the anharmonicity constant is probably of less importance due to the smaller magnitude of the second term compared to the first one in eqn. 1.

It should be noted that the approximation had different impact on the moments of inertia for the five compounds being largest for chlorobutatriene and 4-chlorobutenyne. This is an unfortunate circumstance since for these two molecules the microwave data were used to add credibility to models which represented the best fit to the electron diffraction data but which contained, as it was pointed out, unreasonable values for the C=C–H valence angles (Models IV and II, respectively).[1,4] The results presented in this paper make it necessary to correct the support given to these models as comparisons of moments of inertia now favour models with the C=C–H angles fixed at reasonable values, *i.e.* models III and I, respectively, for chlorobutatriene and 4-chlorobutenyne (see Table 1). In the case of 4-chlorobutenyne information about the Cl···H nonbond distances is also available from the microwave investigation.[9] The Cl···H (etylynic) distances obtained from micrawave data (r_s-values [10]) and electron-diffraction data (r_a-values [10]) compare favourably for *cis*- and *trans*-1-chlorobutenyne.[2,6,7] For 4-chlorobutenyne the r_s-values are 5.024, 6.197, and 4.830 Å, respectively, for the Cl···H_1(*cis*), Cl···H_1(*trans*) and Cl···H_2 distances [9] as compared to the r_a-values of Models I and II, respectively: I, 5.046(10), 6.169(9) and 4.762(8) Å; II, 5.142(47), 6.182(41) and 4.861(36) Å.[4] Comparisons seem to support a combination of models I and II with ∠C=C–H_1 = 122° (I) and ∠C=C–H_2 = 114.6(2.6)° (II). The smaller C=C–H_2 angle of Model II is also favoured by the determination of the amplitude of vibration associated with the Cl···H_2 distance as described previously.[4] The moments of inertia (r_α^0) for the combined model (Model II with ∠C=C–H_1 changed to 122°) are I_a = 11.5, I_b = 359.3 and I_c = 370.7 au Å², and they are in good agreement with the corresponding microwave ones given in Table 1.

1. Almenningen, A., Gundersen, G., Borg, A., Granberg, M. and Karlsson, F. *Acta Chem. Scand. A 29* (1975) 395.
2. Almenningen, A., Gundersen, G., Borg, A., Granberg, M. and Karlsson, F. *Acta Chem. Scand. A 29* (1975) 545.
3. Almenningen, A., Gundersen, G., Granberg, M. and Karlsson, F. *Acta Chem. Scand. A 29* (1975) 725.
4. Almenningen, A., Gundersen, G., Granberg, M. and Karlsson, F. *Acta Chem. Scand. A 29* (1975) 731.
5. Karlsson, F., Granberg, M. and Vestin, R. *Acta Chem. Scand. A 28* (1974) 201.

6. Karlsson, F., Granberg, M. and Vestin, R. *Acta Chem. Scand. A 29* (1975) 855.
7. Karlsson, F. and Vestin, R. *Acta Chem. Scand. 27* (1973) 3033.
8. Karlsson, F., Granberg, M. and Vestin, R. *Acta Chem. Scand. A 28* (1974) 206.
9. Karlsson, F., Granberg, M. and Vestin, R. *Acta Chem. Scand. A 29* (1975) 111.
10. Kuchitsu, K. and Cyvin, S. J. In Cyvin S. J., Ed., *Molecular Structures and Vibrations*, Elsevier, Amsterdam 1972, Chapter 12.

Received February 20, 1976.

On the Photochemical Behaviour of Radiation Produced Trapped Electrons in an Alcohol/Water Glass

JOHAN MOAN

Norsk Hydro's Institute for Cancer Research, The Radium Hospital, Montebello, Oslo 3, Norway

Radiation produced electrons are stabilized at low temperatures in a variety of solvents among which alcohols and alcohol/water mixtures are the most frequently studied cases. The processes following an ionization event in an alcohol glass are:[1-4]

$$RCH_2OH \xrightarrow{\gamma, X} RCH_2OH^+ + e^- \quad (1)$$

$$e^- \longrightarrow e_t^- \text{ (electron trapping)} \quad (2)$$

$$RCH_2OH^+ + RCH_2OH \longrightarrow RCH_2OH_2^+ + RC{\cdot}HOH \quad (3)$$

(R = H, CH_3, C_2H_5 *etc.*)

The trapped electron, e_t^-, has an absorption spectrum in the visible part of the spectrum and is easily bleached during exposure to visible light, giving rise to alcohol radicals.[5] The nature of this process is somewhat unclear. One possibility is that the photomobilized electrons (e_m^-) react with $RCH_2OH_2^+$ ions [2,5,6] which probably are trapped within a few Ångströms of the electrons, the reactions being:

$$RCH_2OH_2^+ + e_m^- \longrightarrow RCH_2OH + H \quad (4)$$

followed by

$$RCH_2OH + H \longrightarrow RC{\cdot}HOH + H_2 \quad (5)$$

Another possibility would be that mobilized electrons react with neutral alcohol molecules according to the scheme:[7]

$$RCH_2OH + e_m^- \longrightarrow RCH_2O^- + H \quad (6)$$

followed by (5).

To distinguish between the two processes we studied the dependence of the photobleaching efficiency on the dose of ionizing radiation delivered to the sample. We have carried out such an experiment in the case of an ethylene glycol/water glass (1:1 by volume) at 77 K. The results are, as shown below, definitely in favour of the second hypothesis.

We exposed an ethylene glycol/water glass at 77 K to the radiation from a 4 MeV modified AEI-linear accelerator. The samples were prepared by allowing 20 μl drops of sample solution to fall into liquid N_2. The irradiated samples were analyzed by ESR methods. Fig. 1 shows how the yield of trapped electrons and ethylene glycol radicals varies with the dose. It can be seen that while the yield of ethylene glycol radicals increases practically linearly with the dose, the electron yield reaches a plateau.

A similar dose dependence of the electron yield has been reported for a variety of solvents. Thus, the yields are generally reaching a maximum and then decreasing (see review article in Ref. 8). A number of explanations of this behaviour has been proposed: (1) only a limited number of electron traps exist,[9] (2) reactions of the electrons with radicals in the sample [10] and (3) reactions of mobile electrons with positive ions produced by the radiation, or reactions of mobile positive ions with trapped electrons.[11] The maximum concentration of trapped electrons was found to be of the order of 5×10^{-3} M, which is in correspondence with the findings of others for alcohol matrices (see review in Ref. 8).

The samples could be optically bleached by exposing them to the light of a 200 W high pressure mercury lamp fitted to a Bausch & Lomb grating monochromator. Except for the lowest dose (500 krad) the ESR signals from trapped electrons decreased practically linearly with the exposure time during bleaching. This shows that with exception of the first case the samples are total absorbing thus explaining the apparent low quantum efficiency of bleaching at this dose (Fig. 1). For doses exceeding 2 Mrad, Fig. 1 shows that the quantum efficiency of electron bleaching is practically constant. This is true both for bleaching at 366 nm (3.4 eV) and at 625 nm (2.0 eV). The photomobilization threshold for electrons in the present matrix is 2.2 eV.[12] Hence irradiation at 366 nm causes photomobilization of the trapped electrons, while irradiation at 625 nm causes excitation. Since the quantum efficiency of bleaching is dose independent, and since the concentrations of $RCH_2OH_2^+$ as well as

6. Karlsson, F., Granberg, M. and Vestin, R. *Acta Chem. Scand. A 29* (1975) 855.
7. Karlsson, F. and Vestin, R. *Acta Chem. Scand. 27* (1973) 3033.
8. Karlsson, F., Granberg, M. and Vestin, R. *Acta Chem. Scand. A 28* (1974) 206.
9. Karlsson, F., Granberg, M. and Vestin, R. *Acta Chem. Scand. A 29* (1975) 111.
10. Kuchitsu, K. and Cyvin, S. J. In Cyvin S. J., Ed., *Molecular Structures and Vibrations*, Elsevier, Amsterdam 1972, Chapter 12.

Received February 20, 1976.

On the Photochemical Behaviour of Radiation Produced Trapped Electrons in an Alcohol/Water Glass

JOHAN MOAN

Norsk Hydro's Institute for Cancer Research, The Radium Hospital, Montebello, Oslo 3, Norway

Radiation produced electrons are stabilized at low temperatures in a variety of solvents among which alcohols and alcohol/water mixtures are the most frequently studied cases. The processes following an ionization event in an alcohol glass are:[1-4]

$$RCH_2OH \xrightarrow{\gamma, X} RCH_2OH^+ + e^- \quad (1)$$

$$e^- \longrightarrow e_t^- \text{ (electron trapping)} \quad (2)$$

$$RCH_2OH^+ + RCH_2OH \longrightarrow RCH_2OH_2^+ + RC{\cdot}HOH \quad (3)$$

(R = H, CH_3, C_2H_5 *etc.*)

The trapped electron, e_t^-, has an absorption spectrum in the visible part of the spectrum and is easily bleached during exposure to visible light, giving rise to alcohol radicals.[5] The nature of this process is somewhat unclear. One possibility is that the photomobilized electrons (e_m^-) react with $RCH_2OH_2^+$ ions [2,5,6] which probably are trapped within a few Ångströms of the electrons, the reactions being:

$$RCH_2OH_2^+ + e_m^- \longrightarrow RCH_2OH + H \quad (4)$$

followed by

$$RCH_2OH + H \longrightarrow RC{\cdot}HOH + H_2 \quad (5)$$

Another possibility would be that mobilized electrons react with neutral alcohol molecules according to the scheme:[7]

$$RCH_2OH + e_m^- \longrightarrow RCH_2O^- + H \quad (6)$$

followed by (5).

To distinguish between the two processes we studied the dependence of the photobleaching efficiency on the dose of ionizing radiation delivered to the sample. We have carried out such an experiment in the case of an ethylene glycol/water glass (1:1 by volume) at 77 K. The results are, as shown below, definitely in favour of the second hypothesis.

We exposed an ethylene glycol/water glass at 77 K to the radiation from a 4 MeV modified AEI-linear accelerator. The samples were prepared by allowing 20 μl drops of sample solution to fall into liquid N_2. The irradiated samples were analyzed by ESR methods. Fig. 1 shows how the yield of trapped electrons and ethylene glycol radicals varies with the dose. It can be seen that while the yield of ethylene glycol radicals increases practically linearly with the dose, the electron yield reaches a plateau.

A similar dose dependence of the electron yield has been reported for a variety of solvents. Thus, the yields are generally reaching a maximum and then decreasing (see review article in Ref. 8). A number of explanations of this behaviour has been proposed: (1) only a limited number of electron traps exist,[9] (2) reactions of the electrons with radicals in the sample [10] and (3) reactions of mobile electrons with positive ions produced by the radiation, or reactions of mobile positive ions with trapped electrons.[11] The maximum concentration of trapped electrons was found to be of the order of 5×10^{-3} M, which is in correspondence with the findings of others for alcohol matrices (see review in Ref. 8).

The samples could be optically bleached by exposing them to the light of a 200 W high pressure mercury lamp fitted to a Bausch & Lomb grating monochromator. Except for the lowest dose (500 krad) the ESR signals from trapped electrons decreased practically linearly with the exposure time during bleaching. This shows that with exception of the first case the samples are total absorbing thus explaining the apparent low quantum efficiency of bleaching at this dose (Fig. 1). For doses exceeding 2 Mrad, Fig. 1 shows that the quantum efficiency of electron bleaching is practically constant. This is true both for bleaching at 366 nm (3.4 eV) and at 625 nm (2.0 eV). The photomobilization threshold for electrons in the present matrix is 2.2 eV.[12] Hence irradiation at 366 nm causes photomobilization of the trapped electrons, while irradiation at 625 nm causes excitation. Since the quantum efficiency of bleaching is dose independent, and since the concentrations of $RCH_2OH_2^+$ as well as

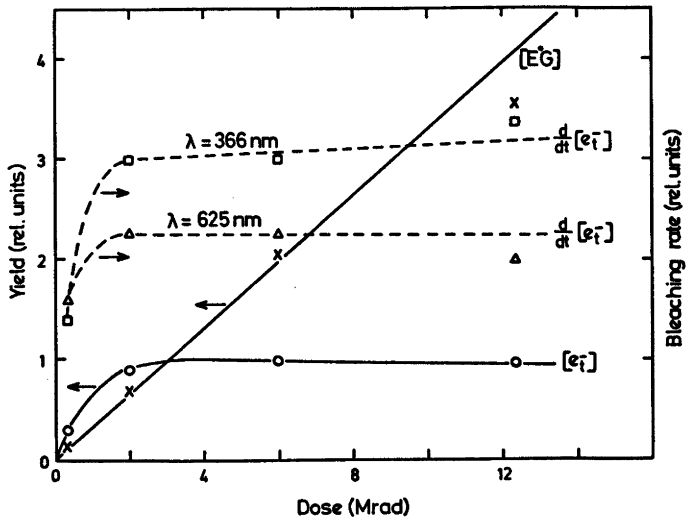

Fig. 1. Ethylene glycol/water mixtures irradiated at 77 K with different doses from a 4 MeV electron accelerator. ○, concentration of trapped electrons; ×, concentration of ethylene glycol radicals; △, quantum efficiency of bleaching at 625 nm; □, quantum efficiency of bleaching at 366 nm.

of RC·HOH is supposed to increase nearly linearly with the dose, the present data strongly suggest that the mechanism of optical bleaching of e_t^- is described by eqn. (6) rather than by eqn. (4). Thus, the electrons probably react mainly with neutral alcohol molecules when being excited. This is what one would expect for excitation with quantum energies below the photomobilization threshold (*i.e.* for excitation at 625 nm). It is a somewhat surprising result that the same mechanism seems to be operative also at 366 nm where the trapped electrons are mobilized and should have the possibility of encountering $RCH_2OH_2^+$ ions.

1. Dainton, F. S., Salmon, G. A. and Wardman, P. *Proc. Roy. Soc. London A 313* (1969) 1.
2. Ayscough, P. B., Collins, R. G. and Dainton, F. S. *Nature (London) 205* (1965) 965.
3. Smith, R. and Pieroni, J. J. *Can. J. Chem. 45* (1967) 2723.
4. Dainton, F. S., Salmon, G. A. and Zucker, U. F. *Proc. Roy. Soc. London A 320* (1970) 1.
5. Dainton, F. S., Keene, J. P., Kemp, T. J., Salmon, G. A. and Teplý, J. *Proc. Chem. Soc.* (1964) 265.
6. Dainton, F. S., Salmon, G. A. and Teplý, J. *Proc. Roy. Soc. London A 286* (1965) 27.
7. Habersbergerová, A., Josimovic, Lj. and Teplý, J. *Trans. Faraday Soc. 66* (1970) 656.
8. Kevan, L. *Adv. Radiat. Chem. 4* (1974) 181.
9. Shirom, M. and Willard, J. E. *J. Am. Chem. Soc. 90* (1968) 2184.
10. Teplý, J., Janovsky, I., Kiss, F. and Vacec, K. *Int. J. Radiat. Phys. Chem. 4* (1972) 265.
11. Ekstrøm, A., Suenram, R. and Willard, J. E. *J. Phys. Chem. 74* (1970) 1888.
12. Moan, J. *Chem. Phys. Lett. 17* (1972) 565.

Received February 24, 1976.

Acta Chemica Scandinavica A 30 (1976) 485—497

Conformational Analysis of Coordination Compounds. III. Tris-diamine Cobalt(III) and Chromium(III) Complexes with Six-membered Chelate Rings

SVETOZAR R. NIKETIC,[a,*] KJELD RASMUSSEN,[a,**] FLEMMING WOLDBYE [a] and SHNEIOR LIFSON [b]

[a] Chemistry Department A, The Technical University of Denmark, DK-2800 Lyngby, Denmark and [b] Chemical Physics Department, The Weizmann Institute of Science, Rehovot, Israel

A fast convergent minimization programme is applied to calculate equilibrium conformations of coordination compounds.

Energy equations containing harmonic bond stretching and angle bending functions, Pitzer-type torsional functions, and Buckingham-type functions for non-bonded interactions (with parameters chosen previously) were used to calculate equilibrium geometries and energies of all possible conformers of the tris(1,3-propanediamine)cobalt(III) system and of ten species of the tris(2,4-pentanediamine)cobalt (III) system.

These calculations demonstrate that various previously suggested conformations of the same type converge to a common equilibrium conformation having the highest possible symmetry. The (C_3)-chair$_3$ conformer represents the global minimum in the force field chosen. Distribution of equilibrium conformations on an energy scale is governed by a delicate balance of all energy contributions. It is suggested that the effect of long range non-bonded interactions is not negligible.

The shapes of chair and twist-boat chelate rings are discussed in detail, and comparison with X-ray structures is made in terms of the deviations from idealized ring geometries.

In previous papers [1] two of us investigated the capability of a steepest-descent energy minimization based on Wiberg's programme [2] for the conformational analysis of tris-diamine metal complexes.

The conclusions of the earlier work were that (1) several energetically almost equivalent conformations should exist in equilibrium in solution; (2) with the steepest-descent method one cannot definitively identify the most stable conformation; (3) different initial conformations of the same gross conformational type did not coalesce during minimization. The main deficiency of the approach is due to the intrinsic limitation of the steepest-descent algorithm, namely the extremely slow convergence when a system is close to its minimum. Therefore the termination criterion adopted was the attainment of identical rates of convergence for different conformations rather than true convergence.

In the present work a more refined energy minimization was employed, leading to true convergence. A programme was developed,[3] based on the Consistent Force Field (CFF) approach of Lifson and Warshel,[4] with a very flexible structure and a minimum of input requirements. The work reported here was undertaken with a twofold aim: (1) to evaluate the performance of the energy minimization part of our version of the CFF system; and (2) to further refine the results of the former calculations,[1] using the same force field. We confined our investigations to complexes with six-membered metal-chelate rings represented by M(tn)$_3$ and M(2,4-ptn)$_3$, where tn = trimethylenediamine = 1,3-propanediamine and 2,4-ptn = 2,4-pentanediamine. Comparisons with

* Present address: Department of Chemistry, University of Beograd, P.O. Box 550, 11001 Beograd, Yugoslavia.

** To whom correspondence should be addressed.

experimental structures were done for M = Co(III) and, in two cases, Cr(III). The results were also compared with other relevant calculations of a similar nature.

THE PROGRAMME

It is our intention to present elsewhere a full documentation of the version [3] of the CFF system [4,5] developed at Chemistry Department A of the Technical University of Denmark. Therefore we shall give here only a short account of the main features.

The types of potential energy functions (the "force field") are chosen automatically by the programme from two control parameters. Harmonic, anharmonic and Morse functions are possible choices for bond stretching; harmonic or Urey-Bradley for angle bending; Pitzer-type for torsions; and Lennard-Jones or Buckingham, plus Coulomb terms, for non-bonded interactions.

The programme reads a molecular formula written in a line notation very close to the usual chemical one, and constructs the topology of the molecule as lists of all types of interactions according to the force field chosen. Chirality symbols *R* and *S* are used for dissymmetric carbon or other atoms; for metal atoms *R* and *S* are interpreted as Δ and Λ.

Molecular geometry in cartesian coordinates is either calculated from a built-in library of standard bond lengths and valence angles, according to the topology, or is taken from a previous calculation or from a crystal structure determination. Transformation from fractional coordinates and unit cell parameters is performed with a separate utility programme.

Conformational energy and analytical first and second derivatives are calculated according to the force field chosen and the type of calculation specified. This part of the programme is usually called an appreciable number of times during a minimization run.

A hierarchy of three gradient algorithms was developed for energy minimization. (1) After investigating various steepest-descent algorithms,[2,6,7] we abandoned all as they either were too slow, became oscillatory or required frequent changes in the programme to optimize their functioning on different types of molecules. We therefore developed an algorithm of our own, which was reasonably fast and would automatically work well on all problems tackled so far. (2) Our next choice was a variable metric method, the Davidon-Fletcher-Powell algorithm.[8] We introduced a few minor changes in a routine, which was a standard one at The Weizmann Institute of Science in 1970. (3) As the most powerful method in terms of convergence rate we used a modified Newton, second-order gradient algorithm (MNA) developed by Gill, Murray, and Picken.[9] It is based on the Cholesky factorisation of the Hessian matrix of second derivatives, and it is both stable and relatively fast. The original ALGOL procedure was completely rewritten to conform with our addressing of the Hessian matrix and with our FORTRAN library.

It may happen that convergence is slow, even with the Newton method. In such cases a separate utility programme is used to scramble the conformation by adding randomly generated increments to all cartesian coordinates of the conformer. Subsequent minimization has not yet failed to converge properly.

Convergence to a true minimum was considered adequate when all partial derivatives of potential energy with respect to cartesian coordinates were reduced to $< 10^{-6}$ kcal mol^{-1} Å^{-1}. A typical minimization of a previously [1] minimized complex molecule of 46 – 64 atoms, using 20 – 50 steepest-descent and 5 – 8 Newton iterations, required 2 – 3 min on an IBM 370/165 and 380K without overlay structure.

CALCULATIONS

Stereochemistry. All structures studied in this work contain three six-membered metal chelate rings in an octahedral environment. Their stereochemistry and nomenclature proposals were previously described in detail.[1a]

There are 16 theoretically possible conformers of the M(tn)$_3$ system [1a] for each of the absolute octahedral configurations Δ and Λ, in which the individual chelate rings adopt any of the three stable conformations: *chair*, *δ-twist-boat*, and *λ-twist-boat*. Three of these: chair$_3$, lel$_3$[= $\Delta(\lambda\lambda\lambda)$ or $\Lambda(\delta\delta\delta)$], and ob$_3$[= $\Delta(\delta\delta\delta)$ or $\Lambda(\lambda\lambda\lambda)$] of idealized symmetries C_3, D_3 and D_3, respectively, will be termed *homoconformational*. The other 13 forms containing two or three rings of different conformations, or

different orientations of chair conformations,[1a] are termed *heteroconformational.*

Among the numerous theoretically possible isomers of the $M(2,4\text{-ptn})_3$ system three species — each of which containing three identical stereoisomers of coordinated diamine (*i.e.*, either 2*R*,4*R*-, or 2*S*,4*S*-, or *meso*-2,4-ptn) — are of chemical interest. Equatorial preference of all methyl groups limits the number of conformers to one for each stereoisomer of 2,4-ptn as shown in Table 1. (See also Fig. 7 of Ref. 1a.) Two other sets of theoretically possible homoconformational forms of $M(2,4\text{-ptn})_3$ comprise four $(eq)_3(ax)_3$ conformers having C_3 symmetry (also shown in Table 1), and three hexa-axial conformers (not shown in Table 1). All other conformers having a distribution of methyl groups different from $(eq)_6$, C_3-$(eq)_3(ax)_3$, or $(ax)_6$ are heteroconformational. They are derived either from heteroconformational forms of the basic $M(tn)_3$ skeleton, or from species containing different stereoisomers of coordinated 2,4-ptn. A set of four conformers of the latter type is exemplified in Table 1. They were investigated in an attempt to study the effect of one methyl group in an axial position.

Initial coordinates. The starting conformations were taken as the "final minimized conformations" obtained from our former calculations.[1a] All distinct forms resulting from various minimizations of the same conformer were subjected to the refinement procedure.

In addition, calculations were carried out on $M(tn)_3$ conformations corresponding to those found by X-ray diffraction studies on $(-)_D$-$[Co(tn)_3]Br_3.H_2O$;[10] $(-)_D$-$[Co(tn)_3]Cl_3.H_2O$;[11] $[Cr(tn)_3][Ni(CN)_5].2H_2O$;[12] as well as on $M(2,4\text{-ptn})_3$ conformations found in $(+)_{546}$-$[Co(2R,4R\text{-ptn})_3]Cl_3.H_2O$ [13a] and $(-)_{546}$-$[Co(2R,4R\text{-ptn})_3]Cl_3.2H_2O$.[13a]

Force field. In the previous work [1a] two force fields were used, FF-1 and FF-2. In the present work, we have used only FF-1. In a series of calculations on $Co(tn)_3$ conformations FF-1 was supplemented with Co···C and Co···H non-bonded interactions with parameter values similar to those used for C···C and C···H interactions, respectively. These modifications produced only insignificant changes in the final results and were not studied further.

RESULTS

Tris(trimethylenediamine) conformations. The initial conformations, on which the present minimizations were carried out, were 41 distinct conformations of the $M(tn)_3$ system, part of which were minimized previously.[1a] They comprised three idealized * homoconformational forms ($chair_3$, lel_3, and ob_3) minimized in FF-1; the same three forms minimized in FF-2;

* The term idealized means that the conformation in question was generated from standard bond lengths and valence angles, with torsional angles chosen to fit the desired conformation.

Table 1. Some of the theoretically possible conformations of $M(2,4\text{-ptn})_3$ exemplified for the overall Δ absolute configuration.[a]

Isomer	Methyl groups		
	$(eq)_6$	$(eq)_5(ax)$	$(eq_3(ax)_3$
Homoconformational			
$M(2R,4R\text{-ptn})_3$	lel_3 (D_3)	—	$chair_3$ (C_3)
$M(2S,4S\text{-ptn})_3$	ob_3 (D_3)	—	$chair_3$ (C_3)
$M(meso\text{-}2,4\text{-ptn})_3$	$chair_3$ (C_3)	—	lel_3,ob_3 (C_3)
Heteroconformational			
$M(meso\text{-}2,4\text{-ptn})_2(2R,4R\text{-ptn})$	—	$chair_3$ (C_1)	—
$M(meso\text{-}2,4\text{-ptn})_2(2S,4S\text{-ptn})$	—	$chair_3$ (C_1)	—
$M(2R,4R\text{-ptn})_2(meso\text{-}2,4\text{-ptn})$	—	lel_3 (C_1)	—
$M(2S,4S\text{-ptn})_2(meso\text{-}2,4\text{-ptn})$	—	ob_3 (C_1)	—

[a] Molecular symmetries are given in parentheses.

two chair$_3$ conformations corresponding to X-ray structures of the Co(tn)$_3$ ion; 10 idealized heteroconformational forms [1a] minimized in FF-1 and FF-2; idealized and X-ray *syn*-chair$_2$lel conformations; *syn*-chair$_2$ob and $(C)_1$-chair$_3$ conformations; and eight (C_3)-chair$_3$ forms of M(tn)$_3$ artificially generated from various ring conformations of complexes containing trimethylenediamine of known X-ray structures; and an average (C_3)-chair$_3$ conformation obtained from minimized idealized and minimized X-ray conformations of Co(tn)$_3$.

Previously [1a] we omitted three of the heteroconformational forms having a pair of *syn*-chair$_2$ rings partly because molecular models indicated that in their *idealized* forms they would be highly unstable. Meanwhile, the *syn*-chair$_2$lel conformation has been found in crystalline [Cr(tn)$_3$] [Ni(CN)$_5$]. $2H_2O$.[12b] Consequently, we have included in our calculations two *syn*-chair$_2$lel conformations: the one found by Jurnak and Raymond [12] and the idealized form which required a modified treatment [1c] in order to be minimized successfully; and the *syn*-chair$_2$ob and (C_1)-chair$_3$ conformers.

All *prima facie* distinct forms of the same gross conformation converged to the unique conformation. The minimization procedure, therefore, led to 16 unique local-minimum conformations of the M(tn)$_3$ system.

Energy contributions for 16 M(tn)$_3$ conformations are given in Table 2, and distributions of bond lengths and valence angles are given in Table 3. Six examples of individual conformations are shown in Fig. 1.

One of the most remarkable results obtained here was that the same minimum-energy chair$_3$ conformation of M(tn)$_3$ was reached from all 13 distinct initial chair$_3$ conformations showing (a) the superiority of the present method, and (b) a proof of our assumption that various chair$_3$ conformations found before [1a] belong to the same energy minimum on the potential energy surface of M(tn)$_3$. Furthermore, the (C_3)-chair$_3$ conformer was found to represent the global minimum of the M(tn)$_3$ system in FF-1 (see Table 2).

Another striking result of the minimizations was that each conformer showed a strong tendency to attain its highest possible symmetry (for the notation, see Table 1 in Ref. 1a) irrespective of the structure of its initial conformation. Thus, all chair$_3$ forms, including the X-ray structures, converged to the chair$_3$ conformation having rigorous C_3 symmetry; all lel$_3$ and ob$_3$ approached rigorous D_3 symmetry, *etc.*

The next lowest conformation minimized in FF-1 was lel$_3$ (< 1 kcal mol^{-1} above the global minimum). The ob$_3$ and the remaining hetero-

Table 2. Energy contributions for M(tn)$_3$ conformations.[a]

Conformer of M(tn)$_3$	E_b	E_t	E_p	E_{nb}	E_T	ΔE
(C_3)-chair$_3$	1.61	9.39	2.80	−1.80	11.99	0.00
lel$_3$	1.56	4.50	7.14	−0.41	12.79	0.80
lel$_2$ chair	1.75	6.75	5.03	0.32	13.86	1.87
(C_1)-chair$_3$	2.08	9.89	2.63	−0.22	14.39	2.40
syn-chair$_2$lel	2.08	8.53	3.32	0.66	14.59	2.60
(C_1)-chair$_2$lel	2.06	8.60	2.91	1.06	14.60	2.61
(C_1)-chair$_2$ob	1.60	9.23	4.86	−0.90	14.79	2.80
anti-chair$_2$lel	1.93	9.28	2.74	1.04	15.00	3.01
trans$_{(\text{chair, lel})}$-chair lel ob	1.65	8.04	6.05	0.09	15.82	3.83
anti-chair$_2$ob	2.39	8.58	3.48	1.56	16.01	4.02
ob$_2$chair	1.76	7.98	6.17	0.35	16.26	4.27
syn-chair$_2$ob	2.36	9.21	3.23	2.02	16.82	4.83
lel$_2$ob	1.48	6.67	8.58	0.59	17.32	5.33
cis$_{(\text{chair, lel})}$-chair lel ob	2.23	8.04	5.38	2.40	18.05	6.06
ob$_3$	2.32	6.11	7.60	2.22	18.26	6.27
ob$_2$lel	1.60	7.76	8.54	0.83	18.73	6.74

[a] All energies are given in kcal mol^{-1}; E_b, E_t, E_p, E_{nb}, E_T, and ΔE are bond stretching, angle bending, torsional and non-bonded contributions, total energy, and energy relative to (C_3)-chair$_3$, respectively.

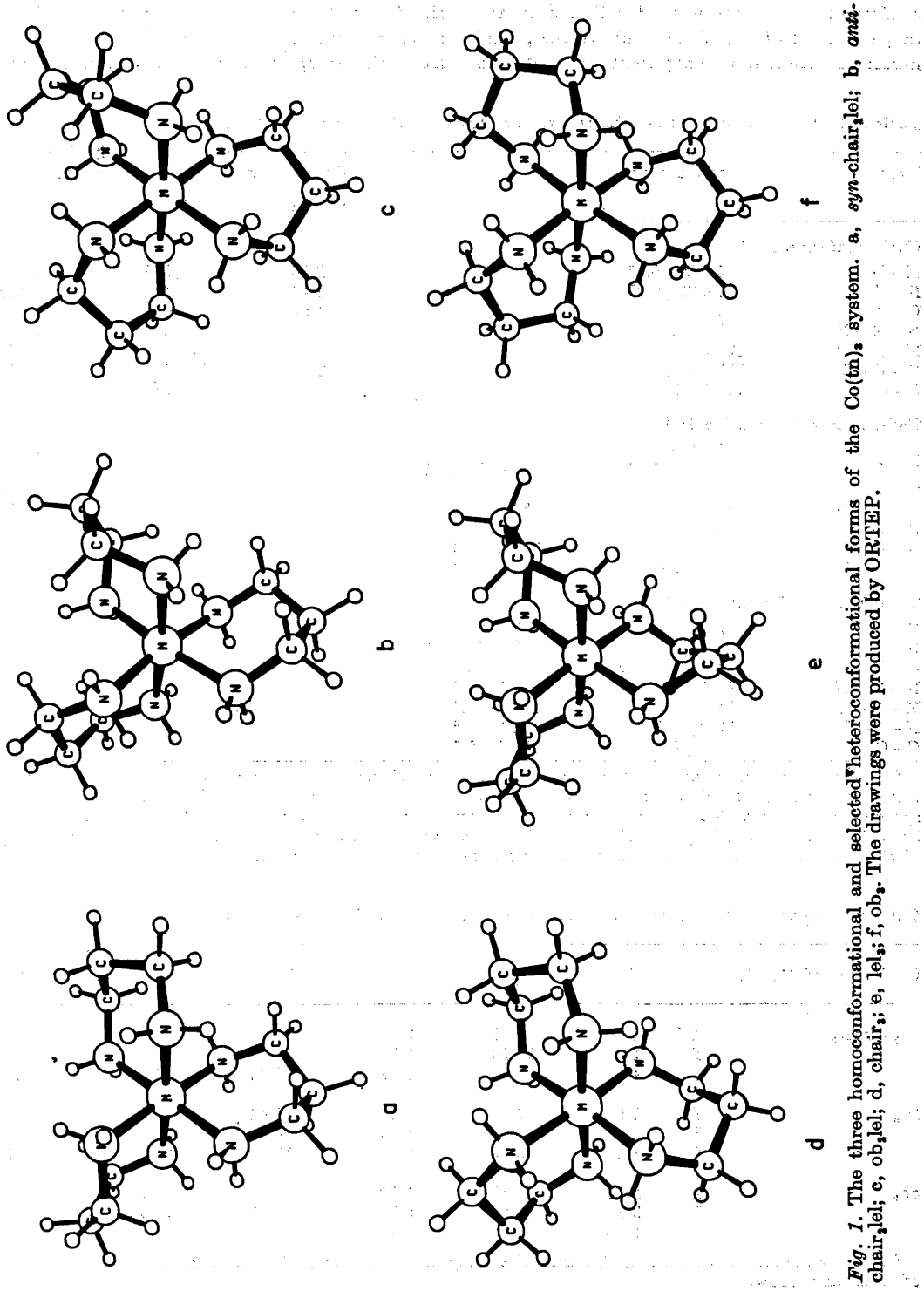

Fig. 1. The three homoconformational and selected heteroconformational forms of the $Co(tn)_3$ system. a, *syn*-chair$_2$lel; b, *anti*-chair$_2$lel; c, ob$_2$lel; d, chair$_3$; e, lel$_3$; f, ob$_3$. The drawings were produced by ORTEP.

conformational forms were distributed in the range of 1.9 to 6.8 kcal mol^{-1} above the global minimum. There are no apparent regularities in the distribution; neither can the energies of the heteroconformational forms be interpolated from the energies of the homoconformational

Table 3. Distribution of bond lengths and valence angles in M(tn)$_3$ conformations.

Type	Distribution [a]		Observed in X-ray structures of		
			Co tn$_3$[b]	Co tn$_3$[c]	Cr tn$_3$[d]
Chair conformation [e]					
M–N	2.045±0.01		2.00	1.979	2.095
N–C	1.477±0.03		1.47	1.484	1.495
C–C	1.543±0.01		1.54	1.499	1.502
N–M–N	90.0±4.0		94.	90.4	89.98
M–N–C	120.0±2.0		118.	122.2	120.72
N–C–C	111.5±0.7		112.	111.8[f]	112.40
C–C–C	110.8±1.0		114.	113.5[f]	114.43
Twist-boat conformation *lel* [g]					
M–N	2.045±0.005	2.042±0.01			2.100
N–C	1.478±0.005	1.479±0.01			1.472
C–C	1.545±0.005	1.549±0.01			1.462
N–M–N	87.8±1.0	88.0±1.2			89.21
M–N–C	114.0±1.0	117.0±3.0			116.59
N–C–C	112.0±1.0	112.2±1.8			119.18
C–C–C	112.0±1.0	112.7±0.8			117.20
Twist-boat conformation *ob* [g]					
M–N	2.050±0.005	2.045±0.02			
N–C	1.476±0.005	1.478±0.02			
C–C	1.545±0.005	1.548±0.01			
N–M–N	88.0±0.5	87.9±1.6			
M–N–C	114.0±0.8	116.0±3.0			
N–C–C	112.0±1.0	112.5±1.6			
C–C–C	113.0±0.5	112.6±0.8			

[a] The distribution means that the values found in all minimum-energy conformations are distributed in the range bracketed by the upper (+) and lower (−) limit indicated. [b] Averaged assuming C_3 symmetry (Nomura, Marumo and Saito [10]). [c] Averaged assuming C_3 symmetry (Nagao, Marumo and Saito [11]). [d] Jurnak and Raymond. [12b] [e] Distribution is given over the averaged values assuming C_s symmetry of chair rings. [f] One anomalous valence angle has been omitted from averaging. [g] See text.

Table 4. Comparison of the present calculations with the results of Geue and Snow.[14]

Conformer of M(tn)$_3$		E_b	E_t	E_p	E_{nb}	E_T	ΔE
(C_3)-chair$_3$	A [a]	1.61	9.38	2.80	−1.80	11.99	0.00
	B	2.61	11.24	2.30	1.42	17.57	0.00
	C	4.25	10.88	2.09	11.77	28.98	0.00
lel$_3$	A	1.56	4.50	7.14	−0.41	12.79	0.80
	B	2.73	5.16	5.92	4.14	17.95	0.38
	C	3.30	5.02	6.02	13.87	28.21	−0.77
ob$_3$	A	2.32	6.11	7.60	2.22	18.26	6.27
	B	3.94	7.56	6.31	7.33	25.15	7.58
	C	5.10	6.90	5.99	16.04	34.04	5.06

[a] A, our calculations with FF-1; B, our results using the force field of Geue and Snow; C, original results of Geue and Snow.

Table 5. Energy contributions for M(2,4-ptn)$_3$ conformations.[a]

Conformer of M(2,4-ptn)$_3$		E_b	E_t	E_p	E_{nb}	E_T	ΔE
chair$_3$	$(eq)_6$	1.82	9.45	3.00	−4.56	9.71	0.00
lel$_3$	$(eq)_6$	1.87	4.64	7.05	−3.49	10.07	0.32
chair$_3$	$(eq)_5(ax)$ [b]	1.91	12.31	3.45	−4.22	13.47	3.74
chair$_3$	$(eq)_5(ax)$ [c]	1.94	11.79	4.11	−4.11	13.73	4.02
ob$_3$	$(eq)_6$	2.75	6.02	7.51	−0.91	15.37	5.66
lel$_3$	$(eq)_5(ax)$	2.08	8.16	8.39	−2.58	16.04	6.33
chair$_3$	$(eq)_3(ax)_3$	2.13	18.53	3.99	−3.18	21.47	11.76
ob$_3$	$(eq)_5(ax)$	2.99	10.46	8.88	−0.18	22.15	12.44
lel$_3$	$(eq)_3(ax)_3$	2.28	15.92	11.51	−1.01	28.70	18.99
ob$_3$	$(eq)_3(ax)_3$	4.12	20.18	11.01	1.79	37.11	27.40

[a] See footnote in Table 2. [b] M(*meso*-2,4-ptn)$_2$(2*S*,4*S*-ptn) species. [c] M(*meso*-2,4-ptn)$_2$(2*R*, 4*R*-ptn) species.

forms. This is not surprising, as there are subtle but important differences in the minimized geometries of a particular gross ring conformer in the various conformational forms. Without exception, the heteroconformational forms have higher energies than what can be found from interpolation; this shows that different ring conformers in the same complex distort each other away from the symmetrical low-energy geometries.

The global minimum found here is different from that found by Geue and Snow,[14] who found the lel$_3$ conformer to be 0.77 kcal mol^{-1} lower in energy than the chair$_3$ conformer. This prompted us to minimize the three homoconformational forms using their force field.[15] The result was that the chair$_3$ conformer is still the global minimum, but that the lel$_3$ conformer lies only 0.38 kcal mol^{-1} above the chair$_3$ conformer. A comparison of these results and those of Geue and Snow is given in Table 4. There are substantial differences, particularly for the bond and non-bonded contributions. The geometries of the three forms as given by Geue and Snow [15] (their Table 8) are very close to those found here, the deviations being for torsional angles 0.3 (av.) and 2.0° (max), and for valence angles 0.4 (av.) and 1.4° (max).

The reason for the discrepancy is most probably that Geue and Snow omit the longer non-bonded interactions.[15] As far as we can check it, this means that, *e.g.*, H···H interactions are omitted for distances longer than 2.78 Å, or more than 300 individual H···H interactions or more than 80 %. Some of the interactions omitted correspond to situations where the two atoms do actually "see" each other directly, and not through other atoms or through bonding regions. The significance of including also the longer non-bonded interactions will be discussed below.

Due to the proximity of lel$_3$ and some of the low-energy heteroconformational forms of M(tn)$_3$ to the global minimum (Fig. 1) the definitive prediction of the most stable conformation requires the choice of a more refined force field, and calculation of conformational entropy contributions to the free energies. These supplementary calculations require a complete consistent force field study of M(tn)$_3$, which will be undertaken after an extension of our programme.

Tris(2,4-pentanediamine) conformations. Initially we considered only the three hexa-equatorial conformers (*cf.* Table 1), since the non-existence of conformations of M(2,4-ptn)$_3$ with axial methyl groups, in aqueous solutions, at room temperature, for M = Co(III), was assumed by Mizukami *et al.*[16] on the basis of NMR studies. Starting with six distinct $(eq)_6$ conformations of M(2,4-ptn)$_3$ systems: two idealized (C_3)-chair$_3$ conformations with acute and obtuse NMN angles; X-ray and idealized lel$_3$; and X-ray and idealized ob$_3$ conformations, the minimization led to three minimum-energy conformations (Table 5). The lowest energy conformations were (C_3)-chair$_3$ and (D_3)-lel$_3$. (D_3)-ob$_3$ was found 5.6 kcal mol^{-1} above the global minimum of the system (Table 5).

In order to investigate the accessibility of conformers with axial methyl groups, we included in our calculations two additional series of $M(2,4\text{-ptn})_3$ conformers. One consisted of four $(eq)_5(ax)$ conformations (Table 1) generated from homoconformational $(eq)_6$ forms by changing the position of one of six equivalent equatorial methyl groups on lel_3 and ob_3, or any of methyl groups from two non-equivalent sets on $(eq)_6$-$chair_3$. The other series consisted of three * $(eq)_3(ax)_3$ conformations (Table 1) generated from $chair_3$, lel_3, and ob_3 homoconformational forms by changing positions of three equatorial methyl groups while preserving the C_3 molecular symmetry.

The conformational distribution of hexa-equatorial $M(2,4\text{-ptn})_3$ forms (Table 5) is similar to that of homoconformational forms of $M(tn)_3$ (Table 2). The presence of equatorial methyl groups does not cause any significant deviation of bond lengths, valence angles, and torsional angles from the values in the corresponding $M(tn)_3$ structures. However, deformations due to the presence of axial methyl groups are appreciable, but almost entirely localized on the ring atom(s) carrying axial substituent(s). Axial methyl groups in $M(2,4\text{-ptn})_3$ conformations increase the conformational energies by about 4, 6, and 7 kcal mol^{-1} per ax-CH_3 group (for $chair_3$, lel_3, and ob_3 forms, respectively) relative to the energies for the corresponding hexa-equatorial forms. It is, therefore, very unlikely to find lel_3 and ob_3 conformations in $M(2,4\text{-ptn})_3$ complexes with *meso*-diamine, or to find $chair_3$ conformations in complexes with optically active diamine. Energy contributions are given in Table 5, and average bond lengths and valence angles in Table 6. The four conformations of lowest energy are shown in Fig. 2.

* Only one of two possible $(eq)_3(ax)_3$-$chair_3$ conformers (*cf.* Table 1) was chosen in order to reduce the amount of computational work, since the preliminary calculations and the results of minimization of two $(eq)_5(ax)$-$chair_3$ conformers indicated only slight differences between two $(eq)_3(ax)_3$-$chair_3$ forms.

ANALYSIS OF ENERGY CONTRIBUTIONS

$Co(tn)_3$ complexes. Analysis of the various contributions from bond, angle and torsional deformations and non-bonded interactions revealed absolutely no correlations between these contributions and the number of rings having chair, lel and ob conformations.

A separate programme was written to allow for histogram analysis of non-bonded distances of all types, H···H, H···N, H···C *etc.* Neither in this way could any correlation be found, *e.g.* between the position on either the total or the non-bonded energy scale and the number

Table 6. Average bond lengths and valence angles in $M(2,4\text{-ptn})_3$ conformations.[a]

Type[b]	$chair_3$[c]	lel_3 Calc.	Obs.[d]	ob_3 Calc.	Obs.[e]
M–N	2.043	2.043	1.985	2.054	1.988
C–N	1.477	1.479	1.489	1.478	1.50
C–C	1.544	1.549	1.516	1.550	1.53
$C-C_{Me}$	1.549	1.548	1.530	1.549	1.50
N–M–N	93.85	88.10	89.1	87.80	87.9
M–N–C	120.13 (124.7)	114.10 (124.4)	118.0	114.62 (124.5)	115.7
N–C–C	110.68 (112.2)	111.83 (114.0)	112.0	111.96 (114.6)	109.0
C–C–C	110.21	112.64	117.3	113.24	116.7
$N-C-C_{Me}$	109.38 (112.8)	110.26 (113.5)	109.4	110.24 (113.6)	112.2
$C-C-C_{Me}$	109.53 (112.6)	109.38 (110.5)	111.0	109.26 (110.2)	105.7

[a] Average values are given for hexa-equatorial conformations. Valence angles involving carbon atoms bearing axial methyl groups are given for comparison in parentheses. For further details see text. [b] M= Co(III); C_{Me}=methyl carbon. [c] Averaged assuming C_s symmetry of chelate rings. [d] In (−)-[Co(2*R*,4*R*-ptn)$_3$]$Cl_3.2H_2O$ (Kobayashi, Marumo and Saito [13b]); averaged assuming D_3 symmetry. [e] In (+)-[Co(2*R*, 4*R*-ptn$_3$]$Cl_3.H_2O$ (Kobayashi, Marumo and Saito [13a]); averaged assuming D_3 symmetry.

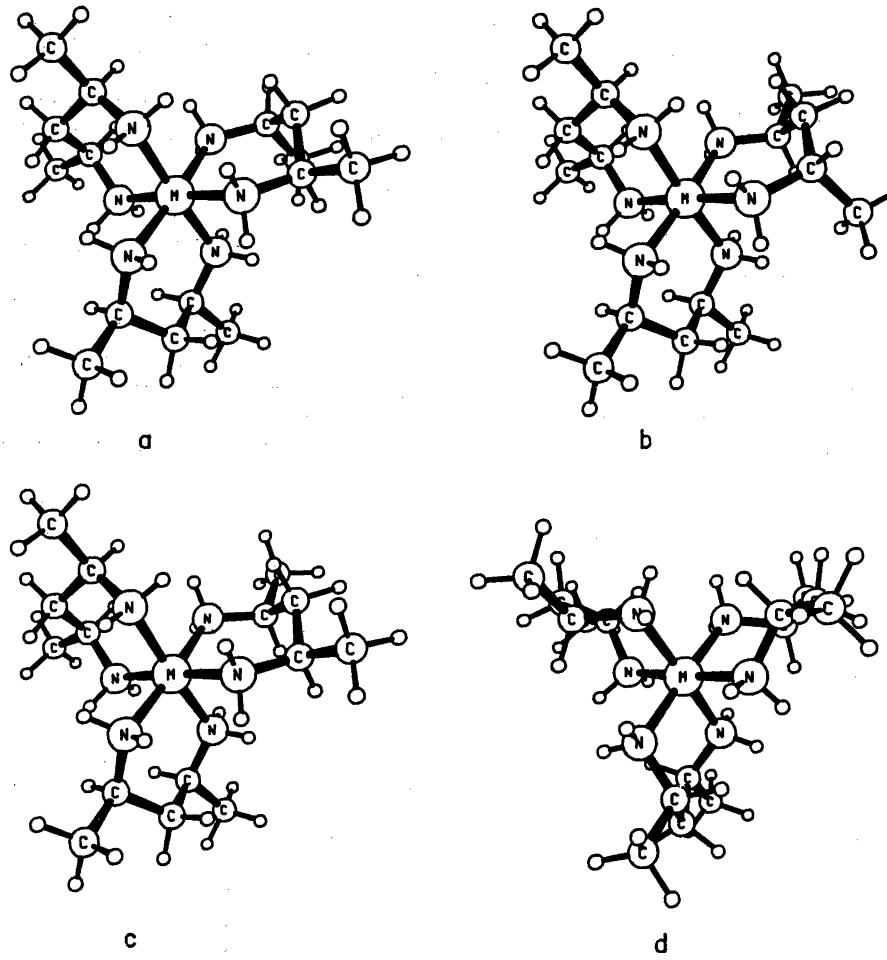

Fig. 2. The four lowest-energy conformations of the Co(2,4-ptn)$_3$ system. a, chair$_3$ (eq)$_6$(ax) (2*R*,4*R*); b, chair$_3$ (eq)$_5$(ax) (2*S*,4*S*); c, chair$_3$ (eq)$_6$; d, lel$_3$ (eq)$_6$. The drawings were produced by ORTEP.

of short non-bonded distances. Three conformers had H···H distances shorter than 2 Å, the lel$_2$chair, the *syn*-chair$_2$ob and the *cis*-chair lel ob.

It must be concluded that the minima are reached by very delicate balancing of all energy contributions through adjustment of practically all internal variables in these flexible molecules.

Co(ptn)$_3$ complexes. Similar analyses of energy contributions revealed the following trends. Chair conformations have relatively high angle deformation and low torsional energies. Ob conformations have relatively high bonded and non-bonded energies. There is, rather unexpectedly, no correlation between the number of equatorial (or axial) methyl groups and either the total energy or the individual contributions.

There is, however, a pronounced additivity in the total energy. An axial methyl group increases the energy of a TB ring by (6.50 ± 0.75) kcal mol^{-1} and that of a chair ring by (3.90 ± 0.15) kcal mol^{-1}.

The histogram analysis gave the same result as for the Co(tn)$_3$ complexes. No contact distances were shorter than 2.00 Å.

For both series the longer non-bonded interactions contributed markedly to the stabilization. As a typical example we may mention

the global minimum conformation of $M(tn)_3$, where non-bonded contributions shorter than 3 Å contribute with 10.074, and the longer ones with -11.880 kcal mol^{-1}. See also the column headed E_{nb} in Table 4, and compare numbers from B and C.

SHAPES OF CHELATE RINGS

We shall here summarize our results on some of the structural features of six-membered chelate rings formed by the coordination of alkanediamines, and compare them with relevant experimental studies.

Chair conformations. Most of the examined 21 individual chair rings in minimum-energy conformations of the $M(tn)_3$ system (Table 2) differ slightly from each other so that they constitute a range of conformations "bracketed" by the following two extreme forms:

(i) chair rings found in the (C_3)-chair$_3$ conformer characterized by obtuse chelate angles (N–M–N = 93.91°) and

(ii) chair rings found in the *anti*-chair$_2$lel conformer characterized by acute chelate angles (N–M–N = 85.52°).

The sequence of endocyclic torsional angles along the chain bonds (starting from Co–N) is 26.6, 49.0, 71.6, 76.7, 57.2, and 30.3° for chair rings in the (C_3)-chair$_3$conformer, and 57.2, 66.0, 64.9, 63.9, 65.7, and 52.0° for chair rings in the *anti*-chair$_2$lel conformer. With respect to their structural features all other distinct chair rings are intermediate between these two extremes.

Comparison of dihedral angles between the NMN, least-square NCCN and CCC planes (as defined by Geue and Snow [14]) reveal (Table 7) interesting conformational features of the chair conformations studied in the present

Table 7. Dihedral angles [a] in chair conformers of Co(III) and Cr(III) tn complexes.

Structure [b]	Source		D_1 (°)	D_2 (°)
(C_3)-chair$_3$-Co(tn)$_3$	highly strained idealized conformation		125	125
anti-chair$_2$lel-Co(tn)$_3$	minimum-energy conformation		136	121
trans-[Co(tn)$_2$(NO$_3$)$_2$]NO$_3$	X-ray [17]		139	121
(C_1)-chair$_2$-[Co(tn)$_2$(CO$_3$)$_2$]ClO$_4$	X-ray [14]	Ring A	147	119
		Ring B	136	122
chair-[Co(en)$_2$(tn)]Br$_3$	X-ray [18]		148	122
(C_3)-chair$_3$-[Co(tn)$_3$]Br$_3$.H$_2$O	X-ray [10]	Ring A	149	122
		Ring B	142	122
		Ring C	146	119
anti-chair$_2$-[Co(tn)$_2$(acac)]$^{2+}$	X-ray [19]	Ring A	145	119
		Ring B	156	113
syn-chair$_2$lel-[Cr(tn)$_3$]$^{3+}$	X-ray [13b]	Ring A	151	119
		Ring B	152	119
trans-[Co(tn)(β-ala)(NO$_2$)$_2$]	X-ray [20]		153	121
cis-[Co(tn)(β-ala)(NO$_2$)$_2$]	X-ray [21]		158	119
syn-chair$_2$lel(C_2) Co(tn)$_3$	minimum-energy conformation		151	118
(C_3)-chair$_3$ Co(tn)$_3$	minimum-energy conformation		155	113

[a] D_1 = dihedral angle between NMN and NCCN planes. D_2 = dihedral angle between NCCN and CCC planes. [b] Structures studied by conformational analysis are shown without ionic charges. Symmetry symbols indicate approximate and rigorous symmetries for X-ray structures and minimum-energy structures, respectively.

work and in most of the known X-ray conformations of the chair rings in Co(III) and Cr(III) complexes of trimethylenediamine. The unique strain relieving mechanism for chair rings appears to be flattening of the inner fragment (C–N–M–N–C) and slight puckering of the outer one (N–C–C–C–N), accompanied by opening of the N–M–N angle and closing of the C–C–C angle. The puckering of chair rings in *anti*-chair$_2$lel is similar to that of idealized chair conformations (see top entries in Table 7) indicating weak interannular interactions. Conversely, pronounced interannular interactions produce flattening of the chairs in *syn*-chair$_2$lel and (C_3)-chair$_3$ (see bottom entries in Table 7) to such extent that the central carbon atom of trimethylenediamine is brought almost to the NMN plane.

The extent of puckering of chair rings in other heteroconformational forms of M(tn)$_3$ (not shown in Table 7) is intermediate between that of *anti*-chair$_2$lel and (C_3)-chair$_3$. In hexaequatorial (C_3)-chair$_3$ Co(*meso*-2,4-ptn)$_3$ the angles D_1 and D_2 are 155.5° and 115.0°, respectively, implying the same mode of flattening of chair rings as in the (C_3)-chair$_3$ Co(tn)$_3$ conformation.

A summary of geometries of tn rings as found by X-ray diffraction has been tabulated by Jurnak and Raymond [12b] (their Table XIX). When we compare our results (Table 3) with those for M(tn)$_3$ complexes, we find that the experimental geometries are reproduced fairly well by our calculations. The largest deviations (experimental data falling outside the ranges of calculated ones) are found for M–N, C–C (partly), C–C–C (partly), and torsional angles, where the calculated values are too large. The remaining conformational quantities are well reproduced, including dihedral angles.

Twist-boat conformations. Twist-boat (TB) conformations of chelate rings found in minimum-energy lel$_3$, ob$_3$ and all heteroconformational forms studied (see Fig. 1) also constitute a range of conformations, but contrarily to the distribution of chair ring conformations, they are clustered around two distinct structural types:

(i) rings with essentially C_2 symmetry, not very different from idealized TB rings, found in lel$_3$, ob$_3$, and a few low-energy heteroconformational forms containing lel rings (Fig. 1) including the *syn*-chair$_2$lel conformer found in the X-ray structure of Cr(tn)$_3$ ion (Jurnak and Raymond [12b]).

(ii) distorted TB conformations found both in lel and in ob rings of high-energy heteroconformational forms (*e.g.*, ob$_2$lel, lel$_2$ob).

The distribution of bond lengths and valence angles in TB rings is shown in Table 3 for

Table 8. Comparison of endocyclic torsional angles in chelate rings of M(2,4-ptn)$_3$ with equatorial and axial methyl groups

Torsional [a] angle	chair (eq)$_2$	(eq) (ax)	lel (eq)$_2$	(eq) (ax)	ob (eq)$_2$	(eq) (ax)
ϕ_1	26.34	22.09	−34.42	−35.41	34.25	41.45
ϕ_2	−48.69	−50.09	75.03	79.46	−74.29	−78.84
ϕ_3	71.60	73.27	−37.80	−51.82	37.44	41.96
ϕ_4	−76.82	−67.46	−37.80	−14.25	37.44	22.97
ϕ_5	57.18	40.80	75.03	55.56	−74.29	−55.11
ϕ_6	−30.20	−17.81	−34.42	−28.21	34.25	21.38

[a] The endocyclic torsional angles are labeled as follows:

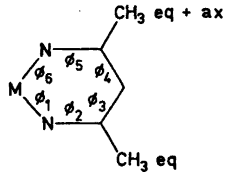

rings of approximate C_2 symmetry (left column) and distorted rings (right column). Chelate angles in both types of TB rings are invariably less than 90°. Also in minimum-energy lel_3 and ob_3 conformations of eq_6-M(2,4-ptn)$_3$ chelate angles are acute and in very good agreement with X-ray data (see Table 6).

NMNC torsional angles in (C_2)-TB rings of lel_3 and ob_3 conformers of M(tn)$_3$ are $34 \pm 1°$. However, in TB rings of approximate C_2 symmetry they vary in the range 30 to 37°.

In distorted TB conformations NMNC torsional angles are found to be in the ranges $5-15$ and $45-50°$, indicating the close resemblance of these structures and idealized boat conformations.

Comparing with the experimental geometry of the only TB ring found [12b] so far, we find that our calculated ranges (Table 3) do not bracket M–N, C–C, N–C–C, and C–C–C; calculated values of MN and NC torsions are too large. The remaining quantities are well reproduced, including the dihedral angles.

Rings with axial substituents. In $(eq)_5(ax)$ and $(eq)_3(ax)_3$ conformations of M(2,4-ptn)$_3$ appreciable flattening of the segments of chelate rings carrying axial methyl groups is observed both in chair and in twist-boat rings. This is reflected both in opening of the valence angles (see Table 7), and in decrease of the values of the corresponding torsional angles (as shown in Table 8).

A comparison between (1) the conclusions on shapes of six-membered chelate rings drawn by Jurnak and Raymond [12b] on the basis of X-ray structures and (2) conclusions drawn from empirical force field calculations will have to await the development of an optimized force field.

CONCLUSION

Our work corroborates the conclusions of others [14,15,22] that energy minimization is successful in predicting detailed geometries of coordination compounds.

It has been clearly demonstrated here that truly convergent minimization methods are imperative for meaningful results.

The scope of this work was not to obtain very accurate geometries. For such purpose we shall need a force field which is optimized on geometries of model compounds, and this means that the full potentiality of the CFF approach [4,5] must be utilized. Revised methods for simultaneous optimization on experimental conformations and vibrational spectra are now being worked out for our new version of the CFF system.

Final cartesian atomic coordinates and corresponding internal coordinates of sixteen M(tn)$_3$ and ten M(ptn)$_3$ conformers may be obtained from the authors upon request. ORTEP drawings of all minimum conformations are also available.

Acknowledgements. SRN wishes to express his gratitude to Statens naturvidenskabelige Forskningsråd for a two-year stipend, and KjR wants to thank The Weizmann Institue of Science, particularly its Chemical Physics Department, for repeated hospitality. We are indebted to Dr. R. Herak for providing the X-ray coordinates in advance of publication. The computations were paid through a grant from Statens naturvidenskabelige Forskningsråd.

REFERENCES

1. a. Niketic, S. R. and Woldbye, F. *Acta Chem. Scand. 27* (1973) 621; b. *Ibid.* 3811; c. *Ibid. A 28* (1974) 248.
2. Wiberg, K. B. *J. Am. Chem. Soc. 87* (1965) 1070.
3. Niketic, S. R. *Force Field Calculations on Coordination Compounds*, Thesis, The Technical University of Denmark, 1974.
4. Lifson, S. and Warshel, A. *J. Chem. Phys. 49* (1968) 5116.
5. a. Lifson, S. *J. Chim. Phys. Physicochim. Biol. 65* (1968) 40; b. In Jaenicke, R. and Helmreich, E., Eds., *Protein-Protein Interactions*, Springer, Berlin 1972, p. 3.
6. Rosen, J. *Brown Univ. Comp. Rev. 1* (1964) 64.
7. Bixon, M. and Lifson, S. *Tetrahedron 23* (1967) 769.
8. Fletcher, R. and Powell, M. J. D. *Comput. J. 6* (1963) 163.
9. Gill, P. E., Murray, W. and Picken, S. M. *Natl. Phys. Lab. Rep. NAC 24* (1972).
10. Nomura, T., Marumo, F. and Saito, Y. *Bull. Chem. Soc. Jpn. 42* (1969) 1016.
11. Nagao, R., Marumo, F. and Saito, Y. *Acta Crystallogr. B 29* (1973) 2438.
12. a. Jurnak, F. A. and Raymond, K. N. *Inorg. Chem. 11* (1972) 3149; b. *Ibid. 13* (1974) 2387.
13. a. Kobayashi, A., Marumo, R. and Saito, Y. *Acta Crystallogr. B 28* (1972) 3591; b. *Ibid. B 29* (1973) 2443.

14. Geue, R. J. and Snow, M. R. *J. Chem. Soc. A* (1971) 2981.
15. Snow, M. R. *J. Am. Chem. Soc. 92* (1970) 3610; *J. Chem. Soc. Dalton Trans.* (1972) 1627.
16. Mizukami, F., Ito, H., Fujita, J. and Saito, K. *Bull. Chem. Soc. Jpn. 45* (1972) 2129.
17. Yasaki, E., Oonishi, I., Kawaguchi, H., Kawaguchi, S. and Komiyama, Y. *Bull. Chem. Soc. Jpn. 43* (1970) 1354.
18. Schousboe-Jensen, H. V. F. *Acta Chem. Scand. 26* (1972) 3413.
19. Matsumoto, K., Kawaguchi, H., Kuroya, H. and Kawaguchi, S. *Bull. Chem. Soc. Jpn. 46* (1973) 2424.
20. Herak, R., Celap, M. B. and Krstanovic, I. *Acta Crystallogr. A 31* (1975) 5142.
21. Herak, R., Jeremic, M. and Celap, M. B. *Acta Crystallogr. A 31* (1975) 5143.
22. Buckingham, D. A., Maxwell, I. E., Sargeson, A. M. and Snow, M. R. *J. Am. Chem. Soc. 92* (1970) 3617.

Received January 19, 1976.

Acta Chemica Scandinavica A 30 (1976) 498—502

The ESR-Spectra of Radical Anions Generated from 5,12-Dihydrotetracene in Dimethoxyethane and in Liquid Ammonia

JORMA ELORANTA, TIMO NYRÖNEN and RAILI KOSKINEN

Department of Chemistry, University of Jyväskylä, Kyllikinkatu 1—3, SF-40100 Jyväskylä 10, Finland

The radical anion of 5,12-dihydrotetracene was prepared by the action of metallic potassium using dimethoxyethane as solvent. The ESR-spectra were recorded at various temperatures and the optical spectra in the visible region at room temperature. The anion radicals of 5,12-dihydrotetracene and tetracene were also generated in liquid ammonia, and they showed identical ESR-spectra.

The cation radical of 5,12-dihydrotetracene in trifluoroacetic acid was oxidized immediately to the tetracene cation radical.

The spectra of 5,12-dihydrotetracene in the UV and visible regions have been investigated earlier; an equilibrium has been observed to form between tetracene and 5,12-dihydrotetracene radical anions in dimethoxyethane.[1]

The mono- and dinegative ions of tetracene can easily be identified on the basis of the spectrum in the visible region.[2]

The purpose of this work is to study whether it is possible to measure the ESR-spectrum of the 5,12-dihydrotetracene radical anion before the possible formations of the tetracene radical anions.

Liquid ammonia was chosen as an alternative solvent, since the concentration of solvated electrons in alkali metal reduction is high,[3,4] and thus the equilibrium might remain on the side of 5,12-dihydrotetracene radical anion.

EXPERIMENTAL

1,2-Dimethoxyethane was purified as described previously.[1] The ammonia was a product of Merck and the degree of purity was 99.9 %. It was distilled in the high vacuum line.

Tetracene was a product of K & K Laboratories, Inc. the visible spectrum we obtained agreed with that presented in the literature.[5,6]

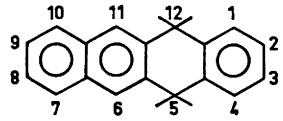

5,12-Dihydrotetracene was a product of Fluka AG. After purification [7] we obtained a spectrum in the UV and visible regions, consistent with that in the literature.[7]

Trifluoroacetic acid and thallium(III) trifluoroacetate were Merck's products for spectroscopy.

The samples were prepared in high vacuum and the same ampoule contained ESR-cuvette and 1 cm and 1 mm optical cuvettes, which were of quartz glass. When liquid ammonia was used as solvent, the optical cuvettes did not tolerate room temperature, but broke down.

The ESR-spectra were recorded with Varian E-9 and E-12 spectrometers equipped with variable temperature control and with Varian 620/L-SS 100 computer facilities.

The spin density calculations and the simulations of the spectra were performed using the Univac 1108 central computer for Finnish universities.[8] In order to perform INDO calculations for tetracene and 5,12-dihydrotetracene, it was necessary to expand the OCPE program to allow the basis set to be more than 80 orbitals. The following parameters were used in the INDO-calculations: $r_{C-C}(\text{arom.}) = 0.140$ nm, $r_{C-H}(\text{arom.}) = 0.1083$ nm, $r_{C-C}(\text{aliph.}) = 0.148$ nm [9] and $r_{C-H}(\text{aliph.}) = 0.1093$ nm. The bond angles in positions 5 and 12 were 109.5°.

Optical spectra were measured with a Beckman DK-2A spectrophotometer.

Table 1. Coupling constants (G) of the radical anion of 5,12-dihydrotetracene in dimethoxyethane at 193 K.

Position	Exp. Anion	Calc. Anion	Calc. Cation
6,11	5.03	−6.5	−6.4
7,10	4.40	−4.6	−5.0
5,12(ax)	3.18	3,3	5.9
5,12(eq)	3.18	0.7	0.9
8,9	1.70	−0.8	−1.0
1,4	0.20	−0.13	−0.06

RESULTS AND DISCUSSION

Dimethoxyethane as solvent. The results of spin density calculations of the 5,12-dihydrotetracene anion by the INDO-method agree satisfactorily with the experimental values (Table 1). If we make comparisons between the anions of the 5,12-dihydrotetracene, naphthalene,[10] and 1,2,3,4-tetrahydroantracene,[11] we can observe that the coupling constants do not change in the equal positions noticeably.

Alternating line width as the temperature was varied between 180 and 233 K, was not observed, but instead some minor changes in intensities occurred.

It is perhaps rather surprising that the coupling constants of axial and equatorial protons were equal even at low temperature, but a similar result has also been observed with the anion of 9,10-dihydroanthracene.[12] The INDO-calculations show that the spin densities in the 1,2,3,4-positions are very small.

The sample was stored under liquid nitrogen between the measurements, although the optical spectra were recorded at room temperature. Immediately after measurements of the optical spectrum, the sample was cooled down and the resulting ESR-spectrum remained unchanged. When the sample was kept a few days at room temperature, a spectrum shown in Fig. 2 was recorded. It is, however, a mixture of different spectra.

The mononegative ion of tetracene has two narrow and very high absorption maxima at the wavelengths 402 nm and 824 nm and the dinegative ion of tetracene has at 619 nm a gently sloping absorption maximum.[2]

The curve labelled 1 in Fig. 3 shows the absorption peaks at 520 nm and 550 nm and they are due to the anion of 5,12-dihydrotetracene [1] and there are no peaks caused by the anions of tetracene. The ESR-spectrum was measured immediately, but there was still no ESR signal. The curve labelled 2 in Fig. 3 shows increasing concentration of the anion of 5,12-dihydrotetracene and immediately we can observe an ESR-spectrum (Fig. 1). In Fig. 3 there is no sign of the mononegative anion of tetracene, but the curve labelled 4 shows the absorption peak of the dinegative anion of tetracene and we can see the decomposition in the ESR-spectrum at the same time (Fig. 2).

When the sample was opened, nothing but tetracene and a small amount of 5,12-dihydrotetracene could be found.

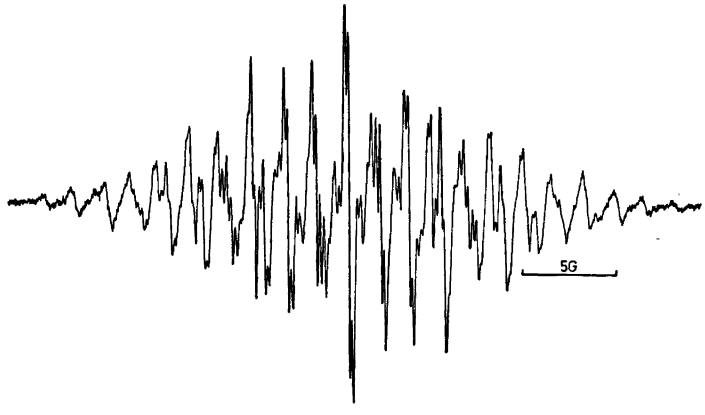

Fig. 1. The ESR-spectrum of the radical anion of 5,12-dihydrotetracene in dimethoxyethane at 193 K.

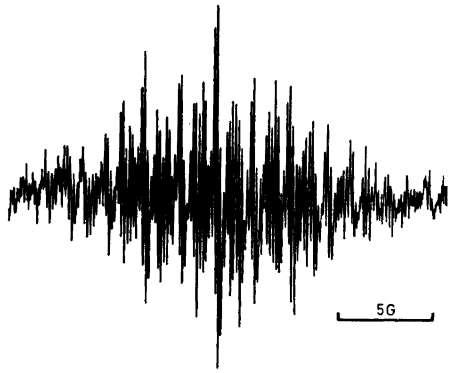

Fig. 2. The ESR-spectra of the radical anions generated from 5,12-dihydrotetracene after the decomposition in dimethoxyethane at room temperature.

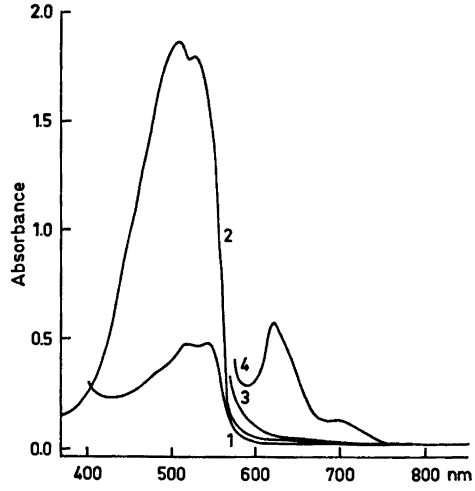

Fig. 3. The optical spectra of the anions generated from 5,12-dihydrotetracene in the visible region in dimethoxyethane at room temperature. Curve 1 is obtained using a 1 cm cuvette and the other curves using 1 mm cuvettes.

When we observe the absorption of the dinegative anion of tetracene in the optical spectrum, the ESR-spectrum simultaneously shows that more than one radical was formed. The dinegative ion of tetracene has no triplet ground state and it cannot give any ESR-signal. This means that there is obviously one (or more) radical(s), whose structure lies between the anion of dihydrotetracene and the dinegative ion of tetracene.

Liquid ammonia as solvent. The radical anions of tetracene and 5,12-dihydrotetracene were generated by sodium-metal reduction. Fig. 4 shows the ESR-spectrum of the anion generated from 5,12-dihydrotetracene and Fig. 5 the ESR-spectrum of the anion generated from tetracene. The peak due to solvated electrons can also be seen in Fig. 4.

On the basis of the ESR-spectra in Figs. 4 and 5, both ions have the same structure; there is, however, a relatively strong noise. The same anion is generated both from dihydrotetracene and tetracene in liquid ammonia even at a low temperature, though the ion is stable also at room temperature. Alternat-

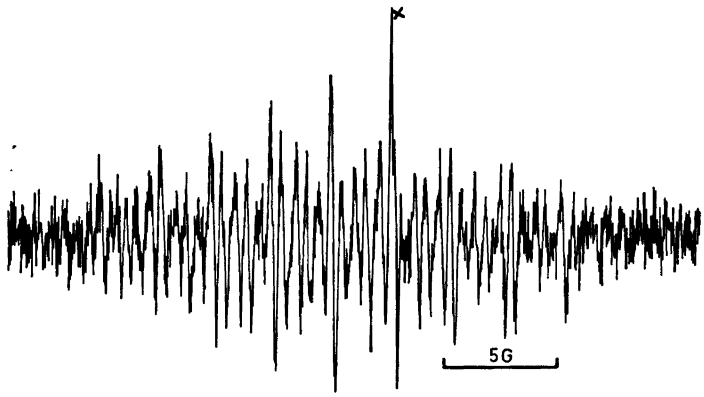

Fig. 4. The ESR-spectrum of the radical anion generated from 5,12-dihydrotetracene in liquid ammonia *via* sodium-metal reduction at room temperature. The peak of the solvated electrons is marked with ×.

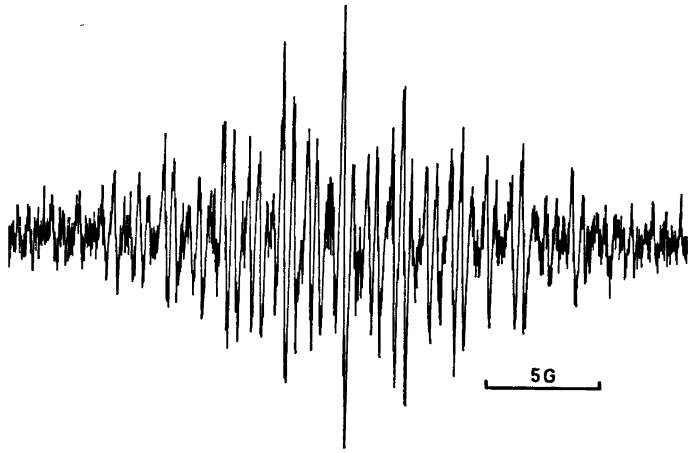

Fig. 5. The ESR-spectrum of the radical anion generated from tetracene in liquid ammonia *via* sodium-metal reduction at room temperature.

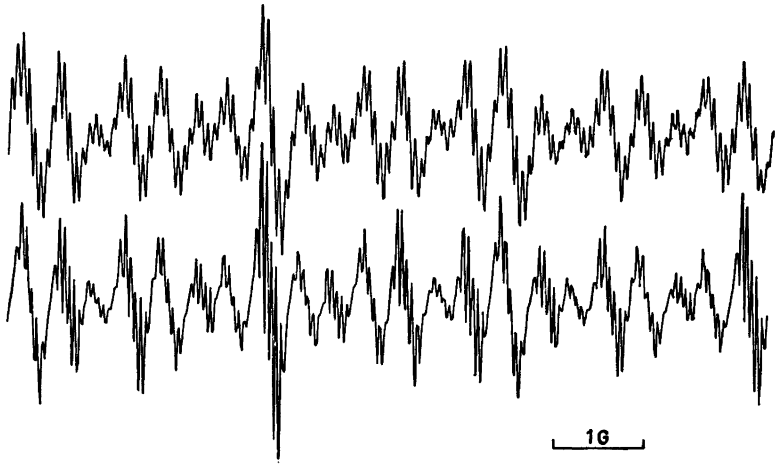

Fig. 6. The part of the ESR-spectrum of the radical anion generated from tetracene in liquid ammonia at 253 K. The lower curve represents a simulated spectrum (the Lorentz line shape) with a line width of 0.03 G and with experimental coupling constants mentioned in Table 2.

Table 2. Coupling constants (G) of the radical anion generated from tetracene and 5,12-dihydrotetracene in liquid ammonia at 253 K.

Position	Exp.	Calc.(dihydrotetracene)	
6,11	5.30	−6.5	−5.5
7,10	5.30	−4.6	
5,12(ax)	2.64	3.3	2.0
5,12(eq)	2.23	0.7	
8,9	1.50	−0.8	
1,4	0.07	−0.13	
Na^+	0.06	—	

ing line width due to the temperature was not observed.

In Fig. 6 the small quartet splitting of sodium ($m_i = 3/2$) can be seen and hence the presence of an ion pair with the radical anion.

The experimental coupling constants presented in Table 2 differ slightly from the values in Table 1. The structure of the anion generated in liquid ammonia has more resemblance to the structure of 5,12-dihydrotetracene anion than to that of the tetracene anion.

The experimental coupling constants of the

axial and equatorial protons differ in positions 5 and 12, but only slightly. This means that the anion is nearly planar and the time averaged value is not concerned, as in dimethoxyethane even at a low temperature.

Trifluoroacetic acid as solvent. An attempt was made to prepare the cation radical of 5,12-dihydrotetracene by oxidation with thallium(III) trifluoroacetate. As a result we obtained the cation radical of tetracene.[13] The same result was obtained using trichloroacetic acid as solvent.[14] In fact, this was expected, since even in reducing circumstances 5,12-dihydrotetracene anion is oxidized to tetracene anion.

REFERENCES

1. Eloranta, J. and Joela, H. *Acta Chem. Scand. 20* (1966) 1626.
2. Eloranta, J. and Linschitz, H. *J. Chem. Phys. 38* (1963) 2214.
3. Hutchinson, C. A. *J. Phys. Chem. 57* (1953) 546.
4. O'Reilly, D. E. *J. Chem. Phys. 35* (1961) 1856.
5. Clar, E. *Chem. Ber. 81* (1948) 70.
6. Clar, E. and Marschalk, C. *Bull. Soc. Chim. Fr.* (1950) 436.
7. Clar, E. *Ber. Dtsch. Chem. Ges. 75* (1942) 1272.
8. *QCPE program 261*, Hase, H. L. and Schweig, A. 1973; *QCPE program 209*, Heinzer, J. 1971.
9. Eloranta, J. and Nyrönen, T. *Finn. Chem. Lett.* (1974) 193.
10. Gerson, F., Weidmann, B. and Heilbronner, E. *Helv. Chim. Acta 47* (1964) 1951.
11. Eloranta, J. and Pasanen, K. *Acta Chem. Scand. 27* (1973) 461.
12. Iwaizumi, M. and Bolton, J. R. *J. Magn. Reson. 2* (1970) 278.
13. Elson, J. H. and Kochi, J. K. *J. Am. Chem. Soc. 95* (1973) 5061.
14. Eloranta, J. and Sippula, A. *Finn. Chem. Lett.* (1975) 170.

Received February 18, 1976.

Acta Chemica Scandinavica A 30 (1976) 503—506

The Crystal Structure of Bis(ethylenediamine)isothiocyanatonitrocobalt(III) Thiocyanate $[Co(NCS)NO_2(en)_2]SCN$

OLLE BÖRTIN

Department of Inorganic Chemistry, University of Göteborg and Chalmers University of Technology, P.O. Box, S-402 20 Göteborg 5, Sweden

The crystal structure of *trans*-bis(ethylenediamine)isothiocyanatonitrocobalt(III) thiocyanate has been determined. The crystals are monoclinic with $a = 16.343(13)$ Å, $b = 16.026(7)$ Å, $c = 11.146(3)$ Å, $\beta = 110.28(4)°$, $V = 2738$ Å^3, $Z = 8$, space group $C2/c$.

Least squares refinement of the structure based on 1970 reflections, gave an R-value of 0.077. The bis(ethylenediamine)isothiocyanatonitrocobalt(III) ions are arranged in closepacked layers which are separated from each other by the thiocyanate ions. The cobalt atoms are octahedrally coordinated by six nitrogen atoms with the bond distances Co—N (to NO_2) 1.914(7) Å, Co—N (to NCS) 1.922(7) Å, and Co—N (to en) 1.959—1.966(7) Å.

In connection with studies of the conversion of nitro and nitrito compounds Adell [1] prepared the two salts $[Co(NCS)NO_2(en)_2]SCN$ and $[Co(NCS)NO_2(en)_2]ClO_4$. When the salts were exposed to sunlight the perchlorate was converted to the nitrito form while the thiocyanate was not. In order to examine whether there are any sterical reasons for this the crystal structure of the thiocyanate has been determined.

STRUCTURE DETERMINATION

Using a thin needle-shaped crystal the intensities of the $hk0 - hk14$ reflections were recorded by a Philips Pailred automatic single crystal diffractometer with Mo$K\alpha$ radiation monochromatized with a graphite crystal. The intensities were corrected for Lorentz and polarization effects using the program DATAP1. The cell dimensions were obtained from powder diffraction photographs taken with a Guinier focusing camera with Cu$K\alpha$ radiation, using lead nitrate ($a = 7.8566$ Å)[2] as an internal standard, and refined by the method of least squares using the program POWDER. Bis(ethylenediamine)-isothiocyanatonitrocobalt(III) thiocyanate was found to be monoclinic with $a = 16.343(13)$ Å, $b = 16.026(7)$ Å, $c = 11.146(3)$ Å, $\beta = 110.28(4)°$, and $V = 2738$ Å^3.

The following reflection conditions were noted: hkl: $h + k = 2n$ and $h0l$: $l = 2n$. Possible space groups $C2/c$ or Cc. The calculated density for a unit cell containing eight formula units is 1.65 g cm^{-3}.

The parameters of the cobalt atoms were deduced from the three-dimensional Patterson function $P(uvw)$ calculated with the program DRF. The other atoms were determined from three-dimensional electron density maps. One of the thiocyanate ions was found along the two-fold axis of $C2/c$ [4(e)] but the other had to be placed perpendicular to and across the axis. This indicates either that this latter thiocyanate ion is statistically orientated in two directions or that the space group is Cc.

The structure was refined by least squares using the program BLOCK. The atomic scattering factors used were those calculated by Doyle and Turner [3] and the structure factors were weighted according to Cruickshank [4] with $a = 80.0$ and $c = 0.005$. When the refinement was performed in the space group Cc the temperature factor of the sulfur atom of the second thiocyanate ion got a high value while the temperature factor of the nitrogen atom was low. This was taken as an indication that the space group was the centric $C2/c$ with the thiocyanate ion statistically distributed in two

Table 1. Final atomic parameters for $[Co(NCS)NO_2(en)_2]SCN$. The anisotropic temperature factor is exp $\{-(h^2(a^*)^2u_{11}+k^2(b^*)^2u_{22}+l^2(c^*)^2u_{22}+l^2(c^*)^2u_{33}+2hka^*b^*u_{12}+2hla^*c^*u_{13}+2klb^*c^*u_{23})\}$. The standard deviations of u_{ij} are $(3-4)\times 10^{-4}$ for Co and $(1-21)\times 10^{-3}$ for other atoms.

Atom	x	y	z	$u_{ij}\times 10^3$ u_{11}	u_{22}	u_{33}	u_{12}	u_{13}	u_{23}
S(1)	0.0	0.0495(3)	0.75	312	33	428	0	341	0
C(1)	0.0	0.1497(10)	0.75	75	55	68	0	48	0
N(1)	0.0	0.2207(8)	0.75	93	43	57	0	28	0
S(2)	0.0829(3)	0.3493(3)	0.3289(6)	35	98	101	−10	14	−39
C(2)	0.0140	0.3493	0.2634	83	87	137	12	59	1
N(2)	0.0829	0.3493	0.3289	117	70	58	17	70	0
Co	0.24784(7)	0.11815(6)	0.23307(10)	27	18	28	0	13	1
S(3)	0.16592(13)	0.13955(13)	0.59582(21)	44	33	37	2	21	−4
C(3)	0.1983(4)	0.1333(4)	0.4730(8)	30	19	36	6	14	5
N(3)	0.2204(4)	0.1283(4)	0.3867(7)	41	33	40	7	21	3
N(4)	0.1920(5)	0.2270(4)	0.1781(7)	44	28	36	5	11	5
C(4)	0.1023(7)	0.2142(7)	0.0835(11)	46	50	64	5	10	10
C(5)	0.0654(6)	0.1381(7)	0.1232(13)	31	50	89	5	15	11
N(5)	0.1321(4)	0.0701(4)	0.1463(7)	26	33	51	−8	13	−4
N(6)	0.3023(4)	0.0089(4)	0.2900(7)	34	28	34	−2	6	−1
C(6)	0.3910(8)	0.0203(7)	0.3768(18)	60	32	165	11	−10	14
C(7)	0.4292(7)	0.0944(7)	0.3576(15)	44	45	123	1	16	15
N(7)	0.3639(4)	0.1652(4)	0.3214(8)	21	35	53	−2	11	−5
N(8)	0.2750(4)	0.1105(4)	0.0796(7)	49	35	36	−6	25	1
O(1)	0.3115(5)	0.1679(5)	0.0486(8)	113	75	64	−34	52	11
O(2)	0.2529(6)	0.0512(5)	0.0119(9)	199	65	89	−63	105	−47

directions across the two-fold axis. The refinement of the ion was then performed so that only the coordinates of the sulfur atom were refined while the nitrogen atom was given the same coordinates as the sulfur atom. The coordinates of the carbon atom were reset so that the ratio between the bond distances N−C and C−S was the same as in the other thiocyanate ion. After the introduction of anisotropic thermal parameters the reliability index $R=\sum||F_o|-|F_c||/\sum|F_o|$ converged to 0.077. The resulting parameters are given in Table 1. A list of observed and calculated structure factors can be obtained from the author on request.

DESCRIPTION OF THE STRUCTURE

The complex ion $[Co(NCS)NO_2(en)_2]^+$ is shown in Fig. 1, and the unit cell in Fig. 2 drawn with ORTEP. Bond distances and bond angles are given in Table 2, together with their

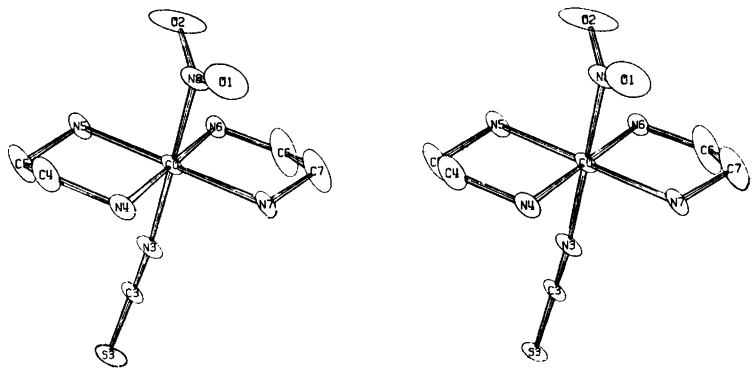

Fig. 1. A stereoscopic view of the ion $[Co(NCS)NO_2(en)_2]^+$.

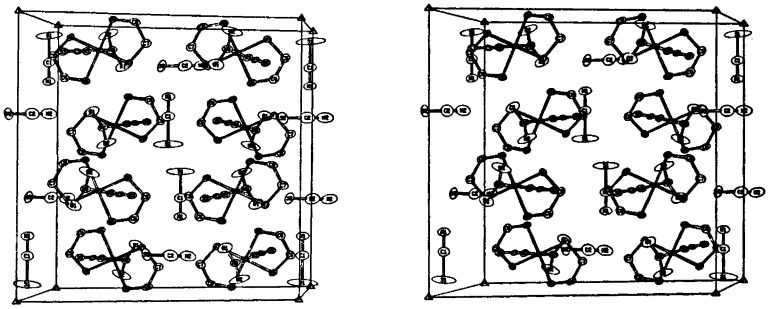

Fig. 2. A stereoscopic view of the structure.

Table 2. Bond distances and angles in $[Co(NCS)NO_2(en)_2]SCN$.

Distance (Å)	
Co – N(8)	1.914(7)
Co – N(3)	1.922(7)
Co – N(5)	1.959(7)
Co – N(7)	1.960(7)
Co – N(4)	1.965(7)
Co – N(6)	1.966(7)
N(3) – C(3)	1.141(11)
C(3) – S(3)	1.633(8)
N(4) – C(4)	1.493(13)
C(4) – C(5)	1.494(15)
C(5) – N(5)	1.498(12)
N(6) – C(6)	1.449(16)
C(6) – C(7)	1.393(17)
C(7) – N(7)	1.514(13)
N(8) – O(1)	1.210(11)
N(8) – O(2)	1.189(11)
S(1) – C(1)	1.606(17)
C(1) – N(1)	1.137(21)
Angle(°)	
N(4) – Co – N(5)	86.0(3)
N(4) – Co – N(7)	94.5(3)
N(5) – Co – N(6)	93.5(3)
N(6) – Co – N(7)	86.0(3)
Co – N(3) – C(3)	175.3(6)
N(3) – C(3) – S(3)	179.3(7)
Co – N(4) – C(4)	109.5(6)
N(4) – C(4) – C(5)	107.5(9)
C(4) – C(5) – N(5)	107.4(8)
C(5) – N(5) – Co	108.7(6)
Co – N(6) – C(6)	109.9(6)
N(6) – C(6) – C(7)	113.7(12)
C(6) – C(7) – N(7)	111.6(9)
C(7) – N(7) – Co	108.4(6)
The other angles round Co are 88.6 – 91.0° or 178.8 – 179.3°.	

standard deviations. The cobalt atom is octahedrally coordinated by the nitrogen atoms of the nitro and isothiocyanato groups in *trans* position and the nitrogen atoms of two ethylenediamine groups. The Co – N bond distances are 1.914(7) Å (to NO_2), 1.922(7) Å (to NCS), and 1.959 – 1.966(7) (to en). The bond distance. C6 – C7 in one ethylenediamine group is rather short, 1.393(17) Å. The explanation of this is probably that the refined coordinates of the carbon atom C6 are the mean values of two possible positions of the atom. This is indicated by its large anisotropic temperature movement and also by the fact that the bond angles involving C6 are larger than other bond angles in the ethylenediamine groups. Very large anisotropic temperature movements are also shown by the atoms of the thiocyanate ion lying along the two-fold axis, especially by the sulfur atom S1.

The structure may be visualized as close packed layers of bis(ethylenediamine)isothio-

Table 3. Packing distances (Å) less than 3.5 Å in $[(Co(NCS)NO_2(en)_2]SCN$.

O(1) – N(4)	3.02
O(1) – C(4)	3.03
O(1) – O(1)	3.26
O(2) – N(3)	3.08
O(2) – C(3)	3.16
O(2) – N(6)	3.01
O(2) – C(6)	3.32
N(7) – N(1)	3.19
N(6) – S(3)	3.46
N(5) – S(3)	3.48
N(5) – S(1)	3.38
N(4) – N(2)	3.45

cyanatonitrocobalt(III) ions parallel to the plane [100] at $x = 0.25$ and $x = 0.75$. The packing distances given in Table 3 indicate that there might be weak hydrogen bonds within the layers. The shortest distances between an oxygen atom and a nitrogen atom of an other complex ion are 3.01 – 3.02 Å. The thiocyanate ions are situated in the space between these layers. This investigation was carried out to see if there are any sterical reasons for the observed inability of the nitro group to be converted to the nitrito form when exposed to sunlight. There do not seem to be any sterical obstacles to such a conversion. The oxygen-nitrogen distances indicating hydrogen bonds are longer than in, *e.g.*, $[CoNO_2(NH_3)_5]Cl_2$[5] for which this conversion has been observed.

Acknowledgements. I wish to thank Dr. Birger Adell for placing the crystals at my disposal. This work has been supported by Chalmers University of Technology, which has supplied a grant to cover the costs of the computer work performed at the Göteborg Universities' Computing Centre.

REFERENCES

1. Adell, B. *Z. Anorg. Allg. Chem. 386* (1971) 122.
2. *International Tables for X-Ray Crystallography*, Kynoch Press, Birmingham 1962, Vol. III, p. 122.
3. Doyle, P. A. and Turner, P. S. *Acta Crystallogr. A 24* (1968) 390.
4. Cruickshank, D. W. J. *The Equation of Structure Refinements*, Glasgow 1964.
5. Börtin, O. *Acta Chem. Scand. 22* (1968) 2890.

Received January 20, 1976.

Acta Chemica Scandinavica A 30 (1976) 507—514

The Crystal Structure of $[(UO_2)_4Cl_2O_2(OH)_2(H_2O)_6].4H_2O$, a Compound Containing a Tetranuclear Aquachlorohydroxooxo Complex of Uranyl(VI)

MÄRTHA ÅBERG

Department of Inorganic Chemistry, Royal Institute of Technology, S-100 44 Stockholm 70, Sweden

The title compound crystallizes in the monoclinic space group $P2_1/n$ (No. 14) with $a = 11.645(1)$ Å, $b = 10.101(1)$ Å, $c = 10.206(1)$ Å, $\beta = 105.77(1)°$, and $Z = 2$. The crystal structure determination was based on 1900 independent reflections collected by the Weissenberg multiple film method. The structural parameters were refined by least squares methods to a conventional R value of 0.12.

The structure is built up from discrete uncharged molecules containing four U atoms at the corners of two approximately coplanar equilateral triangles sharing one edge. Each uranyl group is surrounded by one Cl and four O atoms, the uranium coordination polyhedron being a pentagonal bipyramid. The four U atoms are linked through double bridges of three types: one double O bridge, two HO/O bridges, and two Cl/O bridges. The corresponding U–U distances are 3.693(2), 3.787(2), and 4.036(2) Å, respectively. The mean bond lengths are: U–O(uranyl) = 1.77 Å, U–O(oxo) = 2.23 Å, U–O(aqua or hydroxo) = 2.42 Å, and U–Cl = 2.89 Å.

Hydrolysis of aqueous uranyl salt solutions leads to the formation of polynuclear complexes. Different suggestions have been made as to the compositions of these complexes.[1] Most investigators seem to agree that the dinuclear complex $(UO_2)_2(OH)_2^{2+}$ is present in all solutions regardless of the ionic medium. Additional complexes have also been suggested, *e.g.*, $(UO_2)_3(OH)_4^{2+}$, $(UO_2)_3(OH)_5^{+}$, and $(UO_2)_4(OH)_6^{2+}$.

Clarification of the structures involved in the hydrolysis was carried out using X-ray diffraction studies of concentrated hydrolyzed and acidic uranyl(VI) chloride solutions.[2] The results indicate that the predominant species are dinuclear and triangular trinuclear complexes. Two solid phases have been isolated as single crystals from the hydrolyzed solutions. Knowledge of the structures of these phases, especially the coordination of the uranyl group and the type of bridging between the U atoms in the polynuclear complexes, has been valuable for the interpretation of the X-ray scattering data from the solutions. The crystal structure of $[(UO_2)_2Cl_2(OH)_2(H_2O)_4]$, containing a dinuclear aquachlorohydroxo complex of uranyl(VI), has been reported.[3] The crystal structure of the second phase, built up from tetranuclear aquachlorohydroxooxo uranyl(VI) complexes and previously published in a short communication,[4] will be fully described in the present paper.

EXPERIMENTAL

Preparation of crystals. One of the uranyl(VI) chloride solutions studied by X-ray diffraction was hydrolyzed to the maximum extent (bound HO/U = 1.11 for [U(VI)] = 3.1 M). When this solution crystallized, small amounts of a new phase were obtained in addition to large quantities of the already known compound $[(UO_2)_2Cl_2(OH)_2(H_2O)_4]$.[3] The separation of the two phases was possible as the new one was found to be insoluble in ethanol.

Analysis. A weighed amount of the compound was dissolved in hydrochloric acid of known concentration. The uranium content was determined by precipitation with 8-hydroxyquinoline.[5] The amount of chloride was obtained by passing a portion of the solution through an H^+-saturated cation exchanger and titrating the eluate (dilute HCl) with standardized NaOH. The density of the crystals was cal-

culated from the apparent loss of weight in benzene. Found: UO_3 80.4; HCl 5.0; H_2O 14.6 (difference). Calc. for $(UO_3)_4(HCl)_2(H_2O)_{10}$: UO_3 81.9; HCl 5.2; H_2O 12.9.

From a preliminary structure determination it was known that some of the water molecules were not coordinated to U. An attempt to determine this part of the water content was made by heating the substance at 105 °C to constant weight. The weight loss was 5.1 %. The theoretical value was 1.3 % per water molecule in $(UO_3)_4(HCl)_2(H_2O)_{10}$.

After the heating the crystals were soluble in pyridine-methanol, and a Karl Fischer titration [6] was carried out to estimate the total number of non-uranyl O atoms, *i.e.*, O^{2-} and HO^- as well as water O atoms. The titrations gave an average value of 2.6 such O atoms per uranyl group. Thus the crystals with the stoichiometric composition $(UO_3)_4(HCl)_2(H_2O)_{10}$ have four water molecules of crystallization and ten uranyl-coordinated O atoms in each formula unit. It will be shown that the crystal structure determination indicates that the formula should be written as $[(UO_2)_4Cl_2O_2(OH)_2(H_2O)_6].4H_2O$.

Crystal data. Weissenberg photographs taken around *b* and *c* showed that the symmetry was monoclinic. Systematically absent reflections were $h0l$ for $h+l=2n+1$ and $0k0$ for $k=2n+1$. This is characteristic of the space group $P2_1/n$.

Values of the lattice parameters were obtained by a least squares refinement (unit weights) using the line positions on a powder photograph taken in a Guinier focusing camera. Cu$K\alpha_1$ radiation ($\lambda=1.54051$ Å) was used with KCl as internal standard ($a=6.2929$ Å at 25 °C). Crystal data for $[(UO_2)_4Cl_2O_2(OH)_2(H_2O)_6].4H_2O$ are:

a = 11.645(1) Å	Z = 2
b = 10.101(1) Å	D_m = 4.02(2) g cm^{-3}
c = 10.206(1) Å	D_x = 4.02 g cm^{-3}
β = 105.77(1)°	μ(Cu$K\alpha$) = 871 cm^{-1}
V = 1155.3 Å^3	Space group $P2_1/n$ (No.14)

Intensity data. Intensity data were collected in a Weissenberg camera with Cu$K\alpha$ radiation ($\lambda=1.5418$ Å). Photographs were taken around *b* ($h0l$ to $h8l$) and *c* ($hk0$ to $hk8$) using the multiple film technique. Intensities were estimated visually by comparison with a calibrated intensity scale and were corrected for Lorentz and polarization factors as well as for absorption, but not for secondary extinction effects. About 1650 and 1850 independent reflections were collected around *b* and *c*, respectively.

The crystals used were roughly prismatic *c* with the maximum dimensions (along a^*, *b*, and *c*) 0.060 mm × 0.054 mm × 0.176 mm ($V=2.28\times10^{-4}$ mm^3) for the data taken around *b*, and 0.153 mm × 0.124 mm × 0.166 mm ($V=1.14\times10^{-3}$ mm^3) for the data taken around *c*. The number of faces needed to describe the shapes of the crystals was 14 and 8, respectively. The maximum ratio between the calculated transmission factors, A_{max}/A_{min}, was approximately 10.

Computer programs. The following programs, written or modified for a CDC 3600 computer and briefly described previously,[3] were used for the calculations: CELSIUS, DATAP2, DRF, LALS, DISTAN, PLANE (called PLNJO on IBM 370/155 in Uppsala).

For IBM 360/75 modified versions of DRF, LALS, and DISTAN (B. G. Brandt and A. G. Nord, Stockholm, Sweden) were also used.

Two additional programs were used on IBM 360/75: LIST, Listing of structure factor data. Written by I. Carlbom and modified by A. G. Nord, Stockholm, Sweden; ORTEP2, Thermal-ellipsoid plot program for crystal structure illustrations. Written by C. K. Johnson, ORNL, USA and modified for IBM 360/75 and a CALCOMP 835 micro film plotter by A. G. Nord and B. G. Brandt, Stockholm, Sweden.

STRUCTURE DETERMINATION

Patterson maps $P(u,p,w)$ and $P(u,v,p)$ showed that the eight U atoms in the unit cell must occupy two of the general fourfold positions $\pm(x,y,z)$, $\pm(\frac{1}{2}+x,\frac{1}{2}-y,\frac{1}{2}+z)$ in the space group $P2_1/n$. Two possible sets of parameter values for the U atoms were deduced, and one of these led to a reasonably low conventional R value (0.22).

The positions for all light atoms coordinated to U were found from a subsequent difference map. Least squares refinement of the parameters of all atoms gave an R value of 0.184 before and 0.152 after absorption corrections had been applied to the data taken around *b*. Individual scale factors and isotropic temperature factors were included in the refinement. A further least squares refinement series using an overall scale factor and anisotropic temperature factors for the U atoms lowered R to 0.143.

The data taken around *c* were treated similarly, and the following R values were obtained: 0.211 before and 0.185 after absorption corrections, and 0.167 when the overall scale factor and anisotropic temperature factors for U had been refined. The two sets of data were then analyzed simultaneously in a new series of refinements to an R value of 0.163.

Table 1. Final positional parameters and isotropic thermal parameters (Å²) in the form exp $[-8\pi^2 U(\sin^2\theta/\lambda^2)]$. The positional parameters given are referred to atoms in the same tetranuclear complex. The other half of the complex is obtained from the centre of symmetry at $(0,0,\frac{1}{2})$. O(10) and O(11) are oxygen atoms in water molecules of crystallization.

Atom	x	y	z	U
U(1)	0.12337(12)	0.06018(13)	0.64236(14)	
U(2)	0.11325(13)	0.13620(13)	0.25114(15)	
Cl(1)	0.2735(11)	0.2085(12)	0.5136(13)	0.052(3)
O(1)	0.0414(37)	0.1968(41)	0.6598(44)	0.066(10)
O(2)	0.2187(30)	−0.0772(33)	0.6326(36)	0.050(8)
O(3)	0.0632(38)	0.2929(42)	0.2644(45)	0.069(10)
O(4)	0.1799(32)	−0.0246(38)	0.2315(39)	0.058(9)
O(5)	0.0426(21)	0.0630(22)	0.4147(26)	0.027(5)
O(6)	0.0788(21)	−0.0283(24)	0.8392(26)	0.029(5)
O(7)	0.2839(40)	0.1400(43)	0.8282(48)	0.073(11)
O(8)	0.0675(28)	0.1582(31)	0.0085(34)	0.046(7)
O(9)	0.3026(40)	0.2097(46)	0.2102(47)	0.076(11)
O(10)	0.4501(45)	−0.0810(49)	0.5847(54)	0.083(13)
O(11)	0.0636(81)	0.5313(92)	0.4366(91)	0.16(3)

Table 2. Final anisotropic thermal parameters (Å²) in the form exp $[-2\pi^2(h^2a^{*2}U_{11}+\ldots+2hka^*b^*U_{12}+\ldots)]$.

Atom	U_{11}	U_{22}	U_{33}	U_{12}	U_{13}	U_{23}
U(1)	0.0364(8)	0.0291(7)	0.0292(8)	−0.0059(10)	0.0172(11)	−0.0015(10)
U(2)	0.0430(9)	0.0272(7)	0.0328(8)	−0.0056(10)	0.0301(13)	−0.0032(10)

On comparing the two sets of F_o's with each other and with F_c, it was noticed that the intensities of some weak reflections were overestimated by more than 100 %. Such reflections were discarded when they had been observed on only one film and for just one setting. It was also noticed that the intensities of some reflections at $\sin\theta/\lambda$ values > 0.6 Å^{-1} were underestimated by more than 100 %, mainly due to spot deformation which was not corrected for in this region. These reflections were also discarded. For all other reflections the arithmetic mean of F_o for the two settings was taken. Thus 1900 independent reflections out of 2100 remained. These were used in a least squares refinement of the positional and thermal parameters of the 12 atoms (two U, one Cl, and nine O atoms). An overall scale factor and anisotropic temperature factors for the U atoms were included, and the R value dropped to 0.132. A new difference map was calculated, and two peaks there could be interpreted as the water molecules of crystallization. The positional and thermal parameters of all the 14 atoms were then refined, and an R value of 0.129 was obtained. In a final series of least squares refinements 21 strong low order reflections assumed to be affected by secondary extinction were given zero weight. R then dropped to 0.120. In the last cycle all parameter shifts were less than 0.1 % of the calculated standard deviations. A final difference map was then calculated. No peaks there were larger than about 4 electrons Å^{-3}. None of the residual peaks could be interpreted as remaining O atoms owing to improbable O – U, O – Cl, or O – O distances.

The final parameter values are given in Tables 1 and 2. A listing of the observed and calculated structure factors is available from the author on request.

The scattering factors used were those given by Cromer and Waber [7] for neutral atoms. The real part of the anomalous dispersion correc-

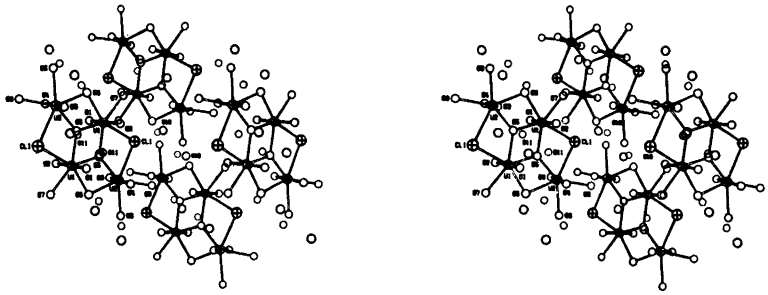

Fig. 1. Stereoscopic perspective projection of the structure parallel to the *b* axis.

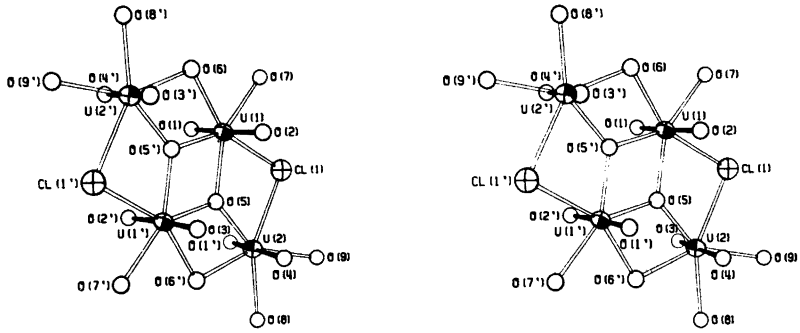

Fig. 2. Stereoscopic perspective picture of one tetranuclear complex as viewed parallel to the *b* axis. The numbering of the atoms is shown. The molecule has a centre of symmetry. The thermal ellipsoids for U(1), U(2), Cl(1), O(5), and O(6) are scaled to include 50 % probability. For the other atoms $U = 0.025$ Å^2 has been chosen arbitrarily for clarity.

tions for U and Cl, according to Cromer,[8] was included. The weighting scheme for the refinements was that suggested by Hughes.[9] The function minimized was $\sum w(|F_o| - |F_c|)^2$, where $\sqrt{w} = 1$ for $|F_o| \leq 72$ and $\sqrt{w} = 72/|F_o|$ for $|F_o| \geq 72$.

DESCRIPTION OF THE STRUCTURE

A stereoscopic perspective projection of the structure parallel to the *b* axis of the unit cell is shown in Fig. 1. The structure may be regarded as being built up from discrete tetranuclear complexes, one of which is drawn separately in Fig. 2. Some important distances and angles within a tetranuclear complex are given in Table 3.

Each U atom in a tetranuclear complex is surrounded by one Cl and six O atoms at the vertices of a pentagonal bipyramid. The coordination of U is thus similar to that found in the dinuclear complex $[(UO_2)_2Cl_2(OH)_2(H_2O)_4]$.[3]

Two O atoms, O(5) and O(5′), are shared between three U atoms and they are probably O^{2-} oxygens. Two O atoms, O(6) and O(6′), are shared between two U atoms and are probably HO^- oxygens. The Cl atoms, Cl(1) and Cl(1′), are also shared between two U atoms. The remaining O atoms are coordinated to only one U atom: O(7), O(7′), O(8), O(8′), O(9), O(9′) as water O atoms and O(1), O(1′), O(2), O(2′), O(3), O(3′), O(4), O(4′) as uranyl O atoms. Thus the formula of the tetranuclear complex can be written as $[(UO_2)_4Cl_2O_2(OH)_2(H_2O)_6]$.

The U atoms are joined through bridges of three types. Between U(1) and U(1′) there is a double O bridge with a U–U distance of 3.693 Å. U(1) and U(2′) as well as U(1′) and U(2) are joined through an HO/O bridge with a U–U distance of 3.787 Å. Between U(1)

Table 3. Some important interatomic distances (Å) and angles (°). An atom marked with a prime (′) is related by the centre of symmetry at $(0,0,\frac{1}{2})$ to the corresponding atom without the prime (Table 1).

U(1)–U(1′)	3.693(2)		
U(1)–U(2)	4.036(2)		
U(1)–U(2′)	3.787(2)	U(2)–U(2′)	6.902(2)
U(1)–Cl(1)	2.88(1)	U(2)–Cl(1)	2.91(1)
U(1)–O(1)	1.72(4)	U(2)–O(3)	1.71(4)
U(1)–O(2)	1.80(3)	U(2)–O(4)	1.84(4)
U(1)–O(5)	2.26(2)	U(2)–O(5)	2.18(2)
U(1)–O(5′)	2.24(2)	U(2)–O(6′)	2.43(2)
U(1)–O(6)	2.38(2)	U(2)–O(8)	2.40(3)
U(1)–O(7)	2.41(4)	U(2)–O(9)	2.47(4)
Cl(1)–O(1)	3.43(4)		
Cl(1)–O(2)	3.26(3)		
Cl(1)–O(3)	3.13(4)		
Cl(1)–O(4)	3.65(4)		
Cl(1)–O(5)	2.99(2)		
Cl(1)–O(7)	3.25(5)		
Cl(1)–O(9)	3.21(5)		
O(1)–O(5)	2.85(5)	O(3)–O(5)	2.83(5)
O(1)–O(5′)	2.83(5)	O(3)–O(6′)	3.17(5)
O(1)–O(6)	2.88(5)	O(3)–O(8)	2.96(6)
O(1)–O(7)	2.94(6)	O(3)–O(9)	3.10(6)
O(2)–O(5)	2.95(4)	O(4)–O(5)	2.91(4)
O(2)–O(5′)	2.95(4)	O(4)–O(6′)	2.95(4)
O(2)–O(6)	3.03(4)	O(4)–O(8)	2.95(5)
O(2)–O(7)	2.92(6)	O(4)–O(9)	2.80(6)
O(5)–O(5′)	2.56(5)	O(6)–O(7)	2.96(5)
O(5)–O(6′)	2.62(4)	O(6)–O(8′)	2.91(4)
O(8)–O(9)	2.99(6)		
Cl(1)–U(1)–O(5)	70.0(6)	Cl(1)–U(2)–O(5)	70.2(7)
O(5)–U(1)–O(5′)	70(1)	O(5)–U(2)–O(6′)	68.8(9)
O(5′)–U(1)–O(6)	68.9(9)	O(6′)–U(2)–O(8)	74(1)
O(6)–U(1)–O(7)	76(1)	O(8)–U(2)–O(9)	76(1)
O(7)–U(1)–Cl(1)	75(1)	O(9)–U(2)–Cl(1)	73(1)
O(1)–U(1)–O(2)	176(2)	O(3)–U(2)–O(4)	174(2)
U(1)–O(5)–U(1′)	110(1)		
U(1′)–O(5)–U(2)	118(1)		
U(2)–O(5)–U(1)	131(1)		

and U(2) as well as between U(1′) and U(2′) there is a Cl/O bridge with a U–U distance of 4.036 Å. In the dinuclear complex, where the U atoms are joined through a double HO bridge, the U–U distance is 3.944 Å.

The shortest U–O bond lengths are naturally those within the uranyl group. They vary from 1.71 to 1.84 Å but do not differ significantly from the average value 1.77 Å. In the dinuclear complex the mean U–O bond length within the uranyl group is 1.79 Å. The angles O(1)–U(1)–O(2) and O(3)–U(2)–O(4) are 176 and 174°, respectively. The deviation from 180° is not significant.

The U–O bond lengths within the bridges formed by O(5) and O(5′) are 2.18, 2.24 and 2.26 Å with an average value of 2.23 Å. The remaining U–O bond lengths within the pentagonal bipyramids vary from 2.38 to 2.47 Å, mean value 2.42 Å, with no significant difference between O(6) (HO^-) on the one hand and O(7), O(8), and O(9) (H_2O) on the other hand.

Table 4. Least squares planes $Ax+By+Cz+D=0$. For each plane values of A, B, C, and D are given, and, within square brackets, deviations (Å) of atoms from the planes.

Plane 1: 6.254, −8.514, −1.816, 0.908
[U(1) 0.001(2), U(1′) −0.001(2), U(2) 0.001(2), U(2′) −0.001(2), Cl(1) −0.09(1), Cl(1′) 0.09(1), O(5) −0.12(2), O(5′) 0.12(2), O(6) 0.12(2), O(6′) −0.12(2), O(7) −0.01(4), O(7′) 0.01(4), O(8) −0.03(3), O(8′) 0.03(3), O(9) 0.63(5), O(9′) −0.63(5)]

Plane 2: 6.507, −8.351, −2.191, 1.107
[U(1) −0.001(2), Cl(1) 0.02(1), O(5) −0.05(2), O(5′) 0.07(2), O(6) 0.02(2), O(7) −0.03(5)]

Plane 3: −5.586, 8.860, 1.104, −0.852
[U(2) −0.001(2), Cl(1) 0.04(1), O(5) −0.07(2), O(6′) 0.02(2), O(8) 0.18(3), O(9) −0.45(5)]

Plane 4: −9.580, −4.858, −0.696, 1.921
[U(1) 0.001(2), U(2) 0.001(2), O(1) 0.11(4), O(2) −0.24(4), O(3) −0.29(5), O(4) 0.16(4)]

The angles between the planes are: 2.4° (1 and 2), 5.0° (1 and 3), 88.5° (1 and 4), 7.4° (2 and 3), 87.6° (2 and 4), 88.8° (3 and 4).

The U−Cl bond lengths are 2.88 and 2.91 Å. The average value 2.89 Å is greater than the U−Cl bond length of 2.75 Å in the dinuclear complex. In the dinuclear complex, however, the Cl atoms are coordinated to only one U atom.

The four pentagonal bipyramids in a tetranuclear complex are linked together by sharing edges. The U(1) bipyramid shares the edge Cl(1)−O(5) of 2.99 Å with the U(2) bipyramid, the edge O(5)−O(5′) of 2.56 Å with the U(1′) bipyramid, and the edge O(5′)−O(6) of 2.62 Å with the U(2′) bipyramid. The U(2) bipyramid shares only two edges with neighbouring bipyramids: Cl(1)−O(5) with U(1) and O(5)−O(6′) with U(1′).

The pentagons around the uranyl groups are roughly planar. The degree of planarity has been tested by fitting least squares planes to selected atoms within a $[(UO_2)_4Cl_2O_2(OH)_2(H_2O)_6]$ molecule. The results are shown in Table 4. Four least squares planes have been tried: (1) through all four pentagons U(1), U(1′), U(2), and U(2′), (2) through the U(1) pentagon, (3) through the U(2) pentagon, and (4) through the uranyl groups of U(1) and U(2). The weights which have been used are based on the calculated standard deviations of the positional parameters in Table 1. The largest deviations from the least squares planes occur for atom O(9) (planes 1 and 3 in Table 4). The angles between the planes have also been calculated, and they are given in Table 4. Here the largest deviation from the expected values 0 or 90° occurs for the angle between the planes through the U(1) and U(2) pentagons.

As all the Cl atoms are included in the uncharged tetranuclear complex, only hydrogen and van der Waals bonds hold the different complexes together. The water molecules of crystallization, O(10) and O(11), situated in the holes of the structure, are most probably an important part of the hydrogen bond system. Several intermolecular O−O distances are short enough to be hydrogen bond distances (Table 5). However, a more detailed discussion is not meaningful due to the comparatively high standard deviations, especially for distances involving O(11).

Table 5. Short (<3 Å) intermolecular oxygen-oxygen distances (Å). The symmetry codes are: $(\frac{1}{2}-x,\frac{1}{2}+y-1,\frac{1}{2}-z+1)$ (*a*); $(\frac{1}{2}-x,\frac{1}{2}+y-1,\frac{1}{2}-z)$ (*b*); $(x,y,z-1)$ (*c*); $(\frac{1}{2}-x,\frac{1}{2}+y,\frac{1}{2}-z)$ (*d*); $(-x+1,-y,-z+1)$ (*e*); $(-x,-y+1,-z+1)$ (*f*).

O(2)−O(7*a*)	2.88(5)	O(7)−O(11*a*)	2.79(10)
O(2)−O(10)	2.87(6)	O(8)−O(10*d*)	2.79(6)
O(3)−O(11)	2.98(10)	O(10)−O(10*e*)	2.85(10)
O(4)−O(9*b*)	2.74(6)	O(11)−O(11*f*)	2.31(18)
O(6)−O(8*c*)	2.58(4)		

DISCUSSION

The peak of O(11), about 4 electrons Å^{-3}, is indistinguishable from the background peaks in the difference Fourier map calculated with F_c based on all the atoms except O(10) and O(11). The atom O(10), however, is easily located, even in the difference map where the F_c values are calculated from the U atom positions only. Its peak height does not differ from those of the O atoms coordinated to U. The standard deviations of the atomic parameters of O(10) are only slightly higher than those of the coordinated water oxygens O(7) and O(9). The uncertainty in the position of O(11) has not been considered too important, as the main purpose of the structure determination has been to establish unambiguously the arrangement of atoms within the tetranuclear complex. The high temperature factor of O(11) might indicate an occupation number < 1.0 (statistically distributed water molecules).

As already mentioned, the structures of the dinuclear and the tetranuclear complexes are closely related. They are built up from pentagonal bipyramids, UO_2ClO_4, sharing edges. The uncharged polynuclear complexes are linked to each other through hydrogen bonds and van der Waals forces. Differences in U – Cl and in some U – O bond lengths have been noticed. They are explained by the different types of bridges between the U atoms in the two complexes.

The structure of $[(UO_2)_4Cl_2O_2(OH)_2(H_2O)_6]4H_2O$ is also closely related to that of $Cs_x(UO_2)OCl_x$ ($x \approx 0.9$).[10] This compound is built up from double chains with Cl/O bridges along the chain direction and double O bridges holding the two chains together. Each uranyl group is surrounded by three O and two Cl atoms and has four U neighbours, two at 3.704 Å and two at 4.118 Å. These U – U distances are in good agreement with those obtained in the present work. The arrangement of U atoms at the corners of two approximately equilateral triangles sharing one edge can be recognized as a building element of the double chain in $Cs_x(UO_2)OCl_x$. One O atom inside each triangle is also found, and the Cl atoms act as bridges between the U atoms.

Precise emf titrations covering a broad uranyl(VI) concentration range have been carried out in this institute using many different ionic media.[1] The percentage of uranium bound in the different hydrolysis complexes as a function of n_{HO} (= bound HO/U) is dependent on the ionic medium. In, *e.g.*, 3 M (Mg)ClO_4 the maximum value of n_{HO} is 0.55 for the highest uranyl(VI) concentration studied (1.2 M).[11] Then 51 % of the total amount of uranium in the solution is bound in dinuclear complexes and only 6 % in higher complexes. In 3 M (Na)Cl the maximum total uranyl(VI) concentration has been 0.080 M.[12] For that concentration about 10, 70, and 14 % of the total uranium amount is bound in dinuclear, trinuclear, and tetranuclear complexes, respectively, at the maximum degree of hydrolysis, $n_{HO} = 1.26$. Provided the stability constants are valid also for a 3.1 M uranyl(VI) chloride solution, the corresponding values are 15, 63, and 7 % for $n_{HO} = 1.11$, *i.e.*, for the solution used to prepare crystals of $[(UO_2)_4Cl_2O_2(OH)_2(H_2O)_6].4H_2O$. Thus it seems that although the emf titration results indicate that trinuclear complexes are by far predominating in strongly hydrolyzed uranyl(VI) chloride solutions, tetranuclear, and above all dinuclear complexes, are more easily crystallized. An anion like Cl^- can be coordinated to one U atom as in $[(UO_2)_2Cl_2(OH)_2(H_2O)_4]$ or, probably more important, bridge two U atoms as in $[(UO_2)_4Cl_2O_2(OH)_2(H_2O)_6]$, and its presence can probably explain why trinuclear complexes are much more stable in hydrolyzed uranyl(VI) chloride than in perchlorate solutions.

On analyzing the X-ray scattering data from hydrolyzed uranyl(VI) chloride solutions, it was suggested that the trinuclear complex was built up from three U atoms joined through double HO/O bridges and with one Cl atom coordinated to each uranyl group.[2] Now, on the basis of the knowledge of the structure of the tetranuclear complex, it seems more likely to assume a structure with double HO(O) or Cl/HO(O) bridges between the U atoms. The average Cl/U ratio and the positions of the Cl atoms cannot be given unambiguously. But if the U – U distances are the same in the trinuclear complex in solution as in the tetranuclear complex in the solid, the average U – U distance of 3.86 Å obtained by analysis of the X-ray scattering data indicates that, on an average, the trinuclear complexes do not contain more than one Cl/HO(O) bridge.

Acknowledgements. I wish to thank Dr. Georg Johansson for his encouragement and interest in this work, Professor Ingmar Grenthe for helpful criticism of the manuscript, Anita Björnemo and my late brother Anders Åberg for their assistance in the intensity estimations, and Ian Duncan for revising the English of the text.

The work has been financially supported by the Swedish Natural Science Research Council. Computer time has been made available by the Computer Division of the National Swedish Office for Administrative Rationalization and Economy.

REFERENCES

1. Sillén, L. G. and Martell, A. (compilers) *Stability Constants of Metal-Ion Complexes*, Chem. Soc. Spec. Publ. No. 17 (1964); Suppl. No. 1, Spec. Publ. No. 25 (1971).
2. Åberg, M. *Acta Chem. Scand. 24* (1970) 2901.
3. Åberg, M. *Acta Chem. Scand. 23* (1969) 791.
4. Åberg, M. *Acta Chem. Scand. 25* (1971) 368.
5. Hecht, F. and Donau, J. *Anorganische Mikrogewichtsanalyse*, Springer, Wien 1940, p. 205.
6. Fischer, K. *Angew. Chem. 48* (1935) 394.
7. Cromer, D. T. and Waber, J. T. *Acta Crystallogr. 18* (1965) 104.
8. Cromer, D. T. *Acta Crystallogr. 18* (1965) 17.
9. Hughes, E. W. *J. Am. Chem. Soc. 63* (1941) 1737.
10. Allpress, J. G. and Wadsley, A. D. *Acta Crystallogr. 17* (1964) 41.
11. Hietanen, S., Row, B. R. L. and Sillén, L. G. *Acta Chem. Scand. 17* (1963) 2735.
12. Dunsmore, H. S. and Sillén, L. G. *Acta Chem. Scand. 17* (1963) 2657.

Received February 18, 1976.

Acta Chemica Scandinavica A 30 (1976) 515—520

EPR Study of Mixed VO_2+ Chelate Complexes

R. LUNDQVIST,* A. PANFILOV, N. KALINICHENKO and I. MAROV

V. I. Vernadsky Institute of Geochemistry and Analytical Chemistry, USSR Academy of Sciences, Moscow B-334, USSR

The stepwise exchange reactions for VO^{2+} chelate complexes $VOL_2 + HB \rightleftharpoons VOLB + HL$ and $VOLB + HB \rightleftharpoons VOB_2 + HL$, where HL and HB are the chelating agents acetylacetone (HAA), thenoyltrifluoroacetone (HTTA), salicylaldoxime (HSAO), and 8-hydroxyquinoline (HOX) were investigated in toluene solutions using EPR. Stability constants were derived and it was found that the reactions had negligible ΔH and ΔS values (5 – 60 °C). It was also concluded that mixed complexes of the type VO(SAO)(β-diketone) were remarkably unstable compared to unmixed VO chelate. The mechanism of the exchange processes was studied by kinetic measurements. Reaction rate constants and activation energies were calculated.

Previously the chelate complexing chemistry of tetravalent metalyl ions PaO^{2+} and HfO^{2+} was studied [1–2] using solvent extraction. In order to extend the investigations with another metal and to complement the liquid-liquid distribution studies with an independent method, electron paramagnetic resonance EPR studies of VO^{2+} was carried out. EPR studies of ligand substitution of VO^{2+} have been reported for nonchelate complexing [3,4] (Cl^-, SCN^-) and recently of chelating agents [5] (thio-oxine and 1-phenyl-3-methyl-4-benzoylpyrazolone-5 in $CHCl_3$ + 0.66 M CH_3COOH).

EXPERIMENTAL

Chemicals. Benzoylacetone (HBA, Merck *p.a.*), thenoyltrifluoroacetone (HTTA, Merck *p.a.*), and toluene (Reakhim, *p.a.*) were of highest purity whereas the other chemicals were of ordinary quality. The chelate complexes of VOL_2, where L = HBA, HTTA, 8-hydroxyquinoline (HOX), acetylacetone (HAA), or salicylaldoxime (HSAO), were prepared by mixing a water-alcohol solution of $VOSO_4.3H_2O$ with an alcoholic solution of HL.[6] The recovered VOL_2 was dried and stored in a cold place (especially important for $Vo(SAO)_2$ and $VO(OX)_2$). The $VO(OX)_2$ was poorly recovered and was very unstable [oxidation of V(IV) to V(V)].

Apparatus. The EPR studies were carried out in the X-band microwave region with a Varian V4502 equipped with a variable temperature controller V4540, and the spectra were recorded with an X-Y-recorder PDP 4-002.

Procedure. The solution of the VO^{2+} chelates were mostly freshly prepared (one day in advance) because it was observed that precipitates of destroyed VO^{2+} complex were formed, after some days or weeks. Concentrations of V(IV) down to 10^{-5} M were used in order to optimize the reaction rates, although a very weak EPR signal was obtained. The kinetic measurements were made by first recording two solutions representing the initial and final state and then the spectra of the mixture. The solutions were thermostated (± 3 °C) and spectra were recorded repeatedly after mixing, using a syringe technique (1.3 ml, ± 1 – 2 %).

Resolving the EPR spectra. The mixed spectrum was regarded as the sum of some pure EPR spectra j with individual parameters ΔH, g *etc.* A maximum of three components j were found for the investigated systems and the contribution of each spectra were numerically calculated by matrix solution using a small computer allowing an accuracy of about ± 5 %.

EQUILIBRIA OF MIXED COMPLEXES

The stepwise exchange reactions of chelate ligands between a vanadyl(IV) chelate complex VOL_2 and a free undissociated chelating acid

* Permanent address: Department of Nuclear Chemistry, Chalmers University and Technology, S-402 20 Göteborg 5, Sweden.

Table 1. Stability constants for the stepwise ligand exchange of VO^{2+} chelates, $VOL_2+HB \rightleftharpoons VOLB+HL$ and $VOLB+HB \rightleftharpoons VOB+HL$. Experimental data for toluene solutions at different temperatures are given.

System	Temp. °C	$[VOL_2]^{init} \times 10^3$	$[VOB]_2^{init} \times 10^3$	$[HL]^{init} \times 10^3$	$[HB]^{init} \times 10^3$	$VOLB_2$ %	VOLB %	VOB_2 %	K_1	K_2	β_2
HL = acetyl-	21	0.937	–	–	2.54	7.0	8.8	84.2	2.4	18.1	43.0
acetone	30	0.910	–	–	2.85	4.0	10.5	85.5	3.6	11.2	40.4
HB = salicyl-	30	–	0.718	3.80	–	21.5	15.0	61.5	2.5	38.4	95.0
aldoxime	60	–	0.393	11.7	–	78.9	12.1	9.0	2.5	12.3	30.8
	30	0.538	–	21.6	4.72	44.3	7.1	48.7	0.9	36.7	31.4
	60	0.538	–	21.6	4.72	43.1	12.3	44.5	1.5	19.2	29.2
	100	0.538	–	21.6	4.72	45.1	12.2	42.7	1.4	18.5	26.5
								Mean $\pm\sigma$	2.0 ± 0.8	22 ± 10	42 ± 22
HL = thenoyl-	21	–	0.788	1.49	–	33	–	67	–	–	7.1
trifluoro-	22	–	0.767	2.22	–	53	–	47	–	–	2.6
acetone	21	–	0.757	6.69	–	85	–	15	–	–	3.1
HB = salicyl-	22	0.837	–	–	2.03	31	–	69	–	–	3.9
aldoxime	3	0.522	–	9.12	4.62	68	–	32	–	–	2.3
	90	0.522	–	9.12	4.62	63	–	37	–	–	3.0
								Mean $\pm\sigma$			3.7 ± 1.6
HL = acetyl-	30	0.921	–	–	2.04	3.6	11.5	84.9	14.4	33.3	480
acetone	30	0.804	–	–	0.937	30.9	33.5	35.6	9.6	9.4	89
HB-oxine	30	0.615	–	–	1.87	≤ 2.7	8.1	89.2	≥ 4.7	17.4	≥ 82
								Mean $\pm\sigma$	9.6 ± 4.0	20.0 ± 10	$(2.2\pm1.9)10^2$

HB, $VOL_2+HB \rightleftharpoons VOLB+HL$ and $VOLB+HB \rightleftharpoons VOB_2+HL$, were studied. The reactions were investigated, starting with mixing VOL_2+HB as well as VOB_2+HL. As can be seen from Table 1, where the initial conditions and the final percentages of the different VO^{2+} chelates are listed together with calculated stability constants, true equilibria were reached.

In the case of the reaction between oxine and acetylacetone it must be noted that the equilibria could only be studied from one direction, $VO(AA)_2+HOX$, because pure $VO(OX)_2$ was found to be unstable under the conditions used. Even the mixtures of $VO(AA)_2+HOX$ were destroyed during a day, but the relative percentages of $VO(AA)_2$, $VO(OX)_2$, and VO(OX)(AA) were appreciably constant in the time interval from about 10 min to 15 h after mixing.

During the exchange between ligands of β-diketones and salicylaldoxime the mixed VO^{2+} complex was formed in remarkably small concentration. However, under certain conditions (high reagent concentrations), the formation of mixed complexes could be followed kinetically soon after mixing. At equilibrium no VO(SAO)(TTA) could be registered and only a small fraction of VO(SAO)(AA) could be determined by refined calculation.

The temperature dependency of the equilibria was investigated by taking the EPR spectra at different temperatures of a mixture of $VOB_2+VOL_2+HL+HB$, in which the concentrations of VOL_2 and VOB_2 were set much lower than the concentrations of HL and HB, in order to obtain maximum change in the ratio $[VOB_2]/[VOL_2]$ and to increase the accuracy. It was found that the temperature dependency for the ligand exchange was too small, see Table 1, to be detected. It was also concluded that there was no dimerization of VOL_2 for at least up to 10^{-3} M.

KINETICS AND MECHANISMS OF LIGAND SUBSTITUTION

The unexpected low relative stability of the mixed complexes in equilibrated VO^{2+} solutions of β-diketones and salicylaldoxime raised the question of how the ligand exchange occurred. Therefore an investigation of the reaction mechanisms was undertaken. The following

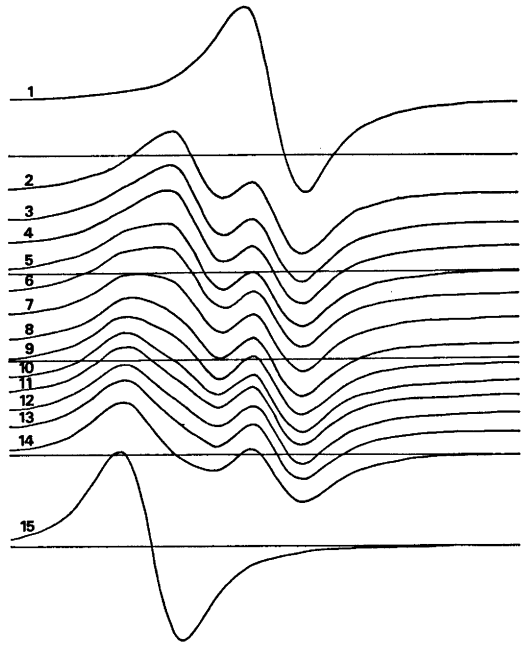

Fig. 1. Kinetics of mixing toluene solutions of $VO(AA)_2+HSAO$ at 60 °C. The EPR spectra of peak group 8 at chronologically increased times shows contribution from the mixed complex VO(AA) (SAO) which has its maximal concentration soon after mixing. 1. Spectra of pure $VO(AA)_2$. 2–14. Spectra within 1–7 min. $[VO(AA)_2]^{init}=0.281\times10^{-3}$M, $[HSAO]^{init}=0.412\times10^{-3}$ M. 15. Spectra of pure $VO(SAO)_2$.

systems were analyzed: $VO(SAO)_2+HAA$, $VO(AA)_2+HSAO$, $VO(SAO)_2+$ HTTA, and $VO(TTA)_2+HSAO$. Thus the reaction leading to equilibria was studied from both sides, (a) VOL_2+HB and (b) VOB_2+HL.

a. The reaction $VO(SAO)_2+$ β-diketone was followed and from spectra analysis it was found that no mixed complex was formed. The rate with which the initial concentration of $VO(SAO)_2$ decreased, was found to be proportional to the concentration of the initial concentrations of β-diketone and $VO(SAO)_2$. This suggests that one molecule $VO(SAO)_2$ reacts with one molecule β-diketone. The kinetic constant for the reaction k_1 is obtained from the relation

$$-\lim_{t\to0}\partial[VO(SAO)_2]/\partial t = k_1[VO(SAO)_2]^{init}[\beta\text{-diketone}]^{init}$$

Table 2. Kinetic constants k_1 and k_2 and activation energy values E_{A1} and E_{A2} for the reactions $VOL_2+HB\rightarrow$ and $VOLB+HB\rightarrow$, respectively. Experimental conditions for toluene solutions are given.

System	Temp. °C	$[VOL_2]^{init}$ M × 10^3	$[HB]^{init}$ M × 10^3	$-\partial\,\%VOL_2/\partial t$ $t\rightarrow 0$, min^{-1}	$\partial\%VOB_2/\partial t$ $t\rightarrow 0$, min^{-1}	k_1 s^{-1} mol^{-1}	k_2 s^{-1} mol^{-1}
HL = acetyl-	5	0.128	0.423	50	3.1	20	1.2
acetone	5	0.281	0.412	36	1.7	14	0.7
	5	0.076	0.423	48	3.2	19	1.3
HB = salicyl-	30	0.283	0.412	59	3.8	24	1.5
aldoxime	30	0.0847	0.424	67	6.4	26	2.5
	60	0.281	0.412	77	6.2	31	2.5
	60	0.0847	0.424	71	21	28	8.3
	$E_{A1}=7.5\pm1.6$ kJ mol^{-1}; $E_{A2}=20.6\pm5.4$ kJ mol^{-1} K^{-1}						
HL = salicyl-	5	0.393	11.66	17	—	0.25	
aldoxime	30	0.718	34.44	67	—	0.33	
	30	0.718	11.66	29	—	0.42	
HB = acetyl-	60	0.718	3.80	12	—	0.53	
acetone	60	0.393	11.66	36	—	0.51	
	$E_{A1}=10.1\pm1.5$ kJ mol^{-1}						
HL = thenoyl	5	0.620	4.12	42	17	1.7	0.67
trifluoro-	5	0.155	5.09	50	21	1.7	0.70
acetone	5	0.375	5.12	45	23	1.5	0.76
	21	0.837	2.03	31	13	2.6	1.0
HB = salicyl-	30	0.155	5.09	77	50	2.5	1.6
aldoxime	30	0.176	2.88	63	33	3.6	1.9
	$E_{A1}=17.4\pm3.5$ kJ mol^{-1}; $E_{A2}=24.0\pm3.4$ kJ mol^{-1} K^{-1}						
HL = salicyl	5	0.393	9.00	6.4	—	0.12	—
aldoxime	21	0.852	3.97	5.2	—	0.22	—
HB = thenoyl	21	0.757	6.69	10	—	0.25	—
trifluoro-	60	0.393	9.00	42	—	0.78	—
acetone							
	$E_{A1}=26.0\pm1.2$ kJ mol^{-1}						

The reaction product could not be recorded, as it instantly reacts further to the final product $VO(\beta\text{-diketone})_2$.

b. The second case, VOB_2+HL, was consequently studied with the systems $VO(\beta\text{-diketone})_2+HSAO$. The EPR spectra (Fig. 1) of such mixtures showed a contribution from a third transition complex which was quickly built up to its maximum concentration (within a minute) and then decreased to near zero. The position of this transition complex lay between that of $VO(\beta\text{-diketone})_2$ and $VO(SAO)_2$, which suggested that the composition was $VO(\beta\text{-diketone})(SAO)$. The initial step leading to the production of $VO(\beta\text{-diketone})(SAO)$ was determined to be $VO(\beta\text{-diketone})_2+HSAO\rightarrow VO(\beta\text{-diketone})(SAO)$, in analogy with the case (a) above. The consecutive reaction $VO(\beta\text{-diketone})(SAO)+HSAO\rightarrow$, with the rate constant k_2, was studied by its product $VO(SAO)_2$. If the consecutive reactions $VO(\beta\text{-diketone})_2\rightarrow VO(\beta\text{-diketone})(SAO)\rightarrow VO(SAO)_2$ can be regarded as initially irreversible then k_2 can be obtained from the relation $\partial\,\%[VO(SAO)_2/100]/\partial t=k_2[HSAO]^{init}$. The reaction constants k_1 and k_2 for different temperatures are collected in Table 2.

In order to derive the Arrhenius activation energies, the kinetic constants for the rate-determining steps were determined at various temperatures between ±0 and 60 °C (Table 2).

DISCUSSION

The direct measurements of the relative complexing power toward VO^{2+} of the chelating agents, made it possible to arrange them in the following order of increasing complexing ability: HAA, HTTA, HSAO, and HOX. This order may also be expected from the stability constants.[7] For bivalent ions like Mn^{2+}, Zn^{2+}, and Ni^{2+} the same order of

complexing ability is reported for complexing reactions in aqueous media. No direct measurements in organic media seem to have been reported.

From the stability constants obtained (Table 1) it is possible to calculate the stability constant for the reaction $VO(AA)_2 + 2HTTA \rightleftharpoons VO(TTA)_2 + 2HAA$ explicitly to log $\beta_2 = 1.1 \pm 0.4$. This reaction could only roughly be studied directly by the method used, because of the too small differences in EPR spectra of the two similar chelates, giving an estimate of the overall stability constant of log $\beta_2 = 1.2 \pm 0.1$.

The neglible temperature influence on the equilibrium between different VO^{2+} chelates in the toluene solution is expected as the number of molecules is constant, *i.e*, the ΔS term is small. The ΔH term is probably also small as the bonding energies of the different chelates

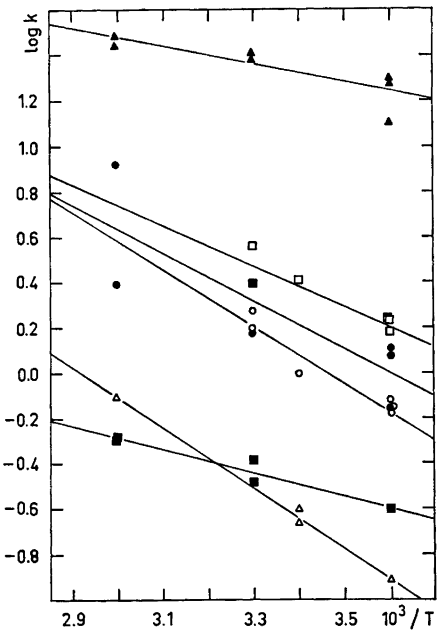

Fig. 2. The rate constants k_1 and k_2 for the reactions $VOL_2 + HB \rightarrow$ and $VOLB + HB \rightarrow$ as a function of the temperature.

System	Rate constant
■ $VO(SAO)_2 + HAA$	k_1
△ $VO(SAO)_2 + HTTA$	k_1
□ $VO(TTA)_2 + HSAO$	k_1
○ $VO(TTA)_2 + HSAO$	k_2
▲ $VO(AA)_2 + HSAO$	k_1
● $VO(AA)_2 + HSAO$	k_2

are of comparable strength and as no interaction with the solvent molecules is expected (especially for HSAO-HTTA).

The stability of the mixed VO^{2+} complexes of β-diketones and salicylaldoxime was significantly lower than is expected on statistical grounds and it was also low compared with that of acetylacetone and oxine and of thio-oxine and 1-phenyl-3-methyl-4-benzoyl-pyrazolone-5.[5] The reason for this may be explained by assuming some sterical hindrance in the formation of the mixed complex. Such hindrance could be the result if the oxygen on the donor nitrogen of salicylaldoxime also participated (through H-bonding) in the bonding of VO^{2+}.

The reaction rates for the substitution reactions studied might be related to the ratio of complexing power of the free and bound chelating agent. The exchange of HAA in $VO(AA)_2$ with HSAO is faster than the corresponding exchange of HTTA in $VO(TTA)_2$ with HSAO, *i.e.* $k_1[VO(AA)_2 + HSAO] > k_1[VO(TTA)_2 + HSAO]$. However, by similar comparison of $k_1[VO(SAO)_2 + HTTA]$ and $k_1[VO(SAO)_2 + HAA]$ it is suggested that HAA gives weaker complexes than HTTA with VO^{2+} only at higher temperatures than 30 °C. It was not possible to compare HSAO and HAA, *i.e.* k_2 $[VO(AA)_2 + HSAO]$ against k_2 $[VO(SAO)_2 + HAA]$ and k_2 $[VO(TTA)_2 + HSAO]$ against k_2 $[VO(SAO)_2 + HTTA]$, as the reaction constants k_2 $[VO(SAO)_2 + \beta\text{-diketone}]$ could not be measured. It is also possible to check some of the obtained rate constants by calculating already obtained stability constants. Thus for the reaction $VO(AA)(SAO) + HSAO \rightleftharpoons VO(SAO)_2 + HAA$, the ratio between the forward and backward rate reactions obtained at 30 °C (see Table 2 and Fig. 2) is $10^{0.32 \pm 0.08}$ $10^{-0.44 \pm 0.02} = 10^{0.76 \pm 0.10}$ which is of the same order as the previously calculated value of the stability constant $k_2 = 10^{1.3 \pm 0.4}$ It should, however, be emphasized that the value of the forward reaction is more uncertain than is reflected by the standard deviation only (experimental difficulties). For the analogous reaction $VO(TTA)(SAO) + HSAO \rightleftharpoons VO(SAO)_2 + HAA$ the ratio between the rate constants is $10^{0.21 \pm 0.04}/10^{-0.44 \pm 0.02} = 10^{0.65 \pm 0.06}$. Here the stability constant k_2 is not known but might be estimated from the observed overall stability constant $\beta_2 = 10^{0.8}$. Because of the very small

stability of the mixed complex it should follow that $k_2 \leq \beta_2$.

The intermediate complexes formed during the reactions of mixing $VO(SAO)_2$ with β-diketones, are not observed as they rapidly undergo further reactions to final products. The reaction rate k_2 for the system $VO(SAO)_2$ + β-diketone could therefore not be directly determined but can be estimated as it should be comparable to (or somewhat less than) k_3 for $VO(\beta\text{-diketone})_2$ + HSAO. Such an estimation makes it probable that $k_2 \geq k_1$ for the reaction $VO(SAO)_2$ + β-diketone and hence no mixed complex will be built up.

The measured activation energy for the reactions may be tested against each other by deriving ΔH for the two equilibrium reactions above. Thus ΔH for the forward and backward reactions of VO(TTA) (SAO) + HSAO $\rightleftharpoons$ $VO(SAO)_2$ + HTTA is $24.0 \pm 3.4 - 26.0 \pm 1.2 = -2 \pm 4.6$ kJ mol^{-1} degree^{-1}. Such a small ΔH value is expected from the observed negligible temperature influence of similar reactions measured directly. In the same way ΔH for VO(AA)(SAO) + HSAO $\rightleftharpoons$ $VO(SAO)_2$ + HAA is $20.6 \pm 5.4 - 10.1 \pm 1.5 = 10.5 \pm 6.9$ kJ mol^{-1} degree^{-1}. This ΔH value is, however, too large to be in accordance with the negligible temperature influence, but as was stated above the value of k_3[$VO(AA)_2$ + HSAO] was very uncertain. If the upper point in Fig. 2 is excluded then E_{A_2} is 13.5 ± 4.9 which solves the dilemma.

Finally, as the present investigation of ligand exchange reactions was made using the EPR method only, another independent method should be used in order to make more detailed and definite conclusions. In particular the insensitivity of the EPR signal of VO^{2+} chelates of similar chelating agents is a drawback. The method of liquid-liquid distribution seems to have certain advantages in this respect and studies of various metals, including VO^{2+}, is planned.

Acknowledgement. One of us (R. L.) wishes to express his gratitude for support from the scientist exchange between the Swedish Engineering Science Academy/Academy of Science and Akademia Nauk SSSR. Ph.D. Richard Warren made linguistic corrections.

REFERENCES

1. Lundqvist, R. *Aqueous Chemistry of Protactinum(IV)*, Dissertation, University of Gothenburg, Oct. 1974.
2. Lundqvist, R. *Acta Chem. Scand. A 29* (1975) 231.
3. Kalinichenko, N. B., Marov, I. N. and Ermakov, A. N. *Zh. Neorg. Khim. 17* (1972) 3250.
4. Kalinichenko, N. B., Marov, I. N. and Ermakov, A. N. *Zh. Neorg. Khim, 18* (1973) 1260.
5. Marov, I. N., Beljaeva, V. K., Melchakova, N. V. and Peshkova, V. M. *Zh. Neorg. Khim. In print.*
6. Bielig, H. J. and Möllinger, H. *Justus Liebigs Ann. Chem. 605* (1957) 117.
7. Sillén, L. G. and Martell, A. E. *Stability Constants of Metal Ion Complexes*, Special publication Nos. 17 and 25, The Chemical Society, London 1964 and 1971.

Received January 26, 1976.

Acta Chemica Scandinavica A 30 (1976) 521—526

A Double-bridged Binuclear Chromium(III) Complex with 2-Picolylamine. Preparation, Resolution and Stereochemistry of the Di-μ-hydroxo-bis{bis(2-picolylamine)chromium(III)} Ion

KIRSTEN MICHELSEN

Chemistry Department I (Inorganic Chemistry), University of Copenhagen, H. C. Ørsted Institute, Universitetsparken 5, DK-2100 Copenhagen Ø, Denmark

A new binuclear chromium(III) complex of the double-bridged type $[(C_6H_8N_2)_2Cr(OH)_2Cr(C_6H_8N_2)_2]^{4+}$, where $C_6H_8N_2$ = 2-picolylamine, has been prepared and investigated. The compound, a racemate, has been resolved into its catoptric forms.

Starting from these optically active compounds, *cis*-complexes, $(+)_D$- and $(-)_D$-$[Cr(C_6H_8N_2)_2Cl_2]ClO_4$, have been synthesized. They belong to the earlier described α-series, and their configurations are suggested to be *cis*, *trans*, *cis* because of their origin.

Based on circular dichroism spectra $(-)_D$-$[(C_6H_8N_2)_2Cr(OH)_2Cr(C_6H_8N_2)_2]Cl_4$ and $(-)_D$-α-*cis*-$[Cr(C_6H_8N_2)_2Cl_2]ClO_4$ are assigned the absolute configurations *ΔΔ* and *Δ*, respectively.

In a previous work by the present author [1] concerning octahedral bis(2-picolylamine) complexes of chromium(III) (2-picolylamine = 2-aminomethylpyridine) synthetic methods for the preparation of compounds belonging to two of the possible three series of complexes of the general formula *cis*-$[Cr(C_6H_8N_2)_2X_2]^{n+}$, where X = F, Cl, Br, and H_2O, were described. At that time it was possible to give only a partial assignment of the isomers. In the preparation of one of the compounds, β-*cis*-$[Cr(C_6H_8N_2)_2Br_2]I$, a by-product assumed to be di-μ-hydroxo-bis{bis(2-picolylamine)chromium(III)} iodide, $[(C_6H_8N_2)_2Cr(OH)_2Cr(C_6H_8N_2)_2]I_4.5H_2O$ was isolated. As this di-μ-hydroxo complex reacts with hydrochloric acid to α-*cis*-dichlorobis(2-picolylamine)chromium(III) salts establishing thereby an informative structural relationship between the two types of compounds, a further investigation was considered worth while. In addition, there has been noticeable recent interest in the spectroscopic, kinetic, structural and magnetic properties of binuclear complexes of exactly this type.[2–10]

EXPERIMENTAL

Reagents. 2-Picolylamine was purchased from Aldrich Co. Inc. Chromium(II) chloride was prepared in small portions from electrolytic chromium from Schmelztechnik G.m.b.H., Munich 42, Germany, following the ideas of Lux and Illmann.[11] As a modification the solution containing the chromium(II) ion was evaporated to *dryness* in a vacuum rotatory evaporator, and the precipitated salt was further heated (oilbath, 110 °C) in the same equipment until it looked grayish-green and dry. All other chemicals were of reagent grade and were used without further purifications.

Analyses. The chromium analyses were performed on a Perkin Elmer 403 Atomic Absorption Spectrophotometer. The microanalytical laboratory of this institute carried out the carbon, nitrogen, hydrogen, and halogen analyses by standard methods.

Physical measurements. Electronic absorption spectra were recorded on a Cary 14 spectrophotometer. The spectra are characterized by their maxima and minima (ε,λ), where the molar extinction coefficient ε is in units of l mol^{-1} cm^{-1} and the wavelength λ is in nm. Optical rotation was measured on a Perkin Elmer 141 polarimeter, and circular dichroism on a Roussel-Jouan Dichrographe I. In all cases the solvent was 0.1 M hydrochloric acid. The magnetic susceptibility of a powdered sample was measured by the Faraday method in the temperature

range 49 – 290 K at a field strength of 15 000 G. The magnetic field was calibrated with $Hg[Co(NCS)_4]$.[12] A more detailed description of the equipment is published elsewhere.[13,14]

Preparations

1a. *Di-μ-hydroxobis{bis(2-picolylamine)chromium(III)}bromide*, $[(C_6H_8N_2)_2Cr(OH)_2Cr(C_6H_8N_2)_2]Br_4.nH_2O$. 4.00 g $[Cr(H_2O)_4Br_2]Br.2H_2O$ (10 mmol) was suspended in 5 ml 2-methoxyethanol, and a spatula of $CrCl_2$ and 2.20 ml 2-picolylamine (21 mmol) was stirred in. After 15 min, ethanol (50 ml 99 %) was added, and the red-violet precipitate was filtered and washed with ethanol and ether; 3.32 g. The crude product was recrystallized by dissolving in water (10 ml) and adding ethanol and ether. Yield 2.82 g (58 %). Anal. $[Cr(C_6H_8N_2)_2OH]_2Br_4.5H_2O$: Cr, C, N, H, Br. In other experiments the complex crystallized with 4 and 4.5 mol of crystal water, respectively. $(\varepsilon,\lambda)_{max}$: (197,540), (117,380). $(\varepsilon,\lambda)_{min}$: (27,436), (59,350). The following two compounds were prepared from 1a by a simple conversion.

1b. *Di-μ-hydroxobis{bis(2-picolylamine)chromium(III)}iodide*, $[(C_6H_8N_2)_2Cr(OH)_2Cr(C_6H_8N_2)_2]I_4.5H_2O$. 1.20 g bromide (*1a*, 1.25 mmol) was dissolved in water (10 ml). 2 g NaI (13 mmol) was added. The solution was heated for a moment and then cooled on ice. Filtering and washing with ethanol; 1.10 g. The crude product was dissolved in boiling water (10 ml), and the filtrate added to a solution of 2 g NaI in water (2 ml). Cooling on ice. Washing with ice-cold water, ethanol, and ether, Yield 1.02 g of shining, flaky, red-violet crystals (70 %). Anal. $[Cr(C_6H_8N_2)_2OH]_2I_4.5H_2O$: Cr, C, N, H, I. $(\varepsilon,\lambda)_{max}$: (198,540), (119,380). $(\varepsilon,\lambda)_{min}$: (29,436), (68,350).

This compound apparently lost all 5 mol of crystal water when heated in an oven for 2 h at 100 °C. The anhydrous complex appeared with a much more bluish colour than the hydrated salt, but the drying had nevertheless left the cation intact, as proved by the absorption spectrum: $(\varepsilon,\lambda)_{max}$: (196,540), (120,380). $(\varepsilon,\lambda)_{min}$: (27,438), 69,350).

1c. *The perchlorate*, $[(C_6H_8N_2)_2Cr(OH)_2Cr(C_6H_8N_2)_2](ClO_4)_4.5H_2O$, was prepared similarly to 1b from the bromide (2.50 g, 2.60 mmol) dissolved in water (10 ml) and $NaClO_4.H_2O$ (4.0 g, 28.5 mmol) dissolved in boiling water (5 ml) 1.05 g (91 %). The crude product was recrystallized from boiling water (15 ml). Washing with ethanol. Yield 1.84 g (67 %). Anal. $[Cr(C_6H_8N_2)OH]_2(ClO_4)_4.5H_2O$: Cr, C, N, H. $(\varepsilon,\lambda)_{max}$: (197,540), (120,380). $(\varepsilon,\lambda)_{min}$: (26,438), (64,350). This compound was used for the magnetic measurements.

2. *Di-μ-hydroxobis{bis(2-picolylamine)chromium(III)}chloride*, $[(C_6H_8N_2)_2Cr(OH)_2Cr(C_6H_8N_2)_2]Cl_4.3\frac{1}{2}H_2O$. The compound was prepared by the same method as the bromide. From 2.66 g $[Cr(H_2O)_4Cl_2].2H_2O$ (10 mmol) and 2.2 ml 2-picolylamine (21 mmol) 1.44 g (37 %) was obtained. Anal. $[Cr(C_6H_8N_2)_2(OH)]_2Cl_4.3\frac{1}{2}H_2O$: Cr, C, N, H, Cl. $(\varepsilon,\lambda)_{max}$: (198,540), (117,380). $(\varepsilon,\lambda)_{min}$: (26,436), (58,350).

3. *Di-μ-hydroxobis{bis(2-picolylamine)chromium(III)} tetrachlorozincate*, $[(C_6H_8N_2)_2Cr(OH)_2Cr(C_6H_8N_2)_2][ZnCl_4]_2.4H_2O$. In this preparation Cr(II) was replaced by zinc powder. 1.33 g $[Cr(H_2O)_4Cl_2]Cl.2H_2O$ (5.0 mmol) was suspended in 3 – 4 ml 2-methoxyethanol, and a spatula of zinc powder and 1.1 ml (11 mmol) 2-picolylamine were stirred in. After 15 min, ethanol (70 ml, 99 %) was added. Filtering and washing with ethanol. The crude product was recrystallized from boiling water. The cooled filtrate directly gave 0.264 g of glistening, red crystals, and the addition of ethanol yielded another crop of 0.166 g. Total yield 16 %. Anal. $[Cr(C_6H_8N_2)_2OH]_2[ZnCl_4]_2.4H_2O$: Cr, C, N, H, Cl. $(\varepsilon,\lambda)_{max}$: (195,540), (114,380). $(\varepsilon,\lambda)_{min}$: (24,438), (57,350).

4a. $(-)_D$-*Di-μ-hydroxobis{bis(2-picolylamine)chromium(III)} antimonyl (+)$_D$-tartrate*, $(-)_D$-$[(C_6H_8N_2)_2Cr(OH)_2Cr(C_6H_8N_2)_2]\{(+)_D$-$SbOC_4H_4O_6\}_4.9H_2O$. 4.00 g $[(C_6H_8N_2)_2Cr(OH)_2Cr(C_6H_8N_2)_2]Br_4.5H_2O$ (4.08 mmol) was dissolved in 30 ml hot water (70 °C). 5.00 g $(+)_D$-$NaSbOC_4H_4O_6$ (16.2 mmol) was dissolved in 20 ml hot water (70 °C). The solutions were mixed, gently heated for a moment and then left in a covered beaker for some hours. By then large, deep red crystals had deposited. They were filtered, thoroughly washed with several portions of ice-cold water and finally with ethanol and ether; 3.45 g (45 %). Anal. $[Cr(C_6H_8N_2)_2OH]_2(SbOC_4H_4O_6)_4.9H_2O$: Cr, C, N, H.

4b. $(+)_D$-*Di-μ-hydroxobis{bis(2-picolylamine)chromium(III)} antimonyl (+)$_D$-tartrate*, $(+)_D$-$[(C_6H_8N_2)_2Cr(OH)_2Cr(C_6H_8N_2)_2]$-$\{(+)_D$-$SbOC_4H_4O_6\}_4.nH_2O$. The mother liquor was set aside for 7 days and then filtered from another crop of 4a (about 75 mg). From the filtrate the desired compound was precipitated by dropwise addition of ethanol (50 ml, 99 %). Filtering and washing with ethanol. The crude product was recrystallized from boiling water (20 ml). Washing with a mixture of ethanol and water (50:50) and with ethanol. Yield 2.17 g of dark, red-violet crystals (29 %). Anal. $[Cr(C_6H_8N_2)_2(OH)]_2(SbOC_4H_4O_6)_4.7H_2O$: Cr, C, N, H.

In other experiments the compound crystallized with 5 or 8 mol of crystal water, respectively.

5a. $(-)_D$-*Di-μ-hydroxobis{bis(2-picolylamine)chromium(III)} chloride*, $(-)_D$-$[(C_6H_8N_2)_2Cr(OH)_2Cr(C_6H_8N_2)_2]Cl_4.4H_2O$. 1.00 g $(-)_D$-$[(C_6H_8N_2)_2Cr(OH)_2Cr(C_6H_8N_2)_2]$-$\{(+)_D$-$SbOC_4H_4O_6\}_4.9H_2O$ (0.533 mmol) was suspended in 7 – 8 ml hot 4 M hydrochloric acid. Stirring for 15 min. By then the originally

coarse crystals had transformed into a fine powder, presumably a tetrachloroantimonate. Filtering and careful washing with conc. hydrochloric acid and ethanol. This powder was then treated with boiling water, whereby a white antimony-compound precipitated, leaving a filtrate from which a sticky red-violet compound would deposit when sufficient ethanol and ether were added. The crude product was recrystallized twice by dissolving in boiling water (3 – 4 ml, slightly acidified with hydrochloric acid), filtering and precipitating with ethanol (50 ml, 99 %) and ether. Washing with ether. Yield 0.363 g (87 %). Anal. $[Cr(C_6H_8N_2)_2OH]_2Cl_4.4H_2O$: Cr, C, N, H, Cl. $(\varepsilon,\lambda)_{max}$: (198,540), (116,380). $(\varepsilon,\lambda)_{min}$: (27,437), (59,350). $[M]_D = -3.19 \times 10^3$ (c = 0.3 g/l).

5b. *(+)$_D$-Di-μ-hydroxobis{bis(2-picolylamine)chromium(III)} chloride,* $(+)_D$-$[(C_6H_8N_2)_2Cr(OH)_2Cr(C_6H_8N_2)_2]Cl_4.nH_2O$. This compound was prepared by exactly the same method as 5a. From 1.40 g $(+)_D$-$[(C_6H_8N_2)_2Cr(OH)_2Cr(C_6H_8N_2)_2]\{(+)_D$-$SbOC_4H_4O_6\}_4.5H_2O$ (0.776 mmol) a yield of 0.470 g (78 %) was obtained. Anal. $[Cr(C_6H_8N_2)_2OH]_2Cl_4.3\frac{1}{2}H_2O$: Cr, C, N, H, Cl, $(\varepsilon,\lambda)_{max}$: (198,540), (116,380). $(\varepsilon,\lambda)_{min}$: (27.437) (59,350). $[M]_D = +3.11 \times 10^3$ (c = 0.3 g/l). In other experiments the compound crystallized with 6 mol of crystal water. The transformation of the compounds 4a and 4b to 5a and 5b could be performed in a more interesting way. An example is given below.

0.70 g of red-violet $(+)_D$-$[(C_6H_8N_2)_2Cr(OH)_2Cr(C_6H_8N_2)_2]\{(+)_D$-$SbOC_4H_4O_6\}_4.5H_2O$ (0.388 mmol) was dissolved in 3 ml 2 m sodium hydroxide. The solution became green, perhaps because of the formation of a di-μ-oxo compound. Ethanol (40 ml, 99 %) was added while stirring to precipitate $NaSbOC_4H_4O_6$. Filtering. Then conc. hydrochloric acid (2 ml) was added to the filtrate recreating the originally red-violet colour of the diol. Sufficient ethanol and ether precipitated a sticky chloride, which was recrystallized as 5a. Yield 0.229 g (72 %). Anal. $[Cr(C_6H_8N_2)_2OH]_2Cl_4.6H_2O$: Cr, C, N, H, Cl. $(\varepsilon,\lambda)_{max}$: (199,540), (118,380). $(\varepsilon,\lambda)_{min}$: (28,437), (60,350). $[M]_D = +3.12 \times 10^3$ (c = 0.3 g/l).

6a. *(−)$_D$-α-cis-Dichlorobis(2-picolylamine)chromium(III) perchlorate,* $(-)_D$-$[Cr(C_6H_8N_2)_2Cl_2]ClO_4.H_2O$. 0.330 g $(-)_D$-$[(C_6H_6N_2)_2Cr(OH)_2Cr(C_6H_8N_2)_2]Cl_4.4H_2O$ (0.421 mmol) was kept in a stoppered flask with conc. hydrochloric acid (3 ml) for 7 days. A very small amount of gray-green powder was then removed by filtration, and perchloric acid (2 ml, 70 %) was added to the filtrate. Cooling on ice gave large red crystals. These were recrystallized from boiling water (10 ml) and washed with ethanol-water (50:50) and with ethanol. Yield 0.132 g (34 %). A careful washing of the compound and a great loss of material in the equipment were responsible for the relatively meagre yield. Anal. $[Cr(C_6H_8N_2)_2Cl_2]ClO_4.H_2O$: Cr, C, N, H, Cl. $(\varepsilon,\lambda)_{max}$: (96,540), (88,402). $(\varepsilon,\lambda)_{min}$: (21,458), (8.7, 353). $[M]_D = -90$ (c = 1 g/l).

6b. *(+)$_D$-α-cis-Dichlorobis(2-picolylamine)chromium(III) perchlorate,* $(+)_D$-$[Cr(C_6H_8N_2)_2Cl_2]ClO_4.H_2O$. The compound was prepared by exactly the same method as 6a. From 0.440 g $(+)_D$-$[(C_6H_8N_2)_2Cr(OH)_2Cr(C_6H_8N_2)_2]Cl_4.3\frac{1}{2}H_2O$ (0.567 mmol) a yield of 0.141 g (27 %) was obtained. Anal. $[Cr(C_6H_8N_2)_2Cl_2]ClO_4.H_2O$: Cr, C, N, H, Cl. $(\varepsilon,\lambda)_{max}$: (96,540), (86,402). $(\varepsilon,\lambda)_{min}$: (21,458), (9.7, 353). $[M]_D = +90$ (c = 1 g/l).

RESULTS AND DISCUSSION

Synthesis and resolution. As the yield of di-μ-hydroxo-bis{bis(2-picolylamine)chromium(III)} iodide in the synthesis intended for *β-cis*-dibromobis(2-picolylamine)chromium(III) iodide was very small,[1] and because the prevalent synthetic method for diols [2,15,16] was unsuccessful in our case, a new preparation method had to be developed. This was partly founded on the preceding experience [1] that chromium(II), present in catalytic amounts, might be responsible for the diol formation, and that an organic solvent was preferable to water. Instead of chromium(II), zinc dust could be used as a catalyst, presumably because of its ability to form chromium(II), but then it was inconvenient because the diol was inevitably precipitated as a tetrachlorozincate.

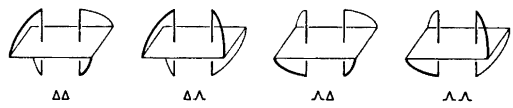

Fig. 1. Configurational isomers for binuclear, double-bridged complexes.

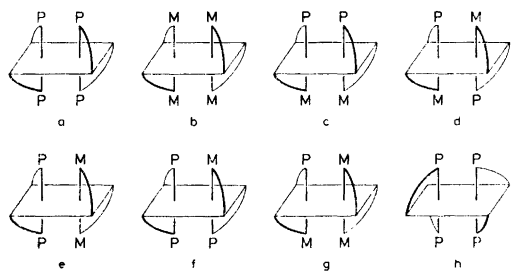

Fig. 2. $[(C_6H_8N_2)_2Cr(OH)_2Cr(C_6H_8N_2)_2]^{4+}$ P symbolizes the pyridine-nitrogen, M the methylaminenitrogen. a – g. ΛΛ isomers. h. A ΔΔ isomer, the optical antipode of a.

Table 1. CD-spectral parameters for some complexes of chromium(III) with 2-picolylamine, 1,10-phenanthroline, 2,2′-bipyridine, ethylenediamine, and trimethylenediamine.

Compound	Ligand = L	$\lambda_{ex}(1)$ nm	$\Delta\varepsilon_{ex}(1)$	$\lambda_{ex}(2)$ nm	$\Delta\varepsilon_{ex}(2)$	$\lambda_{ex}(3)$ nm	$\Delta\varepsilon_{ex}(3)$	$\lambda_{ex}(4)$ nm	$\Delta\varepsilon_{ex}(4)$	Ref.
$(-)_D$-$[L_2Cr(OH)_2CrL_2]^{4+}$	2-picolylamine	588	+0.37	508	−5.55	376	+1.62			
$(+)_D$-$[L_2Cr(OH)_2CrL_2]^{4+}$	2-picolylamine	588	−0.38	508	+5.53	376	−1.65			
$\Delta\Delta$-$(-)_D$-$[L_2Cr(OH)_2CrL_2]^{4+}$	1,10-phenanthroline			~520	~−6.3	~400	+2.6			4
$\Delta\Delta$-$(-)_D$-$[L_2Cr(OH)_2CrL_2]^{4+}$	2,2′-bipyridine	~620	~+0.02	~520	~−6.3	~400	~+1.3			4,22
$(-)_D$-$[CrL_2Cl_2]^+$	2-picolylamine	576	+0.65	513	−0.88	409	+0.17			
$(+)_D$-$[CrL_2Cl_2]^+$	2-picolylamine	575	−0.66	513	+0.88	409	−0.17			
Λ-$(+)_D$-$[CrL_2Cl_2]^+$	ethylenediamine	590	−0.5	520	+0.6	425	+0.25	385	−0.15	20
Λ-$(+)_D$-$[CrL_2Cl_2]^+$	trimethylenediamine	590	−0.36	511	+0.33	419	+0.10	370	+0.10	21

Like the corresponding diols with 1,10-phenanthroline and 2,2′-bipyridine, our compound could be resolved with sodium antimonyl $(+)_D$-tartrate as a resolving agent.[4] In all cases the $(-)_D$-isomer formed the less-soluble diastereoisomer.

The reaction between the catoptromers and conc. hydrochloric acid gave optically active *cis*-dichloro complexes of the so-called α-type. The yields were moderate probably owing to great losses of material during the isolation of the compounds rather than to side-reactions. The complexes were identified as belonging to the α-series[1] by means of their absorption spectra (Fig. 5).

Constitution and stereochemistry of the di-μ-hydroxobis{bis(2-picolylamine)chromium(III)} ion. Alternative formulations of the compound assumed to be $[(C_6H_8N_2)_2Cr(OH)_2Cr(C_6H_8N_2)_2]$-$I_4.5H_2O$ are for instance $[Cr(C_6H_8N_2)_2(H_2O)$-$(OH)]I_2.1H_2O$ and $[(H_2O)(C_6H_8N_2)_2Cr(OH)Cr$-$(C_6H_8N_2)_2(OH)]I_2.4H_2O$. They would be equally consistent with the chemical analyses, and the "anhydrous", watersucking salt (M = 1078) could not be analyzed sufficiently precisely to preclude the possibility of an additional water molecule unambiguously. Nevertheless, we have the following evidence for the double-bridged structure. Firstly: The absorption spectra of the compound dissolved in water and in 0.1 M hydrochloric acid (visible region) are the same. A terminal hydroxo-group would transform fully into an aqua-group under the acid conditions causing a spectral change.[1] Secondly: Measurements of the magnetic susceptibility gave experimental data fitting the Heisenberg-Dirac-Van Vleck model $H = J \times S_2 \times S_2$ for a singlet triplet splitting J of 38 ± 1 cm^{-1} ($\langle g \rangle = 2.00$). As a comparison the value of J is 34 ± 1 cm^{-1} for di-μ-hydroxoxybis{bis-(2,2′-bipyridine)chromium(III)} salts.[17]

The binuclear ion $[(C_6H_8N_2)_2Cr(OH)_2Cr$-$(C_6H_8N_2)_2]^{4+}$ in principle exists in several isomers owing to geometrical and configurational isomerism. The four classes of configurational isomers for dinuclear double-bridged complexes in general are shown in Fig. 1.[18] Molecular models indicate, however, that all the *meso*-isomers in our case would be grossly hindered sterically. Considering now one of the optically active classes, $\Lambda\Lambda$ for instance, we find that seven different isomers

may exist, at least theoretically (Fig. 2a–g). But again we recognize from molecular models that six isomers (Fig. 2b–g) would be grossly hindered, whereas the seventh isomer (Fig. 2a) is relatively free from steric constraints. The seven *ΔΔ* isomers, of course, behave analogously. From this it appears that we are left with a possibility of finding two isomers only (the catoptromers shown in Fig. 2a and h) instead of the theoretical twenty-four (10 *ΔΛ* + 7*ΔΔ* + 7*ΛΛ*). Our experiments agree nicely with this theory. We found exactly one kind of di-μ-hydroxo complex, a racemate that could be resolved, the $(-)_D$-isomer accounting for at least 45 % of the starting material. The two optically active ions are remarkable because they belong to the rarely occurring point group D_2 (one 2-fold axis with two 2-fold axes perpendicular to it).

Stereochemistry of the α-cis-*dichlorobis-(2-picolylamine)chromium(III) ion.* On the assumption that the acid cleavage reaction of the di-μ-hydroxobis{bis(2-picolylamine)chromium(III)} ion proceeds largely with retention of configuration as experienced for diols with 1,10-phenanthroline and 2,2′-bipyridine,[6,4] the catoptromers, Fig. 2a and h, should react with conc. hydrochloric acid to form *cis*-complexes with a 2-fold axis of symmetry as illustrated in Fig. 3.

In fact, our optically active diols did react solely forming *cis*-dichlorobis(2-picolylamine) complexes of the symmetrical α-type, supporting our assumptions about their symmetry properties. *cis*-Complexes of the α-type are earlier shown to have the configuration *cis,trans,cis* or *cis,cis,trans*.[1] The isomers were named by considering first the spatial relationship of the two monodentate ligands, then of the two pyridine-nitrogen atoms and finally of the two methylamine-nitrogen atoms. On the basis of the reactions above, we now conclude that *cis,trans,cis* is the most likely configuration.

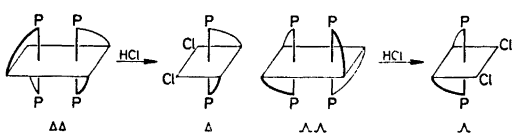

Fig. 3. The reaction of $[(C_6H_8N_2)_2Cr(OH)_2Cr(C_6H_8N_2)_2]^{4+}$ with conc. HCl to *cis*-$[Cr(C_6H_8N_2)_2Cl_2]^{2+}$.

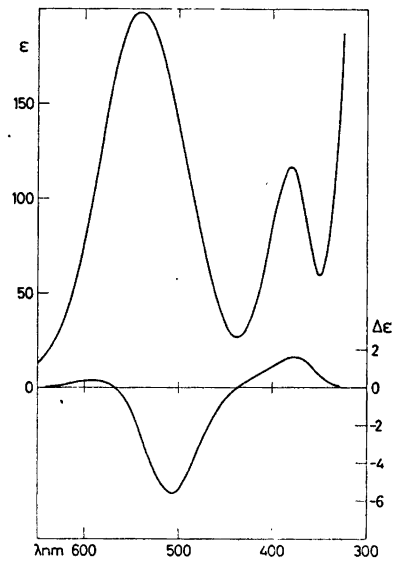

Fig. 4. The absorption spectrum (top) and the circular dichroism spectrum (bottom) of $(-)_D$-$[(C_6H_8N_2)_2Cr(OH)_2Cr(C_6H_8N_2)_2]^{4+}$.

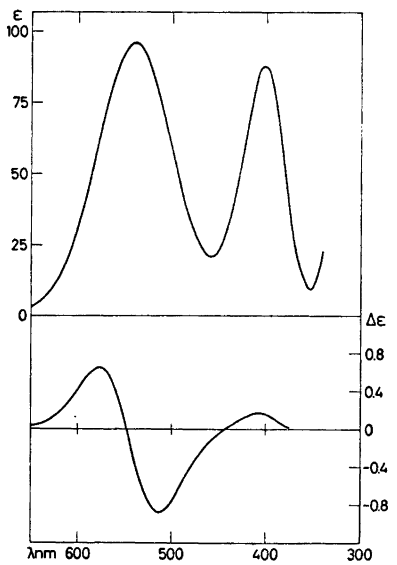

Fig. 5. The absorption spectrum (top) and the circular dichroism spectrum (bottom) of $(-)_D$-α-*cis*-$[Cr(C_6H_8N_2)_2Cl_2]^+$.

Configuration and optical activity. The absorption and circular dichroism (CD) spectra of $(-)_D$-$[(C_6H_8N_2)_2Cr(OH)_2Cr(C_6H_8N_2)_2]^{4+}$ are shown in Fig. 4, and a comparison with CD-spectral data for corresponding compounds appears in Table 1. If the empirical rules [19] relating chirality to the sign of the dominant CD-band in the region of the cubic $^1A_{2g} \rightarrow {}^4T_{2g}d-d$ absorption of the chromium(III) ion can be applied to our compounds, the configurations of $(-)_D$- and $(+)_D$-$[(C_6H_8N_2)_2Cr(OH)_2Cr(C_6H_8N_2)_2]^{4+}$ should be $\Delta\Delta$ and $\Lambda\Lambda$, respectively. Consequently, the configurations of $(-)_D$- and $(+)_D$-α-*cis*-$[Cr(C_6H_8N_2)_2Cl_2]^+$ are Δ and Λ.

The absorption and CD-spectra of $(-)_D$-$[Cr(C_6H_8N_2)_2Cl_2]^+$ are shown in Fig. 5, and the CD-spectral data are listed in Table 1 for this ion, for the catoptromer and for some analogous compounds. The CD-spectrum of $(+)_D$-α-*cis*-$[Cr(C_6H_8N_2)_2Cl_2]^+$ has the same main features as the CD-spectra of Λ-$(+)_D$-$[Cren_2Cl_2]^+$ [20] and Λ-$(+)_D$-$[Crtn_2Cl_2]^+$ [21] with a slightly dominant positive band in the region 510 – 520 nm indicating that this ion, too, has the configuration Λ. This agrees with the assignment suggested above.

Acknowledgement. The author is grateful to Dr. Erik Pedersen for providing the magnetic data.

REFERENCES

1. Michelsen, K. *Acta Chem. Scand. 26* (1972) 1517.
2. Inskeep, R. G. and Benson, M. *J. Inorg. Nucl. Chem. 20* (1961) 290.
3. Ferraro, J. R., Driver, R., Walker, W. R. and Wosniak, W. *Inorg. Chem. 6* (1967) 1586.
4. Mason, S. F. and Wood, J. W. *Chem. Commun.* (1968) 1512.
5. Josephsen, J. and Schäffer, C. E. *Acta Chem. Scand. 24* (1970) 2929.
6. Wolcott, S. D. and Hunt, J. B. *Inorg. Chem. 7* (1968) 755.
7. Earnshaw, A. and Lewis, J. *J. Chem. Soc.* (1961) 396.
8. Morishita, T., Hori, K., Kyono, E. and Tsuchiga, R. *Bull. Chem. Soc. Jpn. 38* (1965) 1276.
9. Veal, J. T., Hatfield, W. E. and Hodgson, D. J. *Acta Crystallogr. 29* (1973) 12.
10. Scaringe, R. P., Singh, P., Eckberg, R. P., Hatfield, W. E. and Hodgson, D. J. *Inorg. Chem. 14* (1975) 1127.
11. Lux, H. and Illman, G. *Chem. Ber. 91* (1958) 2143.
12. Figgis, B. N. and Nyholm, R. S. *J. Chem. Soc.* (1958) 4190.
13. Pedersen, E. *Acta Chem. Scand. 26* (1972) 333.
14. Cotton, F. A. and Pedersen, E. *Inorg. Chem. 14* (1975) 388.
15. Dubsky, J. V. *J. Prakt. Chem. 90* (1914) 61.
16. Pfeiffer, P. and Stern, R. *Z. Anorg. Allg. Chem. 58* (1908) 272.
17. Pedersen, E. *To be published* (1976).
18. Thewalt, U., Jensen, K. A. and Schäffer, C. E. *Inorg. Chem. 11* (1972) 2129.
19. Mason, S. F. *Quart. Rev. Chem. Soc. 17* (1963) 20.
20. McCaffery, A. J., Mason, S. F. and Norman, B. J. *J. Chem. Soc.* (1965) 5094.
21. Pedersen, E. *Acta Chem. Scand. 24* (1970) 3362.
22. Mason, S. F. *Inorg. Chim. Acta Rev. 2* (1968) 89.

Received January 28, 1976.

Acta Chemica Scandinavica A 30 (1976) 527—530

The Crystal and Molecular Structure of Cyano(methylisocyanide)gold(I)

STEINAR ESPERÅS

Department of Chemistry, University of Bergen, N-5014 Bergen-Univ., Norway

The crystal and molecular structure of cyano(methylisocyanide)gold(I), $AuCN(CNCH_3)$, has been determined by three-dimensional X-ray methods. The crystals are orthorhombic, *Pbcm*, unit cell $a = 10.989(6)$ Å, $b = 6.899(6)$ Å, $c = 6.359(5)$ Å, $Z = 4$. The structure analysis is based on 325 intensities collected on a Syntex $P2_1$ diffractometer using Mo$K\alpha$ radiation. Patterson and Fourier syntheses were used to solve the structure, and full-matrix least squares refinement gave an R-value of 0.068.

The gold atom is almost linearly coordinated, the C–Au–C angle being 176(2)° and the Au–C (CN) and Au–C ($CNCH_3$) distances 2.01(5) and 1.98(5) Å, respectively. The molecules, except for the hydrogen atoms, are situated on crystallographic mirror planes. The structure is built up from monomeric units linked together in two-dimensional polymeric layers parallel to the *bc*-plane, through very weak metal-metal interactions.

Univalent gold is mainly found to have a linear coordination, even when the analogous copper and silver complexes show a tetrahedral geometry.[1] Most of the Au(I) compounds like the majority of the Ag(I) and Cu(I) compounds appear to be appreciably covalent. The univalent coinage metal complexes often occur as polymers, (discrete low polymers, infinite polymers or metal atom cluster compounds) either with bridging groups connecting the metal atoms or with weak metal-metal interactions.[2] Few crystal structures of univalent gold compounds have been determined, and the only X-ray work done on isocyanide complexes of coinage metals (I) is on $CuI(CNCH_3)$, a complex with relatively short Cu···Cu distances.[3] As the present gold(I) complex was insoluble in water and all the usual organic solvents, some kind of polymeric arrangement was also expected to be found here.

EXPERIMENTAL

The crystals were prepared by a reaction between methyl iodide and tetraphenylarsonium dicyanoaurate(I).[4]

$$CH_3I + Au(CN)_2^- \xrightarrow[\text{room temp.}]{14\ \text{d}} AuCN(CNCH_3)$$

The crystalline product was obtained as colourless plates elongated along the c axis.

Data were collected with a Syntex $P2_1$ four-circle diffractometer in the $\theta - 2\theta$ mode with graphite monochromator. Accurate cell constants were obtained by means of least squares calculations based on the reflecting positions of 15 high angle reflections. The cell data are $a = 10.989(6)$ Å, $b = 6.899(6)$ Å, $c = 6.359(5)$ Å, $Z = 4$ and $dc = 3.64$ g cm^{-3}. The systematic absences are $0kl$ for $k = 2n+1$ and $h0l$ for $l = 2n+1$ in the orthorhombic crystal system. The space group is *Pbcm* (No. 57) as the alternative group, $Pca2_1$, was discarded during the structure determination.

The data were collected with Mo$K\alpha$ radiation. Within $\angle\theta = 25°$, 325 reflections were found to have intensities stronger than three times the standard deviations. Variable scan rates, between 1.5 and 29.3°/min in 2θ, depending on the intensity of a pre-scan, were used. Three standard reflections were measured at intervals of 50 reflections. No decomposition of the crystal was observed during the data collection.

The data were corrected for Lorentz and polarization effects. Absorption correction, calculated by the analytical method with program ABSCOR [5] was also applied ($\mu = 313$ cm^{-1}). No extinction correction was found necessary.

STRUCTURE ANALYSIS

Of the two possible space groups, *Pbcm* and $Pca2_1$, the centrosymmetric, *Pbcm*, was the first choice. A three-dimensional Patterson map, calculated on basis of the 325 observed reflections, revealed the gold atoms in crystallographic mirror planes at $z = +\frac{1}{4}$. Consequently, all non-hydrogen atoms had to be located in these planes, and a Fourier synthesis confirmed this. Full-matrix least squares refinement with anisotropic temperature factors for the gold atom and isotropic temperature factors for the lighter atoms (hydrogen not included) gave a final value of the reliability index, $R = \sum||F_o| - |F_c||/\sum|F_o|$, of 0.068. There was, however, a possibility that the complex was $NC-Au-NC-CH_3$, *i.e.* a methylcyanide instead of a methylisocyanide. A parallel refinement based on the N-bonded complex yielded a slightly higher R-value (0.069) and rather unreasonable temperature factors.

Attempts to refine the structure in the noncentric space group were not successful.

A final difference electron density map showed several large peaks near the gold position, the highest of these was 2.6 e/Å^3. No peaks above 1.0 e/Å^3 appeared elsewhere in the map.

The atomic scattering factor curves used were taken from the *International Tables*.[6] Those for the gold atom were corrected for anomalous dispersion, using $\Delta f'$ and $\Delta f''$ values calculated by Cromer,[7] and letting f equal the magnitude of the complex scattering factor.

Observed and calculated structure factors following the last refinement cycle can be obtained from the author, upon request.

All calculations were carried out on an ICL 4130 computer at the University of Warwick, England. Apart from the local initial data processing program and ABSCOR (a local version), all programs were made by Dr. D. R. Russel, University of Leicester.

RESULTS AND DISCUSSION

The final positional and thermal parameters are listed in Tables 1 and 2. Interatomic distances and angles are listed in Table 3. Bond lengths and bond angles with atomic numbering in the cyano(methylisocyanide)gold(I) molecule are shown in Fig. 1, and a stereoscopic drawing showing the packing of molecules is given in Fig. 2.

Table 1. Final atomic coordinates in fractions of cell edges with standard deviations in parentheses.

	x	y	z
Au	0.4672(1)	0.1095(2)	0.25
C1	0.285(4)	0.097(7)	0.25
C2	0.647(4)	0.103(7)	0.25
C3	0.890(6)	0.083(9)	0.25
N1	0.180(3)	0.078(5)	0.25
N2	0.755(4)	0.102(6)	0.25

Table 2. Atomic thermal parameters ($\times 10^2$) with standard deviations in parentheses. For Au the expression is $\exp[-\frac{1}{4}(h^2a^{-2}B_{11} + k^2b^{-2}B_{22} + l^2c^{-2}B_{33} + 2hka^{-1}b^{-1}B_{12} + 2hla^{-1}c^{-1}B_{13} + 2klb^{-1}c^{-1}B_{23})]$ and for C and N the expression is $\exp(-B\sin^2\theta/\lambda^2)$.

Au	251(8)	319(9)	622(11)	(B_{11}, B_{22}, B_{33})
	0	0	−4(9)	(B_{23}, B_{13}, B_{12})
C1	404(86)			(B)
C2	429(92)			
C3	697(149)			
N1	409(75)			
N2	505(89)			

Table 3. Bond lengths (Å) and bond angles (°) in the cyano(methylisocyanide)gold(I) molecule. Standard deviations in parentheses.

Au−C1	2.01(4)	C1−Au−C2	176(2)
Au−C2	1.98(5)	Au−C1−N1	175(4)
C1−N1	1.15(6)	Au−C2−N2	179(4)
C2−N2	1.18(6)	C2−N2−C3	175(5)
N2−C3	1.50(8)		

The crystal structure consists of discrete $AuCN(CNCH_3)$ molecules. The gold atom is, as usual for Au(I), linearly coordinated with a C−Au−C angle of 176(2)°. Each gold atom is, however, in addition to the two carbon ligand atoms, surrounded by six more distant gold atoms, situated approximately at the corners of a regular hexagon. The Au−Au distances are 3.524(4), 3.593(3), and 3.724(3) Å. Thus the metal atoms link the molecules weakly together into two-dimensional polymeric layers parallel to the *bc*-plane.

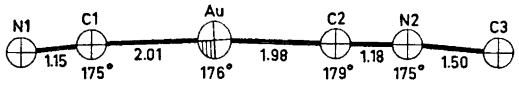

Fig. 1. The cyano(methylisocyanide)gold(I) molecule with bond lengths (Å) and bond angles(°) indicated.

In each layer the metal atoms form a central sheet surrounded on both sides by the ligands. There are no contacts shorter than the sum of van der Waals radii.

The molecular structure of $AuCN(CNCH_3)$ resembles those found for other univalent gold complexes, although the type of metal-metal interaction pattern found in the present investigation has not been found before. Several authors report polymeric structures of gold (I) compounds often with rather short Au – Au distances.[1,8–12] It is, however, not clear when a metal-metal distance can be interpreted as corresponding to an interaction.

Whether the gold – gold separations of 3.52 – 3.72 Å in the complex reported here, $AuCN(CNCH_3)$, represent weak bonding is difficult to decide. However, on the basis of the insolubility of the crystals in water as well as in all the usual organic solvents,[4] this is possibly the case.

The linear coordination of the metal atom is common for univalent gold complexes. Copper(I) compounds on the other hand are mostly found in a tetrahedral arrangement and quite rarely take part in linear coordination. Silver(I) complexes have a strong tendency to occur in both tetrahedral and linear coordination.

Dunitz and Orgel [13] have suggested that the linear two-coordination of univalent gold is due to the formation of *sd*-hybrids on the central atom. Charlton and Nichols [14] report, however, on basis of [197] Au Mössbauer spectroscopy on Au(I) complexes that the hybrids most likely contain a substantial degree of *p*-character. This view is supported by Machmer *et al.*[15] who studied gold(I) chloride by NQR spectroscopy.

The Au – C (CN) and Au – C ($CNCH_3$) coordination distances are 2.01(5) and 1.98(5) Å, respectively. They may be compared with the corresponding distances in i-$C_3H_7NH_2AuC{\equiv}CC_6H_5$ of 1.94 Å[8], in $PPh_3AuC_6F_5$ of 2.07 Å,[16] and in $KAu(CN)_2$ of 2.12 Å [10] and are in the expected range. Also the other bond lengths are normal. All the bond angles are approximately 180° and thus the molecules are almost linear.

In the present complex the IR spectrum shows absorptions at *ca.* 2160 and *ca.* 2290 cm^{-1}, the first is assigned to the cyanide group, the latter to the isocyanide group. While ν_{CN}(CN) is in the expected range,[18] ν_{CN}(CNR) is about 120 cm^{-1} above the corresponding frequency in the free ligand.[19] This increase indicates a

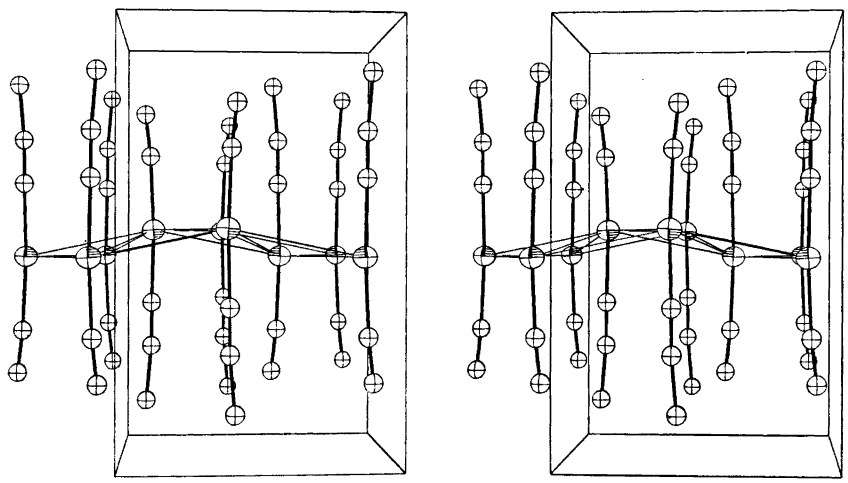

Fig. 2. A stereoscopic drawing showing the packing of molecules as seen along the *c* axis. The *a* axis is vertical and the *b* axis is horisontal.

higher bond order for C≡N in the complex than in the free isocyanide molecule. This is, however, not unusual when the metal is in an intermediate or high oxidation state.[20] A slight increase (*ca.* 5 – 10 cm^{-1}) is caused by a kinematic coupling of the M – C and C – N oscillators.[21] Of much more importance, however, is the effect of coordinating the isocyanide carbon to the positive metal ion. Coordination may be expected to increase the CN bond order and raising the frequency.

When an isocyanide coordinates to a transition element in a low oxidation state (mainly zero), the CN stretching frequency may be lower in the complex than in the free ligand.[20,22] This corresponds to a substantial transfer of electron density from the metal *d*-orbitals to suitable π^* orbitals of the ligand. A metal-carbon π-bond thus established should result in a shorter M – C distance and a longer C – N distance. The former has been confirmed by X-ray structure determinations.[20]

The present investigation does not support the idea of any appreciable amount of back-donation from the gold atom to the cyanide group either. The π-accepting tendency of CN^- does not seem as high as for CNR which is of course reasonable in view of its negative charge.[23] It is reported, however, that in some cases the π-acidity of CN^- and CNR are comparable.[24]

Acknowledgements. The author wants to thank cand. real. Jon Songstad, Department of Chemistry, University of Bergen, for a sample of crystals and Dr. N. W. Alcock, University of Warwick, England, for advice on computing matters. This investigation has been supported by a grant from The Royal Norwegian Council for Scientific and Industrial Research.

REFERENCES

1. Arai, G. *Recl. Trav. Chim. Pays-Bas 81* (1962) 307.
2. Cotton, F. A. and Wilkinson, G. *Advanced Inorganic Chemistry. A comprehensive text*, 3rd Ed., pp. 903 and 1044.
3. Fischer, P. J., Taylor, N. E. and Harding, M. M. *J. Chem. Soc.* (1960) 2303.
4. Songstad, J. *To be published.*
5. Alcock, N. W. In Ahmed, F., Ed., *The Analytical Method for Absorption Correction in Crystallographic Computing*, Munksgaard, Copenhagen 1970.
6. *International Tables for X-Ray Crystallography*, Kynoch Press, Birmingham 1962, Vol. III, p. 204.
7. Cromer, D. T. *Acta Crystallogr. 18* (1965) 17.
8. Corfield, P. W. R. and Shearer, H. M. M. *Acta Crystallogr. 23* (1967) 156.
9. Rundle, R. E. *J. Am. Chem. Soc. 76* (1954) 3101.
10. Ruben, H., Zalkin, A., Faltens, M. O. and Templeton, D. H. *Inorg. Chem. 13* (1974) 1836.
11. Hesse, R. and Jennische, P. *Acta Chem. Scand. 26* (1972) 3855.
12. Lawton, S. L., Rohrbaugh, W. J. and Kokotailo, G. T. *Inorg. Chem. 11* (1972) 2227.
13. Dunitz, J. and Orgel, L. E. *Adv. Inorg. Chem. Radiochem. 2* (1960) 34.
14. Charlton, J. S. and Nichols, D. I. *J. Chem. Soc. A* (1970) 1484.
15. Machmer, P., Read, M. and Cornil, P. *C. R. Acad. Sci. Ser. B 262* (1966) 450.
16. Baker, R. W. and Pauling, P. J. *J. Chem. Soc. Dalton Trans.* (1972) 2264.
17. Rosenzweig, A. and Cromer, D. T. *Acta Crystallogr. 12* (1959) 709.
18. Jones, L. H. and Penneman, R. A. *J. Chem. Phys. 22* (1954) 965.
19. Stephany, R. W. *Thesis*, Utrecht 1973.
20. Bonati, F. and Minghetti, G. *Inorg. Chim. Acta 9* (1974) 95.
21. Cotton, F. A. and Zingales, F. *J. Am. Chem. Soc. 83* (1961) 351.
22. Bonati, F. and Minghetti, G. *Gazz. Chim. Ital. 103.* (1973) 373.
23. Ref. 2, pp. 721 – 722.
24. Sarapus, A. C. and Fenske, R. F. *Inorg. Chem. 14* (1975) 247.

Received February 16, 1976.

Acta Chemica Scandinavica A 30 (1976) 531—539

The Vibrational Spectra of Succinimide and *N*-Deuteriosuccinimide

T. WOLDBÆK,[a] P. KLÆBOE [a] and D. H. CHRISTENSEN [b]

[a] Department of Chemistry, University of Oslo, Oslo 3, Norway and [b] Chemical Laboratory V, The H. C. Ørsted Institute, DK-2100, Copenhagen, Denmark

The infrared spectra (4000 – 200 cm^{-1}) of succinimide as a vapour (160 °C), melt (~130 °C), oriented polycrystalline film, KI-pellet, Nujol mull and dissolved in CCl_4, CS_2, CH_2Cl_2, and CH_3CN were recorded. Additional spectra were obtained in the region 400 – 30 cm^{-1}. Raman spectra of the crystalline solid and saturated solutions in various polar solvents were recorded and semiquantitative polarization ratios were measured. Infrared and Raman spectra of *N*-deuteriosuccinimide in the solid state were recorded.

The fundamental frequencies were tentatively assigned in terms of C_{2v} symmetry based upon Raman polarization data, dichroism of the oriented film and analogies with the spectra of the *N*-halogenated succinimides. Force fields were derived by initially transferring force constants from maleimide and succinic anhydride, and the data were fitted together with those of the N-halogenated succinimides by a least square method.

We have recently reported the vibrational spectra of maleic anhydride,[1] maleimide,[2] and *N*-chloromaleimide.[3] These studies have now been extended to the corresponding saturated cyclic imides. In the present communication we shall report our results for succinimide (SIM) and the *N*-deuterated species (SIMD), while the *N*-halogenated derivatives will be treated in a forthcoming paper.[3] Previously, infrared studies of SIM and SIMD as solids have been restricted to the KBr region [5] and oriented crystals in the NaCl region.[6] No melt or solution data have been reported and the Raman spectra have to our knowledge not been recorded.

In the present study we have obtained as complete infrared and Raman data as possible within the limitations imposed by the low vapour pressure and restricted solubility of SIM. The assigned fundamentals were compared with the results of a normal coordinate analysis, using a generalized valence force field, and treating SIM and SIMD together with the *N*-halogenated succinimides.[4]

EXPERIMENTAL

The sample of SIM was a commercial product from Fluka AG, which was purified by repeated sublimation on a cold finger (m.p. 126 °C, b.p. 287 °C). The deuterated compound (SIMD) was prepared by successive treatments with D_2O and evaporation of the water. Although most of the sample handling took place in a dry box, a slight exchange of deuterium from moist air was observed in the infrared spectra.

The infrared, far infrared, and Raman (using the 4880 and 5145 Å lines from an argon ion laser (CRL 52 G)) spectrometers,[1] cells, and general procedures [2] have been described.

Dimethylformamide (DMFA) was used as solvent for the Raman spectra because of the low solubility of SIM in non-polar solvents.

RESULTS

SIM and certain *N*-halogenated succinimides have been studied by X-ray crystallography and the ring skeleton reported [7,8] to be nearly planar. Furthermore, the same holds true for the related succinic anhydride in the vapour phase.[9]

The fact that SIM forms dimeric molecules in the crystal and probably in solution because of two N – H···O = C hydrogen bonds (contrary to the *N*-halogenated derivatives) presumably do not perturb the fundamentals significantly. As previously noted for the maleimides [2,3] the comparatively weak intermolecular bonds result in coinciding a_g and b_u as well as a_u

and b_g modes (C_{2h} symmetry of the dimer). Only the N–H stretching and bending modes are highly affected by the hydrogen bonding. Therefore it seems appropriate to assume that SIM and SIMD (like the corresponding maleimide [2] and maleic anhydride [1]) have C_{2v} symmetry in all the states of aggregation. The 30 fundamentals will then divide themselves into the symmetry species: $10a_1+5a_2+6b_1+9b_2$ in which a_1 and b_2 represent in-plane, a_2 and b_1 out-of-plane modes. All the fundamentals are active in the Raman effect while those of species a_2 are forbidden in the infrared spectra.

A vapour IR spectrum of SIM was recorded at *ca.* 160 °C, but due to the low vapour pressure, the vapour contours gave no relevant information for the assignments. Instead, infrared measurements of the dichroic ratio of oriented polycrystalline films gave in many cases direct information about the species. This method, particularly suitable for orthorhombic crystals, has previously been applied to succinimide by Hayashii [6] and will therefore not be described here. Our dichroic measurements of various oriented polycrystalline films of SIM were much more complete in terms of spectral resolution and frequency range than the earlier work [6] employing NaCl-optics, but confirmed the earlier results.

Under the assumption of C_{2v} symmetry for the molecules, the transition moments will be directed along the X-, Y- and Z-axes (Fig. 2) for the b_1 b_2 and a_1 modes, respectively. If an oriented gas model can be applied, the dichroic ratio should be equal for all vibrations belonging to the same species. In accordance with Hayashii's [6] determination of the crystal axes, the following infrared intensity ratios should be expected for SIM:

(a) $I_b > I_c > I_a$ for a_1

(*b*) $I_c > I_a > I_b$ for b_2

(c) $I_a > (I_b$ and $I_c)$ for a_1 vibrations.

I_a, I_b and I_c denote the relative intensities for the three mutually perpendicular axes *a*, *b* and *c* of the orthorhombic unit cell.

Additional support for the assignments was provided by the Raman polarization data obtained in saturated solutions in dimethylformamide and water. Also, the force constant calculations of SIM and SIMD were of considerable aid. Moreover, the striking similarity between the spectra of SIM and those of *N*-chloro-, *N*-bromo-, and *N*-iodosuccinimide [4] was of great help for the assignments.

Spectral interpretations. As an illustration, the infrared spectra of two oriented polycrystalline films of SIM are shown in Figs. 1A (*E* vector parallell with the *c* and *a* axes) and 1B (*E* vector parallell with the *b* and *a* axes). The Raman spectrum of the solid is given in Fig. 1C, while the observed infrared and Raman frequencies are listed in Tables 1 (SIM) and 2 (SIMD). Our assigned fundamentals for both compounds are given in Table 3 together with the calculated frequencies.

The broad, intense bands at 3150 (solid), 3270 (melt) and 3280 cm^{-1} (CH_3CN solution) were interpreted as the hydrogen bonded N–H stretch (ν_1). In CCl_4 solution an infrared band at 3423 cm^{-1} was considered as the "free" ν_1 (Table 1.) An intense infrared band at 3070 cm^{-1} (solid) (absent for SIMD) disappeared in dilute solution and was assigned [5] as $\nu_{23}+\nu_{24}$ in Fermi resonance with ν_1. In SIMD the hydrogen bonded ν_1 was found at 2326 cm^{-1} in the solid. The present data suggest that the hydrogen bonding is stronger in SIM than in maleimide since the N–H frequency shifts from dilute solution to melt and further to the solid state were larger for SIM. The two CH_2 groups of SIM and SIMD will give rise to four C–H stretching frequencies (one of each species) which were attributed to bands between 3000 and 2940 cm^{-1} in SIM, SIMD and the *N*-halogenated succinimides.[4]

It is well known from the maleimides,[2,3] maleic,[1,10] and succinic anhydride [10] that the C=O stretch of species a_1 is invariably at higher frequency than the b_2 mode. The same rule applies to SIM, SIMD and the *N*-halogenated succinimides and will be discussed in the forthcoming paper.[4] In SIM ν_2 and ν_{22} were found at 1772 and 1697 cm^{-1}, whereas in SIMD they were situated at 1771 and 1674 cm^{-1}, respectively. A strong Raman band at 1766 cm^{-1} in SIMD was interpreted as $\nu_5+\nu_{10}$ in Fermi resonance with ν_2. The present molecules as well as the corresponding maleimides [2,3] and anhydrides [1,10] have several strong or medium intense bands in the region assigned

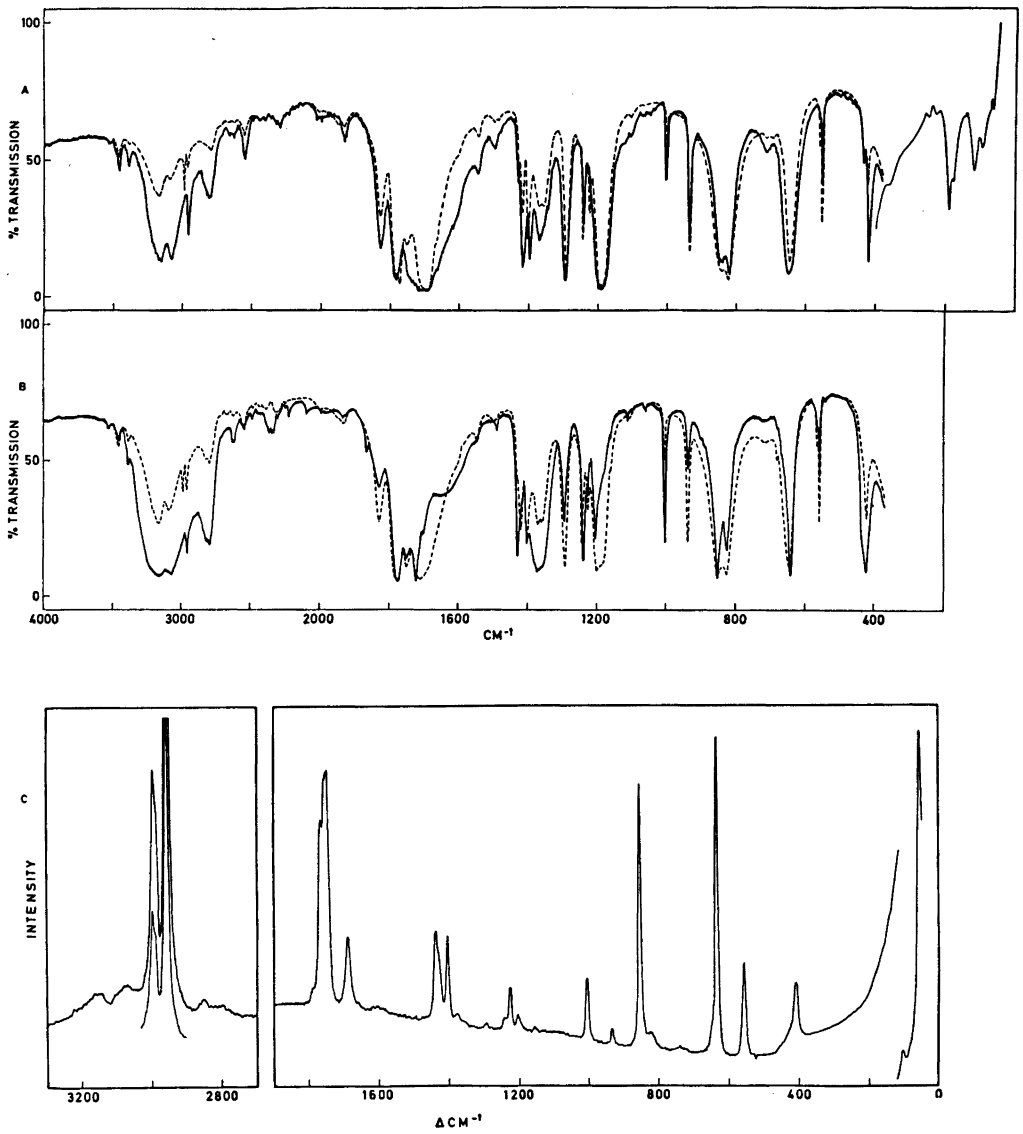

Fig. 1. Infrared and Raman spectra of succinimide in the solid state: A. (upper curve) 4000 – 400 cm^{-1}: the infrared spectrum of oriented crystals between KBr plates; solid line, *E* vector along *c* axis; dotted line, *E* vector along *a* axis. 400 – 30 cm^{-1}: polyethylene pellet; B. (middle curve) the infrared spectrum of oriented crystals between KBr plates; solid line, *E* vector along *b* axis; dotted line, *E* vector along *a* axis; C. (lower curve) the Raman spectrum.

to combination bands or overtones, partly enhanced by Fermi resonance to the a_1 and b_2 fundamentals.

The two methylene groups of SIM and SIMD will give rise to two scissor (a_1, b_2), wag (a_1, b_2), twist (a_2, b_1) and rock (a_2, b_1) fundamentals of which the scissor and wag are generally localized vibrations situated around 1450 and 1300 cm^{-1}, respectively. All the succinimides [4] had intense infrared and Raman bands around 1425 cm^{-1} assigned to an a_1 mode. The corresponding b_2 scissoring modes (ν_{25}) were assigned

Table 1. Infrared and Raman spectral data for succinimide.

Infrared [a]						Raman		Assignments [b]
Solid	Oriented crystals			Melt	Solution	Solid	Solution	
Nujol	*a*-axis	*b*-axis	*c*-axis	~130 °C	CCl_4		DMFA [d]	
3447 w [c]	3451 w	3451 w l	3449 w i					$\nu_3+\nu_{23}=3469\ B_2$
					3423 s			ν_1 free a_1
3375 w	3374 vw l	3378 w	3375 w					$2\times\nu_{23}=3394\ A_1$
3150 s	3155 s l	3155 s i	3150 s	3270 s	3280 s [e]			ν_1 H bonded a_1
3070 s [f]	3075 s l	3075 s i	3075 s	3075 m sh	3070 vw	3070 vw	3081 w	$\nu_{23}+\nu_{24}=3113\ A_1$ FR
						3000 s	3000 s D [g]	ν_{11} fund. a_2
	2981 w	2982 vw sh		2995 w sh		2990 sh	2994 sh	ν_{16} fund. b_1
						2960 vs	2965 s P [g]	ν_2 fund. a_1
2946 m [f]	2951 w	2954 w l	2949 m	2944 w	2954 w sh			ν_{22} fund. b_2
	2920 vw sh		2918 vw i		2924 w			$\nu_6+\nu_{23}=2935\ B_2$
	2820 w sh l	2815 m	2820 w sh				2825 sh [g]	$2\times\nu_{24}=2832\ A_1$
	2788 m l	2795 m i	2795 m	2740 w		2800 w		$\nu_4+\nu_5=2801\ A_1$
2536 w	2540 w	2540 w l	2532 m	2510 w		2527 w		$_5+\nu_{27}=2565\ B_2$
2000 vw	2012 vw		2015 w	1980 vw	1977 w [e]			$\nu_5+\nu_{29}=2023\ B_2$
1930 w	1930 w	1930 vw	1927 w i	1912 vw	1915 w [e]			$\nu_7+\nu_{28}=1936\ B_2$
1860 w		1862 w sh i	1860 w sh			1865 w	1820 w P	$2+\nu_{28}=1870\ A_1$
1827 m	1826 m	1826 m l	1826 s	1800 sh	1800 w			$\nu_9+\nu_{27}=1832\ B_2$ FR
1781 sh	1782 s sh		1782 s i		1727 s	1790 sh		$\nu_8+\nu_{28}=1785\ B_2$ FR
1772 s	1770 s	1773 s l		1775 s	1779 m	1768 s	1776 s P	ν_3 fund a_1
						1746 s		
1747 sh	1745 m	1746 m l	1740 s sh					$\nu_{12}+\nu_{30}=1780\ B_1$
1697 vs	1700 s	1700 m sh	1700 s i	1705 s	1752 s	1690 m	1710 w D [g]	ν_{23} fund. b_2
		1721 m		1710 sh	1717 m sh			$\nu_{17}+\nu_{20}=1743\ A_1$
	1682 sh	1682 sh						$\nu_8+\nu_{18}=1694\ B_1$
	1665 sh	1650 sh				1665 sh		$2\times\nu_{18}=1688\ A_1$
1600 vw sh	1600 sh		1600 sh	1560 w bd				$\nu_{10}+_{27}=1619\ B_2$
1545 w	1544 w	1545 w sh l	1542 w i					$\nu_7+\nu_{30}=1557\ B_2$
	1495 vw	1495 vw	1497 w					$\nu_8+\nu_{29}=1500\ B_2$
	1487 vw l	1487 vw i	1485 vw sh					$\nu_8+\nu_9=1490\ A_1$
1428 s	1429 w	1428 s	1427 w	1429 s	1432 m	1438 m	1432 s P [g]	ν_4 fund. a_1
1416 m	1417 m	1417 sh l	1415 s			1428 sh	1417 s D	ν_{24} fund. b_2
1402 m sh	1402 m	1402 m	1395 s	1390 m sh	1390 s sh [h]	1402 m		ν_{25} fund. b_2
1396 m								

Table 1. Continued.

1373 s[h]	1369 m	1370 s i	1368 s	1345 s	1337 s	1376 w	1380 w P[g]	ν_5 fund. a_1
1355 sh[f]	1355 m sh	1355 sh	1355 sh l		1350 sh			$\nu_{17}+\nu_{21}=1370$ A_1
1294 s	1290 s	1293 s l	1292 s i	1291 s	1287 s[h]	1294 w	1301 vw[g]	ν_{26} fund. b_2
					1282 w[i]			$2\times\nu_{29}=1300$ A_1
1238 s	1242 s l	1238 s i	1242 s	1238 s	1240 s[h]	1240 sh	1240 sh P	ν_6 fund. a_1
1224 w	1223 w i	1225 w		1225 w sh	1226 w[i]	1227 m	1228 m D	ν_{12} fund. a_2
1192 s	1195 s	1200 sh l	1192 s i	1170 s	1154 s	1205 w	1159 w D[g]	ν_{27} fund. b_2'
	1180 s	1180 s l	1180 s i		1175 sh[i]		1180 vw D	ν_{17} fund. b_1
					1115 w[i]			$\nu_{13}+\nu_{21}=1125$ B_2
1109 vw	1105 w l	1109 w	1105 w					
1001 m	1000 m l	1001 s	1003 m	999 m	999 m[h]	1005 m	1005 s P	ν_7 fund. a_1
993 sh								$\nu_{10}+\nu_{20}=990$ B_1
935 s	935 s	935 m	936 s i	913 s		934 w	919 w	ν_{28}/ν_{13} fund. b_2
850 s	850 s	850 s i	850 s	850 s	849 m[h]	857 s	850 s P	ν_8 fund. a_1
844 sh	840 s sh		840 s					ν_{18} fund. b_1
823 s	822 s	823 s l	821 s	818 s	787 s[i]	822 w	825 w sh D	ν_{19} fund. b_1
				760 w bd	765 w sh[i]			$\nu_9+\nu_{21}=830$ B_1
						739 w	717 vw	$\nu_{21}+\nu_{30}=746$ A_2
720 w[f]	715 vw	715 vw l	715 vw i			725 w sh		$\nu_{14}+\nu_{21}=727$ B_2
669 vw sh	678 w i	678 w l	678 w	676 vw	668 w[h]			$\nu_{12}-\nu_{30}=667$ B_1
650 s	644 s		650 s i			650 sh		ν_{29} fund. b_2
640 s	644 s l	640 s i	638 s	633 s	632 s[h]	635 s	630 s P	ν_9 fund. a_1
563 w sh	563 w i	562 w	562 vw	565 vw	550 sh[h]	563 sh	564 sh D[g]	ν_{20} fund. b_1
556 m	556 s	556 m l	555 m	545 s	545 m[h]	555 m	547 s D	ν_{30} fund. b_2
537 vw	538 vw	538 vw i				530 w		ν_{14} fund. a_2
	434 w l	434 m sh i	434 w		415 m sh[h]			$\nu_{15}+\nu_{21}=455$ B_2
427 s	420 s l	418 s i	419 s		400 s	408 m	415 w[g]	ν_{10} fund. a_1
360 m[j]					360 w[k]		360 vw bd[g]	$2\times\nu_{21}=380$ A_1
						267 w		ν_{15} fund. a_2
190 s					160 s[k]			ν_{21} fund. b_1
177 m }								
146 vw }								lattice modes
						105 m		

[a] The weak infrared and Raman bands in the regions 5000–3500 and 2900–2000 cm^{-1} are omitted.
[b] When available the combination frequencies and overtones are calculated from infrared solid data.
[c] w, weak; m, medium; s, strong; v, very; bd, broad; sh, shoulder; P, polarized and D, depolarized; Fr, Fermi resonance, i and l denote intensified and lowered absorptions with polarized radiation.
[d] Dimethylformamide. [e] CH_3CN solution. [f] KBr pellet). [g] H_2O solution. [h] CH_2Cl_2 solution. [i] CS_2 solution. [j] Solid state frequencies below 200 cm^{-1} are from polyethylene (Rigidex pellet). [k] C_6H_6 solution.

Table 2. Infrared and Raman spectral data for *N*-deuteriosuccinimide.

IR Solid Nujol	Raman Solid	Assignments [b]		IR Solid Nujol	Raman Solid	Assignments [b]	
3146 m [c]		H [d]			1213 vw	$\nu_{10}+\nu_{24}=1239$	B_2
3060 m		H		1190 s		H/ν_{17} fund.	b_1
	2998 s	ν_{11} fund.	a_2	1150 w	1150 vw	$\nu_{9}/_{29}+\nu_{19}=1160$	B_1/A_2
	2989 s	ν_{16} fund.	b_1		1115 w	$2\times\nu_{20}=1126$	A_1
	2958 vs	ν_3/ν_{22} fund.	a_1/b_2	1101 w sh		$\nu_{13}+\nu_{21}=1103$	B_2
2398 s sh	2400 vw	$\nu_4+\nu_7=2424$	A_1	1096 s	1100 vw sh	ν_{28} fund.	b_2
2386 s		$\nu_{25}+\nu_{26}=2388$	A_1 FR		1060 w	$2\times\nu_{14}=1080$	A_1
	2331 m sh			1045 w sh		$\nu_{10}+\nu_{29}=1054$	B_2
2326 s	2317 m	ν_1 fund.	a_1	1002 w sh		H	
	2284 w sh	$\nu_7+\nu_{26}=2291$	B_2	999 m	1005 m	ν_7 fund.	a_1
2245 w sh	2245 vw	$\nu_7+\nu_{27}=2271$	B_2	973 vw	974 vw	$\nu_{10}+\nu_{20}=982$	B_1
2205 m		$\nu_6+\nu_7=2230$	A_1 FR	932 w		H	
2180 sh		$\nu_3+\nu_{10}=2190$	A_1	916 vw	915 vw bd	ν_{13} fund.	a_2
1900 vw		$\nu_5+\nu_{30}=1906$	B_2	890 vw		$\nu_{15}+\nu_{29}=903$	B_1
1822 w		$\nu_{26}+\nu_{30}=1840$	A_1	846 s	852 s	ν_8/ν_{18} fund.	a_1/b_1
	1766 s	$\nu_5+\nu_{10}=1777$	A_1 FR	832 sh	837 m	$2\times\nu_{10}=838$	A_1
1771 s	1752 s	ν_3 fund.	a_1	820 s	825 m sh	ν_{24} fund.	b_2
	1743 s sh			754 w		$\nu_{15}+\nu_{19}=793$	B_2
1695 s		H		635 s	634 s	ν_9/ν_{29} fund.	a_1/b_2
1674 s	1667 m	ν_{23} fund.	b_2		589 vw	$\nu_{10}+\nu_{21}=606$	B_1
1655 sh		$\nu_{15}+\nu_{25}=1670$	B_1	563 w	564 w	ν_{20} fund.	b_1
1522 vw sh		$\nu_{15}+\nu_{27}=1540$	B_1	556 w		H	
	1468 w	$\nu_8+\nu_9=1480$	A_1	548 m	548 s	ν_{30} fund.	b_2
1425 m	1428 m	ν_4 fund.	a_1		543 w sh	ν_{14} fund.	a_2
1402 w	1406 m	ν_{25} fund.	b_2	525 m	480 w bd	ν_{19} fund.	b_1
1395 vw sh		$\nu_8+\nu_{20}=1409$	B_1	419 s	418 s	ν_{10} fund.	a_1
1358 s	1359 w	ν_5 fund.	a_1	360 w bd [e]		$2\times\nu_{21}=374$	A_1
1335 w sh		$\nu_{17}+\nu_{21}=1367$	A_1		268 vw	ν_{15} fund.	a_2
1292 s		ν_{28} fund.	b_2	187 s		ν_{21} fund.	b_1
1272 s	1281 vw	ν_{27} fund.	b_2	176 s			
1265 s sh		$2\times\nu_{29}=1270$	A_1	130 m			
1247 w	1241 vw sh	$\nu_8+\nu_{10}=1265$	A_1		125 w	lattice modes	
1231 m	1228 m	ν_6 fund.	a_1		105 w		
1222 w sh		ν_{12} fund.	a_2	91 m			

[a] The weak infrared and Raman bands in the regions 5000–3200 and 2800–2500 cm^{-1} are omitted. [b] When available the combination frequencies and overtones are calculated from solid state data. [c] For abbreviations used, see footnotes to Table 1. [d] H = bands assigned to succinimide. [e] Solid state frequencies below 400 cm^{-1} are from polyethylene (Rigidex) pellet.

to bands around 1400 cm^{-1} in accordance with the observed dichroism. Correspondingly, the wagging fundamentals ν_6 and ν_{26} were observed at 1238 and 1294 cm^{-1} (SIM) and 1231 and 1292 cm^{-1} (SIMD).

The 1373 cm^{-1} band which was clearly of species a_1 involves predominantly CNC stretch, close to the corresponding frequencies for the maleimides.[2,3] An infrared band at 1416 (SIM) and 820 cm^{-1} (SIMD) was interpreted as the N–H(D) in-plane bend. In agreement with the observed dichroism and Raman polarization data, the 1225 cm^{-1} band (SIM) is taken as the CH_2 twist of species a_2 (ν_{12}). The corresponding b_1 mode (ν_{17}) is assigned to the band at 1180 cm^{-1} partly overlapping the b_2 fundamental (ν_{27}), which involves the CNC stretch. Similar bands are found for SIMD at 1222, 1190 and 1272 cm^{-1}, respectively.

Three skeletal modes (ν_7, ν_{28}, ν_8) with strong contributions from skeletal C–C stretch are found at 1001, 935 and 850 cm^{-1} for SIM and at 999, 1096 and 846 cm^{-1} for SIMD. For SIMD as well as for *N*-deuteriomaleimide [2] the b_2 modes of the region 1300–800 cm^{-1}, not localized to the methylene groups, are highly

Table 3. Observed (ν_o) and calculated (ν_c) fundamentals for succinimide and *N*-deuteriosuccinimide.

Species and No.		Succinimide ν_o [a]	Succinimide ν_c	*N*-Deuteriosuccinimide ν_o [a]	*N*-Deuteriosuccinimide ν_c
a_1	ν_1	3150	3151	2326	2331
	ν_2	2960	2946	2958	2946
	ν_3	1772	1773	1771	1772
	ν_4	1428	1412	1425	1412
	ν_5	1373	1403	1358	1384
	ν_6	1238	1239	1231	1231
	ν_7	1001	973	999	972
	ν_8	850	839	846	831
	ν_9	640	640	635	637
	ν_{10}	427	414	419	413
a_2	ν_{11}	3000	2998	2998	2998
	ν_{12}	1224	1190	1222	1190
	ν_{13}	935	1064	916	1064
	ν_{14}	537	538	543	538
	ν_{15}	267	292	268	292
b_1	ν_{16}	2990	2988	2989	2988
	ν_{17}	1180	1197	1190	1197
	ν_{18}	844	749	846	768
	ν_{19}	823	860	525	636
	ν_{20}	563	536	563	534
	ν_{21}	190	184	187	177
b_2	ν_{22}	2946	2946	—	2946
	ν_{23}	1697	1698	1674	1687
	ν_{24}	1416	1427	820	814
	ν_{25}	1402	1403	1402	1403
	ν_{26}	1294	1310	1292	1334
	ν_{27}	1192	1173	1272	1234
	ν_{28}	935	941	1096	1140
	ν_{29}	650	666	635	656
	ν_{30}	556	553	548	545

[a] When possible, frequencies are taken from the infrared spectra of the solids.

mixed compared to the parent molecules, and therefore causing erratic isotopic shifts.

The CH_2 rock of species a_2 (ν_{13}) was found between 935 and 908 cm^{-1} for SIMD and the *N*-halogenated succinimides.[4] For SIM this fundamental presumably overlaps the more intense b_2 mode at 935 cm^{-1}.

For SIM three overlapping bands are situated between 850 and 820 cm^{-1}. From comparison with the *N*-halogenated succinimides [4] the bands at 844 cm^{-1} are considered as the CH_2 rock (ν_{18}) of species b_1, while the stronger lines at 823 cm^{-1} are attributed to the N–H out-of-plane bend (ν_{19}). For SIMD the CH_2 rock of species b_1 overlaps the a_1 fundamental ν_8 at 846 cm^{-1}. The N–D bending mode of species b_1, is situated at 525 cm^{-1} and corresponds to the band at 518 cm^{-1} for *N*-deuteriomaleimide.[2]

In complete agreement with the results for the maleimides [2,3] the succinimides have two bands in the region 640 – 680 cm^{-1} taken as ν_9 (a_1) and ν_{29} (b_2), the former being more intense in the Raman spectrum.

Weak bands at 537 and 543 cm^{-1} for SIM and SIMD, respectively, are attributed to a skeletal mode (ν_{14}) of species a_2 while the corresponding b_1 fundamental (ν_{20}) is assigned to the band 563 cm^{-1} for both molecules.

For SIM the 563 cm^{-1} band presumably overlaps a fundamental (ν_{30}) of species b_2, mainly involving the asymmetrical bending of the C=O groups. The corresponding a_1 mode (ν_{10}) is assigned to the strong infrared and Raman bands at 427 cm^{-1} in good agreement with the results from the maleimides.[2] Similar bands are found for SIMD at 548 and 419 cm^{-1}, respectively.

The remaining two fundamentals ν_{15} (a_2) and ν_{21} (b_1) are attributed to the bands at 265 and 190 cm^{-1} for SIM and at 268 and 187 cm^{-1} for SIMD, in good agreement with the results for the maleimides.[2,3]

NORMAL COORDINATE ANALYSIS

Detailed knowledge about the harmonic force constants cannot be obtained for SIM and the *N*-halogenated succinimides [4] independently since the information from the normal vibrations is insufficient for this purpose. Also, the ambiguities in the assignments suggested us to use force constant calculations as a tool for obtaining more reliable assignments rather than determining force constants of general physical significance. Therefore, the scope of this section is to demonstrate that the approximation of transferable force constants may be applied in establishing reliable spectral interpretations of SIM, SIMD as well as the *N*-halogenated succinimides.[4]

The normal coordinate analysis was carried out employing an approximate internal valence force field (IVFF), and the least squares method was applied in adjusting the force constants. As a starting point we used the force fields for maleimide [2] and succinic anhydride.[10] The related structure and spectral similarities of all the succinimides (N–H, N–D, N–Cl,

Table 4. Final valence force constants for succinimide.

Force type	Constants	
	Symbol [a]	Value [b]
stretch	K_a	5.297
	K_s	11.611
	K_r	3.934
	K_d	3.5
	K_l	4.798
	K_b	5.456
stretch-stretch	$K_{a_1a_2}$	1.045
	$K_{a_1s_1}$	1.53
	$K_{a_1s_2}$	−0.04
	$K_{s_1s_2}$	0.3
	$K_{a_1r_1}$	1.087
	K_{r_1d}	0.211
	$K_{l_1l_2}$	−0.079
bend	H_η	1.185
	H_ξ	1.185
	H_ψ	0.574
	H_ϕ	0.574
	H_θ	0.538
	H_α	1.344
	H_s	1.079
	H_β	1.566
	H_μ	0.47
stretch-bend	$F_{a\eta}$	0.17
	$F_{r\xi}$	0.17
	$F_{s\alpha}$	−1.19
	$F_{r\psi}$	0.15
	$F_{d\phi}$	0.15
bend-bend	$F_{\psi_1\psi_2}$	−0.038
	$F_{\phi_1\phi_2}$	−0.038
	$F_{\psi_1\phi_1}$	−0.015
outo [c]	O_{π_1}	0.411
	O_{π_2}	0.363
outo-outo	$O_{\pi_1\pi_2}$	0.086
torsion	T_τ	0.931
outo-torsion	$F_{\pi_1\tau_1}$	−0.118
	$F_{\pi_2\tau_1}$	0.173
torsion-torsion	$T_{\tau_1\tau_2}$	−0.031

[a] For meaning of symbols, see Fig. 2. [b] In units of mdyn Å^{-1} (stretch constants), mdyn rad^{-1} (stretch-bend interaction) and mdyn Å rad^{-2} (bending and torsion constants). [c] outo means out-of-plane bending.

N−Br, N−I) justified the use of transferable force constants. We therefore employed data from all the five compounds simultaneously in the least squares fitting, keeping the force constants concerning the $H_2-C-C-H_2$ part of the molecule at the same value for all. Moreover, we decided to give the C=O bending force constants and some of the interaction constants a common value for all the compounds. To reduce the number of parameters further we have made H_η and H_ξ, H_ψ and H_ϕ, $F_{a\eta}$ and $F_{r\xi}$, $F_{r\psi}$ and $F_{d\phi}$, $F_{\psi_1\psi_2}$ and $F_{\phi_1\phi_2}$ equal. The final force field consisted of 81 parameters. It was reported [11] that for similar molecules the C=O stretching frequencies can be calculated correctly by using interaction terms between the two C=O bonds, the two C−N bonds and between the C=O and C−N bonds. This model force field was also suitable for the succinimides. For the remaining interaction constants we have only introduced terms between neighbouring groups.

Since the most complete data were obtained for the solid state, we have employed these frequencies in the calculations leading to even more approximate force constants due to crystal effects. The agreement between observed

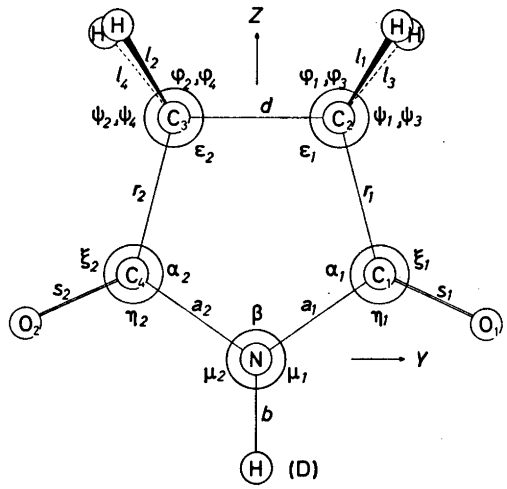

Fig. 2. Internal coordinates for succinimide. The following coordinates are not shown in the figure: out-of-plane bending: $\pi_1 = \pi(NC_2C_1O_1)$, $\pi_2 = \pi(C_3NC_4O_2)$, $\pi_3 = \pi(C_4C_1NH)$; torsion: $\tau_1 = \tau(NC_1C_2C_3)$, $\tau_2 = \tau(NC_4C_3C_2)$. The out-of-plane bending and torsion coordinates are defined as in Wilson, Decius and Cross,[12] where the succession of the letters corresponds to atom 2, 3, 4, 1 in the definition of the out-of-plane bending coordinate. θ_1, θ_2: the bending of the angles HCH. The following structural parameters were assumed: CN: 1.379; C_1-C_2: 1.477; C_2-C_3: 1.520; C=O: 1.220; C−H: 1.09; N−H: 0.99 Å; ∠CNC: 110.0°; ∠NCC: 110.5°; ∠NCO: 122.9° and $\angle C_1C_2H$: 116.1°.

and calculated frequencies was quite good for the a_1 and b_2 species, while some large discrepancies still remained for the out-of-plane modes. This may very well be due to large amplitudes of certain out-of-plane vibrations as mentioned in Ref. 9. For the a_2 and b_1 fundamentals (except those involving the CH_2 groups) we have employed an almost complete force field, using the approximation of keeping some of the interaction constants common for all the molecules. Since the assignments for these species are not as certain as for the in-plane modes and the force constants not as physically interesting, we do not consider it worth while to make any further calculations to achieve a better fit. Later, we will expand the calculations with more data from succinic anhydride and the *C*-deuterated species of both succinimide and succinic anhydride.

The internal in-plane coordinates are shown in Fig. 2, and the out-of-plane coordinates are given in the underlying text. Our calculated fundamentals are listed together with the observed frequencies in Table 3. The final set of force constants for SIM and SIMD are given in Table 4. The results seem physically reasonable, although the restrictions imposed, keeping some of the force constants transferable to the halogenated molecules and using as few constants as possible, are reflected in some of the values. The potential energy distribution (PED) of the fundamentals among the valence coordinates were calculated. These data were not included in Table 3 for the sake of brevity, but can be obtained from the authors on request.

Acknowledgement. The authors are grateful to K. Ruzicka for the preparative work. Financial support was received from the Norwegian Research Council for Science and the Humanities.

REFERENCES

1. Rogstad, A., Klæboe, P., Baranska, H., Bjarnov, E., Christensen, D. H., Nicolaisen, F., Nielsen, O. F., Cyvin, B. N. and Cyvin, S. J. *J. Mol. Struct. 20* (1974) 403.
2. Woldbæk, T., Klæboe, P. and Nielsen, C. J. *J. Mol. Struct. 27* (1975) 283.
3. Woldbæk, T., Klæboe, P. and Nielsen, C. J. *J. Mol. Struct. 28* (1975) 269.
4. Woldbæk, T., Klæboe, P. and Christensen, D. H. *Acta Chem. Scand. A 30* (1976) 547.
5. Uno, T. and Machida, K. *Bull. Chem. Soc. Jpn. 35* (1962) 276.
6. Hayashii, S. *Bull. Inst. Chem. Res. Kyoto Univ. 43* (1965) 355.
7. Mason, R. *Acta Crystallogr. 14* (1961) 720; *9* (1956) 405.
8. Brown, R. N. *Acta Crystallogr. 14* (1961) 711.
9. Brendhaugen, K., Kolderup Fikke, M. and Seip, H. M. *Acta Chem. Scand. 27* (1973) 1101.
10. Di Lauro, C., Califano, S. and Adembri, G. *J. Mol. Struct. 2* (1968) 173.
11. Colthup, N. B. and Orloff, M. K. *Spectrochim. Acta Part A 30* (1974) 425.
12. Wilson, E. B., Decius, J. C. and Cross, C. *Molecular Vibrations*, McGraw-Hill, New York, Toronto, London 1955, p. 56.

Received January 16, 1976.

Acta Chemica Scandinavica A 30 (1976) 540—546

On the Molecular Structure of *N,N'*-Di-*t*-butyl-1,2-ethanediimine, $(CH_3)_3CN{=}CHCH{=}NC(CH_3)_3$, as Studied by Gas Electron Diffraction

ISTVÁN HARGITTAI* and RAGNHILD SEIP

Department of Chemistry, University of Oslo, Oslo 3, Norway

According to a gaseous electron diffraction analysis, the majority of *N,N'*-di-*t*-butyl-1,2-ethanediimine molecules takes a *gauche* form, with respect to the central bond, which is characterized by a rotation of 65° from the *syn* form. The presence of a smaller amount of the *anti* form is also indicated. The arrangement around the double bonds is *trans*. The conformation around the C–N single bond is such that the C=N double bond and one of the C–C bonds of the adjacent *t*-butyl group are in the same plane. The following bond lengths and bond angles were determined with their standard deviations parenthesized: =C–C= 1.496(0.020) Å, C–H 1.117(0.005) Å, N=C 1.283(0.006) Å, N–C 1.468(0.016) Å, C–C 1.537(0.005) Å, =C–C=N 117.3(4.0)°, =C–C–H 116.4(1.5)°, C=N–C 122.8(1.5)°, N–C–C 109.4(0.6)°, and C–C–H 112.1(1.0)°.

Several recent studies show considerable interest toward the conformational properties of molecules with conjugated chains. In addition to the earlier established importance of the *anti* form (torsion angle $\tau = 180°$) in many systems,[1] there are results in increasing number indicating that it is the *gauche* conformer ($\tau \approx 60°$) rather than the *syn* ($\tau = 0°$) that may be present as a second conformer in substantial amounts and even prevail in some cases (for examples and references see DISCUSSION). As the question about the origin of the conformational choice in these systems is not yet well settled, and steric interactions is one of the important effects to be considered, it was found to be of interest to investigate the conformational properties of *N,N'*-di-*t*-butyl 1,2-ethanediimine, $(CH_3)_3C-N=CH-CH=N-C(CH_3)_3$, in the vapour phase.

EXPERIMENTAL

The sample of *N,N'*-di-*t*-butyl-1,2-ethanediimine was kindly supplied by Prof. H. tom Dieck (Institut für Anorganische Chemie, Universität Frankfurt). The electron diffraction patterns were taken with the Balzers apparatus KD-G2 in Oslo [2,3] at the camera distances 50 and 25 cm. The nozzle temperature was about 80 °C and the electron wavelength was 0.05852 Å. Four plates (Kodak electron image) from each camera distance were selected for analysis. The ranges of intensity data used were $1.25 \leqq s \leqq 14.00$ Å^{-1} with $\Delta s = 0.125$ Å^{-1} and $4.00 \leqq s \leqq 28.5$ Å^{-1} with $\Delta s = 0.25$ Å^{-1} corresponding to the two camera distances. The procedure of data reduction was as previously described.[4] The modified experimental molecular intensities are shown in Fig. 1.

STRUCTURE ANALYSIS

The geometry of the models. All models had a twofold symmetry axis perpendicular to the central C–C bond (C_2 symmetry). The rotation angle τ around the central C–C bond was defined in such way that $\tau = 0$ and $\tau = 180°$ correspond to *syn* and *anti* conformations of the N=C–C=N chain, respectively.

In most models the conformation around the C=N double bond was *trans*. The *cis*

* On leave from the Central Research Institute for Chemistry, Hungarian Academy of Sciences, H-1088 Budapest, Puskin utca 11–13, Hungary.

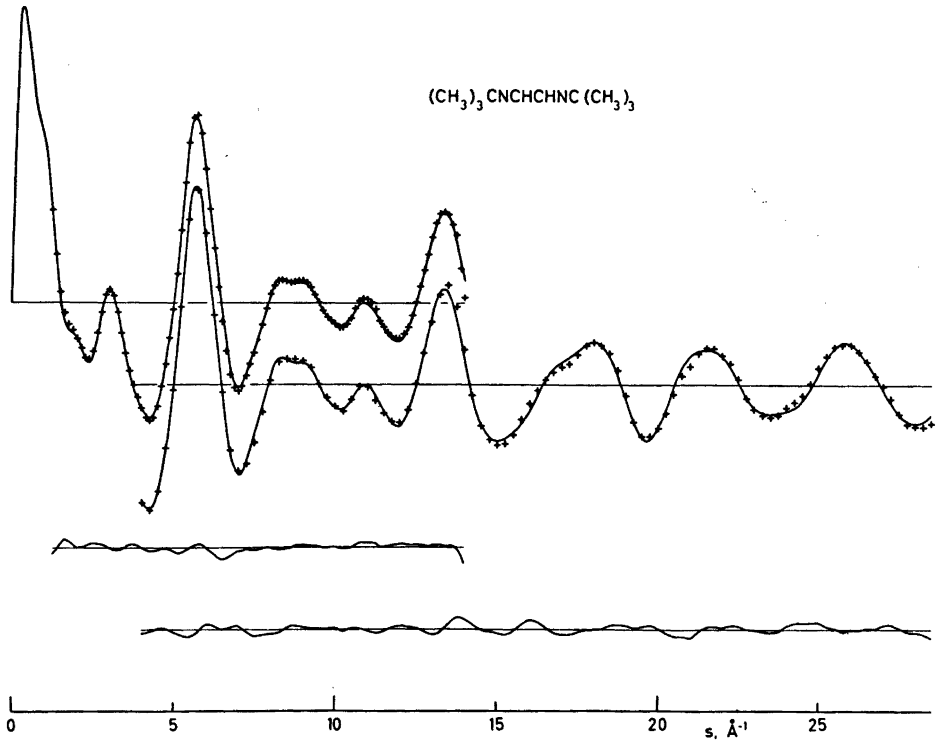

Fig. 1. Modified molecular intensities of *N,N'*-di-*t*-butyl-1,2-ethanediimine. Crosses: experimental (the upper and lower distributions correspond to the 50 and 25 cm camera ranges, resp.) Full lines: theoretical curves calculated from the parameters presented in Tables 1 and 2 for a mixture of 80 % *gauche* and 20 % *anti*. The difference curves are also shown.

Table 1. N,N'-Di-*t*-butyl-1,2-ethanediimine. Results of least squares refinement for the *gauche* ($\tau = 65°$) form (with 20 % *anti* form in the mixture).
Bond lengths (r, Å), bond angles ($\angle$, °), and torsion angles (τ, ϕ, °). The standard deviations for the bond lengths refer to the last digit given.

N	Type	Parameter	$\sigma_{LS}(r,\angle)^a$	$\sigma_{LS}^{corr}(r,\angle)^b$	l	$\sigma_{LS}(l)^a$	$\sigma_{LS}^{corr}(l)^b$
1	=C−C=	1.496	16	20	0.044		
2	C−H	1.117	3	5	0.073	3	5
3	N=C	1.283	3	6	0.029	5	8
4	N−C	1.468	10	16	0.042		
5	C−C	1.537	3	5	0.054	5	8
6	=C−C=N	117.3	3.1	4.0			
7	=C−C−H	116.4	1.3	1.5			
8	C=N−C	122.8	1.3	1.5			
9	N−C−C	109.4	0.6	0.6			
10	−C−C−H	112.1	0.6	1.0			
11	τ(N=C−C=N)	65.0	3.8	3.5			
12	ϕ(C=N−C−C)	0.0					

[a] Standard deviations from the least squares refinement with diagonal weight matrix. [b] Standard deviations from the least squares refinement with off-diagonal elements also included in the weight matrix. [17]

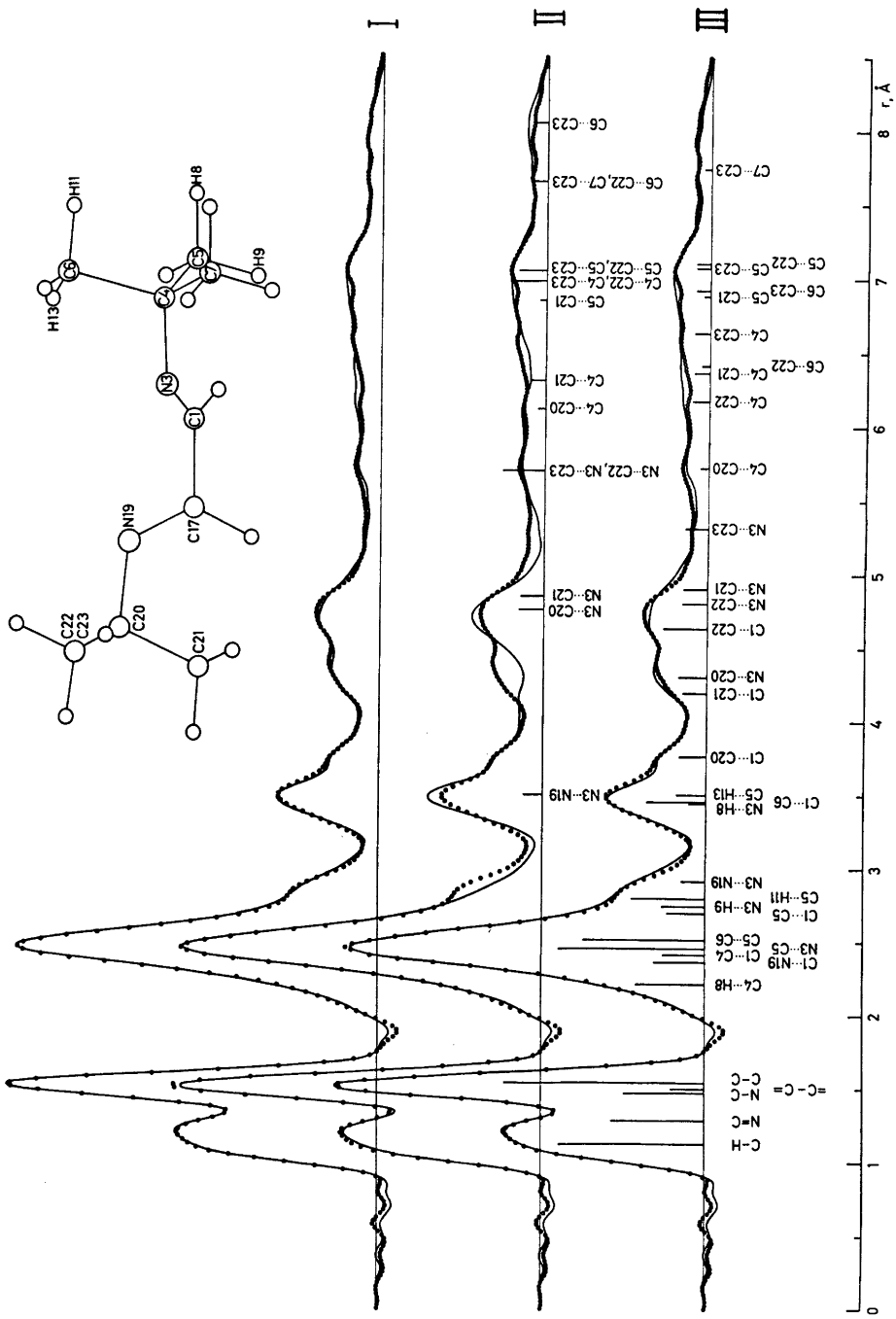

Fig. 2. Radial distribution curves calculated with an artificial damping factor of (exp $(-ks^2)$, $k = 0.002$ Å^2. The experimental curve (circles) is compared to three different theoretical distributions (full lines). I, calculated from the parameters presented in Tables 1 and 2 for a mixture of 80 % *gauche* and 20 % *anti*. II, calculated for the pure *anti* form. III, calculated for the pure *gauche* form. The contributions from the atomic pairs ij are indicated by vertical bars of relative height proportional to $n_{ij}Z_iZ_j/r_{ij}$.

conformation has also been tested but could be rejected with confidence.

Conformations around the C–N single bond were examined. As a result, the rotation form in which the C=N and C–C bonds of the C=N–C–C chain eclipse each other was accepted. The form in which the C=N bond is staggered by two of the C–C bonds of the *t*-butyl group could easily be ruled out by inspecting the experimental and theoretical radial distribution curves.

The following assumptions were made: All C–H bonds are of equal length and have the same mean amplitude of vibration (*l* value). The $-C(CH_3)_3-$ and the CH_3-groups have local C_3 symmetry, and the pyramidal axes coincide with the extension of the N–C bond and the C–C bond, respectively. The C–H bonds of the methyl groups are staggered with respect to the C–C bonds of the *t*-butyl group to which they belong.

The bond lengths, bond angles and torsion angles characterizing the molecular geometry are listed in Table 1.

Experimental radial distribution. The experimental radial distribution curve is presented in Fig. 2. The first two peaks at about 1.2 and 1.5 Å obviously contain the contribution from the bond distances, the former corresponding to C–H and C=N, and the latter to C–N, =C–C–, and C–C. Most of the rotation-independent distances between non-bonded atoms were expected to appear in the next peak at about 2.45 Å. The rotation-dependent distances could appear in this peak and up to very large values of *r* (8–9 Å) on the radial distribution curve. Unfortunately, no information could be read off directly from the experimental radial distribution curve. Its features were, however, instrumental in the analysis for testing models.

Trial structures. Various starting values for the bond lengths and bond angles have been used in the trial structures estimated on the basis of known structures and considering the experimental radial distribution. They were refined using fixed values for the torsion angle τ around the =C–C= bond. Later the constraint on τ was also removed.

REFINEMENTS AND RESULTS

The least squares method was applied to the modified molecular intensities.[4] The modification function was $s/|f_c(s)|^2$. Unit weights were applied for the entire intensity interval.

All bond distances and bond angles together with the torsion angle τ could be refined simultaneously. However, when *l* values were also varied, some of them were kept constant, most often *r*(=C–C=), ∠=C–C–H and/or ∠C–C–H. The *l* values for the bonds =C–C= and C–N were assumed to be 0.044 and 0.042 Å, respectively, and not refined, while those for the other bonds were determined. The *l* values for the most important non-bond distances, N···C, C···C, and C···H, N···H with large occurrence ($n_{ij} \geqq 6$), were allowed to vary in groups in separate refinements together with the geometrical parameters. The groups were formed from distances that occurred in the same peak or were closely spaced, and the *l* values in the group were coupled, *i.e.* the differences between them were kept constant at assumed values. Typical examples of groups of *l* values formed for simultaneous refinement are shown in Table 2. The *l* values for distances C···H and N···H with multiplicities less than six and H···H have not been refined, but in most cases more than one trial value has been tested. Values between 0.10 and 0.35 Å have been utilized in the final calculations.

The outer part of the radial distribution curve, say, $r > 5$ Å, was seen to be little sensitive to the rotation around the =C–C= bond. The distances involving either atoms C5 or C21 remain practically unchanged during rotation around the =C–C= bond since these atoms are very near the rotation axis. Also, the *l* values for these long distances are very uncertain. The interval between $r = 2.8$ and 5 Å seemed to be the most important portion of the radial distribution curve in examining the rotation forms around the =C–C= bond. The rotation-dependent distances occurring in this region (*e.g.* N3---C20) made it possible to identify the *gauche* form with τ(N=C–C=N) around 65° as preferred (Fig. 2).

The theoretical molecular intensity and radial distribution curves calculated for other conformers showed poorer agreement with the experimental data and refined often to un-

Table 2. *N,N'*-Di-*t*-butyl-1,2-ethanediimine. Results of least squares refinement for the *gauche* ($\tau = 65°$) form (with 20 % *anti* form in the mixture). Mean amplitudes of vibration for non-bonded distances in the $C_3CNCCNCC_3$ skeleton and distances C–H and N–H with a multiplicity of six or more. The standard deviations refer to the last digit given.

N	*i*	*j*	n_{ij}	r_{ij}	$\sigma_{LS}(r)^a$	$\sigma_{LS}^{corr}(r)^b$	l_{ij}	$\sigma_{LS}(l)^a$	$\sigma_{LS}^{corr}(l)^b$	Group
21	C4	H8	18	2.213	8	13	0.108	12	17	
22	C1	N19	2	2.362	15	19	0.077	8	9	i
23	C1	C4	2	2.410	16	20	0.077	»	»	»
24	N3	C5	6	2.452	10	12	0.094	»	»	»
25	C5	C6	6	2.510	12	12	0.082	»	»	»
26	C1	C5	2	2.695	19	25	0.092	»	»	»
27	N3	H9	12	2.745	14	19	0.224	25	33	ii
28	C5	H11	24	2.789	13	18	0.224	»	»	»
29	N3	N19	1	2.910	20	26	0.085			
30	N3	H8	6	3.439	12	18	0.098	5	7	iii
31	C1	C6	4	3.453	17	23	0.117	»	»	»
32	C5	H13	12	3.502	11	13	0.098	»	»	»
33	C1	C20	2	3.759	14	15	0.070	13	13	
34	C1	C21	2	4.191	26	30	0.153	51	57	
35	N3	C20	2	4.305	19	21	0.083	16	14	
36	C1	C22	4	4.641	15	16	0.157	21	24	iv
37	N3	C22	2	4.805	24	25	0.197	»	»	»
38	N3	C21	2	4.905	24	28	0.197	»	»	»
39	N3	C23	2	5.317	24	21	0.260	84	82	
40	C4	C20	1	5.731	24	27	0.085	44	30	
41	C4	C22	2	6.179	37	42	0.320	78	71	v
42	C4	C21	2	6.363	22	24	0.280	»	»	»
43	C6	C22	1	6.417	65	76	0.280			
44	C4	C23	2	6.640	24	21	0.280			
45	C5	C21	1	6.885	45	54	0.324			
46	C6	C23	2	6.925	52	44	0.204	26	18	vi
47	C5	C23	2	7.076	22	24	0.165	»	»	»
48	C5	C22	2	7.104	25	27	0.165	»	»	»
49	C7	C23	1	7.750	35	27	0.110			

[a,b] See footnotes in Table 1.

realistic *l* values for some important non-bonded distances.

It was also examined whether a mixture of the *anti* form ($\tau = 180°$) together with the *gauche* ($\tau = 65°$) could be present. Geometrical parameters determined for the *gauche* form and only slightly different from those presented in Table 1 were employed in these calculations. Unfortunately, the theoretical distributions were little sensitive to addition of small amounts of the *anti* form. In fact, the agreement improved somewhat with 10 % *anti*, did not change with 20 %, and became somewhat poorer with 30 % (generalized *R*-factor 0.0765, 0.0775, 0.0801 for mixtures with 10, 20, 30 % *anti* vs. 0.0774 for *gauche* only). In these calculations it was assumed that the *anti* form would have the same structure as the *gauche* form except the torsion angle τ. The *l* values for the rotation-dependent non-bonded distances of the *anti* form were estimated considering the values obtained for the *gauche* form.

Further refinement of some of the *l* values for important non-bonded distances and of some of the bond angles were performed for the mixtures. The results were not very different from those obtained for the *gauche* form only, and depended slightly on the mixture used. It was felt that it would be difficult to give a reliable estimate of the *anti* form content of the mixture. We consider, however, the results obtained for the *gauche* form in a mixture with 20 % *anti* form to be a fair representation of the findings of the present analysis.

Table 1 contains the bond distances, bond and torsion angles and the mean amplitudes of vibration for the bonds. The *l* values for non-bonded distances of the $C_3CNCCNCC_3$ skeleton and distances C···H and N···H that occur at least six times, are given in Table 2 with indicating typical arrangements of the groups in which these *l* values were refined. The standard deviations σ_{LS} (and also σ_{LS}^{corr}) given in Tables 1 and 2 refer to a particular refinement scheme in which the parameters for those σ values are given which were allowed to vary simultaneously.* The σ_{LS} values refer to a refinement with unit weights, while the σ_{LS}^{corr} values were obtained when off-diagonal elements were also included in the weight matrix in order to estimate the influence of correlation between the experimental data on the standard deviations. As for the correlation between the parameters, there were altogether 406 correlation coefficients for the particular refinement scheme for which the results are presented in Tables 1 and 2. Of these coefficients, in order to save space, only those are given in Table 3 whose absolute values are larger than 0.5.

* For the particular scheme the "fudge-factor" was chosen to be nearly zero.

DISCUSSION

The bond lengths and bond angles determined for *N,N'*-di-*t*-butyl-1,2-ethanediimine display no unusual features. A detailed discussion of them, furthermore, would not be justified in the light of the relatively large standard deviations associated with the parameters. Some observations concerning the bond lengths may be of interest, however.

The distance for the central bond =C−C= (1.496(20) Å) has especially large standard deviation. On the other hand, its value is seen to be rather insensitive to the conditions of refinement applied in various schemes. It is larger than those in 1,2,4,5-hexatetraene (1.466(4) Å) [5] and in 1,3-butadiene (1.467(3) Å,[6] 1.463(3) Å [7]). In this connection it is interesting to note that the =N−N= bond in acetaldazin (1.437(13) Å) [8] is larger than in formaldazin (1.418(3) Å).[9]

The length of the double bond C=N in *N,N'*-di-*t*-butyl-1,2-ethanediimine is nearly the same as in formaldazin (1.277(2) Å) [9] and in acetaldazin (1.277(3) Å).[8]

The most interesting structural feature of the *N,N'*-di-*t*-butyl-1,2-ethanediimine molecules is their conformational properties. The majority of the molecules in the vapour takes

Table 3. Correlation coefficients ϱ (associated with the results and corresponding to the notation of Tables 1 and 2) whose absolute value is greater than 0.5.

Parameters 1	2	ϱ_{12}[a]	ϱ_{12}^{corr}[b]	Parameters 1	2	ϱ_{12}[a]	ϱ_{12}^{corr}[b]
r2	r3	0.564	0.618	r4	l5	0.789	0.825
r3	r4	0.663	0.692	r5	l5	−0.739	−0.753
r1	r5	−0.624	−0.598	l5	α7		−0.584
r3	r5		−0.546	r1	l(i)	0.688	
r4	r5	−0.682	−0.720	α6	l(i)	−0.753	−0.746
r1	α6	−0.651		α7	l(i)	−0.588	
r1	α7	−0.785	−0.783	α9	l(i)	0.607	0.596
r5	α7	−0.674	−0.704	α7	l34	−0.545	−0.564
α6	α7	0.651		α8	l34	0.554	
r5	α8	0.585	0.613	α9	l34		0.604
α7	α8	0.526	0.558	l(i)	l(ii)	0.704	0.651
α6	α9		−0.526	α7	l21	−0.531	
α7	α9	−0.625	−0.554	α9	l21	0.513	
α7	τ11	0.657	0.622	l(i)	l21	0.693	0.594
l2	l3	0.517	0.545	l(ii)	l21		0.553
r3	l5		0.510	s(50)[c]	s(25)[c]	0.520	

[a] Refinement scheme with diagonal weight matrix. [b] Refinement scheme with off-diagonal elements also included in the weight matrix. [c] Scale factors for the data sets from the 50 and 25 cm camera ranges, respectively.

a *gauche* form with respect to the central bond and this *gauche* form is characterized by a torsion of 65° from the *syn* form. The presence of a smaller amount of the *anti* form is also indicated by the experimental data. The arrangement around the double bonds is *trans*. The conformation around the C–N single bond is such that the C=N double bond and one of the C–C bonds of the adjacent *t*-butyl group are in the same plane.

We are aware of only one previous investigation of the molecular conformation of *N,N'*-di-*t*-butyl-1,2-ethanediimine, *viz.* that of Exner and Kliegman [10] who suggested a non-planar form on the basis of measurement and calculation of dipole moment. They placed the torsion angle between 90 and 140°, and stressed that the calculations were rather sensitive to the bond angles used. At first sight the present findings seem to be at variance with the conclusions from the dipole moment calculations. However, Exner and Kliegman considered the presence of one conformer only, whereas the dipole moment measurements may be interpreted with a mixture of *anti* form and a *gauche* that is closer to *syn* than to *anti*.

In addition to the *anti* conformer, *gauche* conformers with torsion angles similar to that determined in the present study have been found recently by electron diffraction in several compounds that include oxalyl chloride,[11] oxalyl bromide,[12] formaldazin,[9] acetaldazin.[8] The relative abundance of *gauche* is larger in oxalyl bromide than in oxalyl chloride, and, in fact, the *gauche* is somewhat prevailing in the bromine derivative at the temperatures applied.[12] A *gauche* form was detected only for hexachloro butadiene [with torsion angle 78.1(1.1)°],[13] while all 2,3-butadione molecules were found to take the *anti* form.[14]

Ab initio calculations performed for 1,2-ethanediimine [15] and formaldazin [16] found a minimum for the *anti* forms only.

The steric requirements of the bulky *t*-butyl groups probably play an important role in establishing the conformational properties of the *N,N'*-di-*t*-butyl-1,2-ethanediimine molecules. They are, however, only one of several competing effects that have to be taken into consideration.

Acknowledgements. We express our appreciation to Professor H. tom Dieck for suggesting this investigation and for providing the sample. We are also grateful to Dr. H. M. Seip for useful discussions and to Snefrid Gundersen for technical assistance. One of us (I. H.) thanks Professors O. Bastiansen, S. J. Cyvin and H. Viervoll for an invitation to Norway, and Norges almenvitenskapelige forskningsråd for a Fellowship.

REFERENCES

1. See, *e.g.*, Bastiansen, O., Seip, H. M. and Boggs, J. E. In Dunitz, J. D. and Ibers, J. A., Eds., *Perspectives in Structural Chemistry*, Wiley, New York 1971, Vol. IV.
2. Zeil, W., Haase, J. and Wegmann, L. *Z. Instrumentenkd. 74* (1966) 84.
3. Bastiansen, O., Graber, R. and Wegmann, L. *Balzers High Vacuum Report* (1969) 1.
4. Andersen, B., Seip, H. M., Strand, T. G. and Stølevik, R. *Acta Chem. Scand. 23* (1969) 3224.
5. Trætteberg, M., Paulen, G. and Hopf, H. *Acta Chem. Scand. 27* (1973) 2227.
6. Haugen, W. and Trætteberg, M. In Andersen, P., Bastiansen, O. and Furberg, S., Eds., *Selected Topics in Structure Chemistry*, Universitetsforlaget, Oslo 1967.
7. Kuchitsu, K., Fukuyama, T. and Morino, Y. *J. Mol. Struct. 1* (1968) 463.
8. Hargittai, I., Schultz, Gy., Naumov, V. A. and Kitaev, Yu. P. *Acta Chim. (Budapest). In press.*
9. Hagen, K., Bondybey, V. and Hedberg, K. *To be published.*
10. Exner, O. and Kliegman, J. M. *J. Org. Chem. 36* (1971) 2014.
11. Hagen, K. and Hedberg, K. *J. Am. Chem. Soc. 95* (1973) 1003.
12. Hagen, K. and Hedberg, K. *J. Am. Chem. Soc. 95* (1973) 4796.
13. Gundersen, G. *J. Am. Chem. Soc. 97* (1975) 6342.
14. Hagen, K. and Hedberg, K. *J. Am. Chem. Soc. 95* (1973) 8266.
15. Skancke, A. *Private communication, 1975.*
16. Skancke, A. *Private communication, 1975.*
17. Seip, H. M. and Stølevik, R. In Cyvin, S. J., Ed., *Molecular Structures and Vibrations*, Elsevier, Amsterdam 1972.

Received January 16, 1976.

Acta Chemica Scandinavica A 30 (1976) 547—554

The Vibrational Spectra of *N*-Chloro, *N*-Bromo-, and *N*-Iodosuccinimide

T. WOLDBÆK,[a] P. KLÆBOE[a] and D. H. CHRISTENSEN[b]

[a] Department of Chemistry, University of Oslo, Oslo 3, Norway and [b] Chemical Laboratory V, The H. C. Ørsted Institute, DK-2100 Copenhagen, Denmark

The infrared spectra of the title compounds as solids (Nujol mulls) and in solution were recorded in the region 4000 – 50 cm^{-1}. Raman spectra of the crystalline compounds were obtained, and semiquantitative polarization data were obtained for the chloro-compound from spectra recorded in dimethylformamide solution.

The fundamental frequencies were tentatively assigned in terms of C_{2v} symmetry, partly based upon the striking similarity with the spectra of succinimide. Force fields were derived for the three *N*-halogenated succinimides and the data were fitted together with those of succinimide and *N*-deuteriosuccinimide by a least squares method.

We have for some time been interested in the molecular structure and vibrational spectra of unsaturated and saturated cyclic imides, and have recently published our results for maleimide,[1] *N*-chloromaleimide,[2] and succinimide.[3] In the present communication we shall report data for the *N*-chloro-, *N*-bromo-, and *N*-iodosuccinimides, later to be called SIMC, SIMB and SIMI, respectively. These compounds are widely used as mild halogenating agents in organic chemistry due to the weak *N*-halogen bonds. The crystal structures of these compounds have been studied,[4,5] but the molecular structure has been established for SIMC only. To our knowledge, no infrared or Raman spectra have been reported for the *N*-halogenated succinimides, except for some limited studies of the C=O stretching region.[6–10] We hoped that a comparison between the spectra of these molecules with those of succinimide [3] and the maleimides [1,2] should be illuminating.

EXPERIMENTAL

The samples were commercial products from Koch Light (SIMC) and Fluka AG (SIMB and SIMI). SIMC was purified by repeated sublimation *in vacuo* (M.p. 150 °C). SIMB and SIMI were purified by recrystallization from an acetone-ethyl acetate solution. Both compounds became rapidly discoloured due to free halogen on exposure to light and melted under decomposition.

The infrared, far infrared and Raman spectrometers, cells *etc.* have been described.[11] SIMB and SIMI developed distinct colour in solution, but the infrared solution spectra did not change significantly within a few hours. Under laser illumination the solutions very rapidly became discoloured and therefore no Raman solution spectra or polarization ratios were obtained for SIMB and SIMI. However, satisfactory Raman spectra were obtained in the solid state.

RESULTS

In accordance with the results from X-ray studies on crystalline succinimide [12] and SIMC,[4] we have assumed that all the present molecules have a planar cyclic entity. The spectra have therefore been interpreted in terms of C_{2v} symmetry. The 30 fundamentals will accordingly divide themselves into the symmetry species: $10a_1 + 9b_2 + 5a_2 + 6b_1$. The a_1 and b_2 fundamentals represent in-plane, the a_2 and b_1 out-of-plane modes.

With no infrared spectra of the vapour the assignments were partly based upon the incomplete Raman polarization data. Further support was provided by the normal coordinate analysis as well as comparison with maleimide,[1] *N*-chloromaleimide,[2] and succinimide.[3]

Table 1. Infrared [a] and Raman spectral data for *N*-chlorosuccinimide.

Infrared		Raman		Assignments [b]	
Solid	Solution	Solid	Solution		
Nujol	CCl_4	−180 °C	DMFA		
3481 m [c]	3520 vw			$\nu_2+\nu_{23}=3485$	B_2
		3123 w		$\nu_3+\nu_{23}=3138$	B_2
		3037 sh			
		3000 s		ν_{11} fund.	a_2
2993 m		2991 s	2992 m	ν_{16} fund.	b_1
2957 m [d]	2947 w	2956 vs	2953 s	ν_1 fund	a_1
		2951 s sh		ν_{22} fund.	b_2
	2928 w			$\nu_{12}+\nu_{23}=2943$	B_1
1895 vw				$\nu_2+\nu_{21}=1915$	B_1
1865 sh				$\nu_{23}+\nu_{30}=1884$	A_1
1817 m	1811 m	1810 m sh		$\nu_9+\nu_{25}=1822$	B_2
		1790 sh		$\nu_5+\nu_{14}=1801$	A_2
1780 sh 1772 m sh	1791 m	1780 sh 1776 vs	1776 s P	ν_2 fund.	a_1
1713 vs	1745 vs	1712 m		ν_{23} fund.	b_2
	1726 w sh	1741 w sh	1726 w P	$\nu_3+\nu_{10}=1763$	A_1
	1715 vw sh			$\nu_{17}+\nu_{19}=1752$	A_1
1696 sh		1695 sh		$\nu_{26}+\nu_{29}=1727$	A_1
1592 vw		1594 vw		$\nu_{27}+\nu_{28}=1608$	A_1
1549 w		1545 vw		$\nu_{24}+\nu_{30}=1577$	A_1
1530 vw				$\nu_6+\nu_9=1534$	A_1
1500 vw				$\nu_8+\nu_{18}=1506$	B_1
		1468 w	1464 w [e]	$\nu_5+\nu_{15}=1478$	A_2
		1449 w		$\nu_{12}+\nu_{20}=1455$	B_2
		1427 s			
1425 s	1433 s		1427 m [e]	ν_3 fund.	a_1
		1421 s			
1406 w		1407 s	1409 m [e]	ν_{24} fund.	b_2
1378 m [d]	1375 w	1370 vw		$\nu_9+\nu_{18}=1382$	B_1
	1336 m [f]	1336 w sh	1347 w	$\nu_7+\nu_9=1343$	A_1
1328 s	1311 s	1325 m		ν_4 fund.	a_1
1315 m sh				$\nu_{26}+\nu_{30}=1336$	A_1
1296 m	1290 w sh [f]	1298 w		ν_{25} fund.	b_2
		1272 w	1271 w	$2\times\nu_{28}=1290$	A_1
1248 s	1237 w [f]	1250 w		ν_5 fund.	a_1
1230 w	1230 w sh [f]	1229 m	1229 w D	ν_{12} fund.	a_2
1225 sh				$\nu_8+\nu_{19}=1223$	B_1
1181 s	1171 w sh	1180 vw	1185 w	ν_{17} fund.	b_1
1165 s	1154 s	1163 w	1156 w	ν_{26} fund.	b_2
1095 w	1089 w [g]			$\nu_9+\nu_{19}=1097$	B_1
1050 vw		1052 vw		$2\times\nu_9=1052$	A_1
		1027 w	1020 w sh	$\nu_7+\nu_{15}=1047$	A_2
		1013 m			
1008 m	1009 w [g]		1005 w	ν_6 fund.	a_1
		1008 m			
1000 w	1000 w [g]			$\nu_{12}-\nu_{20}=1005$	B_2
963 s	955 w [g]	965 m	967 m [e]	ν_{27} fund.	b_2
933 w		932 vw	921 m [e]	ν_{13} fund.	a_2
		909 vw	892 w [e]	$\nu_{10}+\nu_{19}=909$	B_1
854 w		855 vw	851 w	ν_{18} fund.	b_1
817 s	811 s	823 w	820 w	ν_7 fund.	a_1
		738 w	703 w	$\nu_{19}+\nu_{30}=742$	A_2
668 sh				$\nu_9+\nu_{21}=669$	B_1
652 s	643 m	655 s	630 s P	ν_8 fund.	a_1
645 sh	636 sh [g]	636 sh		ν_{28} fund.	b_2
571 m	564 w	571 m	568 w D	ν_{19} fund.	b_1

Table 1. Continued.

562 w	554 w[g]	562 m	548 s D	ν_{29} fund.	b_2
		553 sh		ν_{14} fund.	a_2
548 m		547 sh		$\nu_{10}+\nu_{20}=563$	B_1
526 w	525 w[g]	527 s	491 m P	ν_9 fund. ^{35}Cl	a_1
523 w		523 sh		ν_9 fund. ^{37}Cl	a_1
480 w				$\nu_{10}+\nu_{21}=481$	B_1
			380 w[e]	$\nu_{20}+\nu_{30}=396$	A_2
338 s	332 s[h]	337 s		ν_{10} fund.	a_1
		230 m	233 s D	ν_{15} fund.	a_2
225 m	215 m[h]	224 sh		ν_{20} fund.	b_1
171 m[i]		170 vw		ν_{30} fund.	b_2
143 m	120 s[h]	125 w		ν_{21} fund.	b_1
123 m					
102 w		100 m			
95 w					
84 w		86 m		lattice modes	
		77 m			
65 w		63 s			
50 m		56 s			

[a] The weak infrared and Raman bands in the regions 5000–3100 cm^{-1} and 2900–1900 cm^{-1} are omitted. [b] When available the combination frequencies and overtones are calculated from infrared solid state data. [c] w, weak; m, medium; s, strong; v, very; sh, shoulder; P, polarized and D, depolarized. [d] Hexachlorobutadiene paste. [e] H_2O solution. [f] CH_2Cl_2 solution. [g] CS_2 solution. [h] C_6H_6 solution. [i] Solid state frequencies below 200 cm^{-1} are from polyethylene (Rigidex) pellet.

Spectral interpretations. The observed IR and Raman frequencies are listed in Tables 1 (SIMC), 2 (SIMB) and 3 (SIMI) while the assigned fundamentals for all three compounds are given in Table 4 together with the calculated frequencies. Because of the striking similarity between the present spectra and those of succinimide [3] only the carbonyl region (1800–1600 cm^{-1}) and the region below 600 cm^{-1} will be discussed.

For the maleimides [1,2] and succinimides [3] as well as for the corresponding anhydrides [11,12] the in-phase carbonyl stretching fundamentals (a_1) are invariably at higher frequencies than the out-of-phase modes (b_2). Various explanations have been proposed to account for these features in the imides including: mechanical coupling,[8,14] hydrogen bonding,[15] and electronic effects.[6,10,16,17] The latter include resonance stabilization $^{-}O-C=\overset{+}{N}(X)-C=O \leftrightarrow O=C-\overset{+}{N}(X)=C-O^{-}$, resulting in a lowered out-of-phase C=O stretching frequency.

Hydrogen bonding can obviously give no general explanation for the low frequency of the b_2 mode since the effect is also observed for the halogenated compounds where no hydrogen bonding is possible. Moreover, from the dilute solution spectral data for maleimide [1] and succinimide [3] hydrogen bonding does not seem to be important for the carbonyl stretching frequencies for either of these molecules. From the normal coordinate analysis it is seen that for the maleimides [1,2] the high frequency of the in-phase carbonyl stretch relative to the out-of-phase stretch might be explained by a coupling between the C=C and the in-phase carbonyl stretch, whereas for the succinimides such a coupling is not possible.

For the succinimide electronic effects leading to a lowered out-of phase C=O stretching frequency seem to give the only reasonable explanation to all the experimental data. As expected these effects seem to be most important in the solid state and in polar solutions, leading to large solid-solution shifts towards higher frequency for the b_2 mode. The corresponding a_1 fundamental does not give the same shifts. Since an electronegative substituent (X) on the N-atom will reduce the resonance contributions, the b_2 frequency ought to decrease with X in the order Cl, Br, H, I, exactly what is observed for the succinimides (Table 5). The isotopic shift for this frequency on deuteration can be explained by a weak coupling between the out-of-phase C=O stretching vibration of maleimide [1] and succini-

Table 2. Infrared [a] and Raman spectral data for *N*-bromosuccinimide.

Infrared		Raman	Assignments [b]		Infrared		Raman	Assignments [b]	
Solid Nujol	Solution CCl_4	Solid			Solid Nujol	Solution CCl_4	Solid		
		3019 sh [c]	$\nu_4+\nu_{23}=3030$	B_2	1117 w sh		1125 vw	$2\times\nu_{19}=1138$	A_1
		2997 s	ν_{11} fund.	a_2			1062 w	$\nu_{27}+\nu_{30}=1067$	A_1
2977 w [d]		2986 s	ν_{16} fund.	b_1			1015 sh	$\nu_7+\nu_{15}=1036$	A_2
2947 vw sh [d]	2952 m sh	2950 vs	ν_1/ν_{22} fund.	a_1/b_2	1005 m	1007 w [f]	1005 m	ν_6 fund.	a_1
2932 w [d]	2927 m		$\nu_2+\nu_{17}=2945$	B_1	1000 sh	999 w [f]		$\nu_7+\nu_{20}=1001$	B_1
1883 vw	1862 w		$\nu_2+\nu_{30}=1899$	B_2	933 w	927 w	934 m	ν_{27} fund.	b_2
1857 vw	1852 w	1867 vw	$2\times\nu_{27}=1866$	A_1	916 sh		917 sh	ν_{13} fund.	a_2
	1802 vw		$\nu_6+\nu_7=1820$	A_1	890 w			$\nu_8+\nu_{10}=919$	A_1
1807 m	1780 w		$\nu_8+\nu_{26}=1807$	B_2	870 vw			$\nu_{15}+\nu_{28}=876$	B_1
1772 sh	1769 vw sh	1771 sh	$\nu_{12}+\nu_{29}=1784$	B_1	850 vw		854 w	ν_{18} fund.	b_1
1765 m	1752 m	1762 s	ν_2 fund.	a_1	815 m	811 m [f]	822 w	ν_7 fund.	a_1
1710 vs	1738 s	1697 m	ν_{23} fund.	b_2			739 w	$\nu_{19}+\nu_{30}=745$	A_2
	1728 m sh		$\nu_{17}+\nu_{19}=1749$	A_1	655 s		655 sh	ν_{28} fund.	b_2
1696 sh	1712 w sh		$\nu_3+\nu_{10}=1700$	A_1	640 s	634 s	643 s	ν_8 fund.	a_1
1668 m sh			$\nu_{10}+\nu_{24}=1684$	B_2	569 w	563 m [f]	569 m	ν_{19} fund.	b_1
1650 sh	1632 w		$\nu_6+\nu_{28}=1660$	B_2	564 sh				
1579 vw			$\nu_{27}+\nu_{28}=1588$	A_1	556 sh	537 sh [f]	552 w	ν_{29} fund.	b_2
1491			$\nu_4+\nu_{20}=1506$	B_1	546 w	543 vw sh [f]		$2\times\nu_{10}=558$	A_1
		1469 vw	$\nu_{20}+\nu_{25}=1478$	A_2			531 w	ν_{14} fund.	a_2
1421 s	1433 m [e]	1425 m	ν_3 fund.	a_1	479 m	479 m [f]	482 s	ν_9 fund	a_1
1405 w		1408 m	ν_{24} fund.	b_2	424 w			$2\times\nu_{15}=442$	A_1
1379 w [d]			$\nu_{15}+\nu_{26}=1388$	B_1			380 vw	$2\times\nu_{20}=372$	A_1
1364 w [d]	1338 m		$\nu_{17}+\nu_{20}=1366$	A_1			350 w	$\nu_{15}+\nu_{30}=355$	B_1
1320 s	1300 s	1316 m	ν_4 fund.	a_1			343 w	$\nu_{15}+\nu_{30}=345$	B_2
1292 m	1285 w sh [e]	1293 w sh	ν_{25} fund.	b_2	279 s [g]	271 s [h]	278 s	ν_{10} fund.	a_1
1248 m	1232 w [e]	1248 w	ν_5 fund.	a_1			250 vw	$2\times\nu_{21}=248$	A_1
1228 w		1228 w	ν_{12} fund.	a_2			221 vw	ν_{15} fund.	a_2
1213 sh			$\nu_{10}+\nu_{27}=1212$	B_2	186 m	171 m [h]	187 w	ν_{20} fund.	b_1
1180 s	1180 w sh [e]		ν_{17} fund.	b_1	176 sh				
1167 s	1156 s	1161 w	ν_{26} fund.	b_2	134 m	112 s [h]	135 vw	ν_{30} fund.	b_2
1152 m sh			$\nu_{15}+\nu_{27}=1154$	B_1	124 m			ν_{21} fund.	b_1
1135 w sh			$\nu_6+\nu_{30}=1139$	B_2			80 w	lattice mode	

[a] The weak infrared and Raman bands in the regions 5000–3100 cm^{-1} and 2900–1900 cm^{-1} are omitted. [b] When available the combination frequencies and overtones are calculated from infrared solid data. [c] For abbreviations used, see footnotes to Table 1. [d] KBr pellet. [e] CS_2 solution. [f] CH_2Cl_2 solution. [g] Solid state frequencies below 400 cm^{-1} are from polyethylene (Rigidex) pellet. [h] C_6H_6 solution.

Table 3. Infrared[a] and Raman spectral data for *N*-iodosuccinimide.

Infrared		Raman	Assignments[b]		Infrared		Raman	Assignments[b]	
Solid Nujol	Solution	Solid			Solid Nujol	Solution	Solid		
		2990 m[c]	ν_{11} fund.	a_2	1292 s	1295 m[e]	1293 w	ν_{25} fund.	b_2
		2983 w sh	ν_{16} fund.	b_1	1244 s	1229 w[e]	1245 w	ν_5 fund.	a_1
	2955 m sh	2943 s	ν_1 fund.	a_1	1223 w sh		1226 w	ν_{12} fund.	a_2
	2927 m	2932 s	ν_{22} fund.	b_2	1189 vs		1185 w	ν_{17} fund.	b_1
	2872 w		$\nu_{12}+\nu_{23}=2899$	B_1		1156 s			
	2855 w	2846 w	$\nu_2+\nu_{26}=2896$	B_2	1151 s sh		1149 w	ν_{26} fund.	b_2
1987 w			$\nu_3+\nu_{19}=1992$	B_1	1006 w	1005 w		$\nu_9+\nu_{29}=1026$	B_2
1949 vw			$\nu_{24}+\nu_{29}=1963$	A_1	1002 w	998 w[d]	1004 m	ν_6 fund.	a_1
1905 m	1900 w[d]		$\nu_{10}+\nu_{23}=1909$	B_2	999 m				
1832 m			$\nu_6+\nu_{18}=1859$	B_1	907 w		908 s	ν_{13} fund.	a_2
1813 w sh	1800 w	1813 w	$2\times\nu_{13}=1816$	A_1	902 w sh			ν_{27} fund.	b_2
1776 m	1779 m		$\nu_{12}+\nu_{19}=1792$	B_2	853 vw	848 w[d]	855 vw	ν_{18} fund.	b_1
1745 s	1753 s	1752 s	ν_2 fund	a_1	818 s		818 w	ν_7 fund.	a_1
		1736 s					786 w	$\nu_{10}+\nu_{29}=$ 791	B_2
1708 m	1715 s sh[d]	1720 w sh	$\nu_7+\nu_{27}=1723$	B_2	669 w sh			$\nu_{29}+\nu_{30}=$ 675	A_1
1685 s sh		1677 m sh	$\nu_{13}+\nu_{14}=1694$	A_1	662 s sh			ν_{28} fund.	b_2
1673 vs					648 s	633 m[d]	648 s	ν_8 fund.	a_1
1655 s sh	1727 s	1654 s	ν_{23} fund.	b_2	566 m	567 w	566 w	ν_{19} fund.	b_1
1632 s		1636 s	$\nu_3+\nu_{10}=1662$	A_1	555 w	543 w	555 w sh	ν_{29} fund.	b_2
1612 w		1610 w sh	$2\times\nu_7=1636$	A_1			515 vw sh	ν_{14} fund.	a_2
1572 w		1570 w	$\nu_6+\nu_{19}=1572$	B_1	471 m	400 m	471 s	ν_9 fund.	a_1
1561 vw			$\nu_{27}+\nu_{28}=1567$	A_1	245 s[f]	236 s[g]	245 m	ν_{10} fund.	a_1
1426 s	1433 m	1428 m	ν_3 fund.	a_1	228 s		226 m		
1408 m		1410 m	ν_{24} fund.	b_2	206 w		205 m	ν_{15} fund.	a_2
		1379 vw	$\nu_{21}+\nu_{25}=1386$	A_2	186 s	149 m[g]	179 m	ν_{20} fund.	b_1
1327 s	1338 s	1332 s	ν_4 fund.	a_1	120 m	115 m[g]	125 w	ν_{30} fund.	b_2
1314 s					94 m	73 m[g]	92 m	ν_{21} fund.	b_1

[a] The weak infrared and Raman bands in the regions 5000–3000 cm^{-1} and 2800–200 cm^{-1} are omitted. [b] When available the combination frequencies and overtones are calculated from infrared solid state data. [c] For abbreviations used, see footnotes to Table 1. [d] CH_2Cl_2 solution. [e] CS_2 solution. [f] Solid state frequencies below 400 cm^{-1} are from polyethylene (Rigidex) pellet. [g] C_6H_6 solution.

Table 4. Calculated (ν_{calc}, cm^{-1}) and observed (ν_{obs}, cm^{-1}) fundamentals for *N*-chloro-, *N*-bromo-, and *N*-iodosuccinimide.

Species and No.	*N*-chloro		*N*-bromo-		*N*-iodo-	
	ν_{obs} [a]	ν_{calc}	ν_{obs} [a]	ν_{calc}	ν_{obs} [a]	ν_{calc}
a_1 ν_1	2957	2947	2950	2947	2943	2947
ν_2	1772	1785	1765	1776	1745	1755
ν_3	1425	1416	1421	1414	1426	1415
ν_4	1328	1336	1320	1341	1327	1350
ν_5	1248	1220	1248	1213	1244	1232
ν_6	1008	1001	1005	980	1002	988
ν_7	817	836	815	826	818	819
ν_8	652	636	640	622	648	629
ν_9	526	496	479	458	471	446
ν_{10}	338	344	279	287	236	246
a_2 ν_{11}	3000	3000	2997	3000	2990	3000
ν_{12}	1230	1192	1228	1192	1223	1192
ν_{13}	933	1104	916	1108	907	1097
ν_{14}	553	515	531	514	515	500
ν_{15}	230	246	221	236	206	206
b_1 ν_{16}	2991	2988	2986	2988	2983	2988
ν_{17}	1181	1198	1180	1198	1189	1196
ν_{18}	854	790	850	797	853	764
ν_{19}	571	617	569	624	566	575
ν_{20}	225	218	186	183	186	186
ν_{21}	143	114	124	108	94	95
b_2 ν_{22}	2951	2946	2947	2946	2932	2946
ν_{23}	1713	1710	1710	1703	1673	1670
ν_{24}	1406	1404	1405	1404	1408	1404
ν_{25}	1296	1310	1292	1312	1292	1313
ν_{26}	1165	1153	1167	1155	1151	1163
ν_{27}	963	950	933	911	902	905
ν_{28}	645	656	655	653	662	647
ν_{29}	562	565	556	556	555	554
ν_{30}	171	167	134	133	120	117

[a] When possible frequencies are taken from the infrared spectra of the solid state.

mide [3] with the N–H bending situated at a lower frequency. It is possible that various fundamental frequencies in this region are slightly perturbed due to strong Fermi resonance.

The N–Cl stretching mode (a_1) is found at 527 cm^{-1}. In the Raman spectra of the solid state at low temperature (–180 °C) this band is split probably due to the two isotopes ^{35}Cl and ^{37}Cl. The isotopic shift is about 4 cm^{-1} in agreement with the normal coordinate analysis and this is the only band expected to give an observable isotopic shift.

Due to a strong coupling with the C=O bending mode (a_1) the N-halogen stretching modes are found at 279 and 246 cm^{-1} for SIMB and SIMI. The C=O bending fundamentals (a_1) are situated at 338, 479 and 471 cm^{-1} for SIMC, SIMB and SIMI, respectively.

The N-halogen bending modes (b_2) are very well localized vibrations, situated at 171 (SIMC), 176 (SIMB) and 120 cm^{-1} (SIMI). In agreement with our results for *N*-chloromaleimide,[2] two b_1 modes are observed in the far infrared region, 143 and 225 cm^{-1} (SIMC), 134 and 186 cm^{-1} (SIMB) and at 94 and 186 cm^{-1} (SIMI). The remaining low frequency fundamental ν_{15} (a_2) is found at 230, 221 and 205 cm^{-1} for SIMC, SIMB and SIMI, respectively.

The fundamental frequencies assigned for SIMC, SIMB and SIMI are listed in Table 5

Table 5. Vibrational fundamentals for *N*-protio- (N-H),[a] *N*-deuterio- (N-D), *N*-chloro- (N-Cl),[b] *N*-bromo- (N-Br) and *N*-iodo- (N-I) succinimide.

N-H	N-D	N-Cl	N-Br	N-I	Assignments	Species
3150[c]	2326	526	279	236	N-X[d] stretch	a_1
2960	2958	2957	2950	2943	C-H stretch	
1772	1771	1772	1765	1745	C=O stretch	
1428	1425	1425	1421	1426	CH_2 scissor	
1373	1358	1328	1320	1327	C-N stretch	
1238	1231	1248	1248	1244	CH_2 wag	
1001	999	1008	1005	1002	C-C stretch	
850	846	817	815	818	C-C stretch	
640	635	652	640	648	Skeletal mode	
427	419	338	479	471	C=O bend	
3000	2998	3000	2997	2990	C-H stretch	a_2
1224	1222	1230	1228	1223	CH_2 twist	
935	916	933	916	907	CH_2 rock	
537	543	553	531	515	Skeletal mode	
267	268	230	221	206	C=O outo[e]	
2990	2989	2991	2986	2983	C-H stretch	b_1
1180	1190	1181	1180	1189	$C-H_2$ twist	
844	846	854	850	853	CH_2 rock	
823	525	225	186	186	N-X outo	
563	563	571	569	566	Skeletal mode	
190	187	143	124	94	C=O outo	
2946	–	2951	2947	2932	C-H stretch	b_2
1697	1674	1713	1710	1673	C=O stretch	
1416	820	171	134	120	N-X bend	
1402	1402	1406	1405	1408	CH_2 scissor	
1294	1292	1296	1292	1292	CH_2 wag	
1192	1272	1165	1167	1151	Skeletal mode	
935	1096	963	933	902	Skeletal mode	
650	635	645	655	662	Skeletal mode	
556	548	562	556	555	Skeletal mode	

[a] From Ref. 3. [b] This work. [c] When possible frequencies are taken from the infrared solid state. [d] X denotes H, D, Cl, Br, I respectively. [e] outo means out-of-plane bend.

and correlated with those of succinimide and *N*-deuteriosuccinimide.[3] The vibrational modes were described in terms of localized atomic motions, although the potential energy distribution (PED) calculated from the present force fields (not published for the sake of brevity) indicate this approach to be a very rough approximation. As apparent many vibrational modes were only slightly shifted (*e.g.* CH_2 stretch, scissor, wag, twist, rock and partly C–C and C=O stretch) while others vary quite monotonically with the heavier mass X.

NORMAL COORDINATE ANALYSIS

The force constant calculation was carried out employing an approximate internal valence force field as already described.[3] With the exception of the N-halogen bonds, we have used common structural parameters in all the succinimides (N–Cl, 1.69; N–Br, 1.80 and N–I, 1.90 Å). This approximation is considered to be of minor importance compared with the approximation of transferable force constants. Like in succinimide the agreement between the observed and calculated frequencies is best for the in-plane modes.

The internal coordinates are given in Fig. 2 of Ref. 3. Our calculated fundamentals are listed together with the observed frequencies in Table 4. The final set of force constants is given in Table 6. The potential energy distribution (PED) of the fundamentals among the valence coordinates were also calculated

Table 6. Final valence force constants for *N*-chloro- (N-Cl), *N*-bromo- (N-Br), and *N*-iodo- (N-I) succinimide.

Force Constants	Value [b]			Force Constants	Value [b]		
Symbol [a]	N-Cl	N-Br	N-I	Symbol [a]	N-Cl	N-Br	N-I
K_a	3.151	3.248	3.216	H_s	1.079	1.079	1.079
K_s	12.072	12.261	11.567	H_β	1.566	1.566	1.566
K_r	3.632	3.79	3.975	H_μ	0.447	0.401	0.365
K_d	3.5	3.5	3.5	$F_{a\eta}$	0.170	0.170	0.170
K_l	4.798	4.798	4.798	$F_{r\xi}$	0.170	0.170	0.170
K_b	3.512	3.337	2.588	$F_{s\alpha}$	−1.190	−1.190	−1.190
$K_{a_1a_2}$	0.789	0.886	1.167	$F_{r\psi}$	0.150	0.150	0.150
$K_{a_1s_1}$	1.472	1.700	1.616	$F_{d\phi}$	0.150	0.150	0.150
$K_{a_1s_2}$	−0.04	−0.04	−0.04	$F_{b\beta}$	−0.982	−0.982	−0.982
$K_{s_1s_2}$	0.15	0.15	0.2	$F_{\psi_1\psi_2}$	−0.038	−0.038	−0.038
$K_{a_1r_1}$	0.266	0.199	0.103	$F_{\phi_1\phi_2}$	−0.038	−0.038	−0.038
K_{r_1d}	0.487	0.520	0.422	$F_{\psi_1\phi_1}$	−0.015	−0.015	−0.015
$K_{l_1l_2}$	−0.079	−0.079	−0.079	O_{π_1}	0.223	0.202	0.148
H_η	1.185	1.185	1.185	O_{π_2}	0.359	0.335	0.312
H_ξ	1.185	1.185	1.185	$O_{\pi_1\pi_2}$	−0.027	−0.052	−0.013
H_ψ	0.574	0.574	0.574	T_τ	1.219	1.247	1.225
H_ϕ	0 574	0.574	0.574	$F_{\pi_1\tau_1}$	−0.118	−0.118	−0.118
H_θ	0.538	0.538	0.538	$F_{\pi_2\tau_1}$	0.173	0.173	0.173
H_α	1.844	1.360	1.743	$T_{\tau_1\tau_2}$	−0.031	−0.031	−0.031

[a] For meaning of symbols, see Fig. 2 and Table 4, Ref. 3 [b] In units of mdyn Å^{-1} (stretch constants), mdyn rad^{-1} (stretch- bend interaction) and mdyn Å rad^{-2} (bending and torsion constants).

and can be obtained from the authors on request.

Acknowledgement. The authors are grateful to K. Ruzicka for the preparative work. Financial support was received from the Norwegian Research Council for Science and the Humanities.

REFERENCES

1. Woldbæk, T., Klæboe, P. and Nielsen, C. J. *J. Mol. Struct. 27* (1975) 283.
2. Woldbæk, T., Klæboe, P. and Nielsen, C. J. *J. Mol. Struct. 28* (1975) 269.
3. Woldbæk, T., Klæboe, P. and Christensen, D. H. *Acta Chem. Scand. A 30* (1976) 531.
4. Brown, R. N. *Acta Crystallogr. 14* (1961) 711.
5. Yardley, K. *Proc. Roy. Soc. London 108 A* (1925) 542.
6. Matsuo, T. *Bull. Chem. Soc. Jpn. 37* (1964) 1844.
7. Fayat, N. M. C. and Foucaud, A. *C. R. Acad. Sci. 261* (1965) 4018.
8. Buczkowski, Z., Lange, J. and Urbanski, T. *Rocz. Chem. 39* (1965) 231.
9. Abramovitch, R. A. *J. Chem. Soc.* (1975) 1413.
10. Popov, E. M., Khomenko, A. Kh. and Shorygin, P. P. *Izv. Akad. Nauk SSSR, Ser. Khim. 1* (1965) 51.
11. Rogstad, A., Klæboe, P., Baranska, H., Bjarnov, E., Christensen, D. H., Nicolaysen, F., Nielsen, O. F., Cyvin, B. N. and Cyvin, S. J. *J. Mol. Struct. 20* (1974) 403.
12. Mason, R. *Acta Crystallogr. 14* (1961) 720; *9* (1956) 405.
13. Di Lauro, C., Califano, S. and Adembri, G. *J. Mol. Struct. 2* (1968) 173.
14. Bellamy, L. J., Connelly, B. R., Philpotts, A. R. and Williams, R. L. *Z. Electrochem. 64* (1960) 563.
15. Uno, T. and Machida, K. *Bull. Chem. Soc. Jpn. 35* (1962) 276.
16. Lee, C. M. and Kumler, W. D. *J. Am. Chem. Soc. 83* (1961) 4586.
17. Bellamy, L. J. and Williams, R. L. *J. Chem. Soc.* (1957) 4294.

Received January 16, 1976.

Acta Chemica Scandinavica A 30 (1976) 555—562

Brønstedian Energetics, Classical Thermodynamics and the Exergy. Towards a Rational Thermodynamics. I.

TORBEN SMITH SØRENSEN

Fysisk-Kemisk Institut, Technical University of Denmark, DK-2800 Lyngby, Denmark

A comparison between the process-oriented energetics of Brønsted and the system-oriented classical thermodynamics is carried out. It is shown that a unification can be made in terms of the exergy concept. The exergy is generally defined as the maximum available energy in the thermodynamic system which may be completely general with several temperatures, pressures, phases *etc.* The exergy is shown to be a non-additive energy function when subsystems are united. Under appropriate simplifying conditions the exergy specialises into the well-known Gibbsian Legendre-transformed energy functions. The "active variables" of the Legendre-transformations correspond to Brønstedian "neutral transports".

As is well known the foundation of phenomenological thermodynamics were laid by Sadi Carnot with his famous treatise over cyclically operating heat engines in 1824.[1] Historically, the Carnot cycle was used in developing a statement of the second law of thermodynamics and to create the concept of entropy.[2,3] This procedure cannot be said to be particularly expedient in chemical thermodynamics, however, and therefore the Carathéodory version of the second law is sometimes preferred.[4–6] The present author does not feel, however, that an understanding of Carathéodory's theorem about Pfaffian forms is of much help in overcoming the didactic problems in teaching thermodynamics to chemists.

The reason is that there are a number of logical flaws and weaknesses in the definitions of "heat" and "work" of traditional thermodynamics, as pointed out by J. N. Brønsted many years ago. Brønsted tried to reformulate classical thermodynamics into a more precise and symmetrical structure named *energetics* by himself.[7–12] I would especially recommend the Philosophical Magazine article [12] as a short-hand introduction to Brønstedian energetics. The Brønsted energetics has obvious pedagogic advantages and permits replacement of lengthy considerations by short statements of immediate transparency.

In 1971 the author wrote an article [13] trying to reconcile the *process-oriented* Brønstedian energetics with the *system-oriented* Gibbsian approach. Especially the connection between Brønsted's "neutral transports" and Gibbs' derived energy functions was pointed out. In the author's Ph. D. dissertation [14] the analysis was carried somewhat further in an effort to establish a general *exergy* function (generalised free energy) on the basis of Brønsted's energetics. Actually, Brønsted never did integrate his work principle explicitly, although the mere mentioning of a work *loss* assumes the existence of a work *function*. Colmant has once pointed out [15] that Brønstedian energetics in many respects is very similar to the "energetique" advocated earlier by Le Chatelier.[16] The latter author bases, however, his entire theory on the "puissance motrice" which can be regarded as an exergy function.

The term "Exergie" was apparently introduced by Z. Rant in 1953 and has been used within the field of power station and refrigeration techniques.[17] A quantity named "essergy" has been defined through the information theory by R. B. Evans in 1969,[18] and this is also essentially an exergy function. Very recently a book about irreversible thermodynamics utilising the exergy concept has appeared.[19] None of the above-mentioned exergy functions

Table 1.

Type of basic process	Potential	Quantity	Conserved/Not Conserved
Mechanical	Force (f)	Length (x)	C
Kinetic	$v^2/2$ (v = velocity)	Mass (M)	C
Gravitational	Gravitational potential (Φ)	Mass (M)	C
Spatial	Negative pressure ($-p$)	Volume (V)	C
Elastic	Stress tensor	Strain tensor ("length")	C
Interface	Interfacial tension (σ)	Interfacial area (A)	NC
Thermal	Temperature (T)	Entropy (S)	C Rev. processes NC Produced in irrev. processes
Chemical	Chemical potential (μ)	Number of moles (n)	C Physical transport NC Chemical reactions
Electric	Electric potential (Ψ)	Electric charge (q)	C
Dielectric	Electric field ($\mathscr{E}$)	Dielectric polarisation ($\mathscr{P}$)	NC
Magnetic	Magnetic field ($\mathscr{H}$)	Magnetisation ($\mathscr{M}$)	NC

have the generality and simplicity of the function defined on the basis of the work principle of Brønsted.

In the present article I shall try to formulate the main content of Brønstedian energetics and its extensions in the pious hope that there will be a renewed interest in this concise representation of the body of thermodynamic facts.

POTENTIALS, QUANTITIES AND THE WORK PRINCIPLE

Brønsted wished to expand the meaning of the term "work" beyond the narrow definition (force times length) in mechanics and classical thermodynamics. Just as the work done by lifting a weight may be calculated as the product of the mass and a difference in gravity potential, a number of other processes in nature may be described as transfer of quantities of an extensive nature between two potentials of an intensive nature (basic process of the first type) or the creation or destruction of a quantity at a single potential (basic process of second type). The work done by those basic processes is given by

$$\text{Type 1: } \delta W = -\Delta P \delta K \tag{1a}$$

$$\text{Type 2: } \delta W = -P \delta K \tag{1b}$$

δK represents a virtual variation of the amount of a quantity and P the conjugated potential. A list of some dual quantities and potentials is given in Table 1. Processes of type 1 may be considered to be the sum of a destruction and a creation process of the second type with the net result that quantities participating in processes of the first type are conserved. The *work principle* of Brønsted now states that when two or more of such basic processes are coupled together and when the transformations are reversible – that is their directions may be reversed without any supplementary help from outside – the sum of all the work done must be zero

$$\sum \delta W_i = -\sum P_i \delta K_i = 0 \tag{2}$$

The summation has to be carried out over all quantities and all localities with distinct potentials in the considered closed system. In case of continuous systems the summation must be replaced by an integration over the volume of the system.

Taking our departure in a simple mechanical basic process such as the lifting of a weight, we may define work done by thermal, electric, or other basic processes by successive coupling of the basic processes under study with the mechanical process. We notice that in cases

where we have already established the extensive quantity the intensive potential will be defined through the work principle. For example, with K being equal to the number of moles of a substance (n_i) we have a direct definition of the chemical potential μ_i. There is no need to make a *detour* over the internal energy or its Legendre-transforms as did Gibbs in his "Equilibrium of Heterogenous Substances" [20] in order to define this fundamental potential. On the other hand, for the thermal basic process the work principle uniquely defines the thermal quantity which is not heat, but entropy when some temperature scale has been established. The only net result of a Carnot cycle is a transfer of entropy from a heat reservoir (better: entropy reservoir) at one temperature to a reservoir at another temperature. A general Carnot cycle may be carried out with any reversibly functioning device with thermal communication during a part of the cycle with two thermal reservoirs. With this general definition of a Carnot cycle we have included cooling techniques such as the cyclical magnetisation and demagnetisation of paramagnetic salts.[21] The definition from Brønsted's work principle of the entropy * reveals that quantity to be the real thermal quantity corresponding to other quantities in physical chemistry such as electric charge, volume, number of moles, mass and surface area.

The basic spatial process consists of moving a piston corresponding to an infinitesimal volume δV when the pressure on one side is p_1 and on the other side p_2. If the piston is moved towards the p_2 side, the process may be characterised as a transfer of δV from p_2 to p_1. The work done is

$$\delta W_{\text{spatial}} = (p_1 - p_2)\delta V$$

Comparison with eqn. (1a) shows us that the potential in the spatial basic process should be put equal to the negative pressure.

One striking example of the fundamental manner in which Brønstedian energetics differ from traditional thermodynamics may be given at this stage. Consider an ideal gas confined in a cylinder with piston in thermal contact with an entropy reservoir. On the other side of the piston is vacuum, but a weight is placed on the piston. Now, traditional thermodynamics would maintain that the conversion of heat taken from a single reservoir into work is possible in a *non-cyclical* process. Heat flows into the gas and the piston with the weight goes up. As the internal energy of the gas remains constant in the isothermal expansion, the potential energy taken up by the weight corresponds to the heat absorbed. Brønsted finds this untenable. He maintains that the conversion of thermal energy at a single temperature into other kinds of energy is impossible under all circumstances. The two basic processes which are coupled together in the present example are the transfer of δV from zero pressure to p and the transfer of mass M from the gravitational potential ϕ to $\phi + \mathrm{d}\phi$. The transfer of entropy from the entropy reservoir to the ideal gas is just a *neutral transport* without any energetic significance, because the transfer occurs between regions with the same temperature. The absorption of entropy is only a consequence of the special *constitutive relation* of the ideal gas (the ideal gas law). Consider that the material enclosed in the cylinder were water at 2 °C. Now, when heat is absorbed, the piston goes down! The "tragicomedy of thermodynamics" – as Truesdell has put it [22] – has been the persisting tendency to entangle in special constitutive relations, so that the purely *energetic* content of the theory becomes invisible.

We notice also that there is no need to speak about "heat" in reversibly coupled processes. Entropy is the useful thermal quantity which can be defined both when it is reversibly or irreversibly transported and as a static entropy

* Actually, Brønsted did first define the entropy and thereafter an "energetic temperature scale", see *e.g.* section 3 in Ref. 12. His arguments are somewhat circuitous, however, because he first defines a calorimeter as an energetic system with uniform potentials which is only in thermal contact with the surroundings. Then he measures some preliminary temperature of the calorimeter by any conventional thermometer and defines the change in entropy as being proportional to the change in temperature when they are both infinitesimal. Finally, he establishes the energetic temperature scale by means of the work principle. The arguments are much shortened and clarified if the order of definitions are reversed giving rise to an "energetic entropy definition" corresponding to any arbitrary temperature scale.

content of a body. The "heat" defined in traditional thermodynamics can only be defined when it is transported and it is not conserved in the basic thermal process: the Carnot cycle. Heat enters into Brønstedian energetics only in connection with *irreversible* processes as we shall see in the next section.

EXERGY AND BRØNSTED'S HEAT PRINCIPLE

We shall now proceed to define the exergy of an isolated thermodynamic system. By isolated we mean that it has no communication of work or any energetic quantities with the outside world. Such a system may be characterised by the set of two vectors $(\mathbf{P},\mathbf{K})$ denoting the amount of different quantities at different "positions" (be it in physical space or in more abstract reaction spaces) and the conjugated potentials. Furthermore, there will be a set of *constitutive relations* given by the vector eqn. $\mathbf{C}(\mathbf{P},\mathbf{K})=\mathbf{0}$. By a constitutive relation we mean a relation between potentials $\mathbf{P}$ and quantities $\mathbf{K}$, such as given by the dependence of heat capacity (better: entropy capacity) on temperature or the dependence of pressure on volume and temperature (eqn. of state). The constitutive relations for general thermodynamic systems will depend both on the materials constituting the system and on the specific arrangement of the quantity exchange and the energy conversion between the subsystems within the system. Most of such constitutive relations will possess what might be called the *local property*, *i.e.* only $\mathbf{P}$'s and $\mathbf{K}$'s at the same physical locality enter into the constitutive relation. Sometimes it will be necessary, however, to operate with quite complicated non-localised constitutive relations. For example when a charge distribution produces an electric field according to the eqn. of Poisson. This will be the case for, *e.g.*, electrokinetic phenomena [23] or in electrolyte diffusion zones.[24]

Imagine now that we allow for interaction of the system with an outside mechanical basic process. We proceed to move quantities between the different localities in a reversible manner by coupling with the exterior mechanical reservoir until the potential differences in the system cannot be further equalised. At that point – the *energetic zero point* of the system – the state of the system will be $(\mathbf{P}_0,\mathbf{K}_0)$. The state is not necessarily a state with all potentials of the same kind being identical at all localities. Different quantities are often linked together in fixed proportions in so-called *transport complexes*. For example, one mol of a given ionic species is linked to a charge z_iF and a mass M_i, z_i being the number of elementary charges on the ion with sign, F the Faraday constant and M_i the ionic weight in Daltons. Thus, in electrical and gravitational fields equilibrium will be reached with the equalisation of the compound *electro-gravi-chemical* potential

$$\tilde{\mu}_i=\mu_i+z_iF\psi+M_i\Phi \tag{3}$$

in all regions of the system to which access of the i'th ion is possible.

When the system has reached the energetic zero point some work has been received by the external mechanical reservoir and we shall term this work the *exergy* of the system and designate it by the symbol Ex. By the work principle we have

$$Ex=-\int_{\mathbf{P},\mathbf{K}}^{\mathbf{P}_0,\mathbf{K}_0}\sum_{\text{system}}P_i\delta K_i \tag{4}$$

We can only carry out the integration having a knowledge of the set of constitutive relations $\mathbf{C}(\mathbf{P},\mathbf{K})=\mathbf{0}$. On the other hand it should be clear from the fundamental theorem of energy conservation in nature that the exergy of a given system must be independent of the integration path. Thus, the exergy must be a function of state of the system, a state being defined by the set $(\mathbf{P},\mathbf{K})$. Clearly, this requires that the constitutive relations satisfy the requirement

$$\frac{\partial P_j}{\partial K_i}=\frac{\partial P_i}{\partial K_j} \tag{5}$$

When the constitutive relations possess the local property, eqn. (5) will be automatically satisfied for quantities and potentials which refer to two different regions, because the cross derivatives will be zero. *Within* the same region eqn. (5) will yield relations of the usual Maxwell type.

To give a specific example of an exergy calculation consider two blocks of the same material at atmospheric pressure and tempera-

tures t_2^i and t_1^i on any arbitrary temperature scale (superscript i stands for "initial"). We may put as constitutive relation

$$\delta S = c\,\delta t \tag{6}$$

where S is the entropy conjugate to the chosen temperature scale and c is an entropy capacity of the material which we for simplicity consider independent of temperature. By means of a Carnot cycle we transfer entropy from the upper temperature t_2^i to the lower t_1^i. When the amount of entropy transported has reached the value S, the two temperatures will be, respectively,

$$t_1 = t_1^i + S/c$$

$$t_2 = t_2^i - S/c$$

At the energetic zero point $t_1 = t_2$ and the transfered entropy equals to

$$S^0 = (c/2)(t_2^i - t_1^i)$$

The exergy can now be calculated from eqn. (4)

$$Ex = \int_{S=0}^{S^0} (t_2 - t_1)\mathrm{d}S = \frac{c}{4}(t_2^i - t_1^i)^2 \tag{7}$$

We notice that the exergy is a minimum when the initial temperature difference is zero *if* $c > 0$ which is the condition of thermal stability of the material.

The exergies of subsystems have a remarkable property: they are *not additive*.[14] Imagine a subsystem I with an exergy $Ex(\mathrm{I})$ and another subsystem II with an exergy $Ex(\mathrm{II})$. When the two subsystems are fused together after their exergies have been extracted, it will often be possible still to extract additional exergy from the total system, because there will still be unexploited potential differences *between* the two subsystems even if an *internal* equalisation of potentials (or transport complex potentials) has been carried out in each system *per se*. Symbolically we have

$$Ex(\mathrm{I}+\mathrm{II}) = Ex(\mathrm{I}) + Ex(\mathrm{II}) + Ex(\mathrm{I}_0 + \mathrm{II}_0) \tag{8}$$

a subscript 0 denoting that the system is at its energetic zero point. Thus, thermodynamics is *holistic* in its very nature, a feature which has been totally neglected in all traditional expositions of the subject.

Until now we have only considered reversible transformations. When irreversible processes have occurred in an isolated system, this is reflected by the fact that the system cannot be carried back to its initial state without mechanical and thermal manipulations from outside. The quantitative description is given by Brønsted's *heat principle*

$$-\mathrm{d}Ex = \mathrm{d}Q \geq 0 \tag{9}$$

In words: the loss of exergy – Brønsted spoke about the loss of work – equals the *energetic heat evolution*. This quantity is always positive (zero only for strictly reversible transformation). It is called heat evolution, because it is accompanied by a *production* of the thermal quantity

$$\mathrm{d}Q = T\mathrm{d}S_{\mathrm{prod}}, \qquad \mathrm{d}S_{\mathrm{prod}} \geq 0 \tag{10}$$

For small changes there will be a simple proportionality between the heat evolution (or exergy loss) and the production of entropy. The proportionality constant T in eqn. (10) has the dimension temperature and it is found to vary with the arbitrary temperature t. Actually, it might quite as well be used as a measure of temperature as the arbitrary temperature. The positivity of T is assumed by the simultaneous positivity of the energetic heat evolution and the entropy production. The advantage of using T instead of t as a measure of temperature is, of course, that we now have an *absolute energetic temperature scale* defined solely through eqn. (10) and with no reference to statistical mechanics, extrapolation of ideal gas properties or properties of materials at very low temperatures. The arguments presented here are not circuitous, since the entropy produced may be measured using the work principle and the arbitrary temperature scale, and the loss of exergy may also be uniquely defined using the arbitrary temperature scale, *cf.* eqn. (7).

It is of course important not to confuse the energetic heat evolution with intuitive considerations, *e.g.* whether there is an increase in temperature or not. Brønsted [9] investigated the heat concept in a number of monographs upon thermodynamics and found that it varied from author to author and from situation to situation. Vague words from the daily life are not suited to build a science upon, perhaps

it would be better to avoid the word "heat" altogether and use instead the word *anergy* which is actually already in use.[17] Anergy is the "low quality" thermal energy into which exergy degrades during irreversible transformations. Further utilisation of this energy is not possible, if the system under consideration remains isolated from its surroundings. Utilisation is possible, however, if the gates open up to other systems with lower temperatures than the temperature prevailing in the original system. Then, suddenly, anergy is converted to new exergy.

INTERNAL ENERGY, NEUTRAL TRANSPORTS AND CONDITIONED EXERGY

An energy quantity as important as the exergy is the *internal energy* of the system (**P**,**K**). We shall designate that quantity by the letter E, but our internal energy is more generally defined than the one usually discussed in thermodynamics. Besides the system considered we need some standard reservoirs of the conserved energetic quantities (C) with fixed conjugate potentials. We start with an empty system and then slowly transfer the conserved quantities in a reversible manner from the standard reservoirs to their positions in the system. The work done in order to perform the operations described can be found from the work principle, and from the principle of conservation of energy we may also find it as a sum of the gain in internal energy of the system and the gain of the standard reservoirs

$$\sum(P-P_{st})\mathrm{d}K(C)+\sum P\mathrm{d}K(NC)=\mathrm{d}E+\mathrm{d}E_{st} \quad (11)$$

The summation over non-conserved quantities (NC) represents the work absorbed by the reversible creation of quantities in the system itself, *e.g.* interfacial areas or mol of a chemical component produced from other components in internal chemical equilibria. The division of the internal energy between the system and the reservoirs is quite arbitrary, but it appears natural to take

$$\mathrm{d}E=\sum_{\text{system}} P\mathrm{d}K \quad (12a)$$

and

$$\mathrm{d}E_{st}=\sum_{\text{reservoirs}} P_{st}\mathrm{d}K_{st}=\sum P_{st}(-\mathrm{d}K) \quad (12b)$$

The definition of the internal energy of a system is thus taken to be

$$E=\sum_{\text{system}} \int_0^{K_i} P_i\mathrm{d}K_i \quad (13)$$

Clearly, we must assume a knowledge of the internal constitutive relations as the case is with the exergy, too. From the principle of conservation of energy or by comparison of eqns. (4) and (13) we immediately find the following connection between the exergy and the internal energy of a system

$$Ex=E-E_0 \quad (14)$$

where E_0 is the internal energy of the system at its energetic zero point. In contrast to exergy the internal energy *is* additive as a result of conservation of energy. Therefore, the fact that the total exergy is often greater than the sum of the exergies of the subsystems [*cf.* eqn. (8)] merely reflects the fact that the energetic zero point of the combined system is at a lower internal energy than the sum of the internal energies of the subsystems at *their* energetic zero points. It is also important to notice another fundamental difference between internal energy and exergy. When we differentiate eqn. (14) we have to take

$$\mathrm{d}Ex=\mathrm{d}E-\mathrm{d}E_0 \quad (15)$$

because the energetic zero point will change when irreversible processes are occurring in the system. This is so, because the system will not be the same before and after some irreversible transformations have taken place, since more entropy has been produced in the system. The change in internal energy in an isolated system during irreversible transformations will be zero, but the internal energy at the energetic zero point will be greater after the transformations than before, and therefore there has appeared a loss in exergy according to (15).

From the very general considerations given here it is possible to make a bridge to the specialised – but for chemists very useful – Gibbsian thermodynamics based upon Legendre transforms of the internal energy. We shall introduce the concept *conditioned exergy* of a thermodynamic system (**P**,**K**) which is permitted to exchange certain quantities with

outside reservoirs of infinite magnitude. Hereby the corresponding potentials – or transport complex potentials – at the localities where the exchanges occur will be fixed at the values $\mathbf{P}_{fix}$ of the external reservoirs. From eqn. (12a) we observe that terms $P_{fix}dK$ will contribute to the changes in internal energy of the system, but there can be no alterations in exergy, since all the transfers of quantities through the boundaries of the system take place over zero potential differences. This is precisely what Brønsted called *neutral transports*. It is interesting to observe neutral transport processes to be on the borderline between reversible and irreversible processes in Brønstedian energetics. They are processes which are not coupled to any other process, but their driving forces must of course be slight differences in potentials. So in a way they are irreversible processes, but the loss of exergy is zero because the difference in potentials is infinitesimal and the processes may equally well be reversed.

If we subtract the contributions $P_{fix}dK$ from the internal energy, we obtain the conditioned exergy in cases with no irreversible processes. In the general case with both reversible and irreversible processes we may write for the conditioned system instead of eqn. (15)

$$dEx(P_{fix}) = dE - \sum P_{fix}dK - dE_0 \qquad (16)$$

with $Ex(P_{fix})$ being the conditioned exergy. Clearly, the conditioned exergy is the maximum amount of work which can be extracted from the open, conditioned system with the external constraints maintained.

In the very special, but important systems studied by Gibbs, the internal energy has the property of being multiplied by n if the amount of all quantities constituting the thermodynamic phase is multiplied by n. The integration in eqn. (13) may then be carried out by means of Euler's theorem for homogeneous functions of the first degree with the result

$$E = \sum PK \qquad (17)$$

Comparison of eqn. (17) with eqn. (12a) gives us the Gibbs-Duhem formula

$$\sum K dP = 0 \qquad (18)$$

Now, consider the following Legendre transform of the internal energy

$$E(\mathbf{P}') = E - \sum P'K \qquad (19)$$

The technique of Legendre transforms was well known in analytical mechanics before it was introduced into thermodynamics by Gibbs, see *e.g.* Lanczos' book.[25] The selected vector of potentials $\mathbf{P}'$ constitutes the *active variables* of the transformation. Taking the differential on both sides of eqn. (19) and using (17) and (18) we obtain

$$dE(\mathbf{P}') = \sum PdK - \sum P'dK - \sum KdP' \qquad (20)$$

If the $\mathbf{P}'$ is chosen to be the vector of fixed potentials $\mathbf{P}_{fix}$, the third term on the r.h.s. of eqn. (20) will vanish and the second term will accomplish the required correction for neutral transports, so under the given external constraints and when no irreversible processes occur, the Legendre-transformed internal energy in eqn. (19) will be equal to the conditioned exergy, *i.e.* the Legendre transforms will correspond to the maximum work which can be withdrawn from the conditioned systems. Table 2 shows the constraints and the neutral transports in connection with the well-known Gibbsian functions.

CONCLUSION

The present way of presentation has distinct advantages in simplicity, symmetry and strength in comparison to traditional exposi-

Table 2. The Gibbsian Legendre-transformed internal energy functions.

Name	Conditioned exergy	Neutral transport of.	Constraints
Enthalpy	$H = E - (-p)V$	V	p and S const.
Helmholtz' free energy	$F = E - TS$	S	T and V const.
Gibbs' free energy	$G = E - (-p)V - TS$	V and S	p and T const.

tions of thermodynamics. Also, it gives to thermodynamics a much more general structure which might become of value in the analysis of complex thermodynamic systems, *e.g.* for analysis of exergy flow patterns in ecosystems. A paper on the rationalisation of irreversible thermodynamics along the lines of Brønsted energetics will be forthcoming.

Acknowledgement. Professor J. Koefoed from Fysisk-Kemisk Institut is warmly thanked for numerous stimulating discussions about thermodynamics and for his interest in the present work.

REFERENCES

1. Carnot, S. *Reflections sur la puissance motrice du feu*, Chez Bachelier Libraire, Paris 1824.
2. Clausius, R. *Ann. Phys. 79* (1850) 368, 500.
3. Poincaré, H. *Thermodynamique*, Carré, Paris 1892.
4. Carathéodory, C. *Math. Ann. 67* (1909) 355; *Sitzungsber. preuss. Akad. Wiss.* (1925) 39.
5. Born, M. *Phys. Z. 22* (1921) 218, 249, 282.
6. Honig, J. M. *J. Chem. Educ. 52* (1975) 418.
7. Brønsted, J. N. *K. Dan. Vidensk. Selsk. Mat. Fys. Medd. 15* (1937) 4.
8. Brønsted, J. N. *K. Dan. Vidensk. Selsk. Mat. Fys. Medd. 16* (1938) 10.
9. Brønsted, J. N. *K. Dan. Vidensk. Selsk. Mat. Fys. Medd. 19* (1941) 39.
10. Brønsted, J. N. *Principles and Problems of Energetics*, Interscience, New York 1955; (first published in Danish in *Københavns Universitets Festskrift*, Copenhagen 1946).
11. Brønsted, J. N. *J. Phys. Chem. 44* (1940) 699.
12. Brønsted, J. N. *Philos. Mag. Ser. 7 29* (1940) 449.
13. Sørensen, T. S. *Dansk Kemi 52* (1971) 138 (in Danish).
14. Sørensen, T. S. *Studier over Fysisk-Kemiske Systemers Statik, Dynamik, Kinetik.* Ph.D. Thesis, Technical University of Denmark, Lyngby 1973.
15. Colmant, P. *Acta Chem. Scand. 3* (1949) 1220.
16. Le Chatelier, H. *Rev. Quest. Sci. 94* (1928) 363.
17. VDI-Fachgruppe Energietechnik *Energie und Exergie*, VDI-Verlag, Düsseldorf 1965.
18. Evans, R. B. *A Proof that Essergy is the only Consistent Measure of Potential Work (for Work Systems)* Ph.D. Thesis, Dartmouth College, 1969, University Microfilms, Ann Arbor, Michigan.
19. Chartier, P., Gross, M. and Spiegler, K. S. *Applications de la thermodynamique du non-equilibre*, Hermann, Paris 1975.
20. Gibbs, J. W. *Scientific Papers, Vol. I*, Dover, New York 1961, p. 89.
21. Giauque, W. F. *J. Am. Chem. Soc. 49* (1927) 1870.
22. Truesdell, C. *The Tragicomedy of Thermodynamics*, Springer, Wien-New York 1971.
23. Sørensen, T. S. and Koefoed, J. *J. Chem. Soc. Faraday Trans. 2 70* (1974) 665.
24. Sørensen, T. S. and Jensen, K. F. *J. Chem. Soc. Faraday Trans. 2 71* (1975) 1805.
25. Lanczos, C. *The Variational Principles of Mechanics*, 3rd Ed., University of Toronto Press, Toronto 1966.

Received March 3, 1976.

Acta Chemica Scandinavica A 30 (1976) 563—566

The Action of Ionic ^{13}C-Cyanide on Aromatic Thiocyanates in Acetonitrile

TOR AUSTAD and STEINAR ESPERÅS

Department of Chemistry, University of Bergen, N-5014 Bergen-Univ., Norway

The reaction between various X-phenyl thiocyanates (X=H, *o*-NO_2, *p*-NO_2, and *p*-Me_2N) and ionic cyanide has been studied in acetonitrile. On the basis of IR measurements, applying ionic ^{13}C-cyanide, the reaction mechanism is suggested to involve a fast exchange of the cyano group prior to an adduct formation between the substrate and 2 mol of cyanide ions. In the case of *p*-nitrophenyl thiocyanate the tetraphenylarsonium salt of the adduct is isolated, and the space group is determined by means of X-ray crystallography. The rate of adduct formation is drastically decreased in the order: *p*-NO_2 > *o*-NO_2 > H > *p*-Me_2N.

Aromatic thiocyanates may, according to Giles and Parker,[1] be regarded as trifunctional electrophiles.

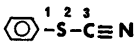

The potential electrophilic centers are; (1) the aromatic carbon atom bonded to the thiocyanate group, (2) the sulfur atom, and (3) the cyanide carbon atom.

If nitro groups are substituents in the benzene ring, Giles and Parker [1] found that only one of the nucleophiles studied, *i.e.*, the thioethoxide ion, did attack at the sulfur atom of the substrate. All the other nucleophiles did attack at the aryl carbon atom and the cyanide carbon atom in different ratios.

In this paper we report the results of the reaction between ionic ^{13}C-cyanide and various aryl thiocyanates in acetonitrile at room temperature. The following reactions resulting from nucleophilic attack of $*CN^-$ on aryl thiocyanates may then be possible;
Reaction A involves an S_NAr process, reaction B involves an exchange of cyanide by means of a substitution on S^{II}, and reaction C is assumed to involve an attack at the cyanide carbon. Cyanogen formed in the latter case is believed to add two cyanide ions in a fast reaction forming the postulated diiminosuccinonitrile dianion, eqn. 1.[2]

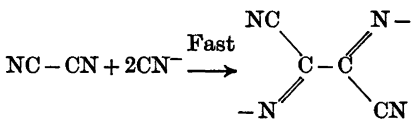

(1)

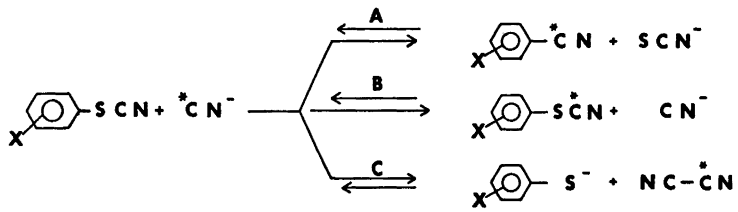

Scheme 1.

Table 1. IR data for aromatic thiocyanates and the corresponding ^{13}C-thiocyanates in acetonitrile.

X	ν(XArSCN) cm^{-1}	ν(XArS^{13}CN) cm^{-1}
p-NO_2	2169	2120
o-NO_2	2165	2115
H	2164	2115
p-$(CH_3)_2N$	2162	2116

The frequency of the nitrile stretching vibration in the 2000 cm^{-1} region has been found to be very sensitive to the mass of the cyano carbon atom. The ^{13}C-pseudohalides, SCN^-, $SeCN^-$, and $TeCN^-$, have been observed to absorb about 50 cm^{-1} lower than did the corresponding ^{12}C-pseudohalides.[2] The sharp cyano-peaks were thus sufficiently apart for both qualitative and quantitative analysis. IR-measurements in the 2000 cm^{-1} region on the present reactions, Scheme 1, were found to be a satisfactory method for characterizing the various components, Table 1.

The p-*nitrophenyl thiocyanate-cyanide reaction.* Upon mixing *p*-nitrophenyl thiocyanate and tetraphenylarsonium cyanide in acetonitrile at room temperature, the reaction mixture turned deep red, and the IR-spectrum of the solution showed a strong peak at 2142 cm^{-1}. A stable deep red tetraphenylarsonium salt was isolated, which according to the molecular weight determination by means of X-ray technique and elemental analysis appeared to be an adduct between *p*-nitrophenyl thiocyanate and two mol of tetraphenylarsonium cyanide. The stoichiometry of the reaction (1:2 in substrate and nucleophile, respectively) was found to be compatible with the results obtained by measuring the absorbance of the reaction mixture in acetonitrile at 2142 cm^{-1} at different cyanide concentrations.

No peak related to ionic thiocyanate, $\nu_{SCN^-} = 2059$ cm^{-1},[2] could be detected in the IR-spectrum which eliminates an S_NAr process (Scheme 1, reaction A).

If equal amounts of the substrate and ionic ^{13}C-cyanide were used, the peak at 2142 cm^{-1}, related to the adduct, split into two peaks ($\nu = 2142$ cm^{-1} and $\nu = 2088$ cm^{-1}) of equal absorbance but each of half the

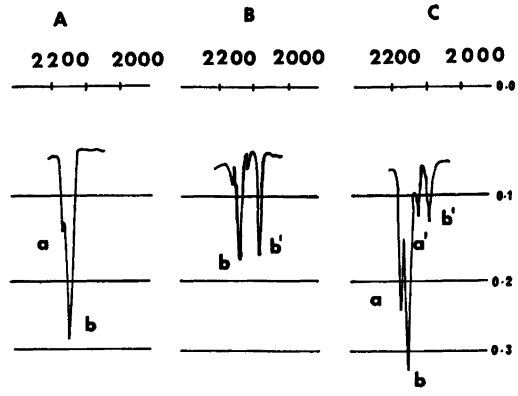

Fig. 1. A and B; IR-spectra of a mixture 3.0×10^{-3} M in *p*-NO_2ArSCN and 3.0×10^{-3} M in Ph_4AsCN or $Ph_4As^{13}CN$, respectively, in acetonitrile. C; IR-spectrum of a solution containing 2.0×10^{-2} M of *p*-NO_2ArSCN and 1.0×10^{-2} M $Ph_4As^{13}CN$.

a and a′ are related to *p*-NO_2ArSCN and *p*-$NO_2ArS^{13}CN$, respectively. b and b′ are related to the adduct. All the spectra were recorded immediately after the reactants were mixed.

absorbance obtained under the same conditions using ^{13}C-cyanide, Fig. 1 A and B. Fig. 1 C shows the IR-spectrum of a more concentrated reaction mixture in which the mol ratio is 2:1 in substrate and ionic ^{13}C-cyanide, respectively. The two new peaks a and a′ are related to the aryl thiocyanate and aryl ^{13}C-thiocyanate, respectively.

Thus, according to these results, a fast exchange of the cyano group appears to take place prior to the adduct formation. The geometrical configuration of the adduct is not known. We suggest, however, that the form represented by (II) is the most reasonable one. This adduct may be formed by an addition of a cyanide ion to the cyano carbon atom of the substrate, forming the intermediate (I), followed by a second cyanide addition to (I). The overall reaction between *p*-nitrophenyl thiocyanate and ionic cyanide may then be represented by Scheme 2.

Evidence for an intermediate of the type (I) has been reported by Hogg [3] and Giles and Parker.[1] The adduct (II) is then of the same type as the postulated diiminosuccinonitrile dianion, eqn. 1.

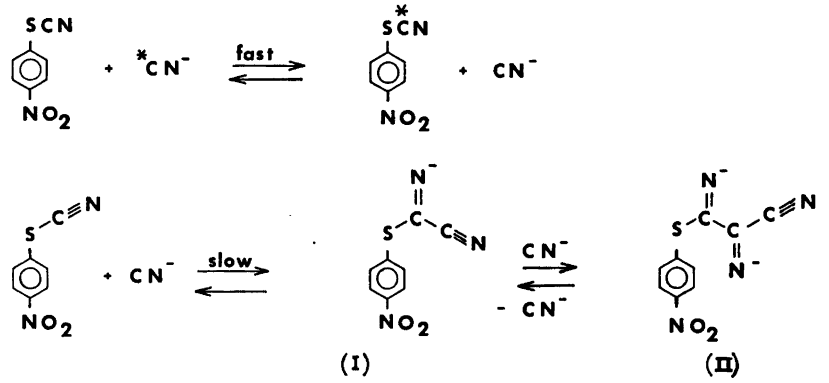

Scheme 2.

Other aryl thiocyanate-cyanide reactions. The other aryl thiocyanates studied, *i.e.*, *o*-nitrophenyl, phenyl, and *p*-dimethylaminophenyl thiocyanate, showed a reaction pattern similar to that outlined above for the *p*-nitrophenyl thiocyanate-cyanide reaction. In all cases a fast exchange of the cyano group was observed, but the rate of adduct formation was drastically decreased in the order; $p\text{-}NO_2 > o\text{-}NO_2 > H > p\text{-}(CH_3)_2N$. Thus, electron withdrawing groups increase the electrophilic nature of the cyano carbon atom.

The IR-spectra in the 2000 cm^{-1} region of a solution of phenyl thiocyanate and ionic ^{13}C-cyanide in acetonitrile at various times after mixing is shown in Fig. 2 (B, C).

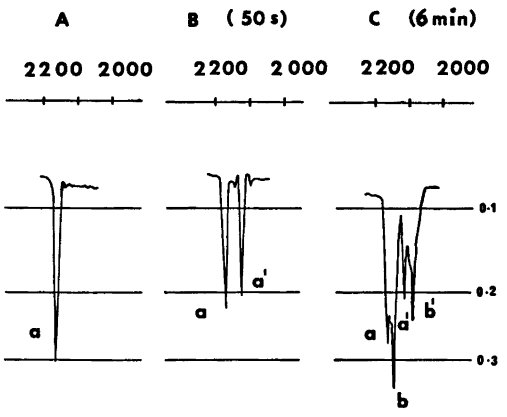

Fig. 2. A; IR-spectra of a 2.0×10^{-2} M solution of ArSCN in acetonitrile. B and C; IR-spectra of a solution containing 2.0×10^{-2} M of ArSCN and 2.0×10^{-2} M of $Ph_4As^{13}CN$ in acetonitrile at various times after mixing.
a and a′ are related to ArSCN and $ArS^{13}CN$, respectively. b and b′ are related to the adduct.

The frequences of the peaks associated with the adduct were found to be the same for all the compounds studied. ($\nu = 2142$ cm^{-1} and 2088 cm^{-1}).

As far as the authors know, there has not been reported any exchange between organic thiocyanates and ionic cyanide previously. In protic solvents total exchange occurs between organic selenocyanates and poltassium ^{14}C-cyanide.[4] Likewise, isotopic exchange between the selenocyanate ion and ionic cyanide in protic as well as in dipolar aprotic solvents is reported,[2,5,6] while no measurable exchange occurs between ionic thiocyanate and ionic cyanide.[2,7] Exchange reaction takes place in acetonitrile between selenium dicyanide and ionic cyanide, but no exchange was found between sulfur dicyanide and ionic cyanide.[2]

EXPERIMENTAL

Acetonitrile was purified by distillation from P_2O_5 and CaH_2.[8] Ph_4AsCN and $Ph_4As^{13}CN$ were prepared from Ph_4AsCl and KCN and $K^{13}CN$ in methanol.[9] $K^{13}CN$ was obtained from British Company Oxygen Limited, and contained more than 90 % ^{13}C.

p-Nitrophenyl thiocyanate [10] and phenyl thiocyanate [11] were prepared from diazotized anilines and copper(I) thiocyanate. *p*-*N*,*N*-Dimethylaminophenyl thiocyanate was prepared from *N*,*N*-dimethylaniline and thiocyanogen in glacial acetic acid.[12]

o-Nitrophenyl thiocyanate was prepared by dissolving 2.0 g of *o*-nitrobenzenesulfenyl chloride and 1.0 g of dry potassium cyanide in 20 ml of acetonitrile. The solution was stirred

for 12 h. The salts were filtered from the solution, and the solvent was removed in vacuum. Pure material was obtained by recrystallization from benzene by addition of some ether. M.p. 116–117 °C.

The p-nitrophenyl thiocyanate–cyanide reaction. 0.40 g of *p*-nitrophenyl thiocyanate dissolved in 15 ml of acetonitrile was added to a solution of tetraphenylarsonium cyanide made by dissolving 0.75 g of the nucleophilic reagent in 10 ml of acetonitrile. The reaction was carried out at room temperature, and the mixture turned deep red immediately after mixing the reactants. The solvent was removed in vacuum, and excess of the substrate was washed away by means of 10 ml of benzene and finally 10 ml of ether. The dark red product was dissolved in 10 ml of acetonitrile at room temperature and placed in a freezer (−15 °C), whereupon the salt crystallized. The amount of pure material was 0.50 g. The crystals were deep red and appeared quite stable in the crystalline form. (Found: C 68.57; H 4.48; N 3.02; S 3,64. Calc. for $C_{5_7}H_{44}N_4O_2SAs_2$: C 68.50; H 4.41; N 5.61; S 3.21.).

The crystals of the product from the *p*-nitrophenyl thiocyanate-cyanide reaction form dark red prisms. The space group was determined by oscillation and Weissenberg photographs, and accurate cell constants were obtained by means of least squares on the basis of the reflecting angles of 15 high angle reflections, using a Syntex $P2_1$ four-circle diffractometer. Density of the crystals was determined by flotation. The following results were obtained:

Space group: $P1$ (or $P\bar{1}$)

Cell constants: $a = 10.086(1)$ Å $\alpha = 76.19(1)°$
$b = 13.243(2)$ Å $\beta = 96.03(1)°$
$c = 9.515(1)$ Å γ $106.51(1)°$
$V = 1182.4$ (0.2) Å^3

Density: Found, 1.402 g/cm^3, calc. for $Z = 1$, 1.403 g/cm^3. Molecular weight calc.: 998.5.

The molecular weight is in good agreement with the weight based on the formula $C_{5_7}H_{44}N_4O_2SAs_2$ (998.9). The space group is probably $P1$, as there is only one molecule in the cell and no centrosymmetry in the molecule.

IR measurements. The IR-measurements were performed using a 2.0×10^{-2} M solution of the aryl thiocyanate and a 2.0×10^{-2} M solution of tetraphenylarsonium ^{13}C-cyanide unless otherwise stated. In all cases the cyanide solution was added to the aryl thiocyanate solution at room temperature.

The stoichiometry of the *p*-nitrophenyl thiocyanate-cyanide reaction was tested by reacting the substrate with various amounts of tetraphenylarsonium cyanide and measuring the absorbance at $\nu = 2142$ cm^{-1} $\frac{1}{2}$ h after the solutions had been mixed. 4.0×10^{-3} M of the substrate and successively 2.0×10^{-3}, 4.0×10^{-3}, 6.0×10^{-3}, and 8.0×10^{-3} M of the nucleophile gave the absorbances 0.085, 0.160, 0.230, and 0.330 respectively, which indicates that 1 mol of the aryl thiocyanate reacts with 2 mol of ionic cyanide.

The IR measurements were performed on a Unicam SP 200 G Infrared Spectrophotometer applying 0.1 cm liquid cells.

REFERENCES

1. Giles, D. E. and Parker, A. J. *Aust. J. Chem. 26* (1973) 273.
2. Austad, T. and Esperås, S. *Acta Chem. Scand. A 28* (1974) 892.
3. Hogg, D. R. and Stewart, J. *J. Chem. Soc. Perkin Trans. 2* (1974) 1041.
4. Schiavon, G. *Ric. Sci. Rend. Ser. A 32* (1962) 69.
5. Belluco, U., Bruno, M. and Schiavon, G. *Ric. Sci. 28* (1958) 963.
6. Belluco, U., Bruno, M. and Schiavon, G. *Ric. Sci. 28* (1958) 111.
7. Adamson, A. W. and Magee, P. S. *J. Am. Chem. Soc. 74* (1952) 1590.
8. Coetzee, J. F. *Pure Appl. Chem.* (1967) 429.
9. Andreades, S. and Zahnow, E. W. *J. Am. Chem. Soc. 91* (1969) 4181.
10. Challenger, F. and Collins, A. D. *J. Chem. Soc. 125* (1924) 1377.
11. Gatterman, L. and Hausknecht, W. *Ber. Dtsch. Chem. Ges. 23* (1890) 739.
12. *Org. Synth. Coll. Vol. 11*, p. 574.

Received February 18, 1976.

Acta Chemica Scandinavica A 30 (1976) 567—571

Electron Diffraction Investigation of Gaseous Chlorocyano-, Chlorobromo-, and Bromoiodoacetylene

ARNE ALMENNINGEN, ODDBJØRN NOR and TOR G. STRAND

Department of Chemistry, University of Oslo, Oslo 3, Norway

Electron diffraction data for the three asymetrically substituted acetylenes confirm their expected linear structures. The following R_α distances, and standard deviations including contributions from systematic errors of 0.001 R_α, were obtained: $R(C\equiv C) = 1.205(3)$, 1.206(4), and 1.206(8) Å for chlorocyano-, chlorobromo-, and bromoiodo-acetylene, respectively. $R(C-Cl) = 1.624(2)$ and 1.636(3) Å in chlorocyano- and chlorobromoacetylene, and $R(C-Br) = 1.784(3)$ and 1.795(6) Å in chlorobromo- and bromoiodoacetylene, for the latter molecule $R(C-I) = 1.972(8)$ Å. For chlorocyanoacetylene, $R(C-C) = 1.364(3)$ and $R(C\equiv N) = 1.160(3)$ Å.

The three asymmetrically substituted acetylenes, chlorocyano-, [1] chlorobromo-,[2] and bromoiodoacetylene [3] were all synthesized by E. Kloster-Jensen. The IR and Raman spectra of the molecules are known.[4–8] The crystal structure of chlorocyanoacetylene has been given,[9] and recently a complete microwave substitution structure was published for this molecule.[10] The results of the microwave structure of chlorobromoacetylene [11] depend slightly on the assumed bond shrinkage values, only for the chlorine-bromine distance was the R_s value obtainable.

The present electron diffraction investigation was carried out to increase the available structural data of substituted acetylenes. In addition it is of interest to compare microwave and electron diffraction distances when the latter distances are corrected for harmonic vibrational effects. To experimentally study the accuracy of computed atomic scattering factors of heavier atoms, the electron diffraction investigation of the simple, linear bromine and iodine containing compounds seemed interesting, as contributions from interatomic multiple scattering to the molecular intensities are expected to be unimportant for linear molecules.[12]

EXPERIMENTAL AND CALCULATION PROCEDURES

Diffraction photographs of the samples [1–3] were obtained from the Oslo apparatus [13] for an electron wavelength of 0.06461(5) Å corresponding to an accelerating voltage of about 35 kV. Values for the long and short camera distances applied, the number of plates for each distance, and the nozzle temperatures are included in Table 1.

Atomic scattering factors were computed for 35 keV electrons by a program originally written by A. C. Yates.[14] For C, N, and Cl the calculations were for analytical expressions for the HF potentials of the atoms [15] while the scattering factors for Br and I were computed from tabulated values of relativistic HFS potentials.[16]

The plates were photometered and the data treated as usually.[17] The first backgrounds were drawn on leveled intensity curves from each plate and the molecular intensities were all modified by $s/|f_C'|^2$. The final background adjustments were achieved by comparing the experimental to the best calculated intensities and were carried out on the data for each plate. These intensities were scaled and averaged, and the average correlation coefficients and the standard deviations at each point were computed.[18] Using $\Delta s = 0.125$ and 0.25 Å^{-1} for the data of the long and short camera distances, the correlation was taken care of by values of the elements p_2 and p_3 of the matrix ϱ^{-1} for the weight matrix [17] of -0.640 and 0.146, and -0.600 and 0.125, for the long and short camera distances, respectively.

Constants for the diagonal part of the weight matrix were estimated from the standard

Table 1. Nozzle temperatures (t_n), camera distances (l), number of plates (n), applied data range, and constants for the diagonal part of the weight matrix (s_1, s_2, w_1, w_2).[17]

Molecule	t_n °C	l mm	n	s(min) Å^{-1}	s(max) Å^{-1}	s_1 Å^{-1}	s_2 Å^{-1}	w_1 Å^2	w_2 Å^2	w [a]
ClCCCN	−3	480.60	5	1.375	19.875	7.0	15.0	1.10	0.41	
		200.60	6	7.00	35.00	12.0	28.0	0.06	0.08	0.14
ClCCBr	−20	480.75	6	1.375	19.125	7.0	16.0	1.75	0.07	
		260.75	6	5.25	30.00	10.5	22.0	1.10	0.20	0.25
BrCCI	12	480.60	6	1.500	19.375	7.0	14.5	1.75	0.29	
		200.60	5	7.00	25.00	9.5	18.0	1.38	0.19	0.24

[a] w is the overall weight factor for the data of the short camera distance relatively to the part of the long camera distance data of unit weight.

deviation of the intensities except for the inner part of the long camera distance data where the differences between experimental and calculated intensities were much larger than expected from the standard deviations of the experimental intensities. In this region the weights were estimated from the differences with the calculated intensities. Also the overall weight of the short camera distance data relative to overall unit weight on the long camera distance data was estimated from the standard deviations of the intensities. The constants applied in the least-squares refinement are included in Table 1, and the molecular intensities with standard deviations are illustrated in Fig. 1.

To the approximation of small vibrations and disregarding the centrifugal distortion term, the distance R_α is defined in terms of the electron diffraction parameter R_a by [19]

$$R_e + \langle \Delta z \rangle \approx R_a + D \equiv R_\alpha \qquad (1)$$

where $D = u^2/R - K$, u being the root mean-square amplitude of vibration, $u = (\langle \Delta z^2 \rangle)^{\frac{1}{2}}$, and K is the perpendicular amplitude correction term, $K = (\langle \Delta x^2 \rangle + \langle \Delta y^2 \rangle)/2R$. Values of u, K, and D were computed by a modified [20] computer program by W. D. Gwinn.[21]

To calculate the normal vibrations of chlorocyanoacetylene [6] with sufficient accuracy, stretch-stretch and bend-bend interaction force constants were included in the force field. For chlorobromo- and bromoidoacetylene the published force fields were applied.[8]

The numbering of the atoms is given in Fig. 2, the applied force field for chlorocyanoacetylene is tabulated in Table 2, calculated u- and D-values for this molecule are included in Table 3, and the same values for chlorobromo- and bromoiodoacetylene are given in Table 4.

The final least-squares refinements were carried out on the average molecular intensities keeping the data for each camera distance separated and applying a nondiagonal weight matrix with constants for the off diagonal elements given above. The constants for the diagonal part of the weight matrix are included in Table 1. The R_a distances were corrected to R_α ones by the computed D values given in Tables 3 and 4, and the linear geometry of the molecules was satisfied by the latter distances, keeping only the bond distances as independent geometrical parameters in the least-squares refinements.

For chlorocyanoacetylene all the u-values were refined along with the geometrical parameters and the two scale factors, however, to make the iteration converge, $u(2,3)$, $u(3,4)$, and $u(4,5)$ were given the same shifts in the refinement starting from the calculated values. In the same way $u(2,4)$ and $u(3,5)$ were refined in one group. u-Values refined in one group got the same standard deviations. The obtained root mean-square amplitudes and standard deviations thus obtained are included in Table 3. For chlorobromoacetylene, the u-values of the bonded distances were fixed on the calculated values, and of the u-values of the nonbonded distances, only $u(1,4)$ could be varied together with the other parameters.

For bromoiodoacetylene the u-values of the nonbonded distances were determined. The experimental u-values for these two molecules are given in Table 4.

Most of the elements of the moment matrix of the parameters were small. Correlation coefficients with absolute values larger than 0.5 were for chlorocyanoacetylene $\varrho[R(2,3), R(1,2)] = -0.62$, $\varrho[R(4,5), R(2,3)] = -0.58$, $\varrho[u(1,2), K(20)] = 0.62$, and $\varrho[K(48), K(20)] = 0.56$, where $K(48)$ and $K(20)$ are the scale factors for the data from the long and short camera distance data, respectively. In the same way for chlorobromoacetylene $\varrho[R(1,2), R(2,3)] = -0.72$, $\varrho[R(3,4), R(2,3)] = -0.72$, $\varrho[u(1,4), K(48)] = 0.59$, and $\varrho[u(1,4), K(20)] =$

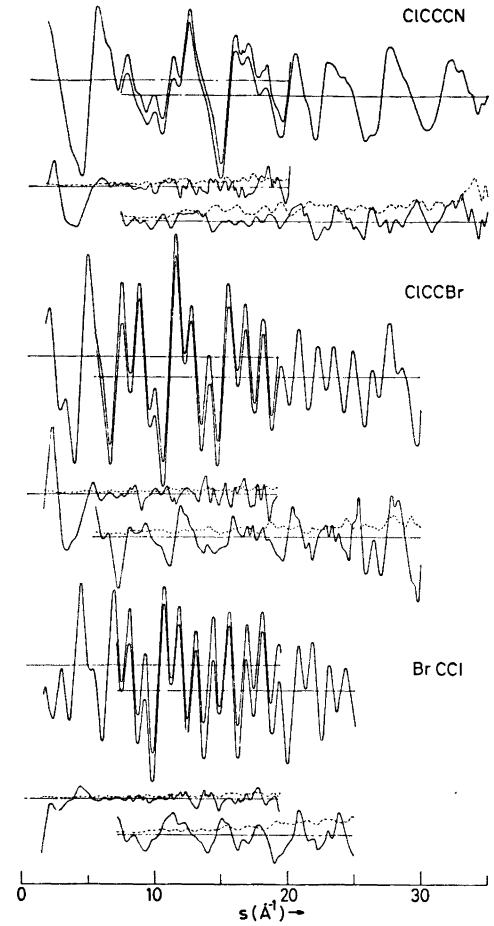

Fig. 1. $s/|f'_{Cl}|^2$-modified average experimental intensities for the long and short camera distance data (two upper curves for each molecule). The corresponding standard deviations of the average intensities (broken curves), and the differences between the experimental intensities and the intensities calculated from the parameters of Table 5 and Table 3 or Table 4 using experimental u-values when possible (solid curves) are given below the molecular intensities for the two camera distances.

0.74, and for bromoiodoacetylene $\varrho[R(3,4), R(2,3)] = -0.74$, $\varrho[R(1,2),R(2,3)] = -0.51$, $\varrho[u(1,4),K(48)] = 0.74$, $\varrho[u(1,4),K(20)] = 0,85$, and $\varrho[K(48), K(20)] = 0.64$. The final results are given in Table 5.

Applying the scale factors from the least-squares refinements, the intensity curves from the two camera distances were connected, calculated intensities were added to the inner part, and radial distribution functions were computed and compared to functions calculated for the parameters of Table 5 and Table 3 or 4, respectively. The radial distribution functions are illustrated in Fig. 3.

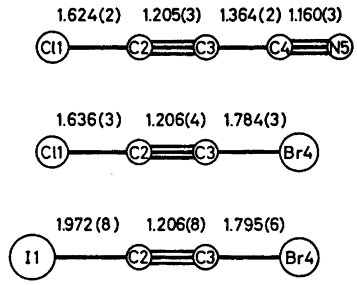

Fig. 2. Numbering of the atoms of the molecules. Final corrected R_α distances and standard deviations are included.

Table 2. Applied force field for chlorocyanoacetylene. Stretching force constants K and stretch-stretch interaction force constants F in mdyn/Å and force constants for bending, H and bending-bending interaction, G, in mdyn Å/rad.[2]

$K(1,2)$	3.7	$F(1,2/2,3)$	1.080
$K(2,3)$	18.0	$F(1,2/3,4)$	0.771
$K(3,4)$	10.0	$F(1,2/4,5)$	0.629
$K(4,5)$	16.1	$F(2,3/3,4)$	1.270
		$F(2,3/4,5)$	0.286
		$F(3,4/4,5)$	0.589
$H(1,2,3)$	0.340		
$H(2,3,4)$	0.286	$G(1,2,3/2,3,4)$	0.044
$H(3,4,5)$	0.255	$G(2,3,4/3,4,5)$	0.044

Table 3. Chlorocyanoacetylene, calculated root mean-square amplitudes of vibration, u, and correction terms between R_a and R_α, D of eqn. 1, at −3 °C. Experimental u-values with least-squares standard deviations are included.

Distance	D (Å)	u (Å) calc	u (Å) exp
1−2	−0.0101	0.046	0.033(4)
2−3	−0.0056	0.035	0.041(3)
3−4	−0.0087	0.039	0.046(3)
4−5	−0.0172	0.035	0.042(3)
1···3	−0.0072	0.047	0.051(4)
1···4	−0.0012	0.049	0.048(4)
1···5	−0.0002	0.051	0.067(4)
2···4	−0.0044	0.044	0.050(4)
2···5	−0.0078	0.047	0.059(8)
3···5	−0.0152	0.044	0.051(4)

Table 4. Chlorobromo- and bromoiodoacetylene, calculated root mean-square amplitudes of vibration, u, and correction terms between R_a and R_α, D of eqn. 1, at 15 and 25 °C, respectively. Experimental u-values with least-squares standard deviations are included.

Distance	ClCCBr D (Å)	ClCCBr u (Å) calc	ClCCBr u (Å) exp	ICCBr D (Å)	ICCBr u (Å) calc	ICCBr u (Å) exp
1–2	−0.0118	0.044		−0.0128	0.045	
2–3	−0.0096	0.036		−0.0112	0.037	
3–4	−0.0086	0.041		−0.0109	0.043	
1···3	−0.0067	0.049		−0.0062	0.050	0.040(31)
1···4	0.0004	0.050	0.048(2)	0.0006	0.055	0.055(3)
2···4	−0.0045	0.043		−0.0091	0.048	0.060(13)

DISCUSSION

For small vibrations, the R_α distance is according to eqn. 1 equal to the equilibrium distance plus an anharmonicity term. These distances should therefore approximately satisfy the molecular geometry and be close to the equilibrium distances. Also the microwave R_s distances should be close to the equilibrium distances and the two types of distances should be comparable.

The R_α distances fit linear structures of the three molecules satisfactorily, and the expected linear geometries are confirmed (Fig. 1). For chlorocyanoacetylene the largest discrepancies between the present result and the microwave R_s structure [10] are for the C3 – C4 and the C2≡C3 distances with differences of 0.005 and −0.004 Å, respectively. These differences are

Table 5. R_α distances with standard deviations, including contributions from systematic errors of 0.001 R_α, in Å.

	ClCCCN	ClCCBr	ICCBr
$R(1-2)$	1.624(2)	1.636(3)	1.972(8)
$R(2-3)$	1.205(3)	1.206(4)	1.206(8)
$R(3-4)$	1.364(2)	1.784(3)	1.795(6)
$R(4-5)$	1.160(3)		
$K(48)$ [a]	0.93(3)	0.95(2)	1.02(3)
$K(20)$ [a]	0.95(4)	0.96(3)	1.03(4)
$R(48)$ [b]	7.0	7.8	9.5
$R(20)$ [b]	13.1	16.2	28.4

[a] Scale factors for the data of the long and short camera distances. [b] Weighted R-factors for the data of the long and short camera distances, $R = 100\{\sum_i w_i[I(\text{exp}) - I(\text{calc})]^2 / \sum_i w_i I(\text{exp})^2\}^{\frac{1}{2}}$.

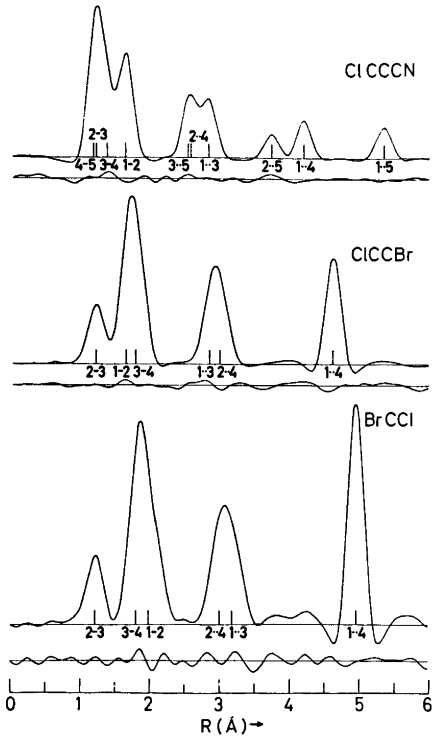

Fig. 3. Experimental radial distribution functions of the molecules obtained from connecting the average experimental intensities of Fig. 1 and adding theoretical intensities inside $s = 4.75$ Å^{-1}. The damping functions were $\exp(-0.005s^2)$ for chlorocyanoacetylene and $\exp(-0.007s^2)$ for chlorobromo- and bromoiodoacetylene. Differences between experimental and calculated functions from the parameters of Tables 5 and 3 or Table 4 multiplied by a factor of 2 are given below each radial distribution function.

not significant. For chlorobromoacetylene $R_\alpha(\mathrm{Cl1\cdots Br4}) = 4.626(5)$ Å is in good agreement with the R_s distance of 4.625 – 4.626 Å of Ref. 11, and also the other structure parameters from the two investigations agree satisfactorily.

The obtained values for the C≡C bonds are the same while the difference of 0.012(4) Å between the carbon-chlorine bonds of chlorobromo- and chlorocyanoacetylene may be significant.

The carbon-bromine distances of the present investigation agree with the R_s value of 1.785 Å for bromocyanoacetylene [10] and the carbon-iodine distance of 1.972(8) Å is not significantly different from the R_0 value of 1.985 Å of iodocyanoacetylene.[10]

As seen from the standard deviations of the intensities of Fig. 1 and the R-factors of Table 5 the data are not very accurate, and the accuracies and the maximum s-values for obtaining meaningful molecular intensities decrease with increasing atomic numbers of the heaviest atom. This is at least partly due to the combined effect of increasing background scattering from the heavier atoms and phase shifts in the atomic scattering. The computed atomic scattering factors are, however, expected to be more than sufficiently accurate to analyze the present data. This is confirmed by the experimental u-values for chlorobromo- and bromoiodoacetylene of Table 4, which are all within one standard deviation of the calculated ones. The scattering factors for bromine and iodine were also computed from an analytical potential which is known to be less accurate for heavier atoms.[22] While the scattering factor for Br agreed relatively well with the function obtained from the tabulated HFS potential, the scattering factor for iodine showed large discrepancies, and the obtained g-functions [17] for bromiodoacetylene differed considerably from the g-functions for the tabulated HFS potential. Applying the former g-functions in the least-squares refinement, about the same overall agreement with the experimental data was obtained. However, the C – Br distance increased by 0.021 and the C – I distance decreased by 0.019 Å with practically no changes in the C≡C and Br···I distances, and the u-value of the Br···I distance converged to 0.042(4) Å. These values for the distances are less reasonable, and the u-value is in poorer agreement with the calculated one, than the results obtained for g-functions based on the more accurate tabulated values for the HFS potential of iodine.

Acknowledgements. The authors wish to thank Dr. Else Kloster-Jensen for samples of the compounds. Thanks are due to Dr. David Liberman for the tabulated values of the potential of Br and I, and siv.ing. Liv Fernholt should be thanked for doing the initial calculations on chlorobromoacetylene.

REFERENCES

1. Kloster-Jensen, E. *Acta Chem. Scand. 18* (1964) 1629.
2. Kloster-Jensen, E. *J. Am. Chem. Soc. 91* (1969) 5673.
3. Kloster-Jensen, E. *Tetrahedron Lett. V* (1969) 5323.
4. Cyvin, S. J., Kloster-Jensen, E. and Klæboe, P. *Acta Chem. Scand. 19* (1965) 903.
5. Klæboe, P. and Kloster-Jensen, E. *Spectrochim. Acta A 23* (1967) 1981.
6. Christensen, D. H., Klæboe, P., Kloster-Jensen, E. and Johnsen, I. *Spectrochim. Acta A 25* (1969) 1569.
7. Christensen, D. H., Klæboe, P., Kloster-Jensen, E. and Johnsen, I. *Spectrochim. Acta A 26* (1970) 1567.
8. Christensen, D. H., Stroyer-Hansen, T., Klæboe, P., Kloster-Jensen, E. and Tucker, E. E. *Spectrochim. Acta A 28* (1972) 939.
9. Bjorvatten, T. *Acta Chem. Scand. 22* (1968) 410.
10. Bjorvatten, T. *J. Mol. Struct. 20* (1974) 75.
11. Bjørseth, A., Kloster-Jensen, E., Marstokk, K. M. and Møllendal, H. *J. Mol. Struct. 6* (1970) 181.
12. Bartell, L. S. *J. Chem. Phys. 63* (1975) 3750, and references therein.
13. Bastiansen, O., Hassel, O. and Risberg, F. *Acta Chem. Scand. 9* (1955) 232.
14. Yates, A. C. *Comput. Phys. Commun. 2* (1971) 175.
15. Strand, T. G. and Bonham, R. A. *J. Chem. Phys. 40* (1964) 1686.
16. Liberman, D., Waber, J. T. and Cromer, D. *Phys. Rev. 137* (1965) 1727.
17. Andersen, B., Seip, H. M., Strand, T. G. and Stølevik, R. *Acta Chem. Scand. 23* (1969) 3224.
18. Seip, H. M., Strand, T. G. and Stølevik, R. *Chem. Phys. Lett. 3* (1969) 617.
19. Morino, Y., Kuchitsu, K. and Oka, T. *J. Chem. Phys. 36* (1962) 1108.
20. Stølevik, R., Seip, H. M. and Cyvin, S. *Chem. Phys. Lett. 15* (1972) 263.
21. Gwinn, W. D. *J. Chem. Phys. 55* (1971) 477.
22. Cox, Jr., H. L. and Bonham, R. A. *J. Chem. Phys. 47* (1967) 2599.

Received February 18, 1976.

Acta Chemica Scandinavica A 30 (1976) 572—578

Short Communications

The Influence of Ammonium Ion on Dissociation Reactions of *trans*-1,2-Diaminocyclohexanetetraacetate Complexes of Alkaline Earth Ions in the pH Range 8—10

JONNA HINDKÆR DAHL,[a] NIELS RHOD LARSEN[b] and ARNE JENSEN[a]

[a] Department of Chemistry AD, The Royal Danish School of Pharmacy, DK-2100 Copenhagen Ø, Denmark and [b] Chemistry Department A, The Technical University of Denmark, Building 207, DK-2800 Lyngby, Denmark

The exchange reactions between the alkaline earth complexes of *trans*-1,2-diaminocyclohexane-*N*,*N*,*N*',*N*'-tetraacetate (CDTA) and Cu(II) or Pb(II) have been studied by several authors.[1–3] Furthermore, the rate of dissociation of these complexes has been studied using the exchange of optically active CDTA instead of metal ion exchange.[4,5] It has been shown in the studies mentioned that the rate of dissociation k_d in the pH range 7 – 9 can be calculated from eqn. (1)

$$k_d = k^{MCDTA} + k_H^{MCDTA}[H^+] \quad (1)$$

A deviation from this equation is observed at pH > 9 for $M = Mg^{2+}$, Sr^{2+}, or Ba^{2+}, but *not* for $M = Ca^{2+}$.[3,4] The mechanism shown in (2) is stated for the dissociation of $MCDTA^{(4-n)-}$, and it is believed that this mechanism is also valid for $M = Ca^{2+}$ (rds≡ rate determining step).

Considerably higher values of k^{MCDTA}, but not of k_H^{MCDTA}, were obtained in the exchange between the MCDTA complex and Cu(II) than in the exchange between the MCDTA complex and CDTA, *cf.* eqn. (1) and Ref. 4. A cause for this difference in the obtained values of k^{MCDTA} has been the use of an ammonium/ammonia buffer when investigating the exchange reactions between the MCDTA complexes and the Cu(II) ion.[3]

The present communication indicates conclusively that the rate of dissociation of the magnesium, calcium, and strontium complexes of CDTA is influenced in a pronounced way by the ammonium ion concentration – and *not* by the ammonia concentration. The overall reactions studied are shown in (3a) ($M = Mg^{2+}$) and (3b) ($M = Ca^{2+}$ or Sr^{2+}). The reactions are pseudo first order with rate constants k_d. The charges, protons, and nomenclature for the optical rotation have been omitted for clarity.

$$M(\text{D-CDTA}) + Ba(\text{D,L-CDTA}) \rightarrow M(\text{D,L-CDTA}) + Ba(\text{D-CDTA}) \quad (3a)$$

$$M(\text{D-CDTA}) + Li(\text{D,L-CDTA}) \rightarrow M(\text{D,L-CDTA}) + Li(\text{D-CDTA}) \quad (3b)$$

The double exchange reactions in eqn. (3) insure a concentration of free CDTA sufficiently low so that ammonium complexes do not in any way interfere in the reaction.

Ba(D,L-CDTA) can be used only in (3a) ($M = Mg^{2+}$) as the change in optical rotation observed with this complex is too small for $M = Ca^{2+}$ or Sr^{2+}. Li(D,L-CDTA) has been used in (3b) since a readily observable change in rotation is obtained. The determination of k_d

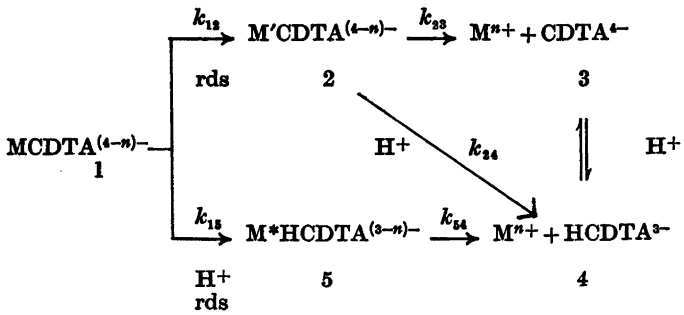

(2)

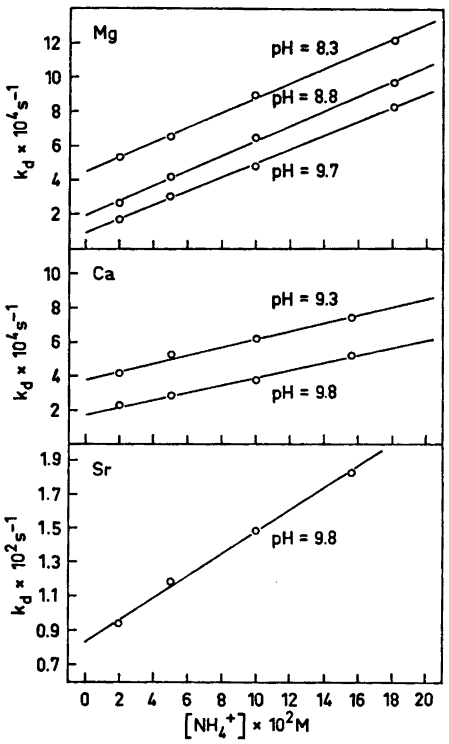

Fig. 1. Ammonium ion dependence on the observed first-order rate constants k_d for, respectively, $MgCDTA^{2-}$, $CaCDTA^{2-}$, and $SrCDTA^{2-}$.

in (3a) and (3b) is feasible only if the rate constants of dissociation of Ba(D,L-CDTA) and Li(D,L-CDTA), respectively, are much larger than k_d, a condition which is shown to be fulfilled. The ionic strength and pH are adjusted using $CsNO_3$ and CsOH.[4] A tenfold excess of the racemic species is used to make the overall reactions go essentially to completion.

A "Perkin-Elmer Model 141" photoelectric polarimeter (with potentiometric read-out) in combination with a "Radiometer Servograph REC 51" recorder equipped with a high sensitivity "Radiometer REA 112" unit was used to monitor the change in optical rotation as a function of time during the reactions.[4]

A plot of k_d *versus* $[NH_4^+]$ for $M = Mg^{2+}$, Ca^{2+}, or Sr^{2+} at constant pH (*cf.* Fig. 1) indicates a linear relationship between k_d and $[NH_4^+]$ for the investigated range of ammonium ion concentration and pH values. Furthermore the results of a linear regression analysis indicate a slope for Mg^{2+} or Ca^{2+} independent of the pH value used. Variations in $[NH_3]$ occurring in conjunction with variations in $[NH_4^+]$ are therefore without effect upon the linear relation between k_d and $[NH_4^+]$. The linear relationships can be expressed by eqn. (4) where C is the pH dependent rate constant of dissociation obtained without NH_4^+ present and $k_{NH_4}^{MCDTA}$ is the rate constant of the ammonium ion assisted dissociation.[4]

$$k_d = C + k_{NH_4}^{MCDTA}[NH_4^+] \quad (4)$$

Table 1. Rate constants for the dissociation of $MCDTA^{2-}$ complexes.

M^{2+}	pH	C s^{-1} [a]	$k_{NH_4}^{MCDTA}$ $M^{-1}s^{-1}$ [a]
Mg	9.7	8.9×10^{-5}	4.1×10^{-3}
Mg	8.8	1.9×10^{-4}	4.3×10^{-3}
Mg	8.3	4.5×10^{-4}	4.3×10^{-3}
Ca	9.8	1.8×10^{-4}	2.2×10^{-4}
Ca	9.3	3.8×10^{-4}	2.4×10^{-4}
Sr	9.8	8.3×10^{-3}	6.5×10^{-2}

[a] Calculated from eqn. (4) by a least squares method; initial $[M(D\text{-CDTA})] = 2.5 \times 10^{-3}$ M; $[M(D,L\text{-CDTA})] = 2.5 \times 10^{-2}$ M; NH_4^+/NH_3 buffer; $\mu = 0.5$ ($CsNO_3$); 25.0 °C.

It may be concluded that NH_4^+ acts on step 1→2 in mechanism (2). This is a consequence of the facts that k_H^{MCDTA} is independent of $[NH_4^+]$ [3,4] and that the relative deviation from the straight line in the $[H^+]$ profile for k_d is the same whether carrying out a metal ion exchange in an ammonium/ammonia buffer or a ligand exchange without ammonium ion. The deviation from the straight line is caused by step 2→4 in mechanism (2).[3,4]

Fig. 1 and Table 1 also show that $k_{NH_4}^{SrCDTA} > k_{NH_4}^{MgCDTA} > k_{NH_4}^{CaCDTA}$ which agrees with $k_{12}^{SrCDTA} > k_{12}^{MgCDTA} > k_{12}^{CaCDTA}$ and *not* with $k_H^{SrCDTA} > k_H^{CaCDTA} > k_H^{MgCDTA}$.[3,4] The accordance between the sequences of $k_{NH_4}^{MCDTA}$ and k_{12}^{MCDTA} therefore supports the conclusion that step 1→2 is influenced by ammonium ion. The sequences of $k_{NH_4}^{MCDTA}$ and k_{12}^{MCDTA} are not on the other hand in accordance with the sequence of the ionic radii of Mg^{2+}, Ca^{2+}, and Sr^{2+}. This discrepency and the special course of the dissociation of the CaCDTA complex described previously [3,4] may be attributed to a different structure of the CaCDTA complex as compared to the structures of the Mg^{2+} and Sr^{+2} complexes as well as those of the BaCDTA and LaCDTA complexes.[3,4] However, circular dichroism measurements and absorption measurements of aqueous solutions of $Mg(D\text{-CDTA})^{2-}$, $Ca(D\text{-CDTA})^{2-}$, $Sr(D\text{-CDTA})^{2-}$, $Ba(D\text{-CDTA})^{2-}$, $La(D\text{-CDTA})^{-}$, and $H(D\text{-CDTA})^{3-}$ in the wavelength range 200 – 325 nm did not demonstrate that

$Ca(D\text{-}CDTA)^{2-}$ possesses a structure of its own, since the effects observed were very small.

It is difficult to explain how the ammonium ion influences step 1→2 in the stated mechanism. It seems reasonable though to assume that this step is very complex consisting perhaps of several steps where an intermediate such as $M''NH_4CDTA$ is found in one of the steps.

It is necessary to control the factors that affect the reaction rates when making use of the kinetic properties of the CDTA complexes of the alkaline earth ions in analytical chemistry.[2] The present investigation has shown that $[NH_4^+]$ has such pronounced influence on the values of k_d that a prior knowledge of $[NH_4^+]$ in the sample to be analysed is essential for the method. Further studies [6] on the differential kinetic analysis of the alkaline earth ions are being carried out with particular emphasis on the use of classical spectrophotometry in automated analyses.

1. Margerum, D. W., Menardi, P. J. and Janes, D. L. *Inorg. Chem. 6* (1967) 283.
2. Pausch, J. B. and Margerum, D. W. *Anal. Chem. 41* (1969) 226.
3. Jensen, A. and Larsen, N. R. *Acta Chem. Scand. 27* (1973) 1838.
4. Larsen, N. R. and Jensen, A. *Acta Chem. Scand. A 28* (1974) 638.
5. Carr, J. D. and Schwartzfager, D. G. *J. Am. Chem. Soc. 97* (1975) 315.
6. Dahl, J. H. and Jensen, A. *To be published.*

Received March 18, 1976.

Analysis of the 100 MHz ^1H NMR Spectrum and Conformation of *trans*-2-*t*-Butyl-*cis*-2-methyl-1,3-dithiane 1-Oxide

KNUT BERGESEN,[a] MICHAEL J. COOK[b] and ALAN P. TONGE[b]

[a] Department of Chemistry, University of Bergen, Allégatan 70, N-5014 Bergen-Univ., Norway and [b] School of Chemical Sciences, University of East Anglia, Norwich NR4 7TJ, England

Recent studies from our laboratories [1–3] and elsewhere [4,5] have demonstrated that the S=O bond of 1,3-dithiane 1-oxides I, II, III favours the equatorial site. In contrast thiane 1-oxide,[6] 1,3-oxathiane 3-oxide,[4,7] and thiane-3-one 1-oxide [3] adopt preferentially the axial S=O conformer. The origin of the equatorial S=O preference in I–III is somewhat unclear but a suggestion [1] that dipolar interactions are involved has recently received support in the form of force field calculations performed by Allinger and Kao.[8] These workers also calculated that conformer Ie is 4.2 kcal mol^{-1} more stable than the lowest energy twist form.

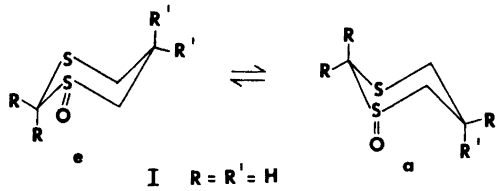

I R = R' = H
II R = Me, R' = H
III R = H, R'R' = O

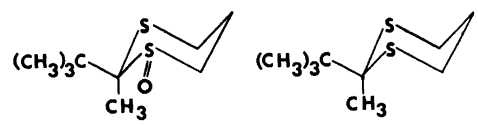

In the present paper we report the analysis of the 100 MHz spectrum of the 2-*t*-butyl-2-

Table 1. 100 MHz spectral parameters (in Hz) of IV and V in $CDCl_3$.

	Chemical shift [a]			Coupling constants	
	IV	V [b]		IV	V [b]
4a	266.60	303.11	4a5a	12.75	11.85
4e	239.38	271.80	4e5e	3.00	4.35
5a	215.07	178.73	4a5e	2.92	3.28
5e	228.88	205.47	4e5a	3.97	3.96
6a	267.13	303.11	5a6a	14.21	11.85
6e	301.85	271.80	5e6e	3.82	4.35
			5a6e	3.39	3.96
			5e6a	3.23	3.28
			4a4e	−14.49	−14.46
			5a5e	−14.54	−13.56
			6a6e	−13.31	−14.46
			4e6e	1.57	0.65
			4a6a	−0.18	0.03
			4a6e	−0.23	−0.05
			4e6a	−0.41	−0.05

[a] Downfield from TMS. [b] Data taken from Ref. 11.

$Ca(D\text{-}CDTA)^{2-}$ possesses a structure of its own, since the effects observed were very small.

It is difficult to explain how the ammonium ion influences step 1→2 in the stated mechanism. It seems reasonable though to assume that this step is very complex consisting perhaps of several steps where an intermediate such as $M''NH_4CDTA$ is found in one of the steps.

It is necessary to control the factors that affect the reaction rates when making use of the kinetic properties of the CDTA complexes of the alkaline earth ions in analytical chemistry.[2] The present investigation has shown that $[NH_4^+]$ has such pronounced influence on the values of k_d that a prior knowledge of $[NH_4^+]$ in the sample to be analysed is essential for the method. Further studies [6] on the differential kinetic analysis of the alkaline earth ions are being carried out with particular emphasis on the use of classical spectrophotometry in automated analyses.

1. Margerum, D. W., Menardi, P. J. and Janes, D. L. *Inorg. Chem. 6* (1967) 283.
2. Pausch, J. B. and Margerum, D. W. *Anal. Chem. 41* (1969) 226.
3. Jensen, A. and Larsen, N. R. *Acta Chem. Scand. 27* (1973) 1838.
4. Larsen, N. R. and Jensen, A. *Acta Chem. Scand. A 28* (1974) 638.
5. Carr, J. D. and Schwartzfager, D. G. *J. Am. Chem. Soc. 97* (1975) 315.
6. Dahl, J. H. and Jensen, A. *To be published.*

Received March 18, 1976.

Analysis of the 100 MHz ^1H NMR Spectrum and Conformation of *trans*-2-*t*-Butyl-*cis*-2-methyl-1,3-dithiane 1-Oxide

KNUT BERGESEN,[a] MICHAEL J. COOK[b] and ALAN P. TONGE[b]

[a] Department of Chemistry, University of Bergen, Allégatan 70, N-5014 Bergen-Univ., Norway and [b] School of Chemical Sciences, University of East Anglia, Norwich NR4 7TJ, England

Recent studies from our laboratories [1–3] and elsewhere [4,5] have demonstrated that the S=O bond of 1,3-dithiane 1-oxides I, II, III favours the equatorial site. In contrast thiane 1-oxide,[6] 1,3-oxathiane 3-oxide,[4,7] and thiane-3-one 1-oxide [3] adopt preferentially the axial S=O conformer. The origin of the equatorial S=O preference in I–III is somewhat unclear but a suggestion [1] that dipolar interactions are involved has recently received support in the form of force field calculations performed by Allinger and Kao.[8] These workers also calculated that conformer Ie is 4.2 kcal mol^{-1} more stable than the lowest energy twist form.

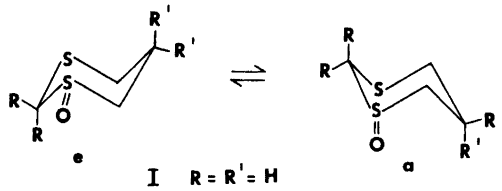

I R = R' = H
II R = Me, R' = H
III R = H, R'R' = O

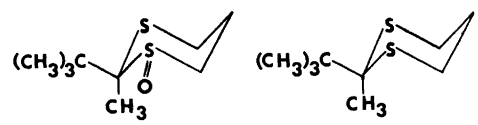

In the present paper we report the analysis of the 100 MHz spectrum of the 2-*t*-butyl-2-

Table 1. 100 MHz spectral parameters (in Hz) of IV and V in $CDCl_3$.

	Chemical shift [a]			Coupling constants	
	IV	V [b]		IV	V [b]
4a	266.60	303.11	4a5a	12.75	11.85
4e	239.38	271.80	4e5e	3.00	4.35
5a	215.07	178.73	4a5e	2.92	3.28
5e	228.88	205.47	4e5a	3.97	3.96
6a	267.13	303.11	5a6a	14.21	11.85
6e	301.85	271.80	5e6e	3.82	4.35
			5a6e	3.39	3.96
			5e6a	3.23	3.28
			4a4e	−14.49	−14.46
			5a5e	−14.54	−13.56
			6a6e	−13.31	−14.46
			4e6e	1.57	0.65
			4a6a	−0.18	0.03
			4a6e	−0.23	−0.05
			4e6a	−0.41	−0.05

[a] Downfield from TMS. [b] Data taken from Ref. 11.

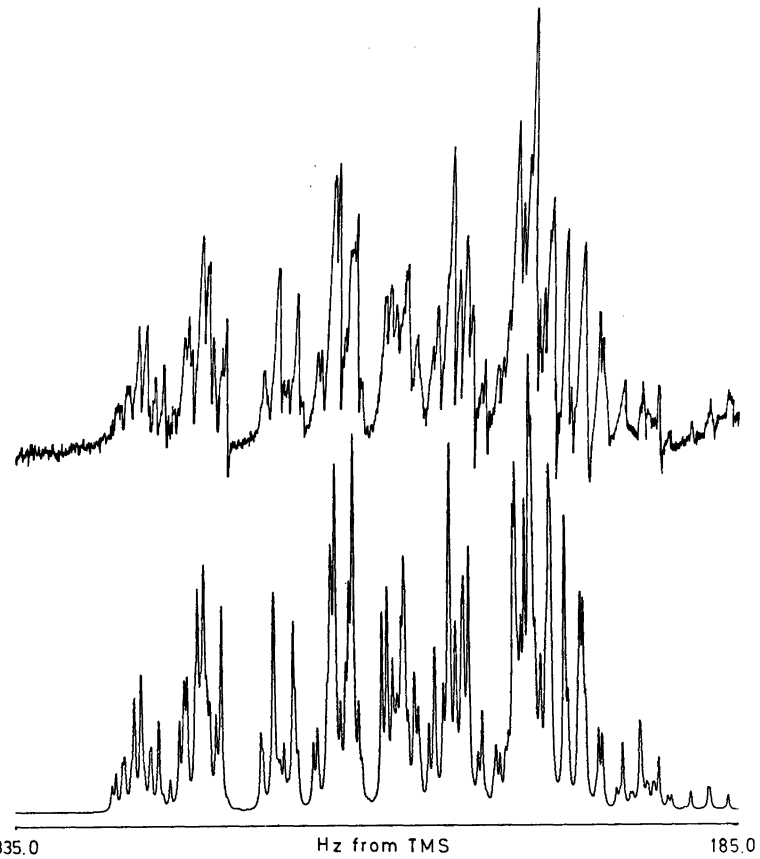

Fig. 1. Experimental (upper trace) and calculated (lower trace) 100 MHz spectrum of *trans*-2-*t*-butyl-*cis*-2-methyl-1,3-dithiane 1-oxide.

methyl derivative IV. Earlier we used [1,2] this compound as a "fixed chair" model in investigations of conformational equilibria of mobile 1,3-dithiane 1-oxides, but our present interest lay in a closer appraisal of its ring shape. The spectrum, Fig. 1, was analysed as an ABCDEF system using the LAOCN 3 program.[9] Input parameters were chosen largely on the basis of data obtained earlier from a crude first order analysis of the 220 MHz spectrum.[2] All parameters were allowed to vary and the values at the final iteration are reported in Table 1. The r.m.s. error of fit of 129 experimental and calculated transitions was 0.083. The calculated "probable error" for each parameter was 0.03 or less. The real errors are expected to be 2.5 times this value.[10] We find that the data obtained from the 220 MHz spectrum [2] are in moderately good agreement with the refined data obtained here.

Recently we reported [11] the analysis of the spectrum of 2-*t*-butyl-2-methyl-1,3-dithiane, V, and the data are reproduced here to facilitate comparison. H-5a, H-5e, and H-6e are deshielded in IV relative to V but H-6a and the protons H-4a and H-4e, which are rather distant from the S=O bond, are significantly more shielded. $^2J_{4,4}$ is much the same in both IV and V but $^2J_{5,5}$ is smaller (more negative) and $^2J_{6,6}$ larger in the former. The vicinal coupling constants are generally typical of those expected for rings "locked" in chair type conformations. However, there are small but significant variations in corresponding vicinal couplings between protons on C-4 and C-5, and on C-5 and C-6 in IV and these differ again from those in V. Such variations may arise from different internal dihedral angles, Ψ, within the rings as well as from different electronegativities of sulfide and sulfoxide sulfur atoms. The Lambert-Buys R-value method [12] provides a means of estimating Ψ from R, the ratio $\sum^3 J_{trans}:\sum^3 J_{cis}$ using the equation $\cos \Psi = 3/(2+4R)^{\frac{1}{2}}$. In this approach

electronegativity effects cancel, at least to a first approximation. By this treatment Ψ_{65} and Ψ_{45} in IV are 59 and 61°, respectively, so demonstrating that the CH_2-CH_2 fragment adjacent to the sulfoxide group is the more puckered. The ring is also marginally more puckered than V in this region ($\Psi = 58°$). The latter value, which is 5° lower than that in 2-phenyl-1,3-dithiane, we earlier interpreted in terms of flattening due to the axial 2-methyl group and/or the presence of twist forms.[11] It seems likely that similar effects occur in IV also.

Experimental, *trans*-2-*t*-Butyl-*cis*-2-methyl-1,3-dithiane 1-oxide IV was prepared as described in Ref. 2.

The NMR spectrum was recorded of a 10 % solution in $CDCl_3$ using a 100 MHz Varian HA-100 spectrometer operating at 35°. Line positions were taken by averaging data from four 100 Hz sweepwidth spectra, calibrated at every 10 Hz. Spectral analysis was performed using a local version of the LAOCN3 program and carried out on a UNIVAC 1110 computer. Graphical presentation of data, Fig. 1, was obtained using a CALCOMP plotter.

Acknowledgement. We thank NATO for providing a research grant to MJC and KB.

1. Cook, M. J. and Tonge, A. P. *Tetrahedron Lett.* (1973) 849.
2. Cook, M. J. and Tonge, A. P. *J. Chem. Soc. Perkin Trans. 2* (1976) 767.
3. Bergesen, K., Carden, B. M. and Cook, M. J. *Tetrahedron Lett.* (1975) 4479.
4. Van Acker, L. and Anteunis, M. *Tetrahedron Lett.* (1974) 225.
5. Khan, S. A., Lambert, J. B., Hernandez, O. and Carey, F. A. *J. Am. Chem. Soc. 97* (1975) 1468.
6. Lambert, J. B. and Keske, R. G. *J. Org. Chem. 31* (1966) 3429.
7. Bergesen, K., Cook, M. J. and Tonge, A. P. *Org. Magn. Reson. 6* (1974) 127.
8. Allinger, N. L. and Kao, J. *Tetrahedron 32* (1976) 529.
9. Castellano, S. and Bothner-By, A. A. *J. Phys. Chem. 41* (1964) 3863.
10. Ewing, D. F. *Org. Magn. Reson. 7* (1975) 520.
11. Bergesen, K., Carden, B. M. and Cook, M. J. *J. Chem. Soc. Perkin Trans. 2* (1976) 365.
12. For a review see Lambert, J. B. *Acc. Chem. Res. 4* (1971) 87.

Received May 6, 1976

Stability Constants for Scandium Thiodiacetate Complexes

INGEMAR DELLIEN

Physical Chemistry 1, Chemical Center, P.O.B. 740, S-220 07 Lund 7, Sweden

Thermodynamic data such as $\Delta G_j°$, $\Delta H_j°$, and $\Delta S_j°$ for complex formation reactions in aqueous solution between lanthanoid(III) ions and carboxylate ligands show that these thermodynamic properties are greatly affected by the geometrical requirements of the ligand and the size of the metal ion. As scandium(III) has a similar electron configuration as the lanthanoids but is considerably smaller (the radii of the lanthanoid ions are in the range 1.06–0.85 Å, while that of Sc^{3+} is 0.73 Å [1]), data on scandium complexes should give additional information on the effects of a variation of the metal ion radius upon the thermodynamic characteristics of complex formation.

The earlier measurements on some lanthanoid thiodiacetate complexes [2] have here been extended to the scandium thiodiacetate system. The main reasons for this investigation are summarized below:

i. For the scandium complexes, the ratio between the consecutive formation constants, K_1/K_2, is low for the bidentate ligands malonate [3] and oxalate [4] (≈ 40), but quite high ($\approx 10^4$) for terdentate ligands such as oxydiacetate [5] and dipicolinate.[3] The lanthanoids are typical hard acids which ought to form poor bonds with sulfur donors. The results obtained from the lanthanoid thiodiacetate systems confirms this expectation, *i.e.* the ligand seems to be effectively bidentate.[2] A determination of K_1/K_2 for the scandium thiodiacetate complexes will indicate how the ligand is bonded.

ii. The stability of acid complexes as MHA^{2+} also gives information on the bonding in and the geometry of the complexes. Thus, acid complexes are not formed when the lanthanoid ion and the ligand form five-membered chelate rings, as in the oxalates [5] and oxydiacetates,[6] or when the coordinating groups are close to each other due to a rigid ligand geometry, as in the maleates.[7] The effectively bidentate ligands malonate and thiodiacetate form weaker chelate complexes,[8,2] and acid complexes are thus formed in appreciable amounts in these systems. The variation pattern of pK_a (MHA^{2+}) *versus* the lanthanoid ion radius can be qualitatively described with simple electrostatic arguments.

This communication reports a determination of the composition and stability constants for scandium thiodiacetate complexes. The measurements have been designed to make it possible to decide if any scandium hydrogen thiodiacetate complex is formed. A potentiometric

electronegativity effects cancel, at least to a first approximation. By this treatment Ψ_{65} and Ψ_{45} in IV are 59 and 61°, respectively, so demonstrating that the CH_2-CH_2 fragment adjacent to the sulfoxide group is the more puckered. The ring is also marginally more puckered than V in this region ($\Psi = 58°$). The latter value, which is 5° lower than that in 2-phenyl-1,3-dithiane, we earlier interpreted in terms of flattening due to the axial 2-methyl group and/or the presence of twist forms.[11] It seems likely that similar effects occur in IV also.

Experimental, *trans*-2-*t*-Butyl-*cis*-2-methyl-1,3-dithiane 1-oxide IV was prepared as described in Ref. 2.

The NMR spectrum was recorded of a 10 % solution in $CDCl_3$ using a 100 MHz Varian HA-100 spectrometer operating at 35°. Line positions were taken by averaging data from four 100 Hz sweepwidth spectra, calibrated at every 10 Hz. Spectral analysis was performed using a local version of the LAOCN3 program and carried out on a UNIVAC 1110 computer. Graphical presentation of data, Fig. 1, was obtained using a CALCOMP plotter.

Acknowledgement. We thank NATO for providing a research grant to MJC and KB.

1. Cook, M. J. and Tonge, A. P. *Tetrahedron Lett.* (1973) 849.
2. Cook, M. J. and Tonge, A. P. *J. Chem. Soc. Perkin Trans. 2* (1976) 767.
3. Bergesen, K., Carden, B. M. and Cook, M. J. *Tetrahedron Lett.* (1975) 4479.
4. Van Acker, L. and Anteunis, M. *Tetrahedron Lett.* (1974) 225.
5. Khan, S. A., Lambert, J. B., Hernandez, O. and Carey, F. A. *J. Am. Chem. Soc. 97* (1975) 1468.
6. Lambert, J. B. and Keske, R. G. *J. Org. Chem. 31* (1966) 3429.
7. Bergesen, K., Cook, M. J. and Tonge, A. P. *Org. Magn. Reson. 6* (1974) 127.
8. Allinger, N. L. and Kao, J. *Tetrahedron 32* (1976) 529.
9. Castellano, S. and Bothner-By, A. A. *J. Phys. Chem. 41* (1964) 3863.
10. Ewing, D. F. *Org. Magn. Reson. 7* (1975) 520.
11. Bergesen, K., Carden, B. M. and Cook, M. J. *J. Chem. Soc. Perkin Trans. 2* (1976) 365.
12. For a review see Lambert, J. B. *Acc. Chem. Res. 4* (1971) 87.

Received May 6, 1976

Stability Constants for Scandium Thiodiacetate Complexes

INGEMAR DELLIEN

Physical Chemistry 1, Chemical Center, P.O.B. 740, S-220 07 Lund 7, Sweden

Thermodynamic data such as $\Delta G_j°$, $\Delta H_j°$, and $\Delta S_j°$ for complex formation reactions in aqueous solution between lanthanoid(III) ions and carboxylate ligands show that these thermodynamic properties are greatly affected by the geometrical requirements of the ligand and the size of the metal ion. As scandium(III) has a similar electron configuration as the lanthanoids but is considerably smaller (the radii of the lanthanoid ions are in the range 1.06–0.85 Å, while that of Sc^{3+} is 0.73 Å [1]), data on scandium complexes should give additional information on the effects of a variation of the metal ion radius upon the thermodynamic characteristics of complex formation.

The earlier measurements on some lanthanoid thiodiacetate complexes [2] have here been extended to the scandium thiodiacetate system. The main reasons for this investigation are summarized below:

i. For the scandium complexes, the ratio between the consecutive formation constants, K_1/K_2, is low for the bidentate ligands malonate [3] and oxalate [4] (≈ 40), but quite high ($\approx 10^4$) for terdentate ligands such as oxydiacetate [5] and dipicolinate.[3] The lanthanoids are typical hard acids which ought to form poor bonds with sulfur donors. The results obtained from the lanthanoid thiodiacetate systems confirms this expectation, *i.e.* the ligand seems to be effectively bidentate.[2] A determination of K_1/K_2 for the scandium thiodiacetate complexes will indicate how the ligand is bonded.

ii. The stability of acid complexes as MHA^{2+} also gives information on the bonding in and the geometry of the complexes. Thus, acid complexes are not formed when the lanthanoid ion and the ligand form five-membered chelate rings, as in the oxalates [5] and oxydiacetates,[6] or when the coordinating groups are close to each other due to a rigid ligand geometry, as in the maleates.[7] The effectively bidentate ligands malonate and thiodiacetate form weaker chelate complexes,[8,2] and acid complexes are thus formed in appreciable amounts in these systems. The variation pattern of pK_a (MHA^{2+}) *versus* the lanthanoid ion radius can be qualitatively described with simple electrostatic arguments.

This communication reports a determination of the composition and stability constants for scandium thiodiacetate complexes. The measurements have been designed to make it possible to decide if any scandium hydrogen thiodiacetate complex is formed. A potentiometric

standard method has been used, *viz.* the determination of the concentration of free hydrogen ion by means of a glass electrode. The measurements were performed at 25.0 °C in an aqueous sodium perchlorate medium with the total sodium ion concentration equal to 1.00 M.

Notations, calculations and experimental. Thiodiacetic acid, $S(CH_2COOH)_2$, is denoted H_2A, the other notations have been defined earlier.[8] The stability constants have been calculated from the experimentally determined E-values by the least squares procedure "Letagrop Etiter".

Scandium oxide (99.9 %) was obtained from Johnson Matthey Chem. Co. The other chemicals used were the same as described earlier.[2,8]

The equipment and experimental procedure in the potentiometric measurements were the same as used earlier. Six titration series were made, giving 76 experimental values of v/ml and E/mV. The titrator solution (T) had the composition $C_H = 63.6$ mM, $C_A = 230.9$ mM, and $C_{Sc} = 0$. The various titrand solutions (S) had $C_{Sc} = 10$ mM or 20 mM, and C_H varied between 3 mM and 50 mM.

The titrations had to be interrupted at $\bar{n}^* \approx 1.3$, due to the formation of a precipitate of the approximate composition $ScOHA(H_2O)_{0.5}$.

Results. Some of the experimental (v/ml, E/mV) data are given in Table 1. From these values the corresponding ($\bar{n}^*$,a^*) values were calculated. Different $\bar{n}^*(a^*)$ curves were obtained in solutions with different values of the hydrogen ion concentration, *cf.* Fig. 1 in Ref. 2. As the extent of hydrolysis is small in the solutions used, it is reasonable to explain this finding by the formation of acid complexes. The highest $\bar{n}^*$ value is 1.3; thus it is probable that at most two thiodiacetate ions are coordinated to the scandium ion in the concentration range investigated. The formation of the solid phase prevents measurements at higher free ligand concentrations. Hence no reliable estimate of $\beta_{1,0,3}$ can be obtained.

The hydrolysis of the scandium ion was accounted for by using stability constants for the species $ScOH^{2+}$ and $Sc_2(OH)_2^{4+}$ from Biedermann *et al.*[9] in the calculations. It was assumed that thiodiacetate complexes of the composition ScA^+, ScA_2^-, and $ScHA^{2+}$ were formed, and a least squares refinement of the corresponding stability constants by Letagrop Etiter gave the following values:

$$\beta_{1,0,1} = (8.60 \pm 0.15) \times 10^3 \ M^{-1}$$
$$\beta_{1,0,2} = (5.5 \pm 1.1) \times 10^5 M^{-2}$$
$$\beta_{1,1,1} = (1.46 \pm 0.12) \times 10^6 M^{-2}$$

(The uncertainties are equal to 3σ, where σ denotes the standard deviation). The standard deviation in the error-carrying variable C_H/C_A was equal to 9.8×10^{-3}. The accuracy of the data is lower than for the lanthanoid systems. Due to this, and the scarcity of data at high concentration of free ligand, the uncertainty in $\beta_{1,0,2}$ is rather high. It is also not possible to detect the presence of the species MHA_2, which is formed in the lanthanoid thiodiacetate and malonate systems.

The stability of the higher lanthanoid thiodiacetate complexes has been discussed earlier in some detail,[2] and it seems safe to conclude from this discussion that the formation of the complex ScA_3^{3-} can be neglected in the concentration range investigated here.

The concentration of scandium hydroxo complexes amounts at most to 0.5 % of C_{Sc} and to 4 % of C_H. There is no indication of any complex formation between hydrolysed scandium ions and the thiodiacetate ion in the pH range studied. If the hydrolysis of the scandium ion is neglected, the standard deviation in C_H/C_A rises to 12×10^{-3}.

Discussion. It has been inferred earlier from thermodynamic measurements that sulfur is a poor donor to rare earth ions.[10,11] This conclusion is validated for scandium by the results obtained here.

Table 1. Experimental results for the scandium thiodiacetate system. The results are given as v/ml, E/mV, $\bar{n}_H$, $(\bar{n}_{H,calc} - \bar{n}_{H,exp}) \times 10^3$. Two of the six titration series are given. The sodium ion concentration is 1.00 M in all solutions.

Series 1. S: $C_H = 0.05050$ M, $C_{Sc} = 0.01860$ M, $C_A = 0$;
T: $C_H = 0.06360$ M, $C_{Sc} = 0$, $C_A = 0.2309$ M;
$V_0 = 20.00$ ml, $E_0 = -631.1$ mV

0.50, −713.8, 1.923, 1.0; 1.00, −720.9, 1.891, 9.5; 1.50, −729.7, 1.855, 5.4; 2.00, −740.1, 1.778, 15.0; 2.50, −752.0, 1.673, 12.9; 3.00, −764.4, 1.548, −4.7; 3.50, −775.6, 1.420, −11.7; 4.00, −785.7, 1.306, −6.8; 4.50, −795.3, 1.208, −0.7; 5.00, −803.7, 1.124, 9.5; 5.50, −811.3, 1.053, 11.8; 6.00, −817.7, 0.991, 12.2; 6.50, −823.3, 0.938, 8.6; 7.00, −828.2, 0.893, 3.2; 7.50, −832.6, 0.852, −3.8; 8.00, −836.3, 0.817, −7.5; 9.00, −842.6, 0.758, −14.4; 10.0, −847.9, 0.710, −22.0;

Series 2. S: $C_H = 0.0058$ M, $C_{Sc} = 0.01970$ M, $C_A = 0$;
T: $C_H = 0.06360$ M, $C_{Sc} = 0$, $C_A = 0.2309$ M;
$V_0 = 20.00$ ml, $E_0 = -631.6$ mV

0.20, −773.8, 1.061, 8.8; 0.30, −778.0, 0.968, 8.0; 0.40, −781.6, 0.888, 9.2; 0.50, −784.8, 0.824, 7.1; 0.70, −790.3, 0.727, 0.8; 0.90, −794.9, 0.659, −1.7; 1.10, −799.1, 0.610, −4.8; 1.30, −803.0, 0.572, −4.8; 1.60, −808.6, 0.530, 1.0; 1.90, −814.4, 0.499, 9.1; 2.30, −822.2, 0.469, 27.4;

The increase in stability for the scandium thiodiacetate complex as compared to the ytterbium complex is smaller than the corresponding increase in stability found with the ligands malonate, oxydiacetate, and dipicolinate. It might be that the gain in the standard Gibbs free energy due to the electrostatic effects of substituting a lanthanoid ion with the smaller scandium ion is partially counteracted by a distortion of the thiodiacetate ion, brought about by the coordination of the carboxylate groups.

For the scandium thiodiacetate system, K_2 has the value 65 M^{-1}, while K_2 is 2×10^4 M^{-1} for the bidentate ligand malonate and is still larger for the terdentate ligands oxydiacetate and dipicolinate. The ratio K_1/K_2 is 130 for scandium thiodiacetate, which is slightly larger than found for the malonate and oxalate complexes, but much smaller than the values found for the terdentate ligands. The magnitude of the K_1 value indicates that an eight-membered chelate ring is formed in the monothiodiacetate complex. It is suggested from the values of K_2 and K_1/K_2 that the ligand in the second complex to some extent is bonded *via* one carboxylate group only. However, definite conclusions cannot be drawn until structural data on scandium thiodiacetate complexes are available.

Acknowledgement. The author wishes to thank Professors Ingmar Grenthe and Ido Leden for helpful criticism of the manuscript.

1. Shannon, R. D. and Prewitt, C. T. *Acta Crystallogr. B 25* (1969) 925.
2. Dellien, I., Grenthe, I. and Hessler, G. *Acta Chem. Scand. 27* (1973) 2431.
3. Grenthe, I. and Hansson, E. *Acta Chem. Scand. 23* (1969) 611.
4. Gårdhammar, G. *Acta Chem. Scand. 25* (1971) 158.
5. Grenthe, I., Gårdhammar, G. and Rundcrantz, E. *Acta Chem. Scand. 23* (1969) 93.
6. Grenthe, I. and Tobiasson, I. *Acta Chem. Scand. 17* (1963) 2101.
7. Dellien, I. and Malmsten, L.-Å. *Acta Chem. Scand. 27* (1973) 2877.
8. Dellien, I. and Grenthe, I. *Acta Chem. Scand. 25* (1971) 1387.
9. Biedermann, G., Kilpatrick, M., Pokras, L. and Sillén, L. G. *Acta Chem. Scand. 10* (1956) 1327.
10. Grenthe, I. *Acta Chem. Scand. 18* (1964) 283.
11. Grenthe, I. and Gårdhammar, G. *Acta Chem. Scand. A 28* (1974) 125.

Received March 15, 1976.

Acta Chemica Scandinavica A 30 (1976) 579—585

Electrophilic Nature of *o*-Nitrobenzeneselenenyl Compounds. A Kinetic Study

TOR AUSTAD

Department of Chemistry, University of Bergen, N-5014 Bergen-Univ., Norway

The rate of reaction between *o*-nitrobenzeneselenenyl bromide, *o*-$NO_2PhSeBr$, and various *para* substituted benzene sulfinates has been studied using stopped-flow and conventional spectrophotometry. The rate constants in methanol are related to σ substituent constants giving a Hammett plot with a slope of -1.0. The rate constants are also related to the asymmetric S—O stretching frequencies in the sodium salts of the sulfinates. It is concluded that the transition state is stabilized by mesomeric electron donating substituents in the nucleophile.

The reaction between *o*-NO_2PhSeX, X = SCN, *p*-$MeOPhSO_2$, $PhSO_2S$, and $(NH_2)_2C{=}S$, and dimethyldithiocarbamate, $Me_2NCS_2^-$, has also been studied kinetically in methanol. The leaving group effects on the rate constants have been discussed in terms of *trans* bond-lengthening effects of ligands bonded to divalent chalcogen atoms.

Upon changing the solvent from methanol to a dipolar aprotic medium, acetonitrile, an extremely large rate enhancing effect on the reaction between *o*-$NO_2PhSeBr$ and $PhSO_2^-$ was observed. The low reactivity of *o*-$NO_2PhSeBr$ in the former medium relatively to the latter is explained by a strong solvation of the nitro group in the protic solvent, protecting the Se atom from an attack *trans* to the leaving group.

It is concluded that the intramolecular three-center arrangement of the substrate, X—Se···O, is maintained in solution for X = Cl and Br, while it breaks down in solution for X = SCN, *p*-$MeOPhSO_2$, $PhSO_2S$, and $(NH_2)_2C{=}S$.

The geometry of *o*-nitrobenzenesulfenyl [1] (selenenyl) [2] compounds in the crystalline state appears to show an intramolecular nearly linear three-center arrangement between one of the oxygen atoms of the nitro group, the chalcogen atom, and the atom of the group attached to the chalcogen atom, (I).

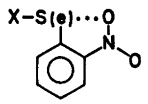

I

Kinetic studies concerning nucleophilic substitutions on *o*-NO_2PhSCl [3] and *o*-NO_2PhSeX,[4] X = Cl and Br, reported previously, appeared to show that the intramolecular three-center arrangement is still maintained in solution. The influence on the rate constant when the leaving group is changed from Cl to Br, when the substrate is changed from *o*-$NO_2PhSeBr$ to PhSeBr, and when the solvent is changed from a protic to a dipolar aprotic solvent, conforms to an attack of the nucleophile *trans* to the leaving group in a synchronous bond formation and bond breaking process.[3,4] The extraordinary high reactivity of *o*-NO_2PhSCl and *o*-$NO_2PhSeBr$ in acetonitrile relative to methanol, is suggested to be due to a strong solvation of the polar nitro group in the protic solvent. The free energy of activation in methanol is then mainly determined by the energy required to desolvate the nitro group. [3] The unusual high stability of the *o*-nitrobenzenesulfenyl (selenenyl) halogenides relative to the unsubstituted substrates in protic solvent has been explained in this way.

In this paper we will report some further data concerning the electrophilic nature of *o*-nitrobenzeneselenenyl compounds. The donor property of the nucleophile is varied systematically by using different *para* substituted aromatic sulfinates. In this way we hope to get information concerning the electronic trans-

mission of substituent effects through the sulfinate group, and to shed further light on the polar effects in the transition state.

So far only halides, Cl and Br, have been used as leaving groups in kinetic studies of substitution reactions on *o*-nitrobenzeneselenenyl compounds. We will also in this paper report some interesting kinetic results obtained by use of other types of leaving groups.

Finally, some data concerning solvent effects on the reaction between benzenesulfinate and *o*-NO_2PhSeBr will be discussed.

RESULTS AND DISCUSSION

The o-NO_2PhSeBr – sulfinate reaction. Aromatic sulfinates react with *o*-nitrobenzeneselenenyl bromide, *o*-NO_2PhSeBr, in a bimolecular substitution reaction as described in eqn. (1).

$$p\text{-XPhSO}_2^- + \text{RSe}-\text{Br} \xrightarrow{\text{MeOH}} p\text{-XPhS(O)}_2-\text{SeR} + \text{Br}^- \quad (1)$$

X = MeO, Me, H, F, and Cl. R = *o*-nitrophenyl.

As indicated by the product the sulfur atom of the sulfinate group is believed to be the nucleophilic atom toward the divalent selenium atom of the substrate. In all cases the products were stable, yellowish-green crystalline compounds, Table 1.

The rate data of reaction (1) at 25 °C in methanol are collected in Table 2. The reactions showed excellent second order kinetics, first order in each of the reactants. The rate of reaction was followed at 430 nm applying a spectrophotometer. Only *para*-substituted nucleophiles were used in order to avoid steric hindrance in the transition state.

The rate constants for the reaction of various aromatic sulfinates with *o*-NO_2PhSeBr show that electron-donating substituents in the

Table 1. Reaction products of the reaction between various substituted benzenesulfinates and *o*-nitrobenzeneselenenyl bromide.

Compound R = *o*-nitrophenyl	M.p./°C	Sulfur % Calc.	Found
p-$MeOPhSO_2SeR$	*ca.* 115 dec.	8.60	8.73
p-$MePhSO_2SeR$	115 (lit. 118)[a]	–	–
$PhSO_2SeR$	106 (lit. 109)[a]	–	–
p-$FPhSO_2SeR$	88	8.88	9.02
p-$ClPhSO_2SeR$	*ca.* 120 dec.	8.50	8.69

[a] Ref. 14.

Table 2. Pseudo first order rate constant, k', and second order rate constant, k_2, for the reaction between *o*-nitrobenzeneselenenyl bromide and different aromatic sulfinates in methanol at 25 °C.

No.	Nucleophile	$[Nu]/10^{-2}$ M	$k'/10^{-2}$ s^{-1}	k_2/M^{-1} s^{-1}
1	*p*-$MeOPhSO_2^-$	0.50	2.67	
		1.00	6.74	6.40
		2.00	12.9	
2	*p*-$MePhSO_2^-$	0.50	1.59	
		1.00	3.20	3.20
		2.00	6.40	
3	$PhSO_2^-$	0.25	0.487	
		0.50	1.08	2.05
		1.00	2.03	
		2.00	4.07	
4	*p*-$FPhSO_2^-$	0.25	0.386	
		0.50	0.835	1.71
		1.00	1.75	
5	*p*-$ClPhSO_2^-$	0.25	0.342	
		0.50	0.623	1.25
		1.00	1.23	

sulfinate increase the rate, while electron-attracting substituents decrease the rate. Thus, the rate depends on the electron density on the sulfur atom. The difference in the rate constant between the strongest and the weakest nucleophile is, however, rather small, *i.e.* $k_2(p\text{-MeO})/k_2(p\text{-Cl}) = 5.1$.

The rate data, except those for p-$MeOPhSO_2^-$ are correlated by the σ values [5] giving a Hammett plot of slope -1.0, Fig. 1. The obvious lack of correlation of p-$MeOPSO_2^-$ may suggest that σ^+ values rather than σ values should be used, but the $\log k_2 - \sigma^+$ plot showed a worse correlation. A combination of σ and σ^+ values, analogous to the Yukawa and Tsuno [6] equation, would probably give the best correlation.

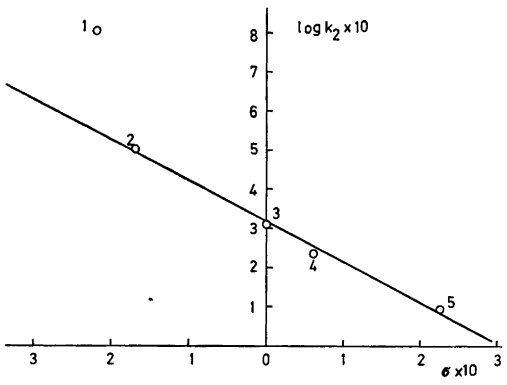

Fig. 1. Hammett plot for the reaction of *o*-nitrobenzeneselenenyl bromide and substituted benzenesulfinates in methanol at 25 °C. σ values from Ref. 5. The numbers correspond to those listed in Table 2.

The sign and magnitude of the slope, $\varrho = -1.0$, Fig. 1, indicate that the sulfur atom in the transition state is more positive charged relatively to the initial state. This is consistent with some degree of bond formation in the transition state.

The asymmetric S – O stretching frequencies of the sodium salts of the various substituted benzene sulfinates are listed in Table 3. It is seen that electron-donating substituents produce frequency shifts to higher wave numbers. Fig. 2 shows that, except for p-$MeOPhSO_2^-$, there appears to be a linear relationship between $\log k_2$ and ν_{as}(S – O). The nucleophili-

Table 3. Asymmetric S – O stretching frequencies, ν_{as}, in sodium salts of aromatic sulfinates, and pK_a values of the corresponding acids.

Compound	ν_{as}/cm^{-1} [a]	pK_a [b]
p-$MeOPhSO_2Na$	1150	2.72
p-$MePhSO_2Na$	1045	2.80
$PhSO_2Na$	1018	2.76
p-$FPhSO_2Na$	1015	–
p-$ClPhSO_2Na$	1000	2.76

[a] The measurements were performed in nujol.
[b] Ref. 7.

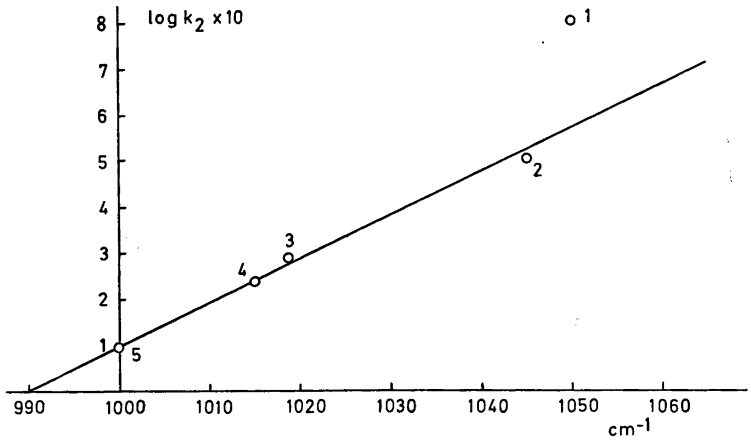

Fig. 2. Logarithm of the rate constants for the reaction of benzenesulfinates with *o*-nitrobenzeneselenenyl bromide as a function of the asymmetric S – O stretching frequencies of the sulfinates. The numbers correspond to those listed in Table 2.

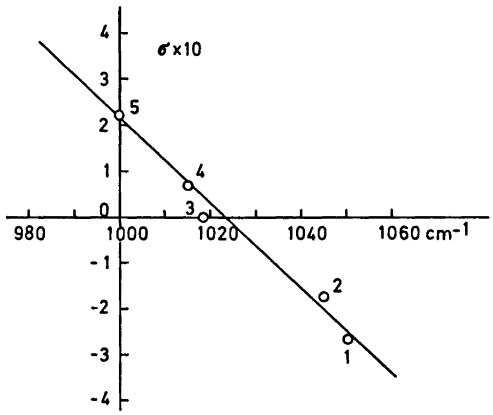

Fig. 3. The Hammett σ values as a function of the asymmetric S – O stretching frequencies of aromatic sulfinates. The numbers correspond to those listed in Table 2.

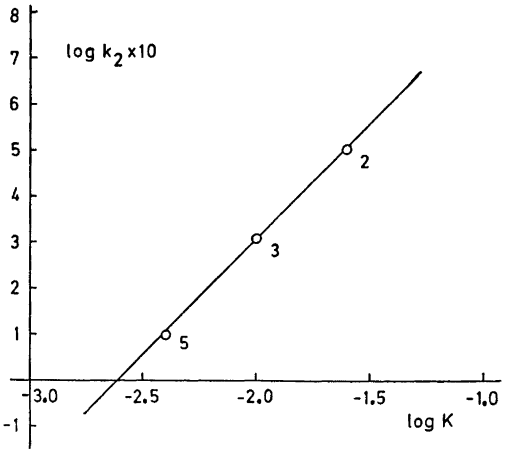

Fig. 4. Logarithm of the rate constants for the reaction between aromatic sulfinates and *o*-nitrobenzeneselenenyl bromide as a function of the logarithm of the equilibrium constant for the sulfinate-iodine reaction. The numbers correspond to those listed in Table 2.

city of aromatic sulfinates toward Se(II) increases as the wave number of the S – O stretching frequencies increases.

As demonstrated in Fig. 3 the Hammett σ values conform to a linear relationship with ν_{as}(S – O).

It has been argued that due to the tetrahedral structure of the sulfinate group, $-\overset{\displaystyle O}{\underset{\displaystyle O}{S}}\!:^{-}$, the "lone electron pair" of the sulfur atom is not available for a conjugation between π electrons of the benzene ring and those of the oxygen atoms.[7] Fig. 3 does, however, show that some mesomeric effects do operate on the sulfinate group in the sodium salts. Furthermore, Figs. 1 and 2 suggest that mesomeric electron donation appears to be a more important factor in stabilizing the transition state relatively to inductive electron donation.

On the other hand, the deviation of the point that corresponds to *p*-$MeOPhSO_2^-$, may perhaps be explained by assuming a transition state analogous to that proposed for the $R_2NCS_2^-$ – *o*-$NO_2PhSeBr$ reaction, (II).[3]

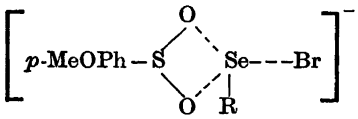

(II)

The sulfinate-iodine equilibria have been studied in aqueous solutions by Foss,[6] eqn. (2)

$$RSO_2^- + I_3^- \overset{K}{\rightleftharpoons} RSO_2I + 2I^- \qquad (2)$$

Concerning aromatic sulfinates, there seems to be a linear connection between the free activation energy for substitution reactions on Se(II) and the free energy of the sulfinate – iodine reaction, Fig. 4.

The pK_a values of the correponding acids of the nucleophiles are also listed in Table 3. By comparing the rate constants and pK_a values, no Brønsted correlation was found. On the basis of infrared and ultraviolet spectra, Detone and Hadze [8] suggested that the proton is bonded to one of the oxygen atoms in the acid, *i.e.* $R\text{-}\overset{\displaystyle O}{\overset{\|}{S}}\text{-}OH$. Consequently, the pK_a values in Table 3 do not represent the proton basicity of the nucleophilic sulfur atom of the sulfinate, and this may explain the lack of linearity in the log $k_2 - pK_a$ plot.

Leaving group effects. The reactions studied are shown by eqn. (3).

$$R-Se-X+Me_2NCS_2^- \xrightarrow[k_3>2\times10^5\ M^{-1}\ s^{-1}]{MeOH} R-Se-S-\overset{\overset{S}{\|}}{C}-NMe_2+X^- \quad (3)$$

X = SCN, *p*-MeOPhSO$_2$, and PhSO$_2$S. R = *o*-nitrophenyl.

In all cases the reaction was too fast to be followed by means of a stopped-flow spectrophotometer. One may then conclude that the second order rate constant is greater than 2×10^5 M^{-1} s^{-1}

Analogous results were also found for the reaction (4)

$$R-Se-\overset{+}{S}-C(NH_2)_2+Me_2NCS_2^- \xrightarrow{MeOH} R-Se-S-\overset{\overset{S}{\|}}{C}-NMe_2+(NH_2)_2C=S \quad (4)$$

The leaving groups and the nucleophile of reactions (3) and (4) are also nucleophilic reagents toward *o*-NO$_2$PhSeBr, and the rate constants for these as nucleophiles at 25 °C in methanol are listed below.[4]

$$R-Se-Br+Nu^- \xrightarrow[25\,^\circ C]{MeOH} RSeNu+Br^- \quad (5)$$

$k_2(SCN^-) = 0.133$ M^{-1} s^{-1}
$k_2(p\text{-}MeOPhSO_2^-) = 6.40$ M^{-1} s^{-1}
$k_2(PhSO_2S^-) = 3.25$ M^{-1} s^{-1}
$k_2((NH_2)_2C=S) = 53.3$ M^{-1} s^{-1}
$k_2(Me_2NCS_2^-) = 2667$ M^{-1} s^{-1}

Thus, concerning nucleophilic substitution reactions on *o*-nitrobenzeneselenenyl derivatives by $Me_2NCS_2^-$, the rate constants of reactions (3), (4), and (5) clearly show that SCN, *p*-MeOPhSO$_2$, PhSO$_2$S, and $(NH_2)_2C=S$ are better leaving groups than Br. Furthermore, Br^- does not react with the substrates of eqns. (3) and (4).

These results, at first sight, appear to contradict the general statement that exchange reactions on Se(II) are thermodynamically controlled. However, the kinetic data can be explained in terms of *trans* bond-lengthening effect of ligands participating in a three-center four electron bonding system around a divalent chalcogen atom (for a review see Refs. 10 and 11).

As pointed out earlier, crystallographic data point to an intramolecular three-center arrangement around the selenium atom in the substrate, (I).[2] The strength of the Se···O bond is, according to *trans* influence of ligands, affected by the group X. If X is more strongly bonded to Se, then the Se···O bond must be relatively weaker. In a thermodynamically controlled reaction, the strength of the X–Se bond in the transition state parallels the nucleophilicity of X toward Se(II). It is therefore reasonable to assume that the *trans* bond-lengthening effect increases in the order: Br < SCN < PhSO$_2$S < *p*-MeOPhSO$_2$ < $(NH_2)_2C=S$. Thus, the rate data can be explained by supposing the intramolecular X–Se···O arrangement to break down in solution for X = SCN, PhSO$_2$S, *p*-MePhSO$_2$ and $(NH_2)_2C=S$. The substrates then undergo a free rotation about the Se–C bond. The *trans* influence is smaller for X = Cl and Br, and the X-Se···O arrangement is for these substrates believed to be maintained in solution. Thus, a nucleophilic attack *trans* to the leaving group of *o*-NO$_2$PHSeBr involves an additional energy term in the free activation energy associated the strength of the Br–Se ···O bonding system, while nucleophilic substitutions on the substrates in eqns. (3) and (4) do not involve such an additional energy term due to free rotation about the Se–C bond.

It is of interest to note that in the crystalline form the thiocyanate salt of $[o\text{-}NO_2PhSe-S-C(NH_2)_2]^+$ forms a nearly linear S–Se···O arrangement,[2] while the present data indicate that the cation undergoes a free rotation about the Se–C bond in methanol.

The transition state in substitution reactions on Se(II) with $R_2NCS_2^-$ as nucleophiles is proposed to be of the type (III).[3]

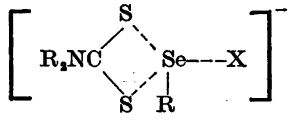

(III)

Both of the donor atoms of the bidentate nucleophile are directed toward the Se atom. In the product, however, only one of the S atoms of the dithiocarbamate is believed to be bonded to the Se atom.

The present results, together with the data of the two previous papers in this series,[3,4] clearly suggest that the nucleophile attacks *trans* to the leaving group, and that the X–Se···O arrangement in solution is strongly affected by the nature of X. Thus, so far both kinetic and structural data are compatible in the description of the mechanism for nucleophilic substitution on S(II), Se(II), and Te(II), as taking place through a linear three-center arrangement of nucleophile, electrophile, and leaving group, based on a single *p*-orbital of the electrophile. Concerning this picture Foss [12] once stated; "Nucleophilic reactivity may then relate to the ability of the reagent to engage the *p*-orbital in bonding, at the expense of the bond at 180°."

Solvent effects. Due to strong solvation of the polar nitro group in protic solvents, *o*-$NO_2PhSeBr$ is expected to be less reactive in this type of medium relatively to dipolar aprotic solvents. An extremely large solvent effect is indeed reported for the *o*-$NO_2PhSeBr-SCN^-$ reaction when going from MeOH to MeCN.[3]

The *o*-$NO_2PhSeBr-PhSO_2^-$ reaction has in the present work been studied kinetically at 25 °C in the solvents; MeOH, MeCN, and $MeNO_2$. The dielectric constant of these solvents is nearly the same. The following second order rate constants were observed;

$k_2(MeOH) = 2.05\ M^{-1}s^{-1}$
$k_2(MeCN) > 2 \times 10^5\ M^{-1}s^{-1}$
$k_2(MeNO_2) \approx 1.4 \times 10^5\ M^{-1}s^{-1}$

Thus, the rate constant increases by a factor greater than 10^5 when going from MeOH to MeCN. It is hard to believe that this large enhancement in the rate constant is only due to a different solvation of the nucleophile in MeOH and MeCN. Acetonitrile which, according to Gutmann,[13] has donor property, $DN_{SbCl_5} = 14.1$, may be involved in the reaction process. A reaction mechanism passing through an equilibrium involving a selenium ion–acetonitrile adduct may be suggested, eqns. (6) and (7).

$$R-Se-Br + MeCN \overset{\text{fast}}{\rightleftharpoons} \overset{+}{R}SeNCMe + Br^- \quad (6)$$

$$\overset{+}{R}SeNCMe + PhSO_2^- \xrightarrow{\text{fast}} RSeS(O)_2Ph + MeCN \quad (7)$$

A mechanism of the type described by eqns. (6) and (7) may be favoured in solvents having large donor numbers. However, nitromethane, which has very poor donor properties, $DN_{SbCl_5} = 2.7$, also gives a large enhancement in the rate constant relatively to methanol (a factor of nearly 10^5). It is therefore difficult to reconcile these results with a mechanism of the type described by eqns. (6) and (7). Thus, as suggested previously, the most reasonable explanation for the tremendous solvent effect on the electrophilicity of *o*-$NO_2PhSeBr$ is to assume a strong solvation of the nitro group in MeOH, which hinders the nucleophile form attacking *trans* to the leaving group.

Conclusion. The electrophilic nature of *o*-nitrobenzeneselenenyl compounds may then be summarized as follows:

1. The intramolecular three-center arrangement, X–Se···O, is believed to be maintained in solution for X = Cl and Br.

2. The X–Se···O arrangement probably breaks down in solution for ligands more strongly bonded to the Se atom, *i.e.* SCN, *p*-$MeOPhSO_2$, $PhSO_2S$, and $(NH_2)_2C{=}S$.

3. Nucleophilic attack appears to take place *trans* to the leaving group.

4. *o*-NO_2PhSeX, X = Cl and Br, is much more stable against nucleophilic attack in protic solvents than in dipolar aprotic solvents.

EXPERIMENTAL

Solvents. Methanol "Merck" *p.a.* was used without further purification. Acetonitrile was purified by distillation from P_2O_5 and CaH_2.[15] Nitromethane "Fluka", (*puriss* ≥ 99.5 %), was used without further purification.

Substrates. *o*-$NO_2PhSeBr$ was prepared and purified as reported previously.[4]

o-$NO_2PhSeSCN$ and *o*-$NO_2PhSeSS(O)_2Ph$ were synthesized by the method described by Foss.[14]

The adduct of *o*-$NO_2PhSeBr$ with $(NH_2)_2C{=}S$, $(NH_2)_2CSSePhNO_2$-*o* Br, was isolated and purified as described previously.[4]

Nucleophiles. Sodium sulfinates, which were recrystallized from methanol/ether, were employed. $PhSO_2Na$ and *p*-$MePhSO_2Na$ were commercial products obtained from "Fluka". The other aromatic sulfinates, *i.e.* *p*-$FPhSO_2Na$, *p*-$ClPhSO_2Na$, and *p*-$MeOPhSO_2Na$, were prepared from the corresponding sulfonyl chlorides and aqueous sodium sulfite as reported by Smiles and Gibson.[16]

$Ph_4AsPhSO_2$ was prepared as described previously,[17] and $Me_2NCS_2Na.2H_2O$ was a gift from Dr. O. Vikane of this Department.

Products. The products of the reactions between the sulfinates and *o*-$NO_2PhSeBr$ were isolated according to the procedure of Foss.[14] *p*-$MeOPhSO_2SePhNO_2$-*o* was recrystallized from ethanol, and the other products in Table 1 were recrystallized from a benzene/methanol mixture.

The products of the reaction between $Me_2NCS_2^-$ and the various selenenyl substrates have been reported previously.[4]

Kinetics. The rate of the reaction between *o*-$NO_2PhSeBr$ and the various aromatic sulfinates in MeOH was followed by measuring the decrease in the optical density, D, at the wavelength 430 nm using a Beckman DB-GT Grating Spectrophotometer. The kinetic runs were performed with matched 1 cm silica cells thermostated by circulating water from a thermostate controlled to ± 0.1 °C.

The runs were performed under pseudo first order conditions applying large excess of the nucleophile. The substrate concentration was about $1-3\times10^{-4}$ M. Values of the first order rate constant, k', were obtained from the slopes of the plots of log $(D_\infty - D_t)$ against time. Plots of k' against [Nu] were linear and passed through the origin. The second order rate constants were calculated from the slope of these lines.

Attempts were made to follow the reaction between *o*-NO_2PhSeX, X = SCN, *p*-$MeOPhSO_2$, $PhSO_2S$, and $(NH_2)_2C=S$, and $Me_2NCS_2^-$ in MeOH using a Durrum stopped-flow spectrophotometer, but the reactions were too fast. The measurements were performed at a fixed wavelength in the range 410 – 430 nm. The concentrations were 2.0×10^{-4} M of the substrate and 5.0×10^{-3} M of the nucleophile. The second order rate constants of these reactions could then be calculated to be greater than 2×10^5 $M^{-1}s^{-1}$.

$Ph_4AsPhSO_2$ was used as the nucleophilic reagent in the kinetic studies of the *o*-NO_2 $PhSeBr-PhSO_2^-$ reaction in MeCN and $MeNO_2$. The measurements were performed at 430 nm. The reaction in MeCN was too fast to be followed by means of the stopped-flow technique, $k_2 > 2\times10^5$ $M^{-1}s^{-1}$.

In $MeNO_2$ a logarithmic curve was observed, and the second order rate constant was estimated to be $\approx 1.4\times10^5$ $M^{-1}s^{-1}$.

REFERENCES

1. Hamilton, W. C. and La Placa, S. J. *J. Am. Chem. Soc. 86* (1964) 2289.
2. Eriksen, R. and Hauge, S. *Acta Chem. Scand. 26* (1972) 3153.
3. Austad, T. *To be published.*
4. Austad, T. *Acta Chem. Scand. A 29* (1975) 895.
5. McDaniel, D. H. and Brown, H. C. *J. Org. Chem. 23* (1958) 420.
6. Yukawa, Y. and Tsuno, Y. *Bull. Chem. Soc. Jpn. 32* (1959) 965.
7. De Filippo, D. and Momicchioli, F. *Tetrahedron 25* (1969) 5733.
8. Detoni, S. and Hadže, D. *J. Chem. Soc.* (1955) 3163.
9. Foss, O. *K. Nor. Vidensk. Selsk. Skr. XIX* (1947) 68.
10. Foss, O. *Selected Topics in Structure Chemistry*, Universitetsforlaget, Oslo 1967, pp. 145 – 173.
11. Foss, O. *Pure Appl. Chem. 24* (1970) 31.
12. Foss, O. *Acta Chem. Scand. 16* (1962) 779.
13. Gutmann, V. *Coordination Chemistry in Non-Aqueous Solutions*, Springer, Wien-New York 1968, p. 19.
14. Foss, O. *J. Am. Chem. Soc. 69* (1947) 2236.
15. Coetzee, J. F. *Pure Appl. Chem.* (1967) 429.
16. Smiles, S. and Gibson, D. T. *J. Chem. Soc.* (1924) 176.
17. Austad, T. *Acta Chem. Scand. A 29* (1975) 241.

Received February 25, 1976.

Acta Chemica Scandinavica A 30 (1976) 586—592

The pH Equilibria of the 3-Bromo-5-sulfosalicylate Ion in Alkaline Solution

YING-HUA LEE

Department of Inorganic Chemistry, University of Göteborg and Chalmers University of Technology, P.O. Box, S-402 20 Göteborg 5, Sweden

The pH equilibria of the 3-bromo-5-sulfosalicylate ion, HC^{2-}, in alkaline solution have been studied at 25 °C and 3 M sodium (perchlorate) medium by means of potentiometric titrations using a glass electrode. The total concentration of HC^{2-} ranged from 5 to 100 mM. An emf correction for the glass electrode has been applied in the pH range 9 − 11.5. The data were evaluated with a "curve-fitting" method, and the results were refined with the generalized least squares computer program LETAGROP ETITR. The systematic errors in E_0 and in the analytical concentrations were adjusted together with the formation constant β_{-11}. The data are best explained by

$$HC^{2-} \rightleftharpoons H^+ + C^{3-}$$
$$\log \beta_{-11} = -10.467 \pm 0.001$$

There was no evidence of the presence of dimeric complexes.

In order to investigate the complexation of the 3-bromo-5-sulfosalicylate ion, HC^{2-}, with metal ions, it is necessary to examine the equilibria between HC^{2-} and hydrogen ions in aqueous solution. In a previous investigation [1] the author determined the acidity constant for the carboxyl group of the acid, H_2C^-, and showed that the dimers $H_4C_2^{2-}$ and $H_3C_2^{3-}$ coexist with H_2C^- in acidic solution. Since the phenolic hydroxyl group is dissociated in alkaline solution only, it is also necessary to investigate the pH equilibria of the HC^{2-} ion in alkaline solution, not only in order to determine the acidity constant of the phenolic group, but also to investigate the formation of dimers.

The most common symbols are listed below for reference:

C	total concentration of disodium 3-bromo-5-sulfosalicylate Na_2HC.
c	concentration of free HC^{2-}.
H	total concentration of hydrogen ion (stoichiometric hydrogen ion concentration in excess of HC^{2-}).
h	concentration of free H^+.
Z	the average number of protons released per HC^{2-}.
β_{-pr}	equilibrium constant for the reaction $pH^+ + rHC^{2-} \rightleftharpoons H_{(p+r)}C_r^{(2r-p)-}$.
U_H	$\Sigma(H_{calc} - H_{tot})^2$.
$\sigma(\beta)$	standard deviation (in β).
V_0, H_0, C_0	volume, H and C in the initial solution S_0.
V_t, H_t, C_t	volume, H and C in the buret solution T.
E	emf in mV.
δH, δH_0	analytical errors in H and H_0.
f_c	analytical error factor for C. $f_c = C_{tot}/C$.

EXPERIMENTAL

Chemicals. Sodium perchlorate and disodium 3-bromo-5-sulfosalicylate solutions were prepared and analysed as described elsewhere.[1]

Perchlorate acid (Merck *p.a.*) was standardized against tris(hydroxymethyl)aminomethane GR or recrystallized borax, $Na_2B_4O_7.10H_2O$.

Sodium hydroxide was prepared from 50 % NaOH by dilution and was standardized against standard perchloric acid and against recrystallized potassium hydrogen phthalate. The results obtained from the two methods agreed to within ±0.1 %.

Borax. A.R. was recrystallized from water under 55 °C.

Table 1. Summary of the titrations in 3 M $Na(ClO_4)$.

Concentrations in mM.[a]

Titr. No.	H_0	C_0	H_T	H_T' (Backtitr.)	C_T	C_T' (Backtitr.)
Series I						
1a	0	12.0	−25.17		12.0	
2a+3a(Backtitr.)	0	20.0	−41.46	50.51	20.0	20.0
4a	0	30.0	−63.67		30.0	
5a	0	40.0	−82.92		40.0	
6a	0	50.0	−109.6		50.0	
Series II						
1b	0.03	5.016	−18.53		5.033	
2b+3b(Backtitr.)	0.03	10.05	−27.70	56.59	9.970	10.06
4b	0.03	19.97	−65.46		20.03	
5b	0.03	29.99	−87.46		29.99	
6b	0.03	99.93	−306.2		99.81	

[a] In each titration V_T ml of the buret solution T, with H_T and C_T, were added to V_0 ml of an initial solution S_0, with H_0 and C_0.

Emf measurements and apparatus. The experiments were carried out as two series (I and II) of potentiometric titrations at 25 °C in a nitrogen atmosphere. New stock solutions were used for each series.

In each titration, the total concentration of disodium 3-bromo-5-sulfosalicylate, C, was kept constant and the total hydrogen ion concentration, H, was varied by the addition of NaOH solution, the pH changing from 9 to 11.5. The values of C ranged from 0.005 to 0.100 M. All solutions were made 3 M in Na^+ by adding $NaClO_4$ to keep activity factors constant so that in the application of the law of mass action concentrations might be used instead of activities. A summary of the titrations is given in Table 1. All solutions listed in Table 1 were prepared from boiled doubly distilled water. The solutions containing NaOH were freshly prepared under N_2 atmosphere.

The cell used for the emf measurements can be described schematically:

+	reference electrode	equilibrium solution	glass electrode	−

The reference half cell had the composition

3 M $NaClO_4$	0.01 M NaCl+ 2.99 M $NaClO_4$	Ag,AgCl

The titration vessel and the "Wilhelm bridge" used were kept in a paraffin oil thermostat at 25.0 ± 0.02 °C. The emf of the cell in series I was measured with a Radiometer PHM 52 (accuracy ± 0.1 mV) and in series II with a digitial voltmeter HP 3450A (sensitivity of 1 μV). The emf measurements for series II were performed with the automatic titrator described by Gobom and Kovács.[2]

The glass electrode was a Jena type U. Since glass electrodes do not usually respond perfectly to changes in pH in alkaline solutions containing high concentrations of Na^+, a correction was necessary. The pH response of the glass electrode was standardized against a hydrogen electrode. If the glass electrode behaved as a hydrogen electrode, the difference between the emf of the hydrogen electrode and that of the glass electrode, ΔE ($=E_H-E_G$), would be constant in the relevant pH range. The method used to determine ΔE was that described by Olin.[3] As is apparent from fig. 1 ΔE varied about ± 0.1 mV at pH < 9 and increased gradually for pH > 9. The correction to E_G, E_{corr}, was then calculated as the difference in ΔE from the value corresponding to pH = 9. A plot of the corrections, E_{corr}, (in mV to be added) as a function of E_G for the Jena type U glass electrode in alkaline solution (pH

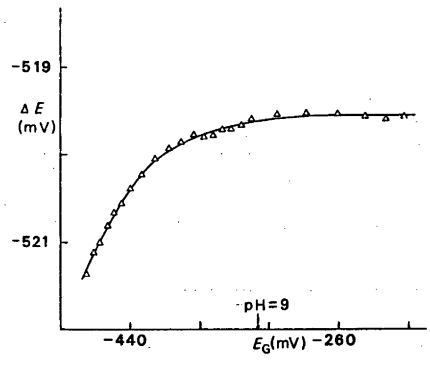

Fig. 1. ΔE ($=E_H-E_G$) as a function of E_G for the Jena type U glass electrode.

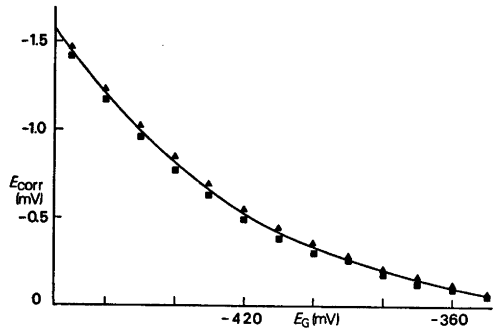

Fig. 2. The corrected emf, E_{corr}, as a function of E_G for the Jena type U glass electrode. $Na^+ = 3$ M. pH from 9 to 11.5. Curves 1 (■) and 2(▲) were obtained before and after the titration series II, respectively.

9 to 11.5) containing 3 M Na^+ is shown in Fig. 2. The correction curves 1 and 2 were obtained before and after titration series II, respectively. Mean values of E_{corr} from curves 1 and 2 were used to correct the measured E_G values in the titration series II (curve 3).

The voltage departures of the glass electrode in alkaline solution are time-dependent and vary with the condition of the surface of the glass electrode. However, as the pH was relatively low (under 11.5) no significant changes in E_{corr} were observed during a month.

From the corrected emf, h was calculated by means of the equation

$$E_G = E_0 + 59.156 \log h + E_j \quad (1)$$

where E_0 is a constant for the electrodes used and E_j is the liquid junction potential, which can be expressed as a function of $[OH^-]$, *i.e.* $E_j = j_{alk}[OH^-]$. Here, j_{alk} is a constant ≈ 8 mV/M in 3 M $NaClO_4$, $[OH^-] = K_w h^{-1}$ and $K_w = 6.03 \times 10^{-15} M^{2}$,[4,5] E_0 was determined by measuring the emf of a buffer solution, which contained 0.01 M borax ($Na_2B_4O_7.10H_2O$) in 3 M $Na(ClO_4)$ medium, after each main titration was finished. As the pH of the buffer solution was known, *i.e.* pH = 9.00, the value of E_0 could be calculated from eqn. (1).

The pH for 0.01 M $Na_2B_4O_7$ in 3 M $Na(ClO_4)$ medium was calculated from the relation $\beta = [H^+]$, where β is the equilibrium constant for the reaction: $B(OH)_3 + H_2O \rightleftharpoons B(OH)_4^- + H^+$ *i.e.*

$$\beta = [B(OH)_4^-]\ [H^+]/[B(OH)_3] \quad (2)$$

According to Ingri [6] only the mononuclear complex $B(OH)_4^-$ is formed in 3 M $Na(ClO_4)$ medium at low boric acid concentrations (≤ 0.025 M). Thus, in the 0.01 M $Na_2B_4O_7$ solution only the $B(OH)_3$ and $B(OH)_4^-$ species are present. From the mass and charge balances:

$$[B(OH)_4^-] = 0.02 + [H^+] - [OH^-] \quad (3)$$

$$[B(OH)_4^-] + [B(OH)_3] = 0.04 \quad (4)$$

As the value of the pH in this solution is about 9, the values of $[H^+]$ and $[OH^-]$ in (3) are small in comparison with 0.02 and can be neglected. Hence

$$[B(OH)_4^-] = [B(OH)_3] = 0.02 \text{ and } \beta = [H^+]$$

As the value of log β obtained by Ingri is $\log \beta = -9.00$ (± 0.02), the pH for 0.01 M $Na_2B_4O_7$ solution is 9.00 ± 0.02.

In the evaluation of the equilibrium constants for Na_2HC in alkaline solution, H^+ and HC^{2-} were chosen as components. The general equilibria and formation constants are

$$pH^+ + rHC^{2-} \rightleftharpoons H_{(p+r)}C_r^{(2r-p)-} \quad (5)$$

$$\beta_{pr} = [H_{(p+r)}C_r^{(2r-p)-}]h^{-p}b^{-r} \quad (6)$$

Since h, C and H are known, it is possible to calculate the auxiliary function, Z, which is the average number of H^+ released per HC^{2-}, from the relation

$$CZ = h - H - K_w h^{-1} \quad (7)$$

TREATMENT OF DATA AND RESULTS

The experimental data were first evaluated by the "curve-fitting" method for determining the formation constant β_{-11}. The results were

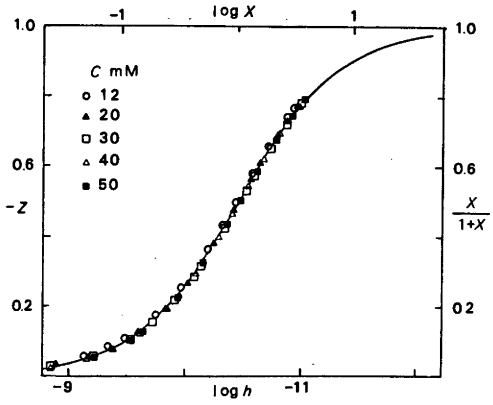

Fig. 3. Experimental data in series I plotted as $(-Z, \log h)_c$. The curve is a normalized curve $(X/(1+X), \log X)$ corresponding to log $\beta_{-11} = -10.46$

then refined with the generalized least squares program LETAGROP ETITR.[7]

Curve-fitting method. As is shown in Fig. 3, the experimental data from series I, plotted as $-Z=f(\log h)_C$, fit the normalized curve $X/(1+X)=f(\log X)$, (where $X=\beta_{-11}h^{-1}$), calculated for the single complex C^{3-} according to reaction (5) with $p=-1$, $r=1$. This indicates that only the mononuclear complex C^{3-} is formed in alkaline solution. The equilibrium constant β_{-11} ($=[C^{3-}]hc^{-}$) was then estimated as $\log \beta_{-11}=-10.46$ from Fig. 3 according to $\log X=\log \beta_{-11}-\log h$

LETAGROP method. β_{-pr} were sought as the values which gave a minimum for the error squares sum $U=\sum(H_{calc}-H_{tot})^2$. The program also permits adjustment of the experimental errors, such as small corrections to H, C, E_0 *etc.* The data in series I and II were treated separately. Initially, β_{-11} was refined with no correction of the experimental quantities, the following results being obtained:

Series I. $\log \beta_{-11}=-10.468\pm0.008$, $\sigma(H)=$ $=0.152\times10^{-3}$ M, $U_H=2.94\times10^{-6}$ M²

Series II. $\log \beta_{-11}=-10.487\pm0.003$, $\sigma(H)=$ $=0.407\times10^{-3}$ M, $U_H=35.94\times10^{-6}$ M²

The presence of the dimeric complex HC_2^{5-} was then investigated. In this calculation both β_{-11} and β_{-12} were varied. Since a negative value was obtained for β_{-12}, it did not seem likely that HC_2^{5-} was present. The calculations were then performed under several conditions for the further refinement of β_{-11}. In each calculation, a number of systematic errors were adjusted alternately with β_{-11}. The resulting "best" set of values for U_H, $\sigma(H)$, β_{-11}, E_0, δH and f_C *etc.* is given in Tables 2 and 3.*

By comparing the values of U_H and $\sigma(H)$ obtained in different calculations (Table 2), it can be seen that the best fit (the lowest values of U_H and $\sigma(H)$) is obtained in calculations 2 and 6, in which the standard deviations of H, δH, are 0.0179 and 0.0449 mM, respectively. The relative errors, $(H_{calc}-H_{exp})/H_{exp}$ or $(Z_{calc}-Z_{exp})/Z_{exp}$, in calculations 2 and 6 are less than 0.5 % for most experimental points (about 93 % of 347 points) and there are no obvious systematic errors.

The adjustment indicated in Table 3 seems to be reasonable. The value of f_C indicates that the correction to C is about 2 % in series I, and 3 % in series II (except for $C=0.005$ M, where it is about 6 %) and that the ratio of δH to C is less than 0.5 % in most titrations. The corrections to C and H are feasible in view of the uncertainties in the chemical analyses.

The adjustment of E_0 (below 1.2 mV for most titrations) shown in Table 3 would appear to be reasonable, considering the accuracy of the E_0 determination.

The final value of β_{-11} is the mean value obtained from calculations 2 (or 3) and 6, *i.e.* $\log \beta_{-11}=-10.467\pm0.001$ This β_{-11} value has been used, together with the constants determined previously,[1] $\log \beta_{11}=2.028$, $\log \beta_{12}=2.537$ and $\log \beta_{22}=4.739$, to calculate the distribution of 3-bromo-5-sulfosalicylic acid present in the different species (*cf.* Fig. 4).

* The output from LETAGROP calculations can be obtained on request.

Table 2. Equilibrium constant for the reaction $HC^{2-} \rightleftharpoons H^+ + C^{3-}$ calculated by LETAGROP with adjustment for E_0, δH_0, δH, and f_C, 25 °C, 3 M $Na(NaClO_4)$, $U_H=\sum(H_{calc}-H_{tot})^2$.

Calculation	$U\times10^6$ (M²)	$\sigma(H)\times10^3$ (M)	$\log \beta_{-11}\pm3\sigma$	Systematic errors adjusted with β_{-11}
Series I (128 points)				
1	0.0765	0.0261	-10.492 ± 0.002	δH, f_C
2	0.0367	0.0179	-10.473 ± 0.002	δH_0, f_C, E_0
3	0.0377	0.0181	-10.473 ± 0.001	δH, f_C, E_0
Series II (219 points)				
4	2.289	0.1028	-10.505 ± 0.004	δH, f_C
5	1.778	0.0939	-10.456 ± 0.020	δH_0, f_C, E_0
6	1.759	0.0449	-10.464 ± 0.001	δH, f_C, E_0

Table 3. E_0, δH_0, δH, and f_C calculated by LETAGROP for the "best fit" for the calculations listed in Table 2.

Titr. No.	E_0 mV (from exp.)	$E_0 \pm 3\sigma$ mV	$\delta H_0 \pm 3\sigma$ mM	$\delta H \pm 3\sigma$ mM	$f_C \pm 3\sigma$
Calculation 1					
1a	198.90			0.165 ± 0.032	1.0311 ± 0.0064
2a	199.15			0.137 ± 0.025	1.0237 ± 0.0031
3a	199.15			0.059 ± 0.042	1.0331 ± 0.0063
4a	198.80			0.168 ± 0.021	1.0190 ± 0.0016
5a	199.00			0.084 ± 0.025	1.0228 ± 0.0015
6a	198.84			0.011 ± 0.042	1.0196 ± 0.0020
Calculation 2					
1a		199.08 ± 0.22	0.103 ± 0.012		1.0231 ± 0.0031
2a		198.73 ± 0.07	0.086 ± 0.058		1.0192 ± 0.0010
3a		198.40 ± 0.43	0.052 ± 0.025		1.0272 ± 0.0073
4a		197.98 ± 0.18	0.131 ± 0.025		1.0192 ± 0.0024
5a		197.91 ± 0.22	0.077 ± 0.039		1.0240 ± 0.0030
6a		197.47 ± 0.26	0.054 ± 0.062		1.0231 ± 0.0033
Calculation 3					
1a		199.10 ± 0.24		0.101 ± 0.013	1.0182 ± 0.0031
2a		198.71 ± 0.27		0.083 ± 0.025	1.0175 ± 0.0037
3a		198.23 ± 1.87		0.052 ± 0.097	1.0268 ± 0.0038
4a		197.91 ± 0.21		0.134 ± 0.028	1.0176 ± 0.0026
5a		197.83 ± 0.26		0.082 ± 0.046	1.0238 ± 0.0034
6a		197.44 ± 0.26		0.053 ± 0.062	1.0228 ± 0.0031
Calculation 4					
1b	201.56			0.062 ± 0.017	1.0617 ± 0.0066
2b	202.77			0.055 ± 0.036	1.0364 ± 0.0066
3b	202.77			0.156 ± 0.046	1.0344 ± 0.0101
4b	200.90			0.159 ± 0.083	1.0374 ± 0.0076
5b	201.13			0.235 ± 0.104	1.0252 ± 0.0060
6b	202.16			0.582 ± 0.181	1.0255 ± 0.0033
Calculation 5					
1b		197.48 ± 0.50	0.097 ± 0.017		1.0772 ± 0.0046
2b		201.13 ± 0.32	−0.034 ± 0.022		1.0358 ± 0.0034
3b		201.58 ± 0.08	0.082 ± 0.005		1.0237 ± 0.0010
4b		199.22 ± 0.24	−0.014 ± 0.036		1.0369 ± 0.0023
5b		199.00 ± 0.41	0.045 ± 0.100		1.0282 ± 0.0035
6b		199.00 ± 0.37	−0.505 ± 0.295		1.0257 ± 0.0034
Calculation 6					
1b		200.82 ± 0.78		−0.005 ± 0.027	1.0581 ± 0.0073
2b		201.54 ± 0.36		−0.029 ± 0.025	1.0362 ± 0.0037
3b		202.05 ± 0.21		0.073 ± 0.012	1.0238 ± 0.0026
4b		199.79 ± 0.25		−0.019 ± 0.038	1.0356 ± 0.0023
5b		199.56 ± 0.42		0.038 ± 0.102	1.0265 ± 0.0037
6b		199.55 ± 0.38		−0.515 ± 0.303	1.0270 ± 0.0035

DISCUSSION

That the dimeric complex HC_2^{5-} does not exist in alkaline solution is to be expected, since it is generally recognized that the intermolecular hydrogen bond is responsible for the association of carboxylic acids, water and phenols *etc.* In acidic solution the formation of the dimers $H_4C_2^{3-}$ and $H_3C_2^{3-}$ can be explained

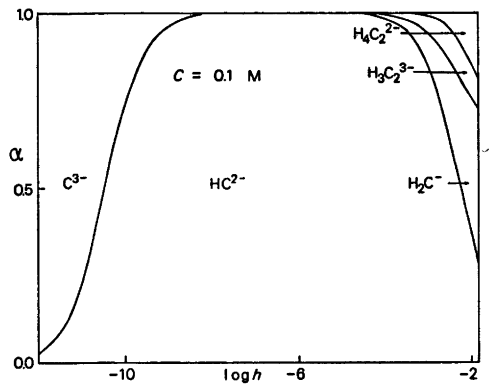

Fig. 4. The distribution of 3-bromo-5-sulfosalicylate between different species plotted *versus* log h. The calculations were performed with HALTAFALL [9] assuming log β_{-11} = −10.467, log β_{11} = 2.028, log β_{12} = 2.537 and log β_{22} = 4.739 At a given log h the fraction of HC^{2-} present in each species is represented by the segment of a vertical line falling within the corresponding area.

by similar reasoning as for salicylic acid.[8] The dimeric hydrogen bonding between the carboxyl groups is strong enough to overcome competition from hydrogen bonding between acid and water molecules, and intramolecular hydrogen bonding between the *ortho*-hydroxyl group and the adjacent carboxyl group. The latter bond has been shown to exist in the salicylate ion.[8] A similar result would be expected for the 3-bromo-5-sulfosalicylate ion HC^{2-}. In alkaline solution, the carboxyl group is completely dissociated. Only the proton in the phenolic hydroxyl group would be available for hydrogen bonding. The absence of dimers in alkaline solution therefore suggests that either intramolecular hydrogen bonding or intermolecular hydrogen bonding between the phenolic hydroxyl group and water molecules is strong. No proton would then be available for dimeric hydrogen bonding.

By comparing the values of the acidity constants, log β_{11} (pKa_1) and $-\log \beta_{-11}$ (pKa_2), for salicylic acid, 5-sulfosalicylic acid and 3-bromo-5-sulfosalicylic acid (Table 4), it is seen that both the substituents −Br and $-SO_3^-$ show an acid strengthening effect on both carboxyl and phenolic hydroxyl groups in the substituted acids. The effect is greater on the phenolic hydroxyl group. This strengthening effect can be explained in terms of the inductive and conjugative (or resonance) effects of the substituents, and by their influence on the intramolecular hydrogen bonding between the carboxyl and phenolic hydroxyl groups.

The −Br group has an electron withdrawing (or attracting) inductive effect (the −I-effect) and an electron releasing resonance effect, (the +M-effect). The $-SO_3^-$ group has the −I effect and an electron withdrawing resonance effect, −M.

The acid strengthening effect of $-SO_3^-$ on the phenolic hydroxyl group in the substituted salicylic acid can be attributed to its electron withdrawing resonance effect and a small inductive effect; the former is a result of an effective conjugation between $-SO_3^-$, a benzene ring and a hydroxyl group (see Fig. 5). Both the resonance and the inductive effects weaken the bonding between O and H of the hydroxyl groups, and consequently

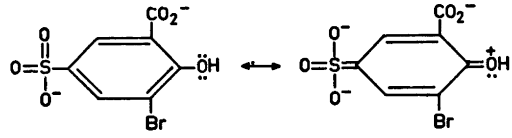

Fig. 5. The conjugation between $-SO_3^-$, a benzene ring and a hydroxyl group.

Table 4. Acidity constants.

	log β_{11} (pK_{a1})	$-\log \beta_{-11}$ (pK_{a2})	Ref.
Salicylic acid	3.173	13.12	8,10
5-Sulfosalicylic acid	2.67	11.74	11
3-Bromo-5-sulfosalicylic acid	2.028	10.467	1

increase the acid strength.

The $-Br$ group in the *ortho*-position to the hydroxyl group shows an apparent acid strengthening effect on the hydroxyl group in the substituted salicylic acid. This effect can be interpreted as due to a greater electron-withdrawing inductive effect. There is no electron-releasing resonance effect, +M, since direct conjugation is not possible.

Both $-SO_3^-$ and $-Br$ groups also show an acid strengthening effect on the carboxyl group, though this effect is a little weaker than that on the phenolic hydroxyl group. The protolysis of the carboxyl group in salicylic acid is dependent on intramolecular hydrogen bonding between the *ortho*-hydroxyl group and the adjacent carboxyl group, since the formation of the intramolecular hydrogen bond makes the anion more stable than the undissociated acid. In the substituted salicylic acid, the hydrogen bond is strengthened by the stabilization of the phenolic hydroxyl ion, due to the $-M$ conjugative effect of the $-SO_3^-$ group and the $-I$ inductive effect of the $-Br$ group on the phenolic hydroxyl group, thereby enhancing the acid strength of the carboxyl group in the substituted salicylic acid. In addition to this indirect acid strengthening effect, a weak electron withdrawing inductive effect of both $-SO_3^-$ and $-Br$ groups situated in the *meta*-position to the carboxyl group would be expected.

Acknowledgements. The author would like to express her gratitude to Professor Georg Lundgren for his encouragement and for many valuable discussions and to Dr. Susan Jagner for revising the English text.

The investigation was supported by a grant from the Swedish Natural Science Research Council (Contract No. 2318).

REFERENCES

1. Lee, Y.-H. *Acta Chem. Scand. 27* (1973) 1807.
2. Gobom, S. and Kovacs, J. *Chem. Scr. 2* (1972) 103.
3. Olin, Å. *Acta Chem. Scand. 14* (1960) 129.
4. Forsberg, O., Johansson, K., Ulmgren, P. and Wahlberg, O. *Chem. Scr. 3* (1973) 153.
5. Ingri, N., Lagerström, G., Frydman, M. and Sillén, L. G. *Acta Chem. Scand. 11* (1957) 1034.
6. Ingri, N. *Acta Chem. Scand. 16* (1962) 439.
7. Brauner, P., Sillén, L. G. and Whiteker, R. *Ark. Kemi 31* (1969) 365.
8. Lee, Y.-H. and Lundgren, G. In Högfeldt, E., Ed., *Contributions to Coordination Chemistry*, NFR, Stockholm 1972.
9. Ingri, N., Kakolowicz, W., Sillén, L. G. and Warnqvist, B. *Talanta 14* (1967) 1261.
10. Ågren, A. *Sven. Kem. Tidskr. 68* (1956) 189.
11. Ågren, A. *Acta Chem. Scand. 8* (1954) 266.

Received March 4, 1976.

Acta Chemica Scandinavica A 30 (1976) 593—598

The Complex Equilibria of Pb^{2+} with 3-Bromo-5-sulfosalicylate Ions

YING-HUA LEE

Department of Inorganic Chemistry, University of Göteborg and Chalmers University of Technology, P.O. Box, S-402 20 Göteborg 5, Sweden

The equilibria between lead(II) and 3-bromo-5-sulfosalicylate ions, HC^{2-}, have been studied at 25 °C in 3 M sodium (perchlorate) medium, by means of potentiometric titrations using both glass and lead amalgam electrodes. The total concentrations of Pb^{2+} and HC^{2-} ranged from 0.25 to 1 mM and from 0 to 35 mM, respectively. The pH range was 3 – 7.

The data have been evaluated with a graphical method, and the results refined with the generalized least squares program LETAGROP ETITR. The four main complexes formed between Pb^{2+} and HC^{-2} are PbHC, $Pb(HC)_2^{2-}$, PbC^-, and PbC_2^{4-} with the following formation constants: $\log \beta_{011} = 1.116 \pm 0.006$, $\log \beta_{012} = 1.931 \pm 0.013$, $\log \beta_{-111} = -4.875 \pm 0.004$ and $\log \beta_{-212} = -11.187 \pm 0.018$. The $PbOH^+$ species was also present in the solutions studied.

The present study was undertaken in order to determine the complex formation constants between Pb^{2+} and 3-bromo-5-sulfosalicylate ion, HC^{2-}, in aqueous solutions. No previous work on the equilibrium in aqueous solutions between Pb^{2+} and salicylic acid or its derivatives has been carried out to the author's knowledge. Owing to the relatively slight solubility of $Pb^{2+} - HC^{2-}$ complexes and the hydrolysis of Pb^{2+}, low concentrations of Pb^{2+} and a high precision method are necessary for such an investigation.

In the present investigation, the potentiometric method with a computerised automatic titrator was employed. The hydrolysis of Pb^{2+} was accounted for. This has been investigated previously by Olin.[1]

The most common symbols are listed below for reference:

B	total concentration of lead.
b	concentration of free lead.
E_g	emf of cell with glass electrode.
E_{am}	emf of cell with lead amalgam electrode.
η	$\log B/b$.
β_{pqr}	equilibrium constants.
U_E	$\sum(E_{am(calc)} - E_{am(exp)})^2$.
V_0, H_0, B_0, C_0	Volume, H, B and C in the solution ($S_0' + S_1$).
V_T, H_T, B_T, C_T	Volume, H, B and C in the buret solution T.
C, c, H, h, σ, (β)	see Ref. 3.

EXPERIMENTAL

Chemicals. Sodium perchlorate, perchloric acid, sodium hydroxide and disodium 3-bromo-5-sulfosalicylate solutions were prepared and analysed as described elsewhere.[2,3]

Lead perchlorate, $Pb(ClO_4)_2$, solutions were prepared by dissolving PbO (Baker *p.a.*) in $HClO_4$ (Merck *p.a.*) as described by Olin.[1] Lead was determined by precipitation as lead sulfate.[1] The analytical hydrogen concentration of the stock solution was determined potentiometrically, using Gran's extrapolation method[4] to evaluate the equivalence point.

Lead amalgam was prepared by dissolving bright lead metal (Merck silberfrei) in mercury. The concentration of lead in the amalgam was 0.4 % (by weight). The amalgam was stored under *ca.* 20 mM $HClO_4$ in a closed vessel filled with nitrogen.

Emf measurements and apparatus. The experiments were carried out as two series (I and II) of potentiometric titrations at 25 °C in nitrogen atmosphere. The two different types of titrations performed were:

1. The total concentration of Pb^{2+}, B, was kept constant and the total concentration of HC^{2-}, C, was increased by addition of Na_2HC solution, while pH varied from 2.5 to 4.

Table 1. Summary of the titrations in 3 M $Na(ClO_4)$. Concentrations in mM.[a]

Titr. No.	H_0'	B_0'	H_1	C_1	$H_{T_1+T_2}$	B_{T_1}	C_{T_2}	C/B
Series I								
1	0.5987	0.3007	−0.0135	0	−0.001	0.5046	179.78	
2	0.6065	0.60175	−0.0135	0	0.0112	1.0049	179.78	
3	1.547	1.1998	0.2995	0	0.3300	2.0010	180.57	
Series II								
1	0.6065	0.60175	−0.0133	179.78	−2.478	1.004	60.00	60
2	0.6065	0.61795	−0.0124	120.06	−2.468	1.004	40.01	40
3	0.6065	0.60175	−0.0127	90.06	−3.099	1.005	29.97	30
4	0.6065	0.60175	−0.0132	60.16	−3.110	1.005	19.95	20
5	0.6065	0.60175	−0.0132	29.95	−4.130	1.004	10.25	10
6	0.5987	0.3007	−0.0133	179.78	−2.490	0.5046	59.89	120
7	0.5987	0.3007	−0.0124	120.06	−2.525	0.5046	39.92	80
8	0.5853	1.2050	−0.0133	179.78	−2.524	2.0100	60.23	30

[a] In each titration equal volumes, V_T ml, of the buret solutions T_1 and T_2 were added to 60.02 ml of an initial solution which consisted of 50.02 ml S_0' and 10 ml S_1 solution.

2. Both B and C were kept constant, while pH was increased from 3 to 6 or 7 by the addition of NaOH solution until precipitation occurred or a desired amount of titrant had been added.

Since a slightly soluble precipitate was formed between Pb^{2+} and HC^{2-} ions at pH < 5, the values of B and C were chosen to be less than 1 mM and 40 mM, respectively, in order to be able to carry out the titrations and to have a sufficient amount of complex formed in the solutions. All the solutions were made 3 M in Na^+ by adding $NaClO_4$ to keep the activity factors constant.

A summary of the titrations is given in Table 1. In the titration series II, the C/B ratio was varied from 10 to 120. All the solutions listed in Table 1 were prepared with boiled doubly distilled water and N_2 gas was passed through the solutions for half an hour before use. The solutions containing NaOH were freshly prepared under N_2 atmosphere.

The hydrogen ion, h, and lead ion concentrations, b, were measured with a Jena type U glass electrode and a lead amalgam electrode (*ca.* 0.4 %), respectively.

The apparatus used for emf measurements is similar to that described in the author's previous work.[3]

From the measured emf, E_g and E_{am}, h and b were calculated using the following relations:

$$E_g = E_{0g} + 59.156 \log h + E_j \quad (1)$$

$$E_{am} = E_{0am} + 29.578 \log b + E_j \quad (2)$$

where E_{0g} and E_{0am} are constants for the electrodes used and E_j is the liquid junction potential, which can be expressed as $E_j = jh$, where j is approximately −17 mV/M in 3 M $NaClO_4$.

Each titration was carried out in three steps: First, E_{0g} and E_{0am} were determined from the potential of the initial solution S_0', containing no HC^{2-} ions, by inserting the analytical concentrations H_0' and B_0' in eqns. (1) and (2). A certain amount of the solution S_1 containing HC^{2-} was then added to the titration vessel to achieve the required $C = C_T/2$ and $B = B_T/2$. In the titration series I, the solution S_1 contains only 3 M $NaClO_4$. It took usually ½ to 1 h to reach equilibrium again. The titrations were then continued by adding equal volumes of T_1 and T_2 solutions until a desired amount of titrant had been added.

In evaluating the complex formation constants, H^+, Pb^{2+}, and HC^{2-} were chosen as components. The general equilibria and the formation constants are

$$pH^+ + qPb^{2+} + rHC^{2-} \rightleftharpoons H_pPb_q(HC)_r^{(2r-p-2q)-} \quad (3)$$

$$\beta_{pqr} = [H_pPb_q(HC)_r^{(2r-p-q2)-}]h^{-p}b^{-q}c^{-r} \quad (4)$$

respectively. Since the pH ranged from 2.5 to 7, both the proton association equilibria of HC^{2-} and the hydrolysis equilibria of Pb^{2+} must be taken into consideration in the calculations of the complex formation constants.

For the $H^+ - HC^{2-}$ equilibria

$$pH^+ + rHC^{2-} \rightleftharpoons H_{(p+r)}C_r^{(2r-p)-} \quad (5)$$

the results obtained in the author's previous work were used.[2,3] The values of β_{101}, β_{102}, β_{202}, and β_{-101} for reactions (5) are given in Table 4.

In the hydrolysis of Pb^{2+}

Table 2. Equilibrium constants for the hydrolysis of Pb(II) calculated by LETAGROP.

	This paper	Olin[1]
$\log \beta_{-110}$	-7.962 ± 0.236	-7.9 ± 0.1
$\log \beta_{-440}$	-19.149 ± 0.010	-19.25 ± 0.1
$\log \beta_{-430}$	-22.629 ± 0.042	-22.87 ± 0.1
$\log \beta_{-860}$	-42.103 ± 0.046	-42.14 ± 0.1

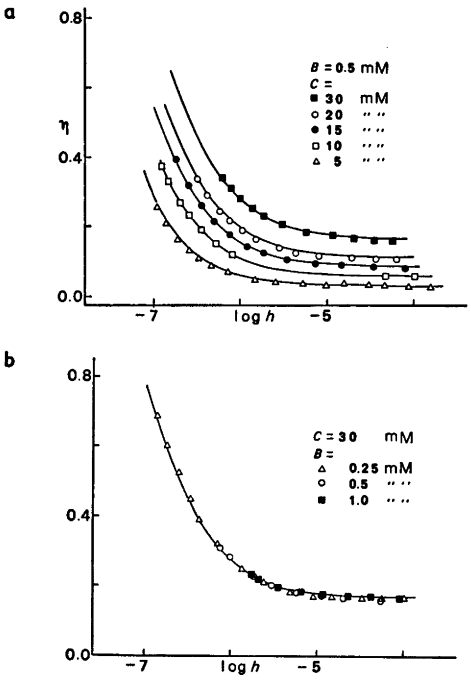

Fig. 1. Experimental data $\eta(\log h)_{B,C}$ in 3 M $Na(ClO_4)$ medium. $\eta = \log B/b$. The curves have been calculated with the final equilibrium constants β_{pqr} (*cf.* Table 4) using HALTAFALL.[10]

$$pH_2O + qPb^{2+} \rightleftharpoons Pb_q(OH)_p^{(2q-p)+} + pH+ \quad (6)$$

the main species are $PbOH^+$, $Pb_4(OH)_4^{4+}$, $Pb_3(OH)_4^{2+}$ and $Pb_6(OH)_8^{4+}$.[1] As a check, emf titrations to investigate the hydrolysis of Pb(II) were performed in a similar way as those described above for the complex formation between Pb^{2+} and HC^{2-}. The values of β_{-pq0} thus obtained were in good agreement with those obtained by Olin (*cf.* Tables 2).

TREATMENT OF DATA

The experimental data plotted as $(\eta, \log h)_{B,C}$, are presented in Fig. 1a–b (where $\eta = \log B/b$).

From Fig. 1a–b it is seen that η is a function of both C and $\log h$ but is independent of the value of B. It is apparent that the mononuclear mixed complexes $H_pPb(HC)_r^{(2r-p-2)-}$ are the predominant species in the concentration region studied.

The formation constants of the main complexes were determined graphically and the results were refined with the generalized least squares program LETAGROP ETITR.[5,6] LETAGROP was also used to investigate the formation of other possible complexes.

Graphical method. It is apparent from Fig. 1b that η varies slightly with pH at pH < 4.5, but increases with the values of C. The most probable complexes at pH < 4.5 are thus $Pb(HC)_r^{(2r-2)-}$, the relevant reactions and equilibrium constants being

$$Pb^{+2} + rHC^{2-} \rightleftharpoons Pb(HC)_r^{(2r-2)-} \beta_{01r} = [Pb(HC)_r^{(2r-2)-}] b^{-1} C^{-r} \quad (7)$$

Preliminary values for β_{01r} were determined by means of Leden's extrapolation method.[7]

When the function

$$F_1 = (B-b)/bc = \sum_1^r \beta_{01r} C^{r-1} =$$

$$\beta_{011} + \beta_{012} c + \sum_3^r \beta_{01r} C^{r-1} \quad (8)$$

with the experimental data B, b, and C ($\approx c$) from series I, was plotted against C, a straight line was obtained (*cf.* Fig. 2). From the intercept and the slope of the line $\beta_{011} = 12.2$ M^{-1} and $\beta_{012} = 83.5$ M^{-1}. The function

$$F_2 = (F_1 - \beta_{011})/C = \beta_{012} + \sum_3^r \beta_{01r} C^{r-2} \quad (9)$$

was calculated from the β_{011} value obtained and plotted against C. A straight line with a slope ≈ 0 (Fig. 2) was obtained, which indicates the absence of complexes $Pb(HC)_r^{2-2r}$ with $r > 2$.

Furthermore, a strong mononuclear pH-dependent complexing between Pb^{2+} and HC^{2-} at pH > 5, is indicated by Fig. 1a–b. As HC^{2-} is a bidentate ligand and the two donor groups (–COOH and –OH) are in a favourable position (*ortho*-position) for chelation of Pb^{2+}, the most likely chelate complexes are PbC^- and PbC_2^{4-}. A similar extrapolation method

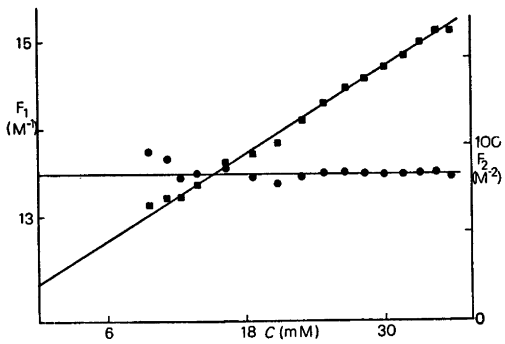

Fig. 2. Determination of β_{011} and β_{012} from eqn. (8). Line 1 (■) gives $\beta_{011}=12.2$ M^{-1}, $\beta_{012}=83.5$ M^{-2}. $B=0.25$ mM. Determination of β_{012} from eqn. (9). The intercept of line 2 (●) gives $\beta_{012}=84$ M^{-2}. $B=0.25$ mM.

was applied to determine β. Using the mass balance condition and the definitions for the equilibrium constants β_{pqr} (eqn. 4), the experimental quantity B may be expressed in the following form

$$B=b+\beta_{011}bc+\beta_{012}bc^2+\beta_{-111}bch^{-1}+\beta_{-212}bc^2h^{-2} \quad (10)$$

Rearrangement of (10) gives

$$F_c=B/b-1-\beta_{011}c-\beta_{012}c^2=\beta_{-111}ch^{-1}+\beta_{-212}c^2h^{-2} \quad (11)$$

As C is constant in titration series II and if $C\gg B$, then $C\approx c$, and the variable F_c is a function of h only. Thus, a set of experimental data from titration series II No. 1 ($B=0.5$ mM, $C=30$ mM) was chosen for plotting F_c as a function of h^{-1}. In the calculation of F_c, the refined values of β_{011} and β_{012} were used. A straight line with no curvature for high values of h^{-1} was obtained (*c.f.* Fig. 3). This suggests that no complex higher than PbC^- is present in the solution at $C/B=60$ and pH <6. However, the complex PbC_2^{4-} ought to be present in the solutions at a higher pH and C/B ratio (*cf.* titration Nos. 6 and 7). The LETAGROP method was used subsequently to investigate the formation of PbC_2^{4-}.

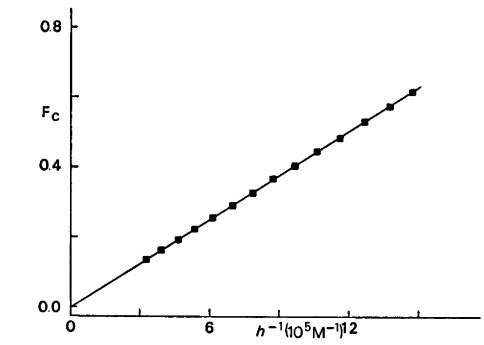

Fig. 3. Determination of β_{-111} from eqn. (11). The value of β_{-111} ($=1.37\times10^{-5}$) was calculated according to $\beta_{-111}=$ slope$/C$. $C=29.95$ mM, $B=0.5$ mM.

The value of β_{-111} obtained as $\beta_{-111}=$ gradient$/C$ was $1.37\cdot10^{-5}$.

LETAGROP method. In this method the β_{pqr} were sought as the values which gave a minimum for the error squares sum $U=\sum(E_{calc}-E_{exp})^2$, where E_{calc} represents a value for the emf of cell with lead amalgam, calculated by assuming a given β_{pqr} set and auxiliary data such as B, C, E_{0am}, E_{0g}, E_{am} and E_g.

Refinement of β_{011}, β_{012} and β_{-111}, and test of the existence of the complexes PbC_2^{4-} *and* $PbOHC^{2-}$. In these calculations, the values of β_{101}, β_{102}, β_{202}, and β_{-101}, together with the equilibrium constants for the hydrolysis of Pb(II) obtained from this work, were given as input information and kept constant. E_{0am} was the main systematic error to be adjusted. For the sake of convenience the data were used in the following three steps:

1. All the experimental data from series I (115 points) were used. Only β_{011} and β_{012} were varied.

2. Part of the data with pH >5 from series II (185 points) were used. β_{-111} and β_{-212} were varied.

3. All the experimental data from series II (343 points) were used. First, β_{011}, β_{012}, β_{-111}, and β_{-212} obtained from calculation 1 and 2 were used as the input information, and the systematic errors E_{0am}, and then H, were adjusted. All the four constants β_{011}, β_{012}, β_{-111}, and β_{-212} were then varied without adjusting the systematic errors.

The main results from the above calculations are given in Table 3.*

In the investigation of the presence of $PbOHC^{2-}$ only the experimental data for

* The output from the LETAGROP calculations can be obtained on request.

Table 3. Equilibrium constants β_{pqr} calculated by LETAGROP 25 °C, 3 M $Na(ClO_4)$.

Calculation No.	U_E	$\sigma(E)$ mV	log $(\beta_{pqr}+3\sigma)$ 011	012	−111	−212
1 (115 points)	0.202	0.043	1.116 ± 0.006	1.930 ± 0.017		
2 (185 points)	1.592	0.0953	1.116	1.931	−4.879 ± 0.003	−11.187 ± 0.003
3 (343 points)	5.635	0.1284	1.116 ± 0.006	1.931 ± 0.013	−4.875 ± 0.004	−11.187 ± 0.018

Table 4. The final equilibrium reactions and equilibrium constants in 3 M $Na(ClO_4)$ at 25 °C.

pqr	Reaction	log $(\beta_{pqr} \pm 3\sigma)$
101	$H^+ + HC^{2-} \rightleftharpoons H_2C^-$	2.028 ± 0.007 [a]
102	$H^+ + 2HC^{2-} \rightleftharpoons H_3C_2^{3-}$	2.537 ± 0.017 [a]
202	$2H^+ + 2HC^{2-} \rightleftharpoons H_4C_2^{2-}$	4.739 ± 0.019 [a]
−101	$HC^{2-} \rightleftharpoons C^{3-} + H^+$	−10.467 ± 0.001 [b]
−110	$Pb^{2+} + H_2O \rightleftharpoons PbOH^+ + H^+$	−7.962 ± 0.236
−440	$4Pb^{2+} + 4H_2O \rightleftharpoons Pb_4(OH)_4^{4+} + 4H^+$	−19.149 ± 0.010
−430	$3Pb^{2+} + 4H_2O \rightleftharpoons Pb_3(OH)_4^{2+} + 4H^+$	−22.629 ± 0.042
−860	$6Pb^{2+} + 8H_2O \rightleftharpoons Pb_6(OH)_8^{4+} + 8H^+$	−42.103 ± 0.046
011	$Pb^{2+} + HC^{2-} \rightleftharpoons PbHC$	1.116 ± 0.006
012	$Pb^{2+} + 2HC^{2-} \rightleftharpoons Pb(HC)_2^{2-}$	1.931 ± 0.013
−111	$Pb^{2+} + HC^{2-} \rightleftharpoons PbC^- + H^+$	−4.875 ± 0.004
−212	$Pb^{2+} + 2HC^{2-} \rightleftharpoons PbC_2^{4-} + 2H^+$	−11.187 ± 0.018

[a] From Ref. 2. [b] From Ref. 3.

pH > 5 from titr. Nos. 4 and 5 in series II were used, since $PbOHC^{2-}$ is most likely to be formed at a high pH value and a low C/B ratio.

RESULTS AND DISCUSSION

It is apparent from Table 3 that the low values of $\sigma(E)$ in calculations 1, 2, and 3 (< 0.13 mV) and the good agreement between these calculations indicate the reliability of the results.

The LETAGROP calculations yielded a negative value for β_{-211}, which means that the complex $PbOHC^{-2}$ is not present in the solutions studied. This is probably due to the fact that precipitation occurred at pH ≈ 6 − 7. The available pH range is thus too restricted to permit formation of $PbOHC^{2-}$. Only four complexes, namely PbHC, $Pb(HC)_2^{2-}$, PbC^-, and PbC_2^{4-}, are formed between Pb^{2+} and HC^{2-} ions. The data are best explained by the equilibria and the corresponding formation constants given in Table 4.

Fig. 4a − b show the distribution of Pb(II) in different species at various pH values. It can be seen from Fig. 4a − b that the main species in the solutions at pH < 4.5 are PbHC and $Pb(HC)_2^{2-}$ (the latter one only when $C \gg B$). The concentration of PbC^- increases rapidly after pH > 5.7 − 6, while both PbC_2^{4-} and $PbOH^+$ exist in minor amounts. The other Pb(II) hydrolysis products at the high C/B ratios are present only in negligible amounts.

It was expected that PbC^- and PbC_2^{4-} would be much more stable than PbHC and $Pb(HC)_2^{2-}$, due to the formation of chelate rings involving the donor groups −COOH and −OH from the same ligand. This chelate effect can be explained in terms of the contribution from the entropy of formation accompanying the metal chelate ring formation.[8]

No direct comparison with β_{pqr} values obtained by others can be made. Nevertheless, it is still of interest to compare the orders of magnitude of β_{pqr} with β_{pqr} for complexes which contain similar ligands with the same donor groups −COOH and −OH, *e.g.* 5-sulfosalicylate ion. As a general rule, Co(II) complexes usually have stabilities comparable with

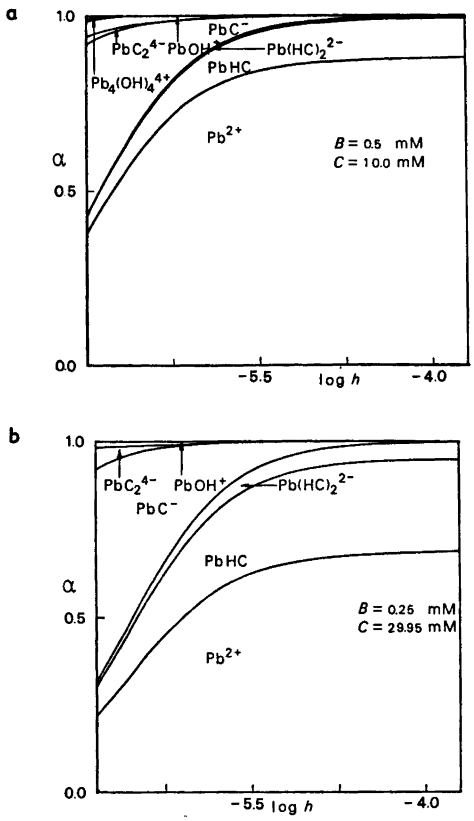

Fig. 4. The distribution of Pb(II) in different species plotted *versus* log h. The calculations were performed with HALTAFALL [10] using the β_{pqr} obtained in this paper (*cf.* Table 4). At a given log h the fraction of Pb^{2+} present in each species is represented by the segment of a vertical line falling within the corresponding area.

those of the corresponding Pb(II) complexes. The stability constants K_1 and K_2 for the chelate reactions $M+L \rightleftharpoons ML$ and $ML+L \rightleftharpoons ML_2$ (where M is metal ion and L is ligand), are related to the value of β_{-111}, β_{-212}, and β_{-101} by the following equations:

$$K_1 = \beta_{-111}/\beta_{-101} \text{ and } K_1K_2 = \beta_{-212}/2\beta_{-101}$$

A comparison of the values of log K_1 and log K_2 for Co(II)-5-sulfosalicylate complexes,[9] namely 6.13 and 3.69, respectively, with those obtained in this paper, namely 5.590 and 4.161, respectively, shows that the constants are of the same order of magnitude.

As mentioned earlier the titrations were interrupted when a white precipitate was formed at pH ≈ 6 – 7.

Acknowledgements. The author would like to express her gratitude to Professor Georg Lundgren for his encouragement and for many valuable discussions, and to Dr. Susan Jagner for revising the English text.

The investigation was supported by a grant from the Swedish Natural Science Research Council (Contract No. 2318).

REFERENCES

1. Olin, Å. *Acta Chem. Scand. 14* (1960) 126.
2. Lee, Y.-H. *Acta Chem. Scand. 27* (1973) 1807.
3. Lee, Y.-H. *Acta Chem. Scand. A 30* (1976) 586.
4. Gran, G. *Analyst (London) 77* (1952) 661.
5. Ingri, N. and Sillén, L. G. *Ark. Kemi 23* (1964) 97.
6. Brauner, P., Sillén, L. G. and Whiteker, R. *Ark. Kemi 31* (1969) 365.
7. Leden, I. *Potentiometrisk undersökning av några kadmiumsalters komplexitet*, Diss., Lund 1943.
8. Schwarzenbach, G. *Helv. Chim. Acta 35* (1952) 2344.
9. Banks, C. V. and Singh, R. S. *J. Inorg. Nucl. Chem. 15* (1960) 125.
10. Ingri, N., Kakolowicz, W., Sillén, L. G. and Warnqvist, B. *Talanta 14* (1967) 1261.

Received March 4, 1976.

Acta Chemica Scandinavica A 30 (1976) 599—608

Reaction Rate Studies of the Acid Hydrolysis of Some Chromium(III) Complexes. VII. The Acid Hydrolysis of Tetraaqua(1,2-ethanediamine)-, Tetraaqua(1,3-propanediamine)- and Tetraaqua(*trans*-1,2-cyclohexanediamine)chromium(III) Ions in Aqueous Perchloric Acid

LENE MØNSTED

Kemisk Laboratorium I, H.C. Ørsted Institutet, Universitetsparken 5, DK-2100 København Ø, Denmark

The acid hydrolysis of the diaminetetraaquachromium(III) complexes of the three chelating diamines: 1,2-ethanediamine (en), 1,3-propanediamine (tn) and *trans*-1,2-cyclohexanediamine (chxn) in perchloric acid solution has been investigated in the temperature range 60 – 80 °C and at an ionic strength of 1.0.

For all the complexes the initial hydrolysis reaction produces a monoaminepentaaqua complex with coordinated monodentate protonated diamine. The reaction rate constants at 70 °C and the activation energies were determined to be:*

(en): $(11.33 \pm 0.14) \times 10^{-6}$ s^{-1},
25.1 ± 0.4 kcal/mol,
(tn): $(0.650 \pm 0.007) \times 10^{-6}$ s^{-1},
25.9 ± 0.3 kcal/mol,
(chxn): $(6.98 \pm 0.14) \times 10^{-6}$ s^{-1},
27.4 ± 0.8 kcal/mol.

Further hydrolysis of the monoamine complexes yields hexaaquachromium(III) ions, and for these reactions the rate constants at 70 °C and the activation energies were determined to be:

(en): $(5.4 \pm 0.3) \times 10^{-6}$ s^{-1},
29.0 ± 1.6 kcal/mol,
(tn): $(0.66 \pm 0.02) \times 10^{-6}$ s^{-1},
29.7 ± 1.0 kcal/mol,
(chxn): $(18.5 \pm 1.1) \times 10^{-6}$ s^{-1},
28.8 ± 1.6 kcal/mol.

In addition to these acid concentration-independent reactions, the monoamine complex with *trans*-1,2-cyclohexanediamine was found to undergo acid dependent hydrolysis and chelation.

An approximately linear correlation of the logarithm of the rate constants for hydrolysis with the statistically corrected pK_1 values for the fully protonated amines is demonstrated for a series of monoaminepentaaquachromium(III) complexes.

A previous qualitative study in this laboratory [1] of the acid hydrolysis of chelated 1,2-ethanediamine complexes of chromium(III) has demonstrated the similarity of the reaction products in this system and in the chromium(III) ammonia system. However, the qualitative observations suggested interesting differences in reactivity between analogous complexes in the two systems. The present work therefore describes an extension of earlier quantitative investigations in this laboratory on bond breaking reactions of chromium(III) non-chelated amine complexes to the acid hydrolysis of the symmetrical diamine chelate complexes: tetraaqua(1,3-propanediamine)- and tetraaqua(*trans*-1,2-cyclohexanediamine)chromium(III).

Garner *et al.*[2] have previously studied the acid-hydrolysis kinetics of the tetraaqua(1,2-ethanediamine)chromium(III) ion in 3 M perchlorate medium. In order to facilitate comparisons with the other diamine system investigated here, the above system has been re-investigated employing a 1 M perchlorate medium.

* 1 kcal = 4.184 kJ.

EXPERIMENTAL

*Chemicals.** *trans*-$[Cr(en)_2(aq)(OH)](ClO_4)_2$,[3] *trans*-$[Cr(tn)_2(aq)(OH)](ClO_4)_2$[4] and *trans*-$[Cr((-)_D\text{-chxn})_2F_2]ClO_4$[5] were prepared according to literature methods. The latter compound was converted to *trans*-$[Cr((-)_D\text{-chxn})_2Cl_2]Cl$ by reaction with concentrated hydrochloric acid.[3]

Tetraaqua(1,2-ethanediamine)chromium(III) and (2-aminoethylammonium)pentaaquachromium(III) ions. Both these ions were prepared from trans-aquabis(1,2-ethanediamine)hydroxochromium(III) perchlorate as described previously.[1]

Tetraaqua(1,3-propanediamine)chromium(III) ion. *trans*-Aquahydroxobis(1,3-propanediamine)chromium(III) perchlorate was dissolved in 0.1 M nitric acid and boiled for 30 min. The resulting solution was charged onto a 2 × 5 cm column packed with Dowex 50 W × 8 200/400 mesh cation-exchange resin. Elution with 2 M sulfuric acid produced separation into three bands. From the visible absorption spectra of their eluates these bands were identified as hexaaqua-, tetraaqua(1,3-propanediamine)-, and a mixture of *cis*- and *trans*-diaquabis(1,3-propanediamine)chromium(III), eluted in that order. The eluate of the second band, containing the tetraaqua(1,3-propanediamine)chromium(III) ion in 2 M sulfuric acid, was purified and the sulfate ion exchanged for perchlorate as described earlier.[6]

(3-Aminopropylammonium)pentaaquachromium(III) ion. A 0.5 M perchloric acid solution of tetraaqua(1,3-propanediamine)chromium(III), prepared as described above, was kept in the dark at 50 °C for 90 h. The (3-aminopropylammonium)pentaaquachromium(III) ion was isolated from the resulting mixture essentially as described previously for the (2-aminoethylammonium)pentaaquachromium(III) ion.[1]

Tetraaqua(trans-1,2-cyclohexanediamine)chromium(III) ion. *trans*-Dichloridobis(*trans*-1,2-cyclohexanediamine)-chromium(III) chloride was boiled for 25 min in 3 M perchloric acid. The resulting mixture was charged onto a 2 × 8 cm column packed with Dowex 50 W × 2 200/400 mesh cation-exchange resin. Elution with 3 M perchloric acid produced separation into three bands. From the visible absorption spectra of the eluates the first band was identified as hexaaqua- and the second as tetraaqua(*trans*-1,2-cyclohexanediamine)chromium(III). The third band, which had a colour characteristic of a tetraaminediaqua complex, was not investigated further. The eluate of the second band, containing the tetraaqua(*trans*-1,2-cyclohexanediamine)chromium(III) ion in 3 M perchloric acid, was purified as described earlier for sulfuric acid eluates.[6]

(trans-*2-Aminocyclohexylammonium)pentaaquachromium(III) ion.* A solution of tetraaqua(*trans*-1,2-cyclohexanediamine)chromium(III) in 3 M perchloric acid, obtained as described above, was kept in the dark at 70 °C for 18 h. The resulting solution, in which equilibrium between the diamine and monoamine complexes was established, contained mainly unchanged diamine complex and only very little monoamine species. The solution was charged onto a 2 × 4 cm Dowex 50 W × 2 column and eluted with 3 M perchloric acid. The hexaaquachromium(III) ion was eluted first, then the diamine- and finally the monoamine chromium(III) complex.

Because of the large amount of diamine complex necessary to get only small amounts of monoamine complex, it was not possible to separate the diamine, monoamine and hexaaqua complexes completely. The tail of the diamine band (which contained about 75 % of monoamine complex) was therefore recovered, diluted three times with water, re-charged onto a 1 × 5 cm Dowex 50 W × 2 column and re-eluted with 3 M perchloric acid. The two species were not completely separated on this short column but from a fractionation experiment the last part of the band was identified as pure (*trans*-2-aminocyclohexylammonium)pentaaquachromium(III) ion.

Due to fast chelation of the monodentate diamine in this complex at lower acid concentrations it was not possible to purify the solution by the Sephadex technique employed for the other Dowex eluates. In order to get satisfactory absorption spectra, especially in the near-UV region, the Dowex resin was thoroughly washed with a hot mixture of a 0.01 M sodium hydroxide solution and hydrogen peroxide. Prior to the final purification of the (*trans*-2-aminocyclohexylammonium)-pentaaquachromium(III) complex the column was washed first with about 200 ml of water and then with 200 ml of 3 M perchloric acid. The molar absorptivity of the second band of the absorption spectrum was still not quite reproducible and consequently only the first part of the spectra (700 − 470 nm) was used in the kinetic calculations for the experiments starting with the (*trans*-2-aminocyclohexylammonium)chromium(III) ion.

The visible absorption spectra of the 1,2-ethanediamine-, the 1,3-propanediamine-, and the *trans*-1,2-cyclohexanediamine complexes prepared by the above methods are given in Ref. 1 and Figs. 1 and 2.

Spectral measurements. All visible absorption spectra were measured on a modified Cary

* The following ligand name abbreviations are used in chemical formulae throughout the paper: a = ammonia, aq = water, en = 1,2-ethanediamine, enH = 2-aminoethylammonium ion, tn = 1,3-propanediamine, tnH = 3-aminopropylammonium ion, chxn = *trans*-1,2-cyclohexanediamine, chxnH = *trans*-2-aminocyclohexylammonium ion, diam = diamine, diamH = protonated monodentate diamine ion, and diam* = unprotonated monodentate diamine.

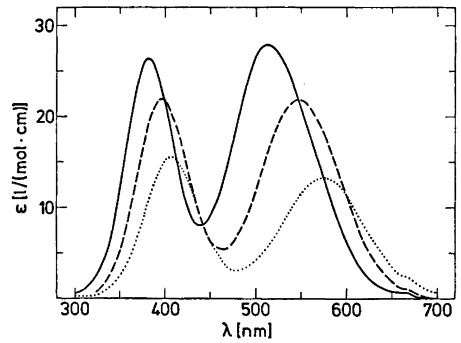

Fig. 1. Visible absorption spectra of compounds prepared as described in the text. ——, $[Cr(tn)(aq)_4]^{3+}$; –·–, $[Cr(tnH)(aq)_5]^{4+}$; ···, $[Cr(aq)_6]^{3+}$.

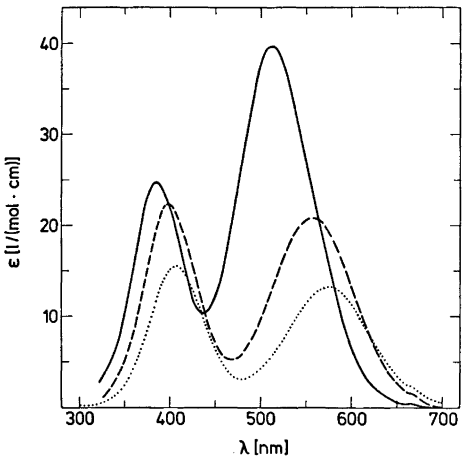

Fig. 2. visible absorption spectra of compounds prepared as described in the text. ——, $[Cr(chxn)(aq)_4]^{3+}$; —, $[Cr(chxnH)(aq)_5]^{4+}$; ···, $[Cr(aq)_6]^{3+}$.

118C spectrophotometer at room temperature (23 ± 2 °C).

Kinetic measurements, determination of chromium and hydrogen ion concentrations, and calculations were performed essentially as described previously.[6]

Determination of acidity constants for the free amines. The diaminedihydrochloride salts in 1.0 M sodium perchlorate solution were titrated at 70 °C with 1 M sodium hydroxide. The titration procedure and the method of calculation have been described earlier.[7] The results are given in Table 1.

Table 1. Acidity constants of some protonated amines in 1 M sodium perchlorate solution at 70 °C.

Amine	pK_1	pK_2
NH_3	8.21 ± 0.03	
en	6.30 ± 0.04	9.00 ± 0.02
tn	7.87 ± 0.03	9.48 ± 0.04
chxn	5.76 ± 0.03	8.84 ± 0.03

RESULTS AND DISCUSSION

Acid hydrolysis of *trans*-bis(diamine)chromium(III) species yields large amounts of diaminetetraaquachromium(III) species. This has previously been demonstrated for the 1,2-ethanediamine-[1] and 1,3-propanediamine [4] complexes and is also the case for the *trans*-1,2-cyclohexanediamine complexes. The further hydrolysis of these diamine species proceeds to give the hexaaquachromium(III) ion *via* an intermediate species with coordinated monoprotonated diamine, but unlike the diamine species the monoamine complexes coordinated with monodentate diamines are not present in large amounts.

The hydrolysis of *trans*-diaquabis(1,3-propanediamine)chromium(III) in aqueous perchloric acid is a very slow process. Preparative hydrolysis was therefore carried out in nitric acid since nitrate ions are known to accelerate the hydrolysis of chromium(III) amine complexes.[8] Cation exchange chromatography of the hydrolysed solutions on Dowex × 8 resin with 2 M sulfuric acid resulted in separation into three bands. From the visible absorption spectra of their eluates these bands were identified as hexaaqua-, tetraaqua(1,3-propanediamine)-, and a mixture of *cis*- and *trans*-diaquabis(1,3-propanediamine)chromium(III) ions.*

* *cis*-Diaquabis(1,3-propanediamine)chromium(III) prepared by mercury(II) accelerated hydrolysis of *cis*-dichloridobis(1,3-propanediamine)chromium(III) exhibits absorption maxima at 486 nm (ε 38.8 l/(mol cm)) and 366 nm (ε 37.9 l/(mol cm)). It therefore appears that an earlier published spectrum [4] of *cis*-diaquabis(1,3-propanediamine)-chromium(III) is, in fact, that of a mixture of the *cis*- and *trans*-diaquabis(1,3-propanediamine)chromium(III) complexes which contains appreciable amounts of the *trans* complex.

Cation exchange chromatography showed that nitric acid hydrolysates of the *trans*-diaquabis(1,3-propanediamine)chromium(III) ion never contained perceptible amounts of tetrapositive species. The (3-aminopropylammonium)pentaaquachromium(III) complex was prepared by heating the tetraaqua(1,3-propanediamine) complex in aqueous perchloric acid at 50 °C for 90 h. This produced a tetrapositive species which was separated from the tripositive species on a SP-Sephadex-C-25 resin column by elution with 0.5 M sodium perchlorate solution. From the mode of formation, the elution behaviour and the visible spectrum this species was identified as the (3-aminopropylammonium)pentaaquachromium(III) ion.

Cation exchange chromatography of a 3 M perchloric acid hydrolysate of *trans*-dichloridobis(*trans*-1,2-cyclohexanediamine)chromium(III) on Dowex X2 resin produced three bands of tripositive species. From the elution behaviour, the mode of formation and the visible absorption spectra of the eluates, the first and second bands were identified as the hexaaqua- and the tetraaqua(*trans*-1,2-cyclohexanediamine)chromium(III) species, respectively. The third band had a tetraamine colour but was not investigated further.

Ageing of the tetraaqua(*trans*-1,2-cyclohexanediamine)-chromium(III) species in 3 M perchloric acid produced mixtures containing minor amounts of a species which was more difficult to elute from the Dowex X2 resin with 3 M perchloric acid than was the unreacted diamine species. From the mode of formation, the elution behaviour and the visible absorption spectrum this species was identified as the (*trans*-2-aminocyclohexylammonium)pentaaquachromium(III) ion. Attempts at further purification of this species at low acidities (~0.001 M) on the Sephadex resin resulted in rapid formation of the tetraaqua(*trans*-1,2-cyclohexanediamine)chromium(III) ion.

In Table 2 the visible absorption spectra of the chromium(III) complexes with the above-mentioned symmetrical diamine ligands are compared with those of the corresponding ammonia complexes. The spectra of the two complexes with a five-membered chelate ring are almost identical and exhibit a molar absorptivity for the first spin allowed absorption band which is substantially larger than that observed for both the tetraaqua(1,3-propanediamine)- and *cis*-diamminetetraaquachromium(III) ion. However, the three chelate complexes resemble each other in that the first spin allowed absorption band is shifted substantially towards the blue relative to that of the corresponding ammonia complex.

Unlike those of the diamine complexes the spectra of the four monoamine species are seen to resemble each other closely. Neither molar absorptivities nor spectral band maxima vary in an apparently systematic manner. The only noteworthy feature of these data is the significant red-shift of the first spin allowed absorp-

Table 2. A comparison of the visible spectra of some symmetrical diaminetetraaquachromium(III)- and of some aminepentaaquachromium(III) complexes.

Complex	Medium [a]	λ_1 max nm	ε_1 max l/(mol cm)	λ_2 max nm	ε_2 max l/(mol cm)	ε_1 max/ ε_2 max	Ref.
Diamine complexes							
cis-$[Cr(a)_2(aq)_4]^{3+}$	A	526	27.0	386	21.3	1.27	6
$[Cr(tn)(aq)_4]^{3+}$	A	514	27.9	382	26.1	1.07	[b]
$[Cr(en)(aq)_4]^{3+}$	B	512	41.3	387	24.7	1.67	1
$[Cr(chxn)(aq)_4]^{3+}$	A	513	39.8	384	24.8	1.61	[b]
Monoamine complexes							
$[Cr(a)(aq)_5]^{3+}$	A	547	19.9	396	18.6	1.07	6
$[Cr(tnH)(aq)_5]^{4+}$	B	546	22.2	395	22.5	0.99	[b]
$(Cr(enH)(aq)_5]^{4+}$	B	551	21.5	397	21.4	1.01	1
$[Cr(chxnH)(aq)_5]^{4+}$	C	556	20.6	398	22.2	0.93	[b]

[a] A, 0.5 M $HClO_4$ + 0.5 M $NaClO_4$; B, 0.25 M $HClO_4$ + 1.0 M $NaClO_4$; C, 3 M $HClO_4$]. [b] This work.

tion band of the (*trans*-2-aminocyclohexylammonium)pentaaquachromium(III) species relative to the corresponding band in the other three complexes. Inspection of molecular models reveals the possibility of substantial interaction between the coordinated water molecules and the hydrogen atoms of the cyclohexanediamine ring in this species. This may result in a distorted octahedral structure and thereby rationalise the observed red-shift.

In the qualitative experiments it was found that the diaminetetraaquachromium(III) complexes hydrolyse to hexaaquachromium(III) *via* monoamine species. It was further found that the amine ligand in the (*trans*-2-aminocyclohexylammonium)pentaaquachromium(III) complex re-chelates even in weakly acid solution to form the diamine complex. For the (2-aminoethylammonium)triaqua(1,2-ethanediamine)- and the (2-aminoethylammonium)-aquabis(1,2-ethanediamine)chromium(III) complexes similar rechelation reactions were found although these were only observed in basic solution.[1,9]

Calculations for the experiments involving the 1,2-ethanediamine and 1,3-propanediamine complexes were consequently carried out in accordance with the reactions:

$$[Cr(diam)\ (aq)_4]^{3+} \xrightarrow{k_{21}(obs)} [Cr(diamH)\ (aq)_5]^{4+} \xrightarrow{k_1(obs)} [Cr(aq)_6]^{3+}$$

This reaction scheme accurately described our kinetic data, and estimated rate constants for the individual kinetic experiments are tabulated in Table 3. As can be seen from this table the rate constants are independent of the hydrogen ion concentration in the acidity range studied. Average rate constants at 70 °C and activation energies are given in Tables 4 and 5.

In experiments starting from tetraaqua(*trans*-1,2-cyclohexanediamine)chromium(III), species coordinated with monodentate diamine were never observed in appreciable amounts. Calculations on the experiments starting with this diaminetetraaqua complex could therefore not be carried out within the framework of a reaction scheme involving an intermediate monoamine species. Consequently the data were parametrised in accordance with the reaction:

$$[Cr(diam)\ (aq)_4]^{3+} \xrightarrow{k_{20}(obs)} [Cr(aq)_6]^{3+}$$

This reaction scheme accurately accommodated the kinetic data, but as shown in Fig. 3 the observed rate constants were dependent on the acid concentration. Such hydrogen ion concentration dependence should be expected if chelation of the diamine ligand in the intermediate monoamine species is important. In order to get further information about the kinetics of this system, experiments with (*trans*-2-aminocyclohexylammonium)pentaaquachromium(III) as the initial reactant

Table 3. Rate constants and initial complex concentrations calculated for individual kinetic experiments with the chromium(III) complexes of 1,2-ethanediamine and 1,3-propanediamine.

Run No.	[Cr(III)] (mmol/l)	[H+] (mol/l)	Temp. (°C)	$10^6 \times k_{21}$ (s^{-1})	$10^6 \times k_1$ (s^{-1})
1,2-Ethanediamine					
1 [a]	0.470 ± 0.003	1.0	79.85	31.8 ± 0.6	18.5 ± 0.9
2 [a]	0.470 ± 0.004	0.5	79.85	28.9 ± 0.6	20.8 ± 1.6
3	0.918 ± 0.002	1.0	70.20	11.77 ± 0.08	5.58 ± 0.19
4	0.474 ± 0.002	1.0	59.65	3.56 ± 0.03	1.41 ± 0.10
5 [b]	0.848 ± 0.002	0.5	79.95	–	17.7 ± 0.3
1,3-Propanediamine					
6	1.100 ± 0.005	1.0	80.05	1.86 ± 0.03	2.32 ± 0.11
7	0.834 ± 0.004	1.0	70.20	0.676 ± 0.009	0.66 ± 0.03
8	1.051 ± 0.004	0.5	70.20	0.675 ± 0.008	0.71 ± 0.03
9	0.833 ± 0.003	1.0	59.65	0.202 ± 0.004	0.166 ± 0.008
10	1.380 ± 0.004	1.0	59.65	0.196 ± 0.002	0.175 ± 0.006

[a] These two solutions were prepared from the same stock solution. [b] This run was started with the monoamine complex.

Table 4. Rate constants at 70 °C and activation energies for the acid hydrolysis of some tetraaquadiaminechromium(III) complexes.

Complex	$10^6 \times k_{21}$ (s^{-1})	E_A (kcal/mol)	Ref.
cis-$[Cr(a)_2(aq)_4]^{3+}$	3.39± 0.08	27.0± 0.4	12
$[Cr(en)(aq)_4]^{3+}$ [b]	11.33± 0.14	25.1± 0.4	[a]
$[Cr(tn)(aq)_4]^{3+}$	0.650± 0.007	25.9± 0.3	[a]
$(Cr(chxn)(aq)_4]^{3+}$	6.98± 0.14	27.4± 0.8	[a]

[a] This work. [b] These results are in agreement with those published earlier for a 3 M perchlorate medium.[2]

Table 5. Rate constants at 70 °C and activation energies for the acid hydrolysis of some aminepentaaquachromium(III) complexes.

Complex	$10^6\ k_1$ (s^{-1})	E_A (kcal/mol)	Ref.
$[Cr(a)(aq)_5]^{3+}$	1.108± 0.011	28.6± 0.2	12
$[Cr(enH)(aq)_5]^{4+}$ [b]	5.4± 0.3	29.0± 1.6	[a]
$[Cr(tnH)(aq)_5]^{4+}$	0.66± 0.02	29.7± 1.0	[a]
$[Cr(chxnH)(aq)_5]^{4+}$	18.5± 1.1	28.8± 1.6	[a]

[a] This work. [b] See footnote in Table 4.

were therefore carried out. The subsequent calculations were performed assuming the following reactions to occur:

$$[Cr(diam)\ (aq)_4]^{3+} \underset{k_{12}(obs)}{\overset{k_{21}(obs)}{\rightleftharpoons}} [Cr(diamH)\ (aq)_5]^{4+}$$

$$\xrightarrow{k_1(obs)} [Cr(aq)_6]^{3+}$$

This scheme accurately accommodated the kinetic data, and it was found that the rate constants for the reactions of the (*trans*-2-aminocyclohexylammonium)pentaaquachromium(III) species were dependent on the hydrogen ion concentration, as illustrated in Fig. 4 for the rate constant for the chelation reaction. This latter result points to the kinetic importance of a deprotonated (*trans*-2-aminocyclohexylammonium)pentaaquachromium(III) species.

In order to describe all accumulated data for the different diamine complexes the reaction scheme presented in Fig. 5 must be used. Assuming a constant hydrogen ion concentration the observed rate constants derived from an interpretation of the experimental data within the earlier presented reaction

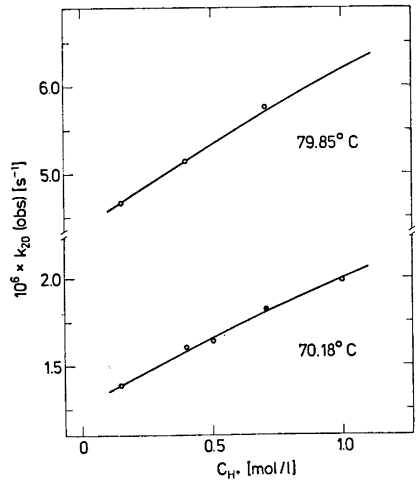

Fig. 3. Hydrogen ion concentration dependence of k_{20}(obs) for the individual kinetic experiments started with tetraaqua(*trans*-1,2-cyclohexanediamine)chromium(III). Experimental values are indicated by circles and the solid curves are calculated from the rate constants and activation energies in Tables 4, 5 and 6 by means of eqns. 1 and 3. The filled circle indicates the experiment used for Fig. 6.

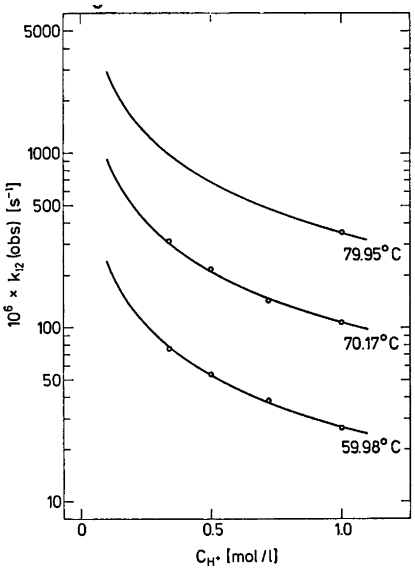

Fig. 4. Hydrogen ion concentration dependence of k_{12}(obs) for the individual kinetic experiments started with (*trans*-2-aminocyclohexylammonium)pentaaquachromium(III). Experimental values are indicated by circles and the solid curves are calculated from the rate constants and activation energies given in Tables 4, 5 and 6 by means of eqns. 2b and 3.

schemes are related to those of Fig. 5 by the following set of expressions:

$$k_{20}(\text{obs}) = (k_{21}(Kk_1^* + k_1[H^+]))/(Kk_{12} + Kk_1^* + k_1[H^+]) \quad (1)$$

$$k_{21}(\text{obs}) = k_{21} \quad (2a)$$

$$k_{12}(\text{obs}) = Kk_{12}/(K + [H^+]) \quad (2b)$$

$$k_1(\text{obs}) = (Kk_1^* + k_1[H^+])/(K + [H^+]) \quad (2c)$$

They are seen to reduce to $k_{21}(\text{obs}) = k_{21}$, $k_{12}(\text{obs}) = 0$ and $k_1(\text{obs}) = k_1$ if $K \ll [H^+]$ and $Kk_1^* \ll k_1[H^+]$. This is in agreement with the experimental results for the hydrolysis of both the 1,2-ethanediamine and 1,3-propanediamine complexes at the acid concentrations employed.

Eqn. (1) was derived assuming a steady state for the concentration of the (*trans*-2-aminocyclohexylammonium)pentaaquachromium(III) species in experiments started from (*trans*-1,2-cyclohexanediamine)tetraaquachromium(III). This assumption was tested in two different ways. In the first method the hydrogen ion dependence and temperature dependence of observed reaction rate constants were parametrised employing eqns. 1, 2a – 2c and an Arrhenius equation of the form:

$$k_T = k_{T_0} \exp[-E_A(1/RT - 1/RT_0)] \quad (3)$$

respectively. Average reaction rate constants at 70 °C and activation energies obtained in this way are tabulated in Tables 4,5, and 6. These constants, obtained using all the experimental data, have been used for the calculation of the solid curves in Figs. 3 and 4 *via* eqns. 1 and 2b combined with eqn. 3. The calculated curves are seen to adequately describe the observed rate constants obtained for both types of experiment. The values obtained for k_{21}(obs) and k_1(obs) in the individual kinetic experiments involving the *trans*-1,2-cyclohexanediamine complex were never particularly well-defined. However, reasonably well-defined rate constants and activation energies for hydrolysis of both diamine and monoamine species were obtained in the final calculations. As demonstrated and discussed at greater length previously [6] this again points to the need for independent experiments when complex kinetic schemes are encountered. The second method employed to test the validity of the steady state approximation is demonstrated in Fig. 6, where the excellent agreement between the experimental and calculated

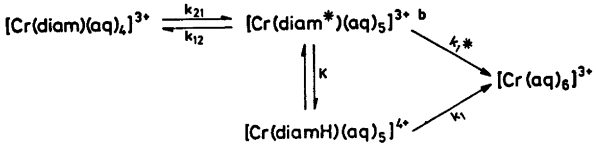

Fig. 5. Reaction scheme for acid hydrolysis of diaminetetraaquachromium(III) species. b. Although the species [Cr(diam*) (aq)$_5$]$^{3+}$ is probably the primary hydrolysis product of the [Cr(diam) (aq)$_4$]$^{3+}$ species, differences in acid strength between coordinated water and coordinated protonated amine make it likely that the monoamine species is probably more accurately described by the formula [Cr(diamH) (aq)$_4$OH]$^{3+}$.

Table 6. "Rate constants" at 70 °C and "activation energies" for reactions of the deprotonated monoamine species containing monodentate *trans*-1,2-cyclohexanediamine.

kK	$10^6 \times kK$ [mol/(l × s)]	E_A (kcal/mol)
$k_{1s}K$ [a]	106 ± 4	30.8 ± 0.4
$k_1{}^*K$ [a]	22.9 ± 1.1	36.4 ± 1.4

[a] With the present data the acidity constant (K) of the (*trans*-2-aminocyclohexylammonium)-pentaaquachromium(III) ion was estimated to be $(2 \pm 2) \times 10^{-2}$ mol/l. A separation of the products $k_{1s}K$ and $k_1{}^*K$ into well-defined constants could therefore not be performed.

concentration-time relationship as well as the minor amounts of monoamine species present in solutions confirm the validity of the approximation employed.

The hydrolysis of the tetraaqua((−)$_D$-*trans*-1,2-cyclohexanediamine)chromium(III) ion was also followed by measurement of optical rotation. This method gave rate constants essentially the same as those obtained by spectral monitoring results, but due to relatively large uncertainty in the measured rotations these experiments gave no additional information about the kinetics of the system.

The complete reaction scheme presented here is similar to an earlier proposed scheme for dechelation of both aromatic [10] and aliphatic [11] amines. However, in our system the rate determining step is *not* proton attack on the uncoordinated free amino group, as demonstrated by the successful isolation of the protonated amine intermediate. It may be envisaged that the scheme presented here also applies to some of these other systems since a hydrogen ion dependence of the observed rate constants of the form given by eqn. (1) is observed for both reaction schemes.

In Fig. 7 rate constants for the monoamine complexes investigated are exhibited as a function of the acidity constants for the fully protonated free amines. Although the reactivity differences may be partly rationalized on this basis it can be seen that there is no quantitative correlation.

For the flexible ligands, 1,2-ethanediamine and 1,3-propanediamine, it is likely that different conformations predominate in the diprotonated, the monoprotonated, and the complex-bound monoprotonated forms, and such an effect could explain the deviations from linearity seen in Fig. 7, but further evidence in support of this suggestion is clearly required. Linear correlations have been observed previously for reactions of the type

$$[Cr(aq)_5X]^{(3-i)+} + aq \rightleftharpoons [Cr(aq)_6]^{3+} + X^{i-}$$

where X is one of a series of anionic ligands (I^-, Br^-, Cl^-, NCS^- or F^-)[13] or one of a series of 3-substituted pyridines.[14] The significant differences in slopes and particularly intercepts for the three correlations are noteworthy, however.

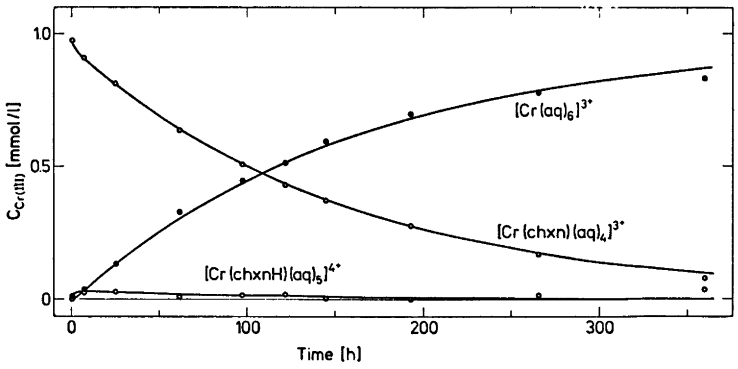

Fig. 6. Kinetic experiment started from (*trans*-1,2-cyclohexanediamine) tetraaquachromium(III) (indicated by a filled circle in Fig. 3) interpreted within the reaction scheme of Fig. 5. Circles indicate concentrations calculated from the spectra of reaction mixtures. The solid curves are calculated from rate constants obtained by eqns. 2a, 2b, 2c and 3 from the data given in Tables 4, 5 and 6.

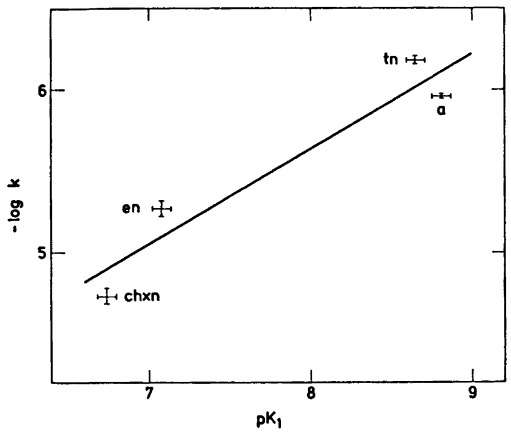

Fig. 7. Correlation between $-\log k_1$ and pK_1 values at 70 °C, statistically corrected for the number of equivalent ionisable hydrogen atoms in the aminogroups (Tables 5 and 1).

For the protonated polyaminepentaaquachromium(III) complexes of 1,4,7-triazaheptane ("dien"),[15] 1,4,7,10-tetraazadecane ("trien")[16] and 1,4,7,10,13-pentaazatridecane ("tetren")[17] the correlation between hydrolysis rate constants and acidity constants for the fully protonated amines is not good. At 70 °C all the complexes react at a rate comparable to that of the 2-aminoethylammonium complex but the free, fully protonated amines are substantially stronger acids than the diprotonated 1,2-ethanediamine. This absence of correlation is believed to reflect the fact that whereas hydrolysis of the coordinated primary aminogroups is responsible for the observed rate constants, it is the protons on the secondary aminogroups which are mainly responsible for the observed acidity constants.

An approach similar to the one outlined above for the monoamine data is not possible for the diamine data since this would require a knowledge of the acidity constants of the protonated, coordinated diamines in the monoamine complexes. Due to rapid chelation and polymerization reactions these constants are not easily measured. A value for the acidity constant of the (2-aminoethylammonium)pentaaquachromium(III) ion similar to those observed for other chromium(III) complexes of the 2-aminoethylammonium ion ligand[9,18] is, however, capable of rationalizing the reactivity difference between the tetraaqua(1,2-ethanediamine)chromium(III) and *cis*-diamminetetraaquachromium(III) species on the same basis as discussed for the monoamine complexes. This makes it reasonable to classify the dechelation of 1,2-ethanediamine as a "normal" substitution reaction. For chelate ligands of higher coordination number numerous examples of deviations from such simple behaviour have been found as may be illustrated by comparing the large difference in reactivity between the isomeric triaqua(1,4,7-triazaheptane)chromium(III) ions.[14]

In Table 7 are given equilibrium constants for 1,2-ethanediamine and *trans*-1,2-cyclohexanediamine as chelate and monodentate protonated ligands. The data show the greater preference of the *trans*-2-aminocyclohexylammonium ligand than of the 2-aminoethylammonium ligand for forming chelate complexes, but it is not immediately apparent whether the large difference is kinetically determined or is the result of a larger acidity constant for the *trans*-2-aminocyclohexylammonium complex. The greater importance of the acid dependent monoamine hydrolysis reaction in the case

Table 7. Equilibrium constants for 1,2-ethanediamine and *trans*-1,2-cyclohexanediamine as chelate and protonated monodentate ligands.

Reaction	K (mol/l)	t (°C)	Ref.
$[Cr(chxnH)(aq)_5]^{4+} \rightleftharpoons [Cr(chxn)(aq)_4]^{3+} + H^+$	$10^{1.2}$	70	*a*
$[Cr(en)_2(enH)(aq)]^{4+} \rightleftharpoons [Cr(en)_3]^{3+} + H^+$	$10^{-3.7}$	24	9
$[Cr(enH)(aq)_5]^{4+} \rightleftharpoons [Cr(en)(aq)_4]^{3+} + H^+$	$<10^{-1.3}$ *b*	80	*a*

a This work. *b* This value is based upon an upper limit for the rate constant for the chelation reaction of the (2-aminoethylammonium)pentaaquachromium(III) ion, estimated from data for experiment 5 in Table 3.

of the (*trans*-2-aminocyclohexylammonium)-pentaaquachromium(III) ion than in the case of the (2-aminoethylammonium)pentaaquachromium(III) ion could be taken as evidence in favour of the latter explanation. Inspection of molecular models, however, reveals significant interaction between the cyclohexanediamine ring and coordinated water molecules in the (*trans*-2-aminocyclohexylammonium)pentaaquachromium(III) ion. This interaction apparently prevents the uncoordinated aminogroup from moving very far away from the first coordination sphere of the complex ion. Such an effect could well result in a larger acidity constant and would at the same time increase the probability of formation of the chelate complex because of the close proximity of the "reactants".

It is clear that further experiments would be of value in throwing more light on many of the points raised in the previous section, and with this in mind an investigation of the hydrolysis of chromium(III) methylamine complexes and of the two isomeric forms of the ammine-triaqua(1,2-ethanediamine)-chromium(III) ion is currently in progress.

Acknowledgement. The author wishes to thank Dr. Martin Hancock for revising the English maniscript.

REFERENCES

1. Mønsted, L. and Mønsted, O. *Acta Chem. Scand. A 29* (1975) 29.
2. Childers, R. F., Vander Zyl, K. G., House, D. A., Hughes, R. G. and Garner, C. S. *Inorg. Chem. 7* (1968) 749.
3. Glerup, J. *To be published.*
4. Couldwell, M. C. and House, D. A. *Inorg. Chem. 11* (1972) 2024.
5. Glerup, J., Josephsen, J., Michelsen, K., Pedersen, E. and Schäffer, C. E. *Acta Chem. Scand. 24* (1970) 247.
6. Mønsted, L. and Mønsted, O. *Acta Chem. Scand. 27* (1973) 2121.
7. Mønsted, L. and Mønsted, O. *Acta Chem. Scand. A 30* (1976) 203.
8. Guastalla, G. and Swaddle, T. W. *Can. J. Chem. 52* (1974) 527.
9. Andersen, P., Berg, T. and Jacobsen, J. *Acta Chem. Scand. A 29* (1975) 381.
10. Basolo, F. and Pearson, R. *Mechanisms of Inorganic Reactions*, 2nd Ed., Wiley, New York 1967, p. 216.
11. Childers, R. F. and Wentworth, R. A. D. *Inorg. Chem. 8* (1969) 2218.
12. Mønsted, L. and Mønsted, O. *Acta Chem. Scand. A 28* (1974) 569.
13. Monacelli, F. *Ric. Sci. 37* (1976) 777.
14. Bakač, A., Marčec, R. and Orhanović, M. *Inorg. Chem. 13* (1974) 57.
15. Lin, D. K. and Garner, C. S. *J. Am. Chem. Soc. 91* (1969) 6637.
16. Kamp, D. A., Wilder, R. L., Tang, S. C. and Garner, C. S. *Inorg. Chem. 10* (1971) 1396.
17. Ranney, S. J. and Garner, C. S. *Inorg. Chem. 10* (1971) 2437.
18. Schwarzenbach, G. and Magyar, B. *Helv. Chim. Acta 45* (1962) 1454.

Received January 29, 1976.

Acta Chemica Scandinavica A 30 (1976) 609—613

An X-Ray Diffraction Study of the Potentially Antidepressant Isomer of 3-(4-Bromophenyl)-*N*,*N*-dimethyl-3-(3-pyridyl)-allylamine

SIXTEN ABRAHAMSSON,[a] ARVID CARLSSON,[b] BERNT CARNMALM [c] and BIRGITTA DAHLÉN [a]

[a] Department of Structural Chemistry, University of Göteborg, S-400 33 Göteborg, Sweden, [b] Department of Pharmacology, University of Göteborg, S-413 46 Göteborg, Sweden and [c] Astra Läkemedel AB, S-151 85 Södertälje, Sweden

An X-ray single crystal analysis has been performed on the dihydrochloride of that isomer of 3-(4-bromophenyl)-*N*,*N*-dimethyl-3-(3-pyridyl)allylamine which selectively inhibits the neuronal uptake of 5-hydroxytryptamine, showing this compound to be the *Z* isomer, formula I.

It is a well-established hypothesis that the tricyclic antidepressants act clinically by inhibiting the neuronal uptake of the transmittor amines noradrenaline (NA) and/or 5-hydroxytryptamine (5-HT), see *e.g.* Iversen.[1] As different types of depressive disorders are known, it is of interest to try to find compounds which normalize the transmittor status in the brain *via* reactions with high selectivity, *cf.* van Praag.[2]

Most of the known tricyclic antidepressants do inhibit the NA uptake, same of them rather selectively, but selective inhibitors of the 5-HT uptake have been lacking. A finding by one of us that some antihistamines of pheniramine type inhibit the neuronal uptake of 5-HT [3] initiated a study of structurally related substances. Among the compounds synthesized was a pair of *cis-trans* isomers, I and II.[4]

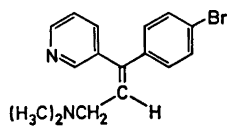

I

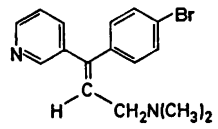

II

As seen from Table 1, they are both inhibitors of the amine uptake, and it is noteworthy that there is a clear difference in the selectivities of their action. Compound I acts more selectively on the 5-HT uptake than does chlorimipramine which has been found earlier to block preferentially this uptake.[5]

Table 1. Inhibition *in vitro* of the uptake of noradrenaline (NA) and 5-hydroxytryptamine (5-HT) [6] by the method of Ross *et al.*[7]

	Astra Reg. No.	EC_{50} μM NA	EC_{50} μM 5-HT	5-HT Selectivity [a]
I. Hydrochloride	A 10124	24.5	1.7	14
II. Oxalate	A 23140	5.5	5.5	1
Chlorimipramine		0.9	0.09	10

[a] Defined as EC_{50} (NA)/EC_{50} (5-HT).

With these figures in mind we considered it of interest to have unambiguous information on the detailed structures of I and II. Attempted interpretation of UV and NMR spectra gave no conclusive evidence of the sterical relationships. An X-ray single crystal analysis of the 5-HT selective isomer was therefore performed.

EXPERIMENTAL

The amines were prepared using the previously described synthetic procedure [4] shown in the scheme:

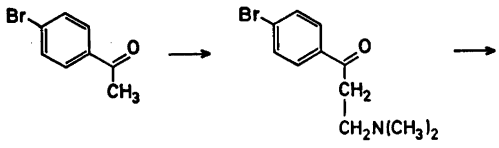

III

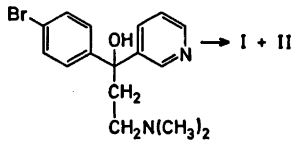

IV

Starting with *p*-bromoacetophenone, a Mannich reaction gives the amino ketone III which reacts with pyridyllithium to the amino alcohol IV. Dehydration with sulfuric acid then gives a mixture of the *cis-trans* isomers I and II. One isomer was isolated by precipitation with concentrated hydrochloric acid from an acetone solution and purified by recrystallization from isopropyl alcohol containing about 2 % of water. The pure isomer was obtained as the dihydrochloride with 1 mol water of crystallization. From the mother liquors the other isomer could be isolated as its oxalate, which was recrystallized from ethanol. The pure salt contains oxalic acid and amine in the molar proportions three to two. The salts analyzed correctly and gave spectra in good correlation with the gross structure of I and II.

CRYSTAL DATA

Molecular formula	$C_{16}H_{21}BrCl_2N_2O$
Unit cell monoclinic	$a = 16.771(8)$, $b = 9.810(4)$, $c = 11.064(7)$ Å $\beta = 98.23(3)°$
V	1801Å^3
M.W.	408.17
Z	4
D_c	1.505 g cm^{-3}
D_m	1.502 g cm^{-3}
Systematic absences	$h0l: l = 2n+1$, $0k0: k = 2n+1$
Space group	$P2_1/c$

The intensity data were recorded on a Picker FACS1 diffractometer with the Vanderbilt software system.[8] 10 steps ($\theta/2\theta$) of 2 s each and a width of 0.2° were used to measure the reflexion intensity with graphite monochromated Cu$K\alpha$ radiation. 10 s background counts were taken on each side of the reflexion. In all 2752 reflexions up to $2\theta = 120°$ were recorded of which only 818 were more than 4 standard deviations above background and considered observed. This limit, though, was consistent with counts obtained for systematically absent reflexions. The data were corrected for Lorentz and polarization effects but not for extinction or absorption. Scattering factors for the non-hydrogen atoms were taken from the International Tables for X-Ray Crystallography [9] and for hydrogen from Stewart *et al.*[10] The scattering curves for bromine and chlorine were corrected for anomalous dispersion (real part). All calculations were performed on a Datasaab-PDP15 dual computer system, using programs developed at the Department of Structural Chemistry.

STRUCTURE DETERMINATION AND REFINEMENT

The bromine atom was located from a sharpened Patterson series. All other non-hydrogen atoms were then found from successive structure factor/electron density calculations. At an R-value of 0.27, it was evident which of the peaks represented the two nitrogen atoms. Cycles of block diagonal least-squares refinement using anisotropic temperature factors for the non-hydrogen atoms reduced the R-value to 0.07. At this stage a difference series revealed all hydrogen atoms except those on the water oxygen and that on the quaternary nitrogen atom. All hydrogen atoms except those of the water molecule were now included in the computations at their calculated positions with isotropic temperature factors corresponding to those of their parent atoms. No hydrogen parameters were, however, refined.

Table 2. Fractional atomic coordinates. The standard deviations (in parentheses) are multiplied by 10^5 for the bromine and chlorine atoms and 10^4 for the other non-hydrogen atoms.

	x	y	z	B (Å^2)
Br(1)	0.41137(12)	0.23240(21)	−0.55741(20)	
Cl(1)	0.94230(26)	0.24402(50)	−0.33309(41)	
Cl(2)	0.25080(29)	0.28251(50)	−0.28388(43)	
O(1)	0.9920(8)	0.0369(14)	−0.1319(11)	
N(1)	0.8458(8)	0.0553(13)	−0.0474(13)	
N(2)	0.8386(8)	0.5758(12)	−0.0366(14)	
C(1)	0.4959(9)	0.2516(20)	−0.4229(16)	
C(2)	0.4998(9)	0.3729(18)	−0.3629(16)	
C(3)	0.5620(10)	0.4013(20)	−0.2636(18)	
C(4)	0.6186(11)	0.2990(19)	−0.2269(13)	
C(5)	0.6131(10)	0.1793(19)	−0.2902(14)	
C(6)	0.5513(10)	0.1525(17)	−0.3881(18)	
C(7)	0.6893(11)	0.3203(17)	−0.1367(17)	
C(8)	0.7304(9)	0.1968(14)	−0.0782(14)	
C(9)	0.7003(9)	0.1137(18)	0.0029(18)	
C(10)	0.7429(11)	0.0090(17)	0.0593(17)	
C(11)	0.8153(14)	−0.0191(17)	0.0293(17)	
C(12)	0.8063(10)	0.1629(17)	−0.1056(16)	
C(13)	0.7114(10)	0.4485(18)	−0.1016(16)	
C(14)	0.7735(12)	0.4846(18)	0.0045(18)	
C(15)	0.8845(13)	0.5028(17)	−0.1236(19)	
C(16)	0.8947(12)	0.6266(17)	0.0701(17)	
H(11)	0.896	0.031	−0.071	2.28
H(12)	0.814	0.654	−0.078	1.96
H(21)	0.460	0.439	−0.040	1.81
H(31)	0.571	0.493	−0.230	4.13
H(51)	0.655	0.116	−0.274	2.47
H(61)	0.553	0.065	−0.422	3.20
H(91)	0.646	0.123	0.019	2.57
H(101)	0.723	−0.044	0.120	2.47
H(111)	0.843	−0.094	0.072	2.19
H(121)	0.828	0.217	−0.165	2.68
H(131)	0.684	0.521	−0.145	2.83
H(141)	0.748	0.532	0.067	2.21
H(142)	0.797	0.403	0.044	2.21
H(151)	0.846	0.473	−0.192	3.08
H(152)	0.909	0.425	−0.084	3.08
H(153)	0.922	0.560	−0.151	3.08
H(161)	0.921	0.551	0.113	2.69
H(162)	0.866	0.676	0.124	2.69
H(163)	0.935	0.684	0.044	2.69

The refinement was terminated at an R-value of 0.058.

RESULTS AND DISCUSSION

The final structure factor list can be obtained from the Department of Structural Chemistry. The atomic coordinates are given in Tables 2 and 3. Interatomic distances and angles for the heavier atoms are given in Fig. 1 which also shows the atomic numbering. The distances and angles show no unexpected features when the standard deviations (all about 0.02 Å) are considered. The molecular configuration and conformation are illustrated in Fig. 2. The analysis definitely establishes that the isomer precipitated as the hydrochloride is (*Z*)-3-(4-bromophenyl)-*N*,*N*-dimethyl-3-(3-pyridyl)allylamine, corresponding to formula I.

There is a slight twist about the double bond. C(4) is thus 0.24 Å and C(8) 0.12 Å on opposite sides of the plane through C(7), C(13)

Table 3. Anisotropic thermal parameters in the form $\exp[-2\pi^2(h^2a^{*2}U_{11}+k^2b^{*2}U_{22}+l^2c^{*2}U_{33}+2klb^*c^*U_{23}+2hla^*c^*U_{31}+2hka^*b^*U_{12})]$. Standard deviations are given in parentheses. All values have been multiplied by 10^4.

	U_{11}	U_{22}	U_{33}	U_{23}	U_{31}	U_{12}
Br(1)	329(9)	403(11)	483(11)	−44(13)	−125(8)	32(13)
Cl(1)	489(26)	337(27)	409(28)	69(28)	43(21)	50(29)
Cl(2)	560(29)	328(26)	391(29)	−69(25)	−77(22)	21(26)
O(1)	523(94)	435(86)	290(90)	133(70)	95(70)	211(76)
N(1)	299(88)	184(80)	355(104)	−360(77)	−132(77)	153(68)
N(2)	209(85)	−11(67)	508(109)	46(71)	−58(74)	−58(62)
C(1)	333(96)	346(121)	357(102)	−95(113)	90(75)	−229(114)
C(2)	142(97)	348(108)	310(118)	−29(96)	43(82)	208(86)
C(3)	327(118)	303(115)	436(139)	−258(100)	−61(98)	110(91)
C(4)	456(108)	442(123)	1(89)	−92(85)	199(77)	−144(97)
C(5)	379(110)	475(124)	5(95)	−57(85)	−43(77)	226(91)
C(6)	249(105)	93(90)	616(150)	−116(96)	266(99)	52(80)
C(7)	377(109)	138(97)	368(118)	−65(90)	−63(94)	19(88)
C(8)	216(85)	25(79)	163(92)	143(67)	3(70)	16(68)
C(9)	92(96)	233(102)	580(140)	84(96)	−259(87)	−93(79)
C(10)	337(114)	208(101)	366(119)	−58(88)	75(89)	−290(90)
C(11)	939(179)	122(97)	196(120)	79(87)	41(107)	−244(108)
C(12)	249(99)	182(94)	236(108)	−110(81)	−31(81)	−75(77)
C(13)	158(94)	272(103)	363(129)	−31(94)	−6(84)	202(85)
C(14)	595(125)	279(111)	156(117)	−15(95)	158(93)	98(98)
C(15)	645(144)	68(101)	473(146)	−271(97)	−10(113)	−15(97)
C(16)	576(133)	85(90)	324(123)	168(87)	−77(100)	−208(93)

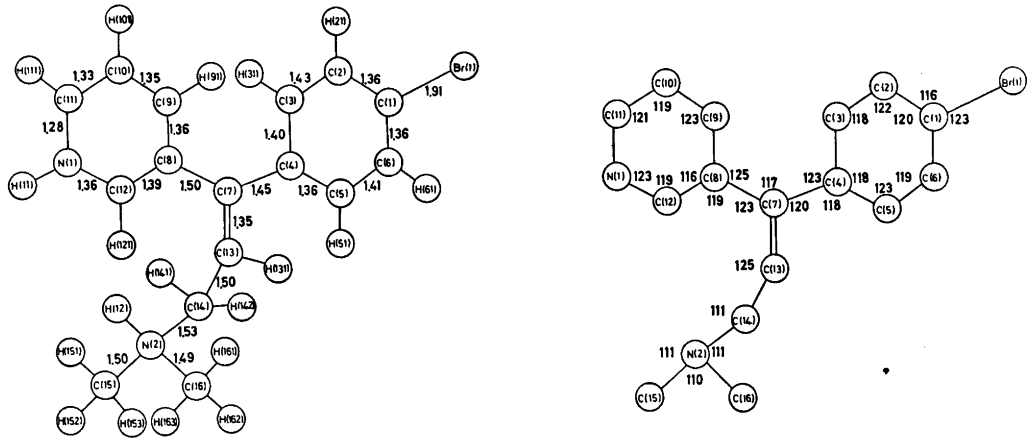

Fig. 1. Bond distances and angles.

and C(14). The benzene ring forms an angle of 23.4° with this double bond plane whereas the angle for the pyridine ring is 78.1°. C(13), C(14), N(2), and C(16) form an extended zigzag chain which is planar within 0.04 Å. C(15) is then 1.26 Å off the plane. The chain plane is inclined 56.7° to the double bond plane.

The molecules are arranged in double layers with bromobenzene rings in the interior and the polar parts on the outside in contact with chloride ions and water (Fig. 3). The hydrogen atom on N(1) points straight towards the water

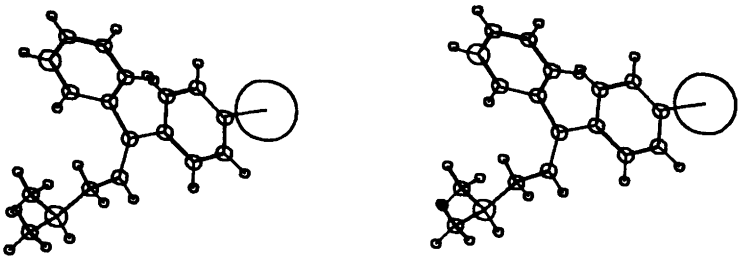

Fig. 2. Stereopair of the molecular ion.

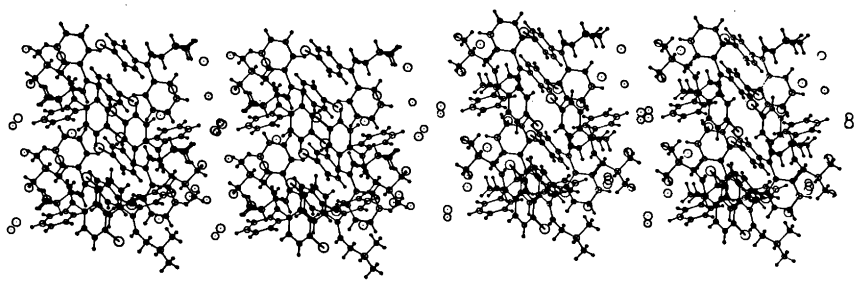

Fig. 3. Molecular packing.

oxygen and the N(1)···O(1) distance of 2.75 Å indicates a fairly strong hydrogen bond. The water oxygen is also close to a symmetry translated oxygen (2.98 Å) and has furthermore two contacts with symmetry related Cl(1)'s (3.04 and 3.12 Å). As the water hydrogens could not be found it is difficult to determine the exact hydrogen bonding scheme around the oxygen. The hydrogen atom on N(2) is involved in a hydrogen bond with the second chloride ion (Cl(2), 3.07 Å) which is thereby forced into a nonpolar neighbourhood. The closest other contacts are Br(1) at 3.41 Å and C(11) at 3.39 Å.

Acknowledgements. We wish to thank Mrs. M. Varju and Mr. G. Rehnberg for skilful technical assistance.

Grants in support of the Department of Structural Chemistry were obtained from the Swedish Medical Science Research Council, the Swedish Board for Technical Development, the U. S. Public Health Service (GM-11653) and the Wallenberg Foundation.

REFERENCES

1. Iversen, L. L. In Vossenar, T., Ed., *Proceed Symp. Depressive Illness*, Excerpta Medica, Amsterdam 1975, p. 55.
2. van Praag, H. M. *Ibid.* p. 71.
3. Carlsson, A. In Schümann, H. J. and Kroneberg, G., Eds., *New Aspects of Storage and Release Mechanisms of Catecholamines*, Springer, Berlin 1970, p. 223.
4. Berntsson, P. B., Carlsson, P. A. E. and Corrodi, H. R. *Belg. Pat.* 781105 (72-04-14), or *Eng. Pat.* 1 366 241 (75-01-08).
5. Carlsson, A., Corrodi, H., Fuxe, K. and Hökfelt, T. *Eur. J. Pharmacol. 5* (1969) 357.
6. Ross, S. B. *Personal communication.*
7. Ross, S. B., Renyi, A. L. and Ögren, S. O. *Eur. J. Pharmacol. 17* (1972) 107.
8. Lenhert. P. G. *J. Appl. Crystallogr. 8* (1975) 568.
9. *International Tables for X-Ray Crystallography*, Kynoch Press, Birmingham 1962, Vol. III, pp. 201 – 209.
10. Stewart, R. F., Davidsson, E. R. and Simpson, W. T. *J. Chem. Phys. 42* (1965) 3175.

Received March 15, 1976.

Acta Chemica Scandinavica A 30 (1976) 614—618

The Crystal Structure of Rubidium and Potassium Dibutyldithiocarbamates

ANDERS WAHLBERG

Institute of Chemistry, University of Uppsala, Box 531, S-751 21 Uppsala 1, Sweden

The crystal structures of the title compounds were determined from three-dimensional diffractometer X-ray data. Crystals of the isomorphous compounds are monoclinic, space group $P2_1/c$, $Z=4$. $a=16.029(1)$ Å, $b=6.487(1)$ Å, $c=13.383(1)$ Å, $\beta=106.22(1)°$, $R=0.078$ for $RbS_2CN(C_4H_9)_2$ and $a=16.085(3)$ Å, $b=6.361(1)$ Å, $c=13.207(2)$ Å, $\beta=106.12(1)°$, $R=0.121$ for $KS_2CN(C_4H_9)_2$. The metal atoms are coordinated to six sulfur atoms with mean distances Rb–S = 3.43 Å and K–S = 3.33 Å. The compounds are layer polymers, the layers being held together by van der Waals forces. The structures are closely related to the cesium and thallium dibutyldithiocarbamates.

Cesium dimethyldithiocarbamate [1] is a chain polymer with metal–sulfur interactions between the chains. The metal atom is eight-coordinated. Cesium dibutyldithiocarbamate [2] is a layer polymer with six-coordinated cesium atoms. The coordination number for thallium in thallium(I) dithiocarbamates lies between five and seven. Dimers are linked to form chain or layer polymers. The crystal structures formed are very sensitive to the size and shape of the alkyl substituents. Related effects are expected in the alkali dithiocarbamates with varying radius of the coordinating cation. The crystal structure of rubidium dibutyldithiocarbamate is expected ($r_{Rb^+} \approx r_{Tl^+}$) to resemble those of cesium and thallium,[3] which are very similar.

EXPERIMENTAL

Rubidium dibutyldithiocarbamate

Crystal preparations. The compound was prepared as described by Uhlin.[4] The solid hydroscopic product was dried *in vacuo* and recrystallized from benzene. The crystals developed as pale orange-yellow flakes elongated along [010] and with faces (100). The density was measured by flotation in mixtures of CCl_4 and C_6H_5Cl. Accurate unit cell dimensions were obtained from a powder photograph taken on an IRDAB XCD 700 camera using Cr$K\alpha_1$ radiation with silicon ($a=5.43054$ Å) as an internal standard. 89 observed θ-values were used in the least-squares refinements of the cell parameters.

Crystal data. Monoclinic crystal system, space group $P2_1/c$, $Z=4$, $a=16.029(1)$ Å, $b=6.487(1)$ Å, $c=13.383(1)$ Å, $\beta=106.22(1)°$, $V=1336.2$ Å^3, $D_o=1.44(1)$ g cm^{-3}, $D_x=1.441$ g cm^{-3}, m.p.$_o$ = 171 – 175 °C, m.p.$_{lit}$[4] = 148 – 150 °C, μ(Mo$K\alpha$) = 41.9 cm^{-1}.

Intensity data. The intensity data were collected at room temperature on a Stoe-Philips four-circle PDP 8/I computer controlled diffractometer with a graphite monochromator using Mo$K\alpha$ radiation and an $\omega-2\theta$ scan technique. The two crystals used were mounted on glass fibres and were protected from air by thin-walled glass capillaries. 436 and 498 intensities were collected on the first ($0.048\times0.140\times0.098$ mm^3) and second ($0.070\times0.356\times0.056$ mm^3) crystals, respectively, $\sin\theta/\lambda \leq 0.40$. The standard reflections were $\bar{4}13$, $2\bar{2}0$, and 006, and 040, 004, and 500. The transmission factor varied from 0.66 to 0.83 and 0.64 to 0.81. The intensities were measured for 176 s (five reflections were measured for 88 s) and the backgrounds for 2×25 s. The orientations of the crystals were repeatedly checked. The standard reflections were measured at intervals of 40 reflections. The intensities were corrected for crystal decomposition by a formula developed from studies of the decrease of the standard reflections (some strong reflections first increased, then decreased). The crystals were used until the intensities of the standard reflections were reduced by ca 20 %. The reflections 100, 001, $\bar{1}01$, and 101 were absorbed in the primary beam stop. Corrections for

Table 1. Atomic coordinates and thermal parameters for rubidium dibutyldithiocarbamate. The anisotropic temperature factor is defined as $\exp(-\beta_{11}h^2-\beta_{22}k^2-\beta_{33}l^2-2\beta_{12}hk-2\beta_{13}hl-2\beta_{23}kl)$.

Atom	x	y	z	B Å^2		
Rb	0.0006(1)	0.2090(3)	0.1100(1)			
S1	0.1754(3)	−0.0443(8)	0.0722(4)			
S2	0.0613(3)	−0.3013(7)	0.1606(4)			
C	0.164(1)	−0.232(3)	0.159(1)	4.3(4)		
N	0.234(1)	−0.308(2)	0.223(1)	5.4(4)		
C11	0.323(1)	−0.240(3)	0.228(2)	6.8(5)		
C12	0.357(2)	−0.344(4)	0.146(2)	8.8(7)		
C13	0.444(2)	−0.239(5)	0.142(3)	11.9(9)		
C14	—	—	—	—		
C21	0.231(1)	−0.449(4)	0.317(2)	7.6(6)		
C22	0.266(2)	−0.654(4)	0.301(2)	8.3(6)		
C23	0.265(1)	−0.792(3)	0.401(2)	7.2(6)		
C24	0.174(1)	−0.881(4)	0.387(2)	6.9(5)		
Atom	β_{11}	β_{22}	β_{33}	β_{12}	β_{13}	β_{23}
Rb	0.0072(2)	0.0219(12)	0.0054(3)	0.0004(2)	0.0019(1)	−0.0009(2)
S1	0.0064(4)	0.0325(20)	0.0070(5)	−0.0026(6)	0.0022(3)	0.0019(7)
S2	0.0061(4)	0.0260(21)	0.0068(5)	−0.0009(6)	0.0022(3)	0.0010(6)

background, Lorentz and polarization effects (including monochromator polarization) and absorption were applied before the data set was reduced, giving 716 independent reflections.

Structure determination and refinements. The metal atom positions were obtained from the three-dimensional Patterson function. The other non-hydrogen atoms, except one terminal carbon atom, C14, were located in difference Fourier syntheses. Scale factors and positional and isotropic thermal parameters were then refined by full matrix least-squares. Attempts were made to include the remaining carbon atom in the refinements, but the large thermal parameters and the unsatisfactory bond distances and angles showed that this atom was disordered. All reflections were included in the final refinement of 65 parameters (anisotropic thermal parameters for the metal and sulfur atoms). The final shifts were less than a tenth of the standard deviations. Resulting positional and thermal parameters are collected in Table 1. A list of squares of observed and calculated structure amplitudes is available on request. $R(F^2)=\sum||F_o^2|-|F_c^2||/\sum|F_o^2|=0.132$, $R_w(F^2)=(\sum w(|F_o^2|-|F_c^2|)^2/\sum w|F_o^4|)^{\frac{1}{2}}=0.183$, $R(F)=0.078$. The expression $w(|F_o^2|-|F_c^2|)^2$ was minimized in the least-squares refinements with the weights $w^{-1}=(1.20\sigma_c(F^2))^2+(0.08|F_o^2|)^2=\sigma(F^2)^2$. Scattering factors [5] were used for the neutral atoms. Corrections for anomalous dispersion [6] were applied for the metal and sulfur atoms. The highest electron density maxima in a difference Fourier synthesis following the refinements were located at three positions reasonable for C14 (0.19, 0.16, and 0.11 e Å^{-3}). The remaining electron density was less than 0.10 e Å^{-3}. The calculations [7] were performed on the IBM 370/155 computer in Uppsala.

Potassium dibutyldithiocarbamate

The experiments were generally performed as for the rubidium compound. The crystals resembled those of the rubidium compound, but the flakes were only a few μm thick. The cell parameters were obtained from 60 θ-angles.

Crystal data, monoclinic crystal system, space group $P2_1/c$, $Z=4$, $a=16.085(3)$ Å, $b=6.361(1)$ Å, $c=13.207(2)$ Å, $\beta=106.12(1)°$, $V=1298.3$ Å^3, $D_o=1.25(1)$ g cm^{-3}, $D_x=1.246$ g cm^{-3}, m.p.$_o$ = 139 − 141 °C, m.p.$_{lit}$[4] = 148 − 150 °C, $\mu(MoK\alpha)=6.8$ cm^{-1}. There were almost no intensities on Weissenberg films at $\sin\theta/\lambda<0.30$. No improvement was obtained by cooling to the temperature of boiling nitrogen.

388 intensities were collected from a crystal of dimensions $0.016\times0.356\times0.182$ mm^3, $\sin\theta/\lambda\leq0.29$. The standard reflections were 004, 500, and 020, and the transmission factor varied from 0.84 to 0.99. The intensities were measured for 69 s and the backgrounds for 2×20 s. At the end of the experiment the intensities of the standard reflections had been reduced by *ca.* 50 %.

Positional parameters from rubidium dibutyldithiocarbamate were refined to fit the potassium dibutyldithiocarbamate data. The refinement was based on F, and 175 reflections ($|F_o|>2\sigma$, $0.25<|F_o|/|F_c|<4.0$) were included in the final cycles to refine 49 parameters. Without introduction of anisotropic thermal param-

Table 2. Atomic coordinates and thermal parameters for potassium dibutyldithiocarbamate.

Atom	*x*	*y*	*z*	*B* Å²
K	0.000(1)	0.201(3)	0.110(1)	6.2(8)
S1	0.167(1)	−0.041(4)	0.066(2)	6.5(10)
S2	0.056(1)	−0.307(4)	0.160(2)	5.8(9)
C	0.151(6)	−0.204(16)	0.156(7)	9(3)
N	0.226(5)	−0.316(10)	0.221(5)	6(2)
C11	0.318(4)	−0.236(11)	0.225(5)	3(2)
C12	0.354(4)	−0.363(11)	0.127(5)	4(2)
C13	0.455(5)	−0.236(14)	0.115(5)	10(3)
C14	—	—	—	—
C21	0.226(6)	−0.423(18)	0.325(8)	12(4)
C22	0.273(5)	−0.644(15)	0.307(7)	8(3)
C23	0.271(4)	−0.798(11)	0.409(5)	4(2)
C24	0.169(5)	−0.895(11)	0.387(5)	5(3)

eters the refinement converged at $R(F) = 0.121$ and $R_w(F) = 0.146$. The weights were $w^{-1} = (1.50\sigma_c(F))^2 + (0.09|F_o|)^2$. Again the atom C14 was found to be disordered. Positional and thermal parameters are collected in Table 2. A list of observed and calculated structure amplitudes is available on request.

RESULTS AND DISCUSSION

General. The crystal structures of the two compounds are very similar. Ionic bonds link the metal atoms and ligands in layers parallel with the *bc*-plane, Fig. 1. The layers are connected by van der Waals forces, the main contacts being between alkyl groups.

The dimeric unit. A plane through the metal and S2 sulfur atoms in the centrosymmetric dimer in Fig. 2 is approximately parallel to the *bc*-plane. The dimer is similar to those found in the dithiocarbamates of monovalent thallium, but it interacts more strongly with neighbouring dimers.

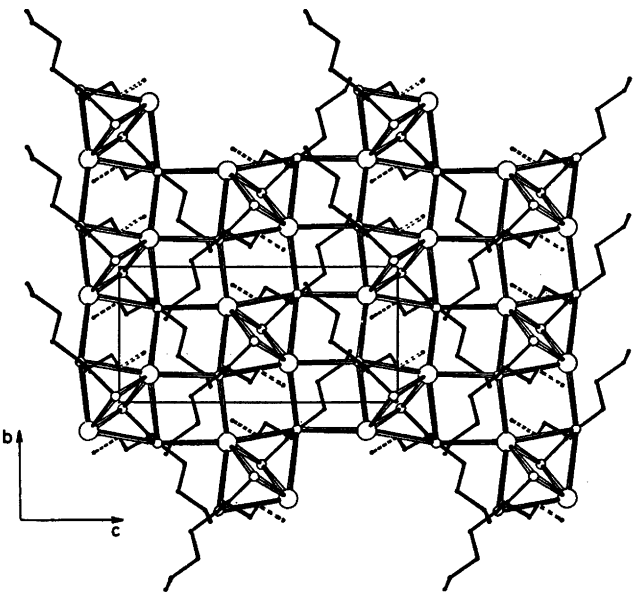

Fig. 1. The layer.

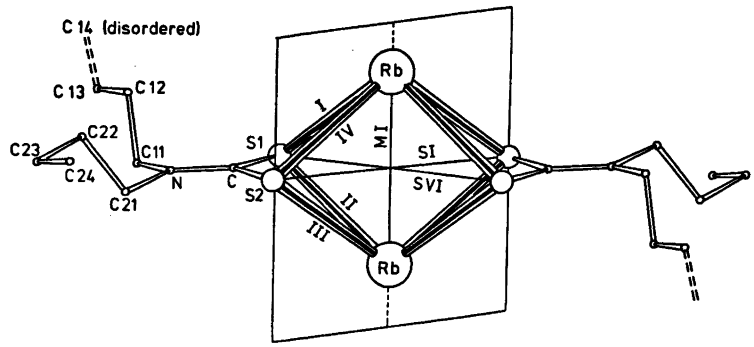

Fig. 2. The centrosymmetric dimeric unit.

The ligand. The atoms in the dibutyldithiocarbamate ligand are defined in Fig. 2. C14 is given a position with normal distances and angles (dashed bonds). The ligand appears normal. Distances and angles are collected in Table 3. The S1–S2–C–N–C11–C21 part of the ligand is planar within experimental error, except C21, which is displaced from the least-squares plane by 0.14(3) Å in the rubidium compound and by 0.30(11) Å in the potassium compound. The figures show that the two butyl groups are located on the same side of the dithiocarbamate plane. It should be noted that the substituents are situated on both sides of the plane in the compounds of cesium and thallium.

Metal–sulfur coordination. The metal atoms are coordinated to six sulfur atoms in four ligands. The average metal–sulfur distance is 3.43 and 3.33 Å in the rubidium and potassium compounds, respectively. Subtraction of Shan-

Table 3. Interatomic distances (Å) and angles (°) for the dibutyldithiocarbamate ligand.

	Rubidium dibutyldithiocarbamate	Potassium dibutyldithiocarbamate
Distance		
S1–S2	2.96(1)	2.96(3)
S1–C	1.73(2)	1.64(10)
S2–C	1.71(2)	1.68(10)
C–N	1.31(2)	1.46(12)
N–C11	1.47(3)	1.55(10)
N–C21	1.57(3)	1.53(12)
C11–C12	1.52(3)	1.76(10)
C12–C13	1.57(4)	1.86(10)
C21–C22	1.49(3)	1.63(14)
C22–C23	1.62(3)	1.67(11)
C23–C24	1.53(3)	1.69(10)
Angle		
S1–C–S2	119(1)	126(6)
S1–C–N	118(1)	118(7)
S2–C–N	123(1)	114(7)
C–N–C11	124(2)	119(6)
C–N–C21	122(2)	123(7)
C11–N–C21	113(2)	110(6)
N–C11–C12	108(2)	109(5)
C11–C12–C13	106(2)	110(5)
N–C21–C22	110(2)	98(7)
C21–C22–C23	112(2)	106(6)
C22–C23–C24	109(2)	108(5)

Table 4. Metal–sulfur, metal–metal and sulfur–sulfur distances (Å) less than 6 Å.

Distance		Rubidium dibutyldithiocarbamate	Potassium dibutyldithiocarbamate
I,	metal–S1	3.347(6)	3.19(3)
II,	metal–S1	3.405(6)	3.28(3)
III,	metal–S2	3.463(5)	3.37(3)
IV,	metal–S2	3.529(5)	3.49(3)
V,	metal–S2	3.336(5)	3.27(3)
VI,	metal–S2	3.480(5)	3.40(3)
MI,	metal–metal	3.998(4)	3.87(4)
MII,	metal–metal	4.784(4)	4.80(4)
MIII,	metal–metal	4.961(4)	4.87(4)
SI,	S2–S2	5.74(1)	5.66(3)
SII,	S2–S2	4.93(1)	4.77(3)
SIII,	S2–S2	4.77(1)	4.63(3)
SIV,	S1–S2	2.96(1)	2.96(3)
SV,	S1–S2	4.74(1)	4.55(3)
SVI,	S1–S1	5.44(1)	5.18(3)
	S1–S2	5.96(1)	5.74(3)
	S1–S2	5.40(1)	5.26(3)
	S1–S2	5.39(1)	5.26(3)

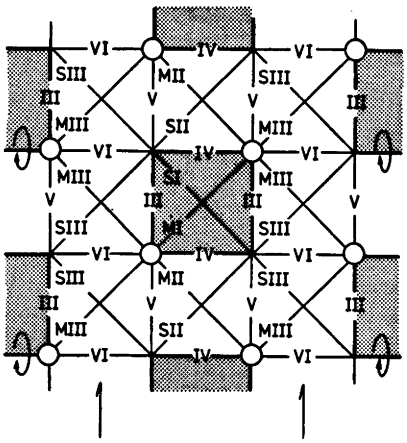

Fig. 3. A schematical representation of the layer.

non and Prewitt effective metal ionic radii [8] from the average distances gives a radius of 1.94 and 1.95 Å for sulfur in the ionic dithiocarbamate ligand. The radius is longer than the Pauling ionic radius for S^{2-} (1.84 Å), but agrees with those derived from cesium dibutyldithiocarbamate (1.92 Å) and cesium dimethyldithiocarbamate (*ca.* 2.00 Å). Table 4 shows that the two-coordinated sulfur atom S1 has shorter average metal–sulfur distances (I, II) than the four-coordinated atom S2 (III–VI). The two shortest metal–sulfur bonds are situated within (I) and outside (V) the dimer, the longest one (IV) being inside. Thus, the structure is a layer polymer.

Potassium is coordinated by six sulfur atoms at the average distance 3.32 Å and by one oxygen atom in the potassium xanthate $KS_2COC_2H_5$.[9] The mean distance is 3.37 Å for another potassium atom, which coordinates to an additional sulfur atom. In the dithioacetate KS_2CCH_3 [10] the average K–S distance for the eight-coordinated metal atom is 3.40 Å. In the dithioformate KS_2CH [11] two independent potassium atoms are each surrounded by eight equivalent sulfur atoms at distances of 3.352 and 3.576 Å.

The layer. Fig. 3 shows how a dimer (shaded) with a centre of symmetry at 0,0,0 is linked to its neighbours. Two dimers at $0, \pm 1, 0$ are each linked by two metal–sulfur bonds, and four at $0, \pm \frac{1}{2}, \pm \frac{1}{2}$ by one bond. By rotations of the shaded area (as indicated in Fig. 3) in every second column, the linkage of four dimers, each by two metal–sulfur bonds, to a central unit is obtained. This layer arrangement is found in the dibutyldithiocarbamates of cesium and thallium.

Acknowledgements. I wish to express by gratitude to Professor Ivar Olovsson for his interest in my work and for the facilities put at my disposal. I am indebted to Dr. Rolf Hesse and Dr. Per Jennische for stimulating discussions. This work has been supported by grants from the Swedish Natural Science Council.

REFERENCES

1. Wahlberg, A. *Acta Chem. Scand. A 30* (1976) 433.
2. Aava, U. and Hesse, R. *Ark. Kemi 30* (1968) 149.
3. Elfwing, E., Anacker-Eickhoff, H., Jennische, P. and Hesse, R. *Acta Chem. Scand. A 30* (1976) 335.
4. Uhlin, A. and Åkerström, S. *Acta Chem. Scand. 25* (1971) 393.
5. Hanson, H. P., Herman, F., Lea, J. D. and Skillman, S. *Acta Crystallogr. 17* (1964) 1040.
6. Cromer, O. T. *Acta Crystallogr. 18* (1965) 17.
7. Lundgren, J.-O. (1974) *Crystallographic Computer Programs* UUIC-B13-4-01, Inst. of Chemistry, Univ. of Uppsala, Sweden.
8. Shannon, R. D. and Prewitt, C. T. *Acta Crystallogr. B 25* (1969) 925.
9. Mazzi, F. and Tadini, C. *Z. Kristallogr. 118* (1963) 378.
10. Borel, M. M. and Ledsert, M. *Z. Anorg. Allg. Chem. 415* (1975) 285.
11. Engler, R., Kiel, G. and Gattow, G. *Z. Anorg. Allg. Chem. 404* (1974) 71.

Received February 24, 1976.

Acta Chemica Scandinavica A 30 (1976) 619—624

Magnetic, Electrical and Thermal Studies of $V_{1-x}Ti_xO_2$ ($0 \leq x \leq 0.06$)

T. HÖRLIN, T. NIKLEWSKI and M. NYGREN

Department of Inorganic Chemistry, Arrhenius Laboratory, University of Stockholm, S-104 05 Stockholm, Sweden

The metal-insulator transition in the $V_{1-x}Ti_xO_2$ system has been studied by NMR, DTA, X-ray diffraction, magnetic susceptibility, and electrical conductivity measurements over extended regions of temperature. Three phases have been shown to exist. A semiconducting VO_2 phase of the M_1 structure exists below a temperature which decreases with increasing Ti content. At temperatures below the transition to the metallic high temperature rutile phase (R) an intermediary phase area exists. This phase is semiconducting and has an almost temperature-independent paramagnetism: it possesses the M_2 type of structure known from the $(V,Cr)O_2$ system. The observed properties of the insulating phases are discussed in terms of a model in which the 3*d* electrons are assumed to be localized on the vanadium atoms, with a Heisenberg exchange coupling between neighbours.

The metal-insulator transition in VO_2 at about 340 K has been subject to considerable interest. The high temperature form is metallic and possesses the rutile structure,[1] named R below. The structure of the low temperature form (hereafter called M_1) is of MoO_2 type,[2] which can be regarded as a monoclinic distortion of the rutile-type structure. In the M_1 structure the V atoms occur in pairs which are tilted somewhat from the c_R axis in such a way that zig-zag chains with alternating shorter and longer V – V distances are formed.

During recent years numerous papers have been published concerning the metal-insulator transition in pure VO_2 and VO_2 doped with various transition elements. Especially the studies of the effects of various dopants have been fertile.

The phase diagrams of the $V_{1-x}Me_xO_2$ systems with Me = W,[3] Mo,[4] Nb,[5] and Re [6] exhibit strong similarities. These metals cause a linear decrease of the $M_1 \rightarrow R$ transition temperature with increasing x value.

Cr, Al and Fe belong to a second class of dopants.[7–10] A partial substitution of any of these metals for V gives rise to a rather complex phase diagram. Besides the R and M_1 phases it displays two more insulating phases; one with a triclinic (T) and one with a monoclinic (M_2) symmetry.

The M_2 structure [7] resembles M_1 in that half of the V atoms form pairs along the c_R direction of the rutile subcell; they are not tilted, however as in the M_1 phase. The other half of the metal atoms are accommodated in zig-zag chains of equally spaced atoms also running parallel with the c_R direction.

The triclinic phase T might be regarded as a transitional phase between M_1 and M_2.[7] Close to the T/M_1 phase boundary the T phase is nearly isostructural with M_1 phase, while near the T/M_2 transition temperature the metal positions in the T phase are close to those in the M_2 phase.

This article reports on X-ray, DTA, NMR, magnetic susceptibility and electrical conductivity studies of the $V_{1-x}Ti_xO_2$ system with $0 \leq x \leq 0.06$. Three phases are observed, namely the M_1 and R phases at low and high temperatures, respectively, and at intermediary temperatures an M_2 phase. In this paper particular attention is paid to the physical properties of M_1 and M_2 phases. The phase relations in and magnetic properties of the entire $VO_2 - TiO_2$ system are presented in a subsequent paper.[11]

EXPERIMENTAL AND RESULTS

Preparation. The starting materials were V_2O_5 (Fisher, Sc.Co., *p.a.*) and TiO_2 (Baker,

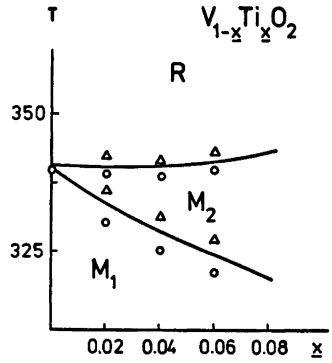

Fig. 1. Transition temperatures plotted *versus* x in $V_{1-x}Ti_xO_2$. The △ and ○ corresponds to data from the heating and cooling, respectively, part of a complete DTA run.

Chem.Co., *p.a.*). VO_2 was prepared by reduction of V_2O_5 at 1275 K. The oxygen equilibrium pressure over V_2O_5 at this temperature is of the order 10^{-3} atmosphere and therefore the reduction proceeded easily as the oxygen was pumped off by an ordinary rotary vacuum-pump. The product was characterized by its X-ray powder pattern and DTA thermogram (see below).

Powder samples of $V_{1-x}Ti_xO_2$ ($0 \leq x \leq 0.06$) were prepared from appropriate mixtures of VO_2 and TiO_2, heated in evacuated silica tubes at 900 °C for 6 days. We observed that slightly oxygen-deficient samples exhibit irregularities of one kind or the other in their DTA thermograms, X-ray patterns and susceptibility curves (see also Refs. 4, 12). The stoichiometry could be reproducibly controlled by addition of a small amount (< 0.5 wt. %) of V_2O_5 to the dioxide mixtures. After the firing, traces of V_2O_5 were found on the walls of the silica tubes. Thus the stoichiometry of the samples should be at the oxygen rich extreme of the dioxide phase area. The accurate position of this phase boundary is not known; however, it is assumed to be close to the true dioxide.

Crystals of Ti-doped VO_2 were prepared by chemical transport reaction techniques using $TeCl_4$ as transporting agent. The method applied has previously been described.[3,4] The transported materials consisted of crystals

Table 1. A summary of experimental results.

x in $V_{1-x}Ti_xO_2$		0.00	0.02	0.04	0.06
Cell parameters at 298 K					
	a (Å)	5.751(± 1)	5.759(± 1)	5.767(± 1)	5.775(± 1)
	b (Å)	4.526(± 1)	4.527(± 1)	4.526(± 1)	4.528(± 1)
	c (Å)	5.382(± 1)	5.381(± 1)	5.384(± 1)	5.385(± 1)
	β (degrees)	122.60(± 1)	122.63(± 1)	122.62(± 1)	122.66(± 1)
Transition temperature (K)	$M_1 \rightarrow M_2$	340 ($M_1 \rightarrow R$)	336	331	326
	$M_2 \rightarrow R$		342	343	344
Latent heat (cal/mol)	$M_1 \rightarrow M_2$	1020[a] ($M_1 \rightarrow R$)	130	126	116
	$M_2 \rightarrow R$		938	886	832
Activation energy just below the transition temp. (eV)	$M_1 \rightarrow M_2$	0.45 ($M_1 \rightarrow R$)	0.38	0.36	
	$M_2 \rightarrow R$		~0.4	~0.4	
Magnetic properties					
$T < 70$	C_{obs} in eqn. (1)	0	0.78×10^{-2}	1.45×10^{-2}	1.73×10^{-2}
	μ_{eff} per Ti atom	–	1.77	1.71	1.52
$T = 338$	$\delta\chi_M$ (emu/mol)	–	1.26×10^{-4}	1.31×10^{-4}	1.17×10^{-4}
Spin exchange coupling constant J (K)		–	410	400	440
ΔH_M (cal/mol)		–	110	110	95

[a] From Ref. 16.

shaped either as octahedra or rectangular rods. The compositions of the crystals were obtained from their cell parameters and also from the transition temperatures. As the DTA thermograms of the starting and transported material and the residue in the hot zone were identical, the DTA measurements on powder samples, which will be described in the following, served to establish the phase diagram necessary for converting a measured transition temperature to a crystal composition.

Phase analysis. DTA studies were performed in the temperature region 100–400 K with an equipment, designed and built at this Institute, which permits simultaneous analysis of five samples.[13]

While pure VO_2 exhibits one DTA peak at 340 K, the Ti substituted material was found to give two peaks. The observed transition temperatures are plotted versus x in $V_{1-x}Ti_xO_2$ in Fig. 1. The DTA curves indicate three phases to be present which can be transformed into one another when the temperature is cycled between 300 and 400 K. The hysteresis was approximately 2 degrees for the transitions at the higher temperature but considerably larger for those at the lower transition temperature, as indicated in the figure.

The X-ray patterns of the powder samples were recorded in a Guinier-Hägg focusing camera, with Cu$K\alpha_1$ radiation ($\lambda = 1.54051$ Å) and KCl as internal standard ($a = 6.2919$ Å). The recording was performed at room temperature and the obtained patterns could be indexed on the basis of the monoclinic unit cell of the M_1 structure. The lattice parameters are given in Table 1. The major effect observed is a slight increase of the a_{M1} axis with increasing content of Ti.

X-Ray powder diffractograms were taken at 355 K of the same samples and the high temperature modification was found to be of the rutile type, R.

The DTA studies indicated that for $x > 0$ in $V_{1-x}Ti_xO_2$ the $M_1 \rightarrow R$ transition takes place *via* an intermediary phase. The X-ray powder diffractogram of the latter phase with $x = 0.06$ could be indexed assuming an orthogonal cell with $a = 12.643$ (± 3) Å, $b = 12.971$ (± 3) Å and $c = 5.807$ (± 1) Å. The NMR data and the magnetic and electrical properties described below suggest that this phase possesses the M_2 type of structure previously found in the $(V,Cr)O_2$ system (see above). (The cell parameters of the monoclinic unit cell are $a = 9.043$ (± 3) Å, $b = 5.801$ (± 1) Å, $c = 4.542$ (± 1) Å and $\beta = 91.44$ (± 3).)

Experimental evidence for the occurrence of an intermediary phase in the $V_{1-x}Ti_xO_2$ system has previously been presented by Umeda *et al.*[14] and by Mitsuishi.[15] They suggested this phase to be triclinic.

The latent heat evolved at the $M_1 \rightarrow R$ transition in VO_2 is 1020 cal/mol.[16] If the DTA peak area is assumed to be proportional to the latent heat, one observed for the $M_2 \rightarrow R$ transition a decrease of the latent heat of the order 36 cal per mol and atomic percent Ti. The latent heats associated with the $M_1 \rightarrow M_2$ transition temperature were found to be about 14 % of the corresponding ones at the higher temperature (see Table 1).

NMR Data. ^{51}V NMR measurements were performed in the temperature interval 100–400 K at the Laboratoire des Physique des Solides, Université Paris-Sud by one of us (M.N.) using a set-up described elsewhere.[7]

The ^{51}V NMR spectra of powder samples of pure VO_2 and of Ti substituted material possessing the M_1 type of structure contained, besides the central line due to the $1/2 \rightarrow -1/2$ transition, the quadrupole satellites due to the $\pm 3/2 \rightarrow \pm 1/2$ transitions of the two principal axes with smallest electrical field gradients, *i.e.* V_{yy} and V_{xx}. Taking $V_{zz} = V_{yy} + V_{xx}$ the following experimental values for the composition $V_{0.96}Ti_{0.04}O_2$ were obtained at room temperature.

$V_{yy} = 121 \pm 3$ kHz $\quad k_y = 0.27 \pm 0.03$ %
$V_{xx} = 365 \pm 4$ kHz $\quad k_x = 0.35 \pm 0.03$ %
$V_{zz} = 486 \pm 5$ kHz

giving a quadrupole frequency $\nu_q = 486$ kHz and anisotropy parameter $\eta = 0.50 \pm 0.02$. K_y and K_x are the Knight shifts in the directions of the respective principal axes. The experimental values given above did not vary with temperature or composition inside the M_1 phase area. Our findings are in agreement with previous NMR results for pure VO_2 [7,14] and for Cr-doped VO_2 possessing the M_1 structure.[7]

As one approaches the $M_1 \rightarrow M_2$ transition temperature the central line starts to broaden. A few degrees below the transition temperature the shape of the central line suggests it to be composed of one narrow line almost unshifted in comparison with its position in M_1 and one negatively shifted, very broad line.

In the region of stability of the M_2 phase the spectrum consists of one central line with nearly the same position as that in M_1 phase and quadrupole satellites with smaller width than observed for the M_1 structure. The intensity of the central line is one half of that observed in the M_1 phase. The following data, representative for all compositions studied, were obtained:

$V_{yy} = 57 \pm 2$ kHz $\quad K_y = 0.29 \pm 0.03$ %
$V_{xx} = 294 \pm 3$ kHz $\quad K_x = 0.35 \pm 0.03$ %
$V_{zz} = 351 \pm 4$ kHz

with $\nu_q = 351$ kHz and $\eta = 0.68 \pm 0.02$, which compares favourably with previous findings for the M_2 phase.[7,14,17]

The NMR spectrum of an M_2 phase should in principle contain two central lines, *viz.* one associated with the vanadium atoms which are paired, the other with the vanadium atoms

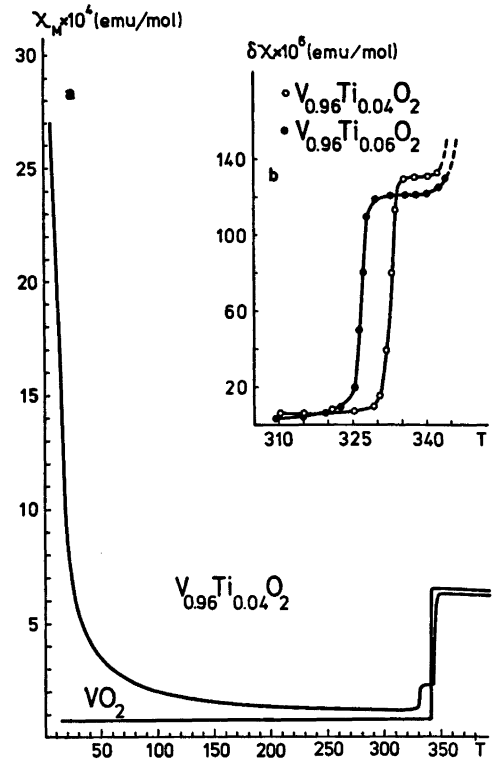

Fig. 2. (a) The molar magnetic susceptibility of VO_2 and Ti-doped VO_2 plotted *versus* the temperature. (b) The remaining susceptibility $\delta\chi_M$, defined according to eqn. 2, plotted *versus* the temperature.

located in the zig-zag chains. Pouget *et al.*[7] report that the latter central line is rather broad for small x values and broadens further for increasing x. The absence of such a line in our spectrum of the M_2 phase is most certainly due to the relatively high Ti content in our samples. The only indication of such a central line is seen close to the $M_1 \rightarrow M_2$ transition temperature.

The intensity of the central line is proportional to the number of V atoms contributing to the NMR line. In the M_1 structure all V atoms are crystallographically equivalent and thus contribute to the intensity of the observed central line. As mentioned above, the observed central line in the M_2 phase area exhibits features very similar to that of the M_1 phase, except that its intensity is only one half of that of the low temperature phase. This agrees with the fact that only half of the number of the V atoms available are paired.

Magnetic susceptibility. Magnetic susceptibility measurements were performed according to the Faraday method in the temperature interval 80 – 400 K. The measurements in the 5 – 100 K region were carried out at the University of Bordeaux by one of us (M.N.).

The molar magnetic susceptibilities of pure VO_2 and of $V_{0.76}Ti_{0.04}O_2$ are given as functions of the temperature in Fig. 2a. The χ_M values are not corrected for the underlying diamagnetism. The monoclinic modification of pure VO_2 is temperature independent paramagnetic ($\chi_M = 65 \times 10^{-6}$ emu/mol). The transition to the rutile structure gives rise to an abrupt increase of the susceptibility to about 10 times the low-temperature value. For $x > 0$ the susceptibility increases with decreasing temperature and at low temperatures ($T < 70$ K) varies according to:

$$\chi_M = \frac{C_{obs}}{T} + \chi_0 \qquad (1)$$

where χ_0 is the susceptibility plateau of pure VO_2. The C_{obs} and corresponding μ_{eff} values are given in Table 1.

ESR studies of Ti-doped VO_2 indicate that the electrons are localized at the V atoms.[18] The agreement between the observed μ_{eff} values and the spin only value of 1.73 μ_B per substituted Ti atom shows that the Ti atoms are not clustered but dispersed.

When one approaches the $M_1 \rightarrow M_2$ transition temperature the temperature dependence of the susceptibility starts to deviate from that given by eqn. 1. The remaining susceptibility, $\delta\chi_M$, defined as

$$\delta\chi_M = \chi_M - \frac{C_{obs}}{T} - \chi_0 \qquad (2)$$

is plotted *versus* the temperature in Fig. 2b. At the $M_1 \rightarrow M_2$ transition temperature $\delta\chi_M$ increases rapidly. In the region of stability of the M_2 phase the $\delta\chi_M$ term is of the order 1.2×10^{-4} emu per mol, approximately independent of temperature and composition (see also Table 1). Our data are in good agreement with previous findings for the M_2 phase in the $(V,Cr)O_2$ and $(V,Al)O_2$ systems.[7,20]

Electrical properties. The conductivity measurements were performed with the four probe technique on rectangular rod-shaped crystals. The logarithm of the conductivity parallel to the c_R direction was continously recorded as a function of the inverse temperature in the temperature range 100 – 400 K.

In Fig. 3 the logarithm of the conductivity is plotted *versus* T^{-1} for pure VO_2 and $V_{0.96}Ti_{0.02}O_2$. The observed data for VO_2 are in good agreement with previous findings.[3,4] The M_1 modification of Ti substituted material exhibits semiconducting properties. Close to the $M_1 \rightarrow M_2$ transition temperature an activation energy of about 0.38 eV for $x = 0.02$ and 0.04 is found compared with 0.45 eV for $x = 0$. The activation energies for both undoped and Ti-doped samples decrease with decreasing

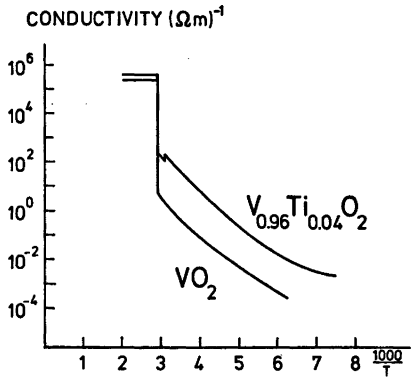

Fig. 3. The logarithm of the conductivity of VO_2 and Ti-doped VO_2 plotted *versus* the inverse temperature.

temperature and more rapidly so for higher x values. This behaviour indicates that impurity conduction dominates at low temperatures, which is in agreement with the findings by Kabashima *et al.*[21]

The conductivity of the M_2 phase is about a factor 0.5 times that of the M_1 phase, while the activation energy appears to be unchanged as seen in Table 1 and Fig. 4. The same figure also illustrates the hysteresis in the $M_1 \rightarrow M_2$ and $M_2 \rightarrow R$ transition temperatures. The crystals showed a tendency to crack when passing the transition temperatures, but the

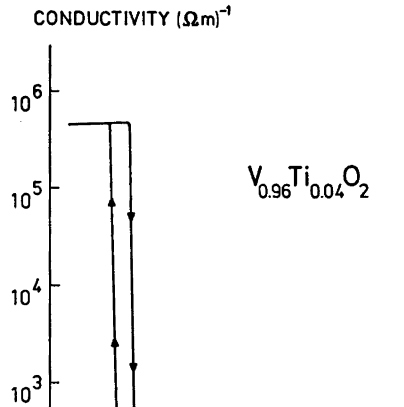

Fig. 4. The logarithm of the conductivity of Ti-doped VO_2 plotted *versus* the inverse temperature close to the $M_1 \rightarrow M_2 \rightarrow R$ transition temperatures.

data presented are from crystals which passed through a complete cycle of heating and cooling without cracking.

Chase [22] has found similar temperature dependence of the conductivity for samples with compositions: $V_{1-x}Ti_xO_2$ with $x = 0.05$, 0.10, 0.15 and 0.20. The reported semiconductor to semiconductor transition temperatures are, however, appreciably higher than ours, while the transition temperatures to the metallic phase are essentially the same.

DISCUSSION

The DTA and X-ray studies of the $V_{1-x}Ti_xO_2$ system presented above revealed a temperature *versus* composition diagram which, besides the M_1 and R phase areas, contained an intermediary phase area. The X-ray powder diffractogram of the latter phase exhibits strong similarities with that of the M_2 phase previously found in the $V_{1-x}Cr_xO_2$, $V_{1-x}Al_xO_2$ and $V_{1-x}Fe_xO_2$ systems.[7-10] Furthermore, a comparison of the magnetic and electrical properties of the intermediary phase of Ti-doped VO_2 with corresponding data for the M_2 phase shows that the two phases most probably are isostructural. The mechanism by which a particular substituent stabilizes the various alternative phases of VO_2 is at present not known. Anyhow, the physical properties of the T and M_2 phases have to be incorporated in any model intended to explain the character of the metal-insulator transition in VO_2.

Several authors have interpreted the $M_1 \rightarrow R$ transition in pure and doped VO_2 in terms of a band model.[23-25] The electrical and magnetic properties of Ti-doped VO_2 possessing the M_1 type of structure reported above might also be elucidated within the framework of such a model.

The NMR data, the magnetic properties and the structural features of M_2 phase of Ti-doped VO_2 suggest the presence of localized 3*d* electrons, and so do the ESR spectra.[19] Since the chains of the paired V atoms are essentially non-magnetic the observed $\delta\chi_M$ values originate from the magnetic moments associated with the equidistant V atoms. The magnitude of the $\delta\chi_M$ values indicates, however, that magnetic interactions between these V atoms have to be present. Following Pouget *et al.*[7] we thus treat these zig-zag chains as a set of noninteracting antiferromagnetic Heisenberg chains with $S = 1/2$.

Bonner and Fisher [27] have calculated the magnetic susceptibility of such a chain. We have determined the spin exchange coupling constants, J, given in Table 1 by fitting our $\delta\chi_M$ values to their data. The magnetic entropy of the M_1 phase is negligible while the magnetic entropy, S_M, of the M_2 phase can be estimated from the calculations by Bonner and Fisher, using the J values given in Table 1. The change in magnetic enthalpy ΔH_M $(=TS_M)$ at the $M_1 \rightarrow M_2$ transition is also given in Table 1.

The change in the lattice latent heat at the $M_1 \rightarrow M_2$ transition, defined as $\Delta H_L = \Delta H_{exp} - \Delta H_M$, is in our case of the same magnitude as that observed for the $T \rightarrow M_2$ transition in the $(V,Cr)O_2$ system.[7] However, in view of the uncertainties in the procedure for obtaining $\delta\chi_M$ and ΔH_M, the only significant conclusion might be that the ΔH_{exp} values do not preclude the possibility of treating the zig-zag chains as antiferromagnetic Heisenberg chains.

The electrical conductivity measurements of Ti-doped VO_2 showed that the activation energies are almost the same in the M_1 and M_2 phases. The insulating M_1, T, and M_2 phases of Cr and Al-doped VO_2 have activation energies of the same order of magnitude.[27] This indicates that the band gap does not originate from the crystal structures of the phases concerned but arises from electron-electron correlation effects.

The magnetic and electrical properties of Ti-doped VO_2 thus support the model proposed by Pouget *et al.*[7] and by Zylbersztejn and Mott [28] which states: (*i*) Pure and doped VO_2 possessing the M_1 type of structure is a borderline case for classical band transport description, and (*ii*) the properties of the M_2 phase cannot be properly described without taking into account the interatomic correlation energy.

Acknowledgements. The authors wish to thank Professor A. Magnéli and Dr. L. Kihlborg for their support of this work.

One of us (M.N.) wishes to express his gratitude to Professor J. P. Friedel and Professor P. Hagenmuller for all facilities placed at his disposal in connection with a research stay in Orsay and Bordeaux.

Drs. J. P. Pouget, H. Launois and G. Villeneuve are thanked for fruitful discussions and invaluable advice in connection with this work.

This investigation has been supported by the Centre National de la Recherche Scientifique and by the Swedish Natural Science Research Council.

REFERENCES

1. Westman, S. *Acta Chem. Scand. 15* (1961) 217.
2. Andersson, G. *Acta Chem. Scand. 10* (1956) 623.
3. Hörlin, T., Niklewski, T. and Nygren, M. *Mater. Res. Bull. 7* (1972) 12.
4. Hörlin, T., Niklewski, T. and Nygren, M. *Mater. Res. Bull. 8* (1973) 179.
5. Villeneuve, G., Bordet, A., Casalot, A., Pouget, J. P., Launois, H. and Lederer, P. *J. Phys. Chem. Solids 33* (1972) 1953.
6. Sävborg, Ö. *Private communication.*
7. Pouget, J. P., Launois, H., Rice, T. M., Dernier, P., Gossard, A., Villeneuve, G. and Hagenmuller, P. *Phys. Rev. B 10* (1974) 1801.
8. Drillon, M. and Villeneuve, G. *Mater. Res. Bull. 9* (1974) 1199.
9. Pollert, E., Villeneuve, G., Ménil, F. and Hagenmuller, P. *Mater. Res. Bull. 11* (1976) 159.
10. Kosuge, K. and Kachi, S. *Mater. Res. Bull. 11* (1976) 255.
11. Hörlin, T., Niklewski, T. and Nygren, M. *To be published.*
12. Hörlin, T., Niklewski, T. and Nygren, M. *Chem. Commun. Univ. Stockholm*, No. 1 (1973).
13. Hörlin, T., Niklewski, T. and Nygren, M. *Chem. Commun. Univ. Stockholm*, No. 9 (1975).
14. Umeda, J.-I., Narita, K. and Kusumotó, H. *Hitachi Rev. 17* (1968) No. 6.
15. Mitsuishi, T. *Jpn. J. Appl. Phys. 6* (1976) 1060.
16. Ryder, E. J., Hsu, F.S.L., Guggenheim, H. J. and Kunzler, J. E. (unpublished): quoted by Berglund, C. N. and Guggenheim, H. J. *Phys. Rev. 185* (1969) 1022.
17. Reyes, J. M., Segel, S. L. and Sayer, M. *J. Solid State Chem. 12* (1975) 298.
18. Goto, T., Nishimura, K., Kabashima, S. and Kawakubo, T. *J. Phys. Soc. Jpn. 28* (1970) 993.
19. D'Haenens, J. P. Quoted in Ref. 28.
20. Villeneuve, G. *Private communication.*
21. Kabashima, S., Goto, T., Nishimura, K. and Kawakubo, T. *J. Phys. Soc. Jpn. 32* (1972) 158.
22. Chase, L. L. *Phys. Lett. 46 A* (1973) 215.
23. Goodenough, J. B. and Hong, H. Y.-P. *Phys. Rev. B 8* (1973) 1323.
24. Hearn, C. J. *J. Phys. C 5* (1972) 1317.
25. Caurthers, E. and Kleinman, L. *Phys. Rev. B 7* (1973) 3760.
26. Bonner, J. and Fisher, M. *Phys. Rev. 135* (1964) 487.
27. Villeneuve, G., Drillon, M., Lannay, J. C., Marquestant, E. and Hagenmuller, P. *Solid State Commun. 17* (1975) 657.
28. Zylbersztejn, A. and Mott, N. *Phys. Rev. B 11* (1975) 4383.

Received February 26, 1976.

Acta Chemica Scandinavica A 30 (1976) 625—633

Conformational Analysis. XII. The Structure of Gaseous 1,3-Dichloropropane, $(CH_2Cl)_2CH_2$, as Determined by Electron Diffraction and Compared with Molecular Mechanics Calculations

SJUR GRINDHEIM [a] and REIDAR STØLEVIK [b]

[a] Department of Chemistry, University of Oslo, Blindern, N-Oslo 3, Norway and [b] Department of Chemistry, University of Trondheim, NLHT, Rosenborg, N-7000 Trondheim, Norway

Gaseous 1,3-dichloropropane has been studied at a nozzle temperature of 38 °C. Three conformers *GG*, *AG* and *AA* were detected. Results are presented with error limits (2σ). The following values for bond lengths (r_g) and bond angles ($\angle_\alpha$) are average parameters for the conformers: r(C−H) = 1.124(12) Å, r(C−C) = 1.531(8) Å, r(C−Cl) = 1.798(6) Å, ∠CCC = 112.9° (1.0), ∠CCCl = 111.6° (0.2). By symmetry *AA* has a staggered conformation, while *AG* and *GG* have torsion angles close to staggered values. The composition at 38 °C is: 73 % (4) of *GG*, 24 % (4) of *AG*, and less than 10 % of *AA*.

An average torsional force constant for the conformers and vibrational frequencies corresponding to the torsional modes have been estimated by combining information from electron diffraction and vibrational spectroscopy. It has been shown that the experimental assignment of low frequencies is most probably wrong.

The conformational energies of the title compound have been compared with the experimentally determined conformational energies of several 1,3-dihalopropanes as well as 1,2,3-trihalopropanes.

This work is part of a systematic conformational study of halogenated propanes by electron diffraction. The title compound is referred to as DCP. Results for 1,3-dibromopropane (DBP) have recently been published.[1] A series of investigations related to these studies are listed in Ref. 2.

Classically the possible number of staggered conformers in DXP is *nine*, as indicated in Fig. 1 of Ref. 1. The four conformers which are distinguishable by vibrational spectroscopy, are characterized as follows:

Conformer	Pointgroup	Symmetry number
XCCCX[*AA*]	C_{2v}	2
X XCCC[*AG*]	C_1	1
X CCC[*GG*] X	C_2	2
CCC[*GG(1:3)*] X X	C_s	1

The classical multiplities [1] of the conformers are 1[*AA*], 4[*AG*], 2[*GG*], and 2[*GG(1:3)*]. The numbering of atoms in *GG* is shown in Fig. 1.

Sheppard *et al.*[3,4] studied 1,3-dihalopropanes and based on ifrared spectra they concluded that DCP crystallized in the *GG* conformation at low temperatures. An extended vibrational spectral study of DCP as liquid, in solution, and in the crystalline state has been published by Klæboe *et al.*[5] They found that the conformers *GG*, *AG*, and *AA* were present in the liquid.

CALCULATION OF STRUCTURAL PARAMETERS, CONFORMATIONAL ENERGIES, TORSIONAL BARRIERS, AND TORSIONAL FORCE CONSTANTS

The semi-empirical energy model corresponds to simple molecular-mechanics calculations, including atom-atom potentials and valence force constants, as described in Ref. 6. Energy parameters were taken from the work of Abraham and Parry.[7] The diagonal force constants in Table 5 were used.

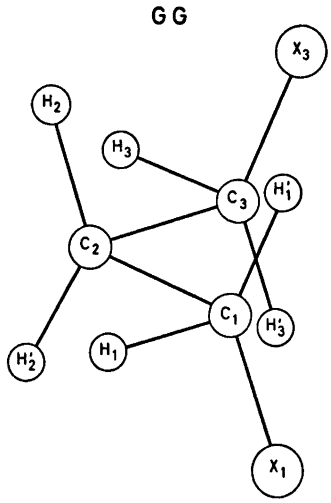

Fig. 1. The numbering of atoms in the *GG* conformer of 1,3-dichloropropane.

The parameter values in Table 1 correspond to the minima found by minimizing the energy. *GG* and *AG* have nearly staggered conformations, while *AA* is exactly staggered and *GG(1:3)* is far from staggered.

According to the calculated conformational energies of Table 2, *AA* is the energetically most stable conformer. Zero-point vibrational energies for the conformers have not been included.

Torsional barriers between the conformers are shown in Table 3. Each energy value has been obtained by adjusting all geometry variables except for the values of ϕ_{1-2} being 60 and 180°, and ϕ_{2-3} being ± 60 and ± 180°. Such values of the torsion angles correspond to (1:2) eclipsed conformations.

The barrier for the transition *anti-gauche* in propyl chloride [8] is 2.78 kcal/mol,* while the *gauche-gauche* barrier corresponds to 2.96 kcal/mol. The calculated barrier for the transition *AA-AG* in DCP is 3.9 kcal/mol, and the fact that this barrier is higher than those in propyl chloride seems reasonable. However, the calculated barrier of 6.5 kcal/mol, corre-

* 1 kcal = 4.184 kJ.

Table 1. Calculated structural parameters in the stable conformers of 1,3-dichloropropane.

Parameter r (Å), ∠(°)	"Normal" value	*AA*	*AG*	*GG*	*GG(1:3)*
r(C–H)	1.094	1.095	1.095	1.095	1.095
r(C–C)	1.513	1.523	1.526	1.529	1.530
r(C–X)	1.760	1.765	1.766	1.767	1.767
∠CCC	110.0	110.2	112.3	114.3	114.1
∠CCX	109.47	110.6	111.0	111.3	112.6
$\angle C_1C_2H$	109.47	109.7	109.8	109.9	109.4
$\angle C_2C_1H$	109.47	109.4	109.1	108.8	108.9
$\angle\phi_{1-2}$	–[a]	0.0	+112.5	+113.3	−100.7
$\angle\phi_{2-3}$	–[a]	0.0	+4.1	+113.3	+100.7

[a] Values (ϕ_{1-2}, ϕ_{2-3}) for exactly staggered conformations are: *AA* (0°, 0°), *AG* (120°, 0°), *GG* (120°, 120°), and (−120°, 120°) for *GG(1:3)*.

Table 2. Conformational energies (kcal/mol) for 1,3-dichloropropane.

Type of energy	*AA*	*AG*	*GG*	*GG(1:3)*
E (bonded)	0.188	0.594	1.103	2.579
E (van der Waals)	1.508	1.764	1.860	1.865
E (polar: X···H)	−5.973	−6.185	−6.313	−5.865
E (polar: X···X)	1.450	1.617	1.858	2.320
E (total) − E (*AA*)	0.0	0.62	1.33	3.72

Table 3. Torsional barriers (kcal/mol) between conformers of 1,3-dichloropropane.

ϕ_{1-2} / ϕ_{2-3}	0°	60°	120°	180°
180°	6.5	14.0	8.7	26.4
120°	0.6(*AG*)	4.2	1.3(*GG*)	8.7
60°	3.9	8.2	4.2	14.0
0°	0.0(*AA*)	3.9	0.6(*AG*)	6.5
−60°	3.9	8.5	4.6	14.0
−120°	0.6(*AG*)	4.6	3.7[*GG*(1:3)]	8.7
−180°	6.5	14.0	8.7	26.4

sponding to the transition *AG*-*AG*, seems unreasonably high.

Clearly *AA*, *AG* and *GG* correspond to well defined minima of the potential energy, while the conformer *GG(1:3)* corresponds to a rather shallow minimum. The barrier height is less than 1 kcal/mol for the transition *GG(1:3)* – *AG*.

The torsional force constants of Table 4 were calculated at the conformational minima. It is noteworthy that the magnitude of the interaction constant ($F_{\phi\phi'}$) is quite small for all three conformers.

CALCULATION OF VIBRATIONAL QUANTITIES

Valence force constants, except for the torsional part, were taken from works of Schachtschneider [9] and Snyder.[10] The final force-constant values used in this work are shown in Table 5. An average torsional force constant has been adjusted to fit the experimental intensities. The normal-coordinate program described by Gwinn [11] was used in computing vibrational frequencies. The fit between observed spectroscopic frequencies [12] and those calculated is shown in Table 6. If the torsional modes are not included, the average relative deviation between observed and calculated frequencies is *ca.* 2 %. Keeping in mind that the non-torsional force constants were not adjusted, the fit is very good for non-torsional

Table 4. Calculated torsional force constants (F_ϕ) in conformers of 1,3-dichloropropane. The values were *numerically* computed according to the definitions given.

[mdyn Å (rad)$^{-2}$]	*AA*	*AG*	*GG*
$F_\phi(1-2)=\partial^2E/\partial\phi^2_{1-2}$	0.125	0.167	0.168
$F_\phi(2-3)=\partial^2E/\partial\phi^2_{2-3}$	0.125	0.126	0.168
$F_{\phi\phi'}=\delta^2E/\partial_{1-2}\partial\phi_{2-3}$	−0.010	−0.043	−0.062

Table 5. Valence force constants for 1,3-dichloropropane.

Stretch (mdyn/Å)
C–C: 4.57
C–X: 3.18
C–H: 4.85 (in C–CH_2X)
C–H: 4.55 (in >CH_2)

Stretch/bend (mdyn/rad)
C–X/CCX: 0.73 (C–X common)
C–X/HCX: 0.33 (C–X common)
C–C/CCC: 0.35 (C–X common)
C–C/CCX: 0.29 (C–C common)
C–C/CCH: 0.26 (C–C common)

Bend/bend [mdyn Å (rad)$^{-2}$]
CCC/CCH: −0.124 (C–C common)
CCH/HCX: 0.105 (in C–CH_2X)
HCX/HCX: 0.097 (in C–CH_2X)

Bend [mdyn Å (rad)$^{-2}$]
CCC: 0.90
CCH: 0.68 (in C–CH_2X)
CCH: 0.67 (in >CH_2)
CCX: 1.17
HCH: 0.45 (in C–CH_2X)
HCH: 0.55 (in >CH_2)
HCX: 0.79

Stretch/stretch (mdyn/Å)
C–C/C–X: 0.730 (C–C common)
C–C/C–C: 0.064 (C–C common)

Torsion [mdyn Å (rad)$^{-2}$]
F_ϕ = 0.17 (all conformers;
$F_\phi = F_\phi(1-2) = F_\phi(2-3)$ and
$F_{\phi\phi'} = 0$).

Table 6. Vibrational frequencies (cm^{-1}) in 1,3-dichloropropane. Observed values are given in parentheses.[12]

Approximate mode	*GG*	*AG*	*AA*
Asym. torsion (ω_1)	60(190)	114	148
Sym. torsion (ω_2)	145(180)	89	116
CCX-bend (ω_3)	225(348)	259	143
CCX-bend (ω_4)	387(362)	285	386
CCC-bend	466(457)	442(431)	307(372)
Asym. C–X	656(641)	668(656)	685(697)
Sym. C–X	680(679)	736(727)	783(780)
CH_2-rock	839(861)	829(793)	807(793)
CH_2-rock	888(867)	901	897
CH_2-rock	992(967)	986	1017
Sym. C–C	1034(1001)	1049(1034)	1061(1034)
Asym. C–C	1034(1077)	1026	1012(1064)
CH_2-twist	1139(1150)	1143	1127(1135)
CH_2-twist	1154(1194)	1155	1165
CH_2-twist	1249(1280)	1254	1259
CH_2-wag	1276(1258)	1282	1285(1270)
CH_2-wag	1297(1316)	1312	1328
CH_2-wag	1388(1357)	1373(1352)	1357(1352)
CH_2-scissor	1436(1421)	1437	1435
CH_2-scissor	1440(1443)	1439	1438
CH_2-scissor	1479(1455)	1482	1485
C–H stretch	2860(2868)	2860	2861
C–H stretch	2915(2918)	2914(2925)	2914(2925)
C–H stretch	2959(2941)	2960(2953)	2960(2953)
C–H stretch	2960(2967)	2960(2953)	2960(2953)
C–H stretch	2998(3001)	2999	2999
C–H stretch	3000(3001)	2999	2999

Table 7. Mean amplitudes of vibration (u) and K values for the *GG* conformer of 1,3-dichloropropane, at 38 °C. The range of values have been indicated [u(C–H): 0.078–92].

Type of dist. (r)	r (Å)	u (Å)	K (Å)
C–H	1.095	0.078-92	0.017-25
C–C	1.529	0.0518	0.0050
C–X (X=Cl)	1.767	0.0530	0.0158
$C_2\cdots X_1$	2.725	0.0712	0.0094
$C_2\cdots H_1'$	2.163	0.1080	0.0162
$C_1\cdots C_3$	2.569	0.0698	0.0042
$C_1\cdots H_2$	2.149	0.1079	0.0123
$X_1\cdots H_1'$	2.353	0.1087	0.0291
H···H	1.76-8	0.127-8	0.021-35
$X_1\cdots X_3$	4.218	0.2745	0.0001
$C_1\cdots X_3$ (*gauche*)	3.268	0.1556	0.0065
$X_1\cdots H_2$ (*anti*)	3.678	0.1041	0.0109
$X_1\cdots H_2'$ (*gauche*)	2.863	0.1659	0.0122
$X_1\cdots H_3'$	2.824	0.2498	0.0199
$X_1\cdots H_3$	4.179	0.1799	0.0850

modes, except for the observed value[12] ω_3 = 348 cm^{-1} which was assigned[12] to the lowest CCX-bending mode within the *GG* conformer. The calculated value is 225 cm^{-1}. The force constants would have to be changed drastically in order to fit this assignment. In Table 1 of Ref. 12 several values in the range 215–221 cm^{-1} have been assigned as CCX-bending modes. Could not a reassignment remove the large discrepancy on this point?

Mean amplitudes of vibration (u) and perpendicular amplitude correction coefficients (K) were computed as described in Ref. 13. K and u values for internuclear distances are found in Table 7. Some of these quantities are quite sensitive to the values of the torsional force constants. In Table 8 are shown values of vibrational quantities corresponding to different values of the average diagonal torsional force constant. The force constant $F_\phi = 0.17$ mdyn Å $(rad)^{-2}$ corresponds to the best value as estimated from the electron diffraction data.

Table 8. Vibrational quantities in 1,3-dichloropropane. (Torsional interaction force constant $F_{\phi\phi'}=0$.)

Torsional force constant			
$F_\phi(1-2)=F_\phi(2-3)=F_\phi$[mdyn Å (rad)$^{-2}$]	0.13	0.17	0.27
Mean amplitudes, u (Å) at 38 °C, for the $X_1\cdots X_3$ distance in			
conformer *AA*	0.101	0.101	0.101
conformer *AG*	0.164	0.160	0.144
conformer *GG*	0.289	0.275	0.222
Torsional frequencies (cm^{-1}) for the conformer *GG*			
asym. mode (ω_1)	57	60	76
sym. mode (ω_2)	139	145	174

EXPERIMENTAL AND DATA REDUCTION

A commercial sample of DCP was obtained from FLUKA. The purity of the sample which was used was better than 99 %.

Electron-density photographs were made at a nozzle temperature of 38 °C in the Balzer[14] apparatus[15] under conditions summarized below.

Nozzle-to-plate distance (mm)	579.7	189.7
Electron wave length (Å)	0.05852	0.05857
Number of plates	4	5
Range of data, in s (Å^{-1})	1.25 – 13.25	6.0 – 39.5
Data interval, Δs (Å^{-1})	0.125	0.25
Uncertainty in s-scale (%)	0.14	0.14

The electron wave length was determined by calibration against ZnO, and benzene. The data were reduced in the usual way[16] to yield an intensity curve for each plate. Average curves for each set of distances were formed. A composite curve was then made by connecting the two average curves after scaling. The final experimental intensity curve is shown in Fig. 2. The intensities have been modified by $s/|f'_{Cl}|^2$.

Scattering amplitudes were calculated by the partial-wave method[17] using Hartree-Fock atomic potentials.[18]

The radial distribution (RD) curve, obtained by Fourier transformation[16] of the final experimental intensity, is presented in Fig. 3.

STRUCTURE ANALYSIS

Radial distribution (RD) curves for the conformers and the final experimental curve are shown in Fig. 4. The conformers *GG* and *AG* are clearly present in considerable amounts, and *GG* is the most abundant conformer. The small peak in the experimental RD curve at *ca.* 5.5 Å might correspond to a small contribution from the conformer *AA*. Approximate composition parameters (α) were estimated from the RD curves: $\alpha(GG)\simeq 70$ %, $\alpha(AG)\simeq 25$ %, and $\alpha(AA)\simeq 5$ %.

According to the calculated energy values in Table 2, *GG(1:3)* is *ca.* 4 kcal/mol less stable than *AA*. If the semi-empirical results are

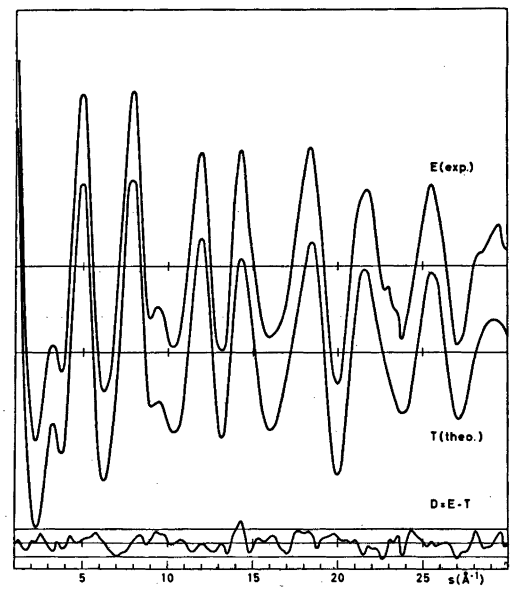

Fig. 2. Experimental (E) and theoretical (T) intensity curves for 1,3-dichloropropane at 38 °C, and D = E – T, corresponding to the final least-squares parameters. The straight lines give the experimental uncertainties (± 3 times experimental standard deviation).

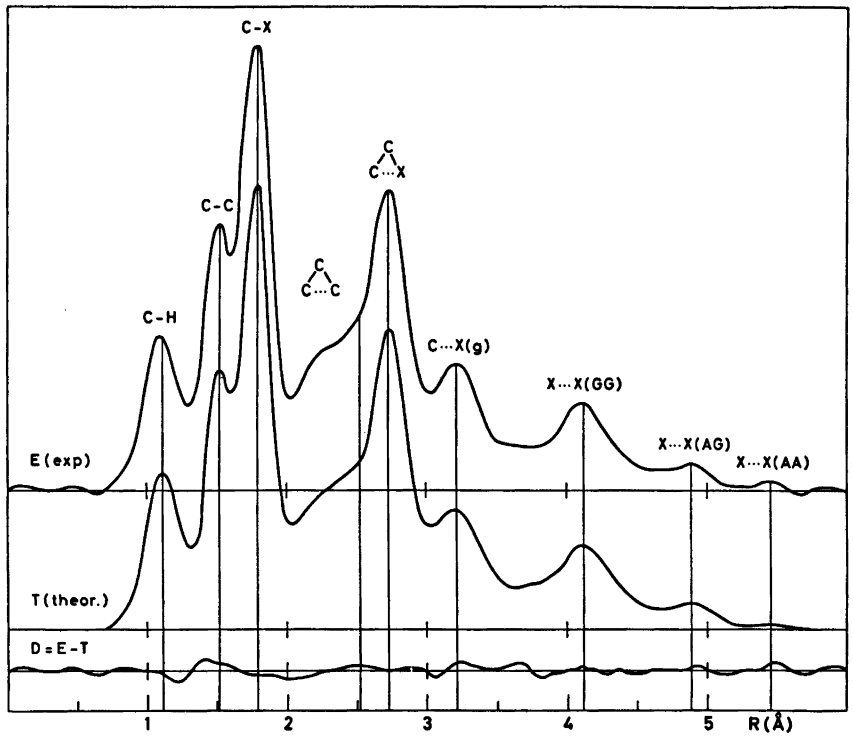

Fig. 3. Experimental (E) and theoretical (T) radial distribution curves for 1,3-dichloropropane at 38 °C, and D = E − T. The curves were calculated from the intensities in Fig. 2 with an artificial damping constant of 0.002 Å².

approximately correct, the percentage of *GG(1:3)* has to be very small (< 1 %).

Least-squares refinements

In calculating theoretical intensities for the least-squares refinements,[16] it was decided not to include a contribution from the *GG(1:3)* conformer. The least-squares program is a modified version of the program explained in Ref. 16. Models for the conformers were constructed as explained in Ref. 1. The models were defined in terms of the following average parameters: r(C−H), r(C−C), r(C−X), ∠CCC, ∠CCX, ∠C_2CH, ∠CC_2H, ϕ_{1-2}, ϕ_{2-3}, and ∠(HC_1H')* which is the projection of the HC_1H' angle on a plane perpendicular to the C_2-C_1 axes. Also adjusted were the composition parameters $\alpha(GG)$ and $\alpha(AG)$ with $\alpha(AA) = 100-\alpha(GG)-\alpha(AG)$. Non-bonded distances were computed as dependant parameters, restricted under the constraints of geometrically consistent r_α parameters.[19,20]

Determination of the torsional force constant

The torsional modes of vibration contribute substantially to the mean amplitudes of several internuclear distances in a molecule like DCP. Since a reasonable force field was known, except for the torsional part, torsional force constants can be adjusted to fit the electron diffraction data. Determination of all torsional force constants is not possible. However, an average value (F_ϕ) for the conformers, assuming $F_\phi(1-2) = F_\phi(2-3) = F_\phi$, were estimated as follows. K and u values were computed for several values of F_ϕ and then included in the least-squares refinements. The structure and composition parameters were adjusted for each new value of F_ϕ. The best fit between theoretical

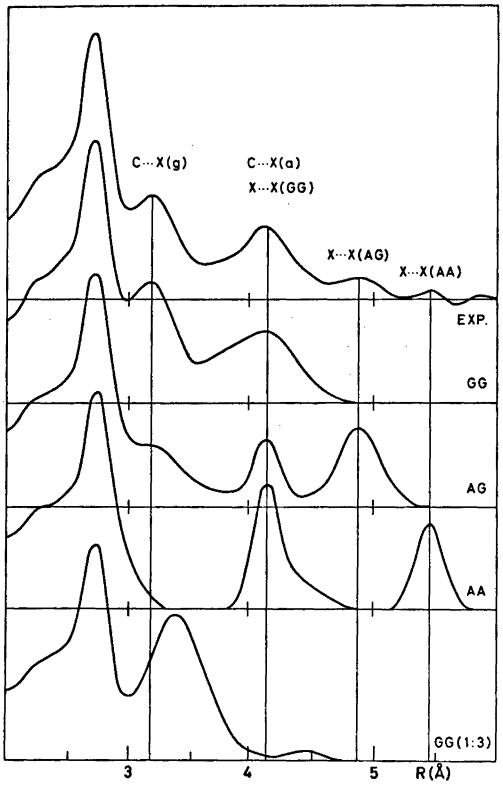

Fig. 4. Radial distribution curves for conformers of 1,3-dichloropropane at 38 °C. Theoretical curves for the conformers *GG*, *AG*, *AA* and *GG(1:3)* are shown together with the final experimental curve. (Damping constant equal to 0.002 Å².)

and experimental intensities was obtained for $F_\phi = 0.17$ mdyn Å (rad)$^{-2}$, with error limits of *ca.* 30 %. The error limits are subjective to a certain degree and do not allow for *systematic* [21] errors. The average experimental F_ϕ value (0.17) is in excellent agreement with the calculated F_ϕ value (0.168) of the *GG* conformer. The calculated average F_ϕ value (0.146) for the *AG* conformer also agrees with the experimental value. The calculated F_ϕ value (0.125) for the *AA* conformer is indirectly supported by the good agreement found for *GG* and *AG*.

In spite of the fact that the torsional interaction constant $F_{\phi\phi'}$ has not been determined in this work, the calculated values of Table 4 are indirectly supported by the agreement found for the diagonal force constants.

FINAL RESULTS

Parameters from the final least-squares refinements [16] and standard deviations (σ) corrected for correlation in the experimental data [22] are given. In the final refinements, intensities beyond $s = 30.0$ Å^{-1} were not included. Using a diagonal weight matrix, all intensities were given equal weight.

Bond lengths and bond angles are found in Table 9. The uncertainty in the s-scale (0.14 %) has been included in the standard deviations for bond lengths.

Composition parameters and torsion angles are found in Table 10. The three torsion angles $\phi_{1-2}(AG)$, $\phi_{2-3}(AG)$, and $\phi_{1-2}(GG) = \phi_{2-3}(GG)$ were not refined independently. However, a common deviation parameter (ϕ_0) was refined. The relationship between ϕ_0 and the torsion angles are given in Table 10. The value of ϕ_0

Table 9. Average bond lengths and bond angles in the conformers of 1,3-dichloropropane. Standard deviations are given in parenthesis (X = Cl).

Bond lengths (r_a in Å)	Bond angle ($\angle_\alpha$ in deg.)
	$\angle$CCC = 112.9(0.5)
	$\angle$CCX = 111.6(0.1)
	$\angle C_1C_2H = 108.8(-)$ [a]
r(C−C) = 1.529(4)	$\angle C_2C_1H = 109.9(-)$ [a]
	$\angle HC_1X = 107.8(0.1)$ [b]
	$\angle HC_1H = 108.3(0.1)$ [b]
r(C−X) = 1.796(3)	$\angle HC_2H = 108.0(0.7)$ [b]
	$\angle(HC_1H')^* = 120.0$ [c]

[a] Calculated value for *GG* (Table 1). [b] Dependent parameter. [c] Assumed value.

Table 10. Composition parameters (α) and torsion angles (ϕ) for 1,3-dichloropropane, with standard deviations in parentheses.

Conformer	*GG*	*AG*	*AA*
α (in %)	73(2)	24(2)	3(3)[a]
ϕ_{1-2} (in deg.)	114.2(0.6)[b]	114.2(0.6)[c]	0(−)[d]
ϕ_{2-3} (in deg.)	114.2(0.6)[b]	5.8(0.6)[c]	0(−)[d]

[a] $\alpha(AA) = 100 - \alpha(GG) - \alpha(AG)$. [b] $\phi_{1-3} = \phi_{2-3} = 120 - \phi_0$. [c] $\phi_{1-2} = 120 - \phi_0$ and $\phi_{2-3} = \phi_0$, ϕ_0 was refined. [d] Assumed value.

is a measure of the deviation from staggered conformations, and the value 5.8° for this parameter is significantly different from 0°. Moreover, calculated values of torsion angles in Table 1 agree with experimental values of Table 10.

An attempt to refine the torsion angles of *GG* and *AG* independently led to the same value of $\phi(GG)$, however, unreasonable values for $\phi_{1-2}(AG)$ and $\phi_{2-3}(AG)$ were obtained with standard deviations six times as large as those reported in Table 10.

As final u and K values are reported those of Table 7 corresponding to the value 0.17 mdyn Å $(\text{rad})^{-2}$ for the torsional force constant. These u values are consistent with the electron-diffraction data.

The following parameter correlation coefficients (ϱ) had $|\varrho| > 0.4$: $\varrho(\text{C}-\text{C}/\angle\text{CCX}) = -0.56$, $\varrho(\phi_0/\angle\text{CCC}) = -0.79$, $\varrho[\alpha(AG)/\alpha(GG)] = -0.77$.

DISCUSSION

The percentages α^* and α of two conformers in equilibrium in the gas phase are related to the expression for the equilibrium constant, as given in eqn. (1):

$$\alpha^*/\alpha = q(M^*/M)\exp(-\Delta E^{\text{m}}/RT) \qquad (1)$$

If Q^{vib} is the vibrational partition function of a conformer referred to the potential-energy minimum of that conformer, then $q = (Q^*/Q)^{\text{vib}}$. $\Delta E^{\text{m}} = E^* - E$ is the potential-energy difference between the two conformers. The difference ΔE^{m} is measured between energy minima. The vibrational energy is included in the quantity Q^{vib}. R and T have their usual meanings. The classical multiplicities [1] of the conformers are: $M(AA) = 1$, $M(AG) = 4$, and $M(GG) = 2$.

If the quantities Q^{vib} are known, then ΔE^{m} may be computed from eqn. (1). Conversely, if the quantity ΔE^{m} is known the q value may be calculated. In eqn. (1) it is assumed that the classical rotational partition functions of the conformers are equal, and that is very nearly true for the conformers *AA*, *AG* and *GG*.

According to the semi-empirical energy model, *AA* is the conformer of lowest minimum energy, while *GG* and *AG* are 1.3 and 0.6 kcal/mol less stable than *AA*, respectively. If the values ΔE^{m} $(AA - GG) = 1.3$ kcal/mol and ΔE^{m} $(AG - GG) = -0.7$ kcal/mol are accepted then the quantities $q(AA/GG)$ and $q(AG/GG)$ have to be quite different from 1.0. On the other hand, if the conformers have equal Q^{vib} values then ΔE^{m} $(AA - GG) = +1.5$ kcal/mol and ΔE^{m} $(AG - GG) = +1.1$ kcal/mol, with *GG* the energetically most stable conformer.

The conformational force fields have to be very different in order that ΔE^{m} $(AG - GG) = -0.7$ kcal/mol. The value of $q(AG/GG)$ would then have to be equal to 0.05. A complete set of reliable experimental vibrational frequencies for each conformer does not exist. However, most probably, the conformational difference in force fields are due to different torsional force constants. If the calculated torsional force constants of Table 4 and the remaining force field of Table 5 are used then $q(AG/GG) = 1.2$ as calculated from the vibrational frequencies. Using equal force constants for the conformers the quantity $q(AG/GG) \approx 1.1$. Thus it seems quite improbable that any reasonable combination of torsional force constants could lead to the very low value 0.05 for $q(AG/GG)$.

As the q values remain unknown at present, the values $q(AA/GG) = q(AG/GG) = 1$ are assumed. The best estimates for the conformational energies are then: ΔE^{m} $(AG - GG) = 1.1 \pm 0.2$ kcal/mol, and ΔE^{m} $(AA - GG) \geq 1.5$ kcal/mol. The last value has to be very uncertain. The percentage of *AA* was 3 % with a formal standard deviation of 3 % which means that only a lower limit of ΔE^{m} $(AA - GG)$ can be estimated.

The conformational energy of *GG(1:3)* remains unknown. However, according to the calculated values of Table 2 this conformer is 3.7 kcal/mol less stable than *AA*, and 2.4 kcal/mol less stable than *GG*. The fact that the fit between calculated and experimental intensities is good does not exclude a small percentage of *GG(1:3)* at the present temperature.

Experimentally determined conformational energies for 1,3-dihalopropanes and 1,2,3-trihalopropanes have been summarized below. The energy values relative to the most stable *GG* conformer are given in kcal/mol.

1,3-Dihalopropanes	X = Cl	X = Br (Ref. 1)
AA: XCCCX	1.5	1.6

AG: XCCCX	1.1	0.9
GG: CCCX X	0	0

1,2,3-Trihalopropanes	X = Cl (Ref. 23)	X = Br (Ref. 6)
AG: XCCCX	0.7	1.5
GG: CCCX X	0	0

For 1,3-dichloro-2,2-dimethylpropane [24] the energy values are 0, 1.1, and 1.3 kcal/mol for the conformers *GG*, *AG*, and *AA*, respectively. In calculating these values it was assumed that conformers of the same molecule have equal vibrational partition functions ($q = 1$). All molecules were studied by electron diffraction, and further details about the conformational equilibria in the gas phase are found in Refs. 1, 6, 23, and 24.

In conclusion, it has been established that for all of these halopropanes, the near-staggered *GG* conformer with nearly parallel C_1-X and C_3-H bonds are more stable than any other conformer in the gas phase.

The extra stability of this type of *GG* conformation awaits a theoretical explanation, which can hardly be obtained quantitatively by simple molecular mechanics calculations, nor by any straightforward modification of such calculations.

The average torsional force constants for 1,3-dihalopropanes (X = Cl, Br) are 0.17 (Cl) and 0.24 (Br) [1] mdyn Å (rad)$^{-2}$, and for 1,2,3-trihalopropanes (X = Cl, Br) the values are 0.25 (Cl) [23] and 0.30 (Br) [6] mdyn Å (rad)$^{-2}$. The value 0.17 mdyn Å (rad)$^{-2}$, as determined in this work, also is reasonable compared to the larger values for the remaining compounds. The final adjustment of force constants for these compounds ought to take into account the information derived from electron-diffraction data.

REFERENCES

1. Farup, P. E. and Stølevik, R. *Acta Chem. Scand. A 28* (1974) 680.
2. Fernholt, L. and Stølevik, R. *Acta Chem. Scand. A 29* (1975) 651.
3. Brown, J. K. and Sheppard, N. *Proc. R. Soc. London A 231* (1955) 555.
4. Dempster, A. B., Price, K. and Sheppard, N. *Spectrochim. Acta Part A 25* (1969) 1381.
5. Thorbjørnsrud, J., Ellestad, O. H., Klæboe, P. and Torgrimsen, T. *J. Mol. Struct. 15* (1973) 61.
6. Stølevik, R. *Acta Chem. Scand. A 28* (1974) 299.
7. Abraham, R. J. and Parry, K. J. *J. Chem. Soc. B* (1970) 539.
8. Radcliffe, K. and Wood, J. L. *Trans. Faraday Soc. 62* (1966) 1678.
9. Schachtschneider, J. H. and Snyder, R. G. *Vibrational Analyses of Polyatomic Molecules, IV*. Project No. 31450, Technical Report No. 122-63 of Shell Development Company.
10. Snyder, R. G. *J. Mol. Spectrosc. 28* (1960) 273.
11. Gwinn, W. D. *J. Chem. Phys. 55* (1971) 477.
12. Thorbjørnsrud, J., Ellestad, O. H., Klæboe, P. and Torgrimsen, T. *J. Mol. Struct. 15* (1973) 61.
13. Stølevik, R., Seip, H. M. and Cyvin, S. J. *Chem. Phys. Lett. 15* (1972) 263.
14. Zeil, W., Haase, J. and Wegmann, L. *Z. Instrumentenk. 74* (1966) 84.
15. Bastiansen, O., Graber, R. and Wegmann, L. *Balzer's High Vacuum Report 25* (1969) 1.
16. Andersen, B., Seip, H. M., Strand, T. G. and Stølevik, R. *Acta Chem. Scand. 23* (1969) 3224.
17. Peacher, J. and Willis, J. C. *J. Chem. Phys. 46* (1967) 4809.
18. Strand, T. G. and Bonham, R. A. *J. Chem. Phys. 40* (1964) 1668.
19. Morino, Y., Kuchitsu, K. and Oka, T. *J. Chem. Phys. 36* (1962) 1108.
20. Kuchitsu, K. *J. Chem. Phys. 49* (1968) 4456.
21. Fernholt, L. and Stølevik, R. *Acta Chem. Scand. A 28* (1974) 935.
22. Seip, H. M. and Stølevik, R. In Cyvin, S. J., Ed., *Molecular Structures and Vibrations*, Elsevier, Amsterdam 1972.
23. Farup, P. E. and Stølevik, R. *Acta Chem. Scand. A 28* (1974) 871.
24. Stølevik, R. *Acta Chem. Scand. A 28* (1974) 455.

Received March 10, 1976.

Acta Chemica Scandinavica A 30 (1976) 634—640

Reinvestigation of the Molecular Structure of *N,N*-Dimethyl Sulfamoyl Chloride by Electron Diffraction

I. HARGITTAI [a] and J. BRUNVOLL [b]

[a] Central Research Institute for Chemistry, Hungarian Academy of Sciences, H-1088 Budapest, Puskin utca 11—13, Hungary and [b] Division of Physical Chemistry, The University of Trondheim, N-7034 Trondheim-NTH, Norway

An electron diffraction reinvestigation of *N,N*-dimethyl sulfamoyl chloride confirmed the conformation with C_s symmetry in which the N–C bonds stagger the S–Cl bond. The geometric parameters determined include: S–Cl 2.064 ± 0.005 Å, S–O 1.421 ± 0.004 Å, S–N 1.618 ± 0.005 Å C–N 1.481 ± 0.012 Å, C–H 1.096 ± 0.010 Å, N–S–Cl 103.0 ± 0.5°, N–S–O 108.8 ± 1.4°, O–S–O 122.7 ± 2.3°, S–N–C 115.8 ± 0.7°, C–N–C 114.6 ± 2.2°. Some geometrical variations in the molecular structures of simple sulfone molecules are discussed.

In the course of our structural studies on molecules containing S–N bond on one hand and sulfone group on the other, a number of compounds have recently been investigated employing electron diffraction.[1–8] The variations in the geometrical configurations of the sulfur bonds showed interesting trends that were interpreted involving both the VSEPR model and non-bonded interactions [9,7,4] (see also comparisons of simple sulfoxides and sulfones [10,11]).

The molecular geometry of *N,N*-dimethyl sulfamoyl chloride, $(CH_3)_2NSO_2Cl$, has also been investigated earlier [12] by electron diffraction. As the determination of the geometrical parameters suffered from severe approximations, it was decided to perform a reinvestigation.

EXPERIMENTAL

The sample of *N,N*-dimethyl sulfamoyl chloride used in this investigation was prepared by E. Páldi.[13] The purity of the sample was confirmed by mass spectrometry. The electron diffractions patterns were taken with the Budapest apparatus,[14,15] a modified EG-100A unit, with essentially the same technique as in some of the other studies mentioned above.[4,6,7] The temperature of the nozzle of the so-called membrane nozzle system [14] was about 105 °C during the exposures. The wavelength of the electron beam was determined from the diffraction pattern of thallium(I) chloride. The ranges of intensity data used were $1.75 \leqq s \leqq 12.50$ Å^{-1} and $7.25 \leqq s \leqq 31.25$ Å^{-1} with $\Delta s = 0.25$ Å^{-1}. The experimental molecular intensities corresponding to the two camera ranges were obtained as before.[4,6,7] The scaled and averaged molecular intensities, $sM^E(s)$, are shown in Fig. 1.

STRUCTURE ANALYSIS

Most of the calculations were performed for conformer I that was earlier established,[12] however, conformers II and III (see Fig. 2) have also been tested. Forms I and III have C_s symmetry (angle of rotation around the S–N bond, $\tau = 0$ and 180°, respectively), form II has no symmetry ($\tau = 120°$ was tested only). The following independent geometrical parameters were chosen; bond distances r(S–Cl), r(S–O), r(S–N), r(C–N), r(C–H), non-bond distance r(O···O),* and bond angles N–S–Cl, N–S–O, S–N–C, C–N–C, N–C–H.**

Spectroscopic calculations were used to obtain the mean parallel amplitudes of vibration (l values). An approximate force field was constructed by means of results from trimethyl-

* For reasons explained later.

** The CH_3 groups were assumed to have local C_{3v} symmetry. A plane through $H_7C_{10}N$ was assumed to halve the C_{11}–N–S angle and a plane through $H_8C_{11}N$ to halve the C_{10}–N–S angle.

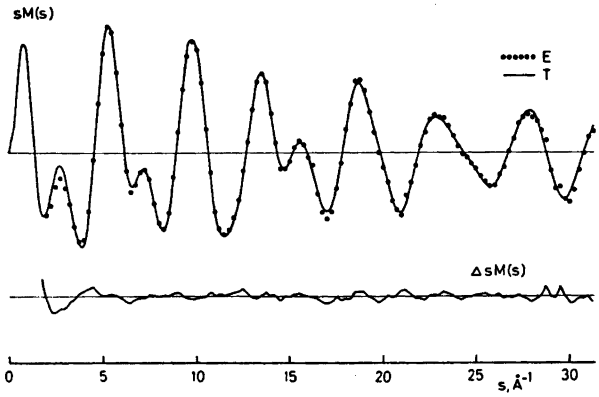

Fig. 1. Molecular intensities. E, experimental; T, theoretical calculated for conformer I with the parameters given in Tables 1 and 2.

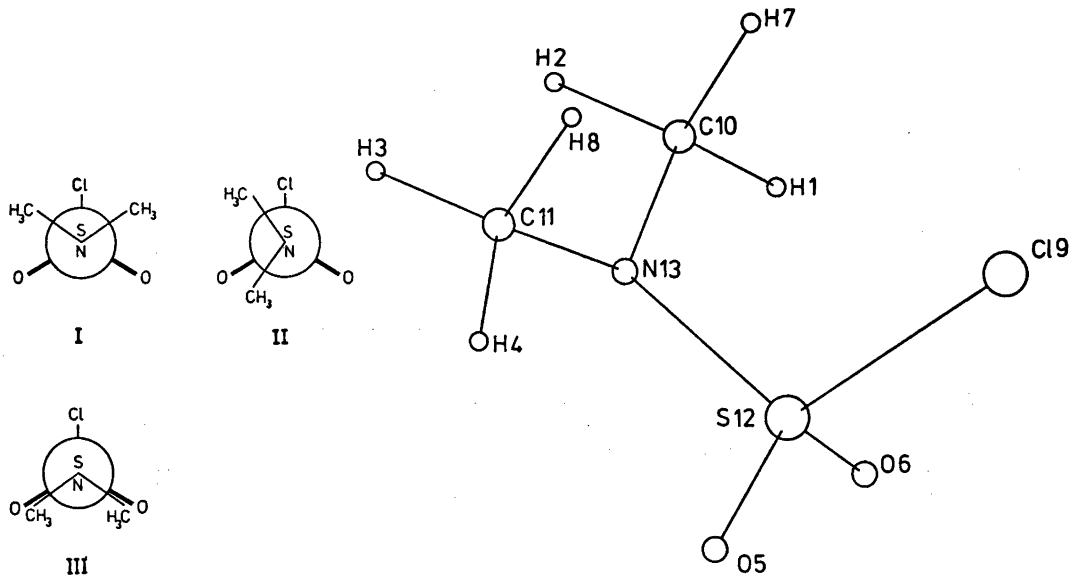

Fig. 2. Newman projections of the molecular models of $(CH_3)_2NSO_2Cl$ representing view along the S–N bond and the numbering of atoms.

amine [16] and the SO_2Cl part of methane sulfonyl chloride.[17] The force field was modified to reproduce the experimental frequencies of Bürger *et al.*[18] Even though the force field was felt to be very tentative, partly because of the low molecular symmetry, the calculated *l* values proved to be very useful. They were first used in the trial structures of the least squares refinements. Most of them, however, were assumed and not varied even in the final stages of analysis because of the strong correlation between the parameters. The *l* values from the spectroscopic calculation that were used in the final structure analysis are given in Tables 1 and 2. Fig. 2 gives the numbering of atoms.

The experimental radial distribution is represented in Fig. 3. The contribution from the S–O, C–N, and S–N bonds appear under the

Table 1. Mean amplitudes of vibration (l) from spectroscopic calculation (for distances that are not listed in Table 2; the labelling of atoms is given in Fig. 2).

Type	Distance (Å)	l (Å)	Type	Distance (Å)	l (Å)
N ···Cl	(2.90)	0.070	C_{11}···H_1	(3.40)	0.103
O ···Cl	(2.81)	0.097	S ···H_1	(2.75)	0.163
O ···N	(2.47)	0.107	H_2···H_3	(2.34)	0.228
C ···C	(2.49)	0.069	O_5 ···H_2	(4.55)	0.138
S ···C	(2.62)	0.093	O_6 ···H_3	(3.86)	0.170
H_1···H_2	(1.81)	0.129	H_3···H_8	(3.07)	0.278
N ···H_1	(2.09)	0.105	Cl ···H_2	(4.35)	0.182
N ···H_2	(2.09)	0.106	C_{11}···H_3	(2.61)	0.158
N ···H_7	(2.09)	0.151	S ···H_3	(3.54)	0.120
H_1···H_3	(3.61)	0.172	O_5 ···H_7	(4.16)	0.254
H_1···H_4	(4.16)	0.139	O_5 ···H_8	(3.27)	0.298
O_5···H_1	(4.04)	0.151	H_7···H_8	(2.63)	0.303
O_6···H_1	(2.44)	0.221	Cl ···H_7	(2.91)	0.303
H_1···H_8	(3.77)	0.223	C_{11}···H_7	(2.79)	0.211
Cl ···H_1	(3.71)	0.268	S ···H_7	(2.92)	0.246

Table 2. *N,N*-Dimethyl sulfamoyl chloride. Results of the least squares refinement. Bond lengths, bond angles and l values that were determined or assumed. The l values for the other distances were taken from spectroscopic calculation and are listed in Table 1. Some dependent parameters are also given.

No.	Type	Geometric parameter r(Å),∠(°)	l value (Å)	$\sigma_{LS}(r,\angle)$	$\sigma_{LS}(l)$	$\sigma_t(r,\angle)^e$	$\sigma_t(l)^e$
1	S−Cl	2.064	0.061[b]	0.002	0.002	0.005	0.003
2	S−O	1.421	0.038[b]	0.0015	0.003	0.004	0.004
3	S−N	1.618	0.051[b]	0.003	0.004	0.005	0.006
4	C−N	1.481	[0.050][c]	0.008		0.012	
5	C−H	1.096	0.079[b]	0.007	0.007	0.010	0.010
6	O···O	2.494	[0.074][b,d]	0.018		0.026	
7	N−S−Cl	103.0		0.4		0.5	
8	N−S−O	108.8		1.0		1.4	
9	S−N−C	115.8		0.5		0.7	
10	C−N−C	114.6		1.6		2.2	
11	N−C−H	107.4		2.4		3.5	
12	O−S−O	(122.7)[a]		1.6		2.3	
13	O−S−Cl	(105.8)[a]		0.3		0.4	
14	$(O\cdots C)_{short}$	(2.89)[a]	[0.155][c]	0.015		0.02	
15	$(O\cdots C)_{long}$	(3.82)[a]	0.08[b]	0.009	0.03	0.02	0.04
16	C···Cl	(3.37)[a]	0.17[b]	0.018	0.04	0.03	0.06

[a] Dependent parameters. [b] The spectroscopic calculations yielded l(S−Cl) 0.071, l(S−O) 0.037, l(S−N) 0.087, l(C−H) 0.079, l(O···O) 0.112, $l(O\cdots C)_{long}$ 0.101, and l(C···Cl) 0.143 Å. [c] Spectroscopic value assumed. [d] Assumed value. [e] Expressions for estimating the total errors

$\sigma_t(r) = [2\sigma_{LS}^2(r) + (0.002r)^2]^{\frac{1}{2}}$

$\sigma_t(\angle) = \sqrt{2}\sigma_{LS}(\angle)$

$\sigma_t(l) = [2\sigma_{LS}^2(l) + (0.02\ l)^2]^{\frac{1}{2}}$

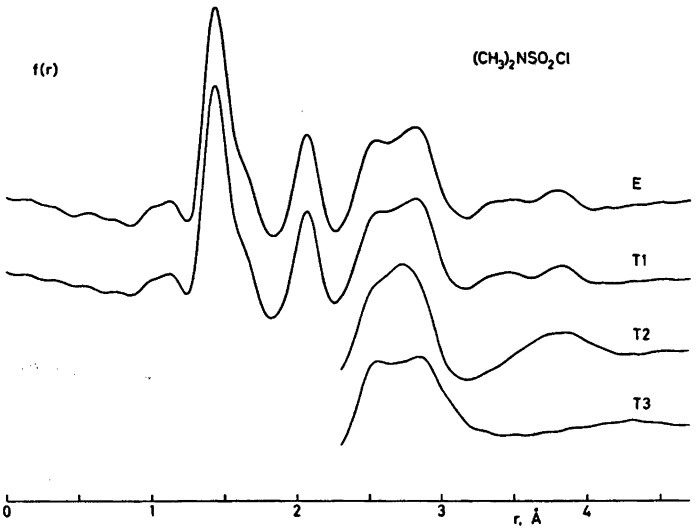

Fig. 3. Radial distributions. E, experimental; T1, T2, and T3, theoretical for conformers I, II, and III, respectively.

same maximum at $r = 1.4$ Å. However, the slight shoulder around $r = 1.6$ Å can readily be assigned to the S–N bond. The maximum at $r = 2.07$ Å originates primarily from the S–Cl bond with a less important contribution from the N···H non-bond distances. All the non-bond distances through one atom in the C_2NSO_2Cl skeleton plus the shortest O···C distances are expected to appear under the double maximum between 2.4 and 3.0 Å. The maxima at about 3.4 and 3.8 Å can be identified primarily with the Cl···C and the longest O···C distances, respectively.

There were two sources for trial structures. A starting set of the geometrical parameters was taken from the results of the earlier investigation.[12] Furthermore, portions of the experimental radial distribution were inverse-Fourier-transformed, and the bond lengths and bond angles refined in separate schemes.

The least-squares method was applied to the molecular intensities.[19] The theoretical background was used as modification function. The coherent and incoherent scattering amplitudes were taken from Cox and Bonham [20] and Tavard *et al.*,[21] respectively.

A diagonal weight matrix was utilized with the following scheme

$W = \exp[-0.1(4.00 - s^2)]$ for $s < 4.00$ Å^{-1}
$W = 1.00$ for $4.00 \leqq s < 30.00$ Å^{-1}
$W = \exp[-0.012 \times (s - 30.00)^2]$ for $s > 30.00$ Å^{-1}

Parameters in selected groups could be refined simultaneously only, because of the strong correlation between the parameters (*cf.* Refs. 8, 22). It was also for this reason that the non-bond distance O···O was treated as independent parameter and kept unvaried in many of the early refinement schemes employing the value of 2.48 Å. A remarkable constancy of this parameter has been observed for a series of simple sulfone molecules.[4,9] This constraint was not used, however, in the final refinements. Likewise, the values 1.47 Å and 109.5° were assumed for r(C–N) and ∠N–C–H in many refinement schemes, but were later allowed to vary. The l values were refined for the bonds S–Cl, S–O, S–N, and C–H and the non-bond distances Cl···C and O···C (longest). The parameters l(C–N) and l(O···O) were adapted from an other study [3] (the calculated values were unrealistically large for them, *cf.* Table 2), and for the rest the spectroscopic values were utilized throughout the entire analysis.

RESULTS

The results of the least-squares refinements are given in Table 2 together with the standard deviations from the least-squares refinement (σ_{LS}) and the total errors (σ_t) which include an estimated 0.2 and 2 % experimental error for the distances and amplitudes, respectively. The σ_{LS} values were obtained in a refinement scheme in which all the independent parameters (geometric and vibrational) were allowed to vary simultaneously with a nearly zero "fudge factor". The correlation coefficients presented in Table 3 are associated with the results given in Table 2. The data of both Tables 2 and 3 should be dealt with caution since they were obtained with many other parameters assumed.

Radial distributions for all three forms are shown in Fig. 3. The experimental distributions could be well approximated with theoretical distributions calculated for conformer I only. Slight deviations from the C_s symmetry of this form (characterized by an angle of rotation around the S – N bond up to about 4°) further improved somewhat the agreement. This was seen not so much in the changes of the generalized R values but in the regions of the radial distributions where the rotation-dependent distances occur. It is stressed also that the other geometrical parameters showed no appreciable changes in the above calculations.

DISCUSSION

The present study confirmed the earlier established form of rotation around the S – N bond in *N,N*-dimethyl sulfamoyl chloride. This form is analogous to those found to be prevailing in the vapours of $(CH_3)_2NSN(CH_3)_2$,[1] $(CH_3)_2NSON(CH_3)_2$,[2] and $(CH_3)_2NSO_2N(CH_3)_2$.[3] In all cases there is at least one symmetry plane and the two N – C bonds plus the lone pair of the nitrogen stagger the sulfur bonds and lone pairs.

The most important differences between the results of the two studies concern the bond lengths. All of them were found shorter than previously. In addition to the possibility of an experimental scale error, was suppose that a $(CH_3)_2NSO_2N(CH_3)_2$ impurity in the first study could account for the differences.

The value found in the present study for r(S – Cl), 2.064 Å, may still be the largest observed for a S – Cl bond. Some results for simple sulfonyl chlorides are (r(S – Cl), r(O···Cl)): $ClSO_2Cl$:[5] 2.011 ± 0.004 Å, 2.781 ± 0.007 Å. CH_3SO_2Cl:[6] 2.046 ± 0.004 Å, 2.816 ± 0.009 Å. $C_6H_5SO_2Cl$:[8] 2.047 ± 0.008 Å, 2.780 ± 0.032 Å. It is of interest to observe that the O···Cl non-bond distances show smaller changes than the S – Cl bonds in the molecules considered. This seems to indicate the importance of the oxygen···chlorine non-bond interactions in the structures of the SO_2Cl fragments.

The length of the S – O bond is intermediate between those in sulfuryl chloride[5] and *N,N'*-tetramethyl sulfamide.[8] It has been noted[4,9] that the changes of r(S – O) and also ∠O – S – O with changing electronegativities of ligands X and Y in simple XSO_2Y sulfones, are consistent with the VSEPR model. Accordingly, as the ligand electronegativity increases, the S – O bond shortens and the O – S – O bond opens

Table 3. Correlation coefficients with absolute values from 0.4 (× 100) associated with the least squares refinement whose results are given in Table 2 (for identification of parameters refer to Table 2, k is the scale factor).

	$r1$	$r2$	$r3$	$r4$	$r6$	∠8	∠9	∠10	∠11	$l1$	$l2$
$r4$		−80									
∠8				−45	−93						
∠9		52		−61							
∠10					−77	73					
∠11	−62			−50		−50		47			
$l2$		68		−82			49				
$l3$		−77		70			−45				−64
$l15$	62			49		−49		−46	−93		
k			49					−44		40	

Table 4. The S – O bond and O···O non-bond distances and O – S – O bond angles in some simple sulfones (vapour phase data).

Compound	Technique[a]	r(S – O), Å	∠O – S – O, °	r(O···O), Å
FSO_2F	MW (i)	1.405 ± 0.003	124.0 ± 0.2	2.481 ± 0.006
FSO_2Cl	MW (ii)	[1.408 ± 0.006]	123.7 ± 1	2.484
$ClSO_2Cl$	ED (iii)	1.404 ± 0.004	123.5 ± 0.8	2.485 ± 0.015
CH_3SO_2F	ED (iv)	1.410 ± 0.003	123.1 ± 1.5	[2.480]
	MW (v)			2.480
$C_6H_5SO_2Cl$	ED (vi)	1.417 ± 0.012	122.5 ± 3.6	2.482 ± 0.039
$(CH_3)_2NSO_2Cl$	ED (vii)	1.421 ± 0.004	122.7 ± 2.3	2.494 ± 0.026
CH_3SO_2Cl	ED (viii)	1.424 ± 0.003	120.8 ± 2.4	2.477 ± 0.013
	MW (ix)	[1.424 ± 0.003]	121.3 ± 0.6	2.483 ± 0.003
$CH_3SO_2CH_3$	ED (x)	1.435 ± 0.003	119.7 ± 1.1	2.482 ± 0.017
	MW (xi)	1.431 ± 0.004	121.0 ± 0.3	
	MW (xii)	[1.425]	122.0	2.493 ± 0.002
	(xiii)	1.433	120.8	2.493 ± 0.002

[a] MW, microwave spectroscopy; ED, electron diffraction. (i) r_o, Ref. 23; (ii) r_o, r(S – O) estimated, Ref. 24; (iii) r_a, Ref. 5; (iv) r_a, r(O···O) assumed from Ref. 25; (v) r_o, Ref. 25; (vi) r_a, Ref. 8; (vii) r_a, present work; (viii) r_a, Ref. 6; (ix) r_o, r(S – O) assumed from Ref. 6; (x) r_a, Ref. 4; (xi) r_o, Ref. 26; (xii) r_o, r(S – O) assumed, Ref. 25; (xiii) r_o, Ref. 25.

somewhat. The relevant data are presented in Table 4. The changes are relatively small, but the trend appears to be real.

Table 4 contains also the r(O···O) distances of the sulfone group. At the same time as the S – O bond lengths and O – S – O angles change as much as up to 0.03 Å and 4°, respectively, the constancy of the O···O distances at 2.48 – 2.49 Å is the more remarkable. This clearly indicates for these structures, that the non-bond oxygen···oxygen interactions may be as much, if not more, important as the electron pair interactions described by the VSEPR model. The geometrical variations may be visualized as the sulfur atom being in the center of a tetrahedron whose two apexes are occupied by the two oxygen atoms of the SO_2 group. As the X and Y substituents are changing, the sulfur atom is moving somewhat up and down in the tetrahedron with the positions of the oxygen atoms unchanged, as determined by their interaction.

REFERENCES

1. Hargittai, I. and Hargittai, M. *Acta Chim. (Budapest) 75* (1973) 129.
2. Hargittai, I. and Vilkov, L. V. *Acta Chim. (Budapest) 63* (1970) 143.
3. Hargittai, I., Vajda, E. and Szöke, A. *J. Mol. Struct. 18* (1973) 381.
4. Hargittai, M. and Hargittai, I. *J. Mol. Struct. 20* (1974) 283.
5. Hargittai, I. *Acta Chim. (Budapest) 60* (1969) 231.
6. Hargittai, M. and Hargittai, I. *J. Chem. Phys. 59* (1973) 2513.
7. Hargittai, I. and Hargittai, M. *J. Mol. Struct. 15* (1973) 399.
8. Brunvoll, J. and Hargittai, I. *J. Mol. Struct. 30* (1976) 361.
9. Hargittai, I. *Second European Crystallographic Meeting*, Keszthely 1974. Collected Abstracts, pp. 441 – 443.
10. Hargittai, I. and Mijlhoff, F. C. *J. Mol. Struct. 16* (1973) 69.
11. Gregory, D., Hargittai, I. and Kolonits, M. *J. Mol. Struct. 31* (1976) 261.
12. Vilkov, L. V. and Hargittai, I. *Acta Chim. (Budapest) 52* (1967) 423.
13. Páldi, E. *Thesis*, Budapest.
14. Hargittai, I., Hernádi, J., Kolonits, M. and Schultz, G. *Rev. Sci. Instrum. 42* (1971) 546.
15. Hargittai, I., Hernádi, J. and Kolonits, M. *Prib. Tekh. Eksp.* (1972) 239.
16. Gebhardt, O. *Thesis*, NTH, Trondheim 1971.
17. Cyvin, S. J., Dobos, S., Hargittai, I., Hargittai, M. and Augdahl, E. *J. Mol. Struct. 18* (1973) 203.
18. Bürger, H., Burczyk, K., Blascheffe, A. and Safari, H. *Spectrochim. Acta 27 A* (1971) 1073.
19. Andersen, B., Seip, H. M., Strand, T. G. and Stølevik, R. *Acta Chem. Scand. 23* (1969) 3224.

20. Cox, H. L. and Bonham, R. A. *J. Chem. Phys. 47* (1967) 2599.
21. Tavard, C., Nicolas, D. and Rouault, M. *J. Chim. Phys. (Paris) 64* (1967) 540.
22. Hargittai, I. and Hedberg, K. In Cyvin, S. J., Ed., *Molecular Structures and Vibrations*, Elsevier, Amsterdam 1972.
23. Lide, D. R., Mann, D. E. and Fristrom, R. M. *J. Chem. Phys. 26* (1957) 734.
24. Holt, C. W. and Gerry, M. C. L. *Chem. Phys. Lett. 9* (1971) 621.
25. Jacob, E. J. and Lide, D. R. *J. Chem. Phys. 54* (1971) 4591.
26. Saito, S. and Makino, F. *Bull. Chem. Soc. Jpn. 45* (1972) 92.

Received March 10, 1976.

Acta Chemica Scandinavica A 30 (1976) 641—648

Equilibrium Studies in the System AgBr—(K,Na)Br—(K,Na)NO_3 at 280 °C and the Significance of Solvation Effects in the Interpretation of Data on Silver Halide Complexation in Nitrate Melts

BERTIL HOLMBERG

Division of Physical Chemistry, Lund University, Chemical Center, P.O.B. 740, S-220 07 Lund, Sweden

The distribution of NaBr between a solid solution (Ag,Na)Br and fused equimolar (K,Na)NO_3 has been studied at 280 °C. The activities of AgBr and NaBr in the solid have been determined from the distribution data and the stability constants for the complexes $AgBr_2^-$, $AgBr_3^{2-}$ and $Ag_2Br_6^{4-}$ in the nitrate melt calculated. As compared to previous conventional solubility measurements the present study gives the same general picture of the complex formation, although the magnitudes of the stability constants for $AgBr_3^{2-}$ and $Ag_2Br_6^{4-}$ are increased as the solid solubility is taken into account.

The influence of variations in the nitrate ion activity on the interpretation of data in terms of complex formation reactions between silver and halide ions has been analysed.

The stability constants exhibit a slight change in magnitude as compared to the case of the more common model of interpretation, where changes in the solvent activity are ignored. It is, however, demonstrated that effects that have been previously ascribed to the presence of AgI_4^{3-} in minor amounts may be eliminated by taking into account solvation of the "free" silver ion by nitrate ions.

The role of solid solution formation in solubility studies on silver halide complex formation in nitrate melts has been treated in two recent papers,[1,2] where the solubility and distribution of α-AgI between solid and liquid solutions was investigated. Earlier papers from this laboratory reported results from a study of the stepwise formation of silver bromide complexes AgBr, $AgBr_2^-$, $AgBr_3^{2-}$ and $Ag_2Br_6^{4-}$ in (K,Na)NO_3 at 280 °C.[3,4]

Later, Sinistri and Pezzati [5] performed similar solubility measurements in this system. The constitution of the solid bromide phase was not checked in either of the investigations.[3–5]

It is well known, however, that AgBr and NaBr are completely miscible in the solid state at elevated temperatures.[6–9] The existence of a miscibility gap was predicted by Kleppa and Meschel.[10]

The system AgBr – KBr is a simple eutectic one, and no solid solutions have been reported.[6,11]

Since molten nitrate solutions have proved to be efficient in equilibrating solid α-AgI with alkali iodide, the experimental part of this study was undertaken in order to find out if a solid-liquid ion exchange reaction

$$AgBr(ss) + Na^+ \rightleftharpoons NaBr(ss) + Ag^+$$

is of importance in the solubility studies. Furthermore, in the system AgBr – NaBr the thermodynamics of the solid solution formation have been studied previously by different methods. Therefore, this system is suitable in testing the applicability of the approach to the solid solution-nitrate melt distribution data, which will be presented in this paper.

In melts rather concentrated in halide ions, where the thermodynamic activity of the solvent changes markedly as the concentrations of solutes are changed, it might be of significance to regard the complex formation equilibria strictly as a reversible exchange of solvent ions coordinated to the central ion for ligand ions, producing "free" solvent ions. Hence, the variable nitrate activity should be taken into account in the definition

of equilibrium constants. The bearing of this "solvation effect" on the interpretation of complex formation data in melts concentrated in ligand ions will be tested on the present experimental material and on previous data on silver iodide complexation in iodide-rich alkali nitrate melts.[1,14]

EXPERIMENTAL

Chemicals. Silver nitrate, sodium nitrate and potassium nitrate (Merck, *p.a.*) were pretreated as described previously.[12] Potassium bromide and sodium bromide (Merck, *p.a.*) were dried at 140 °C for several days prior to use. Silver bromide was prepared from hot aqueous solutions of $AgNO_3$ and KBr.

Apparatus. Large Pyrex test tubes were used as reaction vessels. They were thermostated in a closely fitting aluminium block, which was carefully thermally insulated and furnished with tubes for occasional illumination and observation of the melts. The systems were agitated by vigorous stirring with a Pyrex propeller. A fast cycling regulator, type CR/DHS/PID/SCR from Eurotherm, Worthing, England, controlled the temperature of the system, which was kept at 280.08 ± 0.02 °C (IPTS-68).

Procedure. In the main experiments (series A) systems containing 7.50 g AgBr, 75.00 g equimolar $(K,Na)NO_3$ and various amounts of equimolar (K,Na)Br were equilibrated at 280 °C. Equilibration times of 12 h were shown to be sufficient, but all systems were as a rule run for at least 24 h. Samples from the nitrate phase were then withdrawn, quenched and analysed for bromide and silver (in the range $C_{Br} \geq 1$ mol kg^{-1}).

In another experimental series (B) the equilibrium was approached by precipitating the solid AgBr phase in systems originally containing 6.78 g $AgNO_3$, 70.57 g $(K,Na)NO_3$ and various amounts of (K,Na)Br.

In separate experiments it was ascertained that no loss of bromide could be detected when systems $(K,Na)NO_3$–(K,Na)Br were equilibrated at 280 °C for even ten days or more. It was also checked that variations in the amount of solid AgBr relative to $(K,Na)NO_3$ had no influence on the experimental results.

The study was restricted to the range 0.1 mol kg$^{-1} \leq C_{Br} \leq 2$ mol kg^{-1}.

Analyses. The silver content of melts with $C_{Br} \geq 1$ mol kg^{-1} was determined by electroanalytical precipitation on a rotating platinum cathode from hot aqueous cyanide solutions. For systems with $C_{Br} < 1$ mol kg^{-1} sufficiently accurate values of C_{Ag} were obtained by interpolation in the solubility curve determined by Cigén and Mannerstrand.[3] The alkali bromide content of the melts was determined by titration with standard $AgNO_3$ solution on samples suspended in water. The endpoint was detected potentiometrically.

The composition of the solid phase was calculated from the difference between added and found amounts of alkali bromide in the nitrate melt.

RESULTS AND DISCUSSION

The following notations and symbols will not be specifically defined in the text:

For the solid phase ($i = 1$ for AgBr and 2 for NaBr):

x_i = mol fraction of component i.
a_i = activity of component i.
$f_i = a_i x_i^{-1}$

For the nitrate melt:

All concentrations are expressed in molality units mol kg^{-1}, referring to equimolar $(K,Na)NO_3$ as solvent.
C_{Br}, C_{Ag}, C_0 = total concentrations of bromide, silver and nitrate, respectively.
[A] = concentration of species A.
a(A) = activity of species A.
$\beta_{nm} = [Ag_mBr_n^{(m-n)}][Ag^+]^{-m}[Br^-]^{-n}$.
M, N = maximum value of m and n, respectively.
$X_0 = C_{Ag}[Ag^+]^{-1}$.
$X_n = (X_{n-1} - \beta_{(n-1)1})[Br^-]^{-1}$; $\beta_{01} = 1$.
$\bar{n} = (C_{Br} - [Br^-])C_{Ag}^{-1}$.
$K_1' = [Ag^+][Br^-]a_1^{-1}$.

For the sake of clarity the treatment of data will at first be described without considering the "solvation effect", referred to in the introduction.

The complex formation in the nitrate melt

Following a previously published calculation method,[1] we would have determined the activity a_1 of AgBr in the solid from the equations

$$\mathrm{d} \ln a_1 = -(x_2/x_1)\mathrm{d} \ln a_2 \quad (1)$$

$$\mathrm{d} \ln a_2 = \mathrm{d} \ln ([Na^+][Br^-]) \quad (2)$$

However, the use of molality concentrations for ionic species, which are common with the solvent, in expressions such as eqn. (2) may be

criticized from a thermodynamic point of view.

Consider a nitrate melt with the ion constituents K^+, Na^+, NO_3^-, Br^-, Ag^+ and complexes $Ag_mBr_n^{(m-n)}$. Since activities of all solute species are expressed as concentrations on the molality scale – which lies inherent in the complex formation model used – the Gibbs-Duhem equation may be written for the nitrate melt as (P and T are constant)

$$[K^+]\ d\ln a(K) + [Na^+]\ d\ln a(Na) + [NO_3^-]\ d\ln a(NO_3) + [Br^-]\ d\ln [Br^-] + [Ag^+]\ d\ln [Ag^+] + \sum_{m=1}^{M}\sum_{n=1}^{N} [Ag_mBr_n^{(m-n)}]\ d\ln [Ag_mBr_n^{(m-n)}] = 0 \quad (3)$$

Applying the stoichiometric requirements

$$C_{Br} = [Br^-] + \sum_{m=1}^{M}\sum_{n=1}^{N} n[Ag_mBr_n^{(m-n)}] \quad (4)$$

$$C_{Ag} = [Ag^+] + \sum_{m=1}^{M}\sum_{n=1}^{N} m[Ag_mBr_n^{(m-n)}] \quad (5)$$

and the equilibrium conditions

$$d\ln[Ag_mBr_n^{(m-n)}] = m\ d\ln[Ag^+] + n\ d\ln[Br^-] \quad (6)$$

to eqn. (3) we obtain

$$[K^+]\ d\ln a(K) + [Na^+]\ d\ln a(Na) + [NO_3^-]\ d\ln a(NO_3) + C_{Br}\ d\ln[Br^-] + C_{Ag}\ d\ln[Ag^+] = 0 \quad (7)$$

Since K^+ and Na^+ are the only cations present in the nitrate melt ($[Ag^+]$ is negligible in these alkali bromide containing melts), and since the K:Na molar balance exhibits very small variations, it is felt that more realistic expressions for $d\ln a(Na)$ and $d\ln a(K)$ would be $d\ln y$ and $d\ln(1-y)$, respectively, where

$$y = [Na^+]/([Na^+]+[K^+]) \quad (8)$$

The activity a_1 is then obtained (*cf.* Ref. 1) by

$$a_{1j} = \exp\left[\int_{\ln R_0}^{\ln R_j} (x_2/x_1)\ d\ln R\right] \quad (9)$$

where

$$R = (y[Br^-])^{-1} \quad (10)$$

and R_0 indicates a value of R in a system with $x_2 = 0$. The index j is used to denote corresponding values of different quantities referring to the same actual system. Since the experimental data do not extend to $x_2 = 0$, the integration according to eqn. (9) was started at $[Br^-] = 0.0988$ mol kg^{-1}. The quantities so determined $[\ln a_1([Br^-]_j) - \ln a_1(0.0988$ mol kg$^{-1})]$ were plotted *vs.* $[Br^-]$ and the smooth curve obtained was easily extrapolated to $[Br^-] = 0$ to yield $a_1(0)/a_1(0.0988$ mol kg$^{-1})$. All activities a_{1j} were then calculated setting $a_1(0) = 1$ (*cf.* Ref. 13), and the concentration product $([Ag^+][Br^-])_j$ has been computed as $K_1' a_{1j}$. In doing so we used the value $K_1' = 3.00 \times 10^{-7}$ (mol kg^{-1})^2 which was potentiometrically determined by Cigén and Mannerstrand [4] and which was used in their calculation of stability constants from solubility data.[3] The results are all collected in Table 1.

In the composition range investigated, $AgBr_2^-$, $AgBr_3^{2-}$ and $Ag_2Br_6^{4-}$ appear to be the predominant complexes. The function X_2 was calculated by use of β_{11} from Ref. 3, and β_{21} was easily obtained as the limiting value $\lim_{[Br^-]\to 0} X_2$. Since X_3 was found to vary linearly with $[Ag^+][Br^-]^3$, the constants β_{31} and β_{62} were determined from the linear relationship

$$X_3 = \beta_{31} + 2\beta_{62}[Ag^+][Br^-]^3 \quad (11)$$

All calculations were iterated until no significant change in the parameters could be observed.

When the solid solubility of NaBr in AgBr is taken into consideration, the over-all picture of the complexation is on the whole left unaffected as compared to previous findings.[3,5] As can be seen from Table 2 the value of β_{21} is not influenced, whereas a slight increase in β_{31} and a still more pronounced increase in β_{62} is obtained when the variable composition of the solid phase is accounted for.

It is noteworthy that the discrepancies between the potentiometrically determined values of β_{31} and β_{62} and those obtained from solubility data increase as the solid solution formation is accounted for in the calculations. It is also to be noted that the potentiometrically determined product $[Ag^+][Br^-]$ seems to *increase* as C_{Br} increases in the region C_{Br}

Table 1. Experimental data and calculated quantities. Values of C_{Ag} which are taken from Ref. 3, are printed in italics. Solvation of silver ions is ignored.

Series	C_{Br} (mol kg^{-1})	C_{Ag} (mol kg^{-1})	y	[Na$^+$] (mol kg^{-1})	x_1	a_1	f_1	a_2	f_2	[Br$^-$] (mol kg^{-1})	[Ag$^+$][Br$^-$] × 10^7 (mol kg^{-1})^2	$a(NO_3)$
A	0.1009	*0.0010*	0.500	5.421	0.994	0.998	1.004	0.006	1.0	0.0988	2.99	0.991
A	0.1952	*0.0021*	0.500	5.466	0.989	0.993	1.004	0.011	1.0	0.1903	2.98	0.982
A	0.3906	*0.0055*	0.499	5.560	0.978	0.981	1.003	0.021	1.0	0.3768	2.94	0.964
B	0.3971	*0.0056*	0.499	5.563	0.980	0.983	1.003	0.021	1.0	0.3829	2.95	0.963
A	0.591	*0.0111*	0.499	5.653	0.963	0.971	1.008	0.032	0.86	0.562	2.91	0.947
A	0.807	*0.0187*	0.499	5.750	0.954	0.959	1.005	0.042	0.91	0.756	2.88	0.929
B	0.991	0.0262	0.499	5.839	0.938	0.949	1.012	0.052	0.84	0.918	2.85	0.914
A	0.991	0.0261	0.498	5.838	0.937	0.948	1.012	0.051	0.81	0.919	2.84	0.914
A	0.994	0.0261	0.498	5.841	0.939	0.949	1.011	0.052	0.85	0.922	2.85	0.914
A	1.241	0.0399	0.498	5.952	0.921	0.933	1.013	0.063	0.80	1.129	2.80	0.896
B	1.256	0.0410	0.498	5.961	0.928	0.940	1.013	0.064	0.89	1.140	2.82	0.895
A	1.498	0.0571	0.498	6.066	0.896	0.917	1.023	0.075	0.72	1.343	2.75	0.877
A	1.502	0.0562	0.498	6.069	0.897	0.919	1.024	0.075	0.73	1.337	2.76	0.877
A	1.758	0.0774	0.497	6.179	0.867	0.901	1.039	0.086	0.65	1.537	2.70	0.860
A	2.023	0.1010	0.497	6.295	0.846	0.882	1.042	0.097	0.63	1.732	2.65	0.843
B	2.029	0.1023	0.497	6.300	0.853	0.890	1.043	0.097	0.66	1.732	2.67	0.843
A	2.221	0.1236	0.496	6.371	0.800	0.867	1.084	0.104	0.52	1.862	2.60	0.832

Table 2. A comparison between stability constants obtained by different methods.

Investigation and method	β_{21}/(mol kg^{-1})$^{-2}$	β_{31}/(mol kg^{-1})$^{-3}$	β_{62}/(mol kg^{-1})$^{-7}$
Potentiometric measurements			
Ref. 4, 280 °C Unsaturated melts	$(2.4\pm 0.1)\times 10^4$	$(5.9\pm 0.7)\times 10^4$	$(1.2\pm 0.6)\times 10^{10}$
Solubility studies			
Ref. 5, 275 °C Solid solubility ignored	2.4×10^4	7.8×10^4	–
Ref. 3, 280 °C Solid solubility ignored	2.3×10^4	6.7×10^4	2.2×10^{10}
This study, 280 °C Solid solubility accounted for; $1\leq a_1\leq 0.87$. Solvation effects ignored.	2.3×10^4	$(7.0\pm 0.4)\times 10^4$	$(3.0\pm 0.4)\times 10^{10}$

> 1.00 mol kg^{-1},[4] whereas our analysis of the distribution data indicates a decrease in $[Ag^+][Br^-]$ due to the lowering of the AgBr activity in the solid. These two discrepancies are consistent with each other in the sense that they may both be "explained" by assuming too large apparent values of $[Ag^+]$ from the emf-data due to liquid junction potentials in those melts which are concentrated in (K,Na)Br – provided that halide containing melts exhibit the same ideal thermodynamic behaviour as liquid $AgNO_3$ – (K,Na)NO_3 systems.[12]

For the sake of comparison we calculated the activities a_1 according to eqns. (1) and (2) as well. The maximum difference in a_1, as compared to the values of Table 1, amounts to less than 1 % and there is no change in the determined values of the stability constants. A check of the data pertaining to silver iodide complexes [1] gave similar results, *i.e.* the choice of model for the change of the alkali metal ion activities is of little importance as long as only the complex equilibria in the nitrate melt are considered. The present approach, however, appears to be thermodynamically more sound.

The solid solution (Ag,Na)Br

The activities a_2 for NaBr in the solid have been calculated as follows. According to eqn. (8) an equilibrium constant K_2' for the reaction

$$NaBr(ss) \rightleftharpoons Na^+ + Br^-$$

is defined as

$$K_2' = y[Br^-]a_2^{-1} \quad (12)$$

A polynomial approximation is made, *viz.*

$$x_2/(y[Br^-]) = \sum_{i=0}^{2} b_i x_2^{\,i} \quad (13)$$

and, following a method previously described,[1] a_2 is determined as

$$a_2 = b_0 y[Br^-] \quad (14)$$

since b_0 may be identified as $K_2'^{-1}$. From a least-squares analysis $K_2' = (9\pm 1)$ mol kg^{-1} with the error expressed as three standard deviations. The standard states for NaBr in the solid and for Na^+ in the nitrate melt are chosen to be in accordance with the conditions $\lim_{x_2\to 0} f_2 = 1$ and $a(Na) = y = 0.500$ in pure equimolar (K,Na)NO_3(l), respectively. The values of a_2 and f_2 are included in Table 1. Our experimental data (f_1; x_2) are well described by

$$RT \ln f_1 = A x_2^{\,2} \quad (15)$$

in the range $0.046\leq x_2\leq 0.200$. A value of A may also be derived from the f_2 data. With the present choice of standard state for NaBr in the solid solution the expression consistent with eqn. (15) is

$$RT \ln f_2 = A(x_1^{\,2} - 1) \quad (16)$$

The values of A calculated from literature data are given in Table 3 together with those from this study. The present method appears to

Table 3. Different values of the regular solution parameter A, estimated in the region of dilute solid solutions of NaBr in AgBr.

Ref.	Method	Temperature	A/(kJ mol^{-1})
10	Enthalpy of mixing	350 °C	8±1
8	Emf of the cell	350 °C	
	Ag/(Ag,Na)Br(s)/Br$_2$	400 °C	10±1
9	Miscibility gap studies	280 °C	9±2
This study	Distribution measurements	280 °C	
	$RT \ln f_1/x_2^2$		11±2
	$RT \ln f_2/(x_1^2-1)$		7±2

yield reliable values of the activities of the components in the solid phase.

The nitrate ion activity

The present approach to the problem of deriving reliable values of a_1 leads to a complete model description of the nitrate melt in terms of ion activities, since $a(NO_3)$ is determined by eqn. (7). For the two first terms in the left hand member of this equation we have

$$[K^+]\ d\ln(1-y)+[Na^+]\ d\ln y=0 \qquad (17)$$

Hence, a general expression for the nitrate ion activity is

$$d\ln a(NO_3)=-C_0^{-1}(C_{Br}\ d\ln[Br^-]+ C_{Ag}\ d\ln[Ag^+]) \qquad (18)$$

Furthermore, for systems investigated in this study

$$d\ln[Ag^+]=-x_1^{-1}(x_2\ d\ln y+d\ln[Br^-]) \qquad (19)$$

and eqn. (7) then yields

$$d\ln a(NO_3)=C_0^{-1}[(C_{Ag}x_1^{-1}-C_{Br})\ d\ln[Br^-]+ C_{Ag}x_2x_1^{-1}\ d\ln y] \qquad (20)$$

In the present case the second term of the right hand member of eqn. (20) is negligible. Setting $a(NO_3)=1$ in pure (K,Na)NO_3(l), the nitrate ion activity may be computed according to

$$a(NO_3)_j=\exp\left[\int_{-\infty}^{\ln[Br^-]_j} C_0^{-1}(C_{Ag}x_1^{-1}-C_{Br})d\ln[Br^-]\right] \qquad (21)$$

In the calculation the solubility data of Ref. 3 were utilized in the dilute solution range. The resulting nitrate activities are included in Table 1, which thus contains thermodynamically self-consistent values of activities and concentrations according to the model used.

The influence of variable nitrate ion activity on the interpretation of data

In complex formation studies the solvent activity is generally regarded as constant, an assumption which is justified by the fact that only very dilute solutions are studied. In the present case, however, $a(NO_3)=0.83$ in melts with $C_{Br}=2.2$ mol kg^{-1} as compared to $a(NO_3)=1$ in the pure solvent. The situation is also rather similar in silver iodide systems which have been investigated previously.[1,14]

In calculations aiming at identification of complex species and determination of their thermodynamic stabilities the formation equilibria have been represented as

$$mAg^+ + nX^- \rightleftharpoons Ag_mX_n^{(m-n)}$$

However, from vibrational spectra studies conclusive evidence for strong interaction between silver and nitrate ions in melts has emerged.[15-27] Recently, Clarke and Hartley,[26] in an enlightening study of the features of the low frequency silver nitrate Raman band at 107 cm^{-1}, concluded that specific ionic association between silver and nitrate ions is of significance in such melts. This implies that the formation of silver halide complexes in an alkali metal nitrate melt should rather be regarded as a ligand exchange reaction, the halide ions replacing nitrate ions in the coordination sphere of silver to produce "free" nitrate ions.

For the sake of simplicity the calculations will be restricted to two model cases with $z=2$ and 4, assuming that the over-all formation equilibria can be represented as

$$Ag(NO_3)_z^{(1-z)} + nX^- \rightleftharpoons Ag(NO_3)_{(z-n)}X_n^{(1-z)} + nNO_3^- \quad (\text{for } z \geq n)$$

$$Ag(NO_3)_z^{(1-z)} + nX^- \rightleftharpoons AgX_n^{(1-n)} + zNO_3^- \quad (\text{for } z \leq n)$$

and

$$2Ag(NO_3)_z^{(1-z)} + 6X^- \rightleftharpoons Ag_2X_6^{4-} + 2zNO_3^-$$

This means that effects such as possible changes from bidentate nitrate ions to monodentate as a halide ion enters the coordination sphere (*e.g.* no "free" nitrate ion is produced) are not accounted for in the model although such mechanisms for the complex formation might very well be of significance. As for $Ag_2X_6^{4-}$, it is supposed that silver is coordinatively saturated in the dinuclear complex.

The AgX distribution equilibrium between the solid halide phase and the nitrate melt

$$AgX(a_1) + zNO_3^-(a(NO_3)) \rightleftharpoons Ag(NO_3)_z^{(1-z)} + X^-$$

and hence

$$[Ag^+][X^-] = K_1' a_1 a(NO_3)^z \qquad (22)$$

For the case of a liquid halide phase an analogous expression is easily derived. The over-all stability constants for the complex formation reactions should be defined as

$$\beta^*_{n1} = [AgX_n^{(1-n)}]a(NO_3)^n[Ag^+]^{-1}[X^-]^{-n} \quad (\text{for } z \geq n) \qquad (23)$$

$$\beta^*_{n1} = [AgX_n^{(1-n)}]a(NO_3)^z[Ag^+]^{-1}[X^-]^{-n} \quad (\text{for } z \leq n) \qquad (24)$$

$$\beta^*_{62} = [Ag_2X_6^{4-}]a(NO_3)^{2z}[Ag^+]^{-2}[X^-]^{-6} \qquad (25)$$

In (22) – (25) and all following expressions the possibility of solvated anions has been disregarded, since it has no bearing on the interpretation of the data.

It is easily shown that a very good approximation of the general expression for the nitrate ion activity is (*cf.* eqn. (18))

$$\mathrm{d}\ln a(NO_3) = -(C_0 - C_X + [X^-])^{-1}(C_X\,\mathrm{d}\ln[X^-] + C_{Ag}\,\mathrm{d}\ln[Ag^+]) \qquad (26)$$

for $z \geq n$. (A slight and numerically unimportant modification occurs for $z < n$.) The expression corresponding to eqn. (21) is then

$$a(NO_3)_j = \exp\left[\int_{-\infty}^{\ln[X^-]_j} (C_0 - (\bar{n} - z)C_{Ag})^{-1} (C_{Ag}x_1^{-1} - C_X)\,\mathrm{d}\ln[X^-]\right] \qquad (27)$$

An analysis of the experimental data pertaining to the present AgBr solubility study according to eqns. (22) – (27) reveals that the effects of nitrate solvation do not change the conclusion concerning what complex species exist in the melt. The β^*-values are given in Table 4. From a comparison with Table 2 it is seen that only moderate changes in the constants are obtained when the present solvation model is applied.

A similar check of the silver iodide solubility data of Ref. 1 was performed under the two previous assumptions[1] that either AgI_3^{2-}, AgI_4^{3-} and $Ag_2I_6^{4-}$ (alternative I) or only AgI_3^{2-} and $Ag_2I_6^{4-}$ (alternative II) are the predominating silver containing species in iodide-rich nitrate melts. The results are collected in Table 5. Like the bromide case there is no significant change in the results as z is assumed to take integer values from zero to four.

Finally, the weak indication of the presence of AgI_4^{3-} as it appeared from potentiometric data[14] obtained in unsaturated melts was checked. The evaluation of β_{31} and β_{41} from the f_4^0-function (defined in Ref. 14) was re-examined on the basis of eqns. (23) – (25) for $z=2$ and 4.

Table 4. Apparent stability constants of silver bromide complexes for various silver(I) solvation numbers z.

z	$\beta^*_{31} \times 10^{-4}/(\text{mol kg}^{-1})^{-3}$	$\beta^*_{62} \times 10^{-10}/(\text{mol kg}^{-1})^{-7}$
2	7.0 ± 0.3	2.9 ± 0.3
4	7.8 ± 0.4	3.3 ± 0.3

Table 5. Apparent stability constants of silver iodide complexes for various silver(I) solvation numbers z. Experimental solubility data and other details are given in Ref. 1.

z	Alternative I.[1] $\beta^*_{31}\times 10^{-7}$/ (mol kg^{-1})$^{-3}$	$\beta^*_{41}\times 10^{-7}$/ (mol kg^{-1})$^{-4}$	$\beta^*_{62}\times 10^{-16}$/ (mol kg^{-1})$^{-7}$	Alternative II.[1] $\beta^*_{31}\times 10^{-7}$/ (mol kg^{-1})$^{-3}$	$\beta^*_{62}\times 10^{-16}$/ (mol kg^{-1})$^{-7}$
0 (Ref. 1)	2.4 ± 0.3	3.6 ± 0.7	1.6 ± 0.7	3.8 ± 0.6	3.1 ± 0.6
2	2.5 ± 0.3	3.8 ± 0.7	1.4 ± 0.6	3.8 ± 0.5	3.4 ± 0.5
4	2.6 ± 0.3	4.0 ± 0.7	1.3 ± 0.6	4.0 ± 0.5	3.6 ± 0.5

The data processing produces values of β_{31} which are on the whole the same for different z, *viz.* $(2.2\pm 0.1)\times 10^7$ (mol kg^{-1})$^{-3}$. The value of β_{62} decreases somewhat as z is increased from zero [$(1.2\pm 0.3)\times 10^{16}$ (mol kg^{-1})$^{-7}$ for $z=2$ as compared to $(1.9\pm 0.7)\times 10^{16}$ (mol kg^{-1})$^{-7}$ for $z=0$], whereas β_{41} is effectively zero or apparently slightly negative for $z=2$ and 4.

From the present examination of the solvation effect it becomes evident that the interpretation of potentiometric data is brought into a qualitative agreement with solubility and distribution data as interpreted according to alternative II, if the nitrate solvation of Ag(I) is considered. This means that effects that have been ascribed to the presence of AgI_4^{3-} might very well have their origin in the liberation of NO_3^- ions from the solvated silver ions as the iodide complexation proceeds. A more precise quantitative evaluation of the "solvation effect" cannot be made, since the detailed mechanisms of the complex formation processes are unknown, but it may be concluded that serious misinterpretation of data might result, if species present in only minor amounts are considered in melts where the solvent activity changes significantly.

Acknowledgements. I thank Professor Ido Leden for many inspiring discussions. Fil.mag. Göran Thomé skilfully assisted in the experimental work. I also thank Dr. Peter Sellers for the linguistic revision of the manuscript.

REFERENCES

1. Holmberg, B. *Acta Chem. Scand. 27* (1973) 3657.
2. Holmberg, B. *Acta Chem. Scand. 27* (1973) 3550.
3. Cigén, R. and Mannerstrand, N. *Acta Chem. Scand. 18* (1964) 2203.
4. Cigén, R. and Mannerstrand, N. *Acta Chem. Scand. 18* (1964) 1755.
5. Sinistri, C. and Pezzati, E. *Gazz. Chim. Ital. 97* (1967) 1116.
6. Zemczuzny, S. F. *Z. Anorg. Allg. Chem. 153* (1926) 47.
7. Wynnyckyj, J. R., Schmalzried, H. and Sockel, H.-G. *Z. Phys. Chem. (Frankfurt am Main) 68* (1969) 30.
8. Tsuji, T., Fueki, K. and Mukaibo, T. *Bull. Chem. Soc. Jpn. 42* (1969) 2193.
9. Sinistri, C., Riccardi, R., Margheritis, C. and Tittarelli, P. *Z. Naturforsch. Teil A 27* (1972) 149.
10. Kleppa, O. J. and Meschel, S. V. *J. Phys. Chem. 69* (1965) 3531.
11. Bradley, J. N. and Greene, P. D. *Trans. Faraday Soc. 63* (1967) 424.
12. Holmberg, B. *Acta Chem. Scand. A 28* (1974) 284.
13. Johansson, L. *Acta Chem. Scand. A 28* (1974) 708.
14. Holmberg, B. *Acta Chem. Scand. 27* (1973) 875.
15. Janz, G. J. and James, D. W. *J. Chem. Phys. 35* (1961) 739.
16. Wilmshurst, J. K. and Senderoff, S. *J. Chem. Phys. 35* (1961) 1078.
17. Walrafen, G. E. and Irish, D. E. *J. Chem. Phys. 40* (1964) 911.
18. Janz, G. J. and Kozlowski, T. R. *J. Chem. Phys. 40* (1964) 1699.
19. Wait, S. C., Ward, A. T. and Janz, G. J. *J. Chem. Phys. 45* (1966) 133.
20. Wait, S. C. and Ward, A. T. *J. Chem. Phys. 44* (1966) 448.
21. Devlin, J. P., Williamson, K. and Austin, G. *J. Chem. Phys. 44* (1966) 2203.
22. Li, P. and Devlin, J. P. *J. Chem. Phys. 49* (1968) 1441.
23. Vallier, J. *J. Chim. Phys.-Chim. Biol. 65* (1968) 1762.
24. James, D. W. and Leong, W. H. *J. Chem. Phys. 51* (1969) 640.
25. Clarke, J. H. R. *Chem. Phys. Lett. 4* (1969) 39.
26. Clarke, J. H. R. and Hartley, P. J. *J. Chem. Soc. Faraday Trans. 2, 68* (1972) 1634.
27. Kawamura, K. *Trans. Jpn. Inst. Met. 16* (1975) 281.

Received March 9, 1976.

Acta Chemica Scandinavica A 30 (1976) 649—656

Structural Studies on the Rare Earth Carboxylates. 25. The Crystal Structure of Trisodium Tris(oxydiacetato)-cerate(III) Nonahydrate

INGA ELDING

Physical Chemistry 1, Chemical Center, University of Lund, P.O.B. 740, S-220 07 Lund 7, Sweden

The crystal structure of the triclinic compound $Na_3[Ce(C_4H_4O_5)]_3.9H_2O$ has been determined using X-ray intensity data collected with a four-circle single crystal diffractometer. The space group is $P\bar{1}$ with $Z=2$ and unit cell dimensions $a=10.3597(7)$, $b=11.6189(12)$, $c=12.7957(9)$ Å, $\alpha=113.001(4)$, $\beta=90.227(4)$, and $\gamma=92.065(7)°$. The oxydiacetate ions act as tridentate ligands making the cerium ion nine-coordinated. The coordination polyhedron is a distorted tricapped trigonal prism. The structure is composed of layers of these negatively charged mononuclear tris(oxydiacetato)cerate(III) complexes alternating with layers containing the sodium ions and the water molecules. The sodium ions are surrounded by octahedra and trigonal bipyramids of oxygen atoms belonging to the carboxylate groups and the water molecules. These polyhedra form six-membered chains by sharing corners, edges and faces. The chains are held together by hydrogen bonds and the two layers are connected by carboxylate oxygens and by hydrogen bonds.

The trivalent cerium ion has a single $4f$ electron and ground state $^2F_{5/2}$ which splits in a crystal field. At liquid helium temperatures only the lowest doublet is expected to be populated, which makes it possible to use a fictitious spin $S'=1/2$ to describe the magnetic properties of the ion. A cerium(III) compound with large $Ce^{3+}-Ce^{3+}$ separations will thus have very simple magnetic properties and can be used as a magnetic coolant and thermometer in the mK region. The most widely applied material of this type is CMN: $Ce_2Mg_3(NO_3)_{12}.24H_2O$, but at temperatures below 10 mK the effects of magnetic ordering are complicating its use.

In a search for new materials which might supplement CMN in the ultra-low temperature technique, it was noticed that the solid mononuclear tris(oxydiacetato) and tris(dipicolinato) lanthanoidate complexes all have very long distances (8 – 10 Å) between the central ions.[1–6] The magnetic properties of some of these compounds have been investigated by Wolf and coworkers [7–9] and by Webb and Wheatley.[10] In one attempt to grow large single crystals of the trigonal oxydiacetate compound $Na_3[Ce(C_4H_4O_5)_3].2NaClO_4.6H_2O$ (CDG), single crystals of a new triclinic phase of trisodium tris(oxydiacetato)cerate(III) nonahydrate (TCDG) were obtained. Like the other compounds TCDG has a smaller value of the magnetic heat capacity than CMN.[9] Besides the potential low temperature application of TCDG another reason to determine its structure is the comparatively large water content. As large single crystals are prepared, neutron diffraction can be employed to unravel the hydrogen bond system. In this paper the X-ray investigation of TCDG is reported. The study using neutron diffraction data will be reported separately. To compare the complex in this structure with that in the trigonal CDG the latter compound has been investigated with X-ray diffractometry. This comparison will be the subject of a third communication.

EXPERIMENTAL

Preparation and analysis. A water solution of CDG ($Na_3[Ce(C_4H_4O_5)_3].2NaClO_4.6H_2O$), prepared as described in Ref. 1, was concentrated

at 50 °C and then slowly evaporated in a desiccator over concentrated sulfuric acid at room temperature. A few large crystals of stout prismatic habit were obtained. They were colourless. An analysis for Ce, Cl, C, H, and H_2O gave: 17.6 % Ce, 18.8 % C, 4.3 % H, 22.8 % H_2O and no Cl. Calc. for $Na_3[Ce(C_4H_4O_5)_3].9H_2O$: 18.3 % Ce, 18.8 % C, 3.9 % H, and 21.1 % H_2O. The cerium analysis was carried out using EDTA-titration.

Single crystal work. Weissenberg photographs showed the compound to be triclinic. A crystal of the approximate dimensions $0.15 \times 0.20 \times 0.25$ mm^3 was cut from a larger one. The intensities were recorded at 295 K with a four-circle diffractometer (CAD-4) using graphite monochromated Cu$K\alpha$-radiation. The $\omega - 2\theta$ scan technique was used with $\Delta\omega = 0.80 + 0.50 \tan\theta$. A fast prescan was used to determine the scan speed at which a predetermined minimum number of counts (1000) was received by the detector. However, the recording time for a reflexion was limited to 90 s. The scan interval, $\Delta\omega$, was extended 25 % at both ends for the background measurements. Three reference reflexions were measured after every 50th reflexion to check the stability of the crystal and the electronics. The fluctuation in their intensities was 10 % and could be described by a polynomial of the second degree. This function was used for scaling of the data set. The intensities of 3106 reflexions within the interval $5° < \theta < 50°$ were measured. Of these 308 had negligible intensities (less than 100 in the prescan) and were given zero weight in the subsequent refinements.

The values of I and $\sigma_c(I)$, where $\sigma_c(I)$ is based on counting statistics, were corrected for Lorentz, polarization and absorption effects. In the polarization correction the expression used was $p = (\cos^2 2\theta_M + \cos^2 2\theta)/(1 + \cos^2 2\theta_M)$ with $\theta_M = 13.3°$. The transmission coefficient, evaluated by numerical integration, varied in the interval 0.161 – 0.414.

UNIT CELL AND SPACE GROUP

TCDG, $Na_3[Ce(C_4H_4O_5)_3].9H_2O$, F.W. = 767.6, crystallizes in the triclinic system (space group $P1$ or $P\bar{1}$).

The unit cell dimensions were determined with least-squares refinement of θ-values for 60 reflexions, measured on the diffractometer as described in Ref. 11. The density, D_m, was determined from the loss of weight in benzene. The following crystal data were obtained:

a	= 10.3597(7) Å	α =	113.001(4)°
b	= 11.6189(12) Å	β =	90.227(4)°
c	= 12.7957(9) Å	γ =	92.065(7)°
V	= 1416.6 Å^3	Z =	2

$D_m = 1.78$ g cm^{-3} $\quad \mu(\text{Cu}K\alpha) = 132.6$ cm^{-1}
$D_x = 1.80$ g cm^{-3}

STRUCTURE SOLUTION AND REFINEMENT

The structure was assumed to belong to the centrosymmetric space group $P\bar{1}$. A Patterson synthesis gave the coordinates of the cerium ion. The other non-hydrogen atoms were found in a difference synthesis, and all the coordinates together with a scale factor were refined in least-squares programs, first using a block-diagonal approximation and for the last cycles a full-matrix least-squares refinement. The function minimized was $\sum w(|F_o| - |F_c|)^2$ with weights w calculated using the equation $1/w = (C_1\sigma_c)^2/(4F_o^2) + (C_2F_o)^2$, where C_1 and C_2 are adjustable constants. The refinement was performed with individual isotropic temperature factors (B) for all atoms except cerium, which was given anisotropic temperature coefficients. The convergence was followed by the conventional R-factor ($R = \sum[|F_o| - |F_c|]/\sum|F_o|$) and the weighted R-factor ($R_w = [\sum w(|F_o| - |F_c|)^2/\sum w|F_o|^2]^{1/2}$).

In the first series of refinements one of the water oxygens, OW(4), received a value of B as high as 12. When this oxygen atom was removed, a difference map showed two nearly equal peaks 1.3 Å apart. Half an oxygen atom was placed at each position, resulting in lower B-values and a drop in the R-values. The occupancy factor was also refined assuming a total of one water oxygen in positions A and B and resulted in a factor of 0.49 for position A and 0.51 for position B.

For $C_1 = 4.0$ and $C_2 = 0.05$, which gave the best constancy of $\langle w(|F_o| - |F_c|)^2 \rangle$ in different $|F_o|$-intervals, R was 0.050 and R_w 0.072. 170 parameters were refined. The shifts in the parameters were mostly within 10 % of the e.s.d.'s and never more than 15 %. A final difference map showed a peak of 1.7 e/Å^3 near the position of OW(7). Also this water oxygen might thus be distributed over two positions, as is also indicated by its rather high B-value. However, no attempt was made to investigate this point further using the X-ray data.

The scattering factors for Ce were obtained from Cromer *et al.*[12] and those for Na, O, and C from Hanson *et al.*[13] Correction for anomalous

Table 1. Atomic parameters with e.s.d.'s in parentheses. B denotes the isotropic temperature factor.

Atom	$x/a(\times 10^4)$	$y/b(\times 10^4)$	$z/c(\times 10^4)$	B (Å^2)
Ce	2407.7(5)	2382.9(5)	2451.7(4)	[a]
Na(1)	−1258(4)	6057(4)	2144(4)	3.3(1)
Na(2)	2632(4)	6947(4)	1848(3)	2.6(1)
Na(3)	4006(4)	8594(4)	4336(3)	2.7(1)
O(1)	4171(6)	2012(6)	3568(5)	2.3(1)
O(2)	6185(6)	1611(7)	3882(6)	2.9(1)
O(3)	4577(5)	1667(6)	1455(5)	1.5(1)
O(4)	2565(6)	1960(6)	383(5)	2.1(1)
O(5)	3660(7)	1682(7)	−1187(6)	3.0(1)
O(6)	1218(6)	2361(7)	4119(5)	2.5(1)
O(7)	556(7)	3164(8)	5920(7)	3.9(2)
O(8)	2514(6)	4359(6)	4289(5)	2.2(1)
O(9)	3621(6)	4261(7)	2470(6)	2.9(1)
O(10)	4152(7)	6300(7)	3131(6)	2.9(1)
O(11)	2281(6)	69(6)	1827(6)	2.4(1)
O(12)	1310(6)	−1835(7)	1140(6)	2.9(1)
O(13)	235(5)	1175(6)	1630(5)	1.7(1)
O(14)	544(6)	3576(7)	2308(6)	2.4(1)
O(15)	−1511(7)	3846(7)	1953(6)	3.2(1)
OW(1)	−958(7)	6709(7)	603(6)	3.3(1)
OW(2)	934(6)	5451(7)	1545(6)	2.8(1)
OW(3)	−3587(9)	6175(10)	1914(9)	6.1(2)
OW(4A) [b]	−1971(14)	8422(15)	3022(13)	3.3(4)
OW(4B)	−2307(13)	9549(15)	3127(12)	3.4(4)
OW(5)	4112(6)	8735(7)	2490(6)	2.4(1)
OW(6)	1750(7)	8082(7)	3742(6)	3.0(1)
OW(7)	3147(11)	6046(12)	−80(10)	8.1(3)
OW(8)	6279(7)	9144(7)	4848(6)	2.9(1)
OW(9)	205(7)	10079(7)	3972(6)	3.0(1)
C(1)	5315(9)	1775(9)	3265(8)	1.5(2)
C(2)	5713(10)	1705(10)	2118(9)	2.5(2)
C(3)	4861(10)	1745(10)	393(8)	2.5(2)
C(4)	3617(10)	1795(10)	−169(9)	1.9(2)
C(5)	1185(10)	3235(10)	5091(9)	2.2(2)
C(6)	1934(12)	4455(12)	5319(11)	3.9(2)
C(7)	3091(11)	5547(12)	4365(10)	3.7(2)
C(8)	3658(9)	5336(9)	3236(8)	1.6(2)
C(9)	1311(9)	−667(9)	1449(8)	1.3(2)
C(10)	10(9)	−133(10)	1351(9)	2.3(2)
C(11)	−946(9)	1821(10)	1751(9)	2.5(2)
C(12)	−606(10)	3188(10)	2007(9)	2.1(2)

[a] The anisotropic thermal parameters for cerium, calculated from the expression $\exp[-(h^2\beta_{11}+2hk\beta_{12}+\ldots\ldots)]$, are $\beta_{11}=0.00299(8)$, $\beta_{22}=0.00266(8)$, $\beta_{33}=0.00211(6)$, $\beta_{12}=0.00015(5)$, $\beta_{13}=0.00010(4)$ and $\beta_{23}=0.00134(5)$. [b] The occupancy factor for OW(4A) was refined to 0.49(2) resulting in the value 0.51(2) for OW(4B).

dispersion was made on the scattering factors for Ce and Na. The data for this correction were obtained from Cromer and Liberman.[14]

An isotropic extinction correction (Zachariasen [15]) was applied, $|F_{o,corr}|=|F_o|\ (1+g|F_c|^2\bar{T}\cdot 2.75\times 10^{-3})^{1/4}$, where g is the extinction parameter and $\bar{T}=-\ln A/\mu$. A is the transmission factor. The refined value of g was 2.27×10^4. The extinction coefficient on F_o varied in the interval 1.00 – 1.39, the largest corrections being applied to the reflexions $11\bar{4}$ (1.39), $\bar{2}2\bar{2}$ (1.35) and 130 (1.33).

The final positional and thermal parameters with estimated standard deviations are given in Table 1. Selected interatomic distances and angles are given in Tables 2 and 3. A list of

Table 2. The cerium coordination and the oxydiacetate ligands. Selected interatomic distances (Å) and angles (°) with estimated standard deviations.

Distance		Distance	
Ce – O(1)	2.466(6)	Ce – O(14)	2.464(7)
Ce – O(4)	2.503(6)	Ce – O(3)	2.588(6)
Ce – O(6)	2.476(6)	Ce – O(8)	2.564(6)
Ce – O(9)	2.470(7)	Ce – O(13)	2.597(6)
Ce – O(11)	2.485(7)		
Distance		**Angle**	
Ligand 1			
O(3) – C(2)	1.437(12)	C(2) – O(3) – C(3)	113.2(7)
O(3) – C(3)	1.428(12)	O(1) – C(1) – O(2)	124.0(9)
O(1) – O(2)	2.223(9)	O(1) – C(1) – C(2)	119.5(8)
O(4) – O(5)	2.229(9)	O(2) – C(1) – C(2)	116.6(8)
C(1) – O(1)	1.255(11)	O(4) – C(4) – O(5)	122.8(9)
C(1) – O(2)	1.263(12)	O(4) – C(4) – C(3)	120.2(9)
C(4) – O(4)	1.280(12)	O(5) – C(4) – C(3)	117.0(9)
C(4) – O(5)	1.259(12)	O(3) – C(2) – C(1)	109.1(8)
C(1) – C(2)	1.498(14)	O(3) – C(3) – C(4)	108.0(8)
C(3) – C(4)	1.488(14)		
Ligand 2			
O(8) – C(6)	1.416(14)	C(6) – O(8) – C(7)	112.0(8)
O(8) – C(7)	1.451(14)	O(6) – C(5) – O(7)	124.2(10)
O(6) – O(7)	2.243(10)	O(6) – C(5) – C(6)	119.4(9)
O(9) – O(10)	2.229(10)	O(7) – C(5) – C(6)	116.4(10)
C(5) – O(6)	1.263(13)	O(9) – C(8) – O(10)	124.5(9)
C(5) – O(7)	1.275(13)	O(9) – C(8) – C(7)	119.8(9)
C(8) – O(9)	1.250(12)	O(10) – C(8) – C(7)	115.7(9)
C(8) – O(10)	1.269(12)	O(8) – C(6) – C(5)	107.5(9)
C(5) – C(6)	1.514(17)	O(8) – C(7) – C(8)	107.2(9)
C(7) – C(8)	1.495(15)		
Ligand 3			
O(13) – C(10)	1.429(12)	C(10) – O(13) – C(11)	112.2(7)
O(13) – C(11)	1.435(12)	O(11) – C(9) – O(12)	125.3(9)
O(11) – O(12)	2.234(10)	O(11) – C(9) – C(10)	119.1(9)
O(14) – O(15)	2.234(10)	O(12) – C(9) – C(10)	115.6(8)
C(9) – O(11)	1.259(11)	O(14) – C(12) – O(15)	125.6(10)
C(9) – O(12)	1.256(12)	O(14) – C(12) – C(11)	117.6(9)
C(12) – O(14)	1.262(12)	O(15) – C(12) – C(11)	116.7(9)
C(12) – O(15)	1.249(13)	O(13) – C(10) – C(9)	107.2(8)
C(9) – C(10)	1.528(13)	O(13) – C(11) – C(12)	108.2(8)
C(11) – C(12)	1.519(15)		

structure factors is available, on request, from the author. As the refinement in space group $P\bar{1}$ was satisfactory, no attempt was made to try the non-centrosymmetric $P1$.

DISCUSSION

As shown in Figs. 1 and 2 the structure can be described as composed of layers of the negatively charged mononuclear tris(oxydiacetato)cerate(III) complexes alternating with layers containing the sodium ions and the water molecules. The layers are parallel to the plane $(01\bar{1})$. The cerium ion is nine-coordinated. The sodium ions are surrounded by distorted octahedra or trigonal bipyramids of oxygen atoms belonging to the carboxylate groups and the water molecules, forming finite chains with six sodium ions in each. The sodium chains are held together by hydrogen bonds. The

Table 3. The sodium coordination. Selected interatomic distances (Å) with estimated standard deviations. (i) $-x, 1-y, 1-z$; (ii) $x, 1+y, z$; (iii) $1-x, 1-y, 1-z$; (iv) $1-x, 2-y, 1-z$.

Distance		Distance	
Na(1)–O(7^{i})	2.382(9)	Na(3)–O(2^{iii})	2.391(8)
Na(1)–O(15)	2.488(9)	Na(3)–O(10)	2.515(8)
Na(1)–OW(1)	2.390(9)	Na(3)–OW(5)	2.434(8)
Na(1)–OW(2)	2.439(8)	Na(3)–OW(6)	2.435(8)
Na(1)–OW(3)	2.445(11)	Na(3)–OW(8)	2.436(8)
Na(1)–OW(4A)	2.664(17)	Na(3)–OW(8^{iv})	2.449(8)
Na(1)–OW(4B)	3.946(17)		
Na(2)–O(10)	2.602(8)	Na(1)–Na(2)	4.179(6)
Na(2)–O(12^{ii})	2.415(8)	Na(2)–Na(3)	3.292(5)
Na(2)–OW(2)	2.348(8)	Na(3)–Na(3^{iv})	3.599(8)
Na(2)–OW(5)	2.402(8)		
Na(2)–OW(6)	2.461(8)		
Na(2)–OW(7)	2.345(13)		

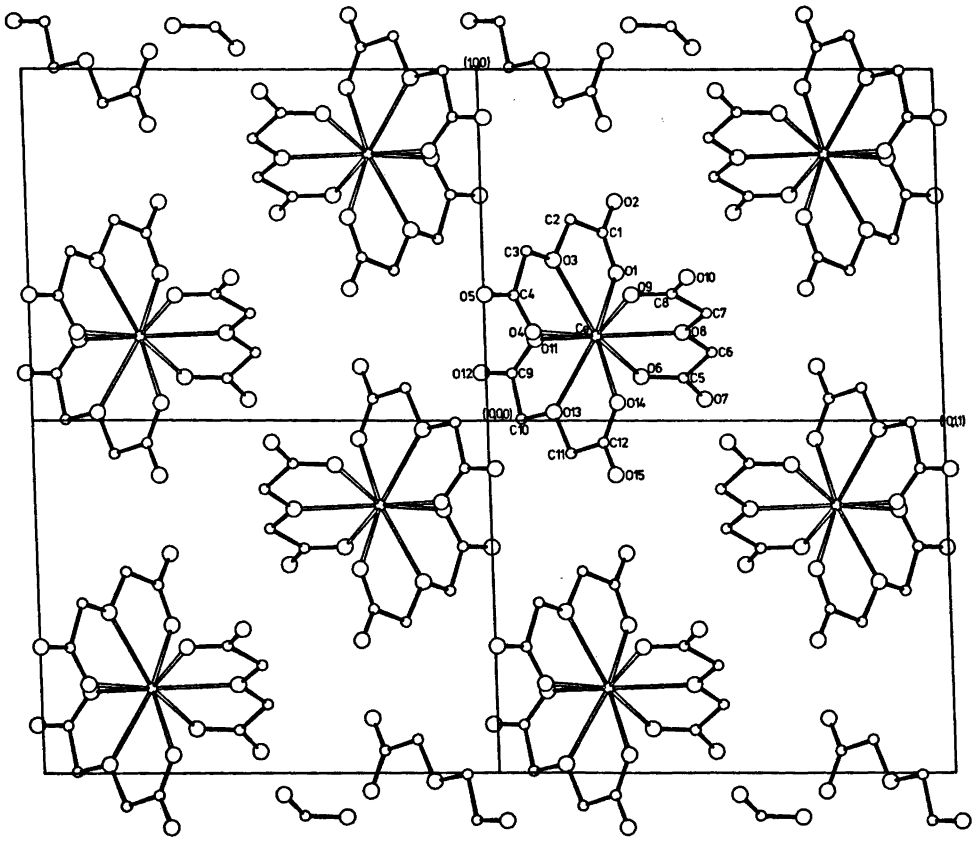

Fig. 1. The layer containing the tris(oxydiacetato)cerate(III) complexes projected on the plane $(0\bar{1}1)$.

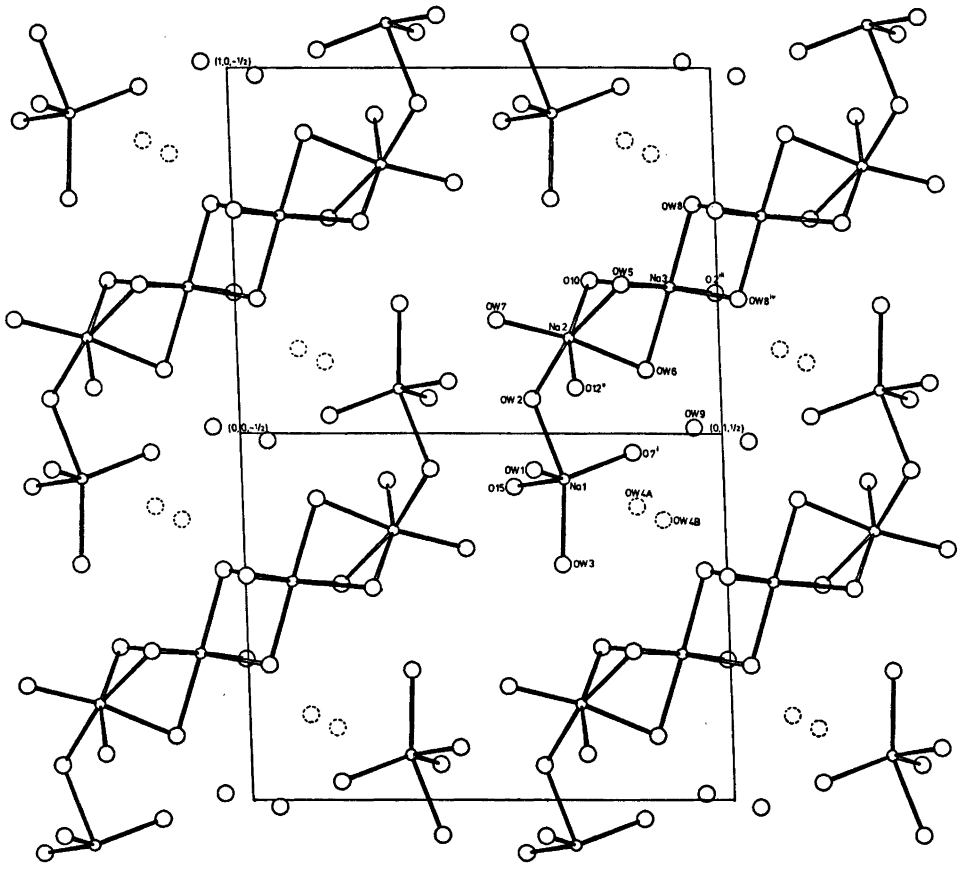

Fig. 2. The layer containing the sodium chains and the water molecules projected on the plane (01$\bar{1}$).

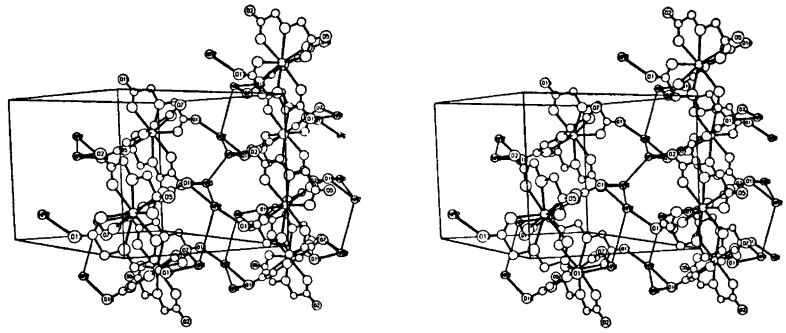

Fig. 3. A stereoscopic pair of drawings showing the connection of the tris(oxydiacetato)cerate(III) complexes by the sodium ions. The sodium chain is shown, but the water oxygens are excluded. The unit cell edges are **b** to the right, **a** upwards and **c** to the left into the figure.

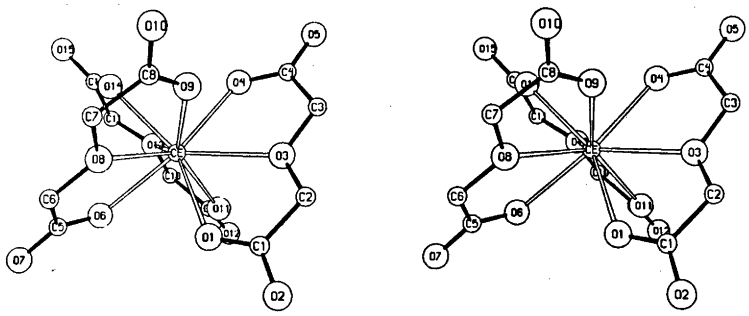

Fig. 4. A stereoscopic pair of drawings of the cerium coordination polyhedron.

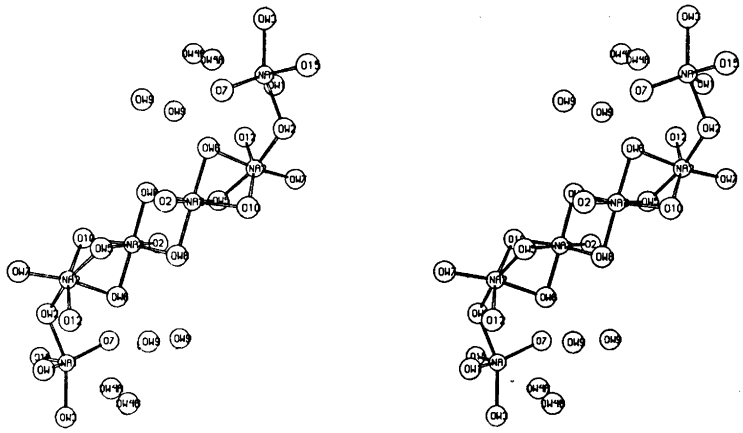

Fig. 5. A stereoscopic pair of drawings of the sodium chain including the water oxygen atoms OW(4) and OW(9).

cerium and sodium layers are connected by the coordination of all outer carboxylate ions of the cerium complexes [except O(5)] to the sodium ions and by hydrogen bonds. Thus the cerium complexes of different layers are held together by the sodium ions Na(2) *via* bonds Na(2)–O(10) and Na(2)–O(12). This gives infinite chains parallel to the **b**-axis as is indicated in Fig. 3. That figure also shows that within each cerium layer each complex is connected to two other complexes *via* bonds Na(1)–O(7), Na(1)–O(15), Na(3)–O(2) and Na(3)–O(10) (one bond of each kind to each complex), in this way forming a zig-zag chain in the **a** direction. The complex ions are thus connected by sodium ions to layers parallel to the *ab*-plane. Between these layers there are only hydrogen and van der Waals bonds.

The coordination polyhedron around the cerium ion is a distorted tricapped trigonal prism of oxygen atoms, very similar to that in CDG.[1,2] The water oxygen atoms in the nona-aqualanthanoid bromates form, *e.g.*, a regular prism of this type.[16,17] A stereoscopic pair of drawings of the coordination polyhedron with designation of the atoms is shown in Fig. 4. The two triangular faces of the prism are formed by the carboxylate oxygens. The mean distance from these to the cerium ion is 2.48 Å (Table 2). The distances from the ether oxygen atoms to the cerium ion are significantly longer than the other oxygen-cerium distances, the average value is 2.58 Å. The contact distances between oxygen atoms belonging to different ligands are in the range 2.99–3.48 Å. A comparison with the geometry of the co-

ordination polyhedron of CDG will be given in a following paper.

The shortest distance between two cerium ions is 8.10 Å. Three more cerium ions are at distances of 8.61 – 8.71 Å and two at 10.36 Å. All these nearest neighbours are in the same cerium layer. Six cerium ions from other layers are at distances of 11.16 – 11.62 Å. The separations of the cerium ions are thus not as large as in CDG, where the shortest distance Ce – Ce is 9.81 Å.

The atoms in each ligand are nearly coplanar. The deviations of the atoms from the least-squares planes through the ligand molecules are less than about 0.1 Å. The distances and angles within the ligand molecules are in good agreement with those found in the acid salts of alkali metal ions.[18,19]

Six sodium ions, Na(1) – Na(2) – Na(3) – Na(3^{iv}) – Na(2^{iv}) – Na(1^{iv}), form a chain across a center of symmetry, the surrounding polyhedra of oxygen atoms sharing corners, edges and faces (Fig. 5). Na(1) and Na(2) share one oxygen atom [OW(2)], Na(2) and Na(3) three [O(10), OW(5) and OW(6)], and Na(3) and Na(3^{iv}) two [OW(8) and OW(8^{iv})]. The sodium-oxygen distances to the six nearest oxygen atoms around each sodium ion range between 2.35 and 2.52 Å (Table 3), except the distance Na(2) – O(10) (2.60 Å) and Na(1) – OW(4A) (2.66 Å). OW(4B) is not coordinated to a sodium ion. The coordination to each sodium ion can be described by distorted octahedra. However, as the occupancy factor of the statistically distributed oxygen atom OW(4) is about the same in both positions in spite of the different distances to Na(1), the interaction between OW(4A) and Na(1) must be very small. This fact and the large deviation of the angle O(7) – Na(1) – OW(1) from the octahedral value (135° compared to 180°) indicate that the coordination polyhedron around Na(1) might be better described by a distorted trigonal bipyramid than by a distorted octahedron. The oxygen-oxygen distances along the edges of the polyhedra are in the interval 3.00 – 4.41 Å.

Acknowledgements. My thanks are due to Dr. Jörgen Albertsson for the supply of a sample of TCDG crystals, and for helpful advice and discussions. I also wish to thank Professor Ido Leden for his kind interest in this work. The Swedish Natural Science Research Council gave financial support, which is gratefully acknowledged.

REFERENCES

1. Albertsson, J. *Acta Chem. Scand. 22* (1968) 1563.
2. Albertsson, J. *Acta Chem. Scand. 24* (1970) 3527.
3. Albertsson, J. *Acta Chem. Scand. 24* (1970) 1213.
4. Albertsson, J. *Acta Chem. Scand. 26* (1972) 985.
5. Albertsson, J. *Acta Chem. Scand. 26* (1972) 1005.
6. Albertsson, J. *Acta Chem. Scand. 26* (1972) 1023.
7. Doran, J. C., Erich, U. and Wolf, W. P. *Phys. Rev. Lett. 28* (1972) 103.
8. Wu, C. Y., Alben, R. and Wolf, W. P. *Solid State Commun. 11* (1972) 1599.
9. Albertsson, J., Chen, P. Y. and Wolf, W. P. *Phys. Rev. B 11* (1975) 1943.
10. Webb, R. A. and Wheatley, J. C. *Phys. Rev. Lett. 29* (1972) 1150.
11. Danielsson, S., Grenthe, I. and Oskarsson, Å. *J. Appl. Crystallogr. 9* (1976) 14.
12. Cromer, D. T., Larson, A. C. and Water, J. T. *Acta Crystallogr. 17* (1964) 1044.
13. Hanson, H. P., Herman, F., Lea, J. D. and Skillman, S. *Acta Crystallogr. 17* (1964) 1040.
14. Cromer, D. T. and Liberman, D. *J. Chem. Phys. 53* (1970) 1891.
15. Zachariasen, W. H. *Acta Crystallogr. 23* (1967) 558.
16. Helmholz, L. *J. Am. Chem. Soc. 61* (1939) 1544.
17. Sikka, S. K. *Acta Crystallogr. A 25* (1969) 621.
18. Albertsson, J., Grenthe, I. and Herbertsson, H. *Acta Crystallogr. B 29* (1973) 1855.
19. Albertsson, J., Grenthe, I. and Herbertsson, H. *Acta Crystallogr. B 29* (1973) 2839.

Received March 12, 1976.

Acta Chemica Scandinavica A 30 (1976) 657—660

On the Crystal Structures of *cis*- and *trans*-Bis(ethylenediamine)-dinitrocobalt(III) Nitrate

OLLE BÖRTIN

Department of Inorganic Chemistry, University of Göteborg and Chalmers University of Technology, P.O. Box, S-402 20 Göteborg 5, Sweden

The crystal structure of *trans*-bis(ethylenediamine)dinitrocobalt(III) nitrate has been refined. The crystals are monoclinic with $a=13.819(5)$ Å, $b=9.680(2)$ Å, $c=9.095(2)$ Å, $\beta=105.83(2)°$, $V=1170.4$ Å^3, $Z=4$ and space group $P2_1/a$. Least-squares refinement of the structure, based on 4212 reflections, gave an R-value of 0.05. The *trans*-bis(ethylenediamine)-dinitrocobalt(III) ions are arranged in a cubic close-packed manner with the nitrate ions in the octahedral holes. The cobalt atom is octahedrally coordinated by six nitrogen atoms with the bond distances: Co—N (to NO_2) 1.937—1.939(2) Å, and Co—N (to en) 1.942—1.959(2) Å.

In connection with studies of nitro and nitrito compounds of transition metals the crystal structures of pentaamminenitrocobalt(III) chloride [1] and *cis*- and *trans*-bis(ethylenediamine)-dinitrocobalt(III) nitrate [2,3] were determined. Some of the bond distances in *trans*-$[Co(NO_2)_2(en)_2]NO_3$ were surprising, *e.g.* Co—N (to NO_2) 1.81 and 2.02 Å. There were also large differences between the N—O bonds in the nitro groups and in the nitrate ions. In order to ascertain whether or not these differences in bond distances were correct a new refinement of the structure has been performed.

trans-$[Co(NO_2)_2(en)_2]NO_3$

Crystal data. $a=13.819(5)$ Å, $b=9.680(2)$ Å, $c=9.095(2)$ Å, $\beta=105.83(2)°$, $V=1170.4$ Å^3, $Z=4$, space group $P2_1/a$, $D_c=1.92$ g cm^{-3}.

Refinement. The refinement was based on the $0kl-26kl$ intensities recorded with a Philips Pailred automatic single crystal diffractometer with Mo$K\alpha$ radiation, monochromatized with a graphite crystal. All intensities were corrected for Lorentz and polarization effects using the program DATAP1. The atomic scattering factors used for Co, N, O, and C were those calculated by Doyle and Turner.[4] The structure factors were weighted according to Cruickshank [5] with $a=30.0$ and $c=0.01$. The scale-factors of the separate layers were refined. It was noticed that, when the scale-factors were plotted against the layer number, those of the even layers yielded a smooth curve while those of the odd layers did not. The scale-factors of the odd layers were assigned values corresponding to this curve and refinement based only on the odd layers was undertaken, an overall scale-factor being refined. This caused the x-coordinate of the cobalt atom to change from 0.1205 to 0.1295, corresponding to a displacement of 0.12 Å. The refinement was continued with anisotropic thermal parameters with the complete three-dimensional data. At this stage a difference syntheses was performed giving the positions of the hydrogen atoms. The electron densities corresponding to the hydrogen atoms varied between 0.6 and 1.1 e Å^{-3}, while the highest spurious peak, which was situated at the position of the cobalt atom, had a height of 1.0 e Å^{-3}. The coordinates and isotropic temperature factors of the hydrogen atoms were refined using the scattering factors for hydrogen calculated by Stewart.[6] Finally separate scale-factors were refined for each layer and the reliability index converged to 0.05. The resulting parameters for the heavier atoms are given in Table 1 and for the hydrogen atoms in Table

Table 1. Final atomic parameters for *trans*-$[Co(NO_2)_2(en)_2]NO_3$ (standard deviations in parentheses). The anisotropic temperature factor is $\exp\{-(h^2(a^*)^2u_{11}+k^2(b^*)^2u_{22}+l^2(c^*)^2u_{33}+2hka^*b^*u_{12}+2hla^*c^*u_{13}+2klb^*c^*u_{23})\}$.

Atom	x	y	z	$u_{ij}\times 10^4$ u_{11}	u_{22}	u_{33}	u_{12}	u_{13}	u_{23}
Co	0.12934(2)	0.25934(3)	0.25261(4)	128(1)	131(1)	137(1)	−1(1)	20(1)	5(1)
N1	0.2719(2)	0.3494(3)	0.3515(3)	178(6)	269(9)	211(8)	−18(8)	21(7)	16(8)
O11	0.3094(2)	0.1238(3)	0.3772(4)	244(9)	379(12)	550(17)	85(9)	−34(11)	112(12)
O12	0.3258(2)	0.3431(3)	0.3864(3)	235(8)	397(12)	463(15)	−107(9)	−1(10)	−48(11)
N2	−0.0126(2)	0.2834(3)	0.1532(3)	177(7)	270(9)	211(9)	49(7)	21(7)	16(8)
O21	−0.0473(2)	0.4000(3)	0.1279(3)	296(10)	334(11)	512(16)	116(10)	−4(11)	80(11)
O22	−0.0675(2)	0.1811(3)	0.1182(3)	193(8)	381(12)	485(15)	−51(9)	−23(9)	−39(11)
N31	0.0969(2)	0.1202(2)	0.3858(3)	248(8)	190(8)	206(9)	−35(7)	35(8)	14(7)
C32	0.1045(2)	0.1805(4)	0.5389(3)	328(11)	356(14)	171(10)	−34(11)	71(10)	35(10)
C33	0.0683(2)	0.3281(4)	0.5143(4)	258(10)	332(13)	272(13)	−19(10)	92(11)	−54(11)
N34	0.1201(2)	0.3919(2)	0.4086(3)	266(8)	213(8)	232(10)	−25(8)	74(9)	−25(8)
N41	0.1381(2)	0.1229(2)	0.0977(3)	184(7)	204(8)	211(9)	2(7)	26(7)	−22(7)
C42	0.1917(2)	0.1840(3)	−0.0058(3)	229(8)	330(13)	231(11)	29(9)	104(10)	−11(10)
C43	0.1569(2)	0.3327(3)	−0.0341(4)	281(10)	312(13)	230(11)	−14(10)	80(10)	32(10)
N44	0.1627(2)	0.3963(2)	0.1170(3)	258(9)	205(8)	223(10)	−31(8)	35(9)	35(7)
N5	0.3838(2)	0.2912(3)	0.7556(3)	385(11)	234(8)	243(9)	18(9)	112(10)	4(9)
O51	0.3807(3)	0.1636(3)	0.7515(4)	970(26)	217(9)	573(19)	46(15)	171(20)	−3(12)
O52	0.4660(2)	0.3545(3)	0.7906(3)	276(10)	531(15)	440(15)	5(11)	42(11)	119(13)
O53	0.3040(2)	0.3609(3)	0.7233(4)	284(10)	385(12)	499(15)	18(10)	38(11)	−97(12)

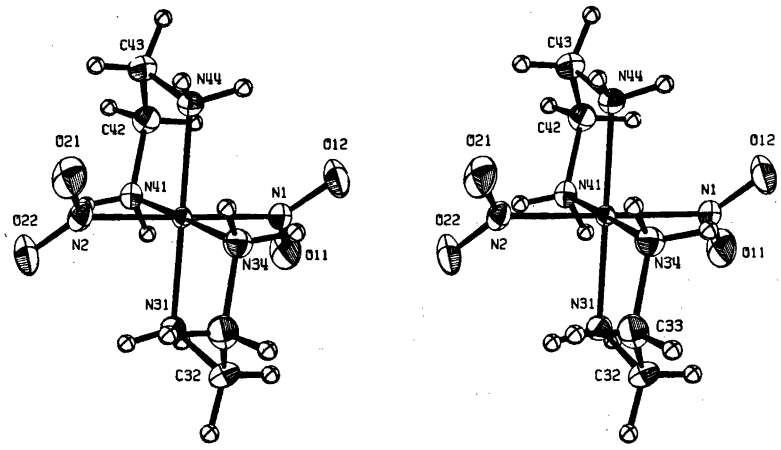

Fig. 1. A stereoscopic view of the ion *trans*-$[Co(NO_2)_2(en)_2]^+$.

2. A list of observed and calculated structure factors can be obtained from the author on request. The *trans*-$[Co(NO_2)_2(en)_2]^+$ ion is shown in Fig. 1, and the unit cell in Fig. 2, drawn with ORTEP. Bond distances and some angles are given in Table 3, together with their standard deviations. Distances and angles for hydrogen bonds are given in Table 4.

cis-$[Co(NO_2)_2(en)_2]NO_3$

Crystal data. $a=11.745(2)$ Å, $b=16.090(3)$ Å, $c=6.512(1)$ Å, $\beta=98.92(2)°$, $V=1215.8$ Å^3 $Z=4$, space group $P2_1/n$, $D_c=1.82$ g cm^{-3}, $D_o=1.85$ g cm^{-3}.

A brief account of the crystal structure analysis of this compound has been published.[2] The *cis*-bis(ethylenediamine)dinitrocobalt(III) ion is shown in Fig. 3 and some bond distances and angles are given in Table 5.

Table 2. Final parameters of hydrogen atoms. The temperature factor is $\exp(-B \sin^2\theta/\lambda)$.

Atom	x	y	z	B
H311	0.037(4)	0.091(5)	0.349(5)	3.7(11)
H312	0.132(3)	0.042(4)	0.391(5)	2.4(8)
H321	0.067(4)	0.128(5)	0.602(5)	3.6(10)
H322	0.167(3)	0.174(5)	0.588(5)	3.2(10)
H331	−0.005(3)	0.336(4)	0.464(4)	1.9(8)
H332	0.082(4)	0.389(5)	0.607(6)	4.2(11)
H341	0.093(3)	0.472(4)	0.371(5)	2.8(9)
H342	0.184(4)	0.426(6)	0.464(6)	5.2(13)
H411	0.078(3)	0.100(4)	0.053(4)	2.2(8)
H412	0.168(3)	0.038(4)	0.152(5)	2.8(9)
H421	0.176(3)	0.122(5)	−0.105(5)	3.4(10)
H422	0.264(3)	0.172(5)	0.049(5)	3.0(10)
H431	0.090(3)	0.344(4)	−0.083(5)	2.4(8)
H432	0.199(3)	0.387(5)	−0.081(5)	2.8(9)
H441	0.129(3)	0.474(5)	0.107(5)	2.9(9)
H442	0.224(3)	0.438(5)	0.164(5)	3.0(9)

Table 3. Bond distances and angles in *trans*-$[Co(NO_2)_2(en)_2]NO_3$ (standard deviations in parentheses). Angles round Co not indicated in the table are 88.6–91.2° or 178.8–179.0°. Bond distances N–H are 0.84–0.99(5) Å, mean 0.90 Å, and C–H 0.86–1.06(5) Å, mean 0.98 Å.

Distance (Å)		Angle (°)	
Co –N1	1.939(2)	N31–Co –N34	86.0(1)
Co –N2	1.937(2)	N31–Co –N41	92.9(1)
Co –N31	1.944(2)	N34–Co –N44	95.0(1)
Co –N34	1.942(3)	N41–Co –N44	86.1(1)
Co –N41	1.959(2)	Co –N1 –O11	120.1(2)
Co –N44	1.950(2)	Co –N1 –O12	120.2(2)
N1 –O11	1.228(4)	O11–N1 –O12	119.8(2)
N1 –O12	1.238(4)	Co –N2 –O21	119.6(2)
N2 –O21	1.224(4)	Co –N2 –O22	119.8(2)
N2 –O22	1.236(4)	O21–N2 –O22	120.6(2)
N31–C32	1.487(4)	Co –N31–C32	110.0(2)
C32–C33	1.509(5)	N31–C32–C33	107.3(2)
C33–N34	1.482(4)	C32–C33–N34	106.9(2)
N41–C42	1.471(4)	C33–N34–Co	109.8(2)
C42–C43	1.517(5)	Co –N41–C42	109.3(2)
C43–N44	1.487(4)	N41–C42–C43	107.3(2)
		C42–C43–N44	107.5(2)
N5 –O51	1.235(4)	C43–N44–Co	109.9(2)
N5 –O52	1.253(4)		
N5 –O53	1.258(4)	O51–N5 –O52	121.2(3)
		O51–N5 –O53	120.6(3)
		O52–N5 –O53	118.2(3)

DESCRIPTION AND DISCUSSION

The cobalt atoms of *cis*- and *trans*-$[Co(NO_2)_2(en)_2]^+$ ions are octahedrally coordinated by the nitrogen atoms from two nitro groups and two ethylenediamine groups. The greater *trans* effect of the nitro group is obvious. The bond distances Co–N (to NO_2) are 1.937–1.939(2) Å in the *trans* compound and 1.887–1.918(17) Å when the nitro groups are in *trans* position to amine nitrogen atoms in the *cis* compound. The bond distances Co–N (to en) are 1.991–1.997(17) Å when *trans* to NO_2 in the *cis* compound, and 1.942–1.959(2) Å and 1.941–1.971(17) Å when *trans* to an other amine nitrogen atom in the *trans* respectively *cis* compounds.

Table 4. Hydrogen bonds N–H···O in *trans*-$[Co(NO_2)_2(en)_2]NO_3$.

Atoms N	H	O	Distances (Å) H–O	N–O	Angle (°) N–H–O
N31	H311	O22	2.36	2.90	121 [a]
N31	H312	O53	2.33	3.15	152
N34	H341	O51	2.24	3.01	143
N34	H342	O11	2.39	2.96	118
N34	H342	O12	2.39	2.94	117 [a]
N41	H411	O22	2.38	2.95	125 [a]
N41	H412	O53	2.03	3.00	166
N44	H441	O21	2.45	3.08	128
N44	H441	O51	2.27	2.98	139
N44	H442	O12	2.32	2.89	119 [a]

[a] All atoms belong to the same complex ion.

Table 5. Bond distances and angles in the *cis*-bis-(ethylenediamine)dinitrocobalt(III) ion (standard deviations in parentheses). Angles round Co not indicated in the table are 88.8–92.5° or 175.7–176.8°.

Distance (Å)		Angle (°)	
Co –N1	1.887(17)	N31–Co –N34	85.9(7)
Co –N2	1.918(18)	N41–Co –N44	85.1(7)
Co –N31	1.941(17)	Co –N1 –O11	122.6(14)
Co –N34	1.997(14)	Co –N1 –O12	121.3(13)
Co –N41	1.971(16)	O11–N1 –O12	116.1(17)
Co –N44	1.991(17)	Co –N2 –O21	121.4(14)
N1 –O11	1.229(22)	Co –N2 –O22	119.5(14)
N1 –O12	1.231(22)	O21–N2 –O22	118.7(18)
N2 –O21	1.211(26)	Co –N31–C32	111.4(13)
N2 –O22	1.226(26)	N31–C32–C33	109.9(19)
N31–C32	1.501(28)	C32–C33–N34	108.2(18)
C32–C33	1.470(34)	C33–N34–Co	108.3(11)
C33–N34	1.528(25)	Co –N41–C42	113.4(13)
N41–C42	1.469(27)	N41–C42–C43	105.9(16)
C42–C43	1.564(31)	C42–C43–N44	109.6(17)
C43–N44	1.505(26)	C43–N44–Co	108.9(12)

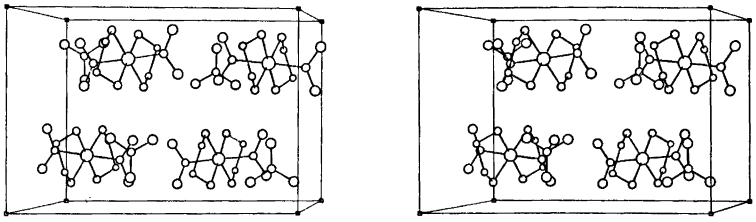

Fig. 2. A stereoscopic view of the structure of *trans*-bis(ethylenediamine)dinitrocobalt(III) nitrate.

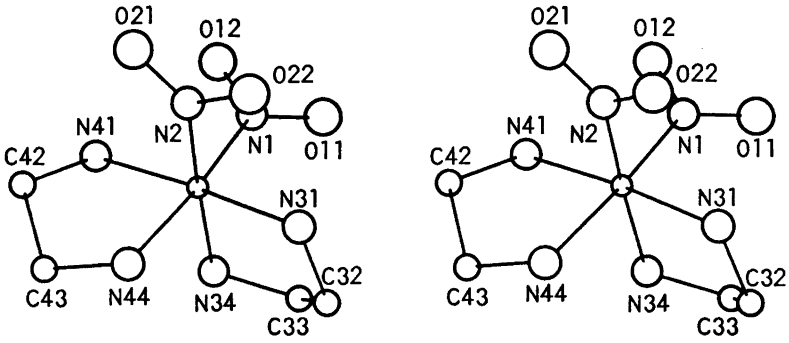

Fig. 3. A stereoscopic view of the ion *cis*-$[Co(NO_2)_2(en)_2]^+$.

When a plane is drawn through the cobalt atom and the nitrogen atoms of an ethylenediamine group, the carbon atoms will be situated on either side of it and at different distances, 0.18 and 0.41 Å for one group and 0.28 and 0.34 Å for the other for the *cis* compound and 0.26 and 0.40 Å for one group and 0.29 and 0.37 Å for the other for the *trans* compound.

The large complex ions are arranged in close-packed manners. In *trans*-bis(ethylenediamine)-dinitrocobalt(III) nitrate the cations are ordered in a cubic close-packed manner and, as the nitrate ions occupy the octahedral holes, the structure can be visualised as a distorted sodium chloride structure. In *cis*-bis(ethylenediamine)dinitrocobalt(III) nitrate the nitrate ions occupy tetrahedral holes between the cations with two nitrate ions fairly close to one another with a separation of 3.23 Å between the nitrogen atoms. The complex ions are linked to one another and to the nitrate ions by means of hydrogen bonds N–H···O. The shortest N–O distance indicating this in the *cis* compound is 2.89 Å. In the *trans* compound there are also hydrogen bonds N–H···O within the complex ions.

Acknowledgements. I wish to thank Professor Georg Lundgren for his stimulating interest in this work.

This work has been supported by Chalmers University of Technology, which has supplied a grant to cover the costs of the computer work, which was performed at the Göteborg Universities' Computing Centre.

REFERENCES

1. Börtin, O. *Acta Chem. Scand. 22* (1968) 2890.
2. Börtin, O. *Acta Chem. Scand. 23* (1969) 3273.
3. Börtin, O. *Acta Chem. Scand. 23* (1969) 3274.
4. Doyle, P. A. and Turner, P. S. *Acta Crystallogr. A 24* (1968) 390.
5. Cruickshank, D. W. J. *The Equations of Structure Refinements*, Glasgow 1964.
6. Stewart, R. F., Davidson, E. R. and Simpson, W. T. *J. Chem. Phys. 42* (1965) 3175.

Received January 20, 1976.

Acta Chemica Scandinavica A 30 (1976) 661—666

Structures of Linear Multisulfur Systems. XI. The Crystal and Molecular Structure of 2-(5-Phenyl-1,2-dithiole-3-ylidene)-6-(5-*t*-butyl-1,2-dithiole-3-ylidene)-cyclohexanethione, $C_{22}H_{22}S_5$

JORUNN SLETTEN

Department of Chemistry, University of Bergen, Allégaten 70, N-5014 Bergen-Univ., Norway

Crystals of the title compound, $C_{22}H_{22}S_6$, are monoclinic, space group $P2_1/c$, with $Z=4$ in a unit cell of dimensions $a=11.289(3)$, $b=23.952(6)$, $c=9.614(2)$ Å, $\beta=126.65(1)°$. 3286 unique reflections were recorded on a four-circle diffractometer. The structure was solved by direct methods and refined by full-matrix least-squares technique to a final R of 0.082. The five sulfur atoms are approximately collinear, all S—S bond lengths being intermediate between a single bond and van der Waals distance; S(1)—S(2) = 2.179(3), S(2)—S(3) = 2.554(3), S(3)—S(4) = 2.582(3), and S(4)—S(5) = 2.149(3) Å. The structure of another modification of this compound has previously been solved. There are only minor differences between the two molecular structures, while the packing of the molecules in the crystal differs appreciably.

A structure investigation of the title compound was first carried out in 1970, and the results were reported in a short note.[1] The crystals originally obtained were of poor quality and the atomic parameters arrived at had low accuracy. In order to improve these results a reinvestigation was planned. It was difficult to get suitable crystals of the original modification (later referred to as mod. 1). However, adequate crystals of another modification (mod. 2) were obtained and used for X-ray investigation.

EXPERIMENTAL

The compound has been synthesized by Stavaux and Lozac'h.[2] Various crystallization procedures were tried. The crystals used in this investigation grew by slow evaporation from a carbon disulfide solution at approximately 5 °C, while crystals of mod. 1 were obtained from DMSO at room temperature.[1] A crystal of dimensions $0.43 \times 0.06 \times 0.32$ mm was chosen for data collection. The space group was derived from photographic Weissenberg and precession data, and unit cell dimensions from diffractometer measurement of 2θ values for 16 reflections with $2\theta > 30°$ [$\lambda_{(MoK\alpha_1)} = 0.70926$ Å]. These measurements were performed with an ω-scan procedure.[3] 3286 unique reflections with $2\theta \leqslant 48°$ were recorded according to the experimental procedure described elsewhere.[4] The intensities of 1100 of the reflections were less than the estimated error in measurements; these reflections were given the threshold value of σ_I and were included in the refinement only if $|F_c| > |F_{threshold}|$. Standard deviations in intensities were calculated as $\sigma_I = k[\sigma_c^2 + (0.01N_{net})^2]^{\frac{1}{2}}$, where k is the appropriate scale factor, σ_c is the estimated error due to counting statistics, N_{net} is the net count of the reflection. The data were corrected for Lorentz and polarization effects and for absorption. Standard deviations in the structure factors were calculated as $\sigma_F = \sigma_I/2(ILp)^{\frac{1}{2}}$.

CRYSTAL DATA

Mod. 2 (present work)	Mod. 1.[1]
$C_{22}H_{22}S_5$; M.W. = 446.74	as mod. 2
Space group $P2_1/c$	as mod. 2
a = 11.289(3) Å	a = 20.009(9) Å
b = 23.952(6) Å	b = 8.066(6) Å
c = 9.614(2) Å	c = 13.457(7) Å
β = 126.65(1)°	β = 103.07(2)°
V = 2085.6(9) Å^3	V = 2116(2) Å^3
Z = 4	Z = 4
$\mu(MoK\alpha) = 5.43$ cm^{-1}	$\mu(MoK\alpha) = 5.35$ cm^{-1}
$D_x = 1.423$ g cm^{-3}	$D_x = 1.403$ g cm^{-3}

D_m not measured due to lack of material.

Table 1. Atomic coordinates and anisotropic thermal parameters with the corresponding standard deviations, referring to the last decimal places, listed in parentheses. The anisotropic temperature factors are defined by: $T_i = \exp[-2\pi^2(U_{11}h^2a^{*2} + U_{22}k^2b^{*2} + U_{33}l^2c^{*2} + 2U_{12}hka^*b^* + 2U_{13}hla^*c^* + 2U_{23}klb^*c^*)]$; the values are multiplied by 10^3.

Atom	X/a	Y/b	Z/c	U_{11}	U_{22}	U_{33}	U_{12}	U_{13}	U_{23}
S(1)	1.06411(20)	0.63622(8)	0.06342(23)	57(1)	61(1)	48(1)	−19(1)	26(1)	−9(1)
S(2)	0.98324(18)	0.57656(8)	0.16007(21)	44(1)	58(1)	37(1)	−10(1)	17(1)	−8(1)
S(3)	0.87710(21)	0.50850(8)	0.26387(21)	48(1)	68(1)	30(1)	−15(1)	16(1)	−10(1)
S(4)	0.78077(19)	0.43869(8)	0.38003(20)	46(1)	67(1)	27(1)	−6(1)	16(1)	−3(1)
S(5)	0.69818(21)	0.37966(9)	0.47117(21)	61(1)	83(2)	35(1)	−12(1)	26(1)	0(1)
C(1)	0.9600(6)	0.6104(3)	−.1443(7)	30(4)	45(4)	46(4)	5(3)	21(3)	6(3)
C(2)	0.8723(7)	0.5669(3)	−.1733(8)	43(4)	47(5)	37(4)	−6(4)	22(3)	−3(3)
C(3)	0.8598(7)	0.5458(3)	−.0448(7)	38(4)	29(4)	36(4)	2(3)	17(3)	−1(3)
C(4)	0.7574(7)	0.5058(3)	−.0760(7)	41(4)	41(4)	26(3)	5(3)	14(3)	4(3)
C(5)	0.7515(6)	0.4844(3)	0.0578(7)	32(4)	46(4)	21(3)	10(3)	7(3)	3(3)
C(6)	0.6454(7)	0.4440(3)	0.0287(8)	47(4)	45(5)	40(4)	−4(4)	22(4)	4(3)
C(7)	0.6483(7)	0.4208(3)	0.1610(7)	47(4)	41(4)	37(4)	3(4)	22(4)	−2(3)
C(8)	0.5472(7)	0.3790(3)	0.1394(7)	46(4)	53(5)	31(4)	−19(4)	15(3)	−10(3)
C(9)	0.5580(7)	0.3554(3)	0.2684(8)	43(4)	48(4)	42(4)	2(3)	27(4)	2(3)
C(10)	0.9691(7)	0.6378(3)	−.2733(8)	41(4)	39(4)	51(4)	2(4)	26(4)	0(3)
C(11)	1.0709(8)	0.6798(3)	−.2268(9)	64(5)	72(6)	54(5)	−10(5)	31(4)	−1(4)
C(12)	1.0749(9)	0.7060(3)	−.3501(13)	80(7)	65(6)	100(7)	−12(5)	53(6)	4(6)
C(13)	0.9802(10)	0.6934(3)	−.5223(11)	95(7)	61(6)	97(6)	8(5)	71(6)	28(5)
C(14)	0.8773(8)	0.6512(3)	−.5721(10)	60(5)	83(6)	61(5)	−1(4)	41(5)	15(4)
C(15)	0.8736(7)	0.6246(3)	−.4491(9)	55(5)	59(5)	57(5)	−13(4)	33(4)	1(4)
C(16)	0.6457(8)	0.4839(3)	−.2583(8)	74(6)	67(5)	36(4)	−13(4)	32(4)	−5(4)
C(171)	0.5083(20)	0.4637(10)	−.2982(25)	18(11)	140(22)	29(10)	−33(11)	−10(8)	57(11)
C(172)	0.5606(22)	0.4343(9)	−.2635(21)	48(14)	102(18)	8(9)	−38(12)	−11(9)	4(9)
C(18)	0.5258(8)	0.4254(3)	−.1568(7)	80(6)	100(7)	19(3)	−58(5)	12(4)	−16(4)
C(19)	0.4600(7)	0.3093(3)	0.2572(8)	48(4)	51(5)	49(4)	8(4)	29(4)	6(4)
C(20)	0.5479(9)	0.2543(4)	0.3236(10)	93(6)	68(6)	101(7)	−2(5)	59(6)	7(5)
C(21)	0.4065(9)	0.3233(3)	0.3642(10)	72(6)	100(7)	78(5)	5(5)	54(5)	9(5)
C(22)	0.3212(9)	0.3009(3)	0.0707(10)	81(6)	62(6)	73(5)	−10(5)	46(5)	2(4)

Table 2. Coordinates and isotropic thermal parameters for hydrogen atoms with corresponding standard deviations in parentheses. $T_i = \exp[-8\pi^2U(\sin^2\theta)/\lambda^2]$. Thermal parameters are multiplied by 10^3.

Atom	X/a	Y/b	Z/c	U
H(2)	0.808(5)	0.548(2)	−.299(6)	6(2)
H(8)	0.492(5)	0.366(2)	0.044(5)	3(1)
H(11)	1.123(6)	0.689(2)	−.122(7)	4(2)
H(12)	1.161(7)	0.733(3)	−.314(8)	10(2)
H(13)	0.977(7)	0.711(3)	−.622(8)	10(2)
H(14)	0.803(6)	0.638(2)	−.720(8)	7(2)
H(15)	0.810(5)	0.598(2)	−.485(6)	4(1)
H(201)	0.630(5)	0.264(2)	0.448(6)	5(2)
H(202)	0.581(6)	0.249(3)	0.257(8)	9(2)
H(203)	0.488(9)	0.230(4)	0.324(10)	15(3)
H(211)	0.465(6)	0.326(2)	0.466(7)	7(2)
H(212)	0.325(6)	0.291(2)	0.367(7)	9(2)
H(213)	0.358(8)	0.358(3)	0.323(9)	10(3)
H(221)	0.254(6)	0.263(3)	0.054(8)	9(2)
H(222)	0.265(6)	0.339(2)	0.029(7)	9(2)
H(223)	0.345(6)	0.283(2)	0.007(7)	5(2)

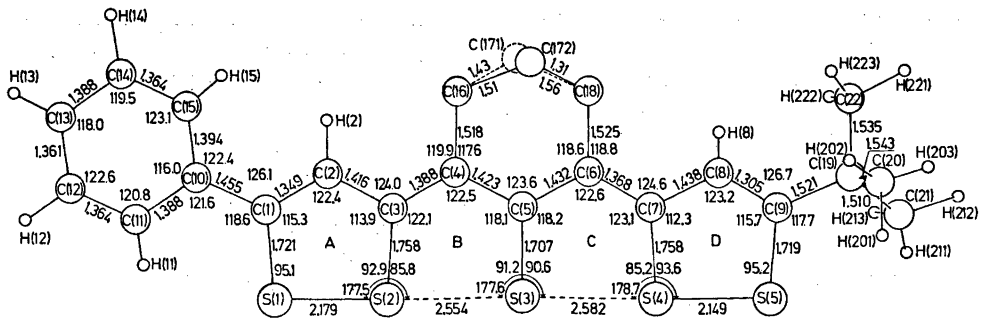

Fig. 1. Bond distances and angles. Standard deviations in S–S, S–C and C–C bonds are 0.003, 0.006 and 0.008–0.016 Å, respectively (0.03 Å in disordered region); in ∠S–S–S 0.1°, ∠S–S–C 0.3° and in angles at C 0.5–1.0°.

Table 3. Bond angles not shown in Fig. 1.

Angle	(°)	Angle	(°)
C(4)–C(16)–C(171)	116(1)	C(9)–C(19)–C(20)	109.2(7)
C(4)–C(16)–C(172)	113(9)	C(9)–C(19)–C(21)	111.3(6)
C(16)–C(171)–C(18)	114(1)	C(9)–C(19)–C(22)	111.5(6)
C(16)–C(172)–C(18)	126(2)	C(20)–C(19)–C(21)	108.8(7)
C(6)–C(18)–C(171)	114(1)	C(20)–C(19)–C(22)	109.4(6)
C(6)–C(18)–C(172)	114(1)	C(21)–C(19)–C(22)	106.5(7)

STRUCTURE DETERMINATION AND REFINEMENT

The structure was solved by direct methods. An E-map based on 289 reflections with $|E| \geq 1.7$ revealed all the non-hydrogen atoms. The refinement indicated disorder in the trimethylene bridge, analogous to what has been observed in two other related structures.[5,6] Two atomic sites for C(17) were refined, C(171) and C(172), each with a population parameter of 0.5. All hydrogen atoms except those in the disordered region were localized in a difference Fourier map, and refined isotropically. No sign of secondary extinction was detected at the end of the refinement. The function minimized in the full-matrix least-squares process was $\sum w(|F_o|-|F_c|)^2$, where $w=1/\sigma_F^2$. Scattering factors were for S and C those of Cromer and Mann,[7] and for H those of Stewart *et al.*[8] The final agreement factor, $R=\sum||F_o|-|F_c||/\sum|F_o|$, is 0.082, $R_w=0.048$, and the standard deviation of an observation of unit weight, $S=\sum w(|F_o|-|F_c|)^2/(m-n)^{\frac{1}{2}}$, is 1.68 ($m$ is the number of reflections included and n the number of parameters refined on).

The final positional and thermal parameters with standard deviations as calculated from the inverse least-squares matrix are listed in Tables 1 and 2. Lists of observed and calculated structure factors are available from the author on request.

All calculations have been carried out on a UNIVAC 1110 computer. The programs concerning data collection and initial handling of the intensity data have been written by cand. real. K. Maartmann-Moe of this Department. For the other calculations the X-ray 72 system has been used.[9]

RESULTS AND DISCUSSION

Intramolecular distances and the most important angles involving sulfur and carbon are shown in Fig. 1. The remaining angles are listed in Table 3. The C–H bond lengths lie in

the range 0.79 – 1.17 Å, the mean value being 0.97 Å. Standard deviations in these bonds are 0.04 – 0.10 Å. The five-sulfur array is almost linear, and each of the five-membered rings A, B, C, D is approximately planar. The molecule is slightly twisted, mainly around C(3) – C(4) and C(6) – C(7), causing a dihedral angle between rings A and D of 10.8°. In the three other linear five-sulfur structures studied (in this paper denoted I, II, III) the molecules are slightly bent around the central S – C bond,[1,10,11] but in the present case no such feature is observed. The phenyl group is twisted 7.5° relative to the plane of ring A, as compared to 6.3° in mod. 1. The high standard deviations in mod. 1(I) prevent a detailed comparison between the two molecular structures. The relative differences between the two outer and the two inner S – S bond lengths are not the same in the two modifications. The differences are, however, hardly significant. The four S – S distances are all longer than the bonds found in cyclic dithioles, but appreciably shorter than van der Waals distance, in agreement with the observations for structures I, II and III.[1,10,11] This feature has also been reproduced in

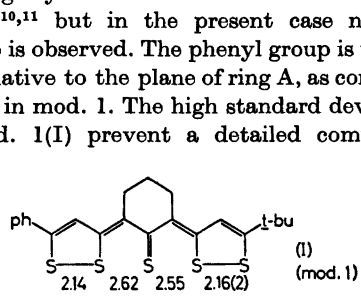

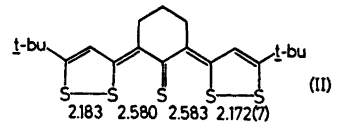

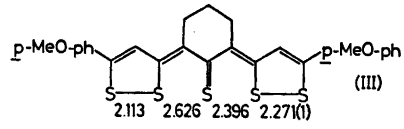

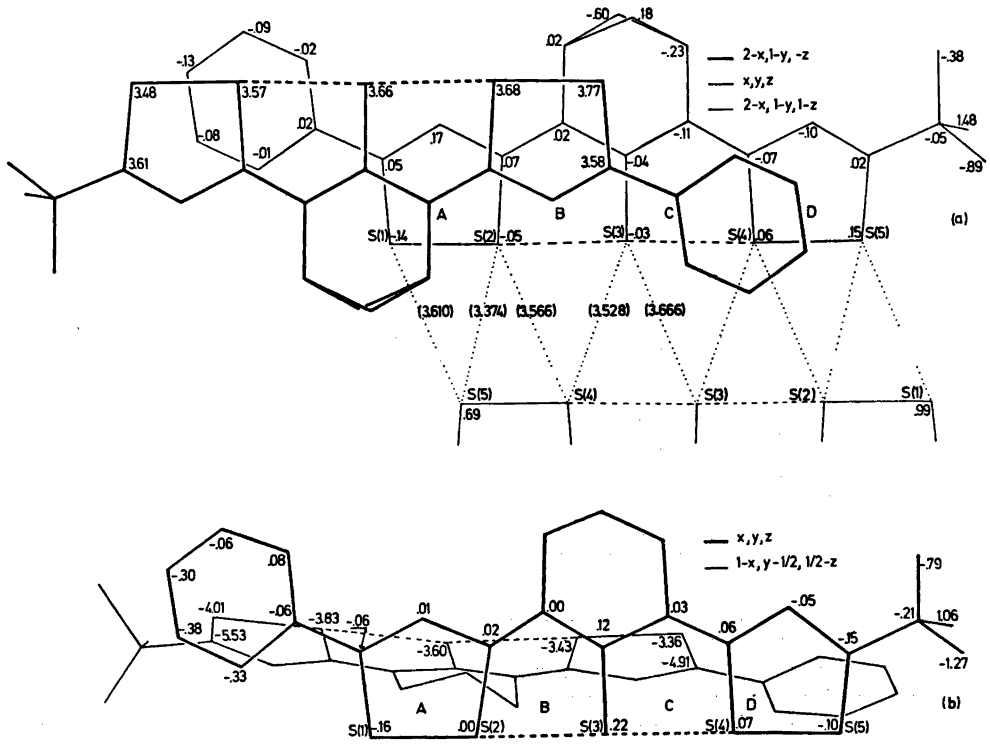

Fig. 2. (Overlap of molecules, (a) in mod. 2, and (b) in mod. 1. Distances from the least-squares plane of rings A + B + C + D of each reference molecule are shown. S···S distances shown in parentheses.

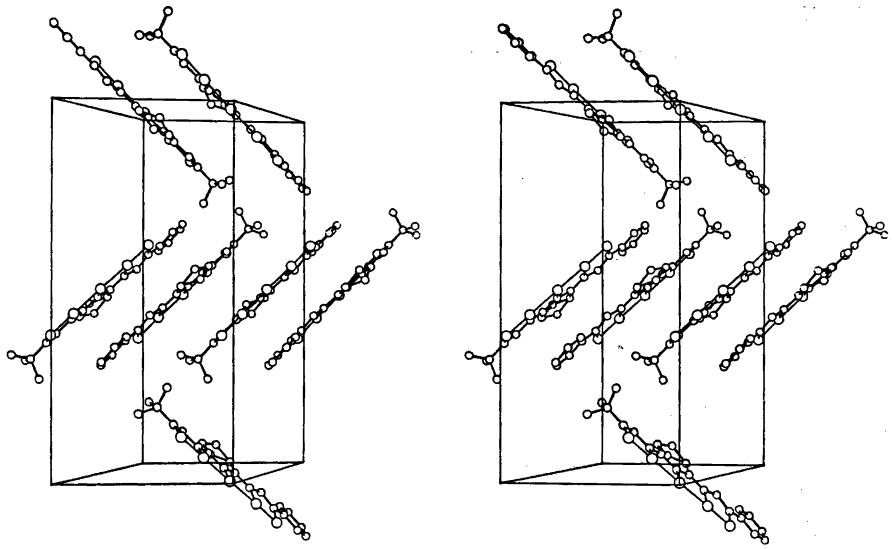

Fig. 3. Stereodrawing showing the packing of molecules in mod. 2. The a-axis runs along the interocular line, left to right, the b-axis vertically and c^* is pointing towards the viewer. Figs. 3 and 4 were drawn utilizing the ORTEP program.[13]

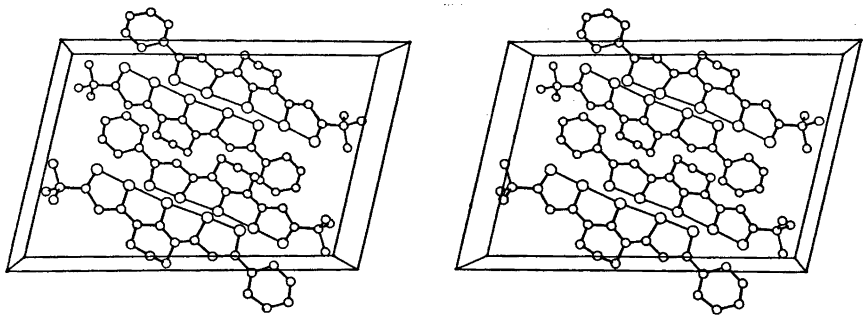

Fig. 4. The packing of molecules in mod. 1 as seen down the b-axis; the a-axis runs horizontally, left to right.

CNDO/2 calculations on model five-sulfur compounds.[12] The pronounced asymmetry in the sulfur sequence of the symmetrically substituted molecule III, together with the variation in lengths of corresponding S–S bonds in the different compounds, suggest that these bonds are easily changed by rather weak forces, intramolecular as well as intermolecular.

The major differences between mods. 1 and 2 are found in the packing of the molecules in the crystals. In the present structure pairs of centrosymmetrically related molecules overlap to a considerable extent, the distance between the molecular planes being 3.6 Å. The shortest intermolecular sulfur-sulfur contacts also occur between centrosymmetrically related molecules (Fig. 2a). In mod. 1 the overlap occurs between molecules related by a screw axis (Fig. 2b). The two molecules are inclined approximately 70° relative to one another. The two types of stacking patterns represented in mods. 1 and 2 are also found in several of the other linear four- and five-sulfur compounds studied. The crystalline packing arrangements are shown in stereodrawings Figs. 3 and 4.

Acknowledgement. The author is indebted to Drs. M. Stavaux and N. Lozac'h for supplying a sample of the compound.

REFERENCES

1. Sletten, J. *Acta Chem. Scand. 24* (1970) 1464.
2. Stavaux, M. and Lozac'h, N. *Bull. Soc. Chim. Fr.* (1968) 4273.
3. Maartmann-Moe, K. *Siemens Review XLI*, Seventh Special Issue *X-Ray* and *Electron Microscopy News* (1974) 54.
4. Sletten, J. *Acta Chem. Scand. A 28* (1974) 989.
5. Sletten, J. and Velsvik, M. *Acta Chem. Scand. 27* (1973) 3881.
6. Sletten, J. *Acta Chem. Scand. A 28* (1974) 499.
7. Cromer, D. and Mann, J. *Acta Crystallogr. A 24* (1968) 321.
8. Stewart, R. F., Davidson, E. R. and Simpson, W. T. *J. Chem. Phys. 42* (1965) 3175.
9. The X-ray system – Version of June 1972. *Technical Report TR-192 of the Computer Science Center*, University of Maryland, June 1972.
10. Kristensen, R. and Sletten, J. *Acta Chem. Scand. 25* (1971) 2366; *27* (1973) 2517.
11. Sletten, J. *Acta Chem. Scand. A 29* (1975) 436.
12. Sletten, J. *Acta Chem. Scand. A 30* (1976) 397.
13. Johnson, C. K. *ORTEP, A Fortran Thermal Ellipsoid Plot Program for Crystal Structure Analysis*, Report ORNL-3794, Oak Ridge National Laboratory, Oak Ridge 1970.

Received March 9, 1976.

Acta Chemica Scandinavica A 30 (1976) 667—672

Short Communications

The Crystal Conformation of 4,4,7,7-Tetramethylcyclononanone at −156°C

P. GROTH

Department of Chemistry, University of Oslo, Oslo, 3, Norway

On basis of dynamic ^{13}C NMR spectroscopy, Borgen and Dale [1] have discussed the asymmetric nature of the conformation of 4,4,7,7-tetramethylcyclononanone ($C_{13}H_{24}O$). Although their conclusions concerning conformational exchange processes are somewhat uncertain, there are strong evidences in favour of an asymmetric triangular ring-conformation [234]* with the carbonyl group in a non-corner position:

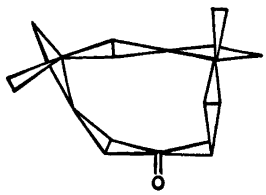

Since the same conformation persists in the solid (shown by IR-spectroscopy [3]), a crystal structure determination has been performed in order to establish the conformation of this nine-membered ring.

The crystals belong to the orthorhombic system with space group *Pbca*, cell dimensions $a = 9.122(2)$ Å, $b = 10.910(2)$ Å, $c = 24.550(7)$ Å, and eight molecules in the unit cell ($D_m = 1.05$ g cm^{-3}, $D_x = 1.06$ g cm^{-3}). 1209 observed reflections were measured on an automatic four circle diffractometer at −156 °C (Mo$K\alpha$-radiation). No corrections for absorption or secondary extinction were carried out [crystal size = (0.25 × 0.30 × 0.32) mm^3].

The structure was solved by direct methods [4] and refined by full-matrix least-squares technique.[5]** Methylene hydrogen positions were calculated. Methyl hydrogens were localized as the twelve largest peaks in a difference Fourier map. Anisotropic temperature factors were introduced for O and C atoms, and weights in least-squares were calculated from the standard deviations in intensities, $\sigma(I)$, taken as

$$\sigma(I) = [C_T + (0.02C_N)^2]^{\frac{1}{2}}$$

where C_T is the total number of counts and C_N the net count. The final weighted R-value was 3.5 % (conventional $R = 4.5$ %) for 1209 observed reflections. The form factors used were those of Hanson *et al.*[6] except for hydrogen.[7]

Final fractional coordinates and thermal parameters with estimated standard deviations are given in Table 1. The principal axes of thermal vibration ellipsoids for the oxygen and carbon atoms were calculated from the temperature parameters of Table 1. Maximum r.m.s. amplitudes range from 0.152 to 0.208 Å (corresponding B-values 1.81 and 3.41 Å^2). No rigid-body analysis has been carried out.

Bond distances and angles and dihedral angles are given in Table 2. The standard deviations (in parentheses) are estimated from the correlation matrix of the final least-squares refinement cycle. Fig. 1 is a schematic drawing of the molecule showing that the nine-membered ring has the [234] conformation. The numbering of atoms is also indicated.

The dihedral angles agree well with those obtained by strain energy calculations for the [234] conformation of cyclononane.[8] The values are given in Table 2. These calculations give [9] the distance between hydrogens at C1 and C6, respectively, as the shortest (1.79 Å). This interaction is thus avoided in the ketone. The next shortest calculated value (1.83 Å) between H-atoms at C5 and C8 corresponds to the shortest contact of the present compound, H51···H81 of (2.04 Å).

As may be seen from Table 2, bond distances are normal. The mean value of C−C bonds (excluding C1−C2 and C1−C9) is 1.536 Å, while the corresponding average for cycloundecanone [10] is 1.532 Å. C1=O is 1.212(3) Å for the present compound and 1.213(3) Å

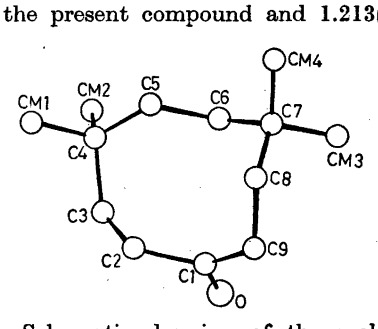

Fig. 1. Schematic drawing of the molecule.

* This notation indicates the number of bonds in each "side" separating the "corner" atoms.[2]

** All programs used, except those for phase determination, are included in this reference.

Table 1. Final fractional coordinates and thermal parameters with estimated standard deviations. The expression for anisotropic vibration is $\exp[-2\pi^2(h^2a^{*2}U11 + \cdots + 2klb^*c^*U23)]$. Hmn is bonded to Cm and HMmn to CMm.

ATOM	X	Y	Z	U11	U22	U33	U12	U13	U23
O	.30619(20)	1.04353(18)	.54105(7)	.0386(12)	.0261(11)	.0375(12)	-.0026(11)	.0051(10)	.0030(10)
C1	.30459(30)	.93556(27)	.54792(10)	.0281(16)	.0292(18)	.0132(14)	-.0029(16)	.0078(12)	-.0016(14)
C2	.16805(30)	.86275(26)	.53295(11)	.0304(18)	.0193(18)	.0174(15)	.0060(16)	-.0005(14)	.0027(13)
C3	.02805(32)	.91436(26)	.55865(11)	.0214(16)	.0229(18)	.0225(15)	.0031(14)	-.0044(14)	.0019(13)
C4	-.03215(27)	.84777(25)	.60998(9)	.0180(14)	.0258(16)	.0184(13)	.0003(14)	-.0005(13)	-.0011(12)
C5	.08970(30)	.79510(26)	.64636(11)	.0214(16)	.0207(15)	.0187(14)	-.0018(15)	.0015(13)	.0021(13)
C6	.20742(28)	.88686(25)	.66473(11)	.0231(17)	.0202(15)	.0174(14)	.0037(14)	.0016(13)	-.0009(14)
C7	.36334(29)	.83448(27)	.67007(10)	.0223(15)	.0222(15)	.0221(15)	.0029(14)	-.0023(13)	-.0032(13)
C8	.42055(32)	.78127(28)	.61609(11)	.0189(16)	.0310(18)	.0298(16)	.0047(16)	-.0037(14)	-.0026(15)
C9	.43915(32)	.86901(29)	.56793(11)	.0242(17)	.0336(19)	.0242(16)	.0015(17)	.0062(14)	-.0028(15)
CM1	-.12875(35)	.74085(30)	.59190(13)	.0253(18)	.0347(19)	.0320(18)	-.0042(17)	-.0031(17)	.0028(17)
CM2	-.12595(33)	.93974(31)	.64141(12)	.0204(16)	.0355(20)	.0279(17)	.0015(17)	.0011(15)	-.0007(16)
CM3	.46418(36)	.93696(32)	.69017(13)	.0272(19)	.0371(20)	.0322(19)	.0033(18)	-.0045(17)	-.0048(16)
CM4	.36205(36)	.73088(29)	.71210(12)	.0309(18)	.0323(20)	.0248(17)	.0058(18)	-.0061(16)	-.0010(14)

ATOM	X	Y	Z	B	ATOM	X	Y	Z	B
H21	.1825(23)	.7757(21)	.5402(8)	.8(5)	H22	.1589(23)	.8748(20)	.4943(9)	1.5(5)
H31	-.0508(25)	.9155(21)	.5324(9)	1.5(5)	H32	.0494(25)	1.0043(21)	.5671(8)	1.3(5)
H51	.1408(23)	.7291(21)	.6255(8)	1.0(5)	H52	.0457(25)	.7567(20)	.6791(9)	1.1(5)
H61	.1752(22)	.9271(19)	.6980(8)	.2(4)	H62	.2113(20)	.9580(20)	.6391(7)	.1(4)
H81	.3567(25)	.7130(23)	.6045(9)	1.8(5)	H82	.5191(26)	.7415(21)	.6242(8)	1.0(5)
H91	.4762(27)	.4237(22)	.5375(10)	2.3(6)	H92	.5163(26)	.9372(24)	.5753(9)	2.2(6)
HM11	-.0708(29)	.6860(24)	.5696(10)	2.5(6)	HM12	-.2156(27)	.7739(23)	.5688(10)	2.7(6)
HM13	-.1679(28)	.6950(24)	.6236(10)	2.9(6)	HM21	-.0648(27)	1.0077(22)	.6559(8)	1.8(5)
HM22	-.1802(26)	.8964(23)	.6720(10)	2.5(6)	HM23	-.2079(25)	.9752(23)	.6178(9)	2.3(6)
HM31	.4312(26)	.9687(22)	.7260(9)	2.2(5)	HM32	.4650(28)	1.0081(24)	.6648(10)	2.7(6)
HM33	.5685(29)	.9052(22)	.6951(9)	2.1(6)	HM41	.3021(26)	.6571(23)	.7009(9)	1.8(5)
HM42	.3229(24)	.7580(20)	.7465(10)	1.3(5)	HM43	.4653(30)	.7001(24)	.7194(10)	3.0(6)

Table 2. Bond distances and angles and dihedral angles with estimated standard deviations. Dihedral angles from strain minimization calculations are also included.

DISTANCE	(Å)	DISTANCE	(Å)
O - C1	1.212(3)	C1 - C2	1.522(4)
C2 - C3	1.532(4)	C3 - C4	1.555(3)
C4 - C5	1.533(3)	C5 - C6	1.529(4)
C6 - C7	1.538(4)	C7 - C8	1.538(4)
C8 - C9	1.531(4)	C9 - C1	1.508(4)
C4 - CM1	1.528(4)	C4 - CM2	1.528(4)
C7 - CM3	1.530(4)	C7 - CM4	1.531(4)

ANGLE	(°)	ANGLE	(°)
O - C1 - C2	119.5(3)	O - C1 - C9	120.8(3)
C1 - C2 - C3	113.0(2)	C2 - C3 - C4	117.2(2)
C3 - C4 - C5	112.8(2)	C4 - C5 - C6	116.3(2)
C5 - C6 - C7	115.7(2)	C6 - C7 - C8	112.4(2)
C7 - C8 - C9	117.8(2)	C8 - C9 - C1	117.5(2)
C9 - C1 - C2	119.6(3)	C3 - C4 - CM1	109.0(2)
C3 - C4 - CM2	107.5(2)	C5 - C4 - CM1	107.9(2)
C5 - C4 - CM2	110.7(2)	CM1 - C4 - CM2	109.0(2)
C6 - C7 - CM3	108.2(2)	C6 - C7 - CM4	108.9(2)
C8 - C7 - CM3	110.5(2)	C8 - C7 - CM4	107.7(2)
CM3 - C7 - CM4	109.1(2)		

DIHEDRAL ANGLE	(°)	(°) *
C1 - C2 - C3 - C4	-101.2(3)	-110
C2 - C3 - C4 - C5	34.4(3)	41
C3 - C4 - C5 - C6	54.2(3)	50
C4 - C5 - C6 - C7	-145.3(2)	-137
C5 - C6 - C7 - C8	59.3(3)	52
C6 - C7 - C8 - C9	62.8(3)	70
C7 - C8 - C9 - C1	-59.9(4)	-58
C8 - C9 - C1 - C2	-53.5(4)	-51
C9 - C1 - C2 - C3	131.3(2)	131

* Values from strain minimization calculations

in cycloundecanone. The C−C−C angles at C2, C4, and C7 are significantly smaller than the other ring angles. No such pattern was observed in the case of cycloundecanone. At C4 and C7 the effect is possibly connected with the methyl substitution. It may also be mentioned that the angle C1−C2−C3 of 113.0(2)° agrees with the result of strain energy calculations [8] where the C−C−C angle at C2 comes out as the smallest one with a value of 113.1°.

C−H bonds range from 0.96 Å to 1.04 Å, while C−C−H and H−C−H angles are obtained between 105 and 113°. No short inter-molecular contacts are observed. A list of observed and calculated structure factors is available on request to the author.

Acknowledgement. The author would like to thank Dr. G. Borgen for preparing the crystals.

1. Borgen, G. and Dale, J. *Acta Chem. Scand. B 30* (1976) 733.
2. Dale, J. *Acta Chem. Scand. 27* (1973) 1115.
3. Borgen, G. and Dale, J. *Chem. Commun.* (1970) 1105.
4. Germain, G., Main, P. and Woolfson, M. M. *Acta Crystallogr. A 27* (1971) 368.
5. Groth, P. *Acta Chem. Scand. 27* (1973) 1837.
6. Hanson, H. P., Herman, F., Lea, J. D. and Skillman, S. *Acta Crystallogr. 17* (1964) 1040.
7. Stewart. R. F., Davidson, E. R. and Simpson, W. T. *J. Chem. Phys. 42* (1965) 3175.
8. Rustad, S. and Seip, H. M. *Acta Chem. Scand. A 29* (1975) 378.
9. Rustad, S. *Personal communication.*
10. Groth, P. *Acta Chem. Scand. A 28* (1974) 294.

Received June 15, 1976.

pH-Independent Hydrolysis of Some 2-Aryloxytetrahydrofurans

HARRI LÖNNBERG and VEIJO POHJOLA

Department of Chemistry and Biochemistry, University of Turku, SF-20500 Turku, Finland

It is well-known that acetals are generally stable under alkaline conditions.[1] However, several hemicyclic carbohydrate acetals, glycosides, are cleaved quite readily in aqueous base solutions.[2] Especially, aryl aldofuranosides exhibit a marked lability to alkali.[3] To further the understanding of the factors influencing the hydrolysis of these compounds the cleavage of the corresponding tetrahydrofuran derivatives in aqueous sodium hydroxide solutions (eqn. 1) has been studied in this work.

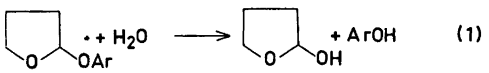

(1)

The kinetic data obtained with the 2-aryloxytetrahydrofurans studied are given in Table 1. The hydrolysis rate of each investigated compound is almost independent of the hydroxide ion concentration. The slight decrease in the first-order rate constants with the increasing base concentration is probably due to specific salt effects. Routes involving rate-limiting nucleophilic attack by hydroxide ion can thus be excluded as the major reaction pathways. In consistence with this conclusion, two kinetically indistinguishable mechanisms can be suggested for the hydrolysis of these compounds; a unimolecular decomposition of the substrate to a phenoxide ion and a cyclic oxo-carbenium ion (eqn. 2), or water, acts as a general acid donating a proton to the *exo* cyclic oxygen atom concerted with the covalent bond rupture (eqn. 3).

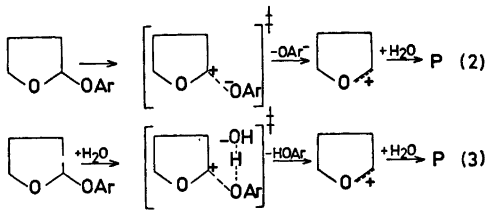

Table 1. First-order rate constants [$k(H_2O)$ and $k(D_2O)$] for the hydrolysis of 2-aryloxytetrahydrofurans in sodium hydroxide and sodium deuteroxide solutions of different concentrations. The ionic strength was adjusted to 0.1 mol dm^{-3} with sodium chloride. $T = 358.15$ K if not otherwise stated; number of runs 2 if not otherwise stated.

Substituent	$C(OH^-)$/mol dm^{-3}			$C(OD^-)$/mol dm^{-3}
	0.1	0.01	0.001	0.1
	$k(H_2O)/10^{-4}$ s^{-1}			$k(D_2O)/10^{-4}$ s^{-1}
None	0.454	0.569		0.345
3-OCH_3	1.054	1.230	1.418	
4-Cl	1.643 [a]	1.952 [a]	1.979 [a]	1.194
3-Cl	5.61 [a]	5.70 [a]	5.77 [a]	3.71
4-$COCH_3$	61.2 [a]	61.2 [a]	59.6 [a]	41.4
	21.9 [b]			
	8.64 [c]			
	2.96 [d]			

[a] Number of runs: 3. [b] $T = 348.15$ K. [c] $T = 338.15$ K. [d] $T = 328.15$ K.

Electron-withdrawing substituents in the aryloxy group greatly accelerate the hydrolysis of 2-aryloxytetrahydrofurans. A plot of the logarithms of the rate constants against the substituent constants σ^- gives a fairly good linear correlation line with a slope of 2.4 ± 0.2 (Fig. 1). If normal substituent constants, σ°, are used instead, a curvilinear Hammett plot is obtained, the point for 4-acetyl group falling far above the straight line the other substituents yield. The need for σ^- values to correlate the hydrolysis rates indicates that resonance inter-

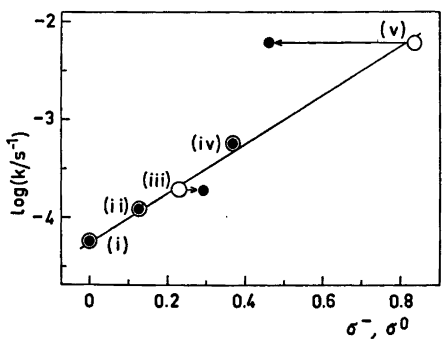

Fig. 1. Hydrolysis of 2-aryloxytetrahydrofurans in aqueous 0.01 mol dm^{-3} sodium hydroxide solution at 358.15 K. Logarithms of the first-order rate constants plotted against the substituent constants of the substituents in the aryl moiety. Open circles refer to σ^- and filled circles to σ° values. Notation: (i) phenoxy, (ii) 3-methoxyphenoxy, (iii) 4-chlorophenoxy, (iv) 3-chlorophenoxy, and (v) 4-acetylphenoxy derivative.

actions between the *exo* cyclic oxygen atom and the substituted benzene nucleus are altered on going from reactant molecule to activated complex. Of the substituents employed, the 4-acetyl group is the only one that exerts a $-R$ effect, or in other words, tends to withdraw electrons by resonance. Because the rate-enhancing effect of this substituent is far greater than predicted by its σ° value, it seems probable that the decomposition of 2-aryloxytetrahydrofurans occurs with formation of an electron-rich center in direct conjugation with the benzene ring. This is what would happen, if mechanism (2) is followed. As the phenoxy group begins to depart a partial negative charge will develop on the *exo* cyclic oxygen atom. Resonance acceptors, such as the 4-acetyl group, will therefore induce a greater through conjugation in the activated complex than in the reactant molecule. In contrast, no marked change in resonance interactions would take place if the *exo* cyclic oxygen atom were protonated by water concerted with the covalent bond fission, and the rate constants would be expected to correlate with σ° rather than with σ^- values. This is the case, for example, in the general acid-catalyzed hydrolysis of 2-(4-substituted phenoxy)tetrahydropyrans.[4]

The activation entropy of -21 ± 3 J K^{-1} mol^{-1} obtained at 298.15 K for the hydrolysis of 2-(4-acetylphenoxy)tetrahydrofuran is also consistent with route (2). According to this mechanism a separation of charges takes place on going from reactant molecule to transition state. Since the developing charges would be solvated, a slightly negative $\Delta S^{\neq}$ value seems reasonable. Participation of water as a proton donating agent would be expected to give rise to a more negative entropy of activation.

One may also consider the possibility that 2-(4-acetylphenoxy)tetrahydrofuran, which exhibits an exceptionally high reactivity, undergoes a spontaneous decomposition, whereas the other investigated substrates, having poorer leaving groups, react by mechanism (3). The values obtained for the kinetic solvent deuterium isotope effect, however, argue against this suggestion. All reactions studied exhibit a ratio $k(D_2O)/k(H_2O)$ of the magnitude 0.7, the differences between separate values being less than experimental errors. Similar values have been reported for uncatalyzed hydrolyses of other acetals.[5] Furthermore, the high positive value of 2.4 for the Hammett ϱ^--parameter conflicts with the proton-transfer catalysis by water. Polar substituents in the leaving group exert opposing effects on the basicity of the *exo* cyclic oxygen atom and on the ease of the carbon-oxygen bond rupture. If water would donate a proton to the *exo* cyclic oxygen atom concerted with the covalent bond cleavage these two influences would, at least partially, cancel each other, and a smaller reaction constant, ϱ^-, would be expected. On this basis it seems probable that the hydrolysis of all the compounds studied occurs with a spontaneous formation of a cyclic oxo-carbenium ion.

Experimental. The 2-aryloxytetrahydrofurans were synthesized by the procedure of Woods and Kramer.[6] The products were purified by repeated distillations under reduced pressure. 3-Chloro-, 4-chloro-, and 4-acetylphenoxy derivatives were further crystallized from dry methanol. The following compounds were prepared:

2-Phenoxytetrahydrofuran, b.p. 346 – 348 K at 0.2 kPa;
2-(3-Methoxyphenoxy)tetrahydrofuran, b.p. 373 – 375 K at 0.2 kPa;
2-(4-Chlorophenoxy)tetrahydrofuran, m.p. 300 – 301 K;
2-(3-Chlorophenoxy)tetrahydrofuran, m.p. 308 – 309 K;
2-(4-Acetylphenoxy)tetrahydrofuran, m.p. 335 – 337 K.

Aqueous sodium hydroxide solutions were prepared from standard Titrisol solutions (E. Merck) by diluting with distilled water. Sodium deuteroxide solutions were prepared from metallic sodium and deuterium oxide under toluene.

Hydrolyses were followed spectrophotometrically at the absorption maxima of the liberated phenoxide ions. The measurements were performed on a Unicam SP 800 spectrophotometer equipped with a scale expansion accessory. The temperature of the cell housing block was adjusted with water circulation from a Lauda thermostat and controlled by a thermoelement. The initial substrate concentration was in the $10^{-4} - 10^{-5}$ mol dm^{-3} range. The first-order rate constants were calculated by the method of Guggenheim.

Acknowledgements. The financial aid from the Finnish Academy, Division of Sciences, is gratefully acknowledged.

1. Cordes, E. H. *Prog. Phys. Org. Chem. 4* (1967) 1.
2. Capon, B. *Chem. Rev. 69* (1969) 407.
3. Green, J. W. *Adv. Carbohydr. Chem. 21* (1966) 95.
4. Fife, T. H. and Jao, L. K. *J. Am. Chem. Soc. 90* (1968) 4081.
5. Fife, T. H. *J. Am. Chem. Soc. 87* (1965) 271; Salomaa, P. *Acta Chem. Scand. 20* (1966) 1263; Anderson, E. and Fife, T. H. *J. Am. Chem. Soc. 91* (1969) 7163; Fife, T. H. and Brod, L. H. *J. Am. Chem. Soc. 92* (1970) 1681; Kankaanperä, A., Oinonen, L. and Lahti, M. *Acta Chem. Scand. A 28* (1974) 442.
6. Woods, G. F. and Kramer, D. N. *J. Am. Chem. Soc. 69* (1947) 2246.

Received June 10, 1976.

Magnetic Structure of $Mn_{0.95}Fe_{0.05}As$

KARI SELTE,[a] ARNE KJEKSHUS,[a] PER G. PETERZENS[a] and ARNE F. ANDRESEN[b]

[a] Kjemisk Institutt, Universitetet i Oslo, Blindern, Oslo 3, Norway and [b] Institutt for Atomenergi, Kjeller, Norway

As the first of a series of ternary arsenides ($T_{1-t}T'_tAs$; T,T' = V, Cr, Mn, Fe, Co) with MnP type structure we investigated $Mn_{1-t}Fe_tAs$.[1] After the data for other $Mn_{1-t}T_tAs$ phases [2,3] have become available, it has turned out that the variation in T_N (Néel temperature) with t for the double, a-axis helimagnetic mode characteristic of Mn-rich samples, appears to have a different trend for T = Fe than for T = V or Co. Since the T_N value for $Mn_{0.97}Fe_{0.03}As$ in Ref. 1 refers to a somewhat inhomogeneous sample with composition close to the phase boundary between the NiAs and MnP type structures, a new determination of T_N for a well defined sample, $Mn_{0.95}Fe_{0.05}As$, is reported here.

Experimental details concerning purity of elements, preparation of sample, neutron diffraction, and data reduction are as in Ref. 1.

The crystal structure of $Mn_{0.95}Fe_{0.05}As$ at and below room temperature is of the MnP type [1] and specified by the parameters given in Table 1.

The magnetic structure of $Mn_{0.95}Fe_{0.05}As$ is confirmed to be of the double, a-axis helical type with the following parameters at 95 K: $\mu_T = 1.45 \pm 0.05\ \mu_B$ (magnetic moment per metal atom), $\tau = (0.142 \pm 0.002) \times 2\pi\mathbf{a}^*$ (spiral propagation vector), $\phi = 72 \pm 5°$ (phase angle between independent spirals), and $\beta = 90°$ (angle between moment and spiral axis). With a value of 211 ± 1 K for T_N of $Mn_{0.95}Fe_{0.05}As$, the $Mn_{1-t}Fe_tAs$ phase fits nicely in with the other $Mn_{1-t}T_tAs$ phases. $Mn_{0.95}Fe_{0.05}As$ differs from $Mn_{0.90}Fe_{0.10}As$ [1] in that β is fixed at 90° in the former sample at all $T < T_N$, whereas β decreases from 90° at $T/T_N = 0.46$ to 60° at $T/T_N \approx 0.3$ in the latter. For the other parameters there is a resemblance between the two samples with respect to magnitude as well as their temperature variation (Fig. 1).

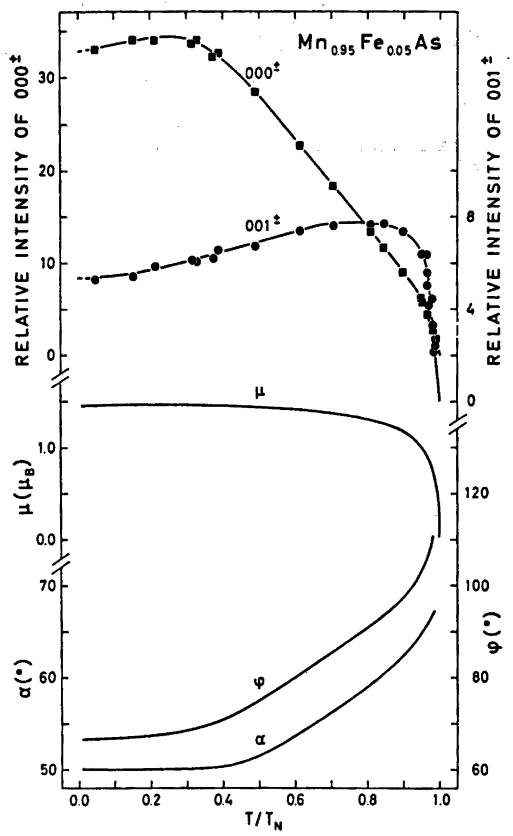

Fig. 1. Phase and turn angles and magnetic moments for spirals in $Mn_{0.95}Fe_{0.05}As$ together with relative intensities of satellite reflections 000± and 001± as functions of reduced temperature.

Table 1. Unit cell dimensions and positional parameters with standard deviations for $Mn_{0.95}Fe_{0.05}As$; space group *Pnma*, positions 4(*c*). (Overall profile reliability factors ranging between 0.033 and 0.046.)

T(K)	11	95	293
a(Å)	5.5384(5)	5.5574(6)	5.6425(4)
b(Å)	3.4863(3)	3.4995(4)	3.6008(4)
c(Å)	6.1472(7)	6.1686(9)	6.2858(8)
x_T	0.0063(21)	0.0056(19)	0.0088(17)
z_T	0.2036(17)	0.2058(20)	0.2120(15)
x_X	0.1971(7)	0.1982(8)	0.2118(6)
z_X	0.5796(8)	0.5804(9)	0.5797(10)

Indication of "doubled 000±" was also found for $Mn_{0.95}Fe_{0.05}As$, although much less pronounced than for $Mn_{0.90}Fe_{0.10}As$.[1] In the case of $Mn_{0.93}Fe_{0.05}As$, sample inhomogeneity is less probable and instrumental imperfections appear to provide the most likely explanation of the phenomenon.

Acknowledgement. This work has received financial support from The Norwegian Research Council for Science and the Humanities.

1. Selte, K., Kjekshus, A. and Andresen, A. F. *Acta Chem. Scand. A 28* (1974) 61.
2. Selte, K., Kjekshus, A., Valde, G. and Andresen, A. F. *Acta Chem. Scand. A 30* (1976) 8.
3. Selte, K., Kjekshus, A., Valde, G. and Andresen, A. F. *Acta Chem. Scand. A 30* (1976) 468.

Received July 1, 1976.

Acta Chemica Scandinavica A 30 (1976) 673—679

Kinetics of the Spontaneous and Catalysed Hydration of Chloral in Aqueous Dioxane

P. E. SØRENSEN

Chemistry Laboratory A, Building 207, The Technical University of Denmark, DK-2800 Lyngby, Denmark

Kinetic orders with respect to water, $n(c_w)$, as well as activation parameters have been determined for both the uncatalysed and catalysed hydration of chloral in mixtures of water and dioxane. The value of $n(c_w)$ for the uncatalysed reaction is found to vary from 4 to 2 when the molar concentration of water, c_w, is gradually changed from 0.25 to 46.3 M. This is interpreted as evidence for a cyclic transition state consisting of the carbonyl compound and four water molecules and the fall in $n(c_w)$ as c_w increases is explained on the basis of association phenomena in the solvent. This picture of the transition state is supported by activation entropy measurements, where large negative values are found in agreement with earlier observations; but the individual values are difficult to explain theoretically. Activation data for a series of acid catalysts seem to indicate a relation between acid strength and degree of association with water molecules and it is concluded that amine catalysts probably enter the cyclic transition state indirectly *via* associated water molecules.

The detailed mechanism for addition of water to the carbonyl group has been the subject of a number of investigations [1] and it has been suggested that the reaction proceeds *via* a cyclic transition state consisting of the carbonyl group and several water molecules. Thus, from hydration experiments with 1,3-dichloroacetone in water-dioxane mixtures, Bell, Millington, and Pink [2] found the order of reaction with respect to water to be approximately three and later studies [3] of the activation parameters for the same reaction supported this picture of the transition state. The role of acid catalysts in the mechanism was investigated by Bell and Critchlow [4] and they concluded that one molecule of catalyst replaces one water molecule in the transition state (for the uncatalysed reaction) in contrast to earlier suggestions [2] that two water molecules were replaced.

The aim of the present work is to investigate reaction orders with respect to water for the hydration of chloral (trichloroacetaldehyde) in water-dioxane mixtures over a wide range of water concentrations and also to look more closely at activation parameters for the process. It was also of interest to study some aspects of the catalysis of the reaction by Brønsted acids and bases, especially to see whether there was any difference between the function of secondary and tertiary amines, the former having one nitrogen bound hydrogen atom, which could form part of the cyclic transition state, like the O – H group of, *e.g.*, a carboxylic acid.

Because chloral is very strongly hydrated [5] over a wide range of water concentrations this compound is particularly suitable for hydration experiments, since the process can be regarded as effectively irreversible without large error.

EXPERIMENTAL

Materials. Chloral, BDH *lab.reag.*, was doubly distilled under dry nitrogen before use. The high risk of oxidation of chloral by atmospheric air was clearly demonstrated by an appreciable increase in the uncatalysed reaction rate if the above precautions were not taken. The following acid catalysts were used without further purification: Trichloroacetic acid, BDH *AnalaR*; dichloroacetic acid, Fluka, *puriss.*; monochloroacetic acid, Merck *purum cryst.*; cyanoacetic

acid, Fluka *puriss.*; glacial acetic acid, BDH *lab.reag.* and formic acid, Merck 98–100 % *krystalliserbar* were distilled before use. The following basic catalysts were purified by distillation before use: Triethylamine, Fluka *purum*; diethylamine, Fluka *purum*; piperidine BDH *lab.reag.*; 2,4,6-collidine, BDH *lab.reag.*; pyridine, Baker *analysed reag.* Dioxane, BASF *technical* was purified as described by Bell and Jensen.[6] This method gives a product which contains less than 0.08 % water, determined by the Karl Fischer titration method. Doubly distilled water was used throughout.

Uncatalysed reactions. The hydration process was followed spectrophotometrically at 294 nm where the carbonyl group has an absorption maximum. At the higher water concentrations ($c_w > ca.$ 0.6 M) the process was too fast to be followed by conventionel techniques and a Durrum-Gibson stopped-flow spectrophotometer was used, provided with an oscilloscope, X–Y recorder, and a paper tape read out system. Solutions of chloral in dioxane (*ca.* 5×10^{-2} M) and of water in dioxane were thermostated and rapidly mixed in the apparatus. The very high water concentrations were established by using a driving syringe of reduced volume for the chloral solution. A Beckman DB-GT spectrophotometer with recorder was used for measuring the reaction rates at water concentrations below 0.6 M. The reaction solution was prepared by injecting pure chloral from a microsyringe into the thermostated water-dioxane mixture in 1 cm silica cells.

Catalysed reactions. Catalytic experiments were only carried out in the region of water concentration where the stopped-flow instrument was used. The experimental procedure was analogous to that described above for the uncatalysed reaction. The catalyst was always dissolved in the water-dioxane mixture to prevent complications from possible side reactions between the catalyst and chloral before mixing.

RESULTS AND DISCUSSION

The observed kinetic curves were in all cases found to be of first order – c_w being much larger than the concentration of chloral – except for the very low values of c_w, where small corrections had to be made to the rate constants. Disturbances due to heat of mixing of water and dioxane in connection with the stopped-flow experiments were not observed. This is consistent with the fact that this enthalpy is a very small positive or negative quantity depending on the composition of the mixture,[7] and with the fact that the activation energy for the hydration is relatively low.

The molar concentrations of water in the reaction chamber of the stopped-flow instrument could be calculated from the dimensions of the driving syringes and the water content of the solutions mixed. For the experiments at low values of c_w, where a conventional technique was used there was good agreement between calculated and titrimetrically obtained values for the water concentration (Karl Fischer method).

Uncatalysed reactions. The results for uncatalysed hydration at some fifty water concentrations (c_w: 0.25–46.3 M) are shown in Fig. 1, where log k_{obs} is plotted against log c_w. Each point represents the mean of at least two experiments which agreed within ± 5 %. The solid curve is a least squares fit of a second order polynomial to the points and is represented by the following expression:

$$\log k_{obs} = -2.379 + 3.582 \log c_w - 0.494(\log c_w)^2 \quad (1)$$

The order of reaction with respect to water, $n(c_w)$, is determined as the slope of this curve and is seen to vary from about 4.0 to about 2.0 in going from the lower to the higher water concentrations. The present results differ to some extend from those reported by Bell, Millington and Pink [2] (Fig. 1) who considered

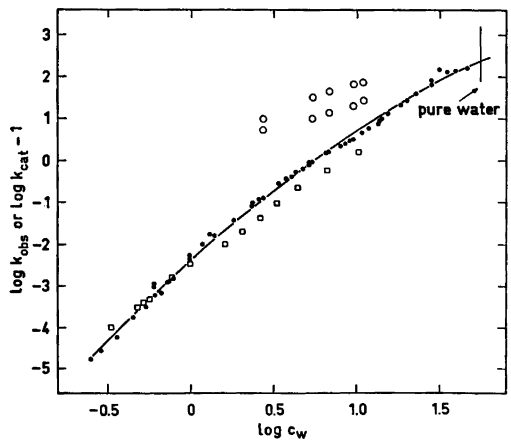

Fig. 1. Kinetic data for hydration of carbonyl compounds in mixtures of water and dioxan at 298.2 K. ● Chloral, present work. ○ Chloral catalysed by diethylamine (upper curve) and triethylamine, present work. □ 1,3-Dichloroacetone, Ref. 2 (log k_{obs} + 3). k_{obs} in s^{-1}, k_{cat} in mol dm^{-3} s^{-1}, c_w in mol dm^{-3}.

the analogous hydration of 1,3-dichloroacetone under very similar conditions. They found a nearly linear dependence of log k_{obs} upon log c_w and determined $n(c_w)$ to be approximately equal to three. However, if the composition of the transition state is independent of water concentration, and medium effects are ignored, it seems likely that a plot of log k_{obs} against log c_w* should show the type of curvature found in the present work. Thus it has been shown by, *e.g.*, cryoscopic measurements [8] that water is unassociated in dioxan only below water concentrations of about 0.3 M and it is easily shown that polymerization of the water leads to a fall in the order of reaction with respect to total water concentration, *i.e.* if the transition state is formed from substrate and four unassociated water molecules, $S + 4H_2O \rightarrow$ t.s., the reaction order with respect to water is clearly four, whereas if the water molecules are dimerized, $S + 2(H_2O)_2 \rightarrow$ t.s., leading to the same transition state, the rate expression is, $v = k[(H_2O)_2]^2[S] = k[\frac{1}{2}[H_2O]_{total}]^2[S]$, which gives a reaction order with respect to water (total concentration) of only two.

The failure of Bell *et al.*[2] to observe considerable curvature may be due to the fact that their water concentrations were not corrected for the presence of small amounts of water in the purified dioxane; *cf.* experimental section. Thus in later work Bell and Critchlow [4] found approximately 40 % lower values for the hydration rate constant of 1,3-dichloroacetone at $c_w = 1.06$ mol dm^{-3} but the range of water concentrations used in their work was too small for the curvature to be observed.

The reaction order with respect to water is approximately four in the concentration range where water exists mainly as a monomer in dioxane. This suggests four water molecules in the cyclic transition state as in (2).

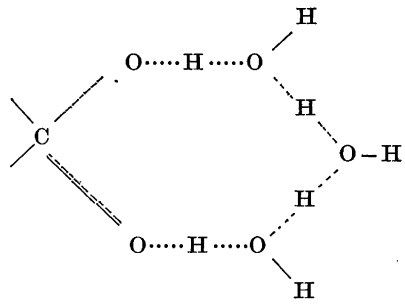

(2)

If the O···H···O bonds are considered to be linear the most stable configuration of (2) is a cyclohexane structure because of the tetrahedral disposition of the carbon and oxygen valencies. The formation of this structure therefore requires a minimum of break down of the ordinary water structure in concentrated water solutions, where, particularly according to a model by Bernal,[9] the so-called V-structure can be described as an irregular network of hydrogen bonded rings with varying numbers of water molecules and therefore varying distortion and stability.

Although the composition of the transition state suggested here may seem more attractive than one involving only three water molecules,[2–4] it is still doubtful whether it is really reasonable to suggest that a single structure operates over a wide range of water concentrations. It is also worth pointing out that it is still a hypothesis that the transition state is of cyclic nature at all and that a number of other questions such as, *e.g.*, the degree of concertedness of the proton transfers are still unsolved.

The type of inert solvent may be expected to affect the observed reaction orders, but it is interesting to see that for the present type of reaction only a small difference is observed if acetonitrile is used instead of dioxane.[2] A solvent such as dimethyl sulfoxide interacts very strongly with water by hydrogen bond formation and this might create a different behaviour for this solvent. Unfortunately there are no experimental data available at present for the hydration of carbonyl compounds in mixtures of water and dimethyl sulfoxide.[15]

Despite a comparatively high inaccuracy for k_{obs} at the very high water concentrations the stopped-flow technique applied in the present work seems to provide a method for obtaining

* A different curvature is found if mol fractions, x_w, are used instead of molar concentrations, *i.e.* the reaction order increases from four to approximately five in going from low to high water concentrations. Application of this concentration unit seems unreasonable in the present case since polymerization of the water on increasing its concentration should lead to lower reaction orders (see below), which is also confirmed by activation entropy measurements.

Table 1. Collected results from acid-base catalysis of the hydration of chloral at 298.2 K, c_w in mol dm^{-3}, k_{cat} in l mol^{-1} s^{-1}.

Compound No.	Catalyst	$-\log K_a$[a]	c_w	Statistical factors p	q	k_{cat}	Linear regression coefficient (number of points)
9	Hydrochloric acid (H_3O^+)	−1.74	2.72	3	2	(32)	− (2)
1	Trichloroacetic acid	0.63	2.73	1	2	2.96 ± 0.06	0.999 (7)
2	Dichloroacetic acid	1.48	2.73	1	2	2.13 ± 0.04	0.999 (7)
3	Cyanoacetic acid	2.47	2.73	1	2	1.62 ± 0.06	0.997 (7)
4	Monochloroacetic acid	2.87	2.73	1	2	1.66 ± 0.04	0.998 (6)
5	Formic acid	3.75	2.73	1	2	0.89 ± 0.01	0.999 (8)
6	Acetic acid	4.76	2.73	1	2	0.99 ± 0.04	0.996 (8)
7	o-Chlorophenol	8.48	< 2.73	1	1	(0.08)	− (3)
8	Water	15.74	2.73	2(3)	1(2)	0.05	−
10	Piperidine	11.13	2.73	2	1	5.8 ± 0.6	0.990 (3)
11	Diethylamine	11.00	2.73	2	1	100 ± 2	0.999 (7)
			5.45			353 ± 6	0.999 (7)
			6.81			446 ± 9	0.999 (6)
			9.57			690 ± 31	0.994 (7)
			10.95			739 ± 21	0.998 (6)
12	Triethylamine	10.73	2.73	1	1	55 ± 1	0.999 (7)
			5.45			47 ± 3	0.987 (6)
			6.81			132 ± 3	0.999 (6)
			9.57			197 ± 8	0.997 (6)
			10.95			268 ± 6	0.999 (5)
13	2,4,6-Collidine	7.45	2.73	1	1	2.0 ± 0.1	0.998 (6)
14	Pyridine	5.22	2.73	1	1	1.5 ± 0.1	0.994 (6)

[a] Taken from Kortüm, G., Vogel, W. and Andrussow, K. *Dissociation of Organic Acids in Aqueous Solution*, IUPAC, Butterworths, London 1961.

values for the hydration rate constants of strongly hydrated carbonyl compounds in pure water using short extrapolations. These constants can be combined with the much slower dehydration rate constants, measured by scavenger techniques, for calculating hydration equilibrium constants, which are unknown or known with little accuracy for many compounds. It is interesting in this context to note that k_{obs} for the hydration of chloral in pure water from Fig. 1, 232 s^{-1}, is comparable with a value, $(4.5 \pm 0.7) \times 10^2$ s^{-1}, determined recently in this laboratory [10] by a polarographic technique analogous to that described by Brdička,[11] making use of the literature value, $K_h = 2.8 \times 10^4$,[5] for the hydration equilibrium constant for chloral.

Catalysed reactions. Catalytic constants were found for a number of acids and bases. The results of these experiments are collected in Table 1 and it is seen from the linear regression coefficients that good linearity was obtained in most cases when the expression $k_{obs} = k_0 + k_{cat}[cat]$ was applied to the primary data. For the basic catalysts there was a risk of a side reaction between chloral and the amine. However, these reactions were shown to be much slower than the rate of hydration. For o-chlorophenol, very high concentrations had to be used to obtain a considerable contribution to k_{obs} from the catalysed reaction. This of course affects the water concentrations; this was allowed for, but the catalytic constant given in Table 1 for this compound is only approximate. The value given for HCl is based on a single experiment with 0.01 HCl.

The Brønsted plots for the acidic and basic catalysts are shown in Fig. 2. Because the pH-

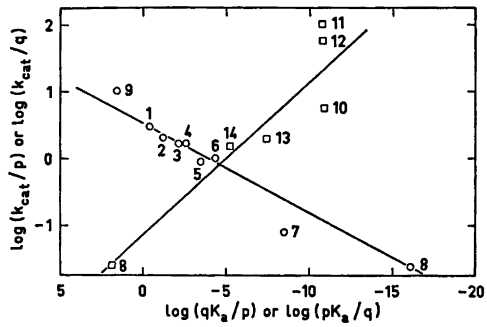

Fig. 2. Brønsted plots for catalysis of the hydration of chloral by a series of acids and bases. Data taken from Table 1. Temperature 298.2 K, $c_w = 2.73$ mol dm^{-3}. The figures are the compound numbers listed in Table 1.

values are not known in the mixed solvent (2.73 M water in dioxan) the values from aqueous solution are used. As was observed by Bell and Jensen [6] for hydration of 1,3-dichloroacetone (2.78 M water in dioxan), using 24 acids, the acid catalysts show good linearity and give an α-value of about 0.13 for the present system. Hydrochloric acid shows clear positive deviation from the plot and, as pointed out by Kresge,[12] this seems to be a typical feature of reactions where all the proton transfers take place between oxygen or nitrogen atoms. The pK-value for H_3O^+ has been used for HCl in the present case. This is reasonable because this species probably exists as the ion pair H_3O^+ Cl^- under the present conditions, and it has been shown [6] that replacement of Cl^- by other inorganic anions such as Br^- or ClO_4^- caused little change in catalytic activity, and that the changes observed were in the direction opposite to the order of strengths of the acids in aqueous solution.

For the basic catalysts, however, the points are very scattered. It may be reasonable, taking into account the point for water, to draw a line as shown in Fig. 2, giving a rough value for β of about 0.2. The values of α and β for the present reaction are somewhat lower than for the hydration of 1,3-dichloroacetone ($\alpha = 0.27$, $\beta = 0.5$). This is in accord with the fact that the hydration of chloral is more exothermic ($\Delta H = -59$ kJ mol^{-1})[5] than that of 1,3-dichloroacetone ($\Delta H = -24$ kJ mol^{-1}).[13]

As seen from Table 1 the catalytic behaviour of diethylamine and triethylamine was examined at several water concentrations, and the logarithm of the observed catalytic constants are plotted against log c_w in Fig. 1. Least squares fits to these two sets of points give reaction orders with respect to water which are indistinguishable and approximately equal to 1.2. This is a considerable decrease compared with the uncatalysed reaction for which $n(c_w)$ is about 2.9 in this region and the value is also somewhat lower than that found by Bell, Millington and Pink [2] ($n(c_w) = 1.85$) for the catalysis of the hydration of 1,3-dichloroacetone by triethylamine. If a transition state similar to (2) is still assumed for the catalysed reaction the above data suggest that the amines are able to replace some of the water molecules in the cyclic transition state. However, since the behaviour of the tertiary and the secondary amine is very similar it seems reasonable to assume that the amine itself is not involved directly in the hydrogen bonded structure, which would be expected to create a difference in behaviour of the two, *cf.* the introduction, but that it operates *via* attached water molecules.

Activation parameters. Table 2 collects the activation parameters obtained by the method of least squares. No detectable curvature was observed within experimental error for any of the plots in contrast to what was reported by Bell and Sørensen [3] for the uncatalysed hydration of 1,3-dichloroacetone where considerable curvature was found. However, this discrepancy may only be apparent because of the comparatively narrow temperature range investigated in the present work.

Considering first the activation energies for the uncatalysed hydration, E_a tends to increase with increasing water concentration. This behaviour was also observed for 1,3-dichloroacetone [3] and can be attributed qualitatively to the increasing degree of association of the water molecules when the water concentration is raised, producing a stabilization of the reactants compared to the transition state. A similar explanation may apply to the series of four acid catalysts. Both experiment and theory suggest (Ref. 4 and references therein) that there is a relation between the strength of an acid in aqueous solution and its degree

Table 2. Collected activation parameters, c_w and c_{cat} in mol dm^{-3}, E_a in kJ mol^{-1}, $\Delta S^{\ddagger}$ in JK^{-1} mol^{-1}. Each Arrhenius plot is based on rate measurements at five different temperatures in the range 285 to 315 K.

Catalyst	c_w	c_{cat}	E_a	$\Delta S^{\ddagger} - nR \ln c_w$ $n=0$	$n=1$	$n=2$	$n=3$	$n=4$	$n=5$
Water	2.72	2.72	7.8 ± 0.6	−243 ± 2	−251	−259	−267	−275	−283
	4.56	4.56	7.7 ± 0.8	−232 ± 3	−240	−253	−265	−278	−290
	6.75	6.75	7 ± 1	−227 ± 3	−243	−259	−275	−291	−307
	9.73	9.73	11.2 ± 0.7	−206 ± 2	−225	−244	−263	−282	−301
					A [a]	B [a]			
Hydrochloric acid	2.72	0.010	21.2 ± 0.4	−192 ± 1	−146	−97			
Trichloroacetic acid	2.72	0.048	18 ± 2	−211 ± 6	−178	−65			
Dichloroacetic acid	2.71	0.111	15 ± 4	−219 ± 12	−193	−50			
Acetic acid	2.74	0.068	6 ± 1	−255 ± 4	−224	−19			
Triethyl amine	6.74	9.40×10^{-3}	9 ± 2	−221 ± 8	−166	−61			
Diethyl amine	6.74	2.28×10^{-3}	9 ± 1	−221 ± 4	−154	−73			

[a] $A = \Delta S^{\ddagger}\ (n=0) - R \ln (c_{cat}/c_w)$; $B = \Delta S^{\ddagger}\ (n=0)$ for water catalysed reaction minus A.

of hydration, *i.e.* the strongest acids are most hydrated. This is in accord with the observation that E_a increases with increasing acid strength throughout the series, although it is worth pointing out that here a stabilization of the reactants will probably partly be cancelled by a stabilization also of the transition state. It is interesting to see that the activation energy is actually higher for the catalysed reactions – except for acetic acid – than for the uncatalysed ones, but this behaviour is overcompensated by a more favorable activation entropy for the catalysed reactions. For catalysis by triethylamine and diethylamine the activation energies are seen to be indistinguishable within experimental error.

Turning now to activation entropies, this parameter (Table 2) exhibits large negative values as was observed for the hydration of 1,3-dichloracetone [3] and this is good evidence for a transition state of highly ordered structure. Considering first the uncatalysed hydration, it is evident that correcting the obtained activation entropy values to a standard state of $c_w = 1$ M by adding $-R \ln c_w$ does not give a common value for $\Delta S^{\ddagger}$ at the four water concentrations investigated. Table 2 shows that a correction involving addition of $-3R \ln c_w$ or $-4R \ln c_w$ is optimal for this purpose, in particular if the value at $c_w = 6.75$, which seems less reliable, is omitted, and this agrees with the conclusion from reaction orders with respect to water that three or four water molecules take part in the transition state ($c_w = 2-10$ M). It has been pointed out [3] that it is probably a good approximation to attribute most of the observed activation entropies in the present type of reaction to freezing of translational degrees of freedom, rotations and internal rotations beeing effectively frozen in the solvents used. Calculation of ΔS (translational) for the reaction, chloral + nH$_2$O → chloral,

nH_2O in the gas phase at 298 K and corrected to a standard state of 1 M gives -430 J K^{-1} mol^{-1} and -574 J K^{-1} mol^{-1}* for $n=3$ and 4, respectively. These figures are much more negative than the experimental values: -268 J K^{-1} mol^{-1} and -283 J K^{-1} mol^{-1} (mean values from Table 2, $n=3$ and 4, respectively). This is not surprising because the calculated values of $\Delta S^{\ddagger}$ are valid only for ideal solution (gas phase) while the experimental ones apply to a condensed phase, where considerable interaction takes place between the solvent molecules. From Dorsey's thermodynamic data for water [14] it is clear that the entropy loss corresponding to "freezing" of three or four water molecules in an "ice-like" transition state as suggested here cannot be larger than approximately 110 and 140 J K^{-1} mol^{-1}, respectively. Thus these figures are too small to explain satisfactorily the observed values for $\Delta S^{\ddagger}$.

However, it is not surprising that the use of a comparatively simple model for the reaction, which neglects, *e.g.*, important effects such as solvent reorganization and low frequency bending and stretching modes of the transition state, does not lead to any exact prediction of the activation entropies and it confirms once more that water is an extremely difficult material to treat theoretically.

Table 2 also contains values for the activation entropies of some catalysed reactions. The figures in the column corresponding to $n=1$ are obtained by adding $-R \ln (c_{cat}/c_w)$ to the column corresponding to $n=0$. This corrects the observed entropy values to a catalyst concentration equal to that for water in each case and makes possible a comparison with the uncatalysed reaction. Both acidic and basic catalysts make $\Delta S^{\ddagger}$ less negative (last column). As pointed out by Bell and Sørensen [3] such behaviour can readily be explained as reflecting the ability of the catalysts to bring with them one or more of the water molecules required for the transition state. A detailed discussion of the individual $\Delta S^{\ddagger}$ values is not possible but it is clear from the series of activation entropies for the acid catalysts that the stronger acids bring more water molecules with them.

Acknowledgment. The author is indebted to Professor R. P. Bell for many valuable discussions.

REFERENCES

1. Bell, R. P. *The Proton in Chemistry*, 2nd Ed., Chapman and Hall, London 1973, pp. 183–188.
2. Bell, R. P., Millington, J. F. and Pink, J. M. *Proc. R. Soc. London Ser. A 303* (1968) 1.
3. Bell, R. P. and Sørensen, P. E. *J. Chem. Soc. Perkin Trans. 2* (1972) 1740.
4. Bell, R. P. and Critchlow, J. E. *Proc. R. Soc. London Ser. A 325* (1971) 35.
5. Gruen, L. C. and McTigue, P. T. *J. Chem. Soc.* (1963) 5217.
6. Bell, R. P. and Jensen, M. B. *Proc. R. Soc. London Ser. A 261* (1961) 38.
7. Goates, J. R. and Sullivan, R. J. *J. Phys. Chem. 62* (1958) 188.
8. Bell, R. P. and Wolfenden, J. H. *J. Chem. Soc.* (1935) 822.
9. Bernal, J. D. *Proc. R. Soc. London Ser. A 280* (1964) 299.
10. Harder, P., Sørensen, P. E. and Ulstrup, J. *J. Electroanal. Chem. In press.*
11. Brdička, R. *Collect. Czech. Chem. Commun. 20* (1955) 387.
12. Kresge, A. J. *Chem. Soc. Rev. 2* (1973) 475.
13. Bell, R. P. and McDougall, A. O. *Trans. Faraday Soc. 56* (1960) 1281.
14. Dorsey, N. E. *Properties of Ordinary Water-Substance*, Reinhold, N.Y. 1940.
15. Note added in proof: Four uncatalysed, kinetic experiments in this solvent mixture at $c_w=1.60$, 2.11, 2.90 and 4.54 M (298.2 K) were carried out recently by the present author and $k_{obs} \times 10^2$ was found to 2.0, 2.5, 8.1 and 17.0 s^{-1}, respectively. These results give a value of $n(c_w)$ only slightly smaller than the one observed for the water-dioxane mixture.

Received April 7, 1976.

* There is a mistake in the calculation of ΔS (translational) for the reaction, $K.H_2O + 2H_2O \rightarrow K.3H_2O$ (K is 1,3-dichloroacetone) in Ref. 3, p. 1743. The value reported as being -206 JK^{-1} mol^{-1} should be -232 JK^{-1} mol^{-1}.

Acta Chemica Scandinavica A 30 (1976) 680—686

Cationic Silver Bromide Complexes in Alkali Nitrate Melts

BERTIL HOLMBERG

Division of Physical Chemistry, Lund University, Chemical Center, P.O.B. 740, S-220 07 Lund 7, Sweden

Potentiometric measurements of the free ligand concentration [Ag^+] and solubility measurements have been used to investigate the formation of cationic complexes between silver(I) and bromide ions in fused equimolar (K,Na)NO_3 at 280 °C. No polynuclear (polybromic) species can be detected potentiometrically. The distribution of AgBr and $AgNO_3$ between solid solutions Ag(Br,NO_3) and the nitrate melt indicates a stepwise formation of complexes $Ag_mBr^{(m-1)+}$ with $m = 2$, 3, and 4. The corresponding stability constants have been evaluated from the solubility data.

The formation and thermodynamic stability of neutral and anionic silver bromide complexes in alkali nitrate melts have been studied previously at this laboratory.[1–3] From studies in aqueous solution – mostly by solubility measurements [4–8] – the ability of silver and bromide ions to form cationic complexes $Ag_mBr^{(m-1)+}$ has become evident. Analogous chloride and iodide complexes with ion charges +1, +2, and +3 have also been suggested in aqueous solution [5–7,9–12] and strong evidence for similar ions in polar organic solvents has emerged as well. [13–15]

Solid compounds of the general formulae $Ag_mXA_{(m-1)}$ (X = Cl, Br or I and A = NO_3, ClO_4, or F) have been prepared from aqueous solutions [7,16–21] and from anhydrous melts.[22–26]

In some binary melts $AgX - AgNO_3$ the existence of cationic silver halide species has been suggested.[26–28] In ternary systems so-called "dinuclear" species Ag_2X^+ have been proposed as an interpretation of emf data obtained in fused alkali or alkaline earth metal nitrates. Thus, evidence for Ag_2Cl^+ and Ag_2Br^+ has been found in a number of nitrate media,[29–35] and Guion [36] explained the results from similar emf measurements in molten eutectic $(K,Li)_2SO_4$ by assuming the presence of Ag_2Br^+. The emf method that was solely used in these investigations [29–36] is, however, not very convenient for studying relatively weak cationic complexes, since – in general – the measured concentration of free ligand, [Ag^+], does not differ very much from the total ligand concentration C_{Ag}. Furthermore, the fraction of halide ion present as Ag_2X^+ has often been small, making an accurate evaluation of the corresponding stability constant impossible.[37,38]

A more convenient method is to study the solubility of a silver halide in melts containing various amounts of, *e.g.*, $AgNO_3$. Seward and Field [39] used this method to indicate the presence of Ag_2Cl^+ in fused $NaNO_3$ and Sinistri and Pezzati [40] have made a more extensive study of silver chloride and bromide complexation in equimolar (K,Na)NO_3 employing the solubility method. They found evidence for complex ions with net charges +1 and +2 and determined the stability constants for the proposed species Ag_2X^+ and Ag_3X^{2+}.

This study of systems $AgBr - AgNO_3 -$ (K,Na)NO_3 has been undertaken in order to complete the picture of the silver bromide complexation in nitrate melts and to compare the results with those from aqueous media with respect to relative stability of different species and to the maximum number of silver(I) ligands attached to a bromide central ion.

The study is restricted to the range 0.2 mol $kg^{-1} < C_{Ag} < 2$ mol kg^{-1}, which is of primary interest as far as only positively charged complexes are concerned. In contrast to what has been found for dissolution of alkali halides in solid AgI [41] and AgBr,[3] it appeared that the

solubility of $AgNO_3$ in solid AgBr was rather small. Nevertheless it was analytically significant and the composition of both phases have been determined. The activity of AgBr in the solid is computed as described recently.[3]

In the region 0.8 mol $kg^{-1} < C_{Ag} \leq 2.4$ mol kg^{-1} the free ligand concentration $[Ag^+]$ has been directly determined from emf measurements.

From the emf data the average ligand number $\bar{n}$ can be calculated with an accuracy good enough to provide a semi-quantitative picture of the complex formation at high ligand concentrations, which assists the interpretation of the solubility data.

EXPERIMENTAL

Chemicals. All chemicals were *p.a.* grade and prepared and stored as described previously.[3,41]

Apparatus. The equipment used for the solubility and emf measurements has been described in Ref. 3 and Refs. 42 and 43, respectively.

Procedure. Solubility measurements: Systems containing 75.00 g equimolar $(K,Na)NO_3$, 12 g AgBr and various amounts of $AgNO_3$ were agitated for at least 50 h until equilibrium was attained (as concluded from constant solubility). Samples were withdrawn from the nitrate phase and analysed for silver and bromide.

Emf measurements: Two general types of cells were used; *cf.* Scheme 1.

In the study of unsaturated melts the electrode function was checked by measuring emfs after adding successive portions of $AgNO_3$ to the left hand compartment of cell II, keeping $C_{Br} = 0$. Silver bromide was then dissolved in the melt, and the titration with $AgNO_3$ was continued to $C_{Ag} \approx 2.4$ mol kg^{-1}.

The measurements on cell I were started with a two-phase system, $Ag(Br,NO_3)(s)$ – nitrate melt, and C_{Ag} was varied by additions of $AgNO_3$ in the range 0.8 mol $kg^{-1} \leq C_{Ag} \leq 2.2$ mol kg^{-1}. In all measurements C^0_{Ag} was kept as high as 2.2 mol kg^{-1} in order to minimize the effects of AgBr-precipitation in the diffusion layer between the half-cells. Stable emf readings were obtained within a few minutes in the study of unsaturated melts, whereas equilibrium times of 2 – 3 h were required when solid-liquid equilibria had to be established.

Analyses. The solubilities were determined by gravimetric analyses for bromide as AgBr. Silver was determined by electroanalytical precipitation of Ag on a rotating platinum cathode from hot aqueous cyanide solutions. The composition of the solid solution was calculated from the difference between added and found amounts of silver nitrate in the melt.

NOTATIONS

A. Quantities referring to the emf measurements.

E_{obs} = the observed electromotive force of cells I and II.

ε = correction term, compensating for deviations from ideal Nernst behaviour.

$E_{corr} = E_{obs} + \varepsilon$

E_0, k = experimental parameters, defined by eqn. (1) below.

B. Quantities referring to the solubility measurements.

For the solid phase:

x_i = mol fraction of component i ($i = 1$ for AgBr and 2 for $AgNO_3$).

a_i = activity of component i.

$f_i = a_i x_i^{-1}$.

For the nitrate melt (all concentrations are expressed in molality units mol kg^{-1}, referring to equimolar $(K,Na)NO_3$ as solvent):

C_{Ag}, C_{Br} = total concentration of silver(I) and bromide, respectively.

[A] = concentration of species A.

I:	Ag $Ag(Br,NO_3)(s)$	C'_{Ag} $AgNO_3$ C_{Br} AgBr (saturated) $(K,Na)NO_3$	asbestos fibre	C°_{Ag} $AgNO_3$ $(K,Na)NO_3$	Ag
II:	Ag	C'_{Ag} $AgNO_3$ C_{Br} AgBr (unsaturated) $(K,Na)NO_3$	asbestos fibre	C°_{Ag} $AgNO_3$ $(K,Na)NO_3$	Ag

Scheme 1.

$a(NO_3)$ = the nitrate ion activity.
β_m = $[Ag_mBr^{(m-1)+}][Ag^+]^{-m}[Br^-]^{-1}$.
K_m = $[Ag_mBr^{(m-1)+}][Ag_{(m-1)}Br^{(m-2)+}]^{-1}\cdot[Ag^+]^{-1}$.
$\bar{m}$ = $(C_{Ag}-[Ag^+])C_{Br}^{-1}$.
M = maximum value of m.

CALCULATIONS AND RESULTS

Electromotive force measurements. In order to minimize the uncertainties in $\bar{m}$ which are due to random errors in E_{obs} the measurements had to be restricted to melts with rather large total concentrations of silver and bromide. In the studied composition range, however, another complication arises, *viz.* that the ideal linear relationship between E_{obs} and log $[Ag^+]$ ceases to be valid when log $[Ag^+] \gtrsim 0$.[43] However, E_{obs} is still well reproducible. If we make the reasonable assumption that the presence of bromide in the melts does not affect the deviations from linearity as compared to halide-free systems, we may use the emf data collected in such melts [43] in the calculation of a correction term ε to be added to E_{obs}, yielding data (E_{corr}; log $[Ag^+]$) which should be rationalized as

$$E_{corr} = E_0 - k \log [Ag^+] \quad (1)$$

The correction, which accounts mainly for liquid junction potentials and possible deviations from thermodynamic ideality, was tested in the bromide-free systems in series 3–5 (Table 1). The resulting parameter values (E_0/mV; k/mV), which were used in the calculations pertaining to bromide containing melts in each series, (37.6; 109.8), (37.4; 109.4), and (37.4; 109.8), respectively. These values of E_0 and k are in excellent agreement with the theoretical Nernst equation parameters RTF^{-1} ln C°_{Ag} = 37.4 mV and RTF^{-1} ln 10 = 109.7 mV, and hence $[Ag^+]$ has been calculated from

$$E_{corr} = (RT/F) \ln (C^\circ_{Ag}/[Ag^+])$$

in series 1 and 2 (systems $Ag(Br,NO_3)(s)$ – nitrate melt). All experimental emf data are collected in Table 1.

In series 1 and 2 the ligand numbers were calculated by use of C_{Br} from the separate solubility data. In Fig. 1 the ligand numbers $\bar{m}$ are plotted *vs.* $[Ag^+]$. The uncertainties in the $\bar{m}$-values are of an order of magnitude of

Table 1. Data from the electromotive force measurements.

C_{Br}/mol kg^{-1}, C_{Ag}/mol kg^{-1}, E_{obs}/mV, E_{corr}/mV;

Series 1, cell type I

0.0162, 0.912, *36.1*, *44.8*; 0.0246, 1.108, *29.0*, *36.5*; 0.0364, 1.325, *22.5*, *28.7*; 0.0470, 1.491, *18.8*, *24.0*; 0.0631, 1.717, *14.3*, *18.4*; 0.0804, 1.927, *10.8*, *13.8*; 0.0977, 2.119; *8.2*, *10.5*;

Series 2, cell type I

0.0128, 0.817, *40.5*, *49.8*; 0.0198, 1.003, *32.6*, *40.7*; 0.0300, 1.214, *25.8*, *32.6*; 0.0426, 1.432, *20.3*, *25.9*; 0.0548, 1.605, *16.6*, *21.3*; 0.0686, 1.788, *13.3*, *17.1*; 0.0815, 1.940, *10.8*, *13.8*; 0.1021, 2.161, *7.8*, *10.0*;

Series 3, cell type II

0, 0.494, *60.2*, *71.1*; 0, 0.701, *44.8*, *54.7*; 0, 0.903, *34.0*, *42.4*; 0, 1.143, *24.6*, *31.2*; 0, 1.356, *18.0*, *23.1*; 0.0352, 1.391, *20.8*, *26.5*; 0.0352, 1.567, *15.8*, *20.3*; 0.0352, 1.710, *12.3*, *15.7*; 0.0352, 1.856, *9.1*, *11.6*; 0.0352, 2.029, *5.5*, *7.0*; 0.0352, 2.188, *2.6*, *3.1*;

Series 4, cell type II

0, 0.766, *40.6*, *50.0*; 0, 0.988, *30.2*, *37.9*; 0, 1.204, *22.5*, *28.6*; 0, 1.422, *16.2*, *20.8*; 0, 1.656, *10.3*, *13.3*; 0.0589, 1.715, *13.9*, *17.8*; 0.0589, 1.844, *11.1*, *14.2*; 0.0589, 1.978, *8.0*, *10.2*; 0.0589, 2.122, *5.3*, *6.7*; 0.0589, 2.350, *1.2*, *1.4*;

Series 5, cell type II

0, 0.893, *34.4*, *42.8*; 0, 1.161, *23.8*, *30.2*; 0, 1.411, *16.5*, *21.1*; 0, 1.652, *10.5*, *13.5*; 0, 1.877, *5.8*, *7.3*; 0.0764, 1.953, *10.0*, *12.8*; 0.0764, 2.101, *6.7*, *8.7*; 0.0764, 2.255, *4.0*, *5.0*; 0.0764, 2.400, *1.4*, *1.6*;

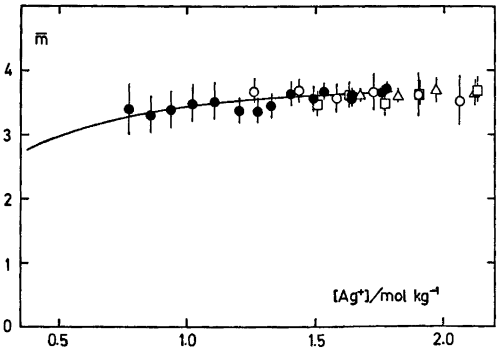

Fig. 1. Ligand numbers $\bar{m}$ determined by emf measurements. Symbols: melts saturated in AgBr (●); C_{Br} = 76.4 mmol kg^{-1} (△); C_{Br} = 58.9 mmol kg^{-1} (□); C_{Br} = 35.2 mmol kg^{-1} (○). The solid curve is calculated by use of the stability constants of Table 3.

Table 2. Solubility and distribution data.

C_{Ag} mol kg^{-1}	C_{Br} mol kg^{-1}	$x_2 \times 10^2$	a_1	f_1	$a_2 \times 10^2$	f_2	$\bar{m}$	[Ag$^+$] mol kg^{-1}	[Ag$^+$][Br$^-$] $\times 10^7$ (mol kg^{-1})^2
0.2860	0.00201	0.03	1.000	1.000			2.57	0.2808	3.00
0.402	0.00297	0.05	1.000	1.000			2.81	0.394	3.00
0.495	0.00440	0.13	1.000	1.001			2.96	0.482	3.00
0.590	0.00662	0.27	0.999	1.002			3.08	0.570	3.00
0.695	0.00924	0.42	0.999	1.003			3.18	0.666	3.00
0.792	0.01195	0.43	0.998	1.002	0.15	0.34	3.27	0.753	2.99
0.900	0.01563	0.83	0.997	1.005	0.17	0.20	3.34	0.848	2.99
1.008	0.02018	0.85	0.996	1.004	0.19	0.22	3.40	0.939	2.99
1.110	0.02470	0.90	0.995	1.004	0.20	0.22	3.45	1.025	2.99
1.200	0.02922	1.40	0.995	1.009	0.20	0.14	3.48	1.098	2.98
1.297	0.03466	1.79	0.993	1.011	0.21	0.12	3.52	1.175	2.98
1.404	0.0419	1.93	0.992	1.012	0.23	0.12	3.55	1.255	2.98
1.501	0.0476	2.37	0.991	1.015	0.26	0.11	3.58	1.331	2.97
1.623	0.0560	2.31	0.989	1.012	0.28	0.12	3.60	1.421	2.97
1.713	0.0627	2.62	0.987	1.014	0.29	0.11	3.62	1.486	2.96
1.824	0.0716	2.70	0.986	1.013	0.30	0.11	3.64	1.563	2.96
1.931	0.0805	2.96	0.984	1.014	0.32	0.11	3.66	1.636	2.95
2.044	0.0914	3.10	0.983	1.014	0.34	0.11	3.67	1.708	2.95
2.186	0.1044	3.32	0.981	1.015	0.36	0.11	3.69	1.801	2.94

± 0.2 as estimated from a reasonable assumption of random errors in E_{corr} of about ± 0.3 mV. As seen from Fig. 1, $\bar{m}$ increases with [Ag$^+$] from 3.3 to 3.7 in the concentration range investigated. Within the limits of experimental errors no systematic dependence of $\bar{m}$ on C_{Br} at constant [Ag$^+$] can be detected. This feature is taken as an indication of the absence of polynuclear complexes $Ag_mBr_n^{(m-n)+}$ in observable amounts with a possible exception for species having $m/n \approx 3.5$.

No attempts at a further quantitative evaluation of the $\bar{m}$-data in terms of definite stability constants have been made, but the important features of Fig. 1 which have been stressed here, give strong support to the interpretation of the solubility data.

Solubility and distribution measurements. All data pertaining to the solubility and distribution measurements are collected in Table 2. As indicated by the magnitude of x_2 there is a small but significant solubility of $AgNO_3$ in AgBr, and the following two heterogeneous equilibria have to be considered in the treatment of the data:

$$AgBr(ss) \rightleftharpoons Ag^+ + Br^-$$
$$K_1' = [Ag^+][Br^-]a_1^{-1} \quad (2)$$

$$AgNO_3(ss) \rightleftharpoons Ag^+ + NO_3^-$$
$$K_2' = [Ag^+]a(NO_3)a_2^{-1} \quad (3)$$

Following the general principles outlined previously,[3] we set d ln $a(NO_3) = 0$, since NO_3^- is effectively the only anion present in the nitrate melt. Taking the standard state for silver bromide to be pure solid AgBr, we arrive at

$$\ln a_{1j} = \int_{\ln [Ag^+]_0}^{\ln [Ag^+]_j} -(x_2/x_1)\, d \ln [Ag^+] \quad (4)$$

(The subscript j is used to indicate different quantities referring to the same actual system, and [Ag$^+$]$_0$ refers to a system with $x_2 = 0$).

Since the experimental study was restricted to a range where K_1' and β_1 cannot be determined these constants have been taken from the thorough investigations of Cigén and Mannerstrand,[1,2] *viz.* $K_1' = 3.00 \times 10^{-7}$ (mol kg^{-1})^2 and $\beta_1 = 267$ (mol kg^{-1})$^{-1}$. The data have been treated according to

$$(C_{Br}K_1'^{-1}a_1^{-1} - [Ag^+]^{-1} - \beta_1)[Ag^+]^{-1} = \sum_{m=2}^{M} k_m[Ag^+]^{(m-2)} \quad (5)$$

From the least squares treatment of the left hand member as a function of [Ag$^+$] it became evident that the summation in the right hand member had to be carried out to $M = 4$, *viz.* complexes with ion charges $+1$, $+2$, and $+3$

Table 3. Over-all stability constants for complexes $Ag_mBr^{(m-1)+}$ in alkali metal nitrate melts at 280 °C. The errors quoted are three standard deviations from the least squares calculations.

	$\beta_1 \times 10^{-2}$ $(\text{mol kg}^{-1})^{-1}$	$\beta_2 \times 10^{-4}$ $(\text{mol kg}^{-1})^{-2}$	$\beta_3 \times 10^{-4}$ $(\text{mol kg}^{-1})^{-3}$	$\beta_4 \times 10^{-4}$ $(\text{mol kg}^{-1})^{-4}$
This work, (K,Na)NO_3	2.67 [a]	1.1 ± 0.4	2.2 ± 0.8	4.5 ± 0.5
Ref. 40, solubility data, (K,Na)NO_3 [b]	3.5	0.8	2.4	–
Ref. 35, emf data, KNO_3 [c]	2.6	2.9	–	–
Ref. 34, emf data, $NaNO_3$ [c]	1.9	1.9	–	–

[a] From Ref. 2. [b] Interpolated values from experimental determinations at 275 and 300 °C. [c] Apparent stability constants, extrapolated from investigations in the range 400–500 °C.

should be considered. Since an existence of polynuclear (polybromic) species $Ag_mBr_n^{(m-n)+}$ would require $m/n \approx 3.5$, to be in accordance with the potentiometric data, such species would have ion charges $\geq +5$. Therefore, it is concluded that only monobromic complexes are present in significant amounts. The solubilities are well reproduced assuming a stepwise formation of complexes Ag_2Br^+, Ag_3Br^{2+}, and Ag_4Br^{3+} and the parameters k_m of eqn. (5) are thus identified as β_m. Starting with $[Ag^+] \approx C_{Ag} - 3C_{Br}$ the calculations were iterated according to eqns. (4) and (5) to yield the final set of stability constants β_m and free ligand concentrations $[Ag^+]$. The constants are given in Table 3.

Since no conclusive evidence is found for specific halide-alkali metal ion interactions in mixed halide nitrate melts,[46–48] and since the calculations indicate that all complexes are present in fairly large relative amounts, no serious errors in the stability constants due to the "solvation effects" should be expected.[3]

The over-all constants $\beta_2 - \beta_4$, which are collected in Table 3, are all of the same order of magnitude. Hence, all complexes Ag_2Br^+, Ag_3Br^{2+} and Ag_4Br^{3+} are present simultaneously in comparable amounts in most of the melts investigated, which is the main reason why the uncertainties in β_2 and β_3 are rather large although the spread in experimental solubility data is fairly low. Table 3 also includes β-values interpolated from the sets of constants determined by Sinistri and Pezzati [40] by solubility measurements at 275 and 300 °C. For β_2 and β_3 the agreement with their data is very good. It is also obvious that Sinistri and coworkers did not extend their measurements to the composition range where Ag_4Br^{3+} had to be considered.

The distribution of Ag(I) between the two phases has been treated as follows. Firstly, the activities a_2 were estimated by integrating the relation

$$\mathrm{d} \ln f_2 = -(x_1/x_2)\, \mathrm{d} \ln f_1 \qquad (6)$$

Since x_1/x_2 appeared to be well approximated by

$$x_1/x_2 = [\sum_{\nu=0}^{2} b_\nu (\ln f_1)^\nu]^{-1} \qquad (7)$$

the integration was performed analytically from the lower limit ($\ln f_2 = 0$; $\ln f_1 = 0$), *i.e.* the standard state for $AgNO_3$ is chosen to be in accordance with the condition $\lim_{x_2 \to 0} f_2 = 1$.

For the most dilute solutions the errors in x_2 and hence in $\ln f_1$ prevent meaningful calculations. For that reason a_2 and f_2 have been omitted in Table 2 for these systems.

Secondly, setting $a(NO_3) = 1$, the heterogeneous equilibrium constant K_2' is calculated as the average value of $[Ag^+]a_2^{-1}$, yielding $K_2' = (5.2 \pm 0.6) \times 10^2$ mol kg^{-1}. From K_1' and K_2' a conditional equilibrium constant K_{12}' for the anion exchange reaction

$$AgBr(ss) + NO_3^- \rightleftharpoons AgNO_3(ss) + Br^-$$

is obtained as $K_{12}' = 5.8 \times 10^{-10}$ mol kg^{-1}.

Table 4. The stepwise stability constants and quotients in molten alkali nitrate and aqueous solution.

Medium	Quantity	$m=1$	$m=2$	$m=3$	$m=4$
H_2O, 20 °C, $I=0$	K_m/M^{-1}	2.4×10^4 [a]	475 [b]	12 [b]	–
(K,Na)NO_3(l), 280 °C	$K_m/(\text{mol kg}^{-1})^{-1}$	267 [c]	40	2	2
H_2O, 20 °C, $I=0$	$K_m/K_{(m+1)}$	50	40	–	–
(K,Na)NO_3(l), 280 °C	$K_m/K_{(m+1)}$	7	20	1	–

[a] Determined at 25 °C, Ref. 44. [b] Ref. 6. [c] Ref. 2.

DISCUSSION

The potentiometric ligand concentration measurements in melts concentrated in solutes have clearly demonstrated the absence of systematic dependence of $\bar{m}$ on C_{Br} in the composition range where a quantitative treatment of the complex equilibria is meaningful. Such a dependence should be expected if polybromic species with ion charges $\leq +3$ were present in significant amounts. The β-values of Table 3 have been used to compute ligand numbers $\bar{m}$, and the corresponding graph of $\bar{m}$ *vs.* $[Ag^+]$ is included in Fig. 1 to illustrate the perfect agreement between the emf and solubility measurements as interpreted in terms of mononuclear complexes only. It might, however, seem reasonable to expect polybromic complex cations to be formed with the bromine atoms joined *via* a Br–Ag–Br linkage – an arrangement which has recently been found in solid Ag_2BrNO_3. This compound contains trigonal bipyramidal Ag_5Br-polyhedra, linked together by edges and corners.[45]

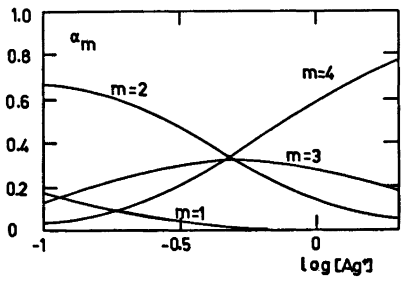

Fig. 2. The distribution of bromide on different complex ions. $\alpha_m=[Ag_mBr^{(m-1)+}]C_{Br}^{-1}$.

The relative distribution of bromide in different species is shown in Fig. 2 and the stepwise stability constants and quotients between them are collected in Table 4, where the relevant comparisons with aqueous solution data can also be made. In water no preference for Br to coordinate a certain number of ligands can be observed, whereas $m=2$ seems to be somewhat preferred at the expense of 3 in fused nitrate media, where Ag_3Br^{2+} amounts to at most about 30 % of C_{Br}.

Finally it should be noted that although three terms in the right hand member of eqn. (5) were found to describe the solubilities sufficiently well in the composition range investigated, there is no obvious reason why the complex formation curve should stop definitely at $\bar{m}=4$. The structures of the solid compounds $Ag_3I(NO_3)_2$[21] and Ag_2BrNO_3[45] suggest that a larger maximum coordination number might be possible.

Acknowledgements. I thank Professor Ido Leden for his support and stimulating interest in this work. Part of the experimental work was skilfully performed by Mrs. Bodil Jönsson. I also thank Dr. Peter Sellers for the linguistic revision of the manuscript.

REFERENCES

1. Cigén, R. and Mannerstrand, N. *Acta Chem. Scand. 18* (1964) 1755.
2. Cigén, R. and Mannerstrand, N. *Acta Chem. Scand. 18* (1964) 2203.
3. Holmberg, B. *Acta Chem. Scand. A 30* (1976) 641.
4. Vouk, V. B., Kratóhvil, J. and Težak, B. *Arh. Kem. 25* (1953) 219.

5. Kratóhvil, J., Težak, B. and Vouk, V. B. *Arh. Kem. 26* (1954) 191.
6. Lieser, K. H. *Z. Anorg. Allg. Chem. 304* (1960) 296.
7. Lieser, K. H. *Z. Anorg. Allg. Chem. 305* (1960) 133.
8. Lieser, K. H. *J. Inorg. Nucl. Chem. 26* (1964) 1571.
9. Pinkus, A., Frederic, S. and Schepmans, R. *Bull. Soc. Chim. Belg. 47* (1938) 304.
10. Berne, E. and Leden, I. *Sven. Kem. Tidskr. 65* (1953) 88.
11. Leden, I. and Parck, C. *Acta Chem. Scand. 10* (1956) 535.
12. Lieser, K. H. *Z. Anorg. Allg. Chem. 292* (1957) 114.
13. Greenslade, D. J. and Symons, M. C. R. *Trans. Faraday Soc. 62* (1966) 307.
14. Luehrs, D. C. and Abate, K. *J. Inorg. Nucl. Chem. 30* (1968) 549.
15. Le Démézet, M., Madec, C. and L'Her, M. *Bull. Soc. Chim. Fr.* (1970) 365.
16. Hellwig, K. *Z. Anorg. Allg. Chem. 25* (1900) 157.
17. Hayek, E. *Z. Anorg. Allg. Chem. 223* (1935) 382.
18. Hayek, E. *Monatsh. Chem. 68* (1936) 29.
19. Lindqvist, I. *Acta Crystallogr. 7* (1954) 635.
20. Lieser, K. H. *Z. Anorg. Allg. Chem. 295* (1958) 106.
21. Birnstock, R. and Britton, D. *Z. Kristallogr. 132* (1970) 87.
22. Berg, L. G. and Lepeshkov, I. N. *Izv. Sekt. Fiz.-Khim. Anal., Inst. Obshch. Neorg. Khim., Akad. Nauk SSSR 15* (1947) 144; *Chem. Abstr. 44* (1950) 7134 i.
23. Lifshits, G. M. *Zh. Obshch. Khim. 25* (1955) 2414.
24. Bergman, A. G. and Tokareva, M. V. *Zh. Neorg. Khim. 2* (1957) 1086.
25. Dombrovskaya, N. S. and Koloskova, Z. A. *Izv. Sekt. Fiz.-Khim. Anal., Inst. Obshch. Neorg. Khim., Akad. Nauk SSSR 22* (1953) 178; *Chem. Abstr. 52* (1958) 3500i.
26. Jacoud, R., Reinsborough, V. C. and Wetmore, F. E. W. *Aust. J. Chem. 19* (1966) 1597.
27. Schwartz, K. G. *Z. Elektrochem. 47* (1941) 144.
28. Hill, S. and Wetmore, F. E. W. *Can. J. Chem. 32* (1954) 864.
29. Hill, D. G., Braunstein, J. and Blander, M. *J. Phys. Chem. 64* (1960) 1038.
30. Hill, D. G. and Blander, M. *J. Phys. Chem. 65* (1961) 1866.
31. Braunstein, J., Blander, M. and Lindgren, R. M. *J. Am. Chem. Soc. 84* (1962) 1529.
32. Manning, D. L., Braunstein, J. and Blander, M. *J. Phys. Chem. 66* (1962) 2069.
33. Gaur, H. C. and Sethi, R. S. *Trans. Faraday Soc. 64* (1968) 445.
34. Manning, D. L., Bansal, R. C., Braunstein, J. and Blander, M. *J. Am. Chem. Soc. 84* (1962) 2028.
35. Alvarez-Funes, A., Braunstein, J. and Blander, M. *J. Am. Chem. Soc. 84* (1962) 1538.
36. Guion, J. *Inorg. Chem. 6* (1967) 1882.
37. Inman, D., White, S. H., Wilmot, I. and Jones, B. *J. Electroanal. Chem. 33* (1971) 225.
38. Braunstein, J. *J. Electroanal. Chem. 33* (1971) 235.
39. Seward, R. P. and Field, P. E. *J. Phys. Chem. 68* (1964) 1611.
40. Sinistri, C. and Pezzati, E. *Gazz. Chim. Ital. 97* (1967) 1116.
41. Holmberg, B. *Acta Chem. Scand. 27* (1973) 3550, 3657.
42. Holmberg, B. *Acta Chem. Scand. 27* (1973) 875.
43. Holmberg, B. *Acta Chem. Scand. A 28* (1974) 284.
44. Berne, E. and Leden, I. *Z. Naturforsch. Teil A 8* (1953) 719.
45. Holmberg, B. and Persson, K. *Acta Crystallogr. A 31* (1975) S 65.
46. Kleppa, O. J. and Meschel, S. V. *J. Phys. Chem. 67* (1963) 669.
47. Janz, G. J. and Kozlowski, T. R. *J. Chem. Phys. 40* (1964) 1699.
48. James, D. W. *Aust. J. Chem. 19* (1966) 993.

Received April 7, 1976.

Acta Chemica Scandinavica A 30 (1976) 687—691

The Ion Pair Formation of Quaternary Ammonium Picrates in Aqueous Methylene Chloride at 25 °C Studied by Conductivity and Distribution

PER BERONIUS and ARNE BRÄNDSTRÖM

Department of Physical Chemistry, University of Umeå, S-901 87 Umeå, Sweden and
Research Laboratory of AB Hässle, Mölndal, Sweden

Electrical conductance measurements of Me_4NPi, Et_4NPi, and Pr_4NPi in water saturated methylene chloride at 25 °C were performed for several concentrations below 5×10^{-4} M. The data were analyzed by means of the expanded Fuoss-Hsia and Pitts' equations for associated electrolytes. Limiting single ion conductances were estimated by means of an indirect method. The data indicate a stronger ion-solvent interaction for Me_4N^+ as compared with Et_4N^+ and Pr_4N^+. Ion-pair association constants, K_A, which increase in the order, $Pr_4NPi < Et_4NPi \ll Me_4NPi$, are discussed in terms of the Bjerrum theory.

The values of K_A according to conductance measurements and distribution measurements in the two-phase system, water/methylene chloride, are in almost complete agreement.

Measurement of electrolytic conductivity is considered to be one of the most accurate methods for determining ion pair association constants, *cf.* Ref. 1. Unfortunately, unequivocal evaluation of the association constant is in general not possible because of the uncertainty concerning proper choice of value for the distance parameter in the conductance equation and in the Debye-Hückel equation.[2-4]

One possibility of attacking this problem might be to investigate the equilibrium between free and paired ions by independent methods. The present study of the association of quaternary ammonium picrates in aqueous methylene chloride by conductance and partition measurements, *cf.* Refs. 5 – 6, constitutes part of such an investigation. By contrast with the present study, previous investigations (Table 3) of quaternary ammonium picrates refer to pure solvents.

EXPERIMENTAL

Water saturated methylene chloride was prepared by shaking the organic solvent (Merck, *p.a.*) with distilled water for 10 min. The system was left for 1 h before separating the two phases. Analysis according to the Karl Fischer method indicated a water concentration of 0.2 % by volume in the organic liquid.

The permittivity, ε, of the water saturated methylene chloride was measured by means of a Ferisol M 803 A Q-meter. The value, $\varepsilon = 8.94$, at 25 °C was obtained. The viscosity, $\eta =$ 0.00416 P at this temperature, was established using an Ubbelohde viscometer. The viscosity of anhydrous methylene chloride is 0.00410 P. This value was calculated [7,8] using the expression, $1/\eta = A \exp -(E/RT)$. The density, $d_4^{25} =$ 1.3147 g cm^{-3}, was determined by means of a Lipkin pycnometer. The electrolytic conductivity was, $\varkappa = 1 \times 10^{-9}$ Ω^{-1} cm^{-1}; $\varkappa = 4.3 \times 10^{-11}$ Ω^{-1} cm^{-1} for anhydrous methylene chloride.[8]

The tetraalkylammonium picrates were prepared from the corresponding bromides or hydrogen sulfates. They were repeatedly recrystallized from 99.5 % ethanol. For the density of the picrates the value 1.4 g cm^{-3} was used in making buoyancy corrections.

Measurements of electrolytic conductivity at 25.00 ± 0.01 °C were performed using a Daggett-Bair-Kraus type conductivity cell,[9] of 1300 cm^3 capacity, connected to a Leeds and Northrup conductivity bridge. The cell constant (~ 0.03 cm^{-1}) was established by several calibrations with aqueous potassium chloride.[10] The cell was thermostated in a kerosene filled constant temperature bath, the temperature of

which was determined using a Leeds and Northrup platinum resistance thermometer.

The conductivity of a predetermined quantity of water saturated methylene chloride was measured. Several portions of the salt under investigation were then successively added by means of a Hawes-Kay salt cup dispensing device.[11,12] The cell content was agitated by a magnetic stirrer to reduce the time required to dissolve the salt. After each addition of a portion of the salt the cell resistance was repeatedly measured until a constant resistance was attained. The time required for this was 2 – 6 h for tetramethyl ammonium picrate and less than 1 h for the other two picrates. Measurements were performed at 5.0, 3.3, 2.5, and 2.0 kHz and extrapolation of the resistance to infinite frequency performed. The correction for the conductivity of the solvent was 0.1 % or less. The densities of the solutions were taken to be the same as that of the solvent.

The distribution measurements were performed as described by Gustavii.[5–6] The concentrations in both layers were determined photometrically by comparison with a standard curve. The molar absorbance for tetramethylammonium picrate in methylene chloride was found to be significantly lower than those of other quaternary ammonium picrates.

From the distribution values both K_A and E were calculated using the equation,

$$c_s = Ec_w^2 + (E/K_A)^{1/2}c_w/\gamma_s \quad (1)$$

where c_s is the concentration in the organic layer and c_w that in the aqueous layer. E is the extraction constant and γ_s the mean activity coefficient of free ions in the methylene chloride layer.

The procedure starts with a calculation of $[Q^+]_s$ and γ_s by iterations in the association equation and the Debye-Hückel equation,

$$\gamma_s = \exp -(30.53[Q^+]_s^{1/2}/(1+30.53[Q^+]_s^{1/2})) \quad (2)$$

$$K_A\gamma_s^2[Q^+]_s^2 = c_s - [Q^+]_s \quad (3)$$

To avoid the difficulties in the least-squares treatment of eqn. (1), which arise from the fact that both c_s and c_w are subjected to errors, which are very different for different pairs of values, an error normalisation was performed in the following way. The "error", F, in the measurement is defined by,

$$F = c_s - Ec_w^2 - (E/K_A)^{1/2}c_w/\gamma_s \quad (4)$$

In this we introduce,

$$c_w = A_w n_w/\varepsilon_w \quad (5a)$$

$$c_s = A_s n_s/\varepsilon_s \quad (5b)$$

where A is the absorbance, n the factor by which the solution is diluted before measurements, and ε the molar absorption coefficient in the solvent indicated. From other measurements we know that the variance in A_w and A_s are equal. We denote them by "Var A". From elementary statistics we have,

$$\text{Var } F = (n/\varepsilon_s)^2 \text{ Var } A \quad (6)$$

where,

$$n^2 = n_s^2 + (n_w\varepsilon_s/\varepsilon_w)^2[2Ec_w + (E/K_A)^{1/2}/\gamma_s]^2 \quad (7)$$

The non-linear least-squares treatment is therefore performed on the normalized "error" function, F/n, where n is calculated for every pair of c_w and c_s. From Var F/n, we can calculate the standard deviations, $\sigma(A)$, $\sigma(E)$, and $\sigma(K_A)$.

RESULTS AND DISCUSSION

In Table 1 corrected values of the molar conductivity, Λ, and the corresponding concentrations, c, are listed. Two independent

Table 1. Molar conductivities of tetraalkylammonium picrates in water saturated methylene chloride at 25 °C.

Run A $c\times10^4$ M	Λ cm² Ω^{-1} mol^{-1}	Run B $c\times10^4$ M	Λ cm² Ω^{-1} mol^{-1}
Me_4NPi			
0.51124	45.175	0.56690	43.740
0.78735	38.456	0.84892	37.503
1.0723	34.111	1.1029	33.814
1.3764	30.901	1.3791	30.935
2.3802	24.752	2.1800	25.688
4.9651	18.289	4.5622	18.945
Et_4NPi			
0.25233	94.630	0.22915	96.096
0.51329	81.950	0.48566	82.947
0.78395	73.866	0.73594	75.023
4.7355	42.610	0.99607	69.250
		1.2601	64.831
		2.2154	54.743
Pr_4NPi			
0.21651	90.009	0.23399	88.863
0.45811	79.538	0.46706	79.167
0.68506	73.118	0.70867	72.517
0.95186	67.657	0.99158	66.958
1.1920	63.942	1.2700	62.877
2.1488	54.437	2.2113	53.965
4.7051	43.043	4.5270	43.535

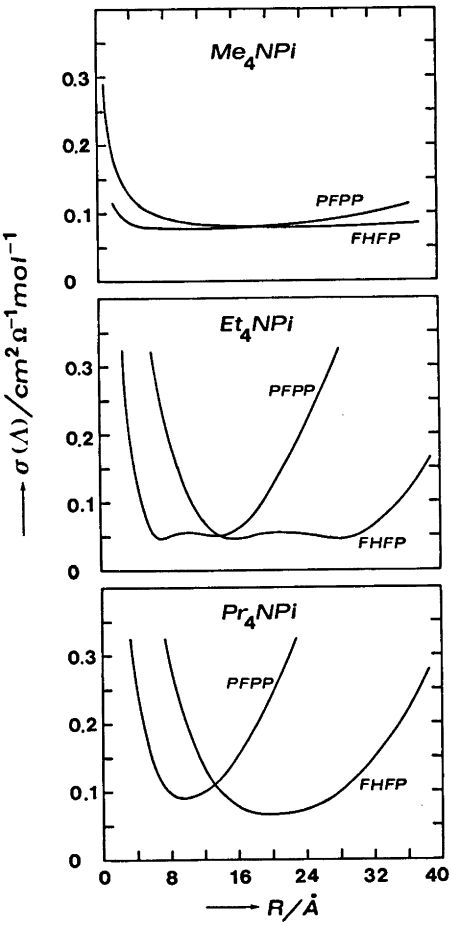

Fig. 1. Conditional minimum $\sigma(\Lambda)$ *vs.* association distance according to FHFP and PFPP equations for quaternary ammonium picrates in water saturated methylene chloride at 25 °C.

series of measurements were made for each picrate.

The conductance data were analyzed by means of the Fuoss-Hsia equation in the form of Fernández-Prini,[13] and the Pitts' equation as developed by Fernández-Prini and Prue.[14] Below these two conductance equations will be denote "FHFP" and "PFPP", respectively. The method of computing the values of Λ_∞ and K_A which minimize $\sigma(\Lambda)$ for some selected value of the distance parameter, R, in the conductance equation, and in the Debye-Hückel equation[15] for the mean activity coefficient of free ions, has been described.[2] (Λ_∞ = limiting molar conductivity; K_A = ion-pair association constant; $\sigma(\Lambda)$ = standard deviation between experimental and computed Λ values; R = maximum distance between centres of charge in the ion-pair.)

The FHFP and PFPP equations fit the experimental data with almost the same precision as is evident from Fig. 1, where $\sigma(\Lambda)$ has been plotted *vs.* R. Especially for Me_4NPi, but also for Et_4NPi, the $\sigma(\Lambda)-R$ curves are quite shallow. The minimum values of $\sigma(\Lambda)$ for the two equations appear at significantly different values of R. It follows that the condition, $\sigma(\Lambda)$ = minimum, is not useful as criterion of "best set" conductance parameters. This is in accord with previous experience.[3,4] In the following calculations R will be set equal to the Bjerrum radius,[16] q.

The conductance parameters derived are within experimental errors independent of the upper limit of the concentration interval studied (Table 2). This independence may be taken as evidence of the absence of significant amounts of higher aggregates than ion-pairs.

In the absence of transference data the limiting molar conductivity of the picrate ion was obtained from the Walden product estimates, $\lambda_\infty(Pi^-)\eta$ in Table 3, derived from conductance data of Bu_4NFBPh_3 and Bu_4NPi in several solvents.[17–22] For each series of conductance measurements Λ_∞ was computed by application of the FHFP equation to the four lowest concentration points. The limiting conductivity of Bu_4N^+ was obtained by assuming[20] equal mobilities of Bu_4N^+ and $FBPh_3^-$. Combination of $\lambda_\infty(Bu_4N^+)$ with $\Lambda_\infty(Bu_4NPi)$ yielded $\lambda_\infty(Pi^-)$. The average value, 0.275 cm² Ω^{-1} mol^{-1} P, of the Walden products in the last column of Table 3 yields 66 cm² Ω^{-1} mol^{-1} for the limiting molar conductivity of the picrate ion in water saturated methylene chloride. Adopting Λ_∞ = 121, 125, and 111 cm² Ω^{-1} mol^{-1} for Me_4NPi, Et_4NPi, and Pr_4NPi, respectively, (Table 2) we arrive at the following ionic conductivities: $\lambda_\infty(Me_4N^+)=55$; $\lambda_\infty(Et_4N^+)=59$; $\lambda_\infty(Pr_4N^+)=45$ cm² Ω^{-1} mol^{-1}.

For a homologous series of tetraalkylammonium ions one might expect that the mobility should decrease with increasing number of carbon atoms in the substituent groups. For the solvent concerned the mobility decreases in the order, $Et_4N^+ > Me_4N^+ > Pr_4N^+$, *i.e.* the mobility of the tetramethyl ammonium ion is

Table 2. Dependence of conductance parameters on concentration interval. The parameters, derived from the data in Table 1, refer to the FHFP equation with R set to $q = 31.34$ Å. N = number of points (c,Λ). Errors listed for Λ_∞ and K_A are standard deviations.

$c_{max} \times 10^4$ M	N	Λ_∞ cm² Ω⁻¹ mol⁻¹	$K_A \times 10^{-4}$ M⁻¹	$\sigma(\Lambda)$ cm² Ω⁻¹ mol⁻¹
Me_4NPi				
4.97	12	121.00 ± 1.38	10.04 ± 0.17	0.08
2.38	10	122.11	10.27	0.08
1.38	8	122.28	10.31	0.10
1.10	6	121.90	10.23	0.13
Et_4NPi				
4.74	10	125.26 ± 0.14	1.763 ± 0.005	0.06
2.22	9	125.34	1.769	0.05
1.26	8	125.42	1.774	0.05
0.78	6	125.34	1.768	0.06
Pr_4NPi				
4.71	14	110.60 ± 0.29	1.270 ± 0.009	0.14
2.21	12	110.93	1.290	0.06
1.27	10	111.02	1.295	0.06
0.99	8	110.99	1.293	0.07
0.71	6	110.88	1.285	0.08

Table 3. Single ion conductivities and Walden products at 25 °C. The data have been calculated from literature data [17–22] by means of the FHFP equation with R set equal to the Bjerrum radius, q.

Solvent	$\lambda_\infty(Bu_4N^+)$ cm² Ω⁻¹ mol⁻¹	$\lambda_\infty(Pi^-)$ cm² Ω⁻¹ mol⁻¹	$\lambda_\infty(Pi^-)\eta$ cm² Ω⁻¹ mol⁻¹ P
Nitrobenzene [17]	11.73	16.15	0.292
Pyridine [18,19]	24.07	33.97	0.300
Ethylene dichloride [20,21]	26.22	31.52	0.247
Acetone [22]	67.17	85.20	0.259

Table 4. Distribution of tetrapropylammonium picrate between buffer (pH = 6.5, $\mu = 0.1$) and methylene chloride at 25 °C.[a]

$c_w \times 10^4$ M	γ_s	n	$c_s \times 10^4$ M	c_s(calc) $\times 10^4$ M
0.6380	0.7877	7.614	1.962	1.970
0.6260	0.7887	7.561	1.924	1.915
0.5260	0.8018	7.119	1.492	1.477
0.4300	0.8174	5.131	1.096	1.102
0.3180	0.8388	3.920	0.709	0.722
0.3110	0.8392	3.881	0.702	0.701
0.3050	0.8393	3.848	0.701	0.683
0.3160	0.8395	3.908	0.698	0.715
0.3040	0.8408	3.839	0.680	0.679
0.2770	0.8461	3.679	0.608	0.600
0.2420	0.8555	3.466	0.496	0.501
0.1720	0.8745	3.047	0.324	0.323
0.1420	0.8847	2.865	0.254	0.255
0.0920	0.9040	2.563	0.155	0.152
0.0390	0.9337	2.236	0.062	0.058

[a] $E = (2.24 \pm 0.06) \times 10^4$; $K_A = (1.31 \pm 0.07) \times 10^4$; $\sigma(\Lambda) = 0.004$.

much too low on the basis of its size. This indicates a much stronger interaction between this ion and solvent molecules as compared with the higher homologues. Similar ion-solvent effects, though not as pronounced as for the present solvent, have been observed for Me_4N^+ in nitrobenzene [17] and ethylene dichloride.[23]

The ion-pair association constants in Table 2 indicate that association increases in the order $Pr_4NPi < Et_4NPi \ll Me_4NPi$, *i.e.* with decreasing radius of the tetraalkylammonium ion (estimated [24] to 3.47, 4.00, and 4.52 Å for Me_4N^+, Et_4N^+, and Pr_4N^+, respectively). This is in accord with ion association theory. Using the Bjerrum equation [16] for K_A the minimum distance between the centres of charge of the ions in the ion-pair are found to be 4.4 Å for Me_4NPi, 5.5 Å for Et_4NPi, and 5.8 Å for Pr_4NPi. These contact distances, which exceed the radii of Me_4N^+, Et_4N^+, and Pr_4N^+ by 0.9,

Table 5. Extraction and association constants for R_4NPi with standard deviations.

R	E_{QX}	$K_A \times 10^{-4}$ Distr.	$K_A \times 10^{-4}$ Conduct.	$\sigma(A)$	$\sigma(\Lambda)$
CH_3	1.40 ± 0.04	10.5 ± 0.8	10.27	0.003	0.08
C_2H_5	164.5 ± 2.2	1.89 ± 0.05	1.769	0.004	0.05
C_3H_7	$(2.24 \pm 0.06) \times 10^4$	1.31 ± 0.07	1.29	0.004	0.06

1.5, and 1.3 Å, respectively, seem quite reasonable taking into consideration the location of the negative charge in the picrate ion.

The results of the distribution measurements are given in Tables 4 – 5. From these it can be seen that the K_A values obtained for tetramethyl- and tetrapropylammonium picrate are, within experimental errors, identical with the values obtained from conductivity measurements. For tetraethylammonium picrate the two sets of values seem not to be significantly different.

Acknowledgements. The authors thank Mrs. Margareta Ögren and Mrs. Ylva Weimar for technical assistance, and AB Hässle, Mölndal, Sweden, and the Swedish Natural Science Research Council for financial support.

REFERENCES

1. Barthel, J. *Angew. Chem. Int. Ed. Engl. 7* (1968) 260.
2. Beronius, P. *Acta Chem. Scand. A 28* (1974) 77.
3. Beronius, P. *Acta Chem. Scand. A 29* (1975) 289.
4. Beronius, P. *Acta Chem. Scand. A 30* (1976) 115.
5. Gustavii, K. and Schill, G. *Acta Pharm. Suec. 3* (1966) 241.
6. Gustavii, K. *Acta Pharm. Suec. 4* (1967) 233.
7. Weissberger, A., Ed., *Technique of Organic Chemistry, Vol. VII, Organic Solvents*, 2nd Ed., Interscience, New York 1955, Chapter II.
8. *Ibid.* p. 192.
9. Daggett, Jr., H. M., Bair, E. J. and Kraus, C. A. *J. Am. Chem. Soc. 73* (1951) 799.
10. Lind, J. E., Zwolenik, J. J. and Fuoss, R. M. *J. Am. Chem. Soc. 81* (1959) 1557.
11. Hawes, J. L. and Kay, R. L. *J. Phys. Chem. 69* (1965) 2420.
12. Kay, R. L., Hales, B. J. and Cunningham, G. P. *J. Phys. Chem. 71* (1967) 3925.
13. Fernández-Prini, R. *Trans. Faraday Soc. 65* (1969) 3311.
14. Fernández-Prini, R. and Prue, J. E. *Z. Phys. Chem. (Leipzig) 228* (1965) 373.
15. Robinson, R. A. and Stokes, R. H. *Electrolyte Solutions*, Butterworths, London 1965, pp. 229 – 230.
16. Bjerrum, N. *K. Dan. Vidensk. Selsk. Mat.-Fys. Medd. 7* (1926) No 9.
17. Taylor, E. G. and Kraus, C. A. *J. Am. Chem. Soc. 69* (1947) 1731.
18. Burgess, D. S. and Kraus, C. A. *J. Am. Chem. Soc. 70* (1948) 706.
19. Luder, W. F. and Kraus, C. A. *J. Am. Chem. Soc. 69* (1947) 2481.
20. Fowler, D. L. and Kraus, C. A. *J. Am. Chem. Soc. 62* (1940) 2237.
21. Mead, D. J., Fuoss, R. M. and Kraus, C. A. *Trans. Faraday Soc. 32* (1936) 594.
22. Reynolds, M. B. and Kraus, C. A. *J. Am. Chem. Soc. 70* (1948) 1709.
23. Tucker, L. M. and Kraus, C. A. *J. Am. Chem. Soc. 69* (1947) 454.
24. Robinson, R. A. and Stokes, R. H. *Electrolyte Solutions*, Butterworths, London 1965, p. 125.

Received April 1, 1976.

Acta Chemica Scandinavica A 30 (1976) 692—696

Isentropic Apparent Molal Compressibilities of Alcohols in Aqueous Solution. Relations to van der Waals Radii and the Scaled Particle Theory

HARALD HØILAND and EINAR VIKINGSTAD

Department of Chemistry, University of Bergen, N-5014 Bg-U, Norway

Isentropic apparent molal compressibilities of the homologous series of 1- and 2-propanol to 1- and 2-hexanol, the diols 1,2-propanediol, 1,2- 2,3-, and 1,4-butanediol, 1,5-pentanediol, and 1,7-heptanediol in aqueous solution at 25 and 35 °C have been determined from ultrasonic measurements. Values at infinite dilution have been evaluated. The additivity of isentropic group molal compressibilities have been investigated.

The isentropic molal compressibilities have been discussed in connection with partial molal volume data for the same alcohols. In relation to two solvation models, one based on the scaled particle theory, the other on van der Waals radii, the isentropic molal compressibilities were seen to be more sensitive to deficiencies in the models than the partial molal volumes.

In this paper we present experimental data for the isentropic apparent molal compressibilities of some alcohols and diols in aqueous solution. This thermodynamic quantity is of interest especially in connection with partial molal volume data. Non-thermodynamic solvation models may be constructed, and their usefulness can be checked against partial molal volume and compressibility data.

It has been demonstrated [1,2] that the partial molal volumes of organic solutes in water may be calculated by adding the appropriate group partial molal volumes. The isentropic molal compressibility data available [3,4] indicate additivity of group molal compressibilities as well. An advantage if such additivity relations can be established, is that different functional groups can be treated individually.

It has recently been shown that the partial molal volumes of organic solutes with more than three aliphatic carbon atoms per polar group can be calculated from eqn. (1).[5]

$$\overline{V}^0 = \tfrac{4}{3}\pi N(r_w + \Delta)^3 \qquad (1)$$

r_w is the van der Waals radius and Δ the thickness of an empty shell enclosing the solute. The value of Δ was on average found to be 0.53 Å.

The isentropic molal compressibility can in principle be calculated from eqn. (1):

$$\left(\frac{\partial \overline{V}^0}{\partial P}\right)_s = -\phi^0_{k(s)} = 4\pi N(r_w + \Delta)^2(\partial\Delta/\partial P)_s \qquad (2)$$

The van der Waals radius is here considered to be independent of pressure.

The partial molal volume can be represented as the sum:

$$\overline{V}^0 = \overline{V}_{int} + \Delta\overline{V} \qquad (3)$$

$\overline{V}_{int}$ is the intrinsic volume, the spherical cavity in which the solute is contained. This quantity can be calculated from the scaled particle theory.[6]

$\Delta\overline{V}$ is the volume change due to solute-solvent interactions. If $\overline{V}^0$ and $\overline{V}_{int}$ are known, $\Delta\overline{V}$ can be calculated from eqn. (3). This has been done for single ions.[6] In this case $\Delta\overline{V}$ was seen to be negative and decreasing with increasing ionic radius.

EXPERIMENTAL

The origin and purity of the alcohols have been described elsewhere.[7]

Isentropic coefficients of compressibility were determined by the "sing-around" principle.[8] Ultrasonic pulses are passed through the solution and the frequencies of these pulses are measured, in this case by a Hewlett-Packard 5326A Time Counter averaging over periods of 10 s. The isentropic coefficients of compressibility are then determined from eqn. (4).

$$\beta_s = 10^6/u^2d \qquad (4)$$

d is the density of the solution, u the speed of sound [eqn. (5)].

$$u = \frac{s}{1/f - \tau} \qquad (5)$$

s is the length of the cell, f the measured frequencies, and τ the delay measured to 300 ns. The cell was calibrated with water as the standard using the data of Del Grosso and Mader.[9] The isentropic apparent molal compressibilities were calculated from the equation:

$$\phi_{k(s)} = \frac{1000(\beta_s - \beta_{s0})}{md_0} + \beta_s\phi_v \qquad (6)$$

The subscript zero refers to pure water, m is the molality, and ϕ_v the apparent molal volume for which values are given.[7]

The cell was thermostated in a water bath The temperature fluctuations were less than 0.007 °C.

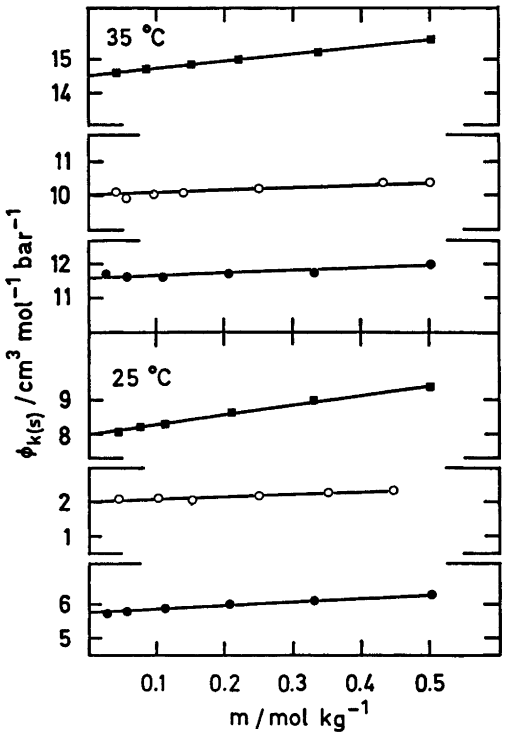

Fig. 1. Isentropic apparent molal compressibilities as functions of concentration. ●, 1-propanol; ○, 2-butanol; ■, 1,5-pentanediol.

Table 1. Isentropic molal compressibilities.

	$\phi^0_{k(s)} \times 10^4$ cm^3 mol^{-1} bar^{-1}		$\phi^0_{k(s)}(CH_2) \times 10^4$ cm^3 mol^{-1} bar^{-1}	
	25 °C	35 °C	25 °C	35 °C
1-Propanol	5.8	11.6		
1-Butanol	4.5	12.2	−1.3	0.6
1-Pentanol	2.3	12.4	−2.2	0.2
1-Hexanol	0.5	13.3	−1.8	0.9
2-Propanol	6.1	11.2		
2-Butanol	2.0	10.0	−4.1	−1.2
2-Pentanol	1.0	11.1	−1.0	1.1
2-Hexanol	−1.2	12.0	−2.2	0.9
1,4-Butanediol	9.0	13.3		
1,5-Pentanediol	7.9	14.5	−1.1	1.2
1,7-Heptanediol	6.0	16.0	−0.6	0.8
1,2-Propanediol	2.4	7.2		
1,3-Butanediol	−0.1	5.7	−2.3	−1.5
2,3-Butanediol	6.9	11.2		
2,4-Pentanediol	4.0	11.3	−2.9	0.1

The total error in the speed of sound measurements was estimated to ± 1 cm s^{-1}.

RESULTS

The isentropic apparent molal compressibilities, $\phi_{k,s)}$, were extrapolated to infinite dilution assuming a linear concentration dependence. Linear extrapolation function have generally been used for partial molal volumes of non-electrolytes, mainly based on empirical findings. Accepting such linearity, the isentropic apparent molal compressibilities should also be linear functions of concentration. Typical plots are shown in Fig. 1, confirming linearity. Results at infinite dilution are presented in Table 1. The error in $\phi^0_{k(s)}$ is estimated to ± 0.3 cm^3 mol^{-1} bar^{-1}, (1 bar $= 10^{-5}$ N m^{-2}).

The data of Nakajama, Komatsu and Nakagawa [3] are apparently the only literature values for $\phi^0_{k(s)}$ of alcohols in aqueous solution. The agreement is good where comparisons can be made.

The basis for calculating group molal compressibilities is the increment in isentropic molal compressibility per CH_2 group. The mean value is $(-1.6 \pm 0.6) \times 10^{-4}$ cm^3 mol^{-1} bar^{-1} at 25 °C. The standard deviation in the group molal compressibility of the CH_2 group is larger than for the corresponding group partial molal volume from these homologous series. The additivity relation is thus less accurate for isentropic molal compressibilities than for partial molal volumes. However, in most cases addition of the isentropic group molal compressibilities given in Table 2, results in values within the experimental error.

2-propanol has exceptionally large $\phi^0_{k(s)}$ values both at 25 and 35 °C. The same was observed for the partial molal volume.[7] The large partial molal volume was explained by a large empty volume due to the closeness of the two methyl groups. This explanation holds for the isentropic molal compressibility if large empty volumes lead to larger compressibilities.

Table 2. Isentropic group molal compressibilities.

	$\phi^0_{k(s)} \times 10^4$ cm^3 mol^{-1} bar^{-1}	
	25 °C	35 °C
CH_3^-	0.8	4.4
CH_2^-	−1.6	0.8
CH_2OH^-	6.5	6.0
CHOH	2.2	0.7

Relations to van der Waals radii. Van der Waals radii for organic solutes can be computed from Bondi's data,[10] and partial molal volumes can be calculated from eqn. (1). This has been done for some alkanes, alcohols, undissociated mono-, and di-carboxylic acids for which experimental data are accessible.[2,7,11] Reasonably good agreement between calculated and experimental data is obtained for the alkanes and higher alcohol homologues. However, when the solutes are of a more polar character, *i.e.* undissociated mono- and di-carboxylic acid, the agreement is poor as expected.

Eqn. (2) can now be used for calculating isentropic molal compressibilities. However, the value of $(\partial \Delta / \partial P)_s$ is not known and must be determined from the experimental data. If such a calculation is attempted, different values are obtained for each alcohol in each homologous series. This solvation model, a solute in a spherical cavity of radius $(r_w + \Delta)$ is no longer capable of representing the experimental results. The reason seems obvious. When pressure is applied the hydration sheath is not uniformly compressed, as indeed is clearly demonstrated by the values of the group molal compressibilities.

The scaled particle theory. The intrinsic volume, $\overline{V}_{int}$, eqn. (3), can be derived as follows: First a point particle is introduced in water. The volume increases due to its kinetic contribution to the pressure. This volume is then expanded against surface forces to make room for the solute of finite size. The reversible work done in this process can be calculated from the scaled particle theory.[12] The expression reads as eqn. (7).

$$\overline{V}_{int} = 2.52r^3 + A'r^2 + A''r + A''' \qquad (7)$$

Values of the constants A', A'' and A''' can be found in the literature for water as the solvent.[6]

The scaled particle theory was originally devised for calculating thermodynamic quantities of hard sphere or simple non-polar fluids, and the extension of the theory to aqueous solution may be questioned. However, it is

still of considerable interest to use the theory for estimating intrinsic volumes. The most interesting quantity in this connection is $\Delta\overline{V}$, the volume change due to solute-solvent interactions. It is determined by the difference $(\overline{V}^0 - \overline{V}_{int})$. Values are given in Table 3. $\Delta\overline{V}$ is seen to be small for the alkanes, in fact zero for methane. It is decreasing in the order alkanes > alcohols > diols ≈ mono-carboxylic acids (undissociated) > di-carboxylic acids (undissociated). In each homologous series $\Delta\overline{V}$ is less negative the more methylene (non-polar) groups the solute contains.

The isentropic molal compressibility can in principle be calculated from eqn. (5); see eqn. (8).

Table 3. Values of $\Delta\overline{V}$ $(=\overline{V}^0 - \overline{V}_{int})$ and $\Delta\phi(=\phi^0_{K(s)} - \phi_{int})$ where the intrinsic volumes and compressibilities have been calculated from the scaled particle theory.

	$\Delta\overline{V}$/ cm³ mol⁻¹	$\Delta\phi \times 10^4$/ cm³ mol⁻¹ bar⁻¹
Methane [a]	0.0	
Ethane	−1.7	
Propane	−2.8	
1-Propanol [b]	−5.8	−51
1-Butanol	−5.0	−61
1-Pentanol	−3.7	−70
1-Hexanol	−2.3	−78
2-Propanol	−4.6	−50
2-Butanol	−5.0	−63
2-Pentanol	−3.8	−71
2-Hexanol	−2.5	−80
1,4-Butanediol	−10.2	−59
1,5-Pentanediol	−8.8	−67
1,7-Heptanediol	−4.0	−82
1,2-Propanediol	−12.4	−59
1,3-Butanediol	−10.1	−51
2,3-Butanediol	−11.9	−68
Acetic acid [c]	−11.1	−43
Propionic	−10.5	−52
Butyric	−9.6	−60
Malonic acid	−20.4	
Succinic	−19.5	
Glutaric	−17.8	
α-Hydroxyacetic [d]	−18.6	−49
α-Hydroxypropionic	−16.1	−58
α-Hydroxybutyric	−14.9	−66

[a] Ref. 11, [b] Ref. 7, [c] Ref. 4, [d] Ref. 14.

$$\left(\frac{\partial\overline{V}_{int}}{\partial P}\right)_s = -\phi_{int} = \left(\frac{\partial A'}{\partial P}\right)_s r^2 + \left(\frac{\partial A''}{\partial P}\right)_s r + \left(\frac{\partial A'''}{\partial P}\right)_s \quad (8)$$

The only additional data required in calculating $(\partial A/\partial P)_s$ is $(\partial\beta/\partial P)$ where β is the coefficient of compressibility. This was calculated from the data of Kell and Whalley [13] assuming linearity between $(\partial\beta/\partial P)$ and P. The value is -1.3×10^{-8} bar^{-2}. Unfortunately, $(\partial A/\partial P)$ consist of two terms of opposing signs and of the same order of magnitude. The values of $(\partial A/\partial P)$ are thus very sensitive to any error in $(\partial\beta/\partial P)$. Numerically eqn. (6) reads as eqn. (9).

$$10^6 \times \phi_{int} = 6.6r^2 + 4.8r + 1.4 \quad (9)$$

ϕ_{int} calculated by eqn. (9) is positive for all the alcohols, and the values are larger than the experimental $\phi^0_{K(s)}$ data by a factor of ten. This means that $\Delta\phi(=\phi^0_{K(s)} - \phi_{int})$ is correspondingly large and negative. Positive values of ϕ_{int} and negative $\Delta\phi$ values seem qualitatively correct. However, the extremely large values suggest that a solvation model based on calculating $\overline{V}_{int}$ and ϕ_{int} from the scaled particle theory fails for the compressibilities. Since this solvation model is basically the same as the van der Waals model outlined above, this is not surprising.

In conclusion these results show that molal compressibilities are more sensitive to deficiencies in proposed solvation models than the partial molal volumes. The reason for this, as mentioned above, must be that the hydration sheath is not uniformly compressed when pressure is applied. If the group molal compressibilities are inspected, Table 2, it is revealed that the hydration sheath around hydrophilic groups are more easily compressed than the sheath around hydrophobic groups, and that end groups have higher groups molal compressibilities than the other groups of the solute molecule.

REFERENCES

1. Traube, J. *Samml. Chem. Vortr. 4* (1899) 255.
2. Høiland, H. *Acta Chem. Scand. A 28* (1974) 699.
3. Nakajima, T., Komatsu, T. and Nakagawa, T. *Bull. Chem. Soc. Jpn. 48* (1974) 788.

4. Høiland, H. and Vikingstad, E. *J. Chem. Soc. Faraday Trans. 1, 72* (1976) 1941.
5. Edward, J. T. and Farrell, P. G. *Can. J. Chem. 53* (1975) 2965.
6. Hirata, F. and Arakawa, K. *Bull. Chem. Soc. Jpn. 46* (1973) 3367.
7. Høiland, H. and Vikingstad, E. *Acta Chem. Scand. A 30* (1976) 182.
8. Garnsey, R., Mahoney, R. and Litovitz, T. A. *J. Chem. Phys. 64* (1964) 2073.
9. Del Grosso, V. A. and Mader, C. W. *J. Acoust. Soc. 52* (1972) 1442.
10. Bondi, A. *J. Phys. Chem. 68* (1964) 441.
11. Masterton, W. L. *J. Chem. Phys. 22* (1954) 1830.
12. Pierotti, R. A. *J. Phys. Chem. 67* (1963) 1840.
13. Kell, G. S. and Whalley, E. *J. Chem. Eng. Data 12* (1967) 67.
14. Høiland, H. and Vikingstad, E. *J. Chem. Soc. Faraday Trans. 1, 71* (1975) 2007.

Received March 22, 1976.

Acta Chemica Scandinavica A 30 (1976) 697—702

Electron-diffraction Study of Gaseous Cyclopentasilane

Z. SMITH,[a] H. M. SEIP,[a] E. HENGGE[b] and G. BAUER[b]

[a] Department of Chemistry, University of Oslo, Oslo 3, Norway and [b] Institut für Anorganische Chemie der Technischen Universität, Graz, Austria

Cyclopentasilane, the first cyclic silicon hydrogen compound to be studied by the electron-diffraction method, was found to have very similar geometry to that of cyclopentane. The ring is puckered, and both models with C_2 and C_s symmetry gave very good agreement with the experimental data. This is consistent with the conclusion of a previous spectral study, namely that cyclopentasilane undergoes pseudorotation. However, from electron-diffraction data alone it cannot be established whether the molecule undergoes dynamic pseudorotation or whether it exists in a single static conformation.

Simple molecular-mechanics calculations yielded virtually no energy difference between C_2 and C_s forms, while the difference between puckered and planar conformations was calculated to be between 1.2 and 2.2 kcal mol^{-1},* depending upon the choice of constants used.

The final structural parameters were $r_a(\mathrm{Si-Si}) = 2.342(3)$ Å $r_a(\mathrm{Si-H}) = 1.496(6)$ Å, $\angle(\mathrm{SiSiSi})_{av} = 104.2°(7)$, $u(\mathrm{Si-Si}) = 0.062(2)$ Å, and $u(\mathrm{Si-H}) = 0.082(7)$ Å. The estimated standard deviations for the distance parameters include corrections for systematic uncertainties.

Cyclopentasilane is the first cyclic silicon-hydrogen compound to have been synthesized [1] and studied by Raman and IR spectroscopy.[2] It was considered desirable to complement the spectroscopic study by the electron-diffraction method and molecular-mechanics calculations in order to obtain a more detailed understanding of the molecular structure, since the molecule is of great importance in understanding silicon chemistry.

EXPERIMENT AND DATA PROCESSING

A sample of cyclopentasilane was synthesized as described previously [1] and placed into an ampoule directly usable in the electron-diffraction apparatus. The diffraction diagrams were recorded with a Balzers' Eldigraph KD-G2 [3,4] on 13 cm × 18 cm Replica 23 Agfa-Gevaert photographic plates at a nozzle temperature of about 80 °C. Four plates exposed at a nozzle-to-plate distance of 500.12 mm and two at 250.12 mm were used in the structural analysis. The electron wavelength determined from zinc oxide diffraction patterns was 0.05845 Å and was adjusted to 0.05851 Å by calibration with the diffraction patterns of gaseous benzene.

The intensity values were recorded while oscillating the plates. The experimental intensities were leveled [5] by using the elastic scattering factors calculated by the partial wave method [6] based upon analytical HF potential for Si-atom [7] and using the best electron density of bonded hydrogen for H.[8] The inelastic scattering factors used were those of Tavard *et al.*[9]

The experimental backgrounds were drawn by hand for each plate, and the average molecular intensities were calculated for each set of plates using a modification function $s/(|f'_{Si}||f'_{Si}|)$.[5] The final background correction of 25 cm data was made on the modified intensities for each plate. The intensities for each plate-set were in the s-range 1.125 to 15.00 Å^{-1} and 4.5 to 29.25 Å^{-1} with increment in s of 0.125 and 0.25 Å^{-1}, respectively (see Fig. 1). The radial distribution function calculated by the Fourier transformation of the composite molecular intensity curve is shown in Fig. 2.

CALCULATION OF MEAN AMPLITUDES OF VIBRATION AND PERPENDICULAR AMPLITUDE CORRECTION COEFFICIENTS

A complete normal analysis was performed previously [2] using symmetry coordinates for a planar ring. In the present work some modifications were made to this force field in order to simplify use of Gwinn's program [10] for calcula-

* 1 cal = 4.184 J.

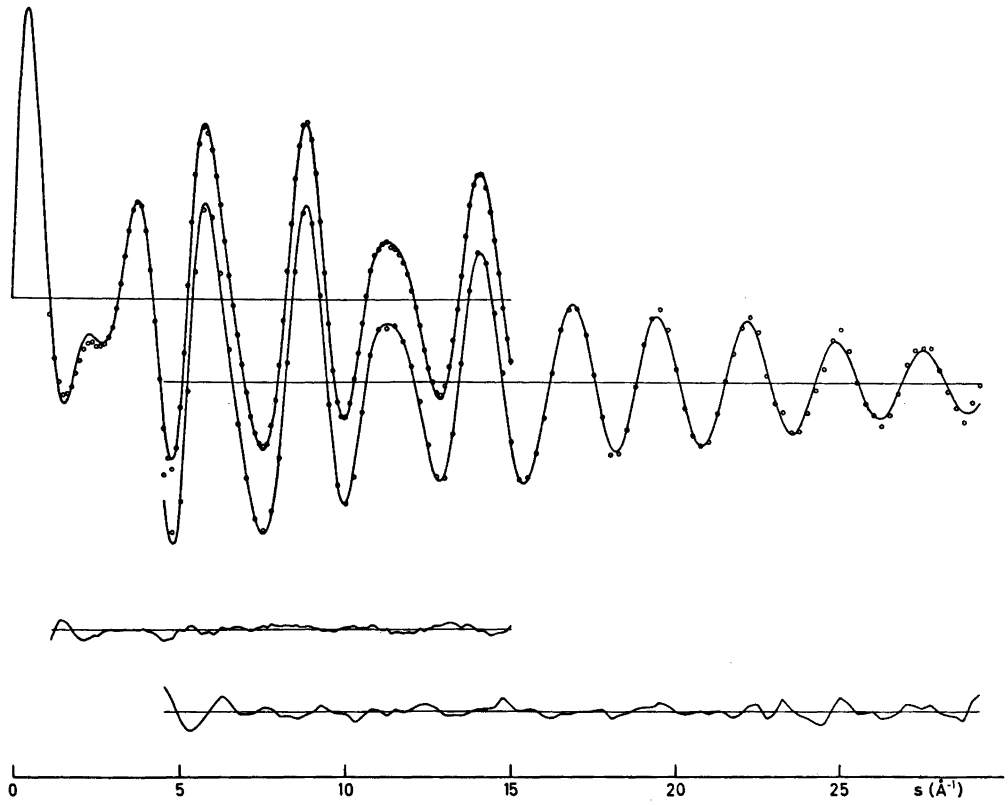

Fig. 1. The experimental intensity data (circles) for cyclopentasilane from the 50 cm ($\Delta s = 0.125$ Å^{-1}) and the 25 cm ($\Delta s = 0.25$ Å^{-1}) nozzle-to-plate distances. The solid line corresponds to the calculated intensities and the lower curves represent the differences between the experimental and calculated intensities. The calculated intensities for models C_2 and C_s are indistinguishable at this scale, therefore only one is shown.

tion of the mean amplitudes of vibration (u^S) and the correction coefficients (K) as described by Stølevik *et al.*[11] Total torsional constants for each Si–Si bond, 0.063 mdyn Å rad^{-2}, were added and two bending force constants were slightly adjusted, namely k_{HSiH} and k_{HSiSi} from 0.54 and 0.52 mdyn Å rad^{-2} to 0.60 and 0.50, respectively, to compensate for the neglection of some coupling constants.

The force field reproduced the observed frequencies sufficiently accurately for calculation of the mean amplitudes of vibration, since they are rather insensitive to moderate changes in the force field. The K-values, however, depend greatly upon the lowest frequency, which was not determined accurately by the experiment;[3] therefore they are less reliable.

The mean amplitudes of vibrations and the correction coefficients were calculated for models C_2 and C_s. Some of the results are given in Tables 1 and 2.

STRUCTURAL ANALYSIS

A comparison of the experimental radial distribution function and the calculated distribution function for a planar (D_{5h} symmetry) model of cyclopentasilane shows the ring to be decidedly nonplanar. The peak corresponding to the Si···Si distance is found at 3.69 Å on the experimental radial distribution function, whereas the expected value for a planar skeleton is about 3.79 Å.

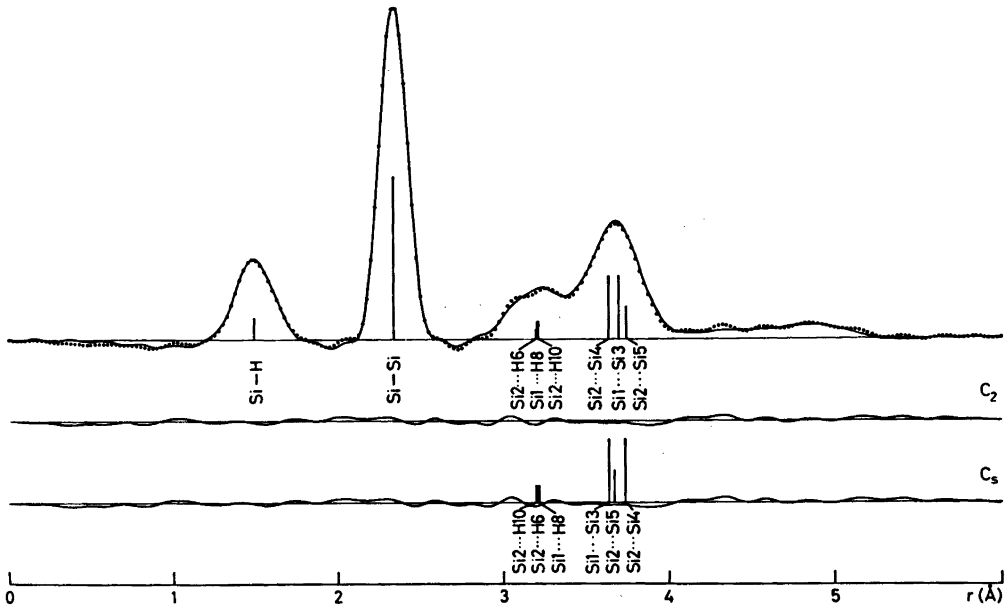

Fig. 2. Experimental (circles) and theoretical (solid line) radial distributions calculated by Fourier transformations of intensity curves composed of the data in Fig. 1. The positions and approximate areas of the most important interatomic distances are indicated for models with C_2 and C_s symmetry. The lower curves represent the difference between the experimental and theoretical curves. Damping constant was 0.0015 Å^2.

Least-squares refinements were carried out for models with C_2 (half-chair) and C_s (envelope) conformations. In both cases the Si–Si bond lengths were assumed equal, as were the Si–H bonds and HSiH angles. The HSiH planes were assumed to bisect the corresponding SiSiSi angles and to be perpendicular to the corresponding SiSiSi plane (for numbering of the atoms see Fig. 3). The constants for the weighting scheme [5,13] are shown in Table 3.

Both C_s and C_2 conformations agree well with the experimental data. The molecular intensities are shown in Fig. 1 and the radial distribution functions in Fig. 2. The theoretical curves are almost identical for the two models; *cf.* the two difference curves given in Fig. 2.

Table 1 shows the final structural parameters determined for Si_5H_{10} when corrections for shrinkage are included. Some non-bonded distances and the corresponding mean amplitudes of vibration for the C_2 model are listed in Table 2. The values of the non-bonded distances correspond to the least-squares refinement with diagonal weight-matrix and corrections for shrinkage (see Table 4, column II) for model C_2. Table 2 should be considered an example of one *possible* instantaneous conformation since only the average Si···Si dis-

Table 1. Structural parameters [a] for Si_5H_{10}.

Parameter	r_a(Å)	u^{ED} (Å)	u^S (Å)	K (Å)
Si–Si	2.342(3)	0.062(2)	0.060	0.008
Si–H	1.496(6)	0.082(7)	0.090	0.027
		Angles (in degrees)		
∠HSiH		105.3(29)		
∠(SiSiSi)$_{av}$		104.3(7)		

[a] For the definition of r_a see Ref. 12. The standard deviations given in parentheses include correction for data correlation [13] and they apply to the last digits given. The deviations for distance parameters are corrected for systematic uncertainties according to $\sigma=[\sigma_{LS}^2+(0.001r)^2]^{\frac{1}{2}}$. The assymmetry constants were (in 10^{-6} Å^3): k (Si–Si)= 2.0 and k (Si–H)= 10.0, zero for non-bonded distances. u^{ED} are mean amplitudes determined by the ED investigation. u^S are mean amplitudes calculated as described in the text for T= 80 °C.

Table 2. Some non-bonded distances and the corresponding mean amplitudes of vibration for the C_2 model.[a]

Parameter [b]	r_a	u^{ED}		u^S	K
Si1···Si3	3.680	0.130	(6)[c]	0.119	0.002
Si2···Si4	3.649	0.131		0.129	0.002
Si2···Si5	3.771	0.124		0.113	0.002
$(Si\cdots Si)_{av}$	3.686				
Si1···H8	3.211[d]	0.151	(8)	0.147	0.023
Si2···H6	3.195	0.151		0.147	0.024
Si2···H10	3.213	0.150		0.146	0.020
Si3···H8	3.210	0.151		0.147	0.022
$(Si\cdots H)_{av}^{short}$	3.208				
Si1···H13	4.303			0.237	0.009
Si2···H13	4.159			0.248	0.010
Si4···H9	4.268			0.248	0.010
$(Si\cdots H)_{va}^{middle}$	4.243				
Si3···H6	4.556			0.222	0.010
Si5···H9	4.649			0.207	0.009
Si3···H7	4.821			0.168	0.010
Si5···H8	4.904			0.174	0.009
Si4···H8	4.938			0.152	0.011
Si1···H12	4.964			0.149	0.009
Si2···H12	4.972			0.150	0.010

[a] The experimental values correspond to the least-squares refinement with diagonal weight-matrix, carried out on a geometrically consistent r_α structure ($r_\alpha = r_a + u^2/r - K$). The distances r_a, amplitudes u, and perpendicular amplitude correction coefficient K are in Å. [b] See Fig. 3 for numbering of the atoms. [c] Parenthesized values are standard deviations from the least-squares refinement in which data correlation is accounted for,[13] and they refer to the last digit given. The indicated parameters were refined in groups. [d] The small difference in the distances Si1···H8 and Si3···H8 originates in the correction for shrinkage of these distances.

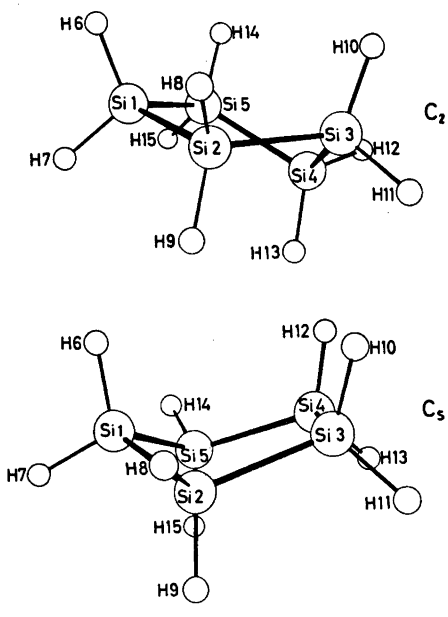

Fig. 3. The C_2 and C_s models of Si_5H_{10}. The numbering of the atoms is indicated.

Table 3. Constants of the weighting scheme.[5,13]

	50 cm	25 cm
s_1 (Å^{-1})	4.5	7.0
s_2 (Å^{-1})	12.5	20.0
w_1	0.12	0.12
w_2	0.05	0.03
P_2	−0.64	−0.60
P_3	0.146	0.125
w	1.0	0.7

tance, $(Si\cdots H)_{av}^{short}$ and $(Si\cdots H)_{av}^{middle}$ can be determined by electron-diffraction. The correlation coefficient between angles Si2Si1Si5 and Si1Si2Si3 is 0.99!

Table 4 shows the most important results obtained in the refinements of the C_2 and C_s models. Again, only the value of the average SiSiSi angle can be relied upon. In fact, the values of ∠Si5Si1Si2 and ∠Si1Si2Si3 can be interchanged (with necessary adjustment of the Si2Si3Si4 angle) and the fit of the data remains the same.

Table 4. Results of various least-squares refinements.[a]

Angle	I C_2	I C_s	II C_2	II C_s
∠Si5Si1Si2	107.7(21)	103.6(19)	104.8(37)	100.5(31)
∠Si1Si2Si3	104.1(15)	102.3(18)	105.7(31)	103.4(27)
∠Si2Si3Si4	102.9(8)	106.6(6)	101.2(9)	105.6(10)
$\angle(SiSiSi)_{av}$	104.3(3)	104.3(2)	103.7(4)	103.7(4)
∠HSiH	105.1(14)	105.4(13)	107.5(12)	107.6(14)
ϕ(Si5Si1 – Si2Si3)	13.3(5)	41.5(9)	14.5(2)	44.1(10)
ϕ(Si1Si2 – Si3Si4)	34.8(11)	25.3(4)	37.7(4)	27.5(8)
ϕ(Si2Si3 – Si4Si5)	43.5(6)	0.0	45.8(18)	0.0

[a] The bond distances were the same in different least-squares refinements within 0.0002 Å. The shrinkage effects were included in calculation I. The parenthesized values are standard deviations from least squares refinements without correction for the correlation between the data. The angles are given in degrees.

Table 5. Conformational energies E (in kcal mol^{-1}) and the corresponding angle parameters calculated by the Westheimer method.[a]

Set	Model	E [b]	E_Θ [b]	E_T [b]	E_V [b]	$(SiSiSi)_{av}$	ϕ_1 [c]	ϕ_2 [c]	ϕ_3 [c]	Angle HSiH
I	C_2	3.86	1.25	3.29	−0.68	105.0	12.1	31.7	39.0	109.9
	C_s	3.86	1.25	3.29	−0.68	105.0	37.2	23.1	0.0	109.9
	D_{5h}	5.07	0.16	5.5	−0.59	108.0	0.0	0.0	0.0	109.1
	$\Delta E = 1.21$ [d]									
II	C_2	3.27	1.26	2.74	−0.73	103.8	14.3	37.3	45.9	110.2
	C_s	3.27	1.26	2.74	−0.73	103.8	43.7	27.2	0.0	110.2
	D_{5h}	5.03	0.12	5.5	−0.59	108.0	0.0	0.0	0.0	109.1
	$\Delta E = 1.76$									
III	C_2	1.93	1.08	2.73	−1.87	103.8	14.3	37.4	46.1	111.0
	C_s	1.93	1.08	2.73	−1.87	103.8	43.9	27.3	0.0	111.0
	D_{5h}	3.94	0.03	5.5	−1.59	108.0	0.0	0.0	0.0	110.0
	$\Delta E = 2.01$									
IV	C_2	1.37	1.03	2.73	−2.39	103.7	14.4	37.4	46.1	112.2
	C_s	1.37	1.03	2.73	−2.39	103.7	43.9	27.3	0.0	112.2
	D_{5h}	3.56	0.00	5.50	−1.94	108.0	0.0	0.0	0.0	111.1
	$\Delta E = 2.19$									

[a] Constants used in all calculations (stretching force constants in mdyn Å^{-1}, bending force constants in mdyn Å rad^{-2}, barrier V^0 and parameter ε in kcal mol^{-1}; natural values are denoted by ^{0}): $r^0_{SiSi} = 2.34$ Å, $r^0_{SiH} = 1.50$ Å, van der Waals radius r^*_{Si} was estimated 1.95 Å by comparing the radii of neighbouring atoms in the periodic table,[16] $\varepsilon_{HH} = 0.042$ (from Ref. 14), ε_{SiH} was assumed to be the same as ε_{SH} which is 0.115 (from Ref. 14), $V^0_{SiSi} = 1.1$ (Ref. 17), $\theta^0_{SiSiH} = 109.4°$, $k_{HSiH} = 0.38$ (Ref. 18), $k_{SiSiH} = 0.46$, the bond stretching constants were $k_{SiH} = 2.72$ and $k_{SiSi} = 1.82$. The values of the following constants were changed in the different sets: k_{SiSiSi} was 0.4 (set I), 0.2 (II), 0.3 (III), 0.35 (IV), θ^0_{SiSiSi} was 109.4 (I and II), 108.0 (III and IV), θ^0_{SiSiSi} was 108.4 (I and II), 109.4 (III), 111.0 (IV), r^*_H was 1.2 (I and II), 1.6 (III) and 1.75 (IV). [b] E is the conformational energy of a single conformation, $E\Theta$ is the sum of bending energies, E_T is the sum of the torsional energies and E_V is the sum of the van der Waals energies (for definitions see Ref. 14). [c] ϕ_1 is a torsional angle ϕ (Si5Si1 – Si2Si3), ϕ_2 is ϕ (Si1Si2 – Si3Si4) and ϕ_3 is ϕ (Si2Si3 – Si4Si5). [d] ΔE is an energy difference between planar conformation and C_2 or C_s conformation.

Because of the uncertainty in the K values, the results obtained both with and without shrinkage correction are presented in columns I and II, respectively.

MOLECULAR-MECHANICS CALCULATION

Simple molecular-mechanics calculations [14] were carried out for models with C_2, C_s and D_{5h} symmetry. The energies of some symmetry-unrestricted models were also calculated, but the geometry always converged close to either the C_2 or C_s model. The difficulty of the calculation in this case lies in the fact that many of the constants needed for the calculation are not available and therefore must be estimated.

The results of some calculations and the constants used are shown in Table 5. The SiH bond distance was assumed 1.50 Å. Assumptions about HSiH angles were the same as before. A computer program [15] calculating energy minima by a combination of the steepest-descent and the Newton-Raphson method was used. It is clear that for any set of constants tried, models with C_2 and C_s symmetry have virtually the same energy. The difference between C_2 or C_s and the planar conformation was estimated to be between 1.2 and 2.2 kcal mol^{-1}.

DISCUSSION

The Si–Si distance in cyclopentasilane, 2.342(3) Å, is appreciably longer than that in disilane,[19] 2.331(3) Å, but in good agreement with the same distance in hexamethyldisilane,[20] 2.340(9) Å. Similar lengthening is observed in cyclopentane,[21] where the C–C bond is 1.546(1) Å, while that in ethane is 1.534(1) Å.[22] The degree of puckering in cyclopentasilane is remarkably similar to that in cyclopentane. The average CCC angle is 104.5° in C_5H_{10} and in Si_5H_{10} the average SiSiSi angle is 104.3°.

An inspection of Fig. 2 shows that although the individual non-bonded distances vary in the two models, the radial distribution function does not. Accordingly, it is not possible to establish by the electron-diffraction method alone whether the molecule undergoes dynamic pseudorotation or whether it exists in a single static conformation. The situation seems to be identical to that of cyclopentane.[21]

Acknowledgement. The authors are indebted to Professor F. Höfler for his assistance in transforming the original force field to a form convenient for our program, and to Siv.ing. R. Seip for recording the electron-diffraction diagrams.

It is gratefully acknowledged that financial support for this research was provided, in part, by the Royal Norwegian Council for Scientific and Industrial Research (NTNF).

REFERENCES

1. Hengge, E. and Bauer, G. *Monatsch. Chem. 106* (1975) 503.
2. Höfler, F., Bauer, G. and Hengge, E. *Spectrochim. Acta. In press.*
3. Zeil, W., Haase, J. and Wegmann, L. *Z. Instrumentenk. 74* (1966) 84.
4. Bastiansen, O., Graber, R. and Wegmann, L. *Balzers' High Vacuum Report 25* (1969) 1.
5. Andersen, B., Seip, H. M., Strand, T. G. and Stølevik, R. *Acta Chem. Scand. 23* (1969) 3224.
6. Yates, A. C. *Comput. Phys. Commun. 2* (1971) 175.
7. Strand, T. G. and Bonham, R. A. *J. Chem. Phys. 40* (1964) 1686.
8. Stewart, R. F., Davidson, E. R. and Simpson, W. T. *J. Chem. Phys. 42* (1965) 3175.
9. Tavard, C., Nicolas, D. and Rouault, M. *J. Chim. Phys. 64* (1967) 540.
10. Gwinn, W. D. *J. Chem. Phys. 55* (1971) 477.
11. Stølevik, R., Seip, H. M. and Cyvin, S. J. *Chem. Phys. Lett. 15* (1972) 263.
12. Kuchitsu, K. and Cyvin, S. J. In Cyvin S. J., Ed., *Molecular Structures and Vibrations*, Elsevier, Amsterdam 1972, Chapter 12.
13. Seip, H. M., Strand, T. G. and Stølevik, R. *Chem. Phys. Lett. 3* (1969) 617.
14. Eliel, E. L., Allinger, N. L., Angyal, S. J. and Morrison, G. A. *Conformational Analysis*, Interscience, New York 1965, p. 446.
15. Rustad, S. *Programmering av regnemaskinprogram for semiempiriske energiberegninger etter Westheimer metoden*, Diss., University of Oslo, Oslo 1974.
16. Pauling, L. and Pauling, P. *Chemistry*, Freeman, San Francisco 1975, Chapter 6.
17. Scott, R. A. and Scheraga, H. A. *J. Chem. Phys. 42* (1965) 2209.
18. Tribble, M. T. and Allinger, N. L. *Tetrahedron 28* (1972) 2147.
19. Beagley, B., Conrad, A. R., Freeman, J. M., Monaghan, J. J., Norton, B. G. and Holywell, G. C. *J. Mol. Struct. 11* (1972) 371.
20. Beagley, B., Monaghan, J. J. and Hewitt, T. G. *J. Mol. Struct. 8* (1971) 401.
21. Adams, W. J., Geise, H. J. and Bartell, L. S. *J. Am. Chem. Soc. 92* (1970) 5013.
22. Bartell, L. S. and Higginbotham, H. K. *J. Chem. Phys. 42* (1965) 851.

Received March 29, 1976.

Acta Chemica Scandinavica A 30 (1976) 703—714

Model Computations on Transition States in the Proton Abstraction from Carbon Acids. Influence of Coupling of Atomic Motions on the Importance of Tunnelling and on the Reduced Mass along the Reaction Co-ordinate

LARS MELANDER and NILS-ÅKE BERGMAN

Department of Organic Chemistry, University of Göteborg and Chalmers University of Technology, Fack, S-402 20 Göteborg, Sweden

When the abstraction of a proton from a carbon acid is accompanied by mesomeric charge delocalization in the carbanion, the latter will attain a conformation which is different from that of the acid, and it seems natural to depict the transition-state force field by a force-constant matrix containing certain off-diagonal elements. The effect of the introduction of such force constants on the imaginary frequency and on the reduced mass along the reaction co-ordinate has been investigated by model computations according to the Schachtschneider-Wolfsberg-Stern method. The results indicate that this kind of coupling of atomic motions will increase the imaginary frequency and hence promote tunnelling in spite of a simultaneous increase of the reduced mass.

Interaction between the proton in flight and a heavy dipole molecule in the solvent has been found to increase the reduced mass along the reaction co-ordinate and to decrease the imaginary frequency. Such a coupling of motions will thus repress tunnelling.

Until recently [1] the tunnelling mass in proton-transfer reactions has been assumed simply to be equal to the mass of the proton. Besides the attractive simplicity of a transition-state model in which the normal mode corresponding to the reaction co-ordinate * consists in a motion of a hydrogen nucleus relative to exclusively heavy, resting atoms, such a model has also the advantage of according with the feeling that the easiest reaction path and hence the fastest reaction should invariably be associated with the smallest conceivable tunnelling mass. Still it is obvious that this kind of model cannot be realistic in general even as a fair approximation. Since atoms other than hydrogen are not infinitely heavy, there must be at least some compensatory motion of these; this is a trivial fact. Also the positions of the heavy atoms relative to each other cannot in general be fixed in the normal mode concerned. This fact is realized in the following way for the simple transfer of a proton between two heavier atoms.

The longitudinal motions in terms of the internal co-ordinates of a linear three-particle system XYZ can be visualized by means of the motions of a mass particle under the influence of gravity on a surface representing the potential energy (vertically) as a function of the two distances X − Y and Y − Z.[2] The two distance co-ordinate axes (which may have to be scaled somewhat differently) should be horizontal and make a certain acute angle to one another in order for the particle to behave properly, and the mass of the particle should bear a certain relation to the masses of the three atoms. (These measures correspond to bringing the kinetic energy into unit matrix form.) From this model, shown in principle in

* In the present paper the term *reaction co-ordinate* will be used in its more precise meaning of the *normal co-ordinate* corresponding to the imaginary normal frequency of the transition state. For the more general concept the term *reaction path* will be used. Thus the reaction co-ordinate coincides with the reaction path in the saddle point corresponding to the transition state.

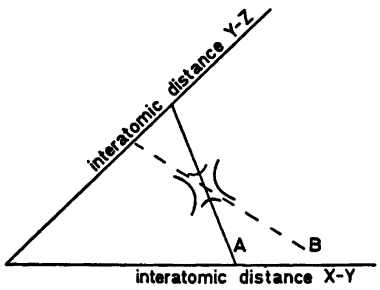

Fig. 1. Simple model used in representing the longitudinal motions of a linear three-atomic system XYZ.[2] The potential energy is represented along an axis perpendicular to the paper. Curved lines join positions of equal potential energy.

Fig. 1, it is obvious that only motions parallel to a certain direction (say A, in case of equal masses for X and Z perpendicular to the bisector of the angle between the distance axes) correspond to a constant sum of the distances X−Y and Y−Z, *i.e.*, to a constant distance between X and Z. This means that the latter distance can be constant in the normal mode corresponding to motion along the reaction co-ordinate only provided that the potential-energy landscape offers the easiest path, the reaction path, with a reaction co-ordinate parallel to A. If there is a lower and/or thinner potential-energy barrier perpendicular to B, the transition state will have its reaction co-ordinate parallel to B, and the corresponding mode will involve a motion of X and Z relative to each other.

If the equation of the potential-energy surface in the immediate vicinity of the saddle point is written

$$2V = F_{11}(\Delta r_{XY})^2 + 2F_{12}\Delta r_{XY}\Delta r_{YZ} + F_{22}(\Delta r_{YZ})^2 \quad (1)$$

where V denotes potential energy, F force constant, and Δr increase in bond length, it is obvious that increased relative importance of the cross term tends to make the angular position of the saddle more and more symmetric with respect to the two displacements Δr_{XY} and Δr_{YZ} and hence to the two co-ordinates r_{XY} and r_{YZ}. Disregarding any possible difference in scaling of the two co-ordinate axes, caused by a difference in mass between X and Z, a large interaction force constant F_{12} may cause the saddle point to take a rather symmetric orientation in Fig. 1 even if F_{11} and F_{22} differ considerably from each other in relative magnitude. Since in proton-transfer reactions the central atom is hydrogen, F_{12} is likely to have a rather large positive value, because hydrogen does not form two stable bonds of covalent character. (The "hydrogen bond" is of low stability, and the ion HF_2^- may be rather exceptional. A positive F_{12} corresponds to a negative contribution to the potential energy when Δr_{XY} and Δr_{YZ} have opposite signs, *i.e.*, for a motion in which one neighbour is approaching and the other leaving the central hydrogen.) This is likely to hold for energetically not too unsymmetric reactions and may be at least part of the explanation why recent experimental estimates of the tunnelling mass [1] have given values so close to the proton mass.

If eqn. (1) is to represent a saddle point it is required that $F_{12}^2 > F_{11}F_{22}$. That a large F_{12} tends to increase the curvature of the potential-energy surface along the reaction coordinate is easily demonstrated for the case $F_{11} = F_{22} = F$. The transformation $\Delta r_{XY} = (\xi + \eta)/\sqrt{2}$, $\Delta r_{YZ} = (\xi - \eta)/\sqrt{2}$ converts then eqn. (1) into eqn. (2).

$$2V = (F_{12} + F)\xi^2 - (F_{12} - F)\eta^2 \quad (2)$$

The expression of $\partial^2 V/\partial\eta^2 = -(F_{12} - F)$ shows the curvature along η in a right-angled co-ordinate system, and the fact that our model requires skewing does not jeopardize the conclusion that an increasing F_{12} increases the absolute magnitude of the (negative) curvature of the skewed surface along the reaction co-ordinate. The importance of tunnelling depends thus strongly on F_{12}. This must be borne in mind in all model computations in which a more or less arbitrary F_{12} is introduced. It is rather common that F_{12} is dealt with merely as a convenient means of securing an imaginary frequency.

From eqn. (2) it is also obvious that the positive curvature along ξ is increased by an increasing F_{12}. This is rather inconsequential in the present context, however, because if the assumption of symmetry is extended to the atomic masses, the corresponding vibrational mode is non-isotopic with respect to hydrogen, which is at rest. Hence the "classical" kinetic

isotope effect would be independent of F_{12}. However, an estimate of the relative importance of tunnelling and the "classical" contribution to the overall isotope effect would lead to an overestimation of the former for too large values of F_{12}.

For energetically very unsymmetric reactions, on the other hand, the possibility exists that F_{11} and F_{22} are rather different in magnitude and even of different signs.[3] The condition $F_{12}^2 > F_{11}F_{22}$ is upheld even for a vanishing F_{12} provided that F_{11} and F_{12} have opposite signs. This is the reason why also negative carbon-hydrogen and oxygen-hydrogen stretching force constants have been tried in the following together with a vanishing off-diagonal force constant representing the coupling between the carbon-hydrogen and the hydrogen-oxygen stretchings.

A more realistic model of the transition state in proton transfer from carbon acids has to include several atoms and force constants. Since there exists no simple algebraic way to express roots of polynomial equations of high degree in terms of the coefficients of the equation, relations between the imaginary frequency and the force constants have to be revealed by means of numerical solution of the secular equation. For this purpose we have used the Schachtschneider-Wolfsberg-Stern method,[4,5] which also affords the "classical" isotope effect when a model for the reactant is introduced. An approximate correction factor [6a] for the tunnel effect can easily be appended afterwards, if desired. In the present investigation we have been chiefly interested in the effect on the imaginary frequency $\nu^{\ddagger}_{H}$ and on $\nu^{\ddagger}_{H}/\nu^{\ddagger}_{D}$ of different off-diagonal force constants in the transition state and of force constants arising from the interaction between the latter and a solvent molecule.

Off-diagonal force constants have not been commonly used in model calculations of, *e.g.*, isotope effects. However, Yankwich [7] and his collaborators have used off-diagonal force constants in the modelling of transition states in the decomposition of, *e.g.*, oxalic acid for the purpose of creating a reaction co-ordinate with a preselected motion and a preselected imaginary frequency. Our approach is in some respects opposite to that of Yankwich *et al.* While their computations provide off-diagonal force constants which correspond to a preselected reaction co-ordinate behaviour but have no obvious physical interpretation, the purpose of our computations is to find out the consequences for the transition-state behaviour of off-diagonal force constants which may be required by the electronic structure of the transition state.

Saunders *et al.*[8] have used off-diagonal elements in connection with model computations on the mechanism of elimination and regarded them in about the same way as they have been regarded in the present paper, *i.e.*, as chemically required features of the force field of the transition state.

It must be remembered that any force-constant model of the transition state is limited in itself to a description of the shape of the col in the multi-dimensional space in terms of a second-degree hypersurface representing the potential energy in the immediate neighbourhood of the saddle point. This is sufficient for the prediction of the normal vibrational modes and their frequencies, the imaginary as well as the real ones. On the other hand, the treatment does not contain any assumption concerning the height of the potential-energy barrier. Thus only isotopic rate ratios but no absolute rates can be obtained, and the tunnel correction [6a] has to be limited to its first term $\frac{1}{2}u^{\ddagger}/\sin\frac{1}{2}u^{\ddagger}$ with $u^{\ddagger} = h|\nu^{\ddagger}|/\mathbf{k}T$, h and $\mathbf{k}$ being Planck's and Boltzmann's constants, respectively, and T the absolute temperature. This simple expression can only be used with rather moderate values of $u^{\ddagger}$, however, and since the tunnel correction factor increases with $|\nu^{\ddagger}|$, the trend in $|\nu^{\ddagger}_{H}|$ will frequently be used in the following as a simple indicator of the trend in the importance of tunnelling. Quantitative estimates of the force constants are very difficult or impossible, and a direct comparison between values of $|\nu^{\ddagger}|$ computed in this way and those obtained from experimental data is hardly warranted.

The term "mass along the reaction co-ordinate" imparts the feeling that the imaginary frequency is settled by a single physically existing mass and a negative force constant corresponding to the curvature of the potential-energy surface. In a polyatomic entity this is no more true for the imaginary normal frequency than for the ordinary real normal frequencies, which in general result from a com-

plicated interplay of several atomic masses and the force field. It is even true that two isotopic systems will in general not have exactly the same reaction co-ordinate, although they correspond to the same potential-energy surface before it is skewed. In the case of the simple three-atomic system discussed above, the latter fact is reflected by the model of Fig. 1 being somewhat different for different isotopic systems. Thus the skewing angle and the scaling of the axes are dependent on the masses of the real atoms, and isotopic substitution will consequently reshape that kind of potential-energy surface. Nevertheless, for a discussion of the degree of participation of heavy atoms in the normal mode of decomposition, the semi-quantitative concept of a "reduced mass along the reaction co-ordinate" may be useful. This is founded on an assumed similarity between the reaction co-ordinates, in virtue of which $(\nu^{\ddagger}_{H}/\nu^{\ddagger}_{D})^2$ could serve as an approximate measure of the ratio $m^{\ddagger}_{D}/m^{\ddagger}_{H}$ between the two reduced masses. The ratios would be equal if the curvature of the potential-energy surface in the direction of the proper reaction co-ordinate were exactly the same in the two isotopic cases. A proton/deuteron in flight among solely much heavier and thus resting atoms would give $\nu^{\ddagger}_{H}/\nu^{\ddagger}_{D}=\sqrt{2}$, and if additional, nonisotopic masses take part in the motion a value between 1 and $\sqrt{2}$ is to be expected. Owing to the finite mass of carbon, oxygen, *etc.*, the upper limit $\sqrt{2}$ is hardly reached. In spite of the uncertainty caused by the difference in reaction co-ordinates it seems hard to devise a more reliable single gauge of the degree of participation of masses other than that of the central hydrogen in the motion along the reaction co-ordinate.

The chemical constitution of most strong carbon acids and, in particular, of their anions makes it interesting to investigate the effect of certain off-diagonal force constants on the degree of tunnelling. Strong carbon acids are frequently strong because splitting off of the proton allows the remaining carbanion to be stabilized by electron delocalization. This rearrangement of the electronic structure is accompanied by some rearrangement also of the relative position of the atomic nuclei, different hybridization and bond orders requiring different bond angles and bond lengths for the overall molecular energy to be at a minimum. The simple carbon acid nitromethane may be taken as an example. In the acid, carbon has four ligands and is approximately tetrahedral, and the carbon-nitrogen bond is a single bond. In its anion, carbon has only three ligands, the carbon-nitrogen bond has considerable double-bond character, while the nitrogen-oxygen bonds have lost most of the fractional double-bond character they have in the acid. The relative positions of the atoms must change in the proton abstraction in such a way that the remaining part of the molecule becomes flat, that carbon and nitrogen approach each other slightly, and that the nitrogen-oxygen distances increase to some extent. The smoothest transition from acid to anion must consequently involve some motion of all the atoms, *i.e.*, the atomic motions must be coupled to each other. In terms of the common valence-force-field treatment of the transition state this corresponds to the existence of several off-diagonal elements in the **F** matrix. It is rather easy to see, for instance, that a simultaneous increase of the distance between carbon and the proton to be abstracted by a base and decrease of the carbon-nitrogen distance must be energetically more favourable than a simultaneous increase (or decrease) of both distances. Hence the expression for the potential energy ($2V=etc.$) ought to contain a term $2F_{HC,CN}\Delta r_{HC}\Delta r_{CN}$ in which the force constant is positive. The same kind of reasoning can be applied to other combinations of co-ordinate displacements. The question is how many finite off-diagonal elements **F** should contain. From the point of view of atomic structure and binding power, it seems natural to include only those elements which correspond to two internal co-ordinates having one atom in common.

The idea of the coupled motions may give the intuitive feeling that the inertial mass along the reaction co-ordinate increases with the introduction of finite off-diagonal force constants, and that this should result in a decreased tunnelling probability. That this is not exactly so in general will be seen in the following.

Recently another kind of coupling has been discussed in connection with experimental results.[1,9] It is quite natural to expect an ap-

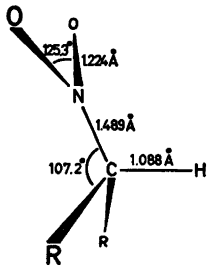

Fig. 2. Bond lengths and bond angles used for nitromethane (R = H).[10] The three atoms H, R and R are assumed to be situated at the corners of an equilateral triangle. One of the NCH planes is assumed to be perpendicular to the plane common to the C, N and both of the O atoms.

preciable interaction with the solvent when the proton is in transit, and this is true about polar solvents in particular. In some of the present computations the transition-state model has been supplemented by the introduction of two atoms, corresponding to a dipole molecule, and the effect of a bending force constant joining it with the proton has been studied. The results seem to corroborate experimental evidence [1] concerning the effect of solvent polarity on tunnelling probability, and this kind of coupling tends to decrease the importance of tunnelling in agreement with intuitive expectation.

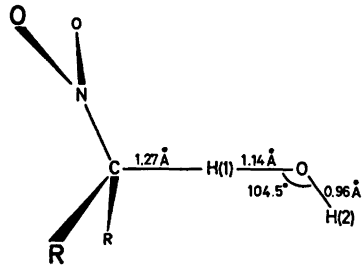

Fig. 3. Bond lengths and bond angles used for the non-planar transition-state model. The C−H(1) and O−H(1) distances are calculated from the corresponding normal bond distances in nitromethane [10] and water,[11] respectively, using Paulings bond number rule [12a] with a bond number equal to 0.5 for the C−H(1) and the O−H(1) bond. The hydroxide O is assumed to be situated on the CH(1) line, and H(2) lies in the NCH(1)O plane. (Angles and bond lengths not given are identical with the corresponding ones in Fig. 2.)

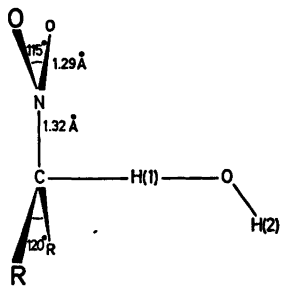

Fig. 4. Bond lengths and bond angles used for the planar transition-state model.[13] The NOO and CRR groups are assumed to be coplanar and perpendicular to the plane of NCH(1)OH(2). The latter plane bisects the ONO and RCR angles. (Angles and other bond lengths not given are identical with the corresponding ones in Fig. 3.)

MODELS AND COMPUTATIONS

The present computations refer to the proton abstraction by hydroxide ion from nitromethane and, in some cases, 2-nitropropane.

Geometry. Bond lengths and bond angles for nitromethane have been taken from Ref. 10 and are shown in Fig. 2.

Bond lengths and bond angles for 2-nitropropane (R = CH_3 in Fig. 2) are assumed to be the same as for nitromethane with the exception that the two methyl groups are treated

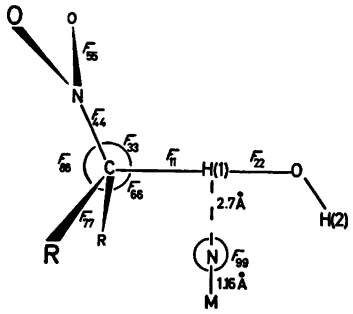

Fig. 5. Transition-state model including a solvent molecule. M and N are situated in the NCH(1)OH(2) plane. M, N and H(1) lie on a straight line, perpendicular to the CH(1)O line. M corresponds to the CCH_3 part of acetonitrile. The H(1)−N distance is equal to the sum of the van der Waals radii [12b] of N and H. The M−N distance is equal to the C≡N distance in CH_3CN.[14] *F* is symbol for (diagonal) force constant. (Distances and angles not given are the same as the corresponding ones in Fig. 3.)

Table 1. Diagonal force constants used in the calculations unless otherwise indicated.

Type of force constant [a]	Value in nitromethane and 2-nitropropane [b]	Value in the transition state [c] and symbol in Fig. 5
C–R, s	5	5
C–H(1), s	5	2.5[d] F_{11}
C–N, s	5.5	5.5, (10) F_{44}
N–O, s	8	8, (6) F_{55}
H(1)–O, s		3.3[e] F_{22}
O–H(2), s		7.2[f]
R–C–R, b	0.5	0.5, (0.35) F_{77}
R–C–H(1), b	0.5	0.25 F_{66}
R–C–N, b	0.7	0.7, (0.5) F_{88}
H(1)–C–N, b	0.7	0.35 F_{33}
C–N–O, b	0.8	0.8
O–N–O, b	0.9	0.9
N–O, b (out of plane)	0.4	0.4
H(1)–O–H(2), b		0.33[e]
C–H(1)–O, b (degenerate linear bending)		0.1[g]
H(1)–N–M, b (degenerate linear bending)		0–0.3[h] F_{99}
ON–CR, t	0.01[f]	0.01[g]
NC–OH(2), t		0.01[g]

[a] s = stretching force constants in mdyn Å^{-1}, b = bending force constants in mdyn Å rad^{-2}, t = torsional force constants in mdyn Å rad^{-2}. [b] Calculated from Ref. 15 with some changes to achieve better consistency with frequency data[16] without using the interactions between non-bonded atoms in Ref. 15. [c] Number in parenthesis indicates value of the force constant used in some computations on the planar transition-state model (Fig. 4). [d] Calculated as half the value in nitromethane. [e] Calculated as half the value in Ref. 17. [f] Calculated as the arithmetic mean of the values for H_2O [17] and OH^-.[18] [g] Estimated value. [h] This force constant is used only in the transition-state model with a solvent molecule included (Fig. 5).

as two mass points with the mass 15 at a distance of 1.54 Å from the central carbon atom.

The geometry of the "carbon acid part" of the transition state is assumed to be the same as for the initial state (nitromethane or 2-nitropropane) in most of the computations, but the hydrogen in transit is moved somewhat towards the hydroxy oxygen. The geometry of the "water part" of the transition state is taken from Ref. 11. The geometry of the transition state has thus been assumed to be the one shown in Fig. 3 with only the exceptions explicitly stated below.

To illustrate the effect of an assumed planarity of the carbanion part of the transition state, the model shown in Fig. 4 was used in some of the computations.

The transition-state model used in the calculations illustrating the coupling between the hydrogen in transit and a solvent molecule is shown in Fig. 5. The solvent interacting with the hydrogen in transit is assumed to be acetonitrile. Thus, M in Fig. 5 corresponds to the CCH_3 part of acetonitrile and is treated as a mass point with the mass 27.

Force constants. The diagonal force constants used in the calculations are given in Table 1. For nitromethane they are based on literature data which have been modified to achieve reasonable agreement with the experimental vibration frequencies when using a simpler force field without non-bonded interactions. The pertinent force constants for 2-nitropropane have been assumed to be the same as for nitromethane. For the transition state the diagonal force constants have been obtained from reactant data using simple assumptions concerning the fractional bonds. In the planar transition-state model (Fig. 4) some of the force constants were varied to account for the change in hybridization. The modified force constants are given in parentheses in Table 1.

The important off-diagonal force constant F_{12} has been so chosen as to afford an imaginary frequency in the same region as obtained from experimental results [1] (order of magnitude

Table 2. Effect of introduction of off-diagonal force constants into the transition state. Transition-state model: non planar (Fig. 3). $F_{12}=3$ mdyn Å^{-1}. Temperature: 25 °C. The nature of the off-diagonal force constants is evident from their indices, related to those in Fig. 5 and indicating their position in the **F** matrix.

Computation number	F_{13}[a]	F_{14}[b]	F_{16}[a]	F_{17}[a]	F_{18}[a]	F_{34}[a]	F_{45}[b]	$\lvert\nu\mp_H\rvert$/cm^{-1}[c] A	B	$\nu\mp_H/\nu\mp_D$[c] A	B	k_H/k_D[c] A	B
1								668.7	664.3	1.377	1.386	7.088	7.516
2	0.2							727.4	720.9	1.359	1.370	6.856	7.283
3	0.2	1.0						853.7	852.2	1.332	1.340	6.410	6.773
4	0.2	1.0	0.2					928.3	896.7	1.320	1.311	6.173	6.553
5	0.2	1.0	0.2	−0.2				1025.5	918.6	1.300	1.294	5.853	6.443
6	0.2	1.0	0.2	−0.2	−0.2			1119.0	989.4	1.283	1.276	5.569	6.196
7	0.2	1.0	0.2	−0.2	−0.2	−0.2		1121.4	992.0	1.281	1.274	5.569	6.195
8	0.2	1.0	0.2	−0.2	−0.2	−0.2	1.0	1123.2	994.3	1.281	1.274	5.563	6.187

[a] Stretching-bending interaction force constant in mdyn rad^{-1}. [b] Stretching-stretching interaction force constant in mdyn Å^{-1}. [c] A: carbon acid: nitromethane, B: carbon acid: 2-nitropropane.

for $\lvert\nu\mp_H\rvert$ 1000 cm^{-1}). The values of F_{12} and of such force constants which are represented in Table 1 but occasionally assigned different values are explicitly stated in connection with each of the Tables 2 – 6.

The other off-diagonal force constants to be used in the following are given below in connection with each table of results. They are always of a rather moderate magnitude, and the condition $F_{ij}^2 < F_{ii}F_{jj}$ is fulfilled in all cases except in the computations 15 and 16 (Table 4) in which F_{11} has been assumed to be equal to or less than zero.

Computations. The computations have been made with a computer program originally devised by Schachtschneider [4] for calculating vibrational frequencies by the **FG** matrix method.[19] The program has been modified by Wolfsberg and Stern [5] to calculate isotope effects. The computations were performed on an IBM 360/65 or an IBM 370/145 computer at Gothenburg Universities Computing Centre.

RESULTS AND DISCUSSION

For our studies we have chosen the simple carbon acid nitromethane in its reaction with hydroxide ion. When considered necessary, the computations have been supplemented by a similar study of 2-nitropropane in order to avoid unexpected consequences of the low masses of the non-reacting hydrogen atoms in the former molecule. As shown below, the behaviour of the two carbon acids is qualitatively the same, although there are differences in the quantitative outcome of the computations.

Effect of introducing off-diagonal force constants. Table 2 shows the effect of introducing non-vanishing off-diagonal force constants other than F_{12} into the transition-state models for nitromethane (A) and 2-nitropropane (B). The magnitudes of all these constants are open to discussion, of course, but their signs are given by the rule that an adjustment towards the final equilibrium conformation of the carbanion should result in a lower potential energy than a motion opposing the rules governing hybridization and the relation between bond order and bond length (*cf.* above).

The successive introduction of these constants is found to invariably raise the imaginary frequency and the apparent mass along the reaction co-ordinate.* The "classical" isotope effect is weakened, probably because of an increase also in the real frequencies of the transition state. The difference between the two carbon acids is quantitative rather than qualitative.

As could perhaps be anticipated, the importance of the off-diagonal force constants decreases with increasing distance from the

* If, however, $F_{12}=A(F_{11}F_{22})^{\frac{1}{2}}$ and A is given a value between 1 and 1.01, $\nu\mp_H/\nu\mp_D$ has been found in a separate set of computations to pass through a minimum when F_{13} is increased. For larger values of A no such behaviour is observed.

reaction centre. Thus it is obvious that the introduction of F_{34} and F_{45}, not directly related to the stretching of the breaking bond, is rather inconsequential. These constants will therefore be dropped in the following.

The effect of introducing separately several of the off-diagonal force constants has also been tested. The results are not given here, since they show the same general pattern.*

In comparing the results it is of some importance to keep in mind that, owing to the symmetry of the model, the symbols "6" and "8" define two angles each, while "7" denotes a single angle.

Influence of conformation of transition state. In the proton-transfer reaction the spatial arrangement around the carbon atom originally carrying the proton undergoes a gradual change from an approximately tetrahedral to a planar one. The transition state is therefore likely to have some intermediate conformation. The exact geometry is not likely to be critical, and in most of the present computations it has been simply assumed that the transition state has the same angular geometry as the reactant. On the other hand, it seemed advisable to make a few computations also on the other limiting conformation (Fig. 4).

Since the sum of the angle symbolized by "7" and the two angles symbolized "8" (Fig. 5) has the value of 360° in the planar conformation, F_{17} and F_{18} cannot both have negative values, because when the proton in transit moves further away from the carbon atom, these angles cannot all increase, nor does any single angle do so at the expense of any other in the conformation of lowest potential energy. Irrespective of its direction, a deviation from planarity of the carbanion will imply a decrease of the angles concerned. Hence there is no longer any natural coupling between the changes in these internal co-ordinates and the change in the internal co-ordinate symbolized "1", and the off-diagonal force constants F_{17} and F_{18} have to vanish.

The same purely geometrical restriction does not apply to the angles "3" and "6", although there seems to be little reason why their equilibrium values should decrease past 90°. The latter kind of reasoning applies also to the distance "4". Since the planar model is used mainly as a representative of "almost planar" transition states, however, the off-diagonal elements F_{13}, F_{16} and F_{14} have still been introduced, and the results for nitromethane are shown in Table 3. Column D and E correspond to the planar model with two different sets of diagonal force constants. Column C corresponds to the previous non-planar transition state and contains results already presented in Table 2 and now reproduced in order to facilitate comparison with column D, which results from the same set of force constants.

It is obvious that the introduction of off-diagonal force constants has a similar effect in the planar transition state as in the non-

* See footnote on the preceding page.

Table 3. Comparison between results from computations using non-planar (Fig. 3) and planar (Fig. 4) transition-state models. Carbon acid: nitromethane. $F_{12}=3$ mdyn Å^{-1}. Temperature: 25 °C.

Computation number	F_{13}[a]	F_{14}[b]	F_{16}[a]	$\lvert\nu^{\ddagger}_{H}\rvert$/cm^{-1} [c]			$\nu^{\ddagger}_{H}/\nu^{\ddagger}_{D}$ [c]			k_H/k_D [c]		
				C	D	E	C	D	E	C	D	E
9				668.7	671.4	671.4	1.377	1.376	1.376	7.088	7.068	7.066
10	0.2			727.4	734.6	734.5	1.359	1.357	1.357	6.856	6.816	6.815
11	0.2	1.0		853.7	843.5	810.8	1.332	1.330	1.346	6.410	6.418	6.581
12	0.2	1.0	0.2	928.3	965.9	941.8	1.320	1.279	1.286	6.173	5.925	6.020

[a] Stretching-bending interaction force constant in mdyn rad^{-1}. [b] Stretching-stretching interaction force constant in mdyn Å^{-1}. [c] C: non-planar transition-state model. This column is identical with column A in computations 1–4. D: planar transition-state model using the same diagonal force constants as for the non-planar transition-state model. E: planar transition-state model using the diagonal force constants in parentheses in Table 1.

Table 4. Effect of strong energetic unsymmetry in the reaction, F_{11} and F_{22} strongly dissimilar. Carbon acid: nitromethane. Transition-state model: non-planar (Fig. 3). Temperature: 25 °C.

Computation number	F_{11}[a]	F_{22}[a]	F_{12}[b]	$\lvert\nu^{\ddagger}_{H}\rvert$/cm^{-1} [c]		$\nu^{\ddagger}_{H}/\nu^{\ddagger}_{D}$ [c]		k_H/k_D [c]	
				F	G	F	G	F	G
13	5	0	2	732.3	766.6	1.131	1.128	3.419	3.374
14	4	−1	0	503.0	494.6	1.033	1.031	1.662	1.641
15	−1	6	0	481.4	721.5	1.025	1.032	1.042	1.063
16	0	6.6	2	518.2	865.4	1.067	1.084	1.956	1.992

[a] Stretching force constant in mdyn Å^{-1}. [b] Stretching-stretching interaction force constant in mdyn Å^{-1}. [c] F: no interaction force constants except F_{12}. G: $F_{13}=0.2$ mdyn rad^{-1}, $F_{14}=1.0$ mdyn Å^{-1}, $F_{16}=0.2$ mdyn rad^{-1}, $F_{17}=F_{18}=-0.2$ mdyn rad^{-1}.

planar one. It seems safe to conclude that the geometry is not critical, nor does the choice of diagonal force constants more appropriate for a carbanion (E) cause any major change in comparison with the outcome from the use of more reactant-like ones (D).

Effect of energetic unsymmetry in the reaction. It seems possible that strongly exo- and endothermic reactions may have so distorted potential-energy surfaces that one of the force constants F_{11} and F_{22} approaches and even passes zero.[3] Some computations have been carried through in order to elucidate the effect of the introduction of off-diagonal force constants in such cases.

In Table 4 sets of F_{11}, F_{22}, and F_{12} have been used which have one of these three constants equal to zero. Computations 13 and 14 correspond to very reactant-like transition states, and 15 and 16 to very product-like ones. In the former case the isotope effect should almost vanish.[20] That there is still a considerable deviation of k_H/k_D from unity is due to the fact that there is no exact matching between the assumed force constants for the transition state and those for the reactant. The assumption [20] of a vanishing interaction between the two fragments is thus not valid in the present case.

The effect of the introduction of the interaction force constants F_{13}, F_{14}, F_{16}, F_{17}, and F_{18} is seen from a comparison between columns F and G in Table 4. With the reactant-like transition state (computations 13 and 14) the effect on $\lvert\nu^{\ddagger}_{H}\rvert$ is small and even uncertain as to its direction. In such a reactant-like transition state the motion along the reaction co-ordinate consists mainly in a relative motion between the carbon acid and the hydroxide ion, and the hydrogen-oxygen distance dominates the reaction co-ordinate. Hence neither the carbon-hydrogen distance "1" nor the other internal co-ordinates of the carbon acid have much to do with this motion.

In the product-like transition state, corresponding to computations 15 and 16, on the other hand, the carbon-hydrogen distance "1" dominates the reaction co-ordinate, and the off-diagonal force constants associated with that co-ordinate have an effect on $\lvert\nu^{\ddagger}_{H}\rvert$ similar to that in the more symmetric transition state treated above.

The influence of the off-diagonal force constants on the reduced mass along the reaction co-ordinate is very weak. This could be expected in view of the large reduced mass which results from a relative motion of two heavy fragments. In the product-like transition state, in which the distance "1" is heavily involved in this motion, the direction of the small effect is opposite to that in the more symmetric case, and the reduced mass seems to decrease slightly. It is impossible to decide whether this is to be considered a "mass" or a "barrier-shape" effect.

Effect of steric hindrance. It is a well-established experimental fact that steric hindrance tends to increase the importance of tunnelling. It is consequently of interest to modify the force field in a direction that would correspond to steric interaction between the reactants. Except for an increase F_{12},[21] corresponding to an augmented potential-energy increase on simultaneous decrease of the carbon-hydrogen

Table 5. Effect of increase in the bending force constants, illustrating possible effect of steric hindrance. Carbon acid: 2-nitropropane. Transition-state model: non-planar (Fig. 3). $F_{12} = 3$ mdyn Å^{-1}.

Computation number	F_{33}[a]	F_{66}[a]	$\|\nu^{\ddagger}_{H}\|$/cm^{-1} [b]		$\nu^{\ddagger}_{H}/\nu^{\ddagger}_{D}$ [b]		k_H/k_D [b]	
			F	G	F	G	F	G
17(=1B, 6B)	0.35	0.25	664.3	989.4	1.386	1.276	7.516	6.196
18	0.50	0.35	663.8	986.7	1.387	1.278	6.769	5.588

[a] Bending force constant in mdyn Å rad^{-2}. [b] F: no interaction force constants except F_{12}. G: $F_{13} = 0.2$ mdyn rad^{-1}, $F_{14} = 1.0$ mdyn Å^{-1}, $F_{16} = 0.2$ mdyn rad^{-1}, $F_{17} = F_{18} = -0.2$ mdyn rad^{-1}.

and hydrogen-oxygen distances, an increase in the forces opposing flattening of the carbanionic part is likely. The former modification is known to increase $|\nu^{\ddagger}_{H}|$.[21] The effect of the latter on the transition state of 2-nitropropane has been investigated in computation 18, the results of which are shown in Table 5 together with those previously obtained in computations 1B and 6B.

The increase in the bending force constants F_{33} and F_{66} is found to have negligible effects on $|\nu^{\ddagger}_{H}|$ and $\nu^{\ddagger}_{H}/\nu^{\ddagger}_{D}$, the former actually decreasing slightly. The importance of tunnelling is thus at least not increased for that reason.

The only obvious effect of increasing F_{33} and F_{66} is a weakening of the classical isotope effect. This was to be expected because of an increase in the transition state of zero-point energy sensitive to the isotopic mass of the proton in flight.

Effect of introduction of a dipole solvent molecule. Tunnelling has been found to be more important in less polar solvents than in more polar ones, and this has been ascribed to a coupling between the motions of the proton in flight and solvent molecules in the latter.[1,9] Such a coupling will increase the reduced mass along the reaction co-ordinate. It seems to be of interest to introduce this kind of coupling in the present study of the vibrational behaviour of a transition state.

A dipole molecule M−N, thought of as a simplified model of acetonitrile, $CH_3C{\equiv}N$, with its negative pole at N, has been introduced into the ordinary transition-state model (Fig. 5). The dipole points with its negative end at the proton in flight, and its direction is assumed to be perpendicular to the line defined by the three reaction centres. The N−H distance is assumed to be the sum of the van der Waals radii of N and H.

Computation 19 (Table 6) was carried through without any force constants pertaining to the atoms M and N and gives the same results as computations 1A and 6A. In computations 20 and 21 the dipole molecule is assumed to exert its action *via* a bending force constant F_{99}, which has the same value in the plane of the paper and in a plane perpendicular to it. The effect is a decrease in $|\nu^{\ddagger}_{H}|$, accompanied by an increase in the reduced mass.

Table 6. Effect of introduction of a dipole solvent molecule into the transition state. Carbon acid: nitromethane. Transition-state model: non-planar (Fig. 5). $F_{12} = 3$ mdyn Å^{-1}.

Computation number	F_{99}[a]	F_{NM}[b]	$F_{H(1)N}$[b]	$\|\nu^{\ddagger}_{H}\|$/cm^{-1} [c]		$\nu^{\ddagger}_{H}/\nu^{\ddagger}_{D}$ [c]	
				F	G	F	G
19				668.7	1119.0	1.377	1.283
20	0.1			653.2	1111.7	1.373	1.281
21	0.3			626.4	1098.0	1.361	1.278
22	0.1	16		653.2	1111.7	1.373	1.281
23	0.1	16	0.5	653.2	1111.2	1.374	1.281

[a] Bending force constant in mdyn Å rad^{-2}. [b] Stretching force constant in mdyn Å^{-1}. [c] F: no interaction force constants except F_{12}. G: $F_{13} = 0.2$ mdyn rad^{-1}, $F_{14} = 1.0$ mdyn Å^{-1}, $F_{16} = 0.2$ mdyn rad^{-1}, $F_{17} = F_{18} = -0.2$ mdyn rad^{-1}.

A comparison between computations 20 and 22 (Table 6) shows that the introduction of a large stretching force constant between M and N has no effect on the magnitudes studied, and the same holds, at least approximately, for the subsequent introduction of a small stretching force constant between the proton in flight and the atom N (computation 23). That the latter force constants should have little or no effect on the imaginary frequency was to be expected, of course, since they act in a direction which is perpendicular to the main component of the reaction co-ordinate.

CONCLUSIONS

Intuitively it seems likely that extra coupling pertaining to the proton in flight, transmitted *via* additional off-diagonal force constants should result in an increased reduced mass along the reaction co-ordinate of the transition state and therefore in a decreased amount of tunnelling. The present results are in some respects at variance with such naive expectations. The introduction of off-diagonal force constants in a fairly symmetric transition state (Table 2) does decrease $\nu^{\ddagger}_{H}/\nu^{\ddagger}_{D}$ but increase $|\nu^{\ddagger}_{H}|$, which means that tunnelling should increase in importance in spite of an increase in the reduced mass. The reason for the fallacy of at least our intuitive thinking is probably that our interest has been concentrated on the reduced mass along the reaction co-ordinate and that the remodelling of the barrier on the hypersurface escapes attention, simply because it is more difficult to imagine. Additional off-diagonal force constants do obviously increase the curvature along the reaction co-ordinate to such an extent that this change overcompensates the increase in reduced mass.

As is evident from Table 4, the results for extremely reactant-like or product-like transition states are exceptional. There are several reasons why tunnelling should be relatively unimportant in such cases. It seems natural to suppose that the curvature of the potential-energy surface along the reaction co-ordinate is smaller than for energetically more symmetric reactions. This together with the large reduced mass and the small energy region available for tunnelling will tend to decrease its importance in such reactions. Nevertheless it should be observed that the contribution from tunnelling to the observable isotope effect must be small also because of the similarity of $\nu^{\ddagger}_{H}$ and $\nu^{\ddagger}_{D}$ (*cf.* Table 4). The reduced mass along the reaction co-ordinate is so large that the difference in isotopic composition is of minor importance.

The result concerning the role of a polar solvent (Table 6) seems to be in accordance with already existing experimental evidence that tunnelling is favoured by low polarity of the solvent or by steric hindrance to solvation in the transition state.

The idea that steric hindrance could possibly promote tunnelling by its resistance to rehybridization and hence prevention of some of the coupled motion is not supported by the present results. Such a steric hindrance would correspond primarily to an increase in the bending force constants concerned, but increments of that kind have turned out to have little effect on $\nu^{\ddagger}_{H}$ also in the presence of several off-diagonal force constants (Table 5).

The inclusion of several off-diagonal force constants corresponds primarily to an attempt at reproducing probable effects of incipient mesomerism in the carbanionic part of the transition state. The question arises how to compare two cases, one with and the other without disposition towards mesomerism. There may be other differences of importance for the shape of the barrier than the existence of off-diagonal force constants. Possible differences in barrier height must be left out of the present discussion, effects from purely conformational differences have been shown above to be inconsequential (Table 3), and thus effects on the diagonal force constants remain to be discussed. Carbanions with localized charge are likely to be pyramidal, while those of the nitronate anion type would be expected to be planar around the central carbon atom. It is not obvious how this difference should affect all the force constants. Stretching force constants should be increased or decreased according to the changes in bond order which have taken place as a consequence of the incipient mesomerism. The bending force constants F_{77} and F_{88} are likely to undergo some reduction when the corresponding angles increase. The combined effect of these force-constant changes has been tested on the planar transition-state

model, Table 3. A comparison of columns D and E indicates that the influence is rather weak, the more carbanion-like force constants giving somewhat lower values of $|\nu^{\ddagger}_{H}|$ but higher values of $\nu^{\ddagger}_{H}/\nu^{\ddagger}_{D}$ in the presence of certain off-diagonal force constants. F_{14} seems to be responsible for this. The direction of a possible change in F_{33} and F_{66}, caused by incipient mesomerism, is uncertain, but a comparison between computations 17 and 18 (Table 5) shows that the magnitude of these force constants is critical neither for $|\nu^{\ddagger}_{H}|$ nor for $\nu^{\ddagger}_{H}/\nu^{\ddagger}_{D}$. In conclusion, differences in diagonal force constants caused by differences in disposition towards mesomerism have little influence on the importance of tunnelling, and they will hardly be able to mask the action of off-diagonal force constants of moderate magnitude.

The conclusion which could possibly be drawn concerning a relation between the disposition towards tunnelling and the degree of incipient mesomerism in the transition state seems to be that mesomerism is likely to promote tunnelling in spite of a probable increase in the reduced mass along the reaction coordinate. From the experimental point of view, tunnelling has been shown, indeed, to take place with some carbon acids the carbanions of which are typically mesomeric. Unfortunately, however, it is hardly possible to make a comparison with carbon acids of the opposite kind. Since the possibility of mesomerism in the anion is the most important structural feature making carbon acids strong, it is difficult to find a carbon acid with little mesomerism in its anion but still strong enough for a meaningful comparison or even amenable to tests concerning the importance of tunnelling. Sulfone and cyano groups seem to acidify neighbouring CH without extensive charge delocalization in the carbanion, but it is questionable whether there actually exists a two-sided barrier of appreciable height with these carbon acids.[6b] Any comparison should perhaps be limited to nitro and carbonyl compounds with carbanions "more or less disposed" to mesomeric charge delocalization.

The main value of the results obtained in the present investigation lies probably in the demonstration that coupling between the motion of the hydrogen in flight and heavy atoms need not invariably lead to decreased importance of tunnelling but may have the opposite effect.

Acknowledgements. Financial support from the Swedish Natural Science Research Council is gratefully acknowledged.

REFERENCES

1. Caldin, E. F. and Mateo, S. *J. Chem. Soc. Faraday Trans. 1, 71* (1975) 1876; *72* (1976) 112.
2. Glasstone, S., Laidler, K. J. and Eyring, H. *The Theory of Rate Processes*, McGraw, New York 1941, p. 100.
3. Marcus, R. A. *Faraday Symposium 10*: Proton-Transfer, Stirling 1975. See also Johnston, H. S. *Gas Phase Reaction Rate Theory*, Ronald Press, New York 1966, p. 242.
4. Schachtschneider, J. H. and Snyder, R. G. *Spectrochim. Acta 19* (1963) 117.
5. Wolfsberg, M. and Stern, M. J. *Pure Appl. Chem. 8* (1964) 225.
6. Bell, R. P. *The Proton in Chemistry*, 2nd Ed., Chapman and Hall, London 1973, a p. 275; b p. 211.
7. Huang, T. T.-S., Kidd, R. W. and Yankwich, P. E. *J. Chem. Phys. 62* (1975) 4757, and references in it to earlier work.
8. Saunders, W. H., Jr. *Chem. Scr. 8* (1975) 27, and references therein.
9. Kurz, J. L. and Kurz, L. C. *J. Am. Chem. Soc. 94* (1972) 4451.
10. Cox, A. P. and Waring, S. *J. Chem. Soc. Faraday Trans. 2, 68* (1972) 1060.
11. Sutton, L., Ed., *Tables of Interatomic Distances in Molecules and Ions*, The Chemical Soc. Publ. 18 (1965).
12. Pauling, L. *The Nature of the Chemical Bond*, 3rd Ed., Cornell University Press, Ithaca 1960, a p. 255; b p. 260.
13. Jonathan, N. *J. Mol. Spectrosc. 7* (1961) 105.
14. Wheland, G. W. *Resonance in Organic Chemistry*, Wiley, New York 1955.
15. Dakhis, M. I., Dashevsky, V. G. and Avakyan, V. G. *J. Mol. Struct. 13* (1972) 339.
16. Wells, A. J. and Wilson, E. B., Jr. *J. Chem. Phys. 9* (1941) 314.
17. More O'Ferrall, R. A., Koeppl, G. W. and Kresge, A. J. *J. Am. Chem. Soc. 93* (1971) 1.
18. Jones, L. H. *J. Chem. Phys. 22* (1954) 217.
19. Wilson, E. B., Jr., Decius, J. C. and Cross, P. C. *Molecular Vibrations*, McGraw, New York 1955.
20. Melander, L. *Acta Chem. Scand. 25* (1971) 3821.
21. Lewis, E. S. In Caldin, E. F. and Gold, V., Eds., *Proton-Transfer Reactions*, Chapman and Hall, London 1975, Chapter 10.

Received April 23, 1976.

Acta Chemica Scandinavica A 30 (1976) 715—718

The Crystal Structure of $Pb_2Cl_6[NH_3(CH_2)_2NH_3]$

IRENE LÖFVING

Division of Inorganic Chemistry 2, Chemical Center, The Lund Institute of Technology, P.O. Box 740, S-220 07 Lund 7, Sweden

Crystals of a lead(II) chloride ethylenediamine complex of formula $Pb_2Cl_6[NH_3(CH_2)_2NH_3]$ are orthorhombic, space group *Pbcm* with $a=9.402(3)$, $b=16.068(4)$, $c=16.887(15)$ Å and $Z=8$. The structure was refined by full-matrix least-squares methods based on 1950 observed reflections to $R=0.031$. The lead atoms, Pb(1), Pb(2), Pb(3), are each eight-coordinated. The coordination polyhedra may be described as distorted bicapped trigonal prisms around the atoms Pb(1) and Pb(3) and as a square antiprism around Pb(2). The polyhedra are linked by sharing faces to infinite layers running parallel to the *bc*-plane. The ethylenediammonium ions, located between the layers, are linked *via* hydrogen bonds to the chloride ions.

The present study of the crystal chemistry of $Pb_2Cl_6[NH_3(CH_2)_2NH_3]$ is part of a research program at our division on negatively charged polynuclear halide complexes of heavy metals in the solid state. It seems reasonable to expect isolated, infinite linear or two-dimensional complexes if the additional cations, necessary to obtain electroneutrality, are large. Such large cations, *e.g.* $NH_3^+(CH_2)_2NH_3^+$, are preferably found among organic compounds.

EXPERIMENTAL

Crystals of the actual compound were prepared by crystallization of stoichiometric quantities of $PbCl_2$ and $NH_2(CH_2)_2NH_2$ from HCl (1:1) solution. The product consisted of colourless plates.

Preliminary Weissenberg photographs indicated orthorhombic symmetry. The conditions limiting possible reflections were $0kl$: $k=2n$ and $h0l$: $l=2n$, indicating either space group *Pbcm* (No. 57) or $Pbc2_1$ (No. 29*).

* Orientation different from that given in the International Tables.

The density, 3.63 g cm^{-3}, was measured by flotation. The unit-cell dimensions, determined from least-squares refinement of the settings of 15 reflections measured on a single-crystal diffractometer, were $a=9.402(3)$ Å, $b=16.068(4)$ Å and $c=16.887(15)$ Å. The volume $V=2551.0$ Å^3. Assuming $Z=8$ the value of the calculated density was 3.58 g cm^{-3}.

A single crystal with the dimension $0.20\times0.15\times0.08$ mm was used for collecting intensity data on a computer-controlled, four-circle diffractometer (Enraf-Nonius CAD-4) with Mo$K\alpha$ radiation and a graphite monochromator. The ω-2θ scan technique was used with a peak scan interval $\Delta\omega=0.90°+0.50°\tan\theta$ and background scans for 1/4 of the peak scan time. A total of 3836 independent reflections was recorded. 1885 reflections with $I<3\sigma(I)$ were considered not significantly different from the background and were excluded from the refinement. The values of $\sigma(I)$ were based on counting statistics. The intensities of two standard reflections, 1 10 6, 1 $\bar{1}$0 6, were measured

Table 1. Atomic coordinates with standard deviations in parentheses.

Atom	X/a	Y/b	Z/c
Pb(1)	0.13687(5)	0.00219(3)	0.08276(2)
Pb(2)	0.03767(6)	¼	0
Pb(3)	−0.08234(8)	0.17649(4)	¼
Cl(1)	0.2063(4)	0.3926(2)	0.0517(2)
Cl(2)	0.8600(3)	0.1086(2)	0.0664(2)
Cl(3)	0.5839(3)	0.4709(2)	0.0957(2)
Cl(4)	0.1966(3)	0.1807(2)	0.1408(2)
Cl(5)	0.8706(3)	0.3164(1)	0.1421(2)
Cl(6)	0.0469(3)	0.0076(2)	¼
Cl(7)	0.6259(5)	0.1555(3)	¼
N(1)	0.5227(12)	0.1514(5)	0.0625(6)
N(2)	0.1774(14)	0.3645(8)	¼
N(3)	0.5759(17)	0.3632(10)	¼
C(1)	0.5326(16)	0.2433(7)	0.0436(7)
C(2)	0.3246(17)	0.4045(9)	¼
C(3)	0.4261(20)	0.3319(11)	¼

Table 2. Thermal parameters. The form of the anisotropic temperature factor is exp $[-(h^2\beta_{11}+k^2\beta_{22}+l^2\beta_{33}+2hk\beta_{12}+2kl\beta_{23}+2hl\beta_{13})]$. The β_{ij} values are multiplied by 10^5 for the Pb and Cl atoms and by 10^4 for the N and C atoms.

Atom	β_{11}	β_{22}	β_{33}	β_{12}	β_{13}	β_{23}
Pb(1)	671(5)	366(2)	193(1)	121(3)	−18(3)	23(2)
Pb(2)	572(6)	184(2)	239(2)	0	0	−11(2)
Pb(3)	813(8)	168(2)	435(3)	3(4)	0	0
Cl(1)	1164(40)	217(10)	181(10)	−181(17)	−125(18)	39(8)
Cl(2)	540(28)	187(9)	272(11)	−7(14)	6(16)	−9(8)
Cl(3)	578(28)	243(10)	277(12)	−37(15)	15(16)	58(9)
Cl(4)	641(31)	265(10)	190(10)	−28(15)	−38(15)	4(8)
Cl(5)	776(32)	152(8)	198(10)	44(14)	62(16)	16(7)
Cl(6)	1386(63)	132(12)	165(12)	−14(26)	0	0
Cl(7)	650(48)	293(16)	234(15)	−26(24)	0	0
N(1)	95(13)	18(3)	25(4)	−5(6)	1(6)	4(3)
N(2)	57(15)	23(5)	17(5)	5(7)	0	0
N(3)	75(18)	49(7)	11(5)	−5(11)	0	0
C(1)	165(20)	20(4)	26(5)	−22(9)	−11(9)	4(4)
C(2)	61(18)	22(6)	16(5)	2(9)	0	0
C(3)	65(21)	33(7)	31(8)	14(11)	0	0

Table 3. Selected interatomic distances (Å) and angles (°) with estimated standard deviations in parentheses.

		Square antiprism around Pb(2)	
		Pb(2) – 2 Cl(1)	2.920(3)
Pb(1) – Pb(1)	3.800(2)	Pb(2) – 2 Cl(4)	3.021(4)
Pb(1) – Pb(2)	4.322(1)	Pb(2) – 2 Cl(2)	3.035(3)
Pb(1) – Pb(3)	4.480(2)	Pb(2) – 2 Cl(5)	3.060(4)
Bicapped trigonal prism around Pb(1)		Bicapped trigonal prism around Pb(3)	
Pb(1) – Cl(1)	2.905(4)	Pb(3) – Cl(7)	2.764(5)
Pb(1) – Cl(1)	3.713(4)	Pb(3) – 2 Cl(5)	2.927(3)
Pb(1) – Cl(2)	3.085(4)	Pb(3) – Cl(6)	2.973(4)
Pb(1) – Cl(2)	3.127(3)	Pb(3) – 2 Cl(4)	3.207(3)
Pb(1) – Cl(3)	2.682(3)	Pb(3) – 2 Cl(2)	3.331(4)
Pb(1) – Cl(4)	3.083(3)		
Pb(1) – Cl(5)	3.150(2)		
Pb(1) – Cl(6)	2.949(3)		
In the ethylenediammonium ions			
C(1) – C(1′)	1.49(2)	C(2) – C(3)	1.51(2)
C(1) – N(1)	1.51(1)	C(2) – N(2)	1.53(2)
		C(3) – N(3)	1.50(3)
Interatomic N – Cl distances less than 3.3 Å			
N(1) – Cl(2)	3.25(1)	N(2) – Cl(6)	3.12(1)
N(1) – Cl(3)	3.12(1)	N(3) – 2 Cl(3)	3.13(1)
Angles in the ethylenediammonium ions			
C(1) – C(1) – N(1)	110(1)		
C(3) – C(2) – N(2)	104(1)		
C(2) – C(3) – N(3)	110(1)		

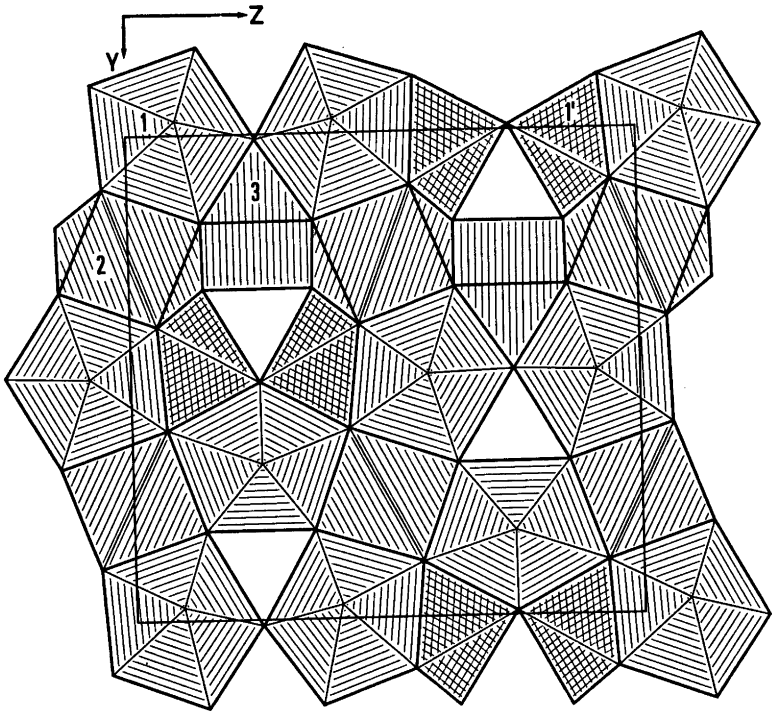

Fig. 1. Projection of a repetition unit of one $(Pb_2Cl_6^{2-})_n$-layer on the *bc*-plane. The positions of the chlorine atoms correspond to the intersections of the lines. The Pb(1) polyhedra are shaded with lines parallel to the heavy lines showing their edges. The Pb(1′) polyhedra are shaded by crossing lines. The antiprisms around Pb(2) are indicated by shading lines parallel to a face diagonal of the square face. The shading lines of the polyhedra of Pb(3) are parallel to the *b*-axis. One polyhedron of each kind is numbered according to the lead atom in the drawing.

after every 50 reflections to check the stability of the crystal and the electronics.

The fluctuations in the intensities of the standard reflections were random and less than 8 %. The intensities were corrected for Lorentz, polarization and absorption effects [$\mu(\mathrm{Mo}K\alpha) = 275\ \mathrm{cm}^{-1}$]; the transmission factors varied from 0.069 to 0.213.

STRUCTURE DETERMINATION AND REFINEMENT

Assuming the centrosymmetric space group *Pbcm*, the positions of the lead atoms were deduced from a three-dimensional vector map. Two of the lead atoms of the asymmetric part of the unit cell occupy special positions. The positions of all other non-hydrogen atoms were obtained from successive difference Fourier syntheses. The positions so obtained were refined by least-squares calculations using anisotropic temperature factors for all atoms. At this stage the R factor was 0.032. The presence of secondary extinction effects in the intensity data was investigated by including an isotropic extinction parameter in the calculations; the refined value of this parameter being $g = 0.14(2) \times 10^4$. The refinement converged to $R = 0.031$ and $R_w = 0.037$ (1951 independent reflections). The goodness of fit, S, was 1.16. The weights w_i were calculated according to $w_i^{-1} = \sigma^2(F_o^2) + 0.00028|F_o|^2$. As a reasonable structure was obtained in this way, space group $Pbc2_1$ was not further considered.

The atomic scattering factors were those given by Doyle and Turner.[1] The final positional and thermal parameters are given in Tables 1 and 2. A list of observed and calculated structure factors is available on request to the Division of Inorganic Chemistry 2.

Selected interatomic distances and angles are presented in Table 3.

All computations were made on the UNIVAC 1108 computer in Lund. A short account of the program system has been given by Stålhandske.[2]

DESCRIPTION AND DISCUSSION

The crystal structure of $Pb_2Cl_6[NH_3(CH_2)_2NH_3]$ is built up of identical layers $(Pb_2Cl_6^{2-})_n$ perpendicular to the *a*-axis and ions $NH_3^+(CH_2)_2NH_3^+$ between them. The repetition unit of such a layer projected on the *bc*-plane is shown in Fig. 1. Each lead atom coordinates eight chlorine atoms (Tables 1, 3). The coordination polyhedra may be described as distorted bicapped trigonal prisms around the atoms Pb(1) and Pb(3) and as a square antiprism around Pb(2). The point symmetries of the sites of the lead atoms are *1*, *2* and *m* for Pb(1), Pb(2), and Pb(3), respectively. Except for the contacts of the polyhedra of Pb(1) and the centro-symmetrically related ones, Pb(1'), all coordination polyhedra are linked by sharing triangular faces (Fig. 1).

The Pb(1) atoms occur in pairs in the structure related by a centre of symmetry at 0,0,0 and the distance between them is 3.800(1) Å. The bicapped triangular prism around Pb(1) has one nearly square, strictly planar face, which is shared by the corresponding Pb(1') prism. The coulombic repulsion between the Pb(1) atoms may explain the remarkably long Pb(1)–Cl(1) distance of 3.713(2) Å. The two short distances Pb(1)–Cl(3), 2.682(2) Å, and Pb(3)–Cl(7), 2.764(2) Å, can be explained by considering that each of the atoms Cl(3) and Cl(7) only forms one coordinative bond while the other chlorine atoms form three or four bonds. The lead-chlorine distances are in good agreement with the value 2.75(4) Å found in bisthiourea-lead(II) chloride reported by Nardelli and Fava.[3] The remaining lead-chlorine distances are fairly close to the value reported as a mean for $PbCl_2$.[4,5]

The positively charged ethylenediamine ions $NH_3^+(CH_2)_2NH_3^+$ connect subsequent $(Pb_2Cl_6^{2-})_n$-layers by means of N–H···Cl hydrogen bonds. The two ethylenediammonium ions I, II in the asymmetric part of the unit cell occur in the *trans* conformation. The non-hydrogen atoms of ion I, including the carbon atoms C(2) and C(3) (Table 1), are strictly coplanar, being situated in the mirror plane $z=\frac{1}{4}$. The ions of this kind extend along the *a*-axis and their projections on the *bc*-plane fall within the non-shaded triangular areas in Fig. 1. The atoms within the ion II are related by the two-fold axis running along $x,\frac{1}{4},0$. The ion contains the carbon atoms C(1) and C(1') and is only approximately planar. These ions are approximately parallel to the plane of the $(Pb_2Cl_6^{2-})_n$-layers. The bond distances and angles within the ethylenediamine ions (Table 3) agree with those reported by Jamet-Delcroix [6] but for the angle C(3)–C(2)–N(2), 104(1)°, which is significantly smaller than for crystalline ethylenediamine, 114.50(2)°. The nitrogen-chlorine (N–H···Cl) distances less than 3.3 Å are given in Table 3. Both ions I and II are in contact with two adjacent layers $(Pb_2Cl_6^{2-})_n$ *via* hydrogen bonds.

The author is much obliged to Professor Bengt Aurivillius for his stimulating and helpful interest, and to Dr. Karin Aurivillius for valuable discussions and comments.

This study has been financially supported by the Swedish Natural Science Research Council.

REFERENCES

1. Doyle, P. A. and Turner, P. S. *Acta Crystallogr. A 24* (1968) 390.
2. Stålhandske, C. *Acta Crystallogr. B 30* (1974) 1586.
3. Nardelli, M. and Fava, G. *Acta Crystallogr. 12* (1959) 727.
4. Sahl, K. and Zemann, J. *Naturwissenschaften 48* (1961) 641.
5. Sass, R. L., Prackket, E. B. and Bracket, T. F. *J. Phys. Chem. 67* (1963) 2863.
6. Jamet-Delcroix, S. *Acta Crystallogr. B 29* (1973) 977.

Received April 27, 1976.

Acta Chemica Scandinavica A 30 (1976) 719—723

The Structures of Two Crystalline Forms of Di-μ-bromobis-{diethylenethioureatellurium(II)} Dibromide

PER HERLAND, MAGNE LUNDELAND and KJARTAN MARØY

Department of Chemistry, University of Bergen, N-5014 Bergen-Univ., Norway

Di-μ-bromobis{diethylenethioureatellurium(II)} dibromide, $[Te_2(etu)_4Br_2]Br_2$, forms two crystalline modifications, one orthorhombic (I) and one monoclinic (II). The former has space group *Fddd* (No. 70), with unit cell $a = 14.454(5)$ Å, $b = 31.258(10)$ Å, $c = 12.057(5)$ Å, $Z = 8$, and the latter has space group $C2/c$ (No. 15), with unit cell $a = 26.734(8)$ Å, $b = 11.437(4)$ Å, $c = 9.321(4)$ Å, $\beta = 101.97(6)°$, $Z = 4$.

The structure determinations were carried out using single-crystal diffractometer data. The refinements, based on 831 non-zero reflections for I and 2349 for II, converged at R values of 0.043 and 0.032, respectively.

Each tellurium atom is bound to two sulfur atoms and two bromine atoms in a distorted square-planar *cis* arrangement. The two bromine atoms are situated on a twofold axis of symmetry, and bridge two tellurium atoms. In the orthorhombic form, the two tellurium atoms are also situated on a twofold axis. The two S—Te—Br systems have the bond lengths S—Te = 2.495(3) Å, Te—Br = 3.042(2) Å in the orthorhombic form, and S—Te = 2.491(2) and 2.481(2) Å, Te—Br = 3.015(1) and 3.079(1) Å in the monoclinic form. The S—Te—Br angles are, in the same order, 175.75(8), 178.68(5), and 170.51(5)°.

In preparing complexes of divalent tellurium with ethylenethiourea, Foss and Fossen [1] isolated four different bromides of which three had the apparent composition $Te(etu)_2Br_2$. The crystal structure of one of these was published together with that of the isomorphous diiodo complex,[2] and these structures have later been refined using diffractometer data.[3] In these crystals the tellurium atoms are situated at centres of symmetry, and the complexes are *trans* square-planar. The crystal structure analyses of the two other $Te(etu)_2Br_2$ complexes have now been carried out. Some features of the structures have been briefly reported earlier.[4] The present work forms part of the extensive studies on linear three-atom systems centered on divalent tellurium, selenium, and sulfur which are being carried out at this department.[5,6]

EXPERIMENTAL

The intensity data, and diffraction angles for unit cell dimensions, were measured on a Siemens automatic single-crystal diffractometer using Mo$K\alpha$ radiation (Nb-filtered) and a scintillation counter.

The crystals used for the measurements were of samples prepared by Foss and Fossen [1] which had been kept in a refrigerator. The crystal used of the orthorhombic form was a prism with (010) predominant, 0.045 mm thick, and 0.115 and 0.195 mm along the a and c axes, respectively. The crystal of the monoclinic form was a prism along the c axis, 0.326 mm long, with distances between the (100), between the (110), and between the $(1\bar{1}0)$ boundary faces of 0.082, 0.095 and 0.095 mm, respectively. Each crystal was mounted with the c axis approximately parallel to the ϕ axis of the diffractometer.

The five-value procedure and $\theta - 2\theta$ scan technique, with scan width of 0.80°, were used. The maximum scan time per degree was 24 s.

Two reflections of medium strength were measured two times each at intervals of 50 reflections. The net intensities were brought to a common scale by means of these reference reflections, which showed no systematic variations.

Reflections with net intensity below three times its standard deviation were assigned an intensity equal to this limit and were labelled as unobserved. These reflections were included in the refinements and the calculation of R values when $|F_c|$ was greater than the observable limit.

Table 1. Atomic coordinates, in fractions of cell edges. Standard deviations in parentheses.

	x	*y*	*z*
Orthorhombic di-μ-bromobis{diethylenethioureatellurium(II)} dibromide. Origin at a centre of symmetry, at 1/8 1/8 1/8 from 222			
Te	1/8	1/8	0.31237(7)
Br	1/8	0.05955(5)	1/8
Br^-	1/8	0.43705(5)	1/8
S	0.11637(22)	0.06835(9)	0.45775(22)
N(1)	0.29695(73)	0.09136(34)	0.49197(95)
N(2)	0.25923(69)	0.02672(30)	0.54806(75)
C(1)	0.23112(67)	0.06248(37)	0.50014(77)
C(2)	0.38628(105)	0.07530(47)	0.53864(131)
C(3)	0.35905(87)	0.02980(37)	0.58013(89)
Monoclinic di-μ-bromobis{diethylenethioureatellurium(II)} dibromide. Origin at a centre of symmetry			
Te	0.06839(1)	0.17088(4)	0.43729(4)
Br	0	0.35462(8)	1/4
Br′	0	−0.00446(8)	1/4
Br^-	0.18045(3)	0.32672(7)	0.27303(8)
S	0.12664(6)	0.31301(15)	0.59152(19)
S′	0.11143(6)	0.00040(14)	0.57482(19)
N(1)	0.07233(24)	0.25228(50)	0.79804(67)
N(2)	0.10756(23)	0.42350(46)	0.82977(60)
N(1′)	0.18975(20)	0.06349(47)	0.43993(58)
N(2′)	0.19708(21)	−0.10821(48)	0.54525(60)
C(1)	0.09982(22)	0.32898(56)	0.74633(67)
C(2)	0.05811(31)	0.29228(65)	0.93738(79)
C(3)	0.08183(28)	0.41411(58)	0.95525(72)
C(1′)	0.16828(23)	−0.01342(54)	0.51320(62)
C(2′)	0.23836(27)	0.02006(63)	0.41211(79)
C(3′)	0.24594(28)	−0.09357(69)	0.50132(89)

Absorption corrections [7] were carried out in addition to Lorentz and polarization corrections.

The scattering factor curves used were those listed in *International Tables for X-Ray Crystallography*,[8] Table 3,3. 1A. The curves for tellurium, bromine, bromide, and sulfur were corrected for anomalous dispersion using the values given by Cromer,[9] and taking the amplitude as the corrected value.

The structures were solved through Patterson and Fourier maps.

The refinements were carried out by means of a full-matrix least squares program, and in the course of the refinements the intensities were corrected for secondary extinction according to Zachariasen.[10] The extinction correction program used has a fixed values of one for the absorption term, and C was found to be 0.54×10^{-7} for I and 1.29×10^{-7} for II.

Difference electron density maps revealed the positions of all the hydrogen atoms in II, but of only two of the six symmetry independent ones in I. The hydrogen atoms are not included in the structure factor calculations.

The final atomic coordinates and thermal parameters are listed in Tables 1 and 2, respectively. Lists of observed and calculated structure factors are available from author K. M. on request.

The program for drawing illustrations is written by C. K. Johnson, Oak Ridge National Laboratory, Oak Ridge, Tennessee, U.S.A. The other programs are partly of a set made available by the Chemical Department of X-Ray Crystallography, Weizmann Institute of Science, Rehovoth, Israel, and partly written at this Department. An IBM 360/50H computer was used for the calculations.

CRYSTAL DATA

Orthorhombic	Monoclinic
$[Te_2(etu)_4Br_2]Br_2$	$[Te_2(etu)_4Br_2]Br_2$
Fddd (No. 70)	*C2/c* (No. 15)
$a = 14.454(5)$ Å	$a = 26.734(8)$ Å
$b = 31.258(10)$ Å	$b = 11.437(4)$ Å
$c = 12.057(5)$ Å	$c = 9.321(4)$ Å
	$\beta = 101.97(6)°$
$Z = 8$	$Z = 4$
$\varrho_{calc} = 2.40$ g/cm³	$\varrho_{calc} = 2.30$ g/cm³
$\mu(MoK\alpha) = 87.5$ cm^{-1}	$\mu(MoK\alpha) = 85.5$ cm^{-1}
2010 refl. within $\theta = 28°$	3397 refl. within $\theta = 28°$
831 refl. with $I > 3\sigma(I)$	2349 refl. with $I > 3\sigma(I)$
$R = 0.043$	$R = 0.032$

RESULTS

Distances and angles are listed in Table 3. A view of the complex cation is shown in Fig. 1, and the unit cell contents are shown in Figs. 2 and 3. The marked and unmarked atoms, used for the monoclinic form, refer to atoms which in the orthorhombic form are related to each other by the twofold axis through the tellurium atoms.

In the earlier published [2] monoclinic modification of $Te(etu)_2Br_2$, the arrangement is *trans* square-planar with the tellurium atoms situated at symmetry centres. Also in the present complexes, two bromine atoms and two sulfur atoms are coordinated to tellurium in an approximately square-planar arrangement. The arrangement is, however, *cis*, and the two bromine atoms are situated on a twofold axis of symmetry and thus bridge two tellurium atoms. The result is a dinuclear cation of

Table 2. Thermal parameters expressed in the form $\exp[-2\pi^2(h^2a^{-2}U_{11}+\ldots+2hka^{-1}b^{-1}U_{12}+\ldots)]$. All values have been multiplied by 10^4. Standard deviations are given in parentheses.

	U_{11}	U_{22}	U_{33}	U_{12}	U_{23}	U_{13}
Orthorhombic di-μ-bromobis{diethylenethioureatellurium(II)} dibromide						
Te	301(5)	299(5)	326(5)	36(6)	0	0
Br	504(10)	347(9)	409(8)	0	0	− 43(10)
Br^-	414(8)	331(8)	462(8)	0	0	− 17(10)
S	414(16)	303(13)	440(15)	−30(15)	79(12)	− 26(15)
N(1)	427(61)	417(64)	805(75)	−122(59)	204(59)	−205(56)
N(2)	568(64)	299(55)	425(53)	55(47)	96(47)	− 67(49)
C(1)	299(55)	413(65)	214(44)	−29(44)	13(46)	24(42)
C(2)	613(97)	514(79)	1095(119)	40(81)	428(82)	−442(99)
C(3)	493(88)	359(60)	479(63)	65(57)	− 10(49)	−160(56)
Monoclinic di-μ-bromobis{diethylenethioureatellurium(II)} dibromide						
Te	306(2)	271(2)	331(2)	26(2)	2(2)	107(2)
Br	498(6)	291(6)	423(6)	0	0	35(5)
Br′	402(6)	297(5)	498(6)	0	0	79(5)
Br^-	585(4)	380(4)	493(4)	5(4)	19(4)	225(4)
S	416(9)	325(9)	469(9)	−81(8)	−47(8)	154(8)
S′	358(9)	312(8)	456(10)	59(7)	92(7)	143(7)
N(1)	642(44)	473(36)	508(39)	−243(31)	−137(30)	304(34)
N(2)	609(39)	293(29)	412(33)	−60(28)	−70(26)	94(30)
N(1′)	408(32)	369(30)	424(33)	28(25)	82(26)	204(27)
N(2′)	482(36)	369(30)	489(37)	−146(28)	−81(27)	227(30)
C(1)	354(32)	259(29)	421(35)	−15(31)	6(32)	86(27)
C(2)	757(56)	455(42)	413(41)	−180(38)	−165(35)	270(41)
C(3)	627(49)	321(36)	331(39)	10(32)	14(29)	120(36)
C(1′)	377(36)	307(33)	280(34)	−26(29)	−11(27)	62(28)
C(2′)	402(39)	475(42)	533(46)	124(34)	99(36)	203(34)
C(3′)	527(49)	526(50)	804(61)	−220(39)	−240(44)	400(46)

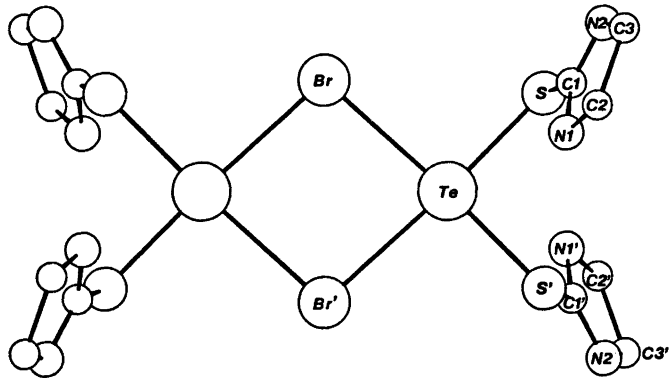

Fig. 1. A view of the di-μ-bromobis{diethylenethioureatellurium(II)} cation as seen normal to the coordination plane of the tellurium atoms.

composition $[(etu)_2TeBr_2Te(etu)_2]^{2+}$. The sulfur atoms are moved slightly out of the $TeBr_2Te$-plane, the angle between this plane and the TeS_2 plane being 4.0° in I and 3.4° in II.

In the orthorhombic crystals the tellurium atoms are also situated on twofold axes of symmetry. The deviations from this twofold symmetry in the monoclinic crystals are

Table 3. Bond lengths (Å) and angles (deg.). Standard deviations are given in parentheses.

	Orthorhombic form	Monoclinic form	
Te – Br	3.048(2)	3.079(1)	3.015(1)
Te – S	2.495(3)	2.491(2)	2.481(2)
∠Be – Te – Br	84.32(5)	84.74(3)	
∠S – Te – S	90.73(9)	92.70(6)	
∠S – Te – Br(*cis*)	92.54(7)	96.23(5)	86.39(5)
∠S – Te – Br(*trans*)	175.75(8)	178.68(5)	170.51(5)
∠Te – Br – Te	95.68(5)	93.93(3)	96.60(3)
S – C(1)	1.745(10)	1.749(7)	1.740(7)
C(1) – N(1)	1.315(15)	1.300(9)	1.316(9)
C(1) – N(2)	1.322(15)	1.323(8)	1.327(8)
N(1) – C(2)	1.495(19)	1.499(10)	1.464(9)
N(2) – C(3)	1.497(16)	1.479(10)	1.457(10)
C(2) – C(3)	1.558(19)	1.526(10)	1.534(11)
∠Te – S – C(1)	103.5(4)	103.3(2)	104.1(3)
∠S – C(1) – N(1)	126.4(8)	126.6(5)	128.0(4)
∠S – C(1) – N(2)	120.6(7)	122.0(5)	120.4(4)
∠N(1) – C(1) – N(2)	113.0(9)	111.4(6)	111.6(5)
∠C(1) – N(1) – C(2)	111.5(10)	112.3(6)	111.3(5)
∠C(1) – N(2) – C(3)	110.8(8)	111.3(5)	110.8(5)
∠N(1) – C(2) – C(3)	102.1(10)	101.5(6)	102.4(6)
∠N(2) – C(3) – C(2)	102.7(9)	103.4(5)	103.0(6)
N(1)···Br^-	3.494(11)		3.374(5)
∠C(1) – N(1)···Br^-	148.4(7)		146.8(4)
∠C(2) – N(1)···Br^-	99.2(7)		101.8(4)
N(2)···Br^-	3.533(10)	3.559(6)	3.368(6)
∠C(1) – N(2)···Br^-	128.1(6)	126.3(4)	127.0(4)
∠C(3) – N(2)···Br^-	120.8(6)	122.3(3)	120.4(4)
N(1)···Br		3.408(6)	
∠C(1) – N(1)···Br		149.5(4)	
∠C(2) – N(1)···Br		97.4(4)	

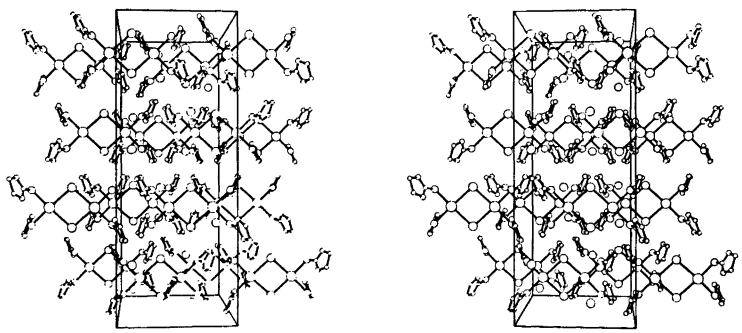

Fig. 2. A stereoscopic view of the cell packing in the orthorhombic crystals of $[Te_2(etu)_4Br_2]Br_2$ as seen normal to the *a* plane.

illustrated by the differences in dimensions in the two halves of the cation; the Te – Br bond lengths differ by 0.064 Å, the Te – S bond lengths by 0.010 Å, the *cis* S – Te – Br angles by 8.17°, and the *trans* S – Te – Br angles by 8.17°, and the Te – Br – Te angles by 2.67°. The averaged dimensions in the monoclinic crystals agree well with the dimensions in the orthorhombic crystals.

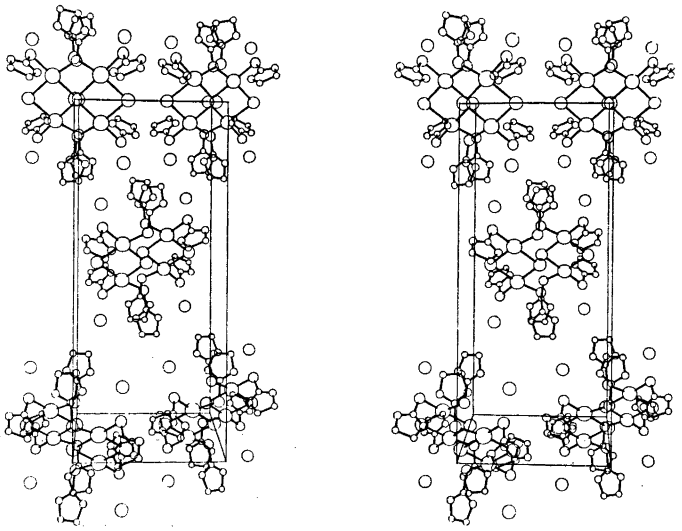

Fig. 3. A stereoscopic view of the cell packing in the monoclinic crystals of $[Te_2(etu)_4Br_2]Br_2$ as seen normal to the c plane.

When the dimensions of the present dimeric *cis* complexes are compared to those of the monomeric *cis* complex $Te(trtu)_2Br_2$,[11] the most obvious difference is found in the Br – Te – Br angle, which is 96.24(7)° in the latter, while in the former they are 84.32(5) and 84.74(3)°, *cf.* Table 3. The bromine atoms are closer together and the tellurium atoms are further apart than in a square arrangement. Since the Te···Te distances are as large as about 4.50 Å, the reason for the distortion is more likely to be the preference of a bond angle at bromine larger than 90°, than the space requirements of the tellurium atoms. The dimerization seems to have a small lengthening effect on the Te – Br bonds, which are 2.994(2) Å in $Te(trtu)_2Br_2$.[11]

As seen from Table 3, each nitrogen atom seems to form a hydrogen bond with a bromide ion or a bromine atom. The bromide ions involved in these contacts are in the orthorhombic crystals at $\frac{1}{2}-x, y-1/4, 1/4+z$ and $x, y-\frac{1}{2}, \frac{1}{2}+z$ relative to the coordinates of Table 1. In the monoclinic crystals, the bromide ions are, in the order listed, at $x, 1-y, \frac{1}{2}+z$; x,y,z; $x,-y,\frac{1}{2}+z$, and Br is at $x,-y, \frac{1}{2}+z$ relative to the coordinates of the table. The sums of the bond angles at nitrogen are in the range 358.2 – 359.9°.

REFERENCES

1. Foss, O. and Fossen, S. *Acta Chem. Scand. 15* (1961) 1618.
2. Foss, O., Kjøge, H. M. and Marøy, K. *Acta Chem. Scand. 19* (1965) 2349.
3. Foss, O. and Marøy, K. *To be published.*
4. Herland, P., Lundeland, M. and Marøy, K. *Acta Chem. Scand. 26* (1972) 2567.
5. Foss, O. In Andersen, P., Bastiansen, O. and Furberg, S., Eds., *Selected Topics in Structure Chemistry*, Universitetsforlaget, Oslo 1967, p. 145.
6. Foss, O. *Pure Appl. Chem. 24* (1970) 31.
7. Coppens, P., Leiserowitz, L. and Rabinovich, D. *Acta Crystallogr. 18* (1965) 1035.
8. *International Tables for X-Ray Crystallography*, Kynoch Press, Birmingham 1962, Vol. III.
9. Cromer, D. T. *Acta Crystallogr. 18* (1965) 17.
10. Zachariasen, W. H. *Acta Crystallogr. 16* (1963) 1139.
11. Fredin, K. S., Marøy, K. and Slogvik, S. *Acta Chem. Scand. A 29* (1975) 212.

Received April 6, 1976.

Acta Chemica Scandinavica A 30 (1976) 724—730

Alkylation Reactions of Triphenylphosphine and Triphenylarsine. A Kinetic Study

TORE THORSTENSON and JON SONGSTAD

Department of Chemistry, University of Bergen, N-5011 Bergen-Univ., Norway

The reactions of triphenylarsine and triphenylphosphine with methyl iodide and various 4-substituted benzyl halides in acetonitrile have been studied kinetically. Triphenylarsine is approximately two powers of ten less reactive than triphenylphosphine at 25 °C, the rate difference being mainly caused by the difference in activation enthalpy.

Hammett plots from the reactions with the various benzyl halides suggest that triphenylphosphine prefers to enter into a more "tight" transition state than does triphenylarsine. Triphenylarsine appears to prefer a "loose" transition state in its reactions with alkyl halides and thus resembles trialkylamines. The effect of the leaving group provides additional evidence for this suggestion.

In recent years several kinetic studies have been performed on reactions of various tervalent phosphorus compounds and alkyl halides.[1–7] With the exception of some reactions where the halogen atom undoubtedly acts as the electrophilic center,[8] alkylation reactions of tervalent phosphorus compounds are considered typical S_N2 reactions on aliphatic carbon.[3]

With regard to the transition state for this class of reactions, Hudson [3] has concluded, from various data, that strong bonding interaction and considerable bond breaking take place in the transition state. Thus, the transition state may be thought to be rather product-like. However, since five-membered cyclic and acyclic phosphites are known to react with alkyl halides with approximately the same rates,[9,10] this view of a product-like transition state for alkylation reactions of tervalent phosphorus compounds is uncertain.

Alkylation reactions of tervalent arsenic species are, as well, considered as usual displacement reactions; but, since very few kinetic studies have appeared,[11–14] no conclusions can be drawn regarding the transition state of this class of reactions. Generally, tervalent arsenic compounds react with alkyl halides with rate constants which are one to two powers of ten smaller than those of the corresponding phosphorus compounds. Toward most inorganic complexes as well, tervalent arsenic compounds are considerably less reactive than are the corresponding phosphorus compounds.[15] The lower reactivity of the tervalent arsenic species is assumed to be due to a number of factors: their lower basicity [16–18] and polarizability,[12,15] their higher ionization potential,[19,20] and a lower energy of bond formation and a higher repulsion energy between the arsenic species and electronically saturated species.[3] Due to the limited number of kinetic studies performed on alkylation reactions of tervalent arsenic compounds, it is not known whether the lower reactivity of these compounds signals a mechanistic pattern different from that of alkylation reactions of tervalent phosphorus compounds.

In the present investigation a kinetic study of various alkylation reactions of triphenylphosphine and triphenylarsine has been performed in an attempt to shed some light on these reactions, with special emphasis on the difference in reactivity of these nucleophilic species and on possible differences in the structure of the transition states. Since alkylation reactions on trialkylamines, Menshutkin reactions, appear to be the only reactions of non-

charged nucleophiles with alkyl halides which have been sufficiently examined to allow conclusions to be drawn with regard to the structure of their transition states,[21,23] some reactions of triethylamine are included in the present study for comparison. These reactions are known to have "early" transition states.

The substrates employed were methyl iodide and various benzyl halides, the classical substrates for studies of "tight" and "loose" transition states in alkylation reactions.[24–27] A dipolar aprotic solvent, acetonitrile, was used to minimize solvolytic side reactions and to allow a future comparison to be made with alkylation reactions of tervalent phosphorus and arsenic species which are unstable in protic solvents.[28]

EXPERIMENTAL

Materials. Acetonitrile, Baker Analyzed Reagent, was purified as previously described [29] and flushed with nitrogen prior to use. Triphenylphosphine and triphenylarsine were purified as reported.[29]

The various benzyl halides were either commercial products or made according to standard procedures. The solid benzyl halides were crystallized from light petroleum (40 – 60 °C) and from acetonitrile and washed with ice-cold acetonitrile prior to use. Benzyl bromide and benzyl chloride, both Fluka *puriss.*, were decanted from anhydrous sodium carbonate and distilled several times at reduced pressure. In this way a sample of benzyl bromide was obtained which could be crystallized at −20 °C from light petroleum. The purified benzyl halides were stored at −20 °C in darkness.

Methyl iodide, Fluka *puriss.*, was treated with silver wool and purified as reported.[12]

Separate experiments on the conductivity of the alkyl halides in acetonitrile showed these compounds to be perfectly stable, even at 50 °C, for long periods, *provided* direct sun-light was avoided. 4-Methoxy-benzyl iodide, however, was too unstable in acetonitrile even at room temperature to allow a kinetic study employing this substrate. The very unstable nature of this compound has been noted.[30]

Rate studies. All kinetic measurements were made by conventional conductivity techniques. The reaction rates were calculated from runs performed under pseudo-first-order conditions. The concentration of the alkyl halides was in the $1.5 - 3 \times 10^{-3}$ M range and was always less than 3 % of the concentration of the nucleophiles, $7.5 - 25 \times 10^{-2}$ M. The reactions were generally followed up to 50 to 75 % completion and the logarithmic rate plots appeared linear throughout. For each reaction studied, the infinity reading was checked with the conductivity of the pure product of exactly the same concentration as that of the alkyl halide. Since the discrepancy was generally less than 3 %, the total error due to the uncertainty in the infinity reading was calculated to be less than 1.5 %

The rate constants listed in the tables are averages from measurements performed in, at least, duplicate from separate weighings of reactants. From the small discrepancy observed between parallel rate determinations the listed rate constants are assumed to have an accuracy of ±3 %.

All solutions were prepared at 25 °C, and the concentrations were corrected for the coefficient of expansion of the solvent at the various temperatures.

Conductance measurements. The measurements were performed with a Conductivity Meter CDM 3 employing an immersion type conductivity cell, CDC 304, with a cell constant of 1.07 cm. The conductivity cell was immersed with teflon fittings into two-arm mixing devices with reaction volumes from 10 to 25 ml. The conductivity of the acetonitrile was less than 1×10^{-7} Ω^{-1} cm^{-1}.

An oil thermostat maintained all temperatures to better than ±0.05 °C, and it was covered to minimize the effect of day-light.

Onium salts. Separate experiments showed that for all reactions studied, the onium salts were obtained in nearly quantitative yield. Since all the bromides and most of the iodides were not sufficiently soluble in acetonitrile for accurate NMR studies and since the methylene signals were significantly dependent upon the anion,[6,31] all onium salts were transformed into their perchlorates according to a previously described procedure.[29] The perchlorates, after being carefully dried, were crystallized twice from acetonitrile/diethyl ether or from acetonitrile alone. The chemical shifts of the methylene protons relative to TMS together with corrected melting points of the onium perchlorates are listed in Table 1.

The NMR measurements were performed on a JEOL NMR C-60 H spectrometer, and a Spin-decoupler JNM-SO 30 counter was used to determine the resonance positions. Acetonitrile was used as the solvent.

RESULTS AND DISCUSSION

In Table 2 are listed the rate constants for the reactions between the various nucleophiles and methyl iodide in acetonitrile. Acetonitrile, an aprotic solvent and slightly more polar than methanol, is a better solvent for these quaternization reactions. The similar rate increase, ~4.3 at 25 °C, from methanol to acetonitrile

Table 1. Melting points and methylene signals in acetonitrile, relative to TMS, of substituted benzyltriphenylphosphonium and benzyl triphenylarsonium perchlorates, $X\text{-}C_6H_4-CH_2.\overset{+}{P}Ph_3\ ClO_4^-$ and $X\text{-}C_6H_4-CH_2.\overset{+}{As}Ph_3\ ClO_4^-$.

X	P+ M.p. °C	P+ δ	P+ J_{H-P}(Hz)	As+ M.p. °C	As+ δ
4-MeO	203	4.69	14.2	155	4.81
4-Me	200	4.76	14.4	167	4.82
4-H	232	4.76	14.7	210	4.84
4-Cl	216	4.76	14.6	191	4.83
4-CN	221	4.84	15.6	221	4.90
4-NO_2	194	4.91	15.3	202	4.95
2-NO_2	218	5.18	14.4	132	5.24

Table 2. Rate constants for the reactions between various nucleophiles and methyl iodide in acetonitrile together with calculated activation parameters at 25.0 °C.

Temp. °C	$k_2 \times 10^3$ M^{-1} s^{-1}	ΔH^* kJ mol^{-1}	ΔS^* J K^{-1} mol^{-1}
Ph_3P + MeI[a]			
25.0	5.94	33	−176
34.0	9.1		
44.0	14.0		
Ph_3As + MeI[b]			
25.0	0.0315	55	−146
34.0	0.0634		
44.0	0.128		
Et_3N + MeI[c]			
25.0	33.5		

$k_2(MeCN)/k_2(MeOH)$ [13] = [a] 4.4, [b] 4.2, [c] 59.

for the reactions of triphenylarsine and triphenylphosphine with methyl iodide, reflects similar enthalpies of solution for the two nucleophiles.[32] Triethylamine on the other hand, being well solvated in methanol due to hydrogen bonding,[21,33] reacts considerably faster in acetonitrile than in the protic solvent.

In agreement with results from previous studies,[11-14] triphenylarsine is found to be considerably less reactive than triphenylphosphine; the latter nucleophile is 200 times more reactive than triphenylarsine toward methyl iodide at room temperature. The rate difference appears to be caused mainly by the difference in activation enthalpies for the reactions, ~5 kcal mol^{-1}.* The activation entropies for both reactions are very negative, but it is significantly less favourable for the triphenylphosphine-methyl iodide reaction. Although the bond angles in triphenylarsine [34,35] and triphenylphosphine [36] are comparable, the large $p-\pi$ conjugation in triphenylarsine,[37,38] mainly absent in triphenylphosphine,[19,37] suggests an enhanced *s*-character for the more diffuse lone pair of the arsine. The lower rates and higher activation enthalpies for the reactions of triphenylarsine are, therefore, as expected.

In Tables 3 and 4 are collected the observed rate constants together with the calculated activation parameters for reactions with various benzyl halides. In Fig. 1 are plotted the logarithms of the rate constants *versus* the Hammett σ-values. The most important results can be summarized as follows:

1. Electron-releasing substituents in the benzyl halides can cause a greater rate enhancement for reactions with triphenylarsine than for reactions with triphenylphosphine. (Table 4 and Fig. 1).

2. Electron-withdrawing substituents reduce significantly the rates of reaction for reactions with both triphenylarsine and triethylamine, while for reactions with triphenylphosphine this effect is negligible. Actually, for reactions between benzyl bromides and triphenylphosphine, a slight rate enhancement is observed. (Table 4 and Fig. 1).

3. Although the activation enthalpies seem to increase slightly from 4-methylbenzyl iodide to 4-nitrobenzyl iodide for reactions with both triphenylarsine and triphenylphosphine, Table 3, the activation parameters do not suggest significant variations in the structure of the transition state with substituents in the benzyl iodides. It is notable, however, that triphenylphosphine reacts with the various benzyl iodides with a higher activation enthalpy, ~8 kJ mol^{-1}, and a more positive activation entropy, ~33 J K^{-1} mol^{-1}, than for its reaction with methyl iodide, while for reactions of triphenylarsine no change is observed. (Tables 2 and 3).

When focusing first on the effect of electron-releasing substituents on reaction rates, Table

* 1 kcal = 4.184 kJ.

Table 3. Rate constants for the reactions between 4-substituted benzyl halides. X-$C_6H_4-CH_2Y$ and triphenylphosphine, Ph_3P, and triphenylarsine, Ph_3As, in acetonitrile at various temperatures together with calculated activation parameters.

X	Y	Nuc.	Temp. °C	$k_2 \times 10^4$ M^{-1} s^{-1}	ΔH^* kJ mol^{-1}	ΔS^* J K^{-1} mol^{-1}
NO_2	Cl	Ph_3P	25.0	0.101	62	−134
			50.0	0.755		
NO_2	Br	Ph_3P	17.0	14.6		
			25.0	23.4	40	−163
			34.0	38.3		
NO_2	I	Ph_3P	17.0	98		
			25.0	163	42	−138
			34.0	276		
H	I	Ph_3P	18.0	121		
			25.0	182	40	−142
			34.0	308		
Me	I	Ph_3P	18.0	205		
			25.0	305	39	−142
			34.0	513		
NO_2	I	Ph_3As	25.0	0.765	57	−134
			44.0	3.18		
			50.0	4.90		
			54.0	6.69		
H	I	Ph_3As	25.0	(1.37)[a]	55	−134
			34.0	2.74		
			50.0	8.31		
			56.0	12.4		
Me	I	Ph_3As	25.0	(2.59)[a]	55	−126
			34.0	5.08		
			50.0	15.4		
			56.0	22.8		

[a] Calculated rate constants.

4 and left hand side of Fig. 1, the greater rate enhancement observed for reactions of triphenylarsine suggests that for reactions of this nucleophile with alkyl halides the formation of fractional positive charge on the carbon atom is more important than for similar reactions of triphenylphosphine. Bond breaking should therefore be more advanced in the transition state for alkylation reactions of triphenylarsine than for alkylation reactions of triphenylphosphine.[24–27]

The effect of the leaving group, as exemplified by the $k_2(RI)/k_2(RBr)$ rate ratios, Table 4, is interesting in this connection. If bond breaking in the transition state were comparable for the reactions of triphenylphosphine, triphenylarsine, and triethylamine, then one would anticipate the following sequence for the $k_2(RI)/k_2(RBr)$ rate ratios: $Ph_3P > Ph_3As \geq Et_3N$.[39,40] The mere fact that the rate ratios are comparable, and even slightly greater, for the reactions of triphenylarsine than for the corresponding reactions of triphenylphosphine may be considered as additional evidence for the suggested difference in the extent of bond breaking in the transition state. In this respect it is interesting to note that reactions between triphenylarsine and alkyl chlorides are strongly catalyzed by small metal cations in aprotic solvents, while the effect is not very pronounced for reactions of triphenylphosphine.[41] Presumably, triphenylarsine, because of the diffusiveness of its lone pair of electrons causing this nucleophile to be a weak base toward both the proton [16–18] and aliphatic carbon,[14,39,42] is only able to displace rapidly a halide ion from an alkyl halide when the carbon-halogen bond is weakened through considerable bond breaking. Electron-withdrawing substituents, destabilizing the positive charge on the benzylic carbon atom, show a distinct

Table 4. Rate constants for the reactions between triphenylarsine, triphenylphosphine and triethylamine and substituted benzyl halides, X-C_6H_4-CH_2Y, in acetonitrile. (Relative rates in parentheses).

X	Y=I	Y=Br	k_2(RI)/k_2(RBr)
Ph_3As; 50 °C; $k_2 \times 10^4$ M^{-1} s^{-1}			
4-CH_3O		9.15 (9.2)	
4-CH_3	15.4 (1.86)	1.71 (1.74)	9.0
4-H	8.3 (1.00)	0.98 (1.00)	8.5
4-Cl	7.0 (0.84)	0.85 (0.86)	8.2
4-CN	4.9 (0.59)	0.62 (0.63)	7.9
4-NO_2	4.9 (0.59)	0.54 (0.55)	9.0
2-NO_2	9.4 (1.13)		
Ph_3P; 25.0 °C; $k_2 \times 10^2$ M^{-1} s^{-1}			
4-CH_3O		0.81 (3.77)	
4-CH_3	3.05 (1.68)	0.350 (1.63)	8.7
4-H	1.82 (1.00)	0.215 (1.00)	8.5
4-Cl	1.82 (1.00)	0.238 (1.10)	8.0
4-CN	1.54 (0.85)	0.221 (1.03)	7.0
4-NO_2	1.63 (0.90)	0.234 (1.09)	7.0
2-NO_2	2.65 (1.46)		
Et_3N; 25.0 °C; $k_2 \times 10^3$ M^{-1} s^{-1}			
4-CH_3	6.82 (1.91)		
4-H	3.57 (1.00)	0.677	5.3
4-NO_2	1.37 (0.38)		

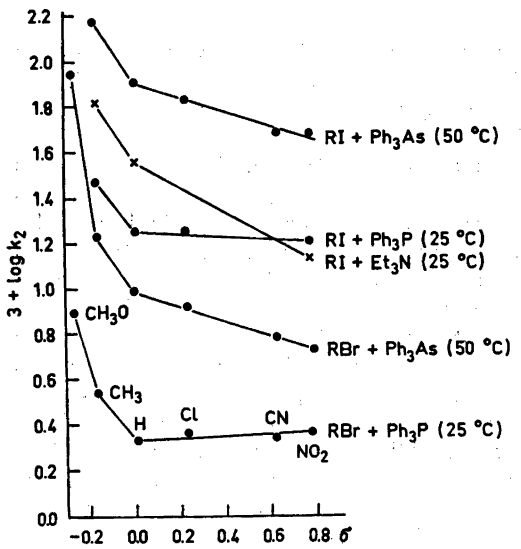

Fig. 1. The logarithms of the rate constant *versus* the Hammett σ constants. (R = *para*-substituted benzyl).

rate reduction for reactions of both triphenylarsine and triethylamine.

The negligible effect of electron-withdrawing substituents in benzylic halides on rates of reactions with triphenylphosphine, clearly suggests that the transition state for this class of reactions is different from that for alkylation reactions of triphenylarsine and trialkylamine. Since electron-releasing substituents show some rate enhancing effect, though less than for the corresponding reactions of triphenylarsine, some bond breaking must necessarily take place in the transition state. Presumably, the energy gain in a "tight" transition state, where some bond making takes place prior to bond rupture,[24,43,44] by delocalization of the negative charge on the central carbon atom through neighbouring orbital overlap, outweighs the anticipated rate diminishing effect due to the electron-withdrawing substituents. A number of reactions are known,[43–48] particularly Finkelstein reactions,[49–51] where 4-nitrobenzyl halides are considerably more reactive than are unsubstituted benzyl halides and U- and even J-shaped Hammett plots are observed. The reaction of triphenylphosphine, however, appears to be the first case of an uncharged nucleophile reacting with a benzyl halide where electron-withdrawing substituents have a negligible effect upon reaction rates.

It is probable that the ability of triphenylphosphine and triphenylarsine to enter into a "tight" transition state, *i.e.* a transition state with some bond making prior to bond breaking, should be related to the stability and the structure of phosphoranes and arsenanes, respectively. Recent NMR [52] and photoelectron studies [53] have shown that the ylidic carbon atom in methylene-triphenylarsorane contrary to the carbon atom in methylene-triphenylphosphorane, is virtually sp^3-hybridized, suggesting that triphenylarsine has a very limited ability to enter into a linear "tight" transition state with some π-bonding contribution. Triphenylarsine should, therefore, in its reactions with alkyl halides closely resemble uncharged nucleophiles derived from first row elements and particularly weakly basic amines. The amount of bond making prior to bond breaking in the transition state for the reactions of triphenylphosphine with alkyl halides cannot, however, be comparable with that in the transi-

tion state for the reactions between triarylphosphines and organic disulfides,[54,55] or triarylphosphines and α-halo sulfones [56] where strictly linear Hammett plots with positive slope have been observed. The structure of the transition state for alkylation reactions of triphenylarsine and triphenylphosphine may thus be visualized as follows:

$$\mathrm{As} \cdots\cdots \overset{\delta+}{\mathrm{C}} \cdots \mathrm{X}$$

$$\mathrm{P} \cdots\cdots \overset{\delta\delta+}{\mathrm{C}} \cdots \mathrm{X}$$

The "tighter" transition state suggested for the triphenylphosphine-alkyl halide reaction would necessarily imply that this class of reactions should be more subjected to steric hindrance than the triphenylarsine-alkyl halide reaction. As mentioned under point 3 above, the activation parameters for the reactions of triphenylphosphine with benzyl iodides are different from that of the triphenylphosphine-methyl iodide reaction while no difference is observed for the reactions of triphenylarsine. Presumably, when triphenylphosphine reacts with alkyl halides and when the steric demands of the reactants do not allow the reaction to go through a "tight" transition state (as is probably the case for triphenylphosphine reacting with benzyl halides) the phosphorus atom adjusts to a "looser" transition state of a less favourable activation enthalpy (Tables 2 and 3). The suggested difference in bond making in the transition state and thus the steric demands of reactants may therefore be the cause for the slightly greater rate enhancement from 4-nitrobenzyl iodide to 2-nitrobenzyl iodide for the reactions of triphenylarsine, ~ 1.9, than for triphenylphosphine, ~ 1.6, Table 4, even though the As–C (alkyl) bond length in alkyltriphenylarsonium cations is slightly longer than the P–C (alkyl) bond length in the corresponding phosphonium cations.

With regard to the non-linearity of Hammett plots for reactions of benzyl systems, Swain and Langsdorf [24] originally suggested that electron-withdrawing substituents might increase the positive character of the carbon atom of the C–X bond and thus render this atom more positive in the ground state than in the transition state. If this were the case, 4-nitrobenzyl halides should be expected to be relatively more reactive than unsubstituted benzyl halides toward basic nucleophiles than weakly basic ones. The data in Table 3 for reactions of trimethylamine and triphenylphosphine clearly indicate the opposite trend.

Finally, some comments with regard to the Hammond postulate [57] and the conclusion arrived at in the present study with regard to the extent of bond making in the transition state when triphenylarsine and triphenylphosphine are the nucleophilic species. This postulate may well be valuable in predicting the structure of transition states in substitution reactions when the leaving group is fixed and the nucleophile is varied provided the nucleophilic atom remains unchanged. However, when special electronic arrangements are possible due to the nucleophile, as in alkylation reactions of tervalent phosphorus compounds and, presumably, Finkelstein reactions,[58] the use of the Hammond postulate should be made with caution.[59]

REFERENCES

1. Buckler, S. A. and Henderson, W. A., Jr. *J. Am. Chem. Soc. 82* (1960) 5795.
2. Aksnes, G. and Aksnes, D. *Acta Chem. Scand. 18* (1964) 38.
3. Hudson, R. F. *Structure and Mechanism of Organophosphorus Chemistry*, Academic, London 1967, p. 131.
4. Borowitz, I. J. and Parnes, H. *J. Org. Chem. 32* (1967) 3560.
5. McEwen, W. E., Kyllingstad, V. L., Schultz, D. N. and Yeh, Y.-I. *Phosphorus 1* (1971) 145.
6. McEwen, W. E., Shiau, W.-I., Yeh, Y.-I., Schultz, D. N., Pagilagan, R. U., Levy, J. B., Symmes, C., Jr., Nelson, G. O. and Granroth, I. *J. Am. Chem. Soc. 97* (1975) 1787.
7. Borowitz, G. B., Schuessler, D., McCornas, W., Blaine, L. I., Field, K. B., Ward, P., Rahn, B. V., Glover, W., Roman, F. and Borowitz, I. J. *Phosphorus 2* (1972) 91.
8. Hoffmann, H. and Diehr, H. J. *Angew. Chem. Int. Ed. Engl. 3* (1964) 737.
9. Hudson, R. F. and Brown, C. *Acc. Chem. Res. 5* (1972) 204.
10. Songstad, J. *Unpublished observations.*
11. Davies, W. C. and Lewis, W. P. G. *J. Chem. Soc.* (1934) 1599.
12. Pearson, R. G., Sobel, H. and Songstad, J. *J. Am. Chem. Soc. 90* (1968) 319.
13. Austad, T., Engemyr, L. B. and Songstad, J. *Acta Chem. Scand. 25* (1971) 3536.

14. Fountaine, J. E. and McEwen, W. E. *Phosphorus 1* (1971) 57.
15. Basolo, F. and Pearson, R. G. *Mechanism of Inorganic Reactions*, Wiley, New York 1967, 2nd Ed., p. 572.
16. Henderson, W. A., Jr. and Streuli, C. A. *J. Am. Chem. Soc. 82* (1960) 5791.
17. Davies, W. C. and Addis, H. W. *J. Chem. Soc.* (1937) 1622.
18. Kolling, O. W. and Mawdsley, E. A. *Inorg. Chem. 9* (1970) 408.
19. Weiner, M. A., Lattman, M. and Grim, S. O. *J. Org. Chem. 40* (1975) 1292.
20. Vilesov, F. I. and Zaitsev, V. M. *Dokl. Akad. Nauk SSSR 154* (1964) 886.
21. Abraham, M. H. *J. Chem. Soc. B* (1971) 299.
22. Bare, T. M., Hershey, N. D., House, H. O. and Swain, C. G. *J. Org. Chem. 37* (1972) 997.
23. Swain, C. G. and Hershey, N. D. *J. Am. Chem. Soc. 94* (1972) 1901.
24. Swain, C. G. and Langsdorf, W. P., Jr. *J. Am. Chem. Soc. 73* (1951) 2813.
25. Ko, E. C. F. and Parker, A. J. *J. Am. Chem. Soc. 90* (1968) 6447.
26. Swain, C. G. and Thornton, E. R. *J. Am. Chem. Soc. 84* (1962) 817.
27. Harris, J. C. and Kurz, J. L. *J. Am. Chem. Soc. 92* (1970) 349.
28. Thorstenson, T. and Songstad, J. *To be published.*
29. Bjorøy, M., Saunders, B. B., Esperås, S. and Songstad, J. *Phosphorus 6* (1976) 83.
30. Spinner, E. *Spectrochim. Acta 17* (1961) 545.
31. Schiemenz, G. P. *J. Organomet. Chem. 52* (1973) 349.
32. Burgess, J. and Peacock, R. D. *J. Chem. Soc. Dalton Trans.* (1965) 1565.
33. Auriel, M. and de Hoffmann, E. *J. Am. Chem. Soc. 97* (1975) 7433.
34. Trotter, J. *Can. J. Chem. 41* (1963) 14.
35. Trotter, J. *Can. J. Chem. 41* (1963) 1187.
36. Daly, J. J. *J. Chem. Soc.* (1964) 3799.
37. Tsvetkov, E. N., Lobanov, D. I., Makhamatkhanov, M. M. and Kabachnik, M. I. *Tetrahedron 25* (1969) 5623.
38. Brill, T. B. and Long, G. G. *Inorg. Chem. 11* (1972) 225.
39. Pearson, R. G. and Songstad, J. *J. Org. Chem. 32* (1967) 2899.
40. Engemyr, L. B. and Songstad, J. *Acta Chem. Scand. 26* (1972) 4179.
41. Halvorsen, A., Thorstenson, T. and Songstad, J. *To be published.*
42. Nesmeyanov, N. A. and Reutov, O. A. *Zh. Organ. Khim. 2* (1966) 1711.
43. Schreck, J. O. *J. Chem. Educ. 48* (1971) 103.
44. Hill, J. W. and Fry, W. H. *J. Am. Chem. Soc. 84* (1962) 2763.
45. Ceccon, A. and Sartori, S. *J. Organomet. Chem. 50* (1973) 161.
46. Hudson, R. F. and Klopman, G. *J. Chem. Soc.* (1962) 1062.
47. Beguin, C. and Delpuech, J.-J. *Bull. Chim. Soc. Fr.* (1969) 378.
48. Ho, T.-L. *Synth. Commun. 3* (1973) 99.
49. Sugden, S. and Willis, J. B. *J. Chem. Soc.* (1951) 1360.
50. Miller, W. T., Jr. and Bernstein, J. *J. Am. Chem. Soc. 70* (1948) 3600.
51. Stein, A. R. *Tetrahedron Lett.* (1974) 4154.
52. Yamamoto, Y. and Schmidbaur, H. *Chem. Commun.* (1975) 668.
53. Starzewski, K.-H. A. O., Richter, W. and Schmidbaur, H. *Chem. Ber. 109* (1976) 473.
54. Overman, L. E., Matzinger, D., O'Connor, E. M. and Overman, J. D. *J. Am. Chem. Soc. 96* (1974) 6081.
55. Overman, L. E. and Petty, S. T. *J. Org. Chem. 40* (1975) 2779.
56. Jarvis, B. B. and Saukatis, J. S. *J. Am. Chem. Soc. 95* (1973) 7708.
57. Hammond, G. S. *J. Am. Chem. Soc. 77* (1955) 334.
58. Robertson, R. E., Annesa, A. and Scott, J. M. W. *Can. J. Chem. 53* (1975) 3106.
59. Farcasiu, D. *J. Chem. Educ. 52* (1975) 76.

Received April 30, 1976.

Acta Chemica Scandinavica A 30 (1976) 731—734

Determination of Partial Gibbs Energies of Mixing of LiCl in the Alk.Cl—LiCl Mixtures from Concentration Cell Measurements

LARS UNO THULIN,* OLE WÆRNES and TERJE ØSTVOLD

Institutt for uorganisk kjemi, Norges tekniske høgskole, Universitetet i Trondheim, N-7034 Trondheim-NTH, Norway

The partial Gibbs energies of mixing of LiCl in the liquid mixtures with KCl, RbCl, and CsCl have been determined by emf measurements of the following cell:

$C(s),Cl_2(g)|LiCl(l)|Li\text{-glass}|(Li-M)Cl(l)|Cl_2(g),C(s)$

where M = K, Rb, and Cs, respectively, and by measurements of transport numbers of the Li^+ ion in the Li-glass membranes used to separate the two half cells in the above concentration cells. The partial Gibbs energies and entropies are calculated.

The results indicate relatively large deviations from regular solution behaviour. The partial excess entropies of mixing are proportional to $(1-X_{LiCl})^2$, indicating that these excess entropies are of vibrational nature.

In the present work the change in the chemical potentials of mixing of LiCl in molten LiCl—MCl mixtures were obtained using a concentration cell with Li-glass membranes, the metal ion M^+ being K^+, Rb^+ or Cs^+, respectively. The emf of this cell depends on the transport properties of the membrane, *i.e.* "the liquid junction potential".

The following galvanic cell was studied:

$C(s),Cl_2(g)|LiCl(l)|Li\text{-glass}|(Li-M)Cl(l)|Cl_2(g),C(s)$

The electrolyte consisted of a fused mixture of LiCl and MCl on the right hand side, and pure fused LiCl on the left hand side of the glass membrane. The membrane is a cation exchange membrane and it contains the mobile Li^+ ion. The chlorine over graphite electrodes are reversible to the Cl^- ions only.

By determining the transport numbers of the Li^+ ion in the glass membranes together with the cell potentials for the above cells, both as functions of composition of the LiCl—MCl liquid mixtures, one is able to determine the difference in Gibbs energy for LiCl in the mixed and the pure fused state.

The transport number of Li^+ ions in glass membranes very similar to the one used in the present work has been determined previously.[1,2] When the galvanic cell contained NaCl and LiCl it turned out that the membrane conducted Na^+ and Li^+ ions over the whole concentration range. For the KCl—LiCl, RbCl—LiCl and CsCl—LiCl systems $t_{Li^+} > 0.9$ for $X_{LiCl} > 0.5$, $X_{LiCl} > 0.3$, and $X_{LiCl} > 0.1$, respectively. When the partial Gibbs energy of sodium chloride obtained from the emf measurements is combined with enthalpy of mixing data to calculate the partial entropies of NaCl in the NaCl—LiCl system it turns out that the calculated entropies are very different from the ones observed in the present LiCl—Alk.Cl mixtures. We believe that this is due to some inaccuracy in the determination of transport numbers for the Li^+ ion in the glass membrane separating NaCl and the NaCl—LiCl mixtures. To obtain a reasonable accuracy in the thermodynamic data calculated from the galvanic cell measurement, we therefore decided to operate in concentration ranges where we could assume $t_{Li^+} \simeq 1$.

* Present address: Det kongelige norske industridepartement, Oslo Dep., Norway.

EXPERIMENTAL

The cell used in the present investigation is similar to the one described in previous papers.[1,3,4] The composition of the glass was: 80 mol % SiO_2, 7.5 mol % Al_2O_3, 7.5 mol % Li_2O, 5 mol % La_2O_3.

All the components of the glass, obtained from E. Merck, Germany, were ground together, pressed to a pill and melted. To assure homogeneity the glass was crushed and remelted. The emf of the above cell was investigated over a concentration range $X_{LiCl}=0.2$ to $X_{LiCl}=1.0$ at 995, 925, and 895 K for the KCl – LiCl, RbCl – LiCl, and CsCl – LiCl mixtures, respectively. The emf and temperature were recorded on a dual channel Watanabe recorder, both compensated by bucking potentials supplied from a Fluke 895A Differentialvoltmeter. The analytical reagent grade salts, LiCl, KCl, RbCl, and CsCl from E. Merck, Germany were dried, melted and slowly crystallized under dry nitrogen atmosphere to remove moisture and impurities. Handling of salts was performed in a drybox at max. 4 ppm water content.

The course of a typical experiment was as follows. The anode compartment, containing the glass membrane at the bottom, was filled with about 5 g of lithium – alkali chloride mixture and then immersed in the pure fused LiCl. Chlorine gas was bubbled over the graphite electrodes and the potential and temperature curves recorded. By adding small crystals of LiCl or the other alkali chloride in the anode compartment the composition of the mixture could be changed. The internal resistance of the cell was in the range 700 – 10 000 Ω. Transport numbers were determined by a modified Hittorf Method described previously.[1]

Table 1. Thermodynamic functions of mixing of liquid LiCl in mixture with KCl from calorimetric measurements of mixing at 1013 K by Hersh and Kleppa and emf measurements at 995 K.

Mol-fraction	Emf	Chemical potentials	Partial enthalpies	Partial entropies	Partial excess entropies
X_{LiCl}	E (mv)	$\Delta\mu_{LiCl}$ (kJ mol^{-1})	$\Delta\bar{H}_{LiCl}$ (kJ mol^{-1})	$\Delta\bar{S}_{LiCl}$ (J mol^{-1}K^{-1})	$\Delta\bar{S}^{E}_{LiCl}$ (J mol^{-1}K^{-1})
0.899	10.6 ± 0.5	−1.02	−0.19	0.84	−0.04
0.801	24.7 ± 0.4	−2.38	−0.72	1.67	−0.17
0.700	42.7 ± 0.9	−4.12	−1.63	2.51	−0.46
0.600	64.9 ± 2	−6.27	−2.89	3.40	−0.85
0.500	90.6 ± 2	−8.75	−4.49	4.28	−1.49

Table 2. Thermodynamic functions of mixing of liquid LiCl in mixture with RbCl from calorimetric measurements of mixing at 1013 K by Hersh and Kleppa and emf measurements at 925 K.

Mol-fraction	Emf	Chemical potentials	Partial enthalpies	Partial entropies	Partial excess entropies
X_{LiCl}	E (mv)	$\Delta\mu_{LiCl}$ (kJ mol^{-1})	$\Delta\bar{H}_{LiCl}$ (kJ mol^{-1})	$\Delta\bar{S}_{LiCl}$ (J mol^{-1}K^{-1})	$\Delta\bar{S}^{E}_{LiCl}$ (J mol^{-1}K^{-1})
0.921	7.9	−0.76	−0.15	0.66	−0.02
0.900	10.6	−1.02	−0.24	0.85	−0.03
0.837	19.3	−1.86	−0.65	1.32	−0.16
0.800	25.3	−2.44	−0.97	1.59	−0.27
0.756	33.9	−3.27	−1.45	1.97	−0.36
0.699	44.8	−4.33	−2.20	2.29	−0.69
0.676	51.2	−4.94	−2.55	2.58	−0.68
0.604	68.6 ± 0.8	−6.62	−3.79	3.07	−1.13
0.531	89.2	−8.61	−5.25	3.64	−1.63
0.501	98.1 ± 0.8	−9.47	−5.90	3.86	−1.89
0.400	132.6 ± 1	−12.80	−8.26	4.91	−2.71
0.324	163.3	−15.73	−10.20	5.99	−3.39
0.300	174.4	−16.84	−10.82	6.51	−3.51
0.199	224.8	−21.70	−13.41	8.96	−4.47

Table 3. Thermodynamic functions of mixing of liquid LiCl in mixture with CsCl from calorimetric measurements of mixing at 943 K by Hersh and Kleppa and emf measurements at 895 K.

Mol-fraction	Emf	Chemical potentials	Partial enthalpies	Partial entropies	Partial excess entropies
X_{LiCl}	E (mv)	$\Delta\mu_{LiCl}$ (kJ mol^{-1})	$\Delta\bar{H}_{LiCl}$ (kJ mol^{-1})	$\Delta\bar{S}_{LiCl}$ (J mol^{-1}K^{-1})	$\Delta\bar{S}^{E}_{LiCl}$ (J mol^{-1}K^{-1})
0.896	10.9	−1.05	−0.29	0.85	−0.07
0.799	25.8	−2.49	−1.15	1.50	−0.37
0.762	32.4	−3.13	−1.63	1.67	−0.59
0.699	46.0	−4.44	−2.65	2.00	−0.98
0.601	70.0 ± 0.7	−6.76	−4.70	2.30	−1.93
0.594	71.4	−6.89	−4.86	2.27	−2.07
0.500	100.2 ± 0.8	−9.67	−7.30	2.66	−3.11
0.415	128.4	−12.39	−9.75	2.95	−4.37
0.398	136.0 ± 0.3	−13.13	−10.26	3.20	−4.46
0.357	151.5	−14.62	−11.50	3.50	−5.07
0.308	172.5	−16.65	−12.96	4.12	−5.67
0.254	199.0	−19.21	−14.53	5.23	−6.17
0.212	221.5	−21.38	−15.68	6.37	−6.53
0.200	227.1	−21.92	−15.99	6.63	−6.76
0.173	245.3	−23.68	−16.67	7.83	−6.76

RESULTS AND DISCUSSION

The emf as function of composition of the galvanic cell

C(s), Cl_2(g)|LiCl(l)|Li-glass|LiCl − MCl(l)|Cl_2(g), C(s)

is given in Tables 1 − 3. The emf is related to the change in Gibbs energy of the cell reaction by eqn. (1).[5]

$$\Delta G = -EF = \Delta\mu_{LiCl} - \int_{\text{over membrane}} t_{M^+}\mathrm{d}(\mu_{Li-sil} - \mu_{M-sil}) \quad (1)$$

Only results for which $t_{M^+} \approx 0$ are recorded in Tables 1 − 3 and eqn. (1) may then be simplified to eqn. (2).

$$\Delta\mu_{LiCl} = -EF \quad (2)$$

$\Delta\mu_{LiCl} = \mu_{LiCl} - \mu^{\circ}_{LiCl}$ which is the change in chemical potential of LiCl on mixing is recorded in Tables 1 − 3 together with the partial enthalpies [6] and entropies of mixing of LiCl.

When calculating the entropy of mixing for a system containing a mixture of fused salts it is common to consider the configurational entropy only. The significant entropy changes observed for reactions of the type (3),[7,8]

$$\tfrac{1}{n}MCl_n(l) + MeBr(l) = \tfrac{1}{n}MBr_n(l) + MeCl(l) \quad (3)$$

however, indicate that other contributions to the entropy of mixing have to be taken into account in a more thorough calculation. Førland [9] has proposed a model for describing the excess entropy change on mixing in systems where ΔH_{mix} is small. He assumes that the excess entropy can be attributed to changes in the environment of the ions by the mixing process. The vibrational entropy can be expressed as a sum of terms assigned to pairs of ions. For a binary mixture of LiCl and CsCl the vibrational entropy of mixing should accordingly be [eqn. (4)]

$$\Delta S_{vibr.} = \tfrac{1}{2}\{(n_{Li} + n_{Cs})(X_{Li}^2 S_{Li-Li} + 2X_{Li}X_{Cs}S_{Li-Cs} + X_{Cs}^2 S_{Cs-Cs}) - n_{Li}S_{Li-Li} - n_{Cs}S_{Cs-Cs}\} \quad (4)$$

where S_{Li-Li} is the contribution to the vibrational entropy from $Li^+ - Li^+$ interactions. The partial molar vibrational entropy of mixing of LiCl is then given by

$$\Delta\bar{S}_{LiCl}^{vibr.} = \text{const. } X^2_{CsCl} \quad (5)$$

In a previous paper this model was tested on the experimental excess entropies in the NaCl − NaBr and KCl − KBr systems.[10] For

these mixtures the enthalpy of mixing is very small and one would assume no deviation from random mixing of anions. The observed partial entropies, however, deviated significantly from the random mixing model and showed good agreement with eqn. (5). For the present systems one might expect deviation from random mixing of cations since the enthalpy of mixing is relatively large. This should, however, result in a positive excess partial entropy of LiCl in the LiCl-rich melts and a negative partial excess entropy at lower LiCl content.[11] The partial excess entropies are all negative, however, and agree with eqn. (5) over the whole concentration range except for very low LiCl content in the LiCl – CsCl system.

In Fig. 1 $\Delta\bar{S}^{E}_{MCl}$ is plotted *versus* $(1-X_{MCl})^2$ for MCl = NaCl in the NaCl – KCl and NaCl – CsCl systems measured by Thulin [1] and for MCl = LiCl in the LiCl – KCl, LiCl – RbCl, and LiCl – CsCl systems. From the experimental data the maximum error in the partial entropies is estimated to be 0.2 J mol^{-1} K^{-1}. The experimental entropies in the NaCl – RbCl system also obtained by Thulin [1] seems to be less accurate and we decided therefore not to use these entropies in the present figure. It is evident from Fig. 1 that there is an increase in the vibrational contribution to the entropy of mixing with an increasing mass ratio of the mixing ions.

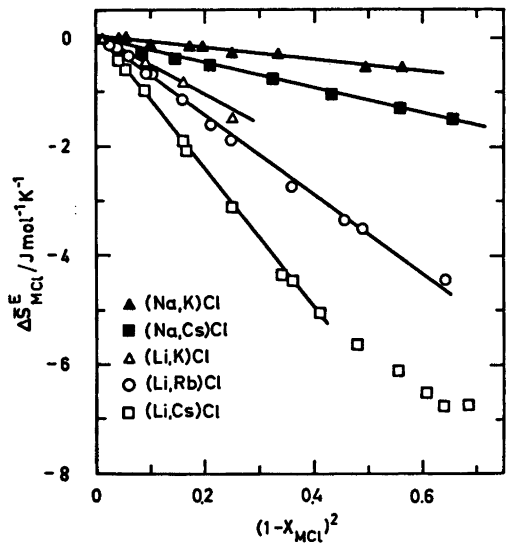

Fig. 1. Partial excess entropies of mixing of MCl as function of $(1-X_{MCl})^2$ in liquid mixtures with KCl, RbCl and CsCl. M = Na or Li. The temperatures of the systems are given in Tables 1 – 3.

This increasing excess partial entropy is negative over the whole concentration range determined. It is thus unlikely that this excess entropy is due to deviation from random mixing of the ions on mixing or that it is due to volume changes on mixing since these are positive for the above systems.[12] In systems where there is even larger difference in electric field strength (Z/r^2) between the mixing cations than in the present systems, deviation from random mixing will occur. In binary mixtures of $MgCl_2$ with KCl, RbCl, and CsCl a positive excess partial entropy of the alkali chloride is observed at low $MgCl_2$ content. At higher $MgCl_2$ content the partial entropy is negative.[3]

A gradual change from predominant vibrational contributions over to configurational contributions to the excess partial entropy is thus observed.

Acknowledgement. This project has been supported financially from Norges tekniske høgskoles fond.

REFERENCES

1. Thulin, L. U. *Acta Chem. Scand. 26* (1972) 225.
2. Hansen, E. L. *Thesis*, NTH, The University of Trondheim, Trondheim 1974.
3. Østvold, T. *High Temp. Sci. 4* (1972) 51.
4. Robbins, G. D., Førland, T. and Østvold, T. *Acta Chem. Scand. 22* (1968) 3002.
5. Førland, T. and Østvold, T. *Acta Chem. Scand. 20* (1966) 2085.
6. Hersh, L. S. and Kleppa, O. J. *J. Chem. Phys. 42* (1965) 1309.
7. Frøyland, K., Førland, T., Lundberg, N. H. and Østvold, T. In Førland, T., Grjotheim, K., Motzfeldt, K. and Urnes, S., Eds. *Selected Topics in High Temperature Chemistry*, Universitetsforlaget, Oslo 1966, p. 27.
8. Østvold, T. *Acta Chem. Scand. 25* (1971) 2302.
9. Førland, T. *Discuss. Faraday Soc. 32* (1962) 122.
10. Østvold, T. *Acta Chem. Scand. 22* (1968) 435.
11. Førland, T. In Sundheim, B. R. *Fused Salts*, McGraw-Hill, New York 1964, p. 88.
12. Holm, J. L. *Acta Chem. Scand. 25* (1971) 3609.

Received April 27, 1976.

Acta Chemica Scandinavica A 30 (1976) 735—739

A Neutron Diffraction Study of $HgCl_2.2KCl.H_2O$

KARIN AURIVILLIUS and CLAES STÅLHANDSKE

Chemical Center, Divisions of Inorganic Chemistry 1, 2, University of Lund, P.O. Box 740, S-220 07 Lund 7, Sweden

The crystal structure of $HgCl_2.2KCl.H_2O$ has been refined from neutron diffraction single-crystal data (2181 reflections) to $R = 0.047$ and $R_w = 0.040$. The crystals are orthorhombic, space group *Pbam* with $a = 8.258(2)$ Å, $b = 11.663(2)$ Å, $c = 8.926(2)$ Å and $Z = 4$.

The structure is built up of $HgCl_2$ molecules, K^+ and Cl^- ions and water molecules, which *via* weak hydrogen bonds are joined to half the chloride ions. The mercury atom is thus two-coordinated, bonded to two chlorine atoms at the distances 2.383(1) Å in a nearly linear way [$\angle Cl(3)-Hg-Cl(3)$ 169.96(4)°]. The distances to next-nearest chlorine atoms indicate that they are mainly ionic in character. In the water molecule the distances O – H and H – H are 0.948(2) and 1.533(3) Å, respectively, with an angle H – O – H of 107.9(3)°. In the hydrogen bond the distance O – H···Cl(2) is 3.249(1) Å with H···Cl(2) 2.329(2) Å and the angle O – H···Cl(2) 163.6(2)°. The water molecules are joined two and two *via* the hydrogen bonds to the chloride ions Cl(2).

The crystal structure of "$K_2HgCl_4.H_2O$" has been the object of several X-ray diffraction studies.[1–3] In Ref. 3 the compound was carefully studied by modern X-ray technique and computation methods. The positions of all non-hydrogen atoms were found and it turned out that the best way to write the formula of the compound is $HgCl_2.2KCl.H_2O$ as no ions $HgCl_4^{2-}$ exist.

In connection with recent NMR and IR studies performed by other authors it seemed advantageous to perform a neutron diffraction investigation to elucidate the hydrogen bonding system and to compare the determined proton-proton distances with those obtained by other methods.

EXPERIMENTAL

Large single crystals of $HgCl_2.2KCl.H_2O$ can be obtained from an aqueous solution of $HgCl_2$ and KCl in the molar ratio 1:2. The single crystal used in this neutron diffraction study was kindly placed at our disposal by Dr. Svanson, University of Gothenburg, Sweden. As the crystal was too large for neutron diffraction measurements it was diminished in size by washing with a saturated solution of the compound. Some crystal data are given in Table 1.

Intensity data were collected at room temperature on a Hilger-Ferranti four-circle diffractometer, located at the DR3 reactor at The Danish Atomic Energy Commission Research Establishment, Risø, Denmark. The wavelength of the monochromatized neutron beam was 1.025 Å and the flux at the specimen about 0.9×10^6 neutrons $cm^{-2}\ s^{-1}$. The reflections were measured by the ω-scan method using the step-scan technique. In the range $0.06 < \sin\theta/\lambda < 0.79$ a total of 2384 reflections were measured. Half the reflection sphere was measured in the $\sin\theta/\lambda$ interval 0.06 – 0.20, a quadrant in the interval 0.20 – 0.50 and an octant above 0.50. One standard reflection was measured after every 15th reflection. Background corrections were made using a method described by Lehmann and Larsen.[4] In this program the peak is separated from the background so that $\sigma(I)/I$ is minimized, where $\sigma(I)$ is the estimated standard deviation based on counting statistics. Squared structure amplitudes were calculated as $F_o^2 = I \sin 2\theta$. An absorption correction

Table 1. Crystal data.

$HgCl_2.2KCl.H_2O$; F.W. 438.6 g mol^{-1}
Orthorhombic, *Pbam* (No. 55)
$a = 8.258(2)$ Å, $b = 11.663(2)$ Å, $c = 8.926(2)$ Å, $V = 859.6$ Å^3, $Z = 4$.
$D_x = 3.39$ g cm^{-3}
Neutrons, $\lambda = 1.025$ Å; $\mu = 1.67$ cm^{-1}.

Table 2. Crystal dimensions. Boundary planes and their distances from an internal origin.

Plane	d(mm)
$(\bar{1}\bar{2}0)$	2.5
$(1\bar{1}0)$	3.4
$(\bar{1}30)$	3.2
$(\bar{1}\bar{3}0)$	3.6
$(\bar{1}00)$	2.1
$(\bar{1}00)$	2.1
$(00\bar{1})$	5.0
$(00\bar{1})$	5.0
Crystal volume 253 mm.^{3}	

was applied using Gaussian numerical integration where the crystal shape was described by 8 boundary planes (Table 2). The linear absorption coefficient was calculated to 1.67 cm^{-1} assuming the incoherent scattering cross-section for hydrogen to be 40 barns and using the values of μ/ϱ for Hg, Cl, K, O, and H tabulated in the International Tables for X-Ray Crystallography.[5] The resulting transmission factors fall in the range 0.34 – 0.56. The symmetry-related reflections were not averaged as the mean-path lengths varied considerably. 203 reflections with $F_o^2 < 2\sigma_c(F^2)$, where $\sigma_c(F^2)$ is based on counting statistics, were considered as unobserved and were excluded in the refinements.

STRUCTURE REFINEMENT

The starting parameters were those from the X-ray study.[3] A subsequent difference Fourier synthesis revealed the positions of the hydrogen atoms. Finally the parameters were refined using full-matrix least-squares with anisotropic temperature factors for all atoms, a scale factor and an extinction parameter.[6] The function to be minimized was $\sum w_i(|F_o| - |F_c|)^2$. Each reflection was assigned a weight w_i, according to

$$w_i^{-1} = \sigma^2(|F_o|) = \sigma_c^2(|F_o|^2)/4|F_o|^2 + a|F_o|^2$$

where $\sigma_c^2(|F_o|^2)$ is based on counting statistics. In the final refinement the constant a was 0.004. In the positional parameters the last shifts were less than 1 % of their standard deviations. The agreement factors were

$$R = \sum(|F_o| - |F_c|)/\sum|F_o| = 0.047 \text{ and}$$
$$R_w = [\sum w_i(|F_o| - |F_c|)^2/\sum w_i|F_o|^2]^{1/2} = 0.040.$$

The standard deviation of an observation of unit weight S, defined by

$$S = [\sum w_i(|F_o| - |F_c|)^2/(m-n)]^{1/2}, \text{ was } 0.92,$$

where m and n are the number of observations and parameters varied. The final isotropic extinction parameter was $1.31(3) \times 10^4$. Calculations with anisotropic extinction correction gave no further improvements.

The coherent scattering factors used were $\bar{b}_{Hg} = 1.27$, $\bar{b}_{Cl} = 0.96$, $\bar{b}_O = 0.580$ and $\bar{b}_H = -0.374$ (all $\times 10^{-12}$) cm.[7] Final positional and thermal parameters are given in Tables 3 and 4. A list of observed and calculated structure factors is available from the authors on request. The calculations were carried out on the UNIVAC 1108 computer in Lund using programs briefly described by Stålhandske.[8]

DISCUSSION

Comparison of the present neutron diffraction results with those obtained from X-ray diffraction (diffractometer data, 843 independent reflections [3]) show no essential differences in the positional parameters or in the bond lengths of the non-hydrogen atoms. The standard deviations in positional parameters of the

Table 3. Final fractional atomic coordinates with estimated standard deviations in parentheses. In brackets are given values according to an X-ray study by Aurivillius and Stålhandske.[3]

Atom	x	y	z
Hg	0	0	0.22921(8)
			[0.22925(8)]
K(1)	0.0823(2)	0.3405(2)	0
	[0.0819(3)]	[0.3410(2)]	
K(2)	0.1054(2)	0.3052(1)	½
	[0.1047(3)]	[0.3047(2)]	
Cl(1)	0.20454(8)	0.07605(6)	0
	[0.2042(3)]	[0.0763(2)]	
Cl(2)	0.24905(9)	0.06027(5)	½
	[0.2489(4)]	[0.0601(2)]	
Cl(3)	−0.11661(6)	0.18606(4)	0.25257(6)
	[−0.1169(2)]	[0.1860(2)]	[0.2520(3)]
O	0	½	0.2310(2)
			[0.231(1)]
H	−0.0869(2)	0.4769(2)	0.2934(2)

Table 4. Final anisotropic thermal parameters, β_{ij}, with standard deviations in parentheses. The expression used is $\exp[-(\beta_{11}h^2+\beta_{22}k^2+\beta_{33}l^2+2\beta_{12}hk+2\beta_{13}hl+2\beta_{23}kl)]$ with $\beta_{13}=\beta_{23}=0$ for the fourfold positions. The β_{ij} values are multiplied by 10^5.

Atom	β_{11}	β_{22}	β_{33}	β_{12}	β_{13}	β_{23}
Hg	1171(9)	346(3)	1605(12)	195(4)	0	0
K(1)	902(24)	422(11)	761(24)	−1(13)	0	0
K(2)	837(23)	418(12)	978(26)	−1(14)	0	0
Cl(1)	663(8)	400(4)	853(9)	−13(5)	0	0
Cl(2)	996(10)	357(4)	1010(10)	71(5)	0	0
Cl(3)	880(6)	345(3)	779(6)	81(3)	56(5)	−19(3)
O	939(18)	863(12)	826(18)	−198(12)	0	0
H	1208(23)	855(14)	1455(29)	−94(15)	188(22)	104(17)

Table 5. Selected interatomic distances (Å) and angles (°). Estimated standard deviations are given in parentheses. Notations of the atoms, *cf.* Table 3.

Mercury to chlorine			
Hg − 2Cl(3)	2.383(1)	∠Cl(3) − Hg − Cl(3)	169.96(4)
− 2Cl(1)	2.797(1)		
− 2Cl(2)	3.251(1)		
Potassium to oxygen or chlorine			
K(1) − 2O	2.859(2)	K(2) − Cl(2)	3.093(2)
− Cl(1)	3.245(2)	− 2Cl(3)	3.187(1)
− Cl(1)	3.263(2)	2Cl(3)	3.189(1)
− Cl(1)	3.268(2)	− Cl(2)	3.209(2)
− 2Cl(3)	3.320(1)	− Cl(2)	3.335(2)
− 2Cl(3)	3.371(1)	− 2O	3.419(2)
Oxygen to chlorine < 3.70 Å			
O − 2Cl(2)	3.249(1)	∠Cl(2) − O − Cl(2)	84.68(4)
− 2Cl(1)	3.315(1)	∠Cl(1) − O − Cl(1)	103.10(4)
		∠Cl(1) − O − Cl(2)	86.12(2)
Distances and angles involving the hydrogen atoms			
O − 2H	0.948(2)	∠H − O − H	107.9(3)
H − H	1.533(3)		
H − Cl(2)	2.329(2)	∠Cl(2) − H − O	163.6(2)
H − Cl(1)	3.195(2)	∠Cl(1) − H − O	88.9(1)

chlorine and oxygen atoms are about one fourth those found in the X-ray work, *cf.* Table 3. The interatomic distances (Table 5), uncorrected for thermal motion, are now determined with a higher degree of accuracy; *e.s.d.*'s in the actual distances being 0.001 − 0.002 Å. Moreover, the positions of the hydrogen atoms are determined accurately.

As stated in the previous paper our opinion is that the best way to describe the compound is that the structure is built up of $HgCl_2$ molecules, K^+ and Cl^- ions and water molecules. The formula should thus be written $HgCl_2.2KCl.H_2O$ instead of $K_2HgCl_4.H_2O$. Half the chloride ions are joined to the water molecules by hydrogen bonds. A projection of the structure on the *xy*-plane is given in Fig. 1. The distances mercury to two chlorine atoms, forming the nearly linear $HgCl_2$ molecule [∠Cl(3) − Hg − Cl(3) 169.96(4)°] are 2.383(1) Å. The next nearest chlorine neighbours are then located about 0.4 and 0.9 Å further away at

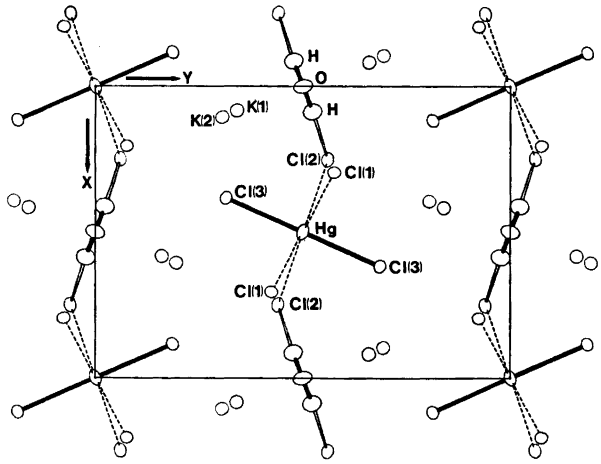

Fig. 1. Projection of the structure of $HgCl_2.2KCl.H_2O$ on the *xy*-plane. The $HgCl_2$ molecule is indicated by heavy lines, weak mercury-chlorine interactions by dashed lines and hydrogen bonds by open lines.

distances indicating that they are most probably ionic in character. The polyhedron around mercury is a distorted octahedron with two mercury-chlorine distances much shorter than the others. The structure can be described as being built up of "chains" of these octahedra, which run along [001], with the polyhedra sharing edges. The "chains" are joined by weak hydrogen bonds to sheets parallel to the *xz*-plane (Fig. 1).

The observed Hg – Cl distances of 2.383(1) Å are close to the values reported for $HgCl_2$[9] (Hg – 2Cl 2.25 Å, ∠Cl – Hg – Cl 180°), Hg_3OCl_4[10] [Hg – Cl 2.31(2) Å, ∠Cl – Hg – O 175.7(8)°] and for the two quasi-molecules $HgCl_2$ in $(C_5H_6N_2)HgCl_2.\frac{1}{2}H_2O$[11] [Hg – 2Cl 2.35(2); 2.37(2) Å; ∠Cl – Hg – Cl ~165°]. The Hg···Cl^- distances 2.797(1) and 3.251(1) Å can be compared to the values 2.99(2) and 3.08(2) Å reported for Hg_3OCl_4.[10] Both potassium atoms K(1) and K(2) are irregularly surrounded by two oxygen and seven chlorine atoms at distances varying from 2.86 to 3.37 Å and from 3.09 to 3.42 Å, respectively. These distances are in agreement with data on the coordination K – O and K – Cl reported in literature.[12]

In the water molecule the uncorrected O – H distance is 0.948(2) Å and the angle H – O – H is 107.9(3)°. The values can be compared to the average values of 0.956 Å and 107.8° given by Ferraris and Franchini-Angela[13] for the water molecule in crystalline hydrates; all structure studies are based on neutron diffraction single-crystal data.

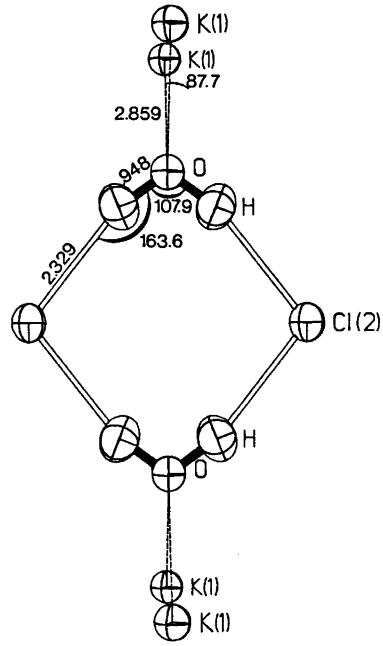

Fig. 2. The tetrahedral environment of the water molecule. The thermal ellipsoids are drawn to enclose 50 % probability.

The O – 2Cl(2) and O – 2Cl(1) distances, 3.249(1) and 3.315(1) Å are both possible donator acceptor distances for hydrogen bonds, the distances nearly equal to the sum of the van der Waals radii, 3.20 Å.[14] The H – Cl(2) and H – Cl(1) distances are 2.329(2) and 3.195(2) Å, compared to the value of the van der Waals radii sum 2.8 Å.[15] The corresponding angles O – H – Cl(2) and O – H – Cl(1) are 163.6(2) and 88.9(1)°. The angle 163.6° and the distance 2.329 Å indicate that the chloride ions Cl(2) are joined to the water molecules by weak hydrogen bonds. The water molecules are linked two by two *via* the hydrogen bonds to the chloride ions Cl(2) (Fig. 2). As each water molecule has a tetrahedral environment, including the two hydrogen-bonded chloride ions Cl(2) and the two potassium ions K(1), situated along the two lone-pair orbitals of the water molecule, the compound belongs to the classification 2*A* of hydrates according to Ferraris and Franchini-Angela.[13] The angle Cl(2) – O – Cl(2) of 84.7(2)° is smaller than the acceptor angles in most other hydrates. A very small angle of this type, 55.1°, was found for the hydrogen bonding system in $HgCrO_4.\frac{1}{2}H_2O$,[16] however.

$HgCl_2.2KCl.H_2O$ has been the object of NMR- and IR-studies by several authors.[17–19] The proton-proton distance found within the molecule, 1.534(3) Å, is as expected [20] shorter than the values derived by NMR measurements, 1.607(3) Å.[17,18]

The O – Cl(2) distance 3.25(3) Å, estimated from IR measurements of the partially deuterated compound,[19] is in excellent agreement with the distance 3.249(1) Å obtained in the present study.

The authors thank professors B. Aurivillius, S. Fronæus and S. E. Rasmussen for the facilities placed at our disposal and for their kind interest in our work. We also thank Dr. F. K. Larsen with co-workers for the data collection and reduction. This work has been supported by the Danish Atomic Energy Commission and the Swedish Natural Science Research Council.

REFERENCES

1. Mac Gillavry, C. H., de Wilde, J. H. and Bijvoet, J. M. *Z. Kristallogr. 100* (1938) 212.
2. Zvonkova, Z. V., Samodurova, V. V. and Vorontsova, L. G. *Dokl. Akad. Nauk. SSSR 102* (1955) 1155.
3. Aurivillius, K. and Stålhandske, C. *Acta Chem. Scand. 27* (1973) 1086.
4. Lehmann, M. S. and Larsen, F. K. *Acta Crystallogr. A 30* (1974) 580.
5. *International Tables for X-Ray Crystallography*, Kynoch Press, Birmingham 1962, Vol. III, p. 197.
6. Zachariasen, W. H. *Acta Crystallogr. 23* (1967) 558.
7. Bacon, G. E. *Acta Crystallogr. A 28* (1972) 357.
8. Stålhandske, C. *Acta Crystallogr. B 30* (1974) 1586.
9. Braekken, H. and Scholten, W. *Z. Kristallogr. 89* (1934) 448.
10. Aurivillius, K. *Ark. Kemi 22* (1964) 517.
11. Authier-Martin, M. and Beauchamp, A. L. *Can. J. Chem. 53* (1975) 2345.
12. *International Tables for X-Ray Crystallography*, Kynoch Press, Birmingham 1962, Vol. III, p. 258 f.
13. Ferraris, G. and Franchini-Angela, M. *Acta Crystallogr. B 28* (1972) 3572.
14. Pauling, L. *The Nature of the Chemical Bond*, Cornell Univ. Press, New York 1960.
15. Baur, W. H. *Acta Crystallogr. B 28* (1972) 1456.
16. Aurivillius, K. and Stålhandske, C. *Z. Kristallogr. 142* (1975) 9.
17. Itoh, J., Kusaka, R., Yamagata, Y., Kiriyama, R. and Ibamoto, H. *J. Phys. Soc. Jpn. 8* (1953) 293.
18. Svanson, S. E. and Almkvist, P. *Ark. Kemi 40* (1969) 165.
19. Falk, M. and Knop, O. *In preparation.*
20. Busing, W. R. and Levy, H. A. *Acta Crystallogr. 17* (1964) 142.

Received April 23, 1976.

Acta Chemica Scandinavica A 30 (1976) 740—744

Product Analysis of Flash Photolysis of Acetone in Gas Phase

PETER AHLFORS, TIMO KAUPPINEN, ARVO MÄKI, MARJA-LIISA POHJONEN and JOUKO KOSKIKALLIO

Department of Physical Chemistry, University of Helsinki, Meritullinkatu 1 C, SF-00170 Helsinki 17, Finland

GLC was used to measure the amounts of methane, ethane, ethylene, biacetyl, and methyl ethyl ketone formed in the flash photolysis of acetone in gas phase at 25 °C and at 2 – 20 Torr pressure of acetone and 0 – 270 Torr of nitrogen. The yields in flash photolysis of biacetyl and azomethane were also measured, and the products formed during irradiation with a constant low intensity light source. The results are discussed in terms of hydrogen abstraction reactions between hot radicals and acetone, collisional deactivation processes, dissociation reactions and addition reactions of thermally equilibrated radicals. As the acetone pressure was increased, small changes were observed in the relative yields, while the yield of biacetyl was found to increase rapidly, indicating an increase in the concentration of thermally equilibrated acetyl radicals produced from vibrationally relaxed singlet or triplet acetone. Ethylene was found in the flash photolysis of acetone, biacetyl and azomethane but not when a continuous light source was used. We suggest that ethylene is formed by hydrogen elimination from hot ethane itself, produced from a combination of hot methyl radicals.

Acetone has a broad [1] $(n-\pi)$ absorption from about 240 nm to 360 nm and a molar absorptivity $\varepsilon = 1.24$ m^2 mol^{-1} at the maximum absorption of about 280 nm. The quantum yields [2,3] for fluorescence and phosphorescence are low for acetone, about $\phi_F = 0.002$ and $\phi_P = 0.02$, respectively, with 313 nm excitation at 40 °C and 50 Torr of acetone. The quantum yield of photolytic decomposition is about $\phi = 0.5$ with 315 nm excitation at 25 °C and 10 Torr of acetone pressure. The quantum yield increases with decreasing acetone pressure and with increasing temperature approaching unity at about 120 °C.

O'Neal and Larson [2] proposed the following mechanism for primary processes in acetone photolysis:

$$A + h\nu \rightarrow {}^1A_m \quad (1)$$

$${}^1A_m \rightarrow {}^3A_m \quad (2)$$

$${}^3A_m \rightarrow CH_3^* + CH_3CO^* \quad (3)$$

$${}^3A_m + M \rightarrow {}^3A_0 + M \quad (4)$$

$${}^3A_0 + M \rightarrow {}^3A_n + M \quad (5)$$

$${}^3A_n \rightarrow CH_3 + CH_3 + CH_3CO \quad (6)$$

$${}^3A_0 \rightarrow A_m \quad (7)$$

A denotes acetone; superscrips 1 and 3 the first electronic excited singlet and triplet states, respectively; subscripts 0 the vibrational ground state and m and n the vibrationally excited states, respectively; and superscript * a hot species with an excess of energy. Experimental values for quantum yields of acetone fluorescence, phosphorescence and primary dissociation at different pressures, temperatures and with different concentrations of hydrobromic acid as quencher were explained [2] by the above mechanism.

Various products have been observed previously [1,3–10] in photolysis of acetone, *e.g.* carbon monoxide, hydrogen, methane, ethane, ethylene, acetaldehyde, ketene, biacetyl, methyl ethyl ketone and small amounts of other ketones of higher molecule weight. These products are expected to be formed from the radicals produced in the primary dissociation of acetone by radical combination and hydrogen abstraction reactions. By flash photolysis high con-

centrations of radicals can be produced and therefore the amounts of products of radical combination reactions should increase relative to the amounts of products formed in hydrogen abstraction reactions between a radical and acetone when compared with respective products formed in photolysis of acetone using a low intensity light source. No results on flash photolysis of acetone have previously been published. The present work was done in order to obtain more information about the mechanism of these reactions.

EXPERIMENTAL

A 1000 J discharge light source of about 15 μs half life, filled with about 100 Torr of krypton and about 10 Torr of nitrogen and connected to a 10 μF condenser was charged at about 12 kV as described earlier.[11] About 1 % of acetone reacted after each flash. The discharge tube and photolysis tube were about 2 m long and 2 cm of diameter. The reaction products of photolysis at 25 °C and at different pressures of acetone and nitrogen were analysed by GLC using Porapak Q or Carbowax 4000 columns and flame ionization detector. The relative amounts of products varied slightly with repeated flashing. The amounts of products corresponding to the first flash were obtained from a linear plot of the relative amounts of products against the number of flashes in each experiment. All materials were degassed in a vacuum line. The products were identified by GLC trough comparison with known substances, and partly by mass spectrometry. Calibration curves were prepared by GLC for quantitative analysis.

The following products were identified by GLC after the flash photolysis of acetone in gas phase; methane, ethane, ethylene, acetaldehyde, methyl ethyl ketone and biacetyl, Table 1. Small amounts of propane were also observed but it is expected to be a secondary product of photolysis of methyl ethyl ketone because by extrapolation to correspond to the first flash the relative amount of propane approached zero. In addition, two unidentified products, amounting to less than 1 % of the main product, ethane, were found. Because a flame ionization detector was used on GLC analysis, carbon monoxide and hydrogen could not be detected. Small amounts of hydrogen have been observed [4,5] in acetone photolysis with ultraviolet light below 200 nm.

The material balance of the products observed in flash photolysis of acetone, Table 1, is not satisfactory, indicating that a product is missing which contains relatively less hydrogen than acetone and hence is formed by a reaction involving hydrogen abstraction. The missing product could be ketene, though we could not detect it among the products. Ketene is difficult to detect in small amounts by GLC method. Ketene has been observed [6,7] in acetone photolysis at temperatures above 100 °C.

RESULTS AND DISCUSSION

The amounts of products observed in flash photolysis of acetone are shown in Table 1 and Fig. 1. The main product, ethane, is formed by combination of two methyl radicals.[11]

Methane is formed by hydrogen abstraction reaction (8) by methyl radical with acetone.

$$CH_3 + CH_3COCH_3 \rightarrow CH_4 + CH_2COCH_3 \qquad (8)$$

Table 1. Products of acetone photolysis formed during one flash at 25°C. Carbowax 4000 and Porapak Q columns were used in the GLC analysis of the first seven and the last four mixtures, respectively. Each column was capable of resolving only a part of the reaction products.

Reaction mixture P/Torr		Products 10^4 P/Torr					
CH_3COCH_3	N_2	CH_4	C_2H_4	C_2H_6	CH_3CHO	$(CH_3CO)_2$	$C_2H_5COCH_3$
2.09	276			136	1.02	2.23	2.36
4.29	16			219	2.70	6.76	2.57
4.23	103			217	3.25	5.78	2.71
9.10	0			314	4.72	24.5	3.66
9.32	35			355	4.08	27.3	4.90
9.08	223			328	4.92	17.9	5.31
19.77	251			471	7.42	54.8	8.25
2.02	283	10.6	2.71	105	1.39		
4.28	290	19.6	3.53	191	3.37		
9.38	274	22.0	3.95	279	5.69		
19.91	271	32.7	5.76	438	6.92		

Owing to the relatively large activation energy [8] $E = 40.1$ kJ mol^{-1}, the hydrogen transfer reaction (8) between thermally equilibrated methyl radicals and acetone molecules at 25 °C and at high concentrations of methyl radical is slow compared with the rate of combination [9,11] of methyl radicals to ethane. Since a primary decomposition of the excited acetone to methane is unlikely, methane is probably produced [9] in collisions between hot methyl radicals and acetone molecules, reaction (9).

$$CH_3^* + CH_3COCH_3 \rightarrow CH_4 + CH_2COCH_3 \quad (9)$$

$$CH_3^* + CH_3COCH_3 \rightarrow CH_3 + CH_3COCH_3^* \quad (10)$$

$$CH_3 + CH_3 + M \rightarrow CH_3CH_3 + M \quad (11)$$

Energy-rich methyl radicals are formed by dissociation of vibrationally excited triplet acetone molecules, reaction (3). The enthalpy of dissociation of acetone [10] is $\Delta H = 334$ kJ mol^{-1}, corresponding to light with $\lambda = 358$ nm. When acetone is excited at about the maximum absorption with 280 nm light, molecules with energy of about 427 kJ mol^{-1} are formed, which is more than is needed to break the C – C bond of acetone. Because we used unfiltered light, excited acetone molecules with even higher excess energy were formed. The zero point level of acetone triplet [2,3] is estimated to be about 314 kJ mol^{-1} and that of acetone singlet about 330 kJ mol^{-1}. The dissociation of acetone from zero point level of the triplet state [3] has an activation energy of $E = 40 \pm 4$ kJ mol^{-1}.

At high acetone pressures of about 20 Torr the relative amounts of methane produced in flash photolysis of acetone approach a constant value (Fig. 1). As the amount of methane is only about 8 % of that of ethane, the energy transfer process (10) is more effective than the hydrogen transfer reaction (9) in collisions between acetone and energy-rich methyl radicals. At low acetone pressures there is a slight increase in the relative amounts of methane. This could be due to the two competing processes (3) and (4), the latter becoming more important at higher pressures, resulting in a decrease in the amounts of energy-rich methyl radicals.

The activation energy is $E = 91 \pm 7.5$ kJ mol^{-1} for the dissociation reaction of thermally equilibrated acetyl radicals.[12] The rate of dissociation at 25 °C and at high concentrations of

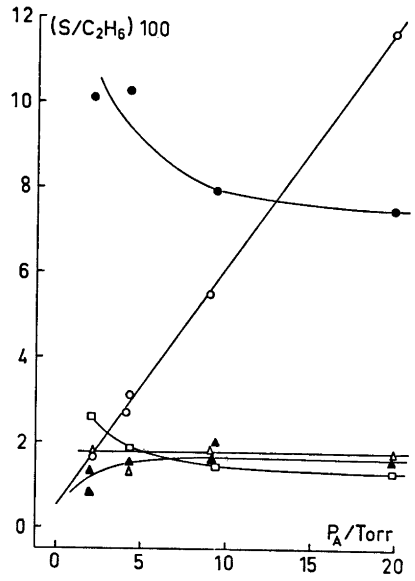

Fig. 1. Relative amounts of different products (S) formed in the flash photolysis of acetone in gas phase at 25 °C and different acetone (A) pressures and about 270 Torr of nitrogen. Symbols for different products (S): ●, CH_4; ○, $(CH_3CO)_2$; ▲, CH_3CHO; △, $CH_3COC_2H_5$; and □, C_2H_4.

acetyl radicals is slow compared with the rates of combination of acetyl radicals with methyl or acetyl radicals. The following reactions of acetyl radicals are expected to be important:

$$CH_3CO^* \rightarrow CH_3 + CO \quad (12)$$

$$CH_3CO^* + CH_3COCH_3 \rightarrow CH_3 + CO + CH_3COCH_3 \quad (13)$$

$$CH_3CO^* + CH_3COCH_3 \rightarrow CH_3CHO + CH_2COCH_3 \quad (14)$$

$$CH_3CO + CH_3COCH_3^* \quad (15)$$

$$CH_3CO + CH_3CO \rightarrow CH_3COCOCH_3 \quad (16)$$

$$CH_3CO + CH_3 \rightarrow CH_3COCH_3 \quad (17)$$

When the acetone pressure is increased the amount of biacetyl formed in flash photolysis of acetone increases rapidly (Fig. 1). As the amount of biacetyl formed is much less than the amount of ethane, the dissociation reactions (12) and (13) of hot acetyl radicals are faster than the reactions (14) and (15) in the pressure

range of 2 to 20 Torr of acetone. This also implies that the dissociation of vibrationally excited acetone triplets, reaction (3), is faster than the energy transfer process (4) which produces acetyl radicals of low energy. The increase in the amount of biacetyl produced when the pressure of acetone is increased is due to the increase in rates of energy transfer processes (4) and (15) relative to the unimolecular rates of dissociation reactions (3) and (12).

Acetaldehyde is probably formed in a hydrogen abstraction reaction (14) between an energy-rich acetyl radical and an acetone molecule. The amounts of acetaldehyde produced are approximately constant at different acetone pressures (Fig. 1) except for a small decrease at low pressures. At low pressures the unimolecular dissociation of hot acetyl radicals, reaction (12), should become more important relative to the bimolecular reaction (14) producing acetaldehyde, resulting in a decrease in the amounts of acetaldehyde produced. As only small amounts of acetaldehyde are produced, the dissociation of hot acetyl radicals (13) is faster than the hydrogen abstraction reaction (15). Equal amounts of methyl and acetyl radicals are produced in dissociation reaction (3), but the amount of methane is about four times larger than the amount of acetaldehyde produced in the photolysis, which indicates that the competing dissociation reaction (13) of hot acetyl radicals is faster than the energy transfer reaction of methyl radicals relative to the hydrogen abstraction reactions of the respective radicals.

Methyl ethyl ketone is most probably produced in an addition reaction between acetonyl and methyl radicals:

$$CH_3 + CH_2COCH_3 \rightarrow CH_3CH_2COCH_3 \quad (18)$$

The acetonyl radical which is formed in hydrogen abstraction reactions between hot methyl and acetyl radicals with acetone, eqns. (9) and (14), may involve an excess energy and dissociate to ketene and methyl radicals:

$$CH_2COCH_3^* \rightarrow CH_2CO + CH_3 \quad (19)$$

As the total amounts of acetonyl radicals formed in reactions (9) and (14) are larger than the amounts of acetonyl radicals disappearing in reaction (18), *i.e.* the yield of methane and acetaldehyde is larger than the yield of methyl ethyl ketone, some additional reaction must occur which consumes acetonyl radicals. One possible reaction is the dissociation of acetonyl radicals to ketene (19).

It has been proposed [11,13] that ethylene is produced in a reaction between two acetonyl radicals in the photolysis of acetone. The amount of ethylene formed does not agree with the amounts of acetonyl radicals produced in our experiments. Ethylene could also be formed *via* a combination of hot methyl radicals, followed by a 1,2-elimination of hydrogen from the energy-rich ethane intermediate:

$$CH_3^* + CH_3 \rightarrow CH_3CH_3^* \rightarrow CH_2CH_2 + H_2 \quad (20)$$

Similar addition elimination reactions were observed by Perona, Bryant and Pritchard [14] in a photolysis of a mixture of 1,1,1-trideuterioacetone and 1,1,3,3-tetrafluoroacetone. With a 250 W medium pressure mercury light source of low intensity, no ethylene was observed in photolysis of acetone (Table 2). At low radical concentrations a bimolecular reaction similar to (20) would be slow compared with reactions

Table 2. Relative amounts of products of photolysis of acetone, biacetyl and azomethane; flash or constant unfiltered light source at 25 °C.

Light source	Reaction mixture P/Torr		Products $10^4\,P$/Torr N_2	CH_4	C_2H_4	C_2H_6	CH_3CHO	CH_3COCH_3	$C_2H_5COCH_3$
Continuous	CH_3COCH_3	1.2	50	5.0		100			14
Continuous	CH_3COCH_3	4.6	18	5.0		100			25
Continuous	CH_3COCH_3	40.0	27	6.2		100			18
Flash	$(CH_3CO)_2$	1.3	216	7.5	2.3	100	6.2	117	
Flash	$(CH_3CO)_2$	3.1	210	9.3	2.5	100	8.8	112	
Flash	$(CH_3)_2N_2$	3.0	30	15.0	0.73	100			
Continuous	$(CH_3)_2N_2$	3.0	23	17.8		100			

(9) and (10). Ethylene was also observed in the flash photolysis of biacetyl and azomethane, the relative amounts being $C_2H_4/C_2H_6 = 0.066$ and $C_2H_4/C_2H_6 = 0.002$, respectively (Table 2). No ethylene was observed in low intensity photolysis of azomethane. At high temperatures of about 400 °C, large amounts of ethylene are produced in photolysis of acetone.[18] Production of ethylene is then favoured by the presence of molecules or radicals of high energy, as is assumed in reaction (20).

REFERENCES

1. Calvert, J. G. and Pitts, J. N., Jr. *Photochemistry*, Wiley, New York 1966, p. 393.
2. O'Neal, H. E. and Larson, C. W. *J. Phys. Chem. 73* (1969) 1011.
3. Cundall, R. B. and Davis, A. S. *Prog. React. Kinet. 4* (1967) 149.
4. Khan, M. A., Norrish, R. G. W. and Porter, G. *Proc. R. Soc. London Ser. A 219* (1953) 312.
5. Wettermark, G. *Ark. Kemi 18* (1961) 1.
6. Ferris, R. C. and Haynes, W. S. *J. Am. Chem. Soc. 72* (1950) 893.
7. Shaw, H. and Toby, J. *J. Phys. Chem. 72* (1968) 2337.
8. Ausloos, P. and Steacie, E. W. R. *Can. J. Chem. 33* (1955) 47.
9. Potzinger, P. and von Bünau, G. *Ber. Bunsenges. Phys. Chem. 72* (1968) 195.
10. Benson, S. W. *The Foundations of Chemical Kinetics*, McGraw-Hill, New York, p. 370.
11. Pohjonen, M.-L., Leinonen, L., Lemmetyinen, H. and Koskikallio, J. *Finn. Chem. Lett. 6* (1974) 207.
12. Watkins, K. W. and Word, W. W. *Int. J. Chem. Kinet. 6* (1974) 855.
13. Mandelcorn, L. and Steacie, E. W. R. *Can. J. Chem. 32* (1954) 79.
14. Perona, M. J., Bryant, J. T. and Pritchard, G. O. *J. Am. Chem. Soc. 90* (1968) 4782.

Received April 5, 1976.

Acta Chemica Scandinavica A 30 (1976) 745—750

The Hydrolysis of the Tin(II) Ion

SYLVIA GOBOM

Department of Inorganic Chemistry, Chalmers University of Technology and University of Göteborg, P.O. Box, S-402 20 Göteborg 5, Sweden

The hydrolysis of Sn(II) has been studied by means of potentiometric titrations at low Sn(II) concentrations, ranging from 0.02 to 2.3 mM, in the pH range 2.7 – 3.7. Tin amalgam and glass electrodes were used as sensors and all measurements were carried out at 25 °C, using 3 M $NaClO_4$ as ionic medium. The emf data could be explained by the following reactions and equilibrium constants.

$Sn^{2+} + H_2O \rightleftharpoons SnOH^+ + H^+$ $\quad \lg {}^*\beta_{11} = -3.70 \pm 0.02$

$3Sn^{2+} + 4H_2O \rightleftharpoons Sn_3(OH)_4^{2+} + 4H^+$ $\quad \lg {}^*\beta_{43} = -6.81 \pm 0.03$

The formation constants were calculated with the least squares program LETAGROP.

This work can be considered as an extension of the study of the tin(II) hydrolysis by Tobias,[1] in which potentiometric titrations of tin(II) perchlorate solutions were carried out in a 3 M $NaClO_4$ medium with tin concentrations varying from 2.5 mM to 40 mM. In the pH range investigated (1.5 – 3.0 for the lowest and 1.5 – 2.4 for the highest tin concentration) Tobias found that $Sn_3(OH)_4^{2+}$ predominated, small amounts of $SnOH^+$ and $Sn_2(OH)_2^{2+}$ also being present. A summary and discussion of the results of hydrolytic tin(II) studies made before 1958 is given in Tobias' paper,[1] and very few studies have been reported since. The existence of $SnOH^+$, in the concentration range used in Tobias' investigation, has, however, been questioned by Liang Chia-Ch'ang and Tu Yu-Ming.[2] After new calculations based on Tobias' data they concluded that the main hydrolysis products were $Sn_3(OH)_4^{2+}$ and $Sn_2(OH)_3^+$ with minor amounts of $Sn_2(OH)_2^{2+}$. Mesmer and Irani [3] measured the solubility of SnO at 25 °C in 1 M perchloric acid – sodium perchlorate mixtures, and, using the equilibrium model proposed by Tobias, calculated the constant for the hydrolysis reaction $SnO(s) + H_3O^+ \rightleftharpoons SnOH^+ + H_2O$, *i.e.* $\lg K_{s1} = -0.28$.

Because of the extensive hydrolysis of tin(II), it is necessary to know the composition and the formation constants of the hydrolytic species when studying complexes with other ligands in aqueous solutions. The formation of $Sn_3(OH)_4^{2+}$ is well established by Tobias.[1] The mononuclear $SnOH^+$ suggested by Tobias,[1] was not formed according to the calculations due to Liang *et al.*, $Sn_2(OH)_3^+$ being introduced instead. The aim of the present work was to investigate the possible formation of $SnOH^+$. For this reason a concentration range in which the formation of $SnOH^+$ ought to be favoured was examined. The results of this work were to be used in a study of acetato – tin(II) complexes in 3 M $NaClO_4$.

SYMBOLS

The following notation is used:

lg	$\log_{10}$
H	analytical hydrogen ion concentration
h	free hydrogen ion concentration
B	analytical concentration of Sn(II)
b	free concentration of Sn(II)
η	lg B/b
E_H	measured emf of the glass electrode (4)
E_B	measured emf of the amalgam electrode (3)
Q	number of ampereseconds passed through the test solution during anodic oxidation
DEH	$E_{H,\mathrm{cal}} - E_H$ (Table 1), where $E_{H,\mathrm{cal}}$ denotes the calculated value of E_H.
DEB	$E_{B,\mathrm{cal}} - E_B$ (Table 1), where $E_{B,\mathrm{cal}}$ denotes the calculated value of E_B.

Emf values are given in mV and equilibrium constants on the molar scale.

METHOD OF INVESTIGATION

The measurements were performed as potentiometric titrations in a paraffin oil thermostat at 25 °C, using the automatic titrator described earlier.[7]

Since a concentration range favouring the formation of $SnOH^+$ was to be used, solutions with a much lower Sn(II) content than that used by Tobias had to be prepared. It thus proved convenient to generate the tin ions by constant current electrolysis. When larger amounts of Sn(II) are required the method used by Tobias, in which a solution of $Cu(ClO_4)_2$ is passed through a tin column, yielding an equivalent amount of tin(II) ions, is, however, preferable.

The free concentrations of Sn^{2+} and H^+, b and h, were measured with a tin amalgam and a glass electrode, respectively. The cells were of the following types

$$-\mathrm{Sn(Hg)} \mid \text{solution S} \mid \text{3 M } NaClO_4 \mid \mathrm{RE}+ \quad (1)$$

$$-\mathrm{GE} \mid \text{solution S} \mid \text{3 M } NaClO_4 \mid \mathrm{RE}+ \quad (2)$$

where GE is the glass electrode and RE the reference half cell:

$$\mathrm{Ag, AgCl} \mid 0.010\ \mathrm{M}\ Ag^+, 2.99\ \mathrm{M}\ Na^+, 3.00\ \mathrm{M}\ ClO_4^-$$

In some titrations (Nos. 1 and 6, Table 1) sodium chloride was used instead of silver perchlorate in the reference half cell (since an investigation of the tin(II) hydrolysis in alkaline solution was carried out simultaneously).[8] No difference in the stability of the two types of reference half cells could be detected.

The emfs of cells (1) and (2) can be written

$$E_B = E_B^\circ - \tfrac{1}{2} \times 59.16 \lg b + E_j \quad (3)$$

and

$$E_H = E_H^\circ - 59.16 \lg h + E_j \quad (4)$$

It was assumed that the activity factors were constant and could thus be included in the constants E_B° and E_H°, respectively. E_j, the liquid junction potential between the test solution and the 3 M $NaClO_4$ in the salt bridge was calculated from $E_j = jh$ mV, $j = 0.017$ mV/mM, according to earlier studies by Biedermann and Sillén.[9]

A description of the electrodes and the equipment used for the coulometric addition of tin ions and other experimental details are given in Ref. 6.

The hydrolysis of tin(II) was studied by introducing tin(II) ions into an acidified solution of 3 M $NaClO_4$, the H level being kept constant in each titration. The initial solution, 3 M $NaClO_4$ containing a slight excess of protons, was prepared from freshly prepared stock solutions. The proton excess was determined by titration with hydrogen ions, generated electrolytically in the solution. A platinum gauze was used as an anode, the other parts of the electrolysis circuit being the same as described in Ref. 6. This type of coulometer was introduced by Biedermann and Ciavatta.[10] Gran's extrapolation method[11] was used to calculate the original H. The stepwise addition of H^+ was continued, until the desired H level was reached, and for each addition the constant E_H° (4) was calculated. The platinum gauze was then replaced by a tin amalgam anode, and the tin ions were generated in steps of *ca.* 0.5 μmol, with a current density of *ca.* 1.2 mA/cm². After each step of electrolysis the equilibrium emf's of the measuring tin amalgam electrode and glass electrode, E_B and E_H, were registered (Table 1). A graphical survey of the concentration ranges covered in these experiments is given in Fig. 1.

Chemicals and analysis

Sodium perchlorate solutions were prepared as described by Biedermann.[12]

Tin amalgams were prepared as described in Ref. 6.

The analytical tin(II) concentration was calculated from the known amount of ampere-seconds that passed through the solution during electrolysis.

CALCULATIONS AND RESULTS

The hydrolytic equilibria can be described by the general reaction

$$q\mathrm{Sn}^{2+} + p\mathrm{H_2O} \rightleftharpoons \mathrm{Sn}_q(\mathrm{OH})_p^{(2q-p)} + p\mathrm{H}^+$$

with the equilibrium constants ${}^*\beta_{qp}$. The mass balances for B and H give

$$B = b + \sum_{pq} q\,{}^*\beta_{qp} b h^{-p} \quad (5)$$

$$h = H + \sum_{pq} p\,{}^*\beta_{qp} b h^{-p} \quad (6)$$

The equilibrium constants were determined from 223 experimental points obtained from six different titrations. Part of the data (Q, E_B, E_H) are listed in Table 1,* and the con-

* A complete list of the experimental data is available from the Department of Inorganic Chemistry, Chalmers University of Technology and University of Göteborg, P.O. Box, S-402 20 Göteborg 5, Sweden.

Table 1. Experimental data. Part of computer output for 6 titrations. For each point Q(coulomb), E_H(≡EH), E_B(≡EB), pH, DEH = $E_{H,\mathrm{cal}} - E_H$ and DEB = $E_{B,\mathrm{cal}} - E_B$ are given. H_0 and B_0 are the initial concentrations of H^+ and Sn^{2+}, respectively. All concentrations are given in mM. V_0 = 49.98 ml. In the calculations the equilibrium constants lg $\beta_{11} = -3.70$ and lg $^*\beta_{43} = -6.81$ were used. E_B and E_H in the table correspond to $E_B°$ and $E_H°$ in eqns. (3) and (4).

SATS 1. E_B = 423.56 ± 0.03 E_H = -216.93; H_0 = 0.1934 B_0 = 0

Q(C)	EH(MV)	EB(MV)	PH	-DEH	-DEB
0.197	1.36	571.28	3.6908	-0.05	0.05
0.247	1.03	568.38	3.6852	-0.04	0.01
0.296	0.71	565.97	3.6796	-0.03	-0.07
0.345	0.48	564.00	3.6739	0.08	-0.09
0.395	0.05	562.38	3.6682	-0.01	-0.02
0.444	-0.17	560.91	3.6624	0.10	-0.01
0.493	-0.52	559.61	3.6567	0.09	0.01

SATS 2. E_B = 816.81 ± 0.03 E_H = 158.53; H_0 = 0.2302 B_0 = 0.0350

Q(C)	EH(MV)	EB(MV)	PH	-DEH	-DEB
0.287	370.58	948.87	3.5823	0.14	-0.03
0.334	370.32	948.00	3.5778	0.14	0.02
0.430	369.78	946.40	3.5690	0.12	0.07
0.526	369.23	945.00	3.5601	0.10	0.12
0.621	368.69	943.66	3.5514	0.07	0.08
0.717	368.15	942.48	3.5426	0.05	0.07
0.812	367.61	941.38	3.5340	0.02	0.05
0.908	367.09	940.35	3.5255	0.0	0.01
1.003	366.57	939.43	3.5171	-0.02	0.01
1.099	366.05	938.55	3.5088	-0.05	-0.02
1.194	365.56	937.74	3.5007	-0.06	-0.02
1.338	364.86	936.58	3.4888	-0.05	-0.05
1.481	364.12	935.54	3.4772	-0.11	-0.05
1.624	363.43	934.56	3.4659	-0.13	-0.07
1.768	362.77	933.65	3.4549	-0.14	-0.07

SATS 3. E_B = 818.51 ± 0.02 E_H = 157.36; H_0 = 0.4731 B_0 = 0.0350

Q(C)	EH(MV)	EB(MV)	PH	-DEH	-DEB
0.191	353.06	949.31	3.3103	-0.13	0.16
0.287	352.94	947.12	3.3077	-0.09	0.11
0.334	352.88	946.15	3.3063	-0.07	0.08
0.430	352.74	944.42	3.3035	-0.05	0.04
0.526	352.57	942.91	3.3007	-0.05	0.02
0.621	352.40	941.56	3.2978	-0.05	0.0
0.717	352.24	940.36	3.2949	-0.04	0.0
0.764	352.17	939.81	3.2934	-0.02	0.0
0.860	352.02	938.77	3.2904	0.01	-0.01
0.956	351.84	937.80	3.2874	0.0	-0.02
1.051	351.69	936.90	3.2844	0.04	-0.04
1.147	351.49	936.08	3.2813	0.02	-0.03
1.242	351.31	935.31	3.2781	0.02	-0.03
1.338	351.11	934.59	3.2750	0.01	-0.03
1.433	350.97	933.90	3.2718	0.06	-0.04
1.529	350.76	933.26	3.2685	0.04	-0.04
1.624	350.61	932.64	3.2653	0.08	-0.05

SATS 4. E_B = 818.90 ± 0.02 E_H = -2.67; H_0 = 0.7674 B_0 = 0

Q(C)	EH(MV)	EB(MV)	PH	-DEH	-DEB
9.142	173.09	912.40	2.9741	-0.19	0.06
9.810	172.52	911.40	2.9639	-0.16	-0.07
10.479	171.97	910.54	2.9539	-0.12	-0.10
11.244	171.34	909.65	2.9429	-0.10	-0.11
12.199	170.59	908.63	2.9296	-0.06	-0.11
13.155	169.87	907.71	2.9168	-0.03	-0.07
14.110	169.17	906.84	2.9045	0.0	-0.05
15.257	168.36	905.87	2.8904	0.03	-0.02
16.404	167.58	904.96	2.8768	0.05	0.0
17.359	166.96	904.24	2.8659	0.07	0.01
18.506	166.22	903.43	2.8534	0.07	0.03
19.461	165.63	902.77	2.8433	0.08	0.03
20.417	165.06	902.16	2.8336	0.08	0.04
21.372	164.53	901.57	2.8242	0.11	0.05
22.232	163.99	900.97	2.8160	0.06	-0.03
22.423	163.90	900.90	2.8142	0.07	0.01
22.615	163.80	900.81	2.8124	0.08	0.04

SATS 5. E_B = 819.44 ± 0.03 E_H = -2.17; H_0 = 1.138 B_0 = 0

Q(C)	EH(MV)	EB(MV)	PH	-DEH	-DEB
0.764	171.63	942.89	2.9394	-0.10	0.06
0.860	171.61	941.40	2.9388	-0.09	0.08
0.956	171.57	940.06	2.9383	-0.09	0.09
1.051	171.59	938.84	2.9377	-0.04	0.09
1.242	171.52	936.68	2.9365	-0.04	0.08
1.433	171.48	934.83	2.9354	-0.01	0.06
1.624	171.42	933.20	2.9342	0.0	0.03
1.816	171.35	931.78	2.9330	0.0	0.03
2.007	171.30	930.49	2.9318	0.02	0.02
2.198	171.23	929.32	2.9306	0.02	0.0
2.389	171.17	928.25	2.9293	0.04	-0.01
2.676	171.06	926.80	2.9274	0.04	-0.02
2.962	170.96	925.49	2.9255	0.05	-0.04
3.249	170.86	924.32	2.9235	0.07	-0.05
3.536	170.76	923.25	2.9214	0.09	-0.05
3.918	170.61	921.96	2.9186	0.11	-0.06
4.300	170.47	920.80	2.9156	0.14	-0.06
4.682	170.29	919.73	2.9126	0.14	-0.07
5.160	170.08	918.53	2.9087	0.16	-0.06
5.638	169.87	917.44	2.9047	0.19	-0.06
6.211	169.61	916.25	2.8998	0.22	-0.06
6.784	169.32	915.18	2.8947	0.23	-0.05
7.453	168.99	914.03	2.8886	0.26	-0.05
8.122	168.64	912.98	2.8824	0.28	-0.05
8.887	168.24	911.90	2.8753	0.30	-0.04
9.747	167.78	910.78	2.8672	0.32	-0.03
10.607	167.33	909.77	2.8591	0.35	-0.01
11.562	166.82	908.73	2.8501	0.37	0.0
12.614	166.27	907.68	2.8404	0.39	0.01
13.760	165.67	906.62	2.8299	0.41	0.02
15.003	165.04	905.57	2.8187	0.44	0.03
16.340	164.36	904.53	2.8070	0.46	0.04
17.774	163.65	903.50	2.7948	0.47	0.06
19.303	162.91	902.48	2.7822	0.47	0.06
21.023	162.11	901.43	2.7685	0.48	0.08
22.838	161.14	900.40	2.7547	0.33	0.10

SATS 6. E_B = 423.69 ± 0.02; E_H = -217.29 H_0 = 0.2033 B_0 = 0

Q(C)	EB(MV)	PH	-DEB
0.296	565.91	3.6603	0.05
0.345	563.95	3.6550	0.05
0.395	562.25	3.6497	0.04
0.444	560.77	3.6443	0.04
0.493	559.43	3.6390	0.02
0.543	558.24	3.6336	0.02
0.592	557.16	3.6282	0.02
0.642	556.14	3.6228	-0.01
0.691	555.24	3.6175	0.01
0.740	554.40	3.6121	0.02
0.789	553.60	3.6067	0.02
0.839	552.83	3.6014	0.0
0.888	552.13	3.5961	0.01
0.938	551.45	3.5909	0.0
0.987	550.85	3.5857	0.03
1.086	549.64	3.5753	0.01
1.184	548.55	3.5652	0.0
1.283	547.55	3.5553	0.01
1.382	546.62	3.5456	0.01
1.480	545.71	3.5360	-0.02
1.579	544.87	3.5267	-0.04
1.727	543.80	3.5132	0.04
1.875	542.70	3.5001	0.0
2.073	541.39	3.4833	0.0
2.270	540.22	3.4672	0.02
2.467	539.12	3.4518	0.03
2.665	538.12	3.4371	0.06
2.862	537.20	3.4231	0.11

centration ranges covered are visualized in Fig. 1 as curves lg B (lg b)$_H$. The evaluation was carried out by means of the least squares computer program LETAGROP ETITR.[13–15] The analytical concentrations of tin and hydrogen ions, B and H, respectively, were assumed to be correct, and the parameters $Typ = 3$ and $val = 6$ in the Letagrop program[15] were chosen. The free concentrations, b and h, were calculated by successive approximation from eqns. (5) and (6), using the measured value of $E_H°$ and the estimated values of $^*\beta_{pq}$ and $E_B°$.

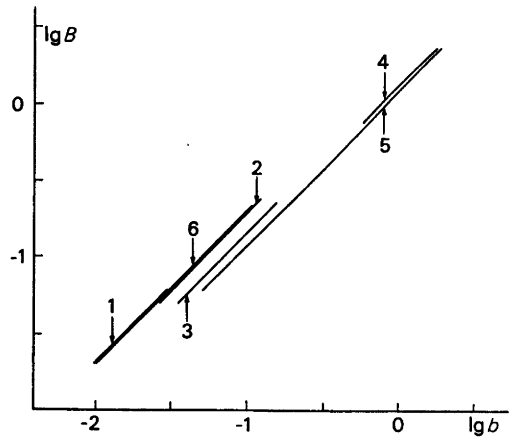

Fig. 1. Survey of concentration ranges studied in 6 titrations, lg B (lg b)$_H$. B and b are expressed in mM (Table 1).

Table 2. Literature survey of hydroxy-tin(II) complexes in 3 M $NaClO_4$.

	Tobias	Liang *et al.* [a]	This work
lg β^*_{11}	-3.92 ± 0.15	–	-3.70 ± 0.02
lg β^*_{22}	-4.45 ± 0.15	-4.58 ± 0.41	–
lg β^*_{43}	-6.77 ± 0.03	-6.85 ± 0.04	-6.81 ± 0.03
lg β^*_{32}	–	-6.66 ± 0.18	–

[a] Recalculation of Tobias data.

As starting values of the equilibrium model, Tobias' values (Table 2) for $*\beta_{11}$, $*\beta_{22}$ and $*\beta_{43}$ were used. These constants were varied (common parameters) together with $E_B°$ (group parameter) to minimize the errors squares sum $U=\sum(E_{B,cal}-E_B)^2$. In these calculations the species $Sn_2(OH)_2^{2+}$ was rejected, and the lowest errors squares sum was obtained for

$$\lg *\beta_{11} = -3.70\pm0.02 \quad (7)$$

$$\lg *\beta_{43} = -6.81\pm0.03 \quad (8)$$

The uncertainties furnished by the program correspond to three times the "standard deviation" of the constant.[16,17] The agreement between the calculated and experimental values $DEB=E_{B,cal}-E_B$ and $DEH=E_{B,cal}-E_B$ is given in the last two columns in Table 1.

To illustrate the complex formation the distribution diagrams $\sum_1^i x_i = f(pH)_B$, i = 1, 2, 3 were constructed (Fig. 2), where x_i represents the fraction of the total amount of tin present in the three species, Sn^{2+} (i = 1), $SnOH^+$ (i = 2), and $Sn_3(OH)_4^{2+}$ (i = 3). The distribution of the complexes was calculated with the Haltafall program [18,19] and plotted [20] with an IBM 370/145 computer.

The diagrams in Fig. 2a – 2d cover the concentrations studied in the present work. In Fig. 2e the curves have been extrapolated to the highest concentration used in Tobias' measurements to enable a comparison between the two investigations.

The agreement of the present results with the equilibrium model proposed by Liang *et al.*[2] was also tested. Theoretical curves, using their values, were compared with the experimental values $\eta(pH)_B$ from Tobias' and the lg B(lg b)$_H$ data from the present work. At low values of B, the theoretical curves deviated markedly from the experimental points, indicating that $SnOH^+$ should not be neglected or replaced by $Sn_2(OH)_3^+$. Letagrop calculations using the equilibrium constants found by Liang *et al.*, as initial values, were also carried out. When these constants and $E_B°$ were varied to find the "best" values, the error squares sum became much higher than that obtained with (7) and (8). This was due to deviations between the calculated and measured E_B values, which were larger the lower the value of B. The "best" value of lg $*\beta_{43}$ also differed considerably from the starting value (*ca.* 0.25 units) and $\sigma(*\beta_{43})$ became *ca.* ten times higher than the value reported in Table 2.

Attempts to interpret the present data in terms of the formation of $SnOH^+$, $Sn_2(OH)_3^+$ and $Sn_3(OH)_4^{2+}$ also failed. On the other hand, an accurate determination of the polynuclear species formed, would require study of a wider range of B. The simplest interpretation of the present data is, however, obtained, by assuming the formation of the single polynuclear complex $Sn_3(OH)_4^{2+}$.

DISCUSSION

In this investigation the formation of the hydrolysis products $Sn_3(OH)_4^{2+}$ and $SnOH^+$

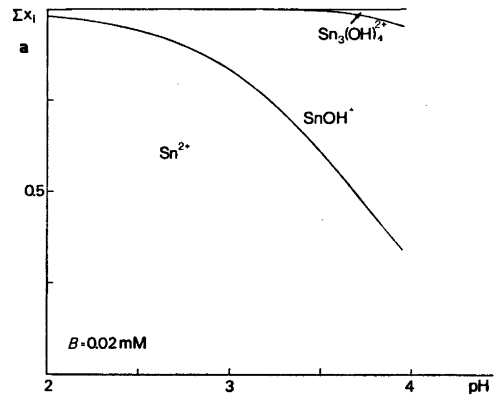

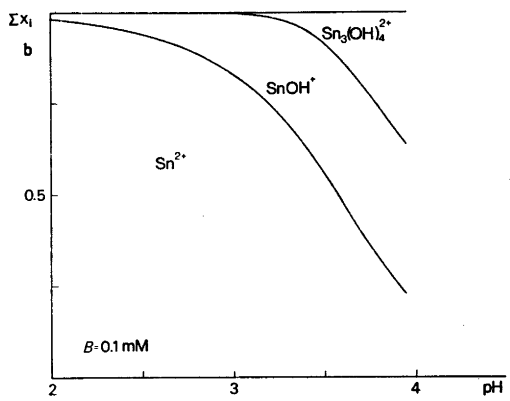

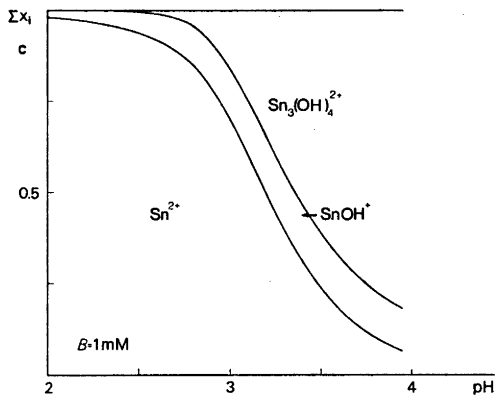

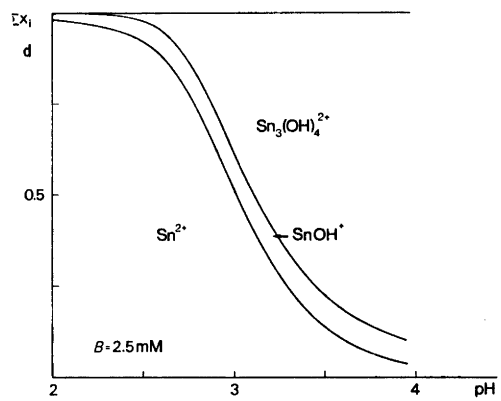

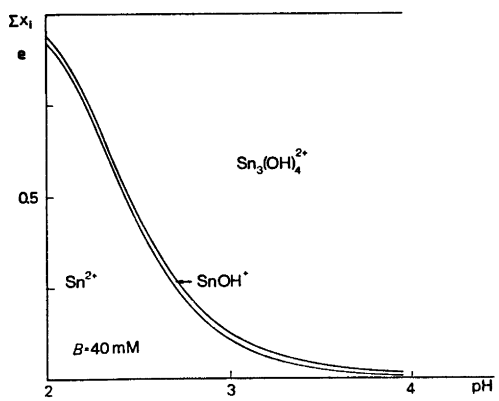

Fig. 2. The distribution of Sn(II) between the species formed, x_i is the fraction of the total amount of tin present in the three species, $Sn^{2+}(i=1)$, $SnOH^{+}(i=2)$ and $Sn_3(OH)_4^{2+}(i=3)$. The curves have been calculated with the equilibrium constants $\lg {}^*\beta_{11} = -3.70$ and $\lg {}^*\beta_{43} = -6.81$.

previously suggested by Tobias[1] has been confirmed, and a more accurate value of $\lg {}^*\beta_{11}$ has been determined. Since low tin(II) concentrations were used, it was possible to study regions where either $SnOH^{+}$ or $Sn_3(OH)_4^{2+}$ were dominant. Tobias worked at rather high tin concentrations, and was therefore restricted to regions where mainly $Sn_3(OH)_4^{2+}$ was formed. In the present work the tin ions were generated through electrolysis, since very low values of B

were required. The titration techniques in the present investigation also differed from those used by Tobias. In Tobias' measurements solutions of $NaHCO_3$ were added, the tin(II) concentration being kept constant. In the present work the titrations were performed at constant H levels, the tin(II) ions being generated *in situ* by electrolysis. In view of the differences between the methods of investigation, the agreement between the values for lg $*\beta_{43}$ is satisfactory.

Whereas $SnOH^+$ was present only in minor amounts in Tobias' work, in the present study it was the predominant complex, especially at low values of B (Fig. 2a–d). It is thus reasonable that lg $*\beta_{11}$ should be obtained with better accuracy in the present work. The lowest tin(II) concentration studied by Tobias was $B = 2.5$ mM, and he has reported experimental values $\eta(\mathrm{pH})_B = 2.5$ from two titrations.[1] If these experimental data are compared with the theoretical curves obtained, using the values in Table 2, a poor fit is obtained, for $\mathrm{pH} < 2.7$, for all the models proposed. On the other hand, a reasonably good fit is obtained for one of his titrations, when $\mathrm{pH} < 2.2$, if the equilibrium model from the present work is used. Tobias has, however, reported that the amalgam electrodes did not function satisfactorily for $B < 2.5$ mM. Even for $B = 2.5$ mM one might suspect erroneous emf values, since there was a marked deviation between the experimental values $\eta(\mathrm{pH})_B = 2.5$ in the two titrations reported. Tobias completed one of these titrations with a back titration. Even here the deviation from the forward titration is evident for $\mathrm{pH} < 2.4$. The problems entailed in working with amalgam electrodes at low Sn(II) concentrations have been overcome in the present work. A possible explanation of these difficulties is given in Ref. 6.

Dimerization of mononuclear monohydroxo complexes is fairly common, and in accordance with earlier investigations[1] $Sn_2(OH)_2^{2+}$ was expected to be formed. When lg $*\beta_{22}$ was varied in the Letagrop calculations, $Sn_2(OH)_2^{2+}$ was, however, rejected. If $Sn_2(OH)_2^{2+}$ was formed, its concentration was too low to evaluate its stability constant.

Acknowledgements. The author is most grateful to Professor Georg Lundgren for all the facilities placed at her disposal, for stimulating discussions and for valuable comments concerning the manuscript. She also wishes to thank many colleagues, especially Drs. Jan Berggren and Olle Börtin, Ing. János Kovacs and Mr. Lars Lagerqvist for fruitful discussions and helpful suggestions during the course of the work. Fil.lic. Ove Lindgren's help with the computer programming is gratefully acknowledged. Thanks are also due to Mrs. Birgitta Carlsson for experimental assistance, to Dr. Susan Jagner for revising the English text of this paper, and to Mrs. Margareta Johansson, who has kindly typed the manuscript.

This work has been partly financed by the Swedish Natural Science Research Council (Contract No. 2318).

REFERENCES

1. Tobias, R. S. *Acta Chem. Scand. 12* (1958) 198.
2. Liang, C.-C. and Tu, Y.-M. *Russ. J. Inorg. Chem. 9* (1964) 727.
3. Mesmer, R. E. and Irani, R. R. *J. Inorg. Nucl. Chem. 28* (1966) 493.
4. Donaldson, J. D. *Prog. Inorg. Chem. 8* (1967).
5. Gmelin, *Handbuch der Anorganischen Chemie, 8 Aufl., Zinn, Teil C1*, p. 54.
6. Gobom, S. *Acta Chem. Scand. A 30* (1976) 771.
7. Gobom, S. and Kovács, J. *Chem. Scr. 2* (1972) 103.
8. Mark, W. *Acta Chem. Scand. To be published.*
9. Biedermann, G. and Sillén, L. G. *Ark. Kemi 5* (1953) 425.
10. Biedermann, G. and Ciavatta, L. *Ark. Kemi 22* (1964) 253.
11. Gran, G. *Analyst 77* (1952) 661.
12. Biedermann, G. *Ark. Kemi 9* (1956) 277.
13. Ingri, N. and Sillén, L. G. *Ark. Kemi* (1964) 97.
14. Arnek, R., Sillén, L. G. and Wahlberg, O. *Ark. Kemi 31* (1969) 353.
15. Brauner, P., Sillén, L. G. and Whiteker, R. *Ark. Kemi 31* (1969) 365.
16. Sillén, L. G. *Acta Chem. Scand. 16* (1962) 159.
17. Dunsmore, H., Hietanen, S. and Sillén, L. G. *Acta Chem. Scand. 17* (1963) 2644.
18. Ingri, N., Kakolowicz, W., Sillén, L. G. and Warnqvist, B. *Talanta 14* (1967) 1261.
19. Dyrssen, D., Jagner, D. and Wengelin, F. *Computer Calculation of Ionic Equilibria and Titration Procedures*, Almqvist & Wiksell, Stockholm 1968.
20. Sjölin, L. *Private communication.*

Received June 10, 1976.

Acta Chemica Scandinavica A 30 (1976) 751—758

Enthalpies of Mixing in Binary Liquid Alkali Carbonate Mixtures

B. K. ANDERSEN* and O. J. KLEPPA

The James Franck Institute and The Department of Chemistry, The University of Chicago, Chicago, Illinois 60637, U.S.A.

The enthalpies of mixing in the binary liquid alkali carbonate mixtures have been determined by direct high temperature calorimetry. The measurements were performed over wide ranges of composition at temperatures from 1130 to 1180 K.

The results are discussed and interpreted in terms of the conformal solution theory for fused salts of Reiss, Katz, and Kleppa as modified by Blander and by Davis and Rice. The enthalpies of mixing at the 50 – 50 compositions are well represented by the semiempirical expression

$$4\Delta H^{M}_{0.5} = U_0{}^{++} + 33.7\ \Delta\alpha\delta_{12} - 3970\ \delta_{12}{}^2, \text{kJ mol}^{-1}$$

In this expression, $\delta_{12} = (d_1 - d_2)/d_1 d_2$, where d_1 and d_2 are characteristic interionic distances in the two salts; $U_0{}^{++}$ represents a numerical estimate of the positive contribution to the enthalpy of mixing, which arises from the London-van der Waals interaction between next nearest neighbour cations; $\Delta\alpha$ is the difference in polarizability between the two cations.

During the last 15 years a large number of binary molten salt systems have been studied by means of direct high temperature calorimetry. So far, however, the study by Østvold and Kleppa [1] of the liquid alkali sulfate mixtures is the only extensive investigation of systems of the charge type $A_2X - B_2X$, where A and B are singly charged alkali metal ions, while X is a doubly charged anion.

Mixtures of molten alkali carbonates, which have the same A_2X charge structure constitute an important and interesting group of solutions, both from a theoretical point of view and because of their technological applications. One of the authors (Andersen [2,3]) has for some time been engaged in a study of the thermodynamic properties of molten alkali carbonates. The present determination of the enthalpies of mixing represents an important contribution to these investigations.

Prior to the present work only a few and not very accurate measurements of the thermodynamic excess properties in $Li_2CO_3 - Na_2CO_3$, $Li_2CO_3 - K_2CO_3$, and $Na_2CO_3 - K_2CO_3$ have been carried out. The enthalpies of mixing in the equimolar mixtures of these systems were determined by Barner and Andersen [4] and by Broers and Ballegoy.[5] The latter also studied two other compositions in addition to the equimolar mixtures as well as some ternary mixtures. In both of these earlier investigations a rather primitive direct calorimetric technique was used. A detailed discussion has been given by Andersen.[3]

Lumsden [6] calculated excess chemical potentials in the systems $Li_2CO_3 - Na_2CO_3$ and $Li_2CO_3 - K_2CO_3$ from the phase diagrams of Janz and Lorenz [7] and the thermochemical data of Janz *et al.*[8] Furthermore, Lumsden concluded from calculations based on the CO_2 equilibrium pressures in the systems $CaCO_3 - Na_2CO_3$, $CaCO_3 - K_2CO_3$, and $CaCO_3 - NaKCO_3$ determined by Førland [23] that Na_2CO_3 and K_2CO_3 form ideal liquid solutions.

So far no thermodynamic investigations have been carried out on mixtures containing the heavier alkali metal ions Rb^+ and Cs^+.

EXPERIMENTAL

Apparatus. All the calorimetric experiments were carried out in a single unit Calvet-type microcalorimeter suitable for work at tem-

* Present address: Fysisk-Kemisk Institut, The Technical University of Denmark, DK-2800 Lyngby, Denmark.

peratures up to about 1400 K. Apart from its single (rather than twin) construction and the higher operating temperature, the calorimeter is similar to that previously described by Kleppa.[9]

Due to the corrosive nature of molten alkali carbonates, these cannot, unlike most other salts which have been studied previously, be handled in fused silica containers and by the usual "break-off" technique. Experience has shown that the attack on Palau (20 % Pd – 80 % Au) in "acid" alkali carbonate melts, that is, in melts kept under a relatively high CO_2 pressure, may be considered as negligible.[3,10] Therefore, this alloy was chosen as the only material in contact with the carbonate melts during the mixing experiments. These were carried out in an atmosphere of pure dry CO_2.

The experimental arrangements inside the calorimeter proper are shown schematically in Fig. 1. The plunger as well as the dipper-crucible could be manipulated from outside the calorimeter proper.

Chemicals. The chemicals used in the present work were: Li_2CO_3, Na_2CO_3, and K_2CO_3, Baker Chemical Co., Analytical Reagent; Rb_2CO_3 and Cs_2CO_3, Kawecki Chemical Co., ≥ 99.8 %.

Semiquantitative spectrographic analysis showed that the metallic impurities in the rubidium carbonate were 0.006 % Na, 0.07 % K, 0.06 % Cs, and others less than 0.01 %; in the cesium carbonate the impurities were 0.08 % Na, 0.01 % K, 0.04 % Rb, and others less than 0.002 %.

The alkali carbonates were dried in a vacuum furnace at about 450 K for a period of 24 h or more. Since some of the alkali carbonates are very hygroscopic, the pick up of water during the weighing process was measured in separate experiments. Under the procedures used this was found to be less than 0.1 % for all salts and could be neglected.

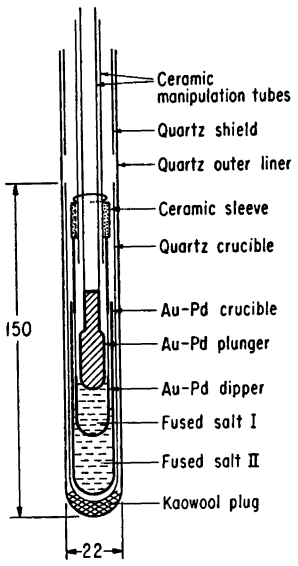

Fig. 1. Schematic diagram of experimental arrangements used for calorimetric measurements.

Procedure. Immediately before insertion into the calorimeter, the fused silica liner with its content was preheated for a period of 15 min about 50 K above the operating temperature of the calorimeter. In typical runs the total time elapsed prior to mixing was about 2 h. Except for $Li_2CO_3 - Cs_2CO_3$ and $Na_2CO_3 - Cs_2CO_3$, which were investigated at 1135 ± 1 K, all systems were studied at 1178 ± 1 K. Under these conditions the weight loss of the most volatile salt, Rb_2CO_3, as determined in blank experiments, was about 0.3 % while that of Cs_2CO_3 was 0.12 %. The weight loss of Li_2CO_3 was of the same order of magnitude as that of Cs_2CO_3. In spite of the relatively small vaporization losses, the attack by the vapours on the fused silica liner and shield was considerable, and the lower parts of these parts of the apparatus had to be rebuilt after ten to fifteen runs.

The mixing of the two salts was achieved by vertical manipulation of the plunger and dipper. After the initial mixing process three additional stirring operations were carried out at one minute intervals to assure complete mixing. Each stirring operation gave rise to a small reproducible heat effect, which had to be corrected for in some of the experiments.

In each run a total of 50 to 100 mmol of salt was used. The calibration of the calorimeter was achieved by dropping weighed pieces of 2 mm gold wire from room temperature into the calorimeter. The evaluation of the resulting endothermic heat effects was based on Kelley's equation for the heat content of gold.[11] Corrections were made for the heat pick-up of the gold pieces during the fall. These were determined in separate experiments and represented 1.7 % at 1135 K and 2.0 % at 1178 K.

The temperature-sensing device of the calorimeter consists of a 54+54 junction Pt – Pt/13 % Rh thermopile, the output of which is amplified by means of a Leeds & Northrup dc amplifier and recorded on a Leeds & Northrup Type H-Azar recorder. The emf *versus* time curves were integrated by means of an Ott precision planimeter. In this way the area between the curve and the "base line", which is proportional to the total heat effect, could be determined with a precision of about ± 0.3 %. The error due to uncertainty in drawing the base line was in most experiments estimated to be about ± 1 %. However, in some experiments, especially those on the $K_2CO_3 - Rb_2CO_3$, $K_2CO_3 - Cs_2CO_3$, and $Rb_2CO_3 - Cs_2CO_3$ systems, which have very small enthalpies of mixing, this relative error was much larger.

RESULTS

All the ten binary alkali carbonates were investigated, and the concentration dependence of the enthalpy of mixing was studied for all the lithium and sodium containing systems. For the three remaining systems ($K_2CO_3-Rb_2CO_3$, $K_2CO_3-Cs_2CO_3$, and $Rb_2CO_3-Cs_2CO_3$) the heat effects were very small and only average values for mixtures close to the equimolar composition were determined.

The experimental results are tabulated in Table 1. In Figs. 2 and 3 the enthalpy interaction parameter, $\Delta H^M/N_1N_2$, is plotted *versus* the mol fraction of the salt with the smaller cation.

An attempt was made to fit the experimental data for the seven systems shown in Figs. 2 and 3 by the least-squares method to expressions of the form

$$\Delta H^M/N_1N_2 = a + bN_1 + cN_1N_2 \qquad (1)$$

Except for $Li_2CO_3-K_2CO_3$, $Li_2CO_3-Rb_2CO_3$, and $Li_2CO_3-Cs_2CO_3$ the straight lines gave the best fits. However, since the uncertainties in the enthalpy data for these three systems are relatively large, they are also represented by straight lines. In Table 2 we give the coefficients a and b as well as the enthalpies of mixing at the 50 – 50 composition.

The temperature dependence of the enthalpy of mixing was tested only for the $Li_2CO_3-Cs_2CO_3$ system, through a single measurement at the equimolar composition at 1198 K. The result showed that the enthalpy of mixing is about 8 % less negative at this temperature than at 1135 K.

DISCUSSION

The enthalpies of mixing are interpreted in light of the conformal solution theories for fused salts developed by Reiss, Katz, and Kleppa (RKK),[12] by Blander,[13] and by Davis and Rice (DR).[14]

We have chosen to represent the enthalpy of mixing for a given binary system by $4\Delta H^M_{0.5}$, *i.e.*, by the calculated value of the interaction parameter, $\Delta H^M/N_1N_2$, at the equimolar composition. To these values we have applied a correction by estimating the values of U_0^{++},

Table 1. Molar enthalpies of mixing of binary liquid alkali carbonate mixtures. N_1 is the mol fraction of the salt with the smaller cation. $\lambda^M = \Delta H^M/N_1N_2$.

Mol fraction N_1	Total mol	ΔH^M kJ mol^{-1}	λ^M kJ mol^{-1}
$Li_2CO_3-Na_2CO_3$ (1178 K)			
0.1003	0.06502	−0.906	−10.038
0.2023	0.06502	−1.710	−10.594
0.2956	0.08346	−2.184	−10.489
0.3882	0.07253	−2.607	−10.975
0.4898	0.09487	−2.864	−11.460
0.6015	0.09248	−2.665	−11.117
0.7479	0.09969	−2.286	−12.125
0.7717	0.09522	−2.054	−11.656
0.8985	0.09008	−1.116	−12.240
$Li_2CO_3-K_2CO_3$ (1178 K)			
0.1134	0.06262	−2.711	−26.966
0.1243	0.06581	−2.995	−27.514
0.2047	0.05878	−5.203	−31.957
0.3012	0.07062	−7.024	−33.372
0.4001	0.07829	−7.750	−32.288
0.4996	0.07876	−8.229	−32.916
0.5343	0.09001	−8.158	−32.786
0.6457	0.07736	−7.705	−33.681
0.7915	0.10488	−5.781	−35.028
0.8459	0.10207	−5.006	−38.401
0.8489	0.09987	−4.661	−36.334
0.8546	0.10678	−4.630	−37.263
$Li_2CO_3-Rb_2CO_3$ (1178 K)			
0.2004	0.06597	−3.849	−24.022
0.3014	0.06776	−6.142	−29.171
0.3978	0.06764	−6.916	−28.871
0.4995	0.09191	−8.326	−33.305
0.5958	0.07184	−7.925	−32.908
0.7498	0.10813	−6.573	−35.037
0.8502	0.10940	−4.937	−38.764
$Li_2CO_3-Cs_2CO_3$ (1135 K)			
0.1000	0.04870	−2.636	−29.289
0.2001	0.04773	−4.879	−30.482
0.3002	0.04651	−7.146	−34.016
0.4002	0.05836	−8.414	−35.052
0.5507	0.08233	−9.966	−40.278
0.7509	0.09194	−8.088	−43.240
0.8498	0.08423	−6.134	−48.057
0.9001	0.08239	−4.460	−49.600
$Na_2CO_3-K_2CO_3$ (1178 K)			
0.1643	0.05879	−0.697	−5.079
0.2627	0.05655	−1.071	−5.531
0.2693	0.05807	−1.076	−5.468
0.3986	0.06681	−1.323	−5.519
0.5995	0.06560	−1.347	−5.611
0.8301	0.06682	−0.846	−6.000
0.8365	0.06725	−0.855	−6.255

Table 1. Continued.

$Na_2CO_3-Rb_2CO_3$ (1178 K)			
0.1970	0.05538	−1.281	−8.096
0.1996	0.05523	−1.352	−8.464
0.3002	0.06601	−1.739	−8.276
0.4360	0.06181	−2.059	−8.372
0.4954	0.07341	−2.134	−8.535
0.4990	0.09195	−2.141	−8.564
0.6994	0.08837	−1.806	−8.590
0.8000	0.07450	−1.351	−8.443
0.8651	0.07985	−0.983	−8.422
$Na_2CO_3-Cs_2CO_3$ (1135 K)			
0.1985	0.03297	−1.389	−8.729
0.3594	0.06057	−2.031	−8.819
0.5524	0.07220	−2.124	−8.590
0.7499	0.07946	−1.622	−8.649
0.8500	0.08457	−1.070	−8.395
$K_2CO_3-Rb_2CO_3$ (1178 K)			
0.699	0.0807	< 0.002	< 0.010
$K_2CO_3-Cs_2CO_3$ (1178 K)			
0.4987	0.06184	0.0719	0.288
0.6967	0.06951	0.0567	0.268
0.8017	0.06128	0.0726	0.457
$Rb_2CO_3-Cs_2CO_3$ (1178 K)			
0.3007	0.04943	0.0387	0.188
0.5009	0.05373	0.0473	0.185

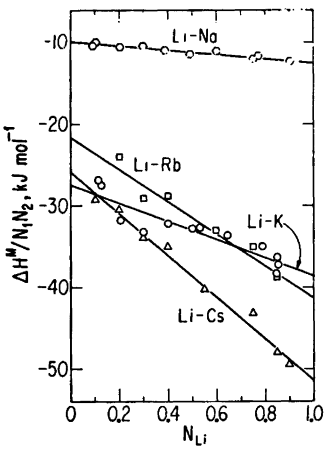

Fig. 2. Plots of $\Delta H^M/N_1N_2$ *versus* N_{Li} for $Li_2CO_3-Alk_2CO_3$ mixtures.

the change on mixing in the London – van der Waals dispersion energy between next nearest neighbour cations. The method of estimating $U_0{}^{++}$ is the same as previously used by Hersh and Kleppa.[15] However, in the present work we have in the London expression adopted the uncorrected values of the ionization potential of the alkali ions, I, rather than the value 0.75 I. We have made use of the ionic radii of the alkali metals given by Melnichak and Kleppa.[16] The same method and values were used also by Østvold and Kleppa.[1] The relevant interatomic distances were calculated from the ionic radii of the ions. For the carbonate anion we adopted the thermochemical radius, $r(CO_3^{2-}) = 1.85$ Å, as given by Kapustinskii.[17] The importance of the choice of ionic radii will be discussed later. The polarizabilities are those reported by Tessman *et al.*[18] Table 3 shows the ionic radii, polarizabilities, and ionization potentials used in the calculations. In Fig. 4 the corrected interaction parameter, $4\Delta H^M_{0.5} - U_0{}^{++}$, is plotted *versus* the square of the distance parameter, δ_{12} ($\delta_{12} = (d_1 - d_2)/d_1d_2$ where d_1 and d_2 are characteristic interionic distances in the two salts). It will be noticed that the points representing the $Li_2CO_3-Na_2CO_3$, $Li_2CO_3-K_2CO_3$, and $Na_2CO_3-K_2CO_3$ systems fall close to a straight line through the origin, while most of the points which represent the rubidium or cesium containing systems fall below this line.

The ionic conformal solution theory of Reiss, Katz, and Kleppa as modified by the perturbation theory of Davis and Rice, predicts that the enthalpies of mixing for families of related fused salt solutions should be of the form

$$\Delta H^M/N_1N_2 = U_0 + U_1\delta_{12} + U_2\delta_{12}^2 \qquad (2)$$

According to the DR theory the leading term in U_1, for a given common anion family, should

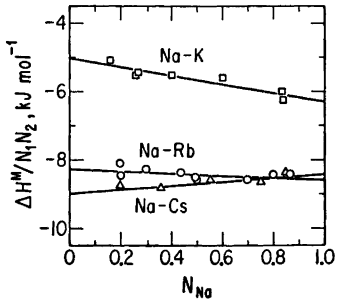

Fig. 3. Plots of $\Delta H^M/N_1N_2$ *versus* N_{Na} for $Na_2CO_3-K_2CO_3$, $Na_2CO_3-Rb_2CO_3$, and $Na_2CO_3-Cs_2CO_3$ mixtures.

Table 2. Integral enthalpies of mixing for binary alkali carbonates ($\Delta H^M = N_1N_2(a+bN_1)$ kJ mol^{-1}; N_1 is mol fraction of salt with the smaller cation).

System	Temp., K	a	b	$4\Delta H^M_{0.5}$	S.D.
Li–Na	1178	−9.90	−2.59	−11.19	0.25
Li–K	1178	−27.56	−11.00	−33.06	1.49
Li–Rb	1178	−21.67	−19.58	−31.46	1.48
Li–Cs	1135	−25.94	−25.30	−38.59	1.03
Na–K	1178	−5.03	−1.27	−5.66	0.16
Na–Rb	1178	−8.26	−0.32	−8.42	0.14
Na–Cs	1135	−8.89	+0.47	−8.66	0.11
K–Rb	1178			≤0.01	
K–Cs	1178			+0.34	
Rb–Cs	1178			+0.19	

be proportional to $\Delta\alpha = \alpha_1 - \alpha_2$, *i.e.*, the difference between the polarizabilities of the two cations. Taking this into account and substituting U_0^{++} for U_0 we may write eqn. (2) as follows:

$$\Delta H^M/N_1N_2 = U_0^{++} + A(\alpha_1-\alpha_2)\delta_{12} + B\delta_{12}^2 \quad (3a)$$

or for $N_1 = N_2 = 0.5$

$$(4\Delta H^M_{0.5} - U_0^{++})/(\alpha_1-\alpha_2)\delta_{12} = A + B\delta_{12}/(\alpha_1-\alpha_2) \quad (3b)$$

In these expressions A and B are unknown coefficients to be determined from experiments.

A plot of the left hand side of eqn. (3b) *versus* $\delta_{12}/(\alpha_1-\alpha_2)$ is presented in Fig. 5, and indicates that the alkali carbonate family is in fact very well represented by this equation. A least square treatment of all the data yields the following values

$A = +33.7$ kJ Å^{-2} mol^{-1}

$B = -3970$ kJ Å^2 mol^{-1}

Table 3. Ionic radii, polarizabilities, and ionization potentials for the alkali metal ions.

Ion	r [a] Å	r [b] Å	α [c] Å^3	I [d] kJ mol^{-1}
Li+	0.57	0.60	0.03	7263
Na+	0.96	0.95	0.41	4544
K+	1.34	1.33	1.33	3059
Rb+	1.49	1.48	1.98	2644
Cs+	1.68	1.69	3.34	2259

[a] Melnichak and Kleppa,[16] [b] Pauling,[19] [c] Tessman *et al.*,[18] [d] *Handbook of Chemistry and Physics*.[24]

According to Davis and Rice the quantity B should mainly reflect the sum of the coulombic energy of mixing predicted by the RKK theory plus a term which arises from nearest neighbour dispersion interactions.

The numerical values of A and B depend greatly on the actual choice of the interionic distances. For example, if we use the original Pauling radii [19] for the alkali metal ions instead of the Melnichak radii we obtain the following constants

$A' = +69.5$ kJ Å^{-2} mol^{-1}

$B' = -5150$ kJ Å^2 mol^{-1}

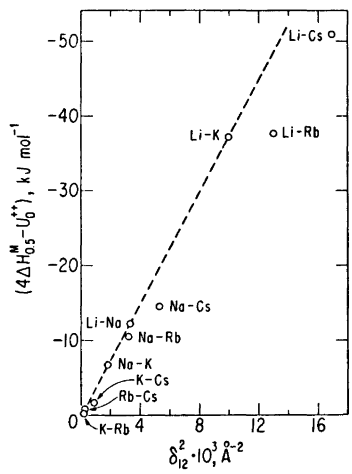

Fig. 4. Dependence of the corrected enthalpy interaction parameter, $4\Delta H^M_{0.5} - U_0^{++}$, on the size parameter δ_{12}^2 in alkali carbonate mixtures.

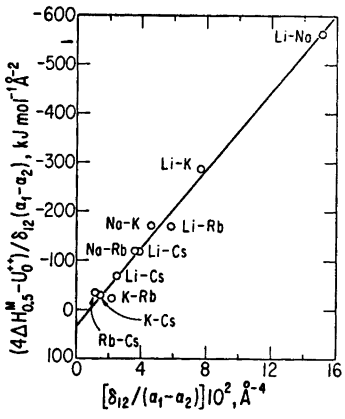

Fig. 5. Dependence of the quantity $(4\Delta H^M_{0.5}-U_0^{++})/\delta_{12}(\alpha_1-\alpha_2)$ on the parameter $\delta_{12}/(\alpha_1-\alpha_2)$ in mixtures of molten alkali carbonates. Melnichak's radii for the alkali metal ions are used.

A plot of the left hand side of eqn. (3b) *versus* $\delta_{12}/(\alpha_1-\alpha_2)$, where U_0^{++} and δ_{12} are calculated by use of the Pauling radii, is shown in Fig. 6. Except for the Li^+-ion, where the Pauling radius is 0.60 Å and the Melnichak radius 0.57 Å, the two set of ionic radii differ by only 0.01 Å or less. In fact very little is known about the interionic distances in the molten alkali carbonates, and it does not seem possible to choose between the two sets of cationic radii. Furthermore, the choice of the thermochemical radius for the CO_3^{2-}-ion also is open to serious question. It was argued by Zarzycki [20] that the larger alkali cations may tend to occupy sites near the corners of the carbonate triangle, while the smaller cations may be located closer to the centre of the carbonate anion. Fortunately, small changes in $r(CO_3^{2-})$ cause relatively small changes in δ_{12}, δ_{12}^2, and U_0^{++}. Therefore the fundamental conclusions in this discussion are not influenced by this choice.

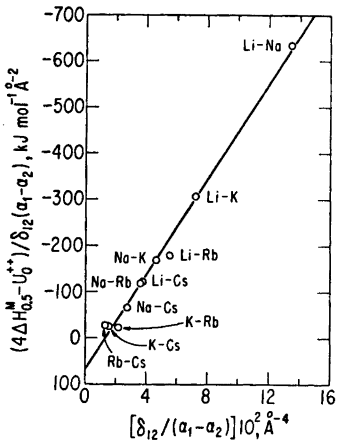

Fig. 6. Dependence of the quantity $(4\Delta H^M_{0.5}-U_0^{++})/\delta_{12}(\alpha_1-\alpha_2)$ on the parameter $\delta_{12}/(\alpha_1-\alpha_2)$ in mixtures of molten alkali carbonates. Pauling's radii for the alkali metal ions are used.

As pointed out in the introduction the only family of charge type A_2X-B_2X which has been thoroughly investigated calorimetrically is the alkali sulfate family. Østvold and Kleppa studied these mixtures using essentially the same calorimetric equipment as we have used in the present investigation. They obtained the following values for the constants in eqn. (3b), based on the Melnichak radii for the alkali metal ions and $r(SO_4^{2-}) = 2.30$ Å

$$A = +68.6 \text{ kJ Å}^{-2} \text{ mol}^{-1}$$

$$B = -5900 \text{ kJ Å}^{2} \text{ mol}^{-1}$$

Clearly, when we take the different anion radii into account the enthalpy of mixing data for the carbonate and the sulfate families show considerable similarity.

Dantzer and Kleppa [21] have expressed doubt whether the small non-zero values of the constant A in the nitrate, chloride, and bromide families are physically significant. However, for the fluorides,[16] sulfates and carbonates it is evident that significant positive values of A are obtained. In these families it seems that the cation-anion dispersion interactions may

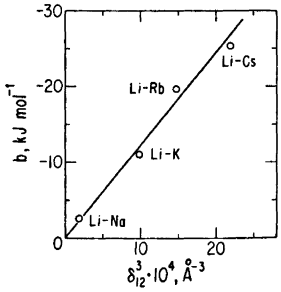

Fig. 7. Dependence of the asymmetry parameter b on the size parameter δ_{12}^3 for the mixtures of lithium carbonate with the other alkali carbonates.

Table 4. Enthalpies of mixing in binary molten alkali carbonates of equimolar composition. The temperatures of investigation are given in parentheses in degrees Kelvin.

	$4\Delta H^{M}_{0.5}$, kJ mol^{-1} Li–Na	Li–K	Na–K
This work	−11.19(1178)	−33.06(1178)	−5.66(1178)
Broers and Ballegoy [5]	−11.7(≃1200)	−33.5(≃1200)	−5.86(≃1200)
Barner and Andersen [4]	−14.6(1153)	−35.1(1189)	−7.37(1189)
Lumsden [6]	−10.0 [a]	−31.0 [a]	0.0 [a](1202)

[a] Indirectly calculated (see Introduction).

give rise to relatively large positive contributions to the enthalpy interaction parameters. These contributions vary linearly with the size parameters δ_{12} and with $(\alpha_1-\alpha_2)$. This effect might account for the deviations from linearity in the plot of corrected interaction parameter *versus* δ_{12}^2 given in Fig. 4.

The data in Table 2 show that the lithium containing carbonate mixtures exhibit quite large values of the asymmetry parameter b, which numerically increase sharply in the sequence Li–Na < Li–K < Li–Rb < Li–Cs. According to Blander's calculation [13] of the higher order terms of the RKK theory it may be expected that this parameter should depend on ionic size through the third power of δ_{12}. Such a behaviour is in fact found for the lithium containing carbonate mixtures as illustrated in Fig. 7. A similar dependence of b on δ_{12}^3 is found also for the lithium sulfate mixtures. However, for the latter the slope is −22 100 kJ Å^3 mol^{-1} while for the carbonate mixtures it is −12 300 kJ Å^3 mol^{-1}. The tendency of increasing negative slope with increasing anionic size is also evident in the lithium containing alkali halide systems. Calculations based on the data reviewed by Melnichak [16] give the slopes (−2000), −4200, −5200, and −9600 kJ Å^3 mol^{-1} for the fluoride, chloride, bromide, and iodide systems, respectively. A similar behaviour is not found in the sodium containing systems.

Influence of the carbonate dissociation. At the high temperatures used in the present investigation the thermal decomposition of the carbonate ions may have to be considered

$$CO_3^{2-} = CO_2 + O^{2-}$$

This dissociation is to some extent prevented by carrying out the experiments in an atmosphere of pure CO_2. The carbonate dissociation depends on the cations present in the melt and the dissociation constant decreases in the sequence Li > LiNa > LiK > Na > NaK > K where the double cation symbol refers to the 50 – 50 mixtures.

When the two salts are mixed, the association process $CO_2 + O^{2-} \rightarrow CO_3^{2-}$ will take place to a limited extent, thus giving rise to a positive contribution to the observed enthalpy. The dissociation constants as well as crude data for the enthalpies of dissociation for Li_2CO_3, Na_2CO_3, K_2CO_3 and their mixtures are given by Andersen.[2,3]* However, since the accuracy of the data is relatively small and no information is available for Rb_2CO_3 and Cs_2CO_3, we have chosen to present the uncorrected enthalpies of mixing only.

Temperature dependence for the enthalpy of mixing. The single measurement on the equi-

* The dissociation constants, K_d, for the process $CO_3^{2-} = CO_2 + O^{2-}$ in Li_2CO_3, Na_2CO_3, and K_2CO_3 at 1178 K are 4.53×10^{-3}, 5.59×10^{-6}, and 1.94×10^{-8}, respectively. ($K_d \approx [N(O^{2-})/N(CO_3^{2-})][p(CO_2)/p^{\ominus}]$ where the standard pressure, $p^{\ominus}$, is 101.325 kPa). The respective standard enthalpies of dissociation are 190.8, 298.7, and 341.8 kJ mol^{-1}.

Example of estimate: Since $p(CO_2)$ is equal to the standard pressure and $N(CO_3^{2-}) \approx 1$, it follows, that the change in the amount of O^{2-}-ions, Δn, during the mixing process, *e.g.*, when half a mol each of Li_2CO_3 and K_2CO_3 are mixed is: $\Delta n \approx K_d(LiKCO_3) - \frac{1}{2}K_d(Li_2CO_3) - \frac{1}{2}K_d(K_2CO_3) = -2.26\times10^{-3}$ mol. Therefore, our estimate of the enthalpy of association is: $\Delta H_{ass} \approx -(2.26\times10^{-3})\times(190\,800 + 341\,800)/2 = -600$ J which is about 7 % of the calorimetrically determined enthalpy of mixing.

The corresponding values estimated for the LiNa- and NaK-systems are −500 and −1 J, respectively. The values for the LiRb- and LiCs-systems are probably of the same order of magnitude as that for the LiK-system, while those for the systems which do not contain Li are of the order −1 J.

molar $Li_2CO_3-Cs_2CO_3$ mixture at 1198 K indicates that the enthalpy of mixing becomes less exothermic with increasing temperature. The change in heat capacity upon mixing, ΔC_p, is calculated to be of the order +12 J K^{-1} mol^{-1}. The positive value of ΔC_p is in accordance with the results of Østvold and Kleppa [1] for the $(Li-Na)_2SO_4$ system and of Hong and Kleppa [22] for the (Li−K)F system. Hong and Kleppa attempt to explain the numerically smaller values in the enthalpy of mixing at the higher temperatures in terms of the thermal expansion of the salts. They propose the following simple approximate relation between ΔC_p and ΔH^M

$$\Delta C_p = -\tfrac{2}{3}\Delta H^M \gamma_1 \qquad (4)$$

where γ_1 is the volume coefficient of expansion of component 1. This gives the right sign and the right order of magnitude of ΔC_p for the (Li−K)F system. However, for the $(Li-Cs)_2CO_3$ system the calculated maximum value of ΔC_p is only 1.5 J K^{-1} mol^{-1}, *i.e.*, nearly one order of magnitude lower than the experimental value. However, the latter value probably is not very accurate since only one measurement was carried out at 1198 K. Also the increased dissociation of the carbonate ions and the increased volatility of the salts at the higher temperature were not taken into account.

Comparison with earlier data. In Table 4 we compare our new results with earlier data, when such data are available. The earlier data are limited to the 50−50 composition. The agreement with the results of Broers and Ballegoy is quite good. However, Broers and Ballegoy concluded from their results that the experimental uncertainties did not allow a closer analysis of the asymmetry in the ΔH^M curves.

Acknowledgements. We are indebted to Dr. J. Ito who carried out the spectrochemical analyses of the rubidium and cesium salts.

This investigation has been supported by a grant from the National Science Foundation and has also benefited from the general support of Materials Science at University of Chicago provided by NSF-MRL.

One of the authors (BKA) wishes to acknowledge financial support from Statens Naturvidenskabelige Forskningsråd (Denmark).

REFERENCES

1. Østvold, T. and Kleppa, O. J. *Acta Chem. Scand. 25* (1971) 919.
2. Andersen, B. K. *Proc. 3rd. Int. Conf. Fuel Cells*, Brussels 1969, p. 87.
3. Andersen, B. K., *Ph.D. Thesis*, The Technical University of Denmark, Lyngby 1975.
4. Barner, J. H. von and Andersen, B. K. *Unpublished work* (1967).
5. Broers, G. H. J. and Ballegoy, H. J. J. van. *Unpublished work* (1970).
6. Lumsden, J. *Thermodynamics of Molten Salt Mixtures*, Academic, New York 1966.
7. Janz, G. J. and Lorenz, M. R. *J. Chem. Eng. Data 6* (1961) 321.
8. Janz, G. J., Neuenschwander, E. and Kelley, F. J. *Trans. Faraday Soc. 59* (1963) 841.
9. Kleppa, O. J. *J. Phys. Chem. 64* (1960) 1937.
10. Janz, G. J. and Conte, A. *Corrosion 20* (1964) 237.
11. Kelley, K. K. *U.S. Bur. Mines Bull. 584* (1960).
12. Reiss, H., Katz, J. L. and Kleppa, O. J. *J. Chem. Phys. 36* (1962) 144.
13. Blander, M. *J. Chem. Phys. 34* (1961) 192.
14. Davis, H. T. and Rice, S. A. *J. Chem. Phys.* (1964) 14.
15. Hersh, L. S. and Kleppa, O. J. *J. Chem. Phys. 42* (1965) 1309.
16. Melnichak, M. E. and Kleppa, O. J. *Rev. Chim. Miner. 9* (1972) 63.
17. Kapustinskii, A. F. *Q. Rev. Chem. Soc. 10* (1956) 283.
18. Tessman, J. R., Kahn, A. H. and Shockley, W. *Phys. Rev. 92* (1953) 890.
19. Pauling, L. *The Nature of the Chemical Bond*, 3rd. Ed., Cornell University Press, New York 1960.
20. Zarzycki, J. *Discuss. Faraday Soc. 32* (1961) 38.
21. Dantzer, P. and Kleppa, O. J. *J. Chim. Phys. 71* (1974) 216.
22. Hong, K. C. and Kleppa, O. J. *J. Chem. Thermodyn. 8* (1976) 31.
23. Førland, T. *On the Properties of Some Mixtures of Fused Salts*, Norges tekniske Vitenskapsakademi Series 2, No. 4, Trondheim 1957.
24. *Handbook of Chemistry and Physics*, 48th. Ed., Chemical Rubber Co., Cleveland 1967.

Received April 2, 1976.

Acta Chemica Scandinavica A 30 (1976) 759—766

Short Communications

Electron-diffraction Study of Gaseous Tetrafluoro-1,3-dithietane

ZUZANA SMITH and RAGNHILD SEIP

Department of Chemistry, University of Oslo, Oslo 3, Norway

The geometry and the low-frequency ring-puckering motion in four-membered rings depend on the relative magnitude of the two opposing forces, the bond angle strain and the torsional strain. It has been reported that all cyclobutane rings unconstrained by adjacent rings are puckered in the gas phase.[1] Harris and Yang,[2] however, interpreted vibrational spectra of perfluorocyclobutane in terms of a planar molecule with D_{4h} symmetry, even though electron-diffraction studies find the ring puckered.[1,3] In a spectroscopic work by Durig *et al.*[4] the authors concluded that tetrafluoro-1,3-dithietane belongs to the D_{2h} symmetry group, while a related molecule, trimethylene sulfide, was found to be puckered [5,6] with a puckering angle of 26°. This study was undertaken in order to determine the structural parameters of tetrafluoro-1,3-dithietane by the electron-diffraction method.

Experimental. A sample of tetrafluoro-1,3-dithietane was purchased from PCR, Incorporated, and purified by distillation. The diffraction diagrams were recorded with a Balzers Eldigraph KD-G2,[7,8] at a nozzle temperature of about 25 °C. Five plates exposed at a camera distance of 500.12 mm and four at 250.12 mm were used in the structural analysis. The electron wavelengths were 0.05865 Å and 0.05857 Å for the two camera distances as calibrated with the diffraction patterns of gaseous benzene. The intensity data spanned the range of $s = 1.625 - 15.50$ Å^{-1} and $5.0 - 28.75$ Å^{-1}. The data processing and the structural analysis were carried out in the usual way.[9] The elastic scattering factors were calculated by the partial wave method[10] based upon analytical HF potentials,[11] and the inelastic scattering factors used were those of Tavard *et al.*[12] The modification function $s/(|f_S'||f_F'|)$ was applied. The average modified molecular intensities [9] for each camera distance are shown in Fig. 1, and the radial distribution function calculated from the composite molecular intensity is shown in Fig. 2.

Structural analysis. A preliminary set of amplitudes of vibration (u) and the correction coefficients (K) were calculated by normal coordinate analysis [13] using the experimental data of Durig *et al.*[4] Due to some discrepancies in fitting the experimental frequencies, more extensive analysis will be necessary.

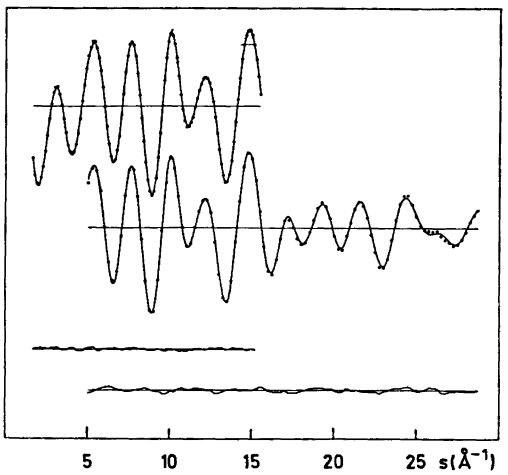

Fig. 1. The experimental intensity data (circles) for tetrafluoro-1,3-dithietane from the 50 cm ($\Delta s = 0.125$ Å) and the 25 cm ($\Delta s = 0.25$ Å) camera distances. The solid line corresponds to the calculated molecular intensities, while the lower curves represent the difference between the experimental and the calculated intensities.

The least-squares refinements were carried out under the assumption that the FCF planes bisect the corresponding SCS angles and are perpendicular to the corresponding SCS plane. As one can see from Table 1, the puckering angle (α) C1S2C3 – C3S4C1, is highly correlated with the CSC angle and with the amplitudes of vibrations u(C1F7) and u(F5F7). When angle α was kept at 0° the values shown in Table 2 were found. When all four parameters were varied simultaneously, least-squares refinement converged to the following values of these parameters: $\alpha = 5.4(18)°$, $\angle CSC = 82.7(2)$, $u(C1F7) = 0.083(9)$ Å and $u(F5F7) = 0.141(43)$ Å, while the other parameters were not significantly influenced. The agreement is nearly identical for α values in the range 0 – 6°; with further increase in the angle the agreement becomes quickly worse. Study of the refined

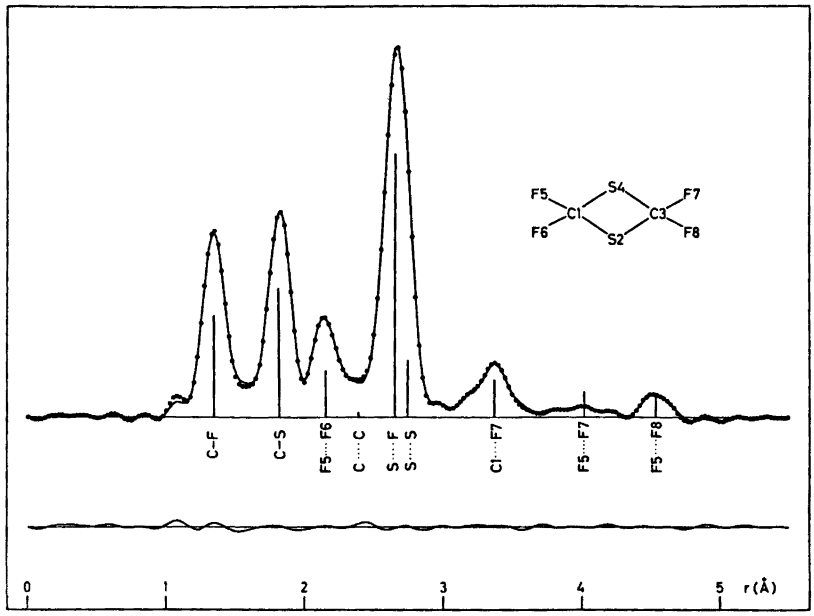

Fig. 2. Experimental (circles) and calculated (solid line) radial distribution curves for tetrafluoro-1,3-dithietane. The lower curve represents the difference between the experimental and calculated curves. The positions and approximate areas are indicated. Damping constant was 0.001 Å².

Table 1. Correlation coefficients, ϱ_{ij}, greater than 0.5, obtained when all parameters were varied and a diagonal weight matrix was used.

i	j	ϱ_{ij}
r(CS)	∠FCF	0.62
∠CSC	α	0.81
∠CSC	u(C1F7)	−0.74
∠CSC	u(SF)	0.53
∠CSC	u(F5F7)	−0.79
α	u(C1F7)	−0.89
α	u(F5F7)	−0.96
u(C1F7)	u(F5F7)	0.84
u(SF)	*scale* (50 cm)	0.51

amplitudes of vibration indicates that the equilibrium angle is very close to zero, since the values u(C1F7) = 0.10 and u(F5F7) = 0.21 were obtained by normal coordinate analysis. When the amplitudes of vibration u(CC) and u(SS) were varied, they converged to unreasonably small values (0.040 and 0.048, respectively), therefore the calculated values were assumed.

The C–S bond distance and the CSC angle in thietane (1.847(2) Å and 77.0(5)°, respectively) were compared with corresponding parameters in analogous molecules,[15] and it was

Table 2. Structural parameters [a] for tetrafluoro-1,3-dithietane.

Parameter	r_a (Å)	u (Å)
C–S	1.820(2)	0.049(2)
C–F	1.344(2)	0.049(2)
∠CSC(°) [b]	82.7(2)	
∠FCF(°) [b]	106.5(2)	
α(°)	0.0	
C···C	2.402(5)	0.069
S···S	2.728(4)	0.056
F5···F6	2.154(4)	0.053(4)
C···F	3.376(5)	0.091(4)
S···F	2.656(3)	0.070(1)
F5···F7	3.991(6)	0.179(14)
F5···F8	4.538(6)	0.082(5)

[a] Results from geometrically consistent r_α-refinements. The standard deviations given in parentheses include correction for data correlation.[13] The deviations for distance parameters are corrected for systematic uncertainties according to $\sigma = [\sigma_{LS}^2 + (0.001r)^2]^{\frac{1}{2}}$. The asymmetry constants used were (in 10^{-6} Å³): k(C–S) = 2.0, k(C–F) = 2.0, and zero for non-bonded distances. [b] When refinement is carried out on the r_a-structure, ∠CSC = 82.4(2)° and ∠FCF = 106.6(2)°.

concluded that the C–S bond lengths in four-membered rings are clearly longer than in other environments. The C–S bond distance in tetrafluoro-1,3-dithietane, 1.820(2) Å, is shorter than that in thietane; however, the CSC angle is larger, 82.7(2)°. The corresponding parameters are 1.804(3) Å and 97.0(19)° in 4-thiacyclohexanone.[16]

The ED-data are consistent with D_{2h} symmetry for tetrafluoro-1,3-dithietane, a result which is in agreement with vibrational [4] and NMR [17] spectroscopy.

Acknowledgement. We would like to thank Dr. H. M. Seip for many helpful discussions and Mrs. S. Gundersen for her assistance with the data reduction. The financial support for this research was provided, in part, by the Royal Norwegian Council for Scientific and Industrial Research (NTNF).

1. Chang, C. H., Porter, R. F. and Bauer, S. H. *J. Mol. Struct. 7* (1971) 89.
2. Harris, W. C. and Yang, D. B. *J. Chem. Phys. 60* (1974) 4175.
3. Alekseev, N. V. and Barzdain, P. P. *J. Struct. Chem. 15* (1974) 171; Lemaire, H. P. and Livingston, R. L. *J. Am. Chem. Soc. 74* (1952) 5732.
4. Durig, J. R. and Lord, R. C. *Spectrochim. Acta 19* (1963) 769.
5. Karakida, K. and Kuchitsu, K. *Bull. Chem. Soc. Jpn. 48* (1975) 1691.
6. Harris, D. O., Harrington, H. W., Luntz, A. C. and Gwinn, W. D. *J. Chem. Phys. 44* (1966) 3467.
7. Zeil, W., Haase, J. and Wegmann, L. *Z. Instrumentenk. 74* (1966) 84.
8. Bastiansen, O., Graber, R. and Wegmann, L. *Balzers High Vacuum Report 25* (1969) 1.
9. Andersen, B., Seip, H. M., Strand, T. G. and Stølevik, R. *Acta Chem. Scand. 23* (1969) 3224.
10. Yates, A. C. *Comput. Phys. Commun. 2* (1971) 175.
11. Strand, T. G. and Bonham, R. A. *J. Chem. Phys. 40* (1964) 1686.
12. Tavard, C., Nicolas, D. and Rouault, M. *J. Chim. Phys. 64* (1967) 540.
13. Stølevik, R., Seip, H. M. and Cyvin, S. J. *Chem. Phys. Lett. 15* (1972) 263.
14. Seip, H. M., Strand, T. G. and Stølevik, R. *Chem. Phys. Lett. 3* (1969) 617.
15. Karakida, K., Kuchitsu, K. and Bohn, R. K. *Chem. Lett.* (1974) 159.
16. Seip, R., Seip, H. M. and Smith, Z. *J. Mol. Struct. 32* (1976) 279.
17. Long, R. C., Jr. and Goldstein, J. H. *J. Chem. Phys. 54* (1971) 1563.

Received June 8, 1976.

Hydrogen Bonding Effects on the Fluorescence of Methyl Salicylate

KJELL SANDROS

Department of Physical Chemistry, Chalmers University of Technology, Fack, S-402 20 Göteborg, Sweden

Some twenty years ago Weller [1] found that salicylic acid and methyl salicylate in methanol solution have unstructured fluorescence spectra both with a Stokes' shift about 5000 cm^{-1} greater than that of the corresponding methoxy compound, *o*-methoxy benzoic acid and its methyl ester. An additional weak fluorescence component with a Stokes' shift similar to that of the corresponding methoxy compound appeared in hydrocarbon solutions. The ratio between the intensities of the short and long wavelength components of the methyl salicylate fluorescence decreased as the temperature was reduced. Partial quenching of the fluorescence with carbon disulfide did not affect the intensity ratio. Weller interpreted the fluorescence properties of salicylic acid and methyl salicylate as a result of the following, at room temperature fully established, protolytic equilibrium in the excited state:

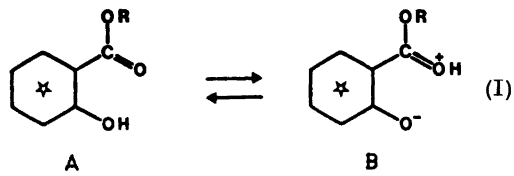

(I)

where R denotes H or CH_3. The short and long wavelength fluorescence components should emanate from A and B, respectively. This interpretation was supported by the fact that phenolic groups are much more acidic in the lowest excited singlet state than in the ground state, while excitation makes aromatic carbonyl and carboxyl groups much more basic. Excitation of intramolecularly hydrogen-bonded salicylic acid or methyl salicylate molecules would thus favour an intramolecular proton transfer. From the measurements on methyl salicylate in methylcyclohexane, Weller calculated the ΔH values for the proton transfer as -1.0 kcal mol^{-1} and 13.5 kcal mol^{-1} in the excited and ground states, respectively.*

A preliminary new study of the methyl salicylate fluorescence has revealed some unexpected effects of solvent and excitation wavelength, which indicate that the hitherto accepted reaction mechanism should be modified. As seen from Fig. 1, the ratio between the intensities of the short and long wavelength

* 1 kcal = 4.184 kJ.

concluded that the C–S bond lengths in four-membered rings are clearly longer than in other environments. The C–S bond distance in tetrafluoro-1,3-dithietane, 1.820(2) Å, is shorter than that in thietane; however, the CSC angle is larger, 82.7(2)°. The corresponding parameters are 1.804(3) Å and 97.0(19)° in 4-thiacyclohexanone.[16]

The ED-data are consistent with D_{2h} symmetry for tetrafluoro-1,3-dithietane, a result which is in agreement with vibrational [4] and NMR [17] spectroscopy.

Acknowledgement. We would like to thank Dr. H. M. Seip for many helpful discussions and Mrs. S. Gundersen for her assistance with the data reduction. The financial support for this research was provided, in part, by the Royal Norwegian Council for Scientific and Industrial Research (NTNF).

1. Chang, C. H., Porter, R. F. and Bauer, S. H. *J. Mol. Struct. 7* (1971) 89.
2. Harris, W. C. and Yang, D. B. *J. Chem. Phys. 60* (1974) 4175.
3. Alekseev, N. V. and Barzdain, P. P. *J. Struct. Chem. 15* (1974) 171; Lemaire, H. P. and Livingston, R. L. *J. Am. Chem. Soc. 74* (1952) 5732.
4. Durig, J. R. and Lord, R. C. *Spectrochim. Acta 19* (1963) 769.
5. Karakida, K. and Kuchitsu, K. *Bull. Chem. Soc. Jpn. 48* (1975) 1691.
6. Harris, D. O., Harrington, H. W., Luntz, A. C. and Gwinn, W. D. *J. Chem. Phys. 44* (1966) 3467.
7. Zeil, W., Haase, J. and Wegmann, L. *Z. Instrumentenk. 74* (1966) 84.
8. Bastiansen, O., Graber, R. and Wegmann, L. *Balzers High Vacuum Report 25* (1969) 1.
9. Andersen, B., Seip, H. M., Strand, T. G. and Stølevik, R. *Acta Chem. Scand. 23* (1969) 3224.
10. Yates, A. C. *Comput. Phys. Commun. 2* (1971) 175.
11. Strand, T. G. and Bonham, R. A. *J. Chem. Phys. 40* (1964) 1686.
12. Tavard, C., Nicolas, D. and Rouault, M. *J. Chim. Phys. 64* (1967) 540.
13. Stølevik, R., Seip, H. M. and Cyvin, S. J. *Chem. Phys. Lett. 15* (1972) 263.
14. Seip, H. M., Strand, T. G. and Stølevik, R. *Chem. Phys. Lett. 3* (1969) 617.
15. Karakida, K., Kuchitsu, K. and Bohn, R. K. *Chem. Lett.* (1974) 159.
16. Seip, R., Seip, H. M. and Smith, Z. *J. Mol. Struct. 32* (1976) 279.
17. Long, R. C., Jr. and Goldstein, J. H. *J. Chem. Phys. 54* (1971) 1563.

Received June 8, 1976.

Hydrogen Bonding Effects on the Fluorescence of Methyl Salicylate

KJELL SANDROS

Department of Physical Chemistry, Chalmers University of Technology, Fack, S-402 20 Göteborg, Sweden

Some twenty years ago Weller [1] found that salicylic acid and methyl salicylate in methanol solution have unstructured fluorescence spectra both with a Stokes' shift about 5000 cm^{-1} greater than that of the corresponding methoxy compound, *o*-methoxy benzoic acid and its methyl ester. An additional weak fluorescence component with a Stokes' shift similar to that of the corresponding methoxy compound appeared in hydrocarbon solutions. The ratio between the intensities of the short and long wavelength components of the methyl salicylate fluorescence decreased as the temperature was reduced. Partial quenching of the fluorescence with carbon disulfide did not affect the intensity ratio. Weller interpreted the fluorescence properties of salicylic acid and methyl salicylate as a result of the following, at room temperature fully established, protolytic equilibrium in the excited state:

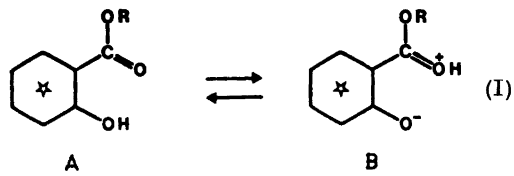

(I)

where R denotes H or CH_3. The short and long wavelength fluorescence components should emanate from A and B, respectively. This interpretation was supported by the fact that phenolic groups are much more acidic in the lowest excited singlet state than in the ground state, while excitation makes aromatic carbonyl and carboxyl groups much more basic. Excitation of intramolecularly hydrogen-bonded salicylic acid or methyl salicylate molecules would thus favour an intramolecular proton transfer. From the measurements on methyl salicylate in methylcyclohexane, Weller calculated the ΔH values for the proton transfer as -1.0 kcal mol^{-1} and 13.5 kcal mol^{-1} in the excited and ground states, respectively.*

A preliminary new study of the methyl salicylate fluorescence has revealed some unexpected effects of solvent and excitation wavelength, which indicate that the hitherto accepted reaction mechanism should be modified. As seen from Fig. 1, the ratio between the intensities of the short and long wavelength

* 1 kcal = 4.184 kJ.

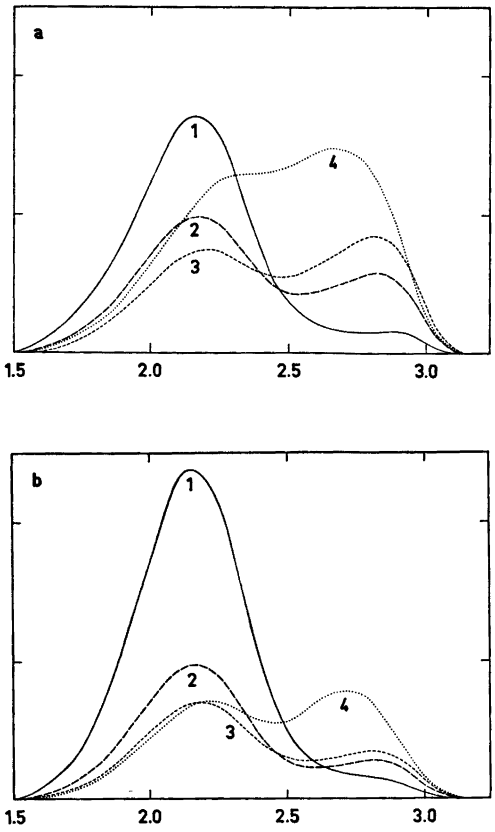

Fig. 1. Fluorescence spectra of 2×10^{-4} mol dm^{-3} methyl salicylate in cyclohexane (——), ethanol (– – –), methanol (- - -), and 2,2,2,-trifluoroethanol (···). The spectra are shown in relative numbers of quanta *vs.* wave number in μm^{-1}. The excitation wavelengths are 286 nm and 316 nm in *a* and *b*, respectively.

fluorescence components depends on the excitation wavelength, and, contrary to the earlier findings, this ratio is much greater in the alcoholic solvents than in cyclohexane. The ratio increases in the same order as do the stabilities of the hydrogen bond complexes between the alcohols and esters. For, *e.g.*, the ethyl acetate complex with ethanol, methanol, or 2,2,2-trifluorethanol, the values of the stability constants are:[2,3] 1.0, 1.4, and 6.9 dm^3 mol^{-1} in carbon tetrachloride at 25 °C. The position of the short wavelength maximum is seen to be solvent dependent. The fluorescence maximum of methyl *o*-methoxybenzoate shows similar solvent shifts.

The fact that the fluorescence spectrum of methyl salicylate depends on the excitation wavelength indicates at least two forms of ground state molecules and that the relative steady state concentrations of the fluorescing species depend on the proportions in which the ground state forms are excited. It seems tempting to assume that the relevant ground state forms are those with and without an established intramolecular hydrogen bond. Yasunaga *et al.*[4] have, by means of ultrasonic absorption measurements, performed a kinetic study of the ground state equilibrium:

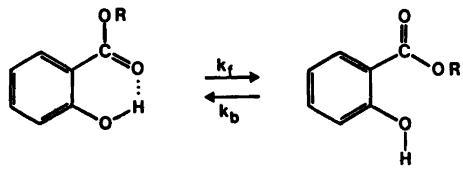

(II)

cis *trans*

The rate constants found in neat methyl salicylate at 25 °C were $k_f = 9.5 \times 10^5$ and $k_b = 2.6 \times 10^7$ s^{-1}. If excited methyl salicylate in cyclohexane solution has a similar value of k_b, the formation of the *cis* form, a prerequisite for the intramolecular proton transfer, cannot efficiently take place during the lifetime of the excited *trans* form. In air saturated solution this lifetime is most probably less than 10^{-8} s. It might well be that the proton transfer in excited *cis* form molecules is very efficient, *i.e.* that equilibrium (I) is almost totally displaced to the right. The temperature effect on equilibrium (II) should then be the main cause of the fluorescence temperature dependence in methylcyclohexane solution found by Weller. In the alcoholic solvents a proton transfer is evidently inhibited by the formation of an intermolecular hydrogen bond between the ester group and the solvent. It may also be noted that for salicylic acid in cyclohexane or benzene, the intensity ratio between the short and long wavelength fluorescence components increases with the acid concentration in a way that may be quantitatively accounted for as caused by dimer formation. The cyclic hydrogen bonding of the carboxyl groups in the dimer inhibits a proton transfer.

It may be expected that spectrally resolved fluorescence lifetime measurements will give more conclusive information regarding the processes which determine the fluorescence behaviour of methyl salicylate.

Experimental. The methyl salicylate was purified by fractional distillation at 1.6 kPa. Gas chromatography of the distilled sample indicate a purity of 99.96 %. The fluorescence spectra at 25 °C obtained with an Aminco Bowman spectrophotofluorometer were transformed to relative quantum spectra on a wave number scale.

Acknowledgement. My thanks are due to Dr. Hans-Dieter Becker for purification and analysis of the methyl salicylate sample.

1. Weller, A. *Z. Elektrochem. 60* (1956) 1144.
2. Becker, E. D. *Spectrochim. Acta 17* (1961) 436.
3. Sherry, A. D. and Purcell, K. F. *J. Phys. Chem. 74* (1970) 3535.
4. Yasunaga, T., Tatsumoto, N., Inoue, H. and Miura, M. *J. Phys. Chem. 73* (1969) 477.

Received June 23, 1976.

NMR Experiments on Cyclic Sulfites. VII. Lanthanide Induced Chemical Shifts in Trimethylene Sulfites with Respect to the Orientation of the S=O Bond

PER ALBRIKTSEN * and
TORE THORSTENSON

Department of Chemistry, University of Bergen, N-5014 Bergen-Univ., Norway

Lanthanide induced chemical shifts (LIS) in sulfoxides have been published.[1] The LIS chemical shift increases linearly with the concentration of the shift reagent for a given sulfoxide concentration. Several workers have attempted to correlate the shifts with the internuclear distance between the proton studied and the lanthanide ion on the basis of assumed models. Apparently the lanthanide induced shifts should make it possible to distinguish between an axial and an equatorial functional group in cyclic compounds since the internuclear distance is changed substantially when the coordination site is moved from one position to the other. Accordingly, the shift induced on complexing the substrate will depend on the relative contributions of rotamers or conformers. The trimethylene (TM) sulfites have been shown to exist in a rigid chair conformation preferably with the S=O group in the axial position.[2-7] However, equatorial S=O groups have been observed for some substituted TM sulfites.[4] A study of LIS of TM sulfites with either S=O equatorial or axial should give additional information with regard to the stereochemistry of cyclic sulfites.

Results and discussion. The following TM sulfites have been prepared and examined with regard to the lanthanide induced shifts of the 4- and 5-protons and 4- and 5-substituted methyl groups: TM sulfite (I), 5-methyl-TM sulfite (II), 5,5-dimethyl-TM sulfite (III), 4-methyl-TM sulfite (IV), 5-phenyl-TM sulfite (V), 5-*tert*-butyl-TM sulfite (VI), 4,6-dimethyl-TM sulfite (with axial S=O bond VII a, with equatorial S=O VII b, and a twisted form VII c) and *trans*-1,3,2-dioxathiadecalin-2-oxide (with axial S=O VIII a, with eq. S=O VIII b).

The compounds I–VI have been reported to be in a 100 % or close to a 100 % rigid chair conformation with axial S=O bond. VII b and VIII b are found to be in a rigid chair conformation with equatorial S=O bond.[5,15]

When the concentration of the LSR is plotted against the chemical shift for the discrete protons, the "shiftslope" will depend on the position of the proton in the molecule. This is shown by Fig. 1 for TM sulfite and *cis*-4,6-dimethyl-TM sulfite (S=O eq. and twisted) and in Table 1 the corresponding slopes are calculated together with the "shiftslopes", K^s, of the other molecules examined.

From each of the three conformational forms in Table 1 and Fig. 1, it is evident that we are able to differentiate between axial and equatorial groups or protons on the same carbon atom. Likewise, we can differentiate between the two rigid chair forms with axial and equatorial S=O bond and the twisted conformer by comparing the Eu-shift for the 4 (6) axial protons.

Under certain conditions for internal rotation or for axial symmetry in the susceptibility tensor, the pseudocontact contribution to the

Table 1. The "shiftslope" K^s (ν/x) for the methyl protons in the rigid chair conformations of the trimethylenesulfites with axial S=O bond, equatorial S=O bond, and the twisted form.

R/K^s (Hz)	S=O ax	S=O eq	Twist
$H_{4,6a}$	8.5 – 11.2	3.7 – 3.8	9.7 (H_{4a})
$H_{4,6e}$	3.5 – 4.4	5.7	4.4 (H_{6e})
H_{5a}	3.8 – 5.6	6.2 – 7.6	–
H_{5e}	3.1 – 3.8	3.2	–
$Me_{4,6e}$	2.1 – 2.6	2.8	5.7 (Me_{4e})
Me_{6a}	–	–	2.2
Me_{5a}	2.4 – 3.7	–	–
Me_{5e}	1.6 – 2.0	–	–

* Present address: Rafinor A/S & Co., N-5154 Mongstad, Norway.

Acknowledgement. My thanks are due to Dr. Hans-Dieter Becker for purification and analysis of the methyl salicylate sample.

1. Weller, A. *Z. Elektrochem. 60* (1956) 1144.
2. Becker, E. D. *Spectrochim. Acta 17* (1961) 436.
3. Sherry, A. D. and Purcell, K. F. *J. Phys. Chem. 74* (1970) 3535.
4. Yasunaga, T., Tatsumoto, N., Inoue, H. and Miura, M. *J. Phys. Chem. 73* (1969) 477.

Received June 23, 1976.

NMR Experiments on Cyclic Sulfites. VII. Lanthanide Induced Chemical Shifts in Trimethylene Sulfites with Respect to the Orientation of the S=O Bond

PER ALBRIKTSEN * and
TORE THORSTENSON

Department of Chemistry, University of Bergen, N-5014 Bergen-Univ., Norway

Lanthanide induced chemical shifts (LIS) in sulfoxides have been published.[1] The LIS chemical shift increases linearly with the concentration of the shift reagent for a given sulfoxide concentration. Several workers have attempted to correlate the shifts with the internuclear distance between the proton studied and the lanthanide ion on the basis of assumed models. Apparently the lanthanide induced shifts should make it possible to distinguish between an axial and an equatorial functional group in cyclic compounds since the internuclear distance is changed substantially when the coordination site is moved from one position to the other. Accordingly, the shift induced on complexing the substrate will depend on the relative contributions of rotamers or conformers. The trimethylene (TM) sulfites have been shown to exist in a rigid chair conformation preferably with the S=O group in the axial position.[2-7] However, equatorial S=O groups have been observed for some substituted TM sulfites.[4] A study of LIS of TM sulfites with either S=O equatorial or axial should give additional information with regard to the stereochemistry of cyclic sulfites.

Results and discussion. The following TM sulfites have been prepared and examined with regard to the lanthanide induced shifts of the 4- and 5-protons and 4- and 5-substituted methyl groups: TM sulfite (I), 5-methyl-TM sulfite (II), 5,5-dimethyl-TM sulfite (III), 4-methyl-TM sulfite (IV), 5-phenyl-TM sulfite (V), 5-*tert*-butyl-TM sulfite (VI), 4,6-dimethyl-TM sulfite (with axial S=O bond VII a, with equatorial S=O VII b, and a twisted form VII c) and *trans*-1,3,2-dioxathiadecalin-2-oxide (with axial S=O VIII a, with eq. S=O VIII b).

The compounds I–VI have been reported to be in a 100 % or close to a 100 % rigid chair conformation with axial S=O bond. VII b and VIII b are found to be in a rigid chair conformation with equatorial S=O bond.[5,15]

When the concentration of the LSR is plotted against the chemical shift for the discrete protons, the "shiftslope" will depend on the position of the proton in the molecule. This is shown by Fig. 1 for TM sulfite and *cis*-4,6-dimethyl-TM sulfite (S=O eq. and twisted) and in Table 1 the corresponding slopes are calculated together with the "shiftslopes", K^s, of the other molecules examined.

From each of the three conformational forms in Table 1 and Fig. 1, it is evident that we are able to differentiate between axial and equatorial groups or protons on the same carbon atom. Likewise, we can differentiate between the two rigid chair forms with axial and equatorial S=O bond and the twisted conformer by comparing the Eu-shift for the 4 (6) axial protons.

Under certain conditions for internal rotation or for axial symmetry in the susceptibility tensor, the pseudocontact contribution to the

Table 1. The "shiftslope" K^s (ν/x) for the methyl protons in the rigid chair conformations of the trimethylenesulfites with axial S=O bond, equatorial S=O bond, and the twisted form.

R/K^s (Hz)	S=O ax	S=O eq	Twist
$H_{4,6a}$	8.5 – 11.2	3.7 – 3.8	9.7 (H_{4a})
$H_{4,6e}$	3.5 – 4.4	5.7	4.4 (H_{6e})
H_{5a}	3.8 – 5.6	6.2 – 7.6	–
H_{5e}	3.1 – 3.8	3.2	–
$Me_{4,6e}$	2.1 – 2.6	2.8	5.7 (Me_{4e})
Me_{6a}	–	–	2.2
Me_{5a}	2.4 – 3.7	–	–
Me_{5e}	1.6 – 2.0	–	–

* Present address: Rafinor A/S & Co., N-5154 Mongstad, Norway.

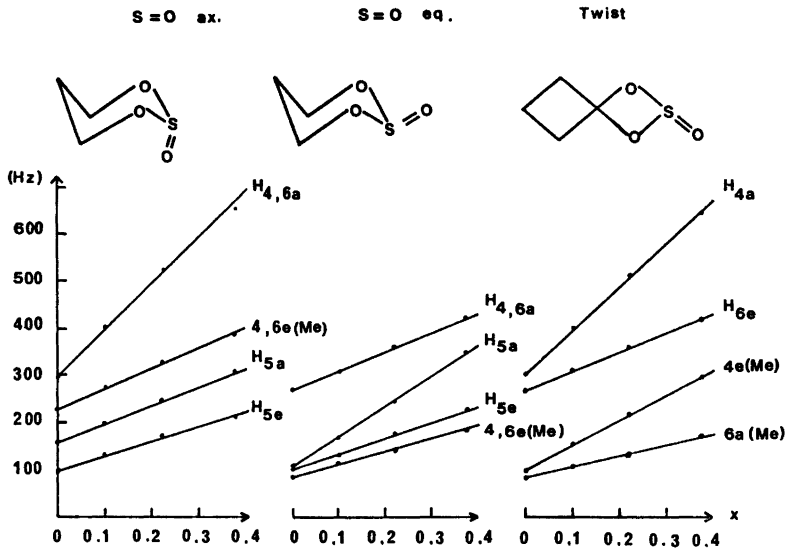

Fig. 1. Lanthanide induced shifts, as a function of the mol fraction, x, for the ring protons (methyl groups) in the rigid chair conformations of trimethylenesulfites with axial S=O bond, equatorial S=O bond, and the twisted form.

^{1}H NMR shift of a proton in a paramagnetic complex can be expressed by eqn. 1. The experimental studies on induced europium shifts can in these cases be analysed in terms of eqn. 1.

$$\Delta\delta_i = k(3\cos^2\theta - 1)/R_i^3 \quad (1)$$

where $\Delta\delta_i$ is the induced shift of the i'th proton, R_i is the proton europium distance, k is a constant and θ is the angle between the radius vector from the europium ion to the i'th proton and the symmetry axis of the complex. The experimental paramagnetic shifts have been shown to depend on $1/R_i^3$.[1] Small discrepancies [9–10] from the $1/R_i^3$ dependency have been assumed to be due to the failure to consider the angular dependency portion of the pseudocontact term.

In this work we have found a good qualitative measure for the distinguishing between a chair form with axial S=O bond, equatorial S=O bond or a twisted form without numerical evaluation of the different terms of eqn. 1.

Application of this method to conformationally mobile sulfites should be made with caution, for it is extremely difficult to predict rotamer populations in the complex with $Eu(FOD)_3$. It has been found for three 5-axial substituted sulfites [11] that on complexing with $Eu(FOD)_3$ the coupling constants are changed towards those of the rigid chair conformation with an axial S=O bond which is assumed [12] to be the most preferable energetically.

Experimental. The synthesis of the unsubstituted and 4- and 5-substituted TM sulfites has been reported previously.[2,7,8,13–15] The compounds I–VI with axial S=O bond were purified by GLC on an Aerograph Autoprep A-700 with a 2.1 m × 6.0 mm column packed with 10 % PDEAS and 10 % Carbowax on Chromosorb W, OMCS A/W, 45/60 Mesh. The compounds VII showed 3 isomers which have been reported to consist of rigid chair forms, with axial S=O (VII a), one with equatorial S=O (VII b) and one twisted (VII c). Compound VIII showed two isomers, also reported [15] consisting of two rigid chair forms, one with axial S=O (VIII a) and one with equatorial S=O (VIII b). The isomer b of these two compounds (with equatorial S=O) was purified by dissolving the reaction mixture, prior to distillation, in ethanol, from which white needles of isomer b were crystallized.

The NMR spectra were obtained on a JEOL-JNM-C-60-H instrument. Carbon tetrachloride was used as solvent. The concentration of the various sulfites were 5 mol % and the mol fractions between $Eu(FOD)_3$ and sulfite were 0.1, 0.22, and 0.375, respectively. 2 vol % tetramethylsilane was added as an internal reference. The $Eu(FOD)_3$ reagent was dried in vacuum at 50 °C for several hours prior to use.

1. Fraser, R. R. and Wigfield, Y. Y. *Chem. Commun.* (1970) 1471.
2. Woerden van H. F. and Havinga, E. *Recl. Trav. Chim. Pays-Bas 86* (1967) 341 and 353.

3. Cazaux, L. and Maroni, P. *Tetrahedron Lett.* (1969) 3667.
4. Cazaux, L., Chassaing, G. and Maroni, P. *Tetrahedron Lett.* (1975) 2517.
5. Wucherpfennig, W. *Justus Liebigs Ann. Chem. 737* (1970) 144.
6. Albriktsen, P. *Acta Chem. Scand. 25* (1971) 478.
7. Albriktsen, P. *Acta Chem. Scand. 26* (1972) 1738 and 3678.
8. Wood, G., McIntosh, J. M. and Miskow, M. H. *Can. J. Chem. 49* (1971) 1202.
9. Farid, S., Ateya, A. and Maggio, M. *Chem. Commun.* (1971) 1285.
10. Briggs, J., Hart, F. A. and Moss, G. P. *Chem. Commun.* (1970) 1506.
11. Albriktsen, P. and Thorstenson, T. *Unpublished results.*
12. Wolfe, S., Rauk, A., Tel, L. M. and Csizmadia, J. G. *J. Chem. Soc. B* (1971) 136, and references therein.
13. Lauterbur, P. C., Pritchard, J. G. and Vollmer, R. L. *J. Chem. Soc.* (1963) 5307.
14. Pritchard, J. G. and Vollmer, R. L. *J. Org. Chem. 28* (1963) 1545.
15. Woerden, H. F. van and Vries-Miedema, A. T. de *Tetrahedron Lett. 20* (1971) 1687.

Received June 14, 1976.

On ^{13}C NMR Spectra of *lel*- and *ob*-Conformations in Tris(diamine)-cobalt(III) Complexes

SVEN BAGGER and OLE BANG

Chemistry Department A, The Technical University of Denmark, Building 207, DK-2800 Lyngby, Denmark

The inert tris(diamine)cobalt(III) complexes with their puckered and flexible rings are often used as test-compounds for the study of theoretical and experimental aspects of conformational analysis.

One well-known stereochemical detail in these compounds is the occurrence of *lel*- and *ob*-rings (Fig. 1).[1]

In the present communication we wish to draw attention to a possibility of distinguishing *lel*- and *ob*-conformations of certain five-membered rings on the basis of proton-decoupled ^{13}C NMR spectra.

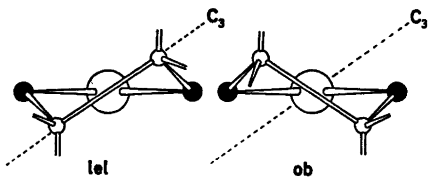

Fig. 1. A chelate ring, $\overline{C-N-M-N-C}$, viewed perpendicular to the C_3-axis (or pseudo C_3-axis) of a tris-complex.

In the following it is assumed that the reader is familiar with the IUPAC nomenclature for conformations and configurations.[2]

A family of complexes, $[Co(en)_x(lbn)_{3-x}]Cl_3.nH_2O$ ($x=0$, 1, 2), where en is 1,2-ethanediamine and lbn is $(-)_D$-(*R*,*R*)-1,2-dimethyl-1,2-ethanediamine, has been separated and resolved by descending paper chromatography.[3]

It is reasonable to assume that the chelated lbn ligand is forced to have the energetically favoured λ-conformation with two equatorially oriented methyl groups.[4] This assumption together with the knowledge of the absolute configuration of lbn makes it possible to deduce if an lbn ligand will adopt a *lel*- or an *ob*-conformation in a tris-complex, where the absolute configuration about the central atom is known.

This possibility of predicting ring conformations makes lbn complexes particularly suited for the present study.

The lbn conformations in complexes I–VI are given in Table 1.

The proton-decoupled 22.63 MHz ^{13}C NMR spectra of the six complexes with known lbn-ring conformations were measured in D_2O solution. The characteristics of the lbn patterns are presented in Table 1.

Two spectral features seem to mark a difference between *lel*- and *ob*-rings.

The linewidths of the methyl peaks from *lel*-conformations are broader than from *ob*-conformations. The half linewidths lie in the two separate intervals 14–26 Hz and 6–10 Hz, respectively. Both categories of peaks appear in the graphical representation as bands without structure and have a chemical shift of *ca.* 18.3.

The chemical shifts of the CH-resonances are different, the position of *lel*-ring peaks being 0.9–1.2 ppm downfield relative to the *ob*-ring peaks. The linewidths are all 2–4 Hz.

These findings are in accordance with a study of 1-propylenediamine complexes by Kojima and Yamasaki.[5] These authors observed that the methyl half linewidths in *fac*-Λ-$[Co(lpn)_3$-$lel_3]_3^+$ and *fac*-Λ-$[Co(lpn)_3ob_3]^{3+}$ were $\sim$27 and $\sim$7 Hz, respectively,[6] and that the shift difference between the CH carbon atoms was 1.3.

3. Cazaux, L. and Maroni, P. *Tetrahedron Lett.* (1969) 3667.
4. Cazaux, L., Chassaing, G. and Maroni, P. *Tetrahedron Lett.* (1975) 2517.
5. Wucherpfennig, W. *Justus Liebigs Ann. Chem. 737* (1970) 144.
6. Albriktsen, P. *Acta Chem. Scand. 25* (1971) 478.
7. Albriktsen, P. *Acta Chem. Scand. 26* (1972) 1738 and 3678.
8. Wood, G., McIntosh, J. M. and Miskow, M. H. *Can. J. Chem. 49* (1971) 1202.
9. Farid, S., Ateya, A. and Maggio, M. *Chem. Commun.* (1971) 1285.
10. Briggs, J., Hart, F. A. and Moss, G. P. *Chem. Commun.* (1970) 1506.
11. Albriktsen, P. and Thorstenson, T. *Unpublished results.*
12. Wolfe, S., Rauk, A., Tel, L. M. and Csizmadia, J. G. *J. Chem. Soc. B* (1971) 136, and references therein.
13. Lauterbur, P. C., Pritchard, J. G. and Vollmer, R. L. *J. Chem. Soc.* (1963) 5307.
14. Pritchard, J. G. and Vollmer, R. L. *J. Org. Chem. 28* (1963) 1545.
15. Woerden, H. F. van and Vries-Miedema, A. T. de *Tetrahedron Lett. 20* (1971) 1687.

Received June 14, 1976.

On ^{13}C NMR Spectra of *lel*- and *ob*-Conformations in Tris(diamine)-cobalt(III) Complexes

SVEN BAGGER and OLE BANG

Chemistry Department A, The Technical University of Denmark, Building 207, DK-2800 Lyngby, Denmark

The inert tris(diamine)cobalt(III) complexes with their puckered and flexible rings are often used as test-compounds for the study of theoretical and experimental aspects of conformational analysis.

One well-known stereochemical detail in these compounds is the occurrence of *lel*- and *ob*-rings (Fig. 1).[1]

In the present communication we wish to draw attention to a possibility of distinguishing *lel*- and *ob*-conformations of certain five-membered rings on the basis of proton-decoupled ^{13}C NMR spectra.

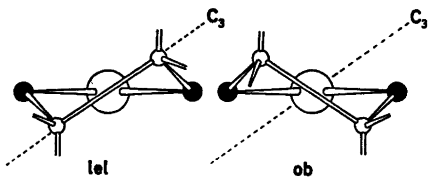

Fig. 1. A chelate ring, $\overline{C-N-M-N-C}$, viewed perpendicular to the C_3-axis (or pseudo C_3-axis) of a tris-complex.

In the following it is assumed that the reader is familiar with the IUPAC nomenclature for conformations and configurations.[2]

A family of complexes, $[Co(en)_x(lbn)_{3-x}]Cl_3.nH_2O$ ($x=0$, 1, 2), where en is 1,2-ethanediamine and lbn is $(-)_D$-(*R*,*R*)-1,2-dimethyl-1,2-ethanediamine, has been separated and resolved by descending paper chromatography.[3]

It is reasonable to assume that the chelated lbn ligand is forced to have the energetically favoured λ-conformation with two equatorially oriented methyl groups.[4] This assumption together with the knowledge of the absolute configuration of lbn makes it possible to deduce if an lbn ligand will adopt a *lel*- or an *ob*-conformation in a tris-complex, where the absolute configuration about the central atom is known.

This possibility of predicting ring conformations makes lbn complexes particularly suited for the present study.

The lbn conformations in complexes I–VI are given in Table 1.

The proton-decoupled 22.63 MHz ^{13}C NMR spectra of the six complexes with known lbn-ring conformations were measured in D_2O solution. The characteristics of the lbn patterns are presented in Table 1.

Two spectral features seem to mark a difference between *lel*- and *ob*-rings.

The linewidths of the methyl peaks from *lel*-conformations are broader than from *ob*-conformations. The half linewidths lie in the two separate intervals 14–26 Hz and 6–10 Hz, respectively. Both categories of peaks appear in the graphical representation as bands without structure and have a chemical shift of *ca.* 18.3.

The chemical shifts of the CH-resonances are different, the position of *lel*-ring peaks being 0.9–1.2 ppm downfield relative to the *ob*-ring peaks. The linewidths are all 2–4 Hz.

These findings are in accordance with a study of 1-propylenediamine complexes by Kojima and Yamasaki.[5] These authors observed that the methyl half linewidths in *fac*-Λ-$[Co(lpn)_3$-$lel_3]_3^+$ and *fac*-Λ-$[Co(lpn)_3ob_3]^{3+}$ were $\sim$27 and $\sim$7 Hz, respectively,[6] and that the shift difference between the CH carbon atoms was 1.3.

Table 1. Information on lbn rings.

	Conformation	Half linewidth of CH_3-peaks (Hz)	Chemical shift [a] of CH-resonances
I. Λ-$[Co(en)_2(lbn)]^{3+}$	*ob*	6	57.6
II. Δ-$[Co(en)_2(lbn)]^{3+}$	*lel*	14	58.7
III. Λ-$[Co(en)(lbn)_2]^{3+}$	ob_2	7	57.6
IV. Δ-$[Co(en)(lbn)_2]^{3+}$	lel_2	14	58.5, 58.8 [b]
V. Λ-$[Co(lbn)_3]^{3+}$	ob_3	10	57.4
VI. Δ-$[Co(lbn)_3]^{3+}$	lel_3	26	58.6

[a] Dioxane (δ 67.40) was used as internal standard. [b] Double peak.

We have at present no satisfactory explanation of the remarkable differences in the linewidths of the methyl resonances.

Acknowledgement. A Bruker WH 90 Fourier transform NMR spectrometer was placed at our disposal by Statens naturvidenskabelige Forskningsråd.

1. Corey, E. J. and Bailar, J. C. *J. Am. Chem. Soc. 81* (1959) 2620.
2. *IUPAC Nomenclature of Inorganic Chemistry*, 2nd Ed., Butterworths, London 1971.
3. Bagger, S., Bang, O. and Woldbye, F. *Acta Chem. Scand. A 30* (1976) 98.
4. Niketić, S. R. and Woldbye, F. *Acta Chem. Scand. 27* (1973) 3811.
5. Kojima, M. and Yamasaki, K. *Bull. Chem. Soc. Jpn. 48* (1975) 1093.
6. Kojima, M. and Yamasaki, K. *Personal communication.*

Received July 5, 1976.

Acta Chemica Scandinavica A 30 (1976) 767—770

Linearly Polarised Spectra, Stark Effect and Uniaxial Stress in the Potassium Dichromate Crystal

JENS H. HØG

Chemical Laboratory IV, H. C. Ørsted Institute, University of Copenhagen, DK-2100 Copenhagen Ø, Denmark

The single crystal absorption spectrum of $K_2Cr_2O_7$ has been recorded in the region 18 000 – 19 000 cm^{-1} and the effects of an electric field and an uniaxial stress have been investigated. The spectrum is interpreted in terms of eight chromophores of the type O_3CrO^- related two and two by inversion. No resonance interaction in the unit cell was observed, neither between the two chromophores of one $Cr_2O_7^{2-}$ ion nor between two chromophores related by inversion symmetry.

Potassium dichromate, $K_2Cr_2O_7$, grows in large orange crystals belonging to the triclinic crystal system.[1] The unit cell contains four molecules related two and two by inversion. There is no other symmetry in the unit cell and it thus contains two asymmetric units and four basically different chromium atoms.

Teltow [2] has given a very detailed experimental description of the single crystal spectrum of $K_2Cr_2O_7$ in the region 18 100 – 19 200 cm^{-1}. A large number of very sharp lines were reported but no assignment was given.

More recently Butowiez [3] reported new measurements of the spectrum in the same region. It should be noted that although Butowiez claims that his spectra have been recorded in the same manner as those of Teltow, it is clear that the spectra denoted as $\vec{E}\parallel\vec{\alpha}$, $\vec{E}\parallel\vec{\beta}$, and $\vec{E}\parallel\vec{\gamma}$ by Butowiez corresponds to $\vec{E}\parallel\vec{\beta}$, $\vec{E}\parallel\vec{\alpha}$, and $\vec{E}\parallel\vec{\gamma}$, respectively, in Ref. 2 ($\vec{\alpha}$, $\vec{\beta}$ and $\vec{\gamma}$ are the crystal optical directions). On the basis of the application of a hydrostatic pressure to the crystal Butowiez assigned several of the lines as pure electronic transitions and the rest as vibrational structure. The exact nature of these electronic transitions were not specified by Butowiez except for saying that they corresponded to transitions to the $^1T_1$ state of the tetrahedral CrO_4^{2-} ion split by the low crystal symmetry.

After the recent success in the application of the pseudo-Stark effect in assignments and the study of resonance interactions in potassium chlorochromate,[4,5] it was thought that a better understanding of the electronic spectrum of $K_2Cr_2O_7$ could be obtained by this method.

EXPERIMENTAL

Large perfect single crystals of $K_2Cr_2O_7$ could easily be grown by slowly lowering the temperature of a saturated solution. The crystals were examined by X-ray crystallography. Crystals exhibiting different faces were used: one shows the natural {100} faces, and others were cut and polished with the crystallographic *b*- and *c*-axis, respectively, perpendicular to the face. Since the angle between the *b*- and *c*-axis is $\alpha \simeq 90°$ the three faces are orthogonal. Crystal thicknesses varied from 0.1 to 1.0 mm.

The spectroscopic measurements were made on a Jena Zeiss 2 m grating spectrograph, using the double pass mode (dispersion $\simeq$ 3.69 Å/mm). Spectra were recorded on Kodak Tri-X and Ilford HP-4 panchromatic film at pumped liquid helium temperatures with the crystals completely immersed in liquid helium. The Stark apparatus was described in Ref. 4 and the stress apparatus in Ref. 6. Both are essentially unchanged.

A D.C. Stark field of 2×10^7 V m^{-1} could be obtained when special care was taken while mounting the crystals. It is important to avoid scratches and dust on the SnO_2-surface since this might cause electrical breakdown.

Table 1. $K_2Cr_2O_7$: Line polarisations, Stark splittings (cm^{-1} at $|V_0| = 10^7$ Vm^{-1}) and stress shifts (cm^{-1} at 4.9×10^7 N m^{-2}). +, observed; −, not observed; w, weak; vw, very weak.

Line frequency (cm^{-1})	Line polarisations						Stark splittings			Stress shifts
	light ⊥ (100)		light ∥ [010]		light ∥ [001]		Field direction			
	$\vec{E}\parallel\vec{\alpha}'$	$\vec{E}\parallel\vec{\gamma}'$	$\vec{E}\parallel\vec{\alpha}'$	$\vec{E}\parallel\vec{\gamma}'$	$\vec{E}\parallel\vec{\alpha}'$	$\vec{E}\parallel\vec{\gamma}'$	$\vec{V}_0\perp(100)$	$\vec{V}_0\parallel[010]$	$\vec{V}_0\parallel[001]$	
18 170.8	+	−	−	w	+	−	2.59	4.92	3.65	1.4
18 361.9	vw	−	−	w	+	−	−	−	3.34	−
18 437.7	+	w	−	w	+	−	2.52	5.12	3.41	1.4
18 503.4	−	+	w	+	+	w	2.74	4.00	2.61	1.5
18 589.6	+	w	+	−	+	−	3.55	3.05	2.30	9.3
18 689.6	+	w	+	−		w	4.75	1.52	4.38	−4.2
18 712.0	+	−	−	+		−	2.34	4.64	−	−
18 713.0	−	+	+	−		+	4.34	0	3.89	−
18 731.6	+	+	+	+		+	2.30	2.32	2.70	−
18 742.0	+	+	+	+		+	1.81	1.02	5.53	−
18 915.7						+	−	−	5.20	−

SPECTRA

Spectra were taken with the light polarised along the extinction directions on each of the three types of crystals. These directions are not the crystal optical directions $\vec{\alpha}$, $\vec{\beta}$, and $\vec{\gamma}$, and the line intensities therefore do not correspond to those of Teltow and Butowiez. Otherwise, the obtained spectra agree completely with those of Refs. 2 and 3. The dispersion of the extinction directions can be neglected over the small wavelength region investigated.

Only the sharp lines of the spectrum have been studied. The results of the polarised spectra are given in Table 1. Here $\vec{\alpha}'$ and $\vec{\gamma}'$ are the extinction directions with the smallest and the largest, respectively, index of refraction on the particular face of the crystal. Notice that $\vec{\alpha}'$ does *not* represent the same direction on two different faces. Polarisation data of two different columns in Table 1 should therefore not be compared directly.

The Stark effect of the crystal was measured with the electric field along three mutually orthogonal directions. All lines were observed to split into two and only two components. As for $KCrO_3Cl$ [4,5] the splitting is symmetric and linear, and the components have equal intensity. The observed splittings are given in Table 1 and are believed to be accurate to within ± 0.15 cm^{-1}.

Spectra were taken with the light propagating perpendicularly to the (100) face when an uniaxial stress was applied along the crystallographic *b*-axis. A stress of 5.9×10^7 N m^{-2} could be obtained before the crystal shattered. None of the lines show a splitting as a result of the stress. Only a linear shift was observed. Table 1 gives the shifts at 4.9×10^7 N m^{-2} obtained from a linear fitting of the experimental points from three different crystals, all giving identical results. The accuracy is ± 0.8 cm^{-1}. Rather thick crystals (~ 0.8 mm) were used in these experiments. The shifts of the high energy lines could therefore not be observed because the lines become obscured by the continuous absorption of the band.

DISCUSSION

Miskowski *et al.*[7] suggest that it is useful to consider the $Cr_2O_7^{2-}$ ion as two separate chromophores of the type O_3CrO^-, and they state that the spectra of $K_2Cr_2O_7$ and $KCrO_3Cl$ are very similar, after due allowance has been made in the $Cr_2O_7^{2-}$ spectrum for the additional complication of the triclinic unit cell with four independent chromium centres. With the present measurements we can see more accurately the content of these ideas.

On closer inspection of Table 1 it is noticed that the lines at 18 170.8, 18 361.9, 18 437.7, and 18 712.0 cm^{-1} show identical Stark effect and polarisation. It is therefore reasonable to assume that the first line is a pure electronic transition and the three other lines are vibrations added onto this origin. The vibrational

intervals are 191, 267, and 541 cm^{-1}. In $KCrO_3Cl$ vibrational intervals at 195, 245, and 568 cm^{-1} were found.

In $KCrO_3Cl$ the site group splitting of the lowest ^1E (C_{3v}) state was 330 cm^{-1}. In $K_2Cr_2O_7$ a line 332 cm^{-1} above the first electronic transition, *i.e.* at 18 503.4 cm^{-1} is found. Its polarisation and Stark effect is different from that of the 0 – 0 transition at 18 170.8 cm^{-1}. The two lines at 18 170.8 and 18 503.4 cm^{-1} could therefore be assigned to the two components of a split ^1E (C_{3v}) state.

Thus we see how similar a part of the $K_2Cr_2O_7$ spectrum is to the $KCrO_3Cl$ spectrum. This indicates that the spectrum must be attributed to a chromophore very similar to the CrO_3Cl^- chromophore, *i.e.* the O_3CrO^- chromophore, with the important implication that the interaction between the two O_3CrO^- chromophores of a $Cr_2O_7^{2-}$ ion is small. If the spectrum were to be interpreted in terms of a $Cr_2O_7^{2-}$ chromophore one would expect to observe the vibrations from the whole $Cr_2O_7^{2-}$ ion and not just those originating from one moiety.

If the idea about the separate O_3CrO^- chromophores is accepted, then the next line in the spectrum at 18 589.6 cm^{-1} together with the line at 18 915.7 cm^{-1} could be the components of the first ^1E (C_{3v}) state of one of the other chromophores. The splitting is 326 cm^{-1} which agrees well with the other values.

The lines at higher energy should be assigned to still other chromophores in the unit cell. It is, however, clear that the higher energy part of the spectrum is very complicated and it is therefore very difficult to make reasonable assignments.

Qualitatively the observed Stark effect can be explained satisfactorily. The eight individual O_3CrO^- chromophores in the unit cell are related two and two by the inversion symmetry. Without the electric field the spectra originating from each member in a pair coincide. The electric field destroys the symmetry of the crystal and the lines will split. Since inversion is the only symmetry in the crystal, the lines will split into two and only two components exactly as observed. The degeneracy of the chromophores related by inversion symmetry shows that there is no resonance interaction across the inversion centre.

The model of individual O_3CrO^- chromophores is confirmed by the stress experiments. Because the site symmetry of each chromophore is C_1, all electronic states will be non-degenerate. The only degeneracy that occurs in the unit cell is the degeneracy with respect to inversion. However, a uniaxial stress does not break down inversion symmetry and will therefore not lift this degeneracy. Instead, the stress will cause a slight change in the crystal field. As a result the lines will shift, but no splitting is expected. This is exactly what is observed. Furthermore, the stress experiment shows that the lines at 18 170.8, 18 589.6, and 18 689.6 cm^{-1} correspond to different electronically excited states because the shifts are different. Also the stress experiment confirms that the line at 18 437.7 cm^{-1} is a vibration built onto the first electronic origin at 18 170.8 cm^{-1}, because these two lines show the same shift.

It is worth noticing the strength of the combined action of polarised spectra and Stark effect as a tool for assignments. Butowiez assigned the line at 18 712.0 cm^{-1} to a separate electronic transition, but our measurements show that this line is a vibration on the first electronic origin at 18 170.8 cm^{-1}. This assignment is in fact confirmed by Butowiez' own measurements of the effect of a hydrostatic pressure which shows that both lines experience the same shift. Furthermore, our measurements show clearly that the two lines at 18 712.0 and 18 713.0 cm^{-1} are indeed separate lines, a fact which both Teltow [2] and Butowiez have been unable to discover because they have only observed the polarised spectra.

In conclusion, the similarity of the $KCrO_3Cl$ and $K_2Cr_2O_7$ spectra should be stressed. In both cases the resonance interaction is very small and the factor group splitting is less than the line width (~ 1.5 cm^{-1}). All data can be explained in terms of orientationally degenerate one-site exciton states.

Acknowledgement. The author expresses his gratitude to Professor C. J. Ballhausen and Professor E. I. Solomon for suggesting this study and for helpful discussions. He also wishes to thank Dr. S. Larsen for help with the crystallographical work, and Dr. J. Rønsbo and Mr. A. Garde, Institute of Mineralogy, for performing the crystal optical measurements.

REFERENCES

1. Brandon, J. K. and Brown, I. D. *Can. J. Chem. 46* (1968) 933.
2. Teltow, J. *Z. Phys. Chem. B 43* (1939) 375.
3. Butowiez, B. *J. Phys. (Paris) 31* (1970) 477.
4. Solomon, E. I., Ballhausen, C. J. and Høg, J. H. *Chem. Phys. Lett. 34* (1975) 222.
5. Høg, J. H., Ballhausen, C. J. and Solomon, E. I. *Mol. Phys. 32* (1976) 807.
6. Ballhausen, C. J. and Trabjerg, I. *Mol. Phys. 24* (1972) 689.
7. Miskowski, V., Gray, H. B. and Ballhausen, C. J. *Mol. Phys. 28* (1974) 729.

Received June 8, 1976.

Acta Chemica Scandinavica A 30 (1976) 771—780

The Complex Formation between Tin(II) Ions and Acetate Ions

SYLVIA GOBOM

Department of Inorganic Chemistry, Chalmers University of Technology and University of Göteborg, P.O. Box, S-402 20 Göteborg 5, Sweden

The equilibria between tin(II) and acetate ions have been studied by means of potentiometric titrations at 25 °C in 3 M $NaClO_4$ medium. The titrations were performed in the approximate pH range 2.0 – 4.2 at total acetate concentrations varying within the limits 80 mM $< c_{Ac} <$ 145 mM. Tin(II) ions were introduced stepwise into the test solution, by constant current coulometry. This study covers the [Sn(II)] range 0.2 to 0.9 mM. The concentrations of the free tin(II) and hydrogen ions were measured with tin amalgam and glass electrodes, respectively. The emf data, which were evaluated with the generalized least squares program LETAGROP, version ETITR, were consistent with the following reactions and equilibrium constants:

$Sn^{2+} + Ac^- \rightleftharpoons SnAc^+$	$\lg \beta_1 = 3.472 \pm 0.004$
$Sn^{2+} + 2Ac^- \rightleftharpoons SnAc_2$	$\lg \beta_2 = 6.042 \pm 0.007$
$Sn^{2+} + 3Ac^- \rightleftharpoons SnAc_3^-$	$\lg \beta_3 = 7.27 \pm 0.05$

Since the hydrolysis of tin(II) was found to interfere with the complex formation, allowance was made for the presence of $SnOH^+$ and $Sn_3(OH)_4^{2+}$.

It would appear that there have been no quantitative studies on tin(II) complexes with acetate ions or other carboxylate ions. Donaldson *et al.*[1–5] have prepared and studied the properties of triacetatostannate(II) compounds with alkali metal, ammonium and alkaline earth metal ions and have found evidence for the existence of $SnCH_3COO^+$, $Sn(CH_3COO)_2$, $Sn_3(CH_3COO)_7^-$, $Sn_2(CH_3COO)_5^-$, and $Sn(CH_3COO)_3^-$ in solution from potentiometric and polarographic measurements.[1,3] Potentiometric and polarographic measurements on the corresponding triformatostannate(II) compounds indicated the presence of $SnHCOO^+$, $Sn(HCOO)_2$, $Sn_2(HCOO)_5^-$ and $Sn(HCOO)_3^-$ in solution.[4] Donaldson *et al.* have studied bonding and structural properties in compounds containing SnX_3^- ions from Mössbauer data (*e.g.* Ref. 5). The expected pyramidal environment of tin has been confirmed by the crystal structure determination of $KSn(HCOO)_3$, in which the three unidentate formate groups form covalent bonds with the tin atom.[6]

SYMBOLS

The following notation is used:

lg	$\log_{10}$
H	total concentration of hydrogen ions, proton excess over H_2O and Ac^-.
h	concentration of H^+.
B	total concentration of Sn(II).
b	concentration of Sn(II).
C	total concentration of Ac^-.
c	concentration of Ac^-.
η	lg B/b
E_B	emf of the cell with amalgam electrode (in mV) (3).
E_H	emf of the cell with glass electrode (in mV) (4).
DA	$H_{cal} - H$ (Table 1).
DEB	$E_{cal} - E_B$ (Table 1), where E_{cal} is the calculated value of E_B.
H_0	analytical hydrogen ion concentration in the starting solution, S_0.
H_T	analytical hydrogen ion concentration in the titrant solution, T.
B_0	analytical tin(II) concentration in the starting solution S_0.
B_T	analytical tin(II) concentration in the titrant solution, T.
C_0	analytical acetate concentration in the starting solution, S_0.
C_T	analytical acetate concentration in the titrant solution, T.

S_0 starting solution.
T titrant solution.
V_0 volume of S_0.
V_T added volume of T.

METHOD OF INVESTIGATION

The measurements were performed at 25 °C as potentiometric titrations using the automatic titrator described previously.[7] The constant ionic medium method [9,10] was applied using 3 M $NaClO_4$ to keep the activity factors constant. The equilibrium conditions can thus be expressed in terms of concentrations instead of activities. The test solutions, S, were obtained by adding tin(II) ions to a solution containing sodium acetate, perchloric acid, and sodium perchlorate.

The tin(II) ions were generated in the test solution by constant current electrolysis.[8] A tin amalgam electrode [7] was used as anode in the following circuit

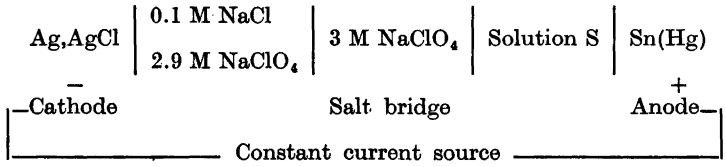

The equilibrium concentrations of Sn^{2+} and H^+ were measured with another tin amalgam electrode and a glass electrode, respectively, in the following cells

$$-\text{Sn(Hg)} \mid \text{solution S} \mid \text{3 M NaClO}_4 \mid \text{RE}+ \quad (1)$$

$$-\text{GE} \quad \mid \text{solution S} \mid \text{3 M NaClO}_4 \mid \text{RE}+ \quad (2)$$

where GE is a glass electrode and RE the reference electrode:

Ag,AgCl | 0.010 M Ag^+, 2.99 M Na^+, 3.00 M ClO_4^-.

The emfs of cells (1) and (2) are related to the concentrations of Sn^{2+} and H^+, b and h, respectively, by the equations

$$E_B = E_B^0 - \tfrac{1}{2} \times 59.16 \lg b + E_j \quad (3)$$

$$E_H = E_H^0 - 59.16 \lg h + E_j \quad (4)$$

where E_j is the liquid junction potential formed between the test solution S and the 3 M $NaClO_4$ of the salt bridge. According to previous investigations,[10] E_j may be assumed to vary linearly with the hydrogen ion concentration. In this work the value determined by Biedermann and Sillén,[11] $E_j = 0.017h$ mV, was used (h in mM).

It has been found that for acetic acid, boric acid and ascorbic acid [12–15] in 3 M $NaClO_4$, E_H^0 is a linear function of the total concentration of the acid. Since the total acetate concentration was kept constant in each titration, E_H^0 was assumed to be constant and was calculated for each titration from the measured value of E_H in an acid solution containing no tin ions.

The reduction of Sn(IV) in the presence of tin

$$\text{Sn(IV)} + \text{Sn(s)} \rightleftharpoons 2\text{Sn(II)}$$

is highly favoured in acid solution,[16] but the process is slow. It was thus important to avoid formation of Sn(IV) in the experiments. To prevent oxidation of the amalgam and tin(II) ions, the solutions and titration vessels were pretreated with argon or nitrogen and the test solutions were kept under argon atmosphere.

The solutions used in the titrations had the following compositions

S_0: H_0 M $HClO_4$, C_0 M NaAc, $(3 - H_0)$ M $NaClO_4$
T: C_T M NaAc, $(3 - C_T)$ M $NaClO_4$.

V_0 ml of S_0 was titrated with V_T ml of T, forming the test solution denoted by S. The tin(II) ions were generated directly into S_0 and S. In order to suppress the hydrolysis of tin and possible complex formation in the starting solution, S_0, the value of H_0 was chosen so that $H_0 - C_0$ was about 10 mM. The titrations thus started at approximately pH = 2. C was kept constant in each titration ($C = C_0 = C_T$) and was chosen sufficiently high to favour the formation of complexes between tin(II) and acetate ions.

In each titration the emf value of the glass electrode, E_H, was first measured in V_0 ml of S_0 in the absence of tin ions. From this value E_H^0 was calculated. The two tin amalgam electrodes, which were to be used to generate and measure the concentration of the tin(II) ions, were then inserted into the solution. The tin ions were added step-wise by constant current electrolysis, until a desired concentration had been attained. The equilibrium value of the amalgam electrode, E_B, was registered after each addition. Using eqn. (3) an approximate value of E_B^0 was thus obtained. V_T ml of the titrator T were then added, and tin ions were generated to compensate for the dilution. The equilibrium values of E_B and E_H were measured for each addition. From

Table 1. Experimental data $\eta(\lg h)$ at different B and C concentrations. For each point E_B, E_G, pH, η, DH = $(H_{cal} - H)$ (in mM), and DEB = $(E_{B,cal} - E)$ (in mV) are given. In calculating H_{cal} and E_{cal} the mean values (Table 3) of the equilibrium constants obtained have been used. The values of E_H^0 and $E_B^0 \pm 3\sigma$ are given at the head of each titration.

SATS 8. H = 109.7, B = 0.773, C = 99.95

E^0_B = 821.10 ± 0.05, E^0_H = 0.05, B = 0, C = 100.0

EA(mV)	EB(mV)	pH	ETA	DH	DEB
117.20	916.48	1.977	0.1135	0.51	−0.20
120.74	917.09	2.038	0.1286	0.42	−0.17
122.68	917.45	2.071	0.1376	0.37	−0.14
124.70	917.82	2.105	0.1476	0.33	−0.13
126.83	918.24	2.141	0.1588	0.30	−0.10
129.14	918.70	2.180	0.1717	0.27	−0.09
131.61	919.23	2.222	0.1865	0.24	−0.06
134.26	919.82	2.267	0.2037	0.22	−0.04
137.17	920.51	2.317	0.2239	0.19	−0.02
140.37	921.31	2.371	0.2482	0.16	0.0
143.88	922.27	2.430	0.2771	0.14	0.04
147.76	923.39	2.496	0.3122	0.12	0.06
152.09	924.75	2.569	0.3554	0.10	0.08
156.91	926.41	2.651	0.4086	0.08	0.11
162.33	928.46	2.743	0.4751	0.06	0.12
168.24	930.94	2.843	0.5560	0.04	0.15
174.64	933.89	2.951	0.6536	0.02	0.14
181.01	937.14	3.059	0.7612	0.01	0.15
187.25	940.59	3.164	0.8766	0.0	0.12
193.03	944.06	3.262	0.9923	−0.01	0.10
198.21	947.36	3.350	1.1028	−0.01	0.06
202.87	950.51	3.429	1.2076	−0.02	0.05
207.05	953.46	3.499	1.3058	−0.02	0.02
210.74	956.16	3.562	1.3956	−0.03	0.0
214.03	958.66	3.617	1.4780	−0.03	0.0
217.04	961.01	3.668	1.5553	−0.03	0.0
219.76	963.18	3.714	1.6265	−0.03	0.0
222.24	965.20	3.756	1.6925	−0.03	0.0
224.55	967.11	3.795	1.7549	−0.04	0.0
226.68	968.90	3.831	1.8131	−0.04	0.0
228.67	970.58	3.865	1.8681	−0.05	−0.01
230.51	972.16	3.896	1.9193	−0.05	−0.01
232.25	973.68	3.925	1.9682	−0.05	0.0
233.87	975.09	3.953	2.0141	−0.05	−0.01
235.41	976.46	3.979	2.0579	−0.06	0.0

SATS 11. H = 89.71, B = 0.823, C = 79.13

E^0_B = 819.48 ± 0.03, E^0_H = 171.51, B = 0.835, C = 79.45

EA(mV)	EB(mV)	pH	ETA	DH	DEB
287.73	913.35	1.962	0.0900	0.12	0.10
288.99	913.48	1.983	0.0942	0.12	−0.22
290.31	913.62	2.005	0.0987	0.12	−0.20
291.62	913.78	2.028	0.1035	0.13	−0.19
293.03	913.95	2.052	0.1088	0.14	−0.16
294.53	914.13	2.077	0.1147	0.13	−0.14
296.12	914.33	2.104	0.1214	0.11	−0.12
297.76	914.54	2.132	0.1285	0.11	−0.11
299.47	914.79	2.161	0.1364	0.11	−0.10
301.32	915.06	2.193	0.1454	0.09	−0.07
303.31	915.36	2.226	0.1557	0.07	−0.06
305.38	915.70	2.262	0.1670	0.06	−0.05
307.55	916.08	2.298	0.1797	0.06	−0.04
309.89	916.52	2.338	0.1942	0.05	−0.03
312.39	917.01	2.380	0.2108	0.05	−0.01
315.09	917.59	2.426	0.2301	0.05	0.0
318.01	918.27	2.476	0.2526	0.04	0.02
321.18	919.05	2.529	0.2789	0.04	0.04
324.63	919.98	2.588	0.3100	0.04	0.06
328.40	921.08	2.651	0.3470	0.03	0.08
332.53	922.39	2.722	0.3914	0.03	0.08
336.97	923.95	2.797	0.4435	0.03	0.11
341.77	925.77	2.878	0.5054	0.02	0.10
346.84	927.88	2.964	0.5769	0.02	0.10
352.03	930.25	3.051	0.6569	0.02	0.11
357.20	932.79	3.139	0.7432	0.02	0.10
362.22	935.43	3.224	0.8334	0.01	0.08
366.89	938.08	3.303	0.9228	0.01	0.08
371.17	940.64	3.375	1.0093	0.02	0.09
375.15	943.12	3.442	1.0935	0.02	0.08
378.78	945.48	3.504	1.1733	0.02	0.08
382.10	947.69	3.560	1.2489	0.02	0.06
385.14	949.77	3.611	1.3200	0.01	0.04
387.96	951.75	3.659	1.3876	0.01	0.02
390.48	953.58	3.702	1.4492	0.01	0.02
392.84	955.30	3.741	1.5080	0.01	0.01
395.05	956.93	3.779	1.5639	0.00	−0.02
397.10	958.48	3.814	1.6165	−0.00	−0.02
399.00	959.94	3.846	1.6658	−0.00	−0.02
400.75	961.33	3.875	1.7117	0.00	0.02
402.40	962.64	3.903	1.7553	0.01	0.04
403.96	963.90	3.929	1.7969	0.01	0.07
405.46	965.07	3.955	1.8371	0.01	0.05
406.89	966.21	3.979	1.8757	0.01	0.05
408.28	967.30	4.002	1.9135	−0.00	0.02
409.60	968.33	4.025	1.9495	−0.01	−0.01
410.83	969.33	4.046	1.9831	−0.01	−0.01
412.00	970.27	4.065	2.0153	−0.01	−0.02
413.10	971.18	4.084	2.0456	−0.00	0.0
414.19	972.06	4.102	2.0757	−0.01	−0.01
415.23	972.90	4.120	2.1045	−0.01	−0.02

SATS 14. H = 155.2, B = 0.387, C = 144.3

E^0_B = 818.07 ± 0.04, E^0_H = 158.000, B = 0.411, C = 144.3

EA(mV)	EB(mV)	pH	ETA	DH	DEB
273.39	923.33	1.947	0.1459	0.14	−0.19
275.52	923.68	1.984	0.1570	0.14	−0.15
277.88	924.10	2.024	0.1702	0.12	−0.10
280.45	924.57	2.068	0.1856	0.09	−0.07
283.26	925.13	2.115	0.2038	0.06	−0.03
286.32	925.78	2.167	0.2253	0.05	0.01
289.78	926.57	2.226	0.2519	0.01	0.03
293.52	927.54	2.290	0.2834	0.01	0.09
298.06	928.81	2.366	0.3257	−0.05	0.12
302.99	930.35	2.450	0.3770	−0.05	0.16
308.70	932.34	2.547	0.4439	−0.05	0.19
315.62	935.05	2.664	0.5358	−0.09	0.20
323.14	938.42	2.791	0.6498	−0.09	0.21
331.20	942.46	2.928	0.7885	−0.08	0.16
339.18	946.96	3.063	0.9426	−0.07	0.11
346.50	951.52	3.186	1.0984	−0.05	0.07
352.88	955.77	3.294	1.2451	−0.04	−0.01
358.77	959.97	3.394	1.3890	−0.08	−0.06
363.45	963.49	3.473	1.5088	−0.06	−0.08
367.55	966.66	3.542	1.6175	−0.04	−0.12
371.15	969.59	3.603	1.7156	−0.03	−0.09
374.33	972.16	3.657	1.8042	−0.01	−0.13
377.20	974.56	3.706	1.8856	0.00	−0.14
379.84	976.81	3.760	1.9616	0.01	−0.13
382.34	978.99	3.792	2.0345	−0.02	−0.10
384.48	980.89	3.829	2.0976	0.01	−0.06
386.51	982.67	3.863	2.1579	0.02	−0.06
388.38	984.35	3.895	2.2139	0.03	−0.04
390.16	985.90	3.925	2.2675	0.03	−0.07
391.80	987.40	3.952	2.3172	0.04	−0.04
393.51	988.89	3.981	2.3693	−0.02	−0.08
394.94	990.22	4.005	2.4129	0.00	−0.04
396.32	991.49	4.029	2.4552	0.01	−0.02
397.62	992.70	4.051	2.4952	0.02	0.02
398.87	993.84	4.072	2.5337	0.03	0.02
400.13	994.98	4.093	2.5725	0.01	0.02
401.27	996.04	4.112	2.6077	0.01	0.04
402.43	997.11	4.132	2.6436	−0.02	0.05
403.47	998.07	4.150	2.6758	−0.01	0.06
404.48	999.01	4.167	2.7071	−0.00	0.08
405.47	999.88	4.183	2.7377	−0.01	0.05
406.43	1000.78	4.200	2.7675	−0.02	0.07
407.37	1001.59	4.216	2.7966	−0.04	0.02
408.23	1002.38	4.230	2.8232	−0.03	0.03
409.10	1003.16	4.245	2.8501	−0.04	0.01

SATS 18. H = 93.25, B = 0.537, C = 101.9

E^0_B = 816.14 ± 0.04, E^0_H = 160.3, E^0_H = 174.82, C = 100.0

EA(mV)	EB(mV)	pH	ETA	DH	DEB
408.25	972.72	3.946	2.0194	−0.16	0.13
407.05	971.77	3.926	1.9853	−0.15	0.13
405.81	970.78	3.905	1.9502	−0.14	0.11
404.54	969.78	3.883	1.9145	−0.13	0.10
403.22	968.76	3.861	1.8776	−0.12	0.11
401.90	967.73	3.839	1.8409	−0.12	0.10
400.54	966.67	3.816	1.8033	−0.12	0.09
399.15	965.57	3.792	1.7652	−0.12	0.06
397.71	964.43	3.768	1.7261	−0.12	0.01
396.20	963.26	3.742	1.6853	−0.12	−0.01
394.63	962.06	3.719	1.6479	−0.16	−0.17
393.06	960.82	3.689	1.6018	−0.13	−0.11
391.29	959.56	3.659	1.5555	−0.12	−0.06
389.43	958.27	3.628	1.5075	−0.11	0.01
387.56	956.90	3.596	1.4598	−0.11	−0.01
385.67	955.45	3.564	1.4124	−0.12	−0.12
383.57	954.02	3.529	1.3605	−0.11	−0.07
381.64	952.54	3.496	1.3136	−0.14	−0.22
379.40	951.00	3.458	1.2602	−0.14	−0.25
376.81	949.43	3.415	1.1999	−0.12	−0.09
374.15	947.80	3.370	1.1395	−0.10	0.01
371.44	946.09	3.324	1.0797	−0.10	0.01
368.59	944.41	3.275	1.0187	−0.09	0.07
365.70	942.71	3.227	0.9588	−0.09	0.08
362.79	940.98	3.176	0.8989	−0.09	0.07
359.64	939.26	3.124	0.8401	−0.10	0.03
356.42	937.54	3.070	0.7808	−0.09	0.0
353.14	935.95	3.014	0.7231	−0.08	0.06
348.77	933.90	2.940	0.6505	−0.07	0.08
344.61	932.11	2.870	0.5860	−0.06	0.12
340.71	930.48	2.804	0.5296	−0.05	0.08
337.06	929.14	2.742	0.4802	−0.05	0.12
333.71	927.97	2.685	0.4379	−0.04	0.13
330.59	926.91	2.633	0.4009	−0.03	0.08
327.74	926.03	2.584	0.3692	−0.03	0.06
325.22	925.33	2.542	0.3428	−0.03	0.07
323.44	924.86	2.512	0.3250	−0.04	0.07
321.76	924.40	2.483	0.3089	−0.04	0.02
320.14	923.99	2.456	0.2940	−0.03	0.0
318.54	923.67	2.429	0.2798	−0.02	0.04

Table 2. Survey of the compositions of the solutions used in the titrations. In titrations Nos. 1–17 $H_T=0$ and in titrations Nos. 18–19 $B_T=0$.

Titr. No.	H_0	B_0	C_0	B_T	C_T
1	110.0	0.535	99.95	0.549	101.5
2	109.9	0.525	99.95	0.541	101.0
3	109.9	0.812	99.95	0.827	100.0
4	110.0	0.862	99.95	0.862	100.0
5	109.7	0.773	99.95	0	100.0
6	108.8	0.213	99.0	0.234	100.0
7	109.0	0.216	99.0	0.241	102.0
8	88.14	0.338	78.37	0.362	78.37
9	88.19	0.884	78.37	0.917	78.37
10	89.48	0.572	79.13	0.578	79.45
11	89.71	0.823	79.13	0.835	79.45
12	89.63	0.337	79.13	0.350	79.45
13	155.4	0.562	144.3	0.590	144.3
14	155.2	0.387	144.3	0.411	144.3
15	152.2	0.798	144.3	0.800	146.0
16	155.1	0.248	144.3	0.305	144.3
17	109.9	0.327	99.92	0.321	101.0
				H_T	
18	93.25	0.537	101.9	160.3	100.0
19	93.05	0.290	101.9	160.3	101.0

these experimental data, the equilibrium model was calculated. Since the amount of data was very large (19 titrations with a total of 690 measuring points), the experimental data from only 4 titrations (Nos. 5, 11, 14, and 18) are represented in Table 1.* The composition of the investigated solutions are given in Table 2. About one third of the experimental points from 9 titrations (Nos. 3–5, 10–14 and 16) are shown in Fig. 1. Back titrations (Nos. 18, 19) showed that the equilibria were reversible. The reproducibility was tested by varying the tin concentration in some titrations (Nos. 5, 18, 19).

The amalgam electrodes normally attained a steady potential almost instantaneously which remained constant within ±0.02 mV for several hours. For each experimental point, the value of E_B was not, however, accepted to correspond to equilibrium, until it had been ascertained that this value was constant within 0.02 mV during 15 minutes. This was an important criterion, because accidental errors in the titrations (*e.g.* a gas bubble in the salt bridge, stop of the gas flow, a poor electrical contact, leakage currents, change in temperature) often appeared as a very slow drift in the

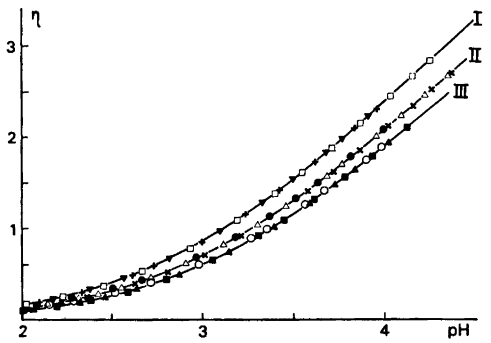

Fig. 1. Survey of measurements: $\eta=\lg(B/b)$ as a function of pH. The theoretical curves have been calculated with the equilibrium constants given in the text. I: $B=0.248-0.562$ mM II: $B=0.639-0.862$ mM III: $B=0.337-0.823$ mM

$C=144$ mM Symbol	Titr. No.	$C=100$ mM Symbol	Titr. No.	$C=79.2$ mM Symbol	Titr. No.
+	13	×	3	▲	10
□	14	△	4	■	11
▼	16	●	5	○	12

* A complete list of the experimental data is available from the Department of Inorganic Chemistry, Chalmers University of Technology and University of Göteborg, P.O. Box, S-402 20 Göteborg 5, Sweden.

emf-values. The glass electrode attained its equilibrium value almost as rapidly as the amalgam electrode.

EXPERIMENTAL DETAILS

The measurements were carried out in a paraffin oil thermostat at 25.00 ± 0.01 °C, the room temperature being 25 °C. The thermostating equipment was the same as described in Ref. 7. The titration cell and the cell used for the generation of the tin ions were of the "Wilhelm" type.[17]

Several *glass electrodes* were tested in order to find electrodes which gave stable emf-values that were not influenced by the magnetic stirrer or other external disturbances. Finally Beckmann 39004 and Jena 9201/71 were chosen. The glass electrodes were checked with hydrogen electrodes in solutions of high buffer capacity in the approximate pH range 2 – 8. These tests were made as titrations with hydroxide ions as described by Olin.[18] The *amalgam* electrodes were prepared by dissolving tin metal (Mallinckrodt, analytical reagent, granular, 20 mesh) in mercury (Merck, *p.a.*). The surface of the tin was first cleaned with diluted HCl, washed with water and dried between filter papers. The tin and mercury were mixed with a magnetic stirrer in a 40 ml wash bottle, under *ca.* 10 mM $HClO_4$, through which nitrogen gas was bubbled to exclude oxygen. With this efficient stirring the amalgam obtained a homogeneous composition almost instantaneously. The amalgam was transferred to the titration vessel by nitrogen gas. It was passed through a capillary tube and to avoid "plugs" only liquid amalgam was used. The solubility of tin in mercury is 1.263 mol % at 25 °C,[19] and the tin content in both electrodes was kept, generally, at ~ 1.25 mol %. In some experiments lower concentrations of tin (*e.g.* 0.5, 0.3, 0.03 mol %) were used in the measuring amalgam. The amalgam was then prepared either from strips of thin tin foil (Merck, *p.a.*) which were dissolved in mercury or by electrolytic reduction of Sn^{2+} in a chloride solution on a mercury cathode. Neither the stability of the electrode potential nor the time required to attain equilibrium seemed to vary with the tin content of the amalgam. In the titration vessel the amalgam was kept in teflon holders. The electrical connection to an amalgam electrode was *via* a platinum wire sealed through a glass tube. This tube also carried the whole electrode. The device was held above the solution when it was filled with amalgam to prevent the platinum needle from coming into contact with the solution, in which case unstable emf-values might be obtained.

It was sometimes difficult to obtain stable, reliable E_B values especially at the lower tin concentrations. In some titrations this was due to a poor contact between the platinum wire and the amalgam in the measuring electrode. The best way of obtaining a good amalgamation of the platinum was to heat the cleaned wire momentarily in a flame and insert it immediately into a small pool of mercury. The small Hg-drop adhered to the Pt gave a perfect contact with Sn(Hg). The generating electrode was inserted into the solution[7] only during the electrolysis and then withdrawn. As the titrations were fairly time-consuming (*ca.* 20 h) the generating amalgam was held above the test solution when not in use. The electrode surface was carefully rinsed by dipping the electrode once or twice into the solution. When the electrode holder was made of a platinum net a slow emf drift, indicating a spontaneous Sn^{2+}-generation, was noticed as soon as the electrode came in contact with the solution. This was due to a lowering of the hydrogen overvoltage on the amalgam where this was in contact with the platinum. On increasing the acidity of the solution it was even possible to see evolution of gas from one or two points on the borderline.

30 – 35 g of *ca.* 1.25 mol % Sn(Hg) was used in the generating electrode, the surface of which was about 2.5 cm^2. The current density was approximately 1.2 mA/cm^2, it not being possible to vary the current strength. The anodic oxidation was carried out stepwise in order to avoid a local excess of tin ions.

The test solution was protected from atmospheric oxygen by the passage of a slow stream of argon, which had been purified by passage through a column filled with an activated copper catalyst (BASF-catalyst R3-11) through wash bottles with 10 % H_2SO_4, 10 % NaOH, 3 M $NaClO_4$[20] and finally through a bottle containing S_0 solution or a mixture of S_0 and T to resemble the test solution. Glass filters were used in some bottles to increase the contact area of the gas. Diffusion-tight high pressure polythene tubing (Samuel Moore "P" Tubing 6 mm) was used to connect the gas cylinder with the titration vessel *via* the wash bottles. The test solution was stirred with a magnetic stirrer, which proved to be more efficient than gas stirring and did not cause any splashing on the glass walls. The digital voltmeter, the constant current source and other instruments in the computerised titrator were those used previously.[7] The reference silver-silver chloride electrode was prepared according to Brown[20,21] and the hydrogen gas electrode as described in Ref. 20.

Chemicals

Sodium perchlorate stock solutions were prepared from recrystallized Na_2CO_3 (Merck, *p.a.*) and ca 70 % $HClO_4$ (Merck, *p.a.*) as described by Biedermann.[22] Using a mixture of bromocresol-green and methyl red[20] as indicator it

was possible to prepare an almost neutral solution. The proton excess was determined by a coulometric titration with hydrogen ions using a Gran plot.[25] The oxygen gas was generated on a cylindrical platinum net anode. The metal content was checked with Eriochrome Black T.[23]

Sodium acetate stock solutions were prepared from recrystallized $NaOCOCH_3.3H_2O$ (Merck, *p.a.*). The sodium content was determined as NaCl by evaporating a known amount of the solution with concentrated HCl.[24] The acetate content was determined by a cation exchanger in the hydrogen form, the resulting eluate being titrated with sodium hydroxide. The results of the two methods agreed to within 0.2 %. The stock solutions were kept in polythene bottles with thick walls. The sodium acetate solution was tested for proton excess by titrating equimolar solutions of $HClO_4$ and NaAc (0.1 M) with $HClO_4$ in 3 M $NaClO_4$ until a suitable proton excess was obtained. The original excess was determined by a Gran extrapolation.[25]

Perchloric acid solutions were prepared by diluting ~70 % $HClO_4$ (Merck, *p.a.*) and were standardized against tris(hydroxymethyl)-aminomethane (Merck, *p.a.*).[26] They were also titrated against recrystallized Tl_2CO_3 (BDH, *p.a.*).[20] The results of the two methods agreed to within 0.1 %. The Sn^{2+} ions were generated by constant current electrolysis and the concentration was calculated from the amount of electricity that had passed through the solution.[7]

CALCULATIONS AND RESULTS

From the experimental values of E_H, E_B, V_T and the analytical composition of the test solutions a series of data sets $\eta(\lg h)_{B,C}$ or $\eta(\lg h)_C$ were calculated (Table 1). The analytical concentrations of H, B, and C for each point in Table 1 were calculated. The titrations can be divided into three groups, each with a different acetate concentration, $C = C_0 = C_T = 79$, 100, and 144 mM, respectively. Experimental values of $\eta(\lg h)_{B,C}$ or $\eta(\lg h)_C$ for some of these titrations are shown in Fig. 1. For the sake of clarity, only about a third of the points from each titration have been included.

E_H^0 was calculated at the beginning of each titration using eqn. (4), assuming h to be known from the composition of the acid solution S_0. By generating tin ions into the solution and neglecting both the hydrolysis and complex formation, an approximate value of E_B^0 could be calculated from eqn. (3), for values of B from about 0.05 mM to the desired value, which was then generally kept constant in the titration. Later, this constant, E_B^0, was adjusted for the presence of $SnAc^+$ and $SnOH^+$ (see Fig. 2).

The titration was interrupted when a black precipitate of SnO became visible on the generating electrode. This compound was identified from its Guinier powder photograph. It was difficult to ascertain when the tin oxide was first formed since there was no sudden change in the emf-values nor any effect on the time required to attain equilibrium. However, the neglection of the precipitate introduced an error which caused the $\eta(\lg h)_{B,C}$ curves to deviate in a non-reproducible way. This generally occurred when pH > 4. Points from this region were not therefore included in the calculations.

The complex formation in the solution may be described in terms of the reactions

$$p\mathrm{Sn}^{2+} + q\mathrm{H_2O} + r\mathrm{Ac}^- \rightleftharpoons \mathrm{Sn}_p(\mathrm{OH})_q(\mathrm{Ac})_r^{2p-q-r} + q\mathrm{H}^+$$

and

$$\mathrm{H}^+ + \mathrm{Ac}^- \rightleftharpoons \mathrm{HAc}$$

The corresponding equilibrium constants are

$$\beta_{qrp} = \frac{[\mathrm{Sn}_p(\mathrm{OH})_q(\mathrm{Ac})_r]h^q}{[\mathrm{Sn}^{2+}]^p[\mathrm{Ac}^-]^r}$$ (the charge of the complex being omitted)

and

$$K_{\mathrm{HAc}} = \frac{[\mathrm{HAc}]}{[\mathrm{H}^+][\mathrm{Ac}^-]}$$

It is assumed that under given conditions the sum of all species $[Sn^{2+}(H_2O)_l(Na^+)_m(ClO_4^-)_n]$ may be written $[Sn^{2+}]$.[27] K_{HAc} was determined by performing titrations in different acetate solutions in the absence of tin ions, evaluation of the data with the Letagrop program yielding

$$\lg K_{\mathrm{HAc}} = 5.018 \pm 0.010$$

This value agrees well with those previously reported under the same conditions.[28,29] For the pure hydrolysis products the values

$$\lg \beta_{101} = -3.70 \pm 0.02$$
$$\lg \beta_{403} = -6.81 \pm 0.03$$

as determined in a separate titration [30,31] (*cf.* Ref. 32) were used.

When $\eta = \lg(B/b)$ was plotted as a function of lg h at a constant C level the curves obtained were independent, within the experimental errors, of the metal ion concentration (Fig. 1). As a consequence the concentrations of $Sn_3(OH)_4^{2+}$ and other possible polynuclear complexes were ignored. Some titrations in which B was varied (Table 1, titrations Nos. 5, 18, 19) were carried out to verify the coincidence of the $\eta(\lg h)_C$ curves with the $\eta(\lg h)_{B,C}$ curves (Fig. 1). In this way a check of the assumed 100 % efficiency of the tin generating electrode was obtained.

The mass balance for total tin, B, hydrogen, H (over H_2O, Ac^- and Sn^{2+}), and acetate, C, gives

$$B = b + \sum_{p,q,r} p\beta_{qrp} b^p h^{-q} c^r \quad (5)$$

$$H = h + K_{HAc} hc - \sum_{p,q,r} q\beta_{qrp} b^p h^{-q} c^r \quad (6)$$

$$C = c + K_{HAc} hc + \sum_{p,q,r} r\beta_{qrp} b^p h^{-q} c^r \quad (7)$$

Inserting into (5) and neglecting polynuclear and possible mixed complexes

$$B/b = 1 + \beta_{101} h^{-1} + \sum_r \beta_{0r1} c_r = 1 + \beta_{101} h^{-1} + \sum_r \beta_{0r1} K_{HAc}{}^r [HAc]^r h^{-q}.$$

Since $C \gg B$ an approximate value of [HAc] and $[Ac^-] = c$ could be calculated from (6) neglecting the b-containing terms. Thus the value of the function

$$F(c) = B/b - 1 - \beta_{101} h^{-1} = \sum_r \beta_{0r1} c^r$$

could be calculated approximately from the corresponding measured values of b and h (eqns. 3 and 4) and the coefficients β_{0r1} could be evaluated by, *e.g.*, Leden's method.[9] According to, *e.g.*, Donaldson [1] the highest mononuclear complex is $SnAc_3^-$. With estimated values of β_{011}, β_{021} and β_{031} – denoted β_1, β_2 and β_3 in the following – the final equilibrium model was calculated with the generalized least squares program Letagrop, version ETITR [33–35] without any of the approximations used in the graphical treatment.

Assuming that E_H, B and C are correct, any errors lie in E_B. Equilibrium constants which minimized the error squares sum $U = \sum w(E_{cal} - E_B)^2$, where E_{cal} is the calculated value of E_B were thus sought. The same weight was assigned to all points ($w = 1$). Using the option denoted $Typ = 3$, $Val = 5$ in Ref. 35, the program calculated b and c from eqns. 5 and 6 by successive approximations using the known or estimated values of $E_H{}^0$, $E_B{}^0$, β_{qrp} and K_{HAc}. The value of H was not utilized for these calculations but $H_{cal} - H = DH$ (Table 1), where H_{cal} was calculated from eqn. 6, was useful as a check of the proposed equilibrium model. The agreement between the calculated and experimental E_B, $E_{cal} - E_B = DEB$ is shown in Table 1.

The formation constants of the tin-acetate complexes were chosen as adjustable common parameters, assuming that K_{HAc}, β_{SnOH^+} and $\beta_{Sn_3(OH)_4{}^{2+}}$ were known. $E_B{}^0$ was used as adjustable group parameter, since, as discussed earlier, only an approximate value of this constant was known. By assuming small errors in H, $E_H{}^0$ and C and varying these as group parameters systematic errors may be compensated for. Since these parameters are interrelated they could not be varied simultaneously. In the version of Letagrop used it was not possible to vary C. Therefore only H or $E_H{}^0$ was varied, which resulted in a closer agreement between experimental and calculated values in some of the titrations. To reduce the risk of systematic errors due to accidental impurities in the reagents, several different batches of the recrystallized salts and several stock solutions of sodium acetate, sodium perchlorate, and perchloric acid had been used.

Since not more than 200 data could be treated at a time with this version of Letagrop, the 690 points were divided into 4 groups. The results of these calculations are shown in Table 3.

The uncertainties provided by the program correspond to three times the "standard deviation" of the constant.[36,37] The standard deviation of the mean values were calculated from

$$\sigma = \sum_i \sigma_i^2 f_i / \sum_i f_i$$

where

σ_i = the standard deviation for each group

f_i = the number of experimental points minus the number of unknown constants for each group.

Table 3. Equilibrium constants, lg β_i, for the formation of $SnAc_i^{2-i}$, i = 1, 2, 3.

Titration No.	lg $\beta_1 \pm 3\sigma$	lg $\beta_2 \pm 3\sigma$	lg $\beta_3 \pm 3\sigma$
1 – 4	3.471 ± 0.004	6.046 ± 0.006	7.25 ± 0.03
5 – 10	3.474 ± 0.004	6.038 ± 0.012	7.30 ± 0.10
11 – 15	3.471 ± 0.003	6.041 ± 0.005	7.26 ± 0.03
16 – 19	3.472 ± 0.003	6.041 ± 0.004	7.27 ± 0.03
Mean value	3.472 ± 0.004	6.042 ± 0.007	7.27 ± 0.05

In Table 1 the "best" value of E_B^0 for each group is given together with three times its standard deviation $\sigma(E_B^0)$. The fit between the experimental and calculated data is illustrated in Fig. 1. For the sake of clarity only a fraction of the titration points have been included. The distribution of the complexes as a function of pH, as calculated with the Haltafall program,[38,39] is shown in Fig. 2. The plotting was carried out on an IBM 370/145 computer.[40]

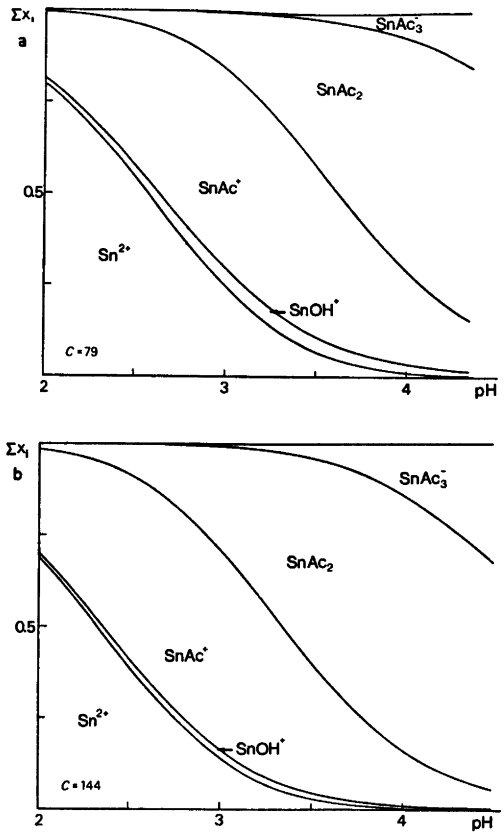

Fig. 2. Distribution diagrams for the tin(II)-acetate system at different acetate concentrations, *i.e.* a, $C = 79$ and b, $C = 144$ mM, respectively. The mol fraction of the total Sn(II) is plotted as a function of pH at constant values of C.

DISCUSSION

The present investigation gives evidence for the formation of the three mononuclear complexes $SnAc^+$, $SnAc_2$ and $SnAc_3^-$. The agreement between the calculated and experimental values

$$DH = H_{cal} - H$$
$$DEB = E_{cal} - E_B$$

is good, although there are systematic trends in some of the titrations (*cf.* Table 1).

The species $SnAc^+$, $SnAc_2$ and $SnAc_3^-$ were also found in the investigation made by Donaldson *et al.*[3] Using the formation constants from the present work, these complexes should, however, not have been formed, in appreciable amounts, in the strongly acid solutions (2 M H_2SO_4) used in their potentiometric and polarographic titrations. Since their experimental data are not given, it is difficult to suggest another interpretation of their measurements. Polarographic and potentiometric studies have been carried out by Elbourne and Buchanan[41,42] on the reactions between Sn(II) and some organic acids, *e.g.* acetic acid. Their calculations seem, however, to have been based on the assumption that only one complex was formed in each solution. The reported values of the mean ligand number for some different compositions do not agree with the equilibrium model given in the present work.

Table 4. Equilibrium constants, lg β_i, for the formation of $InAc_i^{3-i}$ (i = 1, 2, 3), $PbAc_i^{2-i}$ (i = 1, 2, 3, 4) and $SnaAc_i^{2-i}$ (i = 1, 2, 3).

Metal	Medium	lg β_1	lg β_2	lg β_3	Ref.
In^{3+}	2 M $NaClO_4$	3.50	5.95	7.90	46
Sn^{2+}	3 M $NaClO_4$	3.47	6.04	7.26	This work
Pb^{2+}	3 M $NaClO_4$	2.33	3.60	3.59	30

The magnitudes of the formation constants obtained agree well with that expected from consideration of the principle of hard and soft acids and bases.[43–45] The hard acid character of, *e.g.* In^{3+}, Sn^{2+}, and Pb^{2+} should decrease in the given order. Thus the stabilities of the complexes with hard bases, such as the acetate ion, is expected to decrease in the same order. The stability constants of the first three mononuclear complexes are given in Table 4 and the complex formation as a function of pAc is visualized in Fig. 3. It is clear that the harder the acid the lower the acetate concentration at which the third complex starts to dominate.

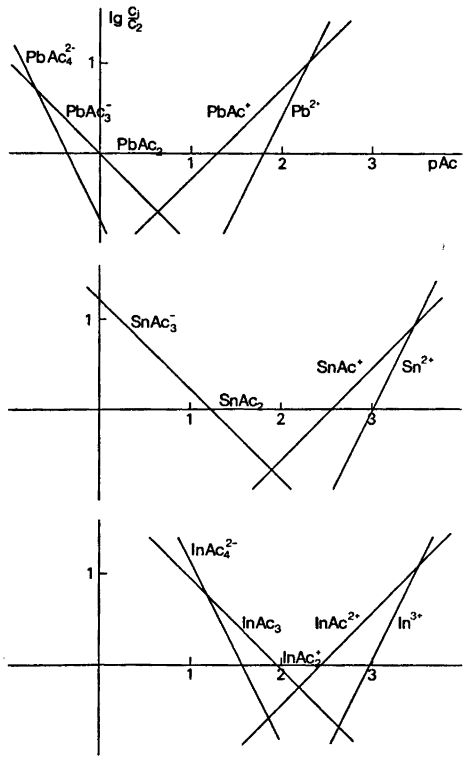

Fig. 3. Distribution diagrams for the $Pb^{2+}-Ac^-$, $Sn^{2+}-Ac^-$ and $In^{3+}-Ac^-$ complexes. lg ($c_i/c_{ref.}$ is plotted as a function of pAc.

The titrations were terminated when a precipitate of black SnO became visible on the generating electrode. This might have indicated the presence of hydrolysed tin-acetate complexes in the solutions. The SnO was, however, only formed on the surface of the electrode, where a temporary excess of Sn^{2+} ion is inevitably built up. As is seen from Fig. 2 a lower acetate concentration would be necessary in order to favour the possible formation of mixed complexes in this pH and [Sn(II)] range.

Acknowledgements. The author is most grateful to Professor Georg Lundgren for all the facilities placed at her disposal, for stimulating discussions and for valuable comments concerning the manuscript. She also wishes to thank many colleagues, especially Drs. Jan Berggren and Olle Börtin, Ing. Janos Kovacs and Mr. Lars Lagerqvist for fruitful discussions and helpful suggestions during the course of the work. Fil.lic. Ove Lindgren's help with the computer programming is gratefully acknowledged. Thanks are also due to Mrs. Birgitta Carlsson for experimental assistance, to Dr. Susan Jagner for revising the English text of this paper and to Mrs. Margareta Johansson, who has kindly typed the manuscript.

This work has been partly financed by the Swedish Natural Science Research Council (Contract No. 2318).

REFERENCES

1. Donaldson, J. D. *Prog. Inorg. Chem. 8* (1967).
2. Donaldson, J. D., Moser, W. and Simpson, W. B. *J. Chem. Soc.* (1964) 5942.
3. Donaldson, J. D. and Knifton, J. F. *J. Chem. Soc. A* (1966) 332.
4. Donaldson, J. D. and Knifton, J. F. *J. Chem. Soc.* (1964) 6107.

5. Donaldson, J. D., Puxley, D. C. and Tricker, M. J. *J. Inorg. Nucl. Chem. 37* (1974) 655.
6. Jelen, A. and Lindqvist, O. *Acta Chem. Scand. 23* (1969) 3071.
7. Gobom, S. and Kovács, J. *Chem. Scr. 2* (1972) 103.
8. Biedermann, G. and Ciavatta, L. *Ark. Kemi 22* (1964) 253.
9. Leden, I. *Diss.*, University of Lund, Lund 1943.
10. Rossotti, F. J. C. and Rossotti, H. *The Determination of Stability Constants*, McGraw, London 1961.
11. Biedermann, G. and Sillén, L. G. *Ark. Kemi 5* (1953) 425.
12. Danielsson, I. and Suominen, T. *Acta Chem. Scand. 17* (1963) 979.
13. Nash, G. R. and Monk, C. B. *J. Chem. Soc.* (1957) 4274.
14. Ingri, N., Lagerström, G., Frydman, M. and Sillén, L. G. *Acta Chem. Scand. 11* (1957) 1034.
15. Wahlberg, O. and Ulmgren, P. *Acta Chem. Scand. 21* (1967) 2759.
16. Latimer, W. M. *Oxidation Potentials*, 2nd Ed., Prentice-Hall, Englewood Cliffs, N. J. 1952.
17. Forsling, W., Hietanen, S. and Sillén, L. G. *Acta Chem. Scand. 6* (1952) 901.
18. Olin, Å. *Acta Chem. Scand. 14* (1960) 126.
19. Haring, M. M. and White, J. C. *J. Electrochem. Soc. 3* (1938) 211.
20. *Some laboratory methods*, Dept. of Inorg. Chem., Royal Institute of Technology, Stockholm, manuscript 1959.
21. Brown, A. S. *J. Am. Chem. Soc. 56* (1934) 646.
22. Biedermann, G. *Ark. Kemi 9* (1956) 277.
23. Lee, Y.-H. *Private communication.*
24. Gobom, S. *Acta Chem. Scand. 17* (1963) 2181.
25. Gran, G. *Analyst 77* (1952) 661.
26. Sjöberg, S. *Acta Chem. Scand. 25* (1971) 2149.
27. Johansson, L. *Coord. Chem. Rev. 12* (1974) 241.
28. Martin, D. L. and Rossotti, F. C. J. *Proc. Chem. Soc.* (1959) 60.
29. Ciavatta, L., Nunziata, G. and Sillén, L. G. *Acta Chem. Scand. 23* (1969) 1637.
30. Gobom, S. *Acta Chem. Scand. A 28* (1974) 1180.
31. Gobom, S. *Acta Chem. Scand. A 30* (1976) 745.
32. Tobias, R. S. *Acta Chem. Scand. 12* (1958) 198.
33. Ingri, N. and Sillén, L. G. *Ark. Kemi 23* (1964) 97.
34. Arnek, R., Sillén, L. G. and Wahlberg, O. *Ark. Kemi 31* (1969) 353.
35. Brauner, P., Sillén, L. G. and Whiteker, R. *Ark. Kemi 31* (1969) 365.
36. Sillén, L. G. *Acta Chem. Scand. 16* (1962) 159.
37. Dunsmore, H., Hietanen, S. and Sillén, L. G. *Acta Chem. Scand. 17* (1963) 2644.
38. Ingri, N., Kakolowicz, W., Sillén, L. G. and Warnqvist, B. *Talanta 14* (1967) 1261.
39. Dyrssen, D., Jagner, D. and Wengelin, F. *Computer Calculation of Ionic Equilibria and Titration Procedures*, Almqvist & Wiksell, Stockholm 1968.
40. Sjölin, L. *Private communication.*
41. Elbourne, R. G. P. and Buchanan, G. S. *Inorg. Nucl. Chem. 32* (1970) 493.
42. Elbourne, R. G. P. and Buchanan, G. S. *Inorg. Nucl. Chem. 32* (1970) 3559.
43. Ahrland, S., Chatt, J. and Davies, N. R. *Q. Rev. Chem. Soc. 12* (1958) 265.
44. Pearson, R. G. *J. Chem. Educ. 45* (1968) 581.
45. Pearson, R. G. *J. Chem. Educ. 45* (1968) 643.
46. Sundén, N. *Sven. Kem. Tidskr. 65* (1953) 257.

Received June 10, 1976.

Acta Chemica Scandinavica A 30 (1976) 781—786

Alkylation Reactions of Tris(dialkylamino)phosphines. A Kinetic Study

TORE THORSTENSON and JON SONGSTAD

Department of Chemistry, University of Bergen, N-5014 Bergen-Univ., Norway

The reactions of methyl iodide with various tris(dialkylamino)phosphines, $(R_2N)_3P$, in acetonitrile at 25.0° C have been studied kinetically. The reactivity order was found to be: Tris(piperidino)phosphine ~ tris(dipropylamino) phosphine ~ tris(diethylamino)phosphine ≥ tris-(dimethylamino)phosphine > tris(morpholino)-phosphine.

With the exception of tris(morpholino)-phosphine which is approximately as reactive as is triphenylphosphine, these aminophosphines are all at least as reactive toward methyl iodide as is tributylphosphine.

The various factors determining the nucleophilicity of tris(dialkylamino)phosphines are discussed.

Within the last decade, a large volume of synthetic work dealing with tris(dialkylamino)-phosphines, $(R_2N)_3P$, has been published. The nucleophilic atom in this class of tervalent phosphorus compounds is generally the phosphorus atom, although, toward methyl trifluoroacetate [1] and when the phosphorus atom is a member of a five-membered ring system,[2] there is some evidence that the nitrogen atoms may be able to compete with the phosphorus atom for the electrophilic center.

Competition experiments [3,4] and numerous semi-quantitative studies [5–11] have shown that these compounds range among the most reactive ones of all the usual tervalent phosphorus compounds. However, this exceptional reactivity is by no means general and toward certain substrates, molecular oxygen and some metal carbonyls,[12] tris(dialkylamino)phosphines are less reactive than are the usual trialkyl phosphites and trialkyl- and triarylphosphines.

Due to the limited ability of tris(dialkylamino)phosphines to act as electrophilic species[7,13], their low reactivity in many reactions can readily be accounted for. However, the complete lack of systematic kinetic studies of reactions of this class of tervalent phosphorus compounds with any substrate leaves much to be known with regard to the factors determining their reactivity.

In this paper the results from a kinetic study of the reactions between some tris(dialkylamino)phosphines and alkyl halides in acetonitrile are presented, eqn. 1.

$$(R_2N)_3P + RX \xrightarrow{MeCN} (R_2N)_3\overset{+}{P}R + X^- \qquad (1)$$

The reactions depicted by eqn. 1 should in principle be well suited for kinetic studies since the products, the phosphonium salts, are obtained in almost quantitative yield and are in most reactions studied easily purified and characterized. However, serious experimental difficulties were encountered in the present study due to the high reaction rates and to the unstable nature of some of the tris(dialkylamino)phosphines (see Experimental Part).

The principle alkyl halide employed in this study was methyl iodide, since several kinetic studies of reactions between this substrate and other tervalent phosphorus compounds have been reported, (for leading references, see Ref. 14), allowing a direct comparison to be made. Furthermore, some reactions between tris-(morpholino)phosphine, Mor_3P, and various 4-substituted benzyl halides were studied in an attempt to obtain information with regard to the structure of the transition state in alkylation reactions of this class of phosphorus nucleophiles.[14]

EXPERIMENTAL

Acetonitrile was purified as described [14] and flushed with dry nitrogen or argon prior to use. Light petroleum (40 – 60 °C), diethyl ether, benzene, and toluene were dried with metallic sodium. The various amines were fractionated from potassium hydroxide pellets. Methyl iodide and the benzyl halides were purified as previously reported.[14]

Tervalent phosphorus reagents. $(Me_2N)_3P$, Fluka prakt., was first distilled under vacuum and then dissolved in a large volume of light petroleum (40 – 60 °C), 500 ml to 25 g compound, and set aside for 24 h at −20 °C to completely precipitate dimethylamine hydrochloride. After filtration, performed in a dry box, the light petroleum was removed in vacuum and the aminophosphine repeatedly distilled in vacuum prior to use.

$(Et_2N)_3P$ and $(Pr_2N)_3P$ were prepared according to standard procedures and purified as $(Me_2N)_3P$.

Tris(piperidino)phosphine, Pip_3P, was prepared and purified in a similar way, but finally crystallized from diethyl ether at dry-ice temperature; m.p. 37 °C.

Tris(morpholino)phosphine, Mor_3P, was prepared and purified as described,[11] m.p. 157 °C (lit.[11] 156 °C).

Mor_2PPh was made according to Hudson and co-workers,[15] m.p. 115 – 116 °C (113 – 115 °C).[15]

$MorPPh_2$, apparently a new compound, was prepared from freshly distilled chlorodiphenylphosphine, $ClPPh_2$, and 2 mol of morpholine in toluene. The product was crystallized from toluene, then from diethyl ether and finally from acetonitrile. Since this compound is very sensitive to moisture, no attempt was made to determine the ultimate yield of the reaction. M.p. 192 °C. (Found: C 71.54; H 6.44; N 4.94; P 11.41. Calc. for $C_{16}H_{18}NOP$: C 70.85; H 6.64; N 5.17; P 11.44).

All operations with the aminophosphines, including the synthesis of the phosphonium salts and the preparations of solutions for the kinetic studies were performed in a dry-box under nitrogen or argon.

Phosphonium salts. The phosphonium salts were prepared in nearly quantitative yield by adding the alkyl halides in slight excess to the aminophosphines dissolved in acetonitrile. The following salts were crystallized from acetonitrile or from acetonitrile/diethyl ether mixture:

Methyl tris(dimethylamino)phosphonium iodide, m.p. > 350 °C (> 350 °C [5]). Methyl tris(piperidino)phosphonium iodide, m.p. 254 °C (242 °C [16]). Methyl tris(morpholino)phosphonium iodide, m.p. 310 °C (dec). Bis(morpholino)methylphenylphosphonium iodide, m.p. 205 – 206 °C. Diphenylmethylmorpholinophosphonium iodide, m.p. 204 – 205 °C. Methyl triphenylphosphonium iodide, m.p. 183 °C (182 – 183 °C [17]). Benzyl tris(morpholino)phosphonium bromide, m.p. 297 °C (dec). 4-Nitrobenzyl tris(morpholino)phosphonium bromide, m.p. 268 – 269 °C (dec). 4-Methylbenzyl tris(morpholino)phosphonium bromide, m.p. 247 – 248 °C.

The phosphonium salts from $(Et_2N)_3P$ and $(Pr_2N)_3P$ and methyl iodide, MeI, could not be obtained as crystalline solids from reactions performed in acetonitrile upon addition of diethyl ether. Only when the reactions were performed in diethyl ether could crystalline phosphonium salts be obtained. All attempts to crystallize methyl tris(diethylamino)phosphonium iodide, m.p. 72 – 92 °C, from the usual dipolar aprotic solvents upon addition of large quantities of diethyl ether or light petroleum failed. Methyl tris(dipropylamino)phosphonium iodide could be crystallized from acetone/diethyl ether mixture after several days at −20 °C. M.p. 135 – 138 °C. These two phosphonium salts, contrary to the phosphonium salts mentioned above, are very hygroscopic.

Kinetic studies. The second order rate constants for most of the reactions were calculated from kinetic runs performed under both pseudo first order and second order conditions. The conductivity method,[14] and, for reactions with methyl iodide, the UV method measuring the rate of formation of iodide ions at 247.5 nm, were applied.

For the reactions of methyl iodide with $(Me_2N)_3P$, $(Et_2N)_3P$, and $(Pr_2N)_3P$, the aminophosphines purified by distillation, none of these methods were entirely satisfactory and the reproducibility of the rate constant was generally poor. The rate constants given in Table 1 for $(Et_2N)_3P$ and $(Pr_2N)_3P$ are therefore assumed to be no better than ± 10 %. $(Me_2N)_3P$ was especially difficult to handle, and the various methods could only give a rough estimate of the rate constant for its reaction with methyl iodide at 25 °C. Competition experiments between $(Et_2N)_3P$ and $(Me_2N)_3P$ toward methyl iodide were therefore performed: To a 1:1 mixture of $(Me_2N)_3P$ and $(Et_2N)_3P$ in acetonitrile, each 3×10^{-3} M, was added an equivalent amount of methyl iodide, dissolved in acetonitrile. After 1 h at room temperature the reaction mixture was evaporated to dryness in vacuum. The residue was washed several times with diethyl ether to remove unreacted aminophosphine, then dissolved in trideuterioacetonitrile, CD_3CN, and the relative amounts of the phosphonium salts from $(Me_2N)_3P$ and $(Et_2N)_3P$ determined by integration of the *N*-alkyl Me-signals in the NMR. Repeating the experiments with varying relative concentrations of the competing nucleophiles showed $(Et_2N)_3P$ to be 1.8 – 2.0 times as reactive as $(Me_2N)_3P$ toward methyl iodide at room temperature, in agreement with the suggested rate constants from the rate studies.

The reactions of Pip_3P, Mor_3P and the various morpholino-substituted phosphines with methyl iodide showed second order kinetics of good

precision and these rate constants are probably well within ± 5 %.

The second order rate constants for the reactions between Mor_3P and the benzyl halides were determined only by the conductivity method under pseudo first order conditions.[14]

All measurements were performed at 25.0 °C maintained within ± 0.05 °C in an thermostated oil-bath.

Comments on the kinetic methods. The conductivity method appeared to be the most reliable one, even though solutions of solely tris(dialkylamino)phosphines in acetonitrile were not entirely stable as viewed from the increasing conductivity of the solutions with time, especially for solutions of the liquid aminophosphines. This instability in acetonitrile appeared to be a function of ageing of the aminophosphines and was kept to a minimum by working with freshly purified samples.

Presumably, part of these difficulties arose from the presence of impurities in the aminophosphines. Regardless of how carefully the liquid aminophosphines, $(Me_2N)_3P$, $(Et_2N)_3P$, $(Pr_2N)_3P$, were distilled, traces of the corresponding amines, R_2NH, were always found to be present as indicated by the red colour of the solutions due to the presence of the corresponding phosphoranes when these aminophosphines were allowed to react with 4-nitrobenzyl bromide.[18]

The solid aminophosphines, on the other hand, which were purified by crystallization, gave colourless solutions of the corresponding phosphonium salts when added to 4-nitrobenzyl bromide. The presence of dialkylamines in the solutions of the liquid aminophosphines in acetonitrile could thus not be due to hydrolysis of these compounds [16,19] by residual water in the applied solvent.

The UV method measuring the rate of formation of iodide ions at 247.5 nm was less reliable due to the extreme dilution necessary and to the high extinction coefficient of the aminophosphines at this wavelength.[20]

RESULTS

In Table 1 are listed the results from the present study for the reactions between the various aminophosphines and methyl iodide in acetonitrile at 25 °C. For comparison, the rates of reaction of triphenylphosphine, Ph_3P, tributylphosphine, But_3P, and trimethyl phosphite, $(MeO)_3P$, for reactions with the same substrate in acetonitrile at the same temperature are included in the table. In column 2 in Table 1, the basicity constants in water for the parent dialkylamines, R_2NH, are listed.

Although the accuracy of the calculated second order rate constants for some of the reactions studied is somewhat limited, the data in Table 1 indicate the following reactivity sequence: $Pip_3P \sim (Pr_2N)_3P \sim (Et_2N)_3P \geq (Me_2N)_3P > Mor_3P \geq Ph_3P$. Thus, $(Me_2N)_3P$, the commonly applied tris(dialkylamino)phosphine and, as shown in the Experimental Part, the most difficult one to handle, is the least reactive one with the exception of tris(morpholino)phosphine, Mor_3P. The data in Table 1 readily suggest that in reactions where a tris(dialkylamino)phosphine is desired, tris(piperidino)phosphine, Pip_3P, is the compound of choice since, being a solid compound at room temperature, its purification and handling is quite simple.

Table 1. Second order rate constants for the reactions between various tervalent phosphorus compounds and methyl iodide in acetonitrile at 25 °C.

	$k_2 \times 10^3$ (l mol^{-1} s^{-1})	pK_a of HNR_2 in water [f]
$(Me_2N)_3P$	~200 [a]	10.73
$(Et_2N)_3P$	480 [b]	10.98
$(Pr_2N)_3P$	530 [b]	11.00
Pip_3P	480	11.11
Mor_3P	22	8.33
Mor_2PPh	11	
$MorPPh_2$	6.1	
Ph_3P	5.9 [c]	
But_3P	240 [d]	
$(MeO)_3P$	0.035 [e]	

[a] Approximate value only. [b] Rate constants only accurate to ± 10 %. [c] Ref. 14. [d] Calculated value (But_3P is ~ 40 times as reactive as is Ph_3P toward MeI in both acetone and methanol).[21,22] [e] Ref. 23. [f] Ref. 24.

Tris(morpholino)phosphine, Mor_3P, is considerably less reactive than are the other aminophosphines studied and is only slightly more reactive than triphenylphosphine. A slight, but smooth increase in reactivity is observed from Ph_3P to Mor_3P with increasing number of morpholino groups attached to the reacting phosphorus atom.

With the possible exception of $(Me_2N)_3P$, the remaining tris(dialkylamino)phosphines are all at least as reactive as is tributylphosphine toward methyl iodide. Since the reactivity of trialkylphosphines toward alkyl halides is only slightly dependent upon the substituents linked to the phosphorus atom,[21] it can thus be concluded that tris(dialkylamino)phosphines range

Table 2. Second order rate constants for reactions between tris(morpholino)phosphine and triphenylphosphine and some benzyl halides in acetonitrile at 25 °C. (Relative rates in parenthesis).

	$k_2 \times 10^3$ l mol^{-1} s^{-1}		
	4-Methylbenzyl bromide	Benzyl bromide	4-Nitrobenzyl bromide
Mor_3P	12 (1.45)	8.30 (1.00)	8.50[a] (1.02)
Ph_3P	3.50 (1.63)	2.15 (1.00)	2.34[b] (1.09)

[a] k_2 for RI = 5.0×10^{-2} l mol^{-1} s^{-1}, k_2(RI)/k_2(RBr) = 5.9. [b] Ref. 14. k_2 for RI = 1.63×10^{-2} l mol^{-1} s^{-1}, k_2(RI)/k_2(RBr) = 7.0.

among the most reactive ones of all tervalent phosphorus compounds toward methyl iodide.

In Table 2 are listed the rate constants for the reactions between tris(morpholino)phosphine and some 4-substituted benzyl halides. For comparison, the results from a recent study on similar reactions of triphenylphosphine [14] are included. Tris(morpholino)phosphine is seen to retain its slightly higher reactivity toward these substrates compared to triphenylphosphine. The effect of the substituents in the benzyl halides on reaction rates are of the same order of magnitude, and as for triphenylphosphine, a slight increase from benzyl bromide to 4-nitrobenzyl bromide is observed. The effect of the leaving group, as exemplified by the k_2(RI)/k_2(RBr) ratios, is slightly lower for tris(morpholino)phosphine, 5.9, than for triphenylphosphine, 7.0.

DISCUSSION

Little is known with regard to the factors determining the nucleophilicity of tris(dialkylamino)phosphines. From several thermodynamic studies, however, two important factors seem to have been established which govern their basicity toward Lewis acids. Since the nucleophilicity is generally closely related to the basicity in a series in which the nucleophilic atom remains constant,[22] it is natural to assume that the nucleophilicity of tris(dialkylamino)-phosphines depends on these two factors as well.

A. The lone pair-lone pair repulsion. The *p*-orbital lone pairs on the nitrogen atoms are interacting with the phosphorus lone pair in a repulsive manner, raising the energy of the latter and rendering it both more basic and nucleophilic.[20] Thus, when the nitrogen lone pairs are not constrained to be orthogonal to the phosphorus lone pair, which is not the case in any of the aminophosphines studied in the present investigation, the basicity and the nucleophilicity of this class of tervalent phosphorus compounds should parallel the basicity of the dialkylamines from which they are derived. The reactivity sequence for aminophosphines found in the present study, Table 1, is in agreement with this theory.

B. The $p_N\pi$-$d_P\pi$ electronic transfer.[20,25,26] This type of electronic transfer should be facilitated by sp^2 hybridization of the nitrogen lone pairs since lone pairs in sp^3 hybrids are expected to be less effective in donating π-density to the phosphorus atom than when contained in a *p*-orbital. Although structural data on tris(dialkylamino)phosphines are scarce, an electron diffraction study of tris(dimethylamino)phosphine [27] and a recent X-ray structure determination of tris(morpholino)phosphine [28] indicate that the nitrogen atoms have considerable sp^2 character. The limited structural data, however, do not allow any conclusions to be made with regard to a possible correlation between the hybridization of the nitrogen atoms and the substituents linked to these atoms.

The π electron transfer should especially be favoured in reactions where considerable positive charge is accumulated on the phosphorus atom in the transition state since the consequent contraction of its *d*-orbitals will render these more available for interaction with the nitrogen orbitals. The very short P–N bond distance of 1.63 Å [29] in dimethylaminodifluorophosphine, Me_2NPF_2, due to the electronegative fluorine atoms is in accord with this suggestion.

However, the data in Table 2 suggest that the transition state for alkylation reactions of tris(dialkylamino)phosphines is quite comparable with that of alkylation reactions of triphenylphosphine. Recently,[14] it has been proposed that this transition state is somewhat "tight" but rather reactant-like with rather small amount of bond breaking, causing the phos-

phorus atom to have only a negligible fractional charge in the transition state. It thus appears conceivable that tris(dialkylamino)phosphines do not owe their high reactivity toward alkyl halides to π-electron transfer in the transition state.

Actually, the lower rate increase from benzyl bromide to 4-methylbenzyl bromide for reactions of Mor_3P than for Ph_3P suggests even less dependence upon fractional charge on the carbon atom and thus less bond breaking in the transition state in alkylation reactions of aminophosphines than for triphenylphosphine. The smaller effect of the leaving group as exemplified by the $k_2(RI)/k_2(RBr)$ ratios accords with this suggestion. The transition state for alkylation reactions of tris(dialkylamino)phosphines should thus be even less ionic and "tighter" than for the corresponding reactions of triphenylphosphine. Presumably, the ability of tervalent phosphorus compounds to enter into a "tight" transition state is related to the stability of the corresponding phosphoranes.[14,23] The very stable nature of phosphoranes derived from tris(dialkylamino)-phosphines is well documented.[30] Tris(dialkylamino)phosphines seem to be the only tervalent phosphorus compounds which can make stable adducts with triphenylmethyl isocyanide, Ph_3CNC.[31]

The π electron transfer may well be the cause for the exceptional reactivity of tris(dialkylamino)phosphines in reactions with highly electron deficient electrophiles or when the reactions go through highly ionic transition states. The NPN bond angles in these compounds, 97 – 98°,[27,28] invalidates the possible argument that tris(dialkylamino)phosphines owe their high reactivity in certain reactions to a large bond angle in their ground state. With Lewis acids like borane, BH_3,[26,32] the triphenylmethyl carbenium ion, Ph_3C^+,[33] and organic azides, RN_3,[20] with which tris(dialkylamino)-phosphines make more stable adducts than do other tervalent phosphorus species, a considerable charge transfer from the phosphorus atom to the accepting atoms is known to take place. The very stable nature of chloro- and bromotris(dialkylamino)phosphonium cations, $XP^+(NR_2)_3$,[34,35] supports this argument.

The results in the present study indicate that the nucleophilicity of tris(dialkylamino)phosphines toward aliphatic carbon is mainly governed by the availability of the free electron pair on the reacting phosphorus atom. Their reactivity toward this class of substrates does not seem to require π electron transfer from the nitrogen atoms to the phosphorus atom. In reactions with alkyl halides these compounds therefore do not appear to act as α-nucleophiles. The α-effect is generally known to be negligible in alkylation reactions.[36,37] By applying the Brønsted equation [38] one can thus speculate that the proton basicity of the phosphorus atom in tris(dialkylamino)phosphines is comparable to that of trialkylphosphines while tris(morpholino)phosphine should be slightly more basic than triphenylphosphine.

Acknowledgement. The authors are indebted to Dr. R. Eliason for valuable comments.

REFERENCES

1. Simonnin, M. P., Charrier, C. and Burgada, R. *Org. Magn. Reson. 4* (1972) 113.
2. Hudson, R. F. and Brown, C. *Acc. Chem. Res. 5* (1972) 204.
3. Freeman, K. L. and Gallagher, M. J. *Aust. J. Chem. 21* (1968) 145.
4. Kren, R. M. and Sisler, H. H. *Inorg. Chem. 9* (1970) 836.
5. Nöth, H. and Vetter, H.-J. *Chem. Ber. 96* (1963) 1109.
6. Downie, I. M. and Lee, J. B. *Tetrahedron Lett.* (1968) 4951.
7. Amonoo-Neizer, E. A., Ray, S. K., Shaw, R. A. and Smith, B. C. *J. Chem. Soc.* (1965) 4296.
8. Harpp, D. N., Gleason, J. G. and Snyder, J. P. *J. Am. Chem. Soc. 90* (1968) 4181.
9. Harpp, D. N. and Gleason, J. G. *J. Am. Chem. Soc. 93* (1971) 2437.
10. Armour, M.-A., Cadogan, J. I. G. and Grace, D. S. B. *J. Chem. Soc. Perkin. Trans. 2* (1975) 1185.
11. Stangeland, L. J., Austad, T. and Songstad, J. *Acta Chem. Scand. 27* (1973) 3919.
12. Thorsteinson, E. M. and Basolo, F. *J. Am. Chem. Soc. 88* (1966) 3929.
13. Strohmeier, W. and Müller, F.-J. *Chem. Ber. 100* (1967) 2812.
14. Thorstenson, T. and Songstad, J. *Acta Chem. Scand. A 30* (1976) 724.
15. Hudson, R. F., Chopard, P. A. and Salvadori, G. *Helv. Chem. Acta 70* (1964) 632.
16. Burgada, R. *Ann. Chim. (Paris) 8* (1963) 347.
17. Blount, B. K. *J. Chem. Soc.* (1932) 337.
18. Vikane, O. and Songstad, J. *Acta Chem. Scand. 27* (1973) 421.

19. Petrov, K. A. and Nifantjev, E. E. *Zh. Obshch. Khim. 31* (1961) 2377.
20. Kroshevsky, R. D. and Verkade, J. G. *Inorg. Chem. 14* (1975) 3090.
21. Henderson, W. A., Jr. and Buckler, S. A. *J. Am. Chem. Soc. 82* (1960) 5794.
22. Pearson, R. G., Sobel, H. and Songstad, J. *J. Am. Chem. Soc. 90* (1968) 319.
23. Thorstenson, T. and Songstad, J. *To be published.*
24. Perrin, D. D. *Dissociation Constants of Organic Bases in Aqueous Solution*, Butterworth, London 1965.
25. Labarre, M.-C., Voigt, D., Senges, S., Zentil, M. and Wolf, R. *J. Chim. Phys. Phys.-Chim. Biol. 68* (1971) 1216.
26. Dorschner, R. and Kaufmann, G. *Inorg. Chim. Acta 15* (1975) 71.
27. Vilkov, L. V., Tsjaikin, L. S. and Jevdokimov, V. V. *Zh. Struct. Khim. 13* (1972) 7.
28. Römming, C. and Songstad, J. *To be published.*
29. Morris, E. D., Jr. and Nordman, C. E. *Inorg. Chem. 8* (1969) 1673.
30. Issleib, K., Lischewski, M. and Zschunke, A. *Org. Magn. Reson. 5* (1973) 401.
31. Songstad, J. *Unpublished observation.*
32. Jugie, G., Jouany, C., Elegant, L., Gal, J.-F. and Azzoro, M. *Bull. Soc. Chim. Fr.* (1976) 1.
33. Dimroth, K. and Nürrenbach, W. *Chem. Ber. 93* (1960) 1649.
34. Nöth, H. and Vetter, H.-J. *Chem. Ber. 96* (1963) 1298.
35. Teichmann, H. and Gerhard, W. *Z. Chem. 14* (1974) 233.
36. Gregory, M. J. and Bruice, T. C. *J. Am. Chem. Soc. 89* (1967) 4400.
37. Oae, S., Kadoma, Y. and Yumihiko, Y. *Bull. Chem. Soc. Jpn. 42* (1969) 1110.
38. Hudson, R. F. *Structure and Mechanism in Organo-phosphorus Chemistry*, Academic, London 1965, p. 131.

Received May 25, 1976.

Acta Chemica Scandinavica A 30 (1976) 787—793

Synthesis of $(-)_{589}$-Di-μ-hydroxo-Λ-bis(ethylenediamine)-chromium(III)-Λ-bis(ethylenediamine)cobalt(III) Perchlorate

JOHAN SPRINGBORG [a] and CLAUS E. SCHÄFFER [b]

[a] Chemistry Department, Royal Veterinary and Agricultural University, Thorvaldsensvej 40, DK-1871 Copenhagen V, Denmark and [b] Chemistry Department I (Inorganic Chemistry), University of Copenhagen, The H.C. Ørsted Institute, Universitetsparken 5, DK-2100 Copenhagen Ø, Denmark

Heating of the cocrystallized dithionates of the cations Λ-*cis*-$[Cr(en)_2(OH)(H_2O)]^{2+}$ and Δ-*cis*-$[Co(en)_2(OH)(H_2O)]^{2+}$ yielded nearly quantitatively $(-)_{589}$-Λ,Λ-$[(en)_2Cr(OH)_2Co(en)_2](S_2O_6)_2$, from which pure $(-)_{589}$-Λ,Λ-$[(en)_2Cr(OH)_2Co(en)_2](ClO_4)_4$ was obtained by a kinetically controlled fractionation procedure.

Di-hydroxo bridged binuclear complexes (diols) with chromium(III) or cobalt(III) have been known for many years and the classical tetraammine and bis(ethylenediamine) diols [1–4] are still among the most studied ones. The structure of these have now been established by single crystal X-ray structural analysis of $[(NH_3)_4Co(OH)_2Co(NH_3)_4]Cl_4 \cdot 4H_2O$ [5,6] and Δ,Λ-$[(en)_2Cr(OH)_2Cr(en)_2]Cl_2(ClO_4)_2 \cdot 2H_2O$ [7] and Guinier X-ray powder diffraction studies.[8] These complexes (and their parent mono-ols, *vide infra*) therefore represent bridged structures of known constitution, whose properties may throw light upon the most common type of hydrolysis products of aqua ions within the whole periodical system.

The kinetics and the thermodynamics of the hydrolysis of the chromium(III) and cobalt(III) diols to their parent mono-nuclear complexes have been studied several times but are still in many respects not understood.[9–14] The proposed reaction mechanisms all involve a mono-hydroxo bridged intermediate (*mono-ol*). The existence of such an intermediate has recently been unambiguously established [15,16] in the chromium(III) bis(ethylenediamine) system in which equilibration between mono-ols and diol is established within minutes at room temperature, *i.e.* long before the occurrence of other reactions confuse the issue. The mono-hydroxo bridged structure of the intermediate has very recently been further established by a single crystal X-ray structural analysis on Δ,Λ-$[(OH)(en)_2Cr(OH)Cr(en)_2(OH)](ClO_4)_3 \cdot H_2O$.[17]

The olation reaction of the mono-nuclear complexes to form bridged complexes, *e.g.* diols, has been less studied.[18–19]

The electronic properties of these bridged systems are of intense current interest. The chromium(III) diols provide simple systems for the study of magnetic interaction between two paramagnetic metal ions.

A super-exchange model $-JS_AS_B (J = -450$ $cm^{-1})$ has been used to account for the magnetic susceptibility [20] and the absorption spectra [21,22] of the related system basic Rhodo, $[(NH_3)_5Cr-O-Cr(NH_3)_5]^{4+}$. This model, which predicts a Landé interval rule to apply to the $S = 0,1,2,$ and 3 levels of the two combined $S = \frac{3}{2}$ systems is at least for the system in question equivalent to the results of the Angular Overlap Model.[21] However, because of the high energy of the $S = 2$ and $S = 3$ levels, their positions have not been established very accurately experimentally. The chromium(III) diol is known to have a weaker magnetic interaction between its two metal ions than have the basic Rhodo. Therefore the $S = 2$ and $S = 3$ levels should be easier to reach and possibly directly observable in electron spin resonance. The present mixed diol should prove an important help in interpreting the ESR spectra of the chromium(III) diol, since it provides the best possible model

system for a chromium(III) ion without magnetic interaction and yet with much the same chemical site as in the chromium(III) diol.

RESULTS AND DISCUSSION

It is a long time since Dubsky [1] and Werner [4] showed that di-μ-hydroxo binuclear complexes of chromium(III) and cobalt(III), so-called diols, are obtained nearly quantitatively from their parent mono-nuclear species by heating of the solid aquahydroxo dithionates, *e.g.*

$$2\ cis\text{-}[Cr(en)_2(OH)(H_2O)]S_2O_6 \rightarrow meso\text{-}[(en)_2Cr(OH)_2Cr(en)_2](S_2O_6)_2 + 2H_2O \quad (1)$$

$$2\ cis\text{-}[Co(en)_2(OH)(H_2O)]S_2O_6 \rightarrow meso\text{-}[(en_2Co(OH)_2Co(en)_2](S_2O_6)_2 + 2H_2O \quad (2)$$

It has recently been shown [7,8] that the diols obtained by these reactions are the *meso* isomers. Similarly the corresponding bis(tetraammine) diols are obtained by heating of the solid sulfates [1,2] or dithionates [8] of their parent mono-nuclear aquahydroxo species. The method seems to be quite general and has been applied on several other diamine complexes.

In our preliminary attempts to prepare a mixed diol, $[(en)_2Cr(OH)_2Co(en)_2]^{4+}$, we therefore used the above method and as starting material used the cocrystallized dithionates of *cis*-$[Cr(en)_2(OH)(H_2O)]^{2+}$ and *cis*-$[Co(en)_2(OH)(H_2O)]^{2+}$. As expected we obtained a mixture of the *meso* isomers of chromium(III) diol, cobalt(III) diol and mixed diol. The formation of mixed diol we could show unambigously, but its isolation as a pure salt we never achieved.

The method which finally led to the isolation of pure mixed diol is based firstly on a modification of the above procedure so as to give mixed diol nearly quantitatively and with only a small contamination of the chromium(III) and cobalt(III) diols and secondly on a kinetically controlled fractionation procedure.

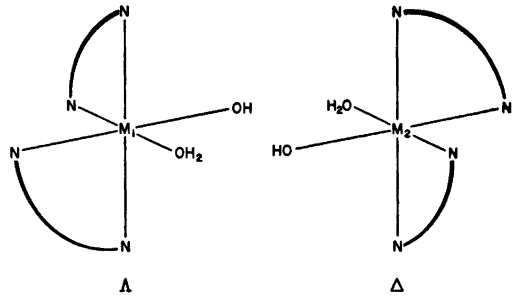

Fig. 1. Assumed packing of the cations in the dithionate of *cis*-$[M(en)_2(OH)(H_2O)]^{2+}$ ion. *A*. $M_1 = M_2 = Cr(III)$ (or Co(III)); mono-nuclear species condense so as to give *meso* chromium(III) diol (or *meso* cobalt(III) diol) as shown recently.[7,8] *B*. $M_1 = Cr$ and $M_2 = Co$; mono-nuclear species condense so as to give $(-)_{589}$-*Λ,Δ*-$[(en)_2Cr(OH)_2Co(en)_2]^{4+}$ as described in the text.

It was assumed that the formation of *meso* diols in the reactions (1) and (2) is facilitated by the packing of the cations in the dithionate, *i.e.* pairwise packing of cations of opposite chirality, oriented much as shown in Fig. 1. This would explain why *meso* diol rather than *racemic* diol is formed. It is then likely that the cocrystallized dithionates of *Λ-cis*-$[Cr(en)_2(OH)(H_2O)]^{2+}$ and *Δ-cis*-$[Co(en)_2(OH)(H_2O)]^{2+}$, if they form an active racemate, will pack also as shown in Fig. 1 and therefore by heating will form mainly the optically active mixed diol, *Λ,Δ*-$[(en)_2Cr(OH)_2Co(en)_2]^{4+}$. Our experiments, based upon these hypotheses, have been successful, and the crude perchlorate salt obtained

Table 1. Analytical data for the different fractions of the mixed diol.

	% Cr 6.64 [a]	% Co 7.53 [a]	% chromium(III) diol [b]	% cobalt(III) diol [c]
Crude perchlorate	6.45	7.70	1.3	4.0
Fraction F_{c1}	6.65	7.51	0.2	0.2
Fraction F_{c2}	6.67	7.50	0.8	0.5
Fraction F_{c3}	6.66	7.50	1.2	1.0

[a] Calculated for $[(en)_2Cr(OH)_2Co(en)_2](ClO_4)_4$. [b] Calculated from ESR measurements. [c] Upper limi for the contamination with cobalt(III) diol, calculated on the basis of an estimated error (± 0.01) on the metal analyses.

Table 2. Kinetic and thermodynamic properties of mono-ols and diols.[a]

	20°C			0.8°C			
	10^2k_f min^{-1}	10^2k_r min^{-1}	K_{eq}	10^2k_f min^{-1}	10^2k_r min^{-1}	K_{eq}	Ref.
$(-)_{589}$-*Λ,Δ*-$[(en)_2Cr(OH)_2Co(en)_2](ClO_4)_4$	24	6	4 ± 1	2.4	0.6	4 ± 1	23[b]
meso-$[(en)_2Cr(OH)_2Cr(en)_2](ClO_4)_4$	23.5	30.8	0.76	2.21	2.54	0.84	15,16

[a] All data refer to the medium 1 M $NaClO_4$. The rate constants k_f and k_r refer to the equilibration reaction

$$[(en)_2M_1(OH)_2M_2(en)_2]^{4+} + H_2O \underset{k_r}{\overset{k_f}{\rightleftharpoons}} [(OH)(en)_2M_1(OH)M_2(en)_2(H_2O)]^{4+}$$

where M_1 and M_2 can both be Cr or Co so that k_f and k_r refer to composite terms as shown in Ref. 23.
[b] Calculated from the data given in the reference. K_{eq} = [aquahydroxo mono-ol]/[diol].

by this method is seen (Table 1) to be nearly pure. The small contamination with chromium(III) diol and cobalt(III) diol is almost certainly due to contamination with racemic aquahydroxo dithionates contained in the starting material, {*Λ-cis*-$[Cr(en)_2(OH)(H_2O)]$, *Λ-cis*-$[Co(en)_2(OH)(H_2O)]\}(S_2O_6)_2$.

Pure mixed diol (99.6 % pure, see Table 1) was then obtained by a kinetically controlled fractionation procedure. This procedure takes advantage of the fact that the kinetics and thermodynamics of the mono-ol/diol systems are different for the three cases, Cr diol, mixed diol, and Co diol. The first two systems enter rather rapidly into equilibrium with their respective mono-ols, but with somewhat different rates and equilibrium constants [23] as shown in Table 2. The cobalt(III) diol's behaviour in this respect is still an unsolved problem. However, important in this connection is the fact that neutral or slightly acid [$[H^+] \leq 10^{-3}$ M] solutions of the cobalt(III) diol after hours at room temperature do not contain any significant amounts of mono-ol and by addition of sodium perchlorate rapidly gives precipitation of cobalt diol perchlorate nearly quantitatively. The fractionation procedure is based upon these properties as described below. An aqueous solution of the crude mixed diol perchlorate (slightly contaminated with chromium(III) diol and cobalt(III) diol) is allowed to equilibrate with respect to mono-ol/diol. Addition of sodium perchlorate then causes nearly instantaneous precipitation of the diols. Upon further standing the mixture reequilibrates, *i.e.* aquahydroxo mono-ol is transformed back into diol, which as a perchlorate is much less soluble than the parent mono-ol. However, the reformation of diol is approximately five times faster for the chromium(III) diol than for the mixed diol (see k_r values in Table 2). Therefore, removal of the precipitate at the time where re-formation and precipitation of chromium(III) diol is essentially complete, gives a solution from which pure mixed diol precipitates (fraction F_{c1}, see Table 1). From the first and impure fraction (F_{a1}) further two fractions (F_{c2} and F_{c3}) were obtained by repeating the kinetically controlled fractionation procedure. These fractions, however, are not as pure as F_{c1}. Obviously the fractionation procedure only gives a very pure product if the contamination with chromium(III) diol is relatively small.

Evidence that the compound actually is a mixed diol is provided in the following.

The compound was analyzed as $[CrCo(en)_4(OH)_2](ClO_4)_4$ which strongly indicated a polynuclear structure with no terminal OH or OH_2 groups. The likely possibility that the compound was an equimolar mixture of chromium(III) diol and cobalt(III) diol could be excluded unambiguously from its absorption spectra (data in Table 3). The compound has no terminal OH^- groups as shown by the visible absorption spectra (at 0 °C and extrapolated back to the time of dissolution), which were identical for the two media {10^{-3} M $HClO_4$, 1 M $NaClO_4$} and {1 M $HClO_4$} (Table 3). These observations strongly suggest a hydroxo bridged structure. It was then shown that the Guinier powder

Table 3. Spectral data for the three diols at 0.8°C. Medium 0.001 M $HClO_4$, 1 M $NaClO_4$.

Compound	$(\varepsilon,\lambda)_{max}$	
$(-)_{589}$-Λ,Δ-$[(en)_2Cr(OH)_2Co(en)_2](ClO_4)_4$	(229, 528) [a]	(149, 383) [a]
	(231, 528)	(148, 383)
Λ,Δ-$[(en)_2Cr(OH)_2Cr(en)_2](ClO_4)_4$	(199, 540) [b]	(107, 386) [b]
Λ,Δ-$[(en)_2Co(OH)_2Co(en)_2](ClO_4)_4$	(298, 525)	(242, 375) sh

[a] Medium 1 M $HClO_4$. [b] Taken from Ref. 16.

diffraction pattern of the perchlorate of the compound is nearly identical to that of *meso*-$[(en)_2Cr(OH)_2Cr(en)_2](ClO_4)_4$ whose cation's structure is known.[7] Also the patterns of the corresponding two dithionates show great similarities. This is evidence that the nuclearity of the mixed diol is two and that the chiralities of the two units building up its binuclear cation are opposite. The cation $[(en)_2Cr(OH)_2Co(en)_2]^{4+}$ comprises four chiral isomers, $\Lambda\Delta$, $\Delta\Delta$, $\Lambda\Lambda$, and $\Delta\Delta$, making up two catoptric (enantiomeric) pairs. The present *meso* mixed diol $\Lambda Cr\Delta Co$ is an internal active racemate which owes its chirality to the lack of intramolecular configurational cancelling caused by the fact that the two central ions are different. As expected the compound showed optical rotation, and the fact that the rotation did not change upon reprecipitation is evidence that the compound is a pure isomer. From the configuration [24,25] of the parent species used as starting materials we therefore find it most certain that the configuration is Λ around the chromium(III) ion and Δ around the cobalt(III) ion.

The results given above do not exclude the possibility that the compound is contaminated with small amounts of chromium(III) diol and cobalt(III) diol in the ratio 1:1. Such a contamination does not alter the elemental analyses and only to a negligible extent affect the other measurements quoted above. ESR spectroscopy, however, provides an excellent tool for the solution of this problem. As shown in Fig. 2 the ESR spectrum of the chromium(III) diol is very complex compared to its corresponding mononuclear species, *cis*-$[Cr(en)_2(OH)_2]^+$. This difference is caused by interaction between the two paramagnetic chromium(III) ions in the diol. In the mixed diol such an interaction would not have much consequence and the ESR spectrum is therefore very similar to that of the parent mononuclear chromium(III) species as shown in Fig. 2. The cobalt(III) diol and the cobalt(III) nucleus in the mixed diol are both diamagnetic and therefore do not give an ESR spectrum. The mixed diol is clearly

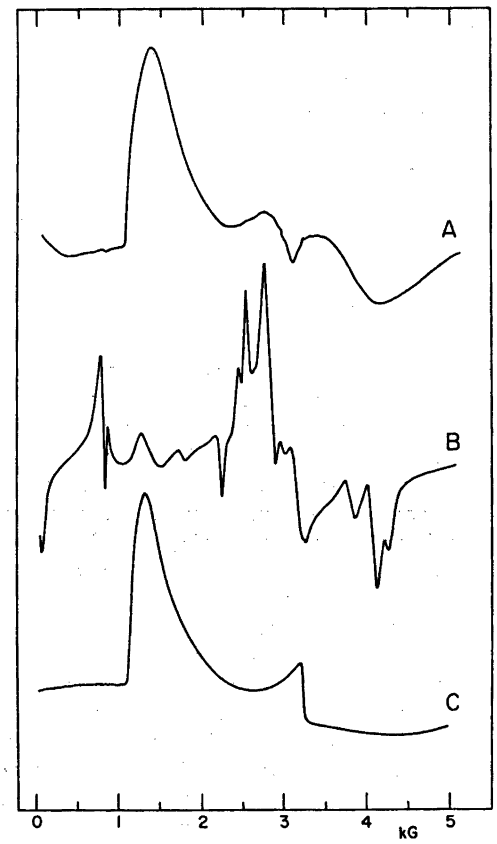

Fig. 2. ESR spectra at −140 °C in glycerol-water (1:1) glass of the cations $(-)_{589}$-Λ,Δ-$[(en)_2Cr(OH)_2Co(en)_2]^{4+}$ (A), Λ,Δ-$[(en)_2Cr(OH)_2Cr(en)_2]^{4+}$ (B), and *cis*-$[Cr(en)_2(OH)_2]^+$ (C).

seen to be almost pure with respect to contamination with chromium(III) diol. The small peak at 0.85 kG, however, was shown to be due to such a contamination. Furthermore, from measurements on samples of the mixed diol artificially contaminated with the chromium(III) diol (up to 5 %) it was shown that the peak height at 0.85 kG relative to the peak height at 1.4 kG can be used as a reliable quantitative measure of the contamination with chromium(III) diol. The results of such an analysis are given in Table 1.

EXPERIMENTAL

Materials. Ammonium bromocamphorsulfonate ($[\alpha]_{589}^{20} = 85°$ for 2 % aqueous solution) was obtained from bromocamphor.[26] *cis*-$[Co(en)_2Cl(H_2O)]SO_4 \cdot 2H_2O$ was obtained from $[Co(en)_2CO_3]Cl$ [27] and then converted to the chloride by treatment with 12 M hydrochloric acid at 0 °C. The resolution of the latter salt into its $(-)_{589}$-*Δ* and $(+)_{589}$-*Λ* isomers was effected by the method of Werner.[28] The $(-)_{589}$-*Δ* isomer was converted to $(-)_{589}$-*Δ*-$[Co(en)_2CO_3]I$ as described by Dwyer, Sargeson and Reid.[29] $(+)_{589}$-*Λ*-*cis*-$[Cr(en)_2Cl_2]Cl.H_2O$ was isolated from racemic [30] *cis*-$[Cr(en)_2Cl_2]Cl.H_2O$ through its bromocamphorsulfonate by a modification of methods previously described.[31,32] The method given here has the advantage that the yield based on the rather expensive ammonium bromocamphorsulfonate has been considerably increased. The *meso*-$[(en)_2Cr(OH)_2Cr(en)_2](ClO_4)_4$, *meso*-$[(en)_2Co(OH)_2Co(en)_2](ClO_4)_4$ and *cis*-$[Cr(en)_2(H_2O)_2]Br_3.2H_2O$ were synthesized as published elsewhere.[8] All other chemicals were analytical grade.

Analysis. Chromium and cobalt analysis determined by atomic absorption spectrophotometry was performed by K. Jørgensen, Chemistry Department I, H. C. Ørsted Institute, and C, N, H, and Cl analyses were made by the microanalytical laboratory at the H. C. Ørsted Institute, Copenhagen.

Instruments. A Zeiss DMR 21 spectrophotometer was used for all spectrophotometric measurements in the visible region. For the spectrophotometric data given below the absorbancy ε has been given in 1 mol^{-1} cm^{-1} and the wavelength λ has been given in nm. The molarity of solutions of the dimers was always defined as the number of mol of dimer and not the number of mol of chromium(III) per litre of solution. The optical rotations were measured on a Perkin Elmer Model 141 polarimeter. Guinier powder diffraction diagrams were measured with a Guinier powder camera with Cu$K\alpha_1$ radiation. ESR spectra were recorded at 9.111 GHz on a JEOL JES-ME-1X spectrometer.

Preparative procedures. 1. $(+)_{589}$-*Λ*-*cis*-Dichlorobis(ethylenediamine)chromium(III) chloride monohydrate. $(+)_{589}$-*Λ*-*cis*-$[Cr(en)_2Cl_2]Cl.H_2O$. To a freshly prepared (within 2 min) solution of *cis*-$[Cr(en)_2Cl_2]Cl.H_2O$ (60.0 g, 0.202 mol) in water (1 l) at 20 °C was added ammonium bromocamphorsulfonate (40.0 g, 0.122 mol) within 5 min and under vigorous stirring. Precipitation of the diastereoisomer commenced during the addition of the ammonium bromocamphorsulfonate and after further 5 min the precipitate was filtered off, washed with 96 % ethanol and then with ether. Drying in air yielded 32 g. This was dissolved in ice-cold 12 M hydrochloric acid (130 ml) and with stirring and cooling in ice added cold 96 % ethanol (260 ml). After 5 min the precipitate was filtered off and washed with 96 % ethanol and then with dry ether. Drying in air yielded 16.5 g of $(+)_{589}$-*Λ*-*cis*-$[Cr(en)_2Cl_2]Cl.H_2O$ (46 % based on ammonium bromocamphorsulfonate). The rotation ($[\alpha]_{589}^{25} = 268 \pm 3°$ for 0.075 % aqueous solutions) was unchanged upon further reprecipitation with 96 % ethanol from 12 M hydrochloric acid ($[\alpha]_{589}^{25} = 271°$) or by repeated reprecipitation with ammonium bromocamphorsulfonate ($[\alpha]_{589}^{25} = 268°$).

2. Cocrystallized dithionate of *Λ*-*cis*-aquabis(ethylenediamine)hydroxochromium(III) and *Δ*-*cis*-aquabis(ethylenediamine)hydroxocobalt(III) cations. $\{$*Λ*-*cis*-$[Cr(en)_2(OH)(H_2O)]$, *Δ*-*cis*-$[Co(en)_2(OH)(H_2O)]\}(S_2O_6)_2$. *Δ*-$(-)_{589}$-$[Co(en)_2CO_3]I$ (22 g, 60 mmol) was dissolved in 1 M nitric acid (130 ml) at 0 °C within 12 min. Then solid silver nitrate (44.2 g, 260 mmol) and *Λ*-$(+)_{589}$-*cis*-$[Cr(en)_2Cl_2]Cl.H_2O$ (17.8 g, 60 mmol) was added and the mixture thoroughly stirred for 10 min. The silver halides were filtered off and to the filtered solution was added, with stirring and cooling in ice, a solution of sodium dithionate dihydrate (40 g, 165 mmol) in water (180 ml, 20 °C). Then pyridine (160 ml, 0 °C) was added and precipitation of the active racemic mixed dithionate of the aquahydroxo complexes commenced within 5 s. After further 50 s the precipitate was filtered off and washed twice with water (40 ml), three times with 96 % ethanol (80 ml), and then thoroughly dried with ether. Drying in air yielded 21.8 g (49 %) of $\{$*Λ*-*cis*-$[Cr(en)_2(OH)(H_2O)]$, *Δ*-*cis*-$[Co(en)_2(OH)(H_2O)]\}(S_2O_6)_2$.

3. $(-)_{589}$-Di-*μ*-hydroxo-*Λ*-bis(ethylenediamine)chromium(III)-*Δ*-bis(ethylenediamine)cobalt(III) perchlorate. $(-)_{589}$-*Λ*,*Δ*-$[(en)_2Cr(OH)_2Co(en)_2](ClO_4)_4$. The crude $\{$*Λ*-*cis*-$[Cr(en)_2(OH)(H_2O)]$, *Δ*-*cis*-$[Co(en)_2(OH)(H_2O)]\}(S_2O_6)_2$ (21.8 g, 0.0294 f.w.) was added to acetic acid anhydride (220 ml). The suspension was heated to reflux within 20 min, kept at reflux for another 30 min and then cooled in an ice bath. The sample was filtered and washed twice with 96 % ethanol (100 ml), twice with 2 M acetic acid (100 ml), three times with 96 % ethanol (100 ml), and finally thoroughly with ether. By the washing with acetic acid, a

small amount of unreacted *cis*-aquahydroxo monomer is removed.* Drying in air yielded 20.3 g (98 %) of crude $(-)_{589}$-*Λ,Δ*-$[(en)_2Cr(OH)_2Co(en)_2](S_2O_6)_2$. This crude dithionate was then added to a saturated solution of ammonium bromide (90 ml) and the suspension was kept at room temperature with stirring for 1 h. The purple crystals of the bromide were filtered off and treated once more with ammonium bromide (45 ml) for half an hour. The sample was filtered and washed with 50 % v/v ethanol (50 ml), twice with 96 % ethanol (50 ml), and then with ether. Drying in the air yielded 20.8 g (95 % based on the dithionate of the aquahydroxo complexes) of crude $(-)_{589}$-*Λ,Δ*-$[(en)_2Cr(OH)_2Co(en)_2]Br_4.2H_2O$. The crude bromide (20.8 g, 28 mmol) was then added to a mixture of a saturated solution of sodium perchlorate (150 ml) and water (150 ml), and the suspension was stirred at room temperature for 1 h. The violet crystals of the perchlorate were collected on a filter, washed with 50 % v/v ethanol (40 ml), twice with 96 % ethanol (80 ml), and thoroughly washed with ether. Drying in air yielded 19.7 g (86 % based on the dithionate of the aquahydroxo complexes) of nearly pure $(-)_{589}$-*Λ,Δ*-$[(en)_2Cr(OH)_2Co(en)_2](ClO_4)_4$ (see Table 1).

Fractionation procedure. Pure mixed diol was obtained by fractional reprecipitation of the above crude perchlorate. As the following fractionation procedure is kinetically controlled the procedure given below must be followed strictly in order to get a successful result.

The crude mixed diol perchlorate (19.0 g, 24.3 mmol) was dissolved in 10^{-3} M $HClO_4$ (270 ml) at 20.0 °C and kept at that temperature for 17 min. Then a saturated solution of sodium perchlorate (270 ml, 20.0 °C) was added with stirring and precipitation of diol perchlorate commenced within a few seconds. After further 9 min at 20.0 °C, with continued stirring, the sample was filtered off within 20 s, washed with 96 % ethanol and then ether. Drying in air yielded 10.6 g (55.8 %) of fraction F_{a1}. The mother liquor was left at 20.0 °C with stirring for 1 h. During this time the precipitation of diol perchlorate became essentially complete. The precipitate was isolated as above to give 4.40 g (23 %) of fraction F_{b1}. Kinetically controlled fractional reprecipitation of F_{a1} (10.6 g) as above yielded 5.9 g (56 %) of fraction F_{a2} and 2.25 g (21 %) of fraction F_{b2}. Finally, fractional reprecipitation of F_{a2} (5.90 g) yielded 3.40 g (58 %) of fraction F_{a3} and 0.99 g (16.8 %) of fraction F_{b3}.

The F_b fractions were reprecipitated in the following way. The diol perchlorate (1.00 g) was dissolved in 10^{-3} M perchloric acid (20 ml, 0 °C) and to the filtered solution was added a saturated solution of sodium perchlorate (20 ml, 20 °C) with stirring and cooling in ice. These operations were performed within 20 s in order to avoid formation of mono-ol. Precipitation of diol perchlorate commenced almost instantaneously. After 3 min the sample was filtered off and washed with 96 % ethanol and then ether. Drying in air yielded 0.80 ± 0.02 g (80 %) of pure $(-)_{589}$-*Λ,Δ*-$[(en)_2Cr(OH)_2Co(en)_2](ClO_4)_4$, fractions F_{c1}, F_{c2}, and F_{c3}, respectively. The yields of these pure or nearly pure (see below) fractions based on {*Λ-cis*-$[Cr(en)_2(OH)(H_2O)]$, *Δ-cis*-$[Co(en)_2(OH)(H_2O)]\}(S_2O_6)_2$ were 16 % (F_{c1}), 8.1 % (F_{c2}), and 3.6 % (F_{c3}).

Purity of the fractions and some properties of the mixed diol. The F_{c1} fraction analyzed as pure mixed diol. *Anal.* calc. for $[(en)_2Cr(OH)_2Co(en)_2](ClO_4)_4$: C 12.27; N 14.31; Cl 18.11; H 4.38. Found: C 12.22; N 14.42; Cl 17.98; H 4.47. Metal analyses for the different fractions are collected in Table 1. The visible absorption spectra changed with time due to formation of mono-ol. However, when measured at 0 °C and with short intervals (2 and 5 min, respectively) after the time of dissolution t_0 the absorptivity ε could be extrapolated linearly back to t_0. These extrapolated spectra were nearly identical for the three F_c fractions. In Table 3 $(\varepsilon,\lambda)_{max}$ values for the F_{c1} fraction are given.

Correspondingly the ESR spectra of the chromium(III) diol and the mixed diol, used for the calculations given in Table 1, and shown in Fig. 2, were taken on freshly prepared solutions. Diol perchlorate was dissolved in 10^{-3} M $HClO_4$ (0 °C) and added one volume of glycerol (0 °C) within 1 min, and then rapidly frozen. The contents of mono-ol in these solutions were therefore negligible. The ESR spectrum of *cis*-$[Cr(en)_2(OH)_2]^+$ was measured on a glass of *cis*-$[Cr(en)_2(H_2O)_2]Br_3.2H_2O$ in a 1:1 mixture of 0.1 M NaOH (aqueous) and glycerol. The optical rotations, $[\alpha]_{589}^{20}$, of freshly prepared solutions changed rapidly with time and became nearly constant after 12 min. Values of $[\alpha]_{589}^{20}$ for the time of dissolution, α_0, and for the time where constant readings were measured, α_∞, were obtained from plots of log $(\alpha_t - \alpha_\infty)$ against time, t. The three F_b and the three F_c fractions showed all nearly identical values for both $\alpha_0 = -214 \pm 4°$ and $\alpha_\infty = -102 \pm 2°$ (0.1 % solutions in 10^{-3} M $HClO_4$, 1 M $NaClO_4$). The observed variations in the α_0 and the α_∞ values were not systematic and mainly due to errors in the measurements.

The Guinier powder X-ray diffraction diagram of $(-)_{589}$-*Λ,Δ*-$[(en)_2Cr(OH)_2Co(en)_2](ClO_4)_4$ was nearly identical to that of *meso*-$[(en)_2Cr(OH)_2Cr(en)_2](ClO_4)_4$. A similar identity was found between the corresponding two dithionates. Pure *Λ,Δ*-$[(en)_2Cr(OH)_2Co(en)_2](S_2O_6)_2$ was obtained by adding a solution of sodium dithionate to a freshly prepared solution at 0 °C of the perchlorate. Thereby $(-)_{589}$-*Λ,Δ*-$[(en)_2Cr(OH)_2Co(en)_2](S_2O_6)_2$ precipitated nearly in-

* It should be noted that mixing of the mother liquor with ethanol is not advisable because of the possibility of a vigorous formation of ethyl acetate.

stantaneously. The salt was not further characterized.

Acknowledgement. The present work was written whilst we were both Visiting Fellows at the Australian National University. We take this opportunity to thank the Research School of Chemistry for support and for excellent working facilities. Grants from Statens Naturvidenskabelige Forskningsråd are further acknowledged.

REFERENCES

1. Dubsky, J. V. *J. Prakt. Chem.* [2] *90* (1914) 61.
2. Werner, A. *Ber. Dtsch. Chem. Ges. 40* (1907) 4820.
3. Pfeiffer, R. and Stern, R. *Z. Anorg. Allg. Chem. 58* (1908) 272.
4. Werner, A. and Rapiport, J. *Justus Liebigs Ann. Chem. 375* (1910) 84.
5. Prout, C. K. *J. Chem. Soc.* (1962) 4429.
6. Vannerberg, N. G. *Acta Chem. Scand. 17* (1963) 85.
7. Kaas, K. *Acta Crystallogr. B 32* (1976) 2021.
8. Springborg, J. and Schäffer, C. E. *Inorg. Synth. 17* (1976). *In press.*
9. Rasmussen, S. E. and Bjerrum, J. *Acta Chem. Scand. 9* (1955) 735.
10. Wolcott, D. *Ph. D. Diss.*, The Catholic University of America, Washington, D.C. 1965.
11. Hoffmann, A. B. and Taube, H. *Inorg. Chem. 7* (1968) 903.
12. El-Awady, A. A. and Hugus, Z. Z., Jr. *Inorg. Chem. 10* (1971) 1415.
13. de Maine, M. M. and Hunt, J. B. *Inorg. Chem. 10* (1971) 2106.
14. Ellis, J. D., Scott, K. L., Wharton, R. K. and Sykes, A. G. *Inorg. Chem. 11* (1972) 2565.
15. Springborg, J. and Toftlund, H. *Chem. Commun.* (1975) 422.
16. Springborg, J. and Toftlund, H. *Acta Chem. Scand. A 30* (1976) 171.
17. Kaas, K. *Acta Crystallogr. To be submitted.*
18. Andersen, P., Berg, T. and Jacobsen, J. *Acta Chem. Scand. A 29* (1975) 381.
19. Andersen, P., Berg, T. and Jacobsen, J. *Acta Chem. Scand. A 29* (1975) 599.
20. Pedersen, E. *Acta Chem. Scand. 26* (1972) 333.
21. Glerup, J. *Acta Chem. Scand. 26* (1972) 3775.
22. Güdel, H. U. and Dubicki, L. *Chem. Phys. Lett. 6* (1974) 272.
23. Springborg, J. and Schäffer, C. E. *Inorg. Chem. 15* (1976) 1744.
24. Matsumoto, K., Ooi, S. and Kuroya, H. *Bull. Chem. Soc. Jpn. 43* (1970) 3801.
25. McCaffery, A. J., Mason, S. F. and Norman, B. J. *J. Chem. Soc.* (1965) 5094.
26. Kipping, F. S. and Pope, W. *J. Chem. Soc. 67* (1895) 356.
27. Springborg, J. and Schäffer, C. E. *Inorg. Synth. 14* (1973) 63.
28. Werner, A. *Helv. Chim. Acta 4* (1921) 113.
29. Dwyer, F. P., Sargeson, A. M. and Reid, I. K. *J. Am. Chem. Soc. 85* (1963) 1215.
30. Pedersen, E. *Acta Chem. Scand. 24* (1970) 3362.
31. Werner, A. *Ber. Dtsch. Chem. Ges. 44* (1911) 3132.
32. Selbin, J. and Bailar, J. C. *J. Am. Chem. Soc. 79* (1957) 4285.

Received May 19, 1976.

Acta Chemica Scandinavica A 30 (1976) 794—796

Disappearance of the Sodium—Electron Pair Formed upon Photolysis of Sodium Pyrenide

GÖRAN RÄMME and KJELL-ÅKE ENGDAHL

Institute of Physical Chemistry, University of Uppsala, P.O.B. 532, S-751 21 Uppsala, Sweden

A reply is given to a suggestion by Giling *et al.* that benzene can trap electrons from intermediately formed e^-,Na^+ in the photolysis of sodium pyrenide at room temperature. The present investigations do not confirm that hypothesis. An alternative possible reaction path for the disappearance of e^-,Na^+, not earlier considered by us, is presented.

Flash photolysis of sodium pyrenide ($\pi^{\cdot-},Na^+$) in tetrahydrofuran (THF) leads to photoejection of electrons, which form e^-,Na^+ ion pairs. The reactions following the flash can be monitored spectrophotometrically at 493 nm for $\pi^{\cdot-},Na^+$ and at 650 nm for e^-,Na^+. Fisher *et al.*[1,2] reported that the e^-,Na^+ pairs disappeared more rapidly than $\pi^{\cdot-},Na^+$ was reformed and that the concentration of the latter species continued to increase even when e^-,Na^+ was no longer detectable. Analysis of the kinetics led to the conclusion that the decay of the 650 nm transient is due to two reactions:

$$e^-,Na^+ + \pi(\text{excess}) \xrightarrow{k_3} \pi^{\cdot-},Na^+, \text{ and}$$

$$e^-,Na^+ \xrightarrow{k_6} X$$

The species X, assumed to have no absorption at 650 nm, must further react with pyrene (π) yielding $\pi^{\cdot-},Na^+$ in order to ensure the observed complete reversibility of the system.

As a possible identification of the species X, a relatively slow collapse of the e^-,Na^+ pair into a Na-atom was suggested, the corresponding rate constant being 4×10^3 s^{-1}. This value seems plausible because the desolvation of the e^-,Na^+ pairs should slow down the collapse process.

The interpretation of these results was questioned by Giling *et al.*[3] They pointed out that benzene is probably present in the experiments as an unavoidable impurity, presumably in the solvent THF, and proposed that the reaction

$$C_6H_6 + e^-,Na^+ \xrightarrow{k_7} C_6H_6^{\cdot-},Na^+$$

is responsible for the decay of the 650 nm transient (due to the disappearance of e^-,Na^+). The latter process is faster than the reappearance of $\pi^{\cdot-},Na^+$ (measured by the decrease of bleaching at 493 nm). In view of the lower electron affinity of benzene as compared to that of pyrene, the $C_6H_6^{\cdot-},Na^+$ radical anions react with pyrene and form $\pi^{\cdot-},Na^+$.

The proposal by Giling *et al.* is kinetically equivalent to the scheme suggested by Fisher *et al.*, but the pseudo-first order rate constant, k_{obs}, governing the decay of the 650 nm transient and given in the treatment by Fisher as

$$k_{obs} = k_3[\pi] + k_6$$

should acquire the form

$$k_{obs} = k_3[\pi] + k_7[C_6H_6]$$

To test the validity of this proposal we initially determined the benzene content in THF both spectrophotometrically and by gas chromatography and found it to be $\sim 10^{-5}$ M. Thereafter, we performed a new series of flash photolysis experiments with the $\pi^{\cdot-}Na^+ + \pi$ system to which increasing amounts of benzene were added. If we consider the last equation above and choose $k_7 = 6 \times 10^6$ M^{-1} s^{-1} (available literature data for the capture of the electron

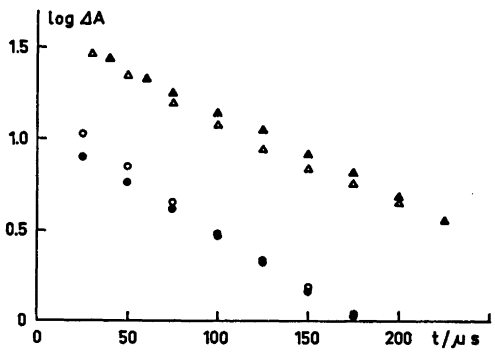

Fig. 1. Logarithmic plot of the change in absorbance as a function of time for the photolysis of $\pi^{\cdot-}$,Na^+ in THF at room temperature in the absence and presence of added benzene as monitored at 493 nm (△, ▲) and 650 nm (○, ●). The solutions were photolyzed in a 60 cm cell and surrounded by a $CuCl_2$ filter solution. ○,△: no benzene added, $[\pi^{\cdot-},Na^+] = 4.1 \times 10^{-7}$ M, $[\pi]_{av} \approx 5 \times 10^{-7}$ M. ●,▲: $[C_6H_6] \approx 10^{-2}$ M, $[\pi^{\cdot-},Na^+] = 3.0 \times 10^{-7}$ M, $[\pi]_{av} \approx 4 \times 10^{-7}$ M.

by benzene in water [4]), $k_3 = 1.7 \times 10^{10}$ M^{-1} s^{-1} and $[\pi] = 5 \times 10^{-7}$ M (a representative value of the pyrene concentration in the previous experiments), a significant increase in k_{obs} can be predicted upon increasing the benzene concentration from 10^{-5} to 10^{-2} M. If we use a value $k_7 = 4 \times 10^8$ M^{-1} s^{-1} calculated from $k_6 = 4 \times 10^8$ s^{-1} and $[C_6H_6] = 10^{-5}$ M, we would expect an even more drastic increase in k_{obs}.

The present experimental results demonstrate that neither the decay of the 650 nm transient nor the reappearance of $\pi^{\cdot-}$,Na^+ monitored at 493 nm is affected by the increase in the concentration of benzene from 10^{-5} to 10^{-2} M, provided the concentration of pyrene is kept constant. This is evident from an inspection of Fig. 1 depicting plots of the logarithm of the change in absorbance at 650 nm and 493 nm as a function of time in two series of experiments in which the concentration of benzene was 10^{-5} and 10^{-2} M, respectively. Moreover, the presence of 10^{-2} M benzene had no effect on the difference spectra recorded at various times after a flash. In particular we found no transient absorption, which could be attributed to the benzene radical anion. Absorption from this species has been reported in the 435 nm region both from its preparation in dimethoxyethane at −70 °C [5] and recently through the use of crown ethers at room temperature in nonpolar solvents in contact with alkali mirrors.[6]

Obviously the presence of benzene even at concentrations of 10^{-2} M do not lead to a faster decay of the 650 nm transient. This is not surprising since the low electron affinity of benzene should make the equilibrium constant of the reaction

$$C_6H_6 + e^-,Na^+ \rightleftharpoons C_6H_6^{\cdot-},Na^+$$

extremely small at room temperature. The equilibrium is shifted to the right at low temperatures and therefore Giling *et al.*, working under such conditions, did observe the formation of $C_6H_6^{\cdot-}$,Na^+ in their photolytic experiments with relatively high concentrations of benzene (10^{-2} to 10^{-1} M). However, even at these low temperatures they found benzene ineffective at concentrations 10^{-4} to 10^{-5} M.

In conclusion, the e^-,Na^+ pair is evidently not trapped by impurity benzene. We can still consider the collapse of the sodium-electron pair as the most feasible reaction path for e^-,Na^+ of the various alternatives discussed in Refs. 1,2 although it has not been experimentally confirmed to date. Thus we can look for further reactions for the disappearance of e^-,Na^+ through routes other than $\pi + e^-,Na^+ \rightarrow \pi^{\cdot-},Na^+$. Recent findings by us in the photolysis of cesium pyrenide [7] and by Levin *et al.* in the photolysis of tetracene [8] have shown that the photolysis of aromatic radical anions is followed, at least partially, by the formation of the corresponding dianions, *i.e.*

$$Ar^{\cdot-},M^+ \xrightarrow{h\nu} Ar + e^-,M^+$$

$$Ar^{\cdot-},M^+ + e^-,M^+ \longrightarrow Ar^{2-},\ 2M^+$$

Electron transfer from the dianion to the hydrocarbon ultimately regenerates radical anions and reverts the system to its initial state.

Acknowledgement. The authors wish to thank Professor Stig Claesson for valuable discussions and encouraging support during the course of this work and Professor Michael Szwarc for constructive comments on the manuscript.

REFERENCES

1. Fisher, M., Rämme, G., Claesson, S. and Szwarc, M. *Chem. Phys. Lett. 9* (1971) 309.
2. Fisher, M., Rämme, G., Claesson, S. and Szwarc, M. *Proc. R. Soc. London Ser. A 327* (1972) 481.
3. Giling, L. J. and Kloosterboer, J. G. *Chem. Phys. Lett. 21* (1973) 127.
4. Hart, E. J., Gordon, S. and Thomas, J. K. *J. Phys. Chem. 68* (1964) 1271.
5. Gardner, C. *J. Chem. Phys. 45* (1966) 572.
6. Kaempf, B., Raynal, S., Collet, A., Schué, F., Boileau, S. and Lehn, J. M. *Angew. Chem. 86* (1974) 670.
7. Engdahl, K.-Å. and Rämme, G. *Chem. Phys. Lett. 41* (1976) 100.
8. Levin, G. and Szwarc, M. *J. Am. Chem. Soc. 98* (1976) 4211.

Received May 13, 1976.

Acta Chemica Scandinavica A 30 (1976) 797—807

Complex Formation between Silver and Iodide Ions in Fused Potassium—Sodium Nitrate. IV. Cationic Complexes

BERTIL HOLMBERG

Division of Physical Chemistry, Lund University, Chemical Center, P.O.B. 740, S-220 07 Lund 7, Sweden

The formation of cationic complexes between silver(I) and iodide ions in fused equimolar $(K,Na)NO_3$ at 280 °C has been studied by potentiometric determination of the free ligand concentration $[Ag^+]$ and by solubility and distribution measurements in two-phase systems formed by $AgI - AgNO_3 - (K,Na)NO_3$, with solid or liquid iodide-based solutions in equilibrium with alkali nitrate melts.

No polynuclear (polyiodic) species can be detected potentiometrically, and the solubility curve and distribution data are well reproduced assuming a stepwise formation of species $Ag_mI^{(m-1)+}$ with $0 \leq m \leq 4$, of which Ag_4I^{3+} has a remarkably high stability. The equilibrium constants, governing the distribution of solvent and solute species between the iodide phase and nitrate melt, are also estimated.

Previous investigations of the complex formation between silver(I) and iodide ions in fused alkali nitrate performed at this laboratory [1–4] have been concerned mainly with neutral and anionic complexes and heterogeneous equilibria between solid or liquid AgI-based solutions and alkali nitrate melts. From studies in aqueous solution the ability of silver and halide ions to form complexes $Ag_mX_n^{(m-n)+}$ has become evident, and subsequent investigations in other media, including ionic melts, have also presented convincing evidence for complex cations of this kind. This topic has been briefly reviewed recently.[5]

For the case of iodide species the mononuclear (monoiodic) complexes Ag_2I^+, Ag_3I^{2+},[6–10] and even Ag_4I^{3+},[7] have been suggested to explain solubility data in aqueous solutions. In addition, results from UV spectroscopy [11,12] and self-diffusion studies [13] support the view that complex cations having iodide as central ion do exist in solution. It should also be noted that a mixed complex $AgHgI^{2+}$ has been reported.[14]

It appears, however, that the information concerning cationic silver iodide complexes in fused salts is restricted to an emf study by Alvarez-Funes and coworkers,[15] considering Ag_2I^+ in liquid KNO_3. The present study aims at a more complete picture of the nature and thermodynamic stability of cationic silver iodide species in fused alkali nitrate. Due to the impossibility of distinguishing between mono- and polyiodic species having the same ionic charge from solubility measurements alone, we have employed both solubility and electromotive force measurements. The emf measurements have been arranged as an ordinary ligand concentration study in a composition range where the difference between the total and "free" silver(I) concentrations is large enough to be determined with an acceptable accuracy. The following cell was used:

$$\mathrm{Ag} \;\Big|\; \begin{matrix} C'_{Ag}\ AgNO_3 \\ C_I\ AgI \\ \\ (K,Na)NO_3 \end{matrix} \;\Big|\; \text{asbestos fibre} \;\Big|\; \begin{matrix} C^\circ_{Ag}\ AgNO_3 \\ \\ \\ (K,Na)NO_3 \end{matrix} \;\Big|\; \mathrm{Ag}$$

From the measured emf the average number of silver ligands bonded to iodide, $\bar{m}$, may be computed. The magnitude of $\bar{m}$ and the variation in $\bar{m}$ with C_I at constant $[Ag^+]$ may then be used to indicate the presence or absence of condensed particles in measurable amounts.

As might be expected, the solubility measurements were complicated by the ability of the high temperature form of silver iodide, α-AgI, to dissolve foreign ions. In preliminary experiments it was observed that α-AgI dissolves

appreciable amounts of $AgNO_3$ at 280° C. Furthermore the solid melts to a yellow-red liquid AgI phase in systems containing more than 0.7 mol kg^{-1} $AgNO_3$ in the nitrate melt. This behaviour, which is analogous to what was observed in the system $AgI-(K,Na)I-(K,Na)NO_3$,[3,4] made it necessary to determine the equilibrium composition of the iodide phase as well as the nitrate phase in the entire composition range under study. The evaluation of the stability constants is based on a formal thermodynamic treatment of the heterogeneous equilibria.

EXPERIMENTAL

Chemicals. All chemicals were *p.a.* grade and were prepared and stored as described previously.[3]

Apparatus. The equipment used for the solubility and distribution measurements and the emf measurements have been described elsewhere.[3,16,17]

Solubility and distribution measurements. Series A: In the major range of $AgNO_3$ concentration the solubilities were measured by a radioassay technique, using AgI labelled with ^{131}I. About 0.1 g AgI was added to 50.00 g equimolar $(K,Na)NO_3$(l) containing a known amount of $AgNO_3$, and the system was agitated until equilibrium was attained (as a rule within 50 h, as indicated by constant solubility). Samples from the nitrate melt were withdrawn with a preheated pipette, solidified, weighed and dissolved in aqueous cyanide solution for the activity measurements.

Series B: The distribution of $AgNO_3$, KNO_3 and $NaNO_3$ between the nitrate melt and the AgI-phase was separately determined in systems containing 8.0 g inactive AgI, 50.00 g $(K,Na)NO_3$ and various amounts of $AgNO_3$. The systems were equilibrated for at least 300 h for solid-liquid equilibria and 50 h for liquid-liquid equilibria to be established. For the systems $Ag(I,NO_3)$(s)-nitrate melt the composition of the solid was calculated from the difference between the added and found amounts of $AgNO_3$ in the nitrate phase. For the systems iodide melt-nitrate melt the compositions were determined by direct analysis of each phase. The phase separation technique has been described elsewhere.[3]

Emf measurements. The procedure was essentially the same as was used in a previous study of bromide complexes.[5] Unsaturated melts were titrated with $AgNO_3$ to a total concentration $C_{Ag} \approx 2.2$ mol kg^{-1}. In some cases further additions of AgI were then made successively up to a maximum value of C_I of about 0.2 mol kg^{-1}. Melts saturated in AgI were studied to a maximum value $C_{Ag} \approx 1.57$ mol kg^{-1}. In all measurements C°_{Ag} was 2.2 mol kg^{-1}, which is high enough to prevent phase separation in the diffusion layer between the half-cells. In absence of iodide phase stable emf's could be read within a few minutes, whereas equilibrium times of 2 – 3 h were required in the study of two-phase systems.

Analyses. Beside the radioassay method gravimetric analyses for AgI(s) were used to determine solubilities greater than 5×10^{-3} mol kg^{-1}. The iodide content of the liquid iodide-rich solutions was determined in the same way.

The silver content of the melts was determined by electroanalytical precipitation on a rotating platinum cathode from hot aqueous cyanide solutions. The contents of sodium and potassium ion in the liquid iodide solution were determined from atomic absorption measurements on samples dissolved in 50 mM aqueous cyanide solutions.

CALCULATIONS AND RESULTS

The following symbols will not be separately defined in the text.

A. Quantities referring to the emf measurements.

E_{obs} = the observed electromotive force.
ε = correction term, compensating for deviations from ideal Nernst behaviour.
$E_{corr} = E_{obs} + \varepsilon$
E_0, k = experimental parameters, defined by eqn. (1)

B. Quantities referring to the iodide phase, marked ' for solid and " for liquid phase.

x_i = mol fraction of component i.
a_i = activity of component i.
$f_i = a_i x_i^{-1}$

The indices 1, 2, 3, and 4 are used for AgI, $AgNO_3$, KNO_3, and $NaNO_3$, respectively.

C. Quantities referring to the nitrate phase.

All concentrations are expressed in molality units, referring to the solvent equimolar $(K,Na)NO_3$.

C_I, C_{Ag} and C_0 = total concentrations of iodide, silver(I) and alkali metal ion, respectively.
[A] = concentration of species A.
a(A) = activity of species A.
[ ]*, ( )* *etc.* denote the values of the quantities in question at the AgI phase transition (s)⇌(l).
$\beta_m = [Ag_mI^{(m-1)+}][Ag^+]^{-m}[I^-]^{-1}$.
$K_m = [Ag_mI^{(m-1)+}][Ag_{(m-1)}I^{(m-2)+}]^{-1}[Ag^+]^{-1}$.
$\overline{m} = (C_{Ag} - [Ag^+])C_I^{-1}$, the ligand number.
$\alpha_m = [Ag_mI^{(m-1)+}]C_I^{-1}$.

Table 1. Data from the potentiometric measurements.

C_I/mol kg^{-1}, C_{Ag}/mol kg^{-1}, E_{obs}/mV, E_{corr}/mV;

Series 1

0.0148, 0.692, *48.8*, *59.2*; 0.0222, 0.842, *41.5*, *51.0*; 0.0317, 0.997, *35.3*, *43.9*; 0.0426, 1.155, *30.8*, *38.6*; 0.0555, 1.318, *26.3*, *33.2*; 0.0692, 1.488, *22.6*, *28.8*;

Series 2

0.0163, 0.720, *47.2*, *57.4*; 0.0234, 0.862, *40.5*, *49.8*; 0.0303, 0.975, *36.2*, *44.9*; 0.0377, 1.081, *32.5*, *40.5*; 0.0464, 1.207, *29.2*, *36.6*; 0.0578, 1.344, *25.7*, *32.6*; 0.0686, 1.462, *23.1*, *29.3*; 0.0796, 1.571, *21.3*, *27.2*;

Series 3

0, 0.899, *34.4*, *42.6*; 0, 1.099, *25.9*, *32.8*; 0, 1.298, *19.7*, *25.1*; 0, 1.497, *14.2*, *18.2*; 0.0699, 1.567, *20.2*, *25.8*; 0.0699, 1.717, *16.3*, *20.9*; 0.0699, 1.867, *12.3*, *15.7*; 0.0699, 2.017, *8.8*, *11.3*; 0.0699, 2.168, *5.8*, *7.4*; 0.0699, 2.318, *3.2*, *4.0*;

Series 4

0, 0.600, *51.1*, *61.7*; 0, 0.799, *38.9*, *48.0*; 0, 0.998, *29.8*, *37.4*; 0, 1.198, *22.4*, *28.7*; 0.03993, 1.238, *26.4*, *33.4*; 0.03993, 1.388, *21.4*, *27.2*; 0.03993, 1.588, *15.9*, *20.4*; 0.03993, 1.786, *10.9*, *14.1*; 0.03993, 1.986, *6.8*, *8.8*; 0.03993, 2.184, *3.0*, *3.8*; 0.0800, 2.264, *5.2*, *6.5*; 0.1201, 2.305, *7.3*, *9.3*; 0.1603, 2.345, *9.6*, *12.4*; 0.2007, 2.385, *11.3*, *14.6*;

Series 5

0, 0.611, *50.5*, *61.0*; 0, 0.841, *36.7*, *45.5*; 0, 0.966, *31.0*, *38.9*; 0, 1.221, *22.0*, *28.0*; 0.0421, 1.263, *25.9*, *32.7*; 0.0421, 1.414, *21.0*, *26.8*; 0.0421, 1.564, *16.7*, *21.4*; 0.0421, 1.720, *13.0*, *16.7*; 0.0421, 1.884, *9.2*, *11.8*; 0.0421, 2.241, *2.3*, *2.8*; 0.0893, 2.330, *4.2*, *5.3*; 0.1342, 2.375, *7.5*, *9.6*; 0.1807, 2.422, *10.2*, *13.1*;

The emf measurements. In the concentration range studied appreciable deviations from linearity in the $E_{obs} - \lg [Ag^+]$ relationship should be expected,[5] and the E_{obs} values were therefore corrected by a term ε to yield data (E_{corr}; $\lg [Ag^+]$) by the same procedure as described previously.[5] The experimental results are given in Table 1.

The parameters E_0 and k were obtained from data pertaining to iodide-free systems (series 3 – 5) according to

$$E_{corr} = E_0 - k \lg [Ag^+] \quad (1)$$

The experimental values of E_0 and k adhere closely to the theoretical $RTF^{-1} \ln C^\circ_{Ag} = 37.4$ mV and $RTF^{-1} \ln 10 = 109.7$ mV, respectively, which were therefore used in the calculation of $[Ag^+]$ in series 1 – 2 (two-phase systems). In these runs C_I was obtained from the separate solubility measurements.

The ligand number $\bar{m}$ has been directly computed from the concentrations of free ligand as calculated from eqn. (1). In Fig. 1 $\bar{m}$ is plotted *versus* $[Ag^+]$. On the assumption of random errors in E_{corr} of about ± 0.3 mV the experimental uncertainty in $\bar{m}$ is estimated to fall in the range 0.1 – 0.3. The following important features of Fig. 1 should be noted:

1. The average ligand number is close to 4 in all investigated melts.

2. All data are collected in a rather limited range of C_{Ag} so the behaviour of $\bar{m}$ should by no means be taken as evidence that the iodide ion is coordinatively saturated at $\bar{m} = 4$ even if this possibility cannot be excluded.

3. C_I is at most varied by a factor 20, but no significant dependence of C_I on $\bar{m}$ at constant $[Ag^+]$ can be observed. This indicates that polynuclear (polyiodic) complexes $Ag_mI_n^{(m-n)+}$ with $m/n \neq 4$ are not present in observable amounts.

These findings have been used in support of the interpretation of the solubility and distribution data.

The solubility and distribution measurements. For reasons previously discussed,[5] the possible effects of alkali metal ion solvation of the un-

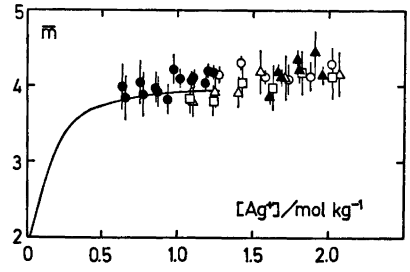

Fig. 1. Ligand numbers $\bar{m}$, determined from the emf measurements. Symbols: melts saturated in AgI (●); $C_I = 0.0699$ mol kg^{-1} (○); $C_I = 0.03993$ mol kg^{-1} (□); $C_I = 0.0421$ mol kg^{-1} (△); C_I variable, 0.08 mol kg^{-1} $\leq C_I \leq$ 0.20 mol kg^{-1} (▲). The full-drawn curve is calculated from the constants of Table 7. It is drawn for the range of $[Ag^+]$ used in the solubility measurements.

Table 2. The constitution of the iodide phase at different C_{Ag}.

Region	Range of C_{Ag}	Iodide phase
I	$C_{Ag} < 0.02$ mol kg^{-1}	"Pure" α-AgI ($x_2' < 0.005$)
II	0.02 mol kg$^{-1} \leq C_{Ag} \leq 0.66$ mol kg^{-1}	Solid solution Ag(I,NO_3)
III	0.66 mol kg$^{-1} \leq C_{Ag}$	Liquid solution (Ag,K,Na) (I,NO_3)

complexed iodide ion have been ignored in the calculations.

For convenience the total range of C_{Ag} studied will be divided into three regions, depending on the constitution of the AgI phase, *vide* Table 2. The conceptual basis for the thermodynamic treatment of the distribution equilibria encountered in regions II and III has been discussed in a recent paper.[16] The activity a_1 and hence the product $[Ag^+][I^-]$ is determined as follows.

In the most general case, which is met in region III, we have to consider the following heterogeneous equilibria, where the species of the right hand members are present in the nitrate melt. The symbol (agi) is used to denote a solid or liquid phase where the solvent is AgI.

$$AgI\ (agi) \rightleftharpoons Ag^+ + I^-$$
$$AgNO_3\ (agi) \rightleftharpoons Ag^+ + NO_3^-$$
$$KNO_3\ (agi) \rightleftharpoons K^+ + NO_3^-$$
$$NaNO_3\ (agi) \rightleftharpoons Na^+ + NO_3^-$$

The thermodynamic equilibrium conditions of relevance are

$$\mathrm{d} \ln a_1 = \mathrm{d} \ln ([Ag^+][I^-]) \quad (2)$$

$$\mathrm{d} \ln a_2 = \mathrm{d} \ln ([Ag^+]a(NO_3)) \quad (3)$$

$$\mathrm{d} \ln a_3 = \mathrm{d} \ln (a(K)a(NO_3)) \quad (4)$$

$$\mathrm{d} \ln a_4 = \mathrm{d} \ln (a(Na)a(NO_3)) \quad (5)$$

Furthermore, at constant T and P the Gibbs-Duhem relation yields for the iodide phase

$$\sum_{i=1}^{4} x_i \,\mathrm{d} \ln a_i = 0 \quad (6)$$

For the nitrate melt the Gibbs-Duhem equation may be written as [16]

$$[K^+]\ \mathrm{d} \ln a(K) + [Na^+]\ \mathrm{d} \ln a(Na) + [NO_3^-]\ \mathrm{d} \ln a(NO_3) + C_I\ \mathrm{d} \ln [I^-] + C_{Ag}\ \mathrm{d} \ln [Ag^+] = 0 \quad (7)$$

In order to solve eqns. (2) – (7) with respect to d ln a_1 we make the following two assumptions:

i. The nitrate ion is virtually the only free anion in the nitrate melt, since practically all iodide is present as neutral or cationic complexes. Hence, the ion activity of NO_3^- may be regarded as constant, *viz.* d ln $a(NO_3) = 0$.

ii. The ion activities of K^+ and Na^+ in the nitrate melt are certainly not constant as these ions are mixed with Ag^+ and $Ag_mI_n^{(m-n)+}$. Since, however, $[K^+] \approx [Na^+]$ in all systems, it may be reasonable to think of a(K) and a(Na) as being affected in the same way by the presence of other cations. The assumption to be made in the calculations is thus d ln a(K) = d ln a(Na) (= d ln a(M)).

Eqns. (3) – (6) may now be combined to yield

$$\mathrm{d} \ln a_1 = x_1^{-1} [x_2\ \mathrm{d} \ln [Ag^+] + (x_3 + x_4)\ \mathrm{d} \ln a(M)] \quad (8)$$

Furthermore,

$$[K^+] + [Na^+] = C_0 \quad (9)$$

The assumptions *i* and *ii* then simplify eqn. (7) to

$$C_0\ \mathrm{d} \ln a(M) + C_{Ag}\ \mathrm{d} \ln [Ag^+] + C_I\ \mathrm{d} \ln [I^-] = 0 \quad (10)$$

Eqns. (2) and (8) – (10) finally yield the general expression for d ln a_1, *viz.*

$$\mathrm{d} \ln a_1 = -\left[\frac{x_2 C_0 - (x_3 + x_4)(C_{Ag} - C_I)}{x_1 C_0 - (x_3 + x_4) C_I}\right] \mathrm{d} \ln [Ag^+] \quad (11)$$

In a similar way an expression for d ln a(M) may be derived:

$$\mathrm{d} \ln a(M) = -\left[\frac{x_1 C_{Ag} - (x_1 + x_2) C_I}{x_1 C_0 - (x_3 + x_4) C_I}\right] \mathrm{d} \ln [Ag^+] \quad (12)$$

Eqns. (11) and (12) are generally applicable irrespective of the constitution of the iodide phase. In region II eqn. (11) takes the simple form

$$\mathrm{d}\ln a_1' = -(x_2'/x_1')\,\mathrm{d}\ln[\mathrm{Ag}^+] \quad (13)$$

since $x_3 + x_4 = 0$. From eqn. (12) expressions (14) and (15) for $\mathrm{d}\ln a(\mathrm{M})$ in regions II and I, respectively, are obtained:

$$\mathrm{d}\ln a(\mathrm{M}) = -C_0^{-1}(C_{\mathrm{Ag}} - C_{\mathrm{I}}/x_1')\,\mathrm{d}\ln[\mathrm{Ag}^+] \quad (14)$$

$$\mathrm{d}\ln a(\mathrm{M}) = -C_0^{-1}(C_{\mathrm{Ag}} - C_{\mathrm{I}})\,\mathrm{d}\ln[\mathrm{Ag}^+] \quad (15)$$

The following heterogeneous equilibrium constants are now introduced in accordance with conditions *i* and *ii*:

$$K_1' = [\mathrm{Ag}^+][\mathrm{I}^-]/a_1' \quad (16)$$

$$K_1'' = [\mathrm{Ag}^+][\mathrm{I}^-]/a_1'' \quad (17)$$

$$K_2' = [\mathrm{Ag}^+]/a_2' \quad (18)$$

$$K_2'' = [\mathrm{Ag}^+]/a_2'' \quad (19)$$

$$K_3'' = a(\mathrm{M})/a_3'' \quad (20)$$

$$K_4'' = a(\mathrm{M})/a_4'' \quad (21)$$

Since $a_1' = 1$ in pure α-AgI, the constant K_1' is identified as the conventional solubility product which is easily determined in region I.

For the sake of clarity eqn. (11) is rewritten as

$$\mathrm{d}\ln a_1 = G\,\mathrm{d}\ln[\mathrm{Ag}^+] \quad (22)$$

Since $K_1'(a_1')^* = K_1''(a_1'')^*$, the concentration product $[\mathrm{Ag}^+][\mathrm{I}^-]$ will be determined as

$$([\mathrm{Ag}^+][\mathrm{I}^-])_j = K_1' \exp\left[\int_{\ln[\mathrm{Ag}^+]_0}^{\ln[\mathrm{Ag}^+]_j} G\,\mathrm{d}\ln[\mathrm{Ag}^+]\right] \quad (23)$$

in regions II and III, and hence the integration of eqn. (22) may be continued irrespective of the discontinuity at the phase transition (*cf.* Ref. 4). In eqn. (23) $[\mathrm{Ag}^+]_0$ refers to a system where $G = 0$. The index j denotes the values of different quantities in the same actual system.

For the solid solution we set $\lim_{x_2' \to 0} f_2' = 1$, and K_2' may thus be estimated from a graphical extrapolation according to eqn. (24):

$$\lim_{x_2' \to 0} (x_2'[\mathrm{Ag}^+]^{-1}) = (K_2')^{-1} \quad (24)$$

The constant K_2' so obtained refers to a constant nitrate ion activity $a(\mathrm{NO_3}) = 1$. The activities a_2' are then determined from eqn. (18).

Taking the hypothetical pure liquid AgI at 280 °C as standard state with $a_1'' = 1$, we define a convenient activity scale for AgI in the liquid AgI phase. For $[\mathrm{Ag}^+]_j \geq [\mathrm{Ag}^+]^*$

$$\exp\left[\int_{\ln[\mathrm{Ag}^+]_0}^{\ln[\mathrm{Ag}^+]_j} G\,\mathrm{d}\ln[\mathrm{Ag}^+]\right] = \lambda_1(a_1'')_j \quad (25)$$

Hence, a quantity $\lambda_1 a_1''$, where λ_1 may be identified as K_1''/K_1', will be directly obtained from the integration process, and it has been included in Table 6. The constant K_1'' may be estimated according to

$$\lim_{x_1'' \to 1} [x_1''/([\mathrm{Ag}^+][\mathrm{I}^-])] = (K_1'')^{-1} \quad (26)$$

For the solutes in the liquid iodide phase the standard states are chosen to give $\lim_{x_1'' \to 1} f_i = 1$ for $i = 2$, 3, and 4. The constant K_2'' is then estimated from an expression analogous to eqn. (24).

The distribution of $\mathrm{KNO_3}$ and $\mathrm{NaNO_3}$ between the two melts has been treated as follows. By use of the general expression (12) activites $a(\mathrm{M})$ were calculated by integration. For convenience an activity scale has been chosen, referring to $a(\mathrm{M}) = 1/2$ in pure equimolar $(\mathrm{K,Na})\mathrm{NO_3}$. From plots of $\lg(a(\mathrm{M})/x_i'' - b)$ *vs.* x_1'' ($i = 3$, 4) at different values chosen for the adjustable parameter b, slightly different intercepts at $x_1'' = 1$ could be obtained, depending on b. From these intercepts rough estimates of K_3'' and K_4'' could be made. The activities $a_i''(i = 1-4)$ are finally computed from eqns. (17) and (19) – (21).

Since the only polynuclear species $\mathrm{Ag}_m\mathrm{I}_n^{(m-n)+}$ that may possibly exist in the alkali nitrate melt should have a ratio $m/n \approx 4$ in order to be in consistence with the emf measurements, they would contribute to C_{I} with terms representing the concentration of species having formal ionic charges $\geq +6$. Preliminary calculations revealed, however, that the solubility and distribution data may be well described by complexes having a maximum charge of $+3$. This leads to the conclusion that a stepwise formation of only monoiodic complexes $\mathrm{Ag}_m\mathrm{I}^{(m-1)+}$ has to be considered, and the stability constants β_m have been evaluated according to

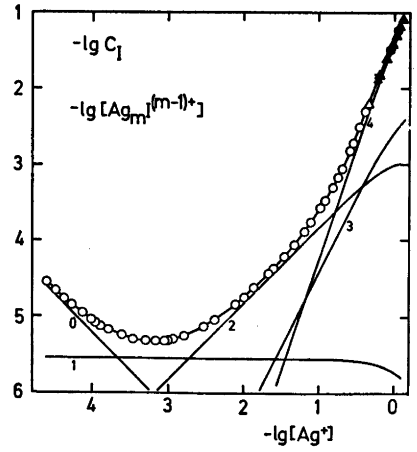

Fig. 2. The solubility curve. Symbols: Radiochemical analyses (○); gravimetric analyses (△). Filled symbols refer to liquid iodide phase. Five curves are included, which show the concentrations of the complexes $Ag_mI^{(m-1)+}$ with m indicated on the curves. The phase transition point is marked (×).

$$C_I \exp\left[\int_{\ln [Ag^+]_0}^{\ln [Ag^+]_j} G \, d \ln [Ag^+]\right] = K_1' \sum_{m=0}^{4} \beta_m [Ag^+]^{(m-1)} \quad (27)$$

where $\beta_0 = 1$.

The C_I values used in the determination of the stability constants were measured by the radioassay technique (series A) over the whole composition range under study and determined gravimetrically in series B in region III and for $C_{Ag} = 0.478$ mol kg^{-1}. Hence, in region II the requisite values of x_1' to be used in the calculation of the product $[Ag^+][I^-]$ were obtained by interpolation between the experimentally determined ones from series B. In region III the experimental data from series B were used directly in the integration according to eqn. (23). In the further calculations on the complex formation in region III the data from series A were incorporated and the corresponding values of $[Ag^+][I^-]$ were obtained by interpolation between those calculated from series B.

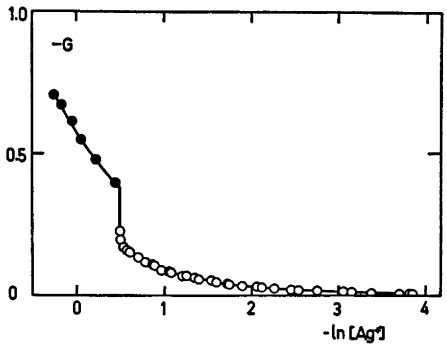

Fig. 3. A plot of G *vs.* ln $[Ag^+]$. The integration is performed along the smooth curve. Symbols: Data from region II (○); region III (●).

The solubility curve, lg C_I *vs.* lg $[Ag^+]$, is given in Fig. 2, where the full-drawn curve is calculated from eqn. (27) by use of the final set of equilibrium constants and the experimentally determined x_i values.

The concentration of free silver ion, $[Ag^+]$, has been calculated iteratively by use of eqns. (28)–(30):

$$[Ag^+] = C_{Ag} - \bar{m} C_I \quad (28)$$

$$\bar{m} \approx 1 + d \lg C_I / d \lg C_{Ag} \quad (29)$$

$$\bar{m} = \left(\sum_{m=1}^{4} m\beta_m [Ag^+]^m\right) / \sum_{m=0}^{4} \beta_m [Ag^+]^m \quad (30)$$

In the first step approximate values of $\bar{m}$ were derived from eqn. (29). The concentrations $[Ag^+]$ so obtained from eqn. (28) were used in eqn. (27) yielding a provisional set of constants β_m and K_1'. Better values of $\bar{m}$ and $[Ag^+]$ were then computed from eqns. (30) and (28) *etc.* until all variables remained unaltered.

Fig. 3 displays a graph of G *versus* the final values of ln $[Ag^+]$. The integration was carried out along the smooth curve.

Tables 3–6 give the experimental and calculated data from all solubility and distribution

Table 3. Solubility data pertinent to region I. All data from series A.

$C_{Ag} \times 10^5$/mol kg^{-1}, $C_I \times 10^5$/mol kg^{-1}, $[Ag^+] \times 10^5$/mol kg^{-1};
2.789, 2.789, 2.48; 3.564, 2.196, 3.26; 4.56, 1.731, 4.26; 5.72, 1.440, 5.41; 7.77, 1.143, 7.45; 10.25, 0.926, 9.93; 11.45, 0.852, 11.14; 13.42, 0.765, 13.11; 16.82, 0.693, 16.48; 24.50, 0.580, 24.14; 34.4, 0.516, 34.0; 50.4, 0.484, 49.9; 69.0, 0.488, 68.5; 90.5, 0.492, 89.9; 101.0, 0.503, 100.4; 116.8, 0.519, 116.2; 161.4, 0.563, 160.6; 297.2, 0.756, 296.0; 413, 0.925, 411; 784, 1.487, 782; 1018, 1.850, 1014; 1371, 2.409, 1367;

Table 4. Solubility and distribution data pertinent to region II. Values in italics are interpolated (further details in the text).

Series	$C_{Ag} \times 10^3$ / mol kg^{-1}	$C_I \times 10^5$ / mol kg^{-1}	x_1'	a_1'	f_1'	a_2'	f_2'	$[Ag^+] \times 10^3$ / mol kg^{-1}	$[Ag^+][I^-] \times 10^{10}$ / (mol kg^{-1})^2
A	21.35	3.69	*0.995*	0.999				21.28	6.15
B	22.09	*4*	0.994	0.999	1.00	0.006	1.0	22.03	6.15
A	24.89	4.30	*0.994*	0.999				24.80	6.14
A	34.30	6.11	*0.992*	0.996				34.20	6.14
B	43.1	*8*	0.989	0.994	1.00	0.013	1.2	42.9	6.12
A	47.3	8.86	*0.988*	0.993				47.1	6.12
A	63.7	13.01	*0.984*	0.989				63.4	6.09
A	78.8	17.46	*0.981*	0.985				78.4	6.07
B	86.0	*21*	0.980	0.984	1.00	0.025	1.2	85.5	6.06
A	104.2	26.78	*0.975*	0.979				103.5	6.03
A	120.2	33.5	*0.971*	0.975				119.3	6.01
B	128.1	*38*	0.968	0.974	1.01	0.037	1.16	126.9	6.00
A	151.1	50.2	*0.966*	0.968				149.6	5.96
B	176.1	*67*	0.963	0.963	1.00	0.051	1.38	173.9	5.93
A	178.6	69.0	*0.960*	0.962				176.5	5.92
A	204.3	89.2	*0.954*	0.956				201.4	5.89
B	218.0	*104*	0.948	0.953	1.00	0.063	1.21	214.6	5.87
B	251.2	*139*	0.945	0.946	1.00	0.072	1.31	246.3	5.83
A	265.2	154.7	*0.940*	0.943				259.9	5.81
A	289.8	190.9	*0.935*	0.937				283.2	5.77
B	304	*218*	0.937	0.935	1.00	0.087	1.38	296.4	5.76
B	348	*305*	0.926	0.926	1.00	0.099	1.34	337	5.70
A	356	309	*0.920*	0.924				345	5.69
B	395	*420*	0.919	0.916	1.00	0.112	1.38	380	5.64
A	426	499	*0.906*	0.910				408	5.60
B	433	*480*	0.902	0.908	1.01	0.122	1.24	415	5.59
B	478	*629*	0.895	0.899	1.00	0.134	1.28	455	5.54
B	525	*870*	0.883	0.890	1.01	0.145	1.24	493	5.48
B	583	*1090*	0.868	0.878	1.01	0.159	1.20	542	5.41
B	605	*1180*	0.864	0.874	1.01	0.165	1.21	560	5.38
B	631	*1290*	0.857	0.868	1.01	0.171	1.20	582	5.35
B	654	*1390*	0.837	0.863	1.03	0.177	1.08	601	5.32
B	658	*1410*	0.815	0.862	1.06	0.178	0.96	605	5.31
B	663		0.81 [a]						

[a] Extrapolated.

Table 5. Data on the distribution of KNO_3 and $NaNO_3$ between the two melts (region III). All data from series B.

C_{Ag} / mol kg^{-1}	a(M)	$x_3'' \times 10^4$	$x_4'' \times 10^4$	$a_3'' \times 10^4$	$a_4'' \times 10^4$	f_3''	f_4''
0.663	0.472	33 [a]	16 [a]				
0.693	0.470	36	17	12	5	0.3	0.3
0.890	0.463	61	31	12	5	0.20	0.16
1.083	0.457	89	43	11	5	0.12	0.12
1.228	0.452	109	55	11	4	0.10	0.07
1.439	0.445	143	70	11	4	0.08	0.06
1.591	0.441	173	90	11	4	0.06	0.04

[a] Extrapolated.

Table 6. Data on the distribution of AgI and $AgNO_3$ between the two melts (region III). Interpolated values are printed in italics.

Series	C_{Ag} / mol kg^{-1}	C_I / mol kg^{-1}	x_1''	x_2''	$\lambda_1 a_1''$	a_1''	a_2''	f_1''	f_2''	[Ag+] / mol kg^{-1}	[Ag+][I$^-$] × 10^{10} / (mol kg^{-1})^2
B	0.663		0.721[a]	0.274[a]							
B	0.693	0.01475	0.714	0.281	0.846	0.43	0.46	0.60	1.6	0.637	5.21
B	0.890	0.02526	0.671	0.320	0.769	0.39	0.57	0.58	1.8	0.792	4.74
A	0.974	0.0323	*0.654*	*0.335*	*0.740*	*0.38*				0.881	*4.56*
B	1.083	0.0377	0.637	0.349	0.706	0.36	0.67	0.56	1.9	0.936	4.35
B	1.228	0.0483	0.611	0.372	0.665	0.34	0.75	0.56	2.0	1.039	4.10
A	1.291	0.0580	*0.604*	*0.377*	*0.647*	*0.33*				1.121	*3.98*
B	1.439	0.0660	0.587	0.392	0.613	0.31	0.85	0.53	2.2	1.180	3.78
B	1.591	0.0815	0.573	0.401	0.583	0.30	0.92	0.52	2.3	1.271	3.59

[a] Extrapolated.

Table 7. Over-all and stepwise stability constants for complexes $Ag_mI^{(m-1)+}$ in $(K,Na)NO_3(l)$ from solubility measurements at 280 °C. The errors quoted are three standard deviations from the least-squares calculations.

Quantity	$m=1$	$m=2$	$m=3$	$m=4$
β_m/(mol kg^{-1})$^{-m}$	$(4.7\pm0.1)\times10^3$	$(2.43\pm0.06)\times10^6$	$(6.3\pm1.1)\times10^6$	$(9.7\pm0.3)\times10^6$
K_m/(mol kg^{-1})$^{-1}$	4.7×10^3	5.2×10^2	2.6	15
$K_m/K_{(m+1)}$	9.1	200	0.17	–

experiments. The composition of the solid iodide phase at the melting point was obtained by extrapolation of x_2' to $C_{Ag}=0.66$ mol kg^{-1}. For the liquid iodide phase the limiting values of x_i'' were obtained by extrapolations of x_i''/x_1'' *versus* ln [Ag+] to yield the limiting quotients $(x_i''/x_1'')^*$ at $[Ag^+]=[Ag^+]^*$ for $i=2$, 3, 4. $(x_1'')^*$ is obtained as $1-\sum_{i=2}^{4}(x_i'')^*$. The limiting values, which are included in Tables 4–6, define the "gap" over which the integration has to be contined at the phase transition point.

The conventional solubility product K_1' and β_1 were obtained by standard methods [18] from data pertaining to region I. Least-squares calculations yield $K_1'=(6.16\pm0.12)\times10^{-10}$ (mol kg^{-1})^2 (the errors are expressed as three standard deviations). This value has been used in the further calculations in regions II and III.

All stability constants are given in Table 7 and the primarily estimated heterogeneous constants are collected in Table 8, where the anion exchange constants K_{12}' and K_{12}'' and the cation exchange constants K_{23}'' and K_{24}'' are also included.

DISCUSSION

The iodide phase and the heterogeneous equilibria. Considering the solid iodide phase, the results from this and previous [3,4,16] investigations clearly illustrate the necessity for careful investigation of the composition of the solid in solubility studies on complex formation at elevated temperatures.

The ideal Temkin behaviour,[19] as indicated by the experimentally verified relation $a_1'=x_1'$ for $0.86\leq x_1'\leq 1$, suggests that the solid phase $Ag(I,NO_3)$ may be regarded as a substitutional solution with the anions mixing at random on the bodycentered cubic iodide sublattice, making the partial molar configurational entropy of AgI take the value $-R\ln x_1'$. Ideal behaviour should then be displayed if the enthalpy of mixing were negligible. In particular, the partial substitution of iodide ions for nitrate

Table 8. The estimated heterogeneous equilibrium constants. The solid and liquid AgI solutions are designated agis and agil, respectively.

Equilibrium reaction	Equilibrium constant	
$AgI(agis) \rightleftharpoons Ag^+ + I^-$	K_1'	$(6.2 \pm 0.1) \times 10^{-10}$ (mol kg^{-1})^2
$AgNO_3(agis) \rightleftharpoons Ag^+ + NO_3^-$	K_2'	(3.4 ± 0.5) mol kg^{-1}
$AgI(agil) \rightleftharpoons Ag^+ + I^-$	K_1''	$(12 \pm 3) \times 10^{-10}$ (mol kg^{-1})^2
$AgNO_3(agil) \rightleftharpoons Ag^+ + NO_3^-$	K_2''	(1.4 ± 0.2) mol kg^{-1}
$KNO_3(agil) \rightleftharpoons K^+ + NO_3^-$	K_3''	$(4 \pm 2) \times 10^2$
$NaNO_3(agil) \rightleftharpoons Na^+ + NO_3^-$	K_4''	$(10 \pm 4) \times 10^2$
$AgI(agis) + NO_3^- \rightleftharpoons AgNO_3(agis) + I^-$	K_{12}'	1.8×10^{-10} mol kg^{-1}
$AgI(agil) + NO_3^- \rightleftharpoons AgNO_3(agil) + I^-$	K_{12}''	8.6×10^{-10} mol kg^{-1}
$AgNO_3(agil) + K^+ \rightleftharpoons KNO_3(agil) + Ag^+$	K_{23}''	3×10^{-3} mol kg^{-1}
$AgNO_3(agil) + Na^+ \rightleftharpoons NaNO_3(agil) + Ag^+$	K_{24}''	1×10^{-3} mol kg^{-1}
$KNO_3(agil) + Na^+ \rightleftharpoons NaNO_3(agil) + K^+$	K_{34}''	4×10^{-1}

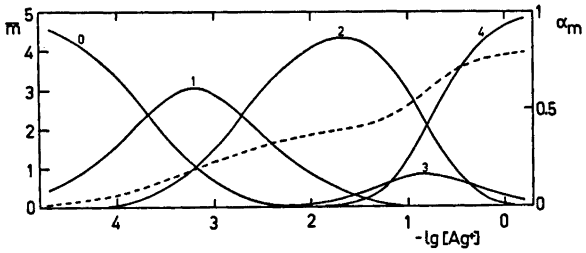

Fig. 4. Ligand numbers $\bar{m}$, calculated according to eqn. (30) (dashed curve), and the distribution of iodide on different species $Ag_mI^{(m-1)+}$ in the nitrate melt (m is indicated on the distribution curves).

Table 9. Stepwise stability constants and quotients in different media.

Medium	Ref.	Quantity	$m=1$	$m=2$	$m=3$	$m=4$
KNO_3(l), 402 °C	15	K_m/(mol kg^{-1})$^{-1}$	5.5×10^2	3.6×10^2	–	–
H_2O, 25 °C, $I=4$ M ($NaClO_4$)	7	K_m/M^{-1}	(1.3×10^8)	(1.7×10^2)	7.1×10^2	5.2
H_2O, 20 °C, $I=0$	9	K_m/M^{-1}	3.8×10^6	2.6×10^4	4.2×10^2	–
KNO_3(l), 402 °C	15	$K_m/K_{(m+1)}$	1.5	–	–	–
H_2O, 25 °C, $I=4$ M ($NaClO_4$)	7	$K_m/K_{(m+1)}$	(10^6)	(2)	140	–
H_2O, 20 °C, $I=0$	9	$K_m/K_{(m+1)}$	140	63	–	–

ions must not change the accessibility of structurally different cation sites, *i.e.* no restrictions must be imposed on the mobility of Ag^+ ions over the cation sublattice. The structural conditions for random anion mixing are, on the whole, advantageous. In the Strock model [20] of α-AgI the closest iodide–iodide distance is 4.36 Å. The nitrate ion, on the other hand, may be roughly approximated with a disc, having an effective diameter of 4.6 Å and a thickness of 2.2 Å.[21] Hence, judging from the dimensions of the anions, the nitrate ion might fit sufficiently well into the structure with only a minor perturbation of the anion sublattice.

The liquid iodide phase displays a pronounced non-ideal behaviour, similar to that of (Ag,K)I melts.[4] It should be noted that – in contrast to what is often found for other silver

halide based melts [23] – the thermodynamic data pertaining to the composition range investigated cannot be rationalized in terms of simple regular solution parameters.

Except for K_1', the relatively large uncertainties in the distribution constants of Table 8 are due to the wide limits of error which are subjectively estimated from the non-linear extrapolations. One relevant comparison of the results with previous findings can be made. The value of K_1'' obtained in this study, $(12 \pm 3) \times 10^{-10}$ (mol kg^{-1})^2, agrees with the recently estimated value [4] $(12.5 \pm 0.8) \times 10^{-10}$ (mol kg^{-1})^2, derived from data on (Ag,K)I melts with a similar extrapolation technique.

The complex formation equilibria in the nitrate melt. The complex formation proceeds rather similarly to that in the $AgBr-AgNO_3-(K,Na)NO_3$ system,[5] and the virtual absence of polyiodic species is rather interesting in view of the well-known ability of silver(I) to coordinate several halide ions in nitrate melts having halide in excess over silver(I). King and coworkers [12] concluded, from light absorption measurements, that polyiodic cationic Ag–I-complexes may exist in aqueous solutions, but the effects observed were very much smaller than the corresponding ones for anionic complexes. Berne and Weill [13] later found no evidence for polynuclear complexes on the cationic side of the silver-iodide system, from self-diffusion measurements on aqueous solutions, whereas clear evidence for polynuclearity on the anionic side was given. The results from this study and from Refs. 3 and 4 are in obvious agreement with these observations; the tendency of condensation in the silver iodide system is much smaller (if any) on the cationic side than on the anionic side in nitrate melts as well.

Fig. 4 gives a survey of the complex formation in the range of free ligand concentrations studied. For $[Ag^+] < 0.01$ mol kg^{-1} the only species of importance besides Ag^+ are I^-, AgI and Ag_2I^+. The solubility product K_1' and the stability constant β_1 for AgI are in good agreement with the values obtained by Elding and Leden [1] from solubility measurements in systems $AgI-(K,Na)I-(K,Na)NO_3$. The emf data of Alvarez-Funes *et al.*[15] on the formation of AgI and Ag_2I^+ in liquid KNO_3 at 402 °C seem to be the only available comparison material on cationic silver iodide complexes in fused nitrate medium (Table 9). Their values of K_1 and K_2 are considerably smaller than those from the present study. This is largely due to the difference in temperature, but may also be attributed in part to the difference in solvent composition in accordance with the general trend for iodide complexes.[23,24]

The second complex, Ag_2I^+, exhibits a remarkable stability relative to AgI and Ag_3I^{2+}. This is evident from the quotients between the successive formation constants of Table 7 and from the flattening out of the $\bar{m}$ curve at $\bar{m} = 2$ (Fig. 4). A similar, although not so pronounced effect was found in the corresponding bromide system.[5]

From the solubility study of Lieser [9] (*vide* Table 9) it becomes evident that there is no such stabilization of Ag_2I^+ in aqueous solution (Leden's solubility data have been discussed in Ref. 4. Anderson and coworkers [25] recently suggested a value of K_2 in water (25°C) which seems to be in conflict with most experience in this field).

From Fig. 4 it is seen that Ag_3I^{2+} contributes at most with about 17 % to C_I (which is also reflected in the large uncertainty in the value of β_3), whereas more than 90 % of the iodide in the nitrate melt is present as Ag_4I^{3+} at $[Ag^+] = 1$ mol kg^{-1}. The fourth complex is undoubtedly strong, but it is an open question whether or not the iodide is coordinatively saturated at $\bar{m} = 4$ in the fused nitrate medium. A close inspection of Fig. 1 reveals that $\bar{m}$ actually seems to exceed 4 in the range 1 mol kg^{-1} < $[Ag^+] < 2$ mol kg^{-1}. A value of, *e.g.*, $K_5 = 10^{-1}$ mol^{-1} kg would give a better fit to the emf measurements than $K_5 = 0$. It cannot be excluded, however, that systematic errors at these high silver ion concentrations are responsible for the observed increase of $\bar{m}$ above 4, and it is also to be noted that the differences $\bar{m} - 4$ are in general not larger than the estimated random errors in $\bar{m}$. Therefore we have abstained from introducing a complex Ag_5I^{4+} (or Ag_6I^{5+}) in our model, even if this would give a better formal description of the emf measurements without violating significantly our model used to describe the solubility data.

It is evident from studies of solution equilibria involving anionic complexes $AgX_n^{(n-1)-}$ that Ag^+ coordinates at most four halide ions. This

is well reflected in the structure of crystalline solids of different general formulae, such as $M_xAg_yX_z$ ($y<z$). The halide ions always seem to be arranged in a more or less distorted tetrahedron around Ag.[26–41]

In the case of cationic complexes there is no similar univocal support from structure determinations to be found when discussing the coordination number. In $Ag_3I(NO_3)_2$ [42] and Ag_2INO_3 [43] every iodine atom is surrounded by six nearest silver atoms, but preliminary results from our structure determinations of Ag_2BrNO_3 and $Ag_2IF.H_2O$ [44] indicate that Br and I have five and four Ag, respectively, as nearest cation neighbours in these compounds. Further structural studies of similar compounds are in progress.

Acknowledgements. I express my sincere gratitude to Professor Ido Leden for his very stimulating support of this work. I also thank Dr. Peter Sellers for revision of the English text.

REFERENCES

1. Elding, I. and Leden, I. *Acta Chem. Scand. 23* (1969) 2430.
2. Holmberg, B. *Acta Chem. Scand. 27* (1973) 875.
3. Holmberg, B. *Acta Chem. Scand. 27* (1973) 3550.
4. Holmberg, B. *Acta Chem. Scand. 27* (1973) 3657.
5. Holmberg, B. *Acta Chem. Scand. A 30* (1976) 680.
6. Kratohvil, J., Tezák, B. and Vouk, V. B. *Arh. Kem. 26* (1954) 191.
7. Leden, I. and Parck, C. *Acta Chem. Scand. 10* (1956) 535.
8. Lieser, K. H. *Z. Anorg. Allg. Chem. 292* (1957) 114.
9. Lieser, K. H. *Z. Anorg. Allg. Chem. 304* (1960) 296.
10. Lieser, K. H. *Z. Anorg. Allg. Chem. 305* (1960) 133.
11. Fromherz, H. and Menschick, W. *Z. Phys. Chem. Abt. B 3* (1929) 1.
12. King, E. L., Krall, H. J. and Pandow, M. L. *J. Am. Chem. Soc. 74* (1952) 3492.
13. Berne, E. and Weill, M. J. *J. Phys. Chem. 64* (1960) 258.
14. Yakhkind, N. D. and Gyunner, E. A. *Zh. Neorg. Khim. 13* (1968) 1005.
15. Alvarez-Funes, A., Braunstein, J. and Blander, M. *J. Am. Chem. Soc. 84* (1962) 1538.
16. Holmberg, B. *Acta Chem. Scand. A 30* (1976) 641.
17. Holmberg, B. *Acta Chem. Scand. A 28* (1974) 284.
18. Johansson, L. *Coord. Chem. Rev. 3* (1968) 293.
19. Temkin, M. *Acta Physicochim. URSS 20* (1945) 411.
20. Strock, L. W. *Z. Phys. Chem. (Leipzig) 25* (1934) 441.
21. Janz, G. J. and James, D. W. *Electrochim. Acta 7* (1962) 427.
22. Lumsden, J. *Thermodynamics of Molten Salt Mixtures*, Academic, London 1966.
23. Braunstein, J. and Hagman, R. E. *J. Phys. Chem. 67* (1963) 2881.
24. Hsu, Y.-T., Escue, R. B. and Tidwell, T. H. *J. Electroanal. Chem. 15* (1967) 245.
25. Andersson, K. P., Butler, E. A. and Woolley, E. M. *J. Phys. Chem. 78* (1974) 2244.
26. Brink, C. and MacGillavry, C. H. *Acta Crystallogr. 2* (1949) 158.
27. Brink, C. and Kroese, H. A. S. *Acta Crystallogr. 5* (1952) 433.
28. Brink, C., Binnendijk, N. F. and van de Linde, J. *Acta Crystallogr. 7* (1954) 176.
29. Hahn, H., Frank, G. and Klingler, W. *Z. Anorg. Allg. Chem. 279* (1955) 271.
30. Meyer, H.-J. *Acta Crystallogr. 16* (1963) 788.
31. Geller, S. *Science 157* (1967) 310.
32. Stomberg, R. *Acta Chem. Scand. 23* (1969) 3498.
33. Geller, S. and Lind, M. D. *J. Chem. Phys. 52* (1970) 5854.
34. Gilmore, C. J., Tucker, P. A. and Woodward, P. *J. Chem. Soc. A* (1971) 1337.
35. Geller, S. *Science 176* (1972) 1016.
36. Geller, S., Skarstad, P. M. and Wilber, S. A. *J. Electrochem. Soc. 122* (1975) 332.
37. Coetzer, J. *Acta Crystallogr. B 31* (1975) 622, 2115.
38. Coetzer, J. and Thackeray, M. M. *Acta Crystallogr. B 31* (1975) 2113.
39. Thackeray, M. M. and Coetzer, J. *Acta Crystallogr. B 31* (1975) 2339, 2341.
40. Coetzer, J., Kruger, G. J. and Thackeray, M. M. *Acta Crystallogr. B 32* (1976) 1248.
41. Thackeray, M. M. and Coetzer, J. *Acta Crystallogr. B 32* (1976) 2197.
42. Birnstock, R. and Britton, D. *Z. Kristallogr. 132* (1970) 87.
43. Persson, K. *Private communication.*
44. Holmberg, B. and Persson, K. *Acta Crystallogr. A 31* (1975) S 65.

Received April 23, 1976.

Acta Chemica Scandinavica A 30 (1976) 808—812

The Crystal Structure Determination of Lithium 2-Hydroxy-3,4-dioxocyclobut-1-en-1-olate Monohydrate, $LiHC_4O_4.H_2O$

DAG SEMMINGSEN

Department of Chemistry, University of Oslo, Oslo 3, Norway

Single crystals of lithium squarate monohydrate have been prepared and studied by X-ray diffraction. The crystals are monoclinic, space group $C2/c$ with unit-cell dimensions: $a=13.627(2)$, $b=7.782(1)$, $c=10.843(1)$ Å, $\beta=120.31(1)°$. The structure was determined by direct methods from 1580 observed intensities measured with counter methods. The structure consists of infinite chains of hydrogen squarate ions joined by strong asymmetric hydrogen bonds [2.431(1) Å]. These chains are tied into a three-dimensional network by weaker hydrogen bonds [2.720(1) and 2.737(1) Å] *via* the water molecules, and $Li^+\cdots O$(squaric acid) electrostatic forces. The refinement terminated with a conventional R-value of 0.041. Standard deviations in bond lengths between carbon and oxygen atoms are 0.001 Å.

Squaric acid (3,4-dihydroxy-3-cyclobutene-1,2-dione) (H_2SQ) was first prepared by Cohen, Lacher and Park [1] and is a member of a series of oxocarbon ring systems with strong acidic properties.[2] The crystal structure of the free acid is now well established by X-ray diffraction methods.[3,4] In the crystal structure the molecules are linked together into infinite planar sheets by short asymmetric hydrogen bonds. The high acidity of H_2SQ [5] and extensive delocalization of the SQ^{2-} ion as suggested by IR and Raman spectroscopy of K_2SQ and X-ray structural investigation of $K_2SQ.H_2O$ implicate that acid salts of squaric acid may form very short hydrogen bonds similar to those found in acid salts of carboxylic acids.[6] The main purpose of the present investigation has been to examine the hydrogen bonding properties of the HSQ^- residue. The acid salt of lithium was chosen in order to minimize the scattering contribution from the cation. While the present investigation was in progress, the crystal structure determinations of $KHSQ.H_2O$[9] and $[H_2NMe_2]^+[H_3SO_3]^-$[10] came to the author's knowledge.

EXPERIMENTAL

Crystals of $LiHSQ.H_2O$ were prepared by dissolving lithium carbonate and squaric acid in a molar ratio 1:2 in water. Colourless, approximately bipyramidal crystals bound by eight faces were formed by slow evaporation. A crystal of dimensions $0.4\times0.5\times0.35$ mm was selected for the data collection. The systematic absences ($h+k=2n+1$ for hkl and $l=2n+1$ for $h0l$) correspond to those of the space groups Cc and $C2/c$. Unit-cell parameters were determined from the diffractometer setting angles of 15 reflexions (Mo$K\alpha$ radiation, $\lambda=0.71069$ Å). Intensity data were collected on a SYNTEX P$\bar{1}$ computer-controlled diffractometer with the crystal arbitrarily mounted. The diffractometer was operated in the $\omega-2\theta$ scanning mode and one quadrant of the reciprocal lattice was examined out to a 2θ limit of 70° with graphite monochromatized Mo$K\alpha$ radiation. A variable scan speed (2—8°/min) dependent on intensity and a 2° symmetrical scan range, corrected for wavelength dispersion, was used. Background counts were taken at the beginning and end of each scan. The ratio of total background to scan time was 0.7.

As a control of crystal and diffractometer stability three reference reflections were measured at regular intervals. A total of 1961 independent reflexions were recorded, of which 1580 had intensities greater than twice their standard deviations estimated from counting statistics. The intensities and their standard deviations were corrected for Lorentz and polarization effects, and a 2 % uncertainty in diffractometer stability was included in e.s.d.'s.

The structure was determined by application of direct methods [11] assuming the space-

group $C2/c$. Full-matrix least-squares refinements with anisotropic thermal parameters for the heavy atoms including Li^+, and isotropic ones for the hydrogen atoms terminated with $R=0.041$, and $R_w=0.050$. The function minimized was $M=\sum w(F_o-F_c)^2$, $w=[\sigma(F_o)]^{-2}$. The positions of the hydrogens for the outset of the final refinements were calculated from the short oxygen-oxygen approach distances. Weight analysis showed that weighting based on standard deviations from counting statistics was satisfactory. Atomic form factors for the heavy atoms were taken from Doyle and Turner,[12] while for the hydrogens those of Stewart, Davidson and Simpson[13] were used. All programs used are written or revised for CD 6600 as described in Ref. 14. No corrections for absorption, extinctions or multiple scattering have been carried out. Tables of observed and calculated structure factors are available from the author on request.

CRYSTAL DATA

LiHSQ monoclinic; $C2/c$

$a=13.627(2)$, $b=7.782(1)$, $c=10.834(1)$ Å,

$\beta=120.31(1)°$, $\varrho_{obs}=1.84$ g cm^{-3}, $\varrho_{calc}=1.85$ g cm^{-3},

$Z=8$, $V=991.4(7)$ Å^3, F.W. = 138.00, $F(000)=560$ $\mu(MoK\alpha)=1.85$ cm^{-1}.

DISCUSSION

Final coordinates and thermal parameters are given in Table 1, while interatomic distances and angles are given in Table 2. A stereo view of the structure is presented in Fig. 1. The atomic numbering scheme and the structure of the HSQ-ion is shown in Fig. 2. The structure is seen to consist of layers extending parallel to the (001) planes, which are related alternately by twofold axes and twofold screw axes. The nearly planar HSQ^- ions form strongly bonded chains along the c glide planes by means of short asymmetric hydrogen bonds. These chains are transversely linked along [010] *via* the water molecules through weaker hydrogen bonds and Li^+---O interactions. The interactions between layers are in the region of the twofold screw axes ($x=\pm\frac{1}{4}$), mainly due to van der Waals forces and dipolar interactions between C – O bonds stacked antiparallel to each other.[16] The shortest distances are O1---C4′ (3.21 Å) and C1---O4′ (3.14 Å), related by screw axes and O2---C2′ (3.22 Å) across centers of inversion.

In the vicinity of the twofold axes ($x=0,\frac{1}{2}$) there are alternately interactions between water molecules and Li^+ ions, and closely stacked pairs of HSQ^- ions. The average distance between the planes of the latter is 3.16 Å and short interatomic contacts occur for C3---C3′ (3.22 Å) and C2---C2′ (3.22 Å). If the thickness of a π conjugated planar system is taken to be 3.4 Å, the layer separation of 3.16 Å may indicate additional attraction possibly of the charge transfer type. Interactions of this kind have been invoked to explain similar short contacts in $K_2SO.H_2O$.[7]

The arrangement close to the water molecules and Li^+ ions around the twofold axes is shown in Fig. 3. There is an almost equidistant distorted tetrahedral environment of oxygen atoms around the Li^+ ions, the Li^+---O distances being only slightly longer than the sum of ionic radii (2.00 Å). An additional, rather long contact from O3 to Li^+ of 2.535(2) Å (not shown in Fig. 3) may, however, also be of some importance. The water molecules and Li^+ ions form a regular, nearly planar ar-

Table 1. Fractional coordinates and thermal parameters with estimated standard deviations. Expression for anisotropic vibration is $\exp[-2\pi^2(U11h^2a^{*2}+\cdots+2U23klb^*c^*)]$.

ATOM	X	Y	Z	U11	U22	U33	U12	U13	U23
O1	.13275(8)	.14538(10)	.10172(9)	.0394(5)	.0159(4)	.0179(4)	-.0001(3)	.0175(4)	-.0023(3)
O2	.12829(8)	.13583(10)	.40291(9)	.0371(5)	.0188(4)	.0175(4)	-.0031(3)	.0154(4)	.0030(3)
O3	.13549(8)	.55581(10)	.40653(8)	.0519(6)	.0168(4)	.0188(4)	.0004(4)	.0249(4)	-.0009(3)
O4	.13527(8)	.55980(10)	.11480(8)	.0489(6)	.0144(4)	.0188(4)	.0005(3)	.0238(4)	.0012(3)
C1	.13492(9)	.25226(13)	.18753(10)	.0236(5)	.0146(4)	.0122(4)	-.0008(4)	.0094(4)	.0004(4)
C3	.13666(10)	.43572(14)	.32593(11)	.0279(6)	.0158(4)	.0128(4)	-.0006(4)	.0123(4)	.0001(4)
C2	.13358(9)	.24666(13)	.32588(11)	.0235(6)	.0161(4)	.0128(4)	-.0009(4)	.0095(4)	.0005(4)
C4	.13658(10)	.43887(13)	.19513(10)	.0274(6)	.0138(4)	.0131(4)	-.0002(4)	.0125(4)	-.0001(3)
OW	.42423(8)	.35541(12)	.30553(10)	.0392(5)	.0152(4)	.0250(4)	-.0011(4)	.0208(4)	-.0003(3)
LI	.40262(22)	.37603(32)	.10605(24)	.0380(12)	.0367(13)	.0201(10)	.0025(10)	.0158(9)	-.0024(9)

ATOM	X	Y	Z	B	ATOM	X	Y	Z	B
HO	.1342(16)	.4973(27)	.5007(20)	5.9(5)	HW1	.4070(20)	.4421(31)	.3347(25)	6.6(6)
HW2	.4065(20)	.2646(28)	.3287(26)	5.6(5)					

Table 2. Interatomic distances and angles.

Distance (Å)		Angle (°)			
a. Within the squarate residue					
C1–O1	1.237(1)	C2–C1–O1	136.0(1)	C4–C1–O1	135.1(1)
C2–O2	1.227(1)	C1–C2–O2	136.9(1)	C3–C2–O2	135.5(1)
C3–O3	1.285(1)	C2–C3–O3	135.8(1)	C4–C3–O3	132.3(1)
C4–O4	1.276(1)	C1–C4–O4	134.7(1)	C3–C4–O4	133.4(1)
C1–C2	1.509(1)	C1–C2–C3	87.5(1)	C2–C3–C4	91.8(1)
C1–C4	1.454(1)	C3–C4–C1	91.8(1)	C4–C1–C2	88.9(1)
C2–C3	1.472(2)				
C3–C4	1.417(1)				
b. Around the Li^+ ion					
Li–OW	2.035(2)	OW–Li–O1	169.8(1)	OW–Li–O2	92.5(1)
Li–O1	2.057(2)	OW–Li–OW	89.0(1)	O1 –Li–OW	94.8(1)
Li–O2	2.057(3)	O2 –Li–OW	105.0(1)	O2 –Li–O1	95.7(1)
Li–OW	2.057(3)				
c. For the hydrogen bonds					
O3–O4	2.431(1)	C3–O3–O4	111.6(1)	C3–O3–HO	109.5(11)
OW–O1	2.737(1)	C4–O4–O3	110.7(1)	C4–O4–HO	112.6(9)
OW–O4	2.720(1)	O3–HO–O4	175.8(19)	HW1–OW–HW2	113.5(24)
O3–HO	1.125(20)	O1–OW–O4	113.3(1)	O1–HW1–OW	178.5(24)
O4–HO	1.307(20)	O4–HW2–OW	178.4(24)		
OW–HW1	0.827(25)				
OW–HW2	0.825(23)				
HW2–O4	1.895(24)				
HW1–O1	1.910(25)				
HW2–HW1	1.382(28)				

rangement, the $Li^+ \cdots O_w$ distances are 2.035(2) and 2.057(3) Å while the angles $O_w \cdots Li^+ \cdots O$ and $Li^+ \cdots O_w \cdots Li^+$ are 89.0(1) and 90.31(2)°, respectively. Apparently this cluster is held together relatively strongly since there are open regions in the structure between the water molecules and the next layer of HSQ^- ions. The coordination around the water molecules is nearly tetrahedral. The two weak hydrogen bonds formed by the water molecule [2.737(1), 2.720(1) Å] (see Table 2) are linear with O–H···O angles insignificantly different from 180°.

Evidence from the bond lengths within the HSQ^- ion as well as the H_O peak in a difference Fourier synthesis, confirm the presence of a

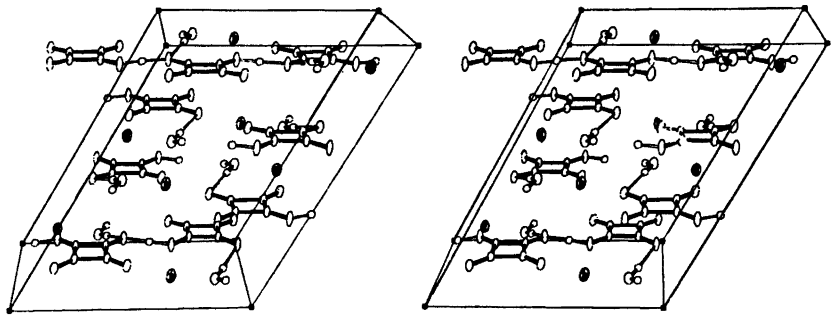

Fig. 1. Stereoscopic illustration[15] of the crystal structure of $LiHSQ.H_2O$, as viewed along the *b* axis. Thermal ellipsoids are scaled to include 50 % probability.

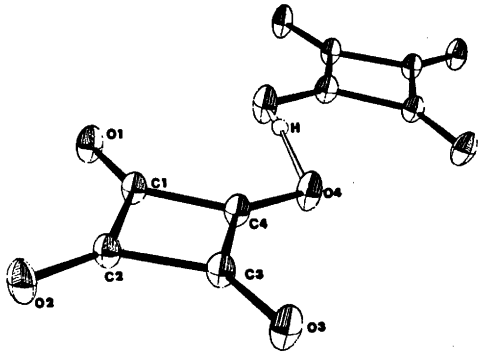

Fig. 2. Perspective drawing of hydrogen-bonded HSQ chain with atom numbering as indicated (50 % probability).

short asymmetric O – H···O hydrogen bond. The length of this bond [2.431(1) Å] compares well with the crystallographically symmetrical hydrogen bond recently determined in $(H_2NMe_2)^+[H_3SQ_2]^-$ (2.435(2) Å).[10] The hydrogen bond in the present study may therefore probably be classified as pseudo type A_2 in the convention adopted by Speakman.[8] This bond is also nearly linear ($\angle O-H\cdots O = 176°$), and with C – O···O angles [111.6(1), 110.7(1)°] close to values found in type *A* hydrogen bonds in acid salts of carboxylic acids [112(2)°].[8] The assymmetry of the hydrogen bond is certainly due to asymmetries in the environments. O4, in particular, participates in one of the weaker hydrogen bonds, whereas O3 is presumably only weakly attracted by the Li^+ ions. However, differences in the more distant surroundings, namely at O1 and O2, may be transmitted through the π conjugated double bond system of the HSQ^- ion and therefore also influence the potential experienced by the proton H_O.

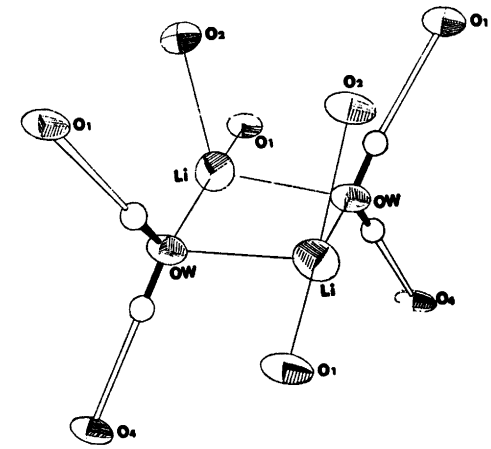

Fig. 3. Perspective drawing of the environment around Li^+ ions and water molecules (50 % probability).

Despite the differences in the environments of the oxygen atoms of the HSQ^- ion there is, in agreement with previous studies of acid salts,[9,10] and the parent molecule,[3] approximate C_{2v} symmetry in the bond lengths of the SQ unit. This may indicate a preference for a localized double bond in the cyclobutene ring in such systems and may be contrasted to the reported fourfold symmetry of the SQ^{2-} ion in the $K_2SQ.H_2O$ structure.[7]

The bond lengths within the HSQ^- ion do not deviate greatly from those found previously in H_2SQ.[3] The average C – O hydroxylic bond of 1.280 Å in $LiHSQ.H_2O$ is similar to, though shorter than that [1.291(1) Å] observed in H_2SQ [3] and the averaged C – O bond in the diketonic group (1.232 Å) is also in agreement with that [1.229(1) Å] found in H_2SQ.[3] Similarly only small though significant deviations are found for the C – C bonds. Thus, although single and double bonds are recognizable, there is in agreement with the H_2SQ investigation appreciable conjugation within the HSQ^- entity.

It appears, however, as if the degree of conjugation along the O1 – C1 – C4 – C3 – O3 diagonal is somewhat higher than that along the other (O2 – C2 – C3 – C4 – O4). This may be due to the fact that O1 is more engaged in external interactions than O2, resulting in a lengthening of the C1 – O1 bond which is transmitted through conjugated system of π electrons. The bond lengths of the present study also agree (within the experimental error for most bonds) to those obtained in the recent study of $KHSQ.H_2O$,[9] while they deviate somewhat from those obtained in the structure determination of the slightly different system of $(H_2NMe)^+[H_3SQ_2]^-$.[10]

There is one significant feature displayed by all the structures involving squaric acid [3] and its acid salts so far investigated.[9,10] That is that the exocyclic angles *cis* to the hydrogen atoms are significantly enlarged irrespective

of the kind of hydrogen bonding scheme adopted. (The hydrogen atoms in these systems are found to be situated close to the mean square plane of the squarate residue). Thus in the present structure these distortions conform to the approximate C_{2v} symmetry of HSQ^- ion, whereas in the squaric acid structure they follow the pseudo fourfold axis of the molecule. The angles within the fourmembered ring system agree well with those previously found in H_2SQ.

Deviations from a least-squares plane through the heavy atoms in the HSQ^- ion have been calculated. The ion is significantly non-planar, since O2 and O4 are displaced about 0.026 Å from the mean plane, while the carbon atoms are displaced approximately 0.017 Å to the opposite side (the mean square displacement is about 0.018 Å). The thermal motions of the atoms in the HSQ^- ion have their largest amplitudes almost perpendicular to the plane through these atoms. The value of the maximum root-mean-squares amplitudes range between 0.23 and 0.20 Å for the oxygen atoms and 0.17 to 0.16 Å for the carbon atoms. A riding-body analysis of the translational, librational and screw motion failed, probably because the atoms of HSQ^- ion lie close to a quadratic curve.[17]

Acknowledgements. The author is indebted to P. Groth at this department for helpful advice during the structure determinations.

REFERENCES

1. Cohen, S., Lacher, J. R. and Park, J. D. *J. Am. Chem. Soc. 81* (1959) 3480.
2. West, R. and Niu, J. In Zabicky, J., Ed., *The Chemistry of the Carbonyl Group*, Wiley, London 1970, Vol. 2, Chapter 4.
3. Semmingsen, D. *Acta Chem. Scand. 27* (1973) 3961. *Ibid. A 29* (1975) 470.
4. Wang, Y., Stucky, G. D. and Williams, J. M. *J. Chem. Soc. Perkin Trans. 2* (1974) 35.
5. Schwartz, L. M. and Howard, L. O. *J. Phys. Chem. 74* (1970) 4374.
6. West, R. and Powell, D. *J. Am. Chem. Soc. 85* (1963) 2577.
7. MacIntyre, W. M. and Werkema, M. S. *J. Chem. Phys. 40* (1964) 3563.
8. Speakman, J. C. In *Structure and Bonding*, Springer, Berlin 1972, Vol. 12, Chapter 3.
9. Bull, R. J., Ladd, M. F. C., Povry, D. C. and Shirley, R. *Cryst. Struct. Commun. 2* (1973) 625.
10. Wang, Y. and Stucky, G. D. *J. Chem. Soc. Perkin Trans. 2* (1974) 925.
11. Germain, G., Main, P. and Woolfson, M. M. *Acta Crystallogr. A 27* (1971) 368.
12. Doyle, P. A. and Turner, P. S. *Acta Crystallogr. A 24* (1968) 390.
13. Stewart, R. F., Davidson, E. R. and Simpson, W. T. *J. Chem. Phys. 42* (1965) 3175.
14. Groth, P. *Acta Chem. Scand. 27* (1973) 1837.
15. Johnson, C. K. *ORTEP*, Report ORNL-3794, Oak Ridge National Laboratory, Oak Ridge 1965.
16. Bernstein, J., Cohen, M. D. and Leiserowitz, L. In Patai, S., Ed., *The Chemistry of the Quinoid Compounds*, Wiley, London 1974, Part 1, Chapter 2.
17. Schomaker, V. and Trueblood, K. N. *Acta Crystallogr. 17* (1964) 142.

Received April 7, 1976.

Acta Chemica Scandinavica A 30 (1976) 813—819

The Crystal Structures of Tris(thiosemicarbazido)nickel(II) Nitrate and its Monohydrate

RITA GRØNBÆK HAZELL

Department of Inorganic Chemistry, University of Aarhus, DK-8000 Aarhus C, Denmark

Tris(thiosemicarbazido)nickel nitrate has been prepared in two crystalline modifications, one of which is a monohydrate. Three dimensional X-ray analyses have shown that the complex ion has the same configuration in the two forms. Nickel is octahedrally surrounded by three sulfur atoms and three terminal nitrogen atoms from the hydrazine groups. The sulfur atoms are *cis* to one another. The average distances in the octahedron are: Ni–S 2.40 Å, Ni–N 2.12 Å. In the anhydrous form one Ni–S bond is significantly longer than the others. The packing of positive and negative ions is different in the two compounds. The unit cell dimensions are for the monohydrate: orthorhombic, $a = 9.43(2)$ Å, $b = 15.71(3)$ Å, $c = 11.77(2)$ Å, space group $Pna2_1$. The anhydrous form: monoclinic, $a = 14.64(3)$ Å, $b = 9.77(2)$ Å, $c = 11.68(2)$ Å, $\beta = 101.6(2)°$. Space group $P2_1/a$. After least squares refinement the R-values are 0.053 and 0.043 for 1273 and 3091 reflections, respectively.

This investigation belongs to a series of structure determinations of nickel complexes with thiosemicarbazide. The purpose is to obtain reliable bond lengths for *trans* planar,[1–3] *cis* planar,[2,3] *trans* octahedral,[4] and *cis* octahedral complexes of the same ligand to support theoretical work on the bonding in such complexes. The occurrence of two different sorts of crystals in one preparation of tris(thiosemicarbazido)nickel nitrate gave a suspicion of *cis-trans* isomerism, and we had to solve both structures to establish what was the actual difference between the two sorts of crystals.

EXPERIMENTAL

Alcoholic solutions of the stoichiometric amounts of thiosemicarbazide and of $Ni(NO_3)_2.6H_2O$ were mixed and left to evaporate. Deep-blue crystals of composition $Ni(CH_5N_3S)_3(NO_3)_2.H_2O$ formed. The water could be removed when the crystals were heated to 150 °C for some hours. The crystals were destroyed by this treatment and the product was not the same as the anhydride mentioned below.

In one preparation some of the crystals that had formed first on the sides of the beaker were of a slightly different colour from that of the main product. There were not enough of these crystals to allow a chemical analysis, and no later preparation contained any of this sort. The structure analysis showed that the formula was $Ni(CH_5N_3S)_3(NO_3)_2$.

Unit cell dimensions and space groups were obtained from rotation and equi-inclination Weissenberg films taken with Cu$K\alpha$ radiation ($\lambda_{Cu} = 1.5418$ Å) and from precession exposures taken with Cu$K\alpha$ and Mo$K\alpha$ radiation ($\lambda_{Mo} = 0.7107$ Å). Intensities were collected by means of an automatic diffractometer of Arndt-Phillips design [5] using Mo radiation and balanced filter technique together with pulse height discrimination. Later another set of data was collected for another crystal of the anhydrous compound using the same diffractometer but crystal monochromatized Mo$K\alpha$ radiation. Data were collected to $\sin\theta/\lambda = 0.7$ giving 1273 significant out of 2942 reflections for the monohydrate, 3091 significant out of 4379 for the anhydrous compound. The linear dimensions of the crystals used were all of the order of 0.2–0.3 mm. No absorption correction was applied because the crystals were so equidimensioned and the absorption factors reasonably small.

CRYSTAL DATA

$Ni(CH_5N_3S)_3(NO_3)_2.H_2O$.

Orthorhombic.

$a = 9.43(2)$ Å; $b = 15.71(3)$ Å; $c = 11.77(2)$ Å; $V = 1742$ Å^3.

$d_c = 1.81$ g/cm^3 for 4 formula units per unit cell.

Table 1. Final coordinates for the monohydrate, $Ni(CH_5N_3S)_3(NO_3)_2.H_2O$, in fractions of the unit cell, standard deviations × 10^4 in parentheses. Hydrogen atom positions were calculated and not refined. Their temperature factor parameters B were kept at 5.0 Å^2.

	x	*y*	*z*
Ni	0.0487(1)	0.0082(1)	0.0021(3)
S(1)	0.0616(3)	0.1335(2)	0.1154(4)
S(2)	0.2257(3)	−0.0666(2)	0.1054(3)
S(3)	−0.1377(3)	−0.0525(2)	0.1150(4)
C(1)	−0.0869(12)	0.1814(7)	0.0614(13)
C(2)	0.3693(12)	−0.0214(7)	0.0413(14)
C(3)	−0.1423(11)	−0.1490(6)	0.0460(11)
N(11)	−0.0950(9)	0.0839(5)	−0.0927(9)
N(12)	0.2282(9)	0.0470(6)	−0.1001(9)
N(13)	0.0107(9)	−0.0981(6)	−0.1019(10)
N(21)	−0.1556(10)	0.1517(6)	−0.0276(10)
N(22)	0.3591(11)	0.0325(7)	−0.0413(12)
N(23)	−0.0641(11)	−0.1648(6)	−0.0453(10)
N(31)	−0.1384(10)	0.2515(6)	0.1106(12)
N(32)	0.4989(10)	−0.0411(8)	0.0810(13)
N(33)	−0.2237(11)	−0.2120(6)	0.0864(11)
N[O(1)]	0.1244(12)	0.3465(6)	0.3055(10)
O(1)	0.2240(10)	0.3115(6)	0.3585(10)
O(2)	0.1519(14)	0.4072(7)	0.2456(13)
O(3)	0.0030(9)	0.3166(6)	0.3192(11)
N[O(2)]	−0.0346(12)	0.7121(7)	0.3163(11)
O(4)	−0.1252(10)	0.7575(6)	0.3634(11)
O(5)	−0.0448(17)	0.6361(7)	0.3253(16)
O(6)	−0.0534(15)	0.7490(11)	0.2568(14)
O(7)	−0.1818(11)	0.4548(6)	0.3387(12)
H(111)	−0.179	0.045	−0.123
H(112)	−0.038	0.111	−0.164
H(121)	0.218	0.114	−0.121
H(122)	0.229	0.011	−0.178
H(131)	0.114	−0.123	−0.129
H(132)	−0.047	−0.078	−0.175
H(211)	−0.255	0.180	−0.050
H(221)	0.450	0.070	−0.064
H(231)	−0.059	−0.230	−0.074
H(311)	−0.100	0.266	0.170
H(312)	−0.230	0.280	0.070
H(321)	0.513	−0.070	0.150
H(322)	0.580	−0.010	0.050
H(331)	−0.270	−0.195	0.160
H(332)	−0.233	−0.270	0.050

$\mu(CuK\alpha) = 132.1$ cm^{-1}, $\mu(MoK\alpha) = 37.8$ cm^{-1}.
Systematic absences: $0kl$ for $k+l$ odd
$h0l$ for h odd
Space group $Pna2_1$ from systematic absences and the piezoelectric effect.

Final atomic coordinates and temperature factor parameters are given in Tables 1 and 2, and bond lengths and angles in Table 5.

$Ni(CH_5N_3S)_3(NO_3)_2$
Monoclinic, b unique.
$a = 14.64(3)$ Å; $b = 9.77(2)$ Å; $c = 11.68(2)$ Å; $\beta = 101.6(2)°$; $V = 1636$ Å^3.
$d_c = 1.85$ g/cm^3 for 4 formula units per unit cell.
$\mu(CuK\alpha) = 138.9$ cm^{-1}, $\mu(MoK\alpha) = 40.1$ cm^{-1}.
Systematic absences: $h0l$ for h odd
$0k0$ for k odd
Space group: $P2_1/a$.

Final atomic coordinates and temperature factor parameters are given in Tables 3 and 4, and bond lengths and angles in Table 5. Structure factor tables can be obtained from the author on request.

Table 2. Temperature factor parameters, u_{ij}, for the monohydrate in $Å^2 \times 10^{-4}$ with standard deviations in parentheses. The expression for the temperature factor is: $\exp[-2\pi^2(u_{11}(ha^*)^2 + \cdots + 2u_{23}klb^*c^*)]$

	u_{11}	u_{22}	u_{33}	u_{12}	u_{13}	u_{23}
Ni	305(6)	318(6)	486(6)	−11(6)	1(10)	1(8)
S(1)	314(14)	344(13)	545(15)	5(11)	−41(16)	13(14)
S(2)	370(14)	404(14)	617(19)	26(11)	−98(17)	24(16)
S(3)	367(14)	321(13)	566(16)	−38(11)	109(16)	−82(15)
C(1)	373(64)	356(58)	784(91)	28(48)	−125(65)	107(62)
C(2)	286(63)	521(69)	886(118)	−66(58)	−55(66)	−48(76)
C(3)	355(61)	273(50)	622(81)	2(50)	−102(63)	−101(54)
N(11)	389(50)	390(50)	538(59)	1(40)	−189(47)	12(46)
N(12)	355(49)	565(59)	403(53)	−101(46)	2(48)	40(48)
N(13)	404(51)	424(50)	538(55)	−58(41)	−43(47)	−29(48)
N(21)	472(58)	421(53)	821(87)	53(46)	−205(61)	51(53)
N(22)	412(60)	663(66)	942(97)	−183(59)	100(66)	156(69)
N(23)	472(58)	394(50)	876(83)	12(44)	132(61)	−168(52)
N(31)	584(62)	491(51)	959(80)	259(52)	−80(74)	−48(71)
N(32)	299(53)	1182(94)	992(116)	71(62)	−41(65)	−31(92)
N(33)	674(68)	494(53)	771(79)	−194(49)	107(64)	−93(56)
N[O(1)]	623(74)	350(55)	613(68)	−71(53)	−30(64)	−35(50)
O(1)	651(63)	807(66)	990(91)	−173(51)	−238(65)	234(61)
O(2)	1344(112)	705(68)	1351(113)	−136(72)	166(89)	474(78)
O(3)	456(54)	511(54)	1194(86)	−41(41)	−21(57)	−59(57)
N[O(2)]	408(66)	693(78)	759(77)	53(58)	−30(65)	−144(63)
O(4)	552(57)	745(61)	1068(79)	−89(50)	120(61)	−171(61)
O(5)	1895(150)	455(65)	2129(169)	245(79)	−1293(139)	−147(79)
O(6)	888(91)	2198(155)	1216(108)	−236(103)	480(89)	−517(119)
O(7)	965(78)	858(68)	1260(102)	485(58)	407(76)	388(70)

Table 3. Final coordinates for the anhydrous compound, $Ni(CH_5N_3S)_3.2NO_3$, in fractions of the unit cell, standard deviations $\times 10^4$ in parentheses. For hydrogen atoms isotropic temperature factor parameters, B, are also given.

	x	y	z	B
Ni	0.3512(0.3)	0.1781(0.4)	0.2185(0.4)	
S(1)	0.1816(1)	0.1997(1)	0.1743(1)	
S(2)	0.3723(1)	0.3474(1)	0.0786(1)	
S(3)	0.3524(1)	−0.0107(1)	0.0870(1)	
C(1)	0.1635(3)	0.0562(3)	0.2494(3)	
C(2)	0.3535(2)	0.4842(3)	0.1597(3)	
C(3)	0.4656(2)	−0.0504(3)	0.1291(3)	
N(11)	0.3216(2)	0.0470(3)	0.3477(2)	
N(12)	0.3619(2)	0.3497(2)	0.3319(2)	
N(13)	0.4944(2)	0.1285(3)	0.2717(3)	
N(21)	0.2301(2)	−0.0039(3)	0.3254(3)	
N(22)	0.3519(2)	0.4757(3)	0.2726(3)	
N(23)	0.5246(2)	0.0197(3)	0.2098(3)	
N(31)	0.0800(2)	0.0004(4)	0.2331(4)	
N(32)	0.3419(3)	0.6085(3)	0.1119(3)	
N(33)	0.5009(2)	−0.1566(3)	0.0809(3)	
N[O(1)]	−0.0492(2)	0.7464(3)	0.4305(3)	
O(1)	−0.1111(2)	0.7406(3)	0.3423(3)	
O(2)	−0.0076(2)	0.6425(3)	0.4705(3)	
O(3)	−0.0328(3)	0.8566(3)	0.4795(4)	

Table 3. Continued.

N[O(2)]	0.1881(2)	0.6634(3)	0.3740(3)	
O(4)	0.1911(2)	0.5396(3)	0.3970(3)	
O(5)	0.1685(2)	0.7003(3)	0.2698(3)	
O(6)	0.2063(3)	0.7498(3)	0.4537(3)	
H(111)	0.359(3)	−0.030(5)	0.348(4)	4.2(1.2)
H(112)	0.333(3)	0.085(5)	0.425(4)	2.4(1.1)
H(121)	0.305(3)	0.351(4)	0.370(3)	2.5(0.9)
H(122)	0.411(3)	0.352(4)	0.382(4)	3.4(1.0)
H(131)	0.537(3)	0.209(5)	0.260(4)	4.9(1.3)
H(132)	0.507(3)	0.098(4)	0.348(3)	2.5(1.0)
H(211)	0.224(3)	−0.077(4)	0.366(3)	2.3(0.9)
H(221)	0.351(3)	0.547(4)	0.316(3)	1.3(0.9)
H(231)	0.587(3)	−0.004(4)	0.239(3)	2.2(0.9)
H(311)	0.073(3)	−0.069(5)	0.270(4)	3.8(1.2)
H(312)	0.029(3)	0.037(5)	0.174(4)	4.9(1.2)
H(321)	0.331(3)	0.673(4)	0.158(4)	3.5(1.0)
H(322)	0.334(3)	0.623(5)	0.031(4)	4.4(1.3)
H(331)	0.462(3)	−0.209(5)	0.014(4)	4.2(1.3)
H(332)	0.557(3)	−0.167(4)	0.106(4)	2.8(0.9)

Table 4. Temperature factor parameters, u_{ij}, for the anhydride in $Å^2 \times 10^{-4}$ with standard deviations in parentheses.

	u_{11}	u_{22}	u_{33}	u_{12}	u_{13}	u_{23}
Ni	238(2)	286(2)	64(2)	28(2)	9(2)	−27(2)
S(1)	250(4)	331(3)	29(5)	47(3)	23(4)	36(3)
S(2)	362(5)	362(4)	81(4)	25(4)	74(4)	−32(4)
S(3)	255(5)	395(4)	388(5)	20(4)	5(4)	−126(4)
C(1)	291(19)	404(16)	436(22)	16(15)	59(16)	65(16)
C(2)	277(18)	302(13)	288(18)	−40(13)	17(14)	−11(13)
C(3)	268(18)	297(13)	357(19)	17(13)	107(15)	25(13)
N(11)	294(16)	356(12)	313(16)	37(12)	−1(13)	38(12)
N(12)	363(17)	295(11)	283(15)	51(12)	13(13)	−10(11)
N(13)	249(15)	393(13)	364(17)	15(12)	−17(13)	−61(13)
N(21)	358(18)	355(13)	489(20)	−38(13)	18(15)	138(14)
N(22)	479(19)	276(12)	292(16)	35(13)	80(14)	−31(11)
N(23)	223(15)	392(13)	456(18)	48(12)	21(13)	−31(13)
N(31)	314(20)	866(26)	1031(34)	−178(20)	−37(21)	473(25)
N(32)	752(26)	340(13)	375(19)	−28(15)	176(18)	22(13)
N(33)	266(19)	426(15)	560(21)	53(14)	146(16)	−101(15)
N[O(1)]	528(22)	346(13)	549(22)	−46(15)	−194(17)	37(14)
O(1)	866(25)	466(14)	559(20)	−121(16)	−355(18)	102(14)
O(2)	648(21)	437(13)	600(20)	127(14)	−119(16)	95(13)
O(3)	1593(45)	454(17)	1617(42)	150(22)	−1133(35)	−334(22)
N[O(2)]	427(20)	507(16)	428(19)	−121(15)	104(16)	15(15)
O(4)	621(20)	473(13)	551(19)	−8(14)	109(15)	37(13)
O(5)	811(25)	736(19)	444(18)	−275(18)	−86(17)	126(16)
O(6)	1209(32)	566(16)	465(19)	−270(19)	306(19)	−100(15)

STRUCTURE DETERMINATION

Both structures were solved by Patterson and Fourier methods. For the monohydrate a few cycles of Fourier refinement were needed before the positions of all the oxygen atoms were determined; temperature factors after refinement show that the nitrate groups in this compound oscillate considerably although they do not have a free rotation.

Refinement proceeded by the method of least squares. With anisotropic temperature factors the R-values. ($R = \sum||F_o| - |F_c||/\sum|F_o|$) decreased to 0.07 – 0.08 at which stage difference Fourier maps were calculated.

Table 5. Bond lengths and angles in tris(thiosemicarbazido)nickel nitrate. M indicates the anhydrous form, O the monohydrate. The three thiosemicarbazide groups of each complex are designated by numbers 1, 2, and 3 corresponding to the second digit of atom identifiers on Figs. 1 and 2.

Bond	M1	M2	M3	O1	O2	O3
Ni–S	2.441(1)	2.389(1)	2.402(1)	2.380(4)	2.376(4)	2.400(4)
Ni–N(1)	2.089(3)	2.123(3)	2.120(3)	2.119(9)	2.163(10)	2.101(10)
S–C	1.703(4)	1.693(3)	1.677(3)	1.712(12)	1.705(13)	1.721(11)
C–N(2)	1.317(4)	1.323(4)	1.333(4)	1.317(18)	1.292(16)	1.326(17)
C–N(3)	1.317(5)	1.333(4)	1.333(5)	1.336(16)	1.344(16)	1.339(14)
N(1)–N(2)	1.404(4)	1.405(4)	1.406(4)	1.430(14)	1.433(14)	1.428(14)
N–O	1.229(4)	1.226(4)	1.220(5)	1.255(15)	1.213(16)	1.247(14)
	1.238(4)	1.247(4)	1.245(4)	1.243(16)	1.202(16)	1.231(20)
N(1)–H(1)	0.93(5)	0.83(4)	0.92(4)			
	0.95(4)	1.02(4)	1.03(5)			
N(2)–H(2)	0.87(4)	0.86(4)	0.93(4)			
N(3)–H(3)	0.82(5)	0.86(4)	0.82(4)			
	0.98(4)	0.94(5)	1.01(5)			
Angle						
S–Ni–N(1)	81.8(1)	82.9(1)	83.0(1)	82.2(3)	82.8(3)	83.2(3)
Ni–N(1)–N(2)	114.3(2)	113.4(2)	114.7(2)	113.0(7)	110.5(8)	113.3(8)
Ni–S–C	94.4(1)	96.1(1)	97.1(1)	96.5(5)	97.1(5)	91.5(5)
S–C–N(2)	122.9(3)	123.0(2)	123.4(3)	122.8(9)	122.2(9)	122.6(8)
N(1)–N(2)–C	121.2(3)	121.6(3)	121.7(3)	119.6(9)	123.4(10)	121.0(9)
N(2)–C–N(3)	117.0(3)	116.6(3)	116.6(3)	117.4(11)	120.5(12)	117.4(10)
S–C–N(3)	120.2(3)	120.4(3)	120.0(2)	119.9(11)	117.2(11)	119.9(9)

They confirmed the presence of hydrogen atoms at approximately the expected positions. The introduction of these hydrogen atoms lowered the R-values considerably and further least squares refinement gave some changes in the positions of the atoms to which the hydrogen atoms were attached. The final R-values were 0.053 for both compounds for 1788 and 1273 significant reflections for the anhydride and monohydrate, respectively. At this point one Ni–S bond in the anhydrous compound seemed definitely longer than the others but since no obvious explanation for this was found, another crystal was selected and a new set of data measured in order to safeguard against accidentally introduced errors. The refinement with the new data proceeded to $R=0.043$ for 3091 reflections and gave nearly the same coordinates as had been found with the first set of data.

In the latest refinements reflections for which $F_o^2 < 2\sigma(F^2)_{count}$ were left out of the R-values and of the least squares totals. The standard deviations found from counting statistics were found not to account for all errors and for the weighting of reflections for the least squares refinement they were modified: $\sigma(F^2)=\sigma(F^2)_{count}+aF^2$; $w=1/\{[\sigma(F^2)+F^2]^{\frac{1}{2}}-|F|\}^2$; a is a parameter which was adjusted so that the average of $w||F_o|-|F_c||^2$ was nearly independent of $|F|$. The final values for a were 0.05 for the monohydrate and 0.024 for the anhydrous, monoclinic form.

The scattering curves used were those of Table A of International Tables.[6] Anomalous dispersion effects for the nickel atoms were taken into account. The data for the acentric monohydrate had been collected from two symmetry related octants and the two possible polarities had to be tried, one gave a significantly better fit than the other.

At the end of refinement an extinction parameter was introduced according to formula 3 in Larson's paper.[7] Little improvement was achieved and the extinction parameters are small in both cases.

DISCUSSION

The $NiThio_3^{2+}$ ions have the all *cis* configuration in both compounds. The average Ni–S distance of 2.40 Å agrees well with that in

Table 6. Intermolecular contacts.

Anhydride		Monohydrate	
N(11)–O(1)	2.982	N(11)–O(7)	3.037
N(11)–O(4)	3.026	N(12)–O(2)	3.069
N(12)–O(3)	2.983	N(13)–O(1)	2.911
N(12)–O(6)	3.037	N(21)–O(4)	2.945
N(13)–O(2)	2.982	N(22)–O(5)	2.860
N(21)–O(6)	2.893	N(23)–O(1)	2.976
N(22)–O(1)	2.910	N(23)–O(3)	2.921
N(23)–O(4)	2.985	N(31)–O(3)	2.980
N(23)–O(5)	2.992	N(33)–O(6)	2.963
N(31)–O(5)	3.199	O (7)–O(3)	2.792
N(32)–O(1)	3.025	N(12)–S(3)	3.460
N(33)–O(5)	2.982	N(13)–S(1)	3.442
N(32)–S(1)	3.409	N(31)–S(1)	3.356
N(31)–S(2)	3.536	N(32)–S(3)	3.453
N(32)–S(3)	3.490	O (7)–S(2)	3.375

$NiThio_3(H_2O)_2(NO_3)_2$ [3] (2.41 Å), and the mean distance in $NiThio_2Cl_2.H_2O$ [8] (2.41 Å). In the latter compound the three sulfur atoms are located in an equatorial plane whereas in both compounds of the present investigation the sulphur atoms are found at the corners of a face of the octahedron. Within the accuracy of the two investigations this does not lead to any differences in bond lengths. In the chloride there are differences between Ni–S bond lengths but standard deviations are so high that no conclusion can be drawn. In the monohydrate the three Ni–S bonds are also equal within experimental error, whereas the anhydrous form has one long and two short bonds. Several unsuccessful attempts have been made to get the structure out of a suspected false minimum but the two different sets of data for this compound gave the same results within the standard deviations. We are thus led to believe that the complex does exist in a symmetric and a slightly distorted form. The difference in colour of the two sorts of crystals may be related to this fact. The dimensions of the thiosemicarbazide are similar in all six independent ligands and are also similar to those found in related complexes,[4,5] thus offering no explanation of the distortion.

The only feature of the structure that would seem to give an indication is the fact that a nitrogen atom is found only 3.41 Å from the sulfur atom of the long bond and with a hydrogen atom pointing exactly towards sulfur. This could indicate some degree of hydrogen bonding, a hypothesis which is corroborated by the fact that this bond forms angles of about 100° with the Ni–S and C–S bonds. N–S

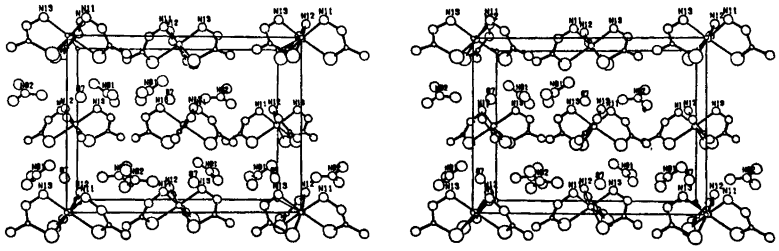

Fig. 1. The structure of nickel tristhiosemicarbazide dinitrate monohydrate viewed along *a*.

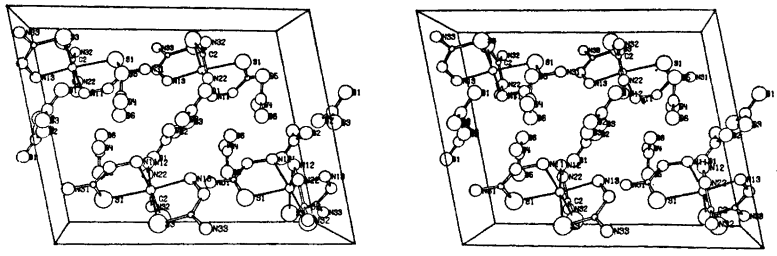

Fig. 2. The structure of anhydrous nickel tristhiosemicarbazide dinitrate viewed along *b*.

contacts of similar length (see Table 6) are found as the other sulfur atoms but in those cases the hydrogen atoms are not so close to the line N–S. The Ni–S bond seems to be sensitive to changes in the coordination of the sulfur atom as evidenced by the difference between the bonds in dichlorotetrakisthioureanickel(II),[9] 2.46 Å, and those in bisthioureanickel(II) thiocyanate,[10] 2.53 Å and 2.56 Å, where each sulfur atom is coordinated to two nickel atoms. We might therefore take the long bond in the present compound as an indication of a relatively strong N–H···S hydrogen bond.

Table 6 also shows that there are a number of weak N–H···O hydrogen bonds in both structures though not all hydrogen atoms are involved in these. The water molecule in the monohydrate is probably contributing to the hydrogen bonding but the hydrogen atoms could not be located in this investigation. The nitrate groups have large thermal movements, but the hydrogen bonding and in the case of the anhydrous compound close distances between nitrate groups prevent actual rotation.

Ballard *et al.*[8] noticed that the S–C bond was longer in octahedral thiosemicarbazide nickel complexes than in planar ones, though barely significantly when only one structure of each sort was considered, but from a comparison of the planar complexes in Refs. 1, 2, and 3 with the octahedral ones in Refs. 4 and 8 and the present investigation and also with free thiosemicarbazide[11,12] it is found that the π-bonding that takes place in the planar complexes leads to a lengthening of the S–C bond by 0.03 Å and the N–N bond by 0.01–0.02 Å, whereas differences between free and octahedrally bonded thiosemicarbazide are insignificant. To decreasing π-bond character in the S–C bond corresponds shorter C–N bonds (Δ(C–N_2)$\sim$0.015 Å, Δ(C–N_3)$\sim$0.03 Å). Although the smaller differences are not highly significant, the effect is probably real.

Both structures contain layers of positive ions alternating with layers of anions. In the monohydrate these layers are only one molecule thick (Fig. 1), whereas those of the anhydrous compound are twice as thick (Fig. 2), the complex cations packing with their sulfur sides together.

Acknowledgements. Thanks are due to Professor S. E. Rasmussen for his continued interest in this work and for excellent working conditions. Carlsbergfonden put the diffractometer at our disposal.

REFERENCES

1. Grønbæk, R. and Rasmussen, S. E. *Acta Chem. Scand. 16* (1962) 2325.
2. Hazell, R. G. *Acta Chem. Scand. 22* (1968) 2171.
3. Hazell, R. G. *Acta Chem. Scand. 26* (1972) 1365.
4. Hazell, R. G. *Acta Chem. Scand. 22* (1968) 2809.
5. Arndt, U. W. and Phillips, D. C. *Acta Crystallogr. 14* (1961) 807.
6. *International Tables for X-Ray Crystallography*, Kynoch Press, Birmingham 1962, Vol. III, p. 202.
7. Larson, A. C. *Acta Crystallogr. 23* (1967) 664.
8. Ballard, R. E., Powell, D. B. and Jayasooriya, U. A. *Acta Crystallogr. B 30* (1974) 1111.
9. Lopez-Castro, A. and Truter, M. R. *J. Chem. Soc.* (1963) 1309.
10. Nardelli, M., Gasparri, G. F., Battistini, G. G. and Domiano, P. *Acta Crystallogr. 20* (1966) 349.
11. Hansen, F. V. and Hazell, R. G. *Acta Chem. Scand. 23* (1969) 1359.
12. Andreetti, G. D., Domiano, P., Gasparri, G. F., Nardelli, M. and Sgarabotto, P. *Acta Crystallogr. B 26* (1970) 1005.

Received May 20, 1976.

Acta Chemica Scandinavica A 30 (1976) 820—824

Low Resolution Microwave Spectra (LRMW) of 1,3-Dichloroacetone, a Conformational Study

HASSE KARLSSON,[a] J. TORMOD NIELSEN,[b] LISE NYGAARD,[b] and KIRSTEN SØRENSEN[b]

[a] Department of Medical Physics, University of Göteborg, S-400 33 Göteborg 33, Sweden and [b] Chemical Laboratory V, University of Copenhagen, The H. C. Ørsted Institute, DK-2100 Copenhagen, Denmark

LRMW spectra of 1,3-dichloroacetone ($C_3H_4Cl_2O$), its perdeuterio- and ^{18}O-species were obtained and analyzed. The observed low intensity of the bands and the (B+C) values are consistent with the presence of one conformer, which is either O-*cis*,*trans*, O-*cis*,*skew* or O-*gauche*,*skew*(−), probably in rather low concentration. No other conformers were observed, and a microwave investigation at high resolution was unsuccessful.

1,3-Dichloroacetone, *sym* dichloroacetone (DCA) was shown by X-ray diffraction [1] to have the O-*cis*,*cis* conformation in the crystal phase, see Fig. 1.

Infrared data [2] showed that two or three conformers of DCA exist in the liquid, in solution and in the gas phase, but the separate conformers were not conclusively assigned.

Parallel to a reinvestigation of the vibrational spectra of DCA and its perdeuterio species [3] it was decided to obtain the microwave spectra and try to find one or more of the conformers in the gas phase. Such independent data would be helpful in the rather complicated vibrational analysis.

EXPERIMENTAL

Compounds. The H_4 sample of 1,3-dichloroacetone was a Fluka *purum* product, which was distilled before use.

The D_4 sample was made by exchange with $(CD_3)_2CO$,[4] as described in Ref. 3, and isolated by single plate distillation. Mass spectra showed the D enrichment to be *ca.* 93 %, consistent with the LRMW result.

The ^{18}O sample was prepared by exchange of 250 mg 1,3-dichloroacetone and 100 μl 90 % enriched $H_2{}^{18}O$ in a high vacuum system. The exchange time was 48 h and the temperature 20 − 22 °C, except that the mixture was heated twice to 45 °C for ½ h to melt dichloroacetone. 220 mg enriched 1,3-dichloroacetone was isolated by single plate distillation. Mass spectra showed the ^{18}O enrichment to be *ca.* 47 %, consistent with the LRMW result.

Spectrometer. The LRMW spectra were measured on a Hewlett-Packard Model 8460A MRR spectrometer, at −10 °C in the region 18 − 40 GHz (in Göteborg) and at room temperature in the region 26.5 − 40 GHz (in Copenhagen), with a sample pressure between 50 and 80 mTorr. Several Stark voltages were used and the measurements were made at 1000 − 1400 V (2000 − 2800 V/cm) at sweep rates of 10 to 2 MHz/s.

LRMW spectra.[5] The three isotopic samples of DCA gave a total of six similar type I spectra,[6] *i.e.* *a*-type *R*-bands. The bands were of rather low intensity, but quite narrow, 150 − 170 MHz, and could be measured to ± 10 MHz. No other band types [6] were observed. The relative intensity of the bands of the $^{35}Cl_2$, ^{35}Cl ^{37}Cl, and $^{37}Cl_2$ species was expected to be 9:6:1, which was confirmed for the two most abundant species, but no $^{37}Cl_2$ bands could be assigned. The bands of the $^{35}Cl(1)^{37}Cl(3)$ and $^{37}Cl(1)$ $^{35}Cl(3)$ species were neither split nor broader than the $^{35}Cl_2$ bands. The two chlorine atoms must therefore be either symmetrically equivalent or the two chlorine positions in DCA must have very similar coordinates, see below.

The following (B+C) values were obtained from the relation (ν MHz)/(J+1): 2038.2, 1990.7, 1992.2, 1947.0, 2024.4, and 1977.6 (all ± 0.5) MHz for the parent ($C_3H_4{}^{35}Cl_2{}^{16}O$), and the ^{37}Cl, D_4, $D_4{}^{37}Cl$, ^{18}O, and $^{18}O^{37}Cl$ species, respectively.

MODEL CONSIDERATIONS

Little is known of the exact geometry of halogenated acetones and their conformation

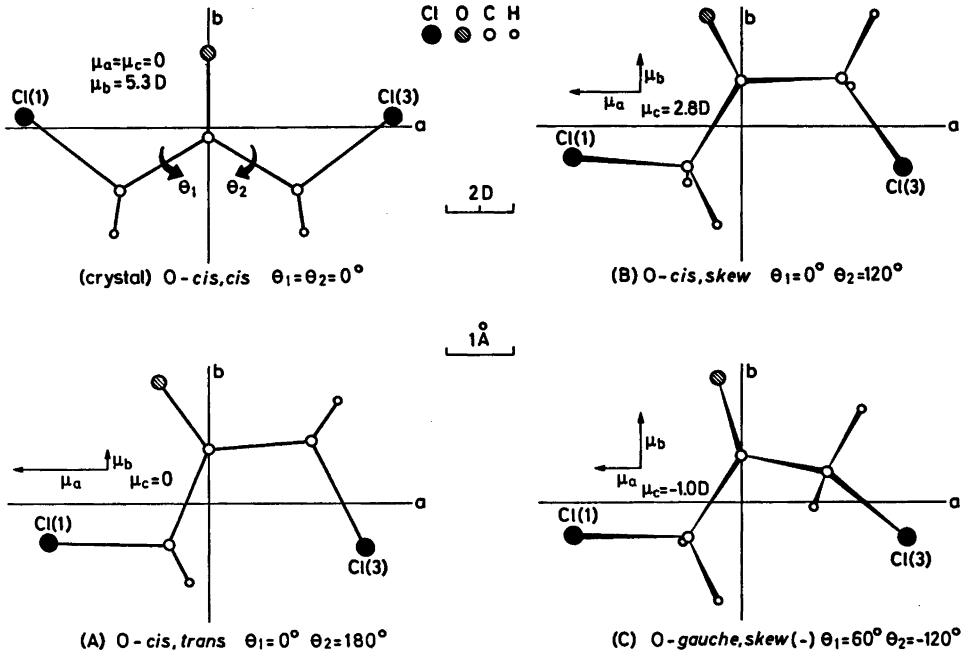

Fig. 1. Some of the possible conformers of 1,3-dichloroacetone and definition of the dihedral angles θ_1 and θ_2.

Table 1. Geometrically possible conformers of 1,3-$^{35}Cl_2$-acetone, their point group symmetry and model values of B+C (MHz), $\varkappa$, μ_a(D), μ_{total}(D), and Cl,Cl distance (Å). The dihedral angles θ_1 and θ_2 (degrees) are defined in Fig. 1.

θ_1[a]	θ_2	Point[b] group	B+C	$\varkappa$	μ_a	μ_{total}	Cl,Cl	Consistent with LRMW
0	0	C_{2v}[b]	(1700)	−0.98	(0)	5.3	5.4	—
0	60	C_1	(1800)	−0.99	(0.7)	4.8	5.3	—
0	120	C_1	2000	−0.94	2.1	3.6	4.9	(B), Fig. 1
0	180	C_s[ab]	2100	−0.88	2.8	2.9	4.7	(A), Fig. 1
60	60	C_s[bc]	2100	−0.95	(0)	4.9	4.6	—
60	120	C_1	(2500)	−0.7	1.7	4.0	4.0	—
60	−120	C_1	2000	−0.93	1.4	2.3	4.9	(C), Fig. 1
60	180	C_1	(2400)	−0.7	2.3	2.5	4.2	—
120	120	C_s[bc]		(+0.9)	(0)	3.3	(2.9)	—
120	180	C_1		(+0.8)	(0.4)	1.7	(2.9)	—
180	180	C_{2v}[a]		(−0.4)	1.1	1.1	(2.0)	—
60	−60	C_2[b]	(1750)	−0.99	(0)	3.7	5.4	—
120	−120	C_2[b]	(2600)	(−0.6)	(0)	0.5	4.1	—
Estimated model uncertainty			±150			±0.5	±0.2	

[a] Models with (θ_1, θ_2) and $(-\theta_1, -\theta_2)$ are mirror images and give the same rotational constants *etc.*
[b] a, b, c are the principal inertial axes.

in the gas phase. A recent microwave paper on 1,3-difluoroacetone [7] showed that the intensity of the observed spectrum is consistent with a 20 – 30 % content of the O-*cis*, *trans* conformer, whereas the spectrum of other conformer(s) could not be assigned, probably due to small dipole moment(s).

Several models were tried in an attempt to assign the LRMW results to one conformer of DCA. The $\varkappa$ correction of (B + C) to $B_0 + C_0$,[8] which is less than 0.5 % (or 10 MHz) when $\varkappa < -0.8$, has been ignored throughout the calculations, since we consider the model uncertainty on B + C to be about 150 MHz or 5 – 10 %. The experimental uncertainty ±0.5 MHz is much less than either of these.

A summary of the model calculations is given in Table 1. Bond lengths and bond angles were assumed to be close to the microwave results for acetone [9] and ethyl chloride [10] and the X-ray results for DCA.[1] The two dihedral angles θ_1 = Cl(1)C(1)C(2)O and θ_2 = Cl(3)C(3)C(2)O were given values of 0, ±60, ±120, or 180°, referred to as O-*cis*, O-*gauche*(±), O-*skew*(±), or O-*trans*, with θ positive when Cl is above the CCC plane, see Fig. 1. The dipole moments and their components were estimated for each model by vectorial addition of partial dipole moments 2.9 and 2.0 D along the bonds C=O (+ → −) and C – Cl (+ → −), respectively.

Of the thirteen geometrically possible models with different combinations of θ_1 and θ_2, see Table 1, ten models could be excluded, since they did not fulfil one or more of the following criteria (i) 1800 MHz < B + C < 2300 MHz, (ii) $\varkappa < -0.7$, (iii) $\mu_a > 1$D, and (iv) a Cl,Cl distance > 3.5 Å (twice the van der Waals radius of chlorine). The excluded model values are given in parentheses in Table 1.

Models for three of the conformers, *i.e.* O-*cis*,*trans*, O-*cis*,*skew*, and O-*gauche*,*skew*(−), fulfil the four criteria, and have (B + C) values rather close to the experimental result given above. Slight variations in bond lengths and angles could bring either of them in perfect agreement with the experimental (B + C).

The experimental values for the relative change in (B + C) by isotopic substitution, Δ(B + C)/(B + C), are consistent with the same three models (within the model uncertainty), an example is given in Fig. 2.

The low intensity of the LRMW spectra could be explained by a low concentration of the conformer and/or a small a-component of the dipole moment.

INFORMATION FROM ISOTOPIC SPECIES

Although only (B + C) values were observed for DCA and for its isotopic species, $(B' + C')_i$, some information on the possible structure of DCA can be obtained in the following way.

The change in the two moments of inertia I_b and I_c by isotopic monosubstitution is $\Delta I_b \cong \mu(a^2 + c^2)$ and $\Delta I_c \cong \mu(a^2 + b^2)$, where μ is the reduced mass and a, b, and c are the coordinates.[11] This is an approximation, since a slight rotation of the axes has been ignored. The

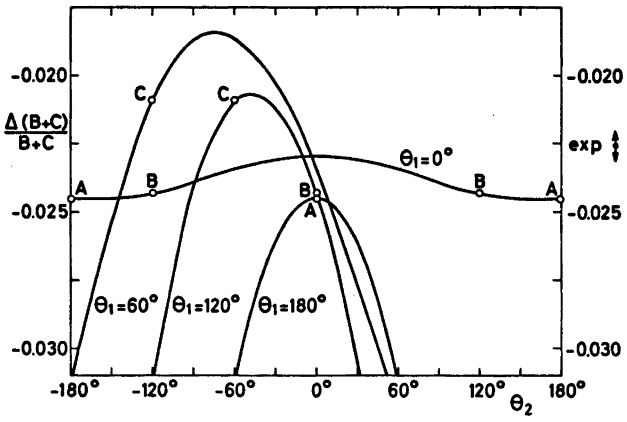

Fig. 2. Relative change in B + C, Δ(B + C)/(B + C), by D_4 substitution in 1,3-$^{35}Cl_2$-acetone as a function of the dihedral angles θ_1 and θ_2.

validity of the approximation was checked with model values. The relative change in (B+C) by substitution is then given by

$$\frac{(B'+C')-(B+C)}{B+C} = \frac{\Delta(B+C)}{B+C} = \frac{-\mu}{B+C}\left\{\left(\frac{B'}{I_b}+\frac{C'}{I_c}\right)a^2 + \frac{C'}{I_c}b^2 + \frac{B'}{I_b}c^2\right\}$$

When model values of the factors to the squared coordinates for ^{37}Cl substitution are inserted, we get the following relation between the chlorine a- and b-coordinates for the (A) conformer (where the c-coordinate is assumed to be zero by symmetry, see Fig. 1), $-(4.1a_{Cl}^2+1.6b_{Cl}^2)10^{-3} = -0.0233 \pm 0.0005$ (exp. value and uncertainty), which gives the correlated coordinates $a_{Cl} = 2.35 \pm 0.05$ Å and $b_{Cl} = 0.6 \pm 0.2$ Å. The coordinate uncertainty includes the estimated model uncertainty in the factors as well as the experimental uncertainty in $\Delta(B+C)/(B+C)$. For the (B) and (C) conformers, see Fig. 1, a similar relation (and the same experimental value) gives the correlated coordinates $a_{Cl} = 2.42 \pm 0.05$ Å, $b_{Cl} = 0.5 \pm 0.2$ Å, and $c_{Cl} < 0.3$ Å. The resulting average chlorine coordinates for the three models are $a_{Cl} = 2.4 \pm 0.1$ Å, $b_{Cl} = 0.5 \pm 0.2$ Å, and $c_{Cl} < 0.3$ Å. This is also an average for the two symmetrically inequivalent but geometrically similar positions in the molecule, since we have only one experimental (B+C) value for the two $^{35}Cl^{37}Cl$ species.

As seen in Fig. 1, the three conformers (A), (B), and (C) have their chlorine atoms in similar positions, and the result can therefore not be used to discriminate between the conformers. An upper limit to the Cl,Cl distance is 4.8 ± 0.2 Å.

For ^{18}O substitution a set of correlated oxygen coordinates derived in a similar way is $a_O = 0.6 \pm 0.2$ Å, $b_O = 1.8 \pm 0.2$ Å, and $c_O < 0.4$ Å. We find again, that this result cannot be used to discriminate between the three conformers.

For D_4 substitution, the relative change in (B+C), $\Delta(B+C)/(B+C)$, was derived exactly for several models, examples are given in Fig. 2. An approximate expression, similar to that given above for monosubstitution, is

$$\frac{\Delta(B+C)}{B+C} = \frac{-\Delta m}{B+C} \times \left\{\left(\frac{B'}{I_b}+\frac{C'}{I_c}\right)\sum_i a_i^2 + \frac{C'}{I_c}\sum_i b_i^2 + \frac{B'}{I_b}\sum_i c_i^2\right\}$$

where a_i, b_i, and c_i are the hydrogen coordinates, $\Delta m = m_D - m_H$, $\Delta I_b \cong \sum_i \Delta m(a_i^2+c_i^2)$, and $\Delta I_c \cong \sum_i \Delta m(a_i^2+b_i^2)$. The approximation is here that the center of mass correction and the rotation of axes are ignored. The validity of the approximation was checked on model values. The expression depends on six hydrogen coordinates for the O-*cis*,*trans* conformer, where C_s symmetry is assumed, and on twelve coordinates for the two other conformers, which do not have a symmetry plane. This can clearly not be used to determine the hydrogen coordinates or even to restrict their values, but only to confirm that a model is reasonable. The experimental result for the D_4 species, $\Delta(B+C)/(B+C) = -0.0226 \pm 0.0005$, is consistent with model calculations for all three conformers.

DISCUSSION

As seen above the information from the measured isotopic species of 1,3-dichloroacetone can set certain limits on the chlorine and oxygen coordinates, and comparison with model calculations has confirmed the effect of D_4 substitution. (It should be noted that two species ($D_4{}^{37}Cl$ and $^{18}O^{37}Cl$) have not been used explicitly, since they give no independent information. Their (B+C) values are, however, consistent with the derivation above).

The exact expression for conversion of (B+C) to (I_b+I_c) is $k/(B+C) = (I_b+I_c)(1-x^2)/4$, where $x = (B-C)/(B+C) = (I_c-I_b)/(I_c+I_b) = (P_b-P_c)/(2P_a+P_b+P_c)$, $P_a = \sum_i m_i a_i^2$, *etc.*, and k is the usual conversion factor $k = BI = 505\,379.1$ MHz uÅ^2.

Taking now the semiquantitative substitution coordinates of the two chlorine atoms and of oxygen and using model coordinates of the hydrogen (and carbon) atoms, we find for the three conformers that the (I_b+I_c) contribution from 2Cl, O, and 4H is 83 ± 3, 6.5 ± 1, and 2.5 ± 1 %, respectively, leaving only *ca.* 8 % to the three carbon atoms.

Since the error in these percentages is rather high, nothing significant can be said of the contribution to (I_b+I_c), or to (B+C), from the three carbon atoms. High resolution results

are needed to find P_c, which could distinguish between the O-*cis,trans* conformer, where P_c (model) is *ca.* 3 uÅ², and the other two possibilities, O-*cis,skew* and O-*gauche,skew*(−), where P_c (model) is about 16 and 20 uÅ², respectively.

Several attempts to obtain a high resolution microwave spectrum of DCA were unsuccessful, which might be explained as follows. For near-prolate molecules ($\varkappa \leq -0.9$) it may be difficult to Stark modulate and thus to observe the ^aR-branch transitions with low K_{-1} values, as well as to resolve the dense bands of ^aR-branch transitions with high K_{-1} values making up the weak LRMW bands observed. The presence of two chlorine isotopes in non-equivalent positions and the expected quadrupole hyperfine structure from these nuclei, together with the supposedly large number of satellite lines from low lying vibrational states adds to the number of lines, and no separate transitions could be assigned.

REFERENCES

1. Sørensen, A. M. *Acta Crystallogr. B 30* (1974) 1366.
2. Bellamy, L. J. and Williams, R. L. *J. Chem. Soc.* (1957) 4294.
3. Sørensen, K. *M. Sc. Thesis*, University of Copenhagen, Copenhagen 1975.
4. Anthonsen, J. W., Christensen, D. H., Nielsen, J. T. and Nielsen, O. F. *Spectrochim. Acta Part A 32* (1976) 971.
5. Scharpen, L. H. and Laurie, V. W. *Anal. Chem. 44* (1972) 378R.
6. Borchert, S. J. *J. Mol. Spectrosc. 57* (1975) 312.
7. Finnigan, D. J., Gillies, C. W., Suenram, R. D., Wilson, E. B. and Karlsson, H. *J. Mol. Spectrosc. 57* (1975) 363.
8. Farag, M. S. and Bohn, R. K. *J. Chem. Phys. 62* (1975) 3946.
9. Nelson, R. and Pierce, L. *J. Mol. Spectrosc. 18* (1965) 344.
10. Schwendeman, R. H. and Jacobs, G. D. *J. Chem. Phys. 36* (1962) 1245.
11. Kraitchman, J. *Am. J. Phys. 21* (1953) 17.

Received April 29, 1976.

Acta Chemica Scandinavica A 30 (1976) 825—828

A New Method for Measuring Transference Numbers

EVEN FØRLAND

The University of Trondheim, Norwegian Institute of Technology, Division of Physical Chemistry, Trondheim, Norway

The transference numbers of cations through a cation exchange membrane are fixed by the composition of the surrounding electrolyte. During electrolysis cations are conducted through the membrane out of the anode side container. Fixed cation fluxes into this container are regulated to compensate for the loss of the same cations through the membrane. Then transference number ratios are found to be equal to the measured cation current ratios.

The validity of the Onsager reciprocal relations is of cardinal importance in the field of irreversible thermodynamics. For the case of isothermal electrical and matter transport this is tested by the numerical equality of the transference numbers determined directly by the Hittorf method and indirectly by the e.m.f.'s of the cells with transference.

For electrolytic conduction processes we define the transference number of an ion as the fraction of current carried by that ion. In order to measure meaningful and accurate transference numbers of ions in membranes, various modifications of the Hittorf method have been tried.[1] This work is concerned with investigating a new method that hopefully will improve transference measurements.

The principle of the Hittorf method is shown in Fig. 1a. The electrolytes on both sides of the membrane should be nearly the same during the electrolysis. The membrane matrix is chosen as frame of reference. From measurements with certain cation exchange membranes it has been found [1] that the anode side electrolyte determines the transference numbers for sufficient high electrical current densities. It is then possible to modify the Hittorf method by omitting one cation species from the cathode side solution. The total gain of this cation to the cathode side after the electrolysis is completed is determined by the usual analytical methods. In this way the analytical difficulties are reduced, but the diffusion problem is larger than for the unmodified Hittorf method.

The new method applied to a cation exchange membrane M is shown in Fig. 1b. During the electrolysis the electrical current from the two anode chambers passes through a small middle chamber before the cathode chamber. The electrolytes on both sides of the membrane

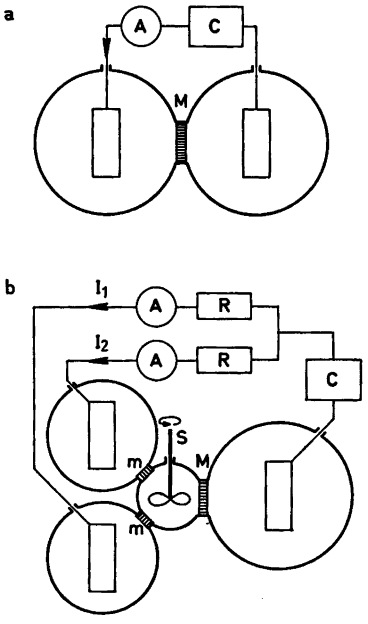

Fig. 1. Methods for measuring transference numbers. a. The Hittorf method; b. The new method. M, membrane for investigation; m, ion exchange membranes; C, constant current source; A, ammeters; R, variable resistors; S, stirrer; I_1, I_2, separate ion currents.

M are the same mixture with components having two different cation species. Thus the transference of ions through the membrane M is fixed by the composition of the electrolyte. The two anode chambers contain electrolytes with each of the two cations from the mixture, respectively. The separate ion currents from the anode chambers into the middle chamber are conducted through the two cation exchange membranes m. The ratio of these ion currents is regulated to compensate for the loss of the same ions through M to keep the composition of the middle chamber unchanged. We have the simple relation (1) between cation transference numbers t_i and separate cation currents I_i.

$$t_1/t_2 = I_1/I_2 \quad (1)$$

Using the relationship (2) we can calculate the transference numbers (3):

$$t_1 + t_2 = 1 \quad (2)$$

$$t_1 = I_1/(I_1+I_2);\ t_2 = I_2/(I_1+I_2) \quad (3)$$

The experiments are carried out by selecting several electrical current ratios close to the expected transference number ratio. After each electrolysis the change in composition in the middle chamber is determined by analyzing a sample. The actual transference number is found by interpolating to the point of balance, where the composition is not changed (Fig. 2).

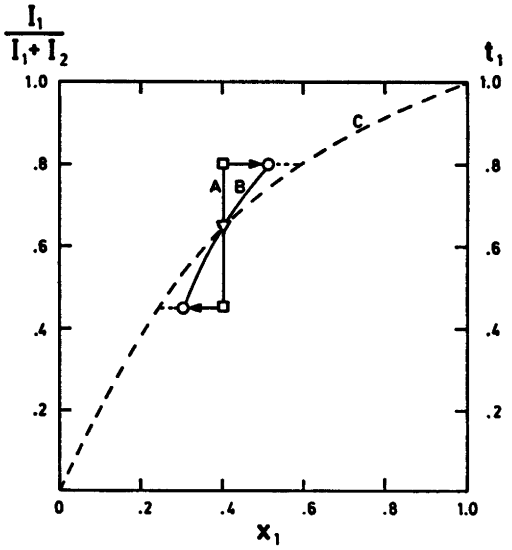

Fig. 2. Interpolation to the point of balance for the transference number t_1. Current ratios $I_1/(I_1+I_2)$ *versus* ionic fraction x_1 and t_1 *versus* x_1. □, composition before electrolysis; ○, after electrolysis; ▽, point of balance. Line A connecting points of selected current ratios with the initial composition; line B connecting the points after electrolysis. Line C: t_1 *versus* x_1.

The cross section areas of the membranes m are much smaller than for the membrane M. This reduces the problem of interdiffusion between the anode chambers and the middle chamber, although the electrical current density through M might still be low. Also to some extent the diffusions into the two anode chambers will counter-balance.

When electrical current is passed the concentration of the solution near the anode side of M will be lowered because both cations and anions are transported away. The diffusion from the bulk of the solution will tend to restore its concentration. Because the anode side solution determines the transference number, the apparent value will be changed, now given by the concentrations at the interface between membrane and solution. The concentration difference between bulk and interface is reduced by fast stirring in the middle chamber.

EXPERIMENTAL

The method was used to determine the transference numbers t_H and t_K for H^+- and K^+-ions through the cation exchange membrane Permaplex C-20 (from Permutit Co. Ltd.) in equilibrium with a solution of 0.2 M HCl and 0.3 M KCl in mixture. It has been found [2] that $1 \geq t_H + t_K > 0.995$.

The middle chamber contained only 2 ml, while the cathode chamber held 550 ml of this solution. The two anode chambers had 300 ml of 0.5 M HCl and 0.5 M KCl, respectively. The cross section areas of the membranes M and m were 1.15 cm^2 and 0.13 cm^2, respectively. The electrodes were Ag/AgCl.

The electrical current densities I over M were varied from 10 to 40 mA/cm^2. For each value of I three experiments were carried out with the cation current ratio fixed at different levels around the expected point of balance. The apparent transference number t_H' connected to the specific value of I was found by interpolation.

The electrolysis lasted for 15 to 20 min. The resulting change of the HCl concentration in a sample from the middle chamber was determined by titration against a solution of NaOH, which was standarized against the original store solution of HCl and KCl mixture.

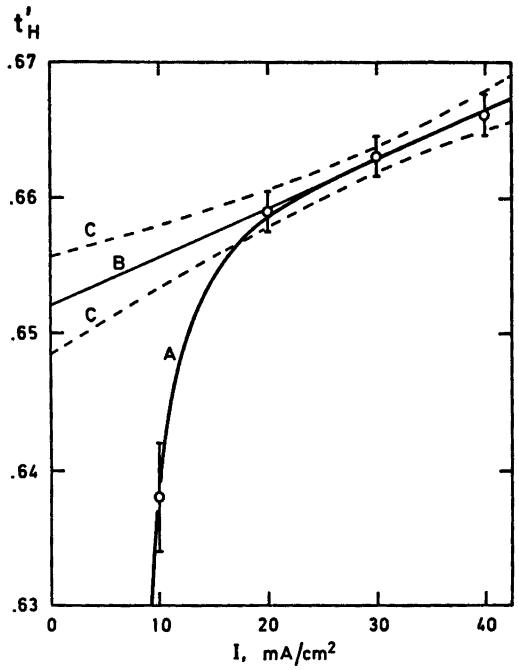

Fig. 3. The apparent transference number t_H' *versus* electrical current density I. O, with vertical bar, experimental; A, apparent transference numbers with diffusion; B, linear regression line; C, 70 % confidence limits.

It has been found [3] that the transference number of water is a linear function of the transference number of protons in this system. Thus the water content in the middle chamber will not change, and it is sufficient to analyze for change in one component only.

RESULTS AND DISCUSSION

The apparent transference numbers t_H' are given in Fig. 3.

The low value for t_H' when having a small value for I was caused by interdiffusion over the two membranes m. The concentration gradient between the middle chamber and the HCl container was larger than over to the KCl container. Thus diffusion alone tended to increase the HCl concentration in the middle chamber. Therefore less electrical current through the HCl container was needed to acquire the point of balance. The apparent transference number t_H' as calculated from the measured electrical current ratio would then be too small.

The concentration profiles through the two membranes m depend upon the electrical current densities I_H and I_K, respectively. Assuming the total cation concentration to be constant through the membrane, the concentration gradient is proportional to the gradient of the ionic fraction.

The excess proton transference caused by diffusion is compensated by potassium ion flux in the opposite direction. The total potassium ion flux density J_K over the membrane m between the middle chamber and the HCl container can be estimated as a combination of electrical transference and diffusion by the following equation.

$$J_K = I_H t_K - D_{HK} \frac{dx_K}{dy} \tag{4}$$

The potassium ion flux J_K, the electrical current density I_H, and the interdiffusion coefficient D_{HK} have equivalent units. The ionic fractions for K^+- and H^+-ions inside the membrane are x_K and x_H, respectively, with $x_K + x_H = 1$. The distance through the membrane is given in relative units y, from 0 (HCl side) to 1 (mixture side). On the membrane surfaces $y=0$ and $y=1$ we have $x_K = x_{K1}$ (very low) and $x_K = x_{K2}$, respectively. The very small contamination of KCl in the HCl container is caused by interdiffusion in between the electrolysis experiments.

The transference number t_K is expressed by the ion mobilities u_K and u_H or by the ratio $m = u_K/u_H$ and by x_K.

$$t_K(x_K) = \frac{x_K u_K}{x_K u_K + (1-x_K) u_H} \tag{5}$$

$$t_K(x_K) = \frac{m x_K}{(m-1)x_K + 1} \tag{6}$$

With no current and assuming a constant gradient $dx_K/dy = (x_{K2} - x_{K1})/(1-0) = x_{K2}$ we find the lower limit for J_K. The upper limit for J_K/I_H is determined by the supply for K^+-ions from the contamination of KCl in HCl solution. We have $t_K(x_{K1}) \approx m x_{K1} \ll 1$. This gives us (7):

$$-D_{HK} x_{K2} < J_K < +I_H t_K(x_{K1}) \tag{7}$$

Introducing eqn. (6) into eqn. (4), assuming D_{HK} to be constant, and integrating between $y=0$ and $y=1$ we find an implicit relation between J_K and I_H.

$$\frac{mI_H D_{HK}}{(mI_H-(m-1)J_K)^2}\ln\left(\frac{mI_H x_{K2}-(1+(m-1)x_{K2})J_K}{mI_H x_{K1}-(1+(m-1)x_{K1})J_K}\right)+\frac{(m-1)D_{HK}}{mI_H-(m-1)J_K}(x_{K2}-x_{K1})=1 \quad (8)$$

We are interested in the asymptotic behaviour when $I_H \gg D_{HK}$ and therefore $|J_K| \ll I_H$. This gives us the explicit relation (9) with (10).

$$J_K(I_H)\approx I_H t_K(x_{K1})[1-\exp(-m\frac{I_H}{D_{HK}})f(x_{K1},x_{K2})] \quad (9)$$

$$f(x_{K1},x_{K2})=\frac{x_{K2}}{x_{K1}}\exp[+(m-1)(x_{K2}-x_{K1})] \quad (10)$$

When I_H is very large the exponential function $\exp(-mI_H/D_{HK})$ will dominate the factor $1/x_{K1}$. Then eqn. (9) gives us eqn. (11) in agreement with eqn. (7).

$$J_K(I_H)\approx I_H t_K(x_{K1}) \quad (11)$$

Then H^+-ions will carry nearly the entire electrical current from the HCl container without significant diffusion. Similarly K^+-ions will carry all but a negligible amount of the electrical current from the KCl container.

It can be shown [4] that the liquid diffusion layer at membrane M will cause a deviation between the apparent transference number t_H' and the true transference number t_H^0, this deviation being proportional to the electrical current density I.

$$t_H' - t_H^0 = \text{constant} \times I \quad (12)$$

The true transference number t_H^0 should be valid for transference through a membrane in equilibrium with the bulk solution having concentrations C_{HCl}^0 and C_{KCl}^0.

The true transference number t_H^0 is estimated by linear extrapolation to zero electrical current density. The linear regression is based on points where diffusion is assumed to be negligible (Fig. 3).

The final result (with standard deviations) is

$t_H^0 = 0.6520 \pm 0.0035$ for

$C_{HCl}^0 + C_{KCl}^0 = 0.500 \pm 0.001$ mol/l with

$x_{HCl}^0 = 0.400 \pm 0.001$

The true transference number t_H^0 for the same type of membrane and the same mixture has been estimated from results with the modified Hittorf method [5,6]

$t_H^0 = 0.665 \pm 0.025$ (Okeyo [5])

$t_H^0 = 0.6417 \pm 0.0048$ (Pongsakorn [6])

Pongsakorn used electrical current densities from 40 to 140 mA/cm^2.

FINAL REMARKS

This method can be generalized by having any convenient combination of electrodes or membranes as ion sources or ion sinks for cations and anions in order to measure transference numbers. Also a modification of this method can be used to determine concentration profiles over the membrane M when the composition of the electrolyte on the two sides are different.

Acknowledgement. The author thanks professor Tormod Førland for stimulating advice and discussions.

REFERENCES

1. Lakshiminarayanaiah, N. *Chem. Rev. 65* (1965) 523.
2. Andresen, I.-L. *Transport Processes in Membranes*, Diss., p. A21, University of Trondheim, Trondheim 1973.
3. Eriksen, E. L. *En studie av strømningspotensialet over en kationbyttermembran*, Diss., p. 35, University of Trondheim, Trondheim 1975.
4. Førland, K. S. *Personal communication.*
5. Okeyo, O. *Cation Exchange Membranes and Transport Properties*, Diss., pp. 169–170, University of Nairobi, Nairobi 1973.
6. Pongsakorn, S. *The Transport of Alkali and Hydrogen Ions due to Diffusion and Charge Transfer across a Cation Exchange Membrane*, Diss., p. A40, University of Trondheim, Trondheim 1975.

Received May 20, 1976.

Acta Chemica Scandinavica A 30 (1976) 829—834

The Crystal and Molecular Structure of the Monomeric *C*-Nitroso Compound *N*,*N*,*N*′,*N*′-Tetramethyl-1,5-diamino-4-nitrosobenzene

H. J. TALBERG

Department of Chemistry, University of Oslo, Oslo 3, Norway

The crystal and molecular structure of the monomeric *C*-nitroso compound *N*,*N*,*N*′,*N*′-tetramethyl-1,5-diamino-4-nitrosobenzene has been determined from X-ray diffraction data collected at −170 °C and refined by least squares methods. The space group is $P2_12_12_1$ with cell dimensions $a = 15.574(5)$ Å, $b = 9.884(2)$ Å, and $c = 6.501(1)$ Å at −170 °C. The final R factor was 4.3 % and the estimated standard deviation in bond lengths is about 0.002 Å and in angles 0.2°. The conformation about the C−NO bond is *trans* with respect to the *ortho* position carrying the dimethylamino group. Sterical interaction between the nitroso group and the *ortho* dimethylamino group causes large (0.64 Å) deviation from planarity in the molecule. The bond lengths indicate a very strong intramolecular charge transfer from the dimethylamino groups to the nitroso group. The C−NO and the N−O bond length are 1.372 and 1.276 Å, respectively.

The present structure determination of *N*,*N*,*N*′,*N*′-tetramethyl-1,5-diamino-4-nitrosobenzene (I) is part of a series of structural investigations of *C*-nitroso compounds and oximes derived from these. Previously, *N*,*N*-dimethyl-*p*-nitrosoaniline (II), its hydrochloride and the oxime tautomer of *p*-nitrosophenol and three of its salts have been investigated.[1–6]

Nitrosobenzenes are found both as monomers and as azo dioxide dimers in the solid state.[7] The monomers are considered to be characterized by a strong intramolecular charge transfer of π-type to the nitroso group. This feature is very pronounced in the *p*-nitrosophenolate ion which may be termed a nitrosonate.[6] Some of the structural results of (II) indicate only a weak charge transfer to the nitroso group, but disorder prevented an accurate structure determination in this case. The structure of three other monomers is also known, but the moderate accuracy in the structural results prevents any conclusions for these compounds.[7]

Since IR spectroscopy indicates that the title compound is monomeric in the crystal and that it possesses an intramolecular charge transfer about as strong as that of (II),[8] it was decided to carry out a structure determination of this compound.

Another initiating factor for the present investigation was the fact that (I) is closely related to the not yet isolated compound *N*,*N*-dimethyl-*o*-nitrosoaniline (III).[8] It has been shown that a benzimidazole derivative is easily obtained from (I), probably by an intramolecular elimination of water.[8] The failure to isolate (III) is thought to be caused by an even more pronounced tendency towards elimination of water for this compound than for (I).[8]

EXPERIMENTAL

The title compound has been synthesized by Knieriem.[8] Suitable crystals were obtained by sublimation. At room temperature and normal humidity they disintegrate rapidly. A freshly sublimized crystal was therefore quickly transferred from the cold finger into the low temperature gas stream at the diffractometer. The crystal was needle formed and of dimensions $0.60 \times 0.25 \times 0.15$ mm. All the data were collected and the unit cell constants determined using this crystal. The measurements were made on a Syntex $P\bar{1}$ diffractometer with monochromatized Mo$K\alpha$ radiation and equipped with an Enraf-Nonius liquid nitrogen cooling device (modified by H. Hope). The temperature at the crystal site was −170 °C. Cell constants were determined by least squares treatment of fifteen general reflections. Intensity data were

collected using the $\omega - 2\theta$ scan technique. Prior to each scan the intensity was measured with moving crystal and stationary counter and the scan speed accordingly adjusted. The scan speed varied between 2.0 and 6.0°/min and the total time for background counts at the scan limits $2\theta(\alpha_1)$ $-1.0°$ and $2\theta(\alpha_2)$ $+1.1°$ was 0.7 of the time of integration. An octant of reciprocal space was examined. All reflections having 2θ less than 45° were measured; between 45 and 70° only reflections having integrated counts larger than a preset value during a 2s scan over the peak were measured. The intensity of three test reflections measured for every 50 reflection showed no significant change during the measurements. Out of 2542 unique reflections 1893 had intensities larger than $2.5\sigma(I)$. They were regarded as observed. $\sigma(I)$ is the estimated standard deviation of the intensity based on counting statistics adding 2 % uncertainty due to experimental fluctuations. The atomic scattering factors for the heavy atoms were those of Doyle and Turner [9] and for hydrogen those of Stewart *et al.*[10] All programs except for the ORTEP program [11] and the MULTAN [12] program applied during the structure investigation are described in Ref. 13.

CRYSTAL DATA

N,N,N',N'-Tetramethyl-1,5-diamino-4-nitrosobenzene, $C_{10}H_{15}ON_3$, orthorhombic, space group $P2_12_12_1$ (No. 19). Dimensions of the unit cell at -170 °C: $a = 15.574(5)$ Å, $b = 9.884(2)$ Å, $c = 6.501(1)$ Å, $V = 1000.7$ Å^3, $M = 193.25$, $F(000) = 416$, D_{calc} $(-170$ °C$) = 1.283$ g cm^{-3}, $Z = 4$.

STRUCTURE DETERMINATION

The structure was determined by direct methods [12,13] and refined by full matrix least squares techniques. Including only heavy atoms anisotropic refinement yielded a conventional R factor of 0.08. At this stage a difference Fourier map revealing the positions of all the hydrogen atoms was calculated. The refinement including all atoms and all observed reflections converged with $R = 0.042$, a weighted R_w factor of 0.039 and a goodness of fit S of 1.77. Using 1439 reflections with $\sin\theta/\lambda$ greater than 0.45 the refinement yielded $R = 0.043$, $R_w = 0.037$ and $S = 1.23$.

The scale factor became larger (3σ), the C2 – C3, C1 – C6, and C6 – C5 bond longer (2.7σ, 2.3σ, 2.3σ, respectively) and the N – O bond shorter (2.0σ) disregarding valence electron scattering. Only the parameters obtained from the refinement with all the observed reflections will be discussed. A final difference Fourier map was calculated in the same manner as for the *p*-nitrosophenolate ions.[6] Also in the present case the highest residual peaks in the map were located in the middle of the bonds and at lone pair positions. The difference synthesis in the plane through the C – N = O group is shown in Fig. 3.

Magnitudes and directions of the principal axis of the vibrational ellipsoids are indicated in Fig. 1. The r.m.s. discrepancy between the atomic vibrational tensor component obtained in the structure determination and those calculated from a rigid body analysis was 0.0009 Å^2 in the benzene ring with the nitrogen atoms and the oxygen atom and 0.0013 Å^2 in the entire molecule. In the last case the translation r.m.s. of vibration along the principal axes are 0.13, 0.11, and 0.10 Å^2 and the r.m.s. librational amplitudes are 3.0, 2.2, and 1.6°. The largest increase in bond length was 1σ when adjusting to this libration. A list of structure amplitudes is available from the author.

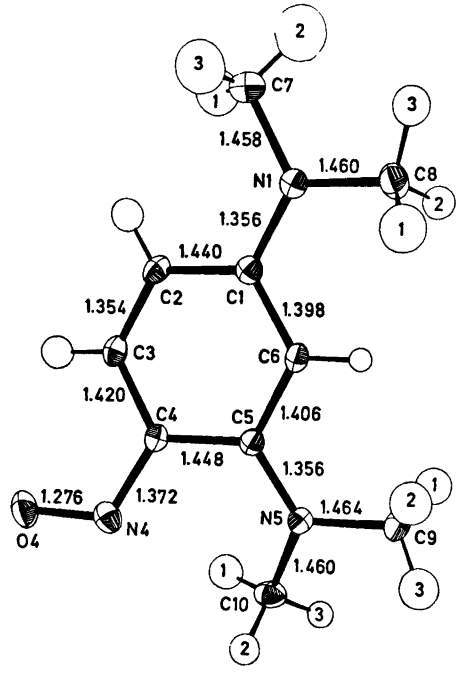

Fig. 1. 50 % probability ellipsoids, bond lengths (Å) and numbering of atoms.

Table 1. Fractional atomic coordinates and thermal parameters. The anisotropic temperature factors are expressed as: $\exp -2\pi^2 (U_{11}h^2a^{*2} + U_{22}k^2b^{*2} + U_{33}l^2c^{*2} + 2U_{12}hka^*b^* + 2U_{13}hla^*c^* + 2U_{23}klb^*c^*)$. Estimated standard deviations in parentheses.

ATOM	X	Y	Z	U11	U22	U33	U12	U13	U23
O4	,66262(7)	,33394(14)	,42882(20)	,0154(5)	,0365(7)	,0264(6)	-,0047(5)	,0016(5)	-,0020(7)
N1	,29988(8)	,34485(14)	,05558(22)	,0172(6)	,0213(6)	,0179(6)	-,0024(5)	-,0008(5)	,0032(6)
N4	,59648(9)	,27284(15)	,49787(22)	,0172(6)	,0229(7)	,0185(6)	,0006(5)	,0006(6)	-,0041(6)
N5	,43892(9)	,15937(15)	,64887(22)	,0161(6)	,0201(6)	,0283(7)	,0005(5)	,0014(5)	,0065(7)
C1	,36805(10)	,34197(17)	,18489(24)	,0158(6)	,0153(7)	,0154(7)	,0015(6)	,0021(6)	-,0012(7)
C2	,43979(11)	,43128(16)	,15118(26)	,0225(7)	,0151(7)	,0159(7)	-,0033(6)	,0014(7)	,0030(7)
C3	,51185(11)	,41396(17)	,26464(28)	,0188(8)	,0159(7)	,0190(7)	-,0039(6)	,0026(7)	,0006(6)
C4	,51881(9)	,31347(15)	,41979(25)	,0157(6)	,0149(7)	,0147(6)	-,0011(5)	,0017(6)	-,0004(6)
C5	,44224(9)	,24028(15)	,47983(24)	,0154(6)	,0122(6)	,0162(7)	,0019(6)	,0034(6)	-,0002(6)
C6	,36958(10)	,25395(16)	,35310(26)	,0153(6)	,0139(7)	,0174(7)	-,0012(6)	,0031(6)	,0007(7)
C7	,29353(13)	,44105(22)	-,11371(31)	,0253(9)	,0323(10)	,0221(9)	-,0001(8)	-,0048(8)	,0073(9)
C8	,23214(11)	,24336(20)	,07508(31)	,0181(7)	,0314(9)	,0206(8)	-,0064(7)	-,0009(7)	,0003(8)
C9	,36451(12)	,07117(21)	,67889(34)	,0211(8)	,0246(9)	,0328(10)	-,0027(8)	,0048(8)	,0109(9)
C10	,49896(12)	,16542(21)	,82031(27)	,0250(8)	,0280(9)	,0161(7)	,0064(8)	,0001(7)	,0020(8)

ATOM	X	Y	Z	B	ATOM	X	Y	Z	B
H2	,4380(11)	,4958(19)	,0497(31)	1,8(4)	H3	,5616(12)	,4705(19)	,2438(31)	1,9(4)
H6	,3214(19)	,2048(16)	,3876(27)	,9(3)	H71	,3279(15)	,4172(25)	-,2196(39)	3,7(5)
H72	,2324(16)	,4373(23)	-,1596(40)	4,3(5)	H73	,3099(13)	,5322(24)	-,0765(38)	3,4(5)
H81	,1949(12)	,2624(20)	,1983(30)	1,7(4)	H82	,2567(13)	,1518(21)	,0861(37)	3,0(4)
H83	,1987(12)	,2449(20)	-,0537(31)	2,0(4)	H91	,3524(13)	,0199(22)	,5517(37)	2,7(4)
H92	,3116(13)	,1202(20)	,7134(32)	2,4(4)	H93	,3765(13)	,0877(23)	,7861(35)	2,8(4)
H101	,5276(12)	,2575(22)	,8246(33)	2,5(4)	H102	,5464(12)	,0949(19)	,8151(31)	1,8(4)
H103	,4650(11)	,1494(18)	,9495(28)	1,5(3)					

Final parameters from the refinement with all the observed reflections are given in Table 1. Bond lengths and angles with their estimated standard deviations are given in Table 2. Fig. 1 shows numbering of atoms and bond lengths. The estimated standard deviations were calculated from the correlation matrix. Deviations from least squares planes are given in Table 3.

DISCUSSION

The crystal structure is characterized by an efficient close packing of the molecules. The packing coefficient (0.82) is somewhat higher than that of (II) (0.76).[14] If one considers the molecule a strong dipole with the negative pole in the vicinity of the nitroso group and the positive pole midway between the dimethyl-

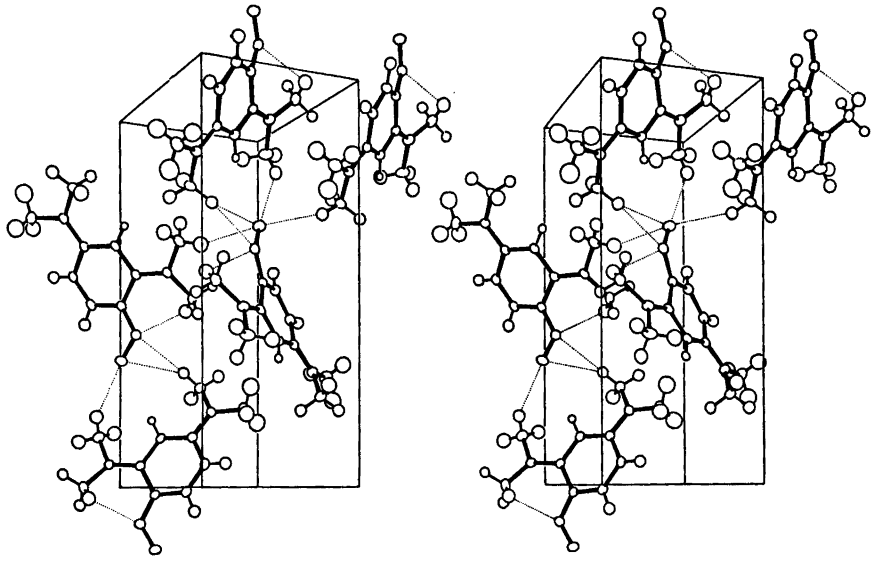

Fig. 2. A stereoscopic illustration of the structure. The unit cell axis y is nearly normal to the paper-plane. The contacts to the nitroso group atoms are indicated by dotted lines.

Table 2. Bond lengths (Å) and angles (°). Estimated deviations in parentheses.

Bond lengths. (Libration corrected bond lengths are given in the second row).

O4–N4	1.276(2)	1.277	N4–C4	1.372(2)	1.373
C1–C2	1.440(2)	1.443	N1–C1	1.356(2)	1.357
C2–C3	1.354(2)	1.355	N1–C7	1.458(2)	1.459
C3–C4	1.420(2)	1.422	N1–C8	1.460(2)	1.463
C4–C5	1.448(2)	1.451	N5–C5	1.356(2)	1.358
C5–C6	1.406(2)	1.408	N5–C9	1.464(2)	1.466
C6–C1	1.398(2)	1.400	N5–C10	1.460(2)	1.461

Bond angles

C1–C2–C3	118.9(2)	N1–C1–C2	120.1(1)	C1–N1–C7	122.3(1)
C2–C3–C4	122.6(2)	N1–C1–C6	120.8(1)	C1–N1–C8	119.8(1)
C3–C4–C5	118.6(1)	N4–C4–C3	122.3(1)	C7–N1–C8	117.7(1)
C4–C5–C6	117.2(1)	N4–C4–C5	118.7(1)	C5–N5–C9	119.5(1)
C5–C6–C1	122.1(1)	N5–C5–C4	122.9(1)	C5–N5–C10	124.8(1)
C6–C1–C2	119.2(1)	N5–C5–C6	119.9(1)	C9–N5–C10	115.2(2)
				C4–N4–O4	116.3(1)

Distances and angles involving hydrogen atoms

C–H		(N)C–C–H		(H)C–C–H	
C2–H	0.92(2)	C1–C2–H	120.8(1.2)	C3–C2–H	120.3(1.2)
C3–H	0.97(2)	C2–C3–H	121.1(1.2)	C4–C3–H	116.3(1.2)
C6–H	0.92(2)	C5–C6–H	117.5(1.1)	C1–C6–H	120.3(1.1)
C7–H1	0.90(3)	N1–C7–H1	111.4(1.6)	H1–C7–H2	109.0(2.1)
C7–H2	1.00(3)	N1–C7–H2	105.4(1.5)	H1–C7–H3	108.4(2.2)
C7–H3	0.97(2)	N1–C7–H3	111.7(1.5)	H2–C7–H3	110.9(1.9)
C8–H1	1.01(2)	N1–C8–H1	110.9(1.2)	H1–C8–H2	109.7(1.8)
C8–H2	0.99(2)	N1–C8–H2	111.1(1.2)	H1–C8–H3	111.7(1.5)
C8–H3	0.99(2)	N1–C8–H3	107.3(1.2)	H2–C8–H3	106.2(1.8)
C9–H1	0.99(2)	N5–C9–H1	110.0(1.3)		
C9–H2	0.98(2)	N5–C9–H2	113.7(1.2)		
C9–H3	0.96(2)	N5–C9–H3	109.6(1.3)		
C10–H1	1.01(2)	N5–C10–H1	109.9(1.2)		
C10–H2	1.02(2)	N5–C10–H2	114.3(1.2)		
C10–H3	1.01(2)	N5–C10–H3	107.3(1.0)		

Intermolecular contact

N1..C7(a) 3.349

Dihedral angles

C1–C6–C5–N5	176.2(2)
C1–C6–C5–C4	4.8(2)
N1–C1–C6–C5	−174.5(2)
C2–C1–C6–C5	6.1(2)
C3–C2–C1–N1	−171.1(2)
C3–C2–C1–C6	−9.5(2)
C4–C3–C2–C1	1.7(3)
N4–C4–C3–C2	−163.1(2)
C5–C4–C3–C2	9.4(3)

Dihedral angles

C4–C5–N5–C10	19.3(2)
C4–C5–N5–C9	−169.6(2)
C6–C5–N5–C10	−161.8(2)
C6–C5–N5–C9	9.3(2)
N4–C4–C5–N5	18.5(2)
N4–C4–C5–C6	−160.4(1)
C3–C4–C5–N5	−168.7(2)
C3–C4–C5–C6	12.4(2)
C3–C4–N4–O4	−2.5(2)
C5–C4–N4–O4	−175.0(1)
C6–C1–N1–C7	176.1(2)
C6–C1–N1–C8	−8.1(2)
C2–C1–N1–C7	−3.3(2)
C2–C1–N1–C8	172.5(2)

Symmetry Code

(a): $\frac{1}{2}-x,\ 1-y,\ -\frac{1}{2}+z$.

Table 3. Deviation (Å) of atoms from least squares planes defined by the benzene ring atoms (A), by the atoms in the fragments C6C1(N1)C2 (B), C3C4(N4)C5 (C), and C4C5(N5)C6 (D) and by the atoms of the dimethyl amino groups (E and F). Asterisks denote atoms defining the planes.

Atom/Plane	A	B	C	D	E	F
C1	−0.063 *	−0.003 *			−0.009 *	
C2	0.048 *	0.001 *				
C3	0.023 *		−0.013 *			
C4	−0.075 *		0.040 *	−0.002 *		
C5	0.059 *		−0.013 *	0.006 *		−0.019 *
C6	0.009 *	0.001 *		−0.002 *		
N1	−0.221	0.001 *			0.021 *	
N4	−0.437		−0.012 *			
N5	0.205			−0.002 *		0.044 *
O4	−0.638		−0.062			
C7	−0.216	0.081			−0.008 *	
C8	−0.496	−0.168			−0.008 *	
C9	0.104			−0.224		−0.016 *
C10	0.644			0.379		−0.017 *

Atom/Plane	A
H2	0.09
H3	0.07
H6	0.06

Atom/Plane	A	E
H71	−0.99	−0.84
H72	−0.12	0.26
H73	0.51	0.61
H81	0.33	0.88
H82	−1.22	−0.72
H83	−0.84	−0.25

Atom/Plane	A	F
H91	−0.71	0.63
H92	0.86	−0.90
H93	0.04	0.22
H101	1.15	−0.46
H102	−0.11	0.89
H103	1.24	−0.55

amino groups the dipole-dipole interactions should stabilize the crystal structure considerably.[14] Fig. 2 shows the content of the unit cell and the coordination about the nitroso group atoms.

A characteristic feature of the molecular structure is the non planarity of the molecule (see Table 3). The only two planar arrangements are those of the atoms in the C2C1(N1)C6 and the C6C5(N5)C4 fragments (Planes B and D). The benzene ring is slightly boat formed with the C1 and the C4 atoms as prow and stern. Considering the locations of the nitrogen atoms bonded to C1 and C4, the boat form becomes even more pronounced. Each of the two dimethylamino nitrogen atoms have a slight pyramidal hybridization and the best plane through the 1-dimethylamino group makes an angle of 5.9° to Plane B while the corresponding angle for the 5-dimethylamino group is 14.2°.

Although the NO bond, as expected, is *anti* to the C4−C5 bond, repulsion between the nitroso group and the methyl group next to it (C10) apparently causes severe conformational strain in the molecule. This is revealed by deviation from trigonal hybridization of the N5 and the C4 atoms, by angular distortions at the N5, C5 and C4 atoms and by a large twist about the C4−C5 bond (ϕ(NCCN) = 18.5°). The C10···N4 distance (2.798 Å) is about 0.20 Å shorter than a normal van der Waals contact. The N5 atom deviates 0.061 Å from the plane through its three bonded atoms while the N1 atom which participates in bonds having lengths about identical to those to N5, deviates only 0.029 Å from a corresponding plane. Usually the nitrogen atom of dialkylamino groups is found to deviate insignificantly from similar planes when the $C_{ar}-N$ bond is as short as the C5−N5 and the C1−N1 bonds (1.356 Å).

The length of the C−NMe_2 bonds corresponds to a π-bond order of about 0.63 and the length of the C5−C6 and the C6−C1 bonds which differ only by 0.008 Å correspond to a π-bond order of about 0.65. As to the O−N−C−CH−CH−C fragment there is a striking similarity in bond lengths between corresponding bonds in (I) and the *p*-nitrosophenolate ions.[5,6] The C−NO bond is only 0.013 Å longer and the

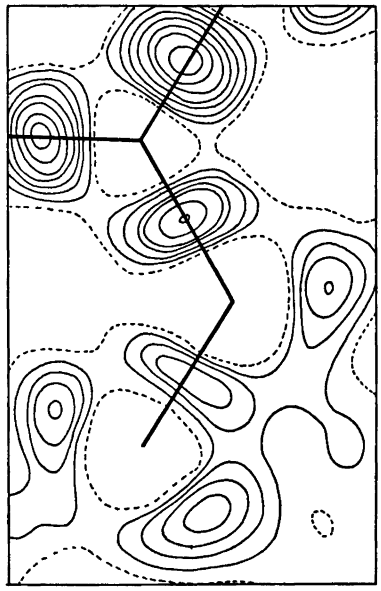

Fig. 3. The final difference Fourier synthesis in the C–N–O plane. A data set with a highest sin θ/λ value of 0.45, positional and temperature parameters from the refinement with high angle data (above 0.45 in sin θ/λ) and a scale factor from a separate refinement using the low angle data and fixing the other parameters on their high angle values were used in the calculation of the synthesis. The dotted line runs through points at 0.0 eÅ^{-3}, and the difference between the contours is 0.05 eÅ^{-3}.

N–O bond only 0.006 Å shorter than the corresponding bond in the anion of the magnesium salt.[6] Hence, the two main zwitterionic VB structures seem to contribute with approximately equal weights to the π-resonance in (I) and apparently the sum of the two weights mounts to about half the total weight.

It is noteworthy that the C–NO bond is longer (5σ) than the C–NMe$_2$ bonds. One would perhaps expect the opposite considering that the two C_{ar}–N bonds in the oxime cation have identical lengths [2] and that the two dimethylamino groups mutually counteract each other as to their electron-releasing effect.

The author thanks Dr. B. Knieriem for supplying a sample of the compound.

REFERENCES

1. Rømming, C. and Talberg, H. J. *Acta Chem. Scand. 27* (1973) 2246.
2. Drangfelt, O. and Rømming, C. *Acta Chem. Scand. A 28* (1974) 1101.
3. Talberg, H. J. *Acta Chem. Scand. A 28* (1974) 910.
4. Talberg, H. J. *Acta Chem. Scand. A 28* (1974) 593.
5. Talberg, H. J. *Acta Chem. Scand. A 29* (1975) 919.
6. Talberg, H. J. *Acta Chem. Scand. A 31* (1977). *In press.*
7. Dietrich, D. A., Paul, I. C. and Curtin, D. Y. *J. Am. Chem. Soc. 96* (1974) 6372.
8. Knieriem, B. *Thesis*, Göttingen 1972.
9. Doyle, P. A. and Turner, P. S. *Acta Crystallogr. A 24* (1970) 2232.
10. Stewart, R. F., Davidson, E. R. and Simpson, W. T. *J. Chem. Phys. 42* (1965) 3175.
11. Johnson, C. K. *ORTEP*, Report ORNL-3795, Oak Ridge National Laboratory, Oak Ridge 1965.
12. Germain, G., Main, P. and Woolfson, M. M. *Acta Crystallogr. A 27* (1971) 368.
13. Groth, P. *Acta Chem. Scand. 27* (1973) 1837.
14. Kitaigorodsky, A. I. *Molecular Crystals and Molecules*, Academic, New York and London 1973, p. 18 and p. 153.

Received May 31, 1976.

Acta Chemica Scandinavica A 30 (1976) 835—844

Short Communications

The Magnetic Structure of β-CrOOD

A. NØRLUND CHRISTENSEN [a] and P. HANSEN [b]

[a] Department of Inorganic Chemistry, Aarhus University, DK-8000 Aarhus C, Denmark and [b] Physics Department, Danish AEC Research Establishment Risø, DK-4000 Roskilde, Denmark

The preparation of beta chromium oxide hydroxide, β-CrOOH, and the isomorphous deuterated compound, β-CrOOD, has been reported recently.[1,2] The magnetic properties of β-CrOOH has been investigated and the compound was found to be antiferromagnetic at temperatures below 120 K.[1] Using neutron diffraction powder methods the magnetic structure of β-CrOOD has been determined. The deuterated compound was used to obtain a better counting statistics of the powder pattern due to the low incoherent scattering of the sample in comparison with that of β-CrOOH.

A neutron powder pattern of β-CrOOD was measured at 6 K using a double axis neutron spectrometer at the DR3 reactor at Risø. The pattern was obtained with an incident neutron wavelength of 1.68 Å. The sample, approximately 30 g, was placed in a 15 mm diameter cylindrical vanadium container and was kept in a He-cryostat. The collimations in front of and behind the sample were defined by Soller slits to be 0.25 and 0.64°, respectively. The Soller slits were made of cadmiated steel. The powder pattern was measured in the 2θ interval 5 to 110° in steps of 0.1°.

The unit cell parameters of β-CrOOD are at 300 K: $a = 4.873(5)$ Å, $b = 4.332(7)$ Å, $c = 2.963(2)$ Å.[2] The space group used is $P2_1nm$ with $Z = 2$. In addition to the nuclear reflections that can be indexed with the above-mentioned unit cell, the pattern had magnetic reflections. Two of these reflections were completely resolved from the nuclear reflections and were observed at lower 2θ values than the nuclear reflections, indicating the magnetic cell to be larger than the chemical cell. All the magnetic reflections were indexed using an orthorhombic cell with $a_M = a$, $b_M = 2b$, and $c_M = 2c$ where a, b, and c are the unit cell parameters of the chemical cell.

The nuclear and magnetic structures of β-CrOOD were refined using the Rietveld least squares refinement program for powder profile intensities.[3,4] The scattering lengths (in 10^{-12} cm) were: $b_{Cr} = 0.353$, $b_O = 0.580$, and $b_D = 0.667$, respectively.[5] The form factor for chromium reported by Delapalme and Sivardiere [6] was used in the calculation of the magnetic intensities. The atomic positions determined previ-

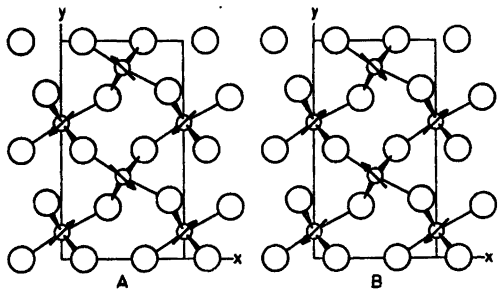

Fig. 1. Projection of the structure of β-CrOOD along 001. For clarity the positions of the deuterium atoms have been omitted. *A* shows the magnetic cell with the spin configuration. The chromium and oxygen atoms have $z = 0$ and $z = 0.25$. *B* shows the spin configuration in the magnetic cell for the chromium atoms with $z = 0.5$ and $z = 0.75$. The oxygen atoms shown in *B* have $z = 0.5$ and $z = 0.75$.

Table 1. Observed and calculated intensities for β-CrOOD. Reading from left to right the columns are: $h\ k\ l\ I_{nucl}\ I_{mag}\ I_{obs}$.

0	1	-1	0	12339	12617	0	6	0	3935	0	3831
0	1	1	0	8895	9240	3	0	2	13294	0	11718
1	1	-1	0	8346	8295	2	4	2	13097	0	10769
1	1	1	0	4697	4668	0	2	4	1568	0	783
1	2	0	5179	0	5053	1	6	0	1388	0	576
0	3	-1	0	367	418	3	2	2	8129	0	6621
0	3	1	0	1805	2054	1	2	4	2206	0	2093
1	0	2	46242	0	42200	3	4	0	7314	0	3244
2	0	0	10049	0	10030	0	6	2	3193	0	1410
0	2	2	43222	0	43346	2	0	4	6772	0	6766
2	1	-1	0	375	400	1	6	2	32336	0	35181
2	1	1	0	1852	1976	2	6	0	15512	0	17232
1	2	2	83314	0	88673	4	0	0	4619	0	4911
0	4	0	2754	0	2834	0	4	4	2225	0	2359
2	2	0	53645	0	55932	2	2	4	44498	0	45922
1	4	0	5947	0	419	3	4	2	41519	0	42170
1	1	-3	0	614	538	1	4	4	5475	0	5920
1	1	3	0	718	629	4	2	0	5345	0	6755
2	3	-1	0	449	433	2	6	2	11640	0	14957
2	3	1	0	322	310	4	2	2	26545	0	24504
0	4	2	3252	0	2580	2	4	4	36087	0	33550
2	2	2	41691	0	38418	0	8	0	11371	0	12372
1	4	2	15954	0	16269	3	6	0	304	0	341
2	4	0	29606	0	29812	4	4	0	28582	0	30982
3	2	0	1102	0	1585	3	2	4	1464	0	1448
0	0	4	45997	0	47663	1	8	0	9105	0	5847

Table 2. Atomic coordinates for β-CrOOD at 6 K. Standard deviations in parentheses.[a] (Refers to the chemical unit cell *a b c*).

Atom	*x*	*y*	*z*
Cr	0.0	0.250(2)	0.0
O1	0.306(3)	0.486(2)	0.0
O2	0.616(3)	−0.009(2)	0.0
D	0.492(3)	0.178(2)	0.0

[a] Overall scale factor = 0.0188. $R(F^2) = 11.0$ %. $R_{nucl} = 8.5$ %. $R_{mag} = 3.7$ %. (For definition of these values see Ref. 3).

ously [2] were transformed to the magnetic cell and used as starting parameters. A non-collinear antiferromagnetic model for the magnetic structure was assumed with spin waves propagating in the direction of the *y*- and *z*-axis and with the spins in planes parallel to the *xy*-plane. Relative to the CrO_6 coordination octahedra in the structure, the spins have directions from the chromium atoms towards oxygen atoms with same *z*-coordinates as the chromium atoms (see Fig. 1). This model of the magnetic structure refined to a magnetic *R*-value of 3.7 % (see Table 1) and gave a magnetic moment $\mu = 2.49(5)\ \mu_B$ for the chromium atom. The spin form angles of $\pm 45(5)°$ with the *x*-axis. The nuclear reflections gave an *R*-value of 8.5 % (see Table 1). Additional scattering contributions to the powder pattern from the cryostat can account for the relatively high *R*-value. The atomic coordinates transformed to the chemical cell (Table 2) are within three standard deviations equal to those of β-CrOOD at at 300 K.[2]

The magnetic structure of β-CrOOD has points of resemblance with that of $CrCl_2$.[7]

1. Christensen, A. N. *Acta Chem. Scand. A 30* (1976) 133.
2. Christensen, A. N., Hansen, P. and Lehmann, M. S. *J. Solid State Chem. 19* (1976) 299.
3. Rietveld, H. M. *J. Appl. Crystallogr. 2* (1969) 65.
4. Rietveld, H. M. *Program F418 – Fortran IV Version*, Reactor Centrum Nederland, Petten, N. H., The Netherlands.
5. Shull, C. G. *Coherent Neutron Scattering Amplitudes*, Massachusetts Institute of Technology, Cambridge, Mass. 1972.
6. Delapalme, A. and Sivardiere, J. *Longeurs de Fermi, Facteurs de Forme Magnétiques, Rayons Ioniques*, Laboratoire de Diffraction Neutronique, C. E. N. G., Grenoble, France.
7. Cable, J. W., Wilkinson, M. K. and Wollan, E. O. *Phys. Rev. 118* (1960) 950.

Received July 12, 1976.

The Crystal Structure of Manganese(II) Diselenite

MARKUS KOSKENLINNA, LAURI NIINISTÖ and JUSSI VALKONEN

Department of Chemistry, Helsinki University of Technology, SF-02150 Espoo 15, Finland

In our investigation of manganese(II) selenites,[1] we found that the equilibrium in aqueous solution shifts towards the diselenite ion when the pH of the solution decreases. Thus, a rose-coloured, crystalline precipitate was obtained from 1 mol/dm³ selenous acid solution at 60 °C. It was identified as $MnSe_2O_5$ by chemical analyses and IR spectroscopy (*cf.* Table 1).

Thermal analysis (TG, DTG, DTA) of the compound was also carried out and the decomposition scheme in air was found to be as follows:

$$MnSe_2O_5 \rightarrow MnSeO_3 + SeO_2 \quad (1)$$

$$2MnSeO_3 \xrightarrow{(O_2)} Mn_2O_3 + 2SeO_2 \quad (2)$$

At a heating rate of 6 °C/min the DTA peak temperatures for reactions 1 and 2 were found to be 420 and 525 °C, respectively.

An X-ray crystallographic study of the crystals was initiated and rotation and Weissenberg photographs indicated orthorhombic symmetry. The accurate unit cell dimensions were obtained by least-squares refinement of Guinier powder data with KCl as the internal standard; *cf.* Table 2.

Table 1. Infrared absorption frequencies in the region 4000 – 250 cm^{-1}.

Observed frequency	Assignment
870 s, 845 m, 830 m, 760 vs, b	ν_{Se-O} (terminal)
585 s, 555 vs, 510 m	ν_{Se-O} (bridge)
445 m, 410 w, 380 m, 330 w, sh	δ_{Se-O} (terminal)

Table 2. Crystal data of $MnSe_2O_5$.

Space group *Pbcn* (No. 60)

$a = 6.797(2)$ Å, $b = 10.617(3)$ Å, $c = 6.300(2)$ Å, $V = 454.6$ Å³;[a] $a = 6.822(3)$ Å, $b = 10.636(4)$ Å, $c = 6.323(3)$ Å, $V = 458.8$ Å³;[b] $Z = 4$, $D_m = 4.2(1)$ g cm^{-3}, $D_x = 4.28$ g cm^{-3};[a] $\mu(MoK\alpha) = 168.8$ cm^{-1}.

[a] Powder data at 20 °C [*a* (KCl) = 6.2927 Å].[12] [b] Diffractometer data at 25 °C.

Table 2. Atomic coordinates for β-CrOOD at 6 K. Standard deviations in parentheses.[a] (Refers to the chemical unit cell *a b c*).

Atom	*x*	*y*	*z*
Cr	0.0	0.250(2)	0.0
O1	0.306(3)	0.486(2)	0.0
O2	0.616(3)	−0.009(2)	0.0
D	0.492(3)	0.178(2)	0.0

[a] Overall scale factor = 0.0188. $R(F^2) = 11.0$ %. $R_{nucl} = 8.5$ %. $R_{mag} = 3.7$ %. (For definition of these values see Ref. 3).

ously [2] were transformed to the magnetic cell and used as starting parameters. A non-collinear antiferromagnetic model for the magnetic structure was assumed with spin waves propagating in the direction of the *y*- and *z*-axis and with the spins in planes parallel to the *xy*-plane. Relative to the CrO_6 coordination octahedra in the structure, the spins have directions from the chromium atoms towards oxygen atoms with same *z*-coordinates as the chromium atoms (see Fig. 1). This model of the magnetic structure refined to a magnetic *R*-value of 3.7 % (see Table 1) and gave a magnetic moment $\mu = 2.49(5)\ \mu_B$ for the chromium atom. The spin form angles of $\pm 45(5)°$ with the *x*-axis. The nuclear reflections gave an *R*-value of 8.5 % (see Table 1). Additional scattering contributions to the powder pattern from the cryostat can account for the relatively high *R*-value. The atomic coordinates transformed to the chemical cell (Table 2) are within three standard deviations equal to those of β-CrOOD at at 300 K.[2]

The magnetic structure of β-CrOOD has points of resemblance with that of $CrCl_2$.[7]

1. Christensen, A. N. *Acta Chem. Scand. A 30* (1976) 133.
2. Christensen, A. N., Hansen, P. and Lehmann, M. S. *J. Solid State Chem. 19* (1976) 299.
3. Rietveld, H. M. *J. Appl. Crystallogr. 2* (1969) 65.
4. Rietveld, H. M. *Program F418 – Fortran IV Version*, Reactor Centrum Nederland, Petten, N. H., The Netherlands.
5. Shull, C. G. *Coherent Neutron Scattering Amplitudes*, Massachusetts Institute of Technology, Cambridge, Mass. 1972.
6. Delapalme, A. and Sivardiere, J. *Longeurs de Fermi, Facteurs de Forme Magnétiques, Rayons Ioniques*, Laboratoire de Diffraction Neutronique, C. E. N. G., Grenoble, France.
7. Cable, J. W., Wilkinson, M. K. and Wollan, E. O. *Phys. Rev. 118* (1960) 950.

Received July 12, 1976.

The Crystal Structure of Manganese(II) Diselenite

MARKUS KOSKENLINNA, LAURI NIINISTÖ and JUSSI VALKONEN

Department of Chemistry, Helsinki University of Technology, SF-02150 Espoo 15, Finland

In our investigation of manganese(II) selenites,[1] we found that the equilibrium in aqueous solution shifts towards the diselenite ion when the pH of the solution decreases. Thus, a rose-coloured, crystalline precipitate was obtained from 1 mol/dm³ selenous acid solution at 60 °C. It was identified as $MnSe_2O_5$ by chemical analyses and IR spectroscopy (*cf.* Table 1).

Thermal analysis (TG, DTG, DTA) of the compound was also carried out and the decomposition scheme in air was found to be as follows:

$$MnSe_2O_5 \rightarrow MnSeO_3 + SeO_2 \quad (1)$$

$$2MnSeO_3 \xrightarrow{(O_2)} Mn_2O_3 + 2SeO_2 \quad (2)$$

At a heating rate of 6 °C/min the DTA peak temperatures for reactions 1 and 2 were found to be 420 and 525 °C, respectively.

An X-ray crystallographic study of the crystals was initiated and rotation and Weissenberg photographs indicated orthorhombic symmetry. The accurate unit cell dimensions were obtained by least-squares refinement of Guinier powder data with KCl as the internal standard; *cf.* Table 2.

Table 1. Infrared absorption frequencies in the region 4000 – 250 cm^{-1}.

Observed frequency	Assignment
870 s, 845 m, 830 m, 760 vs, b	ν_{Se-O} (terminal)
585 s, 555 vs, 510 m	ν_{Se-O} (bridge)
445 m, 410 w, 380 m, 330 w, sh	δ_{Se-O} (terminal)

Table 2. Crystal data of $MnSe_2O_5$.

Space group *Pbcn* (No. 60)

$a = 6.797(2)$ Å, $b = 10.617(3)$ Å, $c = 6.300(2)$ Å, $V = 454.6$ Å³;[a] $a = 6.822(3)$ Å, $b = 10.636(4)$ Å, $c = 6.323(3)$ Å, $V = 458.8$ Å³;[b] $Z = 4$, $D_m = 4.2(1)$ g cm^{-3}, $D_x = 4.28$ g cm^{-3};[a] $\mu(MoK\alpha) = 168.8$ cm^{-1}.

[a] Powder data at 20 °C [*a* (KCl) = 6.2927 Å].[12] [b] Diffractometer data at 25 °C.

The single crystal intensity data in the interval $5° < \theta < 35°$ were collected with a Syntex $P2_1$ automatic diffractometer using the ω-scan technique and graphite monochromatized Mo$K\alpha$ radiation. The scan speed was 1°/min. A total of 599 reflections satisfying the criterion $I > 4\sigma(I)$ were used in the subsequent calculations; the intensities were corrected for Lorentz and polarization effects as well as for absorption from the ϕ-scan data. The structure was solved by direct methods and refined to an R-value of 0.074. In the refinement scattering factors for neutral atoms were used.[2]

The compound $MnSe_2O_5$ was found to be isostructural with $ZnSe_2O_5$, recently prepared by a solid-state synthesis and characterized by single crystal methods.[3] However, as $ZnSe_2O_5$ seems to be the only diselenite whose structure has been reported in the literature, we present, for comparison, the structural data for the manganese compound.

The final positional parameters are given in Table 3. A listing of structure factors and anisotropic thermal parameters is available from the authors upon request. Table 4 lists selected distances and angles for the basic building units of the structure: the diselenite group and the MnO_6-octahedron.

Table 3. Final positional parameters of $MnSe_2O_5$. Standard deviations are given in parentheses.

Atom	x	y	z
Se	0.3717(2)	0.1556(1)	0.5386(2)
Mn	1/2	0.5580(3)	1/4
O(1)	0.3324(16)	0.4317(11)	0.0479(24)
O(2)	0.3045(17)	0.7133(11)	0.1558(23)
O(3)	1/2	0.9283(13)	1/4

Table 4. Selected distances (Å) and angles (°) involving the Se_2O_5 group and MnO_6-octahedron. Estimated standard deviations are given in parentheses. The values are uncorrected for thermal motion.

(a) Se_2O_5-group

Se – O(1)	1.675(11)	O(3) – Se – O(1)	95.8(5)
– O(2)	1.644(13)	O(3) – Se – O(2)	102.6(6)
– O(3)	1.830(7)	O(1) – Se – O(2)	102.9(6)
		Se – O(3) – Se′	121.6(9)

(b) MnO_6-octahedron

$Mn^{[a]} - O(1)^{I,II}$	2.178(13)
$- O(2)^{I,II}$	2.206(12)
$- O(2)^{III,IV}$	2.206(14)

[a] The superscript denotes the symmetry transformation:

I x,y,z III $\bar{x},\bar{y},\bar{z}$
II $\bar{x},y,1/2-z$ IV $x,\bar{y},1/2+z$

The Se_2O_5 group in $MnSe_2O_5$ is in good agreement with the values reported for $ZnSe_2O_5$. The MnO_6-octahedron is almost regular, with Mn – O distances ranging from 2.18 to 2.21 Å, in accordance with literature values.[4] The mean metal-oxygen distances in MnO_6 and ZnO_6 octahedra are 2.20 and 2.11 Å, respectively; the difference (0.09 Å) corresponds rather well to the ionic radii difference of the six-coordinated divalent metals (0.07 Å).[5]

On the basis of IR and Raman spectra, a molecular symmetry of C_{2v} was predicted for both the diselenite [6] and the disulfite [7,8] anion. The structures of $ZnSe_2O_5$ and $MnSe_2O_5$ confirm the symmetry prediction for the diselenite group, but crystal structure determinations [9,10] have shown that the disulfite group is asymmetric with an S – S bond and a C_s symmetry. In vibrational spectroscopy the large number of fundamentals of these compounds makes exact assignment difficult, but different symmetries should be distinguishable through careful analysis, as shown by Herlinger and Long for the disulfite anion.[11]

Regarding the IR spectrum of $MnSe_2O_5$ (*cf.* Table 1), it may be noted that it resembles the spectra of $CaSe_2O_5$ and $BaSe_2O_5$,[8] which may indicate a structural relationship.

1. Koskenlinna, M., Niinistö, L. and Valkonen, J. *Cryst. Struct. Commun. 5* (1976) 663.
2. *International Tables for X-Ray Crystallography*, Kynoch Press, Birmingham 1974, Vol. 4, p. 72.
3. Meunier, P. and Bertand, M. *Acta Crystallogr. B 30* (1974) 2840.
4. Popov, D., Herak, R., Prelesnik, B. and Ribár, B. *Z. Kristallogr. 137* (1973) 280, and references therein.
5. Shannon, R. D. and Prewitt, C. I. *Acta Crystallogr. B 25* (1969) 925.
6. Simon, A. and Paetzold, R. *Z. Anorg. Allg. Chem. 303* (1960) 39.
7. Simon, A., Waldmann, K. and Steger, E. *Z. Anorg. Allg. Chem. 288* (1956) 131.
8. Rocchiccioli, C. *C. R. Acad. Sci. Ser. C 250* (1960) 2347.
9. Lindqvist, I. and Mörtsell, M. *Acta Crystallogr. 10* (1957) 406.
10. Baggio, S. *Acta Crystallogr. B 27* (1971) 517.
11. Herlinger, A. W. and Long, T. V. *Inorg. Chem. 8* (1969) 2661.
12. Hambling, P. G. *Acta Crystallogr. 6* (1953) 98.

Received September 22, 1976.

Crystal Conformation of Cyclotrisarcosyl at —160 °C

P. GROTH

Department of Chemistry, University of Oslo, Oslo 3, Norway

To account for the relatively high observed resistance to ring inversion in cyclic oligopeptides of sarcosine with the general formula

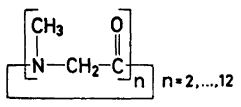

transannular interactions between N and C (carbonyl) were suggested.[1-4] X-Ray crystallographic results for the cases $n=4$, 5, 7, and 8 [5-8] do not support this assumption, and the explanation should be sought in the intrinsic conformation of the peptide chain itself.[8] The NMR-spectrum for cyclotrisarcosyl,[1] consisting of one singlet for *N*-methyl and one quartet for CH_2 (intensity 9:6), shows that all amide groups have the same configuration. Since they cannot all be *trans* in a nine-membered ring, they must all be *cis*. In order to confirm this clear conformational evidence an X-ray crystallographic investigation of cyclotrisarcosyl has been performed.

The crystals of $C_9H_{15}N_3O_3$ belong to the monoclinic system, with cell dimensions $a=12.902(6)$ Å, $b=12.342(6)$ Å, $c=13.213(6)$ Å,

Table 1 A. Final fractional coordinates and thermal parameters with estimated standard deviations for molecule A. The expression for anisotropic vibration is $\exp[2\pi^2(h^2a^{*2}U11+\cdots+2klb^*c^*U23)]$. Hmn is bonded to Cm and HMmn to CMm.

ATOM	x	y	z	U11	U22	U33	U12	U13	U23
O1	1.04361(19)	.79235(28)	.66711(18)	.0368(15)	.0274(15)	.0336(14)	.0041(13)	.0081(12)	-.0006(12)
O2	.74135(25)	.54818(24)	.15767(24)	.0483(23)	.0154(19)	.0383(24)	-.0070(18)	-.0081(19)	-.0043(17)
O3	.68231(19)	.93343(19)	.11529(18)	.0352(17)	.0283(14)	.0455(15)	.0047(13)	-.0081(12)	.0049(12)
N1	.85337(22)	.92812(21)	.14911(21)	.0263(18)	.0183(15)	.0253(16)	.0041(14)	.0038(13)	.0027(13)
N2	.94627(23)	.67447(23)	.15594(24)	.0313(18)	.0168(17)	.0258(20)	.0031(15)	.0020(15)	-.0026(15)
N3	.69913(29)	.71224(28)	.21858(25)	.0275(26)	.0155(21)	.0366(21)	-.0062(21)	-.0024(19)	-.0019(17)
C1	.94346(25)	.87860(27)	.19917(24)	.0234(20)	.0182(19)	.0264(19)	-.0029(17)	-.0005(16)	-.0037(16)
C2	.87903(30)	.64475(28)	.23947(29)	.0379(25)	.0126(19)	.0256(25)	.0017(19)	-.0013(20)	.0002(18)
C3	.72767(31)	.82108(33)	.25547(28)	.0284(26)	.0181(24)	.0264(21)	-.0009(22)	.0023(19)	-.0015(19)
CC1	.98269(28)	.77536(27)	.13679(26)	.0194(21)	.0240(19)	.0219(20)	.0033(17)	-.0034(17)	.0014(17)
CC2	.76777(33)	.63184(35)	.20242(33)	.0378(28)	.0184(25)	.0209(28)	-.0056(23)	-.0031(23)	.0076(23)
CC3	.75448(27)	.89598(28)	.16683(27)	.0315(22)	.0158(19)	.0275(22)	.0017(18)	-.0024(18)	-.0002(17)
CM1	.87478(28)	.99957(28)	.06907(27)	.0408(24)	.0318(20)	.0302(22)	.0055(18)	.0037(18)	.0089(17)
CM2	.97682(32)	.58586(32)	.08937(33)	.0378(27)	.0209(24)	.0418(32)	.0084(21)	.0050(23)	-.0064(22)
CM3	.59247(45)	.69752(42)	.18222(36)	.0289(45)	.0286(36)	.0597(38)	-.0052(34)	-.0065(29)	-.0021(26)

ATOM	x	y	z	B	ATOM	x	y	z	B
H11	.9272(1)	.8585(1)	.2723(1)	.9(5)	H12	1.0884(1)	.9239(1)	.2843(1)	1.2(6)
H21	.8867(1)	.6995(1)	.2952(1)	1.2(6)	H22	.9833(2)	.5734(2)	.2631(2)	1.6(6)
H31	.7829(2)	.8144(2)	.3069(2)	1.1(6)	H32	.6644(2)	.8534(2)	.2862(2)	2.3(7)
HM11	.9421(2)	1.0365(2)	.0845(2)	2.0(11)	HM12	.8177(2)	1.0551(2)	.0678(2)	2.0(8)
HM13	.8716(2)	.9702(2)	.0032(2)	3.2(8)	HM21	1.0049(2)	.6136(2)	.0280(2)	3.4(8)
HM22	.9216(2)	.5293(2)	.0857(2)	2.0(9)	HM23	1.0428(2)	.5588(2)	.1169(2)	2.0(9)
HM31	.5641(2)	.6268(3)	.2086(2)	2.0(7)	HM32	.5885(2)	.6984(2)	.1877(2)	2.0(9)
HM33	.5432(2)	.7535(2)	.2103(3)	3.5(8)					

Table 1 B. Final fractional coordinates *etc.* for molecule B.

ATOM	x	y	z	U11	U22	U33	U12	U13	U23
O1	.91929(19)	.81499(28)	.44378(18)	.0351(15)	.0367(15)	.0280(14)	.0017(13)	.0069(12)	-.0052(12)
O2	.88377(25)	.58271(24)	.76469(24)	.0716(23)	.0488(19)	.0761(24)	-.0118(18)	-.0340(19)	.0342(17)
O3	.85054(19)	.96538(19)	.78431(18)	.0429(17)	.0383(14)	.0280(15)	-.0116(13)	.0002(12)	-.0057(12)
N1	.81848(22)	.93428(21)	.61935(21)	.0327(18)	.0204(15)	.0238(16)	-.0042(14)	.0002(13)	-.0003(13)
N2	.86055(23)	.68816(23)	.55272(24)	.0323(18)	.0207(17)	.0409(20)	.0023(15)	-.0077(15)	-.0014(15)
N3	.78767(29)	.73363(28)	.79199(25)	.0724(26)	.0370(21)	.0346(21)	-.0245(21)	-.0204(19)	.0142(17)
C1	.77140(25)	.86588(27)	.53713(24)	.0272(20)	.0211(19)	.0218(19)	.0025(17)	-.0013(16)	.0004(15)
C2	.78448(30)	.64413(28)	.62265(29)	.0445(25)	.0168(19)	.0456(25)	-.0098(19)	-.0199(20)	.0089(18)
C3	.72670(31)	.82551(33)	.75479(28)	.0453(26)	.0449(24)	.0238(21)	-.0187(22)	.0013(19)	.0028(19)
CC1	.85556(28)	.78601(27)	.58689(26)	.0296(21)	.0233(19)	.0224(20)	-.0022(17)	-.0096(17)	-.0055(17)
CC2	.82244(33)	.65166(35)	.73288(33)	.0508(28)	.0338(25)	.0482(28)	-.0283(23)	-.0182(23)	.0236(23)
CC3	.80162(27)	.91427(28)	.71980(27)	.0299(22)	.0224(19)	.0295(22)	-.0022(18)	.0042(18)	-.0021(17)
CM1	.88156(28)	1.02875(28)	.58957(27)	.0403(24)	.0219(20)	.0295(22)	-.0061(18)	.0068(18)	-.0004(17)
CM2	.94548(32)	.61441(32)	.52778(33)	.0455(27)	.0274(24)	.0644(32)	.0134(21)	-.0238(23)	-.0152(22)
CM3	.82615(45)	.73785(42)	.89694(36)	.1111(45)	.0640(36)	.0410(30)	-.0358(34)	-.0338(29)	.0156(26)

ATOM	x	y	z	B	ATOM	x	y	z	B
H11	.7556(1)	.9088(1)	.4751(1)	1.7(5)	H12	.7857(1)	.8286(1)	.5559(1)	.9(6)
H21	.7777(1)	.5659(1)	.6877(1)	2.4(6)	H22	.7159(2)	.6778(2)	.6181(2)	1.3(6)
H31	.6864(2)	.8608(2)	.8147(2)	4.3(6)	H32	.6789(2)	.8022(2)	.6961(2)	2.4(7)
HM11	.8663(2)	1.0863(2)	.6318(2)	2.0(11)	HM12	.9524(2)	1.0027(2)	.5952(2)	2.2(8)
HM13	.8680(2)	1.0383(2)	.5166(2)	2.0(8)	HM21	.9168(2)	.5473(2)	.4896(2)	2.0(8)
HM22	.9845(2)	.5875(2)	.5880(2)	2.0(9)	HM23	.9974(2)	.6528(2)	.4785(2)	3.2(9)
HM31	.7825(2)	.7868(3)	.9408(2)	2.0(7)	HM32	.8286(2)	.6596(2)	.9285(2)	8.3(9)
HM33	.9004(2)	.7740(2)	.8991(3)	2.0(8)					

Table 2 A. Bond distances, bond angles and dihedral angles with estimated standard deviations for molecule A.

DISTANCE	(Å)	DISTANCE	(Å)
O1 - CC1	1.237(4)	O2 - CC2	1.235(4)
O3 - CC3	1.235(4)	N1 - CM1	1.471(4)
N2 - CM2	1.469(4)	N3 - CM3	1.462(5)
N1 - C1	1.463(4)	N2 - C2	1.468(4)
N3 - C3	1.474(4)	N1 - CC3	1.335(4)
N2 - CC1	1.356(4)	N3 - CC2	1.349(4)
C1 - CC1	1.526(4)	C2 - CC2	1.518(5)
C3 - CC3	1.535(5)		

ANGLE	(°)	ANGLE	(°)
O1 - CC1 - C1	119.4(3)	O2 - CC2 - C2	119.7(3)
O3 - CC3 - C3	118.1(3)	O1 - CC1 - N2	121.3(3)
O2 - CC2 - N3	120.9(3)	O3 - CC3 - N1	122.3(3)
C1 - CC1 - N2	119.2(3)	C2 - CC2 - N3	119.4(3)
C3 - CC3 - N1	119.6(3)	CM1 - N1 - C1	116.6(3)
CM2 - N2 - C2	115.5(3)	CM3 - N3 - C3	116.8(3)
CM1 - N1 - CC3	117.7(3)	CM2 - N2 - CC1	118.8(3)
CM3 - N3 - CC2	118.3(3)	CC3 - N1 - C1	125.7(3)
CC1 - N2 - C2	125.7(3)	CC2 - N3 - C3	124.1(3)
N1 - C1 - CC1	110.2(3)	N2 - C2 - CC2	110.6(3)
N3 - C3 - CC3	110.7(3)		

DIHEDRAL ANGLE	(°)
N1 - C1 - CC1 - N2	-91.7(4)
C1 - CC1 - N2 - C2	-6.7(5)
CC1 - N2 - C2 - CC2	102.1(4)
N2 - C2 - CC2 - N3	-101.3(3)
C2 - CC2 - N3 - C3	10.5(5)
CC2 - N3 - C3 - CC3	87.7(4)
N3 - C3 - CC3 - N1	-104.6(3)
C3 - CC3 - N1 - C1	8.3(5)
CC3 - N1 - C1 - CC1	93.5(4)

Table 2 B. Bond distances *etc.* for molecule B.

DISTANCE	(Å)	DISTANCE	(Å)
O1 - CC1	1.233(4)	O2 - CC2	1.232(5)
O3 - CC3	1.232(4)	N1 - CM1	1.465(4)
N2 - CM2	1.466(5)	N3 - CM3	1.476(5)
N1 - C1	1.466(4)	N2 - C2	1.462(5)
N3 - C3	1.448(5)	N1 - CC3	1.357(4)
N3 - CC2	1.358(5)	N2 - CC1	1.352(4)
C1 - CC1	1.518(5)	C2 - CC2	1.533(5)
C3 - CC3	1.516(5)		

ANGLE	(°)	ANGLE	(°)
O1 - CC1 - C1	118.6(3)	O2 - CC2 - C2	118.5(4)
O3 - CC3 - C3	118.3(3)	O1 - CC1 - N2	122.3(3)
O2 - CC2 - N3	122.3(4)	O3 - CC3 - N1	122.8(3)
C1 - CC1 - N2	119.1(3)	C2 - CC2 - N3	119.2(4)
C3 - CC3 - N1	119.6(3)	CM1 - N1 - C1	115.8(3)
CM2 - N2 - C2	115.8(3)	CM3 - N3 - C3	117.9(4)
CM1 - N1 - CC3	117.4(3)	CM2 - N2 - CC1	119.0(3)
CM3 - N3 - CC2	116.8(4)	CC3 - N1 - C1	125.7(3)
CC1 - N2 - C2	125.9(3)	CC2 - N3 - C3	124.4(3)
N1 - C1 - CC1	109.3(3)	N2 - C2 - CC2	111.7(3)
N3 - C3 - CC3	110.3(3)		

DIHEDRAL ANGLE	(°)
N1 - C1 - CC1 - N2	91.8(4)
C1 - CC1 - N2 - C2	7.3(5)
CC1 - N2 - C2 - CC2	-102.8(4)
N2 - C2 - CC2 - N3	99.7(4)
C2 - CC2 - N3 - C3	-9.9(6)
CC2 - N3 - C3 - CC3	-86.8(4)
N3 - C3 - CC3 - N1	107.8(4)
C3 - CC3 - N1 - C1	-11.9(5)
CC3 - N1 - C1 - CC1	-91.7(4)

$\beta = 90.82(4)°$, space group $P2_1/n$, and eight molecules in the unit cell ($D_m = 1.33$ g cm^{-3}, $D_x = 1.34$ g cm^{-3}). At room temperature the crystals are to some extent destroyed by the radiation and data were therefore collected at -160°C (automatic four circle diffractometer, Mo$K\alpha$-radiation, 2439 observed reflections). No corrections for absorption or secondary extinction were applied (crystal size $0.5 \times 0.3 \times 0.3$ mm^3).

The structure was solved by direct methods [9] and refined by full-matrix least-squares technique.[10] * Methylene hydrogen positions were calculated. Methyl hydrogens were localized in a difference Fourier map. Anisotropic temperature factors were introduced for O, N, and C atoms, and weights in least-squares were calculated from the standard deviations in intensities, $\sigma(I)$, taken as

$$\sigma(I) = [C_T + (0.02C_N)^2]^{\frac{1}{2}}$$

where C_T is the total number of counts and C_N the net count. The final weighted R-value was 4.5 % (conventional $R = 5.0$ %) for 2439 observed reflections. The form factors used were those of Hanson *et al.*[11] except for hydrogen.[12]

Final fractional coordinates and thermal parameters for the two independent molecules (A and B) are given in Table 1 A and Table 1 B. From the temperature parameters of these tables the principal axes of thermal vibration ellipsoids were calculated. Maximum r.m.s. amplitudes range from 0.17 Å to 0.38 Å. No rigid-body analyses have been carried out.

Bond distances and angles and dihedral angles are listed in Tables 2 A and 2 B. The standard deviations (in parentheses) are estimated from the correlation matrix of the final least-squares refinement cycle. The two independent molecules have the same "crown" conformation shown in Fig. 1, which is the only conformation consistent with NMR-data.[4]

Average values of bond distances and two of the bond angles at nitrogen in the *N*-methyl amide groups are compared with earlier findings [6-8,13] in Table 3. It may be seen that the average (C−N−CC) *cis* angle of tricyclo-

* All programs used (except those for phase determination) are included in this reference.

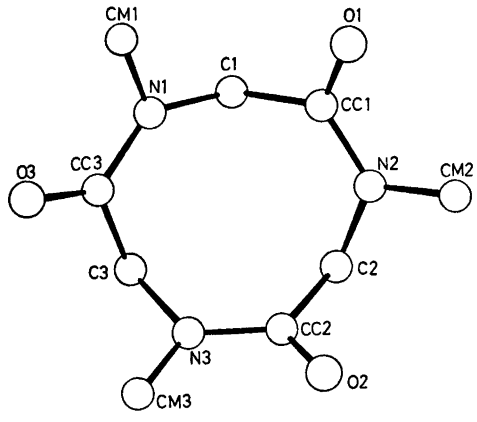

Fig. 1. Schematic drawing showing the molecular conformation.

Table 3. Average bond distances and angles for the cases $n=3,4,^a$ 5,7, and 8.

	$n=$	3	4	5	7	8
Distance (Å)						
CC–C		1.524	1.525	1.527	1.534	1.530
CC–N		1.351	1.346	1.344	1.343	1.345
CC–O		1.234	1.224	1.228	1.221	1.232
C–N		1.462	1.454	1.456	1.449	1.453
CM–N		1.468	1.466	1.483	1.446	1.487
Angle (°)						
(CM–N–CC)*cis*		118.0	117.9	118.7	118.6	118.6
(CM–N–CC)*trans*		–	123.8	123.8	122.8	123.5
(C–N–CC)*cis*		125.3	123.5	123.8	123.7	122.8
(C–N–CC)*trans*		–	116.1	117.2	118.4	117.5

[a] Due to the more accurate data, the values are taken from the cycloalanyltetrasarcosyl structure.[13]

sarcosyl is somewhat greater than those of the larger rings. It should also be pointed out that the significantly longer CM–N bonds of cyclopenta- and cyclooctasarcosyl are possibly connected with the fact that for these compounds methyl hydrogens were not included in the calculations.

There are no short inter-molecular contacts. A list of observed and calculated structure factors is available from the author.

Acknowledgement. The author thanks cand. real. K. Titlestad for preparing the crystals.

1. Dale, J. and Titlestad, K. *Chem. Commun.* (1969) 656.
2. Titlestad, K., Groth, P. and Dale, J. *Chem. Commun.* (1973) 346.
3. Titlestad, K., Groth, P. and Dale, J. *Chem. Commun.* (1973) 646.
4. Titlestad, K. *Acta Chem. Scand. B 29* (1975) 153.
5. Groth, P. *Acta Chem. Scand. 24* (1970) 780.
6. Groth, P. *Acta Chem. Scand. 27* (1973) 3117.
7. Groth, P. *Acta Chem. Scand. 27* (1973) 3419.
8. Groth, P. *Acta Chem. Scand. A 29* (1975) 38.
9. Germain, G., Main, P. and Woolfson, M. M. *Acta Crystallogr. A 27* (1971) 368.
10. Groth, P. *Acta Chem. Scand. 27* (1973) 1837.
11. Hanson, H. P., Herman, F., Lea, J. D. and Skillman, S. *Acta Crystallogr. 17* (1964) 1040.
12. Stewart, R. F., Davidson, E. R. and Simpson, W. T. *J. Chem. Phys. 43* (1965) 3175.
13. Groth, P. *Acta Chem. Scand. A 28* (1974) 449.

Received August 11, 1976.

Crystal Conformation of Cyclodecasarcosyl. $4CH_3OH$ at —160 °C

P. GROTH

Department of Chemistry, University of Oslo, Oslo 3, Norway

With exception for the case $n=6$, the crystal structures of cyclic oligopeptides of sarcosine with the general formula I are known.[1a–f] For

(I) 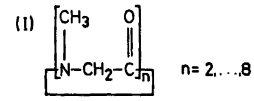

$n=2$, 3, 4 and 8 the conformations could be predicted on the basis of NMR data.[2] For $n=5$,

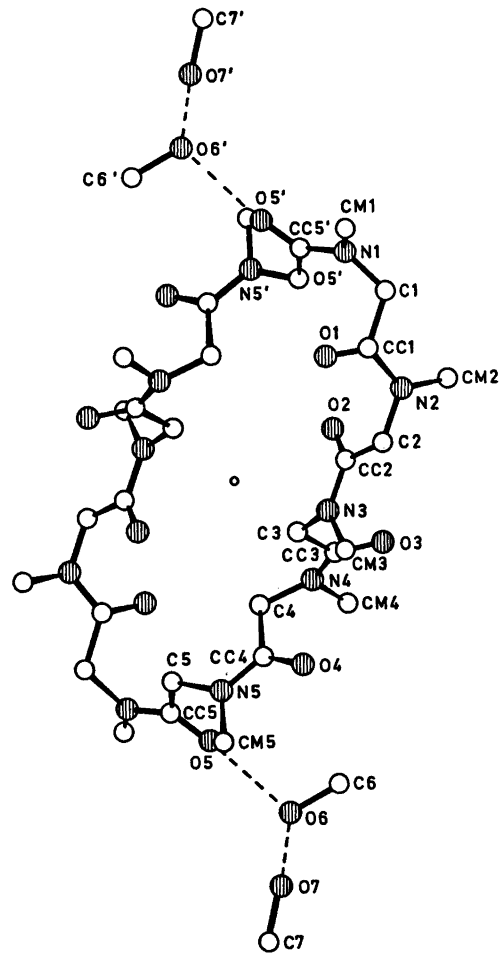

Fig. 1. Schematic drawing of the molecule.

Table 3. Average bond distances and angles for the cases $n=3,4,^a$ 5,7, and 8.

	$n=$	3	4	5	7	8
Distance (Å)						
CC–C		1.524	1.525	1.527	1.534	1.530
CC–N		1.351	1.346	1.344	1.343	1.345
CC–O		1.234	1.224	1.228	1.221	1.232
C–N		1.462	1.454	1.456	1.449	1.453
CM–N		1.468	1.466	1.483	1.446	1.487
Angle (°)						
(CM–N–CC)*cis*		118.0	117.9	118.7	118.6	118.6
(CM–N–CC)*trans*		–	123.8	123.8	122.8	123.5
(C–N–CC)*cis*		125.3	123.5	123.8	123.7	122.8
(C–N–CC)*trans*		–	116.1	117.2	118.4	117.5

[a] Due to the more accurate data, the values are taken from the cycloalanyltetrasarcosyl structure.[13]

sarcosyl is somewhat greater than those of the larger rings. It should also be pointed out that the significantly longer CM–N bonds of cyclopenta- and cyclooctasarcosyl are possibly connected with the fact that for these compounds methyl hydrogens were not included in the calculations.

There are no short inter-molecular contacts. A list of observed and calculated structure factors is available from the author.

Acknowledgement. The author thanks cand. real. K. Titlestad for preparing the crystals.

1. Dale, J. and Titlestad, K. *Chem. Commun.* (1969) 656.
2. Titlestad, K., Groth, P. and Dale, J. *Chem. Commun.* (1973) 346.
3. Titlestad, K., Groth, P. and Dale, J. *Chem. Commun.* (1973) 646.
4. Titlestad, K. *Acta Chem. Scand. B 29* (1975) 153.
5. Groth, P. *Acta Chem. Scand. 24* (1970) 780.
6. Groth, P. *Acta Chem. Scand. 27* (1973) 3117.
7. Groth, P. *Acta Chem. Scand. 27* (1973) 3419.
8. Groth, P. *Acta Chem. Scand. A 29* (1975) 38.
9. Germain, G., Main, P. and Woolfson, M. M. *Acta Crystallogr. A 27* (1971) 368.
10. Groth, P. *Acta Chem. Scand. 27* (1973) 1837.
11. Hanson, H. P., Herman, F., Lea, J. D. and Skillman, S. *Acta Crystallogr. 17* (1964) 1040.
12. Stewart, R. F., Davidson, E. R. and Simpson, W. T. *J. Chem. Phys. 43* (1965) 3175.
13. Groth, P. *Acta Chem. Scand. A 28* (1974) 449.

Received August 11, 1976.

Crystal Conformation of Cyclodecasarcosyl. $4CH_3OH$ at —160 °C

P. GROTH

Department of Chemistry, University of Oslo, Oslo 3, Norway

With exception for the case $n=6$, the crystal structures of cyclic oligopeptides of sarcosine with the general formula I are known.[1a–f] For

(I) 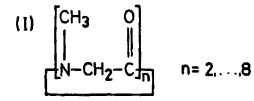

$n=2$, 3, 4 and 8 the conformations could be predicted on the basis of NMR data.[2] For $n=5$,

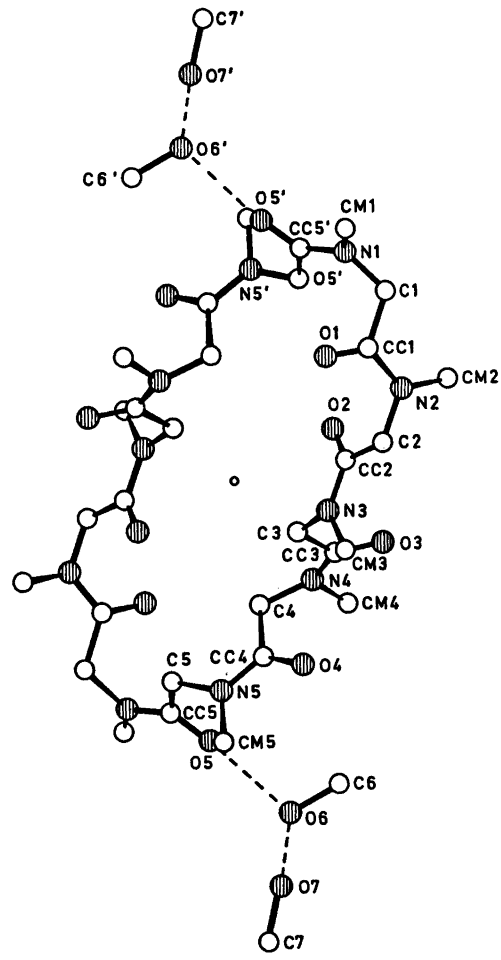

Fig. 1. Schematic drawing of the molecule.

Table 1. Final fractional coordinates and thermal parameters with estimated standard deviations. The expression for anisotropic vibration is $\exp[-2\pi^2(h^2a^{*2}U11+...+2klb^*c^*U23)]$. Hmn is bonded to Cm, HMmn to CMm and HOm to Om.

ATOM	X	Y	Z	U11	U22	U33	U12	U13	U23
O1	-.48717(30)	-.05843(26)	.16415(24)	.0321(16)	.0367(17)	.0486(19)	.0150(14)	.0153(15)	.0087(15)
O2	-.28643(28)	.05991(26)	.44222(23)	.0257(16)	.0355(17)	.0589(19)	.0074(13)	.0045(14)	.0233(15)
O3	-.07281(27)	.34818(26)	.64195(22)	.0186(14)	.0499(17)	.0439(18)	.0163(13)	.0186(13)	.0121(14)
O4	.33845(28)	.47721(25)	.63618(22)	.0246(15)	.0315(15)	.0424(16)	.0152(13)	.0073(13)	.0175(13)
O5	.78578(31)	.44474(26)	.88983(23)	.0585(19)	.0283(16)	.0359(18)	.0205(14)	.0028(15)	.0056(14)
N1	-.76179(36)	-.24623(31)	.14853(28)	.0260(20)	.0269(20)	.0386(22)	.0123(17)	.0089(17)	.0098(17)
N2	-.51474(33)	.10868(30)	.39406(27)	.0187(17)	.0288(19)	.0352(21)	.0086(15)	.0043(16)	.0087(16)
N3	-.09230(34)	.22957(30)	.41988(26)	.0218(18)	.0288(19)	.0362(21)	.0086(15)	.0068(16)	.0111(16)
N4	.14871(34)	.29895(31)	.71484(27)	.0229(18)	.0356(20)	.0332(20)	.0141(16)	.0064(16)	.0129(16)
N5	.53795(32)	.39386(29)	.66925(26)	.0181(17)	.0266(17)	.0366(21)	.0106(14)	.0088(15)	.0147(15)
C1	-.72677(41)	-.10868(36)	.22462(33)	.0229(22)	.0247(21)	.0429(27)	.0149(18)	.0055(19)	.0103(19)
C2	-.35785(43)	.19183(36)	.31808(33)	.0273(23)	.0254(22)	.0384(26)	.0074(19)	.0042(20)	.0128(20)
C3	.02067(42)	.28981(38)	.58492(35)	.0175(21)	.0345(24)	.0462(28)	.0090(19)	.0075(20)	.0102(21)
C4	.28131(41)	.27028(37)	.69369(32)	.0206(21)	.0331(23)	.0321(24)	.0093(18)	.0031(18)	.0154(19)
C5	.59896(40)	.28898(36)	.69666(32)	.0183(20)	.0255(22)	.0366(25)	.0100(17)	.0082(19)	.0075(19)
CC1	-.56628(42)	-.01731(38)	.22799(34)	.0224(21)	.0299(23)	.0348(25)	.0149(19)	.0056(19)	.0146(20)
CC2	-.24214(42)	.15359(38)	.39929(33)	.0235(23)	.0256(22)	.0338(25)	.0076(19)	.0069(19)	.0062(19)
CC3	.02784(40)	.29451(37)	.62574(34)	.0158(21)	.0282(22)	.0387(26)	.0075(18)	.0094(19)	.0132(19)
CC4	.38987(41)	.38947(36)	.66486(30)	.0217(21)	.0279(22)	.0216(23)	.0119(18)	.0053(17)	.0041(18)
CC5	.69272(41)	.33386(39)	.82178(34)	.0224(22)	.0281(23)	.0378(26)	.0089(19)	.0068(19)	.0124(21)
CM1	-.83739(48)	-.27274(45)	.02788(36)	.0436(27)	.0473(31)	.0423(27)	.0204(24)	.0044(22)	.0181(24)
CM2	-.59648(45)	.14931(38)	.39231(34)	.0389(24)	.0287(23)	.0374(26)	.0097(19)	.0045(20)	.0049(20)
CM3	-.03838(47)	.34684(40)	.37535(36)	.0353(25)	.0312(24)	.0479(29)	.0039(20)	.0123(22)	.0146(21)
CM4	.15799(46)	.38984(45)	.82821(35)	.0308(25)	.0668(31)	.0353(27)	.0216(23)	.0133(21)	.0157(24)
CM5	.64497(42)	.50736(39)	.64483(34)	.0219(22)	.0384(25)	.0383(26)	.0095(19)	.0078(19)	.0168(20)
O6	-.74667(35)	-.72861(28)	.07797(25)	.0589(22)	.0365(18)	.0547(21)	.0217(16)	.0091(17)	.0104(15)
O7	-.91039(34)	-.88816(31)	.20122(26)	.0398(19)	.0596(22)	.0447(23)	.0212(17)	.0067(17)	.0228(18)
C6	-.60146(50)	-.73688(50)	.06499(44)	.0637(36)	.0627(34)	.0619(38)	.0338(29)	.0120(30)	.0162(28)
C7	-1.08735(61)	-.96746(58)	.14748(43)	.0687(39)	.0579(34)	.0719(37)	.0273(31)	.0123(31)	.0142(28)

ATOM	X	Y	Z	B	ATOM	X	Y	Z	B
H11	-.7344(35)	-.1116(31)	.3843(26)	1.4(6)	H12	-.8019(35)	-.8675(30)	.1994(26)	1.3(6)
H21	-.3460(36)	.2824(31)	.3418(26)	1.6(6)	H22	-.3296(34)	.1788(30)	.2459(26)	1.2(6)
H31	.1288(32)	.2422(27)	.4862(23)	.4(6)	H32	-.0138(36)	.1122(31)	.5025(26)	1.9(7)
H41	.2578(36)	.1922(31)	.6323(26)	1.7(7)	H42	.3285(34)	.2617(30)	.7638(25)	1.1(6)
H51	.5155(31)	.2837(26)	.6796(22)	.3(5)	H52	.6720(39)	.2788(34)	.6417(28)	2.6(8)
HM11	-.7641(40)	-.2329(35)	-.0117(28)	2.9(8)	HM12	-.9306(45)	-.2484(37)	.0263(31)	3.8(9)
HM13	-.8819(53)	-.3845(47)	-.0137(39)	7.7(12)	HM21	-.5904(43)	.0983(37)	.4535(31)	3.4(9)
HM22	-.5476(36)	.2441(31)	.4322(26)	1.6(7)	HM23	-.6976(42)	.1327(37)	.3617(31)	3.6(9)
HM31	-.1102(47)	.3928(40)	.3643(34)	4.5(10)	HM32	-.0258(42)	.3258(36)	.2953(31)	3.3(8)
HM33	.0548(47)	.4156(40)	.4265(35)	4.9(10)	HM41	.2312(42)	.4822(36)	.8356(31)	3.5(9)
HM42	.0582(43)	.3944(37)	.8420(31)	3.6(9)	HM43	.1959(45)	.3440(39)	.8939(32)	4.0(9)
HM51	.6334(36)	.4946(32)	.5609(27)	2.1(7)	HM52	.6385(43)	.5876(37)	.6819(31)	3.6(9)
HM53	.7538(50)	.5131(43)	.6786(36)	5.3(11)	H61	-.5458(50)	-.6884(45)	.0195(40)	5.4(11)
H62	-.6070(55)	-.8264(50)	.0332(48)	7.2(13)	H63	-.5198(45)	-.6803(39)	.1289(36)	3.8(9)
H71	-1.0931(60)	-1.0484(53)	.0695(45)	7.5(15)	H72	-1.1192(53)	-1.0403(47)	.1927(40)	7.8(13)
H73	-1.1589(60)	-.9262(53)	.1414(43)	7.6(15)	H06	-.7333(52)	-.6325(47)	.8927(39)	6.2(12)
H07	-.8687(63)	-.8513(53)	.1467(45)	8.7(15)					

6, 7 and $n>8$ no conformational evidence is obtainable from NMR spectroscopy. The crystal structure of cyclodecasarcosyl, $C_{30}H_{50}N_{10}O_{10}$, (crystallizing with four molecules of methanol per formula unit) is now reported.

The crystals belong to the triclinic system with space group $P\bar{1}$, cell dimensions (for Dirichlet's reduced cell) $a=9.210(4)$ Å, $b=10.540(5)$ Å, $c=12.211(6)$ Å, $\alpha=103.15(4)°$, $\beta=99.11(4)°$, $\gamma=105.82(3)°$, and $Z=1$ ($D_m=1.28$ g cm^{-3}, $D_x=1.29$ g cm^{-3}). The crystals are unstable at room temperature and data were therefore collected at -160 °C (automatic four circle diffractometer, Mo$K\alpha$-radiation, 2570 observed reflections). No corrections for absorption or secondary extinction were applied (crystal size $0.4\times0.2\times0.3$ mm^3).

The structure was solved by direct methods [3] and refined by full-matrix least-squares technique.[4]* Except for the methylene hydrogens (the positions of which were calculated) all hydrogen atoms were localized in a difference Fourier map. Anisotropic temperature factors were introduced for O, N and C atoms and weights in least-squares were calculated from the standard deviations in intensities, $\sigma(I)$, taken as

$$\sigma(I)=[C_T+(0.02C_N)^2]^{\frac{1}{2}}$$

where C_T is the total number of counts and C_N the net count. The final weighted R-value was 5.3 % (conventional $R=6.4$ %) for 2570 observed reflections. The form factors used were those of Hanson *et al.*[5] except for hydrogen.[6]

Final fractional coordinates and thermal parameters are given in Table 1. The principal axes of thermal vibration ellipsoids were calculated from the temperature parameters of this table, and the maximum r.m.s. amplitudes range from 0.172 to 0.273 Å (corresponding B-values 2.35 and 5.88 Å^2). Due to the size of the molecule no rigid-body analysis has been carried out.

Bond distances and angles and dihedral angles are listed in Table 2. The standard deviations (in parentheses) are estimated from the correlation matrix of the final least-squares refinement cycle.

Fig. 1 is a schematic drawing of the (centrosymmetric) molecule where the positions of the

* All programs used (except those for phase determination) are included in this reference.

Table 2. Bond distances, bond angles and dihedral angles with estimated standard deviations.

DISTANCE	(Å)	DISTANCE	(Å)
O1 - CC1	1.234(4)	O2 - CC2	1.225(4)
O3 - CC3	1.222(4)	O4 - CC4	1.235(4)
O5 - CC5	1.229(4)	N1 - CM1	1.463(5)
N2 - CM2	1.460(5)	N3 - CM3	1.452(5)
N4 - CM4	1.456(5)	N5 - CM5	1.453(4)
N1 - C1	1.451(4)	N2 - C2	1.434(5)
N3 - C3	1.449(5)	N4 - C4	1.453(4)
N5 - C5	1.452(4)	N1 - CC5'	1.337(4)
N2 - CC1	1.344(4)	N3 - CC2	1.345(4)
N4 - CC3	1.362(4)	N5 - CC4	1.345(4)
C1 - CC1	1.517(5)	C2 - CC2	1.536(5)
C3 - CC3	1.524(5)	C4 - CC4	1.523(5)
C5 - CC5	1.528(5)	C6 - O6	1.422(5)
C7 - O7	1.438(6)	O6 - O5	2.753(4)
O6 - O7	2.803(4)		

ANGLE	(°)	ANGLE	(°)
O1 - CC1 - C1	121.8(3)	O2 - CC2 - C2	121.2(3)
O3 - CC3 - C3	128.3(3)	O4 - CC4 - C4	119.8(3)
O5 - CC5 - C5	121.6(3)	O1 - CC1 - N2	122.2(3)
O2 - CC2 - N3	123.4(3)	O3 - CC3 - N4	122.3(4)
O4 - CC4 - N5	121.9(3)	O5' - CC5' - N1	122.8(4)
CM1 - N1 - C1	117.5(3)	CM2 - N2 - C2	117.8(3)
CM3 - N3 - C3	116.4(3)	CM4 - N4 - C4	114.8(3)
CM5 - N5 - C5	116.3(3)	CM1 - N1 - CC5'	119.8(3)
CM2 - N2 - CC1	122.1(3)	CM3 - N3 - CC2	124.3(3)
CM4 - N4 - CC3	118.8(3)	CM5 - N5 - CC4	128.1(3)
C1 - N1 - CC5'	121.1(3)	C2 - N2 - CC1	118.1(3)
C3 - N3 - CC2	118.3(3)	C4 - N4 - CC3	121.7(3)
C5 - N5 - CC4	123.6(3)	N1 - C1 - CC1	111.5(3)
N2 - C2 - CC2	111.9(3)	N3 - C3 - CC3	110.6(3)
N4 - C4 - CC4	110.9(3)	N5 - C5 - CC5	112.8(3)
C1 - CC1 - N2	116.9(3)	C2 - CC2 - N3	115.4(3)
C3 - CC3 - N4	117.2(3)	C4 - CC4 - N5	113.2(3)
C5' - CC5' - N1	115.5(3)	CC5 - O5 - O6	147.4(3)
C6 - O6 - O5	105.6(3)	C6 - O6 - O7	116.6(3)
O5 - O6 - O7	111.5(1)		

DIHEDRAL ANGLE	(°)
N1 - C1 - CC1 - N2	-173.8(3)
C1 - CC1 - N2 - C2	173.5(3)
CC1 - N2 - C2 - CC2	-81.5(4)
N2 - C2 - CC2 - N3	-178.4(3)
C2 - CC2 - N3 - C3	173.8(3)
CC2 - N3 - C3 - CC3	-83.8(4)
N3 - C3 - CC3 - N4	-172.5(3)
C3 - CC3 - N4 - C4	22.6(5)
CC3 - N4 - C4 - CC4	73.9(4)
N4 - C4 - CC4 - N5	165.3(3)
C4 - CC4 - N5 - C5	1.9(5)
CC4 - N5 - C5 - CC5	-181.3(4)
N5' - C5' - CC5' - N1	-175.9(3)
C5' - CC5' - N1 - C1	-18.2(5)
CC5' - N1 - C1 - CC1	-72.2(4)

Table 3. Sequences of *cis* and *trans* configurations of the amide groups for cyclic oligopeptides of sarcosine (formula (I)).

n	sequence (c = *cis*, t = *trans*)
2	c, c
3	c, c, c
4	c, t, c, t
5	c, c, c, t, t
5[a]	c, c, c, t, t
7	c, c, c, c, t, t, t
8	c, c, t, t, c, c, t, t

[a] Cycloalanyltetrasarcosyl hemihydrate.[7]

four methanol molecules and the numbering of atoms are indicated. It may also be seen that the configuration of the ten *N*-methyl amide groups has the sequence *trans, trans, cis, cis, cis, trans, trans, cis, cis, cis*. Corresponding sequences for other cyclosarcosyl molecules with known structure [1a–f] are listed in Table 3. Fig. 1 shows that this 30-membered ring has a remarkably open conformation, and thus (in this respect) resembles that of the corresponding 24-membered ring of cyclooctasarcosyl.[1b] It should, however, be pointed out that in the latter case the inner volume is filled by a cluster of four water molecules, which participate in a network of inter- as well as intramolecular hydrogen bond bridges. In the present compound the solvent molecules are all outside the ring and do not form any intermolecular bridges. Since no direct transannular interactions are present to be held responsible for the rigidity of this rather large and open ring, it must be due to an intrinsic rigidity of the peptide chain itself.[8]

Bond distances and angles are not significantly different from those of earlier findings.[1f]

A list of observed and calculated structure factors is available from the author.

Acknowledgement. The author would like to thank cand. real. K. Titlestad for preparing the crystals.

1. a. Groth, P. *Acta Chem. Scand. 23* (1969) 3155; b. *Ibid. 24* (1970) 780; c. *Ibid, 27* (1973) 3217; d. *Ibid. 27* (1973) 3419; e. *Ibid. A 29* (1975) 38; f. *Ibid. A 30* (1976) 838.
2. Dale, J. and Titlestad, K. *Chem. Commun.* (1969) 656.
3. Germain, G., Main, P. and Woolfson, M. M. *Acta Crystallogr. A 27* (1971) 368.
4. Groth, P. *Acta Chem. Scand. 27* (1973) 1837.
5. Hanson, H. P., Herman, F., Lea, J. D. and Skillman, S. *Acta Crystallogr. 17* (1964) 1040.
6. Stewart, R. F., Davidson, E. R. and Simpson, W. T. *J. Chem. Phys. 43* (1965) 3175.
7. Groth, P. *Acta Chem. Scand. A 28* (1974) 449.
8. Titlestad, K., Groth, P., Dale, J. and Ali, M. Y. *Chem. Commun.* (1973) 346.

Received August 20, 1976.

Crystal Structure of Ethylenediammonium Tetrachloropalladate(II)

ROLF W. BERG and INGER SØTOFTE

Chemistry Departments A and B, The Technical University of Denmark, DK-2800 Lyngby, Denmark

The ethylenediammonium cation (abbreviated enH_2) is structurally interesting because of its possibility in the solid state to adopt different conformations *via* C–C bond rotation. Depending on the type of anion with which the crystal is formed both the *planar* centrosymmetric *trans*-conformation and the C_2-symmetric *gauche*-conformation of the ethylenediammonium ion have been found; *trans* in $[enH_2]Cl_2$,[1] $[enH_2]Br_2$,[2] and $[enH_2][Au(SO_3)_2en]$ [3] and *gauche* in $[enH_2][SO_4]$.[4] In a recent investigation [5] X-ray and infrared data seemed to indicate that $[enH_2][PdCl_4]$ contains $[enH_2]^{2+}$ ions of *trans*-conformation. This work was undertaken to establish the complete structure of $[enH_2][PdCl_4]$ and to see if the structural deductions based on polarized single crystal infrared spectra [5] agree with this structure. Also, it was found of interest to investigate the hydrogen bonding scheme and to see if $[PdCl_4]^{2-}$, one of the typical ions of D_{4h} symmetry in inorganic chemistry, remains square planar in the crystal.

Experimental. Three-dimensional X-ray data were measured at room temperature from a cleaved crystal of size $0.4 \times 0.2 \times 0.05$ mm, obtained as described in Ref. 5 and mounted with its [010] axis as rotation axis. A Stoe & Cie semiautomatic equiinclination diffractometer with ω-scan technique and graphite monochromated Mo$K\alpha$ radiation was used. Harmonics were excluded by means of a pulse height discriminator. Reflections between a cylinder of radius $\gamma = 5.4°$ and a hemisphere with $\sin\theta/\lambda \leq 0.7$ Å^{-1} were measured ($0 \leq k \leq 10$) giving 1304 independent reflections of which 1224 had $I > 2\sigma(I)$, where $\sigma(I) = [(1 + 0.04^2)\mathrm{PC} + \mathrm{BC}]$ (PC = peak count and BC = background count). The diffractometer output was processed by the programme used in Ref. 2 prior to subsequent calculations performed on an IBM 370/165 computer using the X-RAY system [6] and ORTEP.[7] The atomic scattering factors for C, N, Cl^-, and Pd^{2+} were those of Cromer and Mann.[8] No correction was made for X-ray absorption. All symmetry related reflections were averaged and hydrogen atoms were neglected.

Crystal data. Preliminary results [5] were confirmed. $(CH_3NH_3)_2PdCl_4$. $M = 310.33$ g/mol. Monoclinic. $a = 7.34(2)$ Å, $b = 7.66(2)$ Å, $c = 7.91(2)$ Å, $\beta = 91.90(1)°$. $V = 444.49$ Å^3. $Z = 2$. $D_c = 2.318$, $D_o = 2.33$ g/cm^3 (flotation). $F(000) = 300$. $\mu(\mathrm{Mo}K\alpha) = 32.2$ cm^{-1}. Systematic absences: $h0l$ when h odd and $0k0$ for k odd. Space group: $P2_1/a$ (No. 14).

Structure determination. Starting phases were calculated from the scattering of the palladium atom which is in the special position (0,0,0) and which accounts for 31 % of the charge density. Subsequent Fourier maps revealed the chlorine, nitrogen, and carbon atoms and the structure was refined by full matrix least square minimisation of $\sum w(|F_o| - |F_c|)^2$. With anisotropic temperature factors, omission of one reflection, $(00\bar{1})$, nearest to the beam and the use of the weighting scheme $w^{-1} = 2.53 + 0.833|\sigma(F)|^2 - 0.0522|F| + 0.0052|F|^2 - 3.49\sin\theta/\lambda$ the refinement resulted in $R = 0.050$ ($R_w = 0.067$). The correctness of the resulting structure was checked by a difference Fourier map. A listing of observed and calculated structure factors may be obtained from the authors upon request.

Description of the structure. The structure is shown in Fig. 1. Both anions and cations are situated at sites of inversion. This implies that the $[PdCl_4]^{2-}$ anions are planar. The anions are nearly regularly square, having Pd–Cl bond lengths near the normal value 2.31(1) Å found for $(NH_4)_2PdCl_4$ and K_2PdCl_4.[9–11] The angles Cl–Pd–Cl are essentially right, 89.77(7) and 90.23(7)°, and hence the deviation from the regular square planar coordination is dominated by the presence of long [2.323(6) Å] and short [2.300(5) Å] Pd–Cl bonds.

Due to the inversion center the $[enH_2]^{2+}$ cation has a planar N–C–C–N skeleton, and *trans*-conformation. The C–C and C–N bond lengths have the values 1.510(9) and 1.479(8) Å, respectively. These lengths agree well (within 0.02 Å) with previously reported values for other crystals containing *trans*-$[enH_2]^{2+}$.[1–3] The C–C–N angle of 111.8(5)° observed is slightly larger than the tetrahedral angle (found in the chloride salt [1]) and this feature has also been observed for the bromide [2] and the *bis*-[*cis*-ethylenediaminedisulfitoaurate(III)] [3] salts of $[enH_2]^{2+}$, which display C–C–N angles of 112.7(9) and 110.5(7)°, respectively.

The structure found can conveniently be viewed as consisting of essentially square planar $[PdCl_4]^{2-}$ anions stacked in "stripes" along [001], the stripes being mutually twisted in opposite directions due to Cl–Cl repulsions and the formation of N–H···Cl hydrogen bonds. The structure is kept together *via* interleaving $[enH_2]^{2+}$ ions. The shortest N–Cl distances are 3.22(1), 3.27(1), 3.39(1), 3.42(2), and 3.44(2) Å of which the three first ones should be short enough to allow considerable hydrogen bonding. A typical N–H···Cl hydrogen bond is 3.3 Å [12] and Pimentel and McClellan [13] list N–H···Cl hydrogen bonded distances ranging from 2.91 to 3.41 Å. It turns out that the three shortest N–Cl contacts (shown as thin lines in Fig. 1) go from one N to three Cl in different $[PdCl_4]^{2-}$ ions. These N–Cl contacts form approximately tetra-

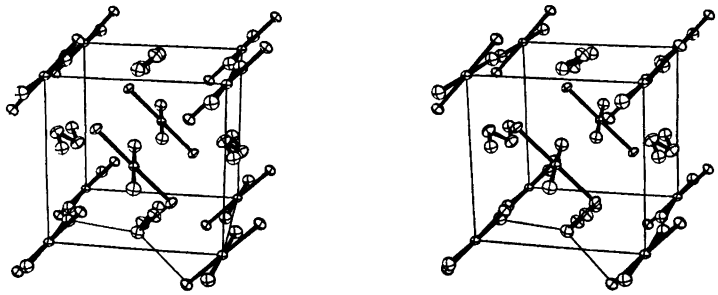

Fig. 1. Stereoscopic view of the structure of ethylenediammonium tetrachloropalladate(II) along the *c* axis. The horisontal axis is *a* and the vertical *b*. Thermal ellipsoids of 50 % charge density are shown. Hydrogen bonds around one N are shown as thin lines.

Table 1. Positional and thermal parameters (U_{ij} in units of 10^{-4} Å^2) with estimated standard deviations. The form of the temperature factor expression is exp $[-2\pi^2\sum_{ij}h_ih_ja_i^*a_j^*U_{ij}]$.

Atom	X/a	Y/b	Z/c	U_{11}	U_{22}	U_{33}	U_{12}	U_{13}	U_{23}
Pd	0.0	0.0	0.0	133(2)	201(3)	230(3)	−4(1)	0(1)	0(1)
Cl1	0.0345(2)	0.0487(2)	0.2892(1)	348(5)	379(6)	211(4)	2(4)	−14(3)	−21(4)
Cl2	0.2217(1)	0.2048(1)	−0.0473(1)	195(4)	262(4)	436(5)	−77(3)	39(3)	22(3)
N	0.5014(7)	0.0268(7)	0.2620(5)	344(21)	383(15)	227(16)	11(17)	−3(14)	34(14)
C	0.4505(7)	0.0461(8)	0.5693(6)	335(20)	414(22)	257(17)	109(19)	37(14)	17(16)

hedral angles with each other and with the C−N bond. Therefore it can be assumed that a 3-dimensional network of hydrogen bonds exists in the crystal.

Discussion. The presence of hydrogen bonds is in accordance with the infrared results,[5] which also predicted that the $[PdCl_4]^{2-}$ square plane was neither parallel nor perpendicular to the *b* axis and that the N−C−C−N plane was not perpendicular to *b*. During the optical examination [5] a contact twinning on (110) (with the present axes) was observed. From Fig. 1 the twinning can be explained predominantly as a $\approx 90°$ rotation of only the $[enH_2]^{2+}$ ions around *c* followed by *very small* adjustments in the Cl parameters. From Fig. 1 it seems quite reasonable that the barrier to the *c*-rotation of $[enH_2]^{2+}$ ions is small and this is also reflected in the shape of the carbon thermal ellipsoids. The marked cleavage [5] along the form (010) is understandable noting that the shortest N−H···Cl contact connects ions along *b*.

1. Ashida, T. and Hirokawa, S. *Bull. Chem. Soc. Jpn. 36* (1963) 704; Koo, C. H., Kim, M. I. and Yoo, C. S. *J. Korean Chem. Soc. 7* (1963) 293.
2. Søtofte, I. *Acta Chem. Scand. A 30* (1976) 309.
3. Dunand, A. and Gerdil, R. *Acta Crystallogr. B 31* (1975) 370.
4. Sakurai, K. *J. Phys. Soc. Jpn. 16* (1961) 1205.
5. Berg, R. W. *Spectrochim. Acta A 32* (1976). *In press.*
6. Stewart, J. M., Kundell, F. A. and Baldwin, J. C. *The X-Ray System, Version 1972*, Chemistry Department, Univ. of Maryland, U.S.A.
7. Johnson, C. K. *ORTEP*, Report ORNL-3794, Oak Ridge National Laboratory, Oak Ridge 1965.
8. Cromer, D. T. and Mann, J. B. *Acta Crystallogr. A 24* (1968) 321.
9. Bell, J. D., Hall, D. and Waters, T. N. *Acta Crystallogr. 21* (1966) 440.
10. Mais, R. H. B., Owston, P. G. and Wood, A. M. *Acta Crystallogr. B 28* (1972) 393.
11. Larsen, F. K. and Berg, R. W. *In preparation.*
12. Hamilton, W. C. and Ibers, J. A. *Hydrogen Bonding in Solids*, Benjamin, New York 1968, p. 184.
13. Pimentel, G. C. and McClellan, A. L. *The Hydrogen Bond*, Freeman & Co., London 1960, p. 290.

Received September 23, 1976.